25th

SLOPE STABILITY

AND LANDSLIDES

Using Effective Engineering and Geological Approaches

to

Identify and Analyze Unstable Slopes

February 20-22, 2002
Los Angeles, California

University of Wisconsin-Madison
Department of Engineering Professional Development
Professor C. Allen Wortley
Course Director

TABLE OF CONTENTS

25th

SLOPE STABILITY AND LANDSLIDES

February 20-22, 2002

TAB	ITEMS
1.	Biographical Sketches, Course Roster, Question/ Problem Form
2.	Tuncer B. Edil Presentations
3.	Elizabeth L. Mathieson and Philip J. Shaller Presentations
4.	Peter J. Bosscher Presentations and Soil Bioengineering for Upland Slope Protection and Erosion Reduction Manual
5.	Alan Kropp Presentation
6.	P. Erik Mikkelsen Presentation
7.	Jonathan Stewart Presentation
8.	Roger P. Heyman Presentation
9.	Horst J. Schor Presentation
10.	Patrick J. Fox Presentation
11.	Introductory Notes - Geotechnical Engineering (C. Allen Wortley)
12.	An Engineering Manual for Slope Stability Studies (J.M. Duncan et al.)
13.	Stabilization of Evolving Slopes (Tuncer B. Edil)
14.	Excerpts from TRB Special Report 247
15.	Miscellaneous
	Note Paper

Please use this Table of Contents as an organizational guide for course materials, including some which will be handed out to you during the course. Not all materials in the course notebook will be presented; however the lecturers will be glad to discuss them with you. Thank you.

TAB 1

Biographical Sketches

Course Roster

Question/Problem Form

PETER J. BOSSCHER

Professor
Civil & Environmental Engineering
University of Wisconsin-Madison

Peter Bosscher received one B.S. degree from Calvin College in Grand Rapids, Michigan and the other from the University of Michigan. He also received his M.S. and Ph.D. degrees in Civil Engineering from the University of Michigan. The topic of his dissertation was "Soil Arching in Sandy Slopes".

He joined the faculty at the University of Wisconsin-Madison in 1980. He teaches in the Geotechnical Engineering Division of the Civil & Environmental Engineering Department. His current research interests are in the areas of cold regions geotechnical engineering, soil dynamics, subsurface exploration, and foundations.

He is a member of the American Society of Civil Engineers, the American Society for Engineering Education, and the Tau Beta Pi Engineering Honor Society.

He enjoys climbing vertical heavily overconsolidated slopes (rock climbing) for a hobby and generally finds the slope much more stable than the person climbing it.

TUNCER B. EDIL

Professor
Civil and Environmental Engineering
University of Wisconsin-Madison
Madison, Wisconsin

Tuncer Edil received his Bachelor's and Master's of Science in Civil Engineering from Robert College in Istanbul, Turkey. He received a Doctor of Philosophy in Civil Engineering from Northwestern University in Evanston, Illinois. He is a licensed Professional Engineer in Wisconsin.

He joined the University of Wisconsin-Madison in 1973 where he teaches in the Department of Civil and Environmental Engineering. His current research interests are in the areas of engineering properties and behavior of soils, mechanics of coastal slumping and erosion (stability of coastal bluffs), pile foundations, compression of peat, and waste disposal and containment.

Prior to joining the University of Wisconsin, he was a lecturer at Northwestern University. He gained experience prior to this in public and private firms in Turkey, Finland, and Chicago. His present consulting activities include engineering properties of glacial soils, shoreline erosion and landslide control, preloading of peat deposits, safety of earth dams, foundation settlements, excavation slopes, retaining walls, and geotechnical aspects of waste disposal and containment.

Tuncer Edil is a member of the American Society of Civil Engineers, the American Society for Testing and Materials, the International Society of Soil Mechanics and Foundation Engineering. He is past Chairman and current Director at large of the Geotechnical Engineering Committee of the ASCE Wisconsin Section. He is past editor of the Journal of Geotechnical Engineering and Chairman of the Publications Committee, a past member of the Embankment, Dams and Slopes Committee, and a current member of the Environmental Geotechnics Committee, all of the national ASCE Geotechnical Engineering Division. He was a member of the Wisconsin State Planning Office Shore Erosion Advisory Group and serves on the Wisconsin Groundwater Research Advisory Council. He is Chairman of ASTM Subcommittee on Peats and Organic Soils.

His papers and publications primarily have been in the field of geotechnical engineering with particular emphasis on soil properties and behavior, coastal slope stability, peat settlement and environmental geotechnics.

He held an American Field Service International Scholarship as an exchange student in high school and spent part of his time in Coronado, California. He held a Fulbright Scholarship between 1963 and 1967 and a NATO doctoral fellowship between 1969 and 1973. In 1972 he received the Student Award of the Year from the ASTM, in 1977 the Young Civil Engineer of the Year Award and in 1988, Merit Award for Individual Achievement as an Engineering Educator, from the ASCE-Wisconsin Section, in 1989, The Journal of Cold Regions Engineering Award for the Best Paper Published in 1988 from the ASCE, in 1980 Dow Outstanding Young Faculty Award in North Midwest Section from the American Society of Engineering Education, in 1972 Outstanding Instructor Award from the UW Polygon Engineering Council, and in 1992 Standard Development Award from the ASTM. He is the current President of the U.S. Universities Council on Geotechnical Engineering Research.

PATRICK J. FOX

Associate Professor
Dept. of Civil and Environmental Engineering
University of California
Los Angeles, California

Dr. Patrick Fox earned a B.S. in geology from the University of Cincinnati, an M.S. in civil and environmental engineering from the University of Wisconsin-Madison and a Ph.D. in Civil and environmental engineering from the University of Wisconsin.

Dr. Fox is an associate professor of geotechnical engineering at UCLA. He teaches courses in advanced soil mechanics, foundation engineering, slope stability, retaining walls, advanced soil testing, groundwater, and environmental geotechnics. Research interests include: slope stability, environmental geotechnics, flow through porous media, geosynthetic clay liners, large strain consolidation, soft soils, soil properties and testing, reinforced soil, and discrete element modeling. He has conducted funded research by National Science Foundation, Air Force Office of Scientific Research, Indiana Department of Transportation, Indiana Cast Metals Association, Purdue Research Foundation, and the geosynthetic clay liner and MSE retaining wall industries.

Dr. Fox has extensive consulting experience in his areas of expertise, and has published numerous papers, and participated in numerous conferences, short courses and workshops. Book contributions include:
Geotechnics of High Water Content Materials (2000), Special Technical Publication 1374, T.B. Edil and P.J. Fox, editors, American Society for Testing and materials, 392p.
Fox, P.J. (1995). "Consolidation and settlement analysis," Chapter 18, *Civil Engineering Handbook*, W.F. Chen, ed., CRC Press, Boca Raton, 742-756.

Society memberships include:
American Society of Civil Engineers
- Member of technical subcommittee on Environmental Geotechnics.
- Manuscript reviewer for ASCE journals and conferences.

American Society for Testing and Materials
- Member of technical subcommittee D18.8, Behavior of Peats and Organic Soils.
- Member of technical subcommittee D35.04, Geosynthetic Clay Liners
- Manuscript reviewer for ASTM journals and conferences.

International Geosynthetics Society
- Member of Editorial Board, Geosynthetics International (1998 - present)

North American Geosynthetics Society
International Society for Soil Mechanics and Geotechnical Engineering
Phi Beta Kappa, Chi Epsilon, Sigma XI

Dr. Fox received the Arthur Casagrande Professional Development Award from American Society of Civil Engineers in 1998 and received a postdoctoral Fellowship from NSF and NATO in 1992.

Roger P. Heyman
Kane, Ballmer & Berkman
515 S. Figueroa Street, Suite 1850
Los Angeles, California
(213) 617-0480

Mr. Heyman is a graduate of the Harvard Law School with over 30 years experience in the prosecution and defense of complex civil litigation in the areas of construction, earth movement, insurance coverage, and real estate law. He has been a Reginald Heber Fellow, a Member of the Attorney General's Los Angeles Area Task Force and a Lecturer on Preventive Law at the UCLA Extension School of Business and Management.

REPRESENTATIVE EARTH MOVEMENT LITIGATION

- Represented developer in defense of $60 million in claims arising out of a landslide in the Hacienda Heights area of Los Angeles County involving 56 homes and a public higheway.
- Served on consolidated defense executive committee in connection with the $400 million Big Rock, California, landslide involving 273 multi-million dollar homes.
- Represented County of San Luis Obispo in litigation with its insurance carriers arising out of the construction and operation of the County's main landfill disposal facilities.
- Represented tract developer/general contractor in suit against the Metropolitan Water District in which relief obtained required MWD to invent, manufacture, and install devices along its major supply lines to cure vibration problems affecting between two and five 500+ unit tracts.

ALAN KROPP

Principal
Alan Kropp & Associates
Berkeley, California

Alan Kropp received the bachelor's degree in civil engineering from California State Polytechnic University, Pomona in 1971. He received a master's degree in geotechnical engineering from the University of California at Berkeley, in 1973.

Mr. Kropp worked for a number of geotechnical consultants in the Bay area after graduation until he formed his own company in Berkeley in 1978. Since that time he has provided geotechnical services to clients on nearly 4000 projects throughout California, along with special assignments in Puerto Rico, Canada, Turkey, and China. Projects have ranged from custom single family homes to high rise structures and industrial complexes. The work has included design recommendations and construction monitoring services for new construction, as well as analyses and remedial work recommendations for distress projects (including hillsides). Mr. Kropp is also a peer reviewer for many cities and counties throughout the greater Bay Area.

Mr. Kropp is a frequent lecturer at seminars, short courses, and extension programs on topics including slope stability, hydrocompression, seismic response, soil bioengineering, and forensic geotechnical engineering. He has also published 25 papers on these and other geotechnical topics. He is a member of numerous organizations including the American Society of Civil Engineers, Earthquake Engineering Research Institute, Seismological Society of America, International Conference of Building Officials, and American Society for Testing and Materials.

Exponent®
Failure Analysis Associates®

Elizabeth L. Mathieson, C.E.G.
Managing Scientist

Professional Profile

Elizabeth Mathieson is an engineering geologist in Exponent's Civil Engineering Practice based in Oakland, California. Ms. Mathieson specializes in landslides and debris flow investigations, fault investigations, sinkhole investigations, hazard mapping, and third party reviews for public agencies.

Prior to joining Exponent, Ms. Mathieson spent more than 17 years in engineering geologic consulting. Her most recent position was as Principal Geologist of D & M Consulting Engineers (formerly Terratech, Inc.). She serves as chairperson of the Enforcement Oversight Committee of the California Board for Geologists and Geophysicists and is past president of the California Council of Geoscience Organizations.

Credentials and Professional Honors

M.S., Engineering Geology, Stanford University, 1983
A.B., Geological Sciences (*magna cum laude*), Harvard University, 1978

Registered Geologist, California, #RG 4025; Certified Engineering Geologist, California, #CEG 1249; Engineering Geologist, Oregon, #E 1589; Registered Professional Geologist, Tennessee, #4576; Instrument-rated private pilot

California Board for Geologists and Geophysicists (Chairman, Enforcement Oversight Committee); California Council of Geoscience Organizations (Past President); Association of Engineering Geologists (Past Director); National Association of Geology Teachers-U.S. Geological Survey Distinguished Student Field Program (1978); Geological Society of America Research Grant with Outstanding Honors (1982)

Association of Engineering Geologists (member); Association for Women Geoscientists (member); Geological Society of America (member); Groundwater Resources Association of California (member); International Conference of Building Officials (member)

Selected Relevant Experience

Evaluated causes of landslides and storm damage including bridge collapses and culvert failures.

Evaluated reported sinkhole-related damage to a large condominium complex in Tennessee. Coordinated work of Exponent staff, geophysical subsconsultant, and construction cost estimator, and served as liaison with local geotechnical consultant.

Evaluated causes of sinkholes that formed above newly constructed storm drain on State highway project in California's Central Valley. Investigation included extensive review of contractor's and inspector's daily logs prepared during construction.

Evaluated claim of earthquake damage to a water main in a highrise building.

Performed down-hole logging of large-diameter drill holes in landslides and beneath distressed houses to examine soil and bedrock for evidence of landsliding, to determine depths and physical characteristics of slide planes, and to collect samples of slide-plane material for laboratory testing and subsequent stability analysis. During construction of foundation underpinning, examined sidewalls of pier holes to determine whether embedment was adequate.

Investigated stability of a large landslide beneath a proposed rocket-fuel mixing facility. Work included literature research, air-photo interpretation, geologic field mapping, and logging and sampling of continuous-core drill holes.

Evaluated causes of earthquake-induced ground failures at government facilities and private residences.

Performed numerous investigations, including: distressed houses, hillside ranch roads, landslide and debris-flow causation, diversion of drainage, over-excavation in quarries, archaeological sites, billing disputes, and a fatal car crash. Work included review of available geologic and engineering information, air photo interpretation, geologic mapping, crawl-space inspections, observation during remedial construction, document review, and presentation of findings.

Prepared geologic and ground movement potential maps for the City of Saratoga, California, and geotechnical hazards maps for the City of Milpitas, California.

Supervised fault-rupture hazard investigations, including logging of exploratory trenches to investigate fault locations and activity. Projects ranged from school sites on faults in Alquist-Priolo Earthquake Fault Zones to single-family houses adjacent to newly mapped faults.

Performed development-feasibility mapping of large ranches proposed for residential development. Prepared geologic maps and cross sections; evaluated fault, landslide, debris flow, and liquefaction hazards; and constructed development feasibility maps. Served as liaison between clients and agency planning departments.

Presentations and Published Abstracts

"Geologists Slowly Regaining Ground in Building Code," Annual Meeting, Association of Engineering Geologists, St. Louis, Missouri, October 4, 2001.

"Earthquake Awareness," presentation to security staff of worldwide corporation at San Francisco headquarters, June 22, 2001.

Testimony on selected proposed changes to 2000, 2001, and 2002 International Building Code on behalf of California Council of Geoscience Organizations, International Code Council Structural Committee Hearings, Costa Mesa, CA, March 19 and 20, 1999; St. Louis, MO, September 15, 1999; Birmingham, AL, April 14 and 15, 2000, and Portland, OR, March 26, 2001.

"Geological Aspects of Slope Stability," in "Slope Stability and Landslides" short course, University of Wisconsin – Madison Department of Engineering Professional Development, University of California Los Angeles, February 21-23, 2001 (with Philip J. Shaller).

"Water, Water Everywhere...and Mostly it Causes Trouble: The Role of Water in Ground Failures," Continuing Legal Education Short Courses, Office of the County Counsel, San Mateo County, California, December 1999; Office of the City Attorney, City and County of San Francisco, May 2000; Office of the City Attorney, Oakland, California, November 2000 (with Exponent Civil Engineering Practice staff).

"Silicon Valley Groundwater Cleanup," MC for Outstanding Environmental and Engineering Geologic Project Award Presentation and Opening Session, Annual Meeting, Association of Engineering Geologists, San Jose, California, September 22, 2000.

"Melange and Minerals – Characterizing Economic Calera Limestone Blocks in the Franciscan Complex," Annual Meeting, Association of Engineering Geologists, San Jose, California, September 22, 2000.

"Impact of Governmental Action on the Engineering Profession and Industry," Panel discussion, Northern California Section, American Institute of Chemical Engineers, Oakland, CA, March 23, 1999.

"Milestones, Mentors, Anecdotes, and Advice," Presentation to San Francisco Bay Area Chapter, Association for Women Geoscientists, April 16, 1998.

"Residential Strain Gauge on an Active Fault," Presentation to Great Basin Section, Association of Engineering Geologists, January 15, 1998.

"Residential Strain Gauge on an Active Fault," Annual Meeting, Association of Engineering Geologists, Portland, Oregon, October 3, 1997 (with J. Michael Cleary).

"Late Quaternary Activity of the Madison Range Fault Along its 1959 Rupture Trace, Madison County, Montana," Annual Meeting, Association of Engineering Geologists, San Diego, October 5, 1983.

"Activity of a Portion of the Madison Range Fault, Madison County, Montana," M.S. thesis, Stanford University, 1983.

"Post-Pinedale Displacement Rate on the Madison Range Fault Along its 1959 Rupture Trace, Madison County, Montana," Annual Meeting, Rocky Mountain and Cordilleran Sections Geological Society of America, Salt Lake City, May 3, 1983.

"Holocene Activity of the Madison Range Fault Along its 1959 Rupture Trace, Madison County, Montana," Presentation to San Francisco Section, Association of Engineering Geologists, Berkeley, California, March 1, 1983.

"Influence of Geologic Conditions on Building Foundation Engineering in Boston, Massachusetts," Senior honors thesis, Harvard University, 1978.

HORST J. SCHOR
BIOGRAPHY

Mr. Schor's professional career included eleven years with a major civil engineering/land planning firm followed by twelve years directing the development of two large scale hillside planned communities in Southern California.

Since 1991 he has been an independent consultant providing land related services to a variety of land developers, mining companies and public agencies. The latter includes the Department of Water and Power of the City of Los Angeles, the State of New Mexico Land Office, The Navajo Nation EPA, the State of Kentucky EPA Water Quality Division, The State of Virginia Division of Mines, Minerals and Energy and The United States Environmental Protection Agency.

In 1999 he was appointed by the United States Environmental Protection Agency and Office of Surface Mining to a six member panel of experts as a landform restoration specialist to develop improvements in the mining reclamation process regarding the mountain top removal/valley fill approach to coal mining in the Appalachian Mountains of West Virginia.

He holds degrees in Civil Engineering and Land Surveying as well as in Geography with a specialization in Urban Planning. He is also a member of the Urban Land Institute, The American Society of Civil Engineers and The International Erosion Control Association.

He is a guest lecturer at The University of Wisconsin College of Engineering, The University of California at Irvine and The University of Dresden in Germany.

H.J. SCHOR CONSULTING • 626 NORTH PIONEER DRIVE • ANAHEIM, CALIFORNIA 92805 • (714) 778-3767 • FAX: (714) 778-1656

Exponent
Failure Analysis Associates®

Philip J. Shaller, Ph.D., R.G., C.E.G.
Senior Scientist

Professional Profile

Dr. Philip Shaller is a member of the Geotechnical, Geological, and Geo-Environmental Group (Geo^3) of Exponent's Civil Engineering Practice and is based in the Irvine, California office. He has worked for 9 years as an engineering geology consultant and has experience in academic research and project management. His expertise includes geological and geotechnical site investigations, slope stability analysis, field mapping, analysis of aerial photographs and remote sensing images, sub-surface characterization, landslide and debris flow identification and mitigation, foundation construction and earthwork observation, rock mass characterization for tunneling, earthquake ground motions, coastal geomorphology, and karst geomorphology.

Dr. Shaller's specialty is in the field investigation and mechanics of large-scale landslides. He also holds bachelors and masters degrees in geochemistry, with a specialty in the chemistry of aqueous- and vapor-phase sulfur.

Credentials and Professional Honors

Ph.D., Geology, California Institute of Technology, 1991
M.S., Geochemistry, Montana College of Mineral Science and Technology, 1985
A.B., Geochemistry, Occidental College, 1983

Registered Geologist, California, #6132; Certified Engineering Geologist, California, #1912

Robert P. Sharp Graduate Teaching Award, California Institute of Technology, Division of Geological and Planetary Sciences, 1990

Geological Society of America (member); South Coast Geological Society (member)

Relevant Experience

Directed an investigation of a potentially life-threatening landslide complex at Lukes Farm, Matahina Reservoir, New Zealand, and a reconnaissance slope stability hazard investigation along the Pacific Coast Highway from Santa Monica to Malibu, California.

Assisted in the development of an emergency response and remediation of a landslide threatening a residential development in Diamond Bar, California, and performed an emergency evaluation and geotechnical investigation of a landslide at the Getty Villa museum complex in Pacific Palisades, California.

Performed a variety of geotechnical site investigation activities, including logging bucket auger borings for a proposed dam near Graybull, Wyoming; mapping stream scour above a heated oil pipeline in Santa Barbara, California; directing a CPT investigation of a bridge crossing of the San Gabriel River in Pico Rivera, California; and investigating and developing cross sections for the proposed expansion of a flood control channel in San Clemente, California. The latter included observing the installation of two slope inclinometers in large fill slopes along the banks of the channel.

Served as a project geologist during construction of The Getty Center museum complex in Brentwood, California, and is the geologist of record for the site's funicular tramway. Developed cross sections, performed computer-aided slope stability evaluations, and logged a combined total of more than 100 test pits, bucket auger borings, drilled pier shafts, drilled slope drains, mass grading cuts, and spread footing excavations at the museum site.

Directed the engineering geologic investigation for a 115-mile railway alignment on the Tongue River, Montana.

Performed construction observation tasks, including the documentation of an approximately 1,000-foot long retaining wall footing in Chino Hills, California, and observed the over-excavation for a water pump plant in San Diego, California. Performed geologic mapping in mass grading cuts at a landslide overexcavation in Diamond Bar, California.

Performed investigations of landslide-related problems for home sites in Malibu, California, and an apartment complex in El Sereno, California.

Investigated vibration issues at a condominium complex in Anaheim, California, and construction defects case for a condominium complex in Lemon Grove, California.

Performed geotechnical and seismic investigations for city agencies. These projects include the revision of seismic safety elements for the City of Monterey Park, California, and the City of West Hollywood, California, as well as the reconstruction of an elementary school in Glendale, California, and the development of a sports park for the City of Chino Hills, California. The latter project included the construction of three groundwater monitoring wells in an area of historically high groundwater.

Served as an instructor at Ranch Santiago Community College in Santa Ana, California, and as a teaching assistant at the California Institute of Technology in Pasadena, California.

Publications

"Review of Proposed Mechanisms of Sturzstroms (Long-Runout Landslides)," *Sturzstroms and Detachment Faults, Anza-Borrego State Park, California*, P.L. Abbot and D.C. Seymour (eds.), South Coast Geological Society, Annual Field Trip Guidebook No. 24, pp. 185–202, October 1996 (with A. Shaller).

"Landslides on Mars," *Landslide News*, No. 8, pp. 18–21, 1994 (with G. Komatsu).

"Analysis of a Large Moist Landslide, Lost River Range, Idaho, U.S.A.," *Canadian Geotechnical Journal*, Vol. 28, pp. 584–600, 1991.

Presentations and Published Abstracts

"Age and Failure Style of a Large Landslide Complex at Matahina Reservoir, New Zealand," Presentation, 40th Annual Meeting of Association of Engineering Geologists, Portland, OR, October 1997, and *Geological Society of America, Abstracts with Programs*, Vol. 29, p. 64, May 1997 (with M. McSaveney, M. Gillon, R. Beetham, and T. Freeman).

"Reinterpretation of Wave-Cut Marine Terraces West of Castellammare Mesa, Pacific Palisades, California," *Geological Society of America, Abstracts with Programs*, Vol. 29, p. 19, May 1997 (with C. Heron).

"Review of Proposed Mechanisms of Sturzstroms (Long-Runout Landslides)," Presentation, 24th Annual South Coast Geological Society Field Trip, October 1996.

"Folds, Faults and Fills: The Geology and Geotechnical Engineering of The Getty Center, Brentwood, California" Presentation, Monthly Meeting of Association of Engineering Geologists, Southern California Section, Los Angeles, CA, June 1996 (with L. Rapp).

"Mechanics of Long-Runout Landslides," Presentation, Monthly Meeting of Association of Engineering Geologists, Southern California Section, Los Angeles, CA, February 1996.

"The Runaway Mountain," Appearance, television documentary program *Horizon*, British Broadcasting Corporation, 1996.

"Last Motion on the Benedict Canyon Fault, Santa Monica Mountains, California," *Geological Society of America, Abstracts with Programs*, Vol. 26, p. 185, October 1994 (with E. Sabins).

"3rd Caltech/U.S.S.R. Schmidt Institute of Earth Physics Conference on Long-Runout Landslides," *Landslide News*, No. 5, pp. 37–38, 1991 (with B. Murray and B. Ivanov).

"Long-Runout Landslides on Mars," Presentation, U.S.S.R. Academy of Sciences, O. Yu. Schmidt Institute of Earth Physics, Moscow, October 1990.

"A Large Composite Landslide/Debris Flow, Lost River Range, Idaho," *Geological Society of America, Abstracts with Programs*, Vol. 21, p. 344, October 1989 (with B. Murray, A. Albee, and J. Shelton).

"Subaqueous landslides on Mars?," Proceedings 20th Lunar and Planetary Science Conference, pp. 990–991, October 1988 (with B. Murray and A. Albee).

Ex

C. ALLEN WORTLEY

Professor (Emeritus)
University of Wisconsin-Madison
Engineering Professional Development Department
Madison, Wisconsin

Allen Wortley received the usual protracted engineering education and after exhaustive study of esoteric subjects of no practical value, received a degree from Caltech.

He is a licensed professional engineer and land surveyor, but ever since he learned from Webster's that the initials P.E. are an abbreviation for physical education, probable error, printer's error, price-earnings ratio, pulmonary embolism, Protestant Episcopal, and lastly, professional engineer, he often does not use them after his name. For similar reasons he doesn't often use L.S., as it stands for U.S. Navy landing ship or place of the seal (locus sigilla). However, he uses C. before his name as most people understand it is an abbreviation for a first name, Charles, rather than capacitance, carat, Centigrade, cent, century, chapter, circa, city, college, copyright, cycle or hundredweight.

He left California and moved east to begin working for a living. As a consulting engineer he inspected old sewer manholes in Pittsburgh. This assignment proved to be very deep but by no means dry.

Later he moved up, north to Wisconsin, where he began to climb the technical professional ladder working on zero-bouyancy floating boat docks, French garbage grinders, and lawn watering systems for penitentiaries. He outraced scientific obsolescence by achieving appointment as chief engineer of his consulting firm.

Then, instead of working for a living, he became a university professor. He pursued the Peter Principle earning a Professional Development degree; and becoming associate dean for engineering outreach and now emeritus professor.

He teaches soil mechanics and foundation engineering and has unearthed the fact that although many people think soil is simply dirt, geotechnical engineers have found it is really bread and butter.

His research has been beautification of water tanks in combination with restaurants, discotheques, and hockey rinks; and ice engineering where he has found that lake water is very cold in the winter, and in fact freezes at all temperatures below thirty-two degrees Fahrenheit.

The most notable accomplishment of Allen Wortley, holder of twenty-two certificates of appreciation and of-the-year awards, is receipt of two Who's Who without purchase of their limited edition directories.

Professor Wortley boasts the usual affiliations that carry arcane Greek letter and acronym designations in return for the payment of annual dues, as well as membership in societies that present awards and offer cheap life insurance.

His hobby is bimonthly golf outings on rainy days, and although not a scratch golfer, he has been scratched while mastering nearly all the Madison areas nineteenth holes.

When not teaching, researching, studying or golfing, he either cuts grass, measures first downs, shovels snow or conducts professional development programs. As program director his main task is to keep speakers on schedule and avoid running over into social hours.

Department of Engineering Professional Development

The College of Engineering
University of Wisconsin-Madison

432 North Lake Street
Madison, WI 53706-1498
Phone: 608-262-2061
FAX: 608-263-3160

QUESTIONS AND PROBLEMS FOR COURSE DISCUSSION

Our speakers and short course leaders want to help you solve specific problems and questions you have about slope stability and landslides. Please complete this form and turn it in to Prof. Wortley as soon as possible. We will appreciate your printing or carefully scripting your responses. Thank you.

PROBLEM STATEMENT (Please describe the situation and problem you wish to solve.)

_____
_____
_____
_____
_____
_____

I think this problem could best be addressed by _____

PROBLEM STATEMENT (Please describe the situation and problem you wish to solve.)

_____
_____
_____
_____
_____
_____

I think this problem could best be addressed by _____

OTHER COMMENTS (whatever . . . perhaps list variations on your problem statement, principles you wish clarified, past approaches that worked or didn't work, etc.

_____
_____
_____
_____
_____

NAME AND AFFILIATION (optional)

_____
_____

TAB 2

Tuncer B. Edil

Presentations

INTRODUCTION TO LANDSLIDES

TUNCER B. EDIL
UNIVERSITY OF WISCONSIN-MADISON

LANDSLIDE

The movement of a mass of rock,debris or earth down a slope.

- Landslides: Investigation and Mitigation, TRB Special Report 247, 1996
- International Decade of Natural Disaster Reduction (1990-2000)
- Recent Developments: personal computers, geosynthetics, improved field investigations and understanding of processes (GIS, instrumentation, research)

SOCIOECONOMIC SIGNIFICANCE OF LANDSLIDES

- Landslides are a significant element of multiple-hazard disasters
- Worldwide landslide activity is increasing due to:
  - Increased urbanization and development
  - Continued deforestation
  - Increased regional precipitation caused by changing climate pattern

ECONOMIC LOSSES

- **Direct** (repair, replacement, maintenance) *versus* **Indirect** (loss of productivity, real estate values, tax revenues, injury, death, trauma, etc.)
- **Public** *versus* **Private**

ECONOMIC LOSSES

- Most severely affected nation: Japan (total losses $4 billion annually)
- USA, Italy and India: total losses $1 to $2 bilion annually
- Losses in smaller geographic areas

Losses in Smaller Geographic Areas

- California
  - Portuguese Bend Landslide (1956-59): $45 million
  - Bluebird Canyon Landslide (1978): $30 million
  - Big Rock Mesa Landslide (1983): $630 million in lawsuits
  - San Francisco Bay Area (1968-69): $90 million
    (1982): >$90 million ($404 million in lawsuits

POTENTIAL FOR LANDSLIDING

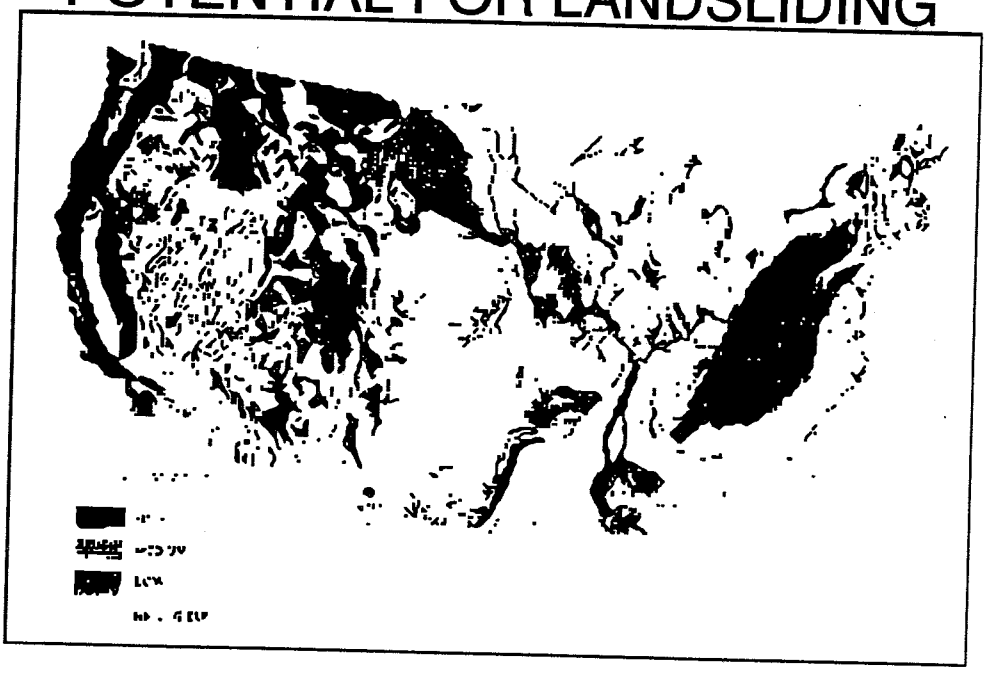

AVERAGE ANNUAL COST OF HIGHWAY LANDSLIDE REPAIRS

(IN THOUSANDS OF DOLLARS)

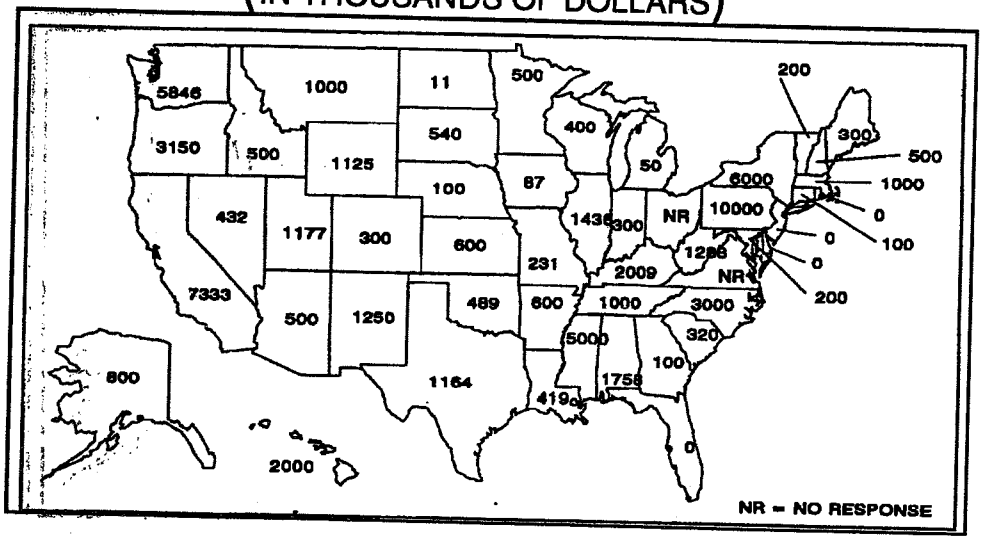

LANDSLIDE CASUALTIES

- Worldwide: 600 people a year (1971-74 data)
- Tens of thousands in individual disasters in the 20th century
- In U.S.A. : 25 to 50 deaths a year
- In Canada: 5 deaths a year

LANDSLIDE TYPES

- Classification (Varnes, 1958 and Hutchinson, 1968)
- UNESCO Working Party: *Multilingual Landslide Glossary*

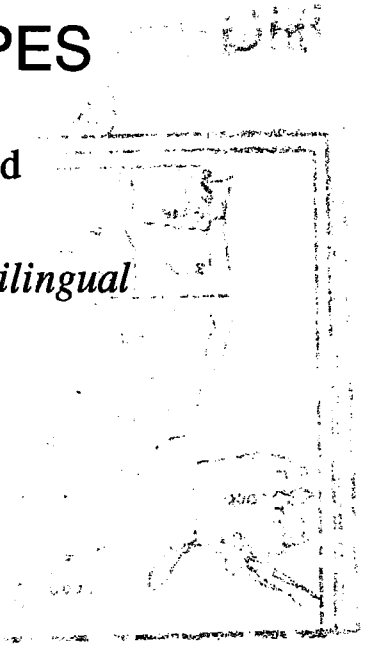

FORMING NAMES

- Type of Material
  - Rock
  - Debri
  - Earth
- Type of Movement
  - Fall
  - Topple
  - Slide
  - Spread
  - Flow

GLOSSARY FOR FORMING NAMES

- **Activity**
  - State (Active, Inactive, etc.)
  - Distribution (Advancing, Retrogressive, etc.)
  - Style (Complex, Multiple, Successive, etc.)
- Description of First Movement
  - Rate (Rapid, Slow, etc.)
  - Water Content (Dry, Wet, etc.)
  - Material (Rock, Soil, i.e. earth or debri)
  - Type (Fall, Topple, Slide, Spread, Flow)

Table 3-2
Glossary for Forming Names of Landslides

ACTIVITY			
STATE	DISTRIBUTION	STYLE	
Active	Advancing	Complex	
Reactivated	Retrogressive	Composite	
Suspended	Widening	Multiple	
Inactive	Enlarging	Successive	
Dormant	Confined	Single	
Abandoned	Diminishing		
Stabilized	Moving		
Relict			
DESCRIPTION OF FIRST MOVEMENT			
RATE	WATER CONTENT	MATERIAL	TYPE
Extremely rapid	Dry	Rock	Fall
Very rapid	Moist	Soil	Topple
Rapid	Wet	Earth	Slide
Moderate	Very wet	Debris	Spread
Slow			Flow
Very slow			
Extremely slow			
DESCRIPTION OF SECOND MOVEMENT			
RATE	WATER CONTENT	MATERIAL	TYPE
Extremely rapid	Dry	Rock	Fall
Very rapid	Moist	Soil	Topple
Rapid	Wet	Earth	Slide
Moderate	Very wet	Debris	Spread
Slow			Flow
Very slow			
Extremely slow			

NOTE: Subsequent movements may be described by repeating the above descriptors as many times as necessary.

Table 3-2
Glossary for Forming Names of Landslides

ACTIVITY		
STATE	DISTRIBUTION	STYLE
Active	Advancing	Complex
Reactivated	Retrogressive	Composite
Suspended	Widening	Multiple
Inactive	Enlarging	Successive
Dormant	Confined	Single
Abandoned	Diminishing	
Stabilized	Moving	
Relict		

DESCRIPTION OF FIRST MOVEMENT			
RATE	WATER CONTENT	MATERIAL	TYPE
Extremely rapid	Dry	Rock	Fall
Very rapid	Moist	Soil	Topple
Rapid	Wet	Earth	Slide
Moderate	Very wet	Debris	Spread
Slow			Flow
Very slow			
Extremely slow			

DESCRIPTION OF SECOND MOVEMENT			
RATE	WATER CONTENT	MATERIAL	TYPE
Extremely rapid	Dry	Rock	Fall
Very rapid	Moist	Soil	Topple
Rapid	Wet	Earth	Slide
Moderate	Very wet	Debris	Spread
Slow			Flow
Very slow			
Extremely slow			

NOTE: Subsequent movements may be described by repeating the above descriptors as many times as necessary.

TYPES OF SLOPE MOVEMENT

(a) Fall

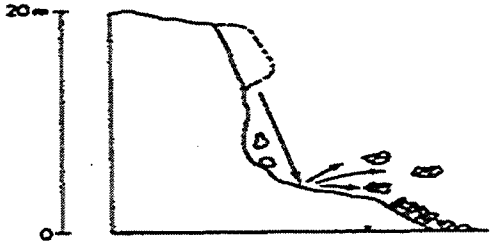

(b) Topple

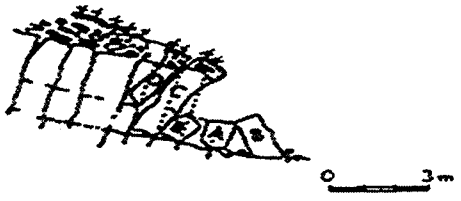

TYPES OF SLOPE MOVEMENTS

(c)

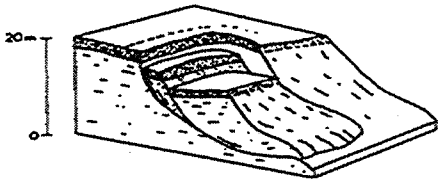

Slide

(d)

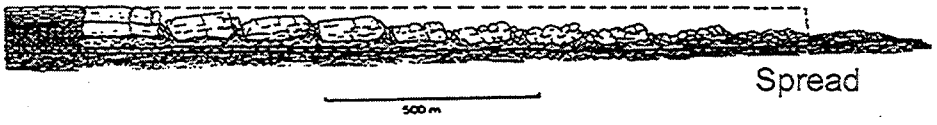

Spread

(e)

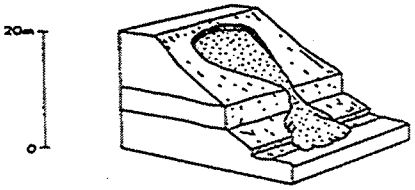

Flow

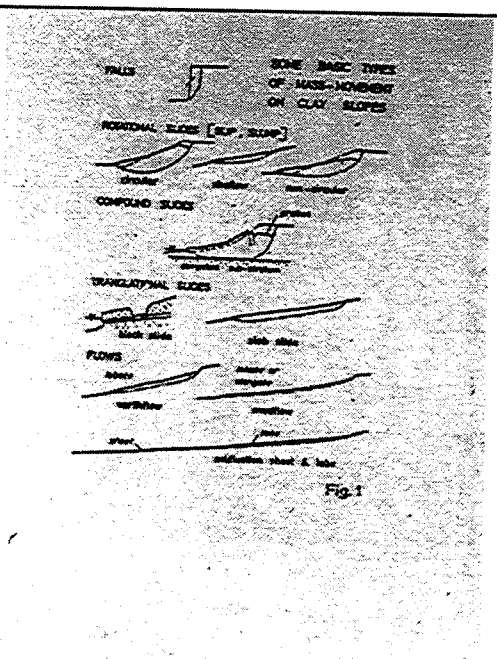

igure Mass Movements in Clay Slopes
(After Skempton and Hutchinson, 1969)

FALL (rock fall)

FALL—Mass travels most of the distance in free fall, by leaps and bounds, and rolling of bedrock or soil fragments.

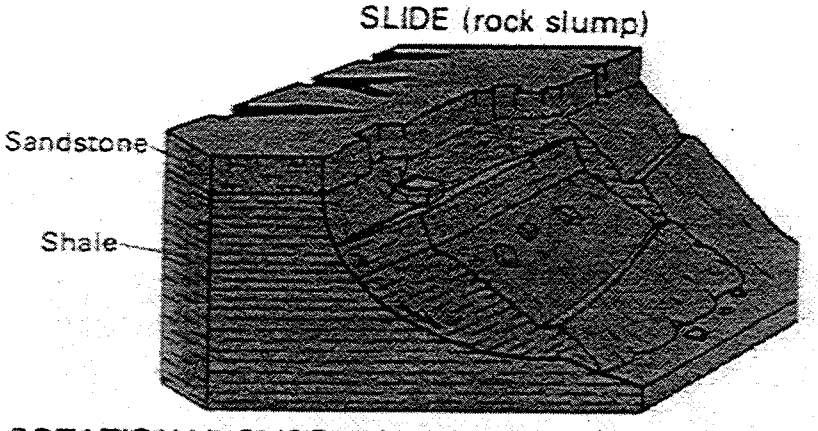

ROTATIONAL SLIDE—Movement involves turning about a point (surface of rupture is concave upward).

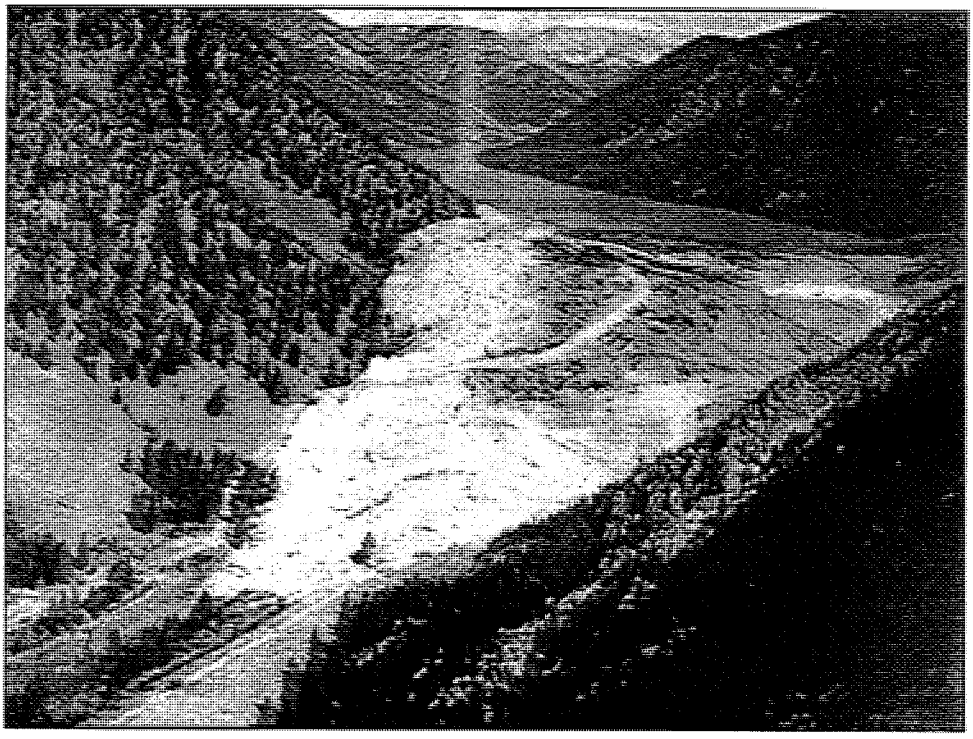

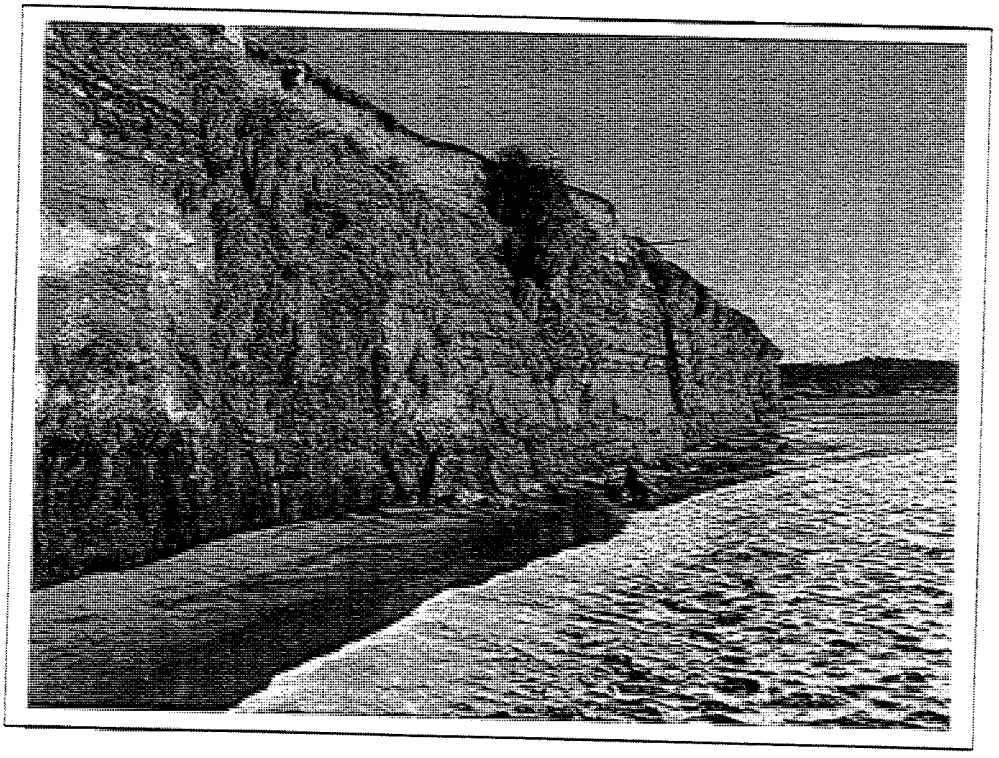

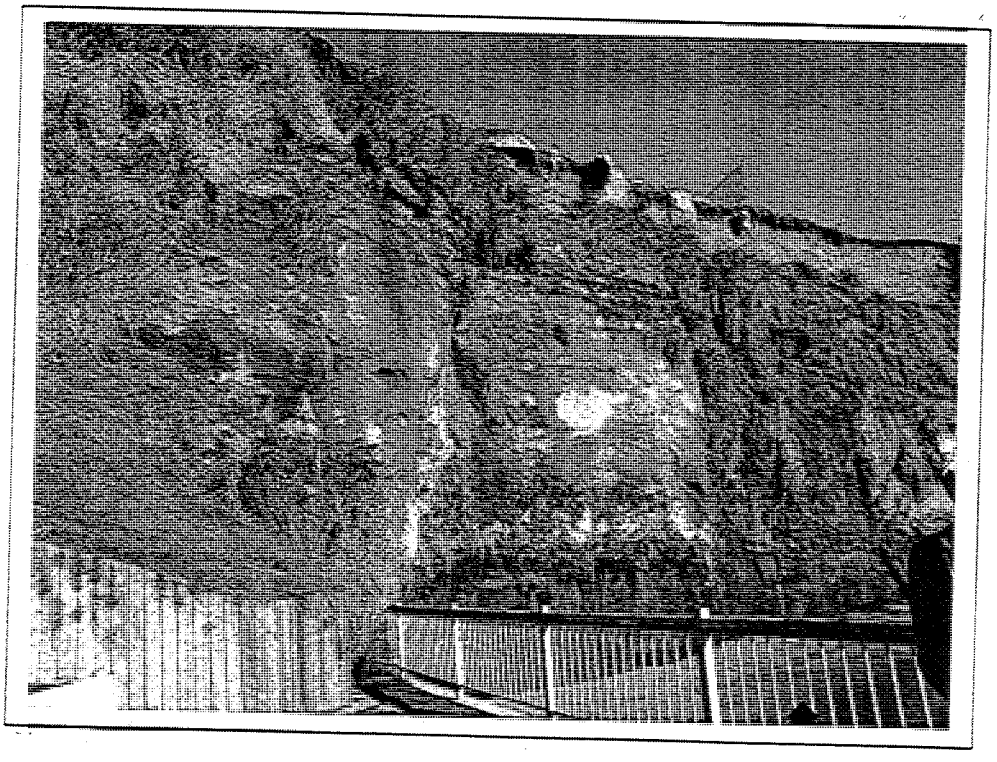

Grand Canyon AZ

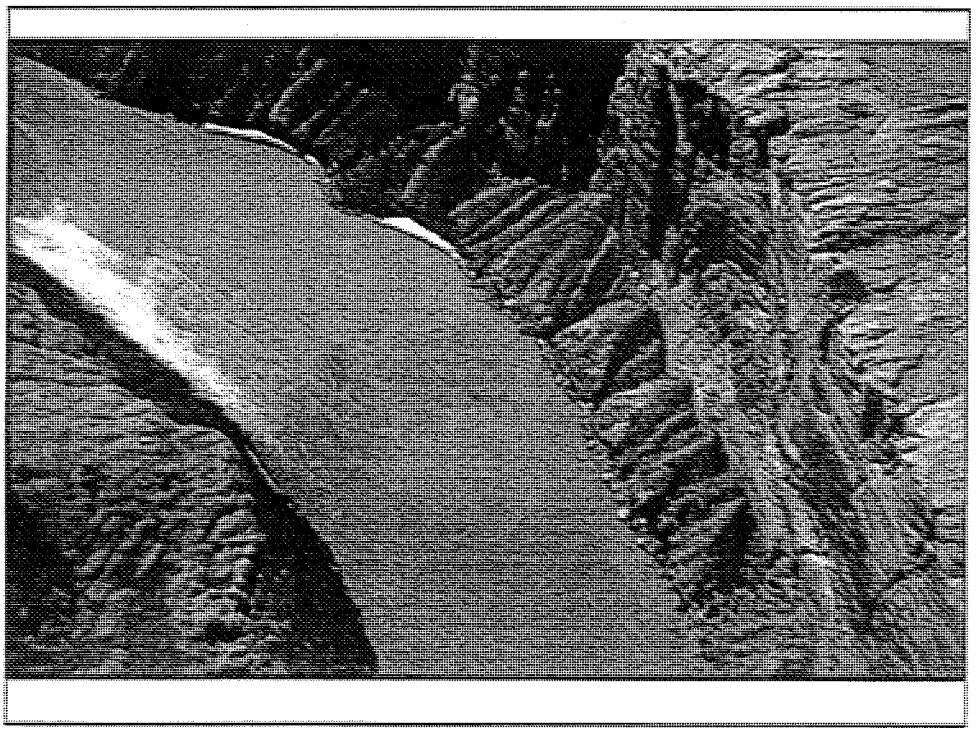

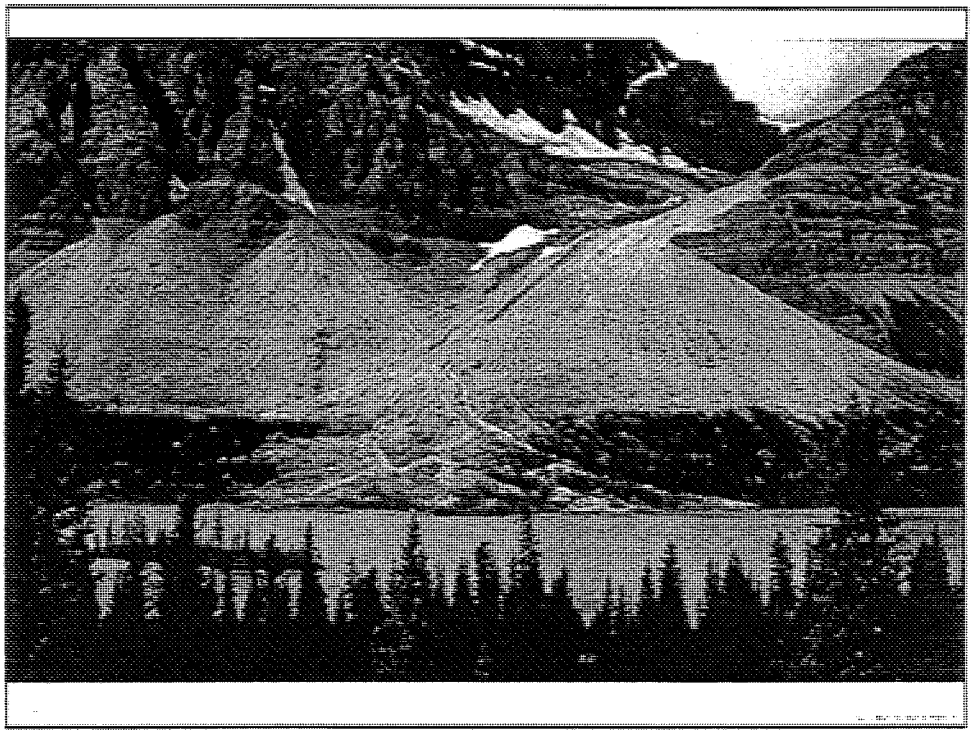

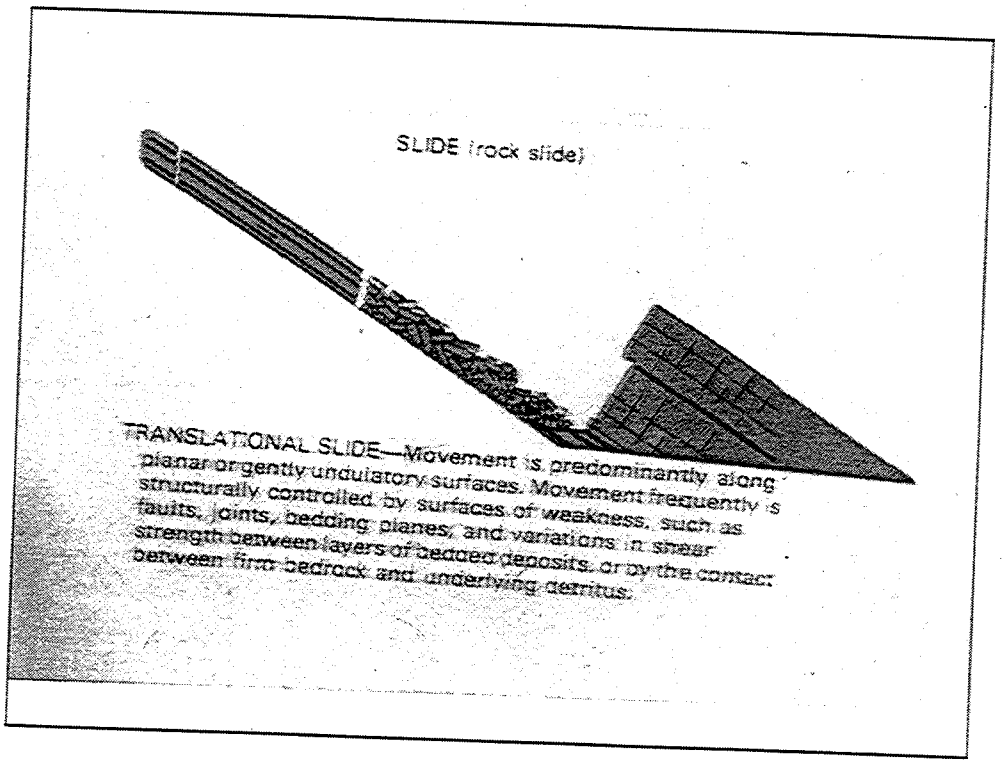
SLIDE (rock slide)
TRANSLATIONAL SLIDE—Movement is predominantly along planar or gently undulatory surfaces. Movement frequently is structurally controlled by surfaces of weakness, such as faults, joints, bedding planes, and variations in shear strength between layers of bedded deposits, or by the contact between firm bedrock and underlying detritus.

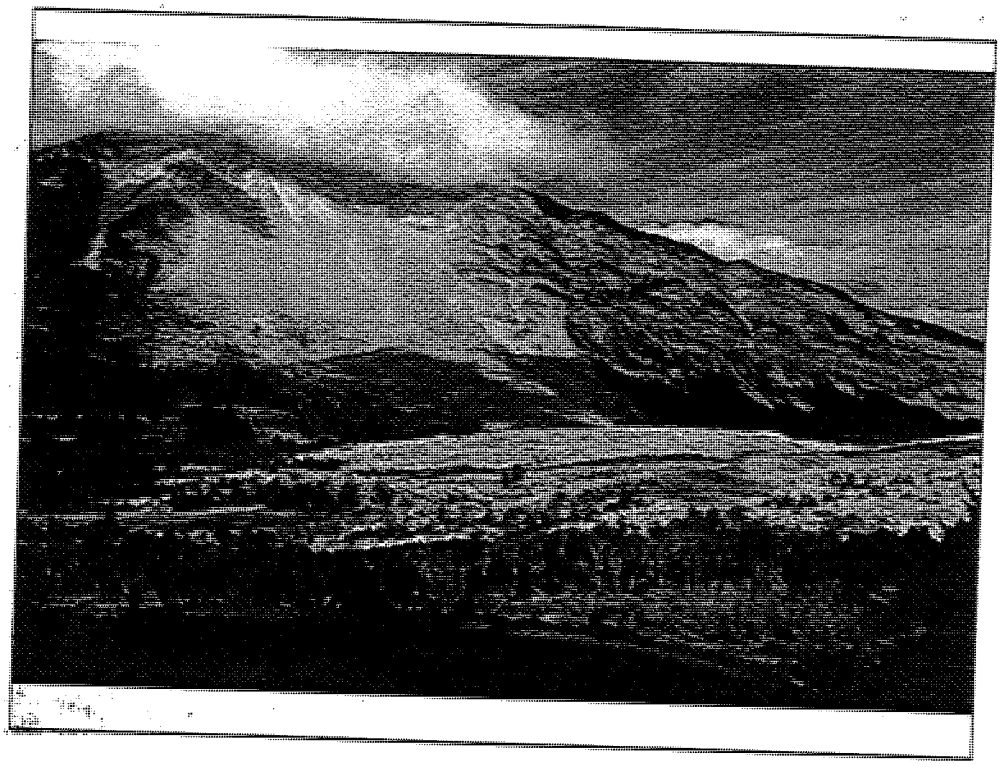

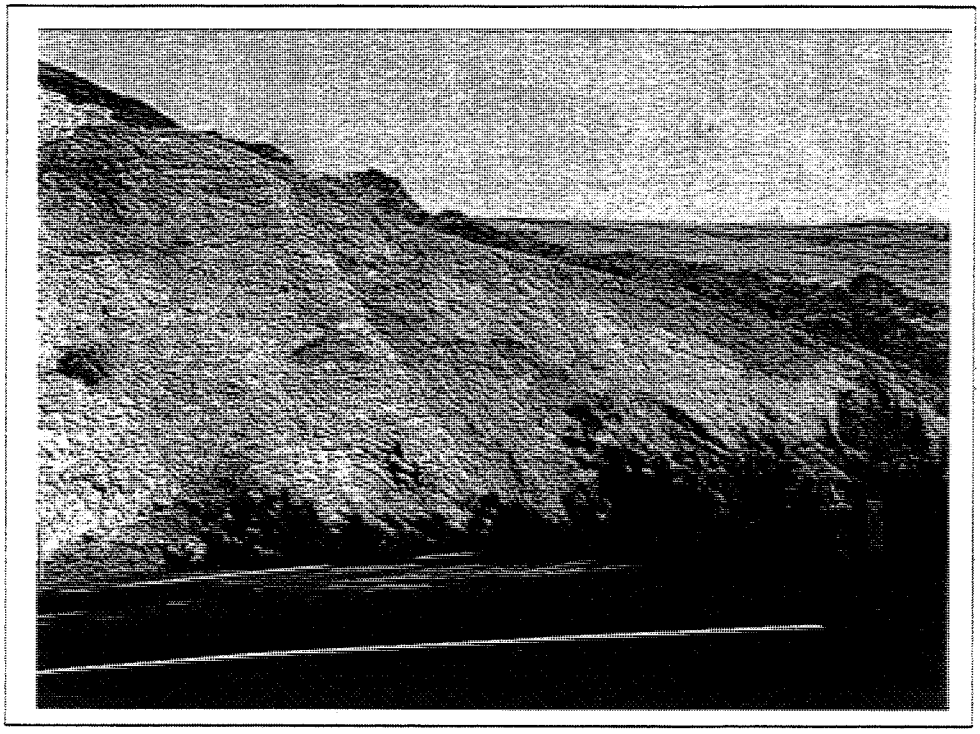

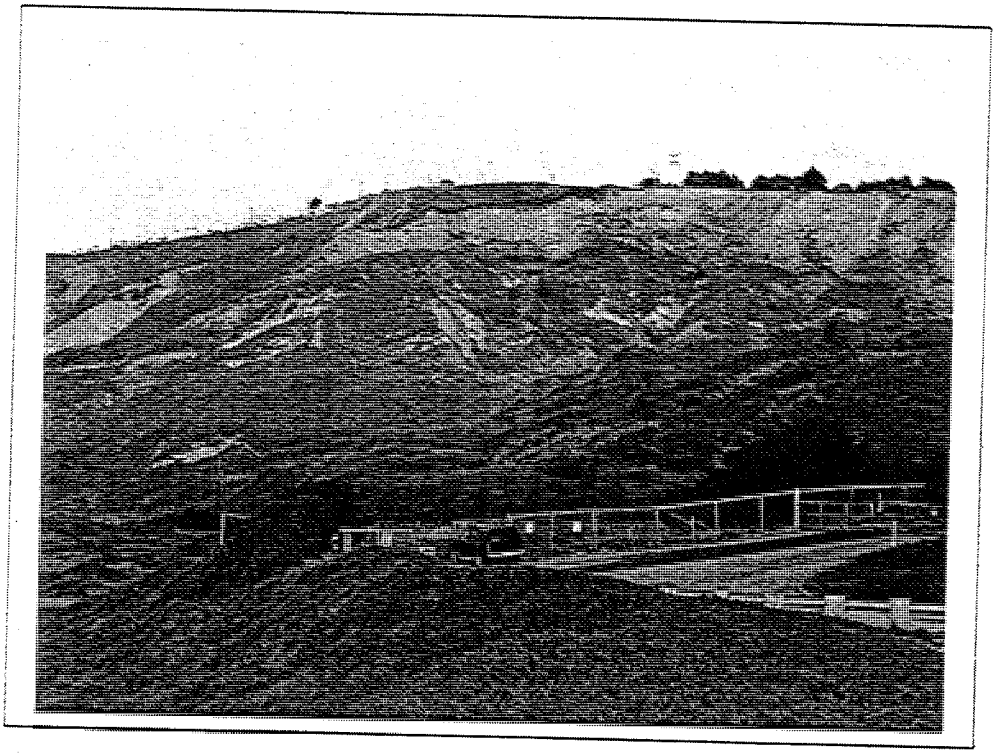

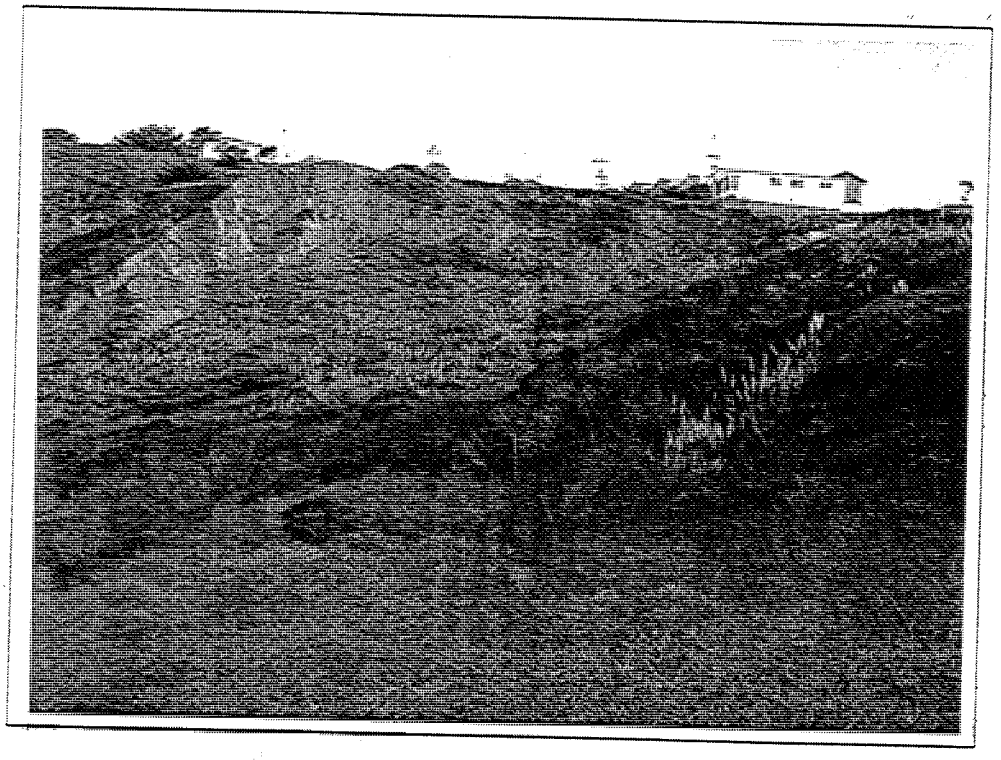

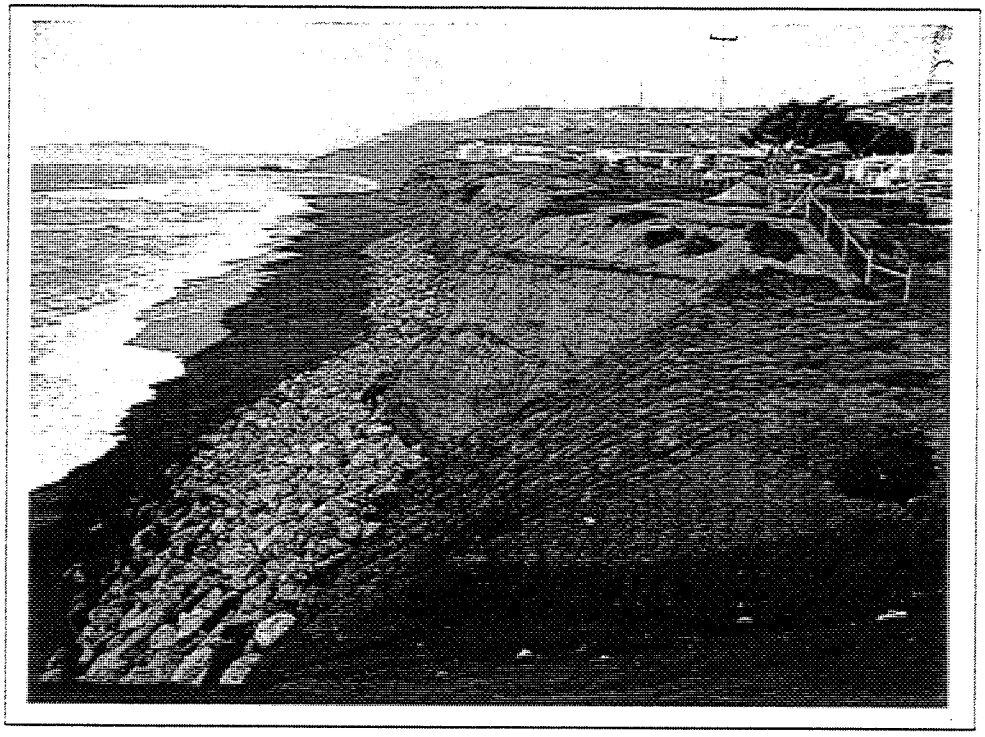

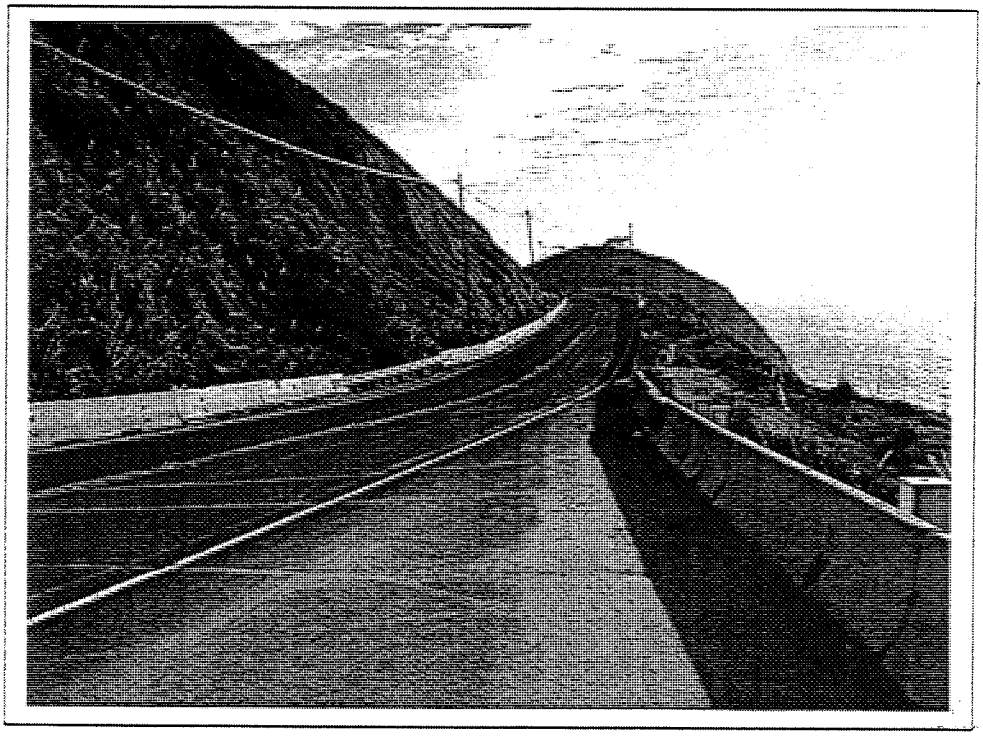

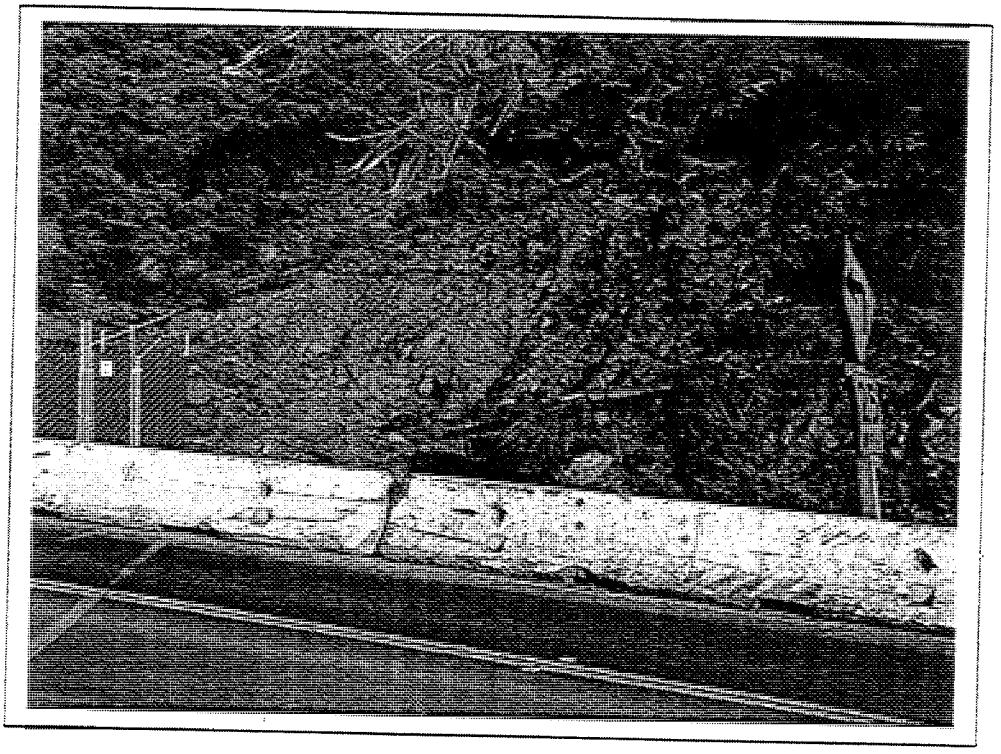

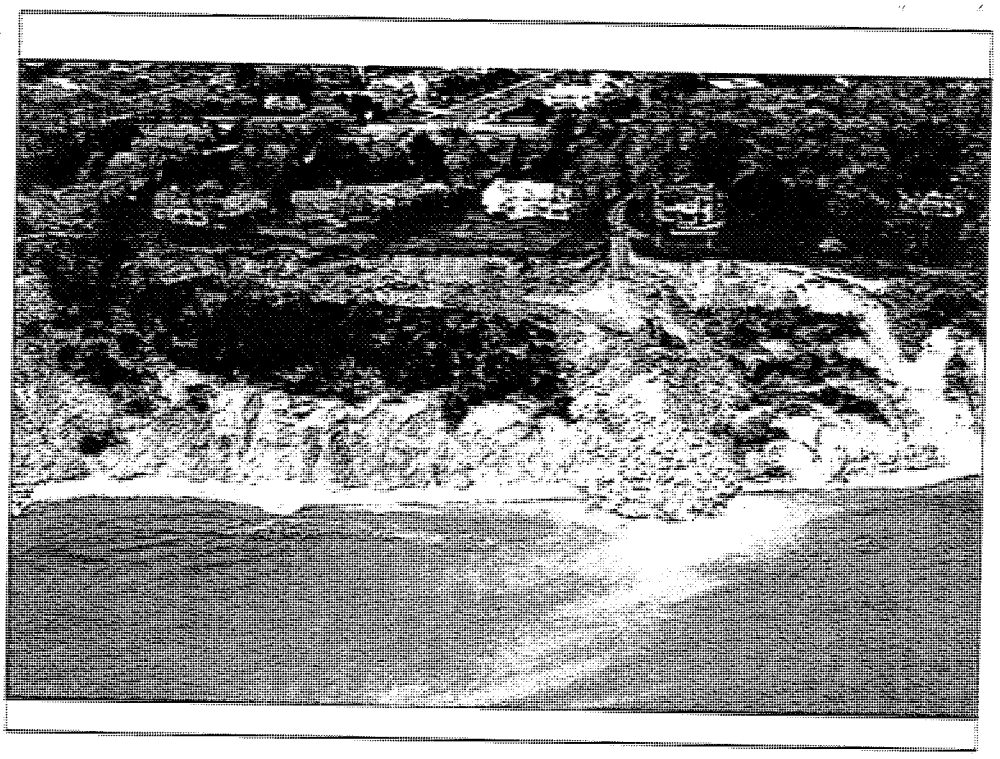

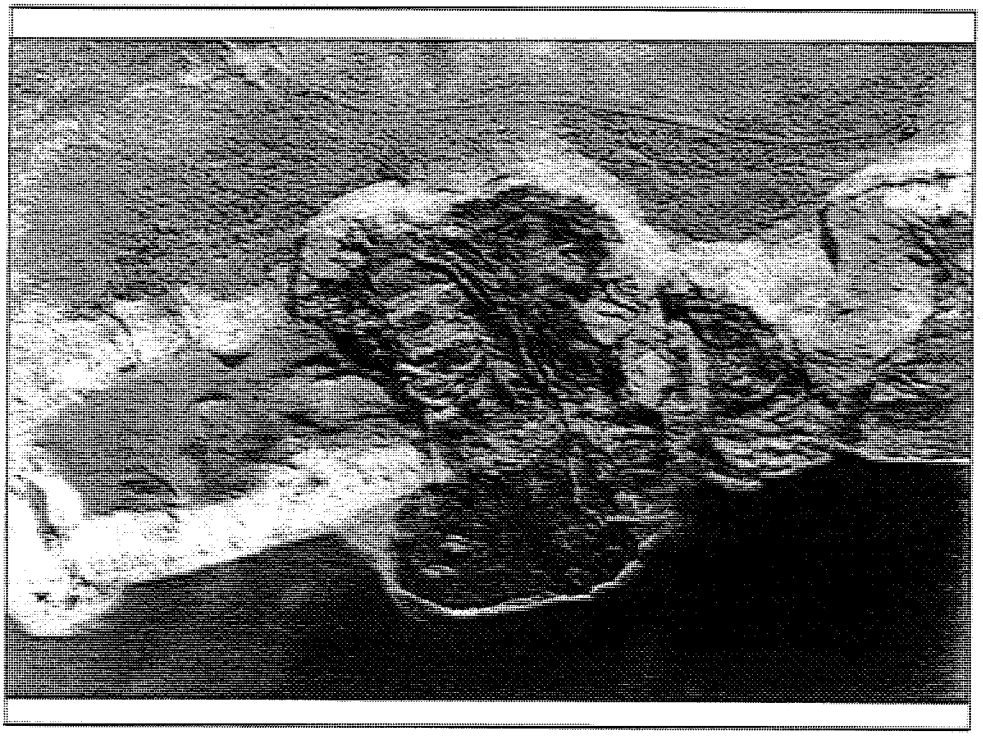

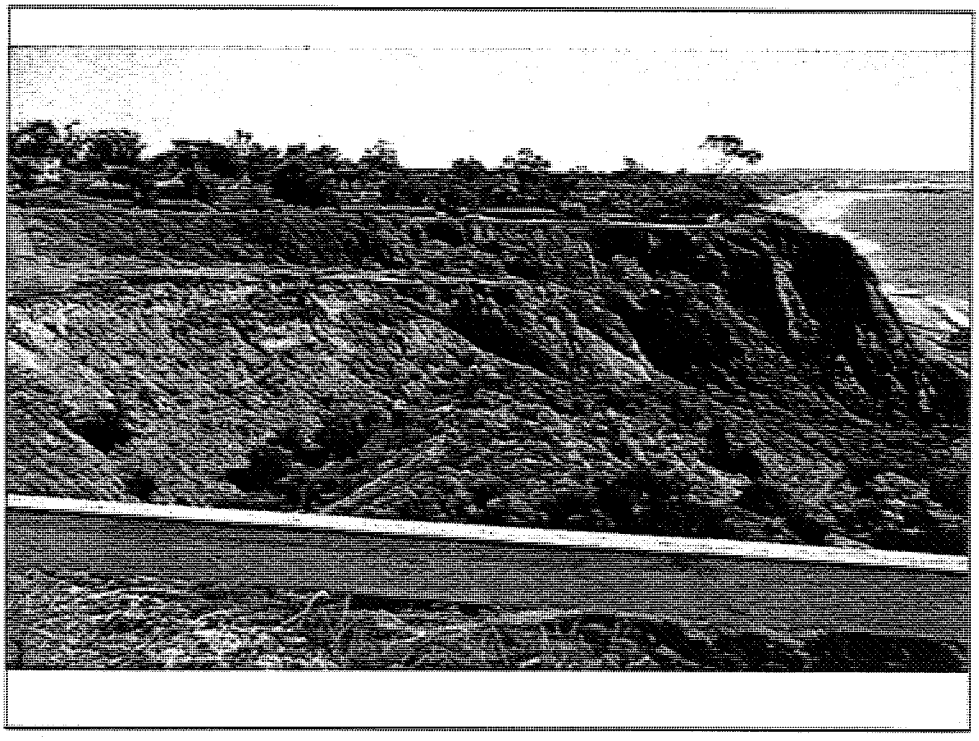

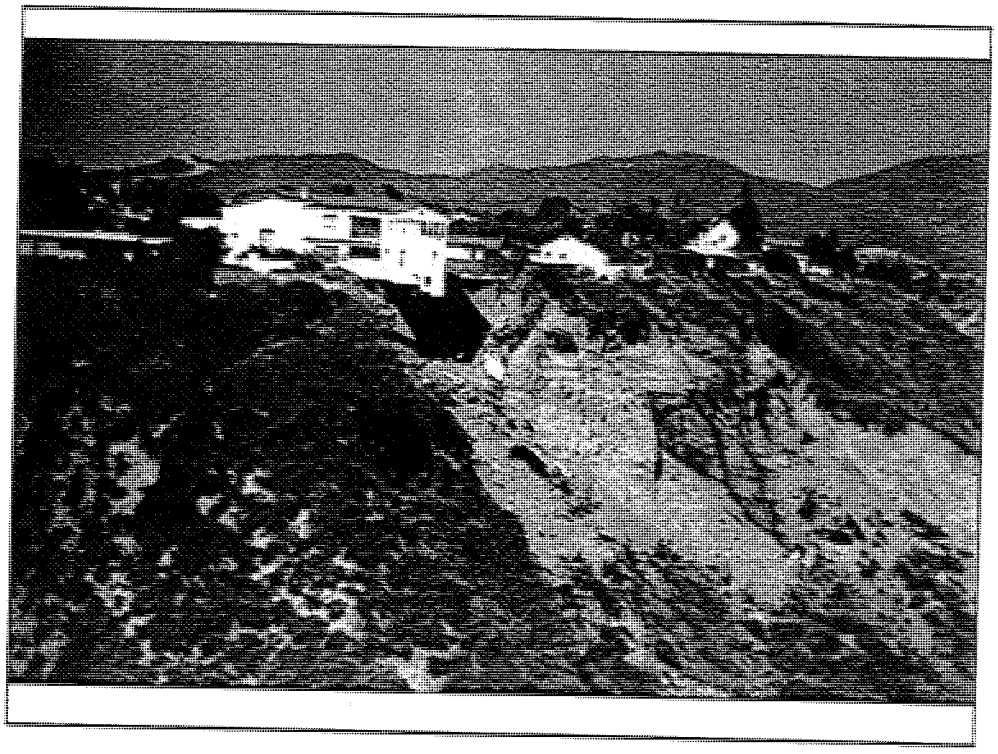

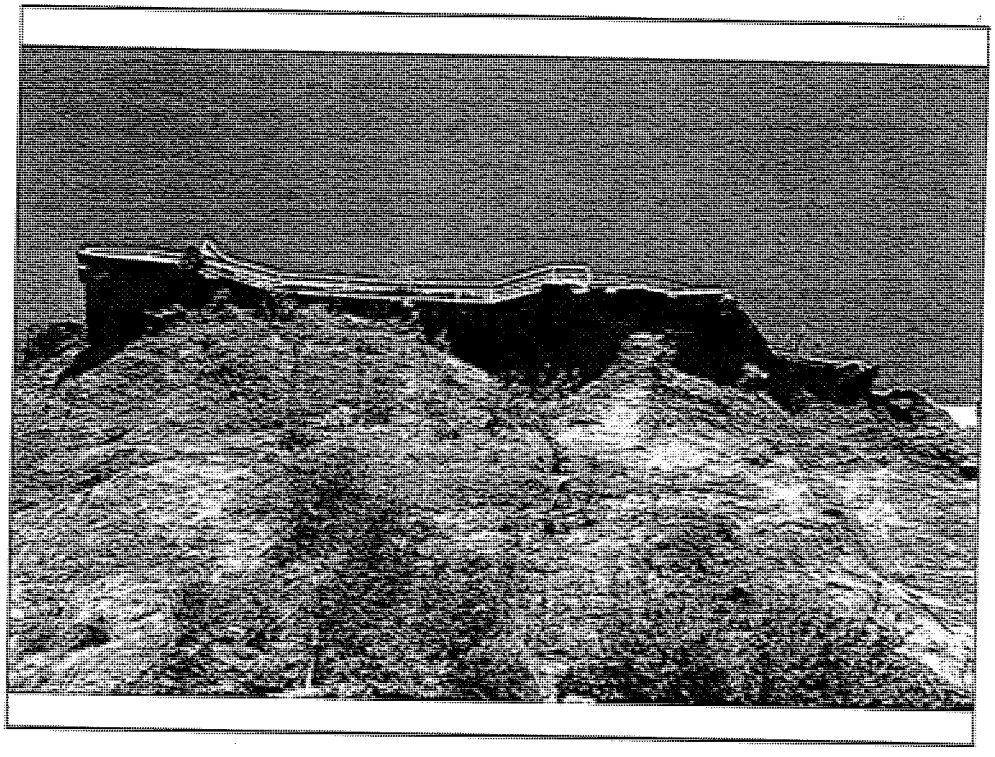

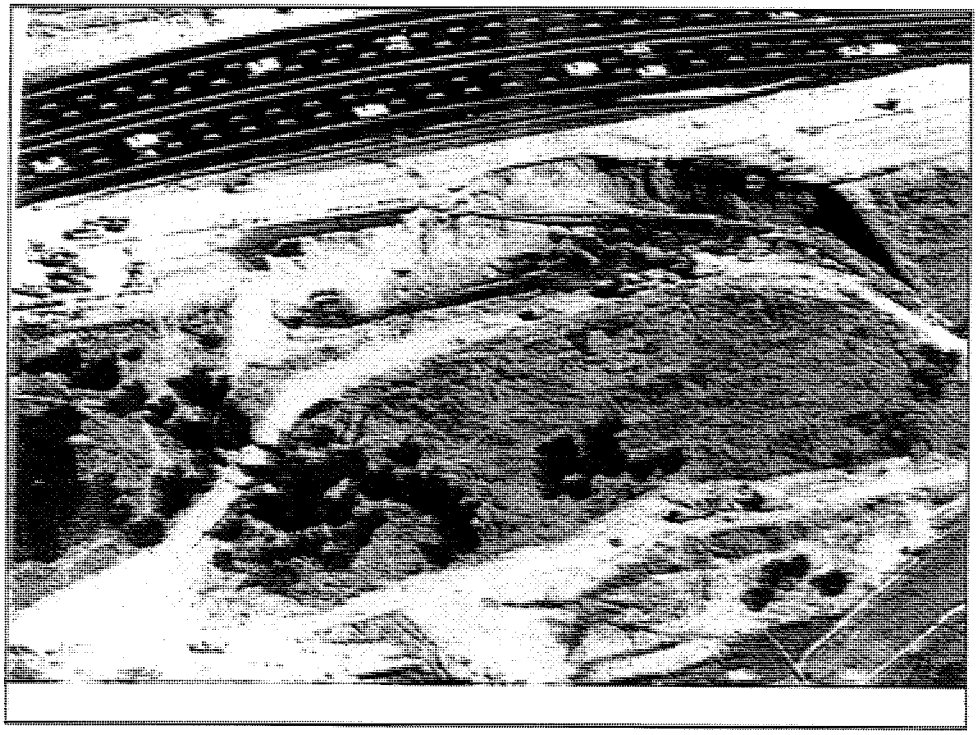

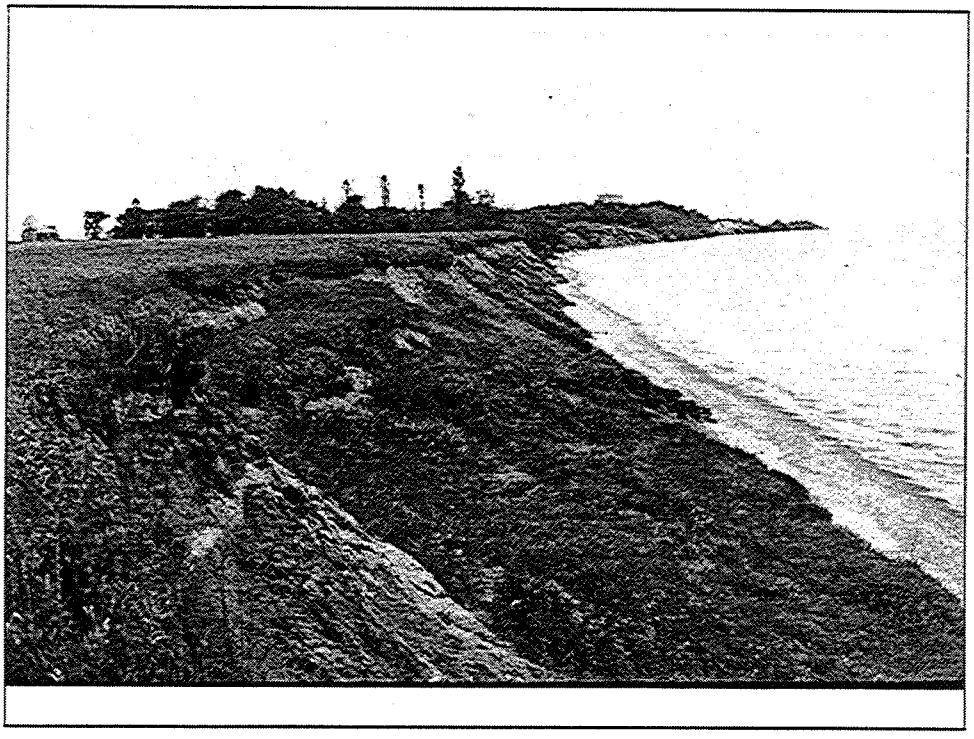

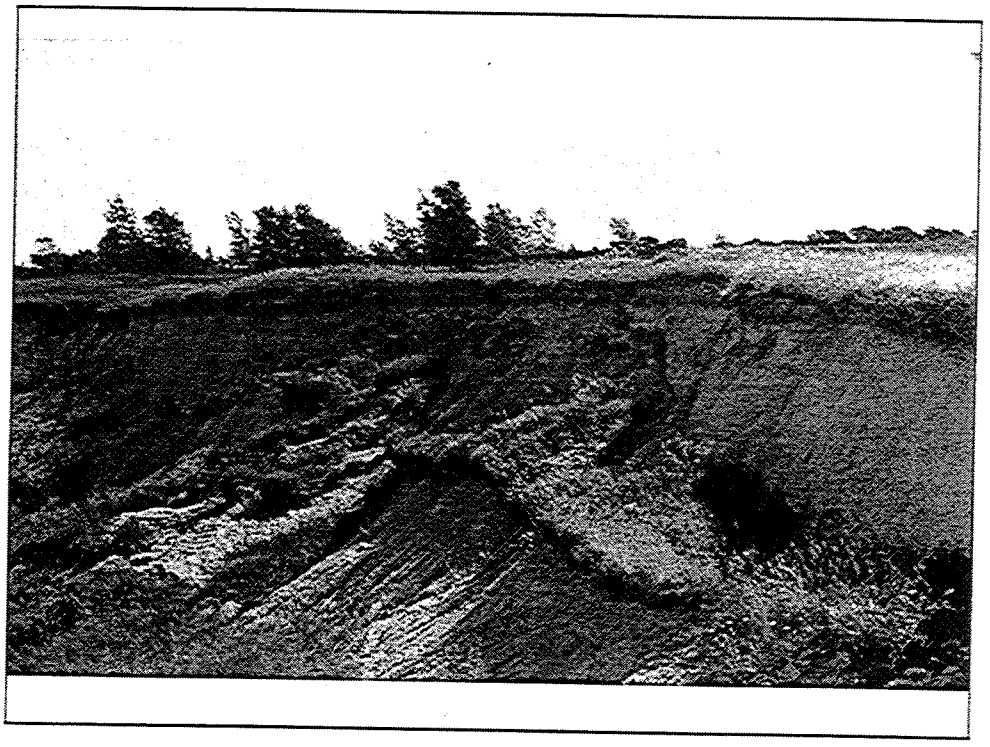

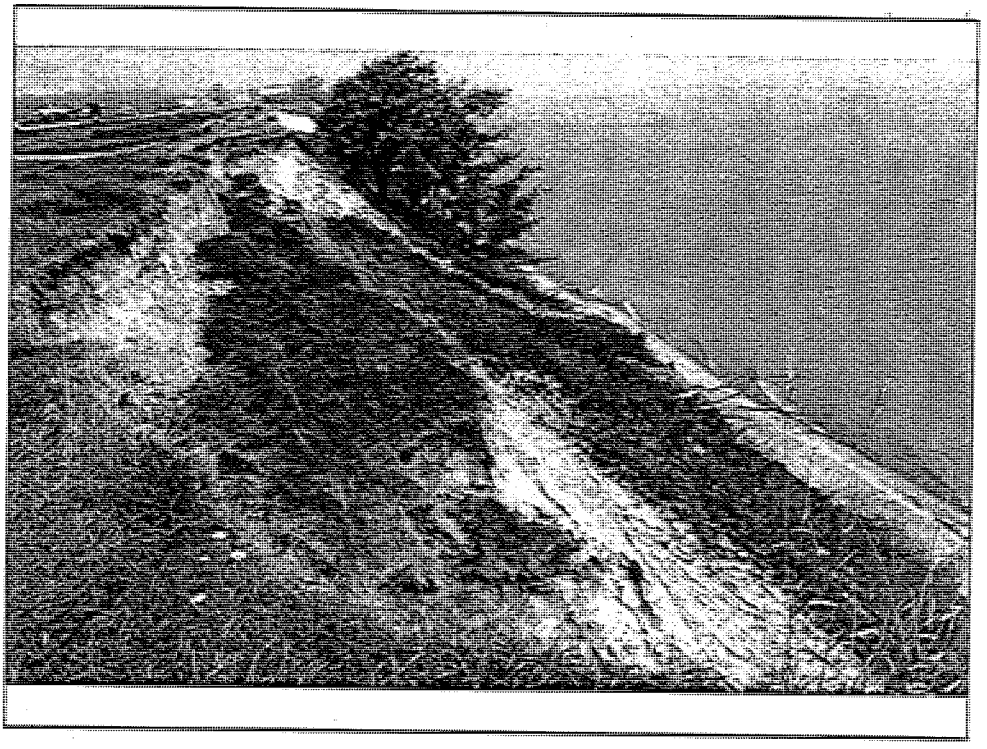

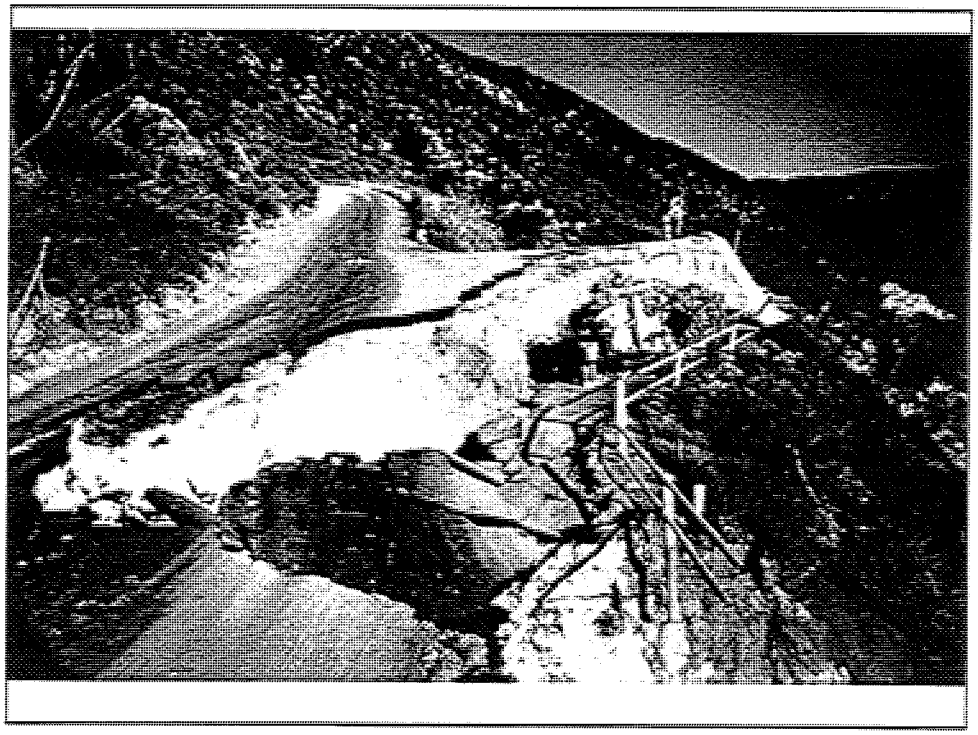

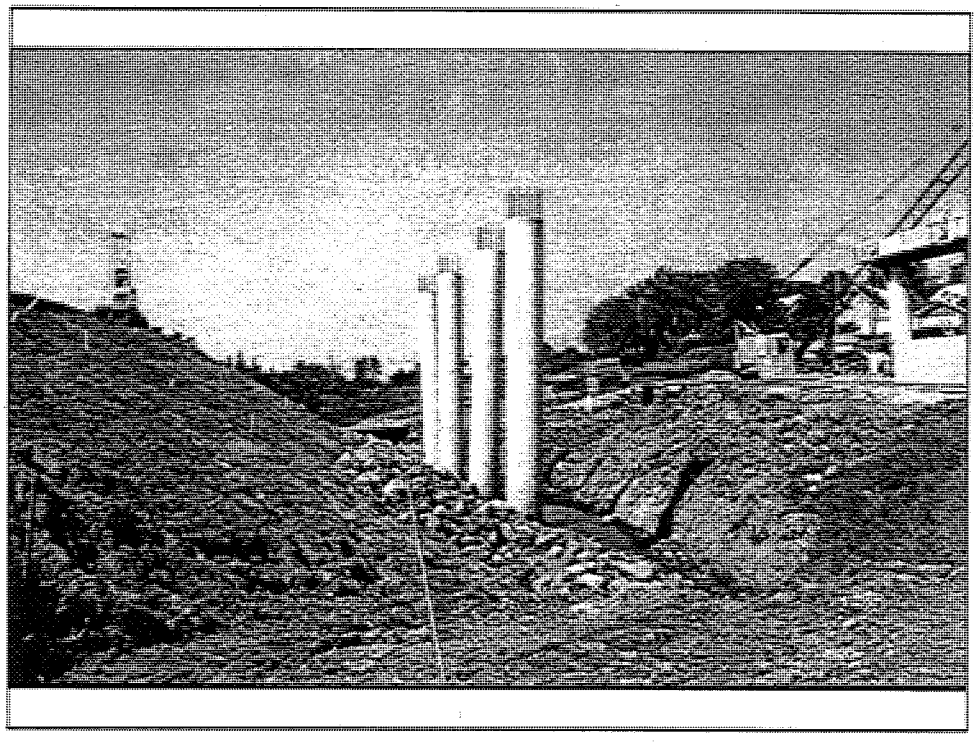

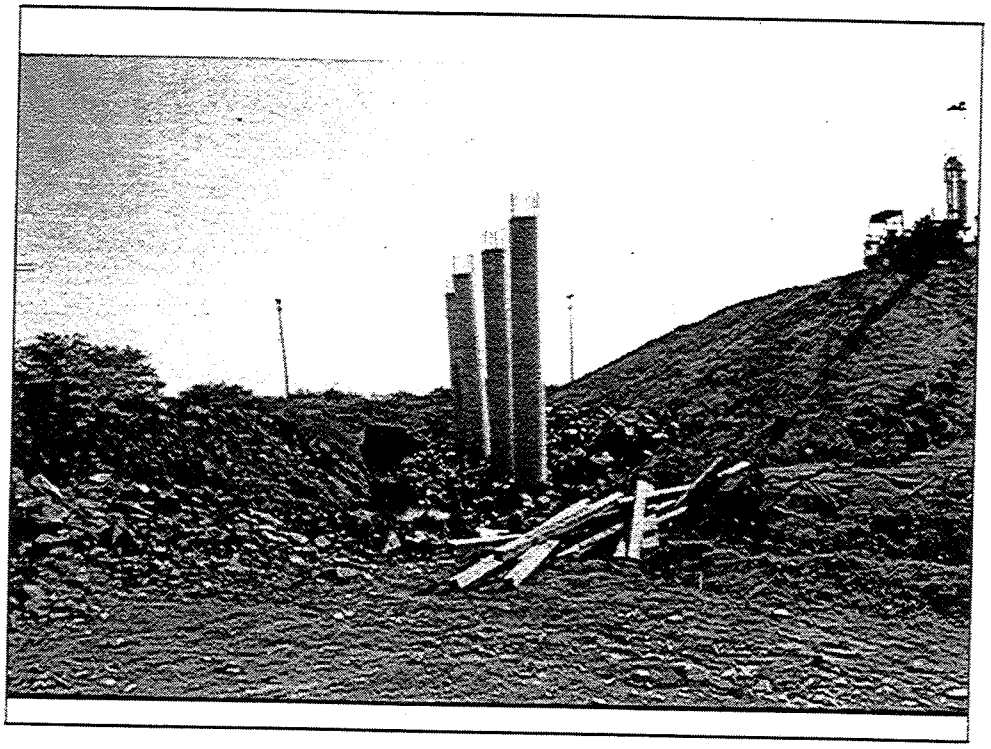

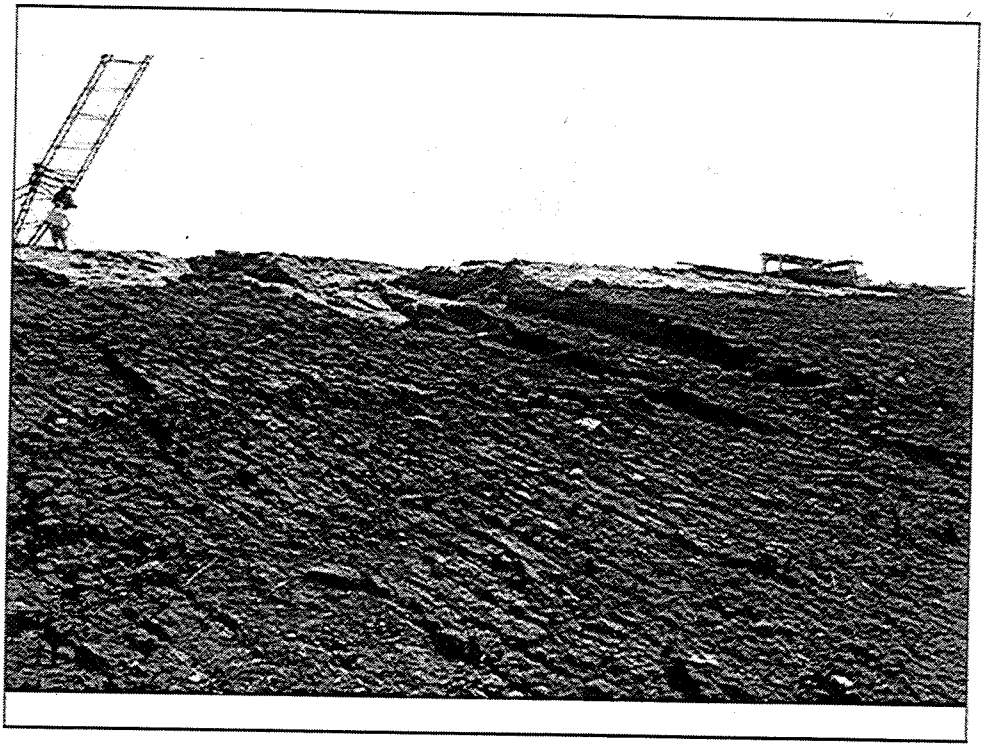

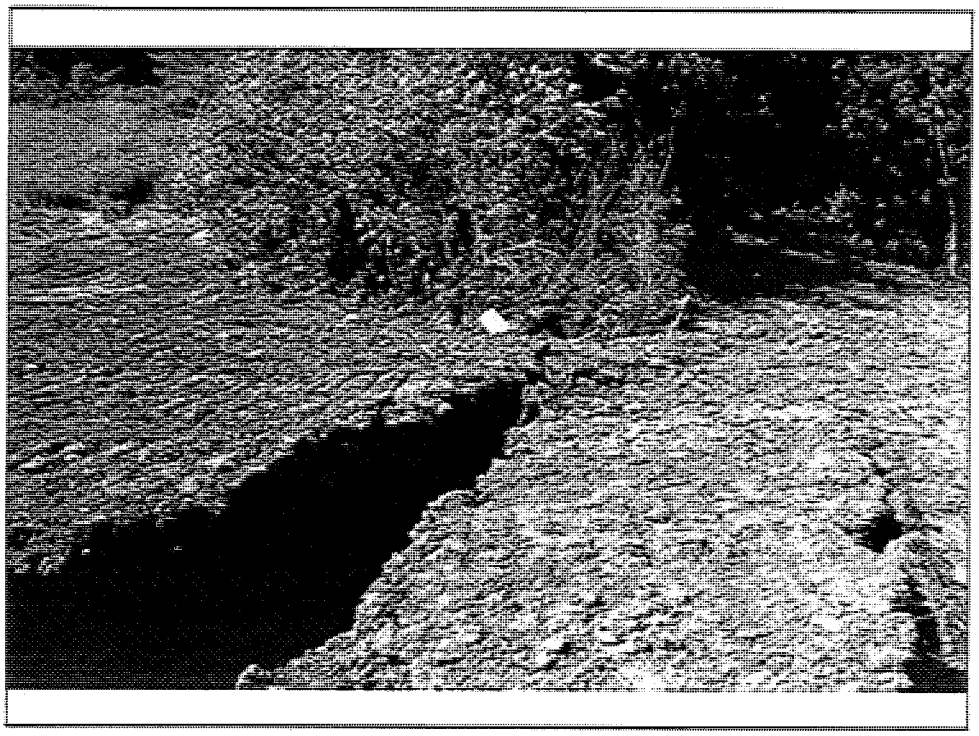

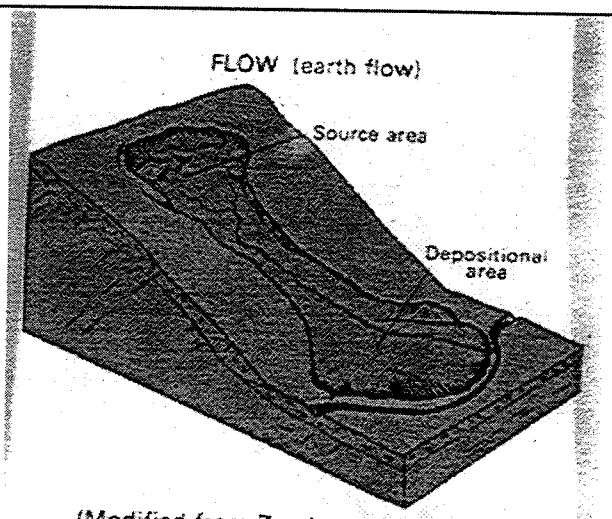

(Modified from Zaruba and Menci, 1969)
FLOW—Movement of mass such that the form taken by moving material or the apparent distribution of velocities and displacements resembles that of viscous fluids; velocity ranges from slow to extremely rapid.

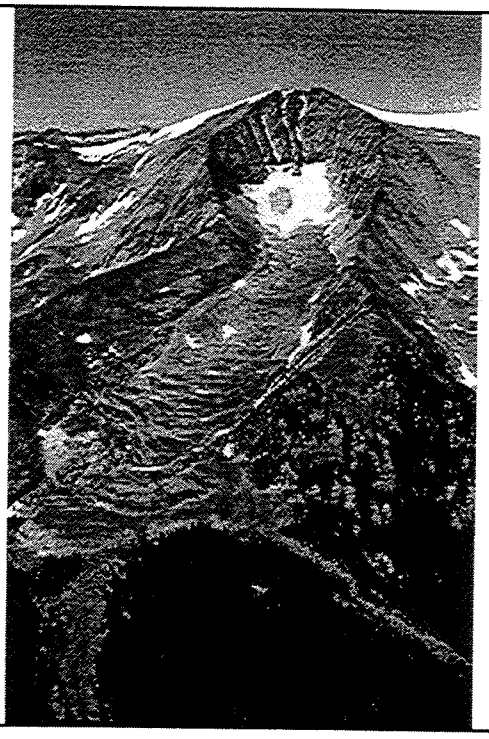

On Aptos Creek in devastated Santa Cruz County, a house bisected by the tide of mud.

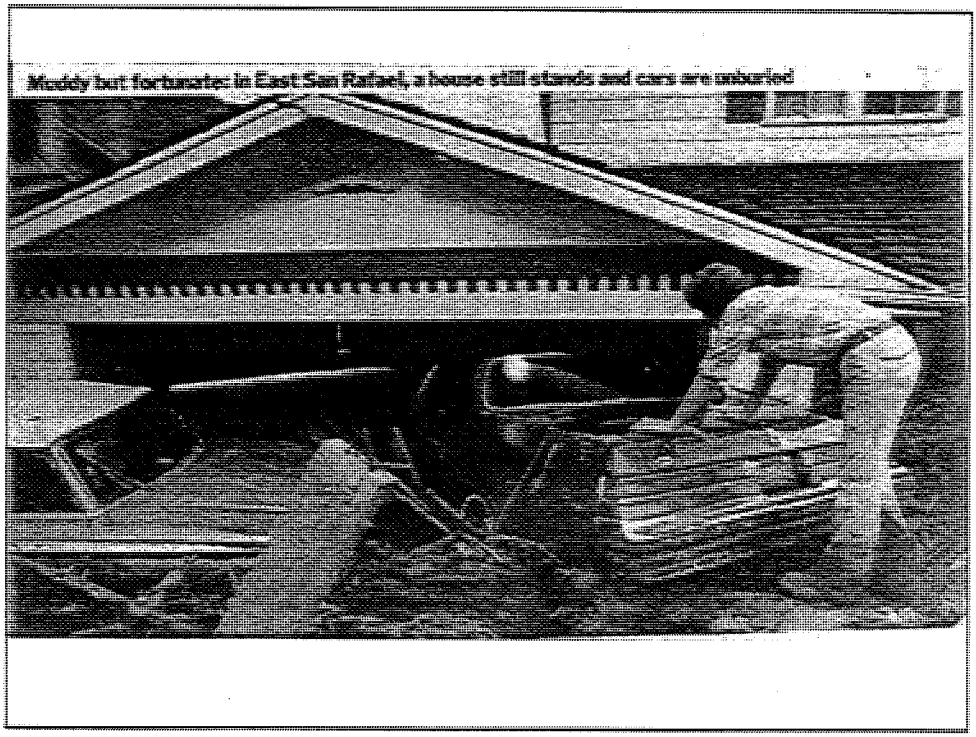

Muddy but fortunate: In East San Rafael, a house still stands and cars are unburied

The Valenz home, below, where Steve died

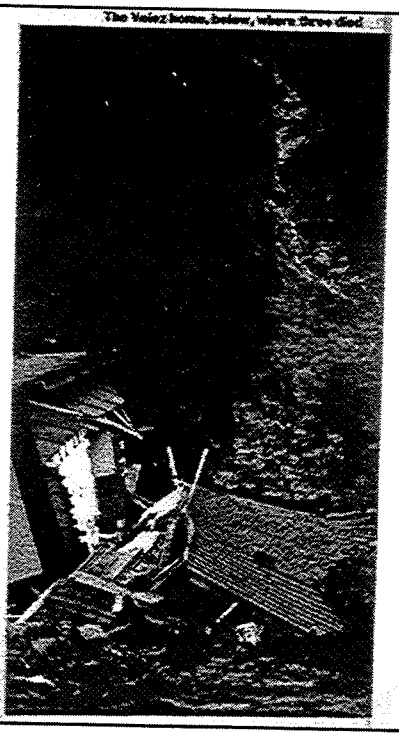

Washed-out highway south of San Francisco

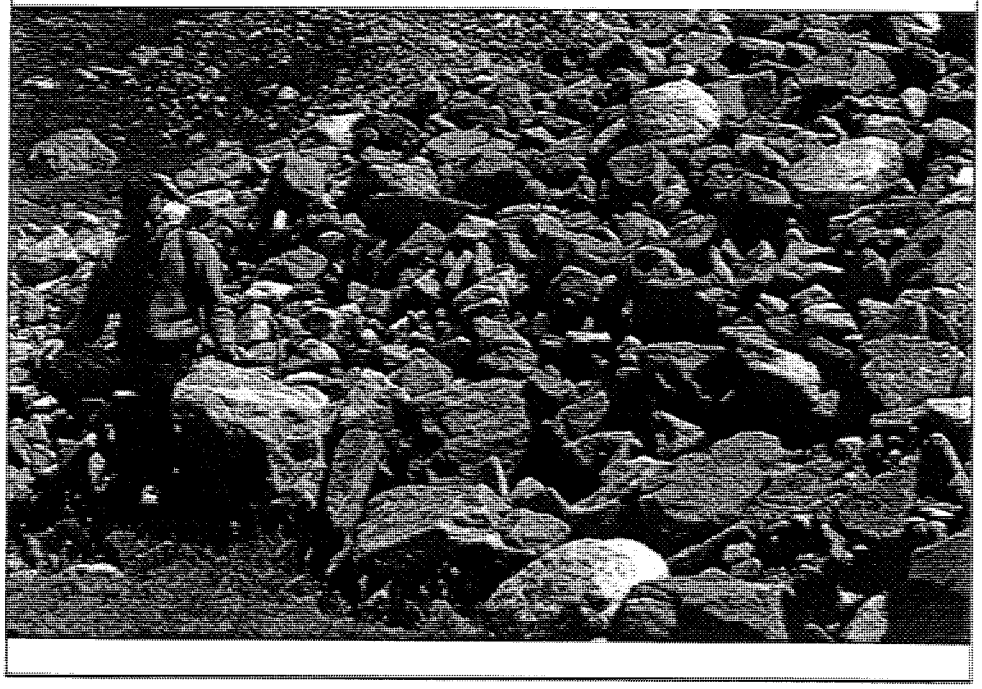

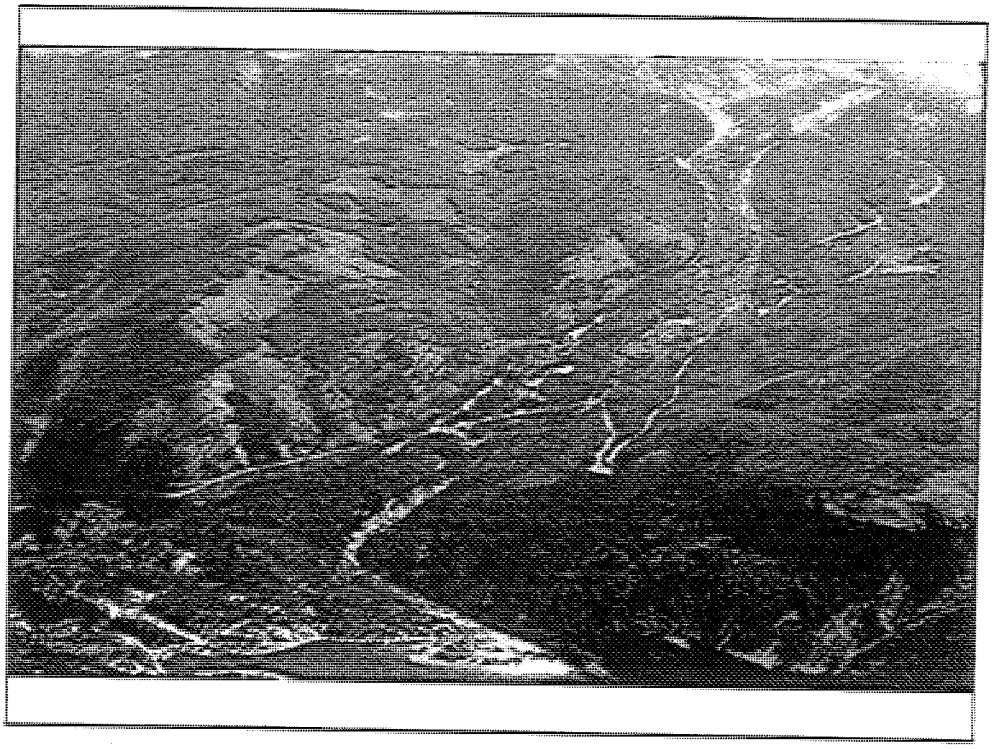

SLOPE CREEP

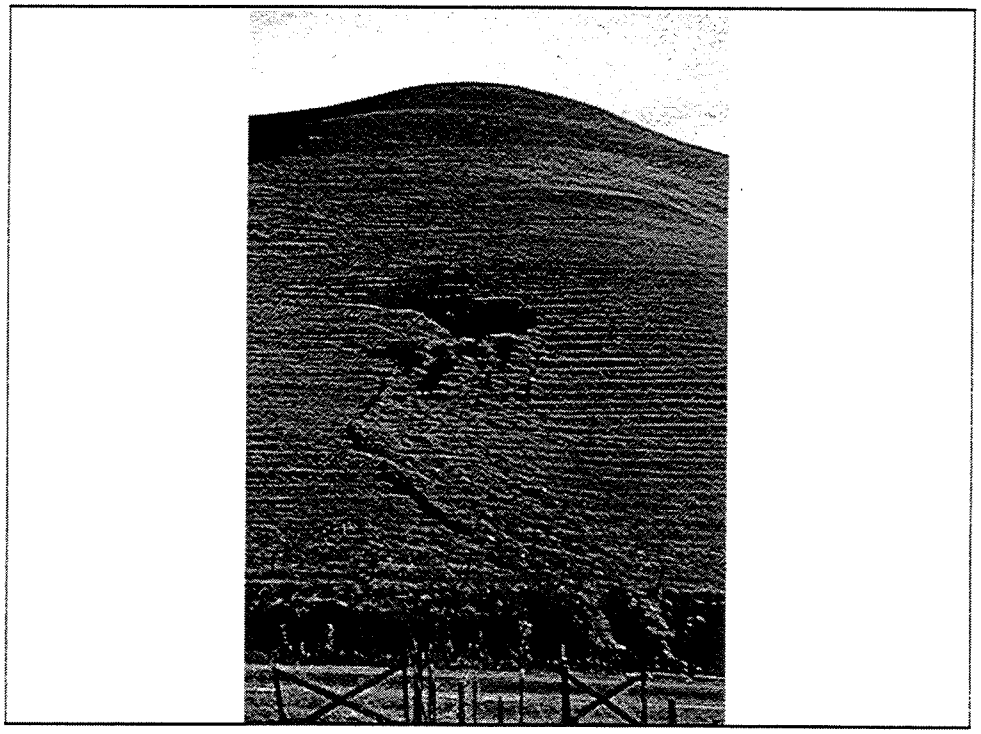

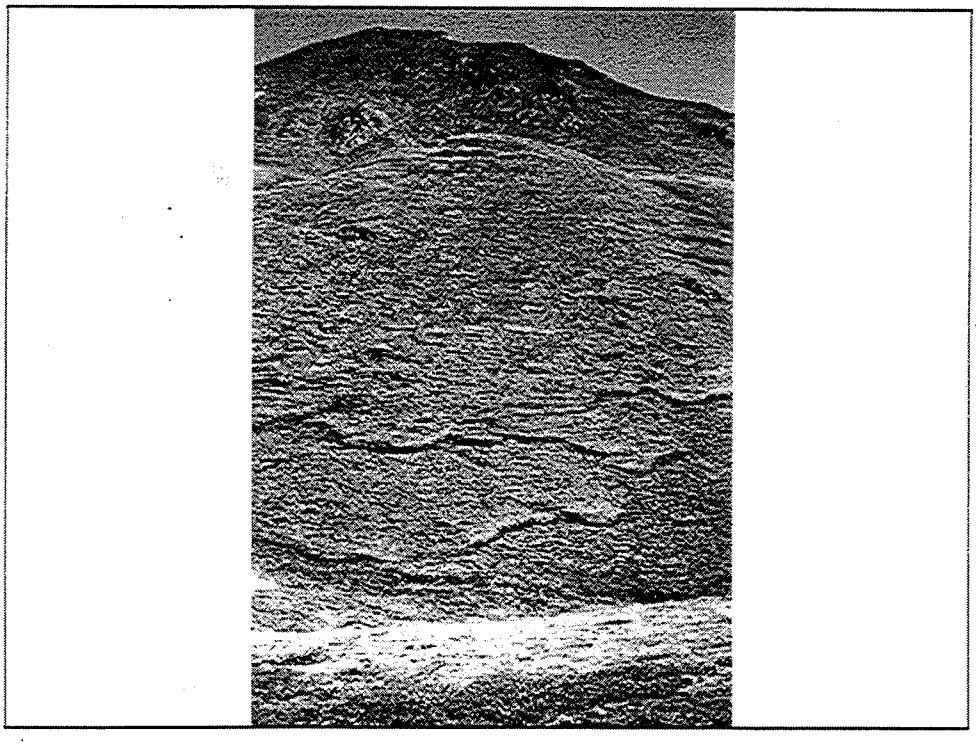

LANDSLIDE FEATURES

- Crown
- Scarp
- Top
- Toe
- Surface of Rupture
- Surface of Separation
- Flank
- Zone of Depletion
- Zone of Accumulation

VARNES BLOCK DIAGRAM OF EARTH SLIDE

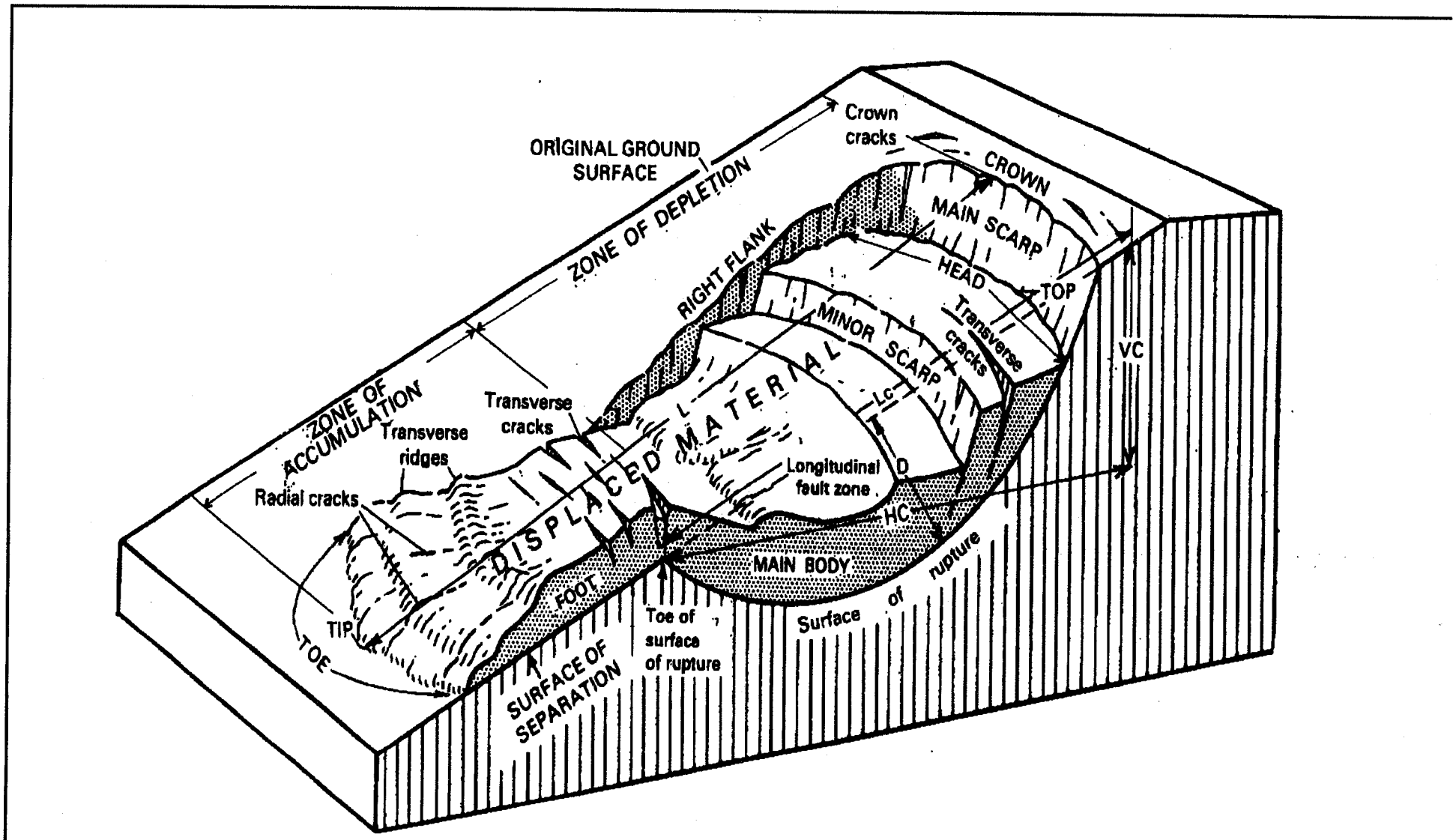

IAEG LANDSLIDE FEATURES

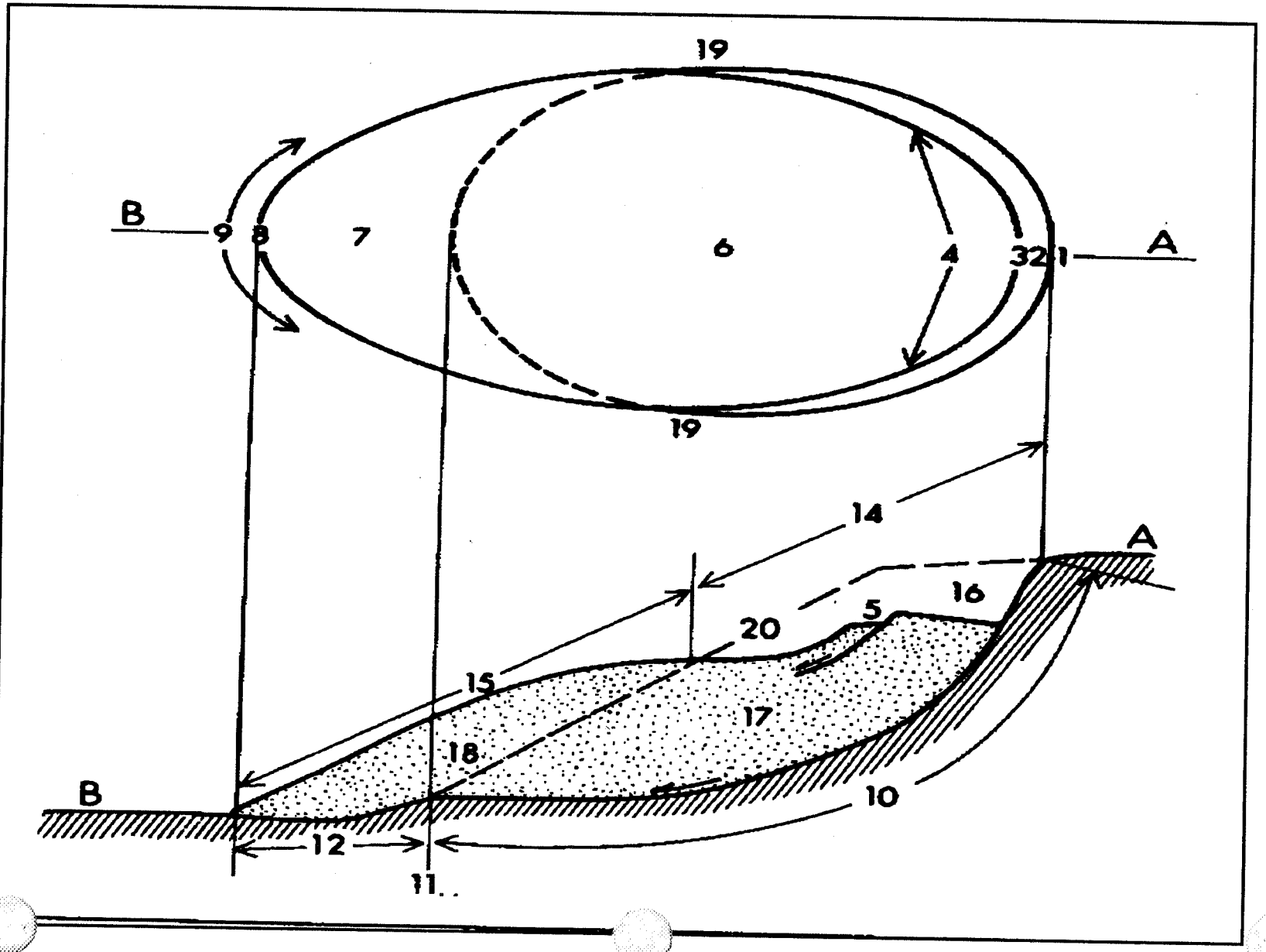

LANDSLIDE DIMENSIONS

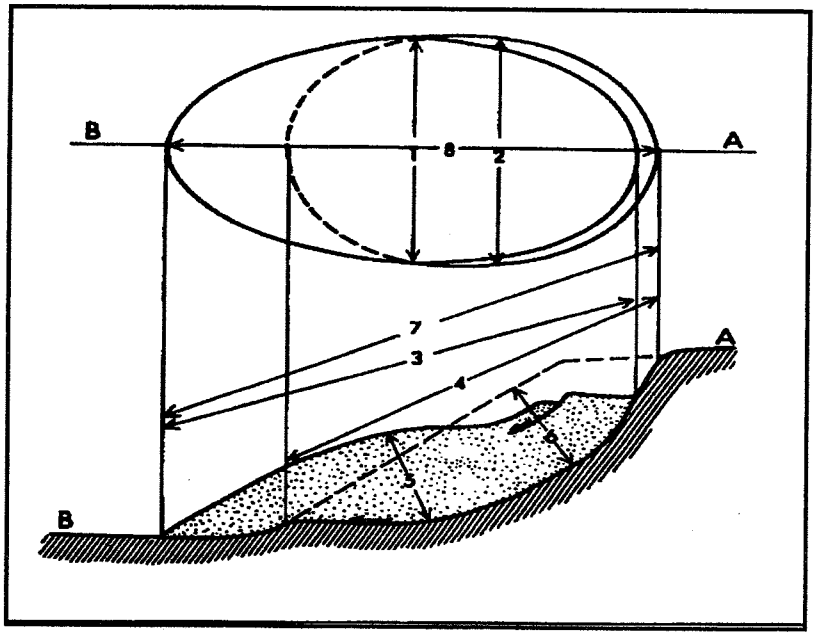

VOLUME OF SLIDING MASS

VOL = 1/6 π D_r W_r L_r before landslide

VOL = 1/6 π D_d W_d L_d after landslide

where

W = width between flanks

D = maximum depth of displaced mass

L = Distance from crown to toe

TRAVEL ANGLE

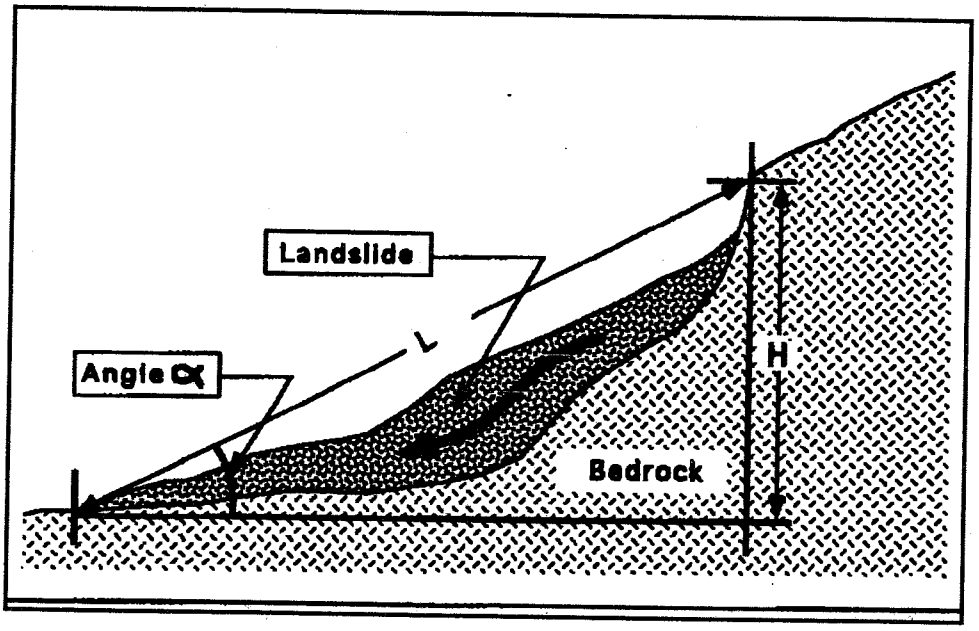

STATES OF ACTIVITY

- Active (erosion at toe)
- Suspended
- Dormant
- Reactivated
- Suspended

STATES OF ACTIVITY

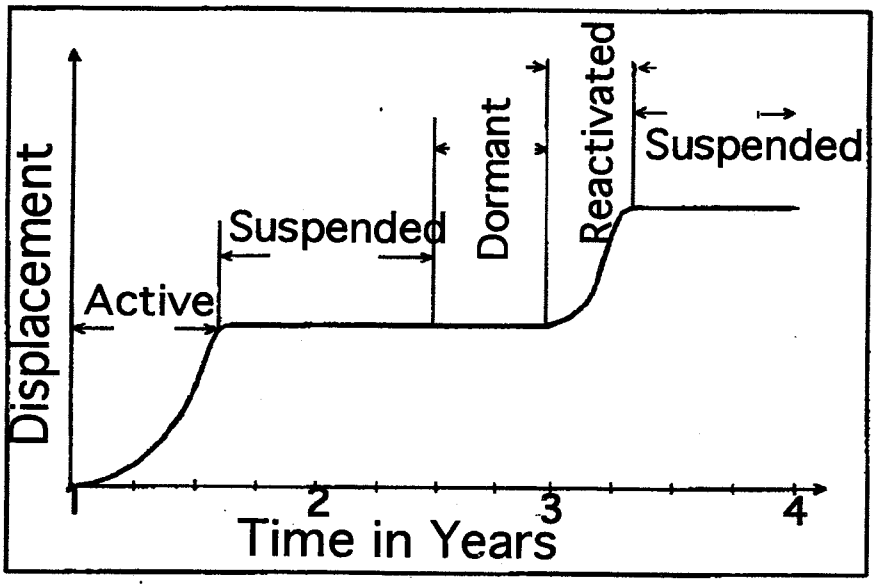

DISTRIBUTIONS OF ACTIVITY

- Advancing
- Retrogressing
- Enlarging
- Diminishing
- Confined

DISTRIBUTIONS OF ACTIVITY

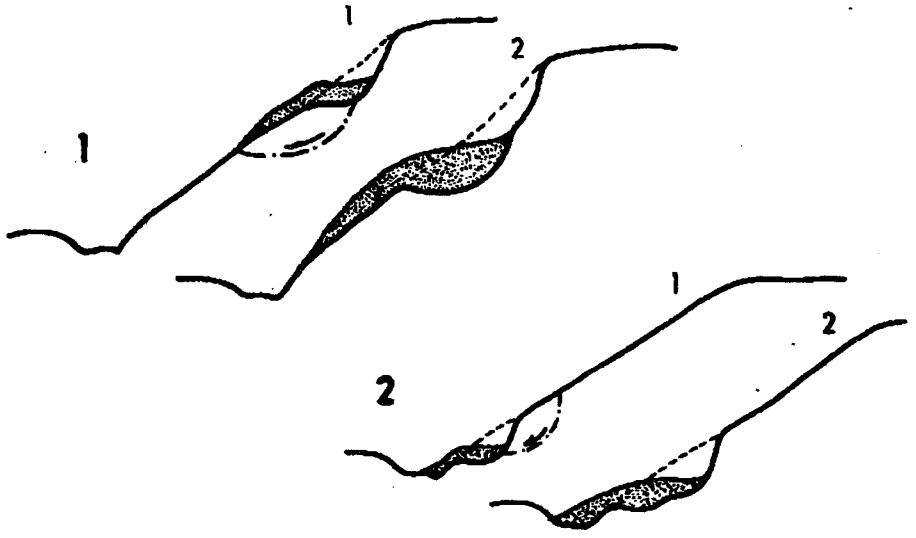

DISTRIBUTIONS OF ACTIVITY

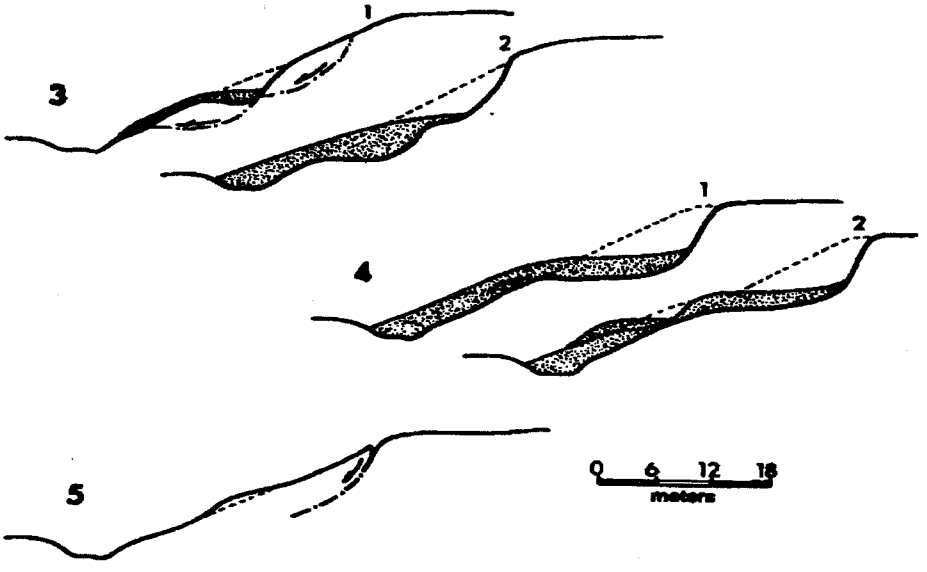

RATE of MOVEMENT

Velocity Class	Description	Velocity (mm/sec)	Typical Velocity
7	Extremely Rapid		
		$5x10^{3}$	5 m/sec
6	Very Rapid		
		$5x10^{1}$	3 m/min
5	Rapid		
		$5x10^{-1}$	1.8 m/hr
4	Moderate		
		$5x10^{-3}$	13 m/month
3	Slow		
		$5x10^{-5}$	1.6 m/year
2	Very Slow		
		$5x10^{-7}$	16 mm/year
1	Extremely Slow		

TYPES OF LANDSLIDES

(a) Fall

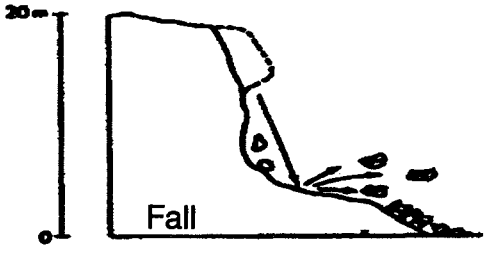

(b) Topple

TYPES OF LANDSLIDES

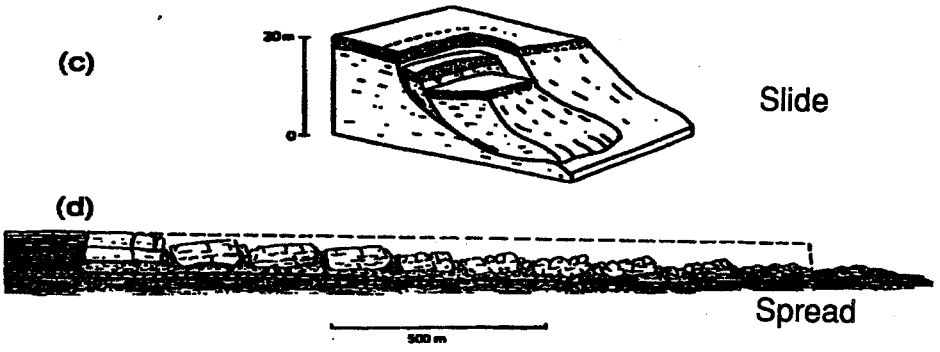

LANDSLIDE TRIGGERING MECHANISMS

- Intense Rainfall
- Rapid Snowmelt
- Water-level Change (rapid drawdown)
- Volcanic Eruption
- Earthquake Shaking

CUMULATIVE RAINFALL
(Southern California)

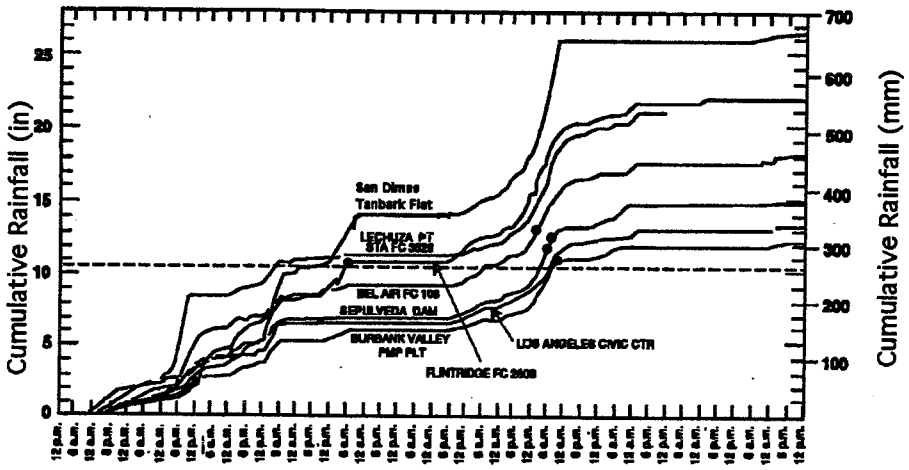

January 1969

RAINFALL THRESHOLDS FOR LANDSLIDES
(San Francisco Bay Region)

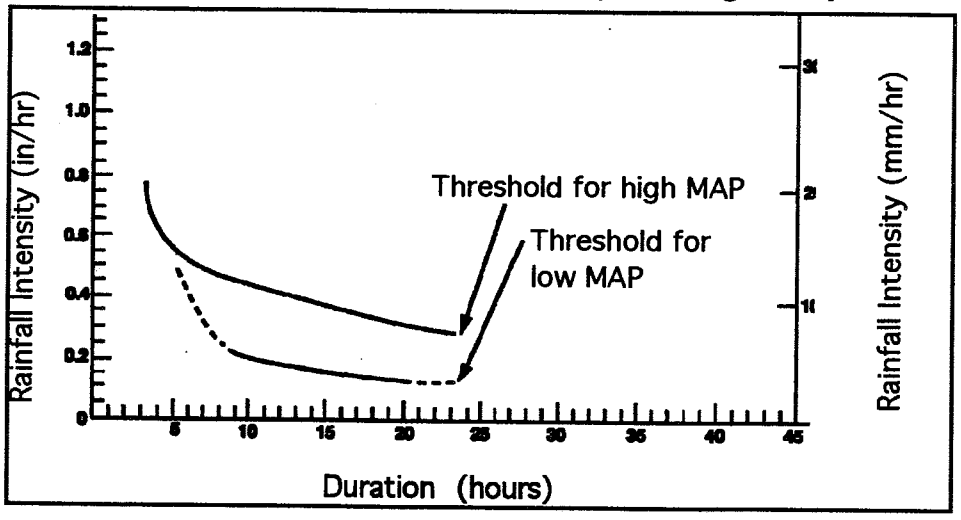

PORE PRESSURE RESPONSE TO RAINFALL

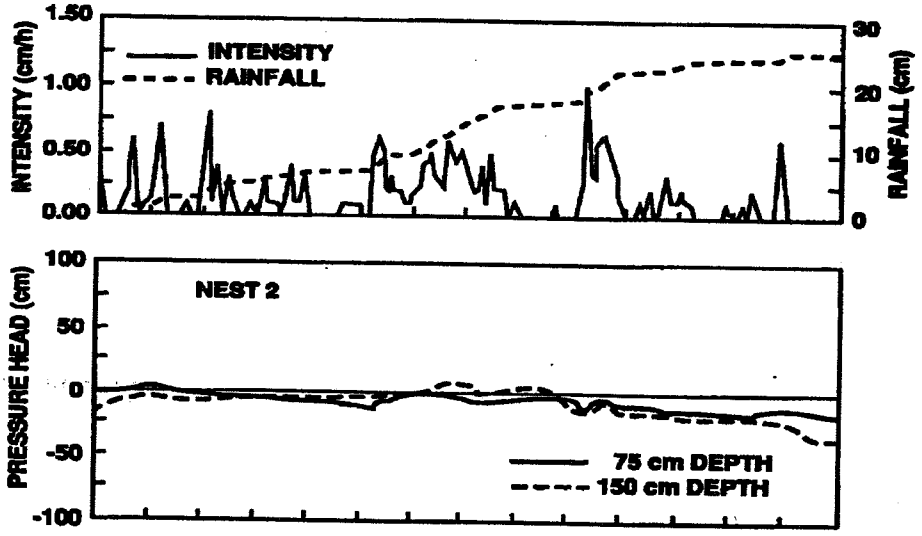

PORE PRESSURE RESPONSE TO RAINFALL

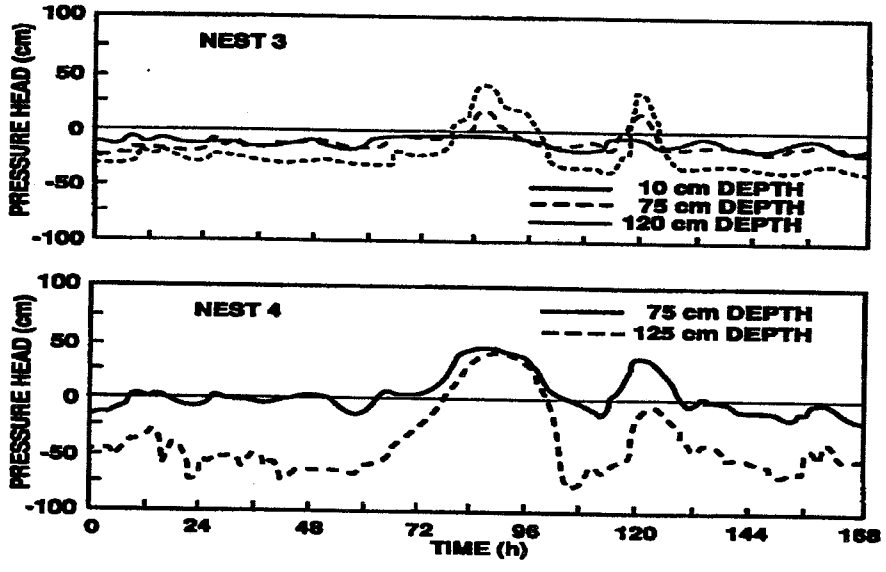

RAPID DRAWDOWN

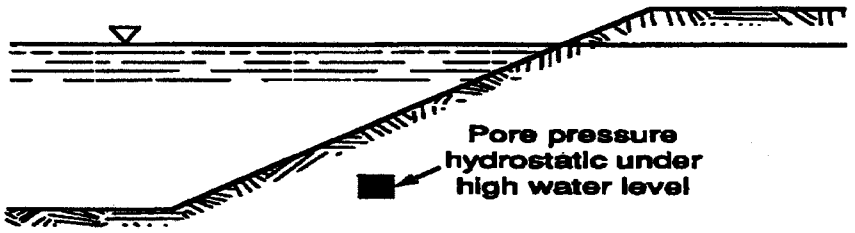

(a)

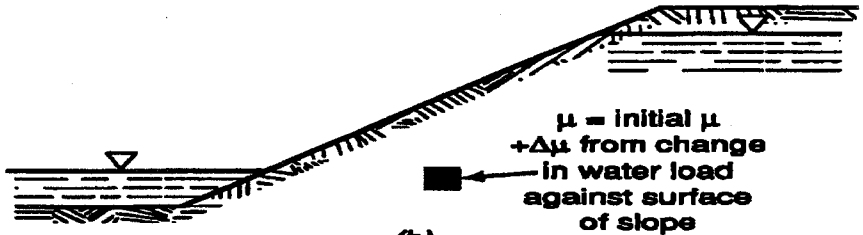

(b)

RAPID DRAWDOWN

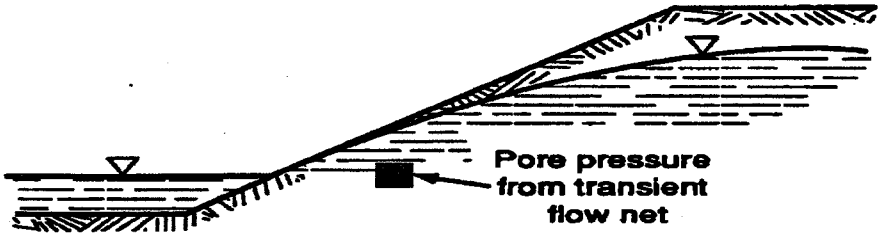

(c)

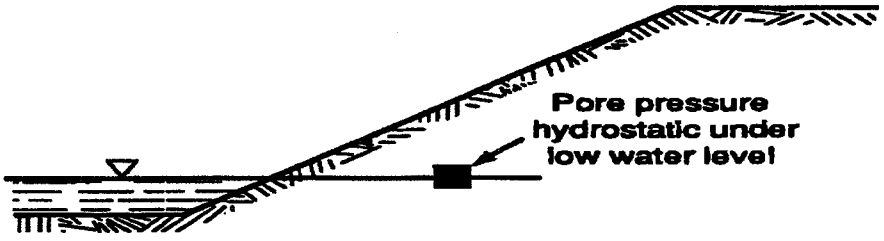

(d)

MAXIMUM DISTANCE TO LANDSLIDES FROM EPICENTER

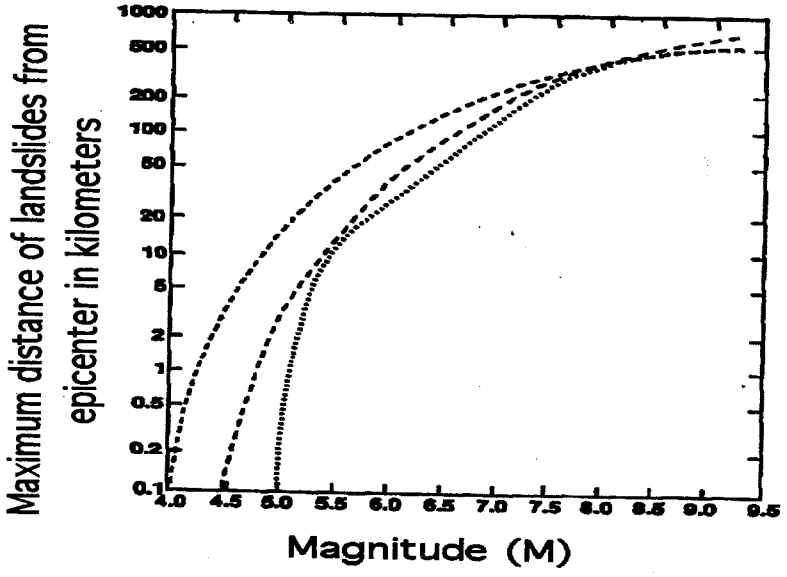

SHEAR STRENGTH OF SOILS

TUNCER B. EDIL
UNIVERSITY OF WISCONSIN-MADISON

STRESSES

Gravity generates stresses (force per unit area) in the ground at different points. Stress on a plane at a given point is viewed in terms of two components:

- Normal stress (σ): acts normal to the plane and tends to compress soil grains towards each other (volume change)
- Shear stress (τ): acts tangential to the plane and tends to slide grains relative to each other (distortion and ultimately sliding failure)

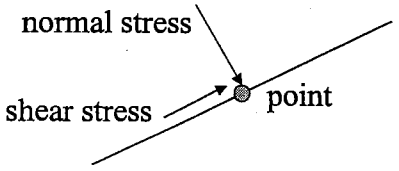

EFFECTIVE STRESS CONCEPT

- Defined as the difference between total normal stress and pore water pressure
- Maybe visualized as "net intergranular normal stress"
- $\sigma' = \sigma - u$
- σ' = effective stress
- σ = total stress
- u = pore water pressure

VERTICAL TOTAL STRESS

- σ_v = vertical total stress = $\Sigma\gamma\,\Delta z + \Delta\,\sigma_v$
- $\Sigma\gamma\,\Delta z$ = geostatic stress due to weight of soil layers above the point where γ is the unit weight of soil and Δz is the layer thickness
- $\Delta\,\sigma_v$ = change in vertical stress (plus or minus) due to surface loads

PORE WATER PRESSURE

- $u = u_o + \Delta u$
- $u_o = h_p \gamma_w$ water pressure due to static or flowing groundwater where h_p = pressure head and γ_w = unit weight of water
- Δu = f(shear and normal stress changes, degree of saturation, stress history,etc) and it is pore pressure change (plus or minus) resulting from stress changes (cut or fill, erosion, etc)

PORE WATER PRESSURE AND TOTAL STRESS

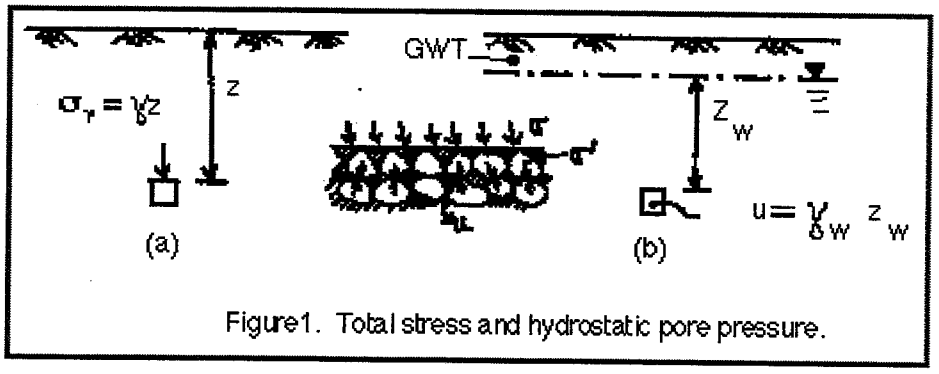

Figure1. Total stress and hydrostatic pore pressure.

STRESS-STRAIN CHARACTERISTICS

- Describes rigidity of soil to shear stresses
- Either a "peaked" or "monotonically increasing" (smooth) curve (Type A or B)
- Failure in peaked curves may be defined either at the peak (peak strength) or at large strains (residual strength) (Points a and c)
- Failure in smooth curves may be defined at a certain strain (typically 15 or 20 %) (Point b)

STRESS-STRAIN CHARACTERISTICS

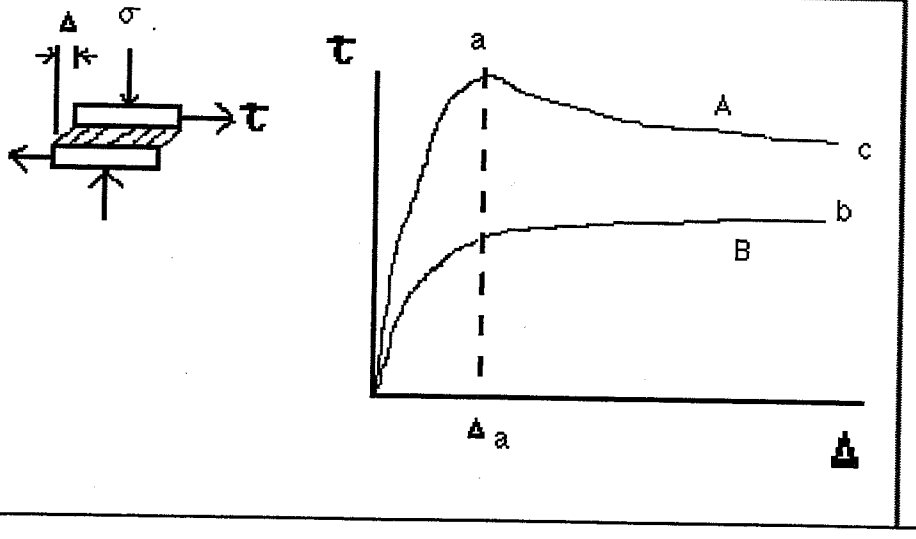

FAILURE CRITERION

- A consistent relationship exists between the shear strength on a plane and the effective normal stress that acts on that plane
- $S = c' + \sigma' \tan \phi'$ where
- S = shear strength on the plane
- σ'= effective normal stress on the plane
- c' = effective cohesion
- ϕ' = effective friction angle

FAILURE ENVELOPE

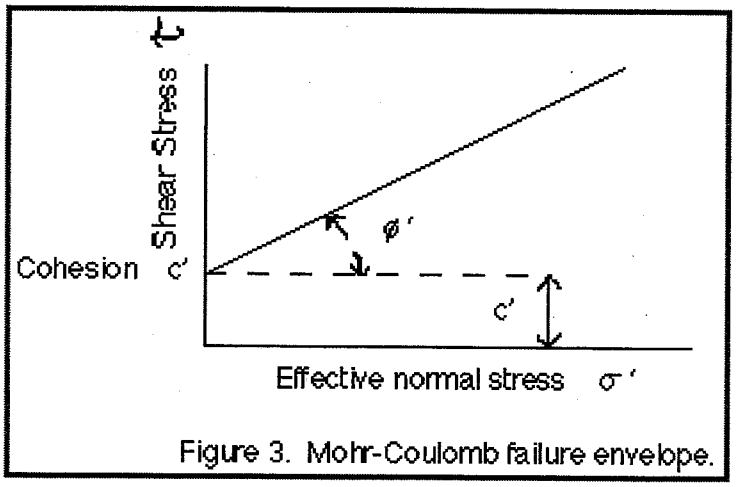

Figure 3. Mohr-Coulomb failure envelope.

DRAINED STRENGTH

- Shear strength defined in terms of effective normal stresses is referred as "drained" or "effective" strength
- To use drained or effective strength, effective normal stresses need to be known which, in turn, requires that pore water pressures are known
- Pore pressures may not be simple to determine in the field

Typically used in analysis of stability of excavation slopes and natural slopes.

UNDRAINED STRENGTH

- In those cases, such as at end of construction in fine-grained soils, where determination of pore pressures are difficult "undrained" or "total" strength is used for convenience
- $S = c_u + \sigma \tan \phi_u$ where c_u = undrained cohesion and ϕ_u = undrained friction angle (zero for saturated soils), and σ = total normal stress

Typically used in foundation, retaining wall, embankment slope design.

LABORATORY MEASUREMENT OF STRENGTH

- Simple Tests (unconfined compression, vane shear, torvane, drop cone, pocket penetrometer)

  used for clays
- Direct Shear Test

  used for sands
- Triaxial Compression Test

  used on important projects and when drained strength parameters are needed

UNCONFINED COMPRESSION TEST

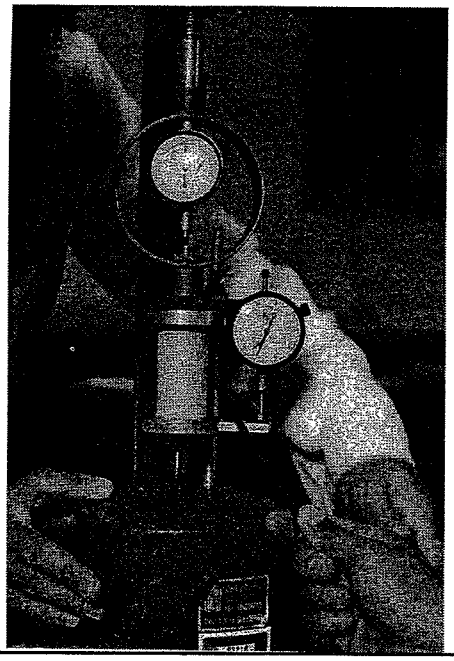

POCKET PENETROMETER

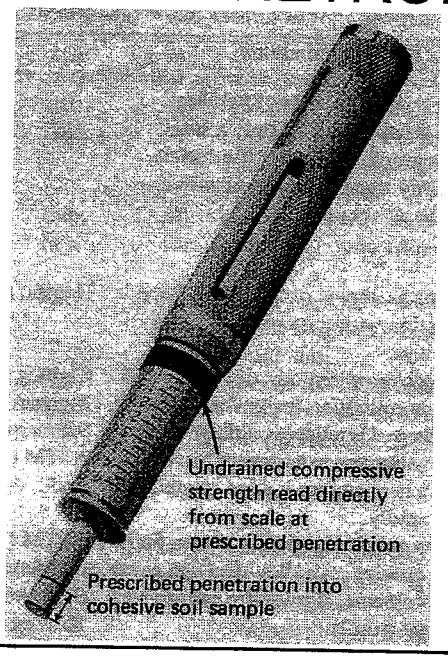

TORVANE

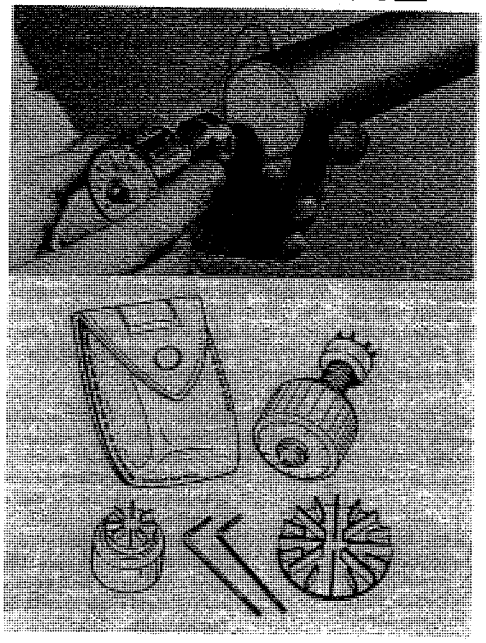

VANE SHEAR DEVICE

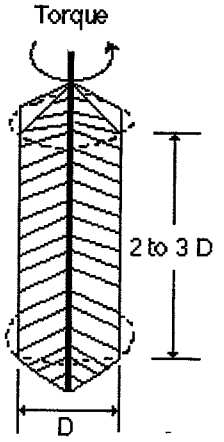

Figure 11. Field vane device.

DIRECT SHEAR BOX

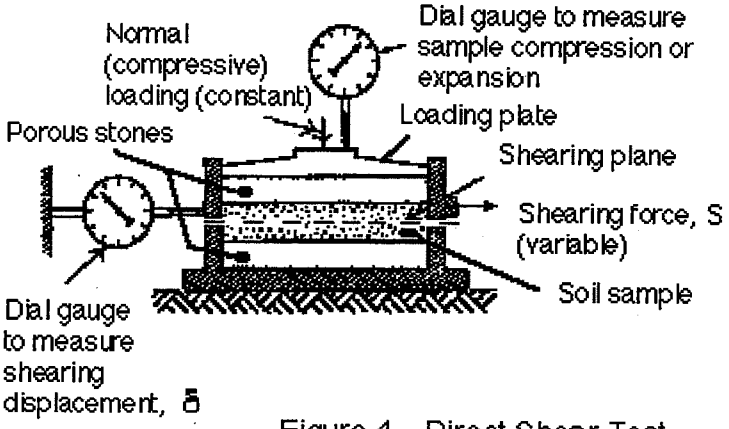

Figure 4. Direct Shear Test.

DIRECT SHEAR TEST FAILURE ENVELOPE

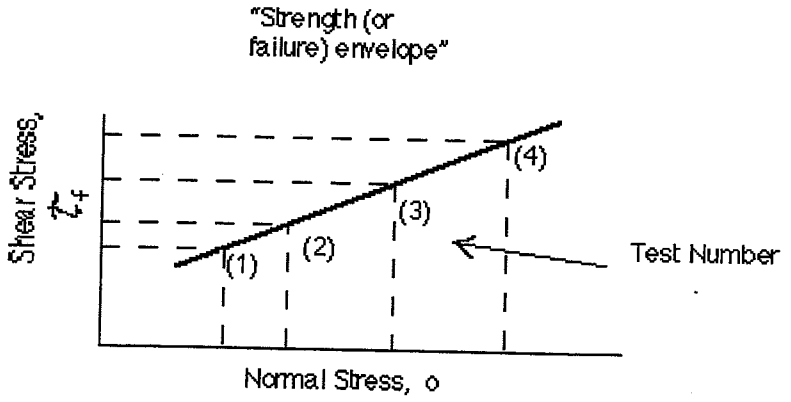

TRIAXIAL CELL

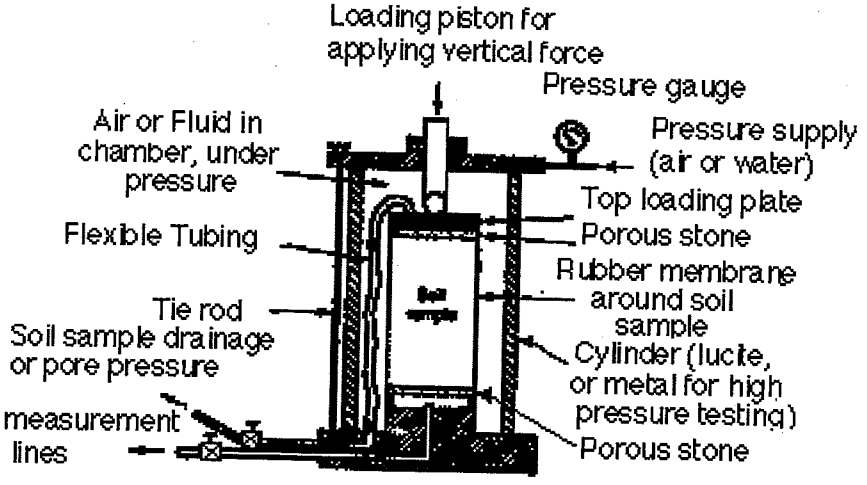

TRIAXIAL COMPRESSION TEST FAILURE ENVELOPE

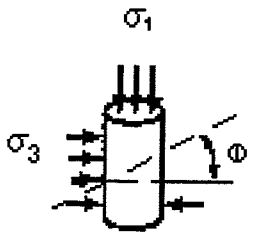

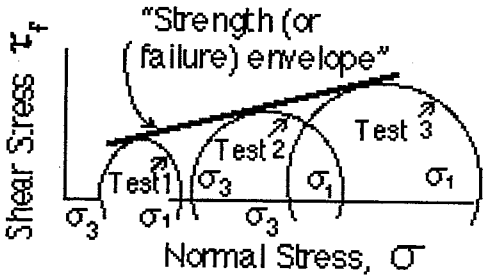

TYPES OF TRIAXIAL COMPRESSION TESTS

- UU (unconsolidated undrained) and UC (unconfined compression): used for undrained strength of clays
- CD (consolidated drained): used for drained strength of sands and silty sands (too slow for clays)
- CU (consolidated undrained) with pore water pressure measurement: used for obtaining drained strength parameters of clays

USE OF UU, CD, CU TESTS

- UU or UC: total strength parameters: EOC case dams, fills, foundations (piles, footings), retaining structures (critical for fill slopes and foundations)
- CD: effective strength parameters: long-term steady seepage case in slopes (critical for cut and natural slopes) and dams
- CU: total strength parameters: rapid drawdown of dams, reservoir, canal, riverbank slopes
- CU with pore pressure measurement: effective strength parameters: same as CD strength parameters

FIELD MEASUREMENT OF STRENGTH

- Standard Penetration Test (SPT)

  very common; main source of strength information for sand
- Field Vane Shear Test

  used with soft clays, peats, and wastes
- Cone Penetration Test (CPT)
- Pressuremeter
- Flat Dilatometer
- Iowa Borehole Shear Test

Standard Penetration Test (SPT)

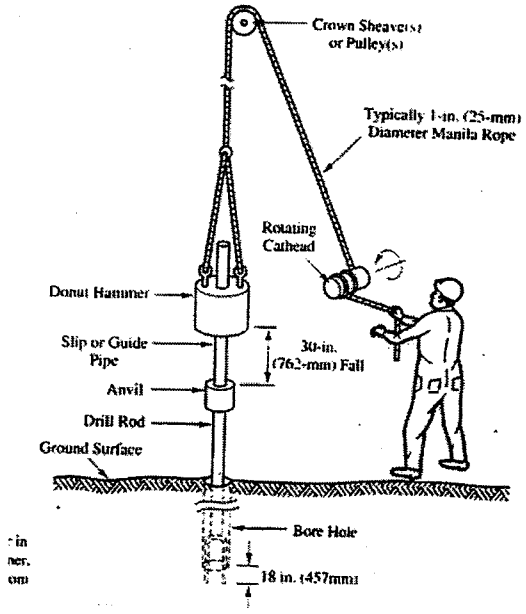

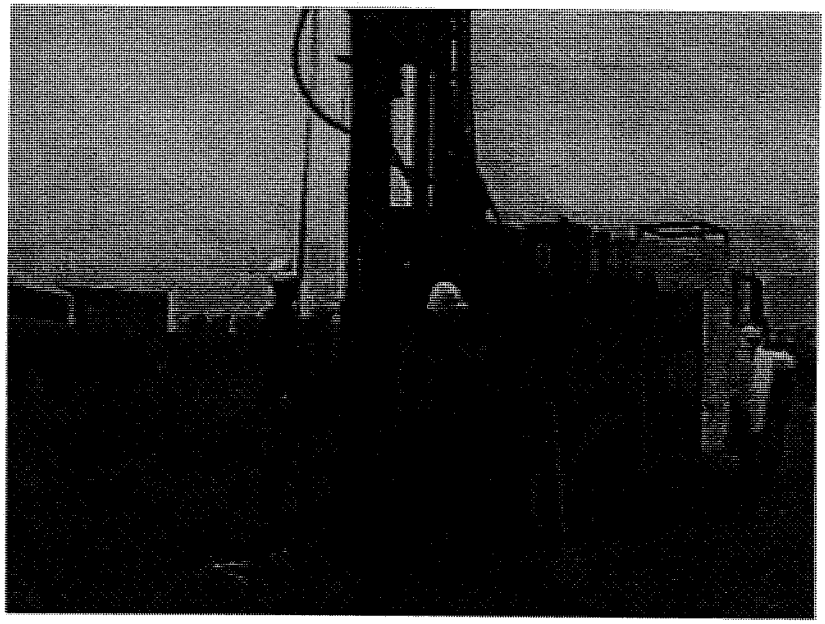

SPLIT SPOON SAMPLER FOR SPT

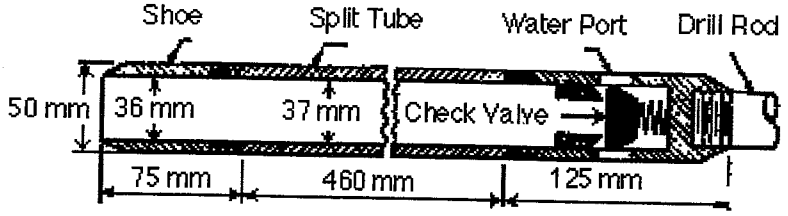

Figure 7. Split-tube sampler for Standard Penetration Test

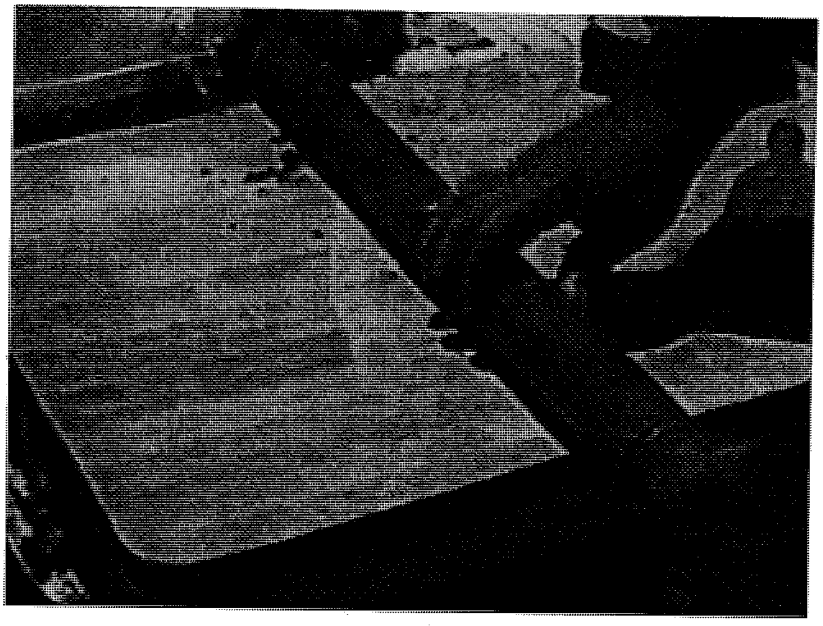

Field Vane Shear Test (FVS)

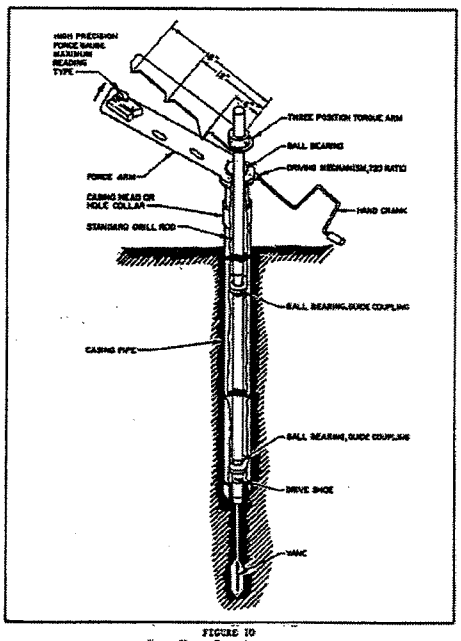

FIGURE 10
Vane Shear Test Arrangement

VANE SHEAR TEST

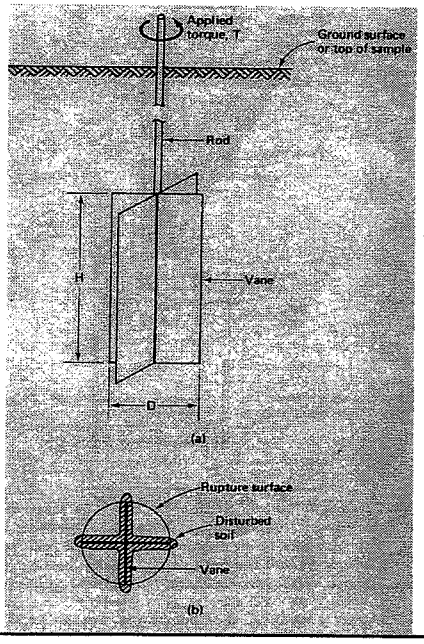

Cone Penetration Test (CPT)

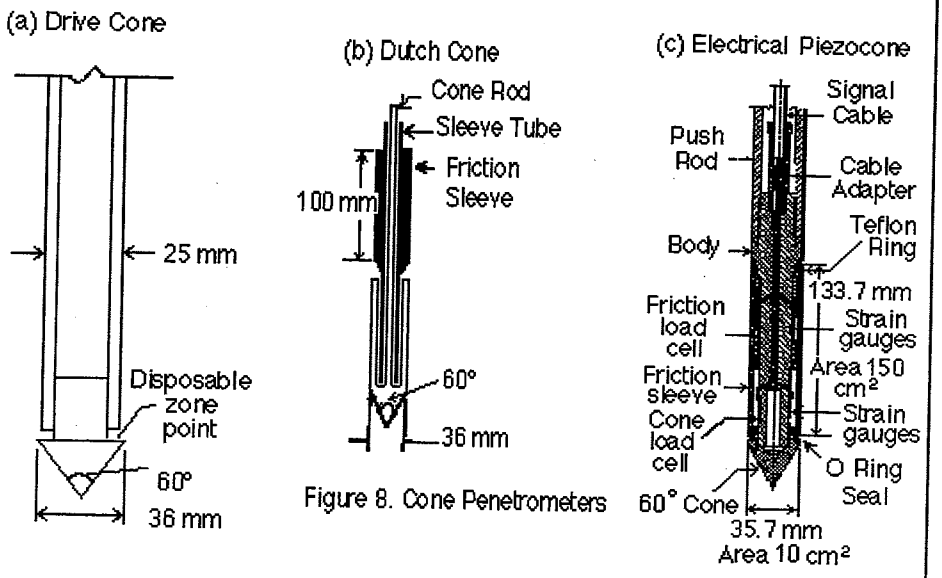

Figure 8. Cone Penetrometers

Borehole Pressuremeter Test

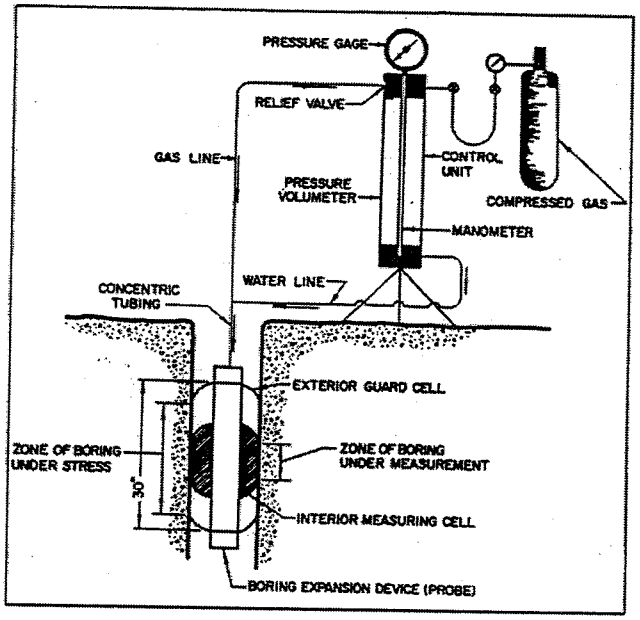

FIGURE 11
Menard Pressuremeter Equipment

Flat Dilatometer Test

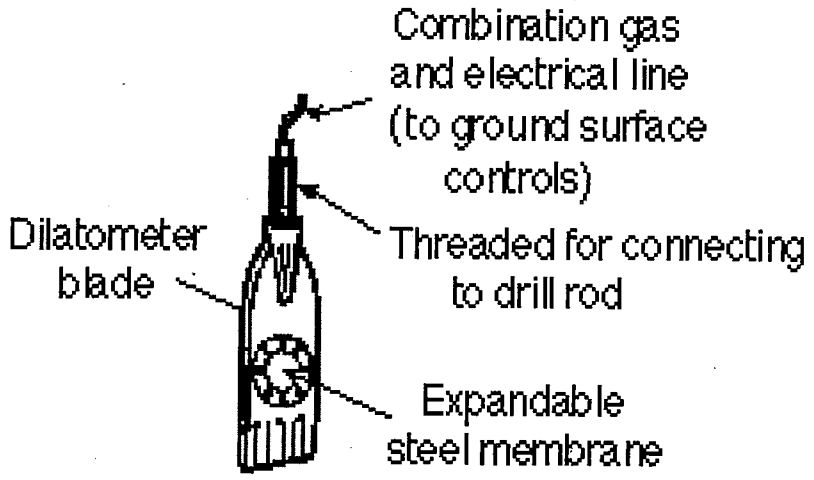

Figure 9. Marchetti Flat Dilatometer

Iowa Borehole Shear Test

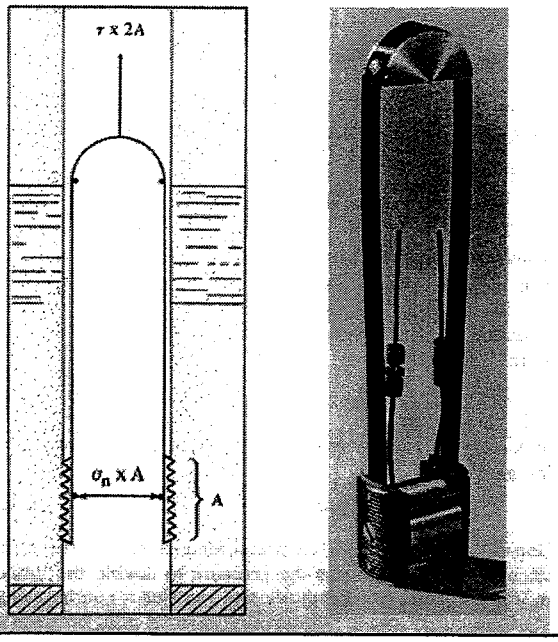

LABORATORY versus FIELD TEST

- Laboratory tests require a sample thus the problems of sample disturbance and representativeness and specimen size
- Drained strength parameters can be determined only in the laboratory
- Field tests minimize sample disturbance but provide strength only at field stresses

SHEAR STRENGTH OF GRANULAR SOILS

- Shearing resistance derived from particle friction and interlocking
- High permeability assures drained conditions in all but dynamic loadings
- $S = \sigma' \tan \phi' = (\sigma - u) \tan \phi'$
- Friction angle, ϕ' depends on relative density (D_r), grain shape (roundness), and grain size distribution (size uniformity)
- Pore pressure, $u = u_o$ for end-of-construction and long-term

DETERMINATION OF Φ' FOR SANDS

- Undisturbed sampling is difficult
- Field tests such as SPT and CPT provide empirical or semi-empirical correlations
- Laboratory tests (direct shear or drained triaxial compression) on specimens reconstituted at estimated field density are also performed on dry or submerged (but freely drained) specimens
- Undrained triaxial compression tests are performed for liquefaction potential

RELATIVE DENSITY vs SPT

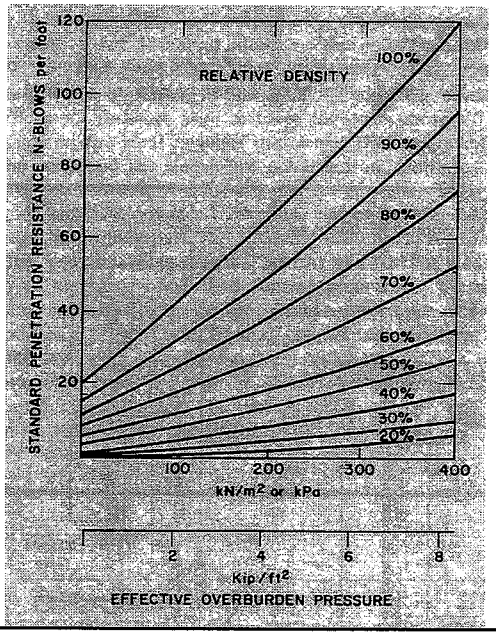

Φ' vs RELATIVE DENSITY

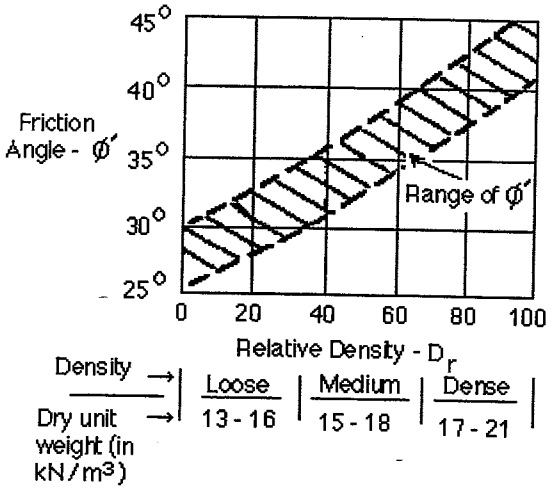

Figure 12. Friction angle as a function of relative density of sand.

SHEAR STRENGTH OF COHESIVE SOILS

- Cohesive soils are fine-grained and has low permeability
- Excess pore pressures are not dissipated during end-of-construction (EOC) and during sudden-drawdown (SDD): $u = u_o + \Delta u$
- Excess pore pressures, however, dissipate in the long-term (LT): $u = u_o$
- EOC and SDD: use either undrained strength with σ
- LT: use drained strength with σ' ($\Delta u = 0$)

DETERMINATION OF UNDRAINED STRENGTH PARAMETERS

- $S = c_u$ for saturated fine-grained soils
- Laboratory tests (unconfined compression, vane shear or simple tests) on highly undisturbed samples
- Field tests (vane shear, cone penetration)
- c_u depends on water content which, in turn, depends on consolidation stress history

UNCONSOLIDATED UNDRAINED TRIAXIAL TEST

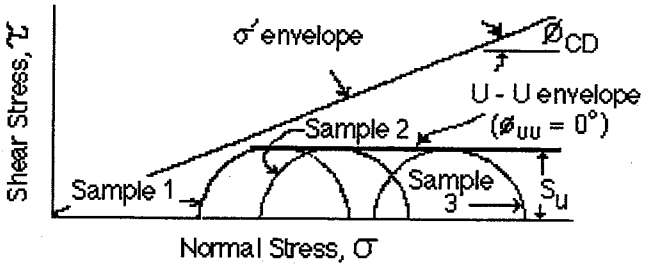

Figure 15. Typical strength envelope from a triaxial test on a normally consolidated clay.

DETERMINATION OF DRAINED STRENGTH PARAMETERS

- $S = \sigma' \tan \phi'$ for normally consolidated soils
- $S = c' + \sigma' \tan \phi'$ for overconsolidated soils
- Triaxial compression test (CD or CU with pore pressure measurements) on highly undisturbed samples
- c' and ϕ' are normalized with respect to σ' and depend primarily on stress history and composition of soil

CONSOLIDATED DRAINED TRIAXIAL TEST

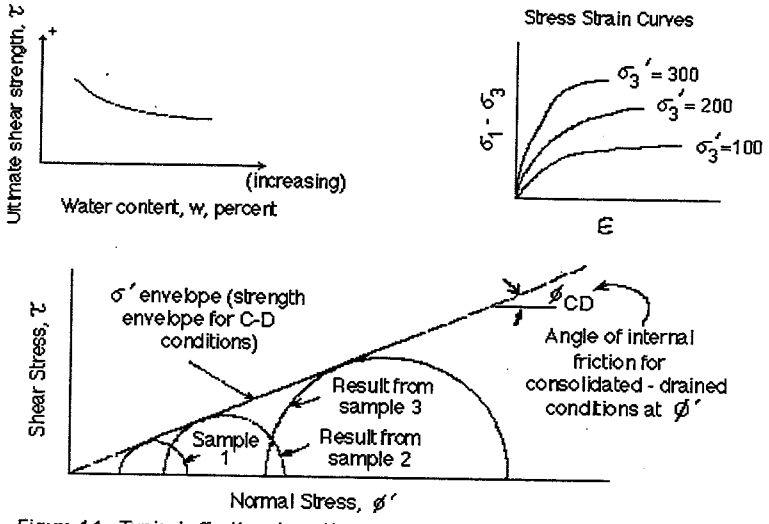

Figure 14. Typical effective strength envelope from a CD triaxial test on a normally consolidated clay.

TYPICAL VALUES FOR STRENGTH PARAMETERS

- Sand: $\phi' = 27$ to 45 (gravel, boulders are higher)
- Clay Drained:
  - Normally consolidated $\phi' = 10$ to 35^o; $c' = 0$
  - Overconsolidated $\phi' = 10$ to 25^o; $c' = 100$ to 400 psf (typically) but could be higher
- Clay Undrained: $c_u = 0$ to more than 8,000 psf
- Municipal Waste : $\phi' = 30$ to 60^o; $c' = 0$ to1,600psf
- Sand-to-Membrane: $\delta = 17$ to 27^o
- Clay-to-Membrane: $\delta = 12$ to 22^o
- Geomembrane-to-Geotextile: $\delta = 6$ to 28^o
- Sand-to-Geotextile: $\delta = 23$ to 30^o

REFERENCES

The following references were used in preparation of these slides:

1. Das, B. M., Principles of Geotechnical Engineering, 3rd Ed., PWS Publishing Co., Boston, MA, 1994.
2. Soil Mechanics Design Manual, NAVFAC DM-7.1, Department of the Navy, 1982.
3. Holtz, R. D. and Kovacs, W. D. An Introduction to Geotechnical Engineering, Prentice Hall, Englewood Cliffs, N.J. 1981
4. Dunn, I.S., Anderson, L.R. and Kiefer, F.W. Fundamentals of Geotechnical Analysis, Wiley, N.Y., 1980

SHEAR STRENGTH OF SOILS

Prepared by

Tuncer B. Edil

Professor

Civil & Environmental Engineering

University of Wisconsin-Madison

I. FUNDAMENTAL CONCEPTS: STRESS AND FAILURE

- EFFECTIVE STRESS CONCEPT
- STRESS-STRAIN CHARACTERISTICS
- FAILURE CRITERION

II. STRENGTH CHARACTERISTICS AND MEASUREMENT

- MEASUREMENT OF SHEAR STRENGTH
  - Laboratory Measurement of Shear Strength
  - Field Measurement of Strength
- SHEAR STRENGTH OF GRANULAR SOILS
- SHEAR STRENGTH OF COHESIVE SOILS
  - Saturated Normally Consolidated Clay
    - Consolidated Drained Test (CD)
    - Unconsolidated Undrained Test (UU)
    - Consolidated Undrained Test (CU)
  - Heavily Overconsolidated Clay
  - Partially Saturated Clays - Compacted Clays
  - Typical Values and Empirical Methods for Strength Parameters of Cohesive Soils
- USE OF DRAINED VERSUS UNDRAINED STRENGTH FOR COHESIVE SOILS

SHEAR STRENGTH OF SOILS
PART I
FUNDAMENTAL CONCEPTS: STRESS AND FAILURE

The analysis of stability problems in Geotechnical Engineering, such as bearing capacity of foundations, retaining structures, and slope stability, requires a knowledge of the shear strength of the soils involved. These analyses are based on conditions of limiting equilibrium which requires a comparison of the state of stress in the soil with the failure state of stress which is defined as soil strength along an assumed failure plane.

EFFECTIVE STRESS CONCEPT

A fundamental principle in soil mechanics is the use of effective stress (σ'), which is defined as

$$\sigma' = \sigma - u \qquad (1)$$

where σ = total stress, and u = pore water pressure. The total load acting on an element of soil is the sum of all loads acting on the mass, including its own weight. Total stress is defined as the total load divided by the gross cross-sectional area of the soil mass. This stress cannot be measured directly at any point; however, the total load can be measured or computed, and when it is divided by the area over which it acts, one can obtain the total stress. Therefore, the vertical total stress due to self-weight of the soil increases, generally in a linear fashion with depth, and it is a function of the unit weight of the soil (γ). The unit weight of soil depends on its density (void ratio), specific gravity of the solids, and the degree of saturation. The vertical total stress due to self-weight can be expressed as

$$\sigma_v = \gamma z \qquad (2)$$

where z is the depth below the ground surface (Fig. 1a).

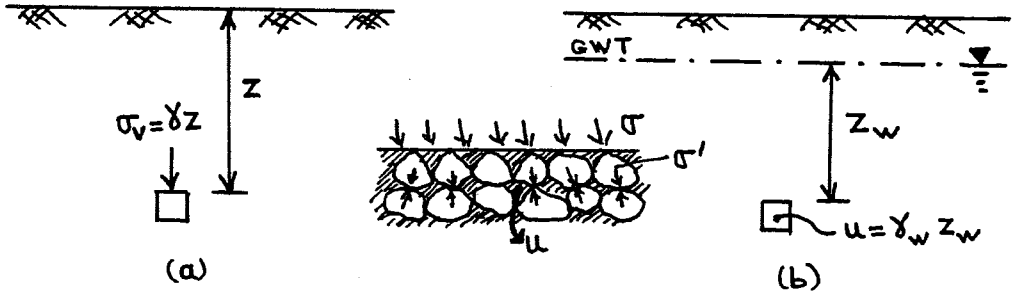

Fig. 1. Total stress and hydrostatic pore pressure.

The weight of structures or other loads applied at the ground surface or excavation of soil cause a change in in situ total stresses.

The actual stress at any point within the soil will depend on the distribution of stresses between the liquid and solid phases for a saturated soil. The water pressure within the soil voids (or pores) is termed pore water pressure (u). In general, pore pressure consists of the pore pressure related to ground water level, u_o, and the **pore pressure change** Δu **(excess pore pressure or pore pressure deficiency)** caused by changing loads on the soil. Therefore;

$$u = u_o + \Delta u \tag{3}$$

The pore pressure related to ground water level can be hydrostatic if the water is not moving; in this case, it can simply be computed from

$$u_o = \gamma_w z_w \tag{4}$$

where z_w is the vertical depth below the ground water table and γ_w is the unit weight of water (Fig. 1b). If the water is moving, the pressure head (hp) can be found from a piezometer or a flow net. In this case, the pore pressure related to flowing ground water can be computed from

$$u_o = \gamma_w \, h_p \tag{5}$$

When soil is loaded by placing a structure or building an embankment, or when it is unloaded by, for example, making an excavation, the tendency to change volume results in pore water pressure change in either case. This change in pressure, Δu may be an increase (excess pore pressure-positive) or a decrease (pore pressure deficiency-negative) depending on the type of soil (its initial density) and the stresses involved. Under the fully drained conditions (such as long-time after imposing stress changes), Δu dissipates and is equal to zero, and pore pressure $u = u_o$. u_o can usually be evaluated without serious difficulty. For partially drained and undrained conditions (such as shortly after imposing stress changes), the evaluation of Δu is often difficult; it depends on the relative rate of loading compared to the rate of drainage within the soil.

Several equations have been proposed to describe the magnitude of the pore pressure change developed as a result of stress changes in undrained soil. For example, one such relationship can be written as

$$\Delta_u = \overline{B} \, \Delta\sigma_v \tag{6}$$

where $\overline{B}$ (sometimes referred to as r_u) is the pore pressure parameter or ratio and $\Delta\sigma_v$ is the change in vertical stress. $\overline{B}$ can be viewed as an empirical coefficient related to the soil's compressibility and degree of saturation. It is not easy to determine $\overline{B}$.

STRESS - STRAIN CHARACTERISTICS

Soils deform under applied stresses. Two stress-deformation curves are shown in Figure 2; stress-strain curves are also of similar form.

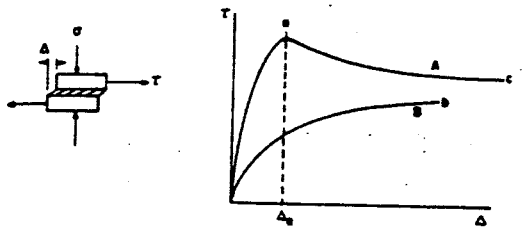

Figure 2. Typical stress-strain curves for soils.

In common practice, the strength of the soil is defined as the peak strength (points and a and b) measured in the test. Many soils demonstrate strain-softening behavior, as illustrated by curve A. it is important in design to account for this decrease. The lower limit to strength (point c) may be called residual strength. For such soils, it is unreasonable to assume that all soil along a failure surface reaches its peak strength simultaneously. In the limit of a large deformation, all strength at all points on the failure surface will be reduced to the residual strength (point c).

The deformation modulus in soils is not constant like in linear elasticity, and it is more complicated. It ordinarily depends on stress field, time and environment.

FAILURE CRITERION

The Mohr-Coulomb criterion is most widely used to define failure in soils. According to this criterion the shear strength can be expressed consistently in terms of effective stress as

$$s = c' + \sigma' \tan \phi' = c' + (\sigma - u) \tan \phi' \qquad (7)$$

where c' and ϕ' are the effective strength parameters: cohesion intercept and angle of internal friction, respectively (Fig. 3).

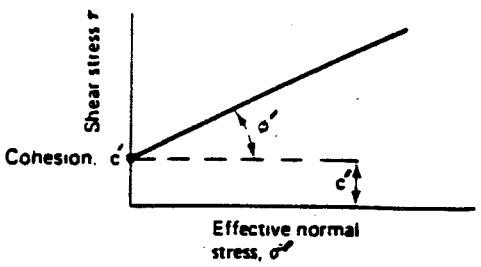

Figure 3. Mohr-Coulomb failure envelope.

As indicated by Eqn. 7, the failure in soils is caused by a critical combination of both shear and normal stresses. Failure is essentially by shear, but critical shear stress is governed by the normal stress acting on the potential surface of failure. The line which plots this critical combination in a τ - σ plot is known as "failure envelope".

The envelope will not necessarily be a straight line, and thus c' and ϕ' would represent a straight line approximation to the actual envelope over the stress range of interest. Furthermore, the envelope will not necessarily have a cohesion intercept, i.e., c' = 0. In fact, the envelope is not a unique quantity for a given soil, but is a function of several variables, the most important being stress history. The use of effective strength parameters requires that the pore pressure ($u = u_o + \Delta_u$) is known so that σ' may be evaluated.

Under fully drained, long-term conditions, the pore pressure change due to applied loads (Δu) is zero, and pore pressure due to ground water flow (u_o) can usually be evaluated without serious difficulty. Hence, analysis with the effective stress description of shear strength (Eqn. 7) is most useful.

For partially drained and undrained conditions, i.e., short-term conditions, the evaluation of Δu is often difficult . In some cases, a total stress description of shear strength may be used as

$$s = s_u \tag{8}$$

One important case is the condition shortly after loading or unloading of saturated fine-grained soils. In this case, the undrained strength (s_u) can be used because of low permeability, where $s_u = c_u$ and $\phi_u = 0$. The shear strength usually changes as drainage occurs. If the change results in a higher strength, the short-term, undrained stability is critical and stability can be expected to improve with time. On the other hand, if drainage produces a decrease in strength, the undrained shear strength can be used only for short-term or temporary situations.

SHEAR STRENGTH OF SOILS
PART II
STRENGTH CHARACTERISTICS AND MEASUREMENT

The shear strength characteristics of different soils and methods used to evaluate shear strength are presented.

MEASUREMENT OF SHEAR STRENGTH

Shear strength is measured both in the **laboratory** and in the **field.** Laboratory tests are made on representative soil samples and must be done in a way that simulates the conditions that will exist in the field as closely as possible; in particular the drainage and the stress conditions. The shear strength of **granular** soils (clean sands and gravels) can generally be made on disturbed samples that are reconstituted in the laboratory to field densities. However, disturbance significantly affects the physical properties of **cohesive** soils (plastic silts and clays, organic soils) even if the field density is maintained; laboratory tests on cohesive soils must therefore be made on undisturbed samples if the strength of a natural soil deposit is to be determined. The strength of proposed **compacted** earth embankments is often required, and for such cases the laboratory samples must be prepared to duplicate the density, water content, and compaction method of the field soil. A variety of field tests available circumvent the problems of sample disturbance attendant to the laboratory tests.

Laboratory Measurement of Shear Strength

The two most commonly used **laboratory shear test** methods are the **direct shear test** (Fig. 4) and the **triaxial compression test** (Fig. 5).

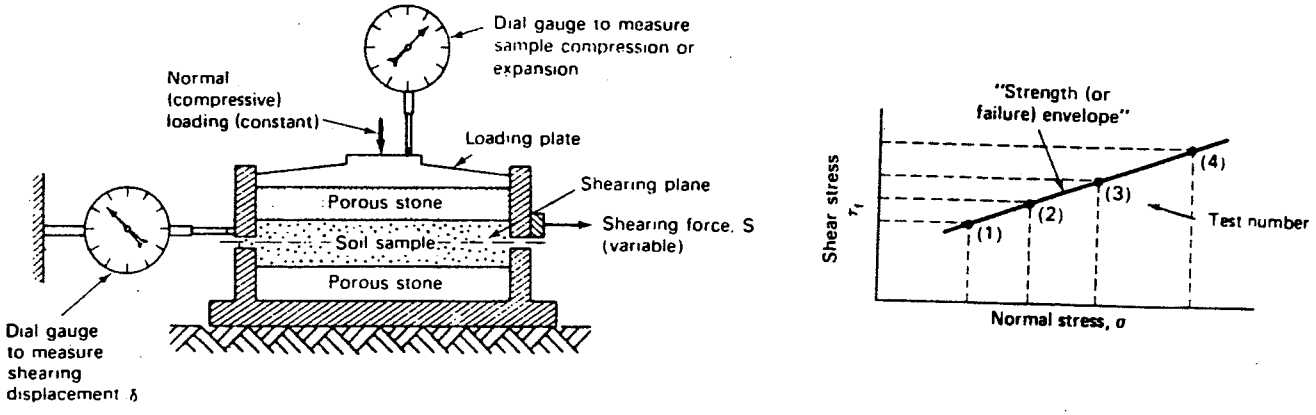

Figure 4. Direct Shear Test.

These tests are capable of establishing the shear strength response defined by Eqns. 7 or 8. These tests allow variation of normal stress and measurement or control of pore pressures. There are also simple methods in the laboratory which are designed to determine the shear strength of a sample in a particular condition, such as the water content or void ratio corresponding to the in situ conditions. These methods are most often used to determine the undrained strength (s_u) of saturated cohesive soils. Simple tests (Fig. 6) include the

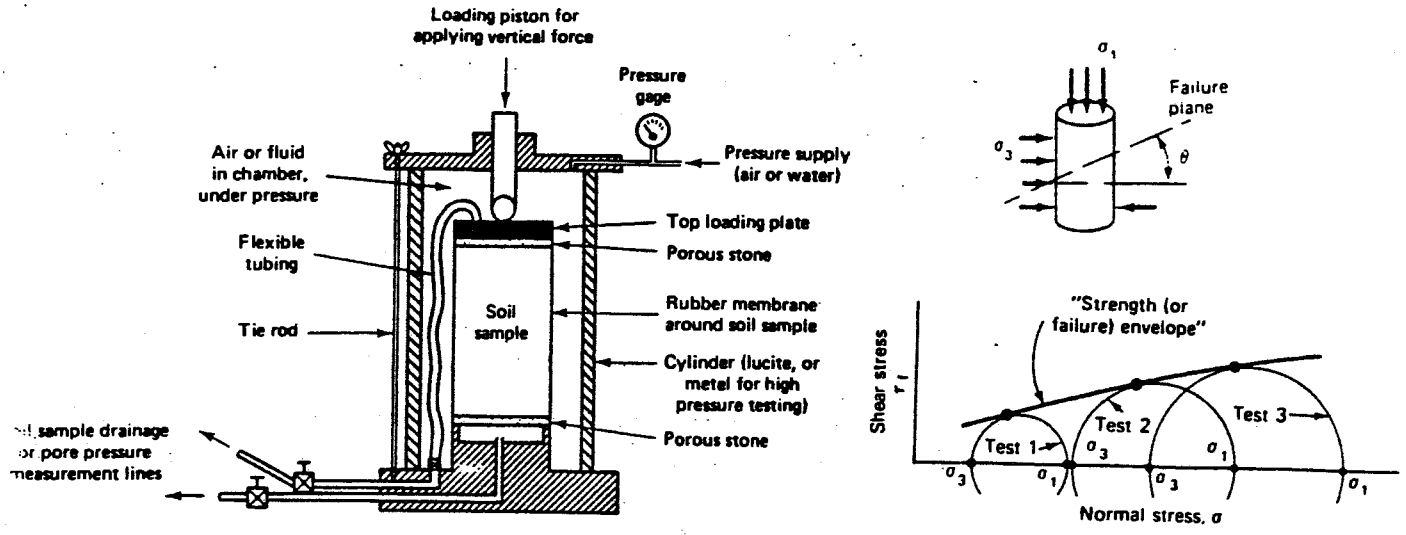

Figure 5. Triaxial Compression Test.

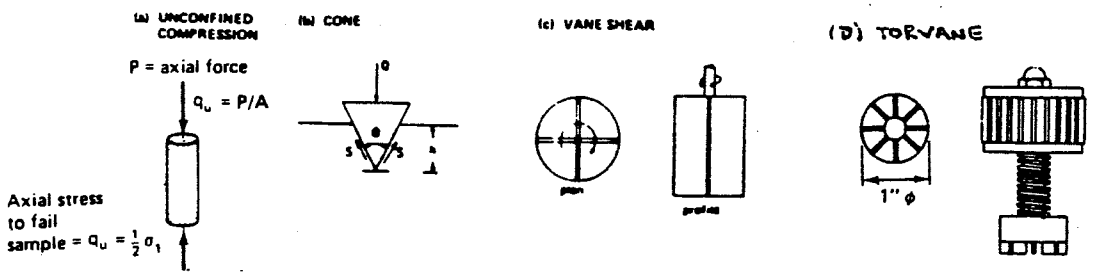

Figure 6. Simple test methods for determining soil strength.

unconfined compression test which is a special case of the triaxial compression test in which no confining pressure is used, the **cone test**, and the **vane test.**

Field Measurement of Strength

To eliminate difficulties arising from sample disturbance, various in-place tests have been devised. An important difference between laboratory and field tests is their relation to the initial in situ state of stress. A laboratory test must often reproduce this state of stress

whereas a field test inevitably begins at this state of stress. Even though the sample disturbance due to the removal of in situ stress is largely eliminated in a field test, the fact that any field test, must be conducted with reference to the existing in situ state of stress is an important limitation in itself. Therefore, field testing usually cannot simulate the large changes in stress that accompany construction activities, cutting, filling, and landslides. In other words, field tests are limited in determining the strength parameters and to establish the shear strength response defined by Eqn. 7.

Certain field tests have been devised to be performed in the same bore holes that are drilled for exploration. More common field tests include **the standard penetration test** (ASTM D 1586), **the cone penetration test, the flat dilatometer test, the pressure meter test, and the field vane shear test.** In the standard penetration test a standard split-tube sample (Fig. 7) is driven 450 mm (18 in.) in three 150-mm (6-in.) increments into undisturbed soil at the bottom of a borehole by blows of a 63.5-kg (140-lb) hammer falling 760 mm (30 in). The sum of the blows for the second and third increments is the standard penetration resistance (N); it is expressed in blows per 300 mm (blow per 1 ft.).

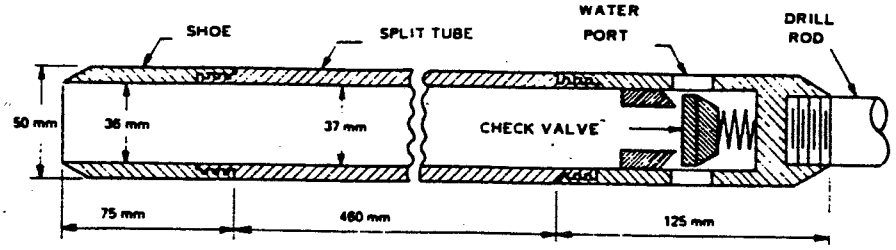

Figure 7. Split-tube sampler for Standard Penetration Test.

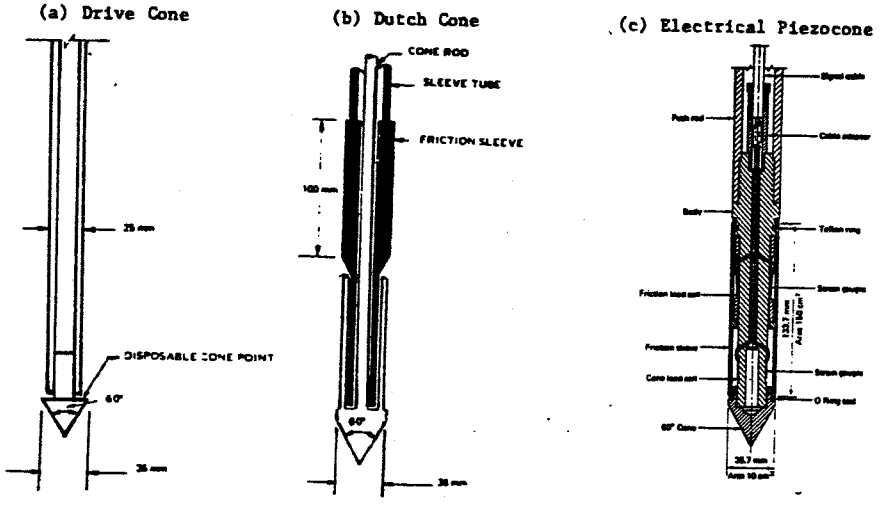

Figure 8. Cone Penetrometers

N is generally correlated empirically with soil properties measured by either laboratory tests or field tests of the same material for calibration. Although many relations between N and soil properties such as strength have been published, these should not be used indiscriminately.

In the quasi-static cone penetration test a conical point (Fig. 8, a, b and c) is forced ahead by a steady force that is measured simultaneously or successively, depending on the design, the frictional resistance of the sleeve against the soil may be measured. The cone does provide detailed information on the relative strength of the soil at small intervals. The ratio of cone resistance to sleeve resistance is an indicator of the type of soil. Several methods are available for evaluating shear strength from cone penetration resistance.

The flat dilatometer (Fig. 9) is a penetrometer that performs a dilation test, whereby resistance to lateral soil deformation is measured. It consists of a pointed blade that has a thin flexible metal membrane centered on one side of the blade and flush with the surface. The blade is advanced into the soil using conventional penetrometer methods (jacking or driving). At the test depth, the membrane is extended 1 mm into the soil by applying pressure. The resistance to membrane expansion relates to soil strength.

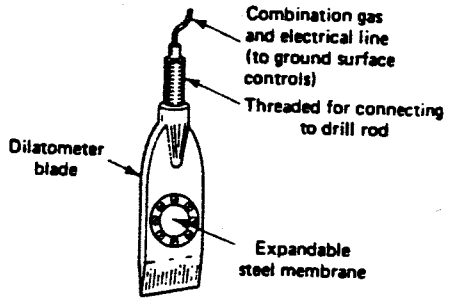

Figure 9. Marchetti Flat Dilatometer

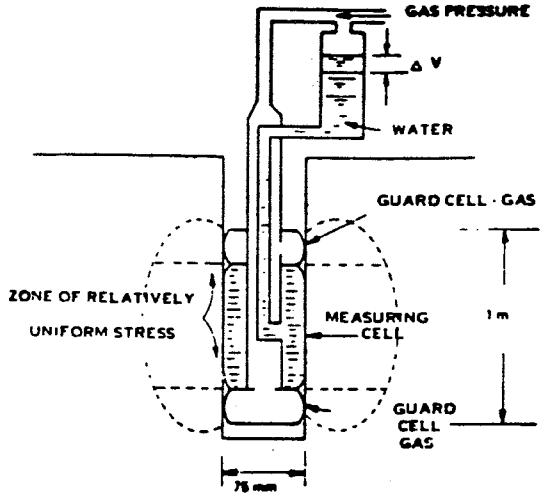

Figure 10. Menard pressure meter for borehole dilation test (not to scale).

The borehole dilation test is another field test (Fig. 10) that can give in situ shear strength. It includes a cylindrical measuring cell that can be pressured and expanded laterally in a borehole. Correlations between applied pressure and resulting soil volume change provide the strength parameters. In the case of the field vane shear test, vertical blades at the end of a thin rod produce a vertical cylindrical surface of shear when rotated (Fig. 11).

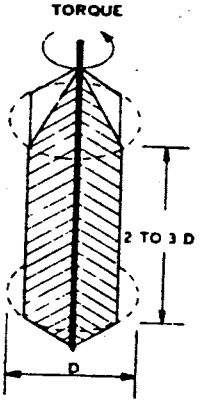

Figure 11. Field vane device.

The torque required to initiate continual rotation is a measure of the peak undrained strength of the clay soil. The strength measured in a vane test has been found to be greater than that measured by other methods.

In addition to the borehole tests, large-scale pit tests are also used. Plate load test and large-scale direct shear test are such field tests.

SHEAR STRENGTH OF GRANULAR SOILS

Clean sands and gravels (fines less than 5-10% by weight) are referred to as **granular** (or sometimes **cohesionless**) soils and are characterized by high permeability. Therefore, their strength is expressed in terms of effective stresses with Δu equal to zero since Δu would dissipate readily under most quasi-static construction activities (drained condition). The only exception to this is dynamic loading such as earthquake or blasting during which in certain sands Δu may build up faster than it can dissipate. For silty cohensionless soils permeability may be sufficiently low that Δu may develop during construction.

In the effective strength computations, only pore pressure due to ground water (u_o) must be estimated since $\Delta u = 0$ (drained). u_o may be positive (due to static or flowing ground water) or negative (due to capillary tension).

There are no cohesive forces (electrical forces) between the grains of **granular** soils. However, if confined, such soils offer resistance to shearing proportional to the effective confining pressure. Shear strength of granular soils can be expressed as

$$s = \sigma' \tan \phi' = (\sigma - u_o) \tan \phi', \quad c' = 0 \qquad (9)$$

Angle of friction has basically two components; one due to **interparticle friction,** the other due to **interlocking.** ϕ' depends, among other factors, on relative density (D_r), grain size distribution, and grain shape (roundness). The value of ϕ' ranges normally from about 27° to 42° or more. The effect of moisture on ϕ' (not on s) is small and amounts to no more than 1° or 2°.

An approximate relationship between ϕ' and D_r is given in Figure 12; angular-grained and well-graded sands would plot close to the upper bound in the plot. The relative density of granular soils may be estimated from the standard penetration resistance using the relationship given in Figure 13.

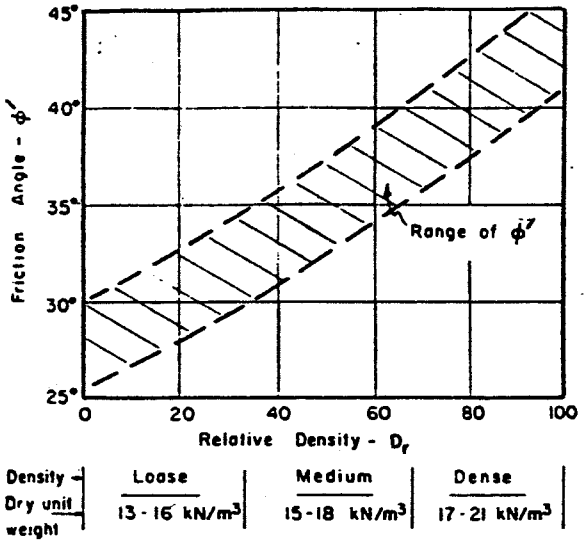

Figure 12. Friction angle as a function of relative density of sand.

The angle of friction for granular soils should, as far as possible, be determined by means of drained triaxial tests or direct shear tests on reconstituted samples of the same density as in situ. The value of ϕ' may be estimated on the basis of standard penetration resistance obtained in the field.

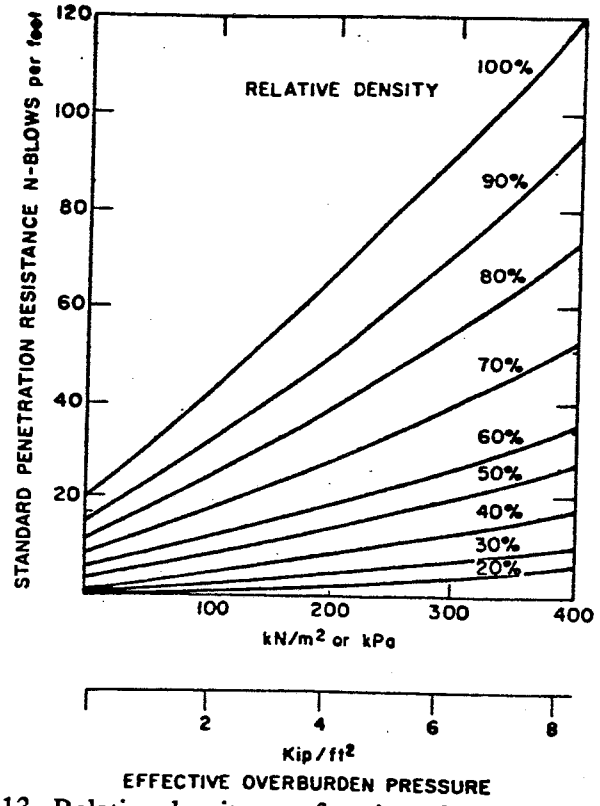

Figure 13. Relative density as a function of standard penetration resistance and overburden pressure.

SHEAR STRENGTH OF COHESIVE SOILS

Soils containing significant amounts of plastic fines (more than 5 to 10% by weight silt and clay) are called **cohesive** soils. Because of the low permeability and high compressibility of clays and plastic silts, the drainage conditions, rate of loading, and the stress history of the soil greatly affect the shear strength properties. A soil that has never been subjected to an effective pressure greater than the existing effective pressure is considered a **normally consolidated** (NC) soil. One that has been subjected to a greater effective pressure is an **overconsolidated** (OC) soil. These terms are used to describe qualitatively the stress history of the soil.

In cohesive soils, clay particles are surrounded by an envelope of water and particle interaction takes place through this water. **Net attraction force between particles, for a given clay-water system, decreases with increasing interparticle distance, i.e., void ratio.** Therefore, upon application or removal of a load, a change in pore pressure, Δu is effected. In response to Δu, pore water tends to flow into (if Δu is negative) or out (if Δu is positive) of the soil. This drainage process results in changing the interparticle distances (void ratio or density) and therefore, the interparticle forces and consequently shear strength. Therefore, the shear strength of cohesive soil changes

(increases or decreases) as a result of construction activity (loading a foundation, building an embankment or making an excavation, etc.) and it is important to take the drainage condition into account. In considering the drainage conditions two limiting cases are usually assumed:

(i) undrained corresponding to the end of construction when full Δu develops and

(ii) drained sufficiently long time after construction when Δu is fully dissipated (because of low permeability of cohesive soils, this may take considerable amount of time).

Undrained or partially drained situations are common in cohesive soils. This is a most important difference between granular soils and cohesive soils. Another important distinction between normally consolidated or lightly overconsolidated and heavily overconsolidated clays is based on the kind of pore pressure change developed in these soils during shear. The general characteristics of **saturated normally consolidated** clays will be discussed first.

In order to simulate the limiting drainage conditions, drained and undrained laboratory tests are performed.

Saturated Normally Consolidated Clays

Consolidated Drained Test - NC Clay

Consider a saturated clay sample placed in a triaxial test chamber and allowed to consolidate under a confining pressure (σ_3) that is equal or greater than its maximum past pressure, σ_c. The axial load on the sample is then slowly increased with drainage at each end of the sample until the failure. In this test, the stress is applied slowly allowing simultaneous drainage of pore water; therefore, the applied stress is equal to the effective stress since pore pressure is nearly zero. When a series of such tests is conducted on a NC soil, the failure envelope is a straight line that passes through the origin (thus, c'=0) as shown in Figure 14.

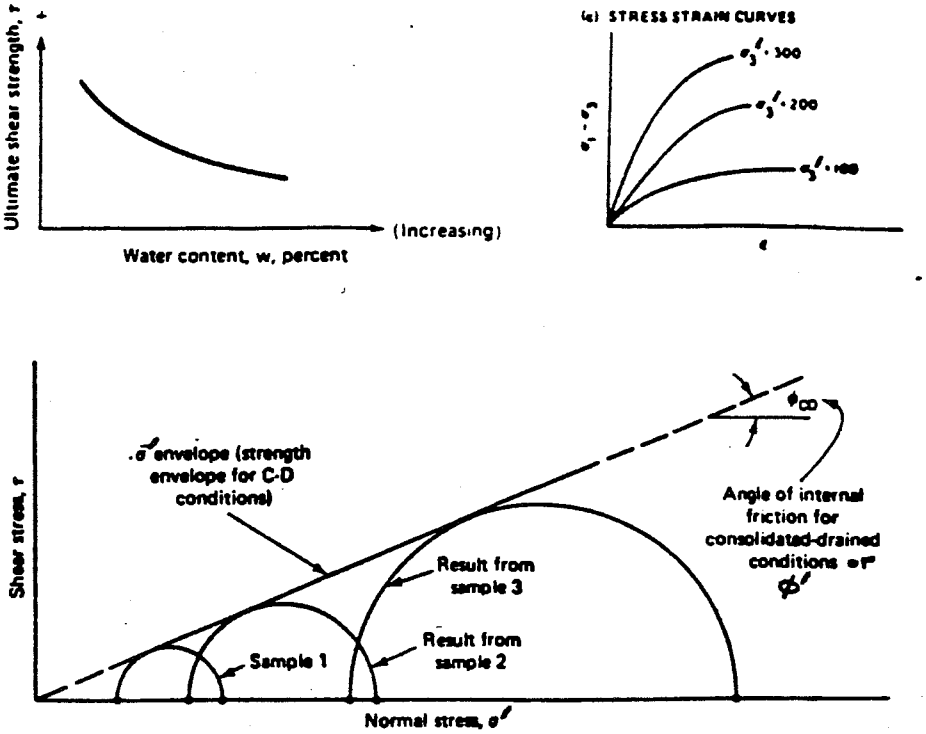

Figure 14. Typical effective strength envelope from a CD triaxial test on a normally consolidated clay.

During the CD test void ratio (or water content) of the sample decreases. The strength envelope is given by

$$s = \sigma' \tan \phi' \qquad (10)$$

in terms of the effective stress.

Unconsolidated Undrained Test - NC Clay

An UU triaxial test is performed by placing a sample in a pressure chamber and applying a confining pressure (σ_3) without allowing any drainage (i.e., no volume change since the sample is saturated) to occur. Following application of the confining pressure, the axial stress is increased without allowing the sample to drain until the failure. Since pore pressures are not measured, the known stresses are the applied total stresses. The failure envelope is a horizontal line as shown in Figure 15 in terms of total stresses. This envelope represents the **undrained strength**, s_u. Since no drainage is allowed in the UU test while stresses are applied, the interparticle distances (or void ratio) remain constant throughout the test at the equilibrium value induced initially in the sample by the in situ stresses prior to sampling. Application of increasing σ_3 does not change this. This test corresponds to undrained field conditions and the effect of Δu on strength due to

loading in the field is accounted for since Δu is allowed to develop in the laboratory test. The unconfined compression test is a special case of the UU test with $\sigma_3 = 0$.

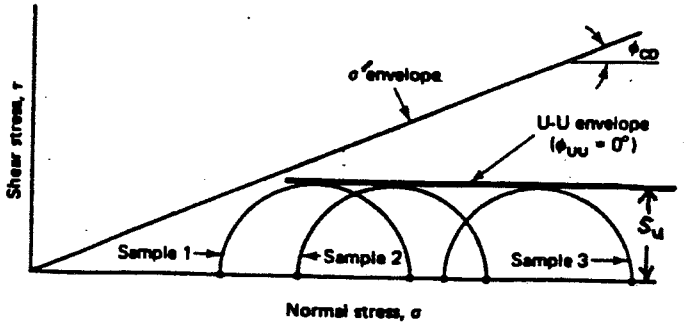

Figure 15. Typical strength envelope from a UU triaxial test on a normally consolidated clay.

Consolidated Undrained Test - NC Clay

The envelope defined in terms of the effective stress, as given in Eqn. 10, can be obtained by performing an undrained test after consolidation, with pore pressure (Δu) measurement. Measured pore pressures during shearing are positive for the NC clay and can be subtracted from the applied stresses (total stresses) to obtain the effective stresses and the relationship given by Eqn. 10. The advantage of the CU test is that it proceeds much faster than the CD test. The relationship of total and effective stress Mohr circles as obtained from a CU test on a NC clay is shown in Figure 16.

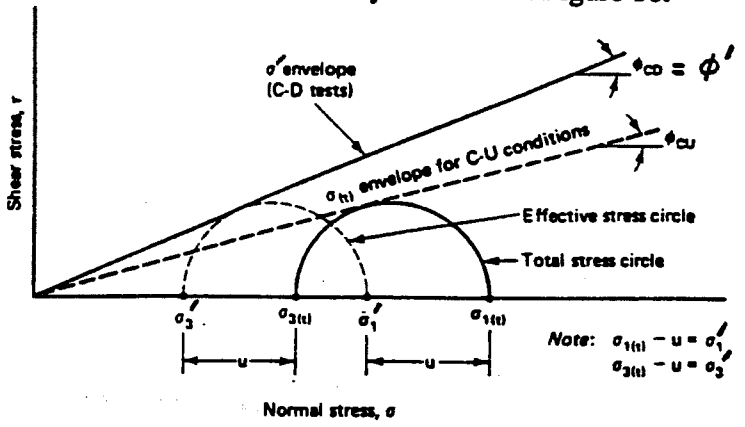

Figure 16. Total and effective stress circles from CU triaxial tests an NC Clay

Heavily Over-consolidated Clays

Most heavily overconsolidated clays show stress-strain relations that suggest general strain-softening (Figure 2, curve A). If the peak strength is used to describe failure, an effective stress failure envelope as shown by line A'B'C in Figure 17 is obtained from a CD test. The failure envelope is approximately a straight line and, if extrapolated to the axis of $\sigma' = 0$, there is a cohesion intercept (c'). Therefore, the **drained** failure envelope is given for the overconsolidated range of stresses ($\sigma_3' < \sigma_c'$) as

$$s = c' + \sigma' \tan \phi' \tag{11}$$

The **undrained** failure envelope of a heavily overconsolidated clay is also a horizontal line like that for a normally consolidated clay (as shown in Figure 15); however, the value of s_u is higher than a corresponding normally consolidated clay.

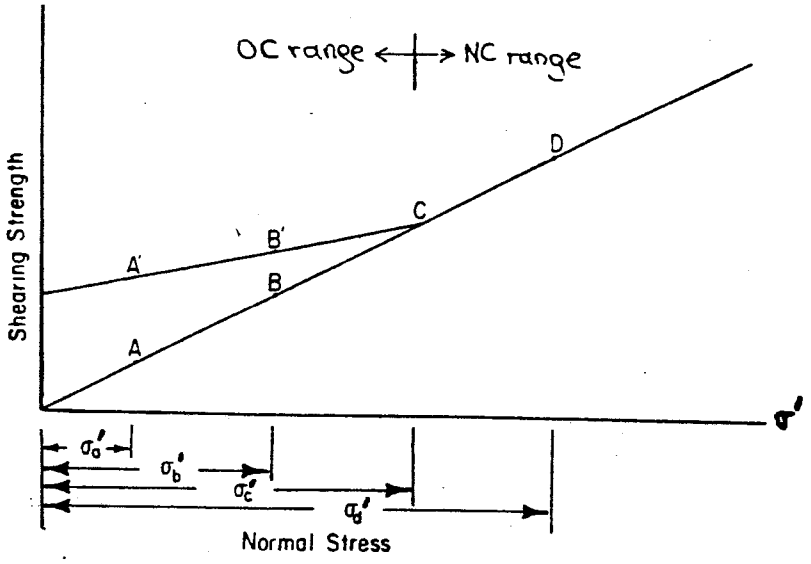

Figure 17. Strength envelope for an overconsolidated clay.

In a CU or UU test, the sample is maintained at constant volume during shearing. Since a heavily overconsolidated clay has a tendency to dilate (similar to a dense granular soil in this respect), the pore pressure change, Δu, will become negative. In other words, coefficient $\overline{B}$ in eqn. 6 may be negative for heavily OC clays while it is positive for NC clays and lightly OC clays. Because Δu becomes negative during undrained shear on a heavily OC clay, the effective stresses are larger than the total stresses, and hence the undrained strength will be greater than the drained strength. In the field the negative pore

pressures over a long period will draw water into the pores, causing an increase in void ratio and a decrease in strength.

Furthermore, many heavily overconsolidated clays contain a network of very small cracks and fissures. Their shear strength is often time dependent and difficult to describe.

Partially Saturated Clays - Compacted Clays

The design of compacted earth embankments and fills requires the determination of the strength of the compacted soils. The strength of compacted cohesive soils is a complex problem, because the compaction moisture content and subsequent changes in the moisture content have a great influence on strength. These soils are generally partially saturated and a total stress analysis is generally used because the pore pressures (u_o) of unsaturated soils are difficult to predict. A UU test does not yield a horizontal failure envelope for the compacted soils due to the compression of air voids under applied confining pressures. Therefore, the undrained strength of such soils is characterized by both c_u and ϕ_u.

Typical Values and Empirical Methods for Strength Parameters of Cohesive Soils

The **undrained shear strength** (s_u) of cohesive soils depends, among other factors, on water content, density, soil texture, clay mineralogy, soil microstructure, stress history, etc. and it may vary from as low as 0.25 tons/ft^2 (25 kPa - very soft) to more than 2 tons/ft^2 (200 kPa - hard). Table 1 gives the empirical relationship between standard penetration resistance (N) and unconfined compressive strength ($q_u = 2s_u$). The undrained strength (s_u) for normally consolidated clays can be estimated from the relationship

$$\frac{s_u}{\sigma'_o} = 0.11 + 0.0037\, I_p \qquad I_p > 10 \tag{12}$$

where σ'_o = effective overburden pressure and I_p = plasticity index. (also designated as PI)

For overconsolidated clays it has been shown that the normalized undrained strength can be estimated from

$$\frac{(s_u/\sigma'_o)_{oc}}{(s_u/\sigma'_o)_{nc}} = (OCR)^{0.8} \tag{13}$$

where OCR is the overconsolidation ratio. The overconsolidation ratio is the ratio of the past maximum vertical effective stress (σ'_c) to the present vertical effective stress (σ'_o) (termed "overburden pressure") at a point in the soil mass:

$$OCR = \frac{\sigma'_c}{\sigma'_o} \tag{14}$$

The **drained** (or effective) cohesion intercept, **c'**, may vary between 0 and 0.2 tons/ft^2 (20 kPa), whereas ϕ' **(drained or effective friction angle)** ranges from more than 30° for clays with low plasticity index to less than 15° for clays with high plasticity index. Peak ϕ' and residual ϕ_r values for normally consolidated clays are given as a function of plasticity index I_p in Figure 18.

Table 1. Empirical Relationship Between SPT and Soil Properties.

N	Consistency	Field identification	γ_{sat}, kN/m^3	q_u, kPa
< 2	Very soft	Easily penetrated several centimeters by fist	16–19	< 25
2–4	Soft	Easily penetrated several centimeters by thumb	16–19	25–50
4–8	Medium	Moderate effort required to penetrate several centimeters with thumb	17–20	50–100
8–16	Stiff	Readily indented by thumb	19–22	100–200
16–32	Very stiff	Readily indented by thumbnail	19–22	200–400
> 32	Hard	Difficult to ident with thumbnail	19–22	> 400

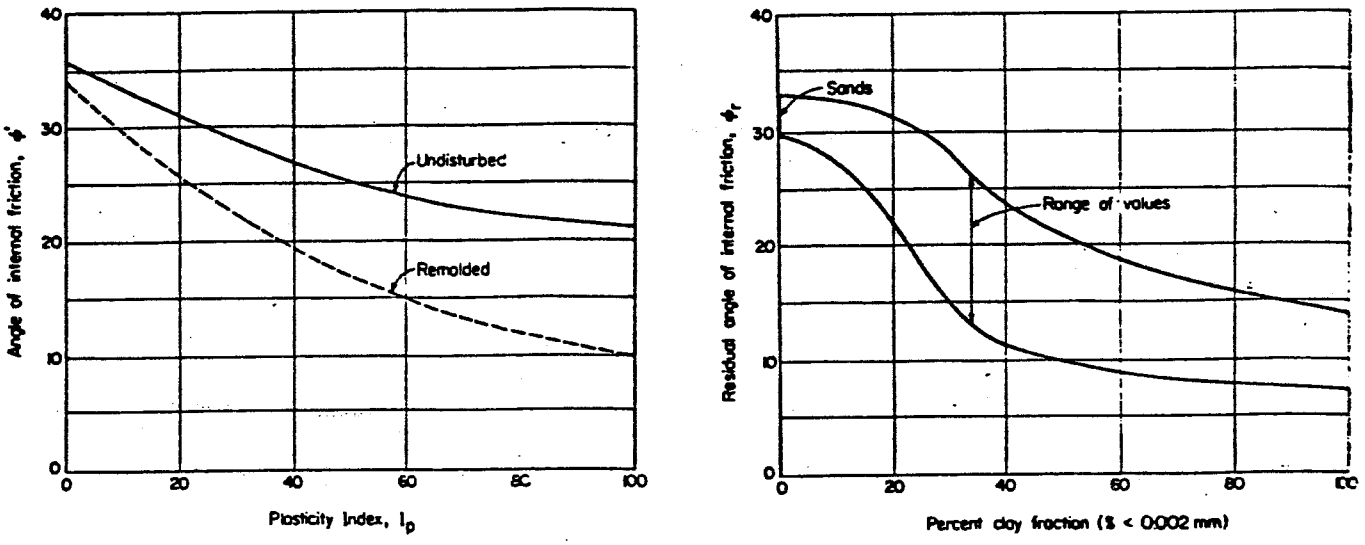

Figure 18. Correlation between: a) ϕ' and plasticity index for normally consolidated clays and b) ϕ_r and percent clay

USE OF DRAINED VERSUS UNDRAINED STRENGTH FOR COHESIVE SOILS

The question of which strength, undrained or drained, to be used for cohesive soils under a given field loading (embankment, building loads, etc.) or unloading (excavation, erosion,e tc.) conditions is of prime importance and the answer depends on the pore pressure generation behavior of the soil in response to stress changes. The pore pressure generation during shear depends, among other things, on the stress history of soil. The stress history is described in quantitative terms by the overconsolidation ratio (OCR). If some depth of soil eroded after deposition or if the weight of glacial ice is removed due to melting, then the material would have OCR > 1. A normally consolidated soil has OCR = 1

The variation of normalized strength with OCR for a typical clay is shown in Figure 19.

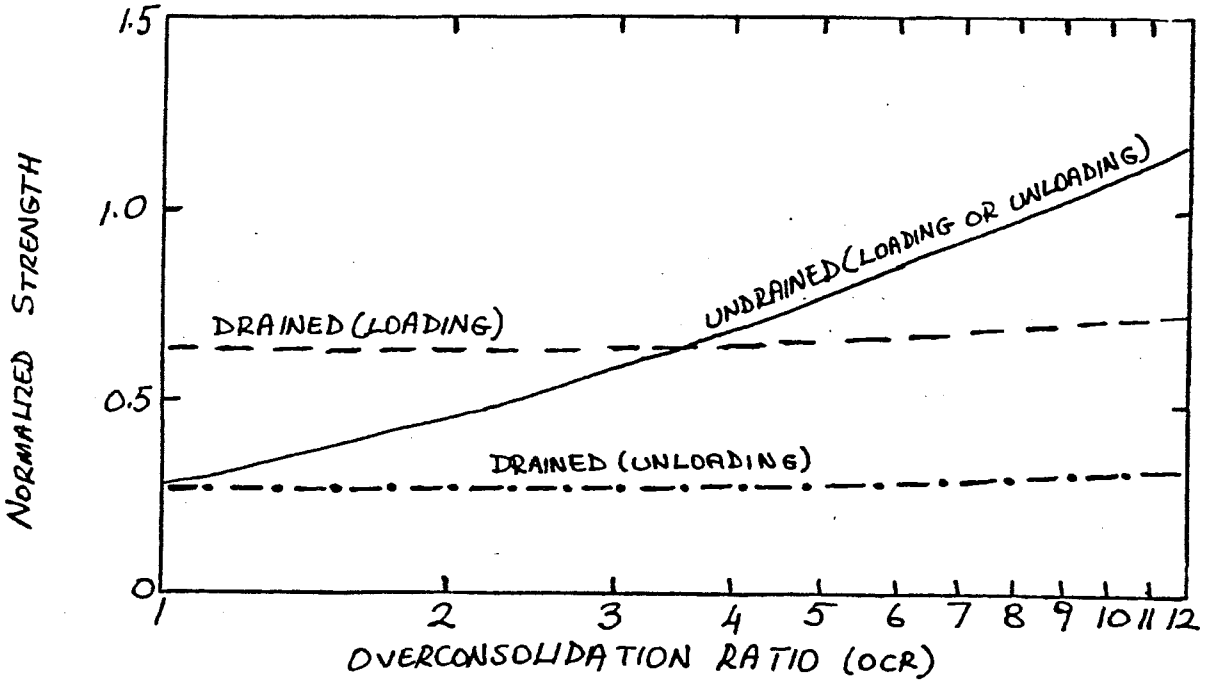

Figure 19. Effect of OCR on drained and undrained strength of clay.

For **unloading** such as in excavations, cuts or river or coastal erosion of slopes, the drained strength is always less (for OC clay, OCR > 1) or equal (only for NC clay, OCR = 1)than the undrained strength. Therefore, in the long-term as the flow of water into soil takes place in response to reduced pore pressures resulting from unloading, the strength drops and the critical strength to be used in the analysis becomes the drained strength. Simple implication of this fact is that an open cut which can be cut to stand initially may cave in after some time.

For **loading** such as embankment construction, foundations, etc., the undrained strength is less than the drained strength for OCR values less than 2 to 4 and therefore, the end-of-construction (short-term) undrained condition is the most critical. As the positive pore pressure dissipate the strength increases to the drained value in the long-term. If OCR is greater than 2 to 4, then the drained strength becomes less than the undrained. In such cases the long-term strength becomes critical similar to the unloading conditions. Table 2 summarizes the critical conditions for stability.

Table 2. Critical conditions for the stability of saturated clays.

Foundation Loading:		
Soil Type:	Soft (NC) clay	Stiff (highly OC) clay
Critical condition:	UU case (no drainage)	Probably UU case but check CD case (drainage with equilibrium pore pressures)
Remarks:	Use $\phi = 0$, $c = \tau_f$ with appropriate corrections (Sec. 11.9).	Stability usually not a major problem
Excavation or Natural Slope:		
Soil type:	Soft (NC) clay	Stiff (highly OC) clay
Critical condition:	Could be either UU or CD case	CD case (complete drainage)
Remarks:	If soil is very sensitive, it may change from drained to undrained conditions.	Use effective stress analysis with equilibrium pore pressures. If clay is fissured, c' and perhaps ϕ' may decrease with time.

REFERENCES

The following publications were referred to in preparing these notes and they can be referred to for a more detailed analysis and understanding.

1. Bowles, J. E. (1979), *Physical and Geotechnical Properties of Soils*, McGraw Hill, NY., N.Y.

2. Dunn, I. S., L. R. Anderson, and F. W. Kiefer (1980), *Fundamentals of Geotechnical Analysis*, Wiley, N.Y.

3. Ladd, C. C., (1971), "Strength Parameters and Stress-Strain Behavior of Saturated Clays," Research Report R71-23, Soils Publication 278, Massachusetts Institute of Technology.

4. Sowers, G. F., (1979), *Introductory Soil Mechanics and Foundations: Geotechnical Engineering*, Fourth Edition, MacMillan Publishing Co., N.Y.

5. Sowers, G. F., and D. L. Royster (1978), "Field Investigation in Landslides," pp. 81-111.

6. Wu, T. H. and D. A. Sangrey (1978), "Strength Properties and Their Measurement," in Landslides: Analysis and Control, Editors: R. L. Schuster and R. J. Krivek, Transportation Research Board Special Report 176, pp. 139-152.

7. Holtz, R. D. and W. D. Kovacs (1981), *An Introduction to Geotechnical Engineering*, Prentice-Hall, Englewood Cliffs, N. J.

8. McCarthy, D. F. (1988), *Essentials of Soil Mechanics and Foundations*, Third Edition, Prentice Hall, N.J.

Table 3.3. Properties of Cohesive Soil Correlated with Standard Penetration Test Results [6]

Clay Consistency	Identification (ASTM D2488-69)	SPT, $\bar{N}$ blows/ft	Undrained Shear Str. lbf/ft^2	Unconfined Compressive Strength lbf/ft^2
Very soft	Easily penetrated several inches by fist. Exudes between fingers when squeezed in hand.	<2	250	500
Soft	Easily penetrated several inches by thumb. Molded by light finger pressure.	2-4	250-500	500-1000
Medium	Can be penetrated several inches by thumb with moderate effort. Molded by strong finger pressure.	4-8	500-1000	1000-2000
Stiff	Readily indented by thumb but penetrated only with great effort.	8-15	1000-2000	2000-4000
Very stiff	Readily indented by thumb nail	15-30	2000-4000	4000-8000
Hard	Indented with difficulty by thumbnail	>30	>4000	>8000

Table 3.4 Relationship between Properties of Cohesionless Soil and Standard Penetration Test Results [21]

Soil Type	SPT, $\bar{N}$ blows/ft	Relative Density D_r%	ϕ (after Peck)	k_a
Very loose sand	<4	0-15	29°	>0.35
Loose sand	4-10	15-35	29-30°	0.35-0.33
Medium dense sand	10-30	35-65	30-36°	0.33-0.26
Dense sand	30-50	65-85	36-41°	0.26-0.21
Very dense sand	>50	85-100	>41°	<0.21

Approximate soil weights are given in Table 4.5.

Note: 1 ft = 0.30 m

Table 3.5 Typical Values of Soil Unit Weight [11]

Soil Type	Moist Unit Weight Above Water Table, $\gamma(lb/ft^3)$	Saturated Unit Weight Below Water Table $\gamma_{sat}(lb/ft^3)$
Poorly graded sand	105-115	115-125
Clean well graded sands	115-125	125-130
Silty or clayey sand & gravel	125-135	130-145
Soft to medium clay	100-115	100-115
Stiff to very stiff clay	110-125	110-125
Organic silt or clay	90-100	90-100

SLOPE STABILITY ANALYSIS

Tuncer B. Edil
University of Wisconsin-Madison

LECTURE OUTLINE

- Infinite Slopes
- Finite Slopes: Plane, Circular and Noncircular Failure Surfaces
- Water Forces on Soil
- Effective and Total Stress Methods
- Critical Conditions for Stability: End-of-Construction, Sudden Drawdown, Long Term

COMMON FEATURES OF SLOPE STABILITY ANALYSIS METHODS

- Safety Factor: $F = S/S_m$ where S = shear strength and S_m = mobilized shear resistance. F = 1: failure, F > 1: safety
- Shape and location of failure is not known a priori but assumed (trial and error to find minimum F)
- Static equilibrium (equilibrium of forces and moments on a sliding mass)
- Two-dimensional analysis

INFINITE SLOPE ANALYSIS

- Translational failures along a plane failure surface parallel to slope surface
- The ratio of depth to failure surface to length of failure zone is relatively small (<10%)
- Applies to surface ravelling in granular materials or slab slides in cohesive materials
- Equilibrium of forces on a slice of the sliding mass along the failure surface is considered

INFINITE SLOPE ANALYSIS

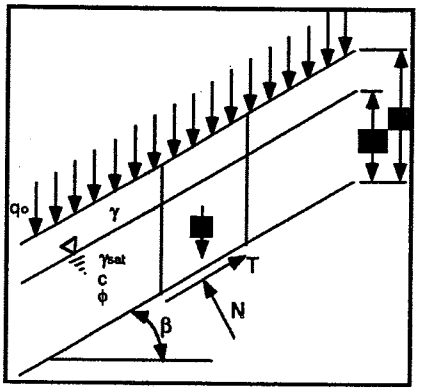

$$F = \frac{\dfrac{c'}{\cos^2\beta\tan\beta} + \left[(q_0 + \gamma H) + (\gamma_{bouy} - \gamma)H_w\right]\dfrac{\tan\phi'}{\tan\beta}}{\left[(q_0 + \gamma H) + (\gamma_{sat} - \gamma)H_w\right]}$$

INFINITE SLOPE

- $F = f(c', \phi', \gamma, \beta, d, u)$
- $F = (c'/\gamma d)\,\sec\beta\,\mathrm{cosec}\beta + (\tan\phi'/\tan\beta)(1 - r_u \sec^2\beta)$
  where $r_u = u/\gamma d$
- For Granular Soil: $F = (\tan\phi'/\tan\beta)(1 - r_u \sec^2\beta)$
  Dry Granular Soil ($r_u = 0$): $F = (\tan\phi'/\tan\beta)$

WATER FORCES ON SOIL

- Water fills voids and increase weight which increases driving forces
- Water also exerts pore pressures which decrease effective stress and therefore strength
- There are mathematically two equivalent ways of taking water forces into account in stability analyses

EQUIVALENT METHODS FOR WATER FORCES

- 1. Boundary water force + total unit weight $u = h_p \gamma_w$; γ_{sat} consider soil element (particles and water filled pores) as single solid mass
- 2. Seepage force + submerged unit weight $F_s = i \gamma_w V$; γ' consider soil element as particle skeleton with water external to it

BOUNDARY WATER FORCE

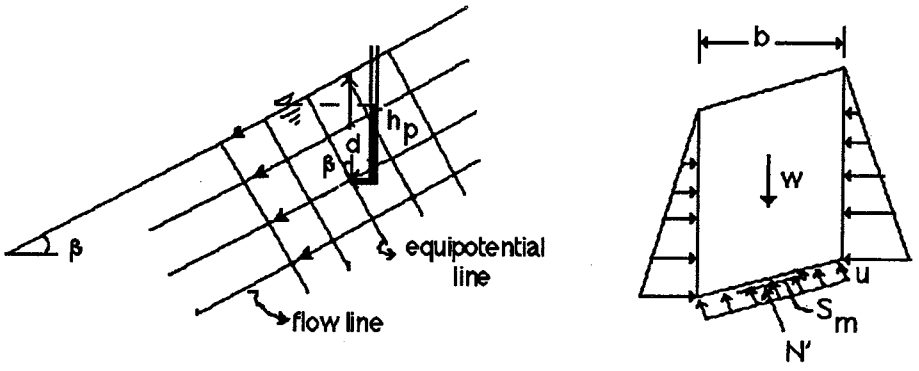

a) Boundary water force

SEEPAGE FORCE

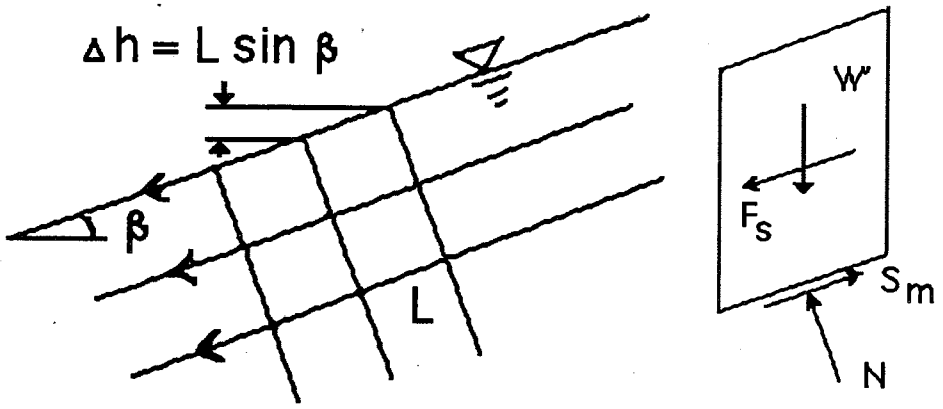

FINITE SLOPES: PLANE FAILURE SURFACE

- Translational Block Slides along single plane of weakness or geological interface
- $F = c'L + (W \cos\theta - uL) \tan\phi' / W \sin\theta + F_w$

BLOCK SLIDES

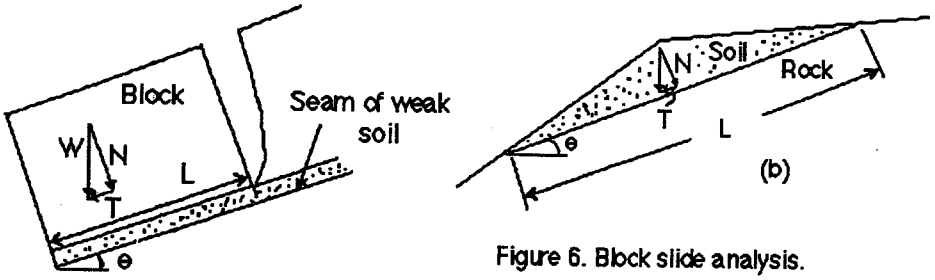

Figure 6. Block slide analysis.

FINITE SLOPES: CIRCULAR FAILURE SURFACE

- Rotational Slides - Method of Slices
- Applies to slopes containing cohesive soils
- Ordinary Method of Slices (Fellenius' Method)
- Bishop's Simplified Method
- Spenser's Method

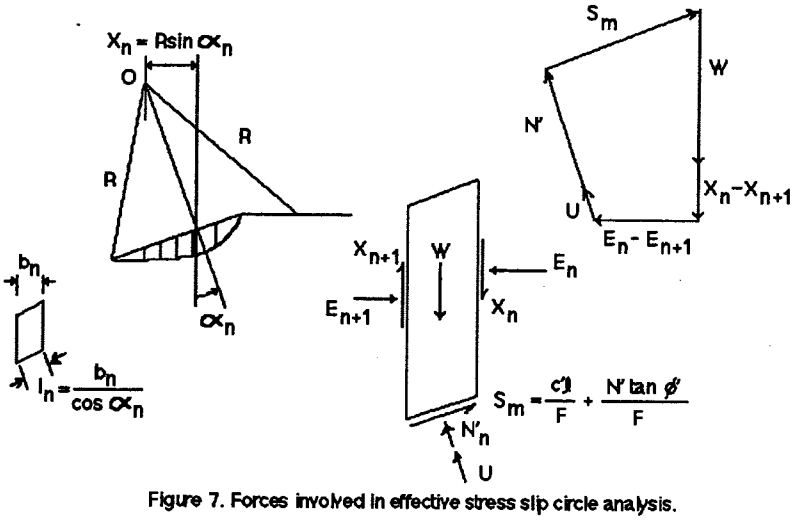

Figure 7. Forces involved in effective stress slip circle analysis.

ORDINARY METHOD OF SLICES

- Assumes that resultant of side forces on each slice are collinear and act parallel to failure surface and therefore cancel each other
- $F = \Sigma[c_n l_n + (W_n \cos\alpha_n - u_n l_n) \tan\phi_n] / \Sigma W_n \sin\alpha_n$
- Undrained analysis: $F = \Sigma[c_n l_n] / \Sigma W_n \sin\alpha_n$

SIDE FORCES IN ORDINARY METHOD OF SLICES

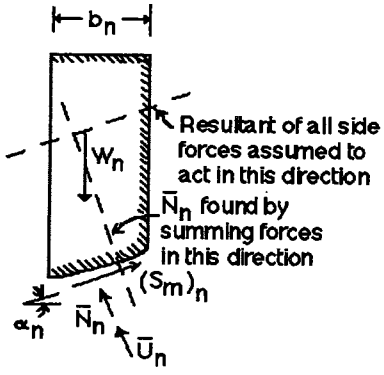

(a)

BISHOP'S SIMPLIFIED METHOD

- Assumes that resultant of side forces on each slice act in horizontal direction and therefore vertical side force components cancel each other
- $F = \Sigma[c_n\, b_n + (W_n - u_n\, b_n)\, \tan\phi_n](1/m_\alpha) \,/\, \Sigma W_n \sin\alpha_n$
- $m_\alpha = \cos\alpha_n + (\sin\alpha_n \tan\alpha_n)/F$
- Undrained analysis: $F = \Sigma[c_n\, l_n] \,/\, \Sigma W_n \sin\alpha_n$

CHART FOR m_α

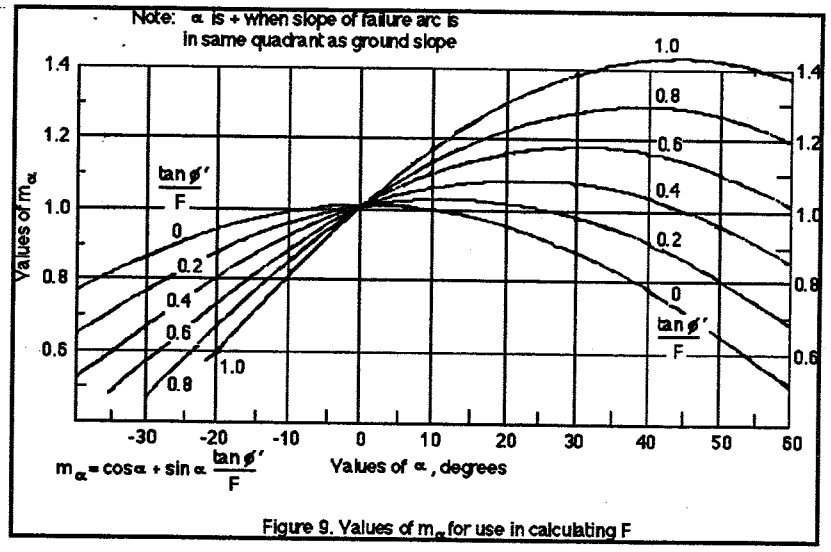

Figure 9. Values of m_α for use in calculating F

SIDE FORCES IN BISHOP'S METHOD

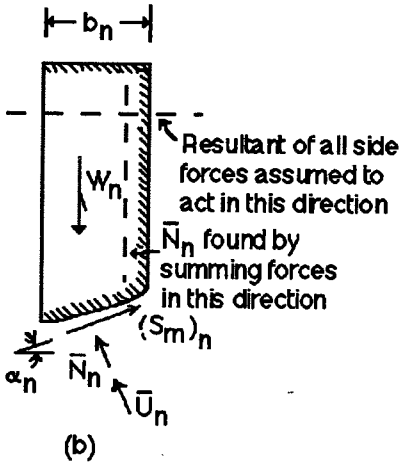

SPENCER'S METHOD

- Assumes that the point of application of resultant of side forces on each slice is at mid-height of each slice but no assumption is made regarding inclination of resultants; inclination is determined as part of the solution
- This method is more exact than Bishop's

FINITE SLOPES: NONCIRCULAR FAILURE SURFACE

- Wedge Method
- Janbu's Simplified Method
- Morgenstern-Price Method

WEDGE METHOD

- Failure surface consists of two or more planes and applicable to slope containing several planes of interfaces and weak layers
- Force equilibrium is satisfied
- Assumes that resultant of side forces on each slice either acts horizontally or at varying angles from horizontal (typically up to 15°)

WEDGE METHOD

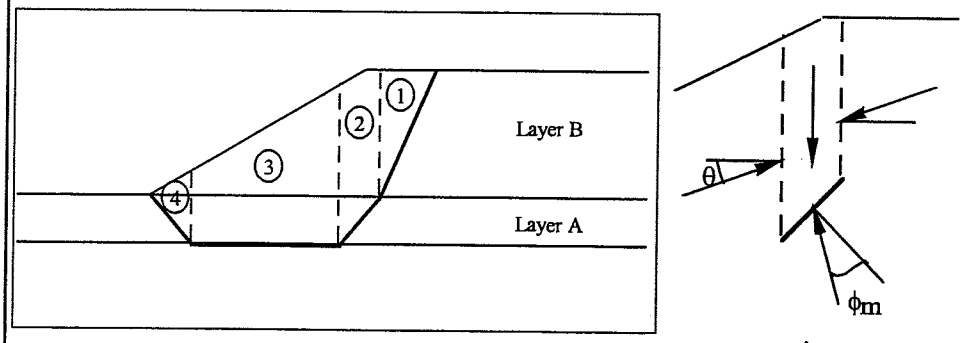

WEDGE ANALYSIS

Equilibrium of Forces in each slice is considered to adjust the inter-slice forces and balance them resulting in a correct solution.

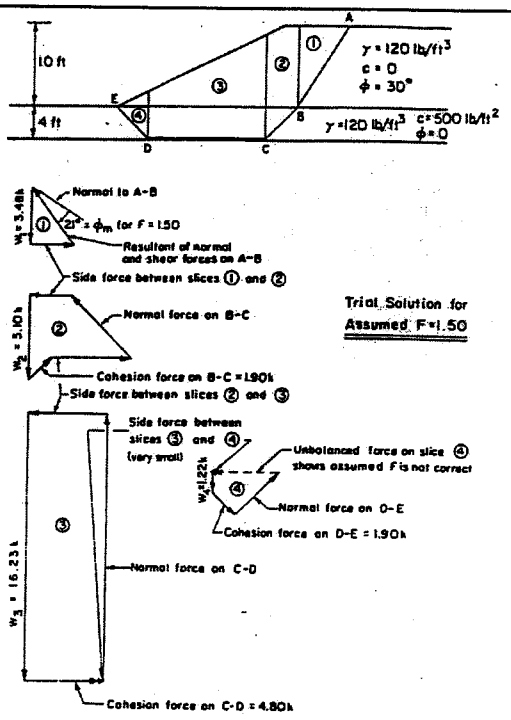

JANBU'S SIMPLIFIED METHOD

- A method of slices applicable to circular and noncircular failure surfaces
- $F = f_o \Sigma\{[c_n b_n + (W_n - u_n b_n) \tan\phi_n](1/\cos\alpha_n m_\alpha)\} / \Sigma W_n \tan\alpha_n$
- f_o is a correction factor that varies with depth to length ratio of sliding mass and type of soil ($\phi = 0$, c, ϕ or c = 0)

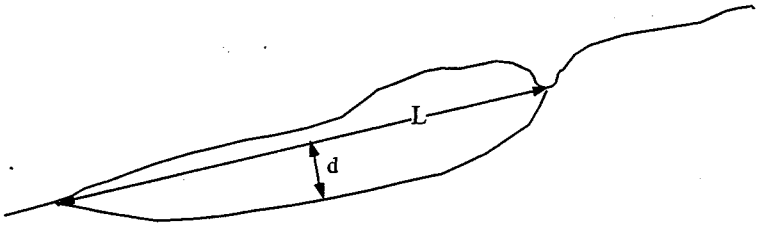

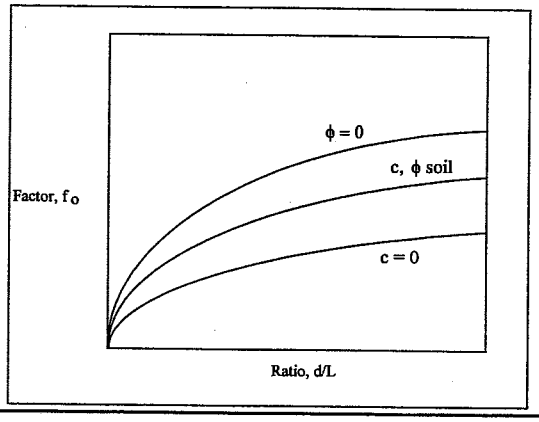

MORGENSTERN-PRICE METHOD

- No assumption is made regarding inclination or point of application of resultants and these are determined as part of the solution
- Requires computers for solving the basic equation
- Exact but not practical

REFERENCES

J.M. Duncan, A.L. Buchignani and M. De Wet (1987), An Engineering Manual for Slope Stability Studies, Virginia Tech Department of Civil Engineering, Blacksburg, Virginia.

L.W. Abramson, T.S. Lee, S. Sharma and G.M. Boyce (1996), Slope Stability and Stabilization Methods, Wiley, N.Y.

Das, B. M., Principles of Geotechnical Engineering, 3rd Ed., PWS Publishing Co., Boston, MA, 1994.

Soil Mechanics Design Manual, NAVFAC DM-7.1, Department of the Navy, 1982.

III

SLOPE STABILITY ANALYSIS

prepared by

Professor Tuncer B. Edil

University of Wisconsin-Madison

- INFINITE SLOPES
- WATER FORCES ON SOIL
- FINITE SLOPES
    - Plane Failure Surface - Block Slide Analysis
    - Circular Failure Surface - Method of Slices
        - Ordinary Method of Slices
        - Bishop's Simplified Method
        - Spencer's Method
    - Noncircular Slip Surface
        - Morgenstern-Price Method
        - Janbu's Simplified Method
        - Wedge Method
- EFFECTIVE AND TOTAL STRESS METHODS
- CRITICAL CONDITIONS FOR STABILITY
- COMPUTER PROGRAMS FOR STABILITY ANALYSIS
- EXAMPLES OF SLOPE ANALYSES

STABILITY OF INFINITE SLOPES

Examples of slopes which can be analyzed using infinite slope analysis:

- embankment formed by end dumping from a truck
- ore or sand stock piling by dropping from a chute
- natural slopes formed in granular materials where the critical failure mechanism is shallow sliding or surface ravelling
- natural slopes formed in cohesive soils with great extent or weak cohesive material on ledge
- slopes in residual soils where a relatively thin layer of weathered soil overlies a firmed soil or rock

Characteristics:

a) thickness of failed material is small compared to the height of the slope,
b) failure surface parallel to slope surface.

The forces acting on a slice of an infinite slope is shown in Fig. 1.

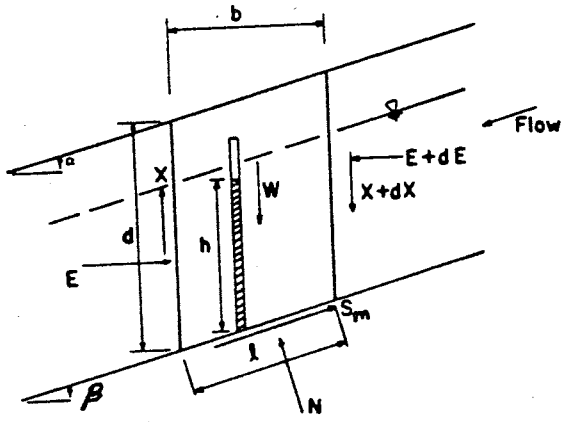

Figure 1. Forces acting on idealized slide of infinite slope.

In an effective stress analysis, the pore pressure distribution is assumed to be known, and in this case steady seepage is assumed to be parallel to the slope surface with the ground-water table as indicated. The forces acting on a slice of width b are shown. Since there is is no internal distortion and the end effects are neglected, $dE = dX = 0$.

The weight of a slice is given by $W = \gamma bl$. The total normal force (N) is related to the effective force (N') and pore pressure (u) by

$$N = N' + ul \qquad (1)$$

and

$$u\bar{l} = (\gamma_w h_p) \sec \beta \qquad (2)$$

where h_p is the piezometric head acting on the slip surface. The mobilized (or "developed") shear resistance acting along the base of the slice (S_m) is

$$S_m = (c'b \sec \beta)/F + (N-u\bar{l}\,) (\tan \phi'/F) \qquad (3)$$

where

c' = cohesion intercept in terms of effect ive stress, and

ϕ' = angle of internal friction in terms of effective stress

F = factor of safety

By resolving W into components parallel and perpendicular to the slope, we get $T = W \sin \beta$ and $N = W \cos \beta$.

Setting $S_m = T$ and N forces can be eliminated between these equations and an explicit relation for F can be found as

$$F = (c'/\gamma d) \sec \beta \operatorname{cosec} \beta + (\tan \phi'/\tan \beta) [1-(\gamma_w h_p/\gamma d) \sec^2 \beta] \qquad (4)$$

F is a function of two dimensionless rations $(c'/\gamma d)$ and $(\gamma_w h_p/\gamma d)$.

The latter, which expresses the relation of the magnitude of the pore pressure at a point and the overburden pressure at that point, has been called the pore-pressure ratio (r_u). With r_{su}, F becomes

$$F = (c'/\gamma d) \sec \beta \operatorname{cosec} \beta + (\tan \phi'/\tan \beta) (1-r_u \sec^2 \beta) \qquad (5)$$

which in the case of *zero cohesion* (clean sands and gravels and normally consolidated or weathered cohesive soilds) becomes

$$F = (\tan \phi'/\tan \beta) (1-r_u \sec^2 \beta) \qquad (6)$$

The value of r_u for different water conditions are as follows:

Deep water table:

$r_u = 0$ (soil dry) or negative due to water tension (can be assumed zero).

Seepage parallel to slope face:

$$r_u = (X/T) (\gamma_w/\gamma) \cos^2 \beta \qquad (7)$$

where X and T are, respectively, the thickness of the seepage zone and the depth of the failure zone measured normal to the slope face.

Seepage emerging from slope:

$$r_u = (\gamma_w/\gamma)\,(1 + \tan\beta \tan\theta)^{-1} \qquad (8)$$

where θ is the angle the seepage emerging from the slope makes with horizontal.

Infinite Slope in Cohesionless Soil (c'=0)

Deep water table:

$$F = \tan\phi'/\tan\beta \qquad (9)$$

Submerged:

$$F = \tan\phi'/\tan\beta \qquad (10)$$

Both the shear stress and the effective normal stress (and therefore, the shear strength) are reduced in this case due to buoyancy in the same proportion resulting in a safety factor same as if the slope is dry.

Seepage parallel to slope face and X = T:

$$F = (\gamma'/\gamma)\,(\tan\phi'/\tan\beta) \qquad (11)$$

where $\gamma' = \gamma - \gamma_w$ (submerged or buoyant unit weight)

Infinite Slope in Cohesive Soil $(c' \neq 0;\ \phi' \neq 0)$

For conditions of parallel see page shown in Fig. 2 the safety factor can be expressed as

$$F = \frac{c' + [d_1\gamma_1 + (d-d_1)\gamma']\cos^2\beta \tan\phi'}{[d_1\gamma_1 + (d-d_1)\gamma]\sin\beta\cos\beta} \qquad (12)$$

Setting F = 1 for the limit equilibrium, we obtain

$$(c'/\gamma d_c) = \cos^2\beta\{[1-(d_1/d_c)(\gamma-\gamma_1)/\gamma]\tan\beta - [(\gamma'/\gamma) + (d_1/d_c)(\gamma_1 - \gamma']\tan\phi\} \quad (13)$$

The ratio $(c'/\gamma d_c)$ is called "stability number".

Deep water table: $d_1 \geq d_c$; $\gamma' = \gamma_1 = \gamma$; use γ.

Submerged: $\gamma_1 = \gamma = \gamma'$; use γ'.

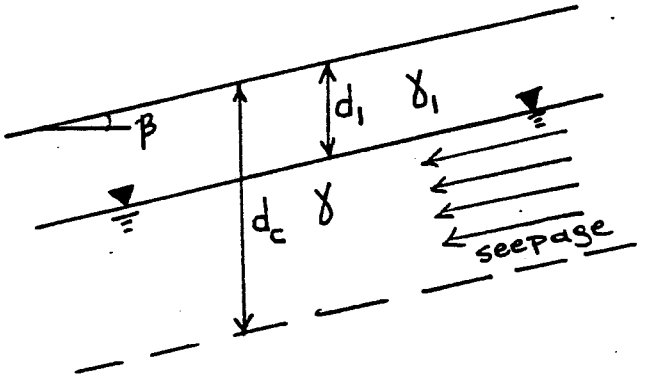

Figure 2. Infinite slope in cohesive soil.

WATER FORCES ON SOIL

In considering the stability of a slice under the influence of seeping water, we can use one of the two equivalent methods:

(1) Boundary water forces acting on a soil element (use the total unit weight).

(2) Seepage and buoyancy forces acting on the solid skeleton (use submerged unit weight).

Water forces acting on a soil sample in the case of upward flow is shown in Fig. 3. The force equilibrium for the same sample is shown in Fig. 4 according to the two methods mentioned above.

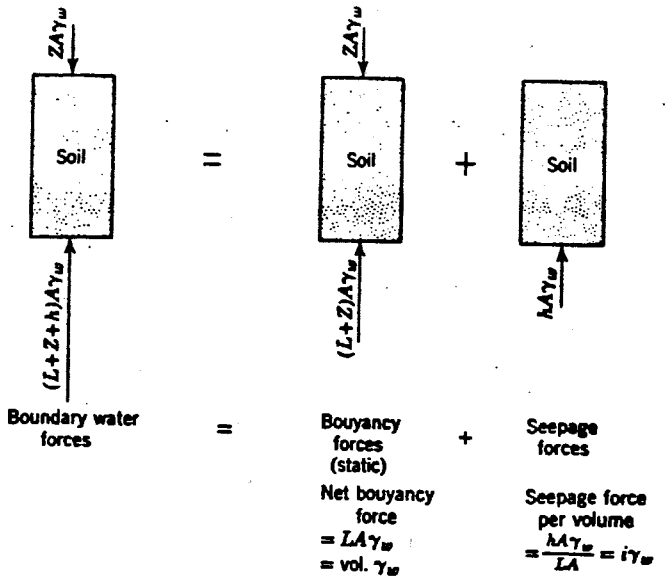

Figure 3. Water forces on soil sample.

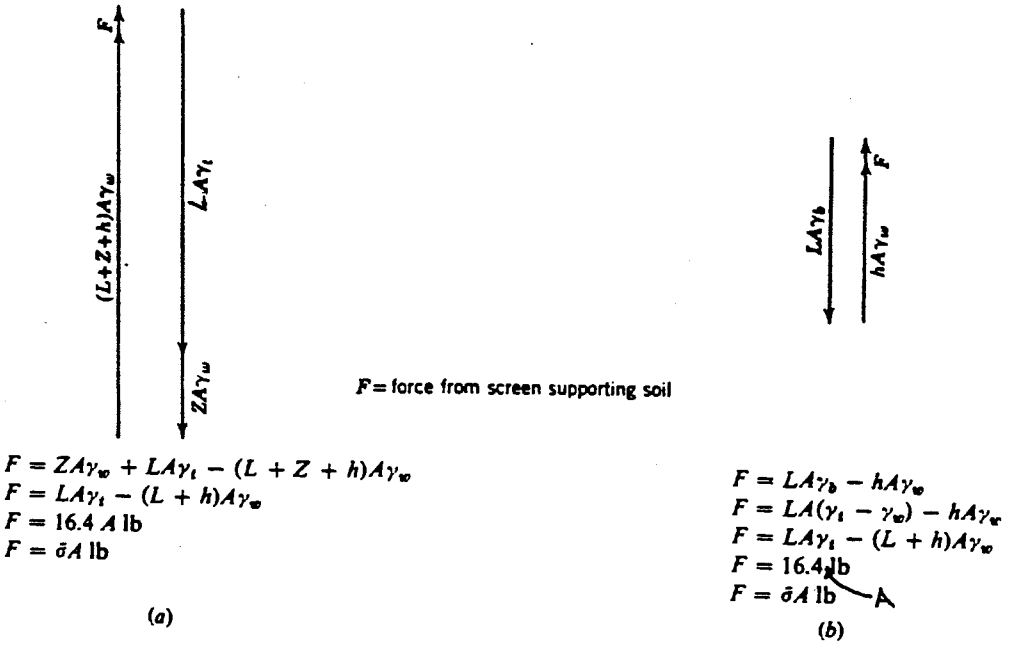

Figure 4. Force equilibrium: (a) Boundary forces plus total weight; (b) Seepage force plus submerged weight.

As seen the two methods give the same result. The principle that we can use either boundary forces with total weights or seepage forces with submerged weights in analyzing the forces acting on an element of soil holds for the most complex flow situations. However, the use of boundary forces with total weights is nearly always the more convenient method. The seepage force per volume is equal to the hydraulic gradient times the unit weight of the permeant. In an isotropic soil the seepage force always acts in the direction of flow.

In order to demonstrate the use of the two methods in slop stability analysis, we can analyze the infinite slope in cohesionless soil with seepage parallel to the slope face. Figure 5 shows the forces according to each method.

In the case of *boundary water forces method*:

pore water pressure $u = h_p \gamma_w = d \gamma_w \cos^2\beta$

boundary pore water force $U = ul = bd \gamma_w \cos \beta$

effective normal force $N' = bd \gamma \cos \beta - bd \gamma_w \cos \beta = bd \gamma' \cos \beta$

shear force $T = bd \gamma \sin \beta$

mobilized shear resistance $s_m = N'(\tan \phi'/F)$

Setting $S_m = T$ and solving for the safety factor we obtain

$$F = (\gamma'/\gamma)(\tan \phi'/\tan \beta) \qquad (14)$$

In the case of the *seepage force method:*

gradient $i = (L \sin \beta)/L = \sin \beta)$

normal force $N = bd \gamma' \cos \beta$

shear force $T = bd \gamma' \sin \beta + F_s$

seepage force $F_s = \gamma_w bd \sin \beta$

setting $S_m = g$ and solving for F we obtain

$$F = (\gamma'/\gamma) (\tan \phi'/\tan \beta) \qquad (15)$$

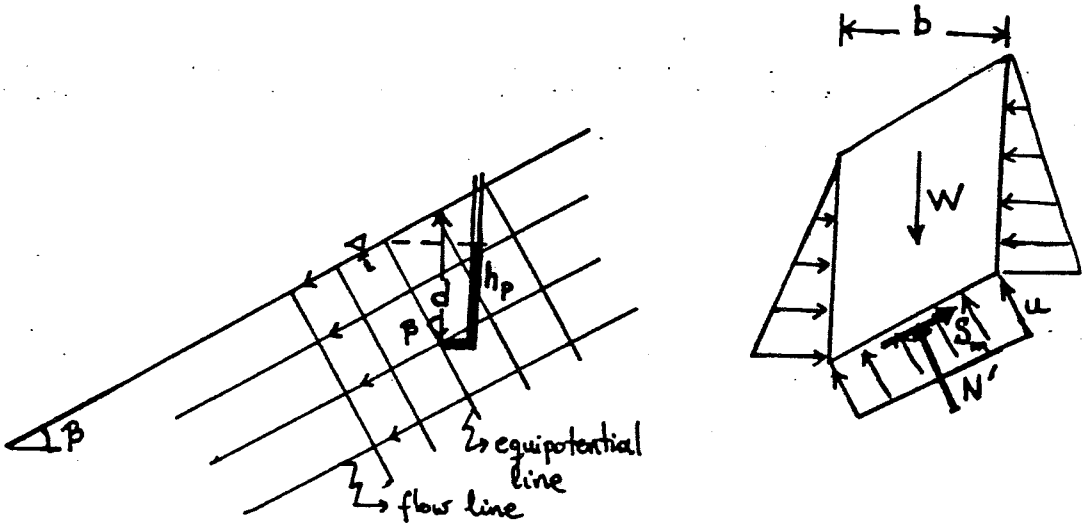

a) Boundary water force

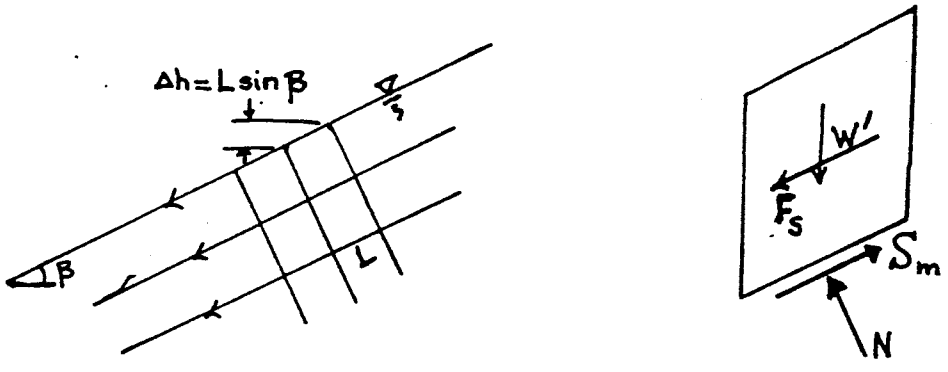

b) Seepage force

Figure 5. Stability of infinite slope in cohesionless soil.

FINITE SLOPES

Plane Failure Surface

This occurs when a soil deposit has a specific plane of weakness. Excavations into stratified deposits where the strata dipping toward the excavation may fail along a plane parallel to the strata. In earthdams along sloping cores of weak material a plane failure may occur. If the failure plane is a complex one, a wedge analysis is needed. This is not a likely failure mode in homogeneous soils unless it is a very steep slope.

Block Slide Analysis. If a mass of soil or rock rests upon an inclined layer of weak or loose soil (Fig. 6(a)) or a mass of soil of finite extent rests upon rock that is less pervious than the soil, failure may occur as a block slide along the inclined plane of contact (Fig. 6(b)).

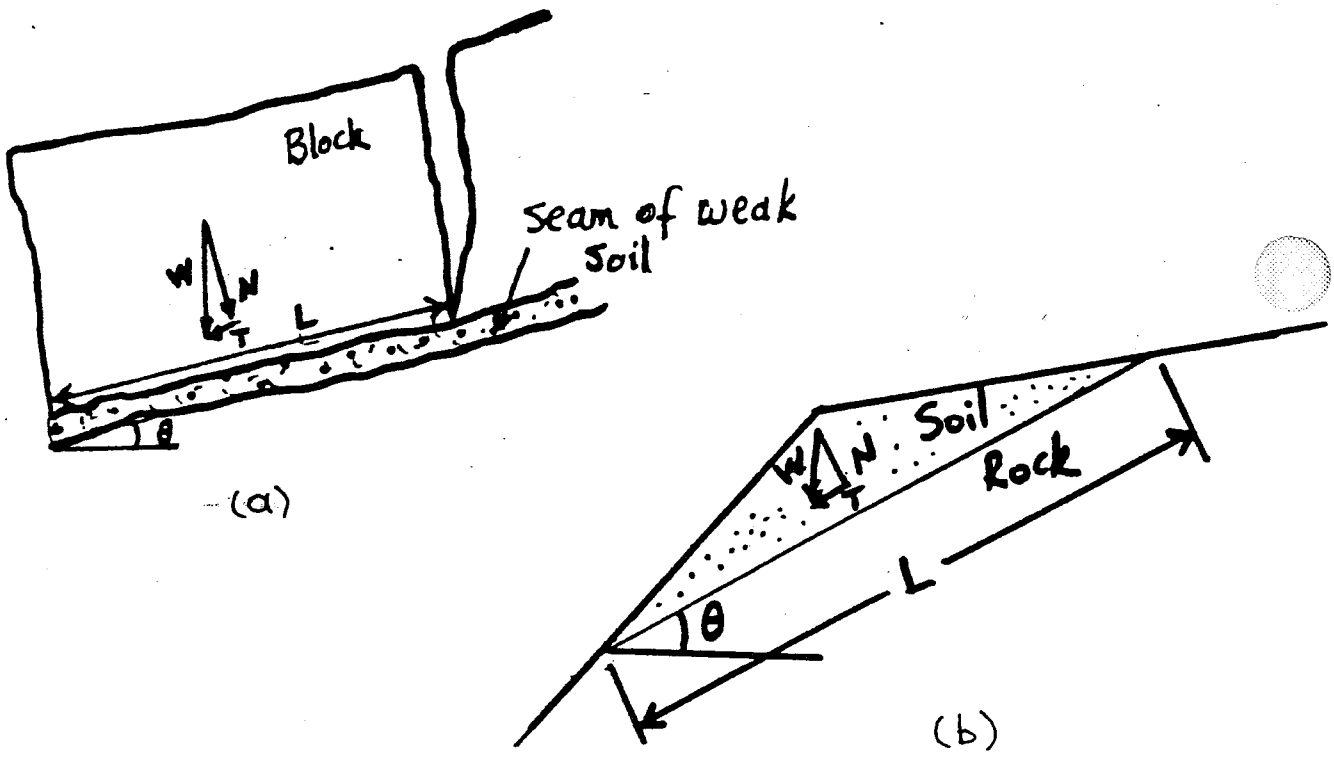

Figure 6. Block slide analysis.

effective normal force $N' = W \cos \theta - uL$

shear force $T = W \sin \theta$

mobilized shear resistance $S_m = (c'/F) L + N' (\tan \phi'/F)$

setting $S_m = T$ and solving for the safety factor we obtain:

$$F = \frac{c'L + (W\cos\theta - uL)\tan\phi'}{W\sin\theta} \qquad (16)$$

Circular Failure Surface

Method of Slices. This method is a versatile and general method for analyzing failures. Circular failures occur in finite slopes (depth of failed material is large compared to the height of the slope) exhibiting cohesion (c only or c and ϕ) and no specific planes of weakness or great strength. Layered soil conditions, irregular slope geometries, and complex water pressure conditions can be handled. With this method the trial slip circle is divided into a reasonable number of slices. The forces acting on a typical slice are shown in Fig. 7.

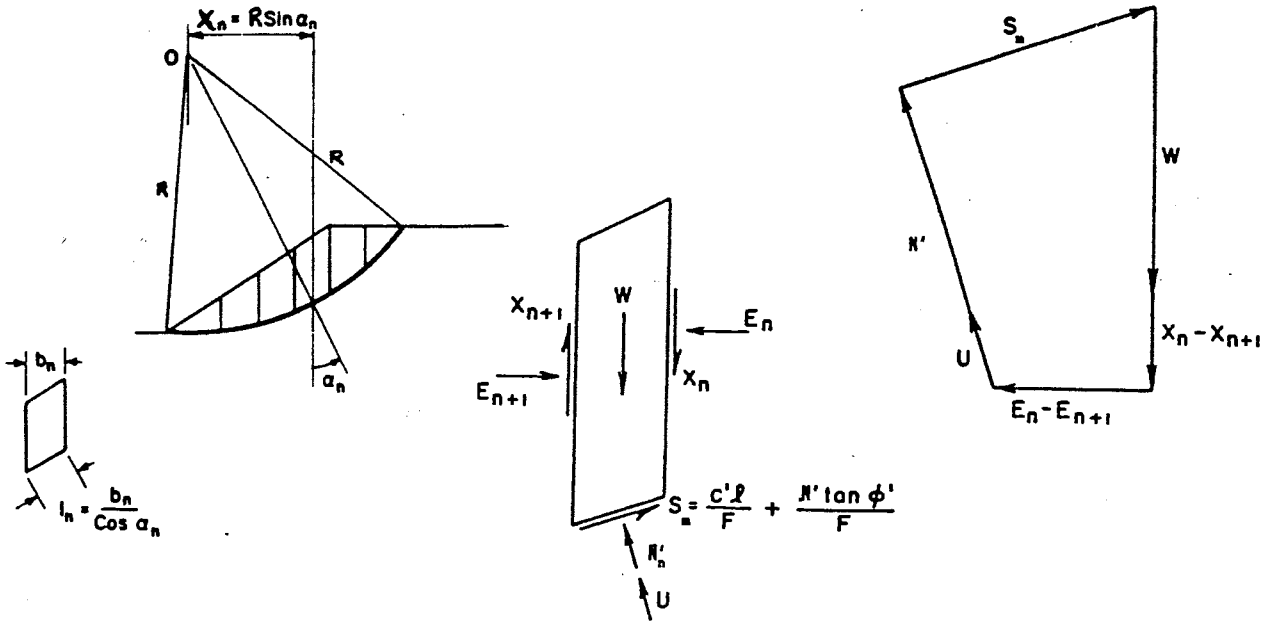

Figure 7. Forces involved in effective stress slip circle analysis.

Moment equilibrium about the center of rotation gives $\Sigma\, Wx = \Sigma\, S_m R$. Substituting for $S_m = S/F$ in this relationship and solving for F gives

$$F = (R/\Sigma\, W_n x_n)\ \Sigma[c_n' l_n + N_n - u_n l_n)\tan\phi_n' \qquad (17)$$

The only unknown in this equation is N_n. If we use force equilibrium, X and E come into the picture and the problem becomes statically indeterminate. Assumptions must be made regarding these side forces.

(A) Ordinary Method of Slices (Fellenius, 1936). Sum forces normal to slice base and assume resultants of side forces are colinear and equal (Fig. 8a).

$$N_n = W_n \cos \alpha_n$$

$$(S_m)_n = T_n = W_n \sin \alpha_n$$

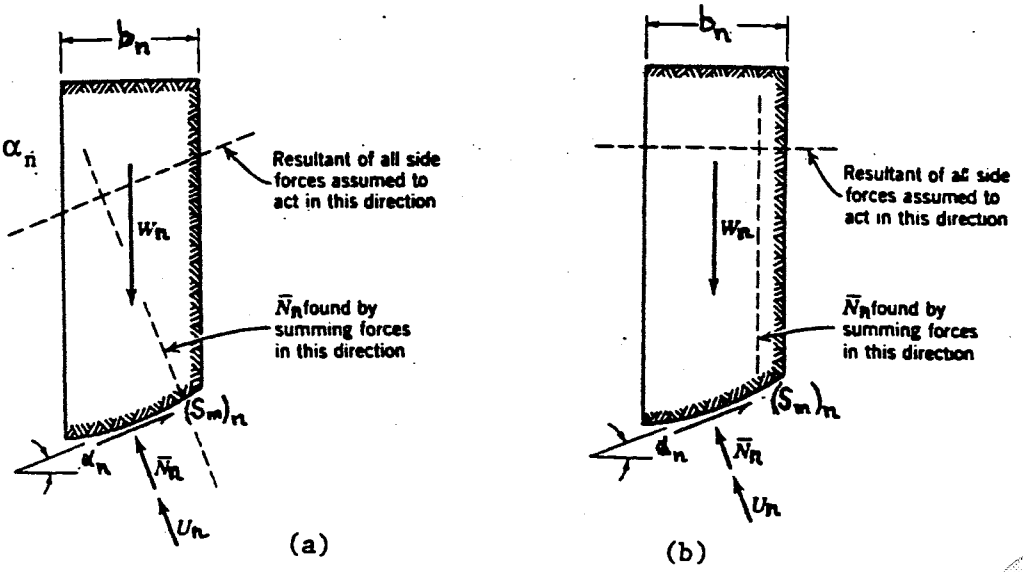

Figure 8. Assumed side forces in ordinary method of slices.

$$F = \frac{\Sigma \left[c'_n l_n + (W_n \cos \alpha_n - u_n l_n) \tan \phi'_n\right]}{\Sigma W_n \sin \alpha_n} \qquad (18)$$

(B) Bishop's Simplified Method (1955). Sum forces in a vertical direction and the variation of X across a slice is ignored, i.e., $X_n - X_{n+1} = 0$ (See Figs. 7 and 8b).

$$F_v = 0 = -N_n \cos \alpha_n - (S_m)_n \sin \alpha_n + W_n + (X_n - X_{n+1}) = 0 \qquad (19)$$

Assume $X_n - X_{n+1} = 0$; substitute S_n/F for $(S_m)_n$; solve for N_n. Substituting N_n in the original equation for F, we obtain

$$F = \frac{\Sigma \left\{\left[c'_n b_n + (W_n - u_n b_n) \tan \phi'_n\right] (1/m_\alpha)\right\}}{\Sigma W_n \sin \alpha_n} \qquad (20)$$

where

$$m_\alpha = \cos \alpha_n [1+(\tan \alpha_n \tan \phi'_n) /F] = \cos \alpha_n + \frac{\sin \alpha_n \tan \phi'_n}{F} \qquad (21)$$

Since F appears on both sides of Eq. 18, it is most convenient to solve for F in an iterative manner. It is useful to have m_α plotted for any assumed value of F, as shown in Fig. 9.

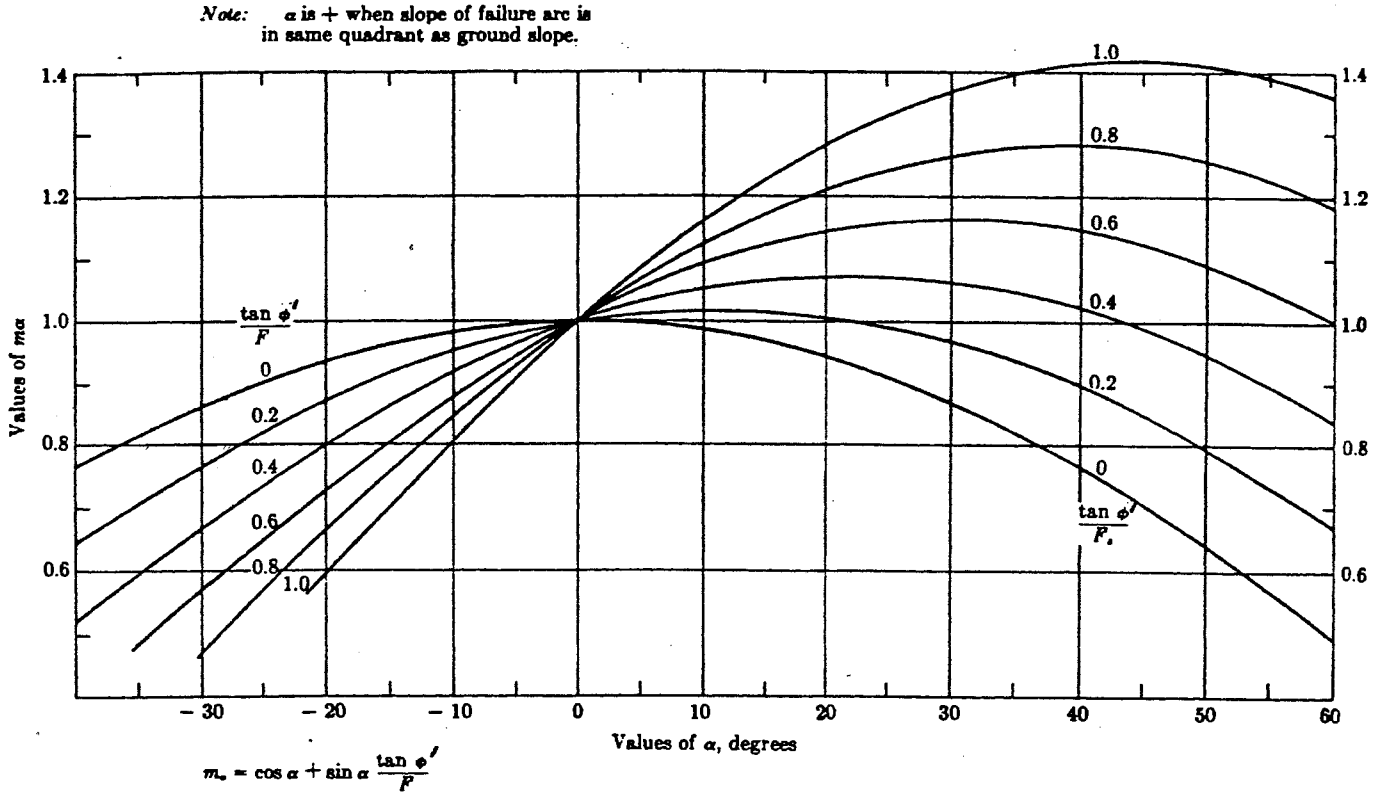

Figure 9. Values of m_α for use in calculating F.

Either effective stress or total stress analysis may be used. For the total stress method set u=0 and use the undrained strength parameters. If $\phi_u = 0$, the equation reduces to

$$F = \Sigma (c_n b_n \sec \alpha_n) / \Sigma (W_n \sin \alpha_n) = \Sigma (c_n l_n) / \Sigma (W_n \sin \alpha_n) \quad (22)$$

Bishop's Simplified Method is one of the most widely used methods for the analysis of rotational slides. Hand calculations are made conveniently by the use of tabular forms. It is basically a trail-and-error method and different slip circles have to be analyzed to find the critical circle and the safety factor. Several versions of efficient computer programs are available for the solution of the basic equation for F and a systematic search for the critical circle.

(C) Spencer's Method (1967). Spencer followed the usual procedures in the method of slices and assumed that the action of the internal forces acting on the sides of a slice can be replaced by their resultant inclined at θ to the horizontal and passing through the midpoint of a thin slice. The value of θ which satisfies both the force and the moment equilibrium equations is determined in the solution. Bishop's simplified method corresponds to $\theta = 0$ in Spencer's method.

Comparison of the Bishop's method and the ordinary method of slices (OMS) with the more rigorous methods (MRM) indicate:

1) For $\phi = 0$: $F_{BISH} = F_{OMS} = F_{MRM}$
2) For $\phi \neq 0$: low u: F_{OMS} 5 to 10% too low
3) For $\phi \neq 0$: high u: F_{OMS} 50% much too low
4) For $\phi \neq 0$: low or high u: F_{BISH} 2% error

Noncircular Slip Surface

When the distribution of shearing resistance within an earth mass is non-uniform, slip can occur along surfaces more complex than a circle. There is theoretical basis for circular failure surface in the case of uniform material.

(A) Morgenstern-Price Method (1965). This method treats a slip surface of arbitrary shape and satisfies all equilibrium conditions. A relation between the side forces on a slice is assumed in the form

$$X = \lambda f(x) E \tag{23}$$

where

λ = factor to be determine in the solution, and

f(x) = arbitrary function concerning distribution of internal forces (choose such that no tension be developed and the failure criterion not be violated). A digital computer is needed to solve the resulting equations for F.

(B) Janbu's Simplified Method (1973). This method follows the method of slices for a non-circular slip surface. The factor of safety is given by

$$F = f_o \Sigma \{[c'_n b_n + (W_n - u_n b_n) \tan \phi'_n] / \cos \alpha_n m_\alpha\} \div \Sigma W_n \tan \alpha_n \tag{24}$$

where m_α is defined as before and given in Fig. 9. The term f_o is a correction factor for the role of the internal forces and is a function of the curvature of the slip surface and the type of soil. Recommended values for this factor are given in Fig. 10 and the method can be performed by hand calculation.

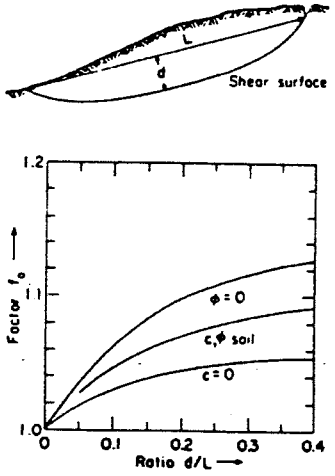

Figure 10. Curves for use in Janbu's Simplified Analysis.

(C) Wedge Method. In this method the potential sliding mass is separated into a series of wedges and the vertical and horizontal force equilibrium of each wedge is

considered in turn. The wedge method is most appropriate for conditions where the failure surface is not likely to be circular and where it can be approximated by a series of planar surfaces, such as in failure by spreading. An assumption must be made regarding the inclination of the force transmitted across the interface between any two wedges. The assumption that the side forces between wedges are horizontal is conservative with an error for most cases no more than 15%. Experience indicates that assuming an inclination of 10 to 15 degrees from the horizontal usually gives reasonable results. F is calculated by trial-and-error. A value of F is assumed, and then checked to determine if the assumed value satisfies equilibrium. The analysis can be performed either graphically or numerically.

EFFECTIVE AND TOTAL STRESS METHODS OF SLOPE STABILITY ANALYSIS

Soil stability and response can be analyzed rationally in terms of effective stresses utilizing the effective, i.e., drained strength parameters (c' and ϕ'). The effective stress method requires the assessment of pore pressures in the field (for computing effective normal stresses). In the long-term (drained) conditions pore pressures are generally governed by steady seepage (u_o). This is the usual condition for *natural slopes* and *permanent cuts and fills* and they should be analyzed using the effective stress method.

It is also possible to analyze slopes under undrained conditions in terms of effective stresses, but the pore pressures due to stress changes (Δu) must be obtained either by prediction in terms of total stress changes (loading or unloading) or from field observations. Undrained conditions correspond to short-term stability cases in low permeability soils, i.e., cohesive soils. For highly permeable granular soils under static stress changes the long and the short term can be considered the same due to rapid dissipation of Δu.

An alternate method of analysis of undrained conditions is the total stress method utilizing the total, i.e., undrained strength parameters. The undrained strength parameters are c_u for saturated soils and c_u and ϕ_u for partially saturated soils such as compacted soils. The total stress method is more properly viewed as a response to the type of test and method of interpretation than as a reflection of basic strength behavior. It is used primarily for the so-called end-of-construction class of problems. The main advantage of the total stress method is that the pore pressure distribution ($u = \Delta u$) along the failure surface is not required; only the undrained strength is needed. Furthermore, strength testing and stability analysis are simpler especially for the $\phi=0$ analysis. However, the interpretation and

selection of the shear strength parameters, in general, are more complex and require greater care than the effective strength parameters.

The use of these two methods will be demonstrated in the case of dam stability.

End-of-Construction Stability in Earth Dam

Effective Stress Method. In order to carry this analysis we should estimate the construction pore pressures. For this purpose we will review excess pore pressure in undrained conditions as developed by Skempton (1954) and Bishop (1954). Skempton proposed that

$$\Delta u = B[\Delta\sigma_3 + A(\Delta\sigma_1 - \Delta\sigma_3) \tag{25}$$

for changes in the principal stress $\Delta\sigma_1$ and $\Delta\sigma_3$. A and B arecalled pore pressure parameters and are measured in the underdrained triaxial test. It has been established that

$$B = \Delta u_a / \Delta\sigma_3 \tag{26}$$

where Δu_a is the pore pressure due to an all-round change in principal stress, $\Delta\sigma_3$.

B = 1 for saturated soils (S = 100%)

B = 0 for dry soils (S=0)

0<B<1 for partially saturated soils; at the Proctor optimum water content and density,B ranges from about 0.1 to 0.5

The pore pressure change during the application of a deviator stress increment $(\Delta\sigma_1 - \Delta\sigma_3)$ is Δu_d

$$\Delta u_d = B \bullet A\,(\Delta\sigma_1 - \Delta\sigma_3) \tag{27}$$

For any given soil, A varies with the stresses and the stress history. At failure, the value of A_f for various clays with positive total stress increments is summarized below:

High sensitivity clays	0.75 to 1.5
N.C. clays	0.5 to 1
Compacted sandy clays	0.25 to 0.75
Lightly O.C. clays	0 to 0.5
Compacted clay-gravels	-0.25 to 0.25
Heavily O.C. clays	-0.5 to 0

Alternative forms of the pore pressure equation:

In laboratory undrained triaxial test

$$\Delta u = B \bullet \Delta\sigma_3 + \overline{A}\,(\Delta\sigma_1 - \Delta\sigma_3) \tag{28}$$

where $\overline{A} = A \bullet b$ $(\overline{A} = A$ for $S = 100\%)$

For earth dam problems

$$\Delta u = B[\Delta\sigma_1 - (1\text{-}A)\,(\Delta\sigma_1 - \Delta\sigma_3)] \quad \text{and} \tag{29}$$

$$(\Delta u/\Delta\sigma_1) = \overline{B} = B\{1\text{-}(1\text{-}A)[1\text{-}\,(\Delta\sigma_3/\Delta\sigma_1)]\} \tag{30}$$

The coefficient $\overline{B}$ is a useful parameter in undrained stability analysis and it can be determined in the laboratory for the relevant values of stress change for a given soil and problem.

An element of soil in the impervious fill of an embankment will be subjected, during construction, to stresses due to the increasing weight of fill placed above this point (Fig. 11).

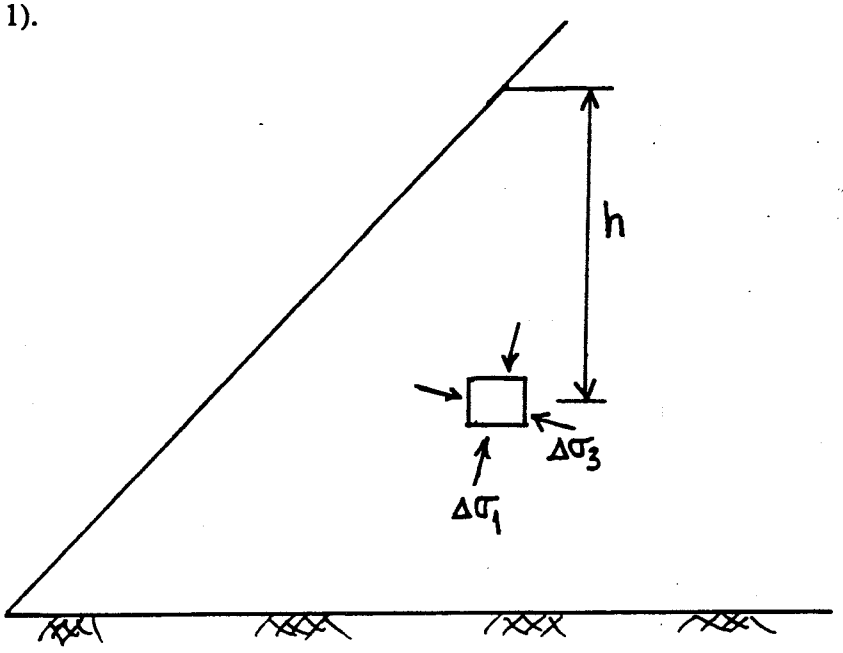

Figure 11. An element of soil in the slope of an embankment.

If we assume a completely undrained condition to take place, the pore pressure becomes

$$u = u_o + \Delta u = u_o + \overline{B} \bullet \Delta\sigma_1 \tag{31}$$

If we assume that $\Delta\sigma_1 = \gamma h$ as a first approximation and ignore u_o (u_o is the pore pressure at the time the layer was placed and it is usually a small negative value unless placed very wet) we obtain

$$u = \Delta u = \overline{B} \bullet \gamma h \tag{32}$$

$\overline{B}$ is a function of $(\Delta\sigma_3/\Delta\sigma_1)$ which is variable in the dam and expressed in terms of total stresses. However, we can study the extent of the effect of $(\Delta\sigma_3/\Delta\sigma_1)$ on $\overline{B}$.

If K is defined in terms of effective stresses as $\Delta\sigma'_3/\Delta\sigma'_1$, then it becomes

$$K = (\Delta\sigma_3 - u)/(\Delta\sigma_1 - u) = (\Delta\sigma_3 - \overline{B}\bullet\Delta\sigma_1)/(\Delta\sigma_1 - \overline{B}\bullet\Delta\sigma_1) \tag{33}$$

We can solve for $(\Delta\sigma_3/\Delta\sigma_1)$ as

$$(\Delta\sigma_3/\Delta\sigma_1) = K - K\bullet\overline{B} + \overline{B} \tag{34}$$

Substituting this back into Eq. 26, we obtain

$$\overline{B} = B\bullet[1-(1-A)(1-K)]/[1-B\bullet(1-A)(1-K)] \tag{35}$$

K varies between the coefficient of earth pressure at-rest, $K_o = 0.5$ (for level ground) and the coefficient of active pressure $K_a = 0.25$ to 0.3 (for steep slopes in a condition of limiting equilibrium.) Since there is small difference between these limiting values, $\overline{B}$ can be assumed constant for a given soil in the failure surface. Average value of $\overline{B}$ for a given soil can be determined by underdrained laboratory tests simulating stress changes in a typical soil element in the field. It should be noted that $\overline{B} = r_u$ in the approximate way it is defined.

Summary

For end-of-construction, pore pressure can be estimated from

$$u_n = \overline{B} \bullet \gamma h_n \tag{36}$$

and entered in the appropriate safety factor equation along with the drained strength parameters. For use in stability charts for $\phi > 0$, P_e can be defined as

$$P_e = (1-\overline{B})\,\gamma H = (1-r_u)\gamma H \tag{37}$$

and can be used along with c' and ϕ'.

Total Stress Method. In this case, the pore pressure term in the safety factor equation is set equal to zero and the undrained strength parameters are used. For the chart solution, if ϕ=0 use the corresponding chart as described; if $\phi_u > 0$, use the chart for $\phi > 0$ with $P_e = \gamma H$ and c_u and ϕ_u.

Stability During Rapid Drawdown

Effective Stress Method. In a manner similar to the one pursued in the case of end-of-construction, pore pressures on rapid drawdown may also be estimated. The total vertical stresses at the base of a slice, before and after the drawdown, are σ_{1b} and σ_{1a}, respectively (Fig. 12).

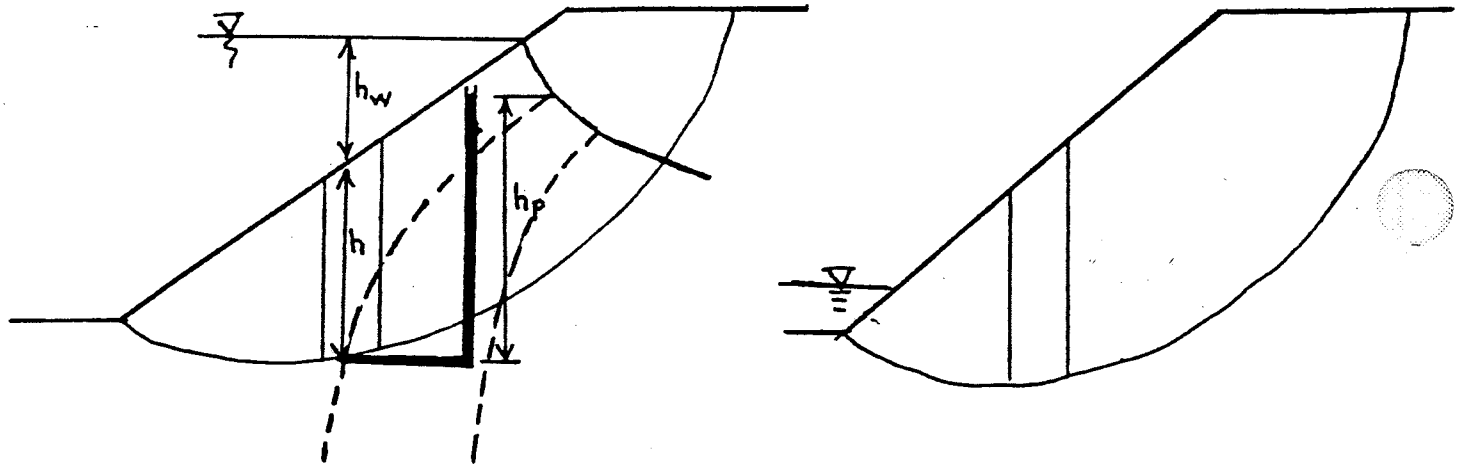

Figure 12. Rapid drawdown.

$$\sigma_{1b} = h_w \gamma_w + h\gamma_{sat} \quad (38)$$

$$\sigma_{1a} = h\gamma_{sat} \quad (39)$$

$$\Delta\sigma_1 = \sigma_{1a} - \sigma_{1b} = -h_w \gamma_w \quad (40)$$

If the pore pressure before rapid drawdown under steady seepage is $u = u_o = h_p \gamma_w$, then the pore pressure after rapid drawdown becomes

$$u = u_o + \Delta u = h_p \gamma_w - \overline{B} \bullet h_w \gamma_w \qquad (41)$$

It can be seen that, on drawdown, the lower the value of $\overline{B}$ the greater will be the residual pore pressure and, therefore, the lower will be the safety factor. For fully saturated soils B = 1 and the upper limit for A, in practice, is also 1; corresponding to $\overline{B} = 1$. For lower values of A, $\overline{B} > 1$. As a safe rule $\overline{B}$ may be taken as unity. Values of $\overline{B} < 1$ are, of course, possible for certain changes in stresses and for S < 100%.

Summary

For rapid drawdown in a dam pore pressure can be estimated from

$$u = h_p \gamma_w - \overline{B} \bullet h_w \gamma_w \qquad (42)$$

and entered into the appropriate equation for safety factor along with the drained strength parameters, c' and ϕ'. For chart solutions, use the chart for $\phi > 0$ with the drained strength parameters:

$$P_d = \gamma H \text{ and } P_e = (1\text{-}r_u)\, \gamma H \qquad (43)$$

Total Stress Method. In this case the pore pressure term of the safety factor equation is set to zero. Total weights along with undrained strengths obtained from the CU triaxial test are used. The undrained strengths are related to the consolidation pressures without using values of c_{cu} and ϕ_{cu} in the laboratory and the field equilibrilum consolidation pressures under seepage are used to determine the underdrained strength at each slice base. Charts for $\phi = 0$ can be used after determining a weighted average undrained strength along an estimated slip circle.

Long-Term Stability Under Seepage in Dams

This condition can be analyzed only by the effective stress method with drained strength parameters. Pore pressures are governed by the seepage condition and can be determined from flow nets or other types of seepage analysis using $u = u_o = h_p \gamma_w$.
Seepage affects stability in two ways:

1) shearing resistance along the slip circle is changed by seepage induced pore pressure relative to the static ground water condition;
2) seepage forces are body forces which affect the driving moment

CRITICAL CONDITIONS FOR STABILITY

Safety of a slope changes with time as the slope adjusts to stress changes induced during construction and to environmental changes. Therefore, the stability corresponding to these various states such as end-of-construction, rapid drawdown, long-term seepage, evolution due to erosion, and other conditions must be considered and the design must be based on the most critical of these conditions. Three examples of changing stability with time are shown in Figs. 13, 14 and 15 for a fill, an excavation cut, and an earth dam, respectively.

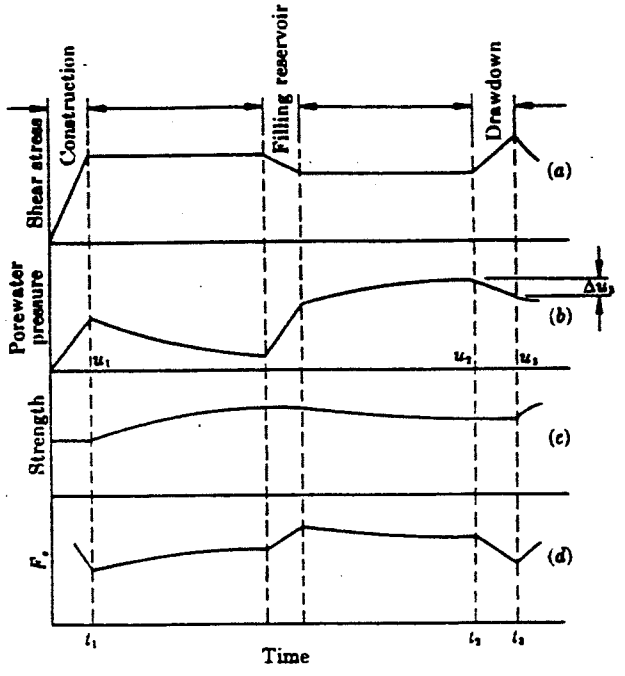

Figure 13. Stability conditions of an earth dam
[After Bishop and Bjerrum, 1960]

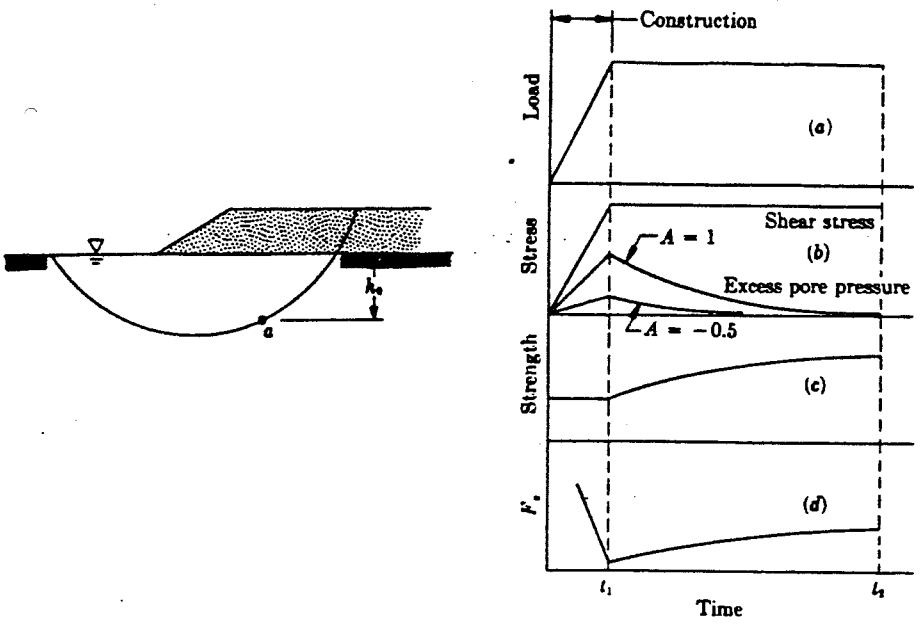

Figure 14. Stability conditions for a saturated clay foundation beneath a fill [From Bishop and Bjerrum, 1960]

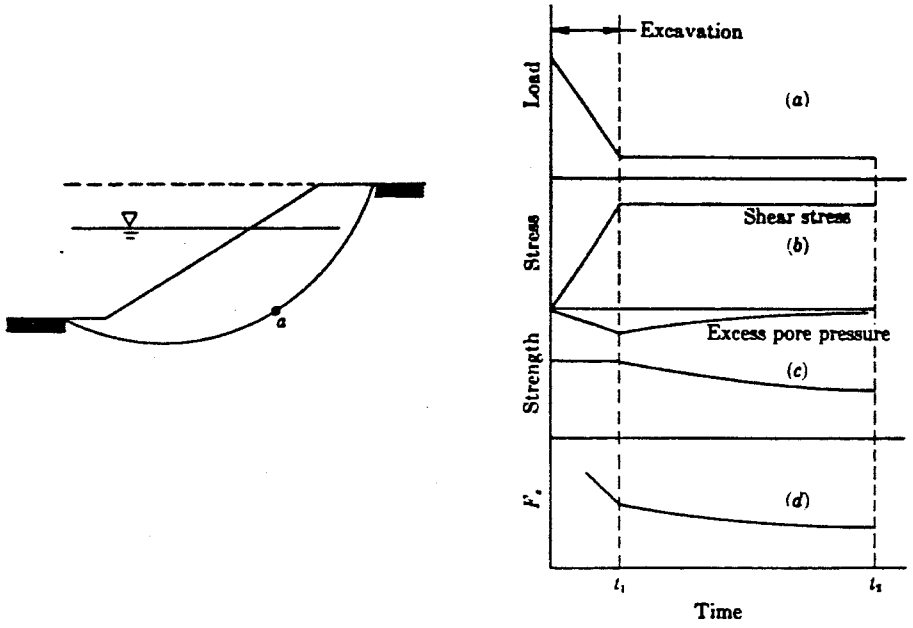

Figure 15. Stability conditions for a cut in clay. [From Bishop and Bjerrum, 1960]

SLOPE STABILITY ANALYSIS EXAMPLES

Ref: Soil Mechanics by Lambe & Whitman

Example 1

Given. The slope, failure surface, flow net, and strength parameters in Fig. 1.

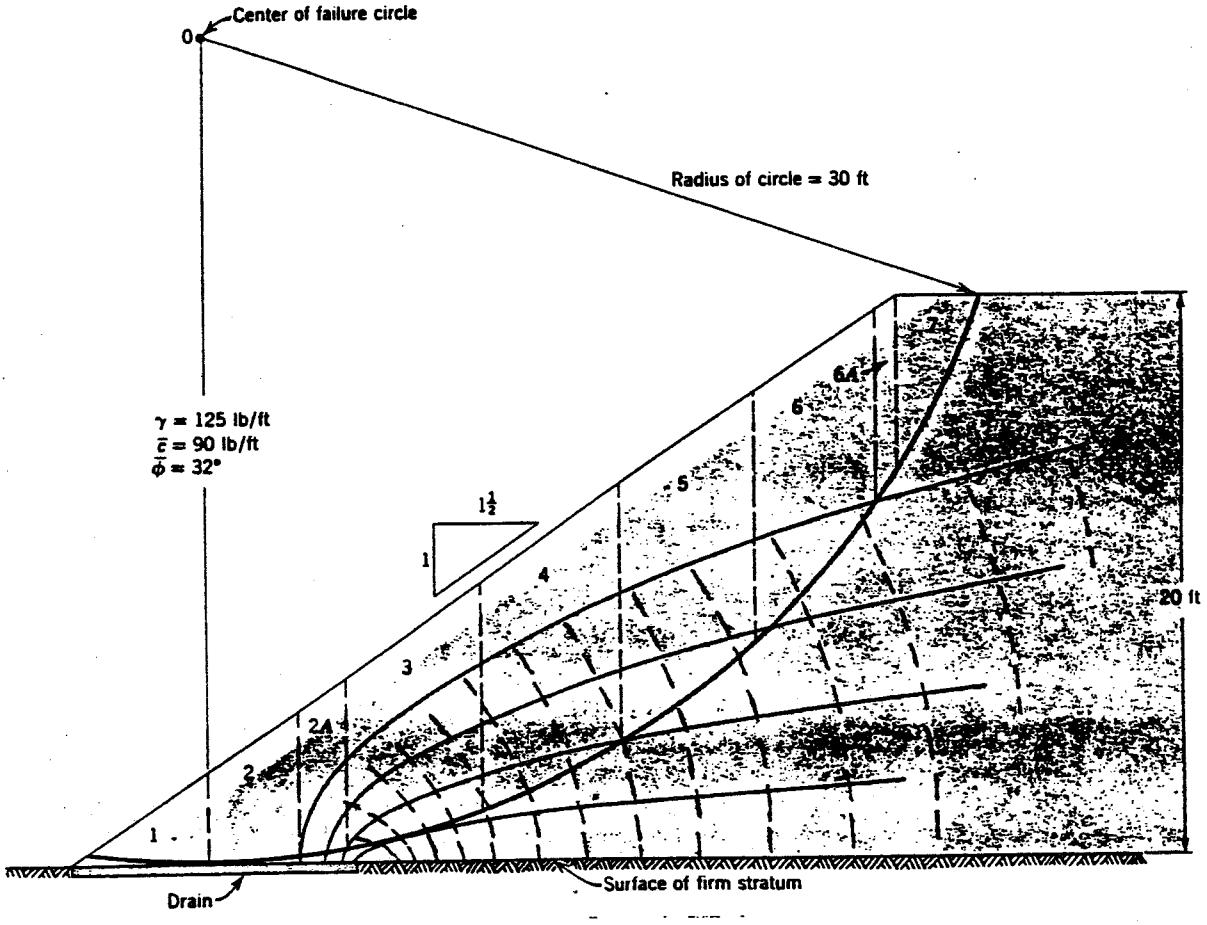

Fig. 1 Downstream Slope of a Dam

Find. The safety factor.

Solution. The first step is to find the weight of the free body above the failure surface. This may be done conveniently by breaking the free body into a series of vertical slices as shown in the figure. Slices 2 to 6A

are approximately trapezoids, and their weight can be computed by multiplying the unit weight of the soil times the width of the slice times the average height of the slice. Slices 1 and 7 may similarly be treated as triangles. The calculation of the resulting weight is given in Table 1. Fig. 2 describes how pore water pressures and forces at the base of each slice can be estimated using the flow net information, i.e. the phreatic surface.

Table 1

Slice	Width (ft)	Average Height (ft)	Weight (kips)	Moment about O (kip-ft)
1	4.5	1.6	0.9	−1
2	3.2	4.2	1.7	3
2A	1.8	5.8	1.3	5
3	5.0	7.4	4.6	34
4	5.0	9.0	5.6	69
5	5.0	9.3	5.8	101
6	4.4	8.4	4.6	104
6A	0.6	6.7	0.5	12
7	3.2	3.8	1.5	39
			$W = 26.5$	366

Resultant lies 366/26.5 = 13.7 ft to right of center of circle.

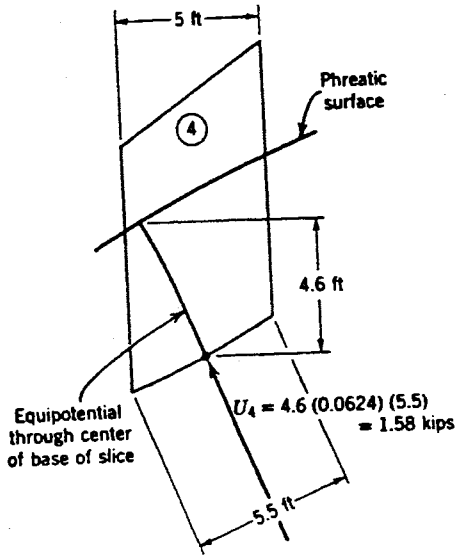

Fig. 2 Computation of Water Force at the Slice Base

Find: Safety factor by ordinary method of slices.

Solution: See Table 2.

Table 2

Slice	W (kips)	sin α	$W \sin \alpha$ (kips)	cos α	$W \cos \alpha$ (kips)	u (kips/ft)	ℓ (ft)	U (kips)	N' (kips)
1	0.9	−0.03	0	1.00	0.9	0	4.4	0	0.9
2	1.7	0.05	0.1	1.00	1.7	0	3.2	0	1.7
2A	1.3	0.14	0.2	0.99	1.3	0.03	1.9	0.05	1.25
3	4.6	0.25	1.2	0.97	4.5	0.21	5.3	1.1	3.4
4	5.6	0.42	2.3	0.91	5.1	0.29	5.6	1.6	3.5
5	5.8	0.58	3.4	0.81	4.7	0.25	6.2	1.55	3.15
6	4.6	0.74	3.4	0.67	3.1	0.11	6.7	0.7	2.4
6A	0.5	0.82	0.4	0.57	0.3	0	1.2	0	0.3
7	1.5	0.87	1.3	0.49	0.7	0	7.3	0	0.7
			12.3				41.8		17.3

$$F = \frac{0.09(41.8) + 17.3 \tan 32^\circ}{12.3} = \frac{3.76 + 10.82}{12.3} = \frac{14.58}{12.3} = 1.19$$

Find: Safety factor by Bishop's simplified method.

Solution: See Table 3.

Table 3

(1) Slice	(2) b (ft)	(3) $c'b$ (kips)	(4) ub (kips)	(5) $W - ub$ (kips)	(6) (5) tan ϕ' (kips)	(7) (3) + (6) (kips)	(8) m_α $F = 1.25$	(8) m_α $F = 1.35$	(9) (7) ÷ (8) $F = 1.25$	(9) (7) ÷ (8) $F = 1.35$
1	4.5	0.40	0	0.9	0.55	0.95	0.97	0.97	1.0	1.0
2	3.2	0.29	0	1.7	1.05	1.35	1.02	1.02	1.3	1.3
2A	1.8	0.16	0.05	1.25	0.80	0.95	1.06	1.05	0.9	0.9
3	5.0	0.45	1.05	3.55	2.25	2.70	1.09	1.08	2.5	2.5
4	5.0	0.45	1.45	4.15	2.55	3.00	1.12	1.10	2.7	2.75
5	5.0	0.45	1.25	4.55	2.7	3.15	1.10	1.08	2.85	2.9
6	4.4	0.40	0.50	4.1	2.65	3.05	1.05	1.02	2.9	2.95
6A	0.6	0.05	0	0.5	0.30	0.35	0.98	0.95	0.35	0.4
7	3.2	0.29	0	1.5	0.95	1.25	0.93	0.92	1.3	1.35
									15.8	16.05

For assumed $F = 1.25$ $\quad F = \dfrac{15.8}{12.3} = 1.29$

$F = 1.35$ $\quad F = \dfrac{16.05}{12.3} = 1.31$

A trial with assumed $F = 1.3$ would give $F = 1.3$. ◀

REFERENCES

The following references were used directly or indirectly in preparing these notes. They can be referred for further information and the listing of the original sources.

Bishop, A.W. (1954); "The Use of Pore-Pressure Coefficients in Practice," Geotechnique, Vol, No. 4, pp. 148-152.

Bishop, A.W. (1955); "The Use of the Slip Circle in the Stability Analysis of Slopes," Geotechnique, Vol. 5, No. 1, pp. 7-17.

Bishop, A.W. and L. Bjerrum (1960); "The Relevance of the Triaxial Test to the Solution of Stability Problems," Proceeding of the ASCE Research Conference on Shear Strength of Cohesive Soils, Boulder, Colorado.

Duncan, J.M. and A.L. Buchignani (1975); An Engineering Manual for Slope Stability Studies, Department of Civil Engineering, University of California, Berkeley.

Dunn, I.S., L.R. Anderson, And F.W. Kiefer (1980); Fundamentals of Geotechnical Analysis, John Wiley and Sons, Inc., New York.

Edil, T.B. (1982); "Causes and Mechanics of Coastal Bluff Recession in the Great Lakes," State-of-the-Art Paper Proceeding of Bluff Slumping Workshop, U.S. Geological Survey and Michigan Sea Grant, Romulus, Michigan, pp. 1-48.

Ladd, C.C. (1971); Strength Parameters and Stress-Strain Behavior of Saturated Clays, Department of Civil Engineering, Massachusetts Institute of Technology, Research Report R71-23, Soils Publication 278.

Lambe, W.T. and R.V. Whitman (1969); Soil Mechanics, John Wiley and Sons, Inc., New York.

Perloff, W.H. and W. Baron (1976); Soil Mechanics: Principles and Applications, The Ronald Press Company, New York.

Schuster, R.L. and R.J. Krizek (1978); Landslides: Analysis and Control, Transportation Research Board, Special Report 176.

Skempton, Q.W. (1954); "The Pore-Pressure Coefficients A and B," Geotechnique, Vol. 4, No. 4, pp. 143-147.

Sowers, G.F. (1979); Introductory Soil Mechanics and Foundations: Geotechnical Engineering, Fourth Edition, MacMillan Publishing Company, Inc., New York.

Taylor, D.W. (1966); Fundamentals of Soil Mechanics, Second Printing, John Wiley & Sons, Inc., New York.

U.S. Department of Labor Occupational Safety and Health Administration (1975); Excavating and Trenching Operations, OSHA 2226.

The first three steps are the same whether the graphical or the numerical method is used.

(1) Select a trial slip surface (an example is shown in Fig. |).

(2) Divide the mass above the slip surface into wedges (or slices). The wedges should be chosen so that the base of any wedge lies wholly within a single soil layer. Three to five wedges are usually sufficient. If there is water outside the slope, it should be represented by a wedge, just as if it was a soil with weight but no strength.

(3) Calculate the weight of each wedge. If the top as well as the bottom of each wedge is a straight line, the weights can be calculated using the tabular computation form described previously for the Ordinary Method of Slices. If the top boundary of a wedge is a broken line, as for wedge 2 in Fig. | , the weight of the wedge can be calculated by dividing it into two parts.

To solve for the factor of safety graphically, follow steps (4) through (9) below.

(4) Assume a value for the factor of safety, and calculate trial values of mobilized cohesion and mobilized friction angles for each soil using the following formulas:

$$c_m = \frac{c}{F} \qquad (1)$$

and

$$\tan\phi_m = \frac{\tan\phi}{F} \qquad (2)$$

To solve for the Wedge Method factor of safety numerically, use the tabular computation form shown in Fig. 3. Steps (1) through (3), as described previously, are the same for the numerical analysis as for the graphical analysis. Steps (4) through (9) proceed as described below. An example is shown in Fig. 5

(4) For each wedge, determine the inclination of the base (α), the length of the base (ℓ), the cohesion of the soil at the base (c), the friction angle of the soil at the base (ϕ), and the pore pressure at the base (u). (If the analysis is being done with total stresses, use u = 0.) Enter these values, along with the weight of each slide, in the tabular computation form shown in Fig.

(5) Calculate the quantities $c\ell/\cos\alpha$, $W\tan\phi$, and $u\ell\tan\phi/\cos\alpha$ for each wedge, and enter these in the table.

(6) Assume a trial value for the factor of safety, and calculate the value of ΔE for each wedge as indicated in the table. ΔE is the difference between the side forces on the left and right sides of each slice, and is given by the equation:

$$\Delta E = \frac{FW\tan\alpha - \frac{c\ell}{\cos\alpha} - W\tan\phi + \frac{u\ell\tan\phi}{\cos\alpha}}{F + \tan\phi\,\tan\alpha}$$

(7) Calculate the sum of the terms ΔE for all slices. If the assumed factor of safety is correct, this sum will be zero. If its value is less than zero, the assumed value of F is too low. If it is greater than zero the assumed value of F is too high.

(8) Assume a new value of F and repeat steps (6) and (7). Try additional values of F until the sum of the ΔE's is negligibly small. Then the assumed value of F is the correct one for the assumed failure mechanism. Usually no more than two trials are needed to determine F. By plotting the assumed factor of safety against the value of $\Sigma\Delta E$ for the first two trials, a value of F can usually be estimated which will be very close to the correct value. If the value of F determined by this procedure differs greatly from both of the first two values, a third trial may be necessary.

(9) Select a new failure mechanism and repeat steps (1) through (8). Try several failure mechanisms in order to find the one with the lowest factor of safety.

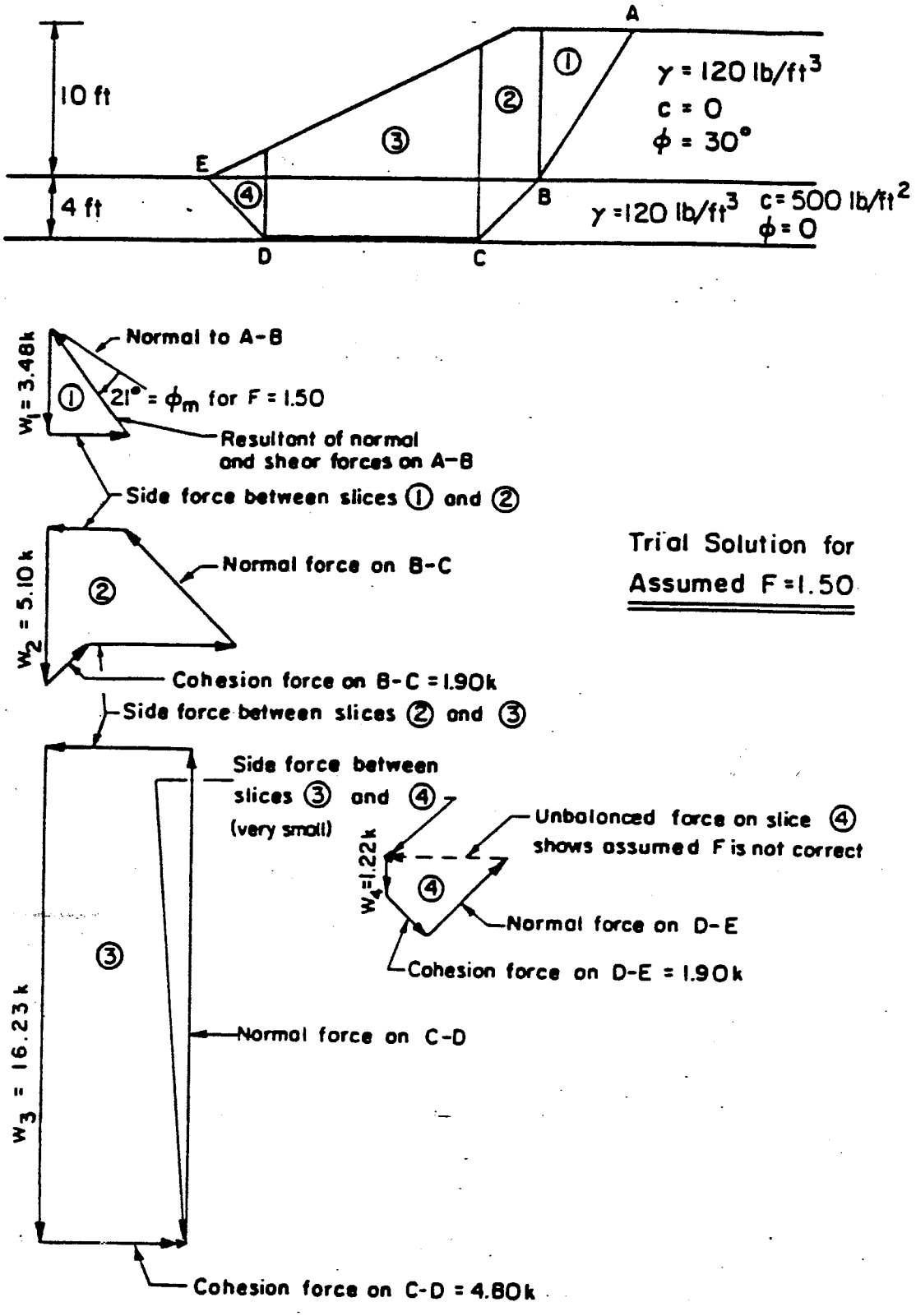

Fig. 1 EXAMPLE OF GRAPHICAL PROCEDURE FOR WEDGE METHOD

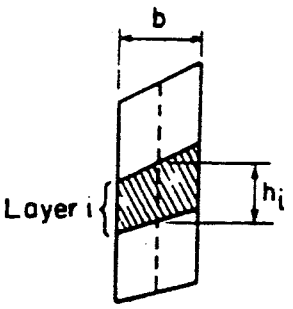

γ_i = unit weight of layer i

h_i = height of layer at center of slice

W_i = partial weight = $b\, h_i\, \gamma_i$

ΣW_i = total weight of slice

Slice No.	b	h_i	γ_i	W_i	ΣW_i

Fig. 2 TABULAR FORM FOR COMPUTING WEIGHTS OF SLICES.

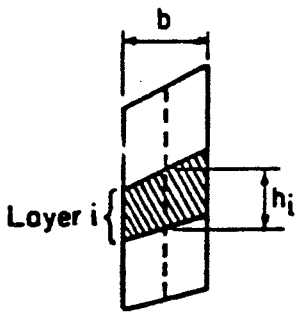

γ_i = unit weight of layer i

h_i = height of layer at center of slice

W_i = partial weight = $b\, h_i\, \gamma_i$

ΣW_i = total weight of slice

Slice No.	$\frac{ft}{b}$	$\frac{ft}{h_i}$	kip/ft^3 γ_i	kip/ft W_i	kip/ft ΣW_i
1	5.8	5.0	0.120	3.48	3.48
2 (right)	1.9	10.0	0.120	2.28	
		1.0	0.120	0.23	
2 (left)	1.8	9.0	0.120	1.94	
		3.0	0.120	0.65	5.10
3	14.4	5.4	0.120	7.33	
		4.0	0.120	6.90	16.23
4	3.7	0.9	0.120	0.40	
		1.85	0.120	0.82	1.22

Fig. 4 EXAMPLE OF USE OF TABULAR FORM FOR COMPUTING WEIGHTS OF WEDGES.

$$\Delta E = \frac{N_4 - N_1 - N_2 + N_3}{N_5}$$

Slice No.	W	α	l	C	ϕ	u	N_1 $\frac{Cl}{\cos\alpha}$	N_2 W tan ϕ	N_3 $\frac{ul\tan\phi}{\cos\alpha}$
1	3.48	60°	11.4	0	30°	0	0	2.01	0
2	5.10	45°	5.7	0.50	0	0	4.03	0	0
3	16.20	0	14.4	0.50	0	0	7.20	0	0
4	1.20	-45°	5.7	0.50	0	0	4.03	0	0

Trial	F	Slice No.	N_4 FW tan α	N_5 F + tan ϕ tan α	ΔE	$\Sigma\Delta E$
1	1.50	1	9.05	2.50	2.81	
		2	7.65	1.50	2.41	
		3	0.00	1.50	-4.80	
		4	-1.80	1.50	-3.89	-3.46
2	2.10	1	12.66	3.10	3.44	
		2	10.71	2.10	3.18	
		3	0.00	2.10	-3.43	
		4	-2.52	2.10	-3.12	+0.07
3	2.08	1	12.54	3.08	3.42	
		2	10.61	2.08	3.16	
		3	0.00	2.08	-3.46	
		4	-2.50	2.08	-3.14	-0.02

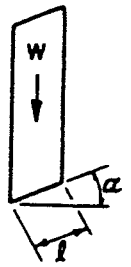

C = cohesion intercept
ϕ = friction angle
u = pore pressure at base of slice

Fig. 5 EXAMPLE OF USE OF TABULAR FORM FOR CALCULATING FACTOR OF SAFETY BY WEDGE METHOD.

$$\Delta E = \frac{N_4 - N_1 - N_2 + N_3}{N_5}$$

Slice No.	W	α	ℓ	C	ϕ	u	N_1 $\frac{C\ell}{\cos\alpha}$	N_2 W tan ϕ	N_3 $\frac{u\ell \tan\phi}{\cos\alpha}$

Trial	F	Slice No.	N_4 FW tan α	N_5 F + tan ϕ tan α	ΔE	$\Sigma \Delta E$

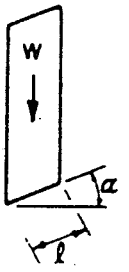

C = cohesion intercept

ϕ = friction angle

u = pore pressure at base of slice

Fig. 3 TABULAR FORM FOR CALCULATING FACTOR OF SAFETY BY WEDGE METHOD.

SELECTION OF METHOD OF ANALYSIS and SELECTION OF STRENGTH PARAMETERS

Tuncer B. Edil

Universwity of Wisconsin-Madison

CHARACTERISTICS OF VARIOUS SLOPE STABILITY PROBLEMS

- FILLS
  - Granular Fills on Firm Foundation
  - Cohesive Fills on Firm Foundation
  - Fills on Soft Subsoils
- EXCAVATIONS
- NATURAL SLOPES
- SLOPES IN SOILS PRESENTING SPECIAL PROBLEMS
  - Stiff-fissured Clays and Shales
  - Loess
  - Residual Soils
  - Highly sensitive Clays

Cohesionless (Granular) Fills on Firm Foundation

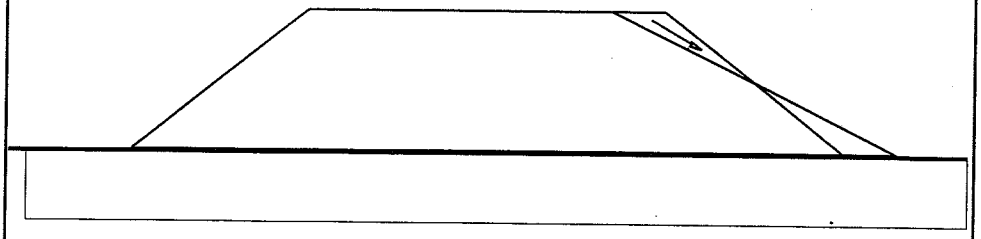

Cohesive Fills on Firm Foundation

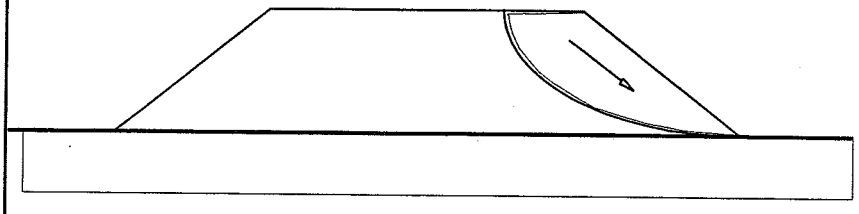

Fills on Soft Subsoil

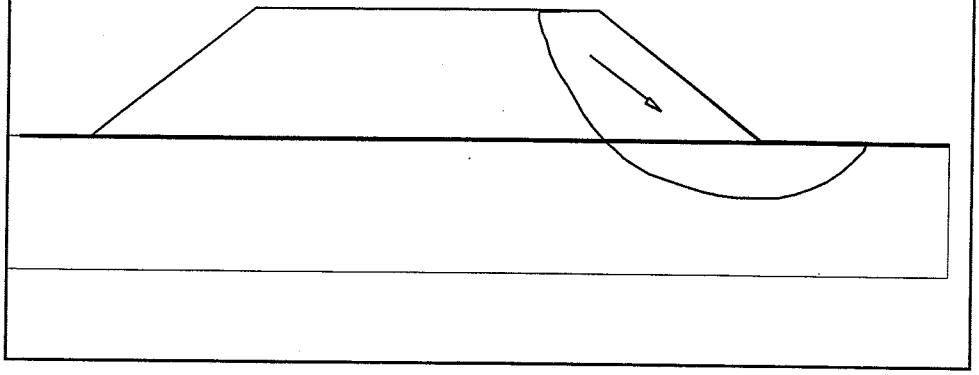

Excavations in Cohesionless (Granular Soil)

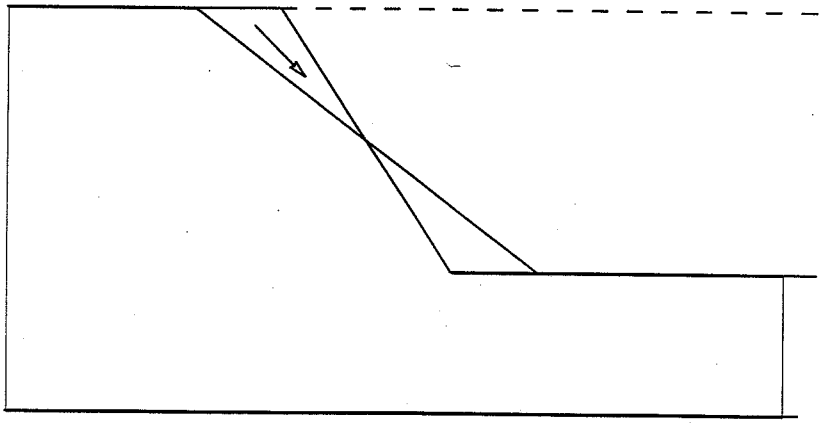

Excavations in Cohesive Soil

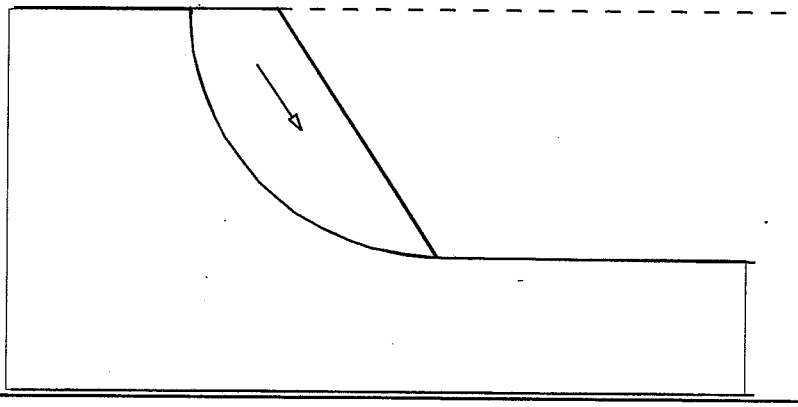

CRITICAL CONDITIONS FOR STABILITY

- Stability of slopes changes with time even if there is no change in slope geometry and soil properties due to changing pore water pressures.
- Critical conditions for slope stability include:
  - End-of-Construction (EOC)
  - Sudden Drawdown (SDD)
  - Long-Term (LT)

ANALYSIS OF CRITICAL CONDITIONS

- For highly drainable slopes in sands and gravels, EOC and LT are essentially the same.
- For slopes in fine-grained soils, the critical conditions need to be individually analyzed.
  - EOC: maximum change in water pressures due to stress; use undrained or total strength
  - SDD: maximum seepage forces
  - LT: no excess pore pressures but groundwater pressures; use drained or effective strength

METHODS OF SLOPE STABILITY ANALYSIS

- EFFECTIVE STRESS METHOD (ESM)
  - Use "drained (effective)" strength parameters
  - Estimate effective stresses using pore pressures for each case ($u=u_o \pm \Delta u$)
  - Typically used for analysis of slopes in granular soils and long -term analysis of slopes in cohesive soils; however, end-of-construction and sudden drawdown analyses in cohesive soils can also be performed.
- TOTAL STRESS METHOD (TSM)
  - Use "undrained (total)" strength parameters
  - Use total stresses
  - Typically used for analysis of end-of-construction and sudden drawdown analyses in cohesive soils; not used for other analyses.

EFFECTIVE AND TOTAL STRESS METHODS OF SLOPE STABILITY ANALYSIS

EFFECTIVE STRESS METHOD

Strength Equation

$$S' = c' + \sigma' \tan \phi'$$

Effective (Drained) Strength Parameters:

c', ϕ'

(c' is usually small, sometimes zero such as in granular soils or normally consolidated clays.)

Effective Stress: $\sigma' = \sigma - u$

Pore Pressure: $u = u_o \pm \Delta u$

u_o = due to hydrogeology

Δu = due to soil loading (positive) or unloading (negative)

States of Stability That can be Analyzed

Short term: $u_o \approx 0$, need Δu

Fill slope: increasing Δu

Cut slope: decreasing Δu

$\Delta u = \bar{B}\, \gamma h \quad (r_u = \bar{B})$

Long term: $\Delta u = 0$, need u_o

$u_o = h_p \gamma_w = r_u \gamma h$

Rapid draw-down:

$$u = h_p \gamma_w - \bar{B}\, h_w \gamma_w = r_u \gamma h$$

$$\left(r_u = \frac{\gamma_w}{\gamma} \frac{h_p - \bar{B}\, h_w}{h}\right)$$

TOTAL STRESS METHOD

Strength Equation

$$S' = c_u + \sigma \tan \phi_u$$

Total (Undrained) Strength Parameters:

c_u, ϕ_u

(ϕ_u is zero for saturated clays or small for partially saturated clays such as compacted soils.)

Total Stress: σ (applied stress)

Pore Pressure: u need not be considered since total stress is used.

States of Stability that can be Analyzed

Short term: constant c_u

Long Term: can't be analyzed

Rapid draw-down:

c_u increasing with depth due to preceeding consolidation.

TBE:lel

Long-Term Steady Seepage

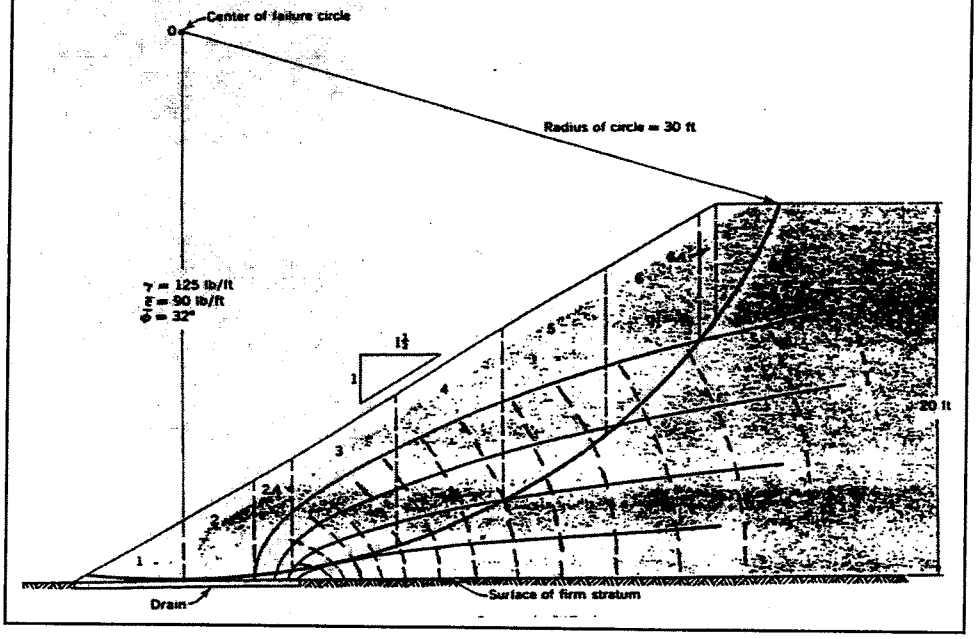

Water Force on a Slice (ESM)

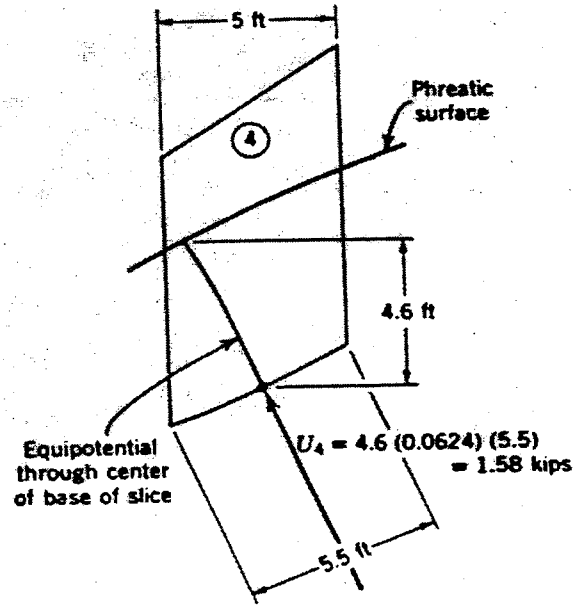

Suddden Drawdown

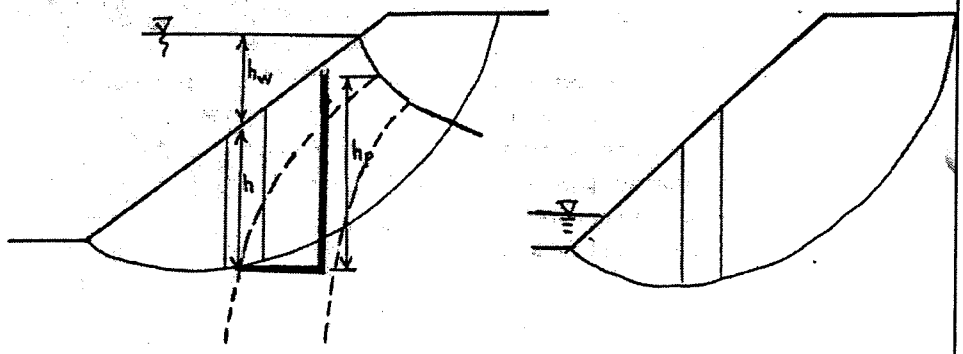

Sudden Drawdown Stresses on an Element

Pore Pressure for ESM: $u=h_p\gamma_w-B\ h_w\gamma_w$ where $B\leq 1$

11).

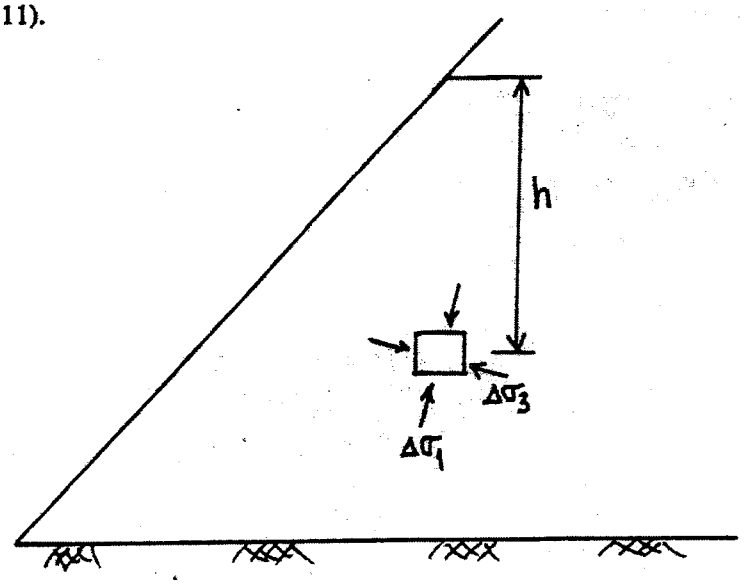

Sudden Drawdown

Undrained Strength for TSM

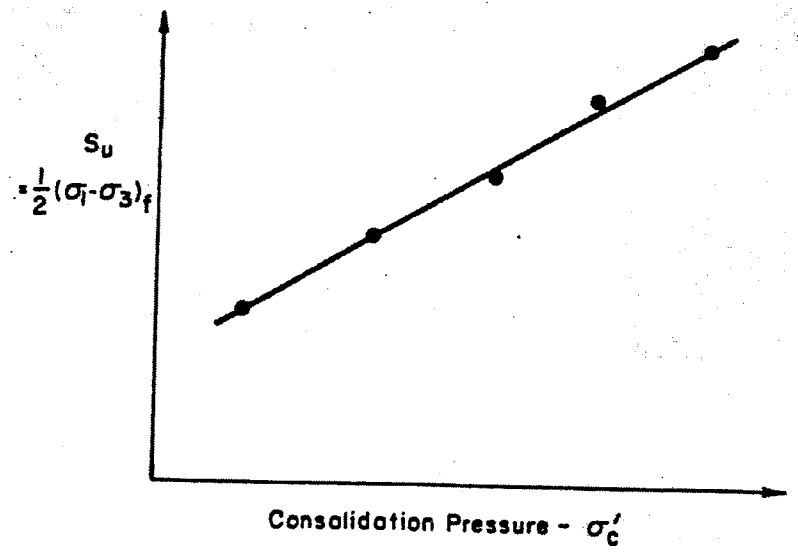

Cohesionless (Granular) Fills on Firm Foundation

Need: ϕ, γ, β, u Infinite Slope Analysis

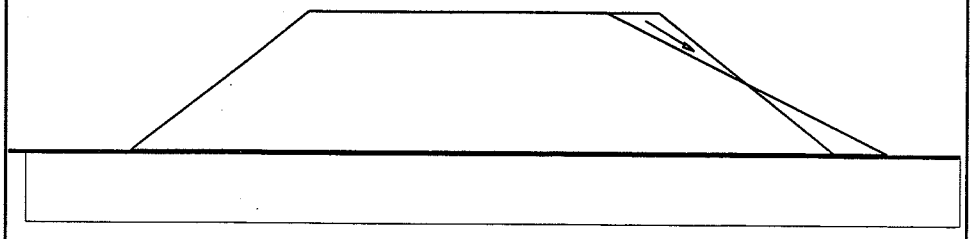

Cohesive Fills on Firm Foundation

Need: ϕ', c', c_u, ϕ_u for fill, γ, H, β, u

Rotational Finite Slope Analysis for EOC, LT, SDD

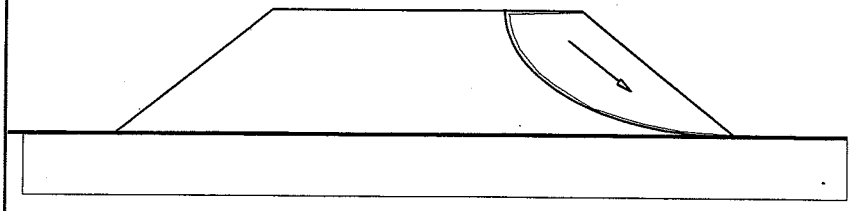

Fills on Soft Subsoil

Need: ϕ', c', c_u, ϕ_u for fill and foundation, γ, H, β, u

Rotational Finite Slope Analysis for EOC, LT, SDD

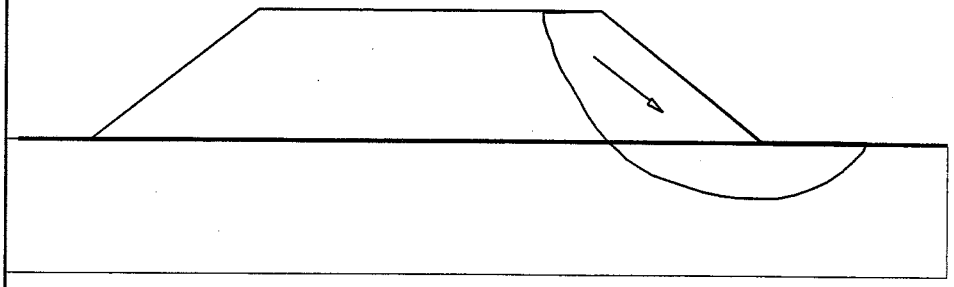

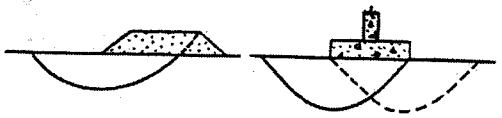

$$(s_u)_{field} = (s_u)_{vane} \cdot \mu$$

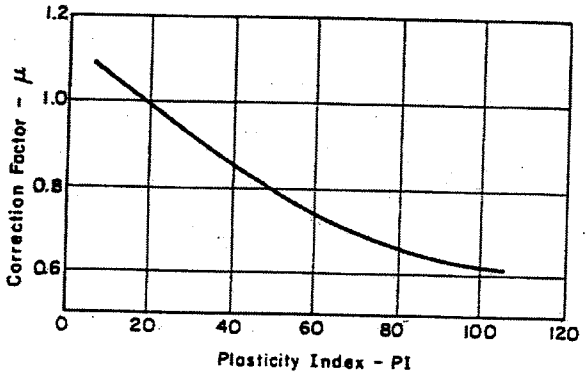

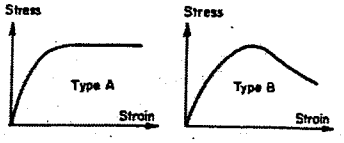

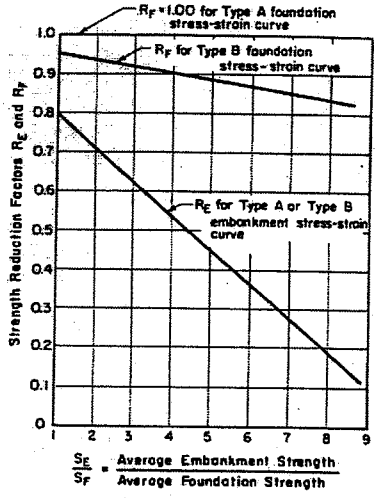

EMBANKMENT HEIGHT FOR TENSION CRACKS, H_T

Maximum Crack Depth, $d_{crack} = 4c/\gamma$ if $H \geq H_T$

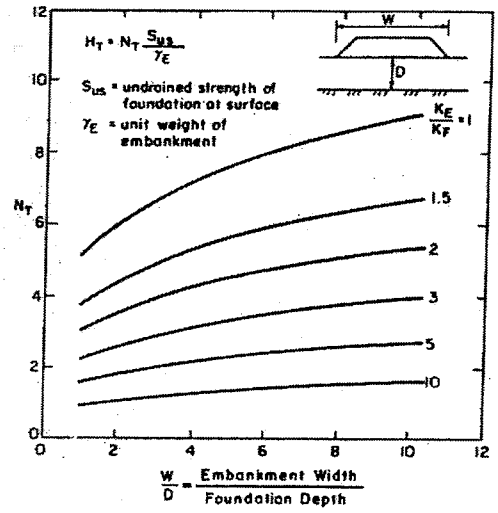

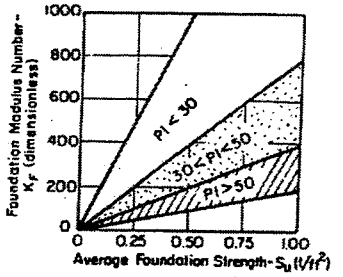

Typical values of K_E for compacted fills

Unified Class.	Compaction Water Content		
	Optimum - 3%	Optimum	Optimum + 3%
GC	300 - 1200	200-500	75 - 300
SP	400 - 1000	400-1000	400-1000
SM	300 - 750	300 - 750	300 - 750
SC	250 - 1000	150-600	50 - 250
ML	250 - 1000	150-600	50 - 250
CL	250 - 1000	100-400	30-200
CH	100 - 400	50-200	20- 100

Values shown apply to fill materials compacted to dry densities from 90% to 95% of the Std. AASHO maximum. In general, the value of K_E increases with increasing dry density at a given water content.

STABILITY FOR A FILL

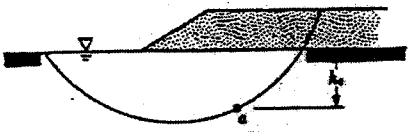

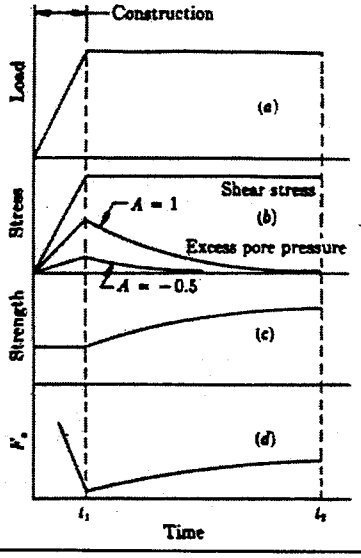

Excavations in Cohesionless (Granular Soil)

Need: ϕ, γ, β, u Infinite Slope Analysis

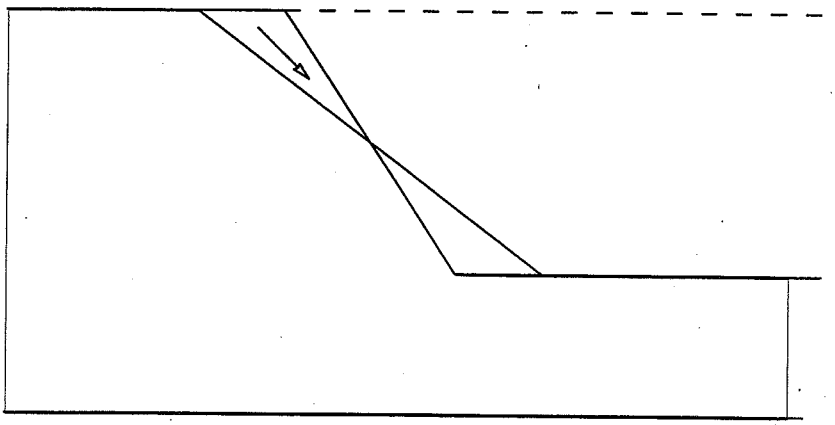

Excavations in Cohesive Soil

Need: ϕ', c', c_u, ϕ_u, γ, H, β, u

Rotational Finite Slope Analysis for EOC, LT, SDD

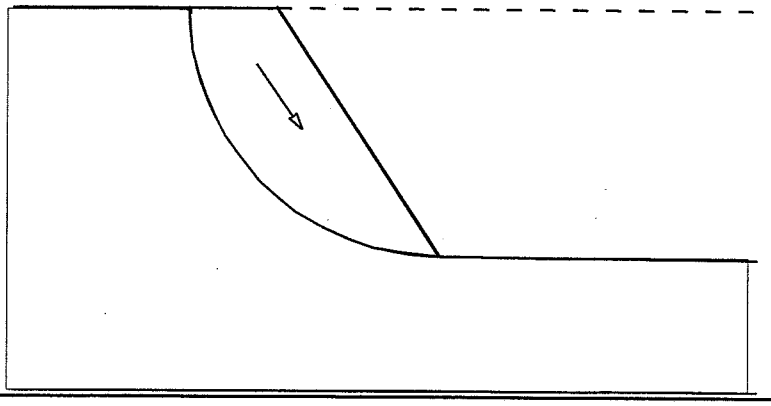

STABILITY FOR A CUT

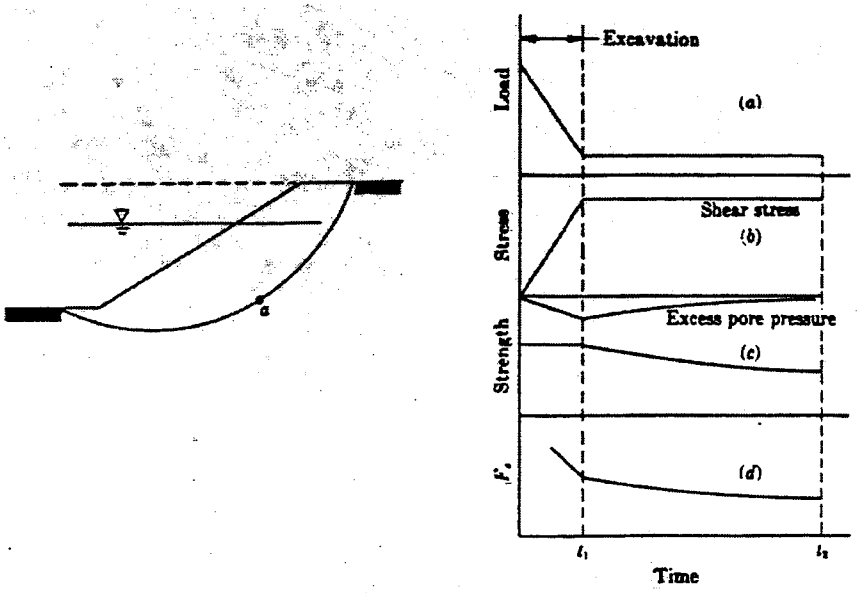

STABILITY FOR A DAM

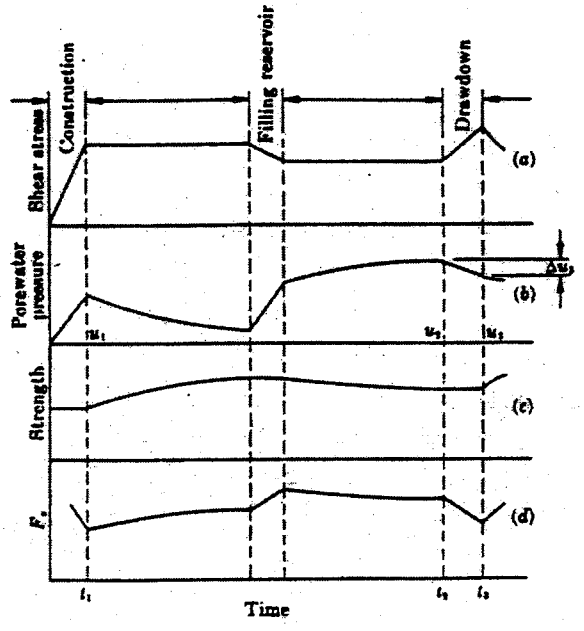

Natural Slopes

Need: ϕ', c',γ, H, β, u

Rotational Finite Slope Analysis for LT only

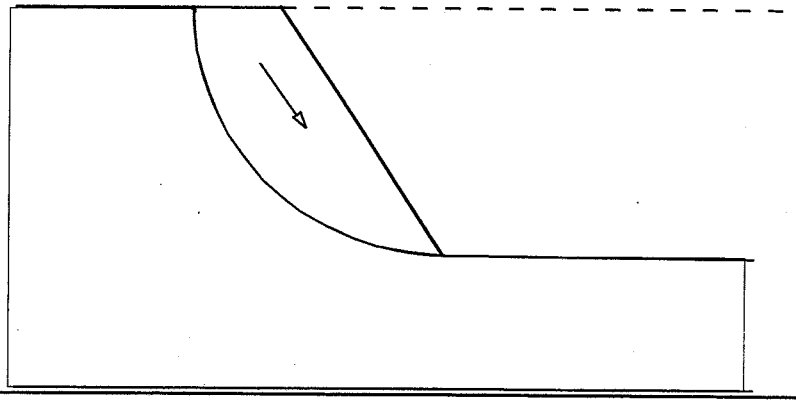

APPROACHES TO SLOPE STABILIZATION

- Understand the cause or causes of instability
- The most common causes:
  - oversteepening of the slope by cutting or filling
  - excess pore water pressures due to:
    - high groundwater level
    - strong seepage or sudden drawdown of external water level
    - blockage of drainage paths
  - undercutting due to erosion from surface water, currents or waves
  - strength loss with time due to creep and weathering

TOOLS FOR DETERMINING CAUSES OF INSTABILITY

- Observation
- Monitoring surficial slope movements
- Use of instrumentation (inclinometers, piozometers, etc.) for subsurface activities
- Thorough geological and hydrogeological exploration

METHODS OF SLOPE STABILIZATION

- Excavation (regrading, benching, lightweight fill)
- Buttress or Berm (including mechanically stabilized embankment)
- Drainage (surface and subsurface drainage including cutoff trenches, horizontal drains, relief wells)
- Reinforcement (soil nailing, stone or deep mixed columns, geosynthetically reinforced slopes, tiebacks
- Retaining Structures (walls, driven piles, drilled shafts)
- Biotechnical Stabilization (root reinforcement, erosion control
- Special Techniques (grouting, chemical injection, lime/cement or fly ash stabilization, freezing, heating, etc.)

TABLE 2.-- METHODS OF STABILIZING SLOPES AND LANDSLIDES (after Turnbull and Hvorslev, 1967)

Scheme	Applicable Methods	Comments
I. EXCAVATION 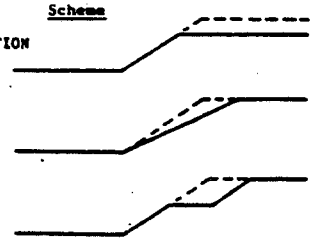	1. Reduce slope height by excavation at top of slope. 2. Flatten the slope angle. 3. Excavate a bench in upper part of slope. 4. Excavate the entire slide mass.	Area has to be accessible to construction equipment. Disposal site needed for excavated soil. Drainage sometimes incorporated in this method.
II. DRAINAGE 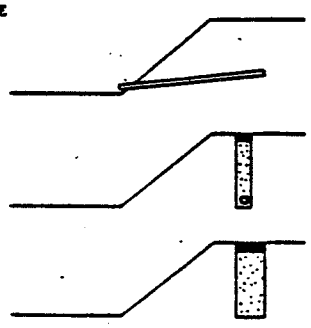	1. Small diameter, horizontal drains (hydraugers). 2. Continuous deep subdrain trench. Generally 5 to 15 feet deep. 3. Drilled vertical wells--generally 18- to 36-inch diameter. 4. Improve surface drainage along top of slope with open ditch or paved gutter. Install deep-rooted, erosion-resistant plants on slope face.	1. Most effective if can tap natural aquifer. Drains are usually free-flowing. 2. Trench bottom should be sloped to drain and be tapped with an outlet pipe. Perforated pipe should be placed on trench bottom. Top of trench should be capped with impervious material. 3. Can be pumped or tapped with a gravity outlet. Several wells in a row, joined at bottom can form a drainage gallery. Top of each well should be capped with impervious material. 4. Good practice for most slopes. Direct the discharge away from slide mass.
III. EARTH OR ROCK BUTTRESS (OR BERM FILL) 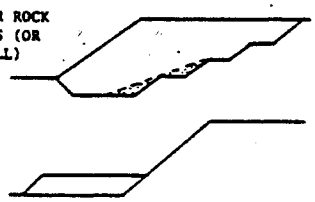	1. Excavate slide mass and replace with compacted earth or rock buttress fill. Toe of buttress must be keyed into firm soil or rock below slide plane. Drain blanket with gravity flow outlet is provided in back slope of buttress fill. 2. Compacted earth or rock berm placed at and beyond the toe. Drainage may be provided behind berm.	1. Access for construction equipment and temporary stockpile area required. Excavated soil can usually be used in fill. Underpinning of existing structures may be required. Might have to be done in short sections if stability during construction is critical. 2. Sufficient width and thickness of berm required so failure will not occur below or through berm.
IV. RETAINING STRUCTURES 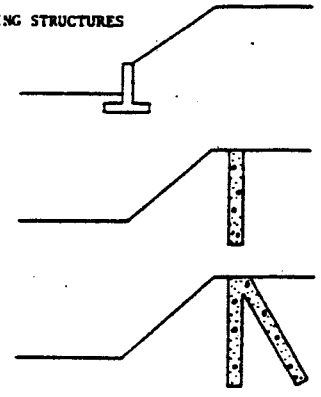	1. Retaining wall - crib or cantilever type. 2. Drilled, cast-in-place vertical piles, bottomed well below bottom of slide plane. Generally 18 to 36 inches in diameter and 4- to 8-foot spacing. 3. Drilled, cast-in-place vertical piles tied back with battered piles or a dead-man. Piles bottomed well below slide plane. Generally 12 to 30 inches in diameter and at 4- to 8-foot spacing. 4. Earth anchors and rock bolts.	1. Usually expensive. Cantilever walls might have to be tied back. 2. Spacing should be such that soil can arch between piles. Grade beam can be used to tie piles together. Very large diameter (6 feet ±) piles have been used for deep slides. 3. Space close enough so soil will arch between piles. Piles can be tied together with grade beam. 4. Can be used for high slopes, and in very limited areas. Conservative design should be used, especially for permanent support.
V. SPECIAL TECHNIQUES	1. Grouting 2. Chemical injection 3. Electroosmosis (in fine-grained soils). 4. Freezing 5. Heating	1. and 2. Used successfully in a number of cases. Used at other times with little success. At the present, theory is not completely understood. 3. Generally expensive. 4. and 5. Special methods which must be specifically evaluated at each site. Can be expensive. All of these techniques should be carefully evaluated in advance to determine the probable cost and effectiveness.

TABLE 7.1 Summary of Methods for Correcting and Preventing Landslides

Method of Treatment and its Effect on Stability of Slide	Treatment	General Use		Frequency of success[a]			Position of Treatment Related to the Actual or Potential Sliding Mass	Posibilities and Limitations
		Prevention	Correction	Collapse	Slide	Flow		
Avoidance	Relocation	X	X	2	2	2	Outside slide limits	The best method if economical
No effect	Construction of viaduct	X	X	3	3	3	Outside slide limits	Applicable to short stretches of sloping hillsides
Movement of earth	Removal from the head	X	X	N	1	N	Upper part and head	Large masses of cohesive material
Reduction in shear stresses	Slope flattening	X	X	1	1	1	In the cut or embankment slopes	More effective in earth fills on frictional soils
	Terracing in slopes	X	X	1	1	1	In the cut or embankment slopes	—
	Removal of all unstable material	X	X	2	2	2	Throughout the slide	In relatively small superficial masses of moving material
Drainage	Surface							
Reduction in shear stresses and increase in shear strength of the soil	Ditches	X	X	1	1	1	Above the crown	Essential in all types
	Slope treatment	X	X	3	3	3	On surface of sliding mass	Rock covering or permeable apron to control the flow
	Subgrade trimming	X	X	1	1	1	On surface of sliding mass	Beneficial in all types
	Sealing of cracks	X	X	2	2	2	Throughout, crest to toe	Beneficial in all types
	Sealing of joint and fissure planes	X	X	3	3	N	Throughout, crest to toe	Applicable to rock formations
	Subdrainage							
	Horizontal drains	X	X	N	2	2	Located to intercept and divert underground water	Large masses of soil with underground flow
	Stabilizing trenches	X	X	N	1	3		Relatively superficial masses of soil with underground flow
	Drainage galleries	X	X	N	3	3		Deep-seated and large masses of soil with significant permeability
	Vertical drainage wells	X	X	N	3	3		Deep-seated sliding masses, underground water in strata or lenses
	Continuous siphon	X	X	N	2	3		Chiefly used as a ditch or drainage well opening
Retaining structures	Support at the base							
Sliding resistance increases	Rock fill	X	X	N	1	1	Base and toe	Sound rock or firm soil at a reasonable depth
	Earth fill	X	X	N	1	1	Base and toe	As counterweight in the toe gives additional strength
	Common or crib retaining walls	X	X	3	3	3	Base	Relatively small moving masses
	Piles							
	Fixed in the slip surface	—	X	N	3	N	Base	The strength of the failure surface is increased by the amount of stress required to make the piles fail
	Not fixed to slip surface	—	X	N	3	N	Base	
	Anchorages in rock	X	X	3	3	N	Uphill from the highway or structure (cuts)	Stratified rock
	Short anchorages in slopes	X	X	3	3	N	Uphill from highway or structure	Eroding slope protected by screen anchored to a solid underlying formation
Other Methods	Hardening of the sliding mass							
Chiefly an increase in shear strength	Cementing or chemical treatment							
	At the base	—	X	3	3	3	Base and toe	Cohesionless soils
	Throughout the mass	—	X	N	3	N	Throughout sliding mass	Cohesionless soils
	Freezing	X	—	N	3	3	Throughout sliding mass	To prevent temporary movement in large masses
	Electro-osmosis	X	—	N	3	3	Throughout sliding mass	Hardens the soil by reducing the water content
	Use of explosives	—	X	N	3	N	In the lower part of the slide	Relatively superficial cohesive mass overlying a mass of rock. Fragmented sliding surface. Explosives may also enable water to drain from the sliding mass

[a] 1: Frequent; 2: occasional; 3: rare; N: not considered applicable.

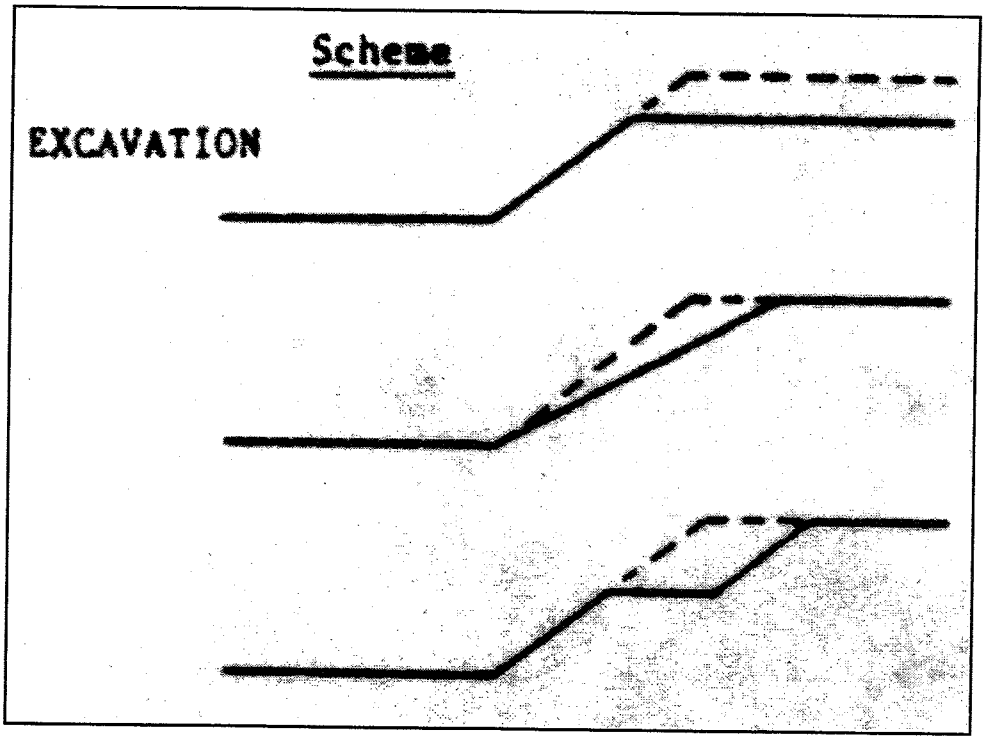
Scheme
EXCAVATION

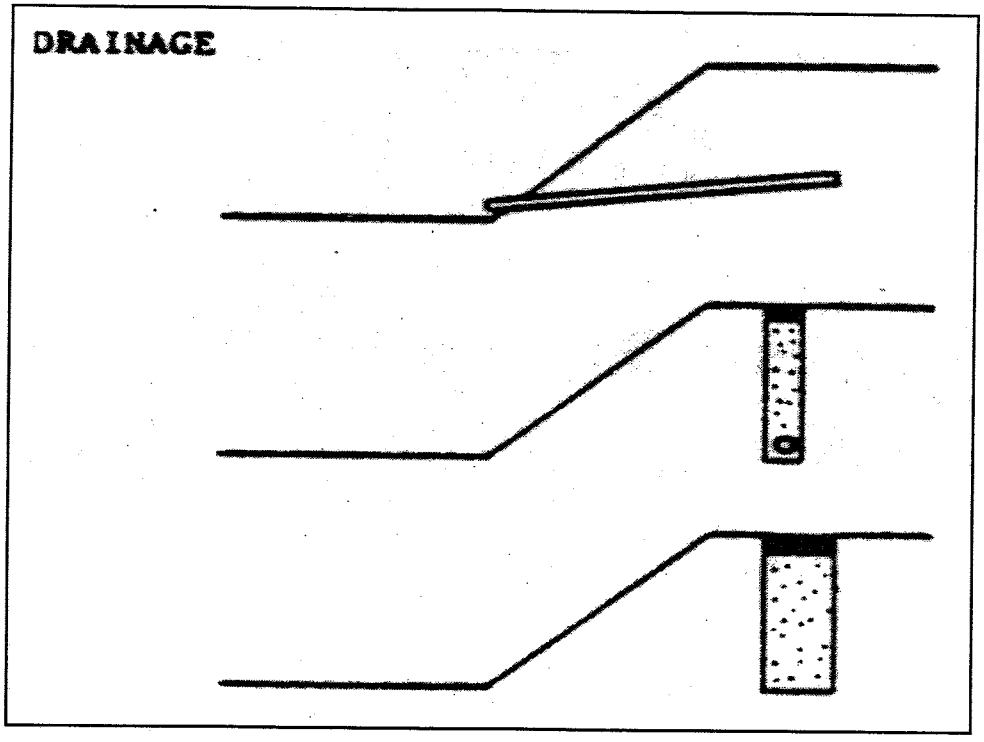
DRAINAGE

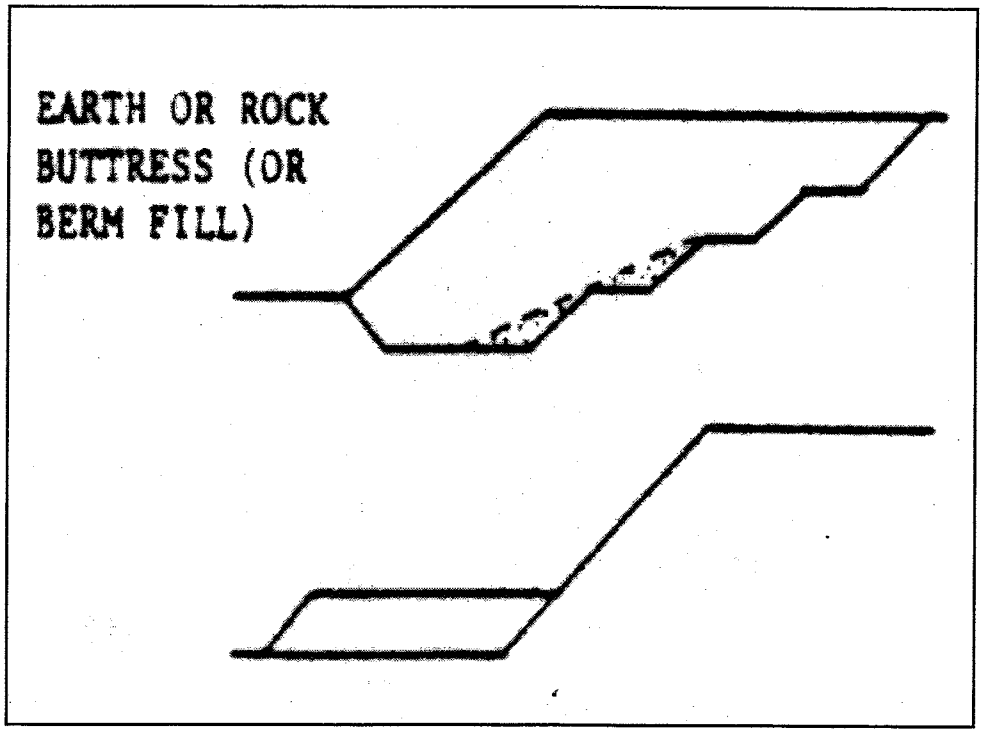
EARTH OR ROCK
BUTTRESS (OR
BERM FILL)

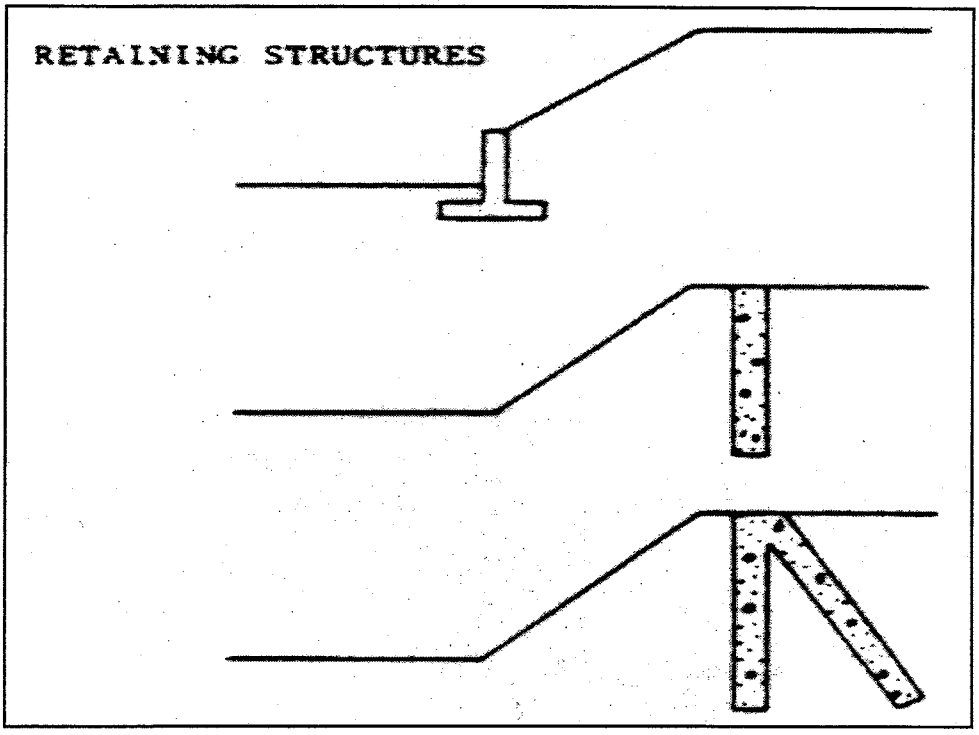
RETAINING STRUCTURES

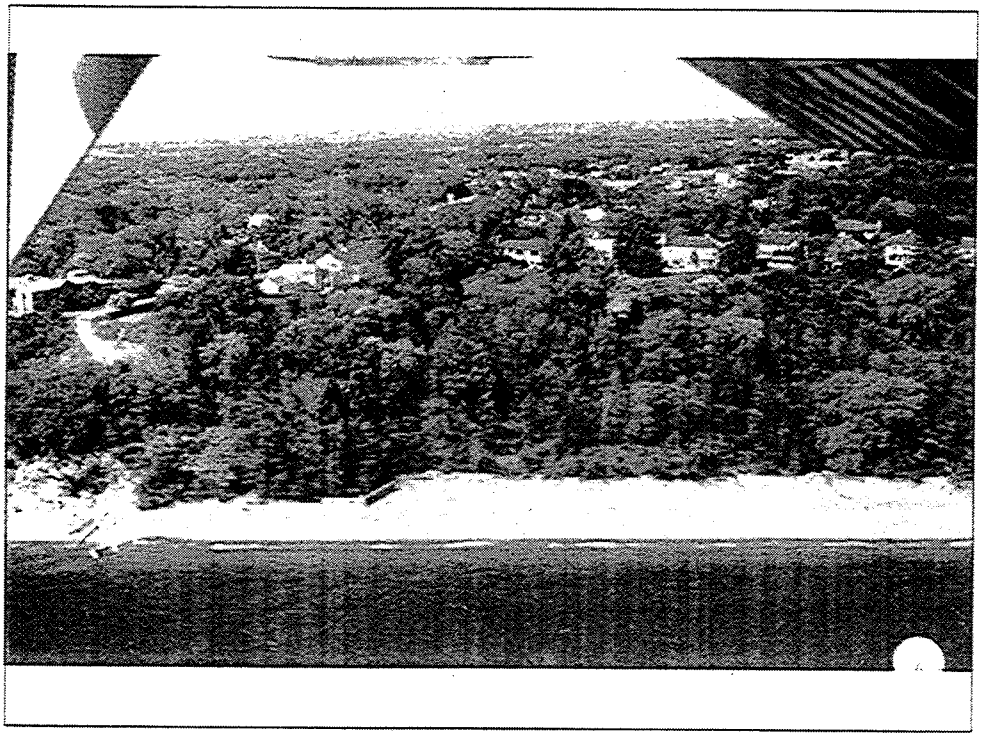

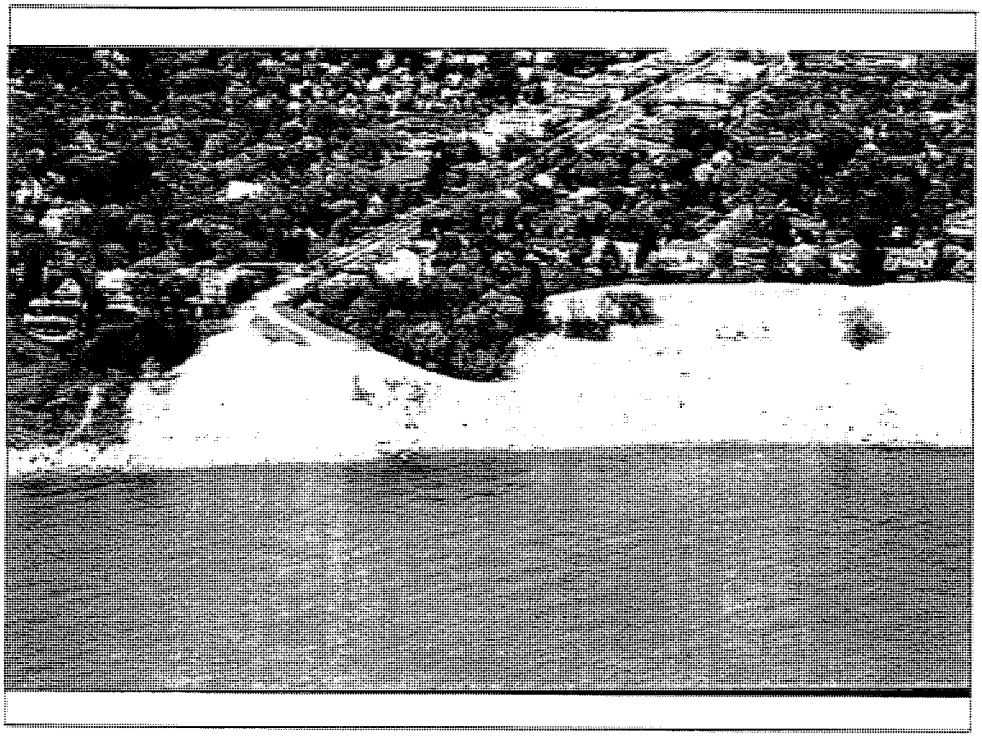

Procedures for Investigation and Design of Slopes

- Field Observations (Field Stability Charts)
- Stability Chart Solutions
- Detailed Analysis

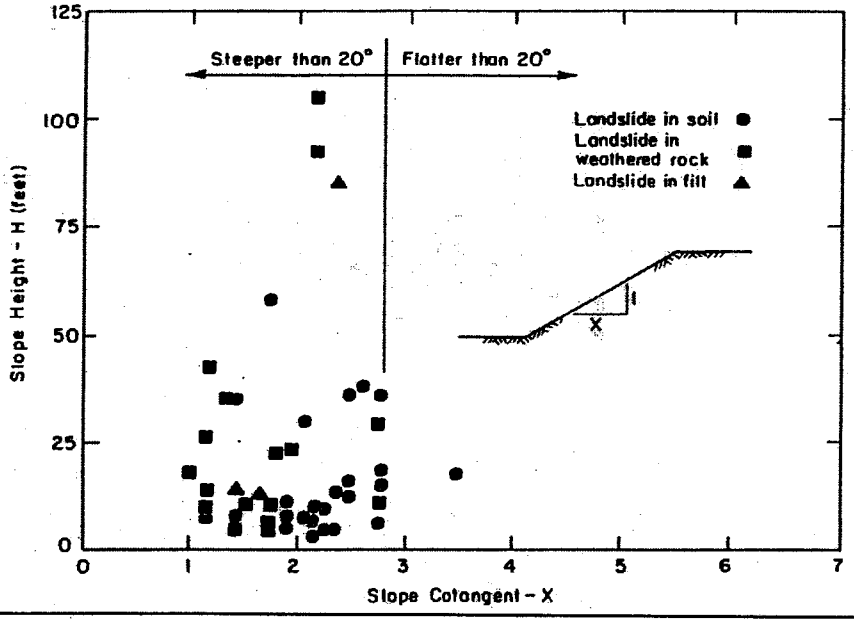

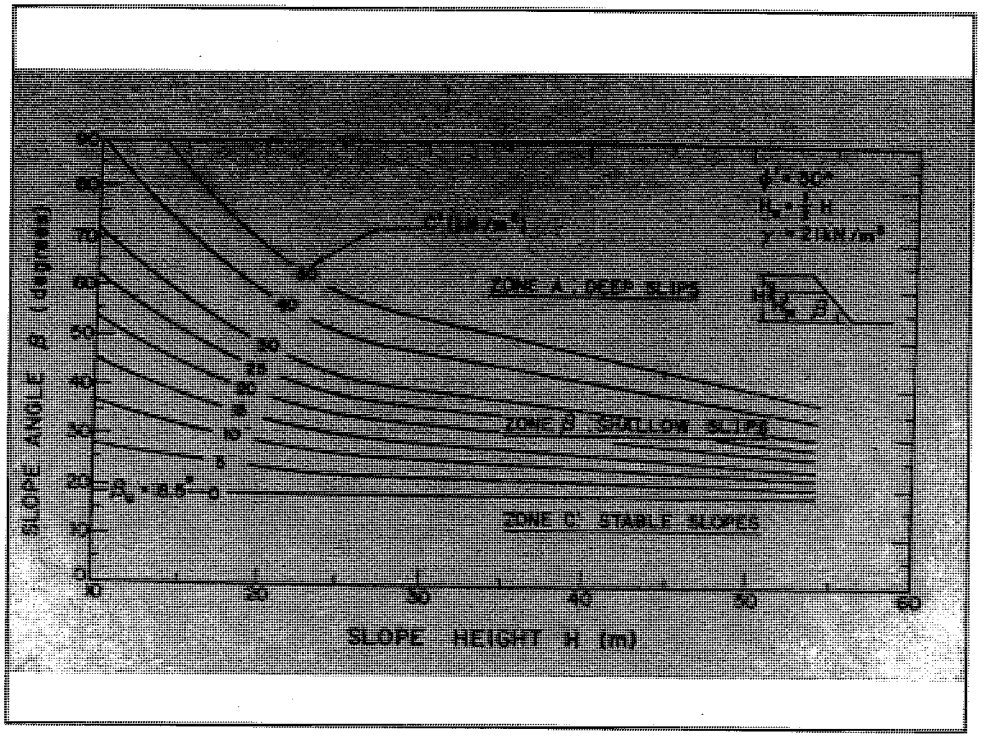

REFERENCES

J.M. Duncan, A.L. Buchignani and M. De Wet (1987), An Engineering Manual for Slope Stability Studies, Virginia Tech Department of Civil Engineering, Blacksburg, Virginia.

L.W. Abramson, T.S. Lee, S. Sharma and G.M. Boyce (1996), Slope Stability and Stabilization Methods, Wiley, N.Y.

U.S. Department of Agriculture, National Engineering Field Handbook Series: Chaptr 18- Soil Bioengineering for Upland Slope Protection and Erosion Reduction, Soil Conservation Service, Washington, D.C.

TAB 3

Elizabeth L. Mathieson

and

Philip J. Shaller

Presentations

Exponent™
Failure Analysis Associates

Geological Aspects of Slope Stability

by Elizabeth L. Mathieson, C.E.G. and Phillip J. Shaller, Ph.D., C.E.G.

February 20, 2002

University of Wisconsin – Madison

"Slope Stability and Landslides"

(ik-spo'nent) ***n.***

1. One who expounds or interprets.

OVERVIEW

- **Stability characteristics of rock and soil depend on their geologic origins and histories**
- **Discontinuities govern strengths of many materials**
- **Slope characterization requires geologic input**

MAJOR TOPICS

1. GEOLOGICAL CONDITIONS PRODUCING LANDSLIDES
2. GEOLOGICAL PROCESSES AND RELATIONSHIPS TO ENGINEERING PROPERTIES
3. LANDSLIDE MECHANISMS RELATED TO GEOLOGY
4. ESTIMATING MATERIAL STRENGTHS AND STABILITY; MASS WASTING POTENTIALS OF EARTH MATERIALS

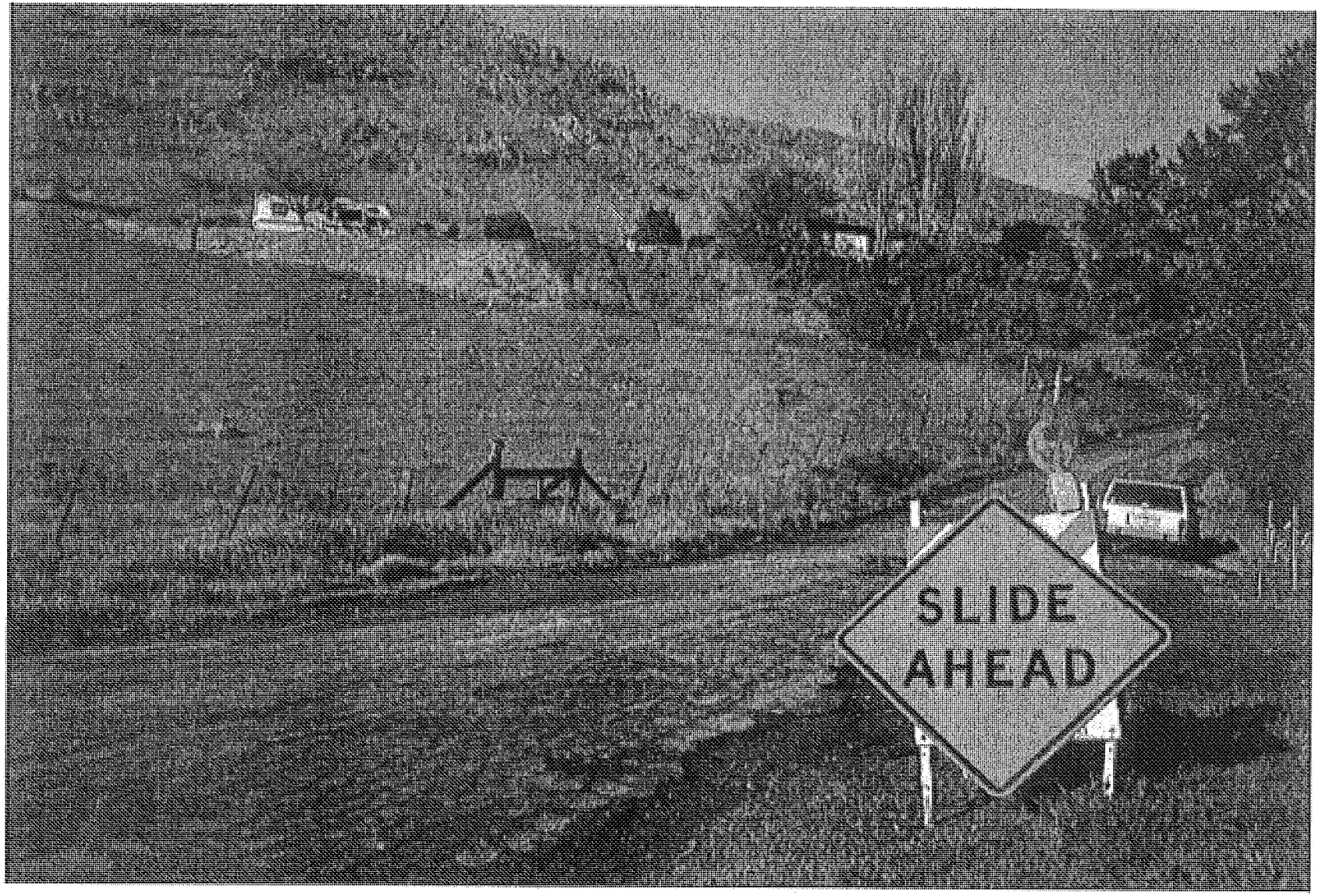
SLIDE
AHEAD

"...important landslide problems call for co-operation between geologist and engineer... the geologist should be familiar with the fundamental principles of soil mechanics, and the engineer should know at least the elements of physical geology."

-- Karl Terzaghi, 1950

GEOLOGICAL CONDITIONS PRODUCING LANDSLIDES

Landslide Overview Map

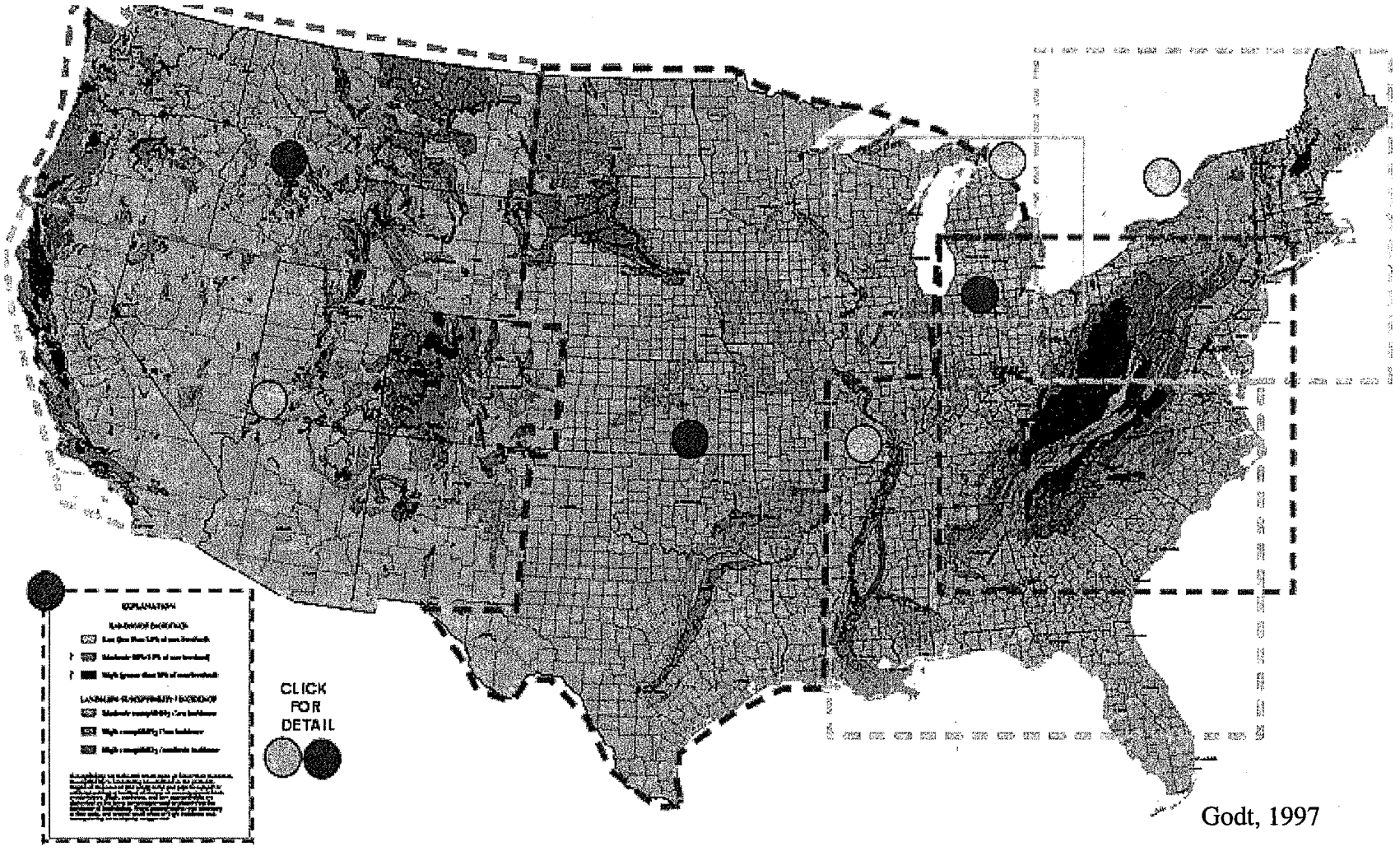

Godt, 1997

Landslide materials

ROCK:

"A hard or firm mass that was intact and in its natural place before the initiation of movement"

SOIL:

"An aggregate of solid particles, generally of minerals and rocks, that either was transported or was formed by the weathering of rock in place."

--Shroder, 1971, and Varnes,1978

Rock Stability vs. Soil Stability

- **Rock slope stability is controlled by the absence or presence of discontinuities**
- **Soil slope stability is controlled by material strength**
- **Both are profoundly influenced by WATER**

The Rock Cycle

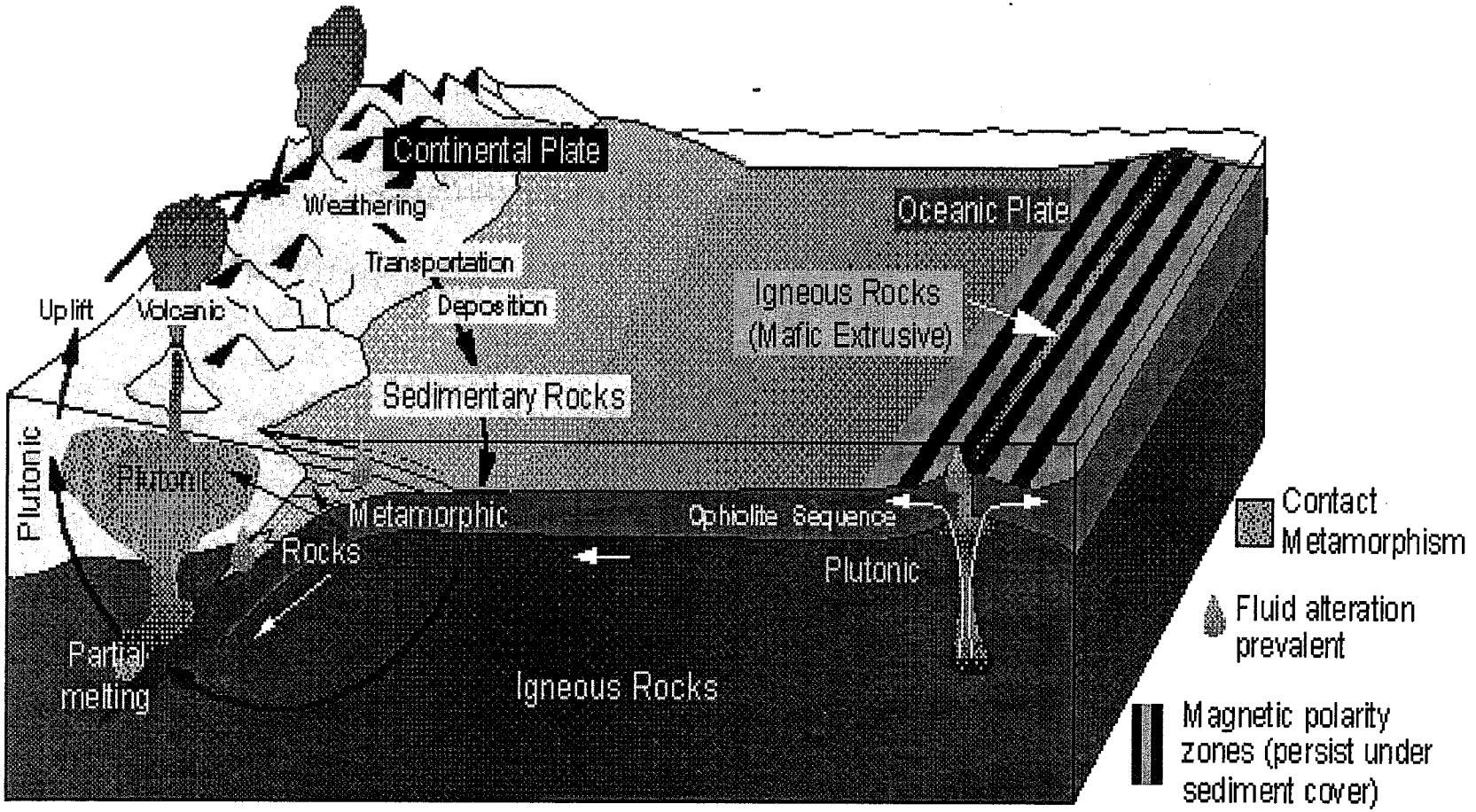

Redrawn by W. Milner, as modified from Montgomery (1990) and Monroe and Wicander (1994).

http://www.science.ubc.ca

Rock Condition

Hardness

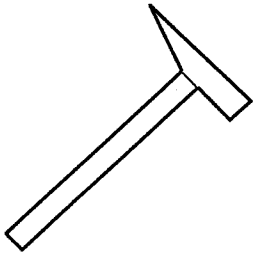

Fracturing

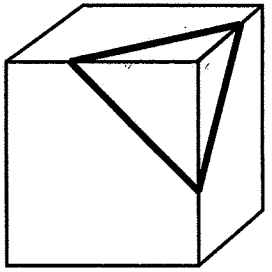

Weathering

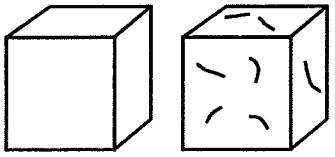

Porosity

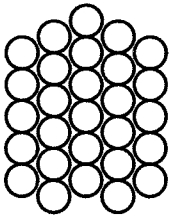

Rock Structure

"The foremost requirements for slide prevention are reliable information on the geologic structure of the ground..."

-- Karl Terzaghi, 1950

Bedding – Grand Canyon

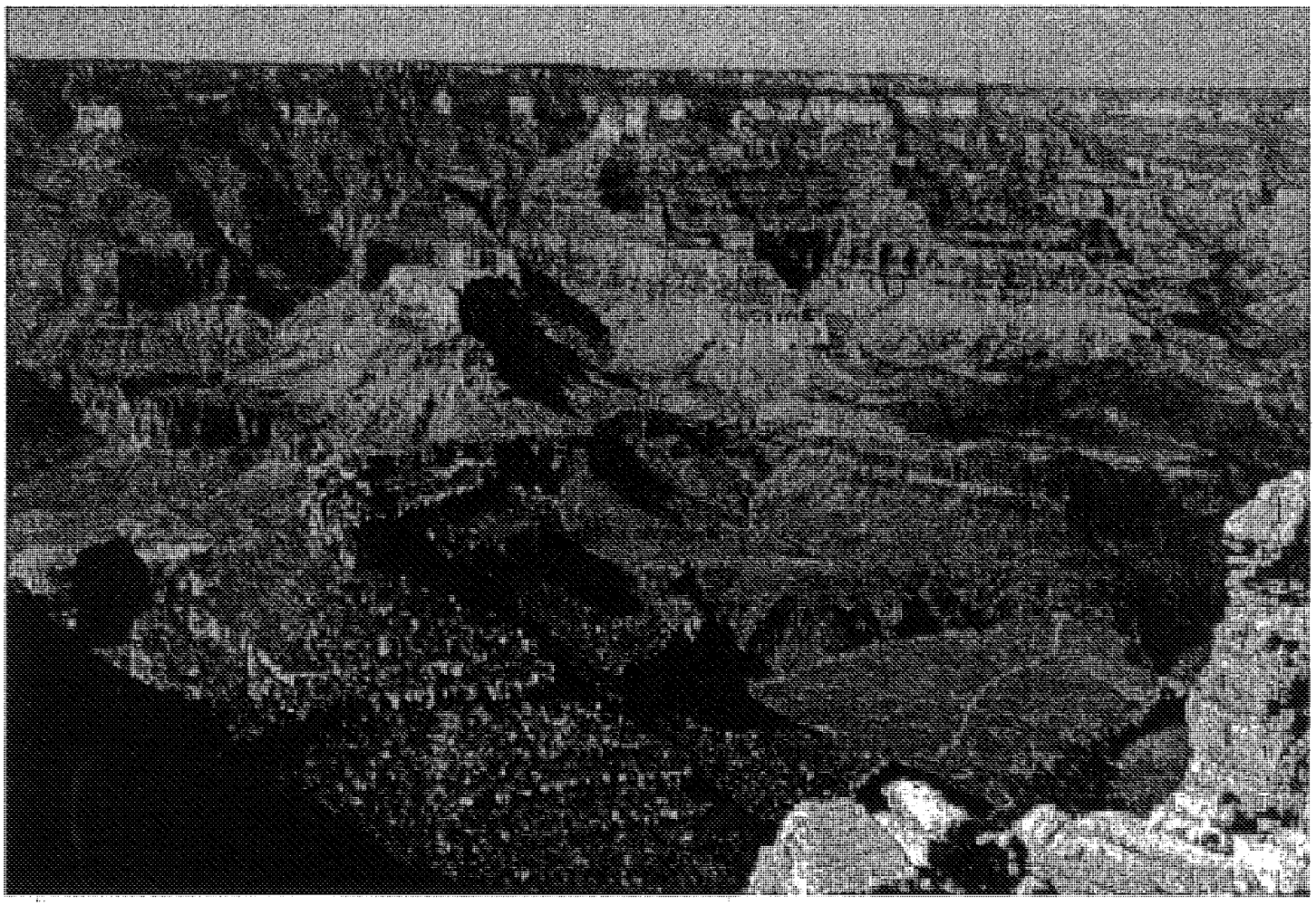

Ruth Eddy

Lakebeds

Martin Miller

Bedding Attitude

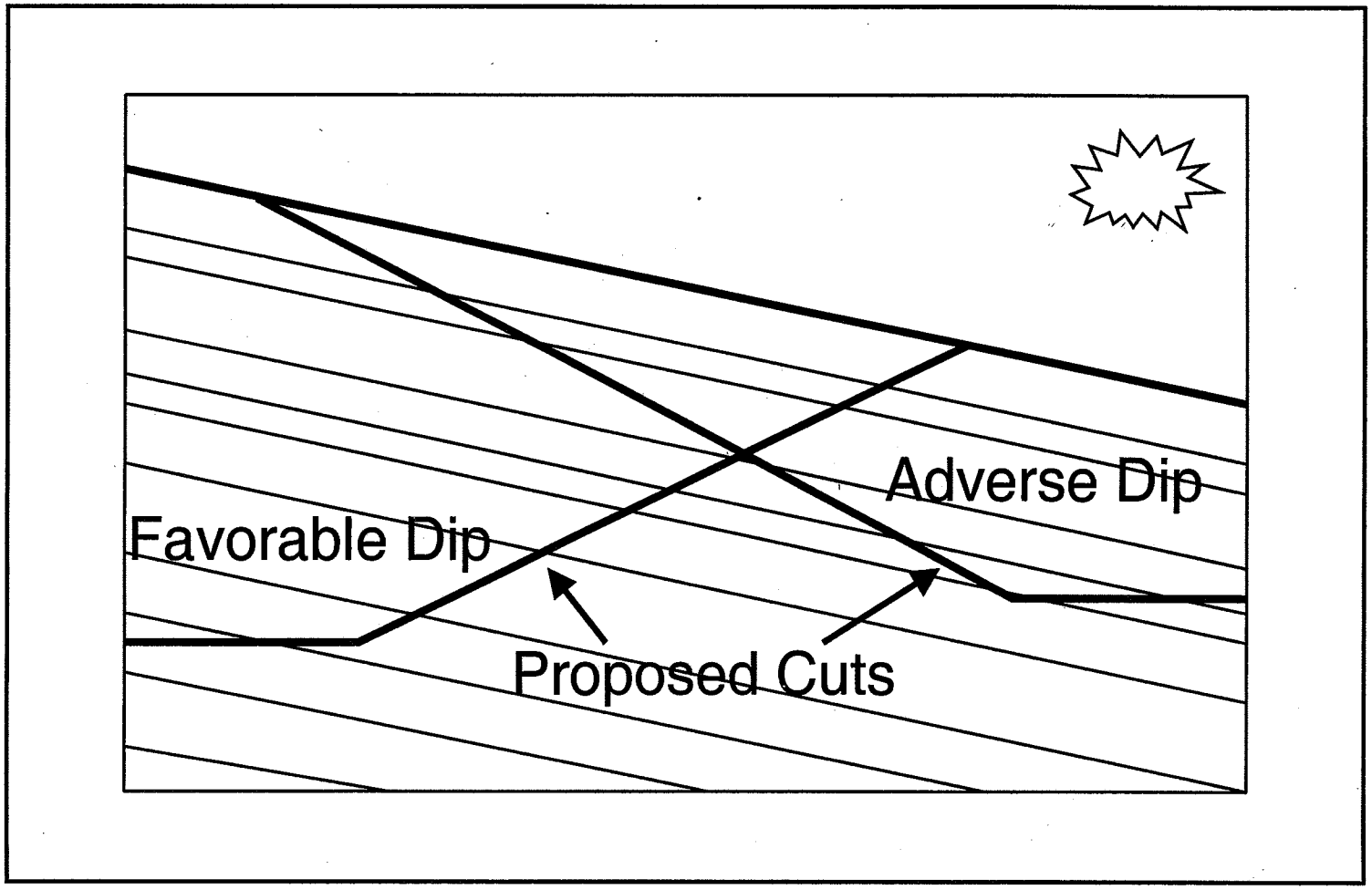

Bedding Thickness

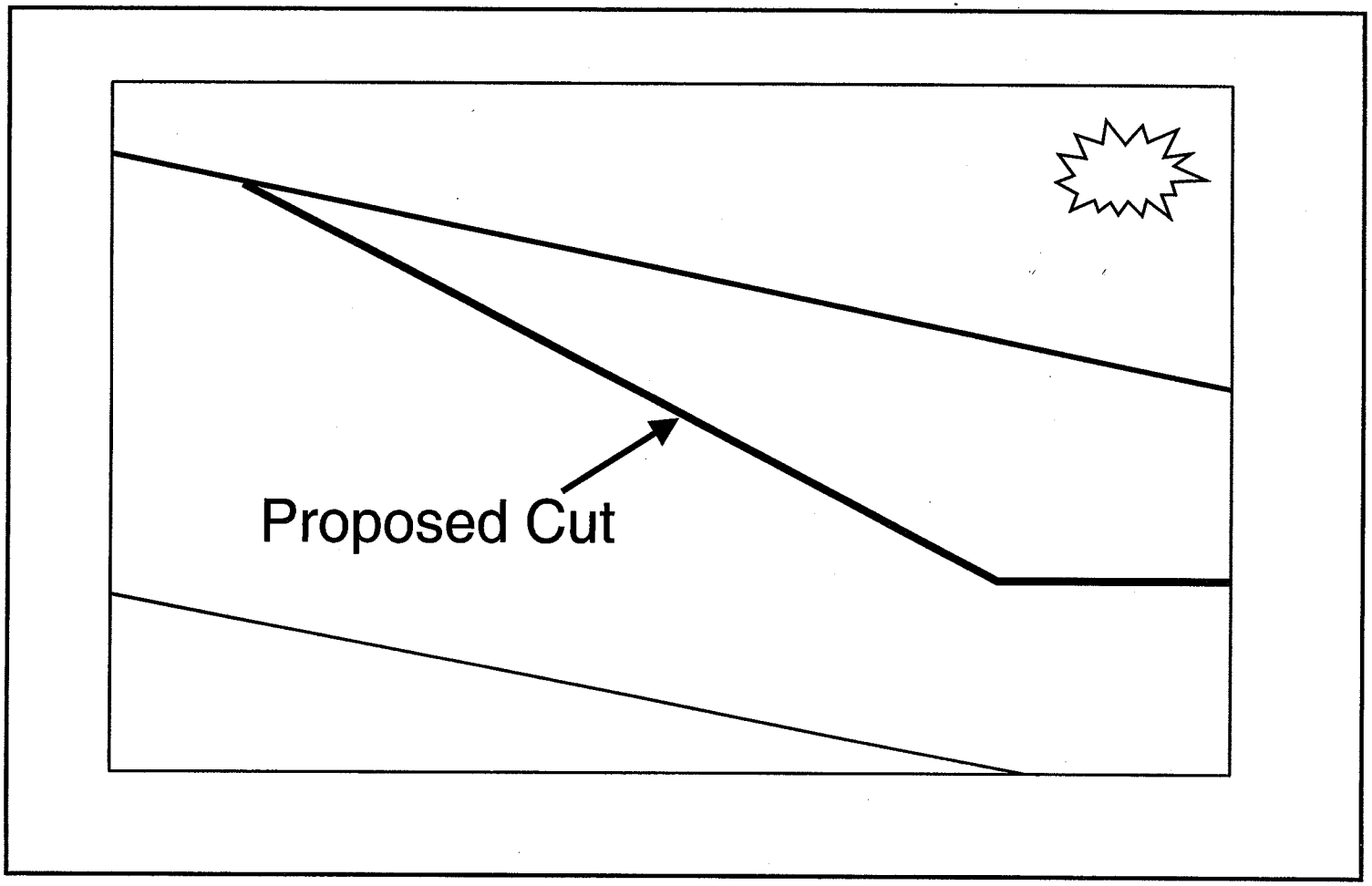

Landslide on Bedding Planes

Connolly, 1997

Folds – Southwest Wales

Martin Miller

Formation of Folds

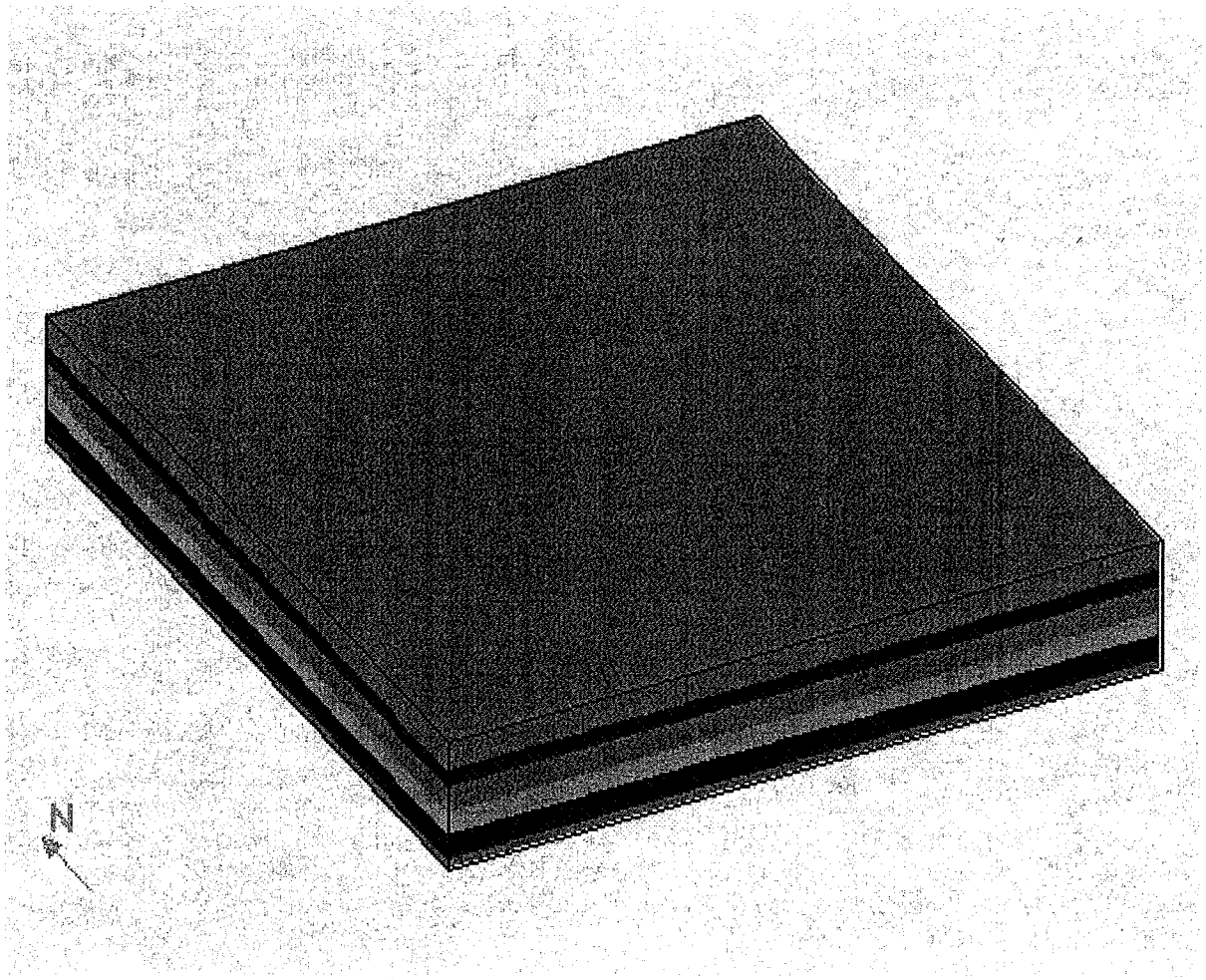

Monash University

Folds

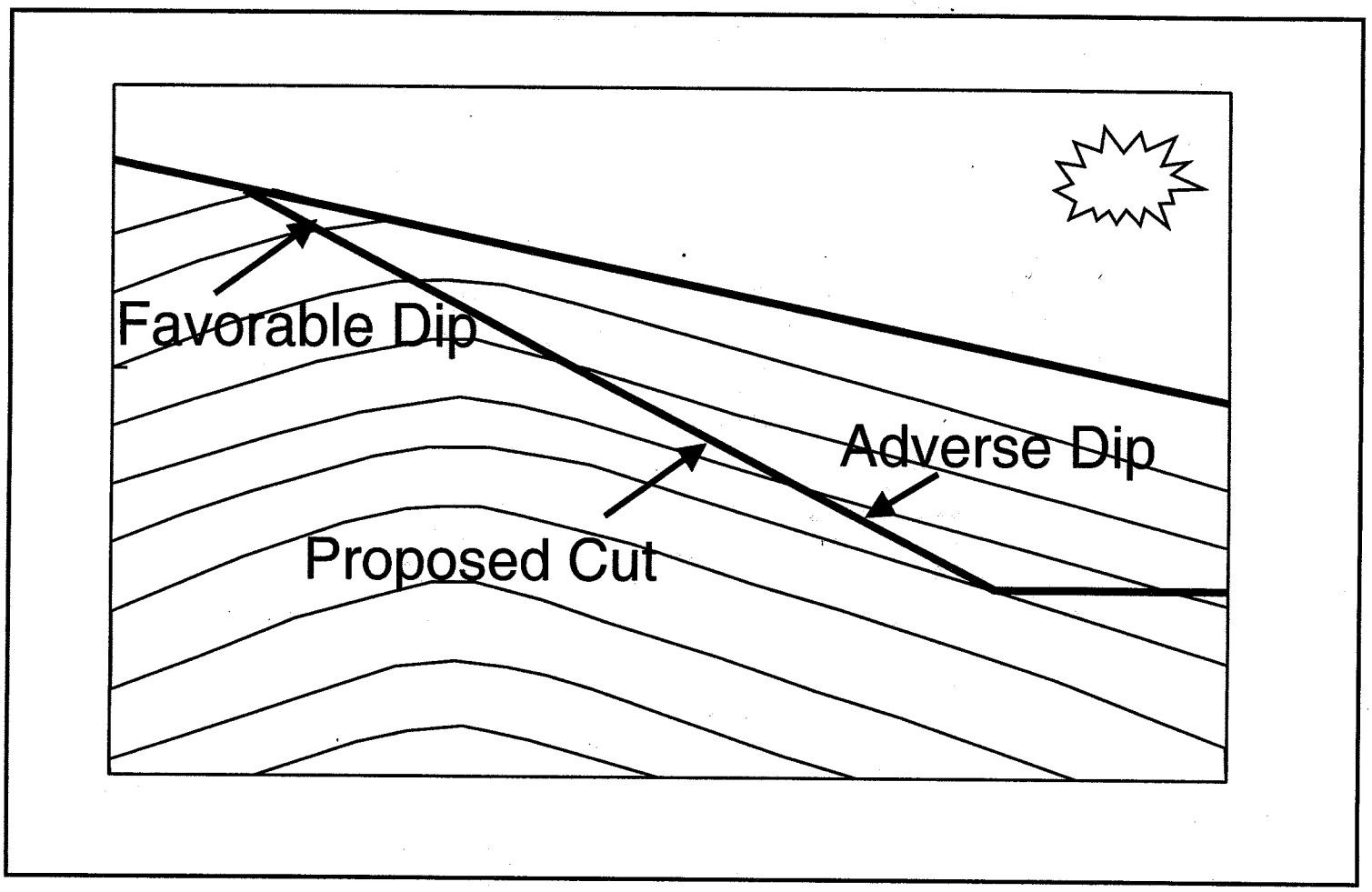

Fractures - Yosemite

Martin Miller

Fault

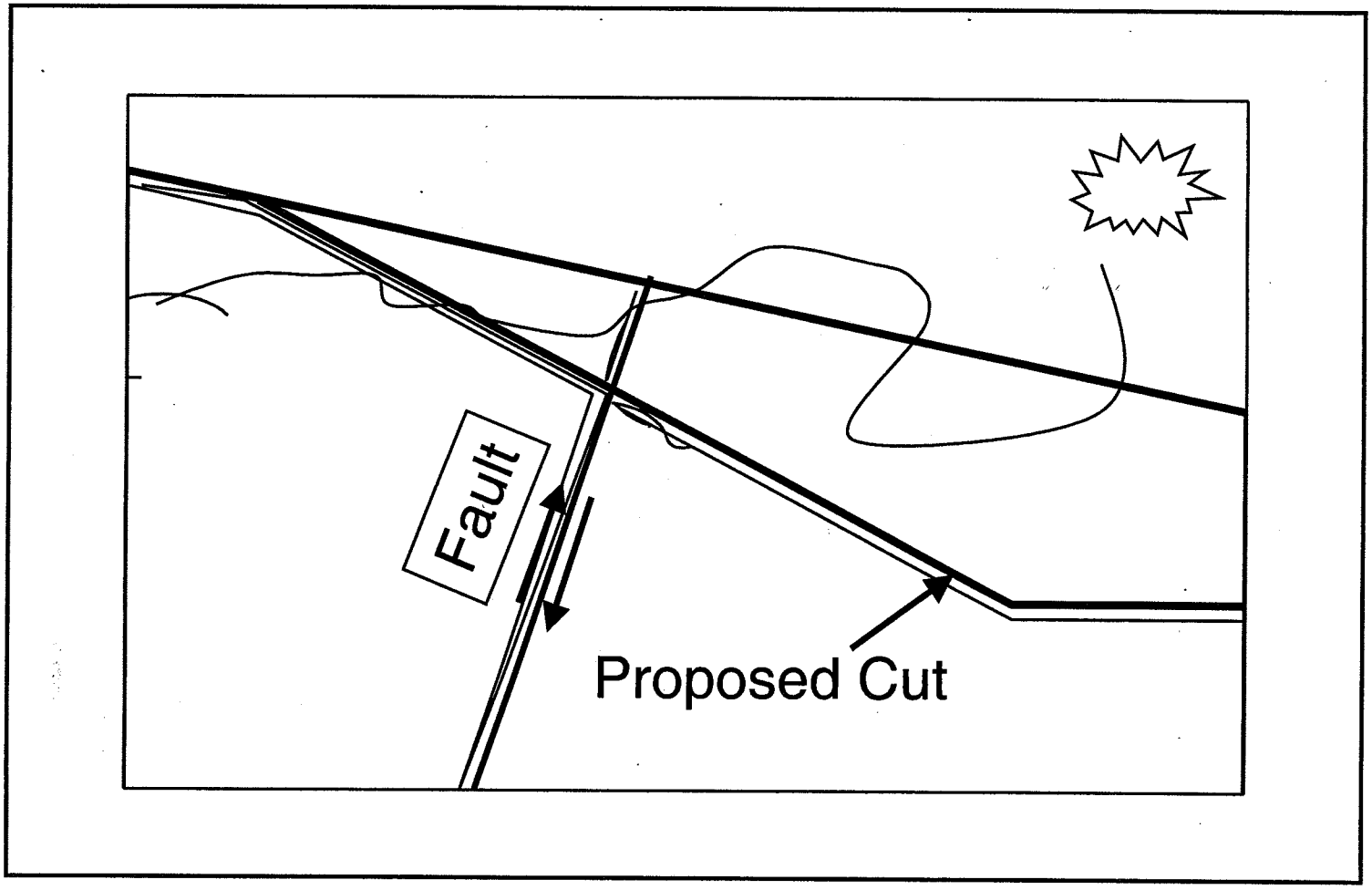

Faults – Canyonlands, Utah

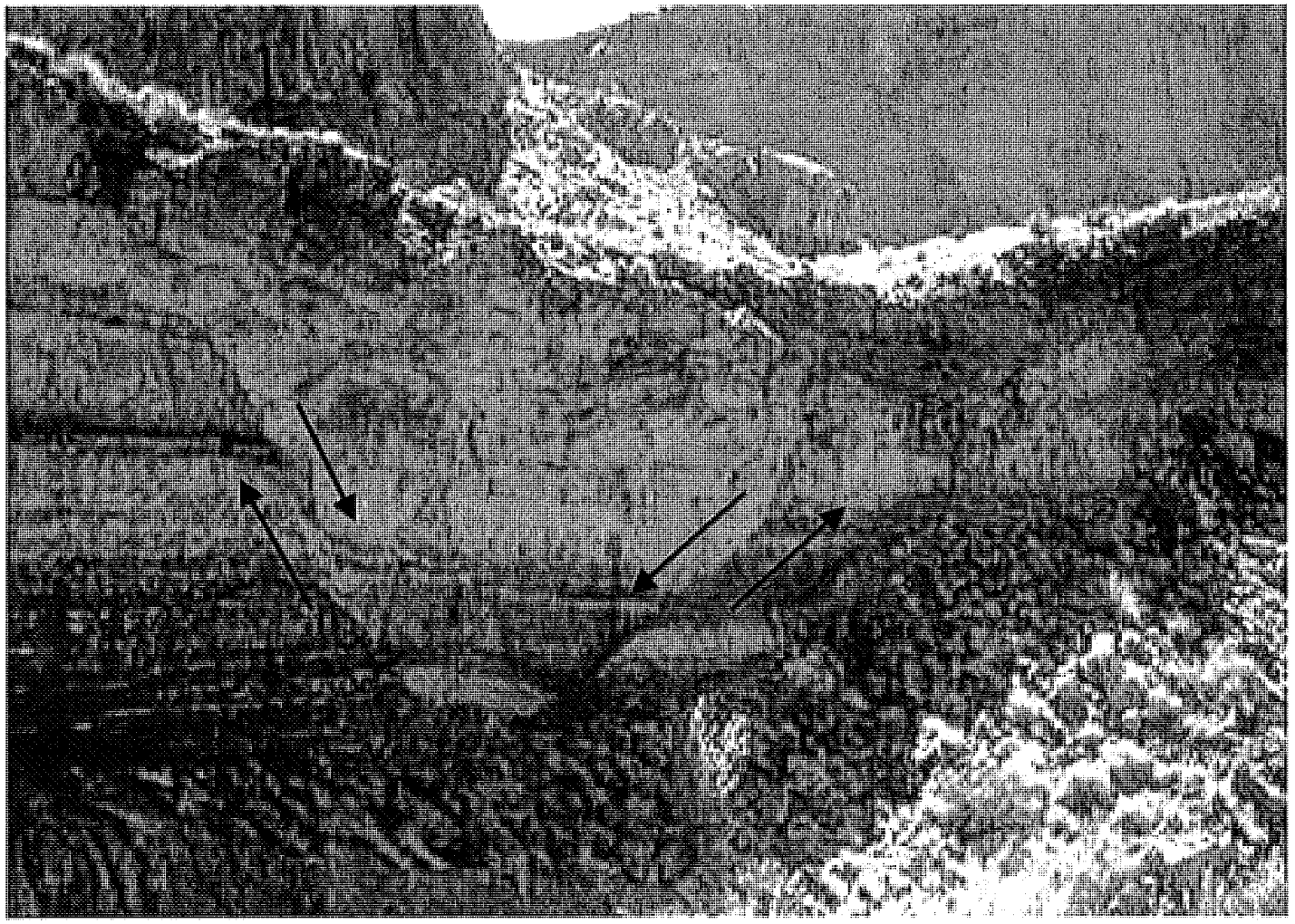

Martin Miller

Fault Breccia

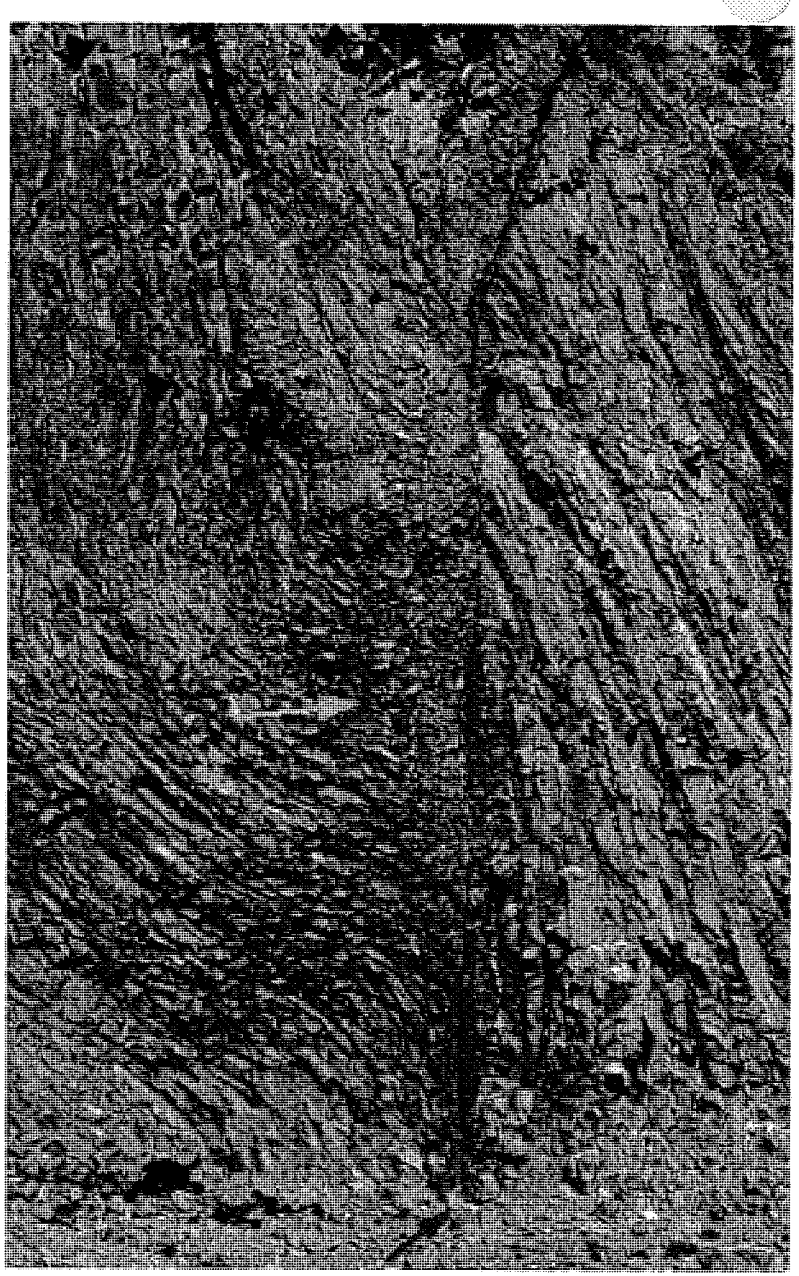

Roy W. Schlische, Rutgers University

Big Rock Mesa Landslide, Malibu

Tvs Vaqueros and Sespe Fms., undiff.

⊙F Fossils

~F Mapped bed with fossils

Screened area represents landslide interpretation in 1961

Boundary of Big Rock Mesa landslide of 1983

0 1000

FEET

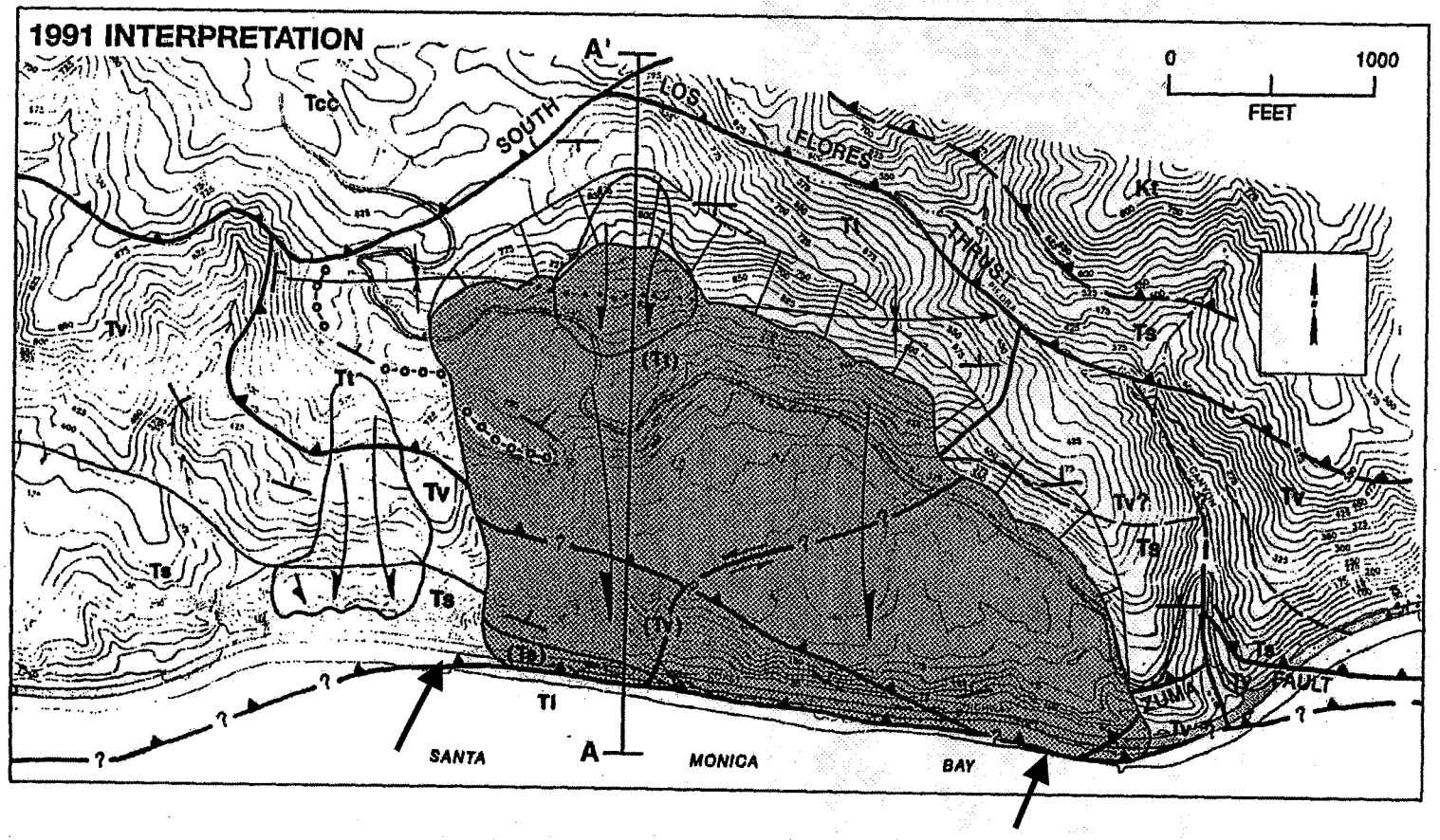

Fault at toe of Big Rock Mesa Landslide

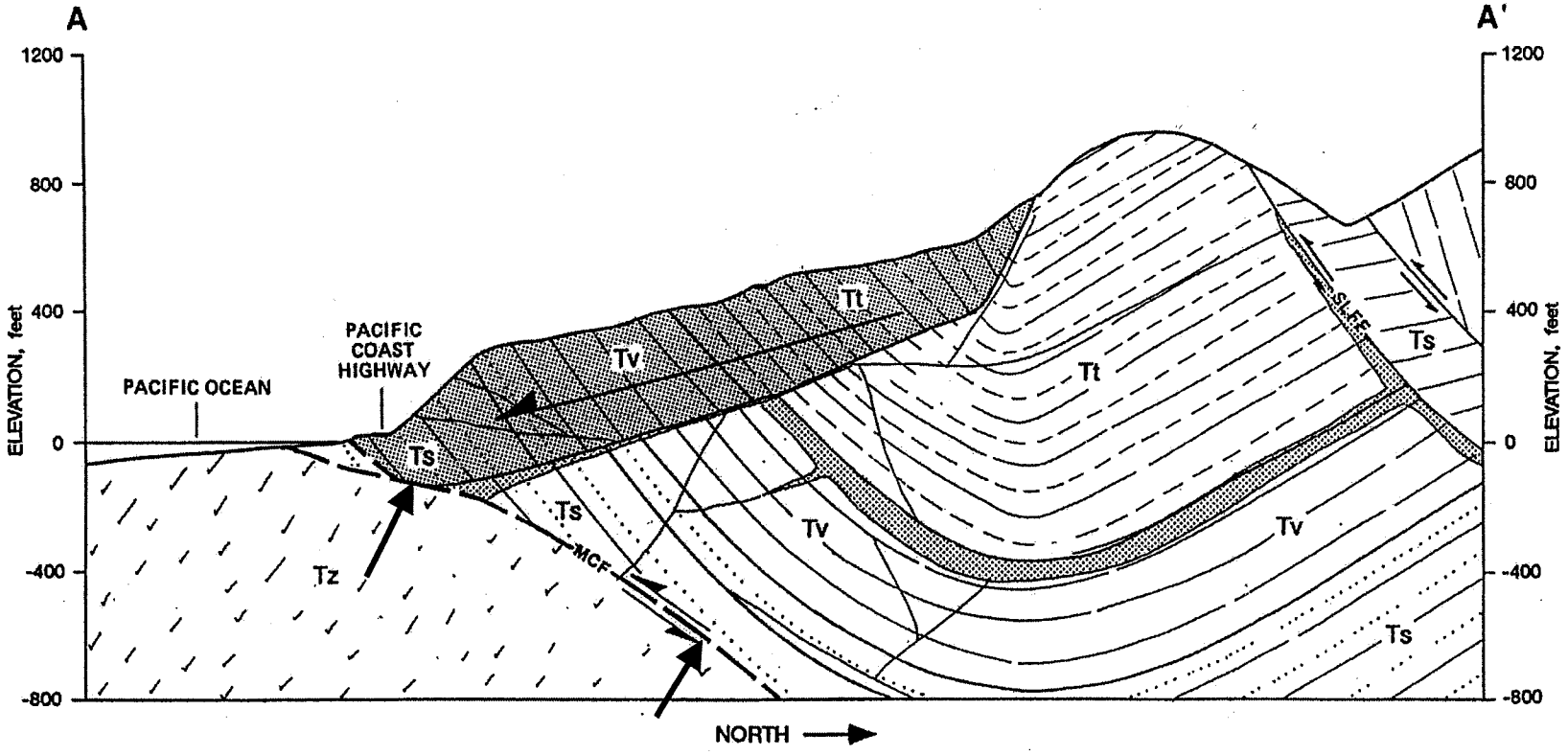

Cotton and Cole, 1992

Foliation

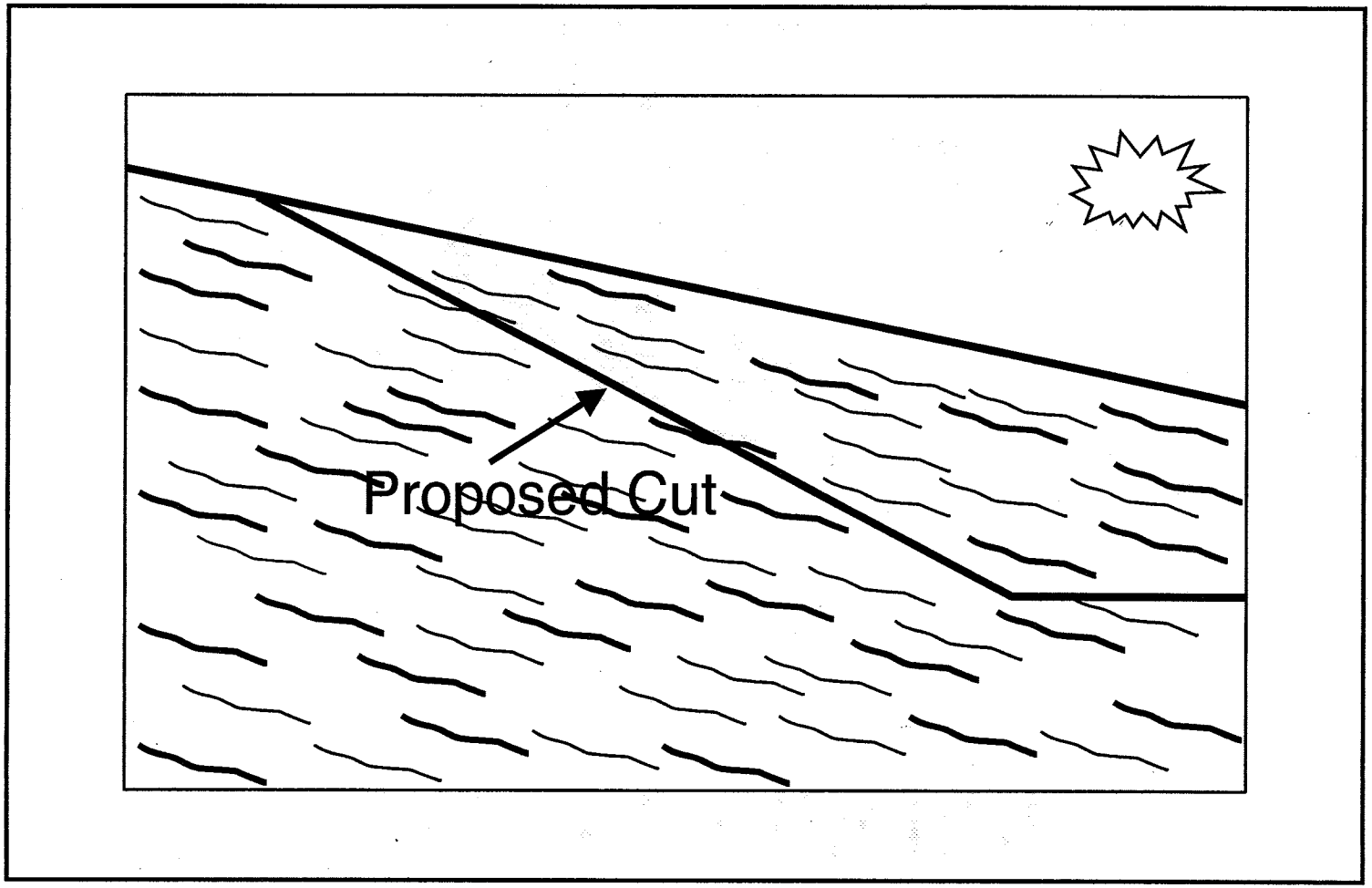

Conglomerate - Montana

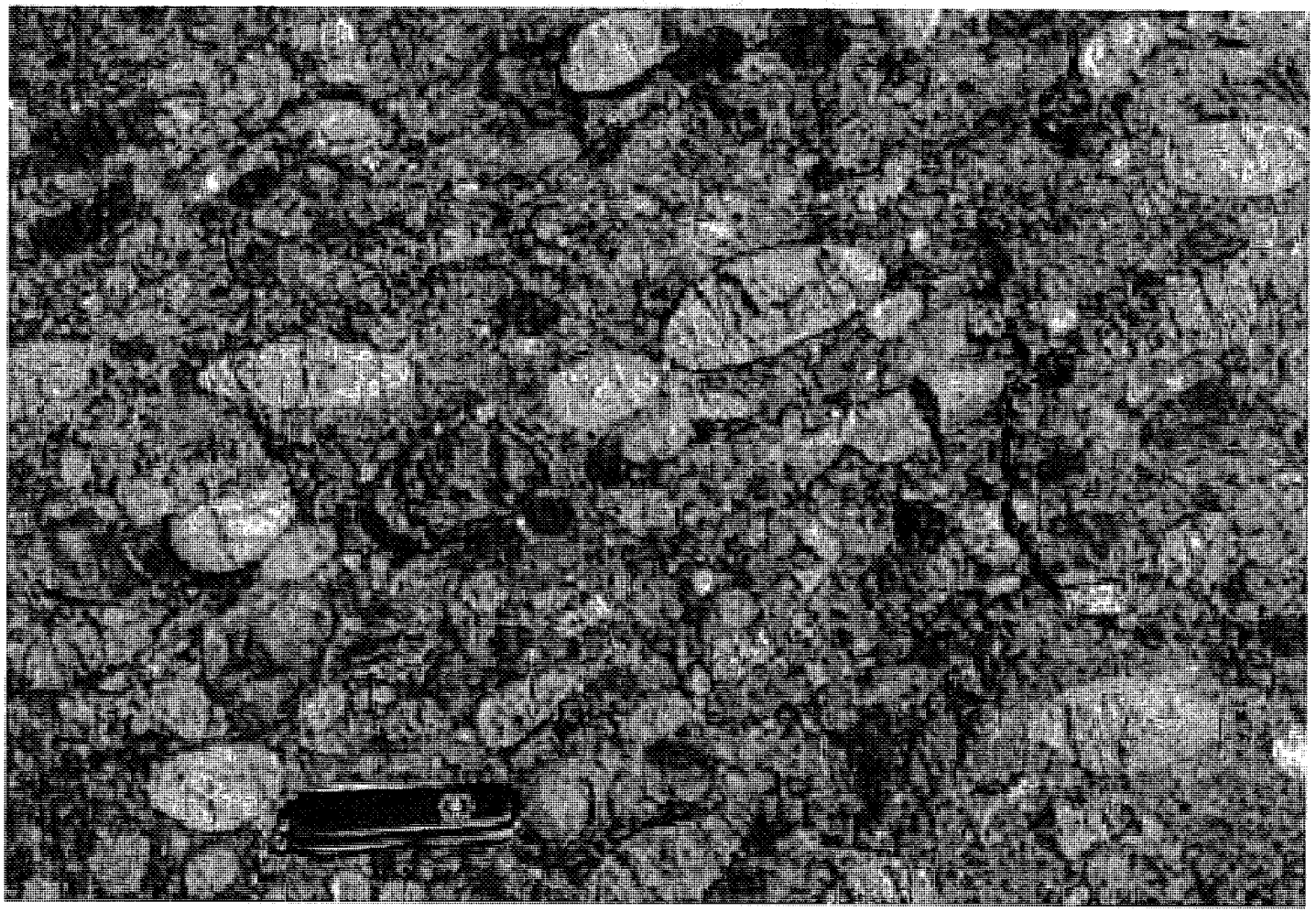

Martin Miller

Foliation – Death Valley

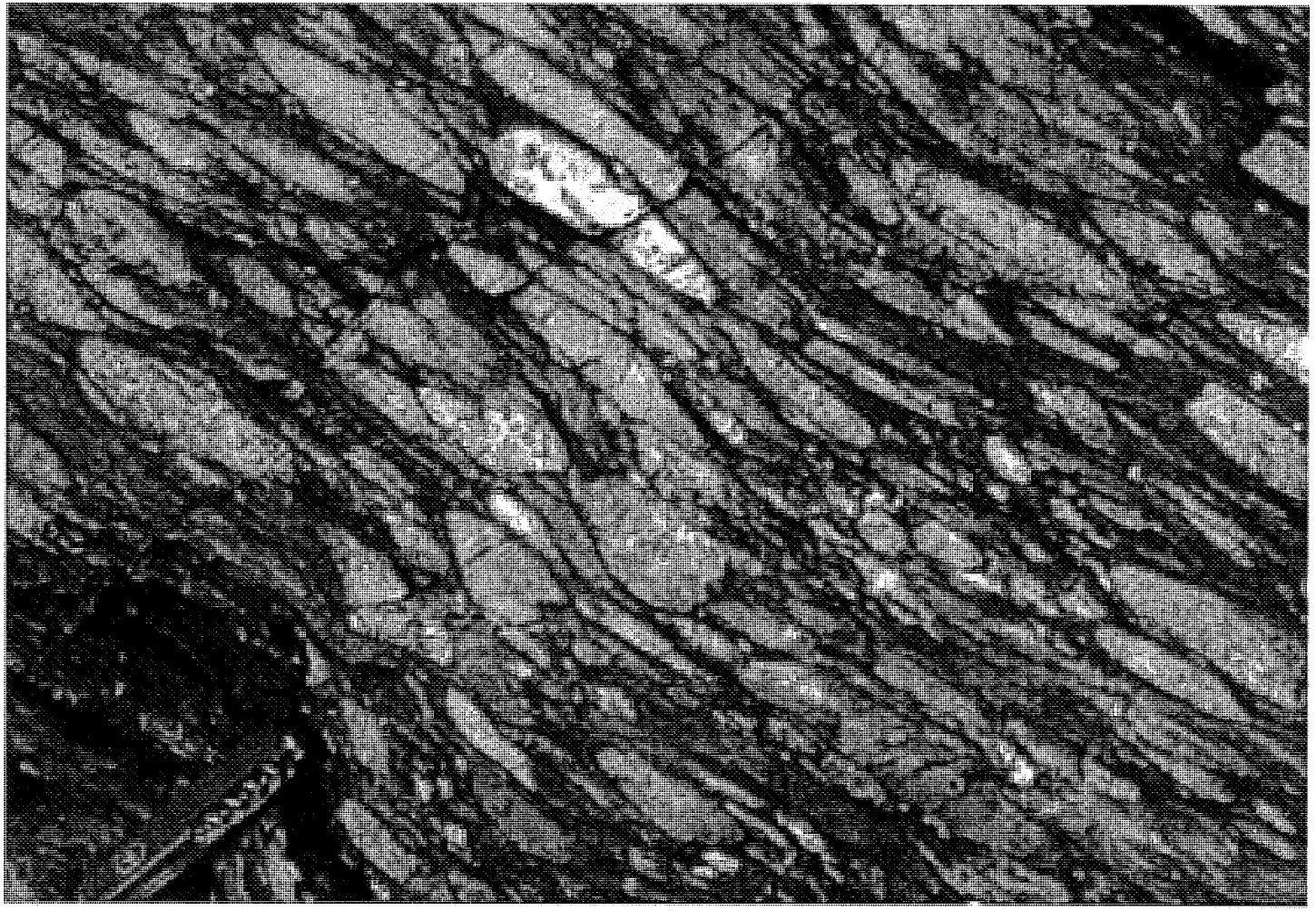

Martin Miller

Evolution of fabrics in a shear zone

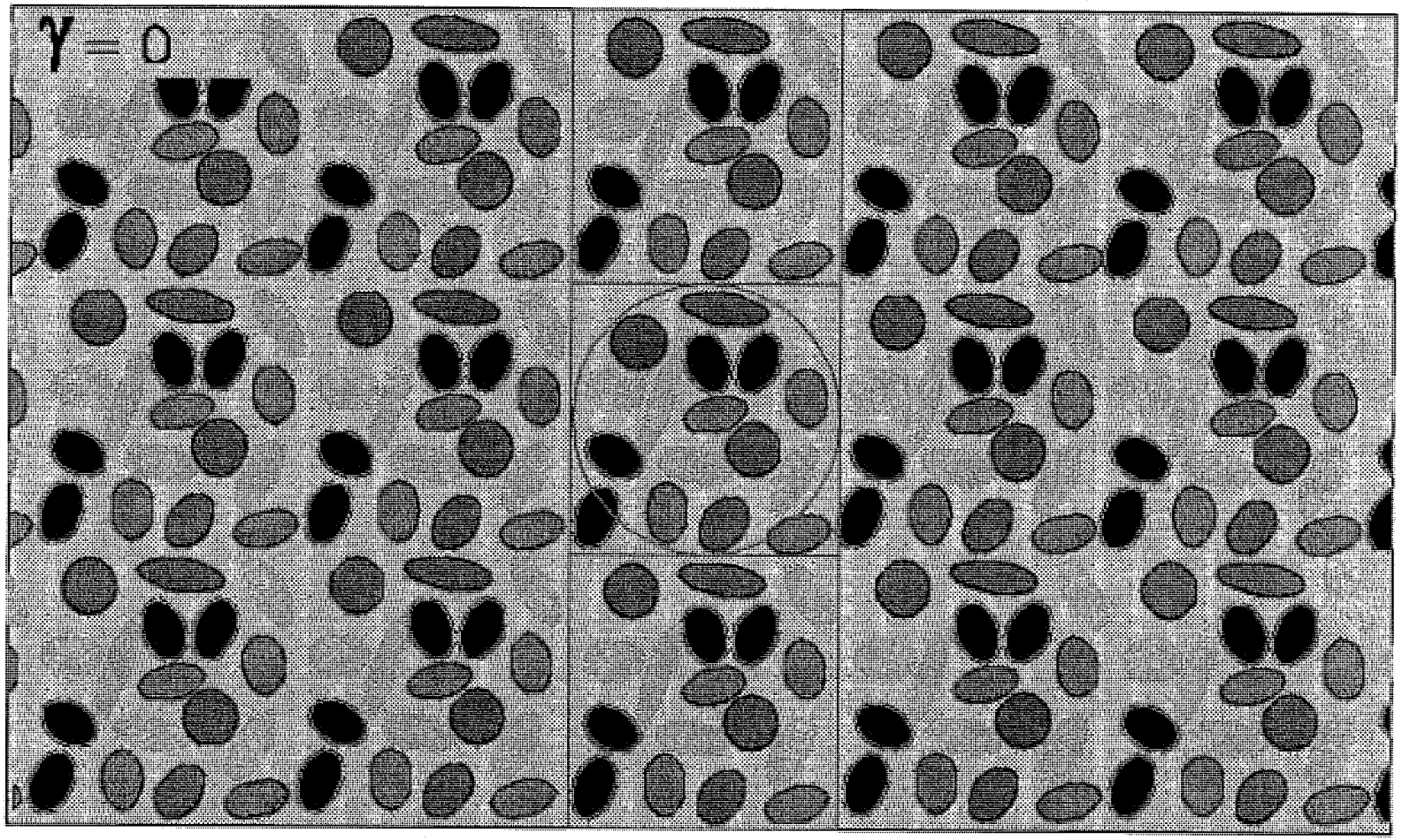

Rod Holcombe, University of Queensland

Henniger Flats Landslide
San Gabriel Mountains, California

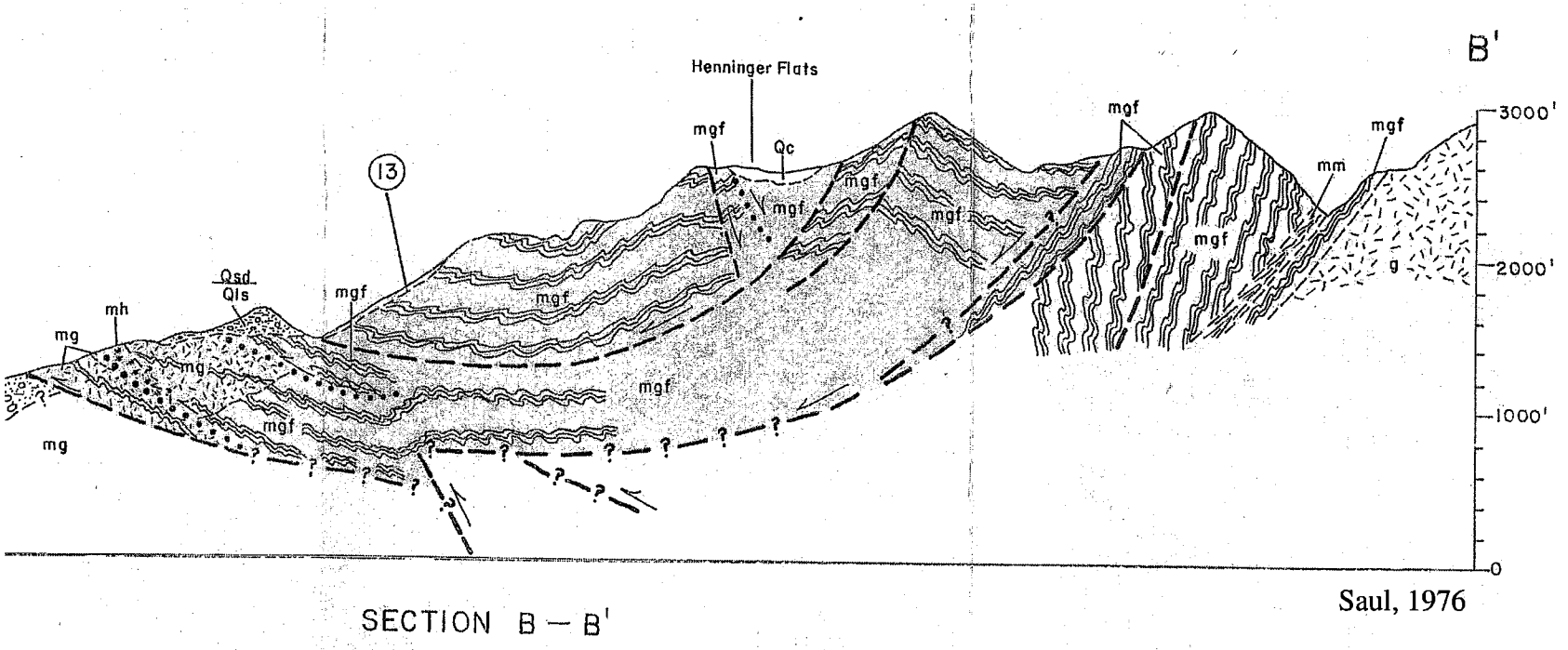

SECTION B — B'

Saul, 1976

"SOIL"

Soil science definition

"earthy material… containing living matter, and supporting or capable of supporting plants"

Engineering geologic definition

"All unconsolidated earthy material over bedrock"

-- AGI, 1974

Soil Type

Granular

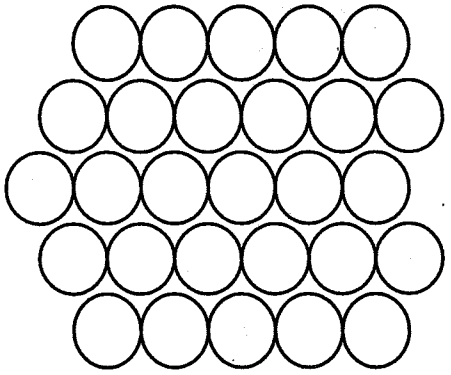

Cohesive

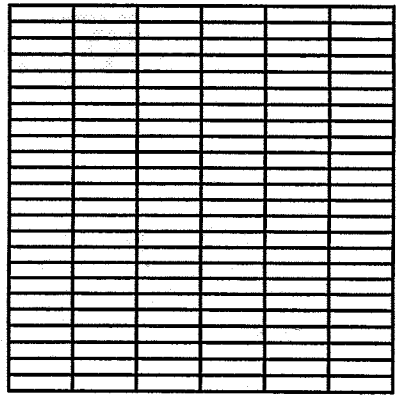

Soil Mineralogy and Chemistry

Influences stability, e.g.:

- **Expansive volcanic clays**
- **Sensitive glacial clays**
- **Weathering profiles**

Santa Tecla Landslide, El Salvador, January 2001

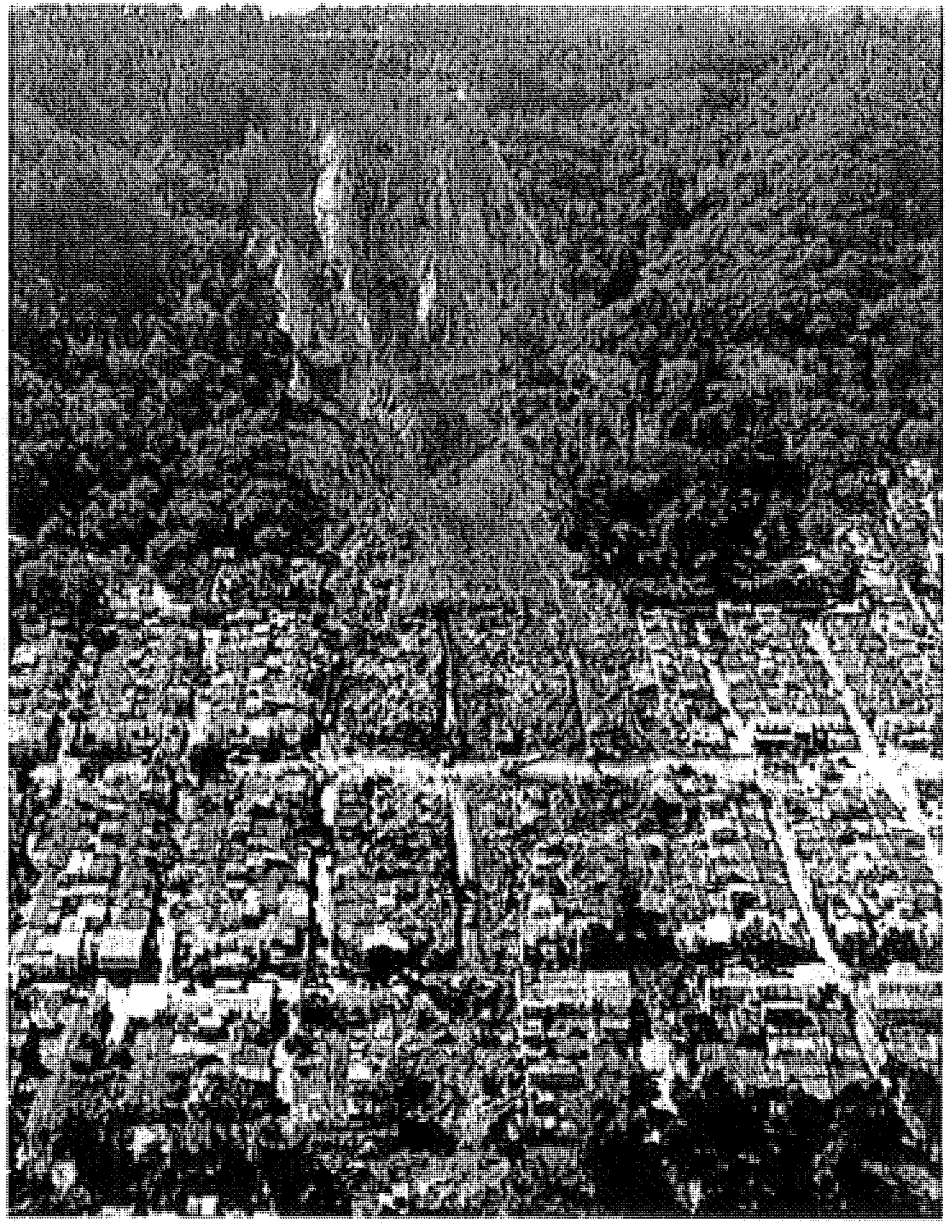

USGS – Harp, 2001

Glacial Clay -- New York

Franklyn Cole

Caliche Soils -- Southern Turkey

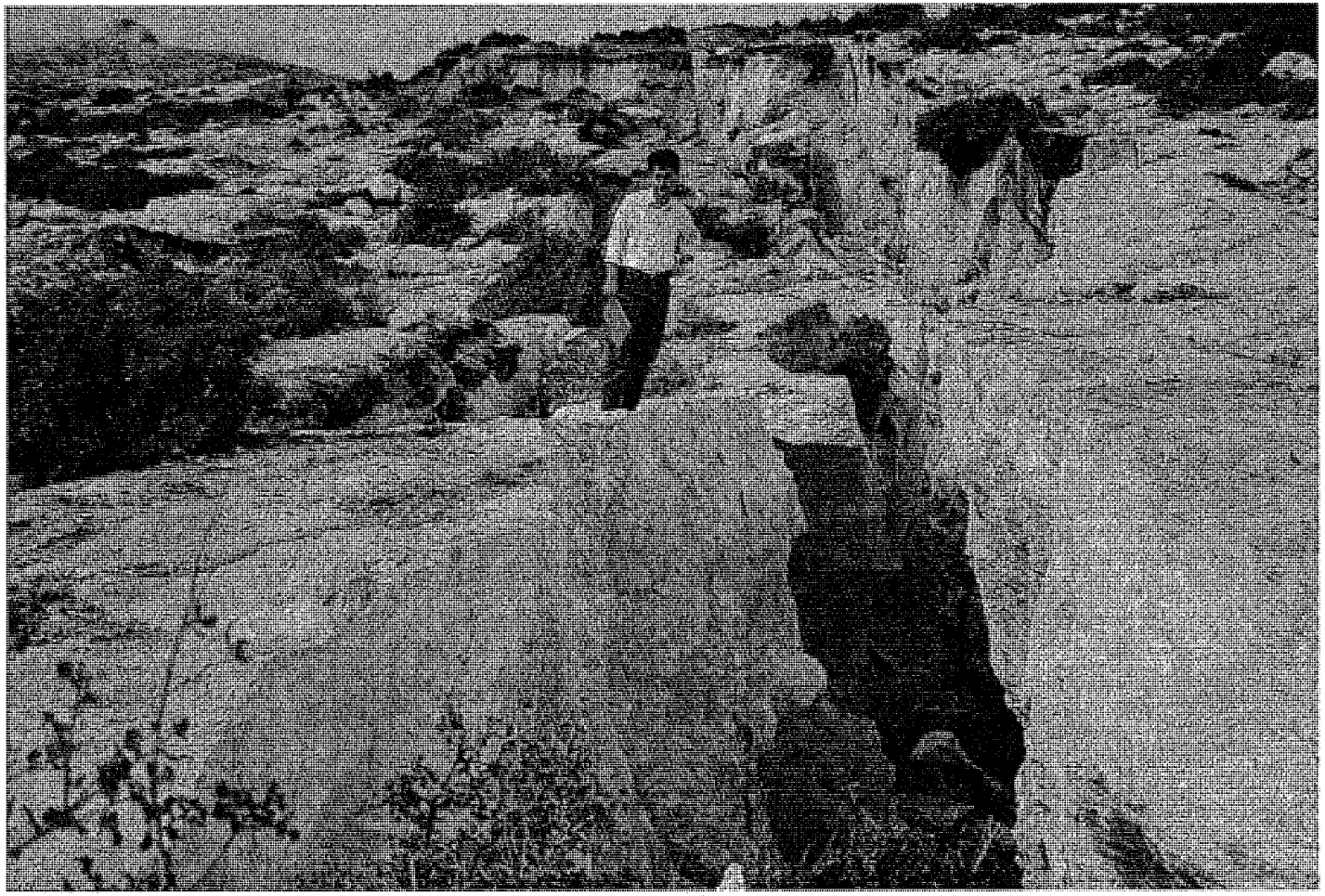

Turkmen and Yilmazer, 1998

Caliche Weathering Profile

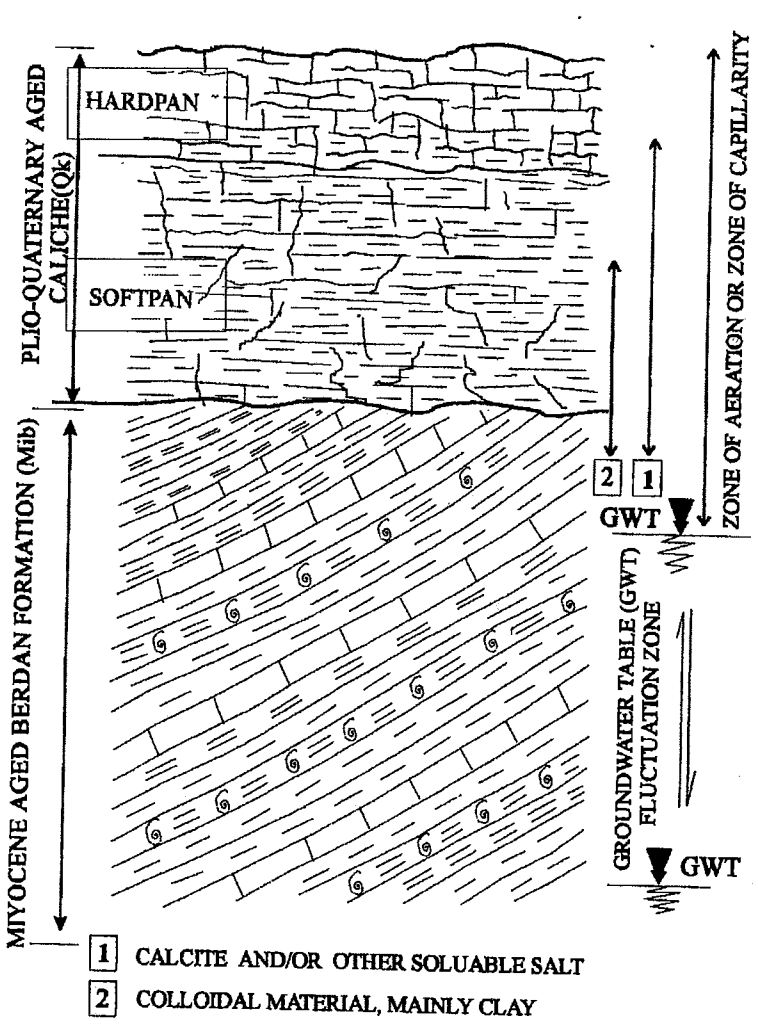

Turkmen and Yilmazer, 1998

Landslide in Caliche Soil

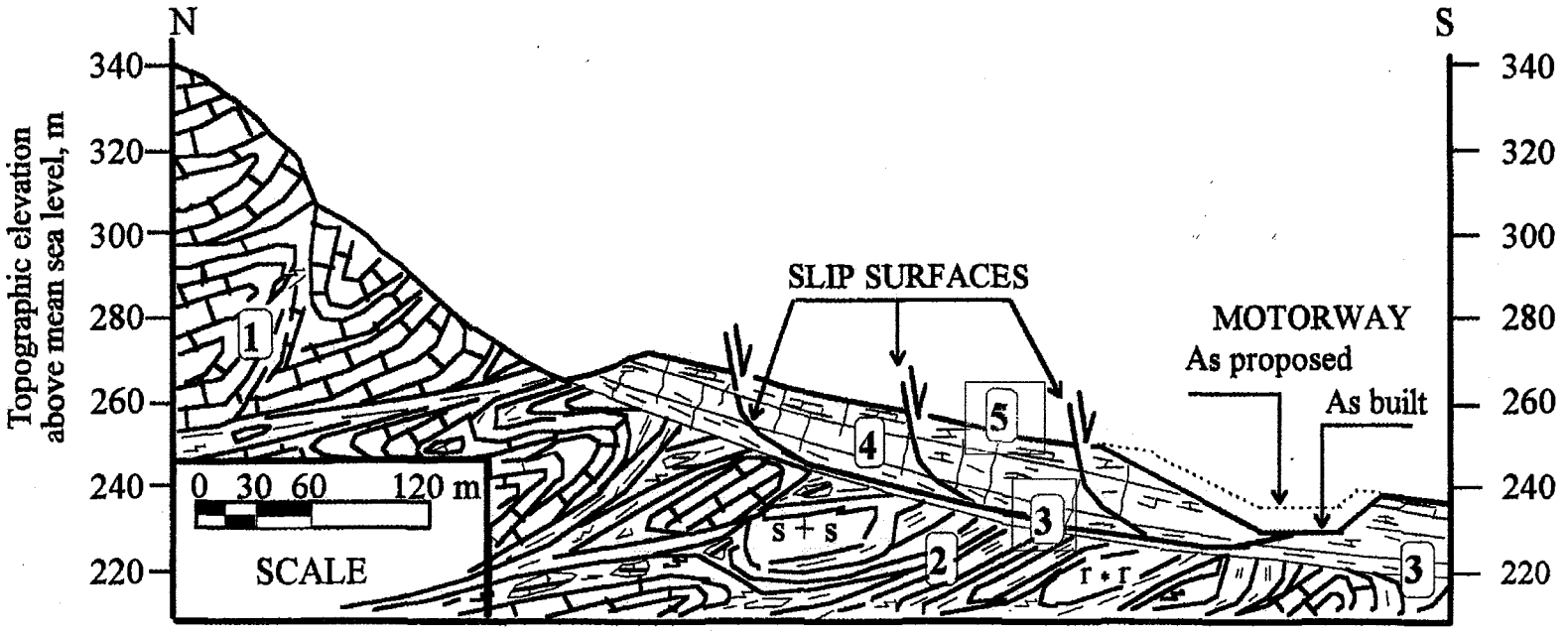

1 LIMESTONE AND DETRITAL COMPONENT OF MELANGE

2 MELANGE OF CRETACEOUS AGE

3 CALICHE SOFTPAN

4 CALICHE

5 CALICHE HARDPAN

Turkmen and Yilmazer, 1998

Soil Density/Consistency

Granular soil:

Very dense to very loose

Cohesive soil:

Very hard to very soft

Soil/Rock Ambiguity

Soft rock?

OR

Hard soil?

Earthflow in Residual Soil

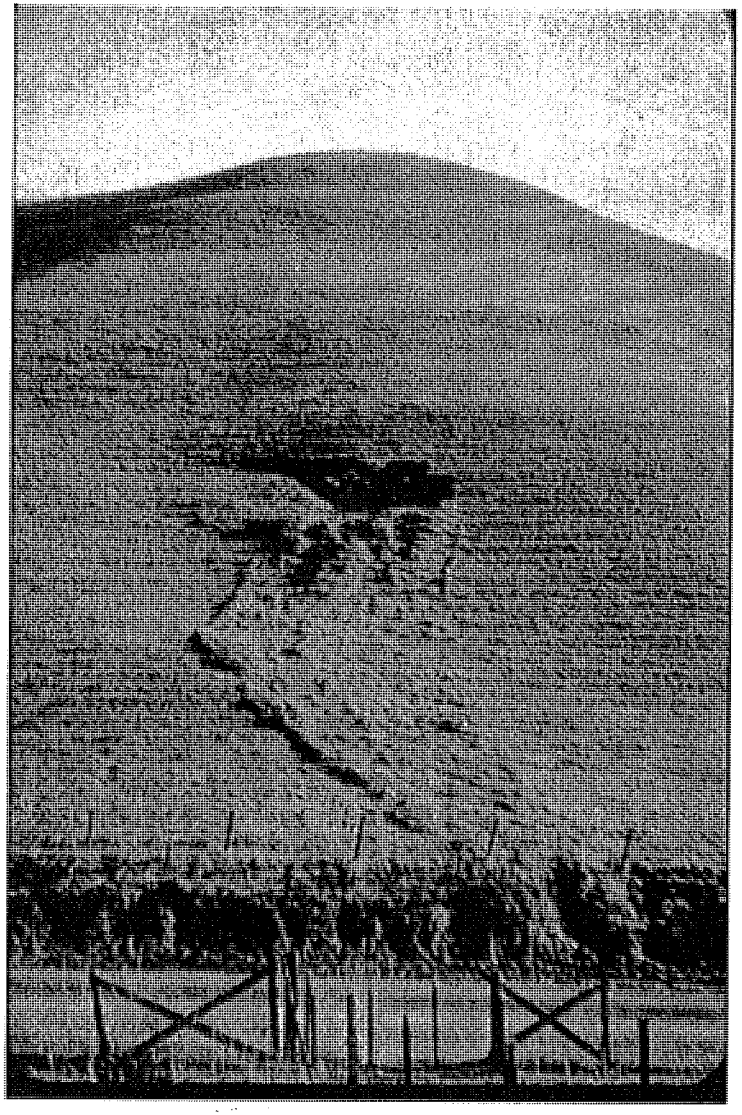

NOAA

Water "Table"

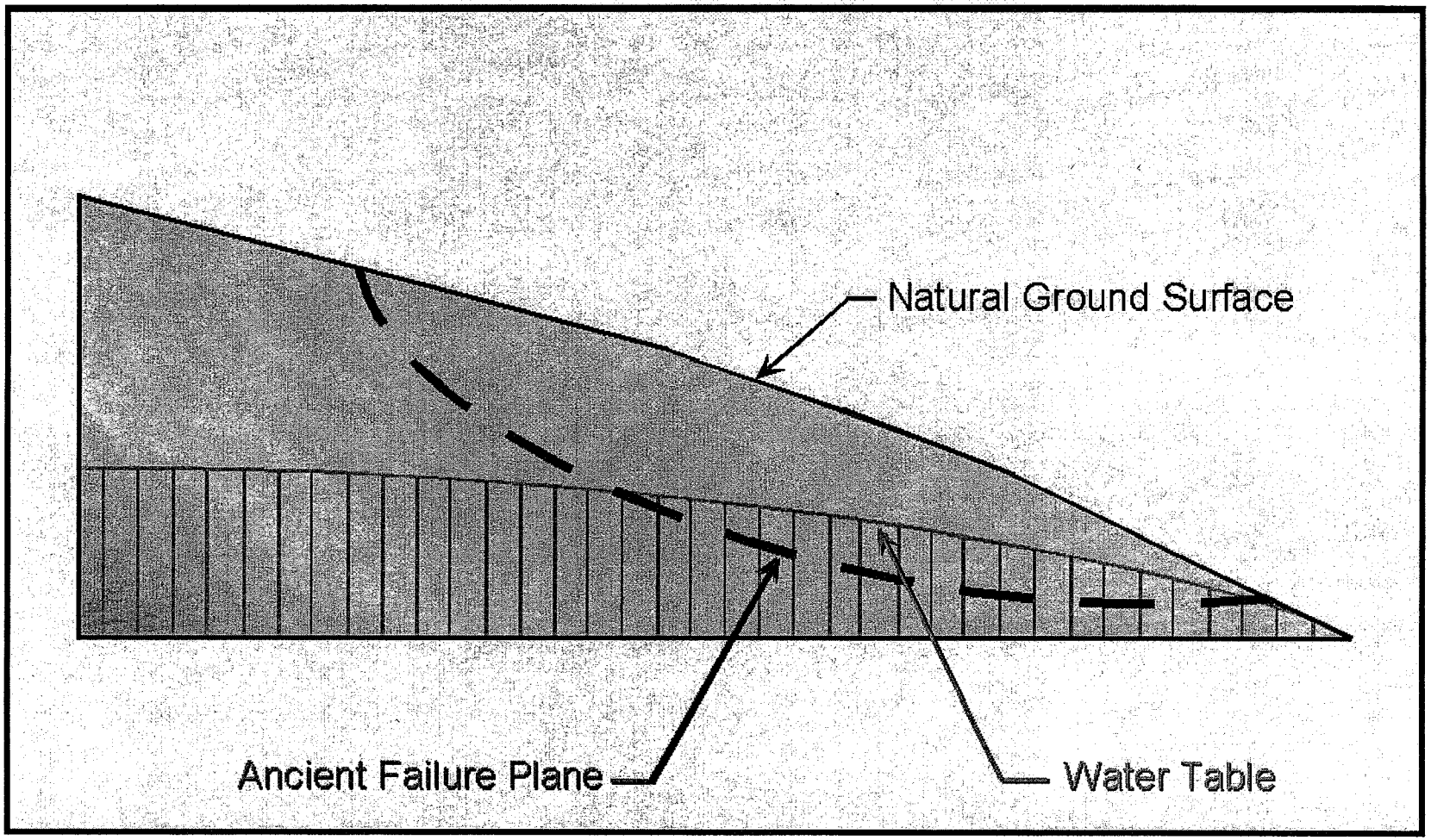

Perched Groundwater

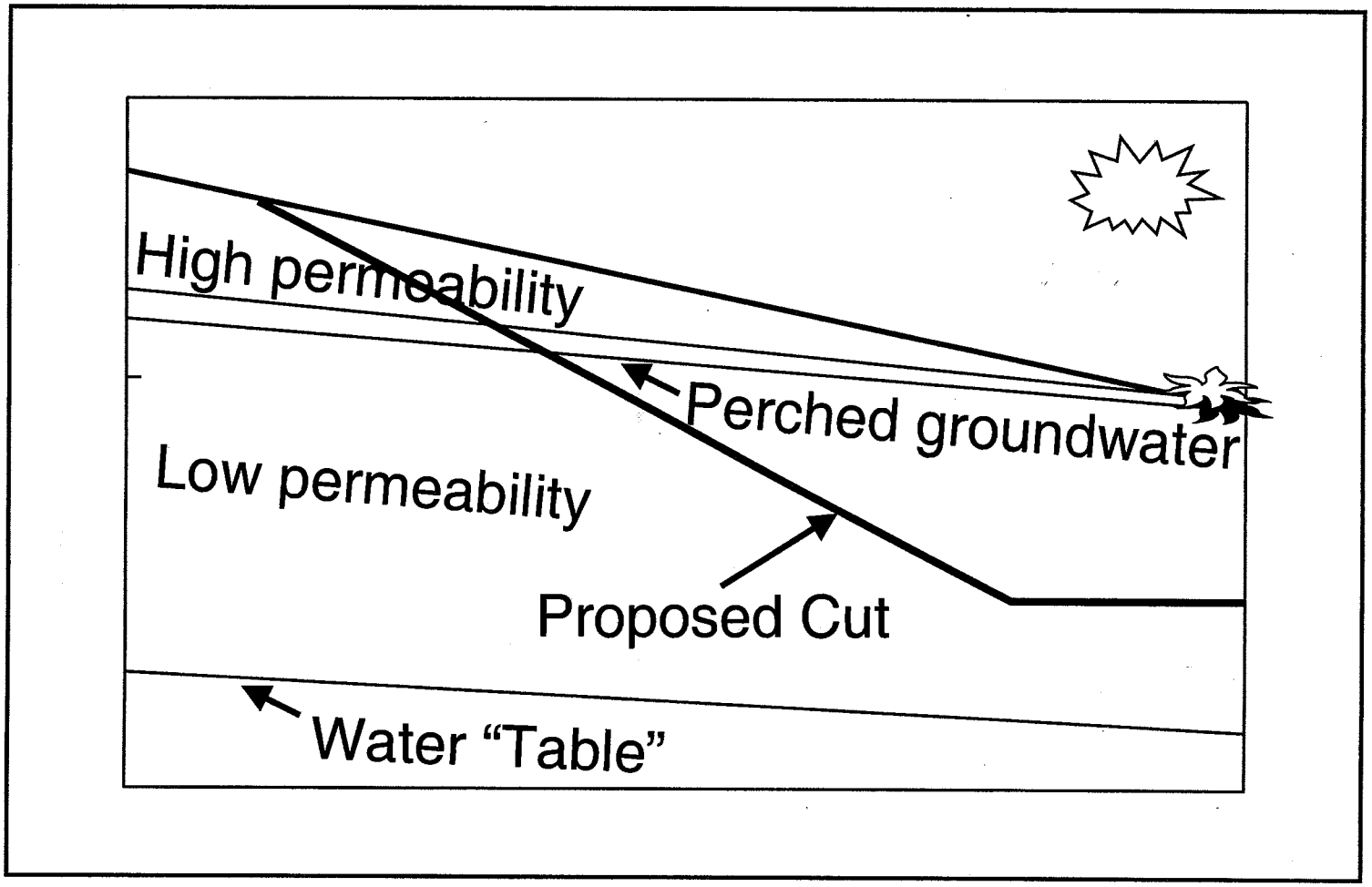

Inhomogeneity/ Discontinuities

Geologic materials are *not* CHILE:

- ***not*** **Continuous**
- ***not*** **Homogeneous**
- ***not*** **Isotropic**
- ***not*** **Linearly Elastic**

Discontinuities in Materials are Zones of Weakness

- Geologic contacts
- Top of bedrock
- Bedding planes
- Fractures
- Faults and shear zones

Highway 50 Landslide, California, 1997

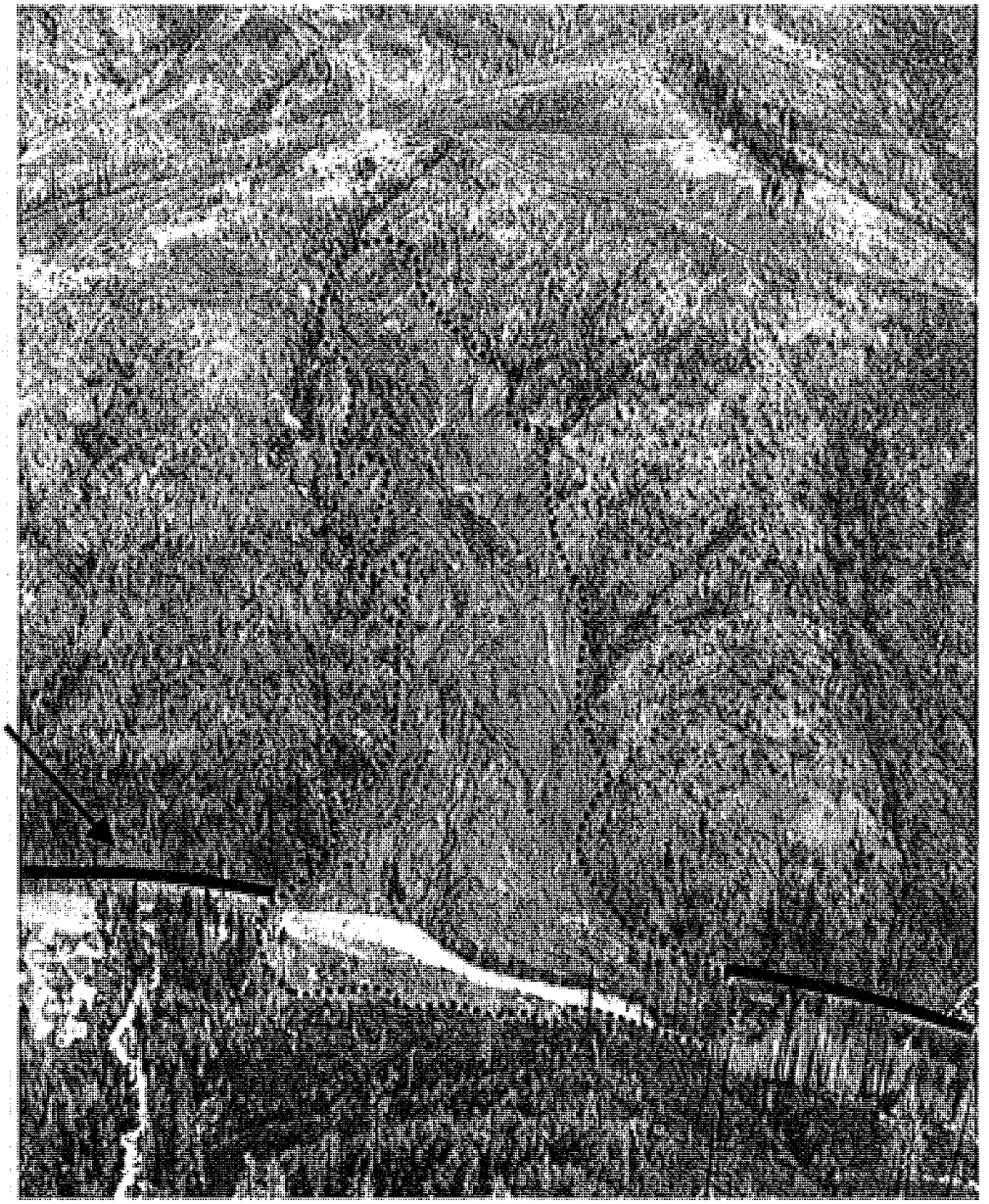

Top of Bedrock

Other Discontinuities

- Fracture infillings
- Folds
- Chilled margin of intrusive rock
- Contact between highly weathered and less weathered bedrock
- Irregular weathering profile
- Block-in-matrix rock

Block-in-Matrix Structure

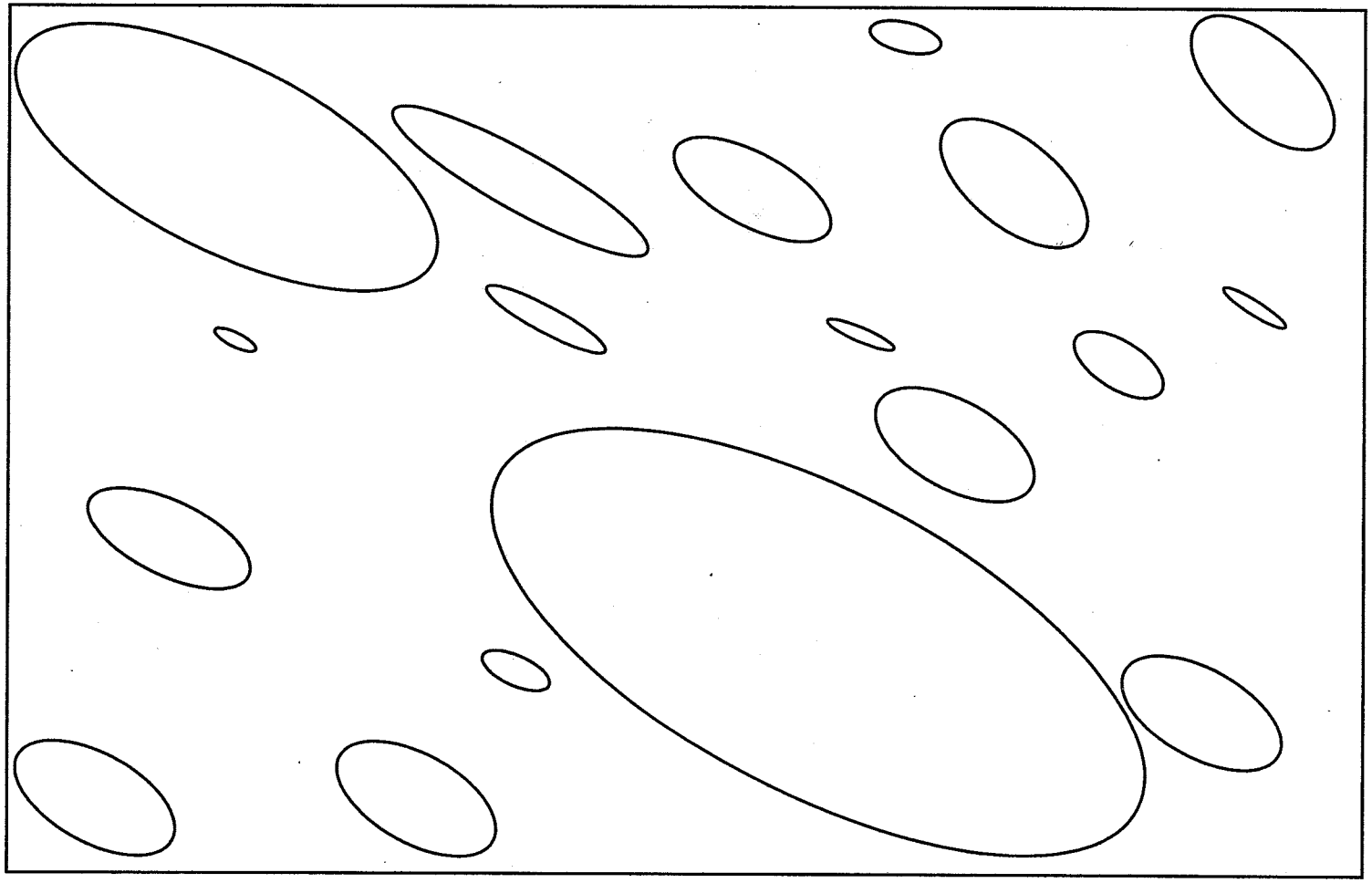

Arizona Inn Landslide, Oregon

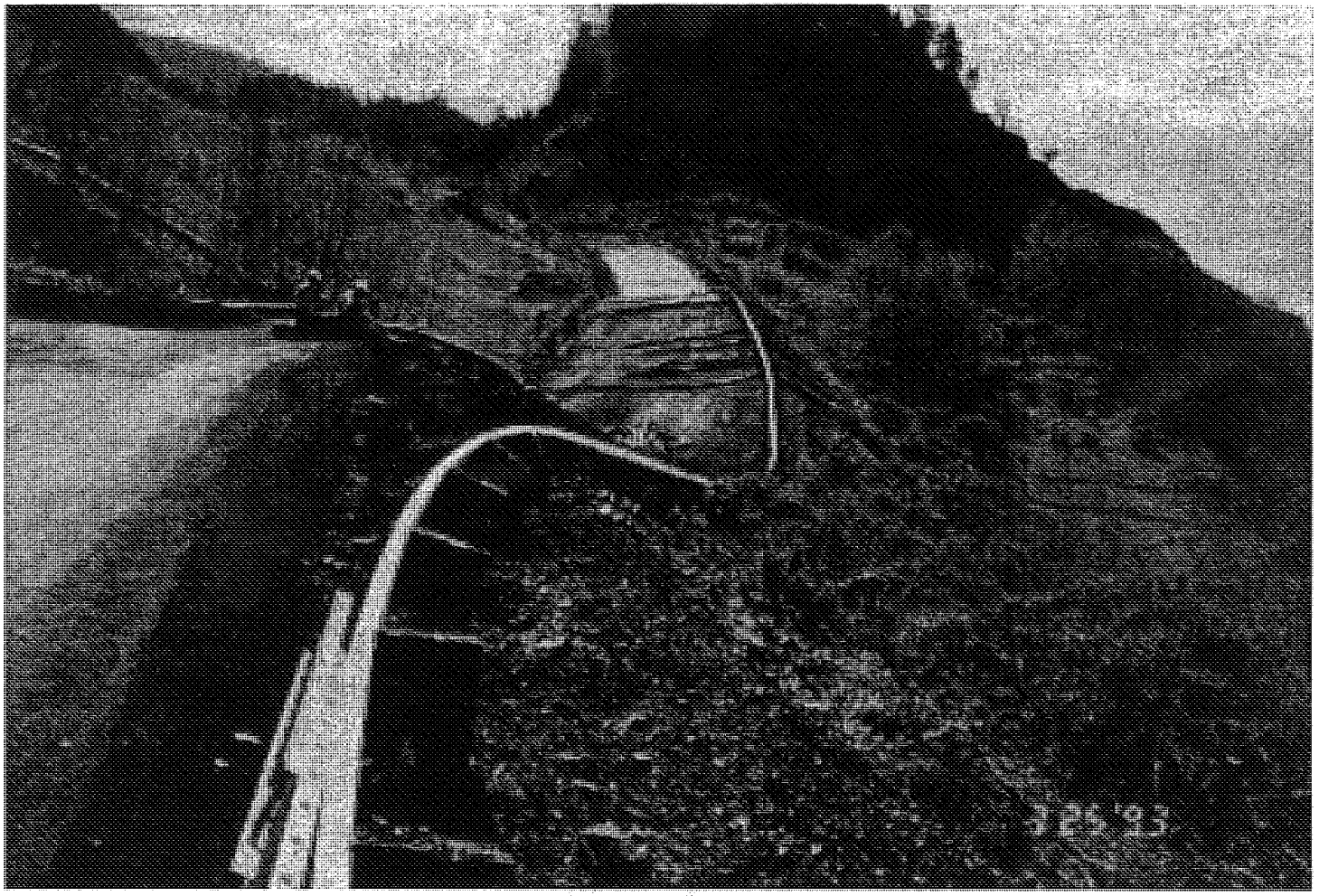

ODOT

More Discontinuities

- Caves and mines
- Old fill
- Buried soil profiles
- Slide planes
- Colluvium-filled swales

Colluvium-Filled Swale

So...

Soil and rock exploration, sampling, and testing programs must take the inhomogeneous, discontinuous character of earth materials into account.

"Engineers imagined that the future science of foundations would consist of…: Drill a hole... Send… samples through a laboratory with standardized apparatus served by… human automatons. Collect the figures, introduce them into equations, and compute the result."

-- Karl Terzaghi, 1936

Reminder...

"The foremost requirements for slide prevention are reliable information on the geologic structure of the ground..."

-- Karl Terzaghi, 1950

GEOLOGICAL PROCESSES AND RELATIONSHIPS TO ENGINEERING PROPERTIES

Rock Formation

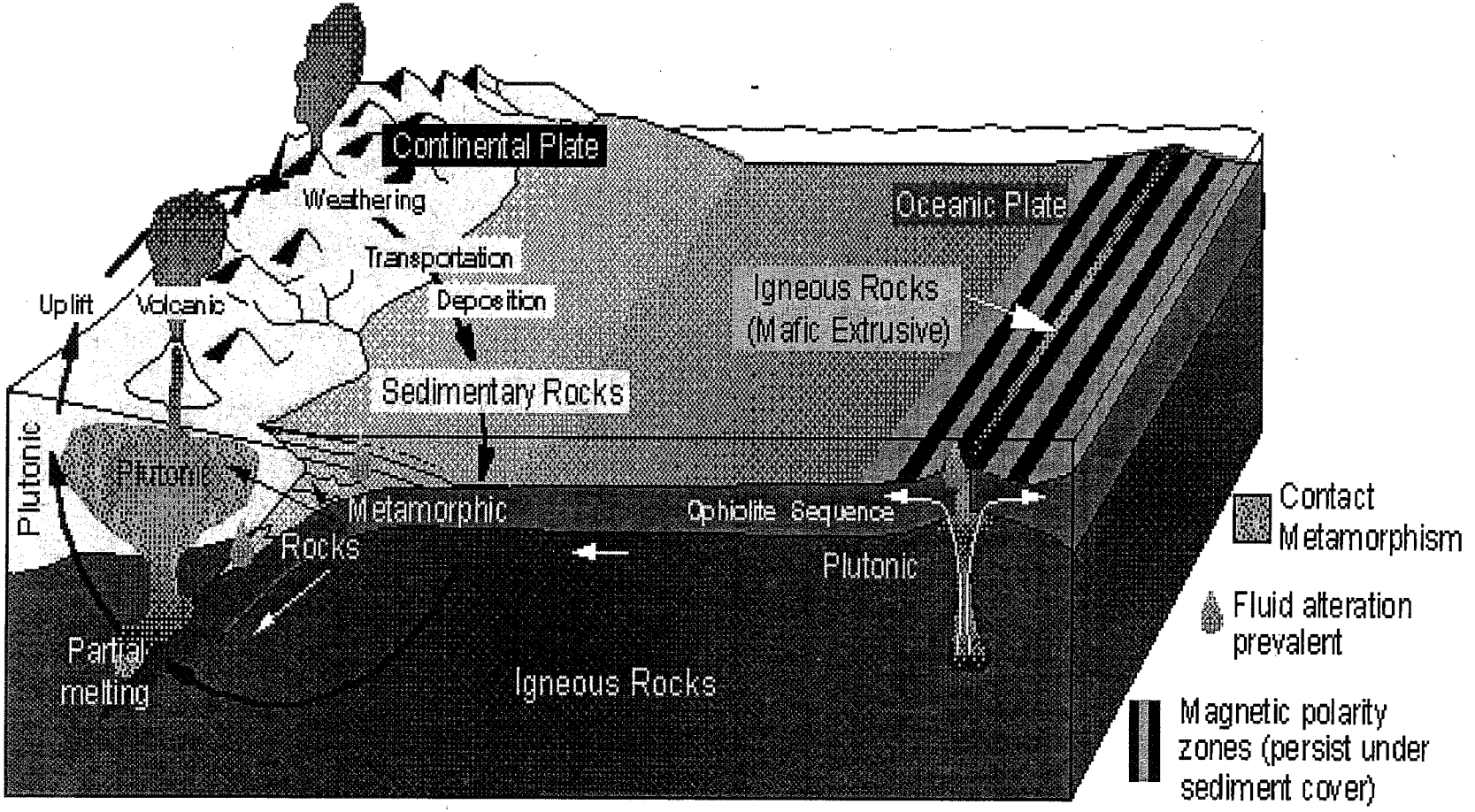

Redrawn by W. Milner, as modified from Montgomery (1990) and Monroe and Wicander (1994).

http://www.science.ubc.ca

Sedimentary Rock

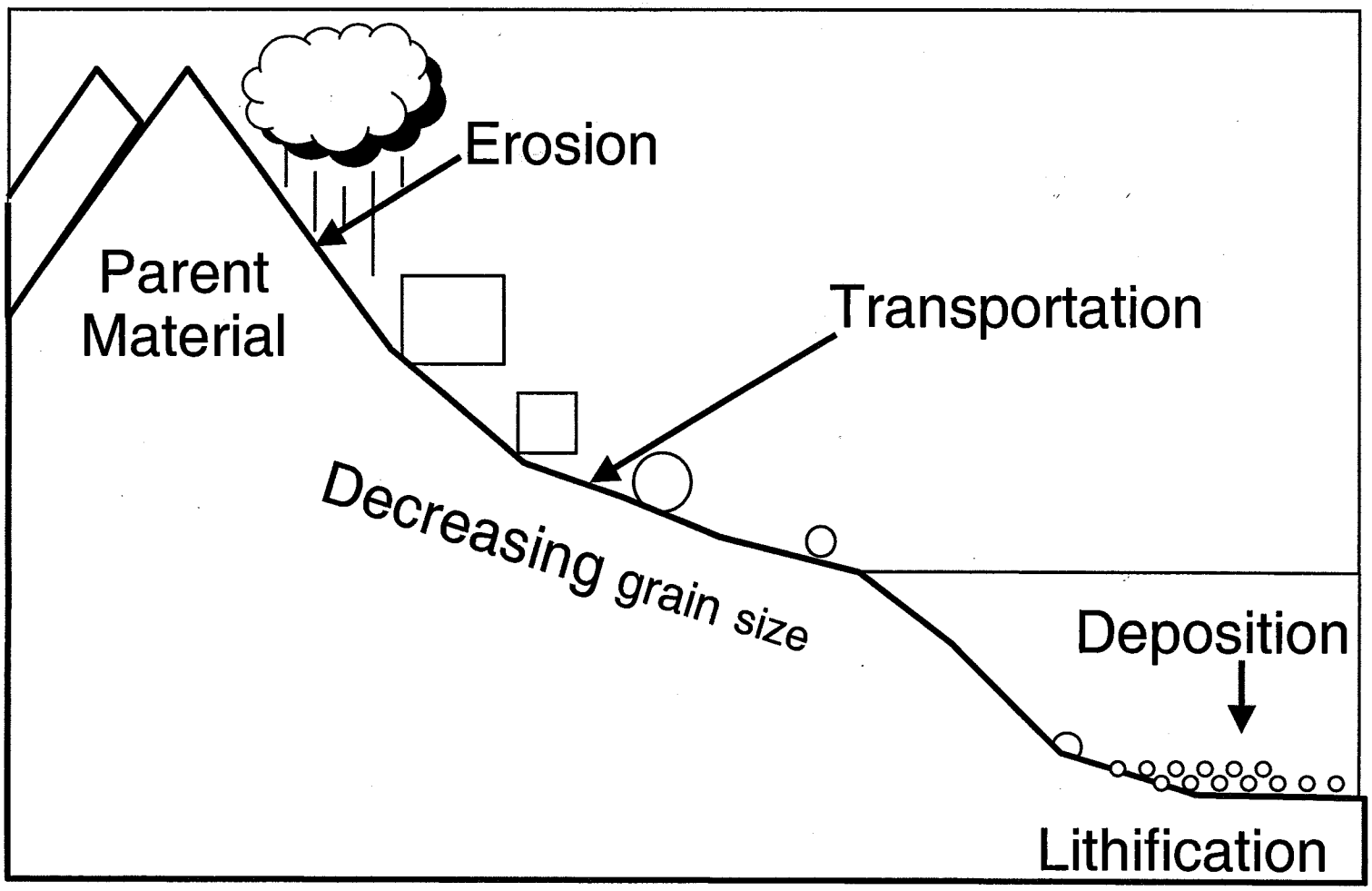

Slump in sedimentary rock

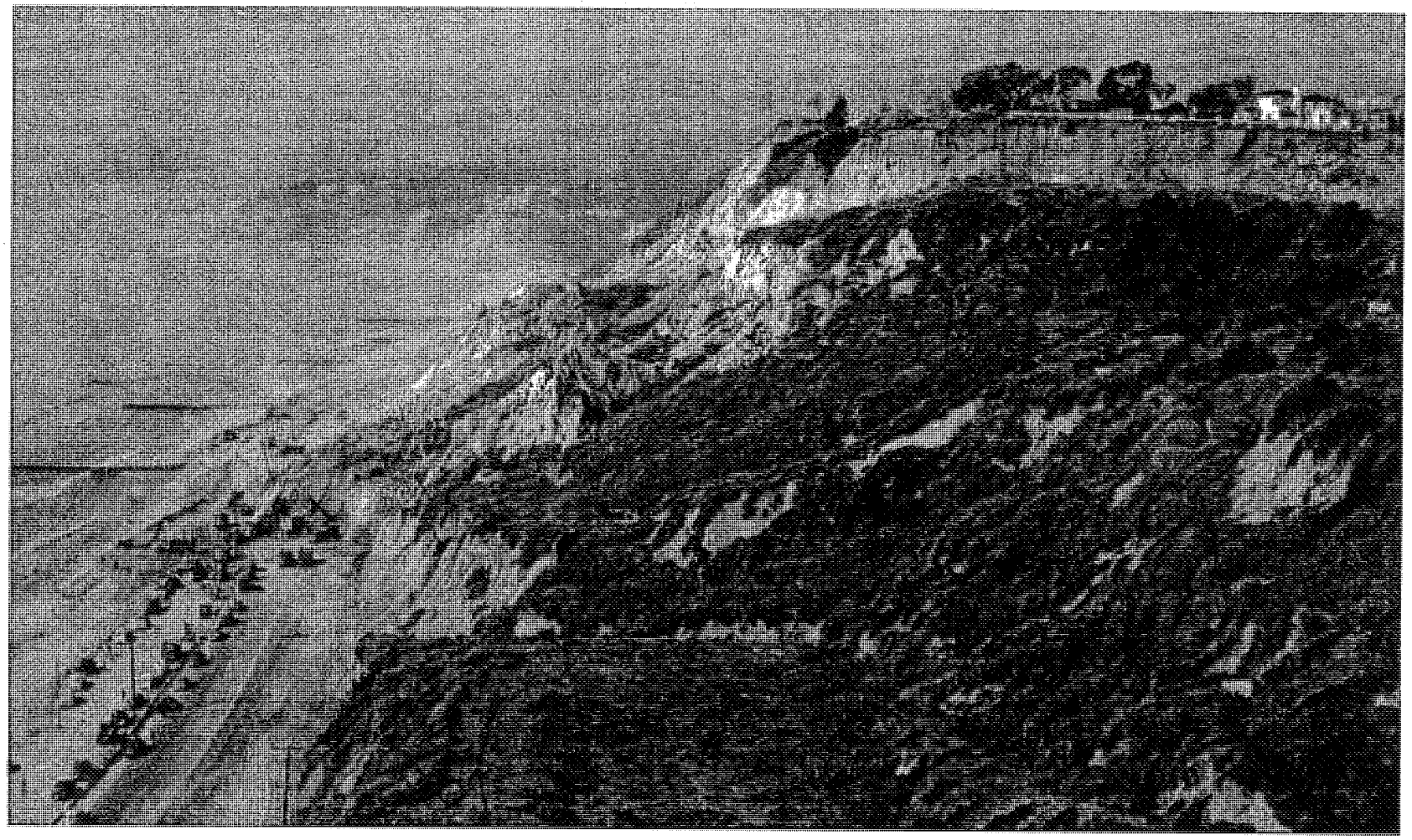

USGS - Morton

Slump in sedimentary rock

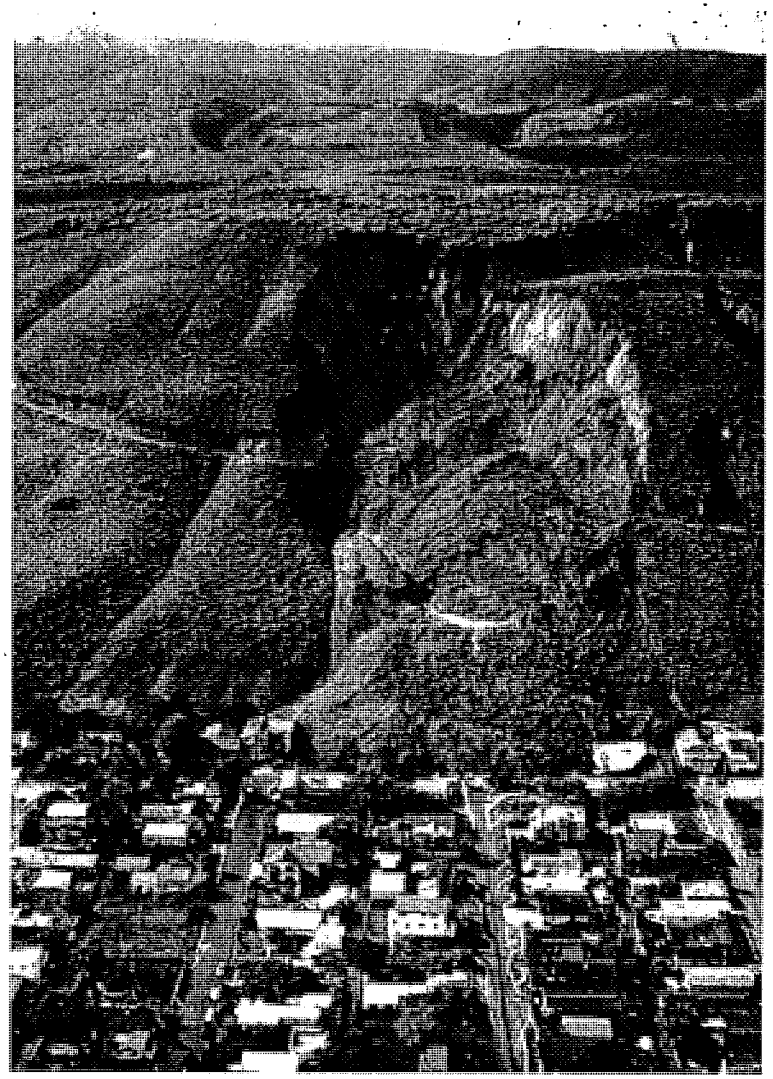

Igneous Rock

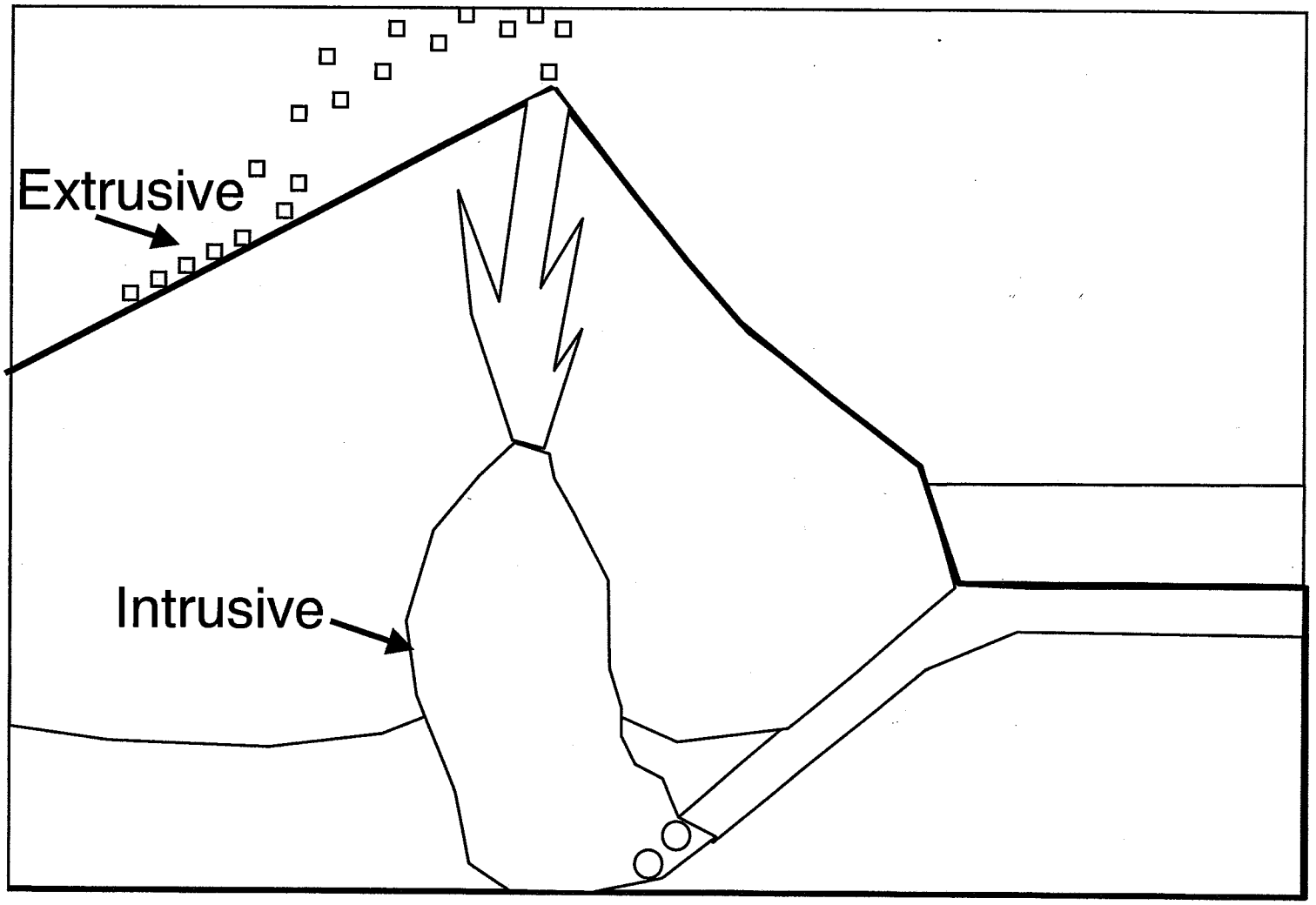

Landslide in Columbia Basalt

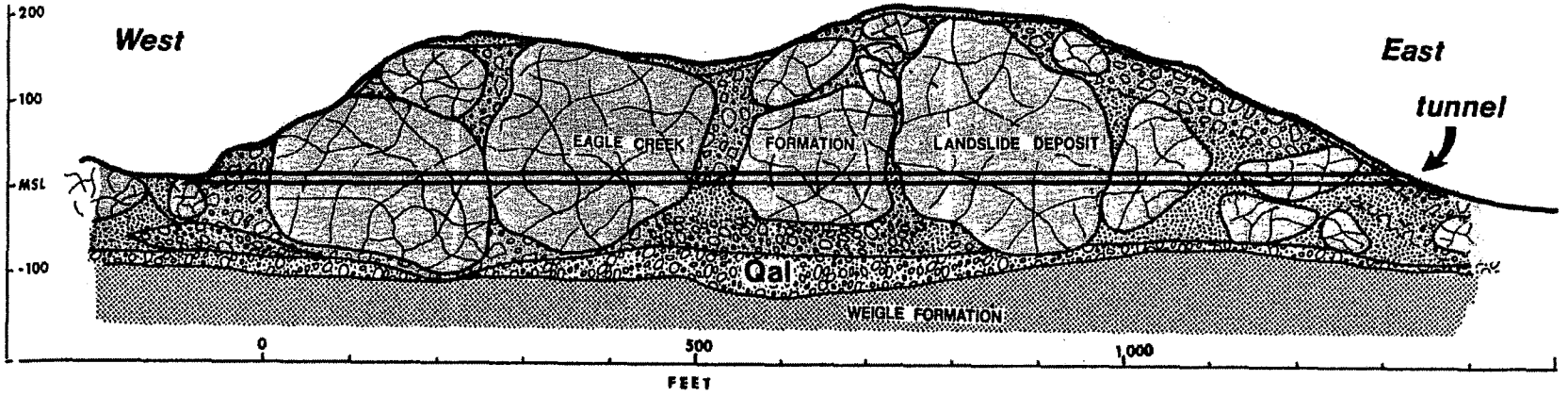

Palmer, 1977

Metamorphic Rock

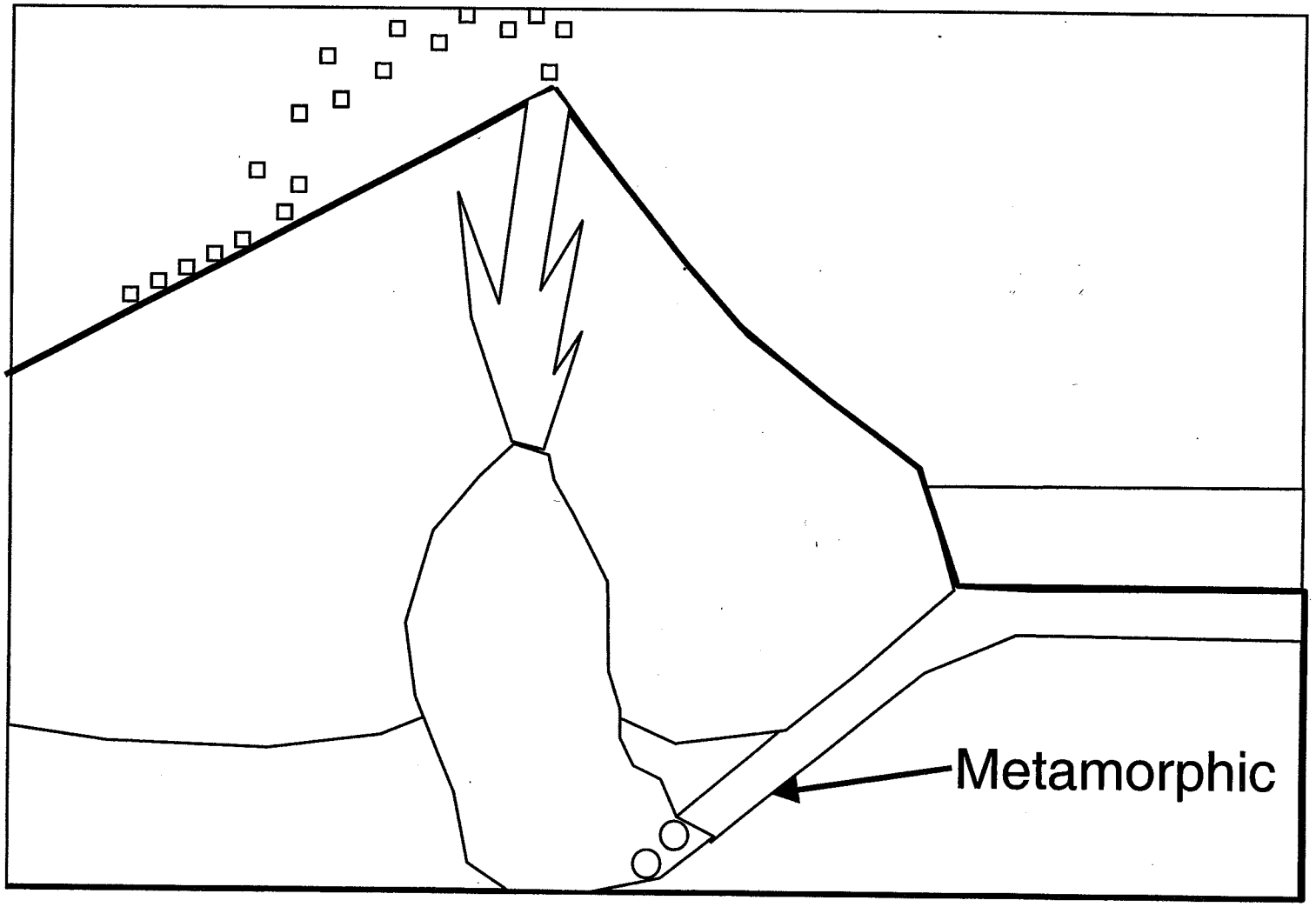

Rock Slide in Metamorphic Rock

MBMG - Hadley

Madison Canyon Slide Cross Section

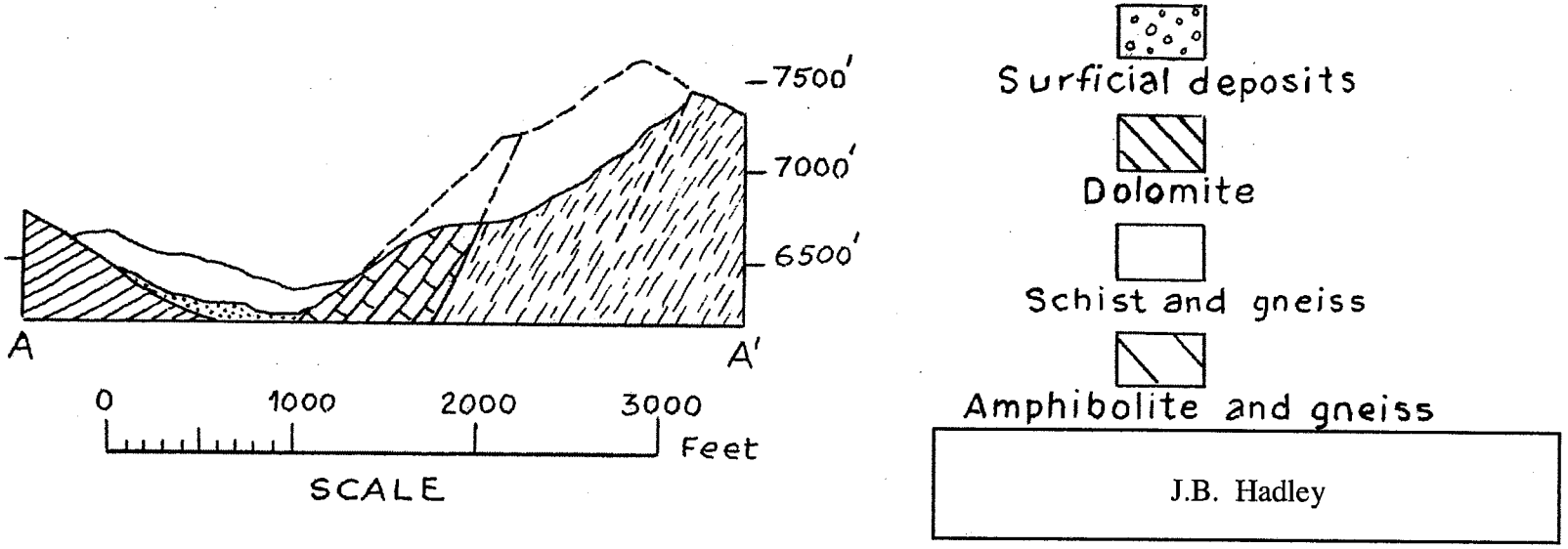

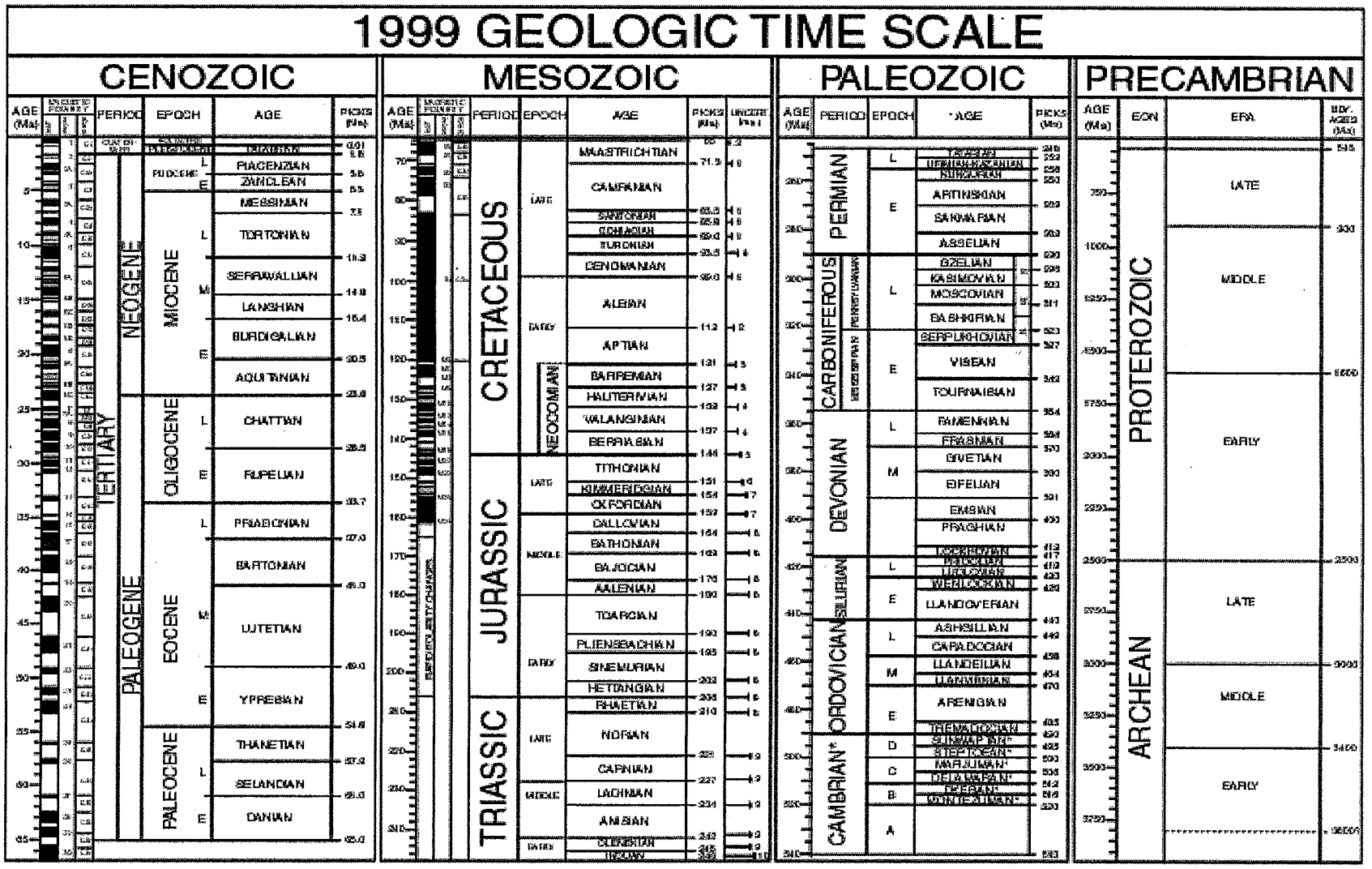

© 1999, The Geological Society of America. Product code CTS00N. Compilers: A. R. Palmer, John Geissman

*International ages have not been established. These are regional (Laurentian) only.

Sources for nomenclature and ages: Primarily from Gradstein, F., and Ogg, J., 1996, *Episodes*, v. 19, nos. 1 & 2; Gradstein, F., et al., 1995, SEPM Special Pub. 54, p. 95–126; Berggren, W. A., et al., 1995, SEPM Special Pub. 54, p. 129–212; Cambrian and basal Ordovician ages adapted from Landing, E., 1996, *Canadian Journal of Earth Sciences*, v. 35, p. 329–338; and Davidek, K., et al., 1998, *Geological Magazine*, v. 135, p. 305–309. Cambrian age names from Palmer, A. R., 1998, *Canadian Journal of Earth Sciences*, v. 35, p. 323–326.

GEOLOGICAL SOCIETY OF AMERICA

"... our present knowledge... does not suggest immediate... developments... like... the change from the Jurassic to the Cretaceous... If such very violent developments... should take place... the issuance or nonissuance of a building permit for a... house on the slope of Fitch Mountain does not seem to be a problem of momentuous (sic) significance."

-- soil engineer, Sonoma County

Tectonics

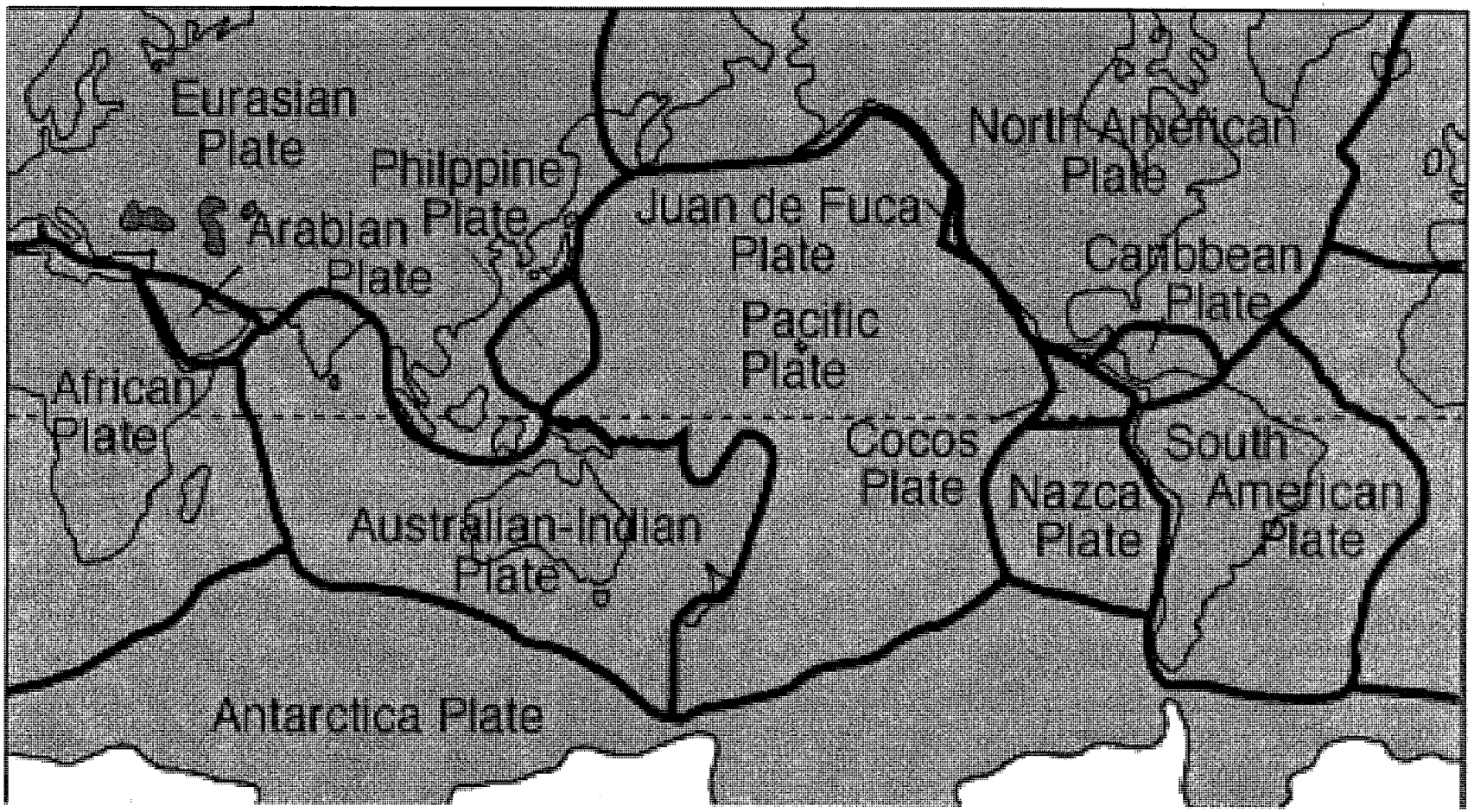
Eurasian Plate
Philppine Plate
Arabian Plate
Juan de Fuca Plate
North American Plate
Caribbean Plate
Pacific Plate
African Plate
Cocos Plate
Nazca Plate
South American Plate
Australian-Indian Plate
Antarctica Plate

Pangea to the present

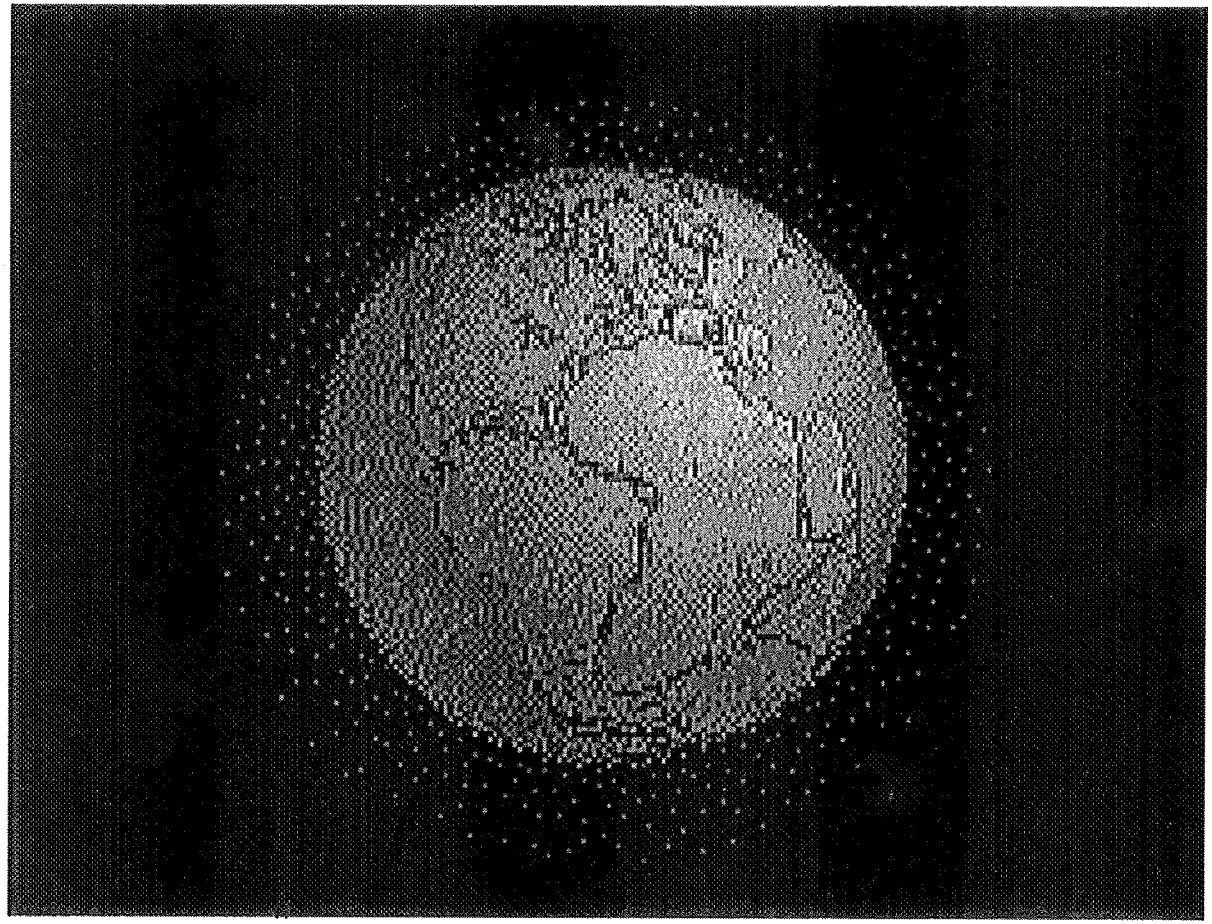

U.S. Geological Survey

Tectonic processes are responsible for:

- Faulting
- Folding
- Fracturing
- Earthquake shaking
- Ridge-top shattering

Effects of the 1994 Northridge Earthquake

USGS

Ridge-top Spreading
1989 Loma Prieta Earthquake

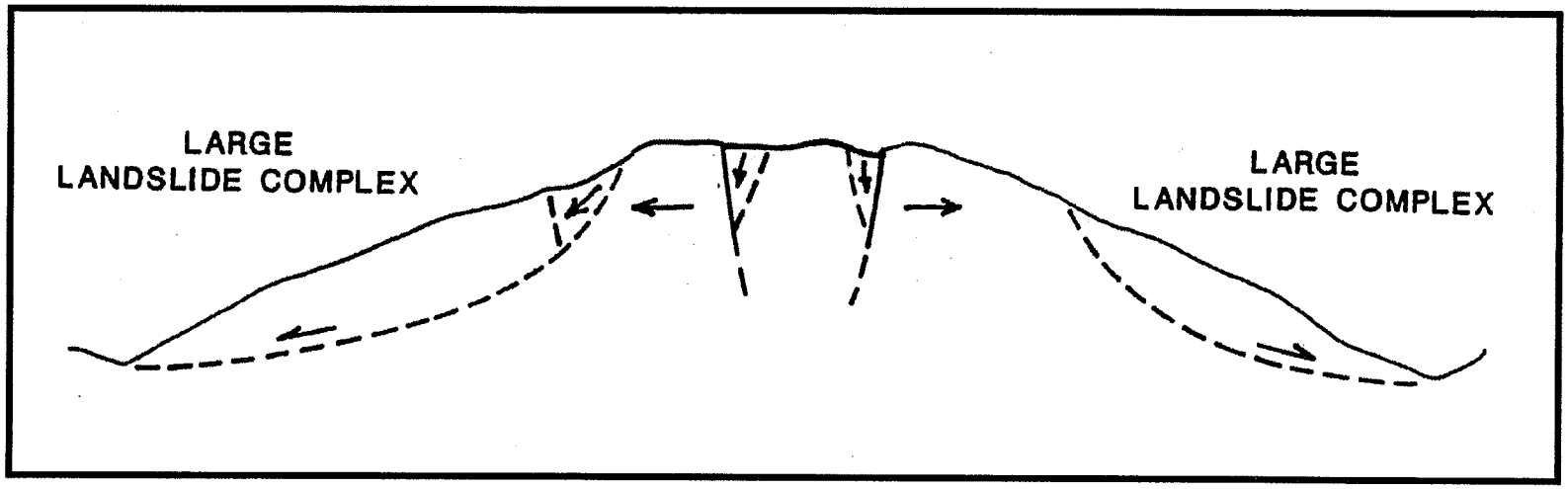

Hart et al, 1990

Rock Weathering and Soil Formation

Weathering of rock:

- Physical
- Chemical

Soil profile development

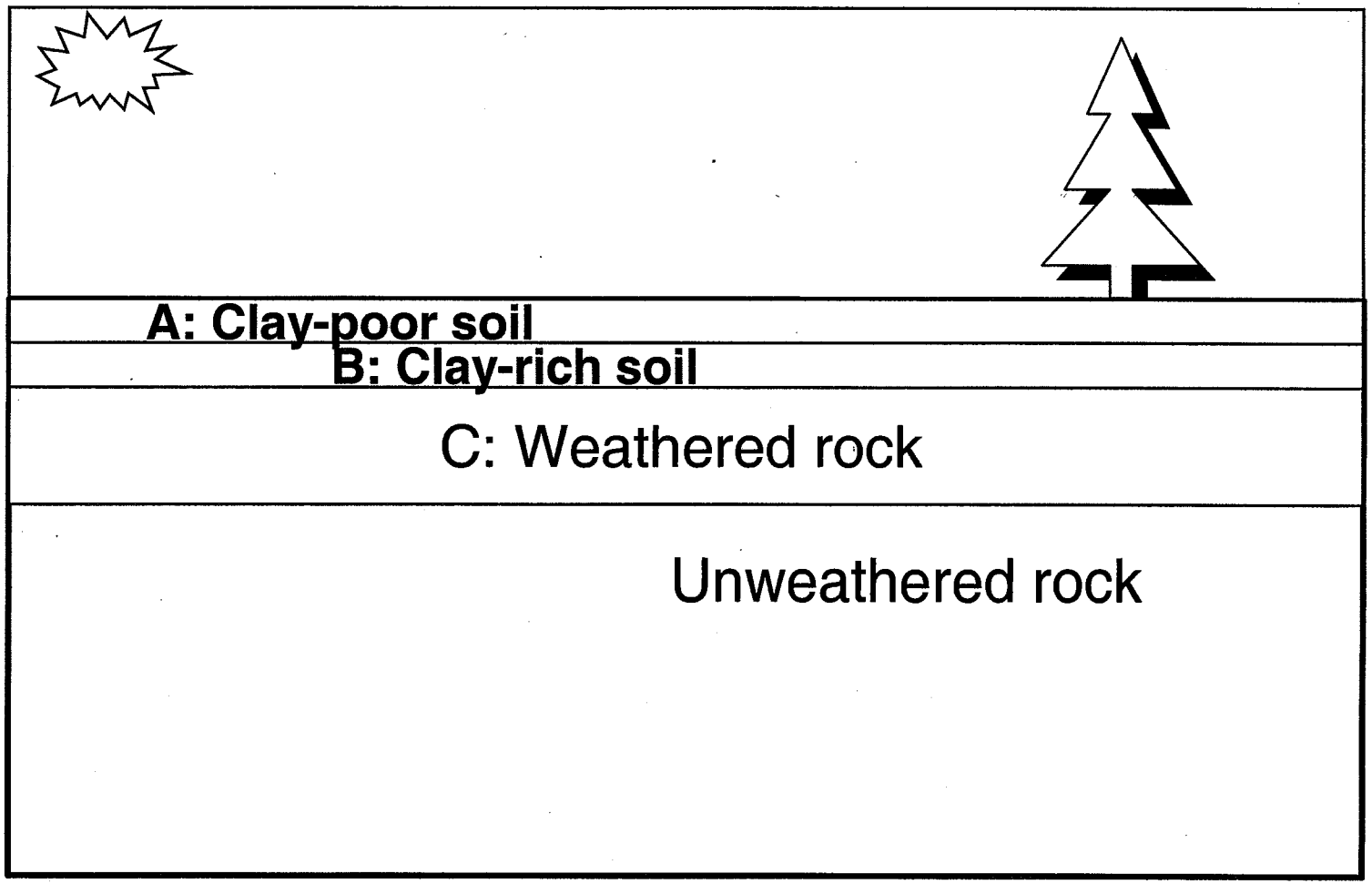

Residual vs. colluvial soil

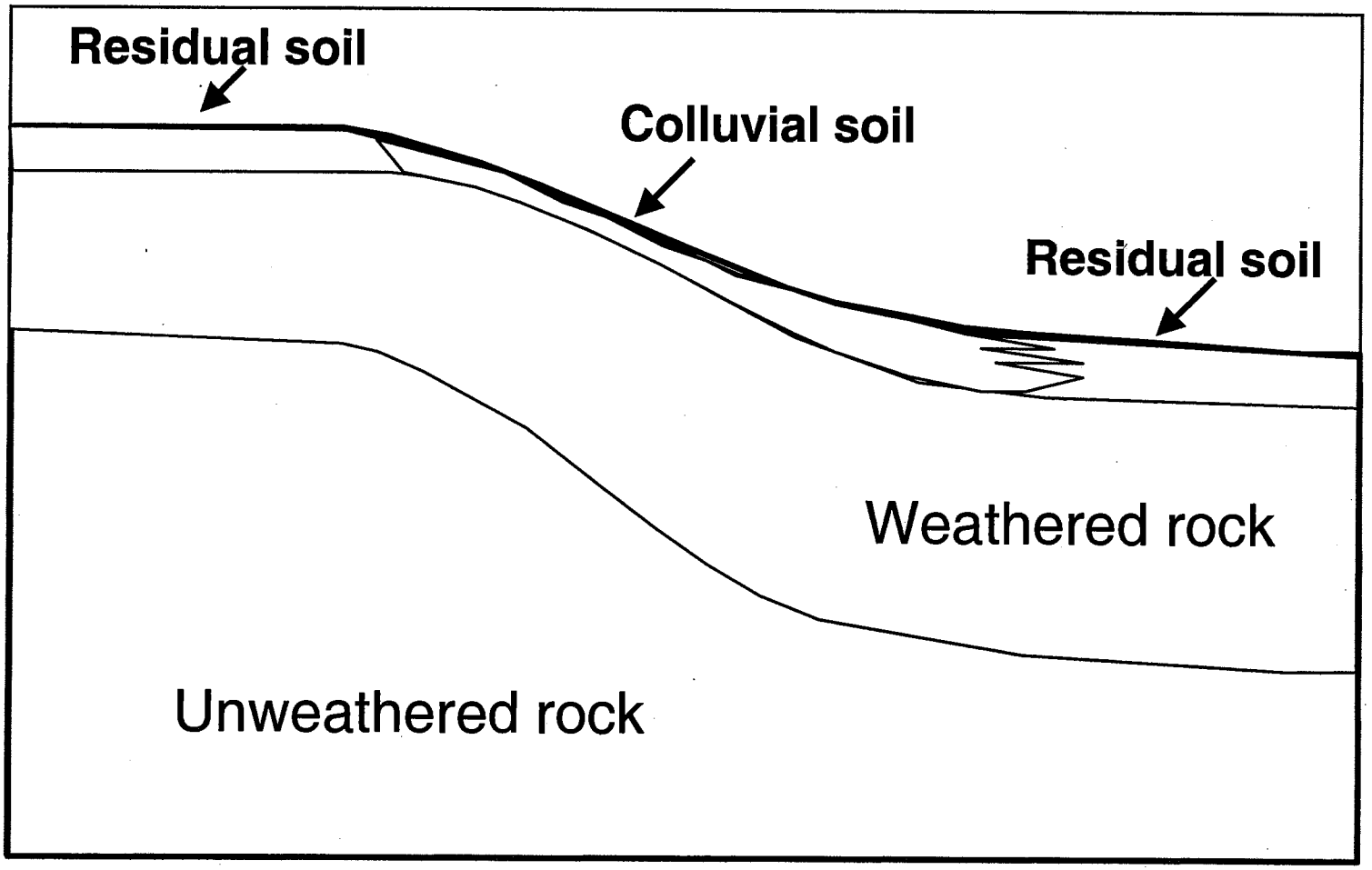

Downslope Movement of Soil

- Erosion
- Soil creep
- Rock creep
- Mass wasting

Erosion

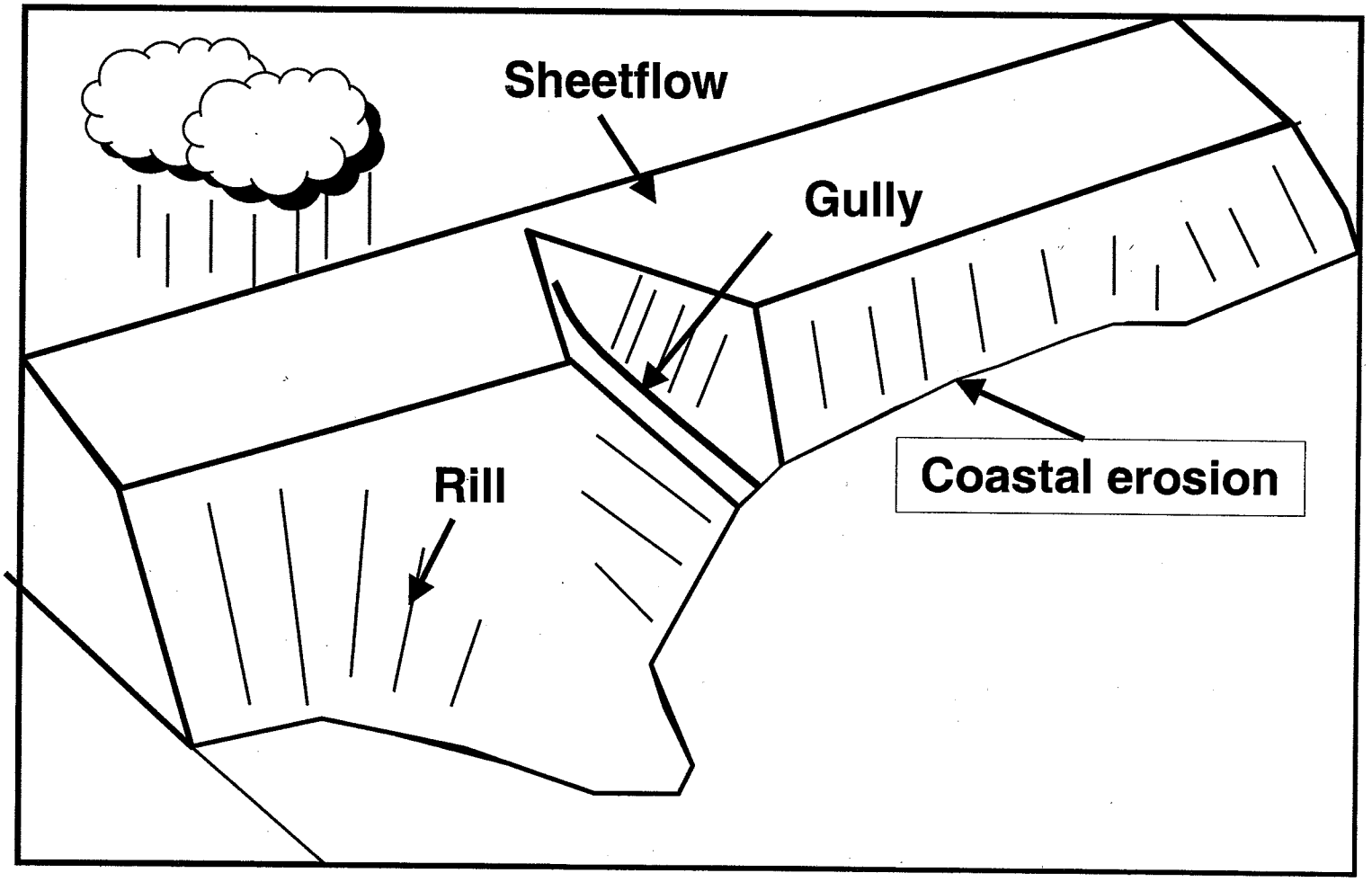

San Mateo County, 1995

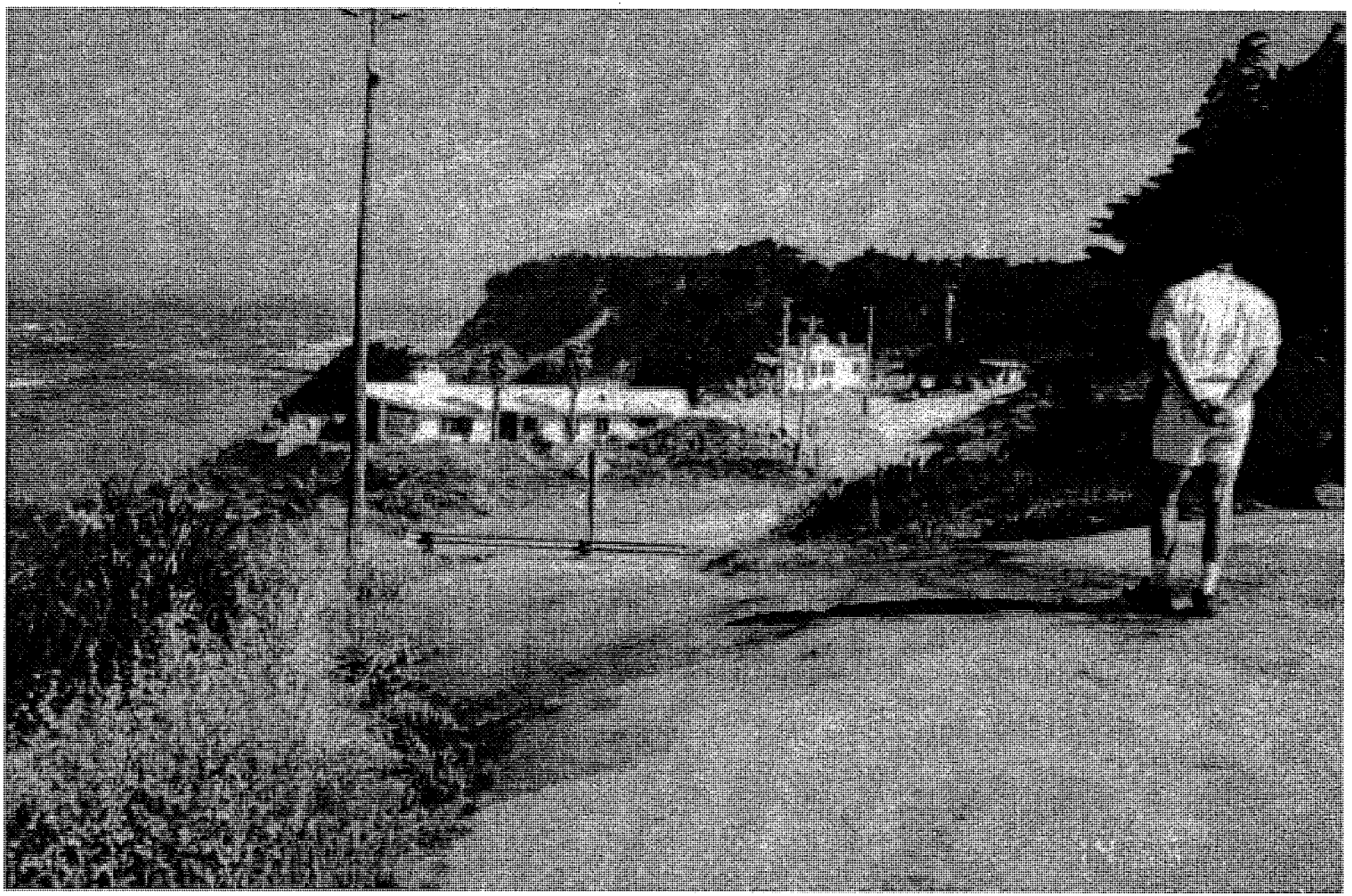

Glacial Erosion and Retreat

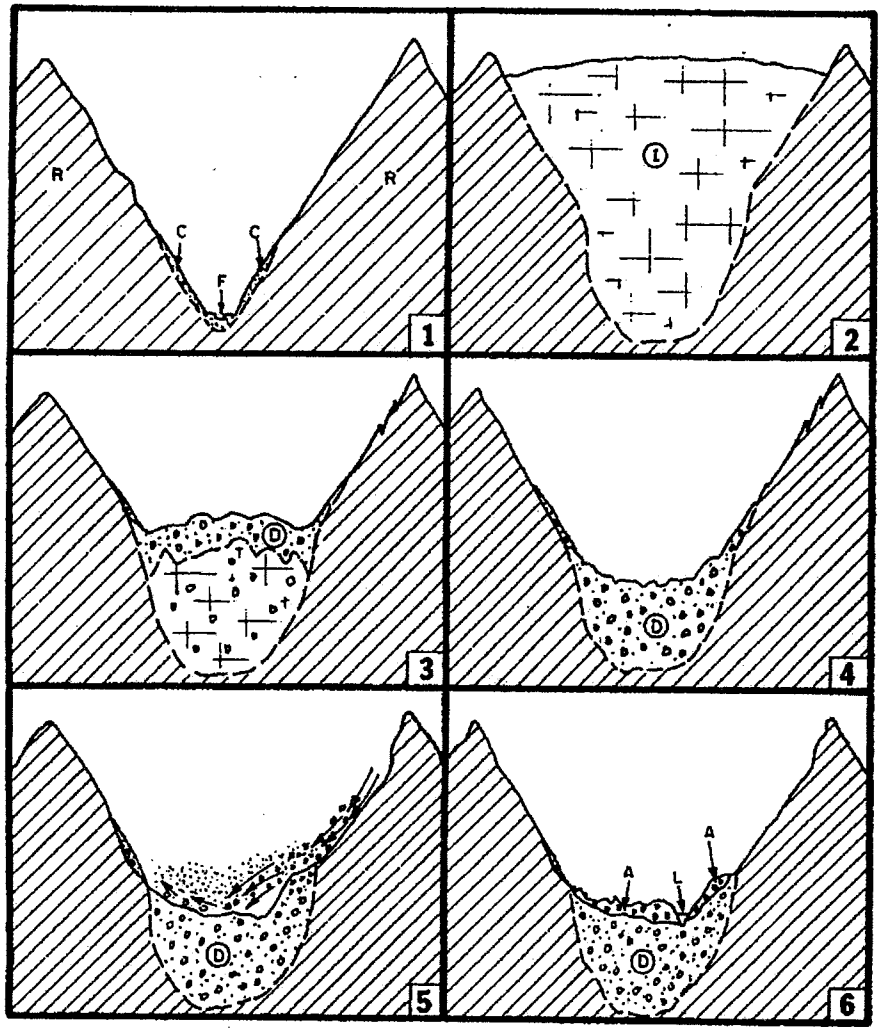

Mollard, 1977

Soil Creep

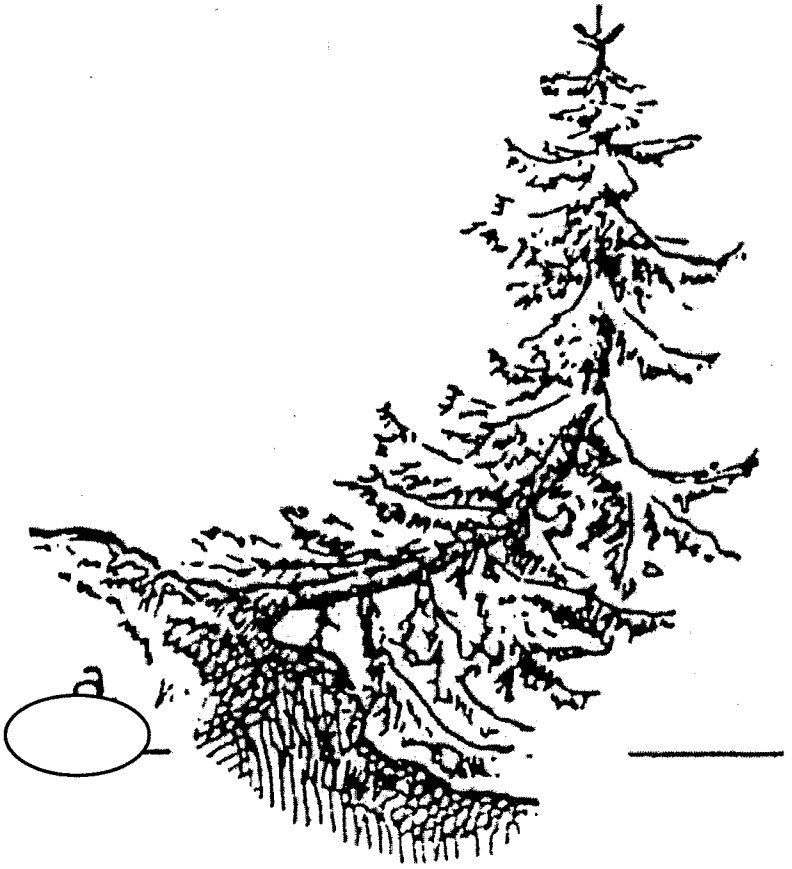

Heim, 1932

Heim, 1932

Rock Creep

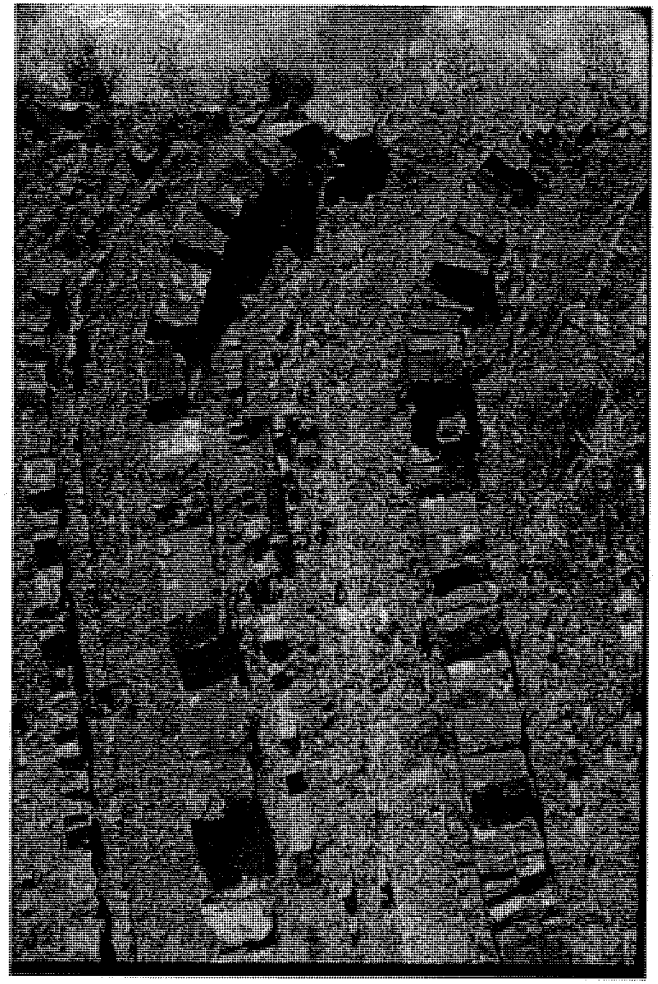

NOAA

Long-Term Geologic Processes

- Relaxation due to unloading
- Eustatic sea level changes
- Fluvial channel meander and incision
- Glacial retreat

Long-Term Climate Change

Comparative precipitation values in Los Angeles, 1877 to 1966 and approximately 15,000 years B.P.*

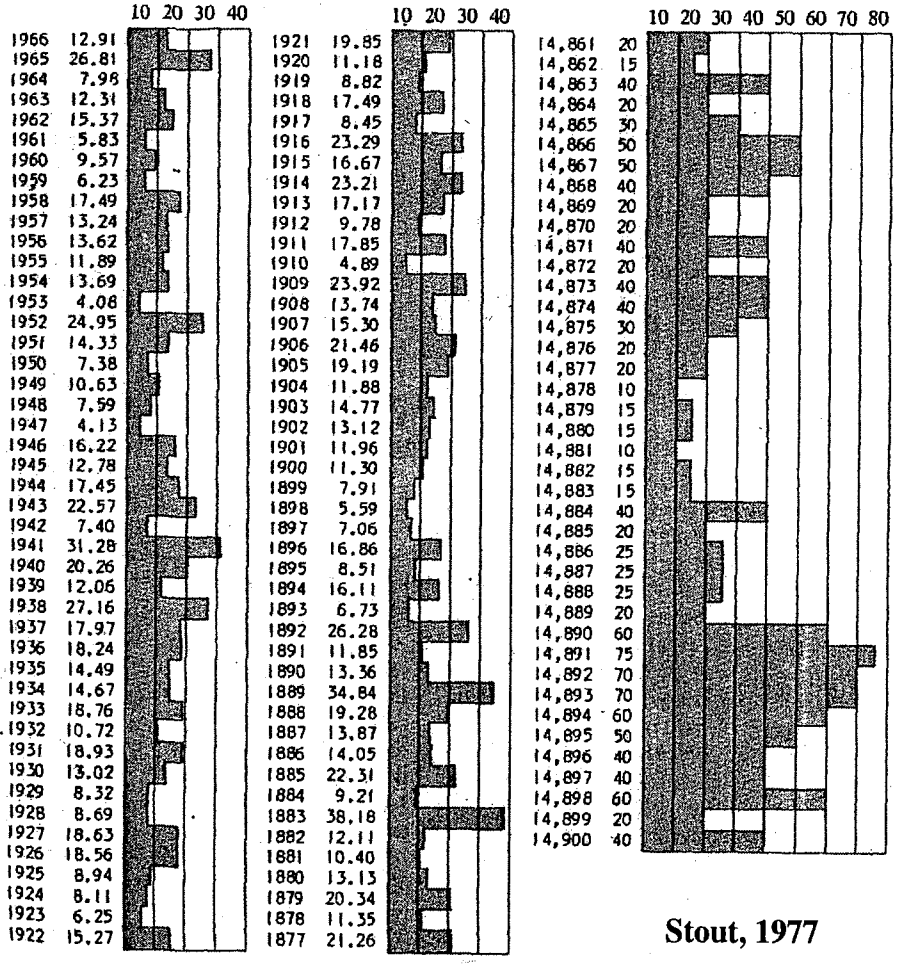

Year	Ppt. (inches)	Year	Ppt. (inches)	Year B.P.	Ppt. (inches)
1966	12.91	1921	19.85	14,861	20
1965	26.81	1920	11.18	14,862	15
1964	7.98	1919	8.82	14,863	40
1963	12.31	1918	17.49	14,864	20
1962	15.37	1917	8.45	14,865	30
1961	5.83	1916	23.29	14,866	50
1960	9.57	1915	16.67	14,867	50
1959	6.23	1914	23.21	14,868	40
1958	17.49	1913	17.17	14,869	20
1957	13.24	1912	9.78	14,870	20
1956	13.62	1911	17.85	14,871	40
1955	11.89	1910	4.89	14,872	20
1954	13.69	1909	23.92	14,873	40
1953	4.08	1908	13.74	14,874	40
1952	24.95	1907	15.30	14,875	30
1951	14.33	1906	21.46	14,876	20
1950	7.38	1905	19.19	14,877	20
1949	10.63	1904	11.88	14,878	10
1948	7.59	1903	14.77	14,879	15
1947	4.13	1902	13.12	14,880	15
1946	16.22	1901	11.96	14,881	10
1945	12.78	1900	11.30	14,882	15
1944	17.45	1899	7.91	14,883	15
1943	22.57	1898	5.59	14,884	40
1942	7.40	1897	7.06	14,885	20
1941	31.28	1896	16.86	14,886	25
1940	20.26	1895	8.51	14,887	25
1939	12.06	1894	16.11	14,888	25
1938	27.16	1893	6.73	14,889	20
1937	17.97	1892	26.28	14,890	60
1936	18.24	1891	11.85	14,891	75
1935	14.49	1890	13.36	14,892	70
1934	14.67	1889	34.84	14,893	70
1933	18.76	1888	19.28	14,894	60
1932	10.72	1887	13.87	14,895	50
1931	18.93	1886	14.05	14,896	40
1930	13.02	1885	22.31	14,897	40
1929	8.32	1884	9.21	14,898	60
1928	8.69	1883	38.18	14,899	20
1927	18.63	1882	12.11	14,900	40
1926	18.56	1881	10.40		
1925	8.94	1880	13.13		
1924	8.11	1879	20.34		
1923	6.25	1878	11.35		
1922	15.27	1877	21.26		

Stout, 1977

*Data are based on U.S. Weather Bureau records, and analysis of tree-ring data (Templeton) is from cypress tree in La Brea tar pits.

LANDSLIDE MECHANISMS RELATED TO GEOLOGY

Fast-Moving Landslides

Primarily in granular materials

- **Debris flows**
- **Rockfalls**
- **Lateral spreads (sands, silts, or sensitive clays)**

Wet Landslides and Debris Flows

Triggering and Runout

Newport Backbay, CA

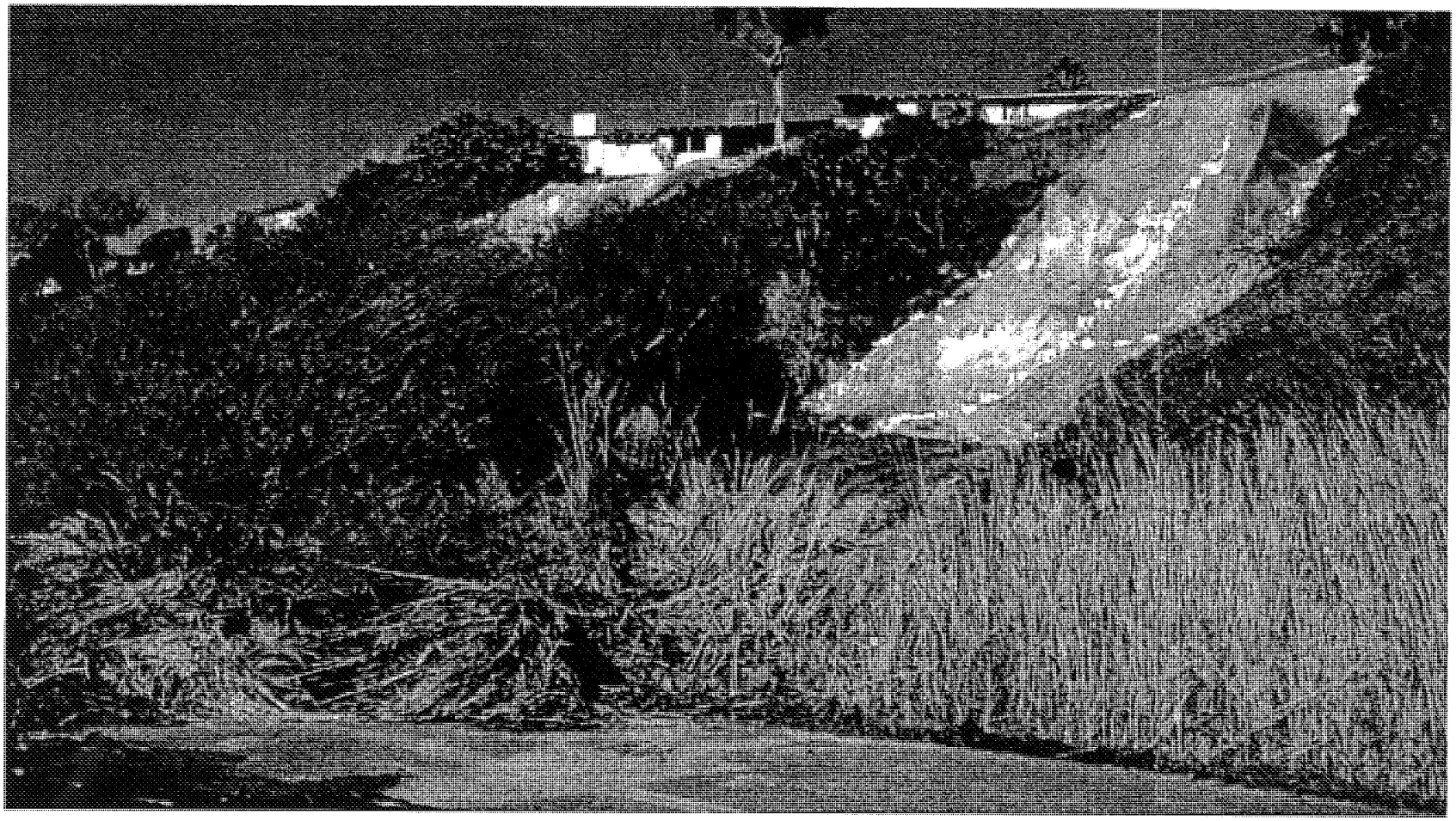

High-conductivity unit conducts groundwater to slope face

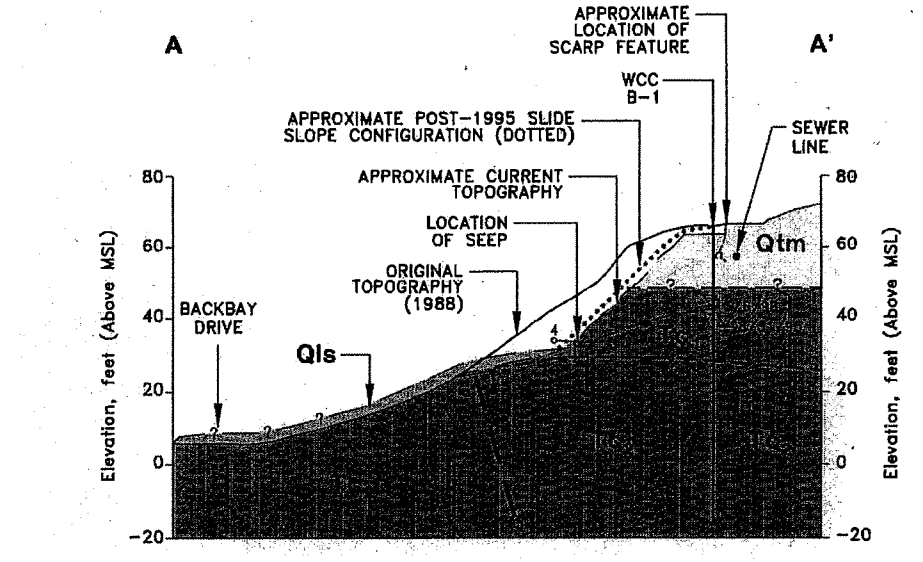

Woodward-Clyde International, 1998

Groundwater Migration

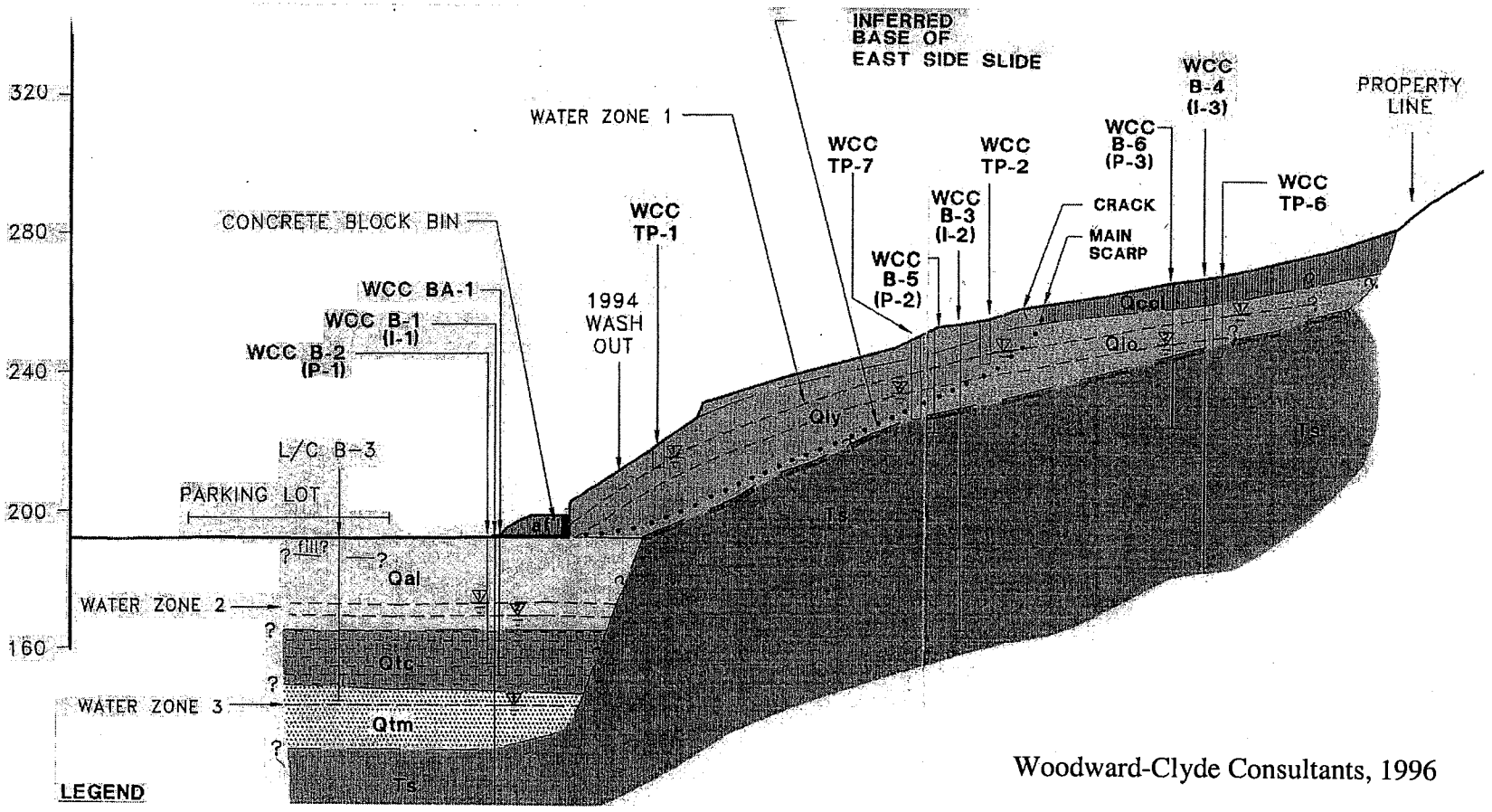

Woodward-Clyde Consultants, 1996

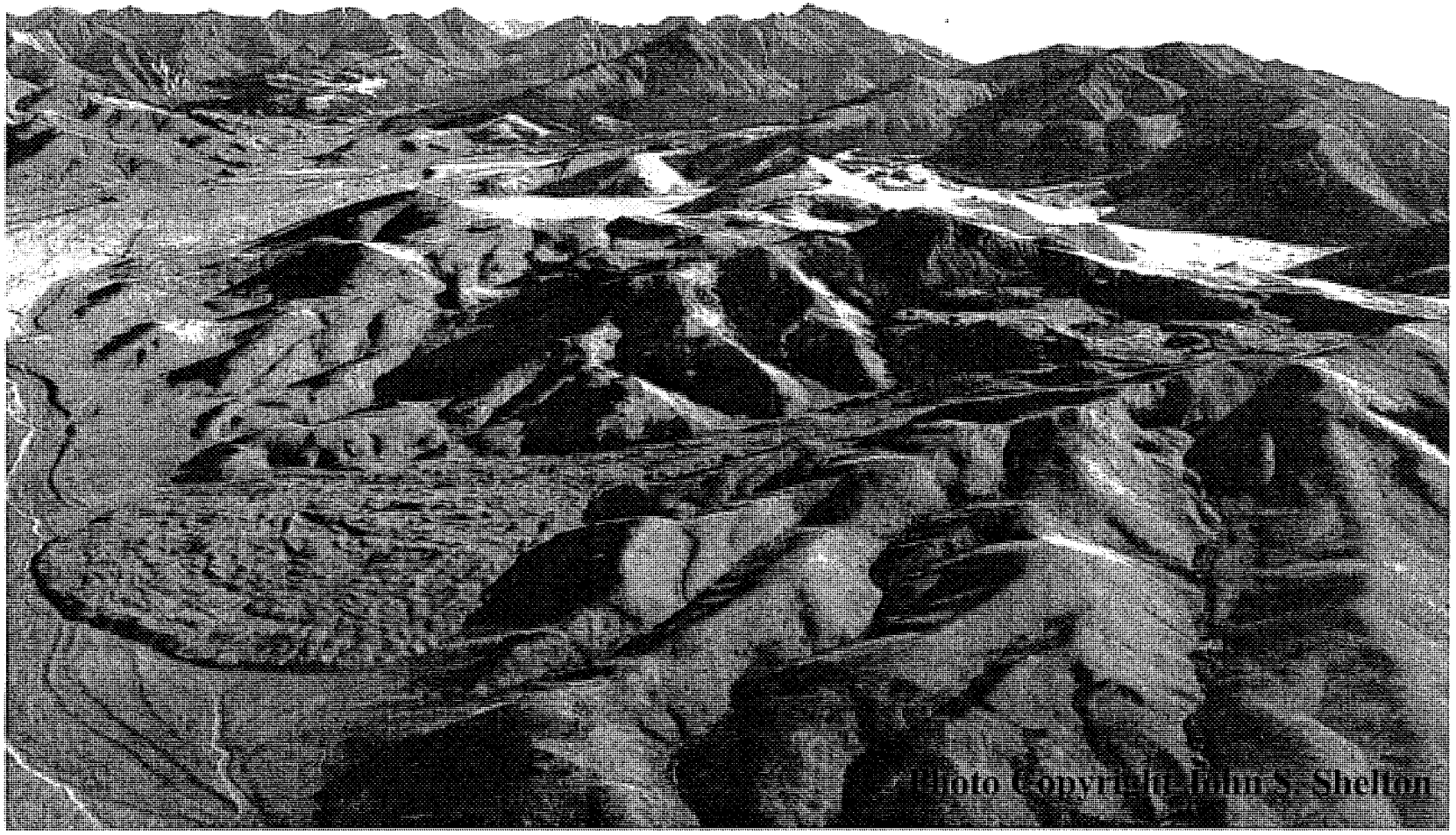

Carlson Landslide, Idaho

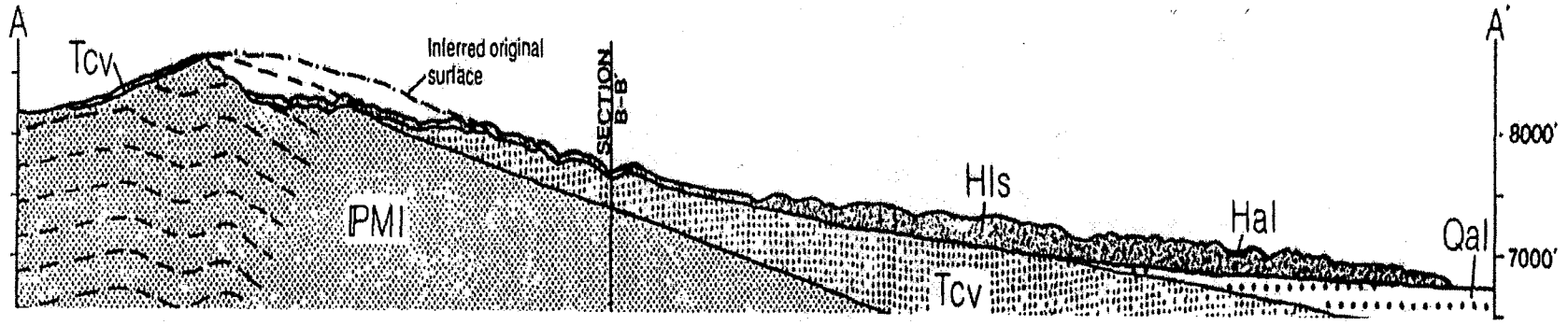
A
A'
Tcv
Inferred original surface
SECTION B-B'
PMI
Hls
Hal
Qal
Tcv
8000'
7000'

Santa Tecla Landslide, El Salvador

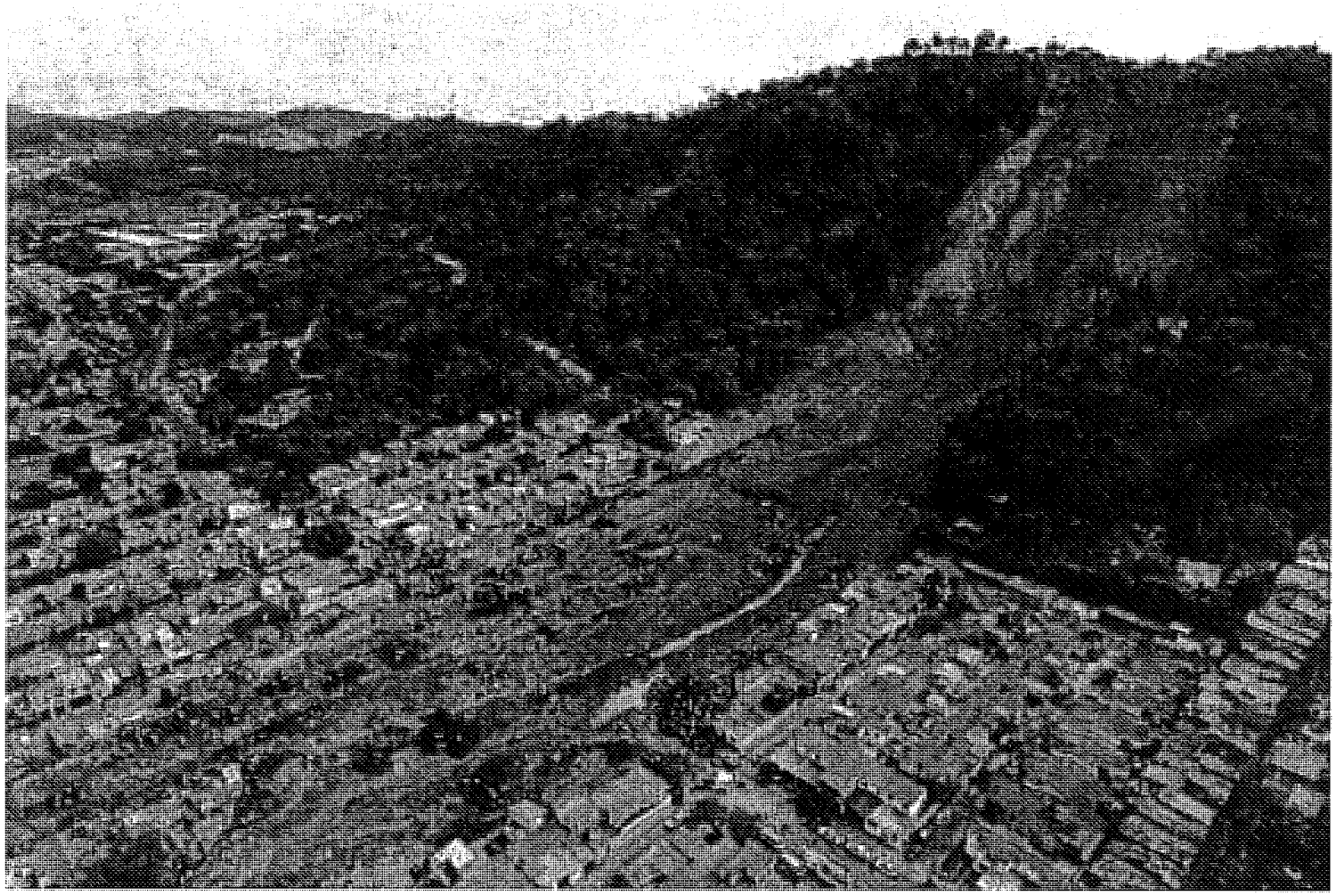

USGS – Harp, 2001

Volcanic Activity

Mt. St. Helens, Washington, May 1980

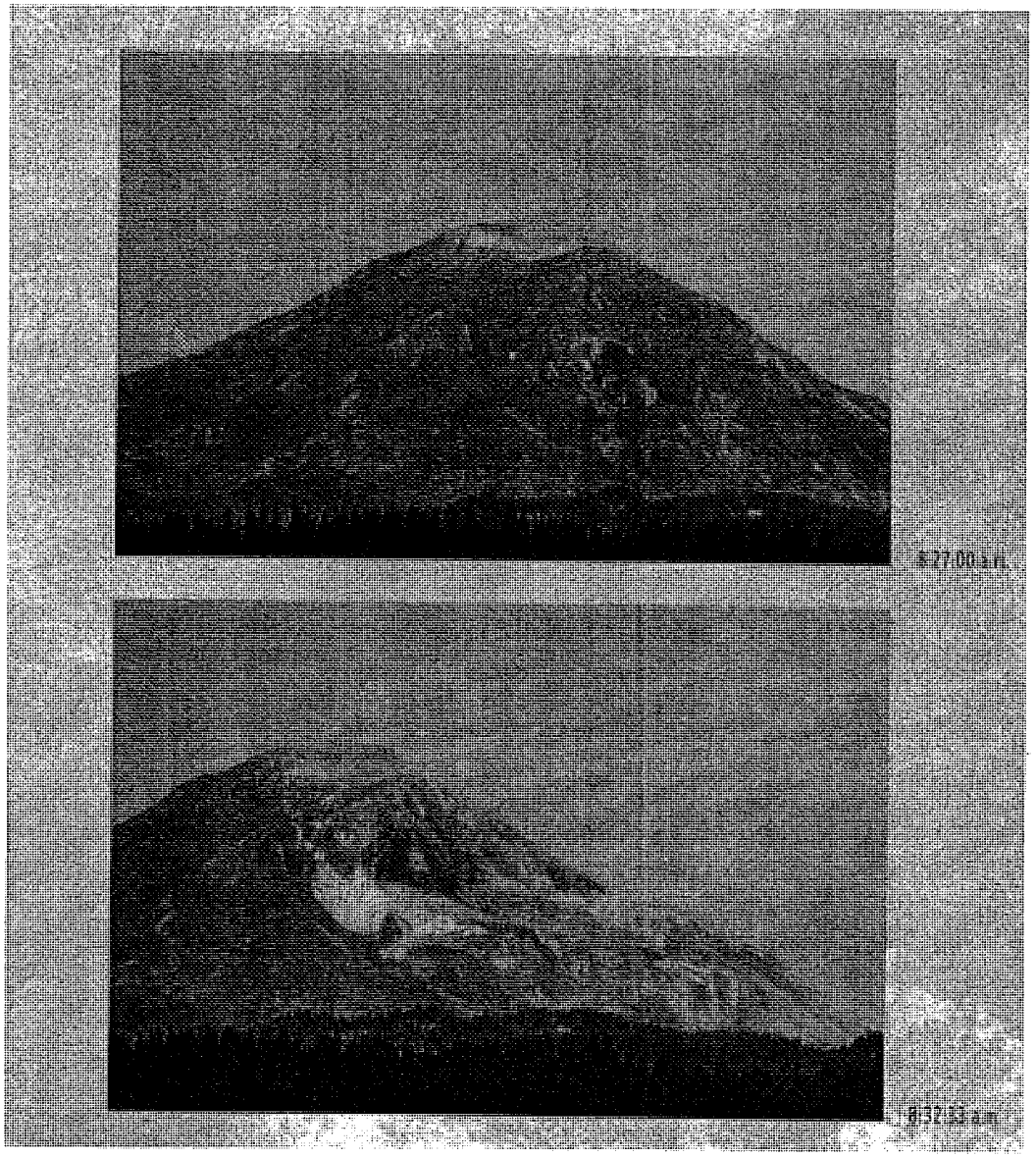

Carson, 1990

Mt. Rainier, Washington, 5,600 b.p.

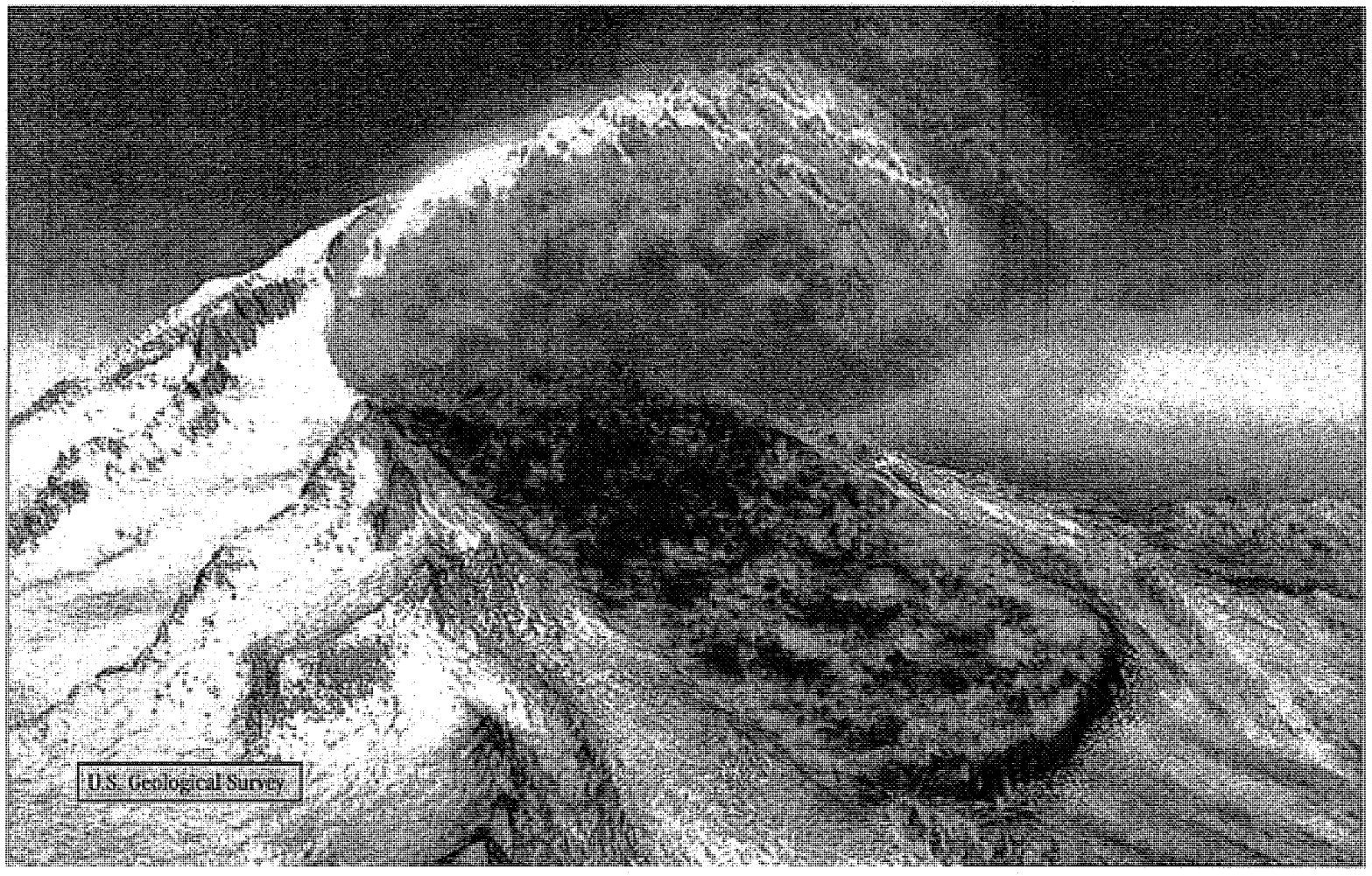

Mudflow Deposits of Mt. Rainier

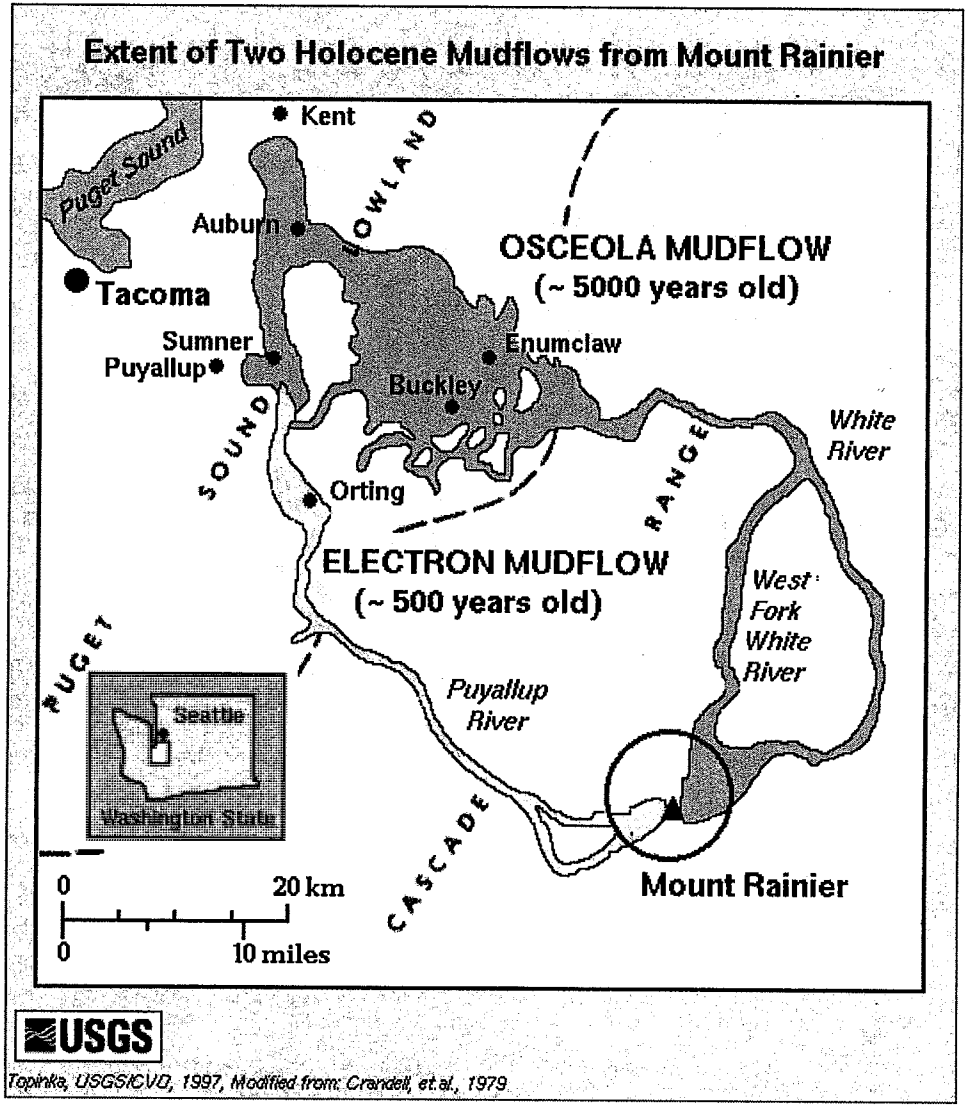

Debris Flows

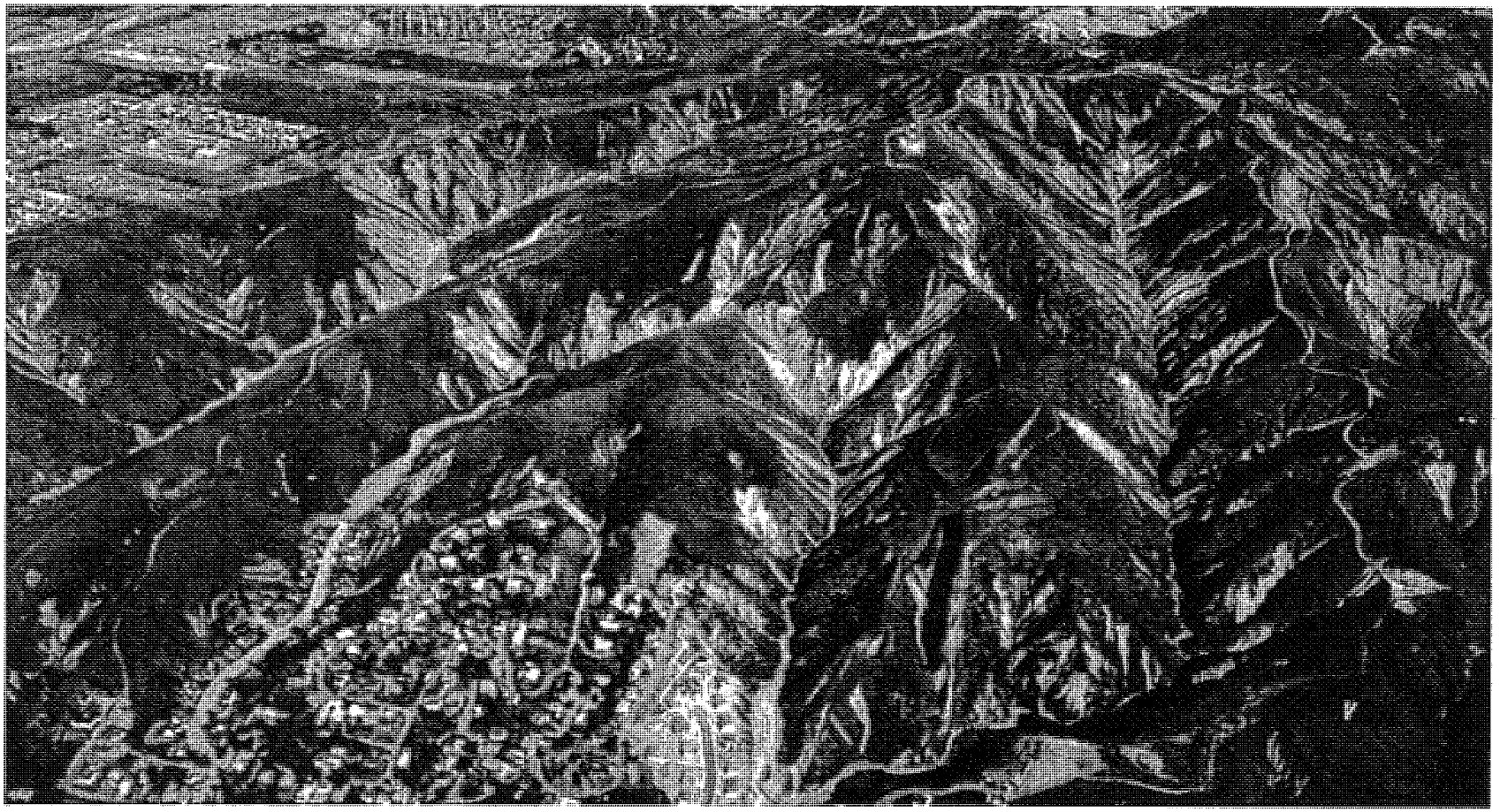

USGS - Morton

Perched Water in Colluvium

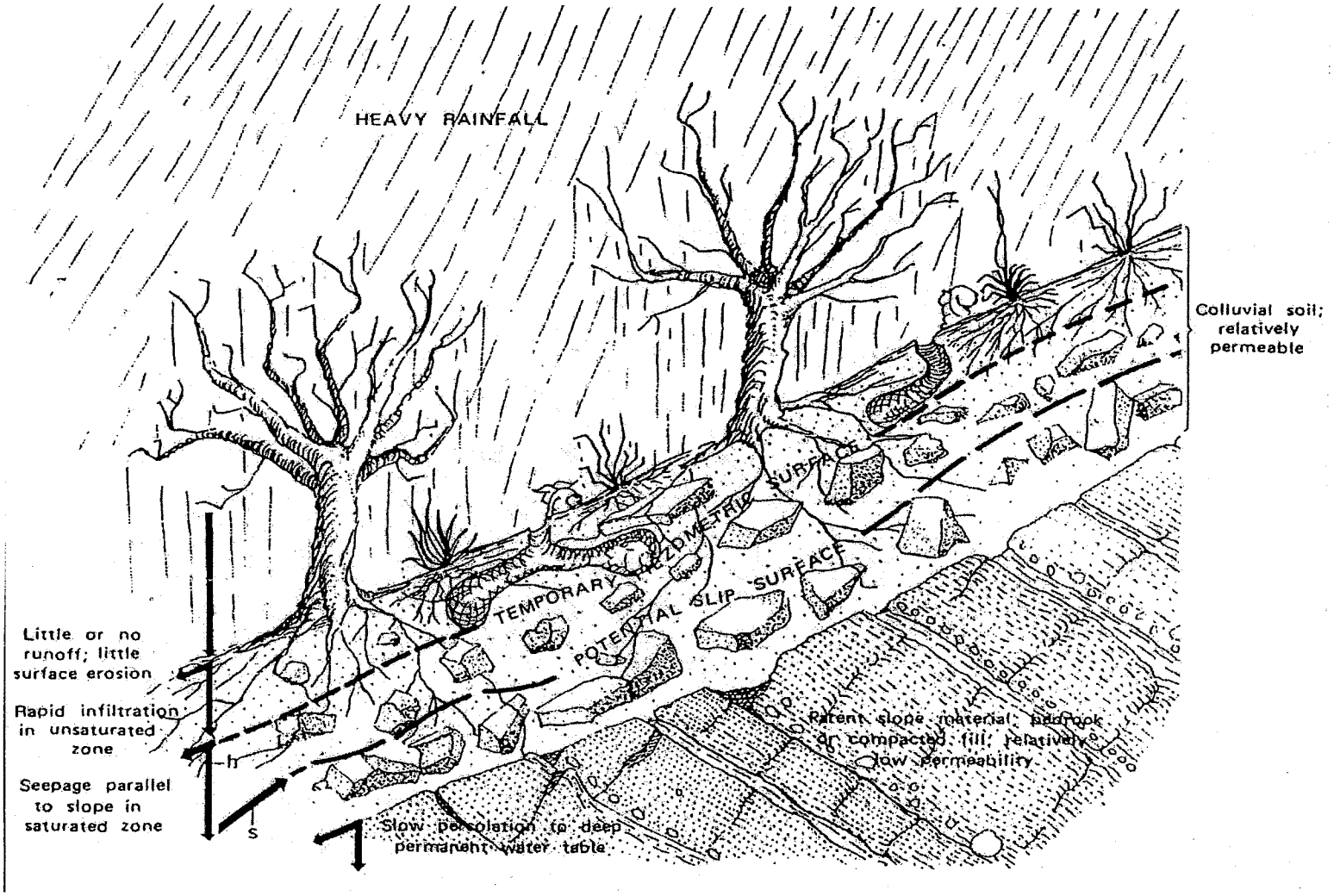

Campbell, 1975, in TRB SR 247

Bainbridge Island, WA, 1997

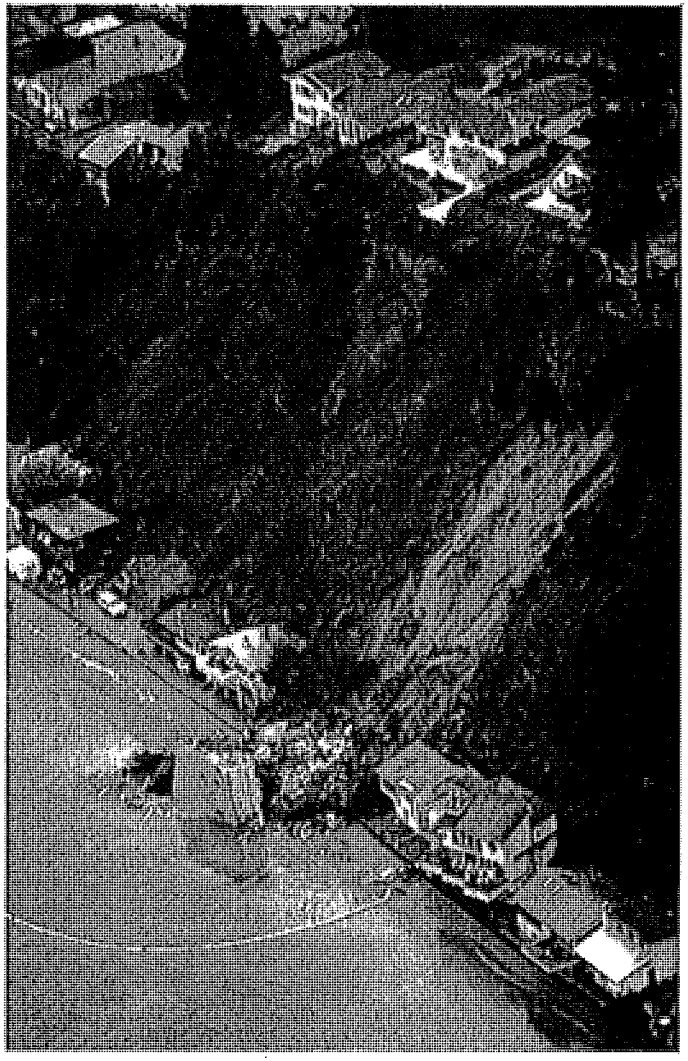

Baum et al, 1998

Debris Flow Scars, Venezuela

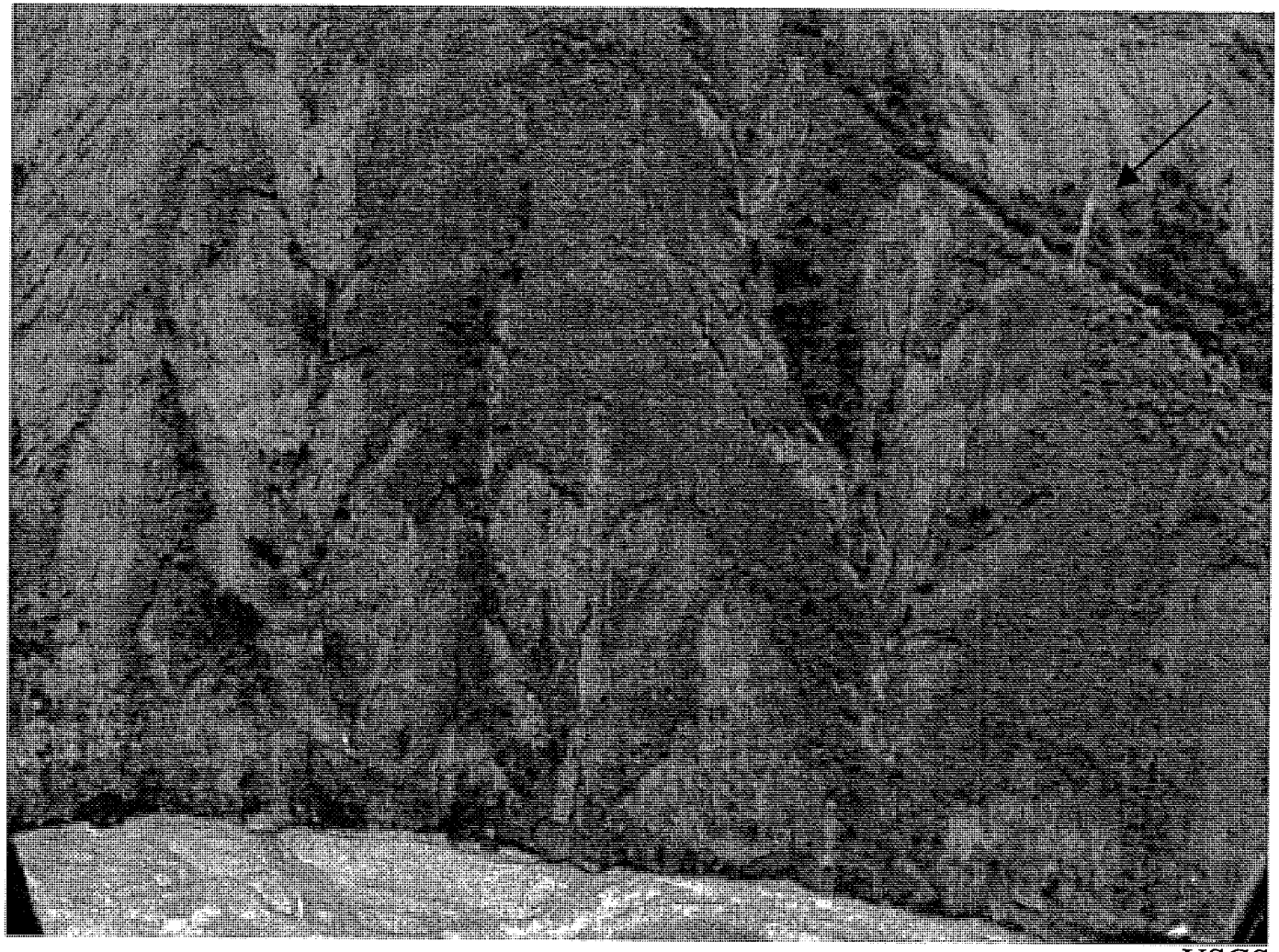

USGS, 2001

Debris Flow Scars, Venezuela

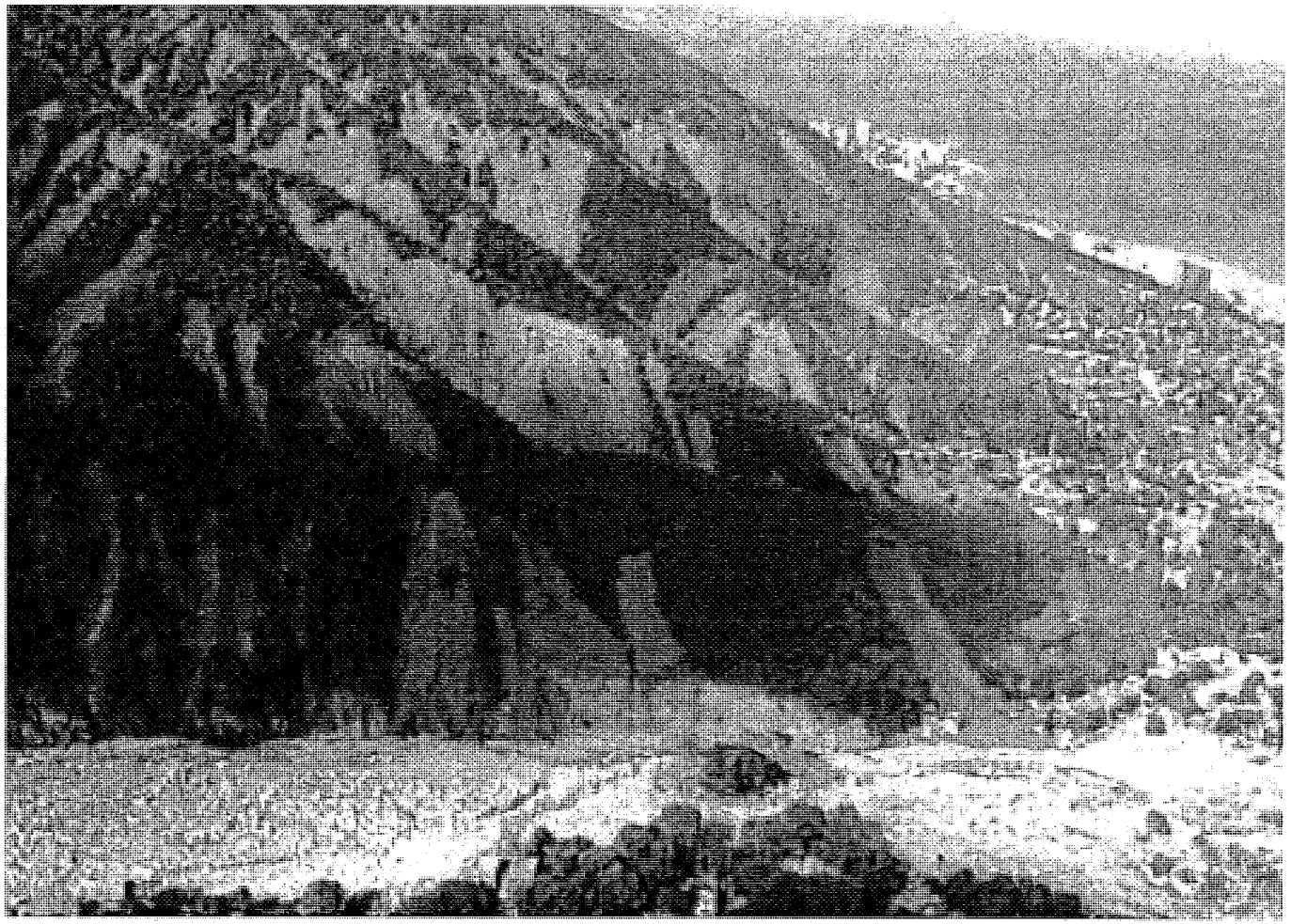

USGS, 2001

Debris-Flow Choked Harbor

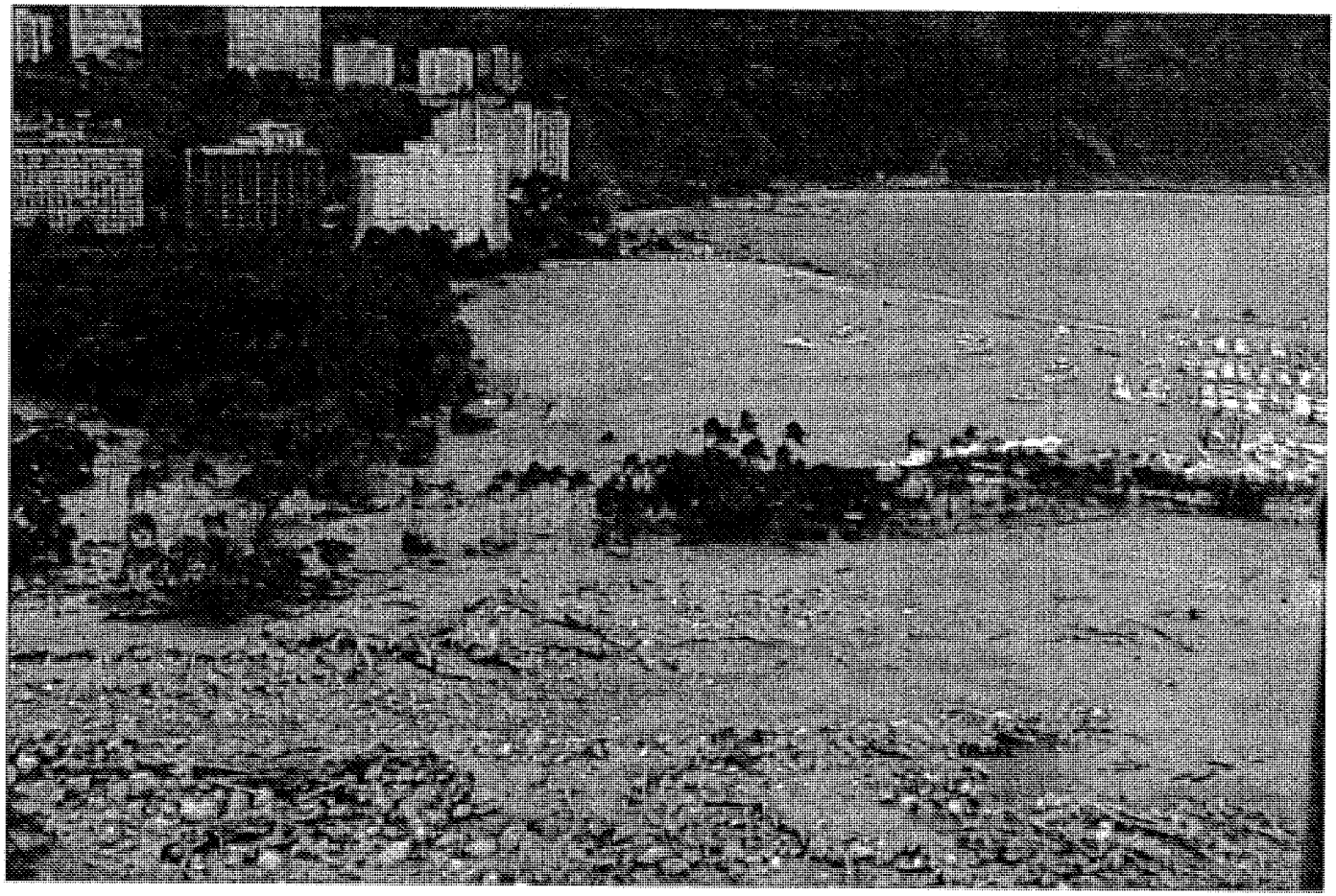

USGS, 2001

Mudflow

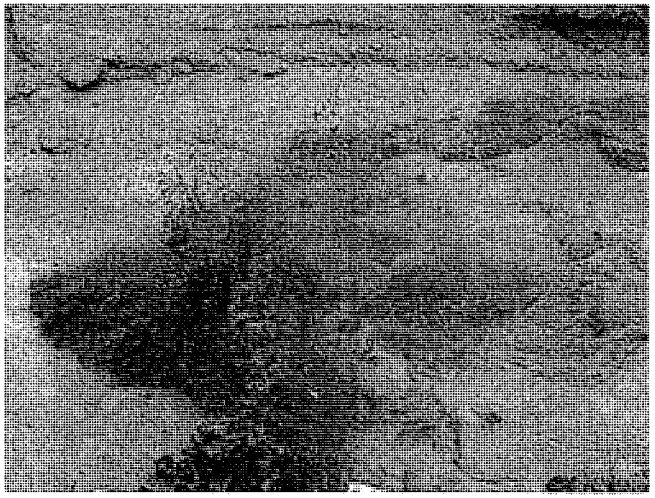

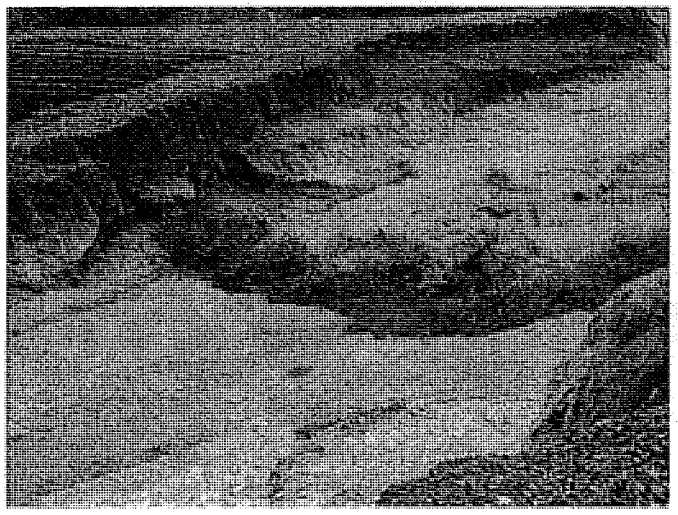

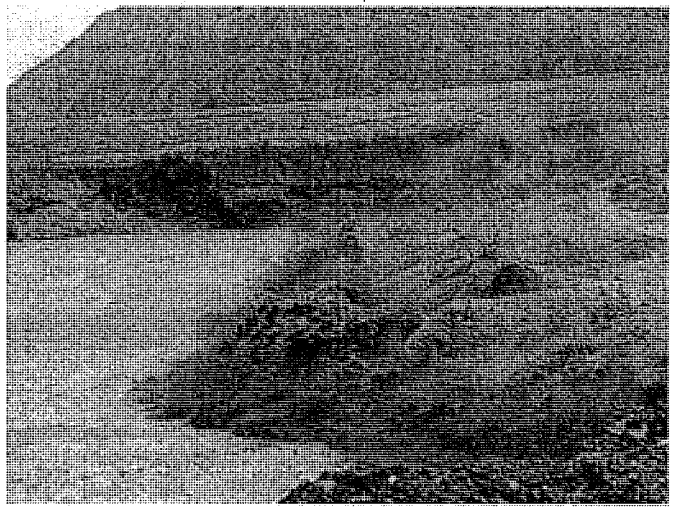

Chinese Academy of Sciences, 1999

Mudflow in Italy, 1998

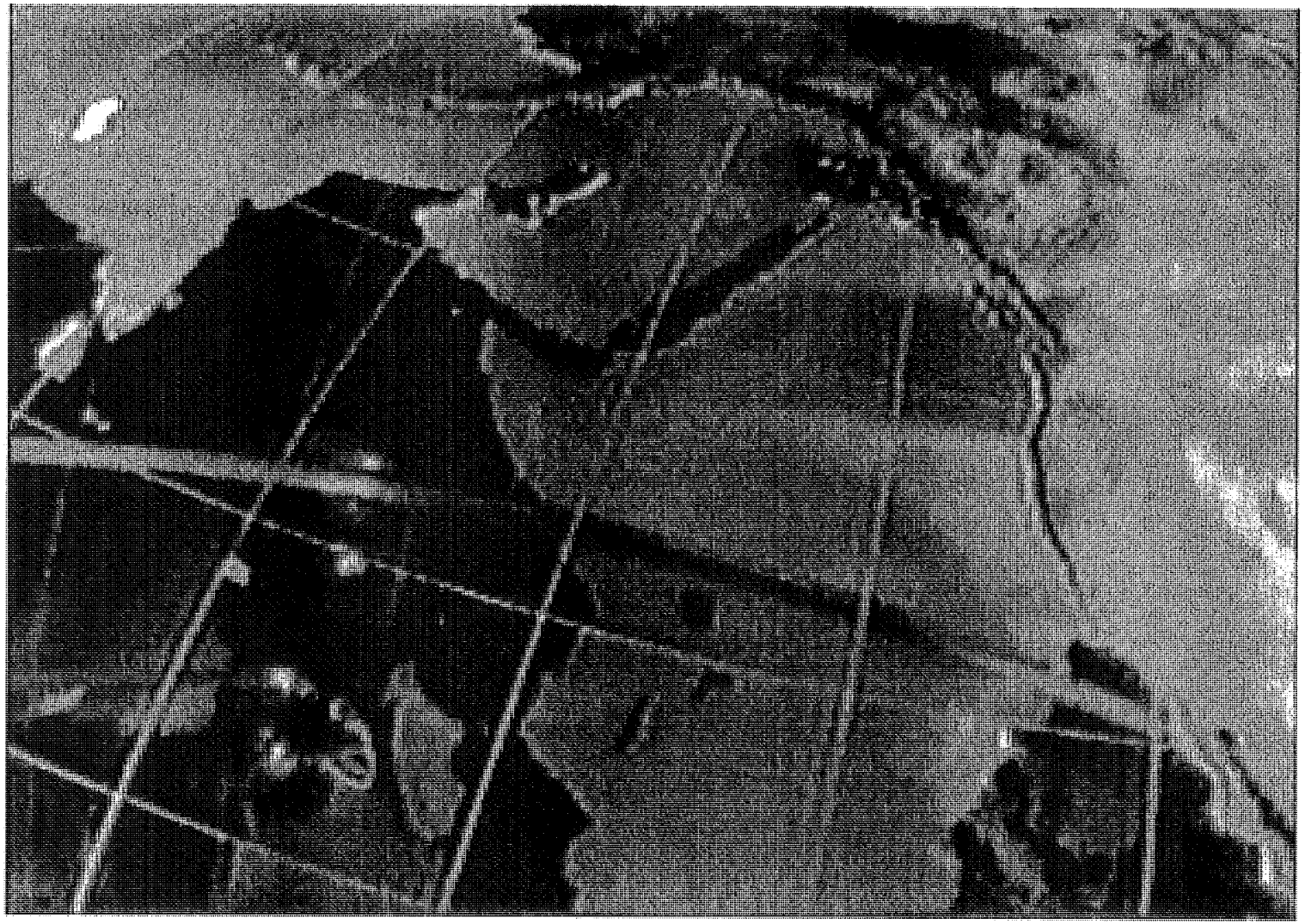

ABC News, 1998

Debris Flow

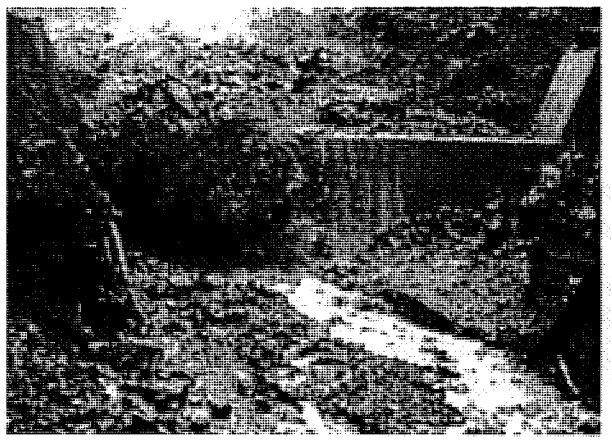

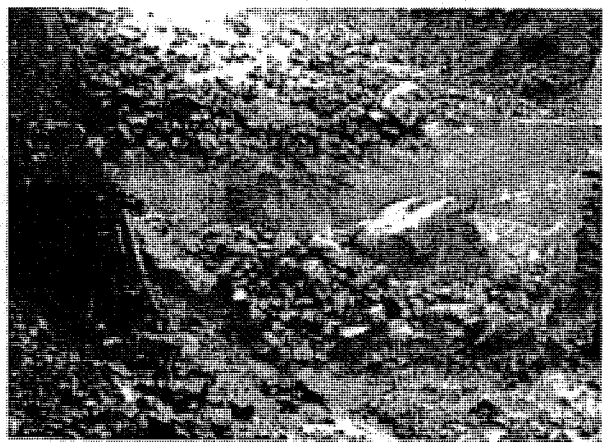

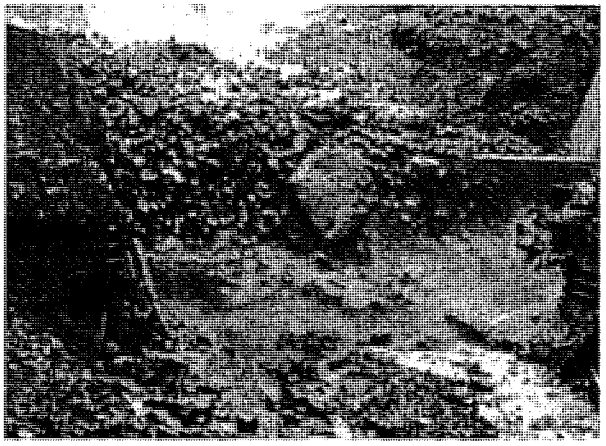

Suwa, 1997

Debris Flow Deposit, Venezuela

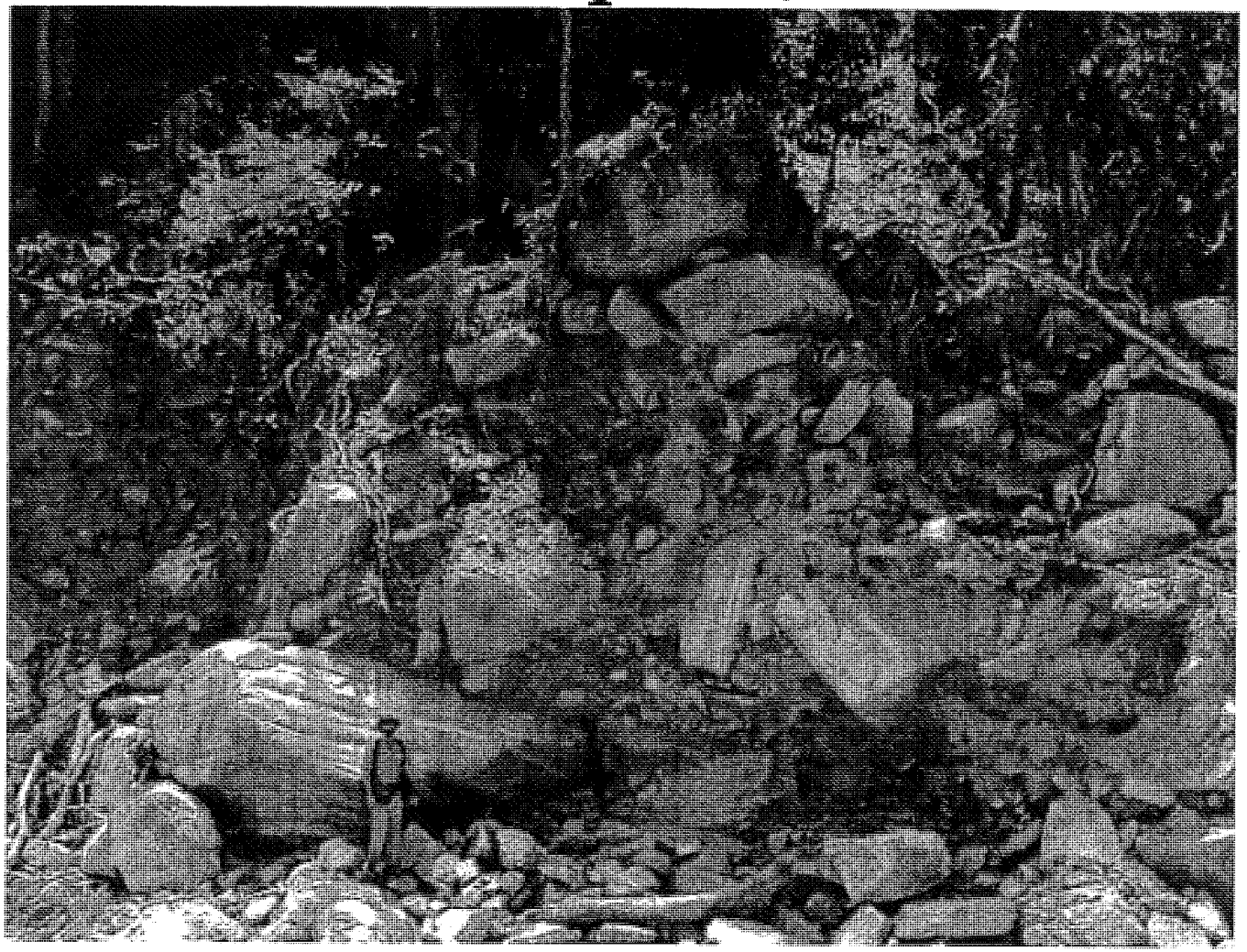

USGS, 2001

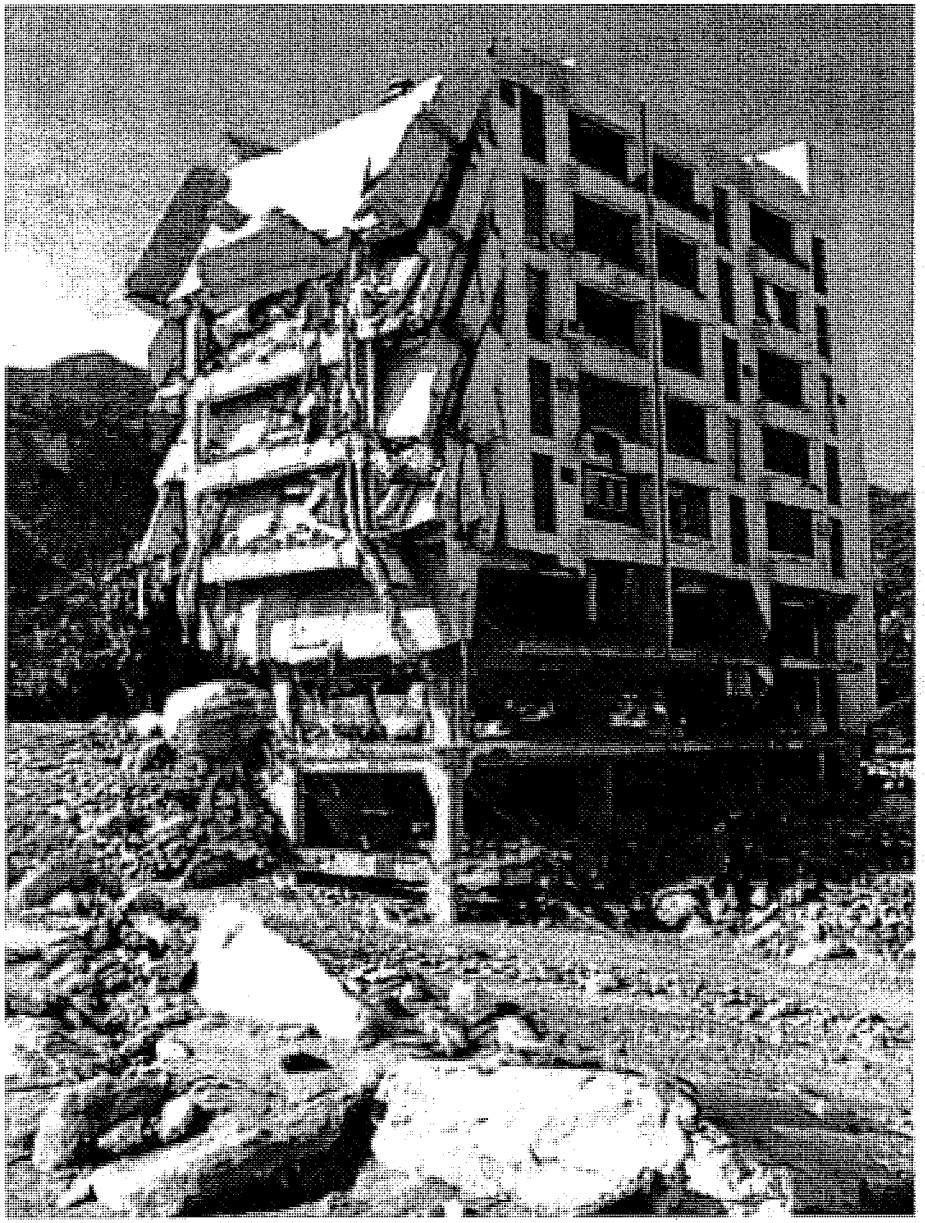

Wrecked Apartment Complex, Venezuela

USGS, 2001

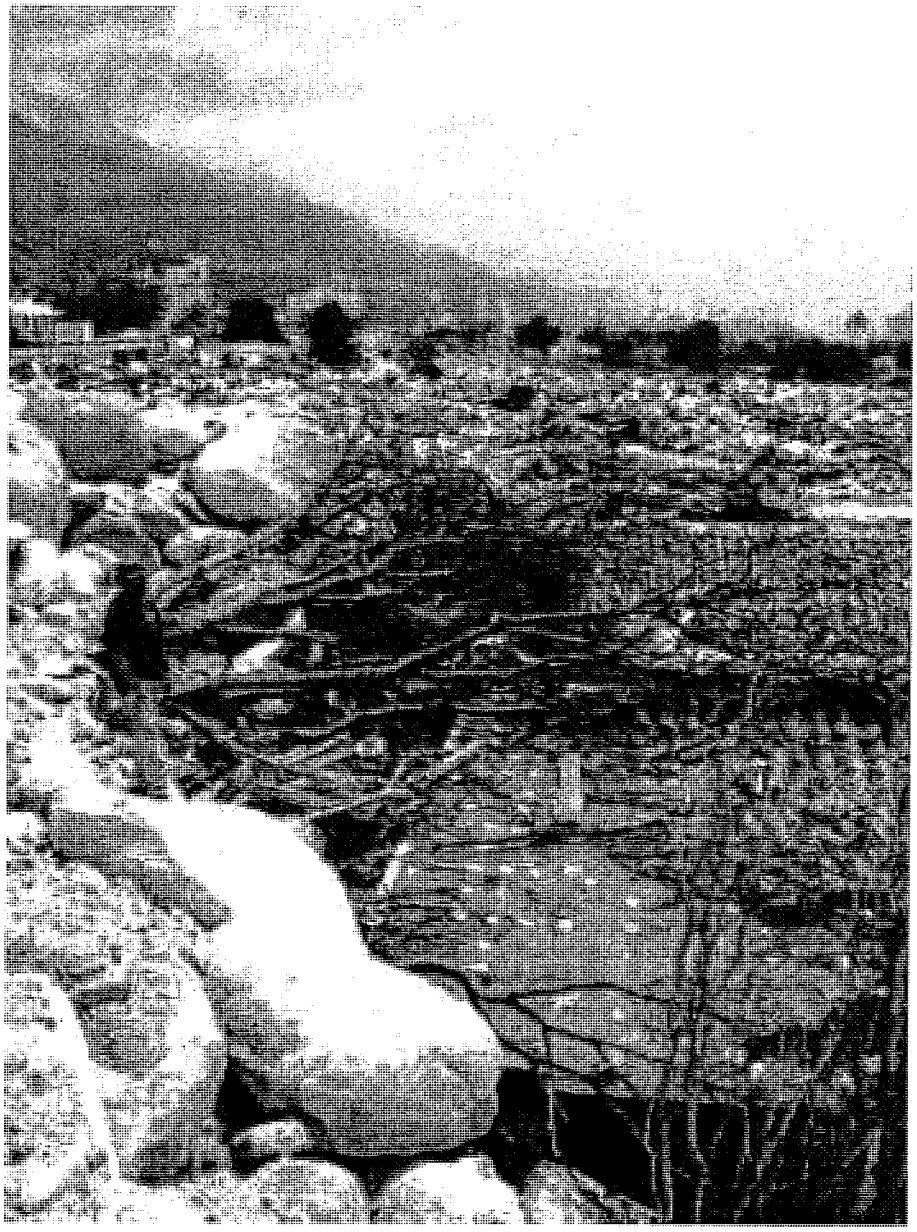

Venezuela December, 1999

USGS, 2001

Rockfall

Mt. Adams, WA, 1997

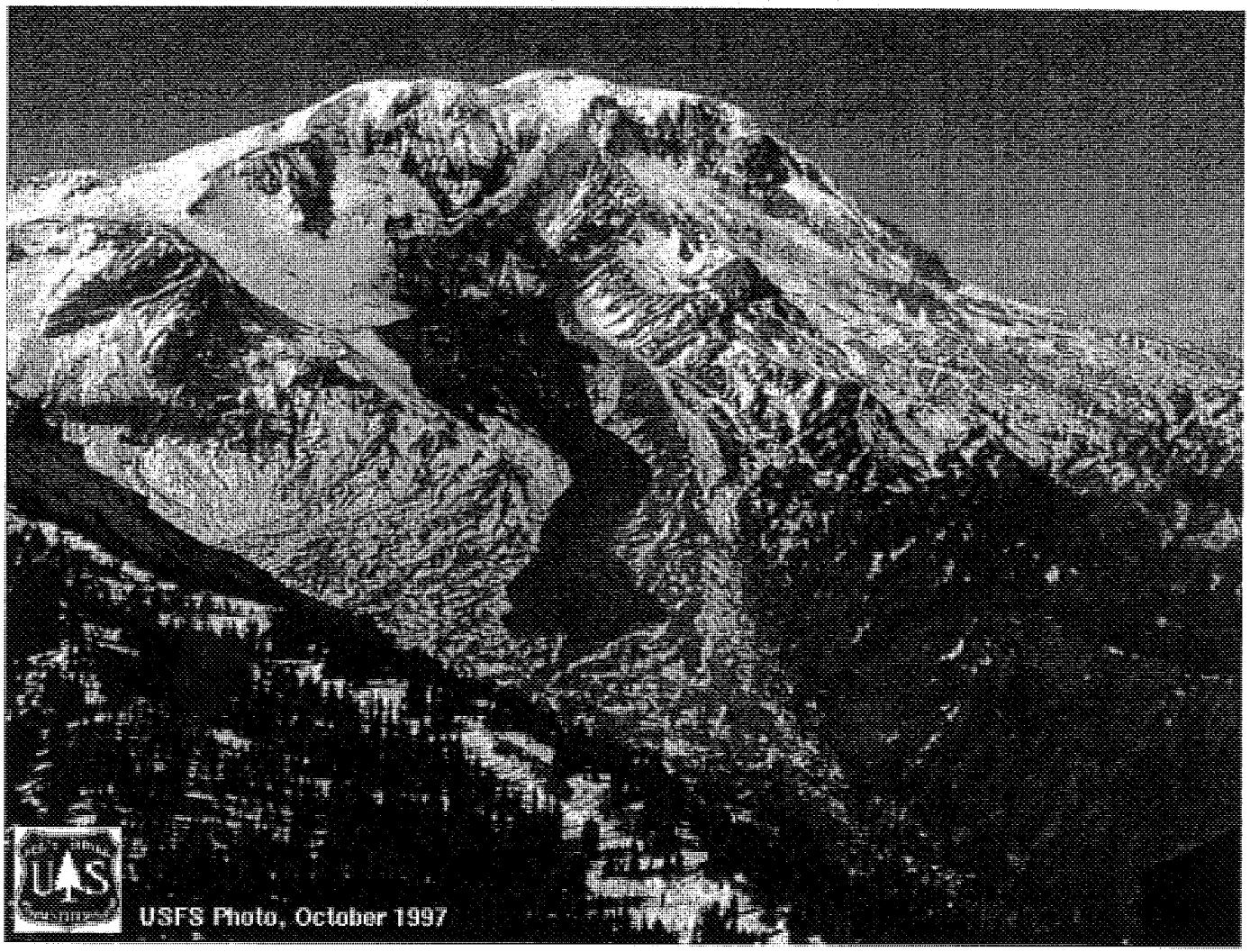

Dust from rockfalls outside of Sylmar after 17 January1994 Northridge Earthquake

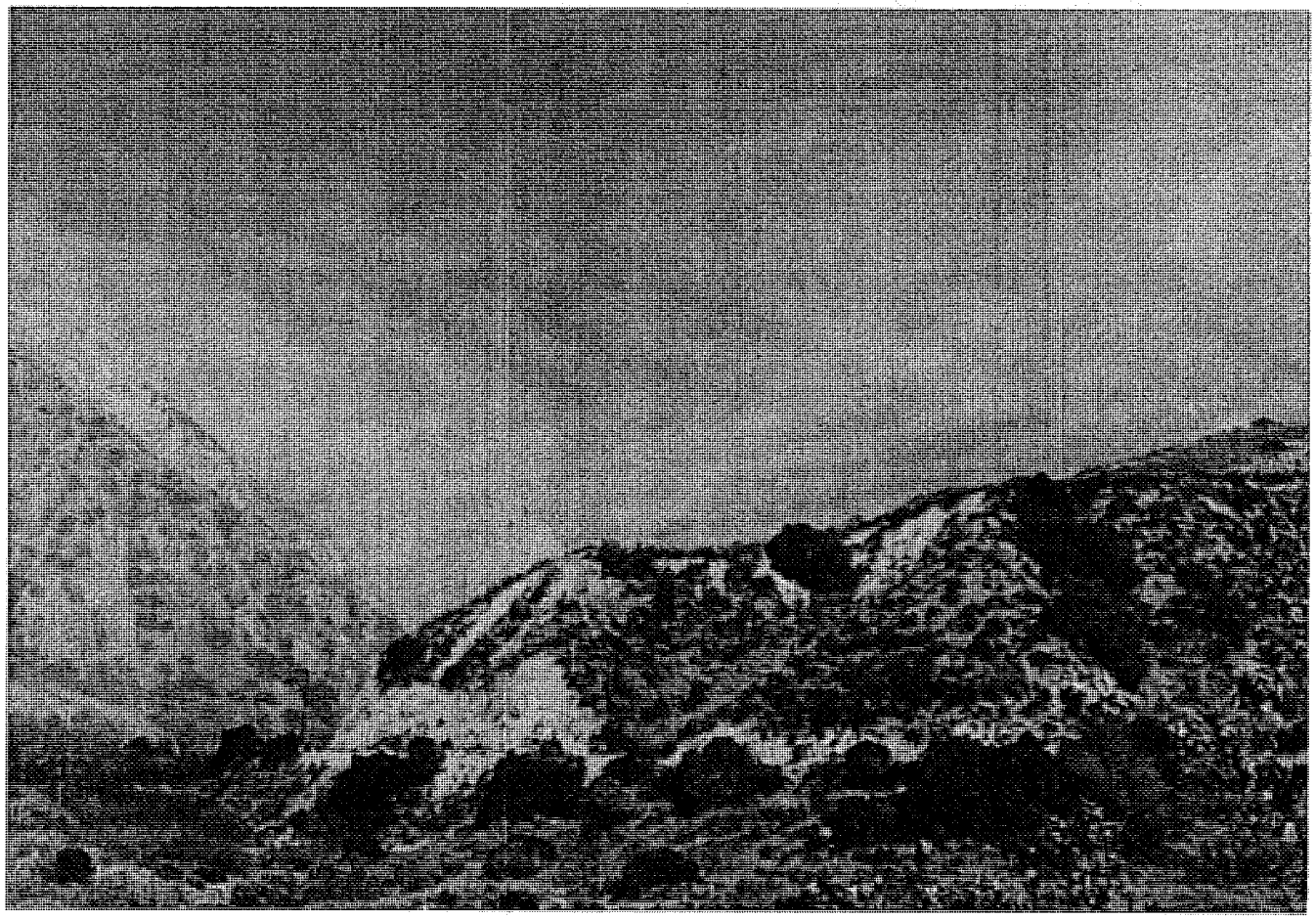

Yosemite Valley, CA

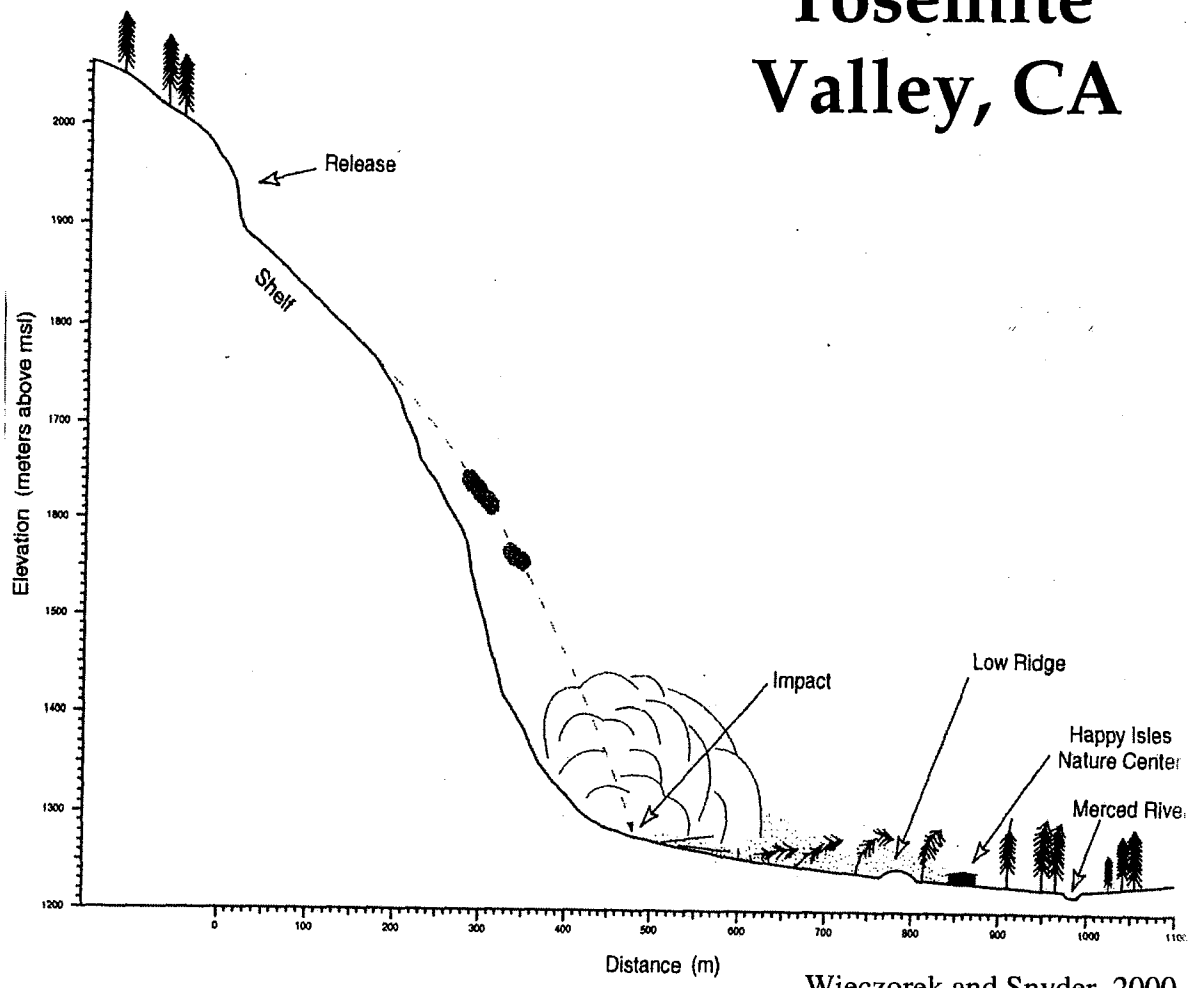

Wieczorek and Snyder, 2000

Rock Avalanches/Long-Runout Landslides

Rock avalanches/long-runout landslides (cont'd)

- **Log Volume vs. H/L characteristics**
- **Proposed mechanisms**
- **Geomorphology**
  - ***Unconfined slides***
  - ***Channeled slides***
  - ***Confined slides***

Rock avalanches/long-runout landslides (cont'd)

- **Hazard potential**
  - ***Destruction/burial of downslope areas***
  - ***Catastrophic displacement of water in reservoirs and other bodies of water***
  - ***Damming of rivers and catastrophic breaching***

Typical landslide with μ=0.64

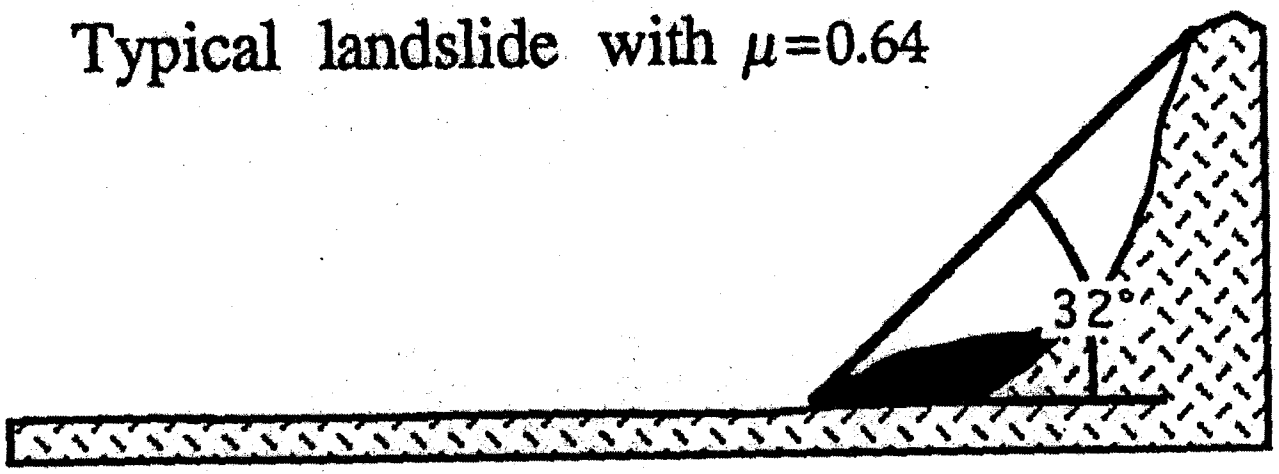

Long runout landslide with μ=0.13

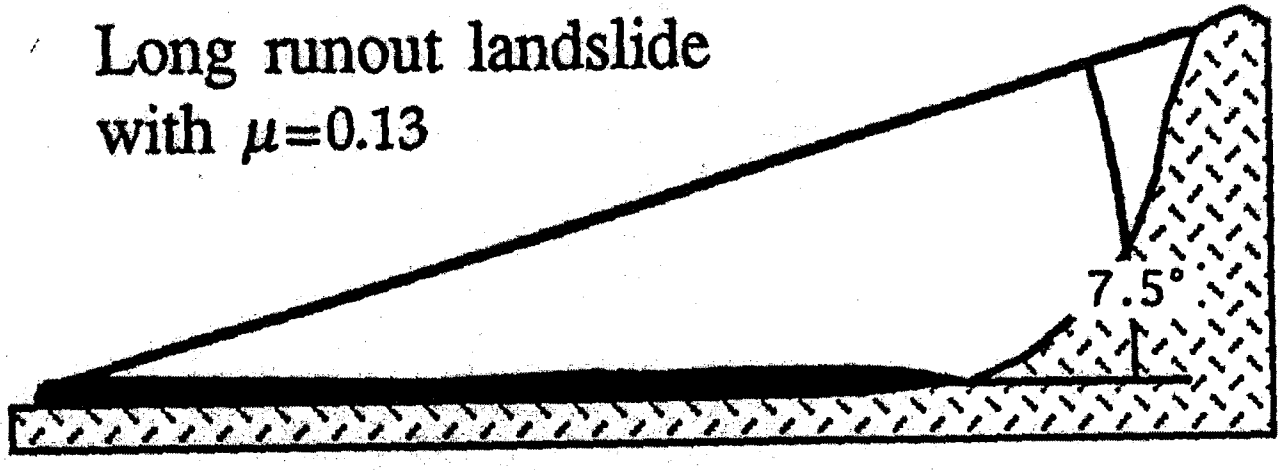

South Coast Geological Society, 1996

Blackhawk Landslide, CA

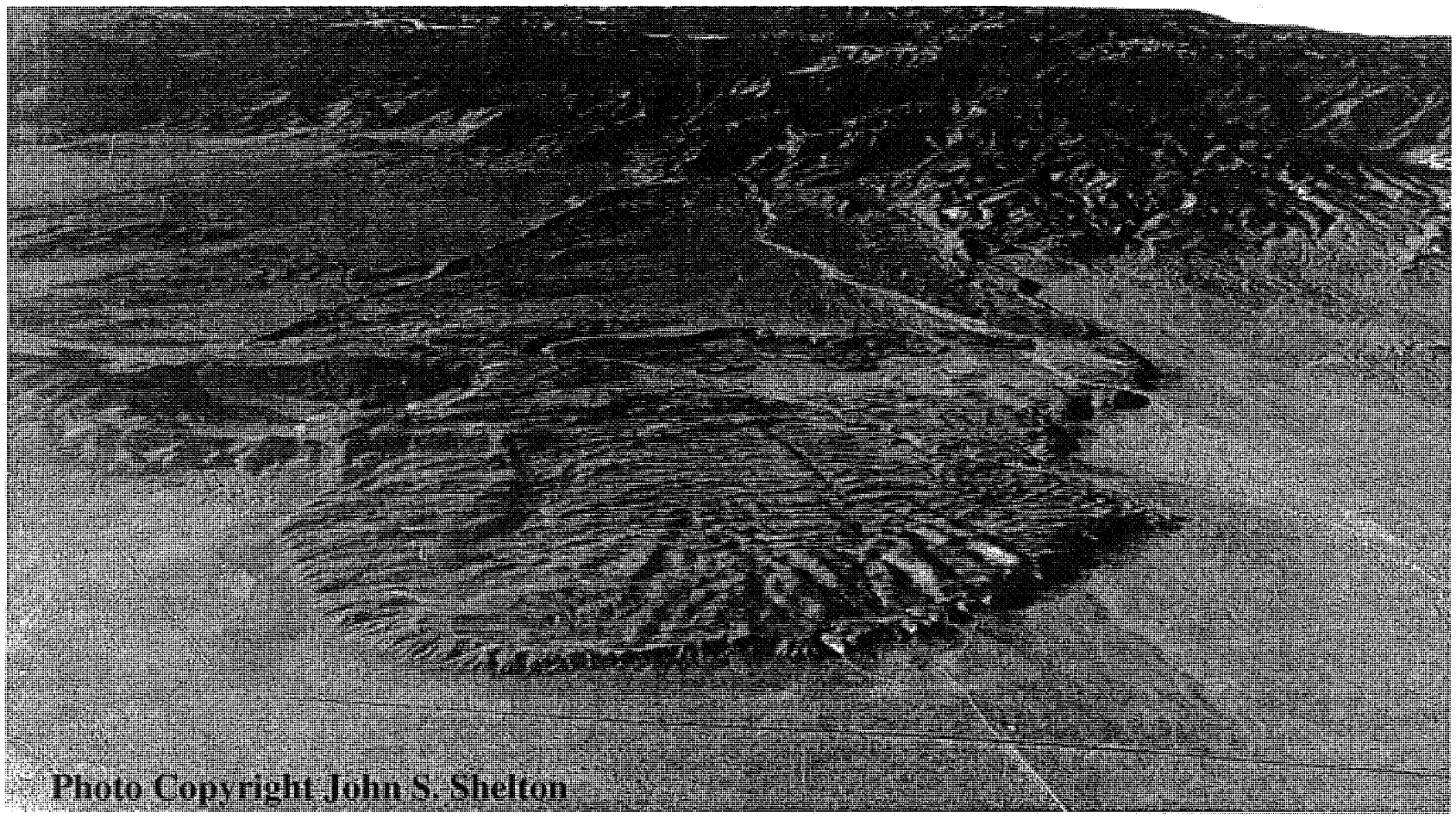

Martinez Mountain Rock Avalanche, CA

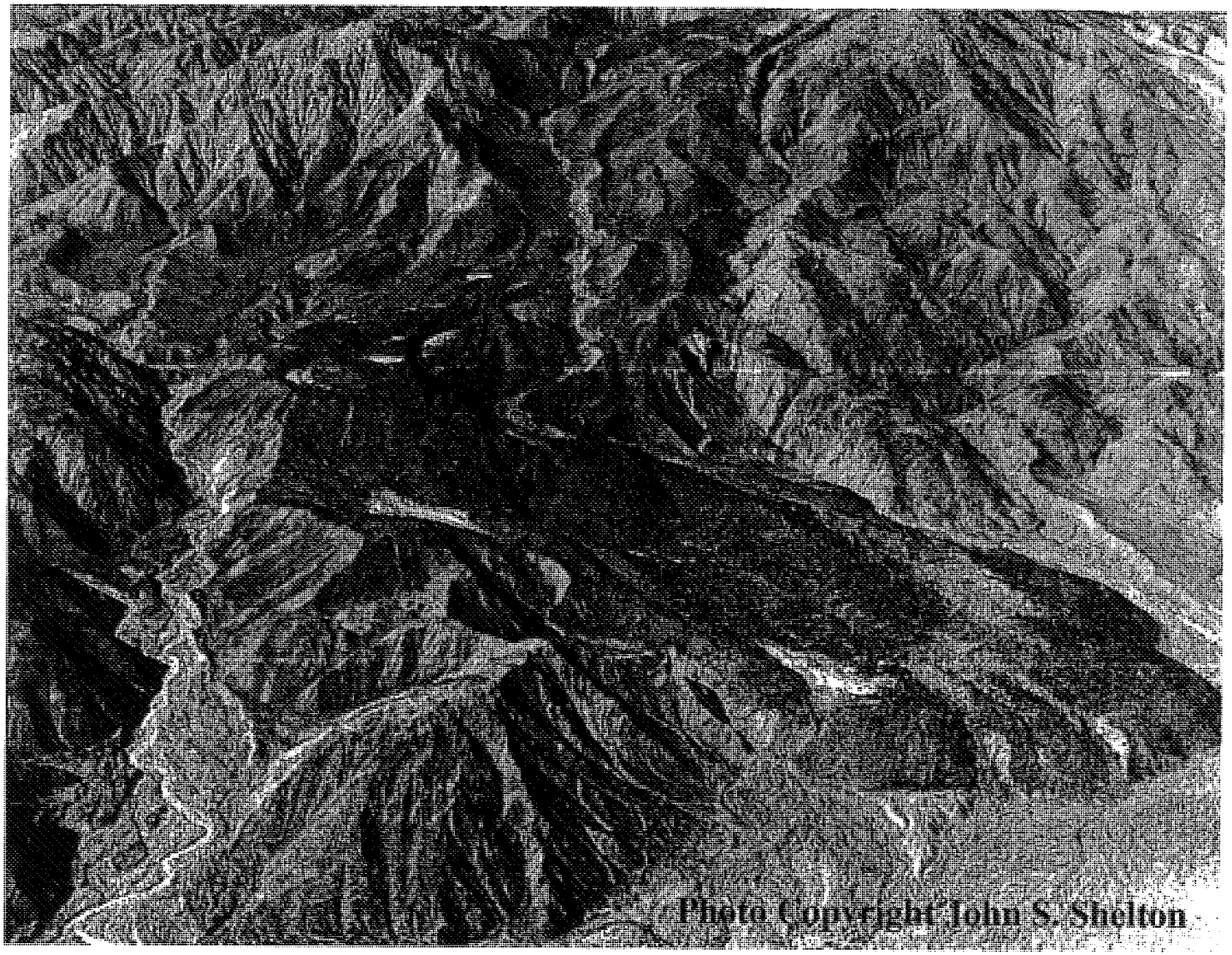

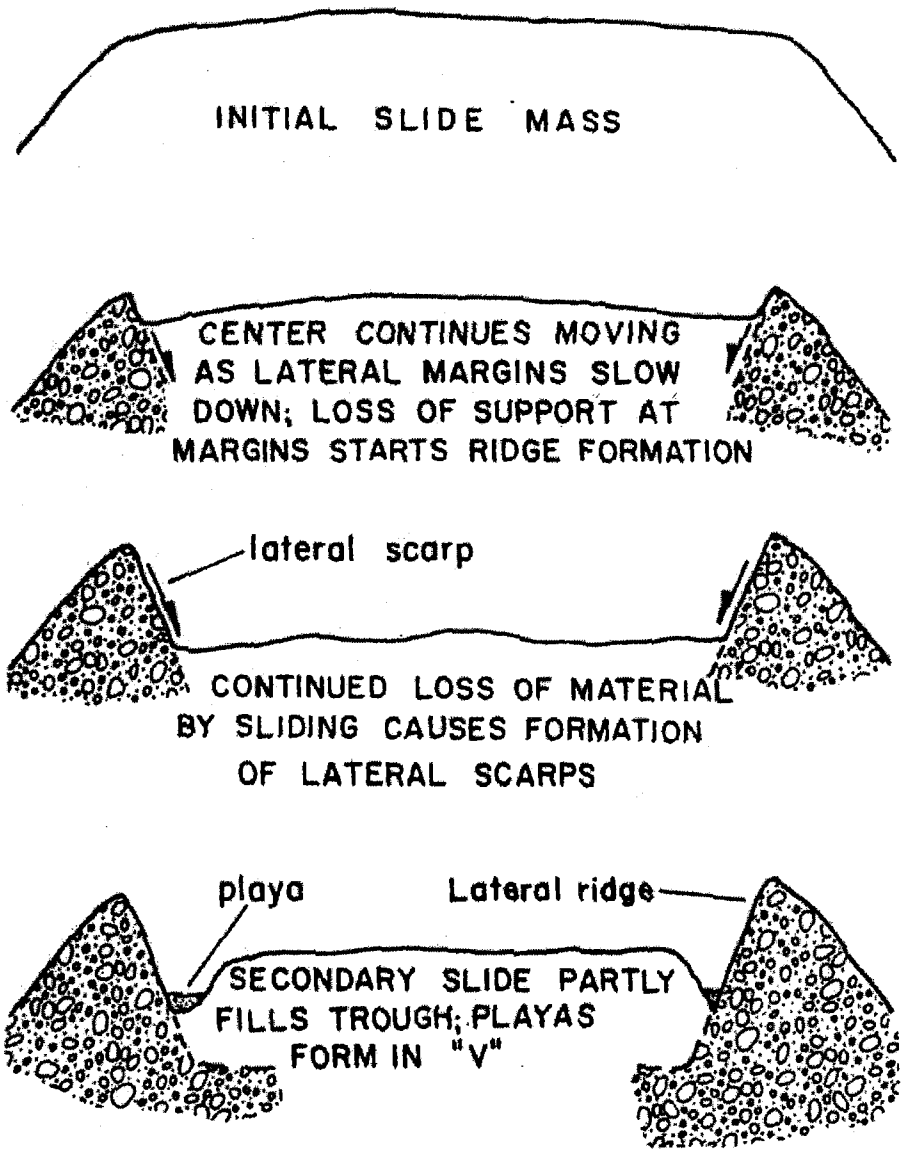

Figure 15. Diagrammatic sections transverse to slide axis, showing formation of lateral ridges.

Bock, 1977

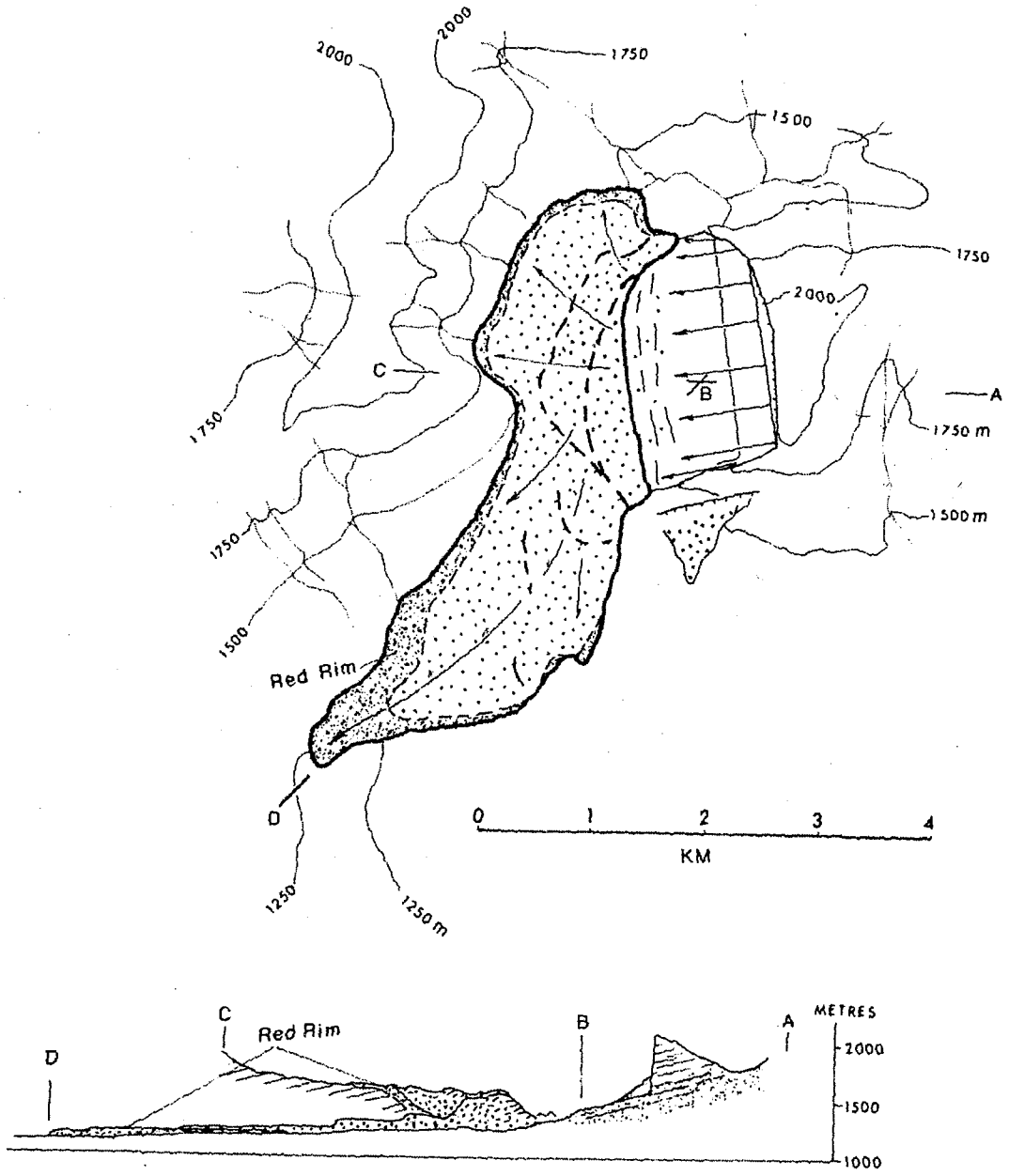

Eisbacher, 1979

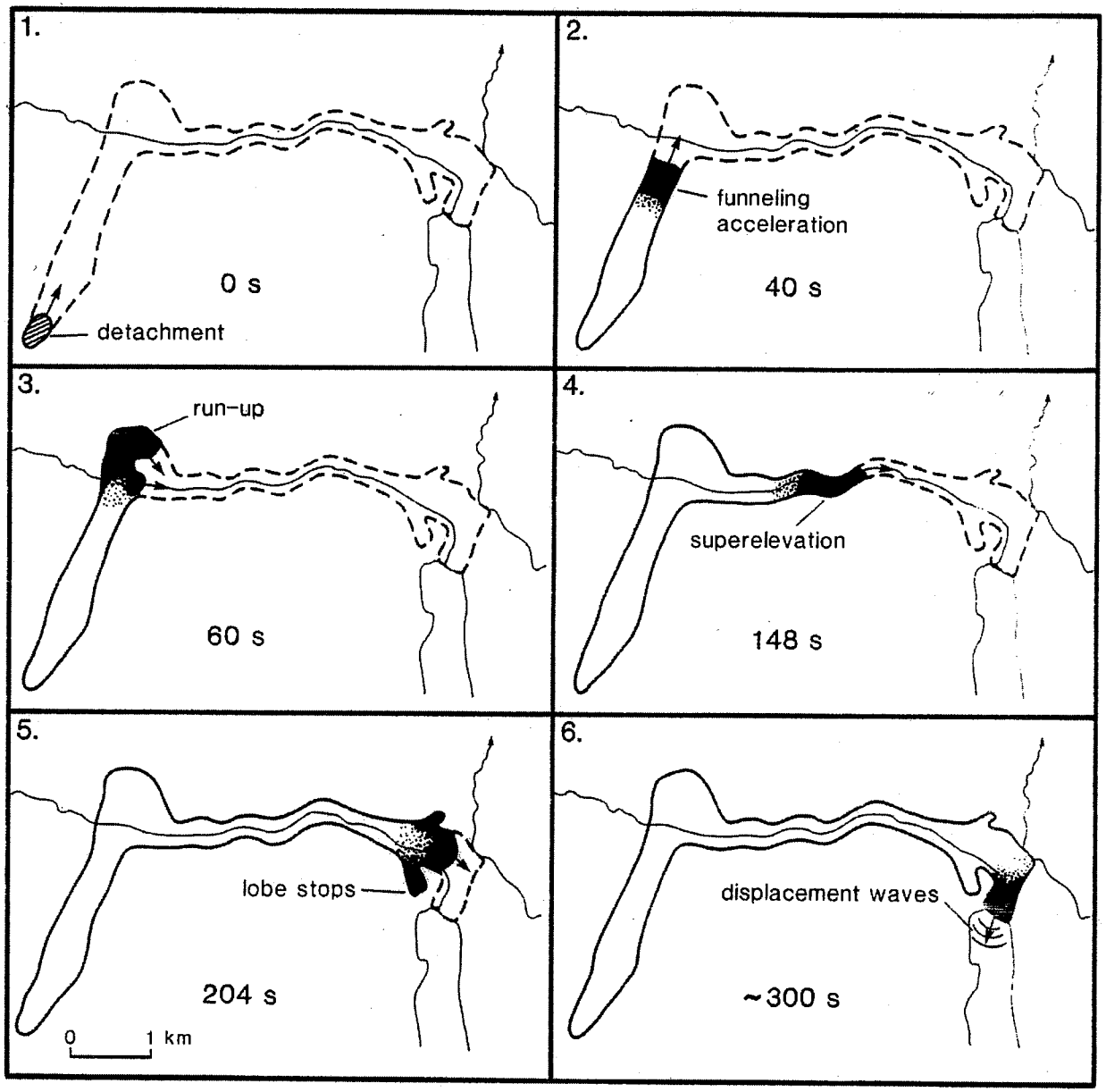

Evans et al, 1989

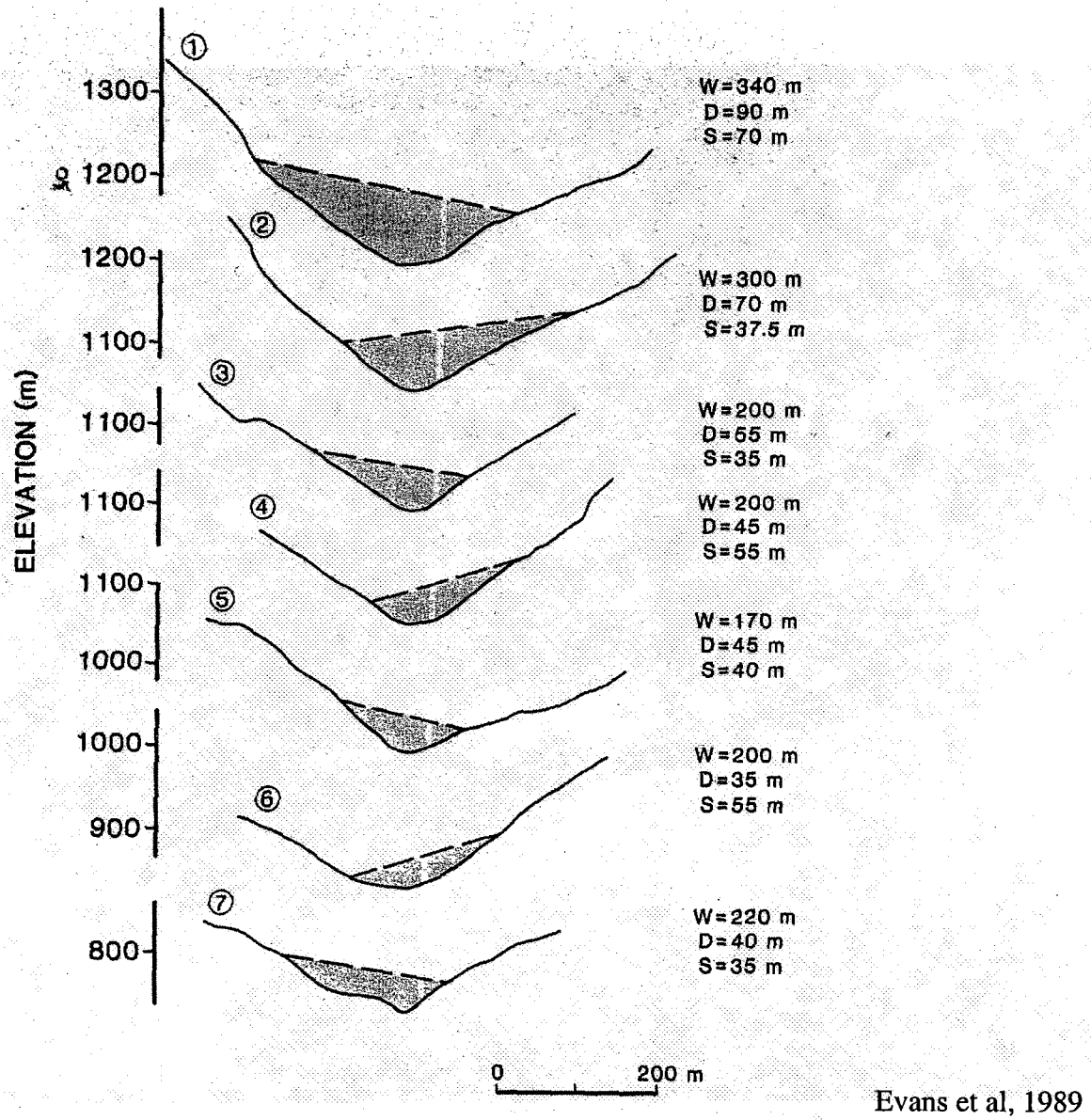

Evans et al, 1989

Vaiont Landslide, Italy

Mueller, 1964

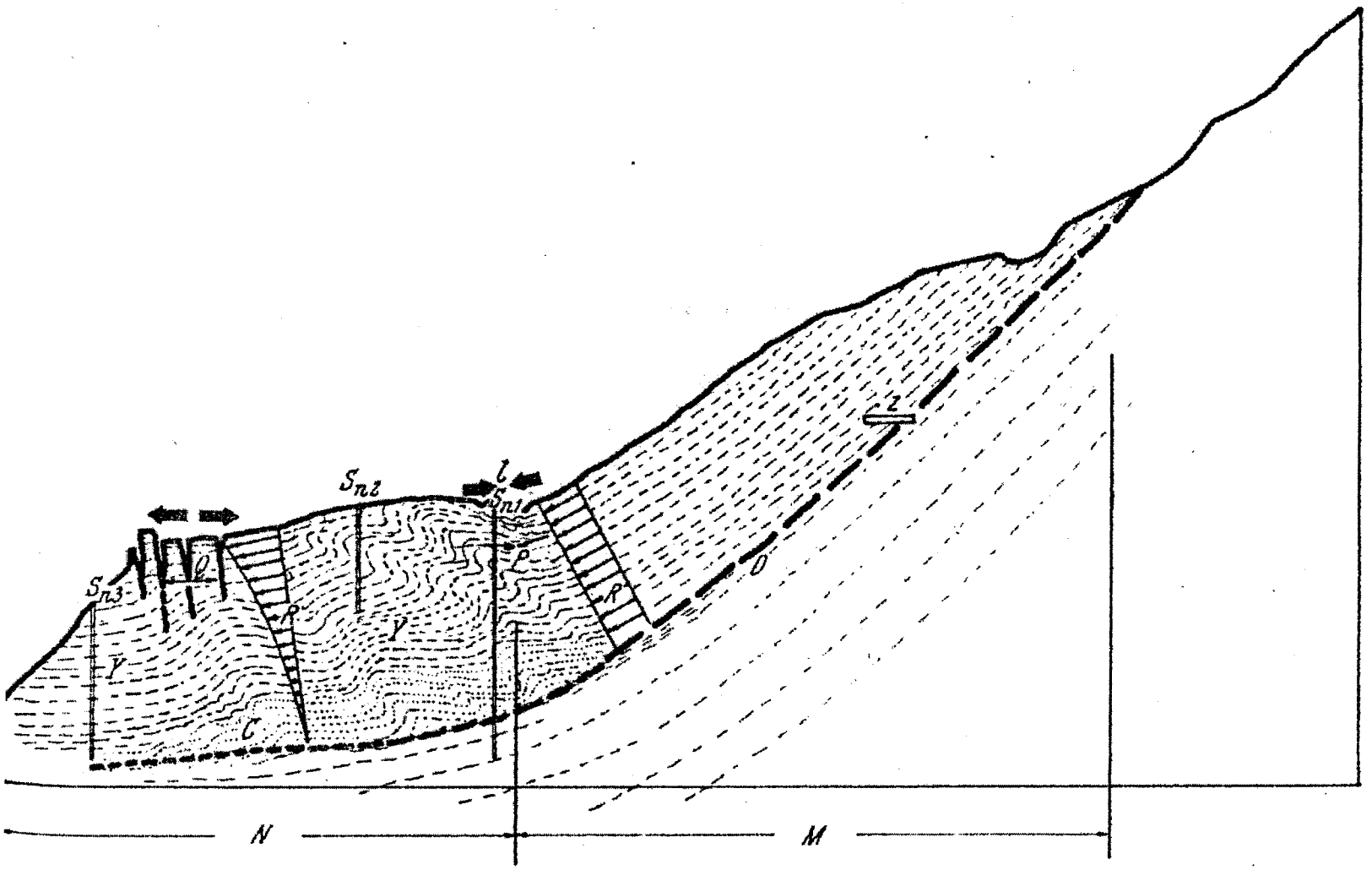

Fig. 16. Outlined section through the west zone of the slide. The arrows indicate the velocity distribution

Mueller, 1964

Plafker, 1992

Slow-Moving Landslides

Primarily in cohesive materials

- Slumps
- Earthflows
- Block slides

Slumps

Blackfoot River, Montana, 1998

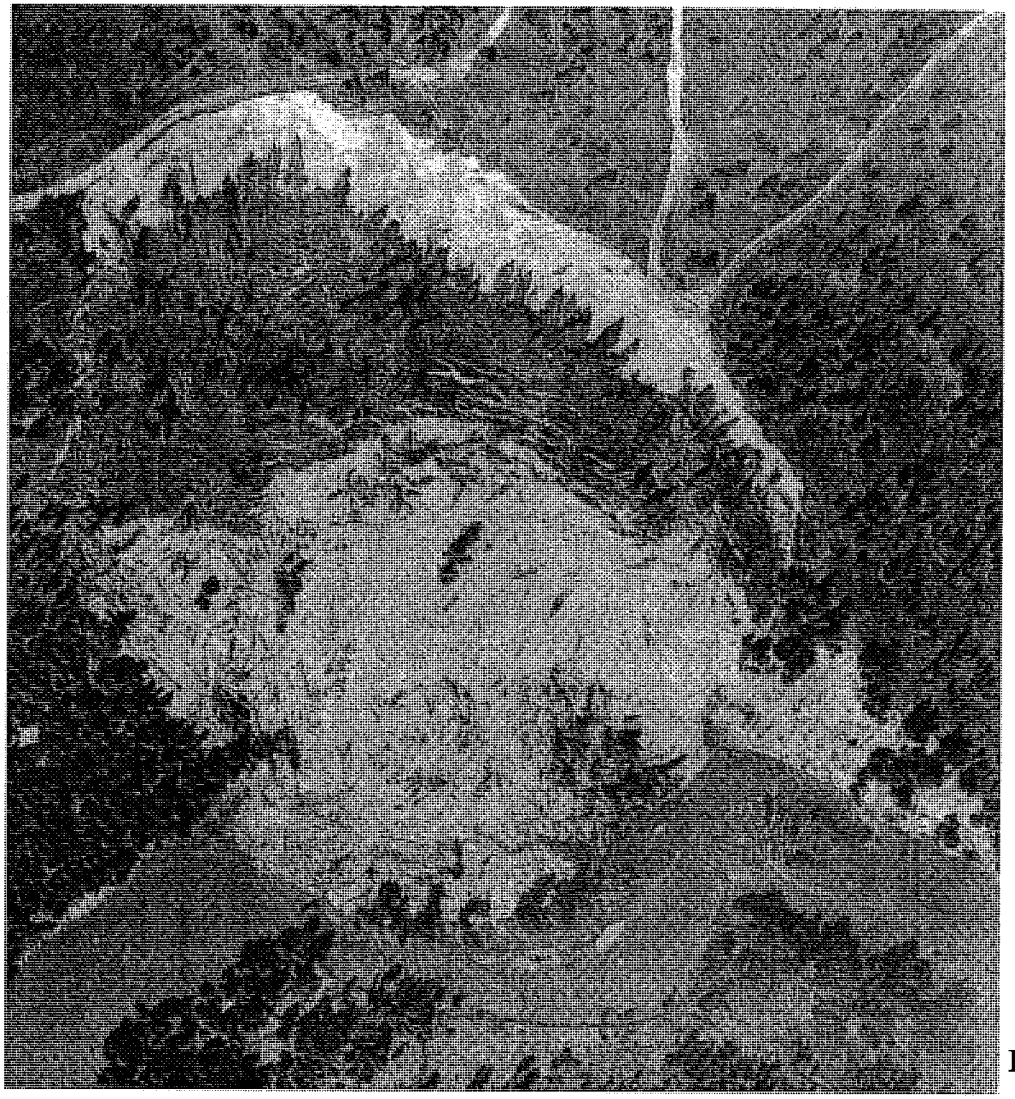

Hyndman and Brown, 2000

Fig. 4. Back tilt of the originally horizontal upper terrace of the slide. Head scarp is on the right. Note person standing at left.

Hyndman and Brown, 2000

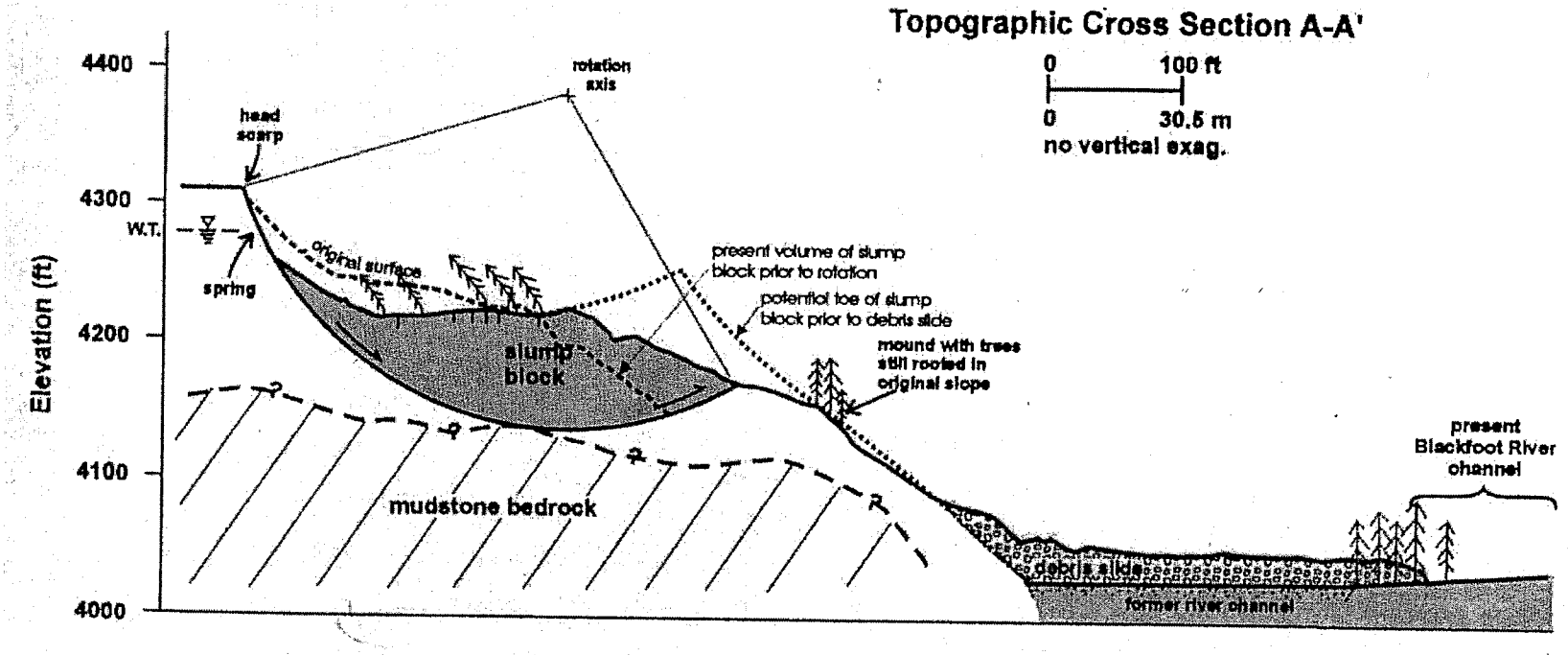

Fig. 3. Cross section through the central part of the slump block and debris slide.

Hyndman and Brown, 2000

Earthflows

Southern Australia

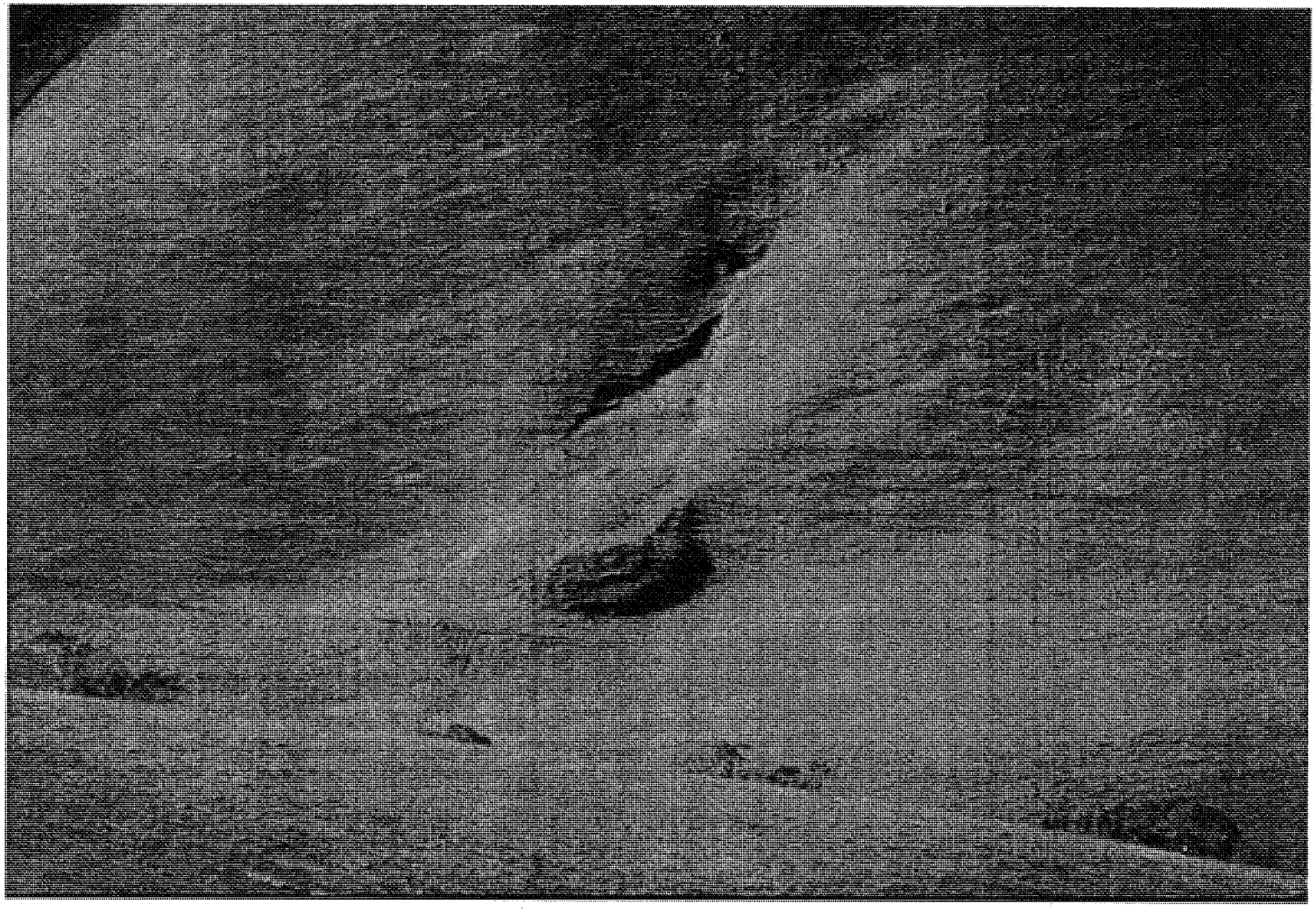

NOAA

Block/Translational Landslides

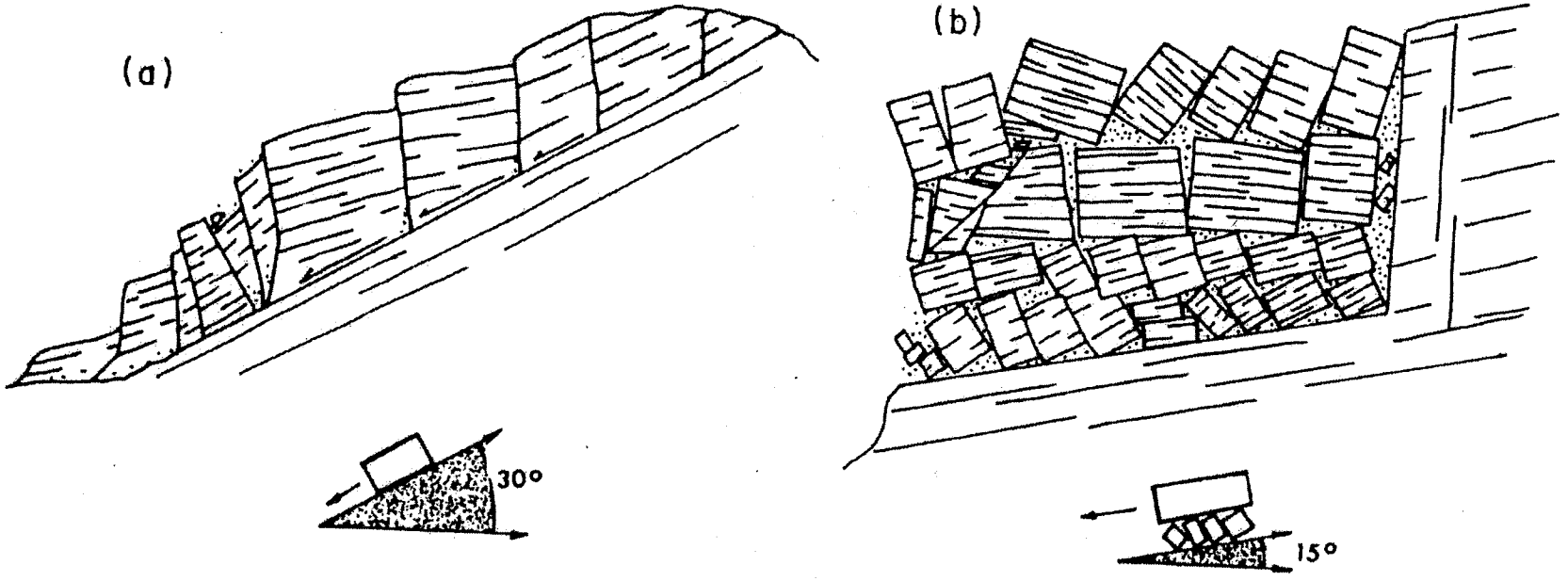

Eisbacher, 1979

Morning Sun Avenue Landslide, Diamond Bar, CA, 1995

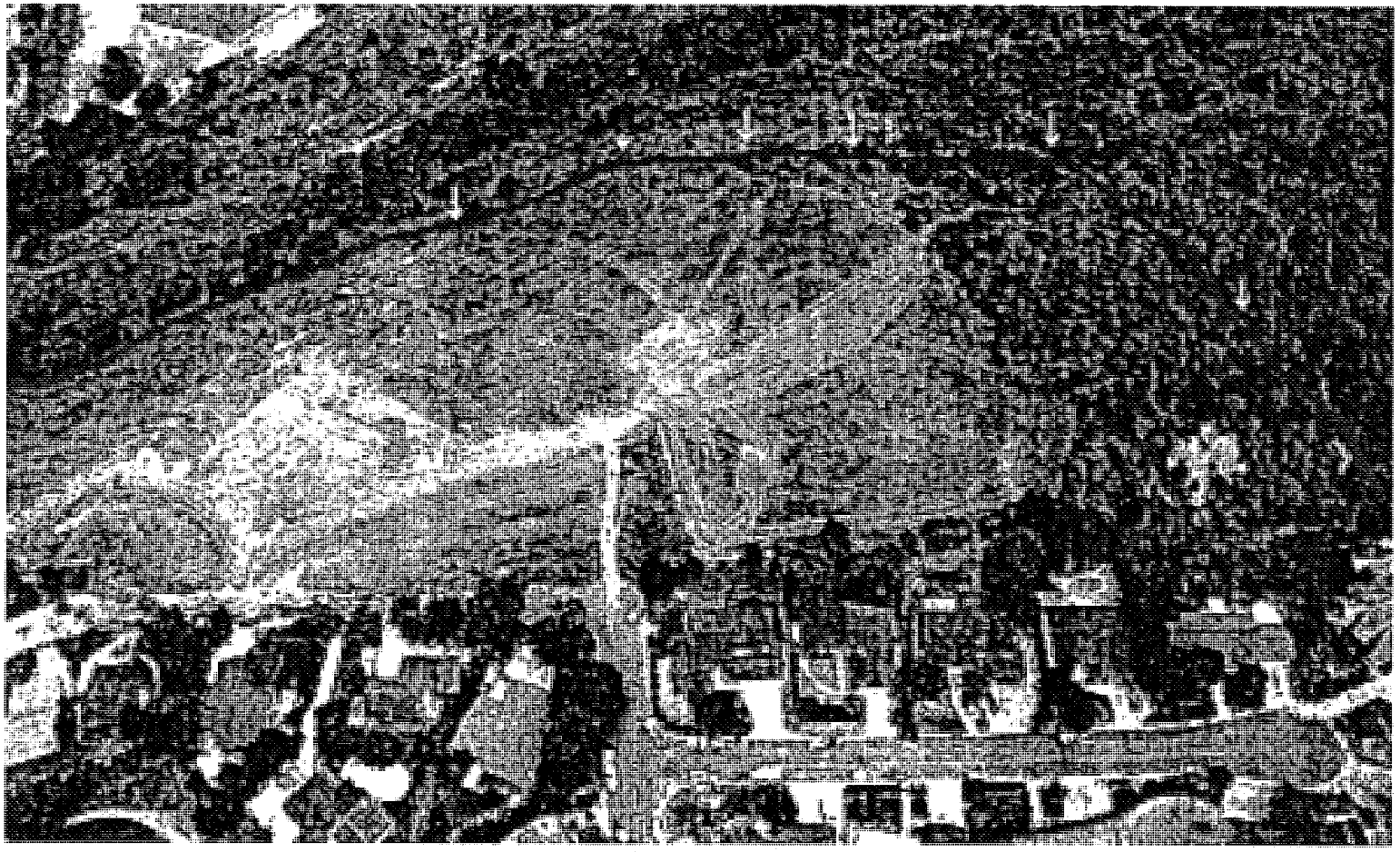

Harp et al, 1995

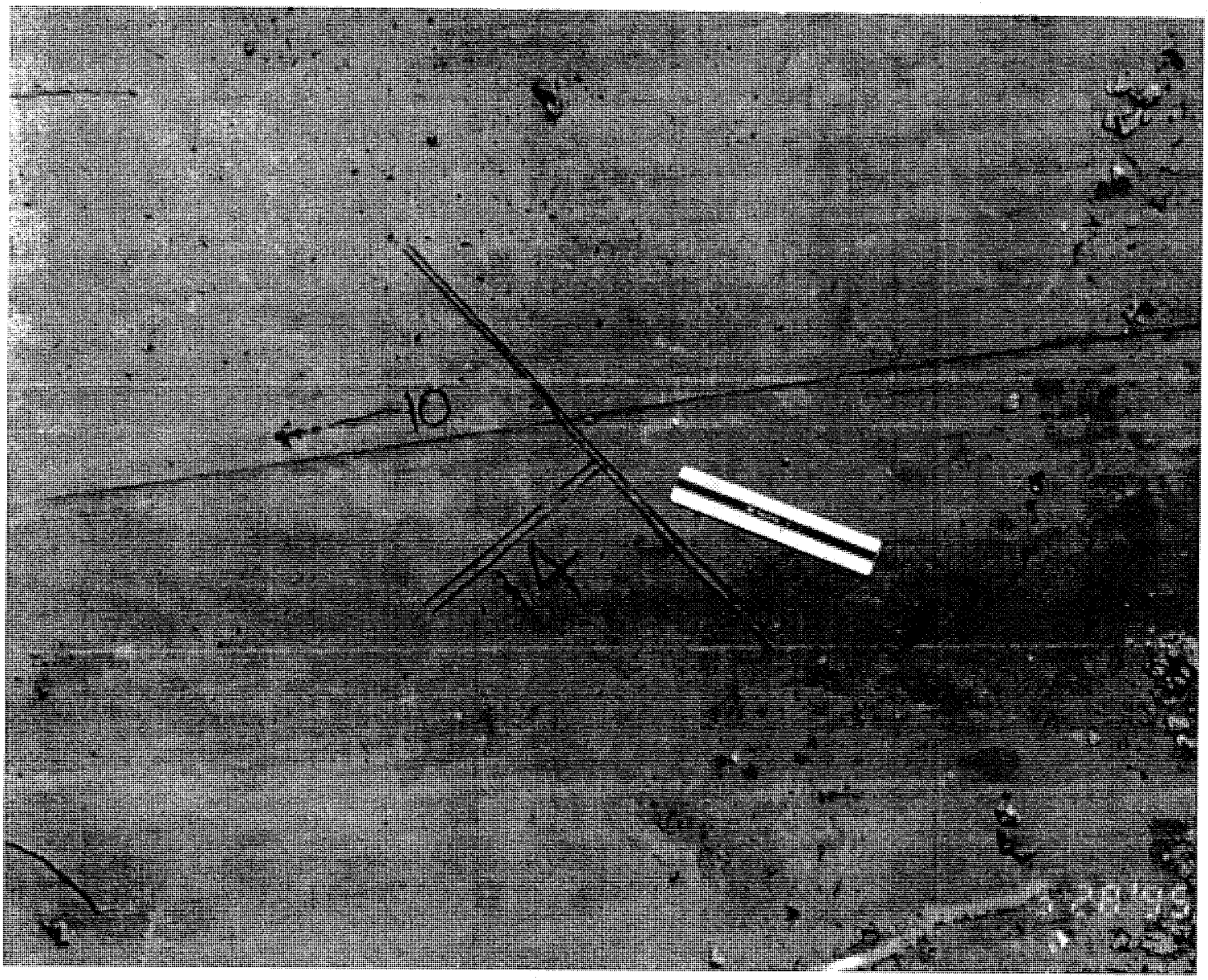
10

ESTIMATING MATERIAL STRENGTHS AND STABILITY;

MASS WASTING POTENTIALS OF EARTH MATERIALS

Bulk Strength Properties

Very weak materials (minimal stability)

- Existing landslide masses
- Loose, granular soil, including volcanic ash
- Thick, clayey soil
- Fault breccia
- Lake deposits/marl
- Mine tailings

Mine Tip Landslide
British Columbia, Canada

Hungr and Kent, 1995

Very weak materials (cont'd)

- Alteration zones
- Volcanic ash
- Loess
- Salt
- Coal
- Permafrost
- Marine or glacial clays

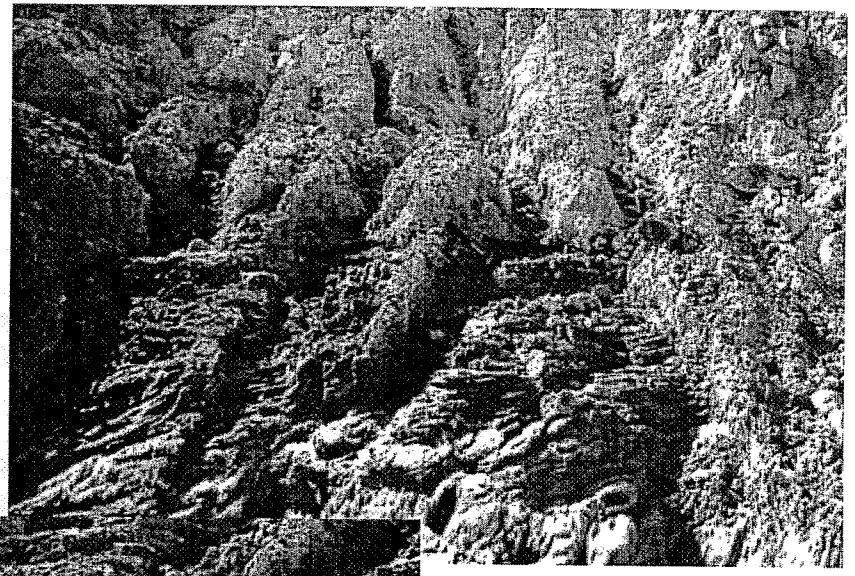

Shear

The Getty Center, Los Angeles

Glacial Clay

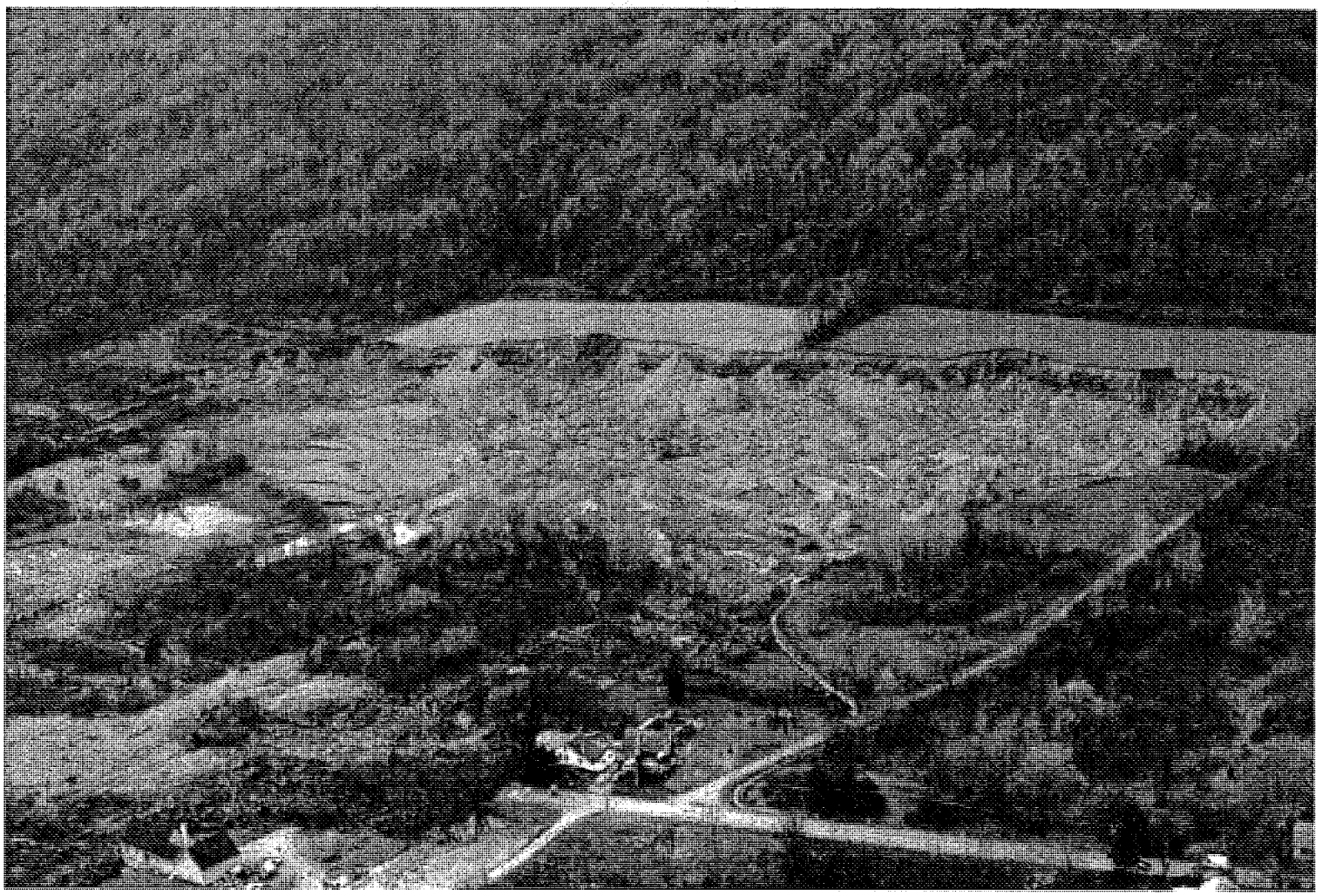

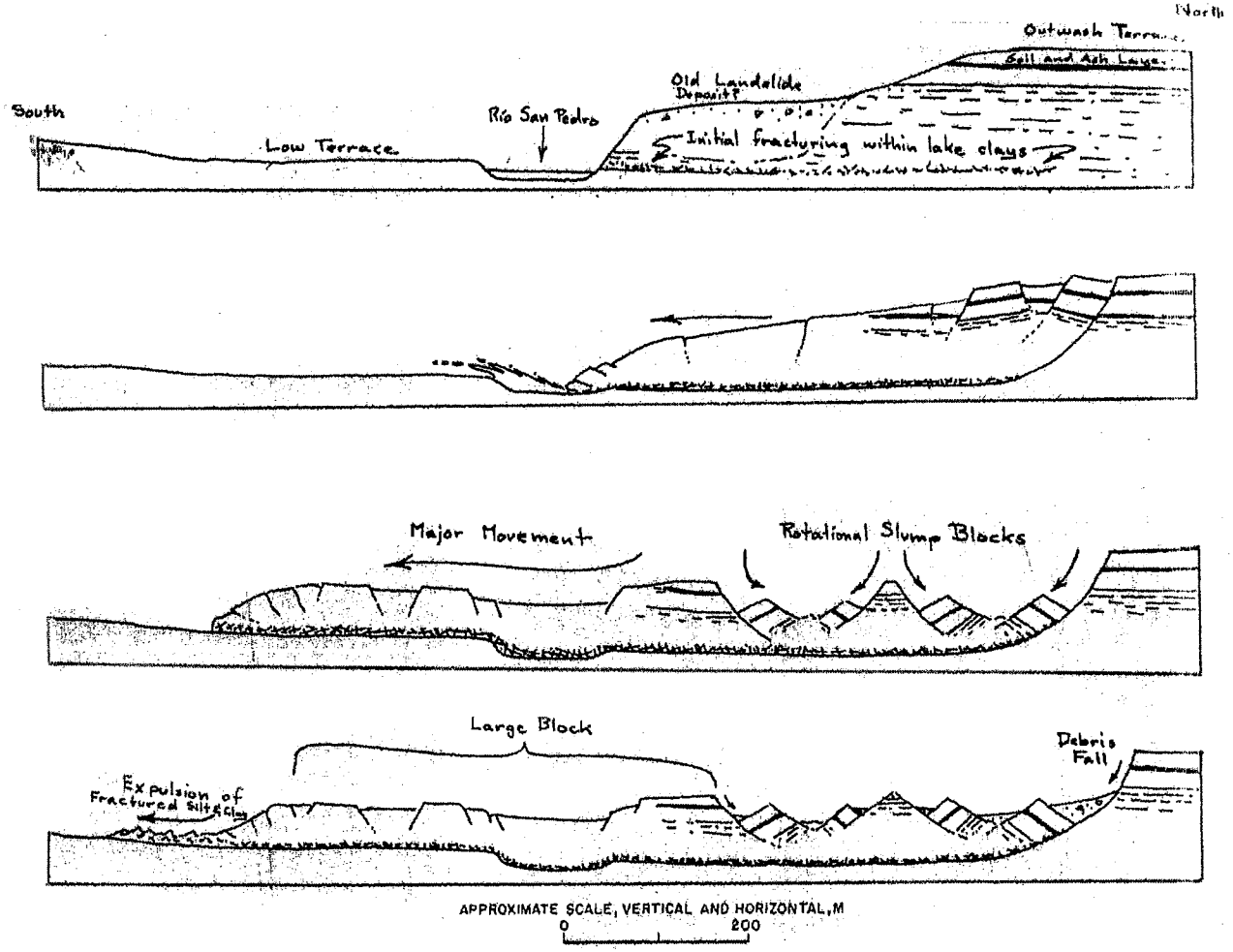

Davis and Karzulovic, 1963

Very weak materials (cont'd)

- Uncontrolled fill
- Soil containing animal burrows
- Bentonite

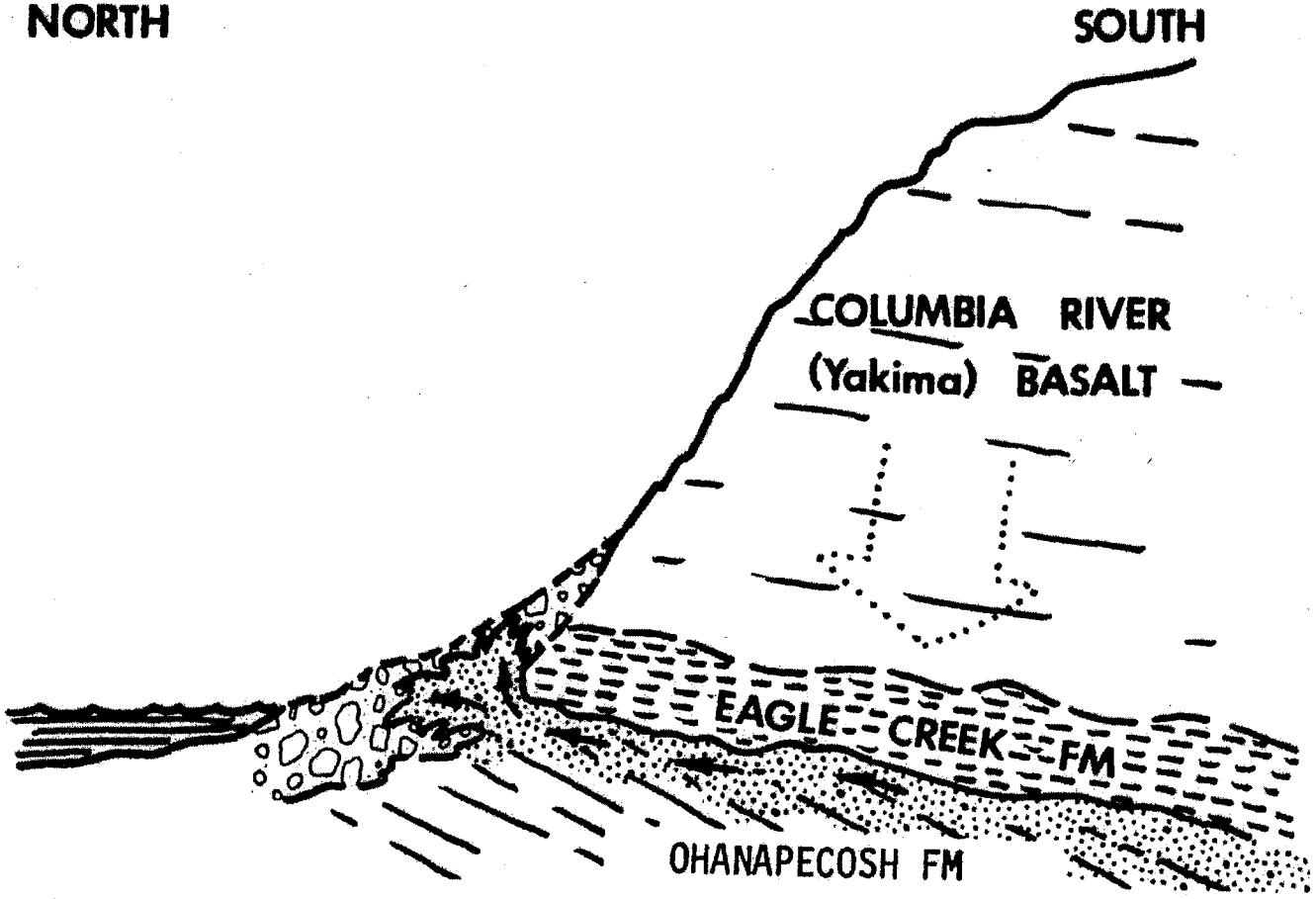

Figure 15. Diagrammatic representation of Waters's (1973) proposed "hydraulic ram" mechanism for some Oregon shore landslides.

Palmer, 1977

Weak materials (fair to good slope stability; susceptible to erosion)

- Shales and claystones
- Thin-bedded rock with adversely dipping bedding
- Serpentinite
- Alluvium
- Fill

Weak materials (fair to good slope stability; susceptible to erosion)

- Massive rock with adversely dipping joint sets
- Block-in-matrix rocks

Shattered Ridge

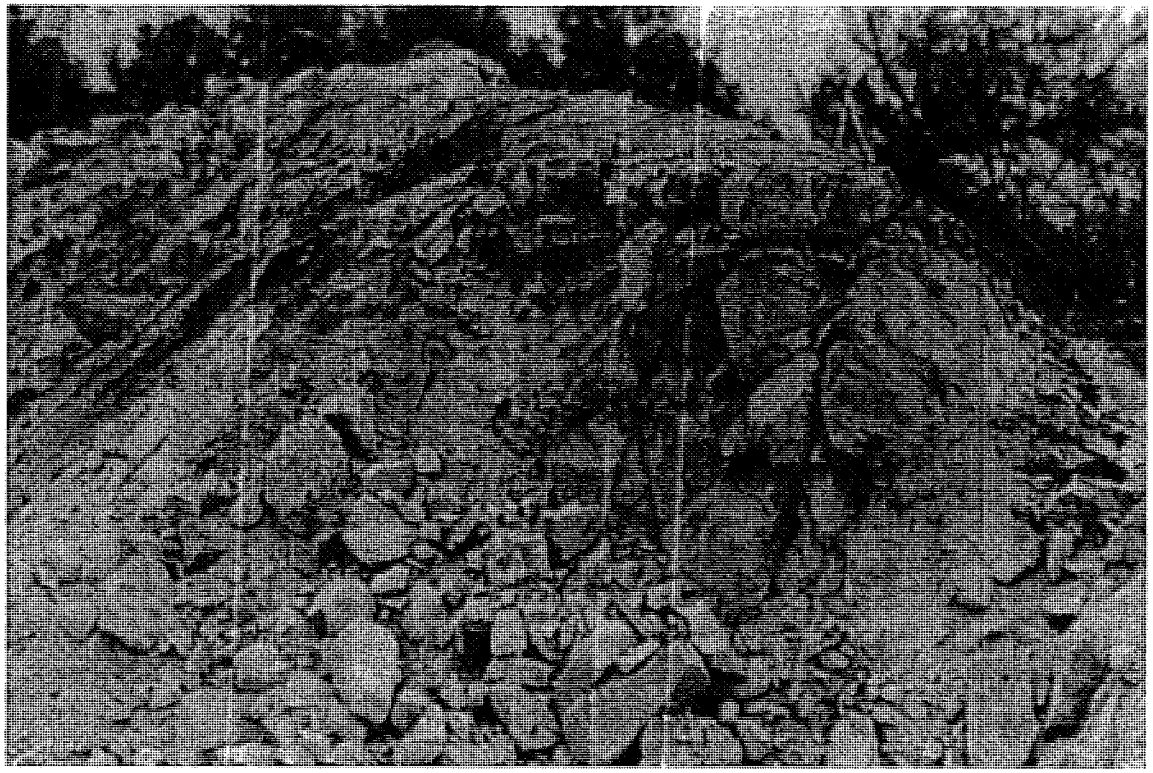

The Getty Center, Los Angeles

17 January 1994

Moderately strong materials (very good slope stability; mild susceptibility to erosion)

- Sandstone
- Weathered/fractured igneous and metamorphic rocks

Three Patriarchs
Zion National Park, Utah

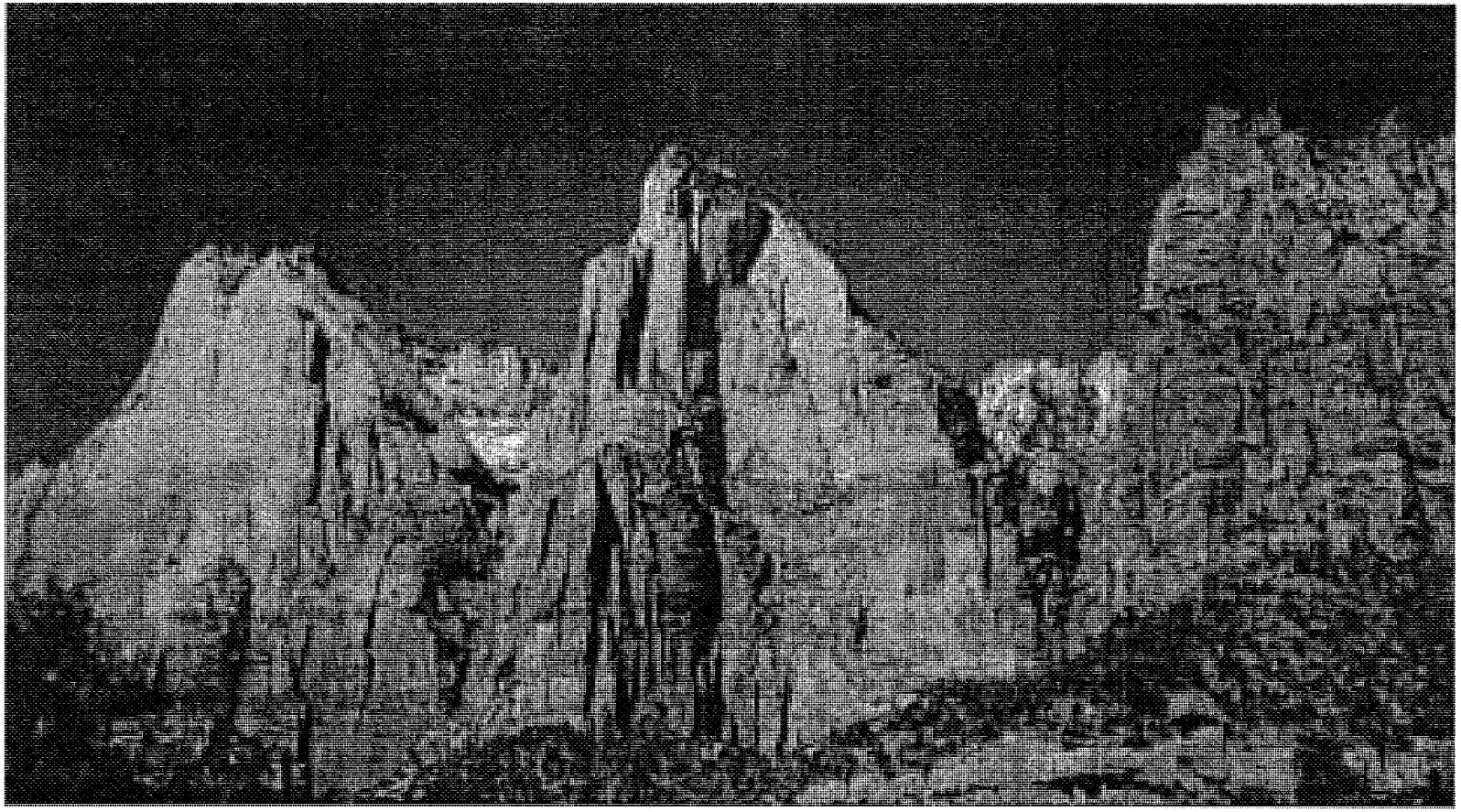

Navajo Sandstone

http://walking.about.com/library/weekly/aa101999.htm

Strong (generally excellent stability)

- Limestone (desert climate)
- Fresh intrusive and metamorphic rocks
- Quartzite
- Conglomerate
- Strong volcanic rock
  - *Basalt*
  - *Welded tuff*

Guadalupe Peak, Texas

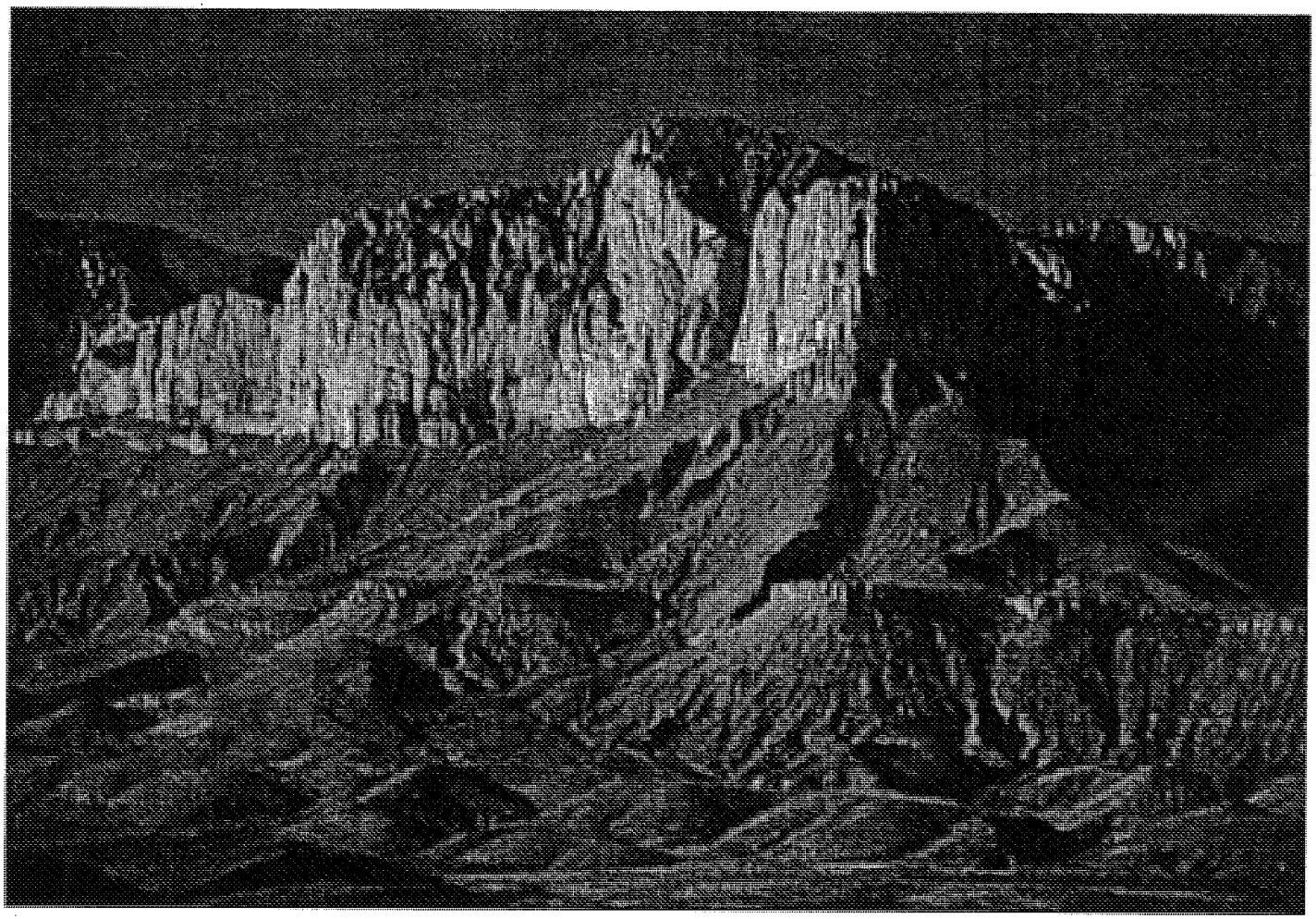

Remnants of Permian Reef Complex UTPB, 2001

Character of Discontinuities

Character of Discontinuities

- Orientation
- Geometry of intersecting surfaces
  - Formation of wedge geometry
  - Slip surface + surface of release
- Spacing between discontinuities (one surface or many parallel surfaces?)

Character of Discontinuities (cont'd)

- **Continuity**
  - **Length (of individual discontinuities)**
  - **Geometry (does a surface retain the same geometry over a significant distance?)**

Character of Discontinuities (cont'd)

- **General Character**
  - **Wavy**
  - **Planar**
  - **Irregular**

Character of Discontinuities (cont'd)

- **Width of opening**
- **Type of Infilling**
  1. **Weak (clay)**
  2. **Strong (cementing agent)**

Fractures – Glacier Point, Yosemite

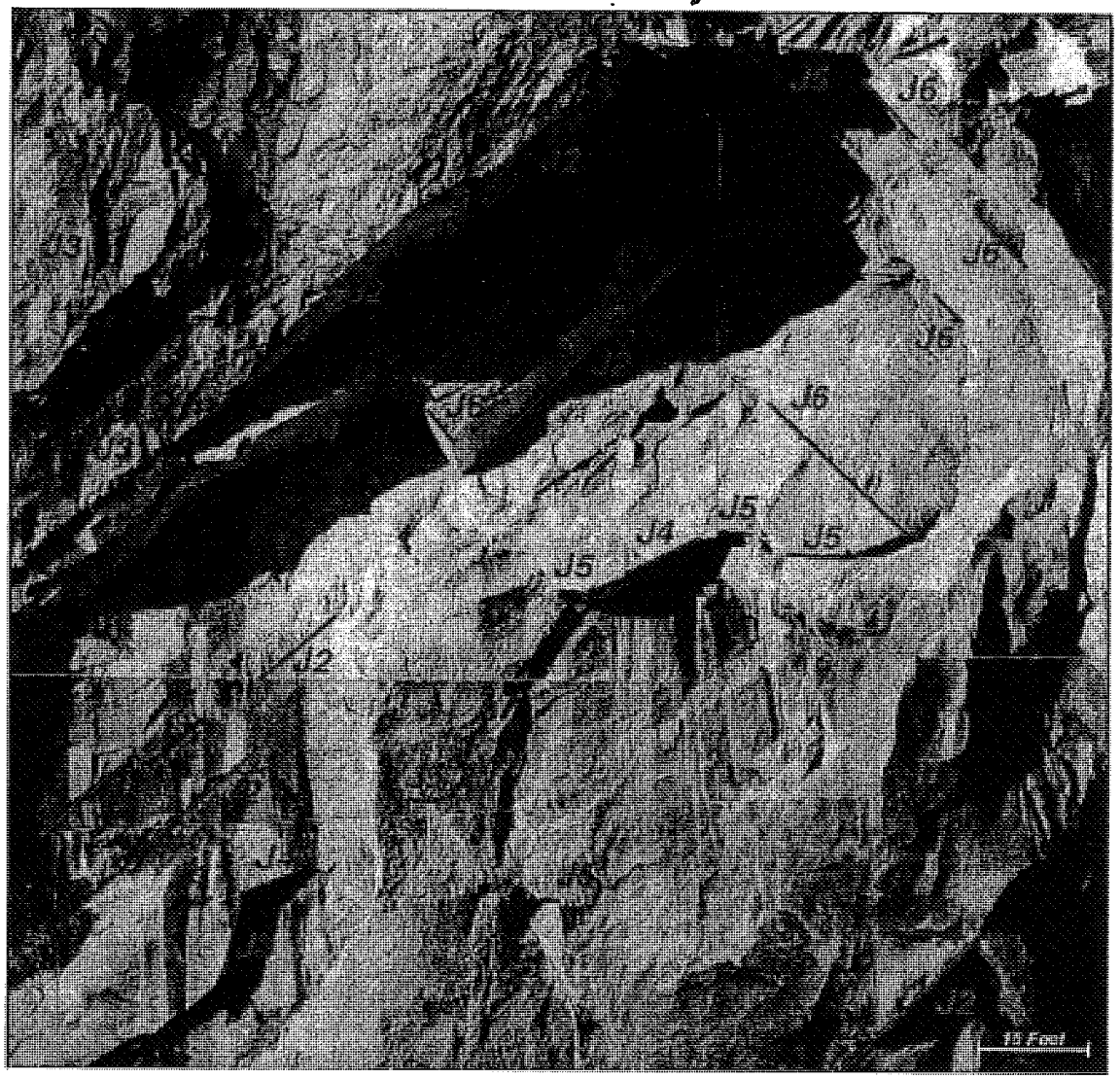

Wieczorek and Snyder, 1999

SUMMARY

- **Stability characteristics of rock and soil depend on their geologic origins and histories**
- **Discontinuities govern strengths of many materials**
- **Slope characterization requires geologic input**

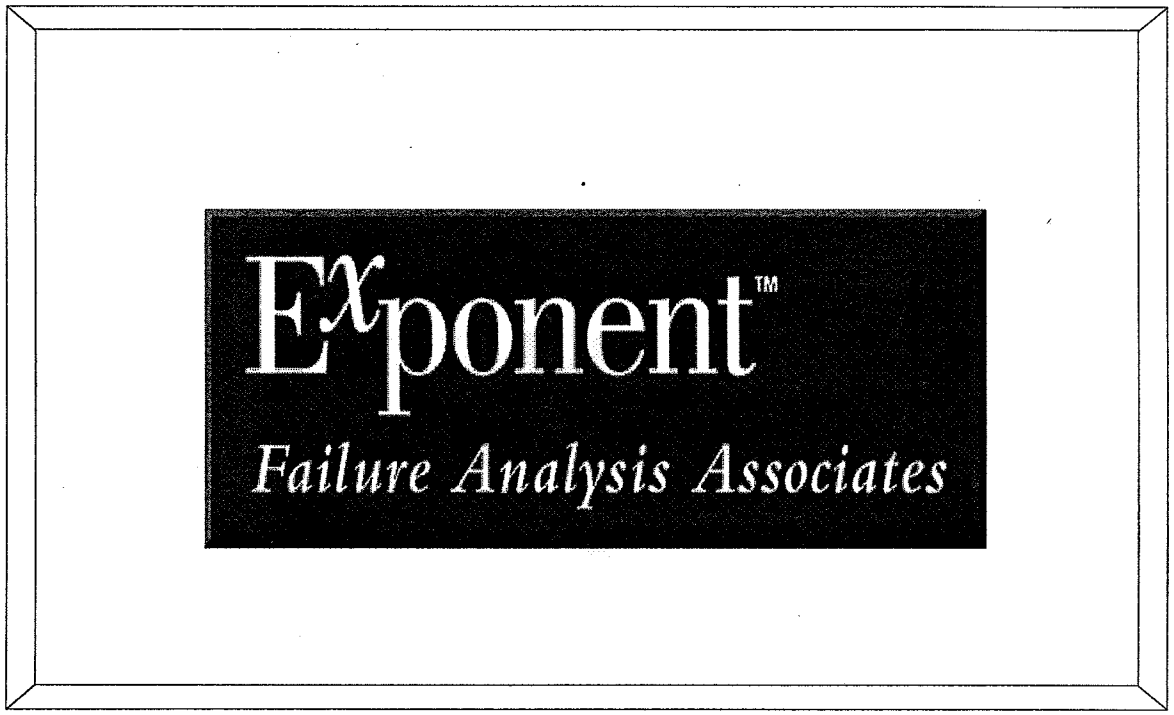
Exponent™
Failure Analysis Associates

Analysis of a large moist landslide, Lost River Range, Idaho, U.S.A.

PHILIP J. SHALLER

California Institute of Technology, Division of Geological and Planetary Sciences, Mail Stop 170-25, Pasadena, CA 91125, U.S.A.

Received July 12, 1990

Accepted March 27, 1991

This paper describes the regional geology, dimensions, morphology, sedimentology, and age relations of the Holocene "Carlson landslide," a large moist landslide composed of basalt breccia located on the eastern margin of the Lost River Range, Idaho. These data are combined to deduce the factors that prompted the slope failure, the kinematics of initiation, travel, and stopping of the landslide, as well as its postemplacement degradation. The landslide is compared with other terrestrial mass movements on the basis of morphology, sedimentology, log(volume) versus fall height – runout length (H/L) relations and estimated Bingham plastic yield strength. Morphology and sedimentology distinguish dry landslides from moist and water-saturated deposits. However, moist and water-saturated landslides plot well within the log(volume) versus H/L envelope for dry terrestrial landslides and exhibit overlapping ranges of estimated Bingham plastic yield strength values with dry landslides, indicating that moist and water-saturated landslides must travel much like dry rock avalanches of similar volume. Thus the mechanism(s) responsible for causing anomalous runout in large dry landslides could operate in moist and water-saturated landslides as well. Morphological comparison of the Carlson landslide with lobate martian landslides suggests a role for water in the martian landslides.

Key words: landslides, debris flows, long runout, morphology, water, Mars.

Cet article décrit les relations de géologie régionale, de dimensions, de morphologie, de sédimentologie et d'âge du glissement Carlson de l'Holocène, qui est un glissement humide de grandes dimensions composé de basalt bréchifié localisé sur le versant est de la Chaîne de montagnes de Lost River, Idaho. Ces données sont combinées pour déduire les facteurs qui ont produit la rupture du glissement, la cinématique du déclenchement, le parcours et l'arrêt du glissement, de même que sa dégradation en place. Le glissement est comparé à d'autres mouvements terrestres de massifs sur la base de la morphologie, de la sédimentologie, des relations de log(volume) versus hauteur de chute – longueur de parcours (H/L) et de la limite de la résistance plastique estimée de Bingham. La morphologie et la sédimentologie différencient les glissements secs de ceux dans les dépôts humides ou saturés. Cependant, les glissements humides et saturés se situent bien dans l'enveloppe log(volume) versus H/L pour les glissements terrestres secs, et chevauchent les plages des valeurs estimées de la limite de la résistance plastique de Bingham pour les glissements secs, ce qui indique que les glissements humides ou saturés d'eau doivent voyager tout à fait comme les avalanches de roche sèches de volume comparable. Ainsi, le ou les mécanismes responsables des parcours anormaux des glissements secs de grandes dimensions pourraient également opérer dans les glissements humides ou saturés. La comparaison morphologique du glissement de Carlson avec les glissements lobaires martiens suggère que l'eau joue un rôle dans les glissements martiens.

Mots clés : glissements, écoulements de débris, long parcours, morphologie, eau, Mars.

[Traduit par la rédaction]

Can. Geotech. J. **28**, 584–600 (1991)

Introduction

A large landslide of Holocene age lies in the upper Pahsimeroi River valley of east-central Idaho, 12 km northeast of Doublespring Pass, at latitude 44°17′N, longitude 133°44′W (Fig. 1). The landslide originated in Tertiary basalts just north of Spring Hill mountain, at the eastern edge of the Lost River Range, and traveled rapidly eastward down a preexisting drainage channel, finishing movement as a giant debris flow. The name "Carlson landslide" is suggested for the deposit because Carlson Lake occupies part of its headscarp. Shelton (1966) published an aerial photograph and brief analysis of the deposit, but no previous field studies have focused on the landslide.

This landslide was investigated as part of a larger study (Shaller 1991) of large ($>10^6$ m^3) martian and terrestrial landslides aimed at determining the role of water in the initiation and travel of large landslides on Mars and the travel mechanics of "long-runout" landslides. Hsü (1975) defined long-runout landslides as those having fall height (vertical distance from crown to toe) to travel length (horizontal distance between crown and toe) ratios of less than 0.6. Hsü (1975) defined this ratio as the "fahrböschung" after Heim (1932); in this paper Hsü's terminology is shortened to H/L. This particular landslide (Fig. 2) was investigated because of its similarity in scale and morphology to a pair of landslides in Mars' Candor Chasma (Fig. 3) (Shaller 1991). Past arguments for and against water in the martian landslides have used morphologies, log(volume) versus H/L relations, Bingham plastic yield strength estimates, and velocities to compare martian landslides with terrestrial mass movements (Lucchitta 1978, 1987; McEwen 1989). These studies have led to contradictory conclusions concerning the nature of martian landslides. Are they analogous to dry rock avalanches on Earth or did they travel in a moist (wet, but not water saturated) or water-saturated condition? The Carlson landslide was studied in an effort to evaluate these arguments, specifically how the presence of water influences the qualitative and quantitative behavior of large bedrock landslides. Study of the Carlson landslide also provides insight into the elusive mechanism responsible for long runout in large landslides.

Regional geology

The Carlson landslide appears on the 1 : 125 000 scale Borah Peak Quadrangle map of Ross (1947), and a portion of its headscarp occurs on the 1 : 62 500 scale Doublespring

Printed in Canada / Imprimé au Canada

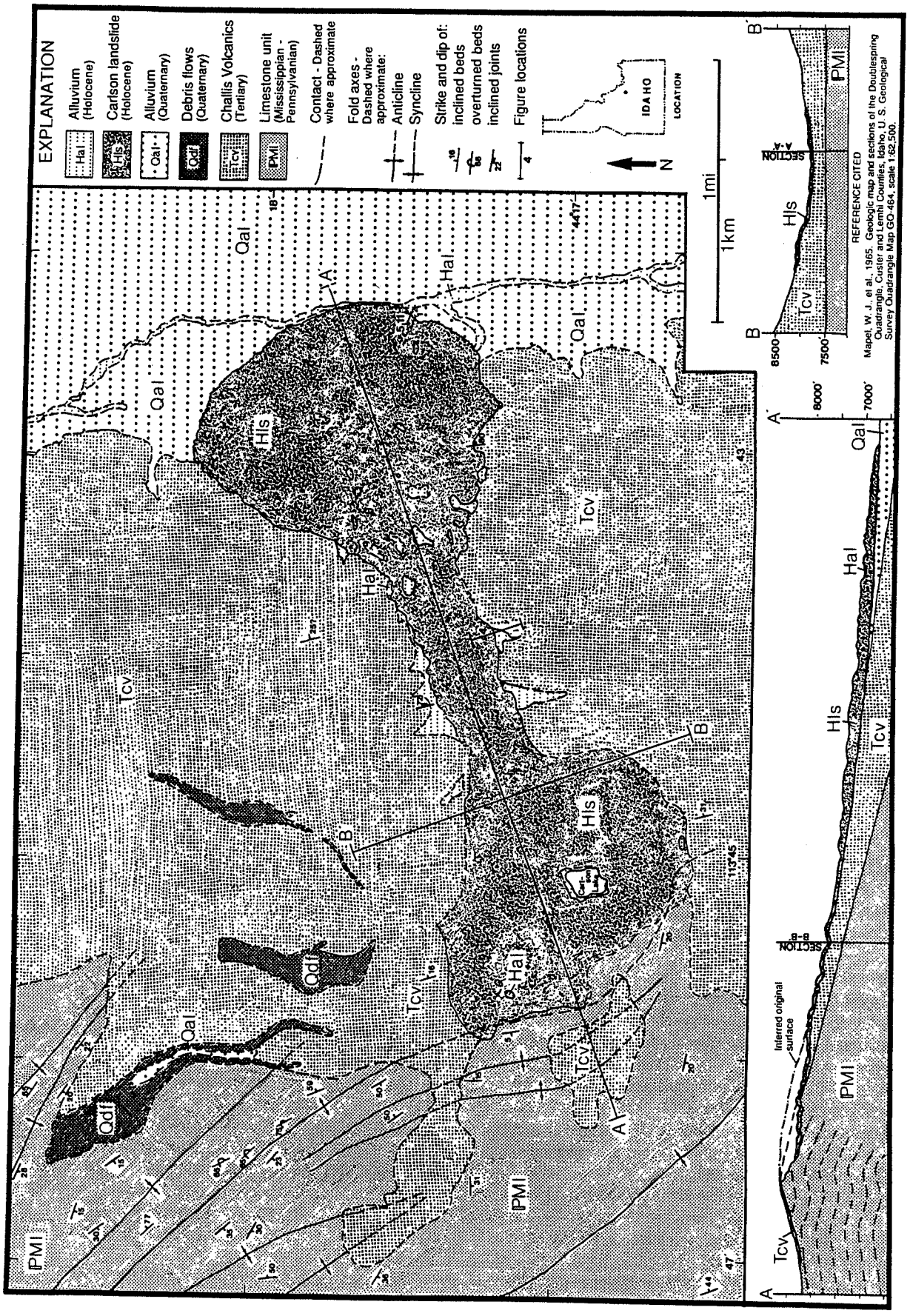

FIG. 1. Geologic map and sections of the Carlson landslide, Idaho.

FIG. 2. Vertical aerial photograph of the Carlson landslide.

Quadrangle map by Mapel *et al.* (1965). The landslide lies at the eastern edge of the northwest-striking Lost River Range, which parallels the Lemhi and Beaverhead ranges to the east. Together these ranges form an area of basin-and-range structure north of the Snake River Plain. The western margins of each range are bounded by normal faults displaying latest Quaternary activity (Scott *et al.* 1985). The Lost River fault broke most recently in the 1983 (M_s = 7.3) Borah Peak earthquake. The Lemhi fault has experienced no historic activity but does exhibit Holocene displacement (Haller 1988). The eastern borders of the Lemhi and Lost River ranges display no Quaternary faulting. The active west-side faulting and lack of east-side faulting together suggest progressive eastward tilting of the three ranges through the Quaternary (Scott *et al.* 1985).

Limestone of Mississippian to Pennsylvanian age underlies most of the central Lost River Range, except on the east where Tertiary Challis volcanics, consisting of basalt, tuff, and agglomerate deposits, overlie the limestone unit. Repeated folding of the core of the range has produced a broad anticlinal form with an axis paralleling the range. The bedrock geology in Fig. 1, borrowed from Mapel *et al.* (1965), shows that the Carlson landslide originated along the folded contact between the limestone unit and the Challis volcanics. The conspicuous terraced river channels near the toe of the Carlson landslide (Fig. 2) were probably cut by Late Pleistocene flood waters enhanced by melting headwater glaciers at the close of the Pleistocene (Ross 1947).

Physical properties of the Carlson landslide

Dimensions

The Carlson landslide measures 4400 m in length from the crown of the headscarp bowl to the tip of the toe. As determined from the movement-parallel surface lineations, the landslide traveled a total distance of 4700 m between these points, associated with a crown to toe elevation drop of 750 m. For comparison with other deposits, these values give the landslide an H/L of 0.17 for the straight-line length and 0.16 for the movement-parallel trajectory.

The headscarp bowl, the area of the landslide above the 8000 ft (1 ft = 0.3048 m) elevation contour, measures 1.88 km across at the lip of the bowl at the 8560 ft contour.

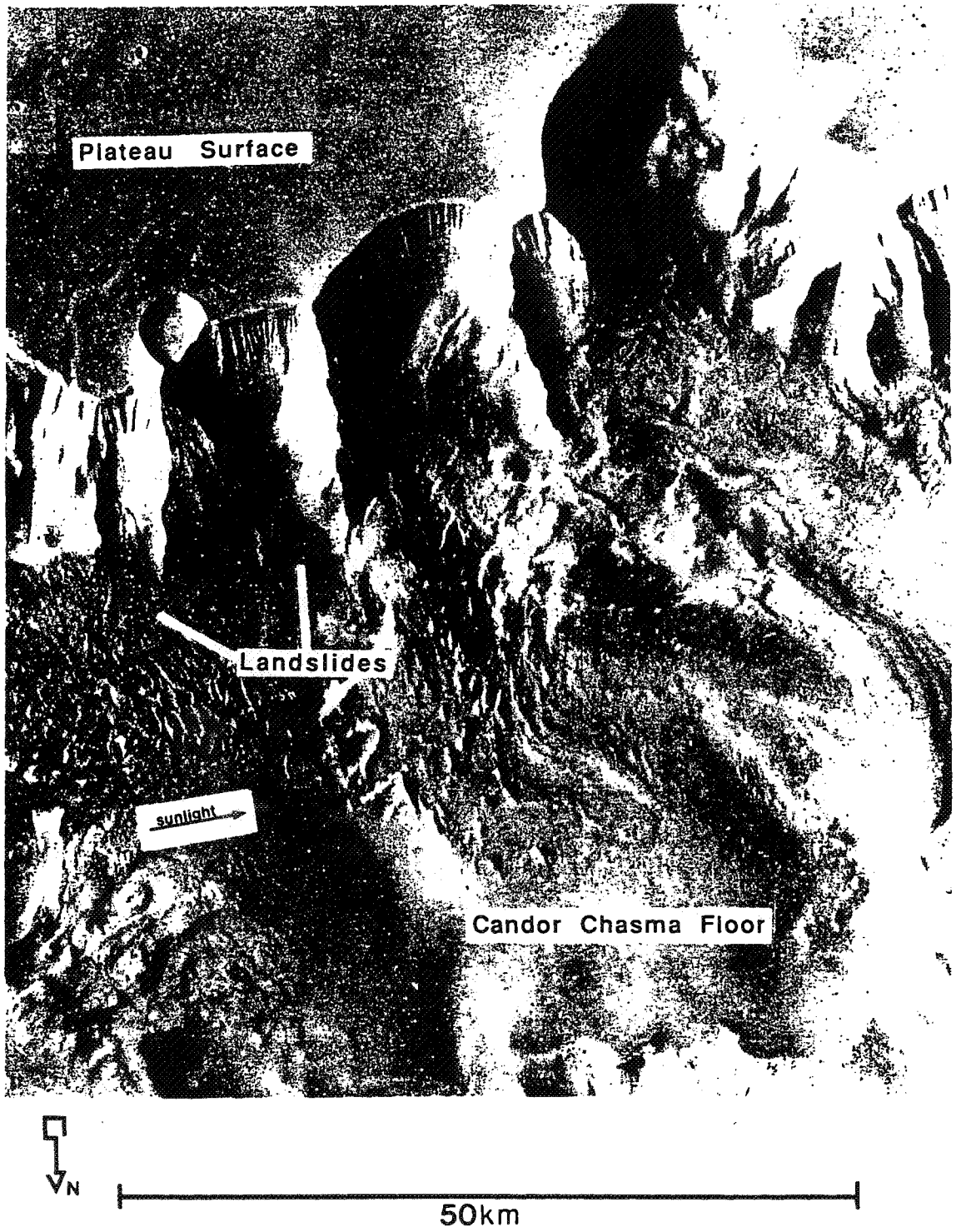

FIG. 3. Viking Orbiter image 909A12 of two martian landslides in Candor Chasma, part of the Valles Marineris canyon system.

Upon collapse of the preexisting slope, debris streamed downhill through a bottleneck only 280 m wide at its narrowest point between 8000 and 7280 ft. Below 7280 ft the debris piled up, forming a basal lobe 1.8 km in width. The Carlson landslide has an area of 5.2 km^2, 3.1 km^2 in the primary depositional region downslope of the 8000 ft elevation contour (Fig. 7) and 2.1 km^2 in the headscarp bowl, the source region for the landslide.

The marginal thickness of the deposit was estimated at three locations, at one point in the neck and at two sites along the toe of the landslide. The thickness of the southside levee in the neck is estimated at ~16 m (Fig. 4) from field measurements of the outer slope of the levee, in combination with the reconstructed prelandslide profile across the drainage basin. Figure 1 shows the location of the profile in Fig. 4. Topographic contours in Fig. 6 allow comparison of the present topography of the landslide with the estimated prelandslide geometry of the buried channel. Profiles of the toe of the Carlson landslide were ascertained using a variable-length staff (7–12 ft) and attached inclino-

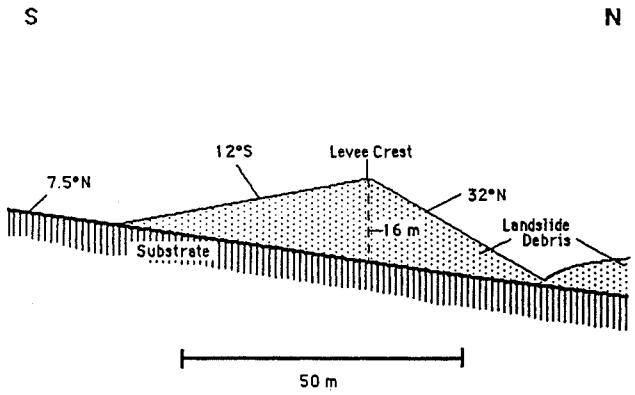

FIG. 4. Calculation of thickness of south-side levee. Location shown in Fig. 1.

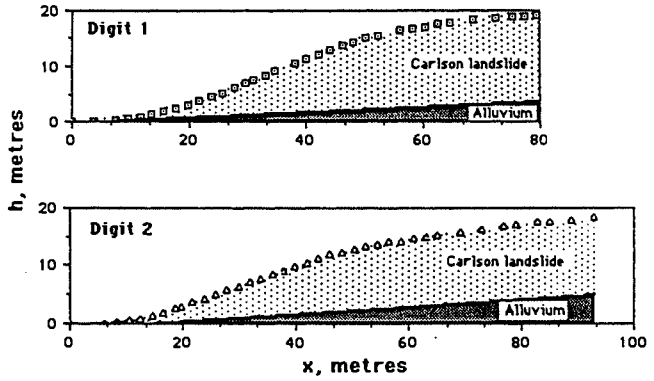

FIG. 5. Profiles of two promontories or digitations at the toe of the Carlson landslide. See Fig. 1 for location.

meter by placing the staff on the ground parallel to the surface and measuring the length and inclination of consecutive segments of the slope. Taking into consideration the 3.5° slope of the underlying alluvial surface, these measurements indicate that the toe of the landslide thickens to 16 m at points 80–90 m from the edge of the deposit (Fig. 5). Figure 1 shows the locations of the profiles along the southeastern margin of the basal lobe.

The volume of the Carlson landslide below the 8000 ft elevation contour is estimated at 100×10^6 m^3. This value is derived from Fig. 6, an isopach map of the landslide developed from the present and reconstructed prelandslide topography of the drainage basin. Longitudinal and transverse channel profiles and piedmont slopes of neighboring drainages in the Challis volcanics, together with the marginal and distal thickness profiles shown in Figs. 4 and 5 allowed reconstruction of the prelandslide topography. Reconstruction of the failed slope made by extension of present slopes into the headscarp bowl gave a compatible estimate for the missing volume, ranging from 50 to 150×10^6 m^3 depending on the degree of gullying of the original slope.

Morphology

The Carlson landslide displays several gradational surficial textures in its headscarp bowl, neck, and basal lobe (Figs. 7, 8). Three gradational morphologies occur from northwest to southeast across the headscarp bowl. These areas are labeled in Fig. 7 as follows: (1) a region of high-amplitude, downstream-aligned ridges and troughs; (2) a pattern of curved ridges and troughs arranged concentrically about Carlson Lake; and (3) an area of low relief southeast of Carlson Lake. Ridges and troughs in the northwestern portion of the bowl display amplitudes of 20–30 m, the highest relief textures on the Carlson landslide.

Headscarp bowl textures grade downhill into movement-parallel ridges and troughs in the neck, labeled 4 in Fig. 7, that vary in spacing and amplitude with lateral and downslope position. The neck ridges and troughs generally consist of straight, parallel, rounded ridges that meet in V-shaped hollows except where the hollows are filled by alluvium. The spacing of ridges averages about 50 m, decreasing slightly from the upper to lower neck. Individual ridges generally stand 25–100 m apart and typically rise 5–10 m above neighboring hollows. In the upper neck (7600–8000 ft), the ridges originating from the northern half of the headscarp bowl (Fig. 7, texture 1) have much greater relief than those coming from the southern part of the bowl (Fig. 2). These differences in relief decrease downslope; below ~7600 ft (Fig. 7) the ridges have a uniform appearance across the deposit. The ridges are of variable length, with none extending the entire length of the neck. Ridges formed by division, with one ridge separating into two crests separated by a trough. They disappeared either when two ridges merged to form a single wider ridge or when the outside pair of three parallel ridges moved together and squeezed out an intermediate ridge and trough. Both processes formed dead-end troughs on the landslide surface that pond water (Fig. 7). Transverse sections at several locations in the neck consistently show seven troughs and six ridges between the lateral levees, indicating a balance in the development and demise of ridges on the landslide in its waning movement stages (Fig. 9).

Marginal levees of variable dimensions bound the Carlson landslide from the lower headscarp bowl to the basal lobe. The north-side levee originates in the headscarp bowl, where it is composed of a series of en echelon ridge segments that step inward and downward until the levee becomes continuous at about 7600 ft (Fig. 7). Below 7600 ft the north-side levee generally displays higher relief than the south-side levee. At points where the landslide encounters side drainages, the north-side levee passes the depressions without deviation, whereas the south-side levee extends some distance up the channels (Figs. 1, 2, 8). In the upper neck, the outer slope of the north-side levee measures 25–30°, much steeper than the 5° outer slope of the south-side levee. The outer slope of the south-side levee steepens downhill, to 5–10° at the first major side drainage, 12° at the second side channel, and finally to 25° along the edge of the basal lobe. The outer slope of the north-side levee, in contrast, remains about 25° along its entire length. The inner scarps of the levees both consistently measure about 32° along their entire length. In the neck they stand well above the interior level of the landslide. The maximum relief observed between crest of the lateral levees and the interior is about 15 m.

Below 7520 ft, the movement-parallel ridges that dominate the neck between the levees give way to a different set of textures (Fig. 7). Below the neck the movement-parallel ridges grade into a hummocky region dominated by closed depressions and a convex-downslope pattern of concentric ridges and troughs, labeled 5 in Fig. 7. The major concentric ridges and troughs in this region exhibit amplitudes of 5–15 m and an average spacing of 80 m, vary-

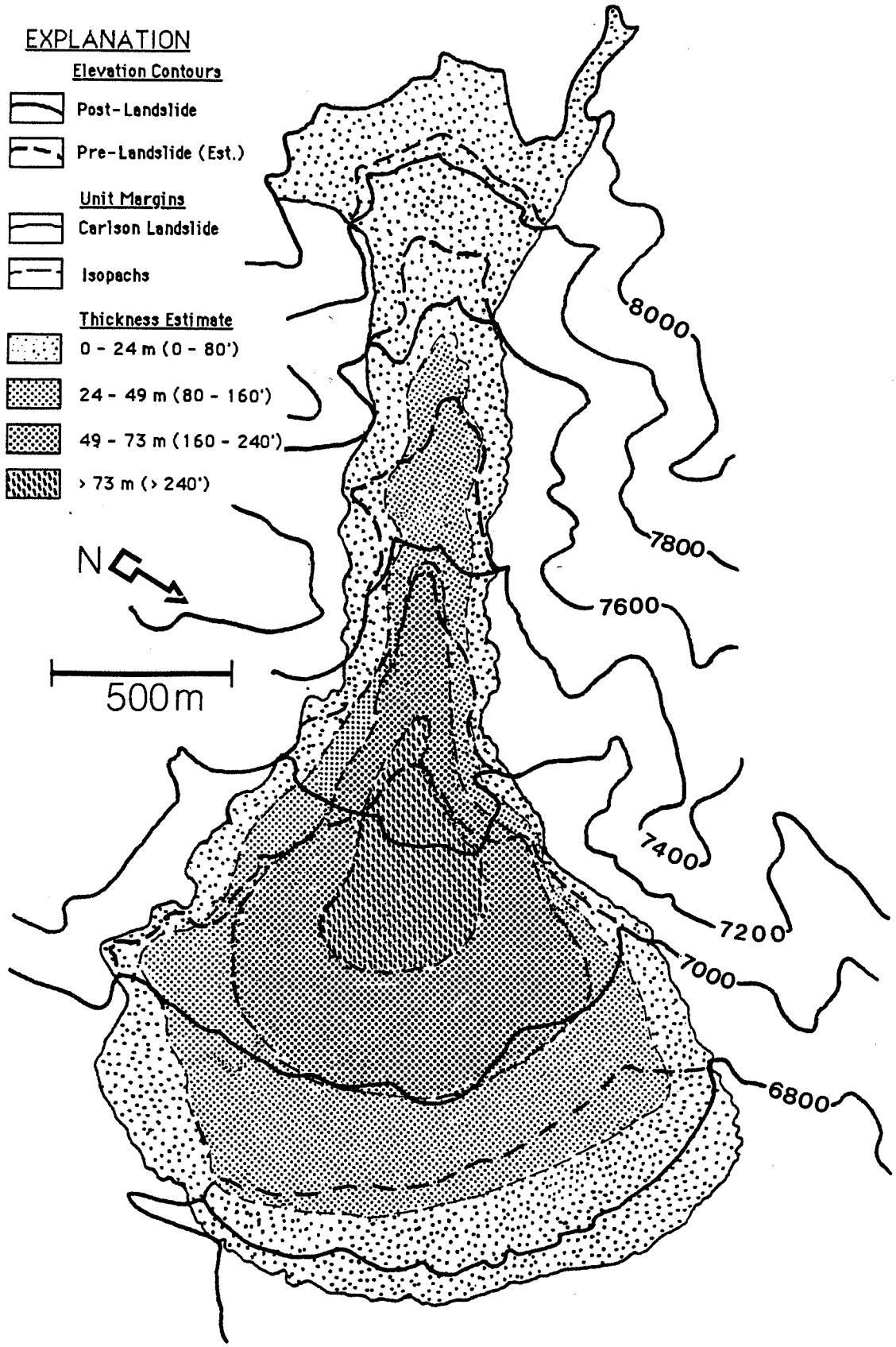

FIG. 6. Isopach map of the Carlson landslide, showing present topography and reconstructed pre-landslide channel geometry. Reconstruction based on comparisons with neighboring drainage basins in Challis volcanics, together with distal and marginal thickness calculations. Elevation contours in feet.

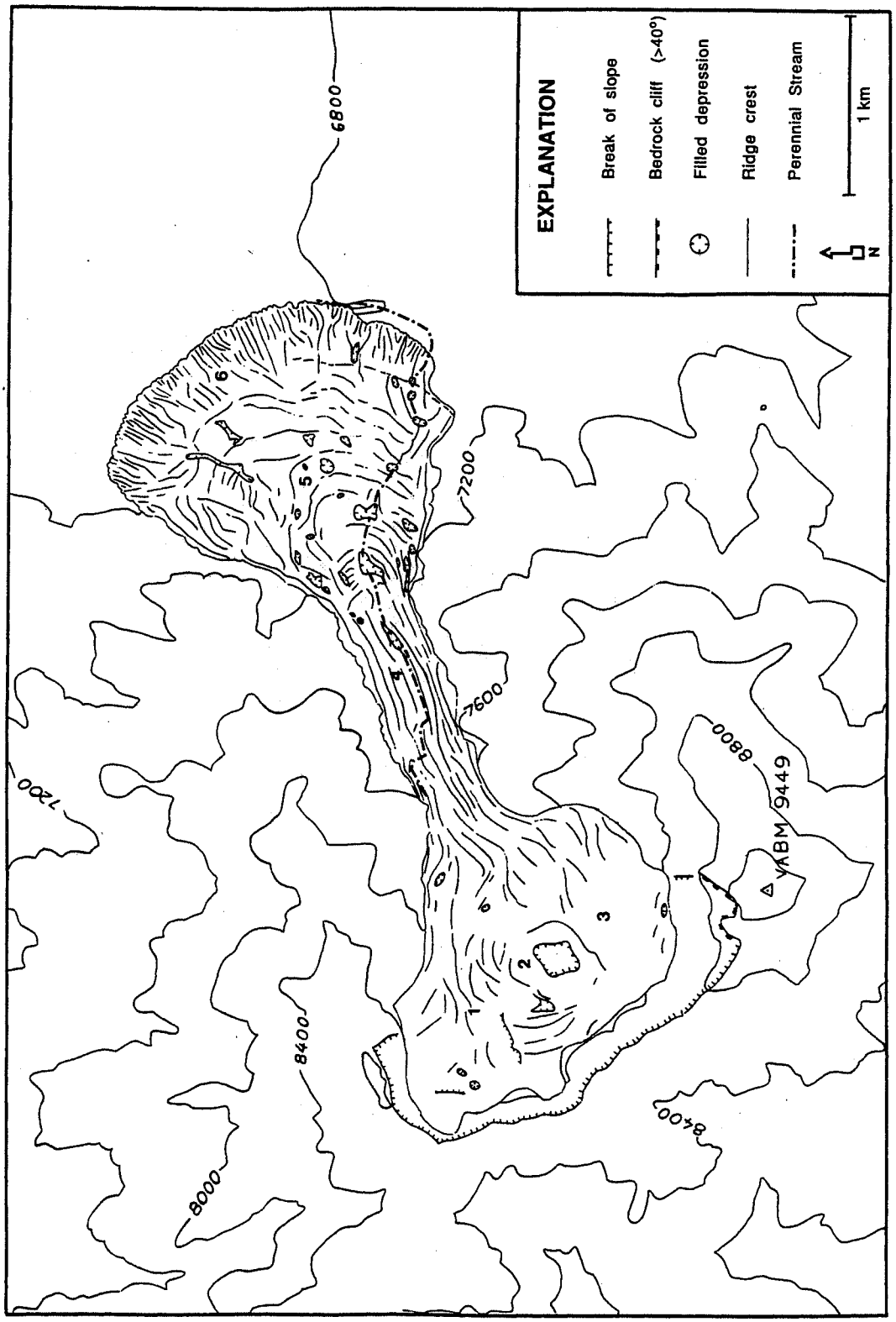

FIG. 7. Generalized morphology of the Carlson landslide. Surficial textures 1–6 described in the text.

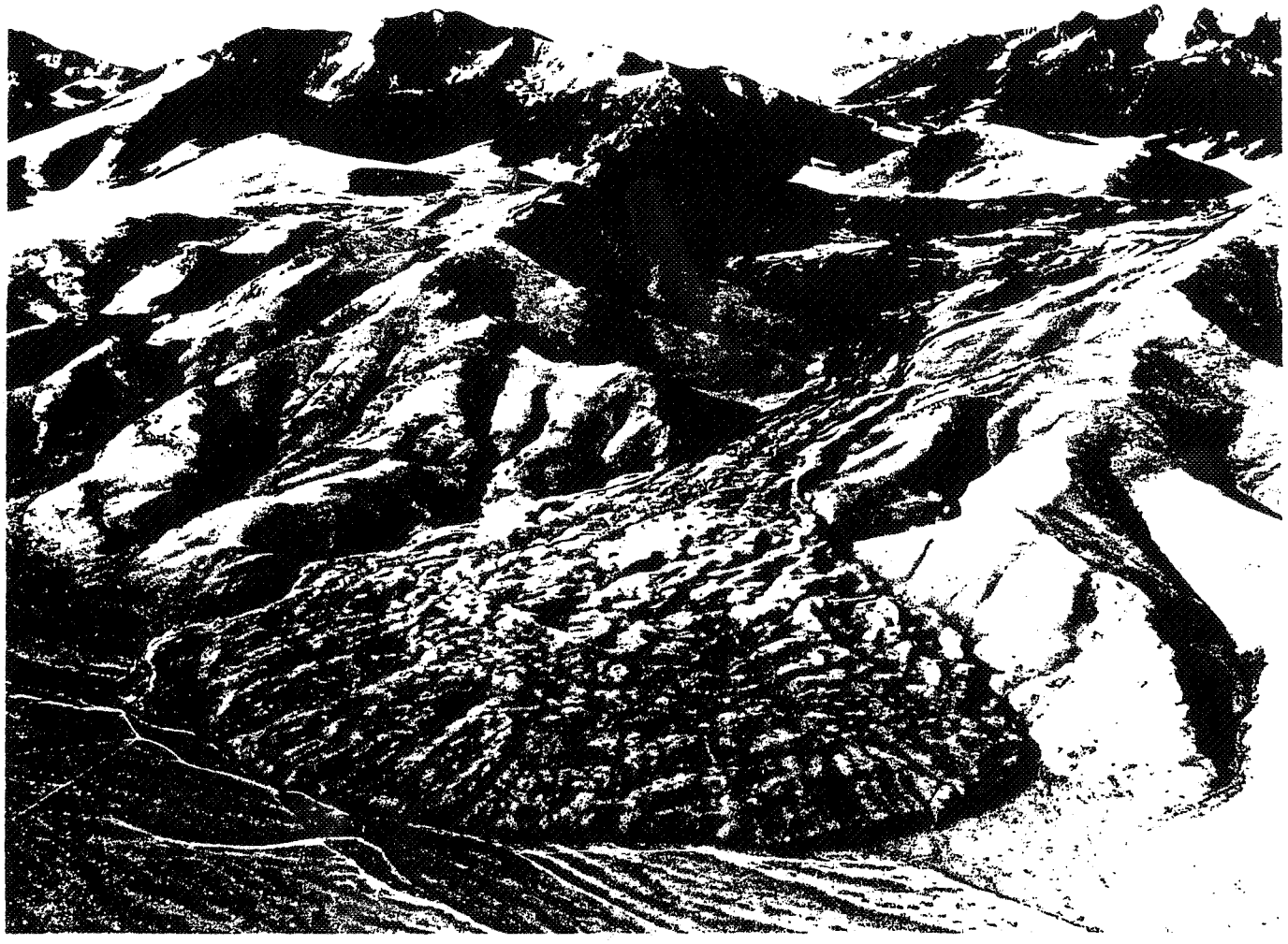

FIG. 8. Oblique aerial photograph of the Carlson landslide (photograph courtesy of J. S. Shelton).

ing between 30 and 110 m. At the distal portion of the basal lobe, this region grades into a radial pattern of about 85 ridges and troughs along the toe of the landslide, labeled 6 in Fig. 7. Like the movement-parallel features in the neck, the toe exhibits rounded ridges and V-shaped troughs except where alluvium fills the troughs. However, the radial ridges are of lower amplitude (2–5 m) and are more closely spaced (30 m) on average than those in the neck. At the leading edge of the landslide the ridges form promontories, and the troughs embayments when observed in plan view.

Sedimentology

The Carlson landslide consists primarily of a very poorly sorted mixture of basaltic rock fragments in a fine-grained matrix of basaltic composition. The matrix is here defined as silt to very coarse sand (1/256–2 mm); the material in this size range generally supports and separates clasts of larger dimensions. Powder X-ray diffraction of the matrix did not resolve a clay signature, indicating a clay content below 5–10% by volume (A. L. Albee, personal communication, 1989). In addition to the basaltic materials, trace quantities of limestone, agglomerate, and quartz rock fragments also occur in the landslide. The rock fragments typically have angular to subangular shapes.

The sedimentology of the landslide varies proximally to distally. In the headscarp bowl, the landslide consists primarily of medium- to coarse-pebble gravel (8–32 mm) of basaltic composition, with few cobbles or boulders and very little matrix. Limestone rock fragments occur mixed with the basalt breccia within about 200 m of the headscarp. Between the headscarp bowl and the basal lobe the deposit grades into a mixture of larger rock fragments and matrix, in the process changing from a clast-supported to a matrix-supported texture. Rock fragment sizes in the basal lobe vary considerably, with very coarse pebble gravel (32–64 mm) quite common, and some fragments of cobble (64–256 mm) and boulder gravel (>256 mm) also evident. A few boulders ranging up to 6 m in length occur on the basal lobe, often lying with their major horizontal axes aligned with the local movement direction.

The matrix-supported texture of the debris in the basal lobe and the observation that the matrix material takes on a malleable, plastic consistency when wetted suggest that in its final movement stages the Carlson landslide probably traveled as a moist debris flow. Unlike water-saturated landslides such as Mount St. Helens (Voight *et al.* 1983) and Mount Shasta (Crandell 1989), the Carlson landslide apparently did not dewater at the termination of movement, suggesting a lower water content for the Carlson landslide. Unlike the larger water-saturated landslides, the moist Carlson landslide appears simply to have dried in place after the cessation of movement.

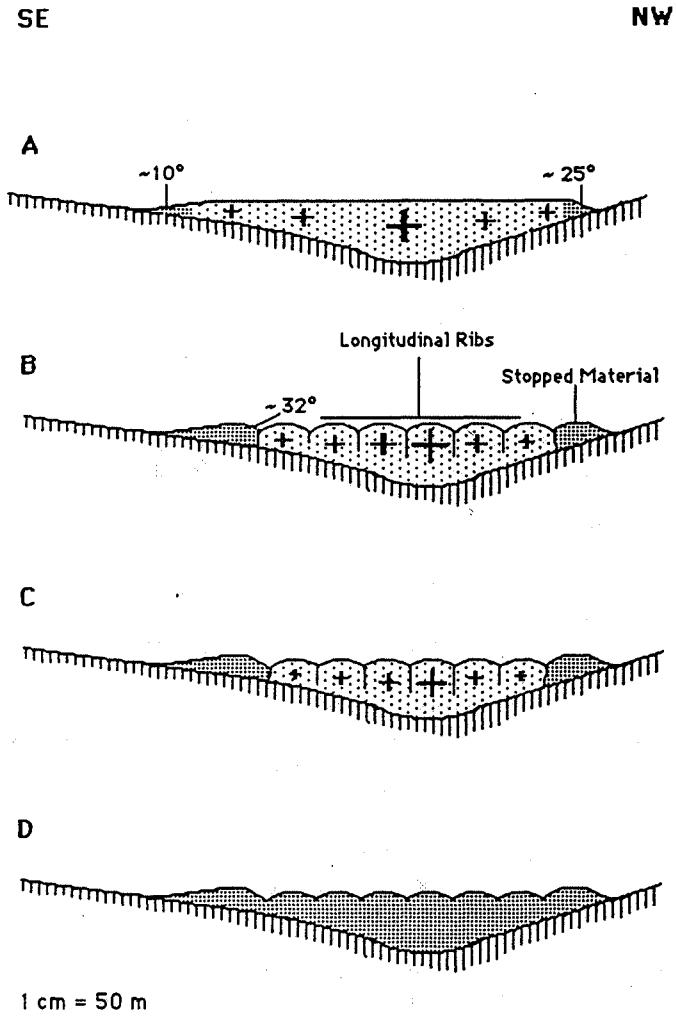

FIG. 9. Conceptualized appearance of cross section through the Carlson landslide at four different times in its evolution. View is upstream with debris approaching viewer. Channel geometry drawn in true scale from channel dimensions at site of Fig. 4 (see Fig. 1 for location). Size of + mark is proportional to debris velocity; darker pattern represents stopped material. (A) Maximum flux conditions. (B) Subdivision of landslide into parallel ribs moving at different velocities; lowering level of debris in the channel oversteepens inner banks of levees. (C) Waning movement continues. (D) Stopped condition.

Age

The Carlson landslide overlies fluvial terraces interpreted by Ross (1947) as marking the terminal melting of ice-age glaciers. An upward-fining fluvial sequence exposed beneath the toe of the landslide also characterizes the Late Pleistocene – Holocene transition (Pierce and Scott 1982). These observations suggest a Holocene age for the landslide. A conventional radiocarbon age of 2420 ± 130BP (M. Stuiver, personal communication, 1990) was obtained from a sample of carbonized peat removed from a small playa atop the basal lobe of the landslide, yielding a minimum age of 420 BC (Stuiver and Becker 1986) for the landslide. The peat occurred 56 cm below the surface of the playa, which had a total depth of at least 86 cm in massive, fine-grained sediments. Assuming a constant sedimentation rate, this gives an estimated minimum age of about 3700 BP, suggesting an early to middle Holocene age for the landslide.

Discussion

Discussion of the Carlson landslide is conveniently separated into five stages: slope preparation, initiation, travel, stopping, and degradation.

Slope preparation

A series of factors played a role in preparing the slope failure that formed the Carlson landslide. The development of steep topography and the progressive eastward Quaternary tilting of the Lost River Range began the distabilization of the slope. Tilting of the Challis volcanics–limestone unit contact and daylighting of the contact at the crown of the headscarp probably provided an avenue for the migration of surface waters into the hillslope, promoting weathering along the contact. Stratigraphy exposed in the headscarp together with rock fragments in the landslide indicate that the original slope consisted of a series of highly jointed lava flows separated in places by thin lenses of volcaniclastic rock. The observation that very few clasts as large as cobbles or boulders occur in the landslide attests to the pervasiveness of the jointing in the failed slope; at failure, the slope disaggregated primarily into very coarse pebble gravel (32–64 mm) and smaller sized material along these joints. The location of the headscarp at the elevation of nearby Pleistocene valley glaciers (Mapel *et al.* 1965) suggests that ice wedging and freeze–thaw processes may have played an important role in widening and loosening the joints and fractures in the slidemass. Considerable *in situ* chemical weathering had probably also taken place along the joints prior to failure, as evidenced by a red silt weathering residuum found sandwiched between the loose rock fragments forming a large basalt boulder on the landslide surface. Headward erosion of the now-buried drainage channel probably provided the critical factor in the destabilization of the slope by removing lateral support from the base of the slidemass in the direction of dip of the bedrock stratigraphy.

Initiation

The slope failure that produced the Carlson landslide apparently began at the lower end of the present headscarp bowl, between 8000 and 8160 ft (Fig. 7), at a point where the original drainage basin reached its steepest gradients. The scarp failure reached headward from this point back to the resistant limestone bedrock at the rear of the present headscarp bowl. Movement of the wedge-shaped mass of Challis volcanics may have begun along its eastward-sloping contact with the underlying limestone unit (section A–A′, Fig. 1). However, once movement had begun, the landslide mass must have rapidly disaggregated into rock fragments because no material exists on the landslide which appears to have simply translated or rotated into position. Rather than beginning motion as a coherent slide or slump that fragmented during runout, the initial motion of the landslide appears to have involved disaggregation of the slidemass.

Because the Carlson landslide took place in a region of Holocene seismic activity, the possibility exists that an earthquake triggered initiation of the landslide. The central Lost River fault experienced a spasm of Holocene activity, producing three scarp-forming earthquakes between about 5500 and 8000 BP. These earthquakes occurred on the Warm Springs, Thousand Springs, and Mackay segments of the fault, all within 30 km of the Carlson landslide. Before this interval, surface faulting on the Lost River had not occurred

since about 12 ka (Schwartz and Crone 1988). Holocene faulting also occurred on the Mahogany Creek segment of the Lemhi fault around this same time, approximately 40 km east of the landslide (Stickney and Bartholomew 1987). The offset produced by the 1983 (M_s = 7.3) Borah Peak earthquake closely mimicked the prehistoric offset on the Thousand Springs segment of the Lost River fault (Salyards 1985), suggesting an equally large magnitude for the prehistoric event. Despite this possible link to seismic activity, no positive evidence exists to link initiation of the landslide to an earthquake. Based on eyewitness accounts of the initiation of large historical landslides, few appear to actually coincide with earthquake shocks (Shaller 1991). More likely the landslide simply failed after a prolonged period of creep initiated by the removal of lateral support from the base of the slope caused by headward erosion of the old stream channel.

Travel

The Carlson landslide exhibited complex, changing behavior during its travel from the headscarp to the alluvial plain. All the available evidence is consistent with the landslide having been a rapid event, emplaced over a period of a few minutes. The primary observations consistent with rapid emplacement are superelevation of the landslide on the south side of its channel in the upper neck and the highly symmetrical plan form of the landslide's basal lobe on the north-dipping alluvial fan surface (Fig. 7). Because the landslide did not clearly run up onto any obstacles that halted its movement, no direct measurement of its velocity is available.

As outlined above, the slidemass appears to have disaggregated into a sliding or flowing jumble of basalt rock fragments soon after initiation. As the landslide moved downslope, its content of moist matrix material appears to have steadily increased until this viscous–plastic material dictated the movement of the landslide in its latter movement stages. At least two possibilities exist to explain the source of moist matrix in the landslide. The most likely possibility is that the *in situ* fractured and jointed slidemass contained a considerable quantity of water along these bedrock discontinuities at the moment of the slope failure. The underlying limestone bedrock, believed by Meinzer (1924) to exhibit cavernous weathering in the nearby Double Springs drainage basin, might have provided a supplementary source of water. Comminution of the basalt rock fragments in the landslide during movement provides the most likely source of sand and silt in the matrix, into which the available water mixed during transport. Brecciation of rock into fine grain sizes is a common process in large landslides and occurs because of either mechanical grinding in the landslides or the shattering of component rock fragments caused by the sudden release of overburden pressure on highly loaded rock (Shaller 1991). Another possibility is that the landslide began as a dry mass of rock fragments that eroded moist sands and silts from its bed as it traveled. Such bed erosion is observed in the geologic relations of large partially eroded rock avalanches in the western United States (Yarnold and Lombard 1989). Also, the Huascaran 2 and 3 landslides are believed to have transitioned from dry rock avalanches to water-saturated debris flows in this manner by traveling over and incorporating wet snow early in their travel phases (Plafker and Ericksen 1978). Because the Carlson landslide traveled down a channel whose drainage basin encompassed only Challis volcanics, sediments incorporated into the landslide from the channel would predominantly have had the observed basaltic composition.

Both the processes described above may explain the observed proximal-to-distal increase in matrix content of the landslide, and indeed both may have occurred during emplacement of the landslide. However, morphological evidence from headscarp bowl and upper neck structures supports the concept that, while the sand and silt in the landslide may have originated either in the substrate or in brecciation of landslide clasts, the water probably originated in the slidemass. At initiation, disaggregated basaltic breccia traveled into the upper neck region between 8000 and 7600 ft, where debris from disparate sources in the headscarp mixed together (Fig. 7). The differing relief of the longitudinal ridges in the upper neck suggests that the material issuing from the headscarp differed somewhat in mechanical properties between different sources in the bowl. Low-relief ridges issuing from the subdued southeast portion of the headscarp bowl (Fig. 7, texture 3) contrast with the high-relief ridges forming the northwestern part of the upper neck. These ridges continue from similar high-relief structures in the northwestern segment of the headscarp bowl (Fig. 7, texture 1). A variation in the initial water content of the slidemass across the headscarp bowl provides the most likely cause for these morphological differences; a higher water content in the southeastern debris source gave this material a more fluid character than the debris originating elsewhere in the headscarp bowl. Below about 7600 ft, however, the landslide debris between the marginal levees becomes quite homogeneous in appearance. Homogenization of the debris seems to have occurred rapidly through this area, probably because the debris moved at its greatest rate as it funneled down the upper neck and through the 280 m wide narrows near 7680 ft (Fig. 7). A cross section through the landslide at this point (section B–B′, Fig. 1) indicates that the south-side levee may have been superelevated as much as 25 m above the north-side levee at the height of the event. This superelevation, together with the discontinuous downward- and inward-stepping north-side levee, indicates that material evacuating the headscarp initially had a strong component of northwest to southeast momentum.

Below 7600 ft, landslide debris slid or flowed through the neck, filling the channel to the height of the lateral levees at the moment of maximum mass flux. Figure 9A gives the estimated appearance of the cross section of the landslide at maximum flux for the channel geometry at the site of Fig. 4 (see Fig. 1 for location). The variation in inclination between the outer slopes of the lateral levees in the neck, 5–12° along the south side of the channel, 25° along the north, appears related to the contrasting fluidity between the landslide debris originating from the different ends of the headscarp bowl. The more fluid debris from the southeast portion of the bowl gave the south-side levee its lower slope, whereas less fluid material from the northwestern portion of the bowl formed the north-side levee. Thus, in contrast with the bulk of the landslide, the material along its margins apparently did not mix well as it moved down slope. The lobate form of the basal portion of the landslide suggests that as landslide debris passed through the channel it developed a transverse velocity profile, with the fastest material moving down the centerline of the channel, grading to stopped material along the margins (Fig. 9A). As the major

pulse of debris waned in the channel, the level of moving debris receded between the halted lateral levees of the landslide. The removal of lateral support from the inner walls of the levees caused them to erode back at an angle of ~32°, the angle of repose of loose granular material (Fig. 9B). Because this angle is consistently steeper than the outer margins of the lateral levees, it appears that the material forming the levees exhibited lower shear strengths when moving than when halted; the debris thus appears to have exhibited thixotropic behavior. The level of moving debris continued to wane in the channel, with recession of the inner banks of the levees, until the debris in the channel came to a halt (Figs. 9C, 9D).

The movement-parallel ridges and troughs in neck (Fig. 7, texture 4) probably formed because of shearing between rapidly moving material at the center of the channel and slower material at its edges (Figs. 9A–9C). The furrows likely formed as high-energy shear zones between the ridges, as inferred for some longitudinal structures of similar geometry observed on the Sherman (Shreve 1966) and Mayunmarca (Kojan and Hutchinson 1978) landslides. The observation that the troughs separated ridges of contrasting lithology in these landslides demonstrated that displacement of the ridges had occurred along the longitudinal grooves. Unfortunately, the monolithologic nature of the Carlson landslide precludes such a demonstration. An alternative explanation for the movement-parallel neck ridges is that they formed from discrete sources of rubble in the headscarp, akin to the formation of longitudinal ridges on rock glaciers (Wahrhaftig and Cox 1959), and became aligned as the rubble mass passed into the narrows below. The primary drawback to this idea is that the ridges are not continuous through the neck region, but rather die out in places and reappear elsewhere, remaining constant in number across the landslide. This observation suggests that their formation was an ongoing, dynamic process as the landslide passed through the neck, possibly related to the relationship between the shear strength and the transverse velocity profile of the moving debris.

At the base of the neck, the landslide slowed, thinned, and spread out where the channel widened and the slope decreased. Because material reached the rear of the basal lobe more rapidly than the flow front advanced, debris backed up into the neck near the end of movement. The concentric ridge and trough pattern (Fig. 7, texture 5) probably formed because of compression between material at the toe of the landslide and faster, trailing material moving down the channel.

The toe of the landslide displays a radial pattern of ridges and troughs (Fig. 7, texture 6) which bears many similarities to the parallel pattern of ridges in the neck. Like the neck ridges and troughs, those at the toe may also have formed as the result of differential movement, as ridges closer to the midline of the basal lobe slipped slightly farther than their neighbors towards the left or right margins. Instead of advancing along a smooth front, the landslide appears to have advanced as a series of tightly spaced fingers. Due to spreading of the lobe, these ridges apparently formed under conditions of longitudinal compression and radial tension. Noncontinuous thinning of the toe, like the necking of a steel rod under tension, may therefore also have played a role in the development of these features.

Stopping

The morphology of the Carlson landslide suggests that it gradually slowed to a halt. This interpretation comes from the observation that the concentric basal lobe ridges indicative of longitudinal compression are rather subdued in comparison with the pronounced pattern of radial ridges and troughs at toe of the landslide. In its final movement stages, therefore, the landslide seems to have been much more strongly influenced by spreading of the basal lobe than by longitudinal compression caused by a rapid halt. This character contrasts markedly with the pronounced transverse ridging observed on dry rock avalanches observed or inferred to have come to an abrupt halt, such as the Elm (Heim 1932) and Blackhawk (Shreve 1968) landslides.

Degradation

The Carlson landslide has undergone only minor post-depositional degradation. Alluvium has been deposited along the margins of the landslide where it blocked off side drainages and has also collected in enclosed basins on the landslide surface (Fig. 1). Also, Carlson Lake has apparently risen at least once, and perhaps several times above the level of the sill at the northeastern margin of the headscarp bowl. Waters that have overtopped the sill have incised a ~3 m deep channel into the steep slope below the edge of the bowl. Slope wash and raveling has degraded the toe of the landslide to a small degree, and one of the radial troughs along the toe of the landslide has experienced minor fluvial incision accompanied by the deposition of a small alluvial cone along the margin of the landslide.

Comparison of the Carlson landslide with other terrestrial mass-movement deposits

In the following, the Carlson landslide is compared with other mass-movement deposits on the basis of morphology, sedimentology, and several quantitative measures of landslide properties. The combined data are then used to access the mechanical behavior of the landslide during runout.

Morphology

The morphology of the Carlson landslide shares some significant similarities and differences with other geologic flow phenomena. For example, detailed similarities exist between the morphologies of the Carlson landslide and a small piedmont glacier photographed on Ellesmere Island (Sharp 1988). Like the Carlson landslide, the glacier funneled through a narrow mountain-front gap and spread out to form a symmetrical basal lobe upon reaching a nearly flat piedmont slope. In addition, surface textures on the glacier closely mimic those on the landslide, including lateral levees in the neck, concentric ridges and troughs on the upper basal lobe, and even a radial pattern of ridges along the toe! Some terrestrial mass movements involving rocky materials also mimic the morphology of the Carlson landslide. A particularly similar, though smaller deposit lies on the north bank of the Columbia River directly opposite Arlington, Oregon (J. L. Anderson, personal communication, 1990). This landslide occurred in lava flows of the Columbia River Basalt and volcaniclastic sediments of the Ellensburg Formation. Like the Carlson landslide, the "Arlington" landslide funneled through a narrow constriction where it deposited a pair of levees. It also built a symmetrical basal lobe at the

base of slope featuring both concentric and radial ridges. Unfortunately, the site has not been visited, so it is unknown whether, like the Carlson, this landslide contained a significant water content at emplacement. The closest known dry rock analog to the Carlson landslide is the Martinez Mountain rock avalanche, which lies along the western margin of the Salton Trough in southern California and contains 380×10^6 m^3 of brecciated gneiss (Shelton 1966; Bock 1977). Like the Carlson landslide, the rock avalanche travelled down a channel and debouched onto a nearly level alluvial fan. It displays paired levees in the channeled portion and a small number of radial ridges on its basal lobe. Unlike the Carlson landslide, however, the Martinez Mountain deposit lacks concentric basal lobe ridges, has a much less symmetrical basal lobe, and exhibits a much more broadly and irregularly spaced pattern of radial ribs on its basal lobe.

The principal connection between the lobate geologic flow phenomena described above is that all experienced channelized transport for significant distances before being discharged onto low-gradient piedmont slopes. In each case, channelized transport apparently gave the moving material a distribution of velocities, from slow at the margins, resulting in the deposition of lateral levees, to a maximum along the center line. The rates of downslope travel of the mass movements relative to their spreading rates controlled the detailed forms of their basal lobes. The Carlson and Arlington landslides and the piedmont glacier all moved downslope and spread at about the same rate, yielding their symmetrical plan forms. The Martinez Mountain dry rock avalanche spread much less rapidly relative to its downhill speed upon leaving its channeled reach, producing a more blunt and irregular plan form.

Sedimentology

The Carlson landslide exhibits sedimentary characteristics akin to other large moist and water-saturated landslides and distinct from dry rock landslides. Together with other large moist and water-saturated landslides (Ui *et al.* 1986; Crandell 1989), the Carlson landslide fails to exhibit reverse grading, a common characteristic of large dry landslides (Cruden and Hungr 1986; Yarnold and Lombard 1989). The surficial textures of large moist and water-saturated landslides also differ considerably from those of dry landslides. Large dry landslides are commonly surfaced by a carpet of cobbles or boulders (Krieger 1977; Bock 1977; Yarnold and Lombard 1989), whereas the surfaces of the Carlson and other moist and water-saturated landslides generally consist of fine-grained matrix punctuated by occasional clasts and boulders of varying scale (Plafker and Ericksen 1978; Crandell 1989). The low internal friction afforded by moist matrix material appears responsible for this behavior. Moist and wet landslides can mix and overturn during runout, whereas dry landslides appear too viscous or rigid to do so (Shreve 1968; Shaller 1991). Moist and water-saturated landslides, including the Carlson, also commonly exhibit a proximal to distal decrease in rock fragment to matrix ratio, corresponding to an overall fining of debris size with travel distance (Ui *et al.* 1986; Crandell 1989). Dry landslides do not generally exhibit this behavior (Heim 1932). Although dry long-runout landslides to develop an increasingly thick basal layer of fine, powdered debris with travel distance,

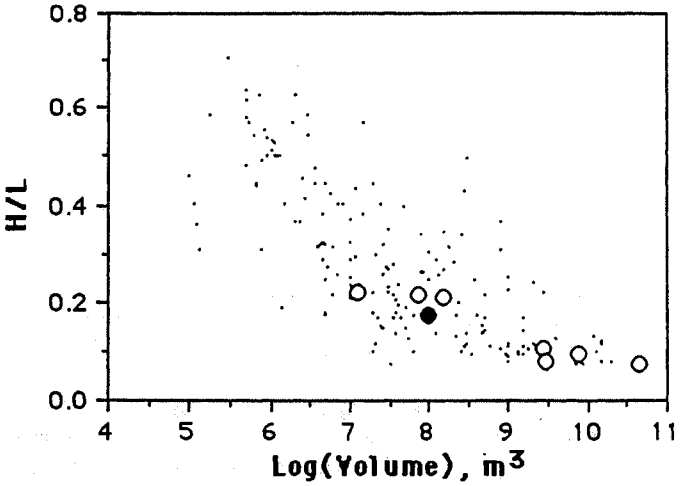

FIG. 10. Plot of log(volume) vs. *H/L* for the Carlson landslide and the seven other moist and water-saturated landslides listed in Table 1 vs. 163 dry terrestrial subaerial landslides (Shaller 1991). ●, Carlson landslide; ○, other moist and wet landslides (Table 2); ·, other subaerial landslides.

this grain-size diminution is not apparent on the surface of a large dry landslide (Yarnold and Lombard 1989). Perhaps homogenization of debris in moist and wet landslides mixes the fine-grained component formed during runout throughout the body of a landslide, so all parts of the landslides appear to decrease in average grain size and block to matrix ratio with distance traveled. The surfaces of moist and water-saturated landslides are also often marked by large-scale hummocks. In water-saturated landslides, these generally represent large buried boulders that experienced partial exhumation during late-stage dewatering and remobilization of surface fines (Ui *et al.* 1986; Crandell 1989). Hummocks on the moist Carlson landslide are often crested by inset clasts having the appearance of paving stones set into the ground. These features may also represent buried boulders, but ones that escaped exhumation because of a lack of post-depositional dewatering.

Quantitative measures of landslide properties

The preceding discussion shows that certain qualitative differences in landslide morphology and depositional characteristics distinguish dry from moist and water-saturated landslides. However, two common quantitative measures of large landslide travel behavior, log(volume) versus *H/L* trends and apparent Bingham plastic yield strength measurements, do not distinguish between landslides of differing water content.

Observational data for large rapid landslides containing over 10^6 m^3 of rock indicate that as their masses increase beyond this threshold volume, the landslides exhibit a rough log-normal group tendency towards decreasing *H/L* with increasing volume (Scheller 1971; Scheidegger 1973; Hsü 1975; Ui 1983; Shaller 1991). Figure 10 compares the log(volume) versus *H/L* trends of eight large moist and water-saturated terrestrial landslides (Table 1) with that of 163 dry volcanic and nonvolcanic terrestrial subaerial landslides (Shaller 1991). The moist and water-saturated landslides plot well within the log(volume) versus *H/L* envelope for dry terrestrial subaerial landslides, indicating that the travel behavior of the moist landslides apparently differs

TABLE 1. Critical characteristics of large moist and water-saturated terrestrial landslides

Name	Volume ($\times 10^6$ m^3)	H/L	Reference
Mt. Shasta	45 000	0.07	Crandell 1989
Mt. St. Helens	25 000	0.11	Voight *et al.* 1983
Pungarehu	7 500	0.10	Ui *et al.* 1983
Galunggung	2 900	0.08	Siebert 1984; Crandell 1989
Huascaran 1	150	0.21	Plafker and Ericksen 1978
Carlson	100	0.17	This paper
Huascaran 3	50–100	0.22	Plafker and Ericksen 1978
Huascaran 2	13	0.22	Plafker and Ericksen 1978

TABLE 2. Bingham plastic yield strengths of landslides and debris flows

Name	Bingham plastic yield strength (Pa)	Reference
Ice	100 000	Nye 1951
Carlson landslide	19 000*	This paper
Mt. St. Helens landslide	2 000 – 20 000*	Voight *et al.* 1983
Chaos Jumbles landslide	6 000 – 10 000*	Eppler *et al.* 1987
Surprise Cyn. debris flow	2 000*	Johnson 1984
Sherman landslide	2 000*	McSaveney 1978

*Calculated using [1]: $k = \rho\, g\, D \sin \beta$.

little from that of dry rock avalanches of similar volume. Thus the mechanism(s) responsible for causing anomalous runout in large dry landslides seem(s) to operate in moist and water-saturated landslides as well.

Many geological flow phenomena experience movement only when subjected to basal shear stresses beyond a certain "yield stress." As a first approximation to their material properties, such substances are often modeled in the geologic and engineering literature as Bingham plastics. Examples include the flow of muds, sludges, and suspensions through pipes (Caldwell and Babbitt 1941), the flow of glaciers (Nye 1951), lava flows (Hulme 1974), debris flows (Johnson 1970, 1984), water-saturated landslides (Voight *et al.* 1983), and dry rock avalanches (Eppler *et al.* 1987; McEwen 1989). Two characteristics cited as indicative of large-scale plastic behavior are halting of motion on a slope and the presence of a parabolically shaped distal profile, or "snout", along the toe of a deposit (Johnson 1970), both features expressed on the Carlson landslide. Equation [1] gives the basic Bingham plastic yield strength formula, which assumes steady flow conditions (Johnson 1984)

$$[1] \quad k = \rho\, g\, D \sin \beta$$

where k is the Bingham plastic yield strength in pascals, ρ is the density in kg/m^3, D is the deposit thickness in metres, g is the gravitational acceleration in m/s^2, and β is the ground slope. Table 2 reports estimated Bingham plastic yield strength values for several moist and dry landslide deposits. Table 2 shows that moist and water-saturated terrestrial landslides exhibit about the same estimated Bingham plastic yield strength as the Chaos Jumbles dry rock avalanches and greater strength than the Surprise Canyon debris flow and the Sherman landslide, a dry rock landslide emplaced onto a snow-covered glacier. Thus, moist and water-saturated terrestrial landslides exhibit Bingham plastic yield strength properties closer to dry rock landslides than to typical desert alluvial fan debris flows.

Comparison of the Carlson landslide with lobate martian landslides

Four large lobate landslides have been located on Mars: two in Candor Chasma (Fig. 3), and two near the base of Olympus Mons (Baker 1983). Lucchitta (1987) believed that the morphologies of the two Candor Chasma landslides and of their source regions provided evidence that these landslides contained considerable amounts of water during transport, and that the deposits must have flowed into place with much the same consistency as terrestrial mudflows. More recently, McEwen (1989) countered this argument by discounting the morphological data and instead using log(volume) versus H/L trends, yield-strength estimates, and velocity estimates of landslides in Valles Marineris (from overtopped obstacle heights) as evidence that all the landslides observed in the chasmas were probably emplaced dry. However, as demonstrated above, log(volume) versus H/L trends and yield-strength estimates fail to provide useful means of separating dry from moist or wet landslides. In addition, dry and water-saturated landslides on Earth exhibit an overlapping range of velocities (Shaller 1991), thus also ruling out velocity estimates as a method of distinguishing dry landslides from those having significant water contents. Thus, morphology remains the only available means of remotely distinguishing landslides of differing water content.

The lobate martian landslides all exhibit morphologies consistent with moist deposition as defined by the lobate Carlson landslide. The Carlson landslide and the lobate martian landslides all began motion as rockfalls and funneled through a narrow constriction in the channel below the headscarp to spread out and form a lobate, flattened, highly symmetrical, finely longitudinally ribbed debris apron. The lobate martian landslides differ from the Carlson landslide in not exhibiting the convex-downslope ridges and troughs texture observed on the Carlson and in having greater characteristic thicknesses than the terrestrial landslide (Table 3) (Shaller 1991).

The debris-apron morphologies exhibited by the lobate martian landslides make them much closer in morphology to the moist Carlson landslide than to any known terrestrial dry rock landslide. Particularly significant on the martian landslides are the very smooth margins of their basal lobes

TABLE 3. Critical characteristics of lobate martian and terrestrial landslides

Name	Volume ($\times 10^6$ m^3)	Basal lobe width (km)	H/L	Thickness (m) Average	Thickness (m) Maximum
Carlson	100	1.8	0.17	30	70
Mars 143	na	4	na	na	na
Mars 84	1 500	5	0.2	60	100
Mars 85	1 500	5	0.2	60	100
Mars 142	26 000	14	0.1	160	160

and the fine spacing of their longitudinal ribs. Although the lobate martian landslides differ from the Carlson landslide in not exhibiting the convex-downslope ridges and troughs texture, there are several reasonable explanations for this difference. One possibility is that the ridges and troughs exist on the lobes but cannot be resolved in the Viking Orbiter images. Conversely, even given the exact same materials for the martian landslides as for the Carlson landslide, the difference in gravity between the two planets might preclude development of the convex-downslope ridges and troughs texture on the martian landslides. On the Carlson landslide, this texture apparently formed because of compression between material at the toe of the landslide and faster, trailing material coming down the channel. On Mars, where deposit velocities must be lower due to the lower gravitational acceleration, the velocity differential might be significantly lower between material at the toe of a deposit and trailing material coming down the channel. In addition, the lobate martian landslides characteristically have greater thicknesses than the Carlson landslide, also making compressional deformation more difficult. The characteristically greater thicknesses of the lobate martian landslides relative to the Carlson landslide probably relate to the difference in gravity between the two planets, rather than to a difference in material properties. This conclusion is based on the fact that the lobate martian landslides have average and maximum thicknesses that average about 2.5 times the thickness of the Carlson landslide (Table 3), a value roughly corresponding to the ratio in gravitational acceleration between Earth (9.8 m/s^2) and Mars (3.72 m/s^2). Other groups of landslides on the two planets of similar volume exhibit an analogous relationship; apparently the shear stresses applied at the base of large landslides control their travel distances during runout (Shaller 1991).

The evidence presented above suggests that the lobate martian landslides were probably moist during deposition, like the Carlson landslide. Other evidence suggests that the Carlson landslide and its martian counterparts may have had rather similar lithologic compositions as well. This speculative argument is based on the fact that the Carlson landslide and a smaller but morphologically similar deposit in the Columbia River valley in Washington State (45°45′N, 120°14′W) both originated in outcrops of weathered basalt (J. L. Anderson, personal communication, 1990). In addition, the landslides from Olympus Mons, a large shield volcano, probably also consist of some form of basalt, as may the two Candor Chasma landslides. The latter two landslides appear to have fallen from bedrock outcrops at the crest of the chasma, outcrops that have been interpreted as mare-type flood basalts (Scott and Tanaka 1986). Because of the instability of water at the surface of Mars in the equatorial latitude range in which the four lobate martian landslides occur (Carr 1981), they must have derived water from the subsurface. Fumarolic activity on Olympus Mons theoretically might have provided the water for two of the deposits, whereas the Candor Chasma landslides most likely obtained water from the high-pressure groundwater aquifers postulated by Carr (1981).

Travel mechanism(s)

The Carlson landslide comprises a composite mass-movement deposit, with morphological and sedimentary properties akin to both large dry long-runout landslides and to much smaller desert alluvial fan debris-flow deposits. With regard to log(volume) versus H/L relations and estimated Bingham plastic yield strength properties, however, the Carlson and other moist landslides exhibit behavior compatible with dry rock avalanches and distinct from debris flows. These facts, together with the observation that large dry rock landslides such as Carlson and the Huascaran landslides (Plafker and Ericksen 1978) transformed gradationally into debris flows during travel, suggest that the processes involved in long-runout landslides and debris flows must be gradational in nature.

Many different theories have been proposed to explain long runout in large rock avalanches. Some have attempted to explain long runout on a case-by-case basis (Habib 1975; Goguel 1978; Johnson 1978; McSaveney 1978; Solonenko 1984), whereas others have approached long runout as a mechanism underlying the behavior of all large landslides. Models proposed to explain long runout as a general property include bulk fluidization theories (Heim 1932; Kent 1966; Hsü 1975; Davies 1982; Krumdieck 1984; Savage 1984; Trunk *et al.* 1986; Melosh 1987; Campbell 1989; Potapov and Ivanov 1991), lubrication theories (Shreve 1968; Erismann 1979), and a mass-loss theory (Van Gassen and Cruden 1989). The process(es) responsible for long runout apparently operate on Mars (McEwen 1989; Shaller 1991) and perhaps on the Moon (Howard 1973), as well as on Earth.

Debris flows of the type commonly associated with desert alluvial fan flood processes have also been described by a variety of mechanical models. These include behavior as a Newtonian fluid (Sharp and Nobles 1953), as a Bingham plastic (Johnson 1970), and as a Coulomb-viscous substance (Johnson 1970, 1984).

Most of the mechanisms proposed to explain both long-runout landslides and debris flows could apply to the Carlson landslide if its behavior is viewed individually. Exceptions include behavior as a Newtonian fluid, air fluidization, and air-layer lubrication. A Newtonian fluid rheology (Sharp and Nobles 1953) can be ruled out because the landslide halted motion on a slope, has a significant thickness, and does not give any indication of exhibiting slow viscous motion at present. Air fluidization (Kent 1966; Krumdieck 1984) also fails because this process generates normal grading (Brown and Richards 1970), whereas the Carlson landslide exhibits a lack of grading, and perhaps some indications of reverse grading as suggested by the smattering of large boulders on its surface. Air-layer lubrication (Shreve 1968) probably also can be ruled out for the Carlson

landslide because the landslide does not appear to have experienced the airborne leap necessary for trapping an air cushion. The weak transverse ridge-and-trough texture on the landslide and its failure to exhibit a raised distal margin provide additional evidence against air-layer lubrication.

Based on comparisons with other large landslides and with debris flows, the Carlson landslide appears to have traveled by means of the flow of its fine-grained matrix material. The homogeneous morphology and sedimentology of the basal lobe of the landslide suggest that in its final movement stages the landslide experienced bulk fluidization and traveled as a giant debris flow whose behavior depended upon the nature of its moist matrix material, perhaps flowing with a Bingham-plastic or Coulomb-viscous rheology (Johnson 1970, 1984). Such rheological properties could, in fact, explain the observed greater thicknesses of the martian landslides relative to the Carlson; for the same material properties, a landslide with either rheology should flow 0.38 times as thick on Earth as on Mars (eq. [1]) (Johnson 1984). The evidence of bulk flow of the Carlson landslide becomes less apparent proximally, however. If the landslide began movement by sliding, it probably developed a basal layer of highly comminuted debris, as often occurs along the basal contacts of large dry landslides (Yarnold and Lombard 1989). Addition of water to this basal material might have led to its mobilization throughout the body of the landslide. Perhaps the gradational behavior between dry rock avalanches, moist landslides, and debris flows results from fine-grained material playing the critical role in each form of mass transport. Sliding of large landslides into place on thin lenses of flowing, comminuted substrate material could explain many of the characteristics of dry long-runout landslides (Shaller 1991). Addition of water to the material might give it considerably different properties, including reduced viscosity, allowing the matrix to mix upwards into the bulk of the landslide, ultimately causing the observed apparent bulk fluidization of the landslide debris. Unfortunately, this model remains speculative because of a lack of information on the viscous properties of powdered dry rock subject to high shear stresses and strain rates at moderate overburden pressures. Nevertheless, it provides a conceptual model for landslide behavior that ultimately may be tested in the laboratory.

Conclusions

The early to middle Holocene Carlson landslide began movement as a dry rock landslide and ended movement as a giant debris flow. Headward erosion of the now buried drainage basin, in combination with eastward tilting of stratigraphy, lava flow jointing, steep topography, and *in situ* weathering of the basaltic bedrock all helped prepare the original slope for failure. The basalt slidemass initially contained a considerable quantity of water along its joints and fractures, especially in its southeast quadrant. At initiation this water became free to mix with fine rock debris generated during movement of the landslide, material that originated either in comminution of the rock debris in the landslide and (or) by incorporation of underlying sediments. The morphologies of the lateral levees reflect the different fluidities of the debris spilling out of the headscarp bowl and provide evidence that the landslide debris had more fluid behavior when halted than when moving. Longitudinal ribs in the neck and at the toe apparently formed by shear between debris trains moving at different speeds, whereas the concentric ridge-and-trough pattern formed by differential velocities between the toe and neck of the landslide. The landslide came to a gradual halt, after which it dried and set like concrete. Since then the landslide has undergone only minor degradation.

The moist Carlson landslide shares its basic lobate geometry with glaciers and with other large landslides. In all cases this lobate geometry appears to result from channelized movement. The Carlson landslide differs in detail with lobate dry rock avalanches because of the relatively greater ability of the moist debris to spread out upon leaving its channel than the dry debris. However, although the morphologies and sedimentologies of large dry and moist landslides differ in detail, their log(volume) versus H/L and apparent Bingham plastic yield strengths do not differ significantly.

The morphologies of lobate martian landslides suggest their emplacement as moist landslides. Detailed differences in deposit thickness and morphology between these deposits and the Carlson landslide probably result from the difference in gravitational acceleration between the two planets. Thus, a limited role for water on the martian surface is supported by the lobate martian landslides.

The geometry and sedimentology of the Carlson landslide rule out Newtonian fluid flow, air fluidization, and air-layer lubrication as likely mechanisms in the travel of the landslide. Rather, the landslide appears to have flowed as a Bingham-plastic or a Coulomb-viscous substance late in its travel history. However, its apparent transition from dry sliding to moist flow and the observed quantitative similarities between moist, water-saturated, and dry landslides suggest that the flow of fine-grained material plays the critical role in each form of mass movement. The flow of basal dry rock powder appears to control the runout of dry rock avalanches, whereas moist fine-grained material controls the travel of water-rich landslides.

Acknowledgements

Support for this project was provided by NASA grant NAGW-1373. I am indebted to John Shelton for encouragement and background information on the Carlson landslide and for the use of his aerial photograph of the landslide in this manuscript. Many thanks to A. L. Albee, Ron Scott, Bob Sharp, and Bruce Murray for their time and help in interpreting the landslide and improving this manuscript and to Murray for unflagging support of this venture. Thanks also to Tom Rockwell for use of the "Livingston corer" and to Danny Hagens for tutorial on same and to Doane Western Co. for permission to cross the old Carlson Ranch property. Finally, I owe overwhelming gratitude to Ann Shaller for field assistance above and beyond the call of duty despite sleet and charging antelopes.

BAKER, V.R., 1983. The channels of Mars. University of Texas Press, Austin, pp. 1–198.

BOCK, C.G. 1977. Martinez Mountain rock avalanche. *In* Landslides. *Edited by* D.R. Coates. Reviews in Engineering Geology, 3: 155–168.

BROWN, R.L., and RICHARDS, J.C. 1970. Principles of powder mechanics. Pergamon Press, Oxford, United Kingdom, pp. 1–223.

CALDWELL, D.H., and BABBITT, H.E. 1941. Flow of muds, sludges and suspensions in circular pipe. Industrial and Engineering Chemistry, **33**: 249–256.

CAMPBELL, C.S. 1989. Self-lubrication for long runout landslides. Journal of Geology, **97**: 653–665.

CARR, M.H. 1981. The surface of Mars. Yale University Press, New Haven, CT, pp. 1–232.

CRANDELL, D.R. 1989. Gigantic debris avalanche of Pleistocene age from ancestral Mount Shasta volcano, California, and debris-avalanche hazard zonation. United States Geological Survey, Bulletin 1861, pp. 1–32.

CRUDEN, D.M., and HUNGR, O. 1986. The debris of the Frank Slide and theories of rockslide–avalanche mobility. Canadian Journal of Earth Sciences, **23**: 425–432.

DAVIES, T.R.H. 1982. Spreading of rock avalanche debris by mechanical fluidization. Rock Mechanics, **15**: 9–24.

EPPLER, D.B., FINK, J., and FLETCHER, R. 1987. Rheologic properties and kinematics of emplacement of the Chaos Jumbles rockfall avalanche, Lassen Volcanic National Park, California. Journal of Geophysical Research, **92**: 3623–3633.

ERISMANN, T.H. 1979. Mechanisms of large landslides. Rock Mechanics, **12**: 15–46.

FAUQUE, L., and STRECKER, M.R. 1988. Large rock avalanche deposits (Sturzströme, sturzstroms) at Sierra Aconquija, northern Sierras Pameanas, Argentina. Eclogae Geologicae Helvetiae, **81**: 579–592.

GOGUEL, J. 1978. Scale-dependent rockslide mechanisms, with emphasis on the role of pore fluid vaporization. *In* Rockslides and avalanches. Vol. 1. Natural phenomena. *Edited by* B. Voight. Elsevier, New York, pp. 693–706.

HABIB, P. 1975. Production of gaseous pore pressure during rock slides. Rock Mechanics, **7**: 193–197.

HALLER, K.M. 1988. Proposed segmentation of the Lemhi and Beaverhead faults, Idaho, and Red Rock fault, Montana—Evidence from studies of fault-scarp morphology. Geological Society of America, Abstracts with Programs, **20**: 418–419.

HEIM, A. 1932. Bergsturz und Menschenleben. Fretz & Wasmuth Verlag A. G., Zürich, pp. 1–217. (English translation by N.A. Skermer, BiTech Publishers, Vancouver, B.C.)

HOWARD, K.A. 1973. Avalanche mode of motion: Implications from lunar examples. Science (Washington, D.C.), **180**: 1052–1055.

HSÜ, K.J. 1975. Catastrophic debris streams (sturzstroms) generated by rockfalls. Geological Society of America Bulletin, **86**: 129–140.

HULME, G. 1974. The interpretation of lava flow morphology. Geophysical Journal of the Royal Astronomical Society, **39**: 361–383.

JOHNSON, A.M. 1970. Physical processes in geology. Freeman, Cooper & Co., San Francisco, pp. 433–459.

_____ 1984. Debris flow. *In* Slope Instability. *Edited by* D. Brunsden and D.B. Prior. John Wiley & Sons, New York, pp. 257–361.

JOHNSON, N. 1978. Blackhawk landslide, California, U.S.A. *In* Rockslides and avalanches. Vol. 1. Natural phenomena. *Edited by* B. Voight. Elsevier, New York, pp. 481–504.

KENT, P.E. 1966. The transport mechanism in catastrophic rock falls. Journal of Geology, **74**: 79–83.

KOJAN, E., and HUTCHINSON, J.N. 1978. Mayunmarca rockslide and debris flow. *In* Rockslides and avalanches. Vol. 1. Natural phenomena. *Edited by* B. Voight. Elsevier, New York, pp. 315–361.

KRIEGER, M.H. 1977. Large landslides, composed of megabreccia, interbedded in Miocene basin deposits, southeastern Arizona. United States Geological Survey, Professional Paper 1008, pp. 1–25.

KRUMDIECK, M.A. 1984. On the mechanics of large landslides. Proceedings, 4th International Symposium on Landslides, Toronto, vol. 1, pp. 539–544.

LUCCHITTA, B.K. 1978. A large landslide on Mars. Geological Society of America Bulletin, **89**: 1601–1609.

_____ 1987. Valles Marineris, Mars: Wet debris flows and ground ice. Icarus, **72**: 411–429.

MAPEL, W.J., READ, W.H., and SMITH, R.K. 1965. Geologic map and sections of the Doublespring Quadrangle, Custer and Lemhi Counties, Idaho. United States Geological Survey, General Quadrangle Map GQ-464, scale 1 : 62 500.

MCEWEN, A.S. 1989. Mobility of large rock avalanches: Evidence from Valles Marineris, Mars. Geology, **17**: 1111–1114.

MCSAVENEY, M.J. 1978. Sherman Glacier rock avalanche, Alaska, U.S.A. *In* Rockslides and avalanches. Vol. 1. Natural phenomena. *Edited by* B. Voight. Elsevier, New York, pp. 197–258.

MEINZER, O.E. 1924. Ground water in Pahsimeroi Valley, Idaho. Idaho Bureau of Mines and Geology, Pamphlet 9.

MELOSH, H.J. 1987. The mechanics of large rock avalanches. Reviews in Engineering Geology, **7**: 41–49.

NYE, J.F. 1951. The flow of glaciers and ice-sheets as a problem in plasticity. Proceedings of the Royal Society of London, Series A, **207**: 554–572.

PIERCE, K.L., and SCOTT, W.E. 1982. Pleistocene episodes of alluvial-gravel deposition, southeastern Idaho. *In* Cenozoic Geology of Idaho. *Edited by* B. Bonnichsen and R.M. Breckenridge. Idaho Bureau of Mines and Geology, Bulletin 26, pp. 685–702.

PLAFKER, G., and ERICKSEN, G.E. 1978. Nevados Huascarán avalanches, Peru. *In* Rockslides and avalanches. Vol. 1. Natural phenomena. *Edited by* B. Voight. Elsevier, New York, pp. 197–258.

POTAPOV, A.V., and IVANOV, B.A. 1991. Landslide motion: Numerical simulation for Earth and Mars. Proceedings, 22nd Lunar and Planetary Science Conference, Lunar and Planetary Institute, in press.

ROSS, C.P. 1947. Geology of the Borah Peak quadrangle, Idaho. Bulletin of the Geological Society of America, **58**: 1085–1160.

SALYARDS, S.L. 1985. Patterns of offset associated with the 1983 Borah Peak, Idaho, earthquake and previous events. *In* Proceedings of Workshop 28 on the Borah Peak, Idaho, Earthquake. *Edited by* R.S. Stein and R.C. Bucknam. United States Geological Survey, Open-file Report 85-290, pp. 59–75.

SAVAGE, S.B. 1984. The mechanics of rapid granular flows. Advances in Applied Mechanics, **24**: 289–366.

SCHEIDEGGER, A.E. 1973. On the prediction and reach of catastrophic landslides. Rock Mechanics, **5**: 231–236.

SCHELLER, E. 1971. Beitrag zum Bewegungsverhalten grosser Bergstürze. Eclogae Geologicae Helvetiae, **64**: 195–202.

SCHWARTZ, D.P., and CRONE, A.J. 1988. Paleoseismicity of the Lost River fault zone, Idaho: Earthquake recurrence and segmentation. Geological Society of America, Abstracts with Programs, **20**: 228.

SCOTT, D.H., and TANAKA, K.L. 1986. Geologic map of the western equatorial region of Mars. United States Geological Survey, Miscellaneous Investigations Series Map I-1802-A, scale 1 : 15 000 000.

SCOTT, W.E., PIERCE, K.L., and HAIT, M.H. 1985. Quaternary tectonic setting of the 1983 Borah Peak earthquake, central Idaho. Bulletin of the Seismological Society of America, **75**: 1053–1066.

SHALLER, P.J. 1991. Analysis and implications of large martian and terrestrial landslides. Ph.D. thesis, California Institute of Technology, Pasadena.

SHARP, R.P. 1988. Living ice: understanding glaciers and glaciation. Cambridge University Press, New York, p. 25.

SHARP, R.P., and NOBLES, L.H. 1953. Mudflow of 1941 at Wrightwood, southern California. Bulletin of the Geological Society of America, **64**: 547–560.

SHELTON, J.S. 1966. Geology illustrated. W.H. Freeman and Company, San Francisco, pp. 124–125, 381.

SHREVE, R.L. 1966. Sherman landslide, Alaska. Science (Washington, D.C.), **154**: 1639–1643.

——— 1968. The Blackhawk landslide. Geological Society of America, Special Paper 108, pp. 1–47.

SIEBERT, L. 1984. Large volcanic debris avalanches: Characteristics of source areas, deposits, and associated eruptions. Journal of Volcanology and Geothermal Research, **22**: 163–197.

SOLONENKO, V.P., DEM'YANOVICH, M.G., and AVDEEV, V.A. 1984. The engineering seismogeology of the northern Muya Interrift Commissure (Baikal Rift Zone). Geologiya i Geofizika, **25**(6): 3–15.

STICKNEY, M.C., and BARTHOLOMEW, M.J. 1987. Seismicity and late Quaternary faulting of the northern Basin and Range Province, Montana and Idaho. Bulletin of the Seismological Society of America, **77**: 1602–1625.

STUIVER, M., and BECKER, B. 1986. High-precision decadal calibration of the radiocarbon time scale, AD 1950 – 2500 BC. Radiocarbon, **28**: 863–910.

TRUNK, F.J., DENT, J.D., and LANG, T.E. 1986. Computer modeling of large rock slides. ASCE Journal of Geotechnical Engineering, **112**: 348–360.

UI, T. 1983. Volcanic dry avalanche deposits—Identification and comparison with nonvolcanic debris stream deposits. Journal of Volcanology and Geothermal Research, **18**: 135–150.

UI, T., KAWACHI, S., and NEALL, V.E. 1986. Fragmentation of debris avalanche material during flowage—Evidence from the Pungarehu Formation, New Zealand. Journal of Volcanology and Geothermal Research, **27**: 255–264.

VAN GASSEN, W., and CRUDEN, D.M. 1989. Momentum transfer and friction in the debris of rock avalanches. Canadian Geotechnical Journal, **26**: 623–628.

VOIGHT, B., JANDA, R.J., GLICKEN, H., and DOUGLASS, P.M. 1983. Nature and mechanics of the Mount St. Helens rockslide-avalanche of 18 May 1980. Géotechnique, **33**: 243–273.

WAHRHAFTIG, C., and COX, A. 1959. Rock glaciers in the Alaska Range. Bulletin of the Geological Society of America, **70**: 383–436.

YARNOLD, J.C., and LOMBARD, J.P. 1989. A facies model for large rock-avalanche deposits formed in dry climates. *In* Conglomerates in basin analysis: A symposium dedicated to A.O. Woodford. *Edited by* I.P. Colburn, P.L. Abbott, and J. Minch. Pacific Section, Society of Economic Paleontologists and Mineralogists, pp. 9–31.

REVIEW OF PROPOSED MECHANISMS FOR STURZSTROMS (LONG-RUNOUT LANDSLIDES)

Philip J. Shallenwith Ann Smith Shaller
Woodward-Clyde Consultants
2020 East First Street, Suite 400
Santa Ana, California 92705

ABSTRACT

No less than 20 mechanical models have been advanced to explain the suite of characteristics associated with high-volume, rapid, long-runout landslides, or sturzstroms. The majority of the proposed models attempt to explain sturzstroms by way of a single unifying theory, while the remainder try to explain the phenomenon on a case-by-case basis. The anomalous nature of sturzstroms is first illustrated with a discussion of a simple block-on-inclined-plane model. Four separate categories of theories are then discussed and evaluated for their ability to explain the variety of unusual phenomena associated with sturzstroms. These categories include: 1) bulk fluidization and flow of landslide debris; 2) special forms of lubrication along the base of the slides; 3) mass-loss mechanisms coupled with normal frictional sliding; and 4) individual-case mechanisms. The theories composing these groups approach the subject with varying degrees of depth, ranging from qualitative, kinematic arguments to highly quantitative mathematical modeling efforts. Although considerable time and energy has been spent over the last century seeking the mechanism of sturzstroms, no one theory has successfully determined the mechanism of all sturzstroms. Computer and experimental simulations offer the promise of ultimately modeling the mechanics of sturzstroms, but continued field study of sturzstroms is essential in order to allow critical evaluation of the veracity of the simulations.

INTRODUCTION

Researchers have struggled to understand how and why large falling masses of rock exhibit their remarkable suite of characteristics ever since Heim (1882) first recognized the unusually great runout lengths of what he later called sturzstroms. In the century since Heim conducted his pioneering studies of the Elm landslide and of a whole population of older and larger landslides in the Alps, researchers have repeatedly revisited the problem using a wide variety of approaches. These efforts have yielded no less than 20 mechanical models for explaining long runout in high-volume rapid landslides, or sturzstroms. These modeling efforts have approached sturzstroms in one of two ways: the majority attempt to explain long runout by way of a single unifying theory while the remainder try to explain the phenomenon on a case-by-case basis. Modelers seeking a unified theory for long runout are supported by the fact that long runout occurs as the rule in large, rapid landslides, rather than the exception. Unfortunately, no one has yet successfully integrated the full spectrum of field observations into a unified theory. In nearly every case, these models have been developed to explain the characteristics of individual landslides or of a small subset of landslides, such as historically observed occurrences, and then have been advanced as general solutions to the problem. This paper will discuss only the major theories that have been advanced for the mechanism of sturzstroms, and will not attempt to be comprehensive in describing every mechanism that has been proposed.

The anomalous nature of sturzstroms is first illustrated with a discussion of a simple block-on-inclined-plane model. Following this discussion, four separate categories of theories are discussed and evaluated for their ability to explain the variety of unusual phenomena associated with sturzstroms. These categories include: 1) bulk fluidization and flow of landslide debris; 2) special forms of lubrication along the base of the slides; 3) mass-loss mechanisms coupled with normal frictional sliding; and 4) individual-case mechanisms. The first three categories include descriptions of mechanisms proposed as unifying theories of long runout, applicable to many or all sturzstroms. The fourth category consists of mechanisms proposed to explain long runout on a case-by-case basis. The theories presented in the fourth category do not attempt to explain long runout as a universal property of sturzstroms, but rather strive to define the phenomenon based on local effects of the depositional environment. The various theories composing these groups approach the subject with varying degrees of depth, ranging from qualitative, kinematic arguments to highly quantitative mathematical modeling efforts.

THE BLOCK-ON-INCLINED PLANE MODEL

A conceptual model of a sliding block on an inclined plane offers the most basic model of landslide runout. This model is most useful in highlighting the difference between "normal" frictional behavior and the character of

In: Sturzstroms and Detachment Faults, Anza-Borrego Desert State Park, California: South Coast Geological Society, Annual Field Trip Guidebook No. 24, 1996, pp. 185-202.

sturzstroms. Figure 1 shows a sketch of the model, including the forces acting on the block during the acceleration (down a slope of length **x**) and deceleration phases of runout. For a rigid block of mass **m**, sliding down an inclined plane at angle β, under gravitational acceleration (**g**) with a constant basal coefficient of sliding friction (μ_k) one finds that the center of gravity of such a block will always end movement when the ratio of fall height (**H**) to runout length (**L**) (which includes the part of the block's travel on the plane (**y**) plus the horizontal component of movement of the block while on the slope), of the center of mass equals the coefficient of sliding friction of the block over its substrate (Shaller, 1991a). In this model, the mass of the sliding block and the acceleration of gravity in the experimental setting cancel out and have no influence on the apparent angle of sliding friction traveled by the block at emplacement. Nearly all sturzstroms vary from this model in some respects, however. Most do not remain rigid blocks during emplacement, while some may experience anomalously low or variable coefficients of sliding friction during runout. The results of these departures from the sliding block model are that both volume (mass) and gravitational acceleration become important factors in determining the distance a sturzstrom will travel during runout for a given value of fall height.

PROPOSED MECHANICAL MODELS

The treatment of sturzstroms in the scientific and engineering literature has often considered these mass movements as traveling by means of a common, but obscure, mechanism. Heim (1932) appears to have been the first to make this implicit assumption after his study of numerous large Alpine landslides. A number of different mechanical theories have been proposed to explain long runout as a group phenomenon. These theories consist of bulk fluidization models (Heim, 1932; Kent, 1966; Hsü, 1975; Davies, 1982; Melosh, 1983; Trunk, et al., 1986; Campbell, 1989; McEwen, 1989; Campbell, et al., 1995), basal lubrication models (Shreve, 1968a; Erismann, 1979) and one mass-loss "rocket" model (Van Gassen and Cruden, 1989).

The various theories outlined above typically address one or more of a number of common geomorphic and sedimentologic characteristics of sturzstroms. Table 1 lists several of the proposed mechanical models of sturzstroms and indicates which common characteristics of sturzstroms are accounted for by each model. The critical characteristics listed on Table 1 were the most commonly shared characteristics of sturzstroms, as determined from a database of sturzstrom deposits on Earth, Mars and the Moon collated by Shaller (1991a). Included among the critical characteristics are their high speed emplacement, their fluid-like morphologies, and their generally sheet-like geometries (except when deposited into deep valleys). Also included is the phenomenon that the headscarp stratigraphy in the source areas of large landslides are typically preserved in sturzstrom deposits, even though the final deposits are much thinned and elongated from the dimensions of the original slide blocks. Sturzstroms also characteristically demonstrate reverse grading, and a group "volume effect," by which is meant that for a given fall height, larger volume sturzstroms, on average, travel further from their source than do smaller ones. The onset volume refers to the observation that, generally, sturzstroms do not occur below the threshold volume of about 1,000,000 cubic meters of rock debris. Landslides smaller than this are typically considered to display "normal" rockfall behavior. Three-dimensional jigsaw puzzle breccia, first defined by Shreve (1968a) for the Blackhawk landslide, is a typical texture observed on sturzstrom deposits, and refers to highly fractured blocks, the component pieces of which are little separated from one another. Sudden halts and distally raised margins are two other moderately common features of sturzstroms. Finally, one column of Table 1 indicates whether the model can explain the presence of sturzstroms on Mars or the Moon.

An alternative means to view the travel of large landslides is to consider their behavior on an individual-case basis. Using this outlook, one may consider the long runout of sturzstroms as an opportunistic phenomenon that occurs under various different conditions for different reasons. Proposals have been made in the literature that individual large landslides have exhibited long runout because of various bulk fluidization or basal lubrication mechanisms. These mechanisms include earthquake fluidization (Solonenko, 1972; Hazlett, et al., 1991), sliding on a vaporized pore fluid gas cushion (Habib, 1975; Goguel, 1978), sliding on a weak stratum in the landslide debris (Watson and Wright, 1969; Johnson, 1978), or sliding over snow (McSaveney, 1978), mud (Evans, pers. comm., 1990), or moist soil (Heim, 1932) in the substrate.

UNIVERSAL BULK FLUIDIZATION MODELS

Bulk fluidization theories form the first large group of models proposed to explain the long-runout of sturzstroms. These models suggest that clasts forming large landslides move with respect to each other during runout throughout the body of a landslide, like molecules in a dense gas or a fluid, and therefore give a large moving landslide the appearance of flowing during runout. Various means of fluidization of landslide debris have been suggested, including upward injection of air into overriding rock masses, energy from the fall, self-generated acoustic energy and energy added from external sources, such as an earthquake.

Heim provided the first analysis of the nature of long runout in sturzstroms. After field study of many old, large, Alpine landslides and extensive interviews with numerous survivors of the Elm landslide of 1881, Heim (1932) concluded that large landslides experience some sort of bulk flow, perhaps akin to the behavior of glaciers and lava flows. In part, this derived from his observation that channeled sturzstrom deposits display many morphological similarities with lava flows and mountain glaciers, including such features as ridges and troughs oriented convex in the downslope direction, consistent with more rapid movement along the center of the sturzstrom than along its margins. The stopping phase of sturzstroms also appears to have given Heim considerable pause. His interviews of Elm survivors seem to have convinced him that large landslides stop with remarkable abruptness, leading him to conceive of a velocity-dependent frictional coefficient for the moving debris.

Heim (1932) also attempted to understand the phenomenon on the scale of the individual clasts within a moving landslide, which he conceptualized as analogous to the molecules in a flowing liquid. This concept provided Heim a means of understanding why larger sturzstroms would exhibit lower apparent friction than smaller landslides, namely that increasing the volume of a landslide would have the effect of reducing the effective sizes and therefore the importance of individual clasts within the moving debris. Thus sturzstroms would become increasingly "fluid-like" at higher volumes.

As with most of the proposed theories of long runout in sturzstroms, Heim's concepts explain some features quite nicely, but others not so well. The preservation of headscarp stratigraphy in all dry multiple-lithology landslides places strict limits on the amount of internal motion a sturzstrom might experience. Turbulent mixing of landslide debris would clearly cause disruption of stratigraphy throughout a landslide mass and must be dismissed. However, bulk laminar flow too would cause the disruption of stratigraphy, because material at the leading edge of a laminar flow would by necessity roll over and mix. This problem is the principle drawback to all proposed mechanisms of long runout which attempt to describe the phenomenon by means of a bulk flow process. The possibility does exist, however, that the basal layer of a sturzstrom might preferentially experience flow during runout without disrupting headscarp stratigraphy in the final deposit, as discussed in Shaller (1991a), in a manner analogous to hypothesized "plug flow" in debris flows (Johnson, 1970) and lava flows (Hulme, 1974).

Heim's (1932) observation of flow structures on channelized landslides indicates that the landslides developed transverse velocity profiles during runout, with material along the centerline moving faster than material along the edges of a channel. However, rather than occurring by way of bulk flow, this velocity distribution may have occurred in a more discontinuous fashion, such as along vertical slip planes, as suggested for the Carlson landslide by Shaller (1991b). Heim's concept of volume dependence related to the relative sizes of clasts in a sturzstrom agrees to some extent with the observation made by Shaller (1991a) that grain size has a critical effect on the apparent angle of sliding friction exhibited by sturzstroms. Smaller clast sizes were found to correlate with a lower apparent angle of sliding friction independently of volume. Heim's volume dependence concept is also apparently consistent with recent computer modeling by Campbell, et al. (1995) who have simulated sturzstroms by following the interactions of thousands of idealized model particles. This model will be discussed in more detail later.

The data on sturzstroms do not show any clear correlation between emplacement velocity (principally derived from the heights of overtopped obstacles), and apparent angle of sliding friction (Shaller, 1991a). Also, velocity data from two Soviet artificially-triggered landslides that exhibited long runout reported in Shaller (1991a) do not support the idea that sturzstroms characteristically stop suddenly from high speed, as suggested by eyewitnesses of the Elm landslide (Heim, 1932). Thus, a velocity-dependent frictional coefficient does not appear universally necessary.

Kent (1966) based his air fluidization theory on geologic relations of the Saidmarreh, Frank and Madison landslides, as well as on eyewitness accounts of the emplacement of Frank and Madison. Referring specifically to Frank, but apparently applying the idea also to the other two deposits, Kent stated:

> ...it seems highly probable that the high speed and high fluidity of the landslip, with its ability to flow uphill without hindrance from normal friction, was due to fluidization with air -- the air entrapped during the first few hundred feet of fall being "entangled" in the rock for long enough to permit the rock to flow as a liquid.

Kent's model was strongly influenced by eyewitness accounts from the Frank and Madison landslides of strong air blasts accompanying passage of the debris. He observed certain characteristics about the sturzstroms including: the fan-like spreading of the landslides, the fact that they ended movement in thin sheets relative to their aerial dimensions, that they traveled at high speeds, exhibited a high degree of fluidity during runout, and were deposited as a chaotic assortment of blocks without gravity sorting. However, Kent did not single out any of the above characteristics for explanation by entrapped air fluidization, but simply noted that: "fluidization by entrapped air appears to be the only mechanism capable of explaining the observed features, and major landslides of sheetlike form thus present a special and perhaps unique case of geomorphological transport."

Several drawbacks exist in Kent's air fluidization theory. One is that it fails to explain the preserved stratigraphy observed in the Saidmarreh and Madison

landslides, as reported by Watson and Wright (1969) and Hadley (1978), respectively, which suggests that these landslides did not experience turbulent flow throughout their interiors during emplacement, as expected with fluidization by escaping air (Brown and Richards, 1970). Another problem with air fluidization is that in industrial use it gives rise to normally-graded bedding so long as a distribution of clast sizes exist (Brown and Richards, 1970). Graded bedding results because air expelled from beneath a landslide should carry smaller particles more readily than larger ones. When the air finally gives out, the larger clasts fall out of suspension first, followed by smaller fragments, leading to a gradation of clast sizes from large at the bottom to small on top. In contrast, each of the Kent's "air-fluidized" landslides exhibit reverse grading, with the largest clasts on top (Watson and Wright, 1969; Cruden and Hungr, 1986; Hadley, 1978). Other sturzstroms either exhibit reverse grading or no grading at all; none are known to show normally graded bedding (Shaller, 1991a). The composite evidence therefore suggests that air fluidization does not provide a reasonable method for achieving long runout in any known sturzstroms.

Several theories which succeeded the air fluidization model of Kent (1966) instead invoked mechanical fluidization to explain the long runout of large landslides.

Hsü (1975) in essence restated Heim's conceptual model of flow in sturzstroms in quantitative terms based on the cohesionless grain flow theory of Bagnold (1954; 1956). This theory describes the turbulent flow of a dispersion of cohesionless grains in a fluid medium (Hsü, 1975). Hsü (1975) pointed out that the flow of mixtures of solid grains and fluid involves a fluid-transmitted stress, t, and a grain-transmitted stress, T; the total stress is the sum of the two.

In an ideally fluidized bed, as envisioned by Kent (1966), the fluid-transmitted stress, t, would provide the dominant component of the total stress, being produced by a rising current of air, and the grain-transmitted stress, T, would ideally equal zero. Hsü (1975) considered this method a highly improbable means of suspending landslide debris. He believed, on the contrary, that the flow motion of the debris of large landslides was propelled principally by the stress transmitted by grains, T, as a result of grain collisions. In this type of flow, kinetic energy transfers through grain collisions, and dissipates by friction during such impacts. The mathematical derivation of "Bagnoldian" grainflow is quite involved and is not pursued here.

Hsü's calculations indicate that flowing grain masses can move down gentle slopes in the presence of an interstitial fluid that reduces the effective normal pressure on grains and consequently reduces the frictional resistance. For wet landslides like the 1970 Huascaran landslide, Hsü (1975) proposed that mud could form the fluid component between clasts, giving rise to the observed fluid-like flow of these landslides. Alternatively, in the case of large dry landslides, Hsü postulated that fine dust might act as the interstitial fluid.

The mechanical fluidization model proposed by Hsü takes as a given the kinematic descriptions of sturzstrom movement by Heim (1932), namely that these landslides flow into place like some sort of viscous fluid. However, the cohesionless grain flow model fails to explain the observation of preserved stratigraphy in dry sturzstroms because the theory presupposes turbulent flowing motion throughout a landslide mass. In addition, Melosh (1983) objected to Hsü's model on conceptual grounds, arguing first that dust suspension in dry rock landslides could not act as the type of interstitial fluid required by Bagnold's theory. He also points out that keeping the rock mass fluidized this way "requires too much energy," especially if the size of the rock fragments is decreased (commonly the debris at the base of a sturzstrom is pulverized into sand-sized and smaller material), because

> ...the average rock velocity and energy density to support the slide are unchanged, but the number of collisions per second in a given volume increases, thus increasing the rate of energy dissipation and making the mechanism still less plausible.

However, under specific circumstances, this energy loss may be much less than calculated by Melosh, evidenced by the results of computer modeling studies including Campbell, et al. (1995), which is discussed later.

Nevertheless, nothing in the cohesionless grain flow model presented by Hsü (1975) can account for the volume dependence of the apparent angle of sliding friction exhibited by sturzstroms, and there is no reason for this mechanism to work only for the large ($>10^6$ m^3) landslides that exhibit long-runout.

Davies (1982) also theorized that mechanical fluidization of the brecciated rock in a moving landslide causes the long runout of sturzstroms. Davies (1982), like Hsü (1975), based his model on the grain-flow theory of Bagnold (1954) and expanded upon Hsü's theory. Davies (1982) hypothesized that:

> ...the debris deposits of sturzstroms are formed by fluidlike spreading of the debris under the action of gravity, and...this spreading occurs due to fluidisation of the debris caused by high basal shear rates as it moves rapidly across the ground...
>
> The mechanism envisaged is thus as follows:
> (i) a debris mass achieves a high velocity by virtue of its fall from a mountain;
> (ii) upon reaching relatively level ground, if the forward velocity is sufficient, shear at the base of the debris causes dilation and reduction of internal friction;

(iii) the debris mass becomes fluidised and spreads out under gravity, retaining forward motion;
(iv) when the forward velocity decreases so that the basal shear is no longer sufficient to maintain the dilation the internal friction increases, the mass becomes rigid and it slides quickly to a halt.

Davies (1982) modeled the process in the laboratory using a quantity of coarse sand in a plastic tray that was surfaced with a coating of glued-on coarse sand, and which could be made to oscillate at frequencies between 4 and 30 Hz. Among his findings, he noted that at frequencies greater than about 10 Hz the inertia of the main grain mass held it stationary while the tray floor and sides oscillated relative to it.

Davies (1982) combined the results of his flowing grain experiment with the mathematical theory of grain flow of Bagnold (1954) and with the apparent angle of sliding friction vs. log(volume) relations of 26 sturzstroms on Earth, Mars and the Moon to attempt to understand the origin of several common characteristics of sturzstroms. The features he considered include: the decrease in apparent angle of sliding friction with increasing volume, the observation of preserved stratigraphy, three dimensional jigsaw-puzzle breccia, reverse grading, and the reported sudden stops of large landslides from high speed. Davies (1982) viewed the effect of volume on the apparent angle of sliding friction as the result of "fluid-like" spreading of sturzstroms during runout into thin sheets; the larger the volume, the larger the area covered by debris, and the longer the runout length for a given fall height. He attributed the preservation of stratigraphy to the observation in the experimental study that the relative motion between a moving mass of grains and the substrate was concentrated near the base, over which unsheared material moved with little disruption. To explain the observation of three dimensional jigsaw-puzzle breccia and reverse grading, he hypothesized that rocks shattered during their fall from the mountain could be carried on the surface "without their constitutive pieces becoming widely separated," due to the relatively low shear rates of the surface. He also interpreted the reverse grading of sturzstrom deposits to have originated by means of migration of large clasts from the interior to the surface as a result of differential shear stresses in the body of a sturzstrom.

Davies (1982) also attempted to explain the sudden stops of sturzstroms reported by eyewitnesses in Heim (1932):

> As a dilated, flowing sturzstrom slows down, a critical velocity seems likely to occur at which the degree of dilation begins to reduce appreciably. This will accordingly cause the internal friction of the shearing layers to increase, and the velocity of flow will thus decrease more rapidly. The result may be to cause the distal edges of the flow to become, quite suddenly, solidified, and to slide to a halt quite rapidly under "normal" frictional effects.

While Davies (1982) addresses many of the most important properties of sturzstroms in his analysis, his proposed model of basal shear-induced mechanical fluidization is based on a number of problematic assumptions and observations. First, the experimental apparatus used to support his theory lacked any consideration of scaling laws for forces or material strengths; rather, the sand grains in this apparatus experienced only minor shear stresses relative to clasts near the base of an actual sturzstrom moving at high velocity with a thickness of tens or hundreds of meters. In addition, the experiment provided a source of vibrational energy to fluidize the grains in the mass, much as is done to sink piers into well-sorted sand in engineering projects (Scott, 1963); the fluidization of the basal materials in the moving sand body therefore did not result from movement-induced shear of the mass of sand along its base, but rather originated from the external energy added to the system. Thus, the experimental apparatus fails to give definitive evidence that the base of a large landslide may be fluidized by its own movement over the substrate, though his interpretations of the nature of the scale effect and three dimensional jigsaw-puzzle effect are consistent with some sort of basal flow phenomenon over which the landslide debris may spread out.

Davies' proposed model also fails to properly explain some important geological relations associated with sturzstroms. One problem is that he attempts to explain the reverse grading of sturzstrom deposits as resulting from the migration of large clasts upwards through a moving breccia mass during transport. The preservation of stratigraphy commonly observed in field relations of sturzstroms suggests that this phenomenon does not occur in these deposits (Shaller, 1991a). It is also inconsistent with Davies own hypothesis of the transport of three-dimensional jigsaw-puzzle blocks, which he interpreted to ride down atop the sturzstrom debris. In addition, the observation of the high angularity of surficial boulders on many sturzstroms suggests that they were never located within the landslides, where the would incur significant impact abrasion (Yarnold and Lombard, 1989; Shaller, 1991a; Yarnold, 1993). Instead, material which begins motion near the base remains near the base for the duration of movement and becomes well sheared during transport, while material beginning near the surface stays near the surface throughout movement. Examples of landslides exhibiting this behavior include El Capitan (Krieger, 1977), Goldau (Heim, 1932) and Martinez Mountain (Shaller, 1991a).

Another troubling aspect of the Davies (1982) model is that it predicts a sudden stop for large landslides, related to the collapse of shear-induced dilation of the flowing breccia during slowing of the landslides. However, as

previously discussed, Soviet data for two sturzstroms fail to show any evidence of sudden stopping, suggesting that collapse of a flowing dilated mass of debris probably does not account for the stopping of sturzstroms.

Campbell is among a number of researchers currently investigating mechanical fluidization by use of computer models of interacting two-dimensional disks (Campbell, 1989; Jenkins, pers. comm., 1990; Savage, pers. comm., 1990; Campbell, et al., 1995). In 1989, Campbell published a model where each particle was modeled a two-dimensional disc, free to translate and rotate, but whose motion was confined to the *x*-*y* plane. The particles were allowed to interact with one another by collision during which energy was dissipated through a coefficient of restitution and through surface friction, and in which both linear and angular momentum were conserved. In this model, particle and bed properties could be manipulated to develop a low-density basal layer of rapidly moving particles that supported an overriding high-density, low-mobility debris "plug" during travel. When set up with the proper initial conditions, this model could yield apparent frictional coefficients of less than 0.1 for the moving mass.

Campbell, et al. (1995) presented a subsequent, much more elaborate modification of this initial model. Computer simulations of granular avalanches were performed using from 5,000 up to 1,000,000 two-dimensional discs (the latter requiring over a year of computer time!). The discs were initially placed tightly packed but without cohesion on simulated slopes angled at 30°, 45° and 60°. The simulations were started with the top edge of the model slope failure located at 1300 particle diameters above the valley floor. This initial elevation was chosen so that if the particle diameter was taken to be 1 m, then this would approximate the initial 1300 m fall height of the Sherman landslide. At the beginning of a model run, the group of particles were allowed to move downslope under simulated gravity and to run out on a flat depositional plane. The discs could be color-coded to permit tracking of individual "layers" in the source slope from start to finish.

In general, the computer simulations showed that the lowermost material on the failed model slopes would accelerate at the highest rate since it was unimpeded by other material. This had the immediate effect of straining and thinning the landslide material in the downslope direction. This is consistent with the thinning of landslide debris observed in all sturzstroms. As in the earlier granular avalanche simulations presented in Campbell (1989), most of the shearing of the modeled sturzstroms took place near the base; hence, after the initial straining and thinning, the landslide debris experienced only minor internal shearing with the result that the headscarp stratigraphy was preserved in the final deposits, consistent with observation. Also, the material that started on top of the slide block ended atop the final debris fragments on the surfaces of sturzstroms. Differing final profiles of the model sturzstroms were achieved by varying the ratio of number of particles to the fall height; a distally-raised profile shape was achieved for model sturzstroms with a relatively low ratio of particles to fall height, while the opposite trend (material piled near the base of slope and tapering toward the toe) was achieved when the particle number to fall height ratio was relatively low. These results are consistent with observed profile relations summarized in Shaller (1991a). The computer simulations also mimicked the decrease in apparent angle of friction with increasing volume that characterize sturzstroms. The origin of the volume effect in the simulations was not, however, immediately apparent. The model results suggest that the basal friction coefficient varies with shear rate; higher shear rates give rise to higher friction coefficients. For sturzstroms with a given fall height to particle diameter ratio, landslides with larger volumes have lower internal shear rates, and thus, lower basal friction coefficients.

The numerical simulations presented in Campbell, et al. (1995) provide a compelling new way of investigating the long-runout phenomenon in sturzstroms. This investigation is particularly significant because the simulations mimic so many aspects of sturzstroms, from the effect of volume on runout length to the preservation of stratigraphy, by means of a repeatable, quantitative method. The results show that many of the significant aspects of sturzstroms can apparently result strictly from the interaction of the very large number of particles comprising a granular avalanche.

The primary drawbacks to the simulations presented by Campbell, et al. (1995) are the necessary simplifications needed to make running the simulations possible in finite time on currently available computer systems. To more closely model actual sturzstroms, future models should incorporate non-circular particles, non-uniform grain sizes, the effects of grain comminution, and effects of topography and substrate. For example, would the simulations provide similar results if basal grains were permitted "fragment" into numerous smaller grains? This type of fragmentation would likely result in many more energy-absorbing grain interactions per unit time than in the uniform grain-size model and could inhibit runout in modeled sturzstroms. Such numerical simulations will become more feasible with ongoing advances in computing power.

Melosh's (1979; 1983; 1986; 1987) acoustic fluidization theory presents yet another approach to modeling long runout as a flow phenomenon. Melosh has proposed the theory as a more geologically and energetically acceptable version of fluidization than the dispersive grain flow model of Hsü (1975). As opposed to Hsü's model, where the fluidization energy is derived directly from the kinetic energy of a falling rock mass via inter-clast collisions, Melosh suggests that acoustic fluidization is produced indirectly by the released fall energy through the propagation of strong sound waves of just the right frequency through a flowing breccia stream. The acoustic energy for fluidization is thought to be broad-

band white noise (hissing) generated by the movement of a landslide as it falls down slope; the acoustic energy, therefore, is generated at the expense of the gravitational potential energy of the debris. The concept behind acoustic fluidization is that if an applied sound field is strong enough, it may relieve the immobilizing overburden pressure in a debris stream and allow separation of the debris fragments for the duration of a sound wave rarefaction, over a region comparable in size to half the pulse wavelength. When the amplitude of the pressure fluctuations approaches the overburden pressure, separation of the debris fragments occur frequently enough to permit the mass of debris to experience relative internal motions under relatively low applied shear stresses.

Melosh proposes that acoustic fluidization requires much less energy than mechanical fluidization, making it a much more energetically attractive alternative for the mobilization of sturzstroms than dispersive grain flow. In theory, at very high sound intensities, acoustically fluidized debris should behave like a Newtonian fluid of viscosity η, where $\eta = \rho\lambda\alpha$. In this equation, ρ is the density of the rock debris, λ is the wavelength of the sound field and α is the speed of sound. At lower sound intensities, flow still occurs, but the debris behaves like a non-Newtonian fluid with a viscosity that is a function of the applied stress.

Melosh (1983) also suggested that some of the unusual geologic aspects of sturzstroms could be explained by acoustic fluidization. Early experimental tests, for example, suggested that when a fluid of this sort flows down a slope, most of the shear strain remains confined to a narrow zone along the bottom boundary (Melosh, 1983). This would support the geologic relations indicating that most of the shear strain in a landslide lobe is concentrated near its base during transport. However, a more recent model of the process (Melosh, pers. comm., 1990) suggests that an acoustically fluidized flow should exhibit flow through most of its interior, not just in a confined zone near the base, a result which may negate the earlier finding. As discussed earlier, bulk flow, whether turbulent or laminar, is not consistent with the presentation of stratigraphy in dry sturzstroms.

Melosh (1983) also noted that acoustic fluidization is critically subject to radiative energy losses, but that radiation losses should become smaller as the ratio of a slide's volume to its surface area increases. He proposed that if the volume to area ratios of sturzstroms increase with increasing volume, it would compensate for decreasing apparent angle of sliding friction. However, Shaller (1991a) indicates that the volume to area ratios of large landslides increase only slightly with increasing volume, and that most of the high values of volume/area correspond to heavily confined landslides which could not easily spread out during emplacement, so the aspect ratios of sturzstroms tend to remain about the same, regardless of volume. In addition, Shaller (1991a) illustrates that the apparent angle of sliding friction values do not vary in any consistent way with the volume to area ratios of subaerial sturzstroms. Thus, the dimensional and geologic relations of large landslides fail to support the acoustic fluidization, as currently understood, to explain the observed long runout in these deposits.

UNIVERSAL BASAL LUBRICATION MODELS

Several theories proposed to explain long runout in large landslides invoke special lubrication along the bases of slidemasses during emplacement.

Shreve's (1959; 1966; 1968a; b; 1987) air-layer lubrication mechanism is by far the best known and durable of these theories. Shreve argued that the low apparent angle of sliding friction ratios of some sturzstroms, as well as certain aspects of their morphologies and internal structures, could be explained by the hovercraft-like sliding of landslide breccia on a layer of compressed air captured under the debris after being launched from a rock ledge. Shreve (1959) developed the theory to explain the long runout and unusual sedimentological and morphological features of the Blackhawk landslide, and later applied the theory to the Sherman, Alaska landslide (Shreve, 1966) as well as to other well-known landslides such as Elm, Frank and Saidmarreh (Shreve, 1968a), which he termed "Blackhawk-type" landslides. Shreve (1968a) turned to the idea of air-layer lubrication because he recognized the failure of bulk flow to explain the preserved stratigraphy in the Blackhawk and Silver Reef landslides. Shreve (1968a) stated his theory as follows:

> According to this idea a landslide of the Blackhawk type starts as a huge rockfall which acquires such high speed in its decent that at a projecting shelf of rock or sudden steepening of slope it leaves the ground, overriding and trapping a cushion of compressed air upon which it traverses the gentler slopes below with little friction, much as the slipper in a thrust bearing slides on a cushion of oil with no metal-to-metal contact. The distance and direction traveled after launching depends upon the initial velocity, the gradient and the smoothness of the land surface, and the amount, redistribution and leakage of the trapped air.

Several characteristics of the Blackhawk and Blackhawk-type landslides were cited by Shreve (1968a) as support for an air-layer lubrication mechanism, including: preserved stratigraphy, bulldozed distal ridges, low apparent angle of sliding friction values, the dust clouds commonly associated with rapid landslides, debris pyramids, high-speed emplacement, three-dimensional jigsaw-puzzle breccia, raised distal rims, lateral levees, and transverse

ridges and troughs. Shreve (1966, 1968a) speculated that the abnormally low apparent angle of sliding friction values provided a measure of the volume of air trapped beneath a large landslide; the larger the fallen mass, the more air was trapped to lubricate the sliding process.

Shreve (1987; pers. comm., 1990) has since stated that the air-layer lubrication model cannot explain the travel of all sturzstroms, only those exhibiting certain special features characteristic of Blackhawk-type landslides. However, these landslides all fail to exhibit one or more of the primary geologic relations deemed critical to the air-layer lubrication mechanism. For example, the Elm landslide (Heim, 1932) experienced an airborne launch and exhibits a pattern of ridges and troughs on its surface. However, it lacks a raised distal rim and has no lateral levees, although the latter observation may reflect the fact that the landslide thinned as it moved (Shreve, 1968a). Cruden and Hungr (1986) also used morphological evidence to argue against air-layer lubrication for the Frank landslide; Frank lacks lateral ridges or levees, has only very poorly developed transverse ridges, and exhibits a raised distal rim in only three short areas along the slide margin. Watson and Wright (1969) found that Saidmarreh lacks a launching platform, a wedge of bulldozed debris, lateral levees, a raised distal rim, original transverse ridges and troughs morphology (one was later developed by erosion), and three-dimensional jigsaw puzzle blocks. The single feature of Saidmarreh consistent with Shreve's model is preservation of stratigraphy between the headscarp and the debris apron. On the basis of this data, Watson and Wright (1969) concluded that little positive evidence exists to support the idea that the Saidmarreh landslide moved on a cushion of air. Shreve (1966) himself had some difficulty in applying air-layer lubrication to the Sherman landslide, which exhibited an air launch, a low apparent angle of sliding friction, lateral ridges and a raised distal rim (argued against by McSaveney, 1978), but lacked the transverse ridges and troughs expected if the toe of the landslide had stopped rapidly from high speed when air at the leading edge gave out. He ended by reasoning that in the case of the Sherman landslide, stopping must have begun at the rear and progressed forward, in contrast to his interpretation of the way he supposed the Blackhawk stopped. These inconsistencies suggest that air-layer lubrication, as defined by Shreve on the basis of specific geomorphic and sedimentologic criteria, is not supported for any sturzstrom aside from Blackhawk, and it seems unlikely there also. Sturzstrom deposits documented on Mars (Lucchitta, 1978; 1979; McEwen, 1989; Shaller, 1991a; b) and subaqueous sturzstroms on Earth (e.g., Moore, et al., 1989) are also problematic for air-layer lubrication and offer additional evidence that another mechanism must prevail for the general population of sturzstroms, and reasonably, for Blackhawk as well.

Erismann (1979) proposed the other lubricated sliding theory, advocating low-friction sliding of sturzstroms on dissociated or melted rock confined along a hypothesized basal slide plane. He believed that self-lubrication could occur in at least two different materials: limestone and gneiss. For sturzstroms composed of limestone, notably Flims (Switzerland), he believed that high temperatures developed along a discrete slip surface would continuously dissociate the carbonate rock into a mixture of lime (CaO) and CO_2 gas during travel. As in the air-layer lubrication model, the carbon dioxide gas would provide a lubricant along a basal slip surface. For large landslides in gneiss such as Köefels, he reckoned that slide-induced heating could melt the crystalline rock locally, generating a fluid lubricant. Erismann realized that the principle drawback to this mechanism was the rapid escape of the gaseous or fluid lubricant away from the slide plane faster than it could be replaced by transformed rock material. In the absence of any data on the temperature/pressure relations along the base, on the permeability or density of the moving debris, or on the viscosities of the proposed lubricants, Erismann (1979) concluded that self-lubrication by such means is "plausible," but that additional work was required to address these unknown parameters.

Field evidence exists to support Erismann's contention that melted rock and calcined rock can form in sturzstroms. Hewett (1988) reported the probable presence of CaO intermixed in the debris of the carbonate-containing Bualtar 1-3 deposits, and Heuberger, et al. (1984) reported amorphous glass along slip surfaces in the Köefels and Langtang landslides. However, Hewett (1988) believed that the calcined rock in the Bualtar deposits probably formed along the bases of the translational slides during the early stages of their sliding motion, and then became mixed into the debris as the landslides disintegrated into brecciated debris streams further down slope. This observation contrasts with Erismann's proposal that lubrication of the base of a limestone landslide could occur by way of carbonate dissociation throughout the duration of its emplacement, even in the brecciated state. However, once a rock mass brecciates, the base of a sturzstrom generally no longer exhibits distinct slip surfaces of any great extent (Yarnold and Lombard, 1989; Shaller, 1991a; Yarnold, 1993), so that vapor production would slow or stop, and any vapor constrained along the slip plane might escape upwards into or through the breccia, turning off the process. However, limestone dissociation might provide a functional mechanism for large coherent slide blocks, allowing them to develop high velocities. Once these landslides reached high speeds, though, even minor disruption of the slide blocks due to movement-related stresses could provide a natural breaking mechanism by stopping the production of gas and allowing accumulated vapor to leak out. The data on melted rock in large landslides from Heuberger, et al. (1984) also fails to support Erismann's theory; the melted rock only occurred along discrete slip surfaces in the largely coherent Köefels and Langtang landslides.

Erismann (1979) based many of the concepts for his model on the assumption that the size effect for large landslides occurred because landslide thickness scales with volume and that the heating energy at the base should

increase with the thickness of the mass. Thus, landslides with greater volumes should travel with greater thicknesses, generate more heat and, by extension, generate more molten or dissociated rock, and therefore should experience lower apparent angle of sliding friction values. However, data presented in Shaller (1991a) fail to support this contention, as apparent angle of sliding friction values fail to show any characteristic decrease with increasing average or maximum thicknesses for terrestrial sturzstroms. Finally, the mechanism fails to deal with the question of lithologies other than gneiss and limestone. Heating of sandstone, granite and quartzite, for example, would require widely different pressure/temperature regimes to generate vapors or melts.

MASS-LOSS ("ROCKET-STAGE") MODELS

Mass-loss models form a third set of mechanisms advanced to explain long runout in sturzstroms. These models propose that the low apparent angle of sliding friction values achieved by large landslides occur because they selectively drop off low-velocity material during movement (Van Gassen and Cruden, 1989; Savage, pers. comm., 1990), in a mechanism analogous to a rocket shedding burned-out stages during its ascent. The ultimate runout length of a sturzstrom traveling by such a mechanism would depend on the rate and timing of the mass loss; the more low-velocity mass lost early in the process, the farther the ultimate runout of the toe of the slide (Van Gassen and Cruden, 1989).

Van Gassen and Cruden (1989) propose a model for long runout in sturzstroms in which the travel distance of the center of gravity of a mass of loose, dry, purely frictional material depends upon momentum transfer within the mass. In this model, landslide debris is deposited gradually from a sliding mass of breccia. The breccia is presumed to maintain a constant angle of sliding friction of 30° throughout the course of movement. Van Gassen and Cruden (1989) outline the model as follows:

> Consider a slide of loose material entering its accumulation zone with a velocity v_o. Friction slows particles at the slide toe to a velocity $v_o - \Delta v$ after a short time, whereas the material behind is still entering the runout zone at a velocity v_o. So the material at the toe and the back interact. The leading particles are propelled forward, while the material behind is slowed down and some of it is deposited. This process continues throughout the accumulation zone. The properties of the material and the geometry of the accumulation zone determine the shape of the resulting deposit.

The model proposed by Van Gassen and Cruden (1989) makes the assumption that the clasts composing a large landslide slow by friction, but come to rest strictly by means of momentum transfer, and that the moving part of the landslide experiences a "normal" coefficient of sliding friction along its base equal to about 0.6. Rocks are only deposited in this model after they give up their momentum to other moving rocks in the mass; they lose no momentum to the ground in the moment they stop, though they can lose momentum to the ground while in motion through friction along the base. Once a landslide mass reaches a depositional area (slope angle below 30°), material at the trailing end of the moving landslide begins to deposit by transferring its energy forward to the moving part of the landslide. The toe of the landslide continues to slide downslope propelled by the input of momentum from stopped trailing clasts until the wave of stopping catches up with the toe, when stopping is complete. The authors propose that this mechanism allows the center of gravity of a landslide to travel farther from its starting point than would occur for a simple sliding block.

The Van Gassen and Cruden (1989) momentum transfer model can explain a number of important aspects of sturzstroms: the cause of stopping from head to toe; the extension of landslide deposits relative to their original slide block dimensions; some aspects of the facies model of sturzstroms; the development of low apparent angle of sliding friction values; and the characteristically high velocities attained by sturzstroms. One of the most useful outcomes of this model is its explanation of the longitudinal extension experienced by sturzstroms during runout. The degree of extension can be quite substantial in some instances, measuring, for example, about 400% in the El Capitan landslide (Krieger, 1977). This extension should naturally occur if a landslide stops in the gradual manner prescribed by Van Gassen and Cruden (1989). The back-to-front mode of stopping required by the model also agrees with the observations made of many large landslides by Heim (1932). In addition, the momentum transfer model can also explain many aspects of the landslide facies model of Yarnold and Lombard (1989) and Yarnold (1993). Material near the head of a landslide would stop rapidly according to the Van Gassen and Cruden model, preventing much interaction between the landslide breccia and the substrate. Material along the toe of the landslide, however, which obtains momentum from trailing clasts, should experience much greater internal shear and interactions with the substrate because of its much greater travel time, in concert with the observations of Yarnold and Lombard (1989) and Yarnold (1993). The model also provides an explanation of the low apparent angle of sliding friction values achieved by many large landslides, their consistently high runout velocities and the fact that the landslides should come to rest gradually, as supported by Soviet landslide velocity data presented in Shaller (1991a), rather than abruptly as suggested by Shreve (1968a) and Davies (1982).

However, the theory fails to account for a number of equally important features of sturzstroms. For example,

the model cannot explain the characteristic trend of decreasing apparent angle of sliding friction with increasing volume. Rather, the theory holds that the apparent angle of sliding friction of a landslide should vary with the profile shape of a landslide. Tapered landslides should, according to the model, experience the lowest apparent angle of sliding friction values, followed by landslides of uniform thickness, and then by those having distally raised profiles. In fact, distally raised landslides consistently have among the lowest apparent angle of sliding friction values of all sturzstroms (Shaller, 1991a). The theory also fails to explain why long runout should only occur in landslides having volumes in excess of ~10^6 m^3. The theory also specifically anticipates that the most distal fragment along the toe of a landslide should be the last to stop moving, as stopping propagates from the head to the toe. In general large landslides exhibit this behavior, but in detail rather large regions of moving landslides appear to come to rest at the same time (Shaller, 1991a). In addition, the mass-loss theory fails to explain the preservation of stratigraphy in sturzstroms. Because the theory does not explain kinematically how mass is lost from a moving landslide, it is unclear whether or not stratigraphy might be preserved during runout.

Certain theoretical objections have been raised about the model. Hungr (1990) argues that the distance traveled by the center of gravity of a landslide should not vary with the mode of deposition. He drew this conclusion from the observation that the change in kinetic and potential energy of the system of particles should equal the total work done on the landslide by external forces in the zone of accumulation. He further states that, "the theory developed in the paper incorrectly implies the existence of a rocket engine, propelling the slide mass along the runout surface. The magnitude of the implied thrust force for the Frank slide is in the order of 10^{11} N, or about 5000 times that of the largest rockets." In Van Gassen and Cruden (1990), the authors agree with Hungr "that the change in kinetic and potential energy of the system of particles should equal the total work done by external forces in the accumulation zone." However, they argue that the total energy of the system is greater than that represented by the kinetic energy of the center of mass of the landslide alone. In response to the second criticism they state that Hungr says the change of linear momentum of a system of particles is equal to the external forces on the system, but that in their model, the expelled particles are those at rest, and that "once the particles are at rest they do not contribute to the changing momentum, they are outside the system."

The momentum transfer model of Van Gassen and Cruden (1989) provides an interesting new view of the process of long runout in large landslides. The model can successfully account for a number of important features of large landslides not properly described by any other theory. However, the model also fails to describe the kinematics of mass loss from the system and makes an incorrect prediction that runout length should vary with the profile shape.

INDIVIDUAL-CASE MECHANISMS

All of the theories discussed to this point have been proposed as general solutions to the problem of sturzstroms. However, a single overriding mechanism may not explain all sturzstroms. Instead, many different mechanisms may operate in large landslides that lead to a common set of characteristics, such as their high velocity, preserved stratigraphy and long runout. As in the general case theories, the individual case models fall into broad categories, which include bulk fluidization theories, basal lubrication theories and one theory which combines facets of both bulk fluidization and basal lubrication.

One individual-case bulk fluidization theory suggests that large landslides may experience fluidization during strong seismic events. Earthquake fluidization can be considered a subset of acoustic or mechanical fluidization.

Hazlett, et al. (1991) suggested earthquake fluidization for the seven large landslides reportedly triggered during the 1944 eruption of Mt. Vesuvius:

> Acoustic fluidization is an appealing mechanism to explain the Vesuvius avalanches because a high level of seismicity existed at the time movement was initiated. It is very likely that a relatively strong acoustic energy field of scattered wave energy existed during the initiation of motion and that this energy supplemented that generated by downslope movement. This may have provided [an] acoustic surcharge to the 1944 block/ash avalanches.

Solonenko (1972) was less specific in detailing by what precise mechanism seismic groundshaking might decrease the apparent angle of sliding friction of large landslides, but seemingly he had a similar idea in mind when he reported the following about the Khait landslide:

> The collapses and landslides produced by strong earthquakes are of specific dynamics. This was clearly expressed during the Khait earthquake (force 10, M=7.5) of December 10, 1949...The distance covered by the collapsed mass was 10.5 km compared to 1.5-2 km involved in the [non-seismogenic] phenomena. This 5-6-fold increase is due to the disturbance of the collapsed mass by seismic oscillations.

McSaveney (1978) also suggested that seismic energy played an important role in the fluidization of the Sherman landslide, but in addition envisioned a role for snow lubrication of the base of the landslide. This model will be discussed later.

Seismic energy fluidization is more energetically favorable than any of the various fluidization theories previously discussed, because it is the only one in which the energy of fluidization is obtained from the depositional environment rather than strictly from the energy of fall of the detached slidemass. Still, there are problems in attempting to model landslide runout according to this model. Hazlett, et al. (1991) noted that each of the supposedly earthquake-fluidized Vesuvius landslides exhibited preserved stratigraphy, ruling out bulk fluidization as an important mechanism for transport of these landslides. It is not known whether the Khait landslide exhibited preserved stratigraphy or not. Also, Shaller (1991a) presented data showing that there was no significant difference in plots of apparent angle of sliding friction versus log (volume) between groups of sturzstroms known to have traveled during earthquakes versus those known not to have been associated with earthquakes. The available evidence therefore argues against earthquake-energy fluidization for sturzstroms.

Three individual-case models have been proposed to explain long runout via special basal lubrication mechanisms. These special case theories include lubrication by vaporized pore fluids (Habib, 1975; Goguel, 1978), by sliding on a weak, clay- or mica-rich stratum in the landslide debris (Johnson, 1978), or by sliding on water-saturated substrate sediments (Evans, pers. comm., 1990).

Habib (1975) and later Goguel (1978) independently developed similar models for long runout in large coherent translational landslides based on lubrication by vaporized pore fluids. They both believed that the rapid velocities and low apparent angle of sliding friction in these landslides resulted from pore fluid vaporization along their bases due to frictional heating produced during sliding. Both authors developed this theory with a quantitative analysis estimating the acceleration a translational slide might achieve down a slope once movement was initiated by some outside influence, e.g., an earthquake. These analyses, not developed here, include both a consideration of the energy dissipated in the slip surface, as well as the influence of speed on the development of gaseous pore pressure. This theory has considerable value for helping to understand the low apparent angles of sliding friction exhibited by large coherent landslides such as Mt. Granier (0.17; Cruden and Antoine, 1984) and Vaiont (0.34; Mueller, 1964).

The theory also appears applicable to the initial movement stages of large translational landslides which became brecciated during movement, such as Saidmarreh (Watson and Wright, 1969) and Flims (Heim, 1932). The theory nonetheless exhibits some major limitations. For example, it might provide a landslide mass too much mobility. Once a cohesive mass of rock began to descend a hill and develop a basal pore pressure, the speed would increase further, increasing frictional heating and developing more pore pressure, producing runaway acceleration once the slidemass became entirely supported by vapor. By the very nature of the boundary conditions of this model, however, the mechanism must break down if the slide mass disaggregates into a sliding or flowing breccia sheet. This ultimately occurs to some extent for almost all large landslides, presumably when stresses placed on a sliding block due to its rapid speed and the changing geometry of its travel path overcome its lithologic strength or the strength of discontinuities in the rock mass. Once this happens, the base of the landslide no longer exhibits distinct slip surfaces of any great extent (Yarnold and Lombard, 1989; Shaller, 1991a; Yarnold, 1993), so that vapor production would slow or stop, and any vapor constrained along the slip plane might escape upwards into or through the breccia, turning off the process. Thus, pore-fluid vaporization might provide a functional mechanism for large coherent slide blocks, allowing them to develop high velocities. Once these landslides reached high speeds, however, even minor disruption of the slide blocks due to movement-related stresses could provide a natural breaking mechanism by stopping the production of gas and allowing accumulated vapor to leak out.

Johnson (1978) proposed basal self-lubrication as an alternative explanation of the low apparent angle of sliding friction and other characteristic features of the Blackhawk landslide that were ascribed by Shreve (1959; 1968a; 1987) to air-layer lubrication. The Blackhawk landslide bulldozed a distal heap of sandstone ahead of it as it progressed down slope at high speed. The sandstone appears to have been derived primarily from sources in Blackhawk Canyon, so that the distal heap was apparently pushed ahead of the landslide for almost its entire runout length. The material also outcrops locally along the base of the landslide, suggesting that bits and pieces of the distal wedge were overrun by the leading edge of the landslide as it traveled down slope (Shreve, 1968a; Johnson, 1978). Johnson (1978) believed that this overrun material may have provided an important lubricating agent for the landslide:

> For example, it may have been that the sandstone "breccia" at the front of the flow was being "smeared out" beneath the overriding marble breccia, providing a zone of high fluidity beneath the front of the debris lobe (i.e., a self-lubricating action). It is hypothesized that when the frontal mass of sandstone "breccia" either diminished in volume or thickness below some critical value or its physical state changed...frictional resistance markedly increased, deceleration increased and the forward motion of the debris flow quickly terminated.

According to Johnson (pers. comm., 1990), the high mica and clay content of the sandstone debris in the bulldozed wedge may have provided a sort of "grease" along which the landslide could readily slide.

This self-lubrication mechanism provides an intriguing explanation for the high velocities and low apparent angle of sliding friction of the Blackhawk landslide, and perhaps others that bulldozed copious quantities of loose, weathered debris ahead of them during runout, including the Silver Reef (Shreve, 1968a), Elm (Heim, 1932) and Sherman (Shreve, 1966) landslides. This mechanism cannot provide a universal mechanism for long runout in large landslides, because not all large landslides bulldozed heaps of material ahead of them during runout. Nevertheless, the model does support the idea that weak substrate materials, whatever their source, may increase the velocities and travel distances of sturzstroms in general.

Watson and Wright (1969) also developed a basal self-lubrication model, to describe the runout of the Saidmarreh landslide. However, instead of proposing a model by which a basal lubricant was entrained from an external source, Watson and Wright (1969) suggested that a weak marl stratum located along the base of the *in situ* slide mass, and along which the initial planar slope failure occurred, formed the basal lubricant for the subsequent runout of the landslide. They stated their conclusion as follows:

> The Saidmarreh landslide mass did not travel with turbulent motion throughout like a mudflow but instead slid forward either on its base or on the comminuted Eocene limestones. The Asmari limestone plate remained on top, breaking and dispersing as blocks...

They also suggested a second possible mechanism, or contributing factor, in the runout of the landslide was sliding on a low-friction gypsum substrate. Thus, both the nature of the landslide debris and the substrate may have played important roles in the runout of the Saidmarreh landslide.

Evans (pers. comm., 1990) proposed that entrained mud lubricated many large landslides in the Canadian Cordillera that traveled down or across stream courses during runout. In addition, Heim (1932) proposed that moist soil may have lubricated the base of the Elm landslide during runout:

> ...the rubble stream of Elm moved along the valley floor from its upper end, scouring the ground deeply all the way...it was the thick, clayey and very wet topsoil that lubricated the base layer to a large extent during the third part of the movement...

McSaveney's (1978) model proposes to explain long runout in large landslides by merging two previously discussed models: mechanical fluidization and sliding of landslide debris on a low-strength or lubricated substrate. He viewed the kinematics of the Sherman landslide as a complex mixture of sliding and flowing. McSaveney (1978) began his analysis of the mechanics of the landslide by assuming that the landslide behaved as some type of fluid during runout. Based on that assumption and on the premise that the landslide debris had reached optimum dilation just after hitting the depositional surface (so that the volume of the landslide did not change significantly during runout), the landslide was viewed as a fluid that uniformly decreased in thickness as it spread out onto the Sherman glacier. By assuming that the leading edge of the landslide slid over the snow substrate with an angle of sliding friction of 0.11, he used the surface slope of the depositional surface to back-calculate a velocity profile for different debris trains on the landslide. McSaveney (1978) believed that the fluid behavior of the landslide resulted from the fact that it experienced mechanical fluidization during runout. He postulated that the Sherman landslide was fluidized by energy derived from its motion and from the vibration of the Great Alaska earthquake.

McSaveney (1978) also noted that the debris:

> behaved as a complex, perhaps dilatent, Bingham plastic with a yield stress of about 2 kN/m^2 and two viscosities. These very high viscosities prevented turbulence and kept deformation in the avalanche largely confined to shear at the base of the debris, so that for the most part, the avalanche slid as a thin flexible sheet, with solid rather than fluid behavior being the more visible. This was particularly so because of the additional effect of a rigid surface crust where the shear stress was low, and because the very rapidly moving fluid flow was supercritical.

McSaveney's (1978) mechanical model of the Sherman landslide allowed him to describe three important depositional characteristics of the deposit: the preservation of headscarp stratigraphy, the presence of three-dimensional jigsaw-puzzle blocks in the final deposit, and the low apparent angle of sliding friction value achieved by the landslide. McSaveney (1978) attributed the first two characteristics to the high viscosity of the landslide, which presumably prevented turbulent mixing of clasts within the flowing landslide. He accounted for the landslides extremely low apparent angle of sliding friction by assuming that most of the movement of the landslide across Sherman Glacier took place by sliding over ice and snow with a low coefficient of sliding friction.

In his calculation of the velocity profile of the landslide, McSaveney (1978) assumed that the landslide only moved forward by sliding over the snow substrate. No forward progress of the landslide by flow was taken into account in this calculation. An implicit tenet of the model was, therefore, that spreading and sliding must have occurred at precisely the same rate and that all of the internal deformation parallel to the ground surface was taken up by sliding at the base. However, while this

concept addresses the qualitative behavior of the landslide, it is unclear how or why this precise choreography of sliding and flowing might have been achieved. McSaveney (1978) viewed the apparent fluidity of the landslide as arising from mechanical fluidization of the mass, a process which results from turbulent motion of constituent clasts in a grain flow. However, he states that the landslide actually experienced very little internal turbulence due to a high viscosity. These two concepts are not readily compatible; the preservation of stratigraphy in the mass, in fact, gives good evidence that the landslide was not fluidized during transport. Thus, though sliding and flowing may indeed occur together in sturzstroms as suggested by McSaveney (1978), the details of the process remain obscure.

CONCLUSION

Although a number of talented researchers have expended tremendous time and energy over the last century seeking to explain the mechanism of sturzstroms, no one theory has been advanced that successfully illustrates the mechanism of all sturzstroms. Modelers seeking a unified theory for long runout are supported by the fact that long runout occurs as the rule in large, rapid landslides, rather than the exception. However, in nearly every case, these models have been developed to explain the characteristics of individual landslides or of a small subset of landslides, such as historically observed occurrences, and then have been advanced as general solutions to the problem. Computer modeling efforts, such as those by Campbell, et al. (1995) offer the possibility that sturzstroms will ultimately be numerically simulated on the basis of pure physical laws. However, even with the current rapid advances in computing power, modern computers still lag far behind the level of speed and complexity needed to adequately model a system as complex as a sturzstrom. Experimental simulations, in which sturzstroms are modeled with flowing granular material, properly scaled by use of exotic materials or by centrifuge techniques, offer a possible means of bridging from present conceptual models to a suitably complex computer model. Continued field study of sturzstrom deposits is also critical to provide the observations needed to test the veracity of the experimental and numerical simulations.

ACKNOWLEDGMENTS

This work forms an important chapter of the author's doctoral dissertation that was edited for this publication. He thanks his Caltech thesis advisors, Bruce Murray and Arden Albee, for their contributions to the original research that went into this work.

REFERENCES

Bagnold, R. A., 1954, Experiments on a gravity-free dispersion of large solid spheres in a Newton fluid under shear: Royal Society of London Proceedings, ser A, v. 225, p. 49-63.

Brown, R. L. and Richards, J. C., 1970, Principles of powder mechanics: Pergamon Press, Oxford, UK, 223 p.

Campbell, C. S., 1989, Self-lubrication for long runout landslides: Journal of Geology, v. 97, p. 653-665.

Campbell, C. S., Cleary, P. W. and Hopkins, M., 1995, Large-scale landslide simulations: Global deformation, velocities and basal friction: Journal of Geophysical Research, v. 100, p. 8267-8283.

Cruden, D. M. and Antoine, P., 1984, The slide from Mt. Granier, Isere and Savoie, France on November 24, 1248: IV International Symposium on Landslides, v. 1, p. 475-481.

Cruden, D. M. and Hungr, O., 1986, The debris of the Frank Slide and theories of rockslide-avalanche mobility: Canadian Journal of Earth Science, v. 23, p. 425-432.

Davies, T. R. H., 1982, Spreading of rock avalanche debris by mechanical fluidization: Rock Mechanics, v. 15, p. 9-24.

Erismann, T. H., 1979, Mechanisms of large landslides: Rock Mechanics, v. 12, p. 15-46.

Goguel, J., 1978, Scale-dependent rockslide mechanisms, with emphasis on the role of pore fluid vaporization, *in* Voight, B., ed., Rockslides and avalanches, v. 1: Elsevier Publishing Company, New York, p. 693-706.

Habib, P., 1975, Production of gaseous pore pressure during rock slides: Rock Mechanics, v. 7, p. 193-197.

Hadley, J. B., 1978, Madison Canyon rockslide, Montana, U.S.A., *in* Voight, B., ed., Rockslides and avalanches, v. 1: Elsevier Publishing Company, New York, p. 167-180.

Hazlett, R. W., Buesch, D., Anderson, J. L., Elan, R. and Scandone, R., 1991, Geology, failure conditions, and implications of seismogenic avalanches of the 1944 eruption at Vesuvius, Italy: Journal of Volcanology and Geothermal Research, v. 47, p. 249-264.

Heim, A., 1882, Der Bergsturz von Elm: Zeitschrift der Deutschen Geologischen Gesellschaft, v. 34, p. 74-115.

Heim, A., 1932, Bergsturz und Menschenleben: Fretz & Wasmuth A. G., Zurich, 218 p. (English translation by Skermer, N. A., 1991: BiTech Publishers, Vancouver, British Columbia).

Heuberger, H., Masch, L., Preuss, E., Schröcker, A., 1984, Quaternary landslides and rock fusion in central Nepal and in the Tyrolean Alps: Mountain Research and Development, v. 4, p. 345-362.

Hewett, K., 1988, Catastrophic landslide deposits in the Karakoram Himalaya: Science, v. 242, p. 64-67.

Hsü, K. J., 1975, Catastrophic debris streams (Sturzstroms) generated by rockfalls: Geological Society of America Bulletin, v. 86, p. 129-140.

Hulme, G., 1974, The interpretation of lava flow morphology: Geophysical Journal of the Royal Astronomical Society, v. 39, p. 361-383.

Hungr, O., 1990, Momentum transfer and friction in the debris of rock avalanches: Discussion: Canadian Geotechnical Journal, v. 27, p. 697.

Johnson, A. M., 1970, Physical Processes in Geology: Freeman, Cooper & Company, San Francisco, 577 p.

Johnson, B., 1978, Blackhawk landslide, California, U.S.A., *in* Voight, B., ed., Rockslides and avalanches, v. 1: Elsevier Publishing Company, New York, p. 481-504.

Kent, P. E., 1966, The transport mechanism in catastrophic rock falls: Journal of Geology, v. 74, p. 79-83.

Krieger, M. H., 1977, Large landslides, composed of megabreccia, interbedded in Miocene basin deposits, southeastern Arizona: U. S. Geological Survey Professional Paper 1008, p 1-25.

Lucchitta, B. K., 1978, A large landslide on Mars: Geological Society of America Bulletin, v. 89, p. 1601-1609.

Lucchitta, B. K., 1979, Landslides in Valles Marineris, Mars: Journal of Geophysical Research, v. 84, p. 8097-8113.

McEwen, A. S., 1989, Mobility of large rock avalanches: Evidence from Valles Marineris, Mars: Geology, v. 17, p. 1111-1114.

McSaveney, M. J., 1978, Sherman glacier rock avalanche, *in* Voight, B., ed., Rockslides and avalanches, v. 1: Elsevier Publishing Company, New York, p. 71-96.

Melosh, H. J., 1979, Acoustic fluidization: A new geologic process?: Journal of Geophysical Research, v. 84, p. 7513-7520.

Melosh, H. J., 1983, Acoustic fluidization: American Scientist, v. 71, p. 158-165.

Melosh, H. J., 1986, The physics of very large landslides: Acta Mechanica, v. 64, p. 89-99.

Melosh, H. J., 1987, The mechanics of large rock avalanches: Geological Society of America Reviews in Engineering Geology, v. VII, p. 41-49.

Moore, J. G., Clague, D. A., Holcomb, R. T., Lipman, P. W., Normark, W. R., Torresan, M. E., 1989, Prodigious submarine landslides on the Hawaiian Ridge: Journal of Geophysical Research, v. 94, p. 17465-17484.

Müeller, L., 1964, The rock slide in the Vajont valley: Felsmechanik und Ingenieurgeologie, v. 2, p. 148-212.

Scott, R. F., 1963, Principles of soil mechanics: Addison-Wesley Publishing Company, Incorporated, Palo Alto, p. 97-98, 330.

Shaller, P. J., 1991a, Analysis and implications of large martian and terrestrial landslides [Ph.D. thesis]: Pasadena, California, Division of Geological and Planetary Sciences, California Institute of Technology, 586 p.

Shaller, P. J., 1991b, Analysis of a large moist landslide, Lost River Range, Idaho, U.S.A.: Canadian Geotechnical Journal, v. 28, p. 584-600.

Shreve, R. L., 1959, Geology and mechanics of the Blackhawk landslide, Lucerne Valley, California [Ph.D. thesis]: Pasadena, California, Division of Geological and Planetary Sciences, California Institute of Technology, 79 p.

Shreve, R. L., 1966, Sherman landslide, Alaska: Science, v. 154, p. 1639-1643.

Shreve, R. L., 1968a, The Blackhawk landslide: Geological Society of America Special Paper 108, 47 p.

Shreve, R. L., 1968b, Leakage and fluidization in air-layer lubricated avalanches: Geological Society of America Bulletin, v. 79, p. 653-658.

Shreve, R. L., 1987, Blackhawk landslide, southwestern San Bernardino County, California: Geological Society of America Centennial Field Guide, Cordilleran Section, p. 109-114.

Solonenko, V. P., 1972, Seismogenic destruction of mountain slopes: 24th International Geological Congress, sect. 13, p. 284-290.

Trunk, F. J., Dent, J. D., Lang, T. E., 1986, Computer modeling of large rock slides: Journal of Geotechnical Engineering, v. 112, p. 348-360.

Van Gassen, W. and Cruden, D. M., 1989, Momentum transfer and friction in the debris of rock avalanches: Canadian Geotechnical Journal, v. 26, p. 623-628.

Van Gassen, W. and Cruden, D. M., 1990, Momentum transfer and friction in the debris of rock avalanches: Reply: Canadian Geotechnical Journal, v. 27, p. 698-699.

Watson, R. A. and Wright, H. E., Jr., 1969, The Saidmarreh landslide, Iran: Geological Society of America Special Paper 123, p. 115-139.

Yarnold, J. C. and Lombard, J. P., 1989, A facies model for large rock-avalanche deposits formed in dry climates, *in* Colburn, I. P., Abbott, P. L. and Minch, J., eds., Conglomerates in Basin Analysis: A Symposium Dedicated to A. O. Woodford: Pacific Section S.E.P.M., v. 62, p. 9-31.

Yarnold, J. C., 1993, Rock-avalanche characteristics in dry climates and the effect of flow into lakes: Insights from mid-Tertiary sedimentary breccias near Artillery Peak, Arizona: Geological Society of America Bulletin, v. 105, p. 345-360.

TAB 4

Peter J. Bosscher

Presentations

and

Soil Bioengineering for Upland Slope Protection

and Erosion Reduction Manual

Microcomputer Applications for Slope Stability

- Slope Stability Analysis & Design
  - Simple Analysis Packages
  - Slope Stability Program Ratings
- Finite Element Methods
  - Seepage Analysis & Design
  - Load-Deformation Analysis & Design
  - Thermal Effects
  - Contaminant Transport
  - Consolidation

Slope Stability Software

- Two major analyses
  - Translational (Infinite Slope)
  - Rotational
- Translational Analyses
  - Relatively simple cases
  - Complex problems involving unique seepage

Translational Slide Example

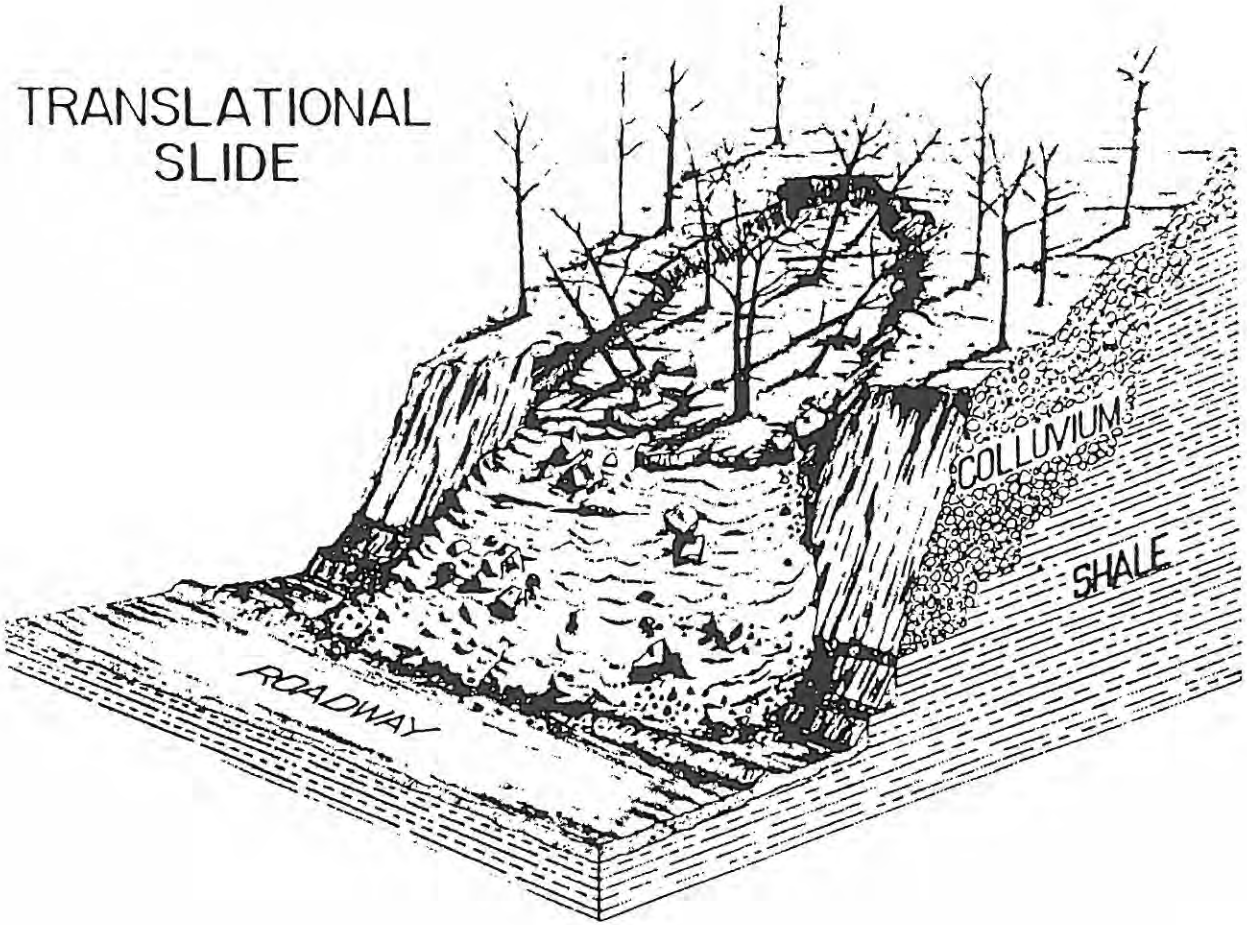

Small Translational Slide

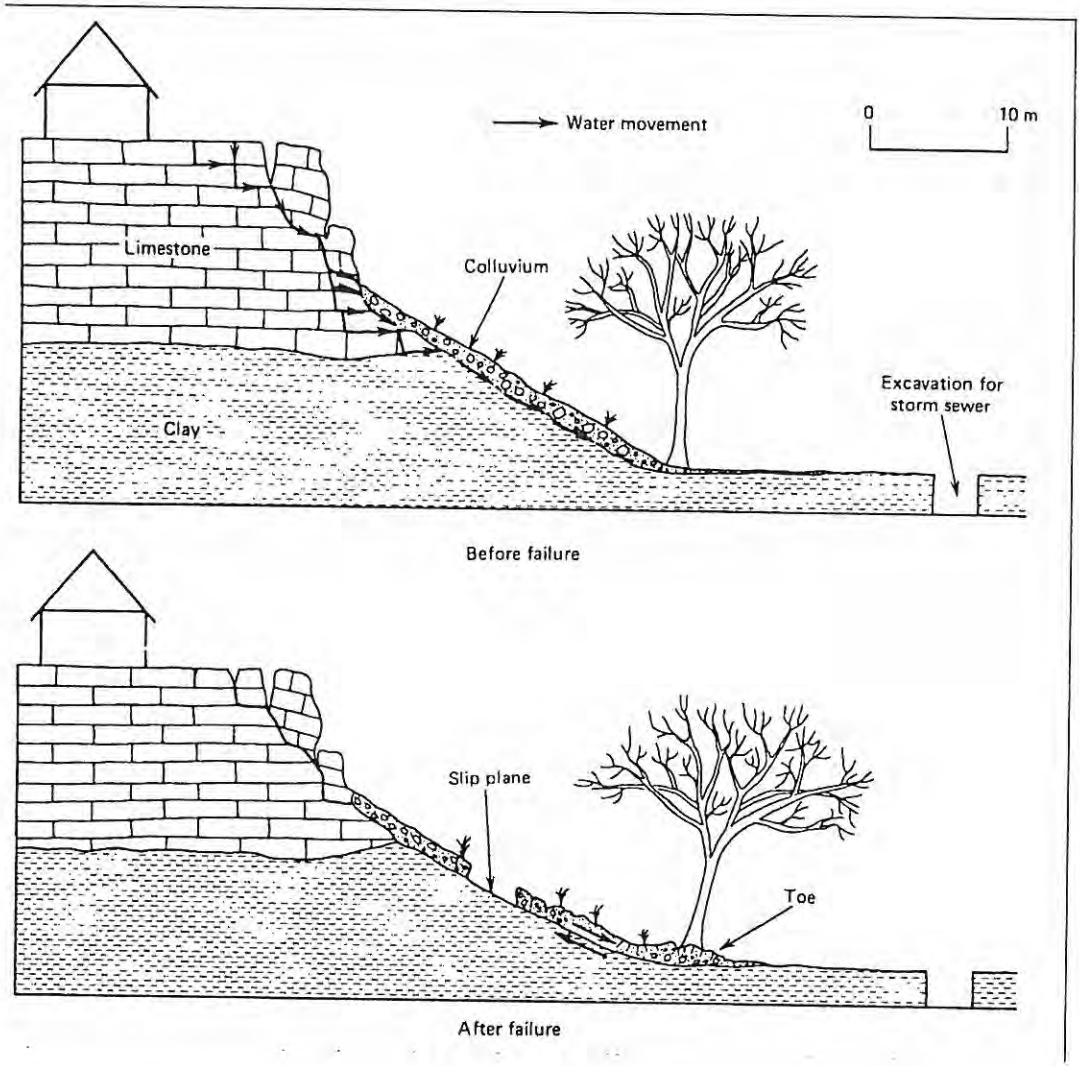

Translational Slope Failures

INFINITE SLOPE (PLANAR SLIP SURFACE)

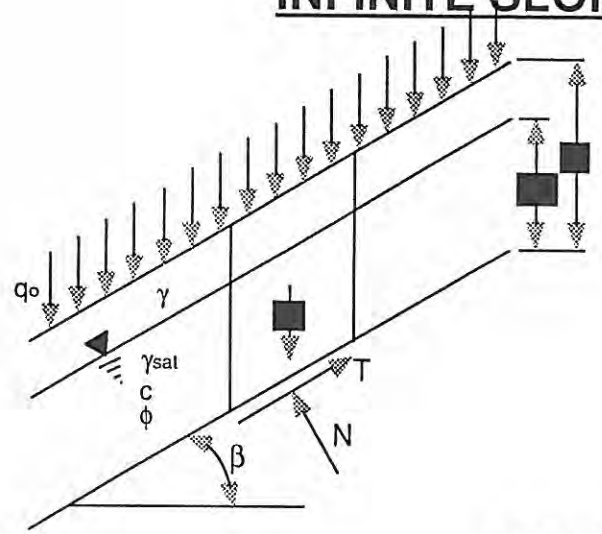

The factor of safety for the generalized infinite slope is:

$$F = \frac{\dfrac{c'}{\cos^2\beta\tan\beta} + \left[\left(q_0 + \gamma H\right) + \left(\gamma_{bouy} - \gamma\right)H_W\right]\dfrac{\tan\phi'}{\tan\beta}}{\left[\left(q_0 + \gamma H\right) + \left(\gamma_{satd} - \gamma\right)H_W\right]}$$

STABILITY OF ROAD FILLS

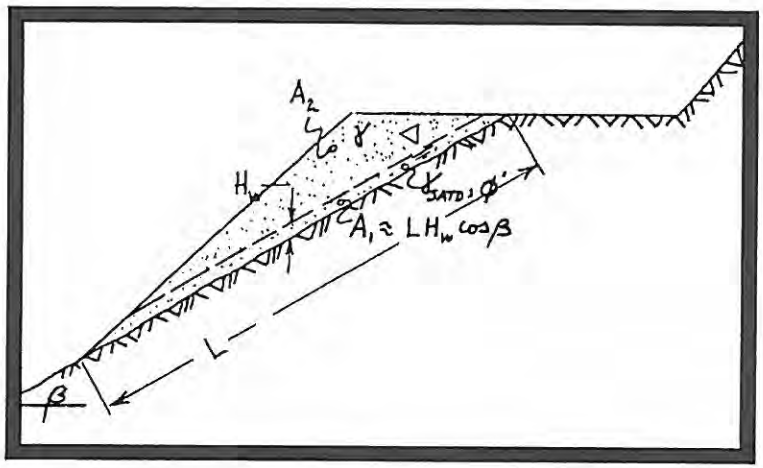

In a fill with a phreatic surface, the factor of safety is:

$$F = \frac{\gamma A_1 + \gamma_{bouy} A_2}{\gamma A_1 + \gamma_{sat'd} A_2} * \frac{\tan\phi'}{\tan\beta}$$

Planar Shear Surfaces

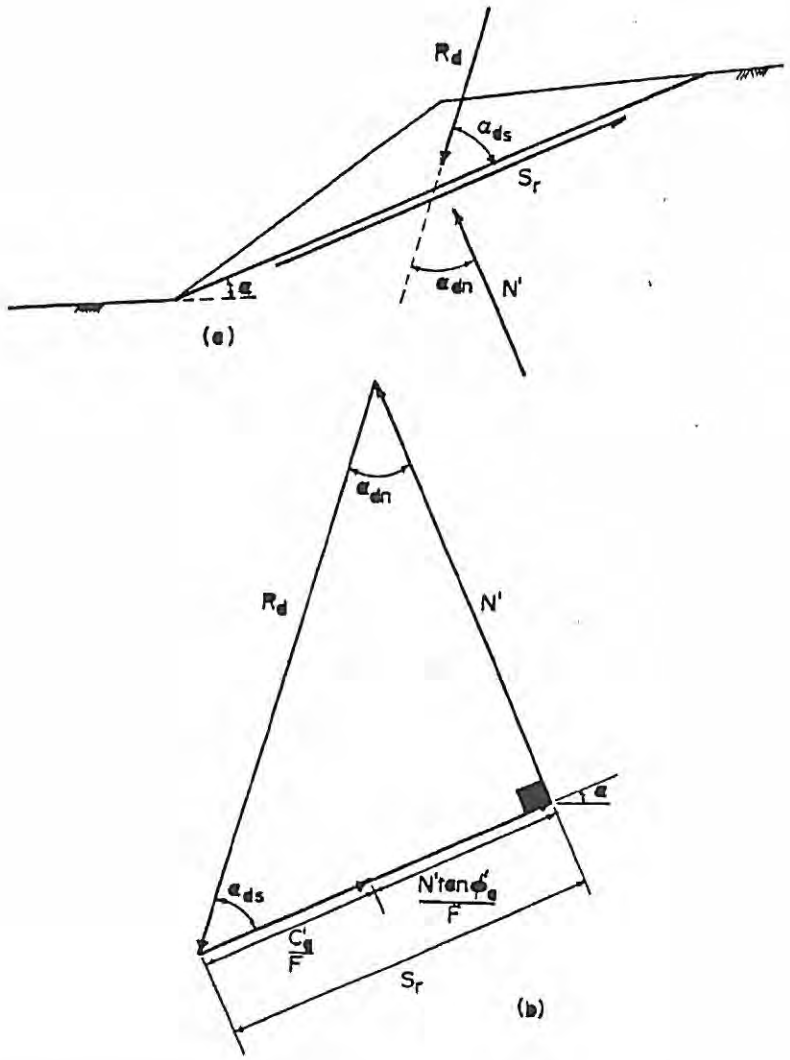

- Rd = driving force (weight, boundary forces, ...)
- N' = normal force (magnitude unknown)
- Sr = resisting shear strength (from friction and cohesion)
- This problem can be readily solved because the failure surface is planar.

Slope Stability Software

- Two major analyses
  - Translational (Infinite Slope)
  - Rotational
- Translational Analyses
  - Relatively simple cases
  - Complex problems involving unique seepage
- Rotational Analyses
  - extensive evaluation of 25 programs
    - 5 for multiuser environments (mainframes)
    - 20 for personal computers
  - minimal standard of performance established

Rotational (Slump) Failure Examples

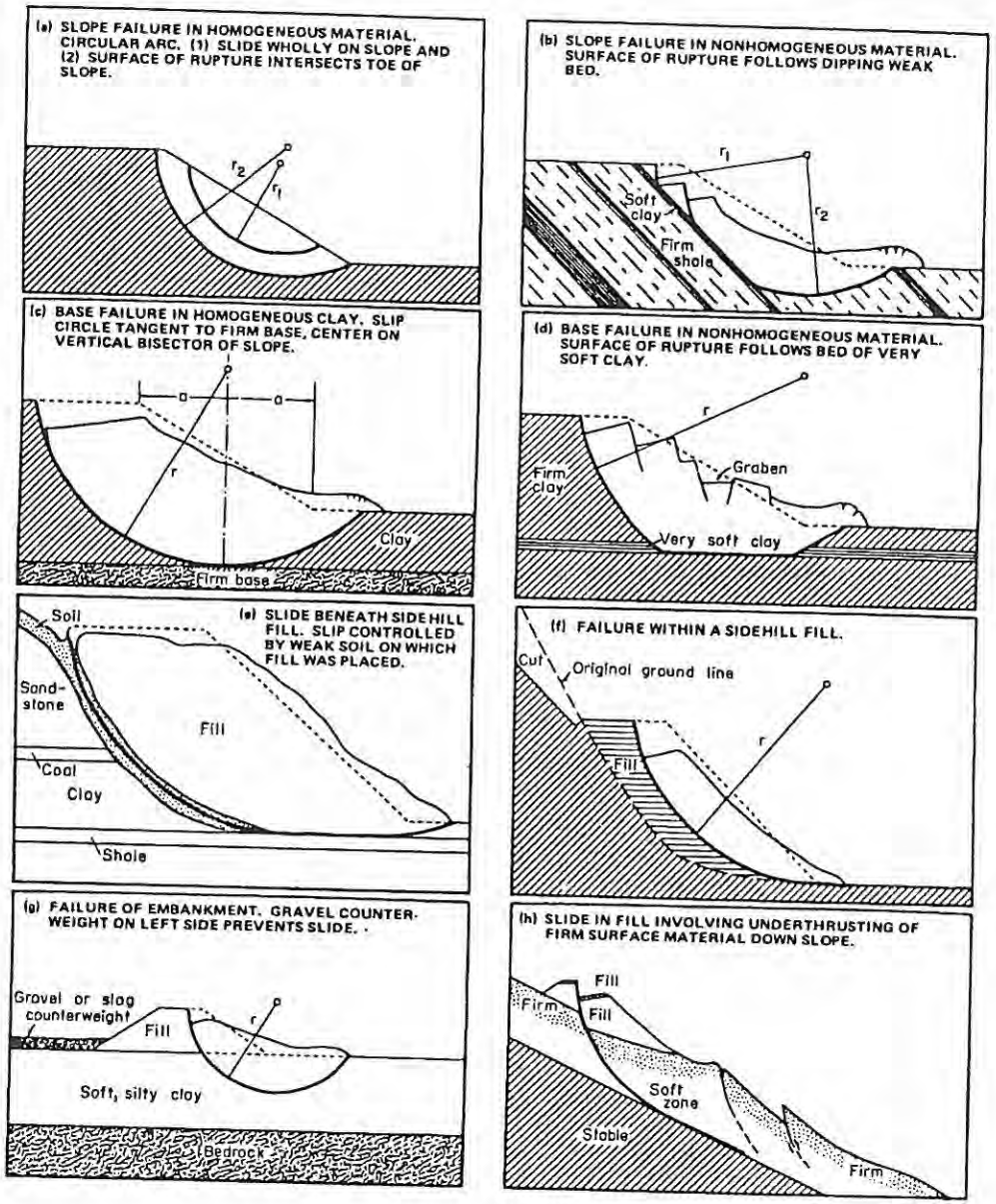

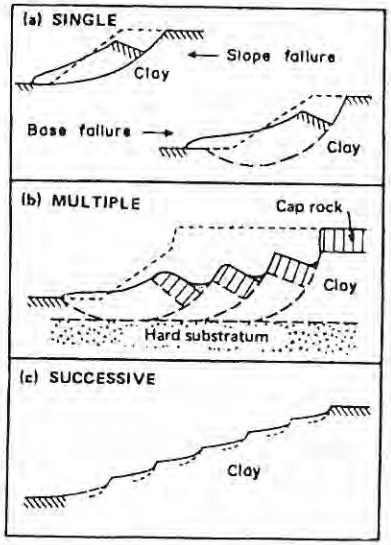

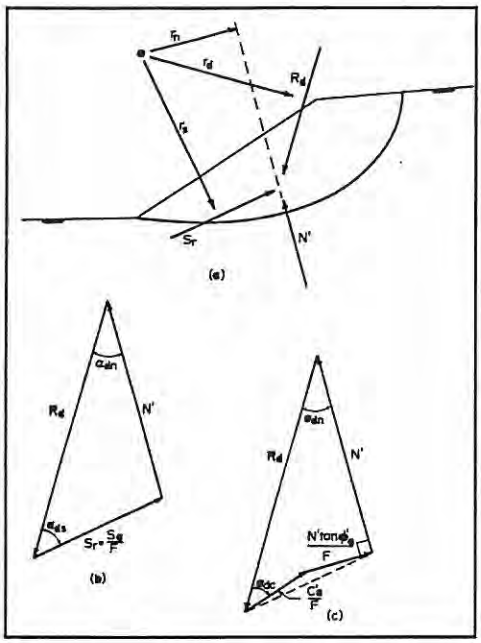

Basic Forces Associated With Limit Equilibrium

- Rd = driving force (weight, boundary forces, ...)
- N' = normal force (line of action and magnitude unknown)
- Sr = resisting shear strength (line of action unknown)
- This problem involves seven unknowns and only three independent equations: therefore it is clearly statically indeterminate.

Software Minimum Requirements

- Type of equilibrium equation
  - Janbu
  - Simplified (Modified) Bishop
- Failure surfaces
  - Bilinear wedge
  - Circular
- Hydrostatic Pressure
  - Piezometric lines
- Search options
  - grid or random
  - specific surface
- Seismic analysis
  - pseudo-static model with seismic coefficients

Software Minimum Requirements

- Stratified soil profiles
  - minimum of 5 lines
- Surcharge
  - line, uniform, irregular or stepped-uniform, concentrated
- Output
  - driving and resisting forces or moments
- Anisotropic soil strength
  - not required
- No known problems in prior use
- Simplified input
- Graphical output
  - desirable, but not essential
- Usefulness of output

Weighting Factors

Matrix Weight	Description
3	Meets all key criteria fully
2	Meets criteria of secondary importance
1	Partially meets all criteria or criteria is of limited importance
0	Does not meet criteria

Weighting Factor Application

	Yes	No
Simplified Bishop	3	0
Janbu	3	0
Other Methods	1	0

	Circular, Wedge, Irregular	Circular, Wedge	Circular, Irregular
Failure Surfaces	3	2	1

	Random, Grid, Single	Grid or Random and Single	Random or Single
Search Options	3	2	1

Weighting Factor Continued

	Yes	No
Seismic Analysis	2	0

	Uniform, Irregular, Line	Uniform, Line	Line or Uniform	None
Surcharge Options	3	2	1	0

	Piez Line, Pore Press, PP Param	Piez Line	PP or PP Param	None
Pore Pressures	3	2	1	0

Weighting Factor Continued

	Yes	No
Soil Layers	3	0
Anisotropic Strength	1	0

	Forces overall, Moments overall	Moments or Forces	FS Only
Output Options	2	1	0
(If external forces are included, add 1)			

	Excellent	Good	Poor
Ease of Input	3	2	1
Output Usefulness	3	2	1

Additional Comments

- Reinforcement option: indicates whether program can analyze/design problems with soil reinforcement.
- In Public Domain: indicates whether the source code is available for public use without restrictions.
- Evaluation: gives a numerical score to each program.

Program Name	Simplified Bishop	Janbu	Other Methods [1]	Failure Surfaces [2]	Search Options [3]	Seismic Analysis	Surcharge Options [4]	Pore Pressures [5]	Soil Layers	Anisotropic Strength	Output Options [6]	Ease of Input [7]	Output Usefulness [7]	Reinforcement Options [8]	In Public Domain	Evaluation	Comments
LEASE	Y	N	O,M	C,I	G,I	Y	U	P	Y	N	S,F,M	G	G	N	N	22	Mainframe
STABL	Y	Y	N	C,W,I	R,S	Y	U	P,U,R	Y	Y	N	G	G	N	Y	25	Mainframe
STABL-4M	Y	Y	S	C,W,I	R,S	Y	U	P,U,R	Y	Y	S,F,M	G	G	N	Y	28	Mainframe
STABL-5M	Y	Y	S	C,W,I	R,S	Y	U	P,U,R	Y	Y	S,F,M	G	G	N	Y	28	Mainframe
STABL-PC	Y	Y	N	C,W,I	R,S	Y	U	P,U,R	Y	Y	S,F,M	G	G	N	Y	28	PC version of STABL (includes tiebacks)
STABL-6	Y	Y	N	C,W	R,S	Y	U	P,U,R	Y	Y	S,F,M	G	G	A	Y	26	Includes reinforcement for embankments and slopes
XSTABL	Y	Y	N	C,W,I	R,S	Y	U	P,U,R	Y	Y	S,F,M	E	G	N	N	29	Pre and Post-processor for STABL; requires coprocessor
STBPRE-STBREF	Y	Y	N	C,W,I	R,S	Y	U	P,U,R	N	N	F	E	G	A	Y	22	Preprocessor and reinforcement analysis with modified STABL
STABL-STS	Y	Y	N	C,W,I	R,S	Y	U	P,U,R	Y	Y	F	G	E	A,D	N	26	Mainframe modified STABL4 to design reinforcement
GEOSLOPE	Y	Y	N	C,W,I	R,S	Y	U	P,U,R	Y	Y	S,F,M	G	G	N	N	28	
STABR	Y	N	O	C	G	Y	U	P	Y	N	S	G	P	N	Y	20	
SLOP8R	N	N	S	I	S	N	N	U	Y	N	S	P	P	N	Y	10	
STABGM	Y	N	O	C	G	Y	U	P	Y	N	S	G	P	A	N	21	
GEOSOFT	Y	N	O,S	C,W,I	G,S	Y	L	P,U,R	Y	N	S,F,M	G	G	N	N	25	Includes STABR/G for circular and SLOPE 8R/G for non-circular
UTEXAS2	Y	N	S,M,L	C,W,I	A	Y	L,U,I	P,U,R,I	Y	N	S,F,M	G	G	A	N	28	
UTEXAS3	Y	N	S,M,L	C,W,I	A	Y	L,U,I	P,U,R,I	Y	N	S,F,M	G	G	A	N	28	
SBSLOPE	Y	N	S	C,I	G,I	Y	L,U	P,R	Y	N	S,F,M	E	G	N	N	26	
PCSLOPE or SLOPE/W	Y	Y	A	C,W,I	G,S	Y	L,U	P,U,R,I	Y	N	S,F,M	G	G	N	N	30	
G-SLOPE	Y	Y	N	C,W,I	G,I	Y	L	P,R	Y	N	S,F,M	G	G	N	N	28	Option for digitizer input
WAGGLE	Y	N	N	W	G	N	U,P	P	Y	N			G	A	N	18	
TENSLO 1	Y	N	N	C	G,R,S	Y	N		Y	N	M	G	E	A	N	21	
TENSLO 2	N	Y	N	W	R,S	Y	N		Y	N	M	G	E	A	N	19	
HOPK-1	N	Y	N	C,W,I	G,S	Y	N	P,U,R	Y	N	N	G	G	N	Y	20	Mainframe
REAM	Y	N	N	C	G,A	Y	N	P,R	Y	N	N	E	G	N	N	18	
GARDS-EPA	Y	Y	N	C,W	G,S	Y	N	P,U	Y	N	N	P	G	N	Y	21	Mainframe and PC versions (focuses on dike stability)
DATA SURGE	Y	N	N	C	G	N	N	P	Y	N	N	E	G	N	N	16	
BISTAT	Y	N	N	C	G	Y	N	P	Y	N	M	G	G	N	Y	17	Allows for stochastic probability analysis

Notes:

1. Spencer, Lowe-Karafiath, Ordinary (or Fellenius), Modified Swedish, Morgenstern & Price, Corps of Engineers, GLE (Generalized Limit Equilibrium), All of above
2. Circular, Wedge, Irregular
3. Single, Random, Grid, Interactive, Automatic Search
4. Point, Line, Uniform, Irregular
5. Piezometric line, U-Pore pressure, R-PP parameter, Interpolation
6. Slice forces, Forces overall, Moments overall
7. Excellent, Good, Poor
8. Analysis, Design

Program Name	Simplified Bishop	Janbu	Other Methods [1]	Failure Surfaces [2]	Search Options [3]	Seismic Analysis	Surcharge Options [4]	Pore Pressures [5]	Soil Layers	Anisotropic Strength	Output Options [6]	Ease of Input [7]	Output Usefulness [7]	Reinforcement Options [8]	In Public Domain	Evaluation	Comments
LEASE	3	0	1	1	2	2	2	2	3	0	2	2	2	N	N	22	Mainframe
STABL	3	3	0	3	1	2	2	3	3	1	0	2	2	N	Y	25	Mainframe
STABL-4M	3	3	1	3	1	2	2	3	3	1	2	2	2	N	Y	28	Mainframe
STABL-5M	3	3	1	3	1	2	2	3	3	1	2	2	2	N	Y	28	Mainframe
STABL-PC	3	3	1	3	1	2	2	3	3	1	2	2	2	N	Y	28	PC version of STABL (includes tiebacks)
STABL-6	3	3	0	2	1	2	2	3	3	1	2	2	2	A	Y	26	Includes reinforcement for embankments and slopes
XSTABL	3	3	0	3	1	2	2	3	3	1	3	3	2	N	N	29	Pre and Post-processor for STABL; requires coprocessor
STBPRE-STBREF	3	3	0	3	1	2	2	3	0	0	0	3	2	A	Y	22	Preprocessor and reinforcement analysis with modified STABL
STABL-STS	3	3	0	3	1	2	2	3	3	1	0.	2	3	A,D	N	26	Mainframe modified STABL4 to design reinforcement
GEOSLOPE	3	3	0	3	1	2	2	3	3	1	3	2	2	N	N	28	
STABR	3	0	1	1	2	2	2	2	3	0	1	2	1	N	Y	20	
SLOP8R	0	0	1	1	0	0	0	1	3	0	1	2	1	N	Y	10	
STABGM	3	0	1	1	2	2	2	2	3	0	1	2	2	A	N	21	
GEOSOFT	3	0	1	3	2	2	1	3	3	0	3	2	2	N	N	25	Includes STABR/G for circular and SLOPE 8R/G for non-circular
UTEXAS2	3	0	1	2	3	2	3	3	3	0	3	2	2	A	N	28	
UTEXAS3	3	0	1	2	3	2	3	3	3	0	3	2	2	A	N	28	
SBSLOPE	3	0	1	1	3	2	2	3	3	0	3	3	2	N	N	26	
PCSLOPE or SLOPE/W	3	3	1	3	2	2	2	3	3	0	3	3	2	N	N	30	
G-SLOPE	3	3	0	3	3	2	1	3	3	0	3	2	2	N	N	28	Option for digitizer input
WAGGLE	3	0	0	1	2	0	3	2	3	0	0	2	2	A	N	18	
TENSLO 1	3	0	0	1	3	2	0	3	3	0	1	2	3	A	N	21	
TENSLO 2	0	3	0	1	1	2	0	3	3	0	1	2	3	A	N	19	
HOPK-1	0	3	0	3	2	2	0	3	3	0	0	2	2	N	Y	20	Mainframe
REAM	3	0	0	1	2	2	0	2	3	0	0	3	2	N	N	18	
GARDS-EPA	3	3	0	2	2	2	0	3	3	0	0	1	2	N	Y	21	Mainframe and PC versions (focuses on dike stability)
DATA SURGE	3	0	0	1	2	0	0	2	3	0	0	3	2	N	N	16	
BISTAT	3	0	0	1	2	2	0	2	3	0	0	2	2	N	Y	17	Allows for stochastic probability analysis

Notes:

1. Spencer, Lowe-Karafiath, Ordinary (or Fellenius), Modified Swedish, Morgenstern & Price, Corps of Engineers, GLE (Generalized Limit Equilibrium), All of above
2. Circular, Wedge, Irregular
3. Single, Random, Grid, Interactive, Automatic Search
4. Point, Line, Uniform, Irregular
5. Piezometric line, U-Pore pressure, R-PP parameter, Interpolation
6. Slice forces, Forces overall, Moments overall
7. Excellent, Good, Poor
8. Analysis, Design

Slope Stability Program Ratings

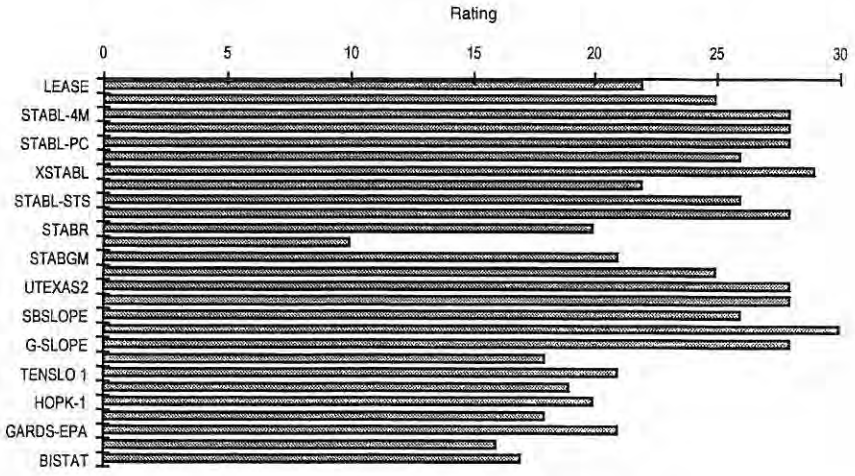

Slope Stability Program Conclusions

- The top-ranked programs are:
  - PC Slope & SLOPE/W
  - UTEXAS2 & UTEXAS3
  - GEOSLOPE
  - STABL 5M & PC
  - X-STABL
- Note that only STABL is in the public domain.

Modeling Procedure

- Progress from the simple to the complex
  - Start with simple, understandable geometry
  - Add additional complexities incrementally
  - Add external loads gradually
  - Changes in factor of safety should take place gradually
- Maintain a consistent set of units
- Adopt an appropriate solution method (see next slide)
- Carefully choose the soil strength parameters
- Validate any slip surface that enters and exits the soil at steep angles (causes numerical problems)

Slope Stability Predictions

- Approaches to Analysis
  - limit equilibrium analysis
  - deformation analysis
- Limit Equilibrium Analysis Procedure
  - 1. slip surface or mechanism is postulated
  - 2. shearing resistance required to equilibrate the failure mass is calculated by means of statics
  - 3. compare the calculated shearing resistance required for equilibrium with the available shear strength
  - 4. iterate until mechanism or slip surface with the lowest factor of safety is found
- Shear Strength Parameters
  - Total Stress Analysis
  - Effective Stress Analysis

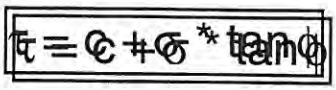

Total Stress Analysis

- When a fully saturated cohesive soil (clay) is rapidly sheared (deformed), the behavior can be analyzed in terms of total stresses. NOTE: This is not a function of the soil type as much as the stress conditions on the soil. The only soil strength parameter needed to describe the behavior of the soil under these conditions is the undrained shear strength. This parameter can be readily obtained from a simple laboratory test called an unconfined compression test.
- The total stress analysis method is used for the analysis of temporary cuts made in uniformly homogeneous clay (not fissured or jointed).
- An important advantage of the total stress analysis method is that it does not require the determination of the pore pressure distribution in the slope.

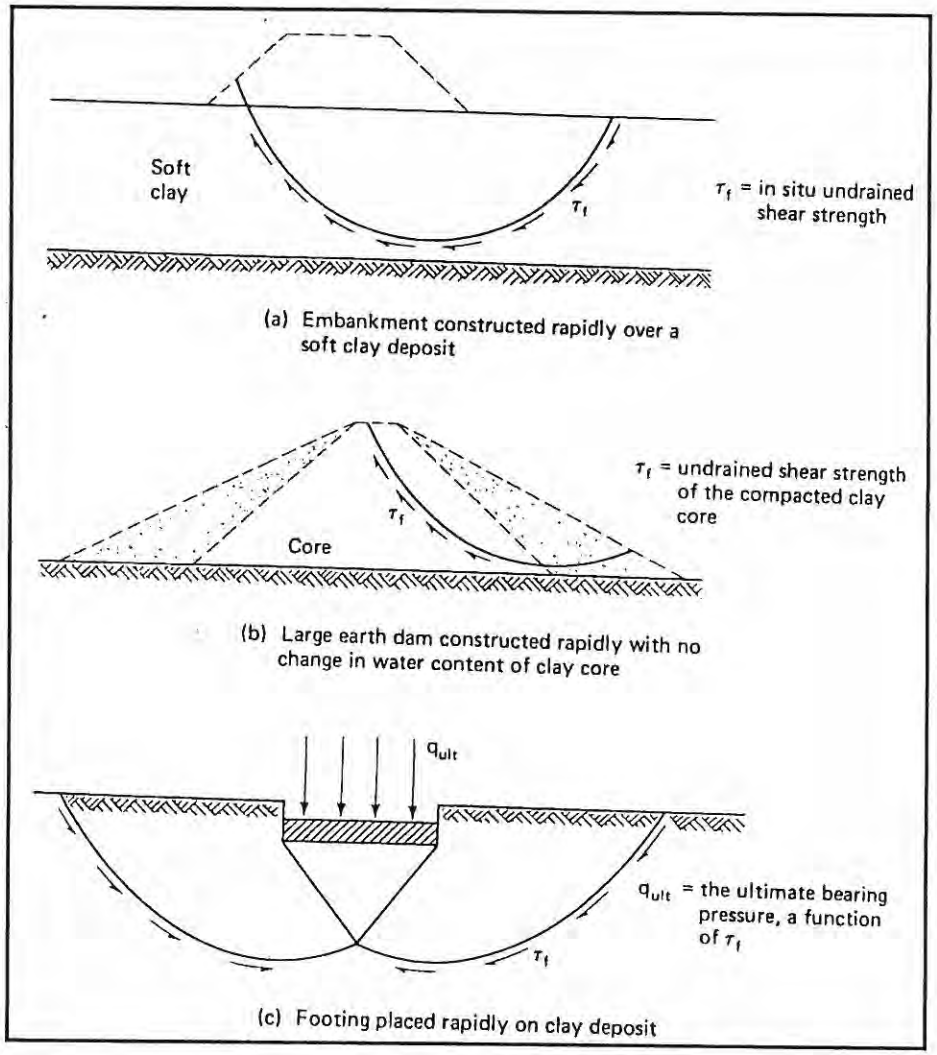

Page 16

Effective Stress Analysis

- If long term stability is important or pore pressures from seepage are present, then an effective stress analysis should be used. This is the usual condition for natural slopes in both rock and soil.
- Effective strength parameters are obtained from either drained triaxial tests or undrained triaxial tests with pore pressure measurements.
- The analysis requires both the effective strength parameters of the soil as well as the distribution of pore pressure in the slope.

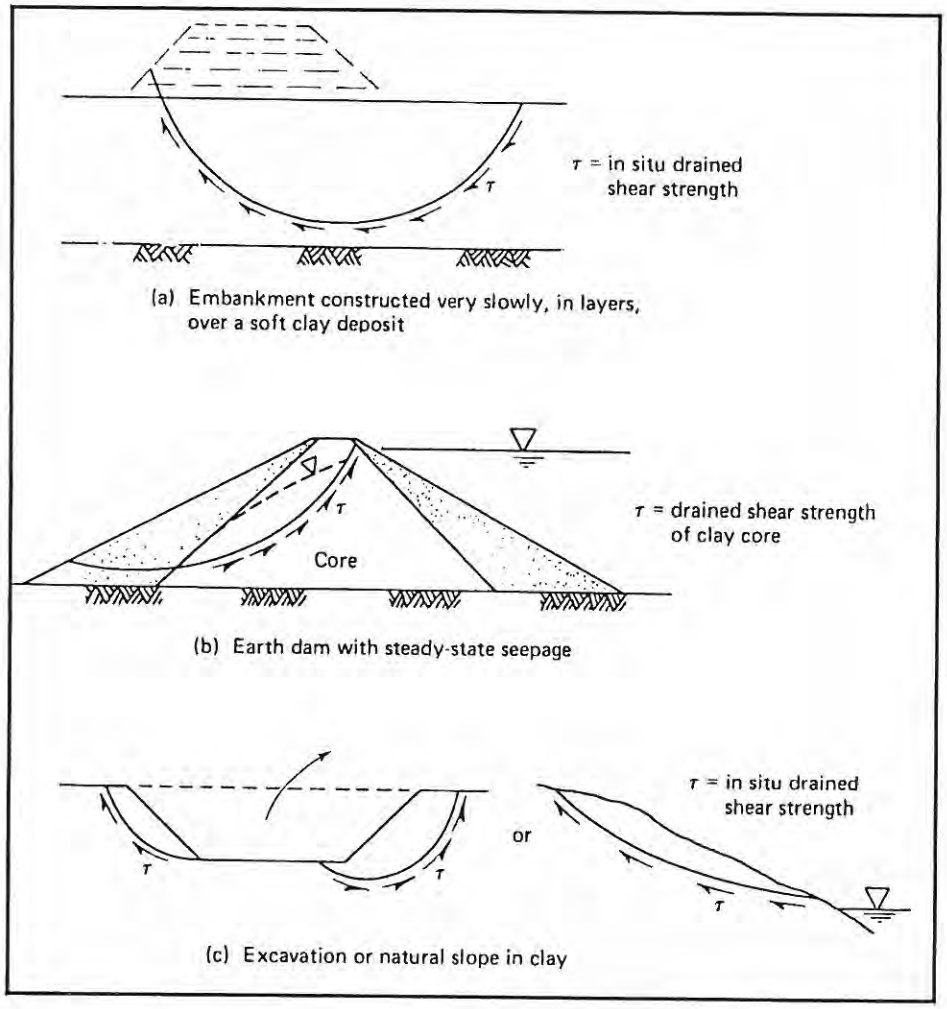

Which Method Gives the Best Value?

- There is no single answer to this question.
- The Ordinary (or Fellenius) method satisfies only moment equilibrium and ignores all interslice forces. Can create errors in FS of 60%.
- From a statics viewpoint, the best method satisfies both force and moment equilibrium (e.g., Spencer and Morgenstern-Price).
- However, all methods make some assumptions about the interslice shear forces.

Methods and Statics

Method	Force Equil (Vertical)	Force Equil (Horiz)	Moment Equil.
Ordinary	Yes	No	Yes
Bishop Simplified	Yes	No	Yes
Janbu Simplified	Yes	Yes	No
Janbu Generalized	Yes	Yes	Used to calc. interslice shear forces
Spencer	Yes	Yes	Yes
Morg-Price	Yes	Yes	Yes
GLE	Yes	Yes	Yes
Corp of Engrs	Yes	Yes	No
Lowe-Karafiath	Yes	Yes	No

Assumptions Used

Method	Assumptions
Ordinary	Interslice forces are neglected
Bishop's Simplified	Resultant interslice forces are horizontal (no interslice shear forces)
Janbu's Simplified	Resultant interslice forces are horizontal. Empirical factor used to account for interslice shear forces.
Janbu's Generalized	Location of the interslice normal force is defined by assumed line of thrust.
Spencer	Resultant interslice forces are of constant slope throughout.

Assumptions Used

Morg-Price	Direction of resultant interslice force is determined using arbitrary function.
GLE	Direction of resultant interslice force is defined using arbitrary function.
Corp of Engr	Direction of resultant interslice force is 1) equal to avg. slope of slip surface or 2) parallel to grnd. surface.
Lowe-Karafiath	Direction of resultant interslice force is equal to the avg. of grnd surface and the base slope of each slice.

www.GS5D.COM

One way to illustrate differences in methods is through the use of lambda (λ).

λ is the percentage of a interslice direction function used to compute the interslice shear force.

Factor of Safety vs Lambda (λ)

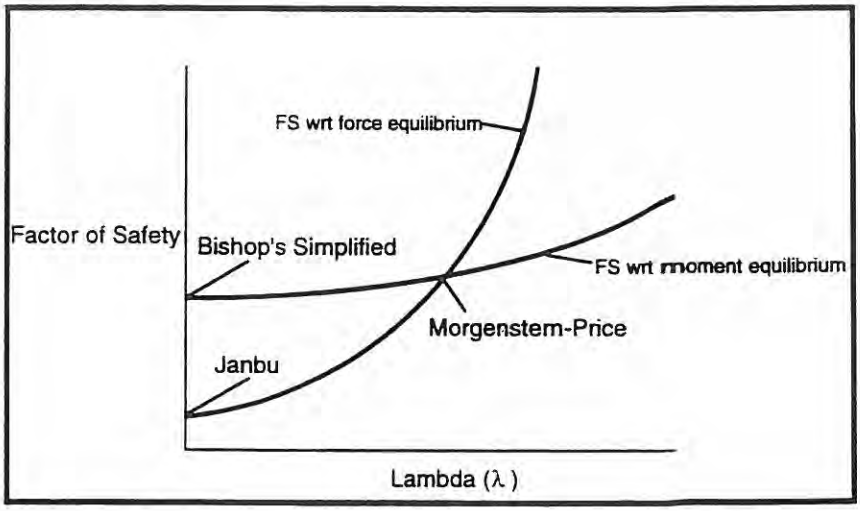

Finite Element Methods

- Numerous analysis/design problems can be solved using this method.
- Based upon simultaneous solution of many equations.
- Problem types:
  - Seepage
  - Load-deformation
  - Thermal
  - Contaminant Transport
  - Consolidation

Seepage Solutions

- Saturated and unsaturated flow analysis
- Steady-state and transient conditions
- Two-dimensional and axisymmetric problems
- Confined and unconfined problems
- Multiple soil types
- Anisotropic hydraulic conductivity coefficients
- Transient boundary conditions

Typical Seepage Problems

- Flow through zoned earth dam
- Migration of the wetting front through a dam after initial impoundment
- Dissipation of excess pore-water pressures after reservoir drawdown
- Dissipation of excess pore-water pressure due to loading or unloading (consolidation)
- Changes in pore-water pressure conditions within earth slopes due to infiltration of precipitation
- Fluctuations in groundwater table elevation due to surface infiltration and evaporation

Load-Deformation Analysis

- Contrast to Limit-Equilibrium
- Solution Relationships

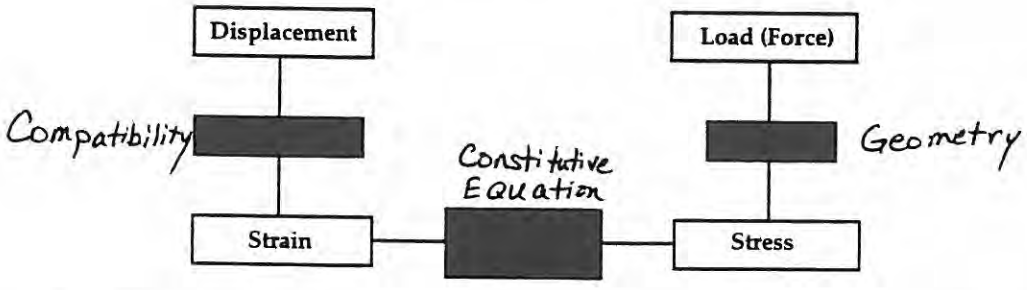

Some Common Constitutive Relationships

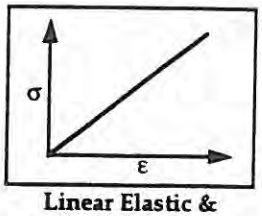

Linear Elastic &
Anisotropic Linear Elastic

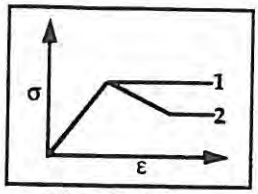

1. Elastic-Plastic
2. Strain-Softening

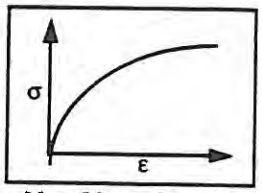

Non-Linear Elastic
(Hyperbolic)

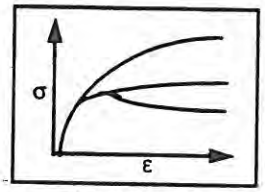

Cam-Clay &
Other Plastic Models

Typical Stress/Deformation Problems

- Settlement of Footings
- Settlement of fluid-filled tanks
- Lateral movement of braced or anchored excavations and surface settlement around the excavation
- Floor rebound of open-pit, sloping excavations
- Consolidation or heave resulting from pore-water pressure changes

Thermal Analysis

- Phase Changes of water to ice and reverse
- Boundary Conditions
  - fixed temperatures or heat flux conditions
  - transient temperature and/or heat flux as function of time
- Soil Properties
  - frozen and unfrozen heat capacities and water content
- Heat Flux Computations

Applications

- Degradation of permafrost beneath warm buildings
- Degradation of permafrost around a warm, buried pipeline
- Slope stability in permafrost areas
- Stability of roadway embankments during freeze-thaw events

University of WisconsinMadison
Geo Engineering Program

Geotechnical • Geoenvironmental • Geological • Geophysical

2228 Engineering Hall 1415 Engineering Drive
Madison, Wisconsin 53706

UNIVERSITY OF WISCONSIN MADISON
150 YEARS

SOFTWARE REQUEST FORM

Name: _____ **(Required)**
Company: _____ **(Required)**
Address: _____ **(Required)**
City and State: _____ **(Required)**
Zip or Postal Code: _____ **(Required)**
Country: _____ **(Required)**
Telephone: _____ Fax: _____ **(Required)**
Email: _____ **(Required)**

ORDER:

_____ *Win*UNSAT-H (Windows 95/98/NT) @ $500.00 each Total $_____
_____ *Win*STABL (Windows 95/98/NT) @ $300.00 each Total $_____
_____ STABL Manual (printed) @ $35.00 each Total $_____
Total $_____

STABL manuals are sent US mail. For FedEx delivery, enter FedEx number here: _____

CHECKS:

Please make checks payable to: **UW-Geoengineering Program.** Mail form and check to:

UW - Geoengineering Program
c/o Craig H. Benson
2214 Engineering Hall
1415 Engineering Drive
Madison, WI 53706

CREDIT CARDS:

Enter all of the information below. Mail form to address listed in section for checks or fax to 608-263-2453 to the attention of **Craig H. Benson**.

Name of Credit Card: _____ **(Required)**
Address for Credit Card Billing (1): _____ **(Required)**
Address for Credit Card Billing (2): _____ **(Required)**
City, State, Country and Zip for Credit Card Billing (3): _____ **(Required)**
Country for Credit Card Billing (4): _____ **(Required)**
Card Type (VISA, MasterCard, AMEX, Discover Only): _____ **(Required)**
Card Number: _____ **(Required)**
Expiration Date: _____ **(Required)**

Credit card orders are processed through Civil Engineering Consultants LLC, a firm in the Madison area. CEC will send credit card receipts directly to purchasers.

SERIAL NUMBERS AND PASSWORDS ARE SENT TO PURCHASERS VIA EMAIL AFTER CONFIRMATION OF THE PURCHASE. SOFTWARE AND OTHER MATERIALS CAN BE DOWNLOADED FROM www.uwgeosoft.org

ALL PROCEEDS FROM SOFTWARE PURCHASES ARE USED TO SUPPORT THE EDUCATIONAL AND RESEARCH MISSIONS OF THE GEOENGINEERING PROGRAM AT UW-MADISON.

Chapter 3 Learning SLOPE/W

3.1 An Example Problem 3-3

3.2 Defining the Problem 3-4

3.2.1 Set the Page Size 3-4
3.2.2 Set the Scale 3-6
3.2.3 Set the Grid Spacing 3-7
3.2.4 Save the Problem 3-8
3.2.5 Zoom the Drawing 3-10
3.2.6 Sketch the Problem 3-11
3.2.7 Identify the Problem 3-13
3.2.8 Specify the Analysis Methods 3-15
3.2.9 Specify Pore-Water Pressure Options 3-16
3.2.10 Specify Slip Surface Options 3-17
3.2.11 Define Soil Properties 3-17
3.2.12 Draw Lines 3-19
3.2.13 Draw Piezometric Lines 3-21
3.2.14 Draw Radius 3-23
3.2.15 Draw Grid 3-25
3.2.16 View Preferences 3-28
3.2.17 Sketch an Axis 3-30
3.2.18 Sketch Text 3-32
3.2.19 Verify the Problem 3-34
3.2.20 Save the Problem 3-35

3.3 Solving the Problem 3-36

3.3.1 Open the Data File 3-37
3.3.2 Start Solving 3-38
3.3.3 Quit SOLVE 3-39

3.4 Viewing the Results 3-40

3.4.1 Open the Data File 3-41
3.4.2 View Selected Slip Surfaces 3-42
3.4.3 View Method 3-43
3.4.4 Draw the Slice Forces 3-45
3.4.5 Draw the Contours 3-46
3.4.6 Draw the Contour Values 3-48
3.4.7 Print the Drawing 3-49

3.5 Graphing Detailed Forces 3-51

3.1 An Example Problem

This chapter introduces you to SLOPE/W by presenting the step-by-step procedures involved in analyzing a simple slope stability problem. By executing each step in the sequence presented, you will be able to define a problem, compute the factors of safety, and view the results. By completing this exercise, you can quickly obtain an overall understanding of the features and operations of SLOPE/W.

Figure 3.1 presents a schematic diagram of a slope stability problem. The objective is to compute the minimum factor of safety and locate the critical slip surface location.

The slope is cut in two materials at 2:1 (horizontal:vertical). The upper layer is 5 m thick and the total height of the cut is 10 m. Bedrock exists 4 m below the base of the cut. The pore-water pressure conditions are depicted by the piezometric line in Figure 3.1. The soil strength parameters are also listed in Figure 3.1.

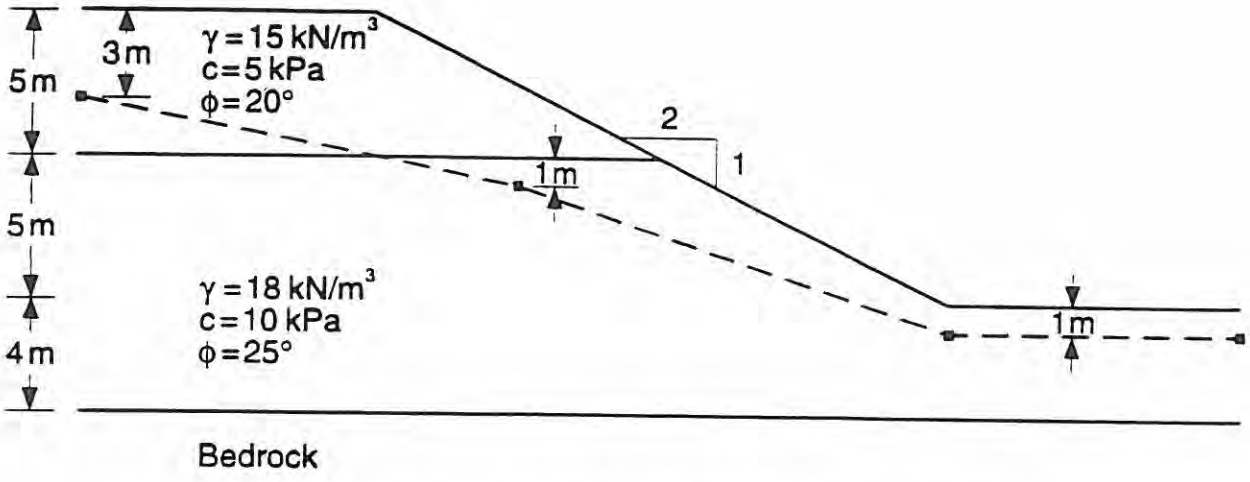

Figure 3.1 A Sample Slope Stability Problem

3.2 Defining the Problem

The SLOPE/W DEFINE function is used to define a problem. To start DEFINE, double-click the DEFINE icon in the SLOPE/W Group window.

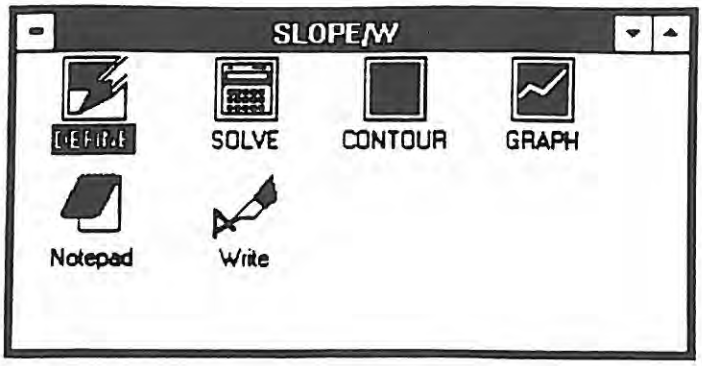

The DEFINE window appears.

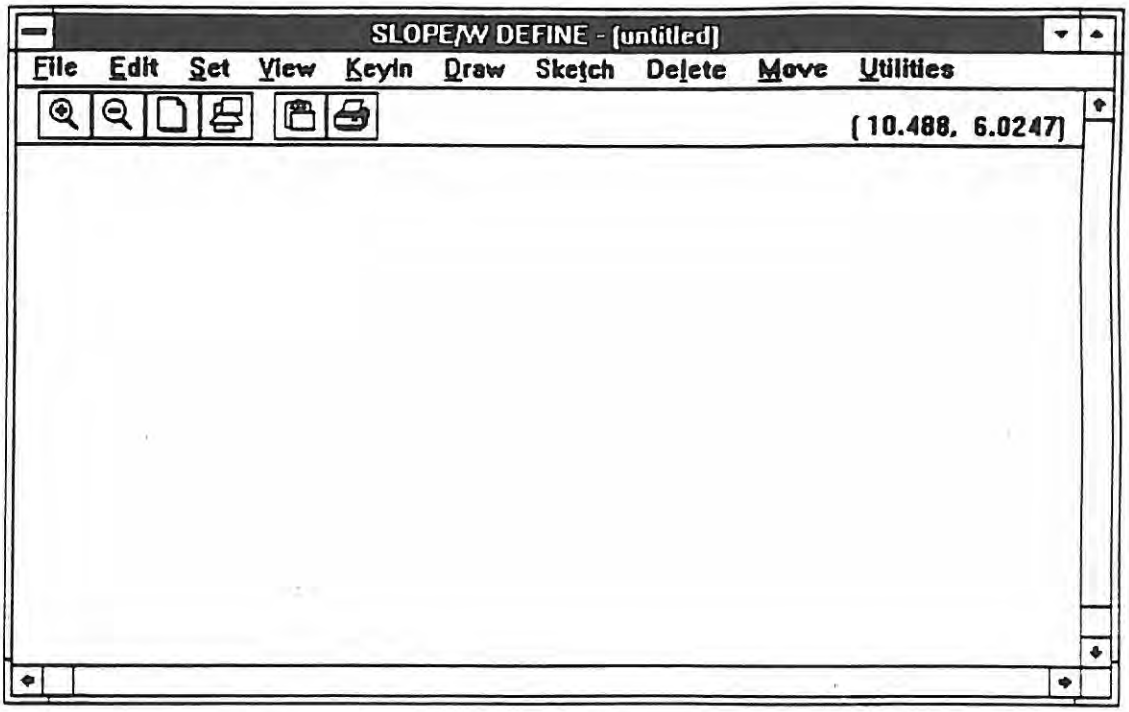

Click the Maximize button in the upper-right corner of the DEFINE window so that the DEFINE window will cover the entire screen. This maximizes the workspace for defining the problem.

3.2.1 Set the Page Size

For this example, the desired page size is 260 mm wide and 200 mm high.

To define the page size:

1. Choose Set from the DEFINE menu.

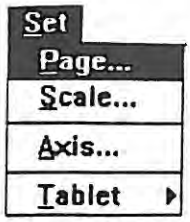

2. Choose Page from the Set menu. The Set Page dialog box appears.

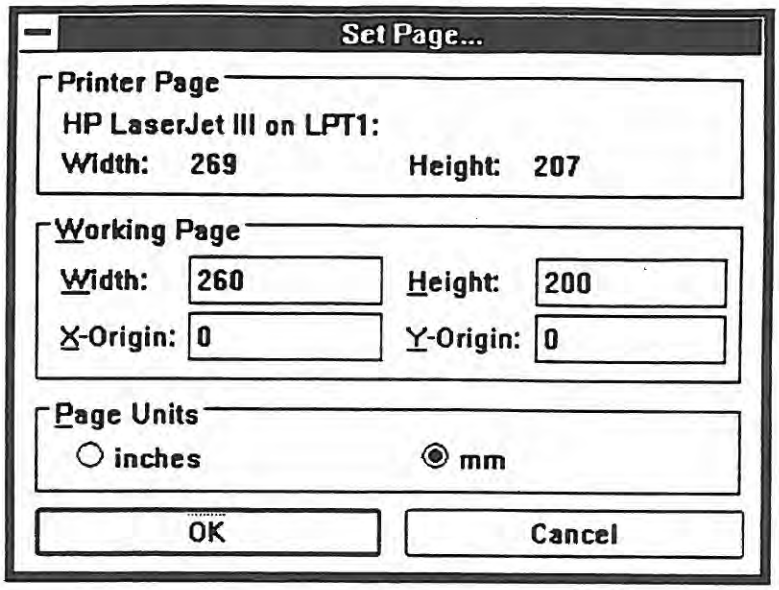

The Printer Page group box displays the name of the printer selected and the printing space available on one printer page. This information is presented to help you define a working page that will print properly.

3. Select **mm** in the Page Units group box.

4. Type **260** in the Working Page Width edit box. Press the tab key to move to the next edit box.

5. Type **200** in the Height edit box.

6. Check that the X-Origin and Y-Origin edit boxes are set to **0**. This sets the origin of the *x-y* coordinate system at the lower-left corner of the page.

7. Select OK.

3.2.2 Set the Scale

The geometry of the problem is defined in meters. A suitable scale is 1:200. This makes the drawing small enough to fit within the page margins.

To set the scale:

1. Choose Set Scale from the DEFINE menu.

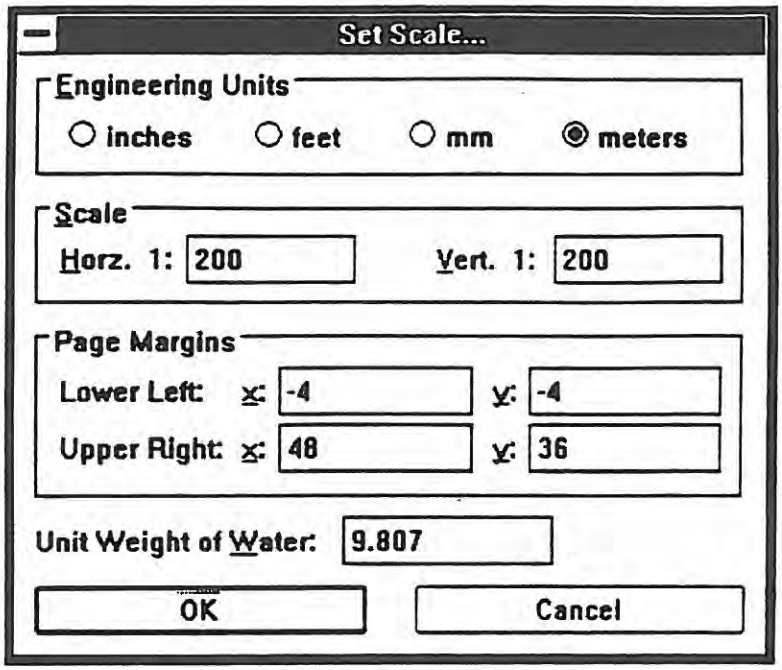

2. Select Meters in the Engineering Units group box.

3. Type **200** in the Horz. 1: edit box and **200** in the Vert. 1: edit box.

   The Page Margins now extend from 0 to 52 meters in the horizontal direction and from 0 to 40 meters in the vertical direction. It is convenient to have the coordinates (0,0) lie some distance in from the lower-left corner of the page. This is specified by setting the lower-left *x*-*y* coordinates to negative values.

4. Type **-4** in the Lower Left X edit box and **-4** in the Lower Left Y edit box.

   The Horz. Scale changes to 215.38 and the Vert. Scale changes to 220 in order to reflect the new engineering dimensions of the page.

5. Re-type **200** in the Horz. 1: edit box and **200** in the Vert. 1: edit box.

The upper-right page margin is recalculated to reflect the new scale. The Page Margins now extend from -4 to 48 meters in the horizontal direction and from -4 to 36 meters in the vertical direction.

6. Select OK.

Since the problem is defined in terms of meters and kN, the unit weight of water must be 9.807 kN/m^3, which is the default value when the engineering dimensions are defined in meters.

3.2.3 Set the Grid Spacing

A background grid of points is required to help you draw the problem. These points can be "snapped to" when creating the problem geometry in order to create points and lines with exact coordinates. A suitable grid spacing in this example is 1 meter.

To define and display the grid:

1. Choose View from the DEFINE menu.

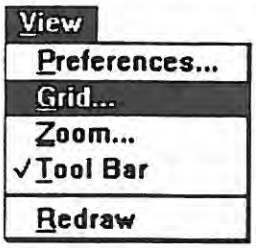

2. Choose Grid from the View menu. The View Grid dialog box appears.

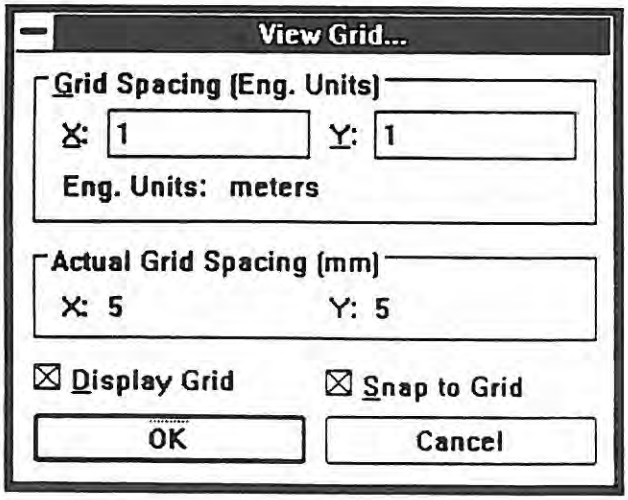

3. Type **1** in the Grid Spacing X: edit box.

4. Type 1 in the Y: edit box.

   The actual grid spacing on the screen will be a distance of 5 mm between each grid point. This value is displayed in the Actual Grid Spacing group box.

5. Check the Display Grid check box.

6. Check the Snap to Grid check box.

7. Select OK.

   The grid is displayed in the DEFINE window. As you move the cursor in the window, the coordinates of the nearest grid point (in engineering units) are displayed in the tool bar.

3.2.4 Save the Problem

The problem definition data must be saved in a file. This allows the SOLVE and CONTOUR functions to obtain the problem definition for solving the problem and viewing the results.

The data may be saved at any time during a problem definition session. It is good practise to save the data frequently.

To save the data to a file:

1. Choose File from the DEFINE menu.

2. Choose Save from the File menu. The following dialog box appears:

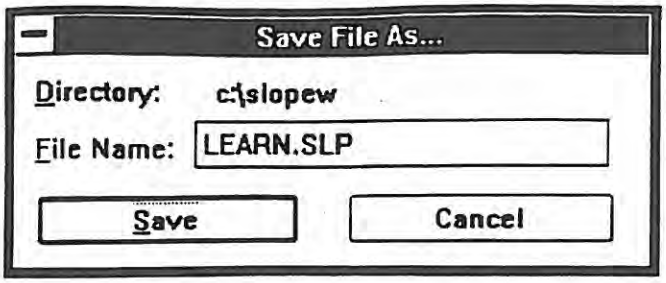

3. Type a file name in the File Name edit box. For example, type **LEARN**.

4. Select Save. The data will be saved to the file LEARN.SLP. Once it is saved, the file name is displayed in the DEFINE window title bar.

   The file name may include a drive name and directory path. If you do not include a path, the file will be saved in the directory name displayed to the right of the Directory prompt.

   The file name extension must be **SLP**. SLOPE/W will add the extension to the file name if it is not specified.

The next time you choose File Save, the file will be saved without first bringing up the Save File As dialog box. This is because a file name is already specified.

It is often useful when modifying a file to save it under a different name. This preserves the previous contents of the file.

To save data to a file with a different name:

1. Choose File Save As. The same dialog box appears.

2. Type the new file name.

   If the file name you type already exists, you will be asked whether you wish to replace the file which already exists. If you select No, you must retype the file name. If you select Yes, the previous copy of the file will be lost.

3.2.5 Zoom the Drawing

Before you sketch the problem dimensions, display the entire page in the DEFINE window by clicking on the Zoom Page tool in the tool bar (located just below the menu bar). Your screen should look similar to the following:

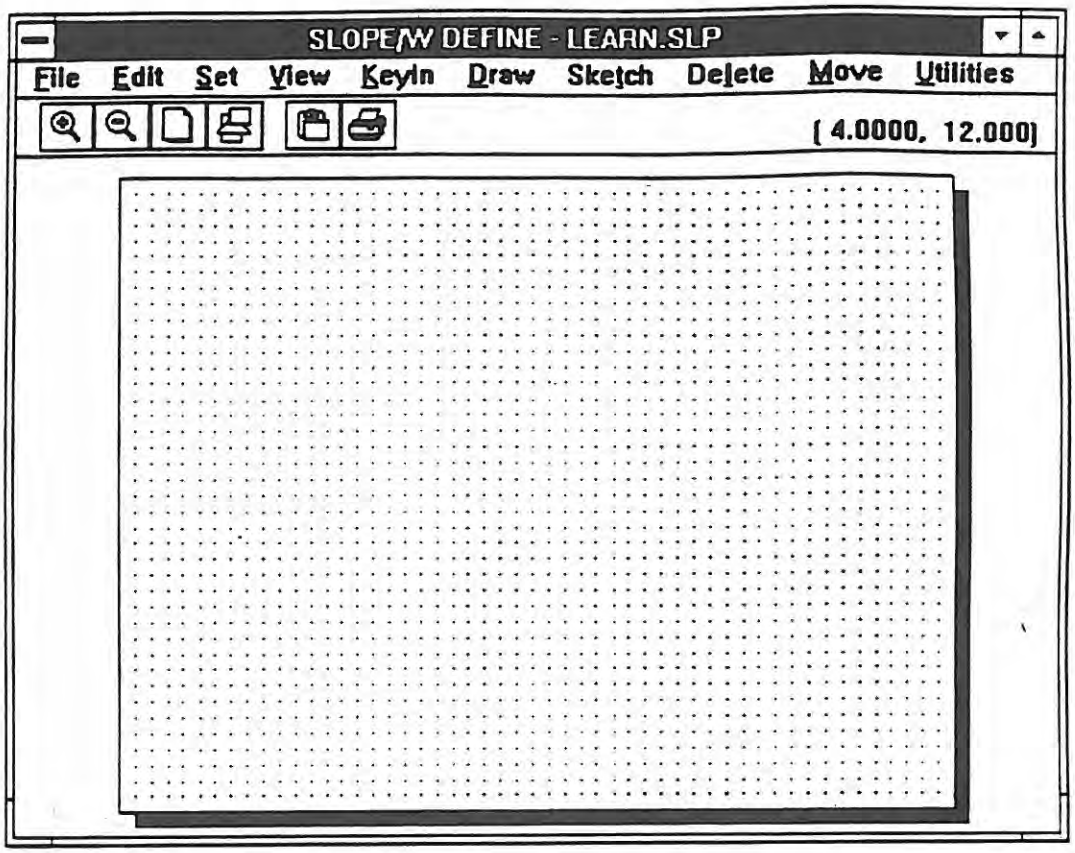

The four zoom commands in the tool bar allow you to zoom in, zoom out, display the entire page, or display all currently defined objects.

To zoom in on a section of the drawing:

1. In the tool bar, click on the Zoom In ( ) tool with the left mouse button.

   The cursor changes to a magnifying glass (), and the Zoom In button appears pushed-in to indicate that you are zooming in on a region.

2. The zoom region is defined by dragging a rectangle around the region. Move the cursor to the top left corner of the area to enlarge. Push the left mouse button down, but do not release it. Now move the mouse to the right, and a rectangle appears. "Drag" the mouse until the rectangle encompasses the desired area.

3. Release the left mouse button.

   The selected region is enlarged so that it fills the entire window. The Zoom In button returns to its normal state.

To display the drawing at the previous size:

- In the tool bar, click on the Zoom Out ( ) tool with the left mouse button.

  The drawing is displayed at the previous size.

See the Tool Bar section in Chapter 4 for a complete description of these commands.

3.2.6 Sketch the Problem

In defining a slope stability problem, it is convenient to first prepare a sketch of the problem dimensions. This sketch is a useful guide for drawing the geometric elements of the problem.

To sketch the slope stability problem:

1. Choose Sketch from the DEFINE menu.

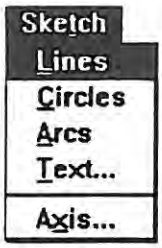

2. Choose Lines from the Sketch menu. The cursor will change from an arrow to a cross-hair, and **<Sketch Lines>** will be added to the DEFINE window title bar. This is to indicate that you are in "Sketch Mode."

3. Using the mouse, move the cursor near position (0,14), as indicated in the Position window, and click the left mouse button. The cursor snaps to the grid point at (0,14). As you move the mouse, a line is drawn from (0,14) to the new cursor position.

4. Move the cursor near (10,14) and click the left mouse button. The cursor snaps to (10,14) and a line is drawn from (0,14) to (10,14).

5. Move the cursor near (30,4) and click the left mouse button. A line is drawn from (10,14) to (30,4).

6. Move the cursor near (40,4) and click the left mouse button. A line is drawn from (30,4) to (40,4).

7. Move the cursor near (40,0) and click the left mouse button. A line is drawn from (40,4) to (40,0).

8. Move the cursor near (0,0) and click the left mouse button. A line is drawn from (40,0) to (0,0).

9. Move the cursor near (0,14) and click the left mouse button. A line is drawn from (0,0) to (0,14).

10. Click the right mouse button to finish sketching a line. The cursor will change from a cross-hair back to an arrow; you are no longer in Sketch Mode.

11. Choose Sketch Lines again.

12. Move the cursor near (0,9) and click the left mouse button. The cursor snaps to (0,9).

13. Move the cursor near (20,9) and click the left mouse button. A line is drawn from (0,9) to (20,9), which is the boundary between the upper and lower soil layers.

14. Click the right mouse button to finish sketching a line. The cursor will change from a cross-hair back to an arrow; you are no longer in Sketch Mode.

15. To display the problem outline in the DEFINE window, click on the Zoom Objects tool in the tool bar.

After you have completed the above steps, your screen should look like the following:

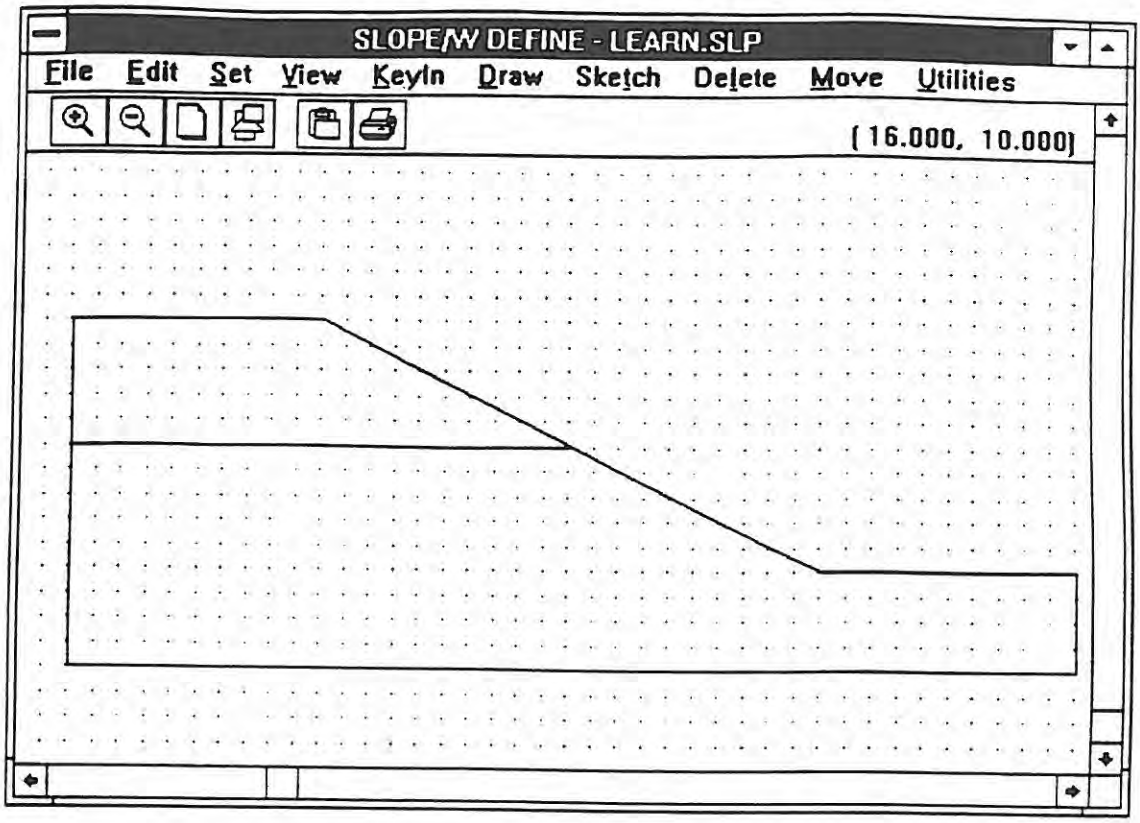

3.2.7 Identify the Problem

To name and identify the problem:

1. Choose KeyIn from the DEFINE menu.

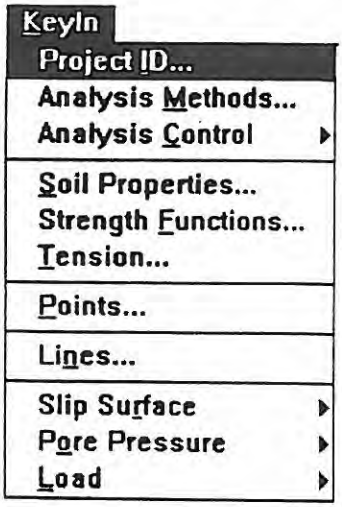

2. Choose Project ID from the KeyIn menu. The following dialog box appears.

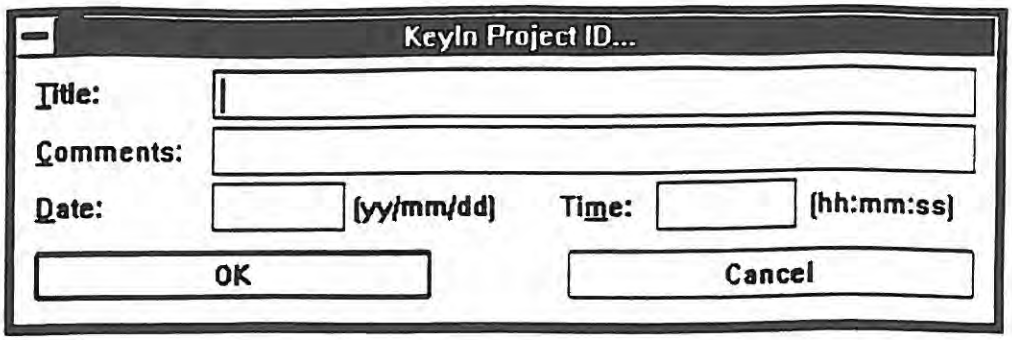

3. Type in any appropriate text in the Title edit box and the Comments edit box.

4. Type the date of the project in the Date edit box. It must be entered in the format **(yy/mm/dd)** where **yy** is the year, **mm** is the month, and **dd** is the day.

5. Type the time of the project in the Time edit box. It must be entered in the format **(hh:mm:ss)** where **hh** is the hour, **mm** is the minute, and **ss** is the second.

6. Select OK.

This information will be written to all data input and output files.

3.2.8 Specify the Analysis Methods

To specify the analysis methods:

1. Choose KeyIn Analysis Methods from the DEFINE menu. The following dialog box appears:

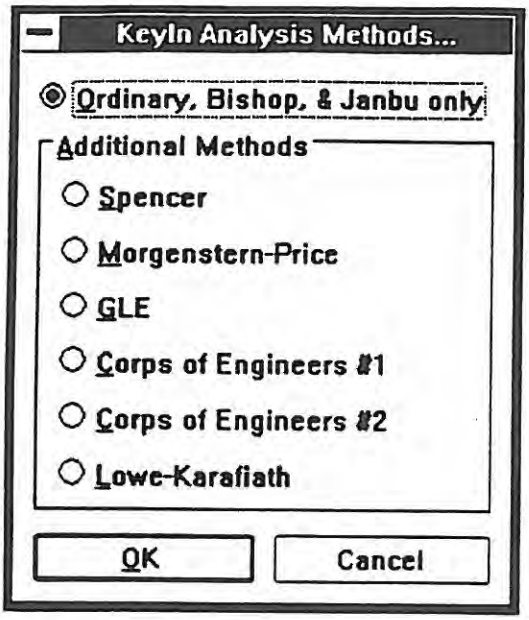

2. Select the Ordinary, Bishop, & Janbu option (this is the default option). No additional methods of analysis are required.

3. Select OK.

3.2.9 Specify Pore-Water Pressure Options

To specify the option for defining the pore-water pressure conditions:

1. Choose KeyIn Analysis Control from the DEFINE menu. A cascading menu appears.

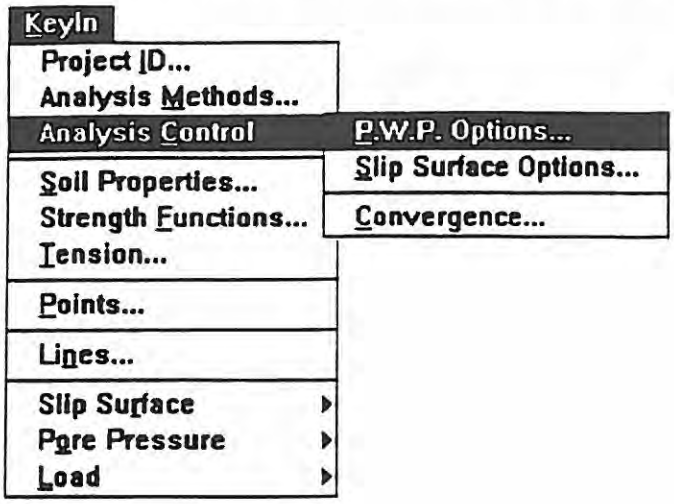

2. Choose P.W.P. Options from the cascading menu. The following dialog box appears:

3. Select the Piezometric Lines / Ru option.

4. Select OK.

3.2.10 Specify Slip Surface Options

The slip surfaces to be analyzed can either be specified manually or be specified by defining a grid of centers and radius lines.

To specify the option for defining the slip surfaces to be analyzed:

1. Choose KeyIn Analysis Control from the DEFINE menu. A cascading menu appears.

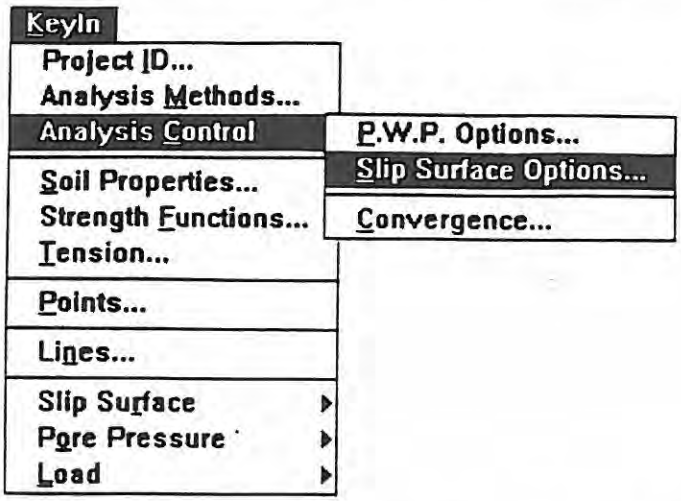

2. Choose Slip Surface Options from the cascading menu. The following dialog box appears:

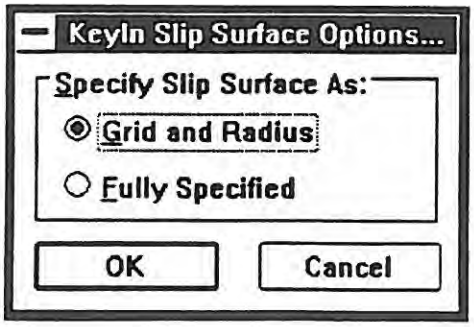

3. Select the Grid and Radius option (this is the default option).

4. Select OK.

3.2.11 Define Soil Properties

The soil properties of this problem are listed in Figure 3.1. The properties must be defined for three materials.

To define the soil properties:

1. Choose KeyIn Soil Properties from the DEFINE menu. The following dialog box appears:

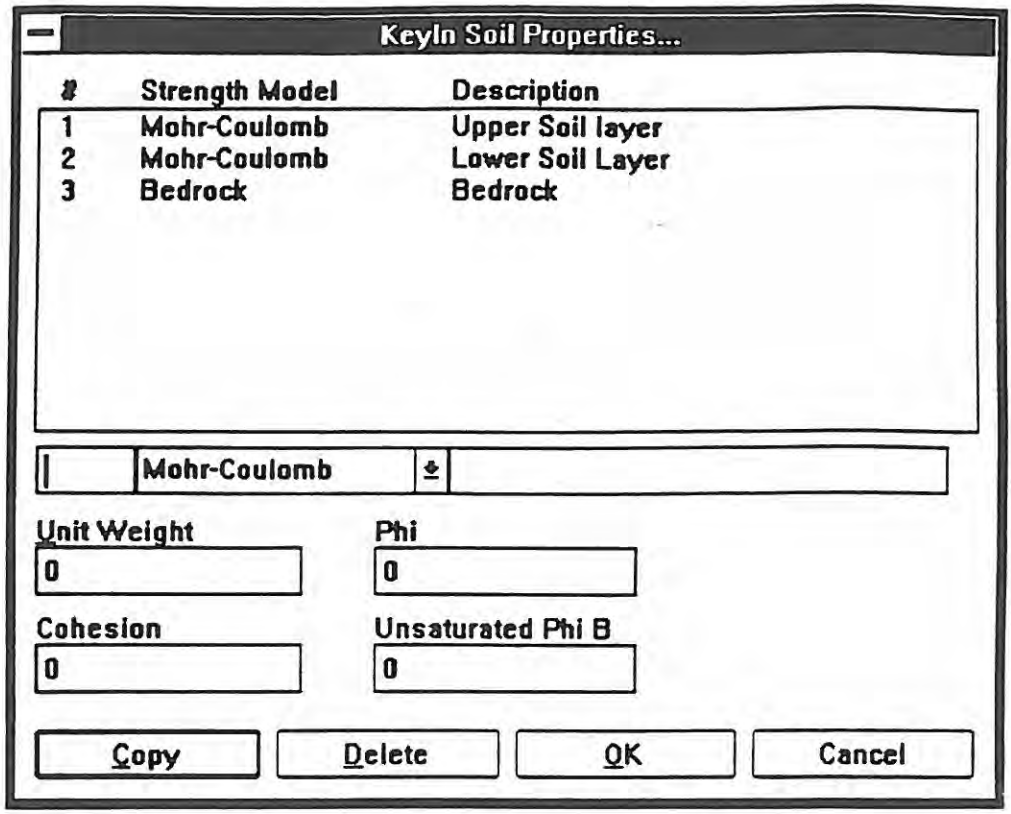

2. Type **1** in the Soil # edit box to indicate that you are defining Soil 1.

3. Press TAB twice to move to the Description edit box (The Strength Model does not need to be selected, since it is the default Mohr-Coulomb model).

4. Type **Upper Soil** in the Description edit box.

5. Type **15** in the Unit Weight edit box.

6. Type **5** in the Cohesion edit box.

7. Type **20** in the Phi edit box.

8. Select Copy. The values contained in the edit boxes are copied into the list box.

9. Repeat Steps 2 to 8 for Soil 2, using the properties shown in Figure 3.1.

10. Type **3** in the Soil # edit box.

11. Click on down arrow to the left of the Strength Model edit box and select the Bedrock strength model. The Soil Description is set to Bedrock and the Unit Weight changes to **-1**.

12. Select Copy to copy the bedrock properties into the list box. The list box should now look the same as the dialog box shown above.

13. Select OK.

3.2.12 Draw Lines

The geometry and stratigraphy are defined by lines connected to points. A line must be defined for each soil layer. All lines must begin at the left-most point and end at the right-most point. The normal procedure is to define the top line first (Soil 1) and then the remaining lines in sequential order.

To draw the lines in the geometry:

1. Choose Draw Lines from the DEFINE menu. The following dialog box appears:

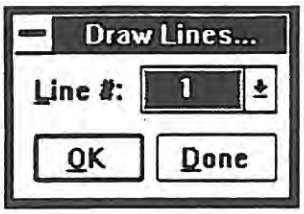

2. Select 1 in the Line # drop-down list box to draw Line 1 (this is the default value).

3. Select OK. The cursor will change from an arrow to a cross-hair, and **<Draw Lines>** will be added to the DEFINE window title bar, indicating the mode in which you are operating.

4. Move the cursor near (0,14) and click the left mouse button (The coordinates (0,14) should be displayed in the tool bar before you click). The cursor snaps to the grid point at (0,14) and creates a point there. As you move the cursor, a line is drawn from the point (Point 1) to the new cursor position.

5. Move the cursor to the crest of the slope (10,14) and click the left mouse button. The cursor snaps to the grid point at (10,14), a point is created (Point 2), and a red line is drawn from Point 1 to Point 2.

6. Move the cursor along the slope to where there is a break between the soil types (20,9) and click the left mouse button. The cursor snaps to the grid point at (20,9), a point is created (Point 3), and a red line is drawn from Point 2 to Point 3.

7. Move the cursor near the toe of the slope (30,4) and click the left mouse button.

8. Move the cursor to the right side of the problem near (40,4) and click the left mouse button. Then click the right mouse button to finish drawing Line 1.

   The Draw Lines dialog box appears again.

9. Click the down arrow to the right of the Line # edit box. A list of available lines (one for each soil number defined) appears:

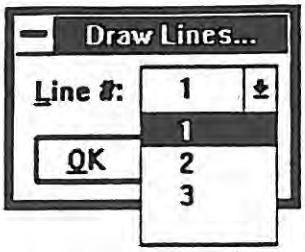

10. Click on 2 in the drop-down list box and then select OK to start drawing Line 2. The cursor will change from an arrow to a cross-hair, and **<Draw Lines>** will be added to the DEFINE window title bar, indicating the mode in which you are operating.

11. Move the cursor to the left side of the problem near the contact between the upper and lower soil layers (0,9) and click the left mouse button.

12. Click the left mouse button near Point 3 (20,9). (The cursor snaps to Point 3 instead of creating a new point at (20,9), since Point 3 already exists at the grid point). Then click the right mouse button to finish drawing Line 2.

    Since the Line 2 endpoint (Point 3) lies in the middle of the previous line (Line 1), SLOPE/W generates the remainder of Line 2 along Line 1 from Point 3 to Point 5. The complete Line 2 appears as a red line, and the Draw Lines dialog box reappears.

13. Click the down arrow to the right of the Line # edit box and click on 3.

14. Select OK to start drawing Line 3. Soil 1 will be shaded yellow. The cursor will change from an arrow to a cross-hair, and **<Draw Lines>** will be added to the DEFINE window title bar, indicating the mode in which you are operating.

15. Move the cursor to the lower-left corner near the contact between the lower soil layer and the bedrock (0,0) and click the left mouse button.

16. Move the cursor to the lower-right corner near the contact between the lower soil layer and the bedrock (40,0) and click the left mouse button. Then click the right mouse button to finish drawing Line 3.

17. Select Done in the Draw Lines dialog box to finish drawing lines. Soil 2 will be shaded light green.

After you have completed the above steps, your screen should look like the following:

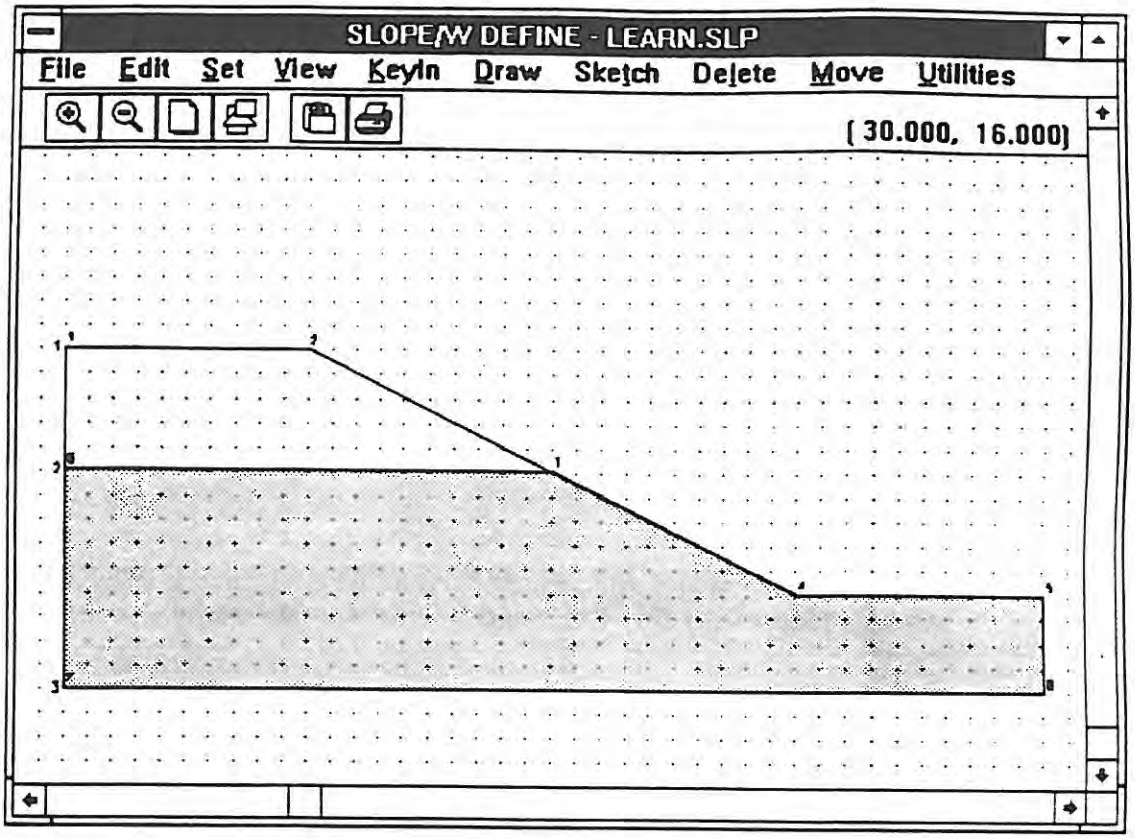

3.2.13 Draw Piezometric Lines

The pore-water pressure conditions in both Soil 1 and Soil 2 are defined by one piezometric line.

To draw the piezometric line:

1. If you have turned off the grid, choose View Grid and select the Snap to Grid option.

2. Choose Draw Pore-Water Pressure from the DEFINE menu. The following dialog box appears:

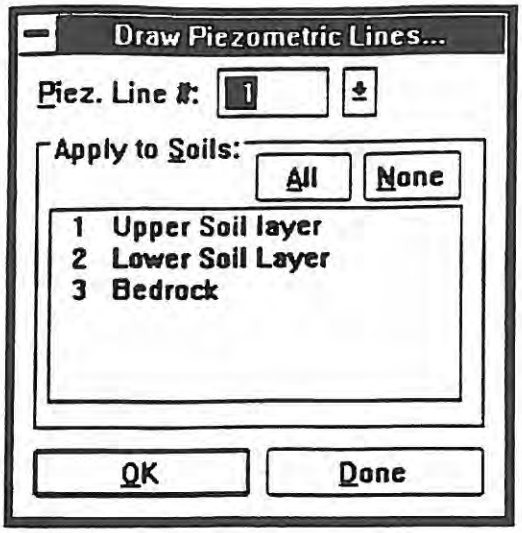

3. Select 1 in the Piez. Line # drop-down list box to draw one piezometric line (this is the default value).

4. Select Soil 1 and Soil 2 in the Apply To Soils list box to apply the piezometric line to Soils 1 and 2.

5. Select OK. The cursor will change from an arrow to a cross-hair, and **<Draw P.W.P.>** will be added to the DEFINE window title bar, indicating the mode in which you are operating.

6. Move the cursor near (0,11) (at the left of the problem) and click the left mouse button. The cursor snaps to the grid point at (0,11) and a point is created (Point 9). As you move the cursor, a dashed line is drawn from Point 9 to the new cursor position.

7. Move the cursor near (15,8) and click the left mouse button. The cursor snaps to the grid point at (15,8), a point is created (Point 10), and a red dashed line is drawn from Point 9 to Point 10.

8. Move the cursor near (30,3) and click the left mouse button.

9. Move the cursor near (40,3) and click the left mouse button. Then click the right mouse button to finish drawing the piezometric line for Soils 1 and 2.

   The Draw Piez. Lines dialog box appears again.

10. Select Done in the Draw Piez. Lines dialog box to finish drawing piezometric lines.

    Since the slip surfaces do not extend into the bedrock, it is not necessary to define a piezometric line for the bedrock.

After you have completed the above steps, your screen should look like the following:

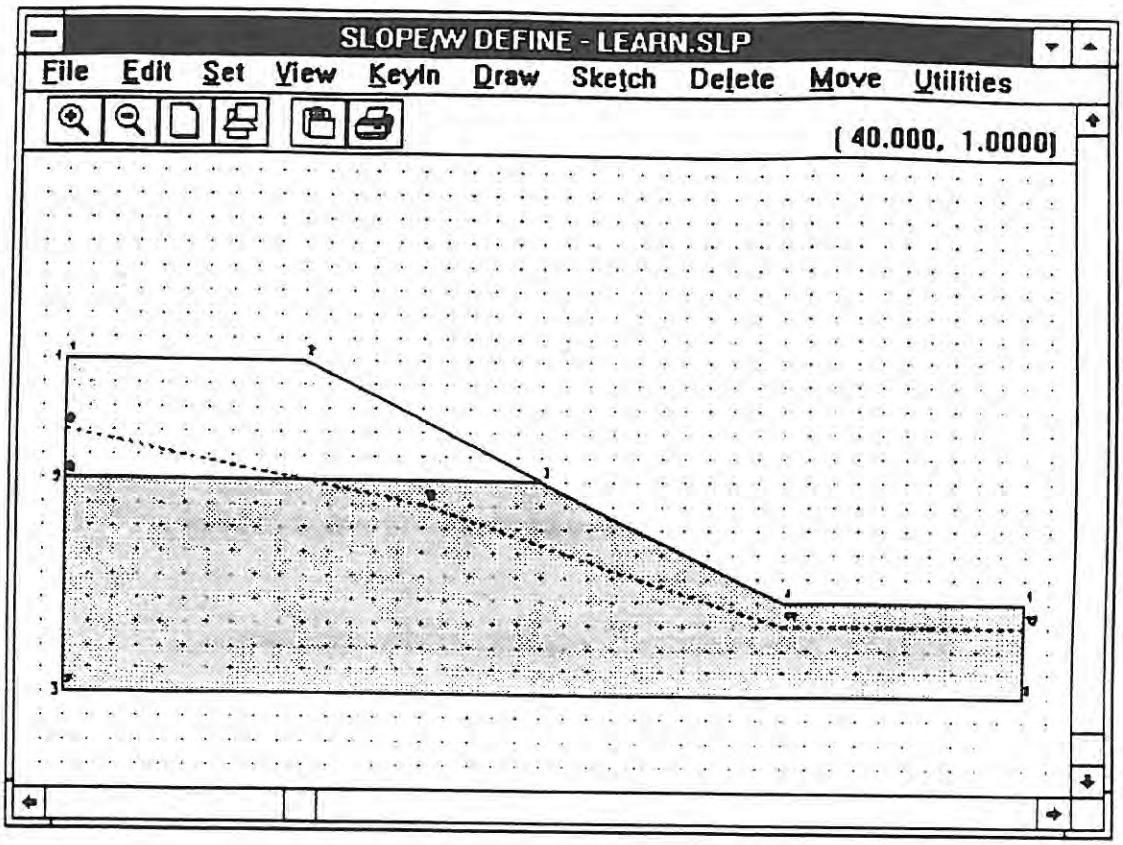

3.2.14 Draw Radius

To control the location of the trial slip surfaces, it is necessary to define lines or points which are used to compute the slip circle radii.

To draw the radius lines:

1. If you have turned off the grid, choose View Grid and select the Snap to Grid option.

2. Choose Draw Slip Surface from the DEFINE menu. A cascading menu appears.

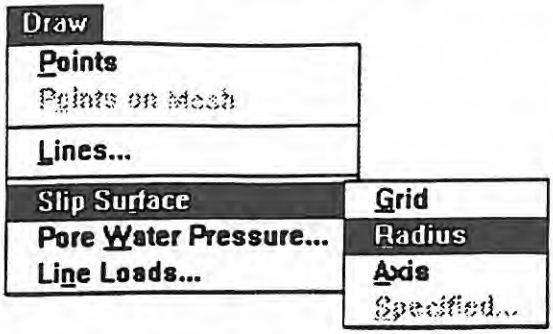

3. Choose Radius from the cascading menu. The cursor will change from an arrow to a cross-hair, and **<Draw Radius>** will be added to the DEFINE window title bar, indicating the mode in which you are operating.

4. Move the cursor near (15,4) and click the left mouse button. The cursor snaps to the grid point at (15,4) and a point is created (Point 13). As you move the cursor, a line is drawn from Point 13 to the new cursor position.

5. Move the cursor near (15,2) and click the left mouse button. The cursor snaps to the grid point at (15,2), a point is created (Point 14), and a red line is drawn from Point 13 to Point 14.

6. Move the cursor near (29,2) and click the left mouse button.

7. Move the cursor near (29,4) and click the left mouse button.

   The region in which the radius lines will be drawn is now outlined. A Divisions dialog window appears.

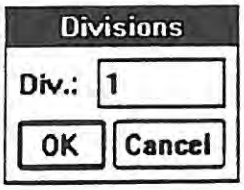

   As you move the mouse in any direction, the cursor only moves along the line between Points 13 and 14. The value in the Divisions edit box also changes. This value represents the number of divisions in which to divide the radius region.

8. Move the cursor up or down until 2 appears in the Divisions window, and click the left mouse button.

A message appears to inform you of how many radius lines will be generated.

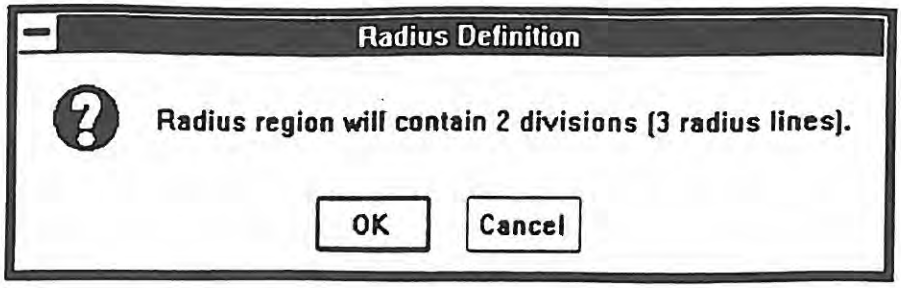

9. Select OK to generate the radius lines.

   Three radius lines are displayed in the DEFINE window. SLOPE/W SOLVE will define slip circles that are tangent to these lines.

After you have completed the above steps, your screen should look like the following:

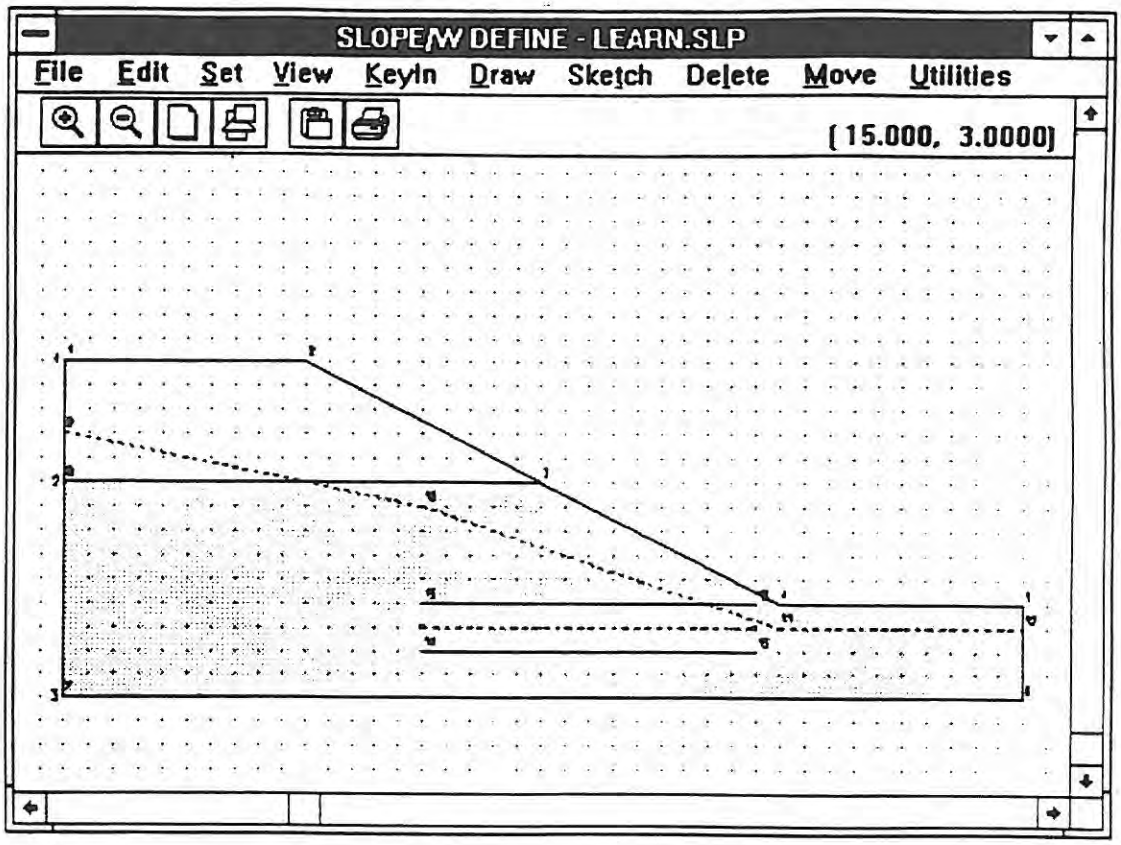

3.2.15 Draw Grid

A grid of rotation centers must be defined to specify and control the location of trial slip surfaces.

To draw the grid of centers:

1. If you have turned off the grid, choose View Grid and select the Snap to Grid option.

2. Choose Draw Slip Surface from the DEFINE menu. A cascading menu appears.

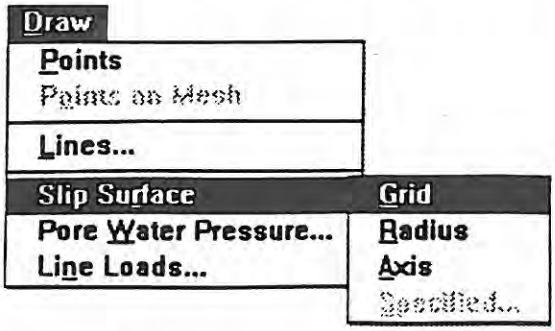

3. Choose Grid from the cascading menu. The cursor will change from an arrow to a cross-hair, and **<Draw Grid>** will be added to the DEFINE window title bar, indicating the mode in which you are operating.

4. Move the cursor near (23,25) and click the left mouse button. (You may need to scroll the window first to get to this position). The cursor snaps to the grid point at (23,25) and a point is created (Point 17). As you move the cursor, a line is drawn from Point 17 to the new cursor position.

5. Move the cursor near (22,19) and click the left mouse button. The cursor snaps to the grid point at (22,19) and a point is created (Point 18). As you move the cursor, a parallelogram is drawn from Point 17 to Point 18 to the new cursor position.

6. Move the cursor near (26,19) and click the left mouse button. A parallelogram is drawn from Point 17 to Point 18 to Point 19.

   The region in which the grid centers will be drawn is now outlined. A Divisions dialog window appears.

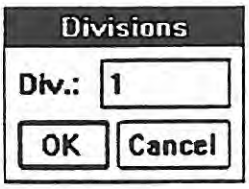

   As you move the mouse in any direction, the cursor only moves along the line between Points 18 and 19. The value in the Divisions edit box also changes. This value represents the number of horizontal divisions in which to divide the grid region.

7. Move the cursor until 2 appears in the Divisions window, and click the left mouse button.

As you move the mouse in any direction, the cursor only moves along the line between Points 17 and 18. The value in the Divisions edit box also changes. This value represents the number of vertical divisions in which to divide the grid region.

8. Move the cursor until 3 appears in the Divisions window, and click the left mouse button.

   A message appears to inform you of how many grid centers will be generated.

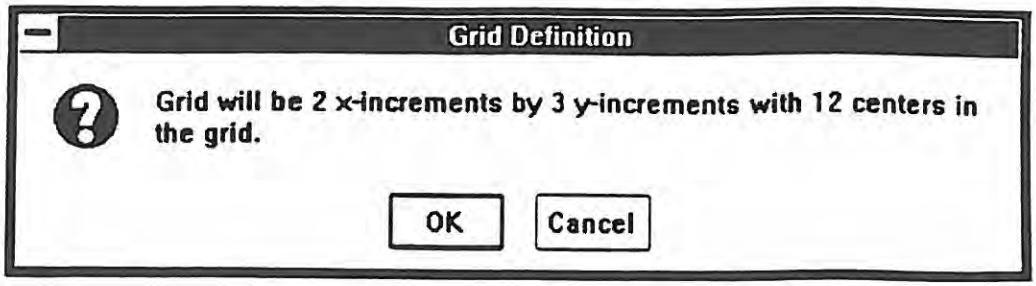

9. Select OK to generate the grid centers.

   A grid of 12 center points is displayed in the DEFINE window. SLOPE/W SOLVE will define slip circles using these center points.

TARAPACA
CAN CITY OF CA
FOR EXHIBITS

After you have completed the above steps, your screen should look like the following:

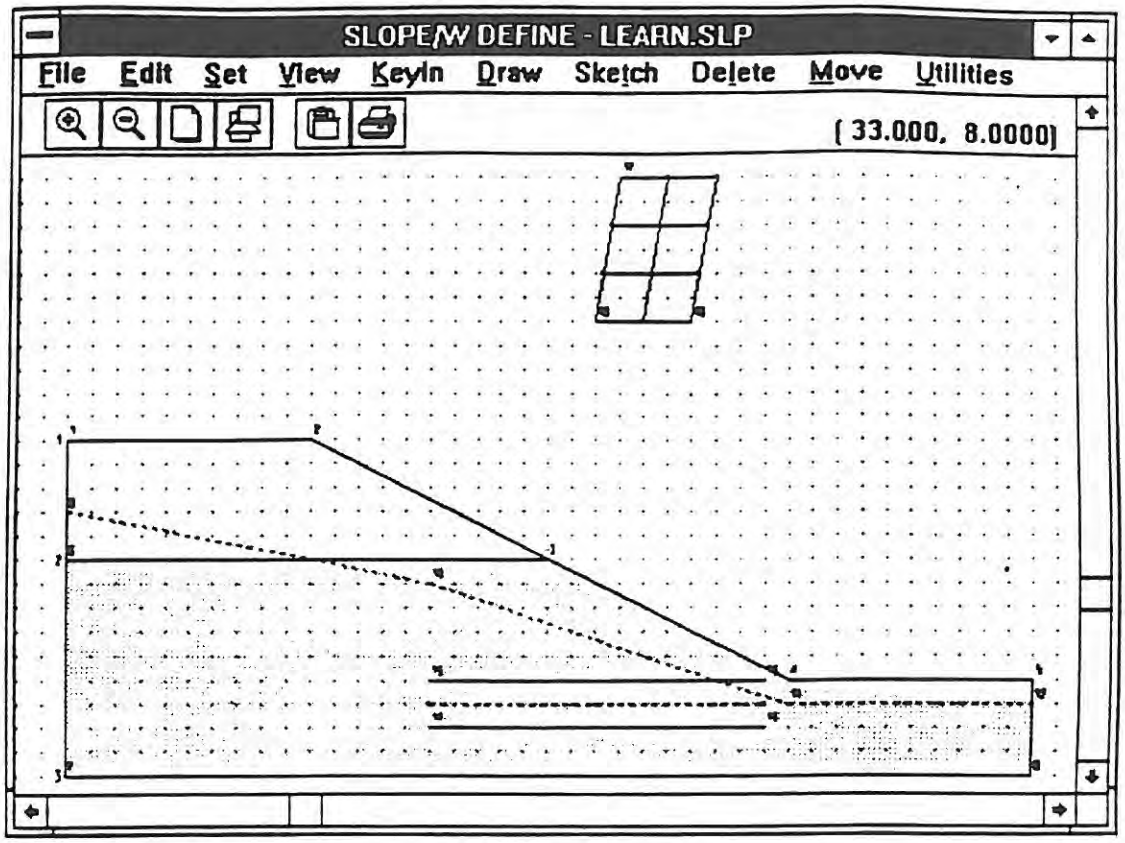

3.2.16 View Preferences

You no longer need to view the point numbers in the DEFINE window. To turn off the point numbers:

1. Choose View from the DEFINE menu.

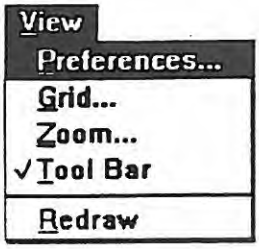

2. Choose Preferences from the View menu. The following dialog box appears:

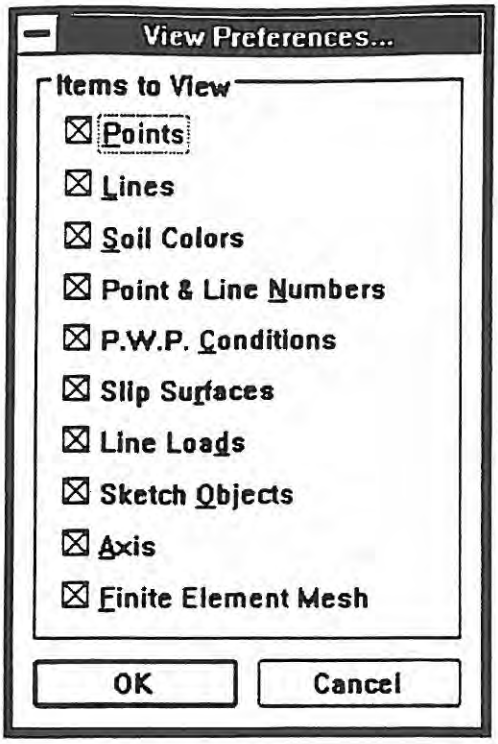

3. Uncheck the Point & Line Numbers check box in order to not display any point or line numbers on the drawing.

4. Select OK.

The problem will be drawn without the point and line numbers displayed.

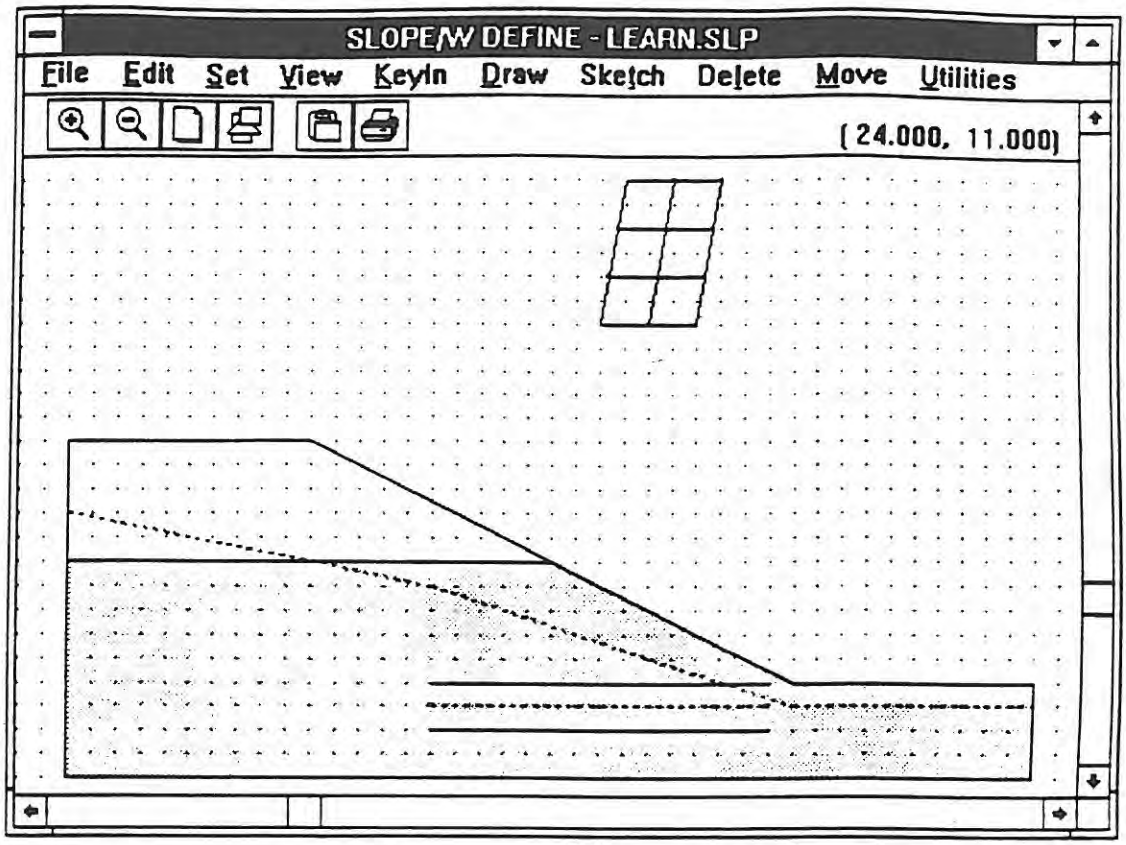

3.2.17 Sketch an Axis

Sketching an axis on the drawing facilitates viewing the drawing and interpreting the drawing after it is printed.

To sketch an axis:

1. If you have turned off the grid, choose View Grid and select the Snap to Grid option. This allows you to define an evenly-spaced region for the axis.

2. Choose Sketch Axis from the DEFINE menu. The following dialog box appears:

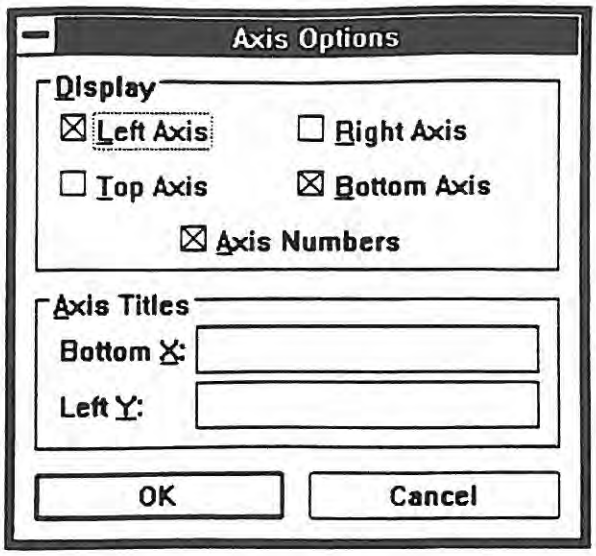

3. Check the Left Axis, Bottom Axis, and Axis Numbers check boxes in the Display group box. The Top Axis and Right Axis check boxes should be unchecked.

   This will cause an X axis to be sketched along the bottom side of the specified region and a Y axis to be sketched along the left side of the specified region.

4. Select OK. The cursor will change from an arrow to a cross-hair, and **<Sketch Axis>** will be added to the DEFINE window title bar, indicating the mode in which you are operating.

5. Move the cursor near position (0,0). Hold the left mouse button down, but do not release it. As you move the mouse, a rectangle appears.

6. "Drag" the mouse near (40,20), and release the left mouse button.

   An axis is generated within the region.

After you have completed the above steps, your screen should look like the following:

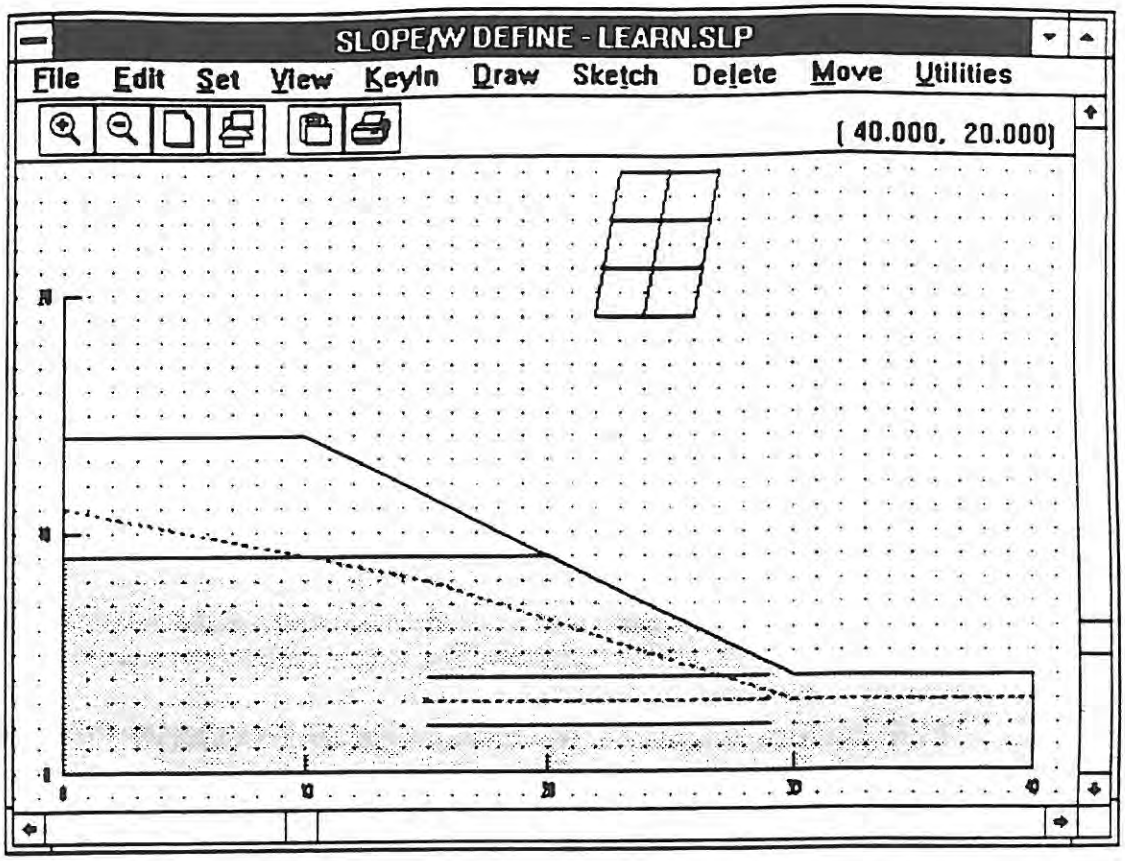

If you wish to modify the axis increments, choose Set Axis. See the DEFINE Reference section for more information on the Set Axis command.

3.2.18 Sketch Text

To clarify the problem, it is helpful to add labels to various parts of the drawing. For this example, the soils will be labelled as Upper Soil and Lower Soil.

To create text labels:

1. Choose Sketch Text from the DEFINE menu. The following dialog box appears:

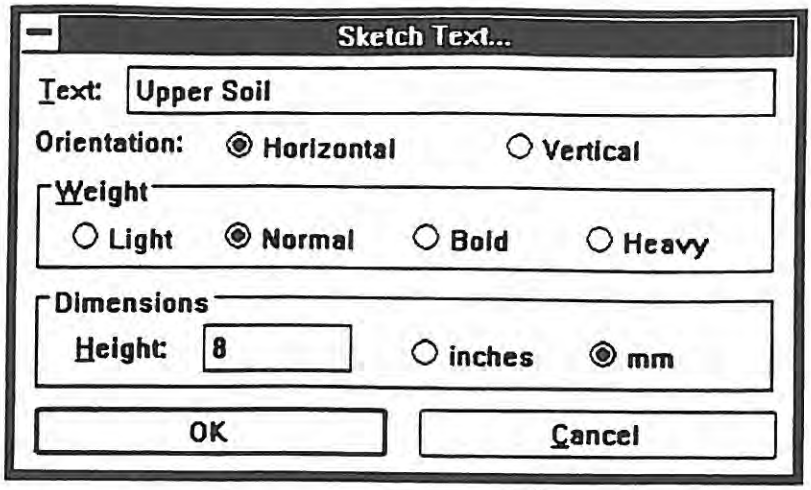

2. Type **Upper Soil** in the Text edit box.

3. Select mm in the Dimensions group box.

4. Type **8** in the Height edit box.

5. Select OK. The cursor will change from an arrow to a cross-hair, and **<Sketch Text>** will be added to the DEFINE window title bar, indicating the mode in which you are operating.

6. Click the left mouse button near position (3,11). The label **Upper Soil** appears on the drawing.

7. Choose Sketch Text again.

8. Type **Lower Soil** in the Text edit box. The dimensions will already be specified as 8 mm.

9. Select OK.

10. Click the left mouse button near position (3,3). The label **Lower Soil** appears on the drawing.

After you have completed the above steps, your screen should look like the following:

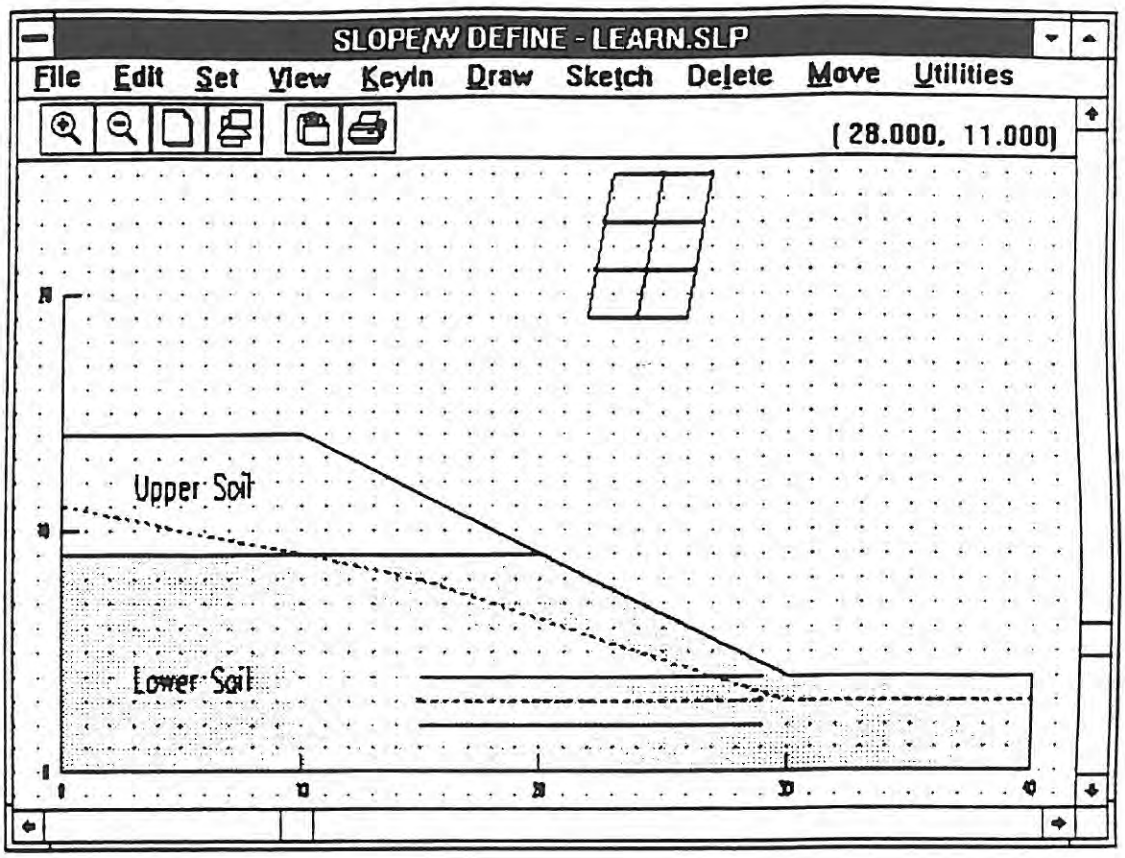

3.2.19 Verify the Problem

SLOPE/W DEFINE performs various checks to ensure that the problem has been correctly defined.

To verify the problem:

1. Choose Utilities Verify from the DEFINE menu. SLOPE/W verifies the problem data and displays the following dialog box:

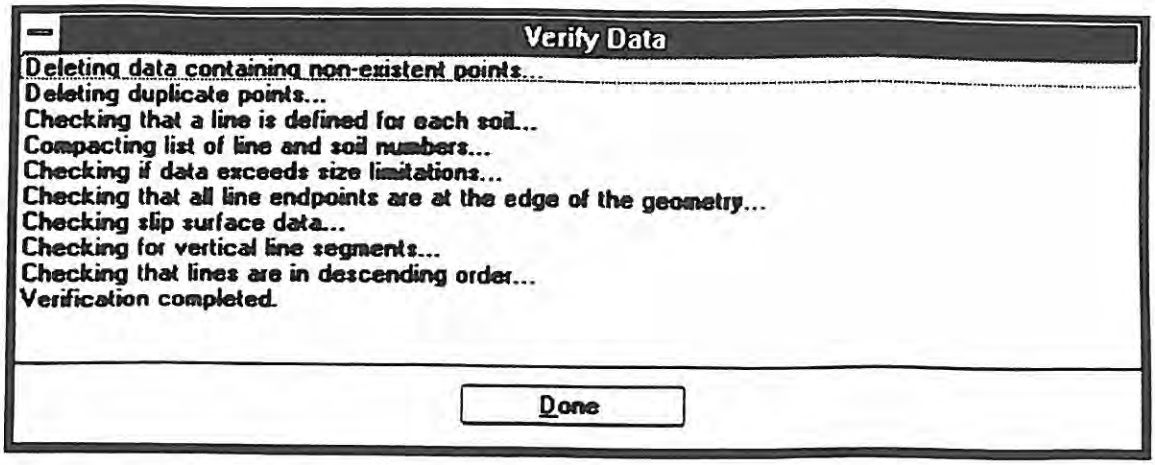

If the data is not acceptable, messages will appear indicating the error found in the data. For example, if one of the endpoints in Piezometric Line 1 does not extend to the edge of the geometry, the following message is displayed:

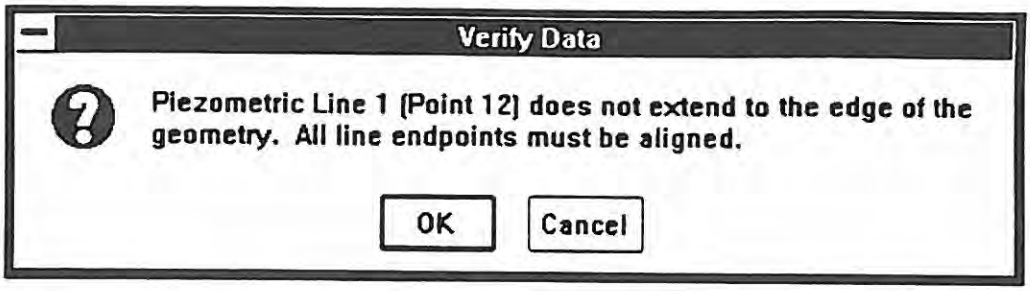

Select OK to continue verifying the data. Select Cancel to abort the verification process.

2. Select Done in the Verify Data dialog box when you are finished viewing the verification messages.

3.2.20 Save the Problem

The problem definition is now complete. Choose File Save to save the problem definition to the same file name it was previously saved to, such as LEARN.SLP. SOLVE reads the problem data from this file to calculate the factors of safety.

Choose File Exit if you wish to quit SLOPE/W DEFINE; otherwise, click the Minimize button in the top-right corner of the DEFINE window to reduce the window to an icon.

3.3 Solving the Problem

The second part of an analysis is to use the SLOPE/W SOLVE function to compute the factors of safety.

To start SOLVE, double-click the SOLVE icon in the SLOPE/W Group window.

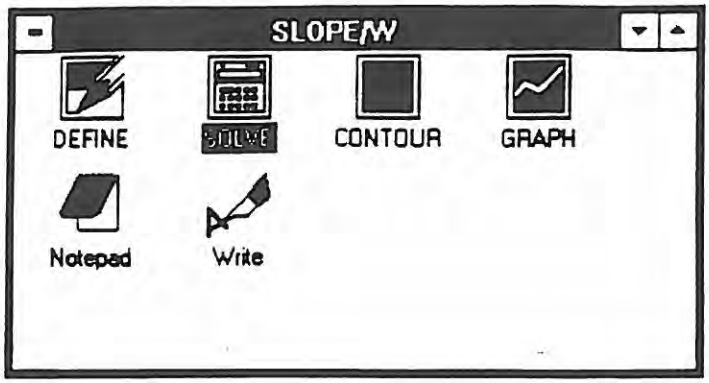

The SOLVE window appears.

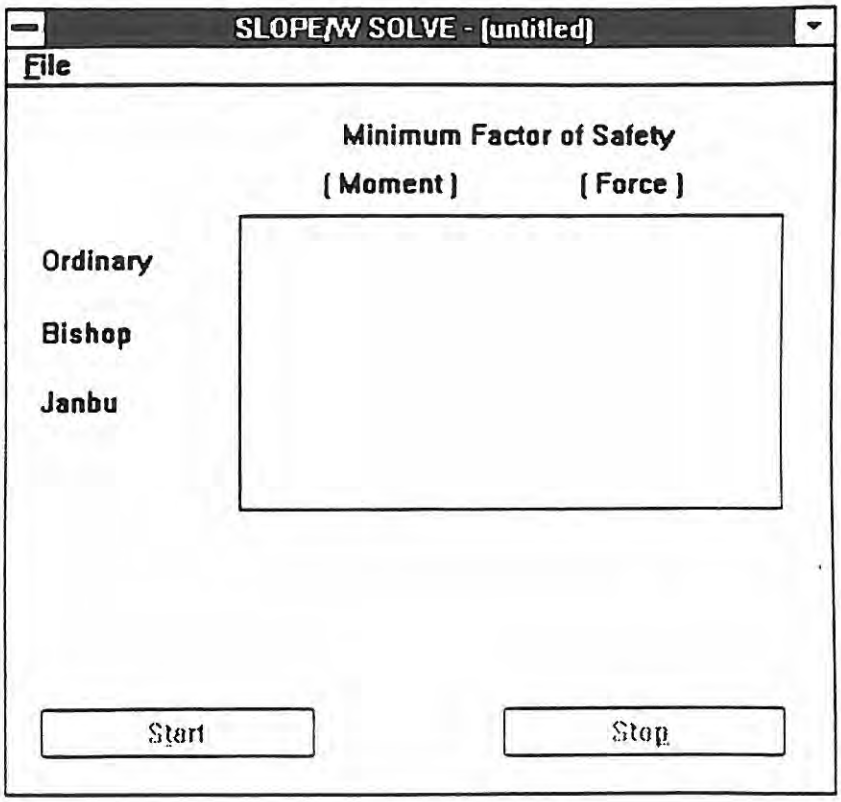

3.3.1 Open the Data File

To open the data file you created in SLOPE/W DEFINE:

1. Choose File from the SOLVE menu.

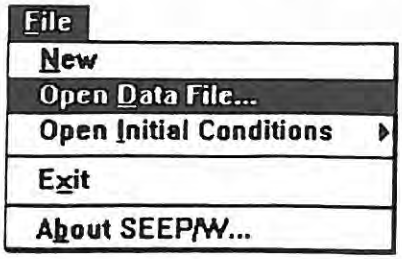

2. Choose Open Data File from the File menu. The following dialog box appears:

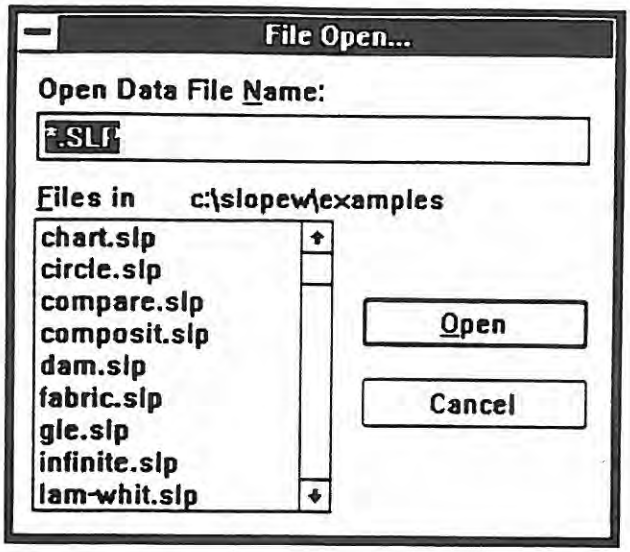

3. Select the data file you created with DEFINE from the Files In list box. For example, select LEARN.SLP.

4. Select Open.

The data file name is now displayed in the SOLVE window.

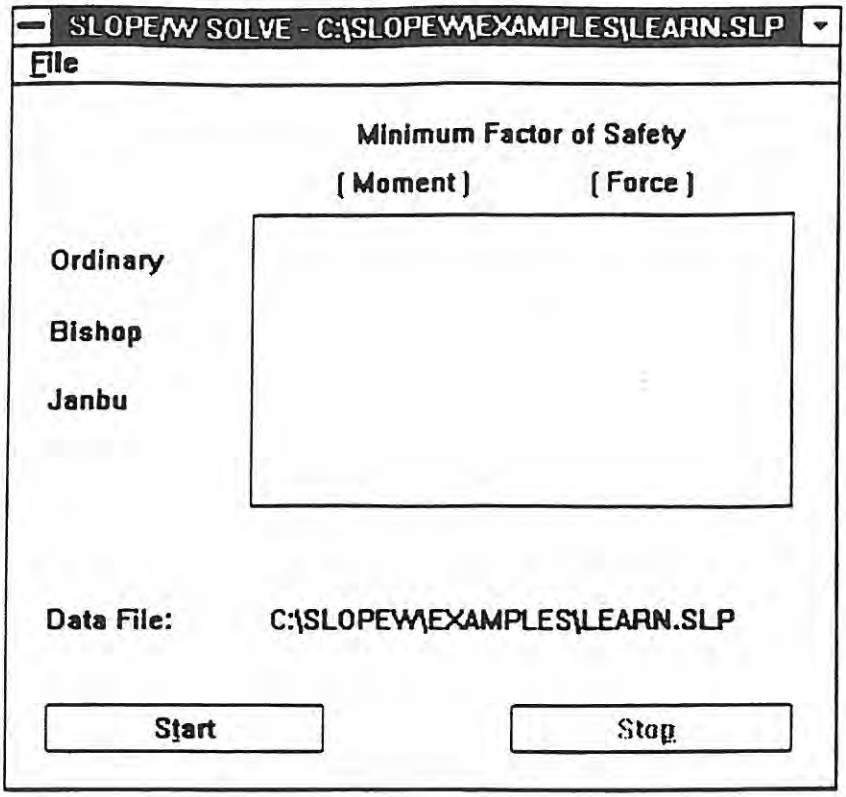

3.3.2 Start Solving

To start solving for the factors of safety, click the Start button in the SOLVE window.

A green dot appears between the Start and Stop buttons; the dot flashes while the computations are in progress.

During the computations, SOLVE displays the minimum factors of safety and the number of the current slip surface being analyzed. For the example problem, a total of 36 slip surfaces are analyzed.

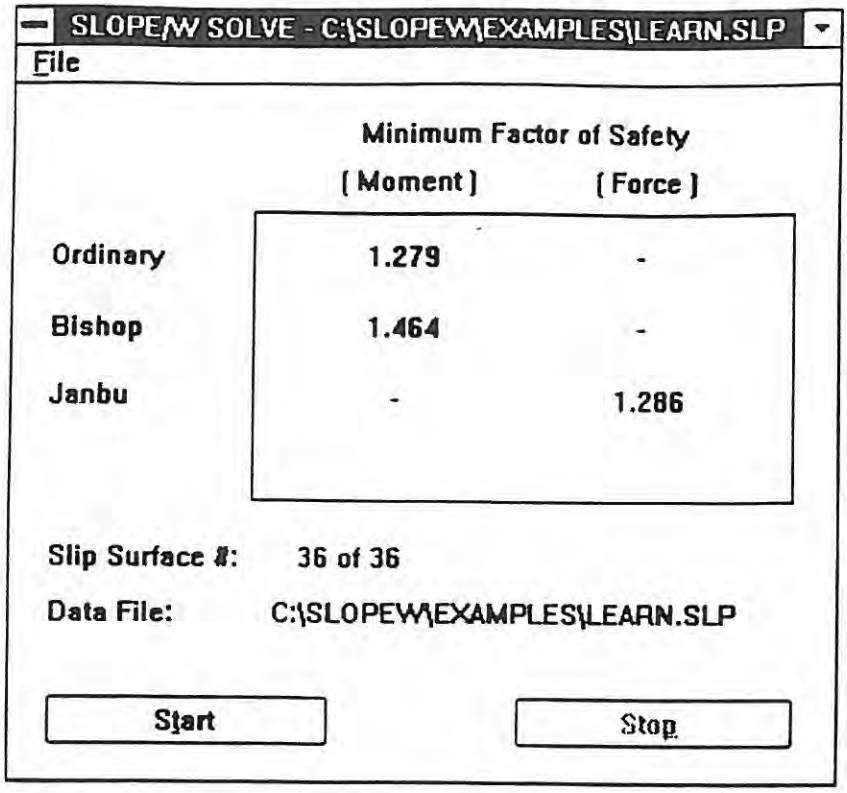

The results of the SOLVE analysis are written to three files with file name extensions of FAC, FRC, and DET. In this example, the file name LEARN.FAC contains the computed factors of safety, the file name LEARN.FRC contains the slice forces on the minimum slip surface, and the file name LEARN.DET contains the detailed forces for the minimum slip surface.

3.3.3 Quit SOLVE

You have now computed the factors of safety. Choose File Exit to quit SLOPE/W SOLVE, or click the Minimize button in the top-right corner of the SOLVE window to reduce the window to an icon.

3.4 Viewing the Results

The SLOPE/W CONTOUR function is used to view and evaluate the results of the problem analysis contained in the SOLVE output files. CONTOUR can display any of the analyzed slip surfaces, along with the associated factors of safety. The factors of safety can also be contoured for presentation purposes.

To start CONTOUR, double-click the CONTOUR icon in the SLOPE/W Group window.

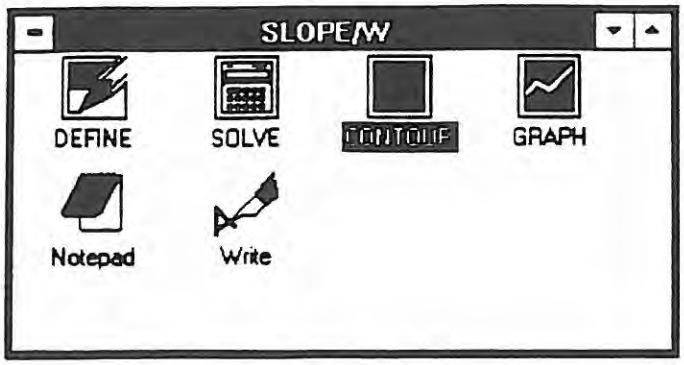

The CONTOUR window appears.

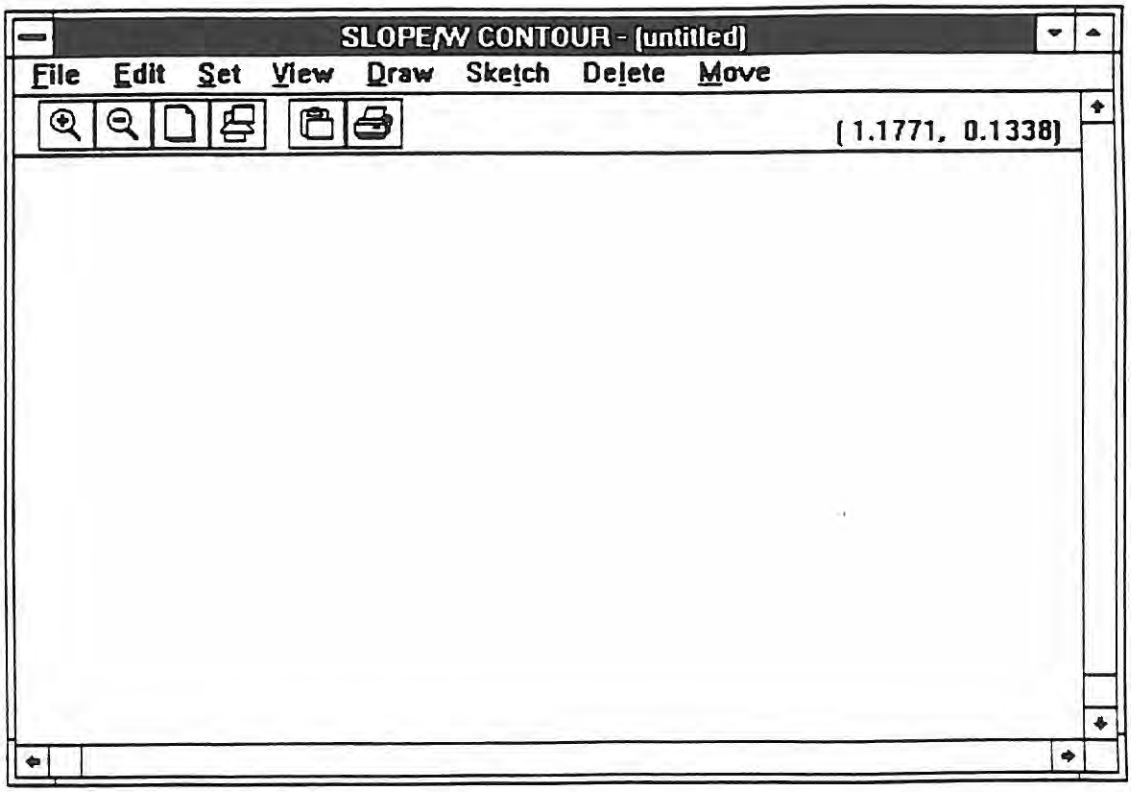

3.4.1 Open the Data File

To open the data file you created in SLOPE/W DEFINE:

1. Choose File from the CONTOUR menu.

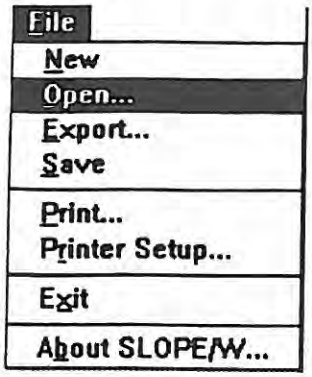

2. Choose Open from the File menu. The following dialog box appears:

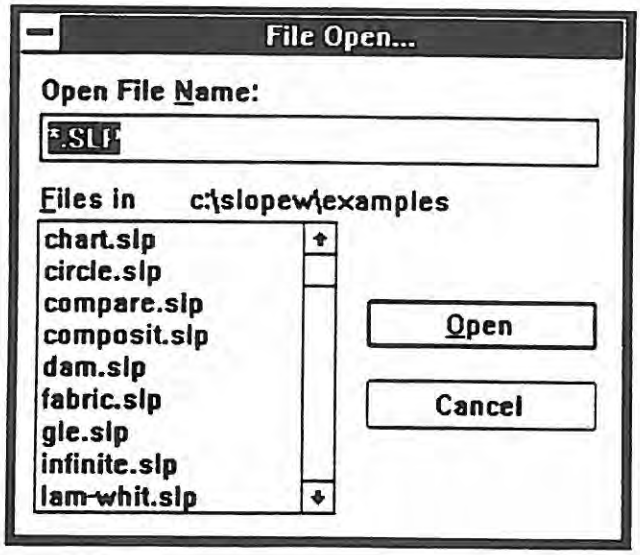

3. Select the data file you created with DEFINE from the Files In list box. For example, select LEARN.SLP.

4. Select Open.

CONTOUR displays the critical slip surface and minimum factor of safety for the problem.

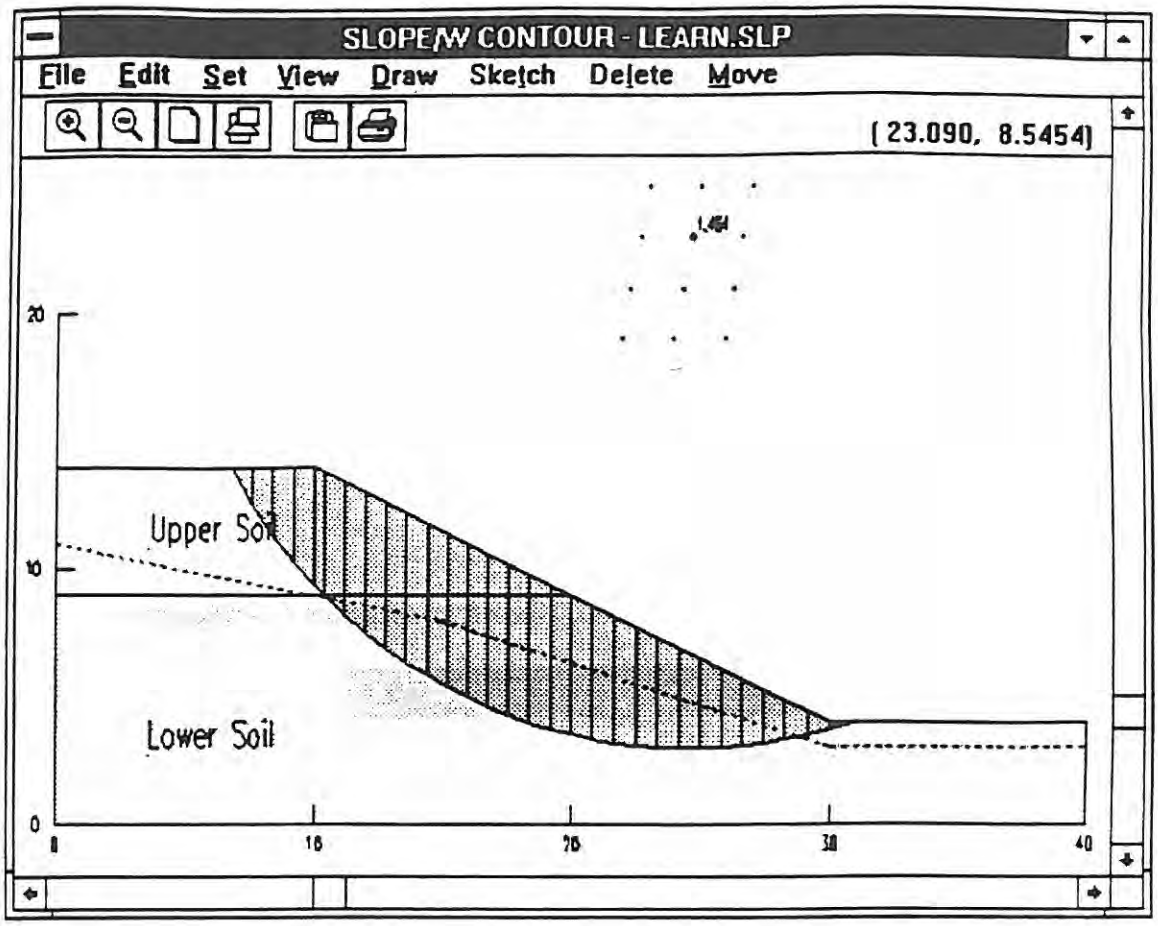

3.4.2 View Selected Slip Surfaces

To view slip surfaces other than the minimum slip surface:

1. Choose Draw from the CONTOUR menu.

2. Select Selected Slip from the Draw menu. The cursor will change from an arrow to a cross-hair, and **<Draw Slip>** will be added to the CONTOUR window title bar, indicating the mode in which you are operating.

3. Click the left mouse button near any grid center point.

   CONTOUR draws the minimum slip surface for this center and displays the factor of safety beside the grid center point. As well, the following dialog box appears:

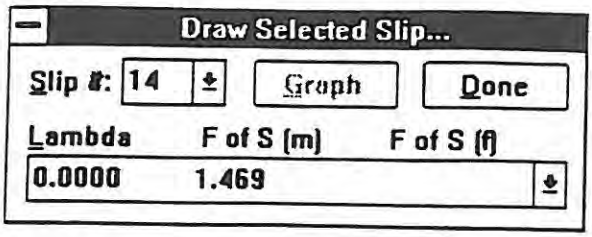

   The dialog box gives information about the slip surface currently displayed – the slip surface number, the Lambda value, and the moment and/or force factors of safety.

4. In the dialog box, click the down arrow to the right of the Slip # edit box. A drop-down menu of other slip surfaces with the same grid center is displayed.

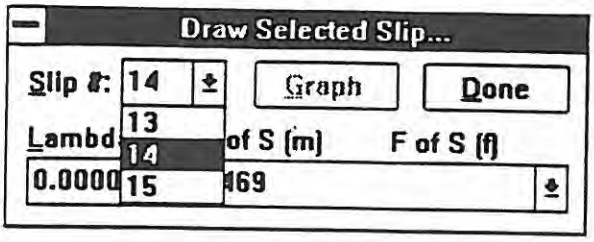

5. Click on any of the other slip surface numbers.

   The selected slip surface and its factor of safety are displayed in the CONTOUR window. The dialog box displays the new slip surface number, its Lambda value, and its moment and/or force factors of safety.

6. View any other slip surfaces by clicking on different grid centers and by selecting the slip surface numbers in the dialog box. When you click on a grid center, the minimum slip surface for the grid center is always viewed by default.

7. To finish viewing slip surfaces, select Done in the dialog box or click the right mouse button.

3.4.3 View Method

In DEFINE, you selected the methods to use when calculating the factors of safety. Since you selected only the Ordinary, Bishop, and Janbu methods, CONTOUR displays the Bishop factors of safety by default. However, the Ordinary and Janbu factors of safety can also be viewed.

To view the factors of safety for another method:

1. Choose View from the CONTOUR menu.

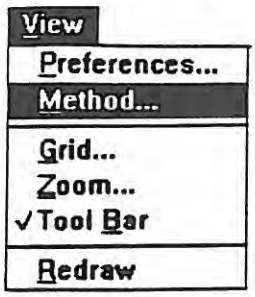

2. Select Method from the View menu. The following dialog box appears:

The current method is displayed in the dialog box.

3. Click the down arrow to the right of the Method edit box. A drop-down menu of the other available methods to view is displayed.

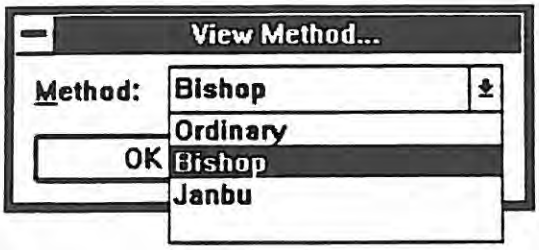

4. Click on one of the other methods (i.e., Janbu).

5. Select OK.

The slip surface currently displayed is redrawn, and the Janbu factor of safety is displayed beside the grid center point. If you wish to view the minimum slip surface for the Janbu method, choose Draw Minimum Slip. To view any other slip surface, choose Draw Selected Slip.

6. Choose View Method again and select Bishop to view the default method.

3.4.4 Draw the Slice Forces

The forces calculated for the minimum slip surface can be displayed as a free body diagram and force polygon of any slice.

To draw the slice forces:

1. Choose Draw Slice Forces from the CONTOUR menu.

   The minimum slip surface is displayed in the CONTOUR window. The cursor changes from an arrow to a cross-hair, and **<Draw Slice Forces>** is added to the CONTOUR window title bar, indicating the mode in which you are operating.

2. Draw the forces on any slice by moving the cursor inside the slice and clicking the left mouse button. The selected slice is highlighted and the following window appears:

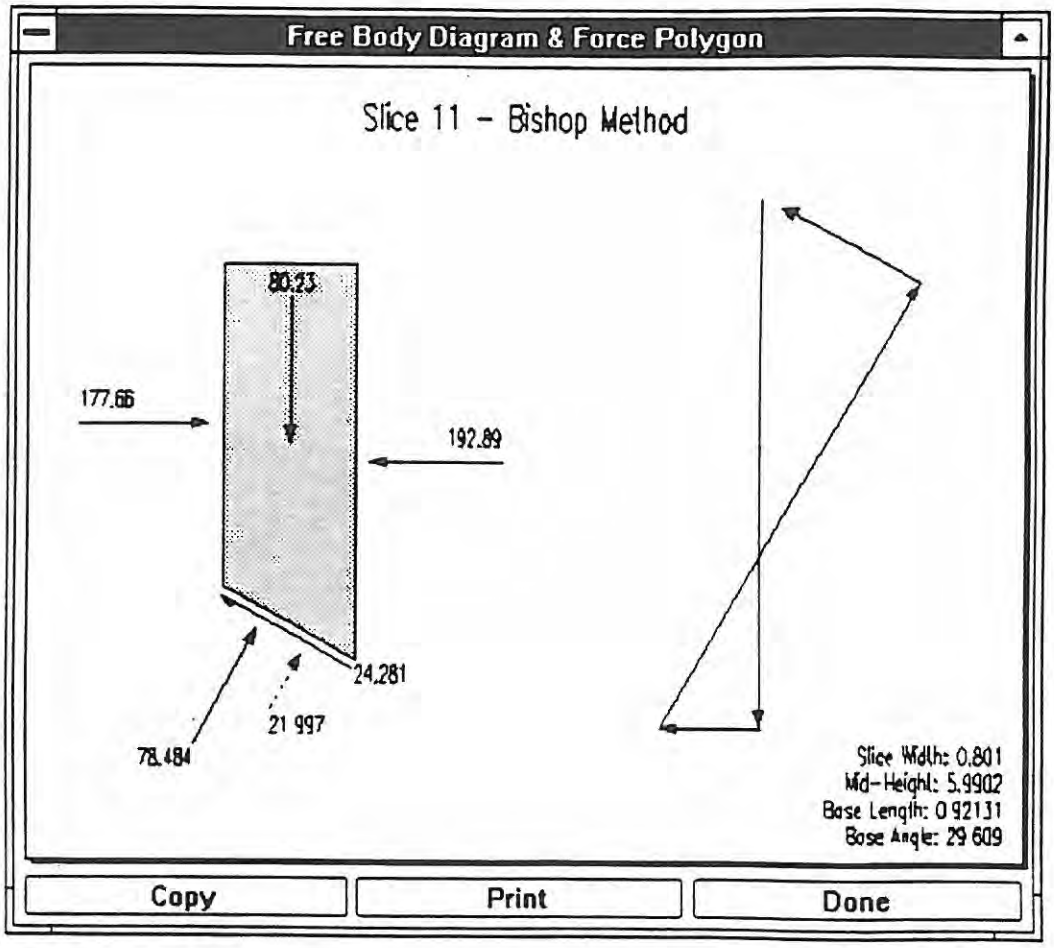

The free body diagram shows the forces for the selected method on the minimum slip surface. The magnitude of each force vector is displayed beside the arrow (the length of the vectors is not drawn to scale), and the direction of the arrows represents the direction

of the vectors. The force polygon shows the summation of all forces acting on the slice. Closure of the force polygon graphically represents the balance of the slice forces.

3. Select Copy if you wish to copy the diagram to the Windows Clipboard for importing into other Windows applications.

4. Select Print if you wish to print the diagram on the selected Windows printer.

5. Repeat Steps 2 to 4 for as many slices as necessary. The Slice Force window can be resized and moved to increase the size of the diagram or to click on a slice that lies beneath the Slice Force window.

6. Select Done.

See the Draw Slice Forces section in Chapter 4 for further information on this command.

3.4.5 Draw the Contours

The minimum factors of safety at each of the grid centers can be contoured.

To contour the factors of safety:

1. Choose Draw Contours from the CONTOUR menu. The following dialog box appears:

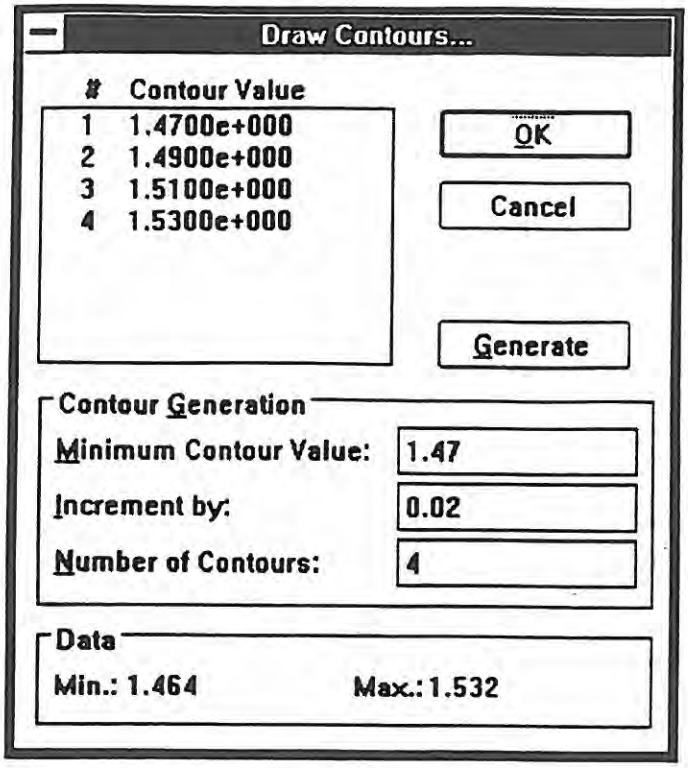

2. Type **1.47** in the Minimum Contour Value edit box.

3. Type **0.02** in the Increment By edit box.

4. Type **4** in the Number Of Contours edit box.

   Note that the range of the Bishop factors of safety is from 1.464 to 1.532, as displayed in the Data group window.

5. Select Generate.

   The contours that will be plotted are displayed in the list box. Seeing the contour values in the list box allows you to check the suitability of the contours. If you wish to plot different contours, change the values in the Contour Generation group window and select Generate again.

6. Select OK.

The factors of safety are contoured as follows:

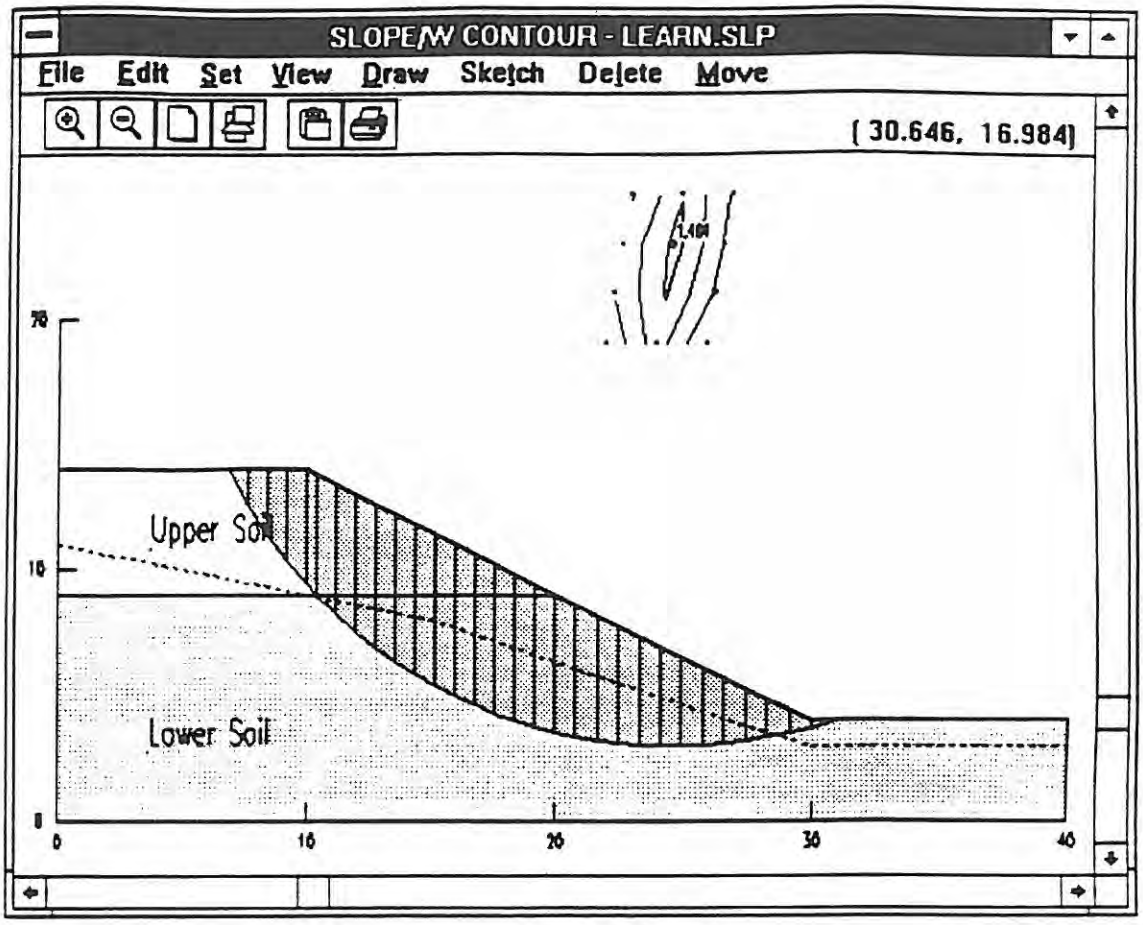

3.4.6 Draw the Contour Values

To label the contours on the drawing:

1. Choose Draw Contour Values from the CONTOUR menu.

   The cursor changes from an arrow to a cross-hair, and **<Draw Contour Values>** is added to the CONTOUR window title bar, indicating the mode in which you are operating.

2. Move the cursor to a convenient point on a contour, and click the left mouse button.

   The contour value appears on the contour. If you wish to remove the contour label, simply re-click on the label, and the label disappears. Click again, and the label will re-appear.

3. Repeat Step 2 for as many contours as you wish.

4. Click the right mouse button to finish labelling contours.

After the contours are labelled, the factors of safety grid should look similar to the following:

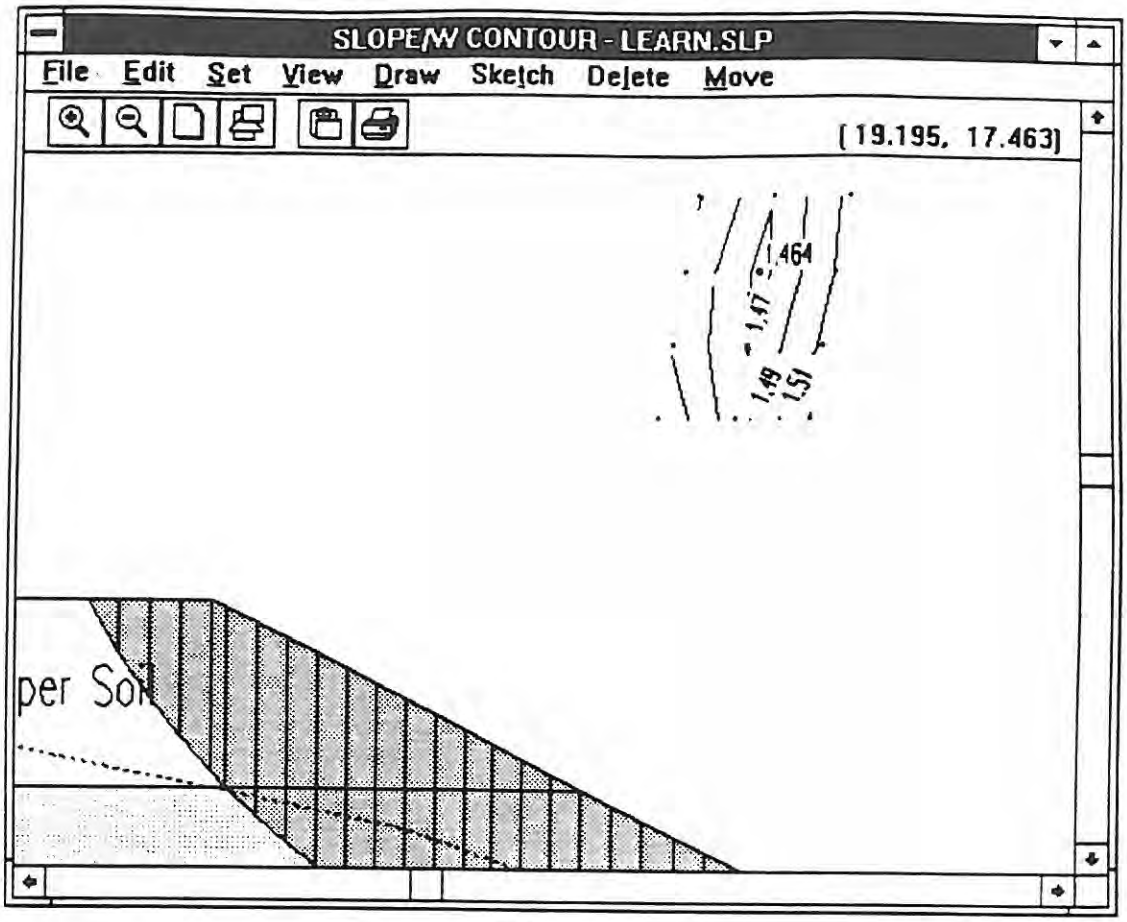

3.4.7 Print the Drawing

To print the drawing:

- In the tool bar, double-click on the Print ( ) tool with the left mouse button.

  The drawing is printed on the default printer at the currently displayed size. To print the drawing at a different size, choose File Print. Select View Zoom or any of the zoom tools from the tool bar if you wish to display the drawing at a different size before it is printed.

Choose File Printer Setup if you wish to change the settings of the default printer. Run Control Panel if you wish to print to a different printer.

You have now finished viewing the factors of safety. Choose File Exit to quit SLOPE/W CONTOUR, or click the Minimize button in the top-right corner of the CONTOUR window to reduce the window to an icon.

3.5 Graphing Detailed Forces

The forces acting on each slice for the critical slip surface are computed and saved in a file with a file name extension of DET. While CONTOUR allows you to display a free body diagram of these forces, you can also view plots of these forces with the SLOPE/W GRAPH function.

To start GRAPH, double-click the GRAPH icon in the SLOPE/W Group window.

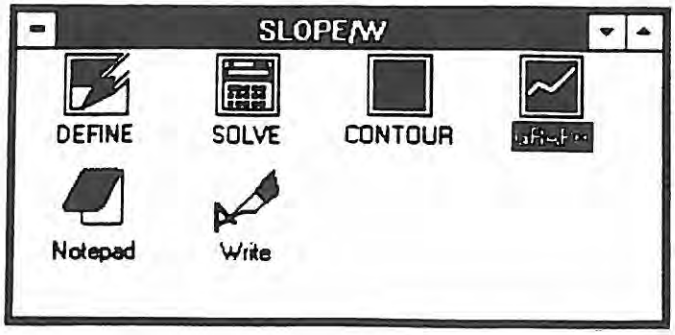

The GRAPH window appears.

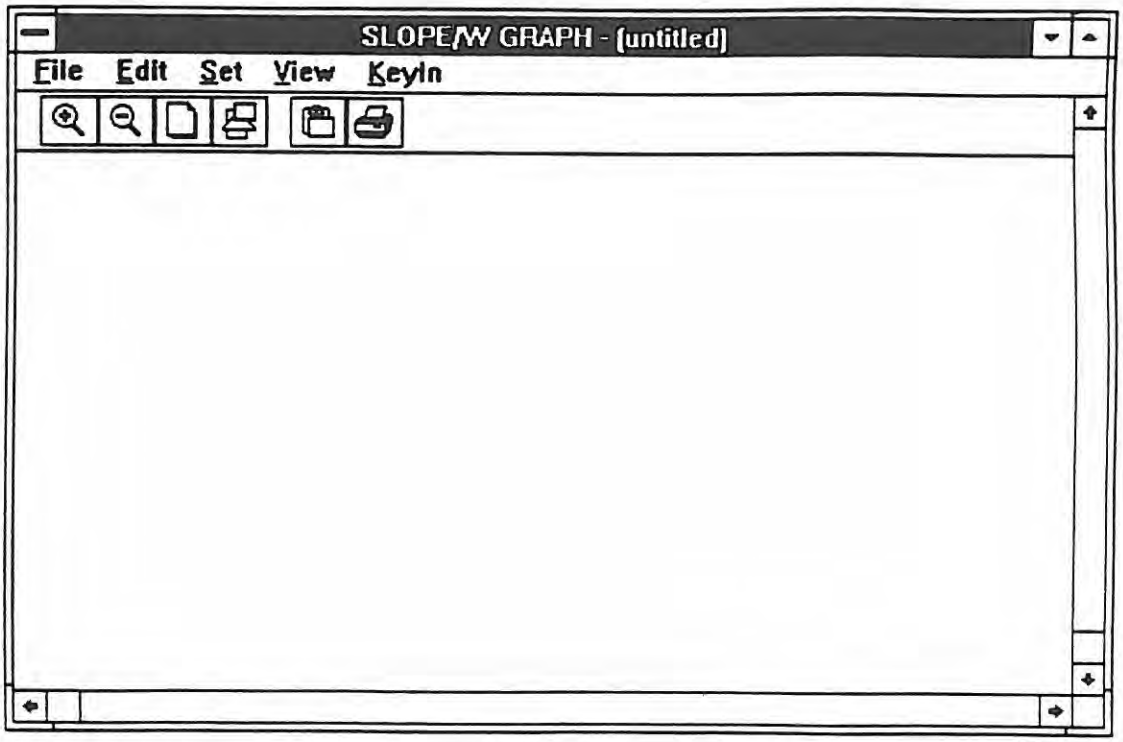

For this example problem, the procedures will be presented for plotting the pore-water pressure distribution from crest to toe along the critical slip surface.

To plot the pore-water pressure distribution:

1. Choose File from the GRAPH menu.

2. Select Open Detailed Forces from the File menu. The following dialog box appears:

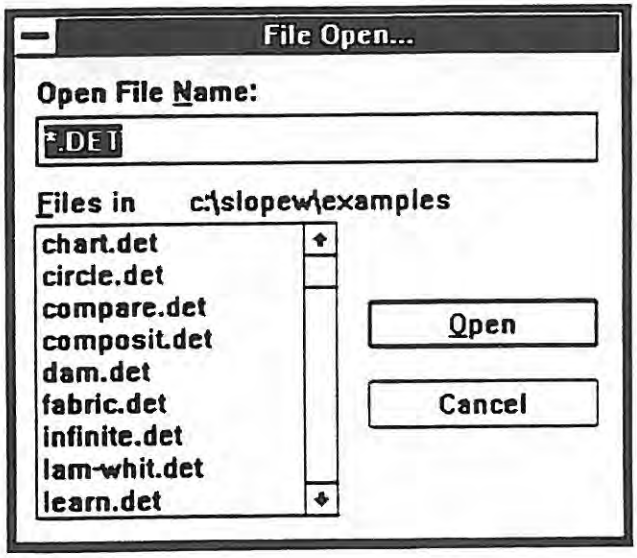

3. Select the detailed forces file you created with SOLVE from the Files In list box. For example, select LEARN.DET.

4. Select Open.

GRAPH displays a plot of Weight vs. X-Coordinate by default.

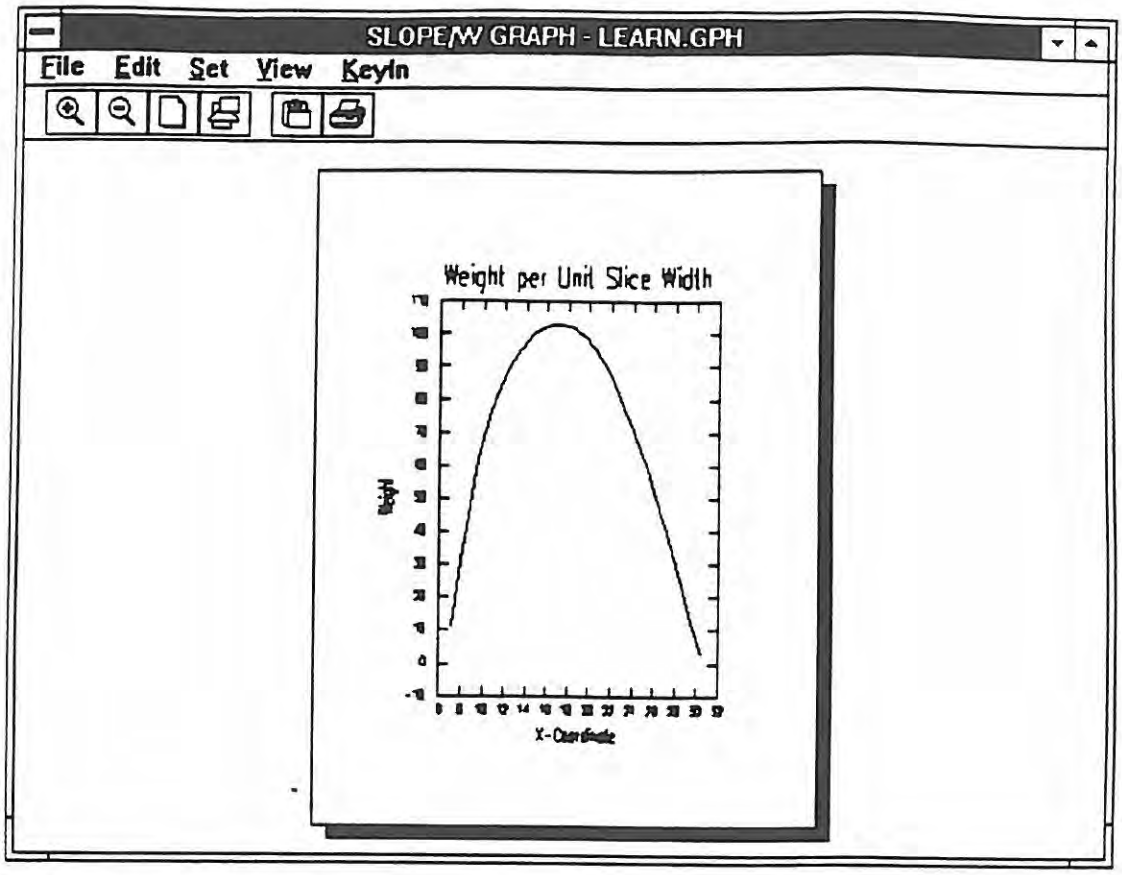

5. Choose View from the GRAPH menu.

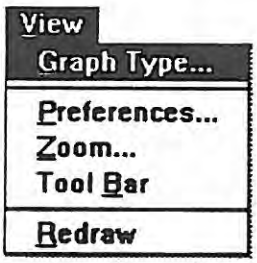

6. Select Graph Type from the View menu. The following dialog box appears:

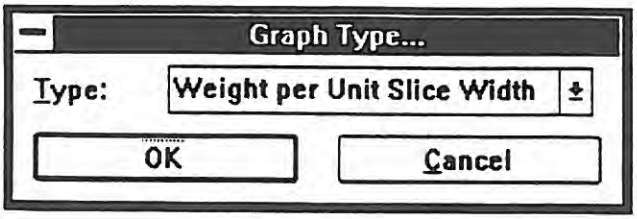

7. Click the down arrow to the right of the Type edit box. A drop-down menu of the other available graphs to plot is displayed.

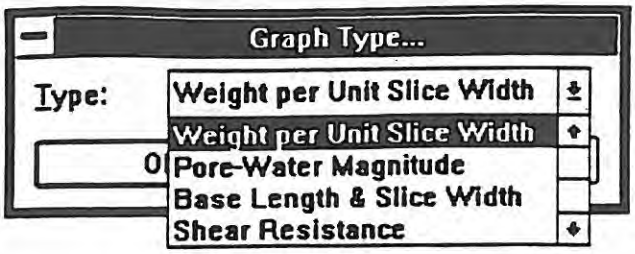

8. Click on the Pore-Water Magnitude graph type.

9. Select OK.

A graph of Force or Pressure vs. X-Coordinate appears in the GRAPH window.

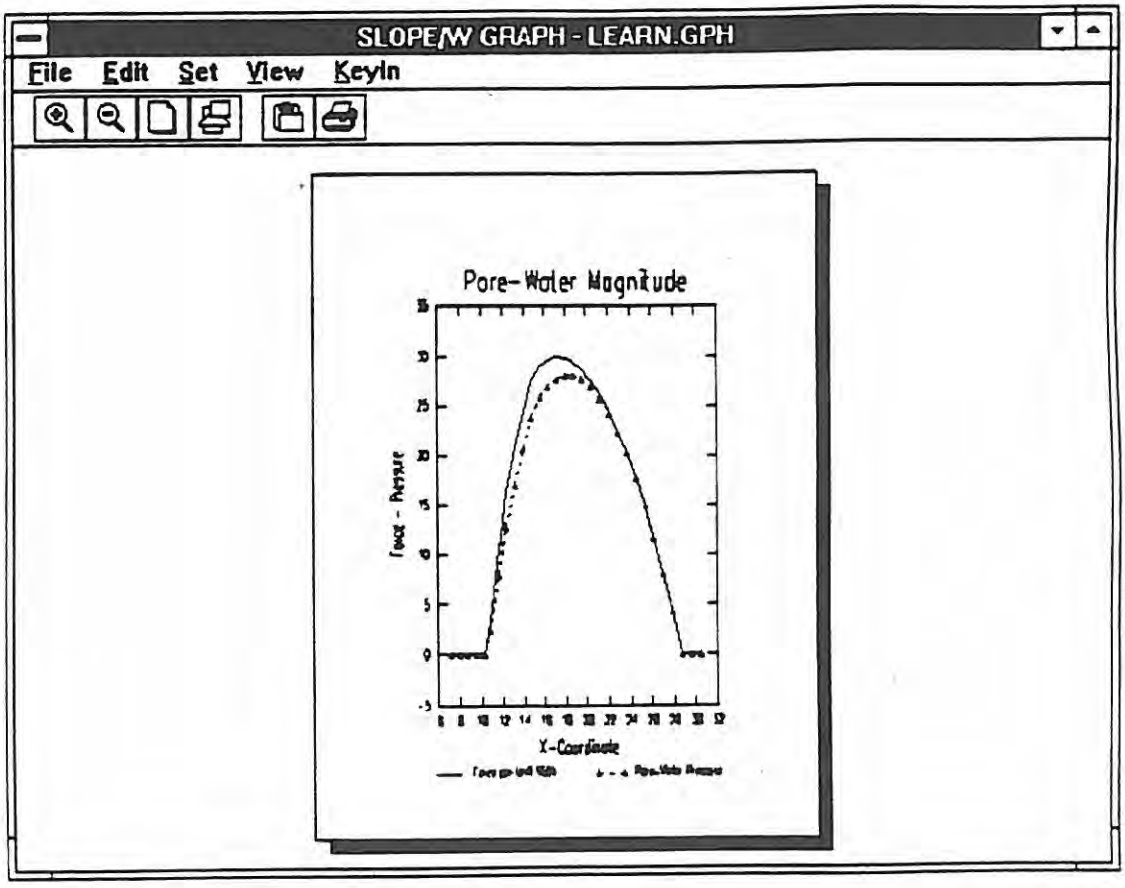

10. To enlarge the graph, choose the Zoom Objects tool or choose the Zoom In tool, hold the left mouse button down, and drag over the region to enlarge.

The red curve with square symbols is the pore-water force at the base of the slice divided by the slice width. The blue curve with triangular symbols is the water force at the base of the slice divided by the base length of the slice.

You may wish to view other graph types by choosing View Graph Type or to experiment with the View Preferences command.

You have now finished graphing the detailed forces. Choose File Exit to quit SLOPE/W GRAPH, or click the Minimize button in the top-right corner of the GRAPH window to reduce the window to an icon.

You have reached the end of this introductory learning session. You have learned sufficient concepts to give you a general understanding of the operation and capability of SLOPE/W. Not all the powerful features of SLOPE/W have been used in this learning session, nor have all the technical details been discussed about the features that have been used. See the Reference chapters in the User's Guide to learn the details about each menu item and command.

UTEXAS3 DEMONSTRATION NOTES

Hardware Requirements

UTEXAS3 requires an IBM[1] PC or IBM Personal System/2[2] (or true compatible) with at least 640KB memory, a hard disk and a math coprocessor.

Diskette Content

The demonstration version of UTEXAS3 is distributed on two 720KB diskettes in MS-DOS[3] format. The first diskette contains the following files:

1. UTEXAS3.EXE: The executable UTEXAS3 demonstration program.
2. UTEXAM1.DAT: An ASCII file containing the input data for Example Problem No. 1 (See user's manual Appendix C).
3. UTEXAM2.DAT: An ASCII file containing the input data for Example Problem No. 2 (See user's manual Appendix C).
4. UTEXAM3.DAT: An ASCII file containing the input data for Example Problem No. 3 (See user's manual Appendix C).

The second diskette contains the following files:

1. OUT1: An output file created by running the full version of UTEXAS3 with the input data for Example Problem No. 1 (UTEXAM1.DAT).
2. OUT2: An output file created by running the full version of UTEXAS3 with the input data for Example Problem No. 2 (UTEXAM2.DAT).
3. OUT3 An output file created by running the full version of UTEXAS3 with the input data for Example Problem No. 3 (UTEXAM3.DAT).

If the diskettes which you receive also contain a file, README.TXT, the file will contain information that was available after this documentation was prepared. If your diskette contains the README.TXT file, examine it first before proceeding.

Installation

To install UTEXAS3 on a hard disk copy the UTEXAS3.EXE file from the diskette onto the appropriate directory on your hard disk. Also if you want to run the example problems, copy the files UTEXAM1.DAT, UTEXAM2.DAT and UTEXAM3.DAT to your hard disk.

---

[1]IBM is a registered trademark of International Business Machines Corporation.
[2]Personal System/2 is a registered trademark of the International Business Machines Corporation.
[3]MS-DOS is a registered trademark of Microsoft Corporation.

If you are planning to run the program from a diskette, first make a copy of the original diskette. You should always use the copy when you are running the program; never run the original.

Running the Demonstration Program

To run the demonstration version of UTEXAS3 you must have a data input file. The input data file must be an ASCII file. You can either create your own input data file or use one of the sample data files for the example problems. The files UTEXAM1.DAT, UTEXAM2.DAT and UTEXAM3.DAT supplied with UTEXAS3 are examples of ASCII input data files. You can create the input data file with any suitable ASCII file editor. The following are examples of file editors that have been successfully used for this purpose:

1. The "Notepad" editor in Sidekick 2.0
2. WordStar operating in the non-document mode.
3. The editor, "M", supplied by Microsoft with the Microsoft FORTRAN language compiler.

The above editors as well as probably many other editors should work provided that they do not introduce special formatting characters. Tabs should NOT be used in the input data; the presence of tabs may cause UTEXAS3 to incorrectly interpret the input data.

Once you have a suitable input data file for UTEXAS3, type the following at the DOS prompt:

UTEXAS3 ***filename***

followed by pressing the "Enter" key on the keyboard. The characters, ***filename***, in the above line of input represent the name of the data input file which you want to run. Once you have entered the above line of information and pressed the Enter key, UTEXAS3 will begin execution. The name of the data input file which you entered will then be shown followed by the names of (1) the file to be used for the output, (2) an "external" input/output file that is presently not used, and (3) the name of the Graphics Input File that will be written for later input to GRAPHIC3, the graphics program for UTEXAS3[4]. Default file names will be offered for each of these three files; the default names will consist of the name of the input file with the extensions: OUT, EXT and ut3, respectively, appended. If these default names are acceptable, you can simply respond to the query with a "Yes" response and UTEXAS3 will then proceed with execution either until it is completed or UTEXAS3 is interrupted (aborted) by you for some reason.

You can omit the file name (***filename***) from the line of input when you first start UTEXAS3. If you omit the file name, you will be prompted for the name

[4]GRAPHIC3 is a separate program that must be obtained separately; it is NOT automatically included as part of UTEXAS3.

of the input file once UTEXAS3 starts. At that point you must type the name of the input file and press the Enter key on the keyboard. UTEXAS3 will then proceed as described above.

Program Output

The demonstration version of UTEXAS3 will read any proper input data file and create all of the output normally created from the input data by UTEXAS3. However, the demonstration program will not perform any slope stability calculations. Instead, at the point where computations would normally be performed the program will issue the following message on the computer screen:

```
DEMONSTRATION VERSION OF UTEXAS3
The value on the following line should be very close to 2.0
  2.0000000000
Press the Enter key to continue
```

The value, `2.0000000000` may not be exactly 2, but should be very close to 2. The above lines of output will be issued every time that UTEXAS3 is requested to perform computations; you may combine several sets of computations in a single input file. For example, the data for Example Problem No. 2 contains data for several sets of computations. The demonstration version of UTEXAS3 will process input data for multiple sets of computations as it normally does. At each point where computations are requested you should press the Enter key to continue as indicated above.

Verification for Your Computer

If UTEXAS3 is executing properly, it should read any correct input data which you supply and issue the output described above. If it does not read the information properly or does not issue the output indicated above, neither the demonstration version or the full working version of UTEXAS3 will work properly on your computer. You should not obtain the full version of UTEXAS3 if the demonstration version does not work properly.

Sample Output Files

The three files, OUT1, OUT2 and OUT3 on the second diskette contain the output that was obtained by running the fully executable version of UTEXAS3 with the sample input data. You may examine these files to see what the output from the fully executable version of UTEXAS3 will look like.

STABLE

User's Manual

A Pre and Post Processor for
STABL
authored by
Peter J. Bosscher

STABL was authored by several persons
associated with the School of Civil Engineering
Purdue University through the support of the
Indiana State Highway Commission

UNIVERSITY OF
WISCONSIN
MADISON

Geotechnical Engineering Program
Department of Civil & Environmental Engineering
University of Wisconsin-Madison
Madison, Wisconsin 53706

STABL USER MANUAL

A Description of the Use of STABL's Programmed Solution for the General Slope Stability Problem

by

Ronald A. Siegel
Graduate Instructor in Research
Purdue University

Joint Highway Research Project

Project No.: C-36-36K

File No.: 6-14-11

Prepared as Part of an Investigation

Conducted by

Joint Highway Research Project
Engineering Experiment Station
Purdue University

In Cooperation with the

Indiana State Highway Commission

Purdue University
West Lafayette, Indiana
June 4, 1975

EXAMPLE PROBLEM

This example concerns the long term stability of a cut in a soft clay material (Figure 17). Without worrying about the validity of such a problem, let it be defined as follows for illustration.

A ground water table is present at a depth of about 17 feet below the existing ground surface which gently slopes toward the cut. An irregular bedrock surface lies at a relatively shallow depth. The variation of the bedrock surface normal to the plane of the profile is insignificant. Therefore a two-dimensional analysis is assumed appropriate.

The shear parameters ($c' = 500$ psf, $\phi = 14^{\circ}$) do not vary significantly with depth, but due to desiccation, tension cracks are assumed to extend to a depth of approximately 11 feet.

By defining the problem geometry with straight lines (Figure 18) the problem can be handled by STABL. The total number of boundaries defined by command PROFIL is six, of which five define the ground surface. A subsurface boundary is used to differentiate a zone containing tension cracks from the remaining clay material. The boundaries are ordered ground surface boundaries first, left to right, with the single subsurface boundary last, satisfying program requirements. The 4th and 5th boundaries on the ground surface are above the tension crack zone, so they are assigned a different soil type number from that assigned to the other boundaries. The clay below the

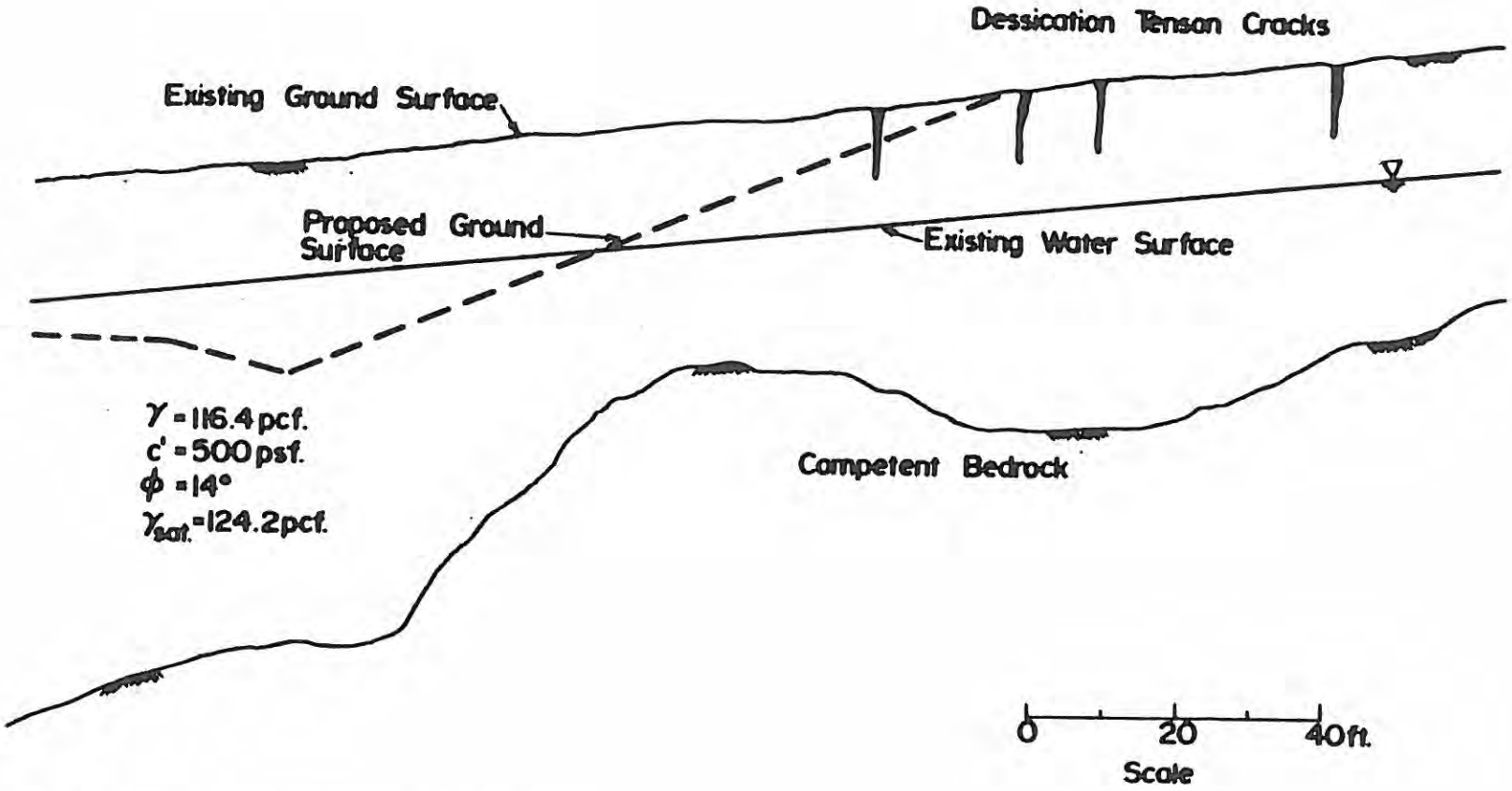

FIGURE 17 - EXAMPLE PROBLEM.

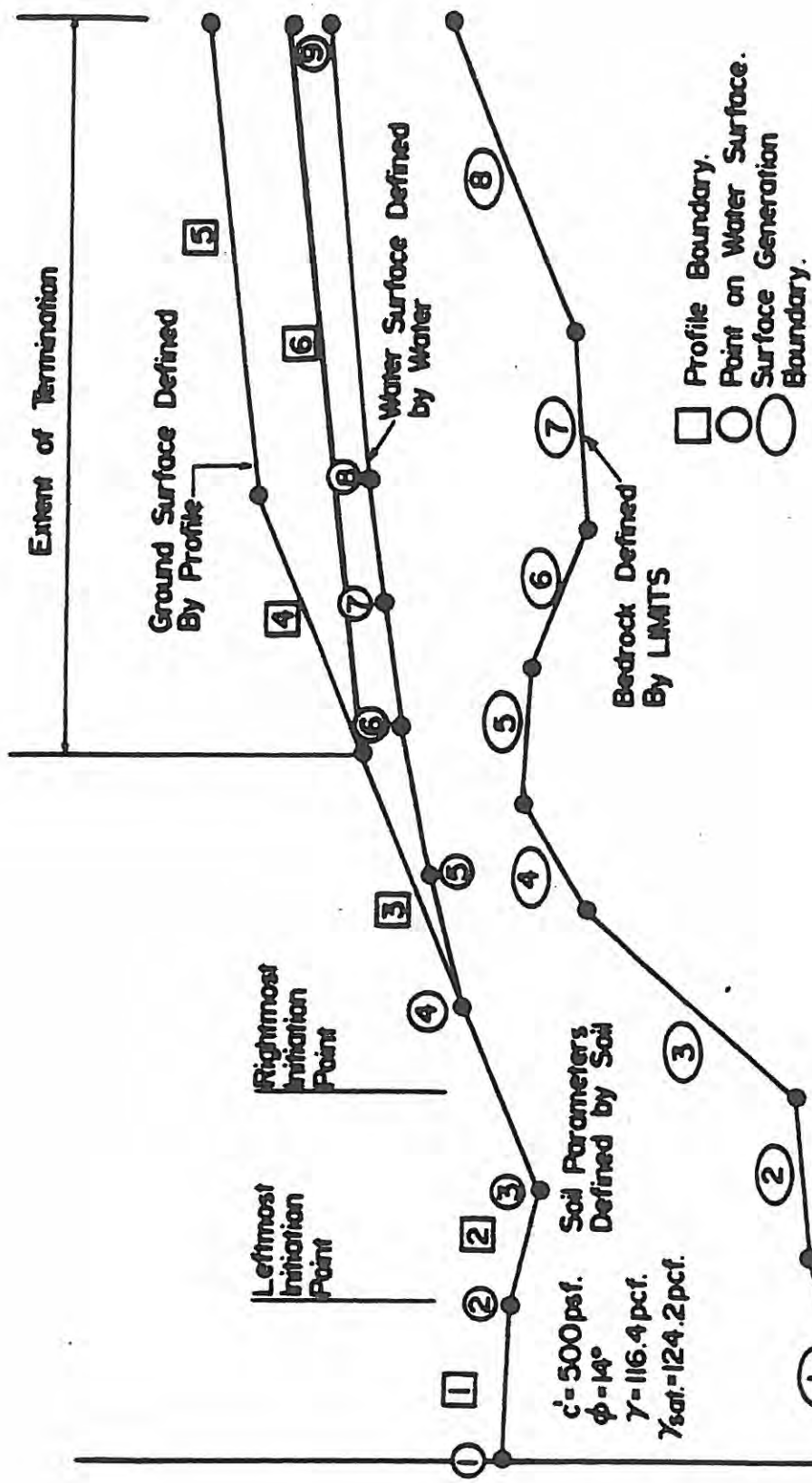

FIGURE 18-LINEAR APPROXIMATION OF EXAMPLE PROBLEM.

tension zone has been arbitarily assigned soil type number 1 and that within the tension zone, soil type number 2.

The bedrock has been assumed competent, with no possibility of failure within it. Therefore, surface generation boundaries, defined by command LIMITS, are used to approximate the bedrock surface. Generation of trial failure surfaces which pass through the bedrock is thus prevented.

It would also have been possible to define the bedrock surface with additional subsurface boundaries defined by command PROFIL. A third soil type with appropriate strength parameters would have been then assigned. The factor of safety of surfaces generated through the bedrock would have been obviously much higher than those above it. The alternative would have been wasteful, and therefore has not been used for this example. However it could have been applicable if the bedrock material was weak.

Of the eight surface generation boundaries which are specified, all eight will deflect generating surfaces upward. The boundaries are therefore not required to be specified in any specific order. However, to maintain consistency, they have been specified in continuous order from left to right.

The water surface is defined by eight points, of which the first four lie at the ground surface. The remaining points have been adjusted to account for response of the ground water table to the change in boundary conditions introduced by the cut.

The two soil types assigned to the boundaries defined by command PROFIL are defined by command SOIL in order of soil type number. Soil

type 1 has shear strength parameters of $c' = 500$ psf and $\phi' = 14$ deg. Soil type 2, since it is in tension, is assigned zero shear strength parameters. The total unit weight of both soil types is 116.4 pcf. The saturated unit weight of soil type 1 is 124.2 pcf, and that of soil type 2 has been arbitarily been assigned 116.4 pcf. The saturated unit weight of soil type 2 will not be used in the analysis however, as soil type 2 is entirely above the water surface. The pore pressure constant and pore pressure parameter for both soil types are not used in this example, so they are assigned zero values.

Searching for the critical surface will be carried out using each of the three trial failure surface generators. Normally, only one generator, or a combination of two, would be used for most problems, but it is instructive to demonstrate the use of each for the same problem. Circular shaped trial failure surfaces are generated and evaluated first by use of command CIRCLE.

It is doubtful that a failure surface would initiate beyond the toe of the slope, because of the controlling influence of the bedrock surface. Since the search is restricted to circular shaped surfaces, the influence of the bedrock may, in fact, force the critical circular surface to pass through a point on the face of the slope, rather than at the toe of the slope or beyond.

Somewhat arbitrarily, it is decided to generate a total of one hundred surfaces; ten surfaces from each of ten initiation points. The leftmost initiation point is positioned at the toe of the slope, $x = 38$ ft, and the rightmost on the face of the slope at $x = 70$ ft.

The termination limits are also somewhat arbitrarily selected. Usually, the critical surface of a slope will pass a short distance behind the crest of a slope. However, the bedrock may force the critical surface to be located short of the crest. The left termination limit is set at x = 120 ft to allow for this possibility. The right termination limit is set at x = 180 ft. If later, the ten most critical surfaces are found to congregate at either limit, the termination limits can be revised for subsequent runs.

The depth limitation is not required, because the bedrock surface, as defined by surface generation boundaries, prevents the generation of deep failure surfaces. It must be specified, however, and for this example, it is set at y = 0.

The length of the line segments defining the circular shaped surfaces is set at ten feet. This is one-fourth of the height of the slope. Lengths one-fourth to one-half the height of the slope are generally reasonable. The length specified for the line segments has a direct influence on computation time. Although short line segments define circular surfaces more accurately, they require more computation time for surface generation and the factor of safety calculation.

No restrictions are placed upon the angle of inclination of the initial line segment. Therefore both the clockwise and counterclockwise inclination limits are specified as zero.

A listing of the raw input data, found on the next page, is shown as it would be prepared for the problem as described. Note that all the data begins in the first column; the commands are on individual lines; the data items on each line are separated by single blank

INPUT FOR FIRST RUN -

```
PROFIL
EXAMPLE PROBLEM
6 5
0. 68. 22. 67. 1
22. 67. 38. 63. 1
38. 63. 101. 88. 1
101. 88. 138. 103. 2
138. 103. 205. 110. 2
101. 88. 205. 99. 1
SOIL
2
116.4 124.2 500. 14. 0. 0.
116.4 116.4 0. 0. 0. 0.
WATER
9
0. 68.
22. 67.
38. 63.
63. 73.
83. 78.
104. 82.
122. 85.
140. 87.
205. 93.
LIMITS
8 8
0. 15. 29. 24.
29. 24. 51. 26.
51. 26. 78. 56.
78. 56. 94. 65.
94. 65. 113. 64.
113. 64. 133. 56.
133. 56. 161. 58.
161. 58. 205. 76.
CIRCLE
10 10 38. 70. 120. 180. 0. 10. 0. 0.
```

OUTPUT FOR FIRST RUN -

--SLOPE STABILITY ANALYSIS--
MODIFIED BISHOP METHOD OF SLICES
IRREGULAR FAILURE SURFACES

PROBLEM DESCRIPTION EXAMPLE PROBLEM

BOUNDARY COORDINATES

5 TOP BOUNDARIES
6 TOTAL BOUNDARIES

BOUNDARY NO.	X-LEFT (FT)	Y-LEFT (FT)	X-RIGHT (FT)	Y-RIGHT (FT)	SOIL TYPE BELOW BND
1	0	68.00	22.00	67.00	1
2	22.00	67.00	38.00	63.00	1
3	38.00	63.00	101.00	88.00	1
4	101.00	88.00	138.00	103.00	2
5	138.00	103.00	205.00	110.00	2
6	101.00	88.00	205.00	99.00	1

ISOTROPIC SOIL PARAMETERS

2 TYPE(S) OF SOIL

SOIL TYPE NO.	TOTAL UNIT WT. (PCF)	SATURATED UNIT WT. (PCF)	COHESION INTERCEPT (PSF)	FRICTION ANGLE (DEG)	PORE PRESSURE PARAMETER	PRESSURE CONSTANT (PSF)
1	116.4	124.2	500.0	14.0	0	0
2	116.4	116.4	0	0	0	0

WATER SURFACE SPECIFIED BY 9 COORDINATE POINTS

POINT NO.	X-WATER (FT)	Y-WATER (FT)
1	0	68.00
2	22.00	67.00
3	38.00	63.00
4	63.00	73.00
5	83.00	78.00
6	104.00	82.00
7	122.00	85.00
8	140.00	87.00
9	205.00	93.00

SEARCHING ROUTINE WILL BE LIMITED TO AN AREA DEFINED BY 8 BOUNDARIES OF WHICH THE FIRST 8 BOUNDARIES WILL DEFLECT SURFACES UPWARD

BOUNDARY NO.	X-LEFT (FT)	Y-LEFT (FT)	X-RIGHT (FT)	Y-RIGHT (FT)
1	0	15.00	29.00	24.00
2	29.00	24.00	51.00	26.00
3	51.00	26.00	78.00	56.00
4	78.00	56.00	94.00	65.00
5	94.00	65.00	113.00	64.00
6	113.00	64.00	133.00	56.00
7	133.00	56.00	161.00	58.00
8	161.00	58.00	205.00	76.00

A CRITICAL FAILURE SURFACE SEARCHING METHOD, USING A RANDOM TECHNIQUE FOR GENERATING CIRCULAR SURFACES, HAS BEEN SPECIFIED.

100 TRIAL SURFACES HAVE BEEN GENERATED.

10 SURFACES INITIATE FROM EACH OF 10 POINTS EQUALLY SPACED ALONG THE GROUND SURFACE BETWEEN X = 38.00 FT.
AND X = 70.00 FT.

EACH SURFACE TERMINATES BETWEEN X = 120.00 FT.
AND X = 180.00 FT.

UNLESS FURTHER LIMITATIONS WERE IMPOSED, THE MINIMUM ELEVATION AT WHICH A SURFACE EXTENDS IS Y = 0 FT.

10.00 FT. LINE SEGMENTS DEFINE EACH TRIAL FAILURE SURFACE.

FOLLOWING ARE DISPLAYED THE TEN MOST CRITICAL OF THE TRIAL FAILURE SURFACES EXAMINED. THEY ARE ORDERED - MOST CRITICAL FIRST.

FAILURE SURFACE SPECIFIED BY 15 COORDINATE POINTS

POINT NO.	X-SURF (FT)	Y-SURF (FT)
1	45.11	65.82
2	55.00	64.30
3	64.97	63.57
4	74.97	63.62
5	84.93	64.47
6	94.00	66.09
7	104.51	68.49
8	114.00	71.65
9	123.21	75.54
10	132.00	80.15
11	140.56	85.45
12	148.60	91.40
13	156.15	97.96
14	163.15	105.10
15	163.63	105.68

*** 1.3250 ***

FAILURE SURFACE SPECIFIED BY 13 COORDINATE POINTS

POINT NO.	X-SURF (FT)	Y-SURF (FT)
1	45.11	65.82
2	54.86	63.58
3	64.80	62.52
4	74.80	62.66
5	84.71	63.99
6	94.39	66.49
7	103.70	70.14
8	112.51	74.87
9	120.70	80.62
10	128.13	87.30
11	134.72	94.83
12	140.35	103.09
13	140.41	103.25

*** 1.3278 ***

FAILURE SURFACE SPECIFIED BY 16 COORDINATE POINTS

POINT NO.	X-SURF (FT)	Y-SURF (FT)
1	41.56	64.41
2	51.49	63.24
3	61.47	62.74
4	71.47	62.89
5	81.44	63.71
6	91.33	65.19
7	101.10	67.33
8	110.70	70.11
9	120.11	73.52
10	129.26	77.54
11	138.12	82.17
12	146.66	87.37
13	154.84	93.13
14	162.61	99.42
15	169.95	106.21
16	170.08	106.35

**** 1.3362 ****

FAILURE SURFACE SPECIFIED BY 15 COORDINATE POINTS

POINT NO.	X-SURF (FT)	Y-SURF (FT)
1	52.22	68.64
2	61.96	66.38
3	71.87	65.00
4	81.86	64.51
5	91.85	64.91
6	101.76	66.20
7	111.53	68.38
8	121.05	71.41
9	130.27	75.28
10	139.11	79.96
11	147.50	85.41
12	155.36	91.58
13	162.65	98.44
14	169.29	105.91
15	169.57	106.30

**** 1.3414 ****

FAILURE SURFACE SPECIFIED BY 13 COORDINATE POINTS

POINT NO.	X-SURF (FT)	Y-SURF (FT)
1	38.00	63.00
2	47.77	60.86
3	57.72	59.86
4	67.72	60.03
5	77.63	61.36
6	87.32	63.83
7	96.65	67.42
8	105.51	72.06
9	113.77	77.70
10	121.31	84.27
11	127.91	91.66
12	133.87	99.79
13	134.96	101.77

*** 1.3419 ***

FAILURE SURFACE SPECIFIED BY 14 COORDINATE POINTS

POINT NO.	X-SURF (FT)	Y-SURF (FT)
1	45.11	65.82
2	55.02	64.50
3	65.01	63.97
4	75.01	64.24
5	84.95	65.30
6	94.78	67.14
7	104.43	69.76
8	113.84	73.14
9	122.96	77.25
10	131.72	82.07
11	140.07	87.58
12	147.95	93.72
13	155.33	100.48
14	159.79	105.28

*** 1.3436 ***

FAILURE SURFACE SPECIFIED BY 13 COORDINATE POINTS

POINT NO.	X-SURF (FT)	Y-SURF (FT)
1	41.56	64.41
2	51.46	63.01
3	61.45	62.54
4	71.43	63.03
5	81.33	64.45
6	91.05	66.79
7	100.51	70.05
8	109.62	74.18
9	118.29	79.15
10	126.46	84.92
11	134.05	91.43
12	140.99	98.63
13	145.06	103.74

*** 1.3446 ***

FAILURE SURFACE SPECIFIED BY 12 COORDINATE POINTS

POINT NO.	X-SURF (FT)	Y-SURF (FT)
1	62.89	72.88
2	72.21	69.26
3	81.96	67.01
4	91.92	66.17
5	101.90	66.75
6	111.70	68.75
7	121.12	72.12
8	129.96	76.79
9	138.05	82.68
10	145.21	89.65
11	151.32	97.57
12	155.41	104.82

*** 1.3544 ***

FAILURE SURFACE SPECIFIED BY 12 COORDINATE POINTS

POINT NO.	X-SURF (FT)	Y-SURF (FT)
1	59.78	70.05
2	65.39	67.29
3	75.29	65.90
4	85.69	65.90
5	95.19	67.29
6	104.89	70.06
7	113.93	74.13
8	122.41	79.45
9	130.06	85.89
10	136.73	93.33
11	142.30	101.64
12	143.22	103.55

*** 1.3557 ***

FAILURE SURFACE SPECIFIED BY 13 COORDINATE POINTS

POINT NO.	X SURF (FT)	Y-SURF (FT)
1	59.38	71.47
2	68.96	68.75
3	78.84	67.19
4	88.88	66.82
5	98.79	67.64
6	108.59	69.64
7	118.09	72.79
8	127.14	77.04
9	135.62	82.34
10	143.41	88.60
11	150.40	95.75
12	156.49	103.68
13	157.29	105.01

*** 1.3643 ***

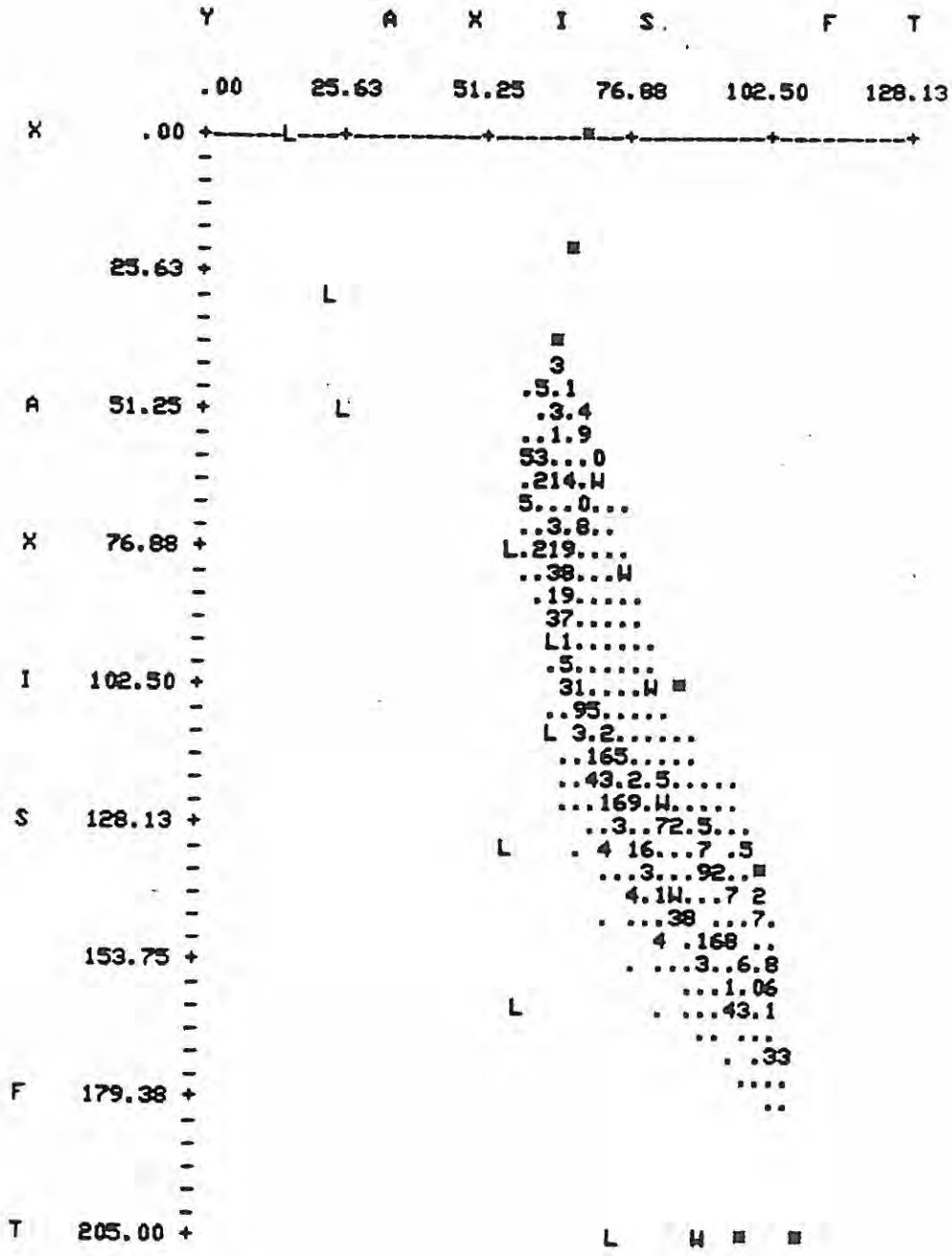
Y A X I S. F T
.00 25.63 51.25 76.88 102.50 128.13
X .00
25.63
A 51.25
X 76.88
I 102.50
S 128.13
153.75
F 179.38
T 205.00

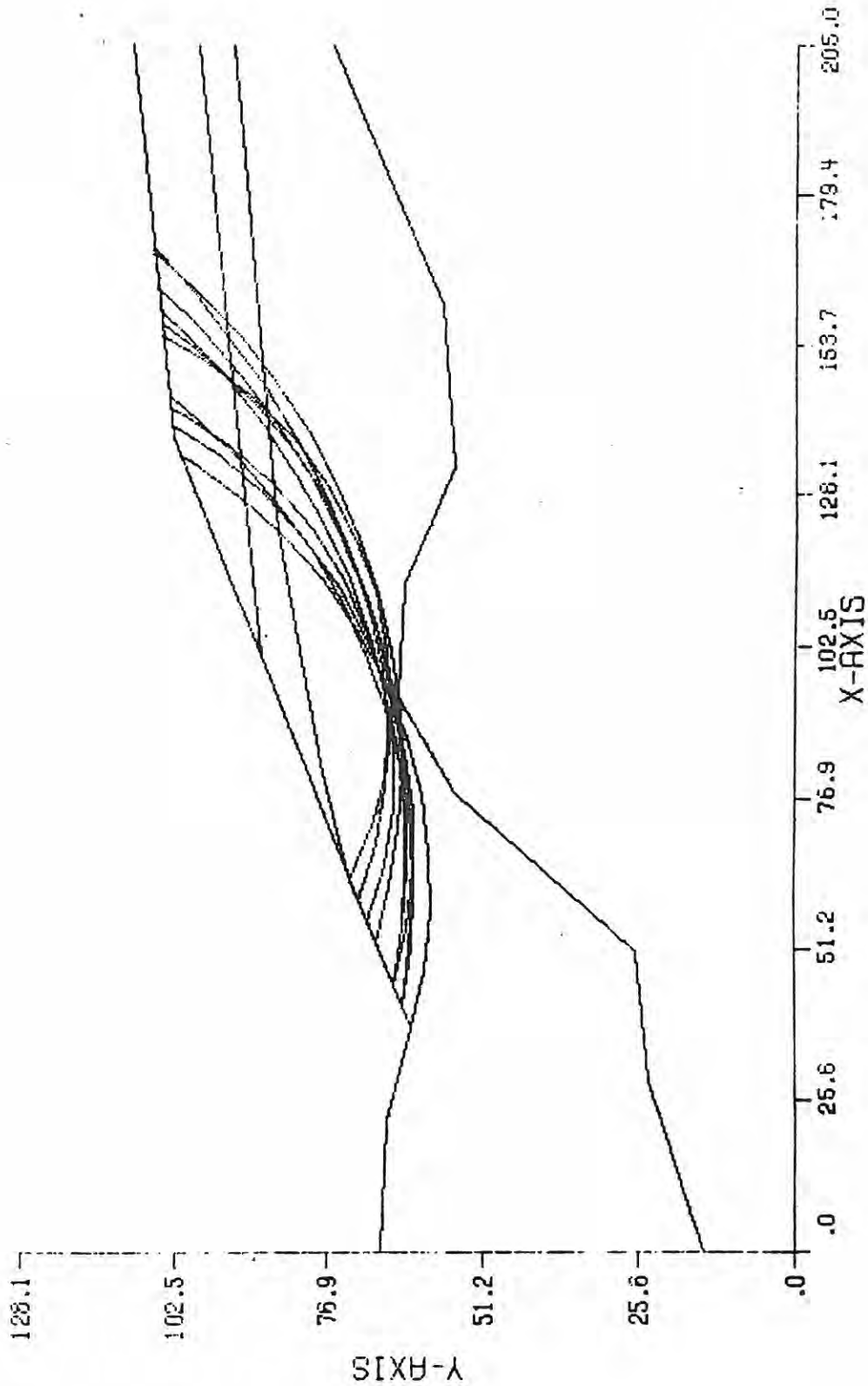
128.1
102.5
76.9
51.2
25.6
Y-AXIS
.0
25.6
51.2
76.9
102.5
X-AXIS
126.1
153.7
179.4
205.0

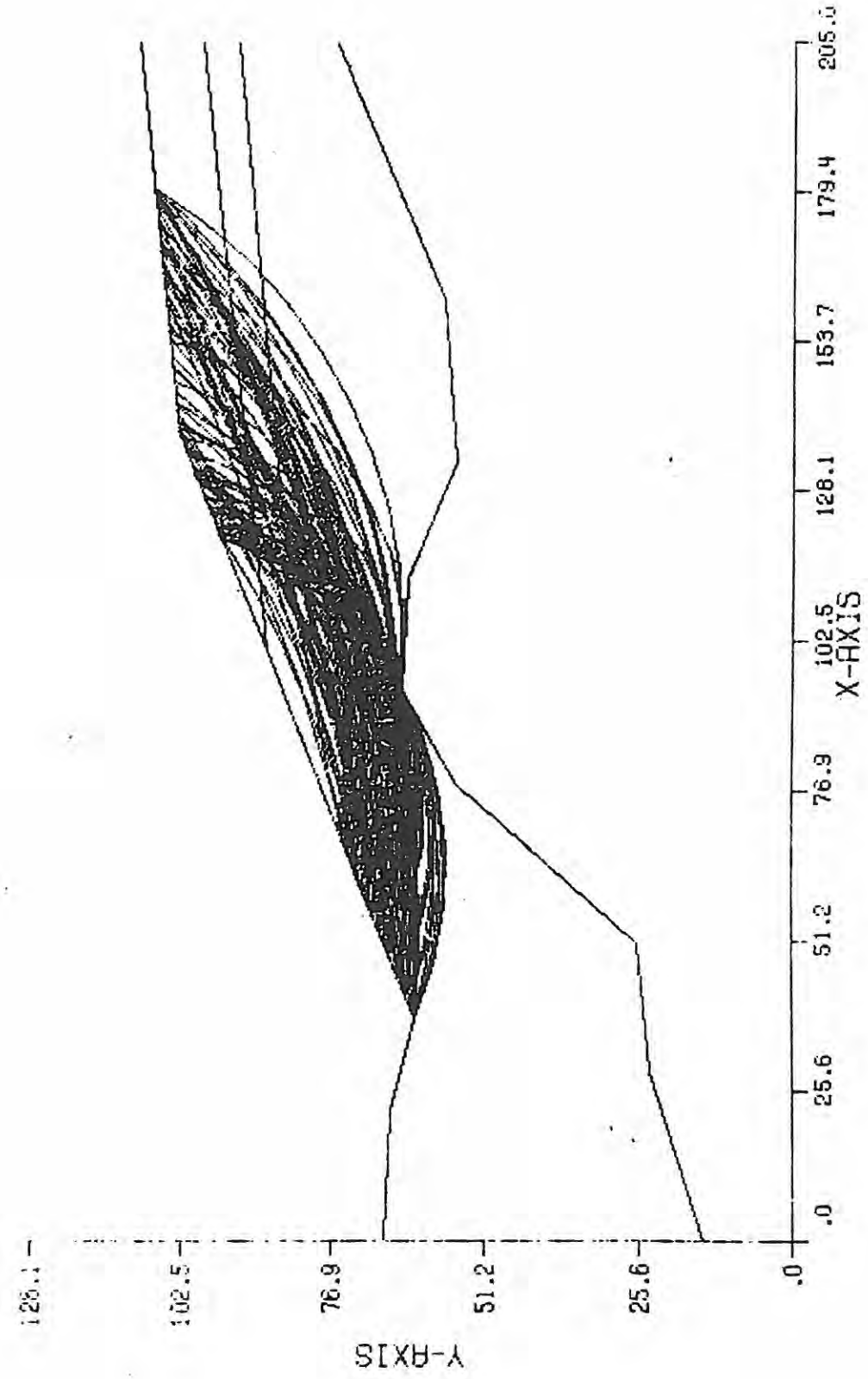
128.1
102.5
76.9
51.2
25.6
.0
Y-AXIS
.0
25.6
51.2
76.9
102.5
128.1
153.7
179.4
205.0
X-AXIS

spaces; and real and integer numeric data, respectively, do and do not contain decimal points.

Following the listing of the raw input data is the output for the commands executed for the first run. The last information printed is the print character plot of the problem resulting from the use of command CIRCLE. Two additional plots, prepared by a Gould electrostatic plotting device, are also included. All the input data, associated with each command used, is displayed with the output. The coordinates of the ten most critical surfaces along with their respective factors of safety are printed when search commands are used.

The print character plot contains information regarding the input data and the surfaces generated. The line segments connecting points can be sketched in for clearer interpretation. The ten most critical of the surfaces generated appear as strings of one digit numbers, while the remaining surfaces generated appear as dots.

From this plot the ten most critical surfaces are found to be located within the extent of all the surfaces generated. This indicates a fairly good choice of initial restraints used to generate the surfaces.

The two Gould plots show basically the same information as the print character plot, but in a form more easily interpreted. The first of these plots shows the extent of the surfaces generated, while the second displays the ten most critical. No distinction is made of the criticality of each surface, so one must refer to the print character plot or to the printed output of the coordinates of these ten surfaces.

The values of the factors of safety of the ten most critical surfaces range from 1.32 to 1.36. This is not a large difference, and the chances of locating a circular shaped surface with a factor of safety much less than 1.32 is probably small. The width of the zone occupied by these critical surfaces at the toe and crest indicates that the bedrock influences the stability of the slope by making the value of the factor of safety relatively insensitive to the position of a circular shaped surface, as long as the surface passes near the bedrock surface.

A tendency can be observed that the more critical surfaces of the ten generated occur nearer the toe of the slope. Therefore, there is a good possibility that the critical surface passes through the toe. A second run is made to check this possibility.

Twenty-five surfaces are generated from each of 3 initiation points; the leftmost again at the toe, and the rightmost at x = 50 ft. The rightmost initiation point is moved, because critical surfaces were not determined for the right initiation points in the first run. If a circular surface through the toe is critical, then most of the critical surfaces subsequently determined should pass through the toe. The total number of surfaces to be generated, 75, should be adequate because the surfaces generated will be required to satisfy stricter requirements. All surfaces to be generated for the second run will lie in a zone somewhat matching that of the ten most critical surfaces of the first run.

All except one of the critical circular surfaces, determined by the first run, lie behind the crest of the slope, so the left

termination limit is moved to the crest at x = 138 ft. Also, all the critical surfaces do not extend beyond x = 170 ft, except one, which does so just barely. Therefore, the right termination limit is changed to that position.

Since the minimum angle of inclination of the initial line segments of the critical surfaces is about -21°, and no angle exceeded 0°, the inclination angle will be restricted between 0° and -25°.

Because the critical surfaces of the first run all lie at or near the bedrock surface, it would be efficient to prevent generation of surfaces at shallower depths. This is accomplished by blocking the generation of such surfaces with downward deflecting surface generation boundaries. One boundary is fixed between a point at the ground surface to the right of the last initiation point (63., 73.) and a point a short distance above the bedrock surface (93., 67.). Another is specified between this last point and the crest.

Having modified the requirements each generated surface must satisfy, the second random search was performed using circular surfaces. The next page contains the listing of the raw input for this run.

Following the listing of the raw input data, the output is partially displayed. Since no changes were made to the input data for commands PROFIL, SOIL, and WATER, the output data associated with these commands are omitted. Also, since the output of coordinates for points defining each of the ten most critical surfaces is somewhat bulky, it is omitted. The print character plot and Gould plots should be sufficient.

INPUT FOR SECOND RUN -

```
PROFIL
EXAMPLE PROBLEM
6 5
0. 68. 22. 67. 1
22. 67. 38. 63. 1
38. 63. 101. 88. 1
101. 88. 138. 103. 2
138. 103. 205. 110. 2
101. 88. 205. 99. 1
SOIL
2
116.4 124.2 500. 14. 0. 0.
116.4 116.4 0. 0. 0. 0.
WATER
9
0. 68.
22. 67.
38. 63.
63. 73.
83. 78.
104. 82.
122. 85.
140. 87.
205. 93.
LIMITS
10 8
0. 15. 29. 24.
29. 24. 51. 26.
51. 26. 78. 56.
78. 56. 94. 65.
94. 65. 113. 64.
113. 64. 133. 56.
133. 56. 161. 58.
161. 58. 205. 76.
63. 73. 93. 67.
93. 67. 138. 103.
CIRCLE
3 25 38. 50. 138. 170. 0. 10. 0. -25.
```

PARTIAL OU UT FOR SECOND RUN -

SEARCHING ROUTINE WILL BE LIMITED TO AN AREA DEFINED BY 10 BOUNDARIES
OF WHICH THE FIRST 8 BOUNDARIES WILL DEFLECT SURFACES UPWARD

BOUNDARY NO.	X-LEFT (FT)	Y-LEFT (FT)	X-RIGHT (FT)	Y-RIGHT (FT)
1	0	15.00	29.00	24.00
2	29.00	24.00	51.00	26.00
3	51.00	26.00	78.00	56.00
4	78.00	56.00	94.00	65.00
5	94.00	65.00	113.00	64.00
6	113.00	64.00	133.00	56.00
7	133.00	56.00	161.00	58.00
8	161.00	58.00	205.00	76.00
9	63.00	73.00	93.00	67.00
10	93.00	67.00	138.00	103.00

A CRITICAL FAILURE SURFACE SEARCHING METHOD, USING A RANDOM
TECHNIQUE FOR GENERATING CIRCULAR SURFACES, HAS BEEN SPECIFIED.

75 TRIAL SURFACES HAVE BEEN GENERATED.

25 SURFACES INITIATE FROM EACH OF 3 POINTS EQUALLY SPACED
ALONG THE GROUND SURFACE BETWEEN X = 38.00 FT.
AND X = 50.00 FT.

EACH SURFACE TERMINATES BETWEEN X = 138.00 FT.
AND X = 170.00 FT.

UNLESS FURTHER LIMITATIONS WERE IMPOSED, THE MINIMUM ELEVATION
AT WHICH A SURFACE EXTENDS IS Y = 0 FT.

10.00 FT. LINE SEGMENTS DEFINE EACH TRIAL FAILURE SURFACE.

RESTRICTIONS HAVE BEEN IMPOSED UPON THE ANGLE OF INITIATION.
THE ANGLE HAS BEEN RESTRICTED BETWWEN THE ANGLES OF -25.0 AND 0 DEG

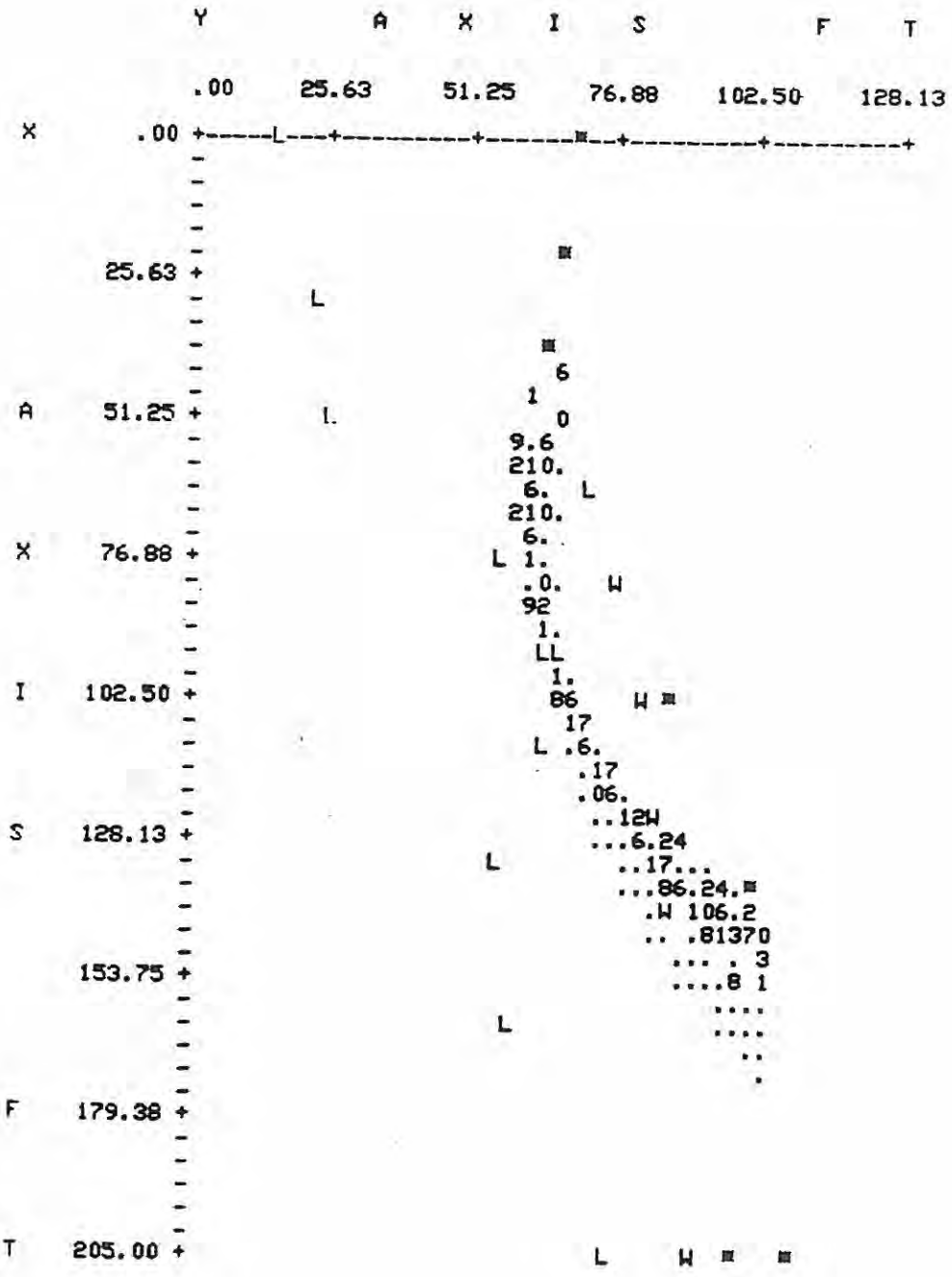
Y A X I S F T
.00 25.63 51.25 76.88 102.50 128.13
X .00
25.63
A 51.25
X 76.88
I 102.50
S 128.13
153.75
F 179.38
T 205.00

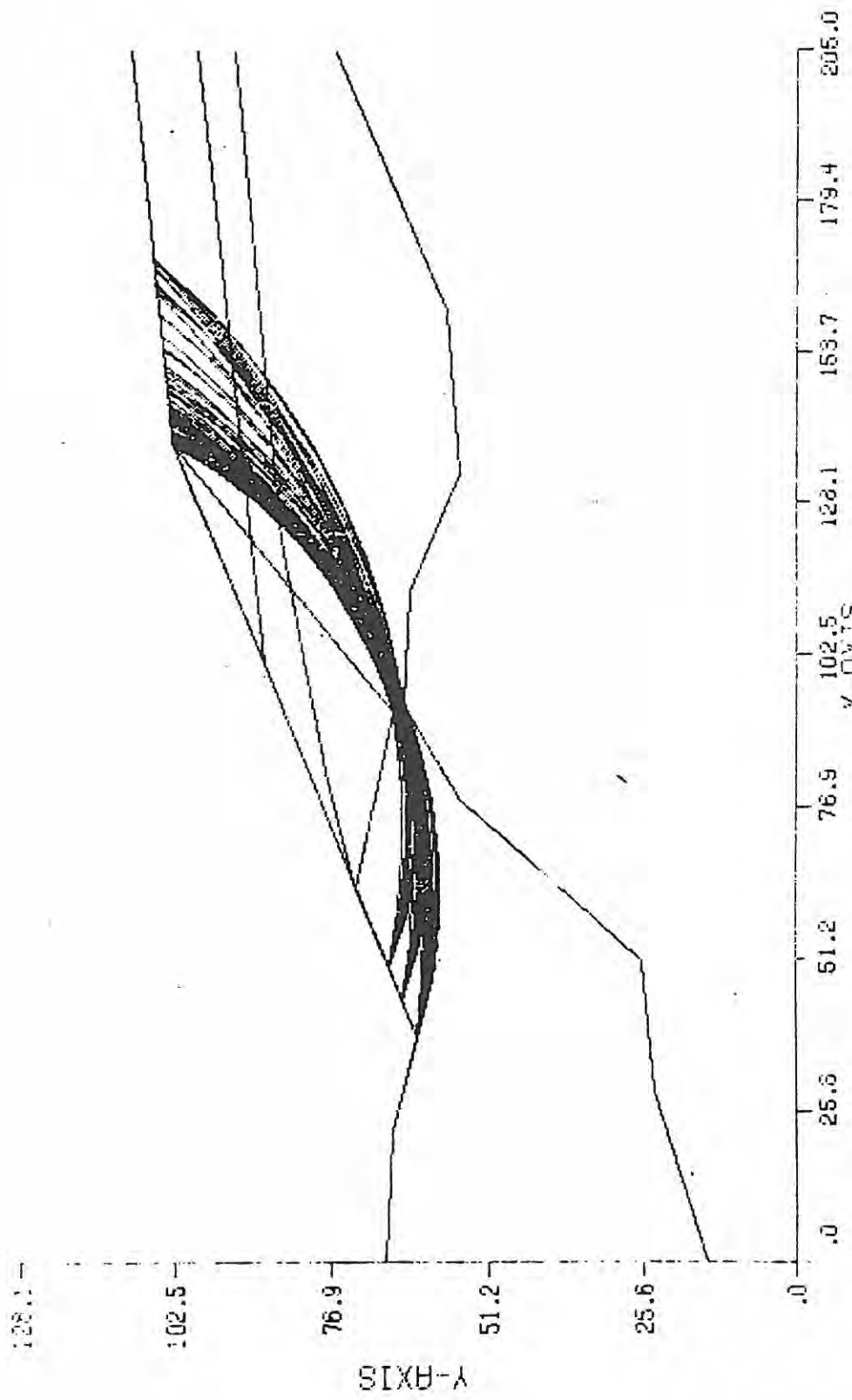
128.1
102.5
76.9
51.2
25.6
.0
Y-AXIS
.0
25.6
51.2
76.9
102.5
128.1
153.7
179.4
205.0
X-AXIS

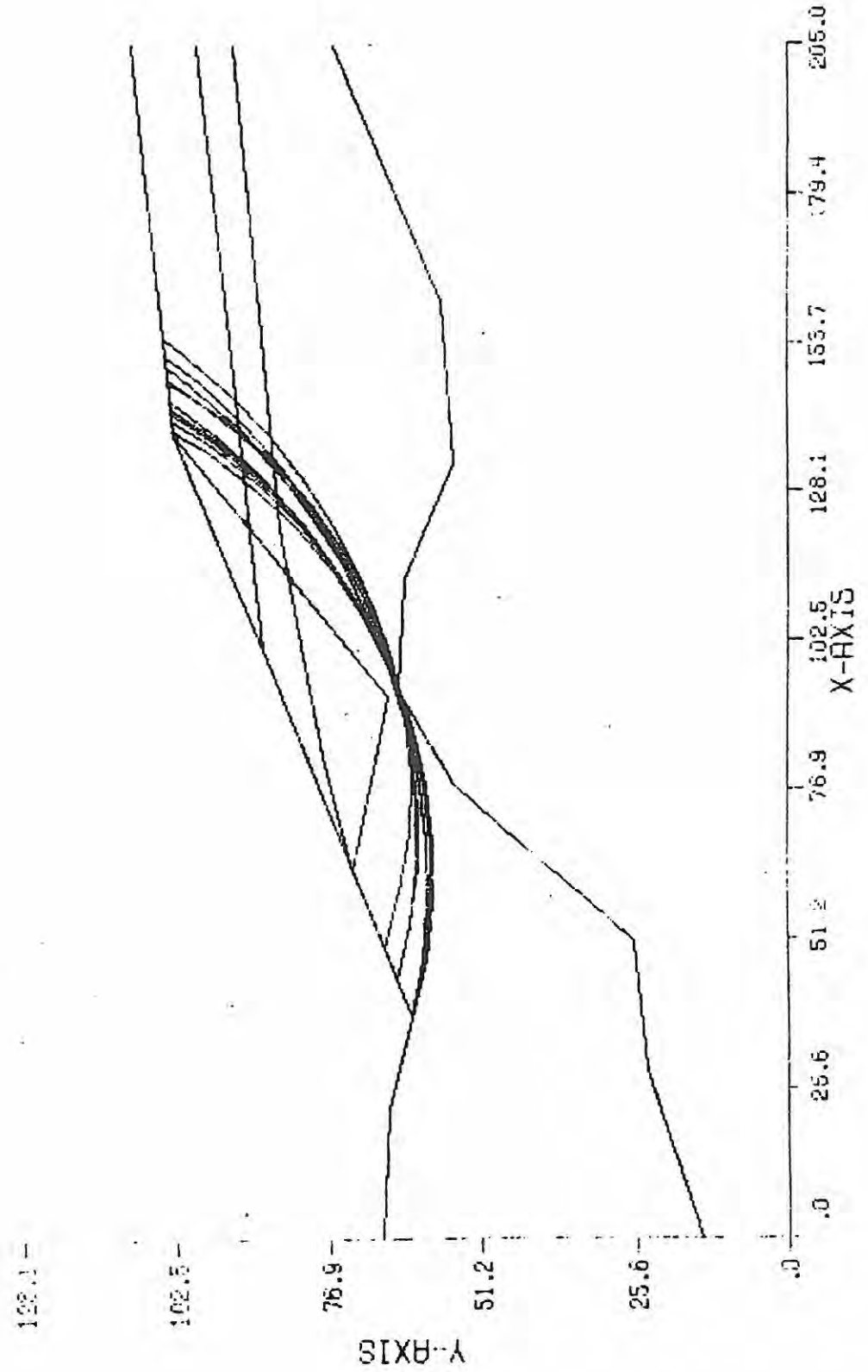
Y-AXIS
128.1
102.5
76.9
51.2
25.6
.0
X-AXIS
.0
25.6
51.2
76.9
102.5
128.1
153.7
179.4
205.0

The range of values obtained for the ten most critical surfaces is 1.25 to 1.28. The difference is smaller, and all values are smaller in magnitude than those obtained from the first run. The ten most critical surfaces form a more compact zone than observed in the plots of the first run. Seven of these surfaces pass through the toe of the slope, and of these seven surfaces, five are more critical than the other three which do not.

There is little justification to refine the search limitations further for another run using circular shape surfaces, so irregular shaped surfaces will be generated and analyzed next.

Using information obtained from analyzing circular surfaces, it is assumed that the critical irregular surface will pass through the toe, and that it will lie near or at the bedrock surface. From the toe of the slope 30 irregular shaped surfaces are randomly generated. Only 30 surfaces may seem inadequate, but it is more than what was generated from the toe of the slope for the second run.

All the critical circular surfaces of the second run terminated to the left of the point x = 160 ft, so the right termination limit is moved to that position. The length of the line segments to define the irregular surfaces is specified as 15 ft. The angle of inclination of the initial line segment is restricted between -15° and -45°. Although the circular search indicated shallower angles of inclination for the critical surface, it is thought that the initial inclination is controlled by the circular shape of the surfaces generated, and if the surfaces were not restricted to this shape, the angle of inclination of the initial line segment of the critical surface could be steeper.

The listing of the raw input data and a portion of the output for the third run follow on the next pages. The range in values of the factor of safety for the ten most critical irregular surfaces is 1.23 to 1.27, a reduction compared to that determined when restricted to circular surfaces.

Viewing the Gould plot of the ten most critical irregular surfaces, it can be observed that these surfaces have steeper angles at inclination for the initial line segments. The initial line segment of the most critical irregular surface is inclined at about 33.5°. Note the fairly compact zone. Tightening the surface generation requirements would be of little benefit for another run using the irregular surface generator. An application of the sliding block generator would be better.

The position of the most critical surface of the third run is used as the probable location of the most critical surface. Nine degenerate boxes are specified along the path of this surface. They are specified from left to right in a manner so they do not overlap.

The first box on the left is specified as a point at the toe of the slope. The next three boxes are specified as vertical lines, 4 feet long, straddling the critical irregular surface. The fifth box is also specified as a vertical line, but its length is specified as only 2 feet. Due to the proximity of the bedrock surface, it is positioned just above the bedrock. The sixth box is specified as a point just above the bedrock surface at the high point. The next two points are again specified as 4 foot vertical line segments, straddling the critical surface. The final box is specified as a horizontal line

INPUT FOR THIRD RUN -

```
PROFIL
EXAMPLE PROBLEM
6 5
0. 68. 22. 67. 1
22. 67. 38. 63. 1
38. 63. 101. 88. 1
101. 88. 138. 103. 2
138. 103. 205. 110. 2
101. 88. 205. 99. 1
SOIL
2
116.4 124.2 500. 14. 0. 0.
116.4 116.4 0. 0. 0. 0.
WATER
9
0. 68.
22. 67.
38. 63.
63. 73.
83. 78.
104. 82.
122. 85.
140. 87.
205. 93.
LIMITS
10 8
0. 15. 29. 24.
29. 24. 51. 26.
51. 26. 78. 56.
78. 56. 94. 65.
94. 65. 113. 64.
113. 64. 133. 56.
133. 56. 161. 58.
161. 58. 205. 76.
40.5 64. 93. 68.
93. 68. 138. 103.
RANDOM
1 30 38. 38. 138. 160. 0. 15. -15. -45.
```

PARTIAL OUTPUT FOR THIRD RUN -

SEARCHING ROUTINE WILL BE LIMITED TO AN AREA DEFINED BY 10 BOUNDARIES
OF WHICH THE FIRST 8 BOUNDARIES WILL DEFLECT SURFACES UPWARD

BOUNDARY NO.	X-LEFT (FT)	Y-LEFT (FT)	X-RIGHT (FT)	Y-RIGHT (FT)
1	0	15.00	29.00	24.00
2	29.00	24.00	51.00	26.00
3	51.00	26.00	78.00	56.00
4	78.00	56.00	94.00	65.00
5	94.00	65.00	113.00	64.00
6	113.00	64.00	133.00	56.00
7	133.00	56.00	161.00	58.00
8	161.00	58.00	205.00	76.00
9	40.50	64.00	93.00	68.00
10	93.00	68.00	138.00	103.00

A CRITICAL FAILURE SURFACE SEARCHING METHOD, USING A RANDOM
TECHNIQUE FOR GENERATING IRREGULAR SURFACES, HAS BEEN SPECIFIED.

30 TRIAL SURFACES HAVE BEEN GENERATED.

30 SURFACES INITIATE FROM EACH OF 1 POINTS EQUALLY SPACED
ALONG THE GROUND SURFACE BETWEEN X = 38.00 FT.
AND X = 38.00 FT.

EACH SURFACE TERMINATES BETWEEN X = 138.00 FT.
AND X = 160.00 FT.

UNLESS FURTHER LIMITATIONS WERE IMPOSED, THE MINIMUM ELEVATION
AT WHICH A SURFACE EXTENDS IS Y = 0 FT.

15.00 FT. LINE SEGMENTS DEFINE EACH TRIAL FAILURE SURFACE.

RESTRICTIONS HAVE BEEN IMPOSED UPON THE ANGLE OF INITIATION.
THE ANGLE HAS BEEN RESTRICTED BETWEEN THE ANGLES OF -45.0 AND -15.0 DG

FOLLOWING ARE DISPLAYED THE TEN MOST CRITICAL OF THE TRIAL
FAILURE SURFACES EXAMINED. THEY ARE ORDERED - MOST CRITICAL
FIRST.

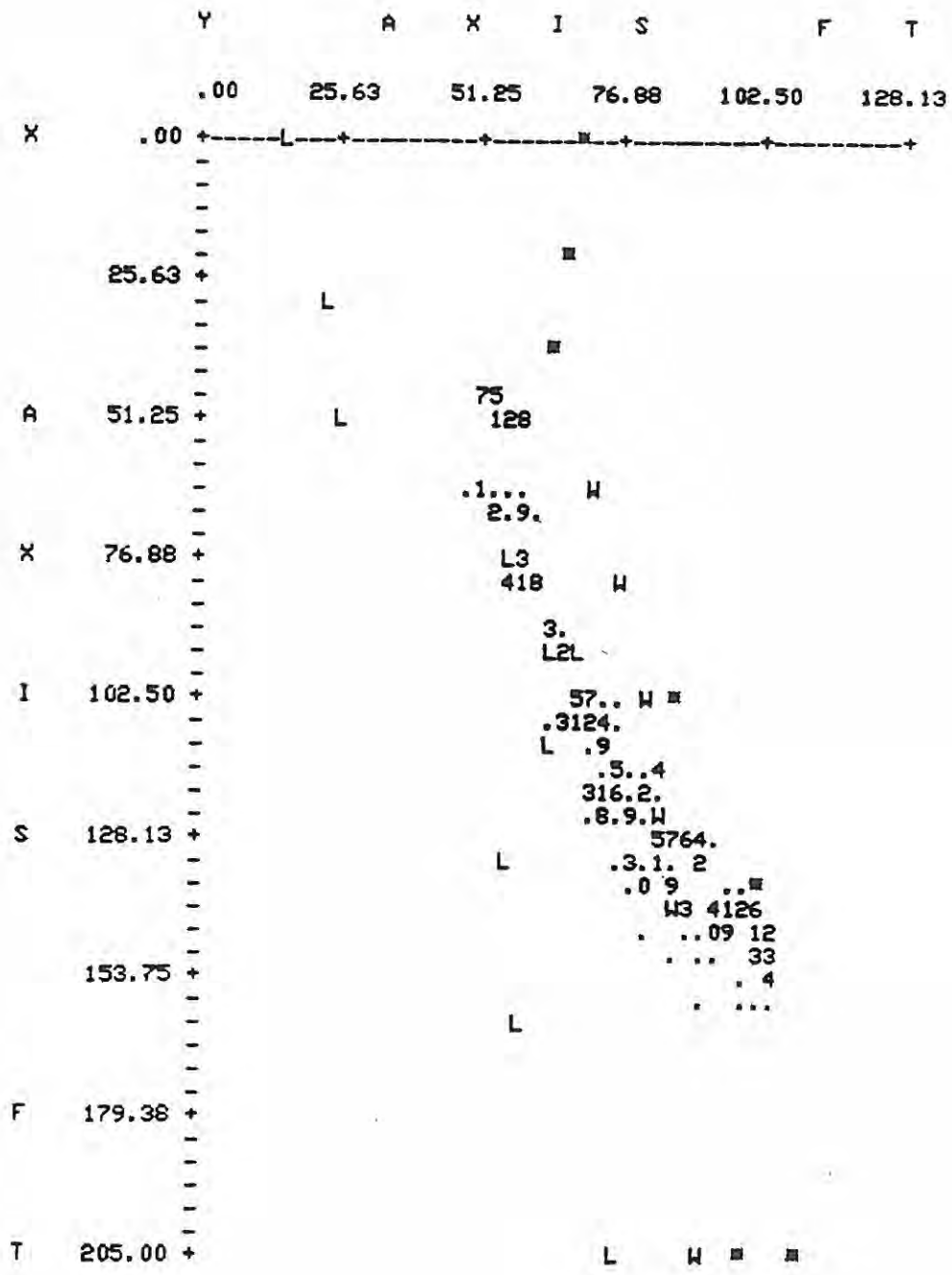
Y A X I S F T
.00 25.63 51.25 76.88 102.50 128.13
X .00
25.63
A 51.25
X 76.88
I 102.50
S 128.13
153.75
F 179.38
T 205.00

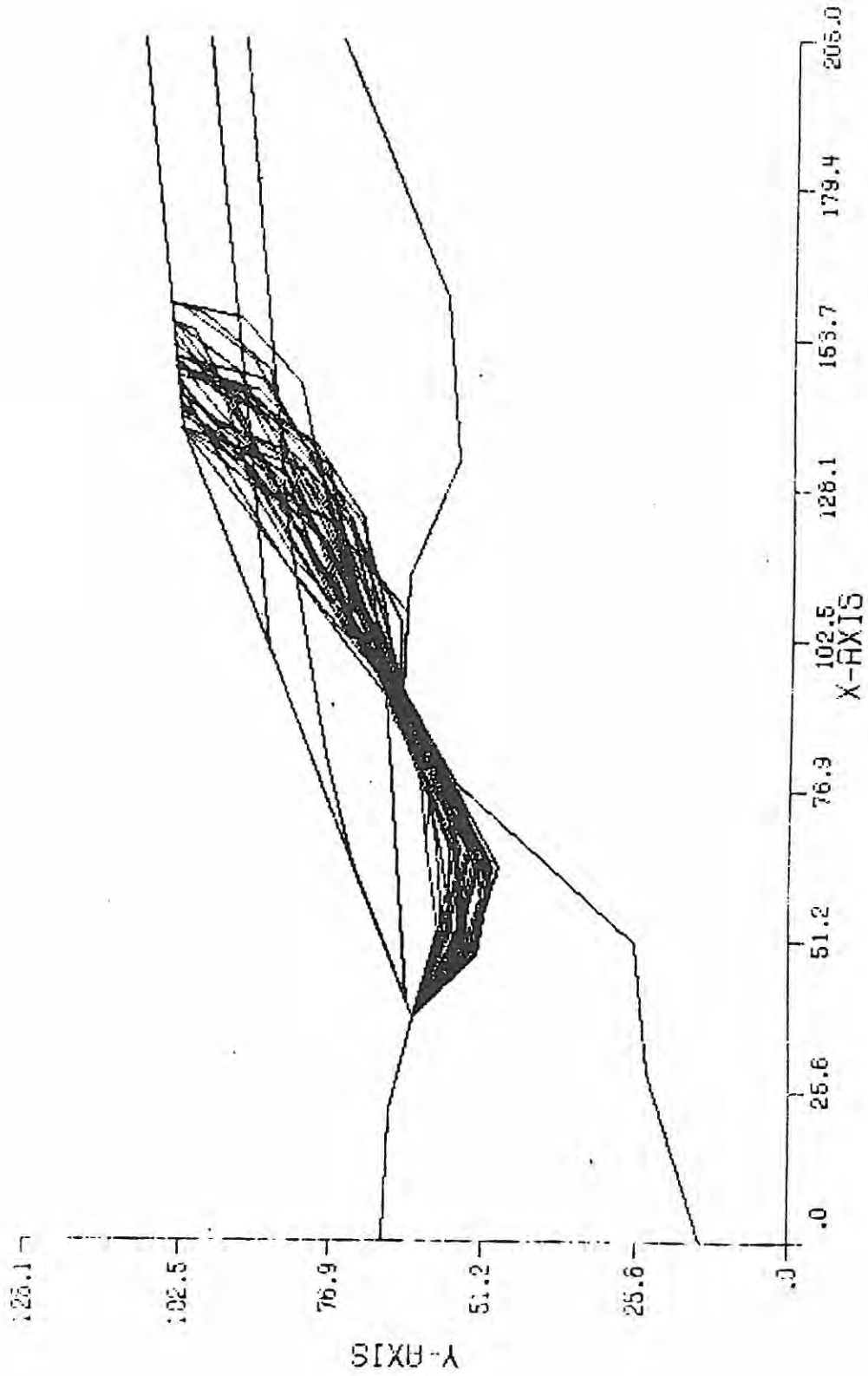
Y-AXIS
128.1
102.5
76.9
51.2
25.6
.0
.0
25.6
51.2
76.9
102.5
126.1
153.7
179.4
205.0
X-AXIS

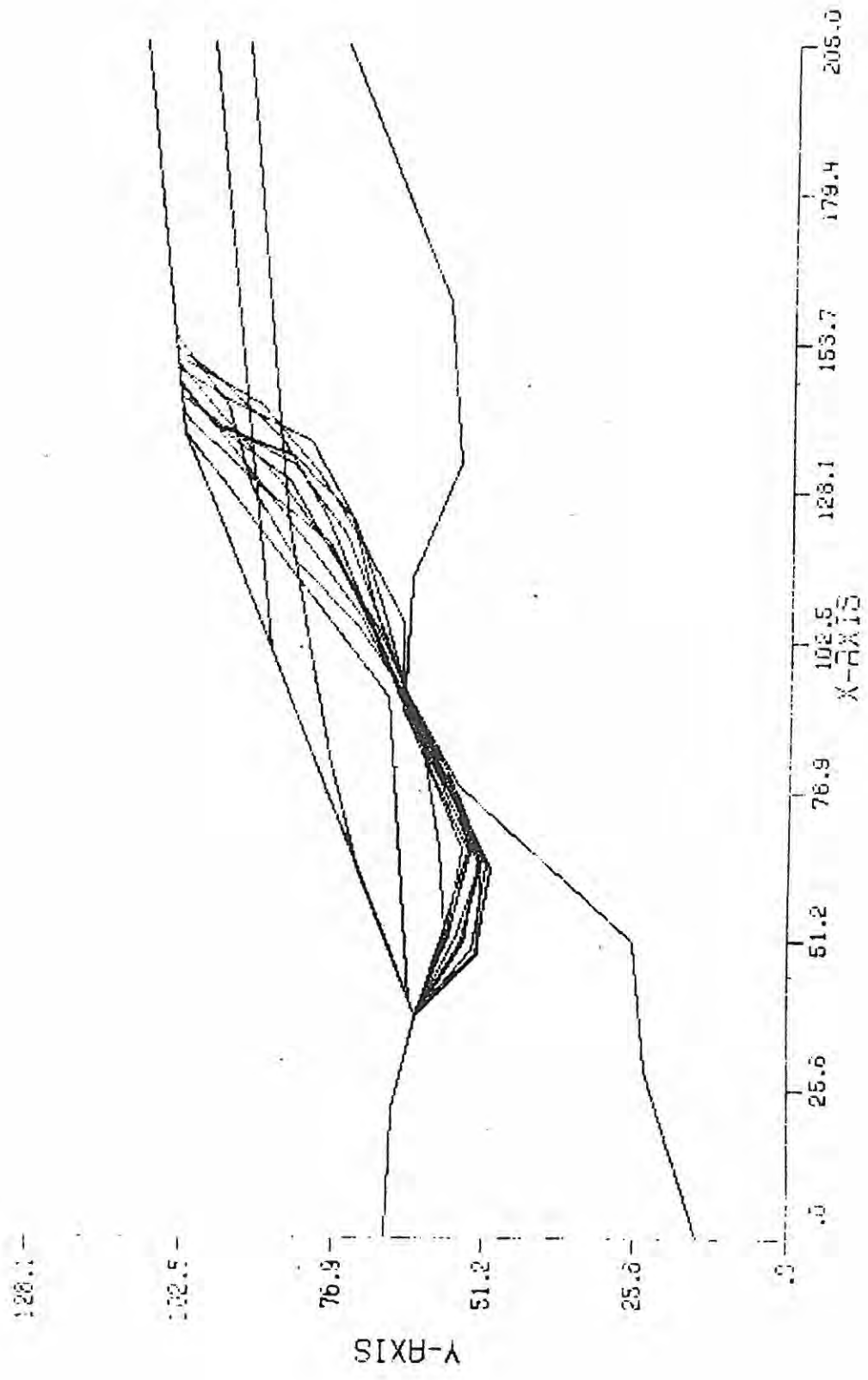
Y-AXIS
128.1
102.5
76.9
51.2
25.6
0
0
25.6
51.2
76.9
102.5
128.1
153.7
179.4
205.0
X-AXIS

segment, 5 feet in length, again straddling the critical irregular surface.

Points are randomly picked from within each box in sequence and connected to form part of a surface. To complete the active portion of a surface, 20 ft line segments are specified. Two-hundred surfaces are generated.

The listing of the raw input data and a portion of the generated output follow on the next pages. The values of the factor of safety ranged from 1.203 to 1.206 for the ten most critical surfaces, and the ten most critical surfaces form a very tight zone. Note the relative position of these surfaces with respect to the boxes, which can be seen in the second Gould plot. Another run would not be justified.

INPUT FOR FOURTH RUN -

```
PROFIL
EXAMPLE PROBLEM
6 5
0. 68. 22. 67. 1
22. 67. 38. 63. 1
38. 63. 101. 88. 1
101. 88. 138. 103. 2
138. 103. 205. 110. 2
101. 88. 205. 99. 1
SOIL
2
116.4 124.2 500. 14. 0. 0.
116.4 116.4 0. 0. 0. 0.
WATER
9
0. 68.
22. 67.
38. 63.
63. 73.
83. 78.
104. 82.
122. 85.
140. 87.
205. 93.
LIMITS
8 8
0. 15. 29. 24.
29. 24. 51. 26.
51. 26. 78. 56.
78. 56. 94. 65.
94. 65. 113. 64.
113. 64. 133. 56.
133. 56. 161. 58.
161. 58. 205. 76.
BLOCK
200 9 20.
38. 63. 38. 63. 0.
48. 55. 48. 55. 4.
58. 52. 58. 52. 4.
68. 53. 68. 53. 4.
78. 57.01 78. 57.01 2.
94. 65.01, 94. 65.01 0.
120. 75. 120. 75. 4.
130. 82. 130. 82. 4.
135. 92. 140. 92. 0.
```

PARTIAL OUTPUT FOR FOURTH RUN -

SEARCHING ROUTINE WILL BE LIMITED TO AN AREA DEFINED BY 8 BOUNDARIES OF WHICH THE FIRST 8 BOUNDARIES WILL DEFLECT SURFACES UPWARD

BOUNDARY NO.	X-LEFT (FT)	Y-LEFT (FT)	X-RIGHT (FT)	Y-RIGHT (FT)
1	0	15.00	29.00	24.00
2	29.00	24.00	51.00	26.00
3	51.00	26.00	78.00	56.00
4	78.00	56.00	94.00	65.00
5	94.00	65.00	113.00	64.00
6	113.00	64.00	133.00	56.00
7	133.00	56.00	161.00	58.00
8	161.00	58.00	205.00	76.00

A CRITICAL FAILURE SURFACE SEARCHING METHOD, USING A RANDOM TECHNIQUE FOR GENERATING SLIDING BLOCK SURFACES, HAS BEEN SPECIFIED.

200 TRIAL SURFACES HAVE BEEN GENERATED.

9 BOXES SPECIFIED FOR GENERATION OF CENTRAL BLOCK BASE

LENGTH OF LINE SEGMENTS FOR ACTIVE AND PASSIVE PORTIONS OF SLIDING BLOCK IS 20.0

BOX NO.	X-LEFT (FT)	Y-LEFT (FT)	X-RIGHT (FT)	Y-RIGHT (FT)	WIDTH (FT)
1	38.00	63.00	38.00	63.00	0
2	48.00	55.00	48.00	55.00	4.00
3	58.00	52.00	58.00	52.00	4.00
4	68.00	53.00	68.00	53.00	4.00
5	78.00	57.01	78.00	57.01	2.00
6	94.00	65.01	94.00	65.01	0
7	120.00	75.00	120.00	75.00	4.00
8	130.00	82.00	130.00	82.00	4.00
9	135.00	92.00	140.00	92.00	0

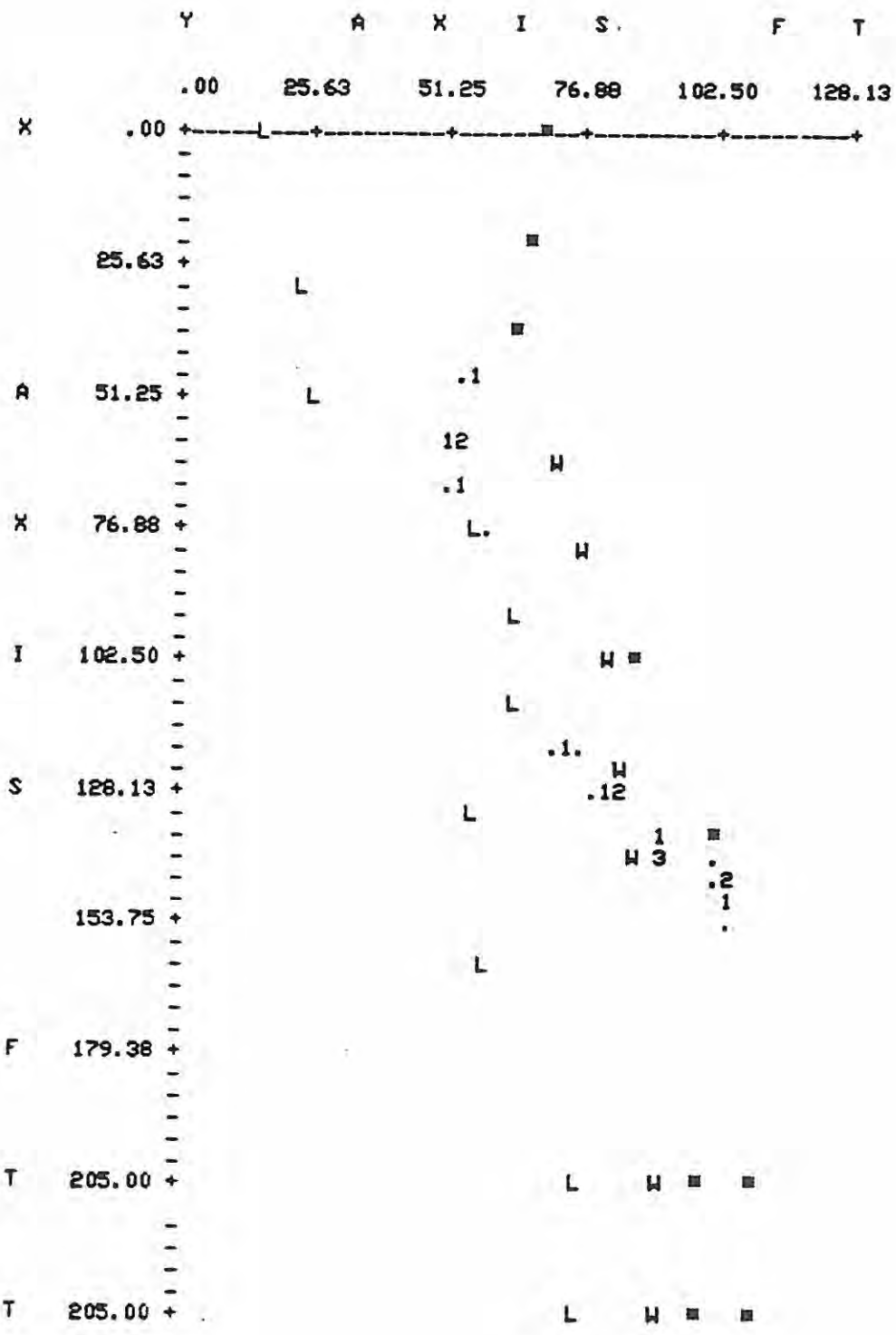
Y A X I S. F T
.00 25.63 51.25 76.88 102.50 128.13
X .00
25.63
A 51.25
X 76.88
I 102.50
S 128.13
153.75
F 179.38
T 205.00
T 205.00

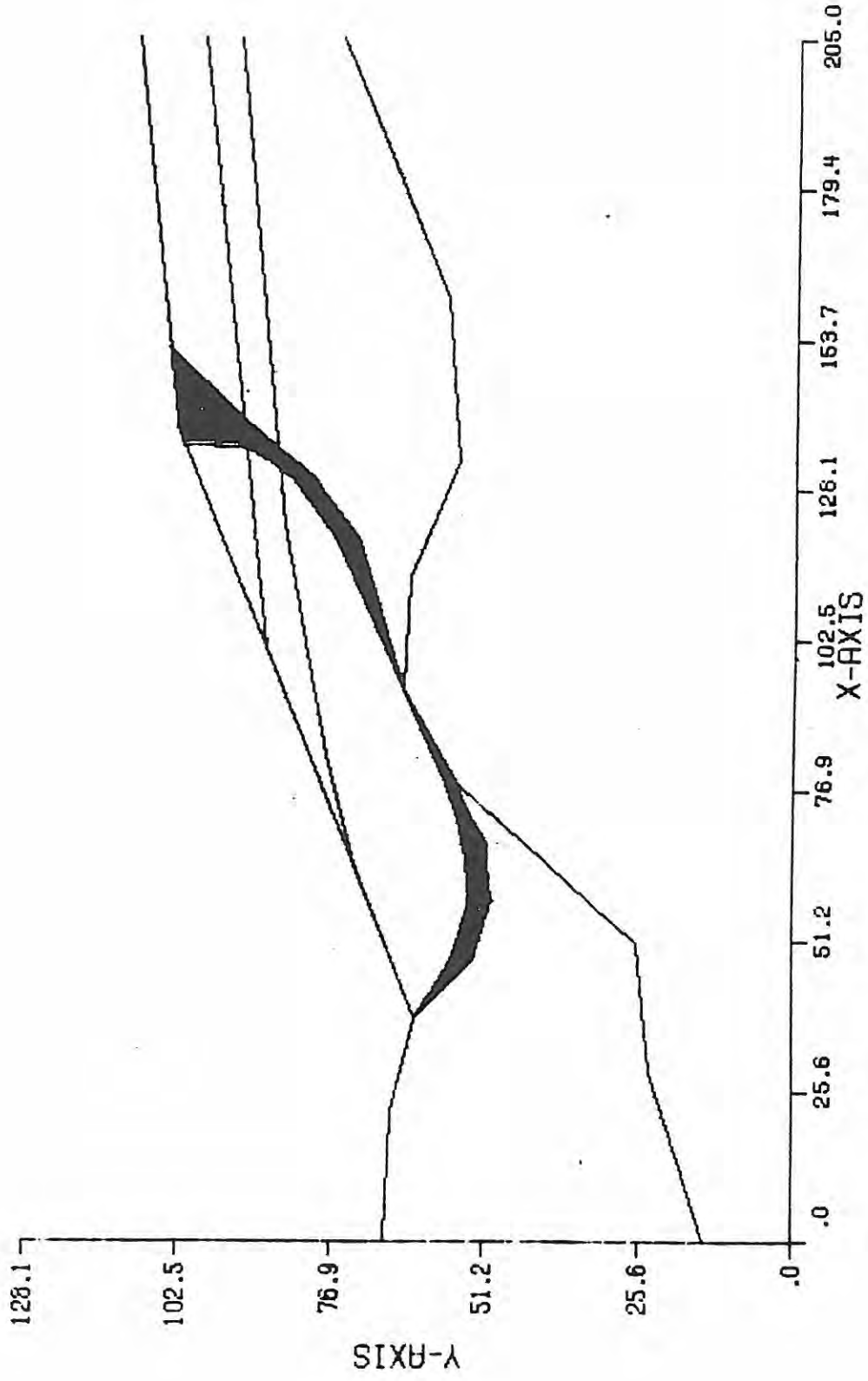
128.1
102.5
76.9
51.2
25.6
.0
Y-AXIS
.0
25.6
51.2
76.9
102.5
126.1
153.7
179.4
205.0
X-AXIS

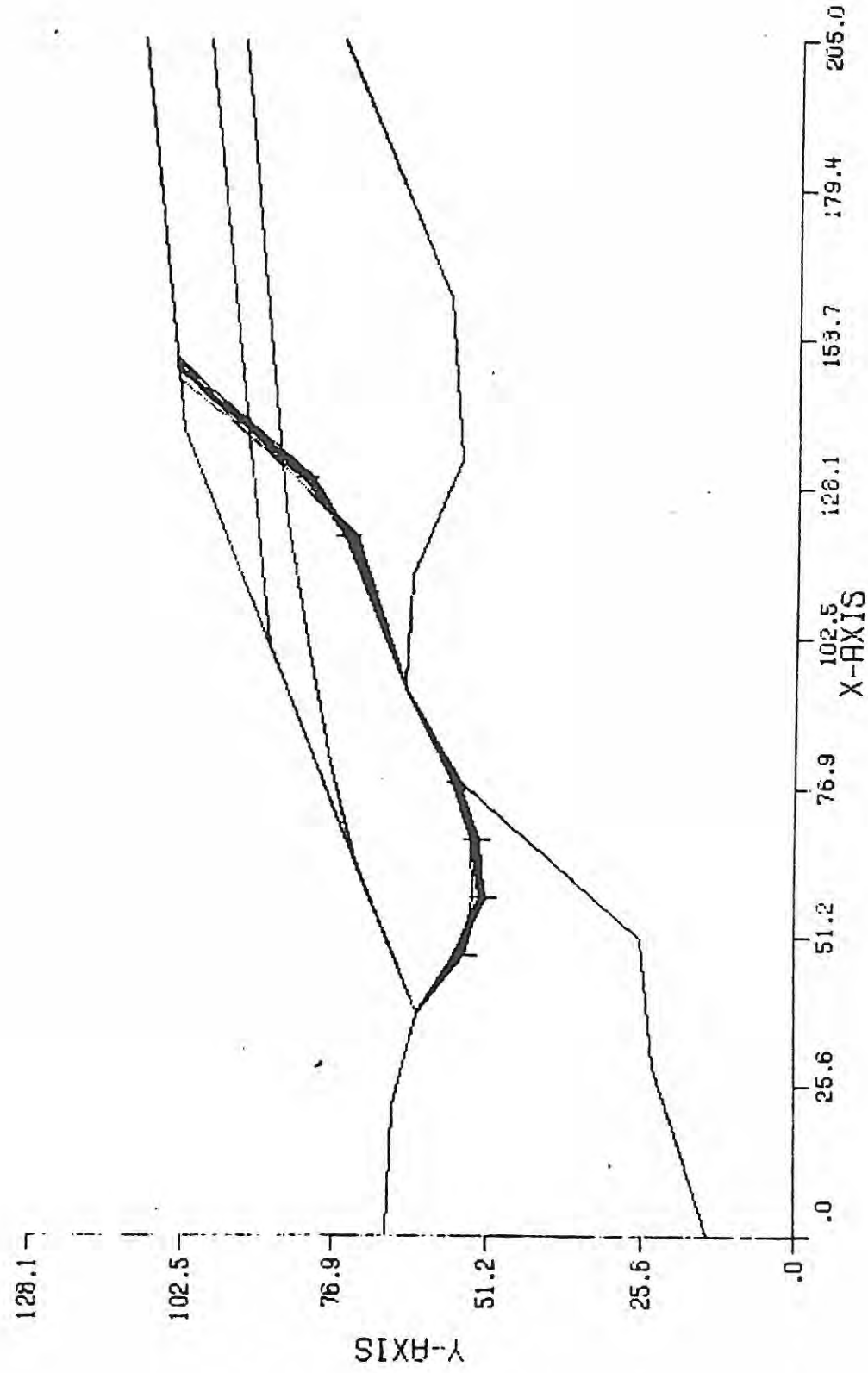
128.1
102.5
76.9
51.2
25.6
.0
Y-AXIS
.0
25.6
51.2
76.9
102.5
128.1
153.7
179.4
205.0
X-AXIS

UNITS

All units used for any one problem must be consistent. The printed output is limited to the following units for dimensioning.

Length	(FT)	feet
Unit Weight	(PCF)	pounds per cubic foot
Stress	(PSF)	pounds per square foot
Direction	(DEG)	degrees

Metric units or any set of consistent units can be used. It must be kept in mind, however, that the printed output will bear the units listed above. A consistent set of metric units for example would be

Length	(M)	meters
Unit Weight	(KG)	kilogram per cubic meter
Stress	(KG/SQM)	kilogram per square meter
Direction	(DEG)	degrees

PROBLEM SIZE LIMITATIONS

STABL as dimensioned in the program listing is capable of handling problems defined as follow.

Data	Maximum Number
profile boundaries (total)	100
*) piezometric surfaces (total)	10
points defining a single water surface	40
points defining specified trial failure surface	100
surface generation boundaries	20
uniformly distributed surcharge boundary loads	10
soil types (total)	20
anisotropic soil types	10
direction ranges of each anisotropic soil type	10
boxes for sliding block surfaces	10

The program can be adjusted to handle larger problems by changing dimension statements. The availability of the computing machine's memory core will take precedence with regard to how large a problem can be ultimately handled.

*) The possibility of defining several piezometric surfaces has been added to the program. This can be used e.g. in cases with artesian water or a perched water table.

Reinforced or Mechanically Stabilized Earth Slopes

by

Peter J. Bosscher

Applications

- steepened slopes
- surficial reinforcement
- compound slopes
- repair of landslides
- embankments over soft ground
- vertical slopes or walls

ROW Savings

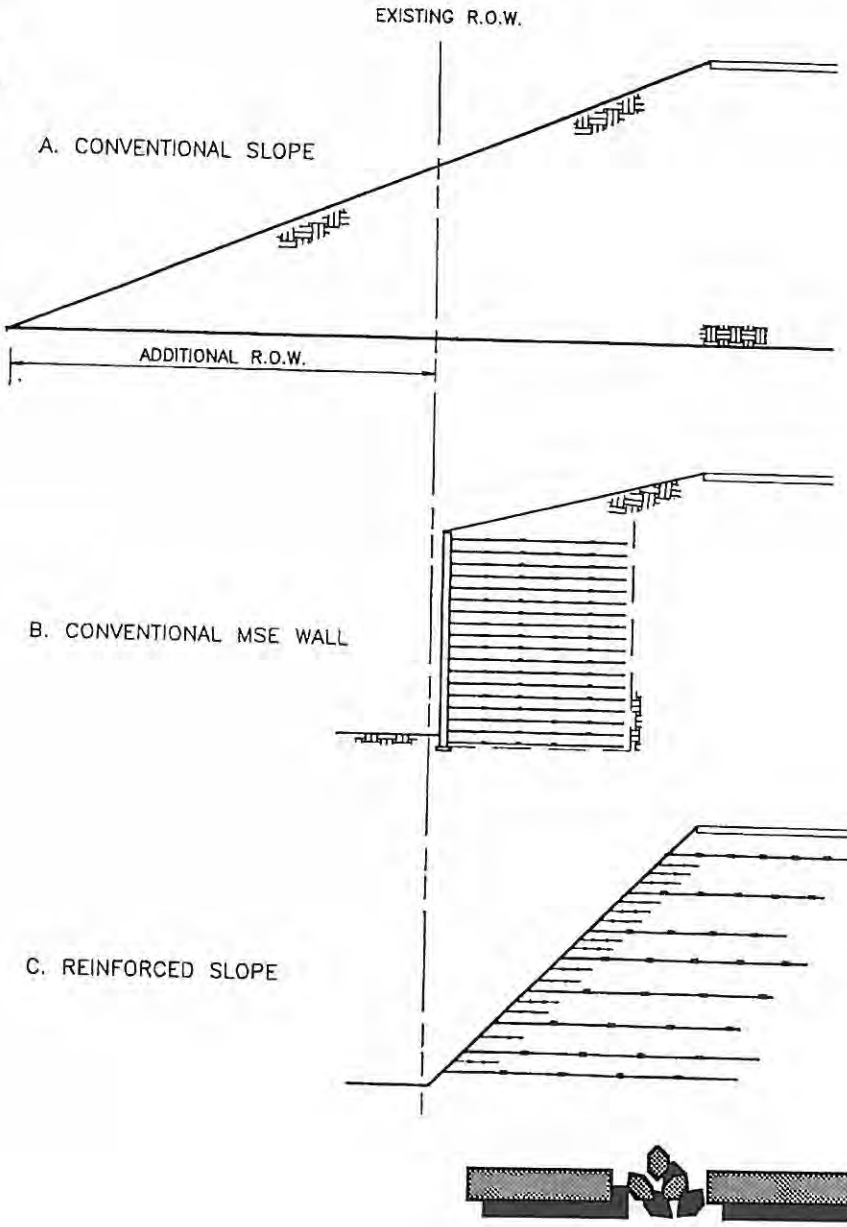
EXISTING R.O.W.
A. CONVENTIONAL SLOPE
ADDITIONAL R.O.W.
B. CONVENTIONAL MSE WALL
C. REINFORCED SLOPE

Principal Components

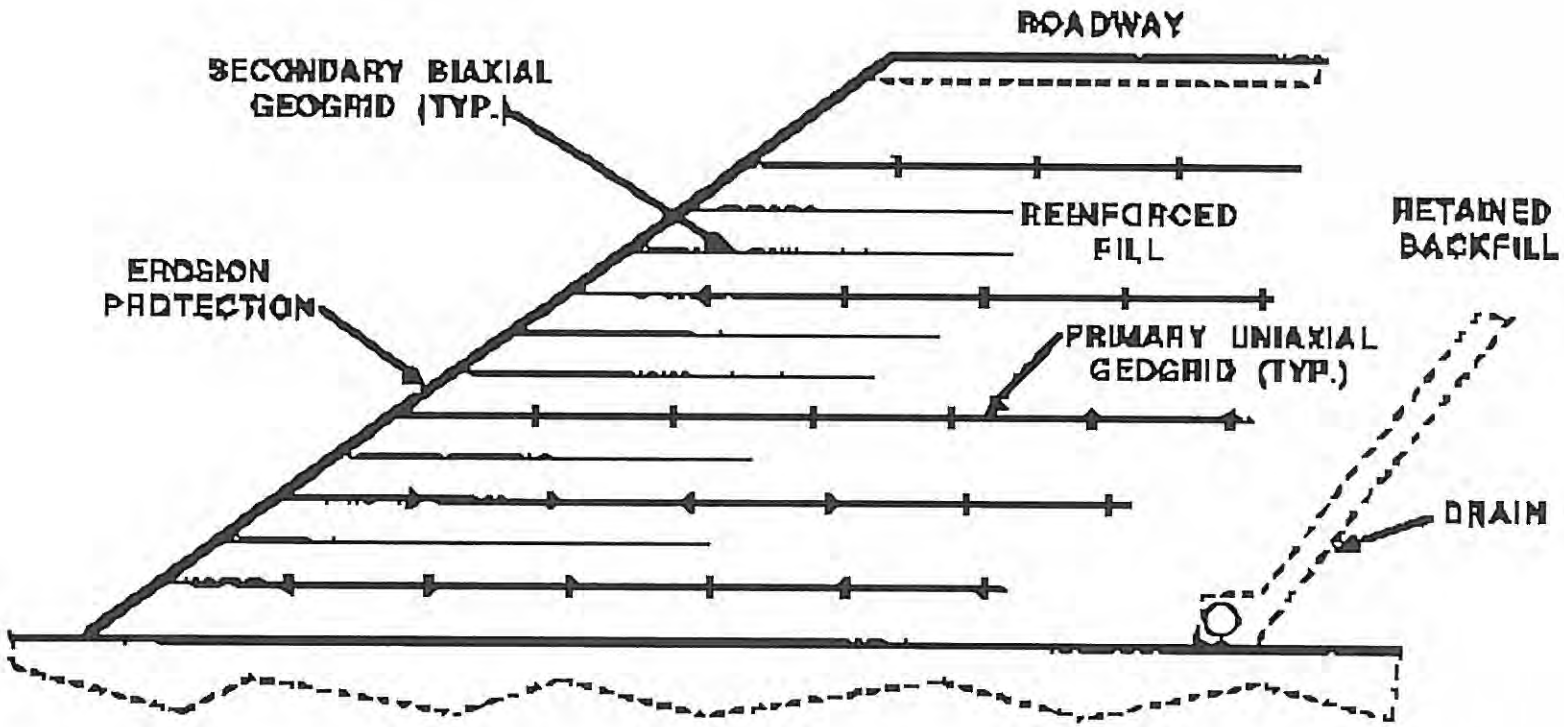

Estimated Costs

Savings are realized from both material and construction time reductions, as well as reduced ROW requirements.

Can also commonly use local on-site fills.

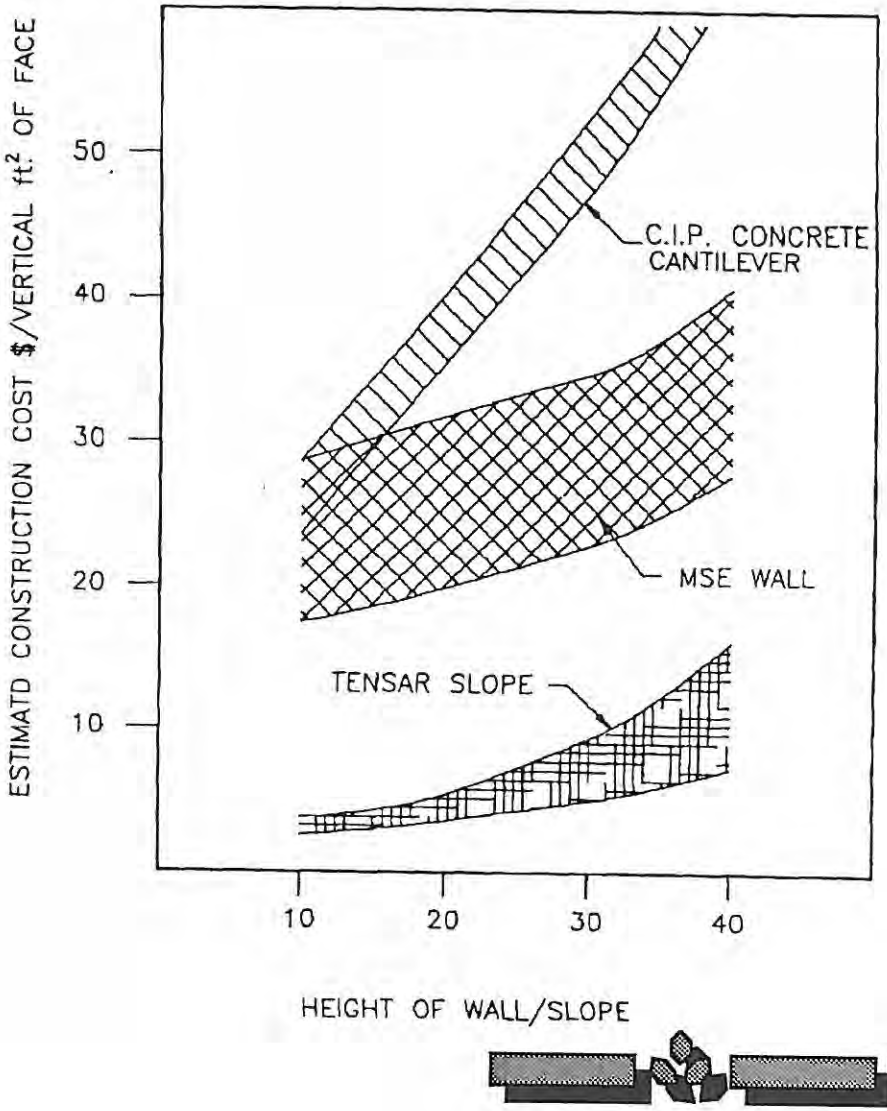

Aspects of Design

- Material Selection
  - Soil
  - Reinforcement
- Stability Analysis
- Additional Considerations
  - Drainage
  - Erosion control
- Specifications
- Field inspection

Failure Modes

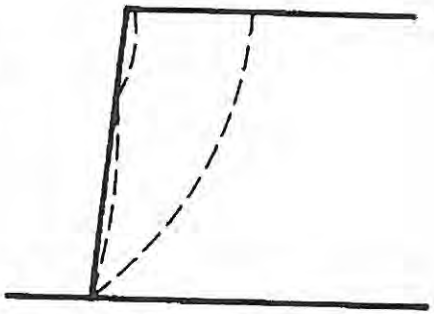

A. UNREINFORCED

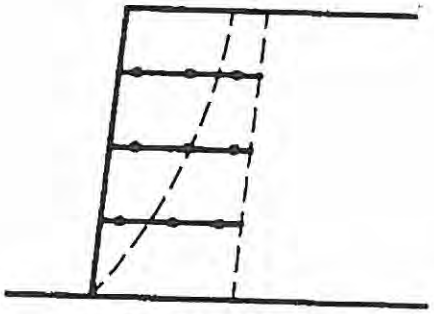

B. INTERNAL

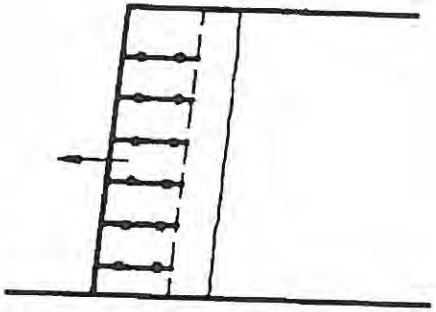

C. PULLOUT/SLIDING

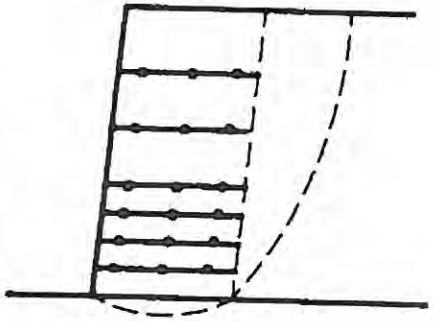

D. GLOBAL

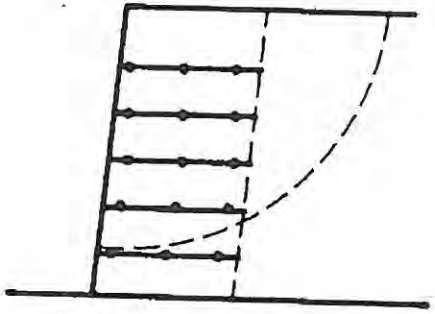

E. COMPOUND

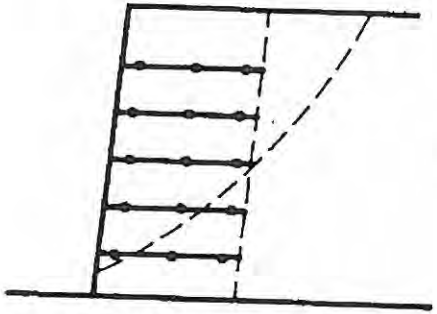

F. COMPOUND

Typical Circular Failure Surface

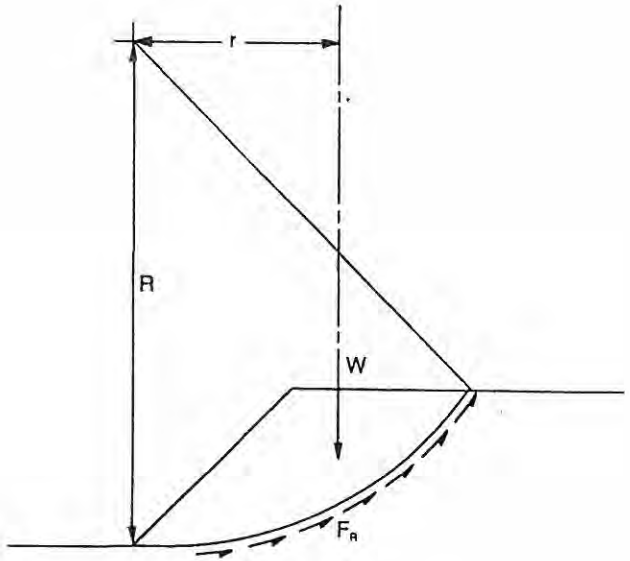

$$FS = \frac{\text{Driving Moment}}{\text{Resisting Moment}} = \frac{rW}{RF_R}$$

Reinforcement Pullout Test

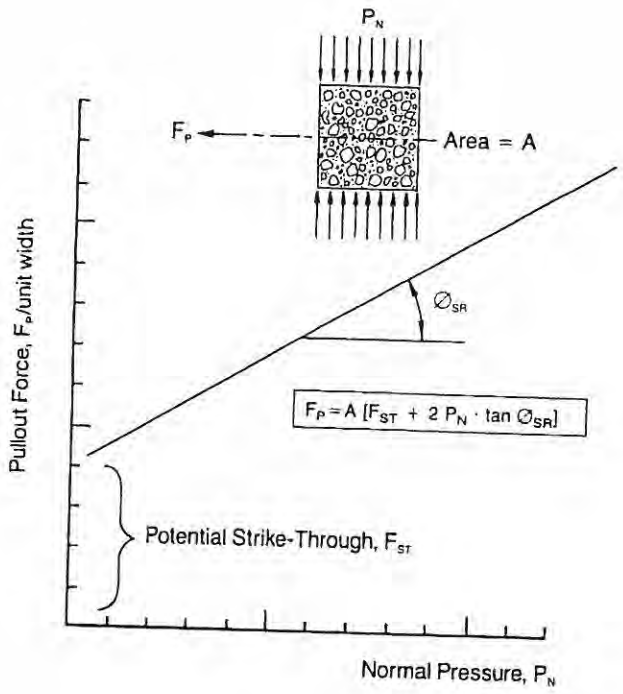

Resisting Forces in Reinforcement

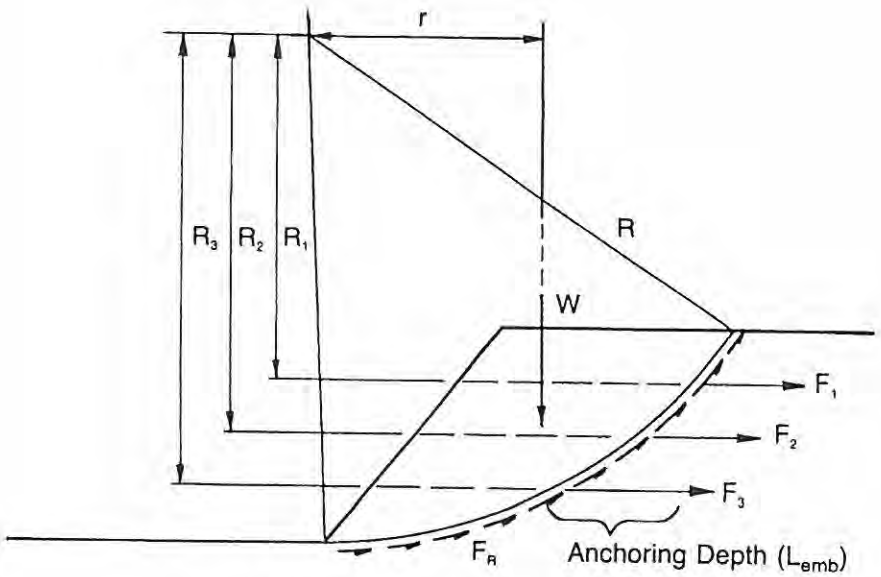

$$FS = \frac{\text{Driving Moment}}{\text{Resisting Moment}} = \frac{rW}{RF_R + R_1F_1 + R_2F_2 + R_3F_3}$$

Slope Stability with Reinforcement

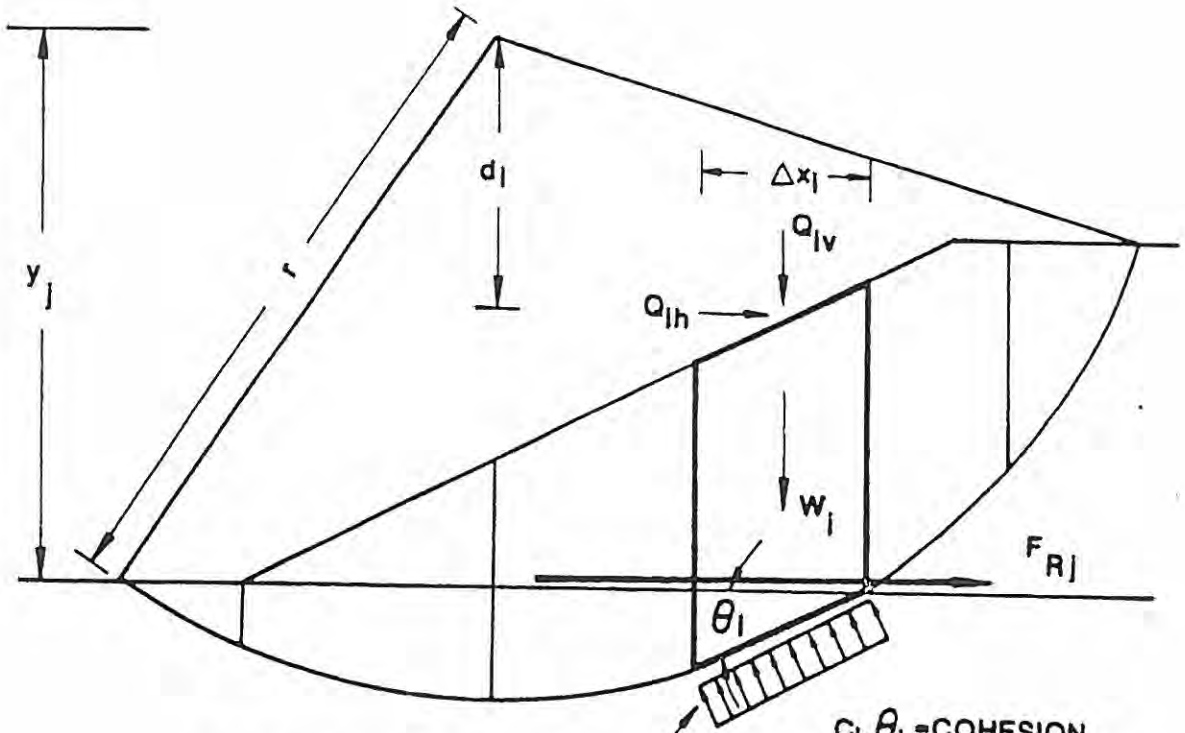

Minimum Reinforcement Length

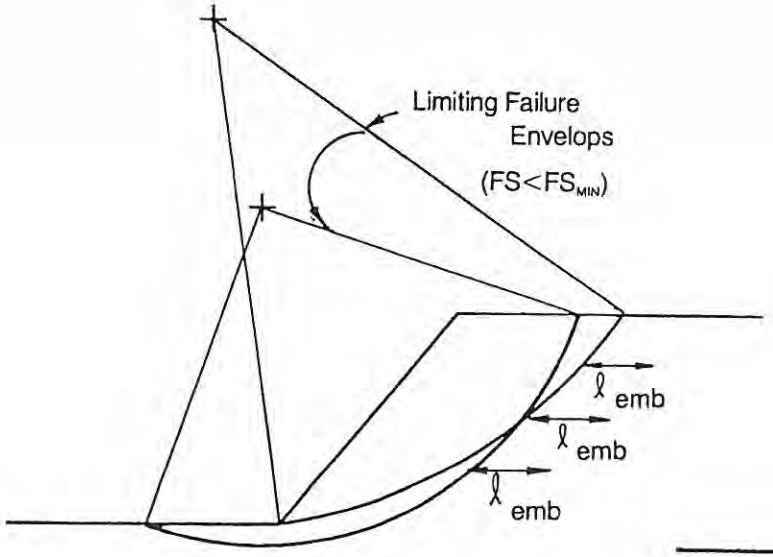

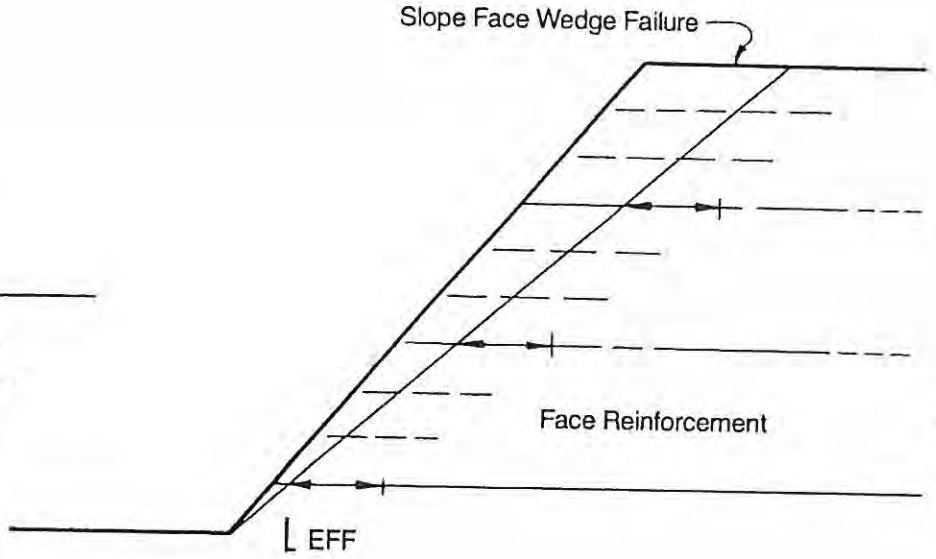

Aspects of Design

- Material Selection
  - Soil
  - Reinforcement
- Stability Analysis
- Additional Considerations
  - Drainage
  - Erosion control
- Specifications
- Field inspection

Reinforced Soil Highway Slopes

RYAN R. BERG, RONALD P. ANDERSON, ROBERT J. RACE, AND VICKY E. CHOUERY-CURTIS

Reinforced soil highway slopes are an economical alternative to conventional grade separations within limited rights-of-way, such as flattened slopes, selected-fill embankments, or vertical retaining walls. Reinforced soil slopes are applied in six main areas of highway construction: steepened slopes, surficial reinforcement, compound slopes for road widening, repair of landslides, embankments over soft foundations, and vertical slopes or walls. Critical applications with a design life of 50 to 75 years and, therefore, grid geosynthetic reinforcement, are emphasized. Those applications are defined and illustrated and their relative economics are reviewed. Steepened embankment slopes are examined in detail. Economics are presented and compared with alternatives. Design of steepened slopes is reviewed with emphasis on stability analysis procedures and appurtenant features. Also, long-term reinforcement material property requirements and specification writing are evaluated. Brief case histories are presented to illustrate applicability, aesthetics, and construction of reinforced soil slopes in highway works, showing that reinforced soil slopes are a proven method of construction having broad applicability in highway construction. It is concluded that highway planners and route layout engineers should consider the reinforced soil slope alternative(s) when faced with grade separations that must fit within limited rights-of-way.

A better angle on highway grade separations is one that provides economic benefits while maintaining or improving safety and aesthetics. Traditionally, separations are created with embankment or vertical retaining wall structures as illustrated in Figures 1a and 1b. An embankment would be at an angle that would be stable against deep-seated and surficial slope failures. Also, embankment slopes are usually constructed flat enough (4H:1V to 2.5H:1V) to allow mowing of grass. Reinforced soil walls, or mechanically stabilized earth (MSE) embankments, have been used extensively in highway construction since the mid-1970s. Reinforced soil walls offer the advantages of precast concrete facing, structural flexibility, and lower cost than does traditional cast-in-place concrete construction. Most of those walls use steel strip or grid-reinforcing elements and a select granular backfill.

A better angle for grade separations is one that lies between the flatter 4H:1V (14 degrees) slope and the vertical (90 degrees) wall, as illustrated in Figure 1c. Aesthetically, the slope may have a vegetated face, which is often more acceptable to the public than are vertical concrete faces. Low-growth, maintenance-free vegetation is typically specified. A steepened, reinforced slope requires less fill and rights-of-way (ROW) than do flat slopes. Steepened slopes eliminate precast or cast-in-place concrete used for facings, thus saving material costs and construction time. The requirement of select granular backfill can also be waived when chemically resistant, structural polymer grid-reinforcing elements are used.

Geogrids, polymer-based grids specifically developed for long-term critical structures, were introduced into North America in the early 1980s (*1*) and typically differ from geotextiles in long-term load carrying definition and in soil interaction characteristics. Critical highway structures reinforced with geogrids are addressed next.

Since the early 1980s, reinforced slopes have typically been used by transportation agencies in problem areas but not as a routine construction alternative for grade separations. The goal of this paper is to familiarize route layout and structural highway engineers with where and how reinforced slopes may be used and with their economic and aesthetic benefits.

COMPONENTS OF REINFORCED SLOPES

The material components of a reinforced slope are labeled in Figure 2. Inclusions of tensile elements in the fill soil create a structurally stable composite mass. Tensile elements used with the reinforced fill to create the stable mass are termed primary reinforcement. Secondary, or surficial, reinforcing elements at the slope face are used to aid in compaction, for alignment control, and to minimize sloughing. The soil at the outer edge of the slope is also faced to prevent or minimize soil erosion. External and internal drainage provisions should also be included in the design.

The reinforcing element typically used is a polymer geogrid. Structural limitations, such as allowable tensile load and design life, are specific to polymer type and product manufacturing process. Extruded, uniplanar geogrids have been used for permanent, critical highway slope and retaining wall construction.

Additional components of reinforced slopes include design, specifications, installation, and inspection. The reinforcement, design, erosion protection, and installation assistance can all be specified to be supplied from one prequalified manufacturer. This is similar to the way "vertical slopes," or MSE walls, are now specified by most transportation agencies. An exception is the supplier should be responsible for all aspects of structural stability and not just internal stability. Alternatively, the specifying agency may provide its own design and specify reinforcing materials. Inspection is routinely conducted by the specifying agency.

R. R. Berg, R. P. Anderson, R. J. Race, Tensar Earth Technologies, Inc., 3000 Corporate Center Drive, Morrow, Ga. 30260. V. E. Chouery-Curtis, Tensar Environmental Systems, Inc., 1210 Citizens Parkway, Morrow, Ga. 30260. Current affiliation for R. R. Berg: Ryan R. Berg and Associates, 7501 S. 80th Street, Cottage Grove, Minn. 55016.

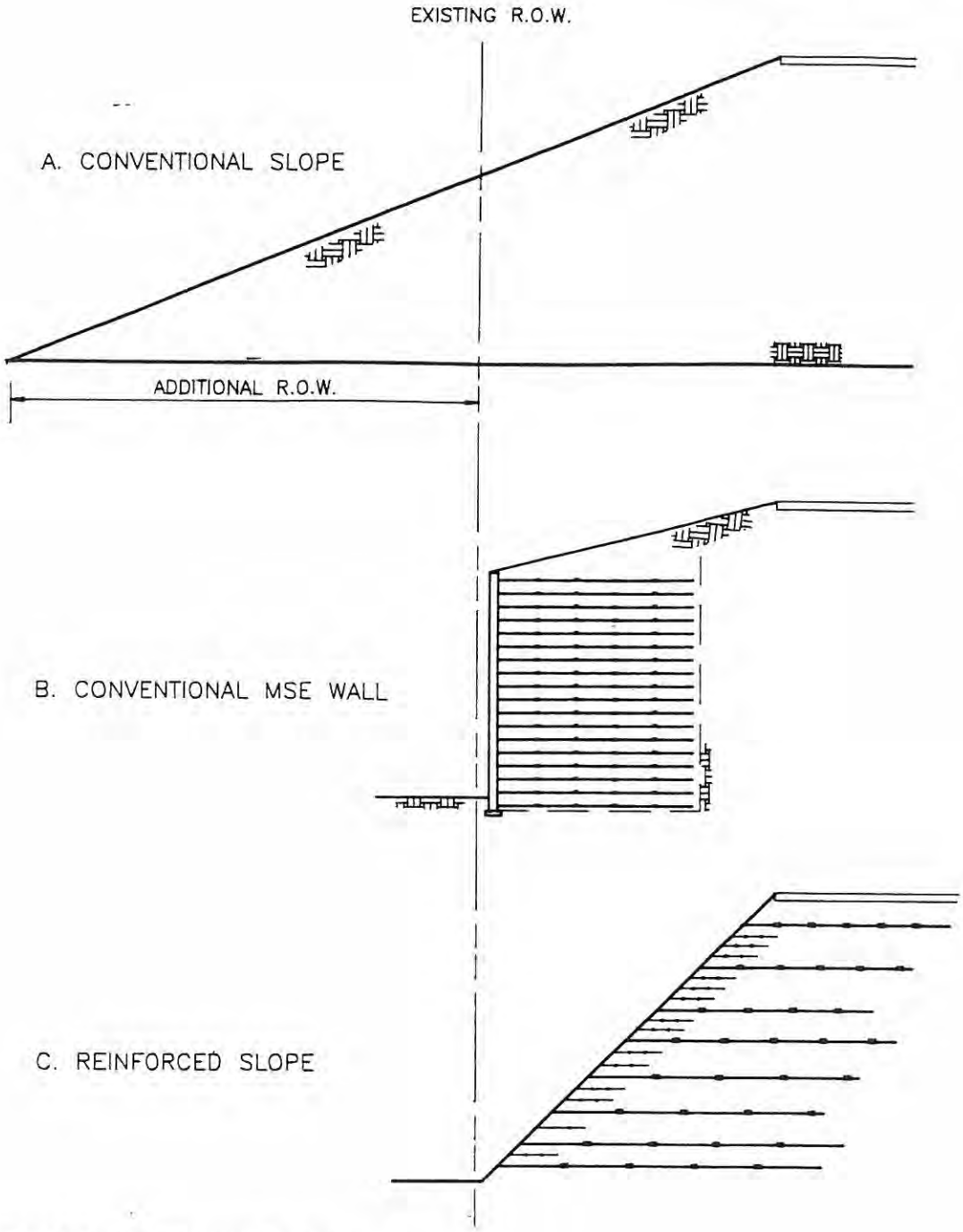

FIGURE 1 Grade separation options.

APPLICATIONS

The primary application of reinforced slopes in highway construction is steepened slopes. Related reinforced slope applications include surficial reinforcement, compound slope construction, landslide repair, and embankments over soft foundations and are briefly reviewed in this and in the Case Histories section.

Steepened Slopes

A steepened slope may be defined as a reinforced mass that would have a factor of safety against slope instability of less than 1 if it were unreinforced. A typical steepened slope is illustrated in Figure 2. On the basis of current design procedures, a structure with a slope angle up to 80 degrees can be classified as a steepened slope. A structure with a slope

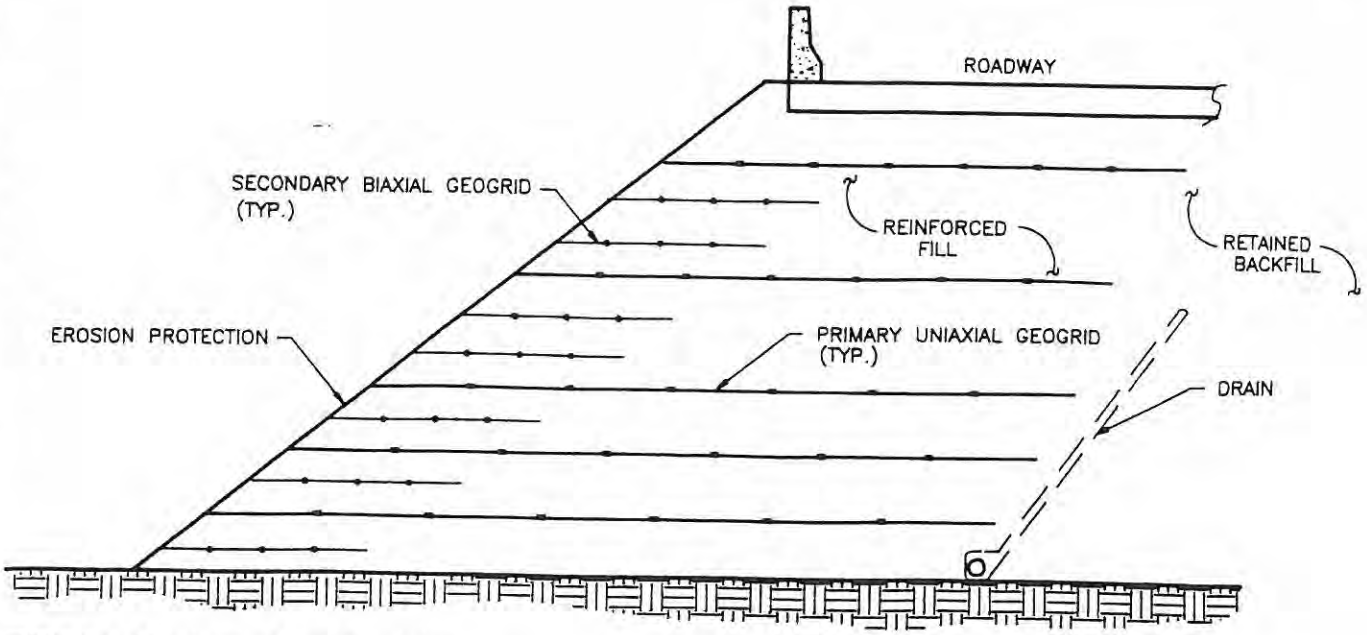

FIGURE 2 Components of a reinforced slope.

angle greater than 80 degrees will typically be classified as a retaining wall. Steepened slopes from 2 : 1 (26.6 degrees) to 0.35 : 1 (70 degrees) are routinely constructed. Construction details and erosion protection requirements vary between those extremes, as is illustrated in the Case Histories section.

Steepened slopes are used in lieu of flatter slopes to create more useable land on top of a slope or to minimize land take or ROW requirements at the bottom of a slope. Cost savings over retaining walls are realized by elimination of concrete facings and, in the case of steel-reinforced MSE walls, by use of on-site or nonselect fill. Aesthetically, a vegetated slope is usually more appealing than the vertical concrete facing.

Related Applications

Surficial Reinforcement

Shallow slope failures are not an uncommon sight along many roadways. Some of those slides can be attributed to lack of soil compaction near the edge of the slope, resulting in a weaker soil that more readily takes in surface water and further weakening the soil and leading to sloughing. Reinforcement allows soil compaction equipment to operate effectively on the slope edge (illustrated in Figure 3), thus achieving desired compaction and preventing future sloughing. Reinforcement for this application is typically 3- to 6-ft long and is spaced at 8- to 36-in. centers, vertically.

Compound Slope Construction

Compound slope construction refers to construction of a steepened reinforced slope into an existing stable, unreinforced slope and differs from the previous applications because

FIGURE 3 Surficial reinforcement on a 1:1 fill.

analysis and construction details vary. Global stability of the overall system may be more difficult to assess.

The most prominent use of this application is in widening of existing roads (see Figure 10). In the near future, many of the nation's freeways and tollways need to be widened, which may either be in the direction of the median, space permitting, or along the exterior lanes. The exterior widening of tall embankments requires large amounts of fill and additional ROW if the new slope is constructed at the same angle as is the existing one. Stability of new fill may be questionable if compaction of the soil at the edge of the existing fill was not achieved during (or maintained since) original construction. The use of a reinforced compound slope to widen roadways facilitates the assurance of global stability, reduces fill requirements, eliminates additional ROW, and often speeds construction.

Landslide Repair

Landslides in soil cut or fill areas can be repaired with a reinforced gravity mass structure that must extend back beyond the slope failure plane and should incorporate drainage provisions. On-site soils are typically used in the reconstruction when tensile-reinforcing elements are incorporated into the reconstructed soil mass. Tensile reinforcement allows the reuse of "failed" soil and reconstruction of the slope to its original lines and grades.

Embankments Over Soft Foundations

Roadway embankment construction over soft soils and high water tables can pose several challenges to the design engineer and contractor. Geogrid reinforcement placed across soft soils increases load distribution and reduces contact pressures and enables the contractor to gain access to place an initial soil lift. Higher strength reinforcement designed to prevent global instability can then be placed on top of this lift. Side slopes of the embankment may also be steepened to reduce weight and therefore decrease consolidation settlements. This method of construction is more economical than dump and displace techniques or pile-supported systems. Soil reinforcement has also been used in conjunction with other techniques, such as deep dynamic compaction, stone columns, geotextiles, and wick drains, to create cost-effective systems.

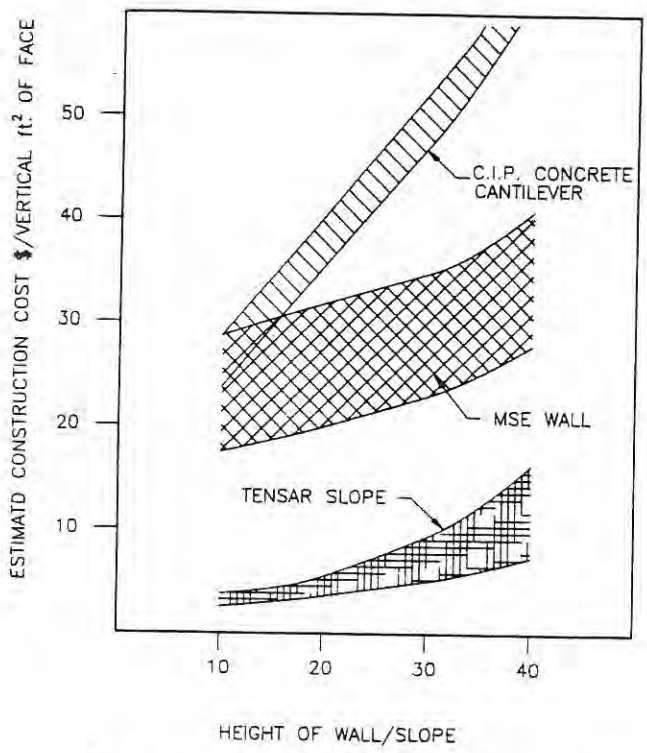

FIGURE 4 Estimated construction costs for grade separation structures.

ECONOMICS OF STEEPENED SLOPES

Steepened slopes are nearly always more economical than retaining wall alternatives and are often more economical than flatter slopes. Savings are realized both from material and construction time reductions and by reduced ROW requirements. Approximately 50 percent of the material cost of an MSE highway wall is in the precast concrete panel facing, which can be eliminated by use of a vegetated, reinforced slope.

Significant material savings over MSE walls in most areas also can be realized by use of local on-site fills. Geogrids were specifically developed to be used with fine or coarse grained soils or both (*1*). Clean, granular fills for use with metal-reinforced MSE walls typically range from $5.00 to $15.00 per cubic yard (in 1990). On-site fill can typically range from $2.00 to $5.00 per cubic yard. This differential will be slightly offset by the additional fill required by a slope, assuming the top of wall/slope is held constant. Therefore, steepened slopes options should be examined during the route layout and cut and fill balancing operations of a project to maximize cost savings.

The cost savings of a geogrid-reinforced steepened slope over other grade separation options is illustrated in Figure 4. The parameters used to develop this graph are listed next. Cost ranges shown for components are in-place costs. Although local economics will vary, it is clear that steepened slopes are a cost-effective alternative to retaining walls.

1. Steepened slope: $\phi' = 28$ to 34 degrees: $\beta = 26$ to 45 degrees; F.S. = 1.5.
   - Erosion protection: $1.25 to $4.00/yd²
   - On-site fill: $2.00 to $3.50/yd³
   - Reinforcement: $0.25 to $9.15/vertical sq. ft. face (no allowance for any additional R.O.W.)
2. MSE Wall: $\phi' = 34$ degrees; F.S. = 1.5; L:H = 0.75.
   - Select fill: $5.00 to $10.00/yd³
   - Facing panels, reinforcement, and design: $17.00 to $26.00/ft² face ($9.00 to $13.50 for materials and design and $8.00 to $13.00 for erection)
3. C.I.P. Concrete Cantilever: $\phi' = 34$ degrees; F.S. = 1.5.
   - On-site fill: $2.00 to $3.50/yd³
   - Reinforced concrete: $300.00 to $400.00/yd³

DESIGN OF STEEPENED SLOPES

As with any earthen structure, several aspects to design exist. Material properties of the different components of the soil structure must be assessed to ensure performance over the life of the structure. Stability analyses should then be performed and appurtenant features designed. Writing the specifications is the next step and is of crucial importance to ensure that the structure built meets the design requirements and functions as intended over the design life. Finally, inspection is required to ensure proper construction. A thorough sum-

mary of soil-reinforcement design with geosynthetics has been presented by Bonaparte et al. (*2*).

Material Properties

Soil

Fill soils may come from designated on-site sources or from undefined off-site borrow locations. In the first case (designated on-site sources), material parameters may be defined by standard geotechnical field exploration and laboratory testing practices before bid. Variabilities may be addressed by using conservative values in design or by parametrically investigating their affects on stability. Soils adjacent to a reinforced mass, which will remain in situ, and phreatic surfaces should also be defined by standard geotechnical practices. In the second case (undefined off-site borrow locations), a material specification for fill must be prepared.

Reinforcement

Two key reinforcement parameters used in design are (a) long-term design strength and (b) soil reinforcement interaction coefficients. Accurate definition of those parameters are required to ensure the slope structure will perform as intended over its entire design life. This is particularly true for critical highway structures.

Procedures for determining long-term design strength of geosynthetic reinforcement are being developed by the AASHTO-AGC-ARTBA Task Force 27 (*3*) and by the Geosynthetic Research Institute (*4*). (Both works were still in draft form and not publicly available when this paper was prepared, though final documents are pending from both organizations.) Other procedures have been presented by Bonaparte and Berg (*5*) and by Jewell and Greenwood (*6*). All procedures are similar and typically address creep of the polymer product, chemical degradation, biological degradation, damage during installation, strength of connections and junctions, and soil-reinforcement interaction characteristics.

Potential degradation of polymer reinforcement over the life of the structure, long-term creep, and long-term soil interaction mechanisms must be quantified. Those are areas that may be glossed over owing to their complexity. Reliance is typically heavily based on manufacturer's recommendations. Polymer materials may be subject to chemical or biological degradation or both in a soil environment. Product-specific studies should be conducted to determine durability reduction or safety factors for application to long-term design strength and to soil-interaction coefficients.

For time-dependent tensile characteristics the general rule in the plastics industry is not to extend creep predictions more than one order of magnitude beyond actual test data. Obviously, this is impractical for highway structures with a design life of 50 to 75 years, because tests of 5 to 7.5 years in duration would be required. Conservative approaches and techniques (*6–8*), such as time-temperature superposition, are used to extend 1.2-year creep data by two orders of magnitude to 120 years. Therefore, it is critical that an acceptable technique for extrapolation of long-term properties be specified and then be accurately documented.

Interaction coefficients between tensile elements and the soil it reinforces are functions of the soil type, soil density, overburden pressure, reinforcement geometry, and long-term load transfer mechanisms of the reinforcement. The geogrid-soil interaction consists of both frictional and passive components. Test procedures used for quantifying the interaction values must therefore account for long-term effects, such as creep and degradation on materials of the grid structure, that are transferring frictional and passive loads.

Analysis Techniques

Limit equilibrium methods are commonly used in analyses of reinforced soil slopes. The designer must be aware of the assumptions used in development of the implemented analysis procedures. Modified Bishop's procedure, Simplified Bishop's procedure, two-part wedge, and three-part wedge methodologies are commonly used in analysis of steepened reinforced slopes. Those methods were existing analysis techniques adapted to analyze reinforced soil structures. Therefore, it is also important to check the assumptions used in adaptation of those procedures, because versions of different design charts and computer programs vary. The reinforcing properties and soil/reinforcement interaction assumptions used also must be checked for validity to the case at hand.

Design charts, such as those presented by Jewell et al. (*9*), Tensar Corp. (*10*), Schmertmann et al. (*11*), and Christopher and Holtz (*12*) may be used for final design if all of the assumptions used in their development are met. It should be noted that those charts are based on specific soil-reinforcement interaction parameters and are especially useful for conceptual cost estimating and for checking reasonability of computerized slope analyses of more complicated slopes.

A computerized search for potential failure planes in steepened highway slope structures is recommended for structures that do not meet design chart assumptions. Some existing slope stability programs have been modified to incorporate tensile reinforcement elements, such as the STABGM (*13*) program modified from STABR. The failure plane search must directly incorporate the reinforcing effects into the factor of safety computation. Further, the search must examine compound type of failures (*14*) in addition to internal and external failures. Internal, external, and compound failure planes are illustrated in Figure 5.

Decisions to use a system such as a reinforced slope often are based on experience. Details such as constructability, construction movements, and site damage factors therefore are based on specifics of those prior projects. Soil type, analysis procedures, reinforcement product, and construction control variances from early projects can affect the performance of the proposed structure. The design and specification process should address possible variances and make allowances for or prevent variances from occurring.

Appurtenant Features

As with any earth structure the design does not end with the stability analyses. The structure must be constructible and must perform over its design life. The stability of the tem-

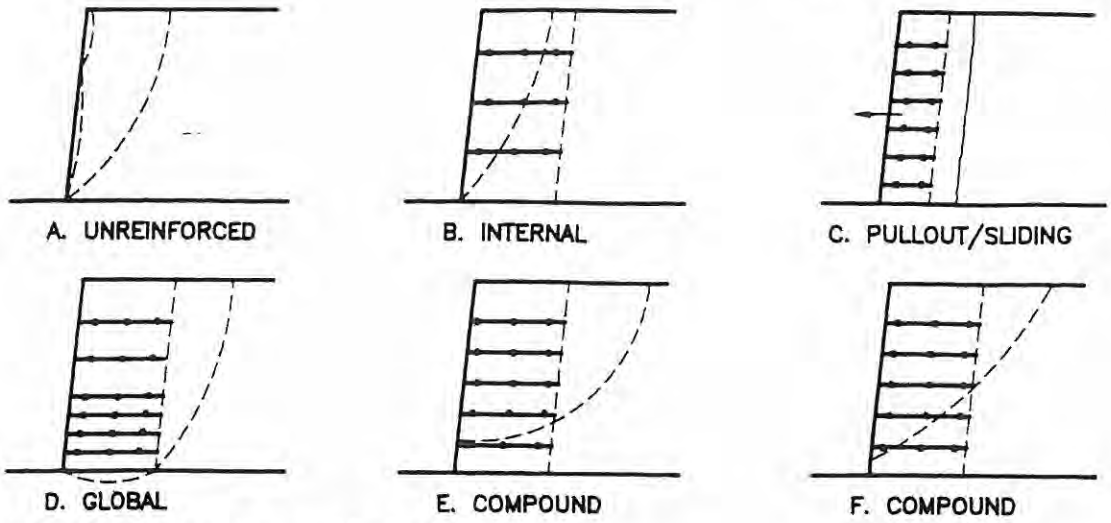

FIGURE 5 Reinforced steepened slope failure modes (*14*).

porary backcut must be assured for cut situations. Either the engineer specifies the maximum cut angle and accepts liability or the backcut stability is specified to be the contractor's responsibility. The backcut should also be benched to interlock the reinforced mass with the retained backfill soils and negate the potential formation of a linear failure plane.

Water or lack of proper drainage is a common culprit of soil structures failing or not performing as designed. Drainage both during construction and for the completed structure is an important detail that should not be overlooked during design. Surface water runoff should be diverted away from open construction cuts to minimize potential erosion and saturation of the reinforced fill soils. Partially completed fills should be sloped away from the face at the end of each work day to minimize water runoff across the slope face. Internal drains behind the reinforced mass should be installed if groundwater is, or may become, present. Often, drains are installed as an added degree of assurance even if groundwater is not anticipated.

Construction forming of some type is required for slopes steeper than about 45 to 50 degrees, depending on cohesiveness of the soil. Details of a forming system may be specified on the construction drawings or be left to the contractor's discretion. Experienced designers and contractors will know if forming is needed and, if so, which systems will work for a particular project.

Erosion control of the face of the finished slope must be considered in design. The authors recommend that a method of erosion protection be clearly specified by the designer and not be left to the discretion of the contractor or reinforcement supplier. Cost and performance of erosion control systems can vary significantly, and lack of tight specification can create a performance problem with the structure.

Specifications

As with MSE highway wall structures, two options exist in specifying reinforced slopes. One option is for the system to be preapproved by the agency and a line and grade approach be used. The system supplier will then be responsible for design, materials, and site assistance during construction. Design should include responsibility of global and compound failure modes (unlike the current MSE practice). The soil profiles and properties, required factors of safety, and analysis method should be supplied by the specifying agency. The other option is for the highway department to fully design the reinforced slope. This, of course, requires some experience of such structures. With this approach the written reinforcement specification is key to achieving desired results.

With either option, long-term design strength and long-term soil interaction characteristics of the reinforcement should be specified by using the proposed Task Force 27 Guidelines (*3*) or the Geosynthetic Research Institute Standard of Practice: GG4 (*4*) or both. The Task Force 27 guideline is specifically written for retaining walls but may be considered for slopes with minor revisions. Fill soil requirements should be modified to allow use of nonselect soils, erosion protection should be addressed, and stability factors of safety should be specified per slope application practice.

Construction Inspection

As with any earthwork construction the soil type, compaction, and moisture content should be monitored during construction. The other materials in a steepened slope (i.e., reinforcement and erosion protection) should also be inspected during construction. The grade of reinforcement, its length, and the elevations at which it is installed should be monitored by the owner's construction inspectors. Proper installation is key to satisfactory performance of an erosion control system and should therefore be closely inspected.

CASE HISTORIES

The following case histories are representative of where geogrid reinforced slopes have been used in highway construction to date. Steepened slope projects are emphasized because

they have the broadest applicability to highway construction. References to technical papers, when available, are provided for further information.

Project Name: Van Duzen, Peanut, California Forest Highway and Federal Lands, Highway 4-1(5)

- *Owner*: USDA Forest Service and Caltrans
- *Specifying agency*: U.S. Department of Transportation, Federal Highway Administration, Central Direct Federal Division
- *Designer*: U.S. DOT, FHWA, Central Federal Division
- *Slope heights*: Approximately 20 to 60 ft
- *Slope angle (H:V)*: 1:1
- *Facing system*: Turf reinforced with a polymer mat
- *Alternative*: Retaining walls/flattened slopes
- *Reinforcement type*: TENSAR UX1600, UX1500, UX1400, BX1100 geogrids
- *Construction date*: Sept. 1987 to Nov. 1988

Five side-hill fills of a new federal roadway through scenic Redwood Forest of northern California were constructed with steepened slopes. The 1 : 1 slopes were constructed with polymer soil-reinforcing geogrids. The steepened embankments range from 100 to 400 ft long and are 20 to 60 ft high. A typical reinforcement layout is illustrated in Figure 6. The fill soils were cohesionless and could ravel during and after construction. Intermediate reinforcing geogrids were used to minimize raveling during construction. The finished slopes were faced with native grasses, which were seeded into a three-dimensional polymer turf-reinforcing mat to prevent post-construction raveling.

The Central Direct Division of the FHWA designed the geogrid-reinforced steepened slopes and administered construction, which was completed in fall 1988. Working in conjunction with the U.S. Forest Service and Caltrans, the FHWA selected geogrid-reinforced slopes over retaining walls for their economy, aesthetics, and safety in this mountainous terrain.

Project Name: Cannon Creek

- *Specifying agency/owner*: Arkansas State Highway and Transportation Department
- *Designer*: Raymond Technical Facilities
- *Slope height*: 76 ft
- *Slope angle (H:V)*: 2:1
- *Facing system*: vegetation
- *Reinforcement type*: TENSAR UX1500 geogrid
- *Alternative*: new geometry and purchase of additional right-of-way
- *Cost savings*: $200,000

A large embankment was planned to carry State Highway 16 over Cannon Creek. The proposed 100,000-yd^3 embankment had a maximum height of 76 ft and was to be constructed with on-site clay soils and 2 : 1 side slopes. A cast-in-place concrete box culvert was first constructed to carry the creek under the embankment. Embankment construction started but was stopped quickly when several small slope failures occurred. It then became apparent that the embankment fill could not be safely constructed at 2 : 1 slopes.

With the box culvert in place there were two options for continuation of embankment construction. A gravelly soil could be used for embankment fill or on-site soils could be used with geogrid reinforcement. Both options were bid as alternatives, and the geogrid option, as illustrated in Figure 7, was used in construction. The geogrid reinforcement option was estimated to be $200,000 less expensive.

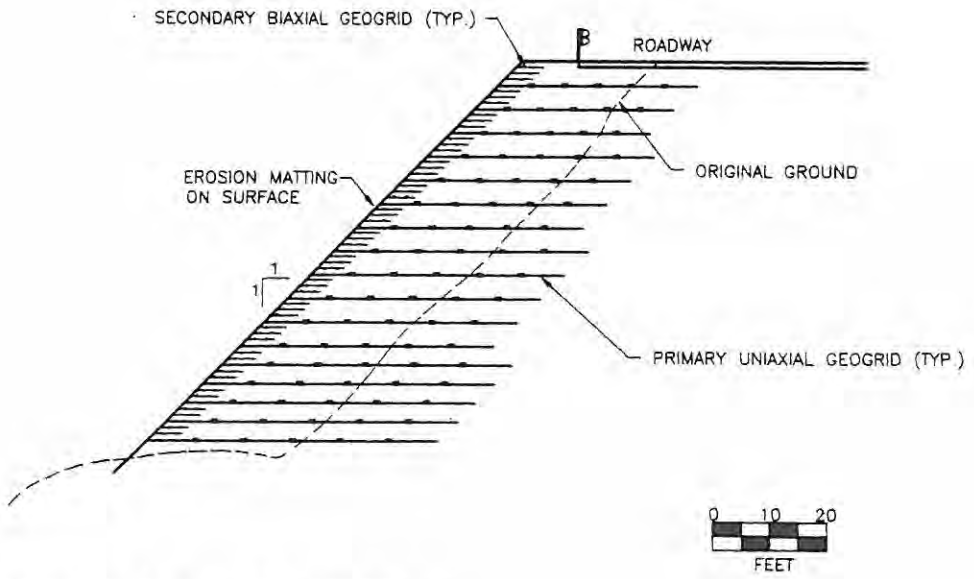

FIGURE 6 Van Duzen-Peanut cross section.

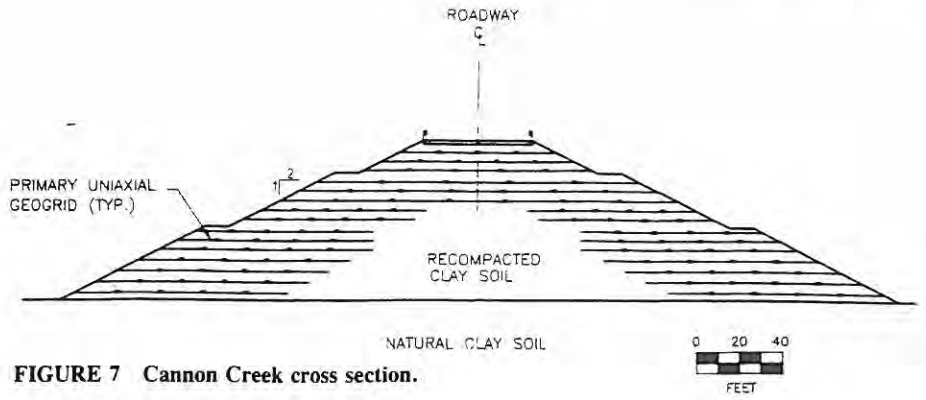

FIGURE 7 Cannon Creek cross section.

Project Name: Maryland Route 410

- *Specifying agency/owner*: Maryland Department of Transportation
- *Designer*: Tensar Engineering, Inc.
- *Slope height*: 48 ft
- *Slope angle* (H:V): 1.5:1
- *Facing system*: vegetation
- *Reinforcement type*: TENSAR UX 1400 and UX 1500
- *Alternative*: imported select fill or retaining walls
- *Construction date*: Summer 1989

A new interchange on U.S. Route 50 at MD Route 410 and MD Route 450 was designed by the Maryland Department of Transportation. Existing ROW were not wide enough to accommodate the new embankments. Embankments at slopes of 2.5 : 1 could be carried to the ROW limits and retaining walls constructed to contain the fill or additional ROW could be purchased. However, part of the existing embankment was an uncontrolled fill that could not be widened by building on top of it. It would need to be excavated and removed or recompacted.

Steepened geogrid-reinforced slopes were selected for construction. The 1.5H:1V slopes stayed within existing ROW limits and eliminated the need for retaining walls (see Figure 8). Some of the original uncontrolled fill was excavated and recompacted during installation of the stabilizing reinforcement. A view of the slope under construction is presented in Figure 9. Slopes were faced with native vegetation and did not require a permanent erosion mat system. Drains were installed behind the reinforced mass to intercept any possible groundwater.

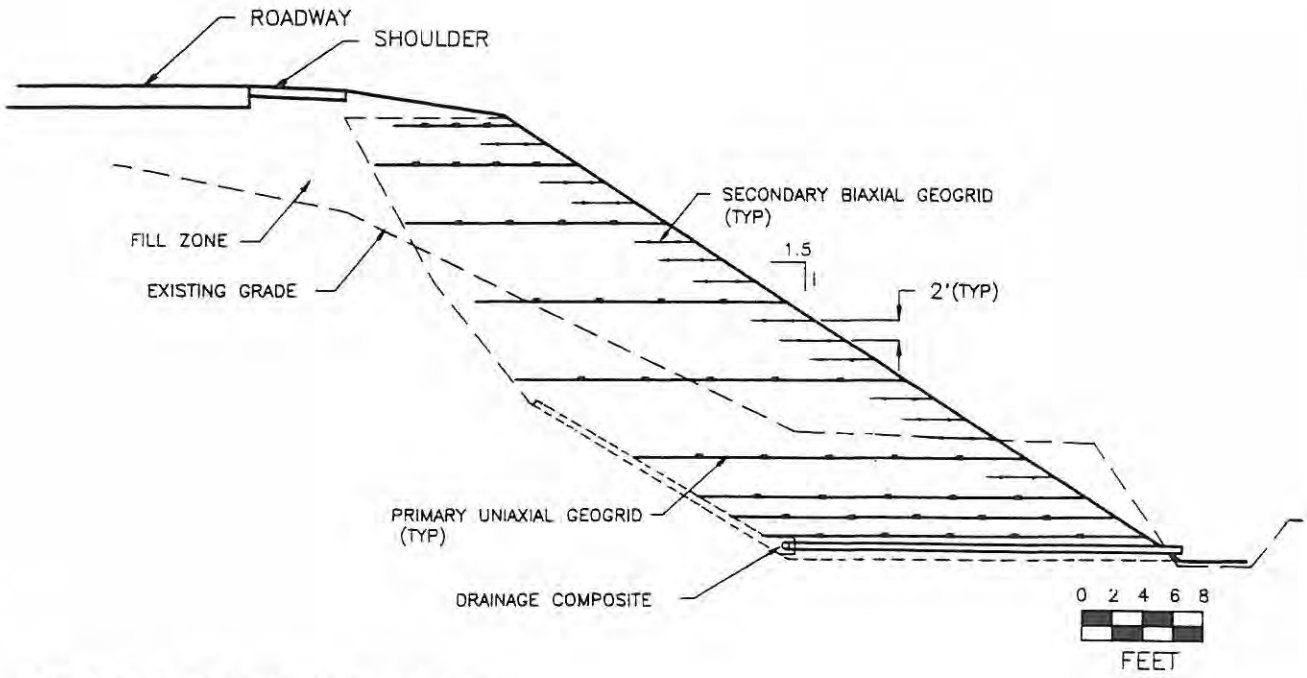

FIGURE 8 Maryland Route 410 cross section.

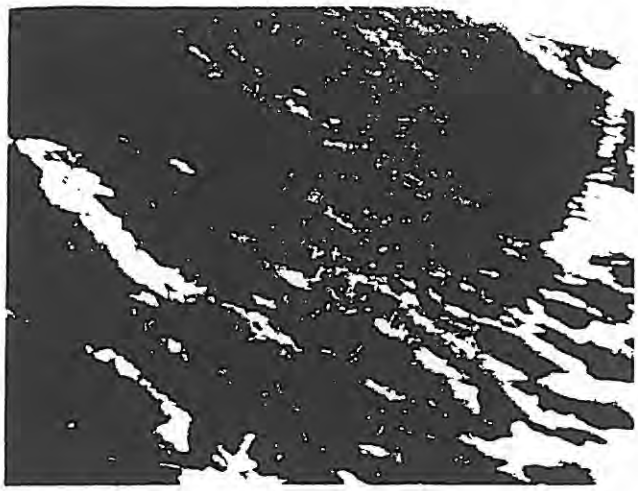

FIGURE 9 Maryland Route 410 project photo.

Project Name: Pennsylvania Turnpike-PTC 6902-86-628

- *Specifying agency/owner*: Pennsylvania Turnpike Authority
- *Designer*: Baker Engineers
- *Slope heights*: 13 ft reinforced; 35 ft total height
- *Slope angle (H:V)*: 1:1 on upper reinforced slope; maximum 1.5:1 on unreinforced slope below
- *Facing system*: geogrid wrap with vegetation
- *Reinforcement type*: TENSAR UX 1600, UX 1400, BX 1100 geogrids
- *Alternative*: retaining wall
- *Construction date*: Summer 1988

The Pennsylvania Turnpike Authority began widening the existing 50-year-old turnpike along the exterior lanes. On this project a geogrid-reinforced slope was used in existing fill sections to add a 10-ft-wide paved shoulder (as shown in Figure 10). A 1 : 1 backcut was used in construction, which allowed traffic to be maintained on the existing traffic lanes.

The reinforced slope option provided an estimated 25 percent cost savings over retaining walls and even a greater savings over a conventional slope. Soil borings from the original construction 50 years ago and performance of existing slopes were used to select soil parameters. This method of road widening has now become a standard procedure with the Pennsylvania Turnpike Authority.

CONCLUSIONS

1. Geogrid-reinforced slopes have broad applicability to highway construction and are (a) an economic alternative to conventional grade separation construction methods; (b) used to build steepened slopes, provide surficial reinforcement, build compound slopes for road widening, repair landslides, construct embankments over soft foundations, and build retaining walls; and (c) a proven method of construction used by a variety of transportation agencies and major design consultants.
2. Steepened slopes can cost up to 50 percent less than retaining walls.
3. Steepened, reinforced highway slopes may be specified as (a) packaged systems, where lines and grades are presented in the bid package and materials, design, and technical assistance are supplied by a single source or (b) designed in-house with the reinforced material a specified item.
4. Geogrid-reinforcement elements should be specified with consideration of installation damage, long-term soil inter-

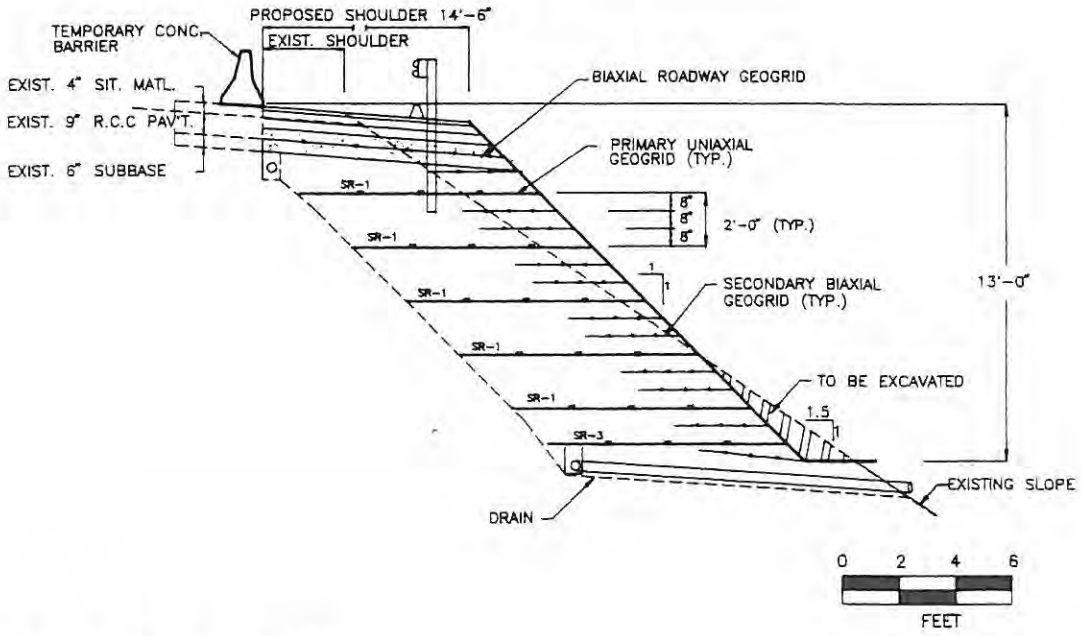

FIGURE 10 Pennsylvania Turnpike cross section.

action characteristics, long-term creep, and chemical and biological degradation potential over the design life of the structure.

5. Steepened, reinforcement slopes may be specified as an alternative grade separation method to retaining walls or flat slopes or both.

REFERENCES

1. F. B. Mercer. *Critical Aspects of Industrial and Academic Collaboration*. Netlon, Ltd., Blackburn, England, 1986.
2. R. Bonaparte, R. D. Holtz, and J. P. Giroud. Soil Reinforcement Design Using Geotextiles and Geogrids. In *Geotextile Testing and the Design Engineer*, ASTM STP 952 (J. E. Fluet, Jr. ed.), American Society for Testing and Materials, Philadelphia, Pa., 1987, pp. 69–116.
3. *Design Guidelines for Use of Extensible Reinforcements (Geosynthetic) for Mechanically Stabilized Earth Walls in Permanent Applications*, Part 2, Draft, Task Force 27, AASHTO-AGC-ARTBA Joint Committee, Feb. 1989.
4. *Determination of the Long-Term Design Strength of Geogrids*. Draft, Geosynthetic Research Institute, GRI Test Method GG4 Drexel University, Philadelphia, Pa., Nov. 1989.
5. R. Bonaparte and R. R. Berg. Long-Term Allowable Tension for Geosynthetic Reinforcement. *Proc., Geosynthetics '87*, Vol. 1, New Orleans, La., Feb. 1987, pp. 181–192.
6. R. A. Jewell and J. H. Greenwood. Long-Term Strength and Safety in Steep Soil Slopes Reinforced by Polymer Materials. *Geotextiles and Geomembranes*, Vol. 7, No. 1 and 2, 1988, pp. 81–118.
7. N. E. Wrigley. The Durability and Aging of Geogrids. *Proc., Durability and Aging of Geosynthetics*, Geosynthetic Research Institute, Drexel University, Philadelphia, Pa., Dec. 1988.
8. R. T. Murray and A. McGown. Assessment of the Time Dependent Behavior of Geotextiles for Reinforced Soil Applications. In *Durability of Geotextiles*, Chapman and Hall, New York, 1988, pp. 52–73.
9. R. A. Jewell, N. Paine, and R. I. Woods. Design Methods for Steep Reinforced Embankments. *Proc., Conference on Polymer Grid Reinforcement*, Thomas Telford, London, March 1984, pp. 70–81.
10. *Slope Reinforcement with TENSAR Geogrids: Design and Construction Guideline*. Tensar Technical Note SR1, Tensar Corporation, Morrow, Ga., May 1986.
11. G. R. Schmertmann, R. Bonaparte, V. C. Chouery, and R. J. Johnson. Design Charts for Geogrid Reinforced Slopes. *Proc., Geosynthetics '87*, Vol. 1, New Orleans, La., Feb. 1987, pp. 108–120.
12. B. R. Christopher and R. D. Holtz. *Geotextile Engineering Manual, Course Text*. FHWA, U.S. Department of Transportation, 1985.
13. J. M. Duncan and K. S. Wong. *STABGM: A Computer Program for Slope Stability Analysis With Circular Slip Surfaces and Geogrid Reinforcement: Users Manual*. Virginia Polytechnic Institute and State University, Blacksburg, Va., Dec. 1984.
14. R. B. Berg, V. E. Chouery-Curtis, and C. H. Watson. Critical Failure Planes in Analysis of Reinforced Slopes. *Proc., Geosynthetics '89*, Vol. 1, San Diego, Ca., Feb. 1989, pp. 269–278.

Publication of this paper sponsored by Committee on Geosynthetics.

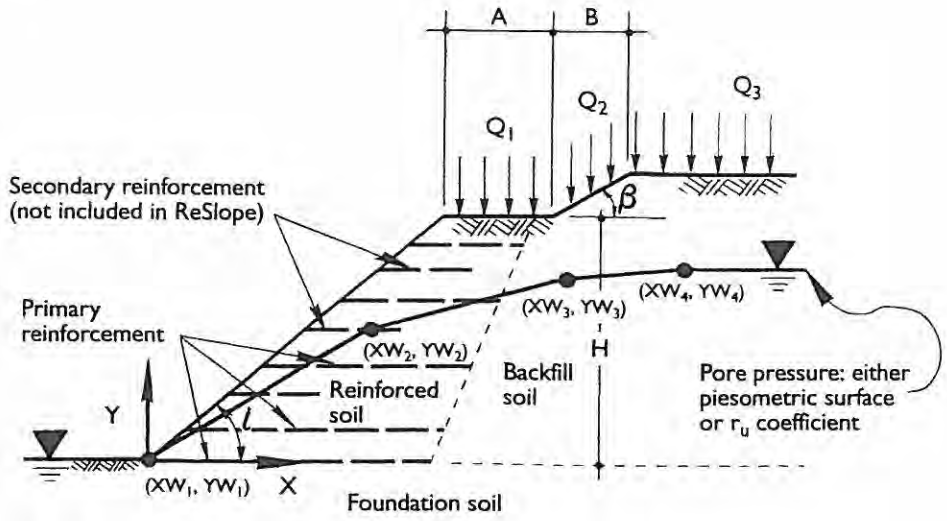

Figure 1. Notation in ReSlope

Software to facilitate design of geosynthetic-reinforced steep slopes

For a given problem, including the ultimate strength of the reinforcement layers, ReSlope yields the optimal length and spacing of the geosynthetics.

By Dov Leshchinsky

SOIL IS AN ABUNDANT CONSTRUCTION MATerial that, similar to concrete, has high compressive strength but virtually no tensile strength. To overcome this weakness, soils, like concrete, may be reinforced.

The materials typically used to reinforce soil are relatively light and flexible, and, though extensible, possess a high tensile strength. Examples of such materials include thin steel strips and polymer sheets commonly known as geosynthetics (i.e., geotextiles and geogrids). When soils and reinforcement are combined, a composite material, "reinforced soil," possessing high compressive and tensile strength (and similar, in principle, to reinforced concrete) is produced. This combined high strength is primarily attributed to the frictional and adhesion interaction between the soil and the reinforcement.

The increase in strength of the reinforced soil structure allows for the construction of steep slopes. Compared with other alternatives, polymer-reinforced soil slopes are cost-effective. Consequently, various earth structures reinforced with geosynthetics are increasingly being constructed worldwide, even in permanent and critical applications (Tatsuoka and Leshchinsky, 1994).

This article describes the various stability analyses associated with the design of geosynthetic-reinforced steep slopes. To facilitate design, these analyses were compiled into a computer program called ReSlope. For a given problem, including the ultimate strength of the reinforcement layers, the software yields the optimal length and spacing of the geosynthetics. This layout satisfies the specified various factors of safety input by the user. Comparisons with case histories, as well as further analytical details, appear elsewhere (Leshchinsky, et al., 1995; Ling, et al.,1996). The original procedure was developed for the U.S. Army Corps of Engineers (Leshchinsky, 1995).

Analysis used in ReSlope

Limit equilibrium (LE) analysis has been used for decades in the design of earth slopes. Attractive features of LE analysis include the experience of practitioners with its application, simple input data, useful (though limited) output design information, and results that can be checked for 'reasonableness' through a different LE analysis method, charts or hand calculations. Due to the simplicity of LE analysis, modeling of reinforcement is tangible; i.e., a tensile force resisting failure. Consequently, extension of LE analysis to the design of geosynthetic-reinforced steep slopes is desirable.

The main drawback of LE analysis is its inability to deal directly with displacements and the potential incompatibility between the soil and the reinforcement. Adequate selection of materials properties and safety factors, however, should

assure acceptable displacements, including a safe level of reinforcement deformation.

The need to know the force in each reinforcement layer at the limit state is a problem in LE analysis of reinforced soil. Physically, this force may vary between zero and ultimate strength when the slope is at a global-limiting equilibrium state. Assuming the actual force is known in advance, as is typically done in *analysis-oriented* computer programs, implies that the reinforcement force is actually an *active* one, regardless of the problem. The designer then assumes the active force of each reinforcement layer so that, overall, a limit equilibrium state is attained. The end result may be an actual reinforced slope in which some layers provide more force than their allowable strength, while other layers are hardly stressed; i.e., tensile-force distribution that satisfies overall equilibrium but is different than the assumed active value.

To overcome this potential problem, a rational methodology to estimate the required (i.e., *reactive*) reinforcement tensile resistance of each layer is introduced via "local stability analysis" or "tieback analysis." Consequently, the designer can verify whether an individual layer is over- or under-stressed—regardless of the overall stability of the slope. Once this problem of 'local stability' is resolved, overall stability of the slope is assessed through rotational and translational mechanisms.

In the rotational mechanism ("pullout failure" or "compound failure"), slip surfaces extending beyond the reinforced soil are examined. The force in the reinforcement layers in this conventional slope stability analysis is taken directly as their allowable value. The translational analysis ("direct sliding") is based on the two-part wedge method in which the passive wedge is sliding over or below any reinforcement layer, or along the interface with the foundation soil. The following is a brief presentation of the various analyses producing a safe layout of reinforcement so as to resist the three potential modes of failure: rupture of the reinforcement, pullout and direct sliding.

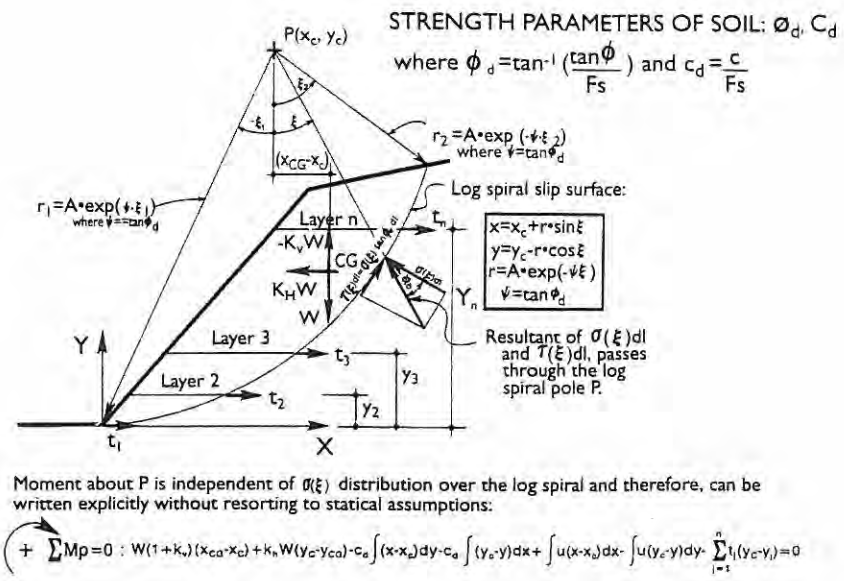

Moment about P is independent of $\sigma(\xi)$ distribution over the log spiral and therefore, can be written explicitly without resorting to statical assumptions:

$$+\circlearrowleft \sum Mp = 0 : W(1+k_v)(x_{cg}-x_c) + k_h W(y_c-y_{cg}) - c_a \int (x-x_a)dy - c_a \int (y_a-y)dx + \int u(x-x_a)dx - \int u(y_c-y)dy - \sum_{i=1}^{n} \tau_i (y_c-y_i) = 0$$

Figure 2. Log spiral slip surface: statical implications

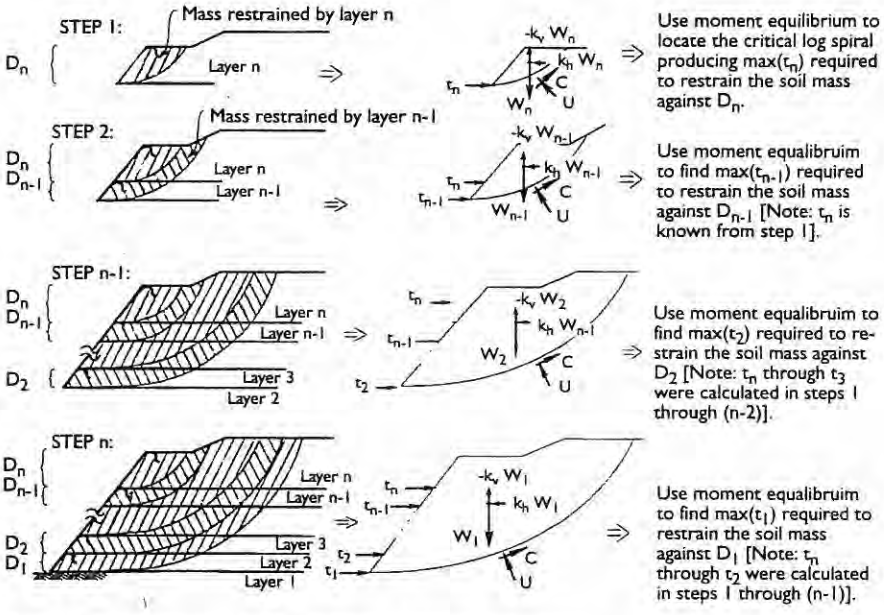

Figure 3. Tensile reaction in reinforcement: computation scheme

Internal stability

Internal stability (also called "local stability analysis" or "tieback analysis") is used to determine the required tensile resistance of each layer needed to assure a reinforced mass that is safe against internal collapse due to its own weight and surcharge. This analysis seeks the reactive tensile force needed to restrain the steep slope from failing at any elevation along its height. The reinforcement tensile force capacity is calculated based on a tied back wedge mechanism in which sufficient anchorage of each layer into the stable soil zone is provided.

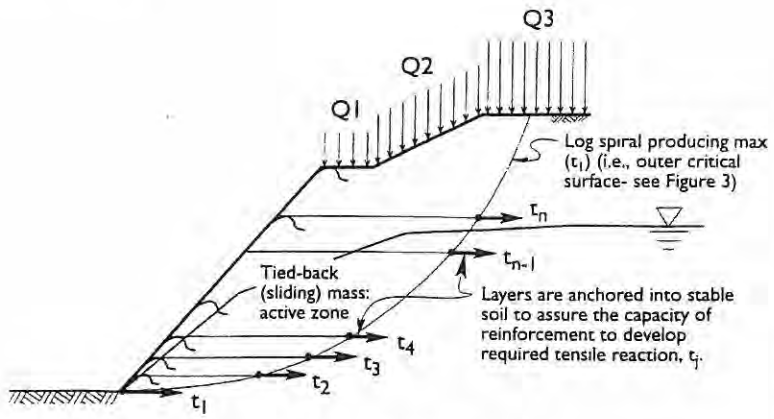

Figure 4. Transfer of tensile reaction into soil adjacent to active zone

GENERAL: In LE analysis one must assure that for all possible slip surfaces, the following F_s is exceeded:

$$\min(F_s) = F_s(\text{design}) = \frac{\tan(\varnothing_{available})}{\tan(\varnothing_{design})} = \frac{C_{available}}{C_{design}}$$

NOTE: $\varnothing_{design} = \varnothing_{mobilized}$, $C_{design} = C_{mobilized}$

STEP 1: Find m so that $\sum_{j=1}^{m} (t_{allowable})j \geq \sum_{j=1}^{n} t_j$

Where m = minimum number of layers, counting from bottom layer #1, capable of developing total tensile resistance equal to the total force, for all reinforcement layers, as obtained from tieback analysis.

STEP 2: Conduct stability analysis according to the following scheme:

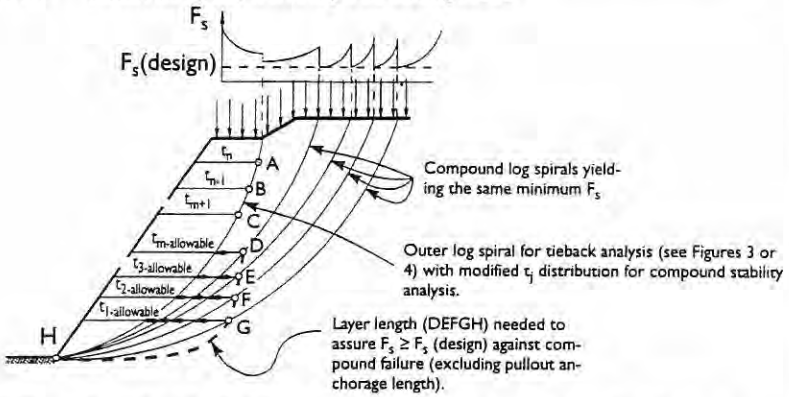

STEP 3: Repeat Step 3 for slip surface emerging at Layer 2, then Layer 3 and so on. Up to Layer n.
STEP 4: The longest length (including anchorage) from Steps 2 and 3 is selected for design, assuring adequate resistance to both tieback and compound failures.

Figure 5. Reinforcement length required to assure compound stability

Figure 1 shows the notation and convention used here and in ReSlope. Reinforcement is comprised of primary and secondary layers. In analysis, however, only the primary layers are considered. At the slope face, layers may be wrapped around or, if some cohesion exists, layers may terminate straight, as shown in Figure 1. The crest is subjected to three different surcharge loads. Pore water pressure can be included through the r_u coefficient or a piezometric surface. Piezometric surface is defined by four nodes, starting at the origin of the coordinate system (i.e., the toe). Each of the soils (i.e., reinforced soil, backfill soil and foundation soil) may possess different shear strength properties.

By definition, steep slopes are inclined at such an angle that they are considered unstable without reinforcement. For example, with granular backfill, a slope would be considered steep if its inclination is steeper than its angle of repose (i.e., $i > \phi_d$ where i and ϕ_d are the slope inclination and angle of repose, or design friction angle, respectively). Consequently, in steep slopes the reactive force in each layer has to contribute to the restoration of an LE state at any elevation. To determine the location of the unstable mass and, subsequently, the necessary reactive force, a log spiral failure mechanism has been selected. This mechanism is frequently used in geotechnical stability problems.

For any assumed log spiral, fully defined by three parameters (e.g., x_c, y_c and A, as **Figure 2** shows, see page 41), the moment equilibrium equation about the pole can be written explicitly without resorting to statical assumptions. Consequently, by comparing the driving and resisting moments, one can check whether the mass defined by an assumed log spiral is stable for the design values of the shear strength parameters: ϕ_d and c_d and the distribution of reinforcement force t_j. This check is repeated for other traces of log spirals until the least stable system is found; i.e., the critical slip surface and the associated maximum required restoring reinforcement force are found.

Note in Figure 2 the terms k_h and k_v are the horizontal and vertical seismic coefficients, respectively, introducing pseudostatic force components. They act at the center of gravity of the critical mass. For clarity of presentation, surcharge is not shown in Figure 2; however, it's straightforward to include surcharge effects in the moment equilibrium equation. In this case, k_h and k_v also multiply the surcharge load, rendering horizontal and vertical pseudostatic forces at the crest, where the surcharge acts.

Figure 3 (page 41) illustrates the computation scheme for estimating the tensile reaction in each reinforcement layer. In Step 1, the soil mass acting against D_n is considered. Note that D_n is signified by a reinforcement layer wrapped around the slope face, thus making it physically feasible for a mass of soil to be supported laterally, resulting in a locally stable mass. That is, D_n is considered as a 'facing unit' allowing for tensile force to be transferred directly into the reinforcement layer from the unstable soil above.

The moment equilibrium equation is used to find the critical log spiral producing $max(t_n)$ employing the free-body diagram shown in Figure 3 while examining many potential surfaces. The resulted t_n counterbalances the horizontal pressure against D_n and thus, signifies the reactive force in layer n. That is, the resulted t_n represents the force needed to restore limit equilibrium and hence stability at elevation n. Note that

D_n was chosen to extend down to layer n. This tributary area implies a 'toe' failure that activates the largest possible reaction force.

In Step 2, the force against D_{n-1} is calculated. D_{n-1} extends from layer n to layer $(n-1)$. Using the moment equilibrium equation, the force $max(t_{n-1})$, required to retain the pressure exerted by the unstable soil mass against D_{n-1}, is sought. When calculating t_{n-1}, the reaction t_n, determined in Step 1, is known in magnitude and point of action. Hence, the reactive force in layer $(n-1)$ is the only unknown to be determined from the moment equilibrium equation.

Figure 3 shows that, by repeating this process, the distribution of *reactive* forces for all reinforcing layers, down to t_1, are calculated while supplying the demand for an LE state at each reinforcement level. Application of appropriate partial safety factors should assure long-term geosynthetic performance at each level.

The outermost critical log spiral defines the extreme surface as dictated by *Layer 1*. In conventional tieback wedge analysis it indicates the extent of the *active zone;* i.e., it is the boundary between the sliding soil mass and the stable soil. Consequently, reinforcement layers are anchored into the stable soil to assure their capacity to develop the calculated tensile reaction t_j (**Figure 4**).

Note that that in Figures 3 and 4, the reinforcement layers are wrapped around to form the slope face. However, in slopes that are not very steep (say, $i < 45$ *degrees*), there typically is no wrap around at the face of the slope. In this case, load transfer from each unstable soil mass to the respective reinforcement layer is feasible due to a "coherent" mass formed at the face. This mass is formed by soil arching, by a trace of cohesion and closely spaced reinforcement layers. The end result is a soil "plug," in a sense similar to the one developed at the bottom of a driven open-end pile.

It should be pointed out that "closely spaced reinforcement" does not necessarily mean closely spaced *primary* reinforcement layers; simply, this "plug" can be created by the combination of secondary and primary layers interacting with each other to create a coherent mass. Since primary and secondary reinforcement layers typically are spaced approximately every foot (30 cm), and since the secondary layers extend at least about 3 feet (90 cm) into the slope, the contribution of secondary layers to the formation of a *"facing"* should not be ignored.

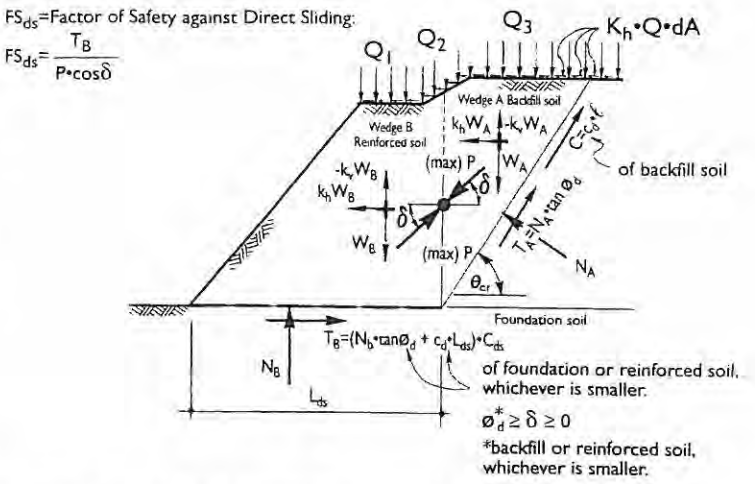

Figure 6. Two-part wedge mechanism for direct sliding analysis

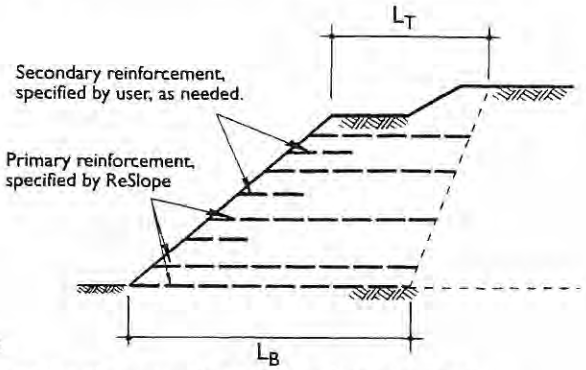

ReSlope options:

(1) $L=L_T=L_B=$ longest length required for tieback analysis, compound failure analysis, and direct sliding analysis.

(2) $L_B =$ same as L in (1)
$L_T =$ longest length required for tieback analysis and compound failure analysis

Figure 7. Reinforcement length specified by ReSlope

With time, surface vegetation and its root mat enhances the effectiveness of this facing. The end result of forming a coherent face (through closely spaced reinforcement and vegetation) is not only an efficient load transfer from unstable deep soil mass to the reinforcement, but also improved surficial stability and erosion resistance.

Pullout or compound stability analysis

For a given geometry, pore-water pressure distribution and (ϕ_d and c_d), the local stability analysis provides the required tensile resistance at the level of each reinforcement layer. It also yields the trace of the outermost log spiral defining the "active" soil zone, a notion commonly used in conjunction with retaining wall analysis. In reinforced soil structures, the capacity of the reinforcement to develop the required tensile resistance depends also on its pullout resistance; i.e., the reinforcement length must be sufficiently anchored into the stable soil zone.

If the boundary of this stable zone is indeed defined by the "active" one, then potential slip surfaces that pass to the right of the outermost log spiral (outside or within the effective anchorage length) will never be critical. However, since such surfaces will render reduced pullout resistance capacity, they may produce an unstable system. Consequently, a conventional slope stability analysis is used to determine the required reinforcement length so that compound failures (or pullout failures) will not be likely to occur.

The tieback analysis results in the required allowable strength of reinforcement at each level. The specified reinforcement, therefore, must possess strength equal to or

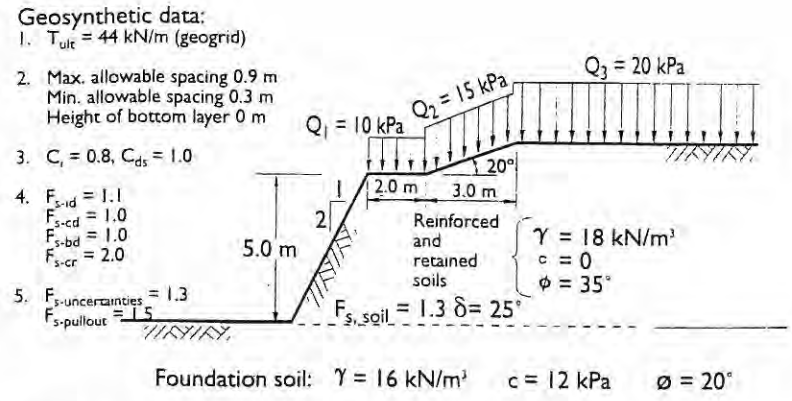

Figure 8: Data for example problem

exceeding this calculated strength. In reality, the allowable strength of most layers will exceed the required value as determined from the tieback analysis. Consequently, if viewed from global stability, only m layers are needed; i.e., reinforcement selected based on tieback analysis may produce more reinforcement than needed for global stability. These bottom m layers may contribute their full allowable strength in the compound analysis where only the aspect of global stability is examined—see Step 1 in **Figure 5.** The upper layers $(m + 1)$ through n are assumed (conservatively) to be capable of contributing only their calculated tieback values.

Embedding the layers immediately to the right of the outermost log spiral obtained in the tieback analysis, so that $t_{allowable}$ for layers 1 through m and t_j for layers $(m + 1)$ through n can develop through pullout resistance, will assure a system that has a factor of safety in excess of $F_{s(design)}$—see Step 2 in Figure 5. Truncating the upper layers $(m + 1)$ through n (points ABC in Figure 5) will decrease the factor of safety. However, since the summation of $t_{(allowable)j}$ for the outermost log spiral equals or exceeds the required overall value, the resulting safety factor is equal to or slightly larger than $F_{s(design)}$. Consequently, these upper layers are sufficiently long.

Following a procedure similar to the one detailed by Leshchinsky (1992), layers 1 through m are lengthened to a test body defined by a log spiral extending between the toe and the crest, deeper than the outermost log spiral. Each layer is embedded beyond the slip surface so that $t_{(allowable)j}$ can develop. F_s will increase as slip surfaces deeper than the critical one are specified. Layer m then is truncated and checked (using the moment equilibrium equation) to see whether F_s has dropped to the minimum design value. If it has, this layer is sufficiently long (see point D in Figure 5); if it is less than the minimum, it is lengthened and calculations are repeated until a satisfactory length is found.

ReSlope repeats this process to determine the required length of layer $(m - 1)$, while considering zero contribution from all layers above since they were already truncated. That is, layers above are not effective for deeper slip surfaces. Subsequently, point E is found. Repeating the process for all layers down to layer 1 yields the length (e.g., curve *DEFGH* in Figure 5) required to assure the minimal value of F_s is met or exceeded for all possible log spiral failure surfaces emerging through the toe.

Compound failure surfaces emerging above the toe are also possible. ReSlope verifies that the length of reinforcement will produce safety factors exceeding $F_{s\,(design)}$ for potential slip surfaces emerging above the toe. As indicated in Step 3 of Figure 5, the scheme shown in Step 2 is repeated for slip surfaces emerging through the slope face. The values of t_j then are taken as determined in Step 2. Subsequently, layers previously truncated will be lengthened, if necessary, to produce a satisfactory safety factor.

Direct sliding analysis

Specifying reinforcement layout that satisfies a prescribed F_s against internal failure does not assure sufficient resistance against direct sliding of the reinforced mass along its interface with the foundation soil or along any reinforcement layer. The length required to assure stability against such failure, L_{ds}, is determined from an LE analysis that satisfies force equilibrium; i.e., the two-part wedge method.

First, an initial value of L_{ds} is assumed (**Figure 6**). Then, a value for δ, the interwedge force inclination, is chosen: δ may be assumed between zero and ϕ_d of the backfill or reinforced soil, whichever is smaller. Subsequently, the maximum value of the interwedge force, P, is found by varying θ while solving the two force equilibrium equations for the active *Wedge A*. This interwedge force signifies the resultant of the lateral earth pressure exerted by the backfill soil on the reinforced soil. Next, the vertical force equilibrium equation for *Wedge B*, which includes the vertical component of the lateral thrust of the active wedge (i.e., $Psin\delta$), is solved. After obtaining N_B, the sliding resisting force, T_B, along the base L_{ds} is calculated.

At this stage, the actual factor of safety against direct sliding of the reinforced mass, $F_{s\text{-}ds}$, can be calculated by comparing the resisting force with the driving force; i.e., $F_{s\text{-}ds} = T_B/Pcos\delta$. This factor of safety corresponds to the assumed value of L_{ds}. ReSlope changes L_{ds}, repeating the process for *Wedge A* and *Wedge B*, until the computed factor of safety against direct sliding equals the prescribed value.

The assumed value of δ may have significant influence on the outcome of the analysis. Selecting $\delta > 0$ implies the backfill soil either will settle relative to the reinforced soil or the reinforced soil will slide slightly as a monolithic block, thus allowing interwedge friction to develop. Since the effects of reinforcement layers—some of which typically will intersect the interwedge interface—are ignored, selecting a value of δ between $(\frac{2}{3})\phi_d$ and ϕ_d should not be viewed as an unconservative choice.

Finally, note that $F_{s\text{-}ds}$ is imposed after reducing the shear strength parameters of the soils by a factor of safety; i.e., using ϕ_d and c_d. In the context of LE slope stability analysis, this constitutes "double taxation." However, in the analysis of reinforced slopes, notions associated with reinforced walls are commonly used, including the value of $F_{s\text{-}ds}$. To be consistent with this practice, ReSlope allows the user to specify $F_{s\text{-}ds}$. For most slopes, its specified value of 1.0 is recommended; however, for a near vertical slope, I recommend using a value of 1.3.

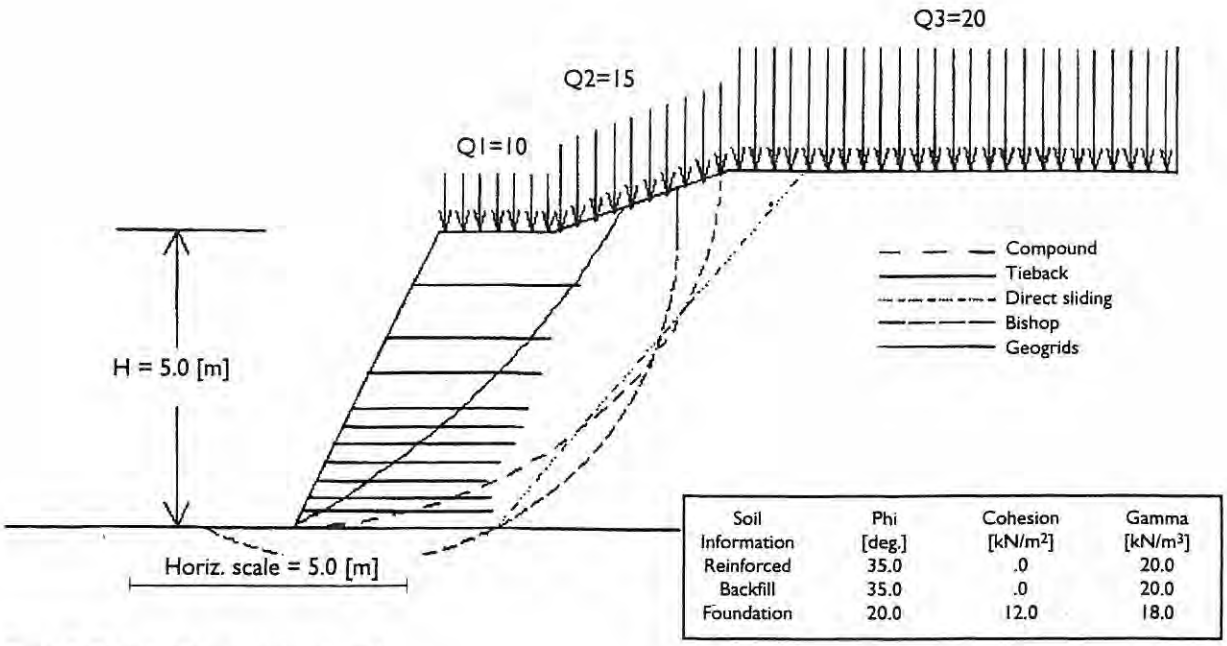

Soil Information	Phi [deg.]	Cohesion [kN/m²]	Gamma [kN/m³]
Reinforced	35.0	.0	20.0
Backfill	35.0	.0	20.0
Foundation	20.0	12.0	18.0

Figure 9. Optimized layout minimum lengths

Deep-seated analysis using Bishop method

ReSlope performs conventional slope stability analysis, using the Bishop method, to assess the minimum factor of safety against deep-seated failure. In a sense, this analysis indicates the bearing capacity of the foundation soil.

The software program examines circular slip surfaces and selects the one rendering the lowest factor of safety. The circles examined, however, are restricted to those passing outside the bottom of the reinforced soil zone. The maximum feasible penetration is set by the user. Circles describing overhanging 'cliffs' are excluded from consideration. In case of a backslope, a tension crack is introduced between the crest and the elevation of the top of the slope. Seismicity is included in the analysis through the coefficients k_v and k_h. That is, I modified Bishop's formulation to include pseudostatic forces due to self weight and surcharge loads.

General guidelines

The supplemental notes accompanying ReSlope provide further details of the analysis described here, along with some limitations. The notes offer guidelines to the selection of the various safety factors used: for the shear strengths of soils, the partial values for each geosynthetic layer, for pullout resistance and against direct sliding. The geosynthetic partial safety factors are consistent with current practice (e.g., Koerner, 1994). Practical information regarding field specifications and contracting is available elsewhere (e.g., Berg, 1992).

Three options for specifying reinforcement length are available in ReSlope (**Figure 7**, page 43, shows two). The first option simplifies construction by specifying that all layers have a uniform length. This length is selected as the longest value obtained from either the tieback analysis, the compound failure analysis, or the direct sliding analysis.

The second safe option is to specify L_B and L_T at the bottom and top, respectively, where L_B is the longest length from all analysis and L_T is the longest length obtained from compound and tieback analysis. Length of layers in between is linearly interpolated. Although this specification is more economical, it may result in misplaced layers at the construction site.

The third safe option is to provide the minimal length of reinforcement so all specified safety factors are met or exceeded. Though this option is not practical for actual field specification, it is extremely instructive. It allows the designer to realize the absolute minimum length of each layer and thus, conduct a design adaptable to local conditions.

Figure 8 shows the details of a given problem. The values of all partial safety factors are marked on this figure. Note that for locating the optimal height of the geogrid layers, the minimum allowable spacing (i.e., minimum thickness of soil layer lift) was specified as 0.3 m; the maximum allowable spacing was specified as 0.9 m (i.e., three lifts of soil layers). Using the data in Figure 8, ReSlope yielded the layout shown in **Figure 9.** Note that this layout shows the minimum required length at each elevation. One can see that the top two geogrid layers correspond to tied back mode of failure; the next six layers underneath correspond to compound failure; and the lower three layers correspond to direct sliding. Hence, this example demonstrates a case where each of the three modes of failure are critical at different elevations. Other options are available using the program and will be demonstrated at Geosynthetics '97. ReSlope will

Curtis "Sure-Grip" Is One Company With An Impressive Grip On Geosynthetics

For Precision Testing of Geosynthetics

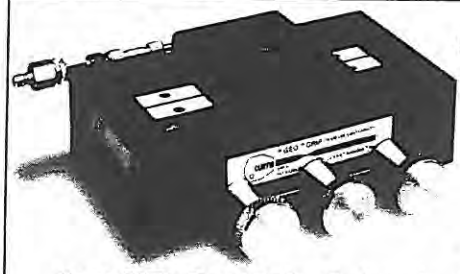

Some of the Most Stubborn Materials on Earth are Clenched Tightest with a Curtis Geo Grip

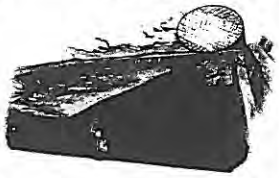

Some Of The Finest Testing Equipment On Earth Is Outfitted With A Curtis Geo Grip

For years now, Curtis engineers have worked with civil engineers across the nation in the testing of geosynthetics. Our experience and expertise in the gripping of geosynthetics have enabled us to engineer grips that not only attain the tightest grip, but help meet budget restraints, ASTM test standards and EPA standards. The Curtis Geo Grip was designed and patented exclusively for testing geosynthetic materials. Call today for our complete product brochure. Get a grip from Curtis!

CURTIS

Curtis "Sure-Grip" Inc.

West Hills Industrial Park
R.D. #8, Box 48C ◆ Kittanning, PA 16201
Phone: (412) 545-8333 ◆ Fax: (412) 545-8334

Document #3037

GSI

When your containment job demands strength, reliability, flexibility and cost efficient installation...
...GSI measures up!

For Fast Service, Specifications or Estimates, Call Toll Free
0/444-5523

Geo-Synthetics, Inc.
428 N. Pewaukee Road
Waukesha, WI 53188

GSI

Document #3050

RESLOPE

be available at the conference and through the IFAI Bookstore (see details in the IFAI Bookstore catalog that was sent with this magazine). GFR

About the author Dov Leshchinsky is a professor at the University of Delaware, Department of Civil Engineering, Newark, Del.

References

Berg, R.R. (1992) "Guidelines for Design, Specification and Contracting of Geosynthetic Mechanically Stabilized Earth Slopes on Firm Foundations," U.S. Department of Transportation, Federal Highway Administration. Publication No. FHWA-SA-93-025, 88 p.

Edris, E.V., Jr. and Wright, S.G. (1992) "User's Guide: UTEXAS3 Slope Stability Package." Vol. IV: User's Manual, Instruction Report GL-87-1, Waterways Experiment Station, U.S. Army Corps of Engineers, Vicksburg, Miss.

Edris, E.V., Jr., Munger, D. F. and Brown, R.A. (1992) "User's Guide: UTEXAS3 Slope-Stability Package," Vol. III: Example Problems, Instruction Report GI-87-1, Waterways Experiment Station, U.S. Army Corps of Engineers, Vicksburg, Miss.

Koerner, R.M. (1994) Designing with Geosynthetics, Third Edition, Prentice Hall Inc., Englewood Cliffs, N.J., 783 p.

Leshchinsky, D. (1992) "Issues in Geosynthetic-Reinforced Soil," Keynote paper, Proceedings of the International Symposium on Earth Reinforcement, Nov. 1992, Kyushu, Japan, Editors: Ochiai, Hayashi and Otani, Balkema, pp. 871–897.

Leshchinsky, D. (1995) "Design Procedure for Geosynthetic-Reinforced Steep Slopes," Technical Report REMR-GT-120 (Temporary No.), Waterways Experiment Station, U.S. Army Corps of Engineers, Vicksburg, Miss.

Leshchinsky, D. and Boedeker, R.H. (1989) "Geosynthetic-Reinforced Earth Structures," Journal of Geotechnical Engineering, American Society of Civil Engineers, Vol. 115, No. 10, pp. 1459–1478.

Leshchinsky, D., Ling, H. and Hanks, G. (1995), "Unified Design Approach to Geosynthetic-Reinforced Slopes and Segmental Walls," Geosynthetics International, Industrial Fabrics Association International, St. Paul, Minn., Vol. 2, No. 5, pp. 845–881.

Ling, H., Leshchinsky, D. and Perry, E.B. (1996), "Seismic Design and Performance of Geosynthetic-Reinforced Soil Structures," Geotechnique, at press.

Tatsuoka, F. and Leshchinsky, D., Ed. (1994) "Recent Case Histories of Permanent Geosynthetic-Reinforced Soil Retaining Walls," Proceedings of Seiken Symposium, November, 1992, Tokyo, Japan, Balkema, 349 p.

Physical Effects of Vegetation

Modification of
Surface Water Regimes
and
Soil Properties

by

Peter J. Bosscher

Associate Professor of Civil
and Environmental Engineering

Role of Vegetation

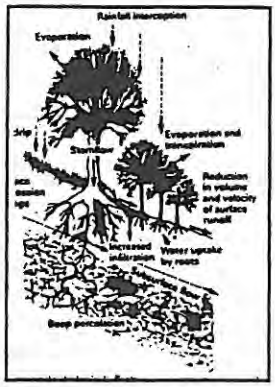

1. Hydrological Effects

2. Mechanical Effects

Modification of Surface Water Regime

- Vegetation intercepts much of the rainfall and emits the water as stemflow or leaf-drip. Some storage of the water may also occur.
- Vegetation reduces the amount of surface runoff by:
    1) increasing the roughness of the ground surface (decreases the runoff velocity and permits more infiltration),
    2) increasing infiltration rate of soil with roots, holes where roots have decayed, reduced soil density (increased porosity),
    3) storing intercepted water (permits more infiltration)
- Vegetation increases lateral drainage (from superficial litter and lateral root mats.

Hydrograph of Various Soil Covers

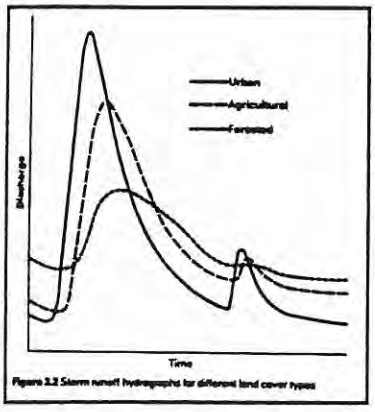

Infiltration of Various Soil Covers

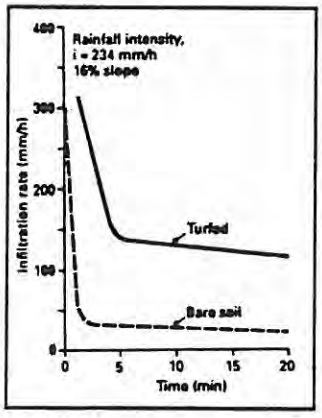

Surface Protection

- The roots of vegetation are very effective at holding soil particles together, preventing detachment and particle transport.
- The canopy of the vegetation intercepts rainfall, reducing its impact velocity. Since the erosion potential of raindrops is a function of the rainfall energy or momentum (related to velocity), the canopy reduces the erosive potential of rainfall.
- Different vegetation types produce different levels of protection from soil detachment. With grasses or low shrubs, the soil loss decreases dramatically with increasing percentage cover. For tall vegetation (> 0.5m) the soil loss decreases with percentage cover but not as dramatically.
- Vegetation litter (dead plant remains) also protects soil from raindrop impact. It also promotes the activity of burrowing insects and animals.

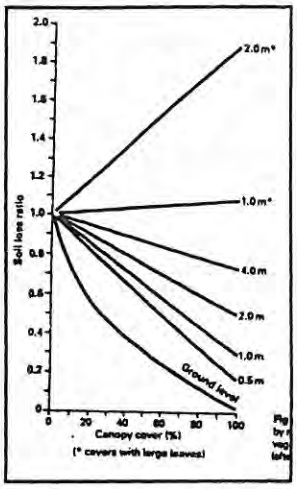

Surface Water Erosion

- Vegetation provides some protection of soil from surface water erosion by retarding the runoff volume and velocity and by physically protecting the soil surface from flowing water.
- Dense uniform vegetation is better than sparse tussocky grasses:
  1) limits channelized flow
  2) reduced flow velocity permits trapping of detached soil (sediment)
- Vegetation in flow channels reduces soil detachment by:
  1) lowering flow velocities near soil surface, and
  2) providing mechanical protection from flattened plant layer.

Mechanical Role

- Vegetation protects the soil mechanically by directly absorbing the impact of human and animal feet and the wheels of vehicles. Relatively little quantitative information is available therefore most recommendations are largely empirically based.
- Vegetation cover insulates the ground reducing variations in soil temperature and moisture. This, in turn, reduces the amount of mechanical and chemical weathering of the soil.
- Relatively large roots of vegetation physically restrain soil particles from moving. The most effective plants for this role are:
  1) resilient
  2) multi-stemmed – with more than one leader
  3) tolerant of burial.

Modification of Soil Water Properties

Evapotranspiration, the removal of moisture from a plant by transpiration, removes great quantities of soil water into the atmosphere.

This in turn depletes soil moisture to a considerable depth and develops large moisture deficits.

Landsliding of steep slopes are strongly correlated with high precipitation and storm activity. Creep movement in slopes is also significantly influenced by precipitation.

The relationship of precipitation to both creep movement and landsliding is due to the relationship of precipitation to the soil moisture and movement of groundwater. The higher or the more prolonged the periods of elevated moisture stress in a slope, the higher will be the creep rates and the greater the danger of landslides.

Soil Moisture Stress in Forested vs. Cutover Slopes

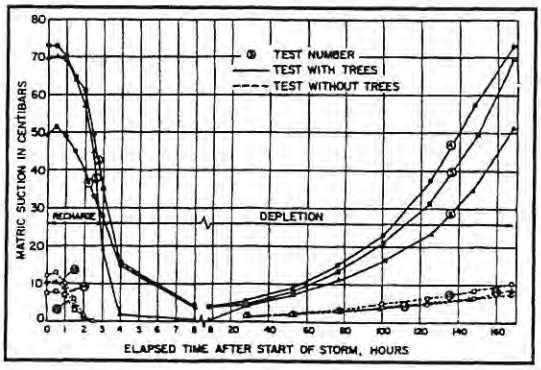

Laboratory Results

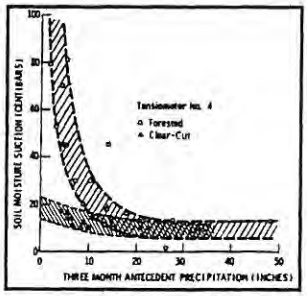

Field Results

Modification of Soil Mechanical Properties

Vegetation modifies the mechanical properties of soil in several ways:

1) Root Reinforcement
2) Anchorage, arching, and buttressing
3) Surface mat effect
4) Surcharge
5) Wind loading
6) Root wedging

Root Reinforcement

- Mechanics of Root Reinforcement
- Theoretical Models of Root-Reinforced Soil
- Root Morphology and Strength
- Root and Fiber Reinforcement Tests
- Root Reinforcement in Sandy, Cohesionless Slopes

Mechanics of Root Reinforcement

A root or fiber reinforced soil behaves as a composite material in which elastic fibers of relatively high tensile strength are embedded in a matrix of relatively plastic soil.

Shear stresses in the soil mobilize tensile resistance in the fibers, which in turn imparts greater strength to the soil.

The net effect of fiber reinforcement on the stress-strain response of soils is to increase the shear strength of the soil. Another important effect is to make some soils tougher (able to resist large deformation without loss of residual strength).

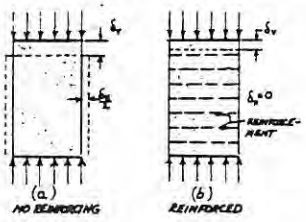

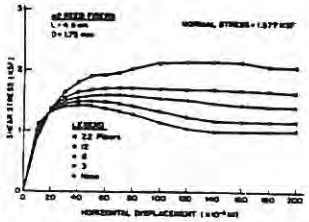

Mechanics (con't)

Two interpretations of increase in shear strength:

- increase in confining pressure in direction of reduced strain
- fibers impart "pseudo-cohesion" to the soil

Increase in Confining Pressure

The fibers anisotropically reduce the strain in the direction of reinforcement. This restraint is equivalent to an increase in confining stress in the direction of the fibers. This equivalent confining stress increase in turn mobilizes additional shear resistance.

The equivalent confining stress increase is essentially proportional to the applied confining stress up to a limit defined as the critical confining stress. At that point the equivalent confining stress levels off, and remains fairly constant with increase applied stress.

The critical confining stress is a function the fiber properties such as strength, modulus, length/diameter, friction, etc.

Mechanics (con't)

Pseudo-Cohesion Concept

This view is theoretically inexact because cohesion is not a directional property whereas the strength increase from fibers is directional. This notion arises from the fact that the friction angle of the soil does not change due to the presence of fibers. The main effect is the upward shift of the failure envelope.

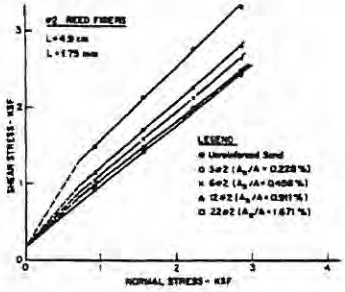

Root Morphology and Strength

Few comprehensive studies of root development, structure, and strength have been done. This figure shows the results of a hydraulic excavation of the root structure of a ponderosa pine.

Generally two nutritional needs dominate root morphology, the need for oxygen (found near ground surface) and the need for water. Some tree species are predisposed by heredity toward development of deep, central sinker roots; others are not. Environmental factors also can effect the root development.

Root Strength

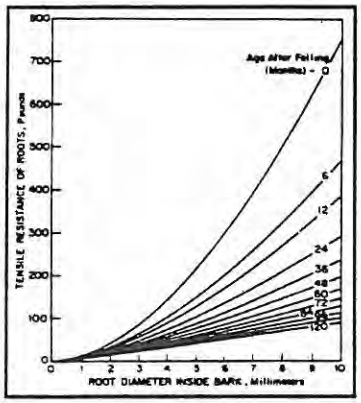

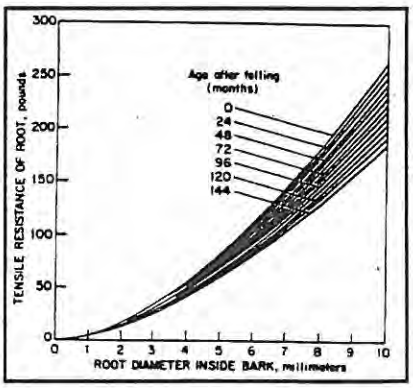

Research showing the decline in root strength with time after cutting. Note the more rapid decline in the Pacific coast vs the Rocky Mountain species.

Root and Fiber Reinforcement Tests

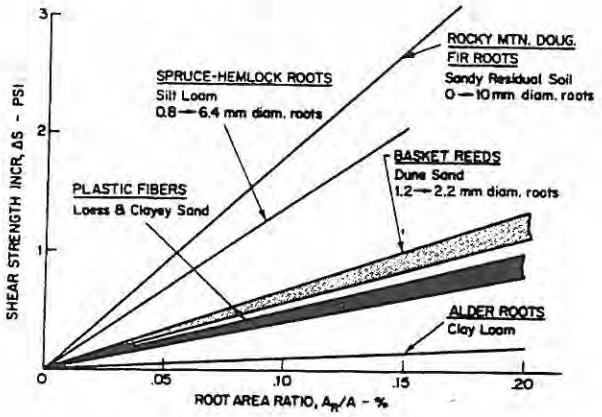

Anchorage, Arching, and Buttressing

If root systems penetrate into deeper soil layers or even weathered bedrock, the trunks and principal roots can act in a similar manner to piles driven into a slope. This has the same action as toothpicks in a layered cake preventing the layers from sliding on the soft frosting in the middle.

The magnitude of the arching effect is influenced by:

1) spacing, diameter and embedment of trees
2) thickness and inclination of the slope
3) shear strength properties of the soil.

Soil Buttressing and Arching

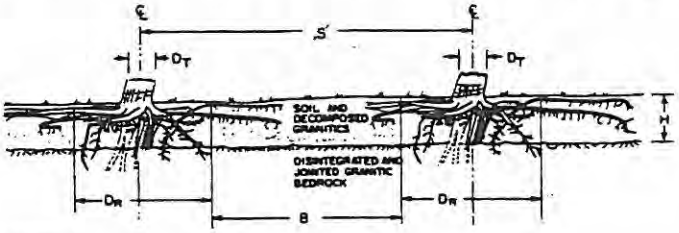

LEGEND

S = Center to center spacing between trees
D_T = Trunk diameter (at breast height)
D_R = Diameter of "vertical root cylinder"
B = Spacing between root cylinders
H = Thickness of soil and decomposed granitic mantle

Scale:
0 1 2 3 4 5 feet

Idealized Model

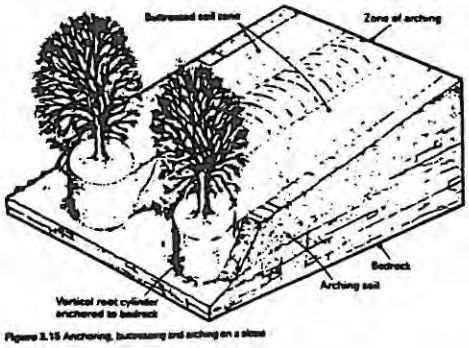

Figure 3.15 Anchoring, buttressing and arching on a slope

Be careful when using the Wang & Yen or Ito and Matsui theories. See attached paper in notes.

Stabilization of Sandy, Cohesionless Slopes

In relatively shallow slopes comprised of cohesionless soils, root reinforcement and buttressing by trees plays a very important role in maintaining stability of the slope.

Surface Mat Effect

A network of intertwined roots at shallow depth form a mat or net having continuity, good anchorage, and a significant degree of in-plane strength, all ow which can make a significant contribution towards reducing soil creep.

Surcharge from Vegetation

Surcharge from the weight of trees is widely believed to have an adverse influence on the stability of slopes. This view is not generally correct; it is only true in special cases.

In some instances surcharge can actually improve stability. A relationship based on a slope stability model indicates that surcharge is beneficial for low cohesion values, high friction, high piezometric levels, and relatively gentle slopes.

Wind Loading

Wind loading is only significant when the wind is stronger than 11 m/s (25 mph). Wind throw or blowdowns can create localized disturbances in the soil mantle. Most of the trees affected in this fashion are the aged or diseased trees. No evaluation on slope stability of the effect of wind blowing through a stand of trees has been done.

Consequences of Vegetation Removal on Slope Stability

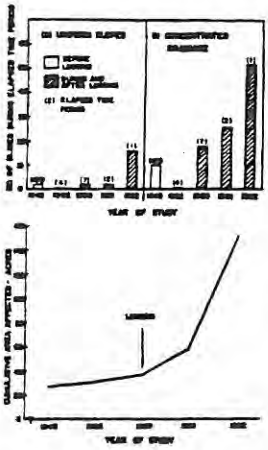

This figure shows the frequency and cumulative area of slides before and after logging in Hollis, Alaska.

Debris-Avalanche Erosion In Forest, Clear-cut, and Roaded Areas

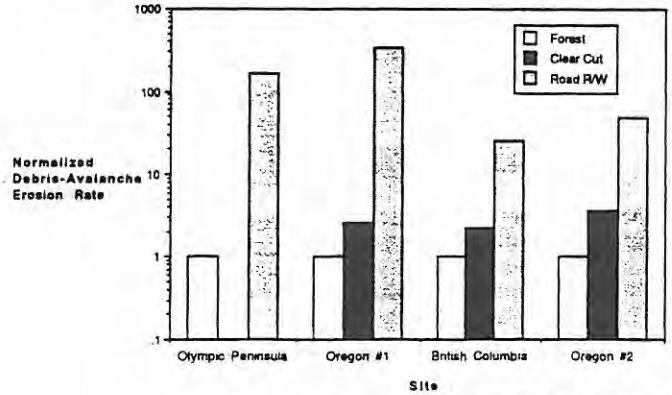

Summary of Hydrological Effects

Foliage intercepts rainfall causing:

1) absorptive and evaporative losses, reducing rainfall available for infiltration B
2) reduction of kinetic energy of raindrops and thus erosivity B
3) increase in drop size through leaf drip, thus increasing localized rainfall intensity A

Stems and leaves interact with flow at the ground surface, resulting in:

1) higher depression storage and higher volume of water for infiltration A/B
2) greater roughness on the flow of air and water, reducing its velocity B
3) tussocky vegetation may give high localized drag, concentrating flow and increasing velocity A

Roots permeate the soil, leading to:

1) opening up of the surface and increasing infiltration A
2) extraction of moisture which is lost to the atmosphere in transpiration, lowering pore-water pressure and increasing soil suction, both increasing soil strength B
3) accentuation of dessication cracks, resulting in higher infiltration A

Summary of Mechanical Effects

Roots bind soil particles and permeate the soil, resulting in:

1) restraint of soil movement reducing erodibility B
2) increase in shear strength through a matrix of tensile fibers B
3) network of surface fibers creates a tensile mat effect, restraining underlying strata B

Roots penetrate deep strata, giving:

1) anchorage into firm strata, bonding soil mantle to stable subsoil or bedrock B
2) support to up-slope soil mantle through buttressing and arching B

Tall growth of trees, so that:

1) weight may surcharge the slope, increasing normal and down-slope force components A/B
2) when exposed to wind, dynamic forces are transmitted into the ground

Stems and leaves cover the ground surface, so that: A

1) impact of traffic is absorbed, protecting soil surface from damage B
2) foliage is flattened in high velocity flows, covering the soil surface and providing protection against erosive flows B

Soil Bioengineering

- Uses:
  - Upland Slope Protection
  - Erosion Reduction
- References:
  - Chapter 18, USDA SCS Engineering Field Handbook
  - TRB paper 950257: "Biotechnical Stabilization of Steepened Slopes" by Gray and Sotir

Overview

- Introduction
- Characteristics of soil bioengineering systems
- Basic principles and design considerations
- Construction techniques and materials

Provides multiple functions and values

Background

- Combines mechanical, biological, and ecological concepts to arrest and prevent shallow slope failures and erosion.
- Two main categories:
  - Living
  - Nonliving

Living Approach

Category	Examples	Appropriate Uses	Role of Vegetation
Vegetative Plantings			
Conventional Plantings	Grass seedlings Transplants Forbs	Control water and wind erosion. Minimize frost effects.	Control weeds. Bind & restrain soil. Filter soil from runoff.
Soil bioengineering			
Woody Plants	Live staking Live fascine Brushlayer Branchpacking Live cribwall Vegetated rockwall	Control of rills & gullies. Control of shallow (translational) slides. Filter sediment.	Same as above, but also reinforce soil, transpire excess water, & minimize downslope movement of earth masses.

Nonliving Approach

Category	Examples	Appropriate Uses	Role of Vegetation
Vegetated structures			
Inert structures with vegetative treatments.	Wall or revetment with slope face planting. Tiered structures with bench planting.	Control erosion on cut & fill slopes subject to scour and undermining.	Stop or prevent erosion & shallow sloughing on or at the slope face above the toe.
Rigid construction (see other texts on Structural solutions)			

Example: Eroding fill slope

Example: Installing measures

Example: 1 Year Later

Applications

- Immediate protection of slopes against:
  - surface erosion
  - shallow mass wasting
  - cut and fill slope stabilization
  - earth embankment protection
  - small gully repair treatment

System Components

- Vegetative components
  - Herbaceous species
  - Woody species
- Structural components
  - Materials
  - Retaining structures
  - Grade stabilization structures

Attributes and Limitations

- Environmental compatibility
- Cost effectiveness
- Planting times
- Difficult sites
- Harvesting local plant material
- Biotechnical strengths
- Maintenance requirements

Basic Principles

- Fit the soil bioengineering system to the site
  - Topography and exposure
  - Geology and soils
  - Hydrology
- Retain existing vegetation whenever possible

Basic Principles

- Limit removal of vegetation
- Stockpile and protect topsoil
- Protect areas exposed during construction
- Divert, drain, or store excess water

Design Considerations

- Earthwork
- Scheduling and timing
- Vegetative damage to inert structures
- Moisture requirements and effects

Construction Techniques

- General considerations
- Soil bioengineering techniques
  - Live stake
  - Live fascine
  - Brushlayer
  - Branchpacking
  - Live gully repair
  - Live cribwall
  - Vegetated rock gabions
  - Vegetated rock wall
  - Joint planting

Live stake

- involves the insertion and tamping of live, rootable vegetative cuttings into the ground.
- Applications and effectiveness
- Construction guidelines
  - Live material preparation
  - Installation

Live stake installation

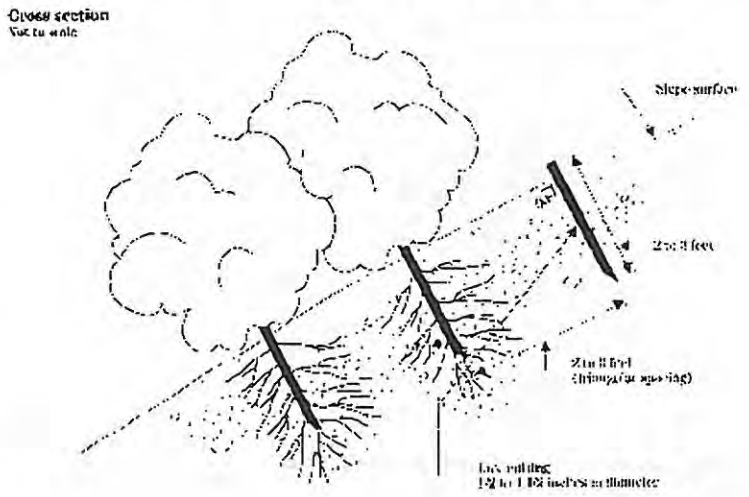

Top growth and root development (7-month old)

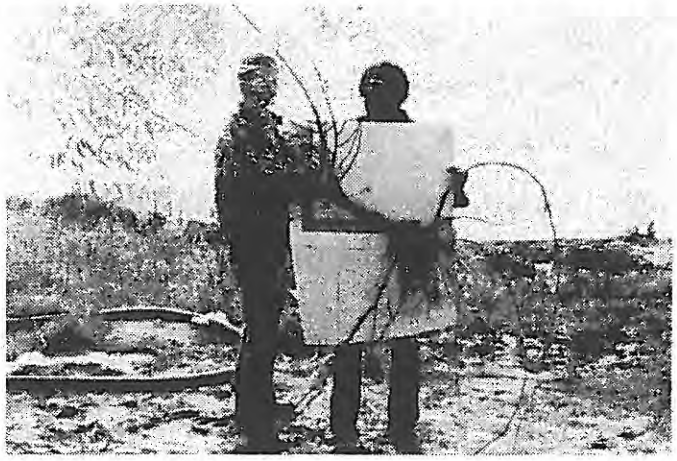

Prepared live stake

A healthy live stake

Live fascine

- long bundles of branch cuttings bound together into sausage-like structures
- Applications and effectiveness
- Construction guidelines
  - Live materials
  - Live material sizes and preparation
  - Inert materials
  - Installation

Live fascine fabrication

Live fascine bundle details

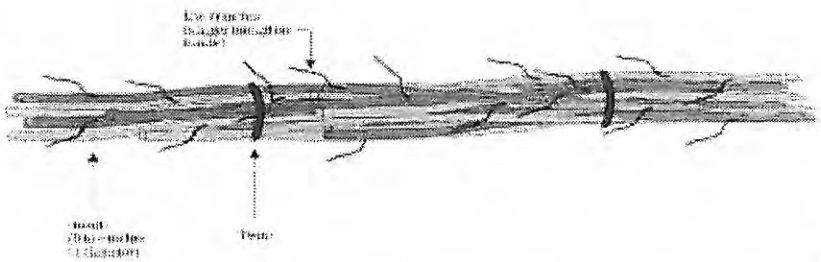

Live fascine installation

Live fascine - 3 months later

Live fascine details

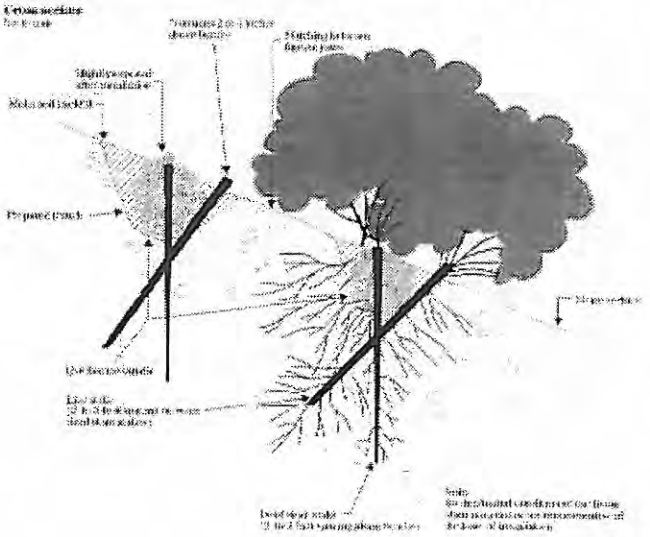

Brushlayer

- similar to live fascine systems; differ principally in orientation and depth of cuttings placement.
- Applications and effectiveness
- Construction guidelines
  - Installation

Brushlayer Details

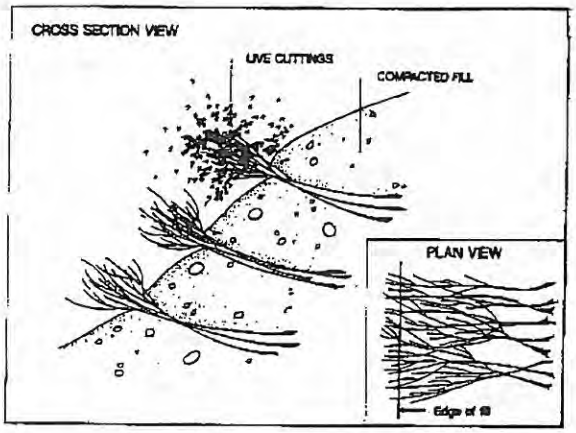

Brushlayer installation

Brushlayer Bench

Brushlayer Branch Placement

Brushlayer - 2 years later

Live cribwall

- consists of a hollow, box-like interlocking arrangement of untreated log or timber members. Filled with suitable backfill and layers of live branch cuttings.
- Applications and effectiveness
- Construction guidelines
  - Live material sizes
  - Inert materials
  - Installation

Live cribwall details

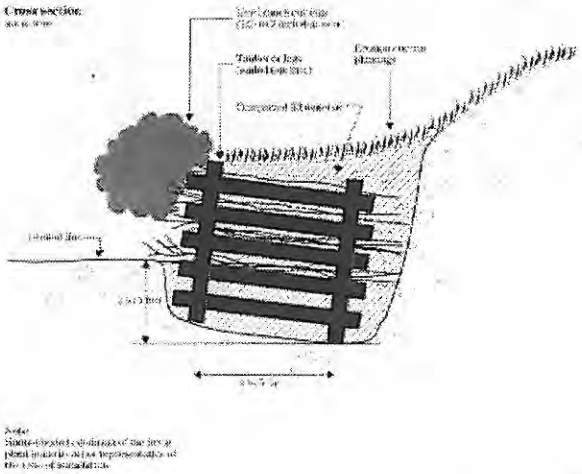

Live cribwall installation

Vegetated rock wall

- combination of rock and live branch cuttings used to stabilize and protect the toe of steep slopes.
- Applications and effectiveness
- Construction guidelines
  - Live material sizes
  - Inert materials
  - Installation

Vegetated rock wall details

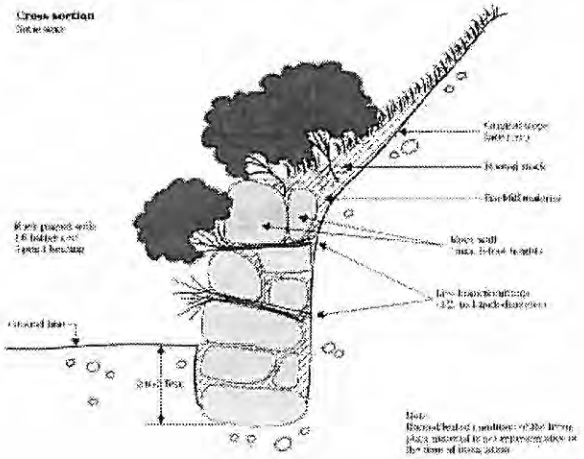

Soil bioengineering materials

- Locating and selecting plant materials
  - Commercial sources
  - Harvesting indigenous species
- Installing plant materials
  - Timing
  - Planting medium
- Quality control
  - Preconstruction
  - Construction

Soil bioengineering materials

- Establishment period
  - Interim inspections
  - Final inspection
- Maintaining the system

Vegetated structures

- Low wall/slope face plantings
- Tiered wall/bench plantings
- Cribwalls with plantings

Low wall with plantings

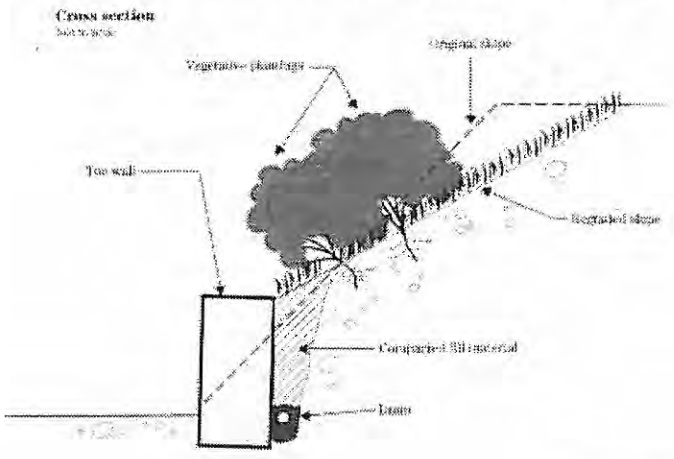

Example of low wall

Open concrete cribwall

Engineering Computations

No Roots

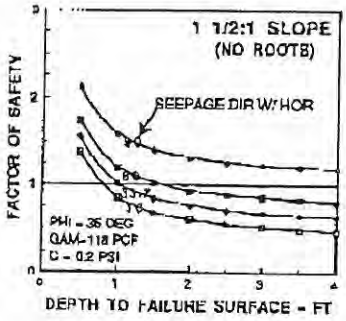

Medium Root Concentration

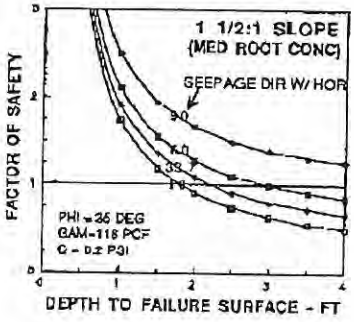

Combined Vegetative-Geosynthetic Systems

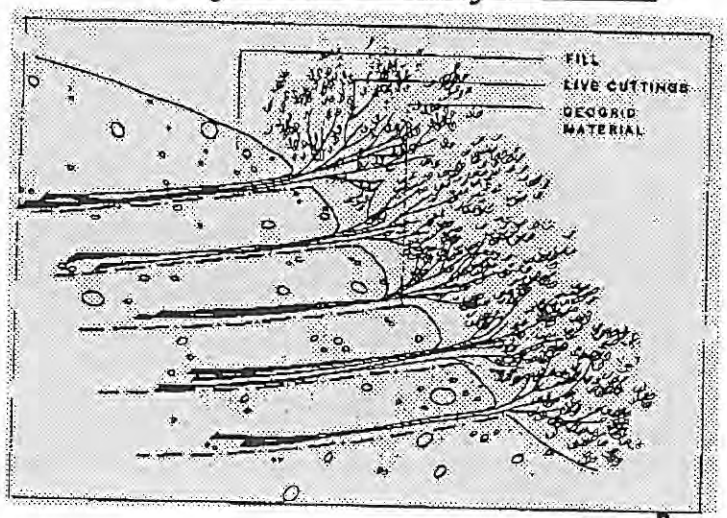

BIOTECHNICAL STABILIZATION OF STEEPENED SLOPES

by

Donald H. Gray[1] and Robbin B. Sotir[2]

ABSTRACT

The use of tensile inclusions makes it possible to repair slope failures or to construct steepened slopes along highway right-of-ways. Live, cut brushlayers can be used in lieu of or in conjunction with synthetic fabrics or polymeric geogrids for this purpose. This approach, which is termed biotechnical stabilization or soil bioengineering, entails the use of living vegetation, primarily cut, woody plant material that is purposely arranged and imbedded in the ground to prevent surficial erosion and to arrest shallow mass movement. In the case of brushlayering the live cut stems and branches provide immediate reinforcement; secondary stabilization occurs as a result of adventitious rooting along the length of buried stems. Unlike most inert reinforcements, imbedded brushlayers also act as horizontal drains and wicks that favorably modify the hydrologic regime in the slope.

The basic principles of biotechnical stabilization are described. Guidelines are presented for analyzing the surficial, internal, and global stability of brushlayer reinforced fills. A case study is reviewed in which live, brushlayer inclusions were used to stabilize steep slopes along a roadway. A brushlayer, buttress fill was used to repair an unstable cut slope along a highway in Massachusetts. Several repair alternatives were considered in this case. Scenic and environmental considerations in combination with stability analyses eventually dictated the use of a composite, drained rock and earthen brushlayer fill. The rock section was placed at the bottom to intercept critical failure surfaces that passed through the toe of the slope. Biotechnical stabilization resulted in a satisfactory and cost effective solution; the treated slope has remained stable and it blends in naturally with its surroundings.

---

1 Professor, Dept. of Civil & Envl. Engr., The *Univ. of Michigan*, Ann Arbor, MI 48109

2 Principal, *Robbin B. Sotir & Associates.*, 434 Villa Rica Road, Marrieta, GA 30064

INTRODUCTION

Reinforced or mechanically stabilized earth (MSE) embankments have been used in highway construction for the past two decades. This approach offers several advantages over more traditional methods of grade separation that employ either vertical walls, on the one hand, or conventional fills with relatively flat slopes (2H:1V or less) on the other. The most prominent use of MSE is probably for widening and reconstruction of existing roads and highways. The use of reinforced steepened slopes to widen roadways improves mass stability, reduces fill requirements, eliminates additional right-of-way, and often speeds construction. Design procedures, advantages, and several case histories of steepened, reinforced highway slopes have been reviewed in detail by Berg et al (1990).

The principal components of reinforced or mechanically stabilized earth embankments are schematically shown in Figure 1. Tensile inclusions (reinforcements) in the fill soil create a structurally stable composite mass. These main tensile elements are referred to as "primary" reinforcement. Shorter, intermediate inclusions may be placed near the slope face. These "secondary" reinforcing elements are used to minimize sloughing or face sliding and to aid in compaction and alignment control. The soil at the outer edge of the slope may also be faced with some kind of netting (e.g., coir or jute) to prevent or minimize soil erosion.

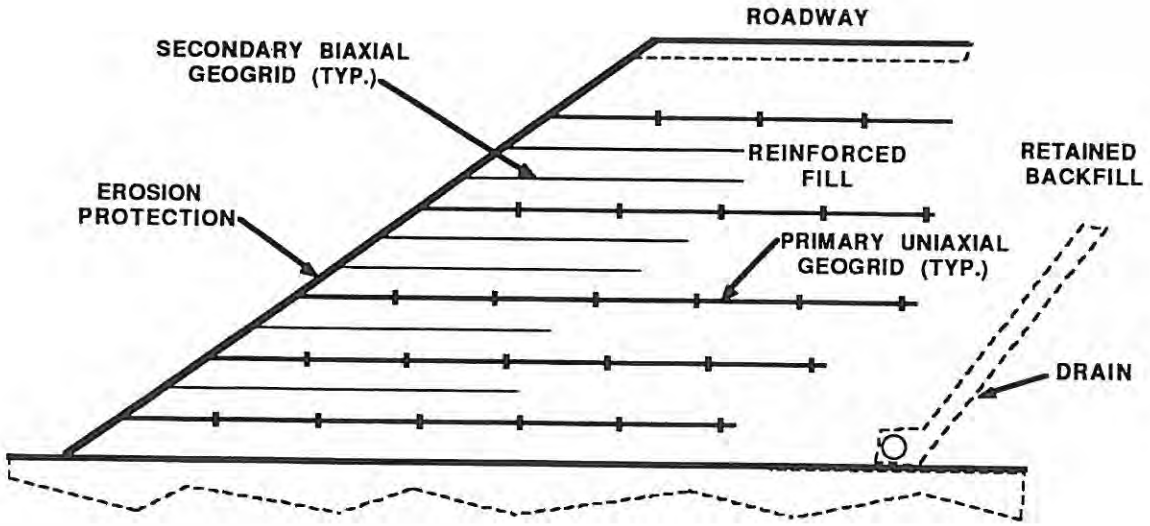

Figure 1. Material and structural components of a typical, reinforced steepened slope (adapted from Berg et al., 1990)

This last component can be eliminated, however, by simply "wrapping" the secondary reinforcement around the slope face of successive lifts or layers of soil as the embankment is raised. Stability considerations also dictate that appropriate external and internal drainage provisions be incorporated in the design.

Metallic strips, geotextiles, and polymer and wire grids have all been used as reinforcing elements in earthen slopes. Higher strength, primary reinforcements are typically used for permanent, critical highway slopes. Lower strength tensile inclusions can be used close to the face as secondary reinforcements. The latter are typically 3 - 6 feet long and are spaced 8 - 36 inches vertically apart as shown in Figure 1. Selection of the appropriate reinforcement depends on the allowable tensile load, deformation, and design life of the structure.

The purpose of this paper is to describe the use of live, cut brushlayers as a supplement or alternative to inert tensile inclusions and to provide some guidelines for the design and installation of brushlayer reinforcements. The live brush can be substituted for the secondary reinforcements or, in some cases, actually replace both secondary and primary reinforcements. Unlike most inert reinforcements, imbedded brushlayers also act as horizontal drains and wicks that favorably modify the hydrologic regime near the face of the slope. This approach which is termed biotechnical stabilization or soil bioengineering, entails the use of living vegetation, primarily cut woody plant material, that is purposely arranged and imbedded in the ground in selected patterns and arrays to prevent surficial erosion and arrest shallow mass movement.

PRINCIPLES OF BIOTECHNICAL STABILIZATION

Live cut brush, woody stems, and roots can be used to create a stable, composite earth mass. The functional value of vegetation in this regard has now been well established (Coppin *et al.*, 1990). *Biotechnical stabilization* refers to the integrated or combined use of living vegetation and inert structural components (Gray and Leiser, 1982). *Soil bioengineering* is a more restrictive term that refers primarily to the use of live plants and plant parts alone (Schiechtl, 1980). Live cuttings and stems are purposely imbedded and arranged in the ground where they serve as soil reinforcements, horizontal drains, barriers to earth movement, and hydraulic pumps or wicks. Live plants and plant parts can be used alone or in conjunction with geotextiles or geogrids. The live cut stems and branches provide immediate reinforcement; secondary stabilization occurs as a result of adventitious rooting that occurs along the length of buried stems. Tech-

niques such as live staking, wattling (fascines), brushlayering, etc. fall into this category. The US Dept. of Agriculture, Soil Conservation Service now includes in its Engineering Field Manual guidelines for the use and installation of these soil bioengineering methods (USDA, 1992).

Brushlayering consists of inserting live, cut branches or brush between successive lifts or layers of compacted soil as shown in Figure 2. This process works best when done in conjunction with the construction of a fill slope. The tips of the branches protrude just beyond the face of the fill where they intercept rainfall, slow runoff and filter sediment out of the slope runoff. The stems of the branches extend back into the slope in much the same manner as conventional, inert reinforcements, e.g., geotextiles and geogrids, and act immediately as tensile inclusions or reinforcements. Unlike conventional reinforcements, however, the brushlayers root along their lengths and also act as horizontal slope drains. This drainage function is very important and can greatly improve mass stability.

Brushlayers alone will suffice to stabilize a slope where the main problem is surficial erosion or shallow face sliding. Sandy slopes with little or no cohesion fall into this category. Deeper seated sliding tends to occur in embankment slopes composed of more fine grained, cohesive soils. This situation may require the use of geogrids in combination with live brushlayers. This latter approaches are illustrated schematically in Figures 3. Guidelines are presented later in the paper for deciding if geogrids must be used in conjunction with live brushlayers.

BIOTECHNICAL STABILIZATION OF HIGHWAY CUT & FILL SLOPES

Biotechnical stabilization has been used successfully to stabilize and repair steep slopes along highways. One of the earliest applications was reported by Kraebel (1936) who used contour wattling to stabilize steep, fill slopes along the Angeles Crest highway in southern California Recent examples of soil bio-engineering solutions for the stabilization of a highway cut slopes are discussed by Gray and Sotir (1992). They also describe the use of brushlayering to repair a high, steep fill slope along a highway in North Carolina (Sotir and Gray, 1989). A earthen brushlayer, buttress fill was used to repair an unstable cut along a scenic highway in Massachusetts as shown in Figures 4 and 5. The cut slope consisted of residual silty sand overlying fractured bedrock. Large amounts of groundwater seeped from fractures in the bedrock and through exposed soil in the cut. Other examples of brushlayer stabilization of a steep, high embankment slope along the Brenner Pass highway in Austria are shown in Figures 6 and 7.

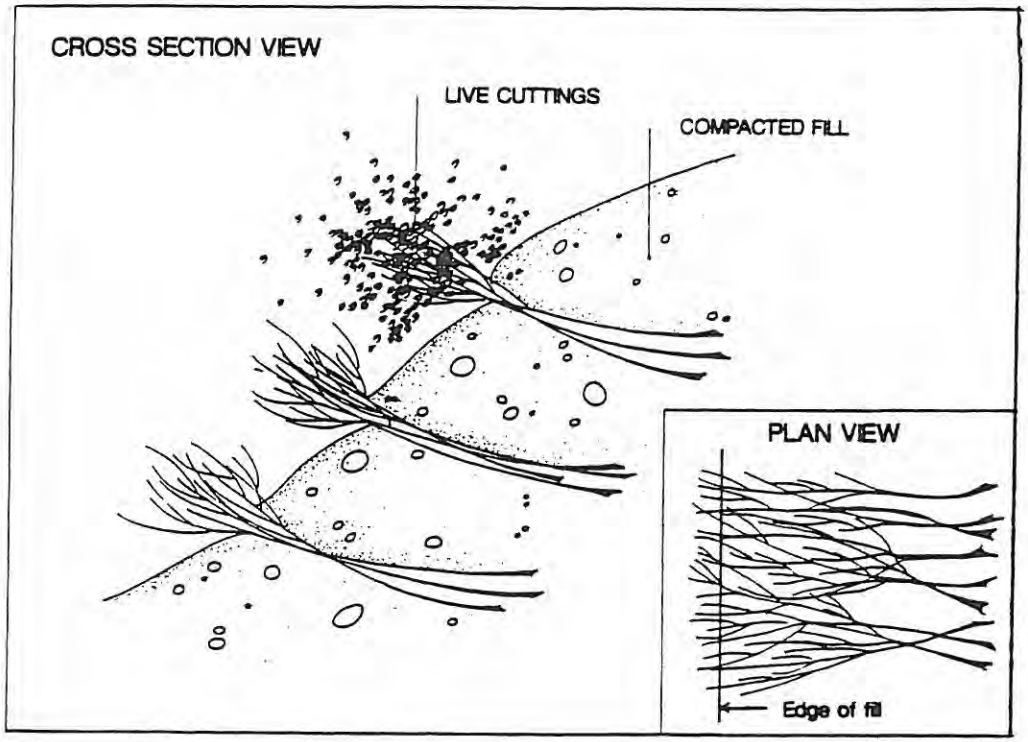

Figure 2. Schematic illustration of fill slope stabilization using live brushlayers place between lifts of compacted soil.

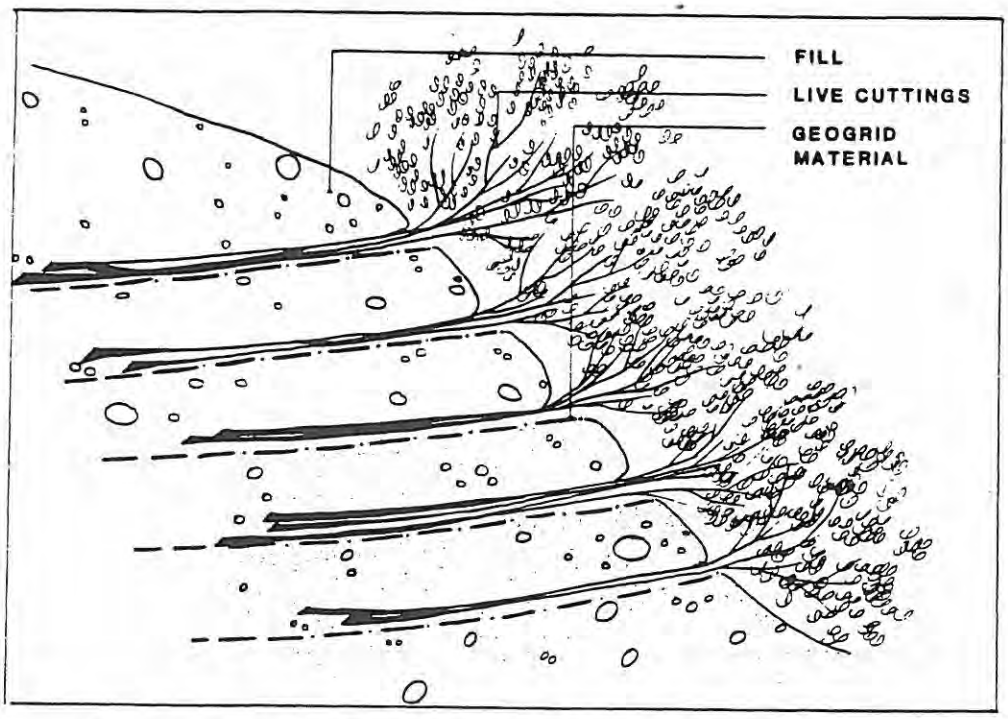

Figure 3. Schematic illustration of live brushlayers used in combination with geogrids or geotextiles.

Figure 4. Brushlayer buttress fill immediately after construction. Winter 1990. Greenfield Rd., nr. Route 112, Colrain, Mass.

Figure 5. Brushlayer buttress fill after two years showing extensive vegetative establishment. Greenfield Road, Mass.

Figure 6. Brushlayer embankment fill stabilization immediately after construction Brenner Pass highway, Austria.

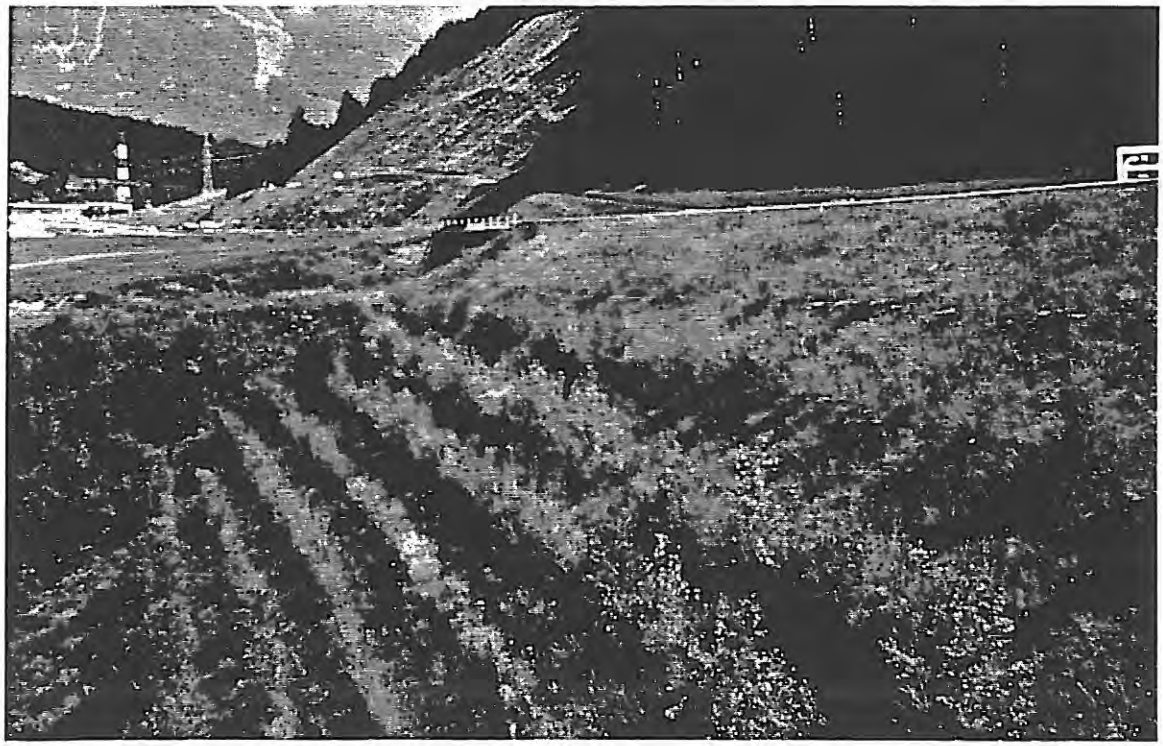

Figure 7. Brushlayer embankment fill stabilization after two years showing both grass and brush establishment. Brenner Pass highway, Austria.

STABILITY CONSIDERATIONS

Surficial Stability

One of the problems with embankment fills is the danger of erosion and sloughing along the outside edge of the fill. Several factors can contribute to this problem, namely, poor compaction at the outside edge and loss of shear strength caused by moisture adsorption and low confining stresses. Attempts to improve compaction may be counterproductive because this impedes establishment of vegetation, which in the long run, provides the best protection against erosion.

Brush layers are very effective in preventing shallow sliding and sloughing for the following reasons: 1) they act as wick and horizontal drains that intercept seepage and favorably modify the hydrologic regime, 2) they root along their length, and these adventitious roots provide secondary reinforcement or root cohesion near the slope face, 3) the growing tips of the brushlayers slow and filter sediment from the slope runoff, and 4) the presence of the brushlayers enhance the establishment of other vegetation on the slope face.

The effectiveness of mechanisms 1 and 2 cited above can be demonstrated by "infinite slope" type analyses which are appropriate for analyzing the surficial stability of slopes. For purposes of discussion consider a marginally stable, oversteepened (1.5H:1.0V) slope in a sandy soil with very low cohesion (γ=118 pcf, ϕ=35^o, c=0.2 psi). Factors of safety can be computed as a function of vertical depth to the sliding surface(H) and seepage direction (θ) with respect to a horizontal reference plane as shown in Figure 8. In the absence of additional root cohesion, the factor of safety drops below unity (F<1) when the seepage either parallels or emerges from the slope face at depths greater than one foot.

Brushlayers and associated roots markedly improve surfcial stability. The presence of fibers (roots) provides a measure of apparent cohesion (Gray and Ohashi, 1983; Maher and Gray, 1990). This fiber or root cohesion can make a significant difference in the resistance to shallow sliding or shear displacement in sandy soils with little or no intrinsic cohesion. Actual shear tests in the laboratory and field on root/fiber permeated sands indicate a shear strength increase per unit fiber concentration ranging from 7.4 to 8.7 psi per lb of root/cu ft of soil or 3.2 to 3.7 kPa per kg of root/cu m of soil (Gray and Ohashi, 1983; Ziemer, 1981).

Root concentrations reported in actual field tests were used to estimate likely root cohesion (c_R) as a function of depth (Riestenberg, 1983; Shields and Gray, 1992). A low to medium root concentration with depth was used in the

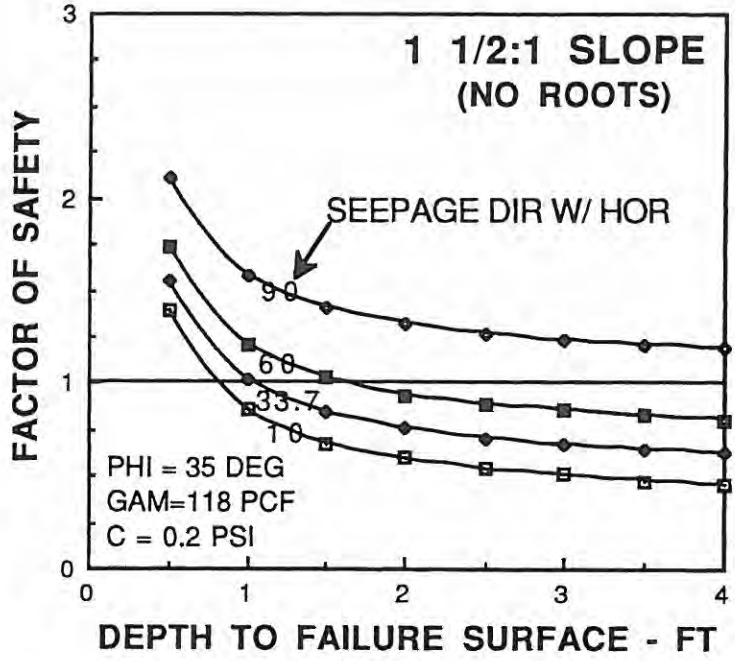

Figure 8. Factor of safety vs. depth and seepage direction for 1.5:1 hypothetical slope without roots in the surface layer.

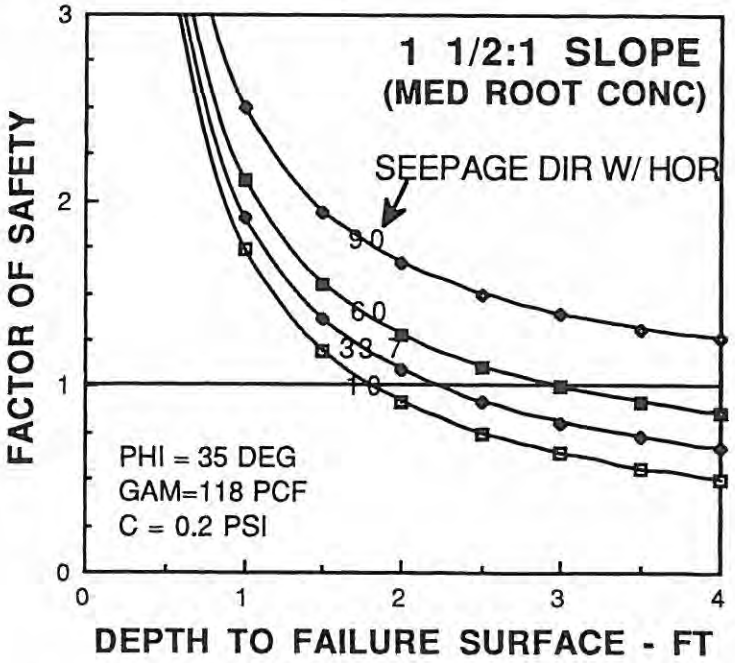

Figure 9. Factor of safety vs. depth and seepage direction for 1.5:1 hypothetical slope with roots in the surface layer.

stability analyses to ascertain the likely influence of slope vegetation on mass stability. Factor of safety is shown plotted as a function of depth and seepage direction in the presence of root reinforcement for the same 1.5:1 slope in Figure 9. With roots present the safety factor is increased significantly near the surface and the critical sliding surface is displaced downward. The results of the stability analyses show that both seepage direction (θ) and presence of root cohesion (c_R) have a significant effect on the factor of safety. Even a small amount of root cohesion can increase the factor of safety substantially near the surface. This influence is pronounced at shallow depths where root concentrations are highest and reinforcement effects therefore greatest.

The brushlayers also act as horizontal drains and favorably modify the hydrologic regime near the face of the slope. They intercept groundwater flowing along the loose, outer edge of a compacted fill, divert the flow downward, and then convey it out laterally through the brushlayer itself. Redirection of seepage flow downward in this manner results in greatly improved resistance to face sliding or sloughing (Cedergren, 1989). Redirection of seepage from parallel flow direction ($\theta=33^o$) to vertical flow ($\theta=90^o$) greatly increases the factor of safety at all depths as shown in Figure 9.

In the case of highly erosive soils (fine sands and silty sands) and very steep slopes (> 1.5H:1.0V) it may be advisable to also use an erosion control netting or mat on the face of the slope between the brush layers. A biodegradable netting with relatively small apertures (e.g., coir netting) placed over long straw mulch will work well in this regard. The netting and mulch provide additional protection against erosion and promote establishment of vegetation on the slope face. The easiest way to install and secure the netting is by wrapping it around the outside edge of successive lifts of compacted fill.

Internal and Global Stability

The internal stability and global stability of a brushlayer fill slope protection system must also be considered. This is especially true when a brushlayer fill is used as a protective "veneer" or buttress fill against an unstable cut or natural slope. Sufficient tensile inclusions, either live brushlayers and/or inert geogrids, must be imbedded in the fill to resist the unbalanced lateral force acting on the earthen buttress. The brush stems and branches reinforce a fill in much the same manner as conventional polymeric grid or fabric reinforcements; accordingly, the internal stability of a brushlayer fill, i.e., the resistance of the brush reinforcement

layers to pullout and tensile failure can be analyzed using conventional methods (Thielen and Collin, 1993; Leschinsky*et al.*, 1985) developed for earth slopes reinforced with geotextiles or geogrids. The required vertical spacing and imbedded length of successive brush reinforcement layers are determined from the specified safety factor, allowable unit tensile strength, and interface friction properties of the reinforcement layer. The allowable unit tensile resistance for a brushlayer can be calculated from the known tensile strength of the brush stems, their average diameter, and number of stems placed per unit width (Gray and Sotir, 1992).

In the case of earthen fills that contain moderate amounts of low plasticity fines the requirement for internal reinforcement is greatly reduced. The total required lateral resisting force approaches zero for fills with moderate cohesion (c=300 psf), slope inclinations less than 1.5H:1.0V, slope heights (H) less than 60 feet as shown in Figure 10. Live brushlayers used alone will suffice in this case to provide some additional internal stability, significantly increase surficial stability, and compensate for possible loss of intrinsic cohesion near the face.

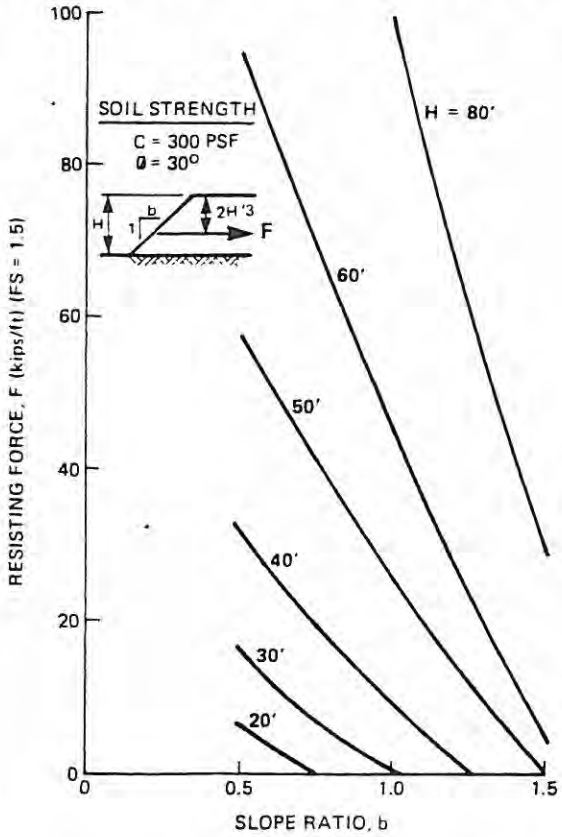

Figure 10. Chart solution for determining the required reinforcement or lateral resisting force for fills constructed from low plasticity soils (from Lucia and Callanan, 1987).

On the other hand, in the case of very high, steep slopes, a conservative design procedure would be to discount the influence of the live brushlayers on internal stability and rely solely on the presence of inert tensile inclusions, e.g., geogrids, used in conjunction with the brushlayers as shown in Figure 3.

Conventional geotechnical analyses can be used to analyze the global or deep seated stability of brushlayer slope protection systems. A brushlayer reinforced outside edge of an embankment fill or alternatively a brushlayer reinforced buttress fill or veneer placed against an unstable cut or natural slope is simply treated as a coherent gravity mass that is part of the slope. An example from an actual case study will be used to demonstrate this analysis procedure.

CASE STUDY EXAMPLE

Project Site: The project site is located along Greenfield Road, just off State Route 112, in northern Massachusetts near the village of Colrain. Widening & improvement of this scenic road resulted in encroachment on an adjacent, unstable hillside which triggered cut slope failures. The slope stratigraphy consisted of a residual soil, a silty sand, overlying a fractured quartz-mica schist bedrock. The cut was excavated back at a design slope angle of 1.5:1; the inclination of the natural slope above the cut was approximately 3:1. Cut slope heights varied in general from 20 to 60 feet. Slope failures were characterized by small slipouts and slumping. A substantial amount of groundwater flowed out of the cut. This water seeped out of both fractures in the underlying bedrock and through the exposed face of the soil mantle.

Alternative Slope Treatments: The initial stabilization treatment of choice was a crushed rock blanket. This system is employed frequently by Massachusetts DOT for cut slope stabilization. The main objection to this system was its stark and harsh appearance which were inconsistent with the scenic nature of the highway. The main design consideration in the case of a rock blanket was to determine the thickness required to provide a specified global safety factor of 1.5. In point of fact, a crushed rock blanket placed the entire length of the slope was not required to satisfy mass stability. Instead, a drained, rock buttress at the toe would have sufficed. A toe buttress, however, would have left upper portions of the slope exposed and vulnerable to piping and surficial erosion.

The soil bioengineering alternative proposed for the site was a drained, brushlayer buttress fill. Reservations were expressed by the project engineer about the ability of an earthen, brushlayer fill to resist large shear stresses at the

base or toe of the slope and to provide a required global safety factor of 1.5. Some concern was also expressed about the possibility of a critical shear surface developing through the earthen fill adjacent and parallel to a brushlayer. In view of these expressed concerns two modified brushlayer fill designs were proposed: (1) a crushed rock blanket with earthen brushlayer inclusions at periodic intervals, and (2) a crushed rock section at the base and brushlayer fill on top. The latter design was ultimately adopted; stability analyses were carried out on various configurations of this hybrid or composite system. The results of stability analyses on this composite system (see Figure 11) showed that it provided the required global factor of safety and that the most critical failure surfaces passed through the basal rock section at the toe of the slope.

Biotechnical Solution: In view of these findings a decision was made to use the composite rock toe and earthen brushlayer buttress fill design to stabilize the cut. An important caveat in this decision was the requirement that the earthen fill remain in a drained condition---a key assumption in the stability analyses. This requirement along with the large quantity of groundwater seeping out of the cut dictated that a suitable filter course or vertical drain be interposed between the earthen fill and cut face. This requirement was met by placing either a gravel filter course or a geotextile filter with adequate in-plain drainage capacity against the cut face during construction. Water from the bottom edge of the filter discharged into the rock toe at the base.

The construction work at the Colrain field site began in November of 1989. A view of the cut slope after installation of the brushlayer, buttress fill is shown in Figure 4. The appearance of the same slope some 2 years later is shown in Figure 5. After this amount of lapsed time the brush had fully leafed out and native vegetation had become well established on the slope. The slope is stable and has an attractive, natural appearance.

Cost Analysis: The costs of several conventional slope stabilization treatments were determined and compared with the soil bioengineering treatment. The conventional treatment costs included a rock blanket and concrete crib wall respectively. Cost analyses for the soil bioengineering treatment were conducted at two different stations or work locations on the project. The cost per square foot for the soil bioengineering treatment only varied by $0.37 per square foot from one location to another.

The rock blanket costs included expenses for transporting, handling, and placing of 1 1/2-inch trap stone in a toe buttress or blanket 10-feet high and 8-feet

Simplified Bishop Slope Stability Analysis

PROJECT: SLOPE REPAIR WITH COMPOSITE DRAINED ROCK ANDEARTH BUTRESS

LOCATION: COLRAIN, MASSACHUSETTS

COMPLETE SLOPE CROSS SECTION

CIRCLE	X	Y	RADIUS	FS
1	32.0	185.0	145.0	1.50
2	50.0	144.0	105.0	1.46
3	65.0	152.0	101.0	1.74
4	42.0	185.0	135.0	1.83

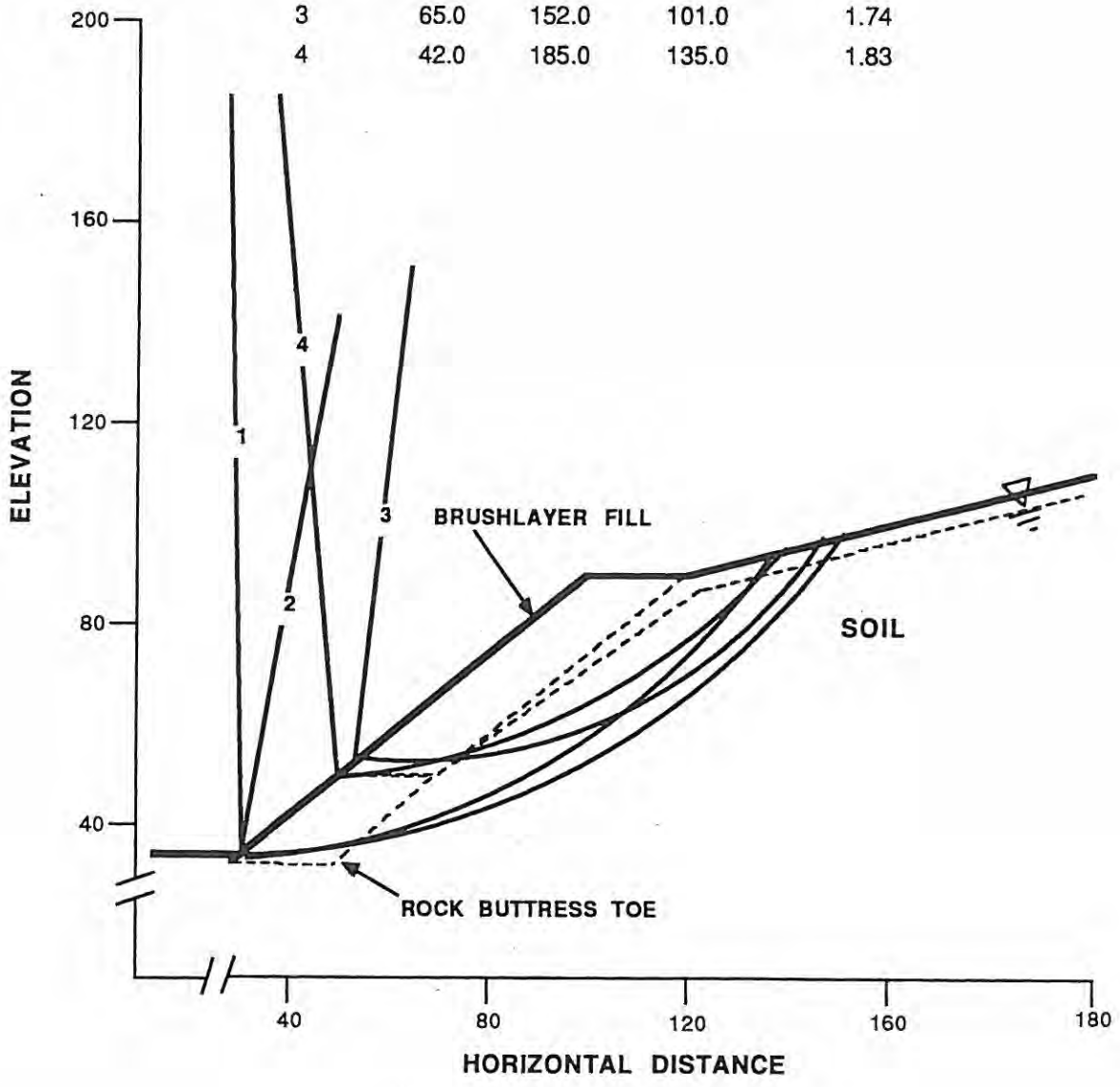

Figure 11. Factor of safety of cut slope stabilized by composite drained rock and earthen brushlayer fill. Colrain, Massachusetts.

wide. Placement of the rock higher up the slope entails greater difficulty and would have increased costs another 5- to 10 percent. The cost per square foot of front face for the crib wall includes footings and an estimated cost for the crib fill. The cost per square foot for the three alternative treatments was estimated as follows:

Rock Blanket (8-ft thick)	$5.60	per sq. ft.
Soil Bioengineering	13.50	" " "
Concrete Crib Walls	34.50	" " "

Accordingly, the soil bioengineering costs were intermediate between those of a rock blanket and a concrete crib retaining wall. It should be kept in mind, however, that the contractor on the project had placed rock blankets on many previous occasions whereas he had no previous experience with soil bioengineering. A cost comparisons between these two methods was thus skewed slightly by unfamiliarity and a learning curve associated with the soil bioengineering method.

INSTALLATION GUIDELINES

Procedures for the harvesting, handling, storage, and installation of live plant material should be followed carefully. Successful biotechnical construction requires that harvesting and placement of live cuttings in the brush layers be carried out during the dormant season.....usually November through April. Harvesting sites with suitable plant materials can be located by means of an aerial survey ahead of time. Stems and branches up to three inches in diameter of willow, dogwood, alder, poplar, and viburnum shrubs are generally suitable for brushlayer treatments. These are cut at the harvesting site, bundled, and transported to the project site on covered flatbed or dump trucks.

Live, cut material should be placed in the ground as soon as possible after harvesting. In the case of brushlayer installations, the cut stems and branches are laid atop successive lifts of compacted soil in a criss-cross fashion as shown schematically in Figure 2. Soil overlying each brushlayer must be worked in between the branches to insure intimate contact between the brush and soil. The vertical spacing between brush layers normally vary from 1 to 3 feet with closer spacings used at the bottom. The length of the cut stems should extend the full

width..... or as far as possible into an earthen buttress fill. A gravel drainage course, vertical chimney drains, or fabric filter with good in-plane drainage capacity must be placed between an earthen buttress fill and the cut face of a slope. Detailed guidelines and instructions for the selection, harvesting, handling, storage, and installation of live, cut plant materials are presented elsewhere (USDA, 1992).

CONCLUSIONS

Soil bioengineering solutions can be used to stabilize and repair slope failures along highway right-of-ways. Live brushlayers can be used in conjunction with or in lieu of inert polymeric reinforcements in over-steepened slopes. The growing tips of the brushlayers filter soil from runoff and mitigate surficial erosion. The stems and adventitious roots in the brush layers reinforce the soil. The brush-layers also act as horizontal drains and hydraulic wicks that favorably modify the hydrologic regime near the face of a slope. Stems and branches of plant species must be used that root easily from cuttings such as willow and alder. In addition construction and installation must be carried out during the dormant season.

REFERENCES

Berg, R.R. Anderson, R.P., Race, R.J., and Curtis, V.E. (1990). Reinforced soil highway slopes. *Transportation Research Record,* No. 1288, NAS-NRC, pp. 99-108.

Cedergren, R. (1989). Seepage, Drainage and Flownets. 3rd Edition. John Wiley & Sons: New York.

Coppin, N., Barker, D., and Richards, I. (1990). Use of Vegetation in Civil Engineering. Butterworths: Sevenoaks, Kent (England)

Gray, D.H. and Leiser, A.T. (1982). Biotechnical Slope Protection and Erosion Control. Van Nostrand Reinhold: New York, N.Y.

Gray, D.H. and Ohashi, H. (1983). Mechanics of fiber reinforcement in sand. *J. of Geotech. Engineering* (ASCE), Vol. 112, No. GT3, pp. 335-353

Gray, D.H. and Sotir, R. (1992). Biotechnical stabilization of a highway cut. *J. of GeotechnicalEngineering* (ASCE), Vol. 118, No. GT10, pp.

Kraebel, C.J. (1936). Erosion control on mountain roads. USDA *Circular No. 380,* 43 pp.

Leshchinsky, D & Reinschmidt, A.J. (1985). Stability of membrane reinforced slopes. *J. of Geotech.Engr.*(ASCE), Vol. 111, No. 11, pp. 1285-1300.

Lucia, P. and Callanan, F. (1987). Soil reinforcement for steeply sloped fills and landslide repairs. Paper presented at 66th Annual Meeting, Transportation Research Board, Symposimum on Earth Reinforcement, Washington, D.C

Maher, M. and Gray, D.H. (1990). Static response of sands reinforced with randomly distributed fibers. *J. of Geotechnical Engineering* (ASCE), Vol. 116, No. 11, pp. 1661-77,

Riestenberg, M.H. and Sovonick-Dunford, S. (1983). The role of woody vegetation in stabilizing slopes in the Cincinnati area. *Geologic Society of America Bulletin*, Vol. 94. pp. 504-518.

Schiechtl, H. (1980). Bioengineering for Land Reclamation and Conservation, The Univ. of Alberta Press, Edmonton, Canada.

Shields, F.D. and Gray, D.H. (1992). Effects of woody vegetation on sandy levee integrity, *Water Resources Bulletin*, Vol. 28, No. 5, pp. 917-931.

Sotir, R.B. and Gray, D.H. (1989). Fill slope repair using soil bioengineering systems. *Proceedings*, XX IECA Conf., Vancouver, B.C., pp. 413-429.

Thielen, D.L. and Collin, J.G. (1993). Geogrid reinforcement for surficial stability of slopes. *Proceedings*, Geosynthetics '93 Conference, Vancouver, B.C. pp.229-244.

USDA (1992). Chapter 18: Soil bioengineering for Upland Slope Protection and Erosion Reduction. Part 650, 210-EFH, Engr. Field Handbook, U.S. Dept. of Agric. Soil Conservation Service, 53 pp.

Ziemer, R.R. (1981). Roots and shallow stability of forested slopes. *Intl. Assoc. Hydrol. Sciences*, Publ. No. 132, pp. 343-361.

United States
Department of
Agriculture

**Soil
Conservation
Service**

Engineering
Field
Handbook

Chapter 18 Soil Bioengineering for Upland Slope Protection and Erosion Reduction

(210-EFH, 10/92)

Issued October 1992

Cover: Live plant cuttings are installed (top photo) on upland slopes to provide soil reinforcement and reduce surface erosion. The bottom photo shows the slope after 1 year. (Photos: Robbin B. Sotir & Associates)

All programs and services of the U.S. Department of Agriculture, Soil Conservation Service, are offered on a nondiscriminatory basis, without regard to race, color, national origin, religion, sex, age, marital status, or handicap.

(210-EFH, 10/92)

Preface

Chapter 18, Soil Bioengineering for Upland Slope Protection and Erosion Reduction is one of the 18 chapters of the U.S. Department of Agriculture Soil Conservation Service (SCS) Engineering Field Handbook, previously referred to as the Engineering Field Manual. Other chapters that are pertinent to, and should be referenced in use with, chapter 18 are:

Chapter 1: Engineering Surveys
Chapter 2: Estimating Runoff
Chapter 3: Hydraulics
Chapter 4: Elementary Soils Engineering
Chapter 5: Preparation of Engineering Plans
Chapter 6: Structures
Chapter 7: Grassed Waterways and Outlets
Chapter 8: Terraces
Chapter 9: Diversions
Chapter 10: Gully Treatment
Chapter 11: Ponds and Reservoirs
Chapter 12: Springs and Wells
Chapter 13: Wetland Restoration, Enhancement, or Creation
Chapter 14: Drainage
Chapter 15: Irrigation
Chapter 16: Streambank and Shoreline Protection
Chapter 17: Construction and Construction Materials

This is the first edition of chapter 18. The science of soil bioengineering is rapidly evolving and improving; therefore, additions to and modifications of this chapter will be made as necessary.

Acknowledgments

This chapter was prepared under the guidance of **Ronald W. Tuttle**, national landscape architect, and steering committee members **David C. Ralston**, national design engineer, and **Curtis W. Sharp**, national plant materials specialist, SCS, Washington, DC.

Robbin B. Sotir & Associates and **Dr. Donald H. Gray** are the principal authors of this manuscript. They supplied original drawings, which were adapted for SCS use, and all photographs. **Carolyn A. Adams**, landscape architect; **Leland M. Saele**, design engineer; **Gary E. Formanek**, agricultural engineer; and **Frank F. Reckendorf**, sedimentation geologist; SCS West National Technical Center, Portland, Oregon, edited the manuscript to extend its applicability to most geographic regions and to fit it to agency programs. Other staff members at the SCS National Technical Centers and State Offices also contributed by reviewing the chapter and providing comments.

Sarah Laurent, editor, SCS, Washington, DC, provided editing assistance, and **Wendy R. Oller**, illustrator, SCS, Fort Worth, Texas, provided desktop publishing in preparation for printing.

Chapter 18 Soil Bioengineering for Upland Slope Protection and Erosion Reduction

Contents:

650.1800	**Introduction**	**18–1**
	(a) Purpose and scope	18–1
	(b) Background	18–1
	(c) Integrated planning and design requirements	18–1
	(d) Applications	18–2
650.1801	**Characteristics of soil bioengineering systems**	**18–4**
	(a) Vegetative components	18–4
	(b) Structural components	18–4
	(c) Attributes and limitations	18–5
650.1802	**Basic principles and design considerations**	**18–7**
	(a) Basic principles of soil bioengineering	18–7
	(b) Design considerations	18–8
650.1803	**Construction techniques and materials**	**18–9**
	(a) General considerations	18–9
	(b) Soil bioengineering techniques	18–15
	(c) Soil bioengineering materials	18–39
	(d) Vegetated structures	18–46
650.1804	**References**	**18–50**
	Glossary	**18–51**

Tables

Table 18–1	Approaches to upland slope protection and erosion control	18–2
Table 18–2	Soil bioengineering plant species	18–9
Table 18–3	Live fascine installation guidelines	18–20
Table 18–4	Brushlayer installation guidelines	18–22
Table 18–5	Plant tolerance	18–39

Figures

Figure 18–1	Soil bioengineering provides soil reinforcement and reduces surface erosion	18–3
Figure 18–1a	Eroding fill slope	
Figure 18–1b	Measures being installed	
Figure 18–1c	Installation 1 year later	
Figure 18–2	Newly established installation provides multiple functions and values	18–6
Figure 18–3	Live stake installation	18–14
Figure 18–4	Top growth and root development of a 7-month-old live stake	18–15
Figure 18–5	A prepared live stake	18–16
Figure 18–6	A live stake that has rooted and is demonstrating healthy growth	18–17
Figure 18–7	Fabrication of a live fascine bundle	18–18
Figure 18–8	A live fascine system	18–19
Figure 18–8a	During installation	
Figure 18–8b	Three months after installation	
Figure 18–9	A dead stout stake	18–20
Figure 18–10	Live fascine details	18–21
Figure 18–11	A brushlayer system	18–23
Figure 18–11a	During installation	18–23
Figure 18–11b	Two years after installation	18–23
Figure 18–12	Installing a brushlayer	18–24
Figure 18–12a	Bench being prepared for a brushlayer	
Figure 18–12b	Placing live branch cuttings	
Figure 18–13	A branchpacking system being installed	18–25
Figure 18–14	Branchpacking details	18–26

Figure 18–15 Completed branchpacking system 18–27

Figure 18–15a Newly installed system

Figure 18–15b One year after installation

Figure 18–16 Live gully repair details 18–28

Figure 18–17 A live cribwall being installed 18–29

Figure 18–18 Live cribwall details 18–31

Figure 18–19 An established vegetated rock gabion system 18–32

Figure 18–20 Vegetated rock gabion details 18–33

Figure 18–21 Vegetated rock wall details 18–35

Figure 18–22 A newly established joint planting stake 18–36

Figure 18–23 Roots improve drainage by removing soil moisture 18–37

Figure 18–23a Root system 7 months after installation

Figure 18–23b Joint planted area after a 2-year growth

Figure 18–24 Joint planting details 18–38

Figure 18–25 A low wall with plantings above 18–47

Figure 18–26 Low wall at the base of a slope with vegetation on face of slope 18–47

Figure 18–27 A tiered wall with bench plantings 18–48

Figure 18–28 Cribwall systems with face plantings 18–49

Figure 18–28a Tiered cribwall system with trees and shrubs planted on benches

Figure 18–28b Open-front concrete cribwall with plantings in openings

Chapter 18 Soil Bioengineering for Upland Slope Protection and Erosion Reduction

650.1800 Introduction

(a) Purpose and scope

Chapter 18 provides field personnel with a guide for soil bioengineering intended primarily for upland slope protection and erosion reduction. It describes characteristics, principles, design, and construction techniques of soil bioengineering. Two approaches to soil bioengineering techniques are presented: woody vegetative systems and woody vegetative systems combined with simple structures. Woody vegetative systems are emphasized. Vegetative plantings and vegetated structures are discussed cursorily to help distinguish them from soil bioengineering techniques.

This chapter is national in scope and should be supplemented with regional and local information. Soil bioengineering measures, such as live cribwalls and brushlayering, are relatively complex and must be tailored carefully to specific soil and site conditions. The contents of this chapter are not directly applicable to massive erosion problems or complex shallow slope failure problems. Additional background on specific designs and sample calculations are available in other sources (Gray, et.al. 1982).

Planning and design of soil bioengineering systems generally require a team of experts. Therefore, the scope of this chapter reflects the interdisciplinary nature of soil bioengineering.

(b) Background

Soil bioengineering, in the context of upland slope protection and erosion reduction, combines mechanical, biological, and ecological concepts to arrest and prevent shallow slope failures and erosion. Basic approaches to upland slope protection and erosion control can be divided into two general categories: living and nonliving (table 18–1).

The **living approach**, which uses live plant materials, can be further divided into two specific categories: vegetative plantings and soil bioengineering. Vegetative plantings are conventional plantings of grasses, forbs, and shrubs used to prevent surface erosion. Soil bioengineering utilizes live plant parts to provide soil reinforcement and prevent surface erosion (fig. 18–1). In soil bioengineering systems, the installation may play the major structural roles immediately or may become the major structural component over time.

Live staking, live fascines, brushlayers, branchpacking, and live gully repair are soil bioengineering techniques that use stems or branch parts of living plants as initial and primary soil reinforcing and stabilizing material. When these vegetative cuttings are placed in the ground, roots develop and foliage sprouts. The resulting vegetation becomes a major structural component of the bioengineering system.

Live cribwalls, vegetated rock gabions, vegetated rock walls, and joint plantings are soil bioengineering techniques that use porous structures with openings through which vegetative cuttings are inserted and established. The inert structural elements provide immediate resistance to sliding, erosion, and washout. As vegetation becomes established, roots invade and permeate the slope, binding it together into a unified, coherent mass. Over time, the structural elements diminish in importance as the vegetation increases in strength and functionality.

Nonliving approaches use rigid constructions, such as surface armoring, gravity retaining walls, and rock buttresses. Vegetation can be used in conjunction with nonliving structures to create vegetated structures. Vegetation enhances the structures and helps reduce surface erosion, but usually does not provide any reinforcement benefits.

(c) Integrated planning and design requirements

Soil bioengineering combines biological elements with engineering design principles. The requirements for both must be considered when planning and designing the measures presented in table 18–1. For example, engineering requirements may dictate highly compacted soil for fill slopes, while plants prefer relatively loose soil. Using a sheep's foot roller for compaction is a solution that would integrate biological and engineering requirements because it compacts the soil, but also allows plant establishment in resulting depressions in the slope. Differing needs can generally be integrated through creative approaches and occasional compromises in planning and design.

(d) Applications

The soil bioengineering techniques in this document are generally appropriate for immediate protection of slopes against surface erosion, shallow mass wasting, cut and fill slope stabilization, earth embankment protection, and small gully repair treatment. Appropriate application of specific measures are discussed in detail in Section 650.1803, Construction techniques and materials.

Other situations where soil bioengineering measures can be employed are not discussed in this chapter. These situations include dune stabilization, wetland buffers, reservoir drawdown areas where plants can be submerged for extended periods, and areas with highly toxic soils. Properly designed and constructed soil bioengineering measures have also been employed with considerable success in stabilizing shorelines and streambanks. This topic is addressed in EFH, Chapter 16, Streambank and Shoreline Protection.

Table 18–1 Approaches to upland slope protection and erosion control

Category	Examples	Appropriate uses	Role of vegetation
LIVING	**Vegetative plantings**		
	Conventional plantings	Grass seedlings Transplants Forbs	Control water and wind erosion. Minimize frost effects.	Control weeds. Bind & restrain soil. Filter soil from runoff. Intercept raindrops. Maintain infiltration. Moderate ground temperature.
	Soil bioengineering		
	Woody plants used as reinforcement, as barriers to soil movements, & in the frontal openings or interstices of retaining structures.	Live staking Live fascine Brushlayer Branchpacking Live cribwall Live gully repair Vegetated rock gabion Vegetated rock wall Joint planting	Control of rills & gullies. Control of shallow (translational) mass movement. Filter sediment. Improved resistance to low to moderate earth forces.	Same as above, but also reinforce soil, transpire excess water, & minimize downslope movement of earth masses. Reinforce fill into monolithic mass. Improve appearance and performance of structure.
NONLIVING	**Vegetated structures**		
	Inert structures with vegetative treatments.	Wall or revetment with slope face planting. Tiered structures with bench planting.	Control erosion on cut & fill slopes subject to scour & undermining.	Stop or prevent erosion & shallow sloughing on or at the slope face above the toe.
	Rigid construction	(see Chapter 6, Structures, of the Engineering Field Handbook).		

Figure 18–1 Soil bioengineering provides soil reinforcement and reduces surface erosion (Robbin B. Sotir & Associates photos)

Figure 18–1a Eroding fill slope

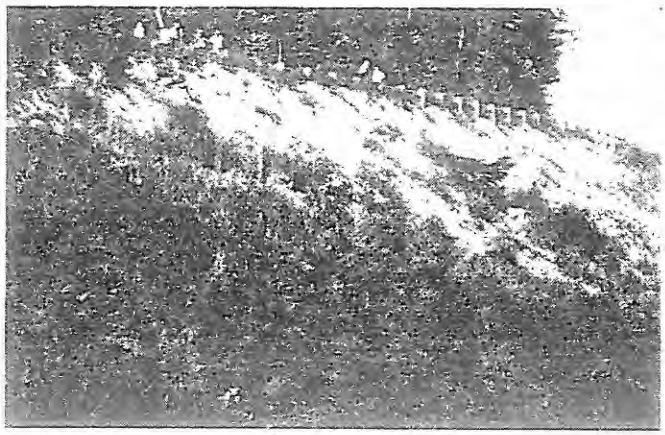

Figure 18–1b Measures being installed

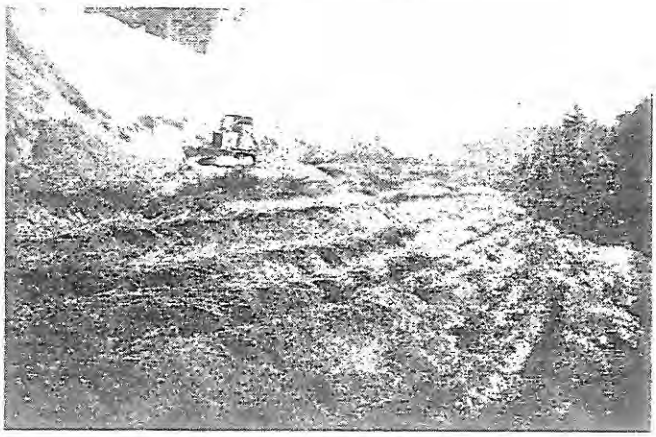

Figure 18–1c Installation 1 year later

650.1801 Characteristics of soil bioengineering systems

Soil bioengineering uses particular characteristics of vegetative components and integrates specific characteristics of structures with vegetation. The resulting systems and their components have benefits and limitations that need to be considered prior to selecting them for use.

(a) Vegetative components

(1) Herbaceous species

Herbaceous vegetation, especially grasses and forbs, offers long-term protection against surface (water and wind) erosion on slopes. It provides only minor protection against shallow mass movement. Vegetation helps to prevent surface erosion by:

- Binding and restraining soil particles in place
- Reducing sediment transport
- Intercepting raindrops
- Retarding velocity of runoff
- Enhancing and maintaining infiltration capacity
- Minimizing freeze-thaw cycles of soils susceptible to frost

Herbaceous species are almost always used in conjunction with soil bioengineering projects to add protection against surface erosion.

(2) Woody species

More deeply rooted woody vegetation provides greater protection against shallow mass movement by:

- Mechanically reinforcing the soil with roots
- Depleting soil-water through transpiration and interception
- Buttressing and soil arching action from embedded stems

Live fascines, for example, provide many of these protective functions. They are fabricated from woody species, such as shrub willow or shrub dogwood, into sausage-like bundles, which are placed with the stems oriented generally parallel to the slope contour. This method of placement and orientation would not be used in slope reinforcement. Live fascines serve to dissipate the energy of downward moving water by trapping debris and providing a series of benches on which grasses, seedlings, and transplants establish more easily. Portions of the live fascines also root and become part of the stabilizing cover. Live fascines provide an immediate increase in surface stability and can further improve soil stability to depths of 2 to 3 feet as roots develop.

In the case of brushlayering, live branches or shoots of such woody species as shrub willow, dogwood, or privet are placed in successive layers with the stems generally oriented perpendicular to the slope contour, as shown in figure 18–1. This orientation is the optimal direction for maximum reinforcing effect in a slope. Brushlayering can improve soil stability to depths of 4 to 5 feet.

(b) Structural components

Properly designed and installed structures help to stabilize a slope against shallow mass movement and protect the slope against rill and gully formation. Structures also play a critical role in the establishment of vegetation on steep slopes or in areas subject to severe erosion. They may make it possible to establish plants on slopes steeper than would normally be possible. Structures stabilize slopes during the critical time for seed germination and root growth. Without this stabilization, vegetative plantings would fail during their most vulnerable time.

(1) Materials

Structures can be built from natural or manufactured materials. Natural materials, such as earth, rock, stone, and timber, usually cost less, are environmentally more compatible, and are better suited to vegetative treatment or slight modifications than are manufactured materials. Natural materials may also be available onsite at no cost.

Some structures are comprised of both natural and manufactured materials. Examples include concrete cribwalls, steel bin walls, gabion walls or revetments, welded wire or polymeric geogrid walls, and reinforced earth. In these cases steel and concrete mostly provide rigidity, strength, and reinforcement, whereas stone, rock, and soil provide mass. These types of

structures have spaces that are often planted with herbaceous or woody vegetation.

(2) Retaining structures

A retaining structure of some type is usually required to protect and stabilize extremely steep slopes. Low retaining structures at the toe of a slope make it possible to grade the slope back to a more stable angle that can be successfully revegetated without loss of land at the crest. Structures are generally capable of resisting much higher lateral earth pressures and shear stresses than vegetation.

(3) Grade stabilization structures

Grade stabilization structures are used to control and prevent gully erosion. A grade stabilization structure reduces the grade above it and dissipates the excess energy of flowing water within the structure itself. Debris and sediment tend to be deposited and trapped upstream of the structure. This, in turn, permits establishment of vegetation behind the structure, which further stabilizes the ground. Grade stabilization structures may range from a series of simple timber check dams to complex concrete overfall structures and earth embankments with pipe spillways.

Gully control provides a good example of the integration of structures and vegetation. Structural measures may be required in the short term to stabilize critical locations. The long-term goal is to establish and maintain a vegetative cover that prevents further erosion. This goal is seldom realized unless the severe gully conditions can be altered immediately. Vegetation alone, for example, will rarely stabilize gully headcuts because of the concentrated water flow, overfalls, and pervasive forces that promote gully enlargement in an unstable channel system. Initially, the vegetation and the structure work together in an integrated fashion. The ultimate function of these structures, however, is to help establish vegetation which will provide long-term protection.

(c) Attributes and limitations

Soil bioengineering measures should not be viewed as a panacea or solution for all slope failure and surface erosion problems. Soil bioengineering has unique attributes, but is not appropriate for all sites and situations. In certain cases, a conventional vegetative treatment (e.g., grass seeding and hydro mulching) works satisfactorily at less cost. In other cases, the more appropriate and most effective solution is a structural retaining system alone or in combination with soil bioengineering.

The following specific attributes and limitations should be considered before applying a soil bioengineering technique:

(1) Environmental compatibility

Soil bioengineering systems generally require minimal access for equipment and workers and cause relatively minor site disturbance during installation. These are generally priority considerations in environmentally sensitive areas, such as parks, woodlands, riparian areas, and scenic corridors where aesthetic quality, wildlife habitat, and similar values may be critical (fig. 18–2).

(2) Cost effectiveness

Field studies have shown instances where combined slope protection systems have proven more cost effective than the use of either vegetative treatments or structural solutions alone. Where construction methods are labor intensive and labor costs are reasonable, the combined systems may be especially cost effective. Where labor is either scarce or extremely expensive, however, soil bioengineering systems may be less practical than structural measures.

Using indigenous materials accounts for some of the cost effectiveness because plant costs are limited to labor for harvesting and handling and direct costs for transporting the plants to the site.

(3) Planting times

Soil bioengineering systems are most effective when they are installed during the dormant season, usually the late fall, winter, and early spring. This often coincides with the time that other construction work is slow.

Constraints on planting times or the availability of the required quantities of suitable plant materials during allowable planting times may limit the usefulness of soil bioengineering methods.

(4) Difficult sites

Soil bioengineering is often a useful alternative for small, highly sensitive, or steep sites where the use of machinery is not feasible and hand labor is a necessity.

However, rapid vegetative establishment may be difficult on extremely steep slopes.

The usefulness of soil bioengineering methods may be limited by the available medium for plant growth, such as rocky or gravelly slopes that lack sufficient fines or moisture to support the required plant growth. In addition, soil-restrictive layers, such as hardpans, may prevent required root growth.

The biotechnical usefulness of vegetation would be limited on slopes that are exposed to high velocity water flow or constant inundation.

(5) Harvesting local plant material

Appropriate vegetation is often obtained from local stands of willows and other suitable species. This stock is already well suited to the climate, soil conditions, and available moisture and is a good candidate for survival. While harvesting may often help a beneficial species proliferate, reliance on the use of local plant materials and gathering in the wild could result in short supplies or unacceptable depletion of site vegetation. Furthermore, some localities have prohibitions against gathering native plants, and materials must be purchased from commercial sources.

Figure 18–2 Newly established installation provides multiple functions and values (Robbin B. Sotir & Associates photo)

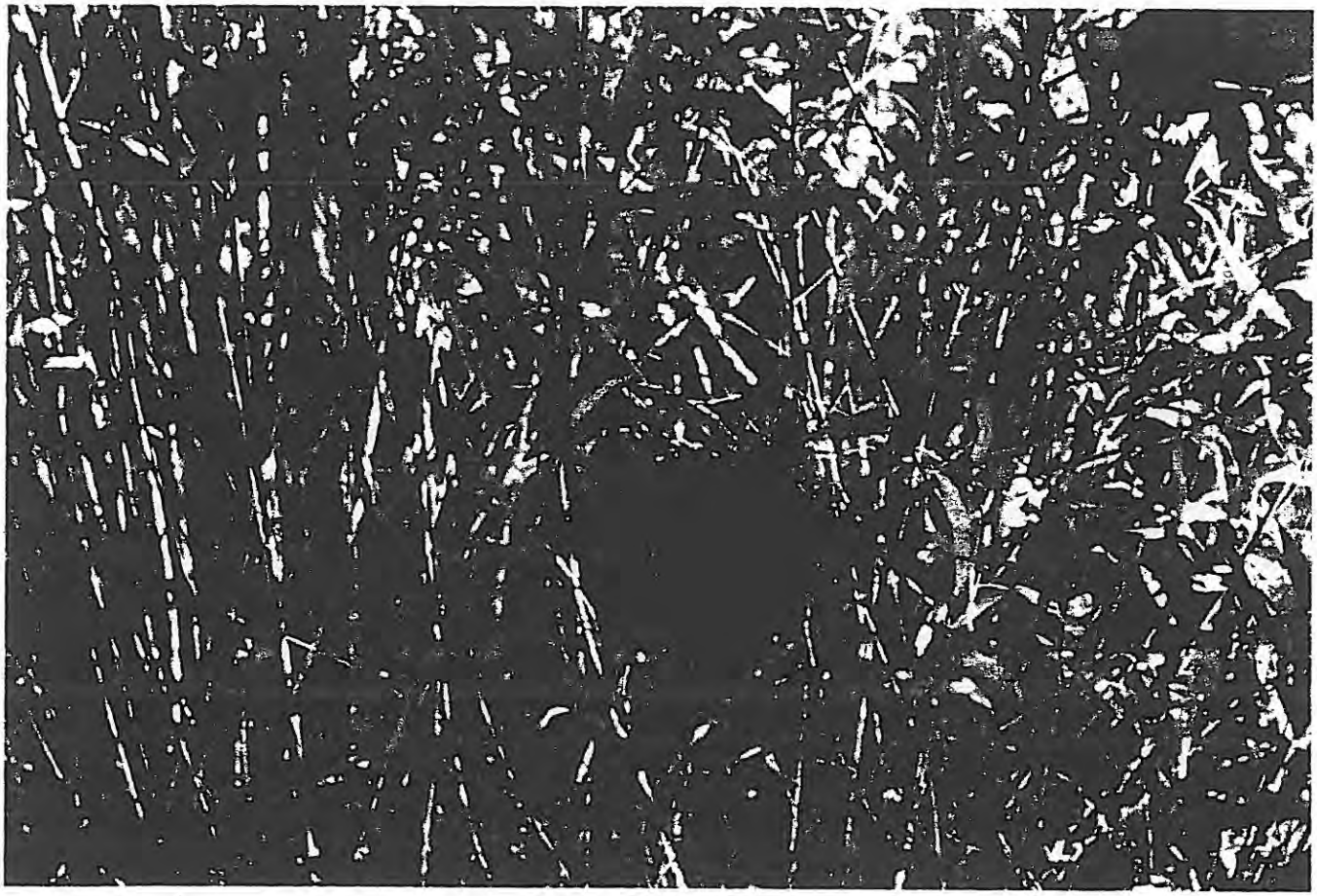

(6) Biotechnical strengths

Soil bioengineering systems are strong initially and grow stronger with time as vegetation becomes established. In some instances, the primary role of the structural component is to give the vegetation a better chance to become established. It has been shown in slope reconstruction projects that soil bioengineering systems can withstand heavy rainfalls immediately after installation. Even if established vegetation dies, the plant roots and surface residue may continue to play an important protective role during reestablishment.

(7) Maintenance requirements

Once vegetation is well established on a soil bioengineering project, usually within one growing season, it generally becomes self-repairing by regeneration and growth and requires little maintenance. However, a newly installed soil bioengineering project will require careful periodic inspections until it is established. Establishing vegetation is vulnerable to trampling, drought, grazing, nutrient deficiencies, toxins, and pests, and may require special management measures at times.

650.1802 Basic principles and design considerations

(a) Basic principles of soil bioengineering

The basic principles that apply to conventional soil erosion control also apply in general to soil bioengineering. These principles are mostly common sense guidelines that involve planning, timing, and minimizing site disturbance rather than the design of individual measures themselves. Applicable principles can be summarized as follows:

(1) Fit the soil bioengineering system to the site

This means considering site topography, geology, soils, vegetation, and hydrology. Avoid extensive grading and earthwork in critical areas and perform soil tests to determine if vigorous plant growth can be supported. At a minimum, collect the following information:

(i) Topography and exposure

- Note the degree of slope in stable and unstable areas. Also note the presence or lack of moisture. The likely success of soil bioengineering treatments can best be determined by observing existing stable slopes in the vicinity of the project site.
- Note the type and density of existing vegetation in areas with and without moisture and on slopes facing different directions. Certain plants grow well on east-facing slopes, but will not survive on south-facing slopes.
- Look for areas of vegetation that may be growing more vigorously than other site vegetation. This is generally a good indicator of excess moisture, such as seeps and a perched water table, or it may reflect a change in soils.

(ii) Geology and soils

- Consult SCS geologists about geologic history and types of deposits (colluvium, glacial, alluvium, other).
- Note evidence of past sliding. If site evidence exists, determine whether the slide occurred along a deep or shallow failure surface. Leaning

or deformed trees may indicate previous slope movement or downhill creep. In addition to site evidence, check aerial photos, which can reveal features that may not be apparent from a site visit.
- Determine soil type and depth. Use the soil survey report, if available, or consult SCS soil scientists.

(iii) Hydrology
- Determine the drainage area associated with the problem area. Note whether water can be diverted away from the problem area.
- Determine the annual precipitation. Are there concentrated discharges?
- Calculate peak flows or mean discharge through the project area.
- If a seep area was noted, locate the source of the water. Determine whether the water can be intercepted and diverted away from the slope face.

(2) Retain existing vegetation whenever possible

Vegetation provides excellent protection against surface erosion and shallow slope failures. Soil bioengineering measures are designed to aid or enhance the reestablishment of vegetation.

(3) Limit removal of vegetation
- Limit cleared area to the smallest practical size
- Limit duration of disturbance to the shortest practical time
- Remove and store existing woody vegetation that may be used later in the project
- Schedule land clearing during periods of low precipitation whenever possible

(4) Stockpile and protect topsoil

Topsoil removed during clearing and grading operations can be reused during planting operations.

(5) Protect areas exposed during construction

Temporary erosion and sediment control measures can be used.

(6) Divert, drain, or store excess water
- Install a suitable system to handle increased and/or concentrated runoff caused by changed soil and surface conditions during and after construction.
- Install permanent erosion and sediment control measures in the project before construction is started if possible.

(b) Design considerations

(1) Earthwork

Typically, sites require some earthwork prior to the installation of soil bioengineering systems. A steep undercut or slumping bank, for example, requires grading to flatten the slope for stability. The degree of flattening depends on the soil type, hydrologic conditions, geology, and other site factors.

(2) Scheduling and timing

Planning and coordination are needed to achieve optimal timing and scheduling. The seasonal availability of plants or the best time of year to install them may not coincide with the construction season or with tight construction schedules. In some cases, rooted stock may be used as an alternative to unrooted dormant season cuttings.

(3) Vegetative damage to inert structures

Vegetative damage to inert structures may occur when inappropriate species or plant materials that exceed the size of openings in the face of structures are used. Vegetative damage does not generally occur from roots. Plant roots tend to avoid porous, open-faced retaining structures because of excessive sunlight, moisture deficiencies, and the lack of a growing medium.

(4) Moisture requirements and effects

The backfill behind a stable retaining structure has certain specified mechanical and hydraulic properties. Ideally, the fill is coarse-grained, free-draining, granular material. Excessive amounts of clay, silt, and organic matter are not desirable. Free drainage is essential to the mechanical integrity of an earth-retaining structure and also important to vegetation, which cannot tolerate waterlogged soil conditions. The establishment and maintenance of vegetation, however, usually requires the presence of some fines and organic matter in the soil to provide adequate moisture and nutrient retention. In many instances,

these biological requirements can be satisfied without compromising engineering performance of the structure. With cribwalls, for example, adequate amounts of fines or other amendments can be incorporated into the backfill. Gabions can be filled with rock and soil drifted into them to facilitate growth of vegetation. Woody vegetative cuttings can be placed between the baskets during filling and into the soil or backfill beyond the baskets. The needs of plants and the requirements of structures must be taken into account when designing a system.

650.1803 Construction techniques and materials

(a) General considerations

Soil bioengineering measures have certain requirements and capabilities. Plant species must be suitable for the intended use and adapted to the site's climate and soil conditions. Consult a plant materials specialist about available cultivars to ensure that appropriate species are used. Species that root easily, such as willow, are required for such measures as live fascines, brushlayer, and live staking or where unrooted stems are used with structural measures. Table 18–2 is a general listing of plant species used in soil bioengineering.

Table 18–2 Soil bioengineering plant species

Name	Location	Availability	Habitat value	Size/form	Root type	Rooting ability from cuttings
Acer negundo Boxelder	N, NE	Common	Excellent	Small tree	Mod. deep spreading	Poor-fair
Alnus rubra Red alder	NW	Very common	Excellent	Large tree	Shallow spreading	Poor
Baccharis glutinosa Water wally	W	Common	Very good	Medium shrub	Fibrous	Good
Baccharis halimifolia Eastern baccharis	S, SE	Common	Very poor	Small-med. shrub	Fibrous	Fair-good
Baccharis pilularis Coyotebrush	W	Very common	Good	Medium shrub	Fibrous	Good
Baccharis viminea Mule fat	W	Very common	Very good	Medium shrub	Fibrous	Good
Betula papyrifera Paper birch	N, E, & W	Common	Good	Tree	Fibrous shallow	Poor
Betula pumila Low birch	N, E, & W	Common	Very good	Medium shrub	Fibrous	Poor

Table 18–2 Soil bioengineering plant species—Continued

Name	Location	Availability	Habitat value	Size/form	Root type	Rooting ability from cuttings
Cornus amomum Silky dogwood	N, SE	Very common	Very good	Small shrub	Shallow fibrous	Very good
Cornus racemosa Gray dogwood	NE	Common	Very good	Med-small shrub	Shallow	Good
Cornus rugosa Roundleaf dogwood	NE	Common	Very good	Med-small shrub	Shallow fibrous	Fair-good
Cornus sericea ssp. stolonifera Red osier dogwood	N, NE, & NW	Very common	Very good	Med-small shrub	Shallow	Very good
Crataegus Sp. Hawthorn	SE	Uncommon	Good	Sm. dense tree	Top root	Fair
Elaeagnus commutata Silverberry	N. Cent.	Very Common	Poor	Medium shrub	Shallow	Fair-good
Ligustrum sinense Chinese privet	S, SE	Common	Fair-good	Small-med. shrub	Shallow fibrous	Good
Lonicera involucrata Black twinberry	E	Common	Poor-fair	Small shrub	Shallow	Good
Physocarpus capitatus Pacific ninebark	NW, W	Common	Fair	Small	Fibrous	Good
Physocarpus opulifolius Common ninebark	NE	Common	Good	Med-high shrub	Shallow lateral	Fair-good
Populus angustifolia Arrowleaf cottonwood	W	Common	Good	Tree	Shallow	Very good
Populus balsamifera ssp. trichocarpa Black cottonwood	NW	Common	Good	Tree	Shallow fibrous	Very good
Populus deltoides Eastern cottonwood	MW, E	Very common	Good	Large tree	Shallow	Very good
Populus fremontii Fremont cottonwood	SW	Very common	Good	Tree	Shallow fibrous	Very good

Table 18–2 Soil bioengineering plant species—Continued

Name	Location	Availability	Habitat value	Size/form	Root type	Rooting ability from cuttings
Populus tremuloides Quaking aspen	NW	Very common	Good	Large tree	Shallow	Fair
Robinia pseudoacacia Black locust	NE	Common	Very poor	Tree	Shallow	Good
Rubus allegheniensis Allegheny blackberry	NE	Very common	Very good	Small shrub	Fibrous	Good
Rubus spectabilis Salmonberry	SW	Very common	Good	Small shrub	Fibrous	Fair-good
Rubus strigosus Red raspberry	N, NE, & W	Very common	Very good	Small shrub	Fibrous	Good
Salix exigua Coyote willow	NW	Fairly common	Good	Medium shrub	Shallow suckering	Good
ssp. interior Sandbar willow	N, SE	Common	Good	Large shrub	Shallow to deep	Fair-good
Salix amygdaloides Peachleaf willow	N, S	Common	Good	Very large shrub	Shallow to deep	Very good
Salix bonplandiana Pussy willow	W & MW	Very common	Good	Medium shrub	Fibrous	Very good
Salix eriocephala ssp. ligulifolia Erect willow	NW	Common	Good	Large shrub	Fibrous	Very good
Salix gooddingii Goodding willow	SW	Very common	Good	Large shrub Small tree	Shallow to deep	Excellent
Salix hookeriana Hooker willow	NW	Common	Good	Large	Fibrous dense	Very good
Salix humilis Prairie willow	N, NE	Very common	Good	Medium shrub	Fibrous	Good
Salix lasiolepis Arroya willow	W	Common	Good	Medium shrub	Fibrous	Very good

Table 18–2 Soil bioengineering plant species—Continued

Name	Location	Availability	Habitat value	Size/form	Root type	Rooting ability from cuttings
Salix lemmonii Lemmon willow	W	Common	Good	Medium shrub	Fibrous	Very good
Salix lucida Shining willow	N, NE	Very common	Good	Med-large shrub	Fibrous	Very good
ssp. lasiandra Pacific willow	NW	Very common	Good	Large shrub Small tree	Fibrous	Very good
Salix lutea Yellow willow	W	Very common	Good	Med-large shrub	Fibrous	Very good
Salix nigra Black willow	N, SE	Very common	Good	Large shrub Small tree	Shallow to deep	Excellent
Salix purpurea Streamco	N, S, E, & W	Very common	Very good	Medium shrub	Shallow	Very good
Salix scouleriana Scoulers willow	NE	Very common	Good	Large shrub Small tree	Shallow	Very good
Salix sitchensis Sitka willow	NW	Common	Good	Very large shrub	---	Very good
Salix X cotteti Bankers willow	N, S, E, & W	Uncommon	Good	Small shrub	Shallow	Very good
Salix discolor Red willow	N, NE	Very common	Good	Large shrub	Shallow	Very good
Sambucus cerulea Blueberry elderberry	W	Common	Very good	Medium shrub	Fibrous	Poor
Sambucus canadensis American elderberry	NE, SE	Very common	Very good	Medium shrub	Fibrous	Good
Sambucus racemosa Red elderberry	NW	Common	Good	Medium shrub	---	Good
ssp. pubens Scarlet elder	NE	Common	Very good	Medium shrub	Deep laterals	Fair-good
Spiraea alba Meadowsweet spirea	N, E	Common	Good	Small dense tree	Dense shallow lateral	Fair-good

Table 18–2 Soil bioengineering plant species—Continued

Name	Location	Availability	Habitat value	Size/form	Root type	Rooting ability from cuttings
Spiraea douglasii Douglas spirea	NW	Common	Fair	Dense shrub	Fibrous suckering	Good
Spiraea tomentosa Hardhack spirea	NE	Common	Good	Small shrub	Dense shallow	Fair
Symphoricarpos albus Snowberry	N, NW, & E	Common	Good	Small shrub	Shallow fibrous	Good
Viburnum alnifolium Hubbiebush viburnum	NE	Fairly common	Good	Large shrub	Shallow fibrous	Good
Viburnum dentatum Arrowwood viburnum	E	Common	Good	Medium shrub	Shallow fibrous	Good
Viburnum lentago Nannyberry viburnum	S, SE	Fairly common	Good	Large shrub	Shallow	Fair-good

Rooted plants and vegetative cuttings are living materials and must be handled properly to avoid excess stress, such as drying or exposure to heat. They must be installed in moist soil and adequately covered. The soil must be compacted to eliminate or minimize air pockets around the buried stems. If soils are not at or near moisture capacity, the installation must be delayed unless deep and regular irrigation can be provided during and following installation.

Installation of soil bioengineering systems is best accomplished in the late fall at the onset of plant dormancy, in the winter as long as the ground is not frozen, or in early spring before growth begins. In some cases installation after initial spring growth may be successful if extreme care is used, but the risks of failure are high. Summer installation is not recommended. Rooted plants can be used, but they are sometimes less effective and more expensive.

All installations should be inspected regularly and provisions made for prompt repair if needed. Initial failure of a small portion of a system normally can be repaired easily and inexpensively. Neglect of small failures, however, can often result in the failure of large portions of a system.

Properly designed and installed vegetative portions of systems will become self-repairing to a large extent. Periodic pruning and replanting may be required to maintain healthy and vigorous vegetation. Structural elements, such as cribwalls, rock walls, and gabions,

Figure 18–3 Live stake installation

Cross section
Not to scale

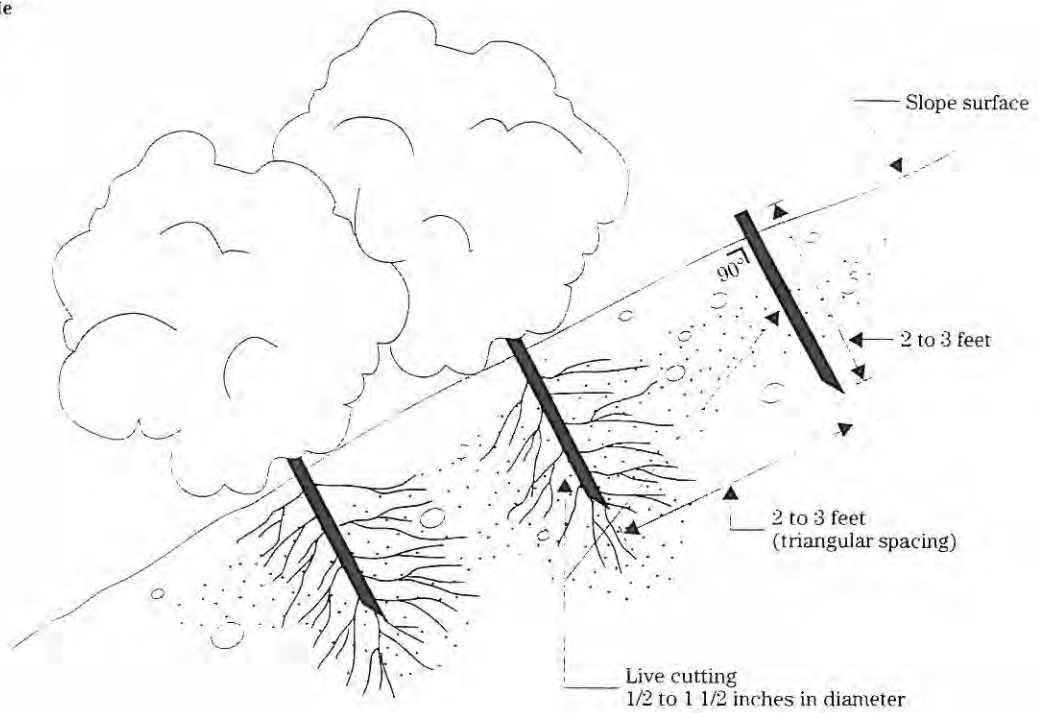

Note:
Rooted/leafed condition of the living plant material is not representative of the time of installation.

may require maintenance and/or replacement throughout their life. Where the main function of structural elements is to allow vegetation to become established and take over the role of slope stabilization, the eventual deterioration of the structures is not a cause for concern.

(b) Soil bioengineering techniques

The following describes soil bioengineering techniques. Their applications, effectiveness, and construction guidelines are also presented.

(1) Live stake

*(i) **Description***—Live staking involves the insertion and tamping of live, rootable vegetative cuttings into the ground (fig. 18–3). If correctly prepared and placed, the live stake will root and grow (fig. 18–4).

A system of stakes creates a living root mat that stabilizes the soil by reinforcing and binding soil particles together and by extracting excess soil moisfure. Most willow species root rapidly and begin to dry out a slope soon after installation. This is an appropriate technique for repair of small earth slips and slumps that frequently are wet.

Figure 18–4 Top growth and root development of a 7-month-old live stake (Robbin B. Sotir & Associates photo)

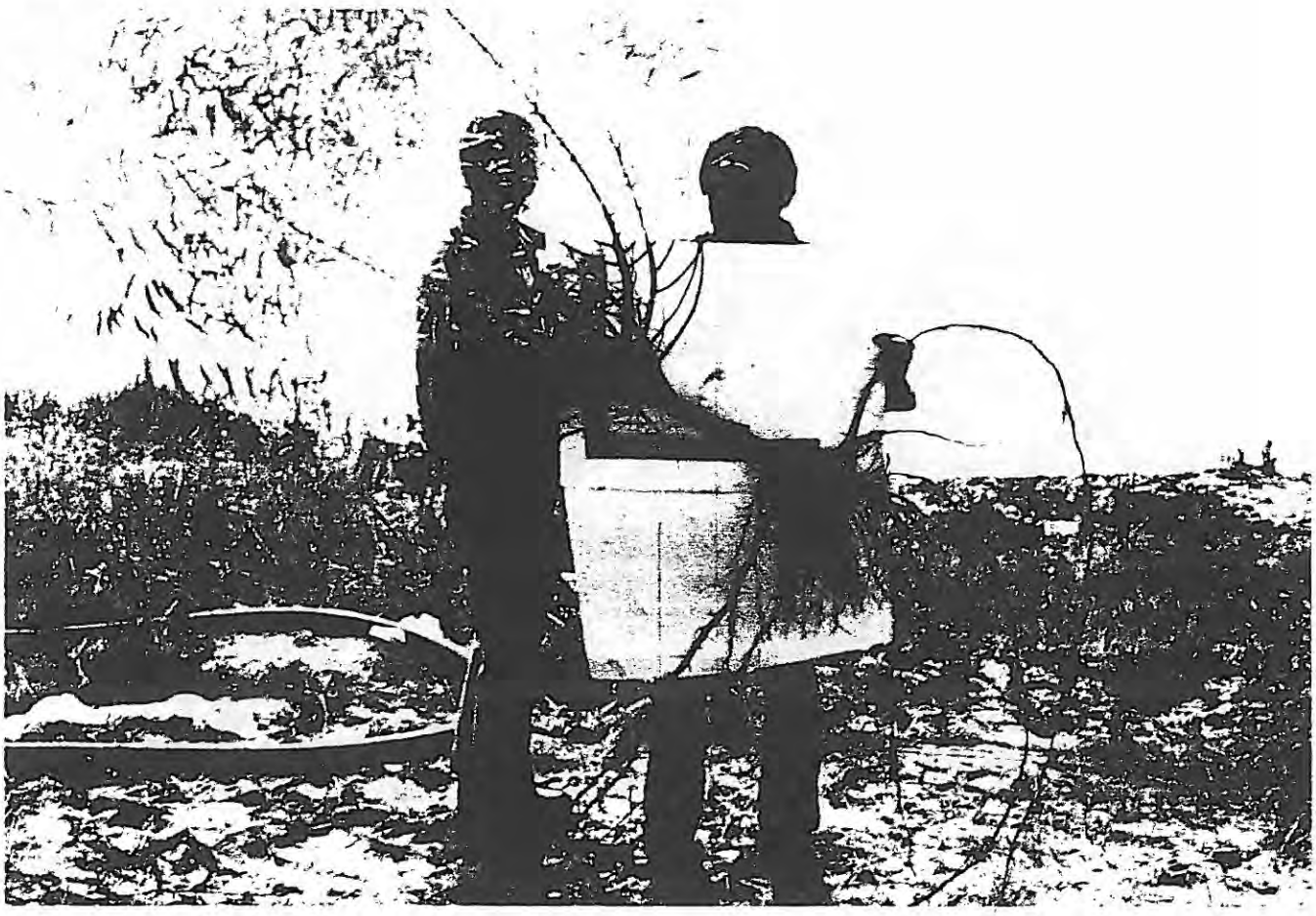

(ii) Applications and effectiveness:

- A technique for relatively uncomplicated site conditions when construction time is limited and an inexpensive method is necessary.
- May be used for pegging down surface erosion control materials.
- Enhances conditions for natural invasion and the establishment of other plants from the surrounding plant community.
- Can be used to stabilize intervening area between other soil bioengineering techniques, such as live fascines.

(iii) Construction guidelines

Live material sizes—The cuttings are usually 1/2 to 1 1/2 inches in diameter and 2 to 3 feet long, as shown in figure 18–5. For final size determination, refer to the available cutting source. Figure 18–6 shows a rooted, healthy live stake.

Live material preparation

- The materials must have side branches cleanly removed and the bark intact.
- The basal ends should be cut at an angle for easy insertion into the soil. The top should be cut square.
- Materials should be installed the same day that they are prepared.

Figure 18–5 A prepared live stake (note angled basal end and flat top end) (Robbin B. Sotir & Associates photo)

Installation

- Tamp the live stake into the ground at right angles to the slope. The installation may be started at any point on the slope face.
- The live stakes should be installed 2 to 3 feet apart using triangular spacing. The density of the installation will range from 2 to 4 stakes per square yard.
- The buds should be oriented up.
- Four-fifths of the length of the live stake should be installed into the ground and soil firmly packed around it after installation.
- Do not split the stakes during installation. Stakes that split should be removed and replaced.
- An iron bar can be used to make a pilot hole in firm soil. Drive the stake into the ground with a dead blow hammer (hammer head filled with shot or sand).

Figure 18–6 A live stake that has rooted and is demonstrating healthy growth (Robbin B. Sotir & Associates photo)

(2) Live fascine

(i) Description—Live fascines are long bundles of branch cuttings bound together into sausage-like structures (fig. 18–7).

When cut from appropriate species and properly installed with live and dead stout stakes, they will root and immediately begin to stabilize slopes. They should be placed in shallow contour trenches on dry slopes and at an angle on wet slopes to reduce erosion and shallow face sliding. This system, installed by a trained crew, does not cause much site disturbance (fig. 18–8)

(ii) Applications and effectiveness

- An effective stabilization technique for slopes.
- Protects slopes from shallow slides (1 to 2 foot depth).
- Immediately reduces surface erosion or rilling.
- Suited to steep, rocky slopes, where digging is difficult.
- Capable of trapping and holding soil on the face of the slope, thus reducing a long slope into a series of shorter slopes.
- Enhances vegetative establishment by creating a microclimate conducive to plant growth.

(iii) Construction guidelines

Live materials—Cuttings must be from species, such as young willows or shrub dogwoods, that root easily and have long, straight branches.

Live material sizes and preparation

- Cuttings tied together to form live fascine bundles vary in length from 5 to 30 feet or longer, depending on site conditions and limitations in handling.
- The completed bundles should be 6 to 8 inches in diameter, with all of the growing tips oriented in the same direction. Stagger the cuttings in the bundles so that tops are evenly distributed throughout the length of the uniformly sized live fascine.
- Live stakes should be 2 1/2 feet long in cut slopes and 3 feet long in fill slopes.

Figure 18–7 Fabrication of a live fascine bundle (Robbin B. Sotir & Associates photo)

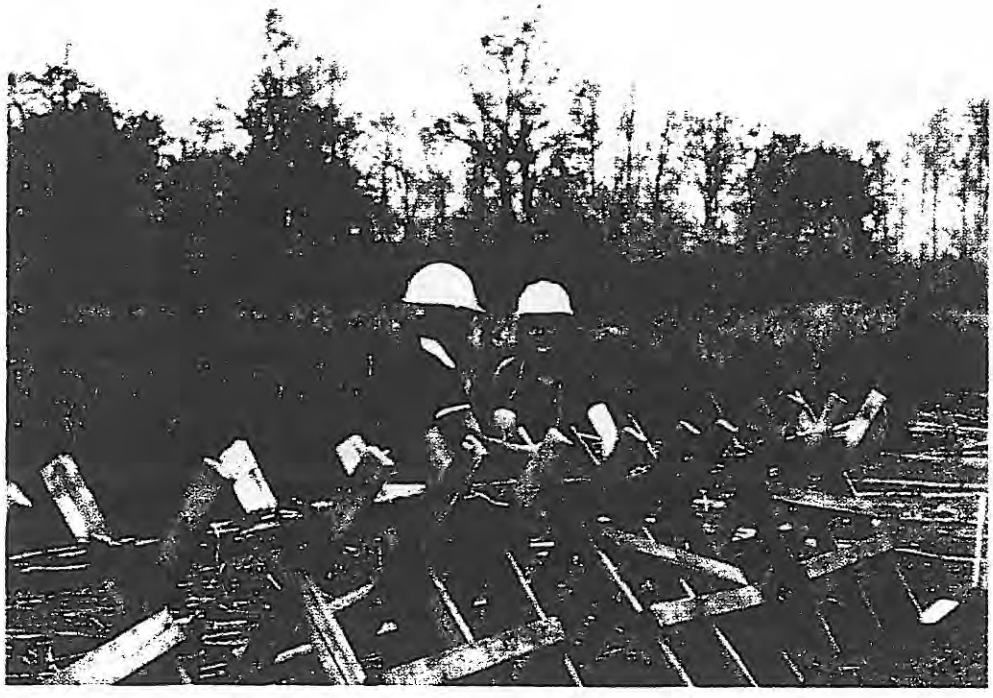

Figure 18–8 A live fascine system (Robbin B. Sotir & Associates photos)

Figure 18–8a During installation (note size and depth of trench to size of live fascine bundle)

Figure 18–8b Three months after installation

Inert materials—String used for bundling should be untreated twine.

Dead stout stakes used to secure the live fascines should be 2 1/2-foot long, untreated, 2 by 4 lumber. Each length should be cut again diagonally across the 4-inch face to make two stakes from each length. Only new, sound, unused lumber should be used, and any stakes that shatter upon installation should be discarded (fig. 18–9).

Installation

- Prepare the live fascine bundles and live stakes immediately before installation.
- Beginning at the base of the slope, dig a trench on the contour just large enough to contain the live fascine. The trench will vary in width from 12 to 18 inches, depending on the angle of the slope to be treated. The depth will be 6 to 8 inches, depending on the individual bundle's final size.
- Place the live fascine into the trench.
- Drive the dead stout stakes directly through the live fascine every 2 to 3 feet along its length. Extra stakes should be used at connections or bundle overlaps. Leave the top of the stakes flush with the installed bundle.
- Live stakes are generally installed on the downslope side of the bundle. Drive the live stakes below and against the bundle between the previously installed dead stout stakes. The live stakes should protrude 2 to 3 inches above the top of the live fascine. Place moist soil along the sides of the live fascine. The top of the fascine should be slightly visible when the installation is completed (fig. 18–10).

Next, at intervals on contour or at an angle up the face of the bank, repeat the preceding steps to the top of the slope (table 18–3). When possible, place one or two rows over the top of the slope.

Long straw or similar mulching material should be placed between rows on 2.5:1 or flatter slopes, while slopes steeper than 2.5:1 should have jute mesh or similar material placed in addition to the mulch.

Figure 18–9 A dead stout stake

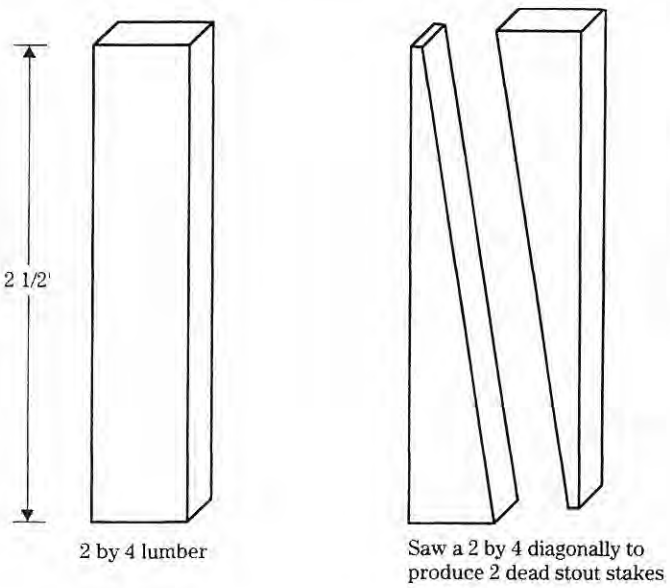

Table 18–3 Live fascine installation guidelines

Slope	Slope distance between trenches (ft)	Maximum slope length (ft)
1:1 to 1.5:1	3 – 4	15
1.5:1 to 2:1	4 – 5	20
2:1 to 2.5:1	5 – 6	30
2.5:1 to 3:1	6 – 8	40
3.5:1 to 4:1	8 – 9	50
4.5:1 to 5:1	9 – 10	60

Figure 18–10 Live fascine details

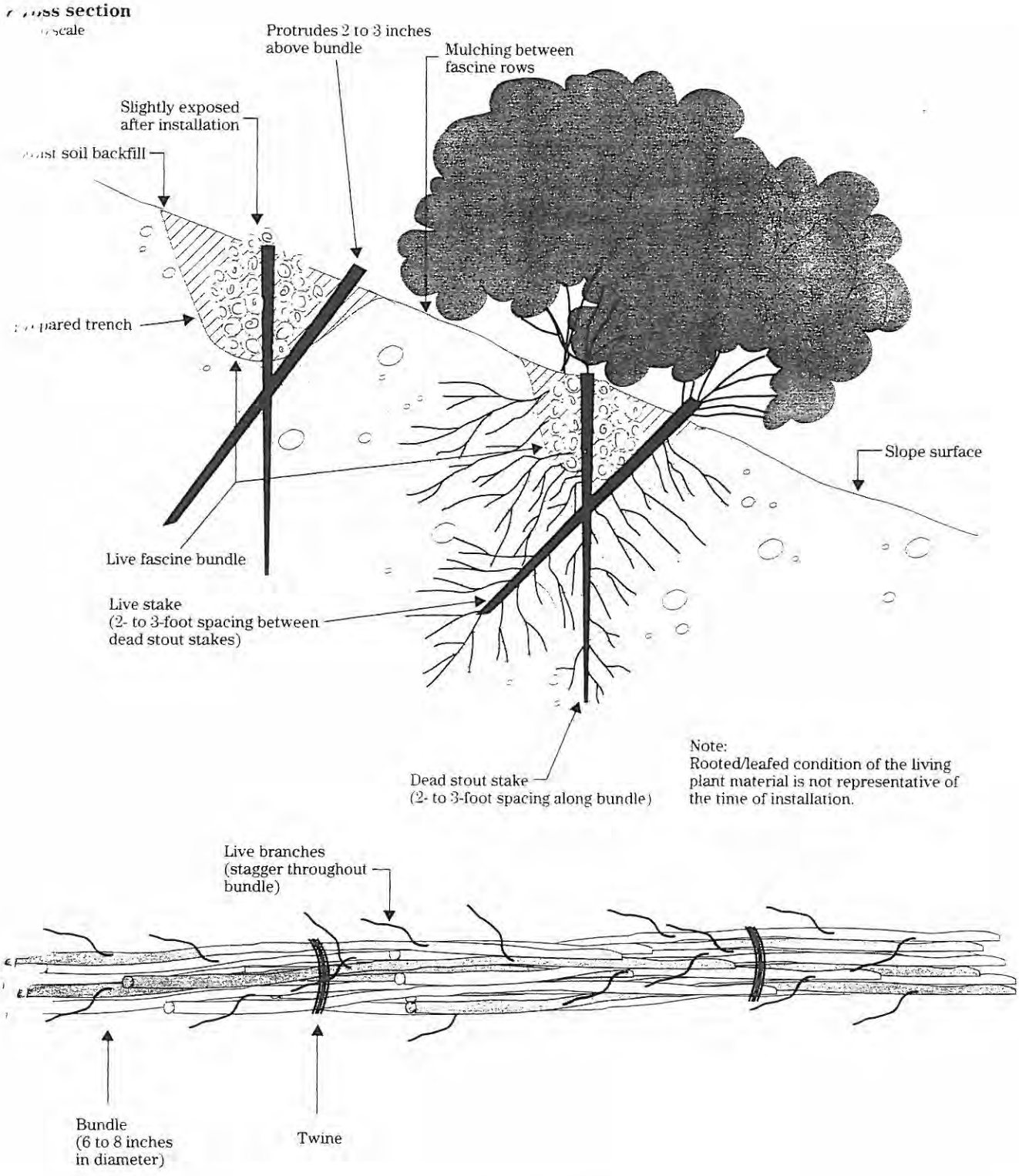

(3) Brushlayer

(i) Description—Brushlayering is somewhat similar to live fascine systems because both involve the cutting and placement of live branch cuttings on slopes. The two techniques differ principally in the orientation of the branches and the depth to which they are placed in the slope. In brushlayering, the cuttings are oriented more or less perpendicular to the slope contour (fig. 18–11). The perpendicular orientation is more effective from the point of view of earth reinforcement and mass stability of the slope.

Brushlayering consists of placing live branch cuttings in small benches excavated into the slope. The benches can range from 2 to 3 feet wide. These systems are recommended on slopes up to 2:1 in steepness and not to exceed 15 feet in vertical height. Brushlayer branches serve as tensile inclusions or reinforcing units. The portions of the brush that protrude from the slope face assist in retarding runoff and reducing surface erosion.

(ii) Applications and effectiveness—Brushlayers perform several immediate functions in erosion control, earth reinforcement, and mass stability of slopes:

- Breaking up the slope length into a series of shorter slopes separated by rows of brushlayer.
- Reinforcing the soil with the unrooted branch stems.
- Reinforcing the soil as roots develop, adding significant resistance to sliding or shear displacement.
- Providing slope stability and allowing vegetative cover to become established.
- Trapping debris on the slope.
- Aiding infiltration on dry sites.
- Drying excessively wet sites.
- Adjusting the site's microclimate, thus aiding seed germination and natural regeneration.
- Redirecting and mitigating adverse slope seepage by acting as horizontal drains.

(iii) Construction guidelines

Live material sizes—Branch cuttings should be 1/2 to 2 inches in diameter and long enough to reach the back of the bench. Side branches should remain intact for installation.

Installation

- Starting at the toe of the slope, benches should be excavated horizontally, on the contour, or angled slightly down the slope, if needed to aid drainage. The bench should be constructed 2 to 3 feet wide.
- The surface of the bench should be sloped so that the outside edge is higher than the inside (fig. 18–12).
- Live branch cuttings should be placed on the bench in a crisscross or overlapping configuration.
- Branch growing tips should be aligned toward the outside of the bench.
- Backfill is placed on top of the branches and compacted to eliminate air spaces. The brush tips should extend slightly beyond the fill to filter sediment.
- Each lower bench is backfilled with the soil obtained from excavating the bench above.
- Long straw or similar mulching material with seeding should be placed between rows on 3:1 or flatter slopes, while slopes steeper than 3:1 should have jute mesh or similar material placed in addition to the mulch.
- The brushlayer rows should vary from 3 to 5 feet apart, depending upon the slope angle and stability (table 18–4).

Table 18–4 Brushlayer installation guidelines

Slope	Slope distance between benches		Maximum slope length (ft)
	Wet slopes (ft)	Dry slopes (ft)	
2:1 to 2.5:1	3	3	15
2.5:1 to 3:1	3	4	15
3.5:1 to 4:1	4	5	20

Figure 18–11 A brushlayer system (Robbin B. Sotir & Associates photos)

Figure 18–11a During installation

Figure 18–11b Two years after installation

Figure 18–12 Installing a brushlayer (Robbin B. Sotir & Associates photos)

Figure 18–12a Bench being prepared for a brushlayer

Figure 18–12b Placing live branch cuttings (Note crisscross configuration)

(4) Branchpacking

(i) Description—Branchpacking consists of alternating layers of live branch cuttings and compacted backfill to repair small localized slumps and holes in slopes (fig. 18–13).

(ii) Applications and effectiveness

- Effective in earth reinforcement and mass stability of small earthen fill sites.
- Produces a filter barrier, reducing erosion and scouring conditions.
- Repairs holes in earthen embankments other than dams where water retention is a function.
- Provides immediate soil reinforcement.

(iii) Construction guidelines

Live material—Live branch cuttings may range from 1/2 inch to 2 inches in diameter. They should be long enough to touch the undisturbed soil at the back of the trench and extend slightly from the rebuilt slope face.

Inert material—Wooden stakes should be 5 to 8 feet long and made from 3- to 4-inch diameter poles or 2 by 4 lumber, depending upon the depth of the particular slump or hole.

Figure 18–13 A branchpacking system being installed (Robbin B. Sotir & Associates photo)

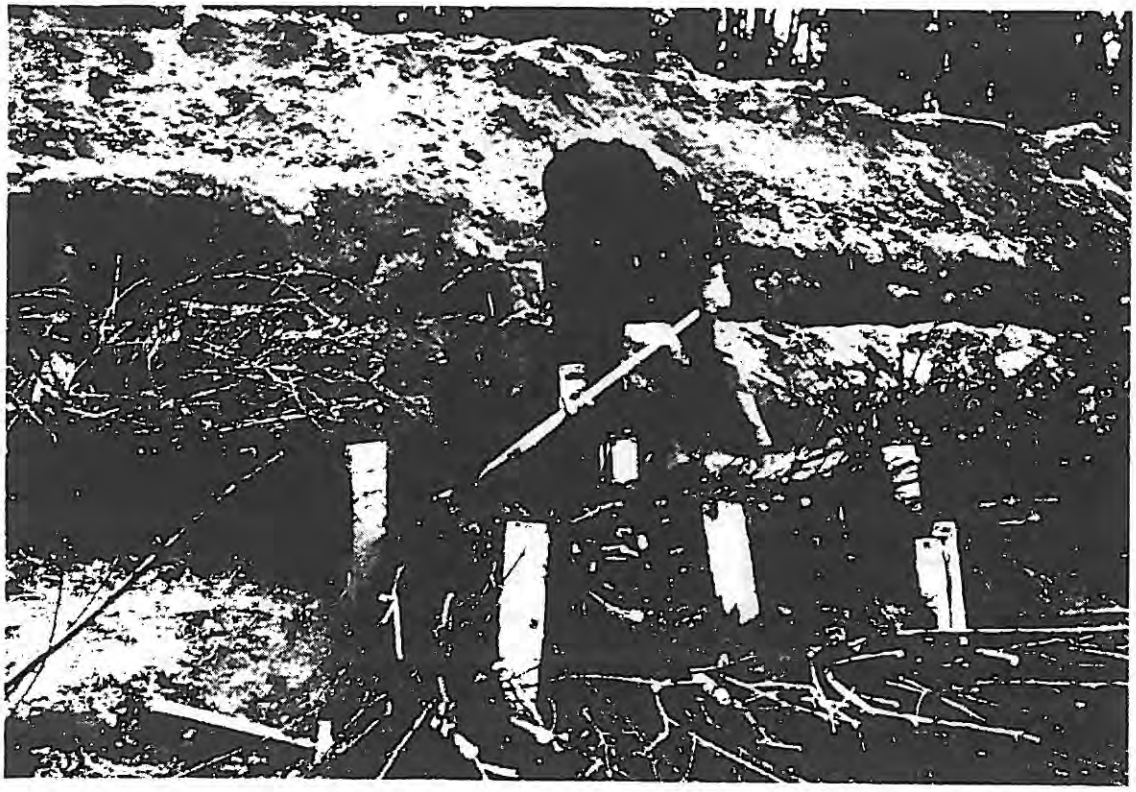

Installation

- Starting at the lowest point, drive the wooden stakes vertically 3 to 4 feet into the ground. Set them 1 to 1 1/2 feet apart.
- A layer of living branches 4 to 6 inches thick is placed in the bottom of the hole, between the vertical stakes, and perpendicular to the slope face (fig 18–14). They should be placed in a crisscross configuration with the growing tips generally oriented toward the slope face. Some of the basal ends of the branches should touch the back of the hole or slope.
- Subsequent layers of branches are installed with the basal ends lower than the growing tips of the branches.
- Each layer of branches must be followed by a layer of compacted soil to ensure soil contact with the branch cuttings.
- The final installation should match the existing slope. Branches should protrude only slightly from the filled face.
- The soil should be moist or moistened to insure that live branches do not dry out.

The live branch cuttings serve as tensile inclusions for reinforcement once installed. As plant tops begin to grow, the branchpacking system becomes increasingly effective in retarding runoff and reducing surface erosion. Trapped sediment refills the localized slumps or holes, while roots spread throughout the backfill and surrounding earth to form a unified mass (fig. 18–15). Branchpacking is not effective in slump areas greater than 4 feet deep or 5 feet wide.

Figure 18–14 Branchpacking details

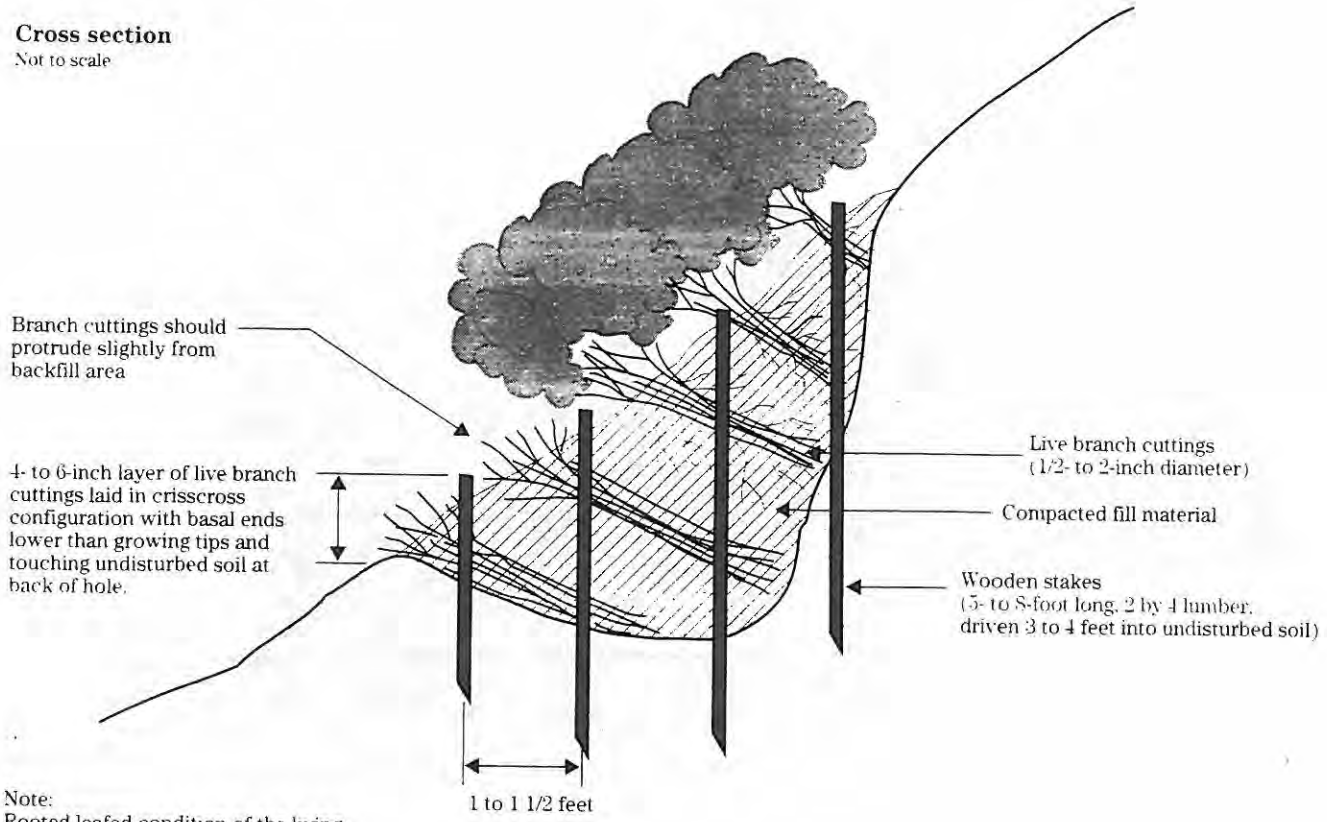

Figure 18–15 Completed branchpacking system (Robbin B. Sotir & Associates photos)

Figure 18–15a Newly installed system

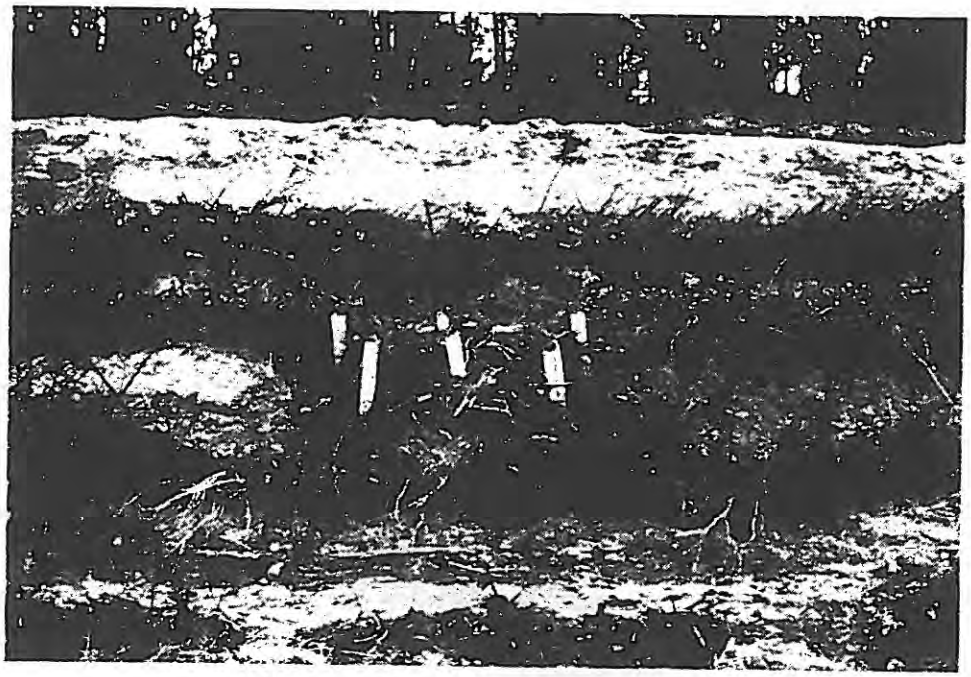

Figure 18–15b One year after installation

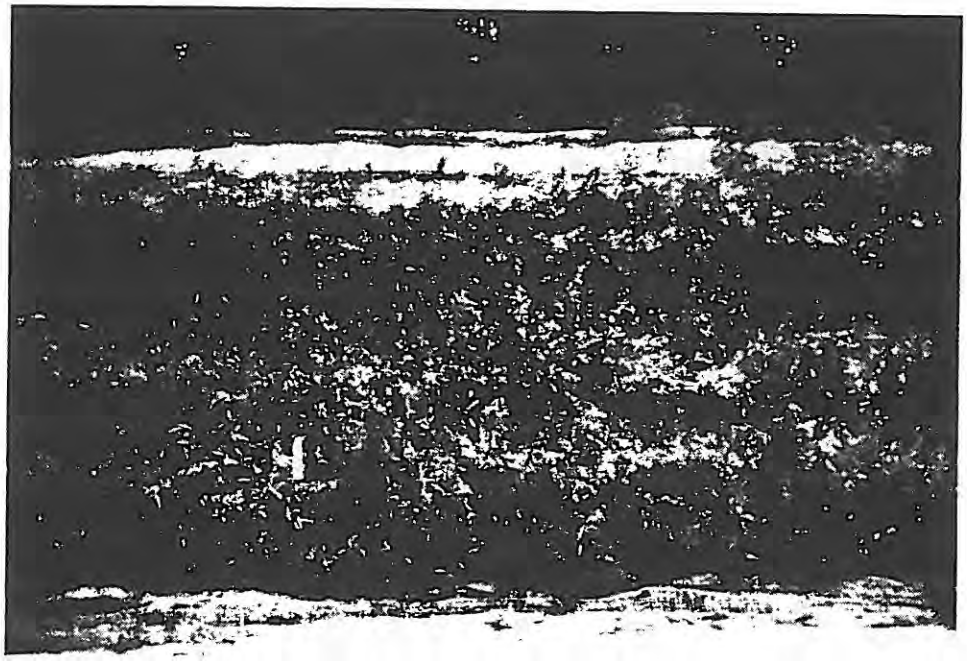

(5) Live gully repair

(i) Description—A live gully repair utilizes alternating layers of live branch cuttings and compacted soil to repair small rills and gullies. Similar to branchpacking, this method is more appropriate for the repair of rills and gullies.

(ii) Applications and effectiveness

- The installed branches offer immediate reinforcement to the compacted soil and reduce the velocity of concentrated flow of water.
- Provides a filter barrier that reduces rill and gully erosion.
- Limited to rills or gullies which are a maximum of 2 feet wide, 1 foot deep, and 15 feet long.

(iii) Construction guidelines

Live material sizes—Live branch cuttings may range from 1/2 inch to 2 inches in diameter. They should be long enough to touch the undisturbed soil at the back of the rill or gully and extend slightly from the rebuilt slope face.

Inert materials—Fill soil is compacted in alternate layers with live branch cuttings.

Installation

- Starting at the lowest point of the slope, place a 3- to 4-inch layer of branches at lowest end of the rill or gully and perpendicular to the slope (fig. 18–16).

Figure 18–16 Live gully repair details

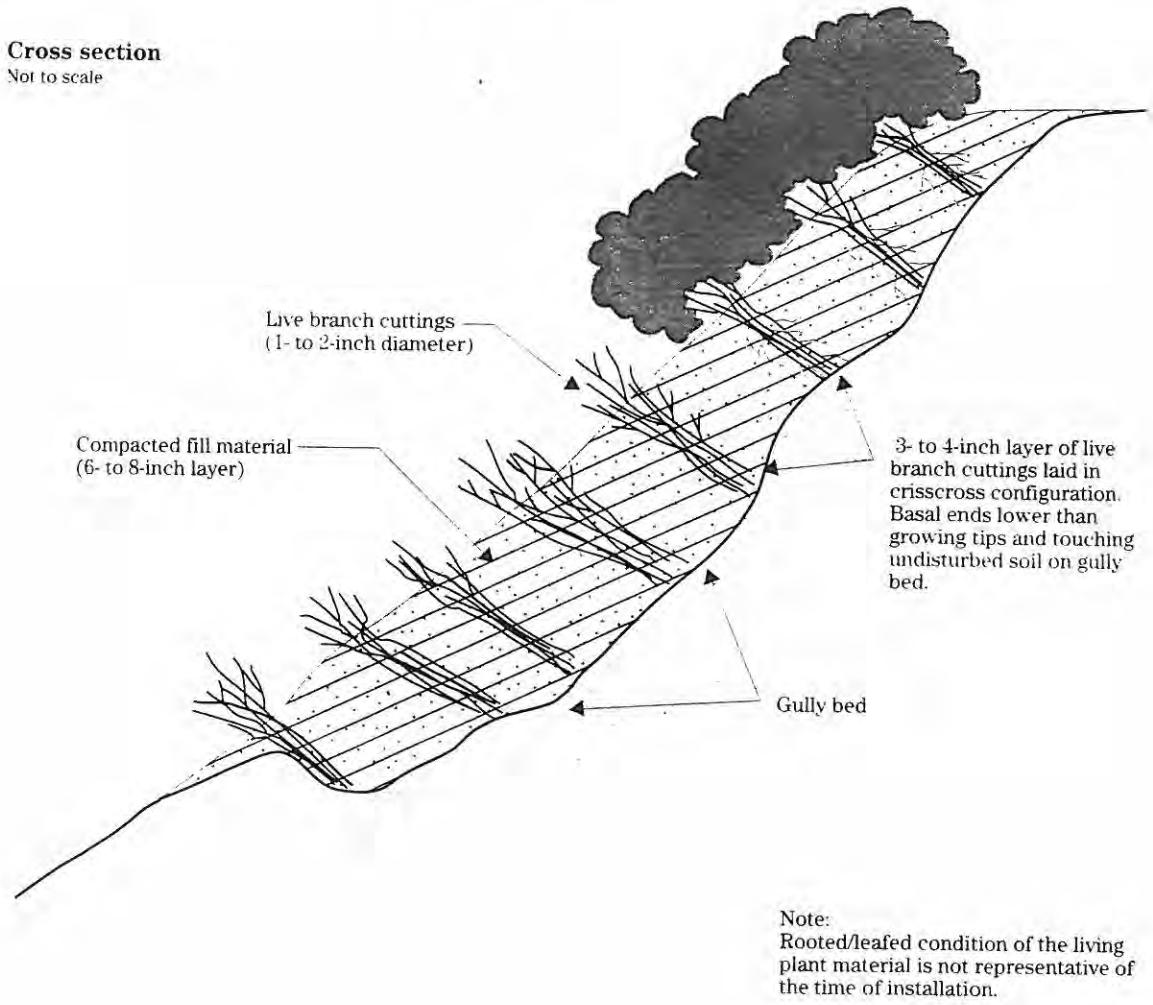

- Cover with a 6- to 8-inch layer of fill soil.
- Install the live branches in a crisscross fashion. Orient the growing tips toward the slope face with basal ends lower than the growing tips.
- Follow each layer of branches with a layer of compacted soil to ensure soil contact with the live branch cuttings.

(6) Live cribwall

*(i) **Description***—A live cribwall consists of a hollow, box-like interlocking arrangement of untreated log or timber members. The structure is filled with suitable backfill material and layers of live branch cuttings which root inside the crib structure and extend into the slope. Once the live cuttings root and become established, the subsequent vegetation gradually takes over the structural functions of the wood members (fig. 18–17).

(ii) Applications and effectiveness

- This technique is appropriate at the base of a slope where a low wall may be required to stabilize the toe of the slope and reduce its steepness.
- Not designed for or intended to resist large, lateral earth stresses. It should be constructed to a maximum of 6 feet in overall height, including the excavation required for a stable foundation.
- Useful where space is limited and a more vertical structure is required.
- Provides immediate protection from erosion, while established vegetation provides long-term stability.
- Should be tilted back or battered if the system is built on a smooth, evenly sloped surface.
- May also be constructed in a stair-step fashion, with each successive course of timbers set back 6 to 9 inches toward the slope face from the previously installed course.

Figure 18–17 A live cribwall being installed (Robbin B. Sotir & Associates photo)

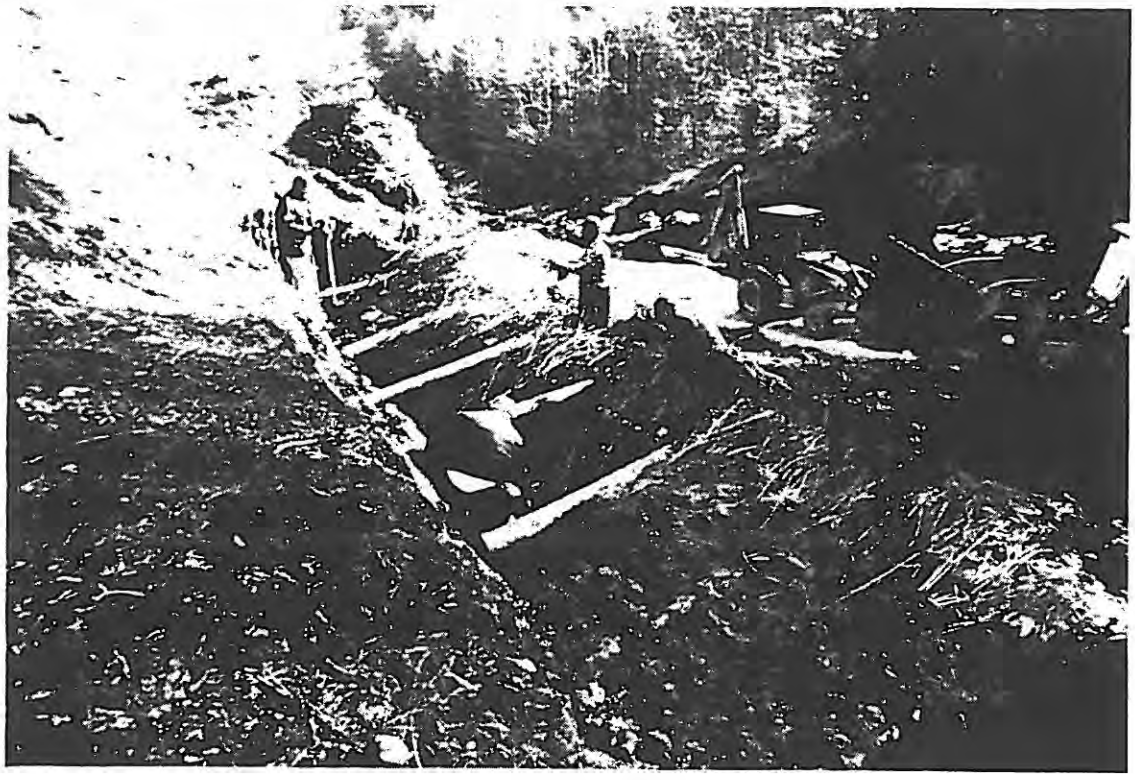

(iii) Construction guidelines

Live material sizes—Live branch cuttings should be 1/2 to 2 inches in diameter and long enough to reach the back of the wooden crib structure.

Inert materials—Logs or timbers should range from 4 to 6 inches in diameter or dimension. The lengths will vary with the size of the crib structure.

Large nails or rebar are required to secure the logs or timbers together.

Installation

- Starting at the lowest point of the slope, excavate loose material 2 to 3 feet below the ground elevation until a stable foundation is reached.
- Excavate the back of the stable foundation (closest to the slope) slightly deeper than the front to add stability to the structure.
- Place the first course of logs or timbers at the front and back of the excavated foundation, approximately 4 to 5 feet apart and parallel to the slope contour.
- Place the next course of logs or timbers at right angles (perpendicular to the slope) on top of the previous course to overhang the front and back of the previous course by 3 to 6 inches.
- Each course of the live cribwall is placed in the same manner and nailed to the preceding course with nails or reinforcement bars.
- When the cribwall structure reaches the existing ground elevation, place live branch cuttings on the backfill perpendicular to the slope; then cover the cuttings with backfill and compact.
- Live branch cuttings should be placed at each course to the top of the cribwall structure with growing tips oriented toward the slope face. Follow each layer of branches with a layer of compacted soil to ensure soil contact with the live branch cuttings. Some of the basal ends of the live branch cuttings should reach to undisturbed soil at the back of the cribwall with growing tips protruding sightly beyond the front of the cribwall (fig. 18–18).

Figure 18–18 Live cribwall details

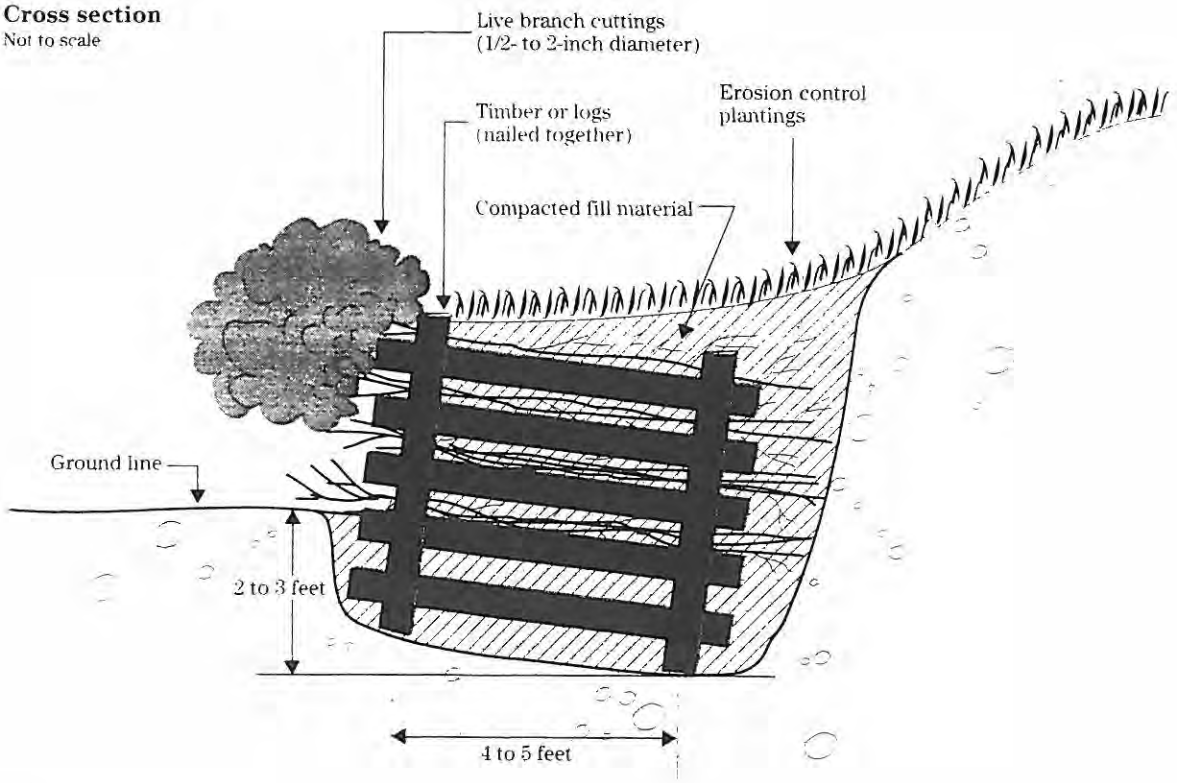

Note:
Rooted/leafed condition of the living plant material is not representative of the time of installation.

(7) Vegetated rock gabions

(i) Description—Vegetated gabions begin as rectangular containers fabricated from a triple twisted, hexagonal mesh of heavily galvanized steel wire. Empty gabions are placed in position, wired to adjoining gabions, filled with stones and then folded shut and wired at the ends and sides. Live branches are placed on each consecutive layer between the rock-filled baskets. These will take root inside the gabion baskets and in the soil behind the structures. In time the roots consolidate the structure and bind it to the slope (fig. 18–19).

(ii) Applications and effectiveness

- This technique is appropriate at the base of a slope where a low wall may be required to stabilize the toe of the slope and reduce its steepness.
- Not designed for or intended to resist large, lateral earth stresses. It should be constructed to a maximum of 5 feet in overall height, including the excavation required for a stable foundation.
- Useful where space is limited and a more vertical structure is required.

(iii) Construction guidelines

Live material sizes—Branches should range from 1/2 to 1 inch in diameter and must be long enough to reach beyond the back of the rock basket structure into the backfill.

Inert materials—Inert material requirements include wire gabion baskets and rocks to fill the baskets.

Figure 18–19 An established vegetated rock gabion system (Robbin B. Sotir & Associates photo)

Installation

- Starting at the lowest point of the slope, excavate loose material 2 to 3 feet below the ground elevation until a stable foundation is reached.
- Excavate the back of the stable foundation (closest to the slope) slightly deeper than the front to add stability to the structure. This will provide additional stability to the structure and ensure that the living branches root well.
- Place the fabricated wire baskets in the bottom of the excavation and fill with rock.
- Place backfill between and behind the wire baskets.
- Place live branch cuttings on the wire baskets perpendicular to the slope with the growing tips oriented away from the slope and extending slightly beyond the gabions. The live cuttings must extend beyond the backs of the wire baskets into the fill material. Place soil over the cuttings and compact it.
- Repeat the construction sequence until the structure reaches the required height (fig. 18–20).

Figure 18–20 Vegetated rock gabion details

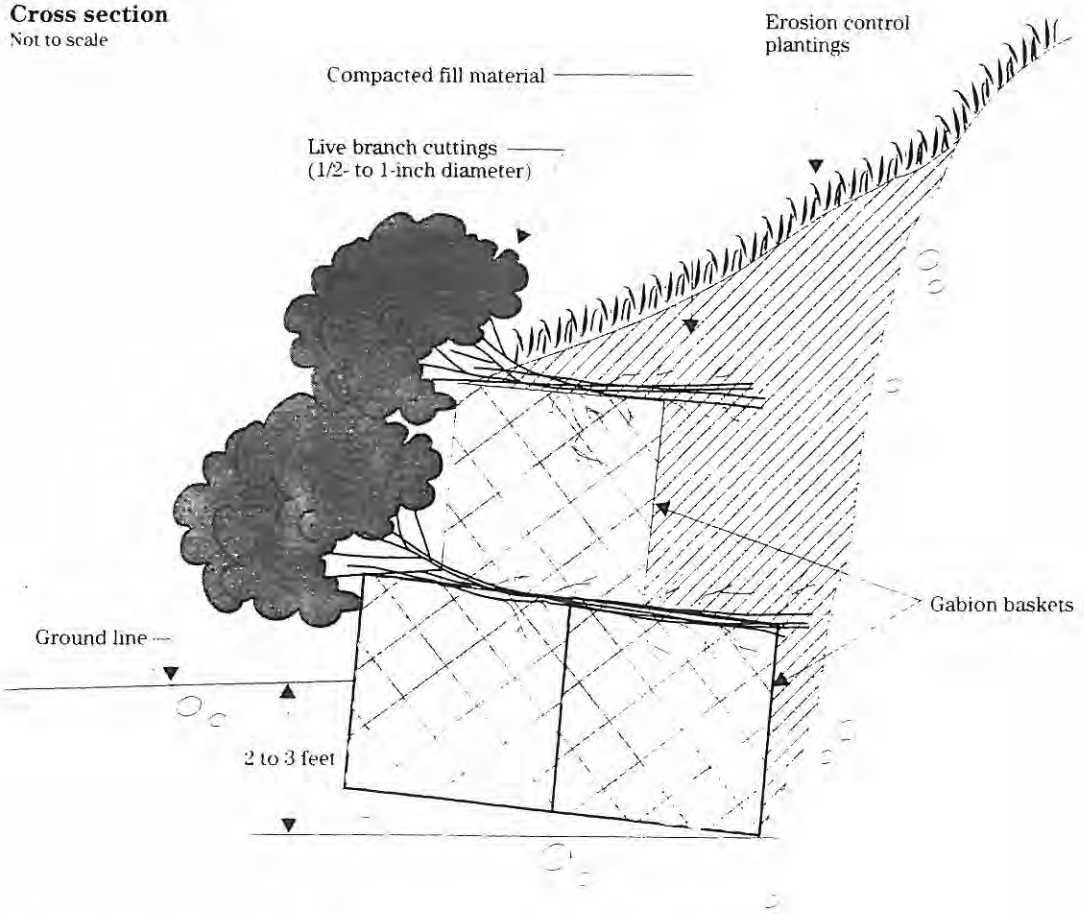

Note:
Rooted/leafed condition of the living plant material is not representative of the time of installation.

(8) Vegetated rock wall

(i) Description—A vegetated rock wall is a combination of rock and live branch cuttings used to stabilize and protect the toe of steep slopes. Vegetated rock walls differ from conventional retaining structures in that they are placed against relatively undisturbed earth and are not intended to resist large lateral earth pressures.

(ii) Applications and effectiveness

- This system is appropriate at the base of a slope where a low wall may be required to stabilize the toe of the slope and reduce its steepness.
- Useful where space is limited and natural rock is available.

(iii) Construction guidelines

Live material sizes—Live cuttings should have a diameter of 1/2 to 1 inch and be long enough to reach beyond the rock structure into the fill or undisturbed soil behind.

Inert materials—Inert materials consist of rocks and fill material for the wall construction. Rock used should normally range from 8 to 24 inches in diameter. Larger boulders should be used for the base.

Installation

- Starting at the lowest point of the slope, remove loose soil until a stable base is reached. This usually occurs 2 to 3 feet below ground elevation. Excavate the back of the stable foundation (closest to the slope) slightly deeper than the front to add stability to the structure.
- Excavate the minimum amount from the existing slope to provide a suitable recess for the wall.
- Provide a well-drained base in locations subject to deep frost penetration.
- Place rocks with at least a three-point bearing on the foundation material or underlying rock course. They should also be placed so that their center of gravity is as low as possible, with their long axis slanting inward toward the slope if possible.
- When a rock wall is constructed adjacent to an impervious surface, place a drainage system at the back of the foundation and outside toe of the wall to provide an appropriate drainage outlet.
- Overall height of the rock wall, including the footing, should not exceed 5 feet.
- A wall can be constructed with a sloping bench behind it to provide a base on which live branch cuttings can be placed during construction. Live branch cuttings should also be tamped or placed into the openings of the rock wall during or after construction. The butt ends of the branches should extend into the backfill or undisturbed soil behind the wall.
- The live branch cuttings should be oriented perpendicular to the slope contour with growing tips protruding slightly from the finished rock wall face (fig. 18–21).

Figure 18–21 Vegetated rock wall details

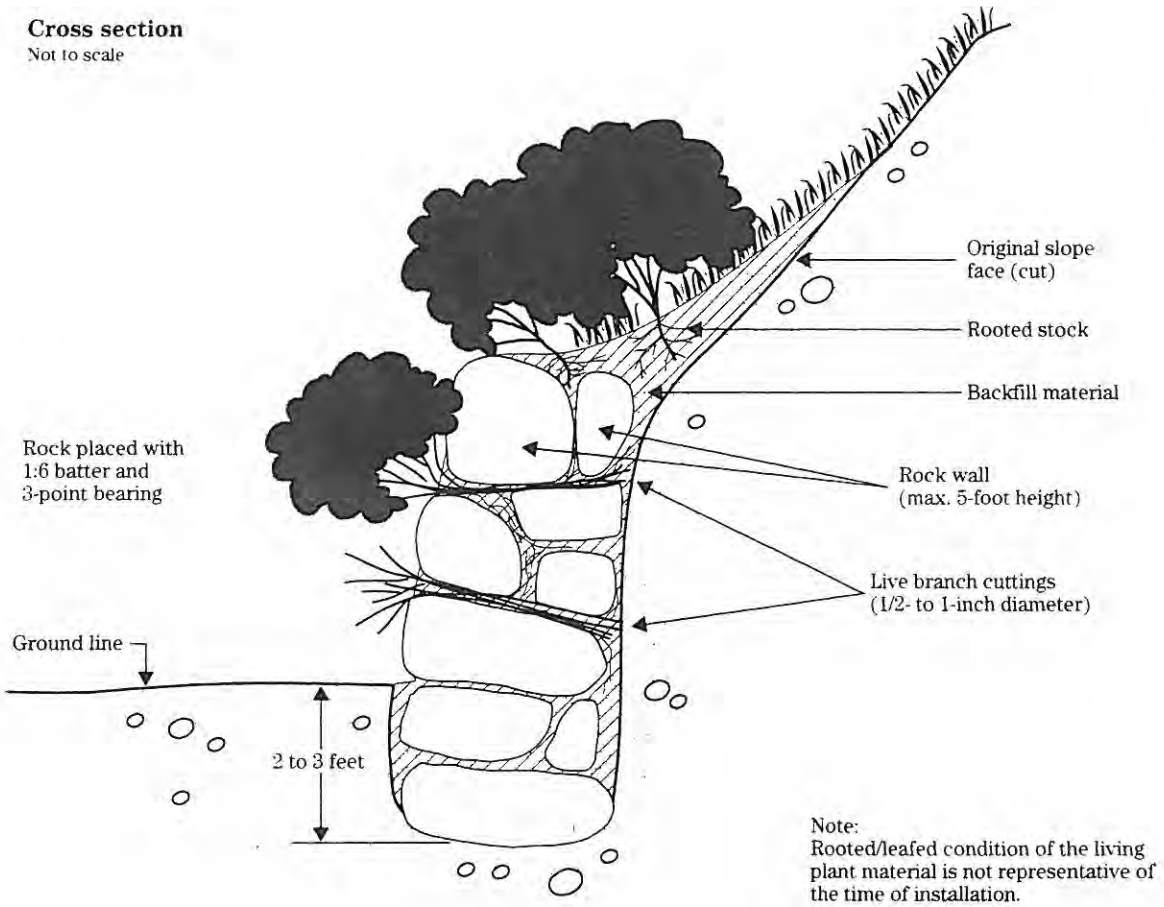

(9) Joint planting

(i) Description—Joint planting or vegetated riprap involves tamping live cuttings of rootable plant material into soil between the joints or open spaces in rocks that have previously been placed on a slope (fig. 18–22). Alternatively, the cuttings can be tamped into place at the same time that rock is being placed on the slope face.

(ii) Applications and effectiveness

- Used where rock riprap is required.
- Roots improve drainage by removing soil moisture. Over time, they create a living root mat in the soil base upon which the rock has been placed. The root systems of this mat help to bind or reinforce the soil and to prevent washout of fines between and below the rock units (fig. 18–23).

(iii) Construction guidelines

Live material sizes—The cuttings must have side branches removed and bark intact. They should range in diameter from 1/2 inch to 1 1/2 inches and be sufficiently long to extend into soil below the rock surface.

Installation

- Tamp live branch cuttings into the openings of the rock during or after construction. The butt ends of the branches should extend into the backfill or undisturbed soil behind the riprap.
- Orient the live branch cuttings perpendicular to the slope with growing tips protruding slightly from the finished face of the rock (fig. 18–24).

Figure 18–22 A newly established joint planting stake (Robbin B. Sotir & Associates photo)

Figure 18–23 Roots improve drainage by removing soil moisture (Robbin B. Sotir & Associates photos)

Figure 18–23a Root system 7 months after installation

Figure 18–23b Joint planted area after a 2 year growth

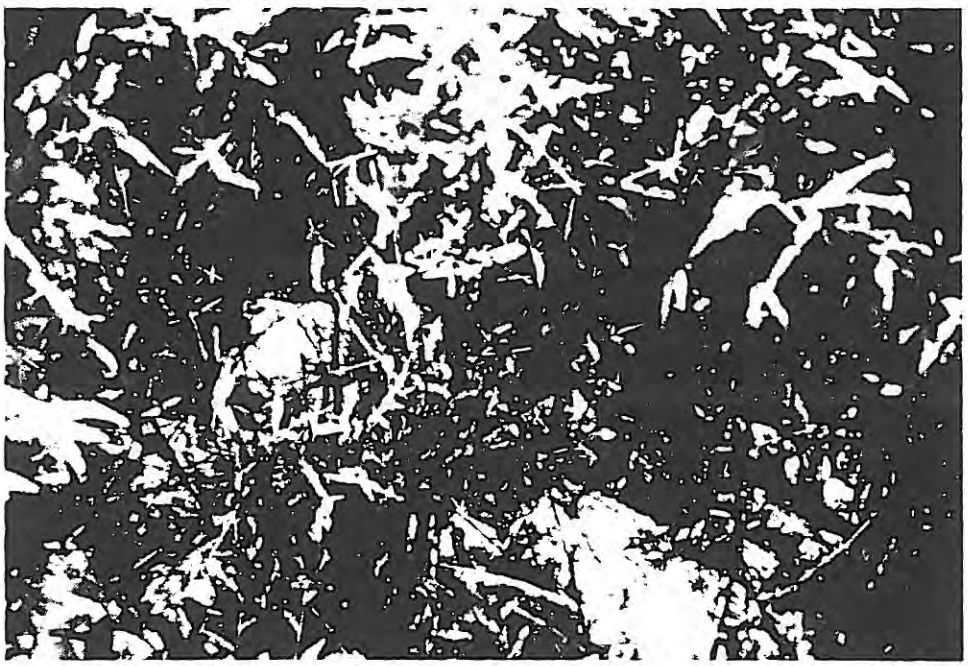

Figure 18–24 Joint planting details

Cross section
Not to scale

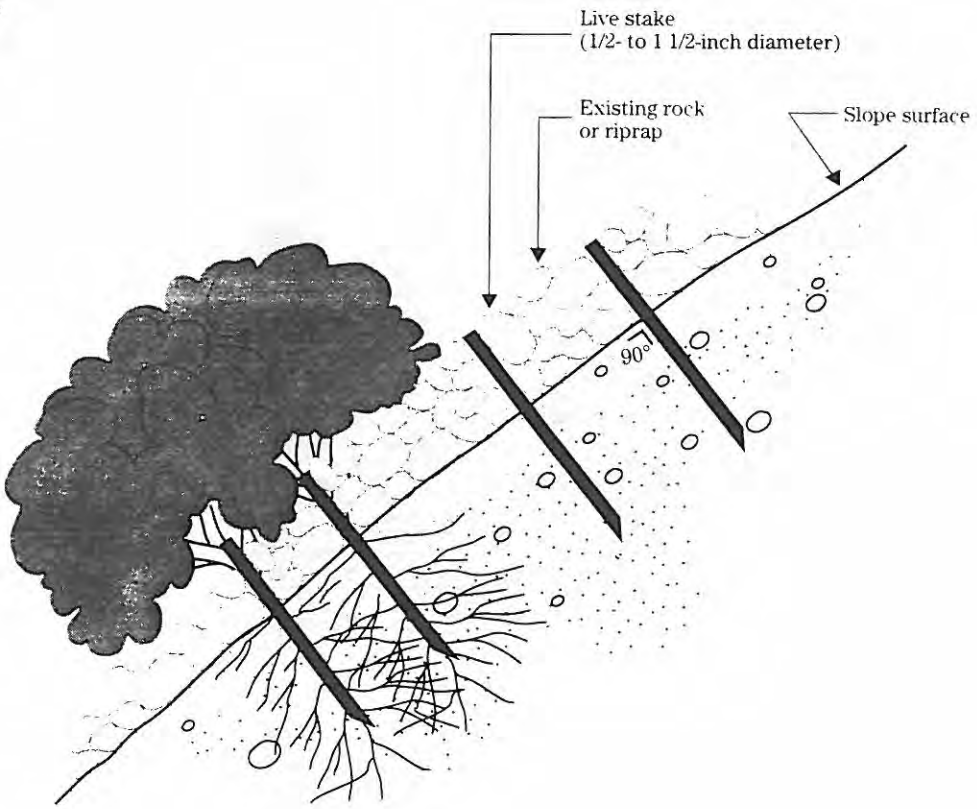

Note:
Rooted/leafed condition of the living plant material is not representative of the time of installation.

(c) Soil bioengineering materials

(1) Locating and selecting plant materials

(i) Commercial sources—Commercially grown plant materials are suitable sources of vegetation for use in soil bioengineering systems; however, it is necessary to allow adequate lead time for their procurement and delivery.

The SCS Plant Materials Program has selected superior cultivars of willows, dogwoods, and other species, which have been evaluated in soil bioengineering systems and are being produced commercially. The most desirable species and cultivars to use can be determined from specifications for critical area stabilization for each state.

The information on plant tolerances in table 18–5 should be used in selecting species appropriate for adverse site conditions. Plant materials specialists are closely involved with the testing of plants and can assist with up-to-date information on cultivar adaptation.

Table 18–5 Plant tolerance

Name	Location	Availability	Tolerance to deposition [1]	Tolerance to flooding [2]	Tolerance to drought [3]	Salt tolerance [4]
Acer negundo Boxelder	N, NE	Common	High	High	High	Medium
Alnus rubra Red alder	NW	Very common	High	Medium	Low	Low
Baccharis glutinosa Water wally	W	Common	Medium	High	Medium	Low
Baccharis halimifolia Eastern baccharis	S, SE	Common	Medium	High	Medium	Medium
Baccharis pilularis Coyotebrush	W	Very common	Medium	Medium	High	Medium
Baccharis viminea Mule fat	W	Very common	High	High	High	Medium
Betula papyrifera Paper birch	N, E, & W	Common	Medium	Medium	Medium	Medium
Betula pumila Low birch	N, E, & W	Common	Low	– – –		Low
Cornus amomum Silky dogwood	N, SE	Very common	Low	Medium	Medium	Low

See footnotes at end of table.

Table 18–5 Plant tolerance — Continued

Name	Location	Availability	Tolerance to deposition [1]	Tolerance to flooding [2]	Tolerance to drought [3]	Salt tolerance [4]
Cornus racemosa Gray dogwood	NE	Common	Medium	Medium	High	Low
Cornus rugosa Roundleaf dogwood	NE	Common	---	---	---	---
Cornus sericea ssp. stolonifera Red osier dogwood	N, NE, & NW	Very common	Low	High	Medium	Low
Crataegus Sp. Hawthorn	SE	Uncommon	Medium	Low	High	Low
Elaeagnus commutata Silverberry	N. Cent.	Very Common	High	Low	High	Medium
Ligustrum sinense Chinese privet	S, SE	Common	High	Medium	Medium	Low
Lonicera involucrata Black twinberry	E	Common	Medium	Medium	Low	Low
Physocarpus capitatus Pacific ninebark	NW, W	Common	Low	Medium	Low	Low
Physocarpus opulifolius Common ninebark	NE	Common	Low	Medium	Medium	Medium
Populus angustifolia Arrowleaf cottonwood	W	Common	Medium	Medium	High	Medium
Populus balsamifera ssp. trichocarpa Black cottonwood	NW	Common	Medium	Medium	Medium	Medium
Populus deltoides Eastern cottonwood	MW, E	Very common	Medium	High	Medium	Low
Populus fremontii Fremont cottonwood	SW	Very common	Medium	Medium	Medium	Medium

See footnotes at end of table.

Table 18–5 Plant tolerance — Continued

Name	Location	Availability	Tolerance to deposition [1]	Tolerance to flooding [2]	Tolerance to drought [3]	Salt tolerance [4]
Populus tremuloides Quaking aspen	NW	Very common	Medium	Low	Medium	Medium
Robinia pseudoacacia Black locust	NE	Common	Medium	Low	High	High
Rubus allegheniensis Allegheny blackberry	NE	Very common	Medium	Medium	Medium	Low
Rubus spectabilis Salmonberry	SW, NW	Very common	Medium	Medium	Medium	Low
Rubus strigosus Red raspberry	N, NE, & W	Very common	Medium	Low	Medium	Low
Salix exigua Coyote willow	NW	Fairly common	High	High	Medium	Low
ssp. interior Sandbar willow	N, SE	Common	High	High	Low	High
Salix amygdaloides Peachleaf willow	N, S	Common	High	High	Low	High
Salix bonplandiana Pussy willow	W & MW	Very common	Medium	Medium	Low	– – –
Salix eriocephala ssp. ligulifolia Erect willow	NW	Common	High	High	Medium	Low
Salix gooddingii Goodding willow	SW	Very common	High	Medium	Medium	Low
Salix hookeriana Hooker willow	NW	Common	High	High	Low	Medium
Salix humilis Prairie willow	N, NE	Very common	Medium	Medium	High	Low
Salix lasiolepis Arroya willow	W	Common	High	High	Medium	Low

See footnotes at end of table.

Table 18–5 Plant tolerance — Continued

Name	Location	Availability	Tolerance to deposition [1]	Tolerance to flooding [2]	Tolerance to drought [3]	Salt tolerance [4]
Salix lemmonii Lemmon willow	W	Common	High	High	Medium	Low
Salix lucida Shining willow	N, NE	Very common	Medium	Medium	Medium	Low
ssp. lasiandra Pacific willow	NW	Very common	High	High	Low	Low
Salix lutea Yellow willow	W	Very common	Medium	Medium	Medium	Low
Salix nigra Black willow	N, SE	Very common	High	High	Medium	Medium
Salix purpurea Streamco	N, S, E, & W	Very common	High	High	Medium	Low
Salix scouleriana Scoulers willow	NE	Very common	High	High	Medium	Low
Salix sitchensis Sitka willow	NW	Common	High	Medium	Medium	Low
Salix X cotteti Bankers willow	N, S, E, & W	Uncommon	High	High	Medium	Low
Salix discolor Red willow	N, NE	Very common	High	High	High	Medium
Sambucus cerulea Blueberry elderberry	W	Common	Medium	Medium	Medium	Low
Sambucus canadensis American elderberry	NE, SE	Very common	High	Medium	Medium	Low
Sambucus racemosa Red elderberry	NW	Common	Medium	Low	Medium	Low
ssp. pubens Scarlet elder	NE	Common	Medium	Medium	Medium	Low

See footnotes at end of table.

Table 18–5 Plant tolerance — Continued

Name	Location	Availability	Tolerance to deposition [1]	Tolerance to flooding [2]	Tolerance to drought [3]	Salt tolerance [4]
Spiraea alba Meadowsweet spirea	N, E	Common	Low	Medium	Medium	---
Spiraea douglasii Douglas spirea	NW	Common	Medium	Medium	Medium	Low
Spiraea tomentosa Hardhack spirea	NE	Common	Medium	Medium	Medium	Medium
Symphoricarpos albus Snowberry	N, NW, & E	Common	Low	Low	High	High
Viburnum alnifolium Hubbiebush viburnum	NE	Fairly common	---	---	---	---
Viburnum dentatum Arrowwood viburnum	E	Common	Medium	Medium	Medium	Low
Viburnum lentago Nannyberry viburnum	S, SE	Fairly common	Medium	Low	Medium	Low

[1] Tolerance to deposition—Regrowth from shallow coverage by soil (stream deposits, soil slips). High, Medium, or Low ability for regrowth.

[2] Tolerance to flooding:
- High—severely damaged after 10 to 30 days of flooding.
- Medium—severely damaged after 6 to 10 days of flooding.
- Low—severely damaged after 1 to 5 days of flooding.

[3] Tolerance to drought—Resistance to drought (relative to native vegetation on similar sites) is High, Medium, or Low.

[4] Salt tolerance—Tolerance (relative to salt tolerant native vegetation on similar sites) is High, Medium, or Low.

(ii) Harvesting indigenous species—Correctly selected indigenous species harvested from existing stands of living woody vegetation are the preferred soil bioengineering materials. The use of indigenous live materials requires careful selection, harvesting, handling, and transporting. They should result in plants that have deep and strong root systems, are relatively inexpensive, are usually effective, and can be installed quickly.

Live plant materials can be cut from existing native or naturalized stands found near the project site or within practical hauling distance. The source site must contain plant species that will propagate easily from cuttings. Cuttings are normally 1/2 to 2 inches in diameter and range in length from 2 to 6 feet.

Chain saws, bush axes, loppers, and pruners are recommended for cutting living plant material. Safety precautions must be followed when using these tools. Onsite plant material should be harvested with great care. In some places a large area can be cut, but other sites require selective cutting. Cuts should be made at a blunt angle, 8 to 10 inches from the ground, to assure that the source sites will regenerate rapidly and in a healthy manner. The harvesting site should be left clean and tidy. Remnant materials that are too large for use in soil bioengineering projects should be chipped or left in piles for wildlife cover. A site may be needed again for future harvesting and should be left in a condition that will enhance its potential for regeneration.

Binding and storage—Live cuttings should be bundled together securely at the collection site for easy loading and handling and for protection during transport. Side branches and brushy limbs should be kept intact.

Transporting—The bundles of live cuttings should be placed on the transport vehicles in an orderly fashion to prevent damage and facilitate handling. They should be covered with a tarpaulin during transportation to prevent drying and additional stress.

Handling—Live cuttings should arrive on the job site within 8 hours of harvest and should be installed immediately. This is especially critical when the ambient temperature is 50 °F or above.

Live cuttings not installed on the day they arrive should be promptly placed in controlled storage conditions and protected until they can be installed. When in storage, the cuttings must receive continuous shade, must be sheltered from the wind, and must be continuously protected from drying by being heeled into moist soils or stored in uncontaminated water. All live cuttings should be removed from storage and used within 2 days of harvest.

(2) Installing plant materials

(i) Timing—Installation of live cuttings should begin concurrently with earth moving operations if they are carried out during the dormant season. All construction operations should be phased together whenever possible. The best time for installation of soil bioengineering systems is during the dormant season, which generally occurs from September to March throughout most of the United States. Each geographic area has a specific dormant season within this broad range, and yearly variations should be taken into account.

(ii) Planting medium—Soil bioengineering projects ideally use onsite stockpiled topsoil as the planting medium of choice. Gravel is not a suitable material for use as fill around live plant materials. Soil bioengineering systems need to be installed in a planting medium that includes fines and organic material and is capable of supporting plant growth. Muddy soils that are otherwise suitable should not be used until they have been dried to a workable moisture content. Heavy clays should be mixed with organic soils to increase porosity. Select soil backfill does not need to be organic topsoil, but it must be able to support plant growth.

Soil samples of the onsite materials should be taken prior to installation of live woody cuttings. Soil samples should also be taken of all fill materials that are brought to the site prior to use. Nutrient testing by an approved laboratory should include analyses for a full range of nutrients, metal contents, and pH. The laboratory reports should also include recommended fertilizer and lime amendments for woody plant materials.

All fill soil around the live vegetative cuttings should be compacted to densities approximating the surrounding natural soil densities. The soil around plants should be free of voids.

(3) Quality control

Maintaining quality control throughout installation and maintenance operations will ensure a successful soil bioengineering project. The following guidelines are recommended:

(i) Pre-construction

- Select plant species for conformance to requirements.
- Locate and secure source sites for harvesting live cuttings or commercial procurement.
- Define construction work area limits.
- Fence off sites requiring special protection.
- Complete and inspect the following preparations:
  - Layout
  - Excavation, systems excavation
  - Bench size, shape, angle
  - Preparation of site; i.e., clearing, grading, and shaping
  - Disposal of excess gravel, soil, and debris
  - Depth of excavation
  - Vegetation to be removed/preserved
  - Stockpiling of suitable soil and/or rock

(ii) Construction

- Inspect each system component, at every stage, for the following:
  - Angle of placement and orientation of the live cuttings
  - Backfill material/rock and stone material
  - Fertilizer, method and quantity applied
  - Lime, method and quantity applied
  - Preparation of trenches or benches in cut and fill slopes
  - Staking
  - Pruning
  - Stock handling and preparation
  - Soil compaction
  - Watering
- Ensure that proper maintenance occurs during and after installation.
- Inspect daily for quality control.
  - Check all cuttings; remove unacceptable material and use fresh stock for replacement installations.
  - Continuously check all items in the preconstruction and construction inspection lists.
  - Inspect the plant materials storage area when it is in use.

(4) Establishment period

(i) Interim inspections—Inspections should be made after the soil bioengineering measures have been installed. The following schedule is recommended:

- Inspect biweekly for the first 2 months. Inspections should note insect infestations, soil moisture, and other conditions that could lead to poor survivability. Immediate action, such as the application of supplemental water, should be taken if conditions warrant.
- Inspect monthly for the next 6 months. Systems not in acceptable growing condition should be noted and, as soon as seasonal conditions permit, should be removed from the site and replaced with materials of the same species and sizes as originally specified.
- Needed reestablishment work should be performed every 6 months during the initial 2-year establishment period. This will usually consist of replacing dead material.
- Extra inspections should always be made during periods of drought or heavy rains. Damaged sections should always be repaired immediately.

(ii) Final inspection—A final inspection should be held 2 years after installation is completed. Healthy growing conditions should exist.

- Healthy growing conditions in all areas refer to overall leaf development and rooted stems defined as follows:

Live stakes	70%-100% growing
Live fascines	20%-50% growing
Live cribwall	30%-60% growing
Brushlayers	40%-70% growing
Branchpacking	40%-70% growing
Live gully repair	30%-50% growing
Vegetated rock wall	50%-80% growing
Vegetated gabion	40%-60% growing
Joint planting	50%-70% growing

- Growth should be continuous with no open spaces greater than 2 feet in linear systems. Spaces 2 feet or less will fill in without hampering the integrity of the installed living system.

(5) Maintaining the system

After inspection and acceptance of the established system, maintenance requirements should be minor under normal conditions. Maintenance generally

consists of light pruning and removal of undesirable vegetation. Heavy pruning may be required to reduce competition for light or stimulate new growth in the project plantings. In many situations, installed soil bioengineering systems become source sites for future harvesting operations. The selective removal of vegetation may be required to eliminate undesirable invading species that should be cut out every 3 to 7 years.

More intensive maintenance will sometimes be required to repair problem areas created by high intensity storms or other unusual conditions. Site washouts should be repaired immediately. Generally, reestablishment should take place for a 1-year period following construction completion and consist of the following practices:

- Replacement of branches in dead unrooted sections
- Soil refilling, branchpacking, and compacting in rills and gullies
- Insect and disease control
- Weed control

Gullies, rills, or damaged sections should be repaired through the use of healthy, live branch cuttings preferably installed during the dormant season. The repair should use the branchpacking system for large breaks and the live gully repair system for breaks up to 2 feet wide and 2 feet deep. If the dormant season has passed, the use of rooted stock may be considered.

(d) Vegetated structures

Vegetated structures consist of either low walls or revetments (concrete or rock and mortar) at the foot of a slope with plantings on the interposed benches. A structure at the foot of a slope protects the slope against undermining or scouring and provides a slight buttressing effect. In the case of low walls, it allows regrading of the slope face to a more stable angle without excessive retreat at the crest. Vegetation planted on the crest of the wall and the face of the slope protects against erosion and shallow sloughing. In the case of tiered structures, the roots of woody plants grow into the soil and backfill within the structure, binding them together. The foliage in front covers the structure and enhances its appearance.

These systems are not soil bioengineering structures, as their plant materials represent little or no reinforcement value to the structure.

(1) Low wall/slope face plantings

(i) ***Description***—A low retaining structure at the foot of a slope makes it possible to flatten the slope and establish vegetation. Vegetation on the face of the slope protects against both surface erosion and shallow face sliding (fig. 18–25).

(ii) ***Materials and installation***—Several basic types of retaining structures can be employed as low walls. The simplest type is a gravity wall that resists lateral earth pressures by its weight or mass. The following types of retaining structures can be classified as gravity walls:

- Masonry and concrete walls
- Crib and bin walls
- Cantilever and counterfort walls
- Reinforced earth and geogrid walls

In addition, each of these can be modified in a variety of ways to fit nearly any condition or requirement. A low wall with vegetated slope is shown in figure 18–26. For further discussion of standard engineering design requirements and specifications see National Engineering Handbook, section 6.

Figure 18–25 A low wall with plantings above

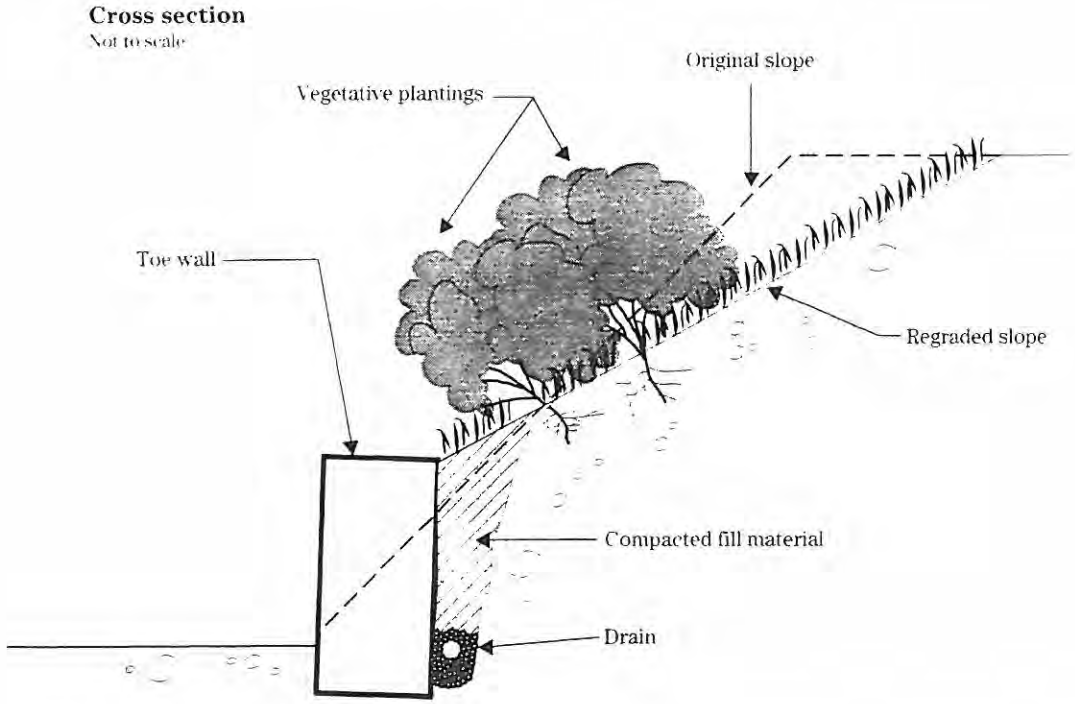

Figure 18–26 Low wall at the base of a slope with vegetation on face of slope (Robbin B. Sotir & Associates photo)

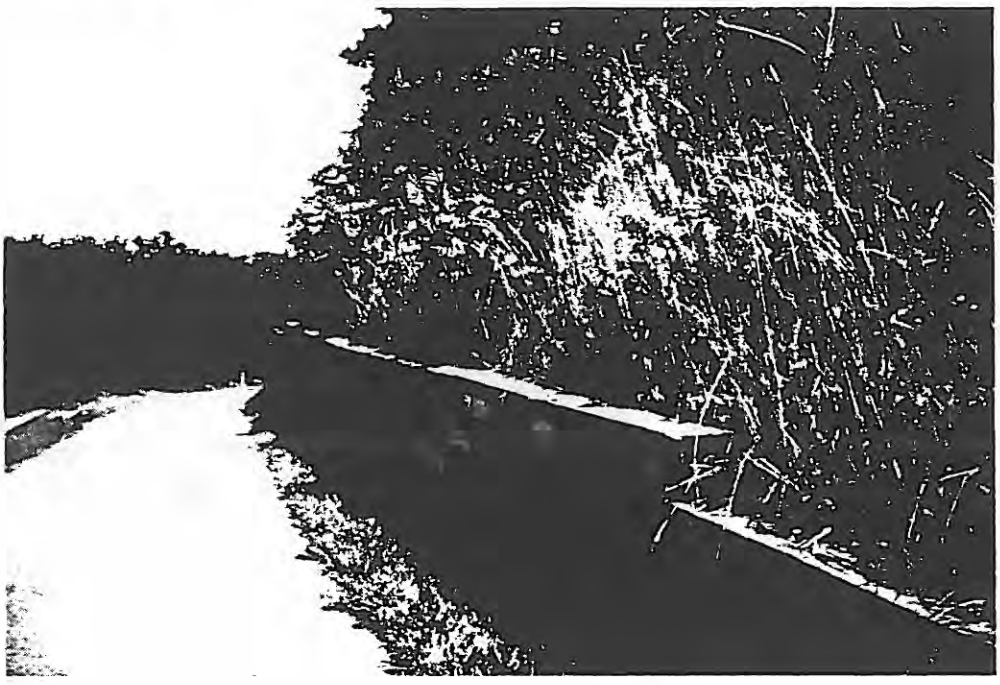

(2) Tiered wall/bench plantings

(i) ***Description***—An alternative to a low wall with face planting is a tiered retaining wall system. This alternative effectively allows vegetation to be planted on slopes that would otherwise be too steep. Shrubs and trees planted on the benches screen the structure behind and lend a more natural appearance while their roots permeate and protect the benches.

Virtually any type of retaining structure can be used in a tiered wall system. A tiered wall system provides numerous opportunities for adding vegetative values on steep slopes and embankments (fig. 18–27).

(3) Cribwalls with plantings

(i) ***Description***—A cribwall is a structure formed by joining a number of cells together and filling them with soil, gravel, or rock to furnish strength and weight. In crib structures, the members are essentially assembled "log cabin" fashion. The frontal, horizontal members are termed stretchers; the lateral members, headers.

The frontal spaces between the stretchers in conventional cribwalls provide openings through which vegetative cuttings can be inserted and established in the crib fill (fig. 18–28).

Figure 18–27 A tiered wall with bench plantings (Robbin B. Sotir & Associates photo)

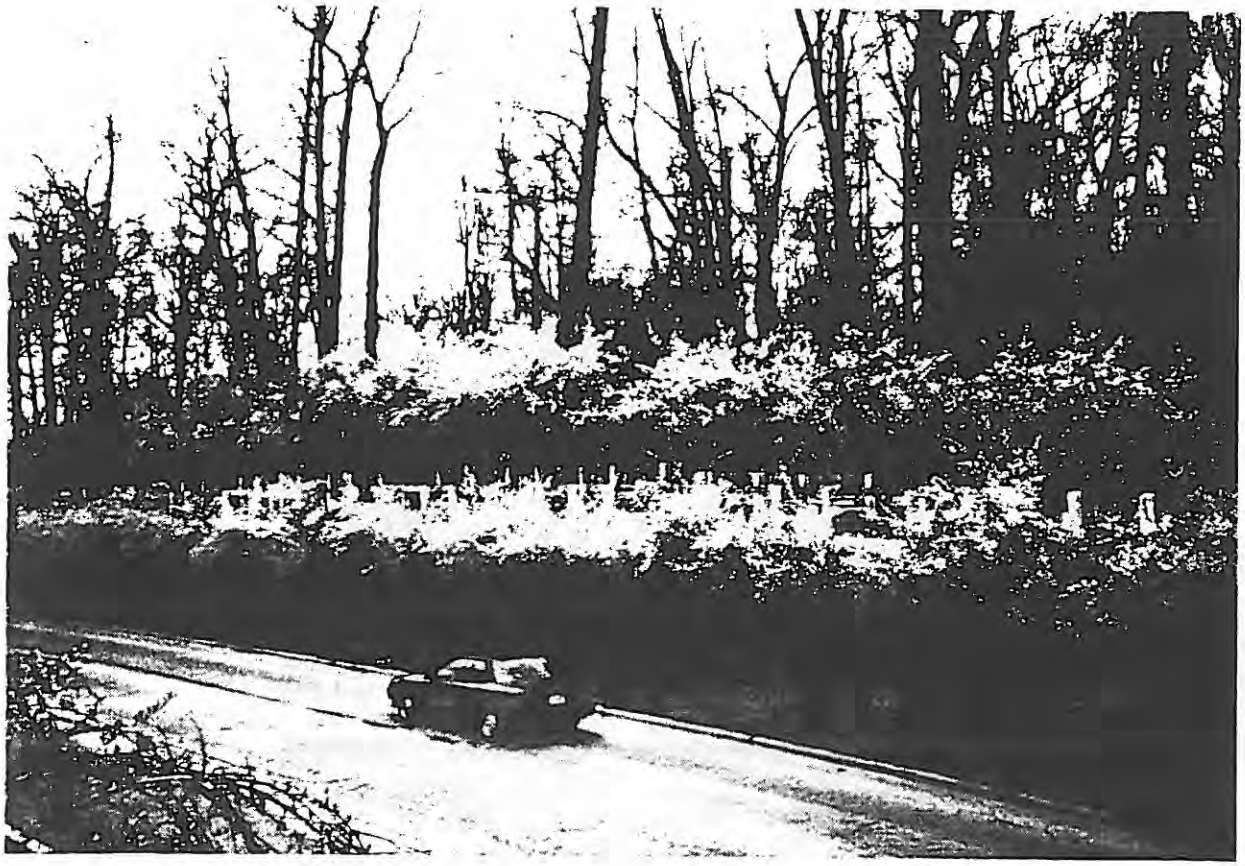

Figure 18–28 Cribwall systems with face plantings (Robbin B. Sotir & Associates photos)

Figure 18–28a Tiered cribwall system with trees and shrubs planted on benches

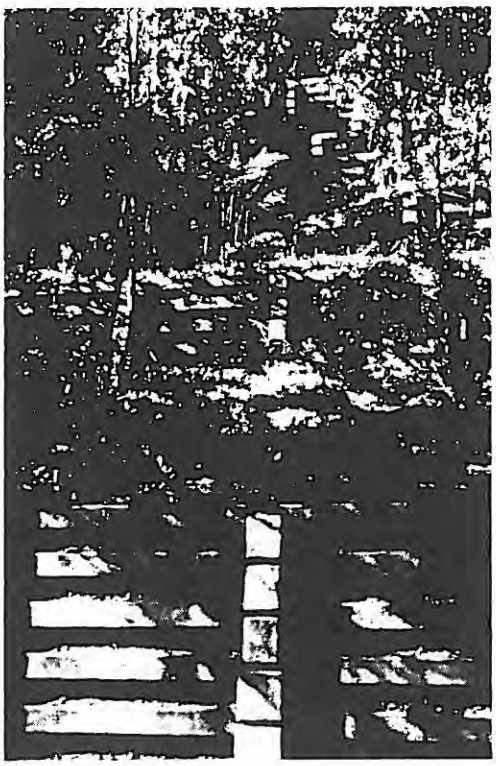

Figure 18–28b Open-front concrete cribwall with plantings in openings

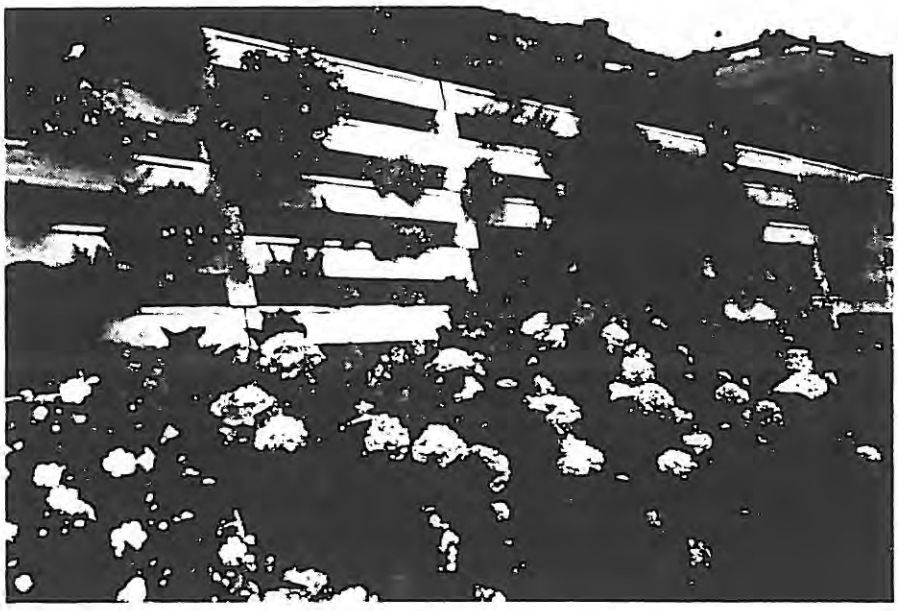

650.1804 References

Coppin, N.J., D.L. Barker, and I. Richards. 1990. Use of vegetation in civil engineering. Butterworths, Sevenoaks, Kent, England.

Fridl, W.F., and P.E. Demetrious. 1982. Biotechnical bank stabilization. Public Works.

Gray, D.H. 1991. Proceedings: Workshop on biotechnical stabilization. The University of Michigan.

Gray, D.H., A.T. Leiser, and C.A. White. 1980. Combined vegetative-structural slope stabilization. Amer. Assoc. Civil Eng., Vol. 50, No. 1, pp. 82-85.

Gray, D.H., and A.T. Leiser. 1982. Biotechnical slope protection and erosion control. Van Nostrand Reinhold, New York, NY. Krieger Pub. Co., Melbourne, FL.

Gray, D.H., and R. Sotir. 1992. Biotechnical stabilization of a highway cut slope. J. Geotechnical Eng. Amer. Assoc. Civil Eng., Vol. 118, No. 9.2.

Gray, D.H., and R. Sotir. 1992. Biotechnical stabilization of cut and fill slopes. Proceedings, ASCE-GT spec. conf. on slopes and embankments. Berkeley, CA.

Hynson, J.R., P.R. Adamus, J.O. Elmer, and T. Dewan. 1983. Environmental features for levee projects. U.S. Army Corps of Eng., Wash., DC, Tech. Rep. E-83.

Kraebel, C.J. 1936. Erosion control on mountain roads. USDA Circ. No. 380, 43 pp.

Kropp, A. 1989. Biotechnical stabilization of a debris-flow scar. Proceedings, XX Intl. Erosion Control Assoc. Conf., Vancouver, BC, pp. 413-429.

Lake, D.W., and J.A. Dickerson. 1989. Cost effective biotechnical slope protection trials in New York. Amer. Soc. Agric.Eng. Pap. No. 892654. 1989 Intl. ASAE meeting, New Orleans, LA.

Reid, G. 1969. How to hold up a bank. A.S. Barnes and Co., New York, NY.

Schiechtl, H. 1980. Bioengineering for land reclamation and conservation. The Univ. Alberta Press, Edmonton, Canada.

Smoltczyk, U., and K. Malcharek. 1983. Living sheets on steep slopes. Proceedings, 2nd Intl. Conf. on Geotextiles, Vol. 2, Las Vegas, NV, pp. 253-257.

United States Navy. 1991. Soil bioengineering major gully washout repair, Silverhill Airfield, Baldwin County, AL, Naval Civil Eng. Lab., Port Hueneme, CA.

Glossary

Batter The angle of the front face of a retaining structure with respect to a vertical plane.

Bench A horizontal surface or step in a slope.

Buttressing Lateral restraint provided by earth or rock masses and embedded structural columns, such as piles and well-rooted tree trunks.

Brushlayer Live branch cuttings laid in crisscross fashion on benches between successive lifts of soil.

Concrete cribwall A hollow, structural wall formed out of perpendicular and interlocking concrete beams.

Cut face The open, steep face of an excavated slope.

Cutting A branch or stem pruned from a living plant.

Crib structure A hollow structure constructed of mutually perpendicular, interlocking beams or elements.

Dead stout stake A 2 by 4 timber that has been cut into a specific shape and length.

Face planting Planting live cuttings and other vegetation in the frontal openings of retaining structures.

Gabion A wire mesh basket filled with rock that can be used in multiples as a structural unit.

Grade stabilization The maintenance of a gentle, noneroding gradient on a watercourse or land surface. This is usually accomplished by means of structural measures or by regrading (lengthening) the slope.

Gravity retaining walls Retaining structures that resist lateral earth forces and overturning primarily by their weight.

Grid wall A lattice or grid-like array of timbers that are fastened or anchored to a slope. The grid spaces are filled with topsoil and then seeded or planted.

Joint planting The insertion of live branch cuttings between openings or interstices of rocks, blocks, or other inert armor units and into the natural ground.

Lateral earth pressure The horizontal pressure exerted by soil against a retaining structure.

Live cribwall A hollow, structural wall formed out of mutually perpendicular and interlocking members, usually timber, in which live cuttings are inserted through the front face of the wall into the crib fill and/or natural soil behind the wall.

Live branch cuttings Living, freshly cut branches of woody shrub and tree species that propagate from cuttings embedded in the soil.

Live fascines	Bound, elongated sausage-like bundles of live cut branches that are placed in shallow trenches, partly covered with soil, and staked in place to arrest erosion and shallow mass wasting.
Live stake	Cuttings from living branches that are tamped or inserted into the earth. The stakes eventually root and leaf out.
Mass movement	The movement of large, relatively intact masses of earth and/or rock along a well defined shearing surface as a result of gravity and seepage.
Mass wasting	See "Mass movement."
Reinforced earth	Strengthening of a soil fill by utilizing tensile inclusions, such as metal strips, woody fibers, wire mesh, or fabric.
Shallow mass movement	Near-surface sliding or movement of earth and/or rock masses usually along planar failure surfaces parallel to the slope face.
Slope flattening	Reduction in slope angle by excavation and regrading in order to achieve a more stable slope.
Soil arching	Restraint of soil movement through an opening or gap as a result of transfer of shear stress from the deforming (or moving) soil mass to adjacent stationary (nonyielding) portions of the soil.
Soil bioengineering	Use of live, woody vegetative cuttings to repair slope failures and increase slope stability. The cuttings serve as primary structural components, drains, and barriers to earth movement.
Steel bin wall	Hollow wall sections constructed of steel that are bolted together and filled with rock or gravel to serve as a gravity retaining wall.
Stepped-back reinforced wall	A reinforced earth retaining wall in which successively higher portions of the wall are set back from the front in stepped fashion.
Surface armoring	Placement of an armor layer, composed of rock, brush matting, gabion mattresses, stabilized earth, etc., on the ground surface.
Tiered retaining wall structures	Retaining structures in which successively higher portions of the structure are set back from the front in stepped fashion. Crib, gabion, and reinforced earth walls can be erected in this fashion.
Toe wall	A low, structural wall erected at the toe or base of a slope to provide support and protect against undermining.
Undermining	The removal of lateral support at the base of a slope by scour, piping erosion, or excavation.
Vegetative cuttings	Live, cut stems and branches of plants that will root when embedded or inserted in the ground.

Vegetated earth buttress	An earthen mass placed against the base or toe of the slope to improve stability. Vegetation can be planted on the face of the buttress or introduced into the buttress in the form of brushlayers.
Vegetative measures	The use of live cuttings, seeding, sodding, and transplanting in order to establish vegetation for erosion control and slope protection work.
Vegetated rock gabions	See "Vegetated structures."
Vegetated rock walls	See "Vegetated structures."
Vegetated structures	A retaining structure in which living plant materials, cuttings, or transplants have been integrated into the structure.
Vegetated structural revetments	Porous revetments, e.g., a gabion mattress or riprap, into which live plants or cuttings can be placed or inserted.

Welcome

What's New
WinStabl Software
WinUnsatH Software
WinStabl FAQ
WinUnsatH FAQ
Bugs
Suggestions
Download
Discussion
Search

Welcome to the University of Wisconsin Geotechnical Software Website. The purpose of this web is to enhance the support services we provide to our donors. We've provided a number of resources here to help you resolve problems, report bugs, and suggest improvements to our products and service.

You may obtain information on our software packages:

- WinStabl
- WinUnsatH
- Gyratory Plate Software
  - PDaqView: software from IOtech for basic operation of data acquisition hardware. This needs to be loaded first.
  - UW Plate (beta version): software from UW which analyzes the plate output and determines the frictional resistance (eccentricity).

You may also obtain information related to our short courses:

- Slope Stability and Landslides
- Foundations
- Pile Foundations

If you cannot open these zip files, you may need to download Winzip. Click here for that program.

Links to other geoengineering software:

- Erosion Software
  - RUSLE website
  - WEPP website
- Other Geotechnical Software Sources

You may also obtain technical support by telephone at 608-262-3491; and by e-mail to our support staff.

University of Wisconsin-Madison

WinStabl

This software provides a Windows-based pre- and post-processor to STABL6 as well as the STABL6 engine. The package supports:

- Simplified Janbu, Modified Bishop, and Spencer's analyses
- Reinforcing layers
- Tiebacks
- Earthquake (pseudo-static) analysis
- Boundary (external) loads
- Anisotropic soils
- Specific failure surfaces
- Circular and irregular surface searching
- Block surface searching
- On-Line Context Sensitive Help (includes full STABL manual)

It offers input screens that resemble spreadsheets, making data input easy. The graphical screen immediately after data entry shows the defined profile permitting rapid input error checking. The output screens are graphical, showing all failure surfaces and highlighting the ten most critical surfaces. Each output screen can be sent to the printer.

The WinStabl package runs under MS Windows (95, 98, ME, NT (4.0), and 2000).

This package is not commercially sold and can only be obtained through a donation to the Geotechnical Engineering Fund at the University of Wisconsin-Madison. The minimum donation required to receive this package is $300. These funds will be used to continue to update this software and to provide additional useful software packages to the geotechnical community. To obtain a fully functioning version of this software, please click here.

This website is dedicated to supporting this program. This website provides information and updates to the WinStabl user community. It also provides a forum to inform us of features you would like to see and any bugs you may find.

Last updated 11/01/01

University of Wisconsin-Madison

WinUnsatH

This software provides a Windows-based pre- and post-processor to UNSAT-H as well as the UNSAT-H engine.

It offers input screens that resemble spreadsheets, making data input easy. A tutorial demonstration of the program is now available.

The WinUnsatH package runs under MS Windows (95, 98, ME, NT(4.0), and 2000).

This package is not commercially sold and can only be obtained through a donation to the Geotechnical Engineering Fund at the University of Wisconsin-Madison. The minimum donation required to receive this package is $500. These funds will be used to continue to update this software and to provide additional useful software packages to the geotechnical community. To obtain a fully functioning version of this software, please click here.

This website is dedicated to supporting this program. This website provides information and updates to the WinUnsatH user community. It also provides a forum to inform us of features you would like to see and any bugs you may find.

Last updated 11/01/01

University of Wisconsin-Madison
Geo Engineering Program

Geotechnical • Geoenvironmental • Geological • Geophysical

2228 Engineering Hall 1415 Engineering Drive
Madison, Wisconsin 53706

UNIVERSITY OF WISCONSIN MADISON 150 YEARS

SOFTWARE REQUEST FORM

Name: _____ **(Required)**
Company: _____ **(Required)**
Address: _____ **(Required)**
City and State: _____ **(Required)**
Zip or Postal Code: _____ **(Required)**
Country: _____ **(Required)**
Telephone: _____ Fax: _____ **(Required)**
Email: _____ **(Required)**

ORDER:

_____ *Win*UNSAT-H (Windows 95/98/NT) @ $500.00 each Total $_____
_____ *Win*STABL (Windows 95/98/NT) @ $300.00 each Total $_____
_____ STABL Manual (printed) @ $35.00 each Total $_____
Total $_____

STABL manuals are sent US mail. For FedEx delivery, enter FedEx number here: _____

CHECKS:

Please make checks payable to: **UW-Geoengineering Program.** Mail form and check to:

UW - Geoengineering Program
c/o Craig H. Benson
2214 Engineering Hall
1415 Engineering Drive
Madison, WI 53706

CREDIT CARDS:

Enter all of the information below. Mail form to address listed in section for checks or fax to 608-263-2453 to the attention of **Craig H. Benson**.

Name of Credit Card: _____ **(Required)**
Address for Credit Card Billing (1): _____ **(Required)**
Address for Credit Card Billing (2): _____ **(Required)**
City, State, Country and Zip for Credit Card Billing (3): _____ **(Required)**
Country for Credit Card Billing (4): _____ **(Required)**
Card Type (VISA, MasterCard, AMEX, Discover Only): _____ **(Required)**
Card Number: _____ **(Required)**
Expiration Date: _____ **(Required)**

Credit card orders are processed through Civil Engineering Consultants LLC, a firm in the Madison area. CEC will send credit card receipts directly to purchasers.

SERIAL NUMBERS AND PASSWORDS ARE SENT TO PURCHASERS VIA EMAIL AFTER CONFIRMATION OF THE PURCHASE. SOFTWARE AND OTHER MATERIALS CAN BE DOWNLOADED FROM www.uwgeosoft.org

ALL PROCEEDS FROM SOFTWARE PURCHASES ARE USED TO SUPPORT THE EDUCATIONAL AND RESEARCH MISSIONS OF THE GEOENGINEERING PROGRAM AT UW-MADISON.

geosoft

Main

Inexpensive Web Hosting for Teachers and Students! If you are a student preparing to apply to college, or a teacher wanting to keep your class informed we have the right package for you.

For whenever your bored or just need something fun to do stop by The Geosoft Network Arcade. The Arcade consists of 11 classic and new games all playable right in your browser.

The Geosoft Network offers 15 megs of free webspace! Your free account comes complete with an online file editor for uploading and updating your site. Along with that your site is easily accessible through an easy URL of http://members.geosoft.org/yourname. Sign up for your free account today.

Free Webspace
15MB of free webspace, with an online file editor for uploading and updating your site.

Message Boards
Free, customizable message boards that allow you to create topics, modify posts, and delete posts.

Search The Web
The power of over 25 search engines at your fingertips!

Arcade
11 new and classic games - all playable right in your browser.

Educational Hosting
Inexpensive web hosting for teachers and students!

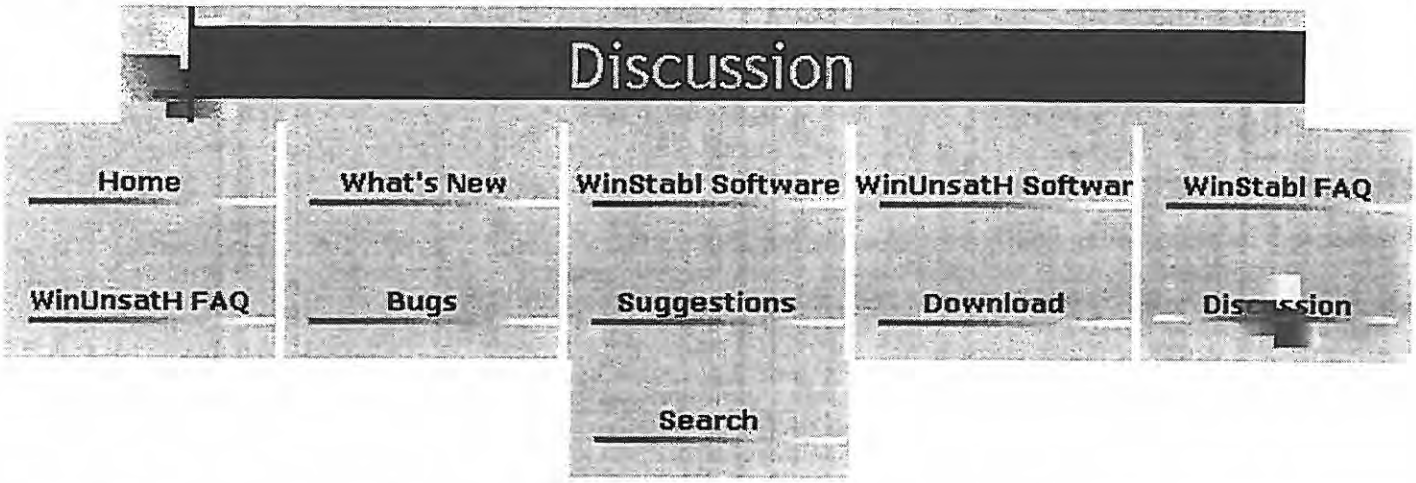

We are providing a discussion group where customers can post articles about problems they encounter, or tips and tricks that other users might want to know about.

The discussion supports threads, so you will be able to post a reply to another user's question. We recommend prefixing the subject of your posting with a "Q:" if it's a question, or an "A:" if it's an answer to a question, or nothing at all if you're just making a comment or observation.

Our support department will be tuned in to this discussion as well, and will reply to questions posted here. Otherwise you can receive customer support by sending e-mail to our support staff for a personal reply; or placing a call to 608-262-3491.

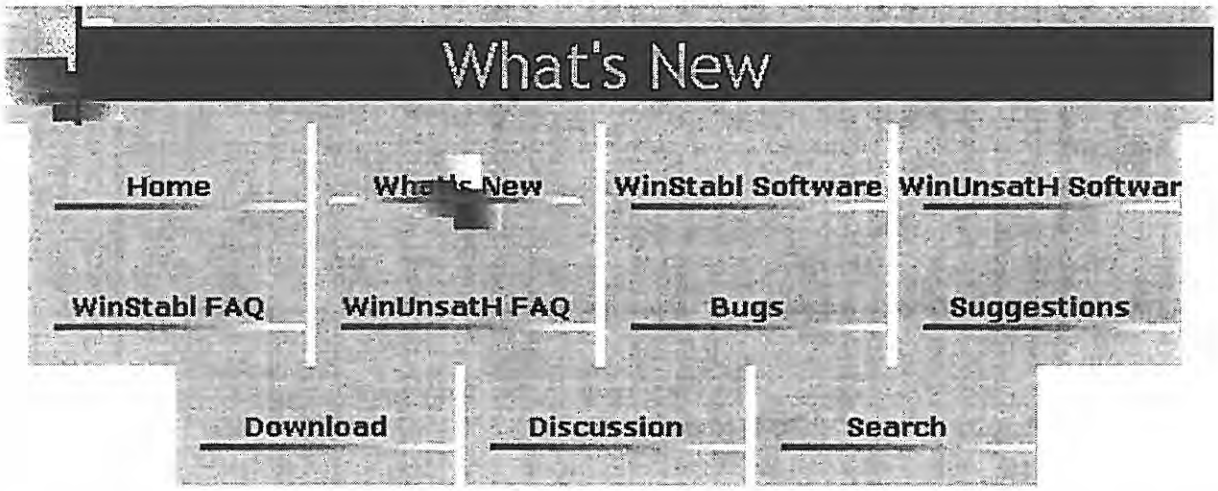

This page displays an up-to-date listing of changes to our customer support web. We'll also place notices here regarding product updates, scheduled releases, or problems and work-arounds that may affect all customers. When bugs reported by our customers get fixed, we'll place a notice here, along with an estimate of when the fix will be shipped.

Feb 14, 2000

- A new tutorial for WinUnsat-H made available
- New installation instructions available

Feb 17, 2000

- A new version (2.08) of WinStabl fixing the help system

Jun 8, 2000

- A new version (2.10) of WinStabl fixing the display of safety factors > 10.0

Aug 8, 2000

- A new version (2.20) of WinStabl better incorporating error messages.

Oct 10, 2000

- A new version (2.30) of WinStabl able to handle European number formats.

Nov 10, 2000

- A new version (2.40) of WinStabl fixes the Limit Generation dialog box.

Jan 17, 2001

- New versions have new passwords. Contact C.H. Benson for new password if software was purchased in last 24 months.

Apr 18, 2001

- A new version (2.50) of WinStabl permits variable graphics scaling via new Results menu item and improves the Help information.

May 17, 2001

- A new installation package for both WinStabl and WinUnsatH to handle issues related to installation on Win95/98/ME systems.

Jul 3, 2001

- A new version (2.60) of WinStabl automatically scales graphics based on display screen sizes. It may still require minor adjustments for your monitor (only needed once).

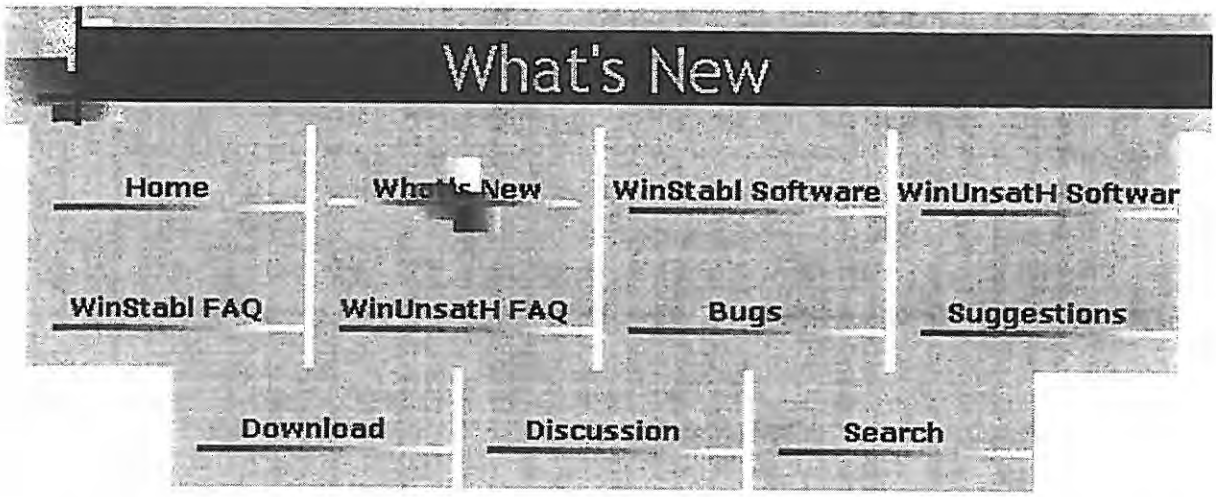

This page displays an up-to-date listing of changes to our customer support web. We'll also place notices here regarding product updates, scheduled releases, or problems and work-arounds that may affect all customers. When bugs reported by our customers get fixed, we'll place a notice here, along with an estimate of when the fix will be shipped.

Feb 14, 2000

- A new tutorial for WinUnsat-H made available
- New installation instructions available

Feb 17, 2000

- A new version (2.08) of WinStabl fixing the help system

Jun 8, 2000

- A new version (2.10) of WinStabl fixing the display of safety factors > 10.0

Aug 8, 2000

- A new version (2.20) of WinStabl better incorporating error messages.

Oct 10, 2000

- A new version (2.30) of WinStabl able to handle European number formats.

Nov 10, 2000

- A new version (2.40) of WinStabl fixes the Limit Generation dialog box.

Jan 17, 2001

- New versions have new passwords. Contact C.H. Benson for new password if software was purchased in last 24 months.

Apr 18, 2001

- A new version (2.50) of WinStabl permits variable graphics scaling via new Results menu item and improves the Help information.

May 17, 2001

- A new installation package for both WinStabl and WinUnsatH to handle issues related to installation on Win95/98/ME systems.

Jul 3, 2001

- A new version (2.60) of WinStabl automatically scales graphics based on display screen sizes. It may still require minor adjustments for your monitor (only needed once).

TAB 5

Alan Kropp

Presentation

DIGITAL RECORDING OF DEEP BORINGS

OPTICAL TELEVIEWER (OPTV)

OPTV attempts to capture the visual details of the subsurface geology via a boring for the attentive eyes of a geologist/engineer. It brings to the site characterization process, a continuous and unbiased record of the subsurface geology that can be presented and preserved on several different media.

The most important feature of the OPTV tool other than its imagery, is the image is oriented to magnetic north. An on board omni-directional orientation package maps the trajectory of the borehole for subsequent recalculation to real geographical coordinates of identified fracture or stratigraphic features.

Borings can be logged with OPTV in alluvial soils and the details are just as prominent as in bedrock so long as the soils do not consist of wet plastic clays which tend to smear the side wall. Loose unconsolidated sandy soils will not generally remain open for geophysical logging. Generally the upper 10 to 15 feet of loose soil is cased off to prevent sloughing and the ultimate loss of a very expensive probe. The differentiation between soft rock and stiff soil from a visual standpoint is very difficult to distinguish.

The boring has to be advanced by a drilling method with the least amount of side-wall disturbance, such as rotary or diamond core bits. Diameters range from 4 to 6 inches. Auger methods are ok, but it is the soil type that determines what the visual integrity of the boring wall and clarity of OPTV image.

The maximum resolution of the OPTV image is 0.5 millimeters by 720 pixels. The later dimension depends on the diameter of the boring. The interpretation slides are available in hard copy color photographic prints or as digital files replayed through a Windows View (Windows OS only). Recording speeds vary from 3 to 5 feet per minute, depending on the desired resolution.

APPROXIMATE COST

Costs for an OPTV logging survey can range from $880 for a shallow (<75') boring in the local area (East Bay, San Francisco, Marin) to $1640/day for several borings up to a cumulative footage of 500 feet plus mobilization outside the local area.

Source of Information:
NORCAL Geophysical Consultants, Inc.
http://www.norcalgeophysical.com/index.html

USGS

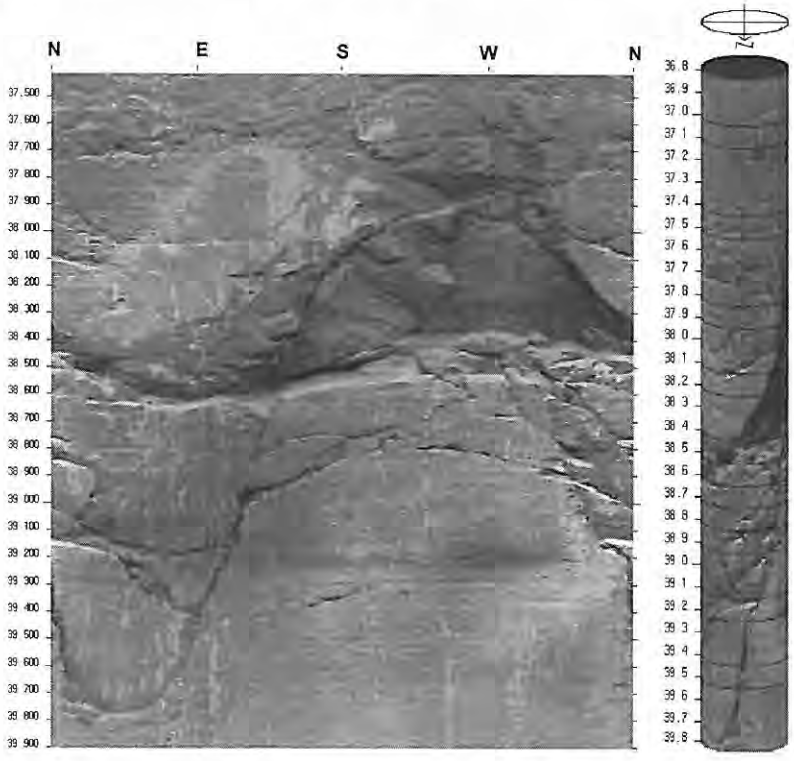

FIELD INVESTIGATION OF LANDSLIDES

A. Review Available Information (Preparation for field)

1. Published maps from state or federal geologic agencies:

Alger & Brabb (1985) have compiled a bibliography of maps and reports for landslides throughout the United States -- 6,500 references are listed on a state-by-state basis.

Within California, USGS (Taylor & Brabb, 1986) has compiled a map of the state showing where landslide inventory and susceptibility maps have been prepared. This reference also lists more than 750 landslide publications for the state. Landslide inventory maps of several states have also been recently published (Pomeroy, 1988, and Fickies and Brabb, 1989, for example). By 1988, 16 states had either published maps or completed substantial work toward a map in a cooperative program between USGS and state geologic agencies. Many state geologic agencies have also prepared landslide maps for their states -- for example, California had released numerous maps in their "Landslide Hazard Identification" map series. A typical example of these is Davenport (1985) which includes a relative landslide susceptibility map, a landslides and related features map, a geologic map, and a relative debris-flow susceptibility map. Some maps, such as Saul (1973), have individual landslides numbered which then provides a table listing the geologic units involved, relative age, probable cause, evidence of movement, and other data regarding type of landslide involved. Many types of generalized maps, such as maps made solely from air photo interpretation, are also available (such as Nilsen, 1975).

The Colorado Geological Survey has compiled a large database of landslide information for that state, as discussed in Jochim, et al (1988). Examples of slide maps for Colorado are presented on Figures 1 and 2.

2. Local agency maps or data:

Many cities, counties, utility districts, flood control agencies, or other local agencies keep records of landslides within their jurisdiction. In Northern California, the record-keeping is quite spotty -- and when records are kept, they are not always available for public review.

3. Other miscellaneous sources:

There are a variety of other sources which may provide useful data in a landslide evaluation including water well logs, agricultural soil survey reports, available unpublished consultant's reports, or miscellaneous geologic literature.

Kockleman (1986) lists a variety of available data sources for landslide hazard maps.

B. Aerial Photographs (Preparation for and response to field)

The evaluation of aerial photographs can help establish "the big picture"; features which are too large or too subtle can be seen in the air photos including primary and secondary scarps, the general limits and geometry of landsliding, apparent surficial anomalies -- this can guide the emphasis in the surficial mapping and subsurface exploration programs.

Historic development and episodes of past landsliding can be identified by the study of air photos taken in different years, particularly if the photos were taken immediately after a very rainy winter.

Black and white photos are the most common type but color or color infrared photos may be helpful. Color photos emphasize differences in vegetation and wet areas through changes in soil color and vegetation vigor. Color infrared photos make water look blue and seeps will often have a bluish tint. Also, springs or sheared zones that hold water will be brilliant red.

Air photos are often available from private companies in urban areas -- a variety of government sources also exist including USGS, Forest Service, and Department of Agriculture.

An excellent summary of the use of aerial photographs in landslide evaluations is presented in Rib and Liang (1978). An example of geomorphic features on a large landslide obtained by air photo mapping is presented on Figure 3. It should be emphasized that the accuracy of aerial photograph interpretation depends on the quality and scale of the photographs as well as the skill and background of the interpreter. Fookes, et al (1991) present a case history in which a number of professional interpreters reviewed aerial photographs of a complex environment and came to dramatically different conclusions regarding landslide susceptibility of the area.

Deformation patterns of a moving landslide can be assessed by making measurements with an analytical stereoplotter on successive sets of air photos (Fleming, et al, 1991). An example of a map produced using this technique is presented on Figure 4.

C. Topographic Map

Topography and geometry of the ground surface are important in determining the nature and extent of landsliding. Therefore, a topographic map should be developed as soon as possible at a reasonable scale.

All key landforms should be located (including scarps, bulges, cracks, etc.) as well as trees, other vegetation, springs, or seepage zones, flow tracks, man-made improvements, or other surficial data.

Reference points outside the limits of sliding should be established so the rate, direction, and magnitude of movement between survey dates can be estimated.

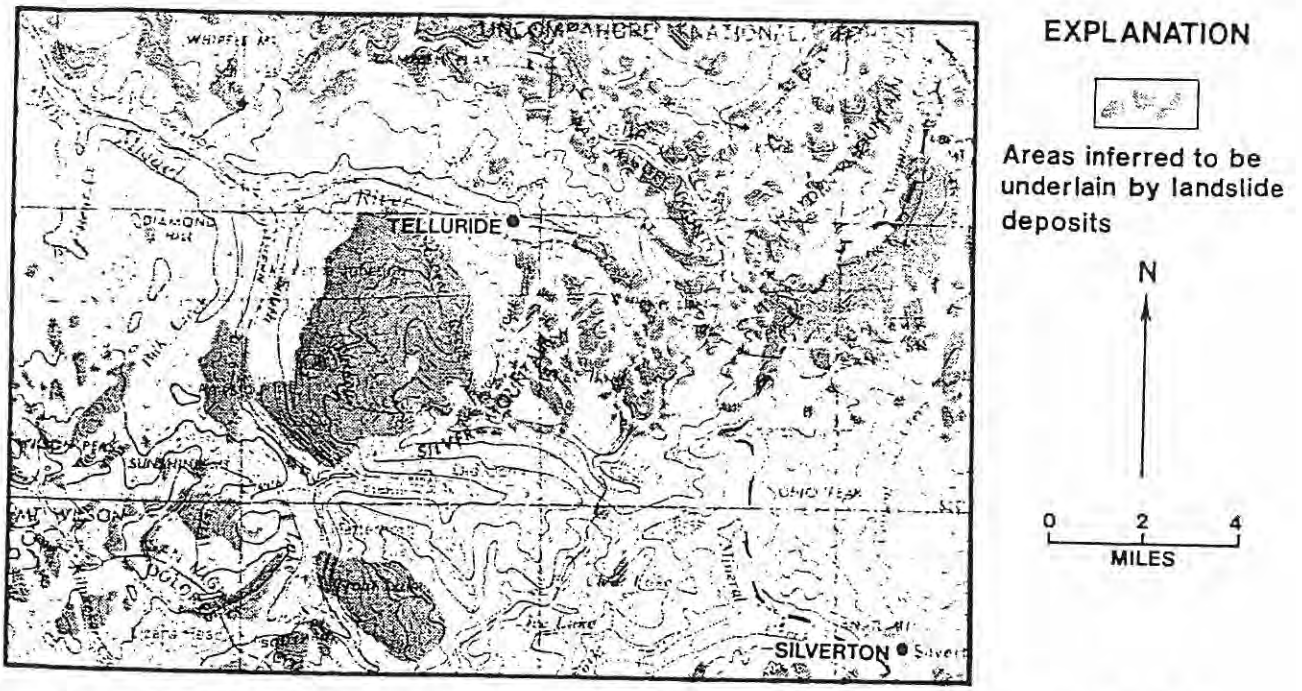

Figure 1 Detail from the landslide inventory map of the Durango 1° X 2° quadrangle, Colorado (Colton and others, 1975).

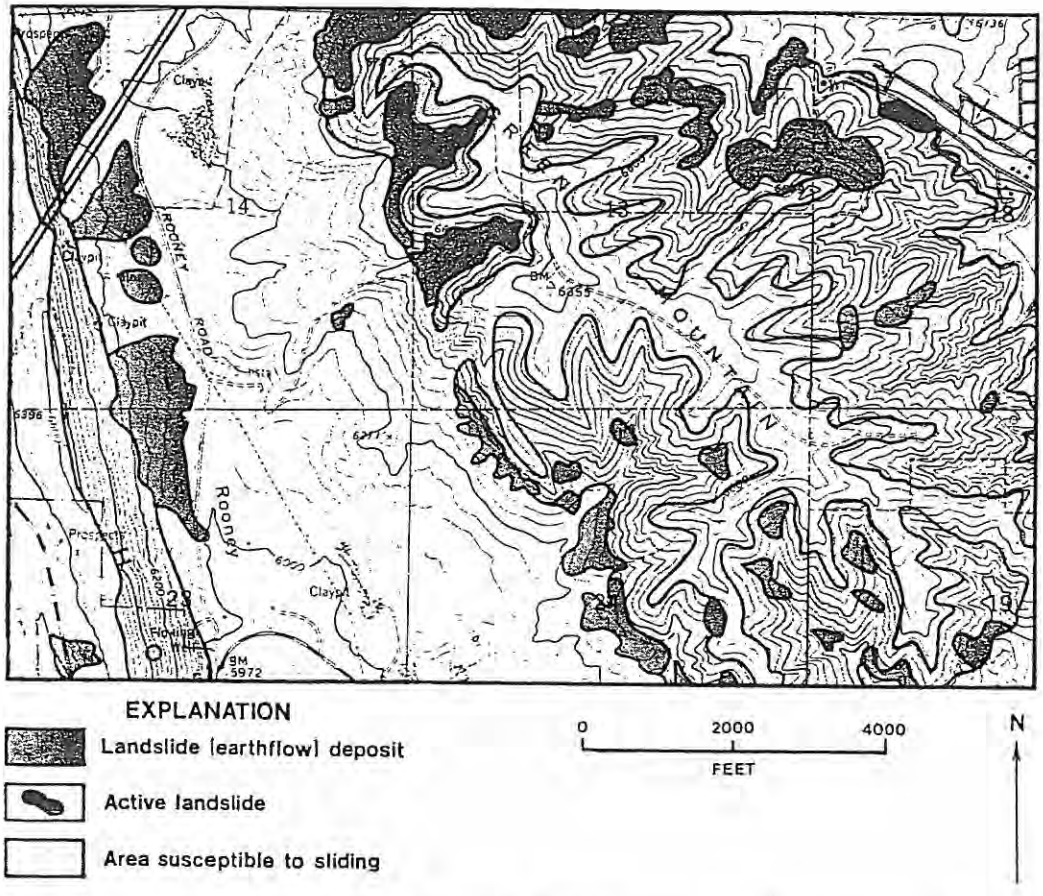

Figure 2 Detail from the Morrison quadrangle folio showing areas susceptible to landsliding (Scott, 1972).

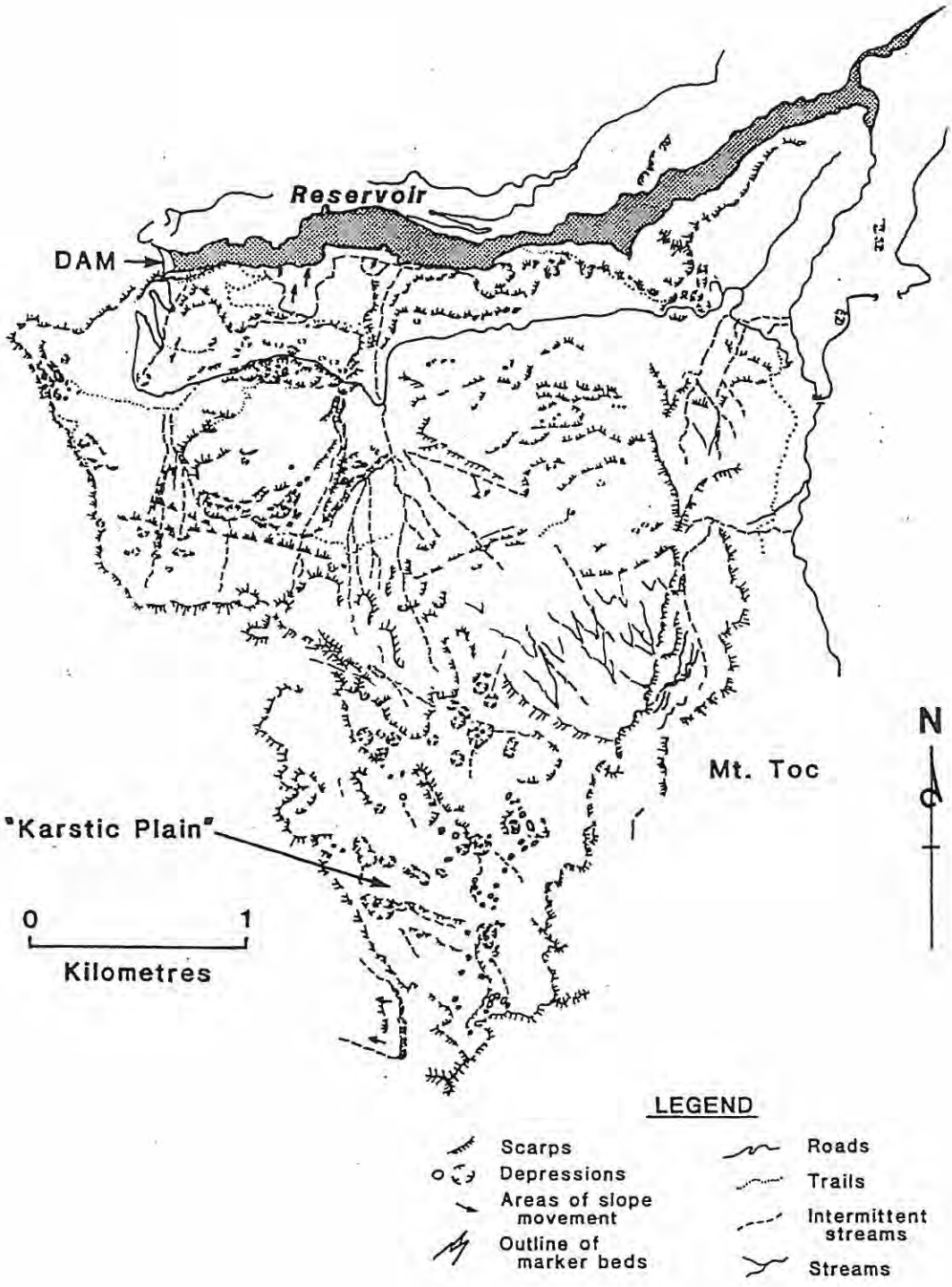

Figure 3 Geomorphic features, Vaiont Slide, delineated from the 1960 airphotos. (Hendron & Patton, 1985)

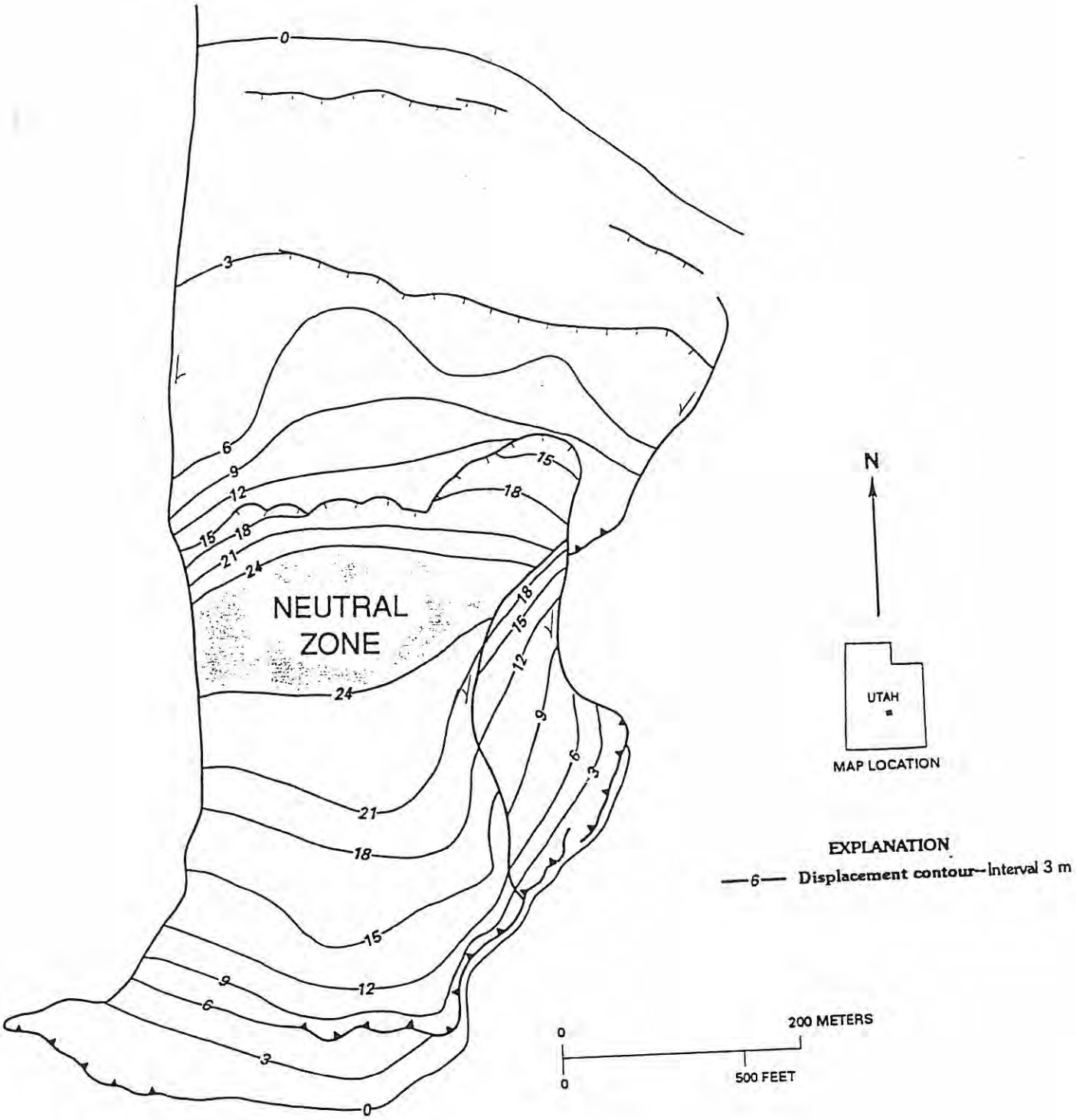

Figure 4. Simplified displacement contours

(after Fleming, et al, 1991)

Illustrations of generalized maps of this type are shown on Figures 5 and 6.

An example of the successful use of survey techniques, in conjunction with aerial photographs, was employed in the evaluation of the Manti Canyon landslide in Utah (Fleming et al., 1988). Examples of data that can be obtained from surveys are presented for moderate-sized landslide features in Hawaii on Figures 7 and 8 and for broad, ridge-spreading features (Sackungen) in Colorado on Figures 9 and 10.

D. Surficial Mapping

Field mapping is perhaps the most important phase of the field investigation. Ideally, the topographic map should be available for the field work so field notes can be recorded directly on a field copy of the map. If the map is not available at the time of the initial mapping, then the geologist or engineer should return to the field after the map is prepared to locate the key features. The topographic map can also be modified as needed based on the field mapping as features need to be added or removed, or relocated.

Key features to observe:

1. All bedrock outcrops within the slide area (often well exposed in the scarp) as well as in surrounding areas (in road cuts, other excavations, etc.): the bedrock structure, lithology, unit thickness, or other geological data should be recorded.

2. Head scarp, lateral scarps, secondary scarps: provides exposures of bedrock, colluvium, residual soils, fill materials -- also slickenside orientation may show direction of movement. Freshness of scarp features should be noted as indicated by the steepness, vegetative cover, crack width, etc.

3. Toe area: is slide mass still intact? is there a large bulging area? did the toe move on top of an undisturbed ground surface?

A field guide to locate various features in relation to landslide type is presented on Table 1. Other guidelines for highway use are presented in Klinedinst, et al (1986).

The recency of movement should also be evaluated -- see Table 2.

Numerous photographs should be taken of the slide area as soon as possible because features may change as continued movement occurs which may obscure key data. Comparisons can be made between the conditions in the same location on different dates. It is strongly recommended that cameras with "data-back" recorders be used to imprint dates on the negatives so confusion does not arise concerning dates of photographs. In some recent cases, continuous videotape recordings have produced dramatic examples of landslide failures in progress.

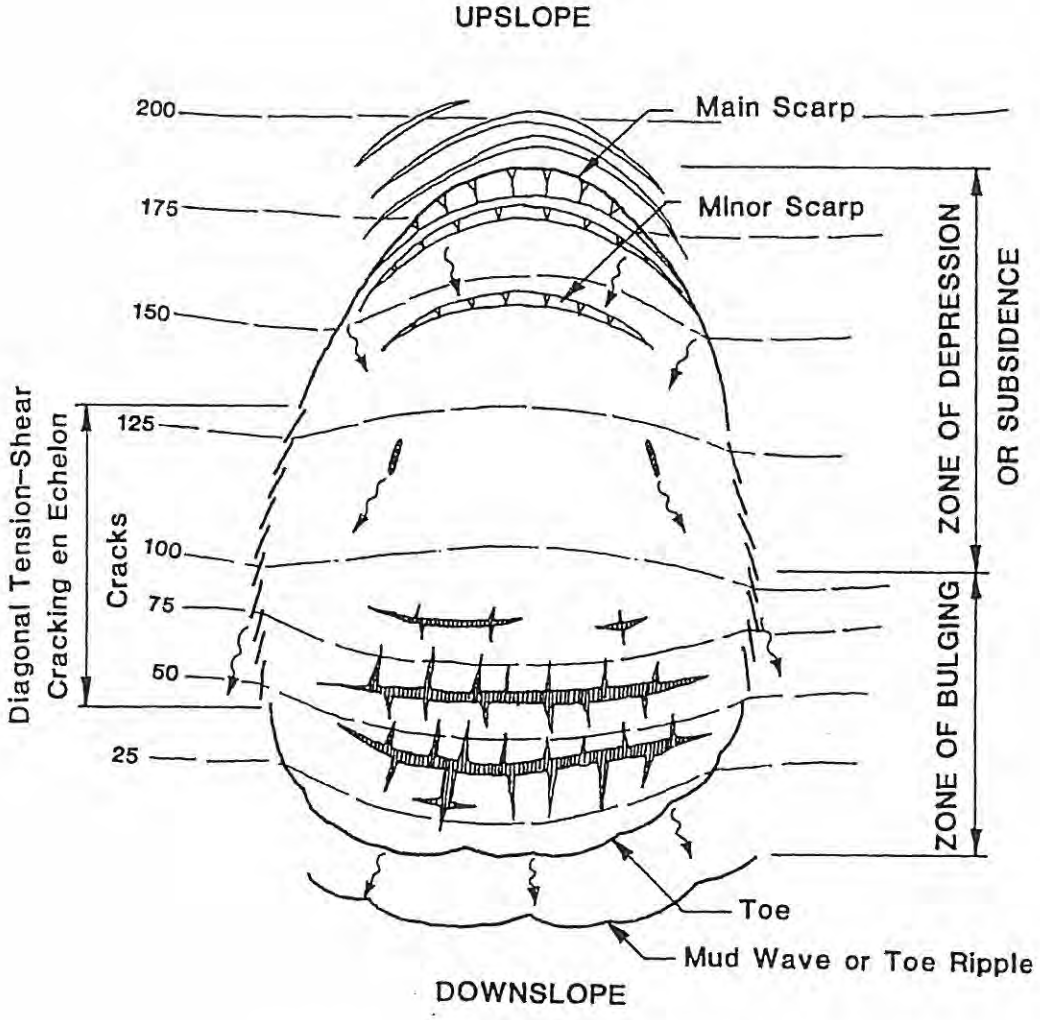

LEGEND

Tension Crack – Possible Shear Displacement Downhill

Tension Crack on Toe Bulge

Springs, Seeps

Figure 5. Landforms on Topographic Map
(after Sowers and Royster, 1978)

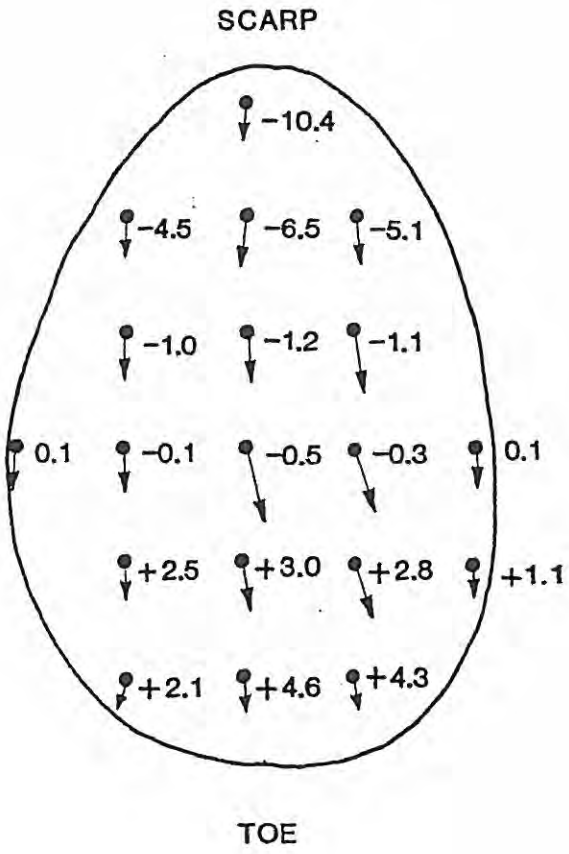

LEGEND

+ 2.1 — Grid Point Vertical Movement (−Subsidence, + Rise, in meters)

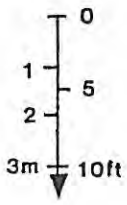

Grid Point Horizontal Movement (with Vector Scale)

Figure 6. Movement Vectors on Topographic Map (after Sowers and Royster, 1978)

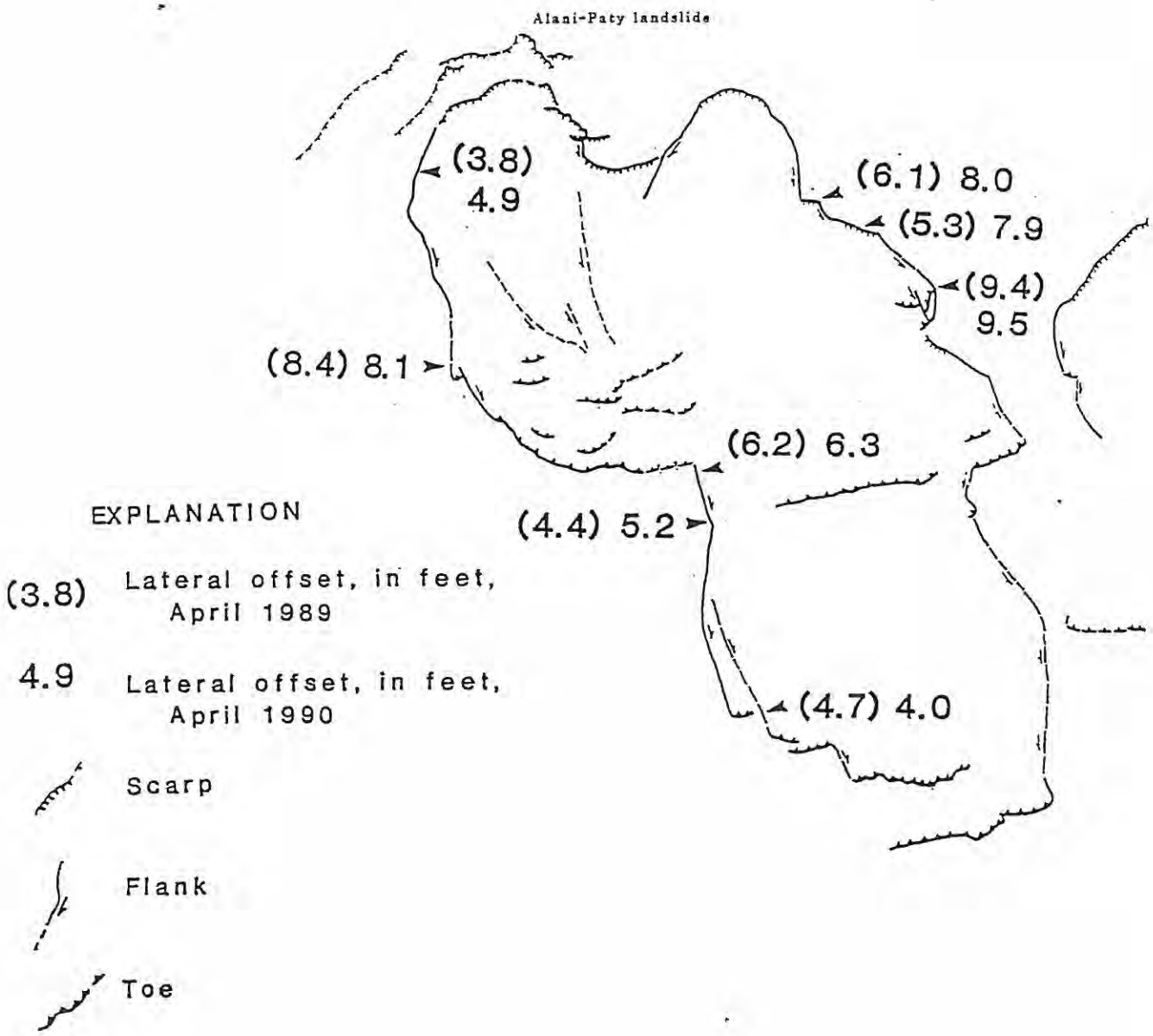

Figure 7. Map showing lateral offsets of curbs and stone walls at boundaries of the Alani-Paty landslide. (Baum, et al, 1990)

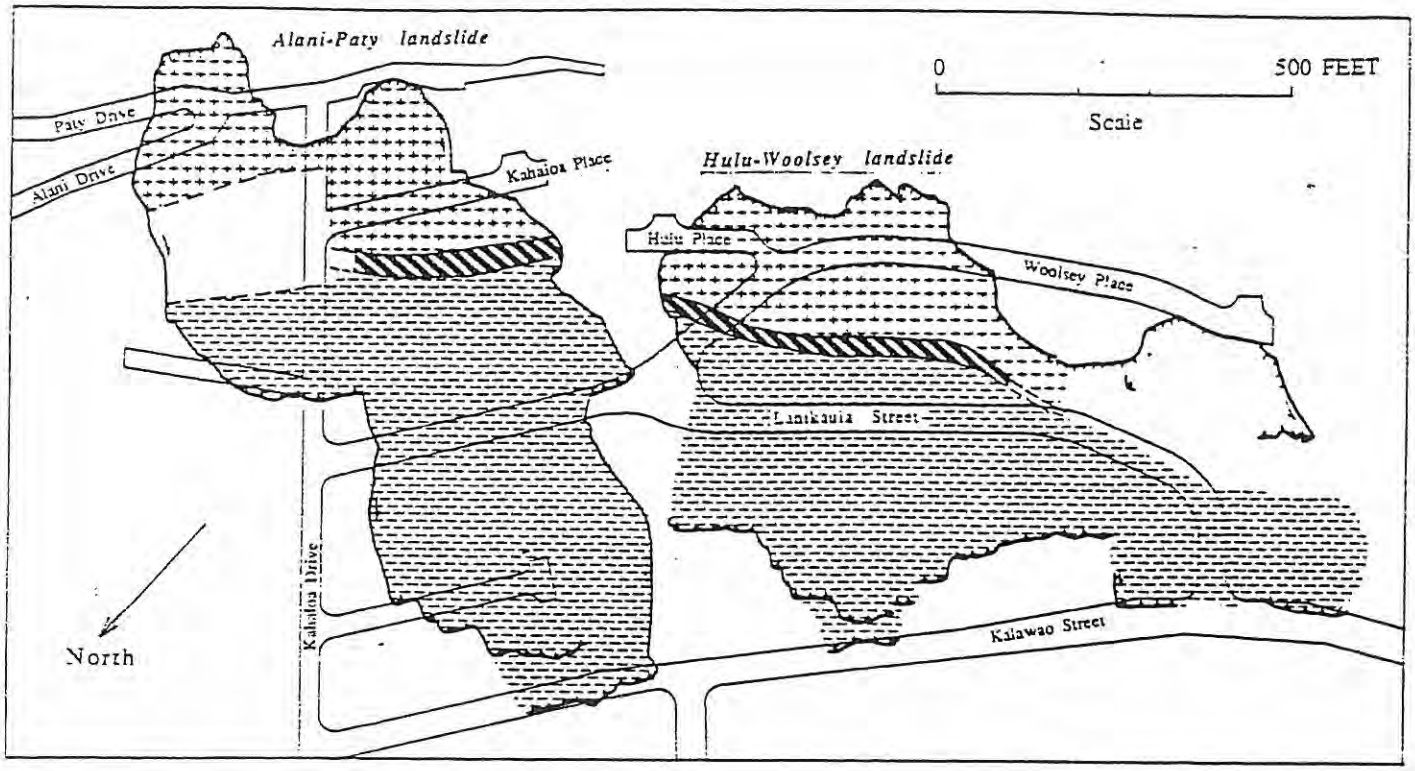

EXPLANATION

Scarp--Hachures on downdropped side

Flank--Arrows on moving ground

Toe--Sawteeth on moving ground

Ground being stretched

Ground being shortened

Moving ground being neither stretched nor shortened

Figure 8. Surveyed Pattern of Deformation in Two Landslides in Hawaii (Baum, et al, 1989)

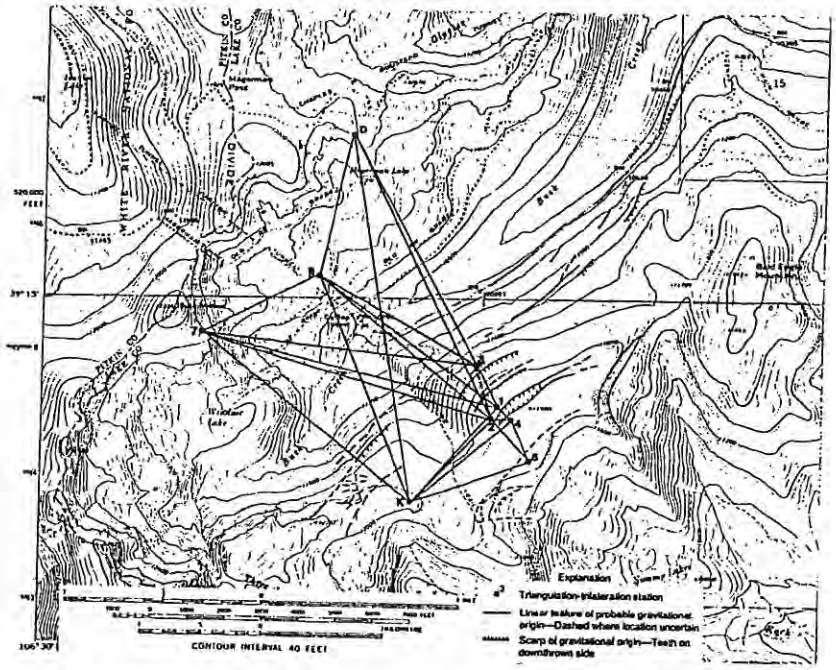

FIGURE 9.--Survey net at Bald Eagle Mountain and valley of Busk Creek, Lake County, Colorado. Base map is from the Homestake Reservoir, 1970, and Mount Massive, 1967, 1:24,000 topographic sheets, U.S. Geological Survey.

(after Varnes, et al, 1990)

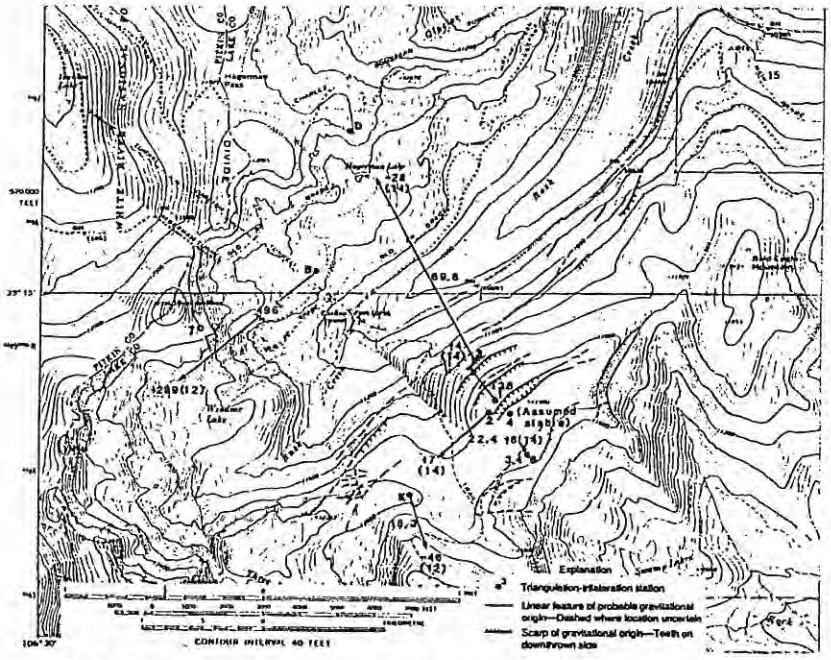

FIGURE 10--Relative movements of the Bald Eagle Mountain survey stations. Arrows show direction of horizontal movement in mm; vertical movement in mm given at end of arrow; period of observation in years, in parentheses. All movements are relative to station 4, assumed stable; the direction of line 4-6 is assumed constant.

(after Varnes, et al, 1990)

TABLE 1
FIELD GUIDE TO LANDSLIDE FEATURES

Type of Motion	Kind of Material	Parts Surrounding Slide			Parts That Have Moved			
		Crown	Main Scarp	Flanks	Head	Body	Foot	Toe
Falls, topples	Rock	Consists of loose rock; probably has cracks behind scarp; has irregular shape controlled by local joint system	Is usually almost vertical, irregular, bare, and fresh, usually consists of joint or fault surfaces	Are mostly bare edges of rock	Is usually not well defined; consists of fallen material that forms heap of rock next to scarp	Falls: Has irregular surface of jumbled rock that slopes away from scarp and that, if large and if trees or material of contrasting colors are included, may show direction of movement radial from scarp; may contain depressions Topples: Consists of unit or units tilted away from crown	Is commonly buried; if visible, generally shows evidence of reason for failure, such as prominent joint or bedding surface, underlying weak rock, or banks undercut by water	Is irregular pile of debris or talus if slide is small; may have rounded outline and consist of broad, curved transverse ridge if slide is large
	Soil	Has cracks behind scarp	Is nearly vertical, fresh, active, and spalling on surface	Are often nearly vertical	Is usually not well defined; consists of fallen material that forms heap of rock next to scarp	Is irregular	Is commonly buried; if visible, generally shows evidence of reason for failure, such as prominent joint or bedding surface, underlying weak rock, or banks undercut by water	Is irregular
Slides Rotational *Slump*	Soil	Has numerous cracks that are mostly curved concave toward slide	Is steep, bare, concave toward slide, and commonly high; may show striae and furrows on surface running from crown to head, may be vertical in upper part	Have striae with strong vertical component near head and strong horizontal component near foot; have scarp height that decreases toward foot; may be higher than original ground surface between foot and toe; have en echelon cracks that outline slide in early stages	Has remnants of land surface flatter than original slope or even tilted into hill, creating at base of main scarp depressions in which perimeter ponds form; has transverse cracks, minor scarps, grabens, fault blocks, bedding attitude different from surrounding area, and trees that lean uphill	Consists of original slump blocks generally broken into smaller masses; has longitudinal cracks, pressure ridges, and occasional overthrusting, commonly develops small pond just above foot	Commonly has transverse cracks developing over foot line and transverse pressure ridges developing below foot line; has zone of uplift, no large individual blocks, and trees that lean downhill	Is often a zone of earth flow of lobate form in which material is rolled over and buried; has trees that lie flat or at various angles and are mixed into toe material
	Rock	Has cracks that tend to follow fracture pattern in original rock	Is steep, bare, concave toward slide, and commonly high, may show striae and furrows on surface running from crown to head, may be vertical in upper part	Have striae with strong vertical component near head and strong horizontal component near foot; have scarp height that decreases toward foot; may be higher than original ground surface between foot and toe; have en echelon cracks that outline slide in early stages	Has remnants of land surface flatter than original slope or even tilted into hill, creating at base of main scarp depressions in which perimeter ponds form; has transverse cracks, minor scarps, grabens, fault blocks, bedding attitude different from surrounding area, and trees that lean uphill	Consists of original slump blocks somewhat broken up; has little plastic deformation; has longitudinal cracks, pressure ridges, and occasional overthrusting; commonly develops small pond just above foot	Commonly has transverse cracks developing over foot line and transverse pressure ridges developing below foot line; has zone of uplift, no large individual blocks, and trees that lean downhill	Has little or no earth flow; is often nearly straight and close to foot, may have steep front
Translational *Block*	Rock or Soil	Has cracks most of which are nearly vertical and tend to follow contour of slope	Is nearly vertical in upper part and nearly plane and gently to steeply inclined in lower part	Have low scarps with vertical cracks that usually diverge downhill	Is relatively undisturbed and has no rotation	Is usually composed of single or few units, is undisturbed except for common tension cracks that show little or no vertical displacement	Has none and no zone of uplift	Plows or overrides ground surface
Rock	Rock	Contains loose rock, has cracks between blocks	Is usually stepped according to spacing of joints or bedding planes, has irregular surface in upper part and is gently to steeply inclined in lower part, may be nearly planar or composed of rock chutes	Are irregular	Has many blocks of rock	Has rough surface of many blocks, some of which may be in approximately their original attitude but lower if movement was slow translation	Usually has none	Consists of accumulation of rock fragments
Flows Dry	Rock	Consists of loose rock, probably has cracks behind scarp, has irregular shape controlled by local joint system	Is usually almost vertical, irregular, bare, and fresh, usually consists of joint or fault surfaces	Are mostly bare edges of rock	Has none	Has irregular surface of jumbled rock fragments sloping down from source region and generally extending far out on valley floor; shows lobate transverse ridges and valleys	Has none	Composed of tongues, may overide low ridges in valley
	Soil	Has no cracks	Is funnel shaped at angle of repose	Have continuous curve into main scarp	Usually has none	Is conical heap of soil, equal in volume to head region	Has none	
Wet *Debris avalanche* *Debris flow*	Soil	Has few cracks	Typically has serrated or V-shaped upper part, is long and narrow, bare, and commonly striated	Are steep and irregular in upper part, may have levees built up in lower parts	May have none	Consists of large blocks pushed along in a matrix of finer material, has flow lines, follows drainageways and can make sharp turns, is very long compared to breadth	Is absent or buried in debris	Spreads laterally in lobes, if dry, may have a steep front about a meter high
Earth flow	Soil	May have a few cracks	Is concave toward slide, in some types is nearly circular and slide issues through narrow orifice	Are curved, have steep sides	Commonly consists of a slump block	Is broken into many small pieces; shows flow structure	Has none	Is spreading and lobate; consists of material rolled over and buried; has trees that lie flat or at various angles and are mixed into toe material
Sand flow *Silt flow*	Soil	Has few cracks	Is steep and concave toward slide; may have variety of shapes in outline, nearly straight, gentle arc, circular, or bottle shaped	Commonly diverge in direction of movement	Is generally under water	Spreads out on underwater floor	Has none	Is spreading and lobate

Note: This table updates Table 1 in book on landslides published in 1958 by Highway Research Board (*3, 10*, chap. 4 by A. M. Ritchie, pp. 58-57).

(after Rib & Liang, 1978)

Table 2. Features indicating active and inactive landslides

Active	Inactive
Scarps, terraces and crevices with sharp edges	Scarps, terraces and crevices with rounded edges
Crevices and depressions without secondary infilling	Crevices and depressions infilled with secondary deposits
Secondary mass movement on scarp faces	No secondary mass movement on scar faces
Surface-of-rupture and marginal shear planes show fresh slikensides and striations	Surface-of-rupture and marginal shear planes show old or no slikensides and striations
Fresh fractured surfaces on blocks	Weathering on fractured surfaces of blocks
Disarranged drainage system; many ponds and undrained depressions	Integrated drainage system
Pressure ridges in contact with slide margin	Marginal fissures and abandoned levée
No soil development on exposed surface-of-rupture	Soil development on exposed surface-of-rupture
Presence of fast-growing vegetation spp.	Presence of slow-growing vegetation spp.
Distinct vegetation differences 'on' and 'off' slide	No distinction between vegetation 'on' and 'off' slide
Tilted trees with no new vertical growth	Tilted trees with new vertical growth above inclined trunk
No new supportive, secondary tissue on trunks	New supportive, secondary tissue on trunks

From Crozier, 1984

E. Distress of Constructed Works

Constructed works are often damaged by landslides, particularly in urban environments. These works may include roadways, sidewalks, driveways, retaining walls, home foundations, utility pipes, telephone poles, fences, or concrete drainage ditches.

All damage should be photographed, described in field notes, and the location should be indicated on the field map.

Although there may be many reasons other than landsliding to explain the damage (poor construction, expansive soils, etc.), the general pattern of damage may be very helpful in establishing the limits of sliding. Also, there are some cases of deep-seated landsliding where little surficial damage within the center of the slide is seen.

Examples of notes from field mapping of distress features are presented on Figure 11. An example of correlating distress features to sliding is on Figures 12 and 13.

F. Vegetation Patterns

Certain types of vegetation often characterize slopes with landslide deposits. Many times these are plants which thrive in a wet environment (cat-tails, alder, etc.) and may be indicators of spring activity, water ponds, or general poor drainage. Other plants thrive in loosened soils, which may have been disturbed by landslide movement.

Tree trunk orientation can often be helpful in assessing the type and recency of movement. Moving ground may push a tree and cause it to lean downhill. A general illustration is shown on Figure 14. If the deflection is not recent, the trunk may curve back in a more vertical position several feet off the ground. In rotational slides, trees that drop in scarp areas or are on the upper portion of a large toe bulge may lean in an uphill direction. Examples are provided in Zaruba and Mencl (1969).

G. Surface Instrumentation

In addition to the monitoring done by a surveyor to evaluate the magnitude of ground movement, extensometers or strain meters can be used on the ground surface in protected locations. These devices often use vibrating invar wire and may be connected to continuously reading devices. A typical system is shown on Figure 15.

Often the ground will slowly move prior to a landslide and then the rate of movement suddenly increases just before the main slide movement occurs (see Figure 16). Rogers (1978) said that expansive clay soils in the Bay Area will slowly creep downhill at up to one inch per year. However, when one inch per year is exceeded, the slope may be moving toward failure. Singh and Mitchell (1969) discuss a method to evaluate the time dependency of creep in various soils and determine if creep toward failure is occurring.

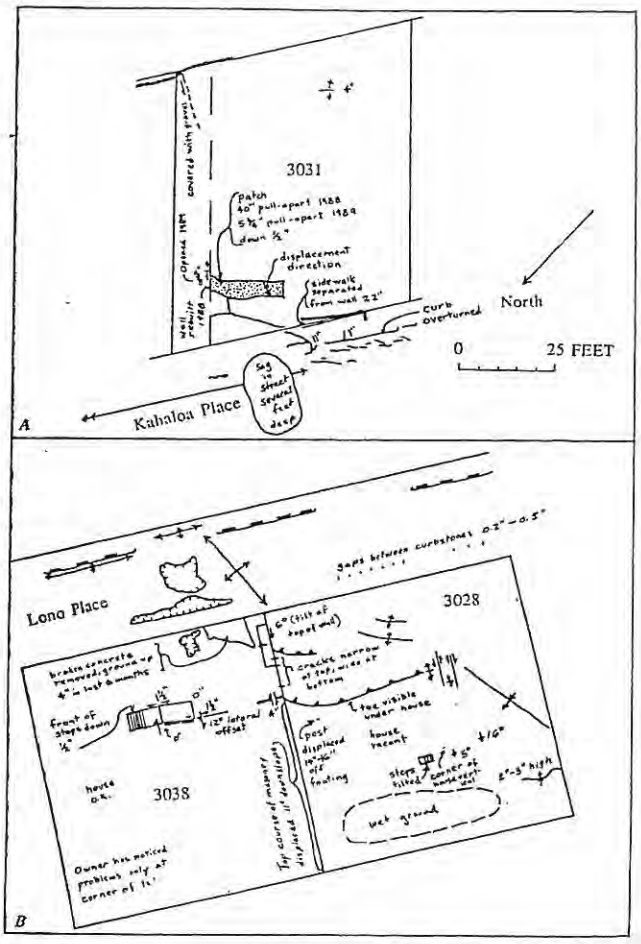

EXPLANATION

- Cracks in pavement, walls, or ground surface--Arrows and number indicate separation in inches
- Patch in wide crack
- Landslide toe--Sawteeth on moving ground
- Concrete slab overriding curb--Rectangles on edge of slal
- Closed depression
- Linear ridge--Large arrows indicate tips of ridge
- Escarpment--Arrows indicate direction of ground slope
- 5° Tilt of an originally horizontal surface--Arrow shows direction of tilt, number indicates tilt angle in degrees
- Lateral offset--Arrows indicate sense of offset, number indicates offset in inches
- Stone or concrete-masonry wall
- Spring or seep

Figure 11. Examples of Urban Field Mapping of Landslide Features (Baum, et al, 1989)

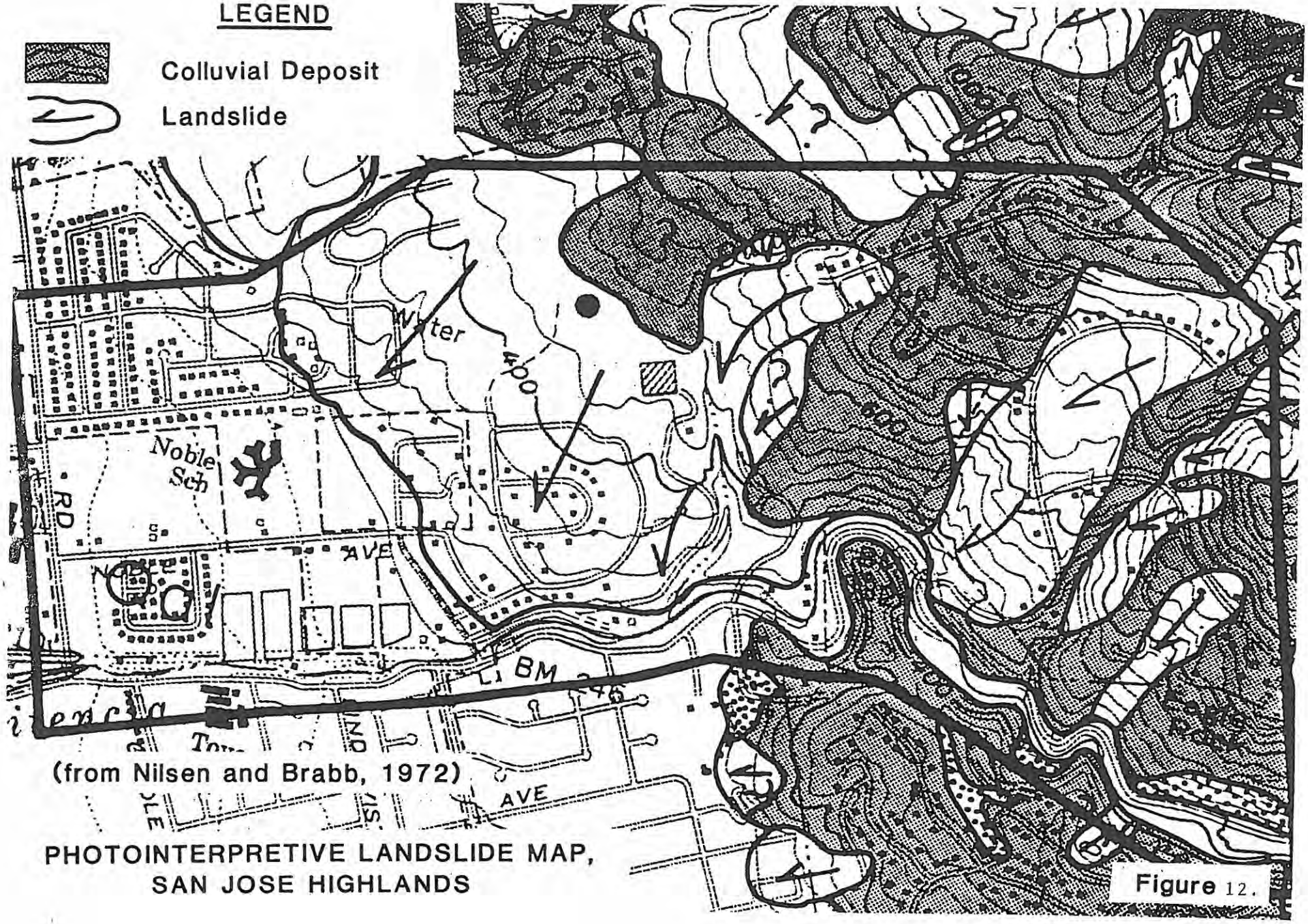

(from Nilsen and Brabb, 1972)

PHOTOINTERPRETIVE LANDSLIDE MAP,
SAN JOSE HIGHLANDS

Figure 12.

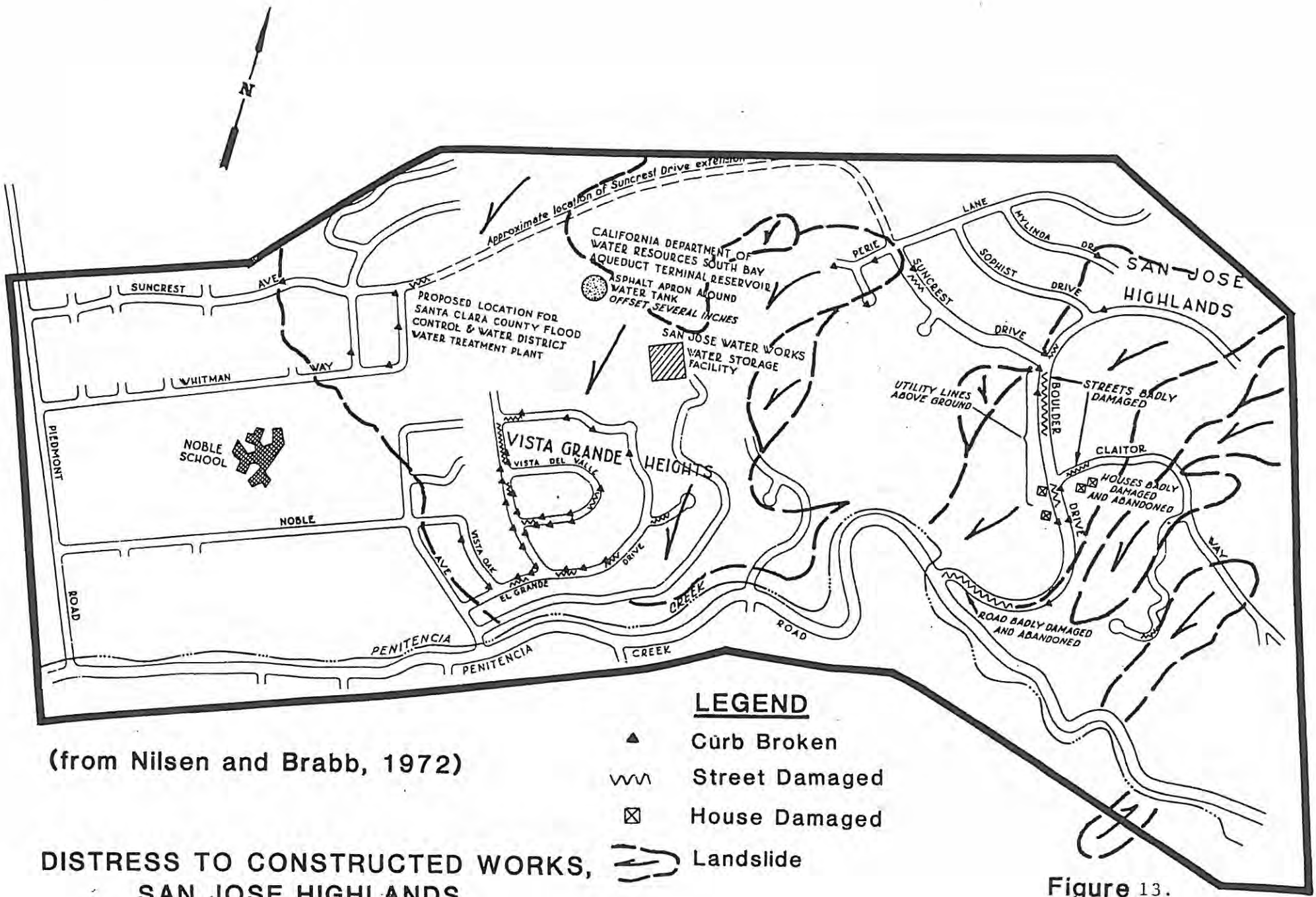

(from Nilsen and Brabb, 1972)

DISTRESS TO CONSTRUCTED WORKS, SAN JOSE HIGHLANDS

Figure 13.

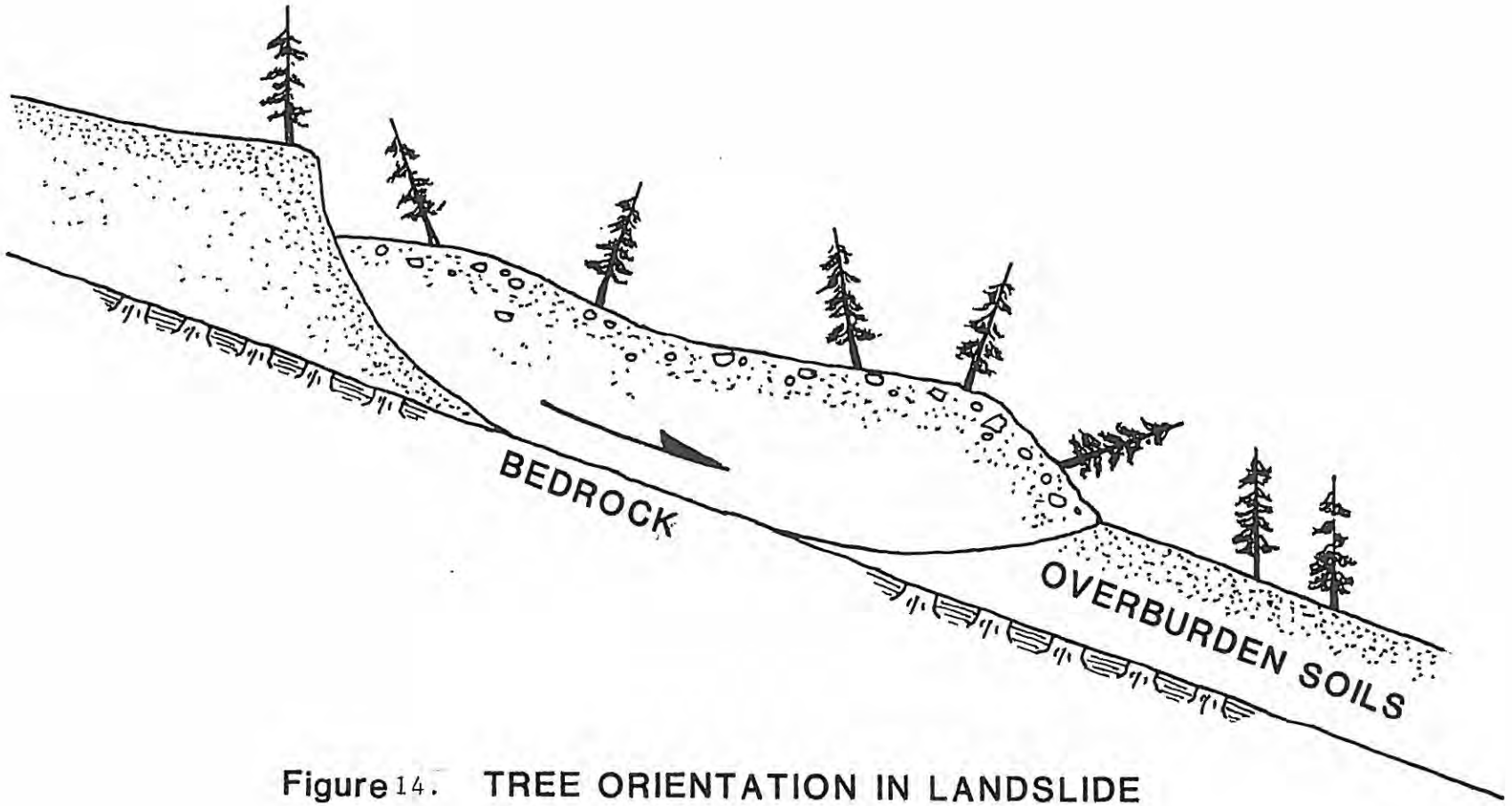

Figure 14. TREE ORIENTATION IN LANDSLIDE

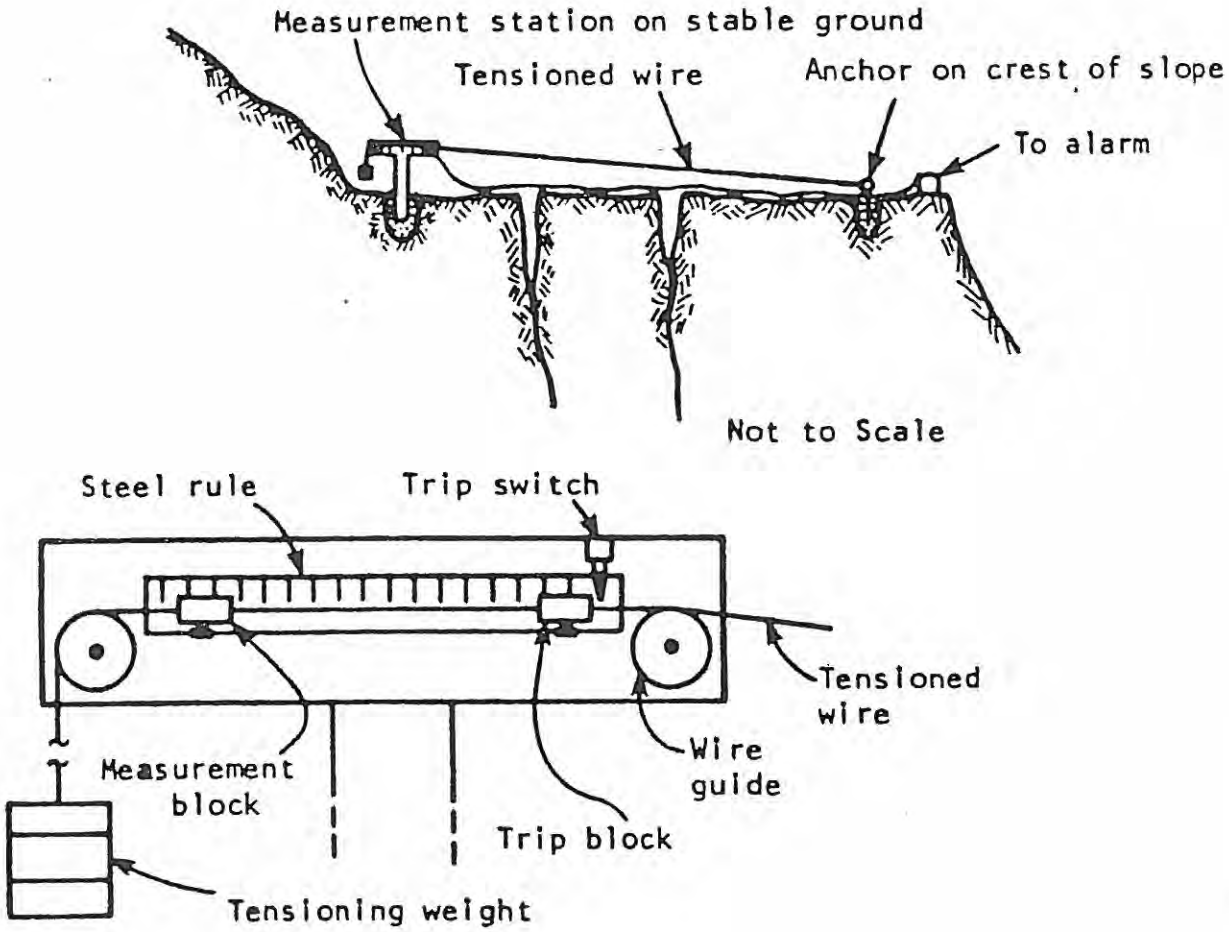

Figure 15. Wire extensometer on crest of slope.
(Golder Associates, 1981)

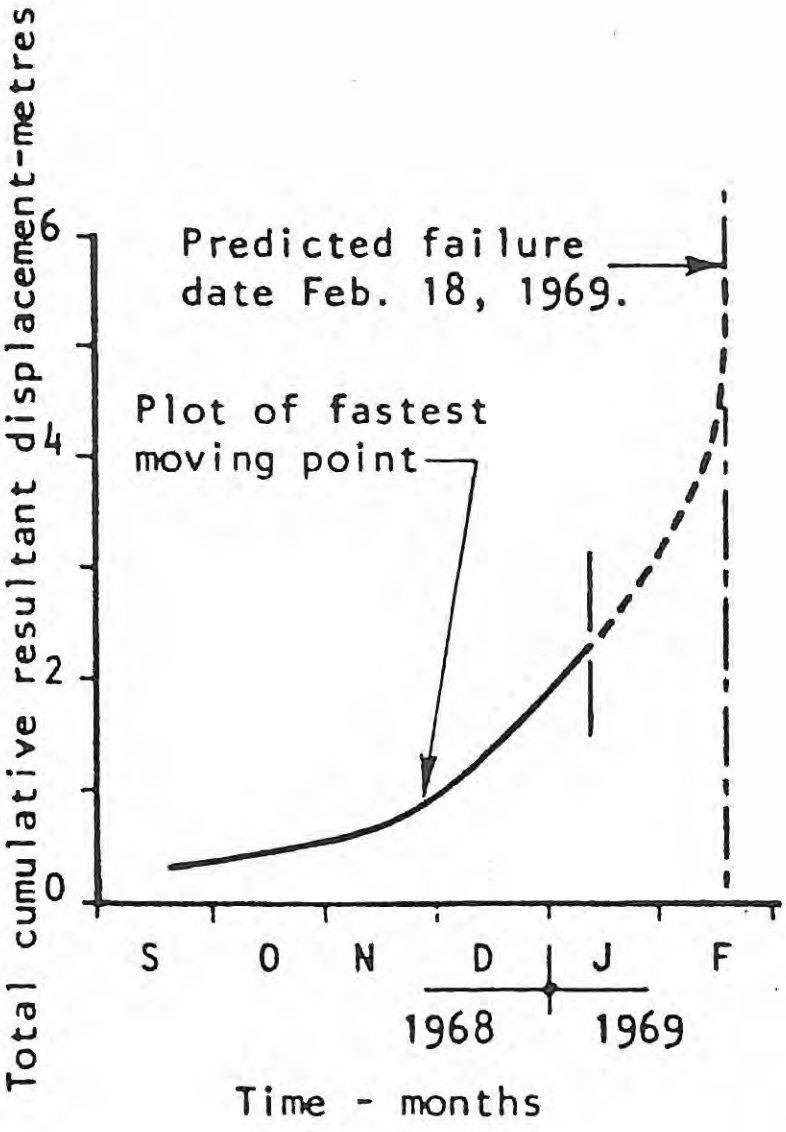

Typical plot of cumulative displacement against time showing acceleration period before failure. (Golder Associates, 1981)

Figure 16.

Hunt (1984) reports on the rate of ground movement just before landsliding at various sites around the world -- see Table 3. Most of these rates were about one-half to one inch per day, and many continued at these rates for several weeks.

The length and time to continue monitoring movement depends on the landslide type and remedial work performed. Guidelines are presented in Dunnicliff (1988). Case histories are presented in Gichaga, et al (1988) and Mehrota (1988).

A more recent surface evaluation tool is the tiltmeter (Egan, et al, 1992). A tiltmeter is a highly precise instrument that measures the rotation of the base upon which it rests. The tiltmeter is extremely precise and can have continuous recording. An example of it successful use is presented in Civil Engineering (1991). It should be noted that tiltmeters can be placed in borings, but the installation is much more complex.

H. Exploratory Borings and Trenches

Subsurface exploration is crucial to the evaluation of a landslide. Borings and trenches generally are used to evaluate the subsurface geology, locate slide plane or planes, recover samples for testing, provide holes for subsurface instrumentation. A general guide to subsurface techniques is presented on Table 4.

Initially, the number and depth of borings or trenches will depend on the anticipated stratigraphy and uniformity of conditions. However, modifications will be needed as the actual conditions are encountered and gaps in the data occur. The borings and trenches should be located both within and outside the slide. Within the slide, the disturbed conditions above and the undisturbed conditions below the slide plane can be studied.

Outside the slide, the undisturbed conditions within the same depth as the slide materials inside the slide can be studied because they may reflect the conditions that existed within the slide mass before failure. The borings and trenches should be located to maximize the ability to draw strategic cross-sections. The depth of the slide may be estimated in advance based on the slide geometry so data collection can be maximized at critical locations.

Skempton and Hutchinson (1969) prepared ratios of depth to length for different types of slides. Rogers (1986) has modified these ratios for Bay Area conditions -- see Figures 17 and 18. One example of similar ratios for mudflows is presented on Figure 19.

Trenches or test pits:

1. Excavated by bulldozers or backhoes
2. Excellent lateral exposures in trench walls
3. Often limited to 10-15 feet deep -- may need shoring
4. Can collect block samples

TABLE 3

MAGNITUDES OF SLIDE MOVEMENTS BEFORE TOTAL FAILURE

Location	Material	Movement velocity
Philippine Islands	Weathered rock (open-pit mine)	2 cm/day
Santos, Brazil	Colluvium (cut)	2.5 cm/day
Rio de Janeiro State, Brazil	Residuum (cut)	0.4-2.2 cm/day
Rio Santos Highway, Brazil	Residuum (cut)	2-3.5 cm/day for first 2 weeks, 30 cm/day during 6th week, then failure
Golden slide	Debris (cut)	2.5 cm/day
Pipe Organ slide	Debris (cut)	5 cm/week
Vaiont, Italy	Rock-mass translation	1 cm/week, then 1 cm/day, then 20-30 cm/day, and after 3 weeks, 80 cm/day and failure
Portuguese Bend	Lateral spreading	1956-1957, 5-12 cm/year 1958, 15-60 cm/year 1961-1968, 1-3m/year 1968, dramatic increase, houses destroyed 1973, 8 cm/day during dry season 1973, 10 cm/day during wet season 1973, 15 cm/day during heavy rains No total mass failure

(Hunt, 1984)

TABLE 4
SUBSURFACE EVALUATION TECHNIQUES

Method and Reference	Procedure	Type of Sample	Applications	Limitations
Auger boring, ASTM D 1452	Dry hole drilled with hand or power auger; samples preferably recovered from auger flutes	Auger cuttings; disturbed, ground up, partially dried from drill heat in hard materials	In soil and soft rock; to identify geologic units and water content above water table	Soil and rock stratification destroyed; sample mixed with water below water table
Test boring, ASTM D 1586 (Figure 4.15)	Hole drilled with auger or rotary drill; at intervals samples taken 36-mm ID and 50-mm OD driven 0.45 m in three 150-mm increments by 64-kg hammer falling 0.76 m; hydrostatic balance of fluid maintained below water level	Intact but partially disturbed (number of hammer blows for second plus third increment of driving is standard penetration resistance or N)	To identify soil or soft rock; to determine water content; in classification tests and crude shear test of sample (N-value a crude index to density of cohesionless soil and undrained shear strength of cohesive soil)	Gaps between samples, 30 to 120 cm; sample too distorted for accurate shear and consolidation tests; sample limited by gravel; N-value subject to variations depending on free fall of hammer
Test boring of large samples	50 to 75-mm ID and 63 to 89-mm OD samplers driven by hammers up to 160 kg	Intact but partially disturbed (number of hammer blows for second plus third increment of driving is penetration resistance)	In gravelly soils	Sample limited by larger gravel
Test boring through hollow-stem auger	Hole advanced by hollow-stem auger; soil sampled below auger as in test boring above	Intact but partially disturbed (number of hammer blows for second plus third increment of driving is standard penetration resistance or N); N-value may be distorted by auger and should be compared with ASTM D 1586	In gravelly soils (not well adapted to harder soils or soft rock)	Sample limited by larger gravel; maintaining hydrostatic balance in hole below water table more difficult
Rotary coring of soil or soft rock	Outer tube with teeth rotated; soil protected and held by stationary inner tube; cuttings flushed upward by drill fluid (Denison—fixed cutter on outer tube; Pitcher—spring-loaded on outer tube; Acker air-mud core barrel—larger clearances for viscous drilling fluid)	Relatively undisturbed sample, 50 to 200-mm wide and 0.3 to 1.5 m long in liner tube	In firm to stiff cohesive soils and soft but coherent rock	Sample may twist in soft clays; sampling loose sand below water table difficult; success in gravel seldom occurs
Rotary coring of swelling clay or soft rock	Similar to rotary coring of rock; swelling core retained by third inner plastic liner	Soil cylinder 28.5 to 53.2 mm wide and 600 to 1500 mm long encased in plastic tube	In soils and soft rocks that swell or disintegrate rapidly in air (protected by plastic tube)	Sample smaller; equipment more complex
Rotary coring of rock, ASTM D 2113	Outer tube with diamond bit on lower end rotated to cut annular hole in rock; core protected by stationary inner tube; cuttings flushed upward by drill fluid	Rock cylinder 22 to 100 mm wide and as long as 6 m depending on rock soundness	To obtain continuous core in sound rock (percentage of core recovered for distance drilled depends on fractures, rock variability, equipment, and skill of driller)	Core lost in fracture or variable rock; blockage prevents drilling in badly fractured rock; dip of bedding and joints evident but not strike
Rotary coring of rock, oriented core	Similar to rotary coring of rock above; continuous grooves scribed on rock core with compass direction	Rock cylinder, typically 54 mm wide and 1.5 m long with compass orientation	To determine strike of joints and bedding	Method may not be effective in fractured rock
Rotary coring of rock, wire line	Outer tube with diamond bit on lower end rotated to cut annular hole in rock; core protected by stationary inner tube; cuttings flushed upward by drill fluid; core and stationary inner tube retrieved from outer core barrel by lifting device or "overshot" suspended on thin cable (wire line) through special large diameter drill rods and outer core barrel	Rock cylinder 36.5 to 85 mm wide and 1.5 to 4.6 m long	To recover core better in fractured rock, which has less tendency for caving during core removal; to obtain much faster cycle of core recovery and resumption of drilling in deep holes	Same as ASTM D 2113 but to lesser degree
Rotary coring of rock, integral sampling method (*4.10*)	22-mm hole drilled for length of proposed core; steel rod grouted into hole; core drilled around grouted rod with 100 to 150-mm rock coring drill (same as for ASTM D 2113)	Continuous core reinforced by grouted steel rod	To obtain continuous core in badly fractured, soft, or weathered rock in which recovery is low by ASTM D 2113	Grout may not adhere in some badly weathered rock; fractures sometimes cause drift of diamond bit and cutting rod
Thin-wall tube, ASTM D 1587	75 to 1250-mm thin-wall tube forced into soil with static force (or driven in soft rock); retention of sample helped by drilling mud	Relatively undisturbed sample, length 10 to 20 diameters	In soft to firm clays, short (5-diameter) samples of stiff cohesive soil, soft rock and, with aid of drilling mud, in firm to dense sands	Cutting edge wrinkled by gravel; samples lost in loose sand or very soft clay below water table; more disturbance occurs if driven with hammer
Thin-wall tube, fixed piston	75 to 1250-mm thin-wall tube, which has internal piston controlled by rod and keeps loose cuttings from tube, remains stationary while outer thin-wall tube forced ahead into soil; sample in tube is held in tube by aid of piston (Osterberg-type activates piston hydraulically; Hong-type by a ratchet)	Relatively undisturbed sample, length 10 to 20 diameters	To minimize disturbance of very soft clays (drilling mud aids in holding samples in loose sand below water table)	Method is slow and cumbersome
Swedish foil	Sample surrounded by thin strips of stainless steel, stored above cutter, to prevent contact of soil with tube as it is forced into soil	Continuous samples 50 mm wide and as long as 12 m	In soft, sensitive clays	Samples sometimes damaged by coarse sand and fine gravel
Dynamic sounding (*4.6, 4.12,* Figure 4.15)	Enlarged disposable point on end of rod driven by weight falling fixed distance in increments of 100 to 300 mm	None	To identify significant differences in soil strength or density	Misleading in gravels or loose saturated fine cohesionless soils
Static penetration (*4.6, 4.12,* Figure 4.15)	Enlarged cone, 36-mm diameter and 60° angle forced into soil; force measured at regular intervals	None	To identify significant differences in soil strength or density; to identify soil by resistance of friction sleeve	Stopped by gravel or hard seams
Borehole camera	Inside of core hole viewed by circular photograph or scan	Visual representation	To examine stratification, fractures, and cavities in hole walls	Best above water table or when hole can be stabilized by clear water
Pits and trenches	Pit or trench excavated to expose soils and rocks	Chunks cut from walls of trench, size not limited	To determine structure of complex formations; to obtain samples of thin critical seams such as failure surface	Moving excavation equipment to site, stabilizing excavation walls, and controlling groundwater may be difficult
Rotary or cable tool well drill	Toothed cutter rotated or chisel bit pounded and churned	Ground	To penetrate boulders, coarse gravel; to identify hardness from drilling rates	Identifying soils or rocks difficult
Percussion drilling (jack hammer or air track)	Impact drill used, cuttings removed by compressed air	Rock dust	To locate rock, soft seams, or cavities in sound rock	Drill becomes plugged by wet soil

(after Sowers & Royster, 1978)

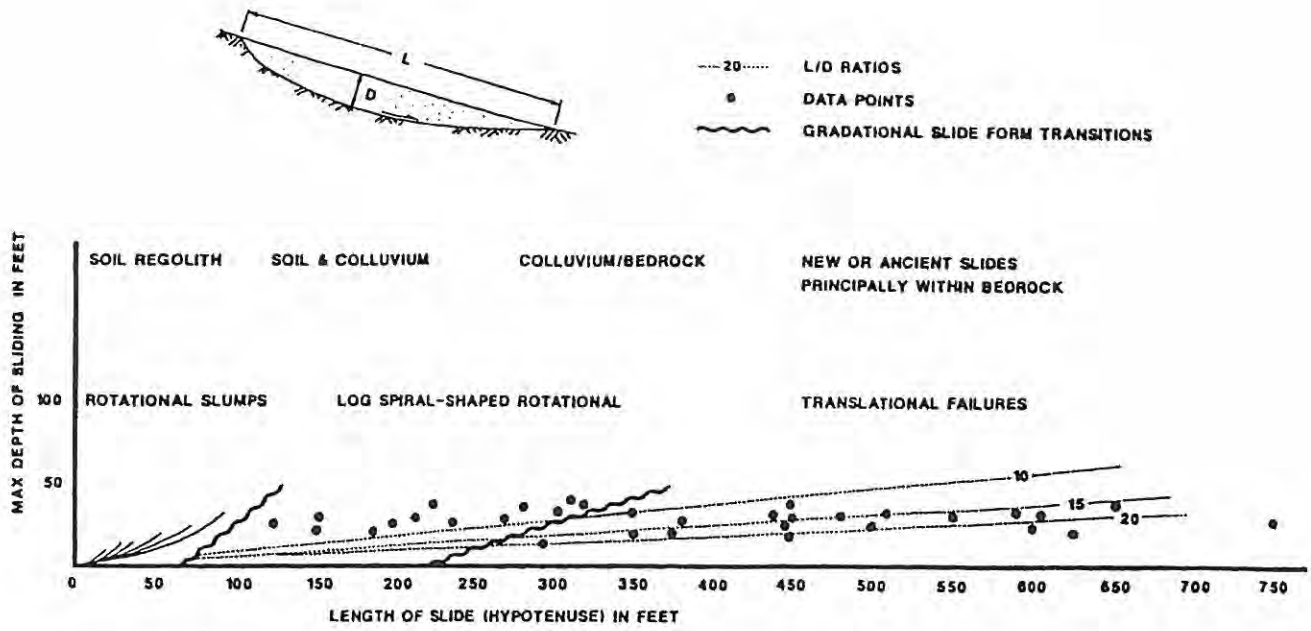

Figure 17.

Length to maximum depth ratios for various types of landslides studied in the East Bay from 1976 - 86. Qualitative distinctions are made in accordance with observations made during various subsurface investigations.

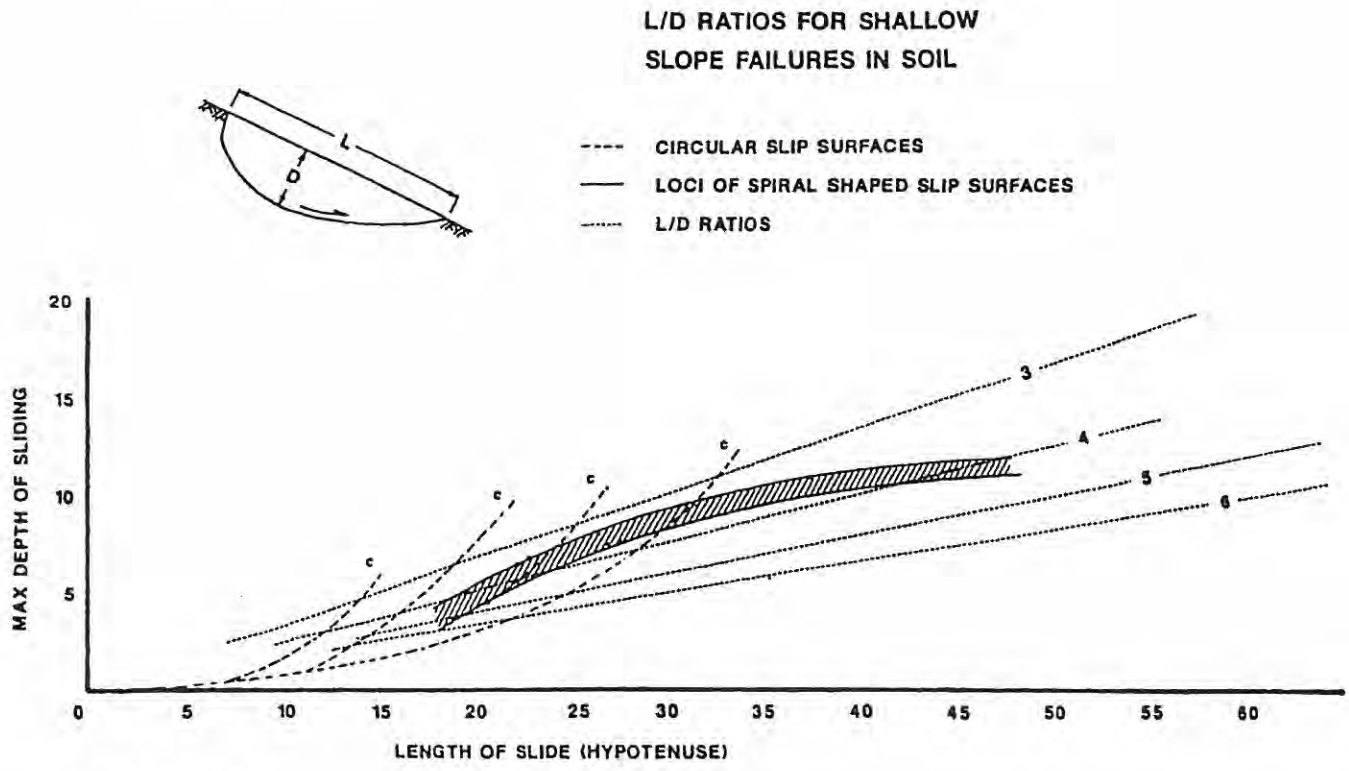

Figure 18.

Length to maximum depth ratios for shallow rotational slump failures in soil. The stippled band delineates log-spiral shaped failure surfaces from $\phi = 10^{o}$ up through $\phi = 45^{o}$.

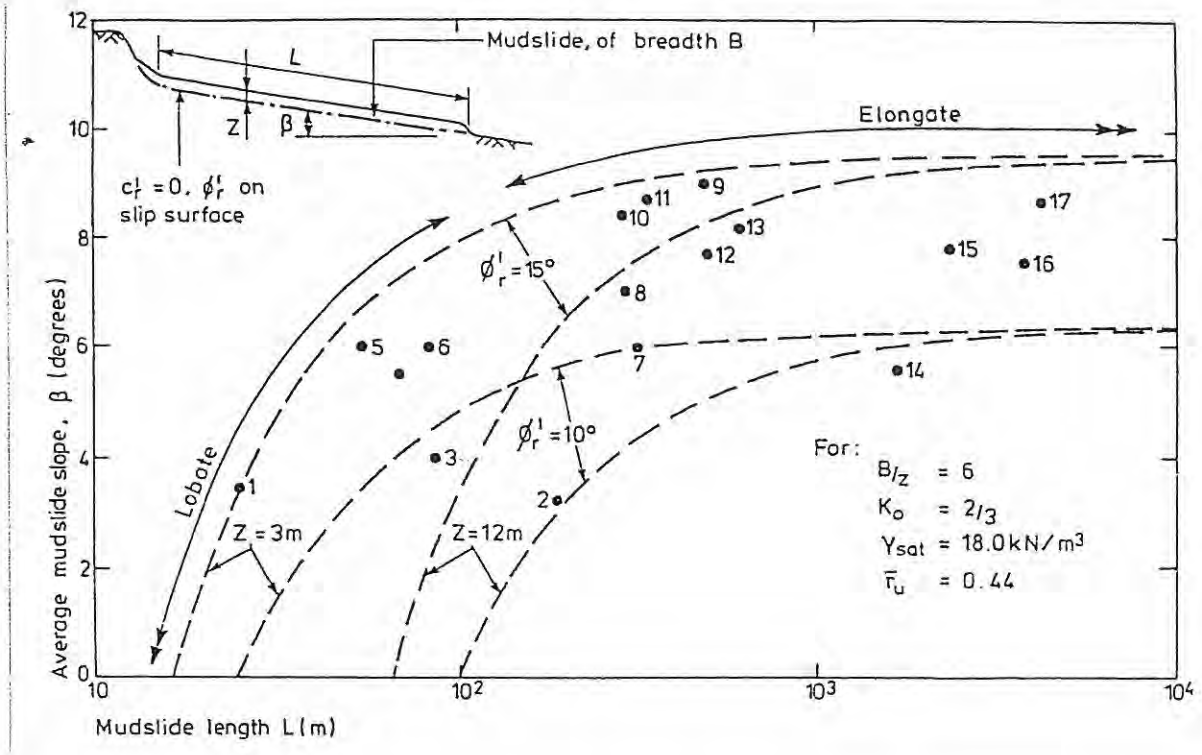

Figure 19. Comparisons of Length to Depth Ratios For Various Mudflows (Hutchinson, 1988)

Small-diameter borings (generally 3-8" diameter)

1. Often drilled 20-100 feet deep
2. Can continuously sample above slide plane for key properties to be measured in lab
3. Can drill without sample for general information, like soft zones, depth to hard bedrock, etc.

Large-diameter borings (generally 24" diameter)

1. Can be entered by geologist for logging
2. Can locate thin slip planes or clay seams
3. Excellent for detailed geologic understanding
4. Slow and expensive

Samplers can be used with small-diameter borings and sometimes with other equipment -- includes split spoon samplers, Shelby tubes, piston-type samplers, Swedish-foil samplers, Denison samplers, or Pitcher barrel samplers. Use core barrel in hard rock (oriented core will be helpful in assessing geologic structure).

Possibly also use in-situ tests to measure properties in-situ and minimize sampling and handling disturbance -- includes standard penetration test, cone penetration test, pressuremeter test, borehole shear test, and vane shear test.

The use of a large-diameter boring to locate a thin slide plane on a large California landslide was discussed in Gardner (1989). Another Southern California example of the use of this technique is presented in Tarricone (1991).

I. Subsurface Instrumentation

Landslides often continue moving slowly on the same slide plane after the major episode of sliding. By monitoring the movement along the slip plane, it can also be estimated whether the rate is increasing such that another large event might occur.

Most common type of instrumentation is the placement of slope inclinometer casing in a hole and then monitoring the movement with readings from an inclinometer probe. The casing is usually 2 to 4 inches in diameter. The probe is inserted in the casing and measurements made ever 2 feet or so. See equipment in Figure 20.

The inclinometer equipment can locate very thin slip planes that otherwise might go undetected. An example of this is shown on Figure 21. Also, some landslide complexes have multiple slide planes (Figure 22), and inclinometer measurements may identify the locations and rates of movement on each. A more detailed discussion of the use of inclinometers is provided in Green and Mikkelsen (1988). Recent innovations regarding monitoring with inclinometers are presented in Mikkelsen (1991).

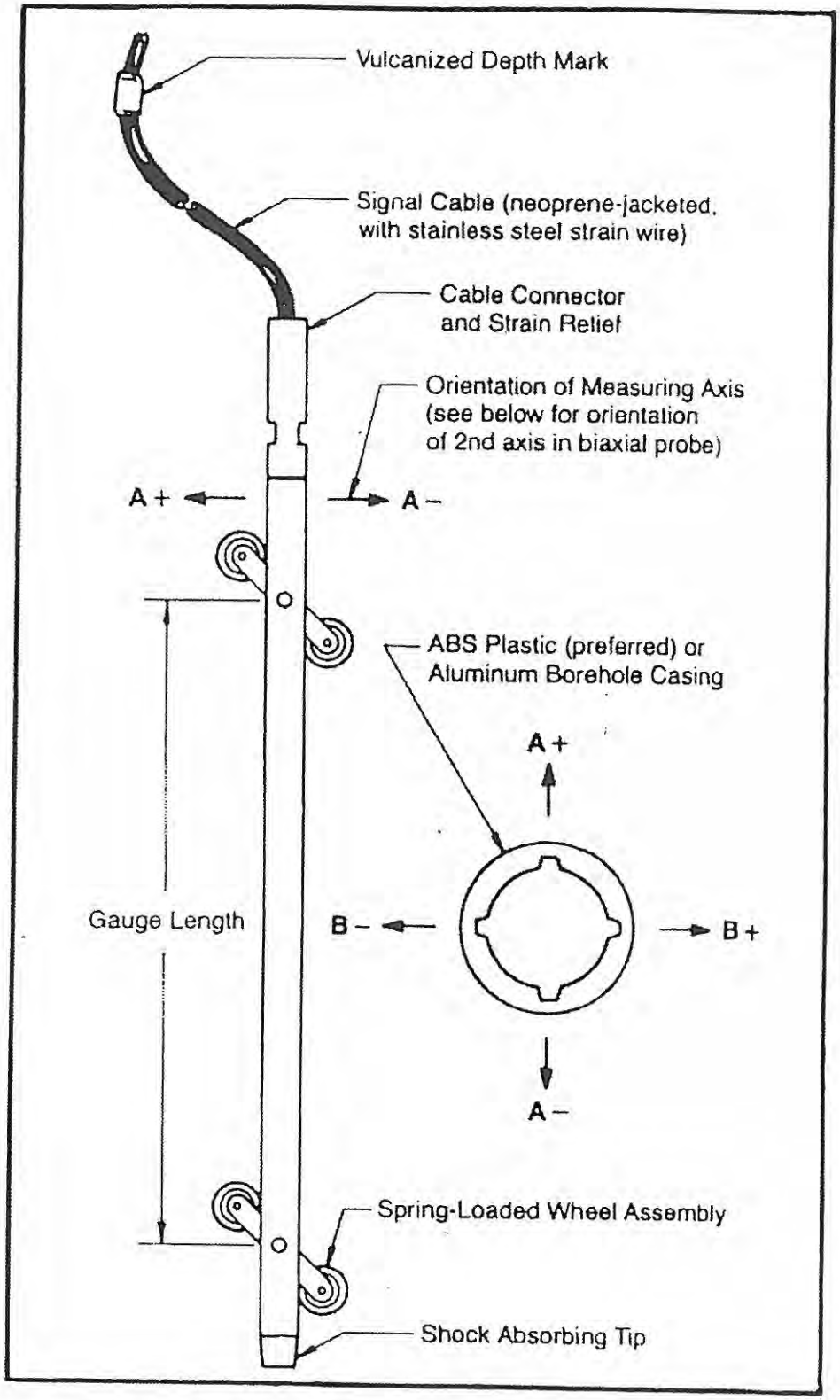

Figure 20. Typical Borehole Inclinometer (Vertical, Traversing)

Geologic Profile and Slope Inclinometer Readings, Minneapolis Freeway (from Wilson 1974)

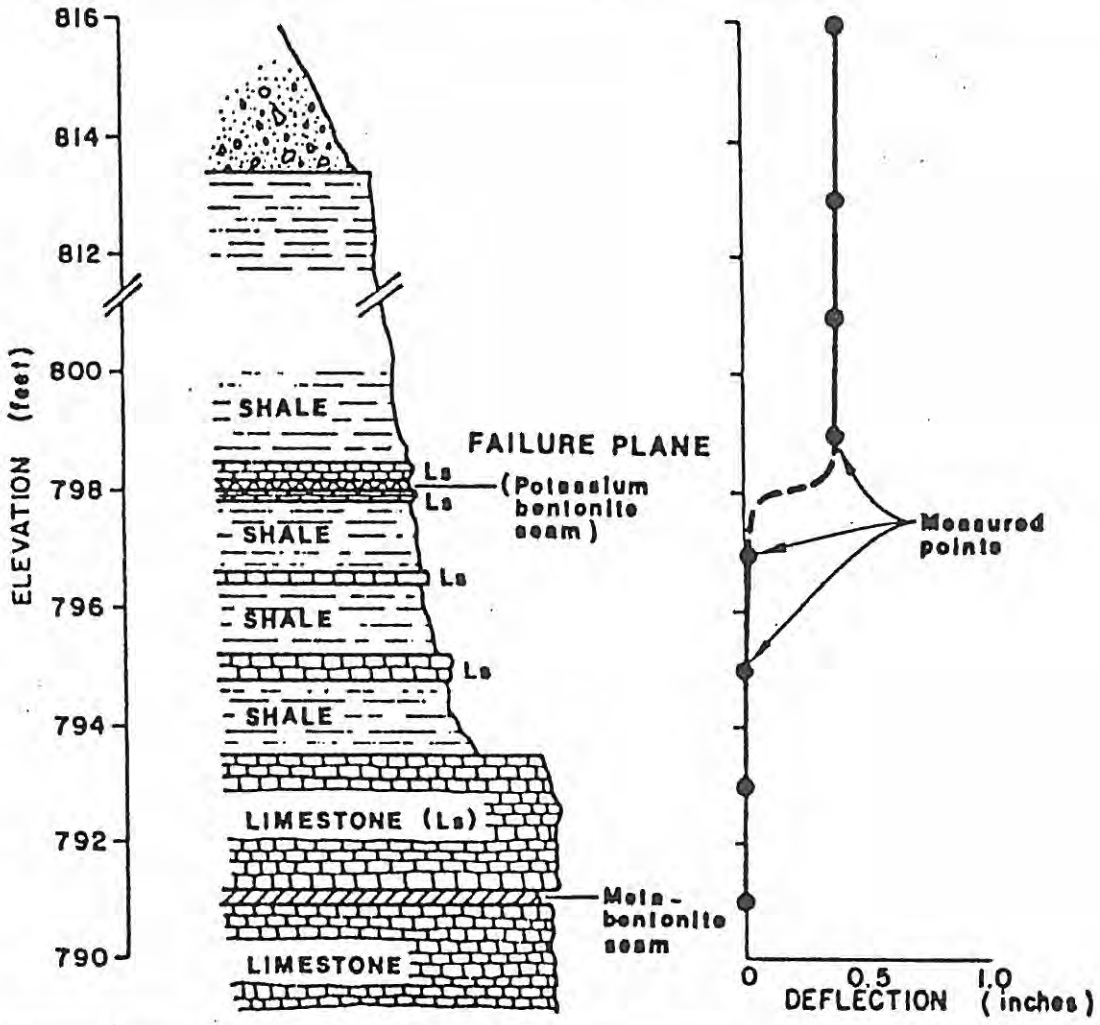

Figure 21.

Backfill of inclinometer casing is important so that it is neither too weak so that the casing can move within the boring or too strong so that small movements are not detected. General recommendations developed by the Slope Indicator Company are presented below.

Types of Backfill and Selected Conditions

	Highly permeable ground	Dry borehole	Water-filled borehole	Bentonite mud filled borehole	Small annulus borehole	Hollow stem auger	Drill casing, 3" annulus
PEA GRAVEL	E	E	E	E	NR	F	E
COARSE SAND	E	E	E	G	NR	NR	G
FINE SAND	E	G	G	NR	NR	NR	G
GROUT	NR	G	E	E	E	E	E

E = Excellent G = Good F = Fair NR = Not Recommended

It is our experience that a good mix design is 3 parts lime to 1 part cement mixed with sufficient water to become soupy.

It is very important that the base of the inclinometer casing is placed before the depth of landsliding because movement readings are referenced to the bottom of the casing. Wilson and Mikkelsen (1978) recommend that the position of the top of the casing be checked by precise survey methods to confirm that the deepest failure planes have been penetrated.

Extensometers are a wire or rod in a vertical or horizontal boring across a slide plane. If slide movement occurs, the change of length of the wire or rod can be recorded. Compensations for friction and temperature are usually made.

Where slopes are moving rapidly and subsurface instruments may rapidly be damaged, more crude (and less expensive) instruments may be used. For example, plain plastic pipe can reveal the depth of the slide plane using a tape measure even if sheared.

A cone penetrometer can sometimes be used to evaluate landslides. The continuous-reading character of the cone may be able to locate very thin landslide slip planes. An example of this use of the cone penetrometer is presented in French and Kropp (1986).

Acoustic emissions are sub-audible noises from deformations in soil or rock. The noises are recorded with sensitive sound equipment inserted in a boring. The type and frequency of recorded emissions have been correlated to stable and unstable slope conditions (Koerner et al., 1978). Successful monitoring of an active landslide in Colorado using acoustic emissions has recently been performed -- see Figure 23.

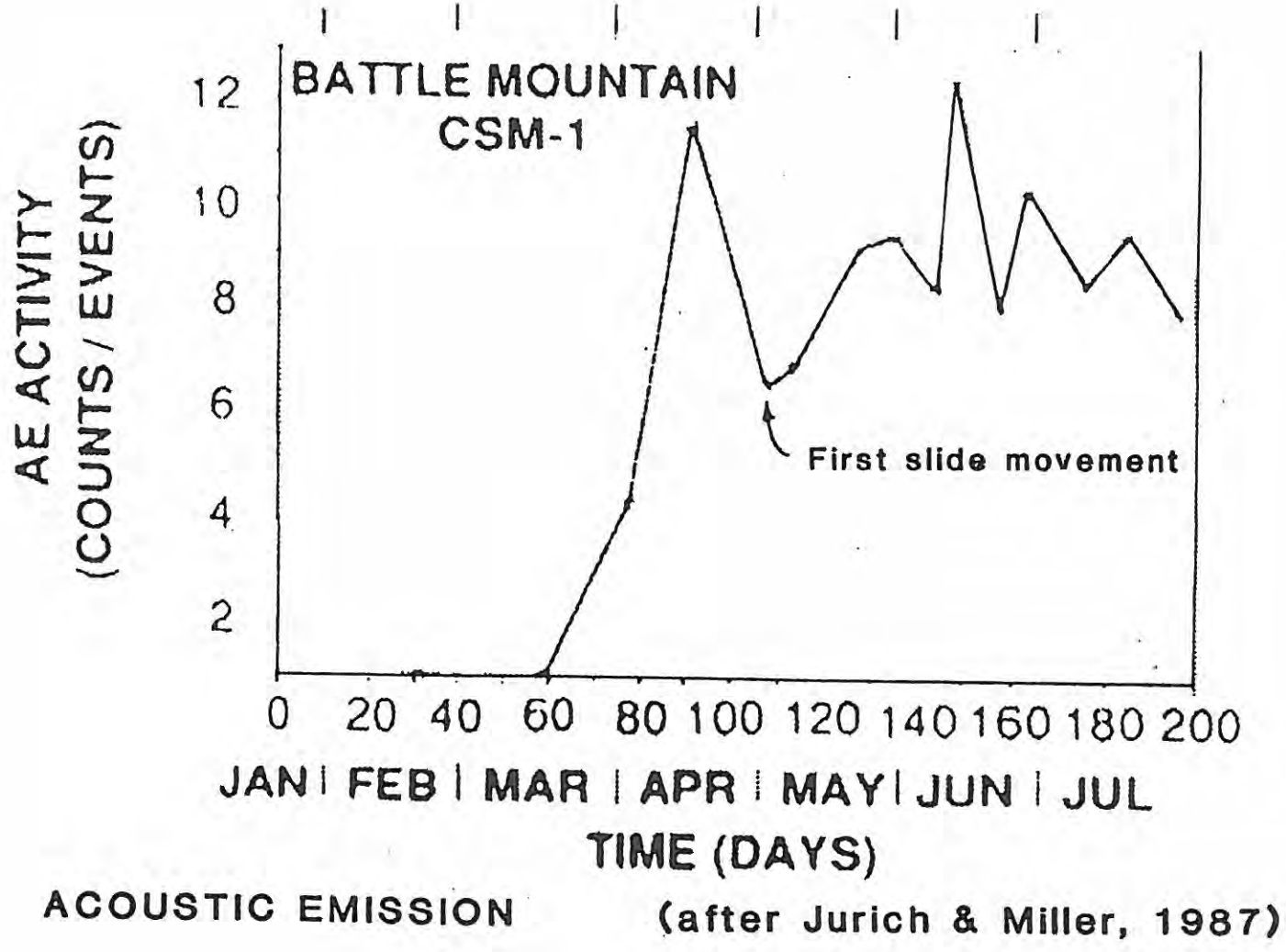
BATTLE MOUNTAIN
CSM-1
AE ACTIVITY
(COUNTS / EVENTS)
12
10
8
6
4
2
First slide movement
0 20 40 60 80 100 120 140 160 180 200
JAN | FEB | MAR | APR | MAY | JUN | JUL
TIME (DAYS)
ACOUSTIC EMISSION
(after Jurich & Miller, 1987)

Figure 22.

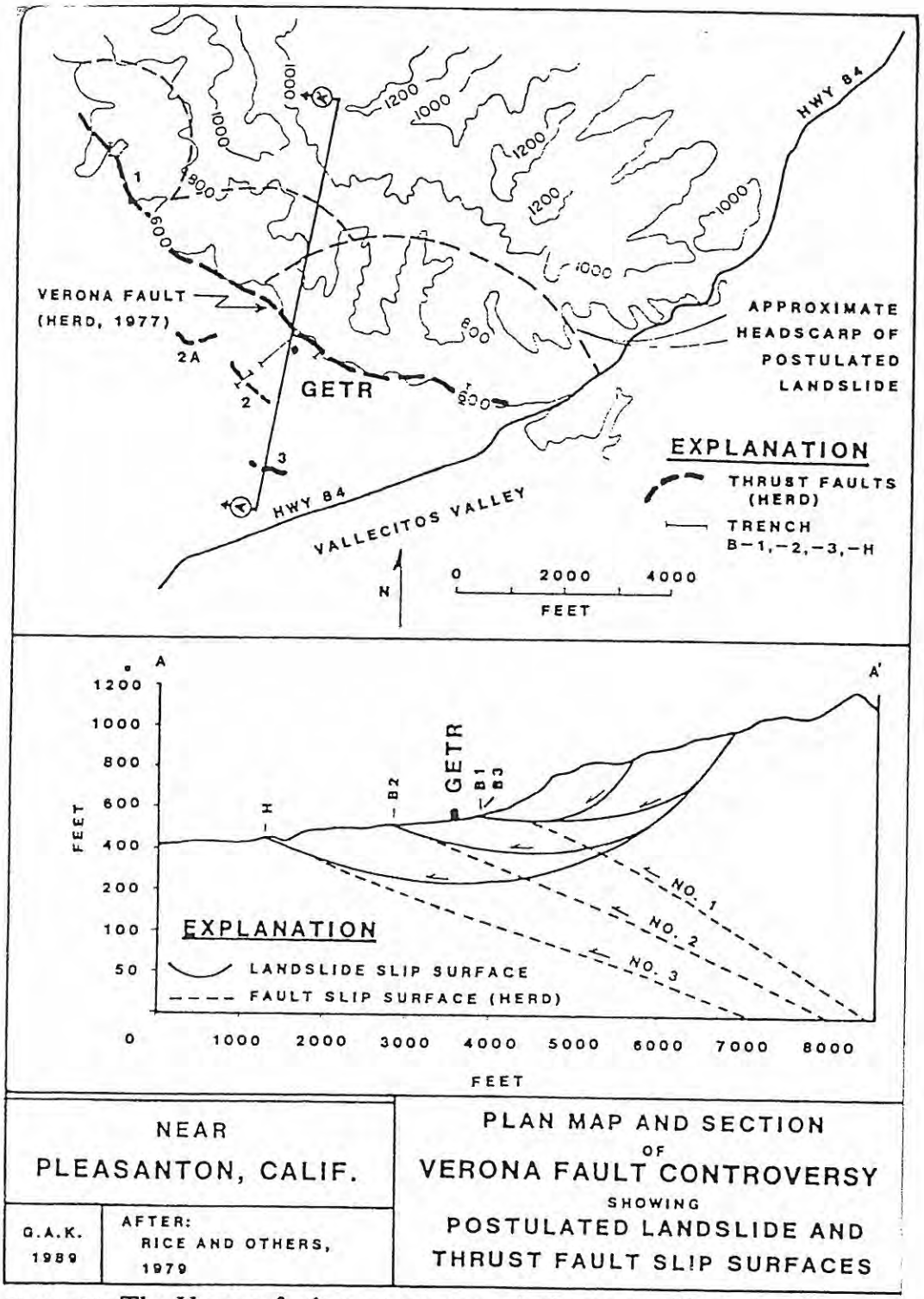

Figure 23 The Verona fault controversy relative to the Vallecito, General Electric nuclear reactor facility. The plan map shows the distribution of postulated thrust faults and headscarps of landslides; the section shows an interpretation of landslide slip surfaces and fault slip surfaces in the vicinity of the GETR facility. **(after Kiersh and James, 1991)**

J. Geophysical Exploration

Geophysical tools can be a rapid means to collect subsurface data to economically supplement other data collected during the field studies.

However, because they often measure properties which are somewhat indirect with regard to landslide evaluation, they must be carefully interpreted and used only to supplement other data from borings or trenches.

Seismic refraction can locate the depth to bedrock or thickness of various layers. Also can help locate water table.

Electrical resistivity can estimate depth to bedrock or to water table but more difficult to interpret.

Gravity measurements may be useful in large slides where disturbed materials are disturbed and less dense.

Gamma radiation was recently used to help locate bentonite seams in a large slide in Palos Verdes (Ray, 1982) - See Figure 23.

Both Cummings and Clark (1988) and Palmer and Weisgarber (1988) provide case histories where seismic refraction and electrical resistivity were used successfully to locate the depth of rupture surface in landslide studies.

K. Groundwater Patterns

Water plays a very important role in causing slides. All water flow features (both natural and man-made) should be shown on the map. Quantities should be estimated during each visit, and changes noted.

The most common tool to evaluate groundwater depth is a piezometer. A general discussion of piezometers in literature prepared by a major manufacturer (Slope Indicator Company) is attached.

Periodic readings should be made to evaluate variations with time.

Because of the relationship between rainfall and groundwater buildup (Wieczorek, 1981; Reid, et al., 1988), the rate and time phase relationship of water level with rainfall may provide prediction tools for estimating future slide movements.

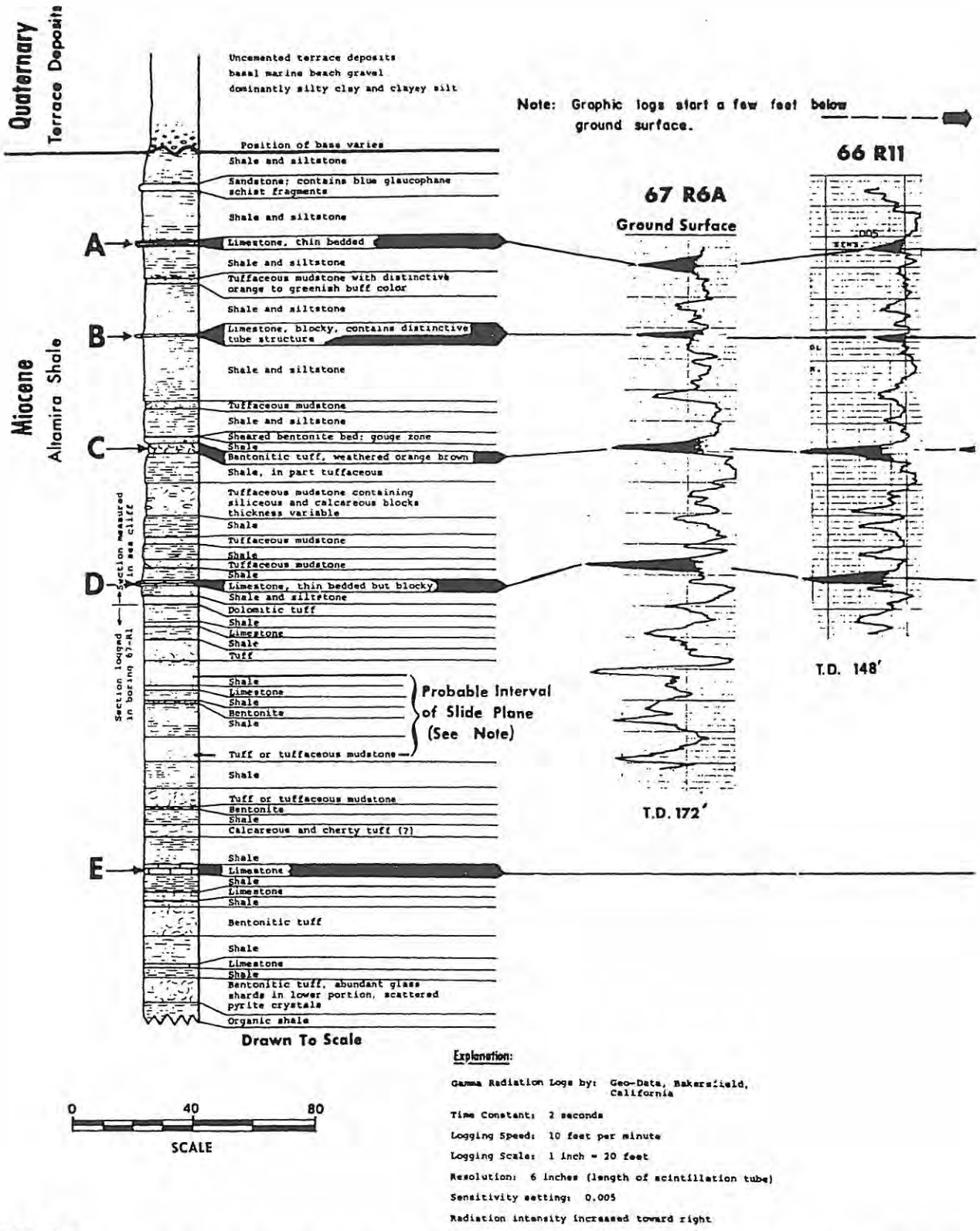

Figure 23. Columnar section showing details of stratigraphy (as exposed in the sea cliff of the South Shores landslide area and correlation with gamma radiation logs. For additional correlations see Figures 6B and 6C.

NOTE: The base of the slide is within this interval. Because the slide is not active, it is not possible to determine precisely which of the bentonite beds within the interval is the actual slide plane. Stability calculations considered the best and worst possibilities within this known interval.

(from Ray, 1982)

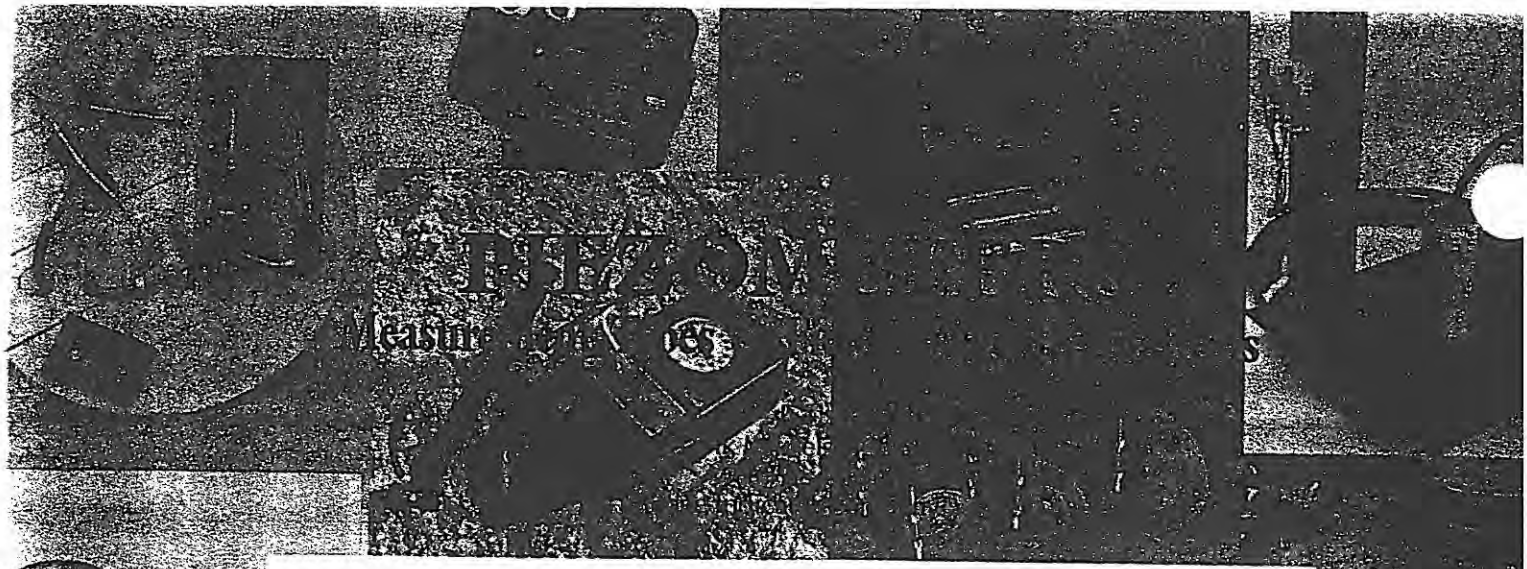

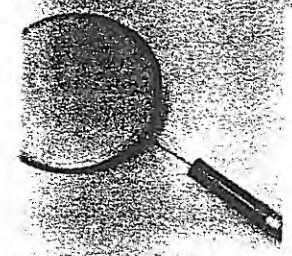

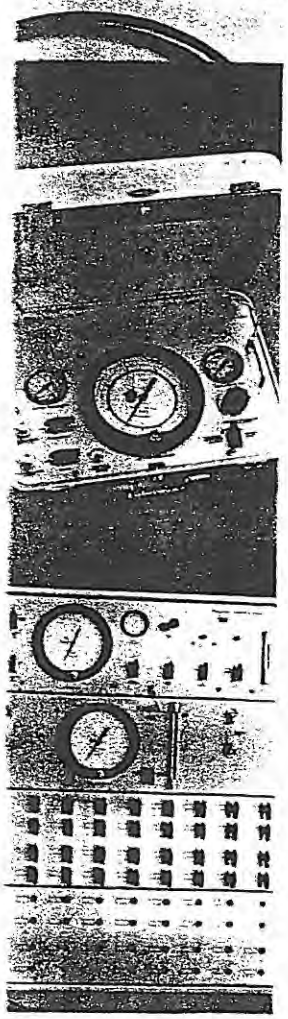

Porewater pressure measurements in soil and rock are fundamental to understanding underground behavior. The data can be used directly in effective stress analyses so that design assumptions may be evaluated; e.g., stability analyses for dams and slopes, and consolidation rates of soft foundation soils.

The basic types of piezometers are:

- Open Standpipe
- Twin Tube Hydraulic
- Pneumatic Diaphragm
- Electrical, Vibrating Wire Diaphragm
- Electrical, Strain Gauge Diaphragm

Open Standpipe

An open standpipe piezometer consists of a pipe terminated by a screen or filter tip. The pipe is installed with the tip at the elevation at which piezometric pressure is to be measured, and the measurement zone is isolated from overlying, and sometimes underlying, zones by packers or bentonite seals. Readout apparatus consists of a water level indicator, which is lowered into the pipe to determine the elevation of the water level in the pipe. The height of the column above the tip indicates the piezometric pressure at tip elevation.

Whenever practical, the open standpipe is used and it is accepted worldwide. It is simple, inexpensive, reliable, and easily manufactured. The main disadvantages are: standpipe interfering with construction; standpipe damage by ground displacements; filter clogging; long hydrostatic time lag in low permeability materials; and freezing problems.

Twin Tube Hydraulic

In twin tube hydraulic piezometers, a chamber in the tip is connected to the ground water through a filter, and to a readout device through two small diameter hydraulic tubes. The tubes, chamber, and readout device are carefully filled with clean, de-aired water, and then closed off. Piezometric pressure, and changes in pressure, are indicated on the readout manometers, bourdon tube gauges, or transducer-type data systems. The data must be corrected for differences in elevation between the tip and the readout.

The twin tube hydraulic piezometer has some attributes that cannot be equalled by diaphragm piezometers in partially saturated soils, but its disadvantages overall are usually higher. When reliable measurements of subatmospheric porewater pressure are critical or hydrofracturing tests and in-situ permeability tests are necessary, no piezometer can do a better job than a twin tube hydraulic piezometer installed properly. However, users of pneumatic and electrical diaphragm piezometers generally do not consider these attributes of the piezometer essential, being mainly concerned with excess positive porewater pressure measured in the most reliable and efficient manner.

Maintenance of the water-filled hydraulic tubing, restrictive elevations for terminals, and maintenance of complicated and corrosion-prone gage houses for hydraulic piezometers are big disadvantages compared to many diaphragm piezometers.

Order Desk # 1-800-331-0703

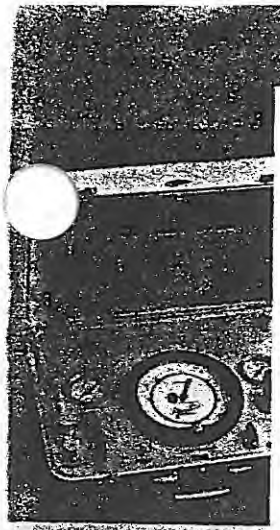

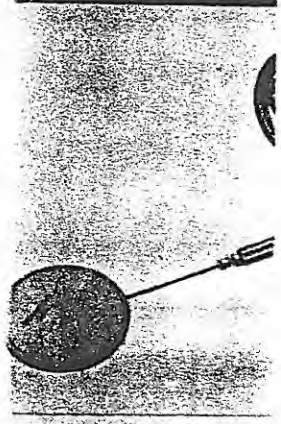

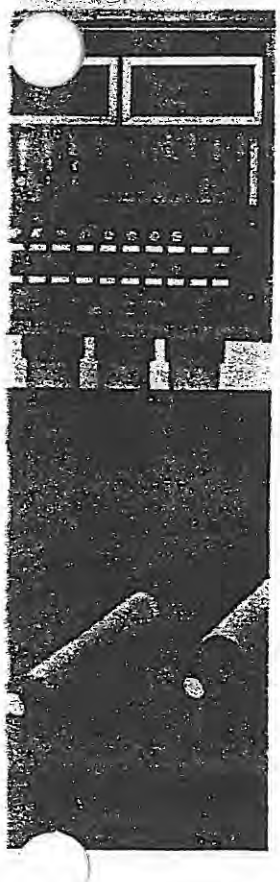

Pneumatic & Electric

In pneumatic piezometers, the external piezometric pressure loads a simple valve, keeping it either open or closed depending on the piezometer design. The valve controls the flow of gas or air in two or more tubes connected to a readout device. There is no connection between the external water and the readout device.

To determine the piezometric pressure, gas or air pressure in the readout lines is slowly increased at a carefully controlled flow rate, until it counter-balances the piezometric pressure acting on the valve. The valve then closes (or opens, again depending on the design), at which point the applied pressures (piezometric and gas/air) are equal.

In electrical strain gage and vibrating wire piezometers, the external piezometric pressure loads a diaphragm, deflecting it by an amount which is proportional to the applied pressure. The diaphragm deflection is measured using either a vibrating wire or electrical resistance strain gage. The output of the strain gage indicates the piezometric pressure.

Pneumatic and electrical transducer terminals are simple, essentially maintenance free, and can be located at any elevation. Pneumatic tubes should be limited to about 1,000 m maximum, but vibrating wire piezometer cables have been installed over several kilometers. Recent model pneumatic piezometers are attractive to many because of simplicity, quick response, and low cost.

The pneumatic piezometer has a simple valve that is either open or closed. There is little or no concern for stability of calibration. It is nearly an ideal gage in that when the gage functions, the reading will tend to be correct. The vibrating wire gage is much more complex. Each gage has a unique range and calibration that may in some cases be subject to drift. Therefore, in-situ calibration of vibrating wire piezometers is desirable, but that also increases the complexity of the gage and the potential for problems.

Currently, the vibrating wire piezometer is the most convenient to use for automatic recording. Automatically recording pneumatic systems are becoming more readily available, and can be converted to an electrical readout at a central surface station. They may well become the future best choice in many circumstances.

A problem common to all diaphragm piezometers is the lack of ability to resaturate the porous filter in-situ. This is a problem area that needs clarification and studies in the field. Twin tubes for circulating water through the filter have been added in some instances. This cumbersome addition functions as a hydraulic piezometer and needs to be maintained as such. Check valves in the twin tubes at the piezometer tip seems to be the best solution to date, but use of this type is not common, and development is needed.

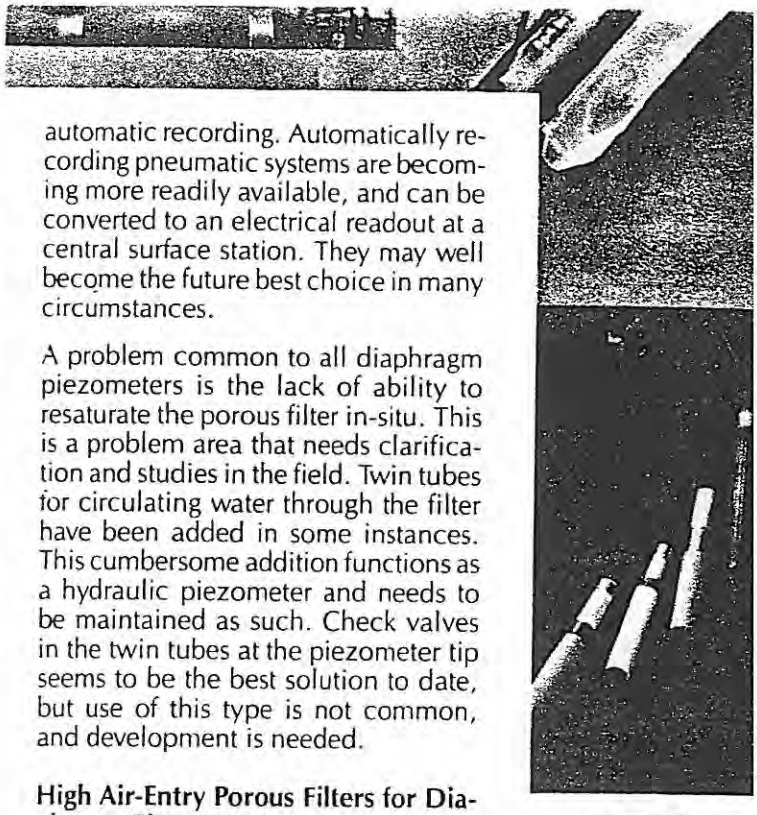

High Air-Entry Porous Filters for Diaphragm Piezometers

High air-entry filters are used to exclude vapor or gas from the piezometer in order for the hydrostatic pressure to be correctly sensed. Despite good intentions by many users, the higher gas pressure still affects the measurements, and in some cases, the high air-entry filter may be an impediment to reliable measurements.

Historically, the use of high air-entry filters was an improvement first made to twin tube hydraulic piezometers so that porewater pressure would be reliably measured in the pressure range below and slightly above atmospheric. Since it is usually possible to remove air from twin tube hydraulic piezometers, it is advantageous to use high air-entry filters. However, it may not be appropriate to use such filters with diaphragm piezometers where water cannot be circulated and the filter resaturated. The most advantageous sizes and types of filters for diaphragm piezometers in this situation have not been determined. Additionally, if a high air-entry filter element is only partly saturated, its air entry value would be reduced. The high air-entry value of the porous ceramic filter is only 100% effective when it is saturated. When dry, the air flows through at low pressure.

Order Desk # 1-800-331-0703

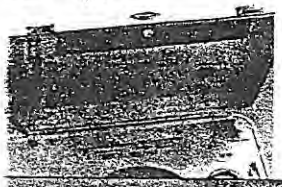

Different piezometer and filter designs combined with various installation procedures are used around the world, and have reportedly resulted in both success, failure, and uncertainty. Some users have optimistic views that if air-entry values are high enough, and proper pre-saturation, installation and testing is carried out in the field, the porewater pressure will be measured correctly. Experience with twin tube hydraulic piezometers does not support this view. Air enters the cavity with time, due to processes which are not fully understood for field conditions in partially saturated soils. If the filter element has dried out and can only be saturated gradually by the surrounding porewater, it is entirely possible that the high air-entry filter may slow down the saturation process of the cavity. The low air-entry filter may still be the best universal choice for diaphragm piezometers, particularly since high excess porewater pressures are the greatest concern of most designers. It may be useful to know that pressures are sub-atmospheric, but knowledge of their actual magnitude may not be essential.

About the Author: P. Erik Mikkelsen has been involved in the field of geotechnical engineering for twenty years. He has gained an international reputation in instrumentation used in embankments, deep foundations and excavations, and landslides. He has been the principal investigator on numerous projects and lectured on a variety of geotechnical topics related to instrumentation selection. Mr. Mikkelsen is frequently assigned to projects involving the planning of field instrumentation and installation, field data acquisition, data processing, instrument data interpretation and evaluation.

Mr. Mikkelsen is currently Vice President of Applications Engineering and Field Services for Slope Indicator Company. As such, he assists clients in instrument selection, special installation problems, trouble-shooting and data interpretation. Mr. Mikkelsen is a member of the American Society of Civil Engineers and the Instrument Society of America.

Piezometer Evaluations

	TYPE	ADVANTAGES	LIMITATIONS AND PRECAUTIONS
Open Standpipe	Observation Well	Simple, inexpensive, universally available. Can be driven in place.	Only applicable to detecting the presence or approximate elevation of the water table or piezometric level in pervious soil.
	Casagrande Type	Simple, inexpensive, reliable, usually has no metallic elements. Long performance record. Can be converted to pneumatic type. Self-deairing.	Porous filter can plug due to repeated water inflow and outflow. Long time lag. Tubing must be raised nearly vertical. Potential freezing problems. Subject to damage by construction equipment and deformation of soil around standpipe.
	Twin Tube Hydraulic	Simple, reliable. Good operating record. Short time lag and ability to purge. Usually a multi-open-tip piezometer. Allows central observation system to be used.	Freezing problems. Tubing must be raised nearly vertical for deairing. Periodic deairing required. Terminal equipment complex and expensive.
	Pneumatic Diaphragm	Stable. Easy to read. Short time lag. Capability of purging lines. Minimum interference to construction. Level of tubes and readout independent of level of tip. No freezing problems. Can be adapted for continuous recording. Allows central observation system to be used. Continuous flow type has moderate dynamic response.	Attention is necessary to several detailed features in making proper selection. More expensive than open standpipe.
Electrical	Vibrating Wire Diaphragm	Easy to read. Usually good long term stability. Can be used to read negative pore pressures. Short time lag. Minimum interference to construction. Level of wires and readout independent of level of tip. Suitable for automatic recording. Allows central observation system to be used. Digital output signal permits data transmission over long distances. No freezing problems. Version available with in-place calibration check. Dynamic response better than pneumatic.	Sensitive to temperature if thermal coefficients of tools and gage are not matched. Some versions subject to zero drift. Not suitable for dynamic readings. Overvoltage protection necessary in regions of electrical storm activity. Cost comparable to pneumatic piezometers. Zero drift may occur if subjected to impact. High accuracy, stable gages are more expensive than vibrating wire types. Range must be specified. Easily damaged if overpressured.
	Strain Gage Diaphragm	Easy to read. Can be used to read negative pore pressures. Short time lag. Suitable for dynamic measurements and automatic recording. Minimum interference to construction. Level of wires and readout independent of level of tip. Allows central observation system to be used. No freezing problems.	Some versions sensitive to temperature. Long term stability not yet verified. Data degraded if transmitted over long distances. Overvoltage protection necessary in regions of electrical storm activity. Similar cost to pneumatic piezometers. Zero drift may occur if subjected to impact. High accuracy, stable gages are more expensive than vibrating wire types. Range must be specified. Easily damaged if overpressured.

Order Desk # 1-800-331-0703

BIBLIOGRAPHY - FIELD INVESTIGATION OF LANDSLIDES

Alger, Christopher S., and Brabb, Earl E., 1985, "Bibliography of United States Landslide Maps and Reports," U.S. Geological Survey, Open-File Report 85-585.

Baum, R. L., Fleming, R. W., and Ellen, S. D., 1989, "Maps Showing Landslide Features and Related Ground Defamation in the Woodlawn Area of the Manoa Valley, City and County of Honolulu, Hawaii", U.S. Geological Survey, Open File Report 89-290.

Baum, Rex, L., Spengler, Steven, R., Torikai, Gill, D., and Liu, Lori Ann S. N., 1990, "Summary of Geotechnical and Hydrologic Data Collected Through April 30, 1991, for the Alani-Paty Landslide, Manoa Valley, Honolulu, Hawaii", U. S. Geological Survey, Open File Report 90-531.

Civil Engineering Magazine, 1991, "Tiltmeters Keep San Diago Church on Firm Footing," April.

Colton, R. B., Holligan, J. A., Anderson, L. W., and Patterson, P. E., 1975, "Preliminary Map of Landslide Deposits, Durango 1° x 2° Quadrangle, Colorado", U. S. Geologic Survey, Miscellaneous Field Studies Map MF-703.

Crozier, M. J., 1984, "Field Assessment of Slope Instability," in Slope Instability, Denys Brunsden and David B. Prior, editors, John Wiley and Sons.

Cummings, David, and Clark, Bruce R., 1988, "Use of Seismic Refraction and Electric Resistivity Surveys in Landslide Investigations," Association of Engineering Geologists Bulletin, Volume XXV, Number 4.

Davenport, Clifton, W., 1985, "Landslide Hazards in Parts of the Diablo and Dublin 7.5' Quadrangles, Contra Costa County, California," California Division of Mines and Geology, Open File Report 86-7 SF (Landslide Hazard Identification Map #3).

Dunnicliff, John, 1988, Geotechnical Instrumentation For Monitoring Field Performance, John Wiley and Sons, New York.

Egan, Howard, and Holzhausen, Gary R., and Samson, Dan, 1992, "Site Qualification for Inclinometer Surveying Using Tiltmeters," in Stability and Performance of Slopes and Embankments II, Edited by Raymond B. Seed and Ross Boulanger, American Society of Civil Engineers, A Specialty Conference, Geotechnical Special Publication, Number 31.

Fickies, Robert H., and Brabb, Earl E., 1989, "Landslide Inventory Map of New York," New York State Geological Survey, Circular 52.

Fleming, R. W., Johnson, R. B., and Schuster, R. L., 1988 "The Manti, Utah Landslide," U.S. Geological Survey, Professional Paper 1311.

Fleming, Robert W., Baum, Rex L., and Johnson, Arvid, M., 1991, "Deformation of Landslide Surfaces as Indicators of Movement Processes," in "For Contributions To: Second Seminar on Landslide Hazards, Cosenza, Italy: March 5 and 6, 1990," U. S. Geological Survey, Open File Report 91-108.

Fookes, P. G., Dale, S. G., and Land, J. M., 1991, "Some Observations on a Comparative Aerial Photography Interpretation of a Landslipped Area," Quarterly Journal of Engineering Geology, Volume 24.

French, James and Kropp, Alan, 1986, "Landslide Investigation Utilizing Electric Cone Penetration Testing," in Use of In-Situ Tests in Geotechnical Engineering, Proceedings of American Society of Civil Engineers Geotechnical Engineering Division Specialty Conference, Blacksburg, Geotechnical Special Publication No. 6.

Gardner, William S., 1989, "Interaction of Geology, Construction Practice and Foundation Design," in Foundation Engineering: Current Principles and Practices, Fred Kulhawy, Editor, Proceedings of American Society of Civil Engineers Congress, Evanston, Illinois.

Gichaga, F. J., Atibu, F. S., and Sahu, B. K., 1988, "Horizontal and Vertical Movements of Red Clay Highway Embankments," in Proceedings, Second International Conference on Case Histories in Geotechnical Engineering, Edited by Shamsher Prakash, St. Louis.

Golder Associates, 1981, "Highway Rock Slope Engineering," Course Manual Prepared for Course Sponsored by Federal Highway Administration.

Green, Gordon E., and Mikkelsen, P. Erik, 1988, "Deformation Measurements with Inclinometers," in Geotechnical Instrumentation, Transportation Research Board, Transportation Research Record 1169.

Hendron, A. J., Jr., and Patton, F. D., 1985, "The Viaont Slide, A Geotechnical Analysis Based On New Geologic Observations Of The Failure Surface", U. S. Army Engineer Waterways Experiment Station, Technical Report GL-85-5.

Hunt, Roy E., 1984, Geotechnical Engineering Investigation Manual, McGraw-Hill Book Company.

Hutchinson, J. N., 1988, "General Report: Morphological and Geotechnical Parameters of Landslides in Relation to Geology and Hydrogeology", 5th International Symposium on Landslides, Lusanne, Switzerland.

Jochim, Candace, L., Rogers, William P., Truby, John O., Wold, Robert L., Jr., Webber, George, and Brown, Sally P., 1988, "Colorado Landslide Hazard Mitigation Plan", Colorado Geological Survey.

Jurich, David M., and Miller, Russell, J., 1987, "Acoustic Monitoring of Landslides," in Geotechnology, Transportation Research Board, Transportation Research Report 1119.

Kiersch, George A., and James, Laurence B., 1991, "Errors of Geologic Judgement and the Impact on Engineered Works," in The Heritage of Engineering Geology: The First Hundred Years, Edited by George A. Kiersch, Geological Society of America, Centennial Special Volume 3.

Klinedinst, Gary, Munoz, Andy, and Niessner, Charles W., 1986, "Guidelines for Slope Maintenance and Slide Restoration," Federal Highway Administration, Report FHWA-TS-85-231.

Kockleman, William J., 1986, "Some Techniques For Reducing Landslide Hazards," Association of Engineering Geologists, Bulletin, Volume XXIII, Number 1.

Koerner, R. M., Lord, A. E., Jr., and McCabe, W. M., 1978, "Acoustic Monitoring of Slope Stability," ASCE Journal of the Geotechnical Engineering Division, Volume 104, No. GT5.

Mehrotra, G. S., and Bhandari, R. K., 1988, "A Geological Appraisal of Slope Instability and Proposed Remedial Measures at Kaliasaur Slide on National Highway, Garhwal Himalaya," in Proceedings: Second International Conference on Case Histories in Geotechnical Engineering, Edited by Shamsher Prakash, St Louis.

Mikkelsen, P. E., 1992, "Instrument Innovations for Monitoring Natural Hazards," Geotechnical News, March.

Nilsen, Tor H., and Brabb, Earl E., 1972, "Preliminary Photointerpretation and Damage Maps of Landslide and Other Surficial Deposits in Northeastern San Jose, Santa Clara County, California," U.S. Geological Survey, Miscellaneous Field Studies Map MF-361.

Nilsen, T. H., 1975, "Preliminary Photointerpretation Map of Landslide and Other Surficial Deposits of the Richmond 7 1/2' Quadrangle, Contra Costa and Alameda Counties, California," U.S. Geological Survey, Open File Map 75-277-47.

Nilsen, T. H., Taylor, F. A., and Dean, R. M., 1976, "Natural Conditions That Control Landsliding in the San Francisco Bay Region - An Analysis Based on Data from the 1968-69 and 1972-73 Rainy Seasons," U.S. Geological Survey, Bulletin 1424.

Palmer, Donald F., and Weisgarber, Sherry L., 1988, "Geophysical Survey of the Stumpy Basin Landslide, Ohio," Association of Engineering Geologists, Bulletin, Volume XXV, Number 3.

Pomeroy, John S., 1988, "Map Showing Landslide Susceptibility in Maryland," U.S. Geological Survey, Miscellaneous Field Studies Map MF-2048.

Ray, Monte E., 1982, "Geologic Investigation, Grading Stabilization Measures, and Development of the South Shores Landslide," in Guidebook and Volume: Landslides and Landslide Abatement, Palos Verdes Peninsula, Southern California, compiled by John D. Cooper, 78th Annual Meeting of the Cordilleran Section of the Geological Society of America, Anaheim, California.

Reid, Mark E., Nielsen, Hans P., Dreiss, Shirley J., 1988, "Hydrologic Factors Triggering a Shallow Hillslope Failure," Association of Engineering Geologists, Bulletin, Volume XXV, Number 3.

Rib, Harold T., and Liang, Ta, 1978, "Recognition and Identification," in Landslides: Analysis and Control, Robert Schuster and Raymond Krizek, Editors, Transportational Research Board, Special Report 176.

Rogers, J. David, 1978, "Shallow Creep Measurements in Landslides," Master of Science Thesis, University of California at Berkeley.

Rogers, J. David, 1986, "Landslide Processes of the East Bay Hills, San Francisco Bay Region, California," Association of Engineering Geologists, Annual Meeting, Field Trip Guidebook.

Saul, R. B., 1973, "Geology and Slope Stability of the S.W. 1/4 Walnut Creek Quadrangle, Contra Costa County, California," California Division of Mines and Geology, Map Sheet 16.

Scott, G. R., 1972, "Map Showing Landslides And Areas Susceptible to Landsliding in the Morrison Quadrangle, Jefferson County, Colorado", U. S. Geological Survey, Miscellaneous Investigation Map, I-790-B.

Singh, A., and Mitchel, K., 1969, "Creep Potential and Creep Rupture of Soils," Proceedings: International Conference on Soil Mechanics and Foundation Engineering, Mexico City.

Skempton, A. W., and Hutchinson, J., 1969, "Stability of Natural Slopes and Embankment Foundations," International Society of Soil Mechanics and Foundation Engineering, Annual Meeting, Mexico City, State-of-the-Art Report.

Sowers, George F., and Royster, David L., 1978, "Field Investigation," in Landslides: Analysis and Control, Robert L. Schuster and Raymond J. Krizek, editors, Transportation Research Board, National Academy of Sciences, Special Report 176.

Tarricone, Paul, 1991, "Treating Soil-Pumping Oil," American Society of Civil Engineers, Civil Engineering Magazine, December.

Taylor, Fred, and Brabb, Earl E., 1986, "Map Showing the Status of Landslide Inventory and Susceptibility," U.S. Geological Survey, Open File Report 86-100.

Varnes, D. J., Radbruch-Hall, D. H., Varnes, K. L., Smith, W. K., and Savage, W. Z., 1990, "Measurement of Ridge-Spreading Movements (Sackungen) at Bald Eagle Mountain, Lake County, Colorado, 1975 to 1989," U.S. Geological Survey, Open File Report 90-543.

Wieczorek, Gerald F., 1981, "Ground Water Levels and Precipitation Data for Slopes Near LaHonda, California," U.S. Geological Survey, Open File Report 81-367.

Wilson, Stanley D., and Mikkelsen, P. Erik, 1978, "Field Instrumentation" in Landslides: Analysis and Control, Edited by Robert Schuster and Raymond Krizek, Transportation Research Board, Special Report 176.

Zaruba, Quido, and Mencl, Vojtech, 1969, Landslides and Their Control, Elsevier, New York.

CASE HISTORIES

Hundreds of landslide case histories exist in the literature and are extremely valuable in providing insights into the evaluation of other landslides. A sample of California landslide case histories published in the past decade are attached. The title page of the document which contains the case history is attached. This is intended to guide the reader to the source volume because additional case histories are usually contained in the document.

A bibliography is also included, which provides a sample of published landslide case histories, most of which include both analyses and remedial work concepts. Additional case histories can also be found in the proceedings of the International Landslide Symposiums and the Case Histories in Geotechnical Engineering Conferences.

TRANSPORTATION RESEARCH

RECORD

No. 1343

Soils, Geology, and Foundations

Rockfall Prediction and Control and Landslide Case Histories

A peer-reviewed publication of the Transportation Research Board

TRANSPORTATION RESEARCH BOARD
NATIONAL RESEARCH COUNCIL

RECEIVED
NOV 17 1992
ALAN KROPP & ASSOC

NATIONAL ACADEMY PRESS
WASHINGTON, D.C. 1992

Accelerated Movement of Large Coastal Landslide Following October 17, 1989, Loma Prieta Earthquake in California

JOAN E. VAN VELSOR AND JOHN L. WALKINSHAW

The January storms of 1982 mobilized an ancient landslide in the coastal bluffs of Marin County, California. Slow, intermittent movement of portions of the large slide mass required periodic maintenance by the local highway district through 1989. A significant increase in the rate of movement occurred following the October 17, 1989, Loma Prieta earthquake. Because the new rate of movement made it impossible to keep the highway open, the highway was closed for 13 weeks following the earthquake. The roadway was ultimately relocated behind the failure plane and the approximately 765 000 m^3 (1,000,000 yd^3) of excavation material placed in the ocean (as an erodible fill) against the lower slope of the landslide. Before the earthquake, approximately 5.5 m (18 ft) of intermittent downslope movement occurred between 1982 and October 1989. During the 17-month monitoring period between the earthquake and landslide repair some 28 m (92 ft) of downslope movement was recorded. The rate of slide movement increased to more than 50 mm/day between October 1989 and the spring of 1990, decreased, and then accelerated to 284 mm/day just before construction began in the spring of 1991.

In 1991, the California Department of Transportation (Caltrans) repaired a large landslide, called the Lone Tree landslide, in the coastal bluffs of Marin County (see Figure 1). Historic landsliding at this site began when the January storms of 1982 mobilized a portion of an ancient landslide. In the years following 1982, the remobilized landslide experienced relatively slow, intermittent, downslope movement.

The steep ocean-fronting cliffs of Marin County have long been associated with landslide processes. The combination of a young, geologically recent, uplifted terrain; active coastal erosion by wind and waves; and an inherently weak geologic foundation material (the Franciscan formation) has resulted in landslides' being the dominant erosional process in the region. The scalloped coastline is formed of overlapping active and dormant landslides and resistant narrow ridges (see Figure 2).

Before the October 17, 1989, Loma Prieta earthquake, movement on the Lone Tree landslide varied from 60 mm to 300 mm/month (2.4 to 12 in./month). After the earthquake, movement increased from 910 mm to 1220 mm/month (3 to 4 ft/month). The rate of slide movement following the earthquake made it impossible to maintain a traversable roadbed and the highway was closed on January 15, 1990.

J. E. Van Velsor, California Department of Transportation, District 4, P.O. Box 7310, San Francisco, Calif. 94120. J. L. Walkinshaw, Federal Highway Administration, Region 9, 211 Main Street, Suite 1100, San Francisco, Calif. 94105.

LONE TREE LANDSLIDE

The Lone Tree landslide extended from just above sea level to approximately Elevation 120 m (400 ft) mean sea level (MSL) and was about 140 m (600 ft) wide and 30 m (100 ft) deep under the roadway. State Route 1 traverses the landslide at Elevation 65 to 70 m (210 to 230 ft) MSL.

Portions of the larger landslide were active during the 1980s (see Figure 3). Between 1982 and 1989, the northern and southern parts of the slide were active. Landslide movement had occurred both above and below the road. The maximum amount of movement occurred in the northern portion, known as the Lone Tree landslide.

A foundation investigation and landslide analysis resulted in a repair strategy of unloading the upper portion of the slide approximately 765 000 m^3 (1,000,000 yd^3) and relocating the highway 70 m (230 ft) inland, behind the slide plane.

Because the project area is surrounded by overlapping and adjacent park land and public agency jurisdictions, selecting a geotechnically suitable and environmentally acceptable disposal site for the excavation material became a major part of the environmental processing of the project. In all, 13 public agencies had jurisdiction or permit authority over the project. Vigorous public debate and the concerns of permitting agencies resulted in about 15 months of environmental evaluation and alternative disposal selections while the highway remained closed.

Hauling the excavation material up to 26 km (19 mi) to existing disposal sites was opposed by the small communities both north and south of the landslide because of the anticipated lengthy community disruption from passing haul trucks. Hauling would also have caused substantial damage to the two-lane state highway. Exclusive of actual hauling costs, it was estimated that the 160-day continuous haul would cause pavement damage equal to 3 years of normal traffic usage, at an equivalent cost of $210,000 to $270,000.

On-land disposal of the material in upland areas was opposed by the adjacent state and federal public park jurisdictions and was geotechnically unacceptable because of the high probability of initiating other slope failures by overloading the already marginally stable slopes.

Ocean disposal was opposed by marine protection agencies because of the anticipated damage to marine organisms from direct burial and from future sedimentation from the eroding fill. A federal marine sanctuary is located approximately 460 m

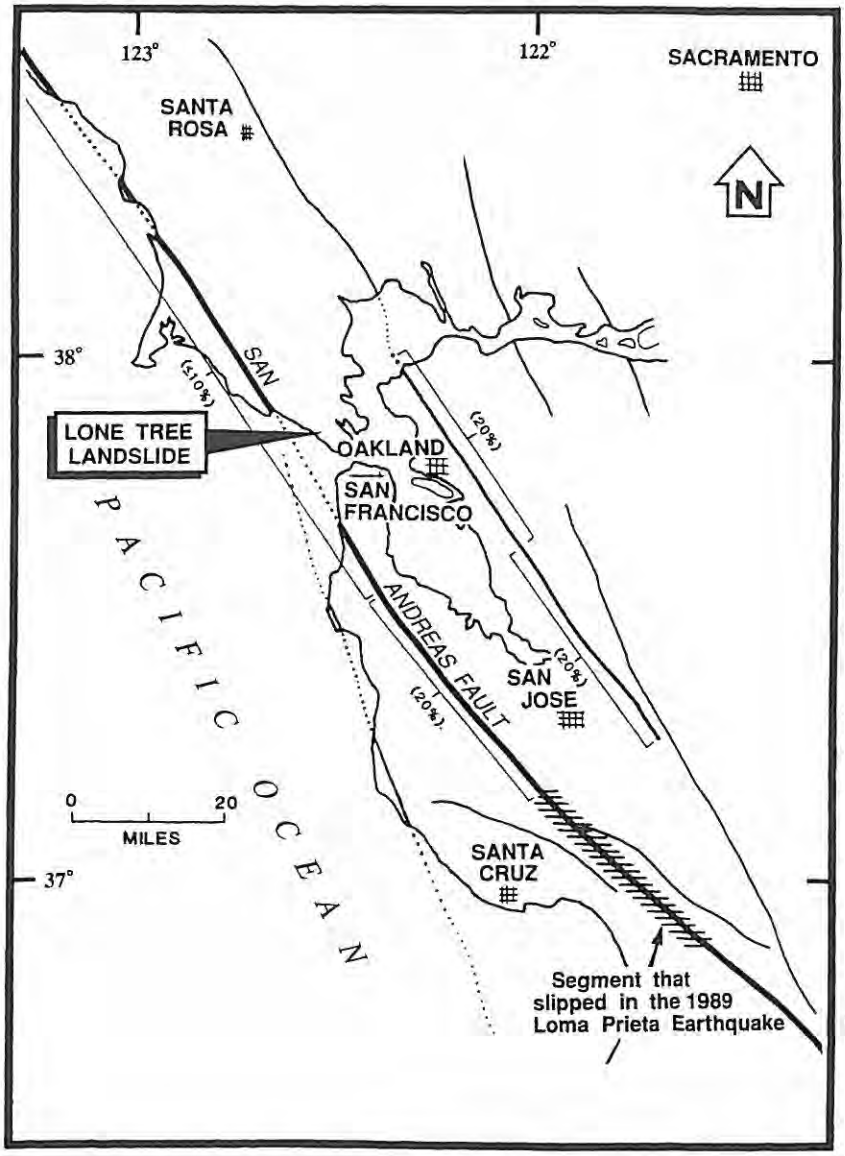

FIGURE 1 Location map; diagram shows conditional probabilities of major earthquakes in Bay Area (*12*).

(1,500 ft) offshore and was a major concern. Before landslide repair, 1525 to 1990 m^3 (2,000 to 2,600 yds^3) of soil and rock were already entering the marine environment each month because of slide movement. It was estimated that 2038 to 2650 m^3 (2,670 to 3,470 yds^3) would be eroded from the proposed fill each month, a 30 percent increase over the expected 25- to 30-year lifetime of the fill.

Lengthy discussions and negotiations with permitting agencies were required. Proposals to remove the excavation material by barges (estimated cost $1.8 million), installation of offshore cofferdams or Longard geotubes, and engineered construction of the proposed fill with a permanent rock revetment (estimated cost $550,000) were evaluated. All these alternatives were rejected on the basis of feasibility or likelihood of causing more environmental damage than was prevented.

Ultimately, approval was obtained to dispose of the 765 000 m^3 of excavation material by placing it on the rocky beach and near-shore area as a lightly compacted fill against the lower slope of the landslide below the highway (see Figure 4). The involvement of elected local, state and federal senators and representatives and the state or national heads of the jurisdictional agencies was required to obtain the needed permits.

The fill extends some 55 m (180 ft) into the ocean and is anticipated to erode gradually over a period of years. Aggressive erosion control on the erodible fill and new cut slope; removal of fill infringing on a coastal stream approximately 2 mi to the south, which had been placed in the past by non-highway agencies to create a parking lot for beach access; and a 5-year offshore sedimentation and biologic community monitoring program in the slide area were conditions required

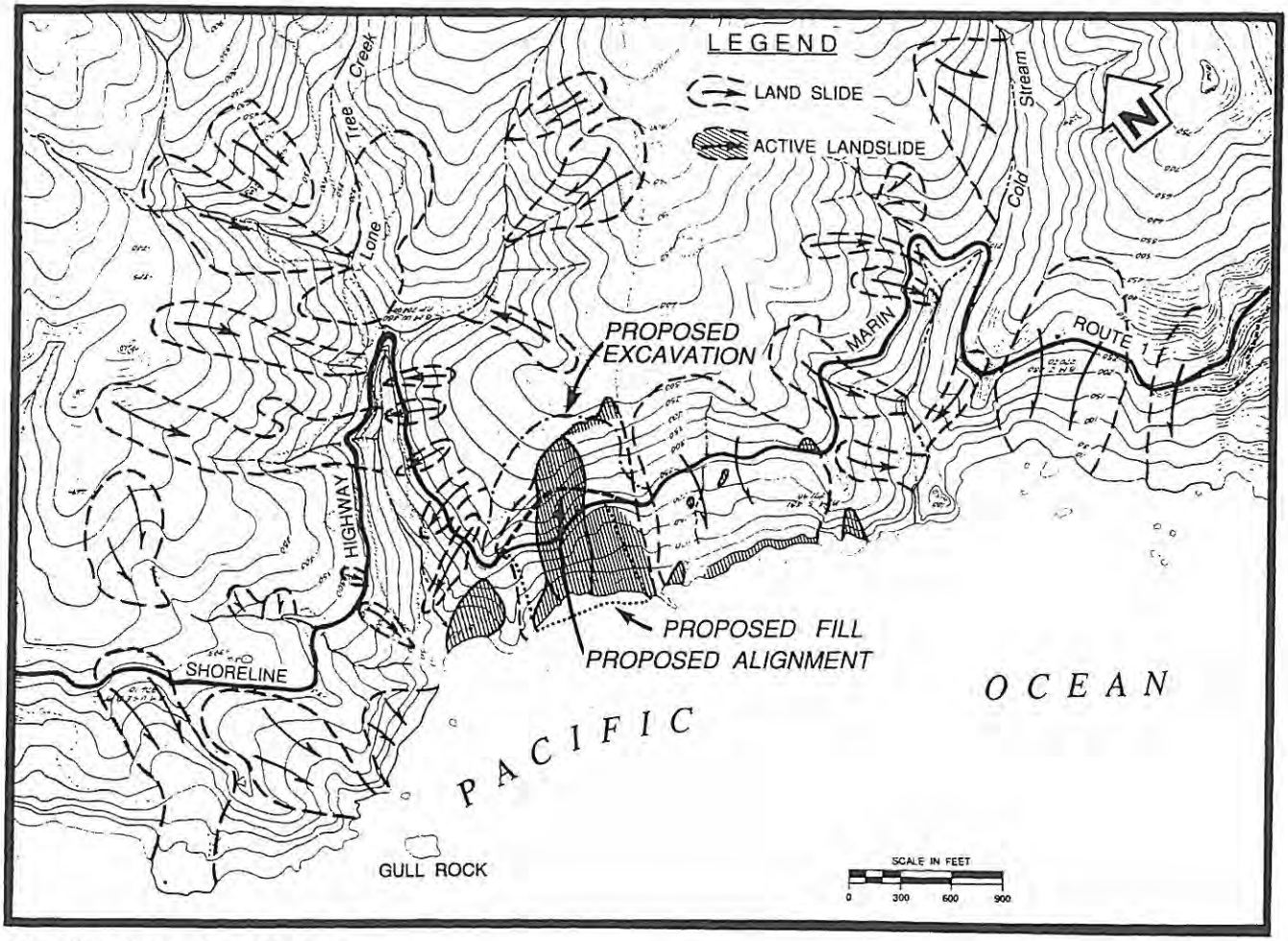

FIGURE 2 Regional landslide map.

by the permitting agencies as mitigation for the landslide repair. Mitigation costs are anticipated to reach at least 50 percent of the $2.1 million expended for actual construction to relocate the roadway to stable ground.

FOUNDATION CONDITIONS

The landslide is within the Jurassic-Cretaceous Franciscan formation. Eugeosynclinal deposits of greywacke, greenstone, chert, limestone, and exotic metamorphic rocks have been profoundly deformed and sheared by regional tectonics (*1*) in this region. The Franciscan formation is widely exposed over much of the California coast ranges and is often associated with large, deep-seated landslides. Landslides of all dimensions are present within the region.

The Franciscan formation is a complex assemblage of sedimentary, volcanic, and metamorphic rocks characterized as a melange—a heterogeneous mixture of disrupted rock masses in a pervasively sheared and crushed matrix material (*2*). Melange is believed to form at shallow depths in subduction zones where compressive forces between moving crustal plates crush and mix rocks of different origins.

Typically, repair of landslides in this type of formation is difficult. The heterogeneous and sheared nature of the Franciscan formation results in disrupted, unpredictable drainage paths, large boulders, and widely varying strengths of material.

Thirteen borings were placed for the investigation of this landslide. Borings SI-1 through SI-6, were placed for groundwater and inclinometer monitoring and were not sampled. Borings P-7 through P-13 were core borings placed to evaluate foundation conditions in the excavation back slope.

The rock recovered in the core borings was primarily highly friable and sheared black shale with sparse clasts [up to 7 m (23 ft) in diameter] of hard gray sandstone and lesser amounts of chert and metamorphic rock. Sieve analyses of core and bulk samples found 24 to 42 percent passing the 0.074-mm (#200) sieve. Dry unit weights averaged 2240 kg/m^3 (140 lb/ft^3) with moisture contents of 4 to 12 percent. Core recovery ranged from 76.5 to 100 percent and averaged 90.4 percent. The high core recovery rate in this difficult-to-sample material is due to the highly skilled state drill crew on staff with the District 4 Geotechnical Section.

The average rock quality designation (RQD), a measure of the degree of fracturing and therefore strength of a rock mass, was recorded for each core sample. RQD is defined as

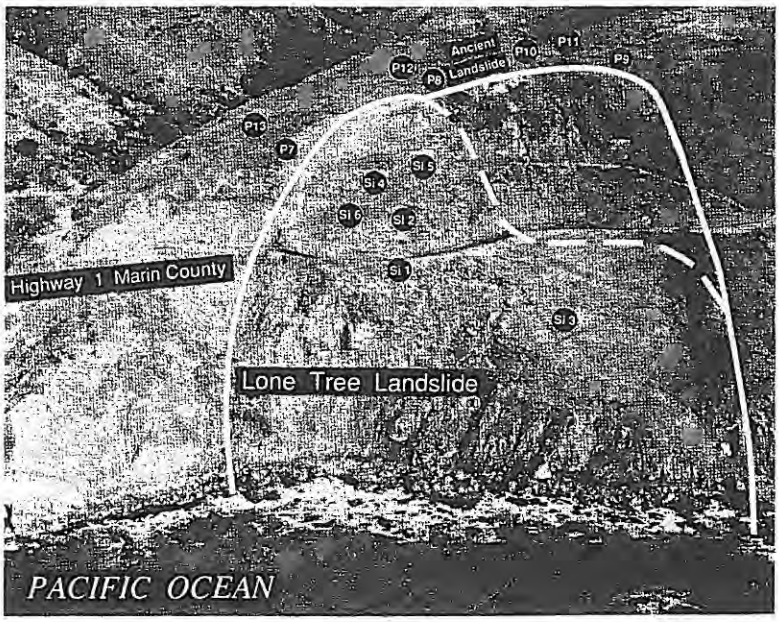

FIGURE 3 Aerial photograph of Lone Tree landslide.

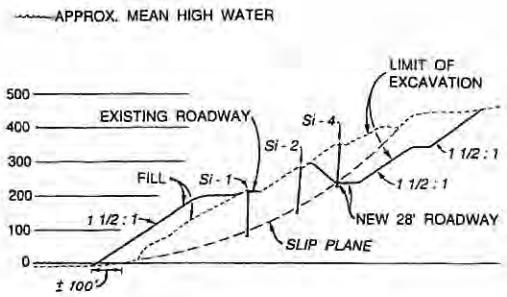

FIGURE 4 Cross section of Lone Tree landslide (Section A-A').

the total length of recovered core pieces greater than 100 mm (4.0 in.) in length expressed as percent of 1.5 m (5 ft) or more of core drilled (*3*). The average RQD was 16 percent but ranged from 0 to 100 percent.

The sheared and fractured state of the rock was also expressed in the frequent severe water loss zones encountered during drilling. For 70 to 80 percent of the coring operation, drilling fluids were not returned to the surface but flowed into the fractured rock.

Samples recovered from the core borings were subjected to soil strength tests. The unconfined tests found cohesion ranging from 29 to 86 kPa (600 to 1,800 psf). Triaxial testing [confining pressures 27 to 90 kPa (4 to 13 psi)] indicated an average ϕ of 24 degrees and cohesion of 50 kPa (1,000 psf).

PRE-EARTHQUAKE SLIDE CONDITIONS

Because of the landslide-prone terrain and the chronic but intermittent and slow rate of slide movement, little documentation of slide movement before the earthquake exists. Available data consists primarily of personal recollection, aerial photographs, snapshots, records of maintenance expenditures, and sparse pavement profiles.

The movement history of this site is typical of many state routes with chronic maintenance problems. For a long time, landslide movement was not documented in any kind of consistent, scientific manner.

The winter of 1981–1982 brought unusually high rainfall to the San Francisco Bay Area (see Figure 5). Unusually high antecedent moisture conditions were aggravated by the storm of January 3–5, 1982, which caused substantial damage throughout the Bay Area and closed State Route 1 at the Lone Tree slide for several months. During the January storm some 300 to 400 mm (12 to 16 in.) of rain fell in the 30-hr storm, which is about equal to the total annual rainfall for the area.

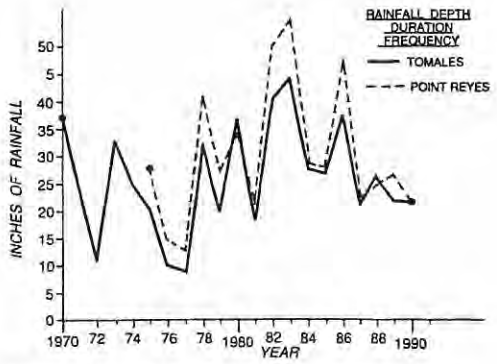

FIGURE 5 Rainfall data, Marin County, California, 1970–1990.

In 1982 it was recognized that the storm had reactivated a portion of an ancient landslide. In addition to landsliding above the road, which had occurred both above the subsiding roadway and to the north, subsidence below the roadway had occurred in the southern portion of the ancient landslide.

An inclinometer was installed at highway level in the southern portion of the landslide in May 1982 at a depth of 47 m (155 ft). The inclinometer was sheared off 8 to 12 months later, at a depth of 12 m (39 ft).

The $500,000 repair implemented in 1982 consisted of high, steep but relatively thin sliver cuts 3 to 4 m (10 to 15 ft) thick; a deep underdrain at highway level; improved surface drainage; and horizontal drains. To buttress the roadway, the excavated material was placed below the road at about Elevation 30 m (100 ft) MSL upward. Because of the steepness of the terrain and the need to minimize impacts to adjacent Mount Tamalpias State Park, the cut slopes were set at 1¼:1 (horizontal:vertical).

During the 1982 construction it was evident that the buttress itself was marginally stable because cracks quickly reappeared in the pavement and movement continued in the slope below the roadway. The 1982 repair was only temporarily effective because the landslide was deeper and laterally more extensive than originally believed. The roadway was reopened to traffic after a 4-month closure.

The northern slide area (the future Lone Tree landslide) began to develop between 1982 and 1983. By 1985 the landslide was clearly defined by cracks in the upper slope and pavement patches where the side scarps crossed the highway.

Unusually heavy rainfall occurred in 1982–1983 and landslide movement continued after the 1982 repair. Movement was generally slow (on the order of several centimeters per month) with brief localized episodes of movement of up to 300 mm/month (12 in./month). Highway maintenance staff repaved the highway periodically to maintain the road surface and highway maintenance expenditures were typically $20,000 to $40,000/year during this time.

During 1985–1986, cumulative subsidence of the roadway in the southern area became so pronounced that a lightweight fill (sawdust) was placed on the roadway in order to restore the highway grade and additional horizontal drains were installed.

The annual maintenance expenditures for this section of highway are graphically shown in Figure 6. About every fourth year there was a major reconstruction, reflecting the accumulation of slow displacement, which required periodic regrading.

In 1989 another increase in the rate of landslide movement was noticed, with almost a foot of vertical drop in August. Cumulative movement had once again lowered the highway profile, which resulted in an unacceptable vertical curve. The highway was once again leveled in August 1989 at a cost of $90,000.

Field reviews were conducted by Caltrans District 4 Geotechnical Section in August and September 1989. An attempt was made to install an inclinometer at roadway grade with a contract drill rig on October 10–11, 1989 because the District 4 state drill crew and rig were already committed to other projects. The contract rig supplied proved to be inadequate. After several equipment failures it was dismissed from the job and plans were made for installation of the inclinometer

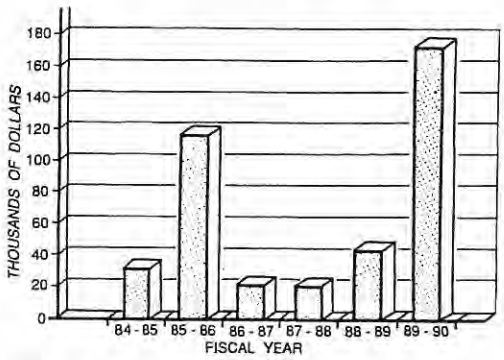

FIGURE 6 Maintenance expenditures at Lone Tree landslide, 1984–1990.

with a different drill rig. In view of the earthquake that followed on October 17, this delay was unfortunate.

The inclinometer was successfully installed on October 23–24, 1989, 7 days after the Loma Prieta earthquake. Inclinometer depth was 33 m (108 ft), and it was initialized on October 26. By November 6, the inclinometer had sheared off at a depth of 31 m (102 ft). Even though the bottom of the hole was no longer accessible, groundwater levels continued to be recorded in the inclinometer on a regular basis. This inclinometer also became the reference point for surface movement recorded by surveys taken from October 30, 1989, until April 9, 1991, when reconstruction of the highway began (see Figures 3 and 4).

On the basis of various highway profiles, topographic maps, aerial photography, and maintenance records we have estimated that 5.5 m (18 ft) of vertical settlement occurred during the 90 months between the January 3–5, 1982, storm and the October 17, 1989, earthquake. The amount of settlement averages to 61 mm (2.4 in.)/month, or 2 mm (0.08 in.)/day. Actual rates varied seasonally and (by some estimates) approached 300 mm/month (12 in./month) during some winter months. In all cases over the 7-year period the intervals of faster movement were brief, lasting 1 to 2 months, and followed by lengthy periods of slower movement.

POSTEARTHQUAKE SLIDE MOVEMENT

In the extraordinarily difficult and busy period that followed the Loma Prieta earthquake, the magnitude of the accelerated movement at the Lone Tree landslide was not immediately reported, nor was it anticipated that the accelerated movement would continue. It took several months to determine that the accelerated movement was not a temporary anomaly (such as had been experienced at brief intervals in the prior 7 years) but instead a permanent change in the slide regime. In the meantime, the roadway was maintained as serviceable through the weekly paving efforts of the local maintenance staff.

On January 15, 1990, after more than 3 months of accelerated movement and a drop of the highway of more than 2.4 m (8 ft), it was recognized that it was no longer possible to keep the road open, and the highway was closed.

On January 17, 1990, a survey monitor line was established across the landslide and periodically monitored until April 9, 1991. In addition, the surface location of the inclinometer placed in October 1989 was monitored. Figure 7 is a plot of total movement from 1982 through 1990; the period from 1982 to 1989 depicts the reconstructed data. The period 1989 to 1991 is from survey data. The total resultant movement (vertical and horizontal) of the top of the inclinometer casing recorded by surveys between October 30, 1989, and April 9, 1991 is shown in Figure 8.

From January 19–21, 1990, five more slope indicators were installed in the landslide: one below the highway, and four in the slope above the highway. Groundwater was found at depths of 7.4 m (24 ft) in Boring SI-3 and 29.6 m (97 ft) in Boring SI-6. In 2 to 6 days, these slope indicators sheared at depths ranging from 14.5 to 23 m (48 to 76 ft).

STABILITY ANALYSIS

Three stability analyses were conducted for this landslide using the computer model PC-STABL4M (Purdue University). The initial analysis used the back-calculated soil strength parameters along the slide plane defined by inclinometer data. The second analysis was conducted to evaluate the stability of the original slide plane after 765 000 m^3 of material were removed from the head of the slide and placed as a temporary buttress against the lower slope. This analysis also used the back-calculated soil strength parameters. The third analysis was conducted to design the back slope for the proposed excavation and used the soil strength parameters obtained by triaxial testing of core samples from the new back-slope material.

Back calculation of safety factors along the failure plane defined by the inclinometers resulted in soil strength values of ϕ = 11 degrees, C = 19 kPa (400 psf), and factor of safety = 0.99. Using these same shear-strength parameters, and adding pseudostatic earthquake forces derived from those measured at the Point Bonita seismograph for the Loma Prieta earthquake (0.11 *g* horizontal, 0.06 vertical), the factor of safety drops to 0.826—a 17 percent drop.

Analysis of the proposed repair strategy yielded an initial factor of safety of 1.6 with the buttress in place. Removal of the buttress, as is anticipated to occur eventually through erosion, yielded a factor of safety of 1.24; therefore, the highway has been relocated behind the slide plane.

The excavation backslope was 60 m (200 ft) high. Stability analysis slope, using soil strength parameters of ϕ = 24 degrees and C = 50 kPa (1,000 psf), resulted in the recommendation of a 1½:1 slope, a midslope bench 15 m (50 ft) wide, and extensive subdrainage (horizontal drains) to achieve a minimum factor of safety of 1.3 to 1.9.

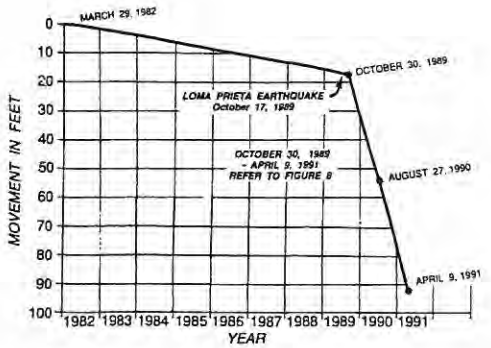

FIGURE 7 Resultant slide movement, 1982–1991, Lone Tree landslide.

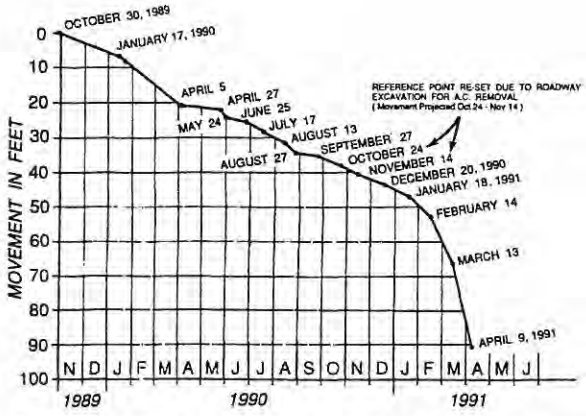

FIGURE 8 Resultant slide movement, October 30, 1989–April 9, 1991, Lone Tree landslide (resultant movement is vectorial summation of horizontal and vertical displacements).

EARTHQUAKE PARAMETERS

The Loma Prieta earthquake, which was 7.1 M_s (surface wave magnitude), occurred along a recently seismically quiescent portion of the San Andreas fault (see Figure 1). The fault segment had been identified as having a relatively high probability for an earthquake of this magnitude because of low microseismicity and the absence of historic earthquakes along this segment. A previous earthquake of a similar magnitude is believed to have occurred in the region in 1865, and the 1906 earthquake rupture zone included this segment.

Primary surface rupture was not found along the San Andreas fault following the Loma Prieta earthquake. The earthquake occurred at a depth of 19 km (11.5 mi), and fault rupture dissipated before it reached the surface. The duration of shaking was 10 to 15 sec; the strongest ground shaking recorded near the epicenter reached 0.64 *g* horizontal and 0.60 *g* vertical (*4,5*).

The Loma Prieta earthquake triggered 131 seismograph stations in the region; 77 recorded ground motion and the remainder were located on buildings. At the Lone Tree landslide, modified Mercalli intensities were estimated at IV. The recording station closest to the Lone Tree slide is the Point Bonita seismograph, located approximately 10 km (6 mi) to the east. The Loma Prieta earthquake recorded 0.11 *g* horizontal and 0.06 *g* vertical at this station. The Point Bonita seismograph is located on a fractured sandstone bedrock.

The epicenter of the Loma Prieta earthquake was located some 113 km (70 mi) southeast of the Lone Tree landslide. The primary wave motion at the site from the 7.1 M_s main shock and the subsequent aftershock swarm would have had

a strong southeasterly component. In addition to the primary southeasterly wave, recorded ground motion also showed a strong transverse wave (Love wave). The direction of the transverse wave (Point Bonita) rotated clockwise from east to west and southwest to northeast, as frequencies increased from 0.4 to 0.8 Hz and 3.2 to 6.4 Hz (*6*).

The Lone Tree landslide is within a southeast to northwest trending ridge, and landslide movement is therefore to the southwest (S15°W). The higher frequency ground motion, (3.2 to 6.4 Hz) was therefore parallel to the direction of slide movement. The earthquake induced ground motion (normal to the free face of the slope) is seen as a factor in the change in the rate of landslide movement observed after the Loma Prieta earthquake.

ANALYSIS OF MOVEMENT AT LONE TREE SLIDE

Before the earthquake, the landslide moved at an average rate of 2 mm/day with brief episodes of 10 mm/day. Immediately after the earthquake, the landslide was moving at 22.8 mm/day (0.9 in.). During the period between October 30, 1989, and January 17, 1990, the landslide averaged 27 mm/day (1.0 in./day).

Varnes (*7*), Hungr (*8*), Morgenstern (*9*), and Cruden (*10*) have presented velocity classifications for landslides and separated them into six or seven classes. Each class covers a range of velocities within two orders of magnitude (see Table 1).

The Lone Tree landslide rate following the earthquake of 27 mm/day, or 3.1×10^{-4} mm/sec in SI units (ASTM E380-89), places this slide in Cruden's (*10*) slow category (Class 3). This rate is close to the middle of Class 3, with a lower limit of 50×10^{-6} mm/sec, or 1.6 m/year (5.25 ft/year), and a high limit of 5×10^{-3} mm/sec, or 13 m/month (42.6 ft/month). In our opinion, the SI units suffer from a lack of logical perception by the public and even the engineering community because of their small scale.

TABLE 1 CLASSIFICATION OF LANDSLIDE MOVEMENT RATES (*10*)

OLD		NEW			
m	mm/sec	CLASS	DESCRIPTION	m	mm/sec (SI Units)
		7	Extremely rapid		
3 m/sec	3×10^{3}			5 m/sec	5×10^{3}
*600 ***		6	Very Rapid	*100 **	
0.3 m/min	5			3 m/min	50
288		5	Rapid	*100*	
1.5 m/ day	17×10^{-3}			1.8 m/hour	0.5
30		4	Moderate	*100*	
1.5 m/month	0.6×10^{-3}			13 m/month	5×10^{-3}
12		3	Slow	*100*	
1.5 m/year	48×10^{-6}			1.6 m/year	50×10^{-6}
25		2	Very Slow	*100*	
0.06 m/year	1.9×10^{-6}			16 mm/year	0.5×10^{-6}
		1	Extremely slow	*100*	

* *Velocity increment between classes*

Fukuzono (*11*) presented the results of the work of a number of authors who have studied the problem of developing predictive models for catastrophic failures. In discussing Salt's work (unpublished paper, Disaster Prevention Research Institute, 1988), Fukuzono reports that Salt's critical limit for the model velocity of a slide that has strained to its residual strength is 50 mm/day (5.8×10^{-4} mm/sec). At this velocity, Salt proposes that a landslide poses a substantial risk for imminent catastrophic failure. This rate is in the middle of the slow class (Class 3). Salt also suggests that the critical limit in terms of acceleration is 5 mm/day/day.

Salt suggests that had his limits been used, several days of forewarning would have been available on several catastrophic slides. The use of these values for real-time hazard prediction requires frequent reading of instrumentation and the immediate interpretation of the results. This is difficult to achieve with conventional instrumentation systems and geotechnical staffing levels in state highway agencies. This monitoring would perhaps lend itself well to some of the automated systems being marketed today.

After closing the roadway on January 15, 1990, a survey monitor line was established across the landslide at approximately roadway level. Between January 17 and April 5, the movement increased to an average of 54.7 mm/day (2.15 in./day), a critical rate by Salt's criteria, indicating possibly imminent failure. From April 5 to August 13 and August 13 to December 20, the average rates slowed down to 34.5 mm/day (1.4 in./day) and 23.8 mm/day (0.94 in./day), respectively. The slowing down gave a false indication of what was to happen over the winter of 1990–1991 (see Figure 7).

Monthly readings over the winter of 1990–1991 show successive rates of 38.9 mm/day (1.5 in./day), 67.7 mm/day (2.7 in./day), 145.6 mm/day (5.7 in./day), and 284.4 mm/day (11.20 in./day) or 3.3×10^{-3} mm/sec [still in the slow class defined by Cruden (*10*)] between December 20, 1990, and April 9, 1991. April 9 is the date of the last reading before any construction activity was started.

Salt's critical acceleration rate was exceeded sometime between February 14 and March 13 approximately a month after exceeding the 50 mm/day rate. The average acceleration for this period was 5.6 mm/day/day, 0.6 mm above Salt's critical acceleration rate. Some additional monitoring was performed during construction and the movement peaked at 800 mm/day (30 in./day) without catastrophic failure.

RAINFALL

Before the earthquake, slide movement responded to winter rains and the subsurface exploration program found zones of high permeability within the slide material. At the time of the earthquake in October 1989, however, it was the end of the summer and this region was experiencing the consequences of its third lower-than-average rainfall season. In October 1989, there were 31 mm (1.25 in.) of rainfall, the first of that rainfall season. Rainfall remained low, 53 mm (2.1 in.) in November and no rain occurred in December 1989, yet the rate of landslide movement did not diminish. The spring of 1990 received 440 mm (17.37 in.) of rainfall, and movement of the landslide continued. There were slight increases or decreases in the rate of landslide movement that

appear to correlate with the seasonal rains; however, there was no change in the overall trend. The landslide continued to move over the summer of 1990, with very little reduction in the rate of movement. The winter of 1990–1991 also experienced below normal rainfall (see Figure 5). Acceleration in the rate of landslide movement occurred in December, when antecedent rainfall was still low [60 mm (2.34 in.)] and continued to accelerate over the spring of 1991. Substantial rainfall in February [105 mm (4.14 in.)] and March [312 mm (12.29 in.)] coincided with continued acceleration.

Because the acceleration of landslide movement began in 1989 and 1990 before substantial antecedent rainfall, and the rate of landslide movement failed to diminish significantly over the summer of 1990, the author believes the more than tenfold increase in rate (2 mm/day to 22.8 mm/day) immediately following the earthquake is not tied to a change in the groundwater regime.

POSTCONSTRUCTION MONITORING

Six inclinometers were placed in the new back slope after construction. Potential slope movement and groundwater are being monitored in the inclinometers. A grid of survey points has been established across the erodible buttress to record its gradual removal by erosion and ocean waves.

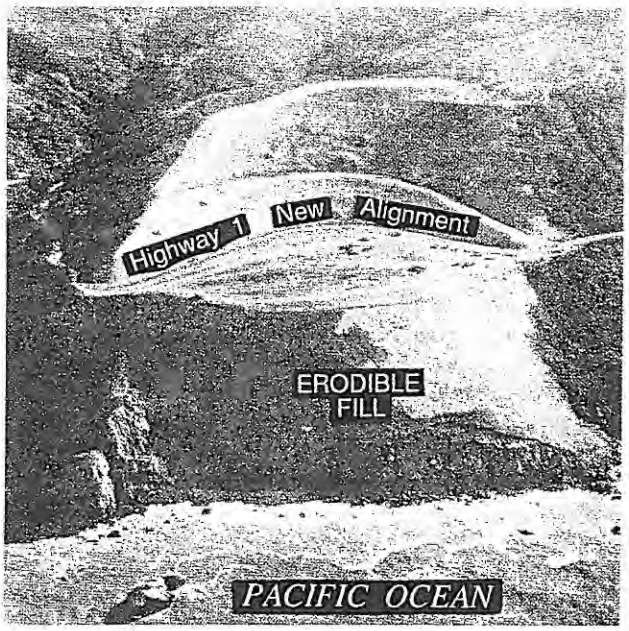

FIGURE 9 Aerial photograph of completed landslide repair, Lone Tree landslide.

CONCLUSIONS

The authors have presented the monitoring and analysis performed to correct a large, slow-moving landslide on State Route 1 in the northern coast of California. Also presented is a comparison of recorded rates of movement with critical velocities and accelerations proposed by others as warnings of imminent catastrophic failure.

Before the Loma Prieta earthquake, the slide was moving at a rate generally manageable by maintenance forces, although road closures were necessary from time to time. After the earthquake, the rate of movement increased to an intolerable, although still subcritical, level, according to published values. After continued movements over a long period, the slide accelerated to the critical values proposed by Salt, although sudden and rapid movements were never reached. Salt's critical velocity was reached in early 1990. Subsequently, there was a decrease in velocity, and the critical velocity threshold was again reached in early 1991, a month or so before reaching his critical acceleration threshold. During the earthwork for landslide repair (Figure 9), the rate of slide movement increased to 16 times the critical velocity and catastrophic failure did not occur.

Continued studies to provide a reliable method for predicting the time of rapid failure of a landslide is necessary. This landslide did not fit existing models.

The authors believe that the accelerated rate of movement at Lone Tree landslide is due to a combination of factors; large movements over the years lowered the shear strength of the material in the failure plane, and earthquake shaking accelerated the process. Other factors include seasonal rainfall and the continued erosion of the toe of the landslide by the ocean, which prevented natural buttressing. The linkage of increased landslide movement with earthquake acceleration is supported by statements in Salt's work, which shows that frictional materials in the fine fraction range are more sensitive to earthquake accelerations than cohesive soils. The lowering of the factor of safety by just a small percentage in these materials can lead to accelerated movement rates.

This case history documents a unique failure by deterioration of the shear zone because of long-term shearing and earthquake shaking. The monitoring program and analysis show that the increase in rate of slide movement coincides with the earthquake event and suggest that it was a major contributory factor.

REFERENCES

1. M. C. Blake, Jr., et al. *Preliminary Geologic Map of Marin and San Francisco Counties, and Parts of Alameda, Contra Costa and Sonoma Counties*. Map MF-484. U.S. Geological Survey, 1974.
2. S. Ellen, D. M. Peterson, and G. O. Reid. *Map Showing Areas Susceptible to Different Hazards from Shallow Landsliding, Marin County and Adjacent Parts of Sonoma County, California*. Map MF-1406. U.S. Geological Survey, 1983.
3. *Manual on Subsurface Investigations 1988*. AASHTO, Washington, D.C., 1988.
4. T. E. Spittler, E. L. Harp, D. K. Keffer, R. C. Wilson, and R. H. Sydnor. *Landslide Features and Other Coseismic Fissures Triggered by the Loma Prieta Earthquake, Central Santa Cruz Mountains California*. California Division of Mines and Geology, Special Publication 104, 1990.
5. S. R. McNutt and T. R. Toppozada. *Seismological Aspects of the 17, October 1989 Earthquake*. California Division of Mines and Geology, Special Publication 104, 1990.
6. J. E. Vidale and O. Bonamassa. Strong Shaking Directions from the 18 October 1989 Loma Prieta Earthquake and Aftershocks in San Francisco and Oakland. *Proc., Seminar on Seismological and Engineering Implications of Recent Strong-Motion Data*, Sacramento, Calif., May 30, 1990.

7. D. J. Varnes. *Special Report 29: Landslide Types and Processes in Landslides and Engineering Practice*. HRB. National Research Council. Washington. D.C., 1958. pp. 20–47.
8. O. Hungr. *Dynamics of Rock Avalanches and Other Types of Slope Movements*. Ph.D. thesis. University of Alberta. Edmonton. Alberta. Canada. 1981.
9. N. R. Morgenstern. Geotechnical Aspects of Environmental Control. *Proc., 11th International Conference on Soil Mechanics and Foundation Engineering*. Vol. 1. San Francisco. Calif., 1985. pp. 155–186.
10. D. M. Cruden. A Simple Definition of a Landslide. *Bulletin of the International Association for Engineering Geology*. 1991.
11. T. Fukuzono. Recent Studies on Time Prediction of Slope Failure. *Landslide News*. No. 4. July 1990. pp. 9–12.
12. *Lessons Learned from the Loma Prieta, California, Earthquake of October 17, 1989* (G. Plafker and J. P. Galloway. eds.). Circular 1045. U.S. Geological Survey.

Publication of this paper sponsored by Study Committee on Landslides: Analysis and Control.

Engineering Geology Practice in Southern California

Edited by

Bernard W. Pipkin and Richard J. Proctor

Special Publication No. 4
ASSOCIATION OF ENGINEERING GEOLOGISTS
Southern California Section

Star
PUBLISHING COMPANY

MAJOR LANDSLIDE REPAIRS IN SOUTHERN CALIFORNIA

Lawrence R. Cann
Principal Engineering Geologist

Edward A. Steiner
Senior Project Geologist

Leighton and Associates
2121 Alton Parkway
Irvine, California 92714

CONTENTS

INTRODUCTION
STAGES OF LANDSLIDE REPAIR
- Emergency Response Stage
- Investigation and Interpretation Stage
- Planning and Design Stage
- Construction Stage
- Methods of Achieving Temporary Stability
- Cost of Landslide Repair

CASE HISTORIES
- Big Rock Landslide, Malibu
- Bluebird Canyon Landslide, Laguna Beach
- Seagate Landslide Repair, Niguel Shores
- Cove Road Landslide, Dana Point

INTRODUCTION

As property values and new home construction costs have risen, mitigation of landslides has become increasingly attractive in contrast to abandonment. In many cases, it is more cost effective to design and implement remediation for a landslide than to abandon and raze a damaged home, and rebuild elsewhere. This is especially true in southern California where costs have made it possible to use remediation techniques which would otherwise be too expensive for a single family home or small structure.

This paper uses four case histories for landslides in Southern California which have been repaired since the 1973 AEG Annual Meeting, the last one held in southern California. These case histories demonstrate a unified approach to landslide stabilization that, in our opinion, provides a high level of benefits when compared to the costs of repair.

The case histories include the Bluebird Canyon landslide in Laguna Beach, the Cove Road landslide in Dana Point, the Seagate landslide at Niguel Shores, and the Big Rock landslide in Malibu.

STAGES OF LANDSLIDE REPAIR

The repair of a complex landslide requires the integrated efforts of people with a wide variety of training and expertise, working as a well-organized team. Like any successful team, there must be considerable advanced planning prior to beginning the repair, and then implementation and coordination of the plan during the repair. A complex landslide repair generally progresses through five stages: the emergency response stage, the geotechnical investigation and interpretation stage, the planning and design stage,the construction stage, and the completion stage.

Emergency Response Stage

Most major landslide repairs begin with a series of emergency earthwork measures taken within a few days after the event to minimize potential for injury or additional property damage. In the interests of expediency, these measures are usually performed before enough information is available to adopt a permanent repair plan. The most important issue at this stage of the slide repair is to halt the landslide by providing temporary stability while a permanent solution is designed. During the emergency the Engineering Geologist and Geotechnical Engineer help to determine the extent of areas which may be influenced by the sliding, help to assess the damage to public and private property, and evaluate the need for heavy equipment. Heavy equipment is used to build temporary access roads, move earth to increase temporary stability, break down dangerously over steepened headscarps, fill in ground fissures and grabens, or construct temporary drainage or run-off control devices. It is important to deal honestly and sympathetically with the affected residents. The loss of a home is also the loss of the largest investment many people will make. The loss of a home is a major crisis for people and the respect and support of all parties is appreciated.

Investigation and Interpretation Stage

Before any landslide repair can begin, the landslide must be thoroughly understood or characterized. Coordination meetings between the client, design civil engineer, engineering geologist, geotechnical engineer, grading contractor and agency are of paramount importance. The main purpose of these meetings is to communicate the geotechnical conditions in sufficient detail and clarity to be understood by the non-technical members the team. Pre-construction planning is absolutely necessary and, if the repair is to involve mass grading, it is very important to develop an earth work logistics plan. Illustrations, including maps and cross-sections depicting the geotechnical conditions, utilities, and easements must be prepared, and thoroughly understood by all the team members prior to commencing the landslide repair.

Time is of the essence because the slide area is in a "metastable" condition, and additional failures, such as headscarp collapses, are common. The investigation stage of a

major landslide repair requires quick response and, in some cases, may involve working around the clock. The geotechnical investigation phase of the landslide repair should include, at least, the following tasks:

- Background research of all available pertinent geologic reports and maps of the specific area. This should be supplemented by collection and review of stereoscopic pairs of aerial photographs taken before and after the slide. Both vertical and oblique photographs in color, black and white, and false color infrared should be reviewed. The infrared photographs are particularly useful to define areas of disrupted drainage, and the margins of the landslide.
- Detailed geologic mapping of existing exposures. The purpose is to understand the root cause of the failure, and geologic conditions are often a factor. This should include existing landslide morphologic features. The surface cracks can be useful indicators of the kinematics of the landslide.
- Subsurface exploration consisting of backhoe or dozer trenches, and large diameter and small diameter borings, if needed. The best results are usually obtained from the large diameter borings which allow the geologist first hand observations of the nature of the landslide rupture surface. The investigator should also collect samples for laboratory testing to determine the strength of the earth materials and the chemical composition of ground water, if present. Care must be taken in this exploration program because the active slide mass is still unstable and may create dangerous subsurface conditions.
- Preparation of maps and cross sections to depict the three dimensional geometry of the landslide. The geometry is critical to accurate analysis of remediation options.
- Detailed geotechnical stability analyses to evaluate the remediation options for stabilization.
- Preparation of a report that summarizes the conditions describes the elements needed to stabilize the slide area.

The Planning And Design Stage

Repair of a landslide is dependent upon the type, size and geometry of the slide, topographic conditions in the vicinity of the landslide, the extent of damage, the surface and ground water conditions, the final stability requirements, the availability of construction material and equipment, and economic constraints.

The planning and design effort is critical to the landslide repair. It requires a synthesis of all of the available data, and it is the point at which the engineering geologist, geotechnical engineer, design civil engineer, and owner must have a clear exchange of ideas. Technical, social and logistical problems must be approached with an open mind and some compromises may be necessary.

The geotechnical issues and design options must frequently be discussed with those trained in other disciplines. These include attorneys, contractors, insurance companies, homeowners, and community leaders.The best results are achieved with a combination of visual and verbal techniques. The geotechnical consultant should make a detailed, written outline of the summary of the findings so that there is a written as well as an oral summation. Sometimes the data and interpretation can be depicted on 3-dimensional models as well as maps and 2-dimensional cross sections. Pictures of the site are beneficial and shorten the otherwise long-winded and detailed descriptions. The best aids to understanding are:

- Maps, drawings, pictures or video tape recordings of existing conditions encountered at the sites.
- Cross-sectional or 3-dimensional views to show the geometry of the landslide and alternative mitigation measures.
- Overlays on maps and cross-sections or sequential models to demonstrate the various remedial alternatives. This makes selection of design options easier and less-time consuming.

The grading contractor can play an important role in this preliminary stage. This is particularly true when repairing landslides in populated areas, such as at the Bluebird Canyon or the Seagate slides discussed below. Both of these slides were successfully repaired with minimal loss to additional property, and at a cost much lower than what would have occurred without good advanced planning.

The land owner is the ultimate decision maker because he/she reaps the rewards or bears the cost of the repair. To have a successful project, the landowner must know and understand the geotechnical problems and their potential impacts. For example, if the landslide material has a high moisture content, it may require specialized and costly treatment before it can be reused as compacted fill. Logistical planning is critical to the success of the project. It should include:

- Frequent meetings between the entire project team
- A proactive, positive attitude toward problem solving.
- Good topographic and other survey data from the design Civil Engineer.
- Clearly illustrate and well understood sequence of the repair project at each anticipated stage including the location of off-site disposal and borrow areas, temporary stability conditions, dewatering requirements, etc.
- A thorough study of the types of equipment and manpower that will be needed on the project.
- A stockpile of supplies needed to complete the repair

- A thorough study of the quantities and topographic conditions involved so that construction traffic patterns can be established to maximize efficiency and minimize handling of earth materials.

Contingency planning for conditions at the site which differ from the interpreted conditions.

Construction Stage

The most critical time during a hillside repair is during the removal of the landslide and construction of the slope stabilization elements. The most common stabilization method is the removal of portions or all of the landslide and their replacement with an earth fill buttress. This requires the excavation of buttress keys and manufacture of temporary cut slopes. In most cases the back slope excavation is only marginally stable with a factor of safety at or less than one. Special precautions must, therefore, be taken to minimize the failure of these back slopes. Great care is needed during this period. A back cut failure may radically increase the total yardage of earth materials moved or threaten adjacent properties.

Methods of Achieving Temporary Stability

A failure of a temporary buttress back slope can easily double or triple the total buttress yardage quantity and can significantly prolong construction and increase grading, geotechnical and civil engineering costs. The potential for failure can be reduced by:

- Excavation of the back slope of the key at the shallowest possible angle, usually no steeper than the dip of bedding or the dip of the landslide rupture surface. In most cases the upslope location of buildings, utilities, and topographic conditions dictate the shallowest back cut slope angle possible.
- Excavation of the key in sections so that the entire key and back slope are not open and unsupported at the same time.
- Time is critical. Subdrain installation and buttress construction should begin and be completed as quickly as possible. If the buttress keyway is wider than about 25 feet, fill may be placed against the back slope first to provide additional temporary support for the slope before placing the fill in the outer portion of the keyway.
- Construction of steel soldier pile walls or reinforced concrete caisson walls may be needed if temporary back slope failures can not be tolerated because existing structures are close to the top of the landslide. Temporary soldier piles can be extracted after the landslide is removed or the back slope is supported by the buttress fill. Or the piles can be designed to be left in place as a part of the permanent fix.
- Ground freezing is a method for strengthening the soil on a temporary basis. It was utilized with limited success in the Seagate slide area in 1981. It has some potential for certain types of excavations in the appropriate soil types.
- Soil cement columns can also be considered for temporary stabilization of back slopes.

Cost of Landslide Repairs

It is difficult to determine the repair costs for a major land slide because of the many variables involved. However, th cost of simply removing slide debris and replacing it as com pacted fill is much higher that normal hillside grading cost For example, to grade a baseball field of compacted fill, i August 1991 cost approximately $1.25 /cubic yard. In con trast, earthwork for landslide repairs can cost from $5 up t 25 or $30/cubic yard.

CASE HISTORIES

Selection Criteria For Accompanying Case Histories

The following case histories demonstrate the methods pre viously discussed. They all contain a common purpose—th restoration of an unstable area to an acceptable degree o safety, to minimize additional damage to nearby properties and to repair the area as efficiently as possible. The repai efforts described in these case histories all share the follow ing common attributes:

1) Thorough planning of the repair effort;
2) Complete and unabiguous communication:
3) Positive attitude among all partners toward the issues and contributions of others;
4) A sense of teamwork by all members;
5) A flexible and creative approach to problem solving; and
6) The resources (equipment, materials, and manpower) to complete the project despite changed conditions.

Each case history was selected because it demonstrates a combination of unique conditions and an innovative method of repair.

Big Rock Landslide, Malibu

Introduction

Repair of the Big Rock landslide required an innovative repair to maintain access along the heavily traveled Pacific Coast Highway in Malibu. The repair incorporated a variety of monitoring methods to warn of incipient failure during construction (Clark, 1986; Evans and Lownes, this volume).

The Big Rock landslide, not to be confused with its much larger active neighbor to the west, the Big Rock Mesa land-

slide, began as a slow moving rock and debris slide during the winter of 1979. The landslide included the upper portion of a natural-over-cut slope excavated for the original Pacific Coast Highway (PCH) some 60 years ago. This designed cut slope was more than 200 feet high with a gradient of about 1:1 (horizontal to vertical). The name "Big Rock" was derived from the highly visible 100-ton boulder perched at the upper portion of the slope. The landslide presented a major challenge to CALTRANS as they sought to protect the row of homes on the Pacific Ocean across PCH from the slope. Adverse conditions included the weather, steep terrain, the limited area in which to work, and the need to keep an important highway open (Fig. 1).

First movement was noted by displacement of the "Big Rock" a few inches to a few feet downhill. After a number of frustrating attempts, CALTRANS finally removed the "Big Rock" by pulling it down onto PCH with a skip loader and cable system. In April, following removal of the rock, three major head scarps with lateral displacements of up to 1.5 feet appeared which, along with sloughing of small rocks and debris onto PCH indicated involvement of a much larger area. The debris was raining down from the toe region of the moving mass, approximately at the top of the cut slope. On April 13, PCH was closed to all traffic. Two lanes were reopened on May 8 after concrete berms were placed on the roadway to protect the open lanes from falling and rolling debris. The containment zone formed behind the berm filled rapidly with debris. A 20-to 30-foot high wall of steel H-beams with heavy wood lagging was driven into the road along its center lane to protect the remaining two open lanes. Within a week the wall was breached by a 30-ton boulder. The barrier remained in place as slide movement slowed, and proved to be an effective but not fail-safe method of keeping PCH open.

Geologic Setting

Preliminary geologic mapping of the slope face showed the slope was breaking across the predominant bedding and was following old fracture surfaces or the contacts between the diabase dikes and country rock. The bedrock consisted of Tertiary sediments of the Vaqueros and Sespe formations which was overlain by the Topanga Formation. These rocks were intruded by irregular shaped bodies of the diabase . All rocks near the ground surface were highly fractured and weathered, especially the diabase dikes.

The geometry of the slide was poorly known. It was estimated to be only 30 feet thick, based on the pattern of scarps and absence of rotational movement. Visual examination of the failure surface by large diameter drilling was precluded by high cost, the very steep slopes, and hardness of the rock. Small diameter core drilling adjacent to the slide mass located several zones of poor quality rock at depths of more than 100 feet. Coring on the slide mass itself could not be completed due to the unsafe slope conditions. Therefore the

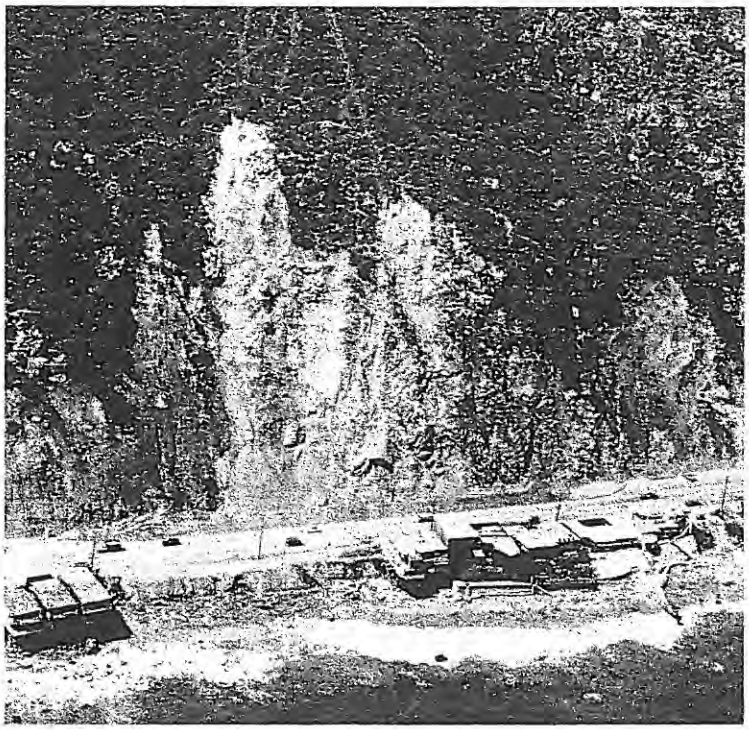

Figure 1. Aerial photograph of the Big Rock landslide, Malibu, California. Pacific Coast Highway and existing homes in foreground.

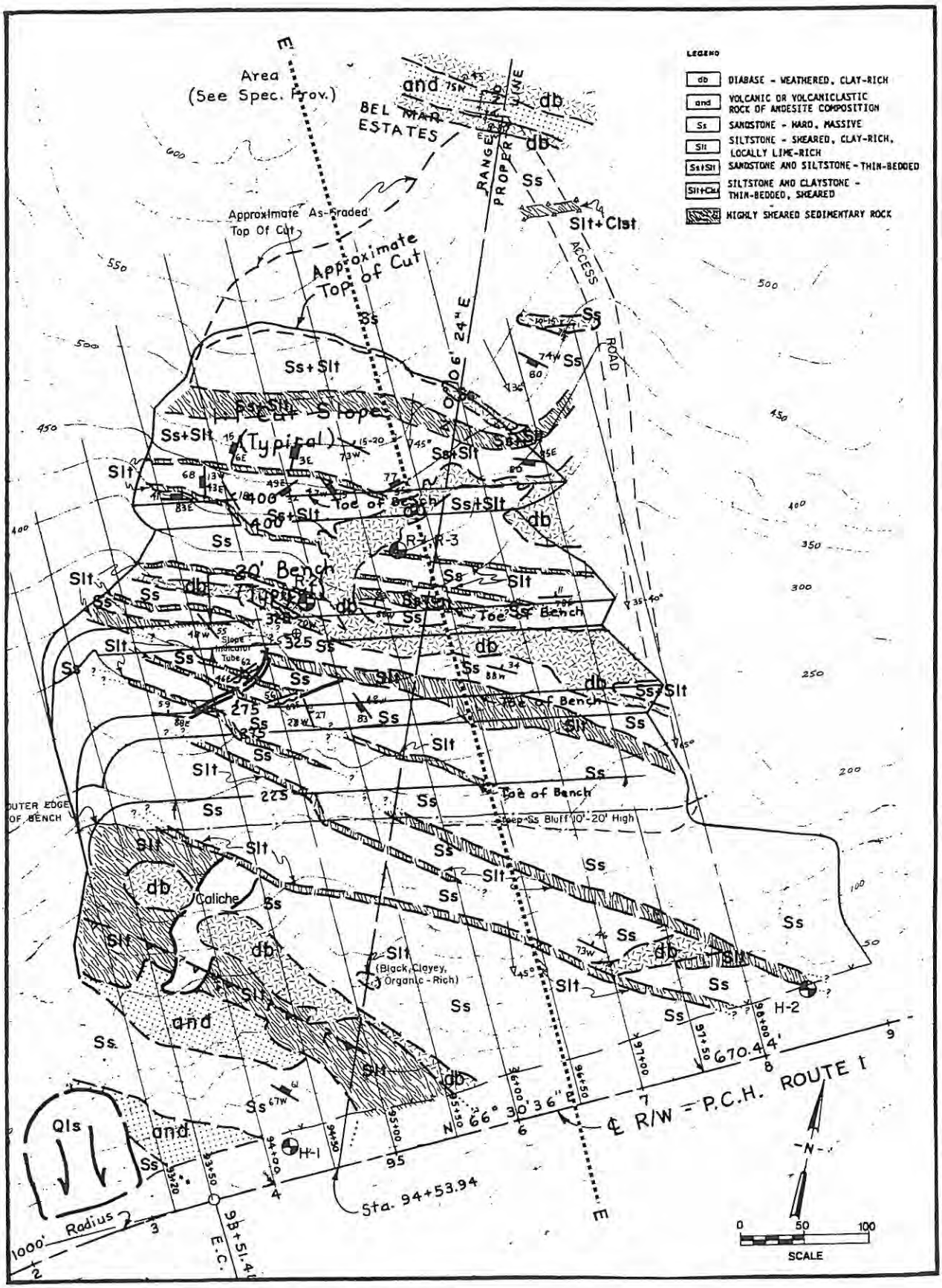

Figure 2. Schematic geologic map of the Big Rock landslide.

limits of the landslide were based primarily on surficial mapping. The generally high degree of weathering and abundant clay content of the diabase bodies made them the likely hosts of the rupture surfaces (Figs. 2 and 3).

Monitoring

The slide presented a continuing hazard to the adjacent highway and homes. As a result, a three-part monitoring program was begun almost immediately. The program was designed as an early warning system for renewed or catastrophic movement. It consisted of: (1) geophones installed at shallow depths in the surface of the slide to detect subaudible rock noises (SARN). The SARN system could effectively detect high levels of micro-seismic activity in the slide, but was less effective in predicting imminent large scale movement. (2) CALTRANS installed a series of long baseline (10 to 25 meter) wire-cable extensometers with an early warning arrangement at highway level. Large movements in the head scarp would set off the signal, allowing closure of PCH to traffic. The system worked well, but the correlation between slide movement and sloughing of debris onto the roadway was poor. In fact, the road was closed several times when birds landed on the cable causing it to stretch. (3) Finally a network of points on the slope face was established and resurveyed to determine which portions of the slope face were actually involved in the slide and to provide a warning of any change in the rate of movement (on a scale of weeks) which could threaten residences along PCH as well as the highway itself. The bulk of the slope face was not involved in the slide, but the uppermost points on the face were slowly moving downslope.

This was an important slide to monitor due to the potential impact of continued or accelerated movement on public safety and property. While it was not possible to predict micro-movements which released debris directly to the base of the slide, the three systems did demonstrate the larger movement pattern and gross changes in rate of movement.

Remediation

Remediation consisted of excavating the loose slide debris and broken rock to a fresh slope face with 1:1 slopes, with wide drainage and slough benches to the top of the existing rock face. Even then designed fresh slope would have had questionable surficial stability because of the deep fracturing. Therefore, the plan included a rock anchor system of #11 steel rebars with an average length of 30 feet drilled perpendicular into the slope face and grouted in place. These were placed at 7 1/2 feet on center over the entire freshly excavated face ands the areas in between dowels were covered with a chain link mesh, welded to the tops of the rebar, to reduce the rockfall hazard.

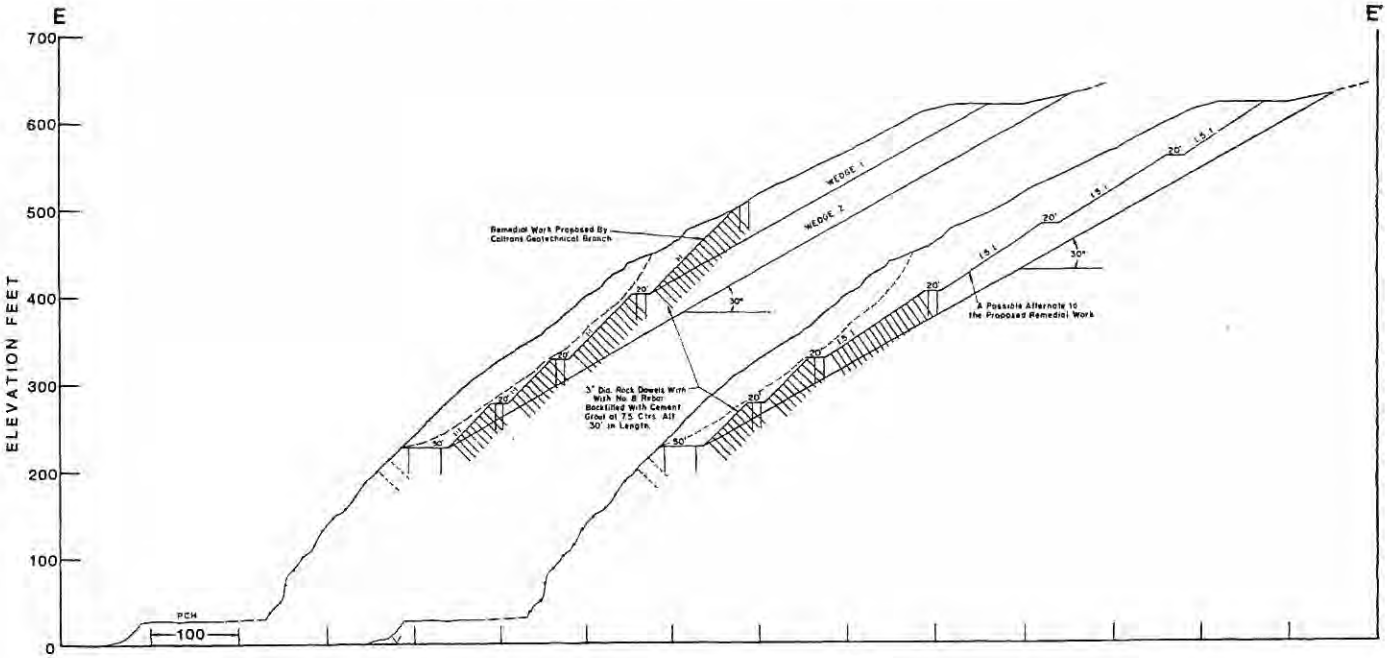

Figure 3. Geologic cross-section of the Big Rock landslide.

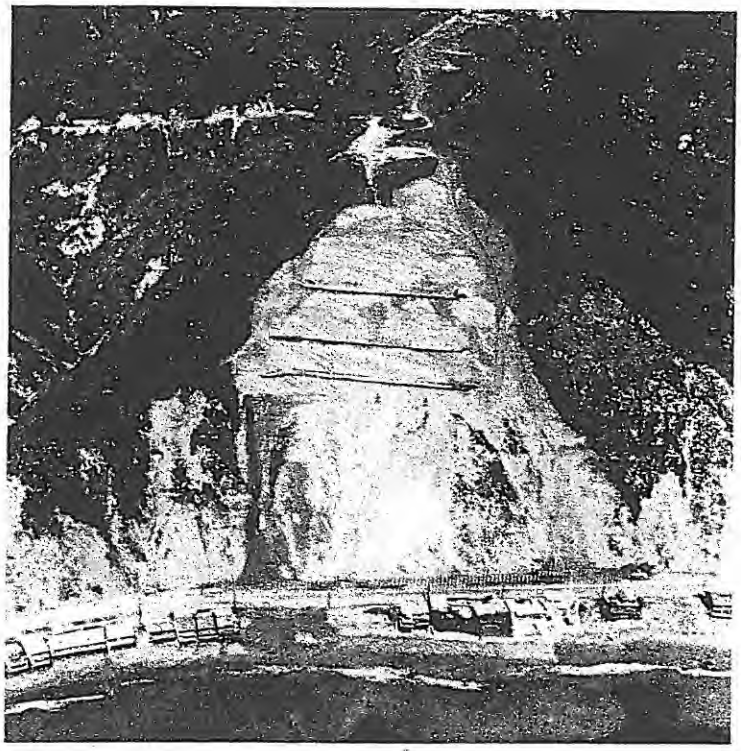

Figure 4. Aerial photograph of the partially completed Big Rock landslide repair.

The grading began in September 1979 with removal starting at the top of the proposed cut slope. The slope cut was begun far enough upslope to remove approximately 60 vertical feet of material in the landslide zone. Since the slide was estimated to be about 30 feet thick, the designed cut would remove the active slide and the weakest, highly broken surficial bedrock.

Steep, locally vertical cuts were made where resistant sandstone layers were encountered. The 1:1 design was continued downslope to near the toe at the road shoulder where a vertical cut 8 feet high was made.

Grading was slowed by loose rock spilling down slope, becoming airborne during descent, and falling onto the highway and adjacent properties; difficult ripping and rock breakage in the cemented sandstone and some diabase. Construction rockfall was mitigated by further lengthening and raising the temporary catchment barrier along the highway. Grading was completed in June 1980 and the lower slopes were sprayed with a hydroseed compound (Fig. 4).

The Bluebird Canyon Landslide, Laguna Beach

Introduction

The successful repair of the Bluebird Canyon landslide (Leighton et al., 1986) required the active participation of city, county, state, and federal officials including the President of the United States. The slide was notable by the support of the entire community for the slide victims, and the efforts of the repair team. This was exemplified by the absence of litigation and hold-harmless agreements signed prior to the repair.

The Bluebird Canyon Landslide (Fig. 5) occurred on October 2, 1978 in a hillside section of the City of Laguna Beach, California (Fig. 5 and 6). This landslide resulted in major devastation and property damage, but no loss of life or injury. The slide dammed the Bluebird Canyon drainage course; ultimately, 24 houses had to be demolished; all major utilities and 775 lineal feet of public roads were destroyed; and nearly 100 residences around the periphery of the slide were threatened or adversely impacted (Fig. 6).

Emergency measures were initiated with reestablishment of access to the slide area which began on October 3, 1978, and the commencement of the installation of a 72-inch diameter storm drain on November 18, 1978 in the Bluebird Canyon drainage course. This storm drain was completed one day before a torrential rainstorm that could have caused major down-stream flooding. All stabilization measures were essentially completed by June 29, 1979, approximately eight months following the occurrence of the landslide. Many phases of the stabilization measures were constructed around the clock on a 6 to 7-day workweek and commencing on October 3, 1978. The remedial stabilization measures included the construction of five principal-engineered devices as fol-

Figure 5. The Bluebird Canyon landslide occurred during the early morning hours of October 2, 1978. Ultimately 24 homes were lost. Miraculously, there were no deaths or serious injuries. (photo courtesy Woody Higdon)

lows:

1) A storm drain in Bluebird Canyon to alleviate damming of the channel.
2) A horseshoe-shaped shear key buttress consisting of a 10-celled prism of compacted fill.
3) Sixty-six soldier piles placed vertically around the perimeter of the buttress excavation, and then interconnected with welded grade beams.
4) A gravity butress, an earthen dam of compacted fill placed in Bluebird Canyon in front of the landslide.
5) A subdrainage system consisting of perforated pipes and permeable materials.

General Geologic Relationships

The Bluebird Canyon Landslide of October 2, 1978 was a block glide that reactivated a prehistoric slide with a history of at least three different episodes of movement. It occurred on a dip-slope that contained a faulted synclinal warp (Figs. 7, 8a, 8b, and 9). The basic conditions for landslide failure were a combination of (1) rock weakness, (2) canyonward-dipping bedding and an ancient slide structure, (3) saturation of the graben area and basal rock units of the landslide resulting in buildup of hydrostatic pressure in at least the graben area and pore pressures along the basal rupture sur-

Figure 6. Index Map

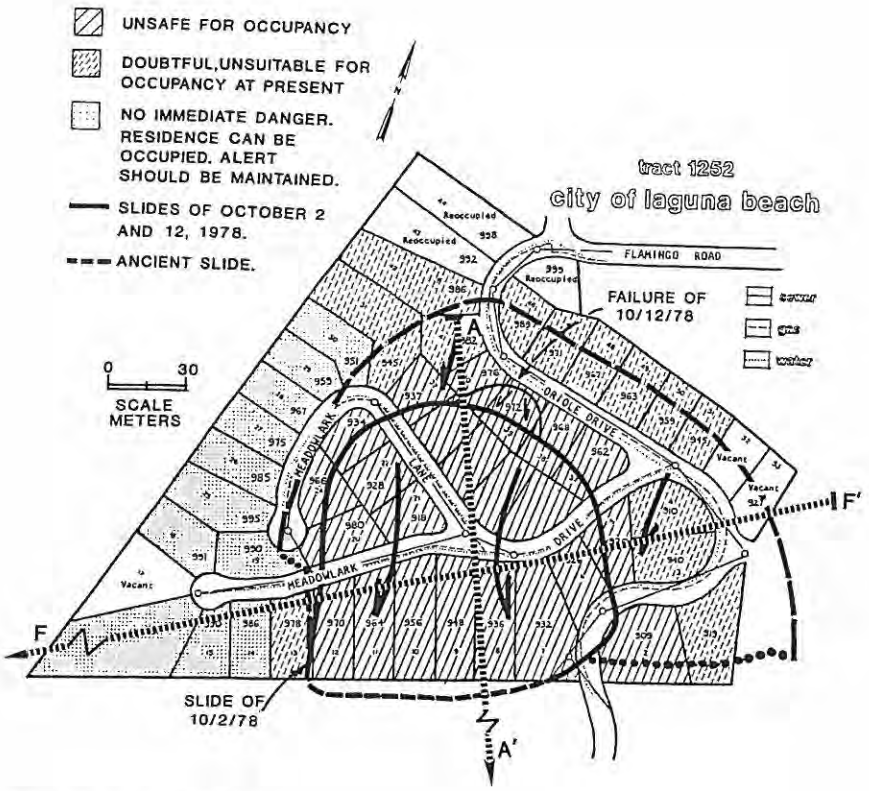

Figure 7. Site Index Map

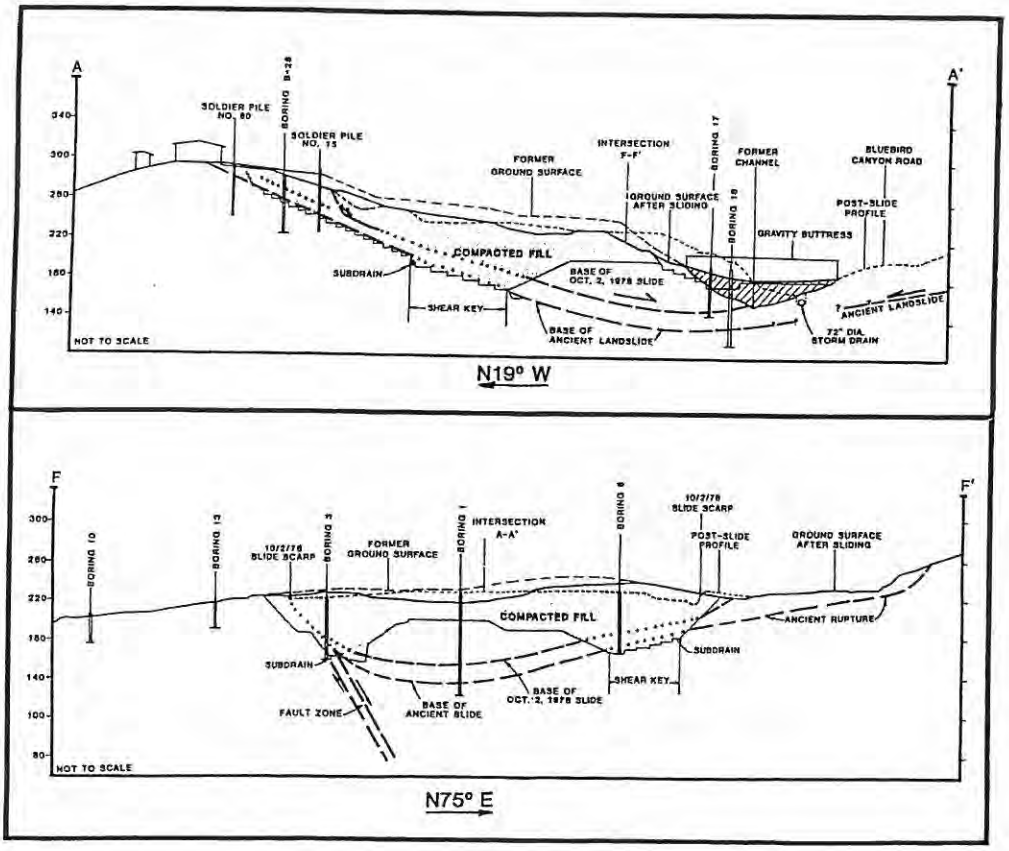

Figure 8. Geologic Cross-sections

face and (4) canyon entrenchment and erosion at the foot of the dip-slope and ancient slide (Figs. 7, 8a, and 8b).

Phase I Emergency Stabilization Measures-Storm Drain Installation

The location and size of the required storm drain were determined by the design civil engineer, Robert Bein, William Frost and Associates (RBF). This determination was based on the area topography, rainfall data, and availability of CSP (Corrugated Steel Pipe). The design called for a 72-inch diameter, 600 foot long storm drain (Fig. 10) to be located at the modified bottom of the Bluebird Canyon channel (see Figs. 11 and 12 for general location).

The main geotechnical concern during the required trenching was reactivation and extension of the slide. The Oriole Drive embankment between Bluebird Canyon Road and Tract 1252 produced a buttressing effect that probably prevented the eastern portion of the October 2nd slide from extending to the eastern margin of the ancient rupture surface. Trenching along the toe of the slide and across Oriole Drive would have undermined the October 2nd slide and breached the buttress created by the Oriole Drive embankment. Consequences of reactivation and extension of the slide would have been:

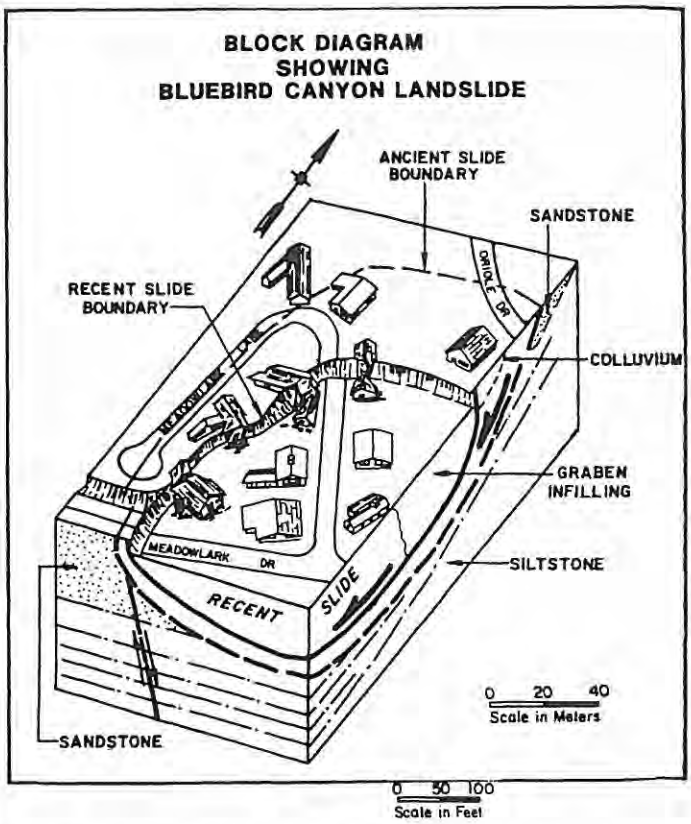

Figure 9. Block diagram showing the Bluebird Canyon landslide.

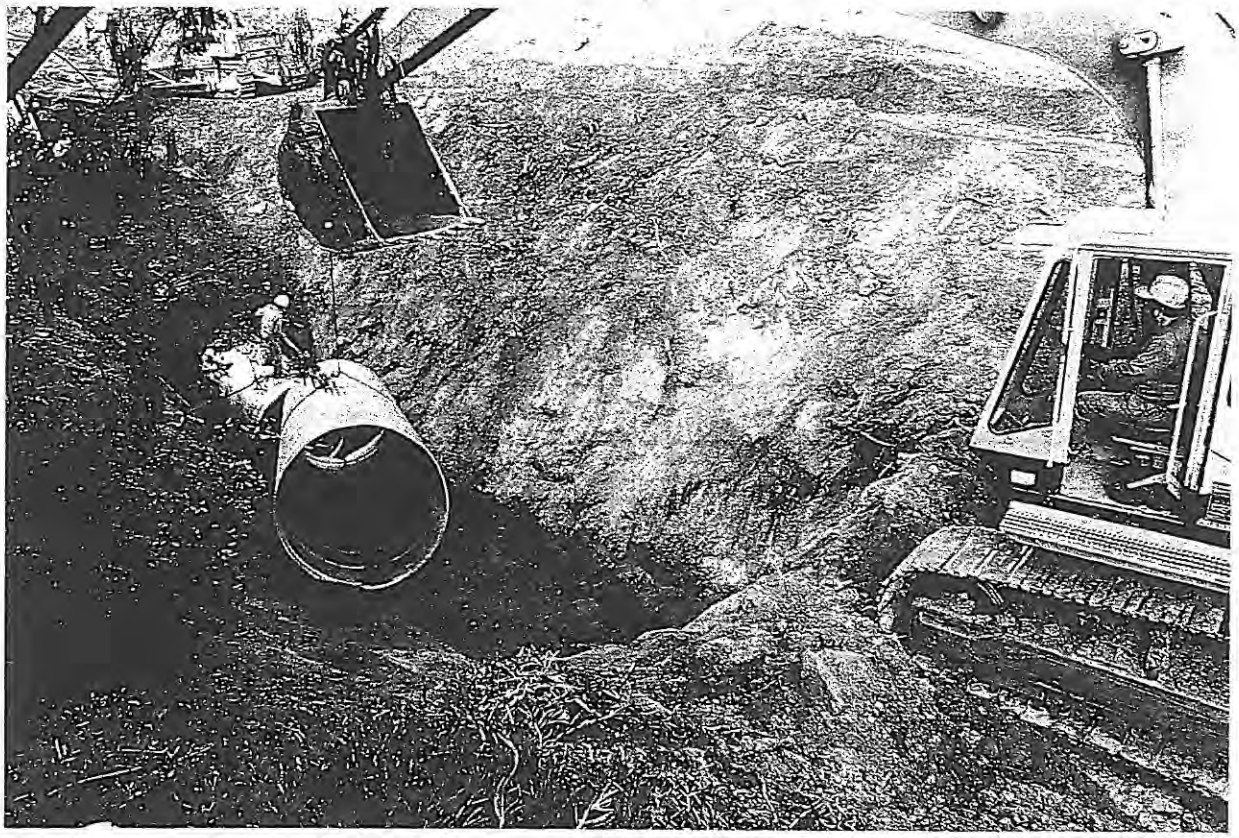

Figure 10. A 72-inch diameter, 600 foot long storm drain pipe was installed during Phase I stabilization construction. Workers were tethered and the city Fire/Rescue squad stood by to provide prompt assistance if needed.

A. Jeopardize the safety of the construction and inspection team.

B. Destruction of approximately 500 additional feet of Oriole Drive, the previously damaged residence at 909 Oriole Drive and three other previously undamaged residences (910, 919 and 940 Oriole Drive).

C. Formation of a lake upstream of the slide and possible breaching of the landslide dam.

To safeguard against the above threats the following was recommended:

A. Trenching for pipe installation be done in small increments (30 feet in length).

B. Prior to trenching across Oriole Drive, a buttress fill be constructed in the canyon bottom, east of Oriole, in order to compensate for the breaching of the buttressing effect of the Oriole Drive embankment.

C. Trenching, pipe installation and backfill of trench across Oriole Drive be accomplished on a round-the-clock schedule to minimize the length of time available for failures.

Installation of the storm drain was completed with no reactivation of the slide.

Phase II Of Stabilization Measures

A very conservative approach was used for evaluation of strength parameters of the slide materials and rupture surface. As a result, a much higher than normal level of confidence could be established in the adopted factor of safety of 1.2 rather than the normally accepted safety factor of 1.5. The main stabilization elements recommended were a drained shear key buttress at the head of the slide and a gravity buttress (Figs. 11 and 12) at its toe. These buttresses, the associated sub-drainage system and ingrading backslope failures are discussed below.

Shear Key Buttress

The shear key buttress consisted of a massive zone of compacted structural fill keyed into firm bedrock underlying the disturbed and slide-involved rock units. The approximate plan location of the buttress key is indicated in Figures 11 and 12. Typical cross-sections of the buttress are shown on Figures 8a and 8b. Earlier geotechnical reports recognized the high potential for backslope failures during the construction of the shear key buttress, and in order to reduce this potential, recommended:

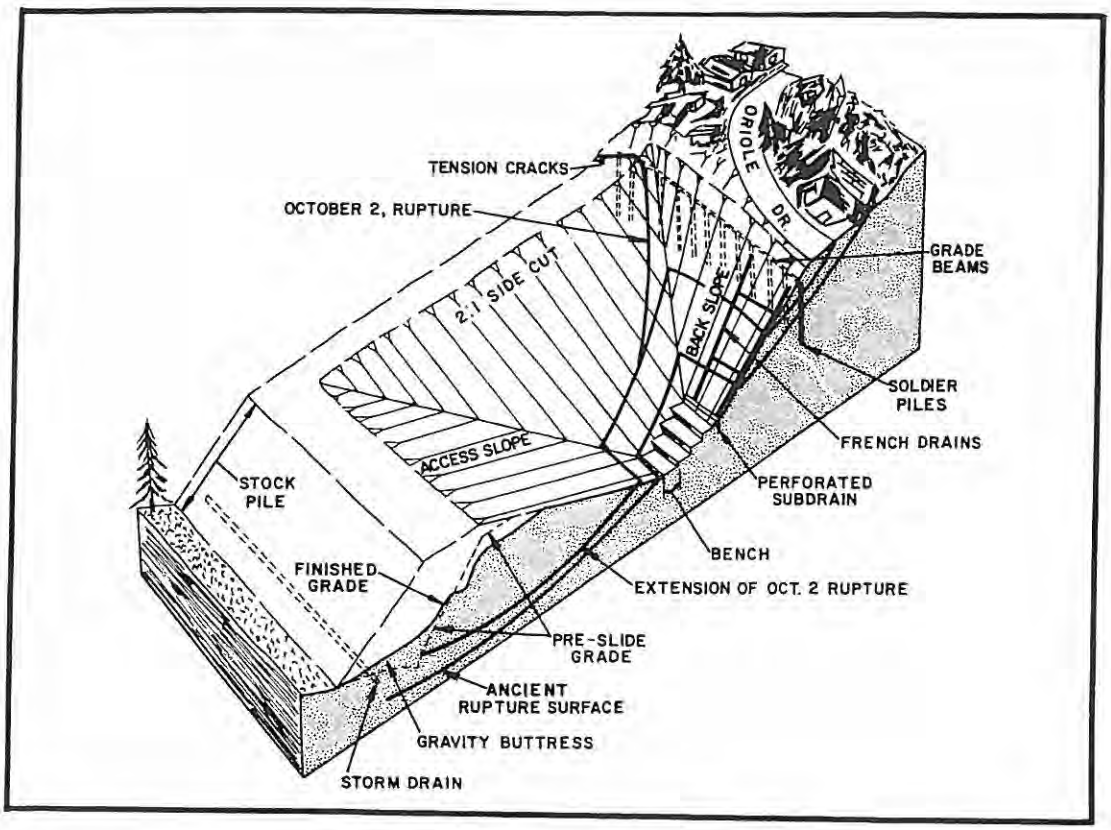

Figure 11. Block diagram showing design and construction elements of the stabilization plan. View is to the northwest.

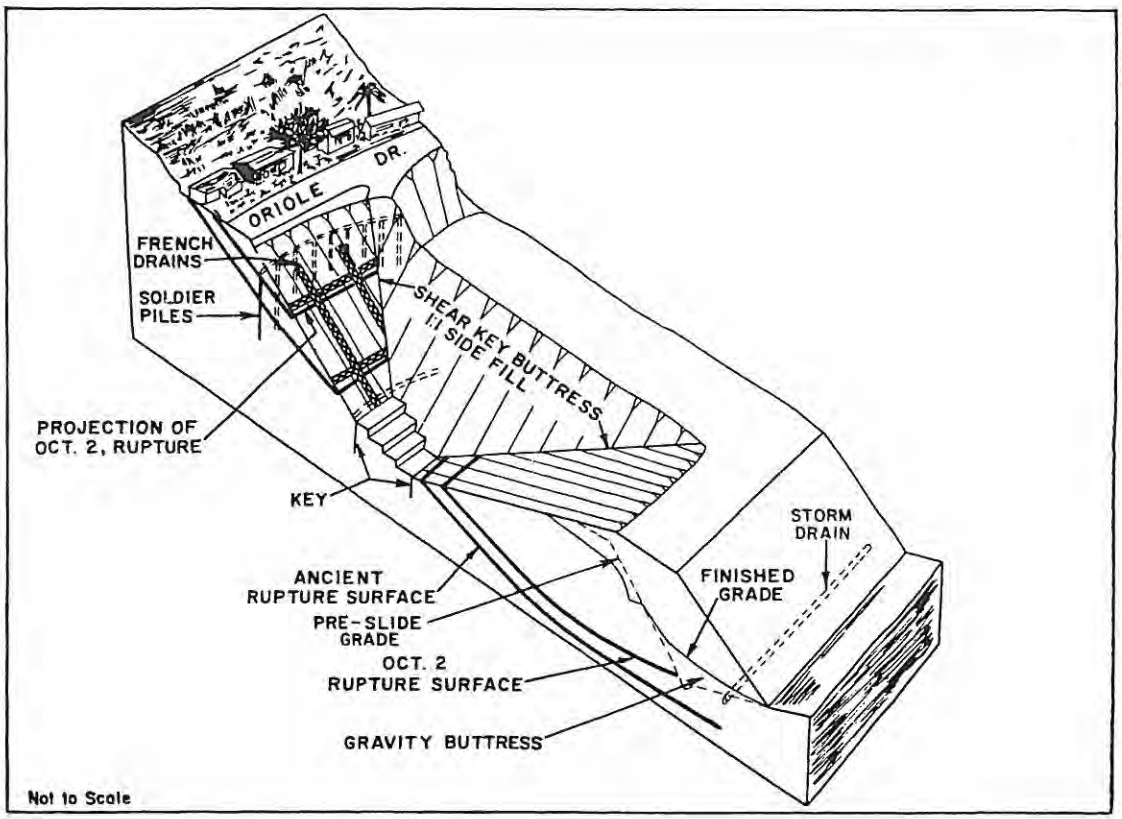

Figure 12. Block diagram showing design and construction elements of the stabilization plan. View to the northeast.

A. Installation of a system of 2-foot diameter reinforced concrete soldier piles.

B. Excavation of the backslope in relatively small sections with round-the-clock grading as necessary.

Forty-eight soldier piles were installed between January 22 and February 6, 1979, at locations indicated on Figures 11 and 12. Availability and economics governed the choice of steel beams used in soldier piles. In order to maximize effectiveness of the soldier piles, they were interconnected at the surface by welded grade beams. Sukut Construction Company, the project contractor, devised a ten-phase grading scheme that combined the geotechnical recommendation of phased backslope excavation with the earthwork constraints. Figures 11 and 12 depict how the combination of soldier piles and the phased backslope excavation reduced the probability of major backslope failures.

Backslope Failures

Geologic mapping and strain monitoring were useful in predicting the location and time of occurrence of backslope failures. As anticipated, numerous backslope failures occurred as a result of the removal of lateral support during excavation of the shear key buttress, particularly during the wet season. Only the failures of April 23, May 12 and May 15 slid on the "ancient rupture surface." All other slides occurred on shallower surfaces. For the most part, the combined effect of soldier piles and phased backslope excavation was successful in containing these failures to the area in front of the soldier piles, preventing further upslope failure in previously undamaged areas. Only the April 23rd failure extended significantly upslope beyond the soldier piles. Despite the extensive counter measures, one residence was destroyed and an 80-foot section of Oriole Drive was lost. As a result of the April 23 backslope failure, eighteen additional soldier piles were recommended and installed, so that buttress stabilization could continue.

Gravity Buttress

The recommended gravity buttress consisted of a compacted earth embankment placed at the slide-modified canyon bottom (Fig. 8a, 8b, and 11 through 14). This feature improved the gross stability of the slide mass by elevating the finish grade of the canyon bottom and effectively reducing the overall height of the south-facing slope. The initial design of this buttress was modified near the end of the construction phase of the shear key buttress. About 15,000 cubic yards of excess soil was placed as compacted fill in the canyon bottom east and west of Oriole Drive.

Subdrainage System

High ground water levels within the ancient graben zone and its role in elevating pore water pressures within ancient rup-

ture zones and triggering the October 2, 1978 slide were documented by subsurface probes. Perched water in the ancient graben zone was also confirmed by numerous seeps and high moisture content observed during the excavation of backslope of shear key buttress. The likelihood of future ground water buildup was reduced by installation of a subdrainage system.

The subdrainage system consisted of a main subdrain and a lacework of french drains (Fig. 11 and 12). The main subdrain is located at the foot of the backslope and consists of a perforated ABS pipe with both 6-inch and 4-inch diameter sections. It was embedded in a 24-inch- wide trench filled to a minimum height of 24 inches with Class 2 filter material. The subdrain is horseshoe-shaped in plan view, with half the drain flowing to the east side of the area and half to the west side. Flow gradient is a minimum of 2 percent toward the 72-inch storm drain to which the subdrain is connected on both the east and west sides of the landslide area. Terminal sections of the subdrain are unperforated in order that water cannot enter the fill and slide materials at the foot of the slide. Class 2 filter material was placed beneath the storm drain to provide subdrainage of the slide material not removed during emergency grading.

At 30-foot intervals french drains radiate from the main subdrain up the backslope. They consist of 2-foot wide trenches filled with a 1-foot minimum thickness of filter material. The radial pattern of french drains is interconnected at 20- to 25-foot vertical intervals by near-horizontal lateral drains. A total of 2,840 feet of 4- and 6-inch diameter ABS pipe and 1,614 tons of Class 2 filter material were used in the subdrainage system.

Earthwork and Quality Control of Fill Compaction

The fill materials used for stabilization consisted of silty clays, clayey silts and fine clayey silty sands. They were spread in thin lifts in approved areas (shear key buttress, gravity buttress and storm drain backfill), moisture-conditioned to near-optimum moisture content and compacted by sheepsfoot rollers and heavy construction equipment. At the base of the shear key buttress, the fill was keyed into firm undisturbed bedrock beneath the basal rupture surface of the ancient slide (see cross-sections). The October 2nd and ancient slide materials were entirely removed from the shear key. All loose slide debris resulting from backslope failures were removed by stripping and/or benching. Brush and loose surficial slide debris were cleared from the base of the gravity buttress; however, most of the October 2nd slide debris and alluvium at the canyon bottom were left in place.

Deep-Seated Stability

The recommended emergency stabilization measures were implemented. The three principal measures for deep-seated stability are: (1) a horseshoe-shaped shear key buttress, (2) a

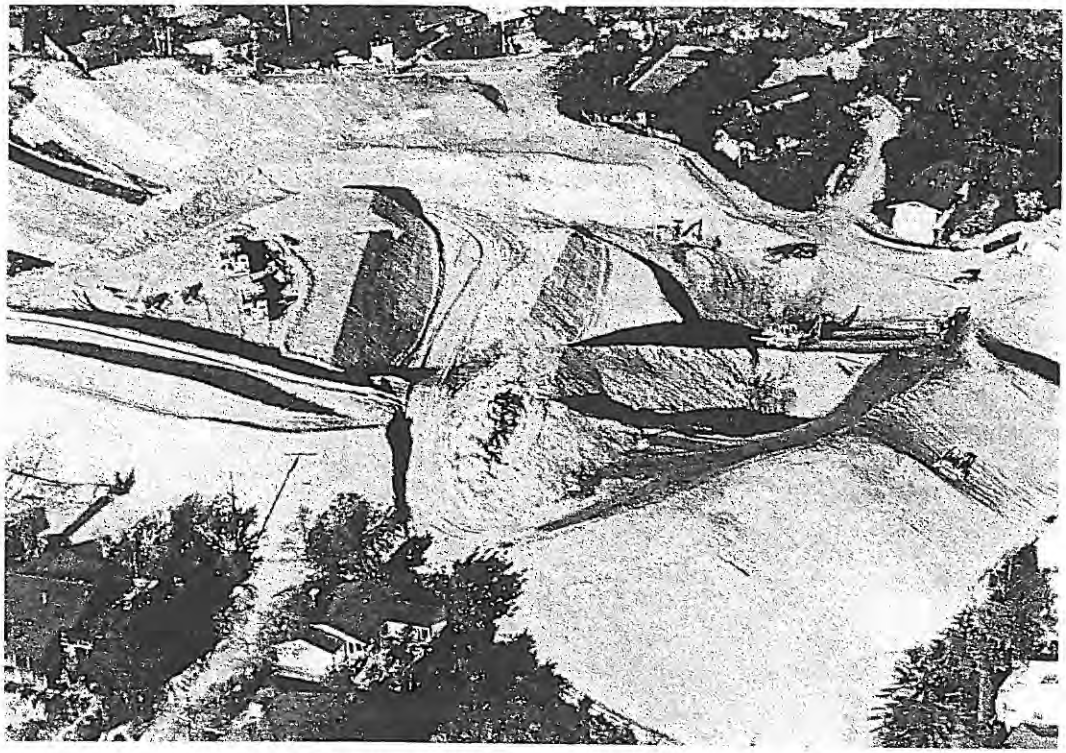

SITE STABILIZATION IN PROGRESS ON BLUEBIRD CANYON LANDSLIDE, MARCH, 1979

Los Angeles Times Photo by Deric Jeannette

Figure 13. Buttress construction in progress, Bluebird Canyon.

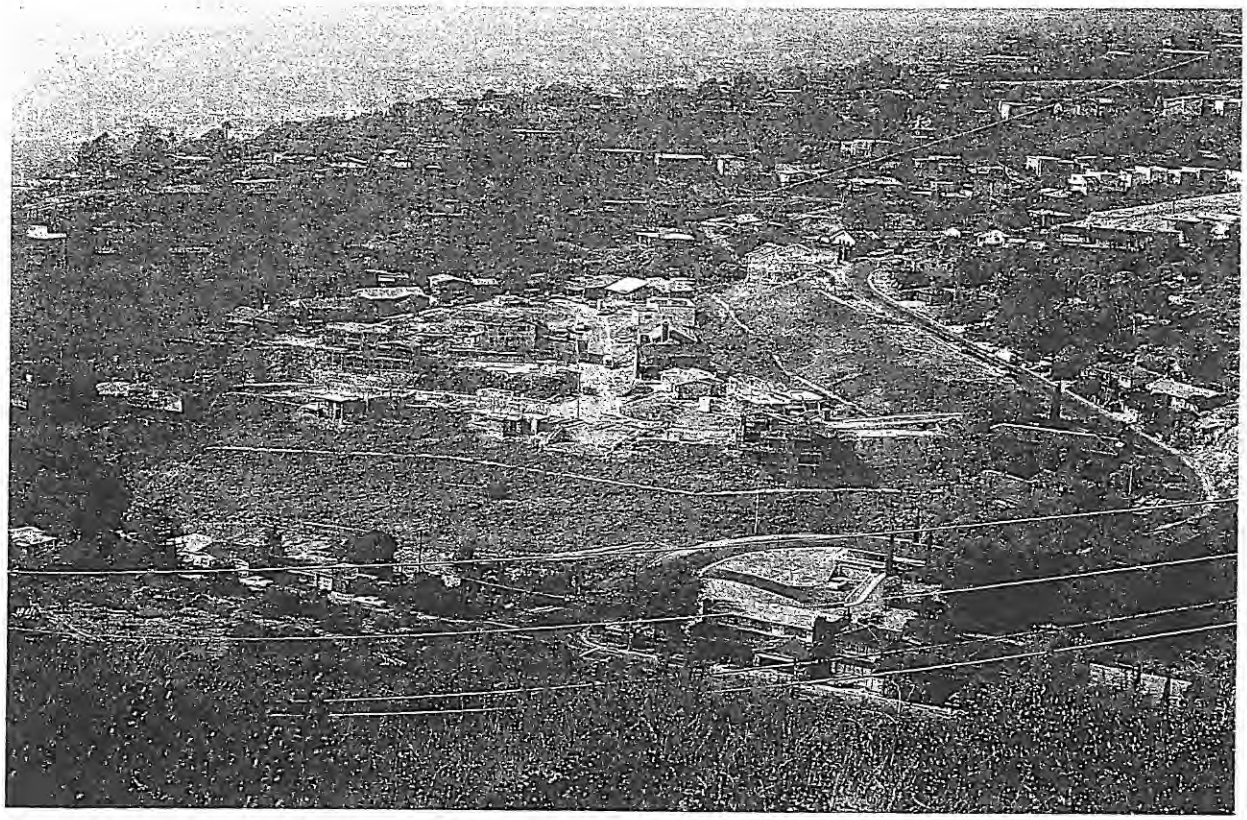

Figure 14. Stabilization of the landslide was essentially completed by June 29, 1979; after only 8 months. Nearly all destroyed homes were

gravity buttress in Bluebird Canyon, and (3) an elaborate integrated subdrainage system.

Analyses of data showed that the adopted criterion of achieving a factor of safety of 1.2 could be met using conservatively estimated strength parameters based on the post-failure geometry of the slide mass. In addition, analyses were also presented which indicate that the factor of safety is 1.5 when strength parameters were back-calculated from pre-failure geometry. In light of the close correlation between strength parameters determined in the laboratory and strength parameters back-calculated from pre-failure geometry, it was the professional geotechnical opinion that the stabilized area meets the normally accepted static stability state of 1.5. Pseudostatic analysis using a lateral earthquake loading of 0.15g (gravitational force) yields a dynamic factor of safety of 1.13 which is normally acceptable.

Conclusions

The Bluebird Canyon Landslide of October 2, 1978 has been successfully stabilized and the blocked drainage course restored. The safety hazards posed to public right-of-way and private properties upslope of the area and downstream of the drainage course have been alleviated. Geotechnical conditions encountered during grading were essentially as anticipated. The major refinements to previous findings were: (1)

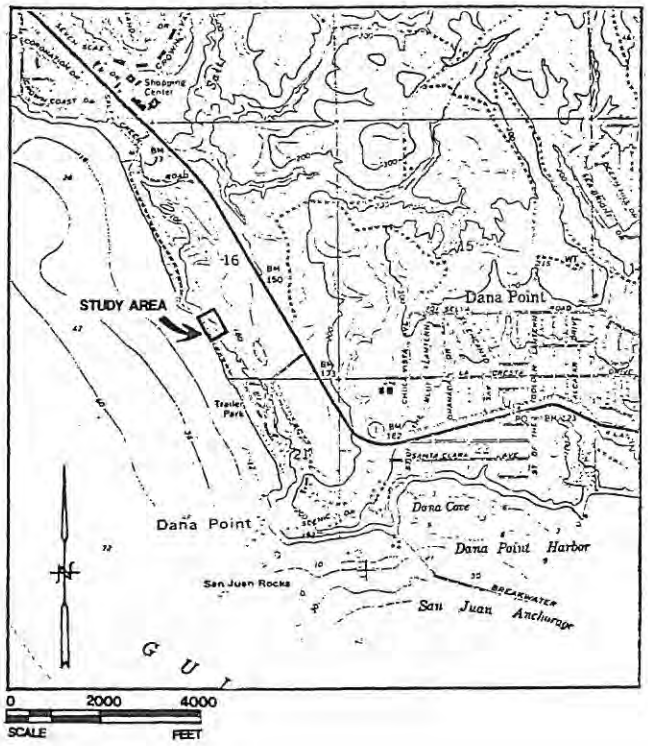

Figure 15. Index Map, Seagate landslide

the "ancient rupture surface" was found to be locally slightly lower than previously inferred, and (2) a north-trending, east-dipping normal fault was found to bound and control the western side of the ancient and October 2nd landslides (Fig. 8a and 8b).

The emergency repair measures completed within the scope of this report have been performed in accordance with FDAA guidelines. Since these guidelines do not allow permanent improvements, further measures are needed to render the emergency stabilization measures permanent.

Seagate Landslide Repair, Niguel Shores

Introduction

The Seagate landslide repair is unique in that it attempted to use a frozen-ground method to stabilize the buttress front cut and back cut. The repair constantly battled the pounding storm surf, unusually high ground water conditions, and geologic mapping while excavating a buttress key more than 20 feet below sea level. Environmental constraints along the Pacific Ocean required the use of a conveyor-belt system to transport the excavated landslide material to a stockpile and return it to the buttress cut. Temporary soldier piles were later installed at the toe and at the head of the landslide to provide emergency backslope stability support. Dewatering was necessary to control subsurface ground water flow upslope of the landslide area and from the Pacific Ocean. Extensive sandbagging and temporary restraining devices were necessary to minimize flooding of the site by high tides and storm surf.

The Seagate landslide occurred in 1977 shortly after the site was rough graded (Fig. 15). The slide occurred during the heavy rains of the winter of 1977 to 1978. Although, the slide took place before expensive coastal view homes had been built, the landslide severely damaged six of the residential lots and a portion of the road. The toe of the landslide extended onto the beach at the toe of the previously graded slope (Fig. 16). The movement of the landslide was temporarily halted by excavation and removal of material at the head of the slide; thus, reducing the driving force.

The slide area was extensively investigated and analyzed prior to commencement of the landslide repair. Numerous large-diameter and small-diameter borings were drilled and geologically logged in addition to the excavation and logging of backhoe trenches. Extensive soil engineering testing and stability analyses were performed in order to arrive at an effective repair plan.

The grading contractor as well as the owner provided valuable input during the design process to assure that the repair alternative selected could be constructed and would be as cost effective as possible. The Seagate landslide repair commenced in mid-September 1980 and was completed by the end of February 1981.

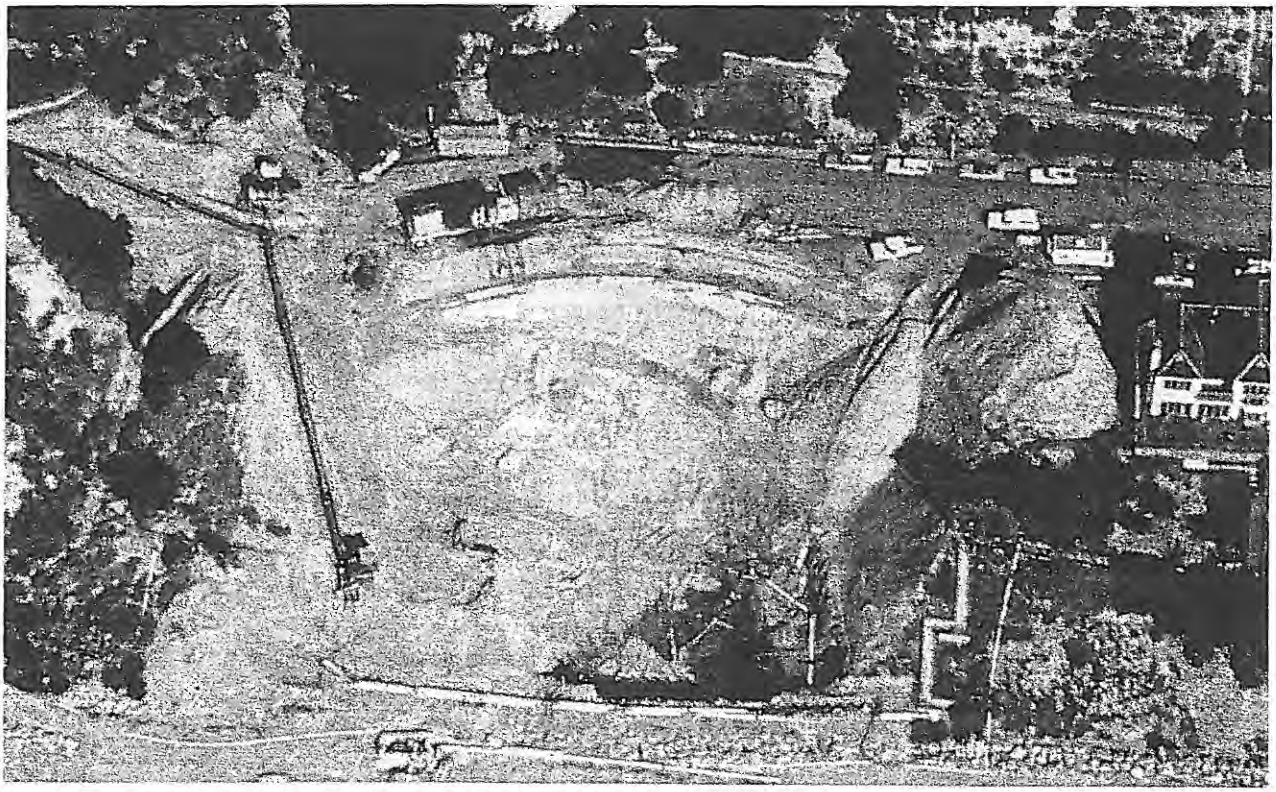

Figure 16. Near-vertical aerial view of the Seagate Landslide repair. The beach and Pacific Ocean are at the bottom of the picture. The conveyor-belt system utilized to remove slide debris from the excavation is shown on the left side of the picture. The buttress key was approximately 75 percent completed at this stage.

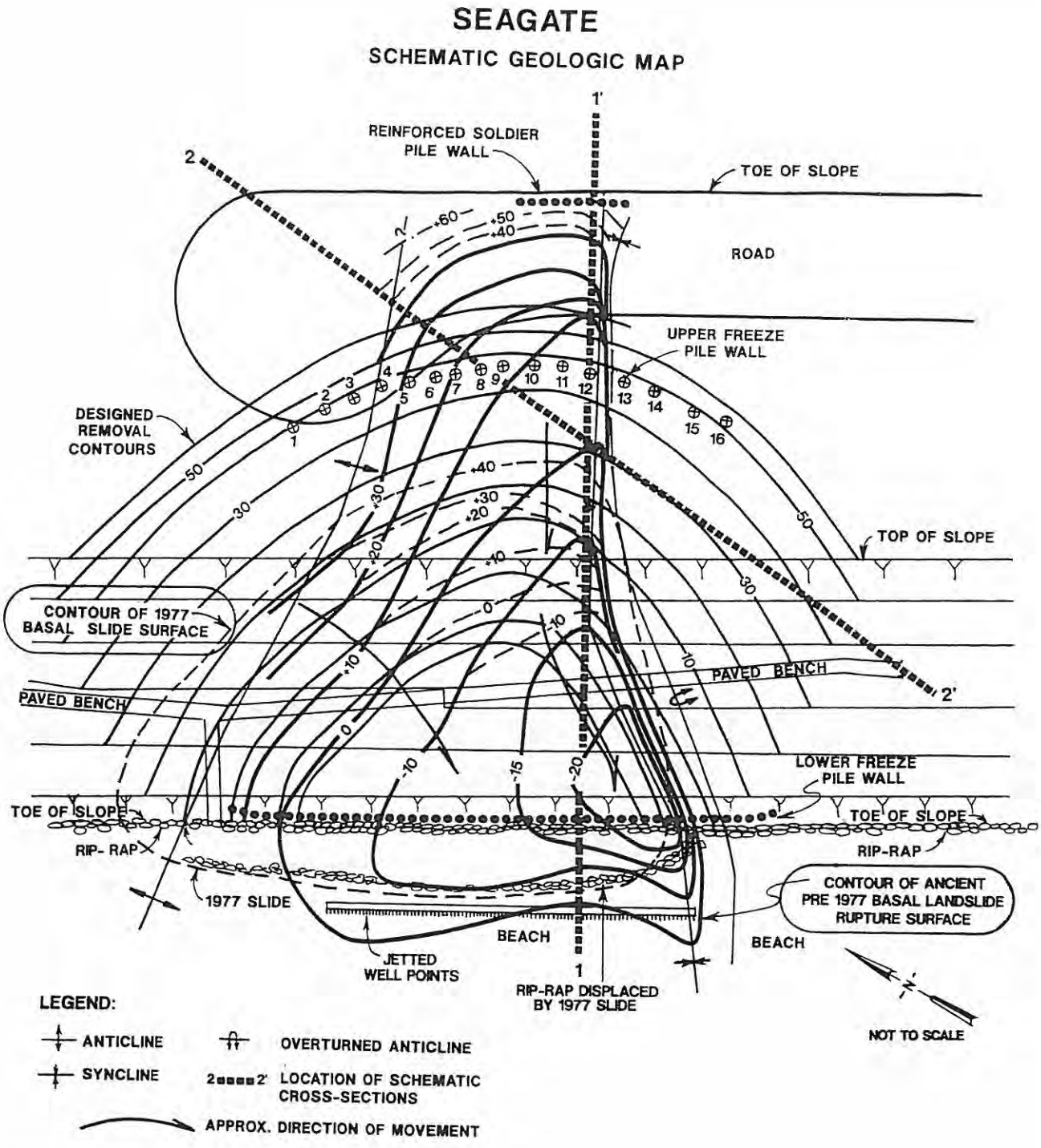

Figure 17. Schematic Geologic Map, Seagate

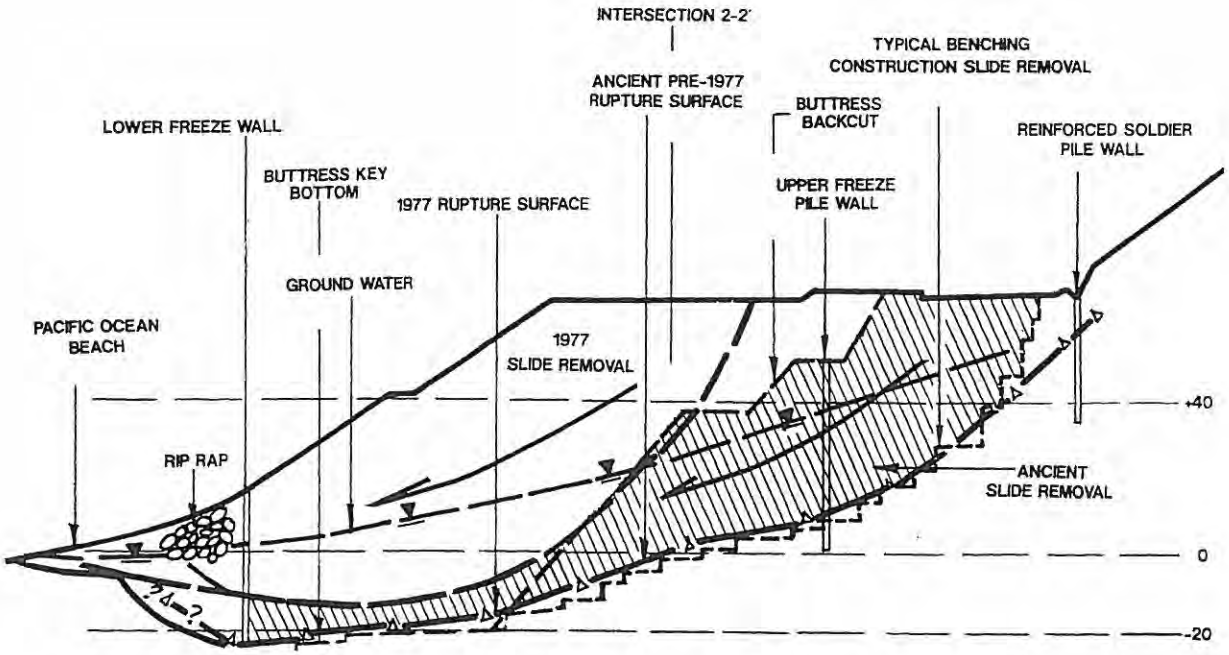

SCHEMATIC CROSS-SECTION 1-1'
(NOT TO SCALE)

Figure 18 a. Geologic Cross-Section 1-1'

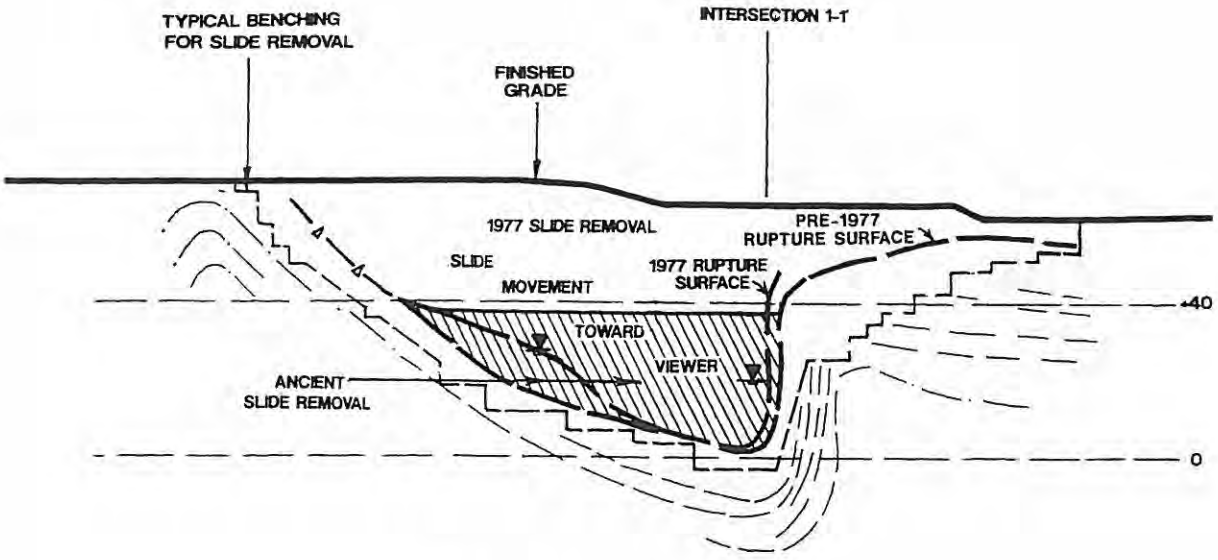

SCHEMATIC CROSS-SECTION 2-2'
(NOT TO SCALE)

Figure 18 b. Geologic Cross-section 2-2'

Summary Of Landslide Conditions-Rupture Zones

The projected 1977 rupture surface of the landslide and the older rupture surface are shown on the Schematic Geotechnical Map (Fig. 17) and Cross-Sections 1-1 and 2-2 (Figs. 18a and 18b). The location of the 1977 rupture surface was mapped essentially as anticipated during shear key excavation. The rupture surface was slightly deeper in the southern area. The rupture surface involved both older terrace deposits and artificial fill as originally interpreted. Additional slide materials encountered during grading consisted of lenses of broken, crumbled siltstone and shale in a silty clayey matrix in various thicknesses up to 6 feet, overlain with terrace deposits. The older rupture surface was parallel to bedding with a 6-foot thick, near-vertical sheared zone forming the southern boundary (Figs. 17, 18a, and 18b).

Several prominent potential rupture surfaces were observed within the bedrock during shear key excavation. These planes are parallel to bedding, 2 to 3 feet beneath the older basal rupture surface. They are polished and slickensided clay surfaces probably formed during past movements (Fig. 19). Because these zones are susceptible to future movement, they were essentially removed during the excavation of the key. These weak layers as well as the 1977 rupture surface were considered during the shear key and buttress design.

Groundwater

The moisture content of earth materials excavated during shear key construction ranged from below optimum in sandier fill and upper sandy landslide debris to saturated in landslide debris below the ground water level. Numerous seepage zones were mapped in the back-cut slopes and landslide debris above the 1977 rupture surface. These occurred near the contacts of: (1) sandier fill layers over silty clayey fill layers, (2) artificial fill over shale and siltstone bedrock, (3) landslide debris above the 1977 rupture surface, and (4) highly jointed and fractured siliceous shale overlying siltstone. Seepage zones below the ground water level generally flowed at 10 to 20 gallons per minute. The seepage zones were confined to porous sands and permeable, fractured siliceous shales. While the porous sands acted as aquifers in the fill and landslide debris, the prominent seepage in bedrock is controlled by secondary structural features (i.e., jointing and folding). Consequently, the wedge-shaped synclinal trough would promote the buildup of pore pressure.

During shear key excavation, ground water infiltration from temporary construction cut slopes presented substantial delays to grading. The phreatic surface was encountered at approximately the 5-foot elevation near the toe and the 8- to 10-foot elevation near the back-cut slope. Numerous sumps, six deep-well points, and a horizontal rock drain were eventually installed within the excavation to remove ground water (Fig. 20). In addition, 60 or more manually jetted well points were installed seaward of the riprap to intercept sea-

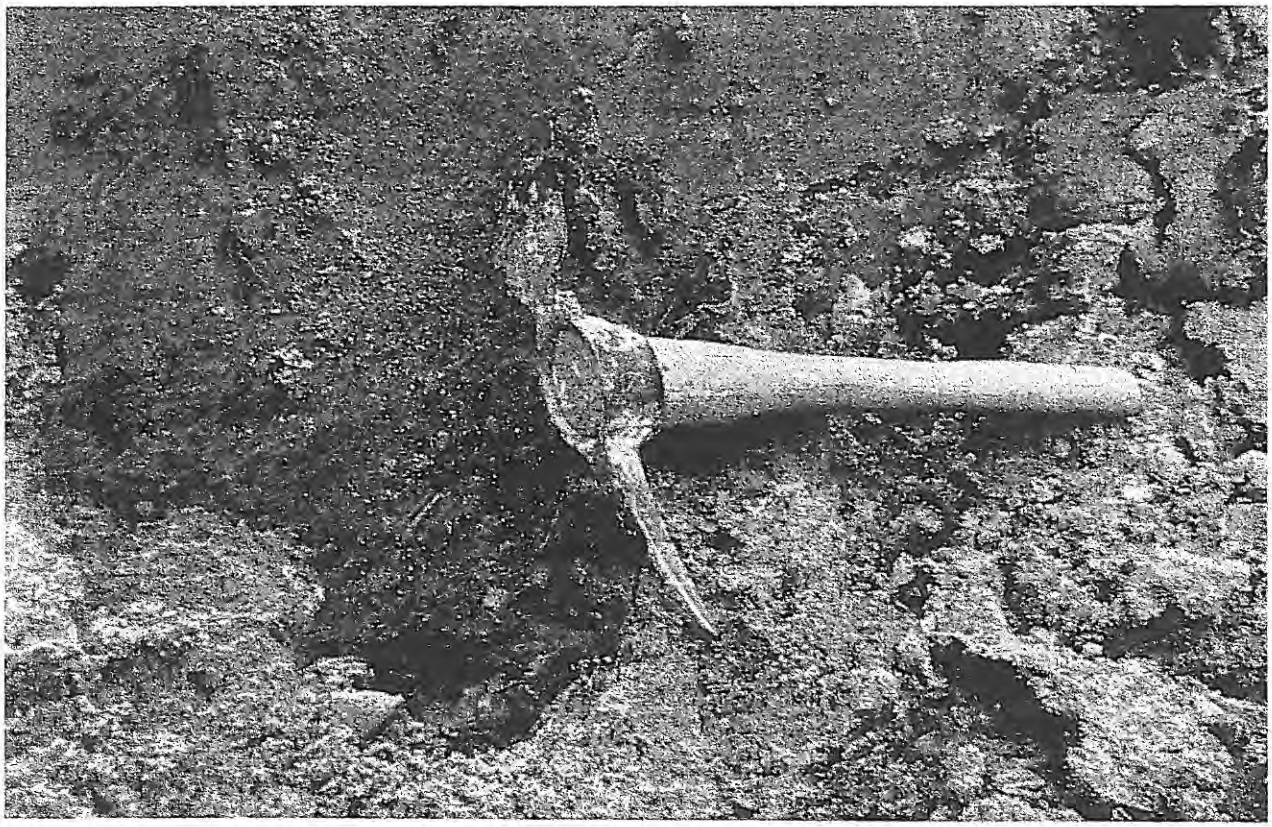

Figure 19. Fat blue-grey clay rupture surface of the ancient landslide. (See Figure 7 for approximate location; left side of backhoe).

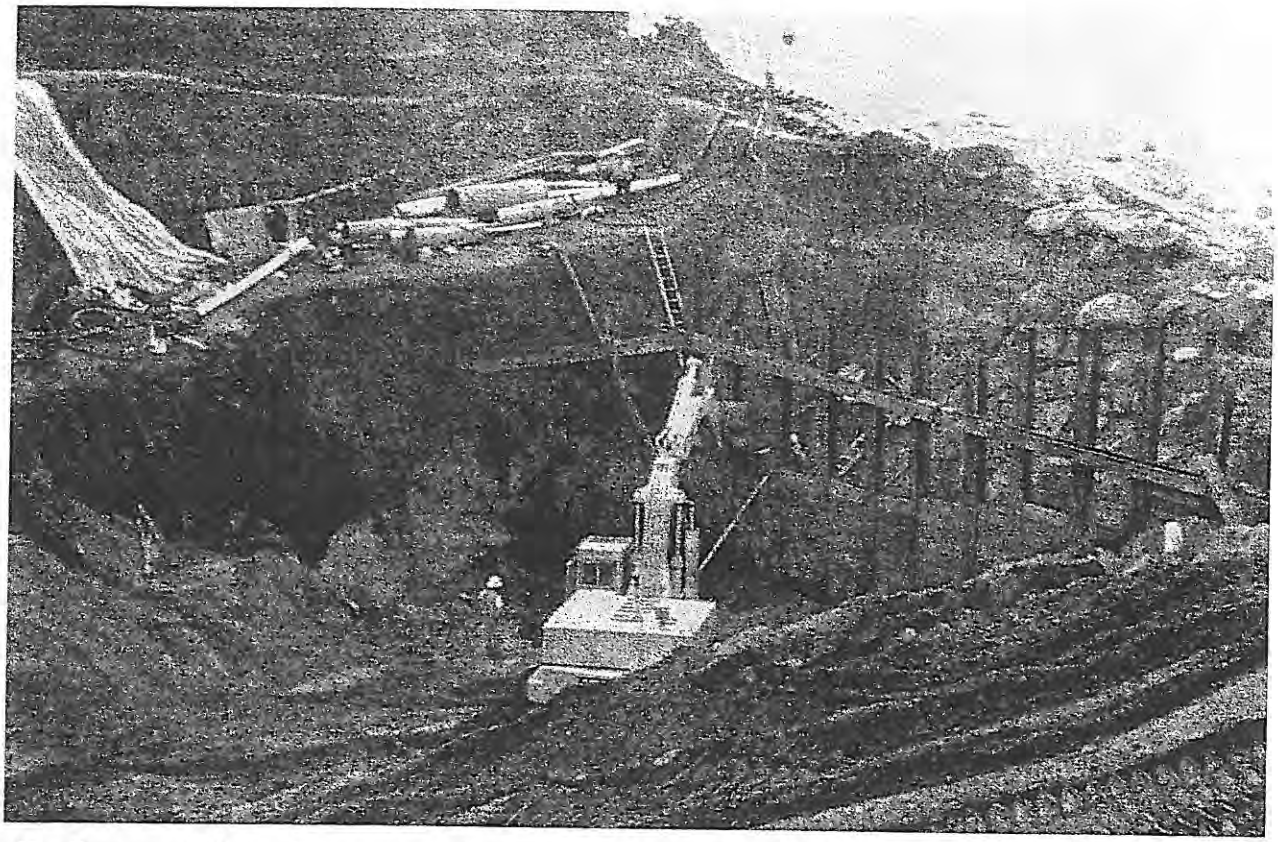

Figure 20. Temporary steel pile wall was constructed at the toe of slope after failure of the lower freeze wall. This was later removed once the

water infiltration into the shear key buttress excavation since the lower freeze wall never froze into a solid impermeable wall (Fig. 21). These were installed to minimize ground water circulation and aid the ground freezing.

The deep well points were drilled below the rupture surface into bedrock, cased with perforated 12-inch ABS pipe, and the bottom backfilled with Class 2 material. Installation of the six well points occurred at various periods during grading (i.e., Deep Wells 1-3, November 11-13, 1980; 4-6, November 25-26, 1980; and 7-8, attempted and abandoned December 2, 1980) as ground water problems continued. Throughout shear key excavation, numerous sumps were established to collect ground water (Fig. 21). All sumps were installed with backhoes (either rubber-tired or track-mounted) in saturated flowing sands using perforated corrugated metal pipe and Class 2 permeable material. The sumps were usually installed less than 10 feet in depth.

A 35-foot-long horizontal french drain consisting of 2-inch rock backfill in a 4-foot-wide trench was excavated below the rupture surface along the southern boundary. Flowing sand required the utilization of a steel shield (4 x 12 x 8 feet) for excavation to a depth of elevation -23 feet. Consecutive segments trending N28°E were excavated, end-to-end, beginning opposite Well Point 5 toward the lower freeze wall (December 17-20, 1980). Near the lower freeze wall, a CMP pipe was installed to an elevation of -33 feet in the final segment to pump the collected ground water. All segments of the trench were immediately covered with existing sands.

The manually jetted well points were installed December 10-13, 1980. Each well point was installed using existing water hydrant pressure to force the pipe through the sands into the shale and siltstone. All well points were connected to a manifold system and a single-suction vacuum pump. Effluent output from all dewatering systems equaled approximately 100 gallons per minute but varied from 100 to 600 gallons per minute depending upon tidal fluctuations. The phreatic surface was eventually lowered 12 to 22 feet below sea level, allowing phased shear key excavation.

Design Considerations And Implementation-Slide Mass Stabilization

Recommendations for slope stabilization called for an all-earth shear key buttress with an associated subdrainage system. This stabilization system was installed in multiple phases to minimize backslope failures and headward progression of the landslide. The buttress, temporary stabilization measures, subdrainage system, and backslope failures during grading are discussed below.

Excavated earth materials were removed from the subject site by means of a system of conveyor belts and trucks (Fig. 22). A hopper was attached at the excavation end to allow nearly

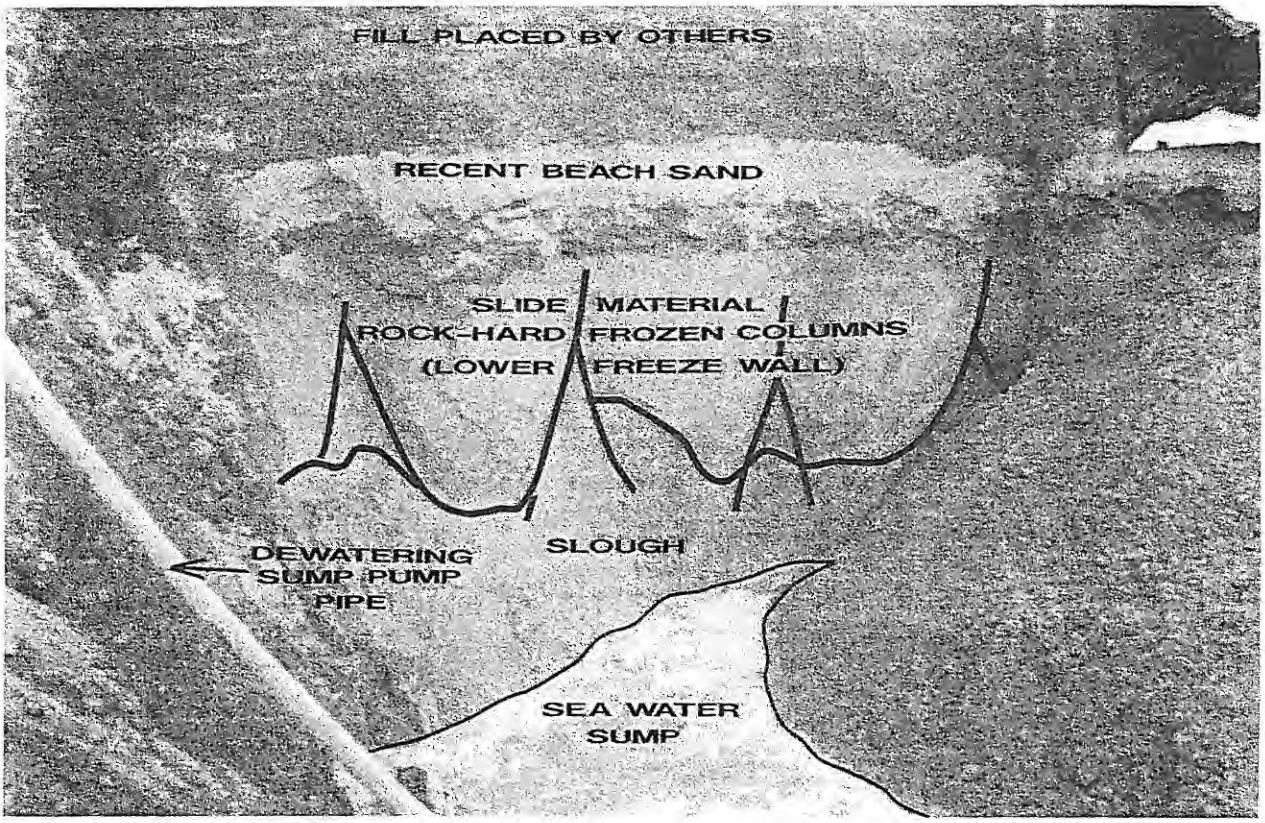

Figure 21. Lower freeze wall that was constructed along the beach at the toe of slope. Upper portions of the frozen columns were rock-hard but these narrowed with depth and sea water seeped into excavation.

continuous feeding of the conveyor-belt system. Earth materials traveled up the interconnected belts along the path of an existing terrace drain bench, finally being stockpiled on the northerly seacliff bluff. Approximately 640 lineal feet of conveyor belt was utilized to lift the material over 150 vertical feet from the excavation to the stockpile area. Each belt section was 40 feet in length (16 total) and each section was powered by an electric motor serviced by an onsite generator. Upon completion of the shear key excavation, the conveyor belts were reversed and the materials were returned to the excavation by the belts and trucks.

Shear Key Buttress

The shear key buttress consisted of a massive zone of compacted structural fill keyed into bedrock once the landslide materials were removed. In both plan and cross-section, the approximate extent of the shear key buttress is shown on Figures 17, 18a, and 18b. The high potential for backslope failures during construction of the shear key had been recognized. Shear key excavation in small successive portions was recommended to reduce this failure potential. Round the clock construction was recommended as an additional option to minimize the period of time the shear key excavation was left unsupported. To accomplish this, Sukut Construction, Inc., the project contractor, devised a multiple-phase grading scheme. This scheme combined geotechnical recommendations with necessary earthwork constraints for phased backslope and toe slope excavations. A temporary system of freeze piles was constructed in a portion of the backslope and the toe area opposite the riprap to provide temporary support for the construction excavations (Fig. 23). In addition to ground freezing, concrete and steel piles were to be installed as an emergency contingency measure should the frozen piles fail. Excavation began in the deeper southwest portion of the subject slide and progressed phase-by-phase along the toe of the subject slide and toward the backslope phase. The base of the shear key buttress was stair-stepped from southwest (-22 feet) to northwest (-4 feet), and southwest (-22 feet) to east (+23 feet) in order to remove the ascending rupture surface.

Strain Monitoring

A system of strain monitoring devices was installed above the back-cut slope to provide early detection of the location and extent of potential failures in the back wall of the excavation. Utilization of these devices improved the general safety of workers in the shear key area and provided information to adopt alternative recommendations for the safety of the surrounding residences above the excavation. The system included three inclinometers and three extensometers installed along the top of the back-cut slope to monitor minu ground movements during excavation. The extensometer con-

Figure 22. Slide material removed was lifted nearly 150 vertical feet to an offsite stockpile area by conveyor-belt system shown in the picture. Once the key had been completed, the earth material was returned to the key by the conveyor and trucks and compacted to form the earth

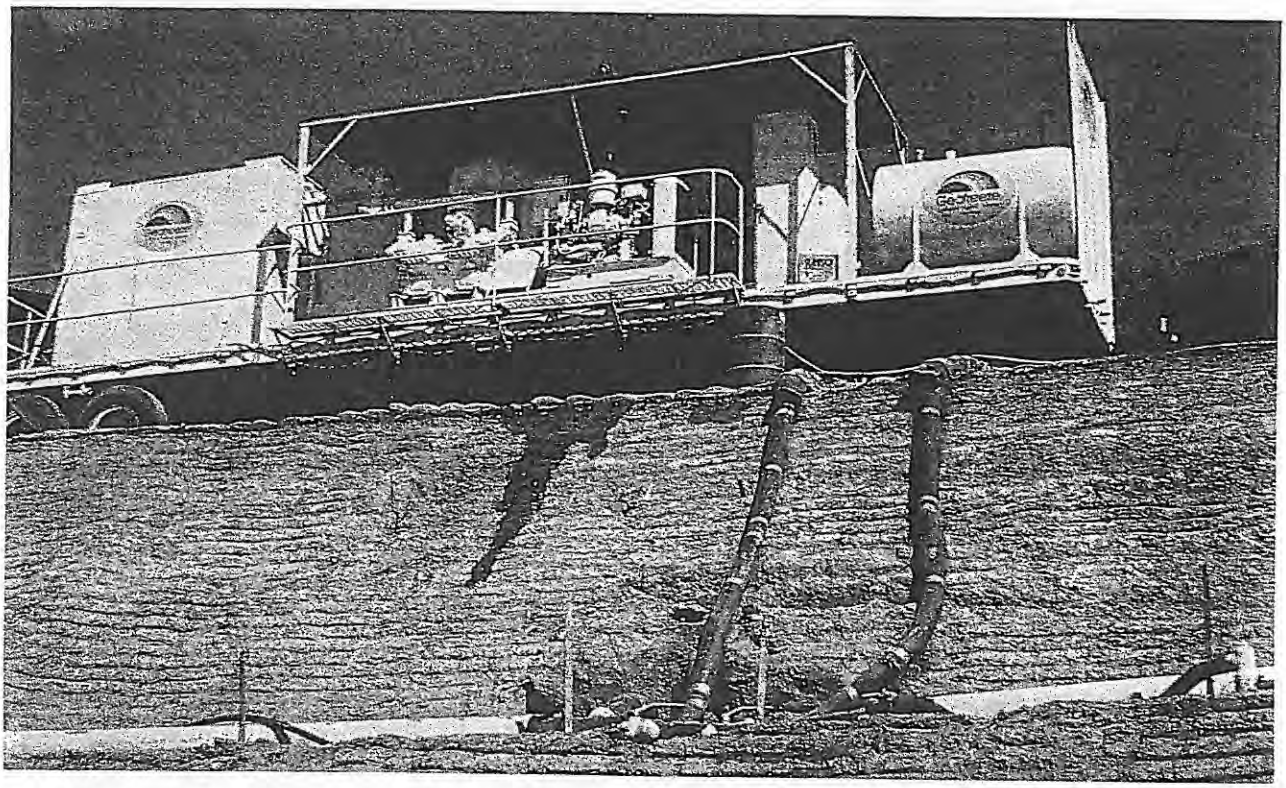

Figure 23. A large compressor unit was situated at side top of the excavation during slide removal. A chilled brine solution was utilized to create the upper and lower free walls. The upper freeze wall is located downslope of the compressor.

sists of a rigid rod, extended between two pins, driven vertically into the ground. Any movement between the pins is detected on a dial indicator connected to the rigid rod. The system is capable of measuring changes as small as a few thousandths of an inch over a baseline length of 10 to 30 feet. Movements of this magnitude are known to precede many backslope failures and serve as good early warning systems.

The inclinometer consists of a longitudinally grooved vertical tube installed in the ground through the depth where the potential for sliding exists (approximately 60 feet at the Seagate landslide). The tube is accurately and regularly monitored at appropriate time intervals to detect minute changes in the position of the tube, reflecting subsurface lateral movements. During shear key grading, the inclinometer was an inexpensive method of detecting the activation of those slide planes prior to back-cut slope failures.

Both the extensometer and inclinometer measurements indicated movement along the potential slide planes beneath the road during shear key excavation prior to backslope failure. They also defined approximate lateral limits of potential backslope failure.

Failures of Temporary Construction Cut Slopes

Several failures occurred in the temporary construction cut slopes during shear key excavation. All failures occurred in the 1977 rupture surface or its projection into the slope from previously activated slide debris. The primary cause of temporary cut slope failures was the necessary removal of lateral support during excavation for the shear key buttress. Locations most susceptible to instability which could endanger the neighboring properties were recognized, and recommendations for temporary shoring were made by Leighton and Associates. A system of frozen ground columns backed up by preparedness for installation of soldier piles was selected by the project contractor for shoring.

One backslope failure was of major proportions, extending almost to the easterly curb line of the road. On January 26, 1981, a portion of the upper frozen pile wall collapsed and the ground upslope of the system moved downward and outward from the road and into the buttress excavation (Figs. 24 and 25). This failure involved the reactivation of old slide material and structural fill that had been placed over the old slide materials by others. The excavated phase was temporarily backfilled to halt the movement of this slide mass, while a concrete and steel soldier pile wall was installed above the developing scarp (Fig. 20). Headward progression of the slide mass continued during shear key excavation but did not breach the soldier pile wall. Consequently, shear key excavation and buttress filling was continued on a dawn-to-dusk work schedule to complete the compacted buttress to a stabilizing level as quickly as possible.

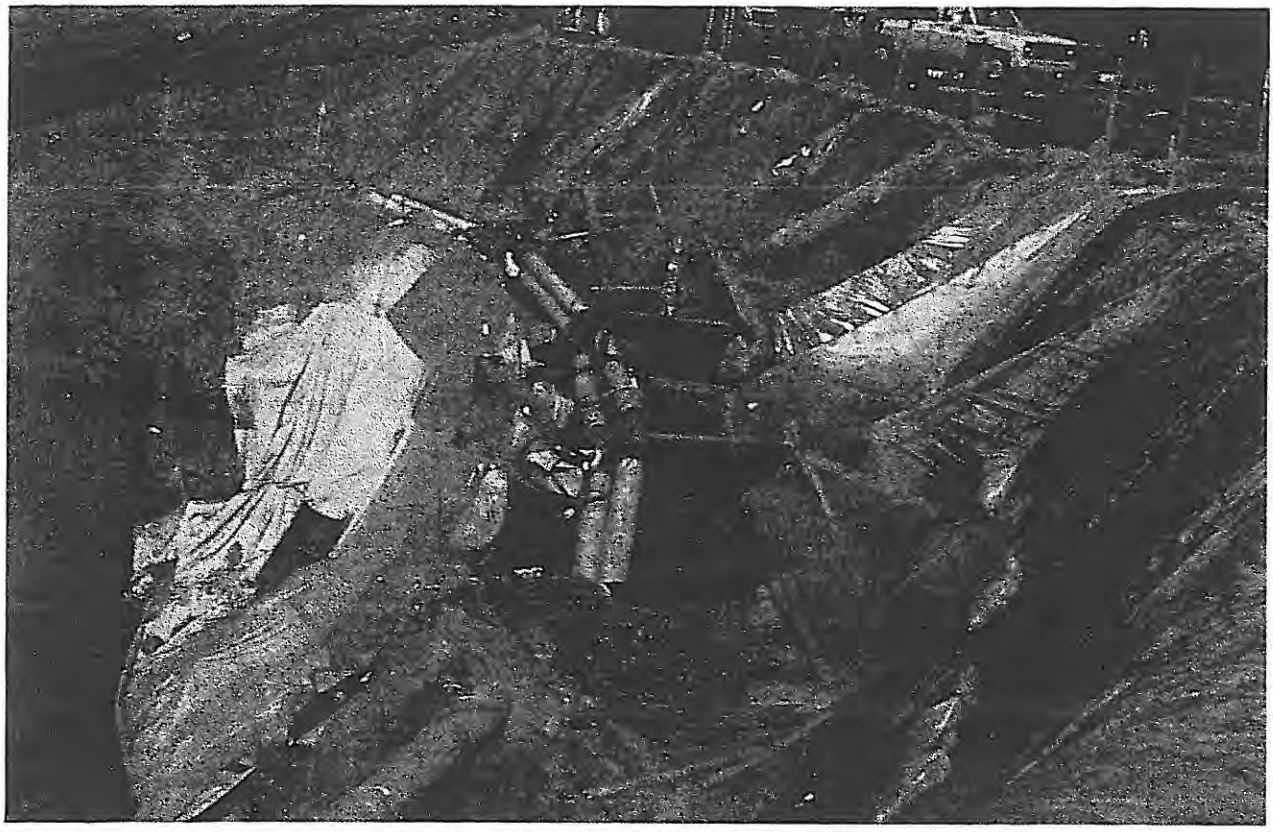

Figure 24. The upper freeze wall failed eventually but provided good temporary support for several months.

Figure 25. Failed frozen columns and freeze pipes of the upper freeze wall. These were found to be of large diameter and rock-hard in some areas and of small diameter and only partially frozen in other areas.

Temporary Frozen Ground Stabilization Measures

Temporary stabilization of the toe cut and a portion of the back-cut slope was attempted, utilizing a system of frozen ground piles. This unique method of temporary stabilization consists of steel casings installed into the ground on appropriate spacings and a specific coolant circulated inside the casings. Progressively, an increasingly larger column of frozen ground (earth materials with frozen pore moisture) forms around the steel pipes. Potentially, the individual frozen columns of earth materials can grow in diameter until they are bonded together as a continuous, solid frozen wall.

Each freeze pipe consists of 3-5/8-inch steel pipe (53 feet long in the upper pile wall and 40 feet long in the lower pile wall), with 1-1/2-inch PVC plastic tubing inside, and capped at the surface. Individual freeze pipes are interconnected and coolant (calcium chloride) is circulated under pressure from the refrigeration unit. The as-built locations of the frozen ground pipes are shown (Fig. 17).

During shear key excavation, both the upper frozen piles and lower freeze wall partially collapsed (Fig. 25). The lower freeze wall bent and failed on December 31, 1980. Excavation halted until a temporary steel soldier pile wall was installed within the excavation (Fig. 17). The upper freeze piles bent and later failed on January 26, 1981 (Fig. 24 and 25). Excavation again halted until a permanent concrete and steel soldier pile wall was installed above the slide scarp. Approximate locations of the upper (16) and the lower (48) freeze piles are shown in Figure 17.

The following three key factors are believed to have contributed to the failure of the frozen columns: (1) overestimation of thermal conductivity of earth materials, (2) insufficiency of soil moisture in some strata, and (3) presence of a high rate of seepage in other strata.

Temporary Soldier Pile Stabilization Measures

Temporary stabilization of a portion of the toe cut and a portion of the back-cut slope was necessary after collapse of the initial freeze wall stabilization. This was achieved by installation of soldier pile walls within the excavation opposite the lower freeze wall and east of the road adjacent to the curb. The soldier pile wall consisted of 34-foot-long steel H-beams (13W120) installed into the ground. Upon the decision to install steel soldier piles, actual installation began immediately. Drilling commenced in the late afternoon and continued throughout the night despite intermittent heavy rain. In less than 48 hours, the holes had been drilled, steel beams placed, concrete poured, and bond beams were being welded.

The lower steel soldier piles were installed January 5-8, 1981, east of the failed freeze pile wall on 5-foot centers. Each steel soldier pile was rooted a minimum of 5 vertical feet below the basal rupture surface in shale and siltstone

bedrock and backfilled with local sands. A grade beam and terminal, lateral braces were welded near the top of the soldier pile wall to maximize strength. An additional H-beam was buried on the beach to act as a dead man. Two 5/8-inch cable tiebacks were connected to the middle of the welded grade beam and the dead man for added support. Wooden planks (6 x 12 inches) were inserted in the webbing between successive H-beams to retard sand flow into the excavation during shear key excavation (see Fig. 20). The soldier pile wall allowed vertical toe cut slopes into bedrock parallel to the pile wall for the deepest phases of shear key excavation. When the level of compacted structural fill had risen to a safe elevation, the dead man, cables, grade beams, and lateral supports were removed and all but one soldier pile beam were extracted from the partially backfilled excavation. The majority of wooden planks were removed as the compacted fill rose; however, some of the planks were not retrievable.

The upper soldier pile wall was installed January 27-28, 1981 along the eastern curb of the road. The 3-foot-diameter concrete reinforced soldier piles were on 6-foot centers with welded grade beams between the tops of individual soldier piles to maximize the integrity and effectiveness of the wall. The soldier pile wall prohibited additional headward progression of old slide debris, allowing excavation of the expanded shear key buttress and placement of the compacted structural fill.

Subdrain System

The subdrain system consisted of a main subdrain and a series of collector french drains. The main subdrain was installed near the base of the backslope in undisturbed bedrock below the projection of the pre-1977 basal rupture surface. It consisted of a perforated 8-inch ABS pipe laid in a 36-inch-wide trench with a minimum of 18 inches of Class 2 permeable material both above and below the pipe. The main subdrain is curved in plan view and drains to both ends. At these two points, terminal sections of solid 8-inch ABS drain the system to the toe of the buttress. A minimum flow gradient of 4 percent is maintained throughout the system to drain water to the riprap. At 30-foot intervals, french drains radiate from the main subdrain up the backslope. They consist of 24-inch trenches excavated into either bedrock or compacted structural fill with a minimum 2-foot thickness of Class 2 permeable material. Two radial extensions were added at the center of the main subdrain system to drain the extended back-cut slope generated during back-cut slope failure. The radial extensions consist of perforated 8-inch ABS pipe laid in a 24-inch trench with a minimum of 12 inches of Class 2 filter material above and below. The radial extensions are installed in compacted structural fill with french drains at their distal termini, installed as described above. In addition, the french drains are interconnected at approximately their mid-height on the back-cut slope by auxiliary drains. The auxiliary drains consist of 24-inch trenches excavated into bedrock with a minimum 2-foot

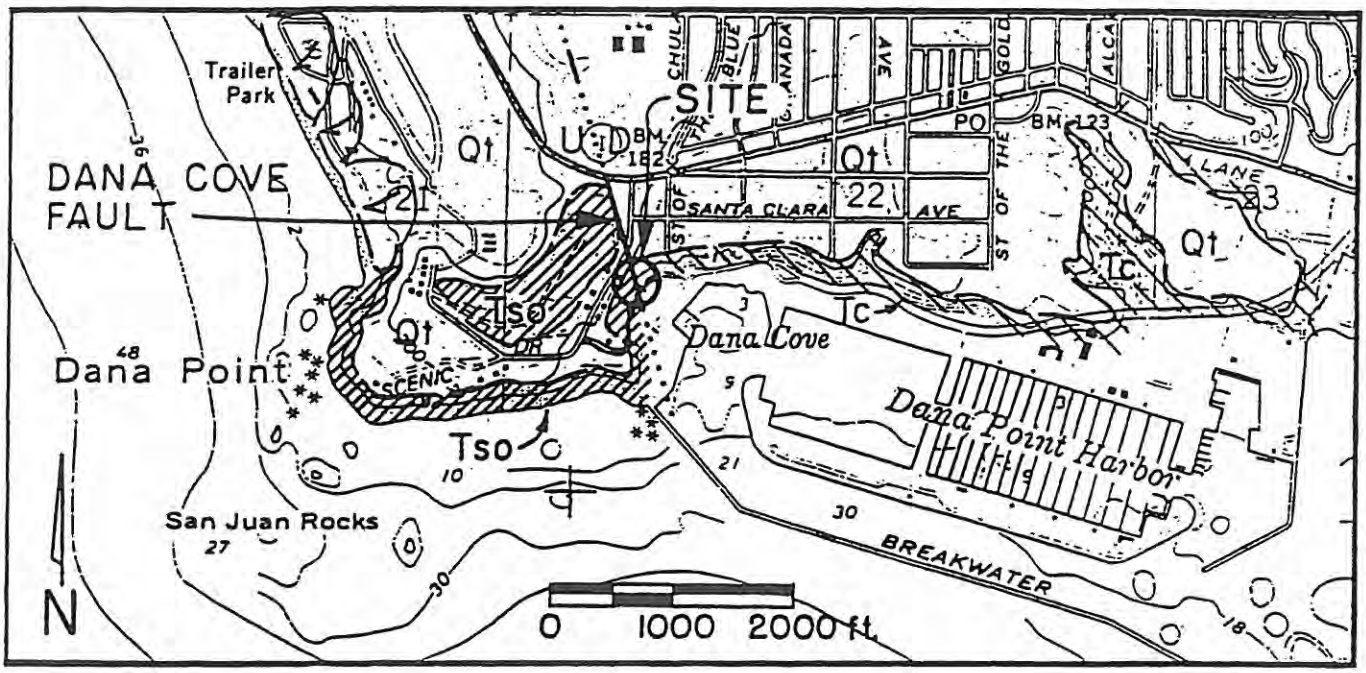

Figure 26. Site Location Map

thickness of Class 2 filter material. From the midpoint, the auxiliary drains maintain a minimum flow gradient of 4 percent toward the interceptor french drains.

A second subdrain system consisted of a nonperforated 4-inch ABS pipe installed in compacted structural fill along the property line of Lots 22 and 23. This subdrain system collected effluent from two existing 4-inch subdrain systems east of the road and drained at the midslope bench drain.

Cove Road Landslide, Dana Point

Introduction

In 1980, a wedge failure in a nearly 150 foot high, 60 degree sea cliff at Dana Point Harbor, California (Fig. 26) undermined a portion of a restaurant on the top of the bluff. Slide material blocked Cove Road, the county road, at the toe of the slope, blocking access to the western end of the harbor and marina. The complicated geologic conditions and a twenty-two million dollar lawsuit filed by the owner of the restaurant required use of sophisticated geotechnical stabilization measures while the restaurant continued to serve its customers. The landslide has been summarized in Kerwin (1989).

The Investigation Phase:

- The limited working area, access problems, and steep terrain necessitated the use of cranes to position drilling and excavation equipment
- The potential failure block extended approximately 40 feet beneath the restaurant structure (Fig. 27).
- The slide block consisted of a weakly cemented, massive silty sandstone with an average unconfined compression strength of approximately 100 psi.
- Shear values of the weaker siltstone bed had an angle of internal friction of 28 degrees and a cohesion of 300 psf. The clay gouge fault and rupture surface clays had an angle of internal friction of 14 degrees and a cohesion of 350 psf.
- Stability analyses of the critical wedge using strength parameters computed from the original failure geometry (i.e., $\emptyset = 28°$ and c = 230 psf) verified the near equilibrium condition of the critical failure wedge. Construction of a restraining structure of adequate size and orientation to apply the rock anchor stabilizing loads necessitated trimming portions of the sandstone scarp to a 1:1 slope. The driving and resisting force for the trimmed configuration of the potential failure block were assumed equal (F.S. = 1.0). In accordance with local practice, a factor of safety of 1.5 against sliding was required for stabilization. Therefore, additional resistance of 1650 kips was required.

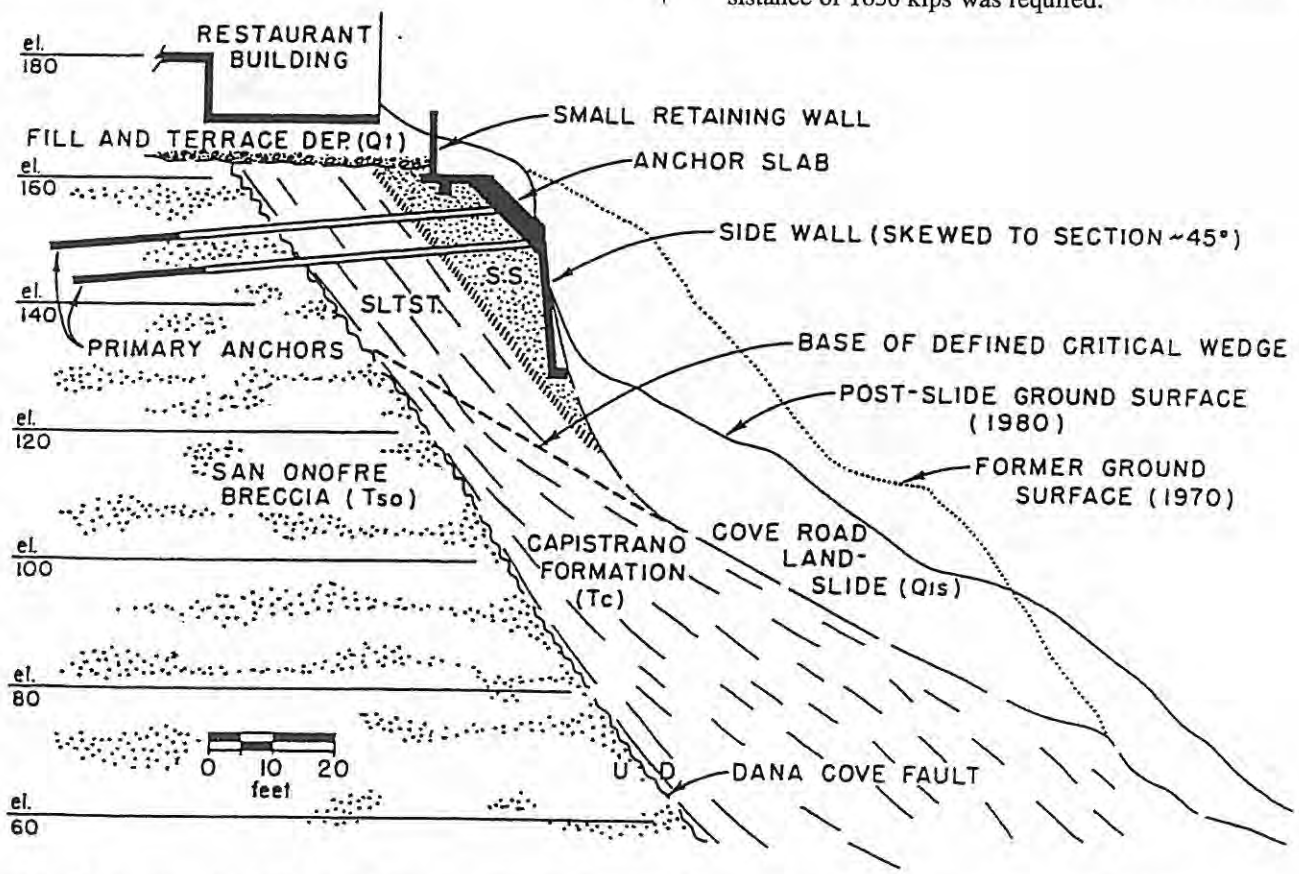

Figure 27. Geologic section of the critical headscarp wedge viewed looking northeast, perpendicular tot he alignment of the primary anchors. (From Kerwin, 1989).

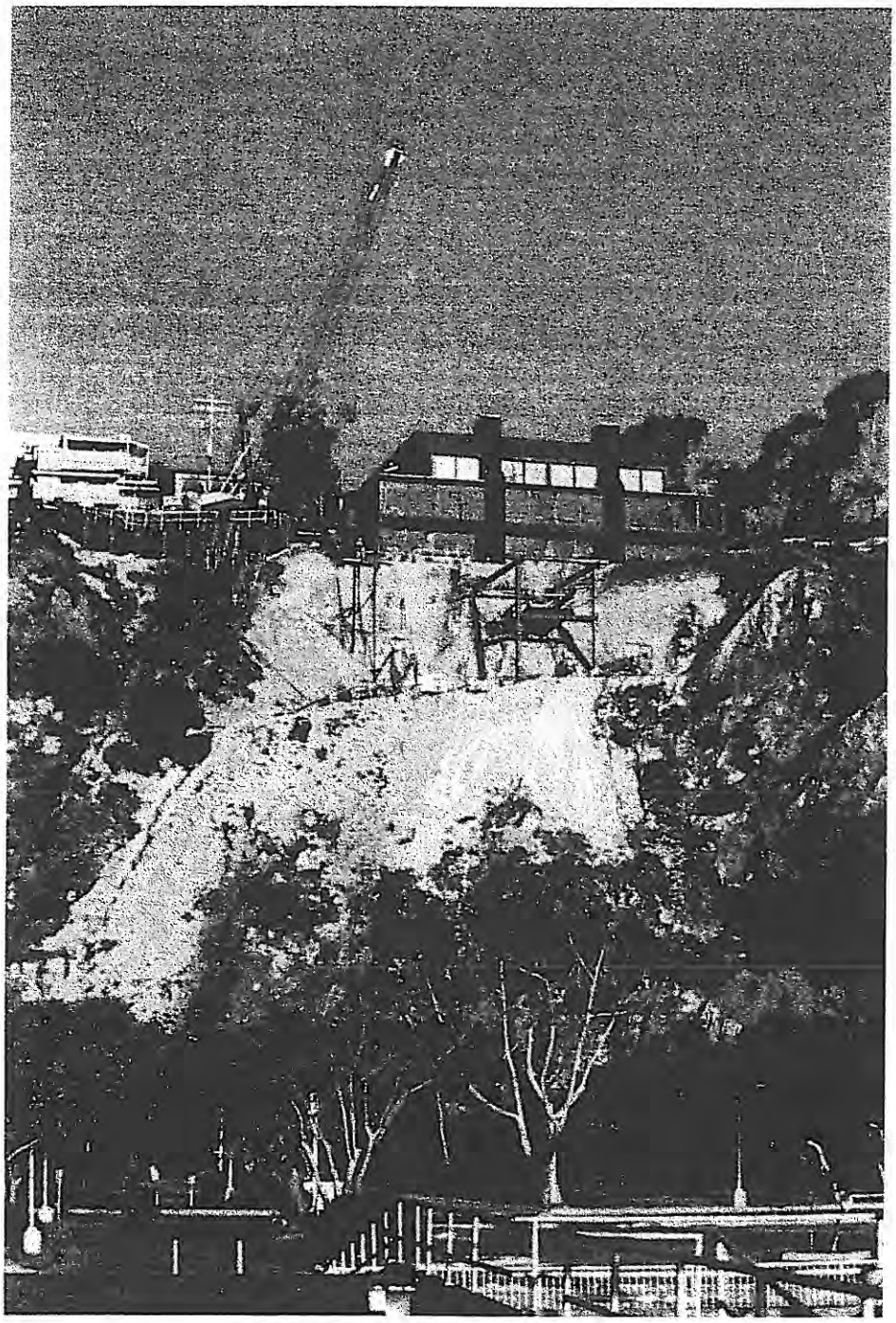

Figure 28. View from the Dana Cove Pier. Construction of a pile supported, temporary crane pad was necessary to provide access and support for drilling and other construction equipment on the site. the 16 primary anchors were drilled from a wooden deck supported by an adjustable steel frame (center of photo). Drilling of the 18 secondary anchors was accomplished from a crane-held platform locked in place with chain binders on shallow, temporary deadmen (not shown). Phase I Construction -January, 1984. (Photograph from Kerwin, 1989).

The Monitoring Phase:

The restaurant owners desired to continue at full capacity during the repair of the failure even though patrons at a few tables appeared to be situated in mid-air. To conclude, a catastrophic failure and automatic alarm system consisting of borehole monitoring system was installed beneath the restaurant. Constant monitoring was needed to evaluate minor movement during construction and to mitigate life threatening smaller failures. Up to 0.06 inch of slopeward displacement was measured on two separate occasions following heavy rains and during the construction of the key structural elements of the repair. No significant damage, deaths or serious injuries occurred during this three year landslide repair.

The Construction Phase (September 1983 to August 1986):

The construction phase was divided into two parts: 1) the repair of the head scarp area; and 2) the repair of the toe of the slide. Construction site access was difficult, because there was virtually no right of way except for foot traffic, a temporary pad for a 65 ton capacity friction crane had was constructed (Fig. 28). Six steel "H" beam columns were built to support the outriggers of the crane.

- The headscarp of the slide had to be trimmed and laid back prior to the construction of any supporting elements. A small dozer and rubber tired backhoe were lowered onto the head of the slide up by the crane. This work had to be done carefully so as to not undermine the restaurant. Much of the work was done by hand and pneumatic clay spades.
- Sixteen anchors with design modes of 175 kips each drilled at 5 degrees from the horizontal were installed from a portable platform lowered and held in place by the crane.
- The length, relatively high loads, and difficult access conditions favored steel cable anchor tendons rather than solid rods. Six 0.6-inch diameter tendons were required to accommodate the 175 kips design load for each primary anchor. Loads of 40 to 105 kips for the secondary anchors necessitated installation of two to four tendons per anchor.
- The first and, possibly most important, is a "side wall" constructed to adjoin the south edge of the primary anchored slab. Supported by anchors bonded in Capistrano Formation sandstone, this wall provides confinement and erosion protection to foundation rock underlying the anchor slab. A second wall covers the headscarp along the exposed fault plane. This "headscarp wall" is supported by anchors penetrating the breccia in a fashion similar to that of the primary system. The "headscarp wall" and a "small retaining wall" to the east provide access around the south corner of the restaurant and prevent possibly damaging degradation of the foundation materials. Open, unreinforced joints were constructed between each of the four elements of the restraining structure to accommodate possible elastic deformation of the rock from anchor loads. The construction joints were not filled and sealed until all anchors had been tested, approved and locked off at the specific loads.
- The aggregate design capacity of the 34 anchors installed for the restraining structure was 2,010 tons. However, the applied stresses are greater because anchors were tensioned and locked off at loads equivalent to 120 percent of the design working capacity to compensate for possible long term losses. The potential for unacceptable future load loss was evaluated prior to final tensioning by routine proof testing of all anchors to 150 percent of design load. Selected anchors were also "lifted off" to determine whether residual loads after selected time intervals were within specified limits (Littlejohn, 1981).
- Surficial stability of the clay siltstone had to be achieved by driving shallow rebar anchors into the material and covering the surface with an interim coating of shotcrete.
- The San Onofre Breccia bedrock was difficult to drill and very abrasive. To help minimize this hard drilling, a larger drill rig had to be utilized and the drilled holes had to be provided with a casing in order to maintain the alignment of the hole and to be able to purge the hole.
- Ultimately, a standard horizontal boring machine with a variable jacking capacity up to 75 kips was used to drill the primary anchor holes. Heavy duty continuous flight auger and a specially fabricated rock drilling bit with retractable "wing" cutters excavated material immediately ahead of the casing, including annular clearance. Casing was advanced the full depth of the hole and was subsequently pulled back approximately 23 feet for placement of the anchor assembly (2 to 3 feet for a packer and the remaining 20 feet for bonding). All anchor borings were initially drilled "dry" in accordance with limitations established during settlement conferences before construction. Subsequent to anchor failures during load testing, holes were redrilled through the casing using essentially the same equipment adapted to rotary wash drilling methods and hardware.

The relatively high jacking forces utilized to drill and advance the casing necessitated design and erection of a larger, stronger drilling structure which incorporated an adjustable platform. A temporary framework of steel "H" beams was constructed above the primary anchor slab. Bearing support was provided by a single pile cast in bedrock at the toe of the critical wedge. Lateral resistance to the jacking force was attained by anchoring the uppermost steel members of the framework to the concrete retaining wall footing cast in sandstone at the top of the anchor slab. Analyses indicated the jacking force applied by the drill rig should be limited to 20 kips to maintain design stability.

- Because of the corrosiveness of the environment, double corrosion protection was specified for the anchor tendons. In addition, the tendons had to be encapsulated in corrugated polyethylene type.
- Ground water and grouting problems necessitated replacing some anchors. It was found that separate feed lines to both the inside and outside of the anchor capsules were needed. It was found that packer assemblies failed to seal out minor accumulations of ground water seepage.
- The final phase of repair was the construction of a 45 foot high, precast concrete crib type retaining wall at the toe of the slope.
- Crucial aspects of this phase of the project included removal and recompaction of the landslide debris and installation of an extensive subsurface drainage system. This portion of the slope restoration work could not have been safely accomplished without prior stabilization of the bluff top.

The entire project required approximately three years to complete and Cove Road was officially re-opened in August 1986.

ACKNOWLEDGEMENTS

The authors wish to thank Scott Kerwin and Jack Eagen of Moore and Taber, Anaheim, California, who kindly provided the photographs of the Cove Road landslide and allowed us to use their report.

REFERENCES

Clark, B.R., 1986, The Big Rock slide, Malibu, California: in Ehlig, P.E., (Compiler), Landslides and landslide mitigation in southern California, Geol. Soc. America, Cordilleran Section Guidebook, p. 71-75.

Kerwin, S.T., 1989, Sea cliff stabilization using long rock anchors: in Cann, L.R., and Steiner, E.A., (compilers), Engineering geology along coastal Orange County: Assoc. of Engineering Geologists, Southern California Section Guidebook, p. 103-116.

Leighton, F.B., 1969, Final geologic report on the general plan study for the City of Laguna Beach.

_____, 1969, Engineering geologic report of storm damage, City of Laguna Beach.

Leighton, F.B., Cann, L.R., and Poormand, I., 1986, Emergency repair operations for the Bluebird Canyon landslide of October 2, 1978: in Ehlig, P.E., (Compiler), Landslides and landslide mitigation in southern California, Geol. Soc. America, Cordilleran Section Guidebook, p. 35-41.

_____, 1984, Verde Canyon landslide, San Clemente, Orange County: Calif. Geology, Calif. Div. Mines and Geology, August.

Leighton and Associates, 1975, Background data and geotechnical information for the seismic safety and safety element: Presented to the City of Laguna Beach.

Littlejohn, G.S., 1981, Accepted criteria for the service behavoir of ground anchorages: Ground Engineering, v. 14, 26-29, Brentware England, Foundation Publishers Ltd.

Morton, P.K., and Others, 1973, Geo-Environmental maps of Orange County, California: Calif. Div. Mines and Geology Preliminary Report 15.

Rex, Robert W., 1972, Origin of the salt of the Imperial Valley and surrounding watershed areas: Report for Bureau of Reclamation Contract #14-06-300-2258, University of California at Riverside (IGPP-UCR-72-33), 38 p.

Tan, S.S., 1976, Geology and engineering geologic aspects of the Laguna Beach Quadrangle, Orange County, California: Calif. Div. Mines and Geology Special Report 127.

Varnes, D.J., 1978, Types of slope movements: Transportation Research Board Committee A2T58, from Spec. Report 176, Chapt. 2.

Vedder, J.G., and Others, 1957, Geologic maps of the San Joaquin Hills-San Juan Capistrano Area, Orange County, California: U.S. Geological Survey Oil and Gas Investigations Map OM 193.

Ziony, J.I., and Others, 1974, Preliminary map showing recency of faulting in coastal southern California: U.S. Geological Survey Miscellaneous Field Study Map MF 585.

EVOLUTION, MECHANICS AND MITIGATION OF THE PORTUGUESE BEND LANDSLIDE PALOS VERDES PENINSULA, CALIFORNIA

Perry L. Ehlig
Department of Geological Sciences
California State University
Los Angeles, CA 90032
and City Geologist
City of Rancho Palos Verdes

ABSTRACT

The 260-acre Portuguese Bend landslide is part of a two-square-mile Pleistocene megaslide on the south flank of Palos Verdes Peninsula. Sliding occurs in weak bentonite beds near the Portuguese Tuff in the middle Miocene Altamira Shale member of the marine Monterey Formation. The megaslide occupies a seaward plunging structural trough in which bedding undulates but dips an average of 7 degrees in the direction of slide movement. The megaslide originated about 120,000 years ago when the sea occupied a marine terrace whose shoreline angle is 140 feet above sea level. Sliding probably started on an uphill ramp where beds dip 15 to 20 degrees seaward and propagated downhill to the beach where the slide base was as much as 200 feet below sea level. The toe propagated to the surface by folding and subsequent thrusting. The head of the megaslide migrated uphill by arcuate slumping on the west and sliding down a west-dipping ramp on the east. The megaslide is broken into a complex of subslides controlled by undulations in the underlying bedrock. Sliding was probably promoted by ground water perched above the Portuguese Tuff in the main part of the slide and by wave erosion and artesian pressure beneath the tuff near the coast.

The megaslide's entire coastal part has reactivated since the start of residential development in this area. The Portuguese Bend landslide reactivated in 1956 when Los Angeles County placed road fill along its head. Its unabated movement destroyed 130 of 160 homes within it. Part of it has moved 800 feet. The 80-acre Abalone Cove landslide started in response to high rainfall in 1978 and part of it moved 30 feet. Several homes were damaged before it was stabilized. The 50-acre Klondike Canyon landslide began in 1980 but moved less than three feet and caused no major damage. The Abalone Cove and Klondike Canyon landslides were stabilized by removal of ground water and control of surface drainage. Mitigation was paid for by establishment of Geologic Hazard Abatement Districts, the first two in California.The Rancho Palos Verdes Redevelopment Agency was established in 1984 to stabilize the Portuguese Bend landslide. A plan was developed to control the slide in phases starting near the head

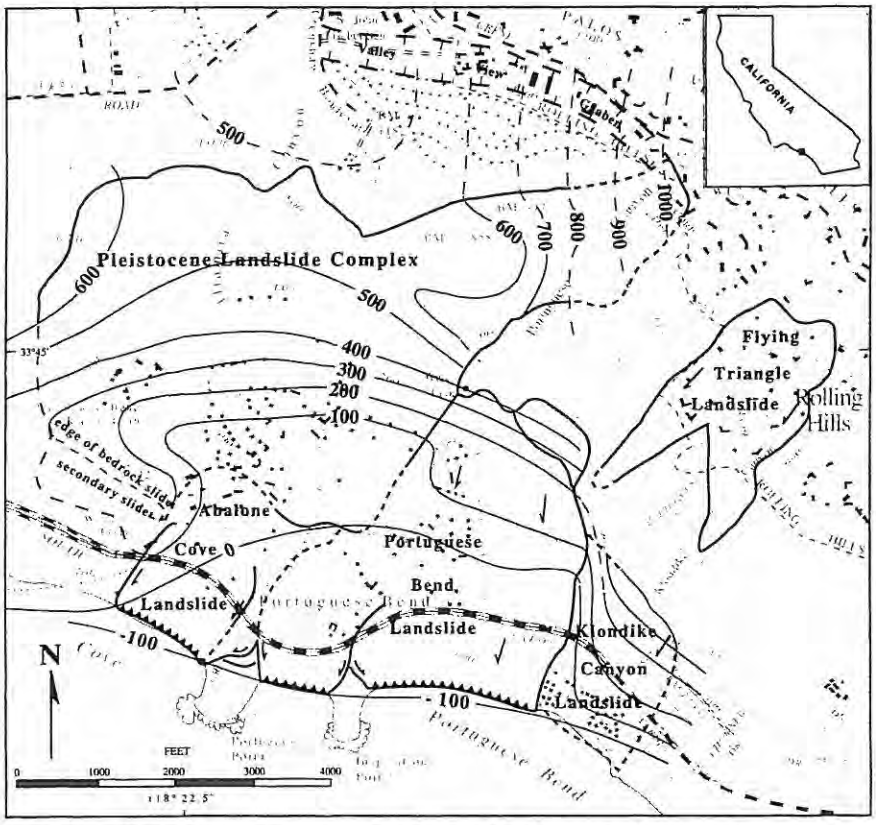

Figure 1. Map showing the Pleistocene landslide complex and the Portuguese Bend, Abalone Cove, Klondike Canyon and Flying Triangle landslides. Structure contours in feet are on the base of the Portuguese Tuff.

and working seaward. Control measures include pumping ground water from wells, restoring surface drainage, and moving earth from where it exerts excess driving force to where it exerts a net resisting force. Because low permeability made ground water removal slower than anticipated, grading was increased to immediately improve stability. The landward part of the slide appears stable and the central part is nearly stable. The seaward part remains active because of wave erosion. Gabions were installed along the toe for temporary shoreline protection but have broken because of percussion and corrosion. A rock revetment and toe berm are needed for permanent stabilization. The project has cost about $3,000,000 to date. After stabilization is complete, undeveloped areas will probably be used for a golf course and public recreation.

HISTORICAL BACKGROUND

The Los Angeles metropolitan area contains few settings more attractive for residential development than the large topographic amphitheater overlooking Portuguese Bend and Abalone Cove on the south flank of the Palos Verdes Peninsula. This area has a generally mild, sunny, smog-free, marine climate and an excellent view of the Pacific Ocean and Catalina Island, located 23 miles offshore. However, its gently rolling terrain, so ideal for residential development, is within the two-square-mile Portuguese Bend landslide complex (Fig. 1).

Development of Portuguese Bend began in 1946 even though the slide complex was recognized by Kew (1926) and Woodring and others (1946). The landslide was ignored because building codes did not require geologic investigations and, even if the landslide had been investlgated, its existence is unlikely to have stopped development. Stability analyses at that time would have shown the area was stable because laboratory tests would have yielded much higher shear strengths for bentonite than the 6^{o} angle of internal friction and 75 psf cohesion obtained by back calculations on the Portuguese Bend landslide. Even today, most test results are too high.

While homes were being built at Portuguese Bend, Los Angeles County was extending Crenshaw Boulevard southward from the crest of the peninsula to Palos Verdes Drive South. In August 1956, cracks appeared in road fill as much as 70 feet thick, which was being placed across the northeast corner of the ancient landslide. Within a month, the cracks propagated westward and seaward to define the part of the Portuguese Bend landslide which moves into Portuguese Bend. During the next several months, movement progressed westward to include the segment of the Portuguese Bend landslide which moves into the cove between Inspiration Point and Portuguese Point. The fully developed slide covered 260 acres and contained about 160 homes within it. All but 30 of the homes were ultimately destroyed.

Studies were performed to determine the feasibility of stabilizing the landslide. Two plans were suggested, one of which involved the building of a buttress along the toe of the slide. This plan required working within the ocean and was rejected because of cost. The other plan involved the installation of shear pins near the toe of the slide where the slide mass was relatively thin. Although this plan received poor reviews, 23 reinforced concrete shear pins, each 20 feet long, were installed. All failed by plucking, tilting or shearing. The unearthed remains of several shear pins are visible in the surf zone at low tide (Fig. 2).

Based on our current knowledge, sliding could not have been stopped solely by installation of shear pins along the toe of the slide. Even if enough pins had been installed to stop movement along the basal slip surface, the thrusting action of the slide would have developed a new slide base above the tops of the shear pins.

In 1961, a legal precedent was set when Los Angeles County was held responsible for starting the slide and, by reason of inverse condemnation, was found liable for the destruction of about 130 homes. In an effort to protect itself from additional liability, Los Angeles County declined further involvement with the slide. Homes which might otherwise have been condemned were allowed to remain in the slide and be repaired at the discretion of the homeowner.

In 1973, the City of Rancho Palos Verdes was incorporated. The Portuguese Bend landslide was included within its boundaries. At the time of incorporation, the city agreed that arrangements within the slide area would remain status quo and that no action would be taken to stabilize the slide. However, the situation was altered by an unusually wet period beginning in 1978.

In April 1978, following the rainiest winter since 1890, the Abalone Cove landslide adjacent to Portuguese Bend began moving within an 80-acre area containing 25 homes. The City of Rancho Palos Verdes took two actions in response to the slide. First, it placed a building moratorium on the entire area containing the Portuguese Bend landslide complex pending investigations to determine which parts, if any, were sufficiently stable to permit development. Second, it commissioned a study to determine what could be done to stop the Abalone Cove landslide.

The study of the Abalone Cove landslide was supervised by the writer, and found a high water table throughout the slide mass. It was anticipated that the slide could be stabilized by removing ground water from as few as six wells. The Abalone Cove Homeowners Protective Association (ACHPA) was formed to install the wells and a pipeline to transport the water to the ocean. The dewatering system was installed using $250,000 in donated funds and production started on March 2, 1980, near the end of the third rainiest winter since 1890. The rate of slide movement abruptly slowed in response to dewatering. High rainfall during the 1982-83 rainy

Figure 2. Reinforced concrete caissons exposed by wave erosion at the toe of the Portuguese Bend landslide in 1981. Pins were installed through the base of the landslide with their midpoints 42 feet below sea level in 1957.

season caused a slight resurgence but only creep has occurred since 1985.

In the meantime, the City of Rancho Palos Verdes sought and received legislation that permitted the establishment of Geologic Hazard Abatement Districts (State of California Public Resources Code, Division 17, Sections 26500 through 26600). Such districts can abate geologic hazards by taxation of the benefiting properties. In 1981, the Abalone Cove Landslide Hazard Abatement District (ACLAD) was established as the first Geologic Hazard Abatement District in California. It includes all properties within the Abalone Cove landslide and all properties within the inactive Portuguese Bend landslide complex located up slope from the active landslide. ACLAD, which took over ACHPA's abatement facilities and activities, has worked well to this time.

Another important event was the filing of a lawsuit by properties owners (Horan et al. vs. County of Los Angeles et al.). Funds were requested to permanently stabilize the Abalone Cove landslide. A panel of experts (David Cummings, Perry L. Ehlig, Richard T. Frankian, John F. Mann, Richard L. Meehan and James E. Slosson) was established to evaluate the feasibility of permanently stabilizing the Abalone Cove landslide and to make recommendations regarding methods and costs of stabilization. In December 1984, the Panel concluded that permanent stabilization was possible and could be accomplished for about ten million dollars. In the subsequent settlement, Los Angeles County agreed to provide ten million dollars in low interest bonds to pay for stabilization of the Abalone Cove landslide and an additional five million dollars in bonds to aid in the stabilization of the Portuguese Bend landslide. The previously established technical panel was retained to recommend and oversee remedial work within the Abalone Cove landslide. An Improvement District has been formed to handle the bond indebtedness. The bonds will be repaid from the tax increment obtained from appreciation of property values as a result of slide abatement.

While dewatering was proving successful in 1980 in abating the Abalone Cove landslide, two other landslides began to move. One was the 50-acre Klondike Canyon landslide adjoining the east side of the Portuguese Bend landslide. Although the area was thought to be underlain by stable bedrock, investigations demonstrated it was an ancient slide whose maximum displacement was only a few tens of feet. In May, 1981, artesian water burst forth from a hole being drilled to install a slope indicator near the toe of the slide. The hole was converted to an artesian dewatering well and became the main method of abating the slide. The Klondike Canyon Geologic Hazard Abatement District was formed to handle abatement activities and is still operating. A survey monument adjacent to the Portuguese Bend slide has moved only 2.5 feet since it was installed in 1957; most of the movement occurred between 1977 and 1981. Another monument near the center of the slide has only moved 1.6 feet since it was installed in 1956. The slide has moved no more than 0.2 foot since 1981 and no homes have been lost because of the movement.

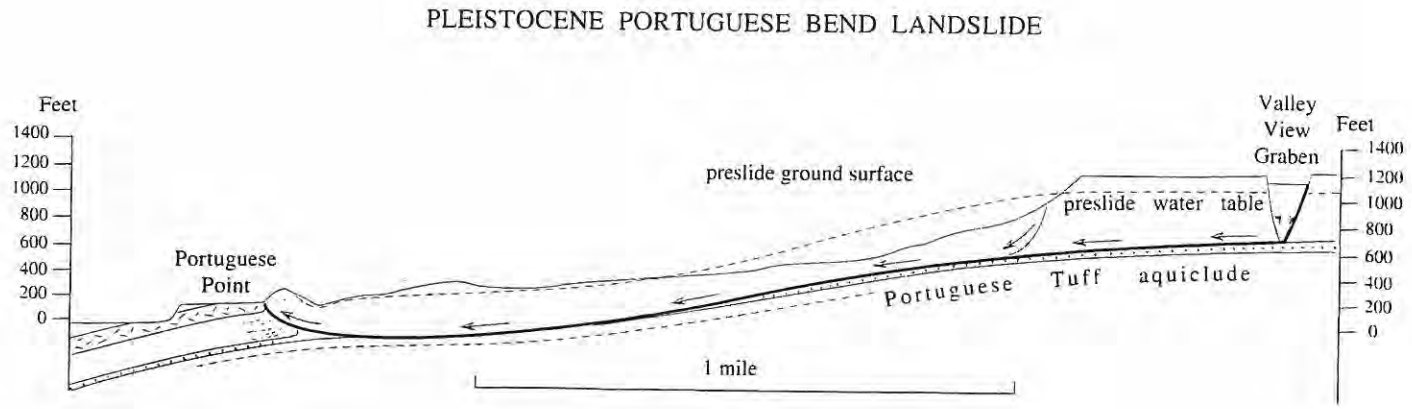

Figure 3. Vertical cross section through the Pleistocene landslide complex showing Portuguese Tuff at slide base and conjectured position of preslide ground surface and water table.

The Flying Triangle landslide also began moving in 1980, initially within an area of 5 acres in the City of Rolling Hills. In late 1983, movement expanded to an area of nearly 90 acres. The down slope part of the slide splits in an inverted V-shaped pattern at the up slope edge of a stable hill called "Flat Top" (Fig. 1). One branch moves southwest into Paintbrush Canyon. The other branch moves south towards Klondike Canyon. Its base passes beneath the bottom of Klondike Canyon to the east of Flat Top but rises and uplifts into the canyon further south. The down slope parts of both branches are in the City of Rancho Palos Verdes. The Flying Triangle landslide is a reactivated ancient slide but is not physically a part of the Portuguese Bend landslide complex. The only abatement activity consists of two horizontal drains installed by the City of Rancho Palos Verdes in order to relieve artesian pressure at the toe of the Klondike Canyon branch.

Starting in 1978, above average rainfall caused a large increase in the rate of movement within the Portuguese Bend landslide. High rates of movement lasted until the start of remedial grading in October 1986. For example, survey monument R-1, located in the east central part of the slide, moved 237 feet horizontally during the 20 year period from October, 1956, to October, 1976. But it moved 382 feet horizontally in the 10 year period from October, 1976, to October, 1986. The accelerated movement greatly increased the cost of repairing the 0.8 mile segment of Palos Verdes Drive within the slide. Prior to 1978, the city spent an average of less than $40,000 per year repairing the road. During the period from 1983 to 1986, the average cost was $250,000 per year and consumed most of the city's total road maintenance budget. This, and the potentially adverse effect of the Portuguese Bend slide on the stability of the slides on either side of it, provided the incentive to evaluate the feasibility of abating the Portuguese Bend landslide. Clearly, the city would benefit if the slide could be slowed or stabilized at a reasonable cost. Success in abating the Abalone Cove landslide gave hope that stabilization was feasible.

During the summer of 1983, I analyzed available data on the Portuguese Bend landslide to learn as much as possible about its mechanics and potential methods of stabilizing it. The results of my study suggested that stabilization of all but the coastal part of the slide could be achieved at a modest cost by removing ground water, reestablishing surface drainage, and moving earth from areas where it produces a high driving force to where it would produce a neutral or negative driving force. At the request of the city, the data was reviewed by a volunteer panel of eighteen geotechnical experts, most of whom had extensive experience in the Palos Verdes Peninsula. The group included several geotechnical engineers, a specialist in ground water geology and a coastal engineer. The panel divided into subcommittees to make specific recommendations on things that might be done to improve stability. The panel concluded that stabilization appeared feasible but more data were needed, specifically a current topographic map and ground water information.

In 1984, the city funded the work requested by the technical panel. It also established the City of Rancho Palos Verdes Redevelopment Agency to carry out the stabilization effort. The City Council serves as the agency's Board of Directors and the agency's boundaries coincide with those of the Landslide Moratorium Area. Thus began the effort to stabilize the Portuguese Bend landslide. The city provided about $200,000 to start the project. A $2,000,000 grant from the state has covered the cost of most grading and additional funds have been provided by the city and small grants to the city. Total expenditures to date approach $3,000,000.

GEOLOGIC SETTING

The Palos Verdes Peninsula is a northwest-trending domical ridge, 9 miles long and up to 5 miles wide. Its crest has gently rolling topography at elevations ranging from 1480 to 1100 feet above sea level. Below this upland, remnants of a flight of Pleistocene marine terraces ring the peninsula and demonstrate it was an island during most of its geomorphic evolution. The peninsula is currently bounded by the Los Angeles coastal plain to the north, by Los Angeles Harbor on the east, and by the Pacific Ocean on the south and west.

The peninsula's shape reflects its Quaternary uplift as a doubly plunging anticline within the hanging wall of the southwest dipping Palos Verdes fault. Wells drilled for oil have established the subsurface position of the Palos Verdes fault along the northeast margin of the peninsula but the fault has not been located at the surface and may not penetrate late Quaternary deposits.

The Mesozoic Catalina Schist forms the core of the Palos Verdes anticline. Schist crops out near the center of the peninsula and is at shallow depth beneath much of its northeast flank. In early middle Miocene, the schist formed an irregular, southwest-sloping sea floor on which the Monterey Formation was deposited. The Monterey Formation is divided into the middle Miocene Altamira Shale, the late middle to early upper Miocene Valmonte Diatomite and the late upper Miocene to early Pliocene Malaga Mudstone. The Altamira Shale is further divided into the tuffaceous, cherty and phosphatic members. The tuffaceous member is of special interest because it contains weak bentonite beds that host the slip surfaces of most large landslides within the peninsula, including the Portuguese Bend landslide complex.

The tuffaceous member comprises all but the uppermost part of the Altamira Shale and represents the infilling of a tectonically formed submarine basin centered south of the peninsula. Its thickness increases in a distance of four miles from as little as 300 feet in the area of schist outcrops in the northeast part of the peninsula to about 4000 feet where penetrated by an exploratory oil well at Long Point to the west of Abalone Cove. It includes cherty and phosphatic shale of largely biogenic origin; siltstone and fine-grained sandstone derived from Catalina Schist and lessor volcanic sources; basalt in the form of pillows, sills and irregularly shaped intrusions; tuff turbidite, and ash fall and debris flow tuff which are largely altered to bentonite; and dolostone formed by diagenesis and geothermal activity. Much of the member contains thin parallel beds giving the false impression that beds should be continuous over long distances. Most beds lens out over short distances and parts of the lithologic sequence, in units as much as 100 feet thick, are affected by syndepositional slumping and debris flow.

In the vicinity of the Portuguese Bend landslide complex, the Portuguese Tuff is the only easily recognized stratigraphic unit within the tuffaceous member. It occurs about 450 feet below the top of the tuffaceous member and consists of about 60 feet of irregularly bedded tuff that appears to have been deposited by turbidity currents during a single eruptive event. Most of it was converted to a nearly pure waxy bentonite. The Portuguese Tuff functions as a zone of low shear strength and as an aquiclude. The base of the Portuguese Bend landslide complex ranges from 50 feet above the top of the tuff to the top of the tuff in most places. Except, along the coast it is near the base of the tuff in the Abalone Cove and Portuguese Bend slides and 70 feet below the tuff in the Klondike Canyon slide.

The cherty member of the Altamira Shale overlies the tuffaceous member along the head of the Portuguese Landslide complex and occurs in rotational slump blocks within the central and western parts of the complex. It is about 50 feet thick and consists of thin bedded chert and porcelanite derived from diatomite. A zone of distinctive chalcedony concretions, unique to this member, makes it easy to identify the cherty member wherever it crops out within the peninsula. The cherty member was deposited across a flat sea floor after cessation of local volcanism and tectonism.

The phosphatic member of the Altamira Shale and the Valmonte Diatomite are present along the head of the landslide complex and highest slump blocks but are not present within the main body of the complex.

During Pleistocene uplift, wave erosion removed the upper part of the Monterey Formation from most of the Palos Verdes Peninsula. The Malaga Mudstone was removed from all but the northern margin. Erosion was greatest along the peninsula's seaward-facing south flank. As a result, the tuffaceous member crops out across the entire south flank. Bedding within the tuffaceous member dips seaward subparallel to the slope of the ground surface. This creates conditions suitable for translational sliding along weak bentonite beds. In addition, wave erosion cut notches into the south flank creating steep wave-cut cliffs in which beds were inclined unsupported out of slope, further favoring formation of landslides.

For a comprehensive coverage of the geology of the Palos Verdes Peninsula refer to Woodring and others (1946). Rowell (1982) presents a detailed chronostratigraphy of the

Monterey Formation; Conrad and Ehlig (1983) provide details on the lithostratigraphy of the Monterey Formation, and Bryant (1987) provides recent information on the marine terraces and Quaternary tectonics of the peninsula.

PORTUGUESE BEND LANDSLIDE COMPLEX

Setting

The Portuguese Bend landslide complex occupies a broad structural, coastal and topographic embayment on the south flank of the peninsula. The structural embayment is shown by contours on the base of the Portuguese Tuff (Fig. 1). It probably formed by differential compaction of sediments deposited in a basin bounded on the east, south and west by thick intrusions and extrusions of basalt, and on the northeast by a basement high of Catalina Schist. The schist and basalt experienced negligible compaction while biogenic and pyroclastic-rich sediments experience extensive compaction. The compaction created a structural bowl beneath the area of the landslide complex. The bowl was subsequently tilted southward during folding of the Palos Verdes anticline. This created steeper south dips beneath the landward part than the seaward part of the complex. The structure is further modified by gentle folds which partly control the boundaries of the slide complex and the development of subslides within it.

The coastal embayment and part of the topographic embayment reflect the greater ease with which the tuffaceous member of the Altamira Shale was eroded in this area compared to the areas on either side. Relatively soft siltstone and shale predominate in the embayment whereas hard basalt and dolostone predominate on either side. Along the present coast, resistant basalt and associated dolostone form the sea cliff to the west of Abalone Cove and resistant dolostone of geothermal origin forms the promontory east of Portuguese Bend. A basalt sill buttresses Portuguese and Inspiration points within the embayment but Holocene wave erosion breached the sill on either side of the points.

In the uphill part of the complex, the basal slip surface is at or slightly above the top of the Portuguese Tuff. At the toe, the basal slip surface is near the base of the tuff. The Klondike Canyon landslide is an exception. Its basal slip surface is 70 feet below the tuff because a monoclinal flexure has raised the bedrock beneath it (Fig. 1). The western edge of the complex occurs where wave erosion removed the Portuguese Tuff from the coastal area prior to development of the complex. The eastern edge occurs where the Portuguese Tuff becomes deeply buried beneath overlying strata near the coast and the seaward part is buttressed by an anticline.

Origin of the complex

In order to properly evaluate the mechanics and stability of the Portuguese Bend landslide complex, it is necessary to know whether the complex originated as a single large megaslide or as a coalescing group of semi-independent slides of variable age. As seen today, the landslide complex is broken into numerous subslides. Based on geomorphic expression, individual subslides might have separate origins from their neighbors, or they might represent parts of a megaslide that started moving as a unit but fragmented as movement progressed.

Jahns and Vonder Linden (1973) believe the complex consists of semi-independent slides formed during three separate time intervals. As interpreted by them, slides in the up-slope part of the complex formed before development of the seventh marine terrace whose shoreline angle is reported to be 650 feet (Jahns and Vonder Linden, 1973, Table 1); slides within the intermediate part of the complex formed before final development of the first marine terrace whose reported shoreline angle is 140 feet, and slides whose toes are along the present coast formed after the first marine terrace. Their interpretation that the headward part of the complex predates the seventh marine terrace is based on several observations. Remnants of a landslide overlie the Portuguese Tuff and occur up slope from the seventh terrace in a bowl-shaped area west of the Portuguese Bend landslide complex. Within the complex, a topographic embayment extends across the slide at the approximate elevation of the seventh terrace. They also report the presence of marine deposits of the seventh terrace resting on inplace bedrock down slope from the exposed base of the landslide on the west side of Portuguese Canyon. I have observed stream gravels which contain reworked marine cobbles but have not found a marine terrace in this area.

Although the south flank of the peninsula contains slides of various ages, I interpret the Portuguese Bend landslide complex to have originated as a single megaslide at the time when the ocean occupied the abrasion platform which caps Inspiration and Portuguese points (terrace 1 of Jahns and Vonder Linden, 1973, but terrace 2 of Woodring and others, 1946, and terrace 2a of Bryant, 1987). My interpretation is based on the following evidence:

1. Subsurface data indicates the deepest slide plane is a relatively smooth surface that extends continuously beneath the entire complex. The slip surface is near the top of the Portuguese Tuff in the upper part of the complex but varies from above the tuff to slightly below the tuff in the central and seaward parts of the complex.
2. The slide base is more than 100 feet below the surface in much of the area where the ground surface is near the elevation of the seventh marine terrace. The topographic embayment is a reflection of the bedrock structure beneath the slide. To the best of my knowledge, no marine terrace deposits occur within the slide in the vicinity of the projected position of the seventh marine terrace.
3. In the western part of the slide, slump blocks containing the cherty member of the Altamira Shale are distributed

from the head of the slide to the coast. The inplace cherty member crops out at an elevation of about 1000 feet in the head scarp of the complex. On the ridge at the west edge of the slide, the cherty member was removed by erosion prior to emplacement of the eighth marine terrace whose shoreline angle is about 950 feet. These observations are in agreement with those of Jahns and Vonder Linden (1973). However, I conclude that the slump blocks containing the cherty member originated near the head of the slide and were transported to the toe as part of a megaslide; whereas, they appear to believe that transport was accomplished by having younger slides develop beneath the toes of older slides.

4. There is no apparent difference between post-sliding landform modification or soil development throughout the parts of the slide not involved in the Holocene Abalone Cove and Portuguese Bend landslides. These two landslides contain the same features as the upslope part of the complex, including a thick soil mantle over old slump blocks and graben deposits, except that these features are disrupted by Holocene sliding.

5. Regarding the timing, the seaward edge of this Pleistocene slide is exposed on the east side of Inspiration Point, as previously recognized by Jahns and Vonder Linden (1973). Here, the Portuguese Tuff was bent upward to a nearly vertical position by up thrusting along the toe of the Pleistocene slide and then unconformably overlain by marine terrace deposits. A similar relationship is present on the inland edge of Portuguese Point but subsequent sliding has thrust the toe of the slide over the seaward part of the terrace and uplifted and back tilted the part of this terrace which overlapped the toe. The age of this terrace is about 120,000 years old (Bryant, 1987).

An important aspect to the difference between my perspective of the evolution of the landslide complex and that of Jahns and Vonder Linden (1973) is that I am concerned with the mechanics of sliding whereas they were concerned with the space-time relationships between sliding and sea level and climatic changes. There is general agreement regarding the interpretation of observable features; of course, more information is available now than when their paper was written. In the case of the Portuguese Bend and Abalone Cove landslides, there is agreement that both are reactivated parts of the Pleistocene landslide. The toes of the two slides are a short distance seaward of the Pleistocene toe and have developed in response to loss of support along the Holocene shoreline angle.

From a mechanical point of view, it is difficult to account for the development of the seaward part of the complex if the complex originated as a series of slides rather than a single slide. The seaward part has a gently sloping base and, at the time it formed, its toe ramped up from as much as 200 feet below sea level. The initial shearing resistance should have exceeded driving force generated within the seaward part of the slide. However, the landward part of the complex could

Figure 4. View of Portuguese Bend area looking north on September 3, 1947. Notice the landslide scarp on the slope inland from the pier. (Spence Aerial Photos)

have provided the extra driving force needed to cause the initial failure (Fig. 3).

The initial slide was probably destabilized by wave erosion and ground water. Its toe is near the axis of a gentle arch in the bedrock. Wave erosion removed weight from the top of the arch. This allowed beds above the incipient slip surface to yield by bending upward in response to the thrusting force produced by sliding further uphill. Instability was probably promoted by development of a perched water table above the Portuguese Tuff in the uphill area, and development of artesian pressure beneath the tuff near the coast. During the early stages of sliding, the toe developed as a slide-propagation fold. Uplift would have been aided by artesian pressure from ground water trapped beneath the Portuguese Tuff. As movement progressed, the slip surface propagated through the fold to form the ramp which is preserved inland from Portuguese Point (Fig. 3).

During initial movement, the head of the megaslide was probably a short distance up slope from the present day 600-foot ground elevation contour (Fig. 1). As movement reduced lateral support, rotational slide blocks developed up slope from the head scarp and slid downhill to form the stepped terraces visible in the northwest part of the complex (Fig. 4 and 5). The northeast arm of the complex and Valley View graben (Fig. 1 and 3) probably also developed at this time due to the combined effects of loss of lateral support and a high water table.

The Pleistocene landslide probably stopped moving because of the combined effects of loss of driving force by displacement of mass away from its head and by drainage of ground water from its up slope area as a result of slide-induced permeability along joints and fissures. Self buttressing by accumulation of debris along the toe after the latest Pleistocene glacio-eustatic lowering of sea level was probably not a factor. Had it been, the entire complex should have reactivated in response to Holocene wave erosion.

The present Portuguese Bend and Abalone Cove landslides coincide with a prehistoric Holocene landslide as interpreted from scarps, closed depressions and displaced landforms visible on aerial photographs that predate historic movement. The Holocene landslide developed from the coastal part of the Pleistocene landslide complex. Movement occurred after wave erosion largely removed strata that buttressed the toe of the Pleistocene slide. Thus, the Portuguese Bend and Abalone Cove landslides are a reactivated part of the Pleistocene landslide complex.

The Holocene landslide is split into three segments by the buttressing effect of Inspiration and Portuguese points. The eastern segment moves into Portuguese Bend; the central segment moves into the unnamed cove between the two points, and the western segment moves into Abalone Cove. The two points are supported by a seaward dipping basalt sill which ranges from about 50 to 100 feet thick within the confines of the points. The sill extends beyond the points but was removed by wave erosion before the start of Holocene sliding. Because Inspiration Point is narrow, the thrust force of the slide mass caused its inland edge to rupture along steeply inclined, conjugate tear faults that diverge at an angle of about 65 degrees. The slide mass cleaves as it pushes against the leading edge of these faults. Because Portuguese Point is wide, the Holocene slide mass initially ramped up onto the point. Subsequent movement caused tear faults to develop on either side of the point but the main tear faults do not join at their inland edge. There is a belt of slide material that is still being thrust up the ramp at the inland edge of Portuguese Point. This belt forms the division between the Portuguese Bend and Abalone Cove landslides.

The most recent prehistoric movement of the Portuguese Bend landslide was less than 4,800 æ 180 years ago based on the C-14 age of carbonized wood taken from pond deposits that were displaced and tilted by prehistoric movement (Emery, 1967). The Abalone Cove landslide moved at the same time as shown by the continuity of a head graben that extends between the two slides, and by the similar youthfulness of scarps, closed depressions and other geomorphic features within the two slides. The Klondike Canyon landslide probably moved at the same time, as suggested by black adobe soil which fills prehistoric fissures, but its displacement was too small to leave well defined geomorphic features.

The part of the Portuguese Bend landslide located between Inspiration Point and Portuguese Canyon was affected by sliding during the period between 1931 and 1947. A well-defined head scarp is visible in a 1947 photograph (Fig. 4) but absent from a 1931 photograph. The scarp is at the same location as the head of the seaward subslide, as described later. This indicates the seaward subslide had a safety factor near 1.00. It may have been creeping when the main slide reactivated in 1956. MacKintosh and MacKintosh (1957) report that the pier, which was built 400 feet east of Inspiration Point in 1946, required repairs before 1956 at the same place where it was offset by sliding in 1956.

PORTUGUESE BEND LANDSLIDE

Boundaries

As described above, Inspiration Point splits the Portuguese Bend landslide into two parts. The eastern part which moves into Portuguese Bend is hereafter referred to as the main Portuguese bend landslide. The western part which moves into the cove between Inspiration Point and Portuguese Point is hereafter referred to a the western segment of the Portuguese Bend landslide. The main landslide has an area of about 190 acres and the western segment has an area of about 70 acres.

Figure 5. View of Portuguese Bend area looking north on September 26, 1956, one month after reactivation of the Portuguese Bend landslide. Road fill where sliding began is on the right central side of photo. (Whitehurse Aerial Surveys)

The main Portuguese Bend landslide has a lobate shape with a length to width ratio of about 1.5:1. Its greatest width is 2700 feet and occurs in the vicinity of Palos Verdes Drive. Its greatest length is 3900 feet.

The head of the main slide occurs where the base of the slide rises to the surface along a structural ramp in the underlying inplace bedrock. After reactivation in 1956, the head was initial marked by a well-defined head scarp and graben but subsequent movement uncovered seaward dipping bedrock along the central part of the head. In 1986, grading uncovered bedrock for a distance of 1,000 feet along the head. Bedrock was also exposed at the northwest corner of the slide but was subsequently covered by fill to provide surface drainage and eliminate a vertical scarp. Bedrock is not exposed along the eastern part of the head because Paintbrush Canyon was incised through the base of the slide prior to placement of fill during construction for Crenshaw Boulevard. The head of the slide has been greatly modified by grading since 1986 and is no longer active.

Along most of the slide's east edge, bedding is upturned by a west-facing monoclinal flexure. As a result, the basal slide plane rises to the surface and forms a sharply defined trace that extends nearly 3000 feet from the head to the toe of the slide. Along much of this length, movement is nearly horizontal and parallel to the trace. Thus, where the trace crosses Palos Verdes Drive, it produces a left lateral offset in the

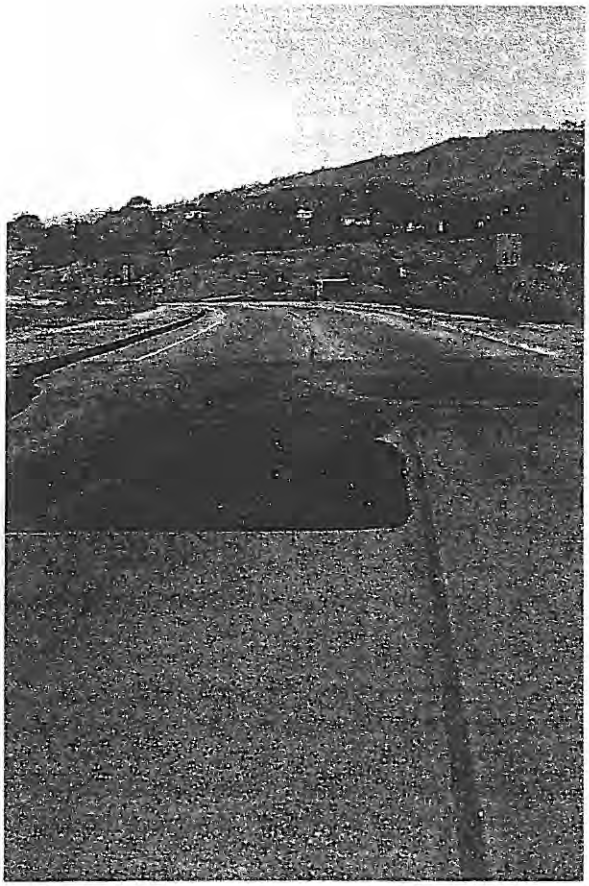

Figure 6. Offset in Palos Verdes Drive at east edge of slide in Oct., 1991.

roadway without noticeable vertical offset or convergence or divergence across the break (Fig. 6).

The western edge of the main slide has a poorly defined boundary. In-between the head of the main slide and the head of the western segment, the gently inclined basal slip surface continues westward beneath the inactive part of the slide complex. Displacement dies out across a broad zone which contains a series of northeast to east trending slices bounded by steeply inclined en echelon faults, fissures and discontinuous half-grabens. The westward decrease in displacement is accommodated by clockwise hinging and rotation of these slices.

Between the head of the western segment and the point where the slide splits into two segments at the inland edge of Inspiration Point, the boundary between the main slide and the western segment is poorly defined. The buttressing effect of Inspiration Point caused a narrow belt of land located directly inland from the point to move less than the land on either side. Since 1956, total horizontal displacement along the axis of this belt ranges from 85 feet at its inland edge to nearly 100 feet at Palos Verdes Drive.

The toe of the main slide is along the beach where the base of the slide rises to the surface. Movement causes the slide mass to thrust over the beach and wave cut bench but wave erosion continually removes material from the toe. Consequently, the position of the toe varies through time due to variations in the rate of slide movement and the rate of wave erosion. In its most advanced position, the toe was as much as 400 feet seaward of its initial 1956 position. Wave storms and the slowing of movement due to slide mitigation have caused the toe to retreat landward as much as 150 feet in recent years.

The western segment of the Portuguese Bend landslide is 1000 feet wide along its toe in the cove between Inspiration and Portuguese points. It extends inland 2000 feet giving it a length to toe-width ratio of 2:1. The east side is transitional into the main Portuguese Bend landslide as described above and is interpreted to be nearly straight. The west side is complex. It is about 300 feet wider at the inland edge of Portuguese Point than in the cove between the two points. The widening is accommodated by thrusting and westward displacement along the slide ramp at the inland edge of Portuguese Point. A survey monument on the hill above this ramp was displaced 2.2 feet west toward Abalone Cove between 1957 and 1963 (elevation changes were not determined during this period). No survey data are available for the period from 1963 to 1976, but it is reasonable to assume that movement continued during this period. Since 1976, the monument on this hill has moved 7.3 feet west and has risen 1.3 feet in elevation. North of Palos Verdes Drive, the west

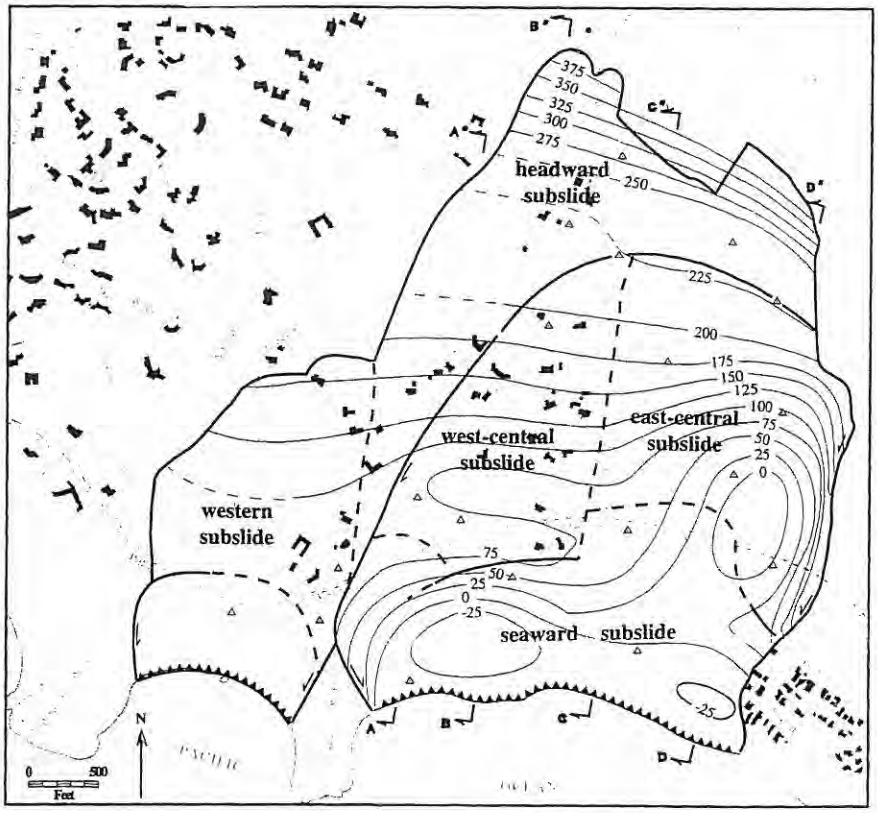

Figure 7. Map of Portuguese Bend landslide showing boundaries of subslides and structure contours in feet on base of slide.

side is marked by northeast-trending fissures and small grabens similar to those along the northwest edge of the main slide. After the Abalone Cove landslide began moving in 1978, movement occurred throughout the zone between the two landslides. Thus, the boundary between the western segment and the Abalone Cove landslide is transitional.

Subslides

Because of its large area and large length to thickness ratio (30:1), and variations in conditions which affect the rate of movement from one part of the slide to another, the Portuguese Bend landslide behaves as a group of semi-independent subslides. As define here, each subslide is controlled by undulations in the slide's base and/or lateral boundary conditions. Therefore, each subslide maintains a fixed location through time as the slide mass translates from one subslide to another. Recognition of these subslide is an essential element in the plan to permanently stabilize the Portuguese Bend landslide.

The main slide is divisible into four subslides. The four are referred to as the headward, east-central, west-central and seaward subslides. The western segment of the slide, which is itself a subslide, is further divided into the landward part of the western segment and the seaward part of the western segment. The subslides and structure contours on the base of the slide are shown on Figure 7.

The headward subslide is crescent shaped and has an area of about 45 acres. It forms the up slope and western parts of the main slide. Its up slope half is controlled by undulations in the underlying bedrock to which its basal slip surface conforms. Along its head, the slide base dips 15 to 25 degrees seaward. The slide mass on this ramp generates a large excess driving force. Further down slope the slide base flattens at the crest of an anticlinal undulation (see Fig. 3) to a seaward dip of only 4 to 5 degrees. In this area the slide mass generates a net resisting force providing the water table is low. The base of the western part of headward subslide has an average dip of only 5 degrees. As a result, its resisting force exceeds its driving force providing the water table is low.

The east-central subslide is nearly rectangular in shape and has an area of about 60 acres. Most of its driving force is generated on the south flank of the anticlinal undulation that controls the adjoining down slope edge of the headward subslide. Here, the slide's base dips between 10 and 18 degrees seaward. Because movement accelerates along this structural ramp, a broad graben has formed by extension across the crest of the anticlinal undulation (C-C', Fig. 8). The graben is included as part of the east-central subslide. The seaward part of the subslide is controlled by a spoon-shaped structural depression where the base of the slide descends to a few feet below sea level and then rises gently on the seaward side. On either side of the depression, the slide's base is subhorizontal in the direction of movement. Consequently, the downhill part of the subslide generates a net resistance to sliding.

The west-central subslide includes about 40 acres within the residential area west of Portuguese Canyon. Its shape is roughly a right triangle with the hypotenuse on the northwest. It is a westward continuation of the east-central subslide except it is partly supported on its downhill side by a subsurface ridge. The slide mass must rise 30 to 40 feet as it moves to the crest of the ridge; this produces a large force resisting movement. The origin of the ridge is undetermined but it may consist of steeply inclined beds along the upturned toe of a deep-seated abandoned part of the Pleistocene landslide. The east end of the ridge is probably terminated by a tear fault. This is suggested by the presence of a steeply inclined right-slip fault which extends for a few hundred feet along the southeast edge of the west-central subslide. The fault is parallel to the direction of slide movement and regenerates at the same location as the slide sheet translates through this area.

The seaward subslide has an area of about 45 acres. Its toe extends eastward from Inspiration Point for a distance of 2,300 feet along the beach. West of Portuguese Canyon, it consists of a single major rotational slump block (cross sections AA' and BB', Fig. 8). Here, its head scarp is about 700 feet inland and is above the ramp on the seaward side of the anticlinal ridge that buttresses the west-central subslide. The head scarp continually regenerates at this location and is in the same place as the scarp visible on the 1947 photograph (Fig. 4). The steep slip surface exposed in the head scarp flattens downward to merge with the base of the main slide near the top of the ramp. From there the slip surface follows the arcuate path of the main slide base. At the base of the ramp it flattens into a bowl-shaped structural depression whose center is about 45 feet below sea level and then rises to the surface at the beach (B-B', Fig. 8).

In the vicinity of Portuguese Canyon, the seaward sublide extends over 1,000 feet inland. Its base dips about 5 degrees seaward in the inland area but flattens to subhorizontal near the coast. The eastern part of the seaward subslide extends about 900 feet inland. Its base has a similar but more subdued shape to that of the western part.

The separation of the western segment of the Portuguese Bend landslide into two subslides is controlled by the buttressing and constricting effects of Inspiration and Portuguese points. Movement of the landward subslide is retarded by these effects while the part of the slide within the slot between the two points is not. Consequently, the seaward subslide moves faster than the landward one and has its head marked by an arcuate graben in the vicinity of Palos Verdes Drive.

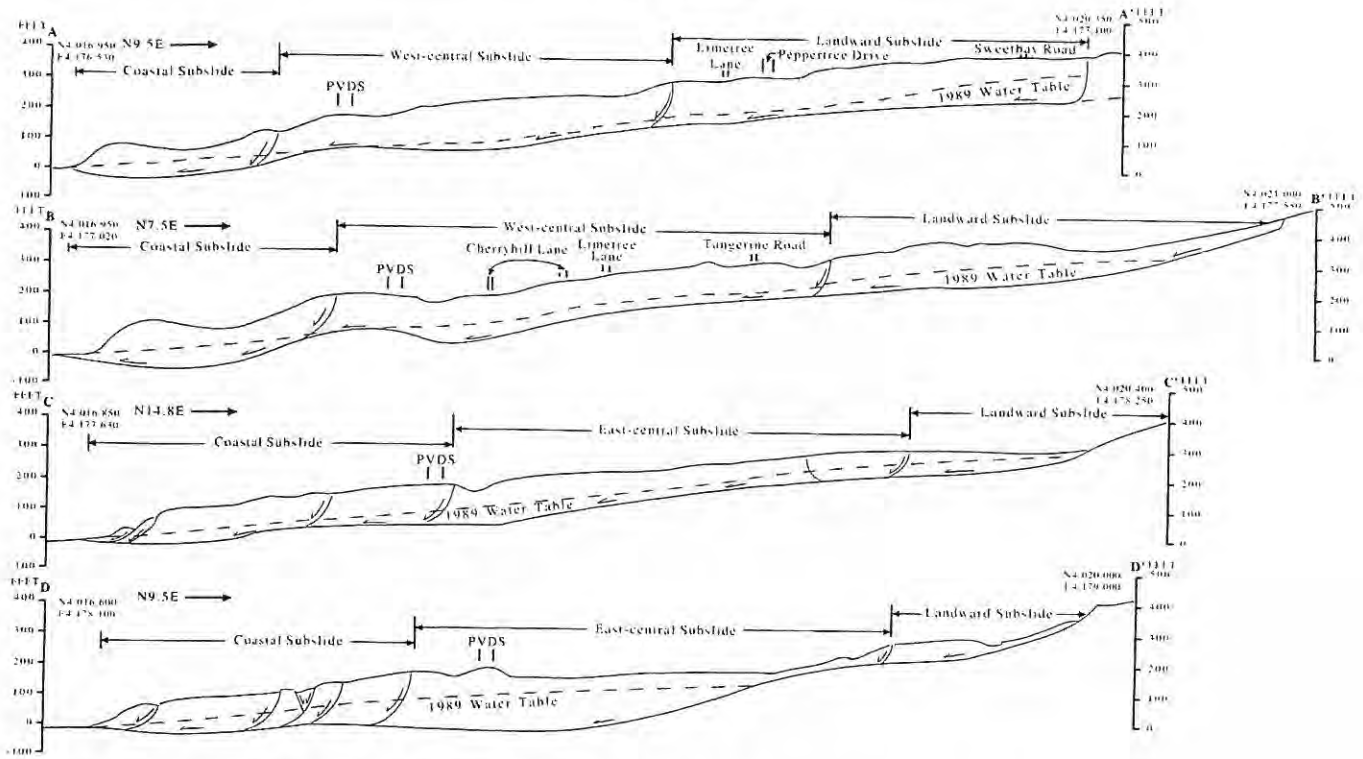

Figure 8. Vertical cross sections through the Portuguese Bend landslide. See Figure 7 for locations of sections.

Mechanics

The main Portuguese Bend landslide probably originated as a simple translational glide sheet driven by excess driving force generated along structural ramps. The earliest movement may have developed along the ramp which extends uphill from the headward subslide. Here, bedding dips as much as 30 degrees seaward. Assuming slippage occurred along a tectonically sheared bentonite bed whose angle of internal friction was 6 to 8 degrees and cohesion near zero, the slide sheet overlying this ramp would have generated three to four times as much driving force as resisting force. As excess driving force was transmitted downhill, it was sufficient to overcome a net resisting force in areas of gentle or reverse dip, at least as far downhill as the shoreline. The toe developed near the then existing shoreline angle because the slide sheet was thinnest at this location. Uplift at the toe was probably promoted by artesian pressure beneath the Portuguese Tuff which is a perfect aquiclude. This is suggested by a change in the stratigraphic position of the slip surface from above the Portuguese Tuff beneath the main body of the slide to within or at the base of the Portuguese Tuff in the vicinity of the toe. The artesian condition could result from surface water entering bedrock beneath the Portuguese Tuff in the area northeast of the slide and along the bottoms of Paintbrush and Klondike canyons. If artesian pressure exceeded overburden pressure, anticlinal uplift could have begun along the shoreline prior to sliding. This would have promoted sliding by reducing support along the toe.

The Portuguese Bend landslide is no longer a simple translational glide sheet. Much of the original slide sheet was displaced to the coast and removed by wave erosion, particularly in the area east of Portuguese Canyon. The present slide mass is a mixture of broken and disoriented bedrock blocks, slide debris, alluvial and pond sediments which were deposited in flat areas and closed depressions, masses of Portuguese Tuff and other slump deposits derived from above the head of the main slide, and fill and debris from human activity. This melange, which has an average thickness of about 125 feet, is weak and parts of it deform like a mass of incoherent earth. The slide still gains a large part of its driving force by translation down inclines in the basal slip surface. However, driving force is also generated by the lowering of mass along normal faults that merge with or terminate at the base of the main slide. There are two styles of normal faulting. One creates nearly symmetrical grabens. The other creates a stair-step arrangement of rotational blocks. Both are capable of causing distention above a subhorizontal slip surface.

Symmetrical grabens form in areas where the slide base and ground surface are subhorizontal and the downhill part of the slide is moving faster than the uphill part. The graben at the head of the east-central subslide is an excellent example (C-C', Fig. 8). This graben is bounded by steeply inclined normal faults that dip toward each other. Numerous normal faults occur between the bounding faults. These create secondary grabens and horsts. The driving force created by

lowering of wedge-shaped blocks helps drive the downhill part of the slide. This type of faulting is capable of causing lateral spreading above a weak subhorizontal slip surface.

The stair-step arrangement of rotational blocks develops where surface elevations rise conspicuously in the uphill direction. The orientation of the main slide base is of minor important. The necessary conditions are well developed within the seaward subslide. Here, as the slide mass moves forward, wave erosion continually regenerates a steep cliff along the toe of the slide. Because of an unbalanced rotational force, a seaward dipping listric normal fault develops landward from the cliff (C-C', D-D', Fig. 8). The fault has a steep inclination near the surface but flattens downward to merge with the base of the main slide. As the block is lowered by backward rotation, a cliff is created on its landward side. This promotes the formation of another rotational block further uphill. Directly east of Portuguese Canyon the series of rotational blocks extends as much as 1,000 feet inland from the coast. The retrogressive growth of rotational blocks has an important impact on the stability of the main slide. Seaward from where the most landward listric normal fault joins the basal slip surface, the rotation of blocks may provide all of the driving force needed to overcome frictional resistance to sliding. Under this condition, the seaward part of the slide does not buttress the landward part, even where the base of the slide dips landward. Only the viscous component of friction resists the thrusting action of the landward part. Because viscous friction is a function of velocity, the landward part will continue to move so long as it has an excess driving force at its downhill edge.

Both absorbed water and ground water play a major role in the mechanics of the Portuguese Bend landslide and were the main causes of temporal variations in the rate of slide movement between 1956 and the start of remedial grading in late 1986. This is shown in Figure 9 by the relationship between rainfall, measured 1 mile northeast of the Portuguese Bend landslide, and the rate of slide movement at Los Angeles County survey monument R-1, located in the east-central subslide. In the vicinity of R-1 all water comes from natural sources. From 1956 to 1963, frequent survey measurements show movement accelerated during rainy months and slowed during dry months. Since 1962, the time between measurements does not permit direct comparison between rate of movement and monthly rainfall but it does permit a direct comparison between the rate of movement and the deviation of rainfall from a long-term average of 12.9 inches per year. Notice that between 1959 and 1978, rainfall deviated only slightly from the long-term average and that the rate of movement has the same pattern as the cumulative deviation of rainfall. Starting in 1978, high rainfall caused a large cumulative deviation from the long-term average and was matched by a large increase in the rate of slide movement. The fact that movement did not slow greatly during periods of below average rainfall in 1981 and 1984, indicates the natural depletion of water is slow.

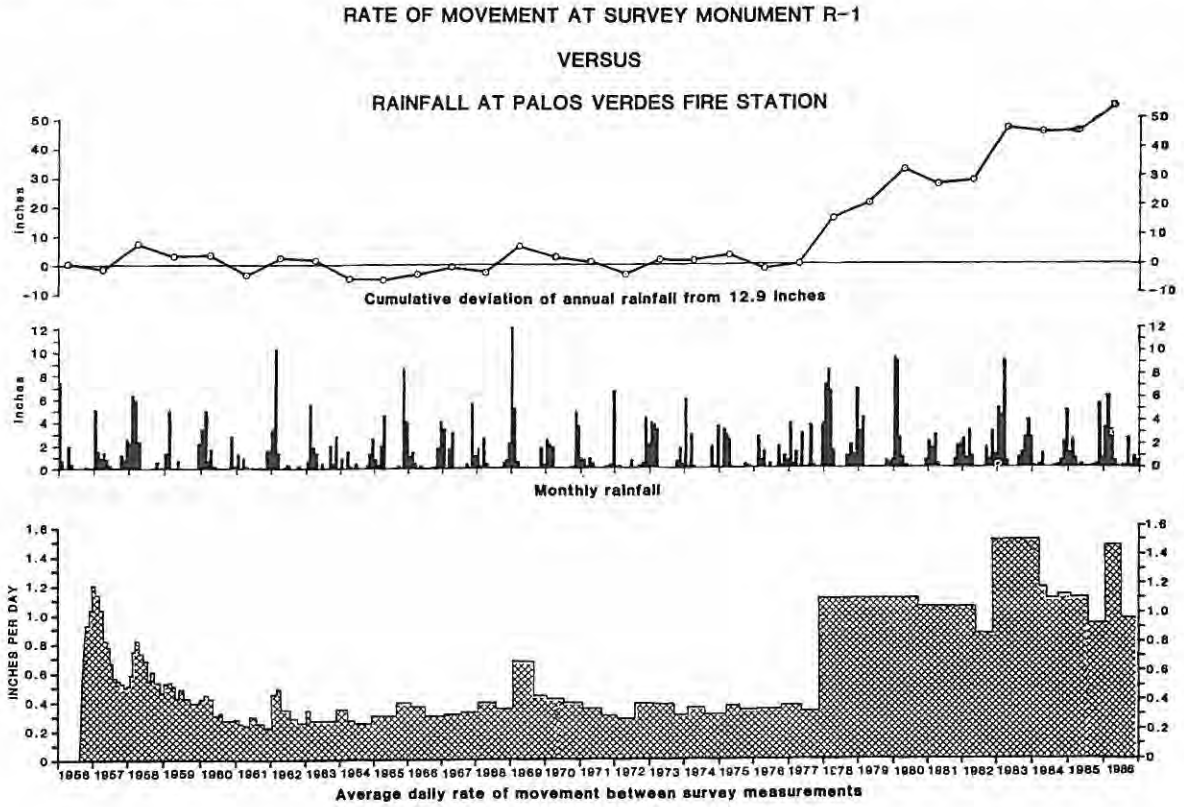

Figure 9. Graph showing relationship of rainfall to rate of slide movement.

Most water within the slide mass is absorbed water. In the zone above the water table, the amount of absorbed water varies seasonally and also annually. Where the slide base is above the water table, the shear strength of bentonite along the basal slip surface varies as a function of its absorbed water content. The strength decreases as the bentonite absorbs water and increases as it loses water. Within the body of the slide, an increases in the amount of absorbed water causes a decrease in the bonding strength between particles and allows deformation to occur more freely. This is especially important in areas where normal faulting and other types of deformation are occurring. Loss of absorbed water makes the slide mass more rigid and resistant to internal deformation. Variations in the absorbed water content account for most of the seasonal variation in the rate of slide movement.

Absorbed water may have played an important role in triggering the Portuguese Bend landslide during placement of road fill in 1956. The bentonite at the base of the slide was probably nearly saturated prior to placement of the fill. Compaction of the bentonite under the added weight of fill probably caused the development of excess pore water pressure, thereby reducing the shear strength of the bentonite. Such an effect was observed in September 1990, when 60,000 cubic yards of earth were moved from the upper part of the slide and placed as a fill in the most easterly part of the slide north of Palos Verdes Drive. Slide displacement is nearly horizontal in the area of the fill and, therefore, must consume more energy than it generates. However, the local rate of movement increased from 0.042 inches per day prior to placement of the fill to 0.077 inches per day upon completion of the fill. Movement subsequently slowed at a decelerating rate for several months until the rate fell below the original rate. This pattern can be explained by a reduction in shear strength due to development of excess pore water pressure during placement of the fill followed by a gradual increase in strength as the pore pressure dissipated.

Ground water reduces the stability of a landslide through its buoyancy effect. In the Portuguese Bend landslide, material below the water table exerts only about half as much normal force causing frictional resistance along the base of the slide as material above the water table. Consequently, in an area where the slide mass is 100 feet thick, a 2 foot rise in the water table will causes a 1% decrease in frictional resistance to sliding. For this reason, ground water played a major role in sustaining the movement of the Portuguese Bend landslide from 1956 to 1978 and was responsible for accelerated movement commencing with high rainfall in 1978. Ground water may also have been an important factor in the enlargement of the original slide beyond the immediate vicinity of the road fill in 1956. Movement in all but the seaward part of the landslide can be stopped by lowering the water table.

Data obtained from monitoring wells installed in 1984 and subsequent years indicate ground water is present above the base of the Portuguese Bend landslide in all but a narrow zone along the slide's northern and eastern margin. The slide mass acts as an unconfined aquifer perched on an impervious slide base. In 1984, the water table was a relatively smooth seaward sloping surface with an average height of about 45 feet above the slide base. The thickness of the saturated zone varied because of undulations in the slide base; it was greatest (as much as 110 feet) above troughs and depressions in the slide's base and least along the crests and seaward flanks of ridges. Since 1984, the water table has been lowered an average of about 10 feet as a result of pumping and low rainfall. Progress in lowering the water table has been slow because of low permeability, particularly in the area east of Portuguese Canyon.

Little reliable data are available regarding ground-water conditions prior to 1984. Based on current knowledge, ground water was present above the slide base in most areas, even in 1956. Unfortunately, no monitoring wells were installed during this period. Data was obtained during the drilling of borings. Most borings which penetrated the water table were filled or abandoned without allowing the water to reach its static level. Monitoring wells drilled since 1984 have shown that it may take many days or even weeks for the water level to stabilize in borings because most slide material has a low storage coefficient (about 5%) and low permeability. Seepage was encountered above the slide base in several bucket auger borings logged by me in 1957, including one located at the northwest edge of the slide. Based on monitoring data and well production, we now know that between 10,000 and 15,000 gallons of water per day enter the northwest corner of the slide as part of the regional ground-water flow. Similar flow probably existed in 1956. If it did, the 1956 configuration of the water table was similar to that in 1984 except much lower.

One question which is often asked is whether artesian pressure exists beneath the slide. If it did, it could explain the unusually low friction angle (6 degrees) determined by back calculations of stability. I have observed no evidence of artesian pressure beneath the main part of the slide. Wherever borings penetrate the slide base, they typically encounter unoxidized bedrock which appears to be impermeable. In 1985, two piezometers were installed beneath the base of the Portuguese Bend landslide, one in the east-central subslide and the other in the seaward subslide. Neither recorded artesian pressure. A multistaged piezometer is installed in the transition zone between the Portuguese Bend landslide and seven are distributed within the Abalone Cove landslide. All extend far below the slide base. None has recorded artesian pressure.

I am aware of only one boring that has encountered artesian water within the Portuguese Bend landslide. It was drilled on the east side of the slide about 200 feet inland from the beach in 1957. Artesian water flowed at a rate of several gallons per minute from beneath the base of a thick zone of sheared bentonite. The water flowed from the hole for many

days. At the time, I assumed the water was coming from beneath the main slide base but it may have come from beneath a seaward dipping listric slip surface associated with a secondary rotational slide. At that time, houses near the beach were disposing of their sewage in pits located up slope from the boring.

In 1981, artesian water was encounter 700 feet further east at the toe of the Klondike Canyon landslide. The water was trapped beneath the Portuguese Tuff. Subsequent pumping has lowered the water table below sea level with no observable effect on the Portuguese Bend landslide. Thus, artesian pressure may occur locally near the beach but there is no evidence of artesian pressure affecting movement of the slide.

PORTUGUESE BEND LANDSLIDE STABILIZATION PROJECT

Plan of Control

During planning of the stabilization project, it was clear that remedial activities would be limited by several constraints. Total funding would be meager and stretched over a period of many years. Therefore, stabilization would have to be carried out in phases. Each phase would have to survive any subsequent slide movement, or be inexpensively repaired, until final stabilization was achieved. It would be impractical to use the common method of stabilizing a large slide by keying a buttress into undisturbed bedrock at its toe and supporting the uphill part by one or more shear keys locked into bedrock beneath the slide. The keyway for a buttress would require excavating below sea level. Any excavation for a shear key would have to extend through 50 to 150 feet of highly unstable slide material with the deep parts well below the water table. Funds would be inadequate to remove a substantial part of the slide and replace it with compacted fill founded on stable bedrock. Stabilization of the seaward part of the slide would require permanent shoreline protection but prerequisite studies and the obtaining permits and funds would take many years. Therefore, uphill stabilization would have to progress without permanent shoreline protection. A final constraint was that abatement activities must be as nonintrusive as possible in developed part of the slide.

A plan of control was developed in accord with these constraints. It had two objectives: (1) permanent lowering of the water table to increase resisting forces, and (2) redistribution of the slide's mass to decrease driving forces and increase resisting forces. The water table would be lowered by removing ground water from wells and restoring surface drainage. A temporary system of culverts would be installed to conduct water to the ocean. Installation of a sewer system was recommended for the developed area but was deemed impractical while the land was moving. Mass-grading techniques were to be used to recontour the undeveloped part of the slide in order to reestablish drainage and redistribute earth to decrease driving force and increase resisting force. Ultimately, the shoreline would be protected by a rock revet-

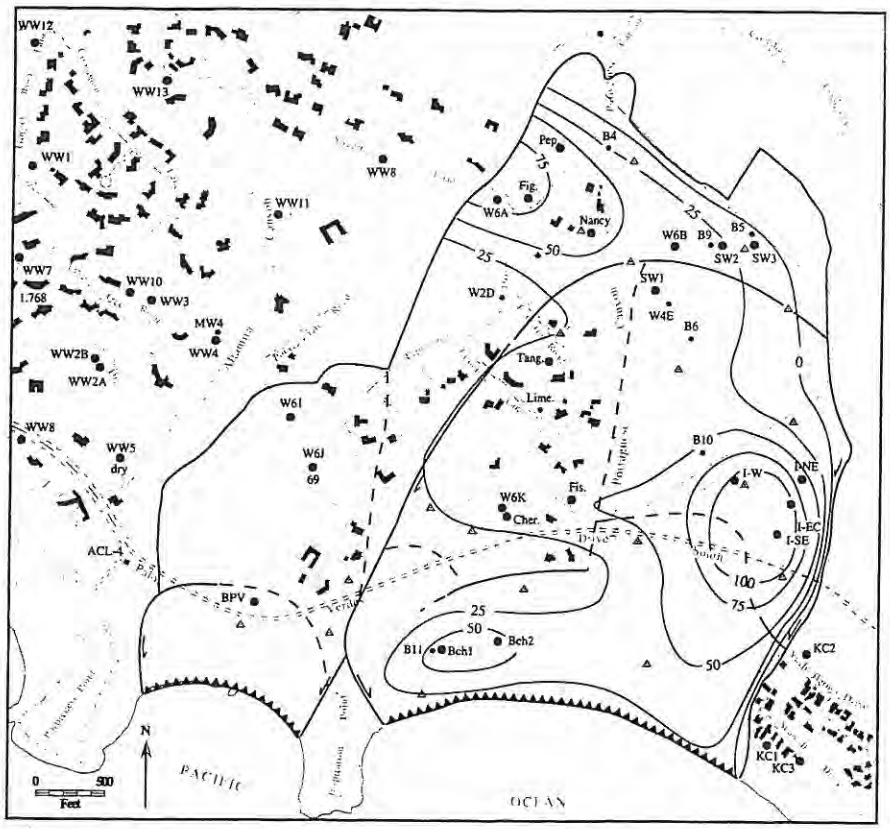

Figure 10. Map of producing and monitoring wells. Isopachs show thickness in feet of saturated zone above slide base in August, 1991.

ment, or other permanent structure, and the stability of the seaward subslide would be improved by construction of a toe berm.

Dewatering System

In 1984, the Redevelopment Agency funded the installation of monitoring wells to determine ground water conditions within the Portuguese Bend landslide. A total of thirteen wells were installed in the area north of Palos Verdes Drive. No wells were installed in the seaward part of the slide because of rapid movement and secondary sliding. Well spacing was nearly uniform but specific sites were chosen in areas most likely to support good producing wells. These included grabens and fissured ground where extension was likely to have increased porosity and permeability, and areas above troughs and depressions in the slide base where the water table was likely to have its maximum height above the slide base. Of the thirteen wells, five showed good potential for production and were fitted with six-inch PVC casing and gravel pack to permit their future use as dewatering wells. The others were fitted with two-inch PVC casing for monitoring.

Of the five wells suitable for production, the three most westerly wells were connected to the Abalone Cove dewatering system and placed into production near the end of 1984. (The water is piped to the ocean because its high sulfate content makes it unusable for domestic or agricultural purposes.) The other two wells and three new wells were placed in production during 1985 and 1986. Additional wells were installed between 1986 and 1991 to increase the total to 19 currently operational wells (Fig. 10). Thus far, only three wells have been rendered unusable for production - one from slide deformation, one from vandalism and one from clogging by bentonite.

Initial production from most wells exceeded 1,000 gallons per day (g/d) and several produced over 10,000 g/d. Production generally declined rapidly during the first few days or weeks and then stabilized to a gradual decline. Total well production peaked at about 30,000 g/d in 1987 due to above average rainfall in 1986 and an increase in the number of producing wells. Production declined below 20,000 g/d in 1989 and has subsequently stabilized at about 17,500 g/d (August, 1991). Of this, over 11,000 g/d comes from two wells at the northwest edge of the slide and an additional 2,000 g/d come from two nearby wells. This production is from perennial inflow of ground water from the northwest and represents interception rather than depletion. Production from the two wells located above the trough in the base of the west-central subslide is currently 2,000 g/d but oscillates through time in a pattern unrelated to rainfall. Most of this water is of domestic origin. Eight wells are present in the undeveloped area east of Portuguese Canyon and north of Palos Verdes Drive. Production from these wells has declined through time to a current total of only 1,700 g/d. Most of this water represent depletion of ground water stored in this area.

The wells are not as effective as originally anticipated. When I first evaluated the possibility of stabilizing the Portuguese Bend landslide, I assumed wells within it would have about the same productivity as wells within and up slope from the Abalone Cove landslide. In the latter, each of the first six wells averaged more than 5,000 g/d during their first two years and two exceeded 30,000 g/d. The present system of eleven wells in the Abalone Cove system currently produces 65,000 g/d of which 50,000 g/d comes from three up slope wells which intercept perennial inflow of ground water from the crest of the peninsula. Based on past performance, the Abalone Cove dewatering system has a proven capacity of over 200,000 g/d.

There are three reasons for the differences in well performance between the two areas. First, the Abalone Cove wells had higher initial production because its water is stored in permeable breccia and course alluvial deposits which form compartments between intact blocks of displaced bedrock. The blocks act like dams that impede the flow of ground water. In the Portuguese Bend landslide, breccia and alluvial deposits are abundant but generally have low permeability because they contain clay derived from Portuguese Tuff exposed within and uphill from the Portuguese Bend landslide. Surface runoff picks up clay from the tuff (bentonite) and transports it down fissures to the water table where it is deposited in pore spaces.. Permeability is exceptionally low in the area east of Portuguese Canyon where most of the slide mass has the properties of clay-rich earth. This material also contains numerous steeply inclined secondary slip surfaces which impede the flow of ground water. Bedrock blocks are present west of Portuguese Canyon but they are highly fractured and form ineffective barriers to ground water migration. A second reason for lower initial production in the Portuguese Bend landslide is that much of the water is stored in basins above troughs and closed depressions in the slide's base. The slide mass is under compression in these areas and removal of ground water promotes compaction which reduces porosity and permeability. The third reason is that the Portuguese Bend landslide receives less than one-third as much inflow from up slope ground water sources and from local sewage disposal. This is beneficial; it means less recharge from these sources.

The stabilization strategy has changed to accommodate the poor performance of wells. The last 4 wells were installed in the headward part of the slide to complete a belt of 8 wells arranged to intercept ground water flowing into the slide and to deplete ground water within the headward part of the slide. This eliminates a major source of recharge into down slope areas. Greater emphasis has also been placed on moving earth to achieve a rapid improvement in stability. This has the added benefit of permanently improving stability over and above that achieved by depletion of ground water.

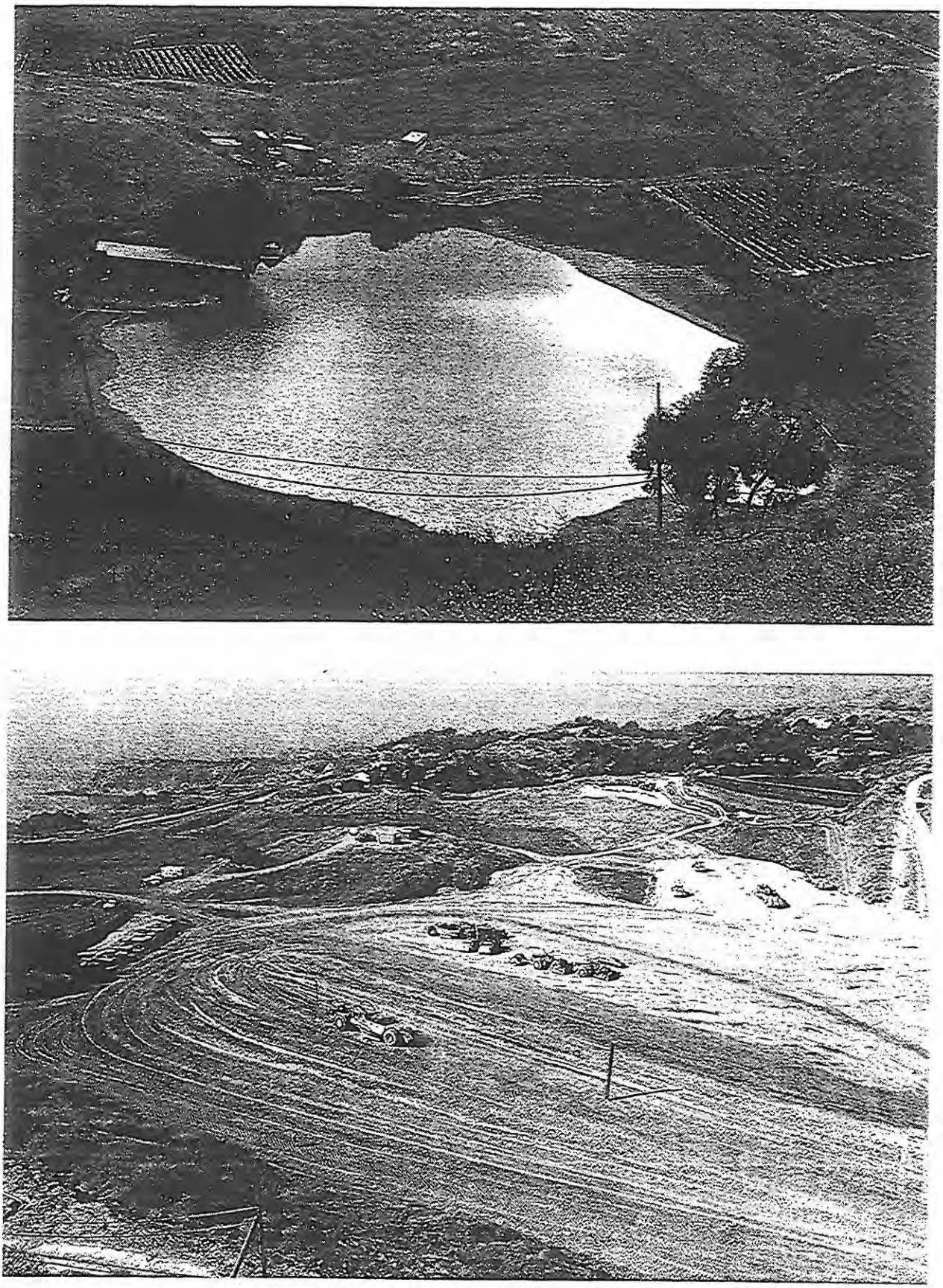

gure 11a. and 11b. Before grading and after grading view of Lake Ishibashi area showing filling of closed depression. Telephone pole at lower ght in Figure 11a is near same location as pipe casting shadow in Figure 11b.

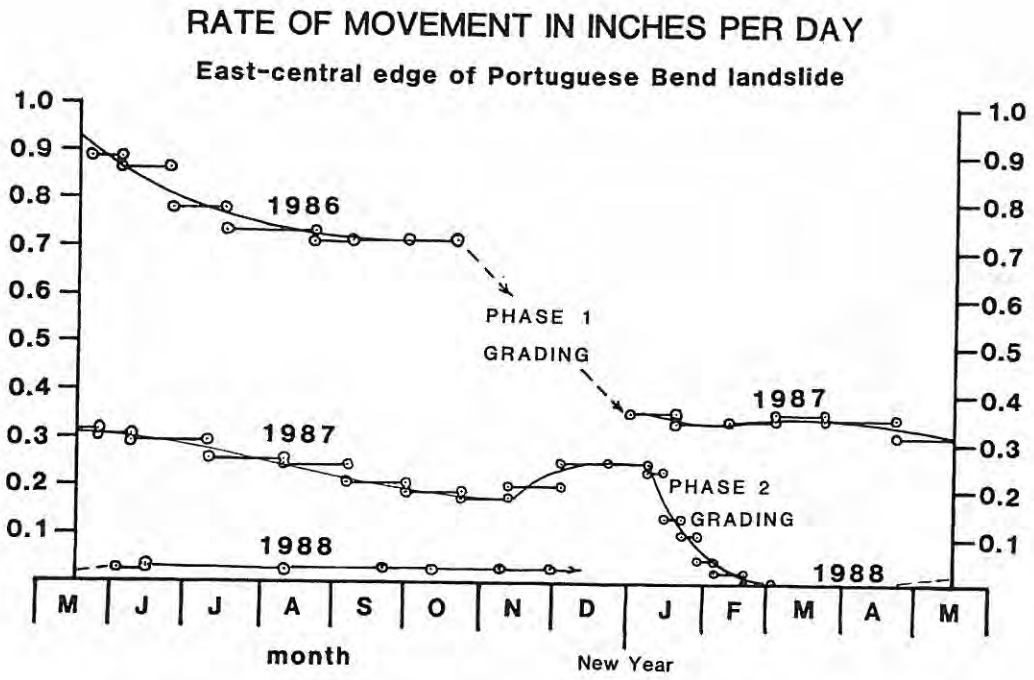

Figure 12. Rate of slide movement at northeast corner of east-central subslide, May 1986 to May 1988. Horizontal bars are average rate of movement between measurements. Continuous line is synthetic curve simulating instantaneous rate of movement.

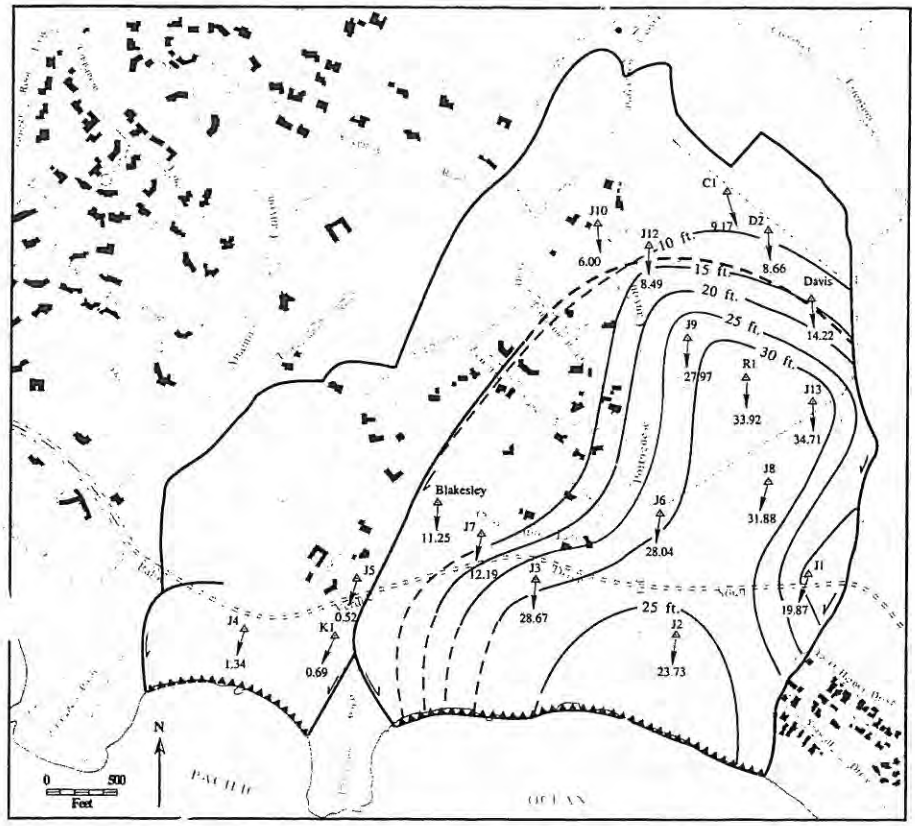

Figure 13. Displacement of Portuguese Bend landslide in feet per year prior to Phase I grading based on survey measurements of 16 January 1985 and 1 October 1986.

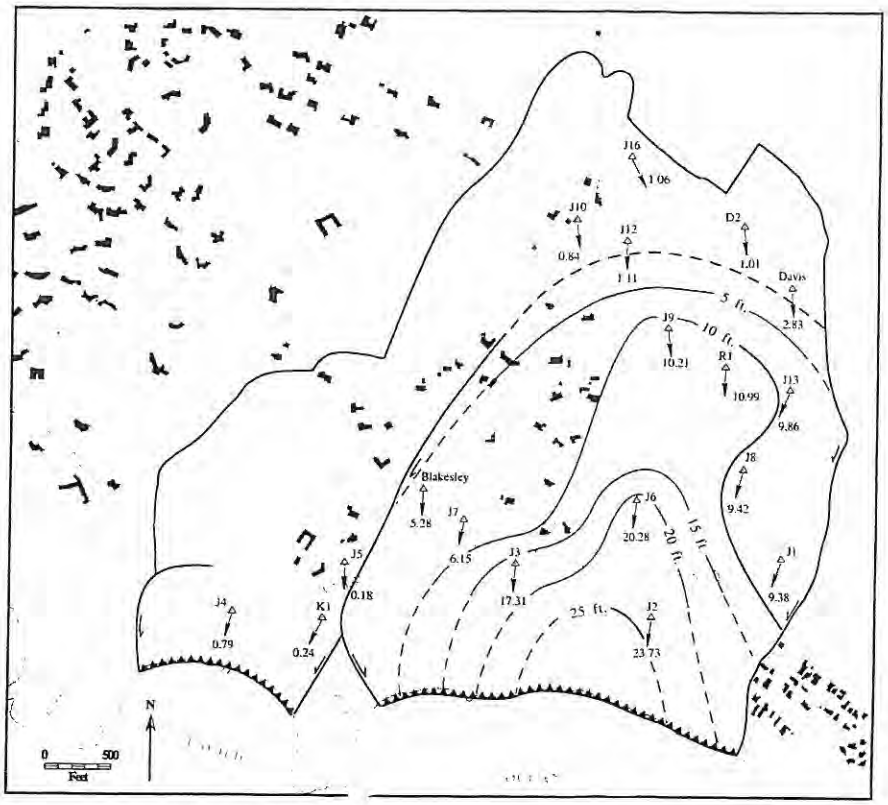

Figure 14. Displacement of Portuguese Bend landslide in feet per year during period between Phase I and Phase II grading based on survey measurements of 25 January 1987 and 4 November 1987.

On a long-term basis, great emphasis will be placed on actions designed to minimize ground water recharge. Phase I Grading and Drainage Improvements

The plan for Phase I grading was devised by me, reviewed by the Panel of Experts and finalized in mid 1986. The plan had two goals: (1) to slow the movement of the headward and east-central subslides by moving earth from above slide ramps where it produces a large net driving force to areas where the slide base is flat, and (2) to reduce ground water recharge by restoring drainage within the undeveloped area north of Palos Verdes Drive and conducting the runoff to the ocean. For aesthetic reasons, the grading plan was designed to create smooth natural-appearing topography and to eliminate steep hazardous slopes.

Grading occurred between mid October and mid December, 1986. A total of 560,000 cubic yards of slide material were moved. Of this, 200,000 cubic yards were moved along the up slope edge of the slide and 350,000 cubic yards were moved from the northeast part of the east-central subslide. The remaining 10,000 cubic yards were moved to extend a drainage trough from the main grading area to the ocean. Most of the earth was placed in the southeast part of the east-central subslide to fill a large depression and restore drainage (Fig. 11).

Prior to Phase I grading, Portuguese Canyon drained into a graben at the northwest corner of the slide where the runoff recharged ground water within the slide. This was corrected by filling the graben and excavating a broad southeast sloping trough along the head of the slide so as to conduct drainage to the east side of the slide. The trough is located where the slide base dips 15 to 25 degrees seaward; thus, the excavation greatly reduced the force driving the headward subslide. On the uphill side of the trough, slide material was removed to inplace bedrock in a belt 1000 feet long with an area of 4 acres. The bedrock surface was ripped and tamped so vegetation could be planted and the bedrock would not act like a paved surface directing runoff to the slide. Where the slide base came to the surface on the downhill side of this area, the slide mass was over-excavated to a depth of 10 feet below final grade and replaced by compacted fill. This provided a stable base for a corrugated steel drainage culvert that was installed to conduct runoff from Portuguese Canyon to a culvert at Paintbrush Canyon on the east side of the slide.

Prior to 1986, divergent slide movement and erosion by runoff down Paintbrush Canyon partially exposed bedrock in a belt about 20 feet wide and 1000 feet long on the northeast side of the slide. During grading, this belt was widened to about 100 feet by removing slide material from inplace bedrock. The bedrock was ripped and tamped to eliminate potential slip surfaces and then overlain by a minimum of 10 feet of compacted fill. This provided a stable surface for the drainage culvert and reduced the likelihood that runoff from the ridge east of the slide would permeate to the slide base.

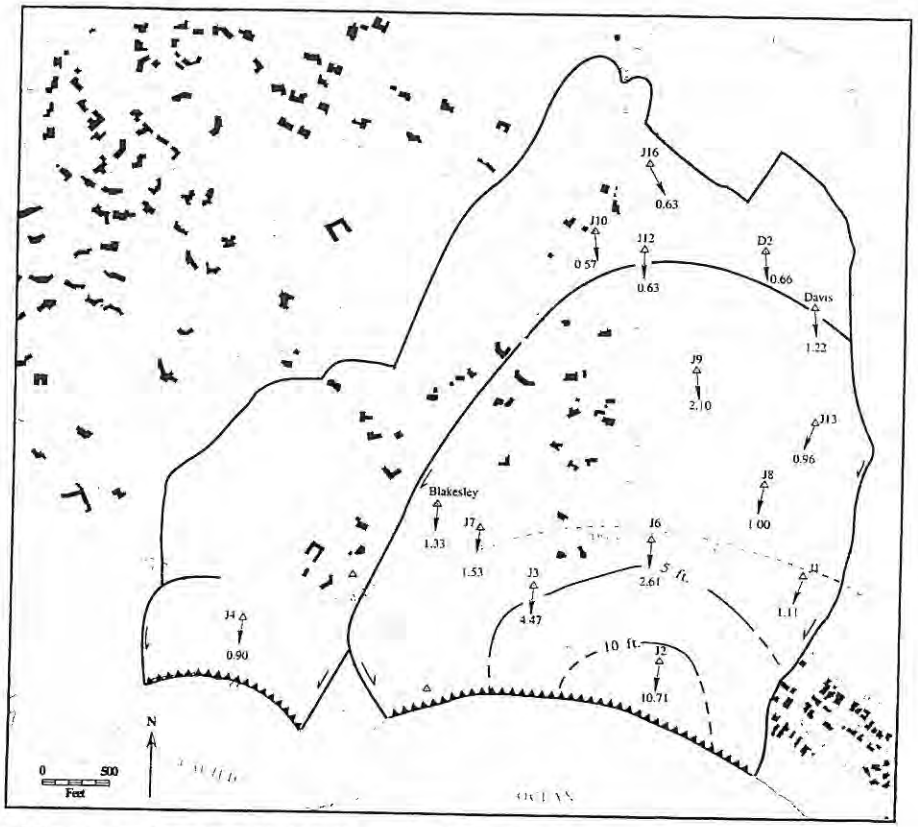

Figure 15. Displacement of Portuguese Bend landslide in feet per year during Phase II grading based on survey measurements of 7 March 1988 and 25 January 1987.

The addition of fill also addressed a public concern that grading would reduce support from the ridge east of the slide.

In order to reduce driving force from the east-central subslide, 350,000 cubic yards of earth were removed from the ramp on its northeast side. Here, the slide base has an average dip of 16 degrees in the direction of slide movement. The earth was moved a short distance seaward to fill the depression and restore drainage in the southeast part of the subslide. The need to reduce driving force was not entirely compatible with the need to restore drainage. Although most fill placed in the depression added resisting force, the northern part did not.

Phase I grading, aided by removal of ground water from wells and low rainfall, caused the headward subslide to nearly stabilize. Monitoring along the northeast edge of the east-central subslide shows movement decreased from 0.72 inches per day (in/d) before grading to 0.36 in/d after grading (Fig. 12). The two central subslides slowed more than 50% as shown by a comparison of Figures 13 and 14.

Phase II Grading and Drainage Improvements

The success of Phase I grading made it desirable to perform additional grading as soon as feasible in order to minimize damage to Phase I drainage improvements and to make drainage improvements along Palos Verdes Drive. At the time, Palos Verdes Drive was in chaotic condition. All storm runoff from the roadway went into nearby fissures. Although the roadway had been moved landward on several occasions, it had migrated into the seaward subslide where secondary rotational slides continually disrupted it. No amount of maintenance work could have restored drain for more than a few days at a time. Therefore, the road would be rebuilt near its 1956 position in order to place it where movement could be controlled and where road fill would be beneficial because of a subhorizontal to landward slope on the slide base.

A cut of 500,000 cubic yards was designed at the head of the east-central subslide in order to reduce its driving force. About 200,000 cubic yards of this earth would be used to reconstruct Palos Verdes Drive and the remainder would be placed as a toe berm in the area east of Inspiration Point where the bases of the slide rises in a seaward direction (cross sections AA' and BB', Fig. 8). The initial plan indicated 40,000 cubic yards of earth would be removed from the headward subslide in an effort to complete its stabilization; however, this was eliminated from the final plan to reduce costs. In fact, the initial bids exceeded available funds. It was necessary to reduce the width of Palos Verdes Drive in order to lower costs. Grading was planned for late fall and early winter to obtain low bids during the slack part of the grading season without excess risk of high rainfall. Rebidding delayed grading but fortunately it was an unusually dry rainy season.

Phase II grading was performed between early January and mid March, 1988. During the first three months after grading, the east side of the slide did not appear to move in the area northward from Palos Verdes Drive. In June, cracks reappeared near a monitoring station at the northeast corner of the east-central subslide. As far as I could tell, the hiatus was real and represented relaxation of compression within the down slope part of the east-central subslide. During the remainder of 1988, movement averaged 0.03 in/d at this station (Fig. 12).

Figure 15 shows the annual rate of movement during the year after Phase II grading. Movement in the central subslides slowed to about 20% of what it was prior to Phase II grading.

September 1990 Grading

During 1989, the central part of the headward subslide continued to move at an average rate of 0.02 inches per day. The rate was gradually decreasing due to removal of ground water but movement would likely increase should rainfall be above average. Therefore, the decision was made to remove 60,000 cubic yards of earth from the up slope edge of the subslide, essentially as originally planned for Phase II grading. The slide base has an average dip of 14 degrees in the removal area. Grading was performed in September, 1990. My monitoring indicates no movement has occurred along the head of the slide since completion of this grading. The headward subslide is not expected to reactivate in the future, even during rainy periods. But only experience will prove if this is correct.

The earth which was removed from the headward subslide was placed as fill on the east side of the slide north of Palos Verdes Drive. Slide movement is nearly horizontal in this area; therefore, the fill should produce a net resisting force. However, the rate of movement increased during emplacement of the fill, as previously described. The rate subsequently slowed asymptotically to 0.040 in/d in mid 1991. The probable cause of the accelerated movement was consolidation of bentonite along the base of the slide and the consequent build up of pore-water pressure along the slip surface. My analysis of movement recorded at my monitoring station indicates the east side of the slide moved about two inches more than it would have if the fill had not been placed. But the increased movement should be compensated for by a decrease in movement after completion of consolidation.

Temporary Shoreline Protection

The need for permanent shoreline protection was recognized during planning for the stabilization of the Portuguese Bend landslide, but temporary protection appeared unnecessary. On January 17 and 18, 1988, while Phase II grading was getting underway, the most severe wave storm of this century eroded an estimated 15 to 25 feet of land from the toe of the slide and removed much of the rock that tended to armor the beach and retard erosion. During the next few months, wave erosion continued at a rapid rate. East of Inspiration Point, the seaward face of the toe berm was oversteepened by erosion and its lower part began to collapse into the surf. Further east, secondary rotational slides accelerated in response to the maintenance of a nearly vertical cliff by wave erosion. This caused a rapid decrease in surface elevation near the coast. At the same time, the slowing of slide movement by Phase II grading resulted in a net landward migration of the shoreline. These two factors had the combined effect of decreasing support to the slide mass further uphill and caused secondary sliding to propagate toward Palos Verdes Drive. Therefore, temporary shoreline protection was recommended.

Gabions were chosen as the least expensive and most environmentally acceptable method of temporary shoreline protection. They consist of plastic coated, galvanized wire mesh in the form of rectangular cages which are filled with beach rock and stacked in a stairstep pattern to form a protective wall along the beach. Near the end of 1988, gabions were installed along the western 800 feet of beach to protect the toe berm. They performed well during the first year and funds were obtained to extend the gabions 1,400 feet to the east side of the slide. However, just as construction of the new gabions began, a storm destroyed many of the original gabions. As soon as the gabion wall was breached, waves eroded behind the gabions and undermined them. Also, the impact of stones cut the plastic coating the wire and, wherever the plastic ruptured, saltwater corrosion weakened the wires and ultimately caused them to break. The 1,400 feet of gabions were installed but are being damaged by impact of stones and by tilting and toppling from upthrusting along the toes of secondary slides. They are likely to last no more than two years.

I have recommended against further use of gabions unless their shortcomings can be corrected. At present, it is unlikely that permission or funding can be obtained to install other types of temporary shoreline protection.

Future Mitigation

Minor funding is available for two projects at the end of this year (1991). First, the channel along Portuguese Canyon will be opened from Palos Verdes Drive northward to the head of the central subslides so runoff from the residential area west of the Canyon can be directed to the canyon and hence to the drainage system installed during Phase I grading. Residents are asked to conduct their runoff to the canyon. At present, most of the residential area drains into fissures. Second, about 30,000 cubic yards of earth will be removed from the head of the east-central subslide in order to reduce its rate of movement. The subslide is not expected to stop but should slow to about 0.01 in/d.

Five major mitigation projects remain: (1) the installation of permanent shoreline protection; (2) construction of a toe berm; (3) regrading of the seaward subslide; (4) redistribution of mass within adjacent parts of the central subslides, and (5) installation of a sewer system in the residential area. Upon completion of the project, each subslide should have a safety factor above 1.00. Thus, uphill subslides will not be pushing on downhill subslides.

The feasibility of constructing permanent shoreline protection is under study by the Army Corps of Engineers. Protection will most likely consist of a rock revetment constructed on inplace bedrock seaward of bedrock disturbed by sliding. A separate but coordinated project will be the construction of a toe berm behind the revetment. The berm will resist the forward movement of the slide and function as a counterweight in areas where the base of the slide ramps up from below sea level. Earth for its construction will come from the inland part of the seaward subslide. The ground surface will be lowered in areas where the base of the subslide dips seaward so as to reduce force driving the main slide. The ground profile between the toe berm and the head of the seaward subslide will be flattened as much as possible to minimize forces tending to cause rotational slumping. Thus, the three projects will be coordinated. These projects will also establish proper drainage seaward of Palos Verdes Drive.

An estimated 200,000 cubic yards of earth will be removed from the ridge north of Palos Verdes Drive and east of Portuguese Canyon in order to reduce the force driving the west side of the east-central subslide and to minimize forces tending to cause rotational slumping. Most of this earth will probably be used in construction of the toe berm. Part of it may be used to fill the hollow on the north side of Palos Verdes Drive to the west of Portuguese Canyon. This area is on the uphill side of the subsurface ridge in the slide base and the added weight of fill will resist slide movement. However, surface elevations will be kept below those existing prior to 1956 as a precaution against subsurface shearing through the ridge.

After slide movement stops, sewers will be installed in the residential part of the slide. Homeowners will pay for the sewers by means of a sewer district. Sewers will eliminate about 8,500 gallons of water per day currently being injected into the landslide. This will eliminate an important source of ground water recharge and will permit wells to lower the water table below existing levels.

Future Land Use

The future use of land within the Portuguese Bend landslide will depend upon the success in completing the proposed mitigation measures. If all proposed mitigation is completed, it should be possible to maintain the slide's safety factor at or above 1.2. This should permit restricted development. If mitigation is not completed and the slide remains unstable or in a quasi-stable condition, the slide area will most likely remain much as it is today. Assuming the slide is stabilized, land users will have to pay the cost of maintaining wells and drainage improvements and permanent monitoring of the slide to assure its continued stability. For this reason, it would be desirable to permit types of land use which generate the tax revenues or user fees needed to maintain slide abatement activities.

The city-owned land seaward of Palos Verdes Drive will most likely be used for recreational purposes. The use is not known at this time but, when determine, can be taken into account during the design of remedial grading. Slide abatement funds could be obtained from users fees.

The undeveloped area north of Palos Verdes Drive is currently under consideration for a golf course. I support such a use because surface drainage and ground water conditions are easily monitored and controlled in a golf course and there is good access for drilling and maintaining wells. The northeast part of the slide provides a suitable area for construction of a club house and related facilities. Here, the slide mass is thin and underlain by gently dipping bedrock. It should be feasible to remove and recompact the slide material to provide a stable base for construction.

Some individuals urge that the undeveloped land north of Palos Verdes Drive be left unimproved so that it can revert to native vegetation for wildlife habitat. Patches of native habitat can be designed into a golf course but I am opposed to leaving the land idle because it will generate no revenues for slide abatement and the uncontrolled growth of brush will create a fire hazard.

Future land use within the existing residential area of the landslide is clouded by several factors. This area, located west of Portuguese Canyon and north of Palos Verdes Drive, was divided into residential lots prior to the start of sliding in 1956. Many of the original homes were destroyed. Most of the 32 residences in this area are on grade beams or other special foundations that permit adjustments to accommodate ground deformation. All present homeowners purchased their homes long after movement began. They moved into the slide because prices and property taxes were low. Most are opposed to anything which will increase their taxes, including sewers. None really know where their land is. Most contend that their houses and landscaping mark their land and, therefore, their land has moved with the slide. But this creates impossible situations. Not only has the land surface been distorted by rotation, tilting, strike-slip faulting, dilation and compression, but, in addition, most of the original boundary monuments have been destroyed. When, in 1988, Palos Verdes Drive was relocated northward toward its preslide position, lot owners sued the city for placing the road on their property. The city won the lawsuit but the dilemma remains. If the homeowner's property has not moved from its original location, most homes are on someone else's land.

The only satisfactory way to resolve this issue is to void the original land descriptions and establish new ones. First priority must go to reestablishing the boundaries of developed lots, but much negotiation will probably be necessary. Lots cannot be restored to their original shaped because the east side of the residential area has moved as much as 400 feet further seaward than the west side. Also, vistas have changed. Some lots that originally had ocean views are now in hollows.

The problem of land ownership is more than academic. A sewer cannot be installed without easements and easements can't be granted without knowing who owns the land. Landowners might be asked to grant a blanket easement but they are unlikely to do so without a financial incentive. The same applies to drainage improvements.

An important unresolved issue is whether the owners of vacant lots will ever be able to build on their lots. At present, the city building code will not permit construction of habitable structures on sites that have a safety factor of less than 1.50 (forces resisting sliding are 1.5 times greater than shearing force tending to cause sliding). It is unlikely the safety factor will be above about 1.25 upon completion of slide mitigation. However, unlike other areas where the true safety factor is imprecisely known and no actions are taken to maintain stability after development occurs, the safety factor of this area will be known with good precision and factors affecting the slide will be monitored and abated when necessary. Therefore, if the slide is stabilized and the factor of safety raised to about 1.20 or higher, the carefully controlled development of vacant lots appears feasible. Most lots would require regrading, and special foundations would be needed. In addition, architectural designs would have to be approved by the Portuguese Bend Homeowners Association. Two things would be accomplished by permitting development. First, it would give the owners of vacant lots an incentive to make drainage improvements and cooperate in all other aspects of slide abatement. Second, it would increase lot values by at least ten times and in some cases as much as 100 times. This would provide the Rancho Palos Verdes Redevelopment Agency with tax funds to carry on abatement activities. Their funding comes from taxes generated by the increase in property values resulting from slide abatement.

Of course, only time will tell what really happens. Excellent progress has been made toward stabilizing the Portuguese Bend landslide but many fiscal, technical and political hurdles remain before the project can be completed.

ACKNOWLEDGMENTS

Special thanks are due to Scott Thompson for preparing computer-graphic illustrations and to Bernard Pipkin for reviewing the manuscript and making helpful suggestions.

REFERENCES

Bryant, M. E., 1982, Geomorphology, neotectonics, and ages of marine terraces, Palos Verdes Peninsula, in Cooper, J. D., comp., Landslides and landslide mitigation in southern California: Assoc. of Engineering Geologists, Southern California Section, p. 15-25.

Conrad, C. L., and Ehlig, P. L., 1983, The Monterey Formation of the Palos Verdes Peninsula, California - an example of sedimentation in a tectonically active basin within the California Continental Borderland, in Larue, D. K., and Steel, R. J., (eds.), Cenozoic marine sedimentation, Pacific margin, U.S.A.: Pacific Section, Soc. Econ. Paleontologists and Mineralogists, p. 103-116.

Easton, W. H., 1973, Earthquakes, rain, and tides at Portuguese Bend landslide, California: Assoc. Engineering Geologists Bull., v. 10, p. 173-194.

Emery, K. O., 1967, The activity of coastal landslides related to sea level: Rev. Geog. Phys. et Geol. Dynam., V. 9, p. 177-180.

Jahns, R. H., and VonderLinden, K., 1973, Space-time relationships of landsliding on the southerly side of Palos Verdes Hills, in Moran, D. E., Slosson, J. E., Stone, R. O., and Yelverton, C. A., eds., Geology, seismicity, and environmental impact: Assoc. Engineering Geologists, Special Pub., p. 123-138.

Kerr, P. F., and Drew, I. M., 1969, Clay mobility, Portuguese Bend, California: Calif. Div. Mines and Geology Special Report 100, p. 3-16.

Kew, W. S., 1926, Geologic and physiographic features in the San Pedro Hills, Los Angeles County, California: Oil Bulletin, v. 12, p. 513-518.

MacKintosh and MacKintosk, 1957, Report of earth movement, Portuguese Bend, California: unpublished technical report, 16 p.

Merriam, R., 1960, Portuguese Bend landslide, Palos Verdes Hills, California: Jour. Geology, v. 68, p. 140-153.

Rowell, H. C., 1982, Chronostratigraphy of the Monterey Formation of the Palos Verdes Hills, in Cooper, J. D., (comp.), Landslides and landslide mitigation in southern California: Assoc. of Engineering Geologists, Southern California Section, p. 7-13.

VonderLinden, K., 1972, An analysis of the Portuguese Bend landslide, Palos Verdes Hills, California: Stanford Univ., unpubl. Ph.D. thesis, 260 p.

Woodring, W. P., Bramlette, M. N., and Kew, W. S. W., 1946, Geology and paleontology of the Palos Verdes Hills, California: U. S. Geol. Survey, Prof. Paper 207, 145 p.

AEG•GRA 2000
FIELD TRIP GUIDEBOOK

FROM THE PACIFIC OCEAN TO THE SIERRA NEVADA: TAMING SHAKY GROUND

ASSOCIATION OF ENGINEERING GEOLOGISTS
GROUNDWATER RESOURCES ASSOCIATION
JOINT ANNUAL MEETING 2000
SEPTEMBER 19 – 26
DOUBLETREE HOTEL
SAN JOSE, CALIFORNIA

LIVING WITH MOVING GROUND –LANDSLIDES AND COASTAL EROSION IN SAN MATEO COUNTY, CALIFORNIA

William F. Cole, Ted M. Sayre, Mark G. Smelser, Edward "Sandy" Hay, and John M. Wallace
(Cotton, Shires & Associates, Inc.), Los Gatos, CA;
Joan Van Velsor and Thomas G. Whitman (Caltrans), Sacramento, CA
Chuck Snell (Gilpin Geosciences, Inc.), Mill Valley, CA; and
D. Scott Kieffer (Jacobs Associates, Inc.), San Francisco, CA

1.0 Geologic Setting

Introduction

This field trip will examine landslides along the margins of the northern Santa Cruz Mountains. We will travel northwestward from San Jose, along the eastern margin of the Santa Cruz Mountains, to the community of Millbrae, and then traverse westward across the Santa Cruz Mountains to Daly City. In the afternoon, we will travel southward along the coast to Half Moon Bay, and return to San Jose along the eastern margin of the mountain range. Figure 1 depicts the regional setting of the field trip, as well as the primary field trip stops.

The Santa Cruz Mountains straddle the San Andreas fault zone for approximately 100 km, from about 30 km south of San Francisco to just east of the community of Watsonville. These mountains are one of the major ranges in the Coast Ranges geomorphic province, and are composed of independent fault blocks with different stratigraphic and structural histories. The northern portion of the range is west of the fault, and the southern portion is east of the fault.

San Andreas Fault Zone

Despite this trip's focus on landslide processes, the terrain through which we will travel is dominated by one of the world's most spectacular tectonic features – the San Andreas fault (SAF). For hundreds of kilometers, the SAF is the boundary between basement rocks of the Francican Complex and the Salinian Block. The Franciscan Complex (Jurassic and Cretaceous) is present to the northeast of the SAF, and consists of mafic and ultramafic basement rocks and sedimentary rocks that were deposited in a deep ocean environment, then accreted at the western margin of the North American plate. Most Franciscan rocks in the field trip area are part the Central tectonic belt (Irwin, 1960; McLaughlin et al., 1988), which is a tectonic melange of late Jurassic to early Cretaceous age. Many of the larger blocks within the Central belt melange are given separate terrane names. The terranes are primarily gently dipping thrust sheets that trend northwesterly and dip northeasterly (Sullivan and Galehouse, 1991).

belt melange are given separate terrane names. The terranes are primarily gently dipping thrust sheets that trend northwesterly and dip northeasterly (Sullivan and Galehouse, 1991).

On the southwest side of the SAF, Cretaceous and Tertiary sedimentary and volcanic rocks were deposited on a continental block of granitic basement rocks (upper Cretaceous), referred to as the Salinian Block (Clark and Brabb, 1978). The Tertiary section consists predominantly of marine classic sedimentary rocks ranging in age from Paleocene to Pliocene (Clark and Brabb, 1978). These deposits include a thick early Tertiary sequence that accumulated in deep marine basins and a thick late Tertiary sequence of predominantly diatomaceous beds that accumulated in sediment-starved basins (Sullivan and Galehouse, 1991). The rocks of the Salinian Block originated south of their present location; however, there has been some debate about the distance traveled by the Salinian Block along the transform (strike-slip) system (Page, 1989). Hill and Dibblee (1953) suggested that the Salinian Block was displaced several hundred kilometers from the southern part of the Sierra Nevada. Evidence for this model includes similarity of the Salinian rocks to granites along the crest of the Sierra Nevada in terms of age, mineralogy, and chemistry.

Approximately 28 million years ago, the Pacific plate first came into direct contact with the North American plate, creating a transform boundary. Since that time, there have slight shifts in both the direction and the rate of movement of the Pacific plate with respect to the North American plate. Geologists concur that one of the more notable of these changes, a shift to slightly oblique movement, caused convergence between the Pacific and North American plates, producing the northwest-oriented mountains of the Coast Ranges beginning approximately 3-4 million years ago. The Coast Ranges are actively being uplifted in the modern tectonic regime. During the Bay Area's most recent major earthquake, the 1989 Loma Prieta event, the Santa Cruz Mountains west of the SAF were uplifted as much as 1.2 meters. The Peninsula Segment of the SAF is estimated to have been initiated between 1 and 2 million years ago. Several paleoseismic studies of the Peninsula Segment yield displacements of approximately 25 kilometers (Wakabayashi and Hengesh, 1995; Jachens, et al., 1996). The most widely reported slip rate estimate, which was determined from studies at the Filoli Estate near Woodside, is 17 +/- 3 mm/year (Clahan, et al., 1995).

Pilarcitos and San Gregorio Faults

The SAF is well defined by seismic activity and dramatic geomorphic expression. However, contrary to the above discussion, the SAF does <u>not</u> form the fundamental boundary between Franciscan rocks and the Salinian Block in the San Mateo County region. The juxtaposition of basement rocks in this region is marked by the Pilarcitos fault (PF), which extends from Black Mountain to the offshore environment at Rockaway Beach in Pacifica (Figure 1). Many geologists have assumed that the PF was the principal strike-slip boundary of the San Andreas fault zone on the San Francisco Peninsula, and that the SAF is the product of a geologically recent (1.e., 1-2 million years ago) eastward shift of tectonism. However, this model has been challenged recently by Wakabayashi (1999), who argues against significant Cenozoic slip on the PF, and suggests that the Peninsula Segment of the SAF represents a shift from faults located east of the San Francisco Peninsula.

The San Gregorio fault (SGF) is a major, right-lateral strike slip fault that forms the principal active tectonic structure west of the SAF in central coastal California (Figure 1.0). Recent

investigation in the Moss Beach-Seal Cove area by Simpson and Lettis (1999) led to recognition of offset alluvial deposits associated with a paleovalley in the uplifted fault block. Simpson and Lettis (1999) estimate a late Pleistocene slip rate of between 3.5 and 4.5 mm/yr. for the eastern, on-land trace of the SGF, and suggest that an offshore (western) SGF trace may contribute a similar amount of slip. Thus, the total slip across the entire zone may be 6 mm/yr. or greater.

Along the San Mateo coastline, the SGF extends for approximately 3 km, from Pillar Point to Moss Beach, (Figure 1). Along this segment, which is sometimes referred to as the Seal Cove fault, the on-land portion of the fault zone forms the eastern margin of an uplifted fault block. The western margin of this block appears to be bounded by a second trace that has been seismically imaged offshore.

Coastal Erosion

The San Mateo County coastline is an abrupt and rugged transition between land and sea. Factors contributing to the shoreline's sense of isolation include prevailing offshore winds, heavy surf, juxtaposition of resistant rock with softer rock, and narrow beaches. The coastline can be divided into several linear coastal segments with endpoints defined by locations where right-lateral faulting has resulted in the juxtaposition of relatively hard bedrock headlands and softer Cenozoic rocks in the surf zone (e.g., Mussel Rock, Point San Pedro and Pillar Point). These relatively straight coastal segments (Daly City, Pacifica and Half Moon Bay shorelines) are locations where weak, relatively young sedimentary rocks are subjected to erosion from wave attack. Rates of cliff retreat in these areas are often on the order of one foot per year. In some places average erosion rates of 5 to 10 feet per year have been recorded (Griggs and Savoy, 1985).

Certain sand-starved, under-nourished beaches are not sufficient to create protective buffer zones between breaking waves and cliff faces. Nearshore currents generally transport sand along the coast to the south. However, various flood control and irrigation projects in the Sacramento delta region have reduced fresh water flow levels and the capacity to transport sediment load through the Golden Gate. In addition, numerous urban storm drainage improvement projects have reduced sediment loads in smaller streams. The combined impact of gradually rising ocean levels (due to global warming) and a reduced capacity to deliver sediment to the coast may be shifting natural balances to favor increased rates of shoreline retreat. We will view and discuss aspects of coastal erosion in the Pacifica and Seal Cove areas.

2.0 CRESTVIEW DRIVE/PINEHURST COURT LANDSLIDE, MILLBRAE

Introduction

During the early morning hours of March 8, 2000, a portion of a very steep, previously graded slope failed between Crestview Drive (upslope) and Pinehurst Court (downslope), in the City of Millbrae, California. The landslide, approximately 250 feet in width, 350 feet in length, and 75 feet in depth, impacted the rear portions of 5 residential structures along Pinehurst Court, with one structure being knocked completely off of its foundation. The landslide occurred on the heels of one of the wettest Februarys on record, with 21 out of 29 days recording measurable rainfall. The landslide gave

earlier indications of failure, when a large headscarp crack developed during the very heavy, "El Nino" winter of 1997-1998. The landslide started moving again in late February-early March 2000, following a period when a nearly continuous parade of Pacific storms dumped approximately 15 inches of rain within a period of approximately 4 weeks. By Monday, March 6, the headscarp had enlarged to nearly 25 feet in height as slow landslide movement continued; however, no obvious toe had developed at the base of the slope. A pronounced bulging and oversteepening of the mid-body of the landslide was evident, prompting City officials to 'red tag' homes along Pinehurst Court with another storm due in on March 7. Nearly one inch of rain fell on the night of March 7 and into the morning of March 8, resulting in the failure of the oversteepened mid-portion of the landslide. No physical injuries were sustained as a result of the landslide.

Geologic materials exposed along the graded hillside are primarily Franciscan Complex interbedded sandstone and shale; however, the landslide debris contains a wide variety of Franciscan Complex melange materials, including sheared shale, greenstone, chert, and sandstone. Pliocene-Pleistocene Merced Formation sandstone is exposed along the upper 6 feet of the headscarp.

History

The Crestview/Pinehurst landslide (CPL) failed within a very steep (30 to 40 degree inclinations), northeast-facing, graded hillside between residential tracts located along Crestview Drive, at the top of the slope, and Pinehurst Court, at the base of the slope (Figure 2). The landslide occurred exclusively on private property, but impacted a City sanitary sewer easement. Initial grading at the site occurred in the 1940's and consisted of quarrying operations to provide fill material for runway construction at San Francisco International Airport. The quarrying operations appear to be concentrated primarily to the east of the hillside between Crestview Drive and Pinehurst Court, apparently due to the presence of the more easily excavated Merced Formation sandstone in this area. The Merced bedrock provides more suitable qualities for engineered fill, in comparison to the Franciscan Complex melange materials. Following quarrying operations, residential development occurred in the late 1950's with the construction of Crestview Drive and Pinehurst Court. Most of the residential structures were constructed by 1959.

The hillside between the two subdivisions, which exhibits nearly 150 feet of relief, was initially cut to slope inclinations of approximately 1.5:1 (H:V) without mid-slope benches or V-ditches. During the first winter, the hillside experienced numerous, shallow landslide failures into the rear yards of the Pinehurst Court residences, prompting mitigation measures which included grading of the slope to develop benches, or terraces, with concrete V-ditches. The graded slope and V-ditches appear pristine in the 1961 aerial photographs. From 1961 to 1997, progressive deformation of the slope can be observed on aerial photographs, as V-ditches were gradually filled with debris or removed by shallow landsliding. The heavy rainfall associated with the El Nino winter of 1997-1998 resulted in the generation of an incipient headscarp in the rear yards of about 5 or 6 Crestview Drive residences. This ground crack was characterized by nearly 3 feet of vertical movement and 1 foot of horizontal movement. Homeowners in the area probed the crack and were able to extend a rod 13 feet into the scarp without hitting bottom. The City retained a geotechnical firm to provide an evaluation of the slope conditions. The preliminary findings of the geotechnical evaluation pointed to several contributing factors to slope instability, including: high groundwater, unfavorable bedding or fracturing, poor drainage conditions due to deteriorating V-ditches, sewer line rupture, and previous

landsliding at the site. Recommendations were provided that included a proposed investigation of the incipient landslide and implementation of winterization measures; neither of which was performed.

Regional Geology

The CPL is located along the San Francisco Peninsula, approximately 10 miles south of the City of San Francisco. The San Andreas fault is located approximately 1,500 feet to the west of the landslide, with the rift basin covered by San Andreas Reservoir (Figure 3). As described in Section 1.0 above, the San Andreas fault in this area does not form the boundary between Salinian rocks and Franciscan rocks, as is the more normal case further north and south. Rather, the Pilarcitos fault to the west controls what is inferred to be the paleo-plate boundary. The Serra fault is located near the toe of the CPL and thrusts Franciscan Complex bedrock over Pliocene-Pleistocene Merced Formation sandstone. At the headscarp of the CPL, a sliver of Merced Formation sandstone can be observed lying unconformably on Franciscan bedrock, with the depositional contact inclined to the west. Prominent seepage occurs at this contact where relatively permeable sandstone provides a conduit for groundwater perched atop the relatively impermeable, sheared melange.

Landslide Failure Mechanisms

Following intense rainfall in February 2000, the landslide began moving on the order of inches to feet per day in early March 2000. Dramatic enlargement of the headscarp was noted during this period without the development of an obvious toe. Subsequently, we observed bulging in the toe region, and up to 5 degrees of tilt in utility poles and trees along the base of the slope on March 6, prior to the March 8 failure which impacted the residential structures. It was apparent on March 6, that significant oversteepening of the mid-portion of the landslide was occurring, with prominent backscarps (compressional thrusting) developing within the landslide mass. In addition, the pre-existing, graded slope angle of 33 degrees was now close to 50 degrees, and it was apparent that the upper portion of the landslide was in full failure mode with the toe of the landslide providing sufficient resistance to prevent catastrophic failure. Heavy rainfall on the night of March 7 resulted in a secondary landslide failure of the oversteepened, mid-portion of the main landslide that was buckling or thrusting into a critically unstable position. The saturated debris flowed into the rear portion of Pinehurst Court residences. At the time of this writing (May 2000), it remains unclear as to whether the toe of the main landslide ever ruptured to the ground surface, because it is now covered with debris from the secondary slope failure (Figure 2).

Consequences

The CPL resulted in destruction, severe damage and economic losses to approximately 10 residential structures. The contributory factors leading to landslide failure are complex and will likely be investigated in upcoming months and years. Full stabilization of the CPL will be very expensive (estimated to be more of 6 million dollars) and, because it is confined to private property, there is no immediate source of available funding. The lack of subsurface investigation and instrumentation during the incipient stages of the failure has prevented the gathering of critically important data on the depth of sliding. Consequently, after-the-fact subsurface investigations will attempt to decipher shears within the Franciscan complex melange from the basal rupture surface of the landslide. Without the aid of inclinometer data gathered during the active failure, this task could be extremely difficult. The success of accurately delineating the deepest landslide failure surface will be

essential to the long-term performance of the selected stabilization design. In addition, when mitigation measures eventually take place, the field geologists monitoring the keyway excavation will not have inclinometer data to aid in determining the depth of landsliding, and will be forced to distinguish between older melange shears from active landslide basal rupture shears.

Of the many legal claims presently being contemplated, one of the more unique is against the City of San Francisco, owner of San Andreas Reservoir. The allegation is that the City, by owning the reservoir, is responsible for subsurface migration of reservoir water to the slope between Crestview Drive and Pinehurst Court, thereby causing saturation of the failed hillside (Figure 3).

3.0 WESTLINE DRIVE, DALY CITY – MUSSEL ROCK LANDSLIDE

Introduction

The Mussel Rock landslide complex comprises 112 acres in the southwest corner of Daly City, California. The landslide complex is a composite of slumps shed from the lower Merced Formation. This area marks the point where the San Andreas fault trends northwestward out to sea just off the coast south of San Francisco (Figure 1). Evidence of the 1906 earthquake rupture is subtly exposed in the Mussel Rock area and the epicenter of the 1957 San Francisco earthquake was in this locality.

In the Mussel Rock area, friable marine sandstone of the Pliocene-Pleistocene Merced Formation nonconformably overlies greenstone and serpentinite of the Jurassic-Cretaceous Franciscan Complex. Wave erosion, earthquake faulting, and composite slumping have reduced the Merced Formation into a large active landslide complex. The composite slumping has created steep scarps that have coalesced to become cliffs and bluffs, up to 120 feet high, that wrap around the area in a horseshoe shape. The landslide debris is a composite mass of hummocky topography, smaller slides and flows, and V-shaped ravines (Figure 4). The volume of landslide debris is estimated at 9 million cubic yards, and the numerous springs within the deposit indicate that the mass is saturated. The toe of landslide complex is generally considered to lie offshore (Smelser, 1987).

The first human occupation of the area is indicated by Ohlone Indian artifacts that are dated to be 1,200 years old (Daly City Department of Community Development, 1984). In 1874, Richard M. Tobin blasted a tunnel through a coastal headland composed of Franciscan Complex greenstone. This tunnel was to be an integral part of a beach road for horses and carriages. However, the seasonal fluctuations of beach sand caused the tunnel floor to be about three feet above the beach during the summer months. Consequently the beach road was abandoned. From 1905 to 1920, the Ocean Shore Railroad route was maintained along the coastline, and part of the route traversed the toe platform of the Mussel Rock landslide complex. Portions of the railroad were destroyed during the 1906 earthquake and the railroad was eventually forced out of business due to financial problems. In 1936, the Coastal Highway was constructed along the former railroad route. The highway was also plagued by landslide activity and was finally abandoned in this area after the 1957 earthquake. During the 1960s, urban development covered the crescent shaped crown surrounding the Mussel Rock landslide. The subdivision grading included fills ranging from about 20 to 40 feet deep in the area of the landslide complex. As shown on Figures 5 and 6, fill was placed within the limits of the landslide identified with aerial photographs.

From 1963 to 1979, a sanitary landfill was operated within the more distal portion of the landslide debris between the highway right-of-way and the zone of wave erosion operation. Consequently, approximately 16 years worth of urban refuse is buried within the landslide debris closest to the ocean. Urban refuse is visible throughout this area and the odor of landfill gas is detectable at several locations around the site. A rip-rap revetment was constructed along the beach to protect the landslide debris and urban refuse from wave attack.

Background

The Westline Drive Landslide Complex (WDLC) has affected many homes comprising a subdivision that was developed in the late 1950's and early 1960's. This area experienced significant landslide movements shortly after the subdivision construction, and movements since that time have continued to afflict the area.

During the winter of 1962-1963, ground movements occurred within several residential lots north of Westline Drive, near the 90-degree bend in the road. A geotechnical report addressing the ground movements concluded that an earthquake on the San Andreas fault could cause 10 feet of sudden ground movement in this area, with potential dire consequences. As a result, in 1972, 11 homes, together with the deep fill on which they were founded, were removed from the site (these homes occupied the undeveloped land adjacent to the northern edge of Westline Drive).

Subsequent ground movements have occurred gradually, with notable deformation during years of heavy rainfall. Landsliding destroyed a house in 1973, and heavy rains during the winters of 1981-1982 and 1982-1983 caused accelerated ground deformations. In the late 1980s, 3 houses were removed from the eastern scarp because of failures along the steep bluff face. Additionally, residents along Westline Drive reported that extensive cracking of the roadway occurred in response to the 1989 Loma Prieta earthquake (peak ground accelerations are estimated to have been on the order of 0.15g in this area). The most significant recent damage occurred in response to the heavy 1997-1998 El Niño rains. Since that time, parts of the street and associated infrastructure have displaced up to several feet. Several more houses have now been declared uninhabitable along Westline Drive.

Site Conditions

Much of the landsliding affecting Westline Drive is along the Alquist-Priolo Zone established along the San Andreas fault (CDMG, 1982). Surface ground rupture from the 1906 San Francisco Earthquake has been mapped as trending northwest through the intersection of Westline and Longview Drives, and through the toe of the WDLC (Figure 5).

The Westline Drive area is underlain by Franciscan Complex rocks at depth, with overlying friable sedimentary rocks of the Pliocene to Pleistocene Merced Formation. The Merced consists of interbedded siltstone, sandstone and claystone that dips moderately steeply (about 40 degrees) to the northeast. A recent subsurface exploration and monitoring program indicates that landsliding is occurring within the Merced and overlying subdivision fill (Figure 6).

Landslide Characteristics and Behavior

The landslide affecting Westline Drive is part of an active complex having an estimated volume of several hundred thousand cubic yards. The WDLC is also damaging the Mussel Rock parking lot and the retaining wall behind the BFI Transfer Station (to the west). In general, these slide movements have occurred along the oversteepened southern flank of the much larger MRLC.

Slope inclinometers along Westline Drive have recorded sliding at depths ranging from 80 to 120 feet beneath the roadway. Triaxial and direct shear tests conducted on highly plastic black clay seams (thin interbeds) retrieved from boreholes, within the interval sliding, yielded residual friction angles of about 12 to 14 degrees. Considering the orientation of bedding in the Merced, it is conceivable that movement is occurring, in part, by oblique sliding along such weak clay beds. Complex block gliding is believed to represent the primary mechanism of sliding, with some elements of classical slumping.

Based on inclinometer data collected over the past year, the rate of slide movement is greatest between March and July, and the sliding rate decreases notably between August and December. The faster rates of movement correlate to higher groundwater elevations in the slope, which have been measured to range from about 25 to 45 feet below Westline Drive.

Conclusions

The WDLC has resulted in tragic socioeconomic losses over several decades. In its present condition, the WDLC will continue to slowly damage public and private improvements, and the boundaries of movement may retrogress over time. Considering the proximity of the San Andreas Fault, seismic slope stability is a major concern for this area. A nearby strong event on the San Andreas could induce very violent ground shaking, and tens of feet of landslide displacement could potentially occur during such an event.

Notwithstanding seismic loading, movement of the MRLC away from the WDLC toe places further demand on stabilization schemes. Long-term stabilization should incorporate measures to effectively decouple these two slide complexes. Such measures could be realized at an extremely high cost, but to fully mitigate the seismic slope stability hazard is considered economically unfeasible.

4.0 ESPLANADE AVENUE, PACIFICA: MITIGATION OF 1998 EL NIÑO SEA CLIFF FAILURE

Background

In February 1998, several residences on the seaward side of Esplanade Avenue were in immediate danger of collapse due to failure of the steep sea cliff. Parts of some of the houses had already fallen over the bluff, others were overhanging the bluff, and a few were intact near the edge of the bluff. House site stability at the top of the bluff is adversely affected by the weak nature of the oversteepened alluvial sediments comprising the lower to middle bluff, the steepness of the bluff face, groundwater seeping from the bluff face, and a 10-foot thick layer of uncemented dune at the top of the bluff upon which the houses were built. In addition, rapid bluff retreat represented a threat to

Esplanade Avenue, so it was essential to implement appropriate coastal protection measures if loss of this public road and associated utilities was to be prevented.

The northern Pacifica coastline has been undergoing progressive sea cliff retreat with a long-term average erosion rate of approximately 0.5 to 2.0 feet per year (Lajoie and Mathieson, 1985). It is not unusual for several years to pass with little noticeable erosion, only to be followed by several feet of the bluff retreat within a single day. In 1949, the length of bluff-top back yards (west of the house sites) was approximately 50 feet. Figure 7 illustrates local retreat of the sea cliff between 1956 and 1998 based on aerial photographs.

Past efforts to stabilize the bluff have been largely unsuccessful. In response to rapid local bluff retreat that occurred during the 1982 El Niño event, a homeowners group funded construction of a rock revetment. Apparently, the lack of adequate maintenance coupled with design flaws (rock size was relatively small and the rock was apparently not keyed into bedrock materials) resulted in a short life span for this structure. Although relatively intact sections of this revetment were still visible in 1996, by March 1998 the revetment had been reduced to an irregular scattering of boulders across the narrow sandy beach.

Increased rates of bluff erosion in early 1998 resulted from severe winter waves and high tides, coupled with a diminishing natural resupply of sand to the shoreline. Snell et al. (2000) conclude that the specific time coincidence of low barometric pressure, southerly winds and wave height, combined with anomalous high tides, resulted in unusually adverse ocean surface factors during the first and third weeks of February 1998 (Figure 8). The result was almost 50 feet of bluff retreat during that month, and the eventual demolition of ten homes. Erosion at the base of the bluffs and landsliding of the undermined upper parts of the bluffs were the primary processes of sea cliff retreat. In addition, increased water seepage from the bluff face softened and loosened bluff sediments, contributing to instability and retreat.

Site Geology

Conspicuous within the City of Pacifica are several broad, relatively flat-floored valleys that open to the ocean suggesting periods of channel incision into bedrock followed by fluvial deposition. Sea level was more than 100 feet lower than present during the last major ice age. During periods of advancing and retreating glaciation, and final melting of the large continental glaciers (initiated approximately 15,000 years ago) sea level rose changing the base levels of coastal drainage channels. Consequent reductions in stream gradients resulted in lower flow velocities and burial of eroded channels with alluvial deposits. Near Esplanade Avenue, subsequent tectonic uplift and coastal erosion has notched sea cliffs into these alluvial deposits. This recent geologic history has resulted in the deposition and exposure of the relatively young, poorly consolidated sediments that form the local bluffs. Periods of rapid bluff retreat can be seen as one consequence of this dynamic geologic setting.

In the study area, 'greenstone' bedrock of the Franciscan Complex lies below the base of the bluff. This rock is a relatively firm to hard, altered submarine basaltic assemblage composed of pillow lavas, flows and breccias. It is overlain partially by beach sand in the tidal zone, and by an approximately 50-foot thick section of poorly lithified Quaternary alluvial fan deposits (coarse basal breccia, intervals of poorly indurated silts, and fine to medium grained sands and gravels) exposed in

the lower portion of the bluff. The alluvial deposits contain a few thin beds of beach sands and are overlain by a clayey, dark brown soil horizon, approximately 5 feet thick. Capping the soil horizon, and extending to the current ground surface, is a 10-foot thick layer of dune sand (Figure 9).

Revetment Design

Selection of a rock revetment design involved consideration of anticipated long-term performance, construction cost, and policies of the California Coastal Commission. Design criteria for the revetment reflect consideration of: nearshore bathymetry, water level, wave height, maximum scour elevation, beach slope, and bedrock material properties according to Chapter 7 of the U.S. Army Corps of Engineers Shore Protection Manual (1984). Both 50-year and 100-year recurrence interval oceanographic conditions were evaluated in our analysis.

The **design water level** is the maximum possible still water elevation and is largely controlled by high tide levels. However, during storm conditions, the sea surface rises along the shoreline (super-elevation) and allows waves to break just before, or at, the revetment structure. Super-elevation of the sea surface was accounted for by: wave set-up (1.0 to 2.5 feet), wind set-up and inverse barometer (0.5 to 1.5 feet), wave group effects (1.0 to 2.5 feet) and El Niño thermal water expansion effects (0.5 to 1.0 feet). These factors are added to the 100-year recurrence interval maximum tide elevation to determine the maximum still water elevation.

Locally, offshore wave heights exceeding 20 feet are not uncommon during winter storms. However, the design wave condition for a shoreline structure is generally not the largest wave, because the largest waves break offshore in water depths approximately equal to the wave's height. The largest **design wave force** will occur when a wave breaks directly on the shoreline structure. The largest wave that can break on the revetment is determined by the depth of water at the toe of the structure. The resulting wave height is 12.0 feet for the 100-year recurrence interval.

As waves encounter a revetment, they break and the water rushes up the face of the structure. Often, wave run-up and overtopping strongly influence the design and cost of coastal projects. **Wave run-up** is defined as the vertical height above the still water level to which a wave will rise on a structure of infinite height. **Overtopping** is the flow rate of water over the top of a revetment as a result of wave run-up. The run-up analysis is performed to determine the design height of the revetment so that no overtopping can occur. Overtopping of the structure would exacerbate erosion of the alluvial deposits comprising the middle of the bluff. The final design elevation of the revetment crest was increased from +20 to +26 feet MSL to allow for settling due to scour at the base of the revetment, dislodging and settling of the armor stone, and to provide some buttressing of a relatively weak sand lens on the bluff face.

The primary factor in determining the stone size is the incident wave energy, which is proportional to the wave height. The calculated individual armor stone size for the 50-year oceanographic conditions is approximately 5 tons. The individual armor stone size for the 100-year wave conditions is approximately 10 tons. Ultimately, an armor stone size of 8 to 10 tons was selected for project design. A second core stone size category was also utilized. Core stone weight ranged from 100 pounds to 5 tons. The smaller size fraction of the core stone was placed deepest within the revetment. The armor stone consisted of select quarry rock free of open fissures and apparent planes

of weakness. Ideally, armor stone should be rough and angular in shape, with the least principal dimension not less than one-third the greatest dimension. Such relative shape dimensions can improve interlocking qualities of the revetment if individual stones are placed in an optimal manner.

Construction Challenges

Construction of the revetment was completed during the summer and fall of 1998. Suitable, large armor stones in the 8 to 10 ton size range were difficult to obtain because significant demands for large rock had been placed on local quarries during El Niño conditions. Rock samples from four quarries, with haul distances of approximately 40 to 100 miles to the site, were delivered for detailed examination. Samples included limestone, graywacke sandstone, welded volcanic tuff and a metaconglomerate. Submitted rock types, other than the limestone, generally had favorable density and durability properties, and were all used to construct the revetment. Stone placement was possible only during periods of low tide, because the revetment keyway was excavated into Franciscan bedrock below mean sea level. Sufficient stone for the construction of a 100-foot segment of the revetment was delivered to a staging area high on the beach, and rock was placed in the keyway segment excavated the previous day.

Engineering efforts employed to arrest coastal erosion processes should be viewed as temporary solutions that are often not free of collateral impacts. In the case of engineered revetments or seawalls, these structures are typically constructed at locations that already have inadequate protective beach or dune buffer zones. The generally deficient beaches seaward of proposed sites for protective engineered structures often become narrower and steeper with time after the protective structure is installed. These changes may result from increased rebound energy of waves reflected off relatively hard, fixed engineered structures and the reduction of cliff detritus descending to the beach. Consequent alteration to the beach and near shore profiles can ultimately undermine foundation support of the protective structure. It is also possible that continued erosion of any adjacent vulnerable coastal bluffs may result in the protective structure being gradually outflanked. With the best revetment or seawall designs, protective success over the time period of a human life span can occasionally be achieved. From a long-term geologic perspective, protective revetments placed within wave impact zones will eventually face inevitable consequences. Utilization of protective design alternatives in dynamic coastal zones should follow full consideration of engineering solution costs and benefits, impacts to beaches and adjacent properties, and alternative hazard avoidance/relocation options.

5.0 Devil's Slide, State Highway 1

Background

Devil's Slide is a large bedrock landslide complex, extending from the ridge crest (at approximately elevation 900') down to at least sea level with a width of approximately 4,000 feet. State Highway 1 crosses the landslide between elevations 450 and 300 feet. Local geologic conditions are characterized by steeply dipping Paleocene and Cretaceous sedimentary rocks and underlying Jurassic-Cretaceous granitic rocks. The relationship between the two rock types is complex due to past faulting, folding and landslide movement. The most active failure surface is approximately 150 feet

below the ground surface; however, a number of discrete failure zones have been identified within the landslide complex by monitoring of slope inclinometers since 1989 (Figure 10). It appears that the granitic rocks are not involved in the landsliding.

The landslide complex is visible on an 1866 topographic map of the coast, and has frustrated all transportation efforts since 1897, disrupting in turn a county road, a railroad and a state highway. The first County road was built across the face of the ocean facing cliffs of Montara Mountain. This road crossed Devil's Slide at approximately elevation 400'. By August 2, 1897 local residents were petitioning the County Board of Supervisors "*The San Pedro Road connecting the Half Moon Bay colony with the Town of Colma is in a most deplorable and dangerous condition...The road...is an abomination and merely an apology for a road...*". The county road was abandoned in 1914, and replaced with a bypass road over San Pedro Mountain.

Ocean Shore Railroad was incorporated in the early 1900's with the intent of constructing a double track electric railroad from San Francisco to Santa Cruz. The railroad alignment began near 12th and Mission streets in San Francisco, and reached the coast near Thornton Beach in Daly City. From that point southward, the railroad alignment clung to the steep and unstable coastline, crossing the numerous gullies and arroyos on trestles and fills/culverts. In the vicinity of Devil's Slide, the railroad alignment pierced San Pedro Point with a 400' long tunnel at approximately elevation 50', then began a long, 2% grade, ascent across the high, ocean fronting cliffs, to reach a high point on the railroad profile at the "saddle cut" of present Highway 1. Severely damaged in the 1906 earthquake, and by chronic landsliding, the railroad was abandoned in the 1920's.

In 1933, 1600 miles of County roads were incorporated into the State Highway system (Chapter 767 of the Statutes of 1933). Consequently, the State Division of Highways acquired the Ocean Shore Railroad right of way by condemnation, and constructed Highway 1 (then known as Route 56) in it's present location. Construction and maintenance of the highway was an arduous task. As described by Construction Engineer E.G. Poss in 1937: "*The location of the highway along the cliff face required men with the agility of mountain goats, courage, experience and a complete lack of nerves...The contractor's pioneering operations in this area are also an epic in themselves. To launch 15 ton cats into space, and carve a precarious foothold in the cliffs could be entrusted only to a few specially skilled and daring cat skinners...On several occasions shovels, cats and compressors were covered by great slides, but only one worker was injured.*"

Following opening of the roadway in 1936, chronic landsliding and road closures plagued this route, and major road closures occurred in every subsequent decade. In the late 1950's, the State Highway Department determined that the alignment across Devil's Slide should be abandoned and that a new bypass route, around the inland margin of landsliding, should be constructed. By 1970, a 6.8-mile inland bypass was ready for construction. The construction contract was halted by a lawsuit filed by the Sierra Club and others, invoking the recently passed CEQA and NEPA. The litigation was successful and the Department was directed to conduct environmental studies for the bypass.

Modern Mitigation Alternatives

In the early 1980's, landsliding and 50 million dollars in Federal funding led to renewed design studies of the highway realignment. In 1986, the Martini Creek Alignment was selected as the preferred alignment by Federal Highway Department as a solution to road failures at Devil's Slide. The bypass was designed to be 4.5 miles long, two-lane facility with climbing lanes, from Pacifica to Montara, and would require extensive grading through environmental sensitive area. For the next 10 years the question of whether the Martini Creek alignment would be built or not was discussed in the legal arena and was not resolved until 1996.

The Marine Disposal Alternative (MDA) was studied as an alternative to the inland bypass. The MDA proposal consisted of unloading the driving force at the top of the landslide and buttressing the bottom of the slide. The project would require the removal of an estimated 1 million cubic yards of material from the head of the landslide and placing it offshore into a non-erodible buttress constructed behind a concrete reinforced tetrahedral breakwater. This type of landslide correction has been implemented at a number of locations along the California coastline but never at the scope and scale proposed at Devil's Slide. The study concluded that even though it was feasible to construct a buttress of this type, too many critical issues were unanswered. Ultimately the creation of a national marine sanctuary immediately offshore removed this alternative from consideration.

In 1996, Measure T was passed overwhelmingly by the voters of San Mateo County. This measure identified the preferred alternative to be a tunnel bypass, and eliminated the Martini Creek alignment alternative. The measure also required voter approval of any other alternative to the tunnel, except repair and maintaining the existing highway.

In November of 1997, Caltrans conducted a study to determine the feasibility of stabilizing the landslide complex using dewatering wells in conjunction with existing horizontal drains. The study concluded that the rock mass has a low hydraulic conductivity and transmissivity. There is no evidence of a pressurized aquifer that could be relieved, and the shallow and moderate failure surfaces are located above the static water levels. In addition, slow landslide movement appears to continue regardless of rainfall patterns and dewatering activities. Consequently, it was determined that dewatering would not be an effective, long-term mitigation measure.

The final environmental document is expected to be approved in spring of 2000 and tunnel design will then begin. The tunnel is planned to be a 1,219-m (4,000-ft) long; double bore facility with one lane in each direction. The north approach will leave the existing alignment of Route 1 onto a 457-m (1,500-ft) bridge structure that crosses the valley at Shamrock Ranch, entering the tunnel facility beneath San Pedro Mountain (Figure 11). The south approach will exit on the south side of San Pedro Mountain onto a 305 m (1,000 ft) approach fill that rejoin Route 1 just south of Devil's Slide. Two tunnel design variations are being considered, one using a 9.1 m (30 ft) wide bore and one using a 11.0 m (36 ft) wide bore. Under the current schedule, project design is anticipated to be completed in early 2001 and construction is scheduled to begin in mid 2001, with a completion date of early 2005.

As part of an ongoing effort to maintain the roadway bench until the tunnel project is completed, continual near-surface and deep dewatering is performed through the use of horizontal drains and the existing drainage wells. The roadway and slope face directly above the roadway bench

are constantly monitored with extensometers, and the roadway will be closed when a certain amount of movement is detected.

6.0 Moss Beach Distillery Restaurant and Seal Cove Landslide Complex

Local Legend

The Moss Beach Distillery (Distillery) was built in the mid 1920s, and is a restaurant and bar located a few miles north of Half Moon Bay. It is known locally as a romantic get-away for lunch and dinner, and also for the legend of "the Blue Lady". The legend holds that during the "flapper" era following World War I, a young married woman and a piano player were involved in a torrid and illicit love affair. The lovers are said to have met often on Moss Beach and at a hotel on the bluffs near the Distillery. Both lovers died a violent death, and according to legend, the woman's spirit haunts the Distillery.

Geologic Setting

The Distillery is located atop a coastal bluff, approximately 100 feet above sea level and 150 feet from the cliff face. Marine terrace deposits that range in thickness from 3 to 40 feet and consist of unconsolidated gravel, sand, and silt underlie the bluff. Underlying the terrace deposits is the Purisima Formation that is composed of poorly to moderately consolidated, interbedded sandstone, siltstone, and mudstone. These rocks are highly fractured and sheared due to regional tectonic uplift and lateral movement along the Seal Cove fault. Approximately 500 feet east of the Distillery, a set of northwest-southeast trending linear ridges mark the surface trace of the Seal Cove fault zone. The Seal Cove fault is generally considered to be part of the active San Gregorio and San Andreas fault systems that mark the boundary between the North American and Pacific plates. In the Moss Beach area, the Seal Cove fault locally forms the contact between granitic bedrock on the east and sedimentary bedrock (Purisima Formation) on the west (Figure 12).

Landslide Hazard

Sheared bedrock materials, tectonic uplift of the coastline, lateral plate movement, and seacliff erosion has destabilized the coastal bluffs in the Seal Cove area, and subsequently created deep-seated, rock slumps. The Distillery sits atop the relatively level unit surface of an active, rotational rock slump (Figure 13). The main scarp is located approximately 100 feet east of the Distillery, exhibits approximately 5 feet of vertical offset, and is associated with recent pavement cracks and structural warping of the house to the east. Several other arcuate scarps are also visible to the east of the Distillery. Historic survey data show that movement of the landslide coincides with heavy winter rainfall years. Continual wave erosion at the base of the landslide, that results in an average rate of cliff retreat of 1.0 to 1.5 feet per year, is considered to be the major destabilizing force.

Landslide Monitoring and Displacement History

Because geologic studies demonstrated that the coastal bluff is subject to deep-seated landslide movements, San Mateo County imposed strict building regulations along the coastal bluff region. These restrictions represented the first time San Mateo County zoned specifically around landslides and faults.

Consequently, these restrictions were considered a bold step in 1971. In addition, because the Moss Beach Distillery lies entirely within the boundaries of a large active landslide, the County required that a detailed surveying network be established to document the yearly movements of the landslide. The County commenced detailed ground surveys in the Moss Beach area in 1972 and performed readings at 1 to 3 year intervals up until the end of the survey in 1986. This ground survey primarily consisted of a network of surface monuments in the roadways both on and off of the landslide terrain. The displacement data verified the geologic conclusion that this landslide has a rotational component, in which the back of the slide drops downward and the toe rises, creating an offshore reef.

In 1995, Cotton, Shires and Associates, Inc. documented landslide movement since 1986, and initiated an annual monitoring program. Based on the historical survey data and field observations over the past 25 years, landslide displacement beneath the Moss Beach Distillery tends to occur in relatively slow (historic average is 2 to 3 inches per year), non-episodic, non-catastrophic increments (Figure 14). In 1997, the active landslide beneath the Distillery was displaced approximately 1 to 2 inches in the horizontal direction, and 1 to 1.5 inches in the vertical direction. These rates are equal to or slightly less than average historical movement rates based on previous surveys. In 1998, following the severe El Nino rainstorms, the active landslide beneath the Moss Beach Distillery moved slightly faster than the historical average and was displaced approximately 2.5 to 5.5 inches in the horizontal direction, and 2 to 3 inches in the vertical direction. If the landslide behaves in the future as it has in the past, we can expect approximately 2.5 feet of vertical and 4.25 feet of horizontal movement over the next 20 years.

Risk Assessment

The active landslide beneath the Distillery is a well-known geologic hazard along the coastal bluff in the Seal Cove-Moss Beach area. Aerial photograph analysis from previous geologic investigations has established that the general morphology of the landslide has been relatively unchanged since the mid 1930's. Consequently, the level of risk imposed by the landslide to structures located upon the landslide is **high**. However, depending upon the location of the structure with respect to the margin of the landslide, this risk may be less severe. The Distillery is not located astride the landslide margin, but instead sits atop the relatively level unit surface. This location represents a high risk of movement, but the entire structure tends to move as a coherent mass, and consequently, only suffers relatively minor distress over time, such as tilting of floors and cracking of walls. In contrast, structures situated astride a landslide margin can expect to sustain gradual and severe damage due to vertical and horizontal separation of the ground surface.

Landslide Mitigation/Foundation Repair

In 1995, the damage to the "flapper" era foundation and walls caused by landslide movement necessitated either extensive repair or demolition and reconstruction. However, because of zoning laws and stringent regulations, rebuilding the structure was not possible. Consequently, the foundation had to be repaired. As part of the foundation repair, the building owner wanted to expand the restaurant slightly. The County did not allow the expansion until the project geologist explained the characteristics of the landslide and rate of movement. In early 1997, the Distillery was shored-up and the entire foundation was replaced. The replacement foundation is a rigid system that allows the restaurant structure to "ride" relatively intact on the surface of the slow-moving landslide. The foundation replacement cost was $2 million and the project was completed in just 15 weeks.

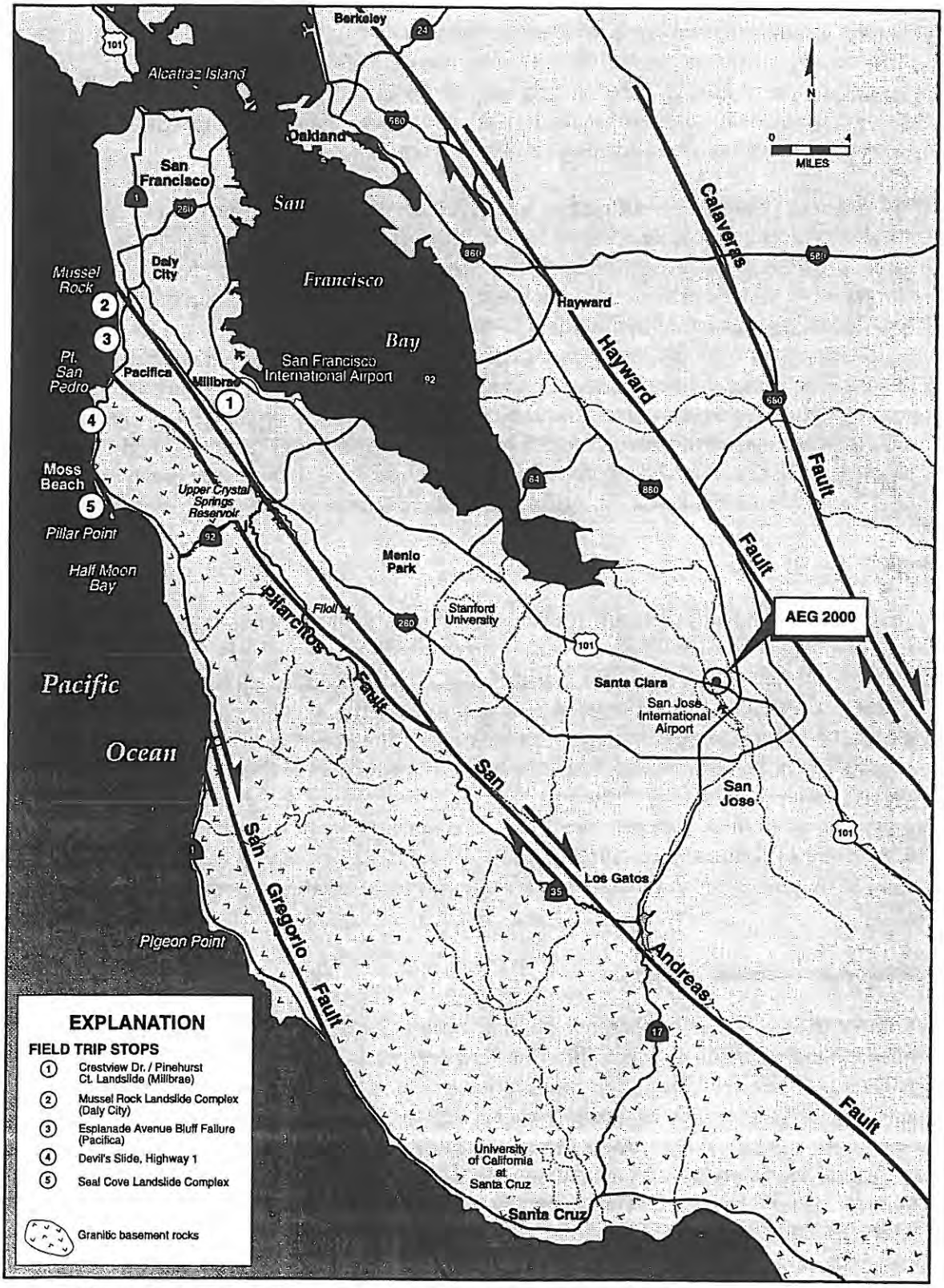

Figure 1. Regional Setting and Field Trip Stops, San Mateo County Area.

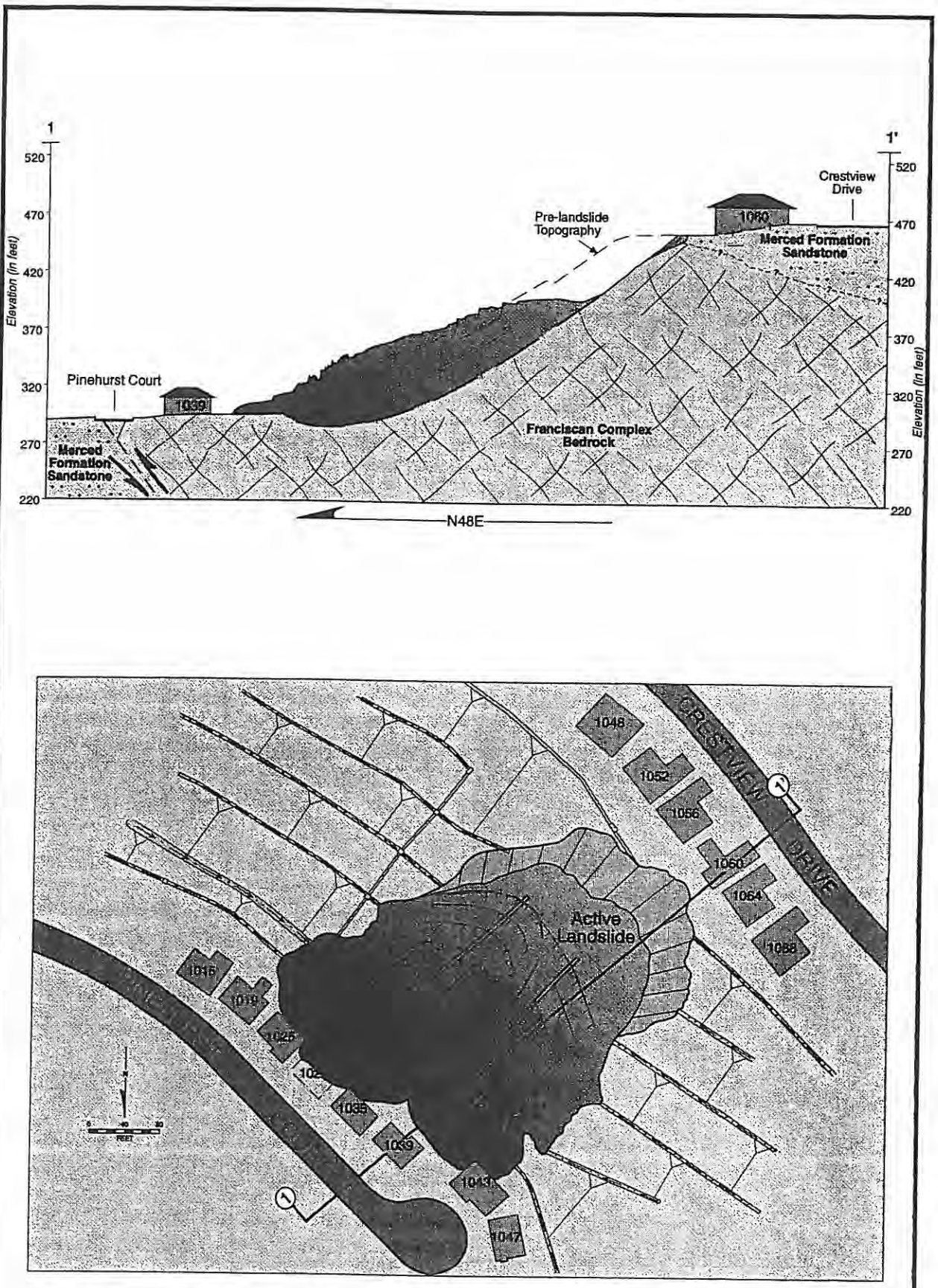

Figure 2. Crestview-Pinehurst Landslide (CPL) Map and Cross Section.

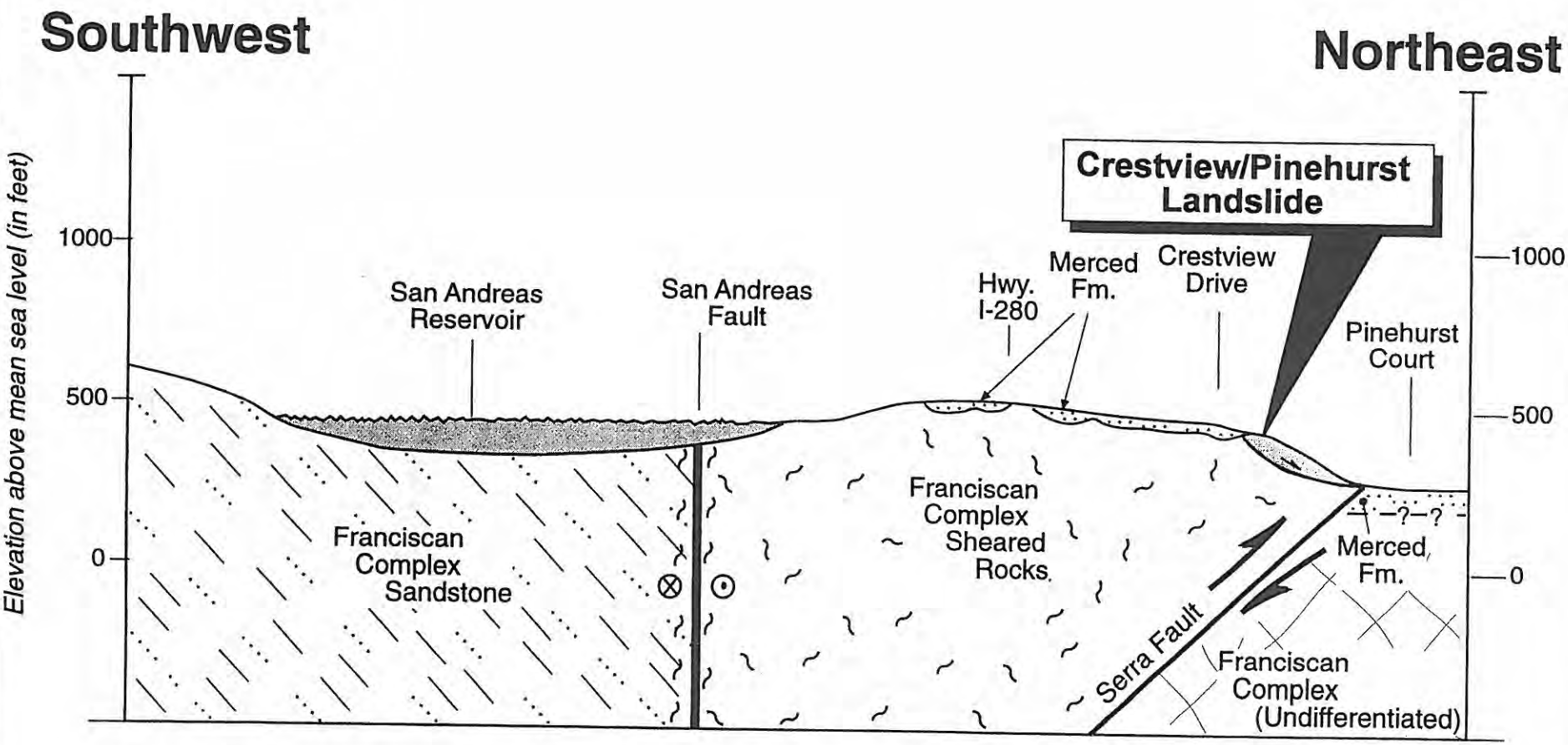

Figure 3. Geologic Cross Section from San Andreas Reservoir to Crestview-Pinehurst Landslide, Millbrae, California.

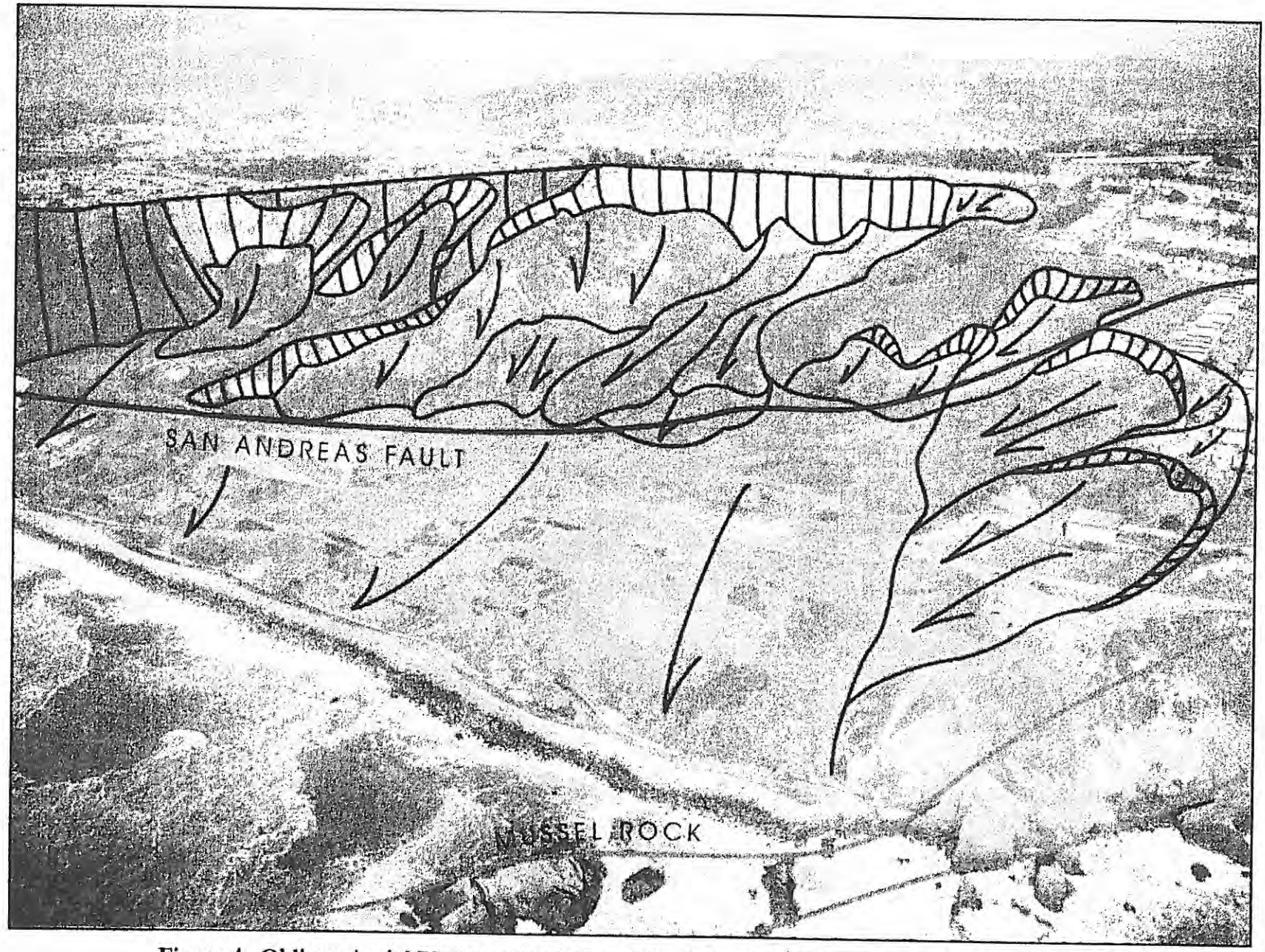

Figure 4. Oblique Aerial Photograph of Mussel Rock Landslide Complex, Daly City, California.

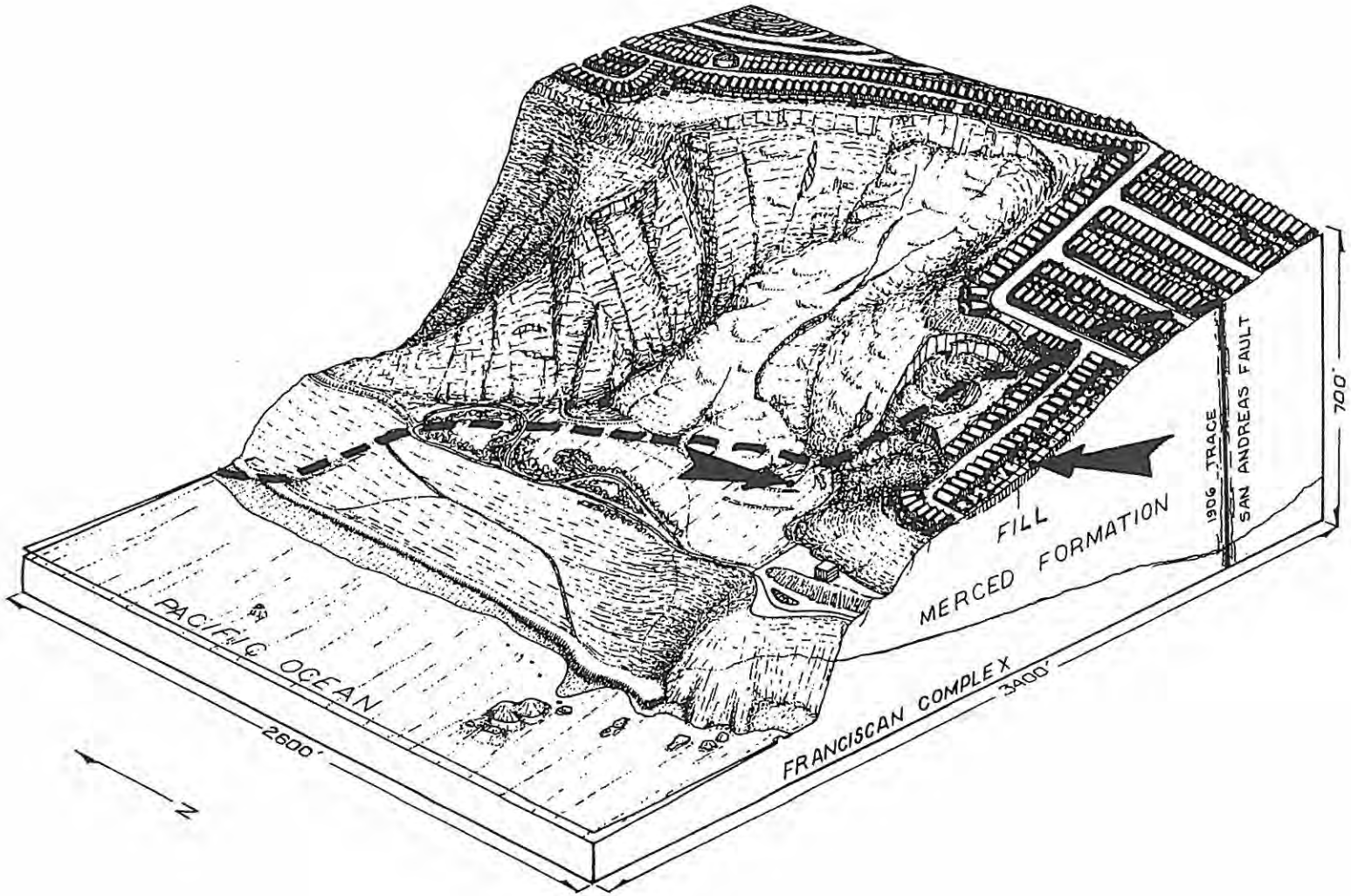

Figure 5. Block diagram of the Mussel Rock Landslide Complex, Daly City, California. The trace of the 1906 earthquake fault rupture is shown as a heavy dashed line and the arrows point to the end points of cross section A-A' depicted in Figure 6.

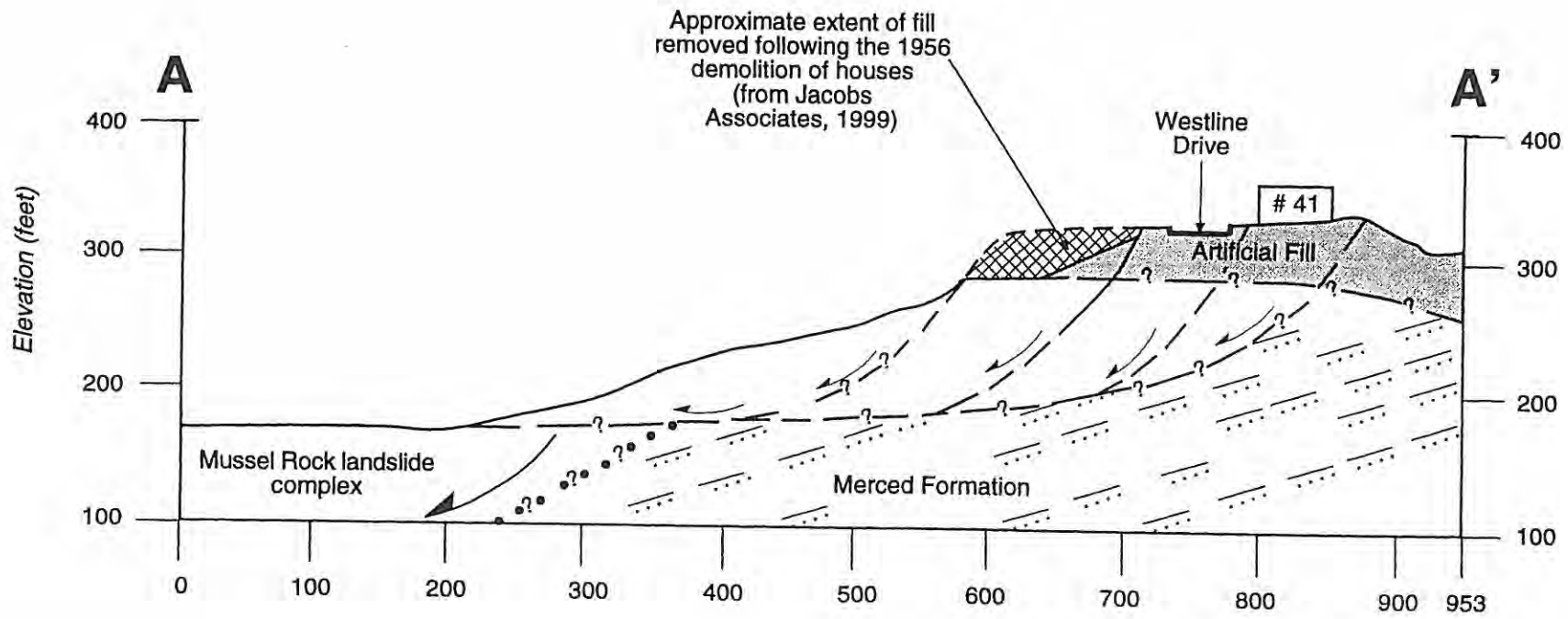

Figure 6. Geologic Cross Section of Westline Drive Landslide Complex, Daly City, California.

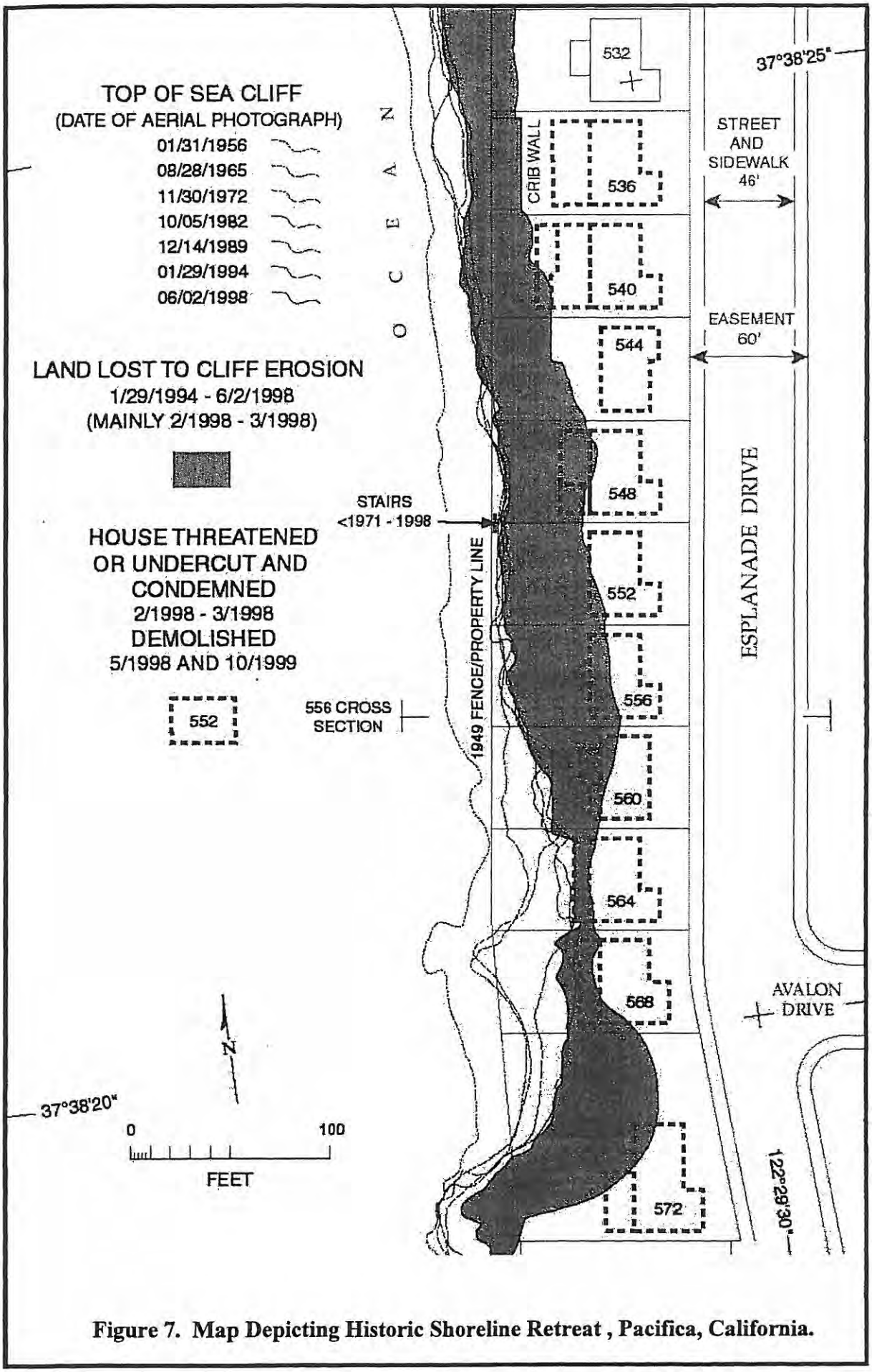

Figure 7. Map Depicting Historic Shoreline Retreat , Pacifica, California.

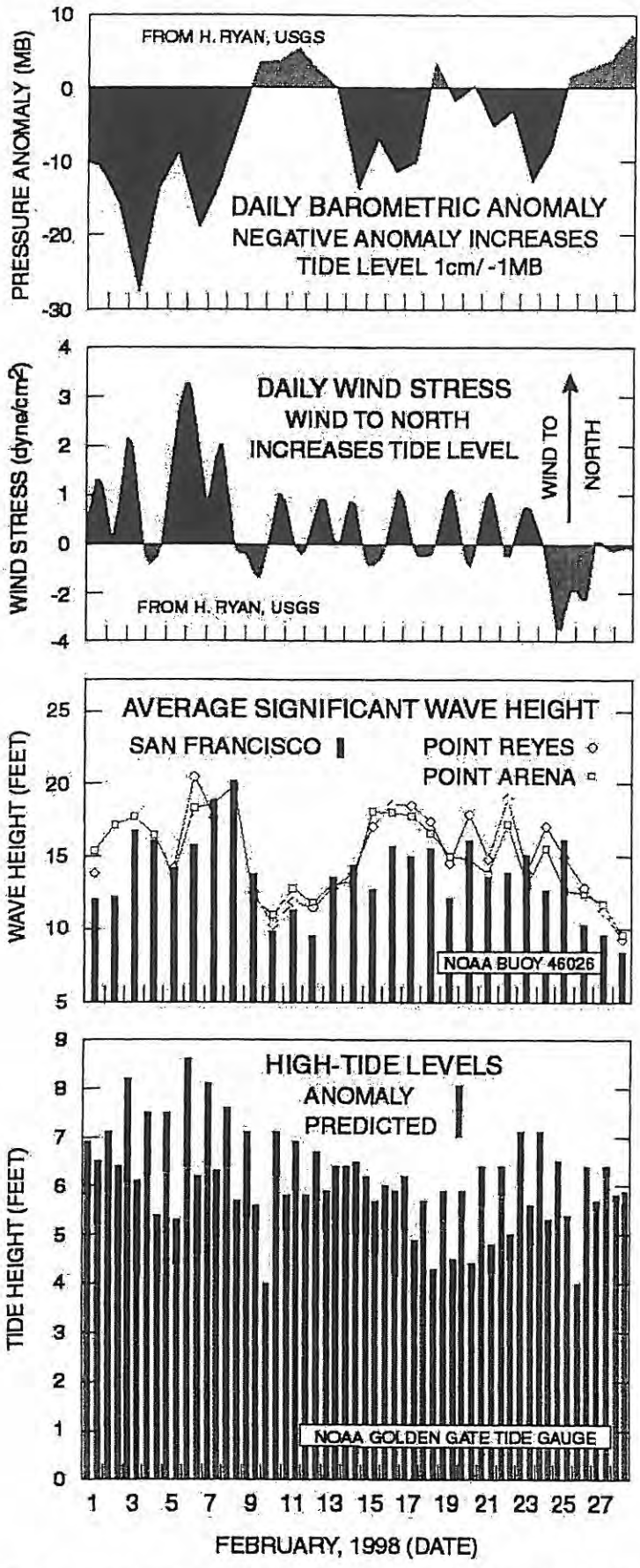

Figure 8. Comparison of Tides, Barometric Anomalies and Wind Stress, San Mateo County Coastline.

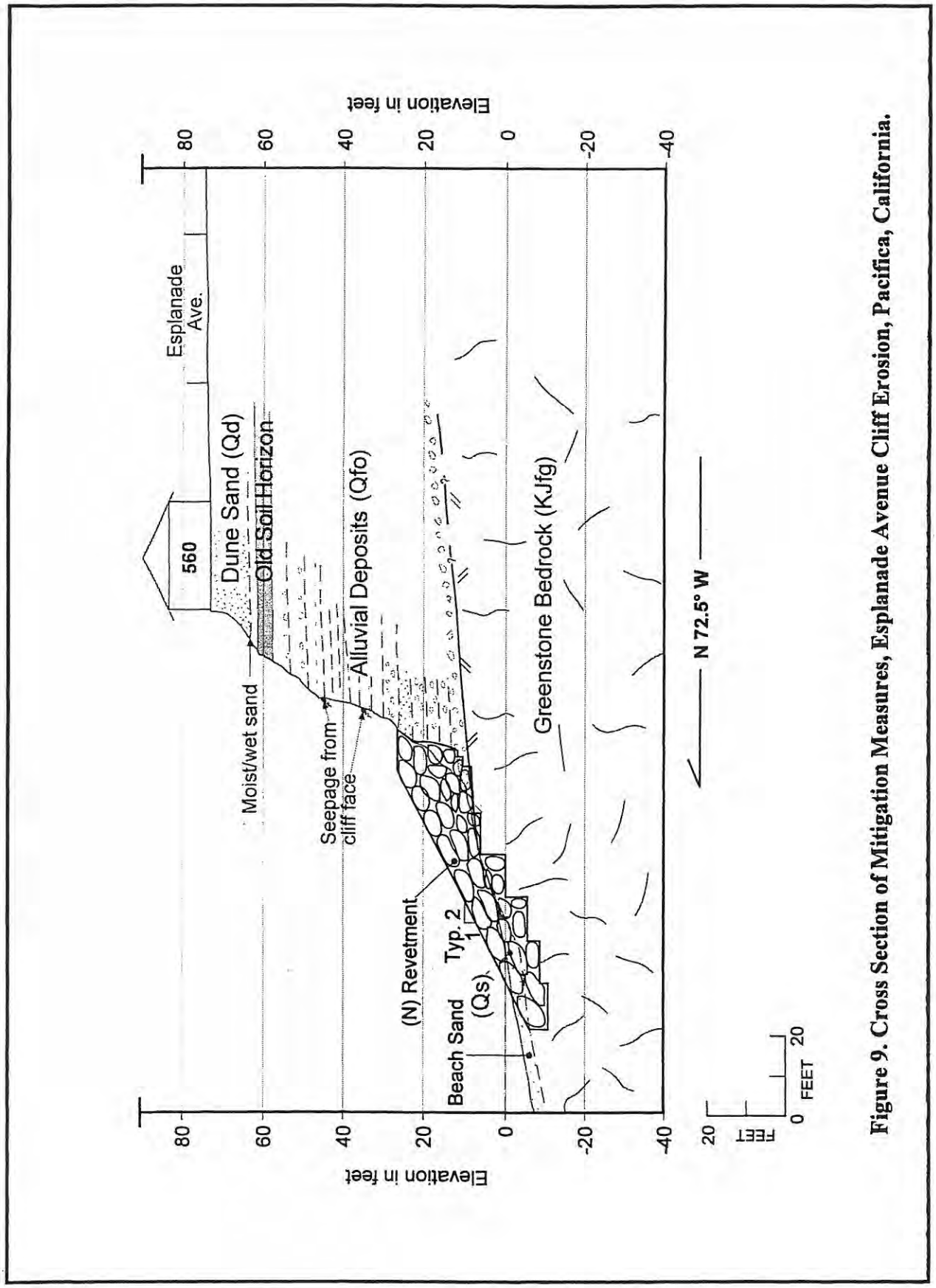

Figure 9. Cross Section of Mitigation Measures, Esplanade Avenue Cliff Erosion, Pacifica, California.

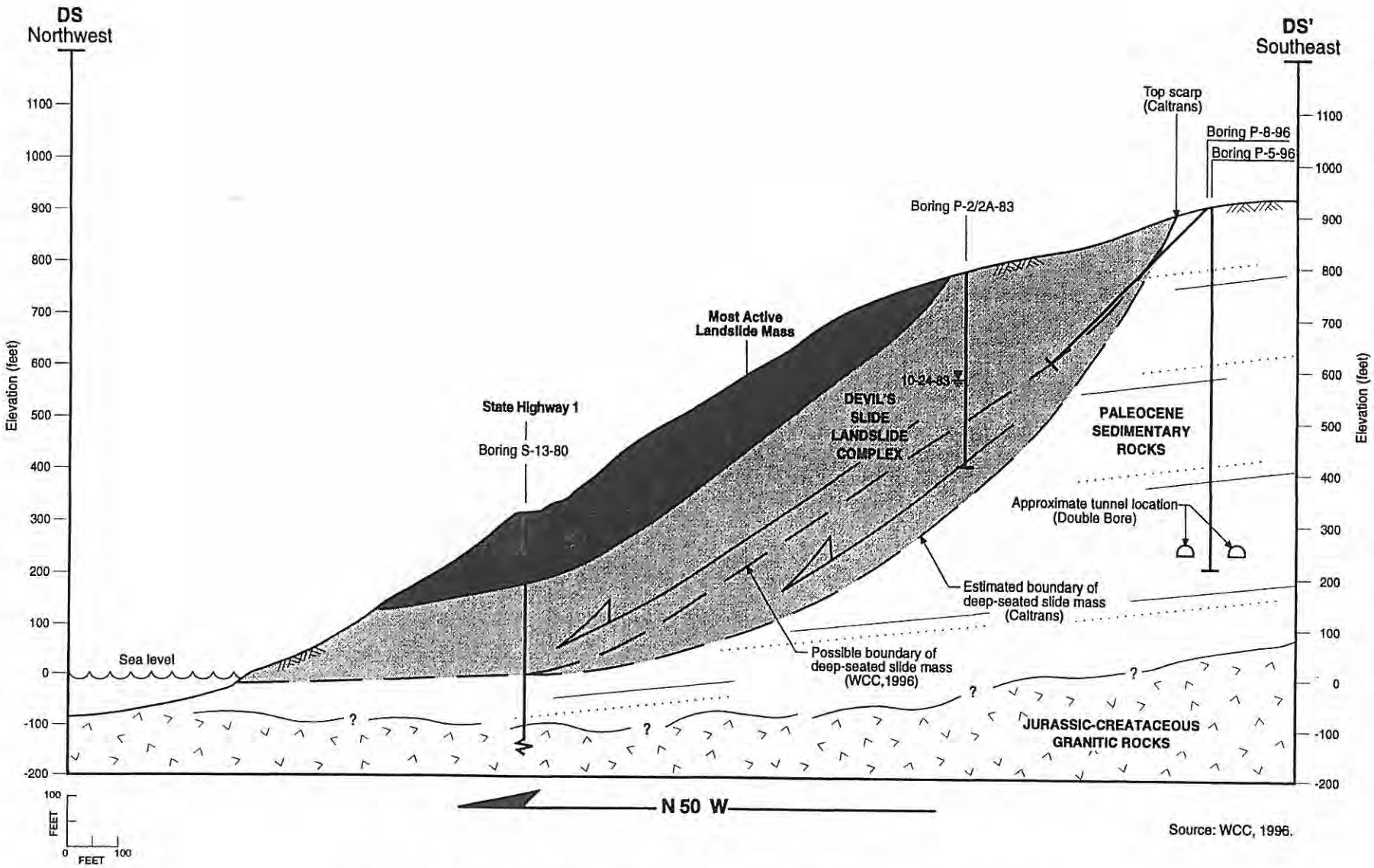

Figure 10. Geologic Cross Section of Devil's Slide Landslide Complex.

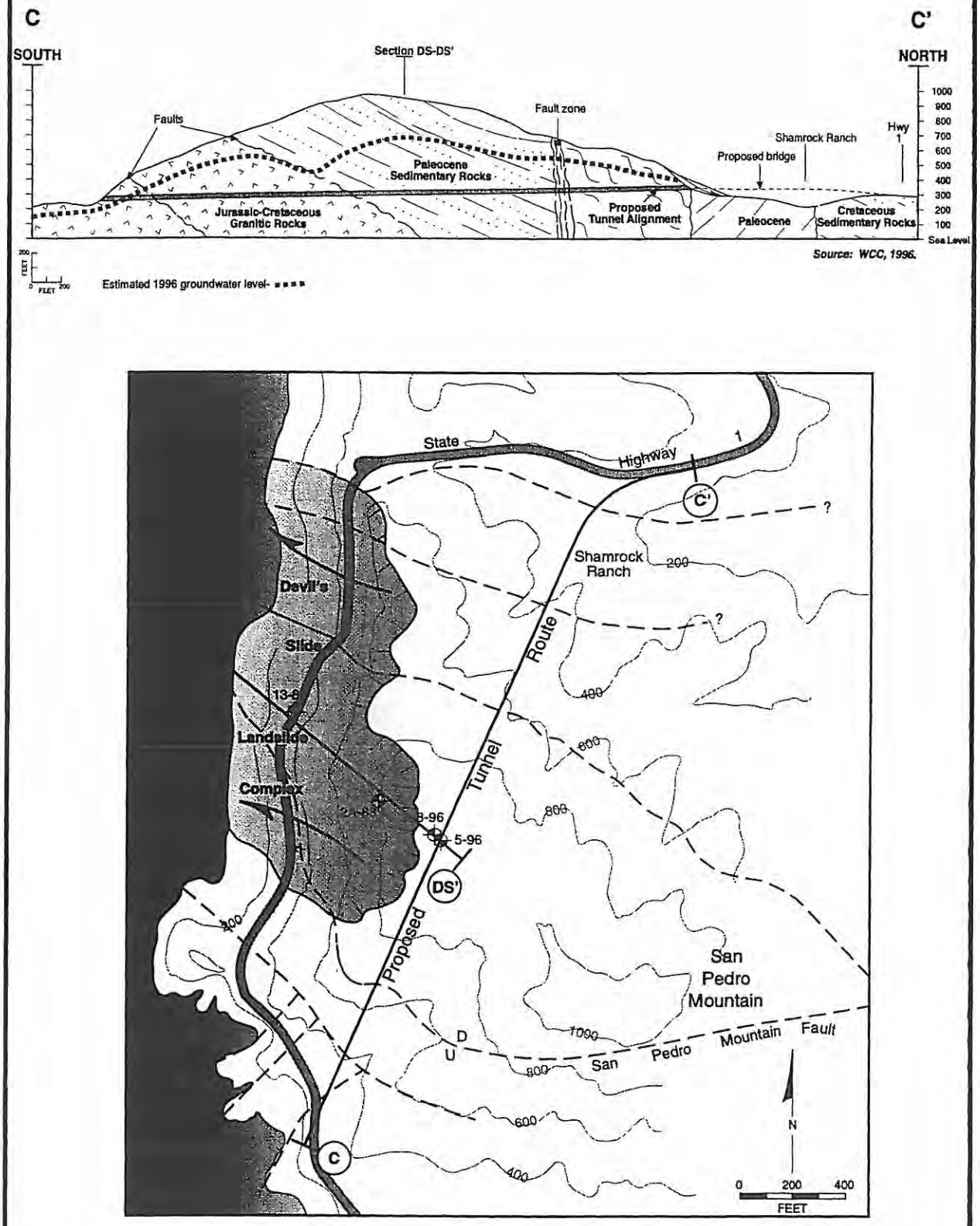

Figure 11. Location Map and Geologic Cross Section, Devils' Slide Tunnel Route.

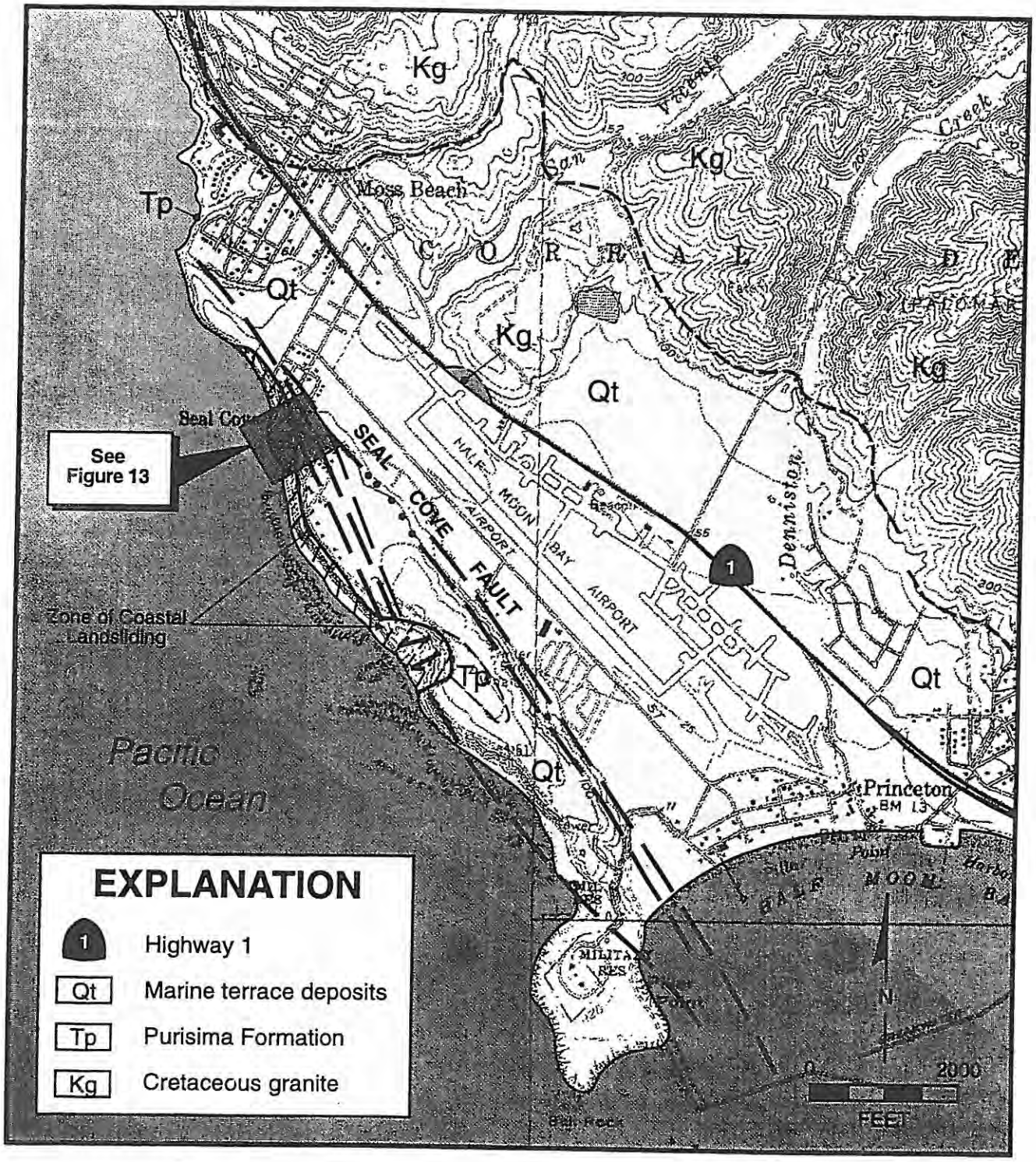

Figure 12. Geologic Map of Moss Beach-Seal Cove Area.

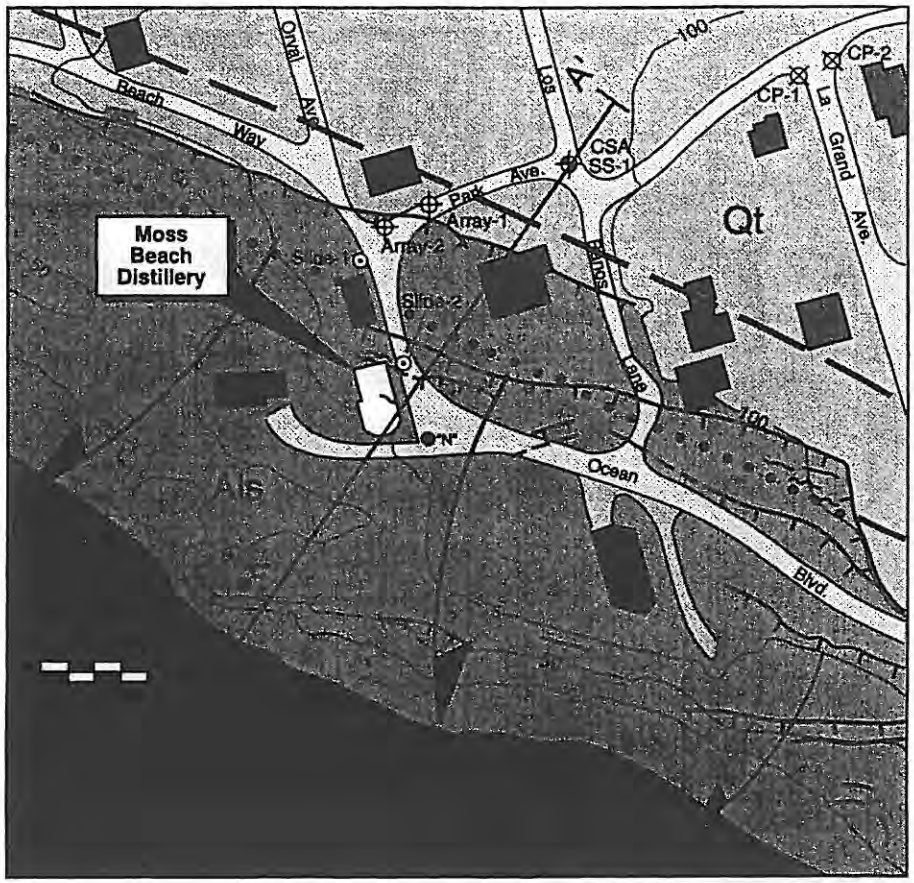

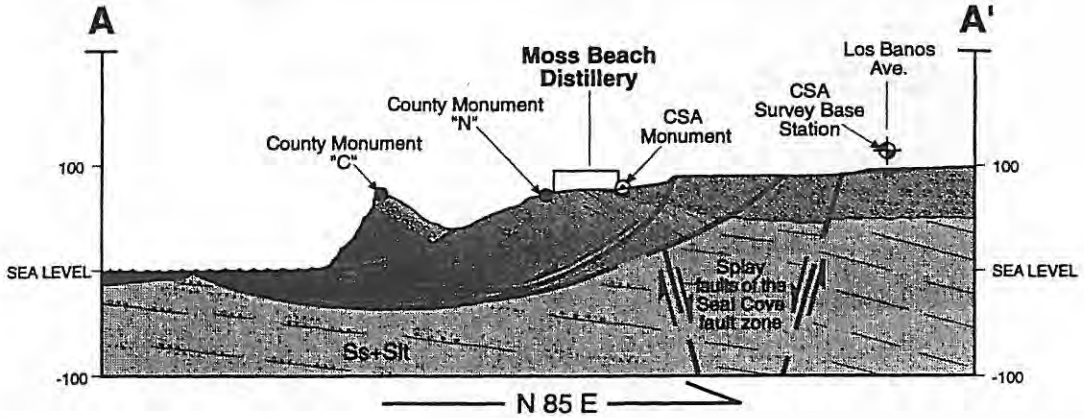

EXPLANATION

EARTH MATERIALS

- Active landslide
- Marine terrace deposits
- Purisima Formation sandstone and siltstone

MAP SYMBOLS

- Concealed fault trace
- Fault trace
- Landslide slip surface
- Active landslide ground cracks (Leighton & Associates, 1971)
- CSA survey base stations
- CSA survey monument
- Landslide nail array monument
- Control point monument
- County survey monument (not found)
- Active landslide movement direction
- Location of Engineering Geologic Cross Section

100 FEET 0 100 FEET

Figure 13. Map and Cross Section of Seal Cove Landslide Complex.

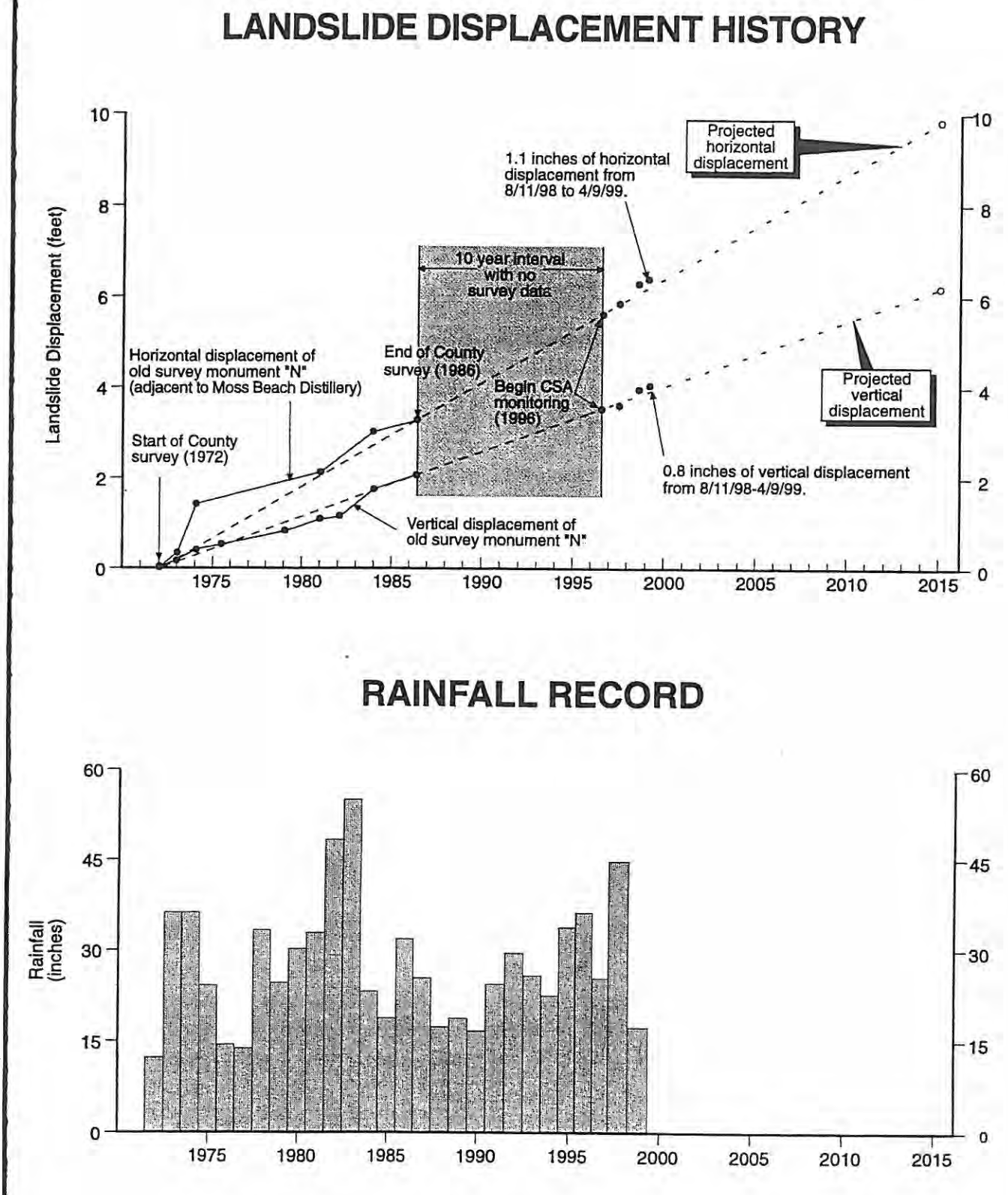

Figure 14. Rainfall vs. Landslide Movement, Seal Cove Landslide Complex.

7.0 REFERENCES

California Division of Mines and Geology, 1982, State of California Special Studies Zones, San Francisco South 7.5 Minute Quadrangle, Revised Official Map.

Clahan, K.B., Wright, R.H. and Hall, N.T., 1995, Paleoseismic investigation of the San Andreas fault on the San Francisco Peninsula, CA, Final Technical Report, Award No. 14-08-001-G2081, National Earthquake Hazards Reduction Program, U.S. Geological Survey, Reston, Virginia.

Clark and Brabb, 1978. Stratigraphic contrasts across the San Gregorio Fault, Santa Cruz Mountains, West Central California, *in* G.E. Weber and G.B. Griggs, *Coastal geologic hazards and coastal tectonics, northern Monterey Bay and Santa Cruz/San Mateo County coastlines*, Field trip guide for San Francisco Section of the Association of Engineering Geologists.

Daly City Department of Community Development, 1984).

Griggs, G. and Savoy, L. (editors), 1985, Living With the California Coast, Duke University Press, North Carolina, 394 p.

Harden, D.R., 1998. *California Geology*, Prentice Hall, Inc., New Jersey, 479p.

Hill, M.L. and Dibblee, T.W., Jr., 1953, San Andreas, Garlock, and Big Pine faults, California-a study of the character, history, and tectonic significance of their displacements, *GSA Bulletin*, v. 64, no. 4, pp. 443-458.

Irwin, W.P., 1960, Geologic reconnaissance of the northern Coast Ranges and Klamath Mountains, California, *California Division of Mines and Geology Bulletin* 179, 79p.

Jachens, R.C., Roberts, C.W., and Zoback, M.L., 1996, Total offset and right-stepping geometry of the San Francisco Peninsula segment of the San Andreas fault, California, defined by aeromagnetic anomalies, Eos Trans. AGU v. 77, p. 46.

Jacobs Associates, Inc., 1999, Westline Drive Site Study, Daly City, California, unpublished consultant report to City of Daly City, California, November 1999.

Lajoie, K. and Mathieson, S., 1985, San Francisco to Ano Nuevo, *in* Griggs, G. and Savoy, L. eds., *Living with the California Coast*, National Audubon Society, Duke University Press, Durham, North Carolina, pp. 140-177.

McLaughlin, R. et al., 1988, Tectonics of formation, translation, and dispersal of the Coast Range ophiolite of California, *Tectonics*, 7(5), pp. 1033-1056.

Page, B.M., 1989, The Salinian Block, *in* Wahrhaftig, C. and Sloan, D., eds., *Geology of San Francisco and vicinity*, Field Trip Guidebook T 105, 28th International Geological Congress, American Geophysical Union, Washington, D.C., p. 16-20.

Ryan, H., 1999, internal U. S. Geological Survey written communication to K. Lajoie

Simpson, G. and Lettis, W.R., 1999, The northern San Gregorio fault zone, Pillar Point to Moss Beach, *in* Weber, G.E. and others, eds., *Neotectonics and Quaternary Geology of the San Gregorio Fault Zone, Santa Cruz and San Mateo Counties, California*, Geological Society of America, Cordilleran Section Annual Meeting, June 2-4, 1999.

Smelser, M.G., 1987, Geology of the Mussel Rock Landslide, San Mateo County. California Geology, March, 1987.

Snell, C. Lajoie, K. and Medley, E., 2000, Sea-cliff erosion at Pacifica, California caused by 1997/1998 El Nino Storms; Proceedings of the GeoDenver 2000 Conference, American Society of Civil Engineers (in press).

Sullivan, R. and Galehouse, J.S., 1991, Geological setting of the San Francisco Bay Area, *in* Sloan, D. and Wagner, D.L., eds., *Geologic Excursions in Northern California: San Francisco to the Sierra Nevada*: Field Trip Guidebook for the Joint Meeting of the Geological Society of America Cordilleran Section, Special Publication 109, California Department of Mines and Geology, 130p.

Wahrhaftig, C. and Sloan, D., 1989, (eds.), *Geology of San Francisco and vicinity*: Field Trip Guidebook T 105, 28th International Geological Congress, American Geophysical Union, Washington, D.C.

Wakabayashi, J., 1999, Distribution of displacement on and evolution of a young transform fault system: The northern San Andreas fault system, California, Tectonics, v. 18, no. 6, pp. 1245-1274.

Wakabayashi, J. and Hengesh, J.V., 1995, Distribution of late Cenozoic displacement on the San Andreas fault system, northern California, in Recent Geologic Studies in the San Francisco Bay Area (ed. By Sangines, E.M., Andersen, D.W., and Buising, A.V.), Soc. Econ. Paleontol. Mineral. Pac. Section, vol. 76, pp.19-30.

Woodward Clyde Consultants, 1996, Devil's Slide Tunnel Study, unpublished consultant report to California Department of Transportation, August 1996.

STABILITY AND PERFORMANCE OF SLOPES AND EMBANKMENTS-II

Volume 2

Proceedings of a Specialty Conference
sponsored by the
Geotechnical Engineering Division of the
American Society of Civil Engineers

co-sponsored by the
San Francisco Section of ASCE, and
The University of California, Berkeley

in cooperation with the
Association of Engineering Geologists
U.S. Committee on Large Dams
ASFE/The Association of Engineering Firms
Practicing in the Geosciences
Association of State Dam Safety Officials

Berkeley, California
June 29–July 1, 1992

Edited by Raymond B. Seed
Ross W. Boulanger

Geotechnical Special Publication No. 31

Published by the
American Society of Civil Engineers
345 East 47th Street
New York, New York 10017-2398

REFERENCES

Bruce, D. A. (1992) "Two New Specialty Geotechnical Processes For Slope Stabilization," ASCE Specialty Conference on Stability and Performance of Slopes and Embankments - II, 15p.

Dash, U. and P. Jovino (1980) "Construction of a Root-Pile Wall at Monessen, Pennsylvania," Embankment Stabilization and Soil Mechanics, Transportation Research Record 749, National Research Council, Washington, D.C., pp. 13-21.

Dash, U. (1987) Pin-Pile Wall Evaluation, FHWA-PA-86-047-84-36, Federal Highway Administration, U.S. Department of Transportation, Washington, D.C., 174p.

Earth, Inc. (1986) Performance Evaluation Report, Existing INSERT Wall, L.R. 69 - Section 255, Armstrong County, Pennsylvania, Report for NCC, 25p.

Fukuoka, M. (1977) "The Effects of Horizontal Loads on Piles Due to Landslides," Proceedings, Specialty Session 10, Ninth International Conference on Soil Mechanics and Foundation Engineering, Tokyo, Japan, pp. 27-42.

Ito T. and T. Matsui (1975) "Methods to Estimate Lateral Force Acting on Stabilizing Piles," Soils and Foundations, Vol. 15, No. 4, pp. 43-59.

Leinenkugel, H. J. (1976) "Deformations und Festigkeitsver Halten Bindiger Erdstoffe," Experimentelle Ergesbnisse und Ihre Physikalische Deutung Veroffentil. Inst. f. Bodenmech. u. Felsmech. 66, Karlsruhe.

Murray, R. (1984) In-Place Roadway Stabilization, New York Department of Transportation, Albany, NY, 19p.

Palmerton, J. (1984) Stabilization of Moving Land Masses by Cast-in-Place Piles, Miscellaneous Paper GL-84-4, Waterways Experiment Station, Vicksburg, MS, 101p.

Reese, L., K. Awoshika, P. Lam, and S. Wang (1987) "Documentation of Computer Program, GROUP1, Analysis of a Group of Piles Subjected to Axial and Lateral Loadings," Ensoft INC., Austin, TX.

Walkinshaw, J. L. (1984) "Correction of a Landslide with a 'Reticulated Root Pile' Structure," Federal Highway Report, Region 9, San Francisco, CA.

Winter, H., W. Schwarts, and G. Gudehose (1983) "Stabilization of Clay Slopes by Piles," Proceedings 8th European Conference on Soil Mechanics and Foundation Engineerings, Helsinki, Vol. 2, pp. 545-550.

HYDRAUGERS AT THE VIA DE LAS OLAS LANDSLIDE

By W.H. Roth[1], Member ASCE, R.H.Rice[2], D.T. Liu[1], Member ASCE, J. Cobarrubias[3]

ABSTRACT

In 1988 a subsurface drainage system consisting of 32 hydraugers was installed to enhance the stability of the 780,000 cubic-foot Via de Las Olas landslide in Pacific Palisades, California. The results of a three-year monitoring program involving measurements of hydrauger discharge and corresponding changes in piezometric levels are discussed in this paper. The presented data demonstrate the effectiveness of the hydraugers through measurable quantities of both discharge and reduction in piezometric levels. The feasibility of dewatering low-permeability siltstone/sandstone bedrock formations by hydraugers has been a controversial issue for some time. This case history should lend additional credence to the concept of dewatering the seemingly "impervious" formations of the coastal bluffs of southern California by small-diameter horizontal drains - as long as these formations are fractured. Because the latter is also a condition for rendering a "rock" formation unstable in the first place, most bedrock slides are likely to benefit from this approach.

(1) Dames & Moore, 911 Wilshire Boulevard, Suite 700, Los Angeles, California 90017

(2) Dames & Moore, 221 Main Street, Suite 600, San Francisco, California 94105

(3) City of Los Angeles, Department of Building & Safety, 200 N. Spring Street, Room 460-A, Los Angeles, California 90012

INTRODUCTION

GENERAL BACKGROUND

The Via de las Olas landslide in Pacific Palisades is typical of the wide-spread stability problems affecting the coastal bluffs of southern California. Located adjacent to a controversial proposed oil drilling site near a popular beach, the implications of possibly reactivating the large slide mass through oil drilling activities played a major role in a nearly 25-year public campaign against oil production at this location. In 1988, after the installation of an extensive drainage system to enhance the stability of the slide area, oil drilling permits were finally obtained. However, coastal oil drilling was banned by a public referendum shortly thereafter and the project was abandoned.

Regardless of the oil drilling issue, the drainage system of the Via de las Olas landslide has been maintained and monitored the past three years. It provides much needed protection against further deterioration of this sprawling slide area whose advancing head scarp has begun to encroach upon the residential area overlooking the coastal bluffs. Continuous monitoring of hydrauger flow rates and piezometric levels over a period of three years has established a valuable data base on the effectiveness of subsurface drainage in the low-permeability clay and siltstone formations typical of the coastal bluffs of southern California.

SITE DESCRIPTION AND HISTORY

A plot plan of the slide area is shown in Figure 1, and a typical cross section is presented in Figure 2. The slide is about 800 feet square in plan dimensions, with a height of approximately 240 feet from the toe to the top of the head scarp. The main head scarp ranges in height from 50 feet in its eastern part, to as much as 130 feet to the west. Reported slope movements at the site date back to 1890, and intermittent slides have been noted since the 1920's, when residential development of the upper mesa began. The last major slope failure occurred in 1958, when approximately 780,000 cubic yards of slide debris forced the relocation of Pacific Coast Highway 200 feet towards the ocean.

Numerous investigations have been performed since the 1958 slide episode. The most extensive studies, however, were performed between 1983 and 1988, in the course of appealing an earlier denial of permit for oil drilling at this site. In this period extensive

geologic mapping and exploratory drilling was performed. A total of 21 borings between 40 and 200 feet deep were drilled using dry auger and continuous coring techniques, some with oriented cores. In addition, extensive geotechnical instrumentation was installed and continuously monitored as described elsewhere in this paper.

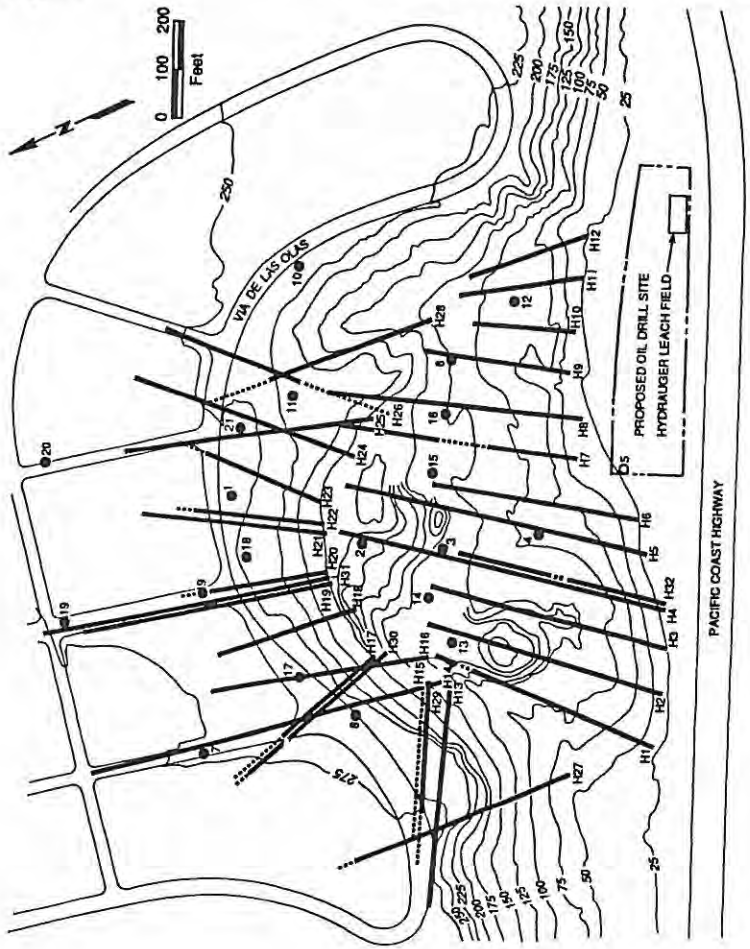

GEOLOGIC CONDITIONS

STRATIGRAPHY

Failure occurred within a sequence of thinly bedded claystones, siltstones, and weakly cemented fine sands of the Modelo formation which constitute the "bedrock" in this area. The bedrock units, also referred to as shales, are of marine origin and Upper Miocene (about 10 million years) in age. They have been planed by marine processes and uplifted to form a wave-cut terrace capped by a thin layer of marine sands. Subsequent deposition of 30 to 50 feet of alluvial deposits on top of these marine sands shaped today's mesa north of the slide's head scarp. The bedrock contact slopes gently toward southeast and, based on visual observation of the head scarp and data from exploratory borings, is believed to be incised by several stream channels filled with terrace deposits.

Bedrock units consist of overconsolidated, moderately plastic, dark gray clays and silty clays, with interbedded layers of poorly cemented fine-grained sands, rarely thicker than about 6 to 12 inches. Based on the interpretation of numerous exploratory borings, including some with continuous oriented coring, the slide mass consists of randomly oriented blocks of varying dimensions lacking coherent or continuous structure. The last major slide movement in 1958 appears to have involved a fairly thick shear zone of 30 to 50 feet. For the purpose of slope stability analysis performed to evaluate the present stability of the slide mass, this shear zone was approximated by the distinct failure plane shown in Figure 2.

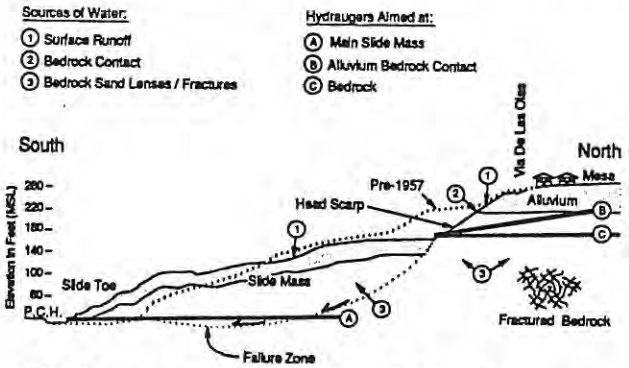

Figure 2. Cross Section with Hydraugers

SLOPE STABILITY

Water is the primary factor affecting slope stability. The increase in unit weight and loss in strength experienced by fractured shales as a result of water saturation, makes these bedrock units particularly susceptible to landsliding. In contrast, bedrock material which is not exposed to saturation by water can form near-vertical bluffs of more than 200 feet in height.

Based on back calculations of the 1958 slope failure, it was concluded that the main slide mass in its present configuration is stable with a comfortable margin of safety. By shifting its weight from the top of the slope to its toe, the stability of the slide mass has improved considerably compared to pre-1958 slope conditions. Hence, future large-scale earth movements are far less likely to occur at this site than at other coastal bluffs between Santa Monica and Malibu, which have not yet failed. Existing slide stability is further evidenced by the fact that no deep-seated slope movements have been detected since the 1958 failure. This, in spite of the extremely wet storm seasons of 1968/69, 1977/78, and 1982/83, which triggered large numbers of major slides in similar geologic formations along the coast. Rainfall amounts of these recent wet seasons were higher than the 1957/58 season which triggered the 1958 slide.

In contrast to the main slide mass, the stability of the rather steep head scarp was evaluated and found to be only marginally stable. Incipient slide movement is evidenced by an extensive crack pattern in the street pavement of Via de las Olas along the crest of the scarp. In addition to possible future damage of adjacent homes on the upper mesa, a slope failure in the scarp area was also seen as a potential threat to the stability of the main slide mass. The debris from a scarp failure loaded onto the head of the main slide mass could considerably reduce the safety factor of the latter. It was, therefore, recommended to enhance the stability of both the main slide mass and the head scarp through the installation of open surface drains and a subsurface drainage system consisting of hydraugers. The purpose of the drainage system is to intercept the active ground water flow before it enters the main slide mass.

GROUND WATER REGIME

The upper mesa extending north towards the Santa Monica Mountains was concluded to constitute a major

recharge area for ground water entering the slide. As indicated in the cross section of Figure 2, there are three water sources which pose potential problems for the site: (1) surface runoff, (2) ground water migrating along the alluvium/bedrock contact at the head scarp, and (3) ground water which approaches the slide mass essentially from below its failure zone, after entering fracture systems in the bedrock below the terrace deposits of the upper mesa.

Recharge in the upper mesa occurs as a result of precipitation during the months between November and April and from irrigation during the summer months. Much of the ground water flowing in the alluvium is apparently concentrated in shallow channels incised into the bedrock surface. Water has been observed discharging from these bedrock channels at the western cliffs and in the central portion of the headscarp following periods of extended rainfall. Established water-loving vegetation evidences these seepage areas.

Deep wells located in the bedrock of the upper mesa experience distinct fluctuations apparently related to rainfall. In contrast, measurements taken over the last 20 years indicate that the ground water levels within the slide mass do not significantly fluctuate with rainfall. In fact, piezometric data and water chemistry indicate that the ground water in the slide mass may be isolated from the surrounding ground water regime. It is likely that this isolation may be due to the shear zone of the slide forming a hydraulic barrier. The migrating ground water from the upper mesa, which probably played a sig-nificant role in triggering the 1958 failure, now appears to find its way around the slide. Concentrated seepage at the slide toe, observed near the western and eastern slide boundaries, supports this interpretation.

DRAINAGE SYSTEM

The drainage system consists of two components: (1) surface drainage (open channel drains), and (2) subsurface drainage (hydraugers). Only the latter is discussed in this paper. The subsurface drainage system consists of horizontal drains (hydraugers), a leachfield at the toe of the slide, and a hydrauger manifold line connecting the hydraugers to the leachfield. The leachfield is designed to return ground water produced by the hydraugers back into the lower ground water regime below the toe of the landslide.

HYDRAUGER INSTALLATION

The basic layout of the installed hydraugers is shown in the plan view and cross section of Figures 1 and 2, respectively. The hydraugers in the main slide mass (A) were designed to drain both perched water within the slide mass and ground water which is migrating through the bedrock underlying the landslide shear zone. At the head scarp, there are two types of hydraugers: (B) inclined hydraugers penetrating and draining the alluvium/bedrock contact of the upper mesa; and (C) near-horizontal hydraugers draining the fractured bedrock underlying the terrace deposits. Type (B) includes hydraugers tapping into the alluvial channels of the western portion of the upper terrace where some of the recharge water is believed to be concentrated.

The hydraugers consist of 1.5-inch diameter slotted PVC pipe inserted in approximately 3-inch diameter holes, which were generally uncased. The holes were drilled through a 20-foot long, 5-inch diameter steel casing grouted in place prior to drilling the deep 3-inch hole. Thirty-two hydraugers were installed, varying in length from 250 to 790 feet at inclinations of 2 to 15 degrees from the horizontal. The total length of installed drainage pipe was 14,455 feet.

Drilling was performed with a rotary-wash horizontal drill rig mounted on a crawler tractor. An attempt was made to drill some of the borings with compressed air, in order to identify saturated zones; however, due to the clayey nature of the bedrock formation, drilling progress was hampered by continuous plugging of the bit. All hydrauger borings were logged by recording the drilling resistance encountered and observations of the drill cuttings. In general, drilling in the main slide area encountered medium and, occasionally, soft resistance, indicative of slide debris. In contrast, drilling in the head scarp was hard, except for four hydraugers, H13, H16, H23, and H30, which encountered moderate resistance. Sand and gravel zones which were large enough to be recognized in the drill cuttings are shown in the hydrauger layout of Figure 1 as dotted lines.

INSTRUMENTATION

Extensive geotechnical instrumentation has been installed within and adjacent to the landslide mass for the monitoring of potential slope movements and ground water conditions. Except for shallow sloughing, none of the slope indicators and extensometers have shown signs

of earth movements which could be interpreted as a reactivation of the main slide mass.

Piezometric levels were collected from an array of instruments which include open-standpipe wells and pore pressure gages. With the exception of a few "average" wells with full-depth screened zones, the standpipes have short isolated screened intervals targeting specific sandy beds within the bedrock, or the alluvium/bedrock contact of the upper mesa. The pore pressure gages consist either of pneumatic or electric-strain-gage type instruments. The locations of the observation wells and pore pressure gages are shown in plan view in Figure 1. A schematic cross section depicting the three typical ground water monitoring devices, (1) average wells, (2) isolated wells, and (3) pore pressure gages, is shown in Figure 3.

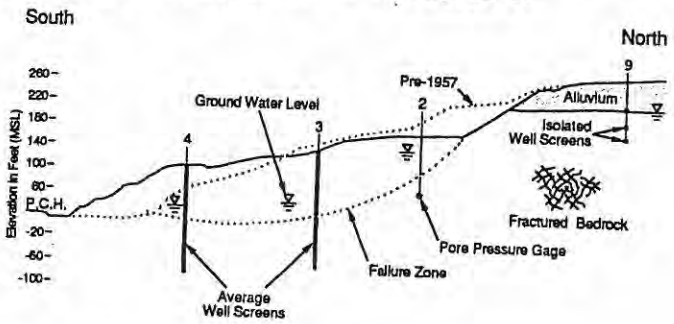

Figure 3. Cross Section with Observation Wells and Pore Pressure Gages

Plans for a fully automated data acquisition system, including computerized warning devices for early detection of threshold ground water levels and rates of slope movement, were abandoned when the oil drilling project was halted in 1988. Nevertheless, the instruments were monitored manually on a rather frequent basis until summer of 1991.

DISCUSSION OF MONITORING DATA

In order to evaluate the effectiveness of the installed subsurface drainage system, hydrauger flow rates and ground water data were recorded for several years. Furthermore, in an attempt to assess the hydraulic connections between alluvium, bedrock, and the slide mass, ground water samples were chemically analyzed and attempt was made to group them by source.

However, the results of the chemical analysis were inconclusive, probably because of the mixing of water types occurring within the contorted slide mass and fractured bedrock formations.

HYDRAUGER DISCHARGE

Plots of hydrauger flow rates and cumulative discharge volumes versus time are presented in Figures 4 and 5, together with a bar graph showing local rainfall data in inches per week. The hydraugers are grouped by the local ground water regions which they tap: (1) the upper-mesa alluvium, (2) the bedrock north of the head scarp, and (3) the main slide mass, respectively. The bottom plot of Figure 5 presents the sum total of all data. Table 1 presents the total discharge volumes accumulated since installation for each of the 31 hydraugers.

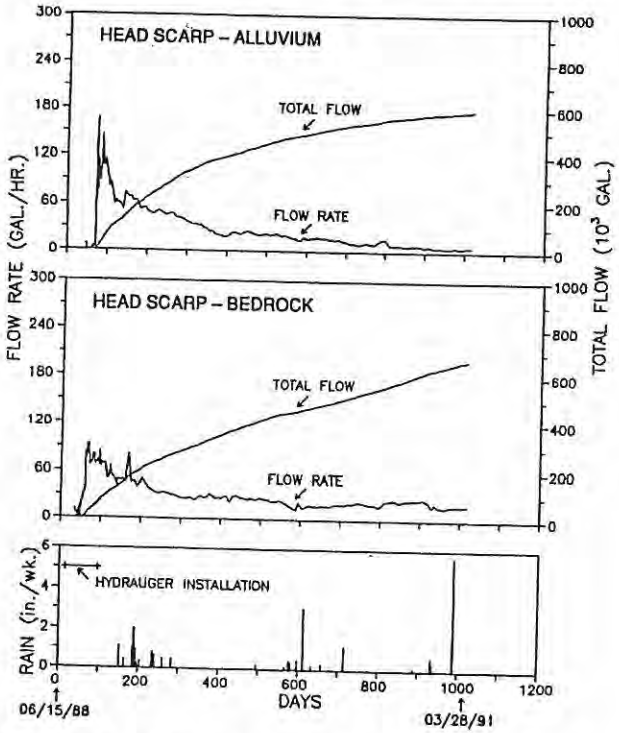

Figure 4. Hydrauger Flow Rates, Head Scarp

Hydrauger H12 which is located at the mouth of a ravine east of the slide area, was excluded from the plotted data, because of its atypically high, and occasionally erratic, flow rates. This hydrauger is thought to have some direct hydraulic connection with surface runoff and/or a leaking storm drain or sewer transversing this ravine.

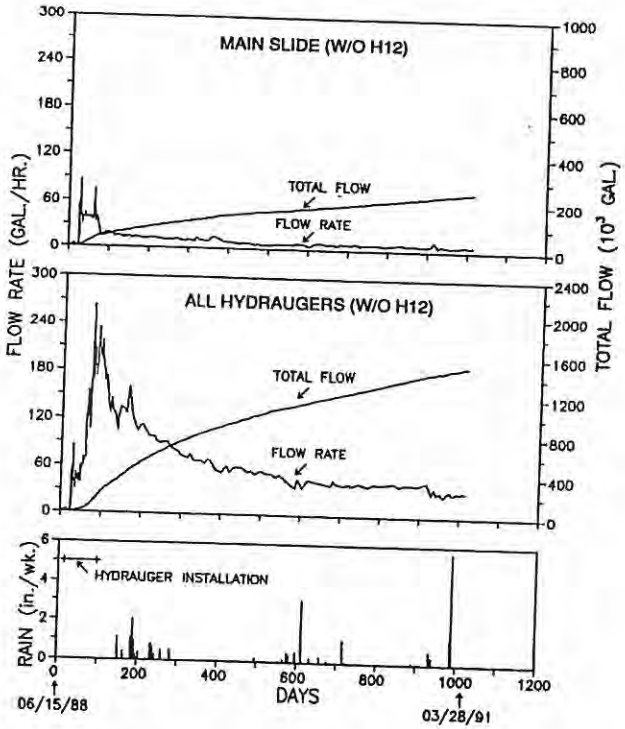

Figure 5. Hydrauger Flow Rates, Main Slide and Total

Of the three groups analyzed, the hydraugers dewatering the bedrock at the head scarp appear to produce most consistently. Starting out with initial flow rates as high as 60 to 90 gallons per hour (gph), discharge has reached a relatively stable rate of 25 to 30 gph. The hydraugers tapping the upper mesa alluvium above the headscarp initially produced at significantly higher rates of 90 to 150 gph, but declined to 25 to 30

gph in the first year, and are presently as low as 5 to 10 gph. Finally, the main slide hydraugers, with the exception of two brief 80 gph peaks in the beginning, only produced about 40 gph for the first 2 months. After that they sharply declined to about 15 gph, and have reached about 10 gph today.

TABLE 1. Total Hydrauger Discharge from 1988 to 1991

Hydrauger #	Total Flow (Gallons)	Hydrauger #	Total Flow (Gallons)	Hydrauger #	Total Flow (Gallons)
1	12999	12	440834	23	42368
2	29617	13	234413	24	35809
3	65714	14	59502	25	31545
4	43910	15	79872	26	4375
5	23005	16	20391	27	178850
6	1432	17	143	28	2772
7	9200	18	252	29	428995
8	69772	19	17292	30	37191
9	90	20	29	31	34378
10	0	21	62501	32	5924
11	2487	22	23144		

The entire hydrauger monitoring period reported herein, of course, coincided with a severe regional drought. Therefore, little insight can be obtained about the interrelationship of rainfall, regional ground water recharge, hydrauger flow rates, and piezometric levels. Notwithstanding this situation, the hydrauger flow rates do not appear to be much affected by rainfall. If anything, it almost seems as if flow rates in the past had decreased in response to rainfall.

The gradual decrease of hydrauger flow rates over time may be related to decreases in permeability of the soil envelope around the hydrauger. This phenomena has been noted in falling-head permeability tests in vertical piezometers, repeated over periods of time. It would not be easy to check this condition in the upward-inclined hydraugers, though air has been used as a testing fluid for in situ permeabilities of soils (Blight, 1971).

PIEZOMETRIC LEVELS

The recorded piezometric levels versus time for the periods before and after the installation of hydraugers are shown in Figures 6 and 7. Only data from those instruments which experienced detectable and consistent changes in response to hydrauger installation are shown. The dotted, dashed, and solid-line plots represent three different types of instruments, (1) pore pressure gages,

JAN.-29'01(MON) 15:25 ALAN KROPP & ASSOC TEL:510 841 8357 P.002

(2) average wells, and (3) isolated wells, as discussed are presented in Table 2.

The head scarp piezometric levels were essentially constant before the installation of the hydraugers, but had shown temporary peaks in response to seasonal rainfall (Figure 6). During hydrauger installation many of these piezometric levels experienced small temporary above. Installation characteristics of these instruments spikes (Figure 7), probably caused by the injection of drilling fluid in the installation process. After these initial spikes, most of the bedrock piezometric levels decreased, over a period of about 1 to 2 months, reaching steady levels up to 15 feet lower than before the hydraugers were installed. In addition, the seasonal peaks typically experienced before the hydraugers, appear to have all but disappeared in the second monitoring period. This behavior, however, must be evaluated in light of the lower rainfall experienced throughout this last period.

The atypical behavior of Gage 7D is likely due to malfunctioning of this instrument which, after some fluctuations beginning at approximately Day 680, broke down completely and was abandoned. Of the observation wells located at the bedrock-alluvium interface of the upper mesa, only 9B experienced a relatively small decrease of 2 feet. The remaining wells in the alluviumdid not show any significant changes; their piezometric levels are not shown here.

TABLE 2. Installation Data of Wells and Pore Pressure Gages

Well #	Location	Type	Installation Date	Ground Surface Elevation (Ft. M.S.L.)	Screen/ Gage Elevation (Ft. M.S.L.)
2	Main slide	Pore pressure gage	01-Jun-83	168	73
3	Main slide	Average well	1987	152	147 to -8
4	Main slide	Average well	03-Apr-83	100	95 to -60
7A	Head scarp	Isolated well	24-Oct-83	274	182 to 160
7C	Head scarp	Isolated well	28-Oct-83	274	192 to 190
7D	Head scarp	Pore pressure gage	01-Sep-87	274	181
9A	Head scarp	Isolated well	19-Oct-83	262	192 to 190
9B	Head scarp	Isolated well	04-Nov-83	262	223 to 221
9C	Head scarp	Isolated well	04-Nov-83	262	188 to 184
9D	Head scarp	Pore pressure gage	02-Sep-87	262	166
12	Main slide	Isolated well	17-Nov-83	100	5 to 1
13	Main slide	Isolated well	27-Aug-87	141	42 to 22
14	Main slide	Isolated well	01-Sep-87	142	43 to 23
19	Head scarp	Pore pressure gage	14-Sep-87	275	78
20	Head scarp	Pore pressure gage	11-Dec-87	270	171
21	Head scarp	Pore pressure gage	05-Dec-87	232	151

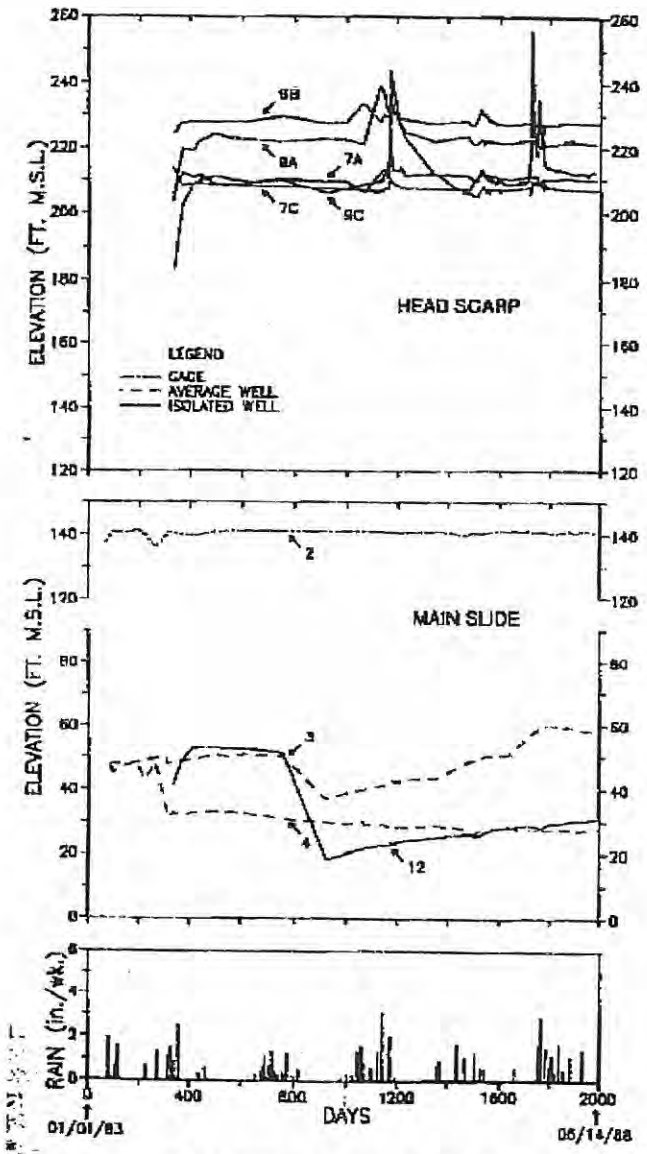

Figure 6. Piezometric Levels, Before Hydrauger Installation

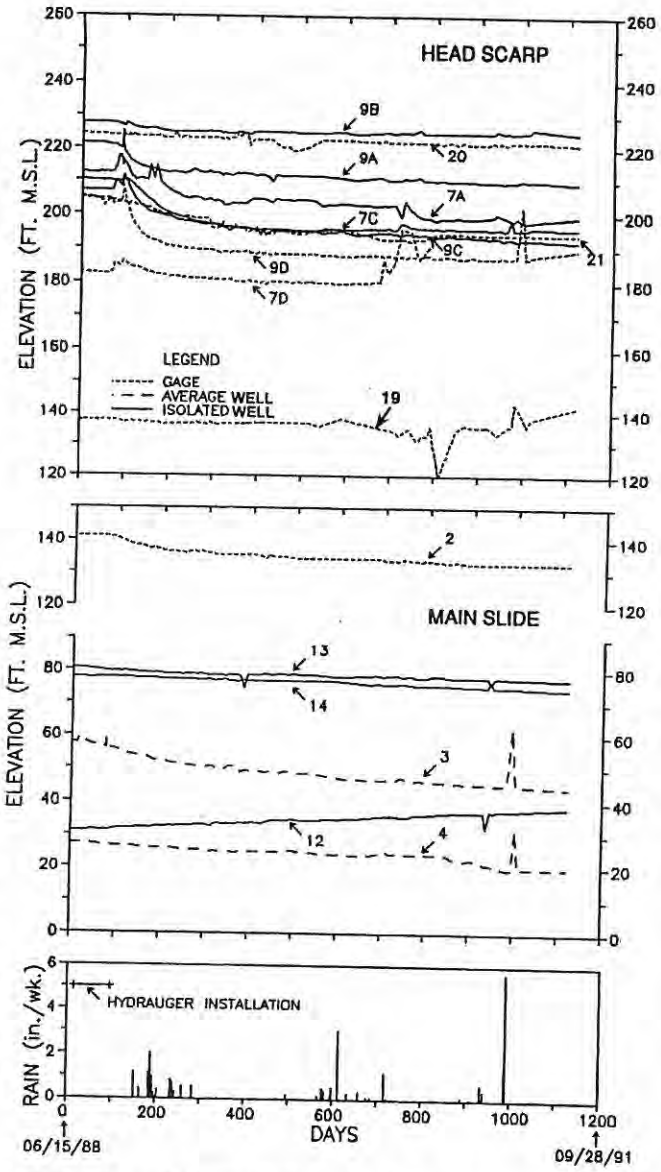

Figure 7. Piezometric Levels, After Hydrauger Installation

In the region of the main slide mass many of the observation wells remained essentially unaffected by the hydraugers. The data from those instruments which did experience changes are presented in the bottom half of Figure 7. The most significant decreases in piezometric levels, about 15 and 8 feet, occurred at Locations 3 and 4, respectively. In addition to these two average-well type instruments, the pore pressure gage at Location 2 showed a decrease of about 5 feet.

The steadily rising piezometric level at Location 12 represents a notable exception from the general trend of constant or decreasing levels across the site. It is situated near the mouth of the same ravine which is thought to be affected by external water influx causing the excess flow rates of Hydrauger H12 as discussed above.

CONCLUSION

Several years of monitoring the drainage discharge and corresponding changes in the ground water regime of the Via de las Olas slide have established a useful data base to evaluate the effectiveness of subsurface drainage in the low-permeability clay- and siltstone formations typical of the coastal bluffs of southern California.

In evaluating the effectiveness of hydraugers, it is important to focus on their main purpose of reducing the pore water pressures within the saturated soil or rock materials. Depending on whether the permeability of these materials is low or high, the pressure reduction is accompanied by small or large volumes of flow, respectively. Hence, in low-permeability materials, such as the bedrock formations of the Via de las Olas slide, even hydraugers which are merely dripping are likely to be effective. Also, the absence of demonstratively dropping piezometric levels is not necessarily a sign of nonfunctioning hydraugers. In the highly contorted and fractured bedrock formations, some of the observation wells may be hydraulically isolated from nearby hydraugers tapping into independent ground water regimes.

Notwithstanding the above, the data presented herein demonstrate the effectiveness of the installed hydraugers through measurable quantities of both discharge and reduction in piezometric levels. Among practitioners dealing with the enormous landslide problems of southern California's coastal bluffs, there have long existed two different schools of thought on this subject. Specifically, the feasibility of

dewatering bedrock slides by hydraugers has been a controversial issue. The case history presented herein should lend additional credence to the concept of dewatering these seemingly "impervious" formations of the coastal bluffs by small-diameter horizontal drains - as long as these formations are fractured. Because the latter is also a condition for rendering a "rock" formation instable in the first place, most bedrock slides are unlikely to benefit from this approach.

APPENDIX

REFERENCES

Blight, Geoffrey E., "Flow of Air Through Soils," Journal of the Soil Mechanics and Foundations Division, ASCE, Vol. 97, No. SM4, Proc. Paper 8026, April, 1971, pp. 607-624.

SI-UNITS CONVERSION

1 in = 0.0254 m;
1 ft = 0.3048 m;
1 cubic yard = 0.7646 m^3
1 gallon per hour = 3.785 liter per hour

STABILIZATION OF TABLACHACA DAM LANDSLIDE

By
Richard A. Millet [1] M. ASCE, Gil M. Lawton [2] M. ASCE,
Pedro C. Repetto [3] M. ASCE, Vinod K. Garga [4] M. ASCE

ABSTRACT

The Tablachaca Dam Landslide exists above the dam of a major hydroelectric power project in Peru. When movement threatened the dam, an emergency comprehensive program of multiple remedial measures designed to act together was developed and successfully implemented. This paper describes the background of the landslide and presents details regarding several of the emergency stabilization measures.

INTRODUCTION

Tablachaca Dam is a 72 m high concrete gravity-arch dam on the Mantaro River in Peru, located approximately 300 km from Lima (Figure 1). Its objective is to divert water from the Mantaro River through a 20 km long pressure tunnel to the Santiago Antunez de Mayolo hydroelectric plant (798 MW). From there water is conveyed through another tunnel to a second power plant (216 MW). These two power plants are owned by the government company ELECTROPERU and provide as much as 50% of the electrical capacity for central Peru. Construction of the dam was completed in 1972.

In September 1972, the reservoir was first filled from river level at about Elevation 2,640 m to a maximum elevation of 2,695 m. During the period when the reservoir was rising, movement was observed in part of an ancient slide on the

1. Executive Vice President, Woodward-Clyde Consultants, Denver, CO 80237
2. Senior Project Engineer, Woodward-Clyde Consultants, Oakland, CA 94607
3. Associate, Golder Associates, Mt. Laurel, NJ 08054
4. Associate Professor, Department of Civil Engineering, University of Ottawa; Ottawa, Canada; Geotechnical Consultant to ELECTROPERU, Lima, Peru

BIBLIOGRAPHY

Baldwin, Joel E., III, Donley, Howard F., Howard, Terry R., and Rodrigues, Roberta, J., 1984, "Distribution, Nature, and Mechanisms of Debris Flow/Avalanches in Pacifica, California" Debris Flows, Landslides and Floods in the San Francisco Bay Region, January 1982, National Academy Press.

Baldwin, Joel, and Cotton, William, 1986, "Landslides and Coastal Processes, San Francisco Peninsula," Association of Engineering Geologists, Annual Meeting, San Francisco, Field Trip Guidebook.

Barrows, Allan G., Tan, Siang S., and Irvine, Pamela J., 1993, "Damaging Landslides Related to the Intense Rainstorms of January - February, 1993, Southern California," California Division of Mines and Geology, California Geology, September/October.

Baum, R. L., Fleming, R. W., and Ellen, S.D., 1989, "Maps Showing Landslide Features and Related Ground Defamation in the Woodlawn Area of the Manoa Valley, City and County of Honolulu, Hawaii," U.S. Geological Survey, Open File Report 89-290.

Baum, Rex, L., Spengler, Steven, R., Torikai, Gill, D., and Liu, Lori Ann S. N., 1990, "Summary of Geotechnical and Hydrologic Data Collected Through April 30, 1991, for the Alani Paty Landslide, Manoa Valley, Honolulu, Hawaii," U.S. Geological Survey, Open File Report 90-531.

Cooley, L. A., Fleming, R. L., Templeton, A. E., Wardlaw, E. G., 1984, "Slide Stabilization with Gravel Trenches," in International Conference on Case Histories in Geotechnical Engineering, University of Missouri Rolla, Rolla, Missouri.

Custenborder, Gene, 1990, "Application of a Polymer Geogrid-Reinforced Buttress in Slope Stabilization, San Diego, California," in Geotechnical Engineering Case Histories in San Diego County, Edited by Hoobs, John H., San Diego Association of Geologists.

Ehlig, Kathleen A., and Bean, Robert T., 1982, "Dewatering of the Abalone Cove, Landslide City of Rancho Palos Verdes, Los Angeles County, California," in Guidebook and Volume: Landslides and Landslide Abatement, Palos Verdes Peninsula, Southern California, Compiled by John D. Cooper, 78th Annual Meeting of the Cordilleran Section of the Geological Society of America, Anaheim, California.

Eisbacher, G. H., and Clague, J. J., 1980, "Urban Landslides in the Vicinity of Vancouver, British Columbia, with Special Reference to December, 1979 Rainstorm," Slope Stability Problems in Urban Areas, Proceedings, Canadian Geotechnical Society Specialty Conference, Toronto.

Ehlig, Perry L., 1986, "Landslides and Landslide Mitigation in Southern California: Guidebook and Volume," Geological Society of America Cordilleran Section Annual Meeting.

Fleming, R. W., Johnson, R. B., and Schuster, R. L., 1988 "The Manti, Utah Landslide," U.S. Geological Survey, Professional Paper 1311.

Hamelehle, Dale, and Rehwoldt, Eric, 1990, "Rockfall Evaluation for Cut Slopes in San Diego County, California," in Geotechnical Engineering Case Histories in San Diego County, Edited by Hoobs, John H., San Diego Association of Geologists.

Hardy, R.M., Clark, J.I., and Stepanek, M., 1980, "A Summary of Case Histories Spanning 30 Years of Slope Stabilization in Calgary, Alberta," in Slope Stability Problems in Urban Areas, Canadian Geotechnical Society, Proceedings of Specialty Conference, Toronto.

Hart, Michael W., 1989, "Engineering Geology in San Diego, California," In Environmental, Engineering, and Urban Geology in the United States, 28th International Geologic Congress, San Francisco, California.

Hungr, O., and Morgan G. C., 1984, "Quantitative Analysis of Debris Torrent Hazards For Design of Remedial Measures," Canadian Geotechnical Journal.

Jochim, Candace L., 1986, "Debris-Flow Hazard in the Immediate Vicinity of Ouray, Colorado," Colorado Geological Survey, Special Publication 30.

Keene, Arthur G., 1992, "Landslide Failure at 20510 Callon Drive, Topanga, California, March 1978," in Landslides/Landslide Mitigation, Edited by Slosson, James E., Keene, Arthur G., and Johnson, Jeffrey A., The Geological Society of America, Reviews in Engineering Geology Volume IX.

Leighton, F. Beach, and Clark, Bruck R., 1989, "Evolution of Landslide Repair in Southern California," in Landslides in a Semi-Arid Environment, Edited by Peter M. Sadler and Douglas M. Morton, Inland Geological Society, Volume 2.

Lung, Richard, and Proctor, Richard, 1966, Engineering Geology in Southern California, Association of Engineering Geologist, Southern California Section.

Martin, Dennis C., 1988, "Remedial Measures for Debris Flows in British Columbia," Association of Engineering Geologist, Bulletin, Vol XXV, Number 2.

Mears, Arthur, 1977, "Debris-Flow Hazard Analysis and Mitigation - An Example From Glenwood Springs, Colorado," Colorado Geological Survey.

Montgomery, David R., Wright, Robert H., and Booth, Tom, 1991, "Debris Flow Hazard Mitigation for Colluvium-Filled Swales," Association of Engineering Geologist Bulletin, Volume XXVIII, Number 3.

Rogers, J. David, 1986, "Landslide Processes of the East Bay Hills, San Francisco Bay Region, California," Association of Engineering Geologists, Annual Meeting, Field Trip Guidebook.

Thomas, Michael, Kropp, Alan, and Lucas, Andrea, 1989, "Biotechnical Stabilization of a Debris Flow Scar," International Erosion Control Association Proceedings, XX Annual Meeting, Vancouver, Canada.

VanDine, D. F., 1985, "Debris Flows and Debris Torrents in the Southern Canadian Cordillera," Canadian Geotechnical Journal, Volume 22.

Wigginton, W. B., and Hickmott, D., 1991, "The Sargent Landslide and Long-Term Groundwater Fluctuations in California Hillsides," in Slope Stability Engineering, Developments and Applications, Thomas Telford, London.

TAB 6

P. Erik Mikkelsen

Presentation

P. Erik Mikkelsen, P.E.
Geoengineering & Instrumentation Consultant
16483 SE 57th Place
Bellevue, WA 98006
Telephone: (425) 746-9577; e-mail: mikkelsen.pe@attbit.com

"Field Instrumentation for Landslides"

by
P. Erik Mikkelsen, P.E.
For
Slope Stability and Landslides
A University of Wisconsin Short Course
At UCLA Engineering Extension, February 20-22, 2002

Abstract
Measuring **displacements and groundwater elevations** are the most commonly used monitoring methods for potentially unstable slopes and active landslides. Monitoring such parameters assists in the assessment of instability, design of remedial measures, and the effectiveness of remedial works. Flow monitoring from drainage works and meteorological observations are also very useful in many instances.

Surface displacements are primarily monitored by landsurveying methods. Horizontal and vertical movement of hubs or monuments can be surveyed from a total station setup or by the increasingly more used and increasingly more accurate GPS methods. **Subsurface** displacements are most often measured by vertical inclinometers, but occasionally it is appropriate to use rod and wire extensometers. Stationary inclinometer sensors and use of automatic recording are improving our understanding of landslide movements. The various methods will be described and discussed.

Groundwater levels are most often observed in well-type installations in exploration boreholes. A large number of "wells" have dual or more purposes, such as water quality sampling, pump testing and water level monitoring. However, the most important parameter for slope stability assessment is to be able to measure the maximum **piezometric level** in the slope usually during a **transient event**. Correct placement of the point or zone of measurement and timeliness of the observations are paramount. Conventional well technology-based design is often inadequate in such instances. Large well diameters, impossible backfilling conditions and manual observations contribute to inconclusive information. Improved installations with piezometer transducers such as pneumatic and vibrating wire pressure sensors will be described and discussed.

Correlation of parameters monitored in a timely manner is now more available than ever. Environmental **data loggers** are gaining wider use, allowing data collection during critical events. Examples from case histories will be presented to illustrate how landslides can be better understood and managed with improved instrumentation and automatic data acquisition.

A revised copy of Chapter 11, "Field Instrumentation" by P. Erik Mikkelsen in "Landslides: Investigation and Mitigation", Transportation Research Board, Special Report 247, Washington D.C.1996, is enclosed for reference to this presentation. Six of the figures were updated with more current information. Some obsolete information was eliminated and an erroneous comment on inclinometer spiral and rotation corrections was corrected.

Also included, is a copy of "Continuous monitoring of the slope above an excavation within a marginally stable landslide", by Derek H. Cornforth and P. Erik Mikkelsen, Proceedings of the 7th International Symposium on Landslides, Trondheim, Norway, June, 1996. It talks about how automated in-place inclinometer and piezometer readings not only improves accuracy, but is superior to conventional observations in collecting timely data for cause and effect correlation.

Another paper, a preprint of "Continuous Monitoring of Groundwater Response to Winter Rainfall", by Derek H. Cornforth and P. Erik Mikkelsen, Proceedings of the 8th International Symposium on Landslides, Cardiff, UK, June, 2000 is included. It talks about the benefits of automated piezometer readings for understanding the time-lag between a precipitation event and subsequent "spiking" in the piezometric levels. Instrumentation costs are also included.

P. Erik Mikkelsen, P.E.

16483 SE 57th Place
Bellevue, WA 98006
Telephone: (425) 746-9577; E-mail: mikkelsen.pe@worldnet.att.net

EDUCATION

1966 B.S. Civil Engineering, University of Utah, Salt Lake City
1967 M.S. Civil Engineering (Geotechnical), University of California/Berkeley

REGISTRATION

1971 California - Civil Engineer
1976 Washington - Civil Engineer

PROFESSIONAL SOCIETIES

Member, American Society of Civil Engineers (ASCE) and the Geo-Institute
Member, International Soc. of Soil Mech. and Foundation Engineering (ISSMFE)
Senior Member, Instrument Society of America (ISA)
Member, US Society on Dams (USSD)
Member, Consulting Engineers Council of Washington (CECW/ACEC)

PROFESSIONAL CAREER

1999 -	Self-employed, Consulting Engineer
1996 - 1999	Cornforth Consultants, Inc./Landslide Tech., Portland, Oregon, Principal/VP
1989 - 1996	Landslide Technology/Cornforth Cons., Bellevue, Washington, Manager/VP
1979 - 1989	Slope Indicator Company; Seattle, Washington, VP Geotechnical Services
1971 - 1979	Shannon & Wilson, Inc.; Seattle, Washington, Senior Associate Engineer
1968 - 1971	Shannon & Wilson, Inc.; San Francisco, California, Geotechnical Engineer

EXPERIENCE SUMMARY

Mr. Mikkelsen has 35 years of geotechnical engineering experience worldwide. He has served as project manager or principal investigator on a variety of projects in the US and abroad. Major project experience includes investigations and instrumentation monitoring for numerous dams, landslide areas, large fills, deep excavations and foundations, buildings and tunnels. Geotechnical instrumentation has been his sub-specialty for a majority of those years. He is especially known for his contribution to inclinometer data management and interpretation. He has worked with automatic data acquisition systems (ADAS) since 1973 and with IBM P/C interfaced ADAS since 1986. Recent projects include investigations for landslides, dam raises, reservoir slope stability and interpretation of dam instrumentation data. Others projects have involved design and installation of strong motion accelerographs and remote communications links. He is steadily involved in troubleshooting and interpretation of inclinometer data. Mr. Mikkelsen routinely serves as an instrumentation specialist/advisor to other consultants and the legal profession. He has published many papers on geotechnical instrumentation and currently gives seminars on instrument monitoring and inclinometer data analysis and interpretation. Mr. Mikkelsen serves regularly as a consultant to Slope Indicator and as a staff consultant to Cornforth Consultants, Inc./Landslide Technology.

Cost examples for labor and materials

One 100-foot inclinometer, two piezometers at 40 and 80 feet.

Cost example	Labor	Materials VWP	Materials Standpipes	Totals VWP	Totals Standpipes	% materials VWP	% materials Standpipes
Inclinometer Casing	$3,156	$1,000	$1,000	$4,156	$4,156	24%	24%
2 piezometers, separarate boring	$2,504	$1,100	$600	$3,604	$3,104	31%	19%
2 piezometers combined w. inclinom.	$230	$800		$1,030			
						Relative Costs	
Totals, Inclin. + separate piezos	$5,660	$2,100	$1,600	$7,760	$7,260	100%	94%
Totals, Inclin. + piezos combined	$3,386	$1,800		$5,186		67%	

Cost example, 6 months total

One 100-foot inclinometer, two piezometers at 40 and 80 feet.

Instrument Type	Cap. Cost	Monthly Charge	Data acquisition		6 months total	
			Monthly	Weekly	Monthly	Weekly
Inclinometer Instrument	$10,000	$1,000	$100	$400	$6,600	$8,400
VWP readout box	$2,000	$200	$25	$100	$1,350	$1,800
2 single ch. dataloggers	$1,200	$120	$25	$25	$870	$870

Method	Install	Monitor Wkly	Monthly Reports	Total	
Conventional manual readings	$7,760	$10,200	$4,800	$22,760	
Manual inclin. + VWP datalogger	$5,186	$9,270	$4,800	$19,256	*)
Conventional manual readings	34%	45%	21%	100%	
Manual inclin. + VWP datalogger	27%	48%	25%	100%	*)

*) - Continuous data

P. Erik Mikkelsen, P.E. 02/20/2002

Field Instrumentation for Landslides

P. Erik Mikkelsen, P.E.
Consulting Engineer
Bellevue, WA

February 21, 2002

The role of Instrumentation in landslides

- Determine topographical extent, depth and geometry of the moving mass
- Determine movements within the slide area
- Determine slide velocities
- Monitor ground water level and pore water pressure
- Provide information for early warning systems
- Monitor the effectiveness of control measures

The challenges

- Many different types of landslides
  - Require different approaches to instrumentation
- Generally there is a lack of definition
  - Lack of historical information, one is usually not aware of a problem before movement is detected
  - Limited knowledge of site conditions and slide geometry
- Time element
  - Triggering events can occur anytime
  - Not always sufficient time to properly design a monitoring system. In an emergency it is usually necessary to improvise.
- Physical limitations and economic constraints limit what can be measured.

P. Erik Mikkelsen, P.E.

Three simple steps to success

For any instrumentation application

1. Know what to measure
2. Know why
3. Know how to do it

P. Erik Mikkelsen, P.E.

Common Approach

- Surface monuments installed and monitored by surveyor
- Borings to get stratigraphy and properties
- PVC standpipe observation wells or piezometers in borings
- Install inclinometers in borings as warranted

P. Erik Mikkelsen, P.E.

Expanded Program

- GPS surveying
- Pneumatic or electrical piezometers
- In-Place Inclinometers
- Rod or wire extensometers
- TDR in borings
- Tilt sensors at ground level
- ADAS and EWS

P. Erik Mikkelsen, P.E.

Surface Surveying

- Get involved in mapping and hub layout
  - topo map may not show important details
  - get selected ground profiles
  - assist in hub layout for monitoring
- Accuracy
  - good conventional survey: +/- 0.5" to 1.0"
  - collimation accuracy: +/- 0.05"
- Topographic mapping
  - select scale and contour interval

P. Erik Mikkelsen, P.E.

Geodetic Total Station

- Surface monuments are surveyed to determine displacements and velocities using either optical or electronic devices
- Advantages: Can be automated, flexible in use
- Accuracy: typically +/- 0.1" + 2 ppm x D over 10,000 ft.

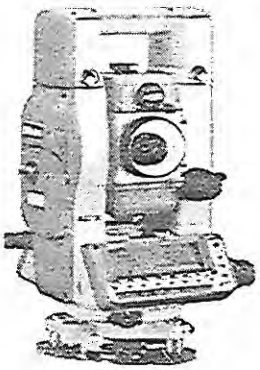

P. Erik Mikkelsen, P.E.

GPS Surveying

- GPS gets around conventional problems such as:
  - setup problems: bad angles and line-of-sight
  - atmospheric disturbance and weather
- First Order Surveying using DGPS
  - requires same attention to precision setup
  - use fixed points around movement area for "calibration"
  - accuracy better than 1 inch, approaching sub-centimeter or 1/3" accuracy

P. Erik Mikkelsen, P.E.

GPS Receiver

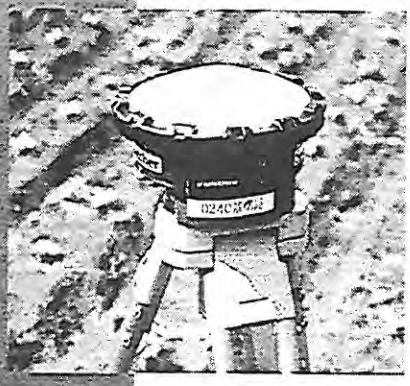

- Method: Measure movements of a GPS station positioned on the slide body.
- Equipment: Commercially available
- Advantages: Automated, economical when used over large areas
- Sensitivity: Depends on equipment used and method of taking measurements

P. Erik Mikkelsen, P.E.

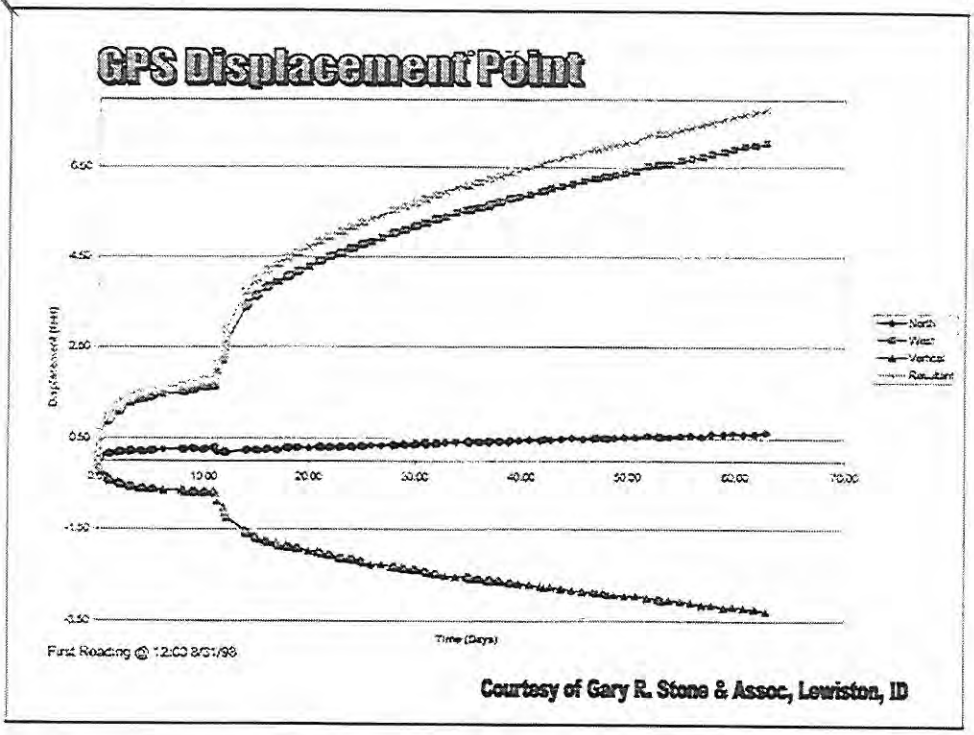
GPS Displacement Point
6.50
4.50
2.00
0.50
-1.50
-3.50
10.00
20.00
30.00
40.00
50.00
60.00
70.00
Time (Days)
North
West
Vertical
Resultant
First Reading @ 12:00 8/31/98
Courtesy of Gary R. Stone & Assoc, Lewiston, ID

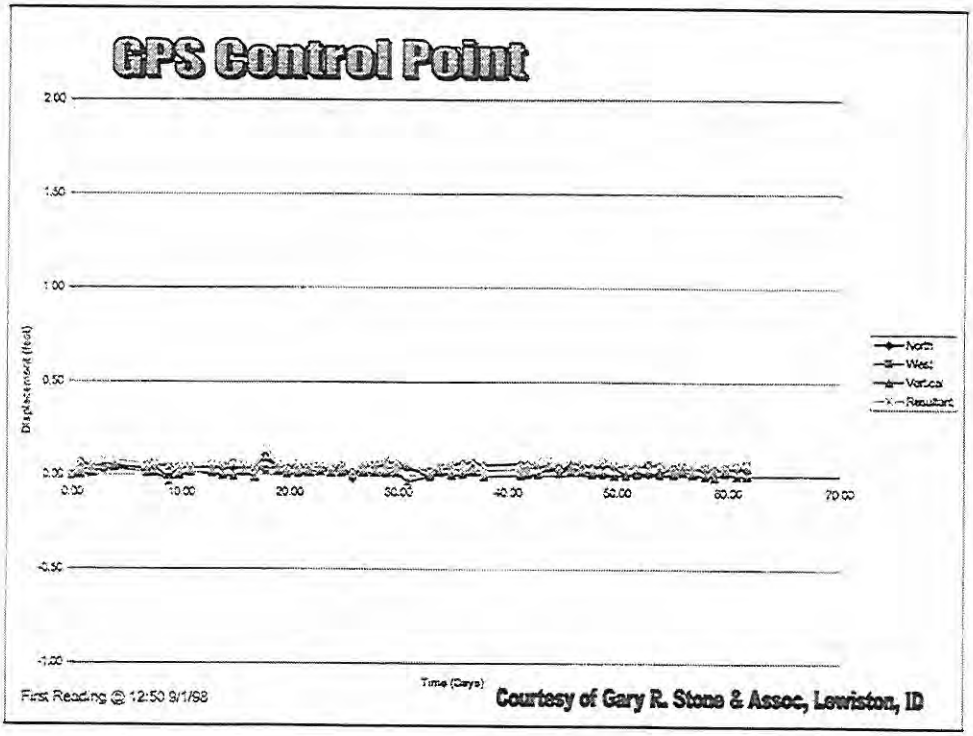
GPS Control Point
2.00
1.50
1.00
0.50
0.00
-0.50
-1.00
10.00
20.00
30.00
40.00
50.00
60.00
70.00
Time (Days)
North
West
Vertical
Resultant
First Reading @ 12:50 9/1/98
Courtesy of Gary R. Stone & Assoc, Lewiston, ID

Surface extensometer

- Function: To measure and monitor surface strain, tension cracks or joint movements
- Types: Numerous
- Advantages: Simple, automatic, reliable
- Precision: <0.01 in.

P. Erik Mikkelsen, P.E.

Surface tiltmeter

Courtesy of Elmo Dibiagio, NGI

- Used to measure slope movements involving a rotational component
- Type: Electrolytic sensors, servo-accelerometers or other gravity referenced sensors.
- Advantages: Small, simple construction, easy to install
- Sensitivity: Typically +/- 10 seconds of arc
- Advantages: Can be automated, flexible in use

P. Erik Mikkelsen, P.E.

Multipurpose Observation Well

- **Obviously economical, but .....**
  - Time-lag
  - Hit and miss manual recording
- **Installation sensitivity/problems**
  - time consuming backfill procedures
  - complicated backfill
  - risk of incomplete backfill
  - regulatory restrictions

P. Erik Mikkelsen, P.E.

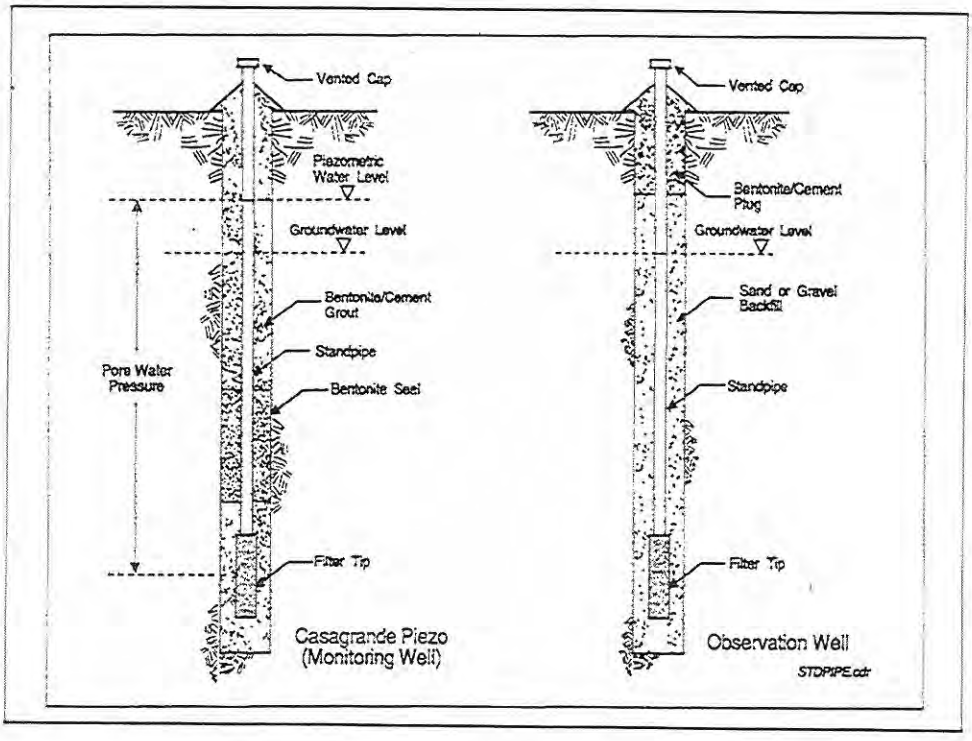

Piezo Sensors or Transducers

- **Advantages**
  - insignificant time-lag
  - remote readout
  - allows automatic recording
  - improved multi-level installation performance
- **Disadvantages**
  - more complexity
  - added hardware cost
  - tubing or cable damage potential

P. Erik Mikkelsen, P.E.

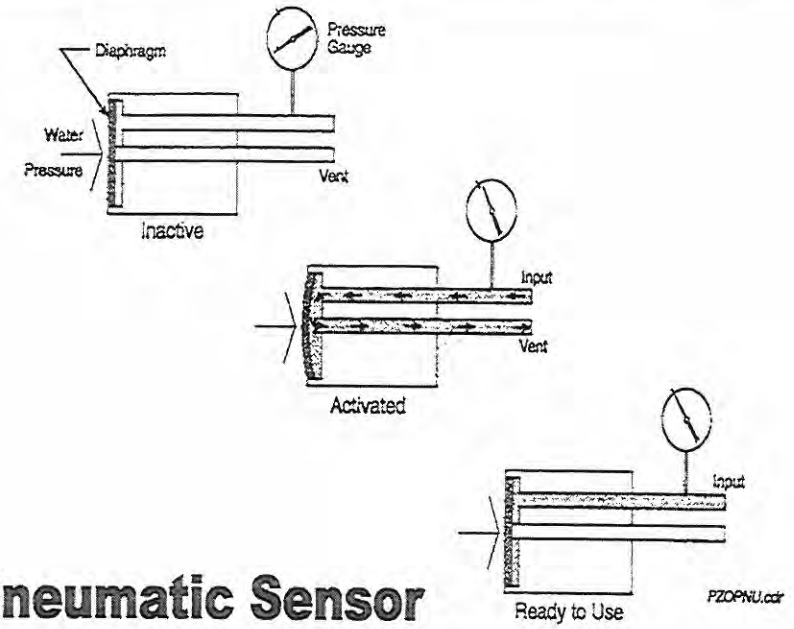

Pneumatic Sensor

Pneumatic Sensors

- **Advantages**
  - lower cost
  - no calibration factors
  - not influenced by overvoltage
- **Disadvantages**
  - slower to read
  - reading is reader influenced
  - not easily adapted to automated readings
  - quality influenced more by low bid

P. Erik Mikkelsen, P.E.

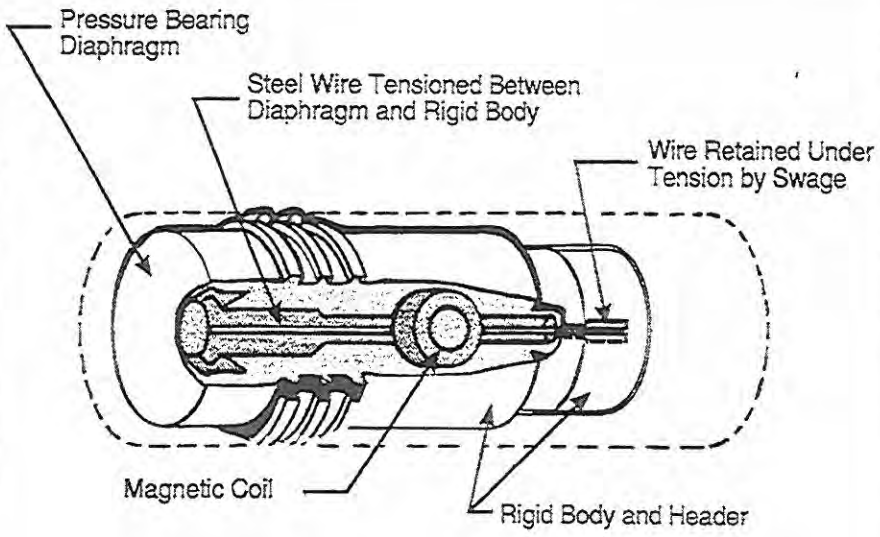

Vibrating Wire Sensor

VWPPIEZO.cdr

VW Piezometer Sensors

- **Advantages**
  - instant reading, not influenced by observer
  - best suited for automated readings
  - calibration not influenced by lead length
  - high zero stability (minimal drift for decades)
- **Disadvantages**
  - vulnerable to overvoltage
  - calibration factors, barometric influence
  - can be damaged by over-pressure
  - higher hardware cost

P. Erik Mikkelsen, P.E.

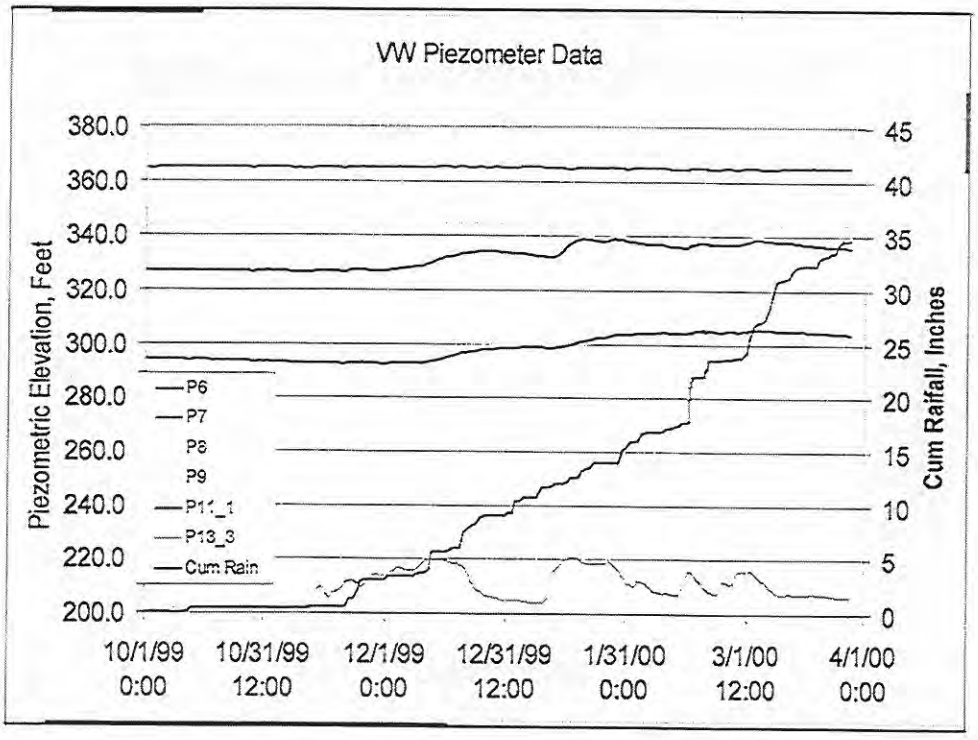

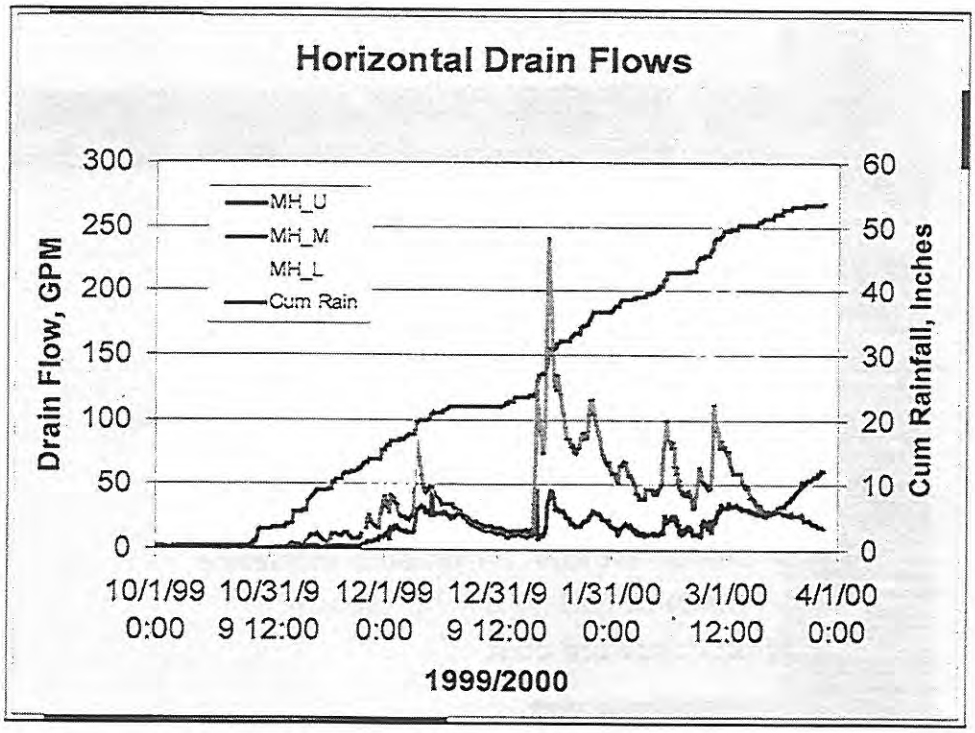
Horizontal Drain Flows
Drain Flow, GPM
Cum Rainfall, Inches
MH_U
MH_M
MH_L
Cum Rain
300
250
200
150
100
50
0
60
50
40
30
20
10
0
10/1/99 0:00
10/31/99 12:00
12/1/99 0:00
12/31/99 12:00
1/31/00 0:00
3/1/00 12:00
4/1/00 0:00
1999/2000

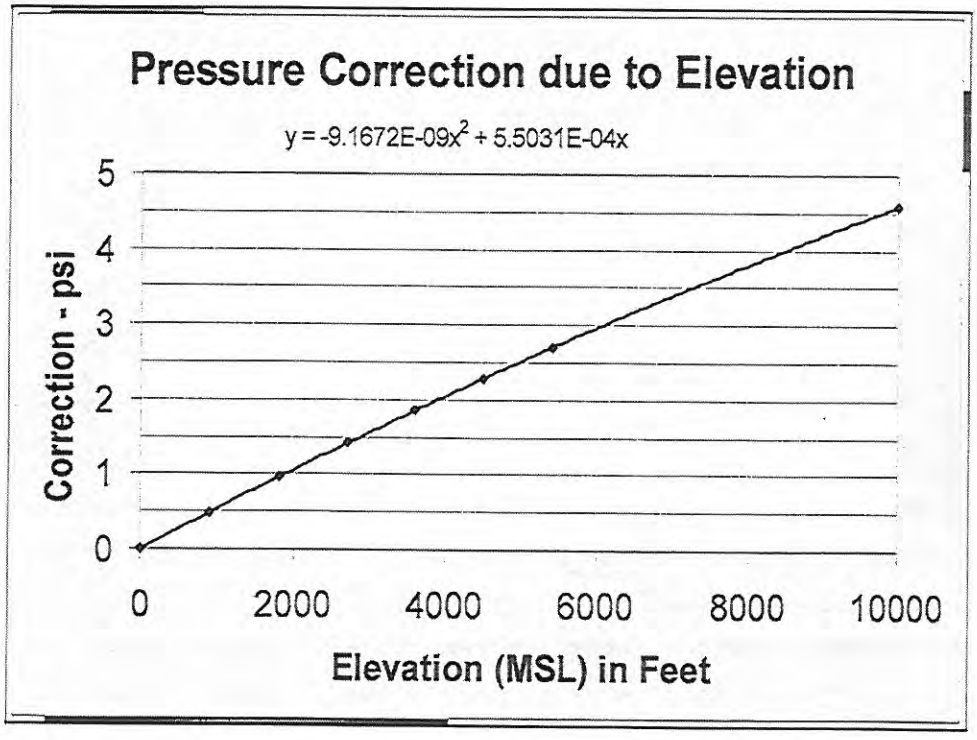
Pressure Correction due to Elevation
y = -9.1672E-09x2 + 5.5031E-04x
Correction - psi
5
4
3
2
1
0
0
2000
4000
6000
8000
10000
Elevation (MSL) in Feet

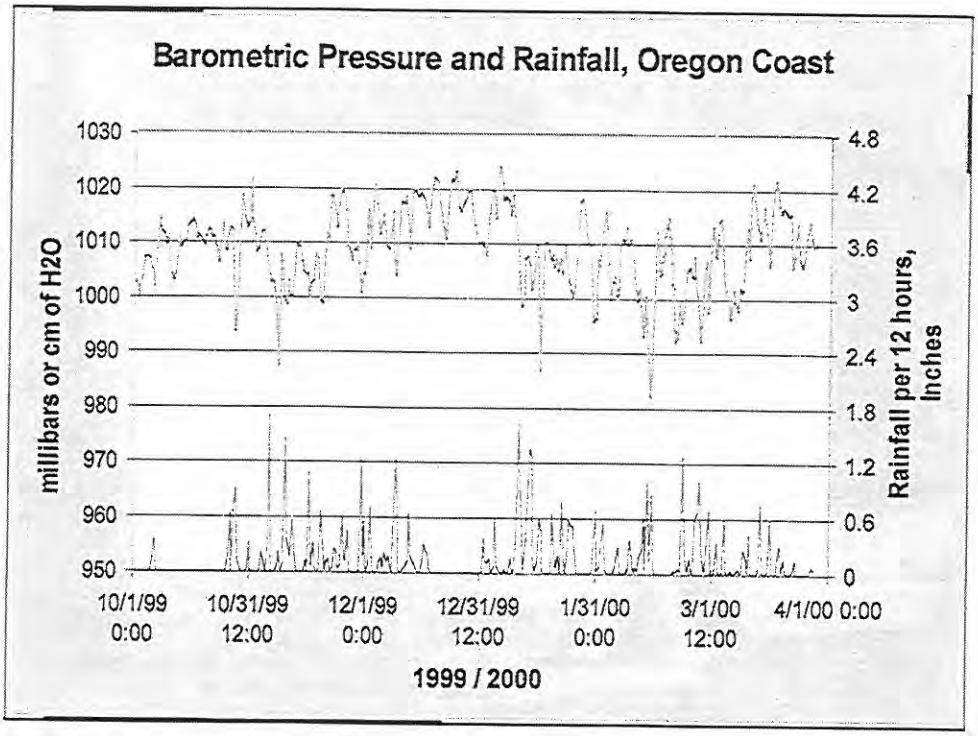
Barometric Pressure and Rainfall, Oregon Coast
millibars or cm of H2O
1030
1020
1010
1000
990
980
970
960
950
Rainfall per 12 hours, Inches
4.8
4.2
3.6
3
2.4
1.8
1.2
0.6
0
10/1/99 0:00
10/31/99 12:00
12/1/99 0:00
12/31/99 12:00
1/31/00 0:00
3/1/00 12:00
4/1/00 0:00
1999 / 2000

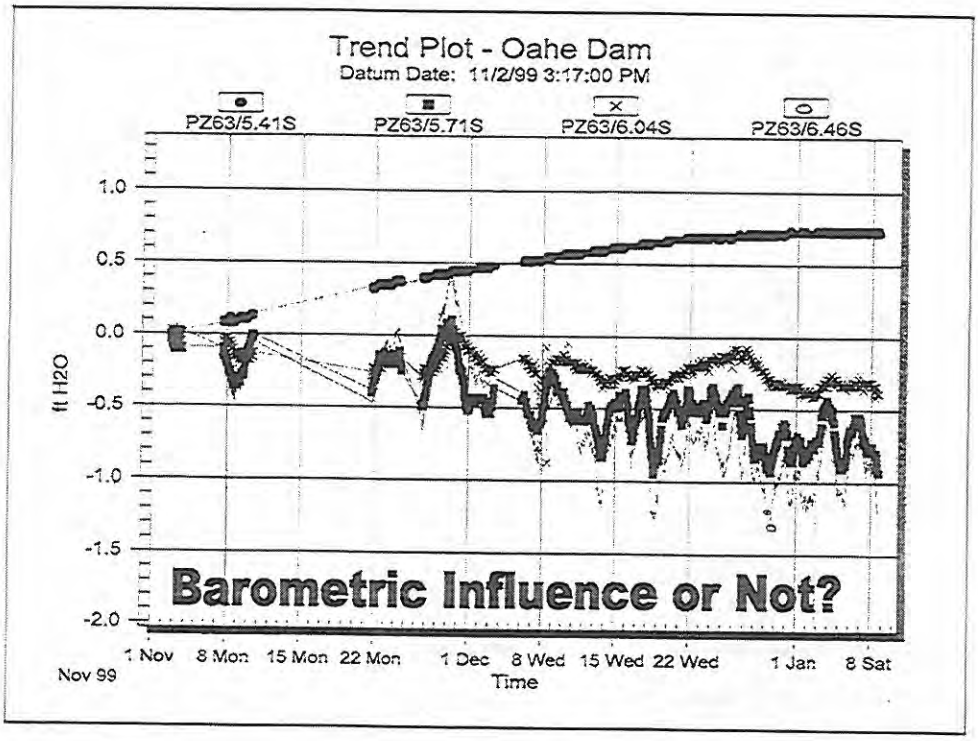
Trend Plot - Oahe Dam
Datum Date: 11/2/99 3:17:00 PM
PZ63/5.41S
PZ63/5.71S
PZ63/6.04S
PZ63/6.46S
ft H2O
1.0
0.5
0.0
-0.5
-1.0
-1.5
-2.0
Barometric Influence or Not?
Nov 99
1 Nov
8 Mon
15 Mon
22 Mon
1 Dec
8 Wed
15 Wed
22 Wed
1 Jan
8 Sat
Time

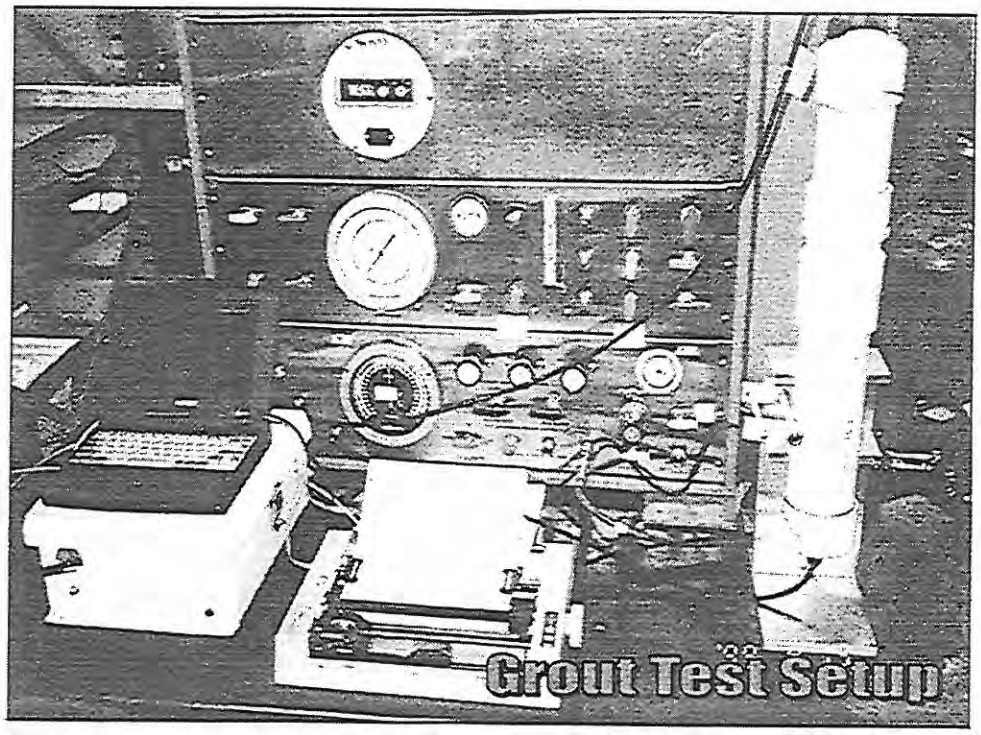
Grout Test Setup

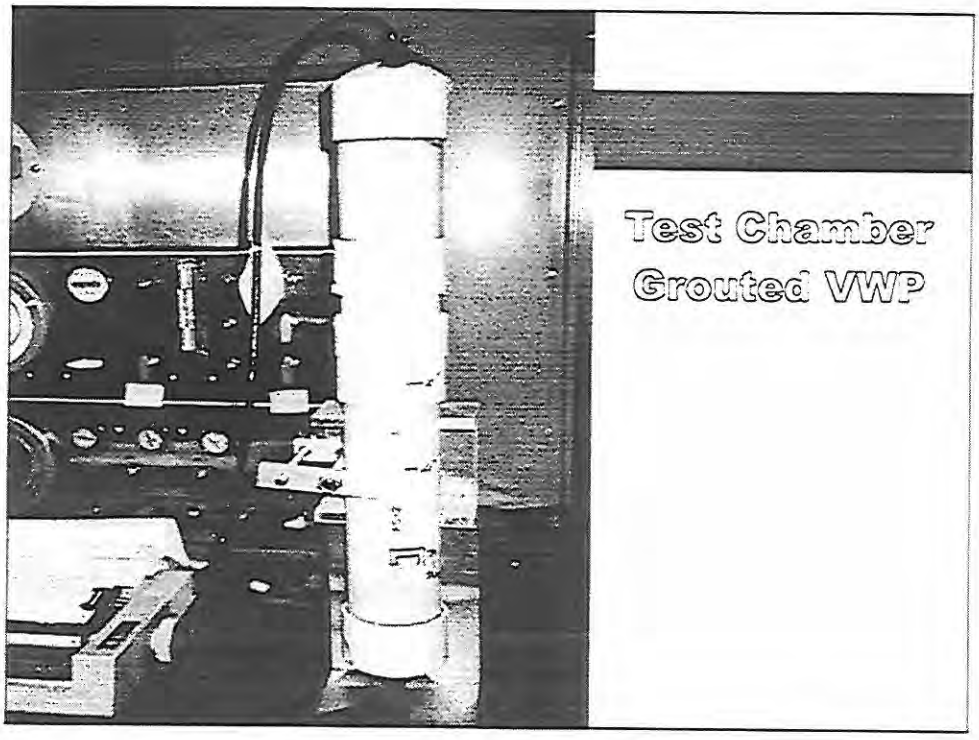
Test Chamber
Grouted VWP

Cement-Bentonite Grout

- Mix ratio by weight - 2.5 water : 1 cem : 0.3 bent
- Mix water and cement first
- Add bentonite slowly under high aggitation to make grout creamy, yet pumpable
- Density - 80 pcf
- Water Content - 78 %
- Modulus - 10,000 psi
- 30- day QU strength - 50 to 100 psi

P. Erik Mikkelsen, P.E.

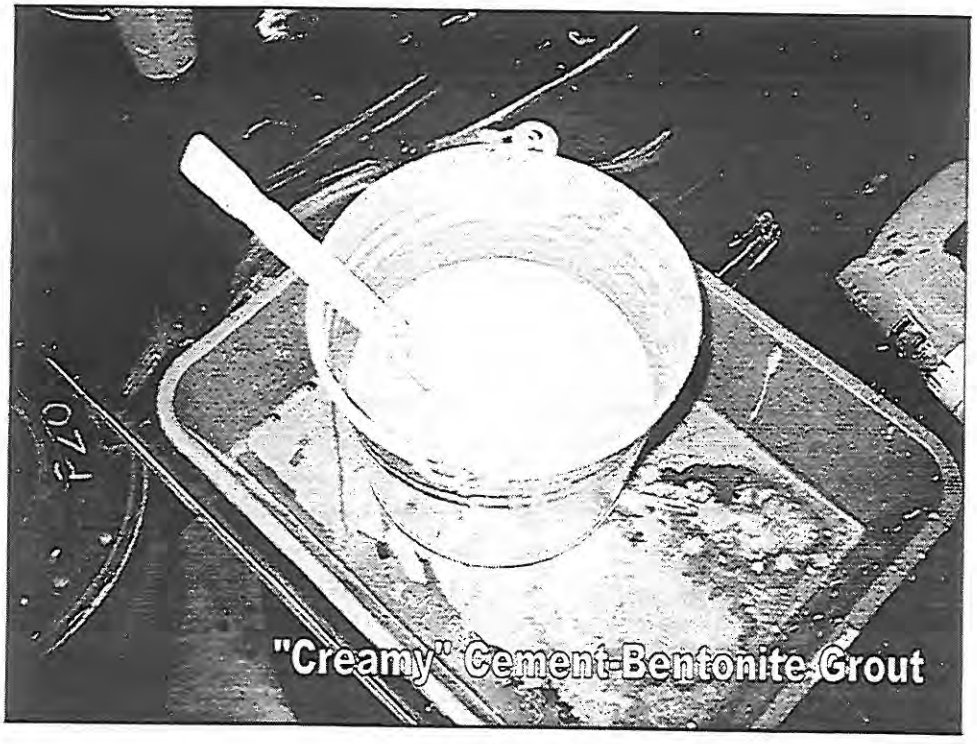

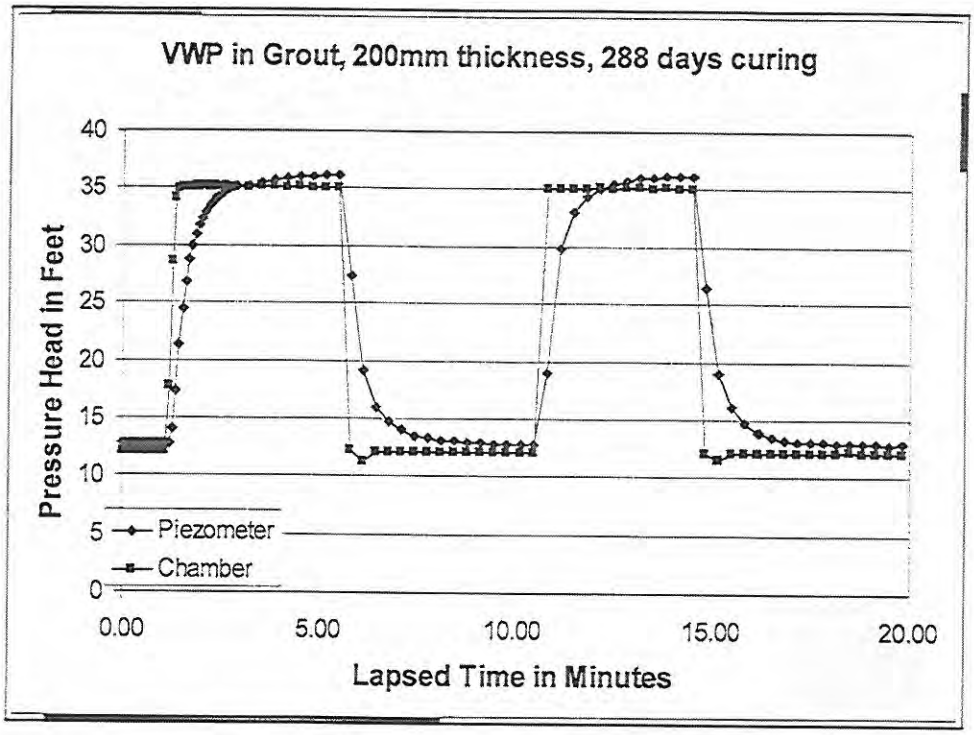
VWP in Grout, 200mm thickness, 288 days curing
Pressure Head in Feet
40
35
30
25
20
15
10
5
0
Piezometer
Chamber
0.00
5.00
10.00
15.00
20.00
Lapsed Time in Minutes

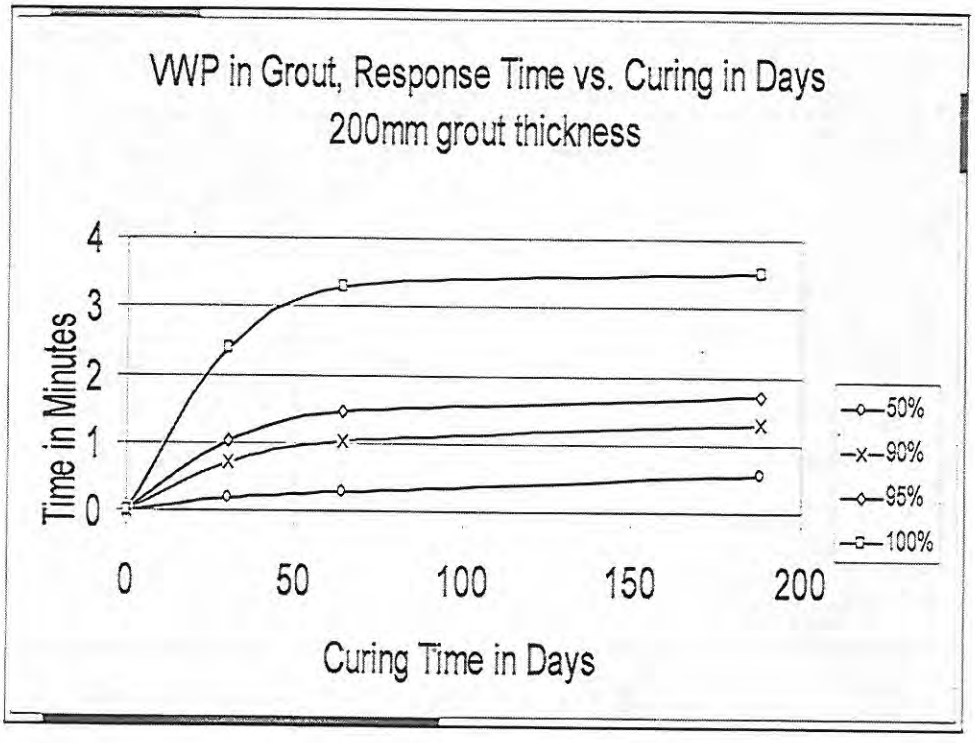
VWP in Grout, Response Time vs. Curing in Days
200mm grout thickness
Time in Minutes
4
3
2
1
0
50%
90%
95%
100%
0
50
100
150
200
Curing Time in Days

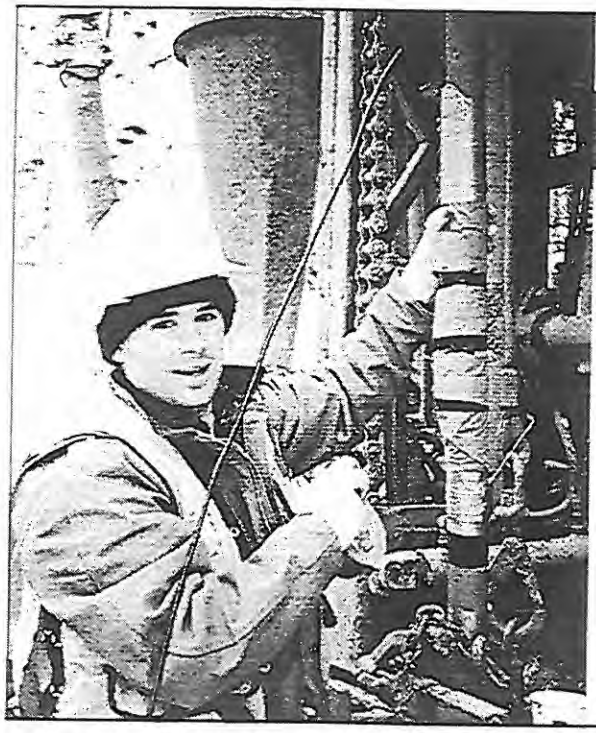

VWP "under wraps" attached to inclinometer casing before grouting

Inclinometer Installations

- Difference between plan and reality
  - size and type of boring
  - backfill: grouted or other, uplift forces
  - verticality and straightness
  - addition of other functions
- Casing Details
  - Size, type, spiral, joint system
  - top reference
  - orientation
  - reading procedures

P. Erik Mikkelsen, P.E.

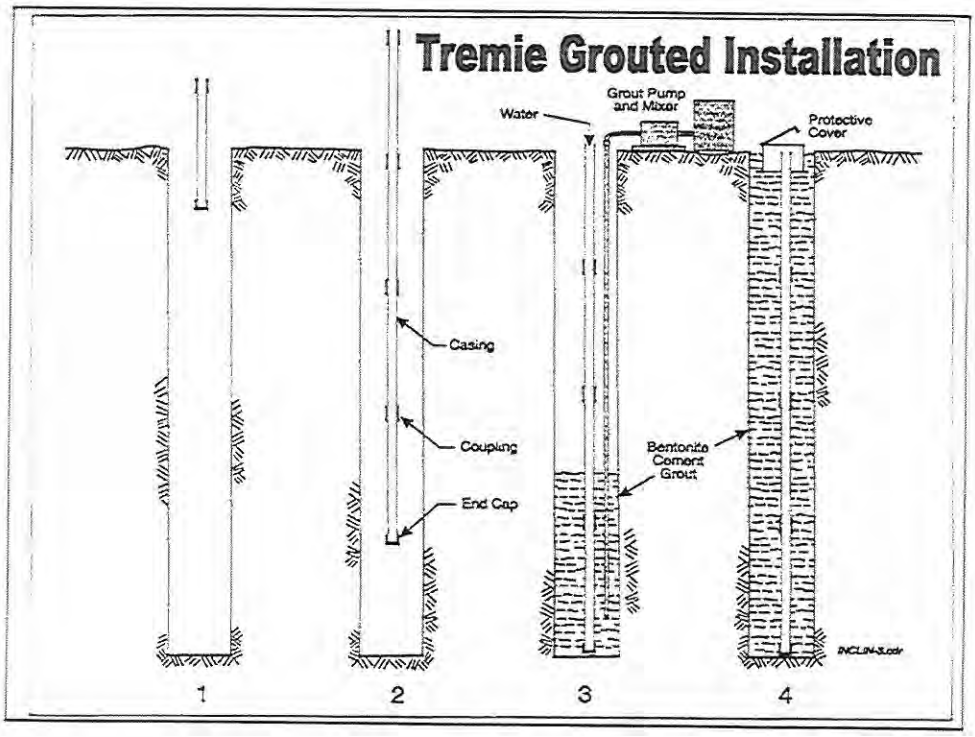
Tremie Grouted Installation
Grout Pump and Mixer
Water
Protective Cover
Casing
Coupling
End Cap
Bentonite Cement Grout
1
2
3
4

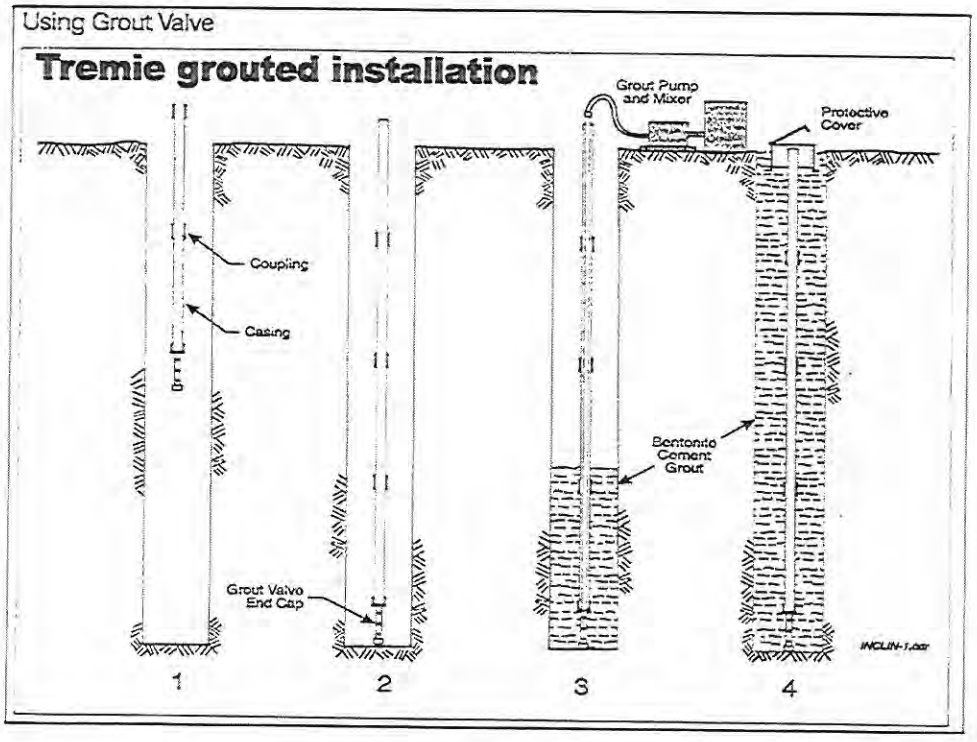
Using Grout Valve
Tremie grouted installation
Grout Pump and Mixer
Protective Cover
Coupling
Casing
Bentonite Cement Grout
Grout Valve End Cap
1
2
3
4

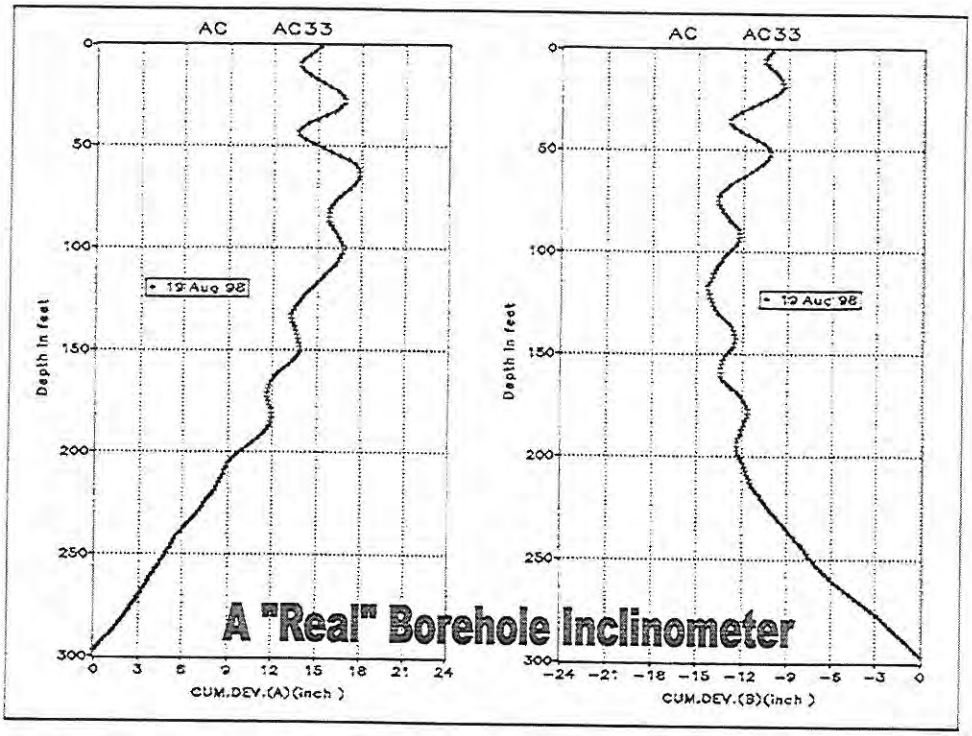

A "Real" Borehole Inclinometer

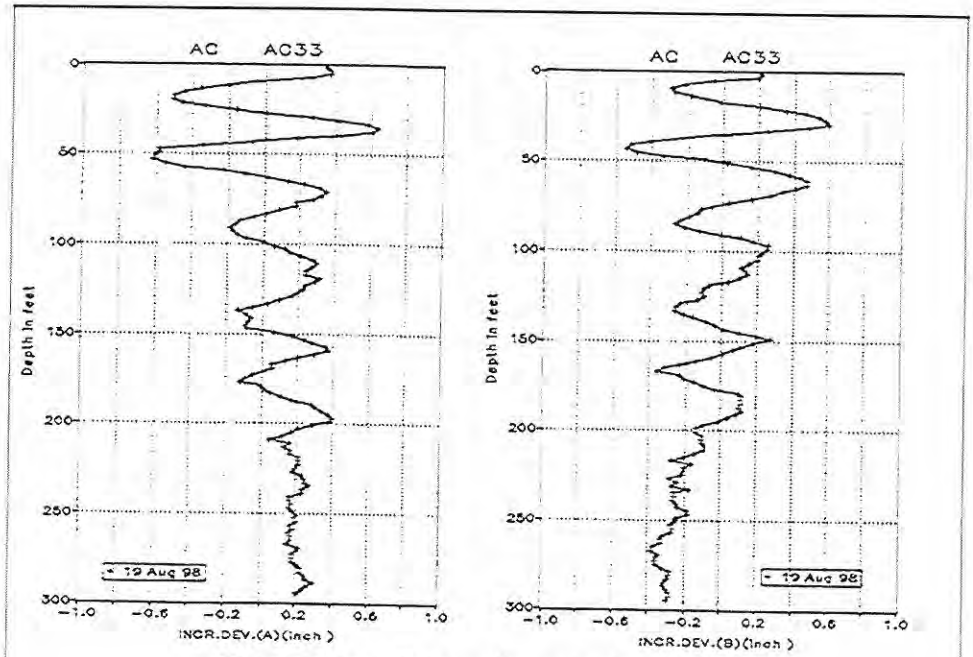

Curvature in Inclinometer Casing

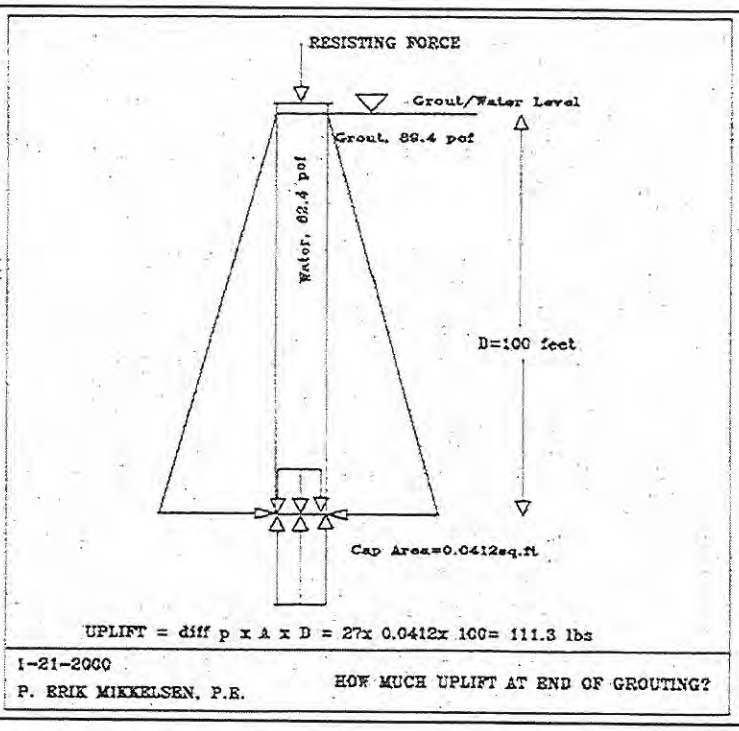

Options for Dealing with Up

- Push down on top of casing
  - high compression, potentially excessive curvature
- Steel pipe to inside bottom of casing
  - pipe needs pulling next day, reinforced bottom
- Special bottom anchor
  - requires special parts, installation risk
- Grout bottom 10 to 20 feet first, stage grout
  - more time consuming
- Set bottom in hydrated bentonite chips
  - seal may fail, some down-force needed

P. Erik Mikkelsen, P.E.

TDR in boreholes

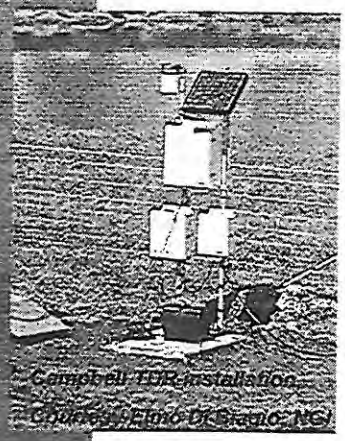

Campbell TDR installation
Courtesy Elmo Di Biagio, NCI

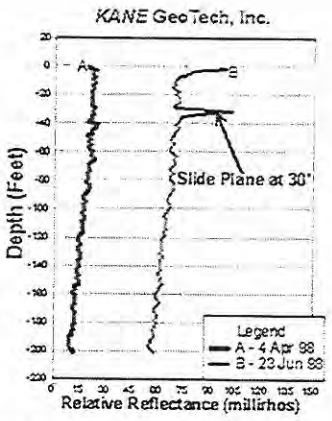

P. Erik Mikkelsen, P.E.

In-Place Inclinometers

- Install after identification of shear zone
  - detail survey of shear zone
  - design single or multiple sensor layout
  - use EL-IPI or VW-IPI sensors
  - suspend assembly on wire
- Data logging
  - grounded j-box at surface with LP
  - surface cable to logger
  - for landslides - mostly CR10X loggers
  - vandal proofing

P. Erik Mikkelsen, P.E.

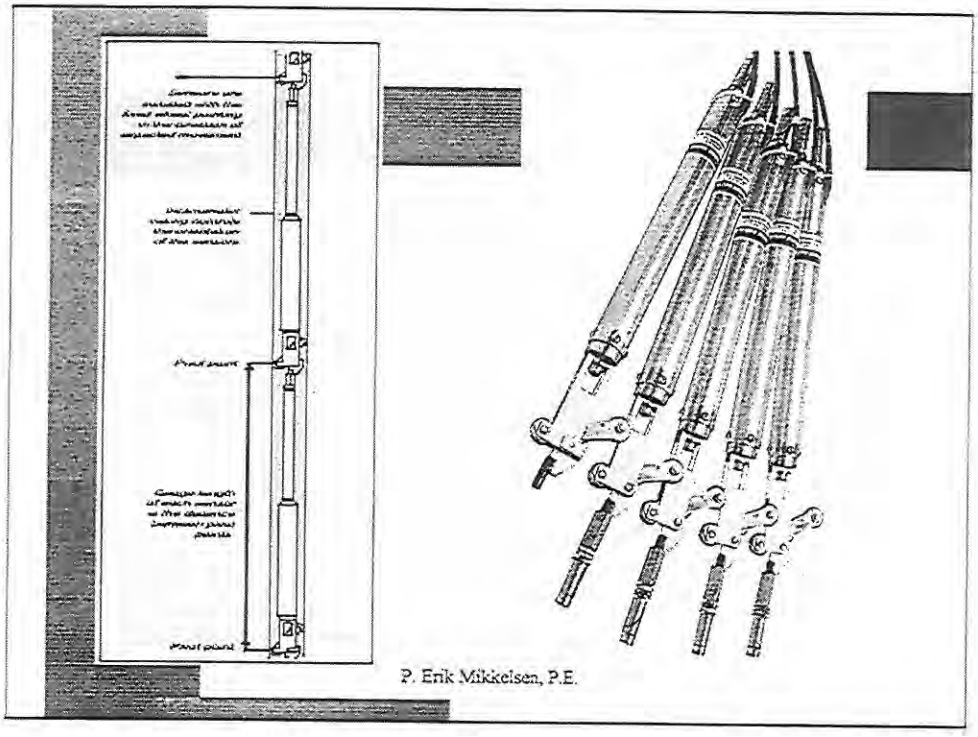
P. Erik Mikkelsen, P.E.

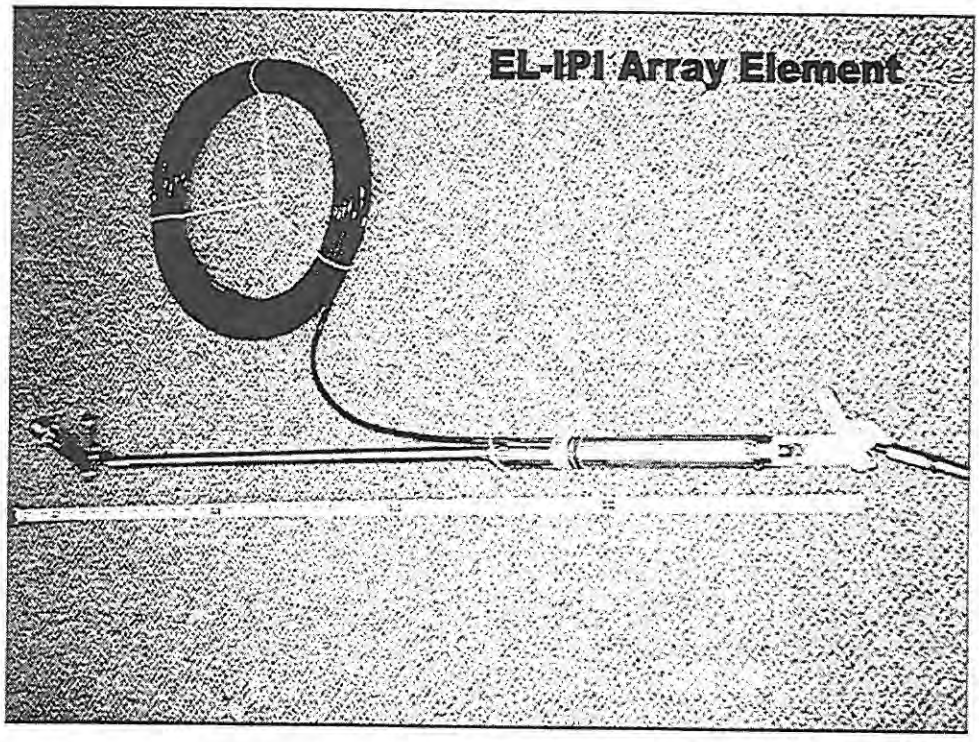
EL-IPI Array Element

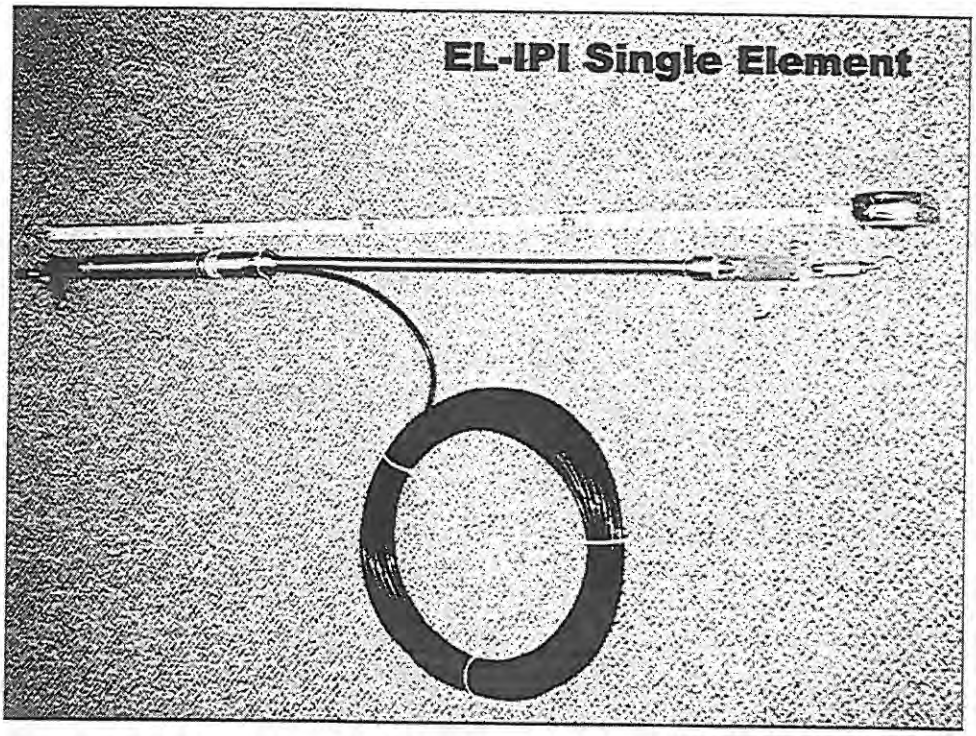
EL-IPI Single Element

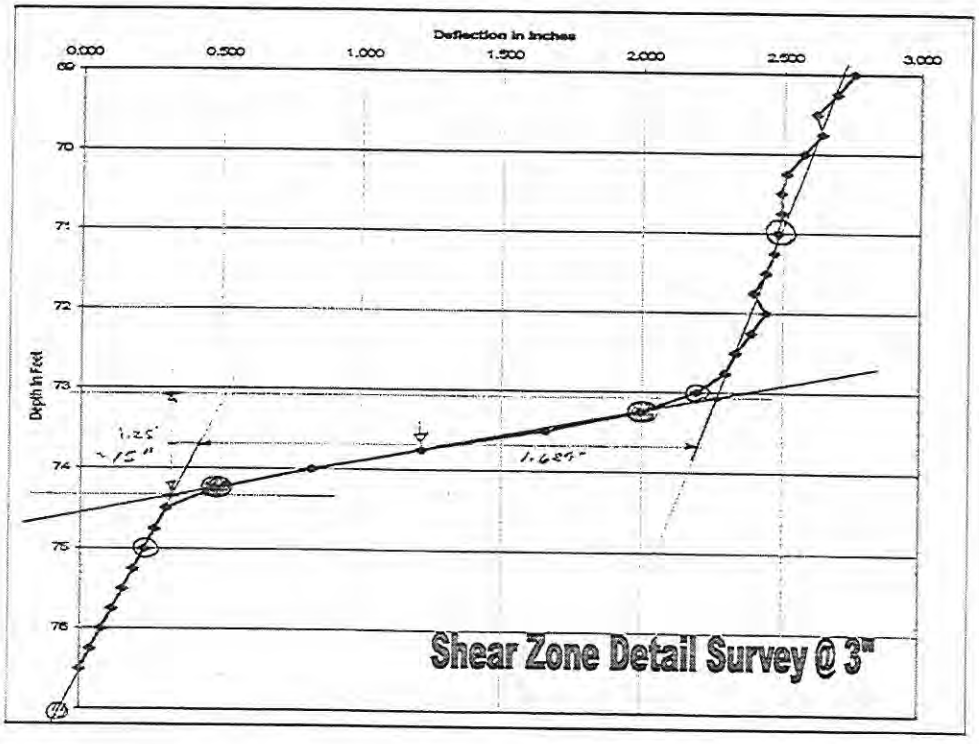
Deflection in Inches
0.000
0.500
1.000
1.500
2.000
2.500
3.000
69
70
71
72
73
74
75
76
Depth in Feet
1.25"
~.15"
1.684"
Shear Zone Detail Survey @ 3"

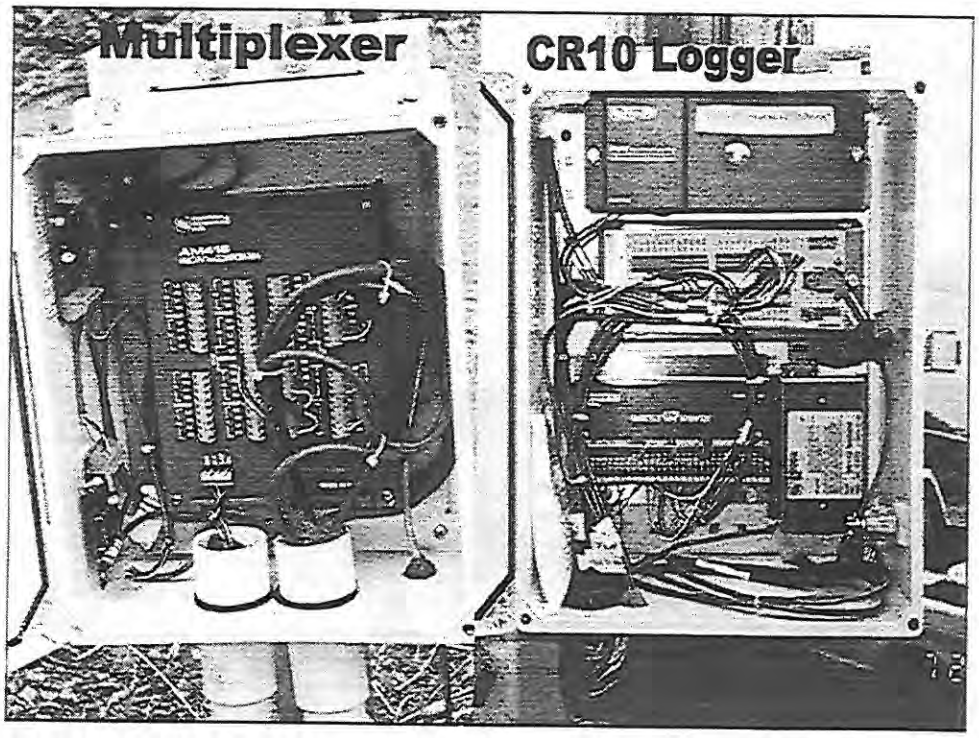
Multiplexer
CR10 Logger

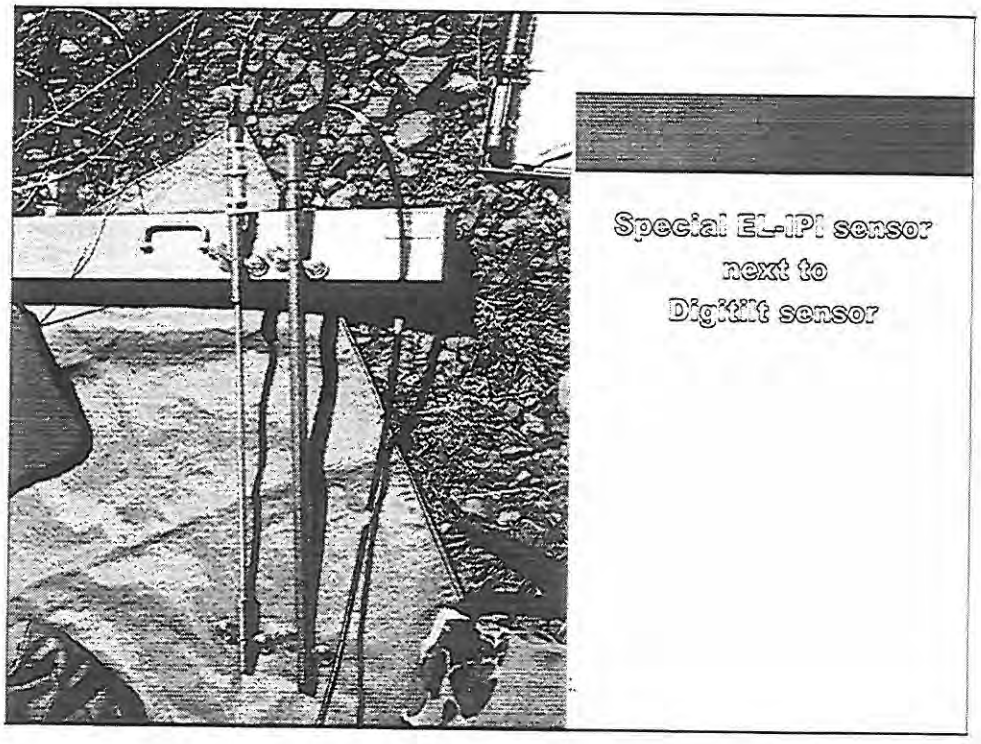
Special EL-IPI sensor
next to
Digitilt sensor

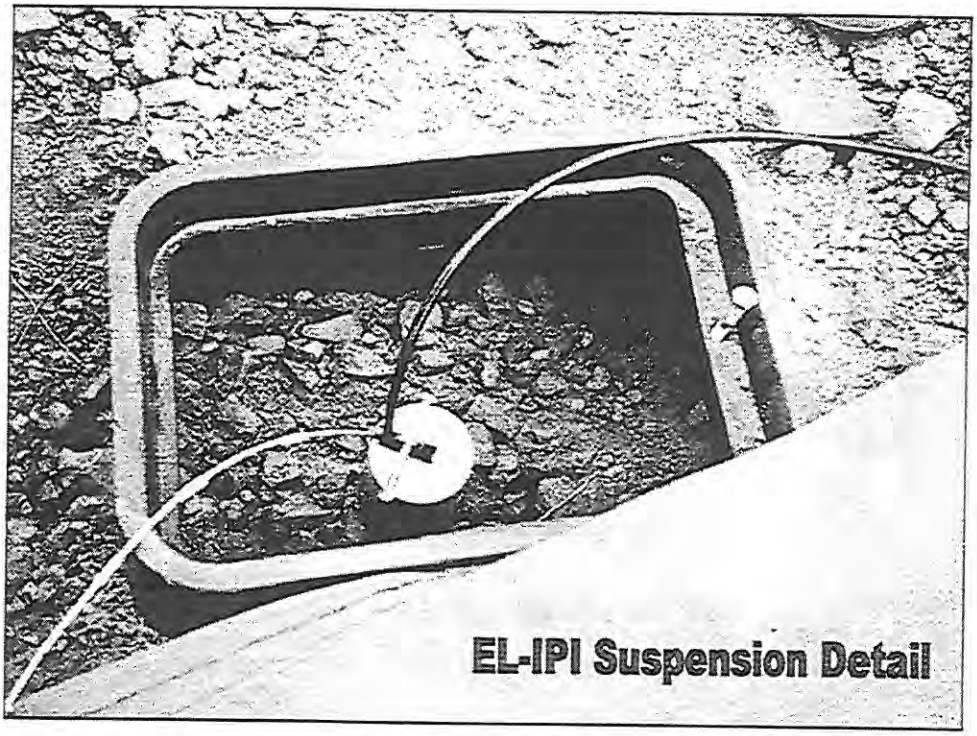
EL-IPI Suspension Detail

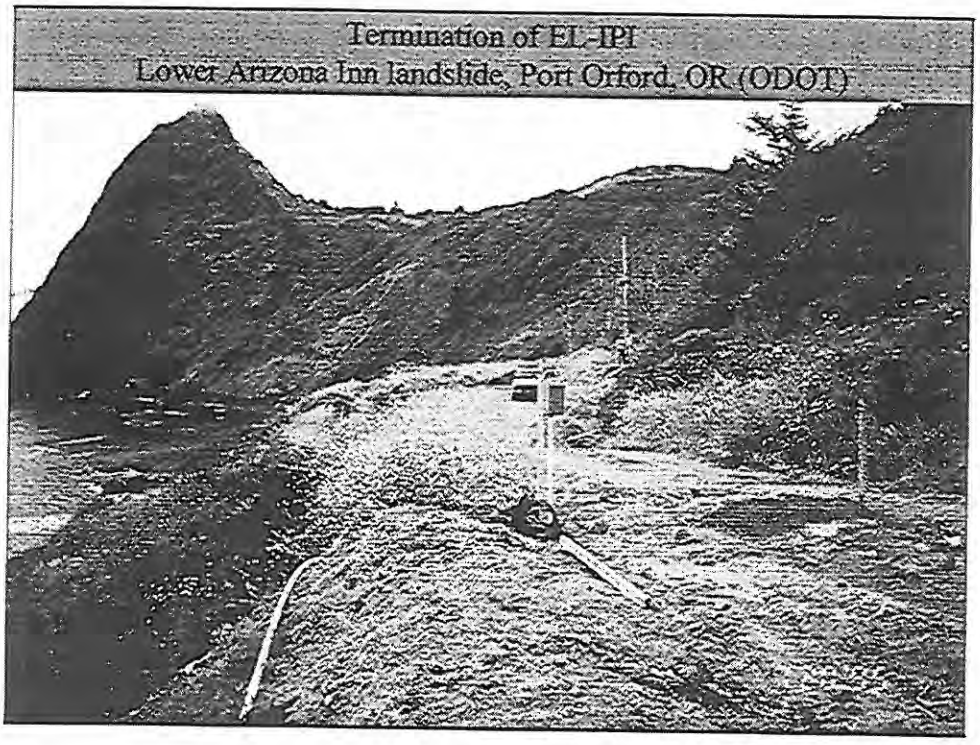
Termination of EL-IPI
Lower Arizona Inn landslide, Port Orford, OR (ODOT)

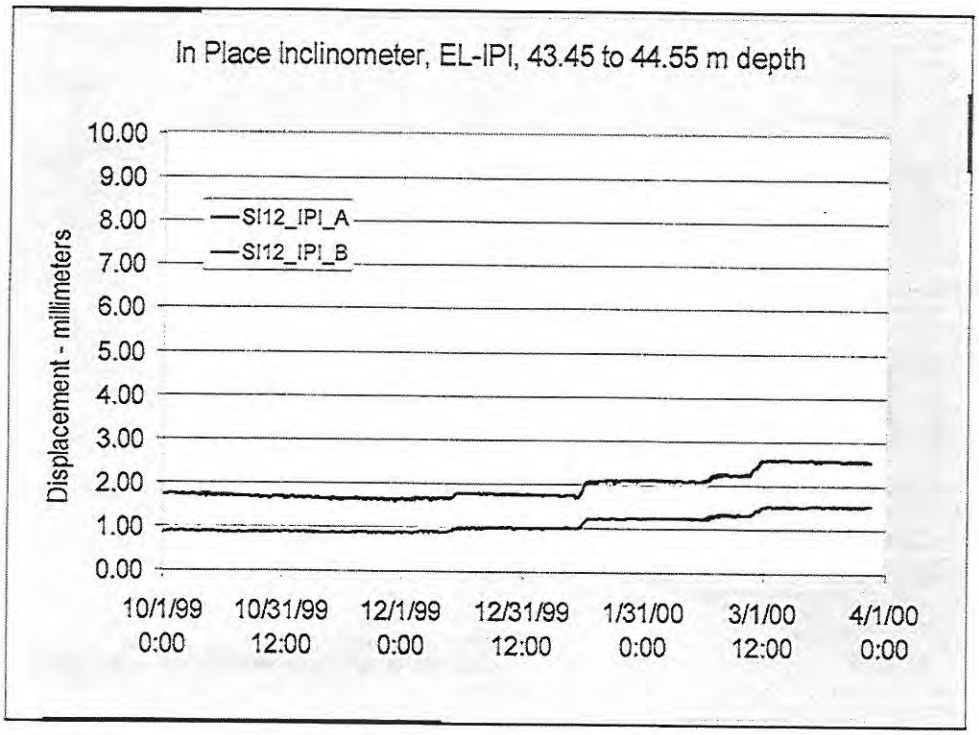
In Place Inclinometer, EL-IPI, 43.45 to 44.55 m depth
Displacement - millimeters
10.00
9.00
8.00
7.00
6.00
5.00
4.00
3.00
2.00
1.00
0.00
SI12_IPI_A
SI12_IPI_B
10/1/99 0:00
10/31/99 12:00
12/1/99 0:00
12/31/99 12:00
1/31/00 0:00
3/1/00 12:00
4/1/00 0:00

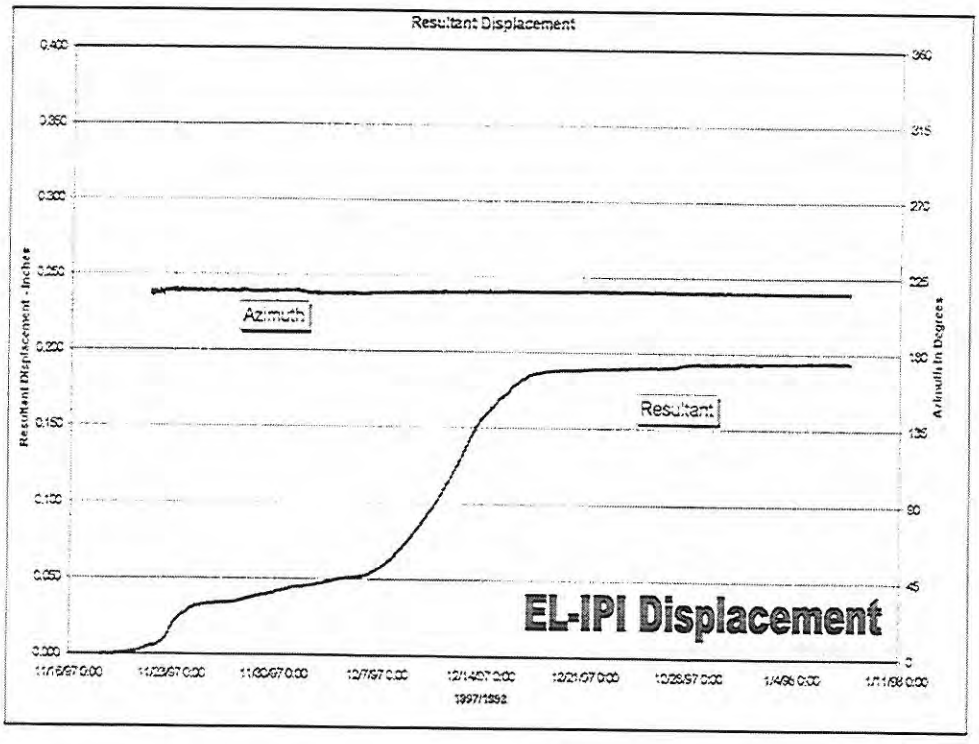
Resultant Displacement
Resultant Displacement - Inches
Azimuth In Degrees
Azimuth
Resultant
EL-IPI Displacement

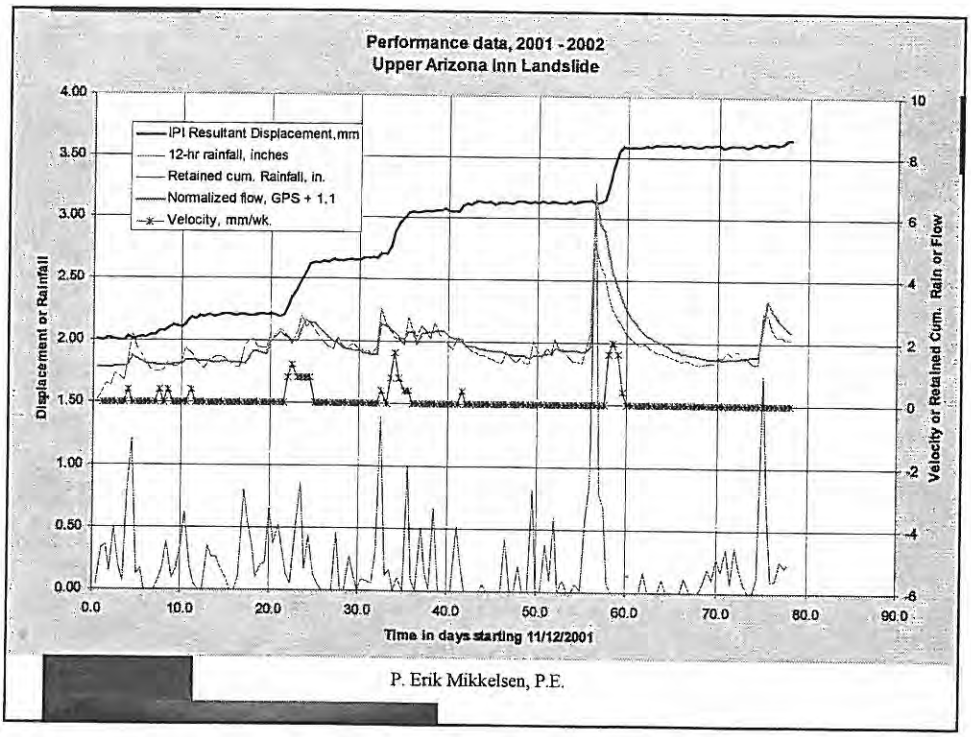

P. Erik Mikkelsen, P.E.

Conclusions

- Surface surveying, conventional & GPS
- Piezometers of some type
- Inclinometers
- TDR in borings for warning
- Occasionally - extensometers
- Increasingly ADAS, timely data
- EWS starting to emerge, but ... beware of liability issues!

P. Erik Mikkelsen, P.E.

LANDSLIDES
INVESTIGATION AND MITIGATION

SPECIAL REPORT 247

A. Keith Turner
Robert L. Schuster
Editors

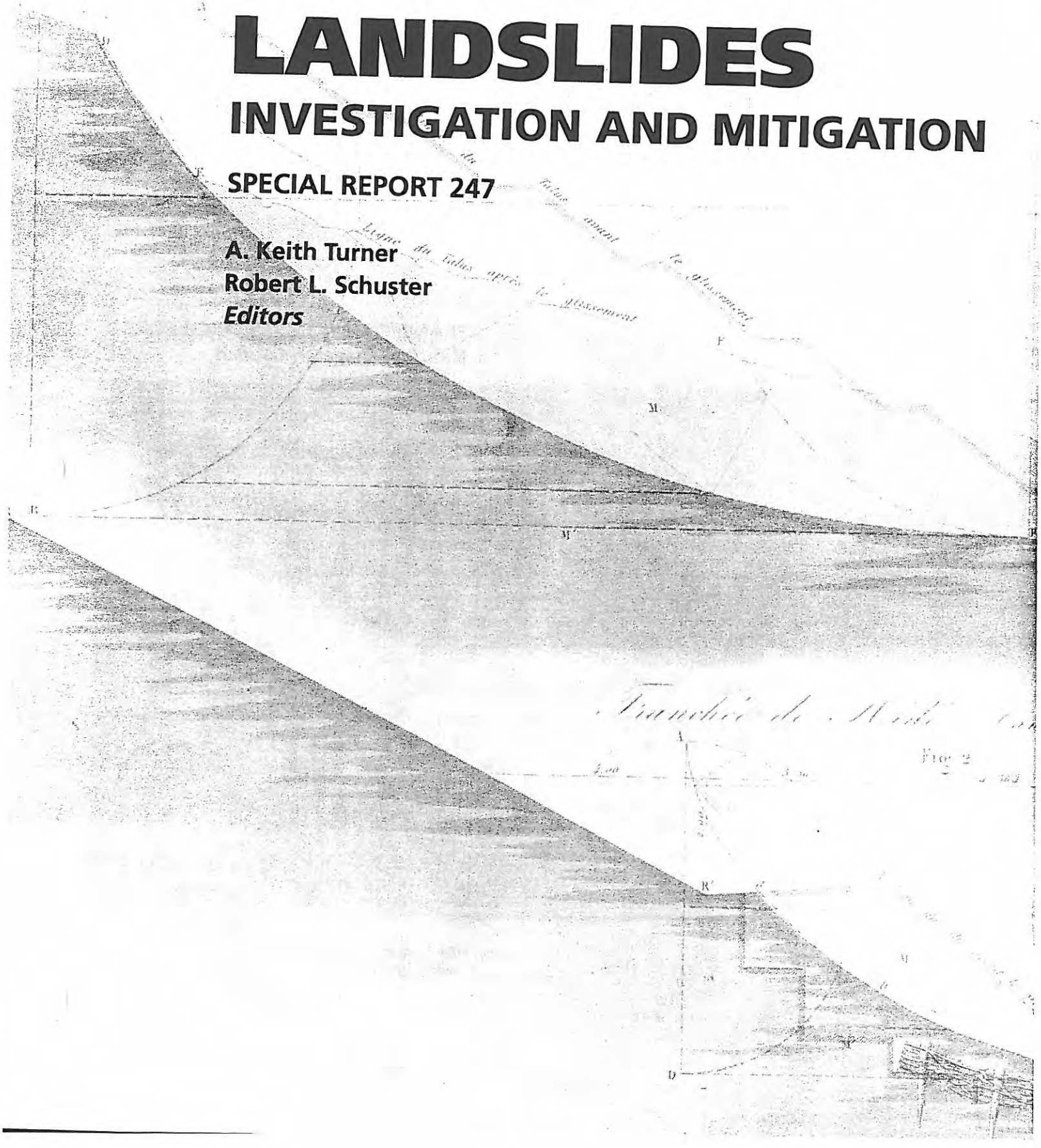

TRANSPORTATION RESEARCH BOARD
National Research Council

National Academy Press
Washington, D. C. 1996

Transportation Research Board Special Report 247

Subscriber Category
IIIA soils, geology, and foundations

NOTICE: The project that is the subject of this report was approved by the Governing Board of the National Research Council, whose members are drawn from the councils of the National Academy of Sciences, the National Academy of Engineering, and the Institute of Medicine. The members of the committee responsible for the report were chosen for their special competence and with regard for appropriate balance.

This report has been reviewed by a group other than the authors according to procedures approved by a Report Review Committee consisting of members of the National Academy of Sciences, the National Academy of Engineering, and the Institute of Medicine.

The Transportation Research Board does not endorse products or manufacturers; trade and manufacturers' names may appear in this Special Report because they are considered essential to its object.

This report was sponsored in part by the National Science Foundation.

Transportation Research Board publications are available by ordering directly from TRB. They may also be obtained on a regular basis through organizational or individual affiliation with TRB; affiliates and library subscribers are eligible for substantial discounts. For further information, write to the Transportation Research Board, National Research Council, 2101 Constitution Avenue, N.W., Washington, D.C. 20418.

Copyright 1996 by the National Academy of Sciences. All rights reserved
Printed in the United States of America

Library of Congress Cataloging-in-Publication Data

Landslides : investigation and mitigation / A. Keith Turner, Robert L. Schuster, editors.
p. cm. — (Special report / Transportation Research Board, National Research Council ; 247)
Includes bibliographical references and index.
ISBN 0-309-06151-2
ISBN 0-309-06208-X (pbk.)
1. Landslide hazard analysis. 2. Landslides. I. Turner, A. Keith, 1941– . II. Schuster, Robert L. III. Series: Special report (National Research Council (U.S.) Transportation Research Board) ; 247.
QE599.2.L36 1996
551.3'07—dc20 95-40780
CIP

Sponsorship of Special Report 247
Division A—Technical Activities
GROUP 2—DESIGN AND CONSTRUCTION OF TRANSPORTATION FACILITIES
Chairman: Michael G. Katona, U.S. Air Force Armstrong Laboratory

Study Committee on Landslides: Analysis and Control
Chairman: A. Keith Turner, Colorado School of Mines
David M. Cruden, J. Michael Duncan, Robert D. Holtz, Jeffrey R. Keaton, Verne C. McGuffey, Victor A. Modeer, Jr., Robert L. Schuster, Tien H. Wu, Duncan C. Wyllie

Liaison Representative
John L. Walkinshaw, Federal Highway Administration, U.S. Department of Transportation

Transportation Research Board Staff
Robert E. Spicher, Director, Technical Activities
G.P. Jayaprakash, Engineer of Soils, Geology, and Foundations
Nancy A. Ackerman, Director, Reports and Editorial Services
Naomi C. Kassabian, Associate Editor
Karen White, Graphic Designer

COVER Damage to railroad line in Olympia, Washington, caused by slope failure after 1965 Seattle-Tacoma earthquake (photograph courtesy of G.W. Thorsen, Washington Department of Natural Resources). *Top inset:* October 1986 reactivation of Cucaracha landslide in Gaillard Cut, Panama Canal, which originally extended across canal (dredges had removed much of toe by time of photograph); white material in upper center is lime added to surface as remedial measure (photograph courtesy of Panama Canal Commission). *Bottom inset:* Recurring landslide on Colorado State Highway 133 at McClure Pass west of Aspen, spring 1993 (photograph courtesy of T.E. Taylor, Colorado State Patrol).

FRONTISPIECE Derailment of *California Zephyr* passenger train near Granby, Colorado, in April 1985 caused by minor landslide (see Figure 2-6, p. 18) (photograph courtesy of R. L. Schuster).

TITLE PAGE *Inset:* Railway and highway at Howe Sound, British Columbia, blocked by October 1990 rock fall, which originated approximately 300 meters above highway (photograph courtesy of D. Howard, *Vancouver Sun*). *Background:* detail from drawing by Alexandre Collin (1846) of landslides in clay slopes along French canals (see Figure 1-5, page 9).

Chapter 11

P. ERIK MIKKELSEN

FIELD INSTRUMENTATION

1. INTRODUCTION

Landslides often present the ultimate measurement challenge, in part because of their initial lack of definition and the sheer scale of the problems. Intuitively, there is a desire to quantify the extent of a potential or real disaster, but what should be measured? The answer can be complicated and should be addressed by drawing on the best available information concerning topography, geology, groundwater, and material properties. The measurement problem usually requires information ranging from a coarse scale down to a fine scale and involving a number of instrumentation techniques. The ultimate goal is to select the most sensitive measurement parameters, the ones that will change significantly at the onset of the landslide event. However, because of physical limitations and economic constraints, all parameters cannot be measured with equal ease and success.

Geotechnical instruments have evolved tremendously during the past quarter-century. Early versions of current instruments were developed and used on various projects beginning in the 1960s. Early reports concerning instrumentation that have retained their value include those by Shannon et al. (1962), Dunnicliff (1971), Gould and Dunnicliff (1971), and Peck (1972). The comprehensive report on geotechnical field instrumentation prepared by the British Geotechnical Society (1974) contains several important papers (Burland and Moore 1974; Dibiagio 1974; Green 1974; Penman and Charles 1974; Vaughn 1974). *Transportation Research Record 482* (Transportation Research Board 1974) includes several documented case histories of geotechnical instrumentation applications. Considerable interest continued during the 1970s concerning the most appropriate methods for using instrumentation (Mikkelsen and Bestwick 1976; Wilson and Mikkelsen 1977). Chapter 5 in *Landslides: Analysis and Control* (Wilson and Mikkelsen 1978) was devoted to landslide instrumentation.

By the late 1980s, geotechnical instrumentation had evolved to the point that a major textbook was devoted to the subject (Dunnicliff 1988), and the Transportation Research Board published a second *Transportation Research Record* containing reports of new applications and methods (Green and Mikkelsen 1988; Hinckley et al. 1988). Other case histories were published during the same period (Patton 1983, 1984). In recent years the full impact of new instruments and computer automation in data collection and data reduction has been reported in numerous papers (e.g., Mikkelsen 1989, 1992; Dunnicliff and Davidson 1991; Tatchell 1991; Gillon et al. 1992; Proffitt et al. 1992; Kane and Beck 1994; O'Connor and Wade 1994). Experiences with large-scale instrumentation and automation of data collection for monitoring slope stability at the huge open-pit mines of Syncrude, Canada, Ltd., in northern Alberta were described by McKenna et al. (1994) and McKenna (1995).

The focus of this chapter is primarily field instrumentation and measurement techniques associated

with permanent borehole installations that serve to measure subsurface behavior. Typical instruments are piezometers for measuring groundwater pressures and inclinometers and extensometers for ground-displacement measurements. Excluded from this discussion are borehole testing and logging techniques that help define structure, lithology, and material properties; these are described in Chapter 10. Surface surveying and other surface measurement technologies, such as seismic monitoring, remote sensing, and aerial photointerpretation, are discussed in Chapters 8, 9, and 10, and so are also not treated in detail in this chapter.

Field instrumentation is most often used on landslides that have already exhibited some movement. In such cases, the overall characteristics of the landslide frequently may be readily observed and noted. However, small movements of a soil or rock mass before or even during incipient failure are usually not visually evident. Thus, the value of the information that can be obtained at the ground surface is limited. Instrumentation can provide valuable information on incipient as well as fully developed landslides. In this respect, use of instrumentation is not intended to replace field observations and other investigative procedures. Instead, it augments other data by providing supplementary information and by warning of impending major movements. Typical situations for which various instruments have been used are the following:

- Determination of the depth and shape of the sliding mass in a developed landslide so that calculations can be made to define the appropriate strength parameters at failure and design remedial treatments,
- Determination of absolute lateral and vertical movements within a sliding mass,
- Determination of the rate of sliding (velocity) and thus provision of a warning of impending danger,
- Monitoring of the activity of marginally stable natural or cut slopes and identification of effects of construction activity or precipitation,
- Monitoring of groundwater levels or pore pressures normally associated with landslide activity so that effective stress analyses may be performed,
- Provision of remote digital readout or information to a remote alarm system that would warn of possible danger, and
- Monitoring and evaluation of the effectiveness of various control measures.

In the last situation, savings are often realized in remedial treatment by a planned and monitored sequence of construction. For example, drainage might be initially installed and its effect monitored to determine whether planned mechanical stabilization is actually necessary.

2. PLANNING AND DESIGN

Adequate planning is required before a specific landslide is instrumented. The plan should proceed through the following stages:

- Determination of types of measurements required;
- Selection of the specific types of instruments best suited to make the required measurements;
- Definition of the location and depth of instrumentation and number of instruments;
- Development of the data acquisition techniques; and
- Decision as to the management and presentation of the data acquired.

Initially the planning process requires development of ideas on the causes of the landslide and the probable limits of the depth and outer boundaries of the movements. Reconnaissance of the area, study of the geology and groundwater seepage, review of rainfall records, and observation of topographic features, especially recent topographic changes, will often provide clues. Unfortunately, no two landslides are alike in all details, and experience alone without the application of judgment may lead to erroneous concepts.

An instrumentation system is a waste of time and money if the instruments do not extend below the zone of movement, were installed at the wrong locations, or are unsuitable. Instruments must collect data accurately, reliably, efficiently, and in a timely manner; otherwise, corrective treatment may be started too late, resulting in even greater economic losses than would have been experienced without it.

2.1 Types of Measurements Required

Landslides by definition involve movement. The magnitude, rate, and distribution of this movement are generally the most important measurements required. Measurements of pore-water pressures within the landslide are important in resolving

many landslide problems. Such measurements are especially important when landslides occur in layered systems in which excess hydrostatic pressures may exist between layers.

As discussed in Chapter 9, if the depth of sliding is readily apparent from visual observations, surface measurements may be sufficient for obtaining the rate of movement. Surface measurements should extend beyond the uppermost limit of visual movement so that any ground movements that might occur before visible surface cracks develop can be monitored. Movement of the ground surface should be measured vertically and horizontally at various locations within the landslide area. Vertical offsets, widening of cracks, and heaving of the toe should be monitored. The direction of movement can often be inferred from the pattern of cracking, particularly by matching the irregular edges of the cracks.

If the depth and thickness of the zone of movement are not apparent, inclinometers or similar devices that can detect the movement with depth must be used. Pore pressures at or near the sliding surface must be measured to support effective stress analysis or to assess the adequacy of drainage measures. Rapid-response piezometers are advantageous, particularly in impervious soils.

2.2 Selection of Instrument Types

Many types and models of instruments are available for measuring the changing conditions in a landslide; they vary in degree of sophistication, particularly with regard to readout capabilities. Instruments have been developed to measure vertical and horizontal earth movements, pore-water pressures, in situ stresses and strains, dynamic responses, and other parameters. However, in most landslides measurements of horizontal movement of the soil or rock and of pore-water pressures are of primary concern. Instruments commonly used for these purposes are described in this chapter.

The types of instruments, layout, and monitoring schedules are usually determined by the specific needs of a project. Several basic requirements, however, should be thoroughly evaluated for any system. Instruments should be reliable, rugged, and capable of functioning for long periods of time without repair or replacement. They must also be capable of responding rapidly and precisely to changes so that a true picture of events can be maintained at all times. High sensitivity is usually a prerequisite when hazard warning is required or landslide performance is monitored during construction, since it is often the rate of change rather than the absolute value that provides the key to proper interpretation.

The location of instruments requires a thorough understanding of geologic and subsurface conditions if meaningful data are to be obtained. Location is particularly crucial for pore-pressure recording devices that are intended to measure pressures in specific zones of weakness or potential instability. Since most measurements are relative, a stable base or datum must be provided so that absolute movements can be determined.

If the movement is known to be along a well-defined shear surface, such as a bedding surface or fracture, simple probe pipes will suffice to determine the depth. If the movement is large and rapid, accuracy is not an essential requirement and even relatively crude inclinometers may suffice. When the rate of movement is small and the depth and distribution are not known, more precise instrumentation is required. Carefully installed precision inclinometers are best in such instances, although there may be cases in which extensometers or strain meters can be used to advantage.

As discussed in Chapter 10, the Casagrande type of piezometer is the most useful general purpose pore-pressure measuring device, but it may give too slow an initial response in fine-grained soils. Therefore, pneumatic or vibrating-wire pressure-sensor types (transducers) may be preferable. High-air-entry, low-flow piezometers may warrant consideration in clays or clay-shales in which permeabilities are low or suction may be present because of unloading.

3. SURFACE MEASUREMENT

Instrumentation that may be used for surface measurement includes conventional surveying equipment, portable tiltmeters, and recently developed differential Global Positioning System (DGPS) location methods.

3.1 Conventional Surveying Equipment

The application of conventional surveying methods to landslide movement measurement and monitoring is discussed at length in Chapter 9. In an

active landslide area, surface movements are normally monitored to determine the extent of landslide activity and the rate of movement. Both optical instrument surveys and electronic distance measurement (EDM) devices are used to determine lateral and vertical movements. Bench marks located on stable ground provide the basis for determination of subsequent movements of established survey points, or hubs, by optical surveys, EDM equipment, or tape measurement. Recent advances in surveying equipment, including the so-called total stations (see Chapter 9, Section 4.2.2.4), increase the automation and productivity of these measurement procedures, especially on the often-rough ground surface found on landslides. Survey lines can be established so that vertical and horizontal displacements at the center and toe of the landslide can be observed. Lateral motions can be detected by theodolite and distance measurements from each hub. When a tension crack has opened above a landslide, simple daily measurements across the crack can be made between two hubs driven into the ground. In many cases, the outer limit of the ground movement is unknown, and establishing instrument setups on stable ground may be a problem.

3.2 Tiltmeters

Portable tiltmeters (Figure 11-1) can be used to detect tilt (rotation) of a surface point, but such devices have had relatively limited use. Their most common application is to monitor slope movements in open-pit mines and highway and railway cuts, but they may be used in any area where the failure mode of a mass of soil or rock can be expected to include a rotational component, such as a landslide area. Tiltmeters utilize either electrolytic sensors or servo-accelerometers. Electrolytic sensors provide greater sensitivity, but servo-accelerometers have greater range. The prime advantages of these instruments are their light weight, simple operation, compactness, and relatively low cost. Stationary electrolytic sensors with automatic data acquisition are gaining wider usage in landslide monitoring.

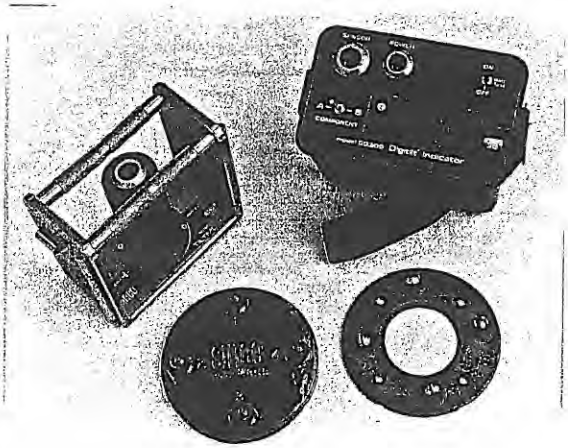

FIGURE 11-1
Portable tiltmeter (Wilson and Mikkelsen 1978).

3.3 Differential Global Positioning System

The DGPS is emerging as a candidate surveying method for monitoring surface movement at landslide sites. A base station at a known location is used to provide corrections and refinements to the computed locations of one or several roving stations (Gilbert 1995). All stations use the same global positioning satellite network. The DGPS relates observations at unknown roving station locations to simultaneous observations at the base stations placed at a known and fixed location. As the satellite signals are monitored, errors may suggest that the base station is moving. Since it is known that the base station is not moving, these fluctuations can be used as corrections to the observations of the unknown roving stations to achieve their accurate location. All measurements are relative to the base station position. As long as that position is defined reasonably precisely, the other measurements will be internally consistent. If its location is very poorly defined, additional errors may arise. An assumed value of the true location (proper latitude and longitude) can be used without affecting the accuracy of the distances within the survey.

The accuracy of the DGPS is now approaching that of conventional surveys. Under favorable conditions, an accuracy of better than 1 cm is possible (Kleusberg 1992; Gilbert 1995). The historically large capital investments for such systems are now dropping (Gilbert 1994), and it appears that these systems already may be economical for monitoring larger landslide areas. However, the accuracy of the DGPS may be degraded in areas where the ground surface is obscured by tree cover or in times of poor weather conditions. Nevertheless, the enhanced productivity of the DGPS approach suggests that it will soon be economically practical for many landslide monitoring applications.

4. GROUND-DISPLACEMENT MEASUREMENT

4.1 Inclinometers

Before some of the sophisticated types of inclinometers are described, one of the simplest subsurface measuring devices deserves mention: the *borehole probe pipe*, also called the "slip indicator" or "poor boy." It typically consists of a 25-mm diameter semirigid plastic tube, which is inserted into a borehole. Metal rods of increasing length are lowered inside the tubing in turn, and the rod length that is just unable to pass a given depth gives a measure of the curvature of the tubing at that point. Use of the borehole probe pipe is an acceptable technique for the location of slip surfaces in unstable slopes. This type of measurement can easily be performed in the riser pipe of an observation well or open piezometer. If there are several shear planes or if the shear zone is thick, a section of rod hung on a thin wire can be left at the bottom of the hole. Subsequently, the rod is pulled up to detect the lower limit of movement.

The development of inclinometers has been the most important contribution to the analysis and detection of landslide movements in the past two decades. Although used most extensively to monitor landslides, the inclinometer has also gained widespread use as a monitoring instrument for dams, bulkheads, and other earth-retaining structures and in various areas of research. Two broad classes of inclinometers may be used: probe inclinometers and in-place inclinometers. Both classes use similar sensors.

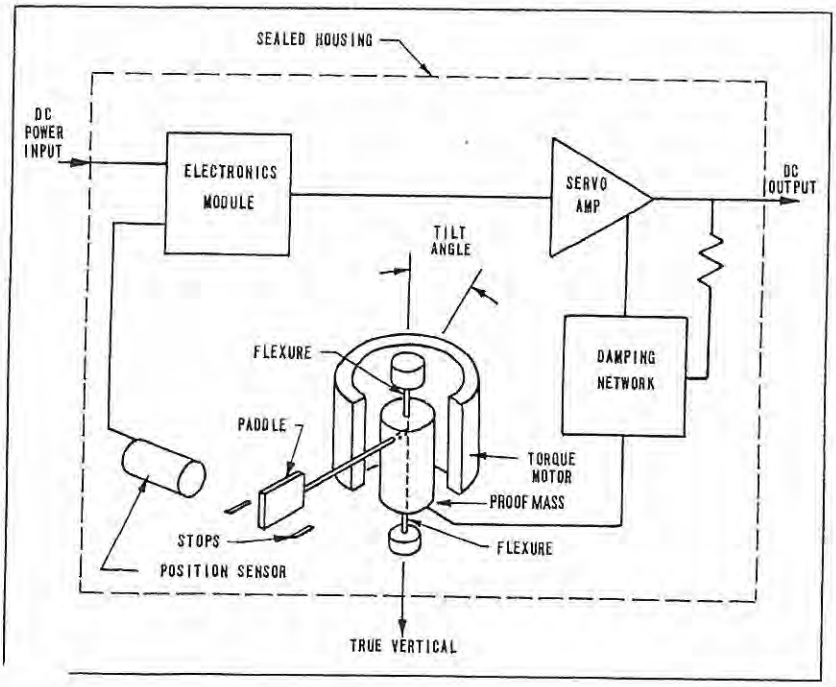

FIGURE 11-2
Servo-accelerometer inclinometer surements ...ilson and Mikkelsen 1978).

4.1.1 Inclinometer Sensors

One basic type of inclinometer sensor is currently in use in the United States, the accelerometer type, which uses a closed-loop, servo-accelerometer circuit. Each sensor measures inclination in one plane, and the use of two sensors per unit (biaxial sensors) is common (Mikkelsen and Bestwick 1976). A few older, obsolete types are also still in use but are gradually being replaced or abandoned because of lower accuracy and efficiency. Most inclinometers rely on commercially available, sensitive servo-accelerometers.

The servo-accelerometer is composed of a pendulous *proof mass* that is free to swing within a magnetic field (Figure 11-2). The proof mass is provided with a coil or *torque motor*, which allows a linear force to be applied to the proof mass in response to current passed through the coil. A special *position sensor* detects movement of the proof mass from the vertical position. A signal is then generated and converted by a restorer circuit, or servo, into a current through the coil, which balances the proof mass in its original position. In this manner, the current developed by the servo becomes an exact measure of the inertial force and thus of the transducer's inclination. The proof mass usually consists of a flexure unit that operates on the cantilever principle. Temperature has only a negligible effect on readings taken with accelerometer transducers. Accelerometer systems have a resolution of approximately 10 arc-sec in ranges from 30 to 50 degrees. A typical example of such measurements is shown in Figure 11-3(*b*).

4.1.2 Probe Inclinometer

The probe inclinometer commonly used today was developed from a device built in 1952 by S.D. Wilson at Harvard University (Green and Mikkelsen 1988). The same basic concepts have been incorporated into instruments now manufactured by several firms. Such an inclinometer consists of a probe containing a pendulum-actuated transducer, which

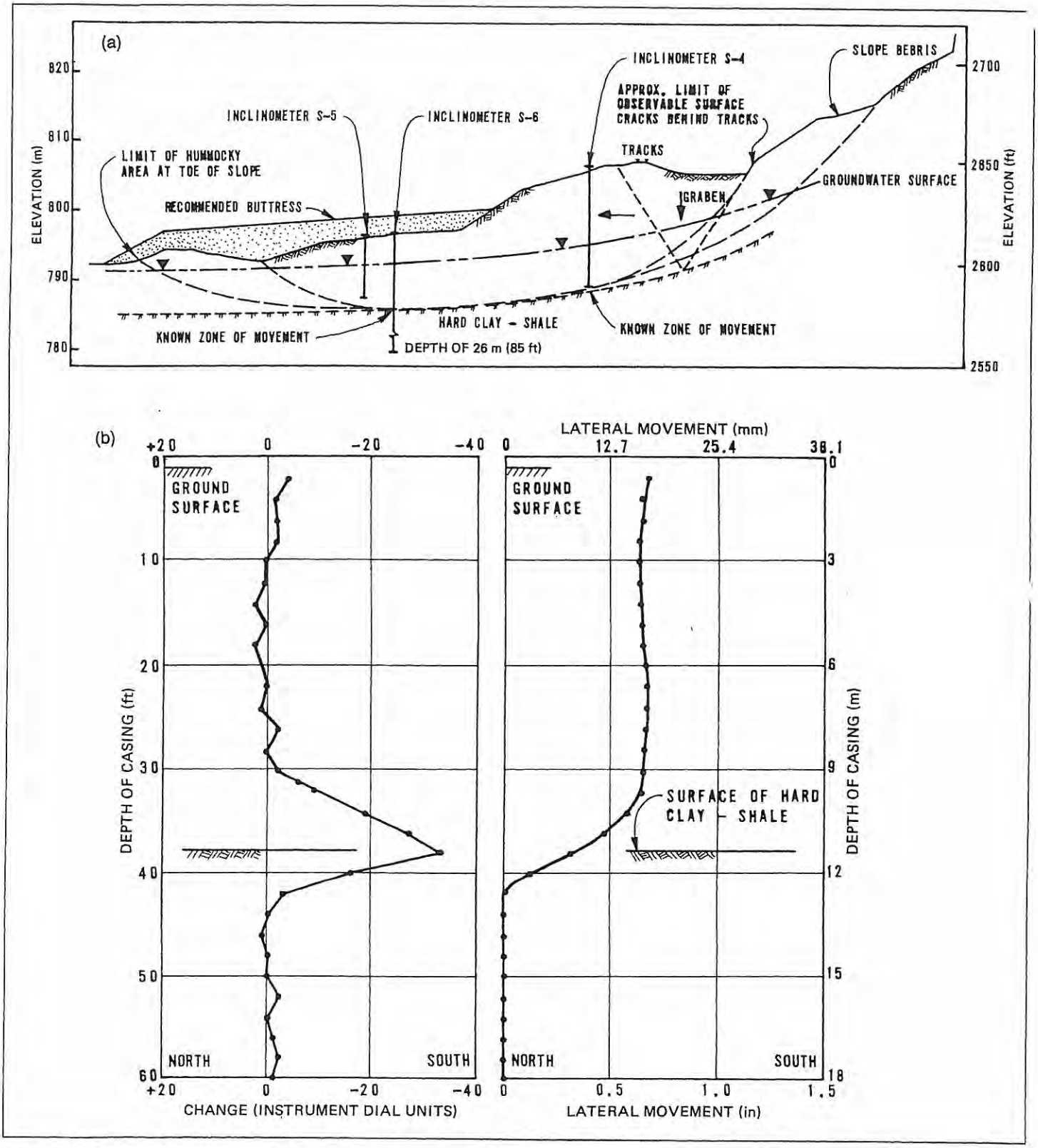

FIGURE 11-3
Inclinometer location and data, Fort Benton landslide, Montana (Wilson and Mikkelsen 1978): (*a*) section through Fort Benton landslide; (*b*) movement of inclinometer S-5 at toe of slope.

is fitted with wheels and lowered by an electrical cable down a plastic casing that is grooved to control alignment. The cable is connected to a readout unit, and data can be recorded manually or automatically (Figure 11-4).

A probe inclinometer system has four main components:

1. A guide casing is permanently installed in a near-vertical borehole in the ground. The casing may be made of plastic, steel, or aluminum. Circular sections generally have longitudinal slots or grooves for orientation of the sensor unit, but square sections are used in some types.
2. A probe sensor unit is commonly mounted in a carriage designed for operation in the guide casing.
3. A control cable raises and lowers the sensor unit in the casing and transmits electrical signals to the surface. For accurate depth control of the sensor unit, the cable is usually graduated or lowered on a separate surveyor's steel tape.
4. A portable control and readout unit at the surface supplies power, receives electric signals, displays readings, and can often store and process data.

The probe inclinometer instrument sensor unit (Figures 11-4 and 11-5) is lowered and raised on an accurately marked cable, its wheels or guides following the oriented, longitudinal slots of the casing. Two sets of grooves in the casing allow the inclinometer probe to be oriented in either of two planes set at 90 degrees to each other. At each installation one set of grooves is designated the A orientation plane, and the other set the B orientation plane. The response to slope changes in the casing is monitored and recorded at the surface. Readings are taken at fixed increments, usually equal to the length of the probe, throughout the entire depth.

The wheels of the inclinometer probe provide points of measurement between which the inclination of the instrument is measured. If the reading interval is greater or less than the probe wheel base, correspondence between the position and orientation of the instrument will be only approximate in determining the total lateral displacement profile. Optimum accuracy is achieved only if the distance between each reading interval equals the distance between the upper and the lower wheels of the probe. Gould and Dunnicliff (1971) reported that readings at depth intervals as large as 1.5 m result in poor accuracy.

Instruments differ primarily in the type of sensor used, the accuracy with which the sensor detects the inclination, and the method of alignment and depth control within the borehole. Probe inclinometers can measure changes in inclination on the order of 1.3 to 2.5 mm over a 33-m length of casing (a precision of 1:10,000).

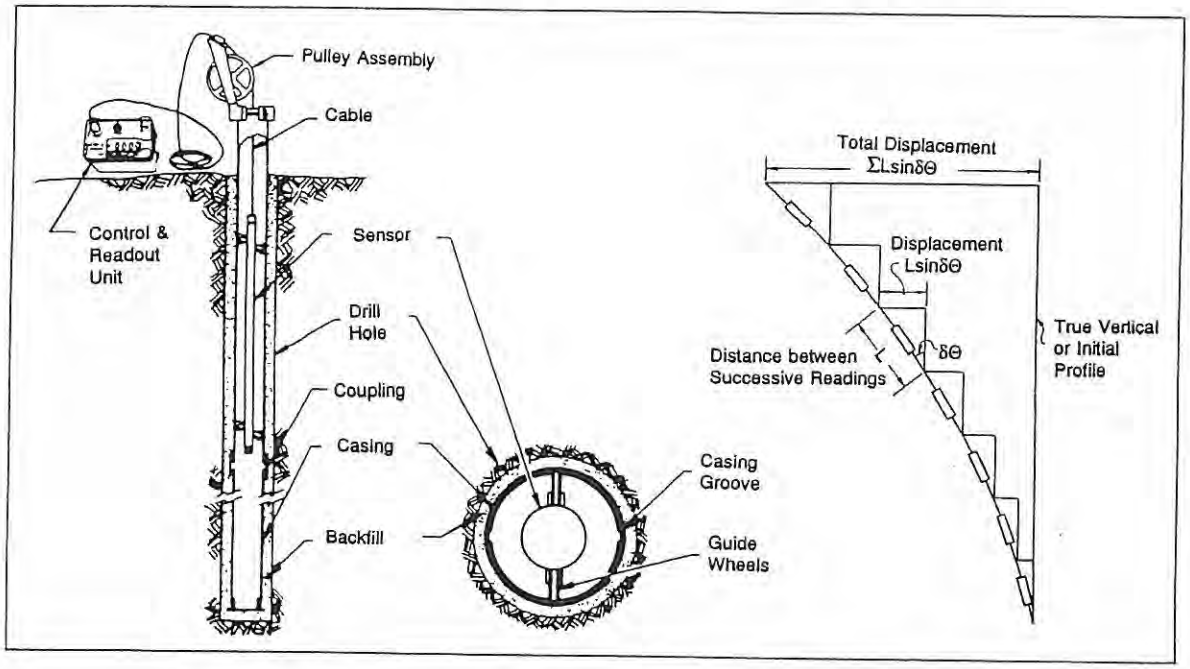

FIGURE 11-4
Principle of inclinometer operation (Wilson and Mikkelsen 1978; Green and Mikkelsen 1988).

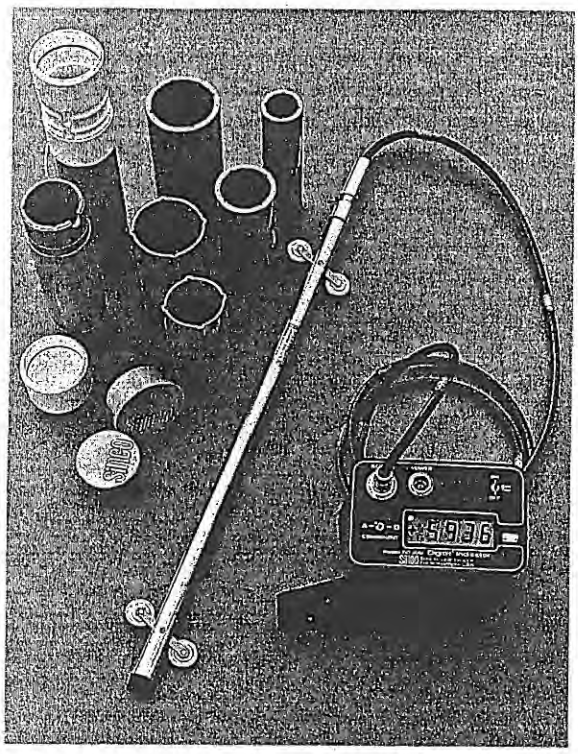

FIGURE 11-5 *(left)* Probe inclinometer with manual readout, inclinometer casing, and couplings (Green and Mikkelsen 1988).

one borehole. The maximum deflection range is ±30 degrees; the precision is reported to be ±0.01 mm in 1 m, but this accuracy is not usually attained because of long-term drift. A more realistic maximum accuracy is about 0.04 mm in 1 m, giving a precision of 1:25,000, or about 2.5 times the precision of a probe inclinometer. Monitor and alarm consoles and telemetry systems are available for use with in-place inclinometers.

Since fixed units often consist of a number of sensors, they are more expensive and complex than

4.1.3 In-Place Inclinometer

The in-place inclinometer (Figure 11-6) employs a series of servo-accelerometer or electrolytic sensors available for both one- and two-axis measurement (Cording et al. 1975). The sealed sensor packages are spaced along a standard grooved inclinometer casing by a series of rods. The rods and sensors are linked by universal joints so that they can deflect freely as the soil and the casing move. The sensors are aligned and secured in the casing by spring-loaded wheels, which fit the casing grooves. They are positioned at intervals along the borehole axis and may be more closely spaced to increase resolution of the displacement profile in zones of expected movement. Use of the grooved casing and guide wheels allows removal of the instrument for maintenance, adjustments, and salvage. Since the casing is a standard inclinometer casing, a probe inclinometer can be used in it after the fixed unit has been removed.

Readings are obtained by determining the change in tilt of the sensor and multiplying by the gauge length or spacing between sensors. The result is the relative displacement of each sensor; these relative displacements can be summed to determine the total displacement at each sensor. Any number of sensors at any spacing can be used in

FIGURE 11-6 *(below)* Installation and detail of multiposition in-place inclinometer

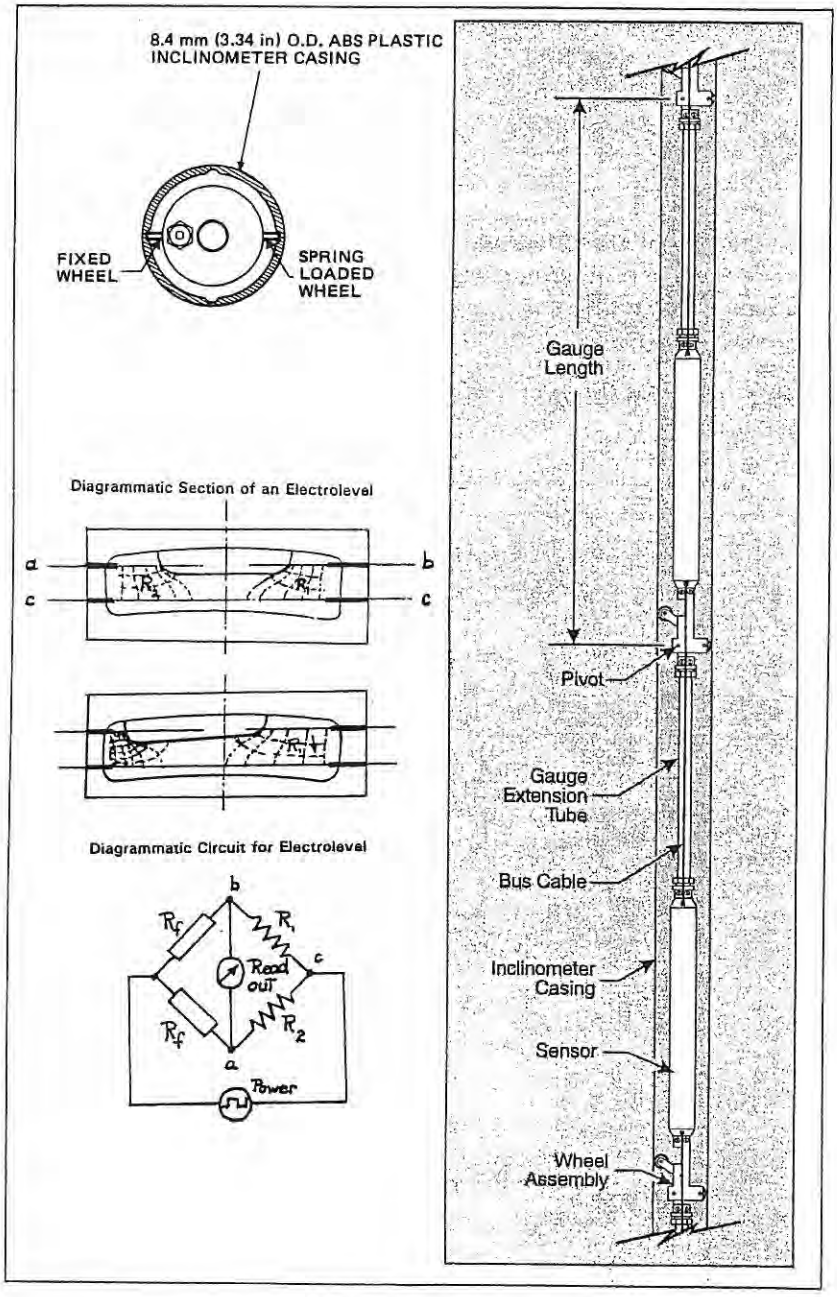

probe inclinometers. However, in-place inclinometers have major advantages over probe inclinometers, including enhanced accuracy and continuous recording capabilities. Fixed units can be monitored remotely by a datalogger or connected to alarm systems. Problems common to probe inclinometers, such as tracking inaccuracies and repeatable positioning (placement error), are eliminated. If the fixed unit is removed for any reason, the overall accuracy will, for the duration, be reduced to no more than that of a probe unit, which can be used in its place. With probe inclinometer units, sensor drift effects are canceled by taking readings in opposite directions. Fixed accelerometer sensors may also drift, and such effects cannot be so easily compensated for. Better long-term performance and resolution are gained by using electrolytic sensor technology. On some projects, an extra inclinometer casing is used so that a probe inclinometer can be used to check readings of the fixed unit.

Because of its potential accuracy (an achievable precision of 1:25,000), an in-place inclinometer can be used to measure small movements in rock and to measure velocity in the hourly time domain. Its adaptability to various remote-monitoring systems allows a continuous record of displacement. By design, most systems are not intended to obtain a continuous profile of deformation. Rather, they measure critical movements of a few sections within the borehole. This instrument, therefore, is not necessarily a replacement for the probe inclinometer unit, but rather has its own purpose and is worthy of consideration for continuous monitoring of movements during critical stages of the landslide.

4.1.4 Principle of Operation

The primary application of the inclinometer to landslides is readily apparent: the definition of slip surfaces or zones of movement relative to stable zones by detection of any change in inclination of the casing from its original near-vertical position. Readings taken at regular incremental depths inside the casing allow determination of the change in slope at various points; integration of the slope changes between any two points yields the relative deflection between those points. The integration is normally performed from the bottom of the boring because the bottom is assumed to be fixed in position and inclination. Repeating such measurements periodically provides data allowing the distribution of lateral movements to be determined as a function of depth below the ground surface and as a function of time (Figure 11-7).

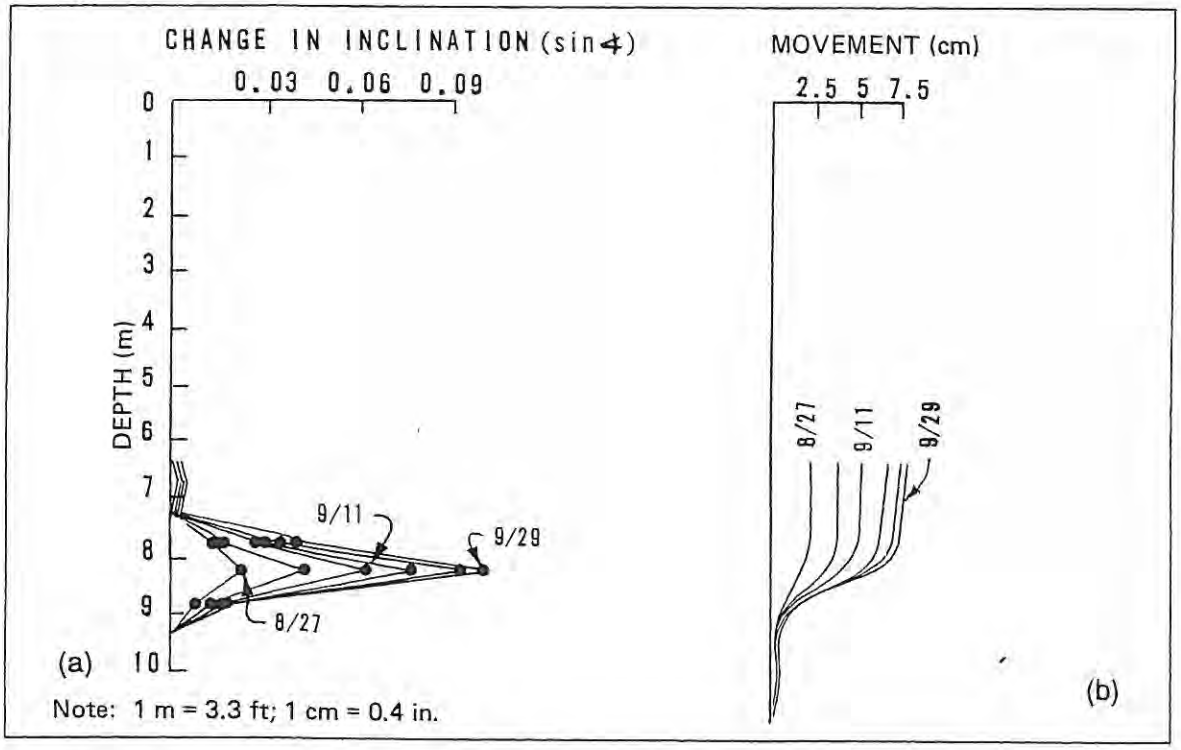

FIGURE 11-7
Measurement of landslide movements with inclinometer: (*a*) observational data, Well A, and (*b*) computed movements, Well A (Wilson and Mikkelsen 1978).

Inclinometers measure the slope of the casing in two mutually perpendicular planes, designated A and B. Thus, horizontal components of movement, both transverse and parallel to any assumed direction of sliding, can be computed from the inclinometer measurements (Figure 11-8). Deviations from this ideal occur because of limitations and compromises in manufacturing and because of installation circumstances. Instruments of different manufacture cannot generally be interchanged without causing discernible effects on the results obtained [Figure 11-8(*a*)]. In the interest of accuracy, the interchange of instruments (probes and cables) of the same manufacture should also be avoided.

Although the principle of operation has remained unchanged, inclinometers have undergone rapid development to improve reliability, provide accuracy, reduce weight and bulk of the instrument, lessen data acquisition and reduction time, and improve versatility of operations under adverse conditions. Use of automatic data recording, personal computers, and data-base software has become standard practice.

4.1.5 Casing Installation

In landslide applications, inclinometer casings are normally installed in exploration drill holes. They must extend through soil and rock suspected of movement and well into materials that, in the best judgment at the time, are assumed to be stable. Some installations extend to depths of more than 200 m (Imrie and Bourne 1981). The annular space between the drill hole and the outer wall of the casing is generally grouted or backfilled with sand. The success of the casing installation depends on the experience and the skill of the personnel; soil, rock, and groundwater conditions; depth of installation; and accessibility to the area.

The accuracy of the inclinometer observations is generally limited not by the sensitivity of the inclinometer sensor, but by the requirement that successive readings be made with the same orientation of the instrument at the same point in the casing. Because the casing must provide a reliable orientation and a continuous tracking for the sensor unit, proper casing installation is of paramount importance.

Since the displacements are referenced with respect to the bottom of the casing, the casing bottom must be extended about 6 m or more into material that will not undergo lateral displacement. If any doubt arises as to the stability of the casing bottom, movement of the casing top should be checked by precise surveying methods. The casing for the inclinometer is usually installed in 1.5- and 3.0-m lengths, which are joined with couplings that are either riveted or cemented, or both, to ensure a firm connection (Figure 11-9). Each coupling represents a possible source of entry for grout or mud, which can seep into the casing and be deposited along the internal tracking system. For this reason, couplings should be sealed with tape or glue. The bottom section of the casing is closed with an aluminum, plastic, or wooden plug, which also should be sealed. If the drill hole is filled with water or drilling mud, the inclinometer casing must be filled with water to overcome buoyancy.

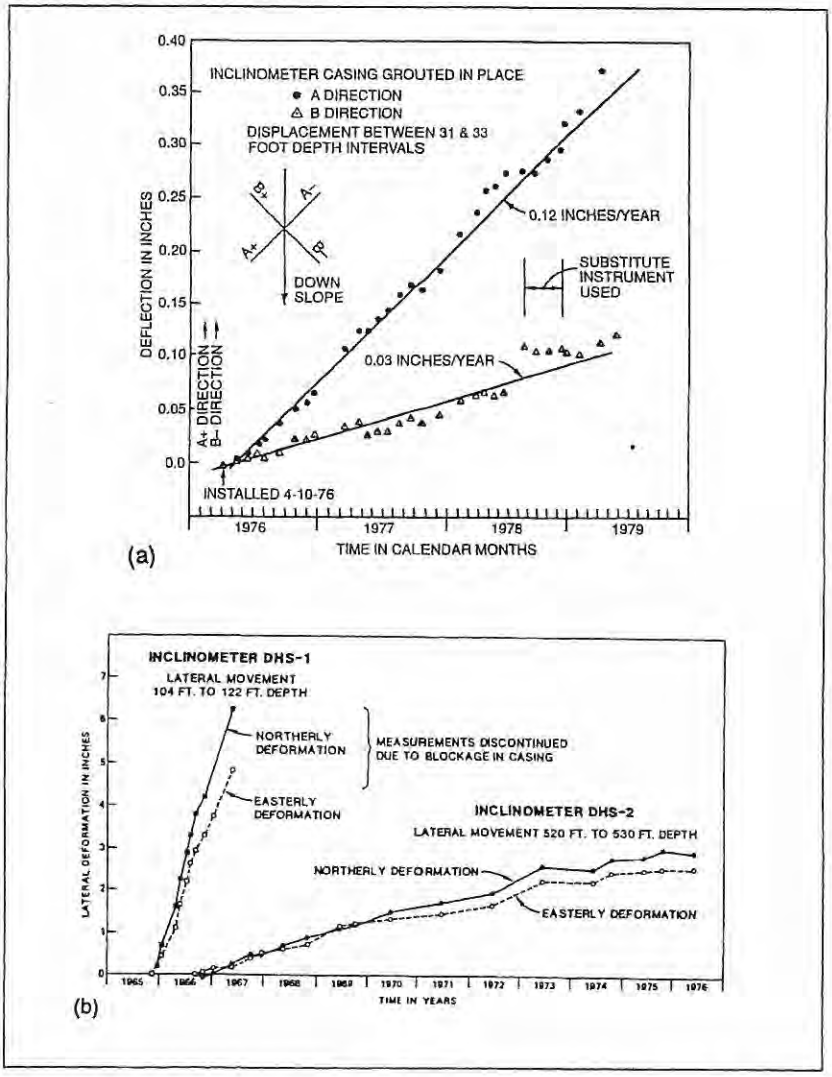

FIGURE 11-8
Typical landslide deformation data from inclinometers (Green and Mikkelsen 1988): (*a*) creep movements on thin shear zone in reactivated ancient landslide; (*b*) deformations measured on deep shear zones on a landslide in Canada.

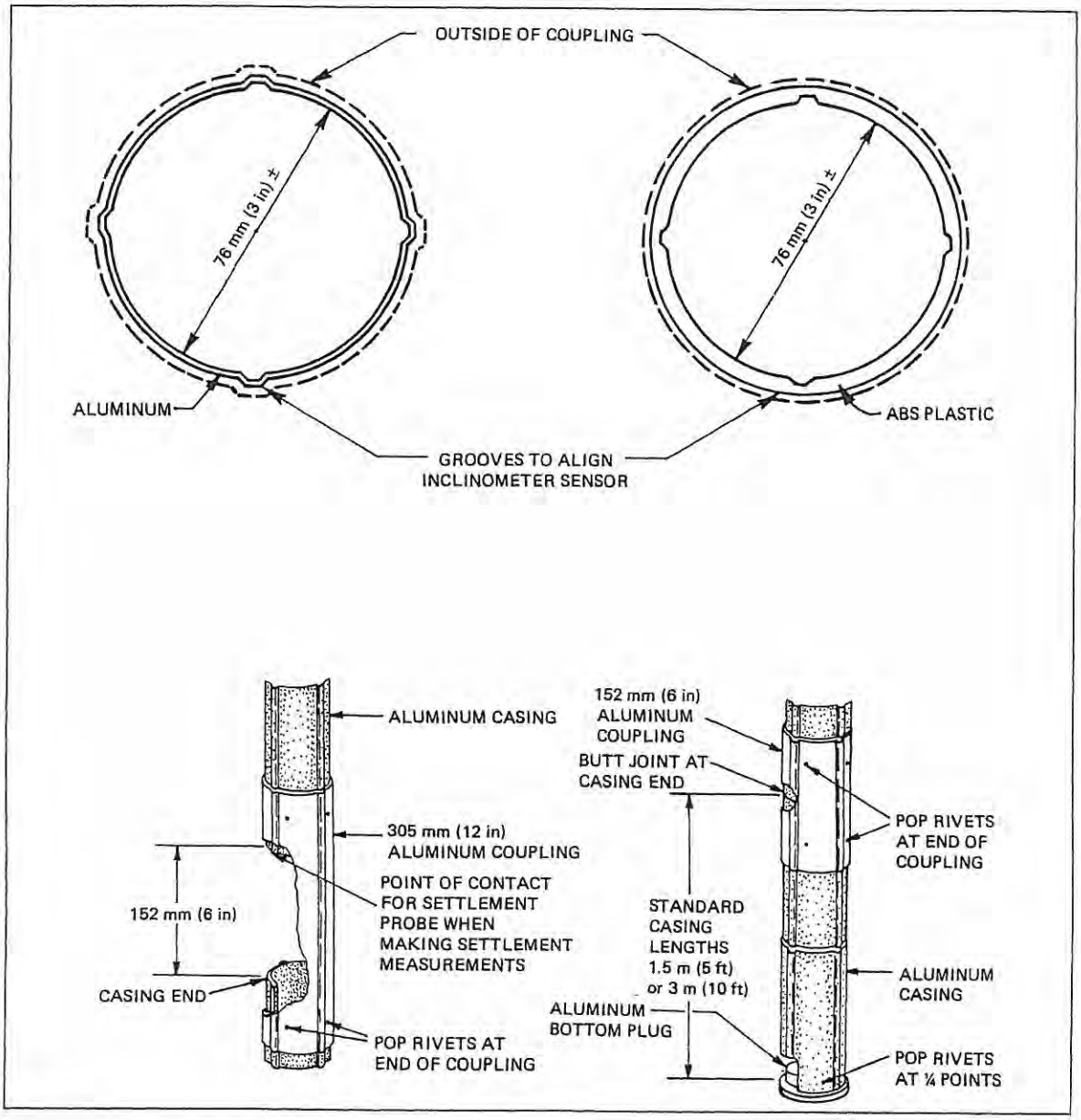

FIGURE 11-9
Details of inclinometer casing (Wilson and Mikkelsen 1978).

Sometimes, extra weight, such as sand bags or a drill stem, may be needed.

The annular space between the boring wall and the inclinometer casing may be backfilled with sand, pea gravel, or grout. The selection of backfill depends mostly on soil, rock, and groundwater conditions (i.e., whether the borehole is dry, wet, caving, or stable without mud). The type of drilling technique (e.g., rotary, hollow-stem, cased holes) is also important. Poorly backfilled casings can introduce scatter into initial measurements. If maximum precision is required, great care should be taken in the selection of the proper backfilling material. Grouting is generally preferred but may not always be possible, particularly in pervious geologic materials such as talus. Grouting may be facilitated by use of a plastic tube with a diameter of 20 to 25 mm firmly attached to the casing bottom through which grout is pumped from the ground surface until the entire hole is filled. In a small-clearance drill hole, grout can be placed (tremied) through drill rods via a one-way valve at the inside bottom of the casing.

In the as-manufactured casing, the grooves may have some spiral. During installation, the casing can become even more twisted or spiraled so that,

at some depth, the casing grooves may not have the same orientation as at the ground surface. Spiraling as great as 18 degrees in a 24-m section of plastic casing has been reported (Green 1974); 1 degree per 3-m section is not uncommon. Because significant error in the assumed direction of movement may result, deep inclinometer casings should be checked after installation by using spiral indicators available from the inclinometer manufacturer. For a particular installation, groove spiraling is generally a systematic error occurring for each section in the same amount and the same direction. In any event, spiraling, whether it is due to manufacture or to torque of the casing during installation, can be measured and is thus not really an error in inclinometer measurement. Spiraling is important only when a determination of the true direction of the movement is required; in such cases, the amount of spiraling should be measured and the results adjusted accordingly.

Small irregularities in the tracking surface of the casing can lead to errors in observation, especially if careful repetition of the depth to each previous reading is not exercised. If plastic casing has been stored in the sun before installation, each section may be locally warped (so that opposing grooves are not parallel), and large measurement errors can occur with minor variations at the depths at which the readings are taken (Gould and Dunnicliff 1971).

Aluminum casings should be used with some caution because severe corrosion may occur if the casing is exposed to alkaline soil, corrosive groundwater, or grout. Epoxy coatings help to minimize this problem. Burland and Moore (1974) recommended cleaning the casing with a stiff brush before taking readings. Frequent flushing with water is also helpful. The top of the casing is generally capped with a tight-fitting plug to prevent intrusion of debris. In addition, the inclinometer casing should be protected and padlocked at the ground surface. When a protective casing or monument covers are selected for use around the top, the need to place a casing-mounted pulley or similar device during inclinometer measurements should be kept in mind.

4.1.6 Observations

Because all inclinometer readings are referenced to an original set of measurements, extreme care must be taken to ensure that the initial set of observations is reliable. Measurements of the original profile should be established by a minimum of a double set of data. If any set of readings deviates from the previous or anticipated pattern, the inclinometer should be checked and the readings repeated. A successful record of measurements generally requires at least two trained technicians, who should be allowed the proper amount of time for setting up, recording observations, and undertaking maintenance of the equipment. Use of the same technicians and instrument for all measurements on a particular project is highly desirable.

When an inclinometer installation is surveyed for the first time with a probe inclinometer to provide the initial set of data, a fixed reference for the probe should be selected so that each time a survey is repeated the same set of grooves is used for alignment orientation and the probe will have the same orientation in the casing. For the typical biaxial inclinometer (Figure 11-5), it is generally recommended that the A component (or sensor) be oriented so that it will register the principal direction of anticipated deformation as a positive change. For example, in an area suspected of landslide activity, the first set of readings is taken by orienting the fixed wheels of the probe in the casing groove closest to the downhill position.

Probe inclinometer measurements generally are recorded as the algebraic sums or differences of pairs of readings. At selected measurement depths, a series of readings in one vertical plane are taken and then repeated with the instrument turned through 180 degrees. Computing the differences of these readings minimizes errors contributed by irregularities in the casing and instrument calibration. One excellent check on the reliability of each measurement is to compute the algebraic sum of each pair of readings. These algebraic sums should be approximately constant except for those readings made while one set of wheels is influenced by a casing joint. Differences between any sum of two readings and the observed constant usually indicate that an error has occurred or that opposite sides of the casing wall are not parallel. This check allows errors resulting from mistaken transcription, faulty equipment, or improper technique to be identified. Thus, the algebraic sum of pairs of readings should be computed on site in the field, so that corrective actions may be taken to resolve transcription errors. However, if the algebraic sum does not remain nearly constant, the sensor unit, readout, and casing should be rechecked before further use.

4.1.7 Data Reduction

Manual computation and reduction of inclinometer data is a tedious and time-consuming operation. A single movement profile for a 33-m casing can involve more than 200 separate computations. Because of the amount of effort involved in taking readings and subsequently computing displacements, a successful measurement program depends primarily on organization and discipline. Field readings must be transposed to discernible measurement, preferably in the form of summary plots indicating successive movement profiles, as soon as possible after the field observation. Successive movement profiles also provide perhaps the best check of instrument reliability. If a record of successive movement profiles is established, the consistency of new measurements can be referenced to previous readings and judged in light of anticipated materials behavior. Because of occasional error in the accumulation of field readings, the data reduction for a particular casing must be performed with the knowledge of both former movement and expected ground behavior.

Manual data recording is adequate for many small projects. A special data sheet is recommended, which can be used to transcribe the data into a computer. Once this is done, the computer can handle the data with any desired degree of sophistication. It must be recognized, however, that in addition to the time delay, this method is subject to two potential sources of error. The first is in recording the data manually, and the second is in transcribing the data. Figure 11-10 shows a special field data sheet formerly used for recording inclinometer data that were subsequently transcribed for computer processing. Major improvements have been made in inclinometer data acquisition and processing during the past few years.

Personal computers may be used as data collection systems that eliminate hand recording of data and prompt the observer to fill in the right data. Most inclinometer manufacturers now provide units that can support automated data collection. These units can record, store, file,

, shown in Figure 11-11.

Software for reducing and plotting the results has also greatly improved and now provides rapid, simple operations (Figure 11-12). Typically such software includes the following features:

- Utilization of simple pulldown menus so that there is very little, if any, need to refer to the instruction manual;
- Allowance for all data sets for each inclinometer, representing readings collected at different times, to be stored in a unique data file; and
- Generation of multiple plots by many types of printers, with color plots possible if appropriate equipment is available.

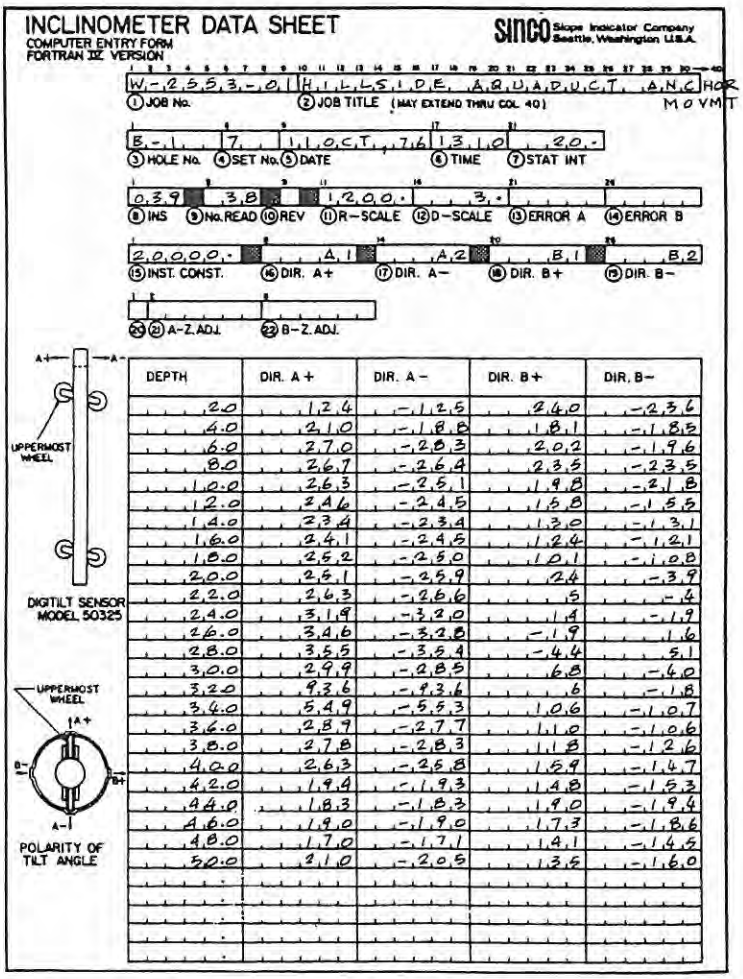

DEPTH	DIR. A+	DIR. A-	DIR. B+	DIR. B-
2.0	1,2,4	-,1,2,5	2,4,0	-,2,3,6
4.0	2,1,0	-,1,8,8	1,8,1	-,1,8,5
6.0	2,7,0	-,2,0,3	2,0,2	-,1,9,6
8.0	2,6,7	-,2,6,4	2,3,5	-,2,3,5
10.0	2,6,3	-,2,5,1	1,9,8	-,2,1,8
12.0	2,4,6	-,2,4,5	1,5,8	-,1,5,5
14.0	2,3,4	-,2,3,4	1,3,0	-,1,3,1
16.0	2,4,1	-,2,4,5	1,2,4	-,1,2,1
18.0	2,5,2	-,2,5,0	1,0,1	-,1,0,8
20.0	2,5,1	-,2,5,9	,2,4	-,3,9
22.0	2,6,3	-,2,6,6	,5	-,4
24.0	3,1,9	-,3,2,0	,1,4	-,1,9
26.0	3,4,6	-,3,2,8	-,1,9	,1,6
28.0	3,5,5	-,3,5,4	-,4,4	,5,1
30.0	2,9,9	-,2,8,5	,6,8	-,4,0
32.0	9,3,6	-,9,3,6	,6	-,1,8
34.0	5,4,9	-,5,5,3	1,0,6	-,1,0,7
36.0	2,8,9	-,2,7,7	1,1,0	-,1,0,6
38.0	2,7,8	-,2,8,3	1,1,8	-,1,2,6
40.0	2,6,3	-,2,5,8	1,5,9	-,1,4,7
42.0	1,9,4	-,1,9,3	1,4,8	-,1,5,3
44.0	1,8,3	-,1,8,3	1,9,0	-,1,9,4
46.0	1,9,0	-,1,9,0	1,7,3	-,1,8,6
48.0	1,7,0	-,1,7,1	1,4,1	-,1,4,5
50.0	2,1,0	-,2,0,5	1,3,5	-,1,6,0

FIGURE 11-10
Simple field sheet formerly used to transcribe inclinometer data before tabulation on punched cards (Green and Mikkelsen 1988).

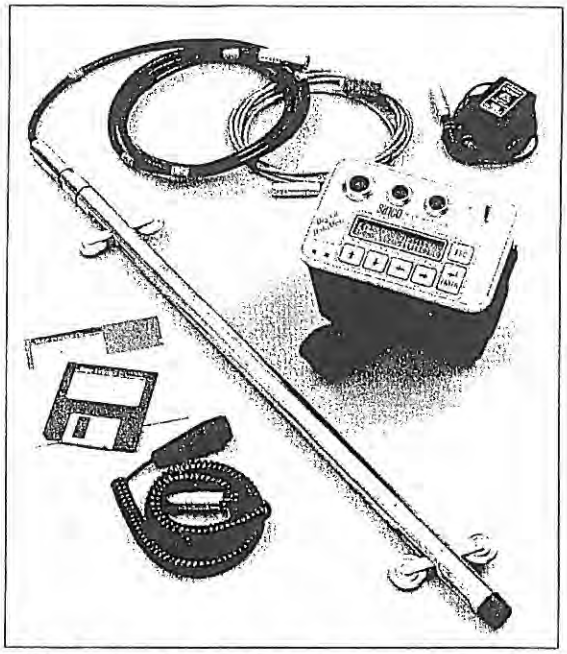

Digitilt DataMate, Digitilt inclinometer probe, and DataMate Manager software for the PC.

Some recently developed software systems incorporate data-base building and management capabilities. Some software allows linkage of inclinometer data with other data automatically collected from other instruments and telemetered from the landslide site. Such software allows the investigator to readily make a coherent assessment of multiple data sources. Routines are included in many systems for performing time-series analyses, correcting systematic errors, and producing illustrations suitable for inclusion in reports.

When combined with the new data acquisition capabilities, such computer programs can in just a few minutes complete the data analysis, a process that previously required hours. Thus, more time is made available to analyze and make systematic error corrections to the data. Since the mid-1970s, it has been possible to make systematic error corrections to inclinometer data.

4.1.8 Evaluation and Interpretation of Data

All too often, confusing or unexplainable results appear because of instrumentation problems. These problems are common to all inclinometers; therefore, they are discussed in some detail so that, even without a detailed understanding of the inner workings of the instruments, these anomalies, the limits of accuracy, and the meaning of the results can be recognized. In simple terms, the person closest to the job should be able to answer the following basic questions:

- Is the landslide active?
- How fast is the landslide moving?
- How deep is the landslide?

By means of repeated surveys, inclinometers measure changes in the orientation of a borehole over certain depth intervals during a period of time. A probe inclinometer records this change in orientation at any depth within the limitations of the cable on which the probe is lowered (i.e., weight, strength, and elongation characteristics). Once the active zone has been detected from successive sets of data, the rate of deformation can be determined by plotting the change versus time. Usually, the major zone of movement is only a few meters thick; hence, the sum of the changes over a few consecutive intervals will often be representative of the magnitude and rate of movement of the entire landslide.

The most commonly encountered errors that affect the quality of inclinometer data are the so-called "zero-shift" error and rotation errors (Figure 11-13). When readings are obtained in a slightly inclined casing, a correction for changes in the servoaccelerometer azimuth orientation may be required. Rotation error produces a false pattern in the displacement-versus-depth profile. Both of these errors may mask shear movements occurring at discrete zones and should therefore be evaluated and compensated for during data processing.

To obtain the greatest observation accuracy, the original installation should be as close to vertical as practicable. The error in inclinometer surveys is proportional to the product of the casing inclination and angular changes in the sensor alignment. As shown in Figure 11-14, angular changes in sensor alignment on the order of 1 degree within inclined casings, corresponding to a sensor rotation value (sin a) of about 0.02, may produce errors of several centimeters per 30 m of casing. Sensor-alignment change occurs from time to time because

FIGURE 11-11
Digitilt inclinometer used with recorder,

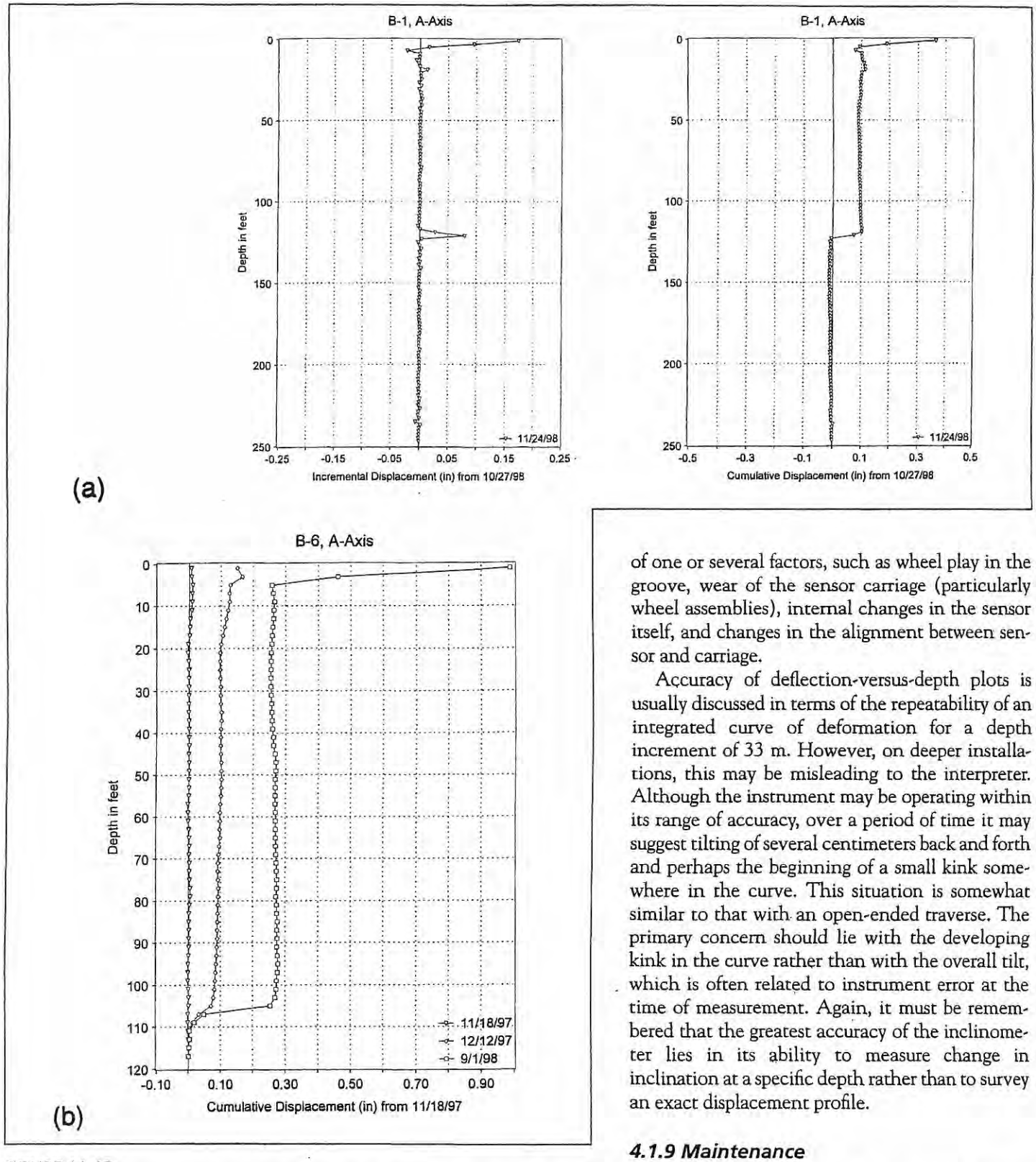

FIGURE 11-12
Graphical computer output of inclinometer data: (*a*) single data set, (*b*) multiple data set

of one or several factors, such as wheel play in the groove, wear of the sensor carriage (particularly wheel assemblies), internal changes in the sensor itself, and changes in the alignment between sensor and carriage.

Accuracy of deflection-versus-depth plots is usually discussed in terms of the repeatability of an integrated curve of deformation for a depth increment of 33 m. However, on deeper installations, this may be misleading to the interpreter. Although the instrument may be operating within its range of accuracy, over a period of time it may suggest tilting of several centimeters back and forth and perhaps the beginning of a small kink somewhere in the curve. This situation is somewhat similar to that with an open-ended traverse. The primary concern should lie with the developing kink in the curve rather than with the overall tilt, which is often related to instrument error at the time of measurement. Again, it must be remembered that the greatest accuracy of the inclinometer lies in its ability to measure change in inclination at a specific depth rather than to survey an exact displacement profile.

4.1.9 Maintenance

Inclinometers are special instruments; consequently, the number of suppliers is limited. Repair

or replacement of an inclinometer can be expensive and time-consuming and can result in loss of important data. The best insurance against damage is careful use and systematic maintenance. The sensor unit should be checked frequently during operation and its wheel fixtures and bearings tightened and replaced as necessary. After each casing has been read, the guide wheels should be cleaned and oiled. Most important, the electric readout should be protected against water at all times. The introduction of a few drops of water into the readout circuitry can cause the galvanometer in a pendulum inclinometer to drift or can induce variations in the numbers on the digital voltage display of an accelerometer instrument. If readings are made too rapidly or if an automatic recorder is used, these variations or drift may not be detected and erroneous measurements may result. When the data are subsequently analyzed, the cause of such results cannot be identified.

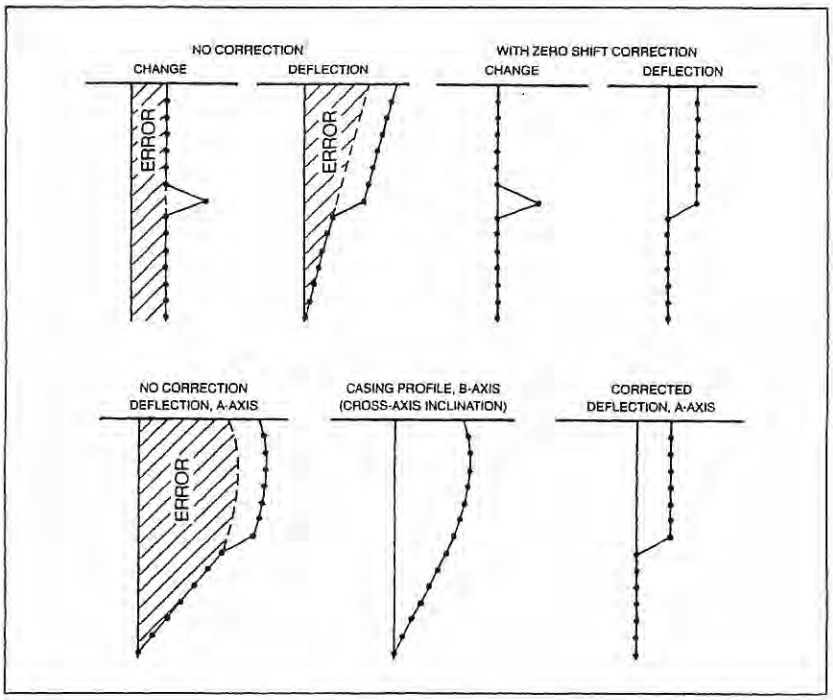

FIGURE 11-13
Typical zero-shift and rotation errors

4.2 Extensometers

Extensometers and strain meters measure the increase or decrease in the length of a wire or rod connecting two points that are anchored in the borehole and whose distance apart is approximately known. One commercially available device is shown in Figure 11-15. When gauge lengths are on the order of a meter or less, these devices are often referred to as strain meters rather than as extensometers. When they are used as extensometers, measurement accuracy and repeatability depend on the type of sensing element and its range of travel and also on the type of connecting wire or rod and the methods used to control the tension. Deadweights are best for maintaining constant tension in wires; if deadweights cannot be used, constant tension springs are acceptable, although there may be some hysteresis. The simplest measurements involve manual readings using a scale or micrometer. Alternatively, linear displacement transducers (potentiometers or vibrating wire) are often used as sensors. These transducers can be monitored by connecting and reading measurements obtained with relatively simple, battery-operated voltmeters. Sensitivity is on the order of 0.1 percent of the range of travel, but repeatability and accuracy may be no better than 0.55 mm, depending on the type of anchor and connecting member. Nevertheless, these parameters are usually sufficient for landslide applications.

4.2.1 Strain Meters

When the above devices are used as strain meters, the repeatability and accuracy are essentially the same as the sensitivity. Thus, for a grouted-in-place 3-m-long extensometer assembly composed of an invar rod with a range of 25 mm, unit strains as low as 0.0001 may be detected with relatively inexpensive instrumentation. Horizontal stretching of embankments has been observed by installing anchors at various positions at a given elevation and attaching horizontal wires to deadweights on the downstream face, as was done at Oroville Dam (Wilson 1967). Care is required to ensure that the wires (or rods) do not get pinched if localized vertical shear movements occur. Other applications are described by Dutro and Dickinson (1974), Heinz (1975), and Gillon et al. (1992).

4.2.2 Rod and Wire Extensometers

Wire extensometers, especially those with long distances between the anchor and the sensor, are particularly responsive to changes in wire tension caused by friction along the wire and to hysteresis effects in the sensor or constant tension spring. The sensitivity of these instruments is controlled by these factors. For example, a typical installation might be constructed with a 16-gauge stainless-

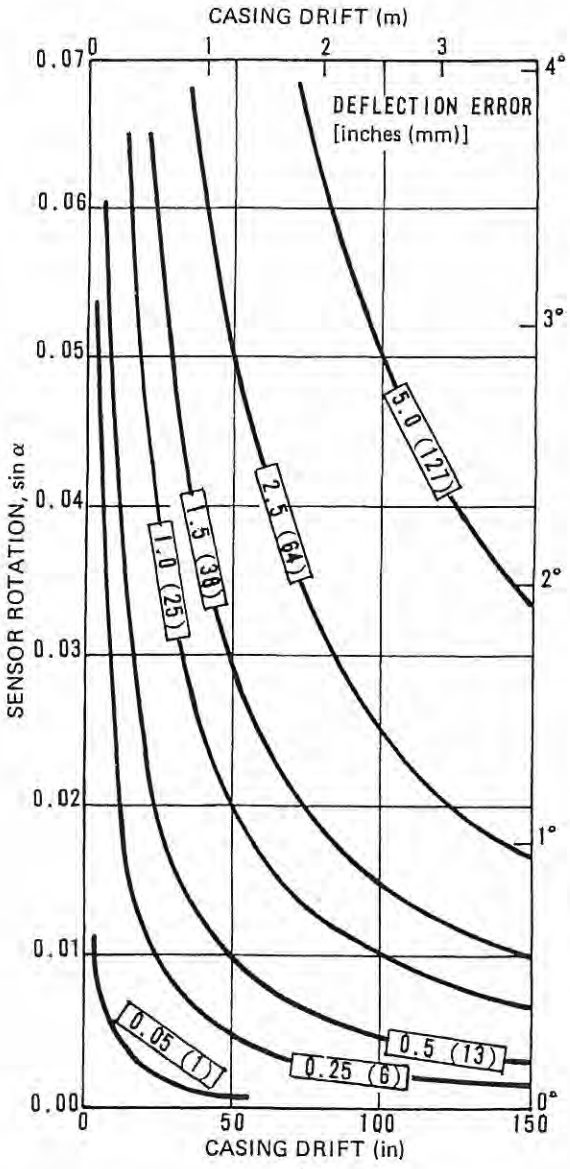

FIGURE 11-14
Measurement error as a result of casing inclination and sensor rotation (Wilson and Mikkelsen 1978).

NOTE: CASING DRIFT OVER ANY DEPTH INCREMENT IS MEASURED AS HORIZONTAL DEVIATION FROM TRUE VERTICAL AXIS IN TWO MUTUALLY PERPENDICULAR PLANES. DEFLECTION ERROR IN ONE PLANE IS RESULT OF DRIFT IN OTHER PERPENDICULAR PLANE.

steel wire 33 m long that is subjected to a pull of 67 N. If the sensor requires 1.11 N to actuate it, the minimum change in length of the wire that can be detected by the sensor is 0.15 mm, which is the effective sensitivity of the extensometer. Up-to-date plots should be kept of changes in length from each anchor to the sensor and of computed changes between anchors. Particular attention should be given to the rate of change in length, because any increase in this rate may be an indication of impending failure.

Extensometer readings are also especially sensitive to temperature changes. If the connecting rods or wires are made of steel, any increase in temperature will result in an increase in their length and thus a reduction in the actual extensometer reading. For example, when the extensometer described in the previous paragraph is subjected to an average change in temperature of 12°C, the same wire will change in length by 3.0 mm. This change in length is about 20 times greater than that detected by the basic sensitivity of the instrument. Daily and seasonal temperature variations are likely to show similar variations in the gauge readings. Not only does the length of the wire change with temperature, but the ground itself expands and contracts as its temperature varies. At a hillside stability project in Montana, rock outcrops were found to expand and contract seasonally by as much as 1.5 mm. Electric lead wires also change their electric resistance with temperature and will cause erroneous readings unless such a change is properly taken into account.

4.2.3 Slope Extensometers

When landslide movements are concentrated along relatively thin shear zones, inclinometers are only capable of measuring movements that are less than 2 to 5 cm. Larger movements exceed the diameter of the inclinometer casing, and the inclinometer becomes useless owing to the inability to access the probe. In such cases, extensometers involving cables and anchors provide a means for continuing the monitoring of the movement. Sometimes extensometer cables and anchors can be installed within the damaged inclinometer casing.

Extensometer cables do not provide accurate measurements until the displacements are greater than the thickness of the shear zone. Before the inclinometer casing becomes crushed, a special detailed survey of the shear zone with the inclinometer probe may be able to determine the thickness of the shear zone, and future slope extensometer results can be corrected accordingly. Alternatively, a completely new subhorizontal extensometer can be installed across the shear zone to provide maximum sensitivity and minimize measurement error.

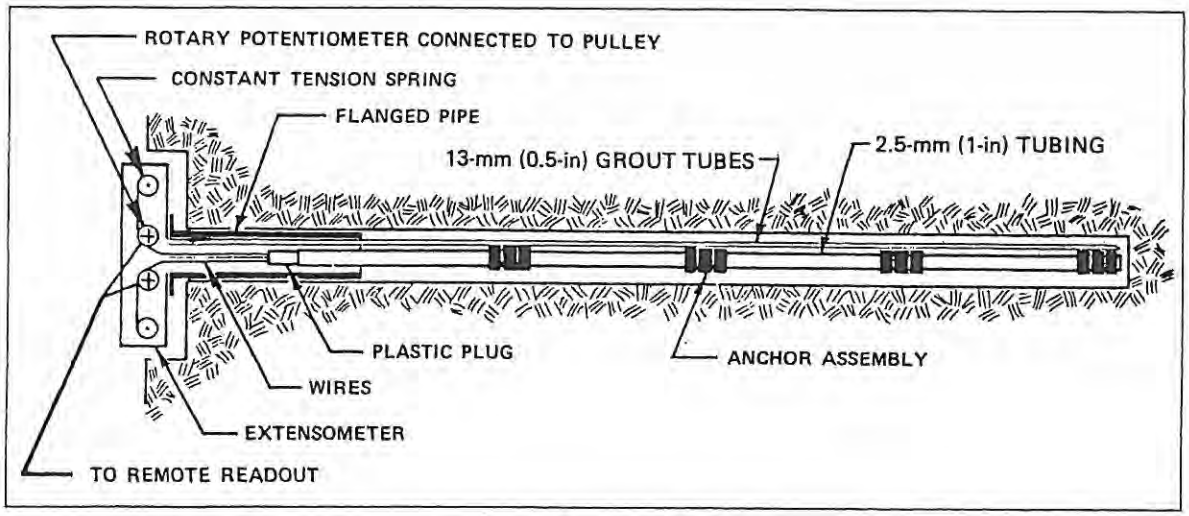

FIGURE 11-15
Extensometer (Wilson and Mikkelsen 1978).

Two types of special extensometers that deserve some mention are designed to measure large movements. The first was invented in Europe in the 1970s for monitoring gross landslide and glacier movements. It was adopted for use in the United States to monitor a natural gas pipeline that moved several feet where it crossed a landslide at Douglas Pass, northwestern Colorado.

The second type, a gravity-tensioned slope extensometer, was developed by the Bureau of Reclamation for use on the Big Bull Elk landslide in Montana (L.R. Carpenter, personal communication, 1995, Bureau of Reclamation, U.S. Department of the Interior). The site is located on the Bighorn Reservoir 16 km upstream from Yellowtail Dam and 72 km southeast of Billings. During initial filling of the reservoir, the landslide slumped 3 to 6 m at its contact with a limestone cliff. Measurement points were installed along two lines established on the landslide. These lines were labeled A and B. Manual readings are taken annually between a point scribed on the cliff and reinforcing bars placed at three points on the landslide.

Determination of the Line A displacements was automated in 1985 by establishing a line parallel to and 2 m uphill from the manually read points. The line was divided into sections 30, 50, and 98 m long. A 10.2-cm diameter polyvinyl chloride (PVC) pipe was buried below the ground surface to protect a surveying tape, which was supported by pulleys placed in the pipe at 17-m intervals or at points where the pipe bent to follow a major slope change. Bellows constructed of rubberized fabric connected the individual sections of pipe at such bends. The bellows allowed both linear and angular displacements of pipe sections and kept the inside of the pipe free of debris. A 30-m extensometer was established in the first section of the line by anchoring the upper end of the surveying tape to an eyebolt installed in the cliff face. This extensometer was tensioned by attaching a weight suspended in a vertical pipe to the lower end of the surveying tape by means of a pulley system installed at the top of the vertical pipe. Two other extensometers were installed in the lower two sections of the line. They were constructed in a similar fashion to the uppermost extensometer. The upper ends of each of these extensometers were anchored by attaching their surveying tape to the axle of the pulley system of the weight-tensioning system of the preceding extensometer.

The displacement of each of these extensometers is determined by monitoring the distance between the lower end of the tape and the position of the lower end of the protecting pipe. This distance is measured by attaching the body of a linear potentiometer to the lower end of the pipe and the sliding potentiometer rod to the tape. The potentiometers exhibit a 5-kΩ electrical change for each 305-mm change in length. The three potentiometer values are monitored by a solar-powered automated data analysis system (ADAS) that transmits the values via a radio link to a personal computer located in the control room at the Yellowtail Dam. These values and other data collected at the dam are relayed through the Geostationary Operational Environmental Satellite (GOES) to a computer at the Bureau of Reclamation office in Denver, Colorado.

5. GROUNDWATER MONITORING

Groundwater levels and pore pressures in a landslide area can be measured by a variety of commercially available piezometers. The selection of the best type for a particular installation involves several considerations, which are discussed in Chapter 10 (Section 9 and Tables 10-6 and 10-7).

5.1 Open Standpipe Piezometers

The most common water-level recording technique, despite the availability of more sophisticated methods, is observation of the water level in an uncased borehole or observation well. A particular disadvantage of this system is that perched water tables or artesian pressures occurring in specific strata may be interconnected by the borehole so that the recorded water level may be of little significance for further analysis. Therefore, at all installations, boreholes between different water-bearing strata should be properly sealed, and each water-bearing zone should be separately monitored. Not only will better measurements result, but unnecessary cross-contamination of groundwater supplies will be avoided and most local regulations concerning well construction will be satisfied.

Sealed, open standpipe piezometers vary mainly in diameter of standpipe and type and volume of collecting chamber. The simplest type (Figure 11-16) is merely a cased well sealed above the monitoring portion. The depth to water is measured directly by means of a small probe. In this case, the static head represents the average conditions over the entire zone being monitored. This measured head may be higher or lower than the free water table, but in the case of moderately impervious soils, it may be subject to a large time lag before a stable water level is observed (Hvorslev 1951). The simplicity, ruggedness, and overall reliability of the open standpipe piezometer dictate its use in many installations. However, it is often a poor choice of instrument for measuring water levels in impervious soils because of the inherent time lag, and in partially saturated soils the significance of the measured head may be difficult to evaluate.

The time lag may be reduced by decreasing the diameter of the riser pipe and increasing the diameter of the inflow screen or porous filter (Hvorslev 1951). The Casagrande type of standpipe piezometer (Figure 11-17) consists of a porous stone tip embedded in sand in a sealed-off portion of a boring and connected with a 1-cm diameter plastic riser tube (Shannon et al. 1962). When properly installed, this type of piezometer has proven successful for many materials, particularly in the long term, because it is self-deairing and its nonmetallic construction resists corrosion. The reliability of unproven piezometers is usually evaluated on the basis of how well their results agree with those of adjacent Casagrande piezometers. However, so that commercial water-level probes can be inserted, larger 1- to 2-cm diameter risers, which increase the time lag, are commonly used with the Casagrande-type piezometers. If rapid piezometer responses are a major concern in a landslide, pressure sensor piezometers should be used.

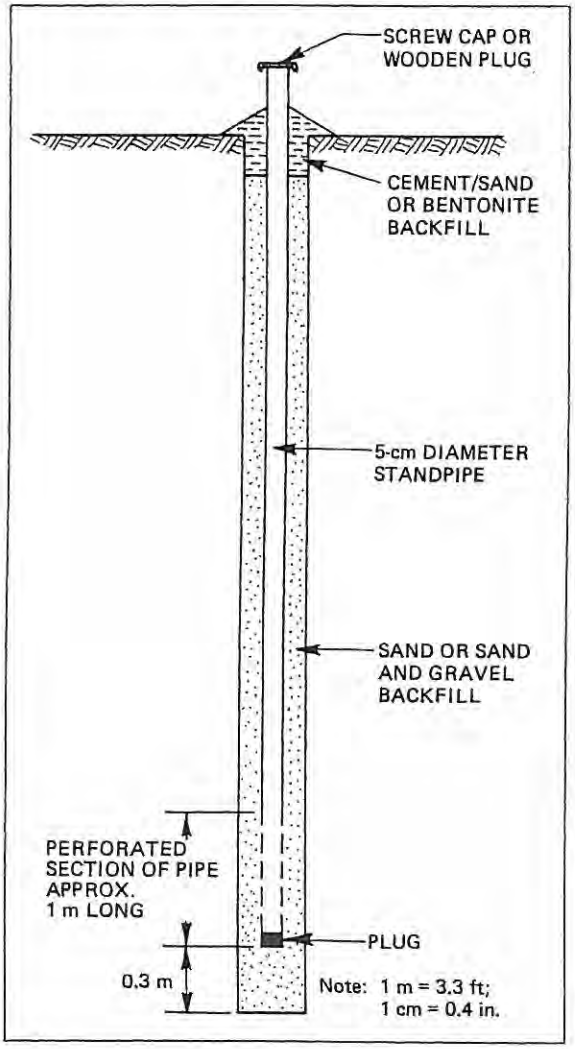

FIGURE 11-16
Open standpipe piezometer (Wilson and Mikkelsen 1978).

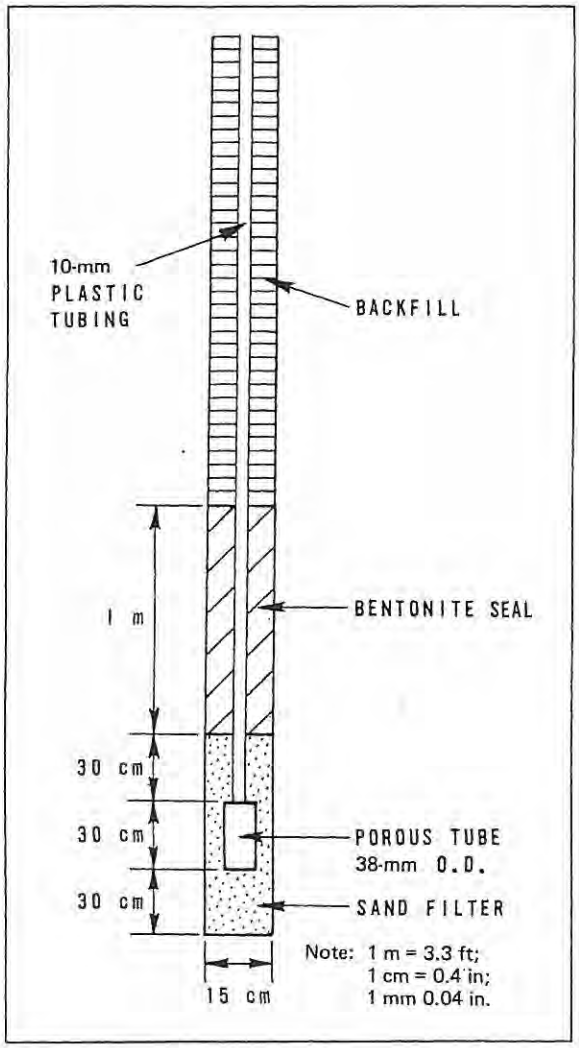

FIGURE 11-17
Casagrande borehole piezometer (Wilson and Mikkelsen 1978).

5.2 Pressure Sensor Piezometers

Electrical vibrating-wire and pneumatic sensors dominate the bulk of the geotechnical piezometer instrumentation market, with the old standby, the Casagrande-style standpipe, as the backup. Considerable improvement in these instruments has occurred during the last decade, and several new commercial products have become available. Each type has distinctly favorable and unfavorable attributes relative to short- and long-term monitoring. Both the electrical vibrating-wire and pneumatic sensors (or transducers) have become less expensive and easier to use.

The pneumatic piezometer consists of a sealed tip containing a pressure-sensitive valve (Penman 1961). The valve opens or closes the connection between two tubes that lead to the surface, or the slope face, at any convenient location and elevation. In the pneumatic piezometer shown in Figure 11-18, flow of air through the outlet tube is established as soon as the inlet-tube pressure equals the pore-water pressure. Pneumatic piezometers have the following advantages: (*a*) negligible time lag because of the small volume change required to operate the valve, (*b*) simplicity of operation, (*c*) capability of purging the lines, and (*d*) long-term stability. Their main disadvantage is the absence of a deairing facility.

Electrical piezometers have a diaphragm that is deflected by the pore pressure acting against one face. The deflection of the diaphragm is proportional to the pressure and is measured by means of various types of electric transducers, the most common being either vibrating-wire or strain-gauge pressure transducers. Such devices have a negligible time lag and are extremely sensitive. However, they cannot be deaired nor can the sensitive electric transducers normally be recalibrated in situ (Dibiagio 1974). For short-term observations at installations where data transmission is over limited distances, standard resistance strain-gauge pressure transducers may be used. Because they are affected by the environment and have poor long-term stability, resistance strain-gauge pressure transducers are generally not recommended for installations in which reliable readings are required over an extended period of time. A typical vibrating-wire electrical piezometer is shown in Figure 11-19. These generally exhibit better long-term stability characteristics. However, not all vibrating-wire types of piezometers have provided consistent long-term stability records.

Although somewhat expensive, the multipoint piezometer offers major advantages for monitoring groundwater in deep landslides. Invented in the mid-1970s and initially used on the Downie landslide located between Mica and Revelstoke on the Columbia River in British Columbia (Patton 1979, 1983, 1984), this system has since become a seasoned and reliable commercial product.

Integrated data gathering and monitoring systems that take full advantage of the latest in microtechnology and single-wire transmission of digital data were launched about a decade ago. These systems, such as the MP System with modular subsurface data acquisition (MOSDAX) developed by Westbay (Patton et al. 1991), are revolutionizing the methods of obtaining and eval-

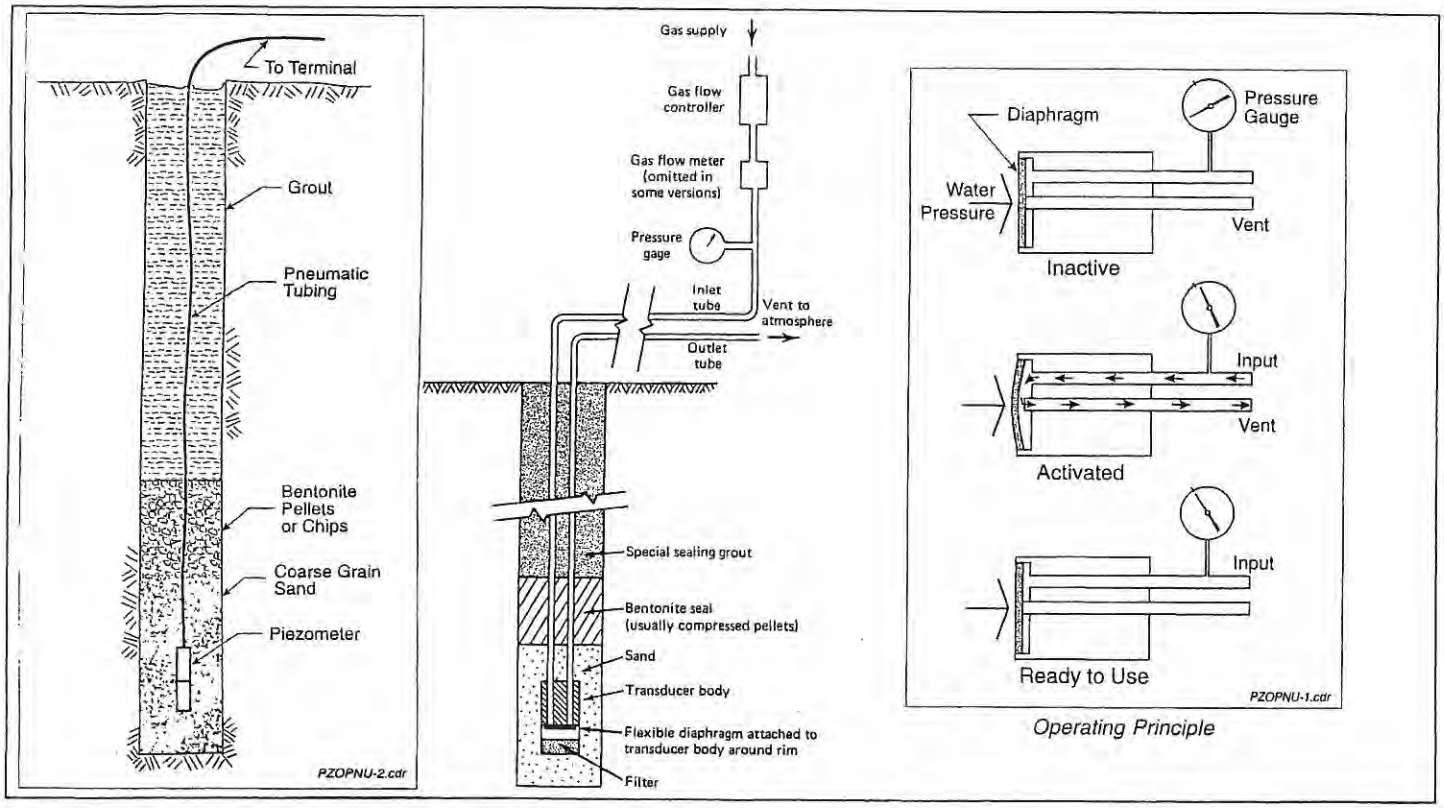

FIGURE 11-18
Pneumatic piezometer

uating groundwater data in complex hydrogeological regimes at reservoirs, dams, and landslide areas.

The MP System facilitates the measurement of groundwater or gas pressure at any number of points spaced as close as 1.5 m apart in a single borehole. Sections of 48- × 38-mm PVC pipe are combined with special valved couplings and packer units to isolate multiple pressure-measuring ports. If desired, ports can serve as monitoring sites or be opened to pump and sample groundwater, or a permeability test may be run from these locations. Installations have extended to depths of more than 300 m. MOSDAX is a pressure-sensing module that can be used to probe any individual port in turn, provided manual data collection is acceptable. Automated data collection is possible, even at unattended sites, when dataloggers are combined with multiple MOSDAX units attached to selected ports.

5.3 Importance of Piezometer Sealing

Piezometers in landslides are commonly installed in boreholes advanced into soil or rock. The depth of the monitoring location for each piezometer is selected on the basis of the drill log and identification of materials encountered in the borehole, the estimated position of the water table, and the estimated location of the sliding surface.

The simplest open standpipe piezometer is constructed by placing a tube within the drilled hole that extends to the ground surface. The monitoring portion of the piezometer installation should be pervious to allow observation of the groundwater pressure. This monitoring section may be constructed of a porous material, or the appropriate portion of the tube can be slotted or constructed from a material with a sufficiently fine screen so that free access of groundwater is permitted but movement of soil into the piezometer is prevented. The piezometer tube assembly is centered in the drilled hole, and a known volume of clean sand is placed around the piezometer monitoring section to create a sand filter between the soil and the piezometer sensor.

Construction of an impervious barrier above the piezometer tip and sand pocket is essential. Casagrande, pneumatic, and electric sensors placed within open standpipe piezometer assemblies in boreholes can be sealed in a similar manner. One

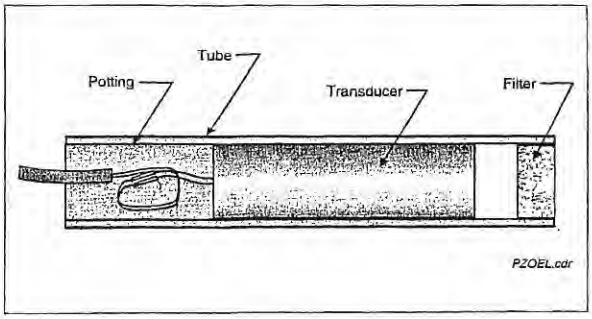

Electrical Piezometer

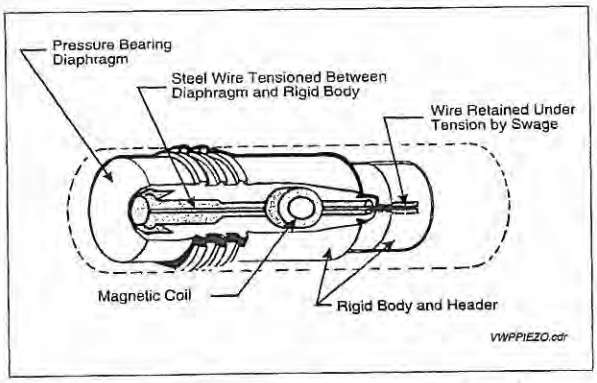

Vibrating Wire Piezometers

well-established procedure is to drop balls of soft bentonite into the space between the piezometer tube and the borehole wall and then to tamp those balls around the piezometer tube by using an annular hammer. Prepared bentonite in chip or pellet form is available commercially; it has a specific gravity that is sufficiently great to allow it to sink through the water in the piezometer hole so that hammering is not necessary. Alternatively, a cement-bentonite grout can be tremied into the hole above the sand filter. Such a seal can be pumped through a 1.3- to 2.0-cm diameter pipe adjacent to the piezometer tube. An alternative method of sealing piezometers in boreholes within fine-grained materials was described by Vaughan (1969). Instead of bentonite being placed above a sand filter, the borehole is completely grouted with cement-bentonite grout. Even if the permeability of the grout is significantly higher than that of the surrounding soil, little error will result because of the relatively large grouted length. In many cases, a sand filter need not be included because the piezometer tip can be grouted directly with little error.

FIGURE 11-19 Electrical piezometer

Installing only one, or at most two, piezometers in a single borehole has generally been found preferable because bentonite seals are sometimes difficult to construct and may leak slightly despite precautions. However, special-purpose, multiple-point piezometers (with up to four tips) have been used successfully by Vaughan (1969) and merit consideration.

In soft and medium-stiff soils, it may be preferable to push the piezometer directly into the ground. Flush-coupled heavy steel pipe is required to allow for the driving of the probe, and the piezometer tip must be robust enough to resist damage and should be designed to minimize disturbance around the tip (Mikkelsen and Bestwick 1976). Casagrande, pneumatic, or, less commonly, electric sensors may be used. These driven piezometers are self-sealing and rapidly installed. If pneumatic sensors are used, these piezometers have a rapid response. Since the piezometer tip cannot be deaired after installation, it should be soaked in deaired water beforehand and kept in the water until it is driven into place. A low-air-entry filter tip can be placed in a saturated sand pocket, but a high-air-entry tip should be pushed into the soil beyond the base of the hole or surrounded by a porous grout such as plaster of paris. This procedure will ensure more rapid pressure equalization, which may be of considerable value in obtaining reliable pore-pressure measurements soon after installation in low-permeability clay. Both electrical and pneumatic piezometers should be checked for malfunction before and during installation, and particular care is needed in pushing electrical piezometers to prevent overpressuring them.

5.4 Presentation of Data

Piezometric heads should be plotted on time graphs showing amounts of rainfall and other data that may influence the pore pressure. If drainage has been installed, the quantity of seepage should also be recorded and plotted. If possible, the response of each piezometer should be checked periodically to determine its recovery rate.

6. DATA RECORDING AND TRANSMISSION

Clearly, the evolution of automated data recording in the field has been the greatest innovation in geotechnical instrumentation during the past decade. The accuracy and speed of data transfer from field to office are increased drastically by electronic recording (Mikkelsen 1992). Methods range in sophistication from data keyed into general-purpose electronic notebooks to fully automated data analysis systems (ADAS). At the heart of this technology are the continuously evolving microchips, which seem to get smaller and faster and have more memory every few months. The versatility, speed, power, portability, and convenience of personal computers provide capabilities that were only dreamed of 10 years ago. Today, some data evaluations can even be conducted in the field with devices that are very simple to use. The day of the slide rule is long gone, and so is the manual recording of numerical readings, with date, time, and comments, for many applications.

Successful instrumentation and data-gathering automation require a blending of expertise from diverse areas, including civil engineering, electronics, communications, instrumentation, and computers (Dunnicliff and Davidson 1991). Much of the necessary synergism was encouraged by those involved in dam instrumentation, in which increased sensitivity to dam safety issues coupled with dramatically improved computer hardware and software offered potential solutions to reductions in monitoring staff and other budgetary constraints. Some of the instruments and much of the experience in the automation of field instrumentation networks developed by those involved in dam monitoring can be applied to other geotechnical applications, including landslide investigations. On the basis of experience with dam instrumentation, Dunnicliff and Davidson (1991) reviewed methods for automating data collection from various classes of geotechnical instruments and the ease with which such automation can be achieved (Table 11-1).

Automated data recording and transmission can be undertaken in several ways, each reflecting different levels of automation, investment, and sophistication. Three broad approaches can be defined:

- Readout boxes with memory,
- Multichannel dataloggers, and
- Integrated computer-based ADAS.

6.1 Readout Boxes with Memory

A variety of dedicated readout boxes containing large volumes of digital memory are appearing on the market from several manufacturers. These readout boxes are lightweight and weather- and splash-proof, have power for at least one work day, and can communicate with a personal computer. Currently available readout boxes are able to process signals from inclinometers and vibrating-wire electrical and pneumatic piezometer sensors. Typically, these readout boxes are carried into the field and manually connected to a series of instruments in a sequential fashion. The data received from each instrument are temporarily stored in the memory of the readout box. At the end of a suitable period, usually no more than a day, the stored data are offloaded from the readout box into a personal computer, with which an appropriate data base is maintained. Expertise in programming is not necessary for this method of electronic recording. An infrequent user is usually guided through the proper recording procedure by menu displays. Some data-entry mistakes are even allowed without the necessity of restarting the reading session.

For example, preparations for a typical field session of reading a series of inclinometers at a landslide would start in the office by connecting the readout box to a personal computer with a serial interface cable and bringing up the data-base management program. A single data-base file would contain information concerning all the inclinometers and all the readings for one project, including special notes and installation parameters. From this file, any of the inclinometer installation parameters and sets of previous readings would be obtained. In an on-going data acquisition program, the installation parameters for each inclinometer would be loaded into the readout-unit memory, but modifications in the parameters would perhaps be required. Deletion of previously transferred data sets is usually necessary to free up memory in the readout box before initiation of a new field reading session. Only a few minutes would be required to accomplish these tasks before the readout box was ready for the field.

In the field, the reading of the individual inclinometers would proceed as usual; the readout box would be connected to the inclinometer probe and activated by selecting the menu option for collection of readings. Then, by scrolling through a list

Table 11-1
Automated Data Collection from Various Geotechnical Instruments (Dunnicliff and Davidson 1991)

INSTRUMENT[a]	CATEGORY[b]	AUTOMATION METHOD	MANUAL BACKUP
Piezometers			
Open standpipe	2	Pressure transducer down standpipe	Usually straightforward, by measuring water surface
Twin-tube hydraulic	2	Pressure transducers connected to lines	Straightforward, by existing pressure gauges
Pneumatic	3	Pressure actuating and measurement system	Straightforward, with manually operated readout
Vibrating-wire	2	Frequency counter	Straightforward, with manually operated readout
Electrical resistance strain gauge	2	Strain gauge completion circuitry	Straightforward, with manually operated readout
4- to 20-mA pressure transmitter	1,2	Electrical current readout	Straightforward, with manually operated readout
Deformation gauges			
Tiltmeter[c]	1,2	—[c]	Straightforward, with manually operated readout
Probe extensometer	4	N/A	N/A
Embankment and borehole extensometer[c]	1,2	—[c]	Straightforward, with manually operated readout
Inclinometer, probe type	4	N/A	N/A
Plumb line and inverted pendulum[c]	3,4	Infrared or light sensor line and position transducers	Straightforward, with manually operated readout
Liquid level gauge[c]	1,2	Pressure transducer	Straightforward, with manually operated readout
Earth pressure cells			
Pneumatic	3	Pressure actuating and measurement system	Straightforward, with manually operated readout
Electrical resistance strain gauge	2	Strain gauge completion circuity	Straightforward, with manually operated readout
Load cells and strain gauges			
Electrical resistance strain gauge	2	Strain gauge completion circuitry	Straightforward, with manually operated readout
Vibrating-wire	2	Frequency counter	Straightforward, with manually operated readout
Hydraulic load cell	2	Pressure transducer	Straightforward, with manually operated readout
Temperature			
Thermistor	1,2	Resistance readout	Straightforward, with manually operated readout
Thermocouple	2	Low-level voltage readout	Straightforward, with manually operated readout
Miscellaneous			
Surface water elevations, rain gauges	1,2	—[c]	Straightforward, with manually operated readout
Weir for measuring water flow	1,2	—[c]	Straightforward, with manually operated readout
Seismograph 4	N/A		Seismograph chart record

[a] For a definition of instument terms, see work by Dunnicliff (1988).

[b] There are four categories in order of increasing difficulty, specialization, and cost of automation:
Category 1, Straightforward: Automation can be done by numerous manufacturers of laboratory and industrial ADAS equipment.
Category 2, More Specialized Requirements: Problems exist in thermally unconditioned environments or with inaccessible power; requires non-standard signal conditioning, low-level voltage measurement, and wide common mode voltage range.
Category 3, Most Specialized Requirements: Problems exist in hostile outdoor environment; radio network communication required if hard-wire communication unavailable; sensors are difficult to automate (e.g., plumb lines or pneumatic piezometers); involves sensors that communicate via serial or parallel interface.
Category 4, Usually Not Practical To Automate: Technical complexity or cost outweighs benefits; significant reliability problems exist in hostile environment; customized automation hardware required or impractical to automate.

[c] Automation method and difficulty depend on type of transducer used.

on the display, the user would select the desired inclinometer. The time and date would be logged automatically, and the stored inclinometer parameters would be retrieved from memory. These parameters would be quickly confirmed by the operator, and the reading session would begin. The readings would be recorded at each depth by pressing a remote hand switch. After a series of field readings was completed, the data would be checked for errors in the field and simple calculations performed. Subsequently, in the office, the new readings would be uploaded into the personal computer, the data base updated, and new displacement plots produced.

6.2 Multichannel Dataloggers

Manufacturers of geotechnical instruments have produced a number of sensor-dedicated dataloggers in the past, but it is only recently that more intelligent field-hardened units that can handle several signal types have emerged. In the early 1980s, Campbell Scientific, a manufacturer of weather and environmental data collection units, produced their initial CR10 instrument, the first significant new data collection unit to be widely utilized by the geotechnical industry in North America (Figure 11-20). The CR10 still forms the heart of most of the small unattended datalogger systems produced by several suppliers.

Because they must remain in the field continuously for extended periods, dataloggers have to be even more rugged than readout boxes, which are only carried into the field during actual reading sessions. Dataloggers have to withstand whatever field and weather conditions are experienced for days, weeks, and months. Sufficient battery power and a great deal of memory are necessary requirements. Continuing improvement in low-power electronics permits dataloggers to be operated unattended from a month to up to a year. Use of solar power for battery recharging can extend unattended use for several years. Dataloggers can monitor from one to a few dozen sensors at a remote site. The sensors can be polled according to a preprogrammed sequence or activated by a triggering event or by manual command.

FIGURE 11-20
Campbell Scientific CR10 datalogger.

6.3 Integrated Computer-Based ADAS

A datalogger may form the heart of an ADAS, but much more powerful and flexible systems are built around personal computers. A computer-based ADAS is generally capable of dealing with a variety of transducer types and instrument-monitoring needs. The use of an ADAS leads to some cost reductions and easier system operation because a single computer can replace several dataloggers. The resulting integrated system is more robust. Computer-based systems generally provide powerful communications capabilities that allow the ADAS to be accessed by several remote users, including the system instrumentation manufacturer for monitoring and evaluation of operational diagnostic tests.

The heart of an ADAS is the central network monitor, which houses the host computer and communications hardware allowing receipt of data from one or several sites. Data are acquired at sites by local monitoring units (LMUs), which are directly connected to the central network monitor, or by remote monitoring units (RMUs), which transmit data to the central network monitor by telemetry (usually radio) links. The individual RMU or LMU systems contain modules for the multiplexing (switching), signal conditioning, power excitation, control, and communications functions required to acquire data from each transducer. RMU and LMU systems can be designed to convert raw data into desired engineering units, to collect data readings according to a preprogrammed sequence, or to be polled from the central network module.

All of the above ADAS components can be located at a remote site, for example, a single landslide or group of nearby landslides. A variety of telephone, microwave, radio, or even satellite data

transmission links have been used to connect remote ADAS installations to a central office computer system. Dunnicliff and Davidson (1991) provided many important recommendations concerning the specification, design, and maintenance of ADAS installations for dam projects, but some further comments are warranted concerning their application to landslide investigations. Economic considerations are most important. These systems were developed mainly for large dam projects and remain relatively costly for many landslide investigation and monitoring activities. Nevertheless, as noted in the case histories presented later in this chapter, they are already in use at several landslide locations, usually those that exhibit considerable potential for having significant economic impacts or pose large safety hazards. The cost of such systems continues to fall, in line with the rapidly declining costs of most electronic components. As the novelty of these automated systems passes and their cost continues to diminish, their increased use at landslide sites can be expected.

Dunnicliff and Davidson (1991) noted that the initial expectation that automation would cut labor costs does not appear realistic. Compared with manual retrieval of readings, automation does not eliminate the need for personnel. Introduction of a new and more sophisticated technology, the need for maintenance of additional components, and processing and evaluating an increased volume of data generally require the same or a greater number of people. However, better and more timely data, and even real-time continuous data, are advantageous because a much better understanding of the landslide problem is provided.

Automated data collection technology is new to most geotechnical engineers; only a few specialists and instrument suppliers have the expertise to carry out successful programs. The technology is better known in other application sectors, such as hydrological and meteorological monitoring, and by the telecommunications industry. Geotechnical practitioners should seek assistance from those in other fields experienced with this technology before attempting to use it for the first time in geotechnical applications.

7. EXAMPLE PROJECTS

Chapter 5 in *Landslides: Analysis and Control* (Wilson and Mikkelsen 1978) contained several brief case histories of landslide instrumentation that had been reported before 1978. Although now somewhat dated, these case histories include several classic examples. These earlier landslide instrumentation applications included those at a rock cut along Interstate-94 in Minneapolis, Minnesota (Wilson, 1970, 1974); in the Potrero Tunnel of the Southern Pacific Railroad near San Francisco, California (Wilson, 1970; Smith and Forsyth, 1971); in the stabilization of glacial till slopes along Interstate-5 in downtown Seattle, Washington (Wilson, 1970; Palladino and Peck, 1972); and at the Fort Benton landslide along the Missouri River in western Montana (Wilson and Hilts 1971). Other early landslide instrumentation case studies were reported by Durr (1974), Muñoz and Gano (1974), and Tice and Sams (1974).

Five recent landslide monitoring projects that feature a variety of instrumentation issues have been selected for inclusion in this chapter. The instrument programs developed, the purposes of the investigations, the measurements achieved, and the lessons learned are described for each case history.

7.1 Downie Slide near Revelstoke Dam and Reservoir, British Columbia, Canada

Investigations in 1956 of alternative dam sites on the Columbia River north of Revelstoke, British Columbia, led to discovery of a large prehistoric rock slide on the west side of the river (Piteau et al. 1978). The volume of this landslide is approximately 1.5 km^3; today its toe extends into Revelstoke Reservoir 66 km upstream from the 160-m-high concrete gravity Revelstoke Dam.

The Downie landslide was first studied in 1965–1966 as part of the design for Mica Dam, located 70 km upstream from the landslide (Imrie 1983). The investigation was undertaken to determine how a blockage of the Columbia River caused by reactivation of the landslide might affect the stability of the downstream toe of the dam. The early investigation consisted of geologic mapping, borings to study the rock layers, and installation of instruments to measure slide movement and groundwater conditions. Five drill holes (three on and two off the landslide) were involved in which core was recovered using double-tube core barrels. Inclinometer casings were placed in the drill holes on the landslide, and measurements were taken. Other early instrumentation included two surface

surveys with 21 monuments, strong-motion seismometer measurements, rock noise surveys, and water-level measurements in the three leaky inclinometer casings. The results of the study, described by Piteau et al. (1978), were helpful in answering questions concerning the stability of Mica Dam but were inconclusive with regard to the nature and depth of the slide (Patton 1983).

Beginning in 1973, a new study was undertaken to evaluate the stability of the landslide and to determine the effect on the landslide of the future reservoir created by the proposed Revelstoke Dam, which would raise the water level 70 m into the toe of the landslide (Imrie and Bourne 1981). This new study proceeded in several stages using instrumentation, stability analysis, and geologic observations. The instrumentation program eventually involved 41 drill holes instrumented with 113 piezometers (both single- and multiple-position) and 10 inclinometer casings (Patton 1983; Moore 1989). Additional instrumentation included 45 surface survey monuments, 2 meteorological stations and 3 snow-course stations, 7 streamflow and adit-flow gauging stations, and 1 seismometer. The combination of surface surveys measured by electronic distance measurement (EDM) and inclinometers cemented vertically into holes that extended as much as 250 m into the landslide monitored movements as small as 2 mm/year (Imrie 1983). The locations of the drainage adits and many of the instrument stations are shown in Figure 11-21.

During reservoir filling in 1983, a continuous surveillance system monitored a microseismic unit, three in-place inclinometer sensors, three extensometers, two automatic flume recorders, and four fluid-pressure transducers (Patton 1983). Some of the instrument readings were telemetered to Revelstoke and Vancouver, British Columbia, to provide constant information on landslide move-

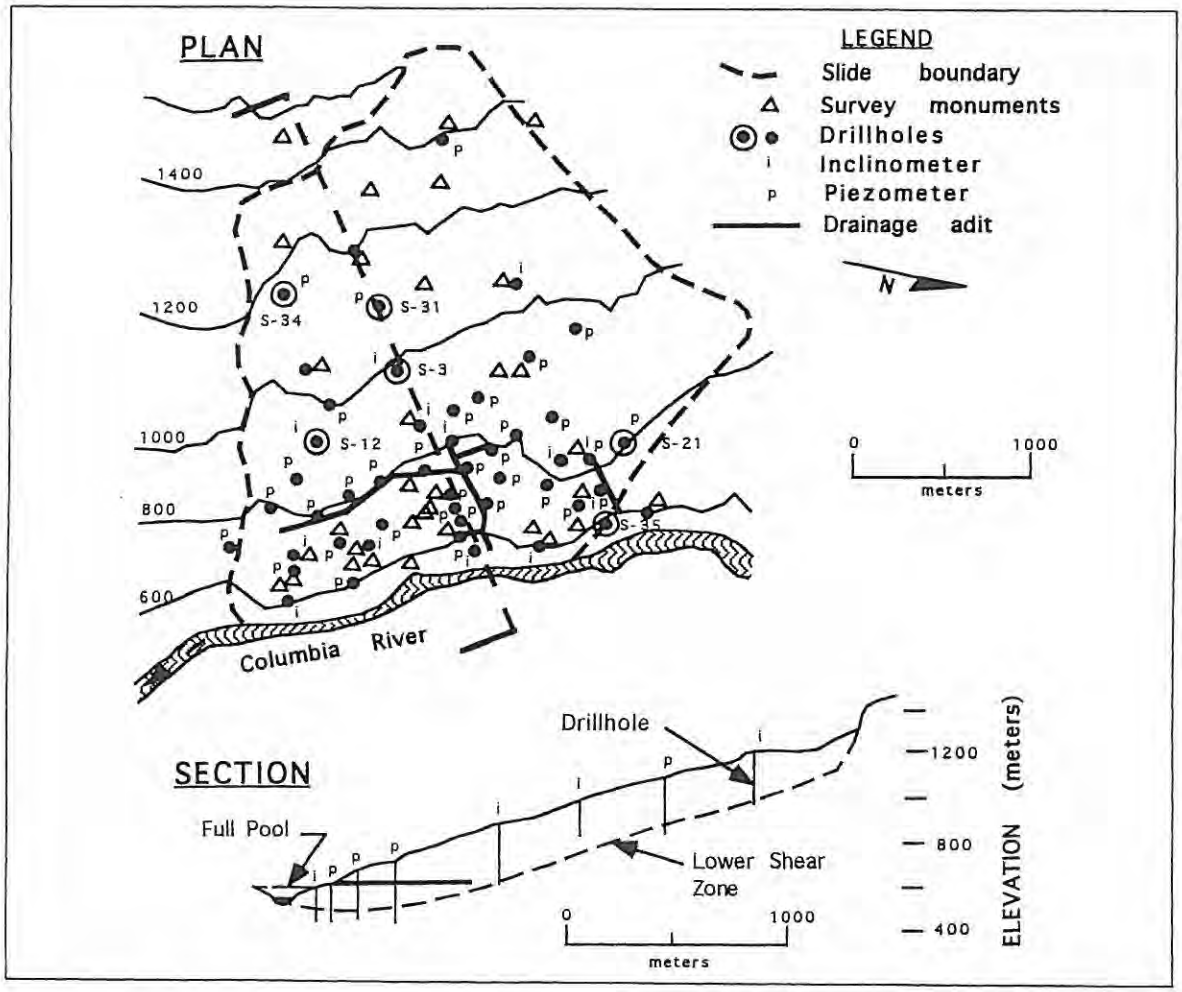

FIGURE 11-21
Plan view and section for Downie slide indicating locations of drainage adits, boreholes, instrumentation, and survey targets (modified from Imrie and Bourne 1981).

ment, seismic activity, and groundwater flow. The telemetry allowed the instruments to serve as a warning system that would allow suitable action, such as lowering the reservoir, to be taken quickly (Imrie 1983).

The Downie slide has been stabilized by means of an extensive drainage system (Imrie et al. 1992). Some 2430 m of exploratory and drainage adits was excavated in and adjacent to the landslide mass in three separate stages between 1974 and 1981. Observations made during initial stages were used to lay out subsequent plans. About 12 200 m of drainholes was drilled from the adits, and a widespread lowering of water pressures at the basal shear zone was achieved (Patton 1983; Moore 1989).

Largely on the basis of the Downie slide studies, Patton (1984) arrived at the following conclusions regarding the collection and use of piezometric data:

- Dormant slides can be affected by maximum long-term piezometric levels and therefore are affected by long-term climatic changes;
- Slope stability analyses should generally consider three classes of piezometric observations: (*a*) short-term measurements, (*b*) seasonal or storm-related maxima over a several-year period of record, and (*c*) estimated long-term maximum piezometric levels;
- Long-term piezometric records are almost always unavailable for slope stability analyses, but they can be estimated for a period to coincide with the expected life of the project using available piezometric records as a basis; and
- Piezometric levels used for slope stability analyses should, as a minimum, be based on the maximum levels recorded over a period of several years.

After 10 to 15 years of use, the monitoring system has begun to decay. Several instruments have become blocked or otherwise inoperable and will have to be replaced (Imrie et al. 1992). The original ADAS, first implemented in 1983 to gather real-time data from key piezometers, inclinometers, extensometers, seismometers, and flow meters (Tatchell 1991), was no longer state of the art and was replaced, beginning in 1991, by advanced telemetry, including hardware and software components (Imrie et al. 1992).

7.2 Cromwell Gorge Landslides, Clyde Dam Project, New Zealand

An extensive network of instruments has been installed to monitor 13 large landslides in Cromwell Gorge of the Clutha River, central Otago, New Zealand (Gillon et al. 1992; Proffitt et al. 1992). The landslides, shown on the map in Figure 11-22, border Lake Dunstan, the reservoir formed by the Clyde Dam, a 100-m-high concrete gravity dam owned by the Electricity Corporation of New Zealand (Gillon and Hancox 1992). Approximately 25 percent of the shoreline of Lake Dunstan is bordered by extensive, deep-seated landslides formed mainly in schist bedrock, schist debris, and colluvium. The total area of landsliding along the shores of the lake is about 20 km^2, and the landslides are composed of about 1.6 km^3 of material.

By mid-1991, more than 2,000 individual points were monitored on or adjacent to these landslides, with the expectation that this monitoring would increase to more than 3,500 points by the completion of lake filling in mid-1992 (Table 11-2). The instruments are distributed over all the landslides along an 18-km stretch of the Clutha River and in more than 16 km of tunnels (Gillon et al. 1992). The elements being measured are deformation, water pressure, water flow rate, and weather. In general, the monitoring techniques are conventional. The challenge is in obtaining data from the great number of monitoring points spread over a large area in steep terrain.

7.2.1 Deformation Measurement

The main deformation-detection instruments being used at Cromwell Gorge are (Gillon et al. 1992)

- Inclinometers for detecting the location and magnitude of small lateral movements;
- Geodetic deformation survey networks for determining the areal extent and magnitude of larger, longer-term movements; and
- Multipoint borehole extensometers installed from tunnels across specific geologic features, such as landslide failure surfaces.

Lower-accuracy techniques include installation of rod extensometers along tunnel walls and across surface scarps and surveying between points in

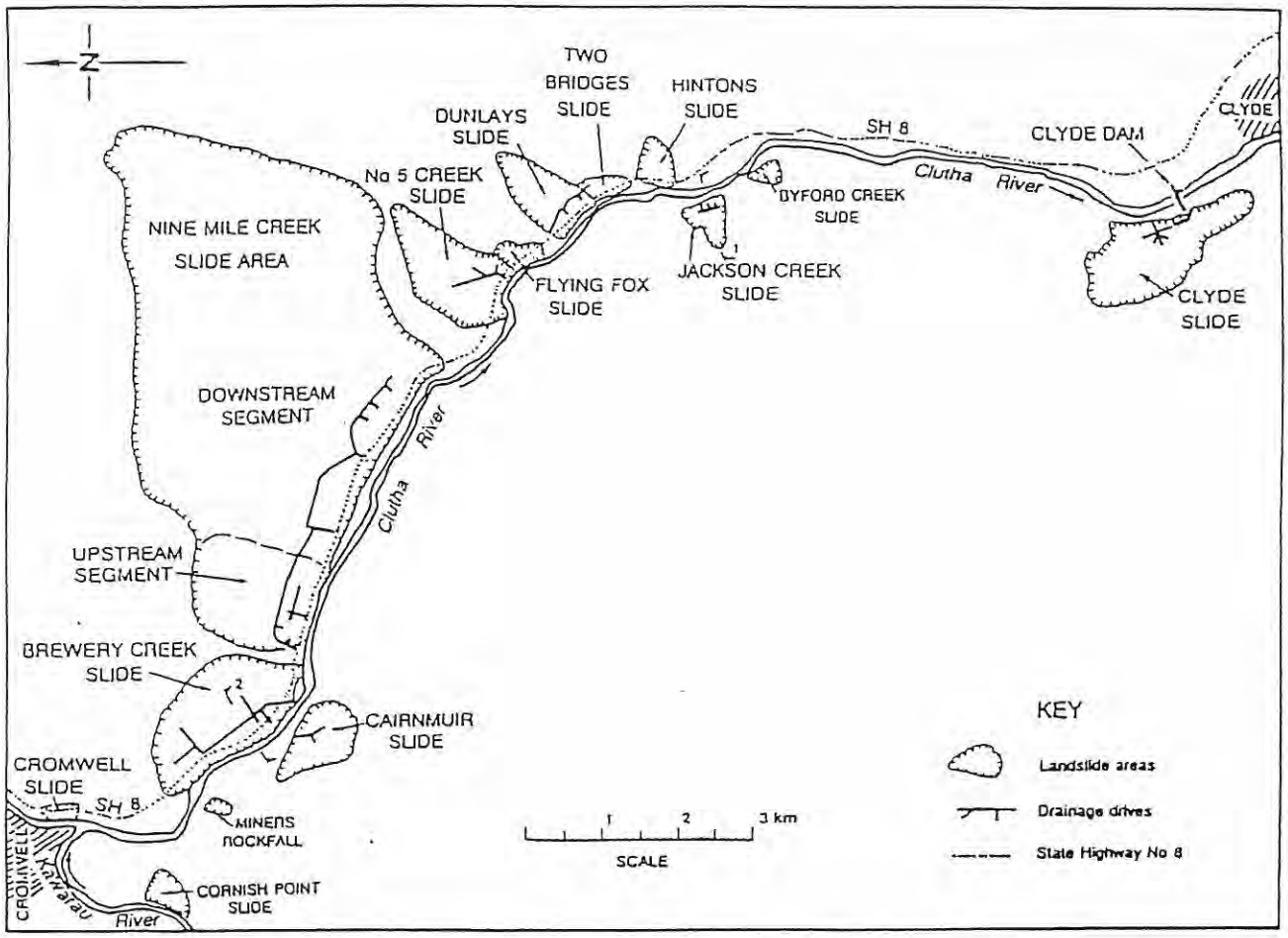

FIGURE 11-22
Map of Cromwell Gorge landslide area, New Zealand, showing locations and extent of drainage adits (modified from Gillon and Hancox 1992).

REPRINTED FROM D.H. BELL (ED.), LANDSLIDES/ GLISSEMENTS DE TERRAIN, *PROCEEDINGS OF THE SIXTH INTERNATIONAL SYMPOSIUM*, CHRISTCHURCH, 10–14 FEBRUARY, 1992, VOLUME 1, 1992–1994, 1800 PP., 3 VOLS., A.A. BALKEMA, OLD POST ROAD, BROOKFIELD, VERMONT 05036

tunnels with EDM equipment. The satellite-based GPS was used on a trial basis on one landslide with relative accuracies similar to those of conventional survey methods.

7.2.1.1 Inclinometers

By mid-1991 there were 180 inclinometer installations. About 150 of these, with an average depth of 90 m and a maximum depth of 300 m, were being regularly monitored (Gillon et al. 1992). During filling of the Lake Dunstan reservoir, inclinometers were monitored twice weekly or weekly at sites showing unusual activity or where construction work could cause instability.

Early in the investigation phase, drilling problems and the practice of combining piezometers with inclinometers caused several poor installations. In general, combining standpipe piezometers with inclinometers tends to create a zone of poor bond at each piezometer sand filter, which may reduce data quality for the inclinometer. However, a recent development has been the use of a Westbay packer, casing components, and pumping port at the bottom of a 70-mm casing to provide an efficient and accurate inclinometer-piezometer. The packer provides a good base bond, and the hole was deliberately drilled deeper to ensure that the piezometer filter avoids any zone of deformation.

7.2.1.2 Multipoint Borehole Extensometers

Before the filling of the Lake Dunstan reservoir, approximately 35 multipoint borehole extensometers were installed from tunnels to intersect basal slide surfaces. Designed and manufactured in house, the extensometers use four untensioned, fully grouted fiberglass rods up to 50 m long. Readings are obtained either manually with a dial gauge or electronically using linear potentiometers linked to a datalogger. These extensometers are accurate to 0.1 mm.

7.2.1.3 Surface Extensometers

Two types of extensometers for measuring surface deformation have been installed across head scarps

Table 11-2
Instruments and Monitoring Points on Cromwell Gorge Landslides (modified from Gillon et al. 1992)

Instruments and Points	July 1991	Future
Standpipe piezometers	760	800
Westbay multipoint piezometer ports	260	400
Inclinometers	180	200
Multipoint borehole extensometers	20	140
Drive leveling points	30	300
Surface monuments	250	280
Surface leveling points	250	350
Drainage flow meters	350	1,000
Weather and miscellaneous monitoring devices	120	120
Total	2,220	3,590

and other surface expressions of slide movement (Gillon et al. 1992). For small movements, rod extensometers were buried in special casings at a depth of 1 m. The rod material is a carbon-fiber composite with a near-zero coefficient of thermal expansion.

For measurement of larger surface movements, a wire extensometer was developed. The 6-mm wire, mounted on 2-m pylons to prevent animal damage, consists of a kevlar core protected against ultraviolet light by a nylon sleeve. The wire runs across an instrumented pulley and is tensioned by weights.

7.2.2 Groundwater-Level Instrumentation

7.2.2.1 Standpipe Piezometers

Standpipe piezometers are the most common instrument on the Clyde Project (Gillon et al. 1992). As of mid-1991 there were 760 standpipe piezometers in about 360 boreholes. Typically, they were installed in cored 96-mm (HQ) diameter boreholes at depths of 100 to 300 m. Multiple standpipe piezometers, normally two or three but sometimes up to five, were installed in each borehole. Most standpipe piezometers are monitored manually at frequencies ranging from daily to quarterly, with weekly being typical.

7.2.2.2 Westbay Multipoint Piezometers

By mid-1991 Westbay multipoint piezometers had been installed in 13 holes, with more installations planned (Gillon et al. 1992). Placement of these instruments began about midway through construction as part of the move to improve data quality and quantity. They have been restricted to critical locations to provide data where complex groundwater conditions exist on high-hazard landslides and to confirm the response of landslides to drainage works.

7.2.3 Drainage Flows

As of mid-1991, drainage flows were measured at about 350 locations, principally at individual drain holes. Ultrasonic pipe-flow meters linked to dataloggers are used when a continuous record is required from individual drain holes.

7.2.4 Data Processing

The use of several software packages, including regional data bases, has facilitated the storage, selective retrieval, filtering, manipulation, quantitative assessment, and analysis of a large and rapidly accruing data base from the Clyde Project landslide instrumentation. The following software packages are being utilized (Proffitt et al. 1992):

- TECHBASE, a relational data base and modeling software package for storage, management, manipulation, statistical evaluation, and output of engineering, scientific, and topographic data;
- TIDEDA, a data base for storing, manipulating, and plotting time-dependent data, including water levels, flows, weather, and surveying information; and
- GTILT, a data-base system used for analysis and plotting of inclinometer surveys. Several types of deflection plots are available in GTILT; however, on the Clyde project graphical output has generally been restricted to cumulative deflection and time-series plots (Figure 11-23).

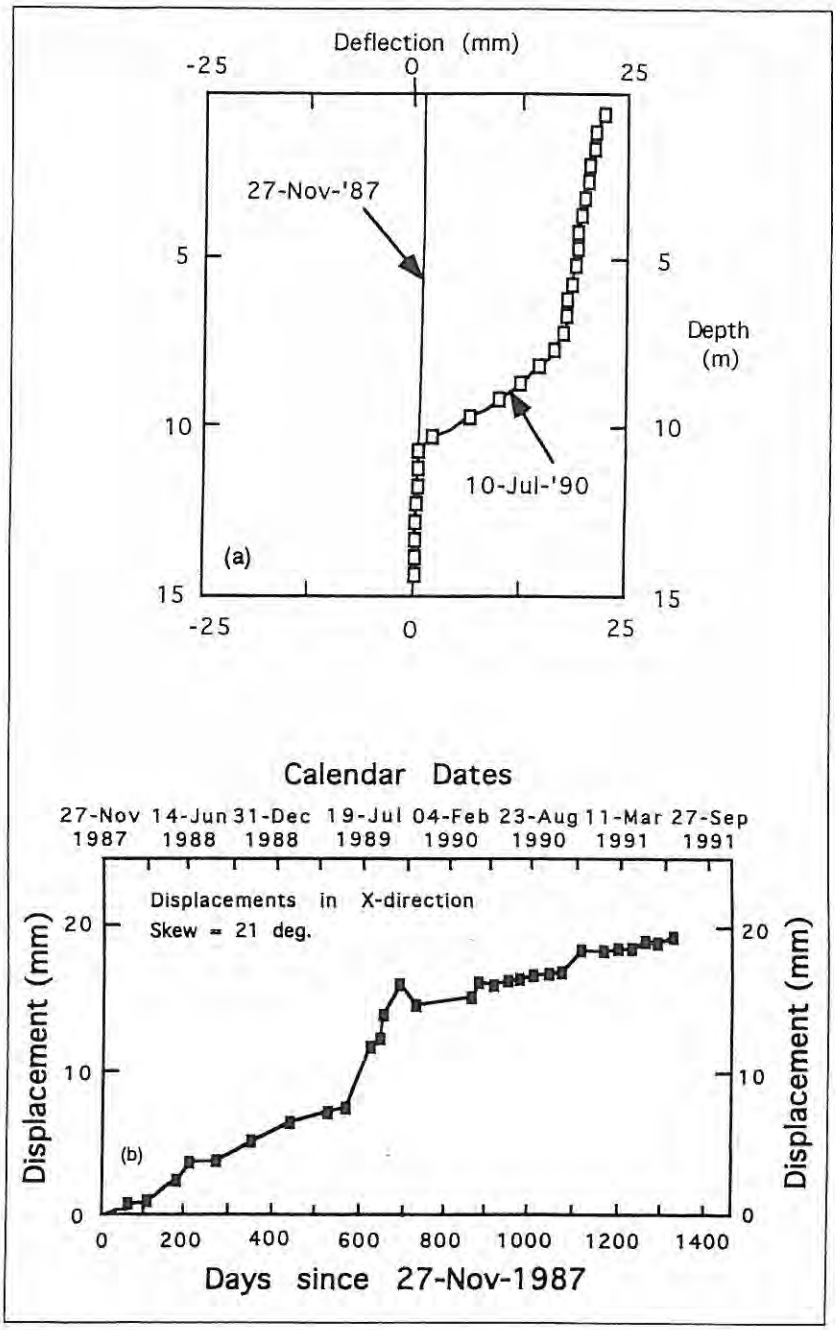

7.3 Arizona Inn Landslide, Oregon

The Arizona Inn landslide (Figure 11-24) on US-101 in the Klamath Mountains of southwestern Oregon has a history of persistent creep and recurring major movements since highway construction in the 1930s. The landslide mass consists primarily of fine-grained, intensely sheared, mylonitized sandstone and mudstone. The landslide area receives an average of 1900 to 2000 mm of rainfall per year. Episodes of major movement correlate with critical rainfall events, each of which generally includes a period of prolonged and high-intensity rainfall of at least 24 hr duration. Catastrophic failure of the 215-m-wide by 580-m-long mass occurred most recently on March 23, 1993, and resulted in closure of US-101 for approximately 2 weeks (Squier Associates, Inc. 1994).

Evaluation of the geologic setting, depth to the failure surface, and high groundwater pressures led to the conclusion that only drainage alternatives would provide cost-effective, long-term stabilization of the landslide. Geotechnical exploration focused on the following key issues (Squier Associates, Inc. 1994):

- Further definition of the artesian zone;
- Measurement of piezometric pressures in the landslide mass, the artesian zone, and the underlying bedrock;
- Relationship of the unconfined water levels to the confined aquifer;
- Relationship of piezometric pressures to precipitation;
- Permeability and variability in the landslide mass and in bedrock;
- Source of artesian pressures; and
- Quantity of groundwater.

Evaluation of these issues has been assisted by drilling of additional exploratory borings and installation of multiple vibrating-wire piezometers in the boreholes, continuous monitoring and evaluation of piezometric pressures and rainfall, and stressing the groundwater system using newly installed wells and pump tests.

The landslide is now being monitored by an instrumentation system incorporating automated monitoring and recording of a number of instruments. Continuous monitoring of one inclinometer, piezometric pressures, and rainfall is being accomplished by an ADAS that allows monitoring of 26 piezometers simultaneously. The locations of borings, test wells, and instrument sites are shown in Figure 11-24.

Six inclinometers were installed by the Oregon Department of Transportation (ODOT) during March through May 1993. Then during early April 1994, ODOT installed (*a*) vibrating-wire transducers in eight open standpipe piezometers, (*b*) a continuous-reading slope inclinometer in one hole,

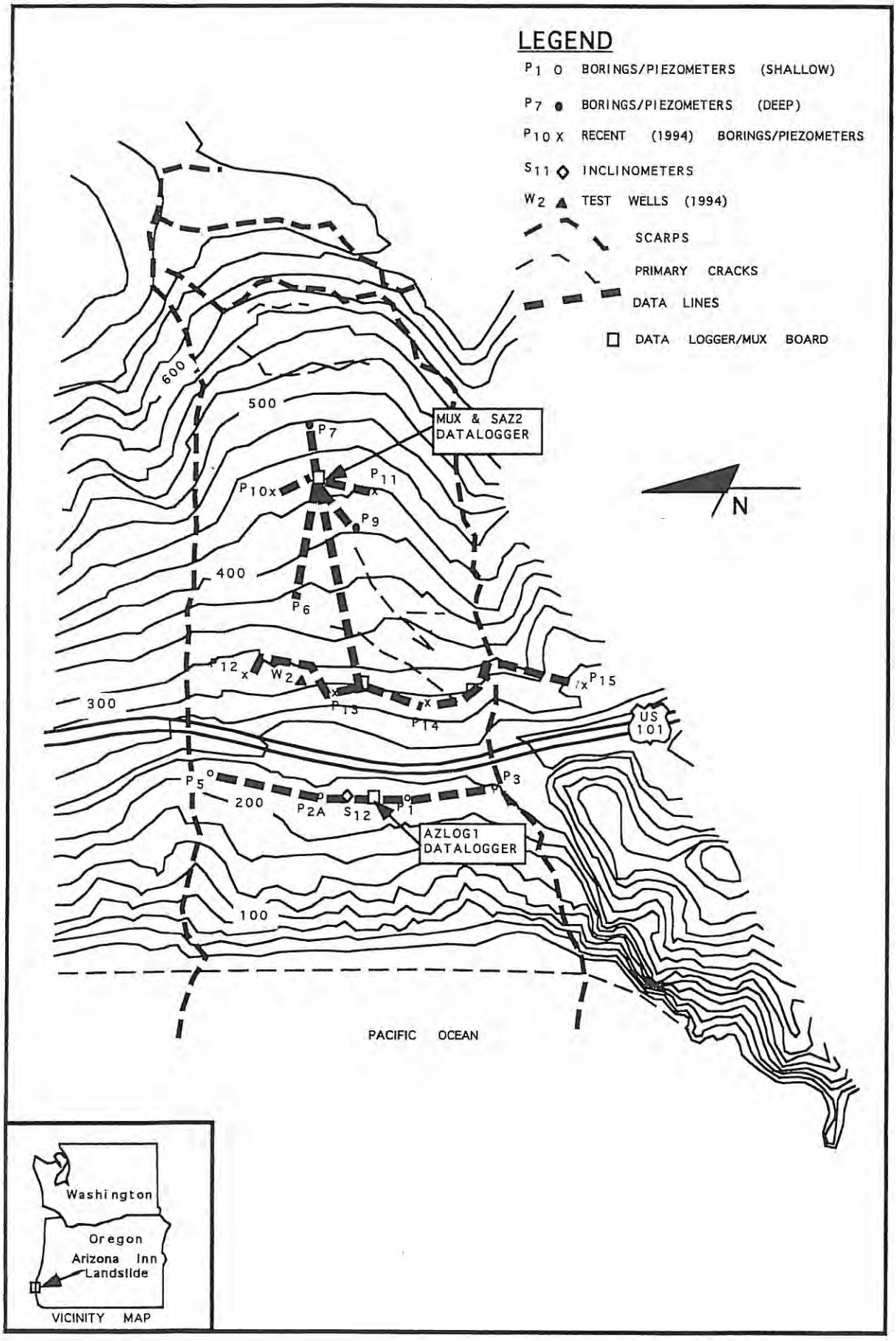

FIGURE 11-23
(opposite page)
Landslide in Cromwell Gorge: (*a*) cumulative deflection in Direction A for Inclinometer RD-6 between November 27, 1987, and July 10, 1990 (July 1990 data include corrections for zero shift and rotations) and (*b*) time-series plot (Proffitt et al. 1992).

FIGURE 11-24
Locations of borings, test wells, and instrument sites on Arizona Inn landslide, Oregon (Squier Associates, Inc. 1994).

and (*c*) an on-site tipping-bucket rain gauge. All of these instruments were connected to the ADAS using two dataloggers. The continuous monitoring system was programmed and placed in operation on April 10, 1994.

Subsequently, 16 vibrating-wire piezometers were connected to a datalogger after the addition of two multiplexing boards. Another datalogger records hourly data for four piezometers and a continuous-reading inclinometer. New software was added; it has three primary routines that monitor and record data from 20 piezometers and from rain gauges as well as system information. The routine includes (Squier Associates, Inc. 1994) daily maximum and minimum piezometric head values, complete hourly data recording of all instruments, and user-selectable reading frequencies during special test periods. Summary plots have been produced for the inclinometers, piezometers, and rain gauges. Zones of shear showed rates of movement of about 2.5 to 7.5 cm/year, with an average rate of about 4 cm/year. Figure 11-25 is a time plot of piezometric readings for the upper part of the landslide.

7.4 Last Chance Grade Landslide, California

The Last Chance Grade landslide, located along US-101 in far northwestern California, is approximately 520 m wide and 460 m long. The landslide, underlain by interbedded shale, sandstone, and conglomerate, is very active; at the road elevation, it moves on the order of 1.5 to 3.0 m/year and affects approximately 235 m of the roadway. Investigation of the Last Chance Grade landslide by the California Department of Transportation (Caltrans) included drilling, borehole logging, geologic mapping, and developing recommendations for stabilizing the highway (Kane and Beck 1994).

Three alternatives are being considered for highway stabilization. The first is to realign the

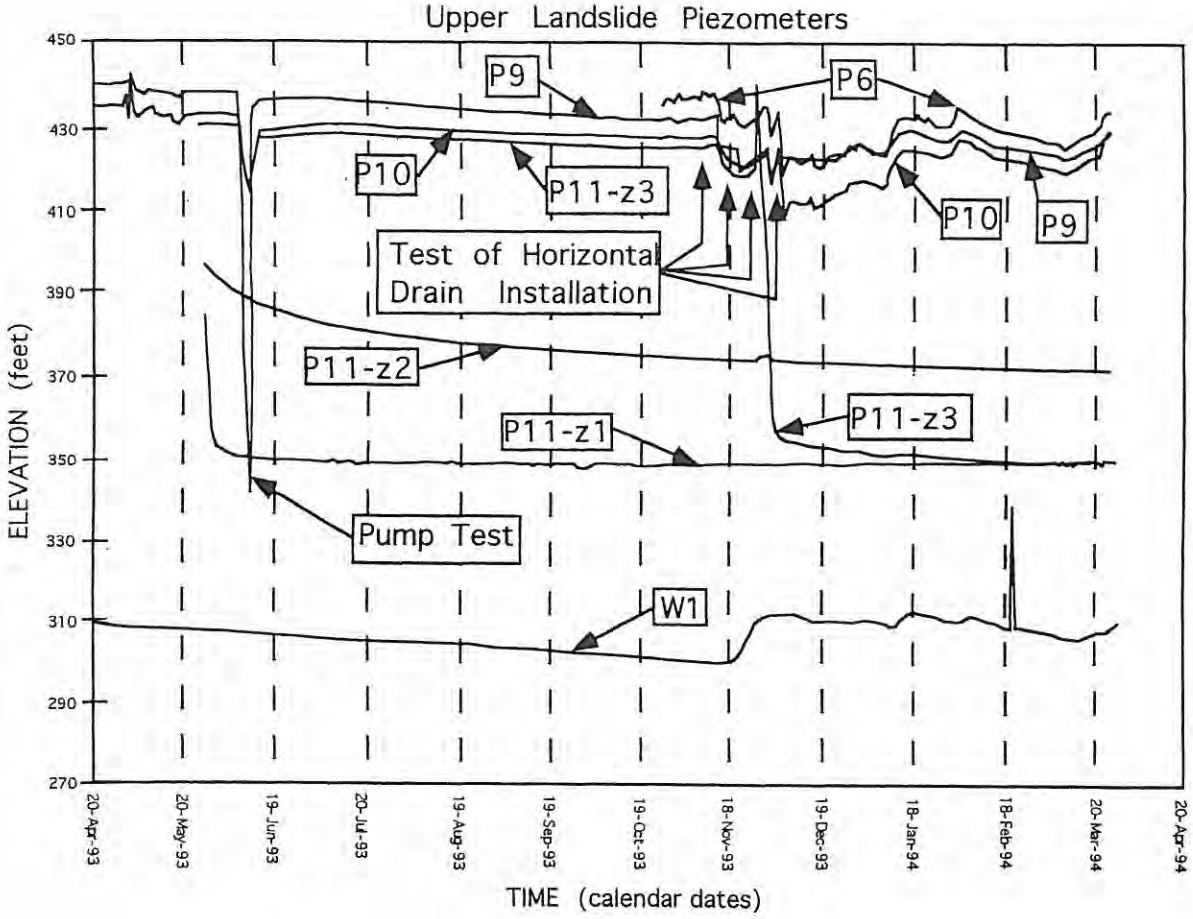

FIGURE 11-25
Time plot of piezometric readings for upper part of Arizona Inn landslide, Oregon; symbols indicate individual piezometers (modified from Squier Associates, Inc. 1994).

roadway in a tunnel excavated behind the sliding surface. The second alternative is to realign the roadway slightly and stabilize the landslide material below the roadway with a soldier-pile and tieback wall and the material above the roadway with several rows of slope reinforcement. The third choice is to realign the highway in a cut excavated behind the sliding surface. Preconstruction determination of the location of the sliding surface will be essential in selecting one of these measures.

Caltrans commonly uses inclinometers to measure landslide movement. The primary disadvantage of the ordinary inclinometer system is the necessity of visiting the site for each set of instrument readings. Because the Last Chance Grade landslide is located far from any Caltrans geotechnical engineering facilities, an alternative method was sought that could be used for denoting zones of landslide movement without actually having to visit the site. For this purpose, as part of the field investigation, while inclinometer casings were installed in two boreholes on the landslide, a coaxial cable was fixed to the outside of one of the casings to allow comparison of time domain reflectometry (TDR) data with standard inclinometer results (Kane and Beck 1994).

TDR is a technique that uses characteristics of returned electrical pulses to determine the amount of strain, or the existence of a rupture, in a coaxial cable. Although developed for cable testing, TDR is finding use in geotechnical applications, especially mining (O'Connor and Wade 1994). Most commonly, a cable tester connected to a coaxial cable installed in a borehole emits a stepped voltage impulse (Figure 11-26). As rock-mass movements deform the cable, its capacitance is changed, and this causes changes in the reflected waveform of the voltage pulse. The time delay between a transmitted pulse and the reflection from a cable deformity determines the damage location (Dowding et al. 1989).

Different wave reflections are received for different cable deformations. The length and amplitude of the reflection indicate the severity of damage. A cable in shear reflects a voltage spike that increases in magnitude in direct proportion to the amount of shear deformation. A distinct spike occurs just before failure. After failure, a permanent reflection is recorded. If the cable is in tension, the wave reflection is a subtle, troughlike voltage signal that increases in length as the cable is deformed. At tension failure, a small necking trough is visible in the TDR signal, which is distinguishable from a shear-failure reflection (Dowding et al. 1989). The cable tester can be connected to a datalogger, which records and stores reflections. The datalogger controls the cable tester and supplies power during measurements. The data can be collected automatically from a remote location using a computer with a telemetering system (Dowding and Huang 1994).

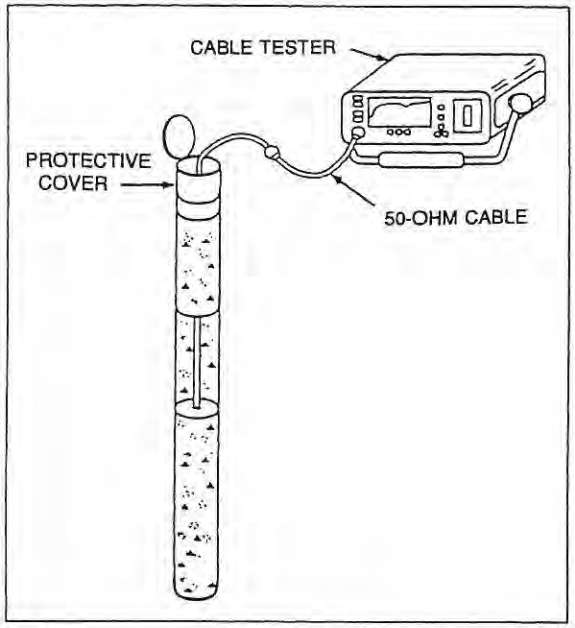

FIGURE 11-26
Diagrammatic sketch of TDR cable installed in borehole (Dowding and Huang 1994)
REPRINTED WITH PERMISSION OF AMERICAN SOCIETY OF CIVIL ENGINEERS

At the Last Chance Grade landslide, an 82-m-long coaxial cable (type RG 59, commonly used for videocassette recording) was attached to the outer, upslope side of an inclinometer casing by means of nylon ties spaced every 1.5 m. Because the inclinometer hole was positioned on the actively traveled roadway of US-101, the cable was continued beyond the highway shoulder in a shallow groove in the bituminous pavement, thus allowing TDR readings to be obtained without interference by traffic. To further explore the possibility of remotely collecting the data and monitoring the landslide, the TDR system was connected to a datalogger operated by a telemetry system that could be activated using a cellular telephone connection. With this arrangement, the TDR data could be directly loaded into a Caltrans computer located in Sacramento, more than 500 km away, and no one would have to visit the landslide site.

At 148 days after installation, the reflection signature for the TDR cable indicated two notable

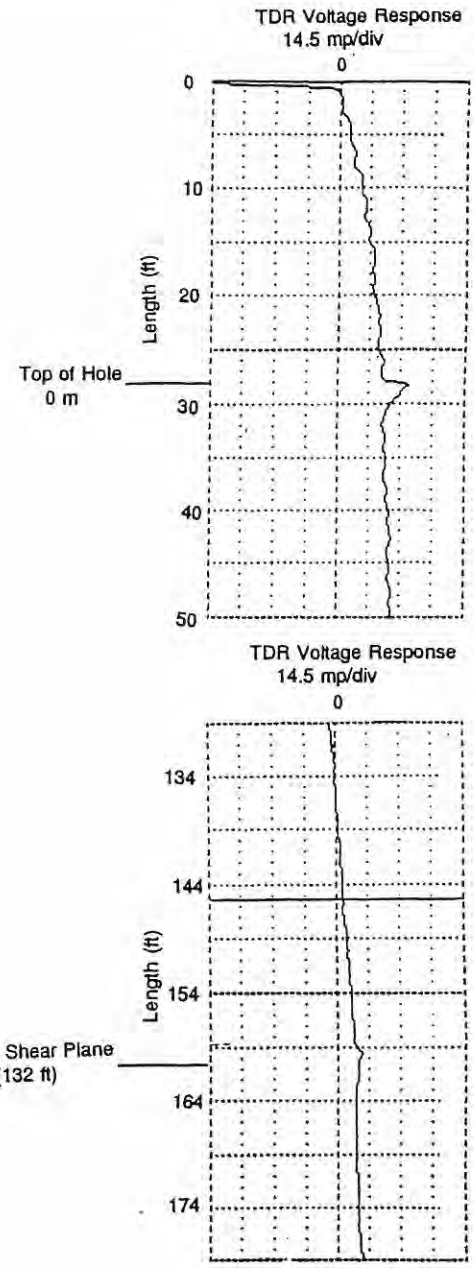

FIGURE 11-27
TDR output for borehole on Last Chance Grade landslide, California; note spikes where cable enters inclinometer hole and in vicinity of surface of sliding (modified from Kane and Beck 1994).

spikes (Figure 11-27). The upper spike, for a depth of 8.6 m, indicated a crimp in the cable where it was squeezed against the lip of the casing. At a depth of approximately 40 m, roughly the same depth as the inclinometer deflections, a trough was visible in the reflection signature, which was interpreted as indicating distress of the cable at the sliding surface (Kane and Beck 1994).

The results of this study indicate that in certain cases TDR may be used instead of, or in parallel with, inclinometers for monitoring landslide movement and that the technology exists to remotely access the TDR installation. The advantages of a remotely accessed system are as follows:

- There is no need to visit the site,
- Debris does not have to be cleaned from the inclinometer casing before TDR readings are taken,
- Cable is inexpensive and readily available, and
- The ability exists to monitor up to 512 holes with one cable tester and multiplexer hookup.

Remote data collection results in cost savings. It also means that hazardous areas can be closely monitored by frequent sampling to determine incipient movements. Another benefit of this technology is that it can be used as part of an early warning system to alert transportation officials of a possible catastrophic highway failure (Kane and Beck 1994).

7.5 Golden Bypass Landslide, Golden, Colorado

In the spring of 1991, during construction of a highway bypass around the city of Golden, Colorado, forming a part of Colorado State Highway 93, an initial minor landslide failure began in one wall of an excavation in Pierre shale (Highland and Brown 1993). Slow movement and enlargement of this earth flow continued until 1994, when the landslide was stabilized by means of a Brazilian-concept tieback panel wall, installation of horizontal drains, and removal of 75 000 m^3 of overburden near the landslide headwall (Ed Belknap, personal communication, 1995, Colorado Department of Transportation, Denver, Colorado).

Seven of the tieback anchor cables were equipped with load cells. In addition, five 12.5-mm-diameter piezometers with vibrating-wire transducers were installed to measure groundwater elevations at the landslide. Automated monitoring of the load cells and piezometers was desired, along with two-way, remote telemetry between the landslide and Colorado Department of Transportation (CDOT) headquarters in Denver, 30 km to the east. Neither power nor communication facilities were available at the site.

As a solution to the problem, an integrated monitoring and telemetry system was installed to remotely automate the load cell and piezometer measurements and provide direct, two-way radio

communication (Dennis E. Gunderson, personal communication, 1995, Geomation, Inc., Golden, Colorado). A network monitor station (NMS) was established at CDOT headquarters. The NMS, an IBM-compatible personal computer running GEONET software, provides the operator interface with the system for programming, alarm announcement and acknowledgment, real-time monitoring, supervisory control, and data logging. An RS-232 cable from a serial port in the NMS connects to a radio gateway unit, which is connected to a high-gain directional antenna mounted on a nearby signal tower. The gateway provides a link between the radio communication from the Golden landslide site and the NMS.

Three measurement and control units (MCUs), which are battery-powered, solar-recharged, and radio-linked, were installed at the landslide (Figure 11-28). MCU1, located at the top of the landslide, automatically monitors three piezometers. MCU2 and MCU3 are located near the bottom of the landslide and automatically monitor (*a*) two load cells and (*b*) five load cells and two piezometers, respectively. All monitoring and telemetry is user-programmable and is currently set at 66-hr intervals. MCU2 and MCU3, both equipped with standard whip antennas, communicate with the networked gateway unit through MCU1, which is equipped with a high-gain directional antenna.

Each MCU has its own microprocessor and is capable of multitasking functions, including

- Automated monitoring of any standard measurement signal (analog or digital);
- Time-and-date stamping of all measurements in the field at the point of capture;
- Conditioning and converting physical-parameter signals to desired engineering units;
- Peer-to-peer communication;
- Acting as a repeater and performing store-and-forward functions for other network nodes;
- Enacting direct or remote-control functions; and
- Accomplishing data reduction in the field, if desired.

The user, at any time without system disruption, can initiate system reconfiguration diagnostics and measurement verification and can enact remote control functions from the NMS.

8. PROBLEMS PREVENTING FURTHER DEVELOPMENT OF NEW INSTRUMENTATION TECHNOLOGY

Instrumentation and associated monitoring techniques have made significant advances during the past decade. The general proliferation of miniature electronics has revolutionized many aspects of data acquisition, processing, and communications, and has profoundly benefited both industry and the public. Personal computers have entered offices and homes, and people have come to expect the speed and convenience of information without delay. However, such progress in the geotechnical field, and in the transportation industry generally, has been less dramatic. Four main reasons govern the slow-paced and uneven gains in geotechnical monitoring relative to other data management technologies.

First, the geotechnical instrumentation industry is relatively small and highly specialized. Its practice and progress are easily influenced by economic conditions, levels of government spending, and existing procurement practices. In the United States, a highly competitive and shrinking heavy construction market has also shrunk the market for instrument suppliers.

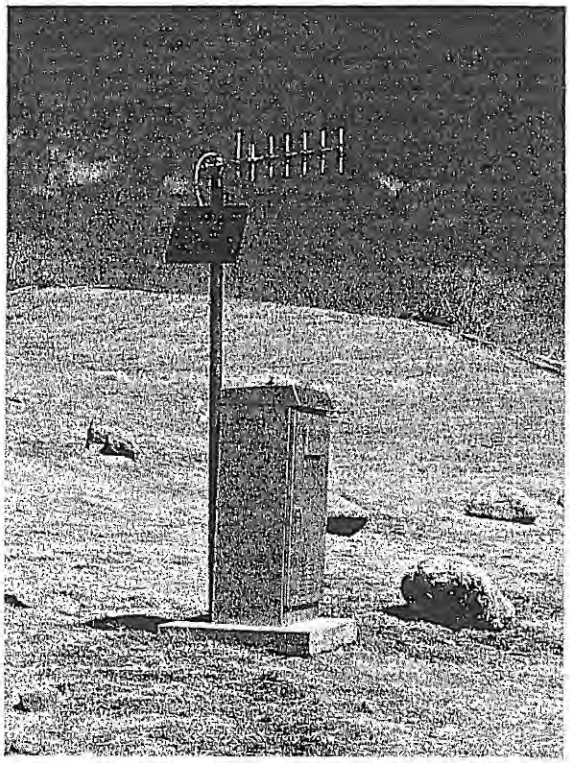

FIGURE 11-28
MCU and solar power supply attached to monitoring well at Golden Bypass landslide.
COURTESY OF GEOMATION, INC.

Second, as overall levels of support for research and development continue to dwindle, less funds are available for government-sponsored instrument development. Property owners concerned with the stabilization of a specific landslide can rarely justify supporting the development and testing of new instruments to further the state of the art of geotechnical knowledge.

Third, geotechnical engineers have frequently underestimated the costs and requirements of a field installation and operation of geotechnical instrumentation, leading to the failure of several monitoring programs. Past bad experiences engender mistrust and avoidance of further instrumentation by geotechnical engineers.

Last, because of current contracting practices and a highly litigious business environment, especially in the United States, designers of all types of transportation facilities have tended to abdicate their responsibilities for requesting and implementing instrument monitoring at landslides. These responsibilities have been allowed to devolve onto general contractors, who may or may not be particularly concerned about what information instruments can provide. Most general contractors are interested in project production efficiency, and instruments are often merely obstacles in the field that should be minimized. However, instruments allow the monitoring of project performance and safety. To place the contractor in charge of the primary source of such monitoring and safety information raises a potential conflict of interest. If instrumentation selection and operation are restored to the chief engineer and those at the project site, landslide instrumentation will more likely become part of broadly expected standard practice during landslide investigations.

REFERENCES

British Geotechnical Society. 1974. *Field Instrumentation in Geotechnical Engineering*. John Wiley & Sons, Inc., New York, 720 pp.

Burland, J.B., and J.F.A. Moore. 1974. The Measurement of Ground Displacement Around Deep Excavations. In *Field Instrumentation in Geotechnical Engineering*, John Wiley & Sons, Inc., New York, pp. 70–84.

Cording, E.J., A.J. Hendron, Jr., W.H. Hansmire, J.W. Mahar, H.H. MacPherson, R.A. Jones, and T.D. O'Rourke. 1975. *Methods for Geotechnical Observations and Instrumentation in Tunneling*. Department of Civil Engineering, University of Illinois, Urbana-Champaign; National Science Foundation, Vol. 2, pp. 293–566.

Dibiagio, E. 1974. Discussion: Session 2—Equipment. In *Field Instrumentation in Geotechnical Engineering*, John Wiley & Sons, Inc., New York, pp. 565–566.

Dowding, C.H., M.B. Su, and K. O'Connor. 1989. Measurement of Rock Mass Deformation with Grouted Coaxial Cables. *Rock Mechanics and Engineering*, Vol. 22, pp. 1–23.

Dowding, C.H., and F.C. Huang. 1994. Early Detection of Rock Movement with Time Domain Reflectometry. *Journal of Geotechnical Engineering*, ASCE, Vol. 120, No. 8, pp. 1413–1427.

Dunnicliff, C.J. 1971. Equipment for Field Deformation Measurements. In *Proc., Fourth Pan-American Conference on Soil Mechanics and Foundation Engineering*, San Juan, American Society of Civil Engineers, New York, Vol. 2, pp. 319–332.

Dunnicliff, C.J. 1988. *Geotechnical Instrumentation for Monitoring Field Performance*. John Wiley & Sons, Inc., New York, 577 pp.

Dunnicliff, C.J., and D. Davidson. 1991. Lessons Learned from Automating Instrumentation at Some U.S. Dams. *Geotechnical News*, Vol. 9, No. 2, pp. 46–51.

Durr, D.L. 1974. An Embankment Saved by Instrumentation. In *Transportation Research Record 482*, TRB, National Research Council, Washington, D.C., pp. 43–50.

Dutro, H.B., and R.D. Dickinson. 1974. Slope Instrumentation Using Multiple-Position Borehole Extensometers. In *Transportation Research Record 482*, TRB, National Research Council, Washington, D.C., pp. 9–17.

Gilbert, C. 1994. Evaluating the Cost of GPS Data Collection. *Earth Observation Magazine*, Vol. 3, No. 7 (July), pp. 42–43.

Gilbert, C. 1995. How to Do Differential GPS Without Known Coordinates for Your Base Station. *Earth Observation Magazine*, Vol. 4, No. 4 (April), pp. 50–51.

Gillon, M.D., P.F. Foster, G.T. Proffitt, and A.P. Smits. 1992. Monitoring of the Cromwell Gorge Landslides. In *Proc., Sixth International Symposium on Landslides*, Christchurch, New Zealand, A.A. Balkema, Rotterdam, Netherlands, Vol. 2, pp. 1135–1140.

Gillon, M.D., and G.T. Hancox. 1992. Cromwell Gorge Landslides—A General Overview. In *Proc., Sixth International Symposium on Landslides*,

Christchurch, New Zealand, A.A. Balkema, Rotterdam, Netherlands, Vol. 1, pp. 83–102.

Gould, J.P., and C.J. Dunnicliff. 1971. Accuracy of Field Deformation Measurements. In *Proc., Fourth Pan-American Conference on Soil Mechanics and Foundation Engineering*, San Juan, American Society of Civil Engineers, New York, Vol. 1, pp. 313–366.

Green, G.E. 1974. Principles and Performance of Two Inclinometers for Measuring Horizontal Ground Movements. In *Field Instrumentation in Geotechnical Engineering*, John Wiley & Sons, Inc., New York, pp. 166–179.

Green, G.E., and P.E. Mikkelsen. 1988. Deformation Measurements with Inclinometers. In *Transportation Research Record 1169*, TRB, National Research Council, Washington, D.C., pp. 1–15.

Heinz, R.A. 1975. In Situ Soils Measuring Devices. *Civil Engineering*, Vol. 45, No. 10, pp. 62–65.

Highland, L.M., and W.M. Brown III. 1993. The Golden Bypass Landslide, Golden, Colorado. *Earthquakes & Volcanoes*, Vol. 24, No. 1, pp. 4–14.

Hinckley, A.L., B.D. Tanner, and E.C. Campbell. 1988. Automation of Monitoring of Geotechnical Instrumentation. In *Transportation Research Record 1169*, TRB, National Research Council, Washington, D.C., pp. 26–29.

Hvorslev, M.J. 1951. *Time Lag and Soil Permeability in Groundwater Observations*. Bulletin 36. U.S. Army Engineer Waterways Experiment Station, Vicksburg, Miss., 50 pp.

Imrie, A.S. 1983. Taming the Downie Slide. *Canadian Geographic*, Vol. 103, No. 3, pp. 47–51.

Imrie, A.S., and D.R. Bourne. 1981. Engineering Geology of the Mica and Revelstoke Dams. In *Field Guides to Geology and Mineral Deposits*, Geological Association of Canada, Calgary, pp. 393–401.

Imrie, A.S, D.P. Moore, and E.G. Energen. 1992. Performance and Maintenance of the Drainage System at Downie Slide. In *Proc., Sixth International Symposium on Landslides*, Christchurch, New Zealand, A.A. Balkema, Rotterdam, Netherlands, Vol. 1, pp. 751–757.

Kane, W.F., and T.J. Beck. 1994. Development of a Time Domain Reflectometry System to Monitor Landslide Activity. In *Proc., 45th Highway Geology Symposium*, Portland, Oreg., August 17–19, Geology Department, Portland State University, Oreg., pp. 163–173.

Kleusberg, A. 1992. Precise Differential Positioning and Surveying. *GPS World*, Vol. 3, No. 7 (July/August), pp. 50–52.

McKenna, G. 1995. Advances in Slope-Monitoring Instrumentation at Syncrude Canada Ltd.—A Followup. *Geotechnical News*, Vol. 13, No. 1, pp. 42–44.

McKenna, G., G. Livingstone, and T. Lord. 1994. Advances in Slope-Monitoring Instrumentation at Syncrude Canada Ltd. *Geotechnical News*, Vol. 12, No. 3, pp. 66–69.

Mikkelsen, P.E. 1989. Geotechnical Monitoring During Construction of Two Highway Embankments on Soft Ground in Tacoma. In *Engineering Geology of Washington* (R.W. Galster, ed.), Bulletin 78, Washington Division of Geology and Earth Resources, Olympia, Vol. 2, pp. 819–829.

Mikkelsen, P.E. 1992. Instrument Innovations for Monitoring Natural Hazards. *Geotechnical News*, Vol. 10, No. 1, pp. 46–49.

Mikkelsen, P.E., and L.K. Bestwick. 1976. Instrumentation and Performance: Urban Arterial Embankments on Soft Foundation Soil. In *Proc., 14th Annual Symposium on Engineering Geology and Soils Engineering*, Boise, Idaho, Idaho Department of Transportation, Boise, pp. 1–18.

Moore, D.P. 1989. Stabilization of Downie Slide and Dutchman's Ridge. In *Proc., 12th International Conference on Soil Mechanics and Foundation Engineering*, Rio de Janeiro, A.A. Balkema, Rotterdam, Netherlands, Vol. 5, pp. 3063–3065.

Muñoz, A., Jr., and D. Gano. 1974. The Role of Field Instrumentation in Correction of the Fountain Slide. In *Transportation Research Record 482*, TRB, National Research Council, Washington, D.C., pp. 1–8.

O'Connor, K.M., and L.V. Wade. 1994. Applications of Time Domain Reflectometry in the Mining Industry. In *Proc., Symposium and Workshop on Time Domain Reflectometry in Environmental, Infrastructure, and Mining Applications*, Evanston, Ill., Sept., Special Publication 19-94, Bureau of Mines, U.S. Department of the Interior, pp. 494–506.

Palladino, D.J., and R.B. Peck. 1972. Slope Failures in an Overconsolidated Clay, Seattle, Washington. *Geotechnique*, Vol. 22, No. 4, pp. 563–595.

Patton, F.D. 1979. Groundwater Instrumentation for Mining Projects. In *Mine Drainage: Proc., First International Mine Drainage Symposium*, Denver, Colo., Miller Freeman Publications Inc., San Francisco, May, Chap. 5, pp. 123–153.

Patton, F.D. 1983. The Role of Instrumentation in the Analysis of the Stability of Rock Slopes. In *Proc., International Symposium on Field Measurements in Geomechanics*, Zurich, Sept. 5–8, pp. 719–748.

Patton, F.D. 1984. Climate, Groundwater Pressures and Stability Analyses of Landslides. In *Proc., Fourth International Symposium on Landslides*, Canadian Geotechnical Society, Toronto, Vol. 3, pp. 43–60.

Patton, F.D., W.H. Beck, and D. Larssen. 1991. A Modular Subsurface Data Acquisition System (MOSDAX) for Real-time Multi-level Groundwater Monitoring. In *Field Measurements in Geotechnics: Proc., Third International Symposium on Field Measurements in Geomechanics* (G. Sørum, ed.), Oslo, Norway, Sept. 9–11, A.A. Balkema, Rotterdam, Netherlands, Vol. 1, pp. 339–348.

Peck, R.B. 1972. Observation and Instrumentation: Some Elementary Considerations. *Highway Focus*, Vol. 4, No. 2, pp. 1–5.

Penman, A.D.M. 1961. A Study of the Response Time of Various Types of Piezometer. In *Pore Pressure and Suction in Soils*, Butterworths, London, pp. 53–58.

Penman, A.D.M., and J.A. Charles. 1974. Measuring Movements of Embankment Dams. In *Field Instrumentation in Geotechnical Engineering*, John Wiley & Sons, Inc., New York, pp. 341–358.

Piteau, D.R., F.H. Mylrea, and I.G. Blown. 1978. Downie Slide, Columbia River, British Columbia, Canada. In *Rockslides and Avalanches* (Barry Voight, ed.), Elsevier Scientific Publishing Company, New York, Vol. 1, pp. 365–392.

Proffitt, G.T., G.J. Fairless, G.G. Grocott, and P.A. Manning. 1992. Computer Applications for Landslide Studies. In *Proc., Sixth International Symposium on Landslides*, Christchurch, New Zealand, A.A. Balkema, Rotterdam, Netherlands, Vol. 2, pp. 1157–1162.

Shannon, W.L., S.D. Wilson, and R.H. Meese. 1962. Field Problems: Field Measurements. In *Foundation Engineering* (G.A. Leonards, ed.), McGraw-Hill, New York, pp. 102–1080.

Smith, T.W., and R.A. Forsyth. 1971. Potrero Hill Slide and Correction. *Journal of the Soil Mechanics and Foundations Division*, ASCE, Vol. 97, No. SM3, pp. 541–564.

Squier Associates, Inc. 1994. *Phase 1—Arizona Inn Landslide Geotechnical Investigation, Curry, County, Oregon*. Geotechnical Services Unit, Oregon Department of Transportation, Salem, 209 pp.

Tatchell, G.E. 1991. Automatic Data Acquisition Systems for Monitoring Dams and Landslides. In *Field Measurements in Geotechnics: Proc., Third International Symposium on Field Measurements in Geomechanics* (G. Sørum, ed.), Oslo, Norway, Sept. 9–11, A.A. Balkema, Rotterdam, Netherlands, Vol. 1, pp. 349–360.

Tice, J.A., and C.E. Sams. 1974. Experiences with Landslide Instrumentation in the Southeast. In *Transportation Research Record 482*, TRB, National Research Council, Washington, D.C., pp. 18–29.

Transportation Research Board. 1974. *Landslide Instrumentation: Transportation Research Record 482*, TRB, National Research Council, Washington, D.C., 51 pp.

Vaughn, P.R. 1969. A Note on Sealing Piezometers in Boreholes. *Geotechnique*, Vol. 19, No. 3, pp. 405–413.

Vaughan, P.R. 1974. The Measurement of Pore Pressures with Piezometer. In *Field Instrumentation in Geotechnical Engineering*, John Wiley & Sons, Inc., New York, pp. 411–422.

Wilson, S.D. 1967. Investigation of Embankment Performance. *Journal of the Soil Mechanics and Foundations Division*, ASCE, Vol. 93, No. SM4, pp. 135–156.

Wilson, S.D. 1970. Observational Data on Ground Movements Related to Slope Instability. *Journal of the Soil Mechanics and Foundations Division*, ASCE, Vol. 96, No. SM5, pp. 1521–1544.

Wilson, S.D. 1974. Landslide Instrumentation of the Minneapolis Freeway. In *Transportation Research Record 482*, TRB, National Research Council, Washington, D.C., pp. 30–42.

Wilson, S.D., and D.E. Hilts. 1971. Application of Instrumentation to Highway Stability Problems. In *Proc., Joint ASCE-ASME National Transportation Engineering Meeting*, Seattle, American Society of Civil Engineers, New York, and American Society of Mechanical Engineers, New York.

Wilson, S.D., and P.E. Mikkelsen. 1977. *Foundation Instrumentation—Inclinometers* (reference manual for 45-min videotape). FHWA, U.S. Department of Transportation.

Wilson, S.D., and P.E. Mikkelsen. 1978. *Field Instrumentation*. In *Special Report 176: Landslides: Analysis and Control* (R.L. Schuster and R.J. Krizek, eds.), TRB, National Research Council, Washington, D.C., Chap. 5, pp. 112–138.

Landslides, Senneset (ed.) © 1996 Balkema, Rotterdam. ISBN 90 5410 818 5

Continuous monitoring of the slope above an excavation within a marginally stable landslide

Derek H. Cornforth & P. Erik Mikkelsen
Landslide Technology, Portland, Oreg., USA

ABSTRACT: A deep excavation for the Portland Zoo station activated shear movements along a pre-existing ancient slip plane below the excavation. A system of in-place inclinometers (placed across the discrete shear zone), vibrating-wire piezometers and an automatic rain gauge was continuously monitored during construction using a data logger. The system was accurate and reliable, and clearly showed the cause-effect relationships of multiple factors (natural and manmade) which could influence the observations. Thus, continuous monitoring provided superior performance to conventional periodic measurements of movements and piezometer levels.

1 INTRODUCTION

Landslides generally are monitored by readings of inclinometers and piezometers taken intermittently. Such measurements show the changes which have occurred during the time interval between readings, but cannot show precisely when the changes occurred. If more than one causative factor is present, the geotechnical practitioner is left to speculate on the relative importance of these causative factors.

Methods for automatically reading inclinometers and piezometers have been developed in recent years (Dunnicliff, 1988; Mikkelsen, 1992). Some early results have shown that comparatively large "spikes" of groundwater levels can occur in certain soils during storms (Prellwitz & Babbitt, 1984). Such transient rises in groundwater levels could be the triggering mechanism of landslide movements and should be included in stability modeling.

The ideal monitoring system for a landslide with a discrete shear zone in which shear movements are controlled by groundwater pressures would be:

- continuous monitoring of the shear zone
- continuous monitoring of the pore water pressure within the shear zone
- local rainfall data for the site

These monitoring devices are now available at a reasonable cost for use on medium to large landslides. This paper describes the installation of a complete monitoring system, and some results and conclusions which can be drawn from the results at a site in which multiple geotechnical factors were present.

2 PROJECT DESCRIPTION

The Portland, Oregon light rail project includes a 5 km tunnel passing through the basalt rock formations on the west side of the city. Near the mid-length of the tunnel, a station is being constructed to serve the Portland Zoo. At this location, the twin tunnels of the light rail system are more than 80 m below the ground surface, and access will occur through two 10 m diameter vertical elevator shafts (Fig. 1). The headhouse pits on the east and west sides of the station require average excavations of 12.3 m and 10.9 m, respectively, below original ground. The open excavations are being supported by soil nail walls, which are installed as excavation progresses. The perimeter of the station excavation has eight inclinometers which penetrate into bedrock (Fig. 1). The inclinometers generally were read twice weekly to monitor the ground movements around the excavation.

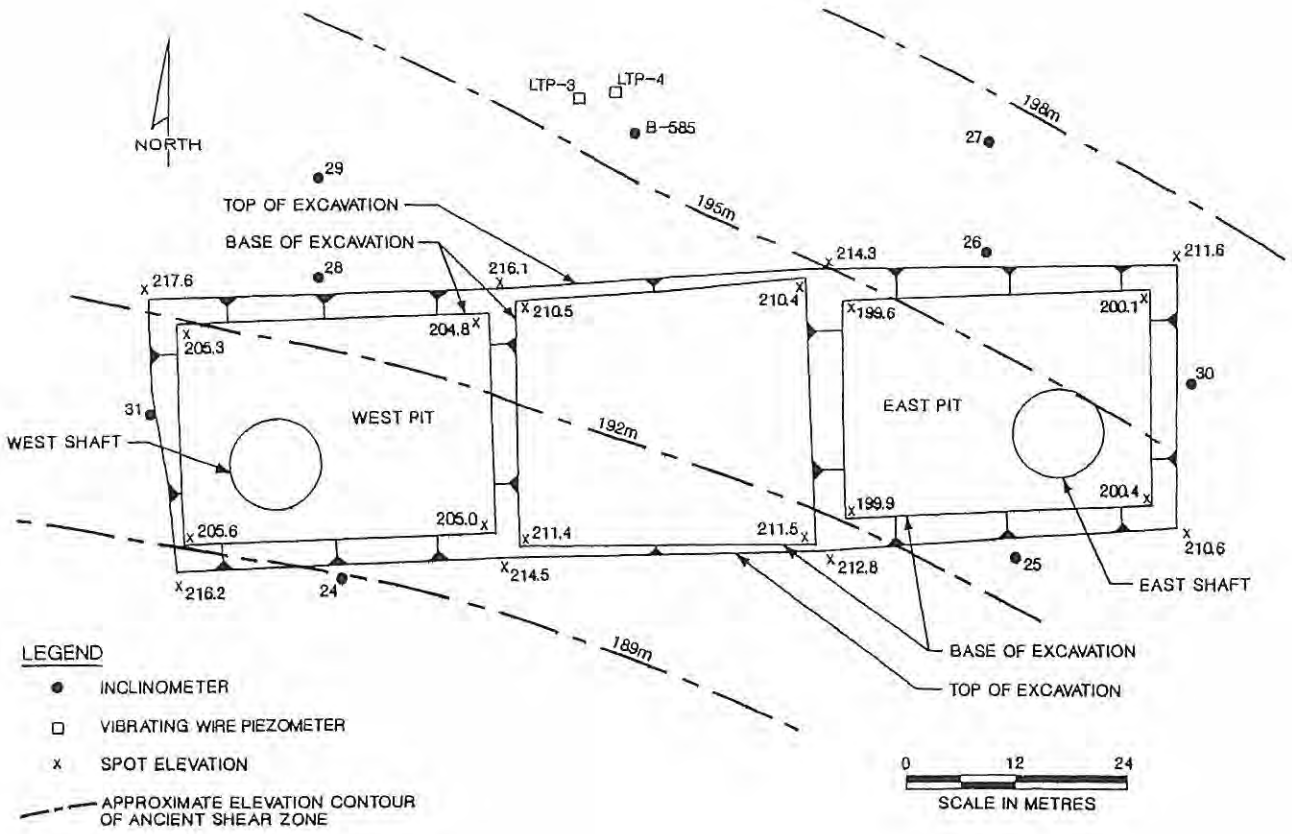

Figure 1. Site Plan at the Portland Zoo Station Excavation

Portland Zoo is located on a long, moderately sloping hillside which has been mapped as ancient landslide terrain. The lower part of the slope was involved in a major landslide when Canyon Road, an arterial road serving Portland, was widened around 1960. The upper part of the slope was generally considered to be stable, but inclinometers installed prior to the Portland Zoo station project showed movements averaging 2 mm over a two-year period. Therefore, the entire slope is marginally stable, and the affected area is about 300 m (on average) wide and has a slope of about 4½° to the horizontal. The Portland Zoo station is very close to the center of the marginally stable slope.

The ground conditions at the station site, from the surface down, comprise:

- Portland Hills silt, a glacial, sandy, slightly clayey silt, generally medium stiff;
- Sandy River Mudstone, a Pliocene stiff clayey silt;
- weathered basalt, grading from a stiff silt, sand and clay (SPT generally > 30) to more rocky relict structure near the bedrock surface; and
- basalt bedrock.

The Zoo station excavation began on January 3, 1995. On January 20, the first set of readings taken in the inclinometers on the north side of the excavation showed significant shear movements occurring along the ancient slip plane located 15 to 27 m below the surface. Extrapolation of the rates of movement indicate that shear movements began close to or coincidentally with the start of the excavation. In boring B-585, where an in-place continuous monitoring inclinometer was subsequently installed, the discrete shear zone of the ancient slip plane is at a depth of 20.7 m below the surface, at the top of weathered basalt bedrock (Fig. 2).

The approximate contours of the discrete shear zone are shown on Figure 1. The depth from the base of the station excavation to the shear zone is estimated to be only 3.7 m at the northeast corner of the east pit.

A back-analysis of the ancient landslide, based on data from numerous piezometers and inclinometers within the slope, provided residual strength parameters of $c_r' = 0$, $\phi_r' = 7.9°$. Several sets of triaxial tests performed on the overburden soils around the station site gave average peak shear strength properties of $c' = 32$ kPa, $\phi' = 33°$.

3 CONTINUOUS READOUT MONITORING

Two locations were selected for continuous readout monitoring: B-585, about 16 m upslope from the center of the excavation, and B-583, about 150 m downslope of the excavation. At each location:

- one shallow piezometer tip was set just below the depth where groundwater was first encountered in the boring;
- one deep piezometer tip was set near the discrete shear zone measured in the adjacent inclinometer casing; and
- one in-place electrolytic inclinometer was installed across the discrete shear zone of the ancient landslide.

In addition, a rainfall gauge was installed near B-585 to continuously monitor rainfall.

3.1 *In-Place Inclinometer*

The depth of the discrete shear zone had been obtained from small movements observed in the earlier two-year period of observations. To obtain a more precise position, inclinometer readings were taken at close intervals of 75 mm and the position of the upper wheel of the inclinometer was plotted. These measurements showed that the shear zone was less than 0.3 m thick and a gauge length of 0.6 m was selected for the in-place inclinometer.

The in-place inclinometer (IPI) supplied by Slope Indicator is a biaxial electrolytic tilt sensor with a nominal linear range of $\pm$ 10°, i.e. about $\pm$ 100 mm horizontal offset from vertical over the gauge length of 600 mm. An 8-conductor polyurethane cable has a waterproof seal at the sensor and runs to the data logger. The sensor is read in a full-bridge configuration using high frequency alternating current. Our measurements indicate a precision of $\pm$ 0.03 mm.

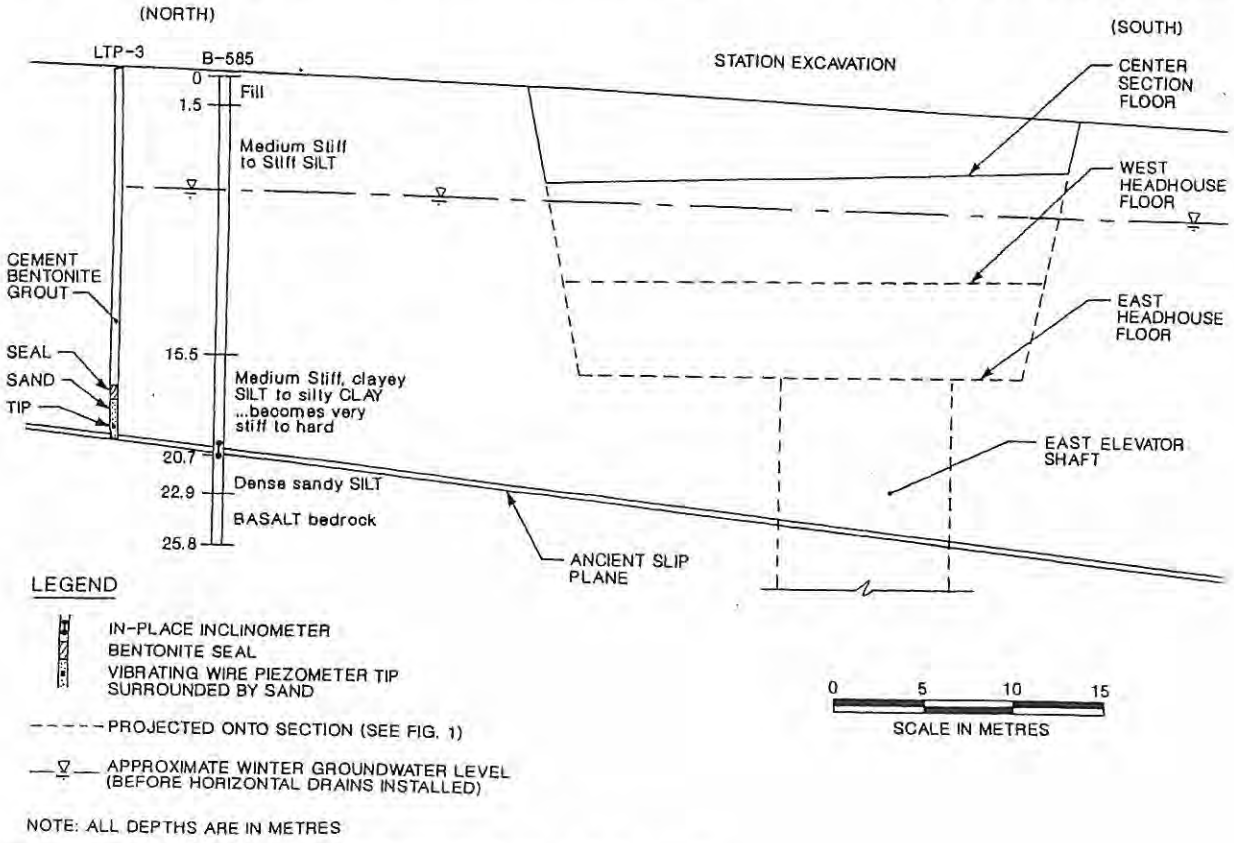

Figure 2. Cross-Section Taken through Center of Excavation

The IPI was installed within the pre-existing grooved inclinometer casing. One wheel was placed below the discrete shear zone and one wheel above it. The IPI has not been disturbed since installation.

3.2 *Piezometers*

The vibrating-wire piezometers were supplied by Geokon with an integral vinyl cable to connect with the data logger. The sensors were installed within a saturated sand backfill which extended to the discrete shear zone (Fig. 2). The sensor tips were located just above the shear zone to avoid damage from shear movements. About 600 mm depth of sand, sealed above by 600 mm of bentonite chips, were placed and saturated. the remainder of the holes were grouted with a weak cement-bentonite to the surface. Each piezometer was placed in a separate hole.

3.3 *Rain Gauge*

A tipping bucket type rain gauge from Texas Electronics was used to measure cumulative rainfall. The gauge was calibrated to tip for every 0.25 mm of precipitation, which is counted as one pulse by the data logger.

3.4 *Data Loggers*

The data loggers are Model CR10, supplied by Campbell Scientific. The cable wires are terminated at a panel on top of the hermetically-sealed, 12-channel data loggers.

An environmental enclosure houses the logger, a 12-volt battery pack and vibrating-wire interface. A 64k byte RAM is used for program and data storage and has 29,000 available data points of storage. Programming, logger communication and data retrieval was accomplished by a laptop PC using software supplied by Campbell. The data loggers were placed in steel cabinets bolted to concrete pads for protection against vandalism.

3.5 *Data Collection*

The project loggers took readings every ten minutes. After each hour, the data was averaged together with maximums and minimums. These were stored permanently in engineering units. Periodically (usually weekly) the data was retrieved using the menu-driven software into the laptop PC and put onto spreadsheets. The spreadsheets generated x-y plots of the data with time.

4 MONITORING DATA RESULTS

The continuous monitoring equipment was installed, and began collecting data on February 18, 1995. The equipment has performed flawlessly from that date to the present (September 1995). To provide examples of its use, the first eight weeks of data collection (February 18–April 15) is presented on Figure 3.

4.1 *Site Activities During Monitoring*

At the start of the data collection, the contractor was excavating from the east and west pits, having already excavated the center portion, which was partly backfilled with a gravel access ramp. On February 23, the owner stopped further excavation of the east pit, at a depth of about 6 m below the surface, because the excavation was getting close to the ancient slip plane on which shear movements were occurring. It was feared that any loss of strength in the overburden soils above the ancient slip plane could lead to a slope failure later in the year. (To prevent such an occurrence, shear piles were installed in October 1995, allowing the excavation to be completed to the design depth.)

The west shaft excavation continued to the full depth and was completed on March 23, 1995. Subsequently, arrays of horizontal drains were drilled upslope at two locations on the north face of the west pit excavation. The 11 drains, 100 to 250 m long, successfully lowered groundwater to the north and northwest of the excavation, where permeable ground was encountered, but had a more limited drawdown to the northeast. The horizontal drains were installed April 4–19, 1995.

4.2 *Shear Zone Deformation*

Deformations measured on the A+ and B+ grooves of the inclinometers are in lockstep with

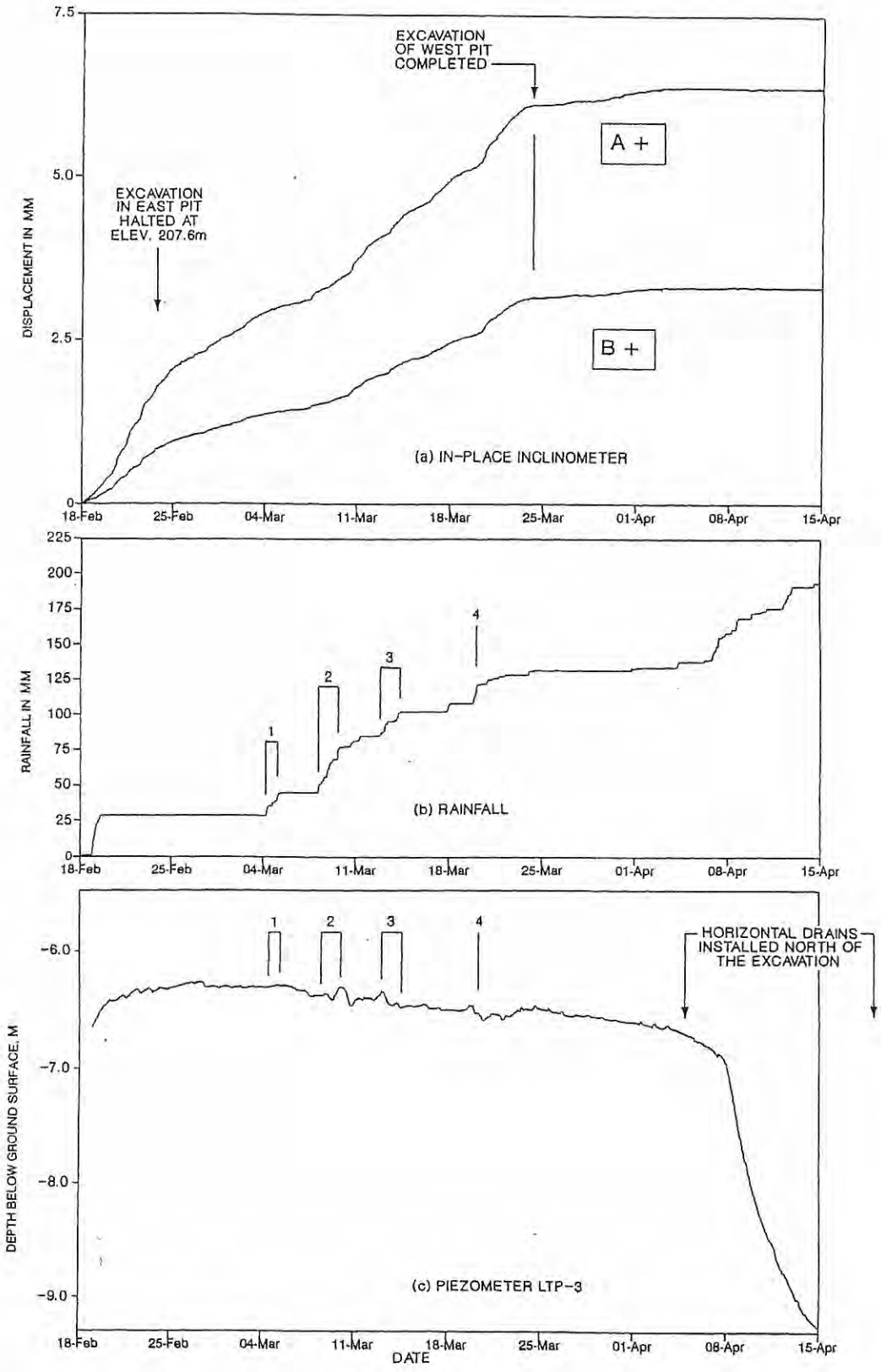

Figure 3. Examples of Continuous Monitoring Data

each other (Fig. 3a), and bear approximately the same proportions throughout the measurement period (i.e. B/A = 0.50). The rate of movement drops sharply after the excavation was completed, and essentially stopped 10 days later. The cessation of movement at the end of excavation clearly demonstrates that the shear zone deformation is an excavation-related event and is not technically a landslide event. A landslide would have continued to move because there was no significant change in groundwater levels during this period.

The excavation of a 'slot' through the middle of the ancient landslide terrain took support away from the ground upslope from the excavation, causing shear movements to occur along the ancient slide plane. Conversely, it also reduced the driving forces downslope from the excavation. Thus, no shear deformations were recorded in the instrument cluster at B-583 to the south of the station.

An important result of the continuous monitoring was to dispell any connection between the observed shear movements and rainfall. The correlation between movement and excavation (Fig. 3a) is self-evident. Some of the fastest movements occurred in the final two weeks of February when there was no rainfall.

4.3 *Velocity of Shear Movement*

Figure 4 shows the velocities of shear deformation measured over a five-day period by the in-place inclinometer. On Sunday, the velocities stayed essentially constant, but on weekdays, the velocities rose to peaks at mid-afternoon during excavation work.

4.4 *Piezometric Head*

Figures 3b and 3c show the rainfall and piezometric head on the deep piezometer at the ancient slip plane. Note that periods of heavy rainfall, identified as 1, 2, 3, 4 on the graph of Figure 3b, had essentially no effect on the observed piezometric head on Figure 3c. Therefore, the continuous monitoring shows that storms do not cause sharp rises in piezometric head at this location.

The piezometer data shows a slow drop in head from mid-February to early April. It probably represents the seasonal drop from late winter to spring. However, the installation of the horizontal drains in April caused a dramatic fall in head.

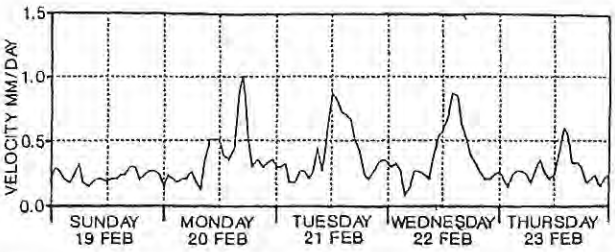

Figure 4. Velocity of Movement Measurements

5 CONCLUSIONS

A continuous readout system of inclinometers, piezometers and local rainfall provides valuable information for geotechnical studies of landslides. Available equipment is reliable and relatively inexpensive to install and read. The system can be used to compare (i) movements with rainfall, (ii) rates of movement with rates of rainfall (for study of coincident or lagging events), (iii) rainfall with spikes of groundwater response (to quantify such spikes), and (iv) movements in relation to construction activities, as described earlier. It is possible to collect the data from remote locations through modems.

The accuracy of an in-place inclinometer far exceeds the performance of conventional inclinometer readings taken at periodic intervals. Once the shear plane has been identified, the in-place inclinometer sensor can provide very accurate measurements of later movements.

REFERENCES

Dunnicliff, J.D. 1988. *Geotechnical instrumentation for monitoring field performance.* Wiley, pp. 108-116.

Mikkelsen, P.E. 1992. *Instrument innovations for monitoring natural hazards.* Geotechnical News, Vol. 10, No. 1, pp. 46-49.

Prellwitz, R. & Babbitt, R.E. 1984. *Long-term groundwater monitoring in mountainous terrain.* Transportation Research Board, Record 965, Soil Reinforcement and Moisture Effects on Slope Stability, pp. 8-15.

Continuous Monitoring of Groundwater Response to Winter Rainfall

DR. D. H. CORNFORTH
Landslide Technology, Portland, Oregon, USA
P. E. MIKKELSEN
Geoengineering & Instrumentation Consultant, Bellevue, Washington, USA

Instrumentation for continuous monitoring of groundwater is becoming increasingly easy to install and is affordable for most major landslide studies. Rainfall can be monitored concurrently at the site so that the direct relationship between rainfall and groundwater response can be analyzed without relying on distant rain gauging stations. This paper presents the continuous record of rainfall and piezometer response at Frog Lake landslide, Oregon during the winter of 1998-99.

BACKGROUND INFORMATION

The Pacific Northwest region of the United States has a wet, temperate climate on the west side of the Cascade mountains. The onset of winter rainfall typically occurs in mid-October and continues until March. Rainfall then tapers off until the end of June; dry summer weather occurs from July to mid-October.

Large areas of western Oregon are covered by ancient landslides which are believed to have originated during the late Pleistocene. Because of the wet climate, most, if not all, of these ancient landslides are marginally stable and manmade changes to the topography can trigger more active movements on portions of the ancient landslide terrain. One such case is at Frog Lake reservoir, situated at about elev. 1,900 feet (580 m) on the western flanks of the Cascades.

In 1953, a 70-foot (21 m) high dam was built to retain water for a Portland General Electric (PGE) hydroelectric project. It reactivated a portion of ancient landslide terrain approximately 3,000 feet (910 m) wide and 5,000 feet (1,520 m) long above the Clackamas River with an average slope of 8 degrees to the horizontal. The shear plane is at least 250 feet (76 m) deep near the head of the active lobe where the Frog Lake reservoir adds weight to the landslide mass. Further details of the landslide are omitted as irrelevant to the scope of this technical paper.

PIEZOMETER INSTALLATION

Piezometer LT-21 was drilled in July 1995 about 65 feet (20 m) north of the embankment toe. The log is reproduced on Figure 1. All materials encountered in the drillhole are landslide debris. The upper 71 feet (22 m) of hole was drilled through sandy silt and sand by the ODEX technique using air feed. The lower 79 feet (24 m) was drilled with HQ coring and passed through highly broken rock.

On removing the drilling rods, the lower part of the hole collapsed. A plastic standpipe piezometer, nominal 1 inch (25 mm) inside diameter, was installed to a depth of 90 feet (27 m) in the remaining open hole. The lower 20 feet (6 m) of the plastic pipe has 0.010 inch (0.25 mm)

wide slots and is surrounded by No. 6 to No. 9 clean sand (approx. 2.2 to 3.4 mm grains). The upper 70 feet (21 m)of the hole is grouted with a cement-bentonite (8:1 mix by weight) slurry.

Drilling took nine days due to the broken rock within the hole. The total cost of drilling, including a full-time geotechnical engineer on site, was around $22,000 (in 1995).

MONITORING EQUIPMENT INSTALLATION

Piezometer

The standpipe piezometer was automated in the spring of 1997. A ¾-inch (19 mm) diameter vibrating-wire pressure sensor was lowered into the standpipe by a cable and suspended at the 90-foot (27 m) depth below the top of the riser. The measured water head is added to the stationary tip elevation to obtain the piezometric elevation.

The PVC riser is enclosed in a 6-inch (150 mm) diameter steel protective casing at the surface. Here, a small junction box with a surge protector for the sensor was installed which serves to terminate the sensor cable, provide lightning protection, and connect to the trenched-in telephone cable. The new trench extends a distance of about 600 feet to another instrument location at the toe of the embankment. From there, wires run another 400 feet up the slope of the embankment to the control house/emergency generator building. All wires were buried in 2-foot (0.6 m) deep trenches. The wire pair was connected to a Campbell Scientific CR10X data logger inside the building.

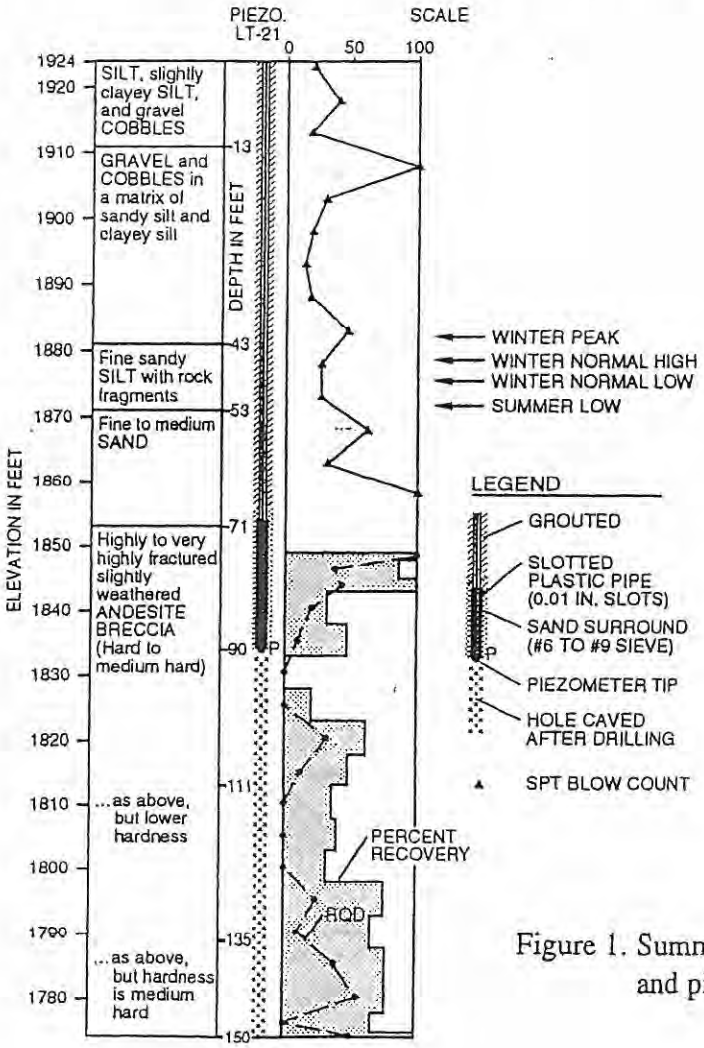

Figure 1. Summary log of drillhole and piezometer LT-21.

The data logger was programmed to store sampled data every hour on the hour. Vibrating-wire frequency readings, heads in feet, and elevations were stored along with other data.

Rain Gauge

Rainfall in inches and intensity in inches per hour were measured with a gauge placed on a steel pole next to the control house. A pair of telephone wires were used to carry the pulse signal from the rain gauge to the CR10X data logger some 200 feet away.

A tipping bucket style rain gauge (Met-One) was installed. Since power was available at the site, a heater for the gauge funnel was included. The thermostatically controlled heater activates below 40 degrees Fahrenheit, melting any snow or ice.

The bucket in the gauge tips for every 0.01 inch (0.25 mm) of accumulated rainfall. Each tip activates a magnet/reed switch and sends a pulse signal to the data logger. The logger keeps track of the number of pulses and the program calculates the cumulative rainfall and intensity. The results are stored each hour.

The approximate additional costs to provide the automated data acquisition system (ADAS) were: instruments: $8,000; design, install: $6,500; total $14,500.

The readings can be downloaded from the site by the owner (PGE) or consultant via telephone lines and graphed in the manner shown in this paper. The installation costs at this site were reasonable, and future monitoring is less expensive than the cost of sending personnel to the site for manual readings.

GROUNDWATER RESPONSE ANALYSIS

In western Oregon, groundwater levels fall steadily through the drier summer months. As winter rainfall begins, groundwater rises and reaches a seasonal high in mid-winter. During the winter, periodic heavy storms provide high intensity rainfall which can temporarily raise groundwater to short-term highs. These spikes usually cannot be caught by weekly or monthly site visits, yet are frequently the triggering event for movements on marginally stable slopes such as ancient landslide terrain. It is of benefit to the geotechnical engineer performing back-analysis slope stability calculations to know the height reached by groundwater during storms because it provides the groundwater model for using factor of safety F = 1.00 in the analysis. In this regard, an in-place inclinometer (Cornforth & Mikkelsen, 1996) can also be included in the ADAS to accurately relate groundwater levels to the onset of shear movements.

At the Frog Lake site, the groundwater levels fall 600 feet (183 m) over a distance of 4,500 feet (1,370 m) from piezometer LT-21 to the Clackamas River, a hydraulic gradient of 13 percent. Groundwater levels within the slope depend upon the rate of infiltration and the groundwater flow regimes.

The groundwater response to winter rainfall has been subdivided into three 13-week periods on Figures 2, 3 and 4. Although one must be cautious in reading too much significance into a single site record, Frog Lake piezometer LT-21 does offer some insights into groundwater response which probably apply to many other sites. For simplicity, an elevation such as elev. 1,875.0 is stated as elev. 75.0; these units are in feet and the conversion of elevation readings to metric units is omitted.

Late Summer, 1998

No rainfall occurred at the site from July 30 to September 18. The end of this period is shown by A on Figure 2 and groundwater levels fell throughout the period at a rate of about ¼ inch/day (6 mm/day).

During the seven-week period from September 18 to November 10, there was sporadic rainfall but no major storms. A total of 7 inches (178 mm) of rainfall was recorded, but groundwater continued to fall, reaching the annual low of elev. 71.5 near the end of September (B, Fig. 2). Therefore, the rainfall infiltration was essentially rewetting the upper 53 feet (16 m) of soil above the groundwater following the dry summer months, and had no influence on groundwater levels.

Winter, 1998-99

The first major storm produced 7.4 inches (188 mm) of rainfall in 6.6 days; the groundwater level rose by 5.1 feet (1.55 m), as shown by CD on Figures 2 and 3. Thereafter, winter storms kept groundwater levels generally within a band fluctuating between about elev. 75.4 and elev. 78.5, a range of 3.1 feet (0.95 m) for about 16 weeks. These limits (Fig. 3) can be termed the 'normal' highs and lows of groundwater during winter and are well above the late summer low of elev. 71.6.

In late December, a groundwater spike reached a peak of elev. 82.0 (E, Figs. 3 and 5). The peak reading was caused by a severe storm with rainfall of 6.0 inches (152 mm) over 1.8 days which raised the groundwater level by 6.1 feet (1.86 m). This peak value is 3.5 feet (1.07 m) above the 'normal' winter high. It is of interest that the peak lasted for only two to three hours (9:00 p.m. to midnight on December 28, see Fig. 5) and the groundwater level declined at almost 2 feet per day (0.6 m per day) for the next two days (F, Fig. 5).

The delay time from the peak rainfall intensity to peak piezometric level was about 25 hours (Fig. 5). In other storms, the delay time was generally about 19 hours.

Spring 1999

Groundwater fell below the 'normal' winter range in late March. However, groundwater fluctuations in the spring appear to be more sensitive to rainfall during this period (G, Fig. 4) than they were in the late summer of 1998 (B, Fig. 2). The spring fluctuations may have been affected by runoff of snowmelt from the high slope above the site.

Continuous vs. Periodic Groundwater Readings

Suppose that winter groundwater observations were being taken at monthly intervals occurring on the first day of each month. The readings for December through March are shown by open

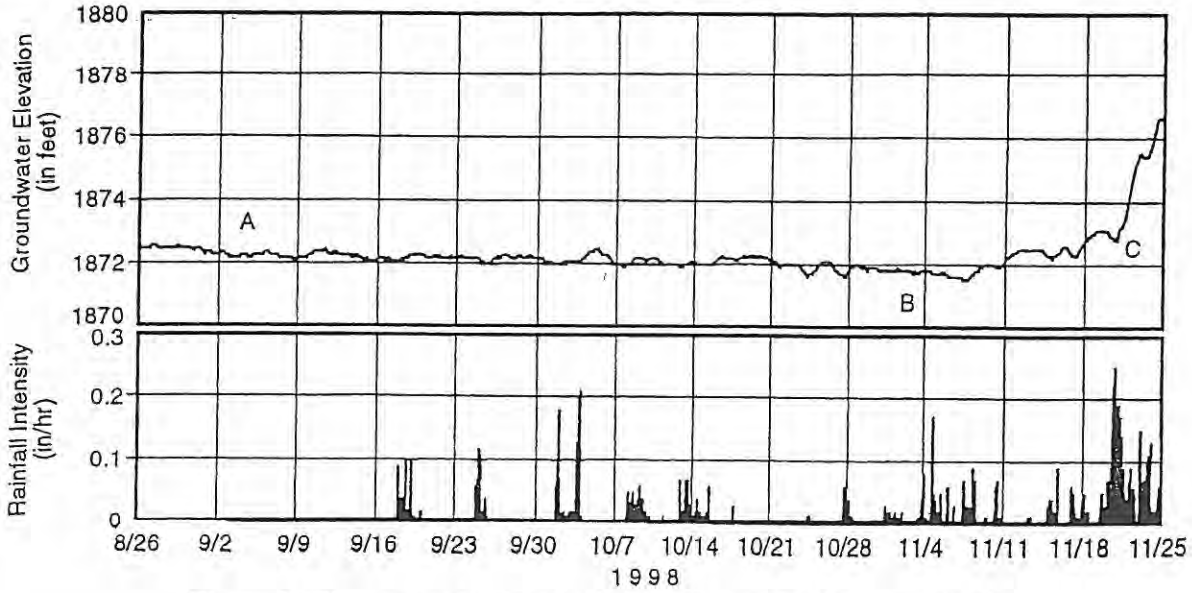

Figure 2. Piezometer data and rainfall intensity 8/26/98 – 11/25/98

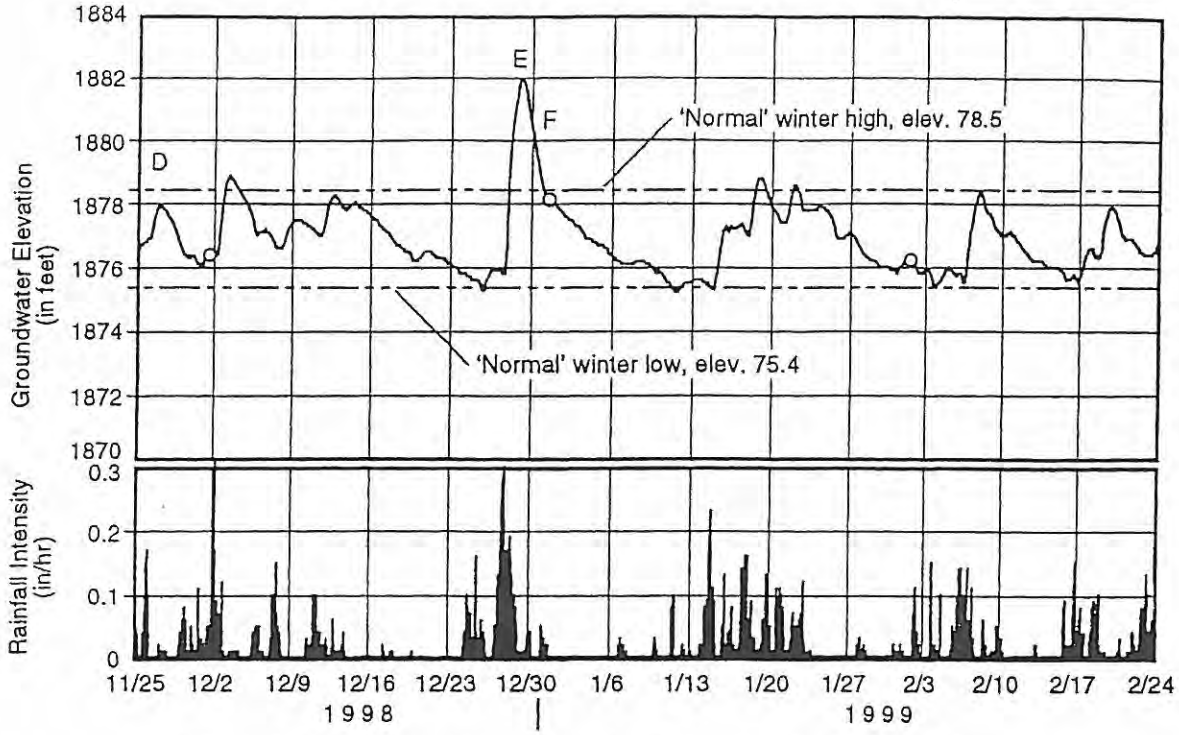

Figure 3. Piezometer data and rainfall intensity 11/25/98 – 2/24/99

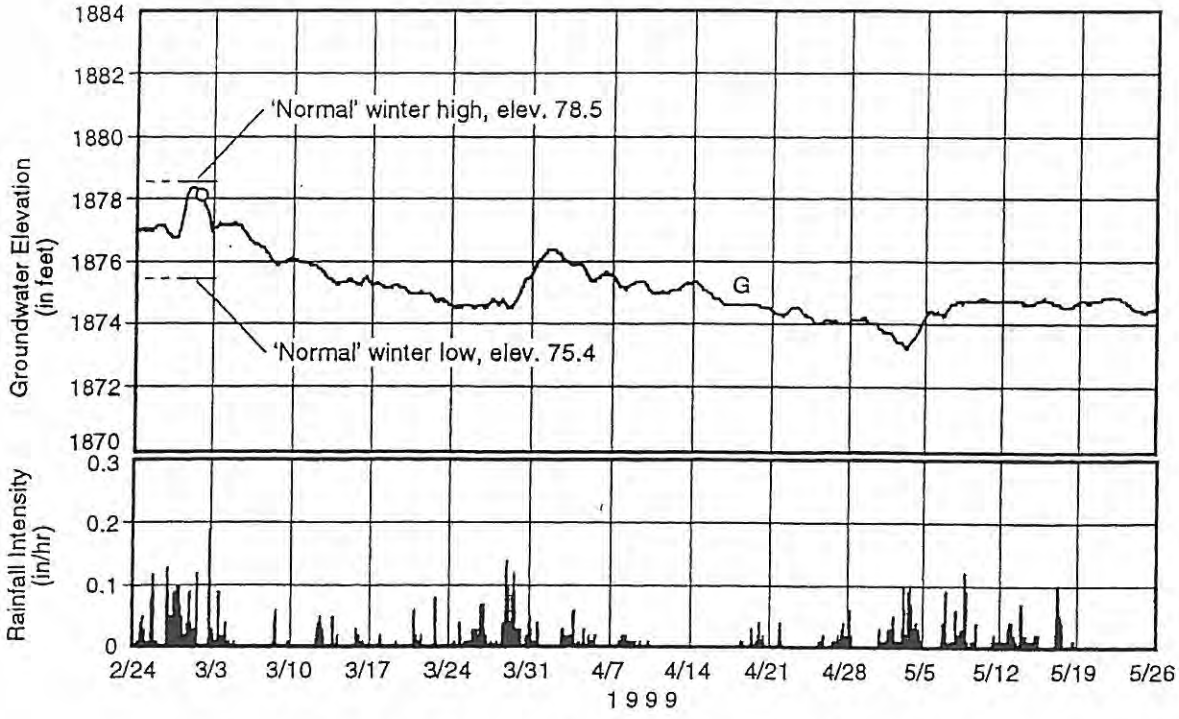

Figure 4. Piezometer data and rainfall intensity 2/24/99 – 5/26/99

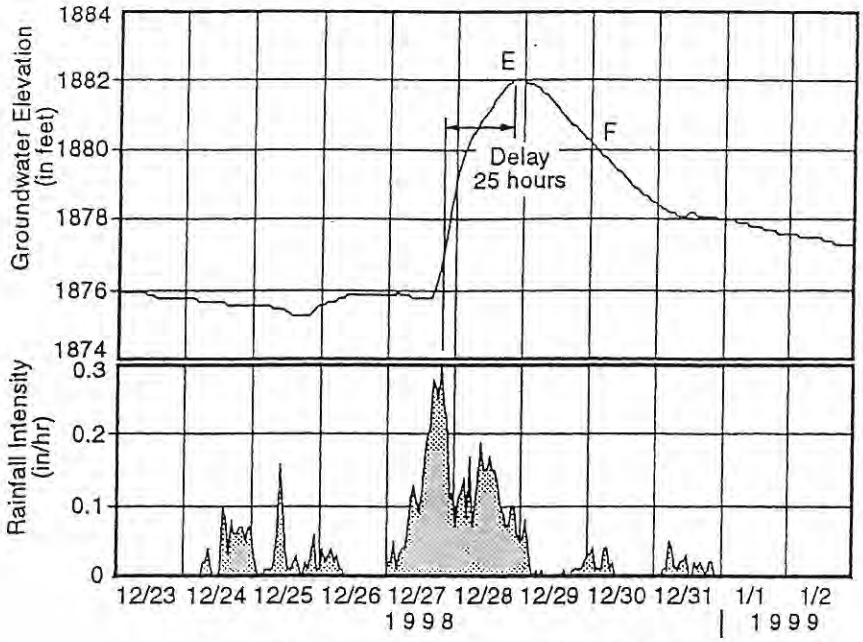

Figure 5. Spike of groundwater in December 1998

circles on Figures 3 and 4. The data shows that the observations would approximately cover the 'normal' range of groundwater levels for the winter, but they would have missed the peak groundwater level (E, Fig. 3).

CONCLUSIONS

1. Continuous groundwater monitoring can measure the precise maximum head occurring during a major storm event. In this case history, the winter peak occurred at around midnight on December 28, 1998 when manual readings would not have been taken.

2. Major spikes of groundwater develop and subside quickly and have a low probability of being recorded by groundwater readings taken on a set schedule, such as weekly or monthly intervals.

3. (i) The groundwater cycle for the winter of 1998-99 at this site was:
   Groundwater slowly declined through the dry summer months to a base elevation of 71.5 feet. The late summer rate of groundwater decline in dry weather is only ¼ inch (6 mm) per week (A, Fig. 2).
   (ii) Rain in the early fall had essentially no effect on groundwater level, and probably is infiltrating the voids and cracks above groundwater (B, Fig. 2).
   (iii) The first major storm caused a sharp rise in groundwater, moving the water level into the winter range (C, Fig. 2 to D, Fig. 3).
   (iv) Winter storms kept the groundwater generally within a range fluctuating from a low of elev. 75.4 to a high of elev. 78.5, for a period of 16 weeks (Figs. 3, 4).
   (v) A severe mid-winter storm of 6.0 inches (152 mm) in 1.8 days caused a spike of groundwater to elev. 82.0, which is 10.5 feet (3.2 m) above the summer low (E, Fig. 3).
   (vi) Groundwater levels generally dropped below the winter range in mid-March and began the seasonal decline to the summer base level (G, Fig. 4).

REFERENCE

Cornforth, D. H. and Mikkelsen, P.E. (1996), "Continuous monitoring of the slope above an excavation within a marginally stable landslide," Proceedings of the 7th International Symposium on Landslides, Trondheim, Norway, Vol. 3, pp. 1539-1544.

TAB 7

Jonathan Stewart

Presentation

Seismic Slope Stability

Jonathan P. Stewart
University of California, Los Angeles

Outline

- Observed slope failures during earthquakes
- Evaluation of dynamic shear strength
- Ground motion parameters for seismic slope stability
- Pseudo-static analysis
- Slope deformation analysis methods
- California Seismic Hazards Mapping Act

Issues Not Addressed

- Liquefaction-related stability problems (e.g., lateral spreading, settlement)
- Ground deformations from volumetric strain (seismic compression)

A. Earthquake-Induced Landslides

- Disrupted slides and falls
- Deep bedrock slides
- Rotational slumps, lurches
- Lateral spreads and flow failures

Rockfalls

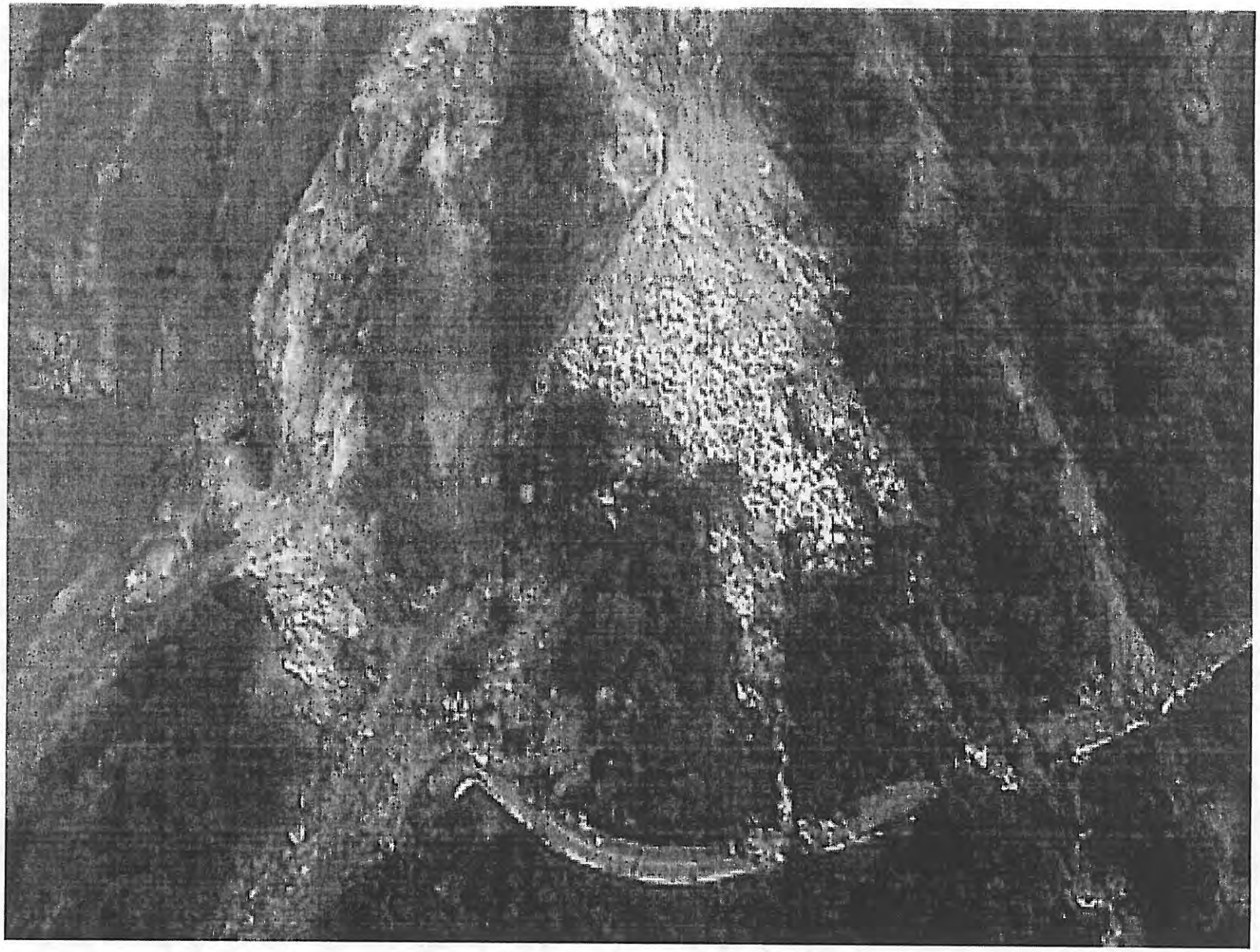

Deep Bedrock Slides

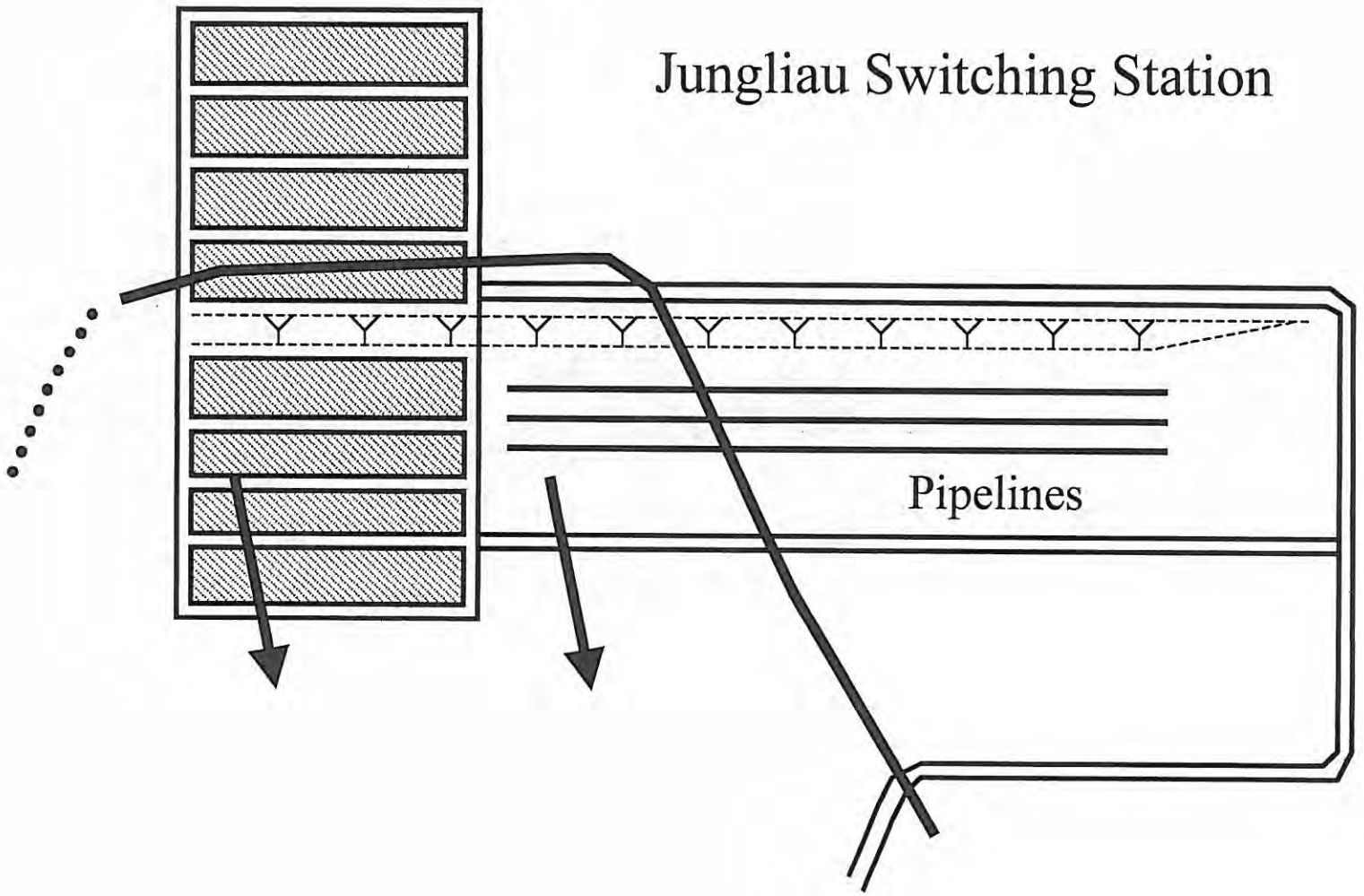

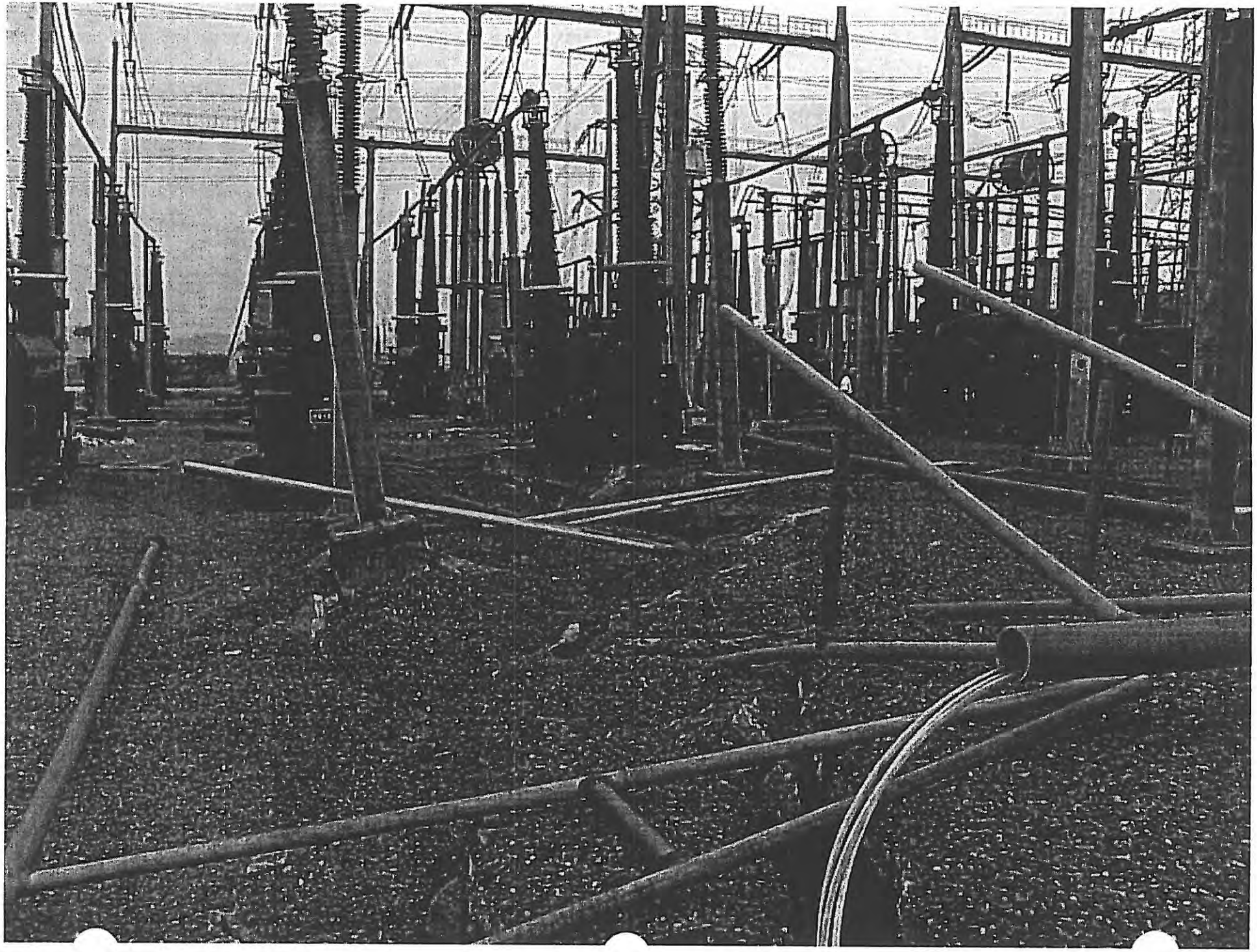

Chaolin Landslide

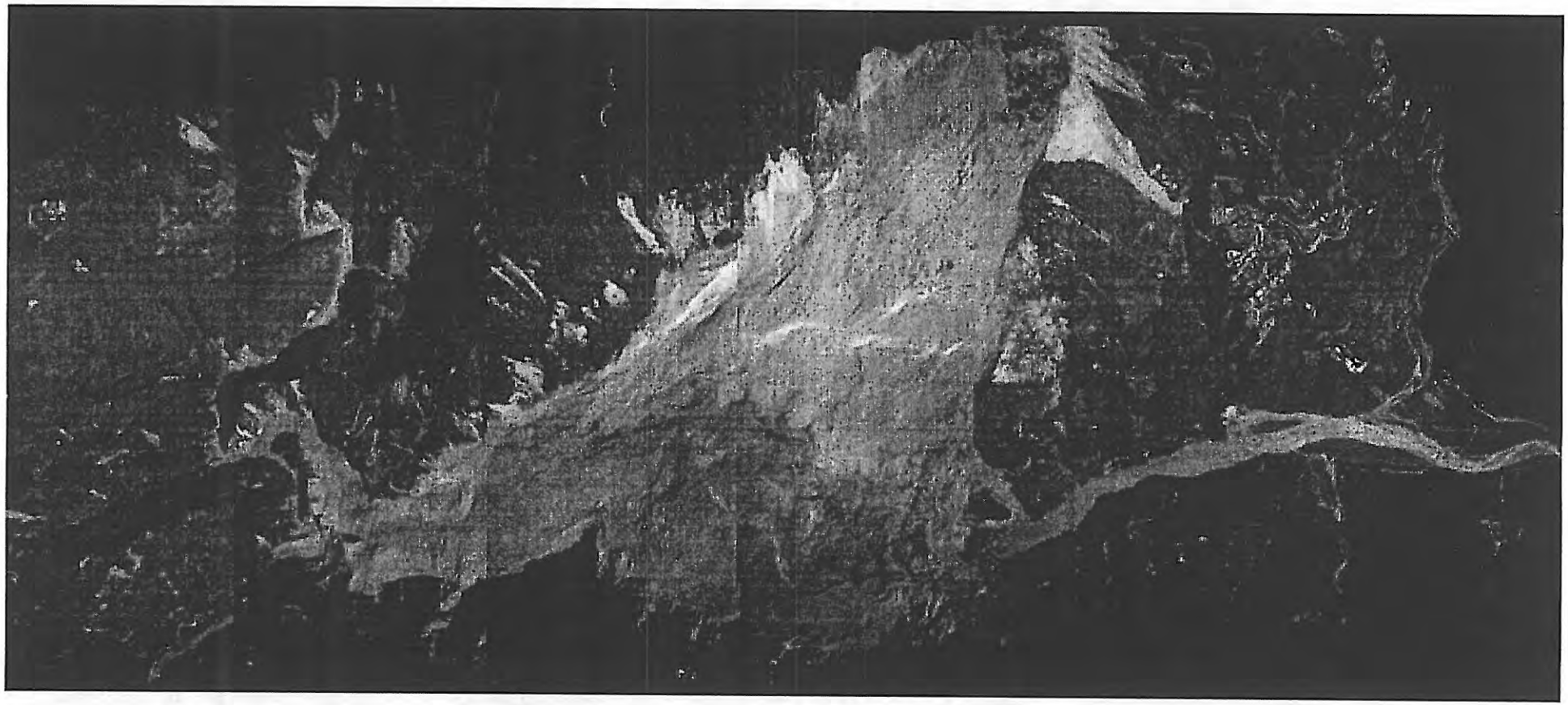

Volume = $120 * 10^6$ m^3

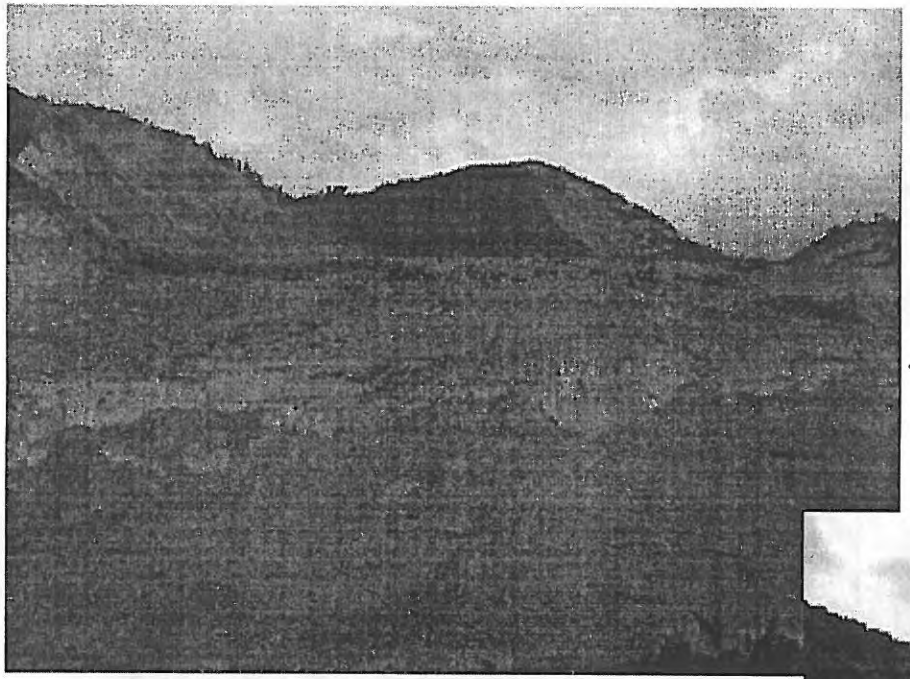

Head Scarp

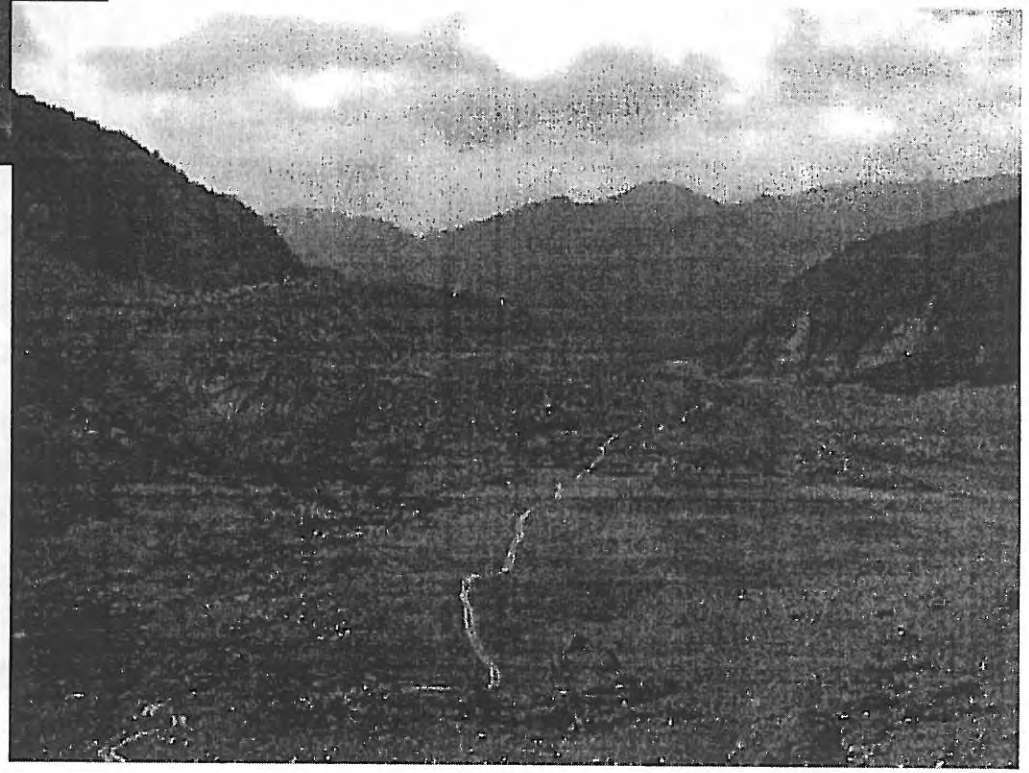

Looking towards toe

Slumps/Lurches in Clay: Navlaki Port, India

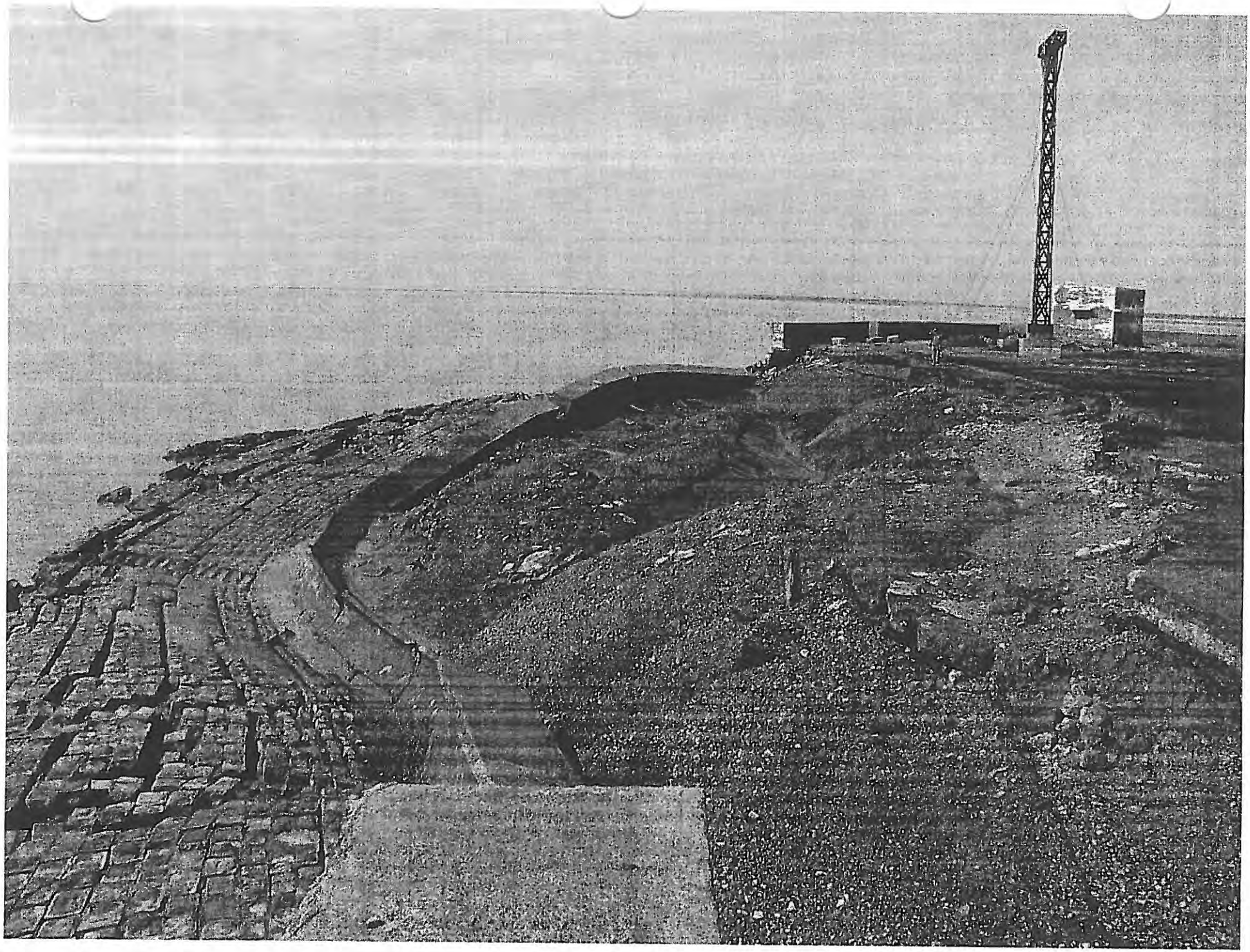

Slope Failures from Liquefaction

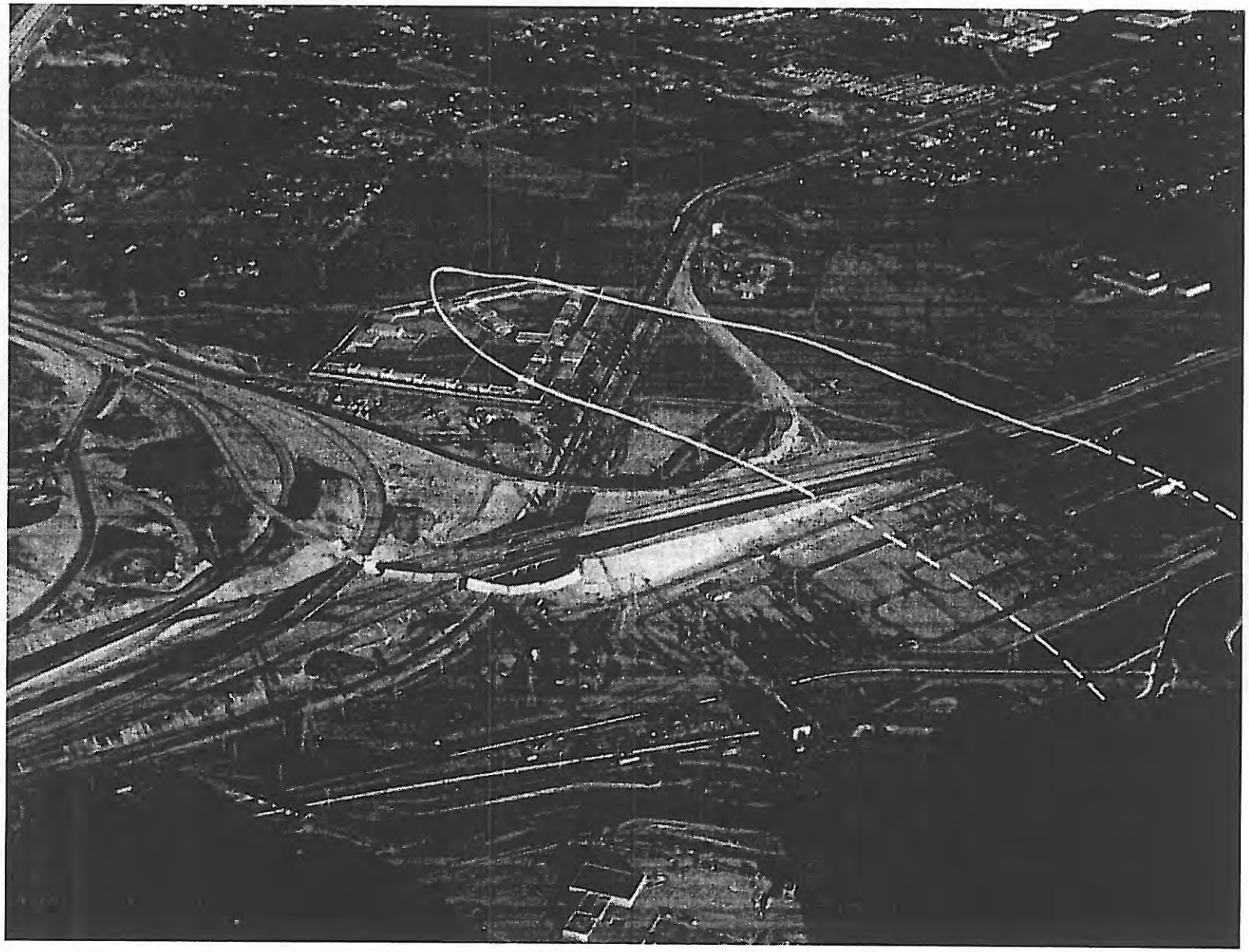

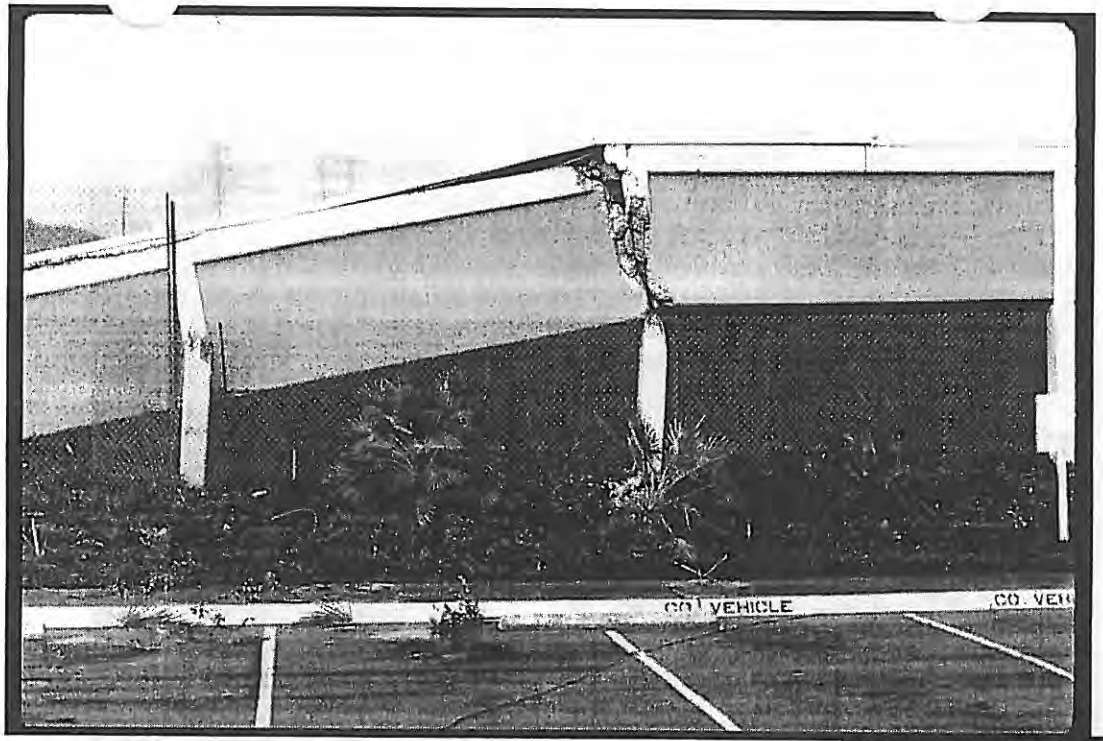
CO. VEHICLE

Flow Failures

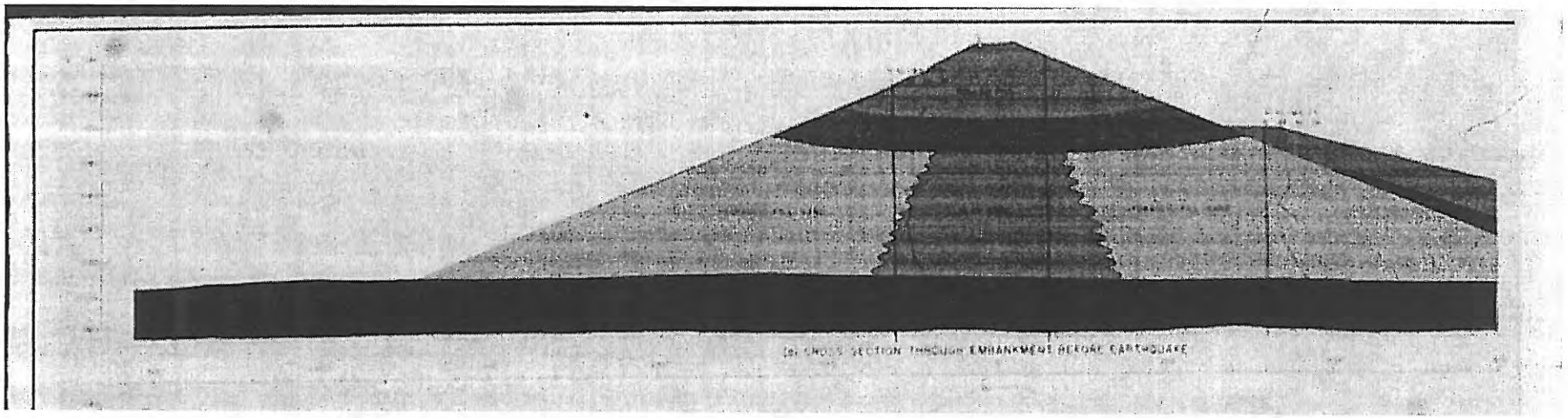

Map: Seed et al., 1973

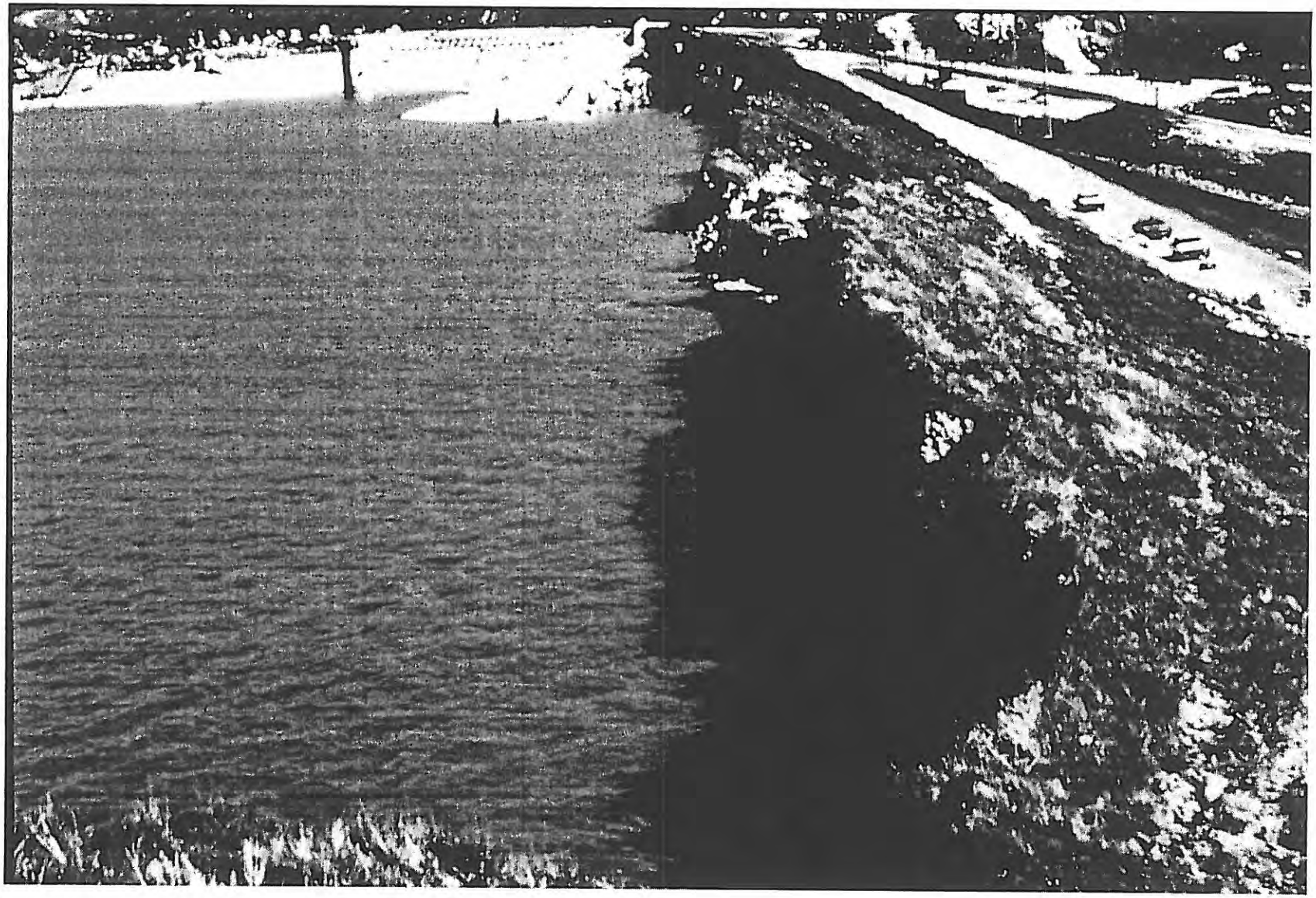

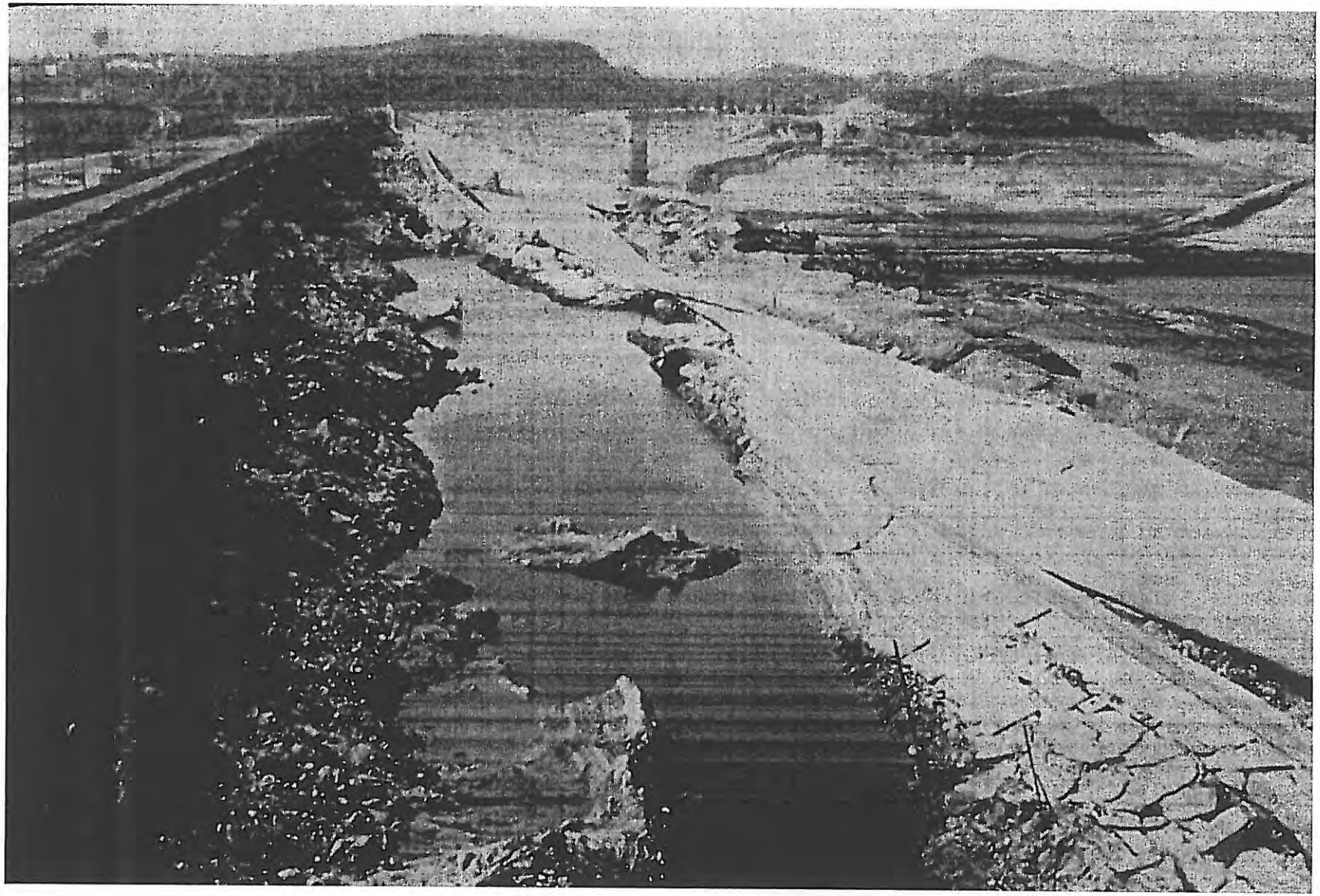

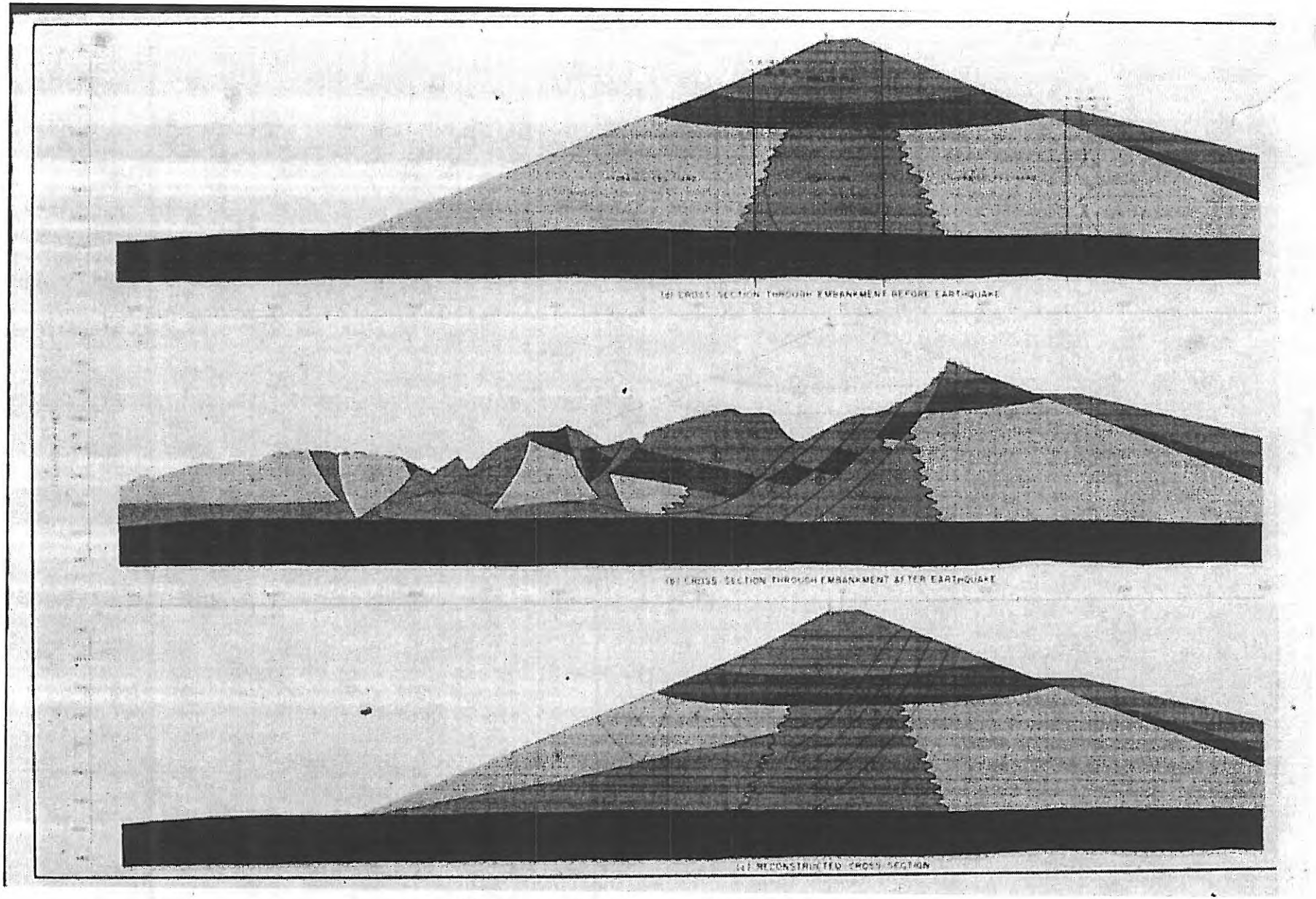

Figure: Seed et al., 1973

B. Strength Evaluation

- Appropriate sampling techniques
- Strength evaluation, considering:
  - Drainage conditions
  - Strain softening
  - Rate effects
  - Cyclic degradation

Soil Sampling

- (Most) current practice:
  - Modified California (driven, large diameter split-spoon sampler) for clays
  - SPT for sands
- Outcome:
  - Drained strength of granular soils from correlations with penetration resistance.
  - Highly disturbed samples for laboratory testing.
  - Unknown relationship between shear strengths derived from laboratory tests and in situ condition.

- Recommendations on sampling:
  - SPT for drained strength of sand (can supplement with CPT, but not replace)
  - Soft to firm clays: pushed tube samples
  - Stiff clays: Pitcher tube or Modified California
  - Gouge zones, slide planes, etc.: hand carved

Soil Strength Evaluation

- (Most) current practice:
  - Direct shear testing of ring samples from Modified California sampler
  - Slow rate of deformation
- Outcome:
  - Drained strength parameters (zero pore pressure).

Dynamic Shear Strengths

- Assess liquefaction potential
  - The following assumes soil is <u>not</u> liquefiable
- Undrained loading ($u \neq 0$)
  - Use undrained strengths (s_u) derived from UU or CU tests
  - Requires triaxial testing (drainage not controlled in direct shear).
  - $s_u > s_d$ for dilatent, saturated soils (dense sands, high OCR clays)
  - $s_u < s_d$ for contractive, saturated soils (loose sands, high OCR clays)

Recommendations:

- Clays: total stress parameters, undrained tests
- Clays at residual: effective stress parameters, drained or undrained test
- Sands, unsaturated: effective stress, drained strength parameters
- Sands, saturated: consider liquefaction susceptibility

- Rapid rate of shearing
  - Small effect for non-plastic materials.
  - Plastic soils: peak shear strength increases with increasing strain rate.
  - Typically 5-15% increase in s_u per log cycle of strain rate, $\therefore (s_u)_{dyn} \approx 1.1\text{-}1.4 \times (s_u)_{static}$ [ref: Sheahan et al., 1996]
  - Strain rate effect not OCR dependant
  - Effect on residual strength is poorly defined, but probably small [ref: Skempton, 1985]

- Cyclic degradation of shear strength
  - Potentially significant for strain softening, contractive soil.
  - Typically related to cyclic pore pressure increase.
  - Requires large number of cycles (large magnitude earthquake).

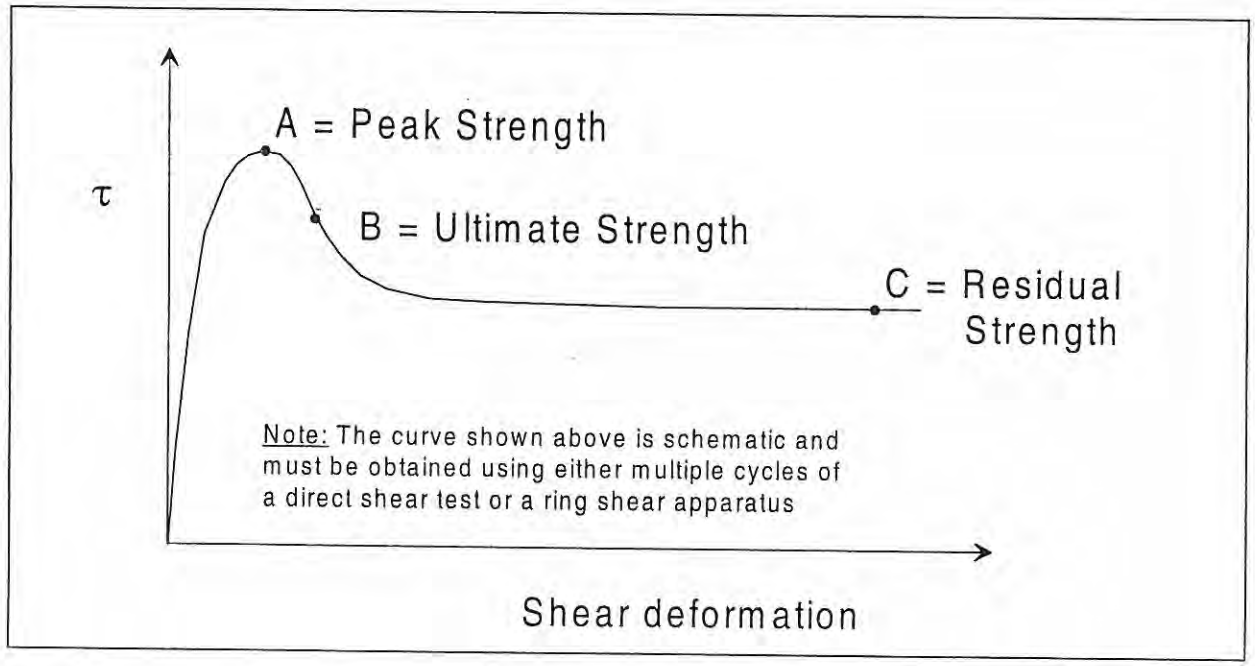

Other factors:

- Soil anisotropy
- Effect of confining stress
- Strain softening

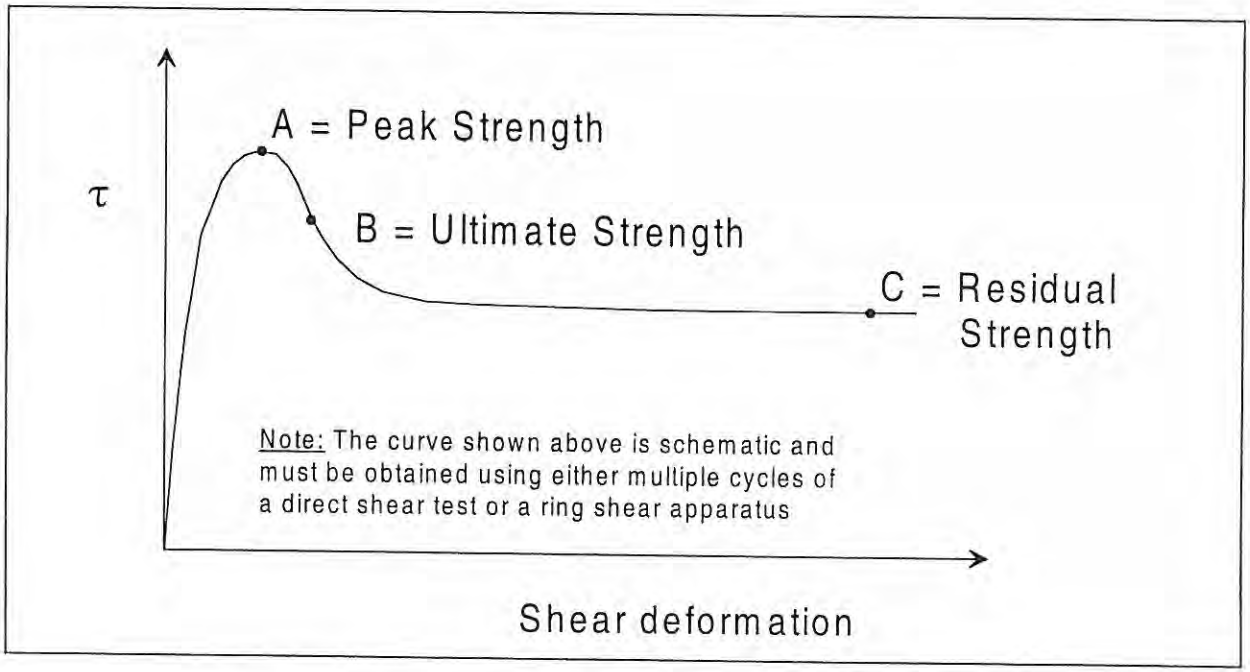

C. Ground Motion Parameters for Seismic Slope Stability

- Amplitude of shaking in slide mass
- Duration
- Frequency content

Amplitude

Objective: spatial average amplitude in slide mass

Dependant on:

- Base motion
- Slide mass amplification
- Wave reversals

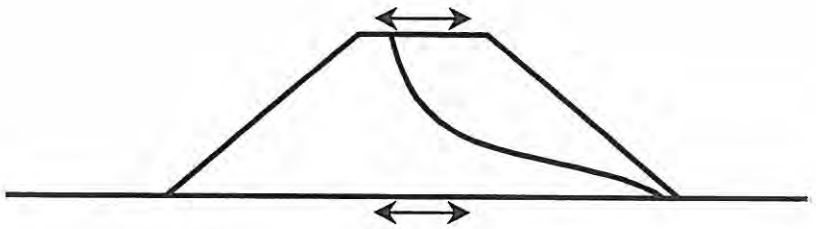

Note: neither base nor crest motion represents average in slide mass

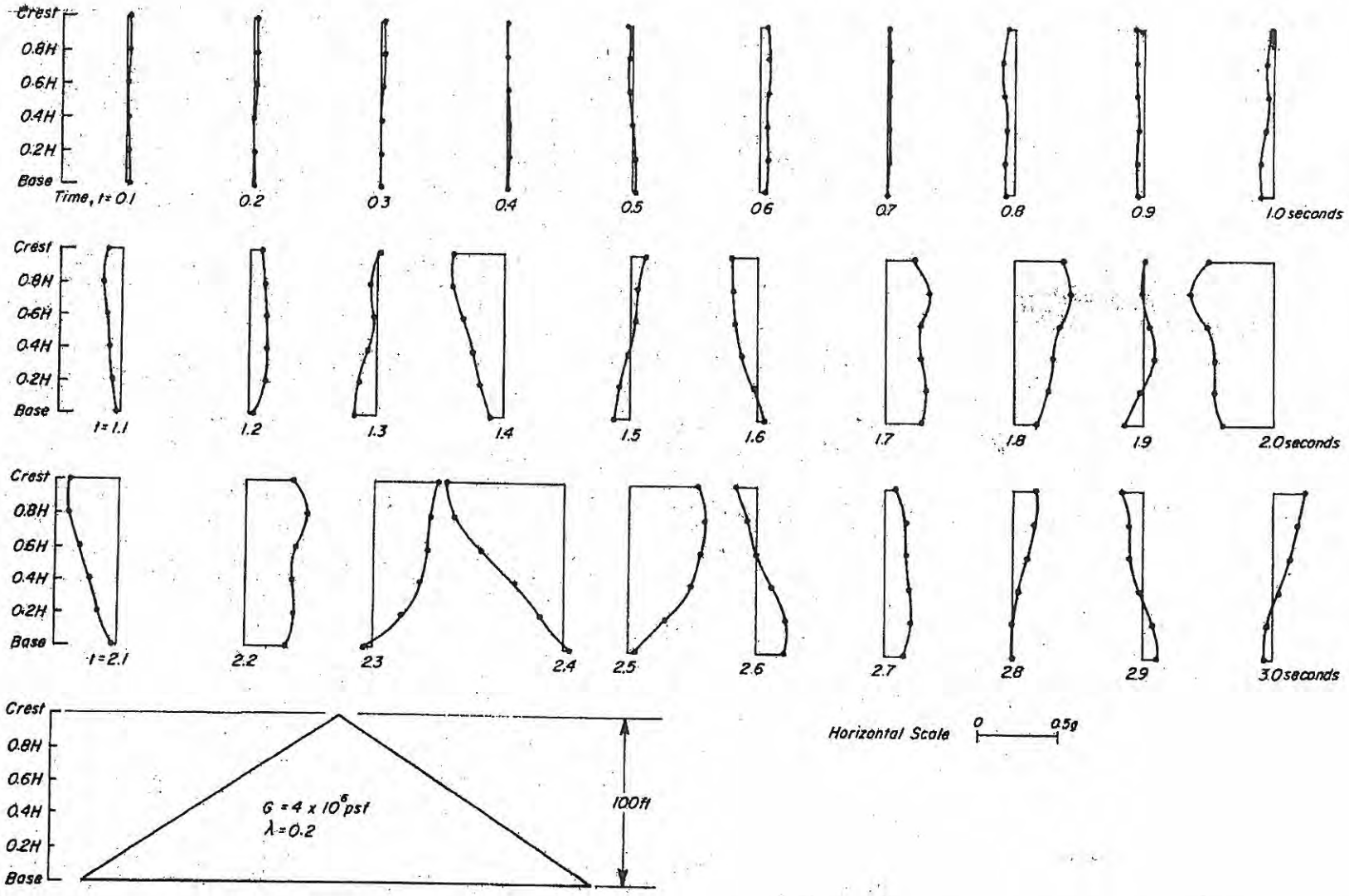

FIG. 10.—ACCELERATION DISTRIBUTION AT 0.1-SEC INTERVALS FOR 100-FT-HIGH DAM SUBJECTED TO EL CENTRO EARTHQUAKE

Ref: Seed and Martin, 1966

Horizontal Equivalent Acceleration (HEA)

Figure: Seed and Martin, 1966

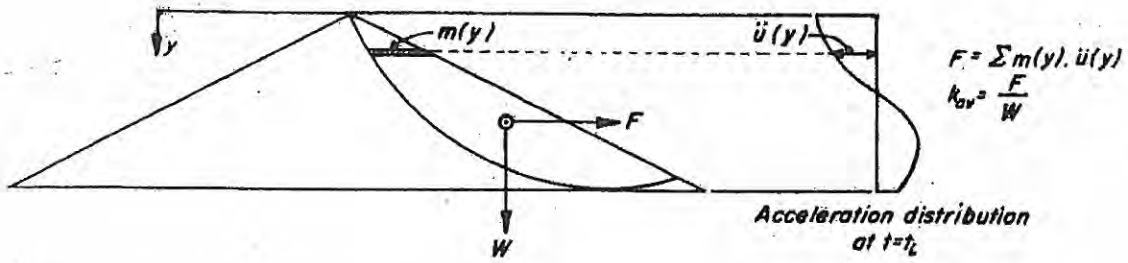

FIG. 11.—CONCEPT OF AVERAGE SEISMIC COEFFICIENT

At each time step:

$F=\Sigma_i m(y)u(y)$

$HEA = (F/W)\times g$

Seismic coefficient, $k = HEA/g$

Maximum values denoted as *MHEA* and *kmax*

If sliding surface is horizontal,

HEA = $(\tau_h/\sigma_v)g$

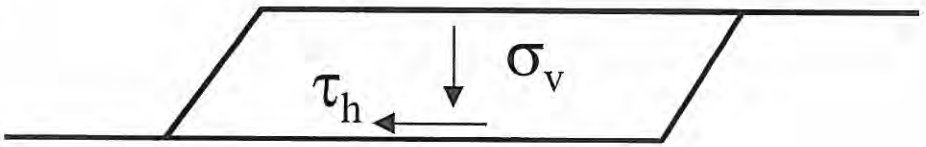

Factors affecting *MHEA*:

- Response of slide mass to input motion (resonance effects)

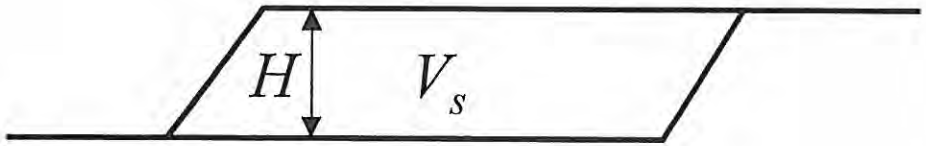

$T_s = 4H/V_s$ (1-D)

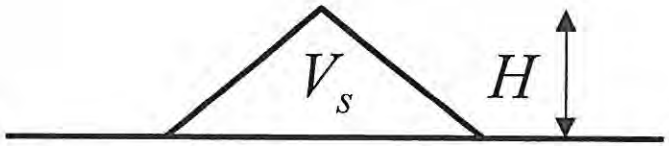

$T_s = 2.6H/V_s$ (2-D)

- Amplitude of base motion

For 1-D sliding mass geometries [Bray et al., 1998]:

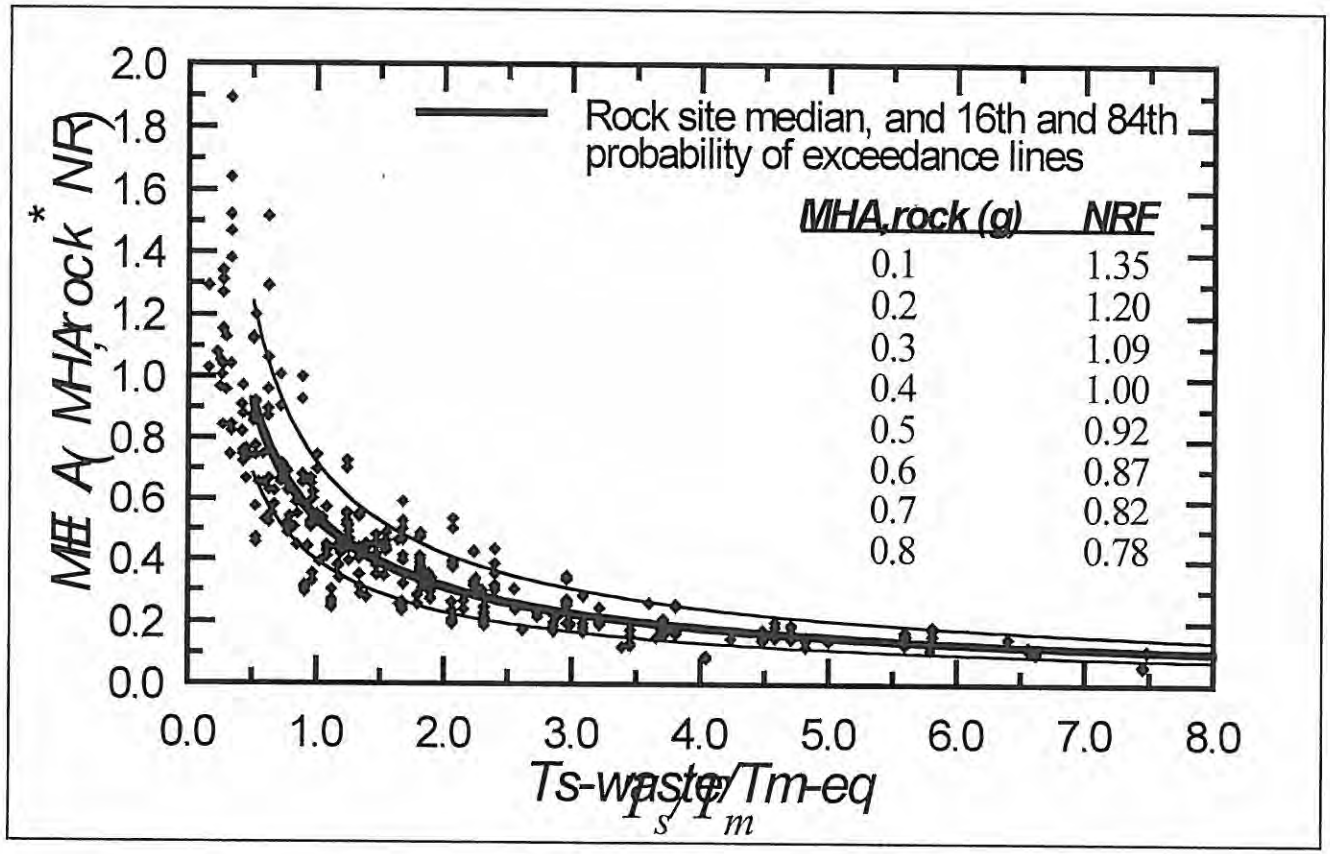

MHA_{rock} = peak horizontal acceleration at base of slide mass for rock site condition (regardless of ground condition)

T_m = mean period of base motion

MHA = PHA

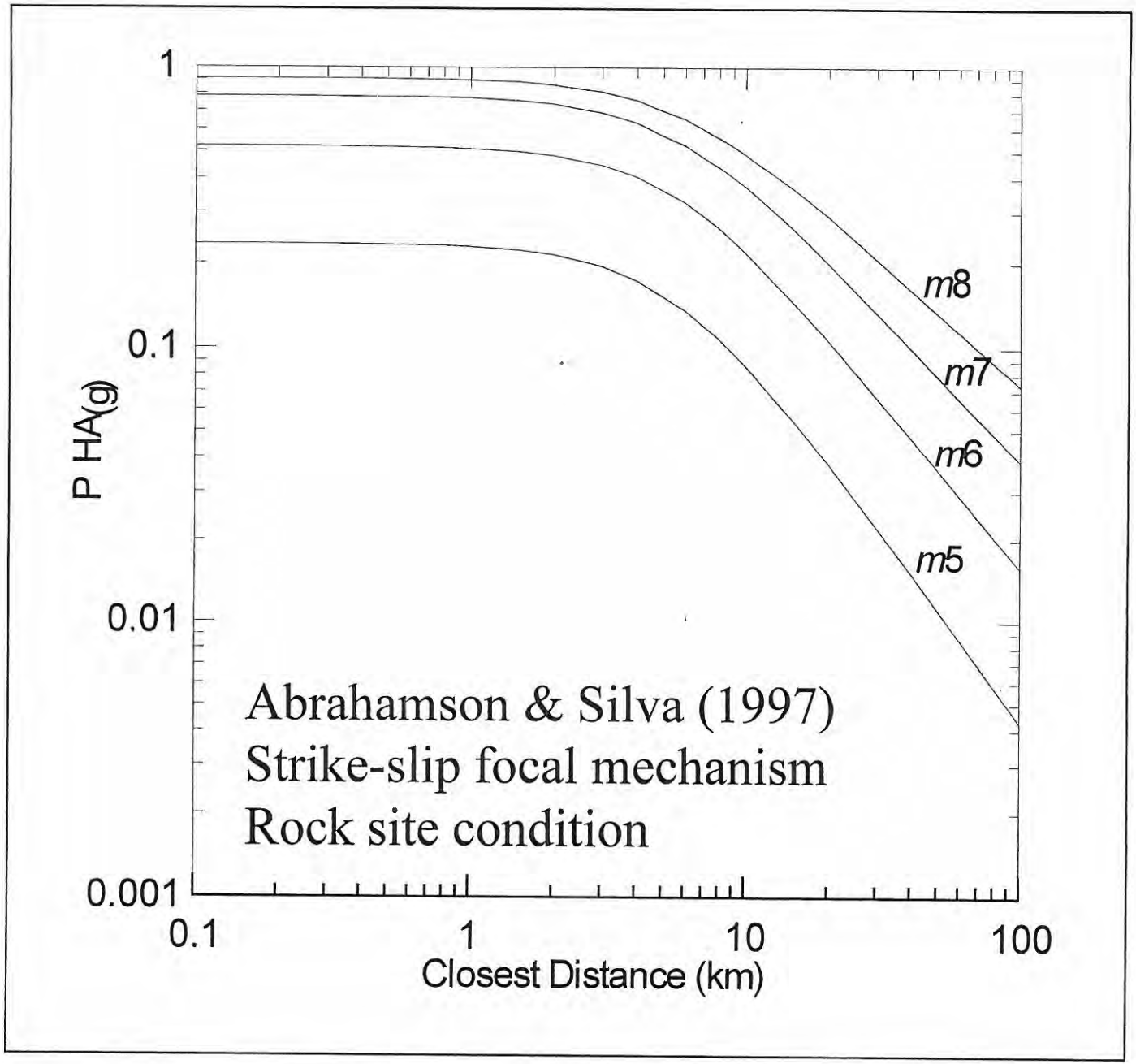
1
0.1
0.01
0.001
P HA(g)
m8
m7
m6
m5
Abrahamson & Silva (1997)
Strike-slip focal mechanism
Rock site condition
0.1
1
10
100
Closest Distance (km)

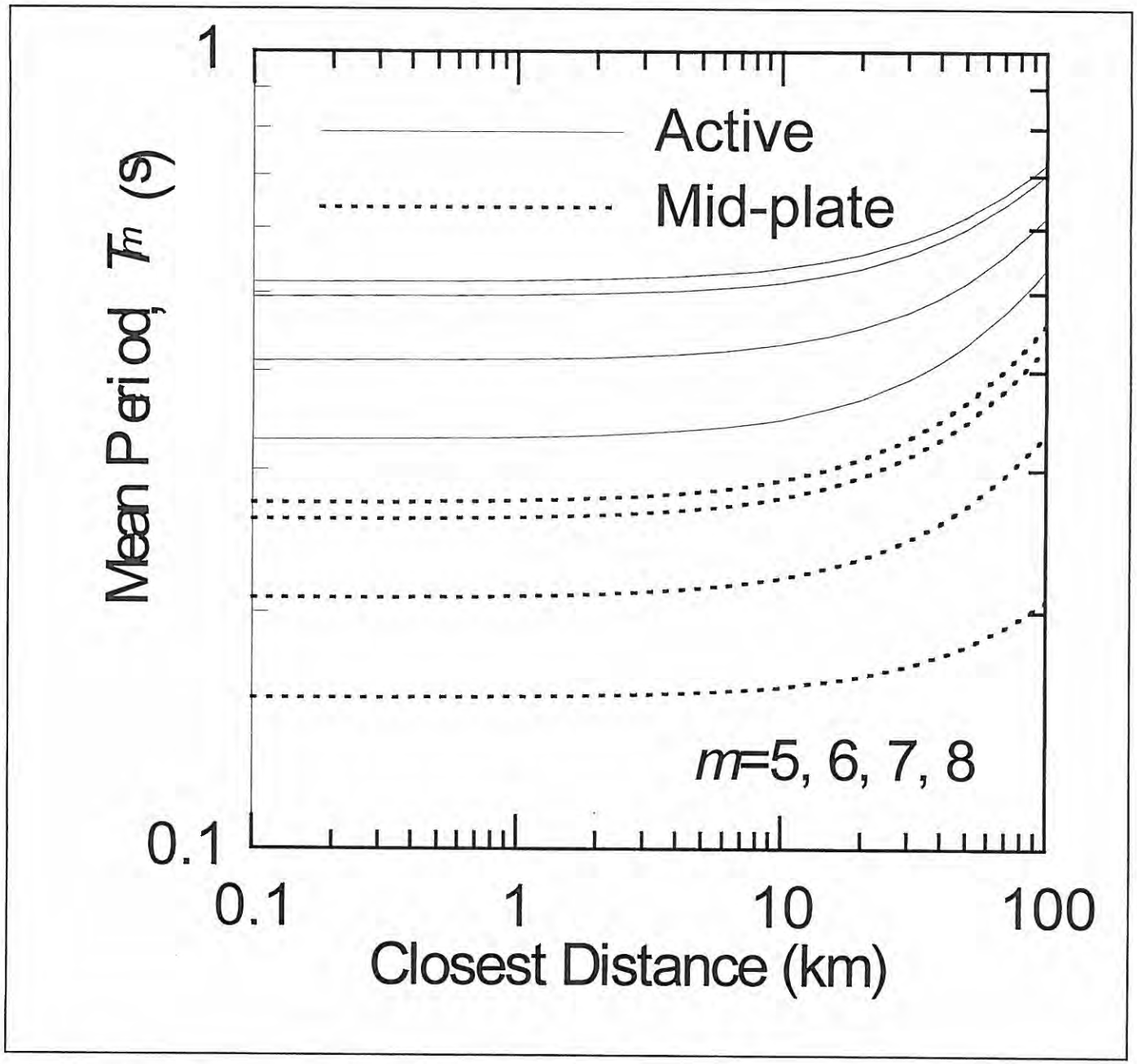

Rock site condition

Ref: Rathje et al., 1998

Duration

Typically taken as 5-95% Arias duration

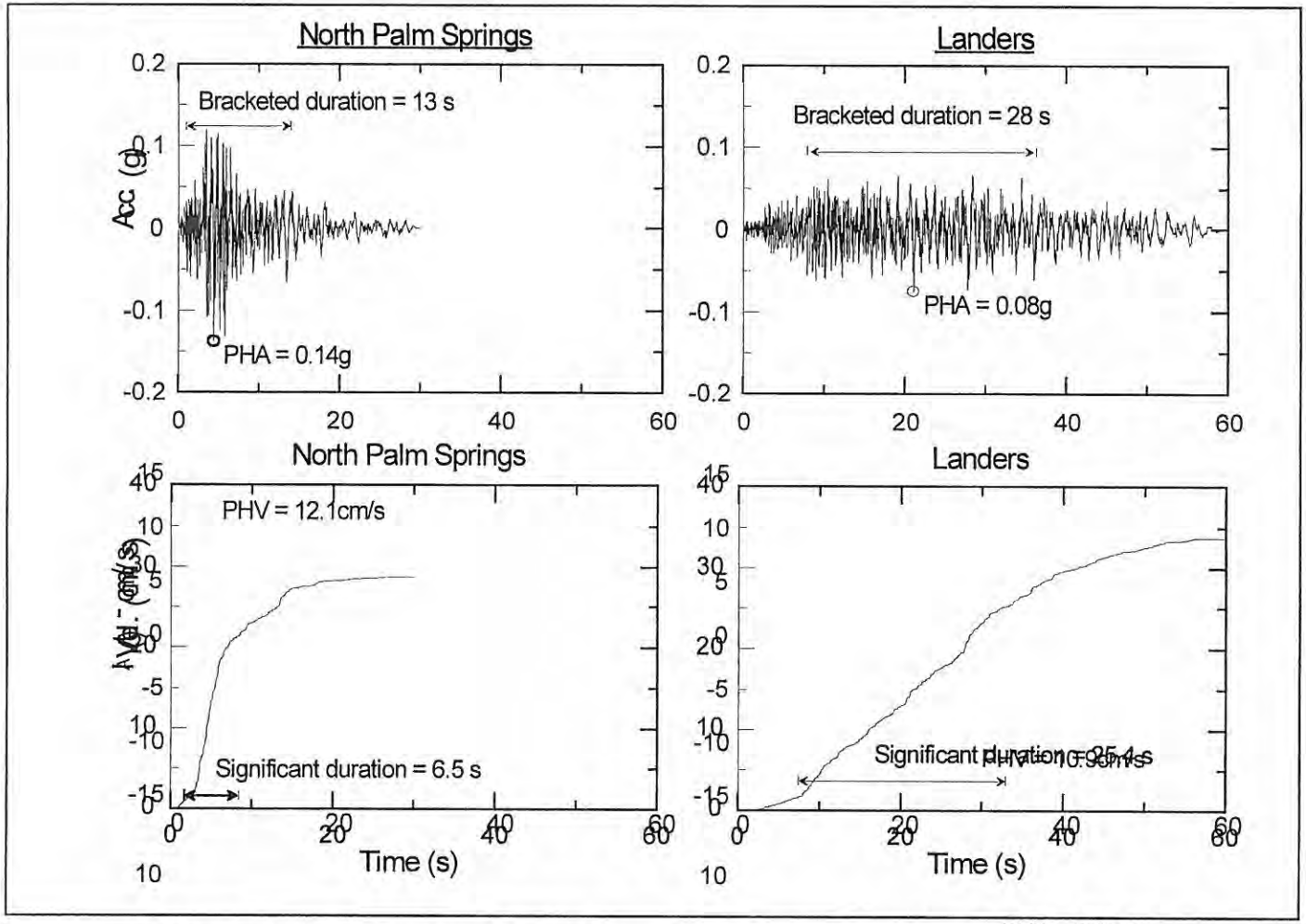

Note: values indicated in bottom frame are 5-75% Arias Duration

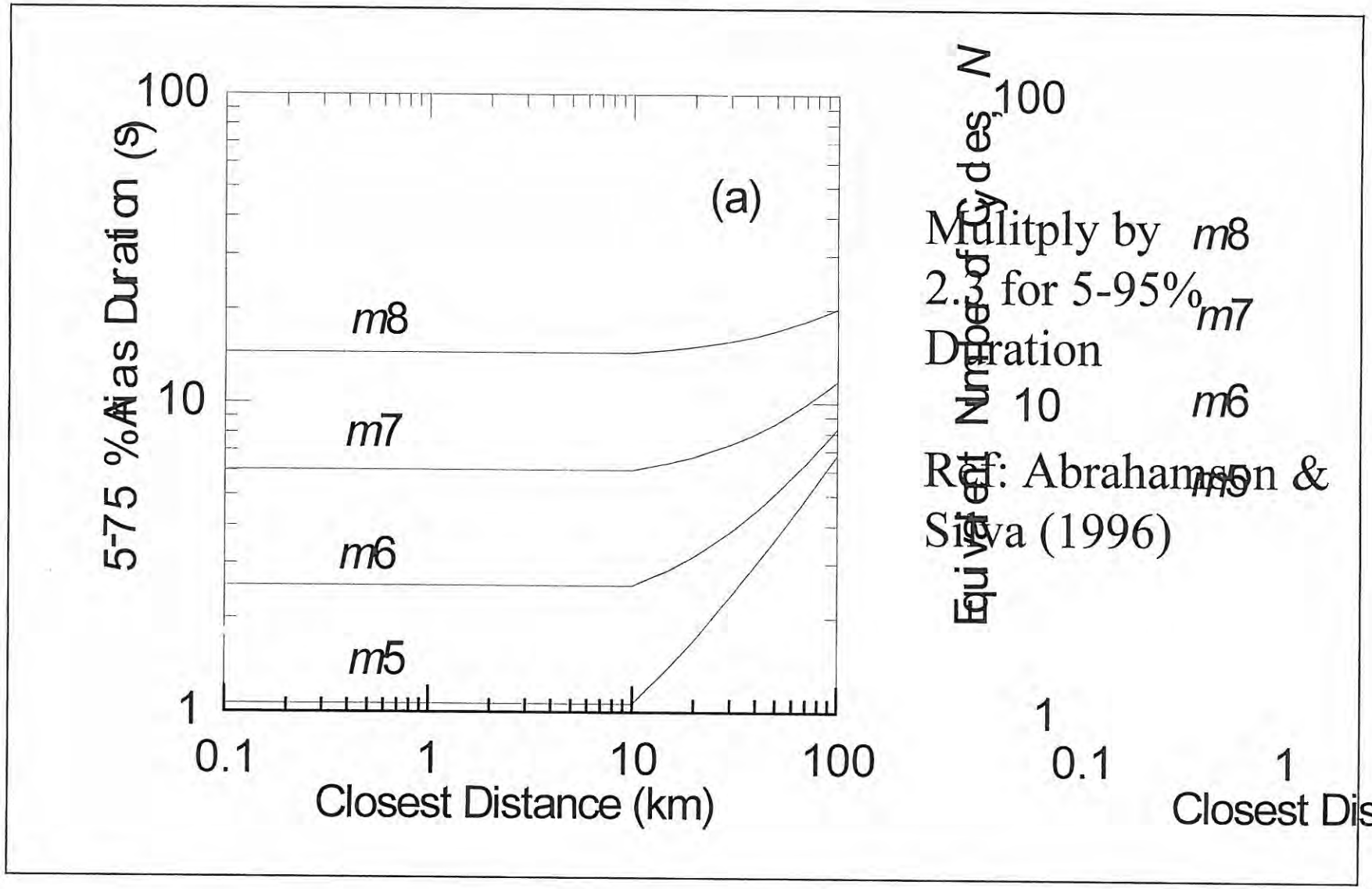
100
10
1
0.1
1
10
100
(a)
m8
m7
m6
m5
5-75 %Arias Duration (s)
Closest Distance (km)
Equivalent Number of Cycles, N
Mulitply by 2.3 for 5-95% Duration
Ref: Abrahamson & Silva (1996)

D. Pseudo-Static Analysis

Effects of earthquake on slide mass represented by equivalent static horizontal force.

Force taken as $k \times W$, where W = weight of slide mass.

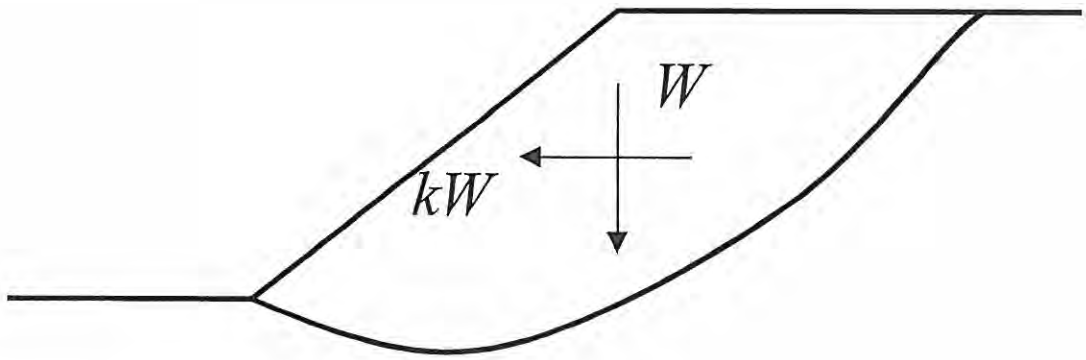

What is *k*?

- Ideally: Representative value of *HEA/g* calibrated to provide specified level of performance

  Note: slope performance strongly dependant on duration as well as amplitude.
- Should be related to seismicity of area.
- Practice: see attached

Calibrated formulations for k

U.S. Army Corps of Engineers (for earth dams):
$k = 0.5 \times MHA_{rock}/g$ with $F.S. \geq 1.0$ and 20% reduction in static material strengths. Calibrated for < 1 m displacements. [ref: Hynes-Griffen and Franklin, 1984]

Landfills:
$k = 0.75 \times MHA_{rock}/g$ with $F.S. \geq 1.0$ and "conservative" strengths (i.e., residual). Calibrated for < 15 cm displacements. [ref: Bray et al., 1998]

Calibrated formulations for k (continued)

<u>California Hazard Act Implementation Committee:</u>

$k = f_{eq} \times MHA_{rock}/g$ with $F.S. \geq 1.0$ and apporpriate dynamic strengths. Calibrated for < 5 cm or < 15 cm displacements.

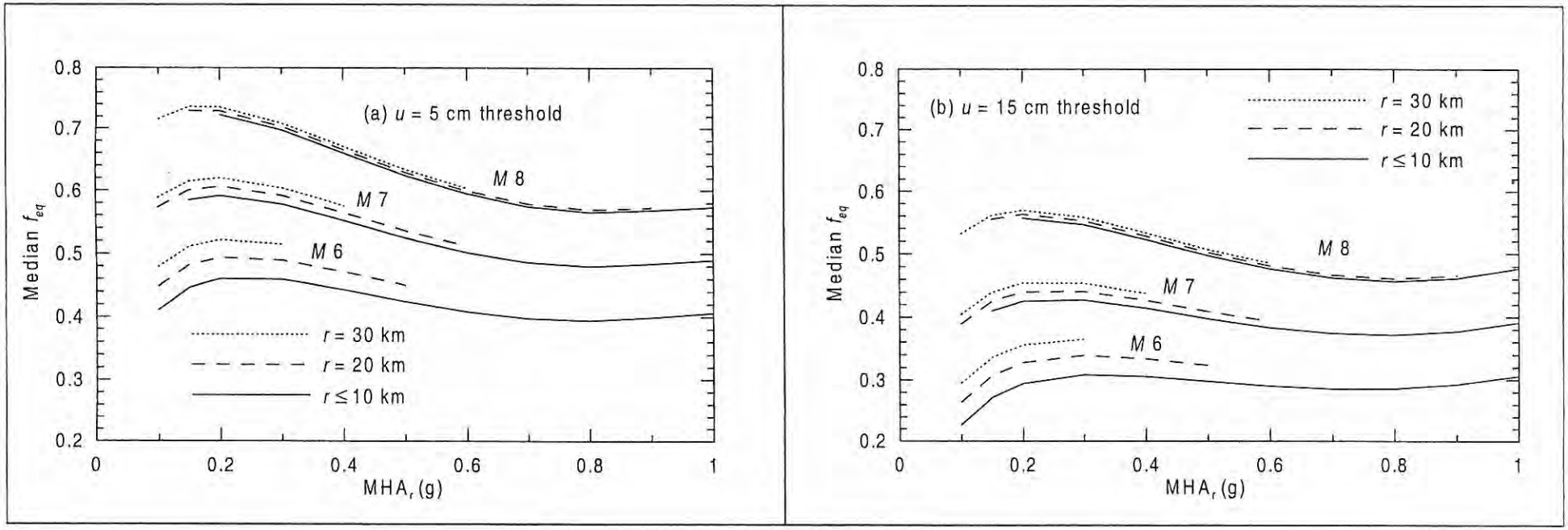

E. Slope Deformation Analysis Methods

- Newmark-type analyses
  - Assumptions
  - Analysis procedure
- Simplified methods
  - Makdisi and Seed, 1978
  - Bray and Rathje, 1998

Newmark Displacement Analysis

Assumptions:

- Well defined slip surface
- Sliding mass is rigid-perfectly plastic

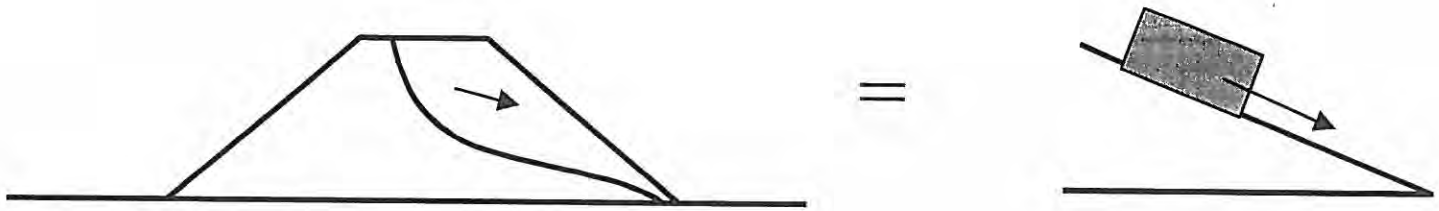

Key parameter: k_y=seismic coefficient that results in $F.S.$=1.0

Mechanics of the Analysis

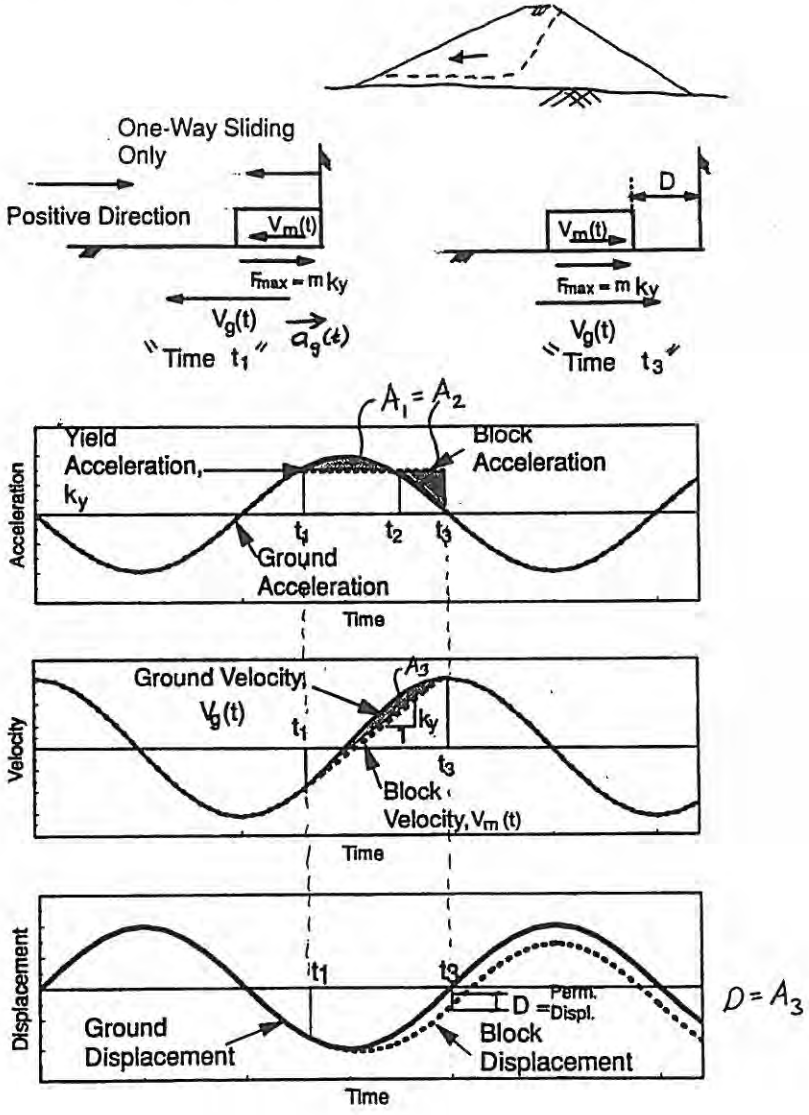

Ref: Franklin and Chang, 1977

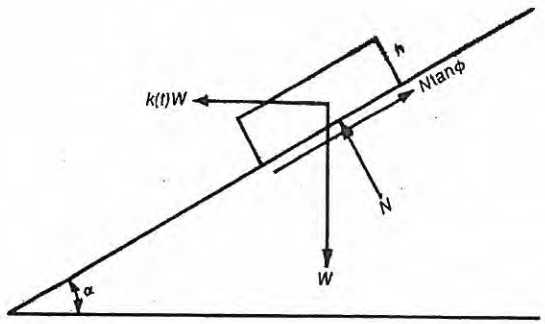

Fig. 16. Forces on sliding block

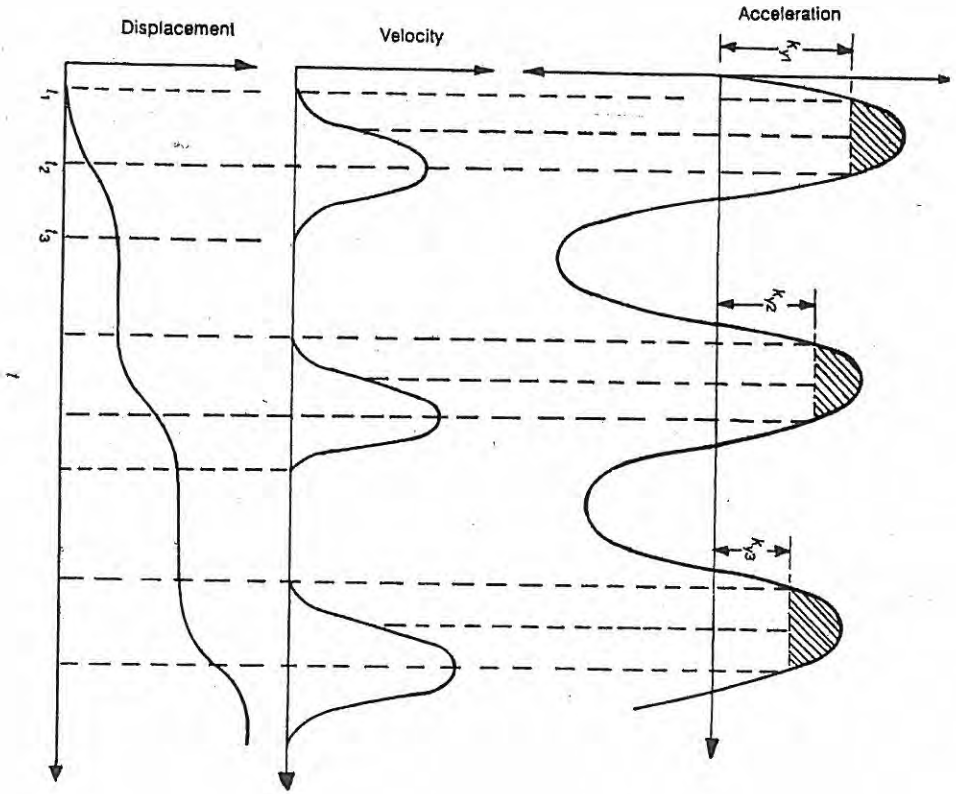

Ref: Seed, 1979

Procedure

- Compute *HEA(t)* for a given trial failure surface.
  - e.g.: QUAD4M, Hudson et al., 1994.
- Calculate k_y for this surface.
- Calculate displacement (u) using Newmark procedure
  - e.g.: TMNM, Pyke and Beikae, 1991.
- Repeat for other potentially critical failure surfaces
  - Use surface with minimum static F.S.
  - Use shallower surfaces as well.

Makdisi and Seed (1978) Simplified Procedure

Simplified slope displacement analysis procedure for earth dams. Based on Newmark displacement concept.

- Evaluate yield coefficient, k_y
- Estimate k_{max} from *MHA* at crest and distance below crest
- Estimate u from k_y/k_{max} and T_s

k_y estimated using "yield strength" of soil, defined as stress level below which material exhibits nearly elastic behavior.

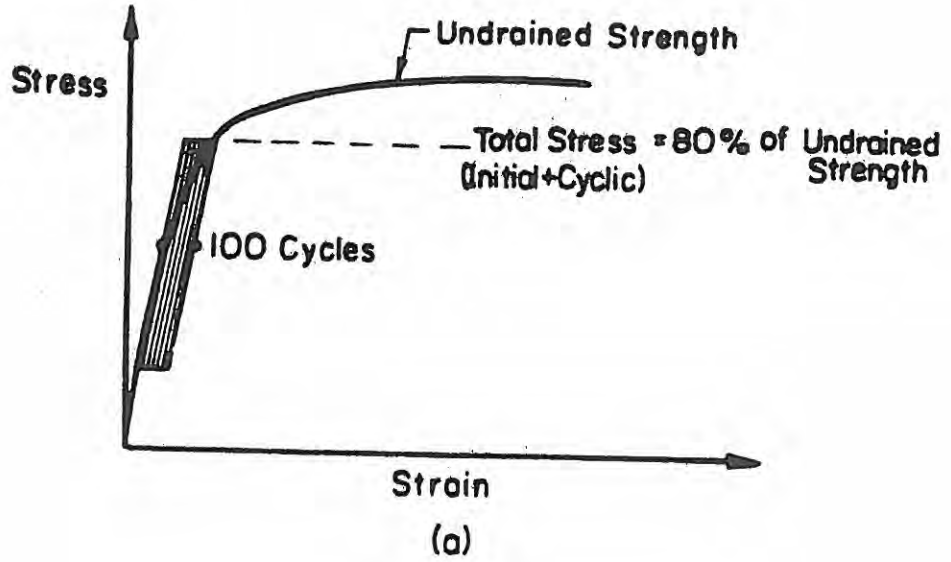

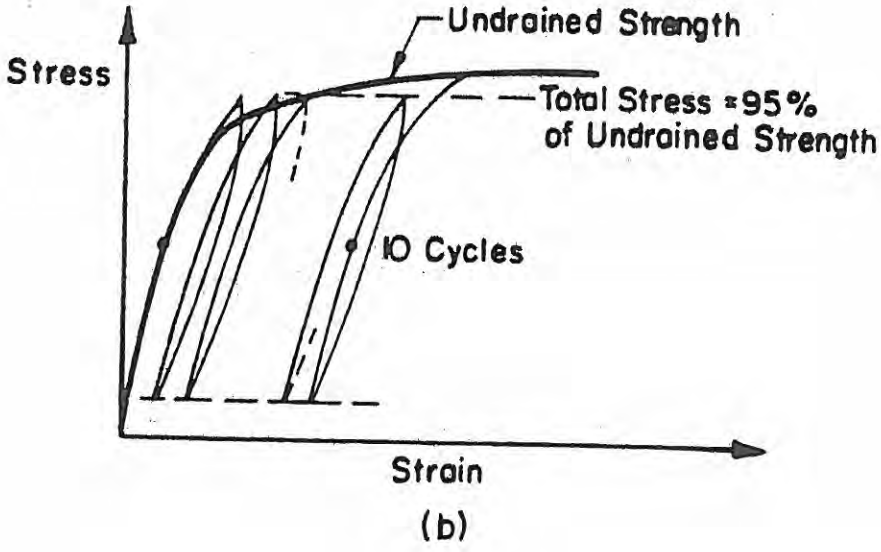

Ref: Makdisi and Seed, 1977

k_{max} evaluated from crest acceleration, MHA_{crest}.
$\rightarrow$ non-trivial analysis [see Makdisi and Seed, 1977 for procedure].

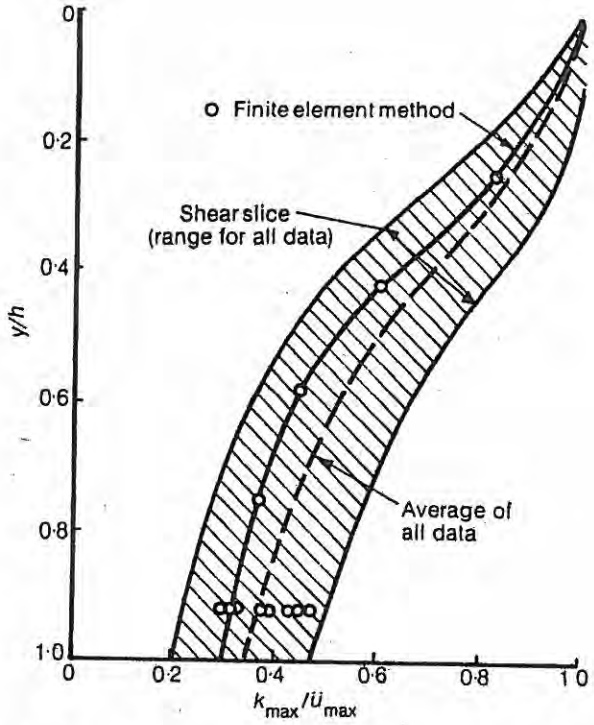

Fig. 19. Variation of effective peak acceleration, k_{max}, with depth of base of potential slide mass (after Makdisi and Seed)

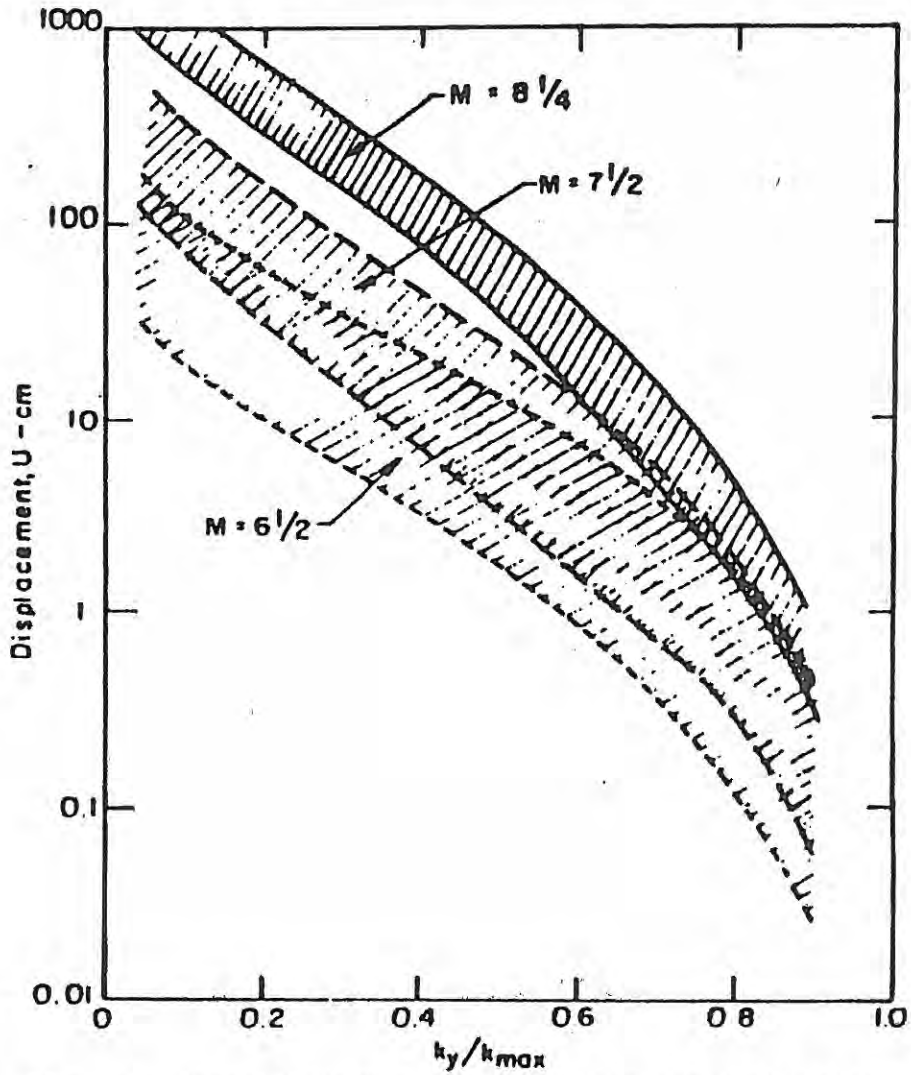

FIG. 14 VARIATION OF PERMANENT DISPLACEMENT WITH YIELD ACCELERATION - SUMMARY OF ALL DATA

Ref: Makdisi and Seed, 1977
NOTE: use 1977 report, not 1978 ASCE journal paper

Bray and Rathje (1998) Simplified Procedure

Similar to Makdisi and Seed, differences:

- Geometry of slide mass

- k_{max} (*MHEA*) evaluated from *MHA* at base
- Displacements u evaluated from k_y/k_{max} and $D_{5\text{-}95}$

Procedure

- Characterize ground motions
  - MHA_{rock} (peak acceleration of base motion)
  - T_m (mean period, evaluated for rock site condition)
  - $D_{5\text{-}95}$ (Arias duration, evaluated for rock site condition)
- Estimate seismic loading in slide mass
  - *MHEA* for base sliding
  - MHA_{top} for shallow surface sliding
  - Use $1.25 \times MHA_{top}$ near crest of slope
- Estimate k_y
- Estimate slope displacement, u
  - Base sliding
  - Shallow sliding (large scatter)

Base Sliding

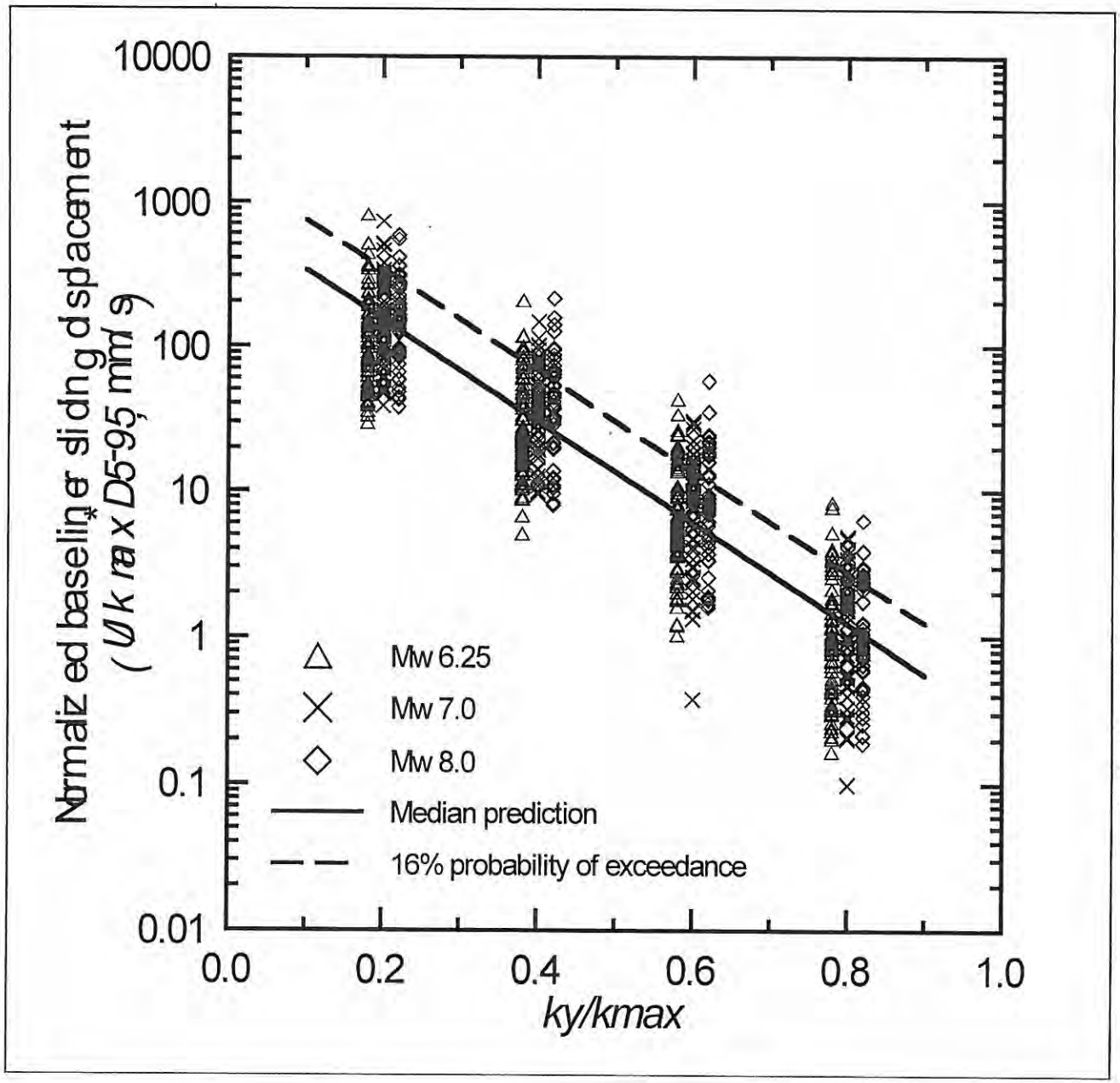

Ref: Bray and Rathje, 1998

Surface Sliding

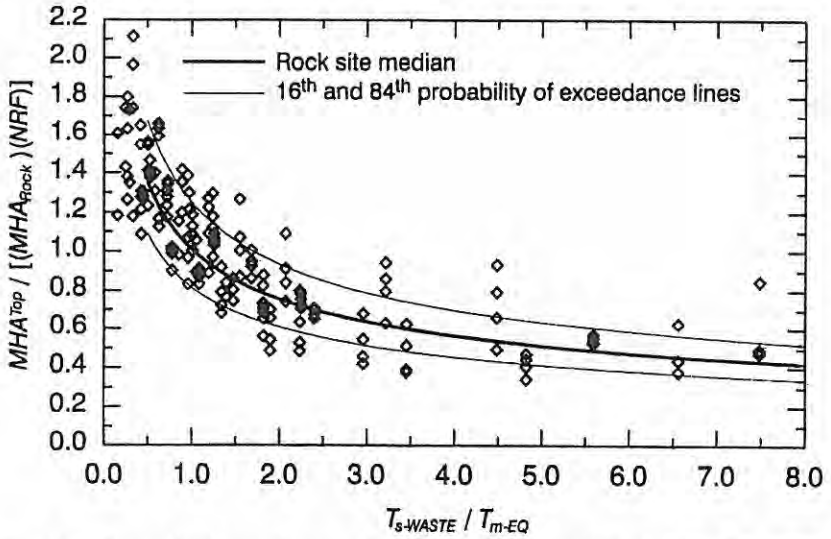

Figure 8. Normalized maximum horizontal acceleration at the top versus the normalized fundamental period of the waste fill (from Bray and Rathje 1998).

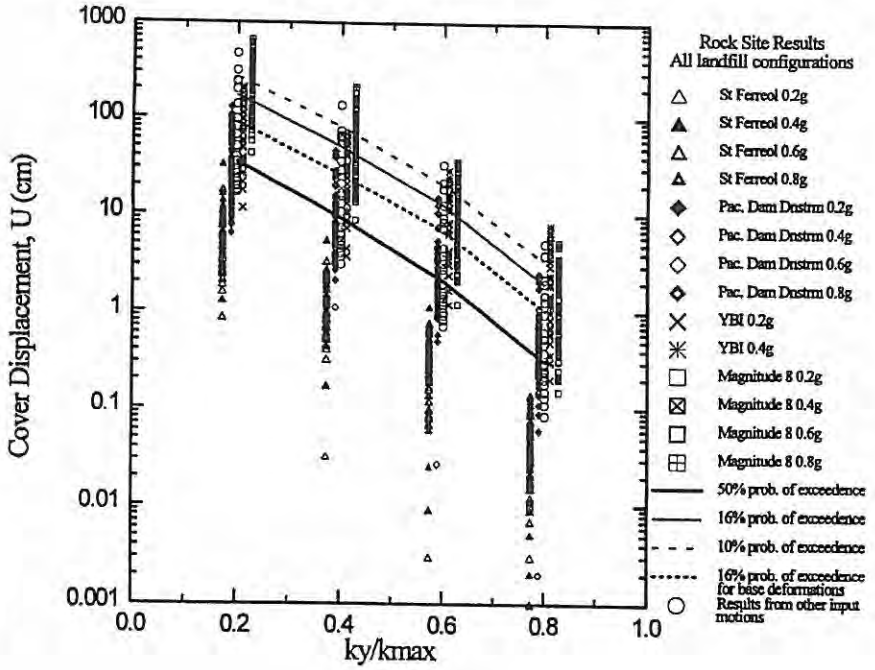

Synthesis

- First critical design issue: Will material undergo significant strength loss?
  - Liquefiable sands
  - Sensitive clays
- Second critical issue: Will earth embankment undergo significant deformation?
  - Screening analysis (pseudo-static)
  - Displacement analysis (Newmark or simplified technique)
  - What is an acceptable deformation?

F. California Hazard Act

- Requires state geologist (CDMG) to establish regulatory zones for seismic slope stability.
- Local agencies (cities, counties) regulate development within zones – generally site specific study to determine fault location required.
- Single family dwellings $\leq$ 2 stories exempt.
- Disclosure during real estate sales required.

BEL AIR COUNTRY CLUB
UNIV OF CALIFORNIA AT LOS ANGELES
Brentwood Heights
St Martin of Tours Sch
Barrington Recreation Center
SUNSET BLVD
BM 329
Hospital
SAN VICENTE BLVD
Brentwood Sch
BRENTWOOD COUNTRY CLUB
University High Sch
West Los Angeles

Sites within Hazard Zones

- Investigation required to assess landslide potential.
- If hazard is identified, appropriate mitigation measures must be taken.

Requires:

- Assessment of ground motion hazard.
- Detailed characterization of soil properties.
- Appropriate engineering analyses.

Guideline Documents

- CDMG Special Publication 117: *Generalized* guidelines for analysis, mitigation (1997) www.consrv.ca.gov/dmg/pubs/sp/117/index.htm
- Recommended Procedures for Implementation of CDMG SP 117 Guidelines
  - Liquefaction Hazards: published March 1999
  - Slope Stability Hazards: published February 2002?

Contents of Recommended Procedures Document for Slope Stability

- Geologic field investigations
- Sampling
- Evaluation of shear strength
- Static slope stability analysis
- Ground motion
- Seismic stability analysis
- Mitigation

REFERENCES

Abrahamson, N.A. and Silva, W.J. (1997). "Empirical response spectral attenuation relations for shallow crustal earthquakes," *Seism. Res. Letters*, 68(1), 94-127.

Bray, J.D. and Rathje, E.M. (1998). "Earthquake-induced displacements of solid-waste landfills," *J. Geotech. Geoenv. Engrg.*, ASCE, Vol. 124 (3).

Bray, J.D., Rathje, E.M., Augello, A.J., and Merry, S.M. (1998). "Simplified seismic design procedure for geosynthetic-lined, solid-waste landfills," *Geosynthetics International*, 5(1-2), 203-235.

Franklin, A.G. and Chang, F.K. (1977). "Earthquake resistance of earth and rockfill dams," *Misc. Paper S-71-17*, U.S. Waterways Experiment Station, Vicksburg, Mississippi, 57 p.

Hudson, M.B., Idriss, I.M., and Beikae (1994). "QUAD4M: A computer program to evaluate the seismic response of soil structures using finite element procedures and incorporating a compliant base," Ctr. for Geotech. Modeling, U.C. Davis.

Hynes-Griffin, M.E. and Franklin, A.G. (1984). "Rationalizing the seismic coefficient method," *Misc. Paper GL-84-13*, Geotechnical Laboratory, Waterways Experiment Station, U.S. Army Corps of Engineers.

Makdisi, F.I., and Seed, H.B., 1977, "A Simplified Procedure for Estimating Dam and Embankment Earthquake-Induced Deformations in Dams and Embankments," *Report No. EERC 77/19*, University of California, Berkeley.

Newmark, N.M., 1965, "Effects of Earthquakes on Dams and Embankments," *Geotechnique*, v. 15, n. 2, pp. 139-160.

Rathje, E.M., Abrahamson, N.A., and Bray, J.D. (1998). "Simplified frequency content estimates of earthquake ground motions," *J. Geotech.& Geoenv. Engrg.*, ASCE, 124(2), 150-159.

Seed, H.B. (1979). "Considerations in the earthquake-resistant design of earth and rockfill dams," *Geotechnique*, 29(3), 215-263.

Seed, H.B. and Martin, G.R. (1966). "The seismic coefficient in earth dam design," *J. Soil Mech. Fndns. Div.*, ASCE, 92(3), 59-83.

Sheahan, T.C., Ladd, C.C., Germaine, J.T. (1996). "Rate-dependant undrained shear behavior of saturated clay," *J. of Geotechnical Engineering*, ASCE 122(2), 99-108.

Skempton, A.W. (1985). "Residual strength of clays in landslides, folded strata, and the laboratory," *Geotechnique*, 35(1), 3-18.

TAB 8

Roger P. Heyman

Presentation

LEGAL ISSUES ASSOCIATED WITH SLOPE STABILITY AND LANDSLIDES:
Considerations for Geologists and Engineers

Presented at

Slope Stability and Landslides

University of Wisconsin-Madison
Department of Engineering Professional Development

February 2002
Los Angeles, California

by

Roger P. Heyman, Esq.
Kane, Ballmer & Berkman
515 S. Figueroa St., Suite 1850
Los Angeles, CA 90017
(213) 617-0480

TABLE OF CONTENTS

Page

I. INTRODUCTION 1

II. SUITS AGAINST PROFESSIONALS 2

A. Theories of Liability and General Rules 2

B. A Certificate Is a Prerequisite for a Suit for Malpractice or Negligence Against an Architect, Engineer or Surveyor in California 2

C. The Bar of the Statute of Limitations 2

III. STANDARD OF CARE FOR NEGLIGENCE LIABILITY 3

IV. LIABILITY FOR SLOPE FAILURE OR LAND SUBSIDENCE ON THE CONSTRUCTED PROJECT 3

A. Liability to the Developer/Owner 3

B. Liability to Subsequent Owners 3

C. Liability for the Intrusion of the Failed Slope Onto an Adjacent Landowner's Property 3

D. Typical Multi-Party/Multi-Plaintiff Lawsuit 3

E. Opportunities for Getting Out of the Mess Early 3

V. LIABILITY TO ADJACENT LANDOWNERS FOR DEPRIVATION OF SUBJACENT OR LATERAL SUPPORT 4

A. General Negligence Liability 4

B. Absolute (Strict) Liability (i.e., Liability Without Fault or Negligence) 4

1. The General Common (Case) Law 4

2. Some State Statutes Have Modified (Both Limiting and Expanding) the Common Law Rule of Absolute Liability for Deprivation of Lateral and Subjacent Support 5

a. California's Statute (Civil Code §832) is an example 5

b. Summary - The Effect of Civil Code §832 6

c. The Application of the Statute 7

d. The Requirements of the Statute 8

VI. ABSOLUTE LIABILITY FOR ULTRA-HAZARDOUS ACTIVITY 9

A. Absolute Liability Also Exists for Any Damage Caused by an "Ultra-hazardous" Activity 9

VII. EXCAVATION AND UNDERGROUND UTILITIES AND FACILITIES 9

A. Most States' Regulations Governing Excavation Contain Common Themes 9

B. Representative of These Statutes Are Those Found in Pennsylvania (Title 73, Section 176-182.3) 10

1. Engineer/Architect Obligations 10

2. Contractor Obligations 10

C. Things to Take Note Of 11

VIII. LIABILITY FOR THE DIVERSION OF SURFACE WATER 11

A. Definitions 11

B. There Are Three Basic Legal Approaches to the Diversion of Surface Waters in the United States, with Many Sub-variations on Each Throughout the Fifty States 11

1. The "Common Enemy Doctrine" 11

2. The "Civil Law Rule" 11

3. The "Rule of Reasonable Use" 12

4. The Modified Civil Law Rule adopted by California 12

IX. PRIVATE EMINENT DOMAIN 13

X. CONTRACTUAL PROVISIONS LIMITING OR IMPOSING LIABILITY 13

A. Contractual Limitation of Liability Clauses for the Professional 13

1. There are two principal contractual methods for limiting or allocating liability for damages due to professional negligence 13

2. Indemnity clauses 14

3. Limitation of Liability Clauses 16

B. Imposition of Liability by Contractual Scope Language 18

LEGAL ISSUES ASSOCIATED WITH LANDSLIDES:
Considerations for Geologists and Engineers

By Attorney Roger P. Heyman
Los Angeles, California

I. INTRODUCTION

Landslides cause property damage and bodily injury. Repairing landslide damage is often expensive. Public and private owners, and the independent geologists and engineers who are involved in excavation, grading, construction of embankments, or preservation of natural slopes, may have liability for the consequences of certain actions or inactions in the event of a landslide. The purpose of this paper is to discuss how such liabilities arise, as a matter of law, and how geologists and engineers can reduce their liability exposure for landslides.[1]

---

[1] This paper is not an exhaustive analysis and an attorney should be consulted as specific legal issues arise.

II. SUITS AGAINST PROFESSIONALS

A. Theories of Liability and General Rules

In general, lawsuits for loss of lateral or subjacent support, diversion of water, subsidence and landslide damage can be brought by the owner against the engineers and geologists retained by him on legal theories of negligence, breach of warranty and breach of contract. Lawsuits can be brought by subsequent owners and neighboring landowners on legal theories of negligence, nuisance and trespass.

B. A Certificate Is a Prerequisite for a Suit for Malpractice or Negligence Against an Architect, Engineer or Surveyor in California

No lawsuit may be brought against an architect, engineer or surveyor in California unless a certificate is filed attesting to the fact that a licensed professional in the defendant's field has concluded that there is a reasonable and meritorious cause for the filing of the action and that the defendant was negligent in the performance of the applicable professional services (or unless the plaintiff's attorney declares that he contacted three such professionals and none would make the requisite statements). C.C.P. §411.35.

C. The Bar of the Statute of Limitations

1. Statutes of limitations bar lawsuits a specified number of years after the subsidence or other damage occurs. Suits arising out of construction are governed by the basic statutes of limitations applicable to the legal theory pled, as well as by overall "outside" statutes of limitation, also known as statutes of repose.

    a. The basic statutes of limitations.

        i. The time period provided by basic statutes depends on the theory pled. It is, for example, one year for personal injury, two years for breach of an oral contract, three years for property damage, three years for negligence, nuisance and trespass and four years for breach of a written contract.

    b. The outside statutes of repose.

        i. The "outside" limits for lawsuits for property damage arising out of construction claims, regardless of when the damage occurs, is four years after "substantial completion" of construction for "patent" defects and ten years after substantial completion of construction for "latent" defects. C.C.P. §337.1 and §337.15.

        ii. Exception, if an owner is sued <u>within</u> the ten-year limit, he can sue the contractor and the consultants for indemnity <u>after</u> the 10-year period C.C.P. §337.15(c).

III. STANDARD OF CARE FOR NEGLIGENCE LIABILITY

A. A professional is liable in negligence only for failure to meet the "standard of care." That standard is the "care and skill ordinarily used in like cases by reputable members of the same profession practicing in the same locality under similar circumstances." BAJI 6.37, 6.32.1, 6.32.2, 6.37.3.

B. Expert testimony is required to establish both the standard and the breach thereof in any suit against a professional. BAJI 6.32.4.

IV. LIABILITY FOR SLOPE FAILURE OR LAND SUBSIDENCE ON THE CONSTRUCTED PROJECT

A. Liability to the Developer/Owner

1. Contractual liability (breach of contract, breach of warranty, indemnity) as well as tort liability (negligence)

B. Liability to Subsequent Owners

1. Tort liability only (negligence)

C. Liability for the Intrusion of the Failed Slope Onto an Adjacent Landowner's Property

1. Tort liability (nuisance, trespass as well as negligence)

D. Typical Multi-Party/Multi-Plaintiff Lawsuit

With any multi-unit development, the lawsuit typically involves claims:

(i) By the ultimate purchasers against the developer for strict liability, breach of contract and negligence

(ii) By affected adjacent landowners for nuisance, trespass and negligence

(iii) Cross-claims by the developer against the engineers and geologists for indemnity, breach of contract, breach of warranty and negligence

(iv) (Sometimes) Directly by the ultimate purchasers /affected adjacent landowners against the engineers and geologists for negligence

E. Opportunities for Getting Out of the Mess Early

1. Policy limit offers

2. Good faith settlements with the most reasonable party (developer/ultimate purchaser)

V. LIABILITY TO ADJACENT LANDOWNERS FOR DEPRIVATION OF SUBJACENT OR LATERAL SUPPORT

A. General Negligence Liability

Excavation done in a negligent manner which deprives neighboring land of its subjacent or lateral support creates liability against the excavating owner and the professionals participating in that excavation for damages to the neighboring land and to any structures thereon. See Section III hereinabove.

B. Absolute (Strict) Liability (i.e., Liability Without Fault or Negligence)

1. The General Common (Case) Law

a. The owner of land who excavates on it has absolute liability for any subsidence to coterminous (contiguous) land in its natural condition resulting from a loss of subjacent or lateral support, even if the excavation is done properly and without negligence.

b. The common law rule of absolute liability applies only to coterminous properties. *Puckett v. Sullivan* (1961) 190 Cal.App.2d 489, 494; *Travelers Indemnity Co. v. City of Redondo Beach* (1994) 28 Cal.App.4th 1432, 1443. There is no liability to non-contiguous properties unless the excavation was done negligently.

c. The common law of absolute liability also applies only to the land in its natural condition; it does not apply to any structures built thereon. There is no liability for damage to the structures unless the excavation was done negligently. *Conlin v. Coyne* (1937) 19 Cal.App.2d 78, 87-88.

i. However, the absolute duty to protect the land in its natural condition is not eliminated by the imposition of structures on the land unless the downward pressure of their artificial weight contributes to the subsidence. The excavator is liable for damages to the coterminous land if the land would have subsided even if the structures had not been built, but he is not liable if the land subsided because of the added weight of the structures. *Platts v. Sacramento Northern Ry.* (1988) 205 Cal.App.3d 1025, 1030. The defendant has the burden of proving that the land would not have subsided had the structures not been built. *Marin Municipal Water Dist. v. Northwestern Pac. R. Co.* (1967) 253 Cal.App.2d 89, 96, 97.

d. The landowner's cause of action against the excavator arises when the land subsides, not when the excavation is made. *Marin Municipal Water Dist. v. Northwestern Pac. R. Co.* (1967) 253 Cal.App.2d 89, 96. Thus, the landowner at time of the subsidence is entitled to sue even if the excavation was made prior to his acquisition of the adjoining land, and the owner at the time of the excavation remains liable even if he sells his excavated property.

2. Some State Statutes Have Modified (Both Limiting and Expanding) the Common Law Rule of Absolute Liability for Deprivation of Lateral and Subjacent Support[2]

a. California's Statute (Civil Code §832) is an example. The Statute provides:

> "§832. Lateral and subjacent support; excavations; degree of care; damages; protection of other structures
>
> Each coterminous owner is entitled to the lateral and subjacent support which his land receives from the adjoining land, subject to the right of the owner of the adjoining land to make proper and usual excavations on the same for purposes of construction or improvement, under the following conditions:
>
> 1. Any owner of land or his lessee intending to make or to permit an excavation shall give reasonable notice to the owner or owners of adjoining lands and of buildings or other structures, stating the depth to which such excavation is intended to be made, and when the excavating will begin.
>
> 2. In making any excavation, ordinary care and skill shall be used, and reasonable precautions taken to sustain the adjoining land as such, without regard to any building or other structure which may be thereon, and there shall be no liability for damage done to any such building or other structure by

---

[2] Rules governing lateral support and excavations are also found in state and local building codes and ordinances. Care should be taken to become familiar with these codes and ordinances.

reason of the excavation, except as otherwise provided or allowed by law.

3. If at any time it appears that the excavation is to be of a greater depth than are the walls or foundations of any adjoining building or other structure, and is to be so close as to endanger the building or other structure in any way, then the owner of the building or other structure must be allowed at least 30 days, if he so desires, in which to take measures to protect the same from any damage, or in which to extend the foundations thereof, and he must be given for the same purposes reasonable license to enter on the land on which the excavation is to be or is being made.

4. If the excavation is intended to be or is deeper than the standard depth of foundations, which depth is defined to be a depth of nine feet below the adjacent curb level, at the point where the joint property line intersects the curb and if on the land of the coterminous owner there is any building or other structure the wall or foundation of which goes to standard depth or deeper then the owner of the land on which the excavation is being made shall, if given the necessary license to enter on the adjoining land, protect the said adjoining land and any such building or other structure thereon without cost to the owner thereof, from any damage by reason of the excavation, and shall be liable to the owner of such property for any such damage, excepting only for minor settlement cracks in buildings or other structures."

b. Summary - The Effect of Civil Code §832

i. The common law provides for absolute liability for damage to coterminous land in its natural state and negligence liability for damage to non-coterminous land and for damage to structures on coterminous or non-coterminous land.

ii. The changes made by the Statute (where it applies):

(1) The Statute <u>eliminates</u> absolute liability to the coterminous land in its natural state where the excavation is above the

"standard depth" -- as long as the statutory conditions of notice and ordinary care are complied with.

(2) The Statute expands absolute liability to damage to the structures where the excavation is below the "standard depth."

(3) The Statute leaves unchanged absolute liability for subjacent support.

(4) The Statute leaves unchanged negligence liability for damages to land or structures on coterminous or non-coterminous land

c. The Application of the Statute

i. The Statute applies only to lateral support, not to subjacent support between surface/subsurface landowners. *Marin Municipal Water Dist. v. Northwestern Pac. Ry. Co.* (1967) 253 Cal.App.2d 83, 91.

ii. The Statute applies only to coterminous properties. *Marin Municipal Water Dist. v. Northwestern Pac. Ry. Co.* (1967) 253 Cal.App.2d 83, 91.

(1) The common law right of absolute liability for deprivation of subjacent support and of negligent liability for non-coterminous properties thus remains the law. *Puckett v. Sullivan* (1961) 190 Cal.App.2d 489; *Travelers Indemnity Co. v. City of Redondo Beach* (1994) 28 Cal.App.4th 1432, 1443.

iii. The Statute does not apply to parcels which were both owned by the excavator at the time of the excavation (because no notice could be given). *Daniels v. McPhail* (1949) 209 P.2d 19.

iv. The Statute Is Not Applicable to Public Entities

(1) A public entity's liability for loss of lateral or subjacent support is not governed by the Statute or by the Common Law. It is governed by the law of Inverse Condemnation under which a public entity must compensate the owner for a "taking" if an excavation causes damage by the deprivation of lateral or subjacent support, without regard to negligence and without regard to notice. *Holtz v. Superior Court* (1976) 3 Cal.3d 296, 301.

d. The Requirements of the Statute

i. The "Standard Depth"

(1) The "standard depth" is defined in the Statute as "nine feet from the adjacent curb level at the point where the joint property line intersects the curb."

(a) This contemplates side by side property on flat land only.

(b) The policy of the Statute, however, would seem to be best served whenever the excavation is nine feet below the natural grade level of the adjoining property.

ii. The Requirements of the Statute When the Excavation is Above the "Standard Depth."

(1) Notice must be given to the owner.

(a) The notice must be reasonable and advance notice and it must state the depth to which the excavation will be made and when it will begin.

(i) Actual knowledge of the excavation does not excuse formal notice unless it is coextensive with the information that the excavator was required to give. *McIvor v. Mercer-Fraser Co.* (1946) 76 Cal.2d 247, 252-253.

(2) The excavator must use "ordinary care and shall take reasonable precautions to sustain the adjoining land."

iii. The Requirements of the Statute When the Excavation is Below the "Standard Depth."

(1) The notice must be at least 30 days in advance of any below standard depth excavation (or "reasonable" notice, whichever is greater).

(a) The purpose of the notice is to permit the adjoining landowner, if he so desires, to protect his land and buildings.

(i) The excavation must allow the adjoining landowner entry on the excavated land to do protective work.

(b) The 30-day notice requirement applies whenever it becomes apparent that excavation will go below the standard depth, even if the original intent was not to do so.

(2) If the depth of the excavation exceeds the "standard depth" defined by the Statute and the foundation or wall of an adjoining building is at or below the "standard depth," then the excavator must, if given the necessary license to enter on the adjoining land, protect the land and structures thereon from any damage, at the excavator's cost and risk, i.e., the Statute creates absolute liability for damage to the land and to the structures for below standard depth excavations.

(3) The owner of the adjacent land is not required to do anything and his failure to protect his land does not relieve the excavator from using ordinary care and from taking the necessary precautions to sustain the adjoining property. *Cornet Stores v. Security Trust & Savings Bank of San Diego* (1953) 120 Cal.App.2d 852, 854.

VI. ABSOLUTE LIABILITY FOR ULTRA-HAZARDOUS ACTIVITY

A. Absolute Liability Also Exists for Any Damage Caused by an "Ultra-hazardous" Activity

1. Blasting in populated areas has been held to be ultra-hazardous.

2. Normal excavation/grading has been held not to be ultra-hazardous.

VII. EXCAVATION AND UNDERGROUND UTILITIES AND FACILITIES

A. Most States' Regulations Governing Excavation Contain Common Themes

1. Generally, these "excavation" statutes require prior notification by the excavating contractor (and in some cases the architect/engineer during design phase) to the owners of underground facilities that excavation will be occurring in the general vicinity of the underground facilities.

2. The majority of the states have adopted a "one call" system, wherein the excavator need only call one number to notify all area underground facility owners of the

excavation. The statutes typically require participation by the various underground facility owners in the "One-Call" system.

3. Upon receipt of notification by an excavator, facility owners must, within a very short period, go out to the site and mark the exact location of the underground facilities.

4. Contractors typically remain liable for their own negligence during excavation (e.g., subsidence of land as a result of the excavation causing damage to underground facilities).

B. Representative of These Statutes Are Those Found in Pennsylvania (Title 73, Section 176-182.3):

1. Engineer/Architect Obligations

All "designers" (defined in the statute as "any architect, engineer or other person who or which prepares a drawing for a construction or other project which requires excavation. . . ."), preparing drawings requiring excavation must request information regarding underground facilities from the owners "not less than ten nor more than ninety working days before final design is to be completed." The location information obtained must be set forth on the drawings and he must make a reasonable effort to prepare the construction drawings to avoid damage to a facility owner's underground facilities "by maintaining an eighteen inch clearance of the facility owner's facilities."

a. A designer is deemed to have met his statutory obligations under the statute if he calls the state's "One-Call" system and shows as proof the serial number of his "One-Call Notice" on the drawings.

1) Any designer who has complied with the Statute, and who is not otherwise negligent, shall not be subject to liability to facility owners for any damage to their property as a result of the excavation.

2. Contractor Obligations

a. Excavating contractors must request the location and type of facility owner lines at each site by notifying the facility owner of upcoming excavation through the state's One Call System, not less than three nor more than ten working days in advance of the excavation.

1) Facility owner must, not more than two working days after receipt of a request from a contractor, mark its underground lines at the site "within eighteen inches horizontally from the outside wall of

such line in a manner so as to enable the contractor, where appropriate, to employ prudent techniques . . ."

2) Any contractor complying with the terms of the Statute, and who is not otherwise negligent, shall not be subject to liability to facility owners as a result of any damage from the excavation.

C. Things to Take Note Of

1. Before starting a project, design professionals and excavators should check, among other things, their individual state's applicable statutes paying special attention to who is required to do what, what depth of excavation activates the statute, what prior notice is required, when the prior notice is required to be given and by what mechanism.

2. Failure to adhere to statutory requirements, that in turn causes damage, will likely be deemed negligence per se.

VIII. LIABILITY FOR THE DIVERSION OF SURFACE WATER AND WATERCOURSE (SURFACE AND SUBSURFACE) WATER

A. Definitions

"Surface water" is defined in California as "water diffused over the surface of land, or contained in depressions therein, and resulting from rain, snow, or which rises to the surface in springs." "Watercourse water" is defined as "water flowing in a fixed channel." *Locklin v. City of Lafayette* (1994) 7 Cal.4th 327, 345. Watercourse water may flow in a channel upon the surface of the land or in an underground channel. *City of Los Angeles v. Pomeroy* (1899) 124 Cal. 597, 693. The diversion of "subsurface water" thus refers to the diversion of an underground watercourse.

B. There Are Three Basic Legal Approaches to the Diversion of Surface Waters in the United States, with Many Sub-variations on Each Throughout the Fifty States

1. The "Common Enemy Doctrine"

a. Each landowner has an unqualified right to deal with and protect himself from surface water as he sees fit, without regard to the effect on his neighbors. This Doctrine is often qualified with concepts of reasonable use or negligence.

2. The "Civil Law Rule"

a. The landowner must accept the surface waters which naturally drain onto his land, but the upper owner is absolutely liable to the lower owner for

any alteration of the natural system of drainage which increases the burden.

3. The "Rule of Reasonable Use"

   a. The courts weigh the reasonableness of the upper and lower landowners' actions and assess liability based upon the facts of each case.

   b. This is a compromise rule between the no liability effect of the Common Enemy Rule and the full liability effect of the Civil Law Rule. It weighs the reasonableness of the upper and lower landowners' actions and assesses liability based upon the facts of each case.

4. The Modified Civil Law Rule adopted by California

   a. California has adopted a Modified Civil Law Rule. *Keys v. Romley* (1966) 64 Cal.2d 396; *Louie v. Gdowski* (2000) 84 Cal.App.4th 1395 for surface water and *Weaver v. Bishop* (1988) 206 Cal.App.3d 1351, 1355-1356 and *Locklin v. City of Lafayette* (1994) 7 Cal.4th 327, 356-357 for watercourses, whether above or below ground. The Modified Civil Law Rule where water, surface or subsurface, is diverted directly onto the lower owner's property is that the upper landowner is liable to the lower owner for damages caused by such diversion under all circumstances except in the case where the upper owner acts reasonably and the lower owner acts unreasonably.

   b. In list form the effect of the Modified Civil Rule for diversion of water directly onto the lower property is:

      i. If both the upper and lower landowners act reasonably, the upper owner is liable to the lower owner.

      ii. If both the upper and lower landowners act unreasonably, the upper owner is liable to the lower owner. *Sheffet v. County of Los Angeles* (1970) 3 Cal.App.3d 720, 727, 729, 730, fns. 6 and 8.

      iii. If the upper owner acts unreasonably, and the lower owner acts reasonably, the upper owner is liable to the lower owner.

      iv. Only if the upper owner acts reasonably and the lower owner acts unreasonably is the upper owner not liable to the lower owner.

   c. In any event, the cost of reasonable steps taken by the lower owner to avoid or diminish the damage to his land are to be borne by the upper owner.

d. "Reasonableness" depends upon such factors as the amount of harm caused, the foreseeability of the harm, the purpose or motive of the diverter and a comparative weighing of the utility of the alteration of the drainage to the upper owner and the burden on the lower owner.

c. Examples of unreasonable behavior by the lower landowner are:

i. Improperly obstructing the flow of the waters over his land.

ii. Altering his property so as to permit the water to damage it.

iii. Failing to take reasonable steps to avoid or reduce his injury.

Burrows v. State (1968) 260 Cal.App. 29, fn. 2.

5. There is one anomaly in this area, and that deals with the liability for the diversion of surface water into a watercourse which increases the flow of that watercourse to the damage of the lower property. Because the diversion of surface water into a natural watercourse was historically governed not by the Civil Law Rule but by the "Common Enemy Doctrine" (Section VIII.A.1.), the upper landowner is not liable for damage to the lower landowner except in the case where the upper landowner acts unreasonably and the lower landowner acts reasonably. *Locklin v. City of Lafayette* (1994) 7 Cal.4th 327, 360. This is the opposite result from the diversion of surface water or watercourse water directly onto the lower property where the upper landowner is liable for damages except in the case where he acts reasonably and the lower landowner acts unreasonably.

IX. PRIVATE EMINENT DOMAIN

If a coterminous landowner refuses an excavator or diverter entry onto his land for the purpose of protecting it and avoiding liability, or attempts to extort an unreasonable sum therefor, there exists a little used civil action for "Private Eminent Domain" to force right of entry upon the payment of reasonable rent onto an adjacent or nearby property when the repair or reconstruction of land or improvement requires entry onto that property. Civil Code §1002.

X. CONTRACTUAL PROVISIONS LIMITING OR IMPOSING LIABILITY

A. Contractual Limitation of Liability Clauses for the Professional

1. There are two principal contractual methods for limiting or allocating liability for damages due to professional negligence.

a. Clauses indemnifying the professional against claims by third parties.

b. Clauses limiting the professional's liability to the owner.

Each will be addressed in turn.

2. Indemnity clauses

a. Under these clauses the owner indemnifies the professional against liability to third parties.

b. Civil Code §2782 and its related provisions set forth the legal parameters for indemnity clauses in design and construction contracts.

(1) Indemnity for Professional's Sole Negligence

(a) Section 2782(a) prohibits indemnity agreements that attempt to indemnify the responsible party for his sole negligence, willful misconduct, or for defects in designs furnished by such party. (There is a similar statute in Washington voiding indemnity for sole negligence. Wash. Rev. Code §4.24.115)

(i) Section 2782 does not preclude the professional from obtaining insurance for his sole negligence.

(2) Partial Negligence

(a) Section 2782 does not preclude a professional from obtaining indemnity for his partial (i.e., comparative) negligence. *Armco Steel Corp. v. Cox* (1980) 103 Cal.App.3d 929, 933.

(i) Example: Engineer Smith is found 60% negligent and Owner Jones 40% negligent in connection with a loss caused to Joe Q. Public. Smith has a valid indemnity clause in its contract with Jones. Both Smith and Jones are 100% responsible to pay J. Q. Public. But, Engineer Smith can recoup any money it has to pay from Jones under the indemnity clause. Only if Smith were solely negligent would indemnity be barred.

(b) Indemnity clauses must be drafted with specific language that conveys the intent to indemnify a party for its own, partial negligence and recognizes the invalidity of sole negligence clauses. *Armco Steel Corp. v. Cox* (1980) 103 Cal.App.3d 929, 934-935.

(c) Typical language would read:

(i) "Owner shall indemnify professional for all liabilities and losses arising from performance, regardless of whether caused in part by professional's passive or active negligence, except if caused by the professional's sole negligence, wilful misconduct or arising from defective designs furnished by professional." This is called a Type I clause.

(d) Absent such a Type I indemnity clause, you will be indemnified only for your passive negligence. (Type II)

(e) Civil Code §2782.6 qualifies the foregoing prohibition by permitting professional engineers and geologists to obtain indemnity for any loss (including those caused by sole negligence or defects in design they furnish) if the services rendered address "subterranean contamination or other concealed conditions caused by hazardous materials."

(i) Such indemnification, however, is not applicable to the first $250,000 of liability or such greater amount as may be agreed upon between the parties and is not applicable to gross negligence or willful misconduct.

(ii) Civil Code §2782.6 does not apply to public agencies as defined in Government Code §811.2 (state, county, city, district, public authority, public agency, Regents and any other political subdivision or public corporation of state).

c. Keep in mind that any indemnity is only as good as the financial ability of the indemnitor to pay for any loss covered by the indemnity.

d. In drafting or reviewing indemnity clauses, other issues to watch for are:

(1) Does the indemnity include an obligation to defend?

(2) Does the indemnity provide a right to attorney's fees for both the defense of a suit by a third party and for the prosecution of a suit to enforce the indemnity if necessary?

(3) Does the indemnity cover all liability and losses?

(4) Does the indemnity cover all types of damages, or only personal injury and property damage? Many indemnity clauses are drafted to cover only these damages, so that they will co-extensive with the indemnitor's insurance coverage. However, this is not a legal requirement.

(5) Does the indemnity cover only losses and liability caused by "fault?" For example, does it also cover breach of contract or other theories of liability?

(6) Does the indemnity give the indemnitee the right to approve of the selection of legal counsel?

e. Another means of obtaining protection through indemnity is to include a contract provision requiring the owner to include an obligation in its general contract that requires the contractor and its subcontractors to provide a defense and indemnity not only to the owner, but to the professional as well. Such extended indemnity obligations are commonly used, for example, by the American Institute of Architects in its standard A-210 General Conditions form.

(1) Be sure to also require that the contractor and subcontractors obtain contractual assumption of liability insurance coverage that would include coverage of their indemnity obligation.

3. Limitation of Liability Clauses

a. These clauses limit the professional's liability to the entity that retained him.

b. Civil Code §2782.5 provides that such provisions are valid if "negotiated and expressly agreed to."

c. Interpreting that Statute liberally, a Court of Appeal has ruled that limitation of liability clauses are enforceable as long as they are not "unreasonable" and as long as each party to the contract had an "opportunity" to accept, reject or modify the clause. *Markborough California, Inc. v. Superior Court* (1991) 227 Cal.App.3d 705.

i. However, in an unpublished opinion, another appellate court reached the conclusion that a limitation of liability clause was not enforceable against a relatively unsophisticated private, residential owner merely based on the "opportunity to negotiate." *Viner v. Brockway* (1994) 30 Cal.App.4th 1307. Rather, the court held the professional's evidence would have to satisfy a number of other tests, including possibly demonstrating that the professional did not

possess superior bargaining strength and that the professional offered the owner the opportunity to buy other protection against negligence (such as insurance).

d. Types of limitation of liability clauses.

(1) There are 5 types of limitation of liability clauses typically used by professionals:

(a) Liability limited to fees: Where the liability of the professional is limited to all or a portion of the fees paid.

(b) Liability limited to fixed sum: Where the liability of the professional is limited to a fixed, not-to-exceed" sum.

(c) Liability limited to insurance: Where the liability of the professional is limited to proceeds of insurance, such as professional liability insurance.

(d) Mixed fee/insurance: Where the liability of the design professional is to limited a portion of fees, plus insurance proceeds. Some clauses will further require that recourse to insurance proceeds be exhausted before there may be recovery against the professional's assets.

(e) Consequential damages waiver: Where the owner waives entirely the right to recover consequential damages, such as loss of income, prospective business opportunity, or the like.

(2) Limitation of liability clauses are tricky to draft an a manner that is enforceable and the rules can vary from state to state. A lawyer should be consulted.

(3) An example of a limitation of liability is that used by the geotechnical firm, Leighton, in the *Viner* case:

> "Unless otherwise negotiated in writing, client agrees to limit any and all liability, claim for damages, cost of defense, or expenses to be levied against Consultant on account of design defect, error, omission, or professional negligence to be a sum not to exceed $25,000 or Consultant's fees, whichever is greater."

B. Imposition of Liability by Contractual Scope Language

1. Every contract provision that creates an obligation on the part of the professional has the potential of creating risk and liability.

2. Care should be taken to be certain that all obligations are subject to the "standard of care." Avoid any language that indicates a warranty or guarantee of results, such as "guarantee," "assure," "ensure," or other wording conveying the message that the engineer will produce a particular result.

   a. Performance specifications can become guarantees, if not carefully worded.

   b. It is advisable to include an express statement in all contracts and reports disclaiming any express or implied warranty or guaranty.

3. Be wary of clauses requiring performance of "inferred" services. Examples would be "all services necessary to complete . . .." Be clear and specific in proposals exactly what you will and will not provide. If you list your services in a proposal, include a provision in the contract that in the event of a conflict between the contract and your proposal, your proposal will control.

4. Express Indemnity Clauses.

   a. Most Owners will want/require some form of express indemnity.

   b. If you cannot eliminate the obligation to indemnify, the goal is to keep the indemnity as narrow as possible. This can be accomplished by:

      (1) Limiting its scope to negligence only.

      (2) Only agreeing to indemnify; do not agree to provide a defense. This may help you avoid having to defend claims for which the Owner may be ultimately found liable

      (3) Limiting the scope of losses to personal injury and/or tangible property damage, other than property damage to the project improvement itself (which may be covered by insurance).

      (4) Not agreeing to indemnity clauses, which would obligate you to indemnify the owner for his own comparative share of negligence, whether active or passive.

   c. A good response to a request for indemnity by an owner is to ask that a reciprocal, "mirroring" indemnity be included in the contract for the benefit of the professional.

TAB 9

Horst J. Schor

Presentation

University of Wisconsin - Madison
Department of Engineering Professional Development

SLOPE STABILITY AND LANDSLIDES

February 20 - 22, 2002

Using Effective Engineering and Geological Approaches to Identify and Analyze Unstable Slopes

Streets and Highway Development

Hillside Development

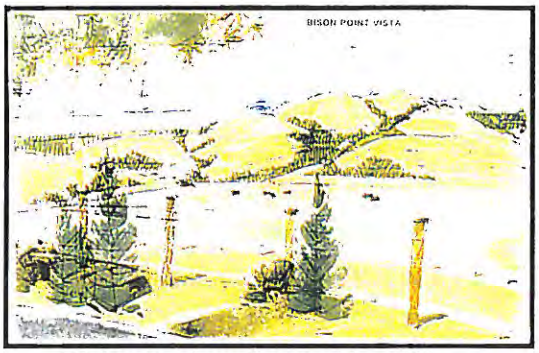

Mining Reclamation and Landfill

Drainage Control

"LANDFORM GRADING AND REVEGETATION"

CREATIVE CONCEPTS IN LAND DEVELOPMENT AND REPAIR

- RE-MANUFACTURED HILLSIDES
- DRAINAGE STRUCTURES
- CONTOUR/LANDFORM GRADING

Horst J. Schor

Materials

American Society of Civil Engineers' Journal of Geotechnical Engineering
"Landform Grading and Slope Evolution"

Landscape Architect and Specifier News
"Landform Grading: Comparative Definitions of Grading Designs"

Urban Land
"Hills Like Mother Nature Makes Them"

Los Angeles Times
"Grading on The Curve"

Pacific Coast Builder
"Landform Grading: Building Nature's Slopes"

H.J. SCHOR CONSULTING
626 NORTH PIONEER DRIVE • ANAHEIM, CALIFORNIA 92805 • (714) 778-3767 • FAX (714) 778-1656

LANDFORM GRADING AND SLOPE EVOLUTION

By Horst J. Schor[1] and Donald H. Gray,[2] Member, ASCE

ABSTRACT: Transportation corridors and residential developments in steep terrain both require that some grading be carried out to accommodate roadways and building sites. The manner in which this grading is planned and executed and the nature of the resulting topography or landforms that are created affect not only the visual or aesthetic impact of the development but also the long-term stability of the slopes and effectiveness of landscaping and revegetation efforts. Conventionally graded slopes can be characterized by essentially planar slope surfaces with constant gradients. Most slopes in nature, however, consist of complex landforms covered by vegetation that grows in patterns that are adjusted to hillside hydrogeology. Analysis of slope-evolution models reveals that a planar slope in many cases is not an equilibrium configuration. Landform-graded slopes on the other hand mimic stable natural slopes and are characterized by a variety of shapes, including convex and concave forms. Downslope drains either follow natural drop lines in the slope or are hidden from view in swale-and-berm combinations. Landscaping plants are placed in patterns that occur in nature as opposed to random or artificial configurations. The relatively small increase in the costs of engineering and design for landform grading are more than offset by improved visual and aesthetic impact, quicker regulatory approval, decreased hillside maintenance and sediment removal costs, and increased marketability and public acceptance.

INTRODUCTION

All slopes are subject to erosion and mass wasting. Various measures can be invoked to slow, if not completely prevent, this degradation. Biotechnical slope-protection methods, for example, have attracted increasing attention as a cost-effective and visually attractive means of stabilizing slopes. This approach has been used to stabilize and revegetate cut-and-fill slopes along highways as well as slopes in residential hillside developments. Kropp (1989) described the use of contour wattling in combination with subdrains to repair and stabilize a debris flow above a housing development in Pacifica, California. Gray and Sotir (1992) described the use of brush layering to stabilize a high, unstable cut slope along a highway in northern Massachusetts. Brush layering and other soil bioengineering measures have likewise been employed (Sotir and Gray 1989) to repair a failing fill embankment along a highway in North Carolina.

Transportation corridors and residential developments in steep terrain both require that some excavation and regrading be carried out to accommodate roadways and building sites. The manner in which this grading is planned and executed and the nature of the resulting topography or landforms that are created affect not only the visual or aesthetic impact of the development but also the stability of the slopes and effectiveness of landscaping and revegetation efforts.

Succinct descriptions and comparative definitions of grading designs are as follows.

Conventional Grading

Conventionally graded slopes are characterized by essentially linear (in plan), planar slope surfaces with unvarying gradients and angular slope intersections. Resultant pad configurations are rectangular.

Slope drainage devices are usually constructed in a rectilinear configuration in exposed positions.

Landscaping is applied in random or geometric patterns to produce "uniform coverage."

Contour Grading

Contour-graded slopes are basically similar to conventionally graded slopes except that the slopes are curvilinear (in plan) rather than linear, the gradients are unvarying, and profiles are planar. Transition zones and slope intersections generally have some rounding applied. Resultant pad configurations are mildly curvilinear.

Slope drainage devices are usually constructed in a geometric configuration and in an exposed position on the slope face.

Landscaping is applied in random or geometric patterns to produce "uniform coverage."

Landform Grading

Landform grading replicates irregular shapes of natural, stable slopes. Landform-graded slopes are characterized by a continuous series of concave and convex forms interspersed with swales and berms that blend into the profiles, nonlinearity in plan view, varying slope gradients, and significant transition zones between man-made and natural slopes. Resultant pad configurations are irregular.

Slope drainage devices either follow "natural" slope drop lines or are tucked away in special swale-and-berm combinations to conceal the drains from view. Exposed segments in high visibility areas are treated with natural rock.

Landscaping becomes a "revegetation" process and is applied in patterns that occur in nature: trees and shrubs are concentrated largely in concave areas, whereas drier convex portions are planted mainly with ground covers.

GRADING APPROACHES

Conventional

Conventional grading practice often results in drastically altered slopes and the replacement of natural hillside forms with artificial, sterile, and uniform shapes and patterns. Conventionally graded slopes can be characterized by essentially planar slope surfaces with constant gradients and angular intersections as shown in Fig. 1. Slope-drainage devices are usually constructed in a rectilinear and exposed fashion.

[1]Prin., H.J. Schor Consulting, 626 N. Pioneer Dr., Anaheim, CA. 92805 (714) 778-3767.

[2]Prof., Dept. of Civ. & Envir. Engrg., Univ. of Michigan, Ann Arbor, MI 48109.

Note. Discussion open until March 1, 1996. To extend the closing date one month, a written request must be filed with the ASCE Manager of Journals. The manuscript for this paper was submitted for review and possible publication on September 14, 1994. This paper is part of the *Journal of Geotechnical Engineering*, Vol. 121, No. 10, October, 1995. ©ASCE, ISSN 0733-9410/95/0010-0729–0734/$2.00 + $.25 per page. Paper No. 9236.

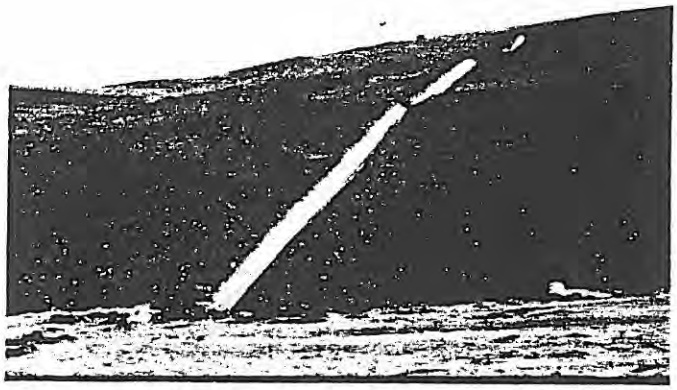

FIG. 1. Conventional Grading with Planar Slopes and Rectilinear Drainage Ditch in Highly Visible and Exposed Location

FIG. 2. Conventionally Graded Hill Slope with Planar Face, Rectilinear Drainage Ditch, and uniformly Spaced Plantings

Grading specifications in southern California, for example, typically call for flat, planar 2:1 (H:V) slopes with a midslope bench and a drainage ditch, commonly placed straight down the slope, that collects and conveys water from brow and midslope bench or terrace drains, respectively. Landscaping and plants are applied in random or geometric patterns as shown in Fig. 2.

Contour Grading

Contour grading offers a slight improvement over the sterile and simple geometry achieved by conventional grading. Some scalloping or curvilinear appearance is introduced onto the slope when seen in plan view; however, the slope gradients or profiles remain planar and unvarying. Transition zones at the bottom and top of slopes may also have some rounding applied. Slope drainage devices are still constructed in the same geometric configuration and exposed position on the slope face as in conventional grading. Landscaping and plants are also applied in random or geometric patterns.

Landform Grading

"Landform grading" essentially attempts to mimic nature's hills. This approach has been largely developed and pioneered by Schor (1980, 1992, 1993), who has successfully applied landform grading to several large hillside developments and planned communities in southern California. It is important to note that very few hillsides are found in nature with linear, planar faces. Instead, natural slopes consist of complex landforms covered by vegetation that grows in patterns that are adjusted to hillside hydrogeology, as shown in Figs. 3 and 4. Accordingly, landform-graded slopes are characterized by a variety of shapes including convex and concave forms interspersed with ridges and elbows in the slope.

Downslope drain devices either follow natural drop in the slope or are tucked away and hidden from view in special concave swale and convex berm combinations as shown in Fig. 5. Landscaping plants are not placed in random or artificial patterns. Instead they are applied in patterns that

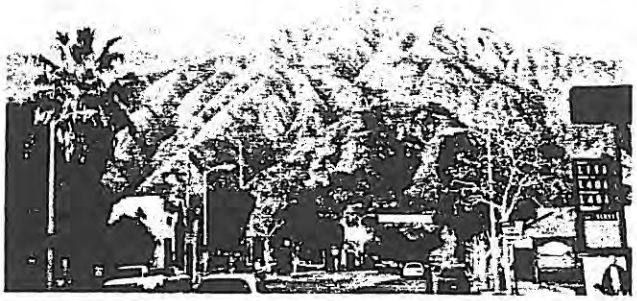

FIG. 3. Natural Hill Slopes with Multiple and Complex Shapes and Profiles

FIG. 4. Natural Hill Slopes Showing Vegetation Patterns

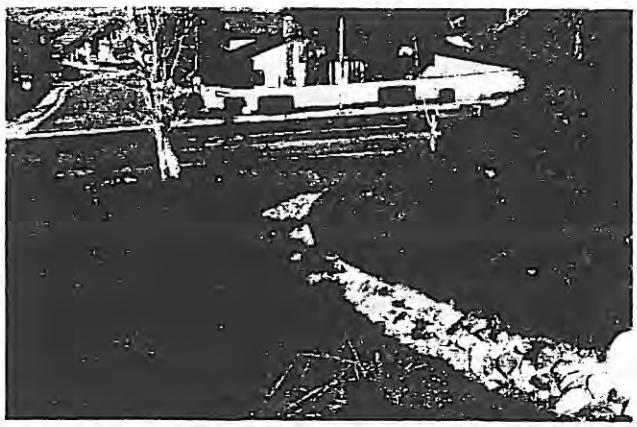

FIG. 5. Example of Landform Grading with Drainageway that is Placed in Special Swale-and-Berm Combination to Conceal it from View

occur in nature (see Fig. 6). Trees and shrubs are concentrated primarily in concave areas, where drainage tends to concentrate, while drier convex portions are planted primarily with herbaceous ground covers. A schematic depiction of conventional site planning versus landform site planning is shown in Fig. 7.

SLOPE-EVOLUTION CONSIDERATIONS

Landform-graded slopes present more than a varied and pleasing visual appearance. They also tend to be intrinsically more stable. The general lack of straight, planar slopes in nature says something. Slopes wear away or degrade over time by gravity-driven forces of erosion and mass wasting. The slopes proceed toward an equilibrium profile, which evidently does not include a linear and unvarying gradient.

Geomorphologists have been interested for some time in various slope-evolution models. The spatial and temporal variation of any point in a slope can be expressed by a number of two-dimensional mathematical models. These models predict the rate of change of elevation (dY/dT) of any point on a slope with elapsed time (T) and coordinate location (X, Y). Examples of these mathematical models are the following:

$$\text{Model \#1 } dY/dT = -A \tag{1}$$

$$\text{Model \#2 } dY/dT = -B\,(dY/dX) \tag{2}$$

$$\text{Model \#3 } dY/dT = -C \text{ (height above base)} \tag{3}$$

$$\text{Model \#4 } dY/dT = -D \text{ (distance from crest)}^{0.6} \tag{4}$$

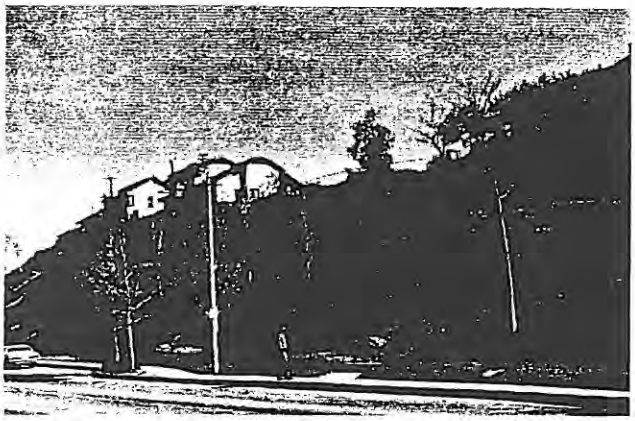

FIG. 6. Example of Landform Grading and Revegetation with Concave and Convex Slope Forms and Nonlinear, Varying Slope Gradients

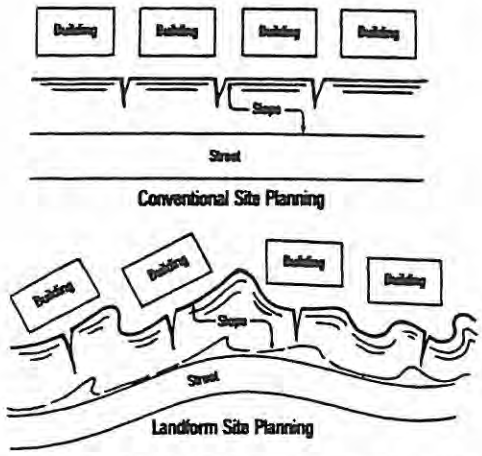

FIG. 7. Plan View of Conventional versus Landform Site Planning

$$\text{Model \#5 } dY/dT = -E\,(d^2Y/d^2X) \tag{5}$$

Graphical illustrations or simulations of these models are shown in Figs. 8–12. Each of these mathematical models has some physical basis. Model #2, for example, describes the "parallel retreat of slope" concept, which postulates that upon reaching its limiting slope angle (angle of repose) a slope retreats back at a constant inclination. A purely frictional, sandy slope whose stability is independent of slope height could conceivably fit this model. Model #4 fits observations from the Universal Soil Loss equation, which indicates that rainfall erosion losses from a slope (all other factors equal) are a function of the slope length. Model #5 is the so-called diffusion model, which postulates that in a transport-limited slope the passage of material down the slope from a point above is limited by the transfer rate at a point below. The slope profile adjusts itself over time to optimize this stepwise or sequential transfer of material downslope by various erosion or mass-wasting processes. Note that in the diffusion model, an initially planar slope evolves over time into a concave-convex slope as shown in Fig. 12.

The diffusion model (#5) was tested as part of a doctoral dissertation on slope evolution models at the University of

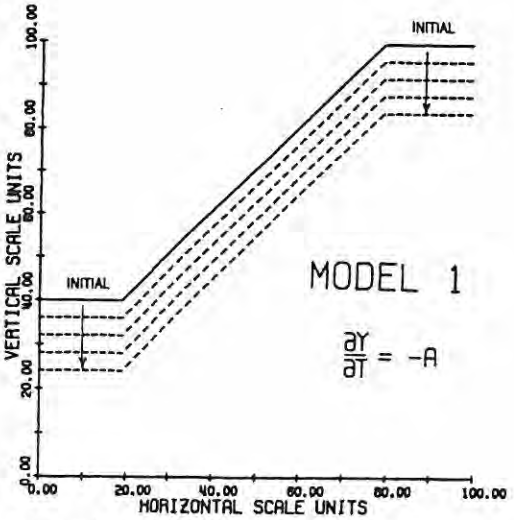

FIG. 8. Evolution of Hillside Slope when Rate of Lowering is Uniform over Entire Slope Profile (Model 1) [from Nash (1977)]

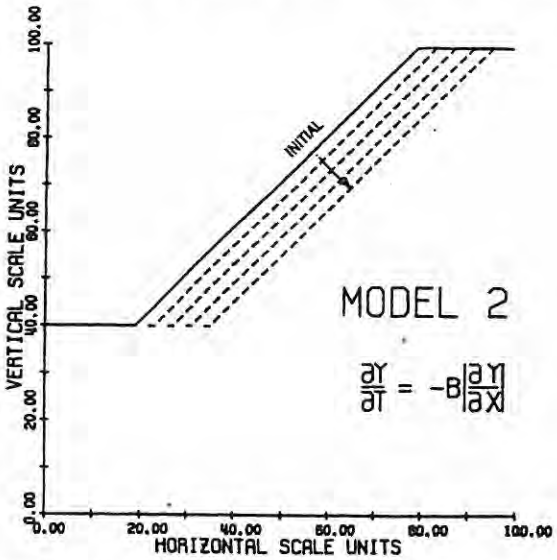

FIG. 9. Evolution of Hill Slope when Rate of Lowering at Point on Slope is Proportional to Profile Gradient at Point (Model 2) [from Nash (1977)]

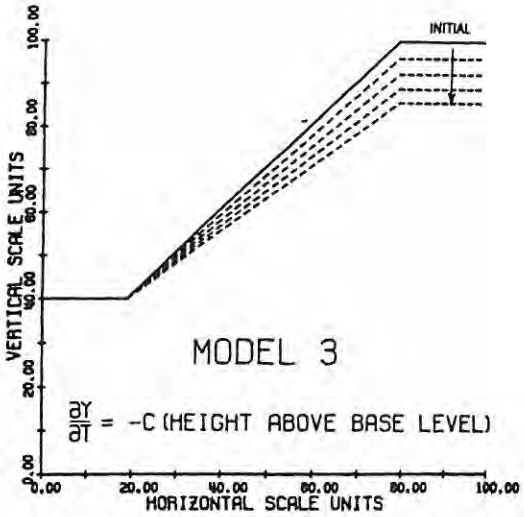

FIG. 10. Evolution of Hillside Slope when Rate of Lowering of a Point on Slope is Proportional to Elevation of Point (Model 3) [from Nash (1977)]

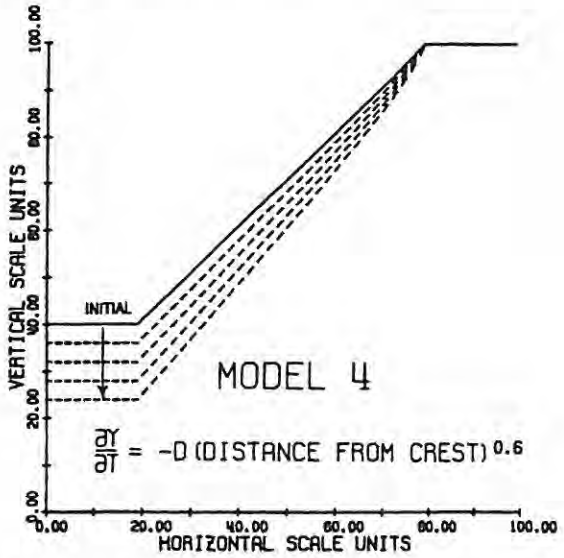

FIG. 11. Evolution of Hill Slope when Rate of Lowering at Point on Slope Profile is Proportional to Distance that Point Lies from Crest or Divide (Model 4) [from Nash (1977)]

Michigan (Nash 1977). The slope profiles of present-day, modern wave-cut bluffs along Lake Michigan and those of ancient, abandoned bluffs marking former glacial lake margins were used for this purpose. The study assumed that slope processes at work on the bluffs have remained relatively constant over geologic time. The ancient bluffs and their ages respectively, are the Nipissing bluffs (4,000 yr) and Algonquin bluffs (10,500 yr). Actual slope profiles for these three bluffs superposed at their midpoint are shown in Fig. 13. The correspondence or fit between the profiles predicted by the diffusion model and the actual profiles was examined for various diffusion constants. The configurations predicted by the diffusion model for an abandoned bluff after 4,000 years and 10,500 years using a diffusion coefficient of 0.012 m^2/yr and an initial, planar profile similar to the profile of the modern bluff are shown in Fig. 14. According to the diffusion model, the slope profiles gradually change over time from a linear to a concave-convex configuration, as illustrated in Fig. 14.

The fit or correspondence between actual and predicted profiles is quite good as can be seen by comparing slope profiles in Figs. 13 and 14. More importantly, this modeling

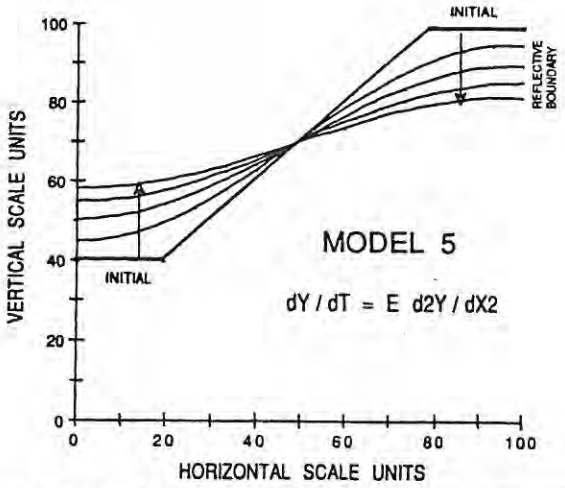

FIG. 12. Evolution of Hillside Slopes when Rate of Lowering of Point on Slope Profile is Proportional to Profile Curvature at that Point, Assuming Reflective Left and Right Boundaries (Model 5) [from Nash (1977)]

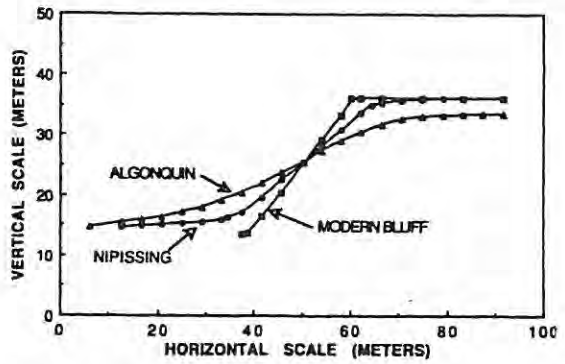

FIG. 13. Modern Bluff Profile, Nipissing Bluff Profile (4,000 yr), and Algonquin Bluff Profile (10,500 yr) Superposed at their Midpoint [from Nash (1977)]

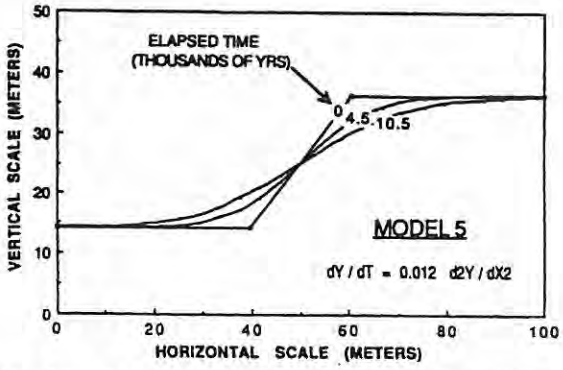

FIG. 14. Slope Profiles Predicted by Model 5 for Initial Planar Slope after 4,000 and 10,500 Years of Elapsed Time Using Diffusion Coefficient of 0.012 m^2/yr and Initial Inclination Similar to Present Wave Cut Bluff [from Nash (1977)]

work indicates that in transport-limited slopes, at least, a planar slope with constant inclination, typical of conventional grading practice, is not a stable, long-term equilibrium slope.

REVEGETATION AND LANDSCAPING

If monotony and uniformity in grading are combined with a uniform or artificial pattern of revegetation, the overall effect is not only sterile and ugly but also ineffective. Successful and attractive revegetation must invoke the same concepts and approaches as landform grading. Vegetation pat-

terns that are found in nature should also be mimicked. Shrubs and other woody vegetation growing on natural slopes tend to cluster in valleys and swales where moisture is more abundant. Random patterns or uniform coverage should be avoided. Instead, the vegetation is placed where it makes sense, i.e., where it has a better chance of surviving and does a better job of holding soil. Trees and shrubs require more moisture, and they also do a better job of stabilizing a soil mantle against shallow mass wasting. Accordingly, it makes sense to cluster them in swales and valleys in a slope (see Fig. 15), where runoff tends to concentrate and evaporation is minimized. Shrubs should also be heavily concentrated along the drainage flow of each swale.

By purposely controlling the drainage patterns on a slope, runoff can be concentrated in concave areas where it is needed or where it can best be handled by woody slope vegetation (see Fig. 16). Conversely, runoff and seepage will be diverted away from convex areas. These areas should be planted with grasses or more drought-tolerance herbaceous vegetation. Irrigation needs are thus reduced by careful control of drainage pattern on a slope and selection of appropriate plantings for different areas.

IMPACT ON DEVELOPMENT COSTS

Design Engineering and Surveying Costs

Design and surveying can be measurably higher if it is initially performed by a team only experienced in conventional methods. Design engineering and construction staking and surveying costs are directly related to the experience, talent, and versatility of the design engineer and his full understanding of the concept. When first implemented with a totally inexperienced staff during pioneering stages, design cost was 15% higher and field cost 10% higher than conventionally designed and surveyed slopes. From that initial experience, design costs quickly decreased to a factor of 1–3%, and surveying to 1–5% over conventional methods and approaches.

A willingness and an open mind to depart from old concepts are essential elements for realizing the benefits of landform grading. In-depth training of the designer, draftsman, and project manager are indispensable, as well, before attempting the landform-grading method. Approving agencies must also be brought into the information dissemination process so that plan check, permitting and, later, inspection can proceed smoothly.

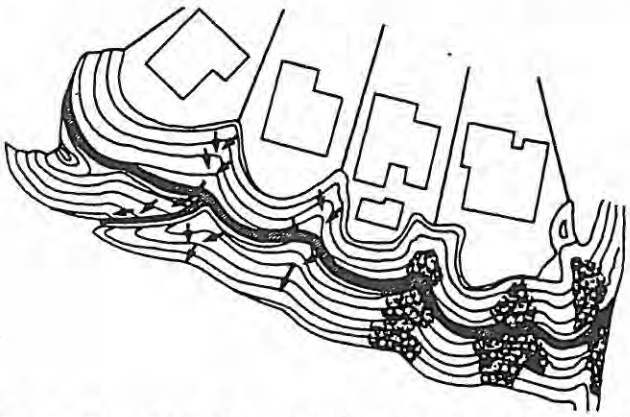

FIG. 15. Topographic Representation of Landform Configuration Showing Radial Flow of Water, Foliage Placement in Swales, and Lots that Conform with Landform Grading Configuration [after Schor (1992)]

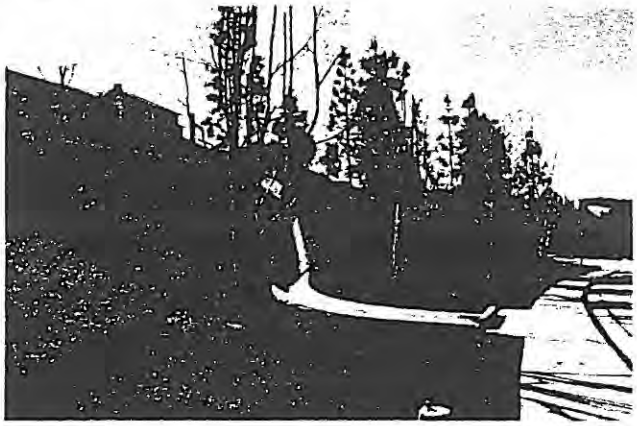

FIG. 16. Landform-Graded Slope with Convex and Concave Slope Shapes, Varying Gradient, Curvilinear Drainage Ditch Concealed in Berm and Swale Configuration, and Clustered Plantings

Construction/Grading Costs

Construction/grading costs are most directly related to the size and volume of earth movement than any other factor. In addition, there is a direct relationship to the competitive marketplace situation at a given time. Competition for larger projects, such as those for 1,000,000 cu yd or more, tends to eliminate adherence to landform-grading standards as a significant factor.

Grading costs in hillsides of largely sedimentary materials and not requiring blasting or extremely heavy ripping range from $0.75 to $1.25 per cubic yard with an average of $1.00 per cubic yard. Variables affecting the unit cost include the quantity of material, the nature of the operating area, i.e., open or confined, the length and steepness of the haul from the cut areas to the fill areas, and the rippability by conventional dozer/scraper equipment.

At first glance it appears that landform-graded projects would be significantly more expensive to construct than conventional ones because of the more intricate details and natural shapes required. However, experience has shown that the differential is minor when compared to the total project cost. This is true because the largest percentage (on average 90%) of the earth volume moved, the mass "X" shown in Fig. 17, can be moved, placed, and compacted in a totally conventional manner. Only the outer slope layers, 20–50 ft thick (or approximately 10% of volume), require specialized shaping. Moreover, even this outer layer can still be placed and compacted with conventional equipment and methods. This outer component needs an additional grade checker for control and a dozer with an experienced operator for final shaping. Accordingly, when costs are reckoned on the basis of the actual additional operations involved they are a minor component, typically on the order of 1% of the total cost.

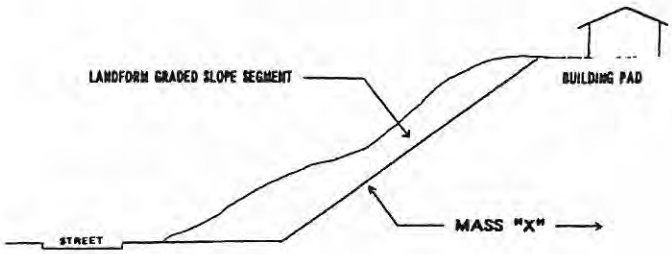

FIG. 17. Relative Amounts and Location of Earth Movement by Conventional as Opposed to Landform Grading

COST-IMPACT COMPARISONS ON VARIOUS SIZE PROJECTS

Large-Scale Projects

On a recently completed hillside project involving 20,000,000 cu yd of earth movement at a cost of some $24,000,000, the total additional cost incurred including design, surveying, construction staking, and grading, was $250,000, or about 1% of the total cost of the grading.

No loss of residential density was encountered, because land planning was done concurrently with the engineering. There was a loss of approximately 1% of commercial pad area due to concave valleys projecting into them. This was offset, however, by the credit given by the governing agency for these indentations toward landscape requirements and coverage calculations for the building pad areas. Furthermore, entitlement approvals were advanced by at least 1 year by being able to mitigate the previous strong community opposition to conventional hillside design and construction methods.

Small-Scale Projects

A 10-acre, 24 custom-lot subdivision requiring 300,000 cu yd of earth movement, initially designed by conventional methods, with little hope for approval, was reconfigured to landform-grading standards. The project applicants had previously proposed conventional grading and had for 2 1/2 years tried to secure permitting agency approvals in a community where grading practices had become a major and highly controversial issue. The governing agency insisted that the applicant apply landform-grading concepts before any further resubmittals. The project was redesigned by adhering to these concepts, and the new layout resulted in 21 lots, a loss of three lots. Design and staking costs also increased by approximately $10,000. However, this revision reduced construction costs by reducing the amount of grading required by 20%. The loss of the lots and additional design costs were further offset by reduced street and storm-drain improvements, tree-removal costs, and an enhanced and aesthetically pleasing project with larger open spaces for each of the lots. This in turn, increased the marketability of the projects. In addition to these benefits, the project received unanimous community approval within 3 months.

APPLICABILITY OF LANDFORM GRADING TO OTHER PROJECTS

In addition to residential and commercial developments the landform-grading concept should lend itself readily to highway slopes. Public objections are often voiced against these highly visible and stark slopes. In addition they are sometimes prone to erosion problems and generation of excess runoff. These problems and objections could be greatly mitigated by the application of this concept, thereby improving public acceptance. This benefit would likely offset any associated additional right-of-way acquisition costs.

Other large earthmoving and shaping projects that result in man-made landforms could also benefit from landform grading. Such projects include sanitary landfills, tailings bankments and mining waste stockpiles, and downstream of earthfill dams.

CONCLUSIONS

Grading considerations are very important to the successful stabilization and revegetation of slopes. Conventionally graded slopes can be characterized by essentially planar slope surfaces with constant gradients. Most slopes in nature, however, consist of complex landforms covered by vegetation that grows in patterns that are adjusted to hillside hydrogeology. Analysis of slope evolution models reveals that a planar slope often is not an equilibrium configuration.

Landform-graded slopes, on the other hand, are characterized by a variety of shapes including convex and concave forms that mimic stable natural slopes. Downslope drain devices either follow natural drop lines in the slope or are tucked away and hidden from view in special concave swale and convex berm combinations. Similarly landscaping plants are not placed in random or artificial patterns, but rather in patterns that occur in nature. Trees and shrubs are clustered primarily in concave areas, where drainage tends to concentrate, while drier convex portions are planted primarily with herbaceous ground covers.

Design and engineering costs for landform grading increase approximately 1–3%, and surveying 1–5% over conventional methods. Construction and grading costs are most strongly affected by the volume of earth movement and the competitive market. Accordingly, a landform-grading specification on a large project is not a significant factor. The relativ small increase in the costs of engineering and design are n than offset by improved visual and aesthetic impact, quick regulatory approval, decreased hillside-maintenance and sediment-removal costs, and increased marketability and public acceptance.

APPENDIX. REFERENCES

Gray, D. H., and Sotir, R. (1992). "Biotechnical stabilization of a highway cut." *J. Geotech. Engrg.*, ASCE, 118(10), 1395–1409.

Kropp, A. (1989). "Biotechnical stabilization of a debris flow scar." *Proc., XX Annu. Conf.*, Int. Erosion Control Assoc. (IECA), Steamboat Springs, Colo., 413–429.

Nash, D. B. (1977). "The evolution of abandoned, wave-cut bluffs in Emmet County, Michigan," PhD dissertation, Univ. of Michigan, Ann Arbor.

Schor, H. (1980). "Landform grading: building nature's slopes." *Pacific Coast Builder*, (Jun.), 80–83.

Schor, H. (1992). "Hills like nature makes them." *Urban Land*, (Mar.), 40–43.

Schor, H. (1993). "Landform grading: comparative definitions of grading designs." *Landscape Arch. & Specifier News*, (Nov.), 22–25.

Sotir, R., and Gray, D. H. (1989). "Fill slope repair using soil bioengineering systems." *Proc., XX Annu. Conf.*, Int. Erosion Control Assoc. (IECA), Steamboat Springs, Colo., 473–485.

Volume 9 • Number 11

November 1993

LANDSCAPE ARCHITECT

AND SPECIFIER NEWS

HILLSIDE DEVELOPMENT

See the LASN Marketplace on pages 26 - 41

Landform Grading: Comparative Definitions of Grading Designs

by Horst J. Schor

The advantages and necessities of hillside living have become more widely evident as flatlands, the traditional building sites, are being consumed rapidly by urban development.

Hillside building, while appealing to the consumer, can require massive grading that may become the focal point of local resistance, thus impending government approval.

However, grading is a necessity to accommodate street and building areas for development, meeting building codes, and safe engineering practices. Grading is also frequently required to correct unstable soils and geologic conditions inherent in many natural hillsides.

The innovative "Landform Grading and Revegetation" concept was conceived to solve negative impressions gained in viewing the typical re-manufactured hillsides using conventional planning, engineering and construction methods. Conventional grading drastically alters a landscape, remanufacturing natural forms and shapes and plant distribution patterns to replace them with artificial, sterile and uniform shapes and patterns.

The concept, as developed and described here, consists of three components:
- Grading
- Drainage Structures
- Revegetation/Landscaping

Grading

In recent years attempts have been made by some to design and construct "LANDFORM grading," while in reality, these efforts can only, at best, be described as contouring or rounding of slopes. Therefore it is necessary to establish proper definitions and characteristics for the three types of grading available: Conventional, Contour and Landform Grading.

Comparative Definitions of Grading Designs

Conventional Grading

• Conventional graded slopes are characterized by essentially linear, planar slope surfaces with unvarying gradients and angular slope intersections. The resultant pad configurations are rectangular.

• Slope drainage devices are usually constructed in a rectilinear configuration in exposed positions.

• Landscaping is applied in random or geometric patter

Contour Grading

• Contour-graded slopes ar basically similar to conventionally graded slop except that: the slopes a curvilinear rather tha the gradients are and profiles ar transition z intersect some r Resultan

To voice your opinion, use the Marketplace Comments Card on page 39.

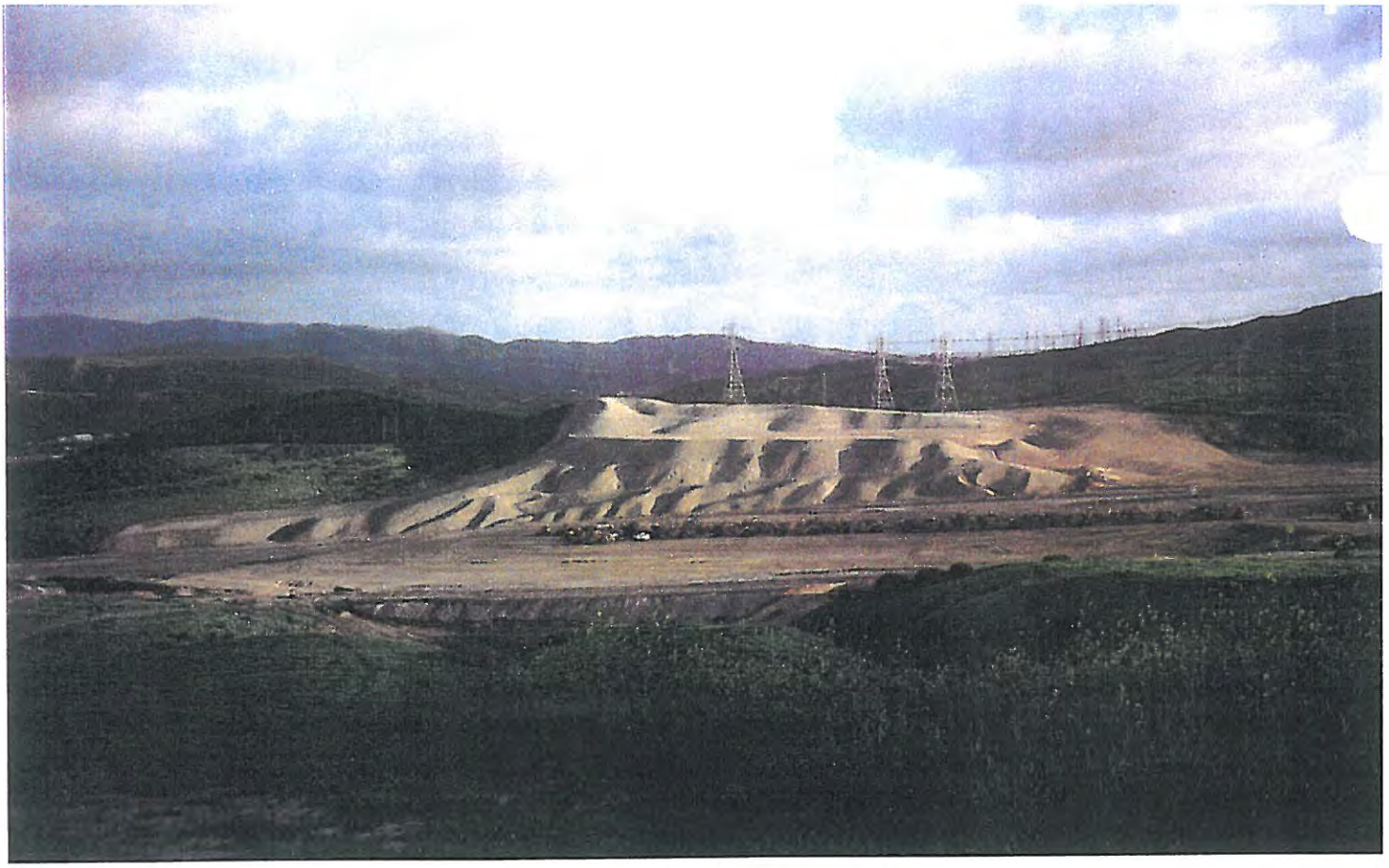

The aerial photo to the left shows a 4,200 acre planned community in which the design revolves around the landform grading and revegetation concept.

The hill above illustrates how landform grading replicates the irregular shapes of natural slopes. The landscaping will be a "revegetation" process emulating the patterns of natural growth.

In high visibility areas, concrete drainage devices are lined with natural river rock to create a stream bed effect (right) in the finished landscape.

are mildly curvilinear.

• Slope drainage devices are usually constructed in a geometric configuration and in an exposed position the slope face.

• Landscaping is applied in random or geometric patterns.

Landform Grading

• Landform Grading replicates the irregular shapes of natural slopes, resulting in aesthetically pleasing elevations and profiles. Landform-graded slopes are characterized by continuous series of concave and convex forms interspersed with mounds that blend into the profiles. Non-linearity and varying slope gradients are significant transition zones between man-made and natural slopes. Resultant pad configuration are irregular.

• Slope down-drain devices either follow "natural" lines of the slopes or are tucked away in special swale and berm combinations to conceal the drains from view. Exposed segments in high visibility areas are treated with natural rock *(see right photo)*.

• Landscaping becomes a "revegetation" process and is applied in patterns that occur in nature. Trees and shrubs are concentrated largely in concave areas,

Continued on page 25

Make the LASN Marketplace Buyer's Guide on page 41 your first choice for all your product inquiries.

The natural hillside above illustrates that vegetation clusters in the swales of the mountain. The goal of landform revegetation is to replicate these natural patterns.

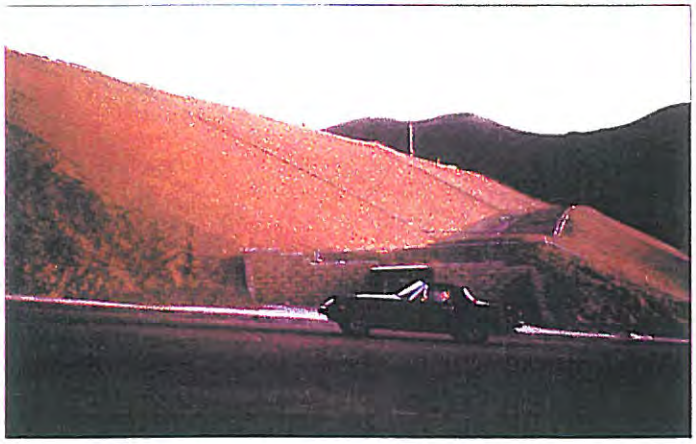

As opposed to the rigid forms of conventional grading (below left), landform grading (below right) provides shadows, depth and a more natural looking hillside.

Continued from page 23

while convex portions are planted mainly with ground covers.

Revegetation/Landscape

Historically, landscaping on manufactured slopes has been applied in uniform patterns, with trees typically spaced 15 feet on center and shrubs 3 feet on center to achieve what has been known in the industry dubiously as "Uniform Coverage."

It is this uniformity that can add to the artificial, man-made look, already created by the uniformity in grading.

In the "Landform Grading and Revegetation" approach, landscaping is applied in patterns that occur in nature.

The approach should be thought of as "Revegetation". Trees and shrubs require more moisture, so it makes sense to cluster them in the swales and valleys where moisture concentrates and evaporation is minimized. Shrubs are heavily concentrated along the drainage flow of each swale and thinned to each side to minimize any erosion.

The result of "Revegetation" is a landscape that does not look "man-made," and, where plant material locations and distributions serve a purpose and make sense.

"Revegetation" in combination with landform grading reduces irrigation's needs: radial drainage patterns that concentrate runoff in concave swales provide the most moisture to plant types that need the most. Flatter slope ratios in swales near the lower half of the slope slow water velocity and thus allow better absorption by plant roots.

Conclusion

Hillside development can be done in an aesthetically pleasing manner. Landform grading and landform revegetation are just two concepts that accomplish this goal. With sensitivity, creativity and the will to improve, we can shape our hillsides by imitating mother nature to recreate a more "natural" habitat for all.

Horst Schor is the principal of H.J. Schor Consulting, Creative Concepts in Land Development, in Anaheim, California. LASN

Make the LASN Marketplace Buyer's Guide on page 41 your first choice for all your product inquiries.

March 1992 $5.00

URBAN LAND

ULI

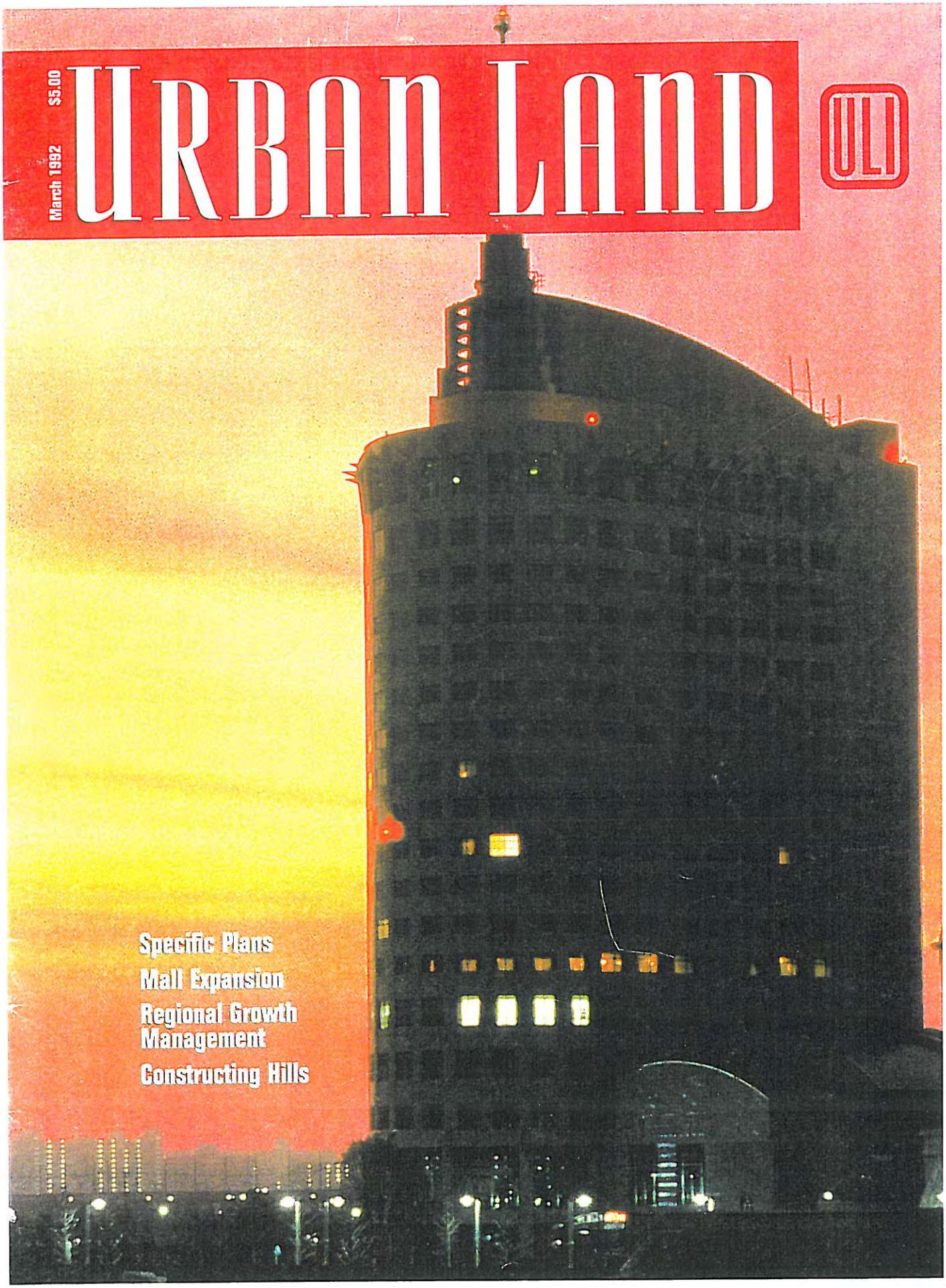

Specific Plans
Mall Expansion
Regional Growth Management
Constructing Hills

Solution File

Hills Like Nature Makes Them

Spending more to replicate the beauty of natural hillsides pays off in the long run.

Urbanizing flatlands is a fairly simple process. Developing hillsides, on the other hand, is a far more complex undertaking. Building pads, extensive circulation systems, and infrastructure facilities like water reservoirs and gravity sewers often have specific location and elevation needs that must be met. When these factors are combined with the need to mitigate adverse soils and geological conditions, massive reshaping of the natural topography is required. This is known as mass grading.

The mass-grading design standards that have been established over the years by regulatory agencies and civil engineering professionals have emphasized stability, runoff control, and the long-term performance of the building sites. Function has taken precedence over aesthetics and environmental sensitivity. Standard mass grading produces flat surfaces and linear and angular forms that bear no resemblance to the original hills—a manmade environment without redeeming aesthetic qualities and totally out of harmony with nature.

Careful study of natural slopes throughout the world has revealed that they are composed of a series of building blocks, various identifiable concave and convex shapes: ridges and swales in different relationships—perpendicular, diagonal, or curvilinear—to the slope face, elbows, pyramids, wishbones, and composite shapes. Applying these natural shapes to a manmade slope in a process known as landform grading can reintroduce the beauty of natural hillsides into urbanized environments.

In conventional grading, slope drainage devices are usually constructed in a rectilinear configuration and in prominent and highly exposed positions. Drain devices on landform graded slopes, on the other hand, either follow the "natural" lines of the slope or are concealed from view between concave swale and convex berm combinations. Exposed segments in high visibility areas are treated with natural rock, giving them the appearance of a stream bed.

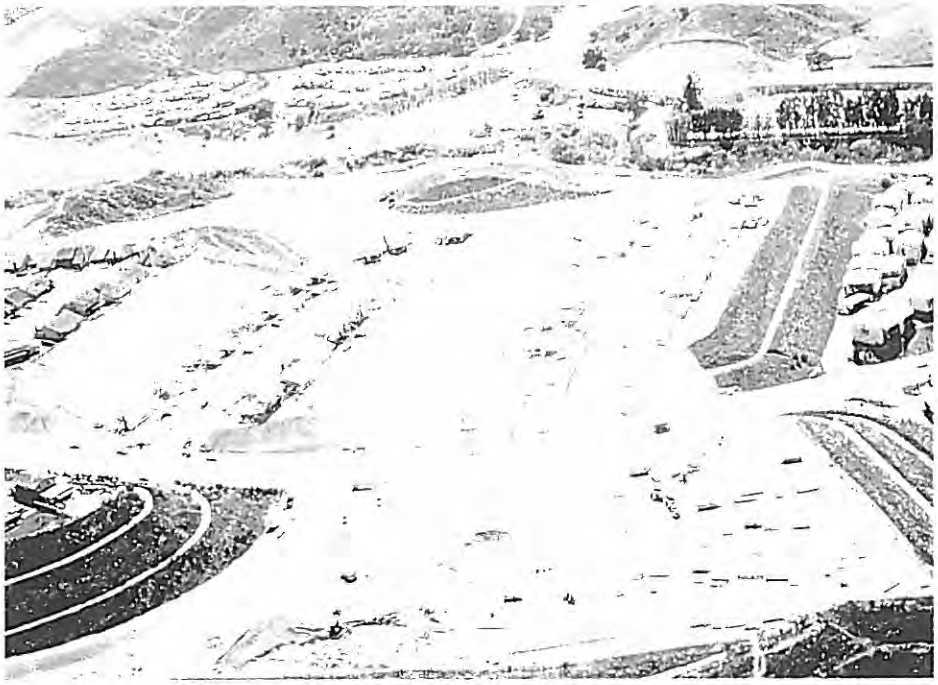

Conventional mass grading of hillsides (top) creates linear, angular, and uniform flat surfaces. Contouring to make the slopes curvilinear in plan offers some improvement to the traditional grading method. Landform graded slopes (bottom) by contrast, are characterized by a continuous series of concave and convex forms interspersed with mounds that blen into the profiles, nonlinear alignment, and varying slope gradients from the top to the bottom of the slope.

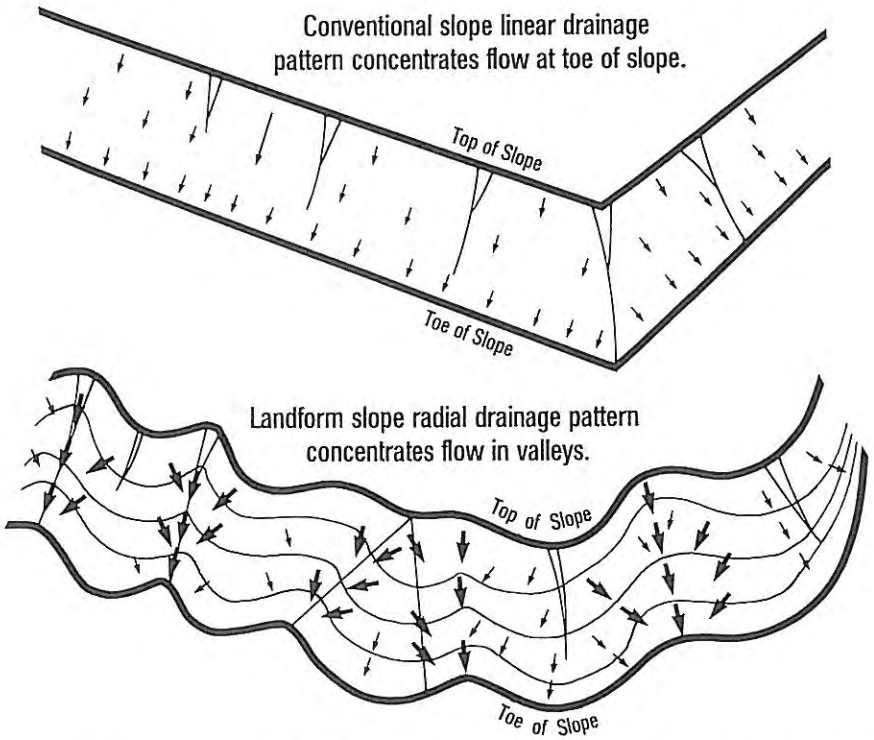

Conventionally graded slopes produce accelerated sheet flow from top to toe, which can erode the slope. Terracing can prevent damage, but looks artificial. Landform grading reconfigures the slope drainage pattern to radial flow, which permits the concentration of rainfall and irrigation runoff into specific areas yet prevents erosion in them by reducing tributary drainage so the amount of drainage is minimal and nonerosive.

Applying plant material to all slope surfaces is the next step after grading, to provide protection from erosion and cover scars. In conventional approaches, landscaping is generally applied in random or geometric patterns. The monotony of landscaping that calls for equal spacing of tree and shrub material and specified numbers of each for a given slope area is apparent.

In the landform approach, landscaping is applied in patterns that occur in nature—trees and shrubs concentrated largely in concave areas while ground covers predominate in convex portions. This approach may be thought of as "revegetation." Trees and shrubs require more moisture, so it makes sense to cluster them in the swales and valleys where moisture concentrates, particularly in semiarid regions. Shrubs are heavily concentrated along the drainage flow of each swale and thinned to each side.

The result of revegetation is a landscape that does not look manmade, where plant material locations and distributions serve a purpose and make sense. Moreover, revegetation in combination with landform grading reduces irrigation needs: radial drainage patterns that concentrate runoff in concave swales provide the most moisture to plant types that need the most; flatter slope ratios in swales near the lower half of the slope slow water velocity and thus allow better absorption by plant roots; and convex shapes

Centrally located, perpendicular, concrete downdrains are an eyesore. Downdrains in landform grading are curvilinear, configured into the concave shapes and partially hidden by convex areas. Made from natural rock, they can become an aesthetic element.

ees and bushes natu-
lly congregate in the
ncave, swaled slope
rtions of hillsides. Natu-
scaping patterns
re pleasing to the
e than the random or
ometric patterns typi-
l of conventional grad-
g/planting schemes.

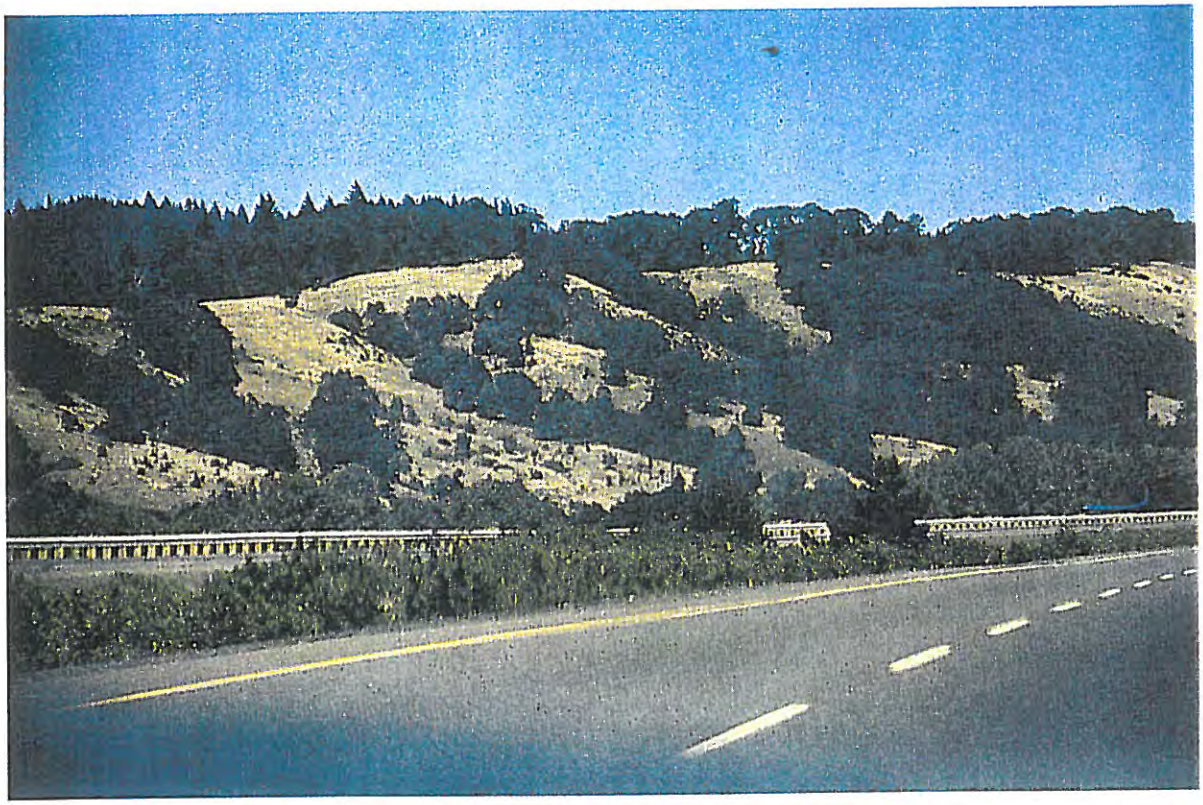

provide prolonged periods of shade, thus reducing evaporation.

Hurdles

The landform grading and revegetation concept was introduced at Anaheim Hills, a 4,200-acre planned community developed by Anaheim Hills, Inc., in Anaheim, California. It is currently being applied on a more extensive scale at Talega, a 3,500-acre planned community under development in San Clemente, California, by the Arvida Company.

The concept's widespread adoption depends on a number of factors, including professional and official attitudes. Civil engineer designers will have to abandon the engineered look and look to nature as their guide. Field surveyors will have to calculate and set different controls for slope construction. Geotechnical professionals will have to take a new approach to slope stability analysis and field testing. Landscape designers will have to think natural. And approval agencies will have to modify ordinances and guidelines and take a flexible attitude to alternative hillside designs.

careful planning, landform grading can produce as
many building lots as conventional grading.

Landform grading can involve additional costs. Perhaps the potential loss of buildable pad area is the most noticeable. Such loss can be minimized by providing for irregular, variable ratio slope patterns in the initial stages of the conceptual design. Concave flatter slope portions should be laid back into the spaces between structures, while convex portions can be steepened in front of building locations to create more pad space.

Engineering costs can be higher. Landform designs by civil engineers inexperienced in the concept can be expected to cost 10 to 15 percent more than conventional designs, but for designs by those with some experience, the difference would be minimal. The same would be true for field survey control costs.

Any additional costs for geotechnical services are difficult to determine, as such costs are highly variable. Additional costs would probably range between 1 and 3 percent. Greater care is required in stability analysis because of the frequent variation in slope orientations and the slope face inclination. These variations can improve stability in adverse bedding conditions. Compaction testing in the field may have to be done at more frequent intervals.

Revegetation does not necessarily entail higher costs than conventional landscaping. Nor does landform grading itself have to cost more than conventional grading. If the volume of earth being moved is great, 1 million or more cubic yards, the difference in cost between the two approaches can be less than 0.3 percent. On smaller projects, landform grading may cost up to 10 percent more. Much depends on the experience of the grading contractor, the experience of the project engineers and developer, and the understanding of the approving and inspecting agencies. With in-depth training of the grade checker and equipment operator, landform grading can be performed almost routinely within the same time frame and at the same cost as traditional grading.

Benefits

Opposition to mass-grading proposals is growing as the aesthetic value of remaining hillsides is recognized. Hillside development proposals face more stringent controls and limitations, all directed toward restricting rather than improving grading.

Landform grading and revegetation represent a concept that can help proposals through the approval process. A project incorporating landscape grading demonstrates concern for the sensitive treatment of the hillside environment. It is more likely to receive approval, and to receive it faster. It may be permitted more density than a conventionally graded project. And objections from neighbors and environmentalists should be reduced.

This is a complex approach to hillside development. Landform grading should be applied where it offers maximum visual and environmental benefits—on slopes along major roads, on other highly visible and permanently exposed slopes, within development projects, and along parks, golf courses, and other open spaces. It should not be applied to slopes below roadway grades, to side slopes between structures, to minor rear yard slopes, and to other slopes that will ultimately be obscured from view. Someday, landform grading should make a major contribution to methods of freeway, dam, and sanitary landfill construction. ❖

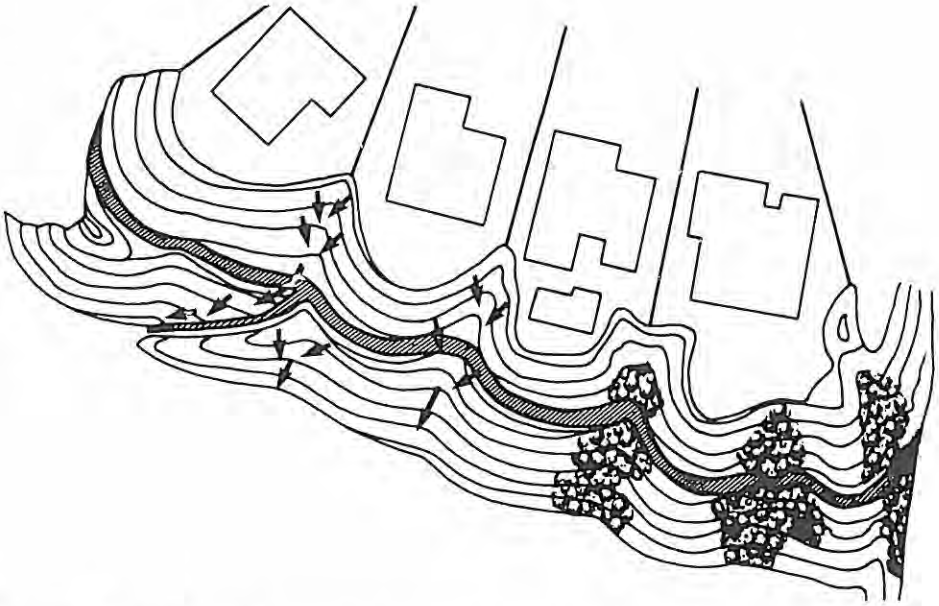

The topographical representation above shows radial water flow, foliage placement in swales, and lots that conform with the landform configuration. (The hatched area is a concrete terrace drain required by building codes.) The sketch below contrasts site planning for conventionally graded and landform graded slopes.

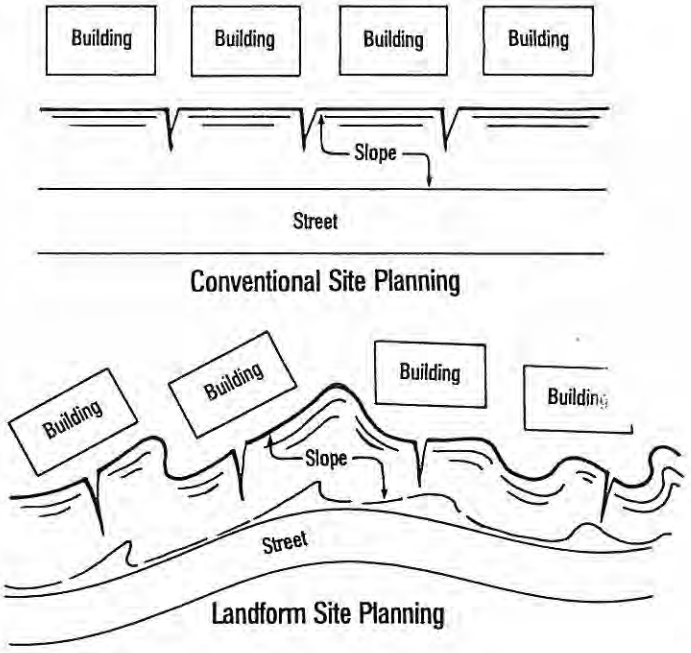

This solution was submitted by Horst Schor, vice president of development and construction for Talega, an Arvida Company master-planned community, and originator of the landform grading and revegetation concept. Schor is based in Anaheim, California.

What's your solution ?

Readers are invited to offer solutions to common (and not so common) development problems for publication in this department. Topic suggestions should be addressed to Karen Schaar/Julie Stern, *Urban Land*, 625 Indiana Avenue, N. W., Washington, D. C. 20004-2930.

Los Angeles Times

MARKETS / MONEY / PERSONAL FINANCE

SECTION D

FRIDAY

JULY 12, 1991 CC1

BUSINESS

ORANGE COUNTY
Los Angeles Times

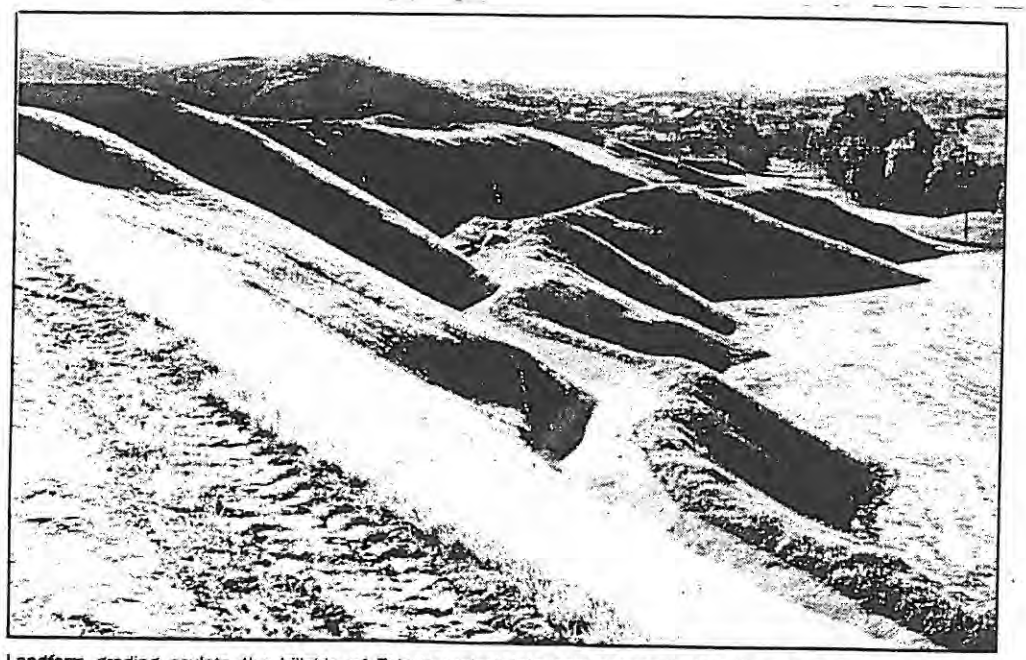

Landform grading sculpts the hillside of Talega project into new shapes in technique created by Horst Schor.

Grading on the Curve

Developer Goes for Natural Look in Sculpting Hills for Talega Project

By JOHN O'DELL
TIMES STAFF WRITER

SAN CLEMENTE

Fred Moeller has been operating bulldozers for almost 40 years now, piling dirt, cutting trenches and grading slopes all over Southern California.

But for all his experience, Moeller has never been on a job quite like this one.

Usually, when preparing hillsides and valleys for a housing project, Moeller and other heavy-equipment operators are asked to prepare a stairstep arrangement of flat-faced slopes with building pads on top.

At Arvida Co.'s Talega development in the hills just inland of Orange County's southernmost city, the rules have changed.

Moeller and fellow operators are being asked to think like sculptors as they follow a complex natural grading plan that calls for them to create slopes, valleys, gullies, hillocks and ridgelines for the homes and commercial buildings that will one day dot the 3,500-acre master-planned community.

In some places they are merely altering existing slopes to accommodate building pads. In others they are creating hills where none ever existed.

The grading process was invented in the late 1970s by Horst Schor, now Arvida's vice president for development. At the time, Schor worked for the Anaheim Hills Co. as it was developing its hillside community on the southern slopes of Santa Ana Canyon.

KEN HIVELY / Los Angeles Times

Fred Moeller guides his 25-ton bulldozer over a mound.

But no one else ever picked up on the idea, Schor said, despite the industry publicity the technique received at the time, when the American Planning Assn. bestowed an award of merit on Anaheim Hills Co. for its innovative natural grading plan.

One reason other developers didn't adopt what Schor calls landform grading is that it costs a little more—adding about 1% to a project's grading costs—and requires a little effort to train the grading crews.

"But Arvida feels the time is really ripe for this," he said. Environmental concerns and complaints about development that destroys natural landscape and ridgelines can delay projects for months, even years. Schor said Arvida's natural grading plan shaved at least 12 months off the time it took to get approval from San Clemente officials for the Talega development—which is located partly within the city and partly in unincorporated county territory. The time saved can more than make up for the extra grading costs.

There are three key elements of landform grading, he said Thursday during a demonstration of the process:

- Building hills and slopes with natural contours;
- Fitting the drainage system into the flow of the land so it follows the valley bottoms like a natural creek system instead of cutting straight down the face of slopes with concrete channels, as is done in a typical stair-step grading plan; and

Please see TALEGA, D7

Los Angeles Times

MARKETS / MONEY / PERSONAL FINANCE

SECTION D

FRIDAY

JULY 12, 1991 CC+

BUSINESS

ORANGE COUNTY
Los Angeles Times

Grading on the Curve

Developer Goes for Natural Look in Sculpting Hills for Talega Project

[continued]

Continued from D6

• Designing a natural landscape plan that mimics nature by placing the trees and shrubs in the valleys and on flat spots, where the heaviest runoff collects, and covers the protruding areas with less-thirsty ground covers.

For Moeller, who spent Thursday morning contouring a small hill with a 25-ton Caterpillar bulldozer, the process isn't much more difficult than building a traditional stairstep.

"It's a lot more challenging, because you're not just going in straight lines."

Russ Churchill, who works with Moeller and the other equipment operators as a grade checker—overseeing their work from the ground to make sure they are following the grading plan—said there is a lot more for him to concentrate on in a landform grading project.

"It's challenging," said Churchill, "but it is very satisfying to see the end result. I didn't really see the whole thing we're working on here until the other day when I was leaving the site about 6 in the evening and I happened to look back up the road and saw it all highlighted with the setting sun and the shadows. It was really awesome."

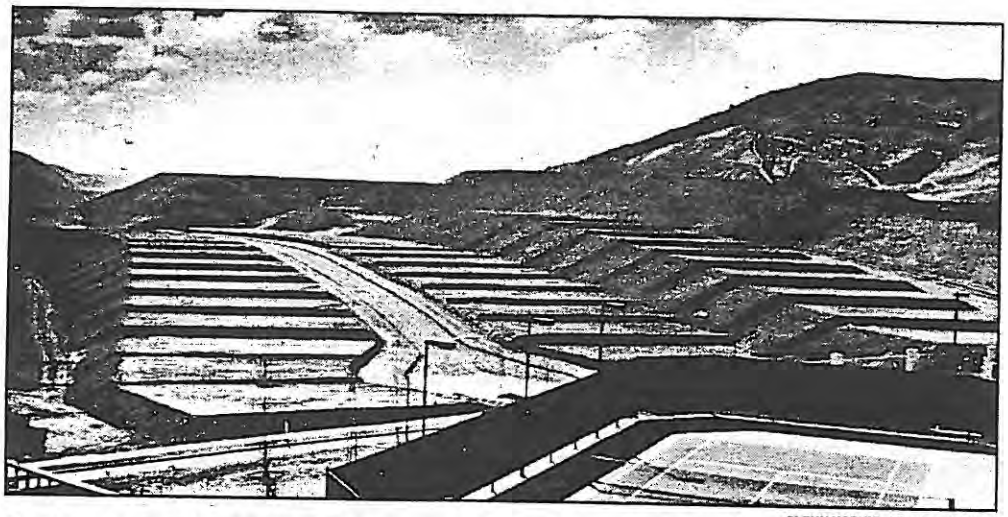

GLENN KOENIG / Los Angeles Times

Traditional grading of sites for homes is shown in picture of Tuscany Hills development in Lake Elsinore area.

Landform Grading: Building Nature's Slopes

By HORST SCHOR
Senior Vice President, Anaheim Hills, Inc.

The advantages and necessities of hillside living are becoming more widely evident as flatlands — the traditional building sites — are consumed by housing, industry and agribusiness.

However, hillside building can require massive grading that may become the focal point of local resistance, thus impeding planning approval. The innovative "landform" grading method was born of negative impressions gained in viewing the conventional, linear slopes commonly manufactured throughout the building industry.

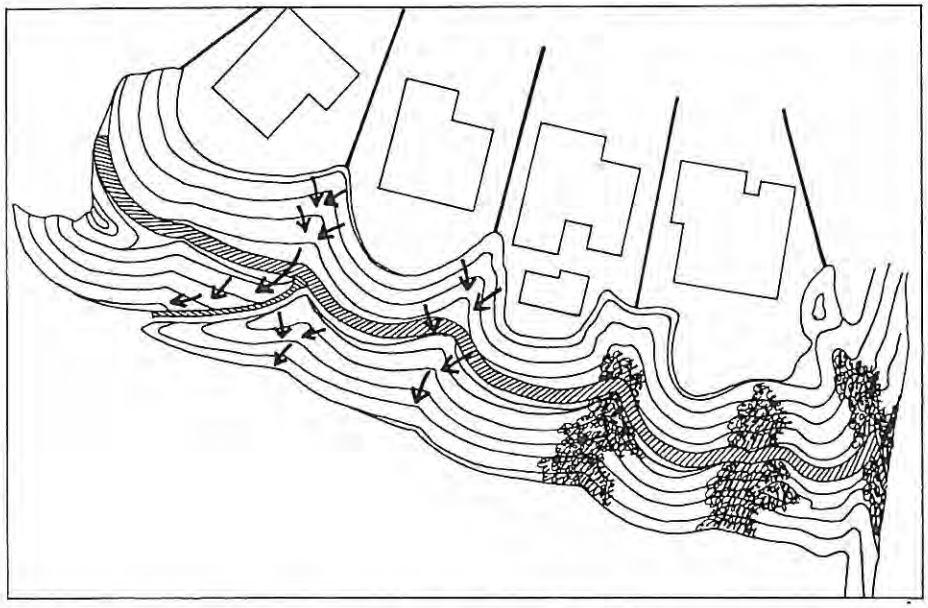

TOPOGRAPHICAL REPRESENTATION of a section of landform-graded slope, showing radial water flow, foliage placement in swales and redistribution of land on lots to conform with landform configurations. Hatched area is concrete terrace drain required by building codes.

Anaheim Hills is situated in 4,300 acres of beautiful, undulating hillsides in northeastern Orange County, California. We, like every other developer, were taking natural terrain and transforming it into rigid, mathematical shapes for building. It was a practice based on the idea: "We've always done it that way." Since there was no specific reason, other than expediency, why it was being done, the time had come to examine ways of changing the accepted thinking about mass grading. The search for an alternative was an attempt to improve the aesthetics of graded hillsides. Anaheim Hills agreed to finance the experimentation and to use the results in the community.

There seemed to be no reason we couldn't grade the slopes to resemble natural slopes. The question then arose: what do natural slopes look like? Curiously, there was no published information about slope shapes as a total unit. We were on our own.

Project research involved study of slopes in such diverse areas as Death Valley, Brazil, Alaska, Hawaii and Anaheim Hills in an attempt to separate distinct features from among the natural slopes and to determine if there was any relationship between climate, soil type and vegetation and slope configuration. Yet it was two years before distinct, repeating patterns emeged from the jumble of forms. Simply stated, cones, pyramids, "elbows," ridges and various combinations of these elements produce natural slope shapes.

The challenge was now to apply these basic shapes to the grading process. Could they be designed and graded? We would have to retrain everyone concerned with the project. Designers, engineers, grading contractors and public officials had always worked in straight lines. Now we were saying, "the more irregular, the better."

Communication of the new ideas was difficult at times. Initially we made clay models in which we combined the basic slope shapes and took them out to the civil engineers and grading contractors. They, in turn, conveyed the ideas to their equipment operators in the field. However, the grading was not shaping up as we expected. We finally had to go into the field and call a bulldozer operator off his machine, show him the drawings and photos and explain the ideas. He then said, "Sure, I can do that. Why didn't you say that in the first place?" With each grading project, we improved and streamlined the operations.

We've now been doing the grading in Anaheim Hills for seven years. Contractors experienced in landform grading prefer it because the finished product doesn't need to meet precise slope-angle measurements, and it affords the operator more leeway in his bulldozing.

There is less finishing cost to the contractor, although there are more engineering, design and field control costs in landform grading. The cut and fill slopes are very complex to design. It is an art to assemble the various shapes on the slopes so they won't look unnatural. They have to blend together and work structurally. Landform grading gets its look not from one component shape or one gully but from a series of them. The landform shapes become a sequence of undulations, peaks and gulleys.

We have to deal with three planning commissions in Aanheim Hills: the cities of Anaheim and Orange and the County of Orange. The planners are delighted with the landform grading idea. At first they were doubtful, but once we'd graded several slopes, we invited them out for a look. They walked over the slopes, viewed them from different angles and saw the value of what we were doing.

The civil engineers were more skeptical. They felt that the shapes we were creating would cause severe erosion. We proved them wrong. Early on, we graded an experimental slope 70 feet high without the artificial drainage interception aids required by the building codes. Rather, we let the curves and elbow shapes of the landforms absorb the im-

pact of the running water, as happens in nature.

The rains from 1977 to this year have been heavy. From September through March 1977-78, it rained more than 31 inches. The same period in 1978-79 gave us more than 21 inches, and 1979-80 during the similar months put more than 22 inches of water on the slope. The slope is still in perfect condition. Nature doesn't follow building codes, but its designs still work.

Ironically, we found that conventional, angular grading tends to encourage erosion. Water generally will sheet flow on a flat surface and will tend to carve swales in the weakest sections of the slope. To compensate, building regulations require terrace drains every 25 feet to break the momentum of the water. Yet there is an entire set of building regulations predicated upon the efficiency of conventional, linear slopes.

On the other hand, the drainage pattern of a landform-graded slope is radial in nature and swales are already provided for the runoff. If the land is formed naturally, as in our process, the water follows the channels, which break its speed by virtue of their energy-dissipating shapes. Further, most foliage occurs in the channels or swales, and its presence breaks the speed of the running water. Our landscaping also follows this natural pattern. We also experimented with such ideas as planting Acacia Rosemary, a lush, low growth, to cushion the impact of rainfall.

Mother Nature is full of surprises. She knows how to control erosion without using the clumsy terrace drains we use in man-made slopes. We've minimized the visual impact of the required concrete drains by running them diagonally and curvilinearly across the slopes, which makes them considerably less visible. We also line them with river rock, so when they are visible they complement the landform slope aesthetics.

AERIAL PHOTO of landform-graded region in Anaheim Hills. Note irregular patterns formed by landform-graded slopes along perimeter of lot pads.

Initially, we and the builders were concerned about the buildable land that would be lost to the landform grading process on each lot. We solved that by reshaping backyards to conform with the grading configurations. The center sections of the lots, which are used most extensively, bulge outward with the ridgelines of the grading. The corners of the yard are taken up by the swales and these edges are characteristically used less often. In effect, we redistributed the lot pad square footage to our advantage.

We are pleased with the results of our experiments. When covered with mature vegetation, our landform graded slopes appear very much like natural slopes. The grading has allowed us to move away from straight lines and abrupt angles in our community planning. The homes are positioned more irregularly, which discourages the monotonous look of row housing. And, importantly, we come very close to restoring the slopes to their natural conditions.

We believe that sooner or later developers will be required to use this type of landform grading. This method of grading is part of the future of land development in this country and eventually in all other countries because most urban and suburban flatland has been built upon in one way or another. Landform grading involves more effort to achieve, design, implement, construct and engineer. However, the cost in time and labor is well worth the results of aesthetics, structural integrity and the value to developers of public acceptance and municipal planning approval.

FRESHLY GRADED landform slopes show ridges, swales and pyramid shapes.

MATURE LANDFORM slopes with vegetation and foliage in swales.

TAB 10

Patrick J. Fox

Presentation

STABILITY OF LANDFILL LINER AND COVER SYSTEMS

University of Wisconsin-Madison 21st National Short Course on Slope Stability and Landslides

Patrick J. Fox

Associate Professor
Department of Civil and Environmental Engineering
University of California
Los Angeles, California USA
(310) 794-4805
pfox@seas.ucla.edu

1. Overview of Landfill Liner and Cover Systems
2. Stability Issues for Landfills
3. Waste and Geosynthetic Materials
4. Stability of Liner Systems
5. Stability of Cover Systems

Landfill Liner and Cover Systems

Design of bottom liner systems and cover systems is governed by:

- RCRA Subtitle C – hazardous waste landfills
- RCRA Subtitle D – municipal solid waste landfills

Primary function: minimize passage of liquids/gases

- instability/large deformations must be avoided

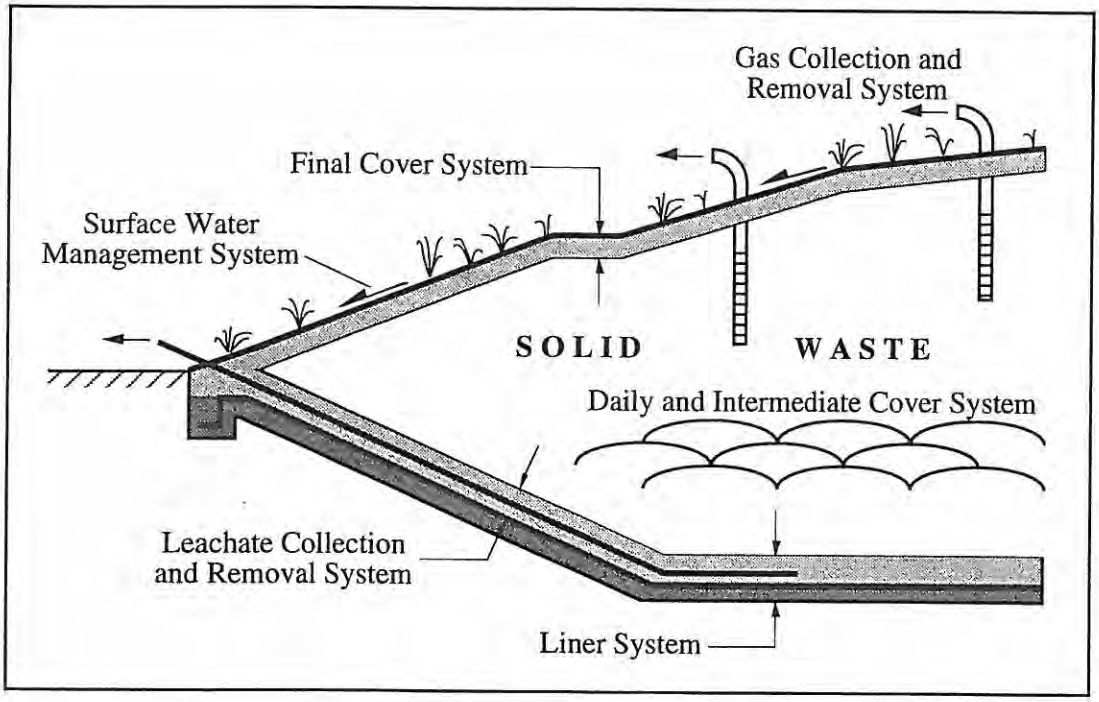

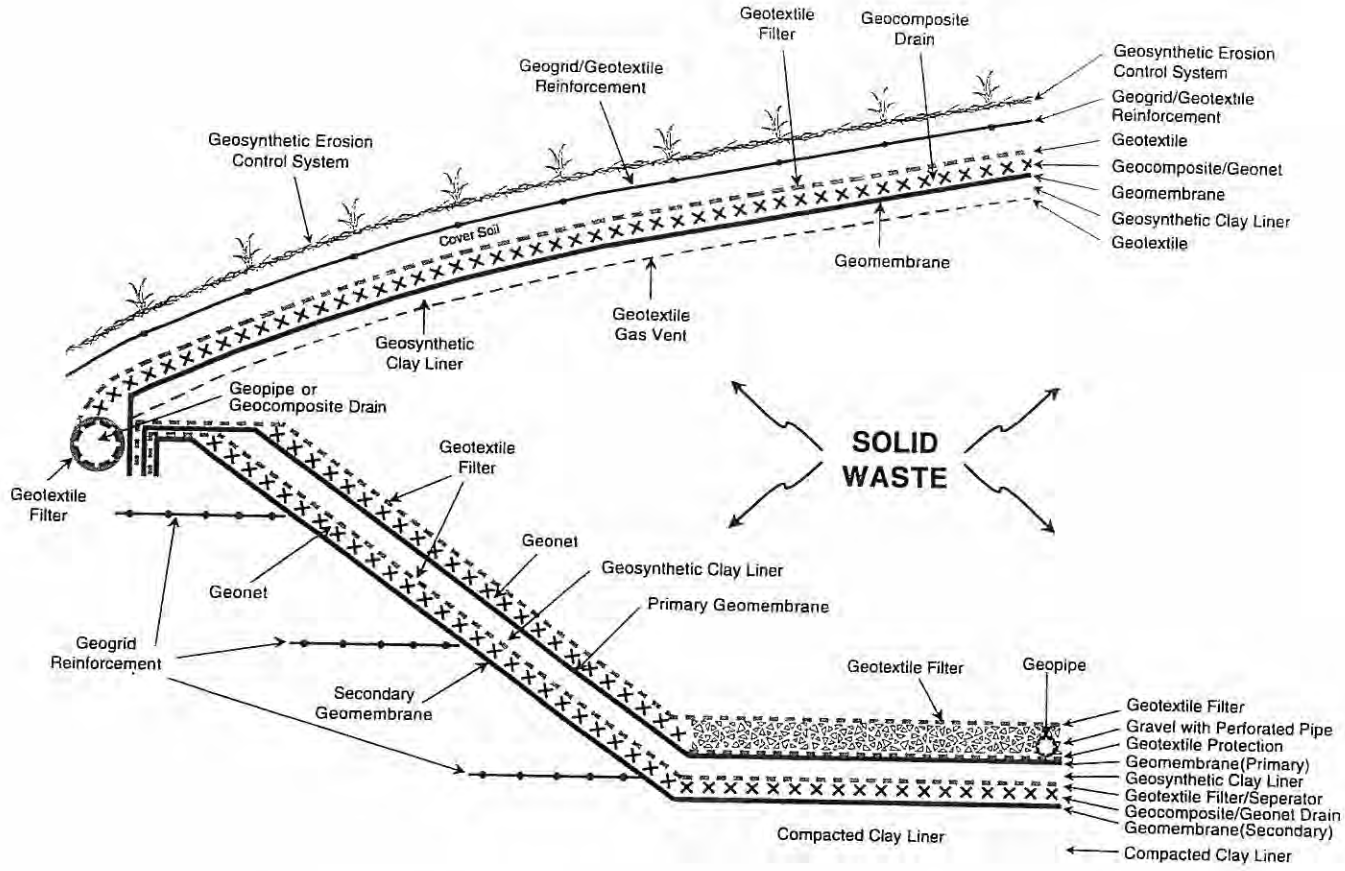

Figure 5.52 Solid waste containment system with high geosynthetic utilization. (Koerner 1998)

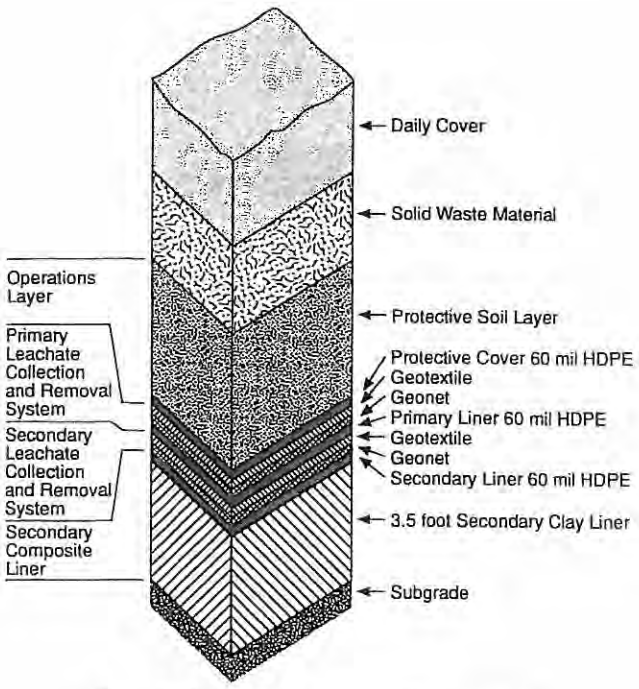

Figure 2a. Schematic Illustration of Sideslope Liner.

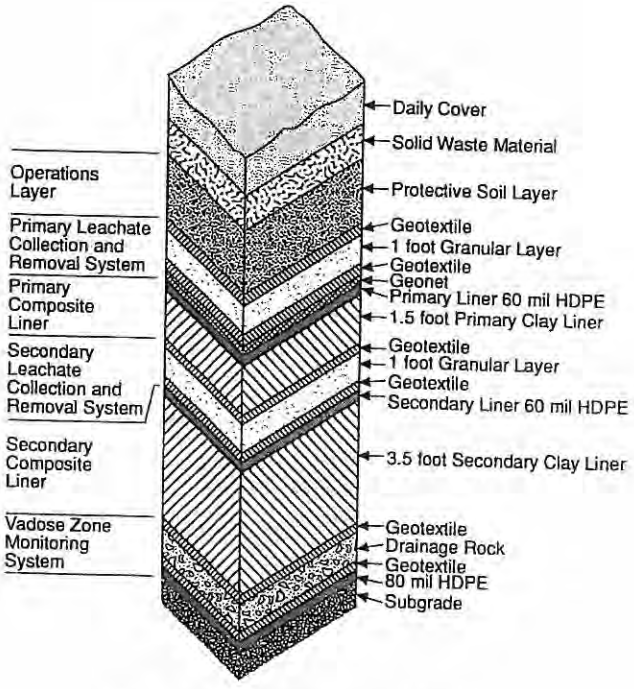

Figure 2b. Schematic Illustration of Base Liner.

(Byrne et al. 1992)

Example: Final Cover System

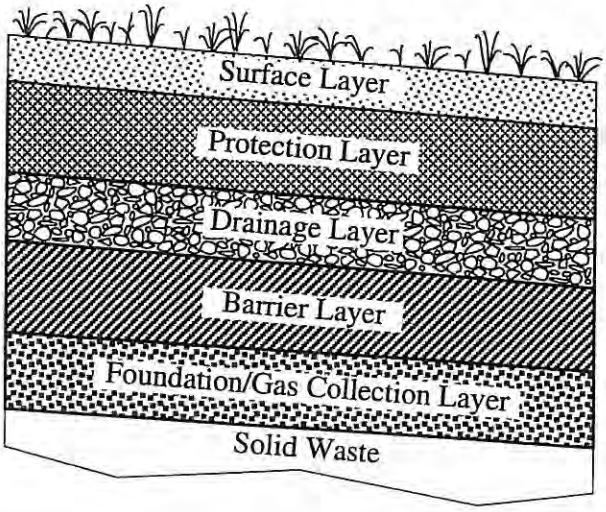

Components

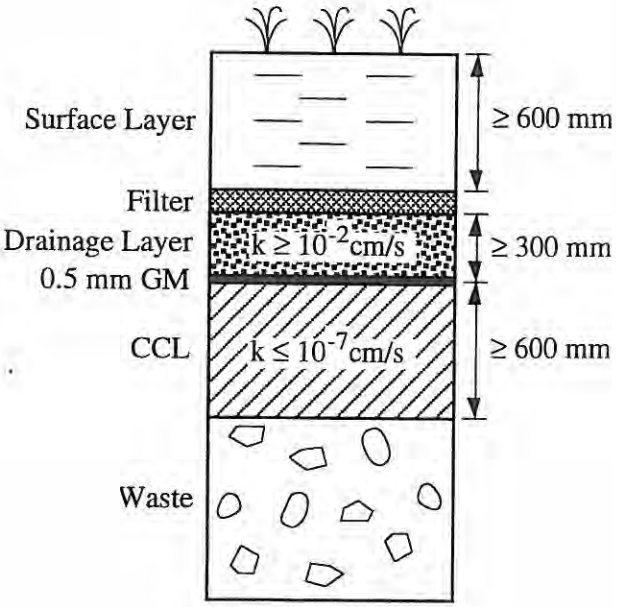

Minimum Subtitle C

Surface Layer: Supports vegetation, minimizes erosion, provides moisture retention, protects barrier from desiccation/freezing

Protection Layer: Provides extra rooting depth, water retention, desiccation/frost protection

Drainage Layer: High k layer; minimizes contact time between infiltrating water and barrier layer

Barrier Layer: Low k layer; minimizes infiltration (CCL, GM, GCL)

Foundation/Gas Collection Layer: Protects barrier from waste, collects landfill gas, reduces gas pressure underneath barrier

CCLs have a number of disadvantages:

- difficult to achieve good compaction on waste materials
- susceptible to desiccation and frost damage
- susceptible to cracking from differential settlement
- difficult to repair if damaged
- time-consuming and expensive to construct
- occupy considerable landfill space
- defects may control k

Geosynthetics are widely used to avoid these problems:

- geomembranes (GMs) and geosynthetic clay liners (GCLs)

Concerns with GMs:

- defects, holes, tears, bad seams
- wrinkles over CCLs, GCLs - impair perf. as composite liner

Concerns with GCLs:

- bentonite migration
- cation exchange
- shear strength
- installation damage

Minimum Final Cover Systems – Subtitle D

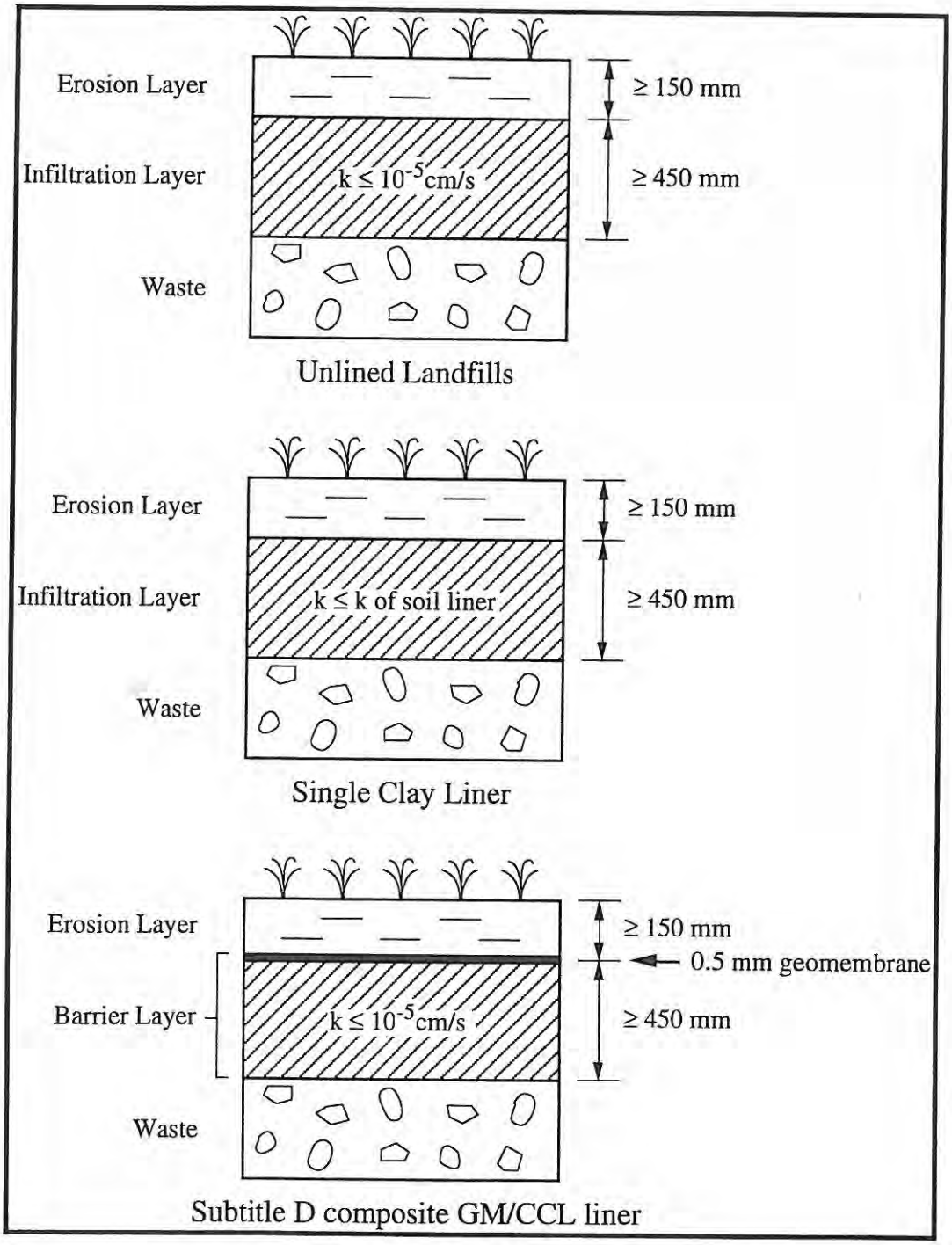

Stability Issues for Landfills

Stability is an important consideration for landfill liner and cover systems because:

- cost and environmental consequences of failure
- steeper slopes provide more landfill volume (3H:1V common, 2H:1V has been used)
- layers are oriented parallel to slope
- barrier layer is designed to minimize liquid/gas flow
  $\Rightarrow$ water flow is parallel to slope
  $\Rightarrow$ condensation may form underneath barrier
- qualities which make a good barrier tend to destabilize slopes (e.g., bentonite, smooth GM for intimate contact, CCL compacted wet of OMC).

Factors affecting stability:

- properties of the foundation soil
- strength, weight, and compressibility of solid waste
- decomposition of waste over time
- strength and weight of liner and cover system components
- slope geometry
- leachate level inside landfill; infiltration within cover system
- construction methods, sequence
- seismic events

Types of Instability

- Foundation failure - most landfills are placed on firm ground to avoid differential settlement of liner system.
  $\Rightarrow$ exception: vertical expansion of old landfills
- Bottom liner failure - serious issue during filling operations
- Failure within solid waste - serious issue during filling operations
- Cover system failure - serious issue after cover construction
- Combination failure

Configurations:

- Open pits, valley/canyon fills, embankment fills
- Cut slopes, fill slopes
- Temporary vs. permanent slopes

Considerations:

- Stability of excavations prior to waste placement
- Stability during filling operations
- Stability of completed landfill

Types of Instability

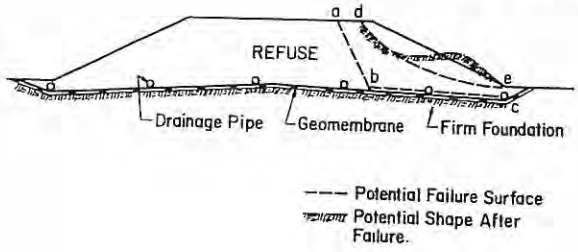

Fig. 11.1 Stability of a landfill on firm base.

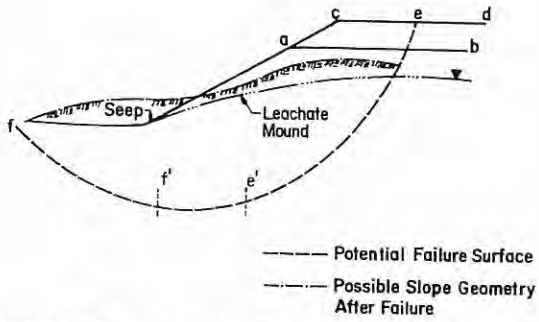

Fig. 11.2 Stability of a landfill expansion on soft base.

(Oweis 1993)

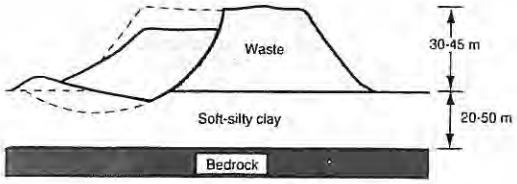

(a) Single rotational failure

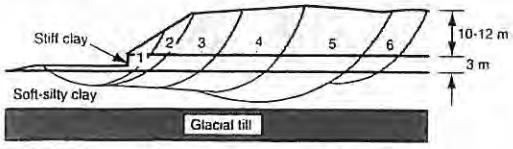

(b) Multiple rotational failures

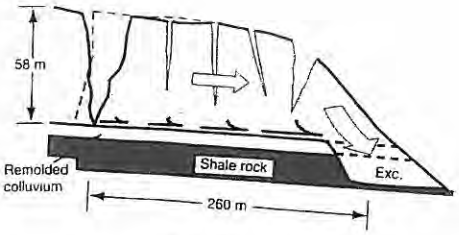

(c) Translational failure

Figure 5.49 Failure of municipal solid waste landfills within the mass itself.

(Koerner 1998)

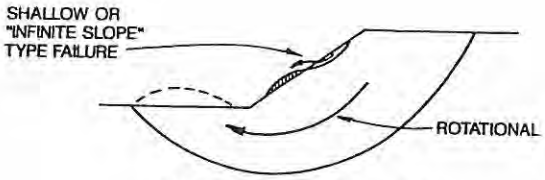

a) Sidewall Slope and Base Failure

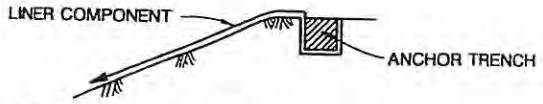

b) Pullout of Liner System Components from Anchor Trenches

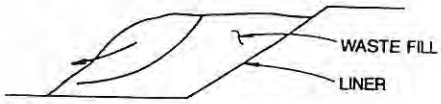

c) Failure Through the Waste Pile

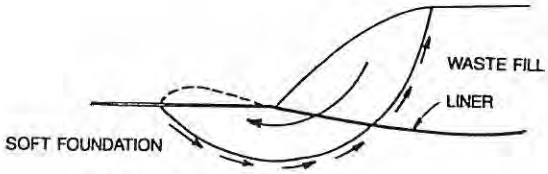

d) Failure Through the Waste, Liner, and Foundation

e) Failure By Sliding Along the Landfill Liner System

FIGURE 4
SCHEMATIC DIAGRAMS OF POTENTIAL FAILURE MODES IN LANDFILLS

(Mitchell and Mitchell 1992)

Waste Materials

Types

- Municipal solid waste (MSW)
- Hazardous waste
- Industrial wastes (e.g., foundry sand, fly ash, papermill sludge)
- Radioactive wastes

Unit weight and shear strength properties of MSW are poorly understood:

⇒ highly variable composition; large inclusions

⇒ conventional sampling and testing methods not applicable

⇒ laboratory tests on large reconstituted specimens; field tests

⇒ parameters back-calculated from failed slopes, slopes with large deformations, or stable slopes assuming FS = 1 (conservative for stable slopes)

MSW has been observed to stand at a vertical cut of 6 m or more (Oweis *et al.* 1985)

- suggests considerable strength ⇒ internal reinforcement
- internal reinforcement ⇒ shear strain at peak >> than for soil

Waste Properties – properties of interest: γ, c, ϕ

Unit Weight, γ

Highly variable depending on initial composition, decomposition, compactive effort, water content, settlement, and depth.

$\Rightarrow$ γ will typically increase with depth

$\Rightarrow$ w% = *f*(climate, initial composition, decomp., cover system, leachate and gas collection systems, type of daily cover)

$\Rightarrow$ typical values: $\gamma = 5$ to 13 kN/m^3 (32 to 83 pcf)

A conservative value should be chosen to avoid underestimating γ.

Table 11.1 Unit weight of municipal refuse

municipal solid waste (MSW) form	*unit weight*	
	kN/m³	*pcf*
MSW, moderate to good compaction	4.7–6.3	30–40
MSW, good to excellent compaction	8.6–9.4	55–60
MSW, baled waste	8.6–14.1	55–90
MSW, active landfill with a leachate mound	6.6	42
MSW, old landfill	9.7	62
MSW, from test pits	8.9–16.2	
MSW, after degredation and settlement	9.9–11	63–70
Incinerator residue as received	7.2–12.7	46–81
Incinerator residue (maximum dry density–standard compaction)	13.5	86
Incinerator residue–old and recent residue (in-place densities)	14.9–16.6	94.7–105.7
Wood chips (dry)	2.3	14.6
Wood chips (with 64% moisture)	3.8	23.9
Leaf compost as delivered	2.6	16.7
In windows (40% moisture)	5.2	33.3
Final product	3.5	22.2

Source: NSWMA (1985), Landva and Clark (1986), Schoenberger and Fungaroli (1971), Poran and Ali (1989), Oweis and Khera (1990).

(Oweis 1993)

Shear Strength Parameters, c and ϕ

Assigning specific c, ϕ to MSW is somewhat speculative

$\Rightarrow c > 0$ is reasonable due to internal reinforcing effect

Estimates of MSW shear strength have been made via:

- laboratory testing – direct shear on reconstituted specimens
- back-calculation from field tests and operational records
  - generally FS = 1.0 must be assumed (conservative)
- *in situ* testing (vane shear, SPT, CPT)
  - results are questionable because test devices small compared to inclusions
  - no published correlations between measured SPT, CPT values and MSW strength

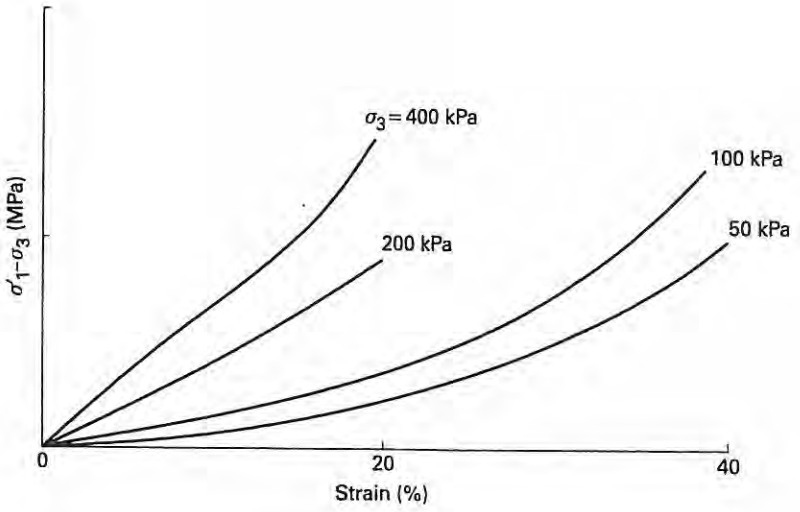

Figure 5.12
Stress–strain behavior of municipal solid waste in triaxial tests (after Jessburger, 1994)

(Oweis & Khera 1998)

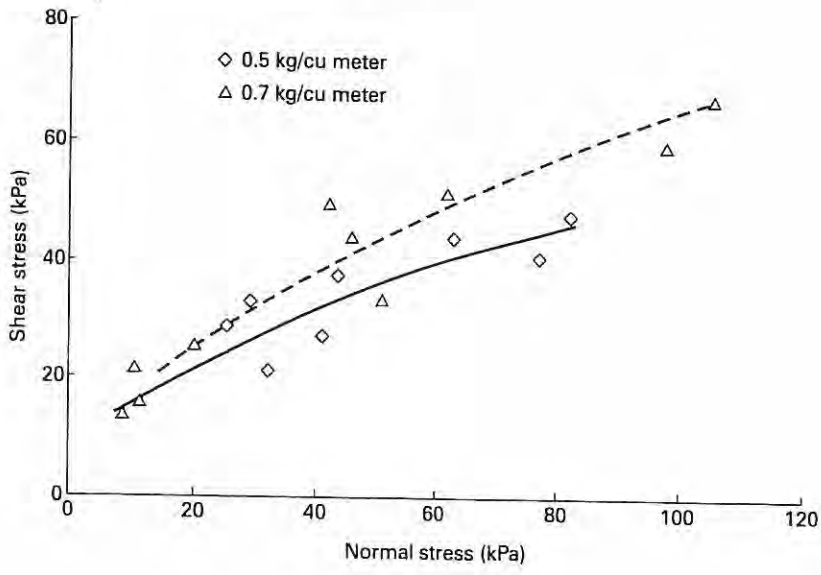

Figure 5.13
Dependence of friction angle on normal stress for municipal waste

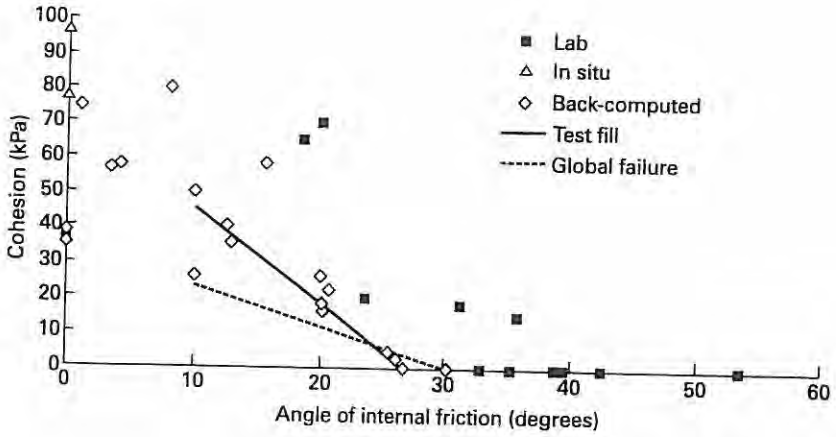

Figure 5.15
Strength parameters for landfill from various methods (Oweis et al., 1985; Landva and Clark, 1990; Siegel et al., 1990; Singh and Murphy, 1990)

Hazardous Waste: Generally placed in containers (steel drums, boxes, etc.). γ can be estimated by considering proportion of containers vs. cover soil. A conservative estimate of fill shear strength is equal to the shear strength of the cover soil at low relative compaction.

Industrial and Mineral Wastes (e.g., fly ash, foundry sand, paper processing wastes): γ, c, ϕ values are generally easier to obtain and more reliable due less heterogeneity of material.

- high water content wastes $\Rightarrow$ disposal ponds
  - empty pond just before filling is critical stability condition

Geosynthetic Materials

Types

- Geotextiles - filter, separation, protection
- Geogrids - reinforcement
- Geonets - drainage
- Geomembranes - barrier
- Geosynthetic Clay Liners - barrier
- Geocomposites - combination

Unit weight and shear strength properties of geosynthetics are well understood:

- manufactured products; MQA/MQC $\Rightarrow$ low variability
- testing methods well established
- direct shear tests typically performed on large specimens

However, geosynthetic products are constantly evolving:

$\Rightarrow$ **it is absolutely essential to obtain product-specific strength parameters under project-specific test conditions for design of landfill slopes.**

Geosynthetic Properties

Properties of interest: μ, c, ϕ

Mass per Unit Area, μ

Obtained from manufacturer, measurements

Wet wt. $\neq$ dry weight for geonets, GCLs, non-woven geotextiles

Shear Strength Parameters: c, ϕ (or c_a, δ)

Direct shear (ASTM D5321) - 12 in. $\times$ 12 in. specimens

Factors that influence test results:

- normal stress, σ_n
- magnitude and rate of horizontal displacement
- drainage and stress conditions during hydration and shear
- hydration and stress history for specimen (GCLs)
- gripping/clamping systems used to hold geosynthetics

Interface Shear Testing

Typically three tests are performed for each interface that bracket the applicable normal stress range.

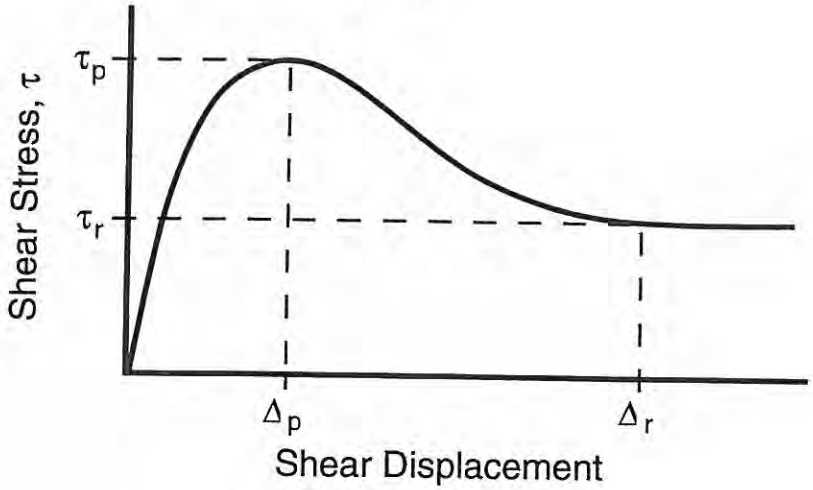

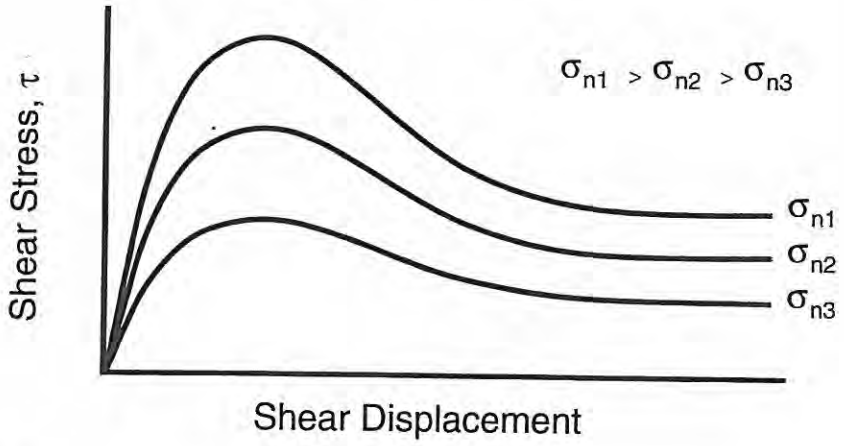

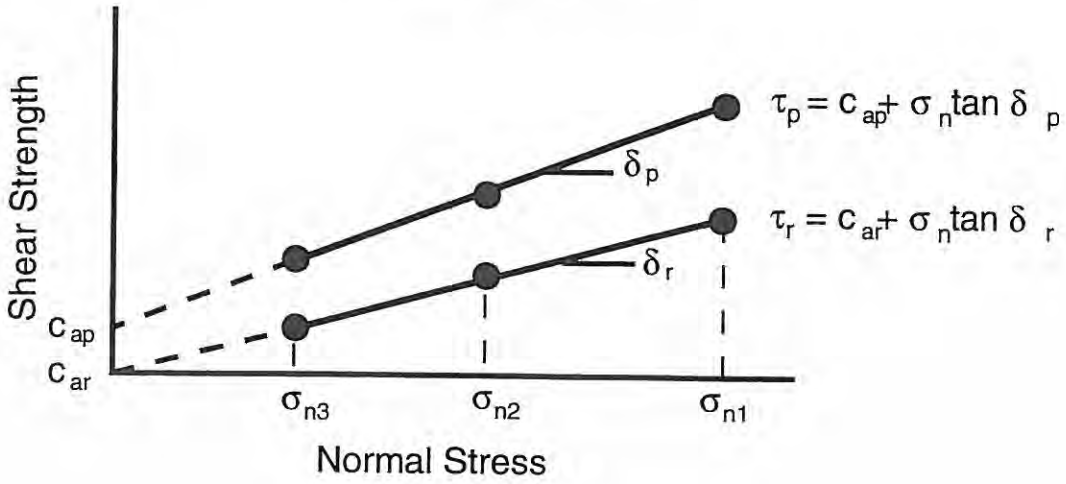

Important Concepts for Shear Strength of Geosynthetics

1. Geosynthetics commonly show significant post-peak strength reduction $\Rightarrow$ due to material damage.

2. Residual shear strength (τ_r) may require Δ = 500 to 750 mm or more.

3. Failure envelopes may be non-linear:
   - $\Rightarrow$ fit using non-linear equation (Giroud *et al.* 1993)
   - $\Rightarrow$ fit using linear equation: c, ϕ values only apply for a given stress range

4. Failure envelopes may or may not have true cohesion.
   - $\Rightarrow$ "Velcro effect" (e.g., textured GM/nonwoven GT)
   - $\Rightarrow$ reinforced GCLs

5. Geosynthetic shear strength is commonly anisotropic in the plane of shearing $\Rightarrow$ even in directions that are 180° apart

Smith and Criley (1995)

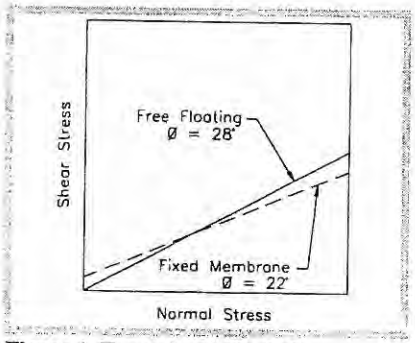

Figure 1. Example of effect of membrane anchorage.

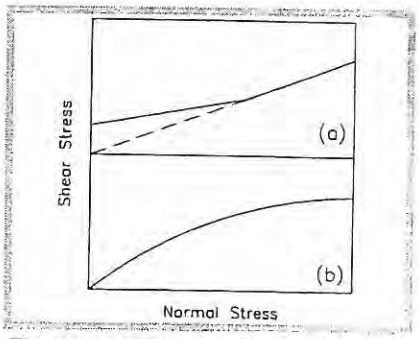

Figures 2a and 2b. Typical bi-linear failure envelopes.

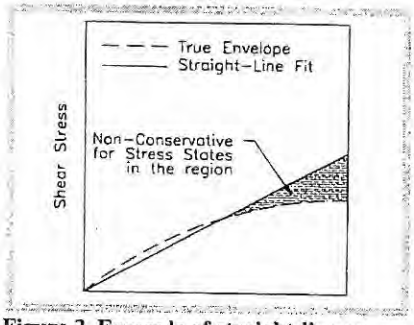

Figure 3. Example of straight-line as nonconservative data fit.

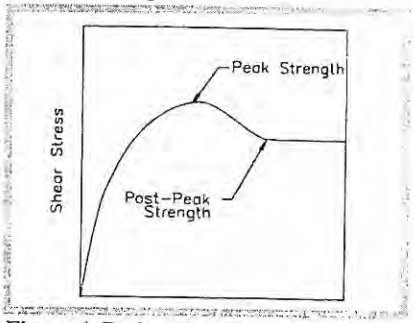

Figure 4. Peak and post-peak envelopes.

GM-CCL Interfaces

Condensation on underside of GM and CCL consolidation may weaken interface strength.

Kettleman Hills: Mitchell and Mitchell (1992) report $S_u = 45 \pm 12$ kPa
Byrne et al. (1992) report $S_u = 30$ to 35 kPa

Seed and Boulanger (1991): smooth HDPE/compacted clayey till

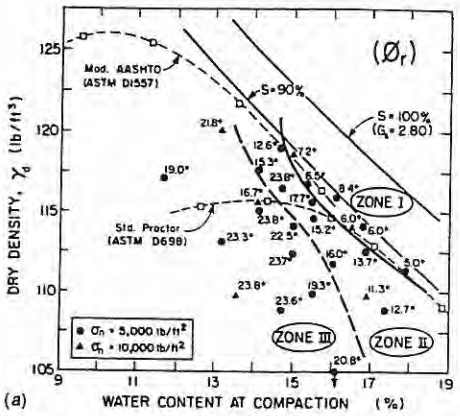

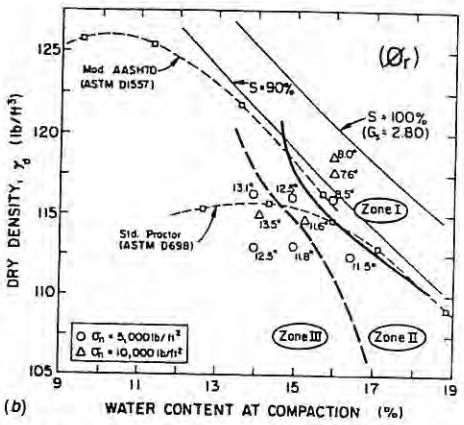

FIG. 2. Measured Shear Strengths for Smooth HDPE-Compacted Clayey Till (with 5% Bentonite) Interfaces as Function of Compaction and Soaking Conditions: (a) Samples Sheared as Compacted; (b) Samples Sheared (UU) after Initial Presoaking

Geosynthetic-Geosynthetic Interfaces

Interface strengths highly variable, depending on products/methods.

Mitchell and Mitchell (1992): smooth GM

Table 1
Summary of Interface-Shear-Strength Tests: Kettleman Hills Repository

Interface Components	Conditions	Direct Shear Tests: Residual Friction Angle: ϕ_r	Pullout-Box Tests: Residual Friction Angle: ϕ_r
HDPE liner/geotextile	Dry, unpolished	9.5° to 12.5°	9.5° (1 Test)
	Dry, partly polished	9.0° to 11.0°	—
	Dry, polished	8.5° to 10.5°	8.0° (1 Test)
	Wet, unpolished	8.0° to 10.0°	7.0° to 10.5°
	Wet, polished	7.0 to 9.5°	6.5° to 9.0°
HDPE liner/geonet (transverse shear)	Dry	7.0° to 8.0° +	–
	Submerged	7.0° to 10.0°	8.0° to 9.0°
HDPE liner/geonet (aligned shear)	Submerged	5.0° to 8.0°	6.0° to 8.0°
Geotextile/geonet	Dry	>20°	–
	Submerged	10° to 14° (+)	–
HDPE liner/HDPE liner	Dry	6.0° to 13.0°	–
	Submerged	6.0° to 11.0°	7.0° to 13.5°

- Variability: $\Delta\phi \approx 2°$-$3°$ most cases
- interface polishing $\Rightarrow$ 1° reduction in ϕ
- dry vs. wet ϕ may differ slightly
- ϕ may be anisotropic in shear plane

Stark *et al.* (1996) - HDPE GM/GT interfaces

- Ring shear tests
- Textured GM strength > smooth GM strength
- Damage/removal of texturing for laminated GM product
- Post-peak strength loss ≈ 50-60% for textured GM/nonwoven GT
- Large displ. required to reach τ_r: $\Delta \approx$ 500-800 mm
- Nonlinear failure envelopes
- Product-specific characteristics (mass/area, polymer composition, fiber type, fabric style, method of construction) can have significant influence on interface shear strength.

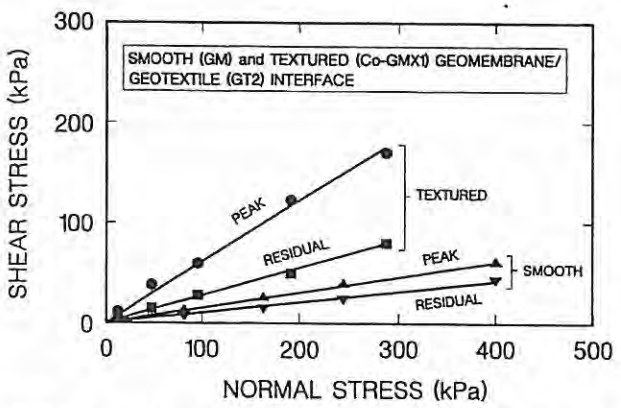

FIG. 1. Comparison of Failure Envelopes for Smooth and Textured Geomembrane/Geotextile Interfaces

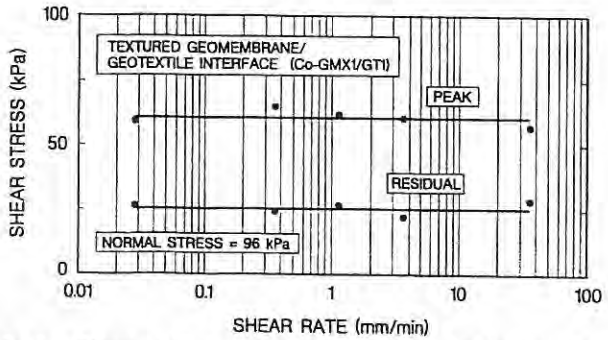

FIG. 2. Effect of Shear Displacement Rate on Textured Geomembrane/Nonwoven Geotextile Interface

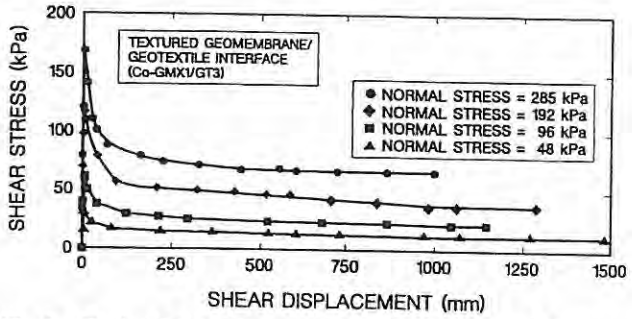

FIG. 3. Typical Ring Shear Test Results for Textured Geomembrane/Nonwoven Geotextile Interface

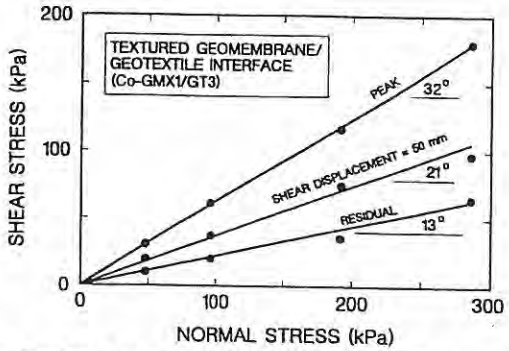

FIG. 4. Typical Failure Envelopes for Textured Geomembrane/Nonwoven Geotextile Interface

Example: Shear Strength of GCLs

Refs: Fox *et al.* (1997), Fox (1998), Fox *et al.* (1998), Triplett and Fox (2000), Fox and Kim (2000)

GCLs: manufactured hydraulic barriers consisting of bentonite clay bonded to a layer, or layers, of geosynthetic material.

- Very low hydraulic conductivity when hydrated with water
- Carrier geosynthetics: uniformly thin layer of bentonite
  tensile strength
- Non-reinforced GCLs: chemical adhesives
  Reinforced GCLs: needle-punched, stitch-bonded $\Rightarrow$ shear strength
- U.S. products: Claymax, Bentomat, Bentofix, Gundseal
  bentonite ≈ 5 kg/m^2
  $k \approx 10^{-10}$ to 10^{-12} m/s, lower for Gundseal

GCL stability is an important issue for design:
- low shear strength of bentonite after hydration
- internal vs. interface shear strength

Advantages for GCLs compared to CCLs:
- better resistance to desiccation and freeze/thaw damage
- better performance under differential settlement conditions
- rapid installation using lightweight equipment
- increased landfill capacity
- generally equal or lower cost, depending on clay availability

GCLs are now widely used and accepted.

Cincinnati Test Plots

Cincinnati test plots (Daniel *et al.* 1998):

- all 3H:1V plots OK
- some 2H:1V plots failed at GCL/GM interface (woven slit film side of GCL with some extruded bentonite)

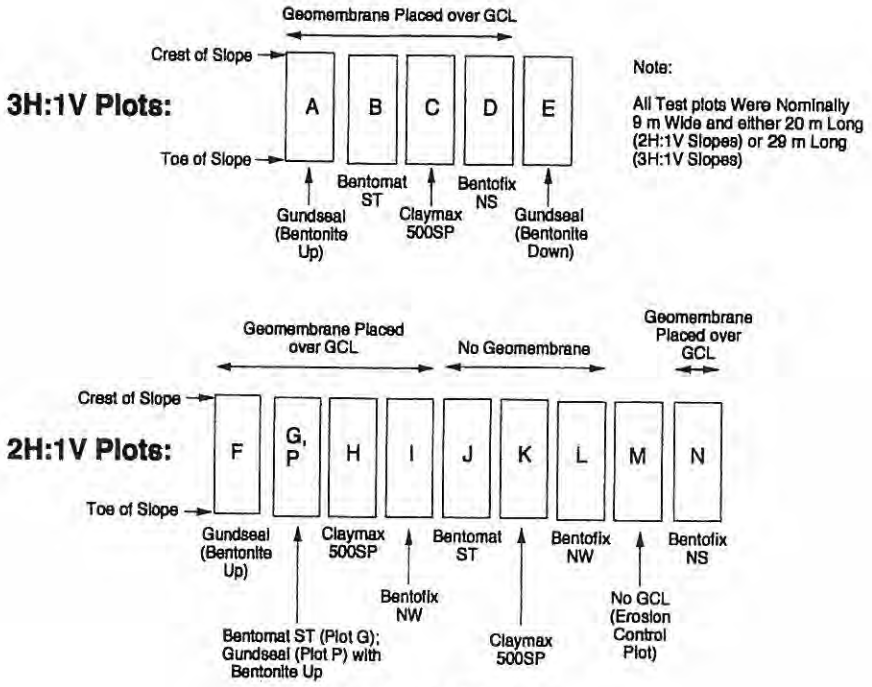

FIG. 1. Layout of Test Plots

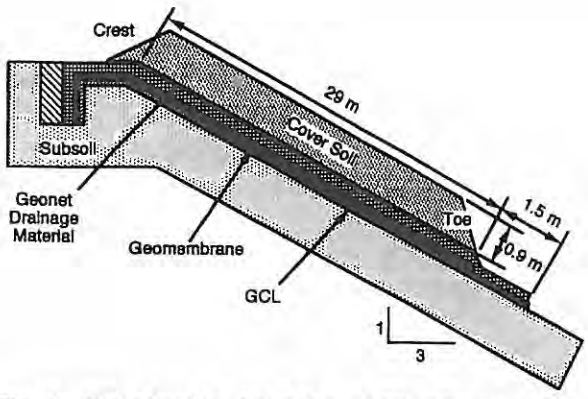

FIG. 2. Cross Section of Test Plots on 3H:1V Slope with Geomembrane Overlying GCL

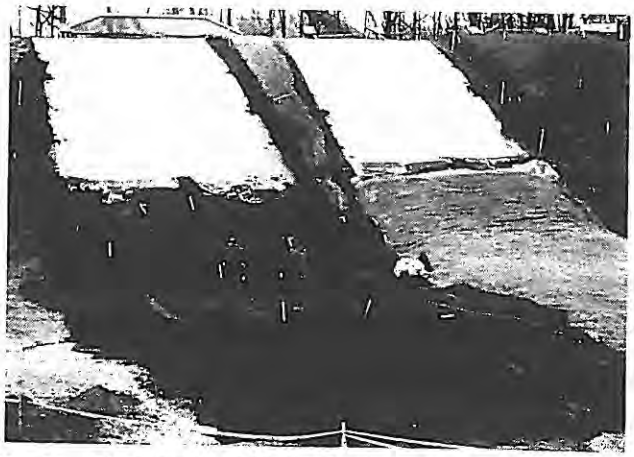

FIG. 15. Photograph of Slides Involving Plot G (Left) and Plot H (Right)

Pullout Shear Machine

- GCL specimens are 1067 × 406 mm ⇒ δ = 203 mm
- High σ_v (up to 483 kPa)
- Aggressive gripping system ⇒ no clamping of geosynthetics
- Vertical displacement
- Pore pressure needles
- No moments created during shear

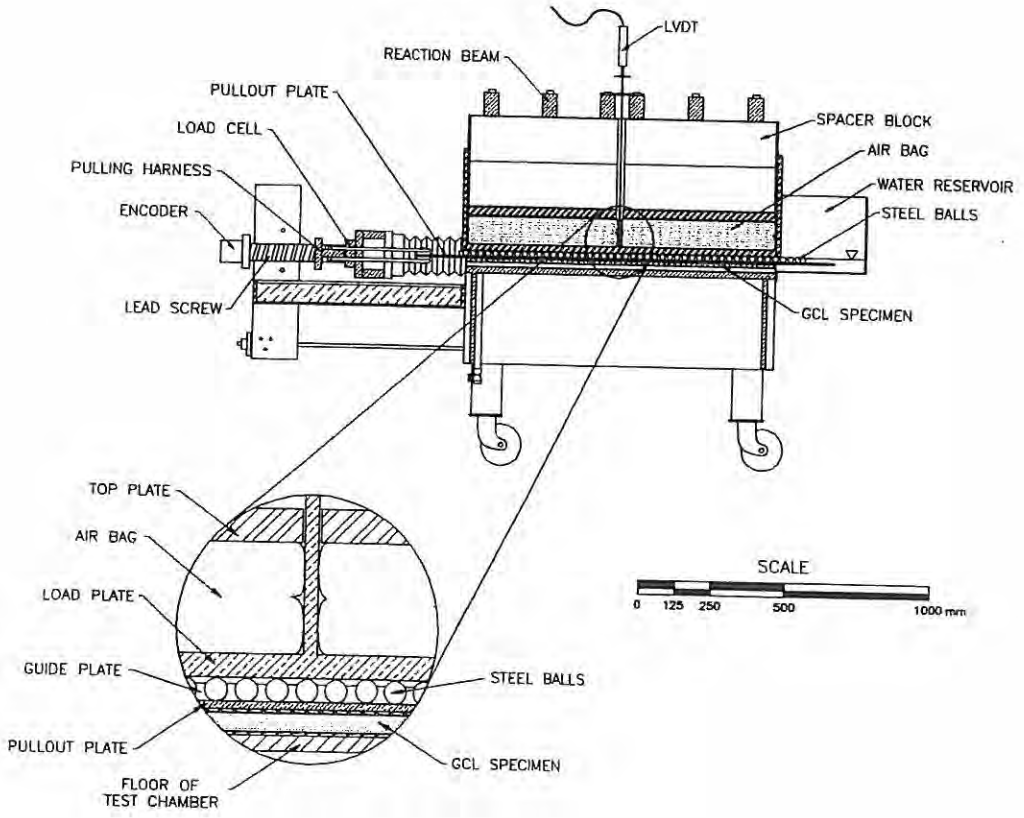

Pullout Shear Machine (cont.)

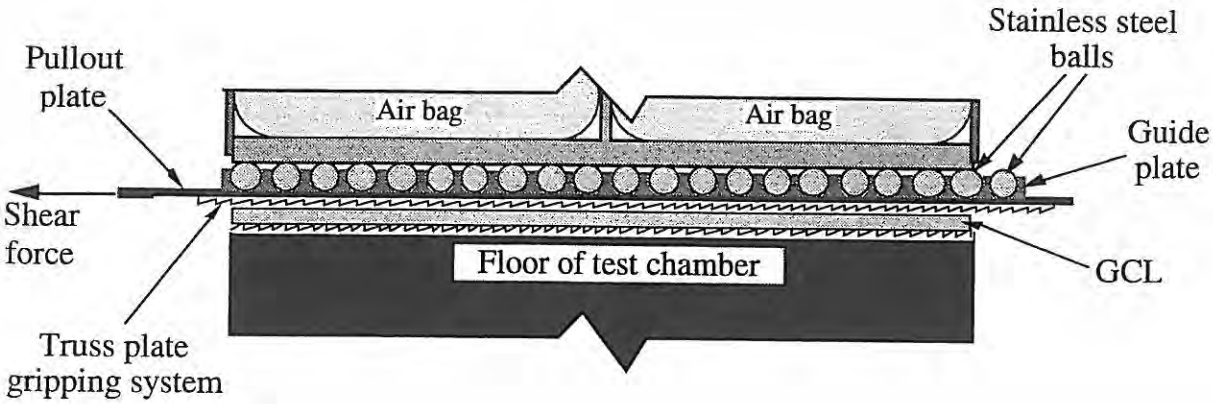

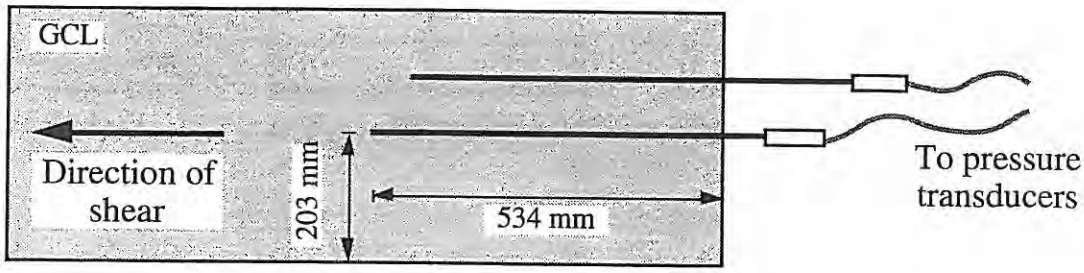

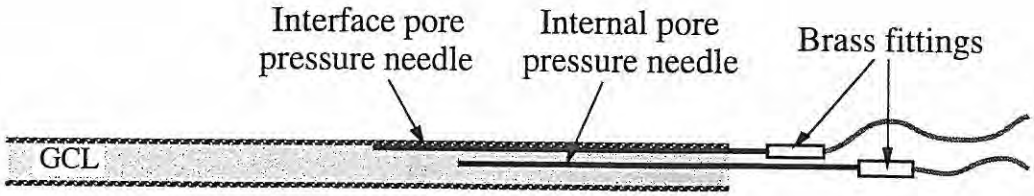

Improved Specimen Hydration Procedure

- 4-day, 2-stage procedure
- reduces required in-machine hydration time

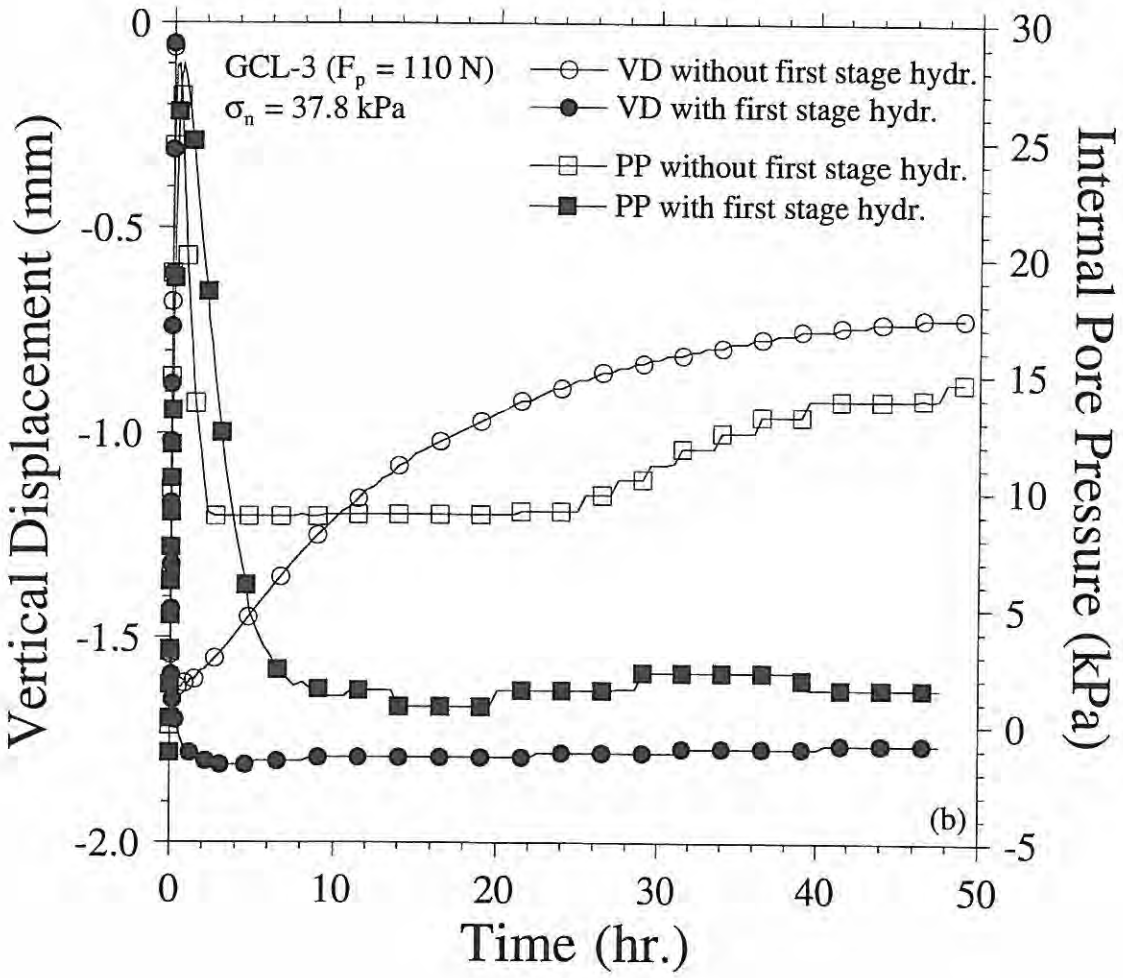

Improved Specimen Hydration Proc. (cont.)

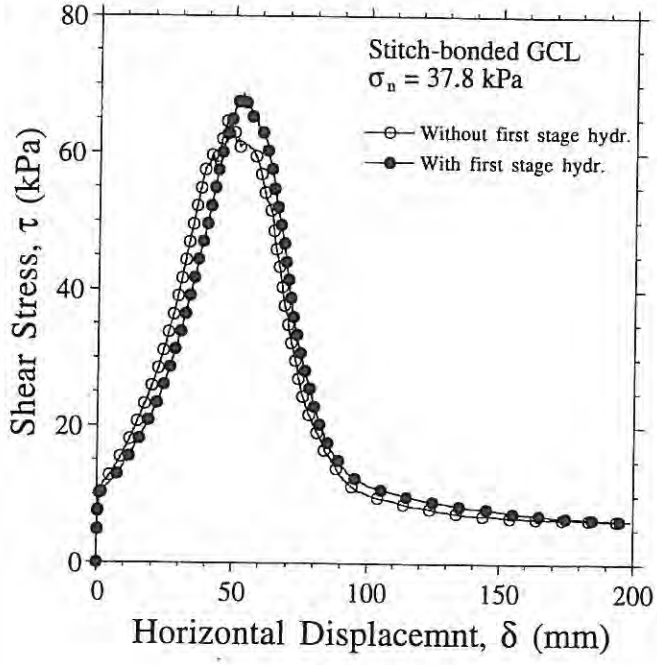

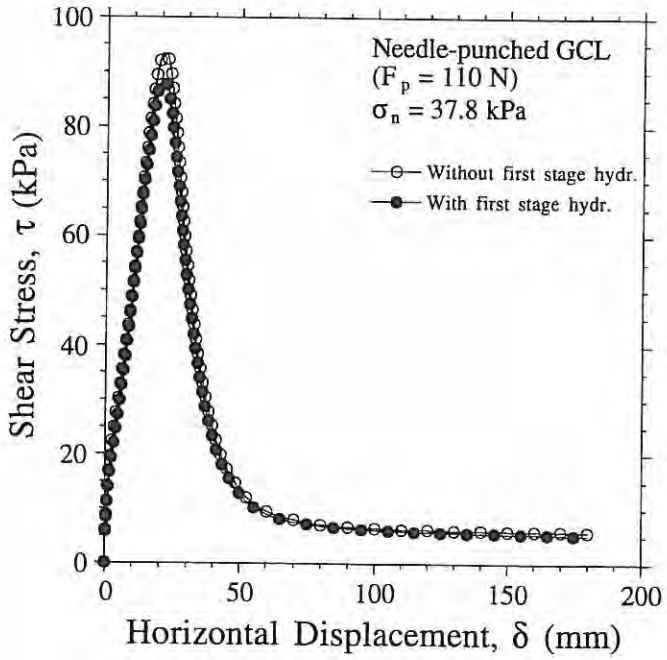

Stress-Displacement Behavior

- Well-defined τ_p and τ_r, τ_r/τ_p as low as 4%
- $\delta \leq 140$ mm needed to reach $1.1\tau_r$

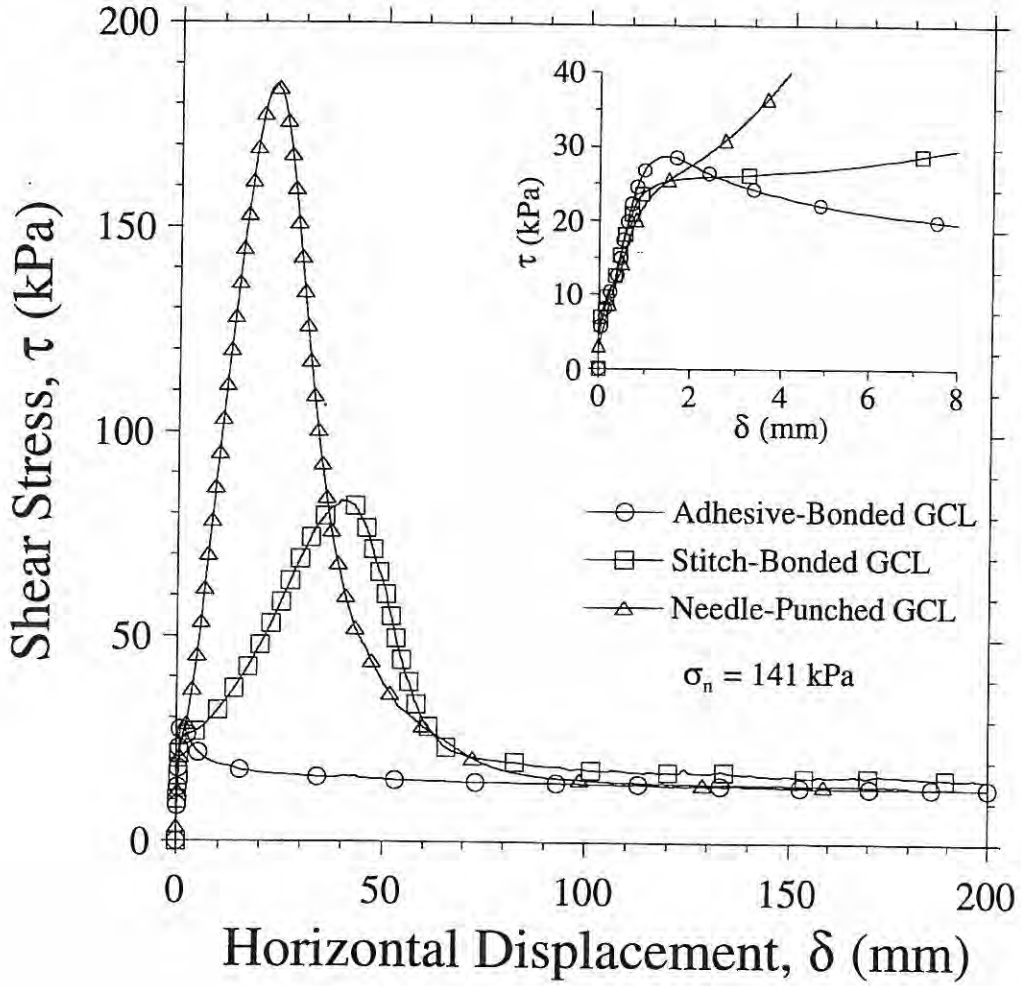

Stress-Displacement Behavior (cont.)

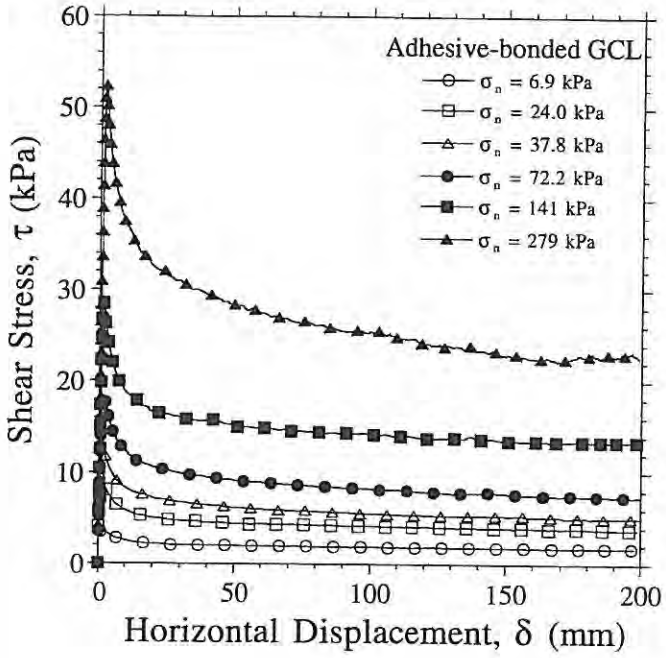

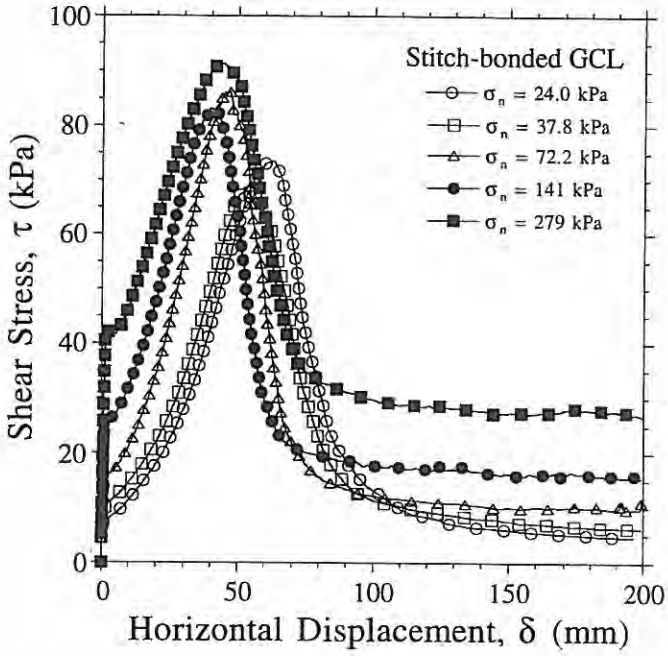

Stress-Displacement Behavior (cont.)

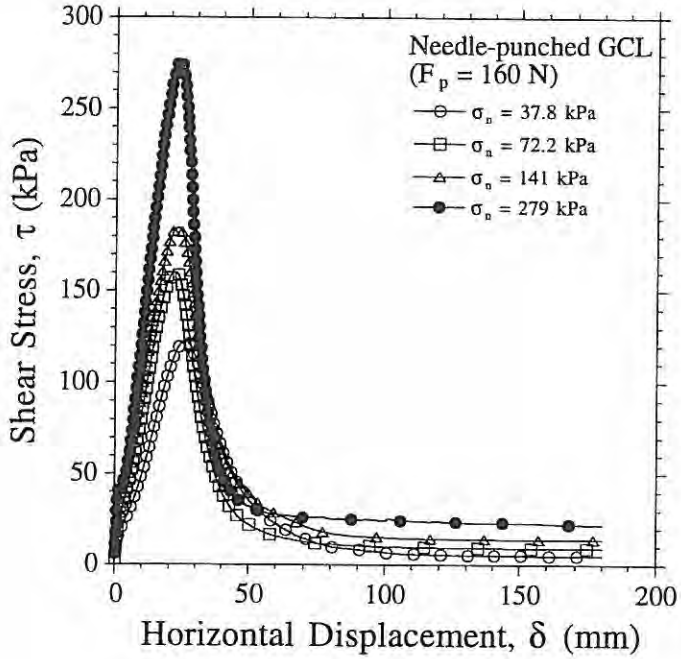

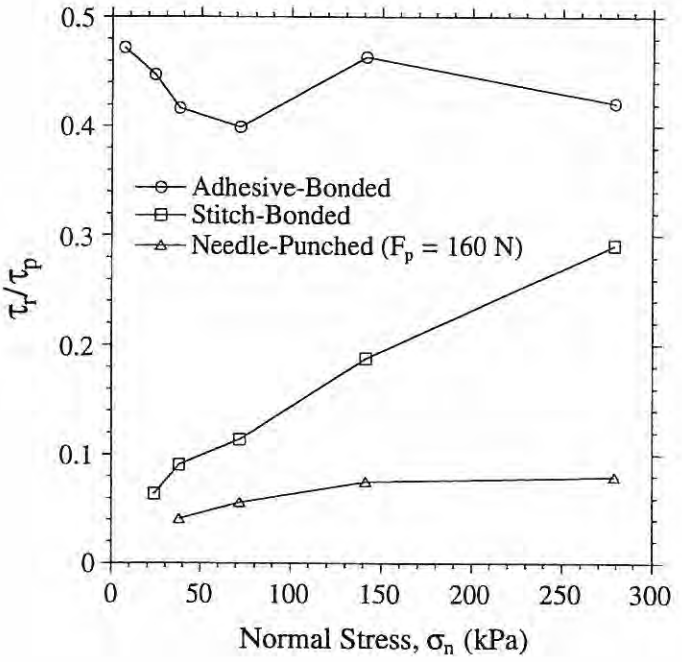

Internal Shear Strength

- Slightly non-linear failure envelopes
- ϕ_p depends on reinforcement type, $\phi_r \approx 4.5°$
- Failure surface not within hydrated bentonite

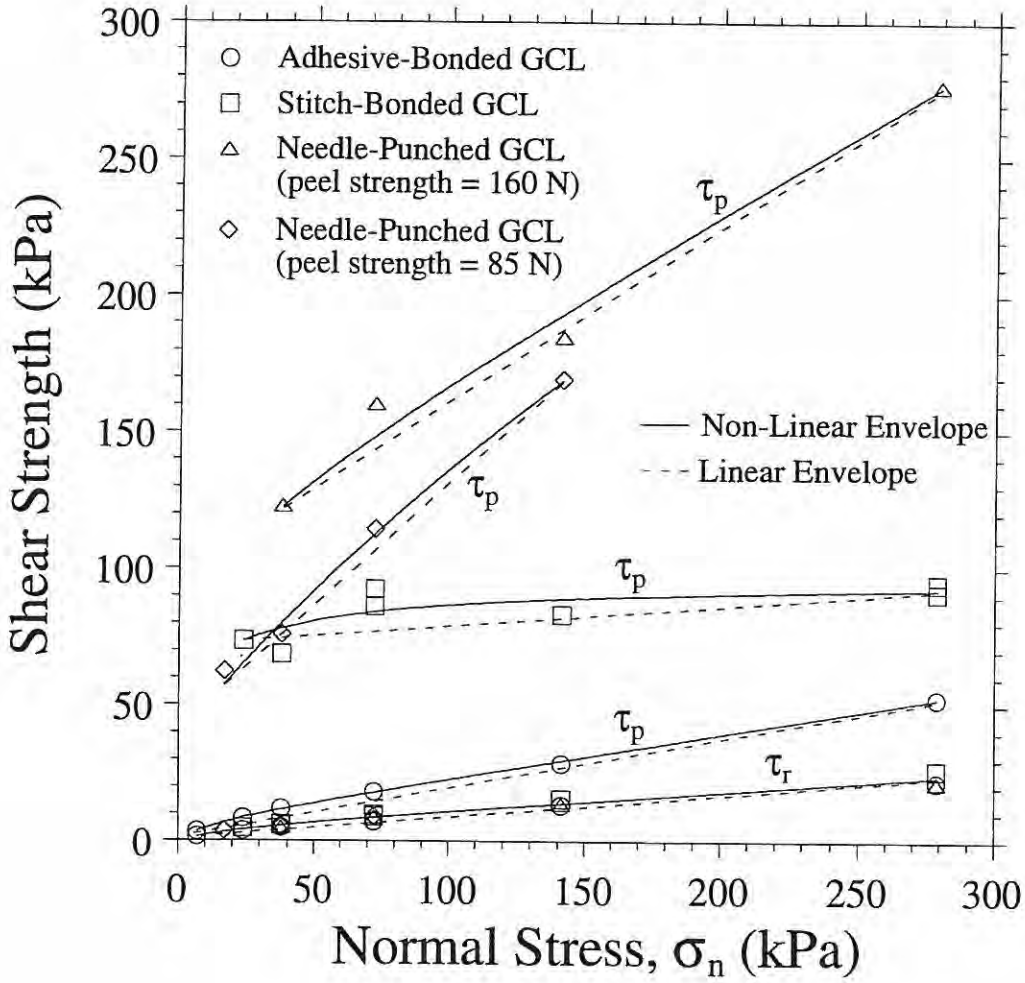

Effect of Displacement Rate

- Both τ_p and τ_r decrease about 3 - 5% per log cycle of displ. rate

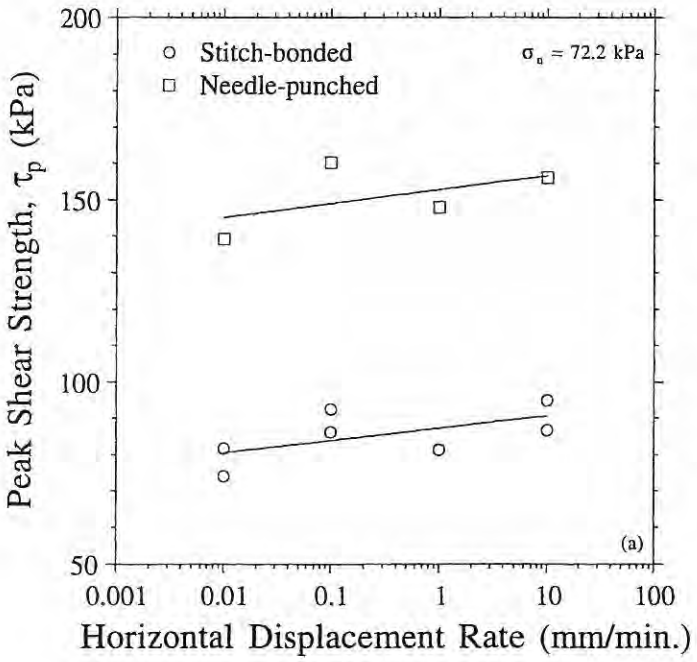

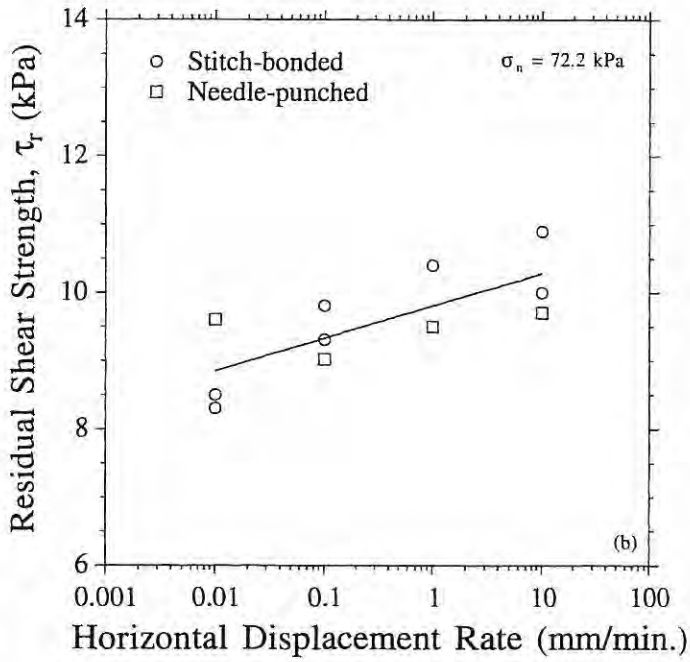

Effect of Shear Direction

- Stitch-bonded GCL
- 101 single-thread chain stitch
- τ_p (standard)/τ_p (reverse) $\approx$ 1.8

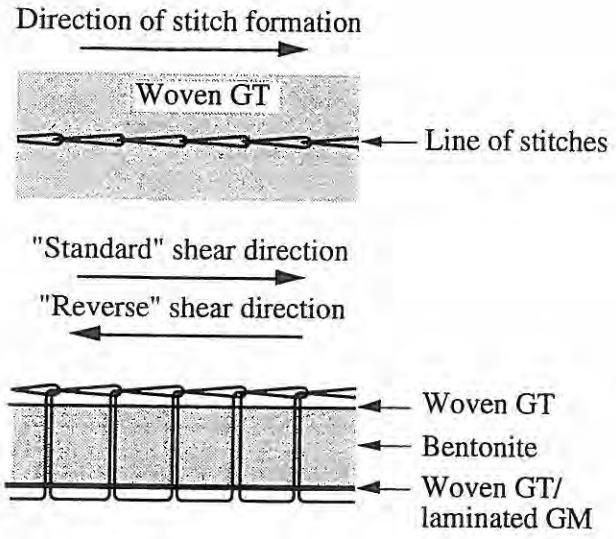

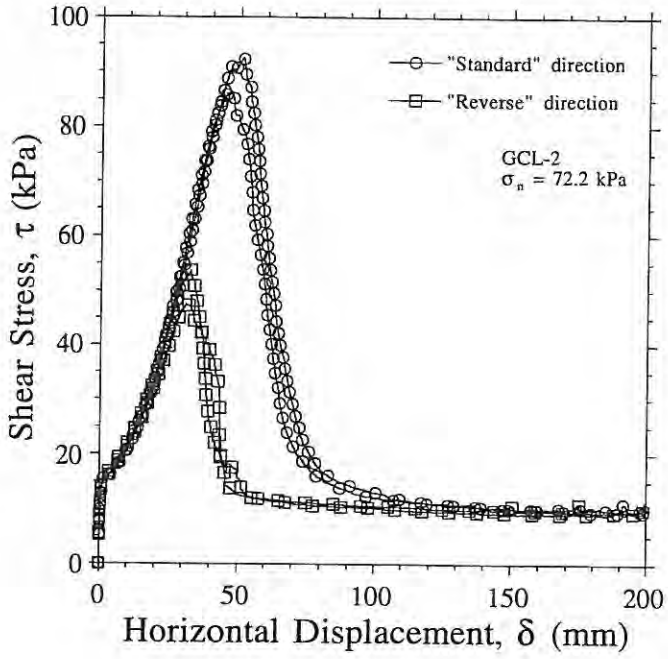

Improved Residual Shear Strength?

- GCL with 75% sand admixture ⇒ no strain softening
- Further investigation warranted

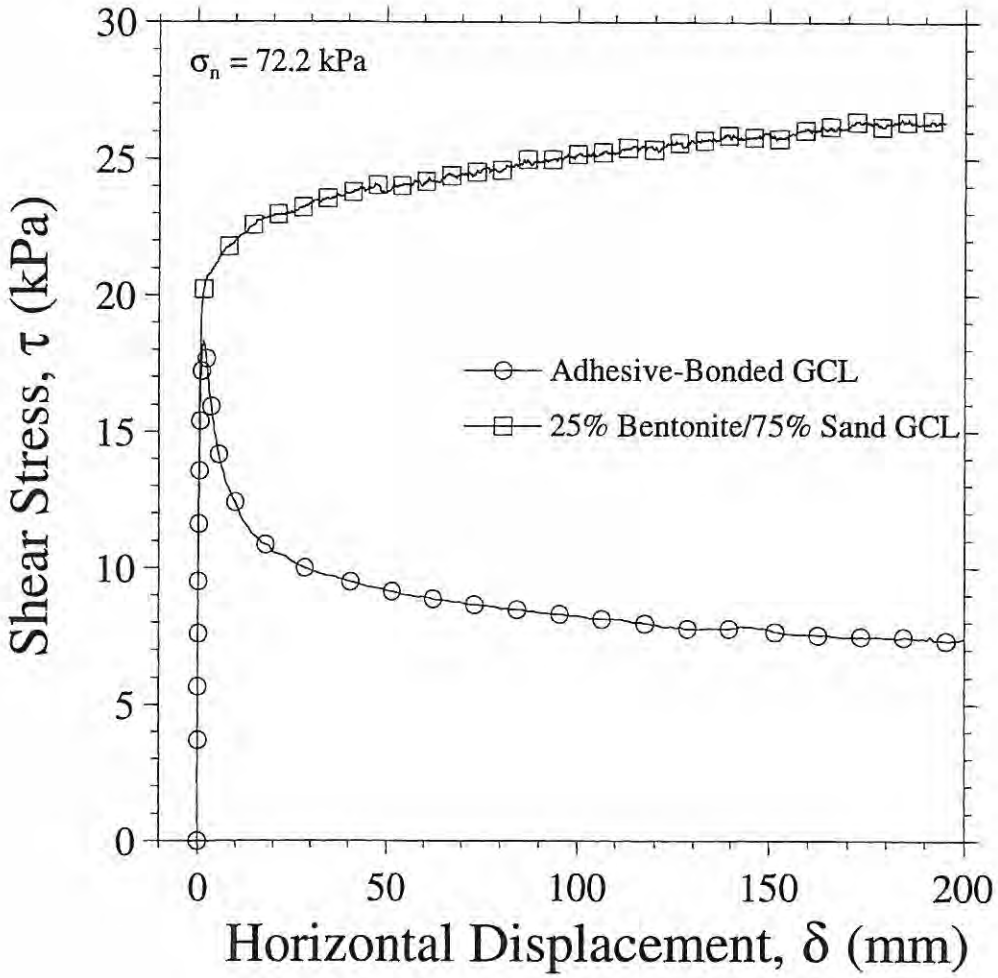

GM/GCL Interface Shear Strength

- Smooth, laminated, coextruded HDPE GMs vs. woven and nonwoven sides of a needle-punched GCL
- Non-linear failure envelopes, true $c \approx 0$

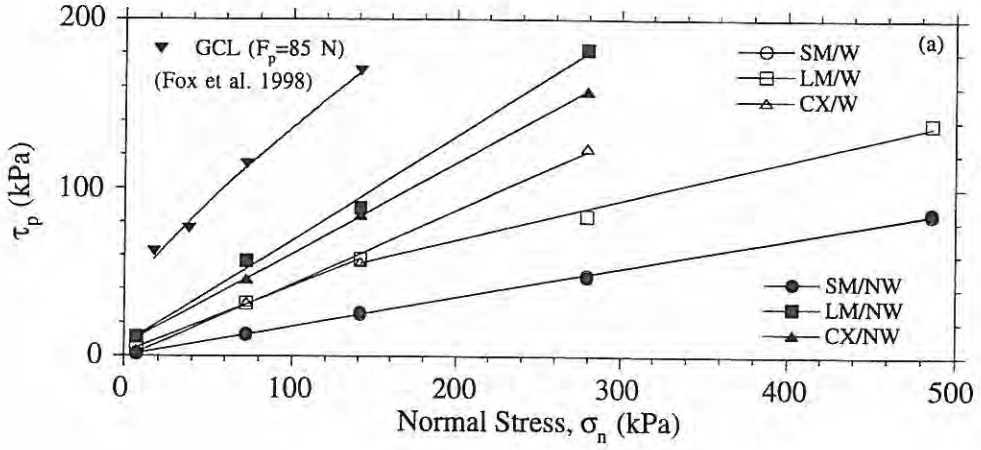

Peak Shear Strength

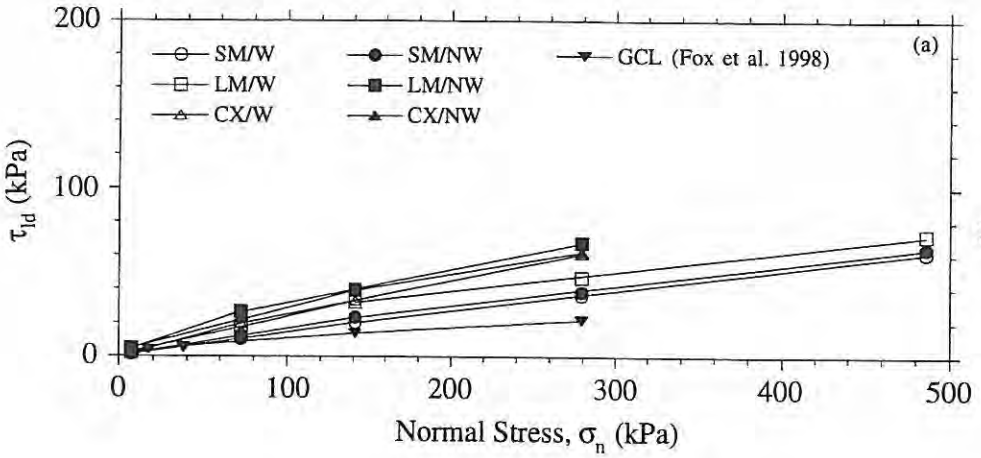

Large Displ. (200 mm) Shear Strength

Reinforced GCLs needed for designs involving slopes:

- internal shear strength of most reinforced GCLs > interface shear strength with typical textured GMs
  $\Rightarrow$ Do we need to design using τ_r for GCL?? Probably not.

Progressive Failure in Direct Shear Tests

- Clamping ends of geosynthetics ⇒ progressive failure

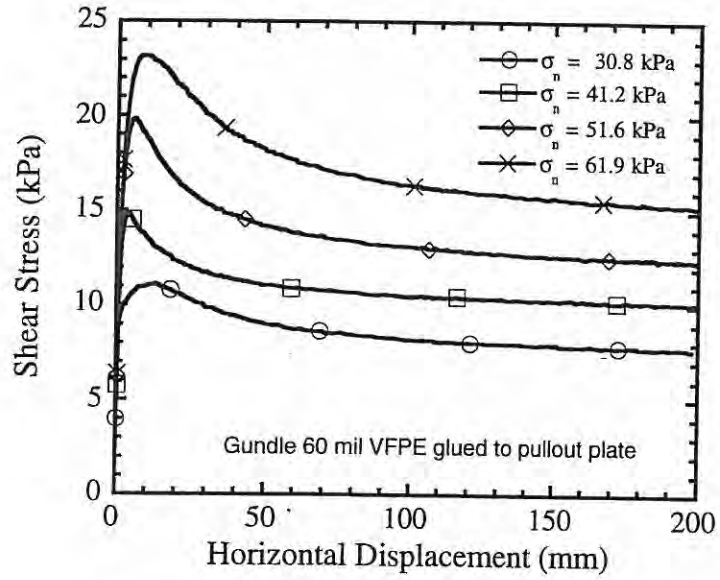

Textured GM/GCL
Without Clamping

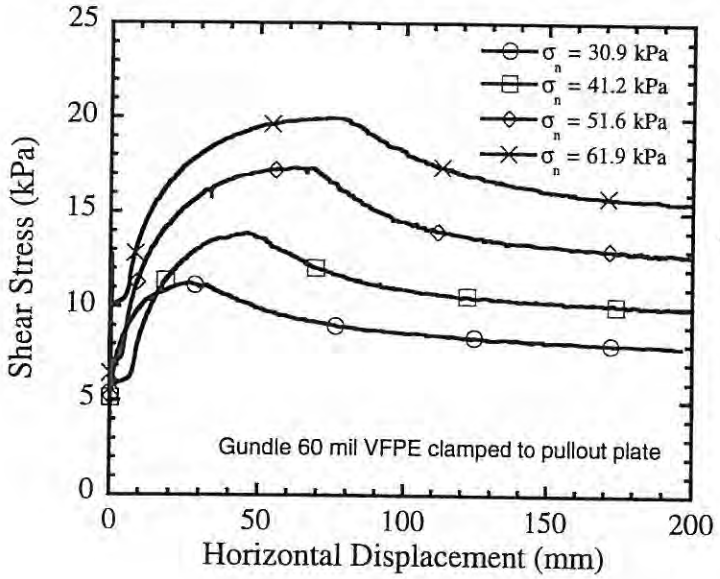

Textured GM/GCL
With Clamping

Numerical model in development to assess the importance of this effect for production testing (Fox and Kim 2000).

Selection of Strength Parameters

Wide variety of materials ⇒ concern over selection of properties

For analysis of existing landfills or failure evaluations:
⇒ use strengths most representative of *in situ* values
⇒ "worst case" conditions should also be considered

For design of new landfills and development of filling plans, use conservative estimates of shear strengths, considering (Mitchell and Mitchell 1992):

- factor of safety (may be prescribed by regulation)
- variability of material properties
- w%, S% of wastes, maximum leachate levels
- variation of properties over time (e.g., MSW degrad./consol.)
- type and consequences of failure
- temporary or permanent slope
- acceptable displacement/deformation (esp. seismic design)
- interface displacements during construction/filling
- waste settlement

IF: positive pore pressures are generated as a result of construction
$\Rightarrow$ short-term is critical stability condition

IF: negative pore pressures are generated as a result of construction
$\Rightarrow$ long-term is critical stability condition

Drained Conditions ($T = t\, c_v/H_{dr}^2 \geq 3$) $u_{ex} \approx 0$

$\Rightarrow$ all free-draining materials, long term for all materials

Use effective stress envelope (c', ϕ'), total γ, and steady state pore pressures on failure surface (hydrostatic or flow net).

Undrained Conditions ($T = t\, c_v/H_{dr}^2 \leq 0.01$) $u_{ex} \neq 0$

$\Rightarrow$ loading sufficiently fast that no drainage can occur

u_{ex} difficult to predict.
Use total stress envelope (c_u, ϕ_u), total γ, u = 0 on failure plane.

For MSW: drained stress conditions are generally assumed or *in situ* undrained strengths must be obtained.

For liner/cover interfaces: drained stress conditions are generally assumed.

Peak vs. Residual Strengths

Large deformations: residual strengths required for interfaces on which slip occurs $\Rightarrow$ strong materials may not fail (don't use τ_r)

Strain-incompatibility: soil and MSW, geosynthetics and MSW

Example: Strain Incompatibility

Failure of waste pile on soft foundation.

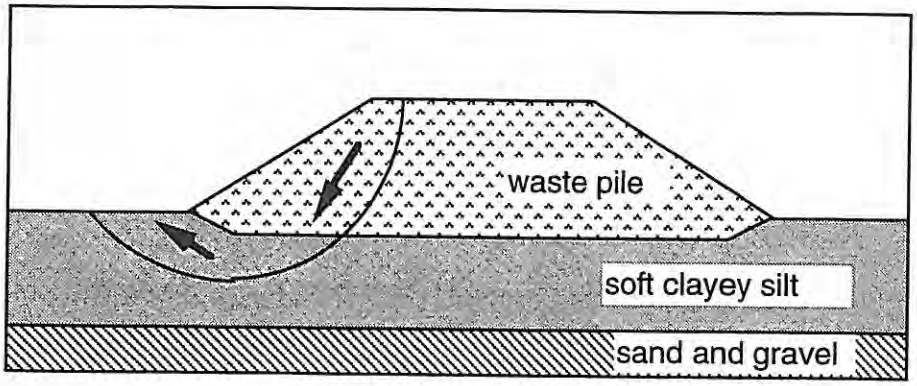

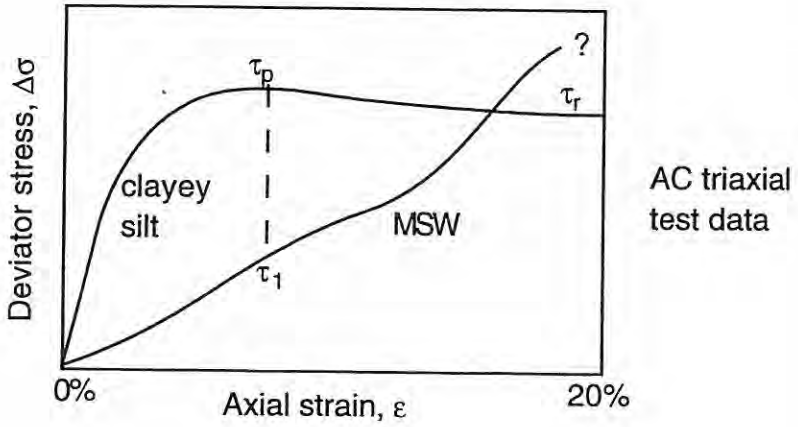

Analysis #1: τ_p for clayey silt, τ_1 for MSW

Analysis #2: τ_r for clayey silt, τ_p for MSW

Stability Analyses

Stability evaluation for landfills is done much the same way as for other types of geotechnical stability problems:

- Limit equilibrium methods typically used
- FEM analyses sometimes used to evaluate stress distributions, deformations
- 2-D analysis is conservative, 3-D analysis performed only for important jobs (e.g., failure evaluation) - section(s) for 2-D analysis must reflect most probable direction of sliding.
- primary uncertainties are in the evaluation of shear strength and deformation properties of the - liner system
  - cover system
  - waste fill

Procedure

1. Assess waste, soil, and geosynthetic properties
2. Assess leachate levels - consider possible clogging of collection system
3. Determine type of analysis required - short term, long term, or both
4. Select mode of failure and analysis method
5. Compute lowest FS value for candidate failure surfaces
6. Repeat for all likely failure modes and conditions

Factor of Safety, FS

Stability of soil/geosynthetic slopes: $FS = \tau_f/\tau = 1.5$ is typical

Stability of refuse: FS > 1.5 needed due to uncertainty of shear strength parameters

Two important considerations for establishing FS:

1) uncertainties associated with problem conditions and chosen shear strengths
2) consequences of failure (liner/waste failure > cover failure)

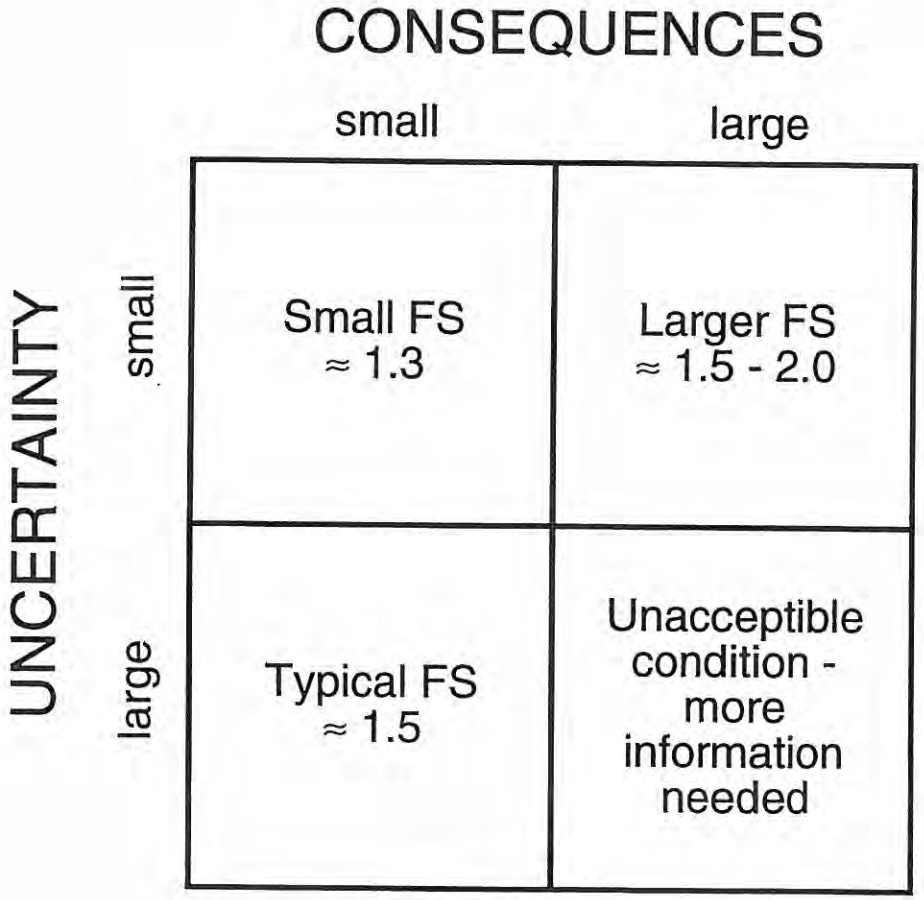

Stability of Liner Systems

Stability evaluation for landfill liner systems is performed:

1. Using circular or non-circular failure surfaces when failure cuts across geosynthetics:
   - ⇒ chart solutions
   - ⇒ slice methods - Bishop's method
     - Janbu's method
     - Spencer's method
   - ⇒ tensile strength of non-reinforcement geosynthetics should be ignored (i.e., don't depend on GM or GCL tensile strength for stability)

2. Using wedge/block methods when failure mode includes planar surfaces - weak layers, geosynthetics

Computer programs (e.g., PCSTABL6, XSTABL, UTEXAS3) are available to carry out these analyses.

DM-7 Wedge Method (NAVFAC DM-7.3 1982, Oweis and Khera 1998)

- force equilibrium method, suitable for hand calculations

Procedure

1. Angles of planar failure surfaces w/r/to horizontal:

   Active wedges: $\alpha = 45° + \frac{\phi}{2}$ Passive wedges: $\beta = 45° - \frac{\phi}{2}$

   $\Rightarrow$ for central wedge, α is dictated by stratigraphy.

2. P_α and P_β are calculated in terms of FS using:

$$P_\alpha = (W - c_m L \sin\alpha - P_w \cos\alpha)\tan(\alpha - \phi_m) - c_m L \cos\alpha + P_w \sin\alpha$$

$$P_\beta = (W + c_m L \sin\beta - P_w \cos\beta)\tan(\beta + \phi_m) + c_m L \cos\beta + P_w \sin\beta$$

where: $\tan(\alpha - \phi_m) = \dfrac{\tan\alpha - \frac{\tan\phi}{FS}}{1 + \tan\alpha \frac{\tan\phi}{FS}}$ $\tan(\beta + \phi_m) = \dfrac{\tan\beta + \frac{\tan\phi}{FS}}{1 - \tan\beta \frac{\tan\phi}{FS}}$ $c_m = \dfrac{c}{FS}$

3. For equilibrium: $\sum P_\alpha = \sum P_\beta \Rightarrow$ find FS by trial and error

4. Depending on geometry, P_α may be positive or negative for center wedge.

5. Find minimum FS value for several (or more) trial failure surfaces. Spreadsheet: can solve entire problem quickly by picking various positions for points d and e (see next page).

Oweis and Khera (1998)

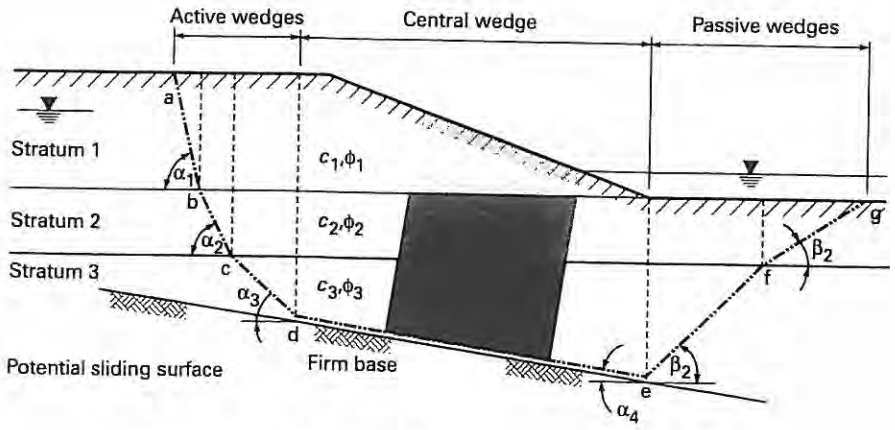

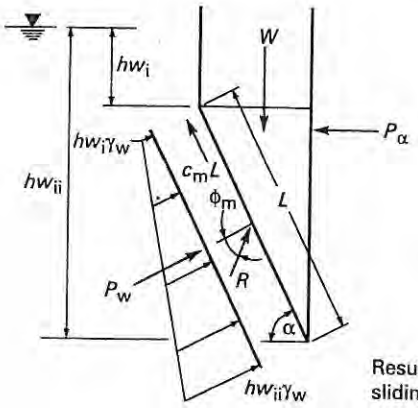

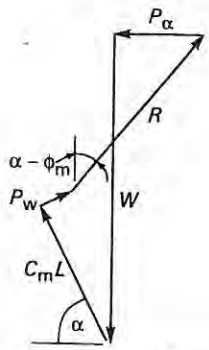

Resultant horizontal force for a wedge sliding along a b c d (P_α) (a general case)

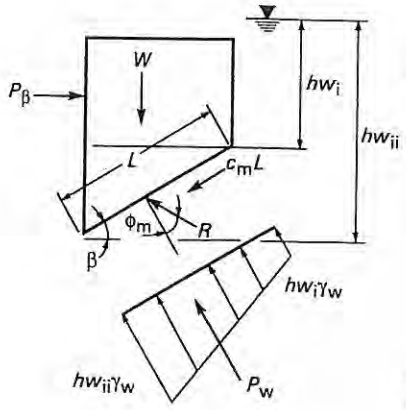

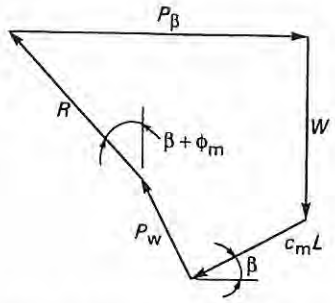

Resultant horizontal force for a wedge sliding along e f g (P_β) (a general case)

Oweis and Khera (1998)

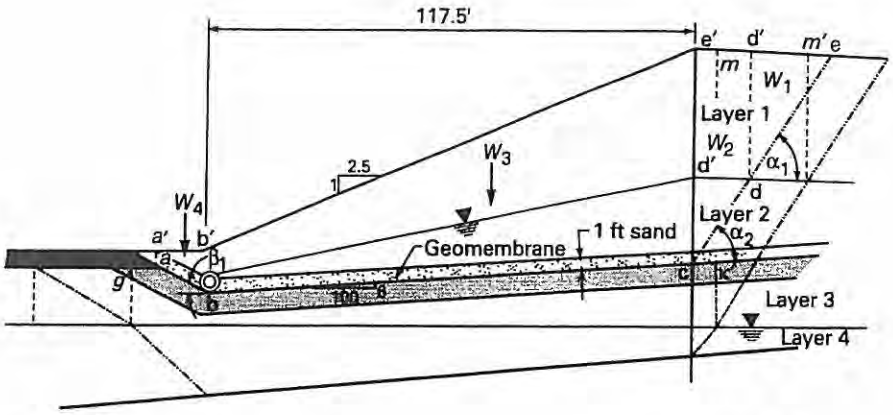

Shallow Potential Failure Surface

Refuse and soil properties

Layer 1, refuse $\phi = 26°$, $c = 100$ lb/ft², $\gamma = 35$ lb/ft³

Layer 2, refuse $\phi = 26°$, $c = 100$ lb/ft², $\gamma = 70$ lb/ft³

Layer 3, sand $\phi = 30°$, $c = 0$, $\gamma = 120$ lb/ft³

Layer 4, soft clay, $\phi = 0$, $c = 500$ lb/ft², $\gamma = 100$ lb/ft³

Geomembrane: interface friction angle with clay liner = 12°

Clay liner: $\phi' = 30°$, $c' = 0$, $\gamma = 120$ lb/ft³

Consider the one ft sand layer above the membrane as part of layer 2.

Consider potential failure wedge along the geomembrane a b c d e

$a'a' = 5'$, $a'b' = 10'$, $bb' = 10'$, $d'e' = 30'$, $d'c' = 20'$

$\alpha_1 = 45 + \phi/2 = 58°$

$W_1 = (30)^2/2 \tan 32 (0.035) = 9.8$ K, $P_{w1} = 0$

$\alpha_2 = 58°$

$$W_2 = (20 \tan 32)(30)(0.035) + \frac{20^2}{2} \times 0.07 \times \tan 32$$

$$= 13.1 \text{ K} + 8.8 \text{ K} = 21.9 \text{ K}$$

$$P_{w2} = \frac{20}{\sin 58} \times \frac{20 \times 0.0625}{2} = 14.7 \text{ K}$$

$$W_3 = \left(\frac{30+10}{2}\right)(117.5)(0.035) + \left(\frac{20+0}{2}\right)(117.5)(0.07)$$

$$= 82.3 + 82.25 = 164.55 \text{ K}$$

$\alpha_3 = \tan^{-1}(0.06) = 3.43$ α

$P_{w3} = 0$ no leakage through membrane

$$= \frac{20(0.0625)(117.5)}{2 \cos 3.43} = 73 \text{ K} \quad \text{with leakage}$$

$\beta_1 = \tan^{-1} 1/2 = 26.56$

$$W_4 = \frac{5+10}{2}(10)(0.035) = 2.6^{\text{K}}, \; P_w = 0$$

$$P_{\alpha 1} = \left[9.8 - \frac{0.1}{F_s}(30)\right]\left[\frac{\tan 58 - \dfrac{\tan 26}{F_s}}{1 + \dfrac{\tan 58 \tan 26}{F_s}}\right]$$

$$-\left[\frac{0.1}{F_s}\frac{30}{\sin 58}\cos 58\right]$$

$$= \left(9.8 - \frac{3}{F_s}\right)\left(\frac{1.6F_s - 0.49}{F_s + 0.78}\right) - \frac{1.88}{F_s}$$

$$P_{\alpha 2} = \left[21.9 - \left(\frac{0.1}{F_s}\right)0.20 - 14.8 \cos 58\right]\left[\frac{1.6F_s - 0.49}{F_s + 0.78}\right]$$

$$-\left[\frac{0.1(20)}{F_s \tan 58} - 14.8 \sin 58\right]$$

$$= \left(21.9 - \frac{2}{F_s} - 7.8\right)\left(\frac{1.6F_s - 0.49}{F_s + 0.78}\right)$$

$$-\frac{1.25}{F_s} + 12.6$$

$P_{\alpha 3}$ = (impervious liner)

$$= [164.55]\left[\frac{\tan 3.43 - \dfrac{\tan 12}{F_s}}{1 + \dfrac{\tan 3.43 \tan 12}{F_s}}\right]$$

$$= 164.55\left[\frac{0.06F_s - 0.212}{F_s + 0.013}\right]$$

$$P_{\beta 1} = 2.6\left[\frac{\tan 26.56 + \dfrac{\tan 12}{F_s}}{1 - \dfrac{\tan 26.56 \tan 12}{F_s}}\right]$$

$$P_{\beta 1} = 2.6\left[\frac{0.5F_s + 0.212}{F_s - 0.106}\right]$$

F_s	$P_{\alpha 1}$	$P_{\alpha 2}$	$P_{\alpha 3}$	ΣP_α	ΣP_β
1.1	3.02	19.68	−21.5	1.2	1.99
1.2	3.73	20.54	−19.0	5.27	1.93

$F_s \simeq 1.12$

Stability of Cover Systems

Stability evaluation for landfill cover systems:

1. Use circular or non-circular failure surfaces when failure cuts across geosynthetics and through waste materials:
   ⇒ computer programs available

2. When failure mode is parallel to slope
   ⇒ infinite slope methods
   ⇒ wedge methods - includes passive block at base

Tensile strength of non-reinforcement geosynthetics should be ignored.

Infinite Slope

Critical case - seepage parallel to slope

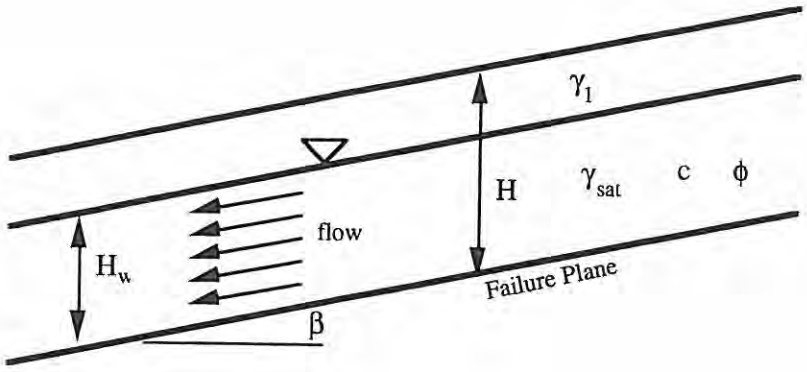

$$FS = \frac{c + \left((H - H_w)\gamma_1 + H_w\gamma'\right)\cos^2\beta\tan\phi}{\left((H - H_w)\gamma_1 + H_w\gamma_{sat}\right)\sin\beta\cos\beta}$$

For c = 0 and $H_w = 0$, $\quad FS = \dfrac{\gamma'\tan\phi}{\gamma_{sat}\tan\beta}$

Seepage-related stability problems have occurred due to:

- failure to design for "worst case" seepage conditions
- inadequate drainage capacity at toe of slope
- clogging of drainage layers with fines over time
- freezing of drainage layer at toe of slope

Finite Slope with Passive Wedge (Koerner and Daniel 1997)

- uniformly thick cover soil (c, ϕ) slides off GM (c_a, δ)
- analysis includes: passive wedge at toe, tension crack at top

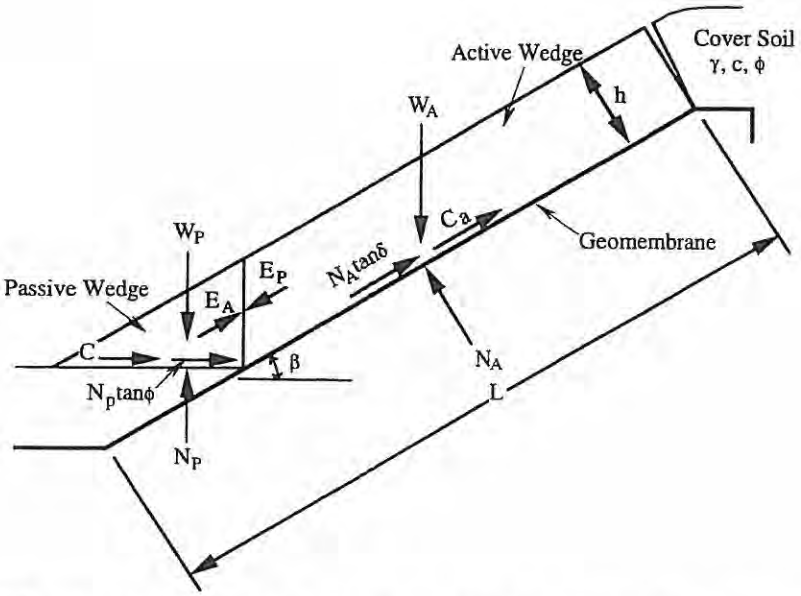

FIG. 5.3. Limit Equilibrium Forces Involved in Finite Length Slope Analysis for Uniformly Thick Cover Soil

W_A = wt. active wedge = $\gamma h^2\left(\frac{L}{h}-\frac{1}{\sin\beta}-\frac{\tan\beta}{2}\right)$

W_p = wt. passive wedge = $\frac{\gamma h^2}{\sin 2\beta}$

$N_A = W_A\cos\beta$

$N_p = W_p + E_p\sin\beta$

$C_a = c_a\left(L-\frac{h}{\sin\beta}\right)$

$C = \frac{ch}{\sin\beta}$

$a = (W_A - N_A\cos\beta)\cos\beta$

$$b = -\left[\begin{matrix}(W_A - N_A\cos\beta)\sin\beta\tan\phi + (N_A\tan\delta + C_a)\sin\beta\cos\beta \\ +\sin\beta(C + W_p\tan\phi)\end{matrix}\right]$$

$c = (N_A\tan\delta + C_a)\sin^2\beta\tan\phi$

Assuming $E_a = E_p$: $a(FS)^2 + b(FS) + c = 0$ $\qquad FS = \frac{-b+\sqrt{b^2-4ac}}{2a}$

Passive Wedge with Seepage (Koerner and Daniel 1997)

- horizontal vs. parallel seepage

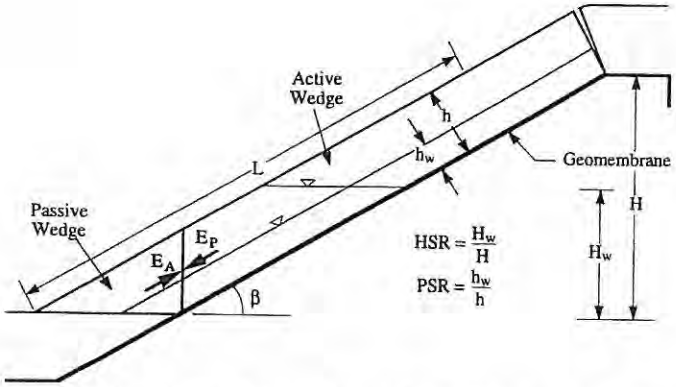

FIG. 5.15. Cross Section of Cover Soil on a Geomembrane Illustrating Different Submergence Assumptions and Related Definitions

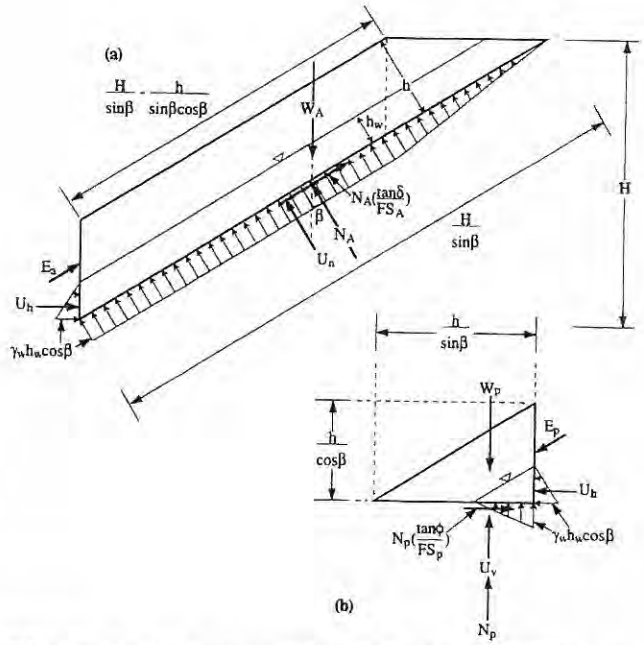

FIG. 5.17. Free Body Diagrams of Cover Soil with Parallel-to-Slope Seepage Buildup

$$W_A = \frac{\gamma_m(h-h_w)(2H\cos\beta-(h+h_w))+\gamma_{sat}h_w(2H\cos\beta-h_w)}{\sin 2\beta}$$

$$W_p = \frac{\gamma_m(h^2-h_w^2)+\gamma_{sat}h_w^2}{\sin 2\beta}$$

$$U_n = \frac{\gamma_w h_w \cos\beta(2H\cos\beta-h_w)}{\sin 2\beta}$$

$$U_h = \frac{\gamma_w h_w^2}{2}$$

γ_m = moist unit wt. of cover soil

$$U_v = U_h \cot\beta$$

γ_{sat} = saturated unit wt. of cover soil

$$N_A = W_A\cos\beta + U_h\sin\beta - U_n$$

$$a = W_A\sin\beta\cos\beta - U_h\cos^2\beta + U_h$$

$$b = -W_A\sin^2\beta\tan\phi + U_h\sin\beta\cos\beta\tan\phi - N_A\cos\beta\tan\delta - (W_p - U_v)\tan\phi$$

$$c = N_A\sin\beta\tan\delta\tan\phi$$

Assuming $E_a = E_p$: $\quad a(FS)^2 + b(FS) + c = 0 \qquad FS = \frac{-b+\sqrt{b^2-4ac}}{2a}$

Finite Slope with Tapered Cover Soil (Koerner and Daniel 1997)

- cover soil thick at toe, thin at crest (h_c) with slope angle ω
- similar analysis to uniform thickness case

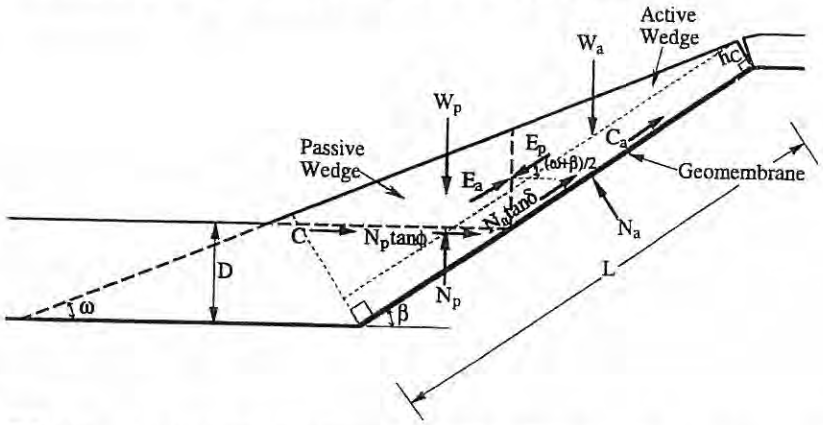

FIG. 5.11. Limit Equilibrium Forces Involved in Finite Length Slope Analysis for Tapered Thickness Cover Soil

$$y = \left[L - \left(\frac{D}{\sin\beta}\right) - h_c \tan\beta\right](\sin\beta - \cos\beta\tan\omega)$$

$$W_A = \gamma\left[\left(L - \frac{D}{\sin\beta} - h_c\tan\beta\right)\left(\frac{y\cos\beta}{2} + h_c\right) + \frac{h_c^2\tan\beta}{2}\right]$$

$$W_p = \frac{\gamma}{2\tan\omega}\left[\left(L - \frac{D}{\sin\beta} - h_c\tan\beta\right)(\sin\beta - \cos\beta\tan\omega) + \frac{h_c}{\cos\beta}\right]^2$$

$$N_A = W_A\cos\beta \qquad N_p = W_p + E_p\sin\left(\frac{\omega+\beta}{2}\right)$$

$$C_a = c_a\left(L - \frac{D}{\sin\beta}\right) \qquad C = \frac{\gamma}{\tan\omega}\left[\left(L - \frac{D}{\sin\beta} - h_c\tan\beta\right)(\sin\beta - \cos\beta\tan\omega) + \frac{h_c}{\cos\beta}\right]$$

$$a = (W_A - N_A\cos\beta)\cos\left(\frac{\omega+\beta}{2}\right)$$

$$b = -\left[\begin{array}{l}(W_A - N_A\cos\beta)\sin\left(\frac{\omega+\beta}{2}\right)\tan\phi + (N_A\tan\delta + C_a)\sin\beta\cos\left(\frac{\omega+\beta}{2}\right) \\ +\sin\left(\frac{\omega+\beta}{2}\right)(C + W_p\tan\phi)\end{array}\right]$$

$$c = (N_A\tan\delta + C_a)\sin\beta\sin\left(\frac{\omega+\beta}{2}\right)\tan\phi$$

Assuming $E_a = E_p$: $\quad a(FS)^2 + b(FS) + c = 0 \qquad FS = \dfrac{-b + \sqrt{b^2 - 4ac}}{2a}$

Finite Slope with Veneer Reinforcement (Koerner and Daniel 1997)

- same as uniform thickness case, but reinforcement force T acting parallel to slope provides additional stability (intentional vs. non-intentional)
- weight of geosynthetic is neglected
- T = available (long term design) strength of geosynthetic
  T_{ult} = ultimate (as manufactured) strength of geosynthetic
  $T = T_{ult}/(RF_{Inst.\ Damage} \times RF_{Creep} \times RF_{Chem/Bio\ Degrad.})$

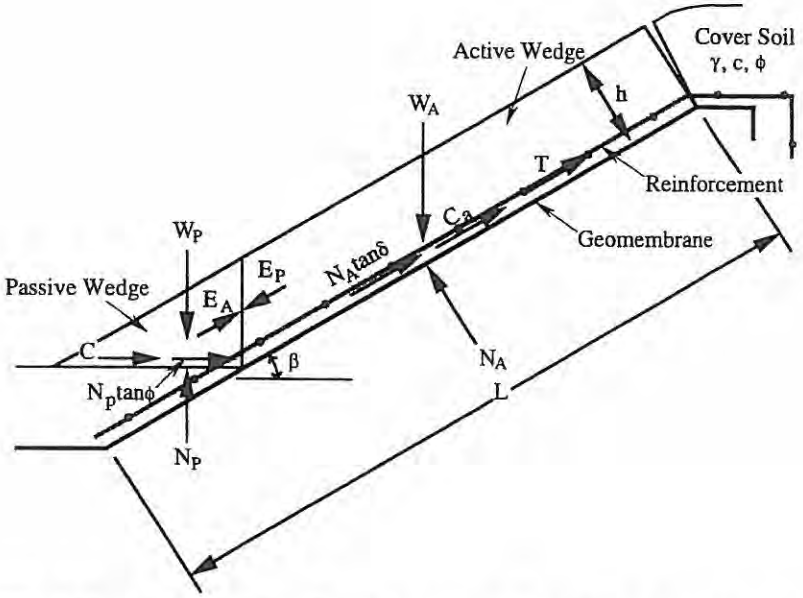

FIG. 5.13. Limit Equilibrium Forces Involved in Finite Length Slope Analysis Including Use of Veneer Reinforcement

$$a = (W_A - N_A \cos\beta - T\sin\beta)\cos\beta$$

$$b = -\left[\begin{matrix}(W_A - N_A \cos\beta - T\sin\beta)\sin\beta\tan\phi + (N_A \tan\delta + C_a)\sin\beta\cos\beta \\ +\sin\beta(C + W_p \tan\phi)\end{matrix}\right]$$

$$c = (N_A \tan\delta + C_a)\sin^2\beta\tan\phi$$

Assuming $E_a = E_p$: $\quad a(FS)^2 + b(FS) + c = 0 \qquad FS = \dfrac{-b + \sqrt{b^2 - 4ac}}{2a}$

Seismic Loading with Passive Wedge (Koerner and Daniel 1997)

- Subtitle D: landfills be designed to resist a peak horiz. ground accel. (PGHA) that will not be exceeded in 250 yrs. (90% probability)
- 2-part analysis: 1) pseudo-static, 2) deformation

C_s = non-dim. seismic coefficient, modified for wave propagation through landfill to cover

Pseudo-static Analysis

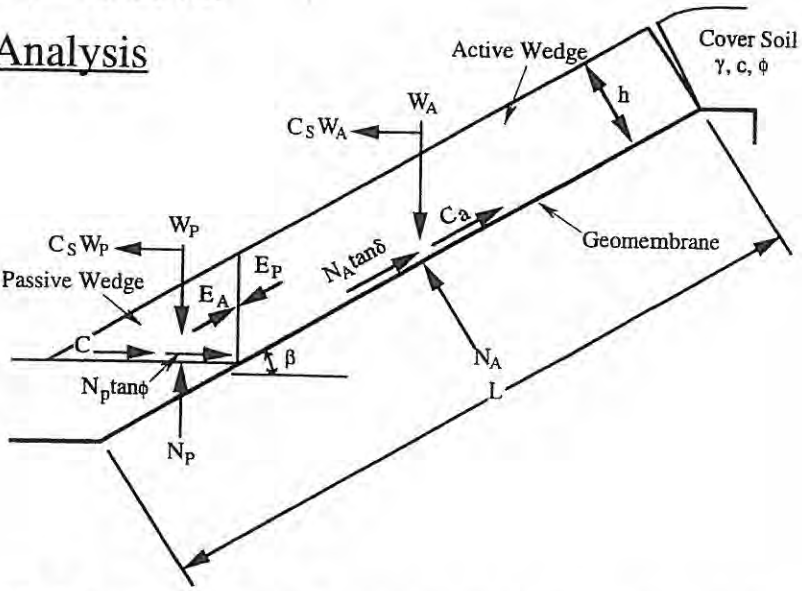

FIG. 5.20. Limit Equilibrium Forces Involved in Pseudo-Static Analysis Using Average Seismic Coefficient

W_A = wt. active wedge = $\gamma h^2\left(\frac{L}{h} - \frac{1}{\sin\beta} - \frac{\tan\beta}{2}\right)$

W_p = wt. passive wedge = $\frac{\gamma h^2}{\sin 2\beta}$

$N_A = W_A \cos\beta$

$C_a = c_a\left(L - \frac{h}{\sin\beta}\right)$

$N_p = W_p + E_p \sin\beta$

$C = \frac{ch}{\sin\beta}$

$$a = (C_s W_A + N_A \sin\beta)\cos\beta + C_s W_p \cos\beta$$

$$b = -\left[\begin{matrix}(C_s W_A + N_A \sin\beta)\sin\beta\tan\phi + (N_A \tan\delta + C_a)\cos^2\beta \\ +(C + W_p \tan\phi)\cos\beta\end{matrix}\right]$$

$$c = (N_A \tan\delta + C_a)\cos\beta\sin\beta\tan\phi$$

Assuming $E_a = E_p$: $a(FS)^2 + b(FS) + c = 0$ $\qquad FS = \frac{-b + \sqrt{b^2 - 4ac}}{2a}$

Deformation Analysis

California: if pseudo-static FS < 1.5, then a deformation analysis must conducted and it must be demonstrated that design can withstand estimated deformations.

1. Select design earthquake.
2. Ground accelerations are transferred horizontally to landfill location and then vertically through the overburden soil and solid waste to the cover (e.g., SHAKE).
3. Plot FS vs. C_s (using τ_r values where appropriate)

   $\Rightarrow$ pick off yield acceleration (C_{sy}) corresponding to FS = 1
4. Compare C_{sy} to estimated acceleration vs. time plot.
5. Double-integrate portions of spectrum that exceed C_{sy}

   $\Rightarrow$ gives velocity vs. time, permanent displacement vs. time
6. If permanent displacement: < 0.3 m $\Rightarrow$ small displ. likely

   > 1 m $\Rightarrow$ large displ. likely, redesign may be necessary

   (Kavazanjian 1998)

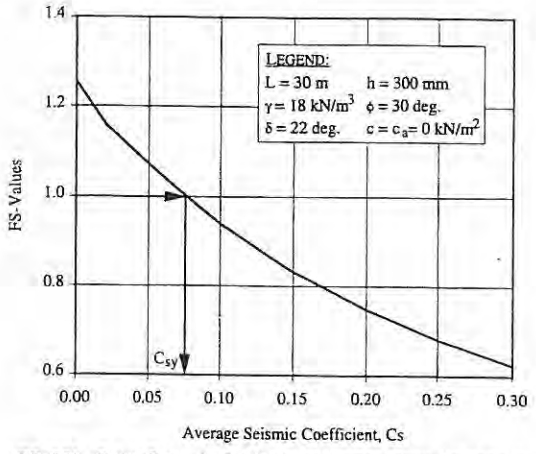

FIG. 5.21. Design Curves for Stability Using Average Seismic Coefficient in Pseudo-Static Seismic Analysis

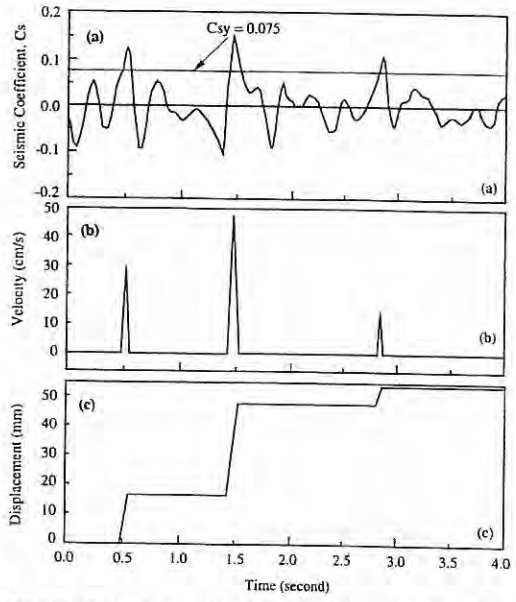

FIG. 5.22. Design Curves to Obtain Permanent Deformation Using: (a) Acceleration; (b) Velocity; (c) Displacement Curves

References

ASTM D 5321 (1999). "Standard test method for determining the coefficient of soil and geosynthetic or geosynthetic and geosynthetic friction by the direct shear method," *Annual Book of ASTM Standards*, ASTM, West Conshohocken, Vol. 04.09.

ASTM D 6243 (1999). "Standard test method for determining the internal and interface shear resistance of geosynthetic clay liner by the direct shear method," *Annual Book of ASTM Standards*, ASTM, West Conshohocken, Vol. 04.09.

Bagchi, A. (1990). *Design, Construction, and Monitoring of Sanitary Landfill*, John Wiley & Sons, 284 pp.

Byrne, R. J., Kendall, J., and Brown, S. (1992). "Cause and mechanism of failure Kettleman Hills landfill B-19, Phase IA," *Stability and Performance of Slopes and Embankments-II*, Geotechnical Special Publication No. 31, R. B. Seed and R. W. Boulanger, eds., ASCE, 1188-1215.

Daniel, D. E., Koerner, R. M., Bonaparte, R., Landreth, R. E., Carson, D. A., and Scranton, H. B. (1998). "Slope stability of geosynthetic clay liner test plots," *J. Geotech. and Geoenvir. Engrg.*, ASCE, Vol. 124, No. 7, 628-637.

Duncan, J. M. (1996). "State of the art: Limit equilibrium and finite-element analysis of slopes," *Journal of Geotechnical Engineering*, ASCE, Vol. 122, No. 7, 577-596.

Fox, P. J. (1998). "Research on geosynthetic clay liners at Purdue University," *Geotechnical News*, 16(1), 35-40.

Fox, P. J., and Kim, R. H. (2000). "Effect of specimen clamping and progressive failure on measured stress-displacement and interface shear strength of geosynthetics in direct shear." *Geosynthetics International*, in preparation.

Fox, P. J., Rowland, M. G., Scheithe, J. R., Davis, K. L., Supple, M. R., and Crow, C. C., (1997). "Design and evaluation of a large direct shear machine for geosynthetic clay liners." *Geotechnical Testing Journal*, ASTM, 20(3), 279-288.

Fox, P. J., Rowland, M. G., and Scheithe, J. R. (1998). "Internal shear strength of three geosynthetic clay liners." *Journal of Geotechnical and Geoenvironmental Engineering*, ASCE, 124(10), 933-944.

Gilbert, R. B., Fernandez, F., and Horsfield, D. W. (1996). "Shear strength of reinforced geosynthetic clay liner," *J. Geotech. Engrg.*, ASCE, Vol. 122, No. 4, 259-266.

Gilbert, R. B., Scranton, H. B., and Daniel, D. E. (1997). "Shear strength testing for geosynthetic clay liners," *Testing and acceptance criteria for geosynthetic clay liners*, STP 1308, L. W. Well, ed., ASTM, West Conshohocken, Pa., 121-135.

Giroud, J. P., Darrasse, J., and Bachus, R. C. (1993). "Hyperbolic expression for soil-geosynthetic or geosynthetic-geosynthetic interface shear strength," *Geotextiles and Geomembranes*, Elsevier, England, Vol. 12, No. 3, 275-286.

Kavazanjian, E. (1998). "Current issues in seismic design of geosynthetic cover systems," *Proc.*, Sixth Int. Conf. on Geosynthetics, Atlanta, Vol. 1, 219-226.

Koerner, R. M. (1998). *Designing with Geosynthetics*, 4th Ed., Prentice Hall, 761 pp.

Koerner, R. M., and Daniel, D. E. (1997). *Final Covers for Solid Waste Landfills and Abandoned Dumps*, ASCE Press, 256 pp.

Lambe, T. W., and Whitman, R. V. (1969). *Soil Mechanics*, John Wiley & Sons, 553 pp.

Mitchell, R. A., and Mitchell, J. K. (1992). "Stability evaluation of waste landfills," *Stability and Performance of Slopes and Embankments-II*, Geotechnical Special Publication No. 31, R. B. Seed and R. W. Boulanger, eds., ASCE, 1152-1187.

Oweis, I. S. (1993). "Stability of landfills," Chapter 11 in *Geotechnical Practice for Waste Disposal*, D. E. Daniel, ed., Chapman & Hall, pp. 244-268.

Oweis, I. S., and Khera, R. P. (1998). *Geotechnology of Waste Management,* 2nd Ed., PWS, 472 pp.

Rowe, R. K., Quigley, R. M., and Booker, J. R. (1997). *Clayey Barrier Systems for Waste Disposal Facilities*, E & FN SPON, 390 pp.

Seed, R. B., and Boulanger, R. W. (1991). "Smooth HDPE-clay liner interface shear strengths: compaction effects," *Journal of Geotechnical Engineering*, ASCE, Vol. 117, No. 4, 686-693.

Singh, S., and Murphy, B. (1990). "Evaluation of the stability of sanitary landfills," *Geotechnics of Waste Fills - Theory and Practice*, ASTM STP 1070, A. Landva and G. D. Knowles, eds., 240-258.

Smith, M. E., and Criley, K. (1995). "Interface shear strength is not for the uninitiated," *Geotechnical Fabrics Report*, Vol. 13, No. 3, 28-31.

Stark, T. D., and Eid, H. T. (1996). "Shear behavior of reinforced geosynthetic clay liners," *Geosynthetics International*, IFAI, St. Paul, Vol. 3, No. 6, 771-786.

Stark, T. D., Williamson, T. A., and Eid, H. T. (1996). "HDPE geomembrane/ geotextile interface shear strength," *J. Geotech. Engrg.*, ASCE, Vol. 122, No. 3, 197-203.

Triplett, E. J., and Fox, P. J. (2000). "Shear strength of HDPE geomembrane/geosynthetic clay liner interfaces." *Journal of Geotechnical and Geoenvironmental Engineering*, ASCE, submitted for review 11/22/99.

TAB 11

Introductory Notes - Geotechnical Engineering

(C. Allen Wortley)

Introductory notes

Geotechnical Engineering

Soil Parameters Review and Principles of Soil Mechanics

Professor C. Allen Wortley
University of Wisconsin–Madison

Contents

General Soil Behavior 1
Basic Weight and Volume Relationships 3
Index and Classification Properties of Soils 5
Soil Classification 7
Soil Structure and Fabric 10
Density and Compaction 12
Water in Soils 16
Consolidation and Settlements 20
Failure Criterion and Shear Strength 22
Earth Pressures 26
Postscript and Acknowledgements 27

Addenda: Bearing Capacity, Field Tests, Boring Log

General Soil Behavior

Soil is composed of discrete particles.

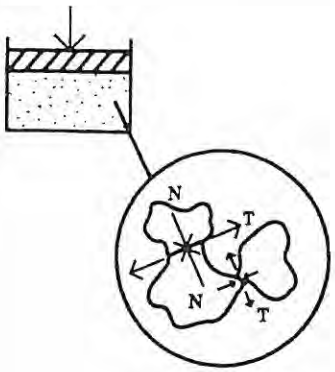

The deformation of a mass of soil is controlled by interactions between individual particles, especially by sliding between particles.

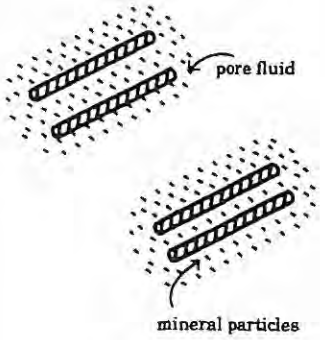

Soil is inherently multiphase, and constituents of the pore phase will influence the nature of the mineral surfaces and affect the processes of force transmission at the particle contacts.

Water can flow through soil and thus interact with the mineral skeleton, altering the magnitude of the forces at the contacts between particles and influencing the compression and shear resistance of the soil.

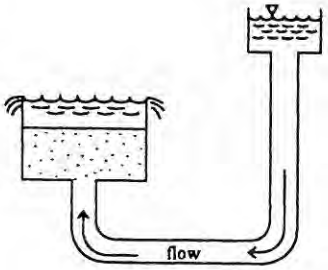

When the load applied to a soil is suddenly changed, this change is carried jointly by the pore fluid and by the mineral skeleton. The change in pore pressure will cause the water to move through the soil, hence the properties of the soil will change with time.

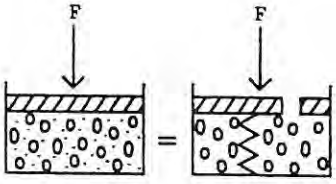

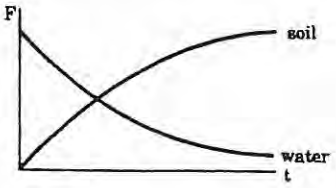

The shear resistance between two particles is the force that must be applied to cause relative movement between the particles.

1. The total shear resistance (the product of the strength of each bond and total number of bonds) is proportional to the normal force that is pushing the two particles together. (If this normal force decreases, either the strength or the number of bonds decreases, and thus the total shear resistance decreases. Hence we say that interparticle shear resistance is *frictional* in nature.)

2. *True cohesion* is when the normal force is decreased to zero and there is still a measurable shear resistance. (Generally, the magnitude of true cohesion between particles is very small, and its contribution to the strength of a soil is also very small—exception would be cementation turning sand into sandstone.

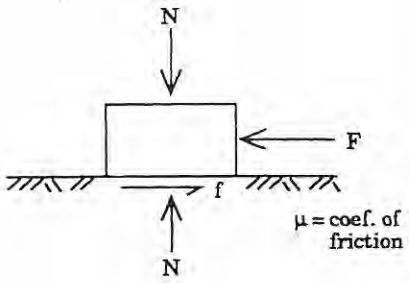

3. Frictional behavior

a. The shear resistance between two bodies is proportional to the normal force between the two bodies.

b. The shear resistance between two bodies is independent of the dimensions of the two bodies.

c. The shear force required to initiate sliding between two surfaces is often greater than the force required to maintain motion; that is the static friction exceeds the sliding (kinetic) friction.

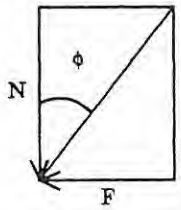

$$\tan\phi = \frac{F}{N}$$

$$F = \tan\phi\, N$$

$$\mu = \tan\phi$$

$$f = \mu N$$

Basic Weight and Volume Relationships

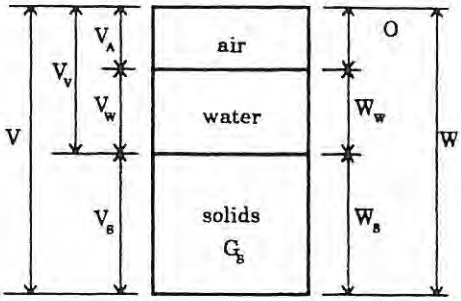

Void Ratio, e

$$e = \frac{V_V}{V_S}$$

Degree of Saturation, S

$$S = \frac{V_W}{V_V} \times 100\%$$

Porosity, n

$$n = \frac{V_V}{V} \times 100\%$$

Water Content, w

$$w = \frac{W_W}{W_S} \times 100\%$$

Unit Weight, γ

$$\gamma = \frac{W}{V}$$

Specific Gravity, G_s

$$G_S = \frac{W_S}{V_S \gamma}$$

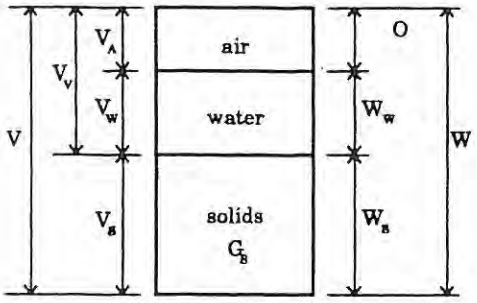

Example Problem

Given: moist soil weight, W = 45 lbs
dry soil weight, W_S = 40 lbs
volume, V = 0.43 cu ft
specific gravity, G_S = 2.67

Find: unit weight, γ
void ratio, e
water content, w
degree of saturation, S

$$W_W = W - W_S = 45 - 40 = 5 \text{ lbs}$$

$$\gamma = \frac{W}{V} = \frac{45}{0.43} = 105 \text{ lbs per cu ft} \qquad \textit{(answer)}$$

$$V_S = \frac{W_S}{62.4\, G_S} = \frac{40}{62.4 \times 2.67} = 0.24 \text{ cu ft}$$

$$V_V = V - V_S = 0.43 - 0.24 = 0.19 \text{ cu ft}$$

$$e = \frac{V_V}{V_S} = \frac{0.19}{0.24} = 0.79 \qquad \textit{(answer)}$$

$$V_W = \frac{W_W}{62.4} = \frac{5}{62.4} = 0.08 \text{ cu ft}$$

$$S = \frac{V_W}{V_V} \times 100\% = \frac{0.08}{0.19} \times 100 = 42\% \qquad \textit{(answer)}$$

$$w = \frac{W_W}{W_S} \times 100\% = \frac{5}{40} \times 100 = 12\% \qquad \textit{(answer)}$$

Index and Classification Properties of Soils

Classification of soils is important because it is the "language" engineers use to communicate certain general knowledge about engineering behavior of the soil at a particular site. It also discusses the engineering properties of soils necessary to the design of foundations and earth structures.

The "solids" part of the soil mass consists primarily of particles of mineral and organic matter in various sizes and amounts. The "texture" of a soil is its appearance or "feel," and it depends on the relative sizes and shapes of the particles as well as the range or distribution of those sizes. Coarse-grained soils (e.g., "sands" and "gravels") are obviously coarse-textured, while a fine-textured soil might be predominantly composed of very thin mineral grains invisible to the naked eye (e.g., "silt" and "clay" soils).

Such textural classification terms—gravels, sands, silts, and clays—are useful in a general sense in geotechnical engineering practice. For fine-grained soils, the presence of water greatly affects their engineering response—much more so than grain size or texture alone. Water affects the interaction between the mineral grains, and this may affect their plasticity and their cohesiveness.

Texturally, soils may be divided into coarse-grained and fine-grained soils. A convenient dividing line is the smallest grain visible to the naked eye. Soils with particles larger than this size (about 0.002 of an inch) are called coarse-grained, while soils finer than that are termed fine-grained. Another convenient way to classify soils is according to their plasticity and cohesion (the sticking together of like materials). For example, sands are nonplastic and noncohesive (cohesionless), whereas clays are both plastic and cohesive. Silts fall somewhere between clays and sands; they are fine-grained yet nonplastic and cohesionless. (If you ever made a sand castle, you know you need damp sand, not dry sand. Why?—mainly because damp sand has a certain amount of cohesion, really "apparent cohesion," due to capillary water tensile stresses. For this reason, some people prefer to call sandy soils "granular" rather than "cohesive" or "fine-grained.")

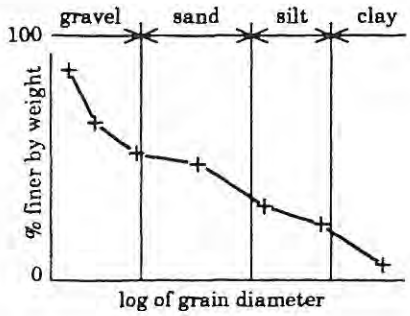

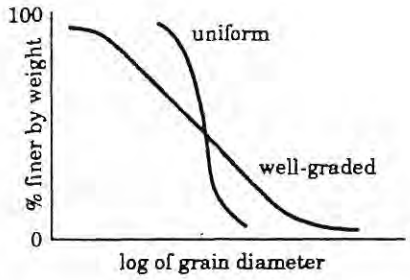

A grain size curve for a given soil sample can be constructed by laboratory tests that identify the percentages, by weight, of the various particle sizes present in the sample. If most of the particles are of the same size, the soil is said to have a uniform gradation (like a bag of pea gravel or beach dune sand); if most sizes are present, the soil is said to be well graded (like a good quality road base mix).

The shape of the individual particles is at least as important as the grain size distribution in affecting the engineering response of granular soils. A qualitative shape determination is made as a part of visual classification. Coarse-grained soils are commonly classified as rounded, subrounded, subangular or angular. Grain shape is very significant in determining the frictional characteristics (shear strength) of granular soils.

Water contents classify fine-grained soils by their Atterberg limits. The methods used relate the natural moisture content to the Atterberg limits water contents. The limits are determined in the laboratory by test methods developed in the early 1900s by Swedish soil scientist A. Atterberg.

Atterberg realized that at least two water contents were required to define the plasticity of clays—corresponding to the upper and lower limits of plasticity. These consistency limits are the liquid limit (LL) and the plastic limit (PL), and the difference between them is the range of moisture contents over which the soil is plastic. This range is called the plasticity index (PI), which equals LL minus PL. (A soil wetter than LL could be described as a slurry, pea soup to soft butter, or a viscous liquid. A soil drier than the PL is a semi-solid, like cheese. A plastic soil will deform but not crack, like soft butter to stiff putty.)

$$\text{Plasticity Index: } PI = LL - PL$$

The limits set by Atterberg are relatively arbitrary; but they are standardized in engineering practice, and many soil properties are indexed to them. We want to be able to compare or scale our water content with some defined limits or boundaries or engineering response. In this way, we would know if our sample was likely to behave as a plastic, a brittle solid, or possibly even a liquid. The index for scaling the natural moisture content of a given soil is the liquidity index (LI), which equals the natural moisture content minus the plastic limit, divided by the plasticity index.

$$\text{Liquidity Index: } LI = \frac{w - PL}{PI}$$

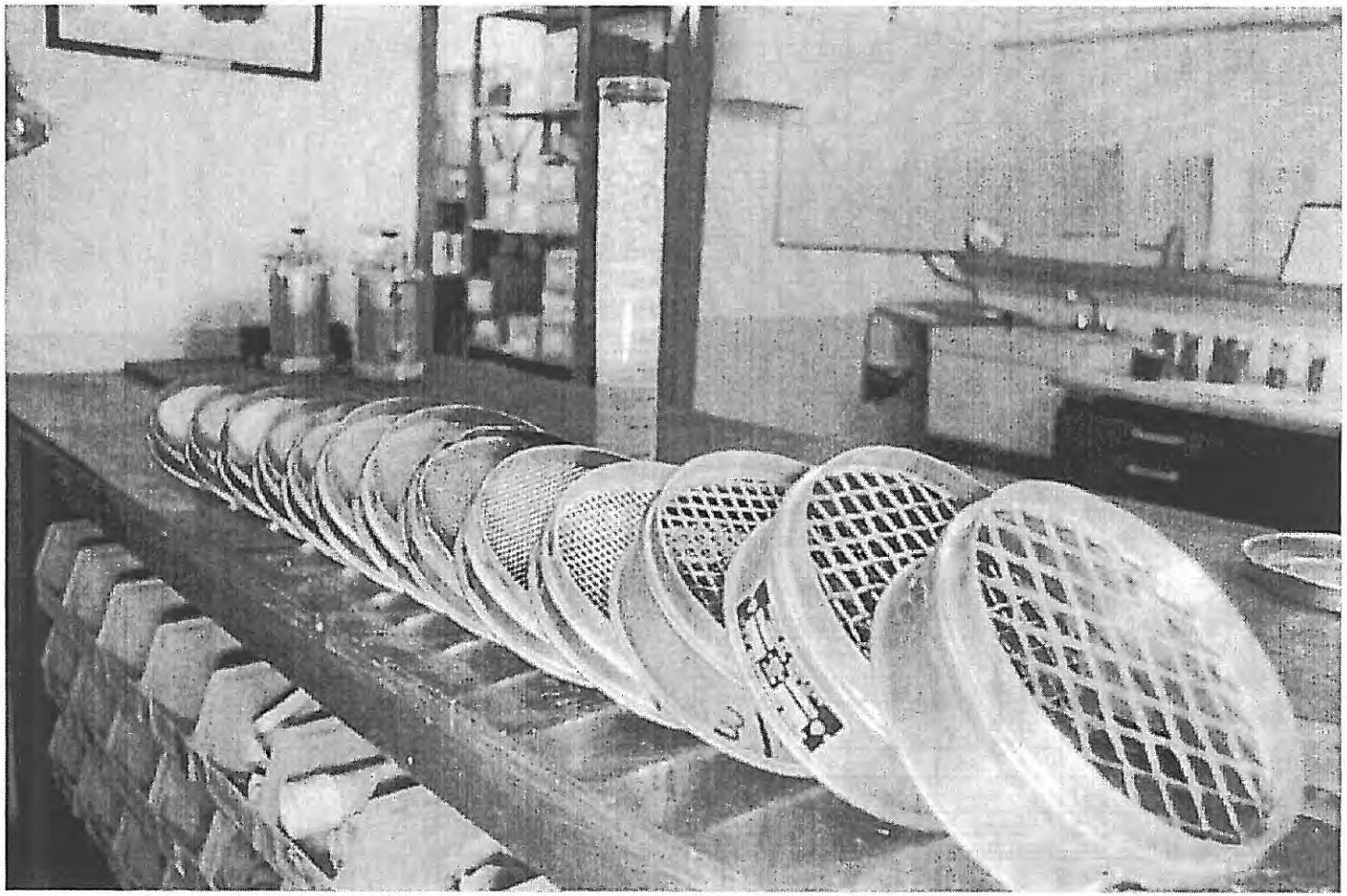

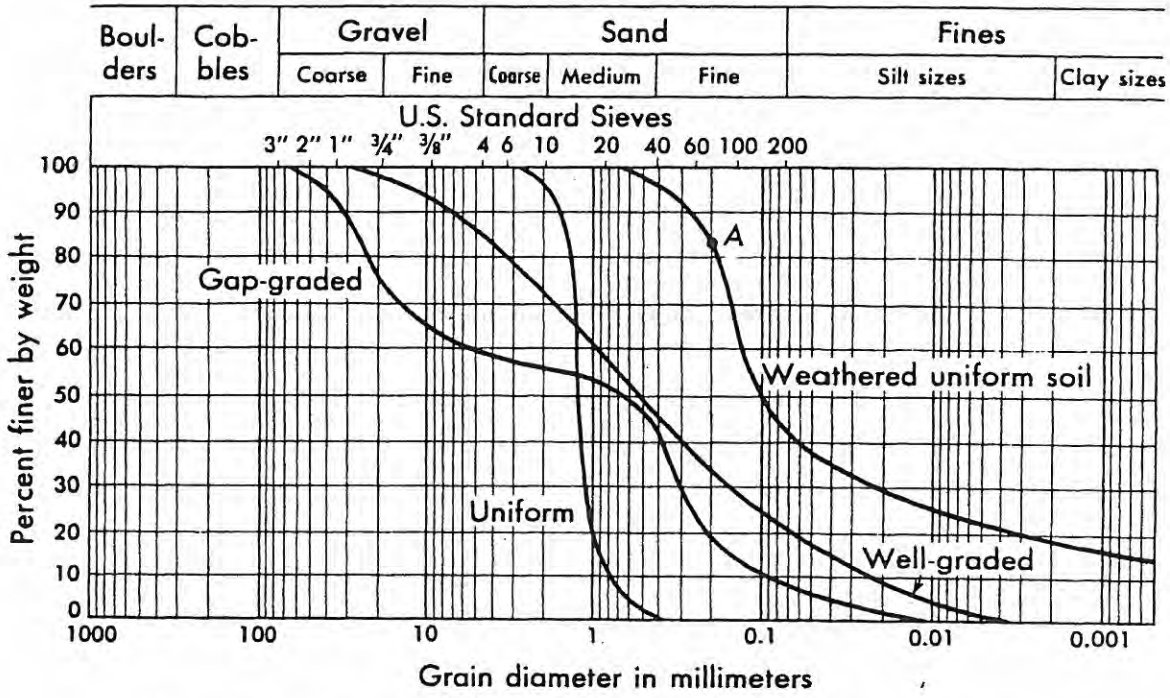

Figure 1.6 *Grain size chart and ASTM–ASCE grain size scale.*

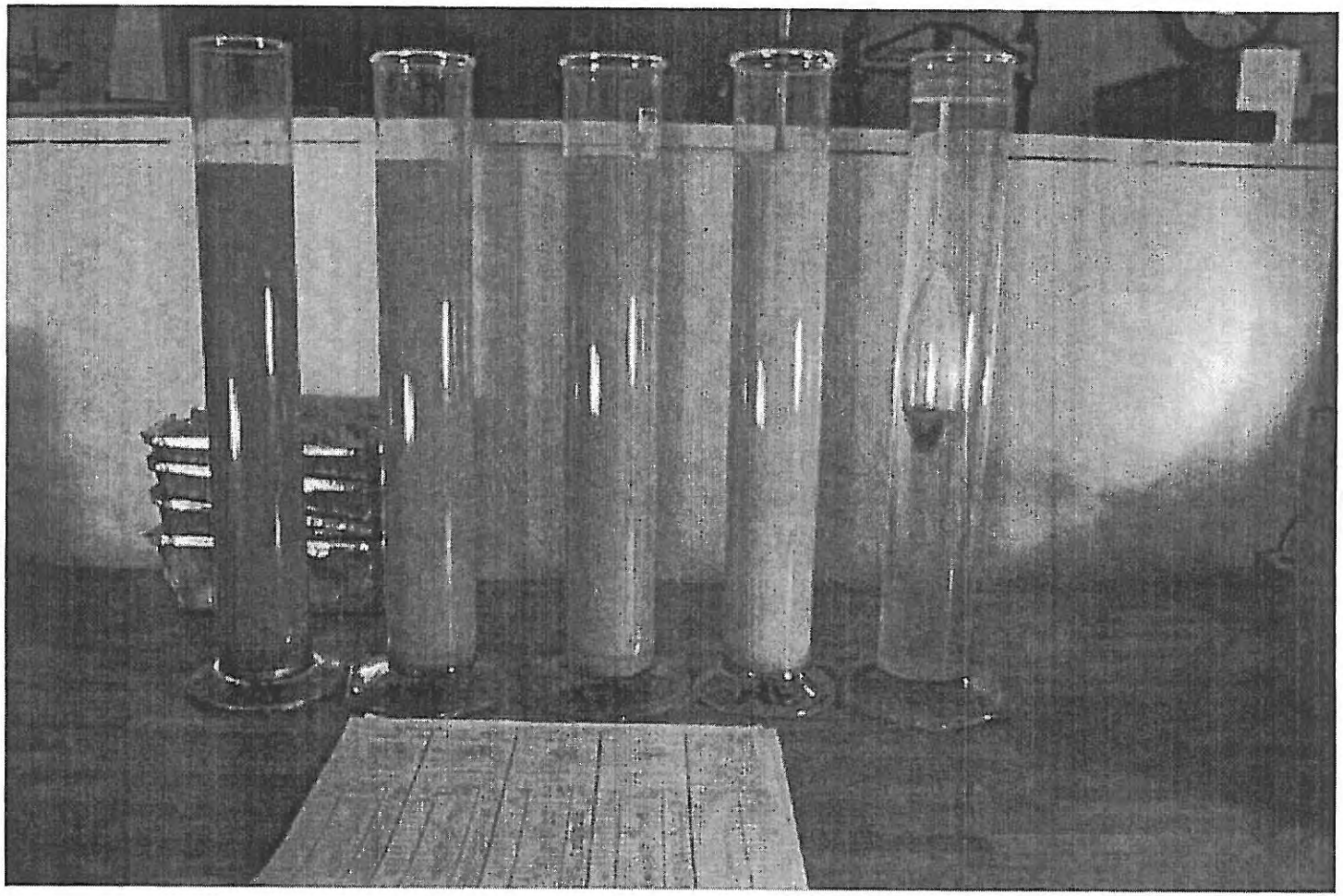

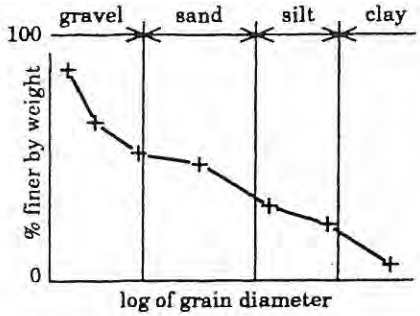

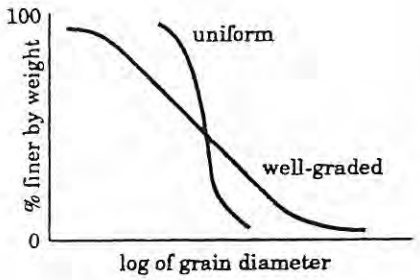

A grain size curve for a given soil sample can be constructed by laboratory tests that identify the percentages, by weight, of the various particle sizes present in the sample. If most of the particles are of the same size, the soil is said to have a uniform gradation (like a bag of pea gravel or beach dune sand); if most sizes are present, the soil is said to be well graded (like a good quality road base mix).

The shape of the individual particles is at least as important as the grain size distribution in affecting the engineering response of granular soils. A qualitative shape determination is made as a part of visual classification. Coarse-grained soils are commonly classified as rounded, subrounded, subangular or angular. Grain shape is very significant in determining the frictional characteristics (shear strength) of granular soils.

Water contents classify fine-grained soils by their Atterberg limits. The methods used relate the natural moisture content to the Atterberg limits water contents. The limits are determined in the laboratory by test methods developed in the early 1900s by Swedish soil scientist A. Atterberg.

Atterberg realized that at least two water contents were required to define the plasticity of clays—corresponding to the upper and lower limits of plasticity. These consistency limits are the liquid limit (LL) and the plastic limit (PL), and the difference between them is the range of moisture contents over which the soil is plastic. This range is called the plasticity index (PI), which equals LL minus PL. (A soil wetter than LL could be described as a slurry, pea soup to soft butter, or a viscous liquid. A soil drier than the PL is a semi-solid, like cheese. A plastic soil will deform but not crack, like soft butter to stiff putty.)

$$\text{Plasticity Index: } PI = LL - PL$$

The limits set by Atterberg are relatively arbitrary; but they are standardized in engineering practice, and many soil properties are indexed to them. We want to be able to compare or scale our water content with some defined limits or boundaries or engineering response. In this way, we would know if our sample was likely to behave as a plastic, a brittle solid, or possibly even a liquid. The index for scaling the natural moisture content of a given soil is the liquidity index (LI), which equals the natural moisture content minus the plastic limit, divided by the plasticity index.

$$\text{Liquidity Index: } LI = \frac{w - PL}{PI}$$

1:10 Plasticity and the Atterberg Limits[1:6c,d]

The Swedish soil scientist Atterberg developed a method of describing quantitatively the effect of varying water content on the consistency of fine-grained soils. He established stages of soil consistency and defined definite but arbitrary limits for each.

Each boundary or limit is defined by the water content that produces a specified consistency; the difference between the limits represents the range in water content for which the soil is in a certain stage or state.

TABLE 1:3 / ATTERBERG LIMITS

Stage	Description	Boundary or Limit
Liquid	A slurry; pea soup to soft butter; a viscous liquid	
		Liquid limit (LL)
Plastic	Soft butter to stiff putty; deforms but will not crack	
		Plastic limit (PL)
Semisolid	Cheese; deforms permanently but cracks	
		Shrinkage limit (SL)
Solid	Hard candy; breaks up upon deformation	

The *liquid limit* (LL) is defined as the water content at which a trapezoidal groove of specified shape, cut in moist soil held in a special cup, is closed after 25 taps on a hard rubber plate. The *plastic limit* (PL) is the water content at which the soil begins to break apart and crumble when rolled by hand into threads 3 mm ($\frac{1}{8}$ in.) in diameter. The *shrinkage limit* (SL) is the water content at which the soil reaches its theoretical minimum volume as it dries out from a saturated condition. This is described in Section 4.5. The limits are customarily expressed as whole numbers of percentage, omitting the percent sign.

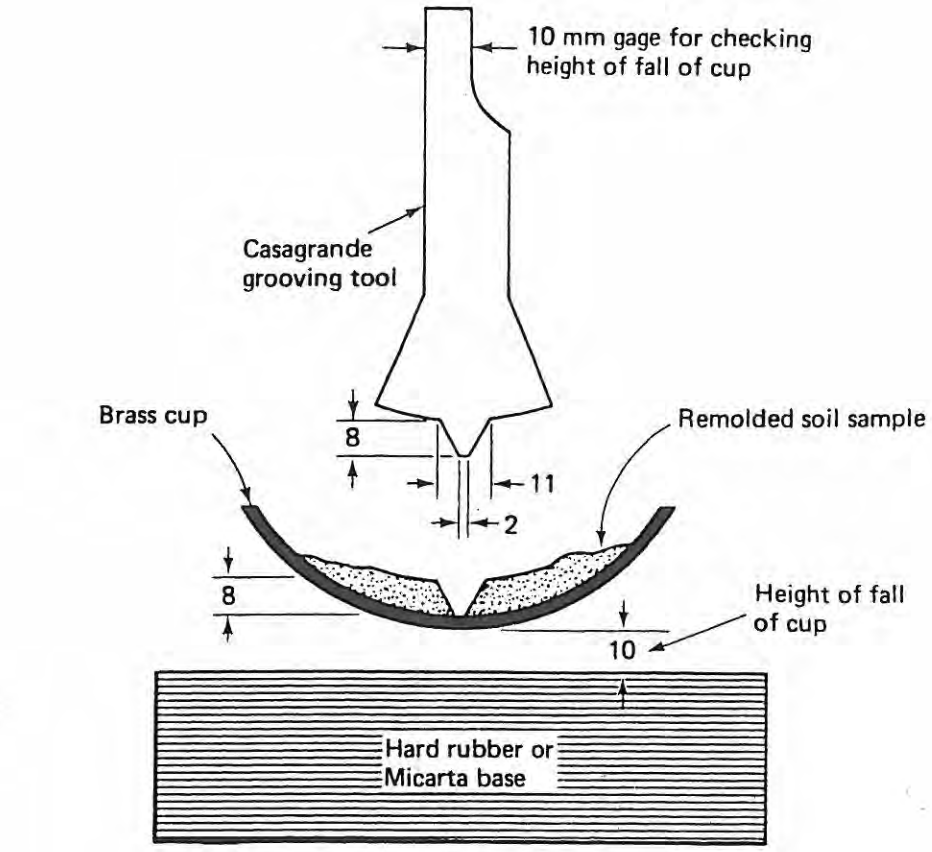

(a)

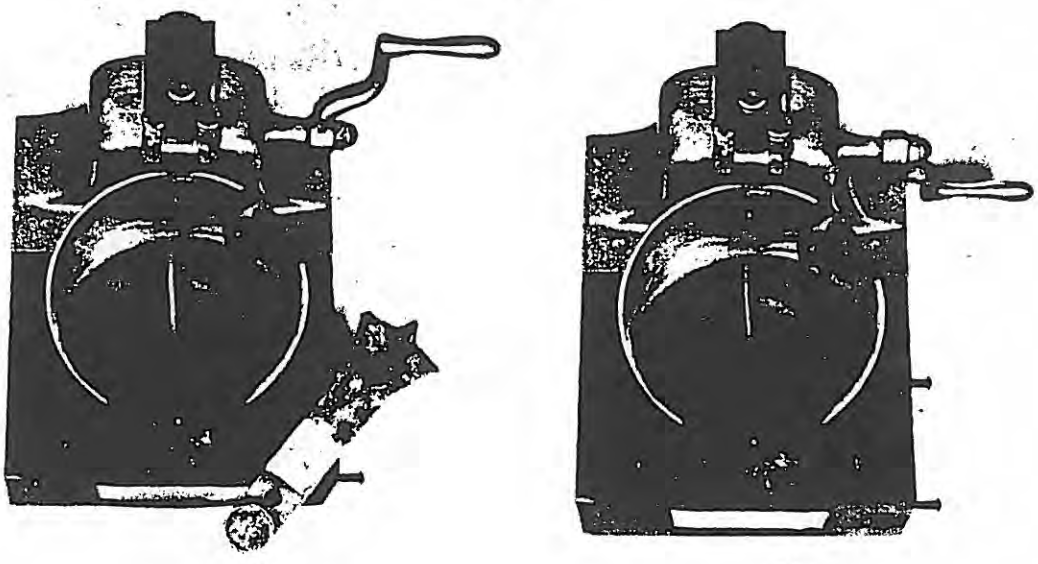

(b)

(c)

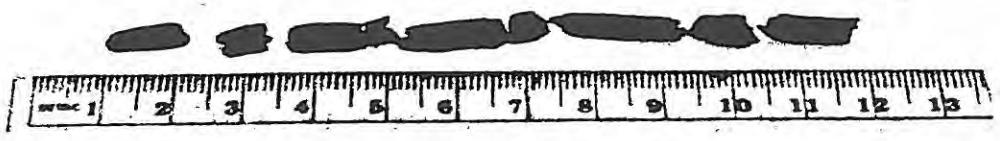

(d)

Fig. 2.8 (a) Schematic diagram of the Casagrande liquid limit device and grooving tool; dimensions in millimetres. (b) Cut groove prior to turning the crank. (c) After turning the crank to apply sufficient blows of the cup to close the groove 13 mm. (d) Plastic limit threads. Parts (a) through (c) after Hansbo (1975). (Photographs by M. Surendra.)

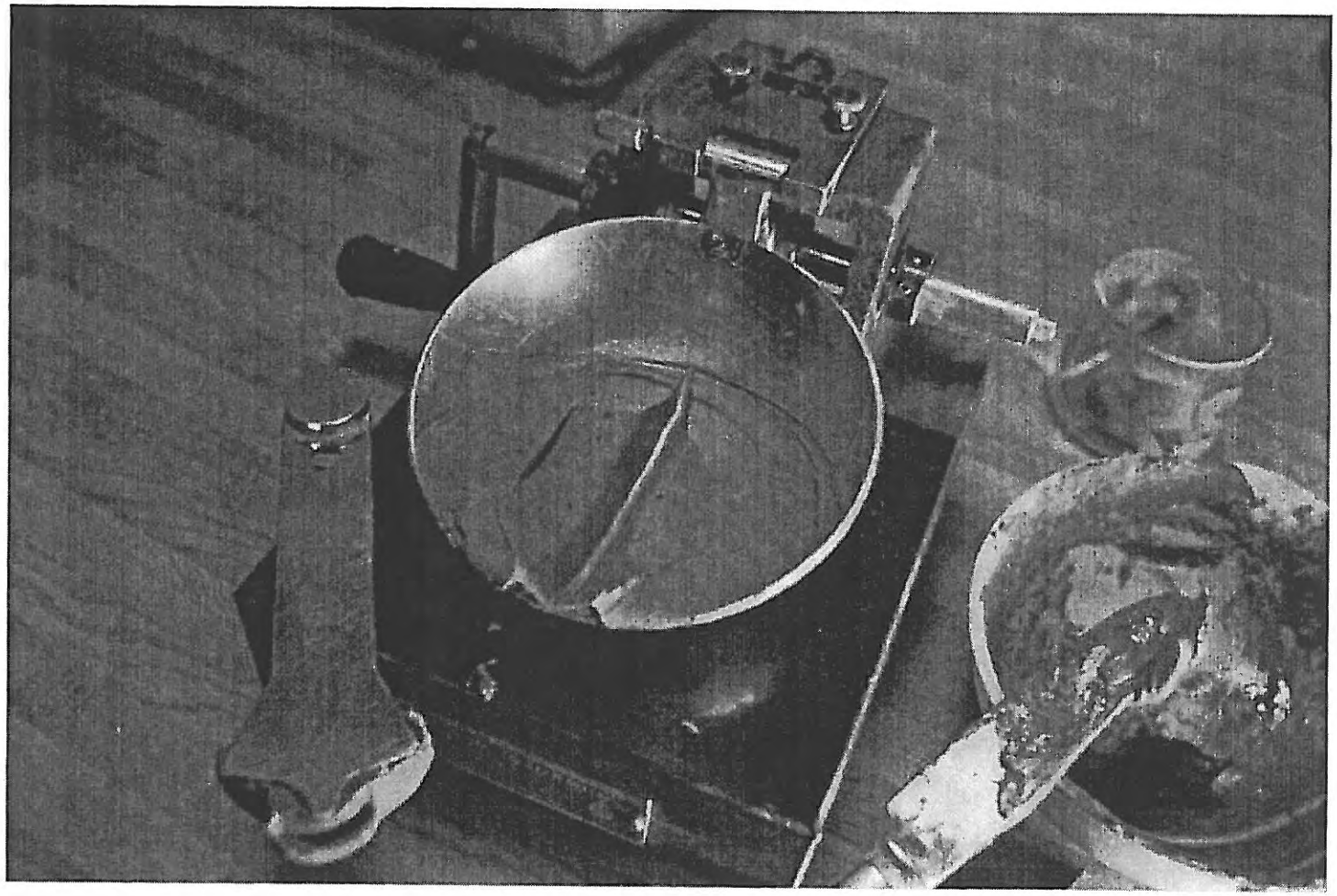

Soil Classification

The preceding discussion gave a general idea about how soils are classified. Usually, however, general classifications like sand or clay include such a wide range of engineering characteristics that additional subdivisions or modifiers are required to make the terms more useful in engineering practice. These terms are collected into "soil classification systems," usually with some specific engineering purpose in mind.

A soil classification system is, in effect, a language of communication between engineers. It provides a systematic method of categorizing soils according to their probable engineering behavior, and it allows engineers access to the accumulated experience of other engineers. A soil classification system does not eliminate the need for detailed soils investigations or testing for engineering properties. But the engineering properties have been found to correlate quite well with the index and classification properties of a given deposit. By knowing the soil classification, then, the engineer already has a fairly good general idea of the way the soil will behave in the engineering situation, during construction, under structural loads, etc.

One classification system widely used by the engineering agencies of the U.S. government, geotechnical engineering consulting firms and soil testing laboratories is the Unified Soil Classification System. There are three major divisions: coarse-grained, fine-grained (including organic soils) and peat.

Coarse-grained soils are subdivided into gravels and gravelly soils (G) and sands and sandy soils (S). These groups are divided into four secondary groups according to the grain size distribution and nature of the fines in the soils. Well-graded (W) soils have a good representation of all particle sizes, wheres the poorly graded (P) soils are either uniform, or skip- or gap-graded (some sizes missing).

Fine-grained soils are subdivided into silts (M, from the Swedish terms "mo," meaning very fine sand, and "mjala," meaning silt), and clays (C), depending on their liquid limit and plasticity index. Organic soils (O) and peat (Pt) are also included in this fraction. The silt, clay and organic fractions are further subdivided on the basis of relative low (L) or high (H) liquid limits. The dividing line has been arbitrarily set at 50. Peat is a separate category of soil containing at least 25 percent organics by weight.

Unified Soil Classification System (abbreviated)

Coarse-Grained Soils

GW Well-graded gravels, gravel sand mixtures, little or no fines.

GP Poorly graded gravels, gravel-sand mixtures, little or no fines.

GM Silty gravels, gravel-sand-silt mixtures.

GC Clayey gravels, gravel-sand-clay mixtures.

SW Well-graded sands, gravelly sands, little or no fines.

SP Poorly graded sands, gravelly sands, little or no fines.

SM Silty sands, sand-silt mixtures.

SC Clayey sands, sand-clay mixtures.

Fine-Grained Soils

ML Inorganic silts and very fine sands, rock flour, silty or clayey fine sands or clayey silts with slight plasticity.

CL Inorganic clays of low to medium plasticity, gravelly clays, sandy clays, silty clays, lean clays.

OL Organic silts and organic silty clays of low plasticity

MH Inorganic silts, micaceous or diatomaceous fine sandy or silty soils, elastic silts.

CH Inorganic clays of high plasticity, fat clays.

OH Organic clays of medium to high plasticity, organic silts.

Pt Peat and other highly organic soils.

Major Divisions			*Group Symbols*	*Typical Names*
Coarse-Grained Soils More than 50% retained on No. 200 sieve*	Gravels 50% or more of coarse fraction retained on No. 4 sieve	Clean gravels −200 <5%	GW	Well-graded gravels and gravel–sand mixtures, little or no fines
			GP	Poorly graded gravels and gravel–sand mixtures, little or no fines
		Gravels with fines −200 >12%	GM	Silty gravels, gravel–sand–silt mixtures
			GC	Clayey gravels, gravel–sand–clay mixtures
	Sands More than 50% of coarse fraction passes No. 4 sieve	Clean sands −200 <5%	SW	Well-graded sands and gravelly sands, little or no fines
			SP	Poorly graded sands and gravelly sands, little or no fines
		Sands with fines −200 >12%	SM	Silty sands, sand–silt mixtures
			SC	Clayey sands, sand–clay mixtures
Fine-Grained Soils 50% or more passes No. 200 sieve*	Silts and Clays Liquid limit 50% or less		ML	Inorganic silts, very fine sands, rock flour, silty or clayey fine sands
			CL	Inorganic clays of low to medium plasticity, gravelly clays, sandy clays, silty clays, lean clays
			OL	Organic silts and organic silty clays of low plasticity
	Silts and Clays Liquid limit greater than 50%		MH	Inorganic silts, micaceous or diatomaceous fine sands or silts, elastic silts
			CH	Inorganic clays of high plasticity, fat clays
			OH	Organic clays of medium to high plasticity
Highly Organic Soils			PT	Peat, muck, and other highly organic soils

Figure 4.9 Unified Classification System, ASTM D-2487-69.

Classification Criteria

More than 12%: GM, GC 5–12% Borderline		$C_u = D_{60}/D_{10} > 4$ $\quad C_z = \dfrac{D_{30}^2}{D_{10}D_{60}}$ between 1 and 3	
		Not meeting both criteria for GW	
Classification on Basis of Percentage of Fines		Atterberg limits plot below *A* line or plasticity index less than 4	Atterberg limits plotting in hatched area are borderline classifications requiring use of dual symbols
Less than 5% pass No. 200 sieve	GW, GP, SW, SP	Atterberg limits plot above *A* line and plasticity index greater than 7	
More than 12% pass No. 200 sieve	GM, GC, SM, SC		
5–12% pass No. 200 sieve	Borderline classification requiring use of dual symbols	$C_u = D_{60}/D_{10} > 6$ $\quad C_z = \dfrac{D_{30}^2}{D_{10}D_{60}}$ between 1 and 3	
		Not meeting both criteria for SW	
		Atterberg limits plot below *A* line or plasticity index less than 4	Atterberg limits plotting in hatched area are borderline classifications requiring use of dual symbols
		Atterberg limits plot above *A* line and plasticity index greater than 7	

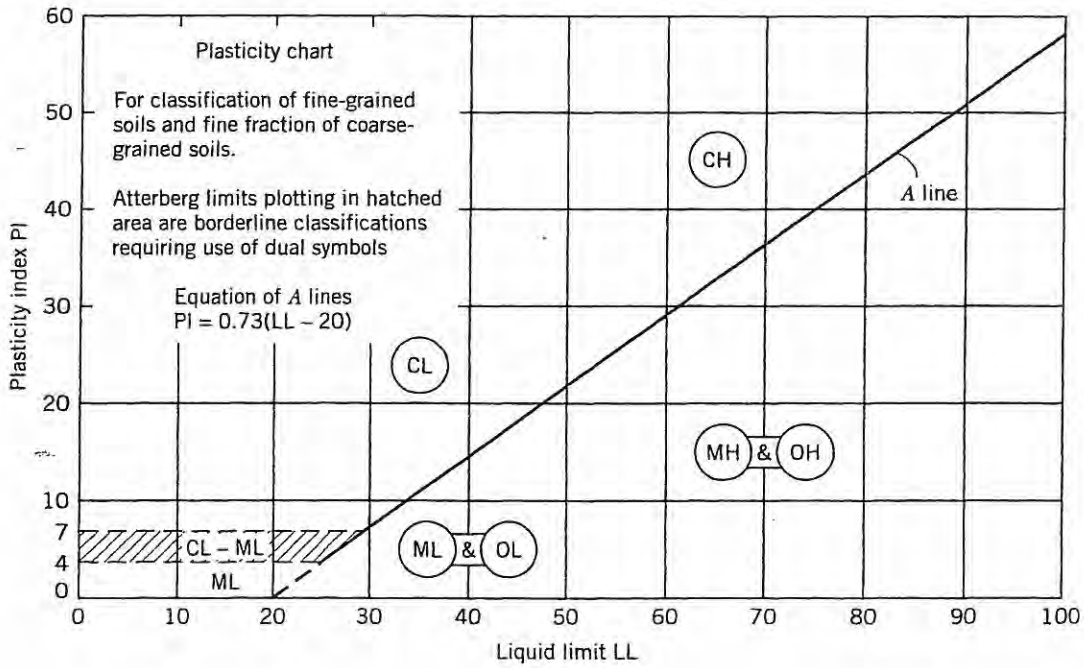

Visual-manual identification, see ASTM D-2488.

* 0.075-mm sieve.

The following soil properties are of significance in most soil problems and therefore form the basis of a complete soil description. They are also a required supplement to the Unified Classification.

1. Shear strength (cohesive soils).
2. Density (cohesionless soils).
3. Compressibility.
4. Permeability.
5. Color.
6. Composition (grain size, shape, plasticity, mineralogy).
7. Structure of soil.

For a precise description many of these properties must be determined by laboratory tests. An experienced soils engineer, however, can estimate most of these by careful field observation and examination of small samples of the soil.[2:14]

SOIL STRENGTH / Shear strength is a fundamental property of undisturbed cohesive soils, a knowledge of which is necessary in solving many problems. It is ordinarily defined in terms of unconfined compressive strength (Section 5:6) but may be estimated from the pressure required to squeeze an undisturbed sample between the fingers. If the soil is *brittle* (fails suddenly with little strain), *elastic* (rubbery), *friable* (crumbles easily) or *sensitive* (loses strength on remolding), these terms should be included in the description. (See Table 2:6.)

TABLE 2:6 / SOIL STRENGTH

Term	Unconfined Compressive Strength (After Terzaghi and Peck)[2:15]		Field Test (After Cooling, Skempton, and Glossop)[2:16]
	Kips/ft^2	kN/m^2	
Very soft	0–0.5	0–25	Squeezes between fingers when fist is closed
Soft	0.5–1	25–50	Easily molded by fingers
Firm	1–2	50–100	Molded by strong pressure of fingers
Stiff	2–3	100–150	Dented by strong pressure of fingers
Very stiff	3–4	150–200	Dented only slightly by finger pressure
Hard	4+	200+	Dented only slightly by pencil point

DENSITY / Relative density is as important for cohesionless soils as strength is for cohesive. It can be found by comparing the soil's actual void ratio with the range in void ratio from loose to dense for that soil. It may be estimated from the ease with which a reinforcing rod penetrates the soil, or from Tables 2:7 and 7:4.

TABLE 2:7 / SOIL RELATIVE DENSITY

Term	Relative Density (%)	Field Test
Loose	0–50	Easily penetrated with 12-mm or $\frac{1}{2}$-in. reinforcing rod pushed by hand
Firm	50–70	Easily penetrated with 12-mm or $\frac{1}{2}$-in. reinforcing rod driven with 2.3-kg or 5-lb hammer
Dense	70–90	Penetrated a foot with 12-mm or $\frac{1}{2}$-in. reinforcing rod driven with 2.3-kg or 5-lb hammer
Very dense	90–100	Penetrated only a few inches with 12-mm or $\frac{1}{2}$-in. reinforcing rod driven with a 2.3-kg or 5-lb hammer

TABLE 7:3 / RELATIVE DENSITY OF SAND—STANDARD PENETRATION TEST
(After Terzaghi and Peck[7:12])

Blows	Relative Density
0–4	Very loose
5–10	Loose
11–20	Firm
21–30	Very firm
31–50	Dense
51+	Very dense

TABLE 7:4 / CONSISTENCY OF COHESIVE SOILS—STANDARD PENETRATION TEST
(After Terzaghi and Peck[7:12])

Blows	Consistency
0–1	Very soft
2–4	Soft
5–8	Firm
9–15	Stiff
16–30	Very stiff
31+	Hard

COMPRESSIBILITY / Compressibility is determined by direct laboratory tests (Section 4:2) or is estimated from the liquid limit and void ratio. (See Table 2:8.)

TABLE 2:8 / COMPRESSIBILITY

Term	Compression Index	Liquid Limit (approx.)
Slight or low compressibility	0–0.19	0–30
Moderate or intermediate	0.20–0.39	31–50
High compressibility	0.40 and over	51 and over

PERMEABILITY / Permeability is determined by direct laboratory and field tests or may be estimated from Table 3:1.

The range in permeability of natural soils is even greater than the range in grain size. Table 3:1 can be used as a standard for describing permeability and as a guide for rough estimates.

TABLE 3:1 / RELATIVE VALUES OF PERMEABILITY
(After Terzaghi and Peck)[3:5]

Relative Permeability	Values of k (mm/sec)*	Typical Formation
Very permeable	1	Coarse gravel, open-jointed rock
Medium permeability	1×10^{-2}	Sand, fine sand
Low permeability	$1\times10^{-2}-1\times10^{-4}$	Silty sand, dirty sand
Very low permeability	$1\times10^{-4}-1\times10^{-6}$	Silt, fine sandstone
Impervious	Less than 1×10^{-6}	Clay, mudstone without joints

*To convert to feet per minute, multiply above values by 0.2.

COLOR / Color, although not an important physical property in itself, is an indication of more important properties. For example, yellow and red hues indicate that a soil has undergone severe weathering, for the colors are iron oxides. A dark greenish brown is often an indication of colloidal organic matter. A change in color encountered during excavation often means a different soil stratum with different properties has been uncovered. Color is usually the easiest property of a soil for persons untrained in soil mechanics to identify; therefore, a practical method of describing a certain soil to workers is by color. Soil color is described visually with the aid of the Munsell color charts.[2:17]

COMPOSITION / Composition includes the grain size, gradation, grain shape, mineralogy (or the coarser grains), and plasticity. Two groups of soils are recognized: predominantly coarse grained (over 0.075 mm) and predominantly fine grained (less than 0.075 mm), as in the Unified Classification. The coarse-grained soils are described primarily on the basis of the grain size, the fine-grained primarily on the basis of their plasticity. The amount of coarse or fine component required to predominate is not fixed, for it depends on the soil structure: If the coarse-grained particles can make contact with one another, the soil behaves essentially as a coarse-grained material; if they cannot touch but are separated by the fines, the fines predominate. The unified Classification arbitrarily defines predominant grain size at over 50% by weight.

However, for soils containing clay minerals, the volume of fines controls soil behavior, although they comprise considerably less than 50% by weight. For example, a well-graded, sand–silt–clay mixture in which the fines exhibit low plasticity may behave like a clayey or fine-grained soil with only 30% fines. If the fine fraction is highly plastic, 10 to 20% fines may be sufficient for the soil to behave as a fine-grained material. Therefore, no fixed percentage of fines can distinguish predominantly coarse-grained or fine-grained behavior, and the engineer must exercise judgment.

The sizes of particles as defined by ASTM–ASCE and their visual identification are given in Table 2:9.

TABLE 2:9 / GRAIN SIZE IDENTIFICATION

Name	Size Limits	Familiar Example
Boulder	12 in. (305 mm) or more	Larger than basketball
Cobbles	3 in. (76 mm)–12 in. (305 mm)	Grapefruit
Coarse gravel	$\frac{3}{4}$ in. (19 mm)–3 in. (76 mm)	Orange or lemon
Fine gravel	4.75 mm(No. 4 sieve)–$\frac{3}{4}$ in. (19 mm)	Grape or pea
Coarse sand	2 mm (No. 10 sieve)–4.75 mm (No. 4 sieve)	Rocksalt
Medium sand	0.42 mm (No. 40 sieve)–2 mm (No. 10 sieve)	Sugar, table salt
Fine sand*	0.075 mm (No. 200 sieve)–0.42 mm (No. 40 sieve)	Powdered sugar
Fines	Less than 0.075 mm (No. 200 sieve)	

* Particles finer than fine sand cannot be discerned with the naked eye at a distance of 8 in. (20 cm).

TABLE 2:10 / PLASTICITY

Term	PI	Dry Strength	Field Test
Nonplastic	0–3	Very low	Falls apart easily
Slightly plastic	3–15	Slight	Easily crushed with fingers
Medium plastic	15–30	Medium	Difficult to crush
Highly plastic	31 or more	High	Impossible to crush with fingers

In forming the description, a predominantly coarse-grained soil is termed either a *gravel* or a *sand*, depending on which component appears to be the more abundant. The less abundant component and the fines (either silt or clay) are used as modifiers, with the least important component first. For example, a soil with 30% fines (silt), 45% gravel, and 25% sand would be described as sandy, silty gravel. The grain shapes and sizes precede the component to which they apply. A predominantly fine-grained soil would be considered either silt or clay and the coarse components would be used as modifiers, with the least important first. For example, a soil with 70% fines (clay), 20% sand, and 10% gravel would be described as gravelly, sandy clay.

Modifiers and suffixes are used by some engineers to quantify grain size components: 0 to 15%, *trace*; 16 to 30%, *some*; 31 to 45%, *-y*; and 45 to 50%, *and*.

DESCRIBING SOIL STRUCTURES / The structure of the soil must be determined by careful observation. The following descriptive terms may be used:

Homogeneous (uniform properties).
Stratified (alternate layers of different soils), including strike and dip.
Laminated (repeating alternate layers less than $\frac{1}{8}$ in. thick), including strike and dip.
Banded (alternate layers in residual soils).

It is important to recognize defects in a soil structure. The following are often observed:

Slickensides (former failure planes), including strike and dip.
Rootholes.
Fissure (cracks, from shrinkage, frost), including strike and dip.
Weathering (irregular discoloration).
Jointed (regular, parallel cracks).

WRITING A SOIL DESCRIPTION / The soil should be described in essentially the order of the significant properties given previously. As many of the properties as are of interest should be included. Examples might be as follows:

1. Hard, moderately compressible, blue-gray, medium-plastic clay.
2. Dense, well-graded, clayey, sandy, well-rounded gravel.
3. Loose, brown, uniform, angular, fine sand.
4. Firm, black, slightly compressible silt and clay; laminated.

Though the letter group symbols in the classification system are convenient, they do not completely describe a soil or soil deposit. For this reason, descriptive terms are also used along with the letter symbols for a complete soil classification. Such characteristics as color, odor and homogeneity of a deposit are observed and included in a description.

For coarse-grained soils, such items as grain shape, mineralogical content, degree of weathering, in-situ density and degree of compaction, and presence or absence of fines are noted. Adjectives like rounded, angular and subangular are commonly used to describe grain shape. Terms like very loose, loose, medium, dense and very dense are used to describe in-situ density.

For fine-grained soils, such items as natural water content, consistency and remolded (disturbed in some way) are noted. Consistency in the natural state corresponds in some respects to the degree of compaction in coarse-grained soils. Terms like very soft, soft, medium, stiff (sometimes the word "firm" is used synonymously), very stiff and hard are used to describe consistency.

Another common classification system is the AASHTO (Bureau of Public Roads) Classification System.

A-1 to A-4	Granular
A-4 to A-7	Silt-Clay
A-8	Organic

General Classification	*Granular Materials (35% or less passing 0.075 mm)*							*Silt–Clay Materials (More than 35% passing 0.075 mm)*			
	A-1			*A-2*							
Group Classification	*A-1-a*	*A-1-b*	*A-3*	*A-2-4*	*A-2-5*	*A-2-6*	*A-2-7*	*A-4*	*A-5*	*A-6*	*A-7-5 A-7-6*
Sieve analysis, percent passing:											
2.00 mm (No. 10)	50 max	—	—	—	—	—	—	—	—	—	—
0.425 mm (No. 40)	30 max	50 max	51 min	—	—	—	—	—	—	—	—
0.075 mm (No. 200)	15 max	25 max	10 max	35 max	35 max	35 max	35 max	36 min	36 min	36 min	36 min
Characteristics of fraction passing 0.425 mm (No. 40)											
Liquid limit	—		—	40 max	41 min	40 max	41 min	40 max	41 min	40 max	41 min
Plasticity index*	6 max		NP	10 max	10 max	11 min	11 min	10 max	10 max	11 min	11 min
Usual types of significant constituent materials	Stone fragments, gravel, and sand		Fine sand	Silty or clayey gravel and sand				Silty soils		Clayey soils	
General rating as subgrade	Excellent to good							Fair to poor			

* Plasticity index of A-7-5 subgroups is equal to or less than LL − 30. Plasticity index of A-7-6 subgroup is greater than LL − 30.

Figure 4.10 The AASHTO Classification of soils and soil-aggregate mixtures.

Description of Classification Groups	
Subgroup A-1a	Includes those materials consisting predominantly of stone fragments or gravel
Subgroup A-1b	Includes those materials consisting predominantly of coarse sand, either with or without a well-graded soil binder
Subgroup A-3	Fine beach sand or fine desert loess sand without silty or clay fines or with a very small amount of nonplastic silt
Subgroups A-2-4 and A-2-5	Include various granular materials containing 35% or less passing the 0.075-mm sieve and with a minus 0.425 mm in having the characteristics of the A-4 and A-5 groups
Subgroups A-2-6 and A-2-7	Include material similar to that described under subgrades A-2-4 and A-2-5, except that a fine portion contains plastic clay having the characteristics of the A-6 or A-7 group
Subgroup A-4	The typical materials of this group are the nonplastic or moderately plastic silty soils
Subgroup A-5	Similar to that described under group 2-4, except that it is usually of diatomaceous or micaceous character
Subgroup A-6	Usually a plastic clay having 75% or more passing the 0.075-mm sieve
Subgroup A-7-5	Includes materials with moderate plasticity indexes in relation to liquid limit
Subgroup A-7-6	Includes materials with high plasticity indexes in relation to liquid limit

Figure 4.11 Description of AASHTO groups.

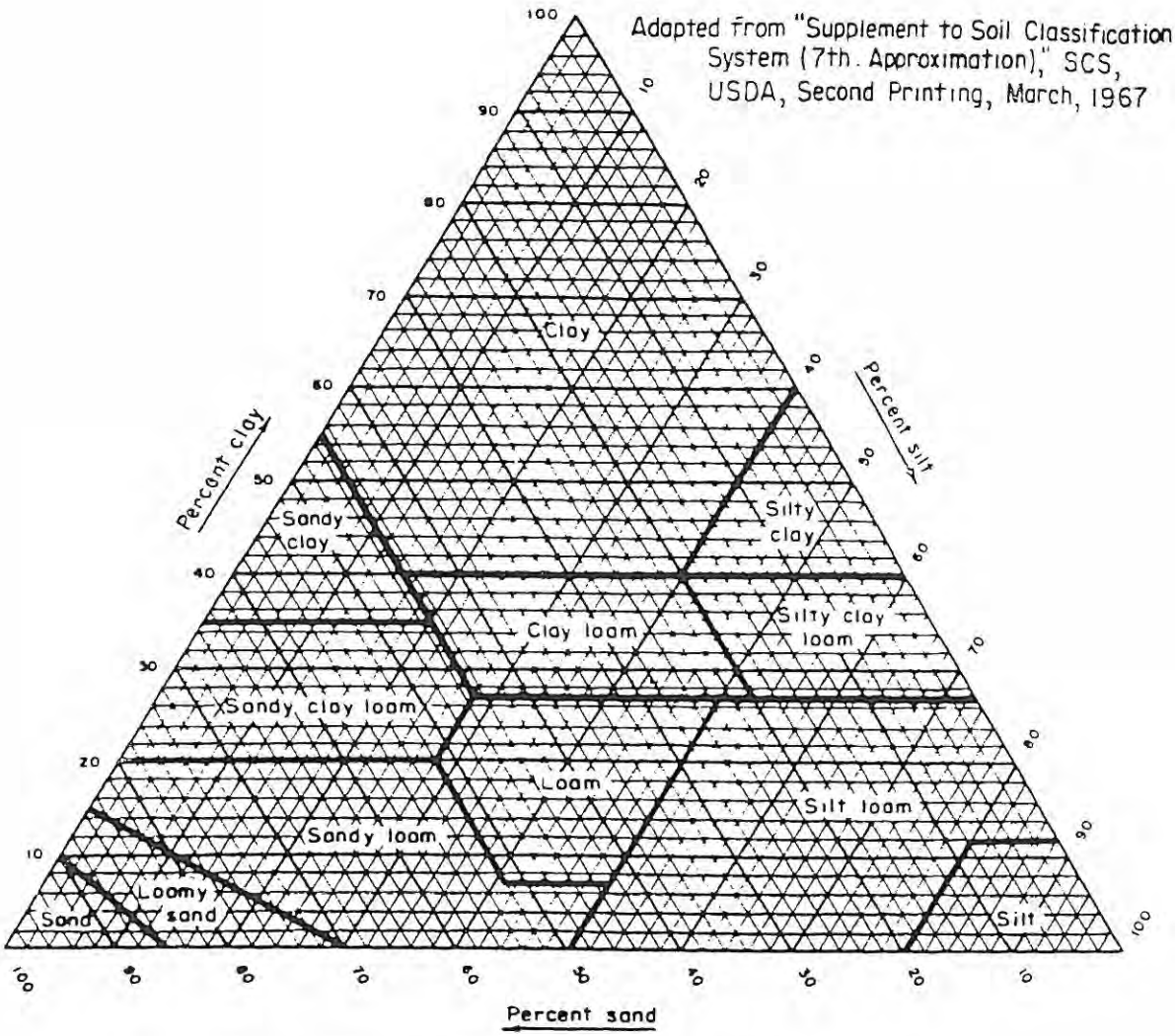

* Very fine sand (0.05 – 0.1) is treated as silt for family groupings; coarse fragments are considered the equivalent of coarse sand in the boundary between the silty and loamy classes.

COMPARISON OF PARTICLE-SIZE SCALES

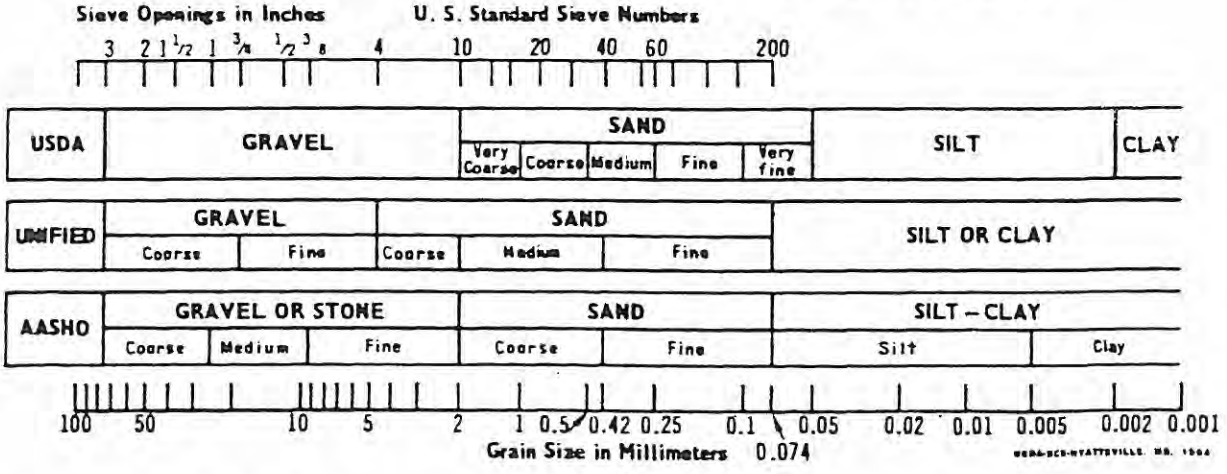

Figure 30.—Soil triangle of the basic soil textural classes. (U.S. Soil Conservation Service.) 288–D–2782.

Soil Structure and Fabric

The term "clay" can refer to specific minerals, such as montmorillonite or kaolinite. But in civil engineering, clay often means a "clay soil"—a soil that contains some clay minerals as well as other mineral constituents, has plasticity, and is "cohesive." Clay soils are fine grained, but not all fine-grained soils are cohesive or clays. Silts are both granular and fine grained. The individual silt grains, like clays, are invisible to the naked eye, but silts are noncohesive and nonplastic.

Certain characteristics of granular soils—such as grain size distribution and the grain shape—affect the engineering behavior of these soils. On the other hand, the presence of water, with a few important exceptions, is relatively unimportant in their behavior.

In contrast, the grain size distribution for clay soils has relatively little influence on the engineering behavior, but water markedly affects their behavior. Silts are an "in between" material. Water affects their behavior—they are "dilatant" (can expand in bulk with change of shape due to the increase of space between rigid particles as they change positions)—yet they have little or no plasticity, and their strengths, like sands, are essentially independent of water content.

Clay minerals are very small particles that are very active electrochemically. The presence of even a small amount of clay minerals in a soil mass can markedly affect the engineering properties of that mass. As the amount of clay increases, the behavior of the soil is increasingly governed by the properties of the clay. When the clay content is about 50 percent, the sand and silt grains are essentially floating in a clay matrix and have little effect on the engineering behavior.

In geotechnical engineering practice, the "structure" of a soil is taken to mean both the geometric arrangement of the particles or mineral grains as well as the interparticle forces that may act between them. Soil "fabric" refers only to the geometric arrangement of the particles.

In granular or cohesionless soils, the interparticle forces are very small, so both the fabric and structure of gravels, sands and, to some extent, silts are the same.

In fine-grained cohesive soils, interparticle forces are relatively large, and thus both these forces and the fabric of such soils must be considered as the structure of the soil.

The structure strongly affects, some would say "governs," the engineering behavior of a particular soil. Geotechnical engineers must consider the soil structure and fabric, at least qualitatively, when cohesive soils are encountered in engineering practice.

The structure of most naturally occurring clay deposits is highly complex. The engineering behavior of these deposits is strongly influenced by both the macrostructure and the microstructure. At present, no quantitative connection exists between microstructure and the engineering properties, but it is important for the engineer to have an appreciation of the complexity of the structure of cohesive soils and their relation to engineering behavior.

Grains of soil, which can settle out of a soil-fluid suspension independently of other grains, will form what is called a "single-grained" structure. This is the structure of a sand or gravel pile, for example. Deposition media include both air (loess deposits, sand dunes) and water (rivers, beaches). Single-grained structures may be "loose" (high void ratio, low density) or "dense" (low void ratio, high density). A wide range of void ratios is possible, depending on the grain size distribution and the packing arrangement of the grains.

The greatest possible void ratio, or loosest possible condition of a soil, is called the maximum void ratio. It is determined in the laboratory by very carefully pouring dry sand from a funnel, with no vibration or free-fall, into a calibrated mold of known volume. The maximum void ratio is then calculated from the weight of the sand in the mold. Similarly, the minimum void ratio is the densest possible condition that a given soil can obtain, which is calculated by vibrating a known weight of dry sand into a known volume.

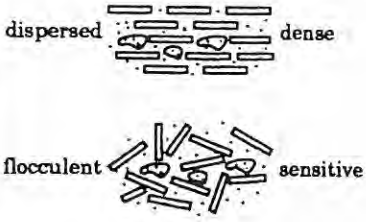

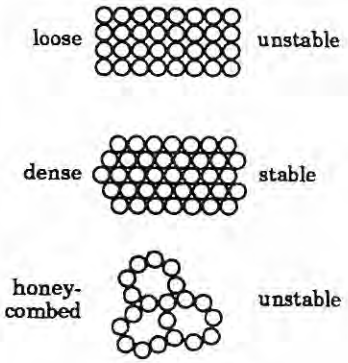

cohesionless soils

Density and Compaction

Relative density (D_r) is useful in comparing the void ratio of a given soil with the maximum and minimum void ratios. Relative density is usually expressed as a percentage, defined as:

$$D_r = \frac{e_{max} - e}{e_{max} - e_{min}} \times 100\%$$

The relative density of a natural deposit very strongly affects its engineering behavior. It is important to conduct laboratory tests on samples of sand at the same relative density as in the field. Sampling of loose granular materials—especially at depths greater than a few yards—is very difficult, if not nearly impossible. Since the materials are very sensitive to even the slightest vibration, you can never be sure the sample has the same density as the natural soil deposit. Consequently, different kinds of penetrometers are used in engineering practice, and the penetration resistance values are roughly correlated with relative density.

An equivalent expression for relative density is as follows:

$$\text{Relative Density, } D_r = \frac{\gamma_{max}}{\gamma} \times \frac{\gamma - \gamma_{min}}{\gamma_{max} - \gamma_{min}} \times 100\%$$

Example Problem

Given: field density, γ = 120 lbs per cu ft
maximum density, γ_{max} = 135
minimum density, γ_{min} = 90

Find: relative density, D_r

$$D_r = \frac{135}{120} \times \frac{120 - 90}{135 - 90} \times 100\% = 75\% \quad \textit{(answer)}$$

The ratio, expressed as a percent, of the in-situ field density of a soil to a density achieved in a laboratory test is known as the percent compaction.

$$\%\ \text{Compaction} = \frac{\text{Field Density}}{\text{Laboratory Density}} \times 100\%$$

Laboratory densities are usually determined by performing Proctor tests on sample materials finer than 3/4 inch and with varying moisture contents. The soil sample is compacted in layers in a 4 inch diameter mold (1/30 cu ft) with a ramming weight. There are two Proctor tests:

Standard Proctor:	ASTM D698 or AASHTO T99 (comparable to light rolling or thorough tamping)
Modified Proctor:	ASTM D1557 or AASHTO (modified) (comparable to the heaviest rollers operating under favorable working conditions)

The Standard Proctor uses 25 blows with a 5 1/2 lb weight falling 12 in., on each of 3 soil layers; and the Modified Proctor is 25 blows with a 10lb weight falling 18 in. on each of 5 layers.

When a graph of the soil densities (on a dry-weight basis) versus the water contents (or so-called moistures) are plotted, a maximum density is observed. The moisture content for this maximum density is referred to as the optimum moisture. Soils compacted dryer or wetter than this moisture content will have lesser densities. In computing the % Compaction, this maximum laboratory density is used in comparison with the field density.

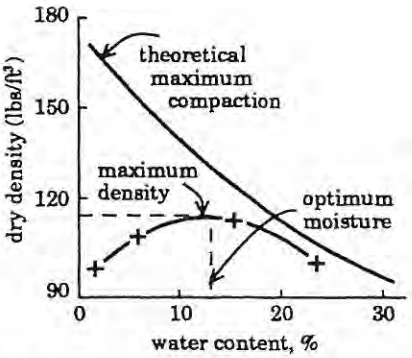

In-situ field densities of soils are determined by using one, or a combination, of the following standardized field testing procedures.

Sand Cone Method	ASTM	D1556
Balloon Method	ASTM	D2167
Nuclear Method	ASTM	D2922

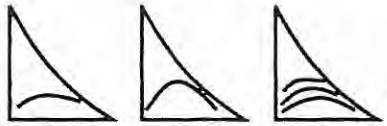

To achieve the required properties of an engineered fill, backfill, or other earth structure application, the character of the soil material must be controlled as well as the moisture/density relationship. Typical required field densities (expressed in lbs per cu ft) for various materials for footings and for floors are as follows:

Material Maximum Dry Density	**Required Field Footing Bearing**	**Dry Densities Under Floor Fill**
110	105	105
115	109	106
120	113	108
125	116	113
130	120	117
135	124	121

Compaction Curves

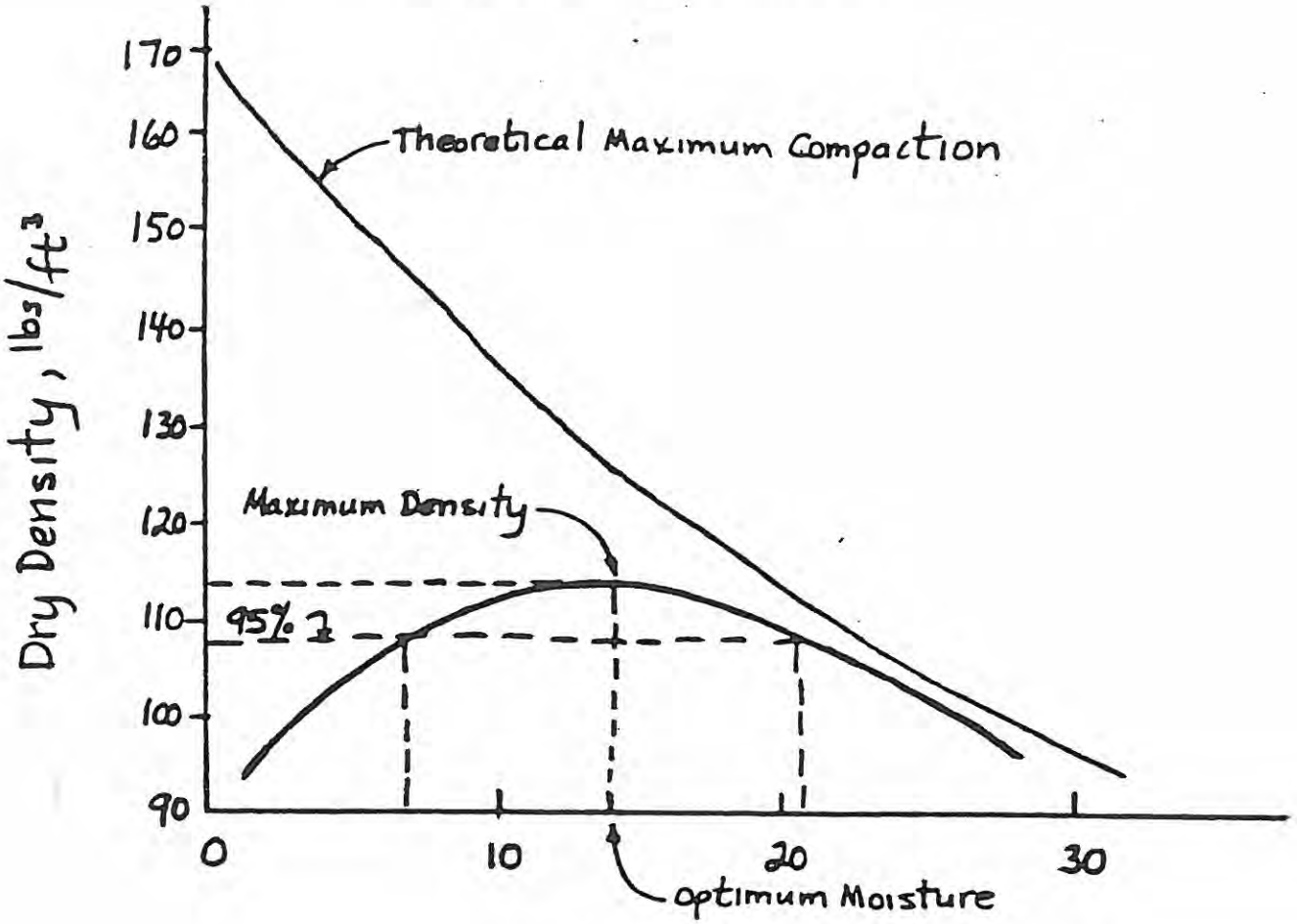

Cohesionless

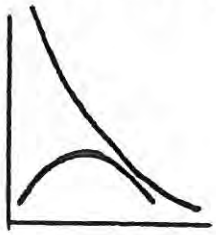

Cohesive

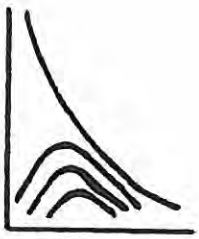

Effort

Sample Specification

Compaction Specifications
for
Granular Fill Materials and General Fill Materials

Granular fill material shall be free of all stones larger than four (4) inches in size and shall be reasonably uniformly graded through the particle size range. Of that portion of the material passing the #4 sieve, not more that 10% shall pass the #200 sieve. When placing fill during wet weather and/or in wet areas, this requirement shall be modified to not more than 5% passing the #200 sieve.

General fill material shall be free from ash, wood, or other foreign materials and free of all stones larger than four (4) inches.

At least two (2) days prior to the start of any filling operations fifty (50) pound representative samples of proposed fill materials shall be submitted to the Engineer for analysis and optimum moisture-maximum density determinations.

The approved fill material shall be placed at optimum moisture content in layers not exceeding eight (8) inches in loose thickness prior to compaction, unless otherwise authorized by the Engineer. Moisture shall be added or the material dried out as required to reach optimum moisture. No frozen material shall be placed nor shall be the fill be placed on frozen ground. No work shall be performed when the air temperature is less than 20° F.

Each layer shall be uniformly spread and compacted to a dry density which is at least the specified percentage of the laboratory determined maximum dry density by ASTM Test Designation D1557. The minimum percent compaction specified may be modified by the Engineer at the construction site under the following conditions.

For Footing Bearing Materials

a) 95% compaction for materials having a maximum dry density of 115 lbs/cu ft or less.

b) 92% compaction for materials having a maximum dry density of 130 lbs/cu ft or more.

c) Proportion between 95% and 92% compaction for materials having maximum dry densities between 115 and 130 lbs/cu ft.

For Underfloor Fill Materials

a) 95% compaction for materials having a maximum dry density of 110 lbs/cu ft or less.

b) 90% compaction for materials having a maximum dry density of 120 lbs/cu ft or more.

c) Proportion between 95% and 90% compaction for materials having maximum dry densities of 110 and 120 lbs/cu ft.

The Contractor shall provide all necessary compaction equipment to attain the specified percent compaction. Compaction by travel of grading equipment alone is not sufficient to achieve uniform compaction. Rollers and compactors are required.

Fill placed adjacent to walls, around footings, in excavated trenches, and in other restricted spaces shall be compacted to the specified percent compaction with small vibratory or hand tamping compactors.

The Engineer, in accordance with standard field methods and with the cooperation of the Contractor, will test every other layer placed at the outset of the project. Thereafter, tests shall be performed as the Engineer deems necessary. Testing costs shall be paid by the Owner.

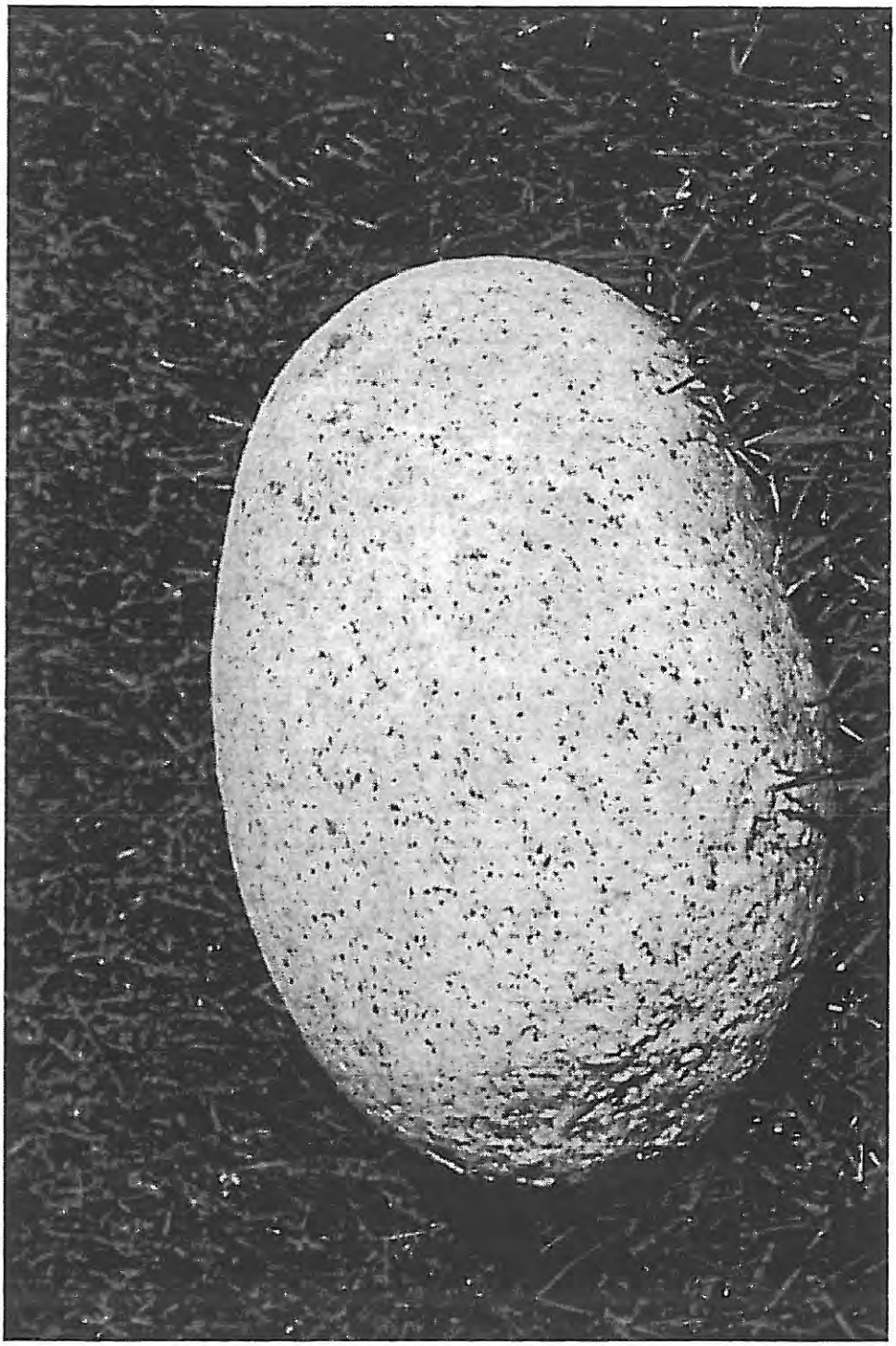

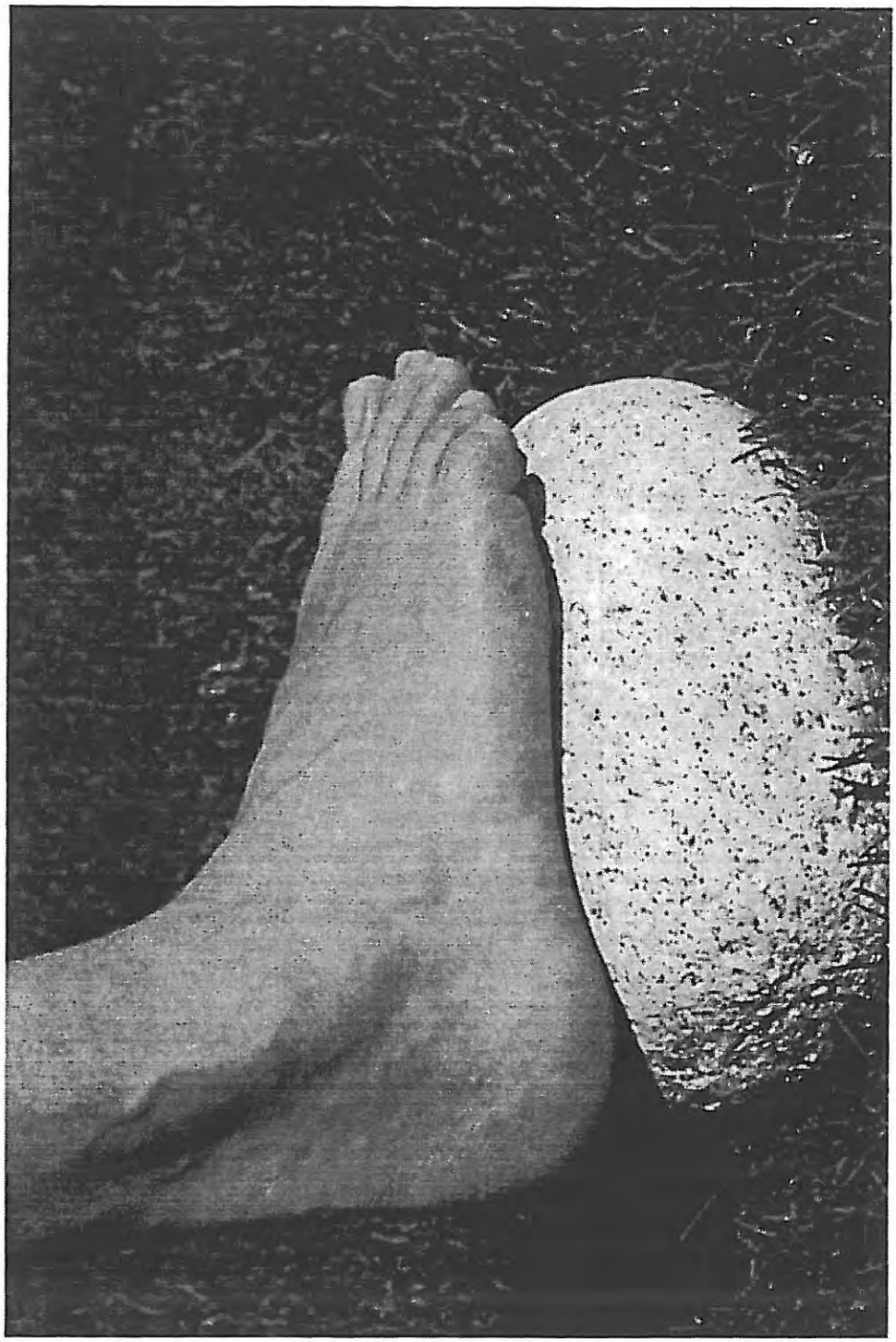

Water in Soils

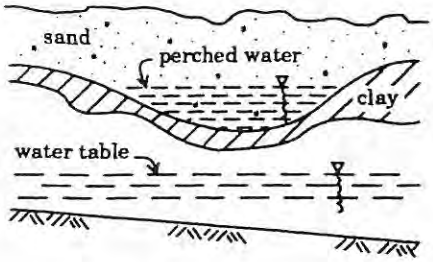

As the preceding discussion of the Atterberg limits, classification of soils and soil structure indicates, water in the soil mass is very important. Water very strongly affects the engineering behavior of most soils, especially fine-grained soils, and water is an important factor in most geotechnical engineering problems. In general, water in soils can be thought of as either static or dynamic.

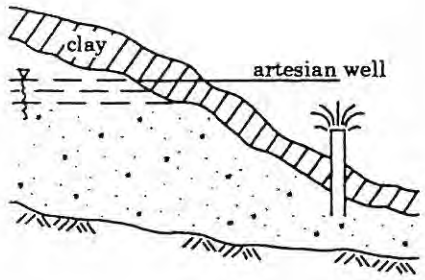

The groundwater table, even though it actually fluctuates throughout the year, is considered static for most engineering purposes. Similarly, capillary water is usually taken to be static, though it too can fluctuate, depending on climatic conditions and other factors. Other static water and phenomena in soils include absorbed water on clay minerals, shrinkage, swelling and frost action.

Water flowing through the voids and pores in a soil mass is dynamic. The ease with which water moves through a soil mass is characterized by its permeability (also referred to as "hydraulic conductivity") as given by Darcy's law. Darcy's law states that the quantity of water flowing in a unit time is equal to the permeability times the hydraulic gradient times the cross sectional area through which it flows. The hydraulic gradient is the driving head divided by the length over which the flow takes place.

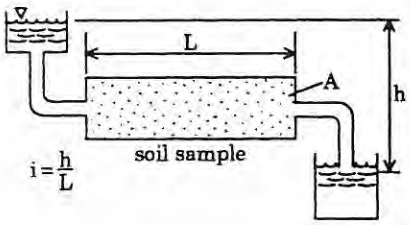

Darcy's Law $q = ki\,A$

where
- q = flow of water (cm^3/s)
- k = coefficient of permeability or hydraulic conductivity (cm/s)
- i = hydraulic gradient or head ÷ length (cm/cm)
- A = area (cm^2)

The concept of intergranular or effective stress is very important to an understanding of soil behavior:

$$\sigma = \sigma' + u$$

where
- σ = total normal stress
- σ' = intergranular or effective normal stress
- u = pore water or neutral pressure

Both the total stress and pore water pressure may readily be estimated or calculated with knowledge of the unit weights and thicknesses of the soil layers and the location of the groundwater table. The effective stress cannot be measured—it can only be calculated!

The total vertical stress (or normal stress) is called the "body stress" because it is generated by the mass (acted upon by gravity) in the body. To calculate the total vertical stress σ_v at a point in a soil mass, simply sum up the unit weight of all the material (soil solids + water) above that point:

$$\sigma_v = \gamma h$$

where σ_v = total vertical stress
γ = the soil unit weight
h = the height of soil above a point

The neutral stress or pore water pressure is similarly calculated for static water conditions. It is simply the depth below the groundwater table to the point in question times the unit weight of water, or:

$$u = \gamma_w z_w$$

where u = pore pressure or neutral stress
γ_w = the unit weight of water (62.4 lbs. per cubic ft)
z_w = the height of water above a point

The stress in the water is called the neutral stress because it has no shear component. Recall from fluid mechanics that by definition a liquid cannot support static shear stress. A liquid only has normal stresses that act equally in all directions. On the other hand, soil stresses can have both normal and shear components. The effective stress is simply the difference between the total and neutral stresses: $\sigma_v' = \sigma_v - u$.

What is the physical meaning of effective stress? In a granular material like a sand or gravel, it is sometimes called the "intergranular stress." However, it is not really the same as the grain-to-grain contact stress, since the contact area between granular particles can be very small and even approach a "point" with rounded grains. Rather, the intergranular stress is the sum of the contact forces divided by the total, or gross, area. The total vertical force, or load, can be considered to be the sum of the intergranular contact forces plus the hydrostatic force in the pore water.

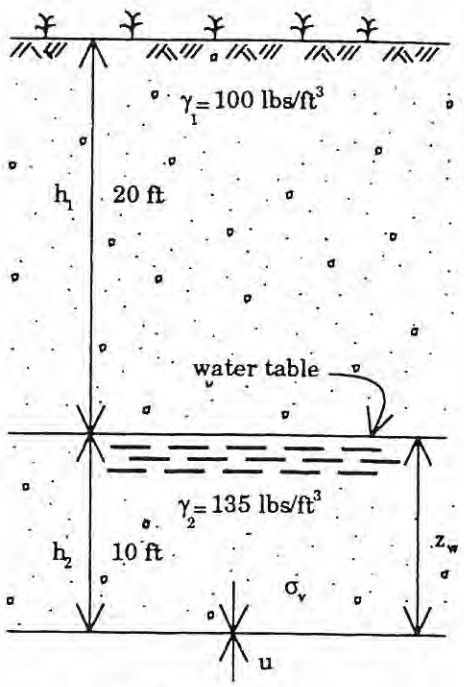

find σ'_v at 30 ft.

$\sigma_v = \gamma_1 h_1 + \gamma_2 h_2$
$= (100)(20) + (135)(10)$
$= 2000 + 1350$
$= 3350$ lbs/ft^2

$\mu = \gamma_w z_w$
$= (62.4)(10)$
$= 624$ lbs/ft^2

$\sigma'_v = \sigma_v - \mu$
$= 3350 - 624$
$= 2726$ lbs/ft^2 (ans.)
= effective vertical stress at a depth of 30 ft.

The response of soil mass to changes in applied stresses (compressibility and shearing resistance) can be explained consistently on the basis of changes in the effective stresses in that soil mass. The principle of effective stress is probably the single most important concept in geotechnical engineering.

What does the concept mean for fine-grained materials? It is doubtful that the mineral crystals are in actual physical contact, since they are surrounded by a tightly bound water film. On the micro scale, the interparticle force fields that would contribute to effective stress are extremely difficult to interpret and philosophically impossible to measure. Any inference about these force fields comes from a study of the fabric of the soil.

In view of this complexity, what place does such a simple equation as $\sigma = \sigma' + u$ have in engineering practice? Experimental evidence and careful analysis has shown that, for saturated sands and clays, the principle of effective stress is an excellent approximation to reality. It is not so good for partially saturated soils or saturated rocks, however.

Whatever it is physically, effective stress is defined as the difference between an engineering total stress and a measurable neutral stress (pore water pressure). The concept of effective stress is extremely useful for understanding soil behavior, interpreting laboratory test results and making engineering design calculations. The concept works, and that's why we use it.

When water flows through soils, it exerts forces called "seepage forces" on the individual soil grains. These seepage forces affect the intergranular or effective stress in the soil mass. Water flows through porous media because of a hydraulic gradient or driving head. As the head increases, the seepage forces increase and gradually overcome the gravitational forces acting in the soil mass. Eventually a quick condition (quick meaning alive) or boiling will occur.

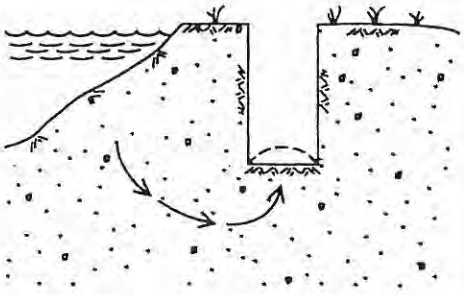

If you dewater a braced excavation pit next to a body of water (e.g., a lake), you create a driving head and seepage forces on the bottom of the excavation because the excavation is surrounded by higher water. There will come a critical head where the bottom will become quick, a condition and not a material, where the effective stresses fall to zero.

Another phenomenon related to quicksand is "liquefaction." This can happen when a loose, saturated deposit of sand is subjected to dynamic loads of very short duration (such as those that occur during an earthquake), pile driving and blasting. The loose sand tries to densify during shear, and this tends to squeeze the water out of the pores. Under static loading, the sand normally has sufficient permeability so that the water can escape, and any induced pore water pressures can dissipate.

But in this situation—because the loading occurs in such a short time—the water doesn't have time to escape, and the pore water pressure increases. Since the total stresses have not yet increased during loading, the effective stresses then tend toward zero, and the soil loses all strength.

Consolidation and Settlements

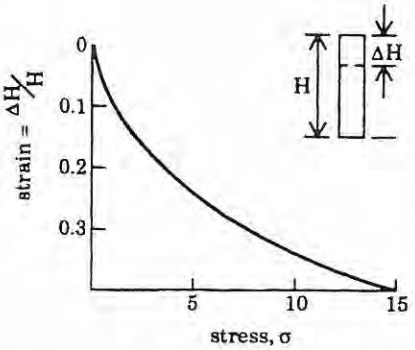

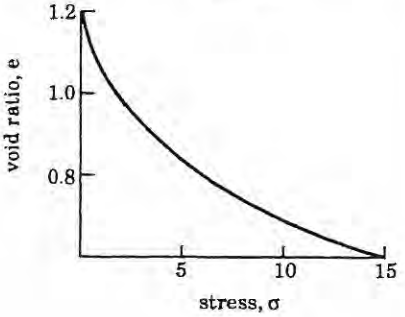

The interrelations between stress, strain and time for soils is not simple and cannot be treated mathematically with present theory. Soils have another property that complicates matters: they have "memory"; consequently, they are "nonconservative." When soils are stressed, they deform, and even when the stress is released, some permanent deformation remains. Deformations in general can be a change of shape (distortion) or a change of volume (compression) or both.

When a soil is loaded, it will compress due to deformation of the soil grains, compression of air and water in the voids, and/or a squeezing out of the water and air in the voids. The amount of compression of the soil mineral grains themselves is small and usually neglected. Soils below the water table are considered to be fully saturated. The water itself doesn't compress. The squeezing out of the water, therefore, contributes most to the volume change of loaded soil deposits.

Squeezing out the water doesn't mean the soil is wrung dry. As the pore fluid is squeezed out, the soil grains rearrange themselves into a more stable and denser configuration, and a decrease in volume and accompanying surface settlement results (i.e., the void ratio gets smaller). How fast this process occurs depends on the permeability of the soil. How much rearrangement and compression takes place depends on the rigidity of the soil skeleton, which is a function of the structure of the soil. Soil structure depends on the geologic and engineering history of the deposit. The character of natural deposits is important.

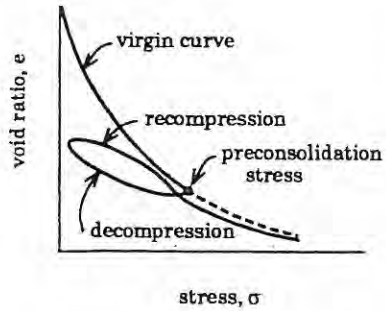

A soil's memory preserves the past stresses and other changes in its structure. When a soil deposit is loaded to a stress level greater than it has ever experienced in the past, the soil structure is no longer able to sustain the increased load, and the structure starts to deform at an increasing rate and to break down. The stress that the soil has sustained in the past is known as the "preconsolidation pressure." The soil is said to be "normally consolidated" when the preconsolidation pressure just equals the existing effective vertical overburden pressure (σ'_v). If a soil's preconsolidation pressure is greater than the existing overburden pressure, then it is said to be "overconsolidated" (or "preconsolidated").

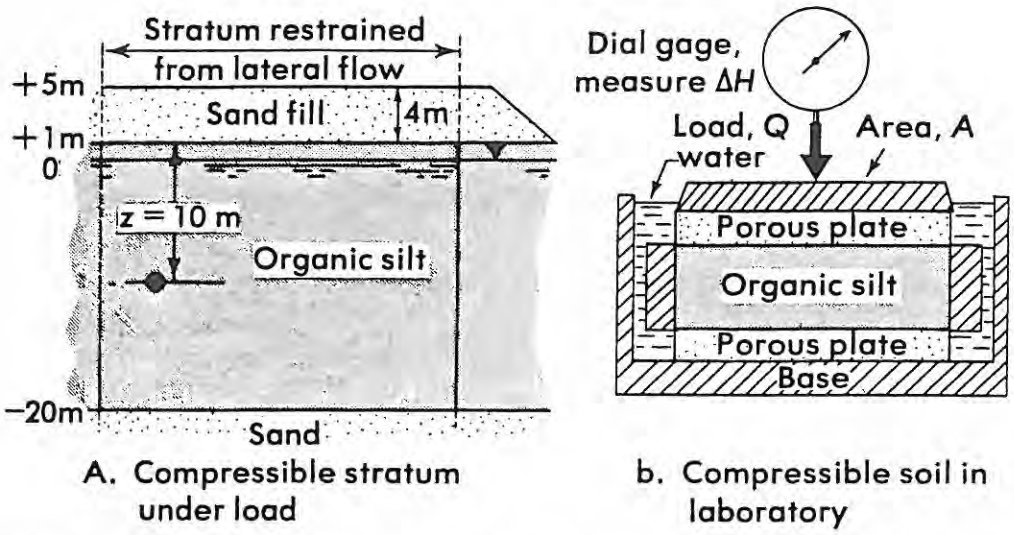

Figure 4.1 *Compressible stratum under load as modeled in a one-dimensional consolidation test.*

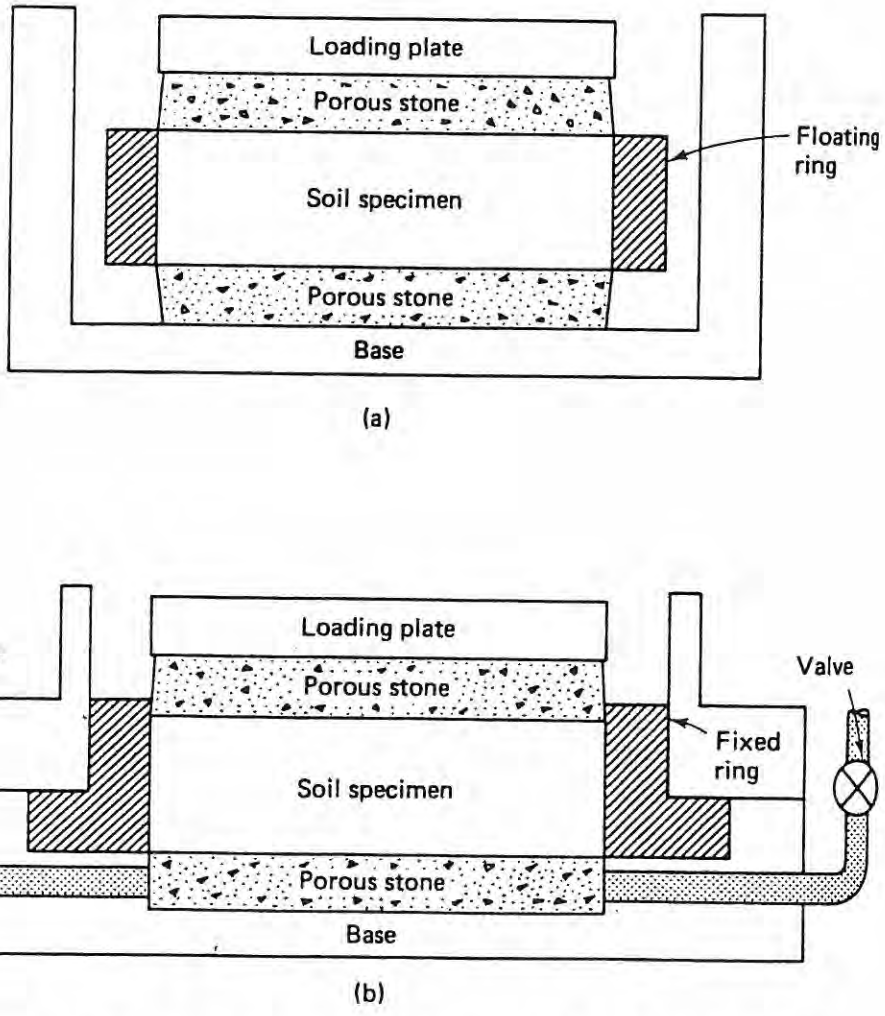

Fig. 8.3 Schematic of an oedometer or consolidation test apparatus: (a) floating-ring oedometer; (b) fixed-ring oedometer (after U.S. Army Corps of Engineers, 1970).

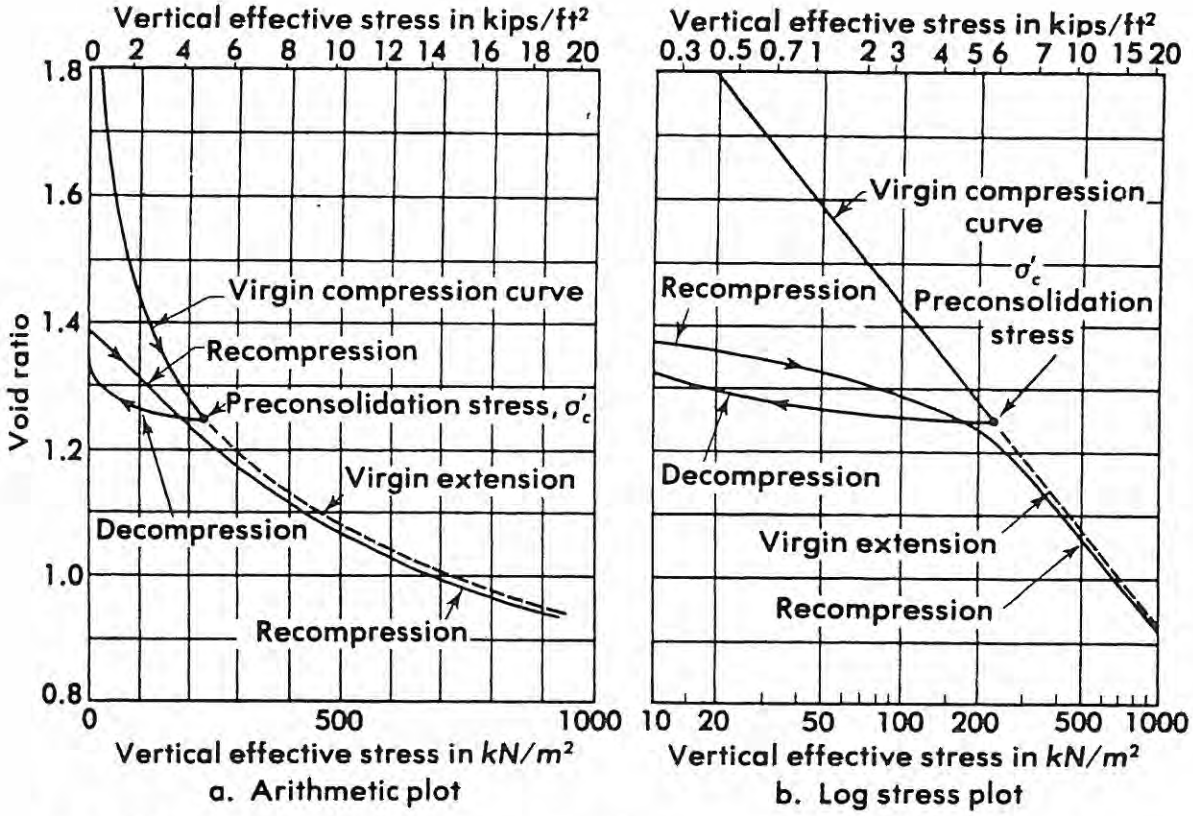

Figure 4.4 *Stress–void ratio: Compression, decompression, and preconsolidation stress.*

The "overconsolidation ratio" (OCR) can be defined as the ratio of the preconsolidated stress to the existing vertical effective stress. Soils that are normally consolidated have an OCR equal to 1; soils with an OCR greater than 1 are overconsolidated.

A soil may be overconsolidated for many reasons. The effective stress could be altered by either a change in the total stress or a change in pore water pressure. Dessication of the upper layers of a deposit, due to surface drying, will produce overconsolidation. Geologic deposition and subsequent erosion, for example, is a change in the total stress that will preconsolidate the underlying soils. This can happen from glaciation and from the removal of overburden naturally or by man.

The settlement and rate of settlement of natural deposits can be computed from laboratory test data, but the purposes at hand do not require an examination of consolidation and settlement theories or a knowledge of exactly how these computations are made.

Failure Criterion and Shear Strength

The theories used to estimate consolidation of deposits are one-dimensional models. This section describes the reaction of sands and clays to types of loading that are not one dimensional. If the load or stress in a foundation or earth slope is increased until the deformations become unacceptably large, the soil in the foundation or slope is said to have "failed"—referring to the "strength" of the soil, which is really the maximum or ultimate stress the material can sustain. In geotechnical engineering, the "shear strength" of soils is the major concern because, for most problems in foundations and earthwork engineering, failure results from excessive applied shear stresses.

The strength of a material is defined as the maximum or yield stress, or the stress at some strain that is defined as "failure." There are many ways of defining failure in real materials—which is to say that there are many "failure criteria." If the material is brittle, its point of failure is obvious. If it is a work-softening material, the peak of the stress/strain curve is sometimes used or a set amount of strain is used.

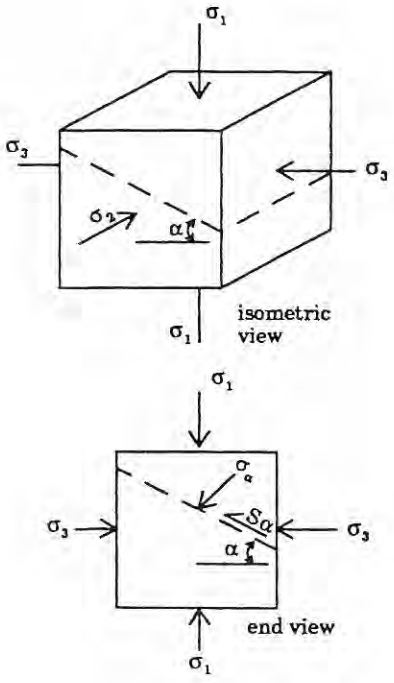

Most failure criteria don't work for soils. In fact, the one used doesn't always work so well either. Nonetheless, the most common failure criterion applied to soils is the "Mohr-Coulomb failure criterion."

About the turn of the century, Mohr (1900) hypothesized a criterion of failure for real materials in which he said that materials fail when the "shear stress on the failure plane at failure reaches some unique function of the normal stress on that plane." The functional relationship between shear stress and normal stress at failure is expressed by a limiting or failure envelope of the shear stress. This envelope is called the "Mohr failure envelope."

Enter Monsieur Dr. Coulomb. Besides his famous experiments with cats' fur and ebony rods, Coulomb (1776) was also concerned with military defense works like reventments and fortress walls. At that time, these constructions were built by rule of thumb, and, unfortunately for the French military, many of these works failed. Coulomb became interested in the problem of the lateral pressures exerted against retaining walls, and he devised a system for analyzing earth pressures against retaining structures that is still used today.

One of the things he needed for design was the shearing strength of soil. Since he was also interested in the sliding friction characteristics of different materials, he set up a device for determining the shear resistance of soils. He observed that there was a stress-independent component of shear strength and a stress-dependent component. The stress-dependent component is similar to sliding friction in solids, so he called this component the "angle of internal friction," denoting it with the symbol ø. The other component seemed to be related to the intrinsic "cohesion" of the material and is commonly denoted with the symbol c.

Who first did so is unknown, but the Coulomb formulation was soon combined with the Mohr failure criterion. Engineers traditionally prefer to work with straight lines, since anything higher than a first-order equation (straight line) gets too complicated. So the natural thing to do was to straighten out the curve in the Mohr failure envelope—or at least approximate the curve by a straight line over some given stress range—then the equation for that line in terms of Coulomb's parameters ø and c (the so-called "strength parameters") could be written (these parameters can also be "primed as c′ and ø′ for effective stress conditions). Thus was born the "Mohr-Coulomb strength criterion," which is by far the most popular strength criterion applied to soils. The Mohr-Coulomb criterion can be written as:

$$s = \sigma \tan\phi + c$$

where
- s = the shear stress on the failure plane
- σ = the normal stress on the failure plane
- ϕ = the angle of internal friction
- c = cohesion

This is a simple, easy-to-use criterion that has many distinct advantages over other failure criteria. It is the only failure criterion that predicts the stresses on the failure plane at failure.

There are several kinds of tests for determining the Mohr-Coulomb strength parameters. The inexpensive, fast and simple direct shear stress is probably the oldest, because Coulomb used a type of shear box more than 200 years ago to determine the necessary parameters for his strength equation. The specimen container or "shear box" is separated horizontally into halves. One half is fixed; with respect to that half, the other half is either pushed or pulled horizontally. A normal load is applied to the soil specimen in the shear box through a rigid loading cap. Dividing the shear force and the normal force by the nominal area of the specimen produces the shear stress as well as the normal stress on the failure plane (which has been forced to be horizontal with the apparatus).

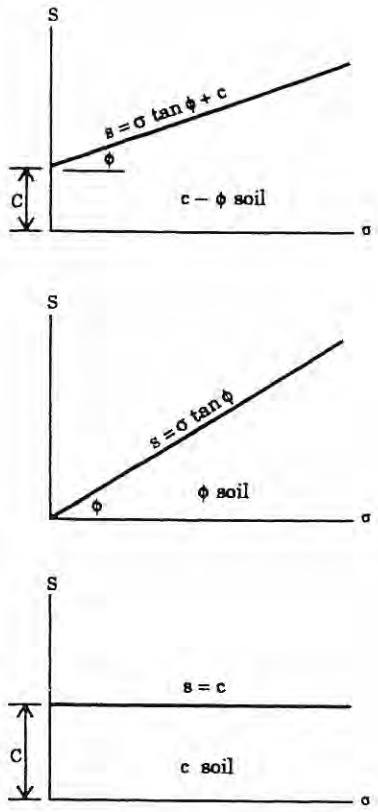

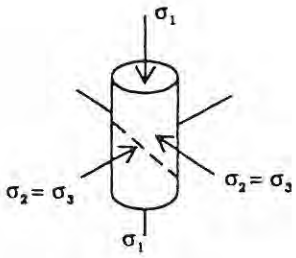

The triaxial test, though more complicated than the direct shear test, is much more versatile. A cylindrical soil specimen, usually encased in a rubber membrane, is placed in a cell chamber that permits pressurizing the sample to replicate in situ conditions. At given pressures, axial loads are applied until failure. Drainage from the sample can also be controlled, and often the volume change of the sample during a drained test, or the induced pore water pressure during an undrained test, is measured. The failure plane is not forced—the specimen is free to fail on any weak plane or, as sometimes occurs, to simply bulge.

Drainage conditions in the triaxial test are models of specific critical design situations for stability in engineering practice. These are commonly designated by a two-letter symbol. The first letter refers to what happens "before shear"—that is, whether the specimen is consolidated. The second letter refers to the drainage conditions "during shear." The three permissible drainage paths in the triaxial test are the consolidated-drained (CD), consolidated-undrained (CU), and the unconsolidated-undrained (UU). The unconsolidated-drained test defies interpretation and is therefore meaningless (it models no real engineering design situation: drainage would occur during shear, and the effects of the confining pressure cannot be separated from the shear stress.)

Before concluding this section on failure criteria and shear strength, a couple more items need to be mentioned. The shear strength of soils is a most important aspect of geotechnical engineering. The bearing capacity of shallow or deep foundations, slope stability, retaining wall design and, indirectly, pavement design are all affected by the shear strength of the soil in a slope, behind a retaining wall or supporting a foundation or pavement. Structures and slopes must be stable and secure against total collapse when subjected to maximum anticipated applied loads.

Thus "limiting equilibrium" methods of analysis conventionally are used for design of structures and slopes, and these methods require a determination of the ultimate or limiting shear resistance (shear strength) of the soil. The deformations needed to mobilize strength must be considered, since structural failures may occur at significantly smaller strains than the 20 percent value often associated with loose sand or normally consolidated clay lab tests.

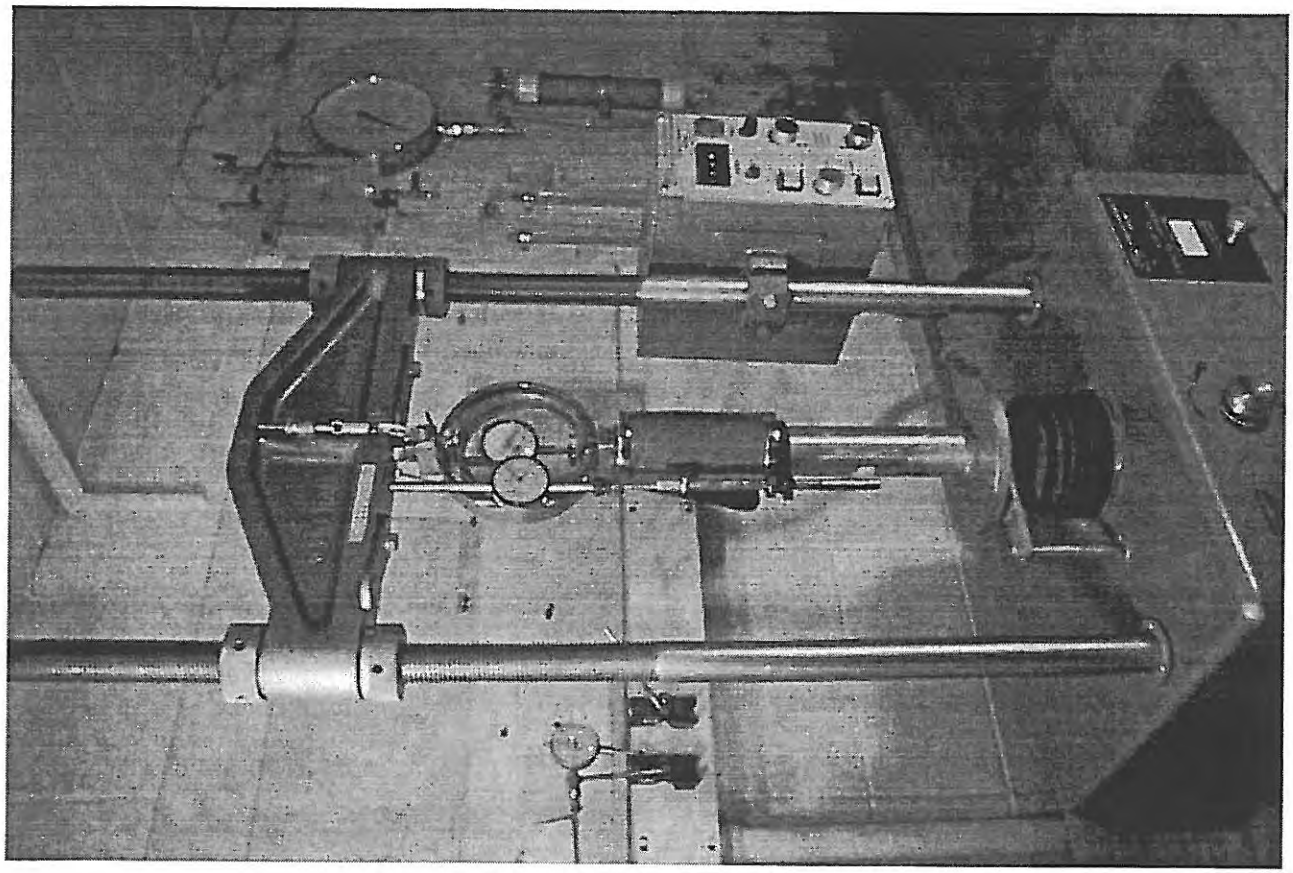

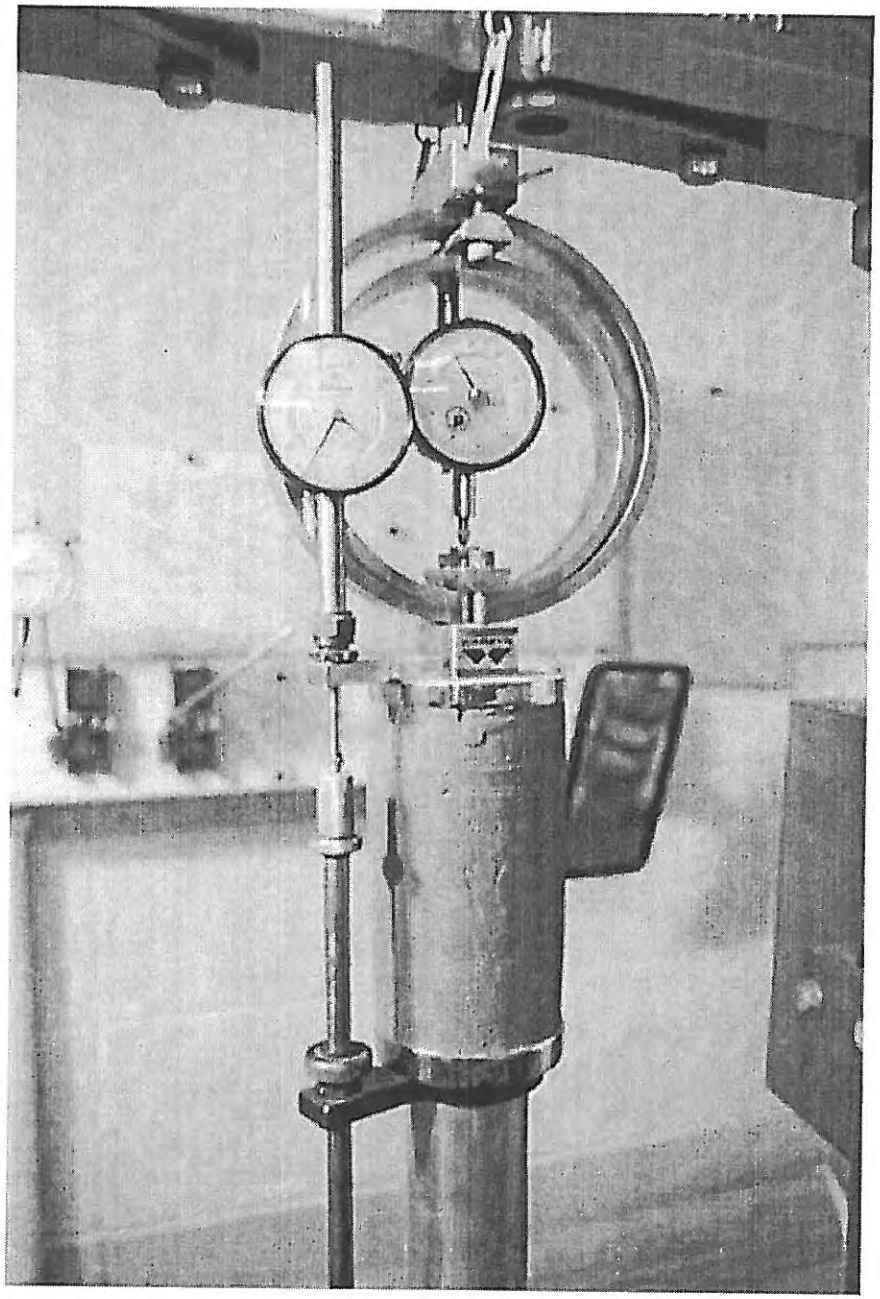

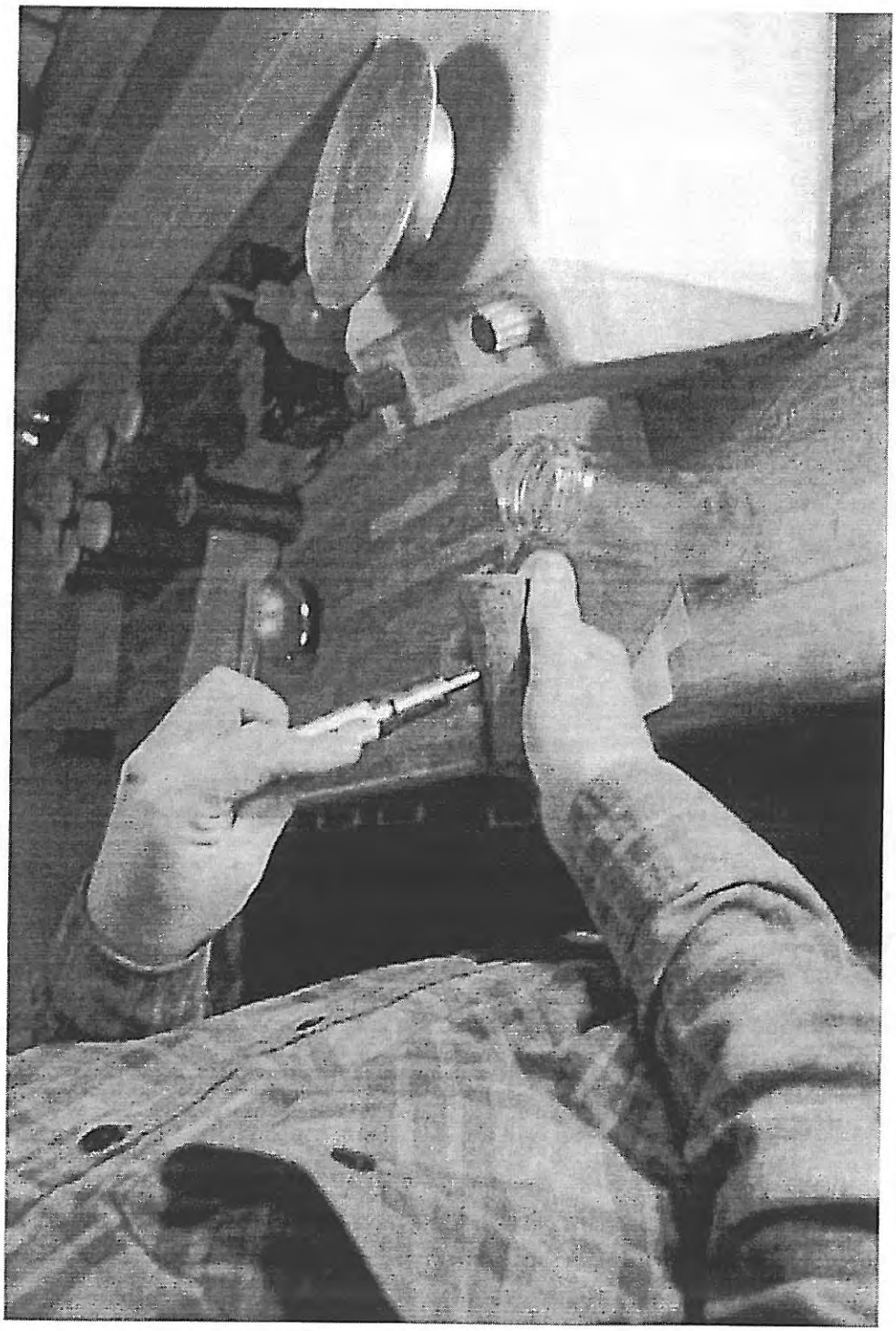

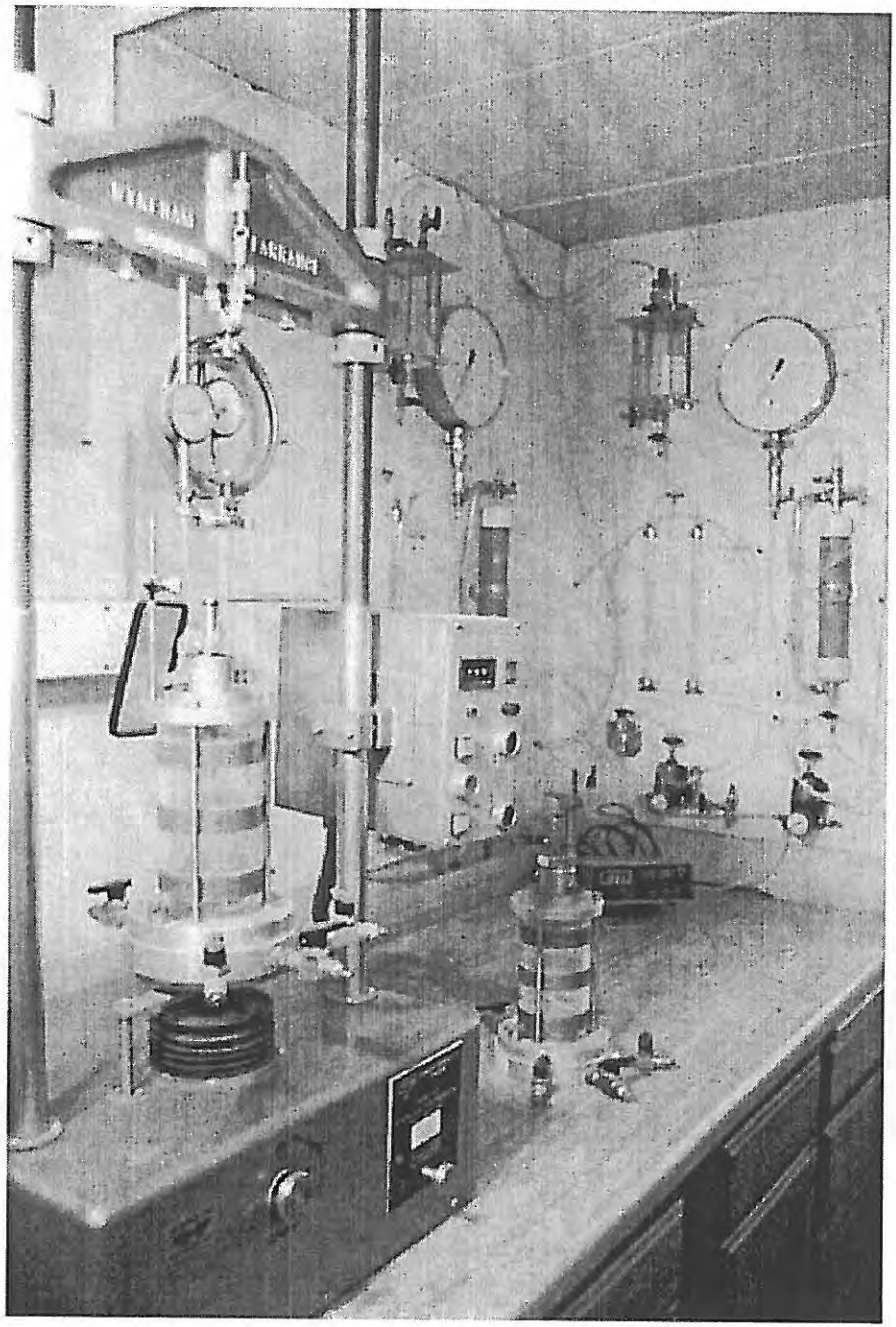

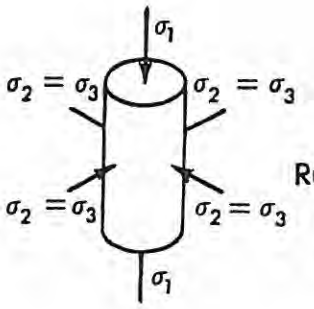

a. Stresses in triaxial shear

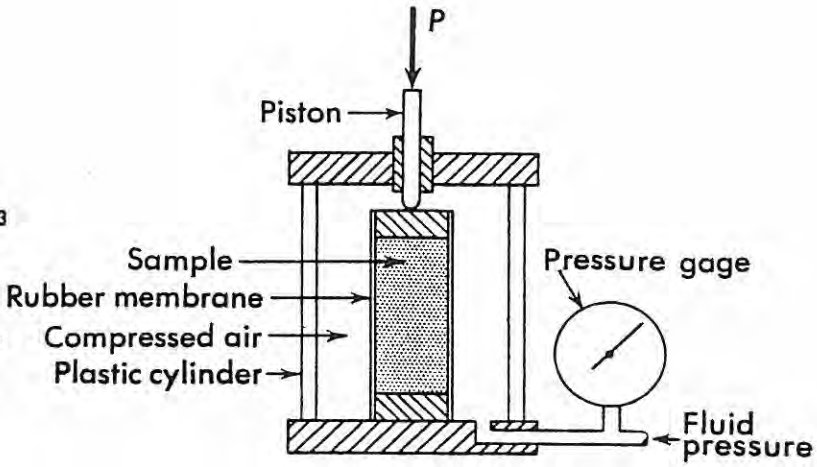

b. Triaxial shear equipment

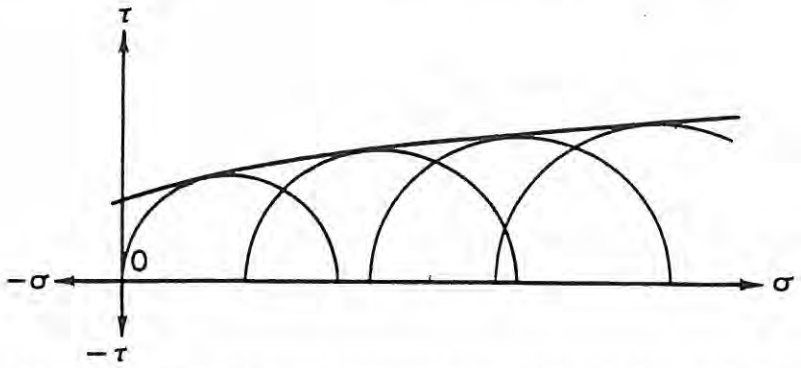

c. Mohr envelope drawn tangent to Mohr's circles of failure (upper half)

Figure 5.12 *Triaxial shear test.*

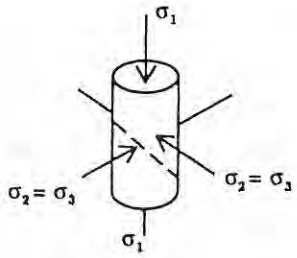

The triaxial test, though more complicated than the direct shear test, is much more versatile. A cylindrical soil specimen, usually encased in a rubber membrane, is placed in a cell chamber that permits pressurizing the sample to replicate in situ conditions. At given pressures, axial loads are applied until failure. Drainage from the sample can also be controlled, and often the volume change of the sample during a drained test, or the induced pore water pressure during an undrained test, is measured. The failure plane is not forced—the specimen is free to fail on any weak plane or, as sometimes occurs, to simply bulge.

Drainage conditions in the triaxial test are models of specific critical design situations for stability in engineering practice. These are commonly designated by a two-letter symbol. The first letter refers to what happens "before shear"—that is, whether the specimen is consolidated. The second letter refers to the drainage conditions "during shear." The three permissible drainage paths in the triaxial test are the consolidated-drained (CD), consolidated-undrained (CU), and the unconsolidated-undrained (UU). The unconsolidated-drained test defies interpretation and is therefore meaningless (it models no real engineering design situation: drainage would occur during shear, and the effects of the confining pressure cannot be separated from the shear stress.)

Before concluding this section on failure criteria and shear strength, a couple more items need to be mentioned. The shear strength of soils is a most important aspect of geotechnical engineering. The bearing capacity of shallow or deep foundations, slope stability, retaining wall design and, indirectly, pavement design are all affected by the shear strength of the soil in a slope, behind a retaining wall or supporting a foundation or pavement. Structures and slopes must be stable and secure against total collapse when subjected to maximum anticipated applied loads.

Thus "limiting equilibrium" methods of analysis conventionally are used for design of structures and slopes, and these methods require a determination of the ultimate or limiting shear resistance (shear strength) of the soil. The deformations needed to mobilize strength must be considered, since structural failures may occur at significantly smaller strains than the 20 percent value often associated with loose sand or normally consolidated clay lab tests.

The converse of strength mobilization involves consideration of allowable strains. The shear strength of a soil was defined earlier as the ultimate or maximum shear stress the soil can withstand. Sometimes the limiting value of shear stress was based on a maximum allowable strain or deformation. Very often, this allowable deformation actually controls the design of a structure because, with the large safety factors used, the actual shear stresses in the soil produced by the applied loads are much less than the stresses causing collapse or failure.

Strength and deformation both must be considered in geotechnical engineering practice.

The two fundamentally different approaches to the solution of stability problems in geotechnical engineering are: (1) the "total stress approach" and (2) the "effective stress approach." In the total stress approach, no drainage is allowed to take place during the shear test, and it is assumed—admittedly it is a big assumption—that the pore water pressure and thus the effective stresses in the test specimen are identical to those in the field. This method of analysis uses the total, "undrained shear" strength of the soil.

The second approach to calculate the stability of foundations, embankments, slopes, etc., uses the shear strength in terms of effective stresses. This approach requires measurements or estimates of the excess hydrostatic pressure, both in the laboratory and in the field. Then, with some knowledge of the initial and applied total stresses, the effective stresses acting in the soil may be calculated. Since shear strength and stress-deformation behavior of soils are believed to really be controlled by effective stress, this second approach is philosophically more satisfying. This method of analysis uses the "drained shear strength" or shear strength in terms of effective stresses. The drained shear strength is ordinarily only determined by laboratory tests.

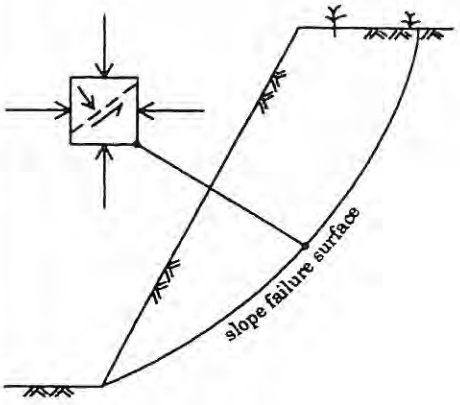

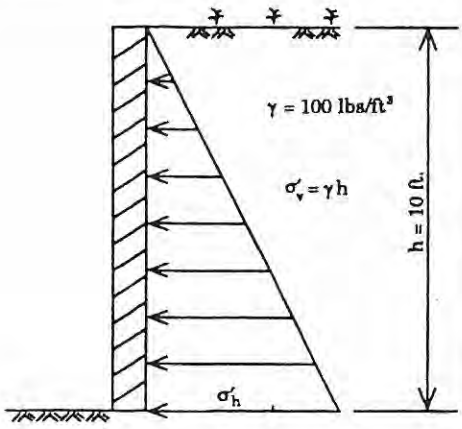

$\sigma'_h = K_o\sigma'_v$

$\sigma'_v = (10)(100)$

$= 1000 \text{ lbs/ft}^2$

active case $K_o = 1/3$

$\sigma'_h = (1/3)(1000)$

$= 333 \text{ lbs/ft}^2$

at rest case $K_o = 1/2$

$\sigma'_h = (1/2)(1000)$

$= 500 \text{ lbs/ft}^2$

passive case $K_o = 3$

$\sigma'_h = (3)(1000)$

$= 3000 \text{ lbs/ft}^2$

Earth Pressures

You will recall from hydrostatics that the pressure in a liquid is the same in any direction—up, down, sideways or any inclination—it doesn't matter. But this is not true in soils. Stresses in situ are not hydrostatic. The ratio of horizontal to vertical stresses can be expressed through the effective stress concept and a coefficient as follows:

$$\sigma'_h = K_o\sigma'_v$$

where
- σ'_h = effective horizontal stress
- σ'_v = effective vertical stress
- K_o = coefficient of the lateral earth pressure at rest

This coefficient is very sensitive to the geologic and engineering stress history, as well as the unit weights of the overlying soil layers. The value of K_o is important in stress analyses, in assessing the shearing resistance of particular soil layers, and in many foundation engineering problems. The K_o in a natural deposit can be as low as 0.4 or 0.5 for sedimentary soils (even less for peat) that have never been preloaded, or as high as 3.0 or more for some very heavily preloaded deposits.

Earth pressures are a function of the material that the retaining structure must support, the loads that the soil behind the structure must carry, the groundwater conditions, and the amount of deflection the retaining structure undergoes.

Earth pressure at-rest—occurs when soil has zero lateral strain, e.g. where a soil element can deform vertically under load, but cannot expand laterally because it is confined by the same soil under the same loading conditions. It is equivalent to the soil being placed against an immovable frictionless wall that maintains the same lateral dimension in the soil regardless of the vertical load.

Active earth pressure—occurs if an unyielding frictionless vertical wall of the at-rest condition is allowed to move away from the soil. Each element of the soil adjacent to the wall can expand laterally. The vertical stress remains constant, but the lateral stress or earth pressure is reduced. The lateral pressure reaches a minimum and the soil mass behind the wall is in a state of shear failure or plastic equilibrium.

Passive earth pressure—occurs if, instead of moving away from the soil, the wall moves toward the soil and the pressure against the wall increases. The maximum pressure against the wall is reached as shear failure again occurs in the soil behind the wall.

Postscripts and Acknowledgements

Karl Terzaghi, generally regarded as the father of soil mechanics, opened the first international conference on soil mechanics and foundation engineering at Harvard University in 1936 by saying, "Since these men (the outstanding executives and experienced construction engineers attending the conference) owe their success and their professional standing to a keen discrimination between reality and fiction, I am sure they will appreciate our feelings against half-baked textbook wisdom and assist us in getting down to tangible facts."

In preparing these introductory notes, I have presented some textbook wisdom that I hope was not too "half-baked." My notes are taken largely (i.e. freely quoted) from the following references:

Holtz, R.D., and W.D. Kovacs. 1981. *An Introduction to Geotechnical Engineering*. Englewood Cliffs, N.J.: Prentice-Hall.

Hough, B.K. 1969. *Basic Soils Engineering*. New York: The Ronald Press Company.

Lambe, T.W., and R.V. Whitman. 1969. *Soil Mechanics*. New York: John Wiley & Sons, Inc.

Sowers, G.F. 1979. *Introductory Soil Mechanics and Foundations: Geotechnical Engineering*, 4th ed. New York: Macmillan Publishing Co.

American Society of Civil Engineers, 1976. *Subsurface Investigation for Design and Construction of Foundations of Buildings*. New York.

Prof. C. Allen Wortley

10:2 Stability—Bearing Capacity

The *bearing capacity* of a soil, often termed its *stability*, is the ability of the soil to carry a load without failure within the soil. It is analogous to the ability of a beam to carry a load without breaking. The load-carrying capacity of soil varies not only with its strength but also with the magnitude and distribution of the load. When a load Q is applied to a soil in gradually increasing amounts, the soil deforms, making a load–settlement curve similar to a stress–strain curve. When the critical or failure load, Q_0, is reached, the rate of deformation increases. The load–settlement curve goes through a point of maximum curvature, indicating failure within the soil mass. Different curves (Fig. 10:1) are obtained, depending on the character of the soil that is loaded. Dense sand and insensitive clay usually show a sharp, sudden failure, whereas loose sand and sensitive clay show a more gradual transition associated with progressive failure.

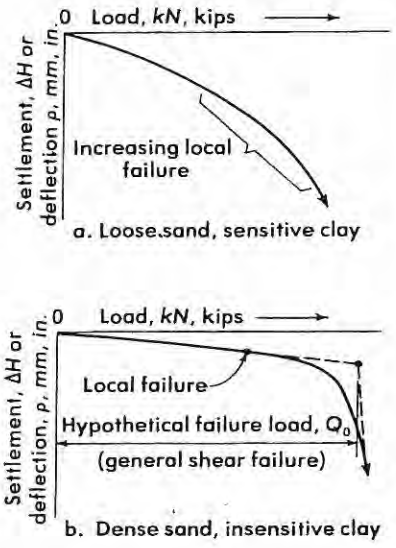

Figure 10.1 *Load settlement curves for foundations.*

If the soil is observed during loading by means of a glass-sided model or by an excavation adjacent to a full-size foundation, it will be seen that there are usually three stages in the development of failure. First, the soil beneath the foundation is forced downward in a cone or wedge (Fig. 10.2a). The soil below the wedge is forced downward and outward. Imaginary lines in the soil that were initially vertical now bulge outward like a barrel. Second, the soil around the foundation perimeter pulls away from the foundation, and surfaces of shear propagate outward from the tip of the cone or wedge (Fig. 10.2b). If the soil is very compressible or can endure large strains without plastic flow, the failure is confined to fan-shaped zones of local shear. The foundation will displace downward with little load increase: one form of *bearing-capacity* failure. If the soil is more rigid, the shear zone propagates outward until a continuous surface of failure extends to the ground surface and the surface heaves (Fig. 10.2c). This is termed *general shear* failure. The failure can be symmetrical, if rotation is restricted by a column attached to the foundation, or it can tilt as in Fig. 10.2d. Such a *bearing-capacity failure* is not common, but it almost always results in a complete failure of the structure.

No exact mathematical analysis has been derived for evaluating such a failure. A number of approximate methods that have been developed are based on simplified representations of the complex failure surface and of the soil properties.

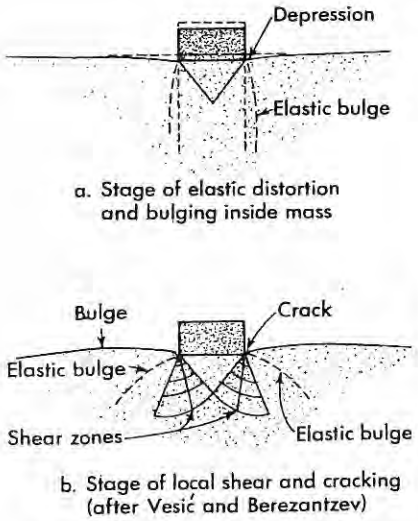

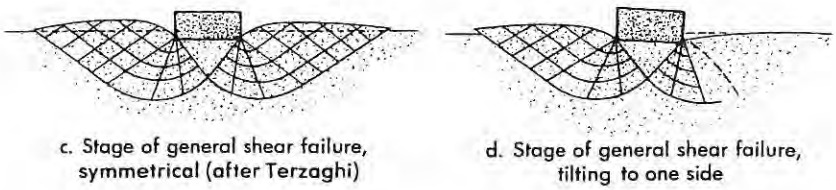

Figure 10.2 *Development of shear failure beneath a foundation.*

BEARING-CAPACITY ANALYSIS / A simple and conservative analysis was developed by Bell, extended by Terzaghi, and further modified by the author. The method approximates the curved failure surfaces with a set of straight lines, as shown in Fig. 10.3.

A foundation having a width of B and an infinite length is assumed, similar to a long wall footing. At the moment of failure the foundation exerts a pressure of q_0, which is the *ultimate bearing capacity*, or simply *bearing capacity*, of the soil. The soil immediately beneath the foundation is assumed to be in compression similar to a specimen in a triaxial shear test. The major principal stress on this zone, II, is equal to the foundation load q_0 if the weight of the soil beneath the footing is neglected. The minor principal stress on zone II is produced by the resistance of zone I to being compressed. Zone I is like a triaxial shear specimen lying on its side with the major principal

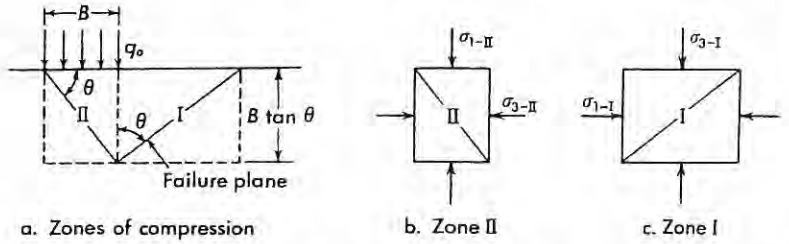

Figure 10.3 *Assumed straight-line failure plane and prismatic zones of triaxial compression and shear beneath a uniform load q_0 of width B.*

stress horizontal. At the moment of foundation failure both zones shear simultaneously, and the minor principal stress on zone II, σ_{3-II}, equals the major principal stress on zone I, σ_{1-I}.

The minor principal stress on zone I is provided by the average vertical stress caused by the soil's own dead weight and any surcharge q_q. The *surcharge* (Fig. 10.4) is any permanent confining pressure above the foun-

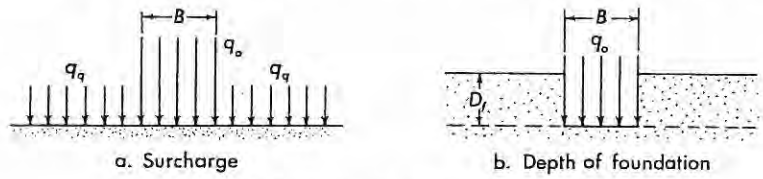

Figure 10.4 *Surcharge and depth of foundation.*

dation level such as the weight of a basement floor or the weight of soil above the foundation level:

$$q_q = \gamma D_f \tag{10:1}$$

The height of the failure zone is B tan θ, where θ is the angle of the failure zone, $\theta = 45 + (\phi/2)$. The average minor principal stress due to soil weight is therefore $(\gamma B/2)$ tan θ. The total minor principal stress is

$$\sigma_{3-I} = q_q + \frac{\gamma B}{2} \tan \theta \tag{10:2a}$$

If the minor principal stress is known, the major principal stress on zone I can be found graphically by a Mohr circle (Fig. 10.5). This is essentially passive earth pressure and it resists the bulging of zone II. Since this is equal to the minor principal stress on zone II, a second Mohr circle will give the major principal stress on zone II, the ultimate bearing capacity:

$$\sigma_{1-II} = q_0 \tag{10:2b}$$

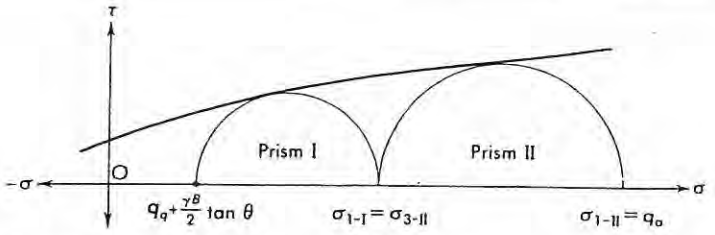

Figure 10.5 *Mohr circle analysis of bearing capacity based on straight-line failure planes and prismatic zones of triaxial compression and shear.*

The graphical analysis can be used in any soil, regardless of the shape of the Mohr envelope. If the Mohr envelope can be approximated by a straight line of the form

$$\tau_{ff} = c + \sigma_{ff} \tan \phi \tag{5:17b}$$

the ultimate bearing capacity can also be derived analytically from the trigonometry of the Mohr circle (Fig. 10.6):

$$\frac{\sigma_1 - \sigma_3}{2} = \left(\frac{c}{\tan \phi} + \frac{\sigma_1 + \sigma_3}{2}\right) \sin \phi$$

$$\sigma_1 = \sigma_3 \left(\frac{1+\sin \phi}{1-\sin \phi}\right) + 2c \left(\frac{\cos \phi}{1-\sin \phi}\right)$$

$$\sigma_1 = \sigma_3 \tan^2 \theta + 2c + \tan \theta \tag{10:2c}$$

$$\sigma_{1\text{-}I} = \left(q_q + \frac{\gamma B}{2} \tan\right) \tan^2 \theta + 2c \tan \theta$$

$$q_0 = \sigma_{1\text{-}II} = \left[\left(q_q + \frac{\gamma B}{2} \tan \theta\right) \tan^2 \theta + 2c \tan \theta\right] \tan^2 \theta + 2c \tan \theta$$

$$q_0 = \sigma_{1\text{-}II} = \frac{\gamma B}{2} \tan^5 \theta + 2c \left(\tan \theta + \tan^3 \theta\right) + q_q \tan^4 \theta \tag{10:2d}$$

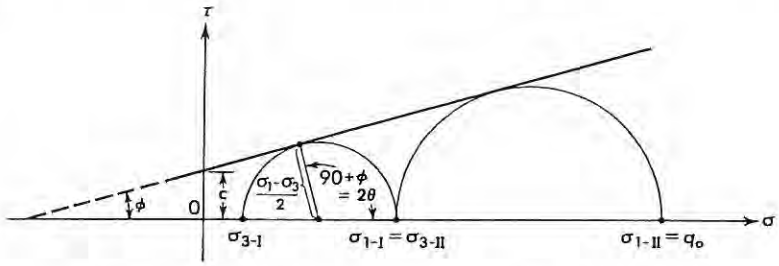

Figure 10.6 *Mohr's circle analysis based on straight-line Mohr envelope.*

This is a general expression for the ultimate bearing capacity for any soil with a straight-line Mohr envelope. It can be used for a cohesionless soil by setting $c = 0$ and for a saturated clay in undrained shear by setting $\phi = 0$, and $\tan \theta = 1$.

GENERAL BEARING-CAPACITY EQUATION—TERZAGHI-MEYERHOF / The equation for bearing capacity can be rewritten in a simple form:

$$q_0 = \frac{\gamma B}{2} N_\gamma + cN_c + q_q N_q \qquad (10:3)$$

The symbols N_γ, N_c, and N_q are *bearing-capacity factors* that are functions of the angle of internal friction. The term containing factor N_γ shows the influence of soil weight and foundation width, that of N_c shows the influence of the cohesion, and that of N_q shows the influence of the surcharge. The values of these factors for different values of ϕ are given in Fig. 10.7.

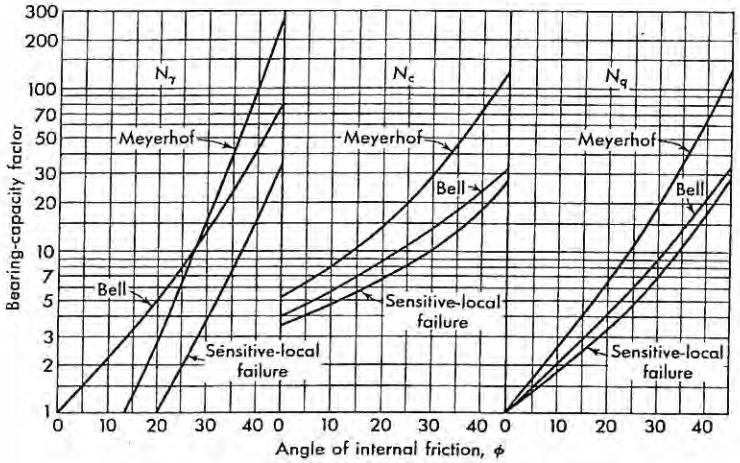

Figure 10.7 *Bearing-capacity factors for general bearing-capacity equation.*

This general expression was also derived by Terzaghi[10:4] from a more rigorous analysis of bearing capacity. It is based on approximating the surface of shear by a combination of straight lines and logarithmic spirals. The analysis was later improved by Meyerhof, but the results are expressed in the same form. Meyerhof's values for the bearing-capacity factors are given in Fig. 10.7.[10:5,10:6]

Both the Terzaghi and the Meyerhof analyses assume the development of the full shear surface and the complete shear failure. However, loose sands and highly sensitive clays fail by *local* or progressive shear when local cracking develops around the foundation or when the cone or wedge of soil under the foundation forms. Terzaghi suggested an empirical reduction to the bearing-capacity factors for this condition. The reduced Meyerhof factors, which apply to sands having a relative density of less than 30 or to clays with a sensitivity of more than 10, are also shown in Fig. 10.7. The factors of the simplified Bell analysis fall between the limiting values of the more accurate ones. Vesic[10:7,10:8] has proposed rational analyses of these conditions, but they have not been verified by full-scale tests.

RECTANGULAR AND CIRCULAR FOUNDATIONS / Both the Bell–Terzaghi and the Terzaghi–Meyerhof analyses assume an infinitely long foundation. When the foundation has a limited length, shear develops on surfaces at right angles to those previously described, and the bearing-capacity factors N_c and N_γ are changed. Correction factors to be multiplied by the bearing-capacity factors are given in Table 10:1, where L is the foundation length and B the width.

TABLE 10:1 / CORRECTION FACTORS FOR RECTANGULAR AND CIRCULAR FOUNDATIONS

Shape of Foundation	Correction for N_c	Correction for N_γ
Square	1.25	0.85
Rectangular $L/b = 2$	1.12	0.90
$L/b = 5$	1.05	0.95
Circular (use diameter D for B)	1.2	0.70

EFFECT OF SOIL PROPERTIES AND FOUNDATION DIMENSIONS / As can be seen by the general equation, the bearing capacity depends on the angle of internal friction ϕ, the soil unit weight γ, the foundation width B, the "cohesion" c, and the surcharge q_q. The angle of internal friction has the greatest influence because all three factors increase rapidly with only small increases in the angle.

If the angle of internal friction is zero, as for a saturated clay in undrained shear, the first and third terms become very small and only the cohesion contributes materially to the bearing capacity. Thus for all practical purposes in a saturated clay,

$$q_0 = cN_c \qquad (10:4a)$$

$$q_0 = 5.2c \text{ (for long footings)} \qquad (10:4b)$$

$$q_0 = 6.5c \text{ (for square footings)} \qquad (10:4c)$$

Both the first term and the third term in the equation depend on the unit weight of the soil. When the shear zone is above the water table (the bottom of the footing a height of about B above the water), the full soil unit weight is used in computations. When the water table is at the base of the foundation, the submerged unit weight, $\gamma' = \gamma - \gamma_w$, must be used in the first term. The effect is to reduce that part of the bearing by about one-half. If the water table is above the bottom of the footing, the surcharge weight is also affected.

The first term of the equation varies in direct proportion to the foundation width. This means that in cohesionless soils such as sands, the bearing capacity of small foundations is low and that of large foundations is very high. Estimating the bearing capacity of sand by small-scale tests can be misleading because the bearing capacity of a full-sized foundation will be much greater. In saturated clays in undrained shear, foundation width has little effect on bearing capacity.

The third term is proportional to the surcharge q_q. For a saturated clay where $\phi = 0$ and $N_q = 1$, the contribution of surcharge to bearing capacity is small. In a soil with a high angle of internal friction, a small amount of surcharge produces a large amount of bearing capacity.

EFFECT OF ECCENTRICITY / If the load is not applied concentrically, the overturning moment reduces the bearing capacity. According to Meyerhof,[10:6] the eccentrically loaded foundation responds as if it had a reduced width, B_r:

$$B_r = B - 2e \tag{10:5}$$

In this expression e is the eccentricity of the resultant of the column load and the foundation weight (Fig. 10.8a). If there is eccentricity in two directions, both the length and width are reduced according to Equation (10:5). The value of q_0 computed from the reduced width is the average, and is used with the reduced width again in computing total capacity, Q.

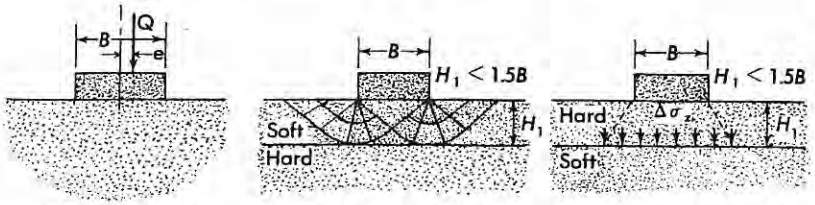

a. Eccentric load

b. Soft layer over hard; restricted shear zone

c. Hard layer over soft, load spread out

Figure 10.8 *Bearing capacity with eccentric loads and stratified soils.*

An older method has been to compute the pressure distribution on the foundation produced by eccentric loading by assuming a linear variation from one side to the other, similar to the stress distribution in an eccentrically loaded column. The maximum pressure is then used in computing the safety factor. This approximation is reasonable for small eccentricities, but the reduced width of Equation (10:5) is more realistic.

EFFECT OF INCLINED LOADING / If the loading is not vertical, the shear pattern is altered. The horizontal component of the load increases the lateral stress on the surrounding zone, leaving less resistance to support the lateral stress generated by the vertical component of the load. Meyerhof had proposed corrections to the bearing-capacity factors to be used in computing the ultimate capacity under the vertical component of load. These are given in Table 10:2.

TABLE 10:2 / CORRECTIONS FOR INCLINED LOAD[10:6]

		Inclination of Load from Vertical			
Factor	D_f	0	10°	20°	30°
N_γ	0	1.0	0.5	0.2	0
N_γ	B	1.0	0.6	0.4	0.25
N_c	0 to B	1.0	0.8	0.6	0.4

NONHOMOGENEOUS BEARING / If the soil is non-homogeneous, the analyses are not directly applicable, but reasonable approximations can be made. When there are random variations in c and ϕ or thin repeating sequences of strata with different ϕ and c parameters within the hypothetical shear zone (Fig. 10.3), the mean of the c and ϕ can be used. If the range in variation is more than $\pm 20\%$ of the mean, somewhat higher safety factors should be used in design.

If a weak stratum overlies a strong one (Fig. 10.3b) the shear will be confined to the weaker material and the stronger will not be involved in the failure. The bearing capacity should be computed from the strength of the weaker stratum. Because the shear zone is restricted, the real bearing will exceed the computed value.

If a stronger layer overlies a weak stratum, the strong layer spreads the load, reducing the bearing pressure on the weaker material (Fig. 10.8c). Failure occurs by shear in the softer stratum as the stronger one bends down under load. The bearing capacity is computed from the strength of the weaker stratum using a reduced bearing pressure $q = \Delta\sigma_z$ computed by the approximation of Equation (10:6).

Factors of Safety

The assessment of adequate safety of a component of a structure is a complex problem of optimization which can be properly resolved only with due considerations of serviceability and economy of the structure, as well as probability and consequences of failure. There are no generally accepted, consistent criteria that can be recommended for use in engineering design today.

The selection of safety factors for design cannot be made properly without assessing the degree of reliability of all other parameters that enter into design, such as design loads, strength and deformation characteristics of the soil mass, etc. Use Table 5.2 as a guide for reasonably homogeneous soil conditions. It is assumed that, where appropriate, all foundations will be analyzed also with respect to maximum tolerable total and differential settlement; if settlement governs the design, higher safety factors must be used. Table 5.2 is for shallow foundations--foundations in which the depth of the footing base below the ground surface is less than the footing width.

TABLE 5.2: Minimum Safety Factor for Design of Shallow Foundations (after Vesic 1975)

Characteristics of the Structure	Soil Exploration	
	Thorough Complete	Limited
Maximum design load likely to occur often; consequences of failure disastrous	3.0	4.0
Maximum design load may occur occasionally; consequences of failure serious	2.5	3.5
Maximum design load likely to occur	2.0	3.0

Net Pressures vs. Gross Pressures

Allowable soil pressures--are they net pressures or gross pressures? You cannot necessarily know which is intended unless it is indicated by the person who makes the allowable soil pressure recommendation.

Net pressure is in excess of the existing overburden pressure that can be safely carried at the foundation depth. Gross pressure is the pressure that can be carried at the foundation depth, including the existing overburden pressure.

The bearing capacity equation is based on gross soil pressure (q_{ult}), which is everything above the foundation level. Settlements are caused only by a net increase in pressure over the existing overburden pressure. So, if the allowable pressure is based on the bearing capacity equation, the pressure is a gross pressure; if it is based on settlement considerations, it is a net pressure.

Approximate Bearing Capacity Relationships for Clay

Note for the clays ($\phi = 0$) the following simple approximate relationships, in terms of c alone, can be made by neglecting the surcharge term ($N_q = 1$) and eliminating the width term ($N_\gamma = 0$):

$q_{ult} = 5c$ long footings near surface

$q_{ult} = 6c$ square footings near surface

$q_{ult} = 9c$ pile point bearing capacity

Also note that the allowable bearing capacity of footings in clay can be "roughed-out" as being equal to the unconfined compressive strength, assuming a safety factor of about 3; then the allowable bearing capacity equals about 2c, or c equals about half the allowable bearing capacity. As previously stated, c also equals about half the unconfined compressive strength, so the unconfined compressive strength is approximately equal to the bearing capacity of a cohesive soil—a statement frequently heard.

Penetration and Other Tests

Besides the unconfined compression or the UU triaxial tests, other methods can be used to obtain the undrained shear strength of cohesive soils. Due to all the problems associated with sampling and laboratory testing, it is sometimes better to measure the strength directly in the field. The two most common field tests for soft clays are the vane shear test (VST), where two crossed blades on a vertical rod are pushed into the clay at the bottom of a bore hole and the rod torqued to fail the clay, and the Dutch cone penetrometer test (CPT), where a 60° cone is pushed into the clay (or sand) and the point resistance and the friction on a friction sleeve attached above the cone are measured. These two tests are not widely used in the U.S.; instead, the standard penetration test (SPT) is most often used for granular and sometimes cohesive soils.

The standard penetration test is a very important procedure used for sampling and penetration testing. A standard "split-spoon" sampler is driven by a 140-pound hammer falling 30 inches. The number of blows required to drive the sampler 12 inches deep is called the "standard penetration resistance," or "blow count" (N). The split-spoon is a cylinder which, when withdrawn from the bore hole, can be uncoupled and opened along longitudinal seams and the "disturbed" soil sample recovered. Split-spoons are used in sand and clays, though better clay samples--so-called "undisturbed" samples—are obtained by pushing an intact thin-wall sampler (a Shelby tube) into the deposit and then bringing it to the surface. The recovered clay sample is later extruded in the laboratory.

There are other field and laboratory tests. One of them the simple pocket penetrometer (PP) test. The pocket penetrometer, which can literally be carried in a pocket, is a small solid cylindrical probe that is pushed a prescribed distance into a cohesive soil sample (or the wall of a test pit, etc.). The penetrometer has a calibrated spring that registers penetration resistance and hence the unconfined compressive strength, usually called the "approximate" unconfined compressive strength.

RECORD OF SUBSURFACE EXPLORATION

Client _____ Boring # B-2 (Page 1 of 2)

Architect Engineer _____ Job # _____

Project Name PROPOSED OFFICE ADDITION Drawn By _____

Project Location _____ Approved By _____

DRILLING and SAMPLING INFORMATION

Date Started 1-13-93 Hammer Wt. 140 lbs.

Date Completed 1-15-94 Hammer Drop 30 in.

Drill Foreman _____ Spoon Sampler OD 2.0 in.

Geologist _____ Rock Core Dia. _____ in.

Boring Method CFA Shelby Tube OD 3.0 in.

Client ID # 8978 Continuous Tube OD _____ in.

SOIL CLASSIFICATION SURFACE ELEVATION 636.4'	Stratum Depth	DEPTH SCALE	SAMPLE NO.	SAMPLE TYPE	% RECOVERY	GROUND WATER	Standard Penetration Test N, Blows/Foot	Unconfined Compressive Strength qu, Tons/sq. ft.	Pocket Penetrometer qu, Tons/sq. ft.	Natural Dry Density lbs.cu. ft.	Water Content %	LL = Liquid Limit PL = Plastic Limit PI = Plasticity Index
Red, very stiff SANDY CLAY (CL)			1	ST	100				3.0		15	33 17 16
-with ferrous stains below 2'			2	ST	100				3.75	107	18	40 16 24
	5.0	5	3	ST	100				4.0		12	
Tan, loose, medium SAND (SP)												
-with red and gray seams below 9'		10	4	SS	100	▽	10				24	
-dense below 13'		15	5	SS	100		36				28	
	17.0											
Gray, very dense, CLAYEY SAND (SC), with seams of gray medium sand		20	6	SS	100		50/5.5"					
	22.0											
Gray, very dense, laminated SANDY SHALE with small seams of sand and silt		25	7	SS	100		50/3"					
			8	SS	100		50/3"					

Continued

SAMPLER TYPE
SS - DRIVEN SPLIT SPOON
ST - PRESSED SHELBY TUBE
CA - CONTINUOUS FLIGHT AUGER
RC - ROCK CORE
HA - HAND AUGER
CU - CUTTINGS
CT - CONTINUOUS TUBE

GROUNDWATER DEPTH
▽ AT COMPLETION 10.00 FT.
▽ AFTER HRS. FT.
● WATER ON RODS 8.00 FT.
+ AT SURVEY FT.

BORING METHOD
HSA - HOLLOW STEM AUGER
CFA - CONTINUOUS FLIGHT AUGERS
DC - DRIVING CASING
RW - ROTARY WASH
ST - PRESSED SHELBY TUBE
HA - HAND AUGER

Figure 1-4A Boring Log.

TAB 12

An Engineering Manual for Slope Stability Studies

(J.M. Duncan et al.)

VIRGINIA TECH

DEPARTMENT OF CIVIL ENGINEERING

AN ENGINEERING MANUAL FOR SLOPE STABILITY STUDIES

by

J.M. Duncan[1]

A. L. Buchignani[2],

and Marius De Wet[3]

March 1987

[1]W. Thomas Rice Professor of Civil Engineering, Virginia Tech, Blacksburg, Virginia

[2]Consulting Engineer, Mill Valley, California.

[3]Instructor, Department of Civil Engineering, University of Stellenbosch, South Africa

Reproduced by the University of Wisconsin-Madison with permission and courtesy of the Virginia Polytechnic Institute and State University.

TABLE OF CONTENTS

	Page No.
INTRODUCTION	1
CHARACTERISTICS AND CRITICAL ASPECTS OF VARIOUS TYPES OF SLOPE STABILITY PROBLEMS	2
Cohesionless Fills Built on Firm Soil or Rock	2
Cohesive Fills Built on Firm Soil or Rock Fills Built on Soft Subsoils	2
Excavation Slopes	4
Natural Slopes	12
Slopes in Soils Presenting Special Problems	17
(1) Stiff-fissured clays and shales	17
(2) Loess	17
(3) Residual soils	18
(4) Highly sensitive clays	18
PROCEDURES FOR INVESTIGATION AND DESIGN OF SLOPES	19
Field Observations	19
Stability Chart Solutions	20
Detailed Analysis	22
GEOLOGIC STUDIES AND SITE INVESTIGATION PROCEDURES	23
SLOPE STABILITY CHARTS	25
Charts for Slopes in Soils with Uniform Strength throughout the Depth of the Soil Layer, and $\phi = 0$	25
Charts for Slopes in Uniform Soils with $\phi > 0$	35
Slope Stability Charts for Infinite Slopes	41
Charts for Slopes in Soils with Strength Increasing with Depth, and $\phi = 0$	45

	Page No.
DETAILED ANALYSES OF SLOPE STABILITY	47
Method of Moments for $\phi = 0$ Soils	47
Ordinary Method of Slices or Fellinius Method for Soils with $\phi = 0$ or $\phi > 0$.	50
Wedge Method for Soils with $\phi = 0$ or $\phi > 0$	53
MINIMUM FACTOR OF SAFETY	70
Locating the Critical Circle	70
Locating the Critical Wedge Mechanism	74
Sources of Inaccuracy in Calculated Factors of Safety	74
Minimum Recommended Values of Safety Factor	74
STABILIZATION OF SLOPES AND LANDSLIDES	77
REFERENCES	80

INTRODUCTION

The purpose of this manual is to provide a simple, practical guide for slope stability studies. It is concerned with (1) the characteristics and critical aspects of various types of slope stability problems, (2) geologic studies and site investigation procedures, (3) methods of designing slopes, including field observations and experience, slope stability charts, and detailed analyses, (4) factors of safety, and (5) methods of stabilizing slopes and slides.

The emphasis of this manual is on simple, routine procedures. It does not include advanced analysis procedures, nor does it deal with specialized problems such as design of dams or the stability of slopes during earthquakes. References are given to the sources of the material contained in the manual, and to more advanced procedures where appropriate, to provide avenues for studies going beyond the scope of this manual.

The first edition of this manual was written under contract with the U.S. Army Corps of Engineers Waterways Experiment Station in 1975. This edition incorporates changes to reflect improvements in the state-of-practice since 1975, and to provide clearer explanations of some of the analysis procedures.

CHARACTERISTICS AND CRITICAL ASPECTS OF VARIOUS TYPES OF SLOPE STABILITY PROBLEMS

Cohesionless Fills Built on Firm Soil or Rock. The stability of fill slopes built of cohesionless gravels, sands, and silts depends on (a) the angle of internal friction of the fill material, Φ' , (b) the slope angle, and (c) the pore pressures. The critical failure mechanism is usually surface ravelling or shallow sliding, which can be analyzed using the simple infinite slope analysis.

Values of Φ' for stability analyses can be determined by drained triaxial or direct shear tests, or by correlations with grain size distribution, relative density, and particle shape. Pore pressure due to seepage through the fill reduces the stability of the slopes, but static water pressure, with the same water level inside and outside the slopes, has no effect on stability.

Slopes in fine sands, silty sands, and silts are susceptible to erosion by surface runoff; benches, paved ditches, and planting on slopes can be used to reduce runoff velocities and retard erosion. Saturated slopes in cohesionless materials are susceptible to liquefaction and flow slides during earthquakes, and dry slopes are subject to settlement and ravelling; relative densities of 75% or larger are required to insure seismic stability under most conditions.

Cohesive Fills Built on Firm Soil or Rock. The stability of fill slopes built of cohesive soils such as clays, clayey sands, and clayey gravels depends on (a) the strength of the fill, as characterized by the parameters c and Φ or c' and Φ', (b) the unit weight of the fill, (c) the height of the fill, (d) the slope angle, and (e) the pore pressures. The critical failure mechanism is usually sliding on a deep surface tangent to the top of the firm foundation.

For fills built of cohesive soils which drain slowly, it may be necessary to analyze the stability for a number of pore pressure conditions:

(1) Short-term or end-of-construction conditions. This can be analyzed using total stress methods, with strengths determined in unconsolidated-undrained (U-U or Q) triaxial compression tests on specimens compacted to the same density and water content as in the field. The tests should be conducted using the same range of stresses as will occur in the field.

Internal pore pressures are not considered explicitly in such analyses; the effects of pore pressures in the undrained tests are reflected in the values of the strength parameters c and Φ. The pore pressures in compacted cohesive soils loaded under undrained conditions depend primarily on the density, the water content, and the applied total stresses. If laboratory specimens are compacted to the field density and water content, and loaded under undrained conditions, the pore pressures induced in the specimen will be the same as the short-term pore pressures in the field at locations where the total stresses are the same. The use of total stress strength parameters therefore accounts properly for pore pressure effects in short-term, undrained conditions.

External water pressures have a stabilizing effect on slopes, and should be taken into account in both total stress and effective stress analyses of all types of slopes.

(2) Long-term conditions. This condition can be analyzed using effective stress methods, with strength parameters determined in drained (D or S) triaxial or direct shear tests, or consolidated-undrained (C-U or $\overline{R}$) tests with pore pressure measurements, on specimens compacted to field density and water content, and tested in the range of stresses that will occur in the field. The measured strengths are related to the effective stresses by means of the strength parameters c' and Φ'.

Pore pressures are governed by the seepage conditions, and can be determined using flow nets or other types of seepage analysis. Both

internal pore pressures and external water pressures should be included in the analyses.

(3) Rapid drawdown condition, or other conditions where the slope is consolidated under one loading condition, and is then subjected to a rapid change in loading, with insufficient time for drainage. This condition can be analyzed using total stress methods, with strengths measured in consolidated-undrained (C-U or R) triaxial compression tests on specimens compacted to field density and water content. The undrained strengths are related to the consolidation pressures as shown in Fig. 1, without using values of c and Φ'.

Stability analyses are performed by determining, for each point through which a trial failure surface passes, the effective stress before drawdown or change in loading. This effective stress is the consolidation pressure, which determines the undrained strength at the point. The undrained strength is determined from the strength diagram. When the undrained strength has been determined for each point along the trial failure surface, the stability is analyzed using total stress methods. See Lowe and Karafiath (1960) for further explanation of the procedure.

Pore pressures are not considered explicitly in such analyses. Pore pressure effects are accounted for by the relationship between undrained strength and consolidation pressure.

Fills Built on Soft Subsoils. The stability of fill slopes built on soft subsoils depends on (a) the strength of the fill, as characterized by the parameters c and Φ or c and Φ', (b) the unit weight of the fill, (c) the height of the fill, (d) the slope angle, (e) the strength of the foundation, as characterized by the parameters c or c' and Φ or Φ', and (f) the pore pressures. The critical failure mechanism is usually sliding on a deep surface tangent to the top of a firm layer within the foundation. A large part of the failure surface usually lies within the foundation, especially in cases where the soft subsoils extend to great depths, and the stability of the embankment depends to a large extent on the strength of

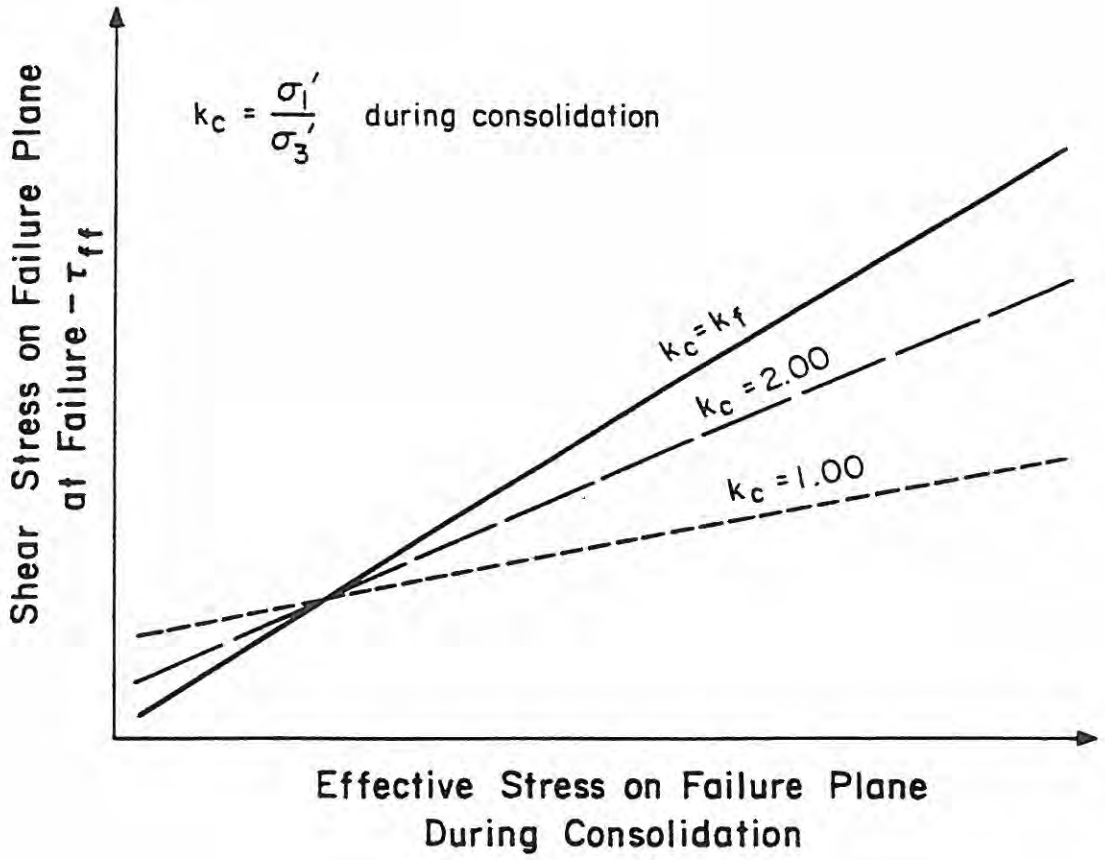

Fig. 1 VARIATION OF UNDRAINED STRENGTH WITH CONSOLIDATION PRESSURE (AFTER LOWE AND KARAFIATH, 1960)

the foundation soils. Surface ravelling may also occur in cohesionless fills.

The short-term stability of embankments on soft subsoils is usually more critical than the long-term stability, because the foundation soil consolidates under the weight of the embankment and gains strength over a period of time. It may, however, be necessary to analyze the stability for a number of pore pressure conditions:

(1) Short-term or end-of-construction condition. If the fill is free-draining sand or gravel, the strength of the fill should be treated in terms of effective stresses. Values of Φ' for use in the analyses should be determined from drained triaxial or direct shear tests, or by correlations with grain size distribution, relative density, and particle shape. Pore pressures in a free-draining fill are governed by the seepage conditions, and can be determined using flow nets or other types of seepage analysis.

If the fill is built of cohesive soil which drains slowly, the strength of the fill for short-term analyses should be treated in terms of total stresses. The strength of the fill material can be determined by performing unconsolidated-undrained (U-U or Q) triaxial compression tests on specimens compacted to the same density and water content as in the field. The test pressures should encompass the range of pressures that will occur in the field.

Soft clay foundations ordinarily drain so slowly that there is little or no dissipation of excess pore pressures during construction. For such conditions, the strength of the clay should be treated in terms of total stresses, and its strength determined using unconsolidated-undrained (U-U or Q) triaxial compression tests on undisturbed specimens, conducted using pressures in the range of pressures in the field.

Under undrained conditions, the strengths of saturated clays can be expressed as

$$S_u = c_u$$

$$\Phi_u = 0$$

in which S_u = undrained shear strength, which is independent of total normal stress, c_u = undrained cohesion intercept of the Mohr-Coulomb failure envelope, and Φ_u = undrained friction angle. The strengths of clays which conform to this $\Phi_u = 0$ failure criterion may be measured using unconsolidated-undrained triaxial tests, unconfined compression tests, or vane shear tests. Strength values measured using field vane shear tests should be corrected for the effects of anisotropy and strain rate using Bjerrum's correction factor, μ, which is shown in Fig. 2.

Embankments on soft foundations may fail progressively because of differences in the stress-strain characteristics of the embankment and the foundation. The strengths of both the embankment and the foundation should be reduced to allow for progressive failure effects, using the reduction factors R_E and R_F shown in Fig. 3. The use of strength parameters reduced by these factors will ensure that neither the embankment nor the foundation are stressed so highly that progressive failure can begin. Even when the strength reduction factors R_E and R_F are used, a factor of safety greater than unity should be used to account for possible inaccuracies in measuring shear strengths.

Internal pore pressures are not considered explicitly in total stress analyses, but the effects of the pore pressures in the undrained tests are reflected in the values of c and Φ. If the laboratory specimens are representative of the soils in the field, the pore pressures in the laboratory specimens will be the same as the pore pressures in the field at locations where the total stresses are the same, and the use of total stress strength parameters from undrained tests therefore accounts properly for pore pressure effects in short-

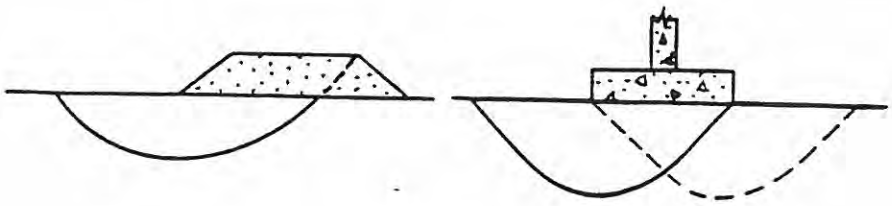

$$(s_u)_{field} = (s_u)_{vane} \cdot \mu$$

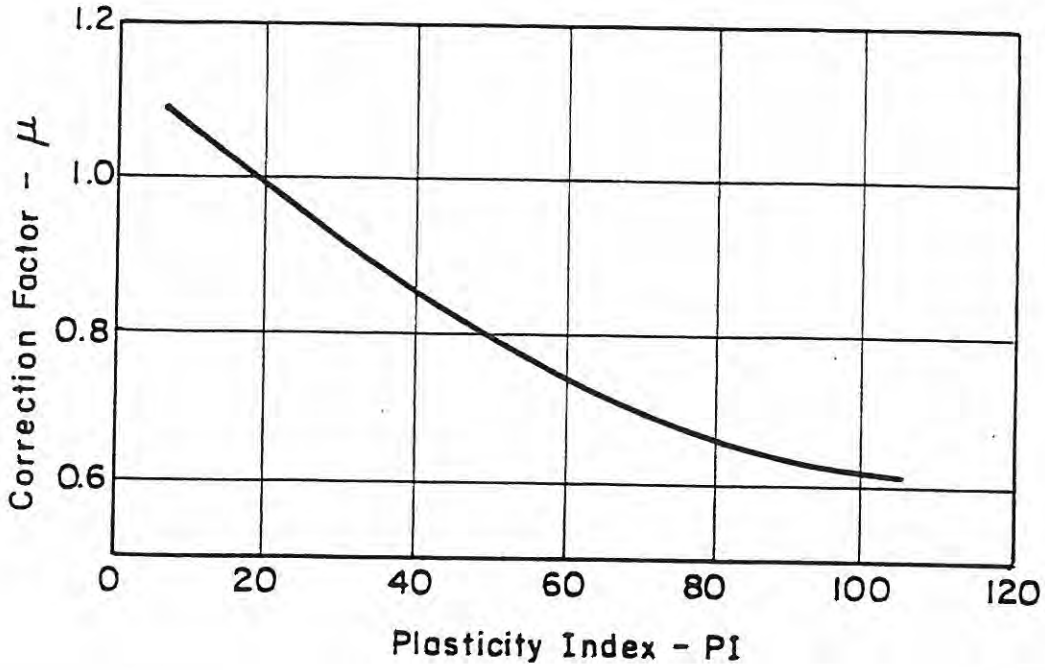

Fig. 2 CORRECTION FACTOR FOR VANE STRENGTH.
(after Bjerrum, 1973)

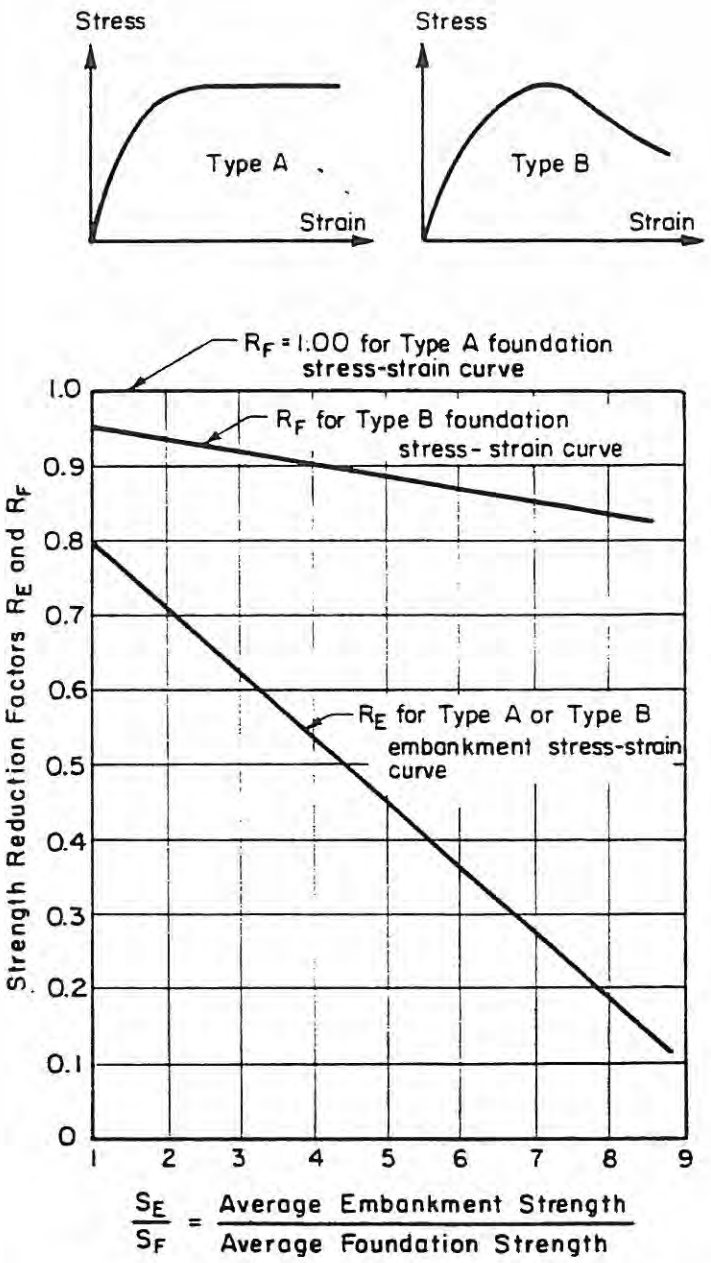

Fig. 3 CORRECTION FACTORS R_E AND R_F TO ACCOUNT FOR PROGRESSIVE FAILURE IN EMBANKMENTS ON SOFT CLAY FOUNDATIONS.
(after Chirapuntu and Duncan, 1975)

term, undrained conditions.

External water pressures should be taken into account in the stability analyses, whether they are performed in terms of total or effective stresses.

If an embankment constructed of cohesive fill is built higher than some critical height, H_T, there will be a tendency for tension to develop in the embankment, and the embankment will crack. The approximate value of H_T can be determined using Fig. 4. Embankments which are built higher than this critical height should be analyzed assuming that the fill is cracked to a depth of

$$H_c = \frac{4c}{\gamma} \tan (45 + \Phi/2)$$

in which H_c = crack height, c = cohesion intercept of embankment fill, Φ = friction angle of embankment, and γ = unit weight of embankment. If H_c exceeds the embankment height, the crack should be assumed to extend through the full height of the fill, but not into the foundation. In performing stability analyses of cracked embankments, it should be assumed that cracks may exist in any part of the embankment. Each trial failure surface analyzed should be assumed to intersect a crack in the embankment, and zero shear resistance should be assigned to the vertical portion of the failure surface which coincides with the crack.

(2) Long-term conditions. This condition can be analyzed using effective stress methods, with strength parameters for both the fill and foundation determined in drained (D or S) triaxial or direct shear tests or consolidated-undrained (C-U or $\overline{R}$) tests with pore pressure measurements. The test specimens of the foundation soil should be undisturbed, and the test specimens of the fill material should be compacted to the field density and water content and tested in the range of pressures that will occur in the field.

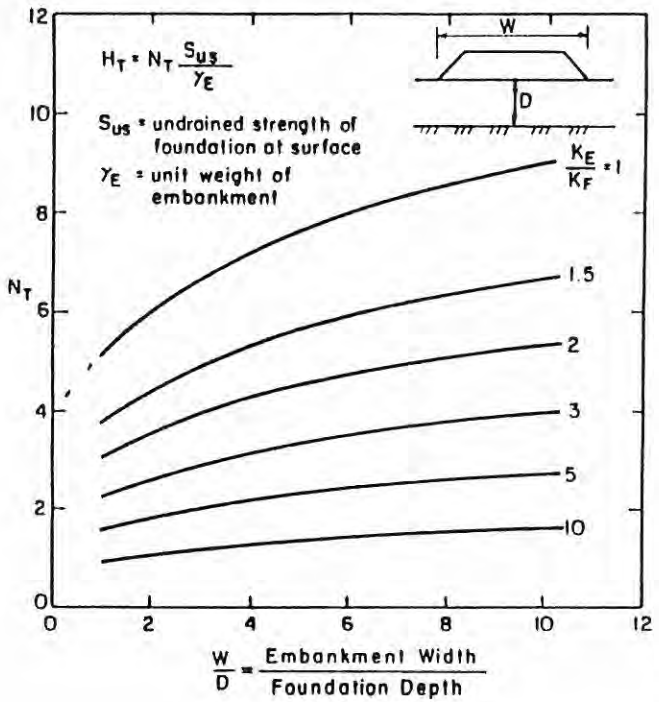

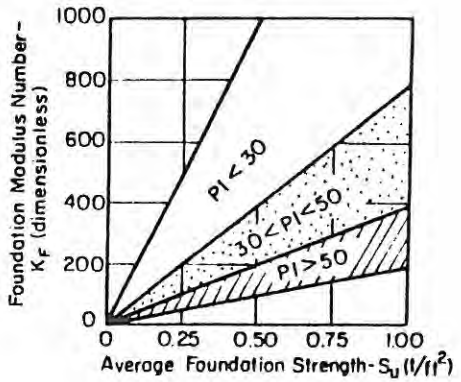

Typical values of K_E for compacted fills

Unified Class.	Compaction Water Content		
	Optimum - 3%	Optimum	Optimum + 3%
GC	300 - 1200	200-500	75 - 300
SP	400 - 1000	400-1000	400-1000
SM	300 - 750	300 - 750	300 - 750
SC	250 - 1000	150-600	50 - 250
ML	250 - 1000	150-600	50 - 250
CL	250 - 1000	100-400	30 - 200
CH	100 - 400	50-200	20- 100

Values shown apply to fill materials compacted to dry densities from 90% to 95% of the Std. AASHO maximum. In general, the value of K_E increases with increasing dry density at a given water content.

Fig 4 CHART FOR ESTIMATING H_T = HEIGHT OF EMBANKMENT WHEN CRACKING WILL BEGIN. (after Chirapuntu and Duncan, 1975)

Pore pressures are governed by the seepage conditions, and can be determined using flow nets or other types of seepage analysis. Both internal pore pressures and external water pressures should be included in the analyses.

(3) Rapid drawdown condition, or other conditions where the slope is consolidated under one loading condition, and is then subjected to a rapid change in loading, with insufficient time for drainage. This condition can be analyzed using total stress methods, with strengths for both the embankment and the foundation measured in consolidated-undrained (C-U or R) tests. Test interpretation and analysis procedures for these conditions have been described by Lowe and Karafiath (1960) and Ladd and Foote (1974).

Table 1 summarizes the important aspects of the stability of slopes in fills, and the applicable analysis procedures.

Excavation Slopes. The stability of excavation slopes depends on (a) the strength of the soil in which the slope is excavated, as characterized by the strength parameters c and Φ or c' and Φ', (b) the unit weight of the soil, (c) the height of the slope, (d) the slope angle, and (e) the pore pressures. The critical failure mechanism is usually a deep surface in homogeneous cohesive soils, and surface sloughing or shallow sliding in homogeneous cohesionless soils. In nonhomogeneous slopes the critical shear surface may be either shallow or deep, depending on the strength characteristics and distributions of the soils within the slope.

The long-term stability of excavation slopes in cohesive soils is usually more critical than short-term stability, because the soil around the excavation swells under the reduced stresses and becomes weaker over a period of time. It may, however, be necessary to analyze the stability of excavated slopes for a number of pore pressure conditions:

(1) Short-term or end-of-construction conditions. If the slope is excavated wholly or partly in free-draining sands or gravels, in which there are no excess pore pressures at the end of construction,

Table 1. Important Aspects of the Stability of Compacted Fills

	Type of fill and foundation		
	Cohesionless fill on firm foundation	Cohesive fill on firm foundation	Any type of fill on weak foundation
Factors that control stability	ϕ' of fill Slope angle Pore pressures External water	Strength of fill γ of fill Slope angle Slope height Pore pressures External water	Strength of foundation Depth of weak foundation layer Strength of fill γ of fill Height of fill Slope angle Pore pressures External water
Failure mechanism	Surface ravelling	Sliding tangent to top of foundation	Deep sliding extending into foundation
Special problems	Surface erosion Liquefaction during earth-quakes	Surface erosion Weathering and weakening of Compacted shales	Embankment cracking Progressive failure Surface erosion
Critical stages for stability	Long-term, or Earthquake	End-of-Construction, Longterm, or Rapid drawdown	End of construction, Longterm, or Rapid drawdown
Analysis procedures	Effective stress, or Dynamic	Total stress, Effective stress or, Combination	Total stress, Effective stress, or Combination

their strengths should be treated in terms of effective stresses. Values of Φ' for these soils should be determined from drained triaxial or direct shear tests performed using an appropriate range of stresses, or by correlations with grain size distribution, relative density, and particle shape. Pore pressures in these free-draining soils will be governed by the seepage conditions, and can be determined using flow nets or other types of seepage analysis.

If the slope is excavated wholly or partly in cohesive soils which drain slowly, their strengths for short-term analyses should be treated in terms of total stresses. The strengths of these soils can be determined by performing unconsolidated-undrained (U-U or Q) triaxial compression tests on undisturbed specimens, and can be expressed in terms of the total stress shear strength parameters Φ_u and c_u.

Under undrained conditions, the strengths of saturated clays can be expressed as

$$S_u = c_u$$

$$\Phi_u = 0$$

in which S_u = undrained shear strength, which is independent of total normal stress, c_u = undrained cohesion intercept of the Mohr-Coulomb failure envelope, and Φ_u = undrained friction angle. The strengths of clays which conform to this $\Phi_u = 0$ failure criterion may be measured using unconsolidated-undrained triaxial tests, unconfined compression tests, or vane shear tests. Strength values measured using field vane shear tests should be corrected for the effects of anisotropy and strain rate using Bjerrum's correction factor, μ, which is shown in Fig. 2.

Internal pore pressures are not considered explicitly in such analyses; the effects of the pore pressures in the undrained tests are reflected in the values of c and Φ. The pore pressures induced

in undisturbed laboratory specimens will be the same as the pore pressures in the field at locations where the total stresses are the same, and the use of total stress strength parameters from undrained tests therefore accounts properly for pore pressure effects in short-term, undrained conditions.

External water pressures should be taken into account in the stability analyses, whether they are performed in terms of total or effective stresses.

(2) Long-term conditions. This condition can be analyzed using effective stress methods, with strength parameters determined from drained (D or S) triaxial or direct shear tests, or consolidated-undrained (C-U or $\overline{R}$) tests with pore pressure measurements, performed on undisturbed test specimens at comparable stress levels.

Pore pressures are governed by the seepage conditions, and can be determined using flow nets or other types of seepage analysis. Both internal pore pressures and external water pressures should be included in the analyses.

(3) Rapid drawdown condition, or other conditions where the slope is consolidated under one loading condition, and is then subjected to a rapid change in loading, with insufficient time for drainage. This condition can be analyzed using total stress methods, with strengths determined in consolidated-undrained (C-U or R) tests on undisturbed specimens. Ladd and Foote (1974) have developed detailed procedures for evaluating the undrained strength of natural soils using C-U or R tests.

Table 2 summarizes the important aspects of the stability of excavated slopes, and the applicable design procedures.

Natural Slopes. If a natural slope is modified by grading operations, it may be necessary to analyze the stability for a number of pore pressure conditions. Fills on natural slopes may be treated in accordance with the

Table 2. Important Aspects of the Stability of Excavation Slopes

	Soil Type	
	Cohesionless	Cohesive
Factors that control stability	ϕ' of soil Slope angle Pore pressures External water	Strength of soil γ of soil Slope angle Pore pressures External water
Failure mechanism	Surface ravelling	Deep sliding, possibly extending below toe of slope
Special problems	Surface erosion Liquefaction during earthquake	Strength loss in stiff-fissured clays Surface erosion
Critical stages for stability	Long-term, or earthquake	End-of-construction, Long-term, or Rapid drawdown
Analysis procedures	Effective stress, or Dynamic	Total stress, Effective stress, or Combination

procedures described previously for fill slopes, and excavations in natural slopes may be analyzed following the procedures described for excavation slopes.

If a natural slope has existed in the same condition for many years, and has come to equilibrium with the prevailing groundwater seepage conditions, it should be analyzed using effective stress procedures. Strengths can be determined using drained (D or S) triaxial or direct shear tests, or consolidated-undrained (C-U or $\overline{R}$) tests with pore pressure measurements. Pore pressures can be determined by field measurements or by using flow nets or other types of seepage analysis. Both internal pore pressures and external water pressures should be included in the analyses.

Slopes in Soils Presenting Special Problems. There are a number of different soil types which present special or unusual problems with respect to the stability of natural or excavated slopes. These include:

(1) Stiff-fissured clays and shales. The shearing resistance of many stiff-fissured clays and shales may be reduced considerably if they are subjected to shearing displacements which are much larger than the shear displacement corresponding to peak strength. There is evidence for some of these soils that slope failures may occur progressively, and that over a long period of time the shearing resistance may be reduced to the residual value--the minimum value which is reached only at extremely large shear displacements. In some cases, however, slopes in these types of soils stand for many tens or hundreds of years at angles which are steeper than would be consistent with mobilization of only residual shear strength. Local experience and local practice is the best guide to appropriate design procedure for such soils.

(2) Loess. Because loess deposits contain networks of interconnected channels formed by plant roots which have decayed, these deposits have high permeability in the vertical direction. Unless vertical infiltration is prevented, water percolating downward through the soil can destroy the weakly cemented bonds between particles, causing

rapid erosion and slope failure. Slopes in loess are therefore frequently more stable when cut vertical to prevent infiltration. Benches at intervals can be used to reduce the effective slope angle. Horizontal surfaces on benches and at the top and bottom of the slope must be paved or planted to prevent infiltration. Local experience and practice are the best guide to procedures for spacing benches and for protecting such slopes against infiltration and erosion.

(3) Residual soils. Depending on rock type and climate, residual soils in many areas may present special problems with respect to slope stability and erosion. Such soils may contain pronounced structural features characteristic of the parent rock or the weathering process, and their characteristics may vary quite significantly over short distances. Under such conditions, determination of design shear strength parameters from laboratory tests may be difficult. It may be possible in such conditions to determine more representative shear strength parameters by back-analyzing slope failures, or to use empirical design procedures based on local experience, without analysis.

(4) Highly sensitive clays. Some marine clays exhibit dramatic loss of strength when disturbed and can actually flow like syrup when completely remoulded. Because of the effects of disturbance during sampling, it may be difficult to measure representative strengths for such soils in laboratory tests. Local experience is the best guide to the reliability of laboratory shear strength values for such clays.

PROCEDURES FOR INVESTIGATION AND DESIGN OF SLOPES

Depending on the type of slope, and the amount of time and effort which can appropriately be devoted to site investigation and analysis, a number of different procedures may be used for investigation and design of slopes. Three frequently used procedures, which represent increasing levels of complexity and cost, are the following:

1. Use of field observations and experience alone, with no test borings, laboratory tests, or slope stability calculations.

2. Use of slope stability calculations by means of charts, in combination with field observations and a minimum number of test borings and laboratory tests.

3. Use of detailed slope stability calculations, in combination with a thorough program of site investigation and laboratory tests.

The use of field observations, slope stability charts, and detailed analysis procedures are discussed in the following sections.

Field Observations. Slopes are often designed based on observation and examination of existing slopes in the same area and the same types of soil. The use of field experience alone implies that no soil strength data from laboratory tests or back analysis is available. This procedure is appropriate when the costs of drilling test borings and making laboratory tests are high compared to the cost of repairing a slope failure.

The first steps in designing a slope based on field observation and experience is to review the available geologic maps and to make a geological reconnaissance of the area. In the geological reconnaissance, particular attention is devoted to evidence of seepage, the characteristics of the existing topography, and the condition of nearby cut or fill slopes. Seepage emerging from the ground indicates unfavorable conditions for cut or fill slopes, and the existence of a hummocky ground surface or old slide

scarps is strong evidence of past instability. The type and condition of vegetation and ground cover should also be noted. Sparse vegetation or steeply leaning trees are often indications of slope stability problems.

A field slope chart, like the one shown in Fig. 5, is a useful tool for slope design based on experience. This type of chart summarizes field data for a particular geologic formation in a form which makes it useful for design of slopes in the same formation. To prepare such a chart, existing landslides and stable slopes are surveyed. Each failed or stable slope is plotted as a point on the chart, which shows slope angle (or cotangent of slope angle) versus height of slope. Each point is identified as stable or unstable. When the number of failures is sufficient, as was the case for the area which Fig. 5 applies, it is only necessary to include data for unstable slopes. When the number of failures is small, however, it is useful to include data for stable slopes, which would be represented by a different symbol. The data for the highest and steepest stable slopes will help to define the limits within which slopes can be expected to remain stable. By comparing these data with the height and slope angle for a planned slope, a prediction of the stability of the planned slope can be made based entirely on experience. For example, the data shown in Fig. 5 indicate that within the area it covers, almost all slope failures were in slopes steeper than 20°.

Stability Chart Solutions. Slope analysis by use of slope stability charts has commonly been used for the preliminary stage of analysis. However, charts are now available which make it possible to perform quite accurate analyses for many conditions. Charts which include the effects of surcharge, tension cracks, submergence, seepage, and increasing strength with depth allow a wide range of variables to be considered in the design of a slope by this method.

Using slope stability charts, the factor of safety for a slope can be calculated within an accuracy of 15% in most cases. Thus, when the available data on site conditions and soil strengths are not extensive, calculations using slope stability charts provide sufficient accuracy for design. Slope stability charts are also very useful for preliminary design

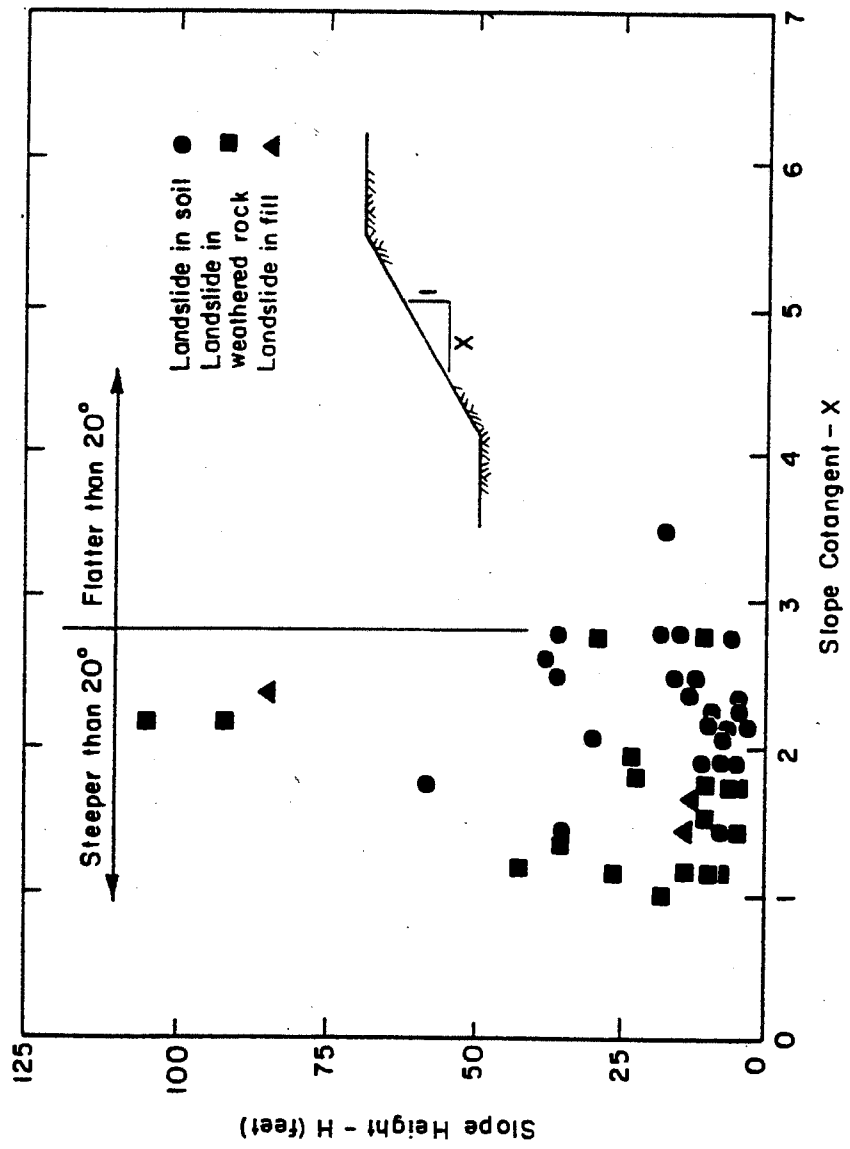

Fig. 5 EXAMPLE OF METHOD OF ESTIMATING SLOPE STABILITY USING FIELD DATA.

calculations, to compare alternatives which can be examined more thoroughly subsequently using detailed analysis procedures. Chart solutions also provide a rapid means of checking the results of detailed analyses.

A further use for slope stability charts is to back-calculate strength values for failed slopes to aid in planning remedial measures. This can be done by assuming a factor of safety of unity for the conditions at failure and solving for the unknown shear strength. Since soil strength usually involves both cohesion and friction, there is no unique value of cohesion (c) and angle of internal friction (Φ) which will give a factor of safety equal to unity; therefore, several pairs of values should be calculated and judgment used to select the most reasonable values. If the material in the slide zone is clay, and the slide occurred under undrained conditions, a unique solution for shear strength can be obtained by assuming $\Phi = 0$ and back calculating a value of cohesion.

Detailed Analysis. A detailed investigation of slope stability includes a geological study; field observations, test borings, laboratory testing, and detailed slope stability calculations. The analysis can be performed using a computer or detailed hand calculations as described in subsequent sections. Slope stability charts may be used for preliminary studies or to check the final analysis.

Field instrumentation studies can be used to monitor the performance of existing slopes, and may be very useful in conjunction with detailed investigations. Data from slope indicators can be helpful for determining potential or existing failure zones. Instrumentation can also be used to monitor the movements of a slope after construction as a check on the design. This is especially useful for sites with very complex soil conditions.

GEOLOGIC STUDIES AND SITE INVESTIGATION PROCEDURES

Detailed geologic studies and site investigations are used to obtain the information required for analysis of new slopes and for planning remedial work on landslides. The first step in a field exploration program is to make a geological reconnaissance, including field mapping of the area. Field notes should be recorded on a large-scale topographic map. The reconnaissance should make note of the uniformity of the topography, seepage, existing landslide scarps, plumbness of trees, and the condition of nearby slopes. Note should also be made of the accessibility of the site to drilling equipment. The locations of the test borings or test pits should be planned and staked in the field during this phase of the investigation.

A sufficient number of test borings should be planned so that detailed surface and subsurface data are obtained throughout the planned slope area. Sometimes, because of rugged topography, equipment access may be difficult and track-mounted equipment may be needed. Large diameter borings are preferable to smaller ones, especially when drilling in a known slide area, because it is often possible to locate the slide plane by examining the cuttings from a large diameter hole. Shear or slickensided zones in the cuttings provide evidence of past movements. Undisturbed samples should be taken at selected depths in the borings, and when a change in soil type is encountered. In the case of an existing slide, samples should be obtained within the failure zone, if possible. In some cases it may be necessary to have a geologist enter a bore hole and examine the sides of the hole for fault zones, evidence of movement or seepage. In this case, as a safety precaution, the hole should be cased. The depths of the borings should extend well below the toe of the slope and, if possible, should extend to a firm soil layer or bedrock.

To obtain water table information, borings should be fitted with perforated casings and backfilled with gravel so that long-term measurements of the fluctuations of the ground water can be made. Piezometers can also be installed at selected locations so that measurements of pore water pressure

can be obtained. Sometimes piezometers can be installed in test borings after sampling has been completed.

Based on the reconnaissance and test boring data, surface and subsurface profiles should be drawn showing the soil conditions and water levels. The unit weights, classification test data, and strength data obtained from laboratory tests should be shown on the profiles.

SLOPE STABILITY CHARTS

The stability of slopes can be analyzed quickly using the stability charts shown in Figs. 6 through 11. Although the charts assume simple slopes and uniform soil conditions, they can be used to obtain reasonably accurate answers for most complex problems if irregular slopes are approximated by simple slopes, and carefully determined average values of unit weight, cohesion, and friction angle are used.

Charts for Slopes in Soils with Uniform Strength throughout the Depth of the Soil Layer, and $\Phi = 0$. The stability chart for slopes in soils with uniform shear strength throughout the depth of the layer, and with $\Phi = 0$, is shown in Fig. 6. Charts giving correction factors for surcharge loading at the top of the slope, submergence, and tension cracks are given in Figs. 7a and 7b.

Steps for use of charts:

1. Using judgment, decide which cases should be investigated. For uniform soil conditions, the critical circle passes through the toe of the slope if the slope is steeper than about 1 (H) on 1 (V). For flatter slopes, the critical circle usually extends as deep as possible and is tangent to some deep firm layer.

   If the conditions are not uniform, or there is water outside the slope, the following criteria can be used to determine which possibilities should be examined:

   - If there is water outside the slope, a circle passing above the water may be critical;

   - If a soil layer is weaker than the one above it, the critical circle may be tangent to the base of the lower (weaker) layer. This applies to layers above as well as below the toe;

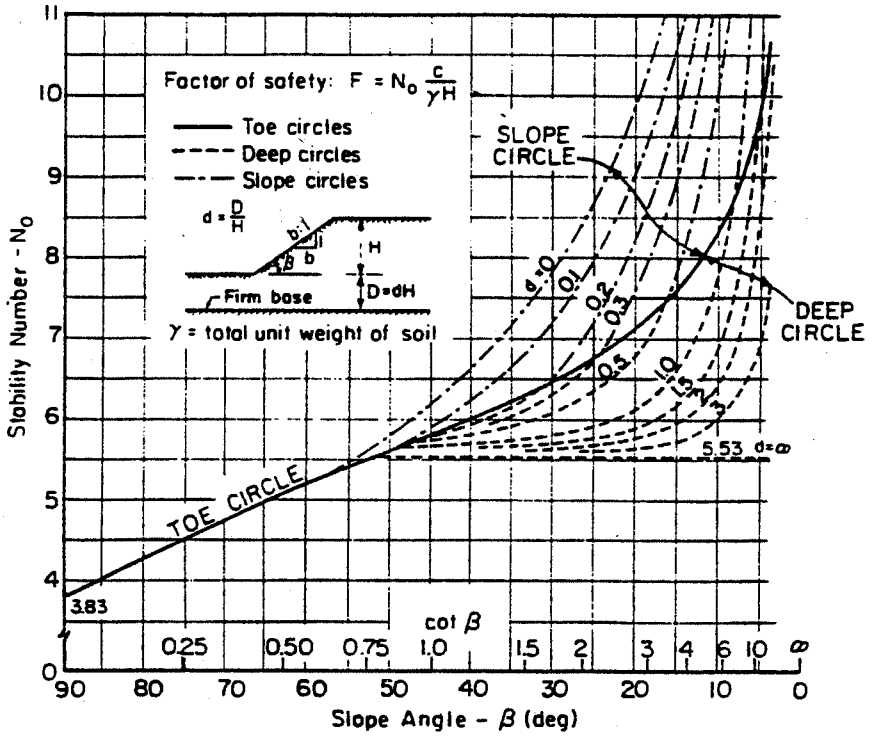

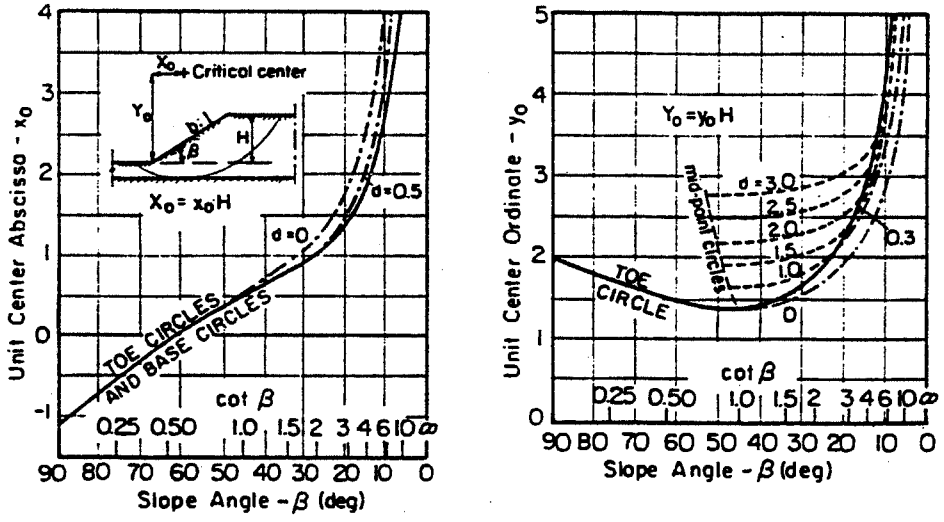

Fig 6 SLOPE STABILITY CHARTS FOR $\phi = 0$ SOILS (after Janbu, 1968)

REDUCTION FACTORS FOR SURCHARGE

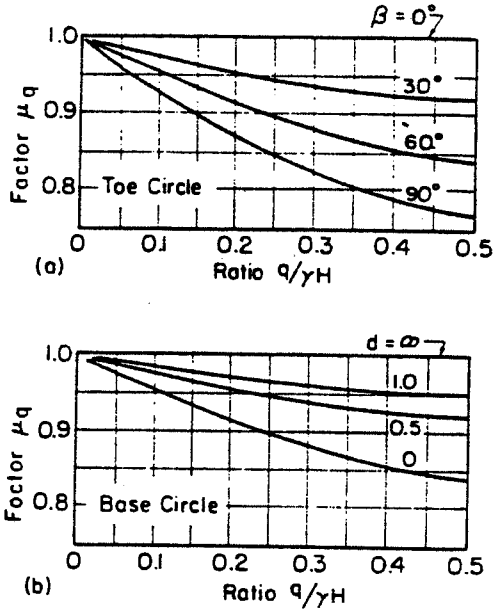

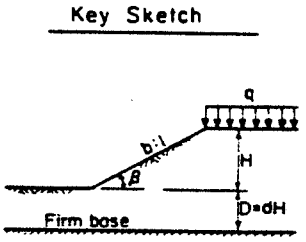

REDUCTION FACTORS FOR SUBMERGENCE (μ_w) AND SEEPAGE (μ'_w)

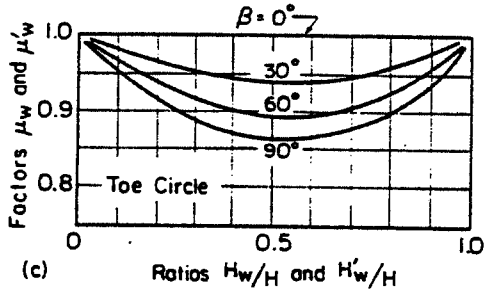

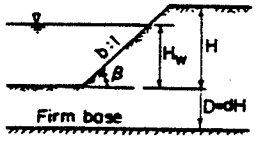

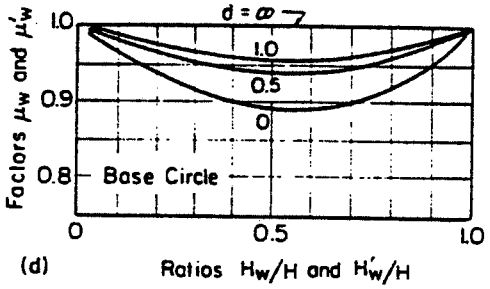

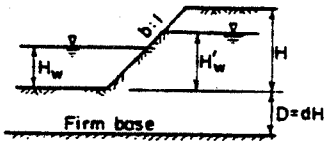

Fig. 7(a) REDUCTION FACTORS FOR SLOPE STABILITY CHARTS FOR $\phi = 0$ AND $\phi > 0$ SOILS. (after Janbu, 1968)

REDUCTION FACTOR FOR TENSION CRACK
No Hydrostatic Pressure in Crack

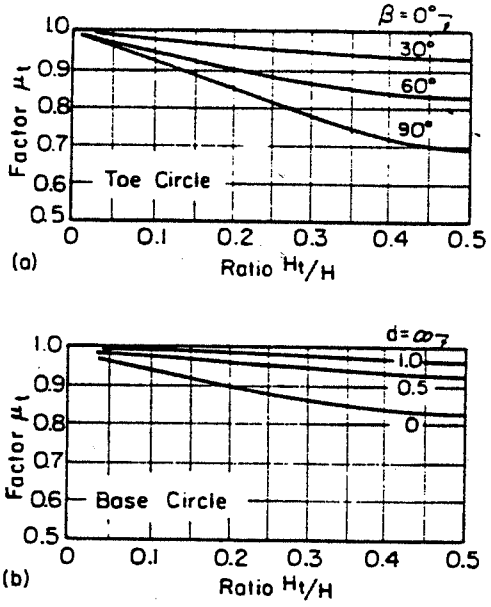

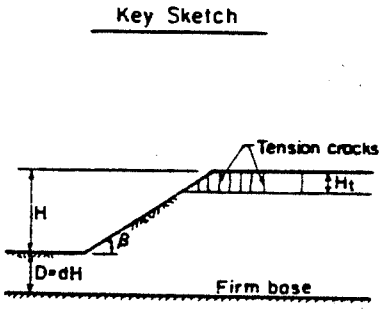

REDUCTION FACTOR FOR TENSION CRACK
Full Hydrostatic Pressure in Crack

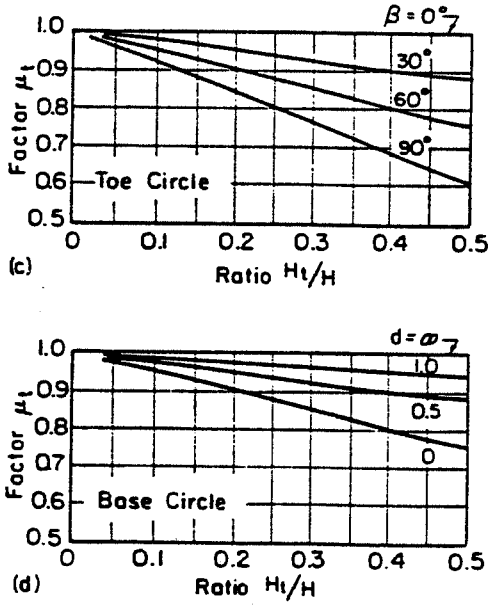

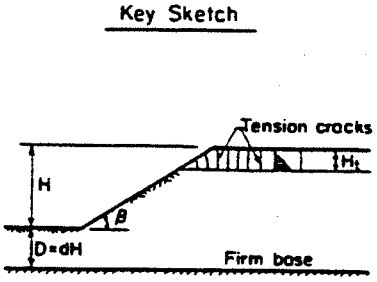

Fig. 7(b) REDUCTION FACTORS FOR SLOPE STABILITY CHARTS FOR $\phi = 0$ AND $\phi > 0$ SOILS. (after Janbu, 1968)

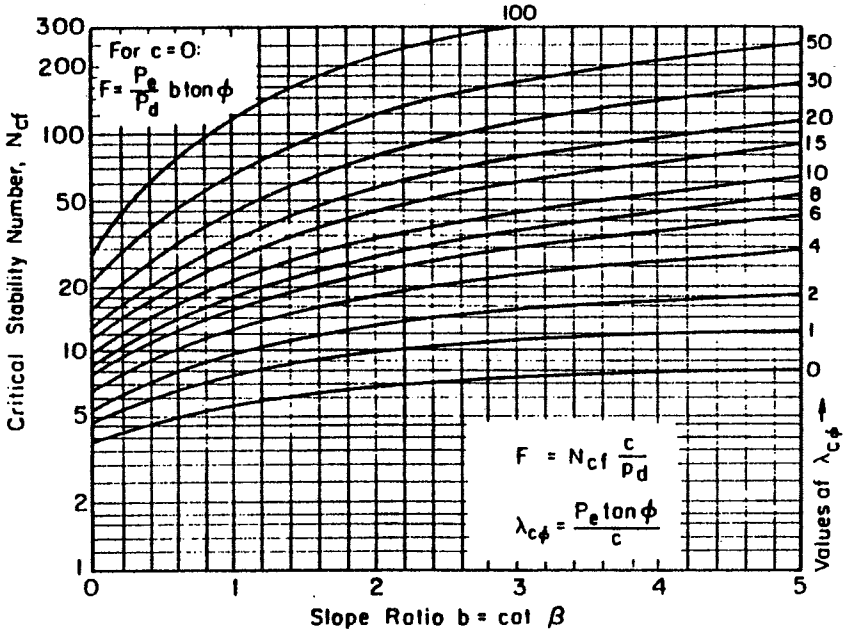

(In formula for P_e take $q = 0$, $\mu_q = 1$ for unconsolidated condition)

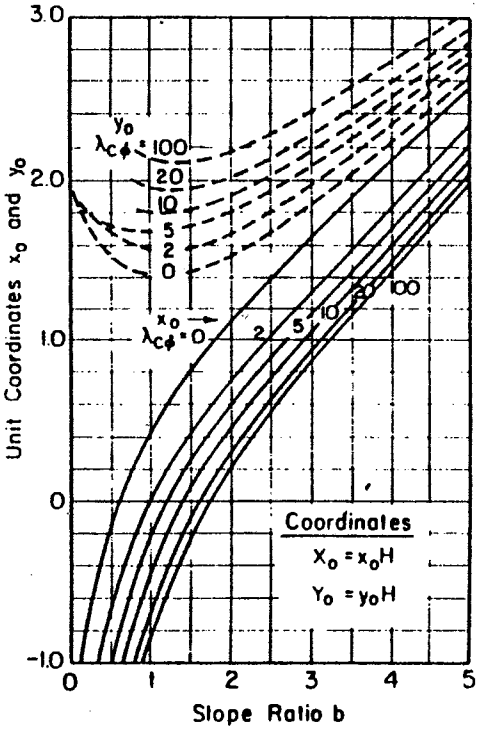

CENTER COORDINATES FOR CRITICAL CIRCLE

Fig.8 SLOPE STABILITY CHARTS FOR $\phi > 0$ SOILS. (after Janbu, 1968)

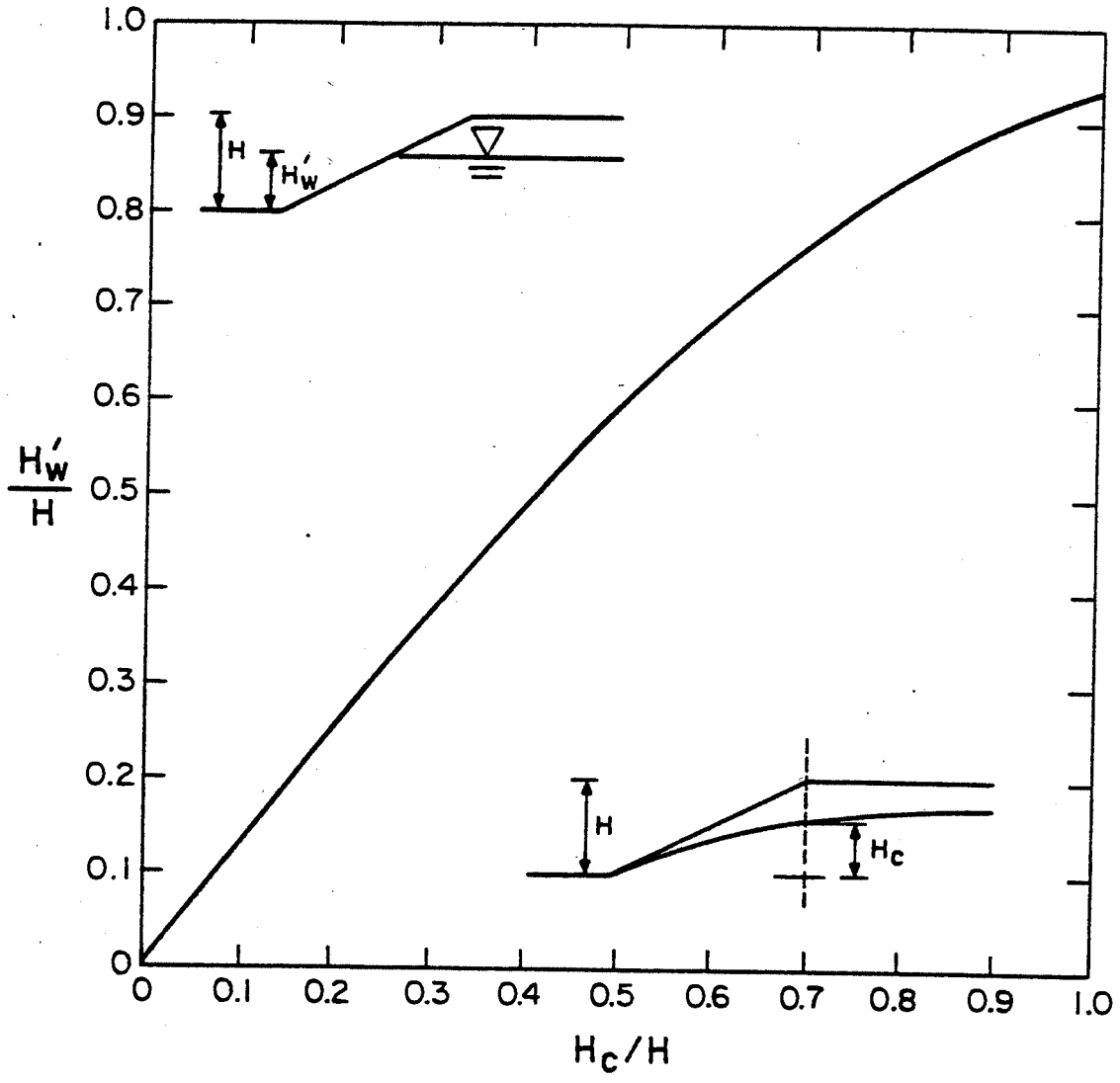

Fig.9 CHART FOR DETERMINING STEADY SEEPAGE CONDITIONS

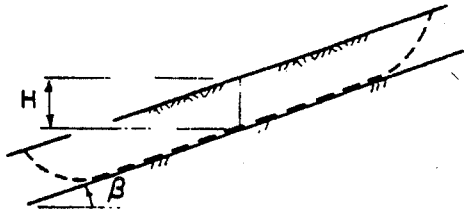

γ = total unit weight of soil

γ_w = unit weight of water

c' = cohesion intercept
ϕ' = friction angle
} Effective Stress

r_u = pore pressure ratio = $\frac{u}{\gamma H}$

u = pore pressure at depth H

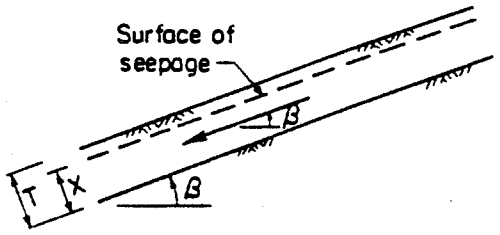

Seepage parallel to slope

$r_u = \frac{X}{T}\frac{\gamma_w}{\gamma}\cos^2\beta$

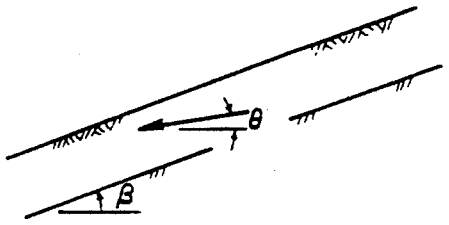

Seepage emerging from slope

$r_u = \frac{\gamma_w}{\gamma}\frac{1}{1+\tan\beta\tan\theta}$

Steps:

① Determine r_u from measured pore pressures or formulas at right

② Determine A and B from charts below

③ Calculate $F = A\frac{\tan\phi'}{\tan\beta} + B\frac{c'}{\gamma H}$

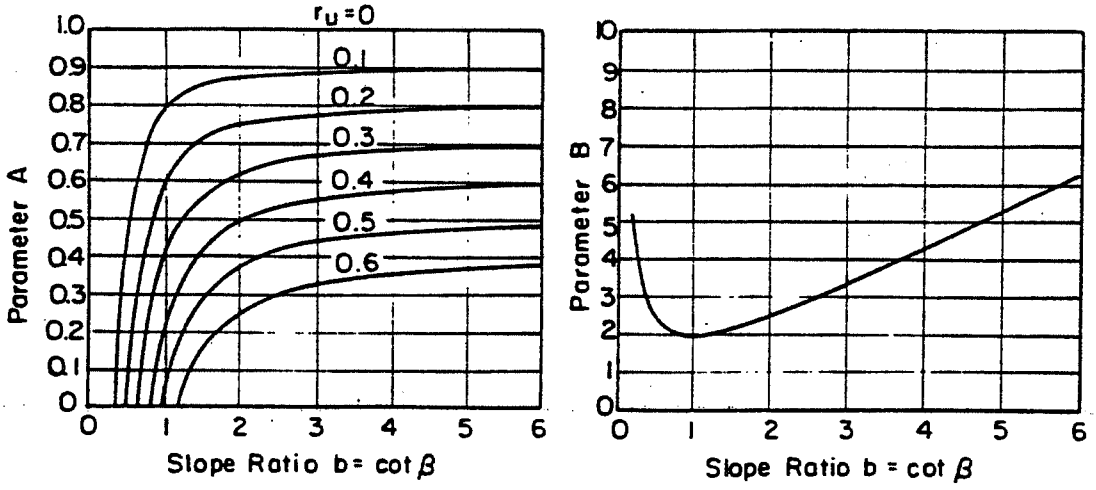

Fig.10 STABILITY CHARTS FOR INFINITE SLOPES.

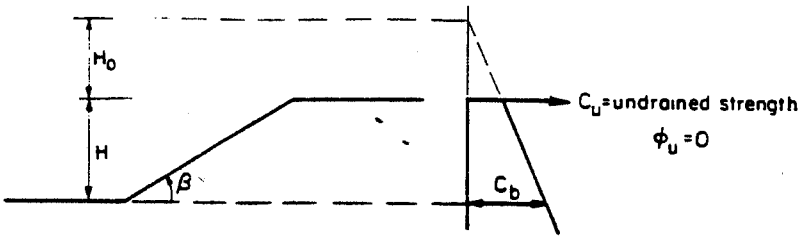

Steps:

① Extrapolate strength profile upward to determine value of H_0, where strength profile intersects zero

② Calculate $M = H_0/H$

③ Determine stability number N from chart below

④ Determine C_b = strength of bottom of slope

⑤ Calculate $F = N \frac{C_b}{\gamma(H+H_0)}$

Use $\gamma = \gamma_{buoyant}$ for submerged slope

Use $\gamma = \gamma_m$ for no water outside slope

Use average γ for partly submerged slope

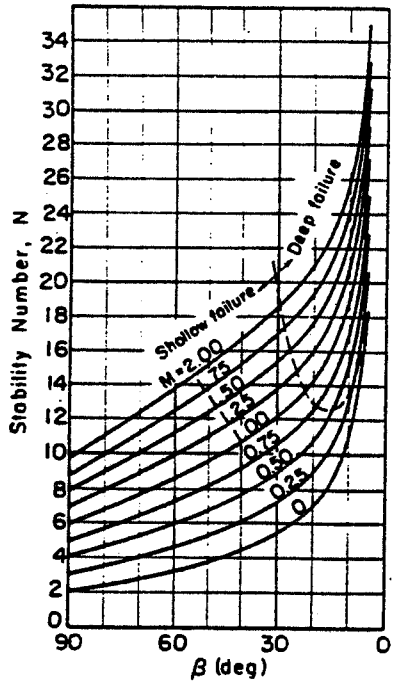

Fig. 11 SLOPE STABILITY CHARTS FOR $\phi = 0$, AND STRENGTH INCREASING WITH DEPTH. (after Hunter and Schuster, 1968)

- If a soil layer is stronger than the one above it, the critical circle may be tangent to the base of either layer, and both possibilities should be examined. This applies to layers above as well as below the toe of the slope.

Once the cases to be investigated have been decided upon, the remaining steps should be performed for each one.

2. This step may be omitted for toe circles.
Calculate the depth factor, d, using the formula

$$d = \frac{D}{H}$$

in which

D = depth from the toe of the slope to the lowest point on the slip circle (L; length)
H = slope height above the toe of the slope (L)

If the circle is entirely above the toe, i.e. $D < 0$, its point of interaction with the slope should be taken as an adjusted "toe", and all dimensions like D, H and H_w adjusted accordingly in the calculations.

3. Find the center of the critical circle using the charts in the bottom half of Figure 6 and draw this circle to scale on a cross section of the slope.

4. Determine the average value of the strength, c, for the circle. This is done by calculating the weighted average of the strengths along the failure arc, using the number of degrees intersected by each soil layer as the weighting factor. An example is shown in Figure 12.

5. Calculate P_d using the formula below

$$Pd = \frac{\gamma H + q - \gamma_w H_w}{\mu_q \mu_w \mu_t}$$

in which

γ = average unit weight of soil (F/L^3)
H = slope height above toe (L)
q = surcharge (F/L^2
γ_w = unit weight of water (F/L^3)
H_w = height of external water level above toe (L)
μ_q = surcharge correction factor (Figure 7a, top)
μ_w = submergence correction factor (Figure 7a, bottom)
μ_t = tension crack correction factor (Figure 7b, top)

If there is no surcharge, $\mu_q = 1$; if there is no external water above toe, $\mu_w = 1$; if there are no tension cracks, $\mu_t = 1$.

6. Using the chart at the top of Figure 6, determine the value of the stability number, N_o, which depends on the slope angle, β , and the value of d.

7. Calculate the factor of safety, F, using the formula

$$F = \frac{N_o \, c}{P_d}$$

in which

N_o = stability number
c = average shear strength (F/L^2)

See Fig. 12 for an example. Note that the charts were used to calculate factors of safety for circles tangent to two different depths. For the case shown in Fig. 12, the deeper circle is more critical.

Charts for Slopes in Uniform Soils with $\Phi > 0$. The stability chart for slopes in soils with $\Phi > 0$ is shown in Figure 8. Correction factors for surcharge loading at the top of the slope, submergence, seepage and tension cracks are given in Figures 7a and 7b. The stability chart in Figure 8 can be used for analyses in terms of effective stresses. The chart may also be used for total stress analysis of unsaturated slopes, if $\Phi_u > 0$.

Steps for use of charts:

1. Using judgment, estimate the location of the critical circle. For most conditions of simple slopes in uniform soils with $\Phi > 0$, the critical circle passes through the toe of the slope. The stability numbers given in Figure 8 have been developed by analyzing toe circles. In cases where $c = 0$, the critical mechanism is shallow sliding. Figure 10 can be used in this case. In cases where there is water outside the slope, the critical circle may pass above the water.

   If conditions are not homogeneous, a circle passing above or below the toe may be more critical than the toe circle. The following criteria can be used to determine which possibilities should be examined:

   - If a soil layer is weaker than the layer above it, the critical circle may be tangent to the base of the weaker layer. This applies to layers above as well as below the toe.

   - If a soil layer is stronger than the layer above it, the critical circle may be tangent to the base of either of the two layers, and both possibilities should be examined. This applies to layers above as well as below the toe.

   The charts in Figure 8 may be used for non-uniform conditions provided the values of c and Φ used in the calculation represent the correct

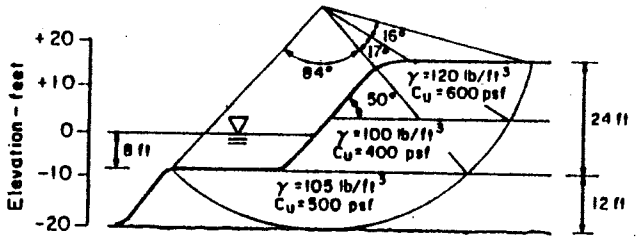

Investigate a deep circle tangent to elevation - 20

$d = \frac{12}{24} = 0.5$ $\quad H_w/H = \frac{8}{24} = 0.33$

From Fig.6, $x_o = 0.35$ $\quad y_o = 1.5$ @ $\beta = 50°$

$X_o = (H)(x_o) = (24)(0.35) = 8.4$ ft
$Y_o = (H)(y_o) = (24)(1.5) = 36$ ft

Plot critical circle on slope above

$$C_{ave} = \frac{(16)(600) + (17)(400) + (84)(500)}{16+17+84} = 499 \text{ psf}$$

From Fig.7a., $\mu_w = 0.95$ for $d = 0.5$ and $H_w/H = 0.33$

$$P_d = \frac{(108)(24) - (62.4)(8)}{(1)(0.95)(1)} = 2203$$

From Fig.6, $N_o = 5.6$ for $d = 0.5$ and $\beta = 50°$

$$F = \frac{(5.6)(499)}{2203} = 1.27$$

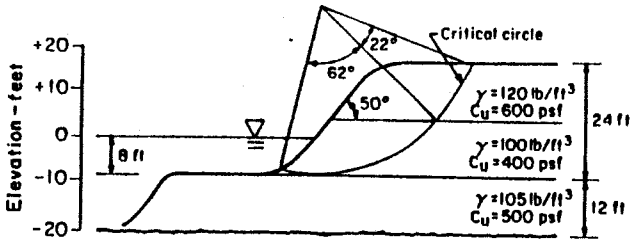

Investigate a circle tangent to elevation - 8 ft

$d = 0$ $\quad H_w/H = \frac{8}{24} = 0.33$

From Fig.6, $x_o = 0.35$, $y_o = 1.4$ critical circle intersects near toe of slope

$X_o = (24)(0.35) = 8.4$ ft $\quad Y_o = (24)(1.4) = 33.6$ ft

Plot circle on slope above

$$C_{ave} = \frac{(22)(600) + (62)(400)}{22+62} = 452 \text{ psf}$$

From Fig.7a., $\mu_w = 0.93$ for $\beta = 50°$ and $H_w/H = 0.33$

$$P_d = \frac{(110)(24) - (62.4)(8)}{(1)(0.93)(1)} = \frac{2640 - 499}{0.93} = 2302$$

From Fig.6, $N_o = 5.8$ for $d = 0$ and $\beta = 50°$

$$F = \frac{(5.8)(452)}{2302} = 1.14$$ (more critical than circle tangent to elevation - 20 ft).

Fig. 12 EXAMPLES OF USE OF CHARTS FOR SLOPES IN SOILS WITH $\phi = 0$.

average values for the circle considered.

Once the types of circles to be investigated have been selected, the following steps should be performed, for each case studied.

2. Calculate P_d using the formula

$$P_d = \frac{\gamma H + q - \gamma_w H_w}{\mu_q \mu_w \mu_t}$$

in which

γ = average unit weight of soil (F/L^3)
H = slope height above slope (L)
q = surcharge (F/L^2)
γ_w = unit weight of water (F/L^3)
H_w = height of external water above toe (L)
μ_q = surcharge correction factor (Fig. 7a, top)
μ_w = submergence correction factor (Fig. 7a, bottom)
μ_t = tension crack correction factor (Fig. 7b)

If there is no surcharge, $\mu_q = 1$; if there is no submergence, $\mu_w = 1$; and if there are no tension cracks, $\mu_t = 1$.

If the circle being studied passes above the natural toe of the slope, the point where the circle intersects the slope face should be taken as the "toe" of the slope for the calculation of H and H_w.

3. Calculate P_e using the formula

$$P_e = \frac{\gamma H + q - \gamma_w H_w'}{\mu_q \mu'_w}$$

in which

H_w' = height of water within slope above toe (L)

μ_w = seepage correction factor (Fig. 7a, bottom)

and the other factors are as defined previously.

H'_w is the average level of the piezometric surface within the slope. For steady seepage conditions this is related to the position of the phreatic surface beneath the crest of the slope as shown in Fig. 9.

If the circle being studied passes above the natural toe of the slope, H'_w must be measured relative to the adjusted "toe" as defined in step 2.

If there is no seepage, $\mu'_w = 1$; and if there is no surcharge, $\mu_q = 1$.

In an effective stress analysis of a slope in soil of low permeability, if the surcharge is applied so quickly that there is not sufficient time for the soil to consolidate under the surcharge, take $q = 0$ and $\mu_q = 1$ in the formula for P_e.

In a total stress analysis, internal pore water pressure is not considered, so $H'_w = 0$ and $\mu'_w = 1$ in the formula for P_e.

4. Calculate the dimensionless parameter $\lambda_{c\Phi}$ using the formula

$$\lambda_{c\Phi} = \frac{P_e \tan \Phi}{c}$$

in which

$\tan \Phi$ - average value of $\tan \Phi$

c - average value of c (F/L^2)

For $c = 0$, $\lambda_{c\Phi}$ is infinite. In this case the charts for infinite slopes are appropriate.

Steps 4 and 5 are iterative steps. On the first iteration, average values of tan Φ and c have to be estimated by inspection of the layers through which the circle under investigation will pass.

5. Using the chart on the right side of Figure 8, determine the center coordinates of the circle under investigation. The coordinates X_o and Y_o are measured relative to the adjusted "toe" of the slope, if applicable.

   Plot the critical circle on a scaled cross section of the slope and calculate the weighted average values of tan Φ and c along the failure arc, using the number of degrees intersected along the arc by each soil layer as a weighting factor.

   Return to step 4 with these average values of the shear strength parameters and repeat this iterative process until the value of $\lambda_{c\Phi}$ becomes constant. See Fig. 13 for two examples.

6. Using the chart on the left side of Figure 8, determine the value of the stability number N_{cf}, which depends on the slope angle, β , and the value of $\lambda_{c\Phi}$.

7. Calculate the factor of safety, F, using the formula

$$F = N_{cf} \frac{c}{P_d} \quad \text{(for } c > 0\text{)}$$

Examples of the use of the $\Phi > 0$ charts for both total and effective stress analyses are shown in Fig. 13.

If $c = 0$, the value of $\lambda_{c\Phi}$ is infinite and the factor of safety is

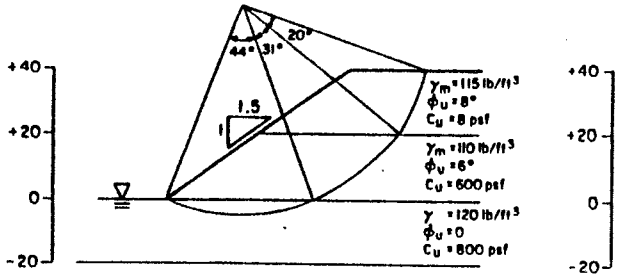

Investigate a toe circle in terms of total stress

$$Pd = \frac{(112.5)(40)}{(1)(1)(1)} = 4500 \text{ psf}$$

$$Pe = \frac{(112.5)(40)}{(1)(1)(1)} = 4500 \text{ psf}$$

Estimate C_{ave} = 700 psf, tan ϕ = 0.122

$$\lambda_{c\phi} = \frac{(4500)(0.122)}{700} = 0.8$$

From Fig 8, x_o = 0.6 and y_o = (1.5)(40) = 60 ft
X_o = (0.6)(40) = 24 ft ; Y_o = (1.5)(40) = 60 ft

$$C_{ave} = \frac{(20)(800) + (31)(600) + (44)(800)}{20 + 31 + 44} = 735 \text{ psf}$$

$$\tan \phi_{ave} = \frac{(20)(\tan 8°) + (31)(\tan 6°) + (44)(\tan 0)}{20 + 31 + 44} = 0.064$$

$$\lambda_{c\phi} = \frac{(4500)(0.064)}{735} = 0.4$$

From Fig.8, x_o = 0.65, y_o = 1.45 for b = 1.5 and $\lambda_{c\phi}$ = 0.4
X_o = (0.65)(40) = 26 ft Y_o = (1.45)(40) = 58 ft

This circle is close enough to the previous iteration, so keep
$\lambda_{c\phi} \approx 0.4$ and C_{ave} = 735 psf

From Fig 8, N_{cf} = 6 for b = 1.5 and $\lambda_{c\phi}$ = 0.4

$$F = \frac{(6)(735)}{4500} = 1.0$$

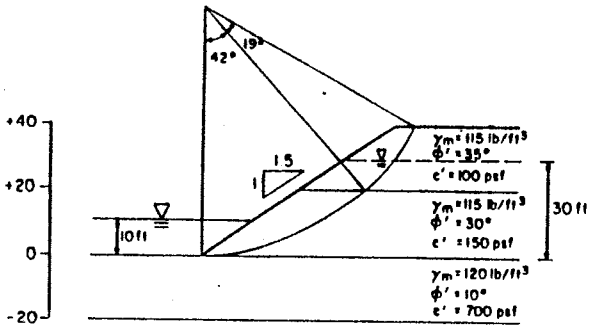

Investigate a toe circle in terms of effective stress

$$Pd = \frac{(115)(40) - (62.4)(10)}{(1)(0.96)(1)} = 4141 \text{ psf}$$

$$Pe = \frac{(115)(40) - (62.4)(30)}{(1)(0.95)(1)} = 2870 \text{ psf}$$

Estimate C_{ave} = 120 psf and tan ϕ_{ave} = 0.64

$$\lambda_{c\phi} = \frac{(2870)(0.64)}{120} = 15.3$$

From Fig.8, x_o = 0.0 and y_o = 1.9 for b = 1.5 and $\lambda_{c\phi}$ = 15.3
X_o = 0 ft, Y_o = (1.9)(40) = 76 ft

$$C_{ave} = \frac{(19)(100) + (42)(150)}{19 + 42} = 134 \text{ psf}$$

$$\tan \phi_{ave} = \frac{(19)(\tan 35°) + (42)(\tan 30°)}{19 + 42} = 0.62$$

$$\lambda_{c\phi} = \frac{(2870)(0.62)}{134} = 13.3$$

From Fig 8, x_o = 0.02 and y_o = 1.85 for b = 1.5 and $\lambda_{c\phi}$ = 13.3
X_o = (0.02)(40) = 0.8 ft and Y_o = (1.85)(40) = 74 ft

This circle is close enough to the previous iteration, so keep
$\lambda_{c\phi}$ = 13.3 and C_{ave} = 134 psf.

From Fig 9, N_{cf} = 35 for b = 1.5 and $\lambda_{c\phi}$ = 13.3

$$F = \frac{(35)(134)}{4141} = 1.13$$

Fig 13 EXAMPLES OF USE OF CHARTS FOR SOILS WITH $\phi > 0$

calculated using the formula

$$F = \frac{P_e}{P_d} \; b \tan \phi \quad (\text{for } c = 0)$$

in which

b = slope ratio = cot β, and the other factors are as defined previously. Fig. 10 can also be used for analysis of infinite slopes.

Slope Stability Charts for Infinite Slopes. Two types of conditions can be analyzed accurately using the charts shown in Fig. 10, which are based on infinite slope analyses. These conditions are:

1. Slopes in cohesionless materials, where the critical failure mechanism is shallow sliding or surface ravelling.

2. Slopes in residual soils, where a relatively thin layer of soil overlies firmer soil or rock, and the critical failure mechanism is sliding along a plane parallel to the slope, at the top of the firm layer.

Steps for use of the charts for effective stress analyses:

1. Determine the pore pressure ratio, r_u, which is defined by the formula

$$r_u = \frac{u}{\gamma H}$$

in which u = pore pressure (F/L^2)

γ = total unit weight of soil (F/L^3)

H = depth corresponding to pore pressure, u (L)

For an existing slope, the pore pressure can be determined from field

measurements, using piezometers installed at the depth of sliding.

For seepage parallel to the slope, which is a condition frequently used for design, the value of r_u can be calculated using the following formula:

$$r_u = \frac{X}{T} \frac{\gamma_w}{\gamma} \cos^2\beta \qquad \left(\begin{array}{c}\text{for seepage} \\ \text{parallel to slope}\end{array}\right)$$

in which X = distance from the depth of sliding to the surface of seepage, measured normal to the surface of the slope (L)

T = distance from the depth of sliding to the surface of the slope, measured normal to the surface of the slope (L)

γ_w = unit weight of water (F/L^3)

γ = total unit weight of soil (F/L^3)

β = slope angle.

For seepage emerging from the slope, which is more critical than seepage parallel to the slope, the value or r_u can be calculated using the following formula

$$r_u = \frac{\gamma_w}{\gamma} \frac{1}{1 + \tan\beta \tan\Theta} \qquad \left(\begin{array}{c}\text{for seepage emerging} \\ \text{from slope}\end{array}\right)$$

in which Θ angle of seepage measured from the horizontal direction, and the other factors are as defined previously.

Submerged slopes with no excess pore pressures can be analyzed using $\gamma = \gamma_b$ (buoyant unit weight) and $r_u = 0$.

2. Determine the values of the dimensionless parameters A and B from the charts at the bottom of Fig. 10.

3. Calculate the factor of safety, F, using the formula

$$F = A \frac{\tan\Phi'}{\tan\beta} + B \frac{c'}{\gamma H}$$

in which Φ' = angle of internal friction in terms of effective stress

c' = cohesion intercept in terms of effective (F/L^2) stress

β = slope angle

H = depth of sliding mass measured vertically (L)

and the other factors are as defined previously.

Steps for use of charts for total stress analyses:

1. Determine the value of B from the chart in the lower right corner of Fig. 10.

2. Calculate the factor of safety, F, using the formula

$$F = \frac{\tan\Phi}{\tan\beta} + B \frac{C}{\gamma H}$$

in which Φ = angle of internal friction in terms of total stress

c = cohesion intercept in terms of total stress (F/L^2)

and the other factors are as defined previously.

An example of the use of the infinite slope charts is given in Fig. 14.

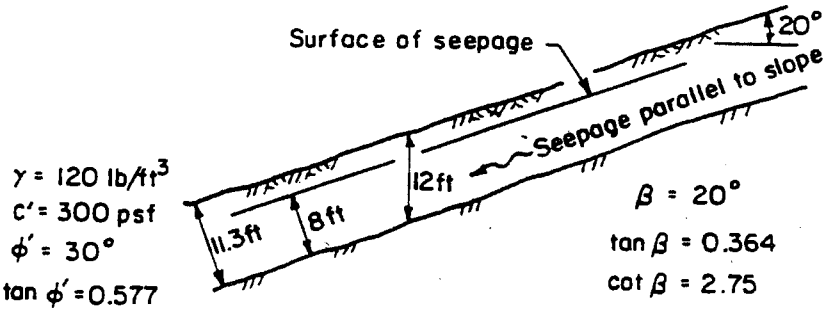

For seepage parallel to slope, with X = 8 ft., T = 11.3 ft. } Formula from Fig. 10

$$r_u = \frac{8}{11.3}\,\frac{62.4}{120}\,(0.94)^2 = 0.325$$

From Fig. 10, A = 0.62 for $r_u = 0.325$ and $\cot\beta = 2.75$

B = 3.1 for $\cot\beta = 2.75$

$$F = 0.62\,\frac{0.577}{0.364} + 3.1\,\frac{300}{(120)(12)} = 0.98 + 0.65 = 1.63$$

For horizontal seepage emerging from slope, $\theta = 0$ } Formula from Fig. 10

$$r_u = \frac{62.4}{120}\,\frac{1}{1+(0.364)(0)} = 0.52$$

From Fig. 10, A = 0.41 for $r_u = 0.52$ and $\cot\beta = 2.75$

B = 3.1 for $\cot\beta = 2.75$

$$F = 0.41\,\frac{0.577}{0.364} + 3.1\,\frac{300}{(120)(12)} = 0.65 + 0.65 = 1.30$$

Fig. 14 EXAMPLE OF USE OF INFINITE SLOPE CHARTS.

Charts for Slopes in Soils with Strength Increasing with Depth, and $\Phi = 0$. The chart for slopes in soils with strength increasing with depth, and $\Phi = 0$, is shown in Fig. 11.

Steps for use of chart:

1. Select the linear variation of strength with depth which best fits the measured strength data. Extrapolate this linear variation upward to determine H_o, the height at which the strength profile intersects zero, as shown in Fig. 11.

2. Calculate $M = H_o/H$, where H = slope height.

3. Determine the dimensionless stability number, N, from the chart in the lower right corner of Fig. 11.

4. Determine the value of strength, c_b, at the elevation of the bottom of the slope.

5. Calculate the factor of safety, F, using the formula

$$F = N \frac{c_b}{\gamma (H + H_o)}$$

in which γ = total unit weight of soil for slopes above water,
γ = buoyant unit weight for submerged slopes, and
γ = weighted average unit weight for partly submerged slopes.

An example of the use of this chart is given in Fig. 15.

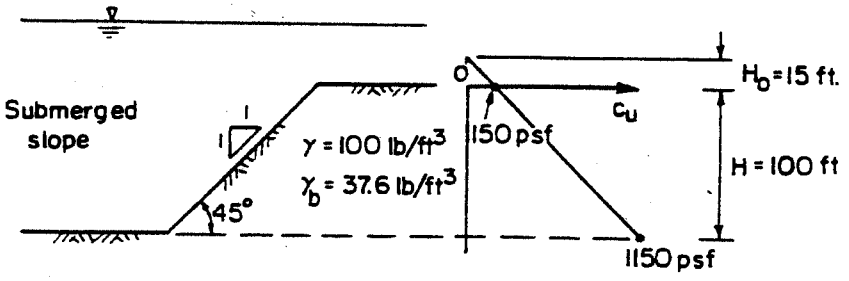

$$M = \frac{15}{100} = 0.15$$

From Fig. 11, $N = 5.1$ for $M = 0.15$ and $\beta = 45°$

$$C_b = 1150 \text{ psf}$$

$$F = (5.1)\frac{1150}{(37.6)(115)} = 1.36$$

Fig. 15 EXAMPLE OF USE OF CHART FOR STRENGTH INCREASING WITH DEPTH, AND $\phi = 0$.

DETAILED ANALYSES OF SLOPE STABILITY

When the site conditions and strength values have been investigated thoroughly and defined accurately, it is appropriate to perform detailed analyses of the stability. Three methods of detailed analysis are described in subsequent sections. These are:

1. The Method of Moments for $\Phi = 0$. This is a very simple but theoretically accurate method for analysis of circular slip surfaces in $\Phi = 0$ soils.

2. The Ordinary Method of Slices. This is a simple and conservative procedure for analysis of circular slip surfaces in soils with $\Phi > 0$. It can also be used for slopes in $\Phi = 0$ soils, and it gives accurate results for this case. For flat slopes with high pore pressures, the factors of safety calculated by this method may be much smaller than values of F calculated by more accurate methods, and it should not be used for such problems.

3. The Wedge Method. This is a simple and conservative procedure for analysis of noncircular surfaces in soils with $\Phi = 0$ or $\Phi > 0$.

Method of Moments for $\Phi = 0$ Soils. For short-term stability problems in saturated soils, the undrained soil strengths can be expressed as

$$S_u = \text{constant} \quad (\Phi_u = 0)$$

with $\Phi_u = 0$, the undrained strength is not dependent on normal stress, and a very simple method of analysis (the $\Phi = 0$ method) can be employed to calculate the factor of safety.

The factor of safety with respect to sliding on a particular circular arc is defined by the equation

$$F = \frac{RM}{OM}$$

in which RM resisting moment due to mobilizing the shear strengths of all of the soils through which the arc passes, and OM overturning moment due to the weight of the soil mass bounded by the circular arc.

The factor of safety defined by this equation can be shown to be exactly the same as the ratio between the shear strength of the soil divided by the shear stress required for equilibrium of the slope. Thus the factor of safety calculated by this method may be considered as the factor by which all of the soil strength values would have to be divided to bring the slope into a state of barely stable equilibrium. The factor of safety should always be at least as large as the margin of uncertainty regarding soil strengths.

The factor of safety of a slope is calculated using the following procedure:

(1) Select a trial circular slip surface (an example is shown in Fig. 16).

(2) Divide the mass bounded by the circular arc into a number of sections, following soil boundaries. If there is water outside the slope, it should be represented by one or more sections just as if it was a soil with weight but no strength.

(3) For each section calculate the area, the weight, the moment arm, and the moment. The areas may be estimated using a planimeter, or by approximating the sections by rectangles and triangles. The moment arms are measured horizontally from the circle center to the centroids of the areas. Note that for a left-facing slope, as in Fig. 16, moment arms are positive to the right and negative to the left. The algebraic sum of the moments of the sections is the overturning moment (OM) of the mass bounded by the circular arc.

(4) For each segment of arc, determine the arc length, the shear strength, the resisting force (product of arc length multiplied by shear

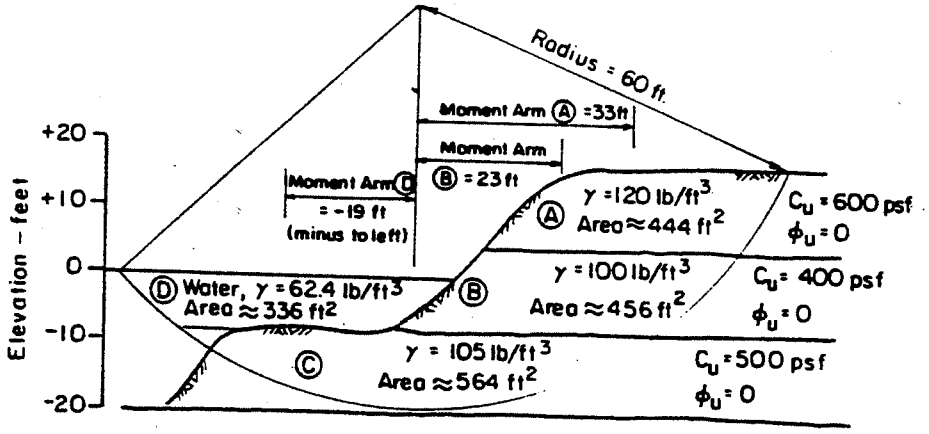

Section	Area (ft^2)	γ (lb/ft^3)	Weight (lb/ft)	Moment Arm (ft)	Moment (ft-lb/ft)
Ⓐ	444	120	53,280	+ 33	$+ 1.76 \times 10^6$
Ⓑ	456	100	45,600	+ 23	$+ 1.05 \times 10^6$
Ⓒ	564	105	59,220	0	0.0
Ⓓ	336	62.4	20,970	- 19	$- 0.40 \times 10^6$
			Total Overturning Moment	=	$+ 2.41 \times 10^6$

Section	Ave. Length (ft)	C_u (psf)	Force (lb/ft)	Moment Arm = Radius (ft)	Moment (ft-lb/ft)
Ⓐ	14	600	8,400	60	0.50×10^6
Ⓑ	16.5	400	6,600	60	0.40×10^6
Ⓒ	69	500	34,500	60	2.07×10^6
Ⓓ	18	0	0	60	0.00
			Total Resisting Moment	=	2.97×10^6

$$\text{Factor of Safety, } F = \frac{\text{Resisting Moment}}{\text{Overturning Moment}} \quad \frac{2.97 \times 10^6}{2.41 \times 10^6} = 1.23$$

Fig. 16 METHOD OF MOMENTS FOR $\phi = 0$.

strength) and the moment (product of resisting force multiplied by circle radius). The sum of the individual moments is the resisting moment (RM) of the soil through which the arc passes.

(5) Calculate the factor of safety for the selected circle, F = RM/OM.

(6) Repeat steps (1) through (5) for a number of circles tangent to the same elevation as the first, until the most critical circle (the one with the lowest value of F) tangent to this elevation has been located.

(7) Repeat for other tangent elevations until the overall critical circle has been located.

Ordinary Method of Slices or Fellinius Method for Soils with $\Phi = 0$ or $\Phi > 0$. The Ordinary Method of Slices can be used to calculate the factor of safety for a circular slip surface in soils whose strengths are governed by any of the following equations:

$$s = c \quad (\Phi = 0)$$

$$s = \sigma \tan\Phi$$

$$\text{or} \quad s = c + \sigma \tan\Phi$$

in which s = shear strength, σ = normal stress on the failure plane, c = cohesion intercept, and Φ = friction angle. To be able to determine the strengths of soils with $\Phi > 0$, the normal stress on the failure plane must be known. Therefore, to analyze the stability of slopes in such soils, it is necessary to determine the normal stress on the shear surface analyzed.

For analysis by the Ordinary Method of Slices, the mass above a trial circular slip surface is divided into a number of vertical slices as shown in Fig. 17. The basic assumption in the method is that the resultant of the side forces on any slice acts parallel to the base of the slice and therefore does not influence the normal stress on the base of the slice. This assumption is conservative, and the method results in factors of

safety which are lower than values calculated by more accurate methods. For most cases the error due to this assumption is no more than 10%. For very high pore pressures and flat slopes, however, the error may be 50% or even more. For high pore pressures and flat slopes, a more accurate method such as Bishop's Modified Method (Bishop, 1955) should be used.

The factor of safety by the Ordinary Method of Slices may be expressed as

$$F = \frac{\Sigma(W\cos\alpha - u\ell)\ \tan\Phi + \Sigma c\ell}{\Sigma W\sin\alpha}$$

in which F = factor of safety, c = cohesion, Φ = friction angle, W = slice weight, α = inclination of base of slice, u = pore pressure on base of slice, and ℓ = length of base of slice.

The factor of safety defined by this equation can be shown to be exactly the same as the ratio between the shear strength of the soil and the shear stress required for equilibrium of the slope. Thus the factor of safety calculated by this method may be considered as the factor by which all of the values of c and tan Φ would have to be divided to bring the slope into a state of barely stable equilibrium. The factor of safety should always be at least as large as the margin of uncertainty regarding soil strengths.

The factor of safety of a slope is calculated using the following procedure:

(1) Select a trial slip surface (an example is shown in Fig. 17).

(2) Divide the mass bounded by the circular arc into a number of vertical slices. The slices should be chosen so that the base of any slice lies wholly within a single soil layer. For hand calculations, 8 to 12 slices are sufficient; for computer analysis 30 or more slices are used. If there is water outside the slope, it should be represented by one or more slices, just as if it was a soil with weight but not strength.

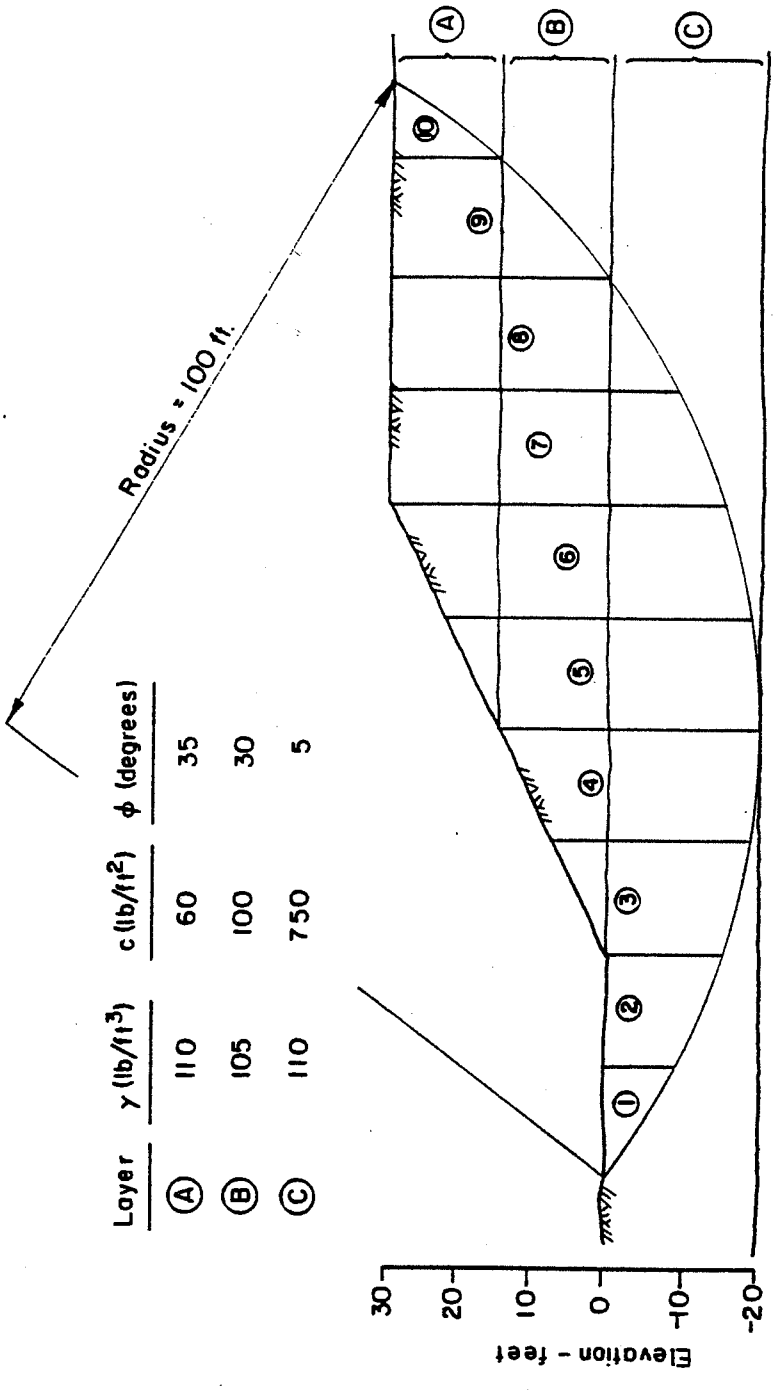

Fig. 17 EXAMPLE PROBLEM FOR ORDINARY METHOD OF SLICES.

(3) Calculate the weight of each vertical slice. When a slice crosses more than one layer having different unit weights, the weights within each layer are summed to determine the total weight of the slice. This may be done conveniently using the tabular computation form in Fig. 18. An example is shown in Fig. 19.

(4) For each slice, determine the length of the base (ℓ), the angle of inclination of the base (α), the cohesion of the soil at the base (c), the friction angle of the soil at the base (Φ), and the pore pressure at the base (u). (If the analysis is being done with total stresses, use u = 0). Enter these values, along with the weight of each slice, in the tabular computation form shown in Fig. 20.

(5) Calculate the factor of safety following the procedure indicated on the computation form. An example is shown in Fig. 21.

(6) Repeat steps (1) through (5) for a number of circles tangent to the same elevation as the first, until the most critical circle (the one with the lowest value of F) tangent to this elevation has been located.

(7) Repeat for other tangent elevations until the overall critical circle has been located.

Wedge Method for Soils with $\Phi = 0$ or $\Phi > 0$. The Wedge Method can be used to calculate the factor of safety for a noncircular slip surface in soils whose strengths are governed by any of the following equations:

$$s = c \quad (\Phi = 0)$$
$$s = \sigma \tan\Phi$$
$$s = c + \sigma \tan\Phi$$

in which s = shear strength, σ = normal stress on the failure plane, c = cohesion intercept, and Φ = friction angle. To be able to determine the strengths of soils with $\Phi > 0$, the normal stress on the failure plane must

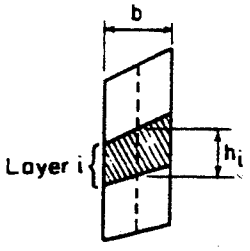

γ_i = unit weight of layer i

h_i = height of layer at center of slice

W_i = partial weight = $b h_i \gamma_i$

ΣW_i = total weight of slice

Slice No.	b	h_i	γ_i	W_i	ΣW_i

Fig. 18 TABULAR FORM FOR COMPUTING WEIGHTS OF SLICES.

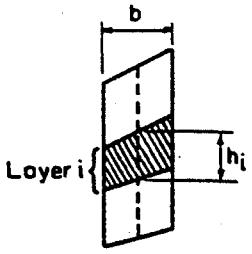

γ_i = unit weight of layer i

h_i = height of layer of center of slice

W_i = partial weight = $b h_i \gamma_i$

ΣW_i = total weight of slice

Slice No.	ft b	ft h_i	lb/ft³ γ_i	lb/ft W_i	lb/ft ΣW_i
1	15	5	110	8200	8,200
2	15	13	110	21400	21,400
3	15	4	105	6300	
		17.5	110	28700	35,200
4	15	11.5	105	18100	
		19.5	110	32200	50,300
5	15	1	110	1600	
		15	105	23600	
		19.5	110	32200	62,400
6	15	11.5	110	19000	
		15	105	23600	
		17.5	110	28900	71,500
7	15	15	110	24800	
		15	105	23600	
		15	110	21400	69,800
8	15	15	110	24800	
		15	105	23600	
		5	110	8200	56,600
9	16	15	110	26400	
		7.5	105	12600	39,000
10	11	7.5	110	9100	9,100

Fig. 19 EXAMPLE OF USE OF TABULAR FORM FOR COMPUTING WEIGHTS OF SLICES.

Slice No.	W	ℓ	α	C	ϕ	u	$u\ell$	$W\cos\alpha$	$W\cos\alpha - u\ell$	$(W\cos\alpha - u\ell)\tan\phi$	$C\ell$	$W\sin\alpha$
										Σ		

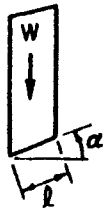

C = cohesion intercept
ϕ = friction angle
u = pore pressure
} at base of slice

$$F = \frac{\Sigma (W\cos\alpha - u\ell)\tan\phi + \Sigma c\ell}{\Sigma W\sin\alpha}$$

$$F = \frac{\qquad\qquad}{\qquad\qquad} =$$

Fig. 20 TABULAR FORM FOR CALCULATING FACTOR OF SAFETY BY ORDINARY METHOD OF SLICES.

Slice No.	W kip/ft	ℓ ft	α degrees	C kip/ft^2	ϕ degrees	u zero for total stress analysis	$u\ell$	W cos α kip/ft	W cos α - $u\ell$	(W cos α - $u\ell$) tan ϕ	C ℓ	W sin α
1	8.2	17.5	-32	0.75	5			6.9		0.61	13.12	-4.35
2	21.4	16.2	-22	0.75	5			19.8		1.73	12.15	-8.02
3	35.2	15.5	-13	0.75	5			34.3		3.00	11.62	-7.92
4	50.3	15.1	-4	0.75	5			50.2		4.39	11.32	-3.51
5	62.4	15.1	4	0.75	5			62.2		5.44	11.32	4.35
6	71.5	15.5	13	0.75	5			69.7		6.10	11.62	16.08
7	69.8	16.2	22	0.75	5			64.7		5.66	12.15	26.15
8	56.6	17.5	32	0.75	5			48.0		4.20	13.12	30.00
9	39.0	22.0	43	0.10	30			28.5		16.45	2.20	26.60
10	9.1	18.5	55	0.10	35			5.2		3.64	1.11	7.45
									Σ	51.2	19.7	26.8

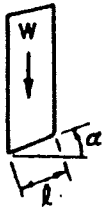

C = cohesion intercept
ϕ = friction angle
u = pore pressure
} at base of slice

$$F = \frac{\Sigma (W\cos\alpha - u\ell)\tan\phi + \Sigma c\ell}{\Sigma W\sin\alpha}$$

$$F = \frac{150.1}{86.8} = 1.74$$

Fig. 21 EXAMPLE OF USE OF TABULAR FORM FOR CALCULATING FACTOR OF SAFETY BY ORDINARY METHOD OF SLICES.

be known. Therefore, to analyze the stability of slopes in such soils, it is necessary to determine the normal stress on the shear surface analyzed.

For analysis by the Wedge Method the mass above the trial slip surface is divided by vertical lines into a number of wedges or slices as shown in Fig. 22. This method satisfies both horizontal and vertical force equilibrium. The basic assumption in the Wedge Method as described in this manual is that the side forces between slices are horizontal. This assumption is conservative, and the method gives factors of safety which are lower than the values calculated by more accurate methods. For most cases the error due to this assumption is no more than 15%. Greater accuracy can be achieved using methods which satisfy all conditions of equilibrium, such as Janbu's Generalized Procedure of Slices (Janbu, 1973), Spencer's Method (Wright, 1969) or Morgenstern and Price's Method (Morgerstern and Price, 1965).

The Wedge Method is most appropriate for conditions where the failure surface is not likely to be circular. For example, the embankment shown in Fig. 22 rests on a thin layer of weak clay, and it is likely that a considerable portion of the critical failure surface will lie within this layer. For this type of problem the wedge mechanism may be more critical than a circular surface.

The factor of safety calculated by the Wedge Method is defined as the ratio between the shear strength and the shear stress required for equilibrium. The factor of safety is the factor by which the strength parameters (c and tan Φ) for each soil would have to be divided to bring the slope into a state of barely stable equilibrium. The factor of safety should always be at least as large as the margin of uncertainty regarding soil strengths.

The Wedge Method factor of safety is calculated by trial and error. A value for F is assumed, and then checked to determine if the assumed value satisfies equilibrium. The analysis can be performed either graphically or numerically. The first three steps are the same whether the graphical or the numerical method is used.

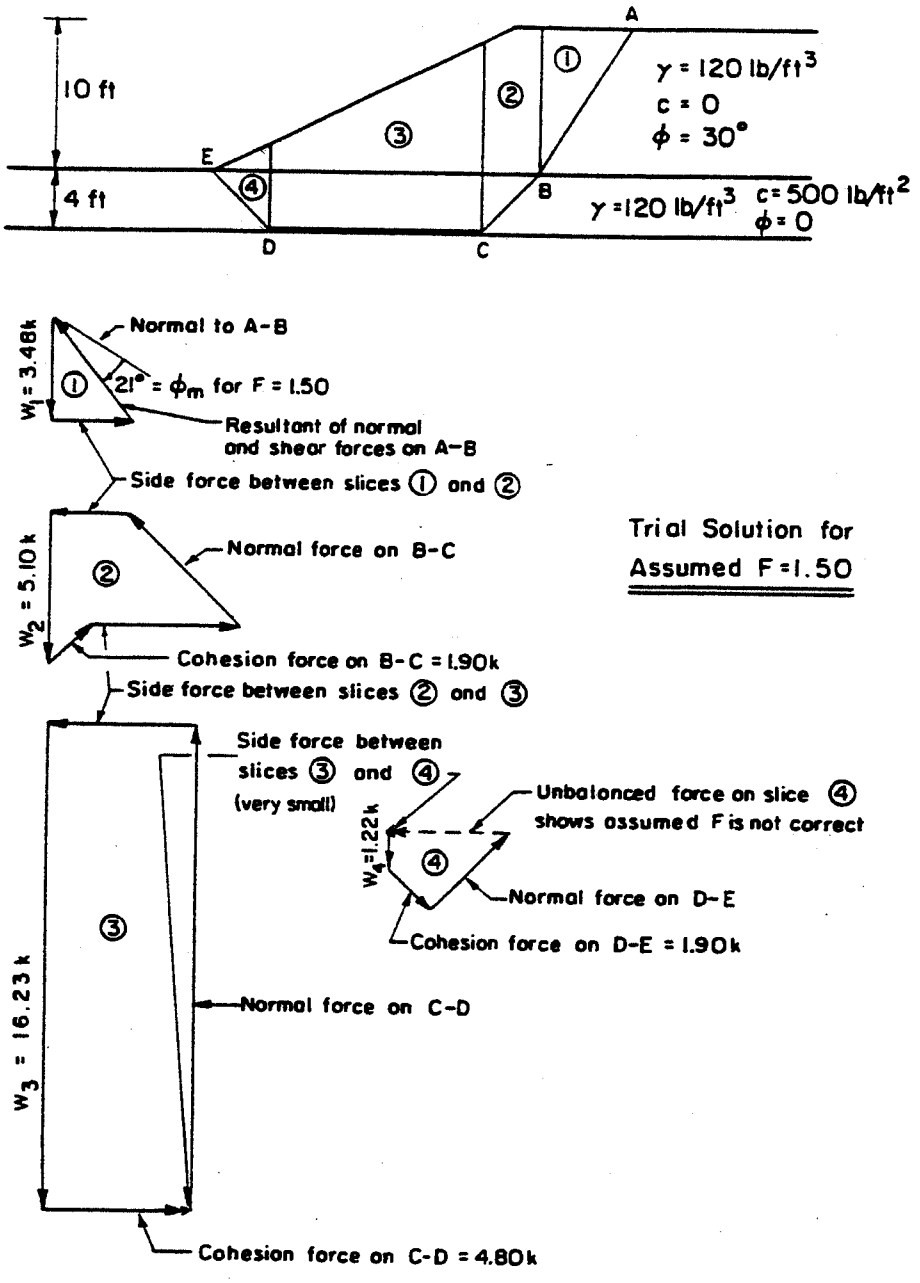

Fig. 22 EXAMPLE OF GRAPHICAL PROCEDURE FOR WEDGE METHOD

(1) Select a trial slip surface (an example is shown in Fig. 22).

(2) Divide the mass above the slip surface into wedges (or slices). The wedges should be chosen so that the base of any wedge lies wholly within a single soil layer. Three to five wedges are usually sufficient. If there is water outside the slope, it should be represented by a wedge, just as if it was soil with weight but no strength.

(3) Calculate the weight of each wedge. If the top as well as the bottom of each wedge is a straight line, the weights can be calculated using the tabular computation form described previously for the Ordinary Method of Slices. If the top boundary of a wedge is a broken line, as for wedge 2 in Fig. 22, the weight of the wedge can be calculated by dividing it into two parts, as shown in Fig. 23.

To solve for the factor of safety graphically, follow steps (4) through (9) below.

(4) Assume a value for the factor of safety, and calculate trial values of mobilized cohesion and mobilized friction angles for each soil using the following formulas:

$$c_m = \frac{C}{F} \qquad (1)$$

$$\text{and} \quad \tan\Phi_m = \frac{\tan\Phi}{F} \qquad (2)$$

in which F = assumed value for the factor of safety, c = cohesion, c_m = mobilized cohesion, Φ = friction angle, and Φ_m = mobilized friction angle.

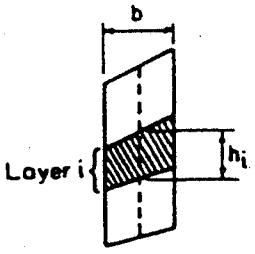

γ_i = unit weight of layer i

h_i = height of layer at center of slice

W_i = partial weight = $b h_i \gamma_i$

ΣW_i = total weight of slice

Slice No.	$\frac{ft}{b}$	$\frac{ft}{h_i}$	$\frac{kip/ft^3}{\gamma_i}$	$\frac{kip/ft}{W_i}$	$\frac{kip/ft}{\Sigma W_i}$
1	5.8	5.0	0.120	3.48	3.48
2 (right)	1.9	10.0	0.120	2.28	
		1.0	0.120	0.23	
2 (left)	1.8	9.0	0.120	1.94	
		3.0	0.120	0.65	5.10
3	14.4	5.4	0.120	7.33	
		4.0	0.120	6.90	16.23
4	3.7	0.9	0.120	0.40	
		1.85	0.120	0.82	1.22

Fig. 23 EXAMPLE OF USE OF TABULAR FORM FOR COMPUTING WEIGHTS OF WEDGES.

(5) Construct the force polygon for wedge 1. An example is shown in Fig. 22. First draw the weight vector vertically, to scale. Next, draw the mobilized cohesion vector, which is equal to the mobilized cohesion multiplied by the length of the base of the slice, and acts parallel to the base of the slice. The tail of this vector connects to the head of the weight vector. (In the example the cohesion is zero on the first slice.) Then, if the analysis is done in terms of effective stress, draw the pore pressure vector, which is equal to the pore pressure on the base of the slice multiplied by the length of the base, and acts perpendicular to the base. The tail of this vector connects to the head of the cohesion vector. If the analysis is done in terms of total stresses, as the example in Fig. 22, the pore pressure is taken as zero, and there is no pore pressure force in any of the force polygons. Next, lay off the direction of the resultant of the normal and frictional forces on the base of the slice. This resultant acts at an angle of Φ_m from the normal direction, and the head of this vector connects to the tail of the weight vector. The remaining force, which closes the polygon, is the side force exerted on wedge 1 by wedge 2. This vector is assumed to act horizontally, as indicated previously. The position of the intersection of the resultant of the normal and frictional forces with the side force determines the lengths of these two vectors, which are unknown until the intersection point is determined.

(6) Construct the force polygon for wedge 2. First draw the weight vector vertically, to scale. Then draw the side force exerted on wedge 2 by wedge 1. Note that this is equal but opposite to the force exerted on wedge 1 by wedge 2, and that the head of this vector connects to the tail of the weight vector. Next, draw the mobilized cohesion vector, which is equal to the mobilized cohesion multiplied by the length of the base of the slice, and acts parallel to the base of the slice, with its tail connected to the head of the weight vector. Then, if the analysis is done in terms of effective stresses, lay off the pore pressure force, from the head of the cohesion force, acting perpendicular to the base of the slice. Next,

lay off the direction of the resultant of the normal and frictional forces on the base of the slice. This resultant acts at an angle of Φ_m from the normal direction, and the head of this vector connects to the tail of the vector, which represents the side force exerted on wedge 2 by wedge 1. (In the example, $\Phi = 0$ for the second slice, and there is therefore no frictional force. In this case the vector consists of only the normal force and acts normal to the base of the slice.) The remaining force, which closes the polygon, is the side force exerted on wedge 2 by wedge 3. This vector is assumed to act horizontally. The position of the intersection of the resultant of the normal and frictional forces with the side force determines the lengths of these two vectors, which are unknown until the intersection point is determined.

(7) Construct the force polygons for the remaining wedges in sequence, using the same procedures as for wedges 1 and 2. If the assumed factor of safety is correct, the force polygon for the last wedge will close, with no unbalanced force. However, if the assumed factor of safety is not correct, an additional force will be required to close the polygon. If the force required to close the polygon would have to act in the direction which would make the slope more stable, the assumed factor of safety is too high. If the required force would have to act in the direction which would make the slope less stable, the assumed factor of safety is too low. This is true for the trial solution with F = 1.50 in Fig. 22.

(8) Assume a new factor of safety and repeat steps (4) through (7). This has been done in Fig. 24. Try additional factors of safety until the unbalanced force on the last slice is negligibly small compared to the magnitudes of the other forces. Then the assumed value of F is the correct one for the assumed failure mechanism. Usually no more than two trials are needed to determine F. By plotting the assumed factor of safety against the magnitude of the unbalanced force for the first two trials, a third trial value of F can usually be estimated which will be very close to the correct value, as shown in Fig. 25. If the value of F determined by this procedure differs

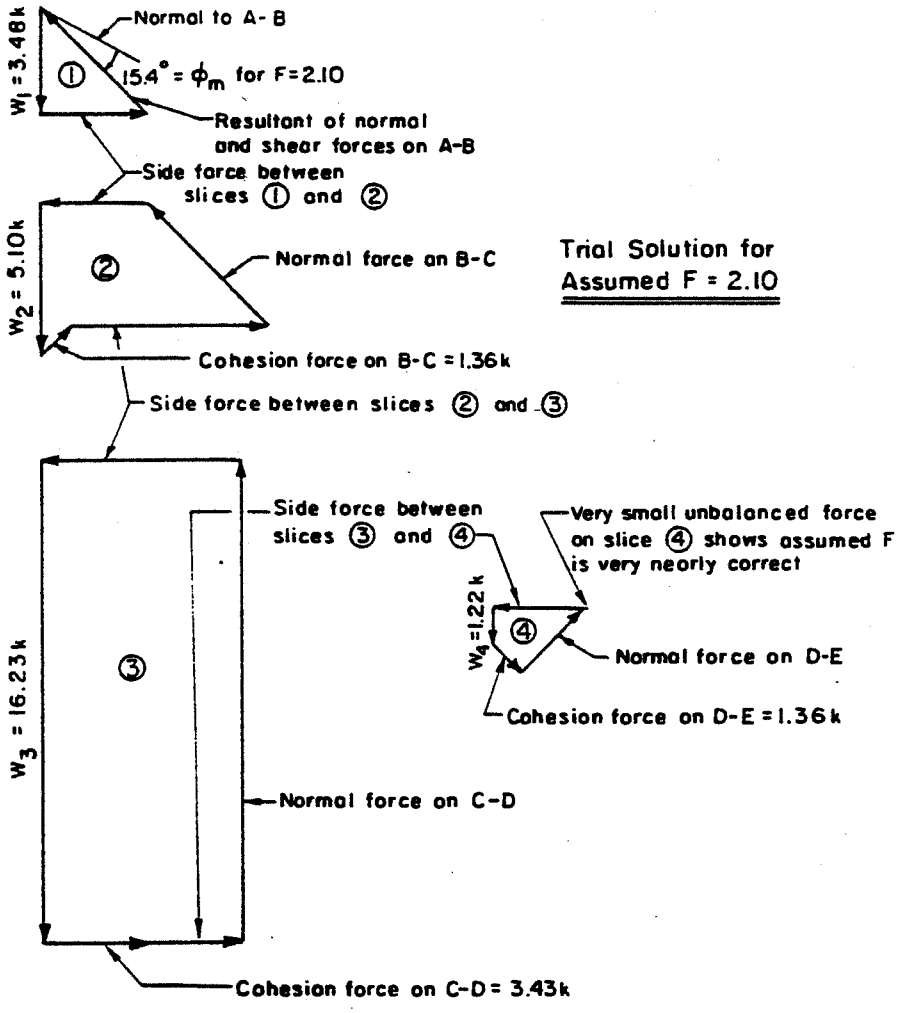

Fig. 24 EXAMPLE OF GRAPHICAL PROCEDURE FOR WEDGE METHOD.
(continued from Fig. 22)

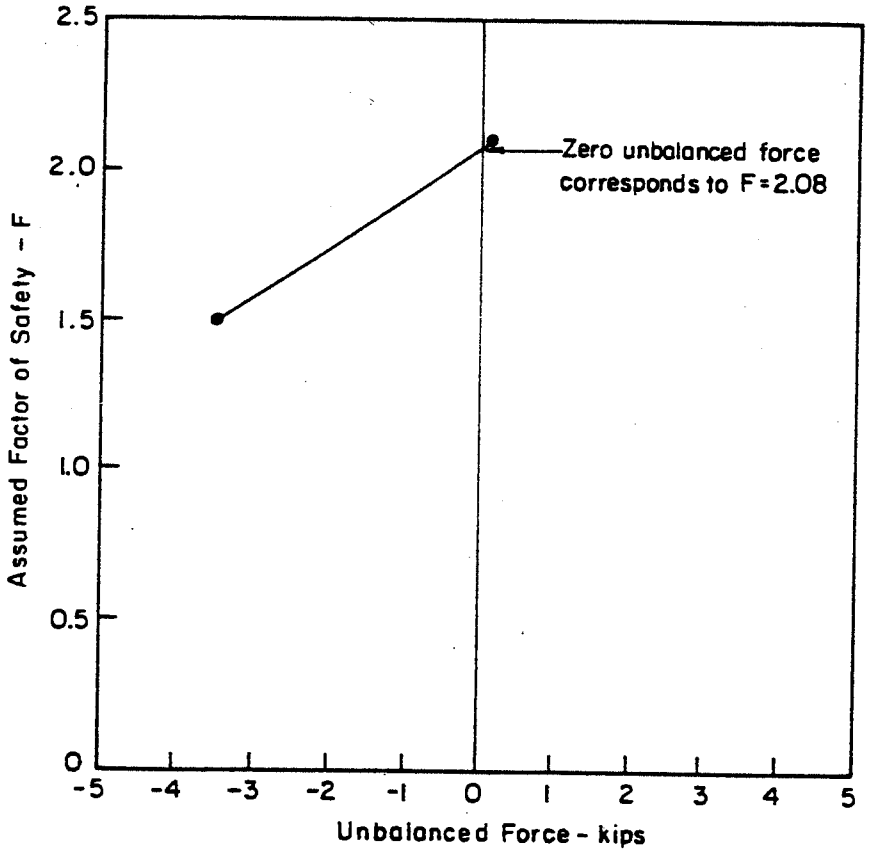

Fig. 25 DETERMINING FACTOR OF SAFETY BY WEDGE METHOD.

greatly from both of the first two trial values, a third trial may be necessary.

(9) Select a new failure mechanism and repeat steps (1) through (8). Try several different failure mechanisms in order to find the one with the lowest factor of safety.

To solve for the Wedge Method factor of safety numerically, use the tabular computation form shown in Fig. 26. Steps (1) through (3), as described previously, are the same for the numerical analysis as for the graphical analysis. Steps (4) through (9) proceed as described below. An example is shown in Fig. 27.

(4) For each wedge, determine the inclination of the base (α), the length of the base (ℓ), the cohesion of the soil at the base (c), the friction angle of the soil at the base (Φ), and the pore pressure at the base (u). (If the analysis is being done with total stresses, use u = 0.) Enter these values, along with the weight of each slide, in the tabular computation form shown in Fig. 26.

(5) Calculate the quantities $c\ell/\cos\alpha$, $W\tan\Phi$, and $u\ell\tan\Phi/\cos\alpha$ for each wedge, and enter these in the table.

(6) Assume a trial value for the factor of safety, and calculate the value of ΔE for each wedge as indicated in the table. ΔE is the difference between the side forces on the left and right sides of each slice, and is given by the equation:

$$\Delta E = \frac{FW\tan\alpha - \frac{c\ell}{\cos\alpha} - W\tan\Phi + \frac{u\ell\tan\Phi}{\cos\alpha}}{F + \tan\Phi\,\tan\alpha}$$

$$\Delta E = \frac{N_4 - N_1 - N_2 + N_3}{N_5}$$

Slice No.	W	α	ℓ	C	ϕ	u	N_1 $\frac{C\ell}{\cos\alpha}$	N_2 W tan ϕ	N_3 $\frac{u\ell \tan\phi}{\cos\alpha}$

Trial	F	Slice No.	N_4 FW tan α	N_5 F + tan ϕ tan α	ΔE	$\Sigma \Delta E$

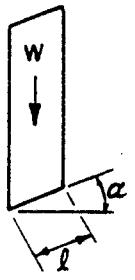

C = cohesion intercept

ϕ = friction angle

u = pore pressure at base of slice

Fig. 26 TABULAR FORM FOR CALCULATING FACTOR OF SAFETY BY WEDGE METHOD.

$$\Delta E = \frac{N_4 - N_1 - N_2 + N_3}{N_5}$$

Slice No.	W (kips)	α	ℓ (ft)	C	ϕ	u	$N_1 = \frac{C\ell}{\cos\alpha}$	$N_2 = W\tan\phi$	$N_3 = \frac{u\ell\tan\phi}{\cos\alpha}$
1	3.48	60°	11.4	0	30°	0	0	2.01	0
2	5.10	45°	5.7	0.50	0°	0	4.03	0	0
3	16.20	0	14.4	0.50	0	0	7.20	0	0
4	1.20	-45°	5.7	0.50	0	0	4.03	0	0

Trial	F	Slice No.	$N_4 = FW\tan\alpha$	$N_5 = F + \tan\phi\tan\alpha$	ΔE	$\Sigma\Delta E$
1	1.50	1	9.05	2.50	2.81	
		2	7.65	1.50	2.41	
		3	0.00	1.50	-4.80	
		4	-1.80	1.50	-3.89	-3.46
2	2.10	1	12.66	3.10	3.44	
		2	10.71	2.10	3.18	
		3	0.00	2.10	-3.43	
		4	-2.52	2.10	-3.12	+0.07
3	2.08	1	12.54	3.08	3.42	
		2	10.61	2.08	3.16	
		3	0.00	2.08	-3.46	
		4	-2.50	2.08	-3.14	-0.02

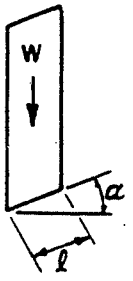

C = cohesion intercept
ϕ = friction angle
u = pore pressure at base of slice

Fig. 27 EXAMPLE OF USE OF TABULAR FORM FOR CALCULATING FACTOR OF SAFETY BY WEDGE METHOD.

(7) Calculate the sum of the terms ΔE for all slices. If the assumed factor of safety is correct, this sum will be zero. If its value is less than zero, the assumed value of F is too low. If it is greater than zero the assumed value of F is too high.

(8) Assume a new value of F and repeat steps (6) and (7). Try additional values of F until the sum of the ΔE's is negligibly small. Then the assumed value of F is the correct one for the assumed failure mechanism. Usually no more than two trials are needed to determine F. By plotting the assumed factor of safety against the value of $\Sigma \Delta E$ for the first two trials, a value of F can usually be estimated which will be very close to the correct value, as shown in Fig. 25. If the value of F determined by this procedure differs greatly from both of the first two values, a third trial may be necessary.

(9) Select a new failure mechanism and repeat steps (1) through (8). Try several failure mechanisms in order to find the one with the lowest factor of safety.

MINIMUM FACTOR OF SAFETY

Locating the Critical Circle. When detailed analyses of slope stability are performed using the Method of Moments for $\Phi = 0$, or using the Ordinary Method of Slices, a number of circles must be examined to locate the most critical circle, with the lowest factor of safety. This can be done conveniently using the following procedure:

(1) Calculate the factors of safety for a number of circles having some common feature. For example:

   (a) all circles tangent to the same elevation, or
   (b) all circles pass through the toe of the slope.

(2) Plot the factors of safety at the locations of the circle centers, and draw contours of F. An example is shown in Fig. 28. If the contours enclose the minimum value of F, the critical circle with the selected common feature can be located readily. If the contours do not enclose the minimum, more circles should be analyzed.

(3) Calculate the factors of safety for additional circles having a second common feature, such as a different tangent elevation, and draw contours of F for these circles. An example is shown in Fig. 29.

(4) Repeat this process until the overall critical circle has been located. A good procedure for many problems is to locate the critical circle passing through the toe of the slope first, and then to examine higher and lower tangent elevations to see if they are more critical.

For complex slopes there may be more than one minimum enclosed by the contours for circles tangent to the same elevation or passing through the toe of the slope. An example is shown in Fig. 30. For these conditions

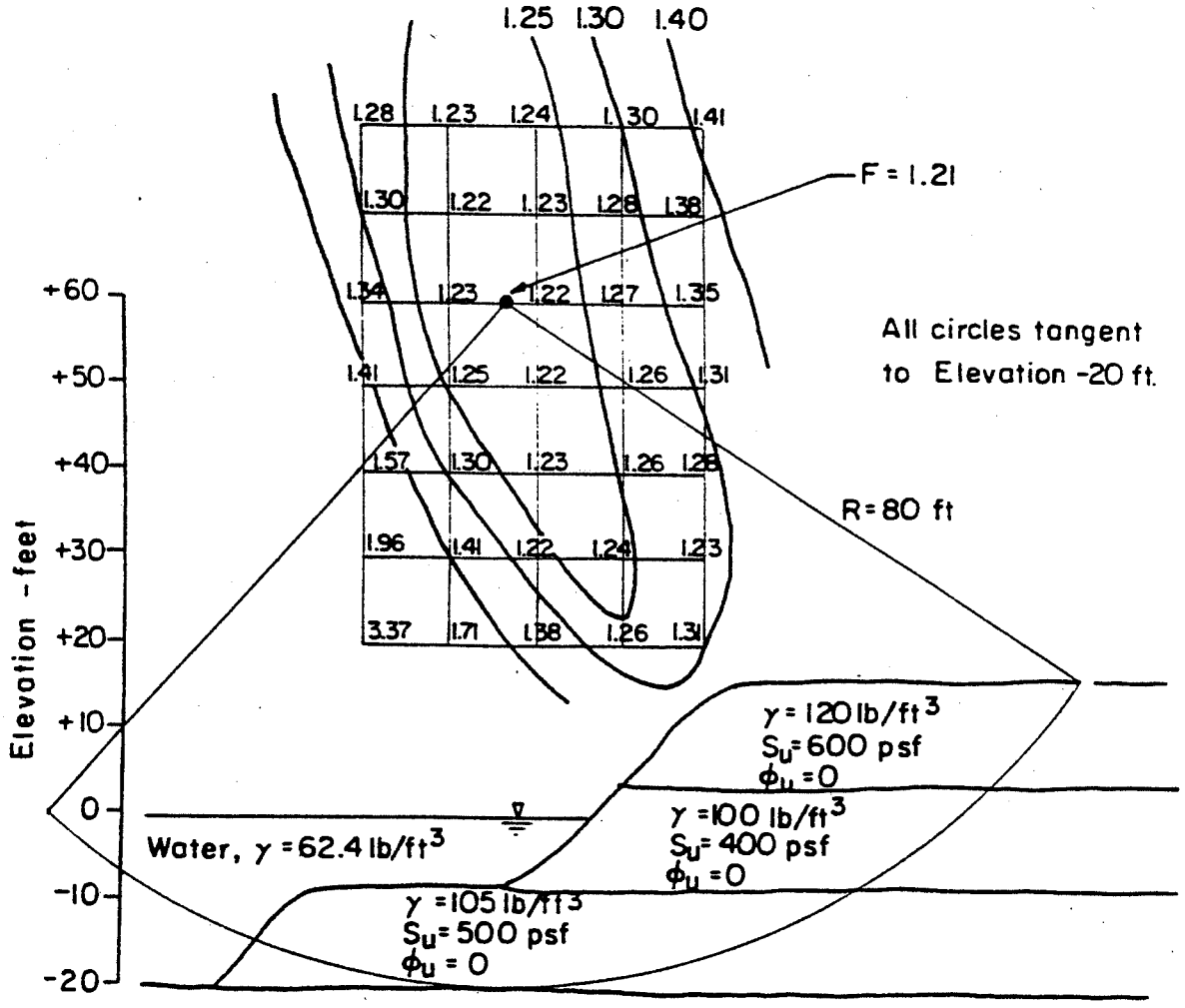

Fig. 28 CONTOURS OF F FOR CIRCLES TANGENT TO ELEVATION -20 FT.

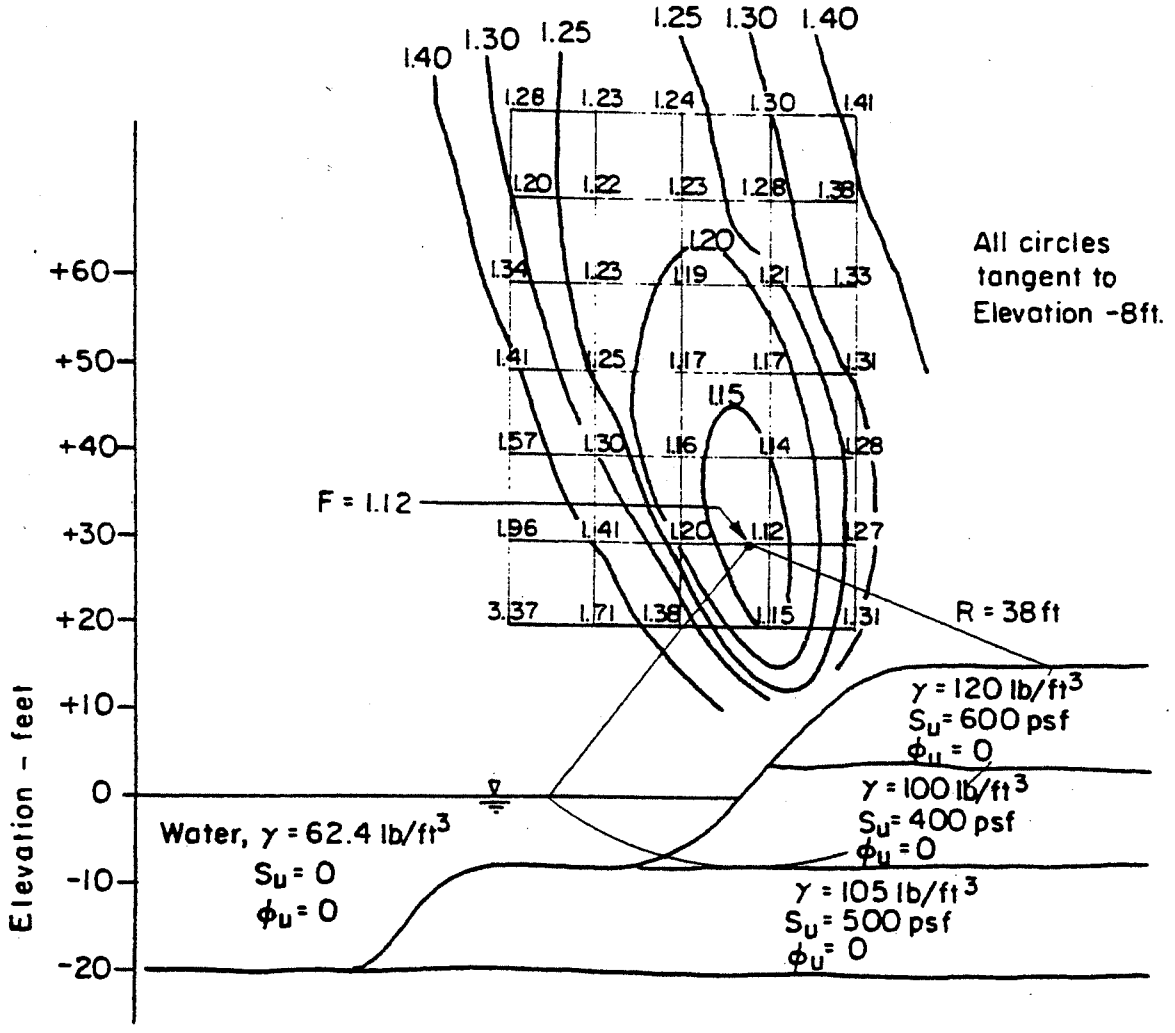

Fig. 29 CONTOURS OF F FOR CIRCLES TANGENT TO ELEVATION - 8 FT.

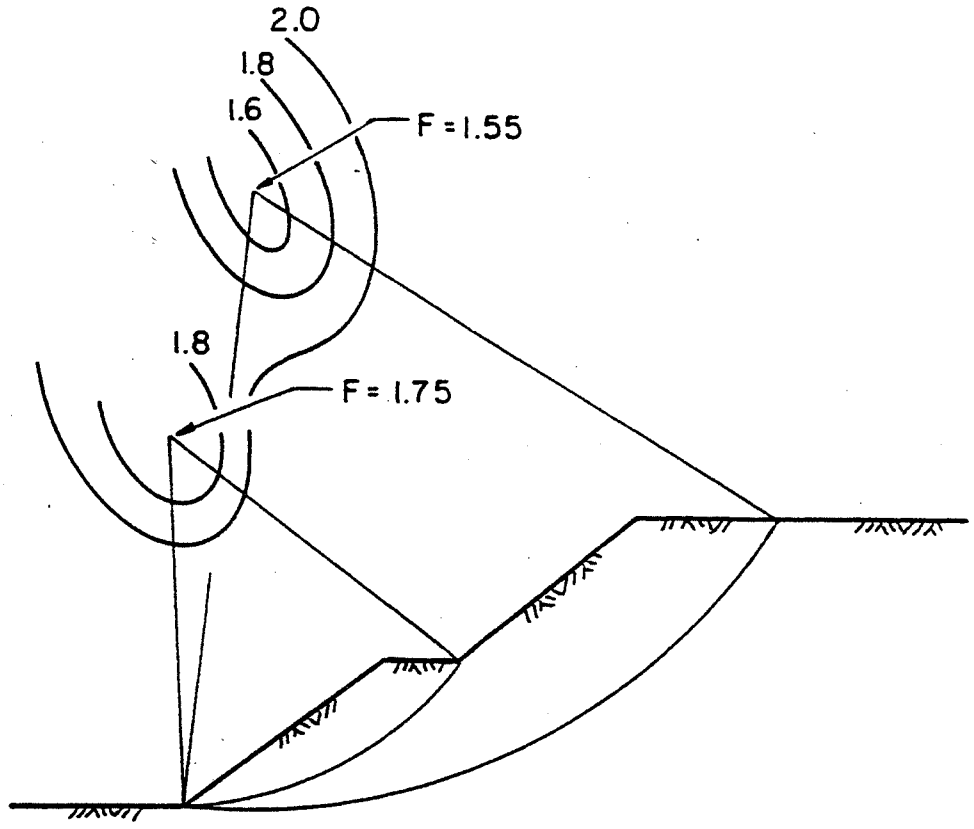

Fig. 30 SLOPE WITH COMPLEX FACTOR OF SAFETY CONTOURS.

widely spaced circle centers should be studied to begin, to be sure that the lowest minimum is located.

Locating the Critical Wedge Mechanism. When detailed analyses are performed using the Wedge Method, enough trial surfaces must be analyzed to determine the minimum factor of safety. The first wedge can be selected as shown in Fig. 31. Then the positions and shapes of the wedges can be varied to find the most critical wedge mechanism.

Sources of Inaccuracy in Calculated Factors of Safety. Under most conditions, the uncertainties due to approximations and assumptions in the method of analysis are smaller than the uncertainties due to inaccuracies in measuring the shear strength. Approximations in the analysis usually amount to 15% or less, but the margin for error in evaluating shear strength may be considerably greater.

Minimum Recommended Values of Safety Factor. The minimum allowable value of F for a slope depends on:

(1) The degree of uncertainty in the shear strength measurements, slope geometry, and other conditions.
(2) The costs of flattening or lowering the slope to make it more stable
(3) The costs and consequences of a slope failure.
(4) Whether the slope is temporary or permanent.

The values of factor of safety in Table 3 are given for guidance.

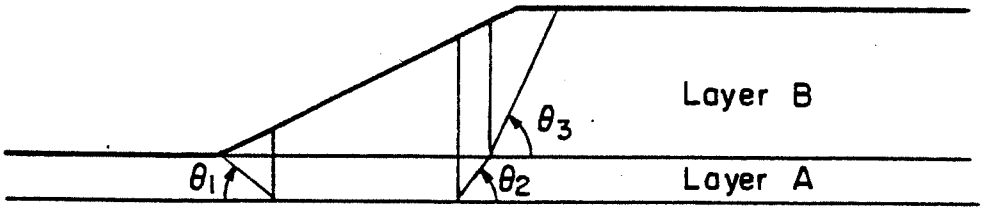

$$\theta_1 \approx 45 - \frac{\phi_{mA}}{2}$$

$$\theta_2 \approx 45 + \frac{\phi_{mA}}{2}$$

$$\theta_3 \approx 45 + \frac{\phi_{mB}}{2}$$

ϕ_{mA} = mobilized friction angle in layer A

ϕ_{mB} = mobilized friction angle in layer B

Fig. 31 TRIAL WEDGE MECHANISM OF FAILURE.

TABLE 3 .-- RECOMMENDED MINIMUM VALUES OF STATIC FACTOR OF SAFETY

Costs and Consequences of Slope Failure	Uncertainty of Strength Measurements	
	Small [1]	Large [2]
Cost of repair comparable to cost of construction. No danger to human life or other property if slope fails.	1.25	1.5
Cost of repair much greater than cost of construction, or danger to human life or other valuable property if slope fails.	1.5	2.0 or greater

[1] The uncertainty of the strength measurements is smallest when the soil conditions are uniform and high quality strength test data provide a consistent, complete and logical picture of the strength characteristics.

[2] The uncertainty of the strength measurements is greatest when the soil conditions are complex and when the available strength data do not provide a consistent, complete, or logical picture of the strength characteristics.

STABILIZATION OF SLOPES AND LANDSLIDES

For purposes of planning effective procedures for stabilizing landslides, it is important to understand the cause or causes of the instability. The most common causes are: oversteepening of the slope by cutting or filling, excess pore water pressure caused by high ground-water levels, strong seepage, or blockage of drainage paths, undercutting due to erosion from surface water, and loss of strength with time due to creep and weathering.

A thorough geological study and a detailed subsurface exploration are the first steps to determine the cause and to plan corrective action for a slope failure. The location of the shear zone within a landslide can sometimes be determined by drilling test borings or by monitoring slope movements using slope indicators which extend beneath the failure zone.

If a slide is being stabilized by flattening the slope, or by use of a buttress or retaining structure, the shear strength of the soil at the time of failure should be determined by calculating what value of strength would correspond to a factor of safety equal to one at failure. This value of strength can be used to evaluate the factor of safety of the slope after stabilization, or to estimate the design loads for retaining structures. Values of shear strength back-calculated from a failure may not agree with values of strength measured in laboratory tests because of difficulties in obtaining representative samples and difficulties in duplicating field conditions in laboratory tests. Usually, the shear strength back-calculated from the field condition is a more reliable value for use in designing remedial measures.

A number of methods of stabilizing slopes and landslides are summarized in Table 4. Often one or more of these schemes may be used together. Schemes 1 through V are listed approximately in order of increasing cost. Excavation (Scheme I) and drainage (Scheme II) are often the most effective schemes for small to medium-sized landslides Buttresses or berm fills (Scheme III), can be used for fairly large slides provided an area is available for equipment access and for temporary stockpiling of excavated

TABLE 2.-- METHODS OF STABILIZING SLOPES AND LANDSLIDES (after Turnbull and Hvorslev, 1967)

Scheme	Applicable Methods	Comments
I. EXCAVATION 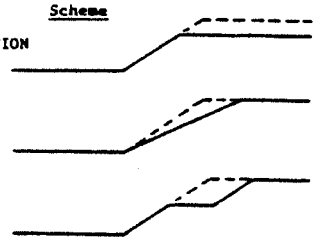	1. Reduce slope height by excavation at top of slope. 2. Flatten the slope angle. 3. Excavate a bench in upper part of slope. 4. Excavate the entire slide mass.	Area has to be accessible to construction equipment. Disposal site needed for excavated soil. Drainage sometimes incorporated in this method.
II. DRAINAGE 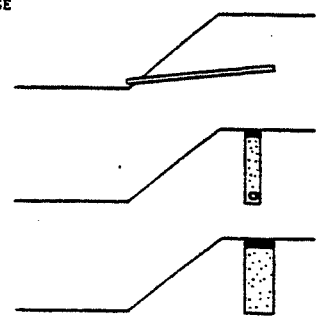	1. Small diameter, horizontal drains (hydraugers). 2. Continuous deep subdrain trench. Generally 5 to 15 feet deep. 3. Drilled vertical wells--generally 18- to 36-inch diameter. 4. Improve surface drainage along top of slope with open ditch or paved gutter. Install deep-rooted, erosion-resistant plants on slope face.	1. Most effective if can tap natural aquifer. Drains are usually free-flowing. 2. Trench bottom should be sloped to drain and be tapped with an outlet pipe. Perforated pipe should be placed on trench bottom. Top of trench should be capped with impervious material. 3. Can be pumped or tapped with a gravity outlet. Several wells in a row, joined at bottom can form a drainage gallery. Top of each well should be capped with impervious material. 4. Good practice for most slopes. Direct the discharge away from slide mass.
III. EARTH OR ROCK BUTTRESS (OR BERM FILL) 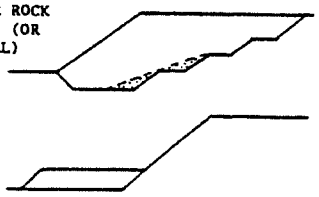	1. Excavate slide mass and replace with compacted earth or rock buttress fill. Toe of buttress must be keyed into firm soil or rock below slide plane. Drain blanket with gravity flow outlet is provided in back slope of buttress fill. 2. Compacted earth or rock berm placed at and beyond the toe. Drainage may be provided behind berm.	1. Access for construction equipment and temporary stockpile area required. Excavated soil can usually be used in fill. Underpinning of existing structures may be required. Might have to be done in short sections if stability during construction is critical. 2. Sufficient width and thickness of berm required so failure will not occur below or through berm.
IV. RETAINING STRUCTURES 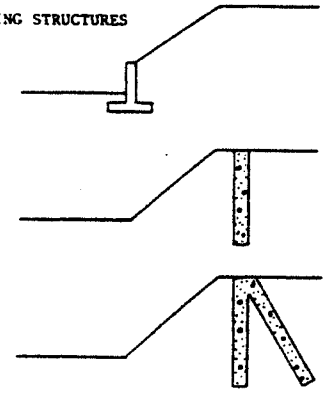	1. Retaining wall - crib or cantilever type. 2. Drilled, cast-in-place vertical piles, bottomed well below bottom of slide plane. Generally 18 to 36 inches in diameter and 4- to 8-foot spacing. 3. Drilled, cast-in-place vertical piles tied back with battered piles or a deadman. Piles bottomed well below slide plane. Generally 12 to 30 inches in diameter and at 4- to 8-foot spacing. 4. Earth anchors and rock bolts.	1. Usually expensive. Cantilever walls might have to be tied back. 2. Spacing should be such that soil can arch between piles. Grade beam can be used to tie piles together. Very large diameter (6 feet ±) piles have been used for deep slides. 3. Space close enough so soil will arch between piles. Piles can be tied together with grade beam. 4. Can be used for high slopes, and in very limited areas. Conservative design should be used, especially for permanent support.
V. SPECIAL TECHNIQUES	1. Grouting 2. Chemical injection 3. Electroosmosis (in fine-grained soils). 4. Freezing 5. Heating	1. and 2. Used successfully in a number of cases. Used at other times with little success. At the present, theory is not completely understood. 3. Generally expensive. 4. and 5. Special methods which must be specifically evaluated at each site. Can be expensive. All of these techniques should be carefully evaluated in advance to determine the probable cost and effectiveness.

soils. Retaining structures (Scheme IV) are generally not used for large landslides because of high cost. The methods shown in Scheme V, special techniques, are generally used under unusual conditions which make them more effective or economical than the other procedures.

REFERENCES

Bishop, A.W. (1955) "The Use of the Slip Circle in the Stability Analysis of Slopes," Geotechnique, Vol. V, No. 1, pp. 7-17.

Bishop, A. W. and Bjerrum, L. (1969) "The Relevance of the Triaxial Test to the Solution of Stability Problems," Proceedings of the ASCE Research Conference on the Shear Strength of Cohesive Soils, Boulder.

Bjerrum, L. (1973) "Problems of Soil Mechanics and Construction on Soft Clays," General Report, 8th Int. Conf. on Soil Mech. and Found. Eng., Moscow, Proc. Vol. 3, pp. 11-159 (also Norwegian Geotech. Inst. Pub. 100).

Chirapuntu, S. and Duncan, J. M. (1975) "The Role of Fill Strength in the Stability of Embankments on Soft Clay Foundations," Geotechnical Engineering Research Report, Department of Civil Engineering, University of California, Berkeley.

Hunter, J. H. and Schuster, R. L. (1968) "Stability of Simple Cuttings in Normally Consolidated Clays," Geotechnique, Vol. 13, No. 3, September, 1968, pp. 372-378.

Janbu, N. (1968) "Slope Stability Computations," Soil Mechanics and Foundation Engineering Report, The Technical University of Norway, Trondheim.

Janbu, N. (1973) "Slope Stability Computations," published in Embankment-Dam Engineering, the Casagrande Volume, John Wiley and Sons, pp. 47-86.

Kenney, T.C. (1963) "Stability of Cuts in Soft Soils," Journal of the Soil Mechanics and Foundations Division, ASCE, Vol. 89, No. SM5, pp. 17-37.

Ladd, C.C. and Foote, R. (1974) "A New Design Procedure for Stability of Soft Clays," Journal of the Geotechnical Engineering Division, ASCE, Vol. 100, No. GT7, pp. 763-786.

Lowe, J. and Karafiath, L. (1960) "Stability of Earth Dams Upon Drawdown," Proceedings of the First Pan American Conference on Soil Mechanics and Foundation Engineering, Mexico City, Vol. 2, pp. 537-552.

Morgenstern, N.R. and Price, V.E. (1965) "The Analysis of the Stability of General Slip Surfaces," Geotechnique, Vol. 15, No. 1, pp. 79-93.

Turnbull, W.J. and Hvorslev, M.J. (1967) "Special Problems in Slope Stability," Journal of the Soil Mechanics and Foundations Division, ASCE, Vol. 93, No. SM4, July, 1967, pp. 499-528.

Wright, S.G. (1969) "A Study of Slope Stability and the Undrained Shear Strength of Clay Shales," Ph.D. Thesis, Department of Civil Engineering, University of California, Berkeley.

TAB 13

Stabilization of Evolving Slopes

(Tuncer B. Edil)

STABILIZATION OF EVOLVING SLOPES

By

Tuncer B. Edil

EVOLVING SLOPES

Evolving slopes are those slopes where there is an ongoing slope shaping process such as *wave action* on coastal slopes or *currents* in river bank slopes modifying slope morphology.

- They are typically natural slopes
- Wave or current action and flooding fluctuates in intensity (climatically-controlled)
- Wave or current action in the slope toe triggers other processes at higher levels in the slope.
- Slope morphology changes in time and so does stability

EXAMPLES OF EVOLVING SLOPES

- Coastal Erosion: Great Lakes Shoreline

  Fluctuating lake levels (up to 2 m in 15-20 years) and storm activity

- River Bank Erosion: Cumberland River, Tennessee

  Fluctuating river stage (up to 6 m) in a short period and sudden drawdown

THE GREAT LAKES SHORELINE

Major Processes:

- Wave Action
- Sliding Slumping
- Flows and Solifluction
- Rain Impact and Rill/Sheet Erosion

Also:

- Groundwater Sapping
- Wind and Ice Erosion

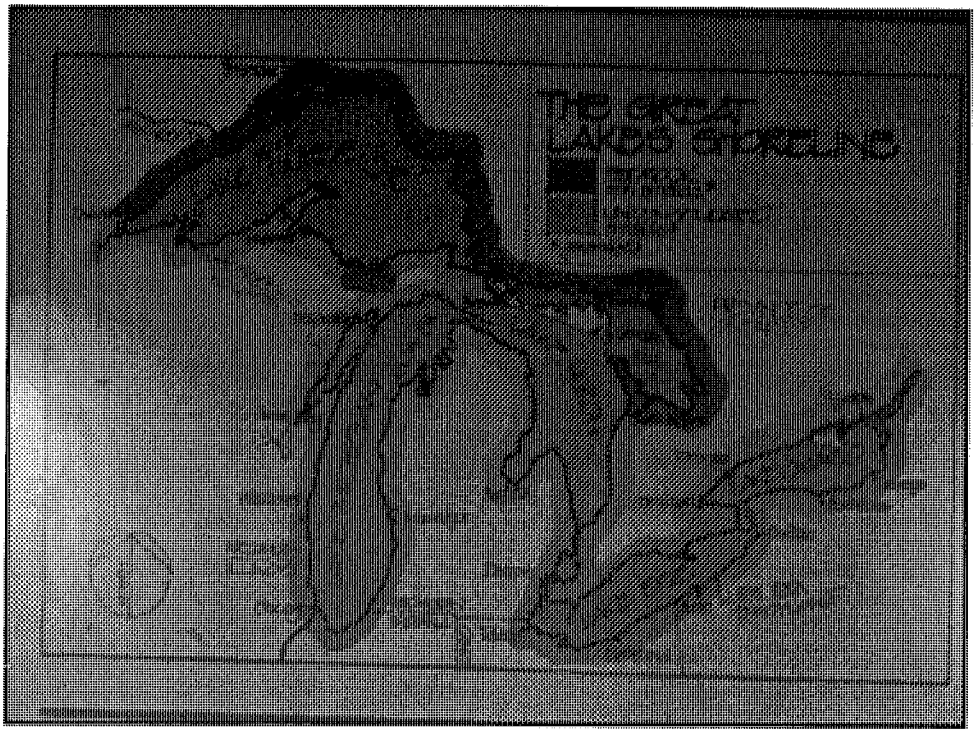

SHORETYPES (USA)

ERODIBLE BLUFFS	1188 MILES	32%
ERODIBLE LOW PLAINS	623 MILES	17%
SAND DUNES	325 MILES	9%
NONERODIBLE	904 MILES	24%
OTHER (FILLS, WETLANDS, ETC.)	675 MILES	18%
TOTAL	3715 MILES	100%

Slope Processes in the Great Lakes

Forces:

- Gravity
- Vibrations
- Climate

Resistances:

- Shear Strength
- Vegetation
- Structural Systems

Processes:

Mass Movement

- Sliding
  - Rotational: Slumps
  - Translation: Block Slide, Slab Slide
- Flow
  - Solifluction
  - Debris Flow

Particle Movement

- Wave Erosion
- Wind Erosion
- Ice Erosion
- Rill Erosion
- Sapping

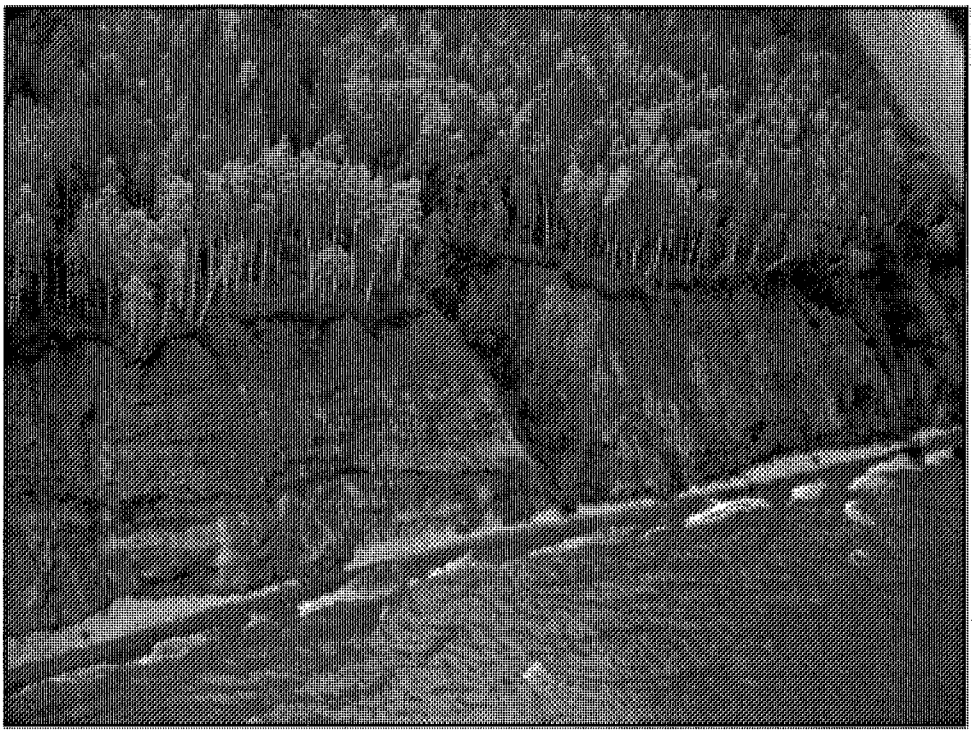

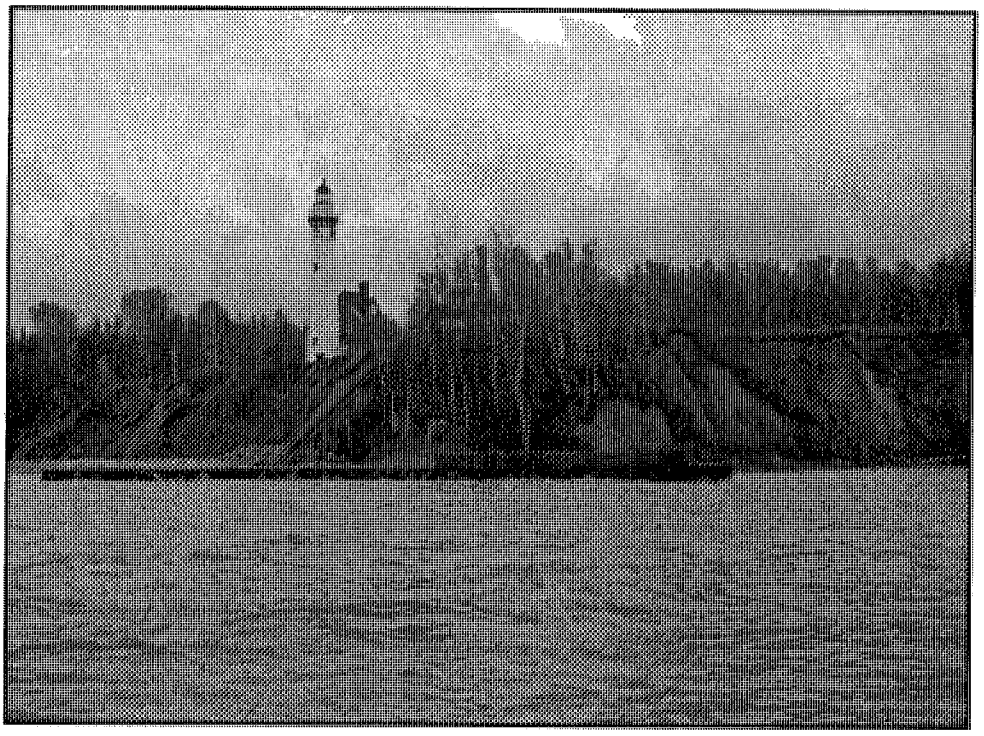

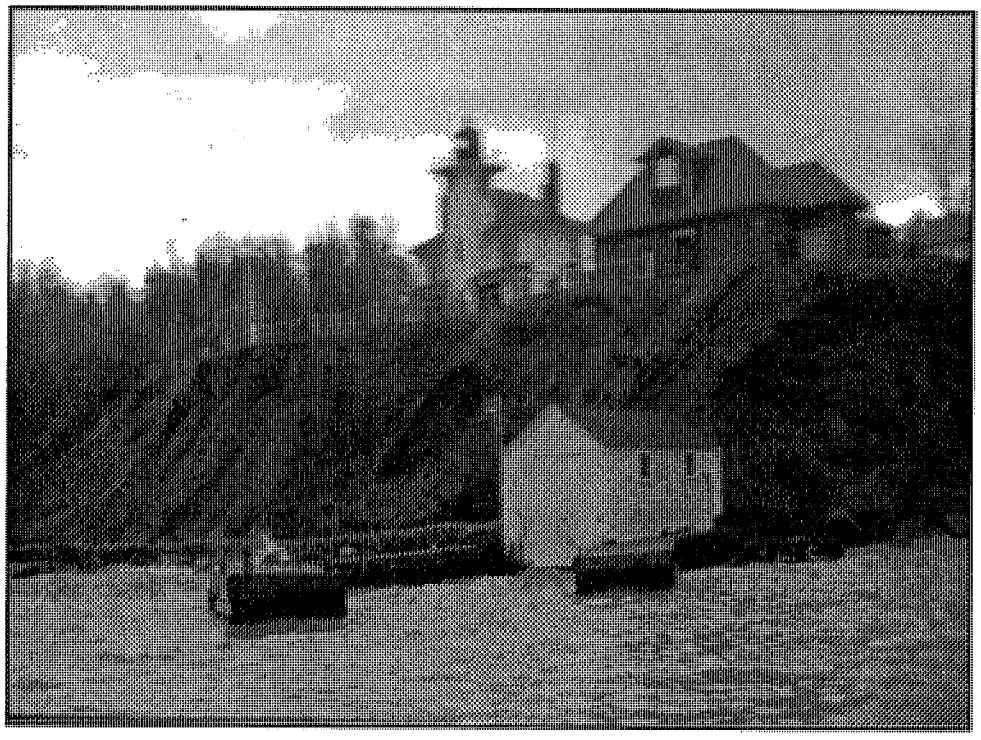

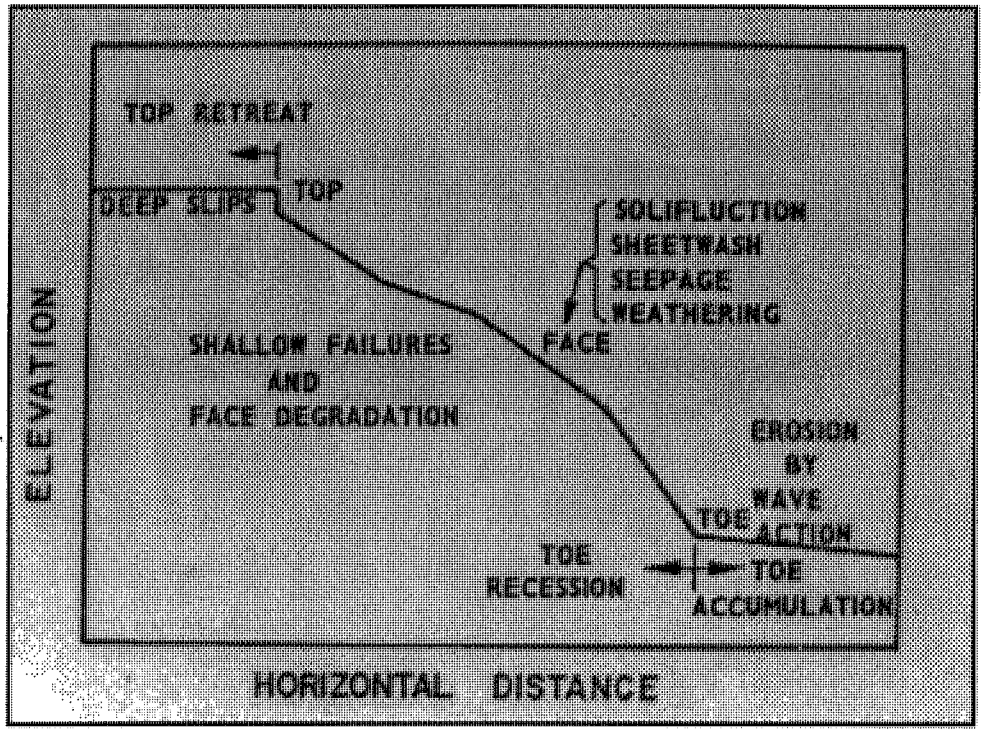

WAVE EROSION

A. Wave Energy

1. Wave Climate (wind velocity, duration, fetch)
2. Water Level
3. Nearshore Bathymetry
4. Shore Orientation

B. Erodibility of Coastal Materials

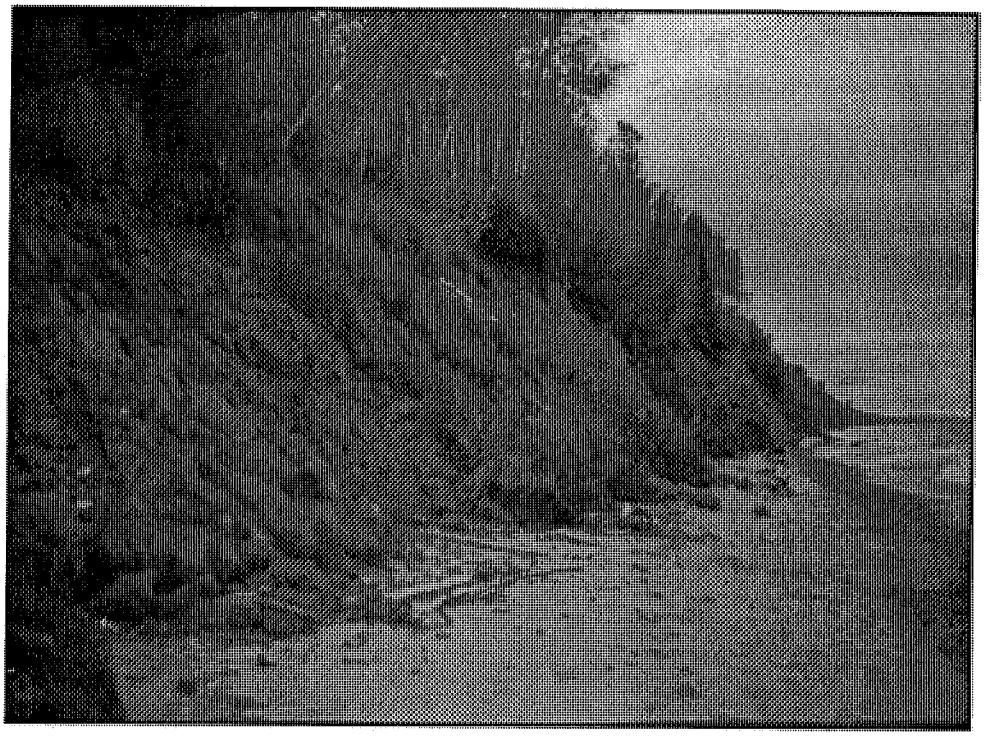

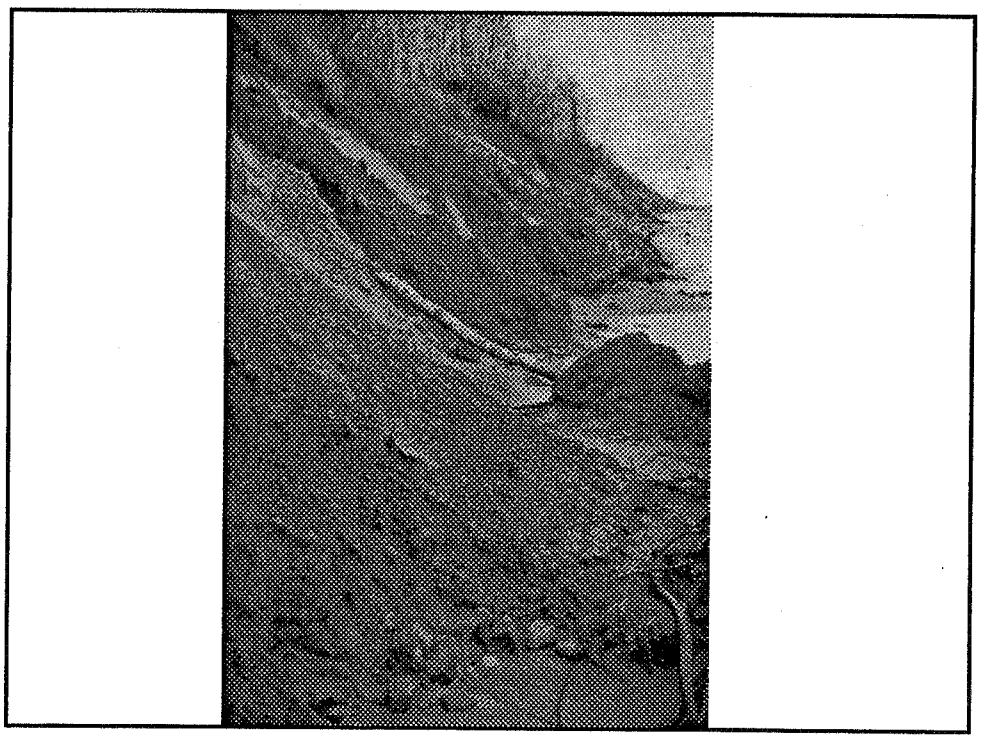

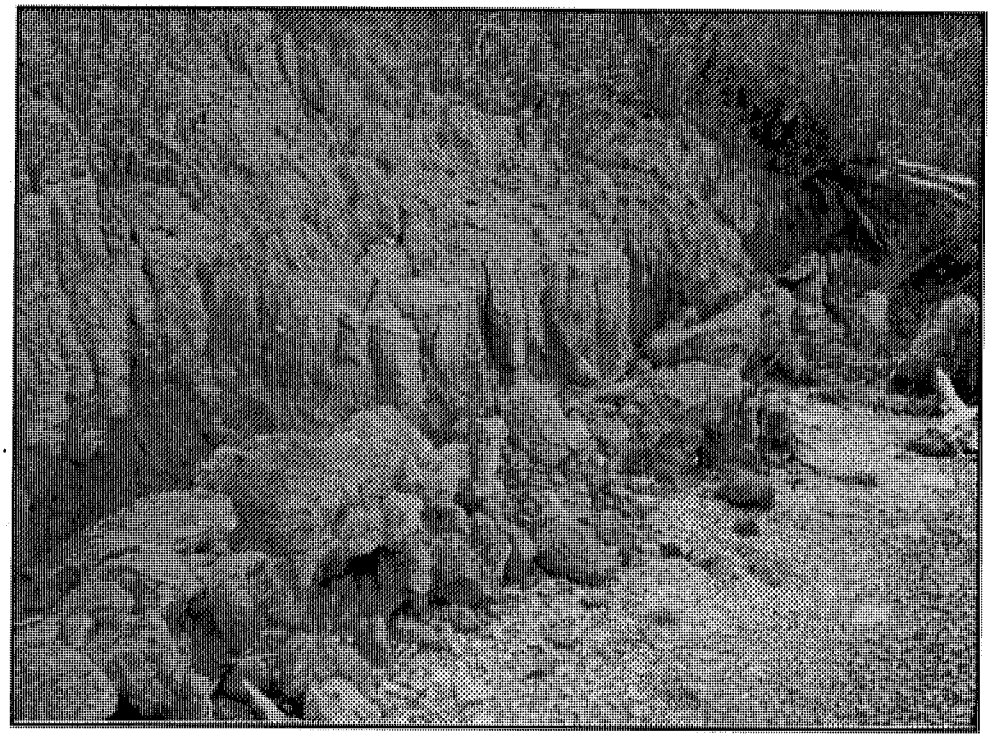

SOLIFLUCTION

"flow of surface soils in seasonally cold regions"

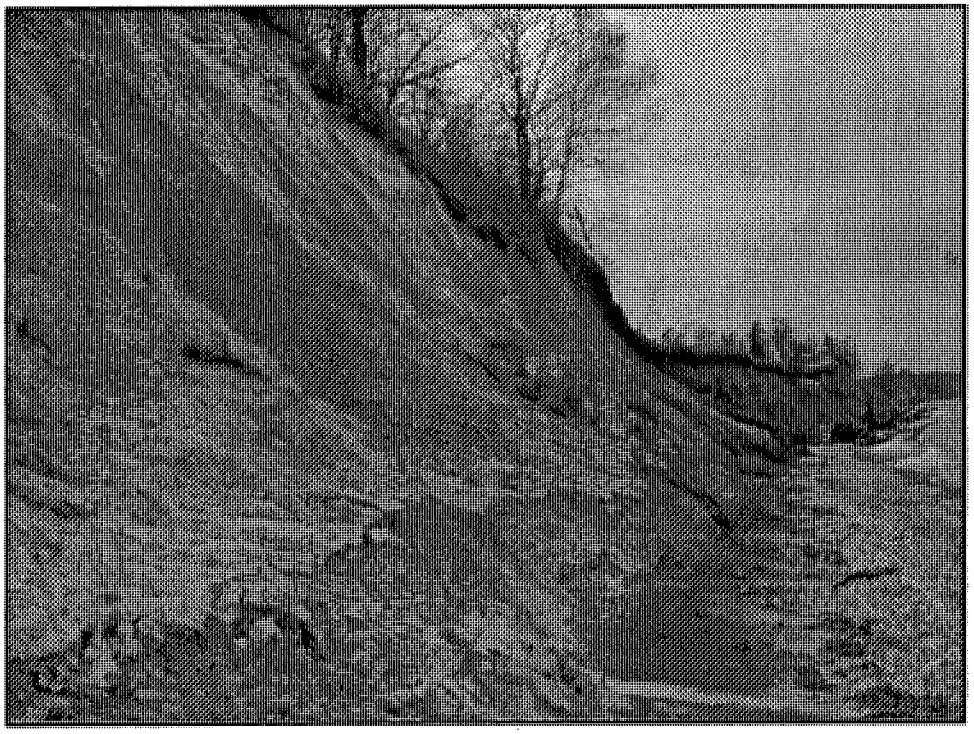

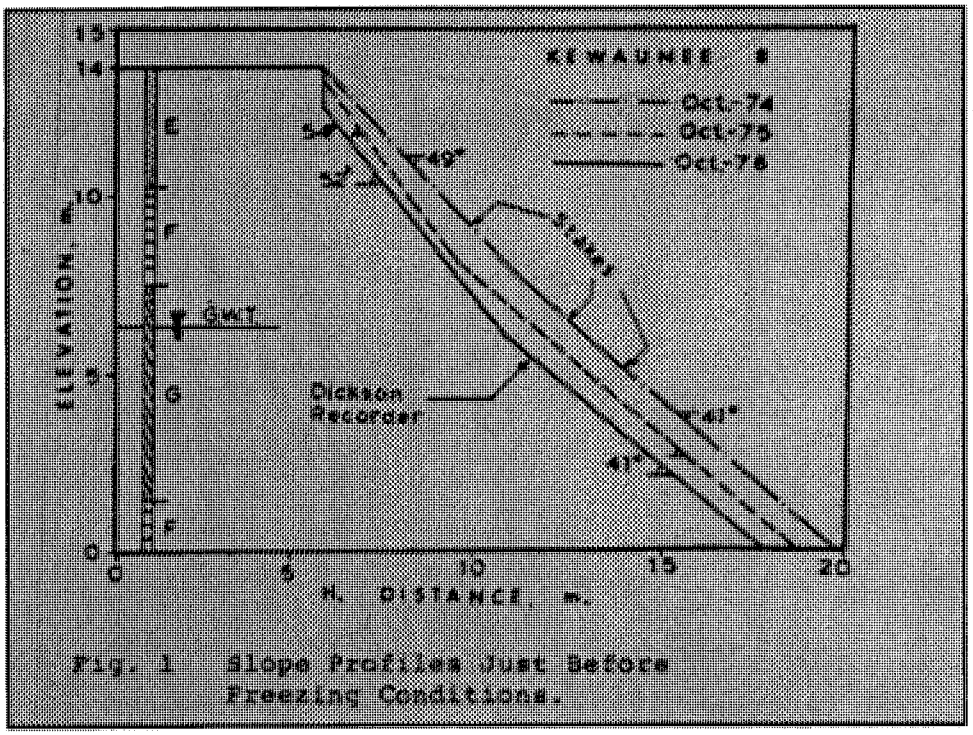

Fig. 1 Slope Profiles Just Before Freezing Conditions.

SHEET/RILL EROSION

"erosion of surficial soils due to rain impact and sheet flow"

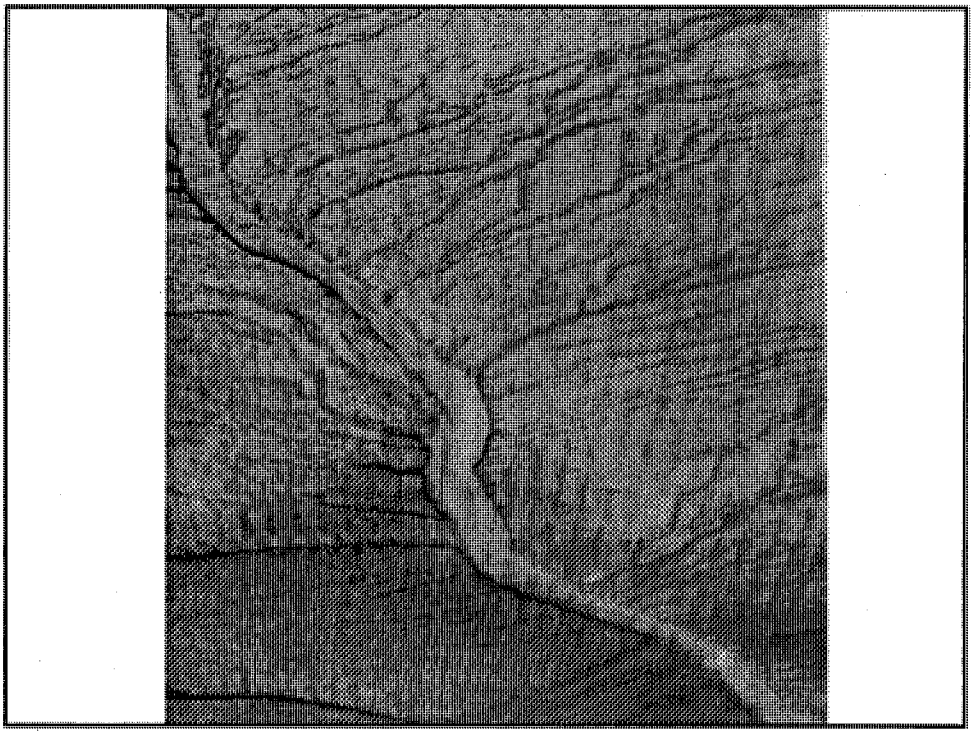

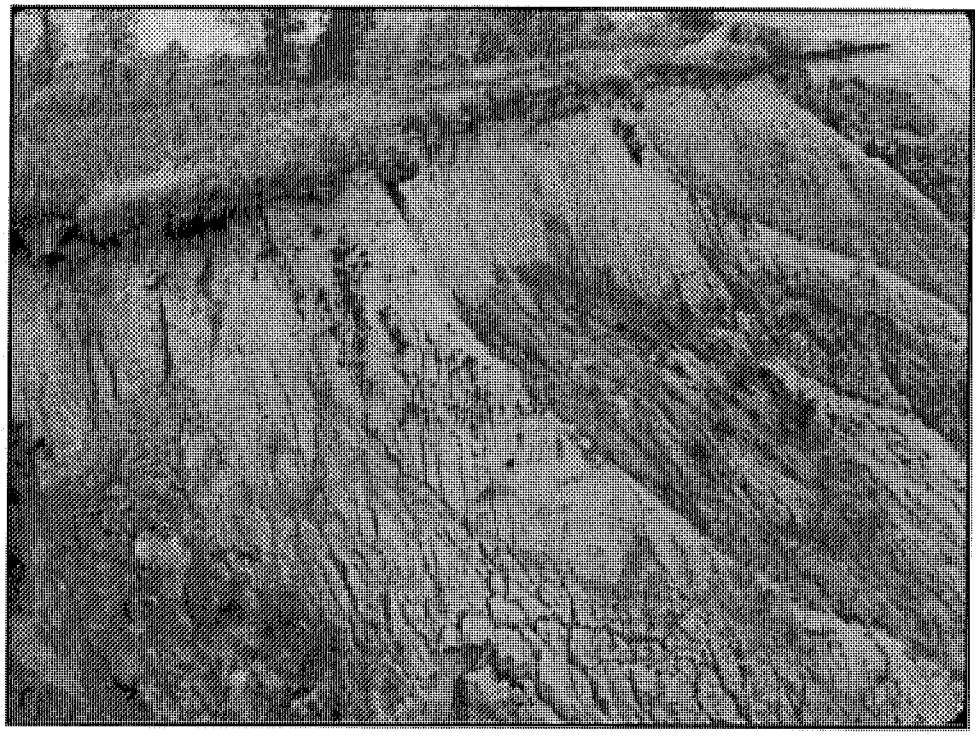

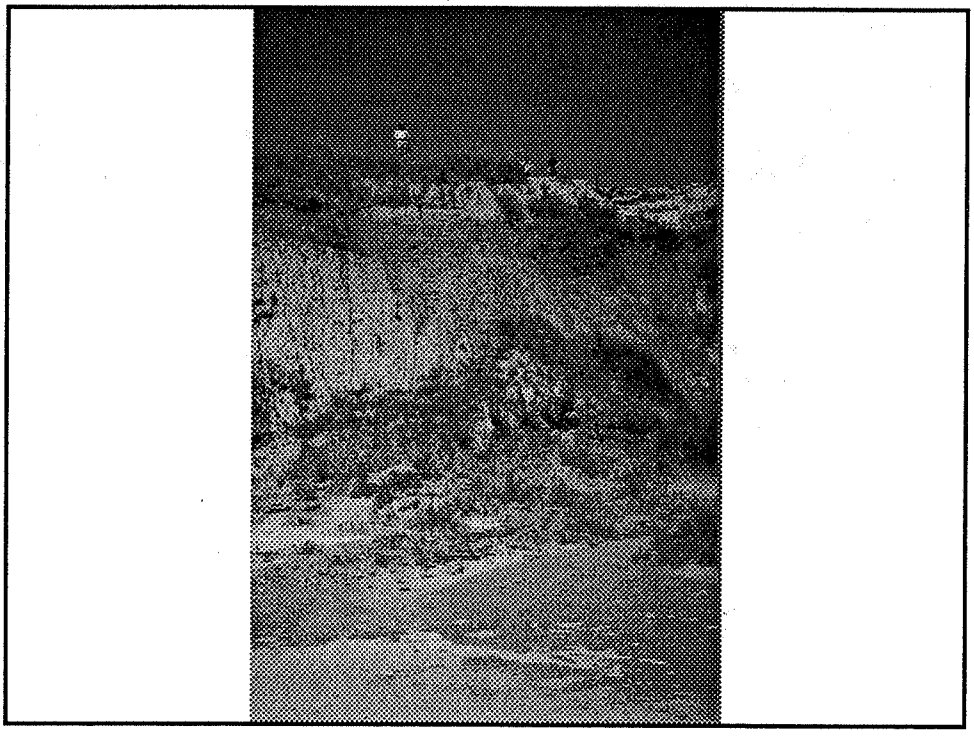

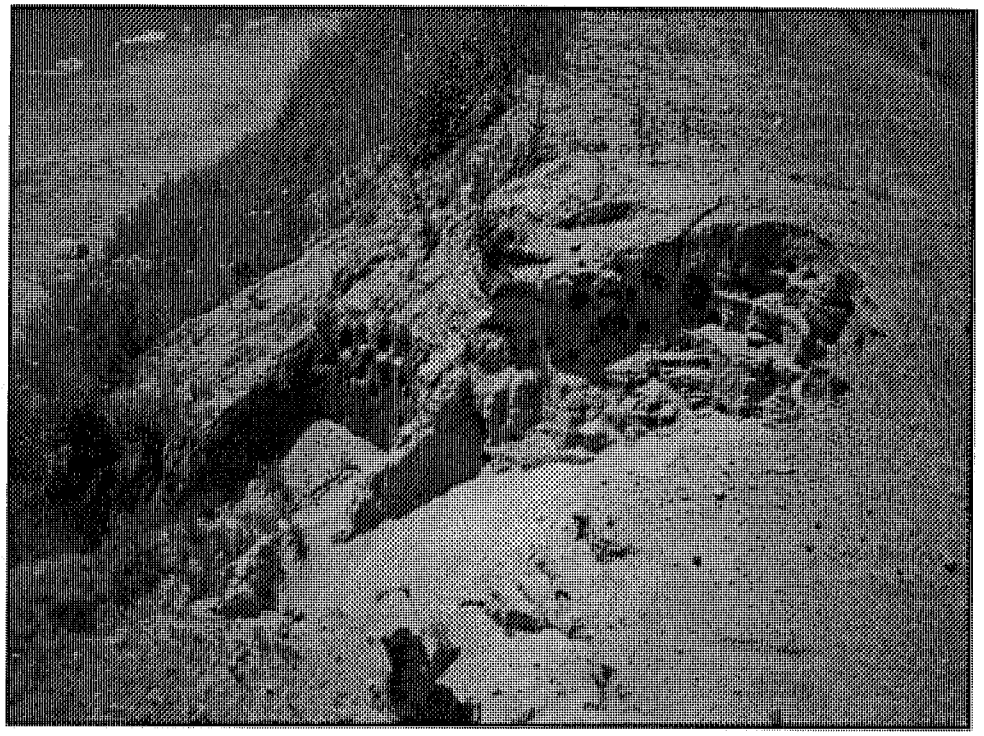

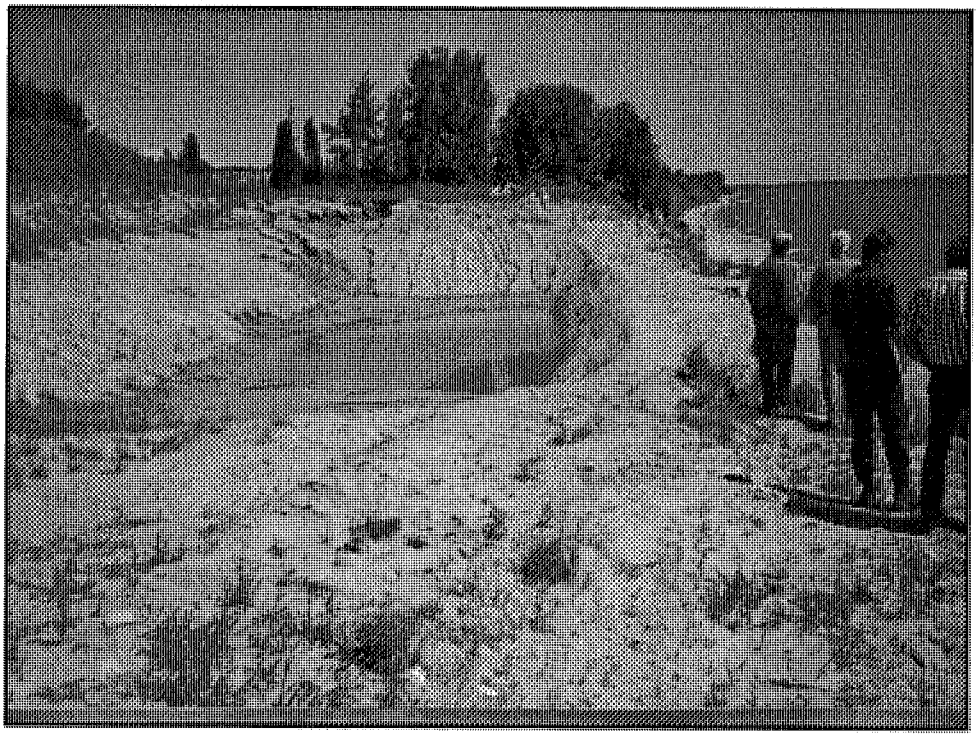

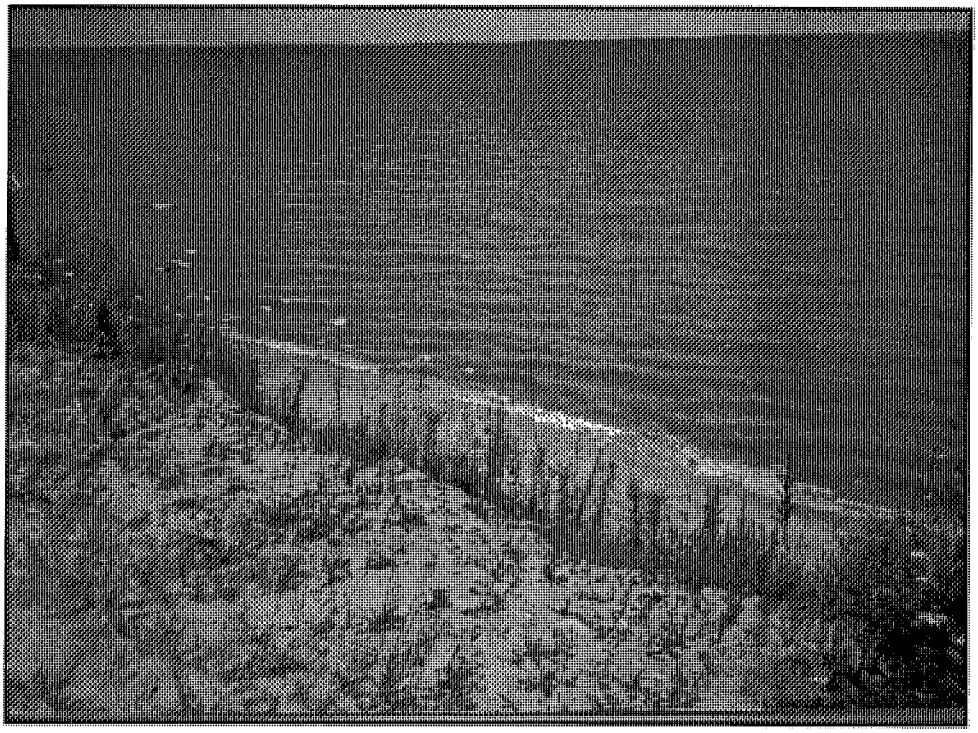

SHEET/RILL EROSION

FOSTER & WISCHMEIER $A = RKCP \dfrac{\sum_{j=1}^{n} s_j x_j^{m+1} - s_j x_{j-1}^{m+1}}{x_n (72.6)^m}$ METHOD

- A = AVERAGE SOIL LOSS PER UNIT AREA PER UNIT TIME
- R: RAINFALL FACTOR
- K: SOIL ERODIBILITY FACTOR
- C: CROPPING-MANAGEMENT FACTOR
- P: EROSION - CONTROL PRACTICE FACTOR
- s_j: SLOPE FACTOR OF THE jTH SEGMENT
- x_j: SLOPE LENGTH OF THE jTH SEGMENT
- x_n: ENTIRE SLOPE LENGTH
- m: COEFFICIENT OF VARIATION = 0.3

SLIDING

- Rotational versus translational sliding
- Shallow versus deep sliding

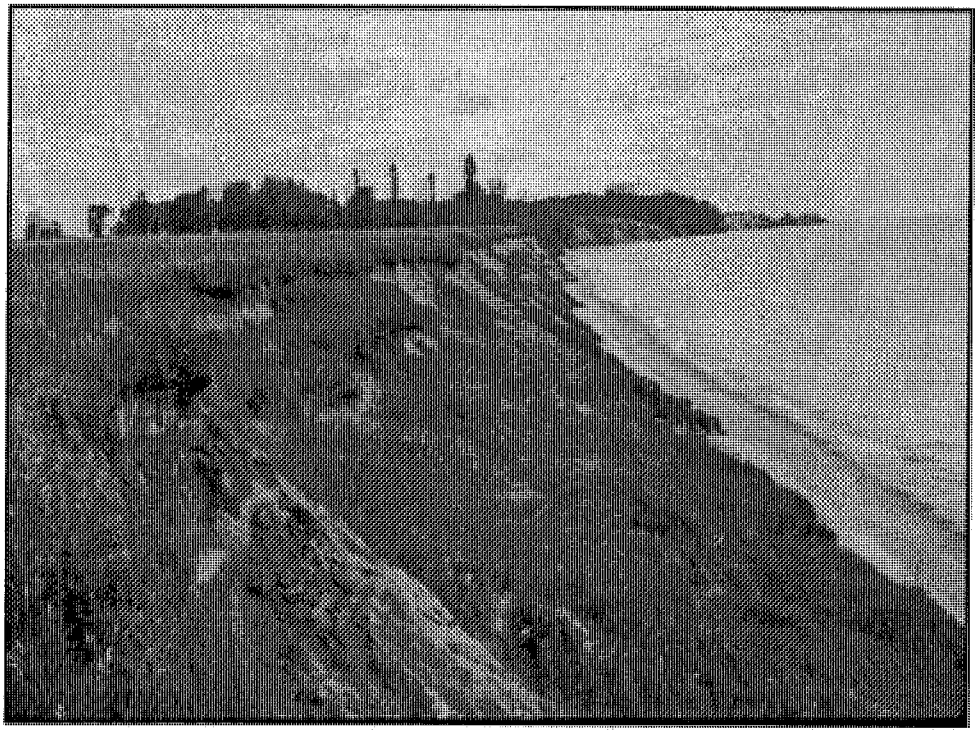

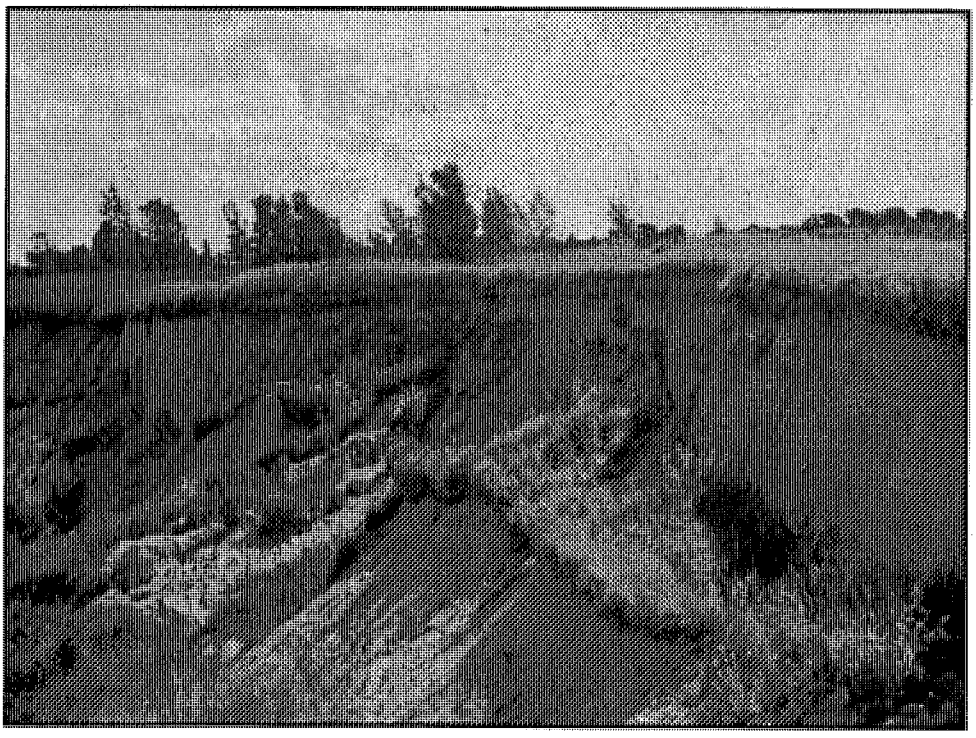

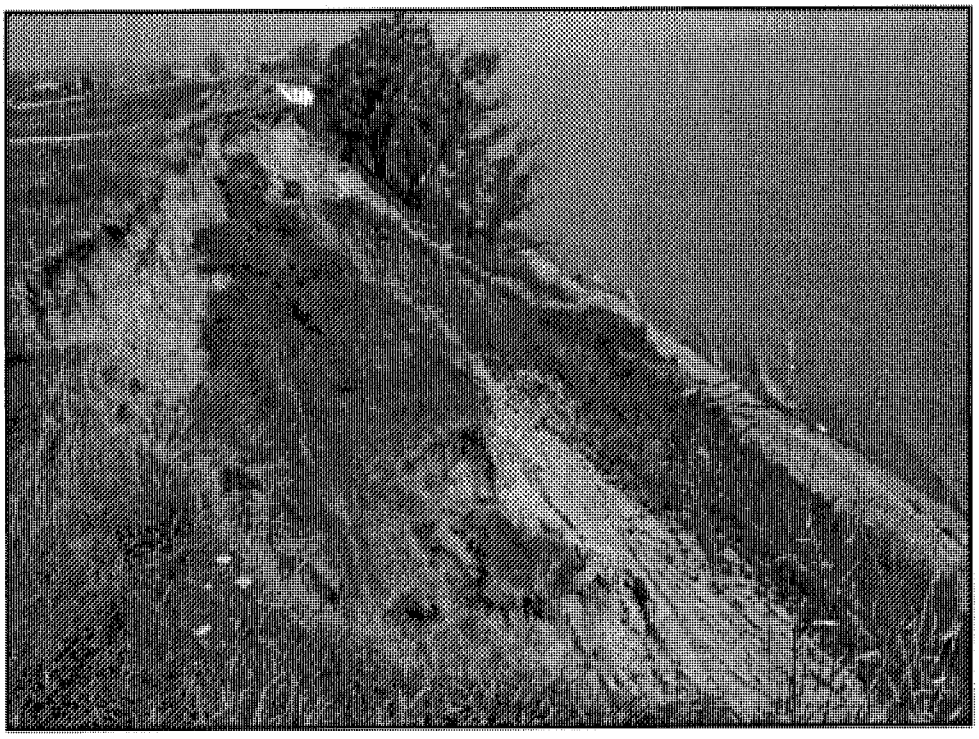

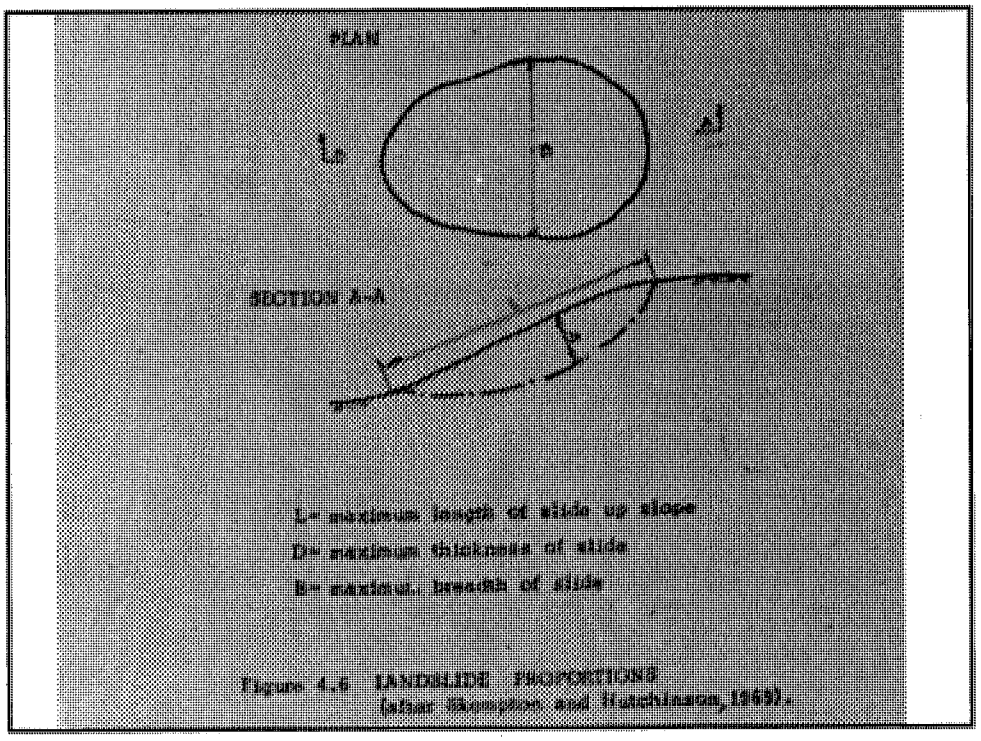

Figure 4.6 LANDSLIDE PROPORTIONS
(after Thompson and Hutchinson, 1969).

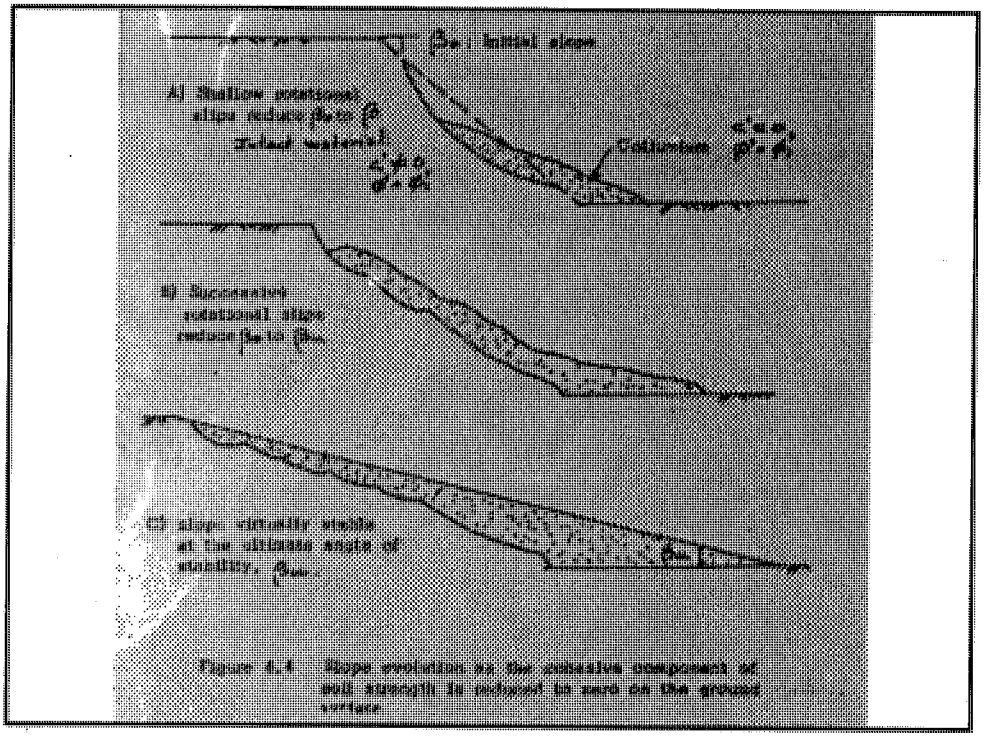

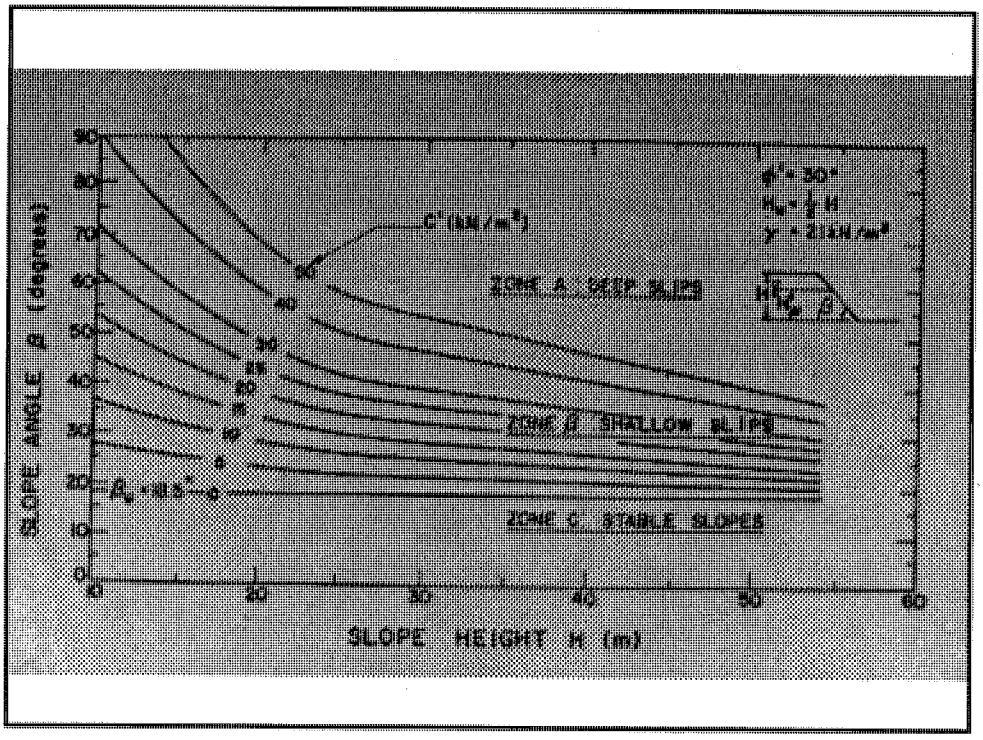
SLOPE ANGLE β (degrees)
SLOPE HEIGHT H (m)
C' (kN/m²)
ZONE A DEEP SLIPS
ZONE B SHALLOW SLIPS
ZONE C STABLE SLOPES
ϕ' = 30°
$r_u = \frac{1}{2}$ H
γ = 21kN/m³
β_e = 18.5°

Table 1. Ultimate Angle of Stability

	H_w/H				
φ°	0	1/4	1/2	3/4	1
25°	25	21.5	16.5	10.5	13
30°	30	28.5	18.5	16	16
35°	35	34	24	21	19

PREDICTIVE CAPABILITY OF STABILITY ANALYSES FOR LAKE MICHIGAN SHORELINE SLOPES

- Evaluation covers a 20-year period
- 175 miles (280 km) shoreline along Lake Michigan coast of Wisconsin
- 435 historical profiles obtained in 1976-78
- 115 available for evaluation in 1995-96

METODS OF SLOPE STABILITY EVALUATED

- Bishop's Deterministic Rotational Circular Failure Method
- Monte Carlo Simulation of Bishop's Rotational Circular Failure Method
- Deterministic Infinite Slope Translational Failure Method
- First Order Second Moment Simulation of Infinite Slope Translational Failure Method

INVENTORY OF GROUND TRUTH INFORMATION

- Historical Profiles measured and monumented in 1976-78
- Geotechnical Data on coastal soil units from borings and surface grab samples
- Geological mapping of shoreline
- Groundwater levels from wells and bluff face seepage lines
- Remeasured profiles in 1995-96
- Oblique aerial photographs taken in 1975 and 1994
- Vertical aerial photographs taken in 1978 and 1992

PROBABILISTIC OUTPUT

- Reliability Index, β

  $\beta = (E[F] - 1.0 / \sigma[F]$

  where

  E[F] : arithmetic mean of factors of safety

  σ[F] : standard deviation of factors of safety
- $\beta = 0$ represents equilibrium (50% chance of failure)
- $\beta > 0$ represents stable slope ($\beta > 2.5$ considered stable)
- $\beta < 0$ represents unstable slope ($\beta < 2.5$ considered unstable)
- β is related to probability of failure if factors of safety have a normal distribution

PREDICTIVE CAPABILITY

Analysis Method	**Percent Accurate Predictions**
Bishop's Deterministic (Rotational Slides)	72
Bishop's Monte Carlo (Rotational Slides)	81
Deterministic Infinite Slope (Translational Failures)	85
FOSM Infinite Slope (Translational Failures)	85
Combination of All Four Methods (All Failure Types)	90

RECOMMENDATIONS

- Perform all for analyses
- Use F = 1.1 for instability criterion in Bishop's deterministic method.
- Use minimum of 25 runs with 100 circles per run for Bishop's Monte Carlo simulations. Use $\beta = 1.1$ for critical circle and 1.8 for unstable circle instability criteria.
- Use corrected (reduced) cohesion for surficial materials in deterministic infinite slope method.
- Use corrected (reduced) cohesion for surficial materials in FOSM infinite slope method. Use $\beta = 0$ for instability criterion.

ESTIMATES OF AMOUNT OF MATERIALS REMOVED FROM BLUFFS BY DIFFERENT PROCESSES (AFTER STERRETT, 1980)

SITE	PROFILE	TOTAL ANNUAL SOIL LOSS ft^3	SLUMP-ING	SOIL-FLUCTION	RILL EROSION/ SHEET-WASH
BENDER PARK	1	452	3%	93%	4%
	2	470	0%	91%	9%
	3	1167	60%	35%	5%
PORT WASH.	1	774	68%	23%	9%
	2	480	3%	96%	1%
	3	381	0%	70%	21%

TIME SCALES OF SLOPE EVOLUTION

1. 2 TO 3 YEARS
2. 50 TO 100 YEARS
3. THOUSANDS OF YEARS

RELATIVE IMPORTANCE OF ENVIRONMENTAL FACTORS

WAVE EROSION
GROUND WATER
VEGETATION

RELATIVE IMPORTANCE OF SLOPE PROCESSES

GRANULAR MATERIALS: EROSIONAL PROCESSES
COHESIVE MATERIALS: SLUMPING AND EROSIONAL PROCESSES

STRATEGIES TO DEAL WITH COASTAL SLOPE INSTABILITY PROBLEMS

- Site-specific Engineering Solutions: Structural Solutions
- Coastal Reach Based Management Solutions: Non-structural Solutions

PROCESSES SOLUTIONS

	STRUCTURAL (STABILIZATION): DESIGN	NONSTRUCTURAL (MANAGEMENT): PREDICTION
TOE EROSION	SHORE PROTECTION (GROINS, SEA WALLS, ETC.)	SHORE RECESSION RATE: (LONG-TERM, CYCLIC)
DEEP ROTATIOAL SLIPS	SLOPE STABILIZATION (REGRADING, DEWATERING, ETC.)	STABLE SLOPE ANGLE AGAINST DEEP SLIPS
FACE DEGRADATION AND SHALLOW SLIPS	SURFACE PROTECTION (VEGETATION, DRAINAGE)	ULTIMATE ANGLE OF STABILITY

STRUCTURAL SOLUTION

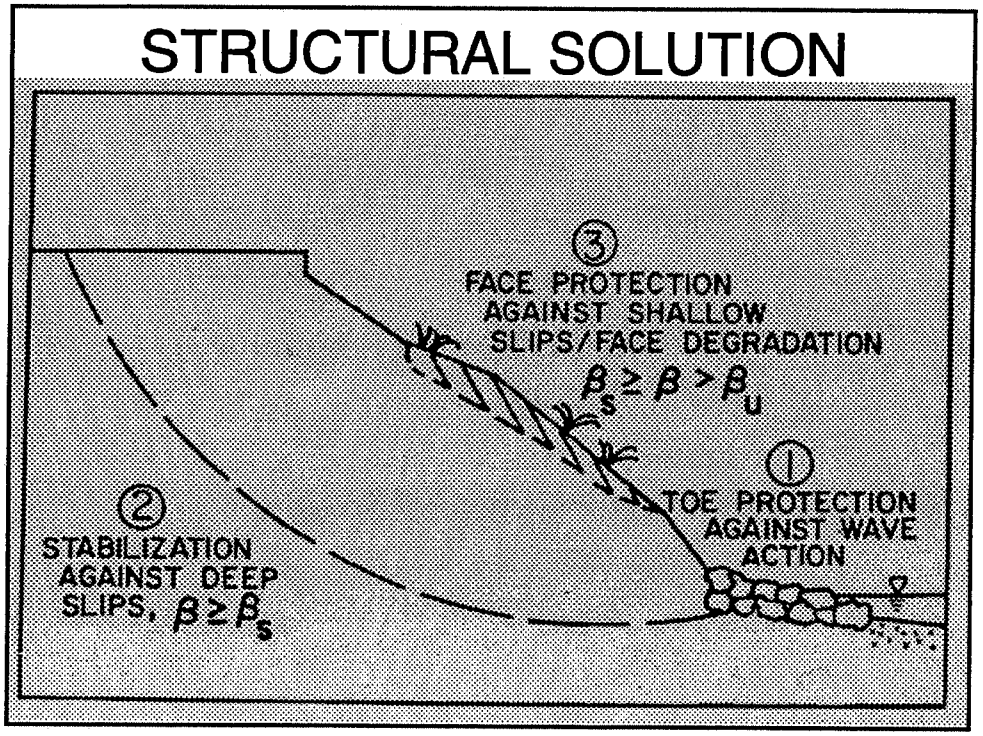

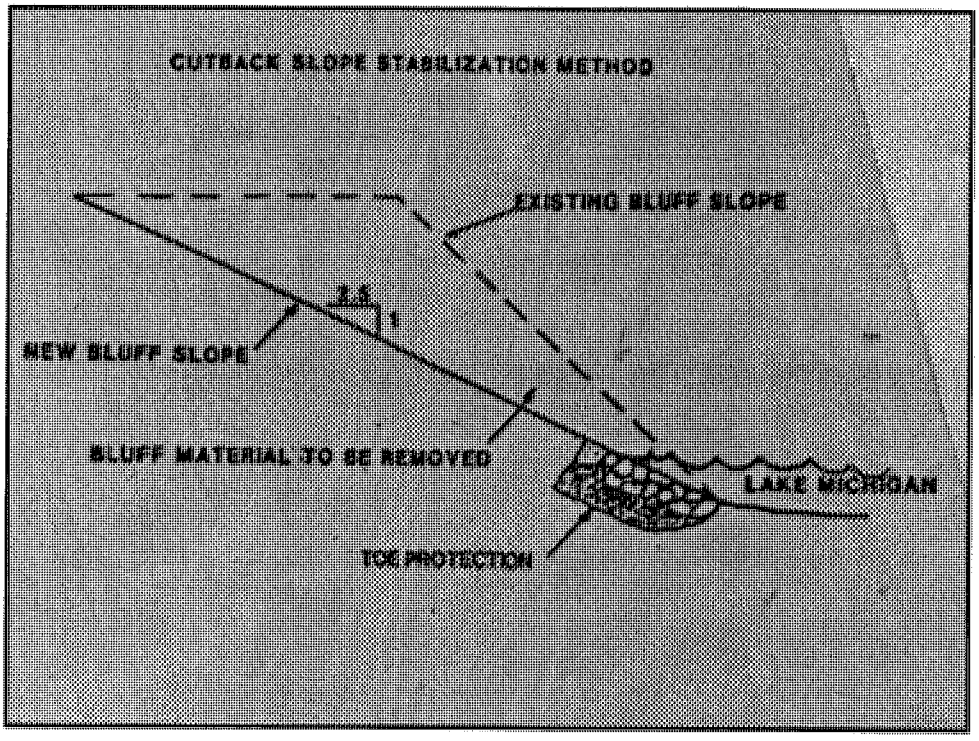

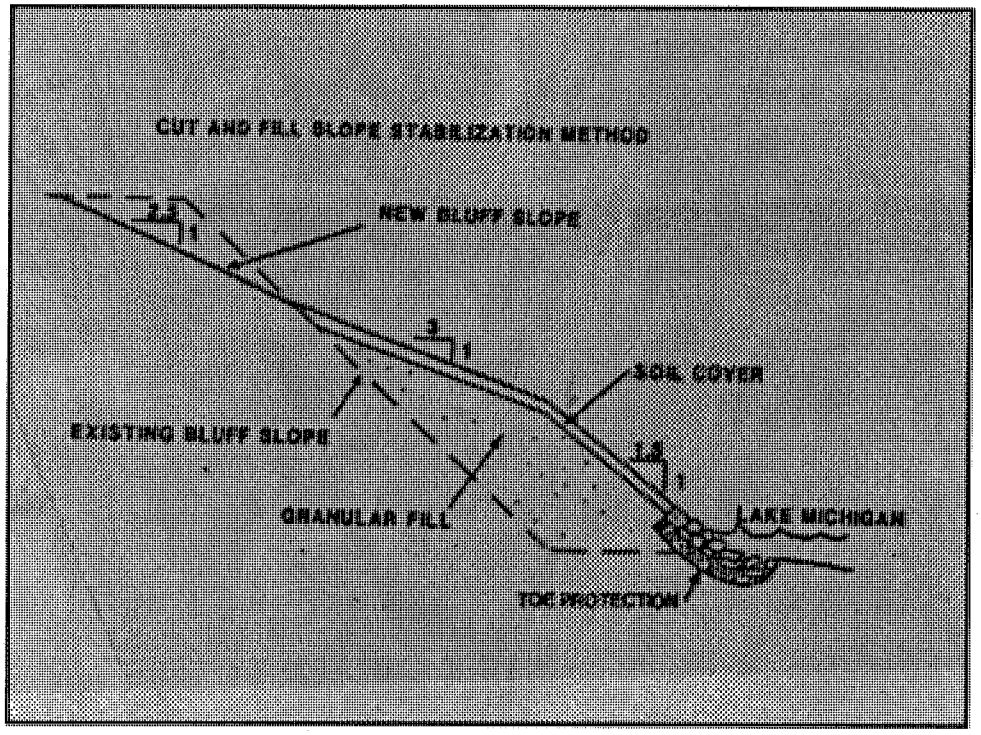
CUT AND FILL SLOPE STABILIZATION METHOD
NEW BLUFF SLOPE
2
1
3
1
SOIL COVER
EXISTING BLUFF SLOPE
1.5
1
GRANULAR FILL
LAKE MICHIGAN
TOE PROTECTION

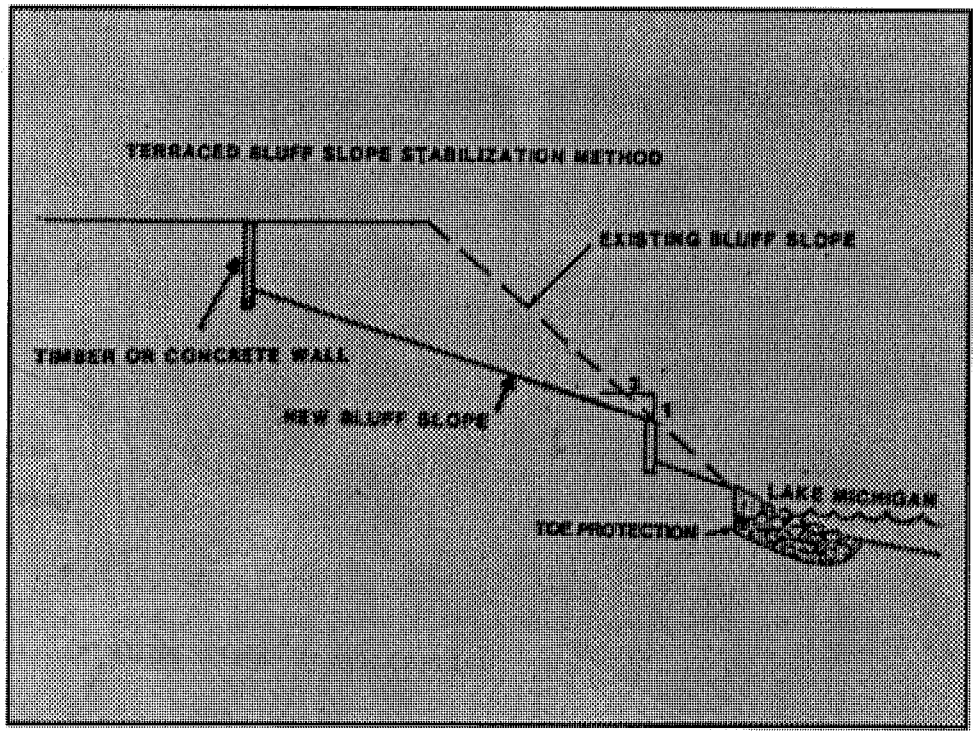
TERRACED BLUFF SLOPE STABILIZATION METHOD
EXISTING BLUFF SLOPE
TIMBER OR CONCRETE WALL
2
1
NEW BLUFF SLOPE
LAKE MICHIGAN
TOE PROTECTION

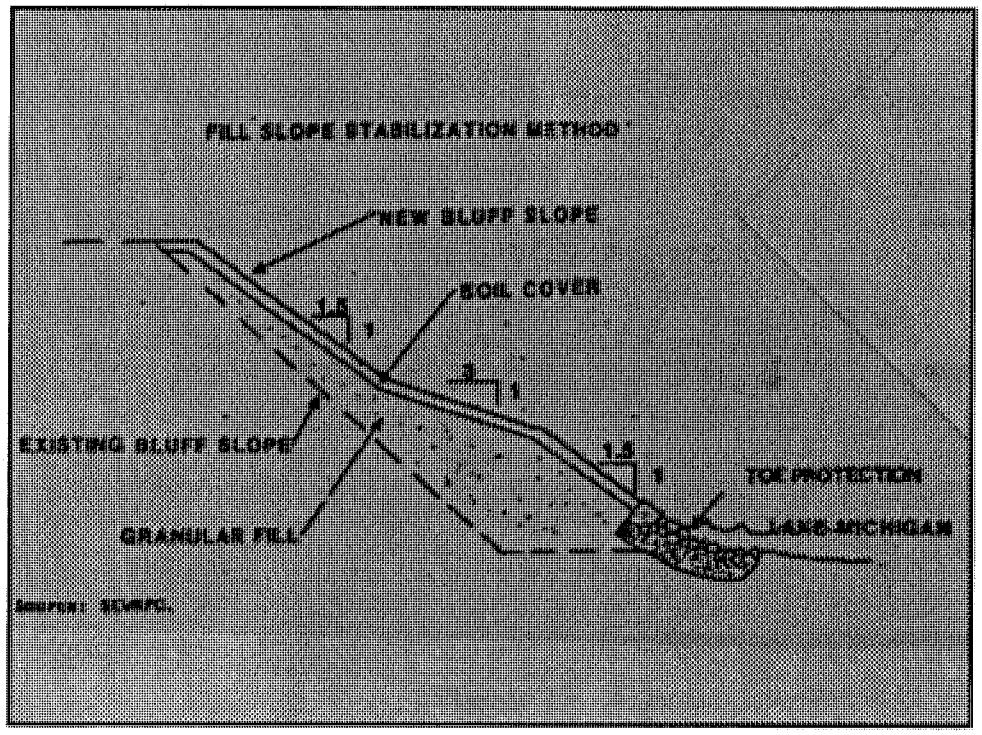

Table 1. Estimated Cost of the Elements of the Shore Erosion Management Plan

Plan Element	Cost: 50 Year Present Worth	Cost: Equivalent Annual Cost
Bluff Slope Stabilization	$ 3,101,000	$ 197,000
Bluff Toe Protection		
Revetment	17,949,000	1,141,000
Beach Nourishment	33,177,000	2,109,000
Offshore Structures	91,525,000	5,269,000
Recommend Plan		
Bluff Slope Stabilization	3,101,000	197,000
Bluff Toe Protection	35,952,000	2,275,000
Total	39,053,000	2,472,000

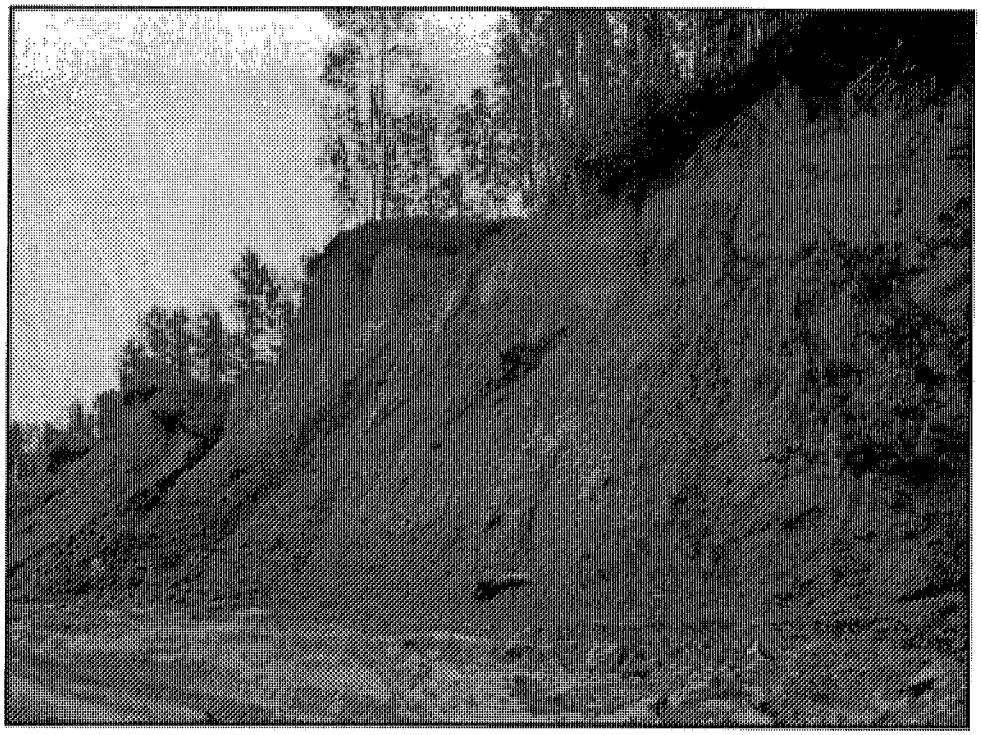

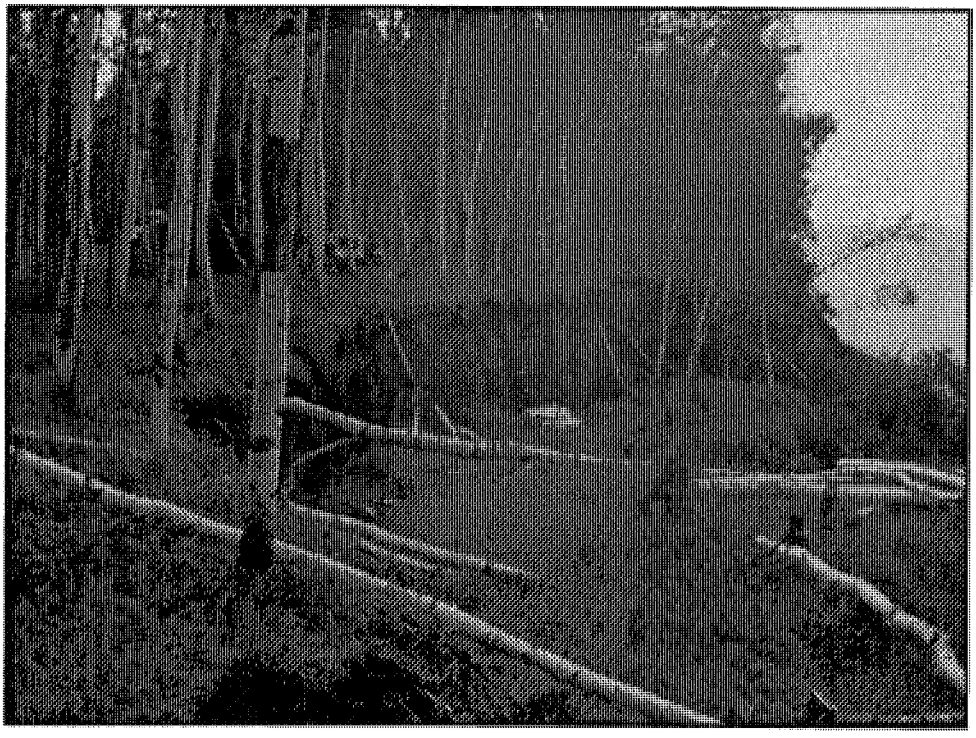

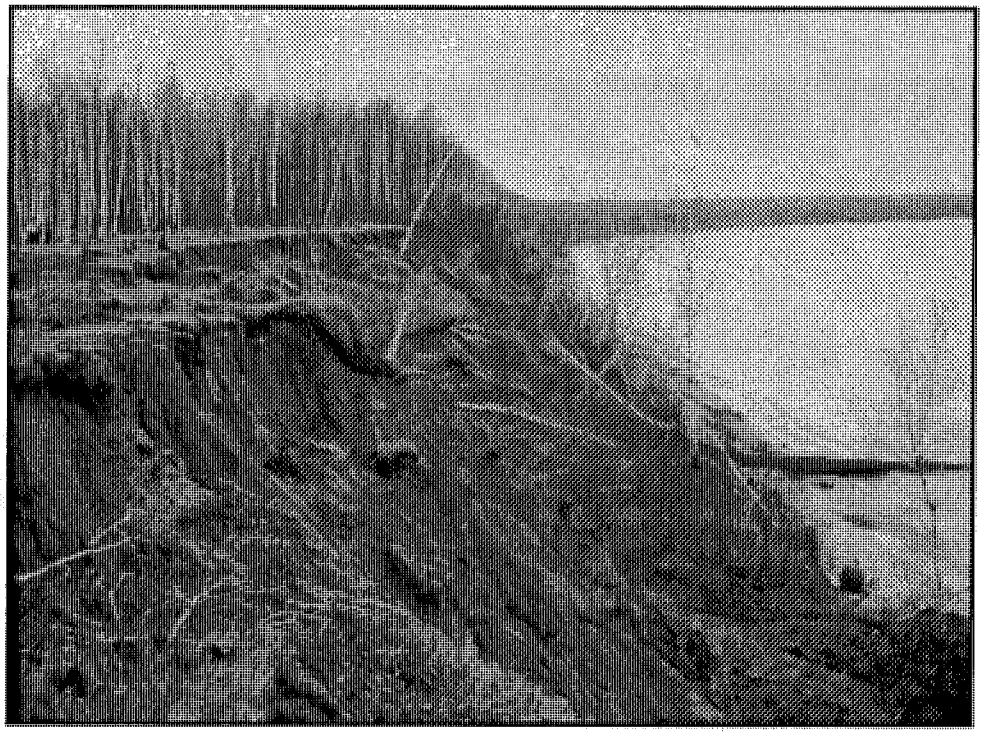

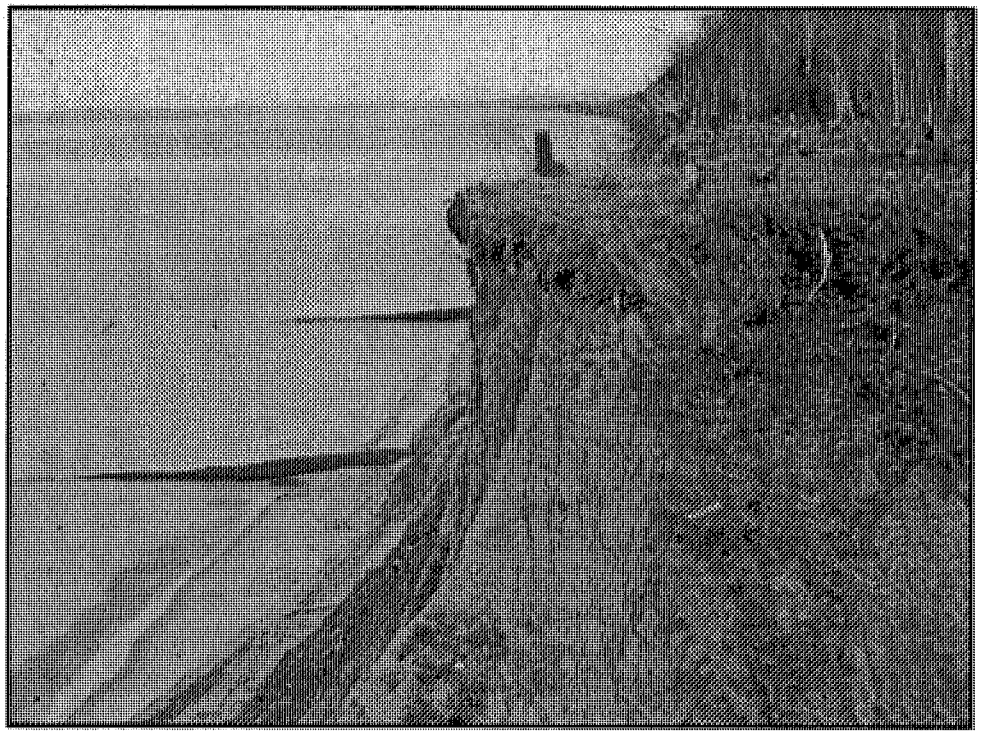

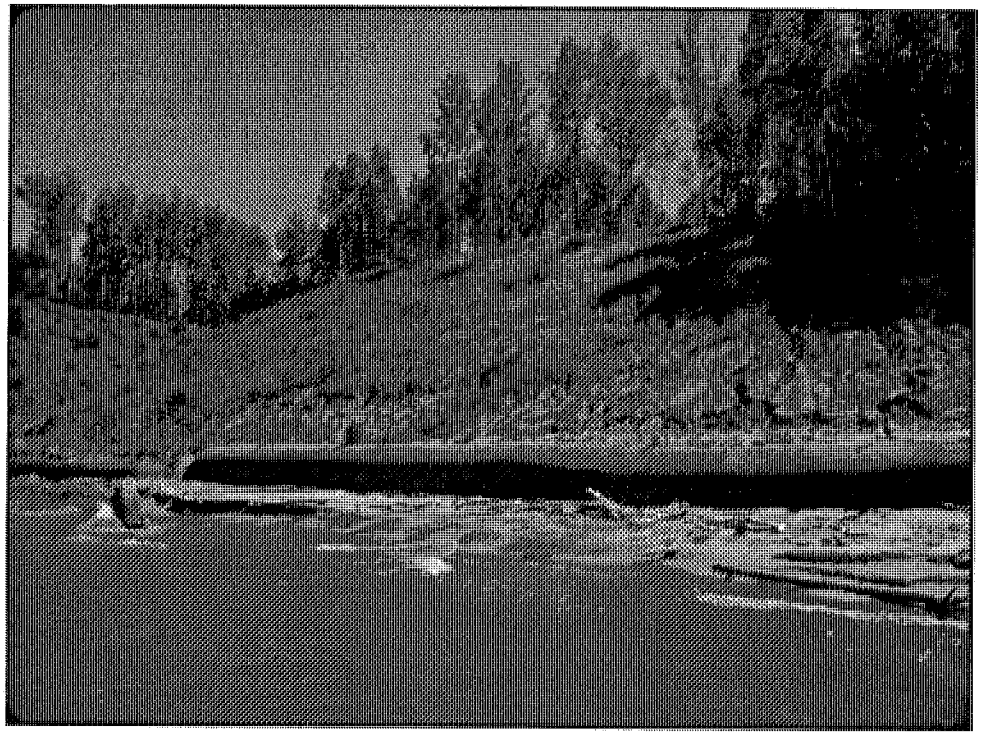

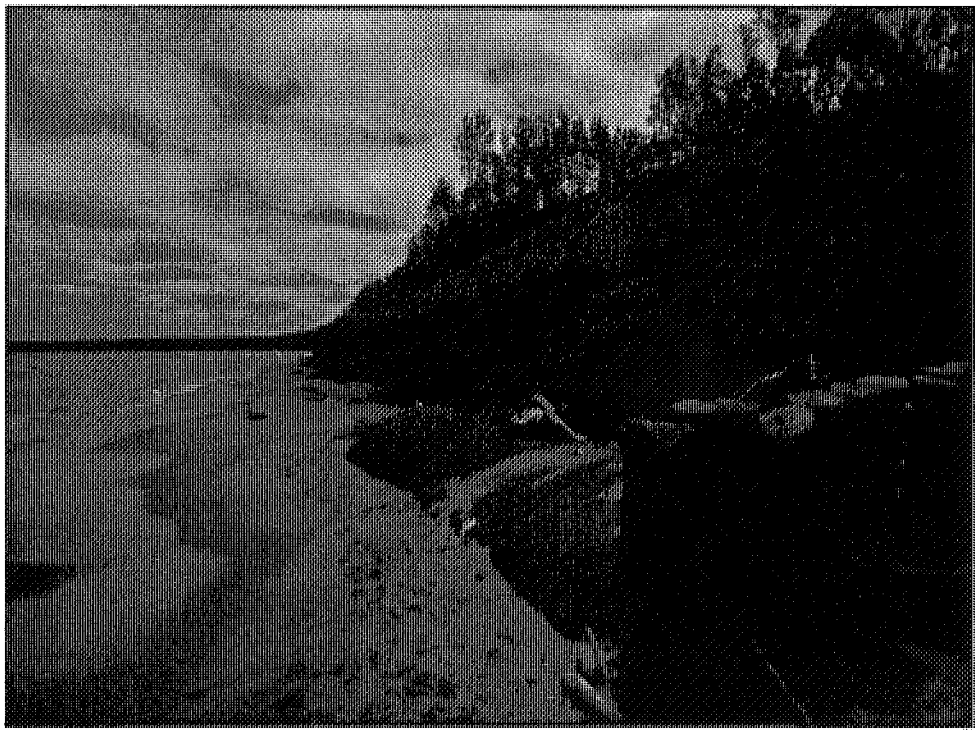

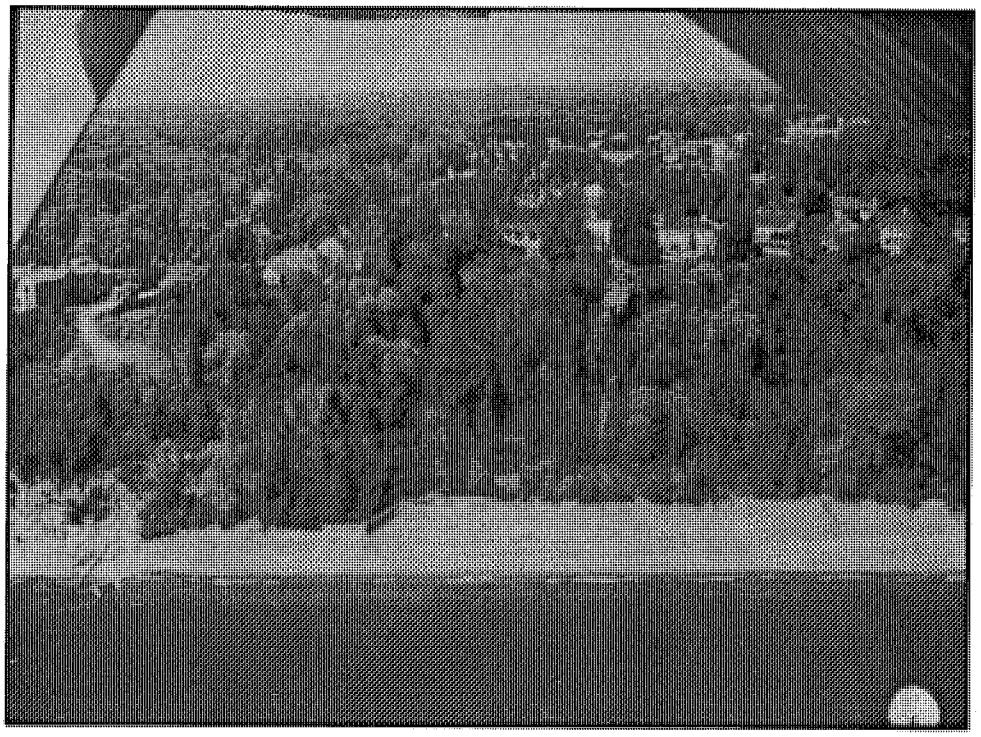

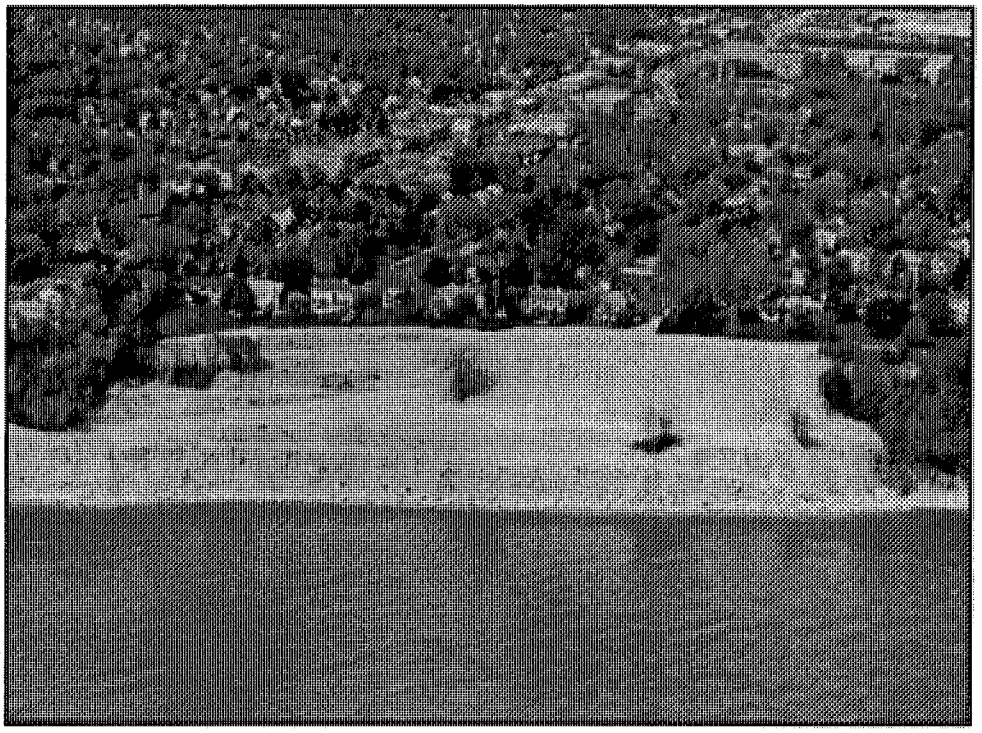

NONSTRUCTURAL (MANAGEMENT) APPROACH

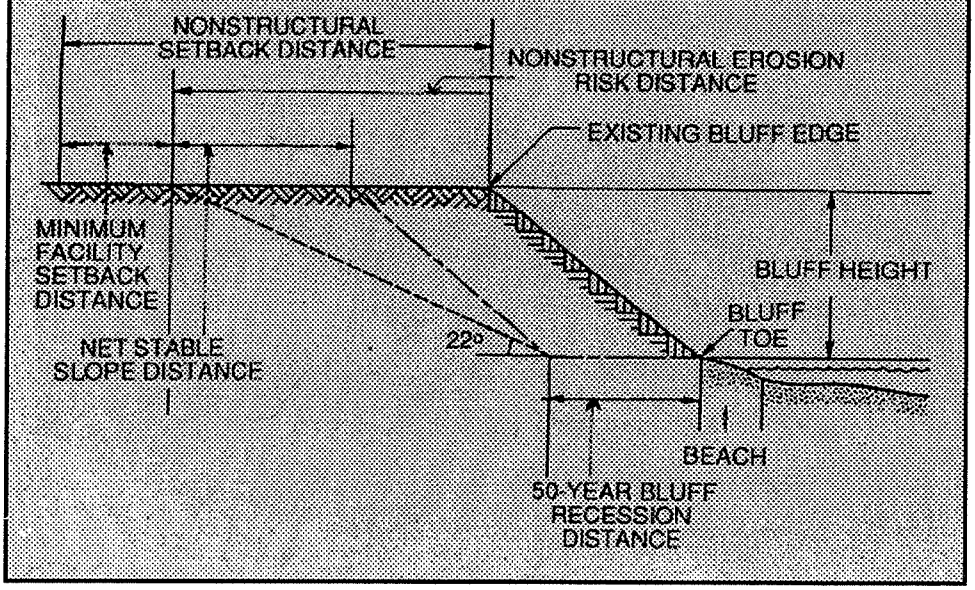

PREDICTION OF FUTURE SHORELINE RECESSION

- Recession due to shore erosion by waves
- Recession due to bluff instability

SLOPE EVOLUTION MODELS-25 YEARS PERSPECTIVE

Slope morphological changes to produce equilibrium are upset by wave erosion

- Decreasing Slope Angle
- Parallel Retreat
- Rotational Slumps: episodic, non-parallel retreat
  - Top Erosion Exceeding Toe Erosion
  - Toe Erosion Exceeding Top Erosion
- No Change

DECREASING SLOPE ANGLE

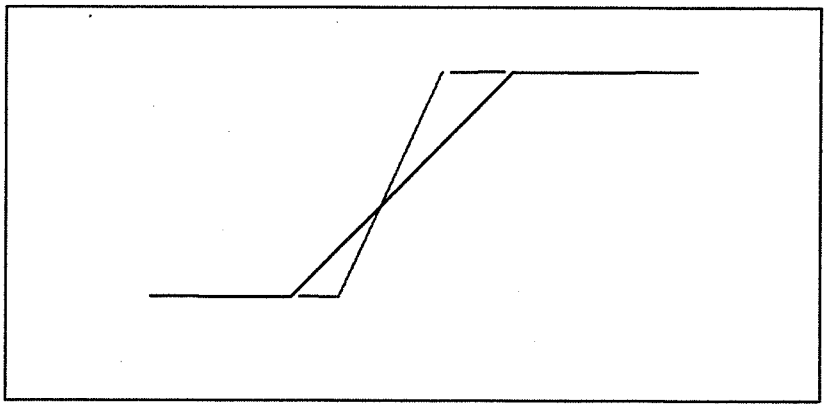

PARALLEL RETREAT

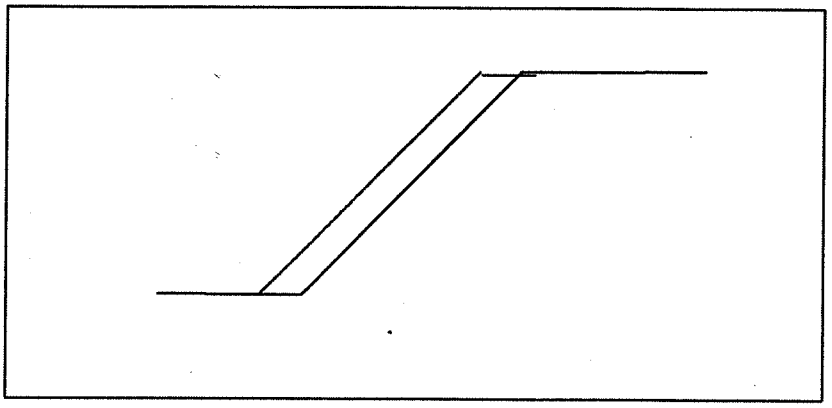

TOP EROSION EXCEEDING TOE EROSION

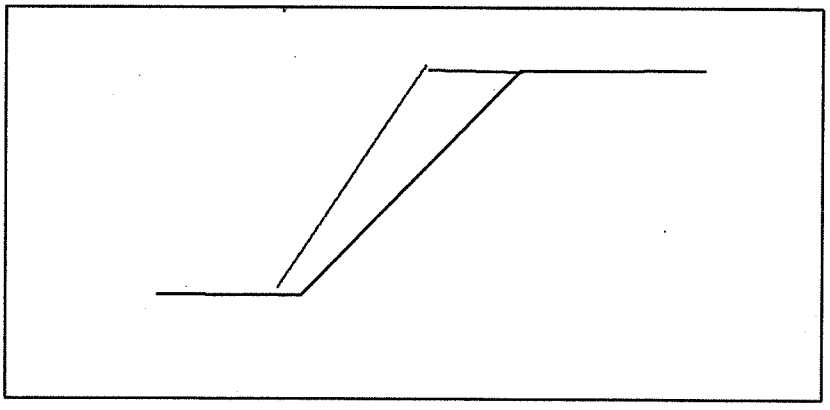

TOE EROSION EXCEEDING TOP EROSION

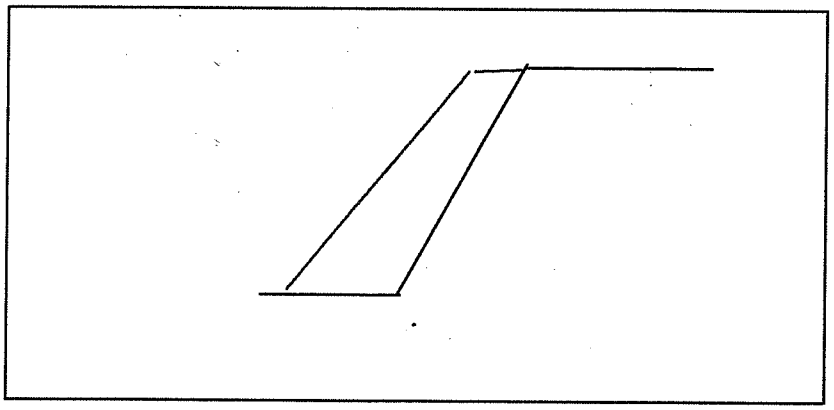

NO CHANGES

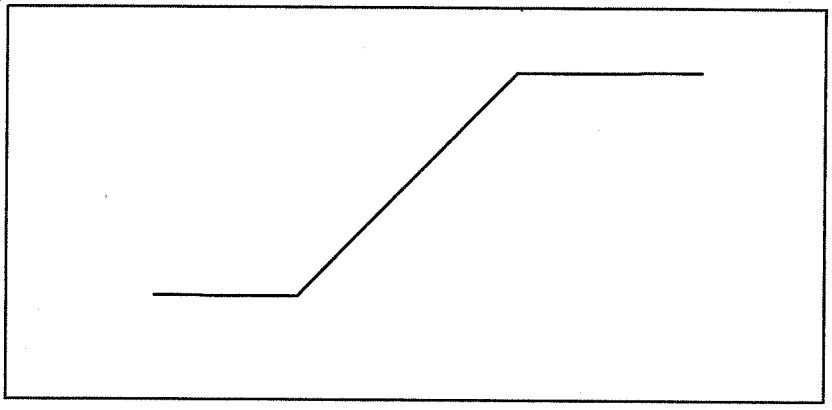

PROPOSED METHODOLOGY FOR INTERPRETING RECESSION RATES AND PREDICTING STABLE SLOPE LINE

ELEMENTS OF THE METHOD

- Divide shoreline into reaches based on evolutionary morphological classes
- Interpret past recession rates based on evolutionary model
  - nearly continuous retreat where annualized average historical recession rate applicable
  - episodic retreat where annualized average historical recession rate not applicable
- For episodic retreat predict expected stable bluff configuration based on morphological class

RIVER BANK EROSION AND FAILURE

Major Processes:

- Scouring action of river currents during floos
- Increase in driving forces (weight) and decrease in strength due to flooding events
- Rapid drawdown following flooding events and consequent slumping and sliding
- Groundwater sapping or piping and subsequent collapse
- Rain Impact and Rill/Sheet Erosion

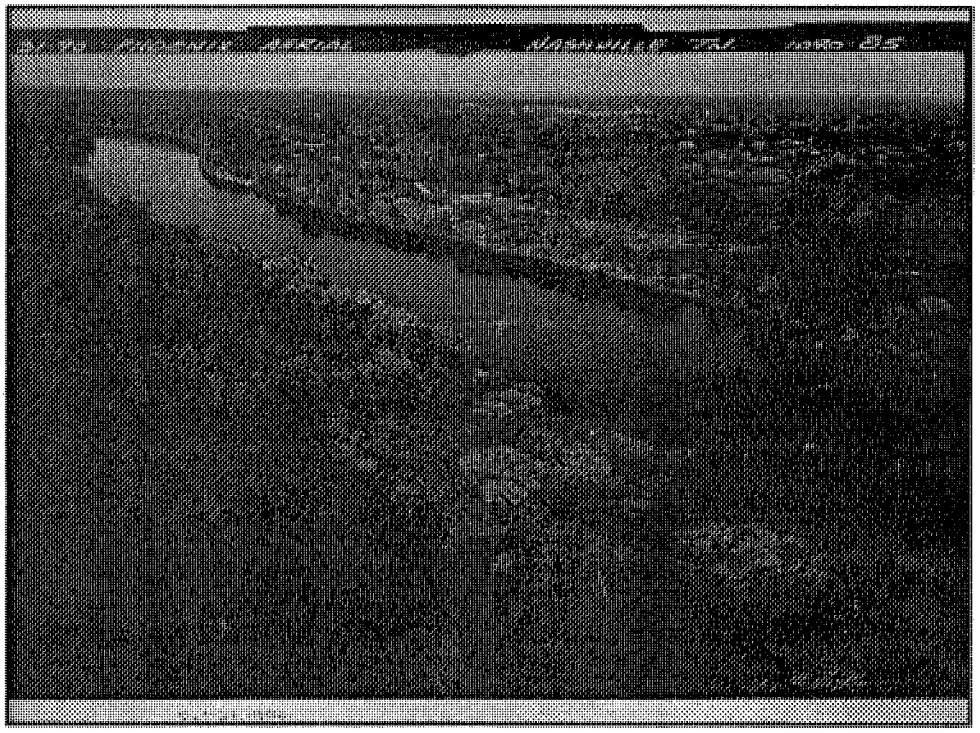

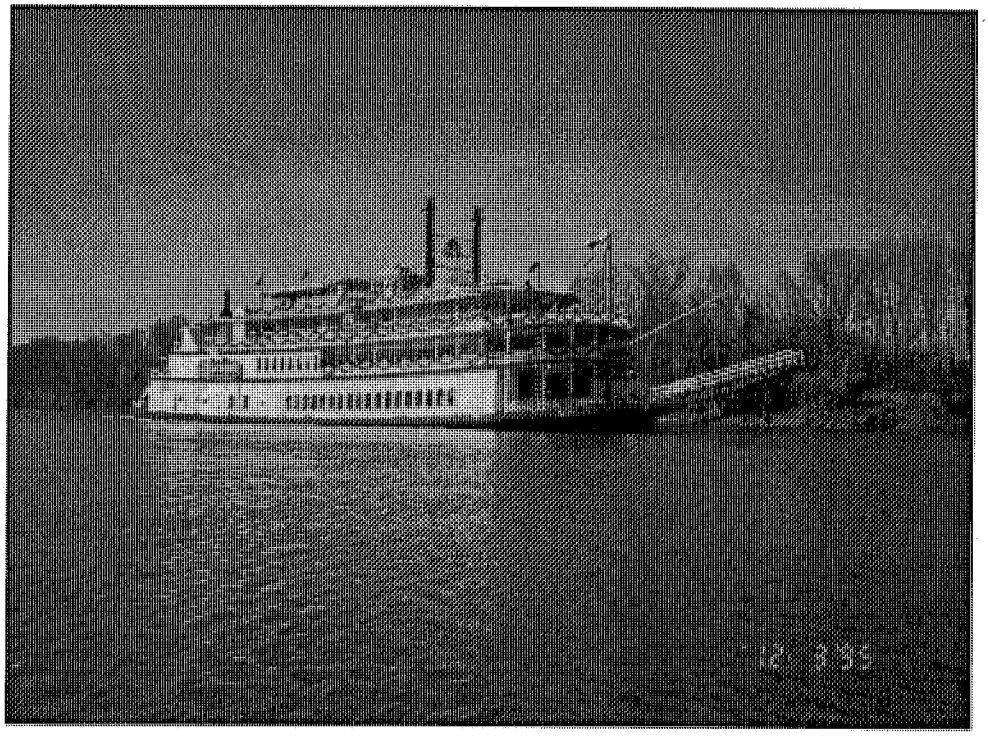

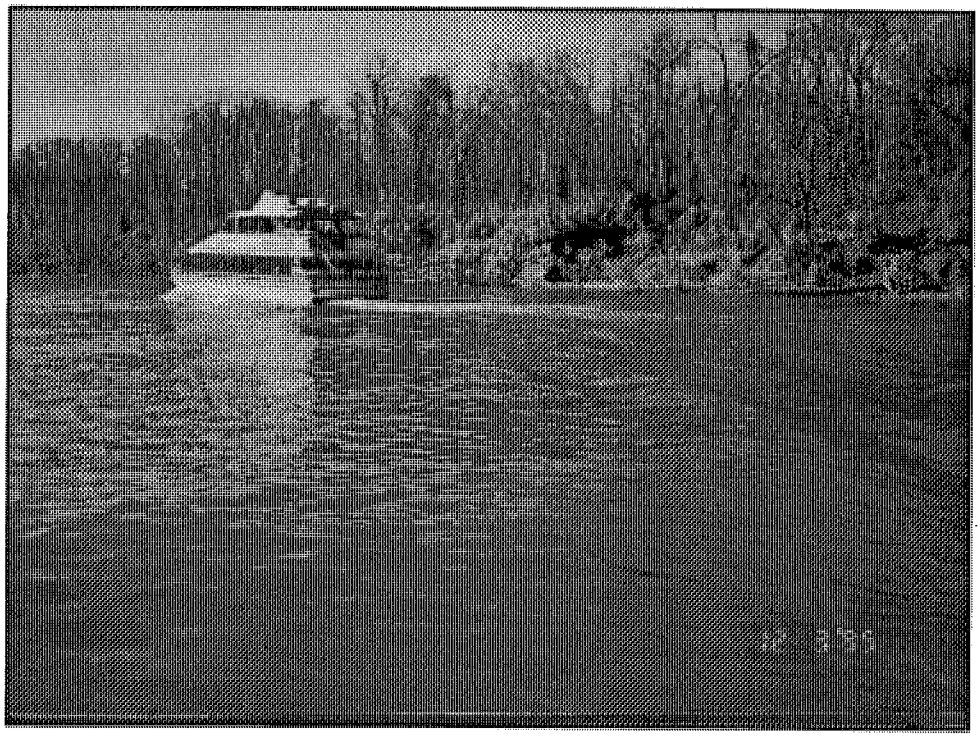

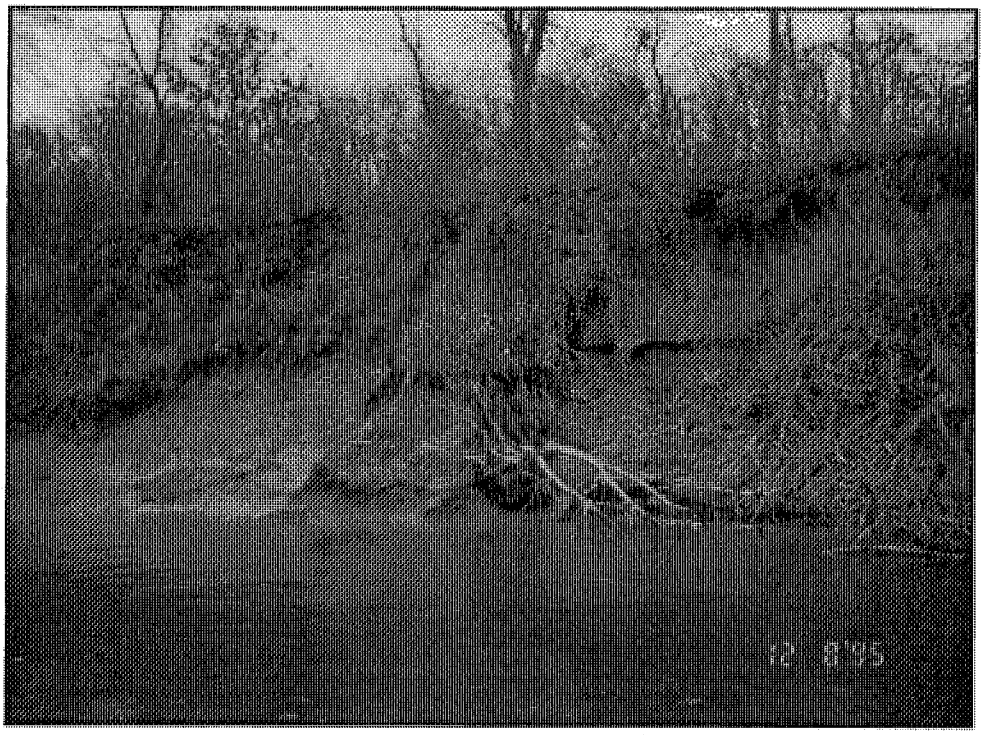

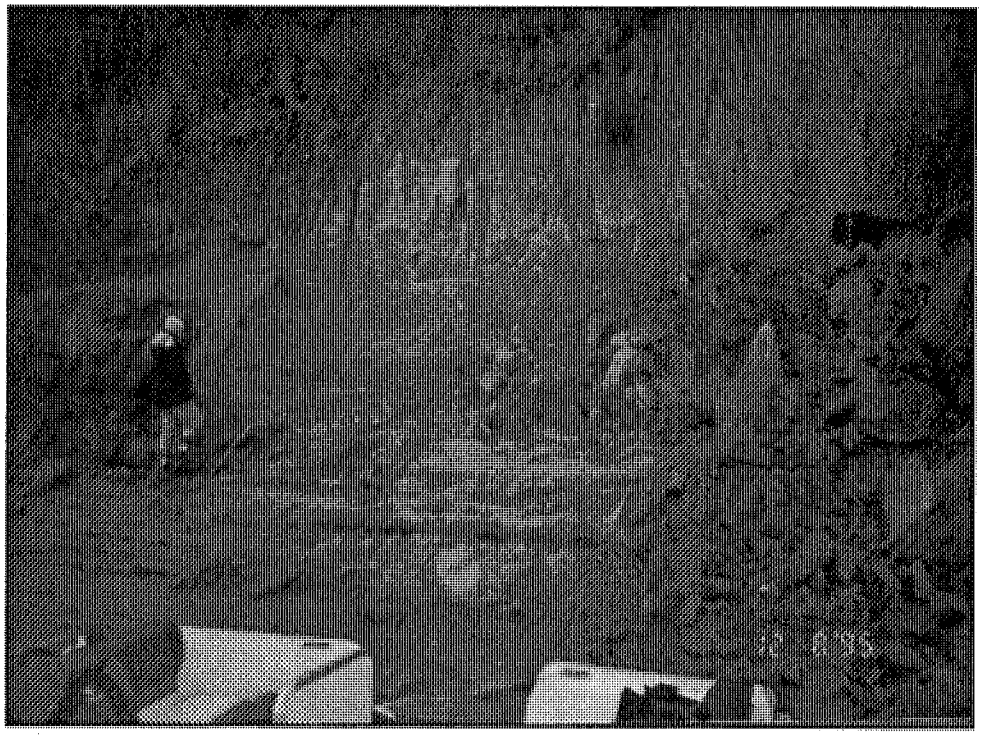

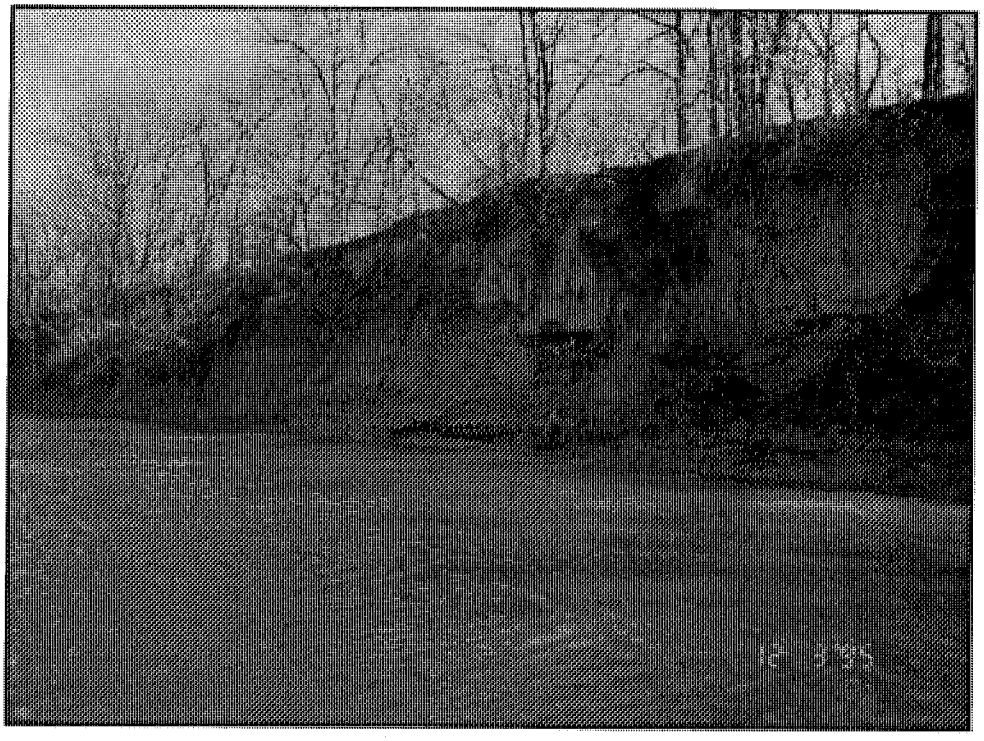

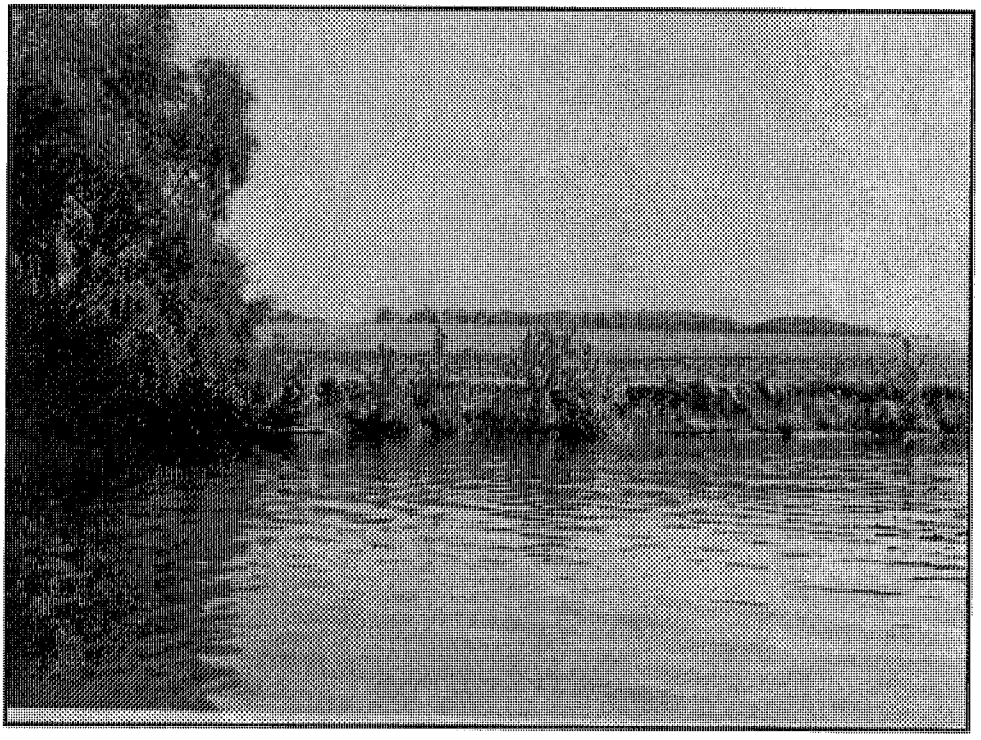

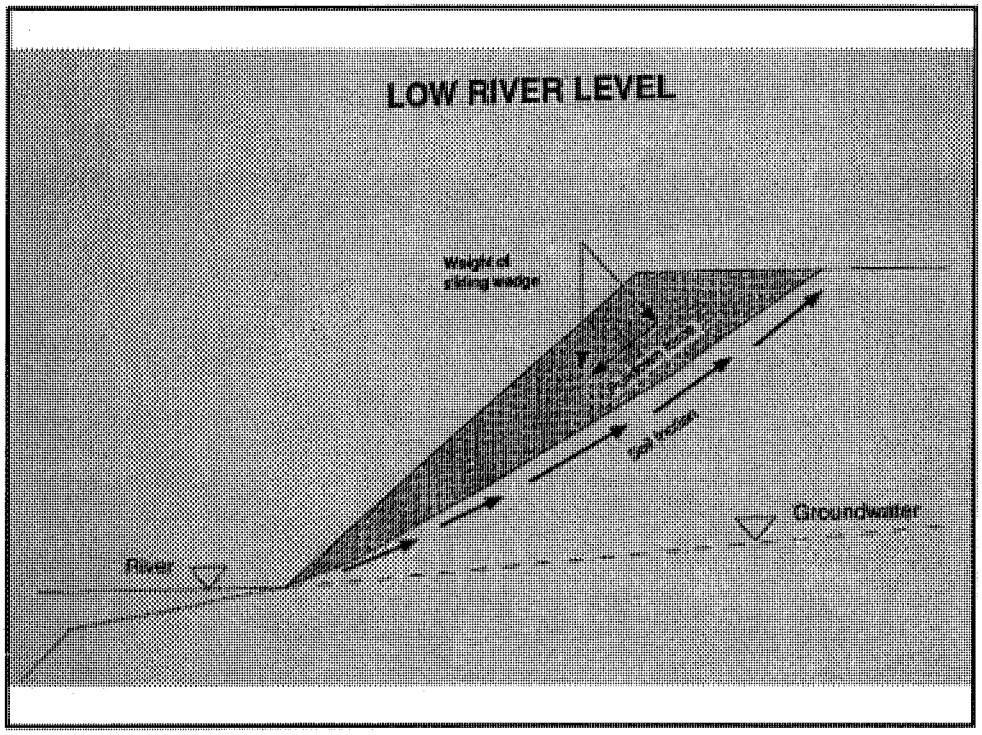
LOW RIVER LEVEL
Groundwater
River

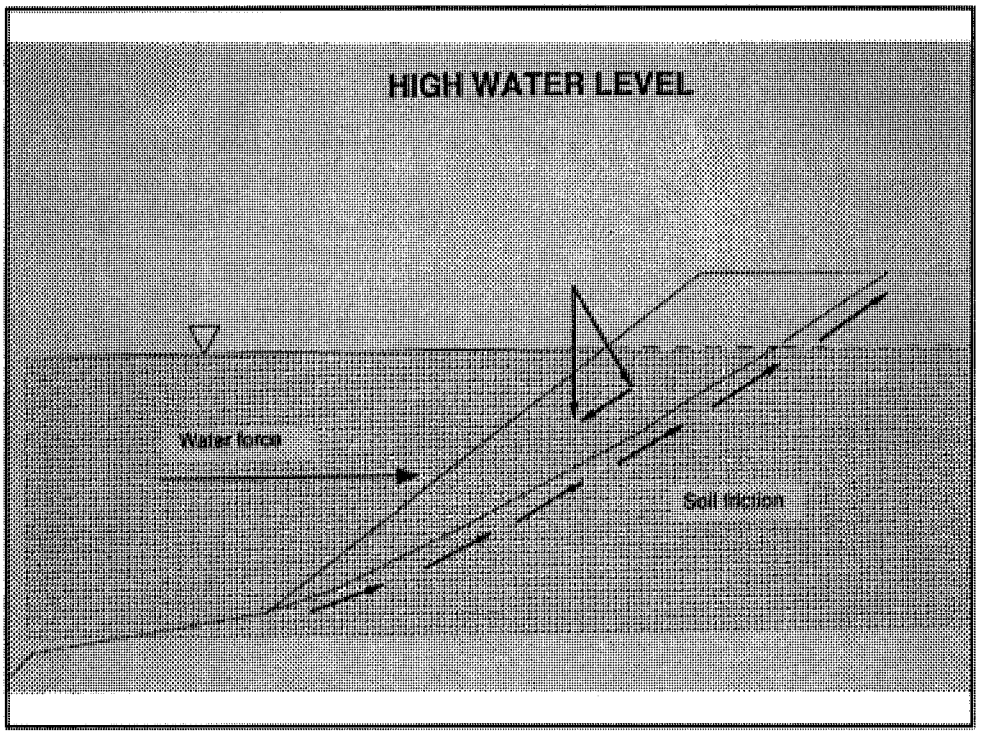
HIGH WATER LEVEL
Water forces
Soil friction

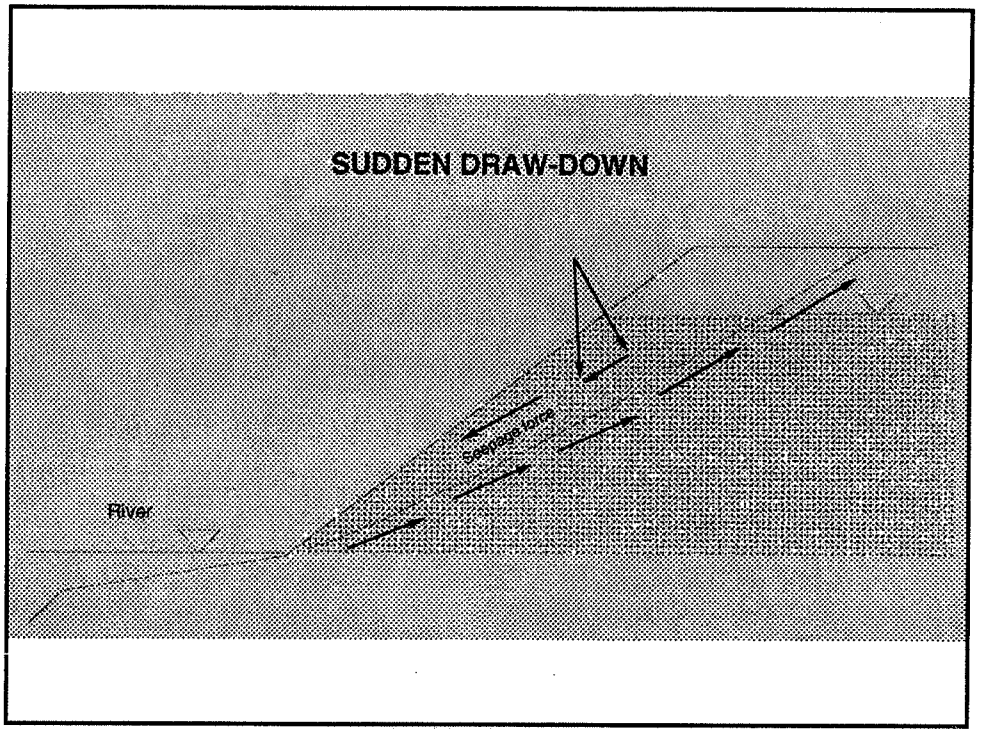
SUDDEN DRAW-DOWN
River
Seepage Line

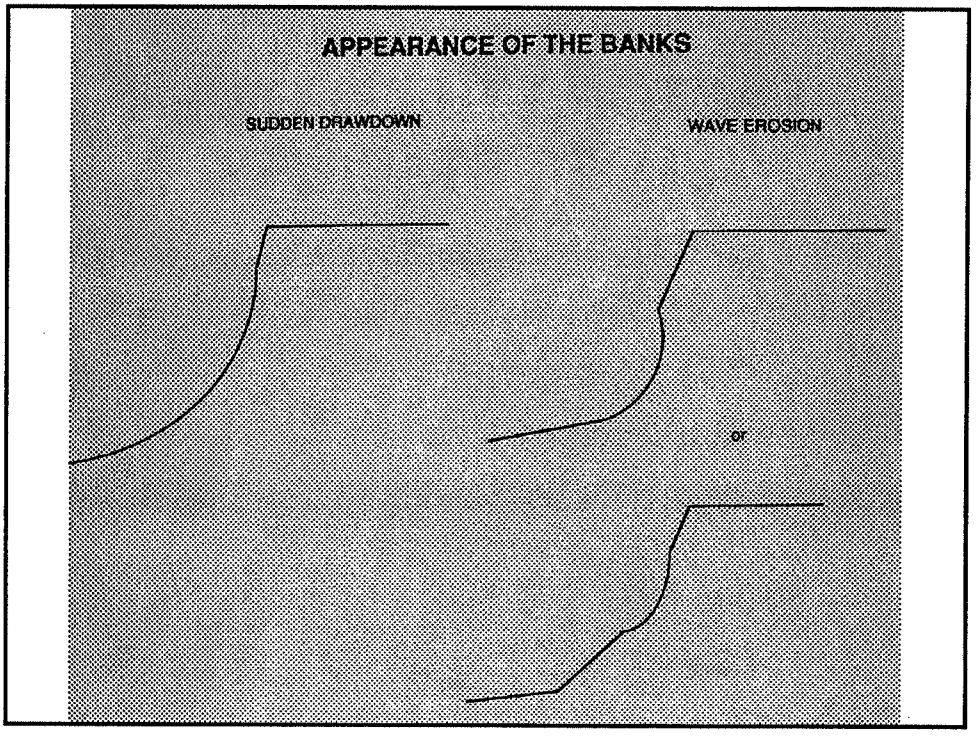
APPEARANCE OF THE BANKS
SUDDEN DRAWDOWN
WAVE EROSION
or

COMPUTATIONS SHOW

For a typical bank in Cumberland River:

- Sudden drawdown causes a reduction of safety factor by 0.4 whereas
- An equal reduction in safety factor due to wave erosion requires an immediate removal of 3 m (9 ft) of material from the bank toe

FACTORS THAT LOWER SLOPE STABILITY

For a given riverbank due to sudden drawdown:

- How high outside water rises
- How long it stays up
- How fast it comes down
- Ability of bank soil to drain water rapidly as outside water comes down

FACTOR THAT LOWERS SLOPE STABILITY

For a given riverbank due to wave/current erosion:

- Amount and size of eroded chunk of soil at the bottom of the slope

BANK EROSION BY PIPING/SAPPING AND COLLAPSE

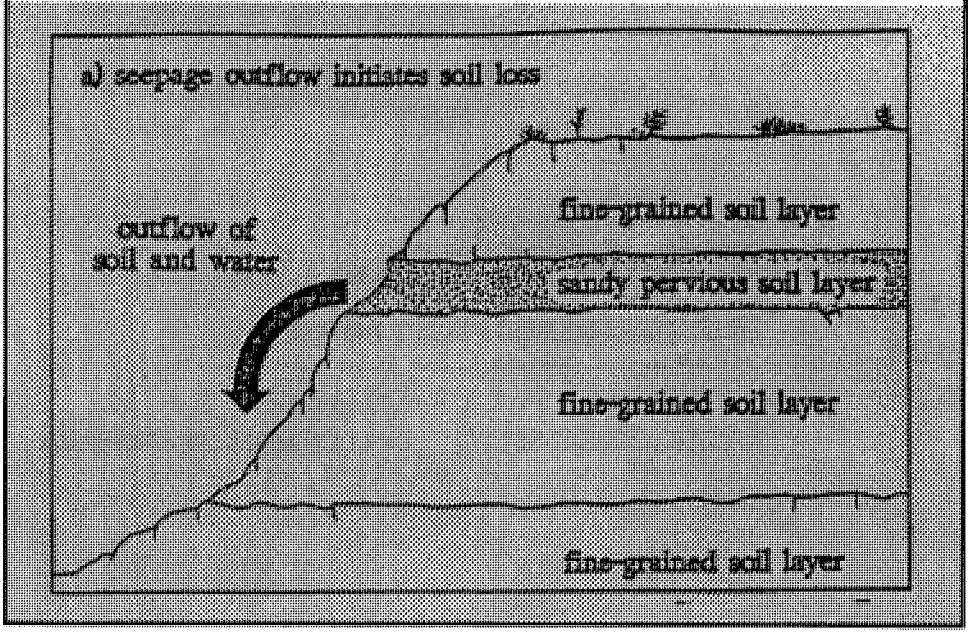

BANK EROSION BY PIPING/SAPPING AND COLLAPSE

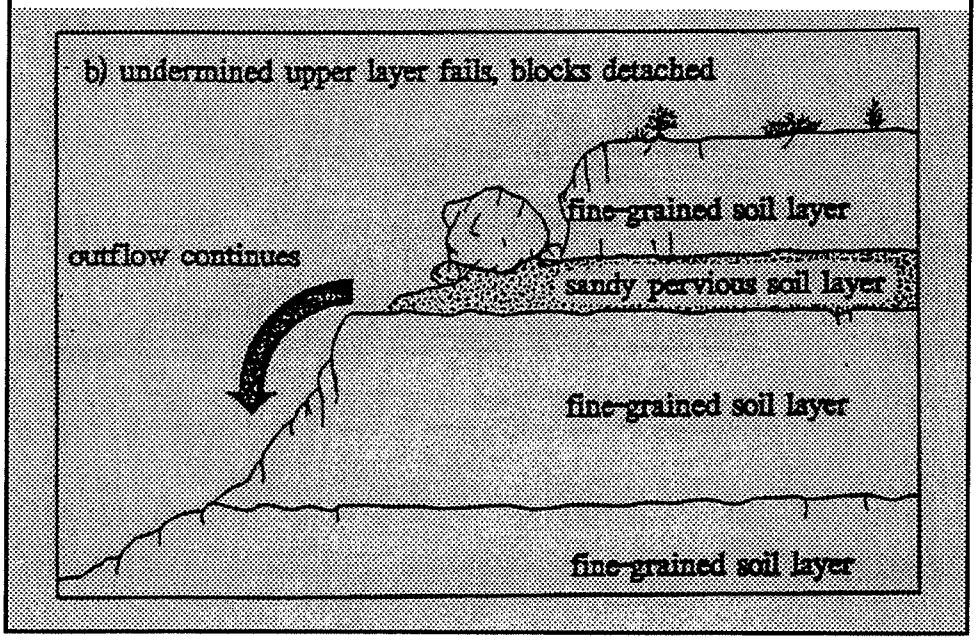

BANK EROSION BY PIPING/SAPPING AND COLLAPSE

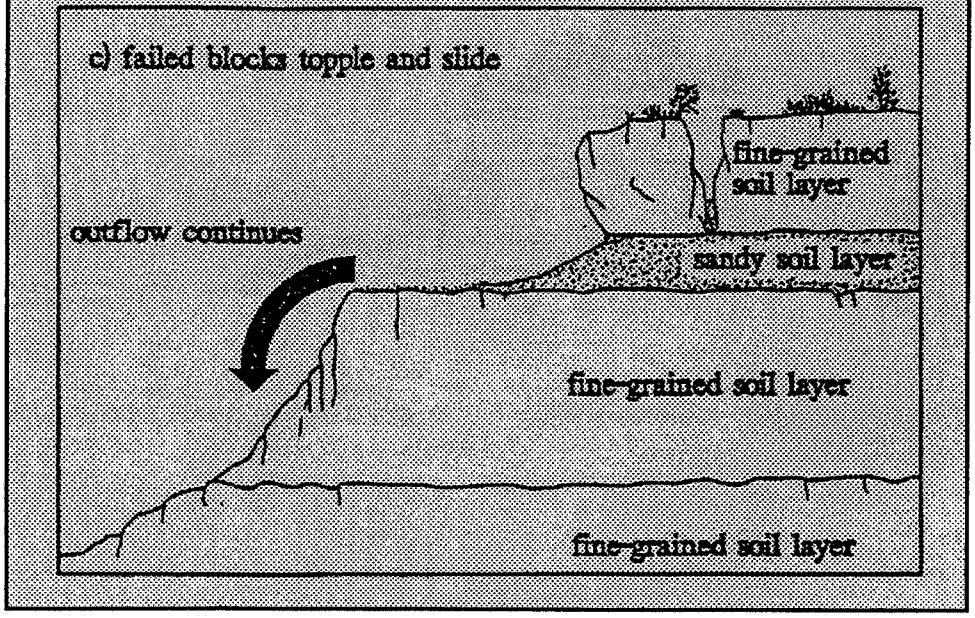

INUNDATION AND RECHARGE TO PERVIOUS ZONES

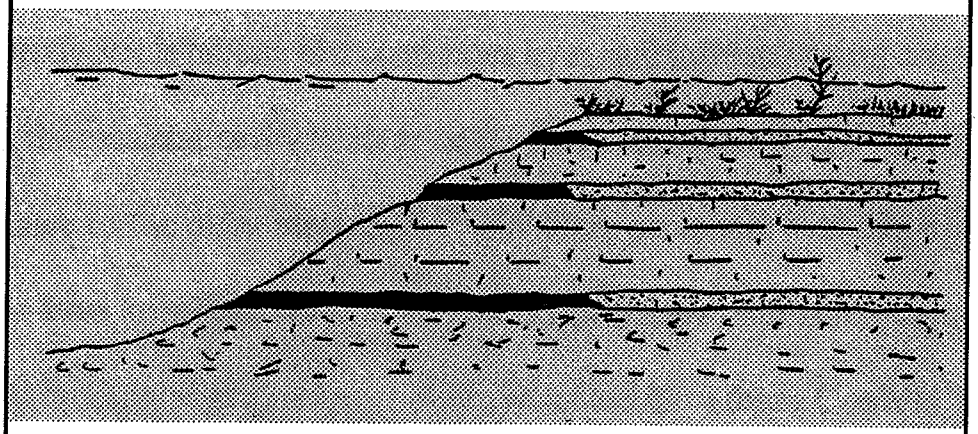

PIPING/SAPPING AND FAILURE OF UNDERCUT ZONES

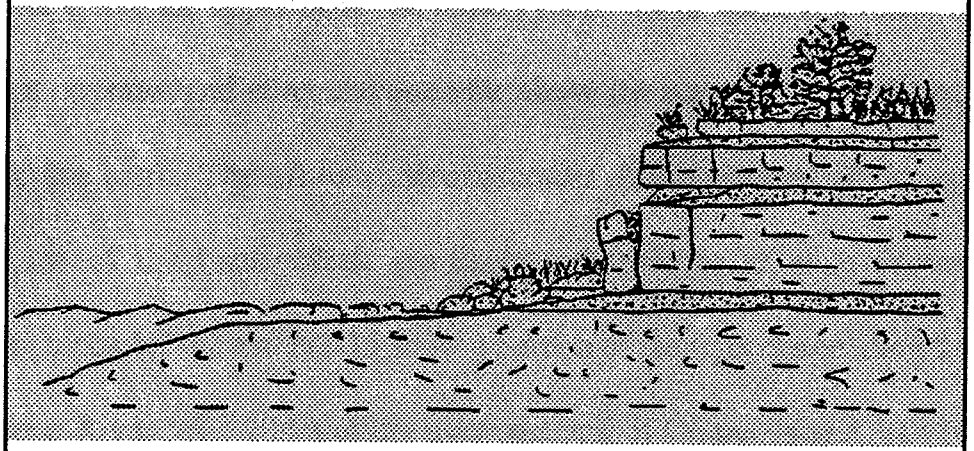

ALTERATION BY WAVES, WINDS, AND CURRENTS

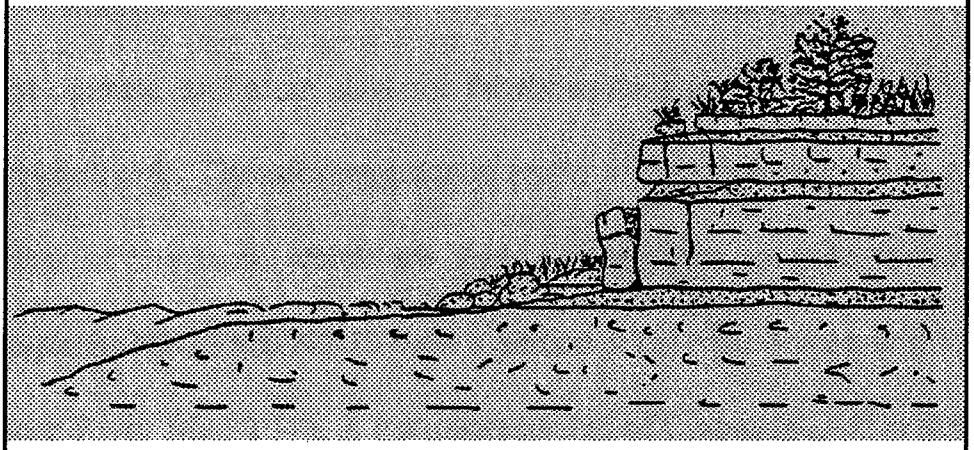

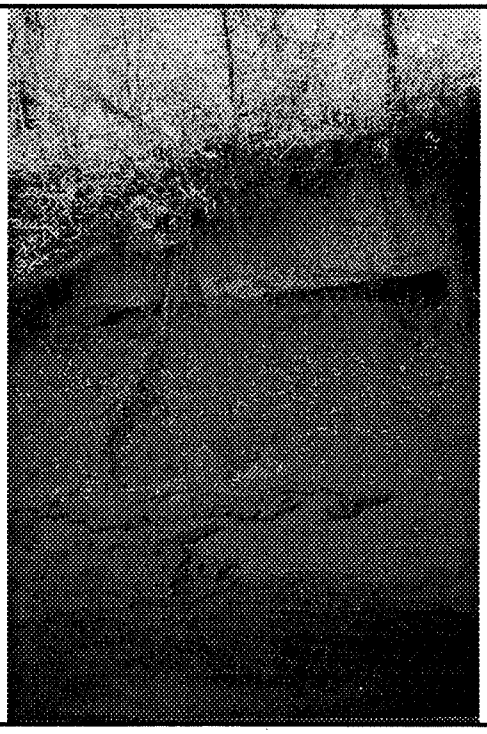

RIVERBANK SLOPE STABILIZATION

- Maintaining stable inclinations consistent with observed safe angles (typically 1V:1H or flatter) for general stability
- Reducing the erosive effect of flowing water:
  - the use of vegetation
  - soil bioengineering
  - the use of rock work in conjunction with plants
  - conventional bank armoring

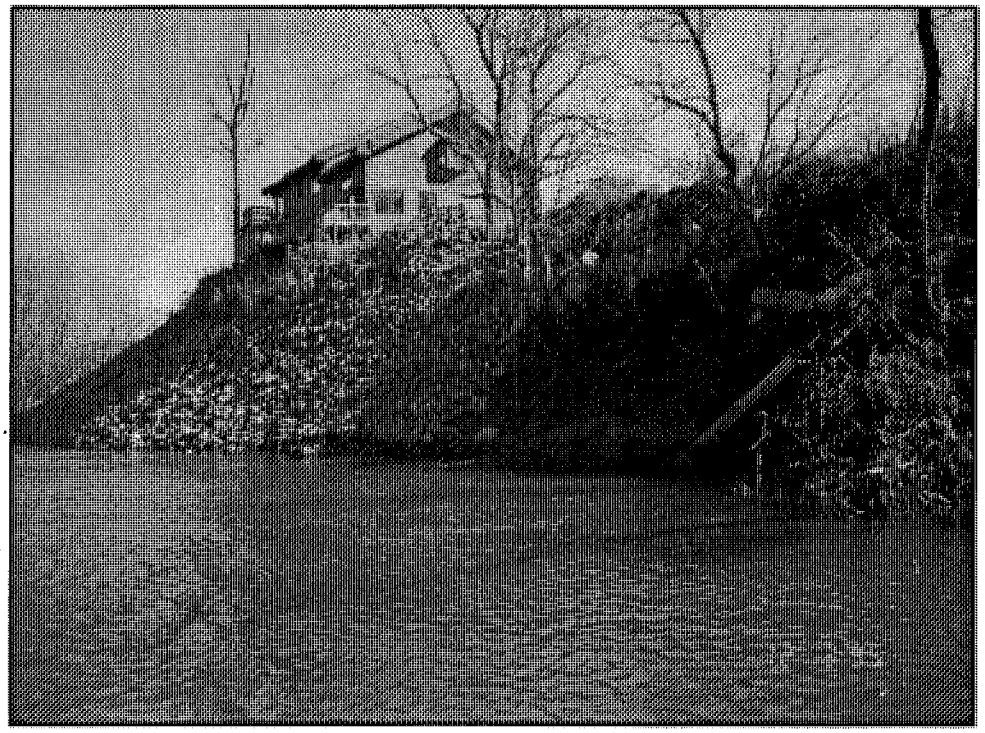

PIPING/SAPPING EROSION. I: BASIC CONSIDERATIONS

By D. J. Hagerty,[1] Member, ASCE

ABSTRACT: Erosion of streambanks and shorelines by exfiltrating seepage is called sapping or piping (because tubular cavities are produced). This mechanism is widespread in occurrence and is very significant to bank and shore stability, but is rarely recognized. The mechanism is complex and acts in concert with other processes of bank and shore erosion and deposition. Operation of those other mechanisms often masks the processes and products of the piping/sapping mechanism. Furthermore, failures caused by this mechanism may occur during periods of stream inactivity long after storm and/or flood events have ended. This paper describes and illustrates characteristic features of piping/sapping erosion and attendant instability. Situations typical of sites where piping/sapping is significant are illustrated. Conditions necessary (but not necessarily sufficient) to cause piping/sapping are presented. Diagnostic procedures are presented in a companion paper. The purpose of this paper is to present the fundamental aspects of this erosion mechanism and to identify those combinations of circumstances under which piping/sapping is likely to be an important process affecting bank or shoreline stability.

INTRODUCTION

Streambank erosion can occur at times and in places not consistent with common theories of tractive force erosion. Banks and shorelines may fail long after periods of high stage and in locations where deposition would be anticipated (e.g., on the convex or bar side of bends). A major cause of such unanticipated erosion may be outflow of seepage, with attendant removal of soil particles in the exfiltration zone, and consequent instability of undercut strata located above the zone of soil loss. Figs. 1(*a*)–(*c*) show a site where seepage flow out of a sandy layer carried sand out of the streambank, and the overlying more cohesive upper bank layer was undermined and collapsed. Collapse of undercut soil layers may partially or totally obscure the exfiltration zone where the internal erosion was initiated (Fig. 2).

Quite often, internal erosion of sandy soil creates approximately cylindrical conduits, or "pipes." Consequently, this form of erosion has been called "piping," defined by Mears (1968) as ". . . subterranean erosion initiated by percolating waters which remove solid particles . . . to produce tubular underground conduits." The term has been in use for more than 30 years (Fletcher et al. 1954). Where the seepage exfiltration takes place over a more extensive area, the term *sapping* has been used to describe the mechanism (Sterrett 1980; Higgins 1984). Fig. 3 shows an area of streambank in which multiple cavities were created by seepage outflow and where soil loss was extensive.

The detrimental effects of concentrated seepage outflow in cohesionless soils has long been recognized (Terzaghi 1929). Instability in soil embank-

[1]Prof., Civ. Engrg. Dept., Univ. of Louisville, Louisville, KY 40292.

Note. Discussion open until January 1, 1992. Separate discussions should be submitted for the individual papers in this symposium. To extend the closing date one month, a written request must be filed with the ASCE Manager of Journals. The manuscript for this paper was submitted for review and possible publication on September 6, 1990. This paper is part of the ***Journal of Hydraulic Engineering***, Vol. 117, No. 8, August, 1991. ©ASCE, ISSN 0733-9429/91/0008-0991/$1.00 + $.15 per page. Paper No. 26066.

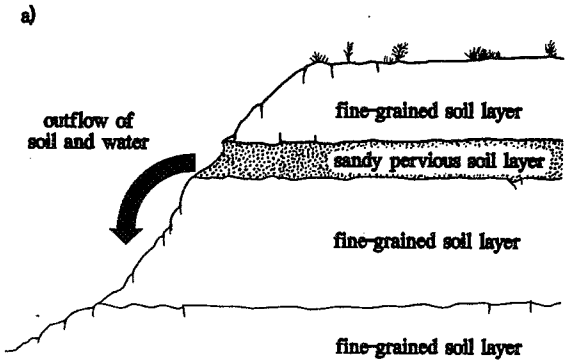

FIG. 1(*a*). Bank Erosion by Piping/Sapping with Subsequent Collapse: Seepage Outflow Initiates Soil Loss

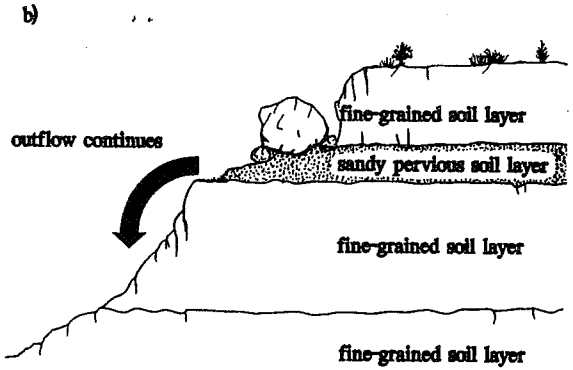

FIG. 1(*b*). Bank Erosion by Piping/Sapping with Subsequent Collapse: Undermined Upper Layer Fail, Blocks Detached

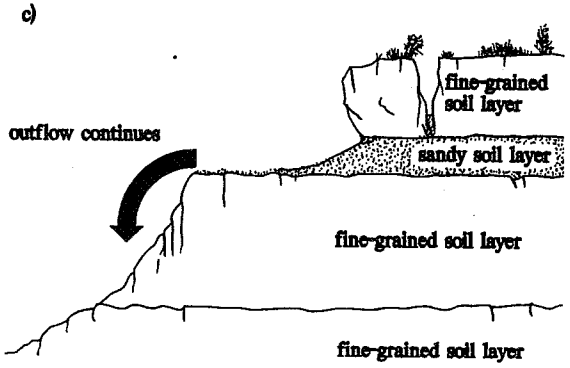

FIG. 1(*c*). Bank Erosion by Piping/Sapping with Subsequent Collapse: Failed Blocks Topple or Slide

FIG. 2. Collapse of Layer Undercut by Piping/Sapping

ments caused by seepage-related internal erosion was described by Casagrande (1936), and the importance of this erosion mechanism to the safety of dams has been demonstrated repeatedly (Terzaghi 1931; Reuss and Schattenberg 1972; Sherard et al. 1972). However, the significance of piping/sapping in bank and shoreline erosion has not been widely recognized.

The important influence of antecedent moisture on the erodibility of soils has long been understood (Wolmann 1959), as has the role of ground-water

FIG. 3. Cavities Typical of Piping/Sapping Erosion; Standard Survey Logbook in Cavity

and pore-water pressures in slope stability (Henkel 1967; Hutchison 1982; Thomson 1970; Williams et al. 1979). Only recently, however, have investigators realized that the formation of soil pipes and cavities can have an important influence on bank and shore stability (Hagerty et al. 1981; Hamel 1983; Jones 1981; Pierson 1983). The destabilizing effects of removal of sandy layers in lower bank zones have been cited repeatedly (Leopold and Miller 1956; Pizzuto 1984), and early investigations documented the removal of sandy layers by seepage outflow (Thomas and Watt 1918), but the significance of this cause of erosion has not been appreciated. This situation has prompted the following comment from Kennedy (personal communication, 1984):

> Most previous work on bank erosion, at least that done by hydraulic engineers, has taken a more global view of the subject, and has been concerned principally with the distributions of local sediment-transport capacity across and along river bends. The question of how the bank material fails and becomes available for transport has been given rather short shrift, at least to the best of my knowledge.

Geologists and geomorphologists have studied piping and sapping processes extensively, and geotechnical engineers have developed comprehensive analyses of the failure mechanics associated with piping/sapping (Springer et al. 1985; Ullrich et al. 1986). A good presentation of theory on the physical processes of sapping has been given by Howard and McLane (1988). Why then should hydraulic engineers be at pains to understand and recognize this erosion mechanism?

This paper has been prepared in the belief that hydraulic engineers should be able to recognize and evaluate piping/sapping erosion for the following reasons:

1. Hydraulic engineers are the persons most likely to be asked to investigate sites where streambank or shoreline erosion has occurred.
2. While investigators with significant expertise easily identify the occurrence of piping/sapping (Clough and Duncan 1986), inexperienced persons may diagnose the operation of this mechanism with only moderate instruction (Luzbetak et al. 1988).
3. Much of the research on piping and sapping done by geologists and geotechnical engineers has not included consideration of the role of this mechanism in bank and shore erosion.
4. Piping/sapping has great inherent significance to streambank and shoreline erosion, and as a terrain-shaping mechanism, as described in the following.

Significance of Piping/Sapping

Piping and sapping are significant erosion mechanisms because of their role in the initiation of drainage patterns. Recognition that throughflow may be important in rill formation is relatively new, especially in the context of experimental demonstration. Piping and sapping are important also because of their widespread geographic occurrence; erosion by seepage outflow has been noted in many different geological settings (alluvial banks, glacial terrain, and residual and colluvial soils), as well as in many different localities.

Finally, piping/sapping is important because of the way this mechanism interacts with other bank and shore processes to influence sediment transport.

Formation of Drainage Patterns

Infiltrating precipitation commonly passes through soil zones of decreasing hydraulic conductivity between the soil surface and the pedological parent material; such layers of lower relative permeability tend to retard vertical flow and promote lateral flow. If this lateral flow emerges at an exfiltration face where the surface elevation is lower, a rill or gully may be initiated. Piping has long been recognized as an important factor in gully formation (Ireland et al. 1939; Buckham and Cockfield 1950), but the mechanism was considered more important in arid climates than in humid zones (Brown 1962; Parker and Jenne 1967). Other and more recent research has shown that piping is significant in the initiation of a total drainage pattern (Bunting 1961; Dunne 1980; Jones 1971, 1987). Much of the emphasis on piping as an initiator of regional drainage has been prompted by the demonstration that throughflow is a very important component in the hydrologic system in a watershed (Born et al 1979; Jones 1987; Kirkby and Chorley 1967; Sloan 1972). Some investigators have even speculated that seepage is the dominant factor in the formation of regional drainage systems (Zaslavsky and Sinai 1981). Piping is considered a major factor in the formation of submarine canyons (Johnson 1939) and has been shown to be the cause of both very large erosional features (Stearns 1936) and minute features in drainage ditches (Sellmeijer 1981).

Geographic Distribution

While piping has been shown to be important in the formation of drainage patterns, it also has been shown to be an erosion mechanism operating on streambanks and shorelines throughout the world. Piping/sapping erosion has been documented in Australia (Twidale 1964), in Canada (Clifton et al. 1981), in China (Hamel 1988), in Northern Ireland (Hill 1973), in Poland (Klimek 1974), and in the Sudan (Berry 1970). In the United States, piping and sapping have been found in the banks of the Ohio, Illinois, Kanawha, Missouri, Monongahela, and Red Rivers (Hagerty et al. 1981; Hagerty 1988; 1990; Spoor and Hagerty 1989), along Chesapeake Bay (Palmer 1973), along rivers in Iowa (Luzbetak et al. 1988), and in bluffs along the Great Lakes (Edil and Vallejo 1977; Lawson 1985). The conditions necessary for piping/sapping to occur, described in a subsequent section, may be found almost anywhere in the world.

Geologic Distribution

The most commonly noted occurrence of piping in streambanks has been in alluvial soil deposits where the natural layering associated with alluvium favors concentration of flow in more pervious strata, and more cohesive layers tend to bridge over cavities, allowing conduits to form (Hagerty and Spoor 1989; Hamel 1983). However, piping and sapping have been noted in glacial terrain where the heterogeneity of the soil deposits may concentrate flow and where secondary features such as joints in precompressed deposits also may lead to localized flow and exfiltration (Hendry 1982; Hill 1973; Lawson 1985). Development of illuviated zones of low hydraulic conductivity in residual soils can cause concentration of flow leading to piping (Jones

and Crane 1984); the presence of fractures or relict structures (derived from the rock parent material) also may cause concentration of seepage and promote piping (Deere 1957). Frozen soil zones can retard and concentrate flow to produce sapping (Kane et al. 1973), and the piping/sapping mechanism may act in concert with freeze-thaw mechanisms to cause destruction of soil structure and loss of soil from a bank or shoreline (Sharp 1976). Numerous instances of piping/sapping operating with other mechanisms have been seen in lakeshore bluffs (Edil and Vallejo 1977; Hadley 1976; Kachugin 1970). Piping occurred even in lacustrine deposits consisting of interbedded silts and varved clays when the lakebed deposits were exposed by excavation below the water table (Leggett and Bartley 1953).

Influence on Sediment Transport

Piping/sapping removes soil grains from exfiltration faces and transports those grains away from the exfiltration zone. If the piping occurs in a streambank or shoreline, the displaced material is particularly susceptible to further transport and working by currents, waves, and other bank/shore phenomena. The structure of the in situ soil mass is disrupted, and the displaced soil grains tend to be loose and erodible. Furthermore, formation of cavities in a seepage outflow zone commonly undermines strata located at higher elevations. Tension and shear stresses are created in the undercut layers, cracks form parallel to the face of the bank or bluff, and blocks or slabs fall from the face. The fallen blocks and slabs are disrupted and weakened, and thus are more erodible. Moreover, the presence of blocks or slabs that have fallen onto the lower bank causes significant interference with flow when the bank is inundated during subsequent periods of high stage. Turbulent flow around the displaced soil masses will be more effective in eroding those masses than would have been the flow over the bank prior to the piping/sapping and consequent collapse of upper strata. Wave action will be more effective in breaking down fallen slabs and blocks than would have been the waves breaking on the shore before the piping/sapping and collapse. Soil loss from a site will be accelerated greatly if piping/sapping is severe there. Piping and sapping also will occur wherever concentrated seepage outflow is sufficiently intense to cause removal of soil grains; piping/sapping is not related by necessity to planform considerations in a stream or to proximity to a body of water (other than the source of the seepage outflow). Piping can be caused by infiltrating precipitation, by lateral flow from a surface impoundment, or by leakage from a pipeline or tank; thus, piping can occur and may even be more likely when the stream itself is relatively inactive. Piping and subsequent collapse of undercut strata can occur at elevations far above the stream or lake level and during periods of low discharge and/or low stage. When the stream floods, or when winds drive waves onto the shore, an irregular configuration of erodible materials may await the onslaught of currents or waves because of the operation of piping and sapping in prior times. Whether or not the erodible failed material is present will depend upon whether or not all conditions necessary for piping/sapping to occur were met.

Conditions Necessary for Piping/Sapping

For internal erosion to produce cavities, there must be a free face or external plane from which seepage outflow can remove soil particles. A source

of water must be available to supply the requisite flow; the source need not be constant since the mechanism can operate intermittently. Generally, flow must be concentrated in order that the intensity of exfiltration, characterized by the exit hydraulic gradient, will be sufficient to remove soil particles. If piping/sapping is to occur, the exit gradient must produce seepage forces sufficient to overcome all the forces and factors that tend to keep particles in place: interlocking with other particles, which interferes with movement; interparticle friction, which resists motion; cohesion between grains derived from physicochemical attractions including capillary forces; cementation; binding by roots; and, in some cases, gravity forces. Finally, the materials displaced by piping/sapping and consequent collapses must be removed from the bank or shore, or net erosion will not occur.

Exposed Face

Piping cavities will not form unless there is an exit point at which water can leave the soil mass, dislodge surface particles, and carry away the dislodged grains. This consideration may seem simplistic but reflection on this requirement can help to indicate why this mechanism is very complex. For example, if collapse of undercut soil layers causes the face of a pervious layer to be covered with relatively impervious soil, any exfiltration and soil removal that was occurring at that face will be retarded or blocked completely. Exfiltration will be retarded until sufficient pore-water pressures build up in the pervious zone to dislodge the impervious cover. However, the cover on one portion of the pervious zone may prevent exfiltration there, but seepage may be diverted to other faces previously inactive. Deposition of sediments over exfiltration zones during high-water periods can produce a blocking layer that retards piping until the exit gradient through the covered face is sufficient to breach the sediment layer. Such short-lived blockages of outflow can change the flow system in the bank or shore so that piping may be seen to occur in certain locations at one inspection, may be inoperative at another inspection, and may be observed at other locations on the same site at a third inspection. Conversely, removal of failed blocks, slabs, or debris piles by waves or scour during floods can re-expose exfiltration faces and facilitate subsequent piping and sapping. Any mechanism that exposes a face in a pervious water-bearing zone can initiate piping/sapping at that exposed face, if a source of water exists to supply continued exfiltration.

Sources of Water

Where piping/sapping takes place on a streambank, the most important source of water for the erosion mechanism may be the stream itself. When the stream rises against and over the face of the bank, water enters the bank soils. Recharge will occur preferentially into those soil zones that have the highest hydraulic conductivity and in which no pre-existing countervailing flow exists. Outflow will cease and recharge will begin when the head in the stream exceeds the head within the outflow zone. The volume of water stored in the bank will depend upon the magnitude of the recharge gradient, the hydraulic conductivity of the exfiltration zone, the area of the pervious layer exposed in the bank, and the time during which recharge occurs, as well as on other less important factors (Ullrich et al. 1986).

Other sources of water include precipitation and depression storage on the floodplain or areas adjacent to the bank or shore. Fig. 4 shows an active

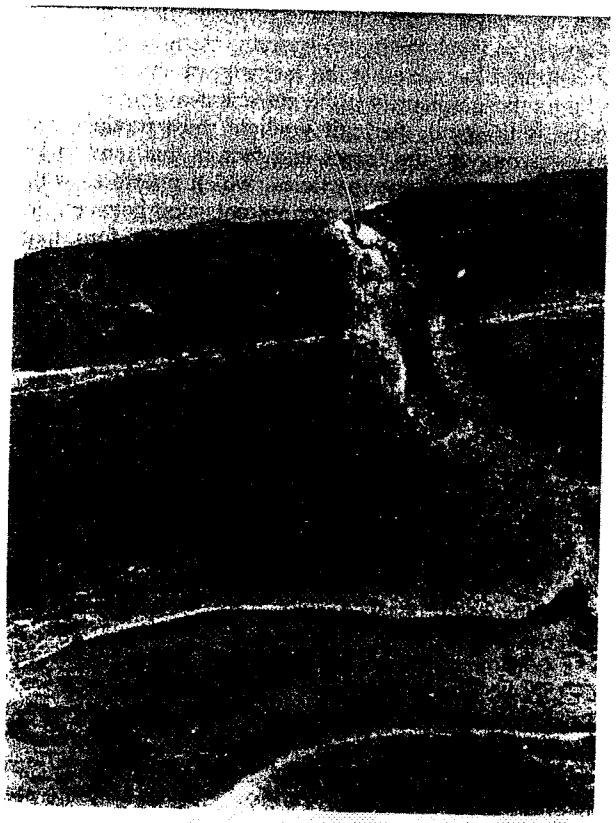

FIG. 4. Piping-Formed Gully (4-m Wide) in Stream Bank (Top), with Adjacent Depression Storage Water Source (Bottom)

piping/sapping zone where the source of much of the exfiltration seepage is an adjacent shallow depression. If undercutting of upper bank or shore soil strata has occurred because of piping/sapping in lower zones, tension in the undercut layers will form cracks parallel to the edges of the layers, and surface water will migrate downward through those cracks into the lower piping zone. Precipitation or water stored in floodplain depressions during floods may enter lower layers (perhaps covered in the bank face by failed soils or sediments) through tension cracks, and piping/sapping may continue as long as the surface supply of water lasts. Overland flow can enter the bank or shore system through cracks in the uppermost soil layers to supply the seepage for piping in lower, more pervious layers. Surface water entering cracks in undercut layers creates pressure (in the cracks), which tends to dislodge blocks and slabs (defined by the cracks) toward the stream or other water body. Irrigation water can enter a bank or shore system through cracks in the upper strata and cause piping/sapping in lower zones when the adjacent stream or lake is inactive (little rise and fall in stage and insignificant wave action). Water collected in agricultural drains also can cause piping

and instability in bank soils around drain outlets. Quite commonly, agricultural drains consist of pipe sections with open joints, placed on and in coarse granular material. Near drain outlets, pipes may fill substantially with sediments so that water emerges from pipe joints. Figs. 5(*a*)–(*c*) show a situation where a very large cusp was eroded in a streambank by piping/sapping around an agricultural drain. The piping/sapping erosion removed support under the drain, the terminal drain section tilted downward opening the last drain joint, and additional outflow from the opened joint intensified the sapping. Six sections of pipe failed and a large cusp formed around the drain during a two-year monitoring period.

The source of water for a piping/sapping process may be subsurface leakage from buried conduits or containment vessels. A very common instance of such leakage is outflow from a septic tank waste-water disposal system. Sewer service is not affordable for many rural dwellings, including those adjacent to streams and lakes, and septic tank systems are common. Instability in banks and shores can be caused by piping/sapping supplied with water by septic tank outflow. A situation very frequently encountered by the writer is piping/sapping in a slope or bank adjacent to a "weekend" residence; the water charged into the soil during occasional occupations seeps into the pervious zones beneath the residence and emerges at exfiltration faces to cause piping erosion and subsequent instability. The piping erosion may operate for much of the time between periods of occupation, and failures can occur when no residents are present to observe the instability and possibly understand the relationships between waste-water discharge and piping collapse. Obviously, leaking water-supply pipes, sewers, or underground tanks also can supply water to activate piping and sapping in adjacent streambanks or shorelines. Leakage from such sources will be localized and concentrated to some degree. Seepage from other sources such as surface depressions will be more widespread, and some concentration of flow may be necessary before piping/sapping will occur.

Concentration of Flow

If nearly cylindrical "pipes" or lenticular sapping cavities are to form in an exfiltration face, flow must be concentrated to some degree. Broad-area seepage certainly can have a detrimental effect on bank or shore stability, but diffuse seepage will not produce the cavities associated with piping and sapping. A number of different conditions can cause concentration of flow. The source of water to supply the internal erosion may be of very limited areal extent as in the case of a leaking underground storage tank. Surface flow in ditches and/or depressions may enter the bank/shore flow system through soil cracks, and only the portion of bank/shore near the ditch or depression may become sufficiently wet for exfiltration to occur. More often, however, concentration of flow occurs because of inequalities in hydraulic conductivity, rather than because of restrictions in the extent of the source of water.

Piping and sapping have been observed most often in alluvial streambanks. This is to be expected partly because of the possibility of recharge into pervious bank soils during high-stage events and because alluvial soils typically occur in layers or lenses so that there is a very definite variation in hydraulic conductivity from one layer to another layer (Deere and Peck 1958; Hagerty et al. 1986; Hamel 1983; Lawson 1985; Ullrich et al. 1986).

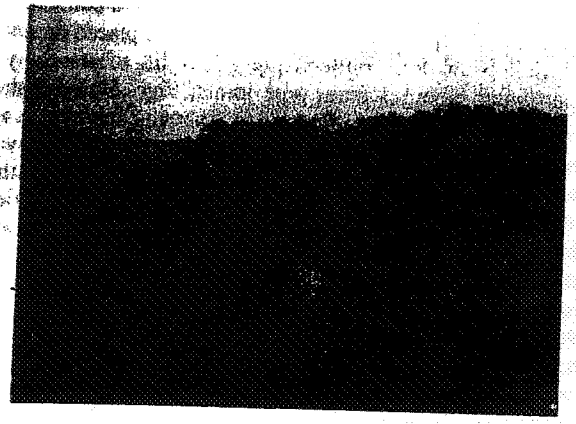

(a)

FIG. 5(a). Bank Erosion Caused by Piping/Sapping around Agricultural Drain, 4 in. (10 cm) in Diameter: Erosion Cusp

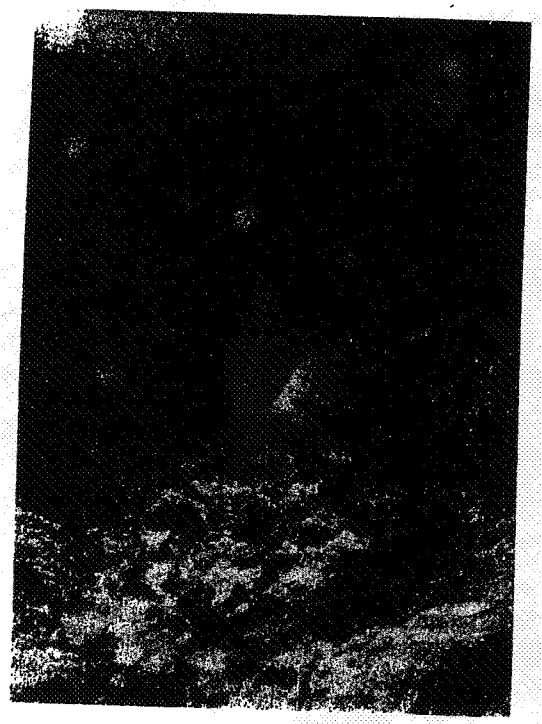

(b)

FIG. 5(b). Bank Erosion Caused by Piping/Sapping around Agricultural Drain, 4 in. (10 cm) in Diameter: View into Cusp

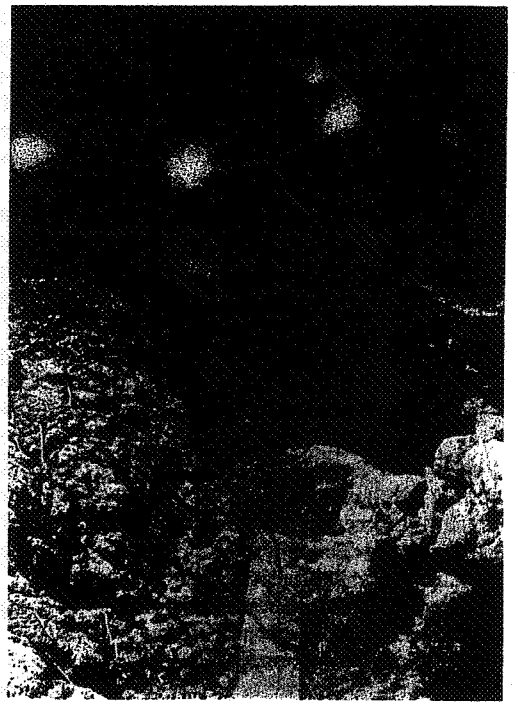

(c)

FIG. 5(c). Bank Erosion Caused by Piping/Sapping around Agricultural Drain, 4 in. (10 cm) in Diameter: Head of Cusp with Drain Exposed

The variations in texture and porosity among alluvial strata in a bank may not be noticeable and may appear to be slight, but even seemingly minor changes in soil texture can change hydraulic conductivity by orders of magnitude. A layer of fine sand containing no silt-sized or clay-sized particles may have hydraulic conductivity of 0.01 cm/s, while a sand layer containing no more than 20% (by weight) silt-sized particles may have hydraulic conductivity of 0.0001 cm/s or less. Likewise, a silty sand may be 100 times more pervious than a sandy silt, even though both soils look and feel very similar. Although piping failures have been noted most often in sandy layers or zones, it is possible for flow to be concentrated in silt layers contained in a sequence of clay strata and for piping to occur where the edges of the silt layers are exposed in a free face (Spoor and Hagerty 1989).

Concentration of flow and consequent piping/sapping can also occur because of variations in hydraulic conductivity in glacial deposits, both water-laid (outwash, esker, etc.) and ice-laid (till, moraine). Very complex flow patterns have been observed in sequences of glacial soils because of differences in texture from one material to another and because of the presence of fractures or joints in ice-contact materials such as glacial till (Grisak and Cherry 1975; Hendry 1982; Lafleur and LeFebre 1980; Williams and Farvolden 1967).

Development of relatively impervious zones because of near-surface eluviation and subsequent deposition of fines at depth can produce relatively impervious zones in residual soils, as well as in relatively old alluvial and lacustrine soils, so that ground water is "perched" and concentrated above the less pervious layers. Piping and sapping can occur in residual soils because of this concentration of flow. The formation of joints or the presence of fractures as relics from the parent rock material also can cause concentration of flow with consequent piping and instability in residual soils (Deere 1957). Flow may be concentrated by the presence of frozen zones with very low effective hydraulic conductivity (Kane et al. 1973) or by the presence of layers in which chemical precipitation has reduced the apparent porosity (Hagerty 1990). For whatever reason, piping/sapping can occur if outflow is concentrated in a particular layer or at a particular location, provided that the hydraulic gradient causing the exfiltration is sufficiently high, and failure debris is removed.

Removal of Displaced Soil

The piping/sapping mechanism can cause undercutting of soil strata above the zone where exfiltration removes soil particles, with consequent failures in those zones (Thorne and Tovey 1981). The slabs or blocks of soil displaced during those failures will accumulate on the lower portions of the bank or shore, together with the soil removed by the piping/sapping directly. In order for this erosion process to continue, the accumulated failure debris must be removed. As noted by Kennedy (1984):

> It is self-evident that in the absence of continued river transport of the material eroded by piping away from the bank toes, the bank eventually would reach equilibrium slopes, become vegetated, and remain stable. Continued bank erosion requires continued transport of the piping-eroded material away from the bank.

This removal of bank failure soil as a requisite for continued instability has been noted by many investigators (Hagerty et al. 1983; Hooke 1979; Klimek 1974; Thomson and Townsend 1979; Twidale 1964). Continuation of piping/sapping depends on sediment transport; initiation of piping depends on the exit hydraulic gradient.

Critical Hydraulic Gradient

The one condition that is absolutely necessary if piping/sapping is to occur is a concentrated flow of intensity sufficient to displace an in situ particle of soil, entrain it, and carry it away from its point of origin. Should particle removal be concentrated in a particular zone, removal of particles will shorten the seepage path and increase the hydraulic gradient at the zone of removal. A local increase in gradient may capture more seepage and intensify erosion. Once started, formation of cavities will tend to accelerate if the supply of water to the exfiltration zone remains constant. But will piping begin?

Removal of soil particles from a piping zone is a very complex phenomenon, dependent upon relative density, structure, and homogeneity of the soil deposit as well as on the shape and mix of sizes of the soil grains (Sherard et al. 1963). In natural deposits, all these factors typically vary significantly even over very short distances. It is practically impossible to predict

in advance the hydraulic gradient at which piping will begin in a given deposit. Laboratory experiments to simulate piping are difficult to accomplish (Luzbetak et al. 1988) and seldom succeed in truly representing field conditions. Even very comprehensive efforts to measure seepage water pressures in the field, and thus to establish hydraulic gradients when piping is observed to begin, are not likely to be meaningful because of the difficulty in monitoring flow conditions at very small scale; piping can be initiated essentially at a single grain only a fraction of a millimeter in size. Thus, it is feasible to identify conditions necessary to the piping process and to assess the potential for piping to occur at a given site but not to predict exactly where and when the mechanism will initiate erosion. Alternatively, a site may be examined for evidence that piping/sapping has occurred there, and then an assessment can be formulated as to the probability that piping will recur. Unfortunately, recognition of the operation of the piping/sapping mechanism often is difficult.

Difficulties in Recognizing Piping/Sapping

Inexperienced investigators may encounter some difficulty in identifying features characteristic of piping/sapping activity or in recognizing this mechanism of erosion, for several reasons. First, the mechanism itself is complex and subtle. At any given time, the effects of piping erosion on a bank or shoreline may not be dramatic. The visual impact of features produced by piping may be much less than the impression created by massive slumps or landslides. Nevertheless, the cumulative effect of this erosion mechanism can be quite significant.

Secondly, piping/sapping erosion on many sites is intermittent. If the principal source of water for the piping/sapping process is bank recharge during floods, piping will take place only after these events. Conversely, the deposits of piped-out soil and fallen blocks and slabs produced during subsequent failures typically are removed from the site during periods of high discharge and high stage. Therefore, an investigator visiting a site immediately after flood recession may observe water and soil flowing out of exfiltration zones, provided that the investigator has been alerted to look for that phenomenon, but no failures in upper bank soils may have occurred so soon after flood recession. A later visit could reveal fallen blocks and slabs, but by then all outflow of soil and water may have ceased. An inspection several months later may reveal little about the mechanics of erosion and failure because of the operation of other bank/shore mechanisms that have altered the evidence of piping/sapping activity. Fig. 6 shows a hypothetical sequence of conditions on a site where piping/sapping caused erosion and consequent collapse of nonpiped layers, and other processes modified conditions after the piping-related collapses.

The interactions among piping/sapping and other bank and shore processes are perhaps the most significant factors that make recognition of piping/sapping difficult. More than one failure mechanism may operate on a given site; piping/sapping may trigger a massive slump, and then the slump debris may be reworked by renewed piping and sapping. On the other hand, sediments may be deposited on a site during a flood while water is being recharged to pervious zones; the pervious zones may remain covered or, if a sufficient gradient is created across the sediment cover, piping may breach

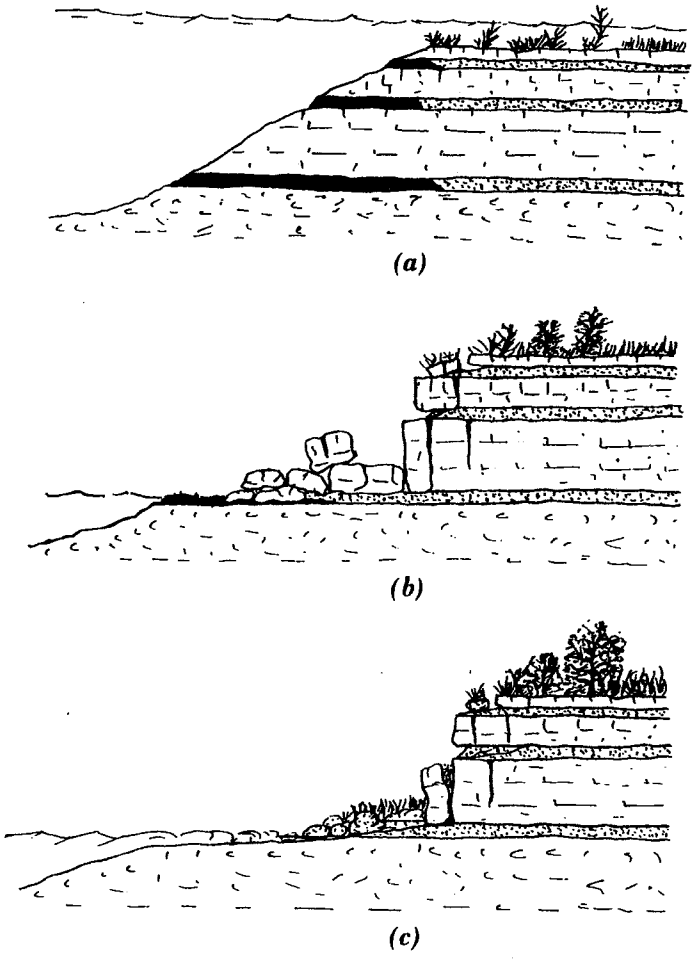

FIG. 6. Hypothetical Sequence of Conditions on Bank Subject to Inundation, Subsequent Piping/Sapping and Collapse, and Reworking of Failed Soils: (*a*) Stage 1—Inundation, Recharge to Previous Zones; (*b*) Stage 2—Piping/Sapping and Failure of Undercut Zones; and (*c*) Stage 3—Alteration by Waves, Winds, and Currents

the sediments. Vegetation may become established on a site during a period of low precipitation or stream inactivity, in piped-out soil or on failed slabs that were displaced earlier when precipitation energized piping/sapping erosion or after the stream had recharged the pervious layers during a flood (Hagerty 1986; Hagerty and Spoor 1989). Waves can degrade and remove fallen blocks and slabs, or selectively remove fine silt and clay particles from deposits of piped-out soil, leaving puzzling deposits of clean sand on a bank consisting of composite-texture soil (Hagerty et al. 1983).

Recognition of piping/sapping is difficult because the mechanism is complex, because this type of erosion often is intermittent, and because interactions with other bank or shore processes tend to obscure or remove the evidence of piping/sapping. Because diagnosis of piping/sapping is difficult, a comprehensive set of guidelines for recognition of piping/sapping is presented in a companion paper.

Summary

1. Piping/sapping is the removal of soil grains by seepage outflow; characteristic cavities are created in the exfiltration face.
2. Soil loss by piping/sapping can be important, but such loss may be overshadowed by instability in other bank or shore zones caused by undercutting in the piped-out zones.
3. Piping/sapping is a very important erosion mechanism because of its widespread geographic occurrence, its operation in many geologic/hydrologic settings, and its impact on other processes of erosion and sediment transport.
4. Conditions necessary for piping/sapping include an open exfiltration face, a source of water, concentration of flow, removal of failed and displaced soils, and a sufficient hydraulic gradient at the exfiltration face.
5. Because the conditions listed are necessary but may not be sufficient, and because piping/sapping is difficult to recognize, guidelines for diagnosis of piping/sapping are presented in a companion paper.

Appendix. References

Berry, L. (1970). "Some erosional features due to piping and subsurface wash with special reference to the Sudan." *Geografiska Annaler*, 52A, 113–119.
Born, S. M., Smith, S. A., and Stephenson, D. A. (1979). "Hydrogeology of glacial-terrain lakes, with management and planning applications." *J. Hydrol.*, 43, 7–43.
Brown, G. W. (1962). "Piping erosion in Colorado." *J. Soil Water Conserv.*, 17, 220–222.
Buckham, A. F., and Cockfield, W. E. (1950). "Gullies formed by sinking of the ground." *Am. J. Sci.*, 248, 137–141.
Bunting, B. T. (1961). "The role of seepage moisture in soil formation, slope development, and stream initiation." *Am. J. Sci.*, 259, 503–518.
Casagrande, A. (1936). "Characteristics of cohesionless soils affecting the stability of slopes and earth fills." *J. Boston Soc. Civ. Engrs.*, 23, 13–32.
Clifton, A. W., Crahn, J., and Fredlund, D. G. (1981). "Riverbank instability and development control in Saskatoon." *Can. Geotech. J.*, 18, 95–105.
Clough, G. W., and Duncan, J. M. (1986). "Ohio River bank stability reconnaissance and evaluation." *Report to Huntington District*, U.S. Army Corps of Engineers.
Deere, D. U. (1957). "Seepage and stability problems in deep cuts in residual soils, Charlotte, North Carolina." *Proc., Am. Railway Engrg. Assoc.*, 58, 738–745.
Deere, D. U., and Peck, R. B. (1958). "Stability of cuts in fine sands and varved clays, Northern Pacific Railway, Noxon Rapids line change, Montana." *Proc., Am. Railway Engrg. Assoc.*, 59, 807–815.
Dunne, T. (1980). "Formation and controls of channel networks." *Prog. Phys. Geography*, 4, 211–239.
Edil, T. B., and Vallejo, L. E. (1977). "Mechanics of coastal landslides and the influence of slope parameters." *Engrg. Geol.* 16, 83–96.
Fletcher, J. E., Harris, K., Peterson, H. B., and Chandler, V. N. (1954). "Piping." *Q. J. Engrg. Geol.*, 35, 258–263.
Grisak, G. E., and Cherry, J. A. (1975). "Hydrologic characteristics and response

of fractured till and clay confining a shallow aquifer." *Can. Geotech. J.*, 12(23), 23–43.
Hadley, D. W. (1976). "Shoreline erosion in southeastern Wisconsin." *Special Report 5*, Wisconsin Geological and Natural History Survey, Madison, Wis.
Hagerty, D. J. (1986). *Summary report on Ohio river site investigations—1986*. Report to Louisville District, U.S. Army Corps of Engineers.
Hagerty, D. J. (1988). "Erosion mechanisms on midwest alluvial streams." *Proc., Nineteenth Annual Conf., Int. Erosion Control Assoc.*, 421–434.
Hagerty, D. J. (1990). *Identification of erosion by piping and sapping*. Report to the U.S. Army Waterways Experiment Station, Corps of Engineers, Vicksburg, Miss.
Hagerty, D. J., Sharifounnasab, M., and Spoor, M. F. (1983). "Riverbank erosion—a case history." *Bull., Assoc. Engrg. Geol.*, 20(4), 411–437.
Hagerty, D. J., and Spoor, M. F. (1989). "Alluvial streambank erosion—a ten-year study." *Proc., Int. Symp. on Sediment Transport and Modeling*, ASCE, 594–599.
Hagerty, D. J., Spoor, M. F., and Kennedy, J. F. (1986). "Interactive mechanisms of alluvial-streambank erosion." *Proc., Third Int. Symp. on River Sedimentation*, 3, 1160–1168.
Hagerty, D. J., Spoor, M. F., and Ullrich, C. R. (1981). "Bank failure and erosion on the Ohio River." *Engrg. Geol.*, 17, 141–158.
Hamel, J. V. (1983). "Geotechnical perspectives on riverbank instability." *Proc., Conf. on Frontiers in Hydraulic Engineering*, ASCE, 212–217.
Hamel, J. V. (1988). "Geotechnical failure mechanisms in alluvial banks." *Mechanisms of alluvial channels*, Water Resources Publications, Littleton, Colo., 369–386.
Hendry, M. J. (1982). "Hydraulic conductivity of a glacial till in Alberta." *Groundwater*, 20, 162–169.
Henkel, D. J. (1967). "Local geology and the stability of natural slopes." *J. Soil Mech. Found. Div.*, ASCE, 93(4), 437–446.
Higgins, C. G. (1984). "Piping and sapping: Development of landforms by groundwater outflow." *Groundwater as a geomorphic agent*, Allen & Unwin, Inc., Boston, Mass., 18–58.
Hill, A. R. (1973). "Erosion of riverbanks composed of glacial till near Belfast, Northern Ireland." *Zeitschrift fur geomorphologie*, 17(4), 428–442.
Hooke, J. M. (1979). "An analysis of the processes of riverbank erosion." *J. Hydrol.*, 42, 39–62.
Howard, A. D., and McLane, C. F. (1988). "Erosion of cohesionless sediment by groundwater seepage." *Water Resour. Res.*, 24(10), 1659–1674.
Hutchinson, J. N. (1982). "Slope failures produced by seepage erosion in sands." *Landslides and mudflows*, A. Sheko, ed., Centre of International Projects, GKNT, Moscow, U.S.S.R., 250–268.
Ireland, H. A., Sharpe, C. F. S., and Eargle, D. H. (1939). "Principles of gully erosion in the Piedmont of South Carolina." *Technical Bulletin 633*, U.S. Department of Agriculture, Washington, D.C.
Johnson, D. (1939). "Origin of submarine canyons." *J. Geomorph.*, 2, 111–236.
Jones, J. A. A. (1971). "Soil piping and stream channel initiation." *Water Resour. Res.*, 7, 602–610.
Jones, J. A. A. (1981). *The nature of soil piping—A review of research*. Geobooks, Norwich, U.K.
Jones, J. A. A. (1987). "The initiation of natural drainage networks." *Prog. Phys. Geography*, 12(2), 207–245.
Jones, J. A. A., and Crane, F. G. (1984). "Pipeflow and pipe erosion in the Maesnant experimental catchment." *Catchment experiments in fluvial geomorphology*, IGU Commission on Field Experiments in Geomorphology, T. P. Burt and D. E. Walling, eds., Geobooks, Norwich, U.K.
Kachugin, E. G. (1970). "Studying the effect of water reservoirs on slope processes on their shores." *Draft Translation 732*, U.S. Army Cold Regions Research and Engineering Laboratory, Hanover, N.H.
Kane, D. L., Carlson, R. F., and Bowers, C. E. (1973). "Groundwater pore pressures adjacent to the subarctic streams." *Proc., North American Contribution to the Second Int. Conf. on Permafrost, Yakutsk, USSR*, National Academy of Sciences, Washington, D.C., 453–458.
Kirkby, M. J., and Chorley, R. J. (1967). "Throughflow, overland flow, and erosion." *Int. Assoc. Sci. Hydrol. Bull.*, 12, 5–12.
Klimek, K. (1974). "The retreat of alluvial riverbanks in the Wisloka Valley (south Poland)." *Geographica Polonica*, 28, 59–75.
Lafleur, J., and LeFebre, F. (1980). "Groundwater regime associated with slope stability in Champlain clay deposits." *Can. Geotech. J.*, 17, 44–53.
Lawson, D. E. (1985). "Erosion of northern reservoir shores," *Monograph 85-1*, U.S. Army Cold Regions Research and Engineering Laboratory, Hanover, N.H.
Leggett, R. F., and Bartley, M. W. (1953). "An engineering study of glacial deposits at Steep Rock Lake, Ontario, Canada." *Economic Geology*, 48(7), 513–540.
Leopold, L. B., and Miller, J. P. (1956). "Ephemeral streams—hydraulic factors and their relation to the drainage net." *Professional paper 282-A*, U.S. Geological Survey, Washington, D.C.
Luzbetak, D. J., Jain, S. C., and Odgaard, A. J. (1988). "Piping as a mechanism of bank erosion along rivers in Iowa." *IIHR Report No. 324*, Iowa Institute of Hydraulic Research, Iowa City, Iowa.
Mears, B., Jr. (1968). "Piping." *Encyclopedia of Geomorphology*, R. W. Fairbridge, ed., Hutchinson & Ross, Inc., Stroudsberg, Pa., 849.
Palmer, H. D. (1973). "Shoreline erosion in upper Chesapeake Bay: The role of groundwater." *Shore Beach*, 41(2), 19–22.
Parker, G. G., and Jenne, E. A. (1967). "Structural failure of western highways caused by piping." *Highway Research Record 203*, Transp. Res. Board, 57–76.
Pierson, T. C. (1983). "Soil pipes and slope stability." *Q. J. Engrg. Geol.*, 16, 1–11.
Pizzuto, J. E. (1984). "Equilibrium bank geometry and the width of shallow sandbed streams." *Earth Surf. Processes Landforms*, 9, 199–207.
Reuss, R. F., and Schattenberg, J. W. (1972). "Internal piping and shear deformation, Victor Braunig Dam—San Antonio, Texas." *Proceedings, Specialty Conf. on Performance of Earth and Earth-Supported Structures*, ASCE, 627–652.
Sellmeijer, J. B. (1981). "Piping due to flow towards ditches and holes." *Proc. Euromech 143*, 69–72.
Sharp, J. M., Jr. (1976). "Groundwater sapping by freeze-and-thaw." *Zeitschrift fur Geomorphologie*, 20(4), 484–487.
Sherard, J. L., Decker, R. S., and Ryker, N. L. (1972). "Piping in earth dams with dispersive clays." *Proc., Specialty Conf. on Performance of Earth and Earth-Supported Structures*, ASCE, 589–626.
Sherard, J. L., Woodward, R. J., Gizienski, S. F., and Clevenger, W. A. (1963). *Earth and earth-rock dams*. John Wiley & Sons, New York, N.Y.
Sloan, C. E. (1972). "Groundwater hydrology of prairie potholes in North Dakota." *Professional Paper 585-C*, U.S. Geological Survey, Washington, D.C.
Spoor, M. F., and Hagerty, D. J. (1989). "Bank failure and erosion on the Illinois Waterway." *Proc., Int. Symp. on Sediment Transport and Modeling*, ASCE, 600–605.
Springer, F. M., Jr., Ullrich, C. R., and Hagerty, D. J. (1985). "Streambank stability." *J. Geotech. Engrg.*, ASCE, 111(5), 624–640.
Stearns, H. T. (1936). "Origin of the large springs and their alcoves along the Snake River in southern Idaho." *J. Geol.*, 44, 429–450.
Sterrett, R. J. (1980). "Factors and mechanics of bluff erosion on Wisconsin's Great Lakes shorelines," thesis presented to the University of Wisconsin, at Madison, Wisconsin, in partial fulfillment of the requirements for the degree of Doctor of Philosophy.
Terzaghi, K. (1929). "The effect of minor geologic details on the safety of dams." *Technical Publication 215*, American Institute of Mining and Metallurgical Engineers, New York, N.Y.
Terzaghi, K. (1931). "Underground erosion and the Corpus Christi Dam failure." *Engrg. News Rec.*, 107, 90–92.

Thomas, B. F., and Watt, D. A. (1918). *The improvement of rivers*. John Wiley and Sons, New York, N.Y.
Thomson, S. (1970). "Riverbank stability study at the University of Alberta." *Can. Geotech. J.*, 7, 157–172.
Thomson, S., and Townsend, D. L. (1979). "River erosion and bank stabilization—north Saskatchewan River, Edmonton, Alberta." *Can. Geotech. J.*, 16(3), 567–576.
Thorne, C. R., and Tovey, N. K. (1981). "Stability of composite riverbanks." *Earth Surf. Processes Landforms*, 6, 469–484.
Twidale, C. R. (1964). "Erosion of an alluvial bank at Birdwood, South Australia." *Zeitschrift fur Geomorphologie*, 8, 189–211.
Ullrich, C. R., Hagerty, D. J., and Holmberg, R. W. (1986). "Surficial failures of alluvial streambanks." *Can. Geotech. J.*, 23(3), 304–316.
Williams, D. R., Romeril, P. M., and Mitchell, R. J. (1979). "Riverbank erosion and recession in the Ottawa area." *Can. Geotech. J.*, 16(4), 641–650.
Williams, R., and Farvolden, R. N. (1967). "The influence of joints on the movement of groundwater through glacial till." *J. Hydrol.*, 5, 163–170.
Wolman, M. G. (1959). "Factors influencing erosion of a cohesive riverbank." *Am. J. Sci.*, 257, 204–216.
Zaslavsky, D., and Sinai, G. (1981). "Surface hydrology: Parts I, II, III, IV, and V." *J. Hydr. Div.*, ASCE, 107(1), 1–93.

Piping/Sapping Erosion. II: Identification-Diagnosis

By D. J. Hagerty,[1] Member, ASCE

Abstract: Although erosion of streambanks and other shorelines by emergent seepage is widespread, this erosion mechanism (termed *piping* or *sapping*) has not been recognized as important to the overall erosion process. The mechanism is complex, and interactions with other bank and shore processes tend to mask the effects of piping/sapping. Direct evidence (water emerging from a soil face and carrying away soil particles) is rarely encountered. Several types of indirect evidence are presented and illustrated in this paper, including cavities formed by piping, deposits of dislocated particles below piping zones, blind gullies, staining produced by persistent seepage outflow, and particular types of localized failures (slab toppling, block shearing, and tensile falls caused by undercutting due to piping/sapping). The interactions of this erosion mechanism with other erosion-deposition processes are described. The purpose of this paper is to facilitate identification and evaluation of piping/sapping erosion, particularly for relatively inexperienced field investigators.

Introduction

Although bank and shoreline erosion by piping and sapping is widespread, little recognition has been given to this mechanism. Seepage outflow can remove soil particles in the exfiltration zone, causing the formation of tubular "pipes" or lenticular cavities, which, in turn, can remove support from overlying soil layers (Hagerty 1991). Piping/sapping has been identified in many localities throughout the world and in many geologic/hydrologic settings, but the mechanism is complex and may not be recognized. Interactions between piping/sapping and other bank and shore processes tend to mask piping cavities and/or to remove features characteristic of piping/sapping activity. For these reasons, it is important to present categories of evidence that indicate that piping/sapping is or was active on a site. The purpose of this review is to assist investigators, particularly those with little experience of erosion mechanics and processes, to diagnose piping/sapping on the basis of visual observations.

Direct Evidence of Piping/Sapping

It is possible to obtain first-hand proof that piping/sapping is operating on a site; outflow of water and soil grains from an exfiltration face can be observed directly. Holes are the end product of such flow. "Dirty water" is the fundamental indicator of piping action (Casagrande 1936). The soil and water shown in Fig. 1 were in motion at the time the photograph was taken. However, such direct evidence is unlikely to be obtained.

In some cases, the outflow of soil and water occurs below stream or lake

[1]Prof., Civ. Engrg. Dept., Univ. of Louisville, Louisville, KY 40292.

Note. Discussion open until January 1, 1992. Separate discussions should be submitted for the individual papers in this symposium. To extend the closing date one month, a written request must be filed with the ASCE Manager of Journals. The manuscript for this paper was submitted for review and possible publication on September 6, 1990. This paper is part of the ***Journal of Hydraulic Engineering***, Vol. 117, No. 8, August, 1991. ©ASCE, ISSN 0733-9429/91/0008-1009/$1.00 + $.15 per page. Paper No. 26067.

FIG. 1. Water and Soil Piped from Stream Bank; Coin Is U.S. Dime, 1.8 cm in Diameter

level; this circumstance is common when water has been recharged into pervious layers in a streambank during a flood, and the pervious layers begin to discharge water back to the stream when the hydraulic gradient in any layer is directed toward the stream. If the gradient reaches a critical value, soil particles can be moved out of the bank and cavities can be formed while those cavities are still covered by receding waters. At times, such subaqueous piping can be detected by the difference in temperature between the seepage outflow and the water in the stream, e.g., cold seepage outflow into a shallow sun-warmed near-bank zone (Hagerty 1990).

If the seepage outflow is particularly vigorous, it may be possible to catch (in cupped hands near the exfiltration face) entrained soil particles in the seepage flow. In other cases, the soil-water mix may be thick and viscous, as was the material shown in Fig. 1, and easily detected. If the source of water for the piping/sapping is constant (such as a pressurized water-supply pipe), the piping erosion may be virtually continuous; piping/sapping associated with such sources therefore is more readily identified than is intermittent erosion. Unfortunately, all too often when an investigator visits a site, intermittent seepage outflow is not occurring, and past operation of piping/sapping can be detected only through indirect evidence.

Indirect Evidence

Several types of indirect evidence of piping/sapping can be identified: (1) Primary indirect evidence consisting of features or conditions that are caused solely or predominantly by the piping/sapping mechanism; (2) secondary indirect evidence consisting of features associated with piping/sapping but that are somewhat removed from the exfiltration zone per se or that indicate

persistent seepage outflow without conclusively indicating that piping has occurred; and (3) tertiary evidence consisting of features or conditions that are associated with a process ancillary to piping/sapping (e.g., collapse of upper bank or shore zones) or that may have been created by another mechanism or process.

Primary Indirect Evidence

Features that are caused solely by piping/sapping include the cavities formed by seepage outflow at the exfiltration face. Fig. 2 shows a group of cavities formed in a streambank approximately 40 ft (13 m) high, at a location near the top of the bank. Fig. 3 shows some of the holes in that bank, in more detail. If a relatively thin pervious zone is exposed in a bank or shoreline, then outflow from that layer can produce a long array of tubular cavities. If the strata over the thin pervious zone possess high shear strength, the individual, nearly circular soil "pipes" may coalesce to form wider lenticular openings. Tubular cavities of nearly circular cross section are more common than lenticular cavities (Hadley 1976; Hagerty et al. 1981; Jones and Crane 1984; Lawson 1985; Palmer 1973). If the outflow occurs through a thick pervious zone, but the flow is perched on a less pervious underlying layer and only the bottom part of the pervious zone carries the flow, the upper part of the pervious layer may dry and lose apparent cohesion so that loose soil grains continually fall in front of, and partially obscure, the piping zone. Where the outflow is concentrated in one spot because of the localized nature of the water source (e.g., a leaking buried tank), piping cavities may appear in several pervious layers near the water source rather than in a wide, relatively short zone at the face of one pervious layer. The height-to-width ratio and size of the cavities depend upon the shear strength of the piping layer and the overlying less pervious layers (if any). Piping cavities as large as 3 ft (1 m) in diameter have been observed in thick silty sand layers overlain by strong clayey silts. The depth of the cavities may vary from several inches (4–6 cm) to as much as 10 ft (3 m), but very long piping cavities have been reported by some investigators (Jones and Crane 1984). Very long piping cavities usually suggest relatively thin pervious soils on the surface, underlain by strong layers of low hydraulic conductivity, but strengthened near the surface by root systems.

Some bird species make nests in holes in banks and shoreline bluffs, and holes formed by piping/sapping have been attributed mistakenly to the activities of these birds. The situation is made more complex by the fact that some birds will move into piping cavities and build nests there. Piping cavities occur in a given horizon and do not extend into adjacent soil layers as bird holes usually do. Marks made by beak and claw also signify holes made by birds. Microstructure (e.g., flow marks) in the soil on the bottoms of the holes, and ratio of depth to diameter (usually less than three for bird holes) also can be used to differentiate piping cavities from holes made by birds.

In addition to characteristic cavities, piping/sapping creates other features that are strong indicators of piping activity. If no other process acts to remove material from a site, the soil particles displaced by piping and sapping will accumulate in front of the cavities from which they were removed. Fig. 4 shows a miniature debris fan, a delta-shaped accumulation of sand particles, which were removed from the cavity shown in the upper part of the figure. When exfiltrating seepage emerges from a cavity, the flow tends to

FIG. 2. Cavities Caused by Seepage Outflow at Piping/Sapping Zone

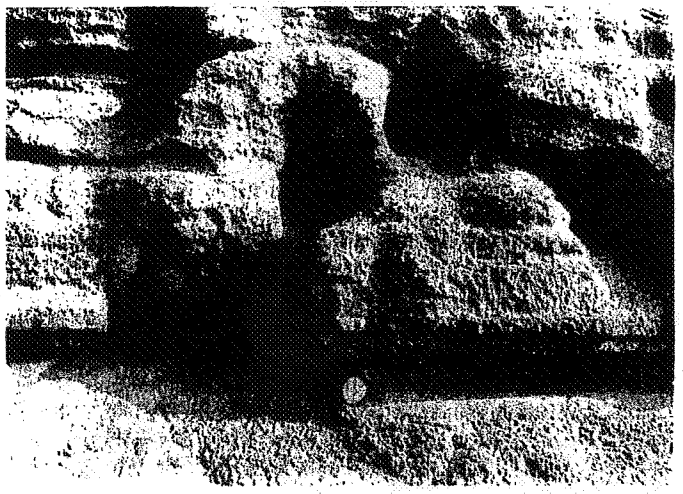

FIG. 3. Close View of Several Cavities from Fig. 2; Coin is U.S. Dime, 1.8 cm in Diameter

spread somewhat, velocity drops, and particles are deposited below the cavity, particularly if the less pervious layer below the outflow zone is resistant and forms a shelf or ledge below the piping zone. If the displaced particles are sand-sized, they usually are deposited in shallow fans with a top surface at an angle of 20° or less to the horizontal. When silt-sized or clay-sized particles are piped out of a "dirty" pervious layer, they may be carried farther than large particles and then deposited in thin films or skins on the faces

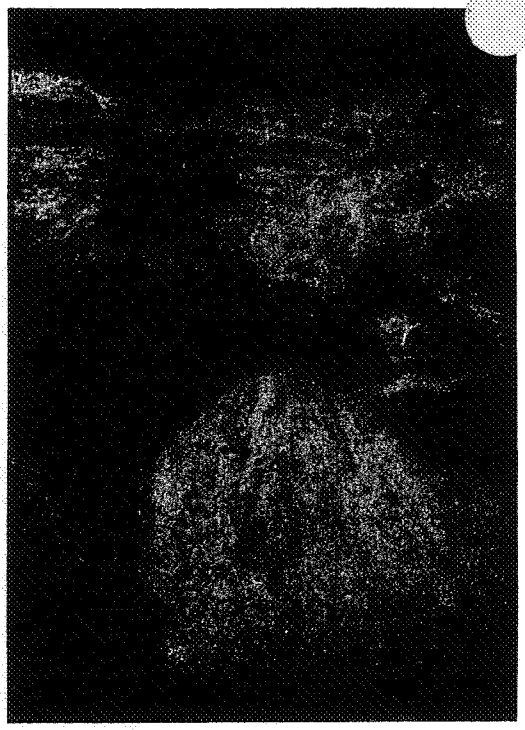

FIG. 4. Fan-Shaped Deposit of Sand Piped from Cavity in Shore (Top of Figure)

of lower soil layers, particularly if those layers are more pervious.

The piped-out particles deposited below and in front of piping cavities accumulate in loose piles and are easily eroded by currents, waves, wind, or surface runoff passing down and over the piping zone. Consequently, these features, while constituting strong evidence that a piping/sapping mechanism has been active, are ephemeral.

Another feature strongly indicative of piping activity is a blind gully or rill. Gullies and rills in a bank or shore simply indicate that water has flowed down the soil face. In order for these features to indicate piping activity, they must show that the water flowed out of the soil face and not down and over the bank or shore; the gullies must be "blind." Figs. 5 and 6 show gullies that originated at or just below an exfiltration zone. In some instances, exfiltration out of pervious bank zones may be sufficient to initiate rills and gullies below an outflow zone (in loose piped-out materials) but not sufficiently strong to create cavities at the exfiltration face itself. In other cases, outflow from the bottom of a thick but weak pervious layer may displace soil particles, but no sizable cavities form because the upper part of the pervious layer collapses and fills the cavities; nevertheless, the outflow may be sufficient to cut gullies below the exfiltration zone. Outflow from a piping zone can saturate more competent lower layers and induce flows or other forms of instability as well as erode gullies (Edil and Vallejo 1977).

FIG. 5. Blind Gully in Loose Soil below Outflow Zone in Stream Bank

FIG. 6. Close View of Blind Gully Initiated in Piping Zone

Rills and gullies are most likely to form in highly erodible in situ soil layers or in loose accumulations of piped-out particles below outflow zones. These erodible materials are vulnerable to other erosion mechanisms such as current tractive scour, reworking by waves generated by wind or vessels, or wind. Thus, these features tend to be short-lived. However, they are more positive indicators of piping action than the features classified as secondary indirect evidence.

Secondary Indirect Evidence

Features included in this category of evidence indicate a significant probability that piping/sapping has occurred at a site, but they lack the strong diagnostic character of the cavities, debris deposits, and blind gullies described in the previous section. Secondary evidence of piping/sapping includes stained zones in a streambank or shoreline and holes where soil pipes have collapsed remote from the seepage exit point in the bank or shore.

Staining and discoloration on the face of a streambank or shoreline is an indirect indicator of potential for piping/sapping. Seeping ground waters can dissolve minerals from the rocks and soils through which they flow. Typically, precipitation is slightly acidic, and water infiltrating humus and surface organic layers tends to become more acidic. This acidic water can dissolve various constituents, including metal species, from the solid matrix. Then, changes in biological and chemical parameters along the flow path can cause precipitation of the species being carried by the seeping water. Typically, this precipitation produces a coating of the soil or rock surfaces in the pervious zones through which seepage is occurring, with some cementation between soil grains and a characteristic coloring or staining produced by the films or precipitated species. Ground-water flow is very slow compared to surface flow, and vivid staining patterns or strong cementation may be the product of many years of persistent seepage. However, the seepage that stained the streambank may have occurred long in the past, and the present subsurface flow regime in and around the stained zone may be very different from the conditions that caused the staining and cementation. These features therefore are indicators of past flow patterns; they do not guarantee that those same flow patterns currently prevail, and they do not indicate that a hydraulic gradient exists sufficient to cause piping/sapping at the exposed face of the stained or cemented zone. In fact, the cementation may prevent removal of soil particles by seepage outflow.

Another secondary indicator of piping/sapping is the presence of holes in the floodplain adjacent to a stream or in a terrace above a shoreline. Piping cavities will elongate to great distances if the soils over the cavities possess high shear strength or are reinforced by root systems (Jones and Crane 1984). Any shortening of the seepage path will increase the hydraulic gradient driving the seepage and will cause the cavities to elongate. Eventually, the soil "pipe" may reach an area where the overlying soil is weak and will breach through to the soil surface. This breaching is likely to occur where the source of water is a ditch or surface depression; when the soil pipe reaches the water source, a breakthrough will occur, with rapid release of any stored water, through the soil pipe system. Fig. 7 shows an area in a field on a floodplain terrace where a soil pipe broke through into a depression approximately 100 ft (30 m) from the streambank where piping cavities had formed. These breakthrough holes are difficult to find if the area adjacent to the exfiltration

FIG. 7. Collapsed Soil "Pipe" in Floodplain Field Remote from Piping Zone

area in a bank or shore is covered with vegetation. Also, care must be taken to determine (as by use of dye tracers) that the hole and underlying cavity were caused by subsurface erosion and not by burrowing animals.

Tertiary Indirect Evidence

In contrast to the types of evidence described previously, some features or circumstances only suggest the possibility that piping/sapping has been active at a site. These features or conditions may be caused by a number of mechanisms, only one of which is piping/sapping. The most common forms of tertiary evidence are the features produced by localized failures caused when piping/sapping undercuts overlying soil strata. The weakest form of evidence of piping/sapping is evidence that other mechanisms were not active on a site where erosion and instability were observed.

Several modes of local failure in banks and bluffs composed of diverse materials have been described by Thorne and Tovey (1981). Undercutting by piping/sapping causes overlying strata to be loaded as cantilevers supporting their own weight as well as any surface loads (e.g., structures). Cantilever action requires the mobilization of tensile stresses in the top planes of the undercut strata. Only cemented soils or soils reinforced by plant roots have true tensile strength, so most natural soils will not support tensile stresses indefinitely, and cracks will begin to develop in the tops of the undercut layers. Formation of such cracks reduces the cross section of the cantilevered layer, and the cracks will tend to propagate downward to the bottom of the layer unless the deflecting cantilever tilts down to rest on the reduced thickness of the piping layer. Slabs or blocks of the cantilevered layer become wholly or partially detached from the layer. If the undercut layer is thick but has only low shear strength, the detached masses tend to be tall, thin slabs which shear off the face of the undercut layer. Thin, very strong layers tend to fail by rotation about the bottom of the crack that defines the failure

FIG. 8. Cracks in and Failure of Blocks from Layer Undercut by Sapping

mass; these cantilever failures produce blocks of more equal dimensions, rather than tall, thin slabs. Soil removal in a piping layer usually is most severe at the exposed face, and undercutting is most extensive at that face, so even slabs that shear off the undercut layer tend to topple outward after shearing. Fig. 8 shows cracks formed above a sapping zone in a cohesive upper layer. Seepage was perched on a clayey silt layer on which the man in the figure is walking. Sapping in a thin sandy zone caused the cracking in the top layer of bank soil and the shearing-falling of the displaced slabs shown in the right foreground of Fig. 8. Collapse of the undercut layer obscured the sapping cavities in the thin sand layer. Fig. 9 shows a situation where piping in a silty sand zone caused undercutting of a clayey silt upper layer, which then cracked and from which slabs tilted and toppled.

When root systems or cementation impart tensile strength to the top part of an undercut layer, that top portion may remain in place while the lower part of the undercut layer falls away. This sort of failure occurred in the streambank shown in Fig. 10. This failure occurred during a prolonged period of severe drought in 1988, when the adjacent stream was inactive and did not rise into contact with the eroding bank. Irrigation water supplied to an adjacent field fed the piping mechanism; the large cavity shown in the figure was formed when the bottom part of the undercut layer fell as the investigator walked up the bank. The upper part of the undercut layer was slightly cemented by mineral deposition, and remained in place (at least temporarily). Root systems can facilitate similar features, as well as promoting shear rather than toppling in detached slabs by providing tensile reinforcement in the top of the undercut layer.

The presence of nearly vertical cracks in an undercut layer facilitates infiltration of surface water. If the crack extends down into the piping layer, infiltrating water can intensify the piping removal in the underlying layer. Furthermore, if the block or slab defined by the crack slipped down to block

FIG. 9. Detached and Rotated Slabs Undercut by Piping

the flow in the piping layer, infiltrating water will fill that layer and rise in the crack, causing uplift on the bottom of the block/slab and outward pressure along the plane of the crack. These pressures can topple or displace the detached block or slab. Fig. 11 shows slabs detached from a soil layer at the top of a bank when piping/sapping in the midheight part of the bank undercut the upper soil layers. This failure occurred when surface runoff from a thunderstorm entered cracks in the uppermost soil layer. The fallen slabs rest on a subaqueous "shelf" that extended out from the bank at a very slight angle to the horizontal (approximately one vertical to 20 horizontal) for about 70 ft (22 m) into the stream.

The failure modes described in the preceding paragraphs are only uncertain indicators of piping/sapping activity since other mechanisms instead of or in addition to piping/sapping can cause these types of failures. Undercutting can be caused by tractive force scour or wave attack on the lower portions of a bank or shoreline [e.g., Brunsden and Kesel (1973)]. Nearly vertical cracks in a bank or bluff face can be caused by mass slumping failures, lateral stress relief, and excavation (Hamel 1983).

Another type of failure that has been encountered in association with piping and sapping activity is lateral spreading and rapid flow of loose pervious soil layers. Sudden rapid spreading can occur by liquefaction of loose, saturated cohesionless soils under the influence of impulse, shock, or earthquake loading. However, investigations at a number of sites have shown

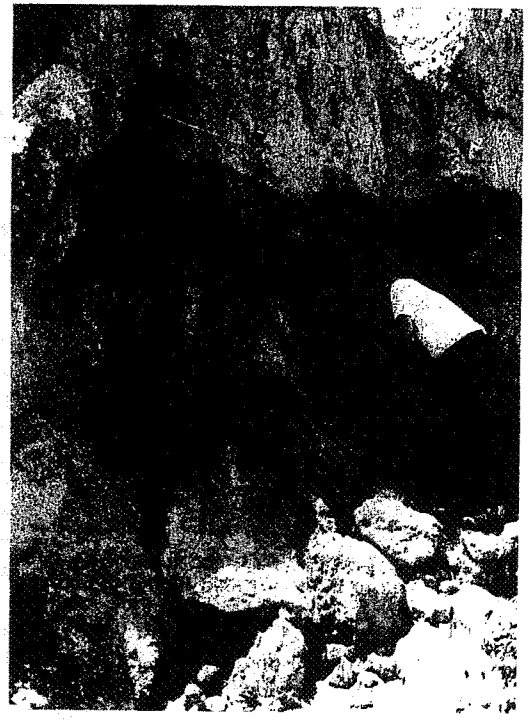

FIG. 10. Tensile Failure Caused by Piping below Partially Cemented Upper Soil Layer

that piping/sapping at the face of a thick, loose pervious layer can produce a sudden, very rapid outflow of a large volume of soil and water from the piping layer. Evidence of spreading and sudden flow failures (e.g. very large cusp-shaped cavities in a bank or shoreline, with active flow of soil and water from the sides of the cavity, and/or gullies along the bottom of the cavity extending toward the exit zone) is only suggestive of piping/sapping activity since spreading failures can be caused by other mechanisms (such as liquefaction during earthquake shocks, and generation of excess pore-water pressure and lateral stress relief from scour during rapid recession of flood waters) as well as by piping.

A third type of feature that is suggestive of piping/sapping activity is the presence of multiple short scarps or nearly vertical faces in a bank or shore. These features may be small erosional berms cut by waves when a lake or stream is maintained at a series of stages, with intermittent periods of falling stage (Lawson 1985), but they also can be erosional faces cut by sapping in thinly bedded alluvial sequences of soil strata. Fig. 12 shows an occurrence of such short multiple scarps. At the site shown in Fig. 12, excavation into the bank face disclosed a sandy layer at each break in the bank slope, overlain by a relatively thin, fine-grained cohesive layer. The combined thicknesses of the sandy layers was much greater than the thicknesses of the strong cohesive layers. The nearly vertical scarps had formed in the cohesive

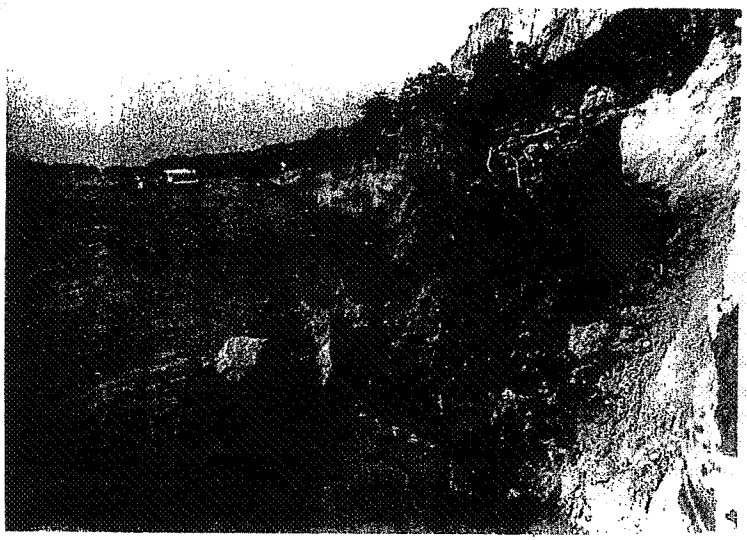

FIG. 11. Slabs Fallen to Base of Bank; Piping in Midheight of Bank

soil when piping/sapping removed underlying sandy zones, causing the cohesive cantilevers to fail. The operation of the failure mechanism was obscured by the abundance of the piped-out sand that partly covered the edges of the cohesive layers. When these accumulations of piped-out grains were

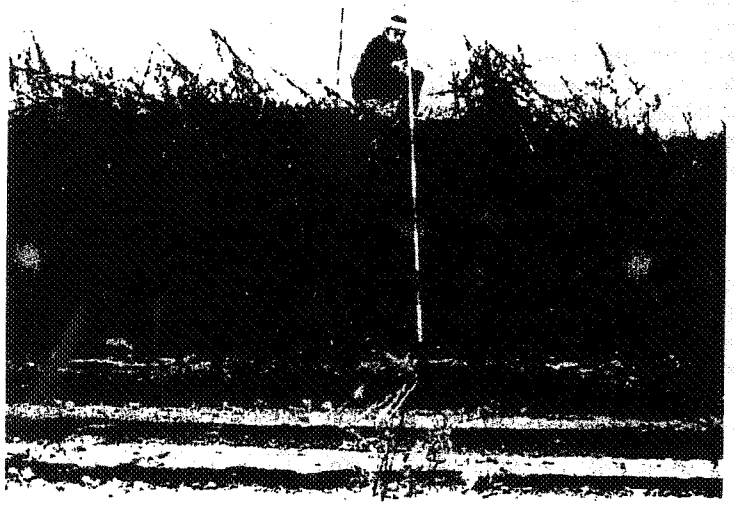

FIG. 12. Multiple Scarps Formed by Sapping in Thin Alternating Cohesive Layers between Sandy Pervious Layers

FIG. 13. Close View of Scarp Formed by Piping/Sapping Activity

excavated, slow flows of water and soil were seen at the faces of the sandy layers.

Close examination of scarps formed by piping/sapping will show the differences in appearance between those scarps and features cut by waves. Fig 13 shows a close view of a scarp caused by piping/sapping. This scarp ha a very irregular alignment; a plan view of the scarp would show many smal cusps or a serrated pattern. Wave-cut benches tend to be much more regula in plan alignment, without the re-entrant angles and sharp limbs on the mul tiple cusps in sapping scarps. However, these scarps are not strong, positive indicators of piping/sapping action unless excavation of failed material i front of a scarp discloses direct evidence in the form of active flow of wate and soil particles out of an exfiltration face. Scarps very similar in appear ance to sapping scarps can be produced by wave action and by deposition When layers of sediments are deposited on a bank or shore, usually wate will tend to drain from the sediments toward the stream or lake. This drain age of water can cause the edges of sediment layers to be undercut and fail This mechanism is very similar to piping/sapping except that the outflow originates from the sediments and not from the underlying bank or shore In any case, the short multiple scarps caused by piping/sapping tend to b very short-lived, especially if the less pervious layers dry and lose cohesio so that the nearly vertical scarps collapse. Wind and wave action can dis place piped-out cohesionless soil grains to obscure short scarps in interbed ded strata. Finally, other processes such as freeze-thaw can degrade thes relatively fragile features.

Negative Evidence

Where the terrain on an eroding bank is complex, it may be difficult t diagnose piping/sapping. However, if the bank topography does not posi tively indicate operation of other mechanisms, piping and sapping appea

more likely to have caused the soil loss than would be the case where evidence of other mechanisms is found. Massive slumps, perhaps caused by rapid recession or drawdown in water level, show characteristic features such as high scarps, rotation and/or translation of a failure mass essentially as a unit, and the formation of a lobe or tongue at the base of the unstable area. Such failures are more prone to occur after a rapid fall in water levels or after periods of intense, prolonged precipitation. Tractive force scour may initiate a mass failure or simply remove soil by direct attack; such erosion will not produce the features typical of piping/sapping and will occur in association with periods of high discharge and at certain planform locations (e.g., outsides of bends). The absence of features typical of other erosion mechanisms is not a positive indication of piping/sapping activity, but (by process of elimination) can suggest that piping/sapping should be investigated more thoroughly.

Summary of Indirect Evidence

The likelihood that piping/sapping will be observed in operation is slight. Some indirect evidence such as characteristic cavities, blind gullies, and deposits of piped-out particles provides strong, positive indications that piping has occurred. Other evidence is only suggestive of erosion by piping/sapping. Diagnosis of this mechanism of erosion is made more difficult, however, by alterations of bank and shore terrain by other erosive mechanisms. Interactions among erosion-deposition mechanisms may remove or obliterate the evidence of piping/sapping erosion.

Interactions with Other Mechanisms

Some interaction with other erosion mechanisms must occur if piping/sapping is to continue on a site. However, many of the interactions among erosion processes are incidental; conditions leading to piping action also may activate other mechanisms, but no interplay among those mechanisms is necessary for piping/sapping to occur.

Necessary Interactions

The end result of piping/sapping in a bank or shore is removal of soil particles from an exfiltration face, with possible concomitant failures in undercut overlying layers. The piped-out soil is moved closer to the adjacent body of water and to lower elevations. If no other process operated, the change in topography would lead to formation of a berm of failed soil, a reduction in the overall slope of the bank or shore, and an elongation in the average length of the seepage paths to exfiltration faces. The hydraulic gradient in the bank/shore area would be reduced and, finally, piping/sapping would cease to be effective. The rate of change in topography would decline steadily so that an equilibrium would be reached only after a very long time.

A net negative material balance must exist at a site in order for piping/sapping erosion to continue. Water originating far from the stream may continue to form and/or elongate cavities in soil masses in or behind a stream bank, without net erosion of the site (i.e., removal of soil from the site limits). A period of high discharge from remote sources may even move copious amounts of soil toward the stream and cause widespread instability at the site, but erosion will still be a function of overall material balance.

FIG. 14. Site Eroded by Piping/Sapping in 1979

However, episodes of instability caused by piping/sapping eventually will cease at the site unless failed and displaced soil is removed by the stream (or some other agency).

Tractive force scour is very effective in removing the products of piping/sapping erosion. Accumulations of piped-out soil are loose and erodible. Fallen blocks and slabs are more erodible than in situ soil because their internal structure and strength have been disturbed to some degree, and because flow around such obstacles will be turbulent and erosive. Overland flow also can move failed soils toward a stream or lake where other processes can remove them. If the net result of all these processes is not removal of material from the site as a whole, piping and sapping will cease.

Incidental Interactions

The net material balance on a site must be negative in order for piping/sapping to continue there, but the variety of interactions to produce that net result can be almost limitless. For example, during a flood, a stream may scour away soil from the lower portions of a bank but deposit sediments on other parts of the same bank, particularly if the bank consists of multiple gently sloping areas between nearly vertical piping-induced scarps. Those sediments may cover exfiltration faces and prevent or retard the piping action that formed the existing bank terrain. A rotational slump in a slope may be triggered by piping/sapping near the base of the slope, but rotation and displacement of strata during the slump may sever the hydraulic connection between the piping zone and the ground-water source that supplied the piping mechanism. Vegetation easily takes root in loose, piped-out soils in front of piping cavities and may act to protect that loose soil against removal by wind, wave, or current action (Hagerty 1986, 1988). Growth of vegetation may promote deposition of sediments over accumulations of loose, piped-

FIG. 15. Piping/Sapping Site Shown in Fig. 14 in 1986

out soils and partial blockage of piping/sapping cavities. Fig. 14 shows a site in 1979 where seepage outflow had caused removal of more than 10 ft (3 m) of bank in a period of five years. The adjacent stream had inundated the bank repeatedly during those five years. Multiple small scarps due to piping/sapping action can be seen in the figure. Fig. 15 shows the same site in 1986 after five years of low discharge in the stream. During minor floods, as much as 18 in. (45 cm) of sediments had been deposited on the lower parts of the bank, and willow trees had grown to a height of 10 ft (3 m). The former operation of vigorous piping/sapping on this site would be very difficult to diagnose from the conditions shown in Fig. 15.

Summary

1. Piping/sapping can be identified by active flow of soil and water from exfiltration zones, but such evidence is encountered only rarely.
2. Strong indications of piping activity are furnished by features produced solely or principally by that mechanism (piping cavities, blind gullies, and accumulations of piped-out soil particles).
3. Stained zones exposed in banks and shores are indirect evidence of piping activity, as are collapsed soil pipes at locations remote from a bank or slope.
4. Other indirect evidence of piping/sapping activity includes features typical of certain localized failure modes associated with undercutting by piping/sapping (cracks, fallen blocks or slabs, and multiple scarps).
5. Piping/sapping will cease if soils displaced by piping are not removed by other transport mechanisms, but interactions with other mechanisms of erosion and sedimentation often obscure the evidence of piping and/or retard or stop piping/sapping activity.

Acknowledgments

The field work upon which this paper is based could not have been done without the assistance of Michael F. Spoor, whose insights are as valuable as his comprehensive knowledge of erosion mechanisms. Support for field investigations was furnished by the Ohio River Division, Corps of Engineers. The writer expresses gratitude to David A. Beatty and Glenn Drummond. Procedures for identifying piping/sapping were developed with support from the Waterways Experiment Station, U.S. Army Corps of Engineers, under Contract No. DACW39-89-K-0027, administered by Bradley M. Comes.

Appendix. References

Brunsden, D., and Kesel, R. H. (1973). "Slope development on a Mississippi River bluff in historic time." *J. Geol.*, 81, 576–597.
Casagrande, A. (1936). "Characteristics of cohesionless soils affecting the stability of slopes and earth fills." *J. Boston Soc. Civ. Engrg.*, 23, 13–32.
Edil, T. B., and Vallejo, L. E. (1977). "Mechanics of coastal landslides and the influence of slope parameters." *Engrg. Geol.*, 16, 83–96.
Hadley, D. W. (1976). "Shoreline erosion in southeastern Wisconsin." *Special Report 5*, Wisconsin Geological and Natural History Survey, Madison, Wis.
Hagerty, D. J. (1986). *Summary report on Ohio River site investigations—1986. Report to Louisville District*, U.S. Army Corps of Engineers.
Hagerty, D. J. (1988). "Erosion mechanisms on midwest alluvial streams." *Proc., Nineteenth Annual Conf., Int. Erosion Control Assoc.*, 421–434.
Hagerty, D. J. (1990). *Identification of erosion by piping and sapping*. Report to U.S. Army Waterways Experiment Station, Corps of Engineers, Vicksburg, Miss.
Hagerty, D. J. (1991). "Piping/sapping erosion. I: Basic considerations." *J. Hydr. Engrg.*, ASCE, 117(8), 991–1008.
Hagerty, D. J., Spoor, M. F., and Ullrich, C. R. (1981). "Bank failure and erosion on the Ohio River." *Engrg. Geol.*, 17, 141–158.
Hamel, J. V. (1983). "Geotechnical perspectives on river bank instability." *Proc., Conf. on Frontiers in Hydraulic Engineering*, ASCE, 212–217.
Jones, J. A. A., and Crane, F. G. (1984). "Pipeflow and pipe erosion in the Maesnant experimental catchment." *Catchment experiments in fluvial geomorphology*, IGU Commission on Field Experiments in Geomorphology Meeting, T. P. Burt and D. E. Walling, eds., Geobooks, Norwich, U.K.
Lawson, D. E. (1985). "Erosion of northern reservoir shores." *Monograph 85-1*, U.S. Army Cold Regions Research and Engineering Laboratory, Hanover, N.H.
Palmer, H. D. (1973). "Shoreline erosion in upper Chesapeake Bay—the role of groundwater." *Shore Beach*, 41(2), 19–22.

EVALUATION OF RISKS OF SLOPE INSTABILITY ALONG A COASTAL REACH

by

Peter J. Bosscher
Tuncer B. Edil
David M. Mickelson

Reprinted From:

Proceedings of the Vth International
Symposium on Landslides, 1988
Lausanne, Switzerland
A.A. Balkema Publishers, Rotterdam/Boston

Geotechnical Engineering Program
Department of Civil & Environmental Engineering
University of Wisconsin-Madison
Madison, Wisconsin 53706

Evaluation of risks of slope instability along a coastal reach
(Etude du risque d'instabilite des falaises)

Peter J. Bosscher
Department of Civil and Environmental Engineering
University of Wisconsin
Madison, Wisconsin

Tuncer B. Edil
Department of Civil and Environmental Engineering
University of Wisconsin
Madison, Wisconsin

David M. Mickelson
Department of Geology and Geophysics
University of Wisconsin
Madison, Wisconsin

ABSTRACT: An appraisal of the risks of instability is made along a reach of the Lake Michigan shoreline in northern Milwaukee County, Wisconsin, based on a geotechnical and geological investigation of slope characteristics and an analysis of the causes and types of erosion. The assessment of risk due to instability was hampered by the lack of stratigraphic information in some sections and properties of some lake sediments. Based on the level of information available regarding the degree of variability of the characteristics of the slopes, each shoreline section was classified into one five probability analysis classes. The evaluation of potential instability is undertaken using a probabilistic approach. In this approach, those factors which are to be estimated based on the limited actual data, are generated in random combinations using the Monte Carlo method. A micro-computer program was developed to carry the necessary computations conveniently. The technique used allows assignment of a hazard potential classification to each shore section and development of appropriate recommendations relative to the slope stabilization measures in a rational way for an extended shoreline reach.

RESUME: Les risques d'instabilite des falaises le long du Lac Michigan au nord de Milwaukee ont ete etudies a partir d'une investigation geotechnique et geologique des pentes et une analyse des causes et types d'erosion. L'evaluation des risques a ete genee par le manique de donnees stratigraphiques a certains endroits et de donnees sur les proprietes des sediments lacustres. Chaque portion de cote a ete classifiee dans cinq categories de probabilite, ceci en fonction de la qualite de e'information disponible. L'evaluation des risques d'instabilite a ete menee par une simulation du type Monte Carlo sur micro ordinateur. Le methode utilisee permet le developpement de recommendations pour les mesures a prendre pour stabiliser les falaises tout au long d'une cote.

INTRODUCTION

Erosion and recession of the coastal bluffs along the Great Lakes shoreline has become a major concern to property owners as well as engineers during the past several decades, but most notably, last year when the lake water levels reached record high levels. The major mass-wasting processes involved are undercutting by wave action, rotational slip failures, translational slides, sheetwash, and solifluction. One, or any combination of the aforementioned phenomena, can act on these bluffs at a given time. In a recent management study of the northern Milwaukee County Lake Michigan shoreline, a 13.4 km-long reach of the shoreline consisting of coastal bluffs has been analyzed to define the risk of erosion damage, to explore alternatives, and to recommend effective, economically feasible, and environmentally acceptable measures for erosion control and slope stabilization.

To achieve this purpose, the study included the inventory of erosion-related characteristics of the shoreline area, the identification of erosion risk areas and shoreline recession rates, the development and evaluation of alternative shore protection measures, and the preparation of a comprehensive shoreline slope stabilization and shoreline erosion management plan. The study area consists of 700 hectares of land adjoining the Lake Michigan shoreline that provides a unique setting for high value residential development and recreational opportunities.

GEOLOGICAL AND GEOTECHNICAL CHARACTERISTICS

The coastal area studied is formed in glacial deposits ranging up to 40 m in thickness. The layer nearest to the surface is known as the Ozaukee Till, consisting of silty clay with a reddish color. The Oak Creek Till is composed of a pebbley silty clay and lies beneath the Ozaukee Till. Lake sediments of various textural characteristics are often found between these two sediments. Directly beneath the Oak Creek Till lies another very stiff till known as the New Berlin Till. It is a coarse-grained till, sandy in texture and dominated by pebbles and cobbles. All of these formations are exposed in the active slopes within the study area. The soil stratigraphy at each profile site is critical to the evaluation of the stability of the slopes. The stratigraphy was identified on the basis of field surveys, historic geological records of soil boring data, and new soil borings performed at selected sections of the shoreline.

The geotechnical properties of the glacial materials forming the bluffs were obtained from historic data and laboratory analysis of the samples collected from the exposed slope surfaces and soil borings. The strength parameters and the unit weights of the bluff material are given in Table 1 in terms of the known values and standard deviations.

The slopes within the study area exhibited a variety of geomorphological characteristics, vegetative cover, and structural protection conditions. These conditions affect the degree and rate of bluff recession along different segments of the study area. Bluffs cover about 75% of the total study shoreline length with heights varying from 23 to 40 m. In the remainder of the study area, a relatively wide terrace exists in front of the bluffs with a height of 1.2 to 3 m above the beach level. Nearly 70% of the shoreline has no significant beach (beach width of 3 m or less); the remainder has sand, gravel or cobble beaches with slopes varying mostly between 4° to 12° (in 1986).

Along the northern Milwaukee County shoreline, ground water generally flows toward the lake and discharges either at or below the base of the bluff

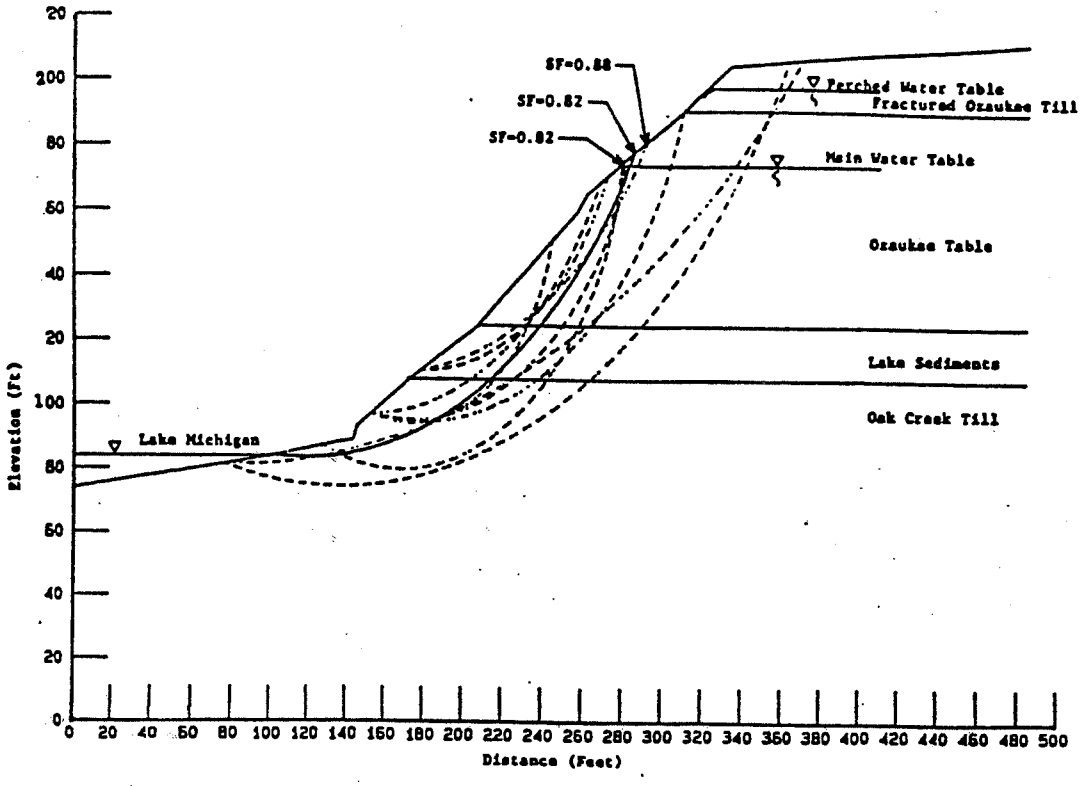

Figure 1. A Typical Bluff Profile from Northern Milwaukee County (1 ft = 0.305 m)

Table 1. Geotechnical properties of soils encountered in the slopes that are used in the analyses

Soil Unit	Unit Weight (kN/m^3)	Friction Angle* (Degrees)	Cohesion Intercept* (kPa)
Tills			
New Berlin	21.7	34 ± 3	0.5 ± 0.25
Oak Creek	21.2	30.5 ± 2	5.0 ± 3.75
Ozaukee	21.1	30 ± 3	7.5 ± 5.0
Fractured Ozaukee	21.1	30 ± 3	0 ± 0.25
Lake Sediments			
Medium Fine Sand	18.9	33 ± 2	0 ± 0.25
Sand and Gravel	18.9	33 ± 2	0 ± 0.25
Silt	20.4	31 ± 2	200 ± 50
Silt and Fine Sand	17.3	31 ± 2	0.5 ± 0.5
Clay and Silt	20.4	27 ± 2	22.5 ± 17.5
Fine Sand and Silt	19.7	33 ± 2	5.0 ± 3.75
Gen'l Lake Sediment	19.7	27 ± 3	5.0 ± 3.75
Fill			
Concrete Rubble/Soil	20.4	35	0

* Values are given as the mean and the standard deviation.

into the lake. The lake sediments consisting of coarse-grained soils may act as water-bearing units. Additionally, a perched water table is usually found within the fractured Ozaukee Till at the top of the bluffs producing seeps on the bluff face. The ground water elevations used in the slope stability analysis at each profile site were based on observed ground water seepage, soil boring data, ground water observation wells, and electrical resistivity analysis. Where no specific ground water data is available, the elevation of the ground water was estimated based on the depth of the permeable soil layers.

The study area shoreline was divided into 36 sections, each with similar physical and erosion related characteristics (Southeastern Wisconsin Regional Planning Commission, 1987). Field surveys were conducted to delineate the section boundaries, to inventory the physical characteristics, and to identify the causes and types of beach erosion and slope failure occurring in each section. An example of a bluff profile from the northern Milwaukee County is given in Figure 1.

The study of slope recession rates conducted by the Southeastern Wisconsin Regional Planning Commission indicated that about 42 and 86 percent of the shoreline measured in 1963 through 1985 and 1978 through 1985, respectively, had recession rates of 0.15 m or less. Less than 2% of the shoreline had slope recession exceeding 0.30 m per year. The highest recession rate measured from 1963 through 1985 was 0.50 m per year. These recession rates are apparently lower than in the other parts of the Wisconsin shoreline along Lake Michigan, perhaps because of the greater extent of the shore protection structures installed in northern Milwaukee County. Slope recession in the 13.4 km-long study area is estimated to result in the loss of nearly 1,115 m^2 of land each year, and nearly 19,822 m^3 of shore material.

A total of 44 slope profiles prepared during the field surveys were used in the slope stability analysis. The location of the profile sites were selected to be representative of shoreline areas with different physical characteristics and different causes and types of soil failure. One to three profiles were prepared for each slope stability analysis section.

SLOPE STABILITY ANALYSIS

Both conventional deterministic slope stability analyses and probabilistic soil stability analyses were conducted to establish the state of stability of the coastal slopes.

Conventional Analyses

The conventional deterministic rotational slope stability analyses using the effective stress method provided the locations of potential failure surfaces and the attendant safety factors based upon the drained strength parameters and the estimated ground water levels. The "worst case" ground water conditions were assumed in these deterministic analyses. Late winter and early spring have been found to be the most critical periods for the stability of Lake Michigan coastal slopes for both deep/seated and shallow slides (Vallejo and Edil, 1979). During this period, ground water levels and flows generally rise, but the surface is still frozen, which decreases its permeability and prevents ground water discharge from the slope face. This creates an inclined artesian effect, resulting in increased pore pressures and reduced slope stability.

Interpreting the stability of coastal slopes is a problem complicated by the dynamic nature of slope geometry. There are forces constantly seeking to achieve slope equilibrium and other forces constantly initiating new slope failures. Since the geometry of the slope changes in response to the slope toe erosion and face stabilization processes, the safety factor, especially for deep rotational slides, varies with time. Slope failure over time is referred to as the evolution of the slope. Two different types of criteria are used in interpreting the results of the slope stability analyses which are based on either the consideration of the lowest safety factor or the consideration of all failure surfaces with a safety factor of less than unity (Edil and Haas, 1980). For each of the profile sites, a slope stability program named STABL was used to generate 100 potential failure surfaces and to calculate the corresponding safety factors (Siegel, 1975). The 10 failure surfaces with the lowest safety factors were identified. An example of the deterministic slope stability analysis results is shown in Figure 1 where the corresponding safety factors for the three most critical failure surfaces are indicated. In the deterministic approach, mean values of soil properties based on the available test results as given in Table 1 were utilized along with the geometrical and geological measurements of the slope at the specific site in computing a safety factor against failure. An assessment of the general stability of slopes of a shoreline section based on the deterministic safety factors of a number of slope profiles located within the section could conceivably be in error if the slope parameters chosen as input for the stability program are not reliable. For example, in this study, adequate information was available at certain sections because of the excellent exposure of slope soil stratigraphy and the rather uniform characteristics of the slopes and the soils within the section. At such locations, adequate information was available for what one may call "reliable" analysis. However, for many other sections, between the borehole locations and with poorly exposed slope faces due to vegetative cover, soil properties, position of stratigraphic unit interfaces, and ground-water table in the slope had to be interpolated or estimated based on an examination of the general slope conditions. In view of the variability of soil properties and other slope parameters which had to be estimated, the computed safety factors would not be as reliable for these profiles as they would be for the profiles at the borehole locations and/or with good exposure.

Probabilistic Analyses

The objective for the probabilistic analysis was to verify the results obtained from the deterministic slope stability analyses, particularly for those profile sites where the slope conditions were not well defined; and to provide an assessment of overall slope stability within slope analysis sections, rather than just for the specific profile sites. The probabilistic model of slope stability analysis, allows us to analyze the general stability condition of a shoreline section in such a way that one can determine the reliability of the safety factors determined by the deterministic slope stability analysis. The variability of the safety factor depends upon the variability of the slope parameters and the method by which the safety factor is computed. At the borehole locations, even though there is a greater reliability, there is, nevertheless, some variability associated with certain slope parameters. For example, soil properties are estimated based on tests on a limited number of samples and they are, in general, highly variable. For profiles between the boreholes or at slope sections without good exposure, however, the variability is even greater since there are no direct measurements of certain slope parameters. Basically, the variability of safety factors depends upon the variability of the soil properties, water table position, and the soil interface lines considered in the analysis. Slope geology was measured in the field for each slope profile representative of the general morphology of slopes in a given section, therefore it is not considered to be a significant source of variability. The probabilistic model used is based on the Monte Carlo method (Benjamin and Cornell, 1970) and described by Edil and Schultz (1983). This method was used because it can artificially derive the probability distribution of safety factors based upon the probabilistic nature of the input random variables. It is a particularly useful method when the relationships among variables are complicated functions involving more than one random variable. Such is the case in dealing with slope stability along the Lake Michigan shoreline. Therefore, one must incorporate into the model the uncertainty and variability of the basic controlling geological, geotechnical, and environmental factors involved insofar as possible. Such factors in the slope instability problem are soil stratigraphy, shear strength, and ground water location.

The dominant component of the shear stress, i.e., the soil unit weight, was found to not significantly alter the resulting safety factor and to be nearly constant for the glacial materials encountered in the Great Lakes, and therefore, it was not considered to be a random variable (Edil and Schultz, 1983). It should further be noted that the geometrical properties of slope height and slope angle which also play an important role in the stability of a slope, were assumed to be measured accurately for the profiles analyzed during the field reconnaissance conducted. Hence, these variables were not classified as being random variables. Furthermore, the profile measured at a given section was assumed to be representative of the general morphology of the slopes in that

shoreline section.

The values that were assumed to vary randomly are: the soil strength parameters, the soil interface locations, and the piezometric surface elevations. The log-normal distribution was used to generate the parameter distributions. Mean values and standard deviations of the soil properties are required to generate log-normal distributions of these properties. The intersection of the stratigraphic unit interfaces with the slope face was designed to permit these intersections to move vertically up or down along the slope face about a mean elevation within a log-normal distribution defined by the assigned standard deviation. The interface lines were also allowed to dip up and down as they move into the slope from the slope face, again, randomly about a mean angle and standard deviation of dip. The spread of these distributions was established on the basis of the expected standard deviations of the soil interface elevations and the dip angles. The elevation of the ground water tables in the slopes could be varied in a similar manner about a mean elevation with a log-normal distribution about it. Many distributions have been proposed for the cohesion intercept as well as for the angle of internal friction. In the program used for the probabilistic analyses, the log-normal distribution was used as the probability density function to represent the strength parameters (Wu and Kraft, 1967) and for the remaining random variables. The beta distribution is presently being incorporated into the program. The degree of variability of these factors differed at each profile site, but, in general, the standard deviation of the elevation of the soil interface lines ranged from 0 to 6 m, and the standard deviation of the angle of inclination ranged from 0° to 3°. The lowest variability of soil interface lines was selected for those sites where the strata were well defined and the representative slope analysis section was small. The standard deviations of soil properties which were used in the probabilistic analyses are given in Table 1. The elevation of the ground water was varied based on available water data and on the type and thickness of the lake sediment layers within each profile site, since in most cases these layers were the water bearing strata. In general, the standard deviation of the elevation of the mean water table ranged from 0.6 to 6 m, and the standard deviation of the elevation of the perched water table, located in the fractured Ozaukee layer, ranged from 0.6 to 2.3 m.

The original STABL program was modified to permit the input of random variables. STABL uses the method of slices (either Bishop's or Janbu's simplified method) in analyzing circular failure surfaces or randomly generated non-circular failure surfaces to determine the stability of a slope. The data in the file for the probabilistic analysis of the slope profile shown in Figure 1 is given in Figure 2. The input defining the geometry of the slope profile and the soil stratigraphy requires the X and Y coordinates of the line segments defining the face of the slope and subsequently the soil interface lines from top to the bottom. There is an index code associated with each line segment defining the slope geometry and the soil stratigraphy. The index code uses two numbers, one to describe the soil below the line segment, and the other to describe the nature of the variability of the line segment. Four possibilities are provided:

1) Surface Coordinates. This option is used to define the bluff surface profile.
2) Randomly vary the angle at which the line segment intersects the bluff face. Keep the vertical elevation of the intersection constant.
3) Randomly vary both the line segment angle and the vertical elevation.
4) No varability in location of this line segment.

The soil input requires information about the unit weights of the various soils referred to in the index code as well as the means and standard deviations of the cohesion intercept and friction angle. The last column of the soil input indicates the piezometric surface with which a particular soil is associated. The Y coordinate, i.e., the elevation of the piezometric surfaces, and the estimated standard deviation of the Y coordinate from the given mean values are provided in the water input. The Y value is used to define a piezometric surface that extends from lake water surface along the bluff face until the Y elevation is reached, at which point the piezometric surface enters the bluff. This models a seep at the specified Y elevation.

A random number generator generates the values of the random variables randomly based on the log-normal distribution and the associated mean and standard deviation of each of the random variables. For each combination of the values of these variables, a slope stability analysis is performed based on a consideration of about 100 random failure surfaces. At least twenty-five such analyses were needed to provide an assessment of the risk of instability (see Figure 3). Running over 100 analyses did not seem to provide any additional information.

CLASSES OF UNCERTAINTY

In order to facilitate the analysis, the shoreline sections were classified into five categories based on the degree of uncertainty and variability of the governing factors. These classes, and the number of slope profiles in each class, are as follows:

CATEGORY I. Well exposed slopes with reasonably uniform stratigraphic and soil conditions within the shoreline section (4 profiles).
CATEGORY II. Well exposed slopes or boring information with varying stratigraphic conditions but reasonably uniform shoreline sections (13 profiles).
CATEGORY III. Poor exposure but borings available with potentially varying stratigraphic and soil conditions within the shoreline section (11 profiles).
CATEGORY IV. Poor exposure and no borings with stable appearance (healthy vegetation cover) (2 profiles).
CATEGORY V. Stabilized slope with a fill berm (14 profiles).

In assigning the slope profiles to these classes, four factors were considered in a qualitative manner. These were slope face exposure (Yes, No, or Fill), availability of borings within the section (Yes or No), variability of the stratigraphy, i.e., the position and thickness of the lake sediments in the slope (Small, Medium, Wide), and variability of material properties, i.e., the textural characteristics of the lake sediments (Small, Wide).

The largest categories were II, III, and V. The stabilized slopes with a rubble fill did not require a significant degree of stability assessment. Therefore, the effort was directed primarily at Categories II and III. The probabilistic technique was useful, essentially in providing verification and confidence for the stability assessed by the conventional deterministic analysis performed in the case of Category II slopes. The potential effect of varying stratigraphic conditions on the assessment of stability could be studied by the probabilistic analysis.

In the case of Category III slopes, the probabilistic method was the primary tool for assessing the stability since there was greater uncertainty regarding most of the governing variables.

Note: INDEX CODE
??
Soil # Coord #

Profile Input

Enter coordinates of profile

X COORDINATE	Y COORDINATE	INDEX	X COORDINATE	Y COORDINATE	INDEX
0.000	74.000	11	5.000	150.000	23
100.000	84.000	11	0.000	0.000	5
104.000	85.000	11	10.000	102.000	13
106.000	89.000	11	0.000	3.000	5
130.000	102.000	11	0.000	0.000	5
142.000	109.000	21	0.000	0.000	5
145.000	114.000	21	0.000	0.000	5
167.000	118.000	21	0.000	0.000	5
183.000	124.000	21	0.000	0.000	5
236.000	150.000	21	0.000	0.000	5
302.000	182.000	31	0.000	0.000	5
334.000	202.000	41	0.000	0.000	5
439.000	202.000	41	0.000	0.000	5
302.000	182.000	32	0.000	0.000	5
0.000	3.000	5	0.000	0.000	5

Figure 2. Slope geometry input data.

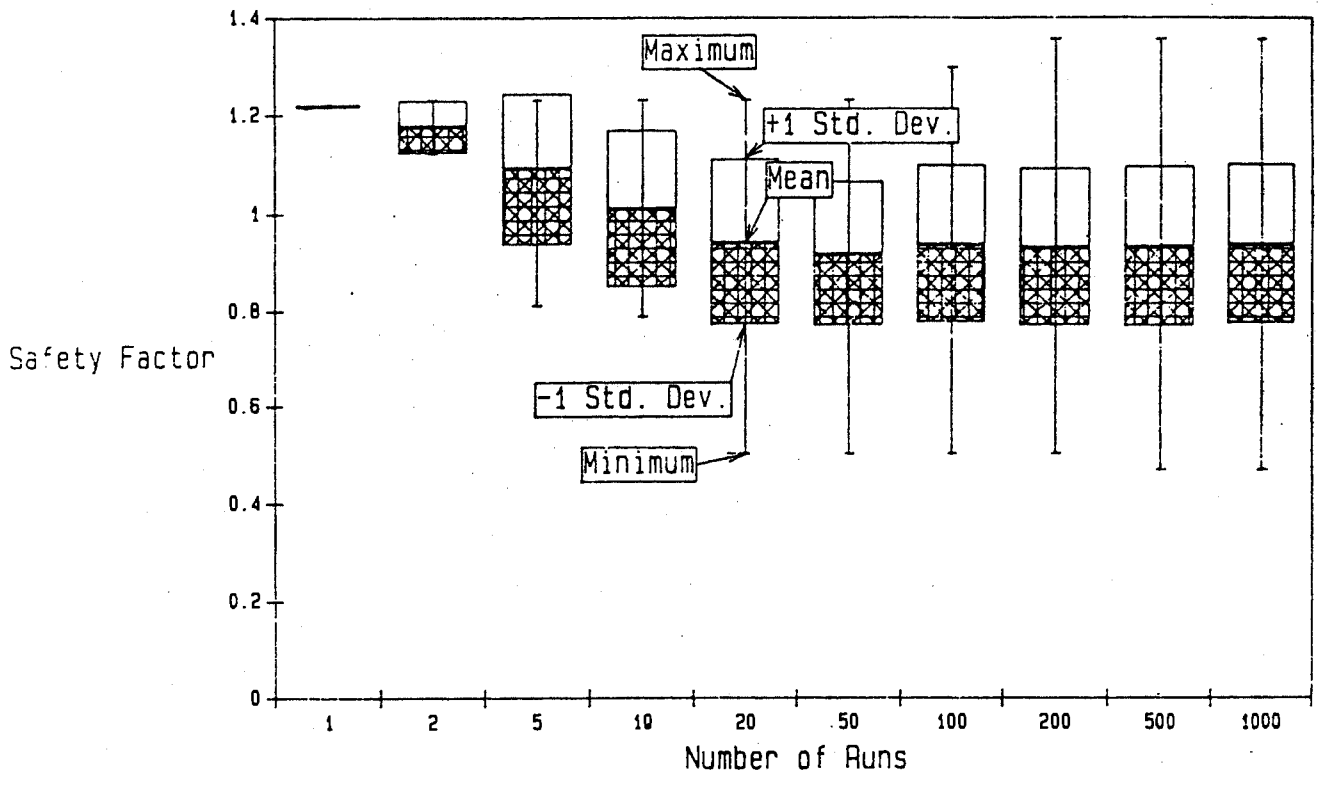

Figure 3. Statistics of safety factor determinations as a function of the number of analyses for Profile 26.

HAZARD CLASSIFICATION

A set of general guidelines was developed to classify the slope sections for rotational slides on the basis of their stability. These guidelines provide a general indication of slope stability by a review of all available data and analysis. The final stability classification was based on both the modeling results and the observed slope conditions in the field. These bluffs being natural slopes often had computed deterministic safety factors around unity. One third of the forty four profiles analyzed had safety profiles in the range of 0.9 to 1.1. The remaining profiles were split between lower ($SF_D < 0.9$) and higher ($SF_D > 1.1$) safety factors. For these latter two groups, the probabilistic method merely served to confirm the stability assessment made on the basis of the deterministic approach. It did not result in a classification change otherwise arrived at on the basis of the deterministic approach. However, for the former group of profiles, with safety factors about unity, the probabilistic method played an instrumental role in assessing the level of instability. A safety factor of about unity (0.9 to 1.1) with the conservative assumptions of the deterministic method implies, at best, a marginal stability. However, it remains problematic to determine the likely landslide hazard potential of these slopes. This judgment was achieved by means of the probabilistic approach.

The cumulative probability of safety factor being less than or equal to unity can be used as a way of assessing the overall landslide hazard potential. Ward (1976) suggested that a probability of more than 60% indicated high landslide hazard, and less than 30% low hazard, with values in between medium hazard potential. Southeastern Wisconsin Regional Planning Commission (1987) adopted 75% and 25% probability levels instead. Based on Ward's values, the landslide hazard classification of twelve profiles with deterministic safety factors between 0.9 and 1.1 is determined as given in Table 2. Based on their cumulative probability, out of 12 profiles, 7 profiles are classified as "unstable" (high landslide hazard), 3 profiles as "marginally unstable" (medium landslide hazard), and 2 profiles as "stable" (low landslide hazard). These results demonstrate the usefulness of the probabilistic approach in delineating the stability classification.

In other efforts, the stability of three profiles was assessed based on only sparse information available using the probabilistic method. Later on, borings provided an enhanced delineation of the stratigraphy and ground water conditions. New analyses were performed using the final information. The results are summarized in Table 3. The initial deterministic safety factors implied unstable conditions for two of the profiles (Profiles 3 and 23) and marginally unstable condition ($SF_D = 0.9$ total) for one (Profile 26). The final deterministic safety factors range between 0.9 and 1.0 implying similar marginal instability for all three profiles. The initial probabilistic analysis indicated all profiles to be unstable. The final probabilistic analyses, based on improved site-specific information about the profiles, resulted in classification of the three slopes into two unstable and one marginally unstable slopes. The comparison of the initial and the final probabilistic analyses indicates that the procedure provides additional information on the stability of a slope even on the basis of limited information. However, it does not replace the need for direct site specific information about stratigraphy and ground water conditions.

SUMMARY AND CONCLUSIONS

An expansion of the classic rotational slope stability analysis to include inputting of random variables, in terms of their probability distributions rather than single deterministic values, is presented. Those factors that are to be estimated based on limited measurements such as strength parameters, positions of stratigraphic unit interfaces, and ground-water table are generated in random combinations from their respective probability distributions. Analysis of twenty five or more such combinations provides a measure of the landslide hazard based on the percentage of combinations yielding a safety factor of equal or less than one. The engineer can exercise his judgment in providing the mean values and standard deviation of the random variables. Thus, this probability approach is found to be a useful tool which minimizes the need to make decisions based upon limited data while not eliminating engineering judgment. It uses all of the existing information. In addition to confirming the results based on the conventional deterministic approach in clearly stable and unstable cases, it is shown that certain delineations of stability in marginal (i.e., the most difficult cases) can be made by the probabilistic technique which is otherwise not possible on the basis of the conventional approach.

The technique was used in the evaluation of risks of instability and the development of appropriate recommendations relative to slope stabilization measures along a coastal reach of Lake Michigan.

ACKNOWLEDGEMENTS

The authors wish to thank the Southeastern Wisconsin Regional Planning Commission for sponsoring this study and developing the data base. Mr. David B. Kendziorski managed the Northern Milwaukee County Shore Erosion Study. Ms. Judy Musich performed the stability analyses.

REFERENCES

Benjamin, J.R. and Cornell, C.A. (1970). Probability, Statistics and Decision for Civil Engineers, McGraw-Hill, New York, N.Y.

Edil, T.B. and Haas, B.J. (1980). Proposed criteria for interpreting stability of lakeshore bluffs, Eng. Geol. 16:97-110.

Edil, T.B. and Shultz, M.N. (1983). Landslide Hazard Potential Determination Along a Shoreline Segment, Sea Grant College Program Reprint, University of Wisconsin, WIS-SG-83-751.

Southeastern Wisconsin Regional Planning Commission (1987). Northern Milwaukee County Lake Michigan shoreline erosion management study. Report, Waukesha, Wisconsin.

Siegel, R.A. (1975). STABL users manual. Joint Highway research project No. C-36-36K, Purdue University, West Lafayette, Indiana.

Vallejo, L.E. and Edil, T.B. (1979). Design charts for development and stability of evolving slopes, J. Civil Eng. Design, 1(3):231-252.

Ward, T.S. (1976). Factor of Safety Approach to Landslide Potential Delineation, Ph.D. Dissertation, Department of Civil Engineering, Colorado State University, Fort Collins, CO.

Wu, T.H. and Kraft, L.M. (1967). The probability of foundation safety, ASCE, J. Soil Mech. Foundation Div., 93(5):213-231.

Table 2. Stability classification of marginal stability cases

Profile	Deterministic Safety Factor	Range* of Safety Factor	Percent* of Safety Factor ≤1.0	Stability Classification
3	0.98	0.62-1.08	65	Unstable
4	0.98	0.81-1.15	55	Marginally Unstable
9	0.99	0.66-1.17	60	Marginally Unstable
19	0.90	0.66-0.93	100	Unstable
23	0.91	0.54-1.06	70	Unstable
25	1.07	0.76-1.44	25	Stable
28	0.95	0.47-1.12	85	Unstable
30	0.96	0.54-1.06	90	Unstable
33	0.91	0.62-1.60	65	Unstable
39	0.99	0.74-1.10	70	Unstable
40	0.99	0.55-1.54	15	Stable
41	0.96	0.60-1.35	40	Marginally Unstable

* Based on 20 random analysis runs.

Table 3. Estimating stability classification based on sparse information

	Initial Analysis			Final Analysis		
	SF_D	$P[SF_p \leq 1]$	Stability Classification	SF_D	$P[SF_p \leq 1]$	Stability Classification
Profile 3	0.80	92%	Unstable	1.00	68%	Unstable
Profile 23	0.49	100%	Unstable	0.91	65%	Unstable
Profile 26	0.98	88%	Unstable	0.96	40%	Marginally Unstable

copy 12-11-91

LANDSLIDE CASES IN THE GREAT LAKES: ISSUES AND APPROACHES

by

Tuncer B. Edil

Professor of Civil and Environmental Engineering
University of Wisconsin-Madison
Madison, WI 53708
Tel: (608) 262-3225 FAX: (608) 262-5199

Currently Visiting Professor at CERMES (Soil Mechanics Research Center)
Ecole Nationale des Ponts et Chaussees, 93167 Noisy-le-Grand Cedex, France

Submitted to the Session on

"Landslide Case Histories: Environmental, Socio-Economic and Technical Issues"

TRB 1992 January Meeting
Washington, D.C.

Final Manuscript

LANDSLIDE CASES IN THE GREAT LAKES: ISSUES AND APPROACHES

by

Tuncer B. Edil

ABSTRACT

This paper presents a review of the experience the author has gained over a decade studying the mechanics of coastal bluff erosion and stability along the Great Lakes shorelines and the approaches to deal with this problem. Extensiveness of the shoreline formed in erodible bluffs and dunes and often complex response of this type of shoreline to wave erosion makes slope processes an important part of the shore recession problem. The shore recession, in turn, affects planning, design, and maintenance of transportation facilities in coastal areas in a significant way. The coastal bluff processes are described, including a discussion and comparison of the role and significance of the causes and the processes. The erosional processes resulting in significant mass wasting include: wave erosion, solifluction, rain impact and rill/sheet erosion, wind erosion, sapping, and ice erosion. Another important process is mass sliding and slumping of bluff materials in response and in conjunction with the erosion processes. The time scale for the impact of these processes on coastal bluff morphology and recession is discussed in view of the important measurements and conceptual models. The methods of approach to this problem are grouped as structural (stabilization) and non-structural (planning and management) solutions. The options and the reqüired information to implement either of these approaches are discussed. Because of the length of the slopes and the variable nature of geology and soil properties, a probabilistic approach to stability analysis has been adopted for planning and managing the stabilization efforts. Two specific cases, one in an undeveloped and another in an urban segment of the shoreline, are presented to demonstrate the stabilization approach.

INTRODUCTION

This paper presents a review of the experience the author has gained over a decade studying the mechanics of coastal bluff erosion and stability along the Great Lakes shorelines and the approaches to deal with this problem. While the author's experience has been primarily along the Lakes Michigan and Superior shorelines of Wisconsin, an extensive literature survey and the available theoretical information are also used in delineating the most likely role and significance of various factors on shore erosion and slope stability in a general sense. Nearly 65% (10,444 km) of the 16,047 km-long Great Lakes shoreline is designated as having significant erosion with about 5.4% (860 km) of it being critical. The total damage to the United States shoreline of the Great Lakes due to wave action during the high lake level period, May 1951 through April 1952, is placed at about $50,000,000 (1952 price level). Nearly 32% of the U.S. shoreline of the Great Lakes, not including the islands, consists of erodible bluffs. Extensiveness of the shoreline formed in erodible bluffs and dunes and often complex response of this type of shoreline to wave erosion makes slope processes an important part of the shore recession problem. The shore recession, in turn, affects planning, design, and maintenance of transportation facilities in coastal areas in a significant way. The coastal bluff processes are described, including a discussion and comparison of the role and significance of the causes and the processes. The methods of approach to this problem are presented along with two specific cases of application.

SLOPE PROCESSES

Slope movement is an expression of force overcoming resistance. Coastal bluffs are examples of systems in which force and resistance are continually opposed. This equilibrium is altered by changing environmental conditions that can initiate down slope movement.

Force requires energy, and all energy in geomorphic systems is ultimately derived from either *gravity* or *climate*. The intensity of shear force is basically a function of gravity and the factors which control it, along the potential failure surface, include slope inclination, height and unit weight of slope forming materials, and included water. Climate, through its control on water, air and temperature, provides energy for the most important forces on bluffs. Climate related forces include wind and wave action, surface and ground-water flow, rain impact, moisture and temperature related ground expansion, and ice action.

Resistance to these forces that tend to move materials down and/or away from the slopes is provided primarily by the shear strength of these materials. Vegetation and man-made structural systems such as shore protection and slope stabilization structures may provide additional resistance. Shear strength is not constant for a given material. It may change in time due to weathering and ground water pressure changes which are, in turn, controlled by certain climatic factors and removal of slope materials due to erosion. Furthermore, use of certain technologies can improve shear strength of soils or minimize the detrimental effects of the climate factors.

The interaction of driving force and soil resistance results in a number of processes leading to debris production and removal. The commonly encountered processes in the Great Lakes coastal bluffs can be separated into two broad groups, namely *mass* and *particle movements*. In the former group, debris begin to move as a coherent unit (rigid body movement or viscous flow). Movements in which particles move individually, with little or no relation to their neighbors, are particle movements. Distinction between these categories is often difficult. The erosional processes caused by waves, currents, rain,

groundwater, and winds seem to be mainly particle movements. The concepts presented above are summarized in Table 1.

Wave Erosion

Probably the most significant geomorphic process along the Great Lakes shoreline is the erosion and removal of shoreline materials by waves. Wave action is important both in itself, and in initiating and perpetuating other geomorphic processes in those segments of the shoreline where bluffs are encountered. The nature and magnitude of wave erosion depends broadly on wave energy and erodibility of materials at the specific location along the shoreline. The most notable factor that affects the wave energy is the water level fluctuations in the Great Lakes. For the long-term water level changes, the intervals vary from 10 to 30 years and the magnitudes are up to 2 meters. These changes are associated with the changes in the volume of water in the Great Lakes constitute the most important factor affecting the rate of erosion of the shoreline in the Great Lakes. When water level is low, wave energy is dissipated on the beach face and the products from mass wasting on the slopes above tend to accumulate at the base of the bluff. Presumably, continued low lake levels would eliminate or greatly decrease the impact of mass wasting on these bluffs, but fluctuations from high to low lake level will probably continue to take place as they have in the past. After the water level falls from a high stand, active mass wasting continues to take place for many years. In fact, probably bluff top retreat reaches a maximum about 4 years after high water level. When the water level rises from a low stand, mass wasting debris that has accumulated at the base of the slope is removed and incorporated into the long shore transport system. This appears to re-initiate slope instability that can continue producing bluff retreat well into the next low water cycle.

The Great Lakes are surrounded by a wide variety of coastal types and deposits, although the coasts are generally dominated by Pleistocene glacial deposits. Each of the lakes has a portion of its coast which is comprised of bedrock. In general, bedrock portions of the shoreline are most resistant to wave action. Most of the recent erosion is confined to the coasts of unconsolidated sediments. These may be in the form of glacial till or out wash, lake sediments, or dunes, which are reworked from glacial sediments. In general, cohesionless material such as sand and silt are the most erodible materials with cohesive soils (clay, silty clay, etc.) having somewhat more resistance to wave erosion due to the cohesion between the particles.

Other factors are superimposed on this long term process that affect slope stability and stable slope angle. The strength of bluff materials is an important factor. Lake sediment, fluvial sand and gravel, and till units having considerably different properties are all present in the bluff face. Groundwater moving toward the fluff face is concentrated on geologic contacts and obvious seeps can be seen in various places along the bluff. Vegetation, offshore bathymetry, and of course the presence of man-made structures also influence the processes that are taking place.

Sliding/Slumping

Slides (both rotational and translational) and flows (including solifluction) are two types of movements that are encountered most commonly in the Great Lakes region. Coastal bluffs are in constant evolution due to the combined effects of toe erosion, slides, and face degradation. These processes, in general, cause a decrease in total lateral normal stress and increase shear stresses along the potential failure surface accompanied by a decrease in pore water pressure. Subsequently, the soil swells as water flows into this zone and shear strength decreases with time and a delayed failure takes place. This situation becomes more critical as the over-consolidation of clays increases. Edil and

Vallejo [1] described bluff stability at two sites on the shore of Lake Michigan. Where unexpected stability occurred, it could be explained in a rational manner by this process of delayed failure.

The observed slides are subdivided into *rotational* slides (slumps) and *translational* slides. Slides in natural slopes tend to be complex or are at least controlled in their mode of movement by internal inhomogeneities and discontinuities such as the presence of a very weak layer or fractures. Barring the presence of such gross inhomogeneities, rotational slides involving approximately circular rupture surfaces have been observed and analyzed in Great Lakes bluffs formed in cohesive soils [1, 2, 3]. Deep-seated rotational slips occur in clay soils but are not observed in sands. One method of analysis of rotational slides that is accurate for most purposes is that advanced by Bishop [2]. The failure arc predicted by the Bishop method has been found to compare well with actual failure surfaces in bluffs on the Great Lakes and other places. Vallejo and Edil [5] developed stability charts for rapid evaluation of the state of stability of actively evolving Great Lakes coastal slopes using the effective stress approach and the Bishop method. These charts indicate the stability status as well as the type of potential failure, whether deep or shallow, to which the bluffs may be subjected. The geometric changes that the bluffs will be subjected to before becoming stable can be discerned from the charts. An example of these charts is given in Figure 1. The family of curves represents height-inclination combination for the limiting long-term safety factor of unity with respect to a deep slip type of failure. Skempton and Hutchinson [6] define the deep slip failures as the ones having the values of the ratio between the maximum thickness of the slide and the maximum length of the slide ranging from 0.15 to 0.33. The slopes with height-inclination combinations falling within Zone A are unstable slopes with potential deep slips in the long term. The stable angle below which no more rapid mass movement will take place (except perhaps creep) is given by the ultimate angle of stability (β_u) [7]. This angle defines the upper limit of Zone C of stable slopes. A slope which is in Zone B (between Zones A and C) will experience shallow failures. The shallow failures are defined by Skempton [8] as those having values of the ratio of the maximum thickness to length of the slide between 0.03 and 0.05. The shallow slips could be planar slides (slab slides), small rotational slips, and flows. For this reason, the slopes in Zone B can be classified as stable slopes with local instability or quasi-stable slopes.

A translational slide in which the moving mass consists of a single unit that is not greatly deformed or a few closely related units, may be called a *block slide*. An example of such a failure involving a block of fractured till in the upper part of a coastal bluff in Milwaukee County, Wisconsin, was reported by Sterrett and Edil [9]. The movement of translational slides is commonly controlled structurally by surfaces of weakness such as faults, joints, bedding planes, and variations in shear strength between layers of bedded deposits, or by contact between firm bedrock and overlying detritus.

Translational slips can also occur in a homogeneous soil mass. In particular, granular materials such as sand and gravel fail in surface ravelling and shallow slides with the failure surface parallel to the slope surface. Similar failures occur in a mantle of weathered or colluvial (granulated) material from clay slopes and are referred to as *slab slides*. An infinite slope analysis is often representative of such failures. Sterrett [10] reported slab slides with a depth of about 0.6 meters from Milwaukee County, Wisconsin. This depth coincided closely with the depth of desiccation cracking and soil structure change from fine to prismatic beds to massive intact blocks. The latter were due to repeated freeze-thaw cycles. Sterrett [10] also observed that frozen slabs of soil measured 0.6m by 10m by 13m failed in early spring. This failure was attributed to differential melting of the bluff face.

Flows and Solifluction

Flows commonly result from unusually heavy precipitation or from thaw of snow or frozen soil. The flows observed in the Great Lakes bluffs take place mostly in spring and result from primarily ground thawing and snow/ice melting. Therefore, they can be classified largely as solifluction. Solifluction is the down slope movement of water saturated materials which follows thawing in previously frozen slopes. Seasonally frozen subsurface layers of soil prevent percolation of water from upper thawed layer (termed "active layer"). The active layer becomes saturated with water from melting of ice lenses within it as well as from melting snow and rainfall. The effects of excess water is to fluidize the active layer reducing its strength and causing it to move down-slope by gravity. The extent of solifluction depends on the grain size of the slope material, availability of water, depth of frost penetration, number and duration of freeze-thaw cycles, inclination of the ground surface, and components of the vegetative cover. Vegetation appears to be the most restraining factor for solifluction. The size of the flows along the western Lake Michigan shoreline varies from 0.3 to 0.6m wide to 15 to 20m wide and 21 meter long. A number of approaches for the analysis of solifluction failures have been suggested. Vallejo [11] introduced a new approach to the analysis of solifluction that reflects the particulate structure of the flowing mass. Vallejo and Edil [12] applied this analysis to a coastal bluff in Kewaukee, Wisconsin, with successful field verification. The critical depth of thaw normal to the slop face) at which failure occurred was measured to be 0.25 meters.

Rain Impact and Rill/Sheet Erosion and Sapping and Wind and Ice Erosion

These processes are also important in general mass wasting that occurs in the exposed coastal slopes of the Great Lakes. In slopes formed in granular material, these processes are dominant. A description of these processes is given by Sterrett [10] who determined, based on field observations, that most of the material removed from the slopes during summer is via sheet-wash and rill erosion. He found that the universal soil loss equation is useful in predicting soil loss from steep slopes in its modified form suggested by Foster and Wischmeier [13].

STRATEGIES FOR DEALING WITH ACTIVELY EVOLVING SLOPES

The most significant characteristic of the coastal slopes in many areas of the Great Lakes shoreline is the fact that they are actively evolving natural slopes. In other words, the slope geometry continually changes. This characteristic sets these slopes apart from other natural slopes in terms of stabilization approaches. There are basically two approaches to the problem of actively evolving coastal slopes. The first approach involves *structural* or *stabilization* solutions on a site-specific basis. The structural approach is similar to other natural slope stabilization efforts with some additional considerations. A proper stabilization program should include: (a) protection against wave action in all cases, (b) slope stabilization against deep slips if needed (important in delayed instability often observed in bluffs formed in stiff clay soils), and (c) stabilization against face degradation and shallow slips. Shore protection is a major component and may be costlier than the slope stabilization in some cases. The problems associated with the execution of this category of solutions seem to be of two types: (i) many attempts are not engineered and fail to cope with the problems; and (ii) those engineered solutions quite often neglect to consider all aspects of the problem. To undertake stabilization works, site-specific studies are undertaken at numerous locations. In these studies, an attempt is usually made to identify and understand slope-stability problems at a single site over a relatively short period of time.

The second approach, that is, *non-structural (planning and management)* approach is particularly suitable in undeveloped tablelands where hazard mitigation to transportation facilities can be planned and managed over an extensive reach of the shoreline, the size of a county or at least several kilometers, are usually considered. These studies are usually aimed at minimizing future losses. In this case the need for understanding bluff processes is more acute because predictions of future recession over a long period of time with changing water-level and climate conditions is necessary. This approach necessitates models of bluff evolution.

Different parts of geomorphic systems respond at different rates to changes in external parameters. In addition, some bluffs appear to pass through an evolutionary sequence which is only interrupted when external variables surpass a threshold level. In other words, it appears that once toe erosion initiates an unstable slope, a predictable progression of failures takes place on the bluff irrespective of water level or the amount of wave erosion [1, 14]. The main problem concerning prediction of slope evolution lies in understanding the response times to environmental changes and the time necessary for bluffs to pass through an evolutionary sequence. Evidence from other areas with evolving slopes such as riverbanks and marine coasts as well as from the Great Lakes suggests that there are possibly three time scales over which the natural cycles of evolution take place. These scales are 2 to 3 years, 50 to 100 years, and thousands of years. It is unfortunate that more information in this area is not available. Without a clear understanding of the time scales of change of coastal bluffs, predictions of future change are likely to be misleading or, in fact, incorrect or overly conservative.

As discussed in a previous section, lake level fluctuation (because of its control on toe erosion) is a primary long-term cause of bluff instability. Given a low water level for long periods of time (100 years) most slopes along the shoreline would become nearly stable. It should be pointed out, however, that along bluffs of cohesive materials, wave erosion is often only the "trigger" that initiates the slope failure. Decrease in lake water levels or toe protection may control wave erosion, but mass wasting on the bluff normally continues to be a problem for a long period of time. Relatively large rotational slides have been observed to take place in areas free of significant wave erosion, for instance during times of low lake levels [15]. A large slide occurred in an area south of Bender Park, Milwaukee County, Wisconsin in 1979. The toe had been protected from wave erosion for at least 20 years by the beach that built up north of a power plant which projected into the lake.

The main tool used in the non-structural or management approach is to establish a setback requirement for new transportation facility development. This requires a knowledge of coastal recession over a long period of time, say 30 to 50 years, and determination of stable slope angle. Typically historical aerial photographs are used to establish the recession rates and geological/geotechnical analyses are used to determine the stable slope angles. Tools for such an analysis are not well-established. However, this does not mean that there has not been any progress. Research conducted primarily during the last decade or two has identified the operating processes and their possible magnitudes [16]. A nonstructural setback distance can be estimated as illustrated in Figure 2 [17]. Setback distance consists of two components. *Erosion risk distance* is the distance from the existing bluff edge which could be affected by recession of the bluff over time, and by the regrading of the bluff to a stable slope angle. *Minimum facility setback distance* is considered to be an additional safety zone intended to prevent facilities from being placed too close to the bluff edge. The solution strategies for active coastal slopes are summarized in Table 2.

TWO CASE HISTORIES

In this section slope conditions and stabilization strategies at two specific sites, respectively, along the southwestern Lake Superior and the western Lake Michigan shorelines are presented.

Madigan Beach - Lake Superior

The bluffs of this site are reached by a 4 km secondary road directed northeastward of U.S. State Highway 2 approximately 25 km east of the town of Ashland, Wisconsin. It is located 610 m west of the mouth of Morrison Creek in the Bad River Indian Reservation. This site provides an example of a situation in which the main highway is quite far from the shore for immediate threat and the upland is undeveloped. The shoreline profile at the Madigan Beach site consists of bluffs rising 18 m above the beach and maintaining temporary steep inclinations in excess of 40° with the horizontal. The processes of undercutting and slumping are evident and the bluff faces are mostly exposed without any of the vegetation and trees which are dominant in the upland. Geologically, northwestern Wisconsin, where Madigan Beach slopes are located is a glaciated area.

The borings and observations of the materials exposed on the bluff face indicated the presence of a 4.5 to 6 m thick reddish-brown stiff, silty, clay layer of low plasticity on the top, underlain by a thick (more than 12 m), very dense brown sandy silt or silty sand. The geotechnical properties of the bluff materials are summarized in Table 3. This highly erodible (cohesionless) sandy silt makes up most of the bluff material and is underlain by a reddish brown, rather stiff, clay layer of high plasticity, mostly below the lake level. A mineralogical analysis of this lower clay layer revealed the presence of quartz, illite, kaolinite, and a small quantity of montmorillonite. The difference in the plasticities of the upper and lower clay layers appears to stem primarily from the difference in their clay fractions (26% and 63%, respectively) rather than a mineralogical difference.

Madigan Beach appears to be subject to severe climatological forces and this, coupled with the erodible (cohesionless) materials forming the bulk of the bluffs, results in a highly active environment for slope evolution. The photo-reconnaissance surveys conducted periodically since 1974 have revealed the action of bluff face degradational processes such as sheet wash, solifluction, and seepage effects, along with the dominant action of waves. The sandy silt material of the bluffs, while highly erodible under surface processes, is strong below the surface when it is confined (the effective angle of internal friction is 37°). This make the bluffs highly stable against immediate rotational slips and they sustain fairly steep inclinations in excess of 40° in many parts of the shoreline. This situation is helped by the presence of clay layers, some 6 m thick, capping the top of the bluffs.

In order to monitor the changes in slope morphology, a number of cross-sections (perpendicular to the shoreline) have been surveyed periodically. The changes in most of the cross sections were indicative of face degradational processes without any deep rotational slips. The bluff top recession measured using 1976 and 1978 aerial photographs indicated a variation of recession on the order of 3 to 11m during this period. In 1977 a shore protection demonstration project was initiated. This project involved placement of longard tubes filled with sand [18] along the beach in different configurations as shown in Figure 3. Longard tubes are constructed of a geotextile and come in various sizes. Those used at Madigan Beach were 1.75 m in diameter weighing about 4,500 kg/m when hydraulically filled with sand. Four of the tubes were placed at the toe of the bluff parallel

to the shoreline acting as a seawall and six 33-m long tubes were placed perpendicular to the shoreline acting as groins. The recession rates measured in the field, as well as discerned from aerial photographs, indicated a significant reduction in the recession from the 1976-77 values. It should be noted, however, that one of the sections experienced a large recession of 2.9m during this period due to a deep slip.

The stability of the bluffs was analyzed using the Bishop method in a conventional manner. The method uses the effective stress analysis of slope stability and utilizes the drained strength parameters of the bluff materials and the measured pore-water pressures as estimated from the piezometer readings. The stability analyses performed on the initially measured profiles of Cross Sections 1, 2, and 3 (Figure 3) resulted in safety factors of 1.36, 1.16, and 1.30, respectively, indicating the general stability of this segment of the site against sliding. Cross Section 2 had already gone through a deep-seated major slide involving a 3.4 m drop of an 8.8m wide section at the top when surveyed in 1976. The initially surveyed profile of Cross Section 4 resulted in safety factors less than unity and, thus, instability. A safety factor of less than unity implies potential instability in the long-term for a currently standing slope since the analysis performed is an effective stress (long-term stability) analysis. It also may imply that some of the assumptions, such as zero pore pressure above the ground water table, are too conservative. The potential circle of failure surface and the corresponding safety factor are shown in Figure 4. This bluff maintained its stability until the latter part of the summer of 1978 when slumping occurred resulting in the recession of the bluff top as marked by the approximate intersection of the predicted failure surface. Another cross section, Cross Section 5, was also analyzed and it was found to have potential for slumping as indicated by the failure surface in Figure 5. The bluff segment in this area was chosen for a slope stabilization demonstration. After considering a number of alternatives, including terracing, berms, and various combinations of these, it was decided to regrade the bluff to a uniform slope of about 25°. This inclination was determined to be safe based on a similar analysis. The bluff stabilization demonstration included surface water diversion in the upland and seeding of the bluff face to prevent surface erosion. The project was completed in the fall of 1977. The toe of the bluff was protected with a longard tube placed parallel to the toe and another longard tube, which was placed perpendicular to the shoreline (see Figure 3), which effectively built up the beach in front of the longard tube acting as a seawall. The six longard tubes which were placed as groins perpendicular to the shoreline were all destroyed by the Spring of 1980. The other tubes which were put as seawalls, however, mostly lasted providing some degree of protection for a while. In 1984, they too were mostly deflated and buried in the beach sand, exposing the stabilized bluff section to renewed wave attack.

Whitefish Bay - Lake Michigan

The topland in the case of these slopes is in a highly developed urban setting in a northern suburb of Milwaukee, Wisconsin. There are expensive homes, behind which a major urban road passes, within 50 m from the edge of the bluffs. A 1983 landslide threatened 6 to 8 homes when the front yard dropped nearly a meter. This coastal area is formed in glacial deposits ranging up to 40 m in thickness. The layer nearest to the surface is known as the Ozaukee Till, consisting of silty clay with a reddish color. The Oak Creek Till is composed of a pebbly silty clay and lies beneath the Ozaukee Till. Lake sediments of various textural characteristics are often found between these two tills. Directly beneath the Oak Creek Till lies another very stiff till known as the New Berlin Till which was deep below the lake level at this location. It is a coarse-grained till, sandy in texture and dominated by pebbles and cobbles. These formations are often exposed in the active slopes along the western shore of Lake Michigan. The stratigraphy was identified on the basis of

field surveys, historic geological records of soil boring data, and new soil borings performed at selected sections of the shoreline.

The geotechnical properties of the glacial materials forming the bluffs were obtained from historic data and laboratory analysis of the samples collected from the exposed slope surface and soil borings. The strength parameters and the unit weights of the bluff material are given in Table 4 in terms of the known values and standard deviations based on the samples collected from different parts of the shoreline.

Along the northern Milwaukee County shoreline, ground water generally flows toward the lake and discharges either at or below the base of the bluff into the lake. The lake sediments consisting of coarse-grained soils may act as water-bearing units. Additionally, a perched water table is usually found within the fractured Ozaukee Till at the top of the bluffs producing seeps on the bluff face. The ground water elevations used in the slope stability analysis at each profile site were based on observed ground water seepage, soil boring data, ground water observation wells, and electrical resistivity analysis.

The study area shoreline, extending nearly 3.7 km, was considered to be a single section, with similar physical and erosion related characteristics. Field surveys were conducted to delineate the section boundaries, and to identify the causes and types of beach erosion and slope failure occurring in the section. Unlike the earlier case, both conventional deterministic slope stability analyses and probabilistic soil stability analyses were conducted to establish the state of stability of this entire section.

Conventional Analyses

The conventional deterministic rotational slope stability analyses using the effective stress method provide the locations of potential failure surfaces and the attendant safety factors based upon the drained strength parameters and the estimated ground water levels for selected bluff profiles. The "worst case" ground water conditions are assumed in these deterministic analyses. Late winter and early spring have been found to be the most critical periods for the stability of Lake Michigan coastal slopes for both deep-seated and shallow slides [5]. During this period, ground water levels and flows generally rise, but the surface is still frozen, which decreases its permeability and prevents ground water discharge from the slope face. This creates an inclined artesian effect, resulting in increased pore pressures and reduced slope stability.

Interpreting the stability of coastal slopes is a problem complicated by the dynamic nature of slope geometry. Two different types of criteria are used in interpreting the results of the slope stability analyses which are based on either the consideration of the lowest safety factor or the consideration of all failure surfaces with a safety factor of less than unity [3].

For a slope profile measured in an adjacent segment of unfailed bluff within the study area, a slope stability program named STABL was used to generate 100 potential failure surfaces and to calculate the corresponding safety factors [19]. The ten failure surfaces with the lowest safety factors were identified. The lowest safety factor calculated was 0.95 and the corresponding failure surface was located within the middle portion of the bluff slope. However, a bluff segment in the study area had already failed in a rotational slide. The safety factor for this failed bluff was calculated to be 1.56 [20].

In the deterministic approach, mean values of soil properties based on the available test results as given in Table 3 were utilized along with the geometrical and geological

measurements of the slope at the specific site in computing a safety factor against failure. An assessment of the general stability of slopes of a shoreline section based on the deterministic safety factors of a number of slope profiles located within the section could conceivably be in error if the slope parameters chosen as input for the stability program are not reliable. For example, adequate information may be available at certain sections because of the excellent exposure of slope soil stratigraphy and the rather uniform characteristics of the slopes and the soils within the section. At such locations, adequate information is available for what one may call a "reliable" analysis. However, for many other sections, between the borehole locations and with poorly exposed slope faces due to vegetative cover, soil properties, position of stratigraphic unit interfaces, and ground-water table in the slope have to be interpolated or estimated based on an examination of the general slope conditions. In view of the variability of soil properties and other slope parameters which have to be estimated, the computed safety factors would not be as reliable for these profiles as they would be for the profiles at the borehole locations and/or with good exposure.

Probabilistic Analyses

The objective for the probabilistic analysis was to verify the results obtained from the deterministic slope stability analyses, and to provide an assessment of overall slope stability within the entire section, rather than just for the specific profile sites. The probabilistic model of slope stability analysis, allows the analysis of general stability conditions of a shoreline section in such a way that one can determine the reliability of the safety factors calculated by the deterministic slope stability analysis. The variability of the safety factor depends upon the variability of the slope parameters and the method by which the safety factor is computed. At the borehole locations, even though there is greater reliability, there is, nevertheless, some variability associated with certain slope parameters. For example, soil properties are estimated based on tests on a limited number of samples and they are, in general, highly variable. For profiles between the boreholes or in slope sections without good exposure, however, the variability is even greater since there are no direct measurements of certain slope parameters. Basically, the variability of safety factors depends upon the variability of the soil properties, water table position, and the soil interface lines considered in the analysis. Slope geometry was measured in the field for the slope profile chosen to be representative of the general morphology of the slopes in the section; therefore, it is not considered to be a significant source of variability.

The probabilistic model used is based on the Monte Carlo method [21, 22, 23]. This method was used because it can artificially derive the probability distribution of safety factors based upon the probabilistic nature of the input random variables. It is a particularly useful method when the relationships among variables are complicated functions involving more than one random variable. Therefore, one must incorporate into the model the uncertainty and variability of the basic controlling geological, geotechnical, and environmental factors involved in so far as possible. The β distribution was used to generate the variable parameter distributions. Mean values and standard deviations of the soil properties and the limits of their variation are required to generate β distributions of these properties. The spread of these distributions was established on the basis of the measured or expected standard deviations of these randomly varying properties. By setting limits on the variation of the parameter, unreasonable possibilities are avoided such as negative cohesion.

The original STABL program was modified to permit the input of random variables [23]. A random number generator generates the values of the variables randomly based on

the given β distribution of the variables. For each combination of these variables, a slope stability analysis is performed based on consideration of about 100 random failure surfaces. At least twenty such analyses are needed to provide an assessment of the risk of instability. Running over 1000 analyses does not seem to provide any additional information [23]. The probabilistic stability analysis performed on the unfailed slope segment in the study area indicated that of the 200 analyses, 159 or 80% gave minimum safety factors of less than 1.0. For the same slope profile, the deterministic safety factor was calculated to be 0.95 as indicated earlier.

Hazard Classification

A set of general guidelines was developed to classify the slope sections for rotational slides on the basis of their stability. These guidelines provide a general indication of slope stability by a review of all available data and analysis. The final stability classification is based on both the modeling results and the observed slope conditions in the field. These bluffs being natural slopes often have computed deterministic safety factors around unity. A safety factor of about unity (0.9 to 1.1) with the conservative assumptions of the deterministic method implies, at best, a marginal stability. However, the determination of the likely landslide hazard potential of these slopes remains problematic. This judgment can be achieved by means of the probabilistic approach.

The cumulative probability of safety factors being less than or equal to unity can be used as a way of assessing the overall landslide hazard potential. Southeastern Wisconsin Regional Planning Commission [17] adopted a hazard classification system in which a probability of more than 75% (75% of the safety factors less than 1) indicated *unstable* or high hazard and less than 25% *stable* or low hazard condition. Based on this classification, this section of Whitefish Bay was classified *unstable*.

Stabilization Effort

In view of the immediate threat presented to the homes and the urban highway immediately behind these slopes, a structural solution was pursued. This solution involved construction of a terraced berm using concrete demolishing debris. Use of a waste material reduced the cost significantly. The berm was constructed from the beach level up the slope. Dumping materials from the slope top was avoided to prevent further movements of existing slump blocks; therefore, an access road to the beach was cut. The configuration of the berm is indicated on Figure 6. The toe of the berm was protected by limestone riprap against wave action. A 0.3 m thick soil cover was placed on the berm surface to provide vegetation. A deterministic slope stability analysis was also performed using the profile after restoration as shown in Figure 6. This analysis indicates a stable bluff slope with respect to rotational sliding. The lowest safety factor calculated was 1.75 with a corresponding failure circle beneath the top portion of the fill layer.

SUMMARY

The processes that operate on coastal slopes are described. These processes often lead to significant mass wasting, instability and recession of the slopes. Transportation facilities existing on the upland are threatened by the slope failures and shoreline recession. Stabilization strategies for long stretches of coastal slopes are presented in terms of management or stabilization approaches. Because of the length of the slopes and the variable nature of geology and soil properties, a probabilistic approach to stability analysis has been adopted for planning and managing the stabilization efforts. Two case histories from the Great Lakes region are presented to demonstrate the low-cost stabilization

approach. Once a hazard classification is established, a variety of methods can be used to stabilize the unsafe or marginally unsafe coastal slopes. Potential slope stabilization measures commonly used include regarding the slope to a stable angle, installing ground water drainage systems to lower the elevation of the ground water and prevent ground water seepage from the face of the bluff, constructing surface water control measures, and revegetating the slope. Figure 7 shows alternative methods of bluff slope stabilization commonly used along the Great Lakes shorelines [17].

The stable long-term inclination used in the cutbacks of the oversteepened bluffs of the western Lake Michigan shoreline is 22° (1V:2.5H). The typical material used in slope stabilization and restoration fills is concrete rubble. Depending on the type of material used for filling, a steeper angle than the usual stable angle of 22° - often approximating 35° - may be utilized for portions of the filled bluff slopes. The restored slopes are normally terraced or contain compound slopes. Filling should begin at the slope bottom, and some bluffs may need to be filled only along the lower portions of the slope. A minimum of 0.3 m thick soil cover is placed over the rubble fill and seeding and mulching would be required to develop a vegetable cover. Adequate toe protection is required for long term stability. Usually a riprap revetment of rock or quarry stones is used for this purpose. trench drains are usually required to intercept and divert the groundwater of the water bearing lacustrine deposits usually found at the mid-height of the bluffs before the placement of the fill materials.

ACKNOWLEDGEMENTS

The author wishes to acknowledge the contributions of his colleagues; Drs. David M. Mickelson and Peter J. Bosscher, and many former students to his understanding of the coastal bluff slumping problem over the years. The financial support provided by the National Oceanic and Atmospheric Administration, U.S. Department of Commerce through the Wisconsin Sea Grant Program and the Wisconsin Coastal Zone Management Program over the years supported the author's research. Southeastern Wisconsin Regional Planning Commission supported the latter developments in probabilistic method and provided the data base for the Whitefish Bay case. Financial support was received from the U.S. Environmental Protection Agency for the Madigan Beach bluff stabilization project.

REFERENCES

1. T. B. Edil and L. E. Vallejo. "Shoreline Erosion and Landslides in the Great Lakes." Proc. 9th Int'l Conf. Soil Mechanics and Foundation Eng., Tokyo, 1977, vol. 2, pp. 51-57.

2. R. M. Quigley and D. B. Tutt. "Stability-Lake Erie North Shore Bluffs." Proc. 11th Conf. Great Lakes Res, 1968, pp. 230-238.

3. T. B. Edil and B. J. Haas. "Proposed Criteria for Interpreting Stability of Lakeshore Bluffs." *Engineering Geology*, 1980, No. 16, pp. 97-110.

4. A. W. Bishop. "The Use of the Slip Circle in the Stability Analysis of Slopes." *Geotechnique*, Vol. 5, No. 1, 1955, pp. 7-17.

5. L. E. Vallejo and T. B. Edil. "Design Charts for Development and Stability of Evolving Slopes." *J. Civil Engr Design*, Vol. 1, No. 3, 1979, pp. 231-252.

6. A. W. Skempton and J. N. Hutchinson. "Stability of Natural Slopes and Embankment Foundations: State of the Art Report," Proc. 7th Int'l Conference Soil Mechanics and Foundations Engrg, Mexico, pp. 291-334, 1969.

7. A. W. Skempton and F. A. Delory. "Stability of Natural Slopes in London Clay." Proc. 4th Int'l Conference Soil Mechanics and Foundation Engrg, London, VOl. 2, 1957, pp. 378-81.

8. A. W. Skempton. Discussion in "Soil Stability Problems in Road Engineering." Proc. Inst Civil Engineering, Vol. 2, No. 2, 1953, pp. 265-268.

9. R. J. Sterrett and T. B. Edil. "Ground-Water Flow Systems and Stability of a Slope." *Ground Water*, Vol. 20, No. 1, 1982, pp. 5-11.

10. R. J. Sterrett. "Factors and Mechanics of Bluff Erosion of Wisconsin's Great Lakes Shorelines." PhD Thesis, Dept. Geology and Geophysics, University of Wisconsin, 1980, Madison, WI.

11. L. E. Vallejo. "A New Approach to the Stability Analysis of Thawing Slopes." *J. Civil Engineering Design*, Vol. 1, No. 3, 1979, pp. 231-252.

12. L. E. Vallejo and T. B. Edil. "Stability of Thawing Slopes: Field and Theoretical Investigations." Proc. 10th Int'l Conference Soil Mechanical and Foundation Engrg, Vol. 3, Stockholm, 1981, pp. 545-548.

13. G. R. Foster and W. H. Wischmeier. "Evaluating Irregular Slopes for Soil Loss Prediction." *Transactions, American Society of Agricultural Engineers*, Vol. 17, 1974, pp. 305-309.

14. C. Peters. "Models of Short and Long-Term Geomorphic Evolution of Bluffs in the Great Lakes." M.S. Thesis, Department of Geology and Geophysics, University of Wisconsin, 1982, Madison.

15. R. M. Quigley, P. J. Gelinas, W. T. Bou and R. W. Parker. "Cyclic Erosion-Instability Relationship, Lake Erie North Shore Bluffs." *Can. Geotech. J.*, Vol. 14, 1977, pp. 310-323.

16. T. B. Edil. "Causes and Mechanics of Coastal Bluff Recession." The State-of-the-Art Paper, Proceedings of the Workshop on Bluff Slumping, Michigan Sea Grant, MICHU-SG-82-901, Ann Harbor, 1982, Michigan, pp. 1-48.

17. Southeastern Wisconsin Regional Planning Commission. A Lake Michigan Shoreline Erosion Management Plan for Milwaukee County, Wisconsin. Report No. 163, 1989, Waukesha, Wisconsin.

18. T. B. Edil and P. L. Monkmeyer. "Demonstration of Shoreline Protection on Lake Superior." Proceedings of the Conference on Voluntary and Regulatory Approaches for Nonpoint Source Pollution Control, EPA-905/9-78-001, Chicago, IL, 1978, pp. 134-157.

19. R. A. Siegel. *STABL Users Manual.* Joint Highway Research Project No. C-36-36K. Purdue University, West LaFayette, IN, 1975.

20. W. T. Painter. Phase I: "Contract Report North Shore Drive Shoreline Landfill." Foundation Engineering, Inc., Milwaukee, Wisconsin, 1983.

21. J. R. Benjamin and C. A. Cornell. *Probability, Statistics and Decision for Civil Engineers*. McGraw-Hill, New York, NY, 1970.

22. T. B. Edil and M. N. Schultz. "Landslide Hazard Potential Determination Along a Shoreline Segment." *Engineering Geology*. No. 19, 1983, pp. 159-177.

23. P. J. Bosscher, T. B. Edil and D. M. Michelson. "Evaluation of Risks of Slope Instability Along a Coastal Reach." Proc. 5th Int'l Symposium on Landslides, Vol. 2, 1988, Lausanne, pp. 1119-1125.

TABLE TITLES

TABLE 1. Forces, Resistances and Slope Processes in the Great Lakes.

TABLE 2. Summary of Strategies for Coastal Bluff Recession.

TABLE 3. Geotechnical Properties of Soil Samples from Madigan Beach Boreholes.

TABLE 4. Geotechnical Properties of Soils Encountered in the Slopes Along Lake Michigan's Milwaukee County Shoreline.

FIGURE TITLES

Figure 1. Stability and Slope Development Chart [5].

Figure 2. Procedure for Estimating Nonstructural Setback Distance [17].

Figure 3. Longard Tube Layout and Bluff Conditions at Madigan Beach. Numbers in Circles Designate Tube Locations.

Figure 4. Bluff Profiles in Cross-section 4.

Figure 5. Bluff Profiles in Cross-section 5.

Figure 6. Bluff Profile from Whitefish Bay [17].

Figure 7. Alternative Methods of Bluff Slope Stabilization [17].

Table 1. Forces, Resistances and Slope Processes in the Great Lakes.

FORCES:	**GRAVITY** **VIBRATIONS** **CLIMATE**	**PROCESSES:**	**MASS MOVEMENT** Sliding Rotational: Slumps Translational: Block Slide Slab Slide Flow Solifluction Debris Flow
RESISTANCES:	**SHEAR STRENGTH** **VEGETATION** **STRUCTURAL SYSTEMS**		**PARTICLE MOVEMENT** Wave Erosion Wind Erosion Ice Erosion Rill Erosion Sapping

Table 2. Summary of Strategies for Coastal Bluff Recession.

PROCESSES	SOLUTIONS	
	STRUCTURAL (STABILIZATION): DESIGN	NONSTRUCTURAL (MANAGEMENT): PREDICTION
TOE EROSION	SHORE PROTECTION (groins, seawalls, etc.)	SHORE RECESSION RATE (long-term, cyclic)
DEEP ROTATIONAL SLIPS	SLOPE STABILIZATION (regrading, dewatering, etc.)	STABLE SLOPE ANGLE AGAINST DEEP SLIPS
FACE DEGRADATION AND SHALLOW SLIPS	SURFACE PROTECTION (vegetation, drainage)	ULTIMATE ANGLE OF STABILITY

Table 3. Geotechnical Properties of Soil Samples from Madigan Beach Boreholes.

Soil Description and Depth	Group Symbol*	Texture**			Liquid Limit %	Plasticity Index	Water Content %	Unit Weight (kN/m^3)	Average+ N	Angle ++ of Internal friction ϕ	Cohesion++ Intercept C (kPa)
		%Sand	%Silt	%Clay							
Reddish brown, stiff silty clay of low plasticity (Upper clay, 0-6m)	CL	10	64	26	31	14	18	21.4	18	19°	80
Brown, very dense sandy silt or silty sand (6-16m)	ML or SM	7-18	78-90	3-4	---	---	18	19.9	>100	37°	0
Reddish brown, rather stiff clay of high plasticity (Lower clay 16m)	CH	11	26	63	51	31	31	19.2	14	21°	0

* According to the Unified Soil Classification (ASTM Designation: D 2487-69 and D 2488-69).

**4.76 mm > Sand > 0.074 mm; 0.074 mm > Silt > 0.002 mm; 0.002 mm > Clay

+ Standard Penetration Resistance, N(ASTM Designation: D 1586-67).

++Drained Shear Strength Parameters.

Table 4. Geotechnical Properties of Soils Encountered in the Slopes Along Lake Michigan's Milwaukee County Shoreline.

Soil Unit	Unit Weight (kN/m^3)	Friction * Angle (Degrees)	Cohesion* Intercept (kPa)
Tills			
New Berlin	21.7	34 ± 3	0.5 ± 0.25
Oak Creek	21.2	30.5 ± 2	5.0 ± 3.75
Ozaukee	21.1	30 ± 3	7.5 ± 5.0
Fractured Ozaukee	21.1	30 ± 3	0 + 3
Lake Sediments			
Medium Fine Sand	18.9	33 ± 2	0 + 0.25
Sand and Gravel	18.9	33 ± 2	0 + 0.25
Silt	20.4	31 ± 2	200 ± 50
Silt and Fine Sand	17.3	31 ± 2	0.5 + 0.5
Clay and Silt	20.4	27 ± 2	22.5 ± 17.5
Fine Sand and Silt	19.7	33 ± 2	5.0 ± 3.75
Gen'l Lake Sediment	19.7	27 ± 3	5.0 ± 3.75
Fill			
Concrete Rubble/Soil	20.4	35	0

* Values are given as the mean and the standard deviation.

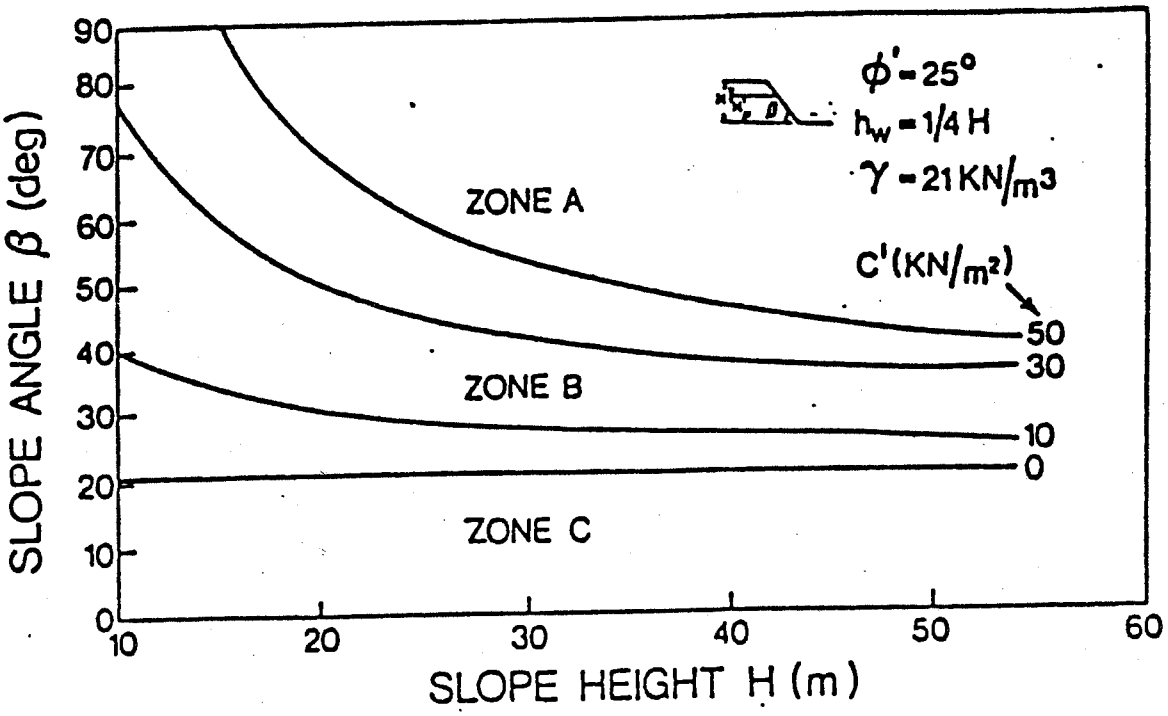

Figure 1. Stability and Slope Develpoment Chart

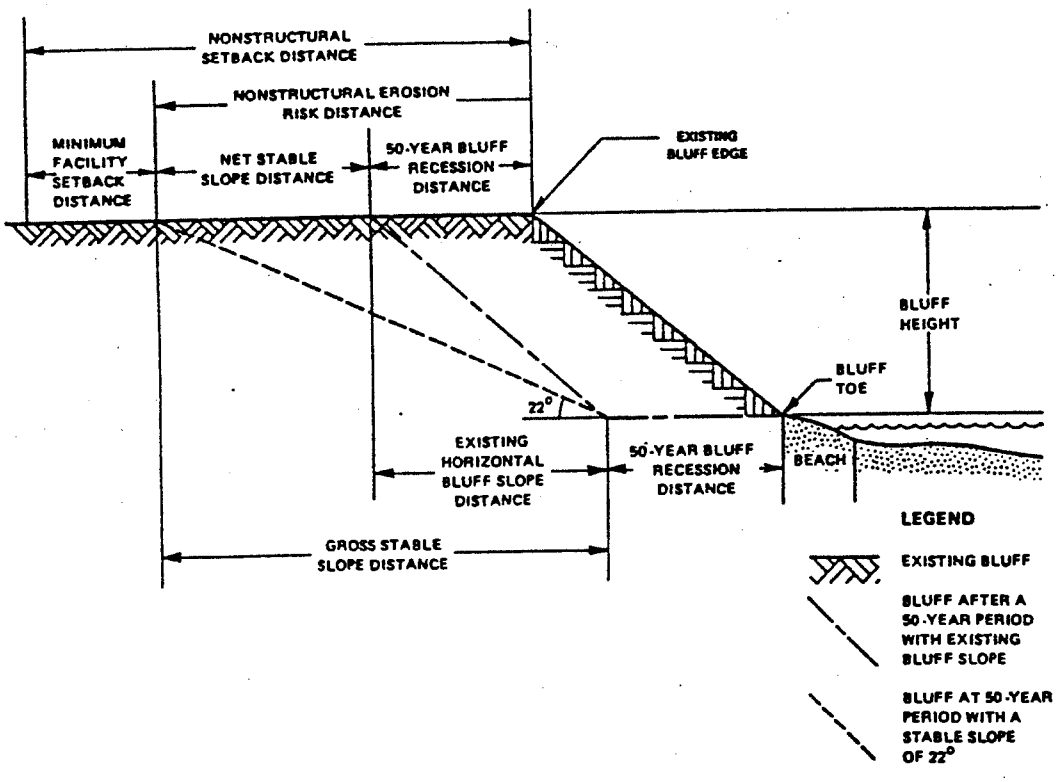

NONSTRUCTURAL EROSION RISK DISTANCE = NET STABLE SLOPE DISTANCE + 50-YEAR BLUFF RECESSION DISTANCE

NONSTRUCTURAL SETBACK DISTANCE=NONSTRUCTURAL EROSION RISK DISTANCE+MINIMUM FACILITY SETBACK DISTANCE

WHERE: NET STABLE SLOPE DISTANCE = GROSS STABLE SLOPE DISTANCE - EXISTING HORIZONTAL BLUFF SLOPE DISTANCE

$$\text{GROSS STABLE SLOPE DISTANCE} = \frac{\text{BLUFF HEIGHT}}{\tan 22^\circ} = \frac{\text{BLUFF HEIGHT}}{0.4}$$

MINIMUM FACILITY SETBACK DISTANCE: INTENDED TO PROVIDE A SAFETY ZONE, PROVIDE AESTHETIC BENEFITS, AND ALLOW PROVISION OF FUTURE SURFACE WATER AND GROUNDWATER DRAINAGE SYSTEMS

Figure 2. Procedure for Estimating Nonstructural Setback Distance [17].

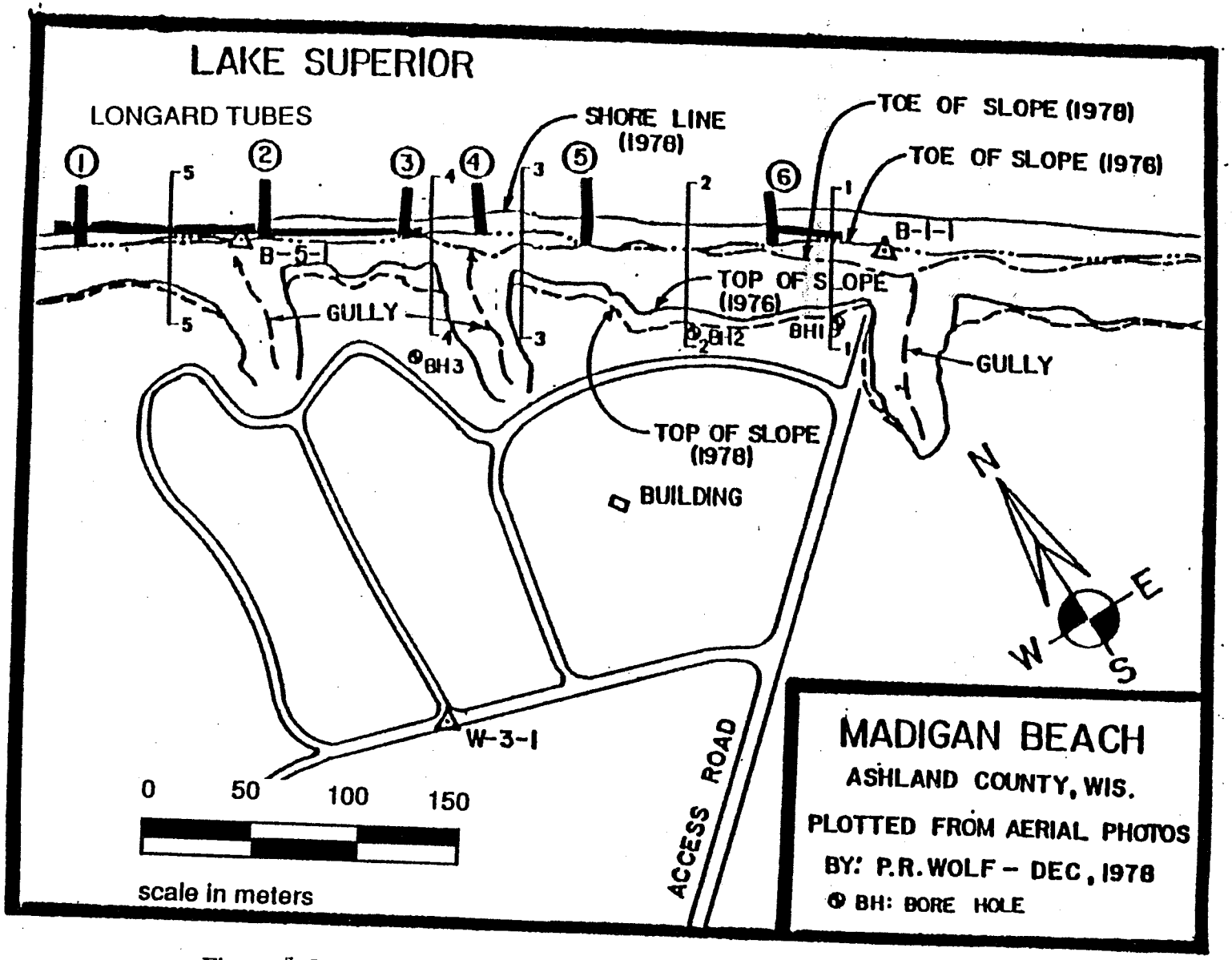

Figure 3. Longard Tube Layout and Bluff Conditions at Madigan Beach. Numbers in Circles Designate Tube Location.

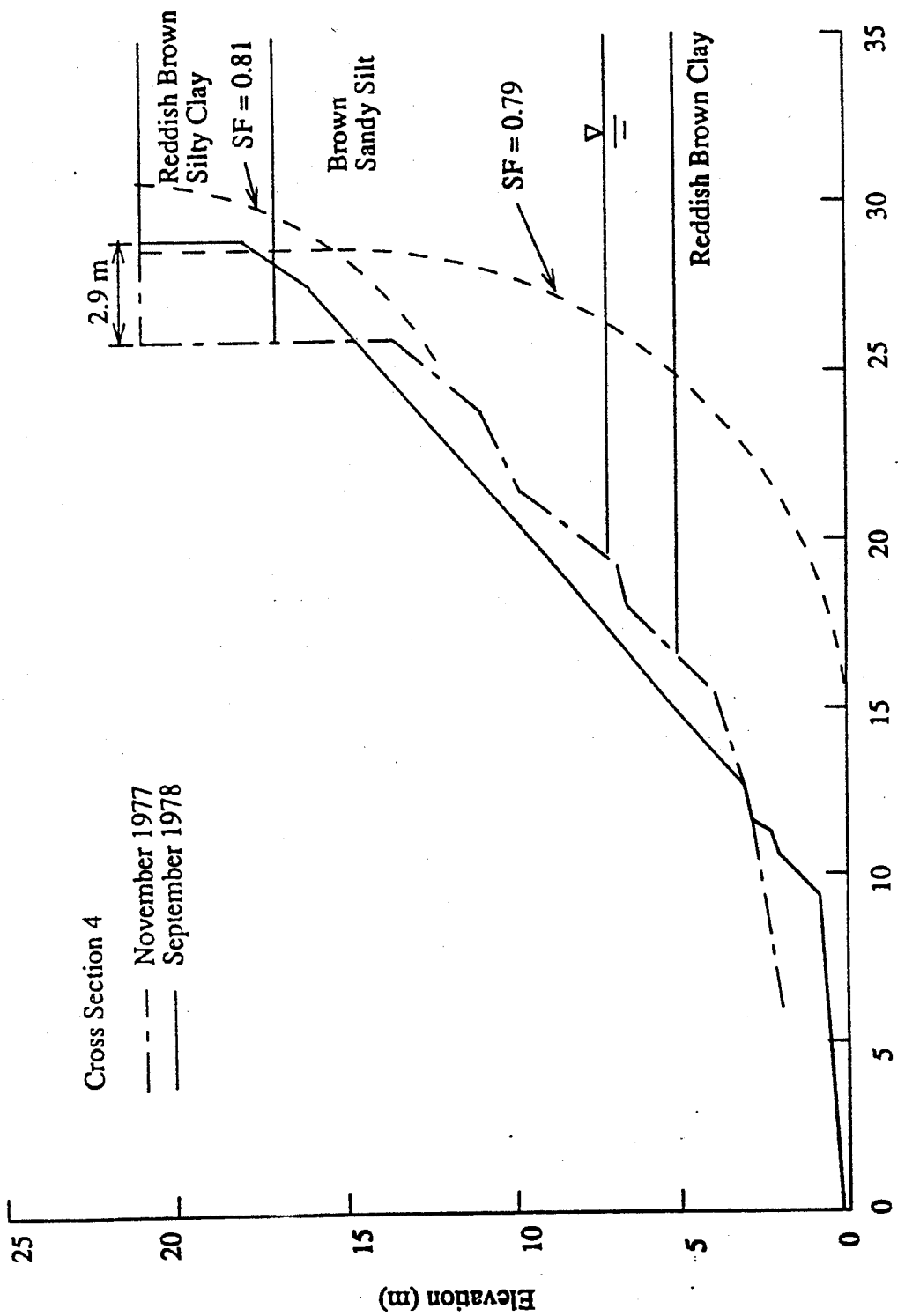

Figure 4. Bluff Profiles in Cross-section 4.

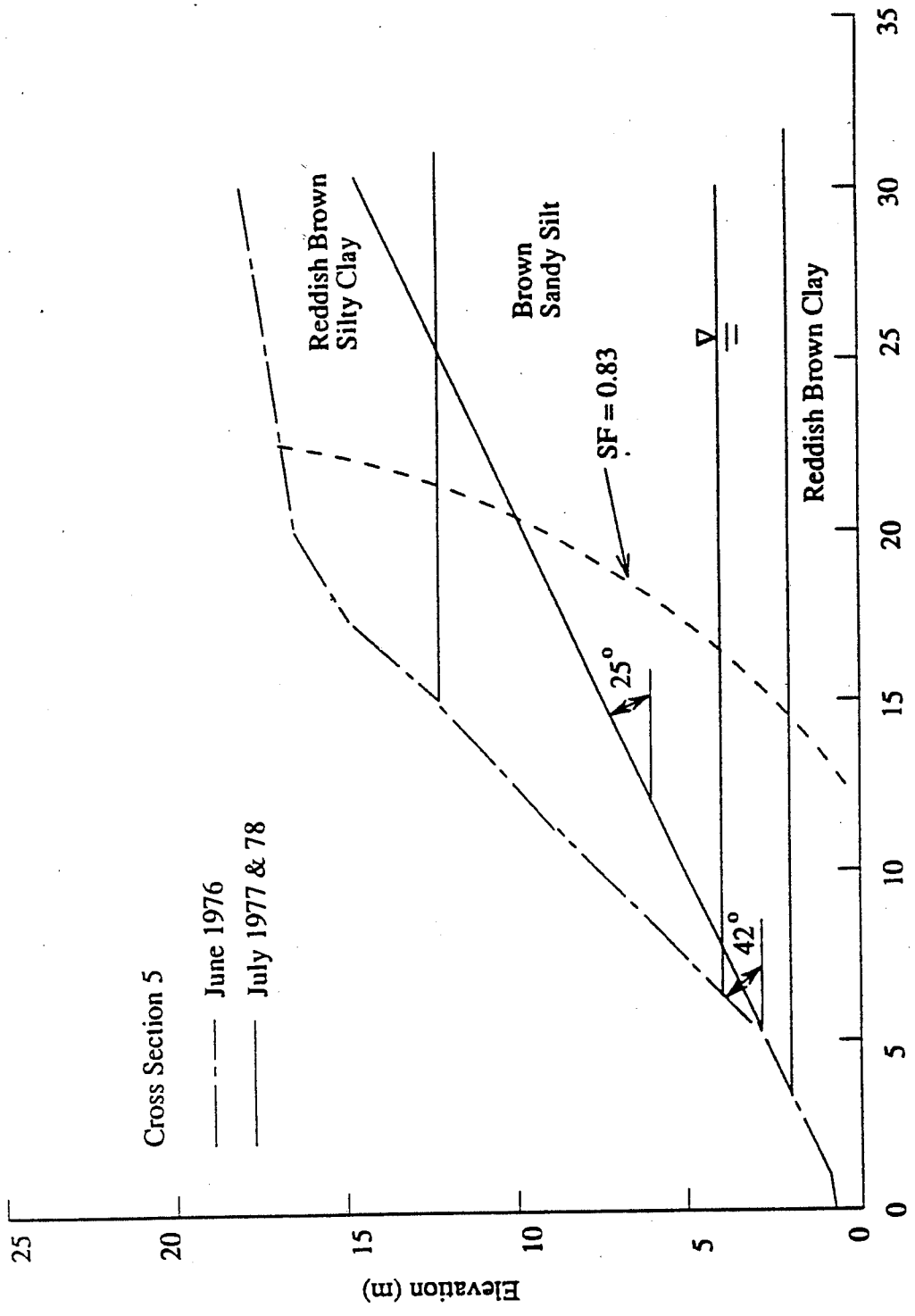

Figure 5. Bluff Profiles in Cross-section 5.

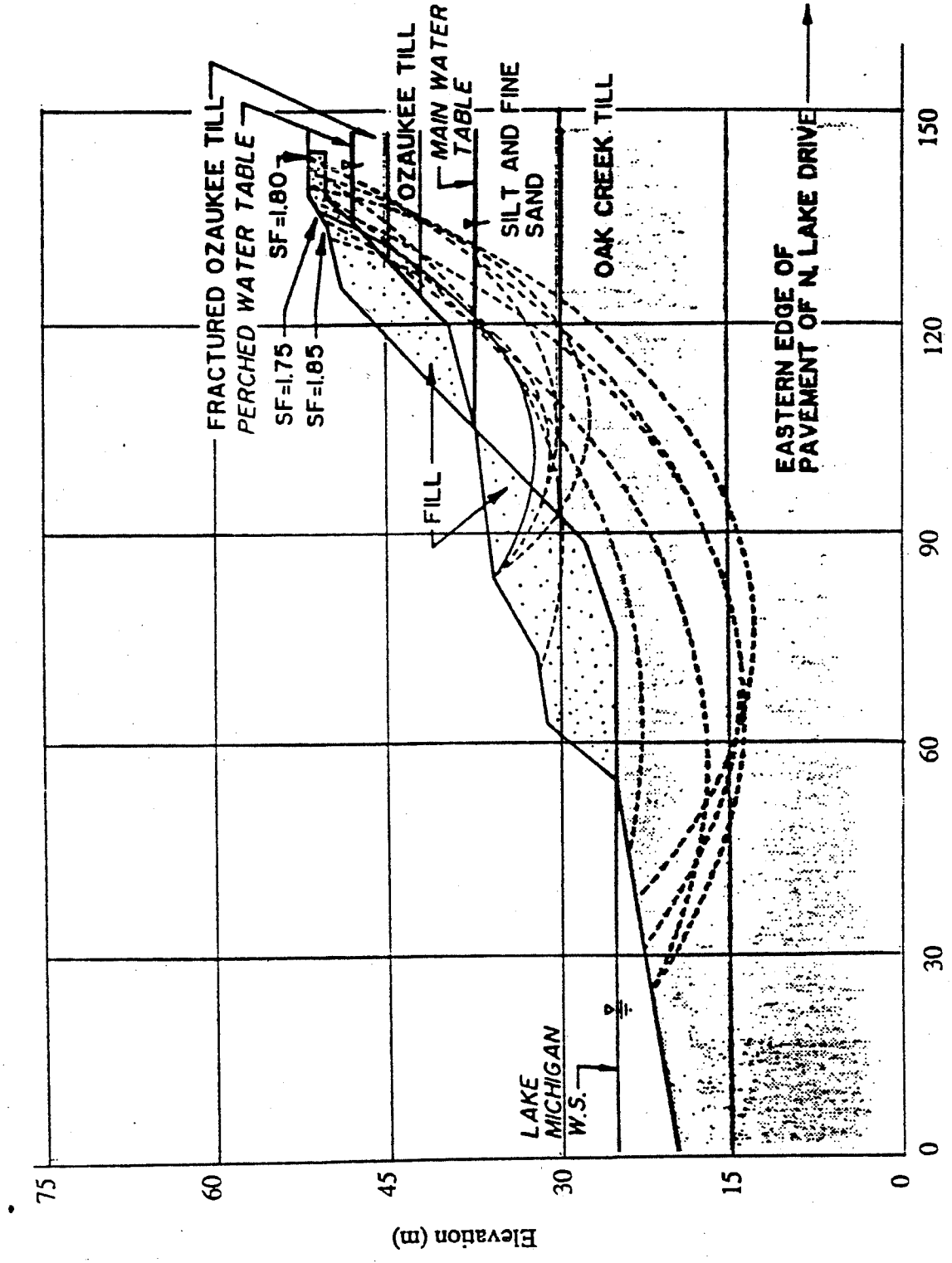

Figure 6. Bluff Profile from Whitefish Bay [23].

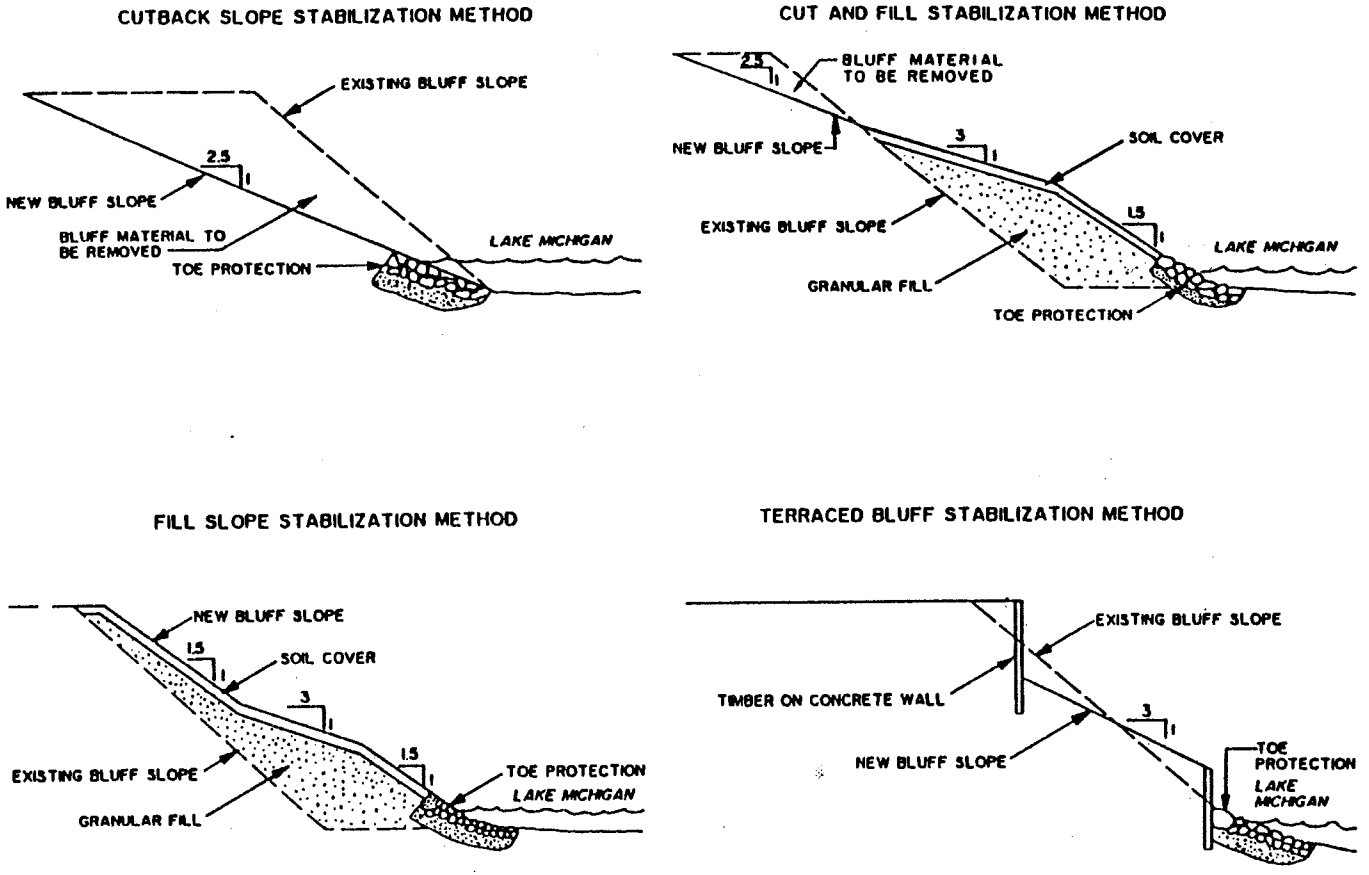

Figure 7. Alternative Methods of Bluff Slope Stabilization [23].

TAB 14

Excerpts from TRB Special Report 247

LANDSLIDES

INVESTIGATION AND MITIGATION

SPECIAL REPORT 247

A. Keith Turner
Robert L. Schuster
Editors

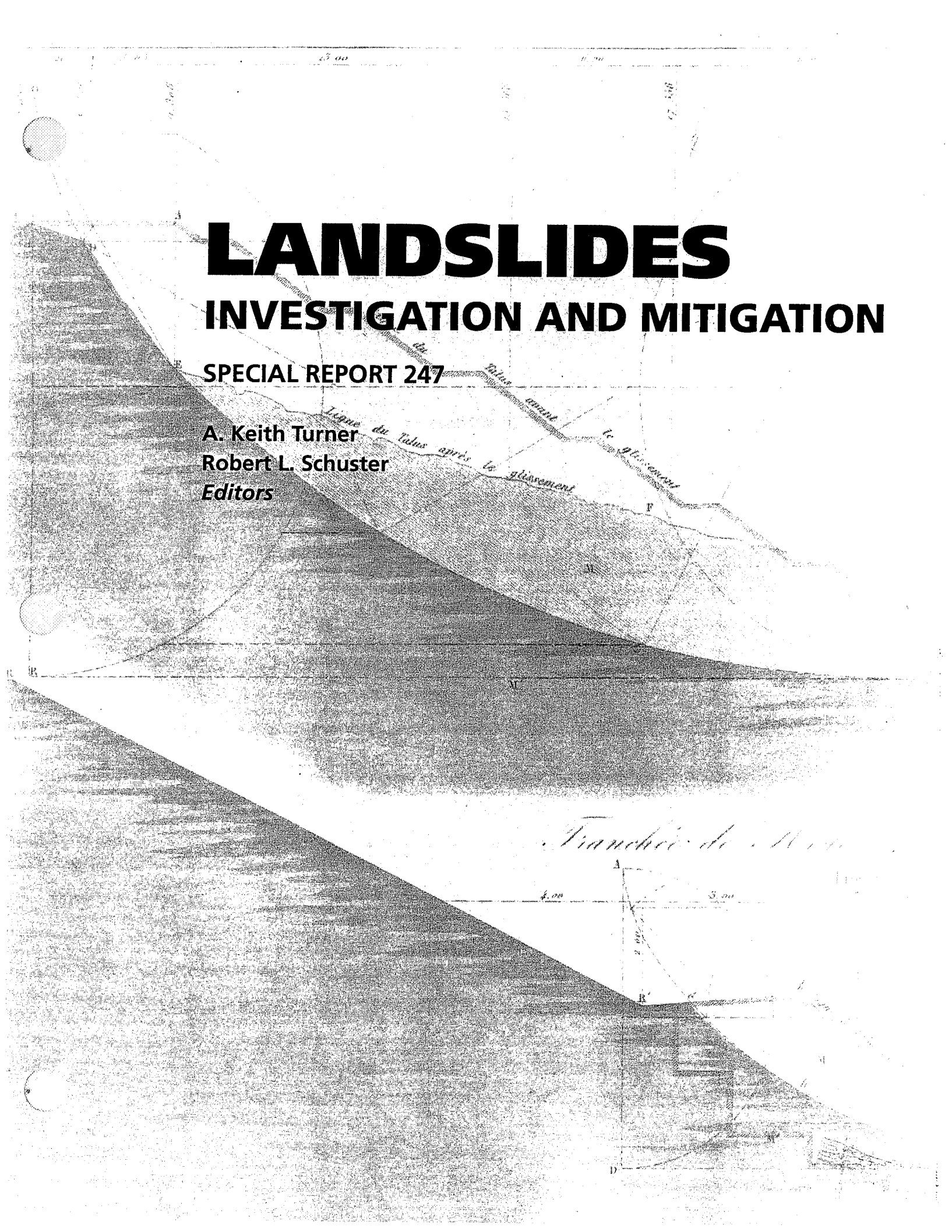

Transportation Research Board Special Report 247

Subscriber Category
IIIA soils, geology, and foundations

NOTICE: The project that is the subject of this report was approved by the Governing Board of the National Research Council, whose members are drawn from the councils of the National Academy of Sciences, the National Academy of Engineering, and the Institute of Medicine. The members of the committee responsible for the report were chosen for their special competence and with regard for appropriate balance.

This report has been reviewed by a group other than the authors according to procedures approved by a Report Review Committee consisting of members of the National Academy of Sciences, the National Academy of Engineering, and the Institute of Medicine.

The Transportation Research Board does not endorse products or manufacturers; trade and manufacturers' names may appear in this Special Report because they are considered essential to its object.

This report was sponsored in part by the National Science Foundation.

Transportation Research Board publications are available by ordering directly from TRB. They may also be obtained on a regular basis through organizational or individual affiliation with TRB; affiliates and library subscribers are eligible for substantial discounts. For further information, write to the Transportation Research Board, National Research Council, 2101 Constitution Avenue, N.W., Washington, D.C. 20418.

Copyright 1996 by the National Academy of Sciences. All rights reserved
Printed in the United States of America

Library of Congress Cataloging-in-Publication Data

Landslides : investigation and mitigation / A. Keith Turner, Robert L. Schuster, editors.
p. cm. — (Special report / Transportation Research Board, National Research Council ; 247)
Includes bibliographical references and index.
ISBN 0-309-06151-2
ISBN 0-309-06208-X (pbk.)
1. Landslide hazard analysis. 2. Landslides. I. Turner, A. Keith, 1941– . II. Schuster, Robert L. III. Series: Special report (National Research Council (U.S.) Transportation Research Board) ; 247.
QE599.2.L36 1996
551.3'07—dc20 95-40780
CIP

Sponsorship of Special Report 247
Division A—Technical Activities
GROUP 2—DESIGN AND CONSTRUCTION OF TRANSPORTATION FACILITIES
Chairman: Michael G. Katona, U.S. Air Force Armstrong Laboratory

Study Committee on Landslides: Analysis and Control
Chairman: A. Keith Turner, Colorado School of Mines
David M. Cruden, J. Michael Duncan, Robert D. Holtz, Jeffrey R. Keaton, Verne C. McGuffey, Victor A. Modeer, Jr., Robert L. Schuster, Tien H. Wu, Duncan C. Wyllie

Liaison Representative
John L. Walkinshaw, Federal Highway Administration, U.S. Department of Transportation

Transportation Research Board Staff
Robert E. Spicher, Director, Technical Activities
G.P. Jayaprakash, Engineer of Soils, Geology, and Foundations
Nancy A. Ackerman, Director, Reports and Editorial Services
Naomi C. Kassabian, Associate Editor
Karen White, Graphic Designer

COVER Damage to railroad line in Olympia, Washington, caused by slope failure after 1965 Seattle-Tacoma earthquake (photograph courtesy of G.W. Thorsen, Washington Department of Natural Resources). *Top inset:* October 1986 reactivation of Cucaracha landslide in Gaillard Cut, Panama Canal, which originally extended across canal (dredges had removed much of toe by time of photograph); white material in upper center is lime added to surface as remedial measure (photograph courtesy of Panama Canal Commission). *Bottom inset:* Recurring landslide on Colorado State Highway 133 at McClure Pass west of Aspen, spring 1993 (photograph courtesy of T.E. Taylor, Colorado State Patrol).

FRONTISPIECE Derailment of *California Zephyr* passenger train near Granby, Colorado, in April 1985 caused by minor landslide (see Figure 2-6, p. 18) (photograph courtesy of R. L. Schuster).

TITLE PAGE *Inset:* Railway and highway at Howe Sound, British Columbia, blocked by October 1990 rock fall, which originated approximately 300 meters above highway (photograph courtesy of D. Howard, *Vancouver Sun*). *Background:* detail from drawing by Alexandre Collin (1846) of landslides in clay slopes along French canals (see Figure 1-5, page 9).

the subsurface investigation and interpreting the results. Measurements made with the instrumentation should be summarized as basic data and then interpreted in a geologic context.

5.3 Engineering-Geologic Maps and Explanations

Engineering-geologic information is most useful when plotted on a topographic base map. An orthophotograph with superimposed topographic contours (Figure 9-37) provides a most useful method for rapidly communicating relevant geologic data to nongeologists if the photograph documents current conditions. The scale of the base map controls the detail that can be shown. Engineering-geologic mapping should be completed at the scale that will be used for design drawings if possible. Detailed geologic mapping, particularly of complex areas, can be accomplished efficiently with the aid of a plane table and alidade, as was done by Fleming and Johnson (1989) for the Aspen Grove landslide in Utah (Figure 9-6).

Three levels of detail may be warranted in landslide assessments: areal assessment, regional evaluation, or site investigation. In urban areas, Leighton (1976) called these levels *regional*, *tract*, and *site*. Areal landslide maps show the general distribution and shape of large landslide deposits. Good examples are a landslide map of Utah (Figure 9-38) by Harty (1991) at a scale of 1:500,000 and a preliminary map of landslide deposits in San Mateo County, California, by Brabb and Pampeyan (1972) at a scale of 1:62,500. Areal landslide maps provide some basis for characterizing large-area suitability; feasibility and design decisions, however, require greater detail.

Increased detail is achieved at the regional evaluation level. Information on the landslide types and their features would be documented on maps for regional evaluation. Baum and Fleming (1989) mapped landslides in central Utah at a scale of 1:12,000 (Figure 9-39). Wieczorek (1982) mapped landslides near La Honda, California, at 1:4,800, and Baum and Fleming (1989) showed the Aspen Grove landslide in Utah at about 1:4,000 (Figure 9-40); these are reasonable scales for site investigations. Fleming and Johnson (1989) mapped the Aspen Grove landslide at 1:200 using a plane table; a portion of this map is shown in Figure 9-41 at 1:833. A smaller part of the Aspen Grove land-

FIGURE 9-37
Part of orthotopographic map of Thousand Peaks landslide area, northern Utah. Photographs at nominal negative scale of 1:12,000 were adjusted to a map scale of 1:4,800. Topographic contours are at 5-ft (1.5-m) intervals. Compare with Figure 9-8.
COURTESY OF KERN RIVER GAS TRANSMISSION COMPANY

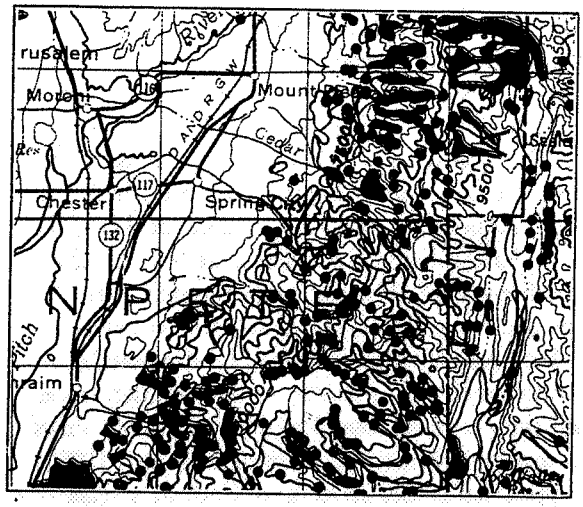

FIGURE 9-38
Example of landslide map for areal assessment, scale 1:500,000 (Harty 1991). Original map is colored and distinguishes between deep-seated, shallow, and undifferentiated landslides compiled from different sources; dots represent landslides smaller than 600 m across, and patches depict landslides larger than 600 m across. Area shown includes Ephraim Canyon, central Utah; increasing detail is shown in Figures 9-39, 9-40, 9-41, and 9-6.

slide mapped in 1983 and 1984 is shown in Figure 9-6 at 1:333.

Regional evaluation maps give sufficient detail for establishing feasibility and some preliminary design. Areas of exposed bedrock should be mapped as bedrock; where surficial deposits are present at the surface, even if bedrock is at a shallow depth, these deposits should be shown. The Unified Engineering Geology Mapping System, described in Section 3.2.2, provides a method for indicating the estimated thickness of surficial deposits overlying bedrock.

The site investigation map is utilized for designing a project and therefore the greatest possible level of detail should be presented. Not only should the information on the bedrock and surficial deposits contained in a regional evaluation map be retained, but greater detail should also be included.

Geologic map explanations should contain brief but complete descriptions of the units mapped and the symbols used. Map units may be correlated with geologic formation names and ages. The locations of sections and reconnaissance instrumentation should also be indicated on the map and included in the explanation.

Comparison of mapped landslides with other physical characteristics of the area may provide insight on conditions influencing stability. A landslide map is essentially a map on which points within an area have been classified as either related to a landslide or not. There is little difficulty in comparing landslide maps with geologic maps where points within an area have been classified according to what geologic material is present. It is more difficult to make a meaningful comparison with contoured data such as elevation on a topographic map or isohyetal lines on a precipitation map. A landslide map can be transformed into contoured data by isopleth mapping (Wright et al. 1974; DeGraff and Canuti 1988), as shown in Figure 9-42. The percentage of a standard area that is underlain by landslide deposits is determined on a grid superimposed on the landslide map. The percentage values determined for all the points on the grid are contoured to show isopleths of landslide deposits.

The isopleth landslide map provides a way to represent landslide activity in an area and improve the understanding of conditions leading to instability (DeGraff 1985), as shown in Figure 9-43. It facilitates comparison of large and small landslides that may be present in different parts of the area. Isopleth maps for different landslide types in an area can be constructed to assess whether their distribution is controlled by different sets of factors. Locations with especially high percentages of landslides may merit more detailed investigation.

5.4 Engineering-Geologic Sections

Engineering-geologic sections should be located so as to provide information that will be needed for planning subsurface investigations and stability analyses. Commonly these positions are perpendicular to topographic contours and aligned longitudinally down active or dormant landslide deposits. The projected shape of sliding surfaces, geologic contacts, and piezometric surfaces should be shown along with the topographic profile (Figure 9-44). Geologic sections should be constructed at the same horizontal and vertical scales. Exaggerated vertical scales do not permit direct measurement of angular relationships and can be misinterpreted. Furthermore, they do not aid in communicating geologic information to nongeologists.

5.5 Three-Dimensional Representations

Communication of geologic information can be enhanced by diagrams of interconnected geologic sections. These interconnected sections (called *fence diagrams*) provide three-dimensional or pseudo-three-dimensional representation of the surface and subsurface conditions (Figure 9-45). *Block diagrams* are created by constructing perpendicular sections and sketching the surface geology in an isometric projection. (Figure 9-7 shows

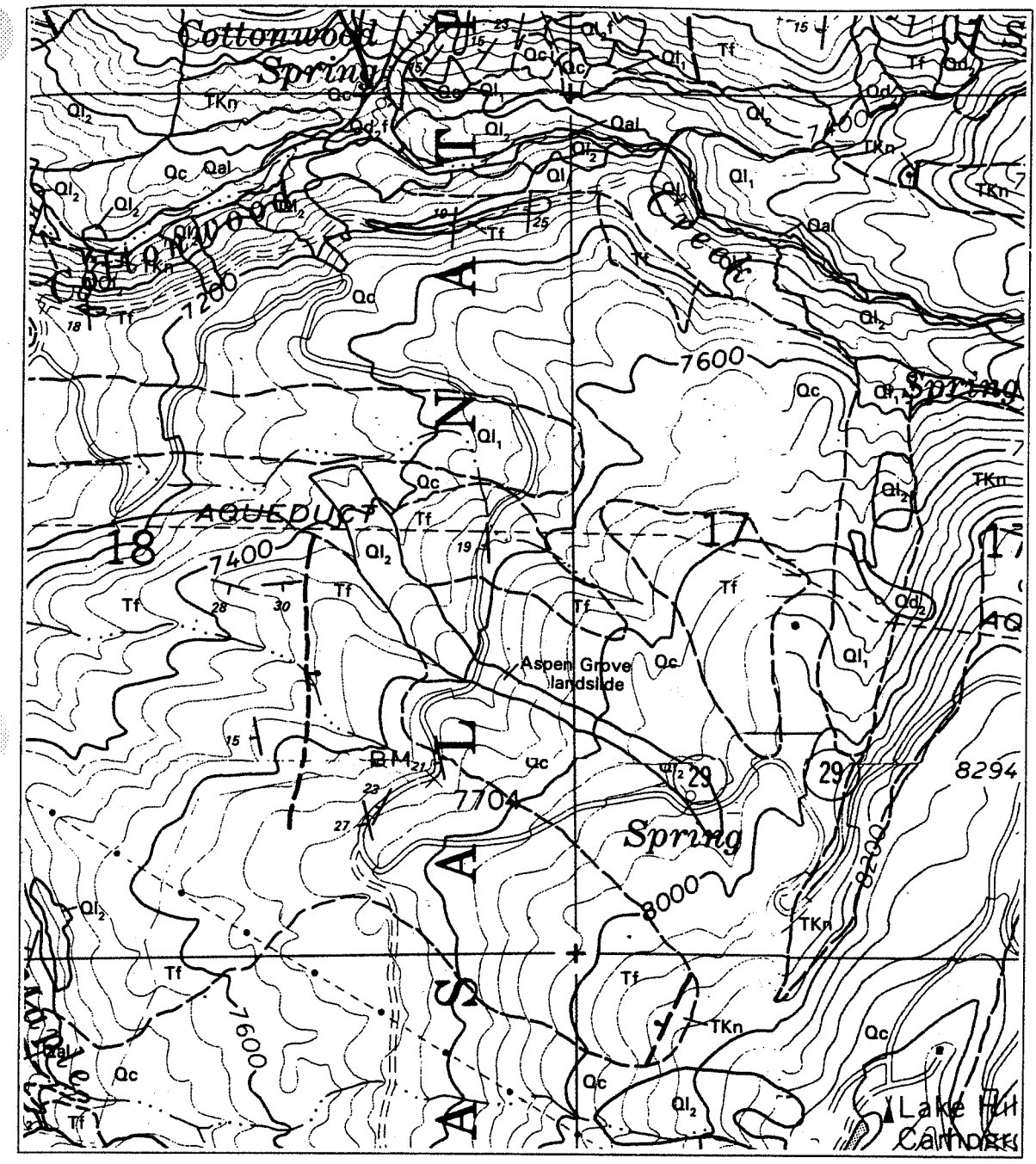

FIGURE 9-39
Example of landslide map for regional assessment, scale 1:12,000 (Baum and Fleming 1989). Aspen Grove landslide, Utah, is identified near center; increasing detail is shown in Figures 9-40, 9-41, and 9-6; less detail is shown in Figure 9-38. Abbreviated explanation: Ql_1, pre-1983 landslide; Ql_2, landslide active in 1983 to 1986; Qd_2, debris flow active in 1983 to 1986; *Qal*, alluvial deposits; *Qc*, colluvial deposits; *Tf*, Eocene-Paleocene Flagstaff limestone; *TKn*, Paleocene–Upper Cretaceous North Horn Formation.

schematic block diagrams of landslide deposits of differing ages.) Scale models constructed from thin sheets of styrofoam (foam-core boards) are the equivalent of orthogonal block diagrams (Figure 9-46). Computer-generated sections, fence diagrams, and block diagrams can be produced routinely with the use of commercially available computer programs. These diagrams can be particularly helpful in communicating geologic information to nongeologists. They are most useful when data from subsurface investigations has been integrated into them.

5.6 Engineering-Geologic Reports

Engineering-geologic reports most likely will be used by nongeologists; therefore, geologic terminology must be minimized and explained in non-

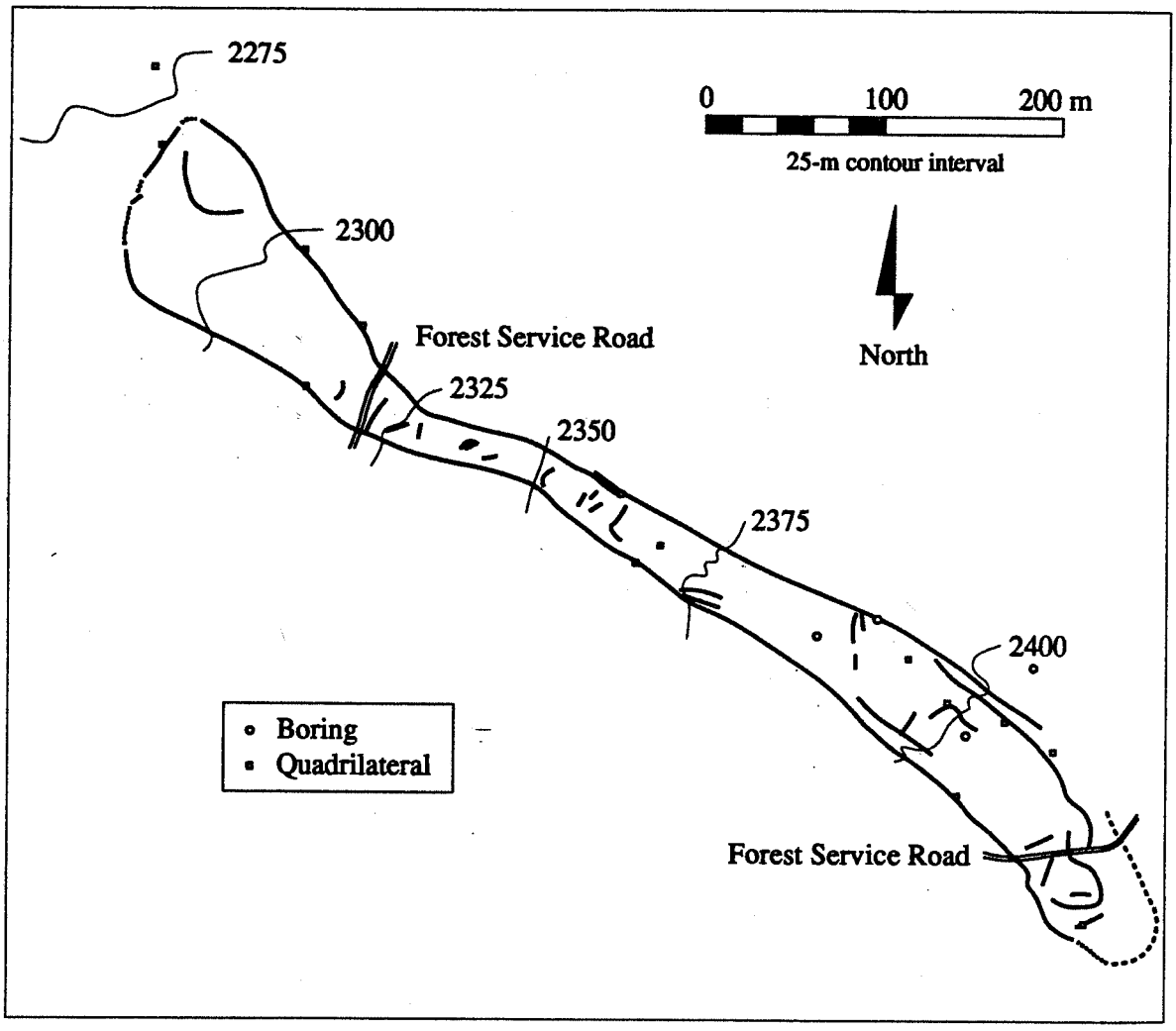

FIGURE 9-40
Example of landslide map for site assessment (Aspen Grove landslide, Utah), scale about 1:4,000 (modified from Baum et al. 1988). More detail of part of landslide is shown in Figures 9-41 and 9-6; less detail is shown in Figures 9-38 and 9-39.

geologic terms. For example, "fossiliferous silty limestone" should be used rather than "biomicrite." Engineering geology essentially is geology that is relevant to an engineering project; geologic information that is not relevant to the project should be omitted or placed in an appendix to the report.

Engineering-geologic descriptions must be quantitative to the greatest extent possible. Phrases such as "moderately weathered," "moderately strong," and "moderately dense" are not meaningful unless they are quantified as in the Unified Rock Classification System (Table 9-4). The basis for geological opinions and recommendations should be clearly stated. As additional information becomes available, such as the results of the subsurface investigation, the basis for opinions can be evaluated, and the opinions can be verified or modified.

6. GUIDANCE FOR SUBSURFACE INVESTIGATIONS

The geologist often is the first technical specialist at a site or the first to spend a substantial amount of time there. Thus, valuable information can be collected regarding logistical issues, such as access to the site for drilling and other equipment, locations and types of utilities in the vicinity, and existing land uses.

The results of the surface observation and engineering-geologic mapping should provide detailed and quantitative information on

- Distribution, modes, and rates of slope movement;
- Positions and geometries of slip surfaces;
- Position of groundwater table and piezometric surfaces;

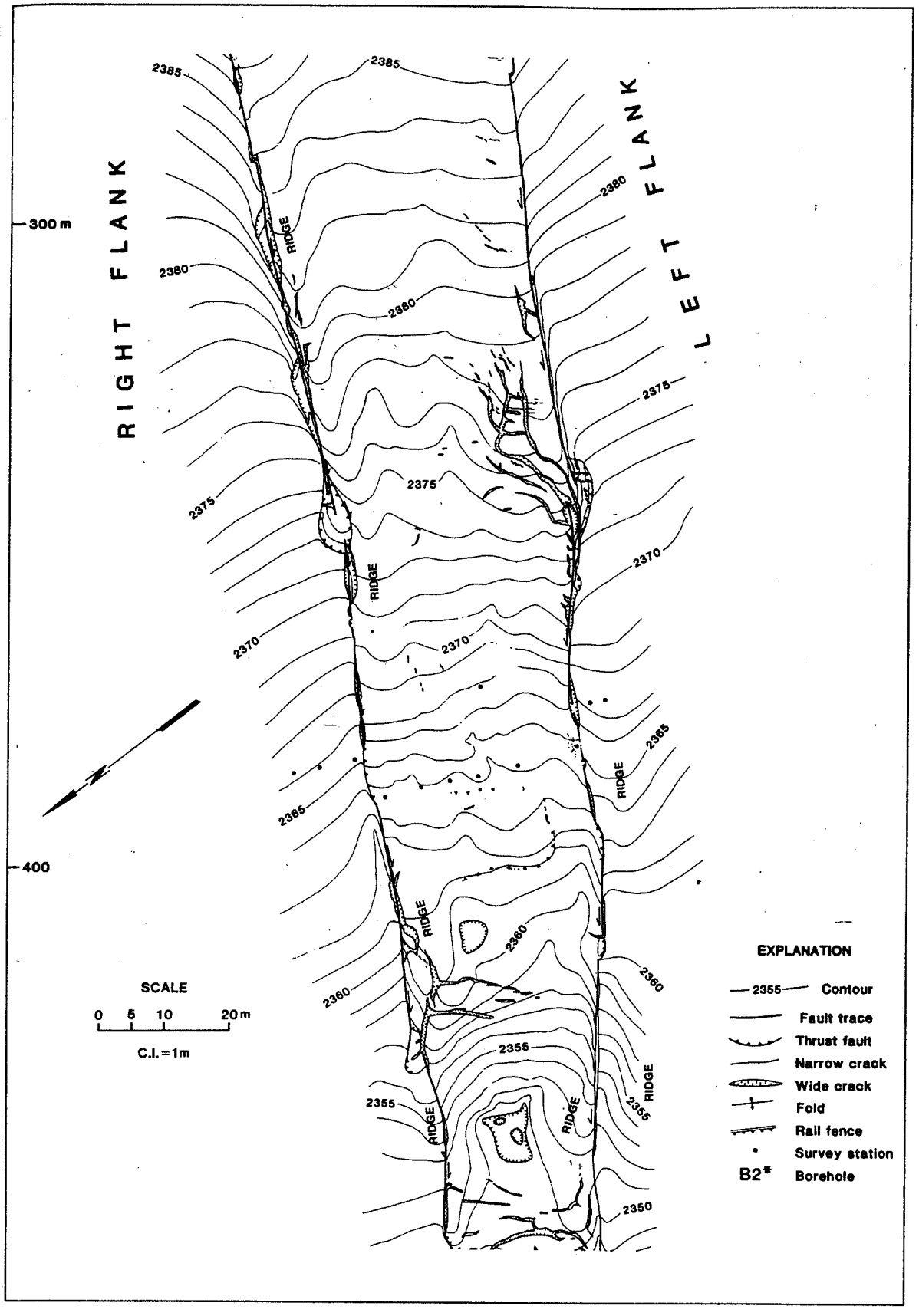

FIGURE 9-41
Example of landslide map for site assessment (part of Aspen Grove landslide, Utah). Fleming and Johnson (1989) originally mapped this landslide at scale of 1:200, but original illustration was published at scale of about 1:833. More detail of part of this landslide is shown in Figure 9-6 at scale of 1:300; less detail is shown in Figures 9-38, 9-39, and 9-40.

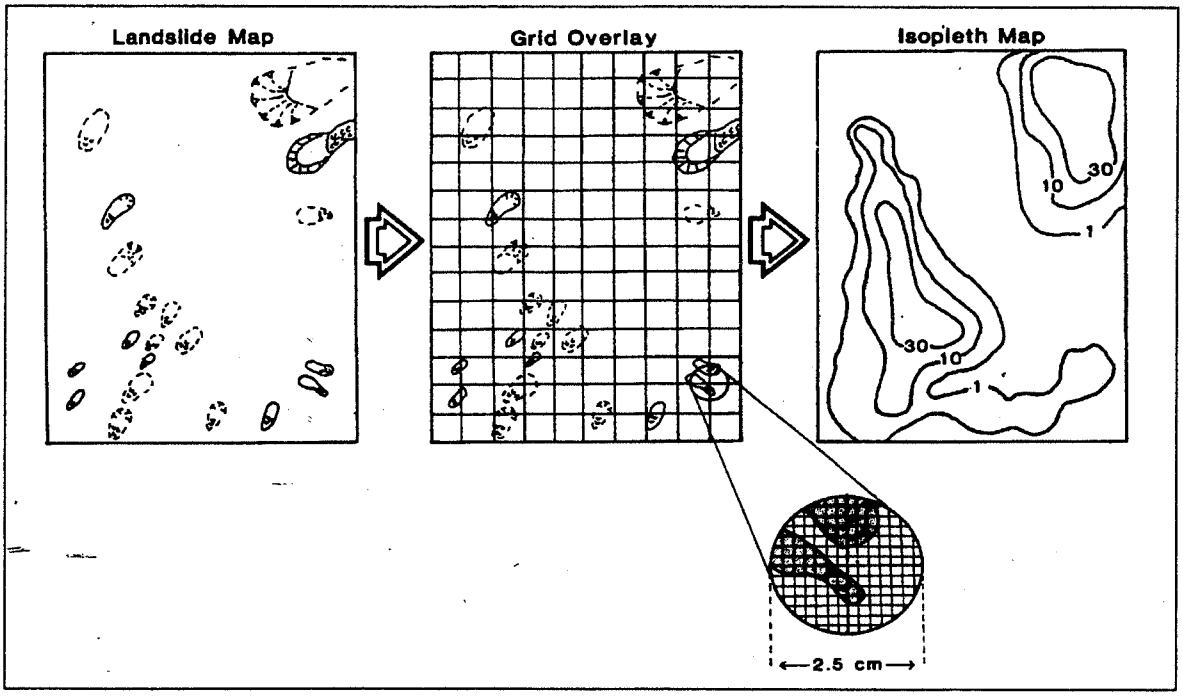

FIGURE 9-42
Steps in constructing isopleth map of landslide distribution (DeGraff and Canuti 1988).

FIGURE 9-43
(below)
Example of isopleth map of landslide distribution (DeGraff 1985).

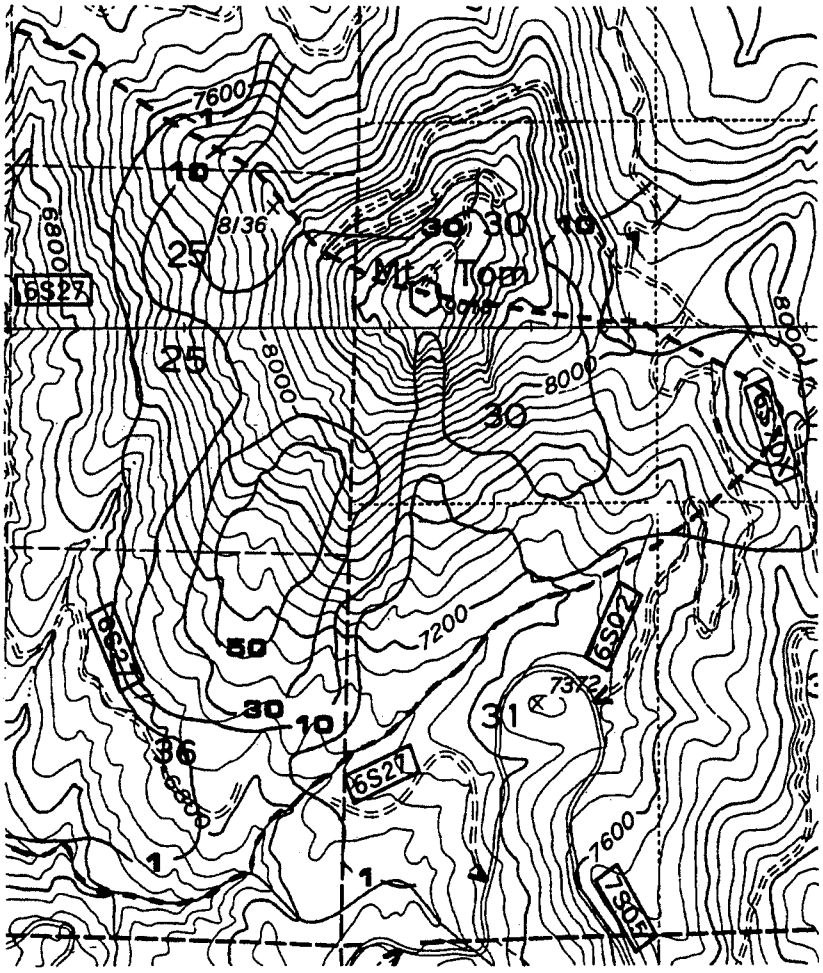

- Potentially difficult drilling or excavation conditions, or both;
- Recommendations for locations of surface geophysics, borings, and test pits; and
- Possible locations and schemes for stabilizing structures.

Of particular importance are the geologist's recommendations concerning the best locations for subsurface investigations. Engineers may plan an investigation program of regularly spaced borings, test pits, or both, hoping to collect sufficient data to adequately characterize the site. However, geology is not random; therefore, borings and test pits at appropriately selected locations are more likely to provide information needed to test geologic-model hypotheses. It must be recognized that additional borings may be needed to collect sufficient samples for laboratory testing.

7. CORRELATION OF SURFACE AND SUBSURFACE DATA

The geologist should observe and log subsurface exposures and samples to provide a basis for correlating surface mapping with subsurface information. Subsurface data generally permit more specific geologic interpretation than do surface data. The geologic interpretation of the site based

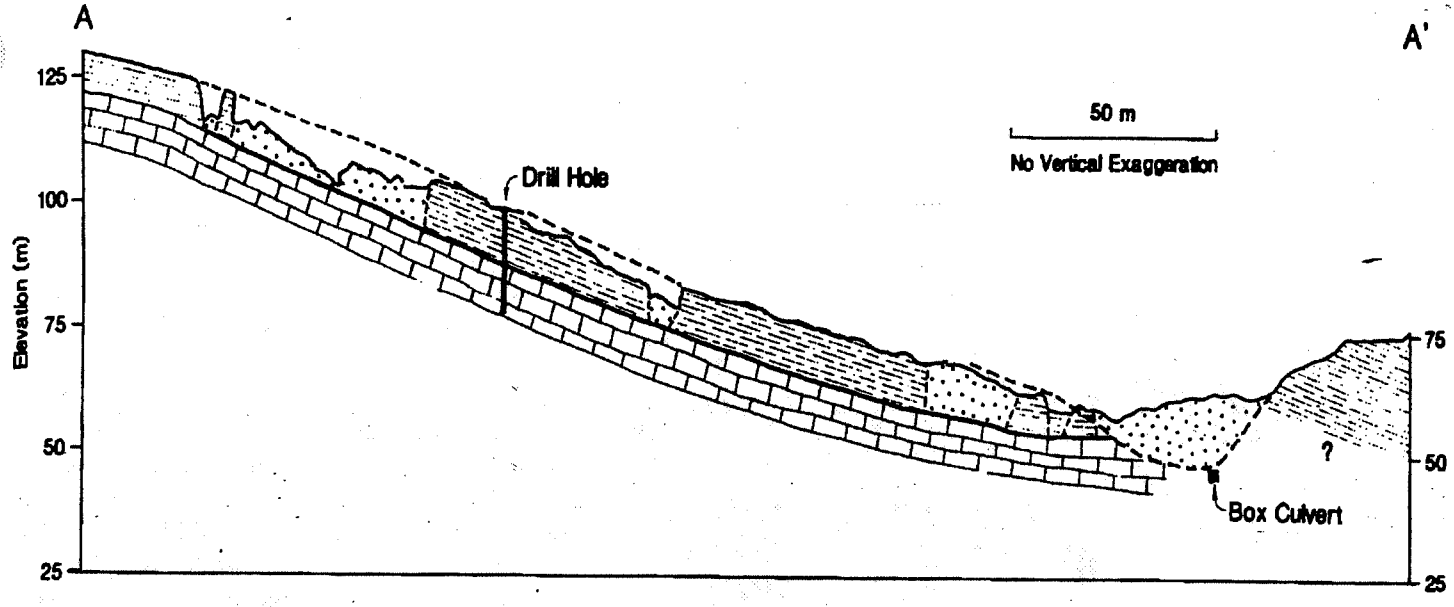

FIGURE 9-44
Example of engineering-geologic section of landslide deposit (Jibson 1992).

on surface mapping must be evaluated in the context of the subsurface data. If appropriate, revisions should be made to the engineering-geologic map and sections. The reevaluation of the geologic interpretation of the site may reveal the need for supplemental subsurface data at locations not initially selected for investigation.

The basic goal of the surface and subsurface investigations is accurate, quantitative characterization of the site. Accurate site characterization permits selection of the best geologic-geotechnical model of the slope system for use in stability analyses. The best model permits the most appropriate design for the project.

8. ADDITIONAL FIELD INFORMATION

Additional field information may be needed to permit prediction of the performance of the slope and the potential risk of damage to the project, adjacent facilities, or both. Long-term monitoring of slope deformation and piezometric levels may be appropriate. The reconnaissance instrumentation can be converted to permanent instrumentation by replacing the rapidly deployed devices with more stable ones.

Adjacent land use strongly influences the consequences of damage. High-value or high-occupancy property adjacent to a slope movement may require a more conservative design and more extensive field monitoring to provide a basis for legal defense in the event of litigation on behalf of the adjacent property. Some adjacent land uses, such as agricultural irrigation, can contribute to stresses causing slope movement at the project site. Repeated surface observations and instrumentation can permit early detection of the beginning of a problem. Alternatively, such observations can provide a legal basis for justifying compensation from the adjacent land owner for part of the damages at the site.

The potential for excessive precipitation, strong earthquake shaking, or both, to occur at a site

FIGURE 9-45
(below)
Example of fence diagram showing subsurface conditions in landslide area (Sowers and Royster 1978).

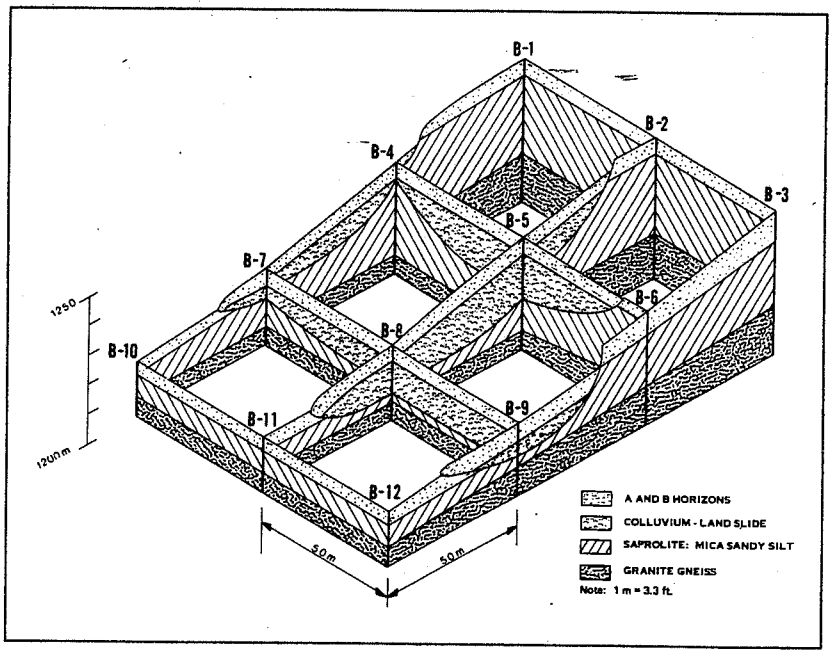

FIGURE 9-46
Example of styrofoam (foam-core) model of Thistle landslide in central Utah made by printing copies of topographic map at scale of 1:2,400 and fixing them onto sheet of styrofoam with spray adhesive. Thickness of each sheet of styrofoam was equal to vertical rise of 40 ft (12 m), and model was made with no vertical exaggeration. Equivalent sun illumination is early to mid-afternoon.

should be recognized early in the investigation. It may be appropriate to consider installing precipitation gauges, strong-motion accelerographs, or both, to collect information that may be of great value in improving design of slope systems. If slope movement occurs in response to precipitation or an earthquake, the intensity or magnitude of the event at the slope will be known. Otherwise, the intensity or magnitude of the event will have to be projected from the nearest recording station, which may be a substantial distance from the site.

9. COST OF SURFACE INVESTIGATIONS

The pre-field investigation involves identifying, collecting, and reviewing available geologic and topographic information and aerial photographs. Usually no more than a few days of a geologist's time is required for this task. Up to several hundred dollars may be needed to purchase maps and available aerial photographs, depending upon the size of the project. It may require six to eight weeks to obtain aerial photographs from government agencies in the United States and Canada; elsewhere it may take much longer. Where aerial photography is produced by the air force of a particular country, its availability requires overcoming major obstacles. However, many smaller countries in the British Commonwealth produce their topographic maps based on aerial photography taken by the Directorate of Overseas Surveys of the Government of the United Kingdom. This is commonly black-and-white photography at a scale of 1:20,000. A project-specific aerial-photograph mission may be warranted for some projects; the cost of such missions varies widely depending upon the size and location of the project, but generally costs at least several thousand dollars.

The amount of time required for a geologist to complete surface observation and geologic mapping depends on the size of the site, the ease of access, the ruggedness of the site, and the degree of geologic complexity. Under most circumstances, however, one to two weeks should be sufficient. The reconnaissance instrumentation usually consists of relatively inexpensive wooden or steel stakes and small-diameter iron pipe. The equipment needed to conduct the monitoring is simple and is probably owned by most geologists so that rental or purchase would not be needed.

The amount of involvement by the geologist during the subsurface investigation can be extensive or minor, depending on the organization of the effort. Often the geologist is assigned to the drilling or excavation equipment to make field observations. In these cases the geologist can be involved for several weeks or even months. If the geologist is not directly involved in the subsurface-data collection, approximately one to two weeks of effort may be required to examine the samples and correlate the subsurface and surface data.

It may be appropriate for the geologist to assist in installing instrumentation and to be involved in long-term monitoring efforts. The geologist can make repeated surface observations at the time the instruments are being read. Long-term monitoring can extend over a period of years, with readings being taken at intervals of weeks or months. The amount of time required for each series of readings varies with the number of instrument locations and the difficulty of access. Generally, a few days to one week is sufficient to read the instruments at a typical site.

Correlation and analysis of surface and subsurface geologic data are commonly done as the data are being collected. It may be appropriate for the geologist to synthesize the data at the end of a major effort. Typically, a few days to one week is sufficient time for such correlation and analysis.

Chapter 12

TIEN H. WU

SOIL STRENGTH PROPERTIES AND THEIR MEASUREMENT

1. INTRODUCTION

Methods of limiting equilibrium are frequently used to analyze the stability of a soil mass (see Chapter 13). In such analyses, the shear strength of the material is assumed to be fully developed along the rupture surface at failure. In this chapter the basic principles that govern shear strength and the methods that may be used for its measurement are outlined. Brief descriptions of the properties of some common soils are provided.

2. GENERAL PRINCIPLES

The basic principles in the description of strength properties are the failure criterion and the effective stress principle. When a failure criterion derived from test data is used to estimate in situ strength, appropriate attention should be given to possible differences between the stress state of the test and that of the in situ soil when subjected to the expected load.

2.1 Failure Criterion

The Mohr-Coulomb criterion is widely used to define failure; it states that the shear strength (s) is

$$s = c + \sigma \tan\phi \qquad (12.1)$$

where

σ = normal stress on rupture surface,
c = cohesion, and
ϕ = angle of internal friction.

In terms of principal stresses, the Mohr-Coulomb criterion becomes

$$\sigma_1 = \sigma_3 \tan^2\left[\left(\frac{\pi}{4}\right)+\left(\frac{\phi}{2}\right)\right]+2c\tan\left[\left(\frac{\pi}{4}\right)+\left(\frac{\phi}{2}\right)\right] \qquad (12.2)$$

where σ_1 is the major principal stress and σ_3 is the minor principal stress.

A more general formulation, which combines failure with stress-strain behavior, is the yield surface (Drucker et al. 1955) and the critical state (Schofield and Wroth 1968). The yield surface is especially useful when evaluation of deformation is required. For limiting equilibrium analysis, the Mohr-Coulomb criterion is still the most convenient failure criterion.

2.2 Effective Stress Versus Total Stress Analysis

Because the shear strength of soils is strongly influenced by drainage conditions during loading, those conditions must be properly accounted for in the use of shear strength in design. A fundamental principle in soil engineering is the use of effective stress σ', which was first defined by Terzaghi (1936a) as

$$\sigma' = \sigma - u \qquad (12.3)$$

where σ is the total stress and u is the pore pressure. The shear strength can be expressed consistently in terms of effective stress:

$$s = c' + \sigma' \tan\phi' = c' + (\sigma - u) \tan\phi' \qquad (12.4)$$

where c' and ϕ' are the strength parameters for effective stress. For a partially saturated soil, the shear strength can be expressed as (Fredlund et al. 1978)

$$s = c' + (\sigma - u_w) \tan\phi' + (u_w - u_a) \tan\phi'' \qquad (12.5)$$

where

u_a = pore-air pressure,
u_w = pore-water pressure, and
ϕ'' = soil property that reflects influence of suction $(u_w - u_a)$ on strength.

When the soil is saturated, $u_a = 0$ and $u = u_w$. For saturated soils, pore pressure consists of the hydrostatic pore pressure related to groundwater level and the excess pore pressure due to applied loads.

When soils are loaded under undrained or partially drained conditions, the tendency to change volume results in an excess pore pressure, which may be positive or negative depending on the type of soil and the stresses involved. General relations between pore pressure and applied stresses have been suggested. For example, Henkel (1960) proposed that

$$\Delta u = B(\Delta\sigma_{oct} + \alpha \Delta\tau_{oct}) \qquad (12.6)$$

where

α = empirical coefficient,
$\tau_{oct} = 1/3[(\sigma_1 - \sigma_2)^2 + (\sigma_2 - \sigma_3)^2 + (\sigma_3 - \sigma_1)^2]^{1/2}$,
$\sigma_{oct} = 1/3(\sigma_1 + \sigma_2 + \sigma_3)$, and
$\sigma_1, \sigma_2, \sigma_3$ = major, intermediate, and minor principal stresses.

For soils tested in the triaxial apparatus or loaded so that $\Delta\sigma_2 = \Delta\sigma_3$, Skempton (1954) proposed that the excess pore pressure be given by

$$\Delta u = B[\Delta\sigma_3 + A\Delta (\sigma_1 - \sigma_3)] \qquad (12.7)$$

where A is an empirical coefficient related to the excess pore pressure developed during shear and B is an empirical coefficient related to the soil's compressibility and degree of saturation. For saturated soils, $B = 1$. For an elastic material, $A = 1/3$. For soils that compress under shear, $A > 1/3$, and for soils that dilate under shear, $A < 1/3$.

Under the fully drained condition, the excess pore pressure is zero, and pore pressure in saturated soils caused by groundwater flow can usually be evaluated without serious difficulty. Hence, analysis with the effective stress description of shear strength (Equation 12.4) is most useful. For partially drained and undrained conditions, the evaluation of excess pore pressure is often difficult. In some cases, a total-stress description of shear strength may be used. One important case is the undrained loading of saturated soils, for which the undrained shear strength ($s = s_u$) can be used. This is the common $\phi = \phi_u = 0$ analysis (Skempton and Golder 1948). The shear strength usually changes as the void ratio changes with drainage. If the change results in a higher strength, the short-term, undrained stability is critical and the stability can be expected to improve with time. On the other hand, if drainage produces a decrease in strength, the long-term, drained stability is critical; the undrained shear strength can be used only for short-term or temporary stability. For partially saturated soils, the prediction of pore-air and pore-water pressures is more difficult. Currently, the only reliable method is in situ measurement.

2.3 Common States of Stress and Stress Change

The Mohr-Coulomb criterion does not indicate any effect of the intermediate principal stress (σ_2') on the shear strength. In practical problems, σ_2' may range from σ_3' to σ_1', depending on the geometry of the problem. The direction of the major principal stress also changes during loading. Experimental studies show that the value of σ_2' relative to σ_3' and σ_1' has an influence on the shear strength.

Several common states of stress are shown in Figure 12-1. In the initial state (*a*), σ_z' is the effective overburden pressure, $\sigma_r' = K_o\sigma_z'$ is the radial or lateral pressure, and K_o is the coefficient of earth pressure at rest. In the stress state beneath the center of a circular loaded area [Figure 12-1(*b*)], the vertical stress is the major principal stress and the radial stress σ_r' is the minor principal stress. The

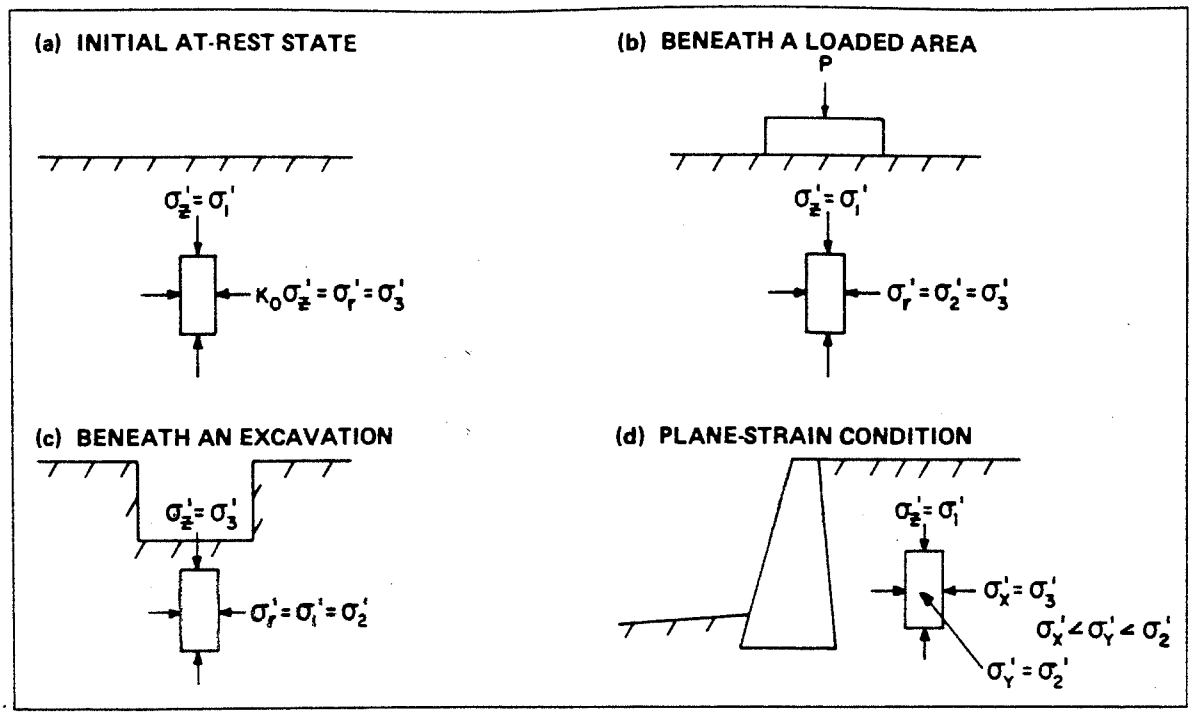

FIGURE 12-1
Common states of stress.

intermediate principal stress (σ_2') is equal to the minor principal stress (σ_3'). In the stress state below the center of a circular excavation [Figure 12-1(*c*)], the vertical stress is the minor principal stress and the radial stress σ_r' is the major principal stress. The intermediate principal stress (σ_2') is equal to the major principal stress (σ_1'). Slopes and retaining structures can be approximated by the plane-strain condition in which the intermediate principal strain (ε_2) is zero. Then the intermediate principal stress (σ_2') is σ_y', oriented as shown in Figure 12-1(*d*), and has a value between σ_1' and σ_3'.

Another important feature in many stability problems is the rotation of the principal axes during loading or excavation and its effect on the shear strength of soft clays (Ladd and Foott 1974). The rotation of principal axes is shown in Figure 12-2. Before the excavation of the cut, the state of stress is represented by that shown in Figure 12-1(*a*). After excavation, the major principal stress is in the horizontal direction at the toe (Point A, Figure 12-2). Thus, the principal axes are rotated through an angle of 90 degrees; at Point *B*, a rotation of approximately 45 degrees occurs. At Point C, the original principal stress directions remain unchanged although the values of the stresses change.

2.4 Stress-Strain Characteristics

Two stress-deformation curves are shown in Figure 12-3. A soil sample is sheared under a normal stress σ and a shear stress τ. The shear displacement is Δ. In common practice, the strength of the soil is defined as the peak strength (Points *a* and *b* in Figure 12-3) measured in the test. When this is used in a stability analysis, the tacit assumption is that the peak strength is attained simultaneously along the entire rupture surface.

FIGURE 12-2
Directions of principal stresses in a slope.

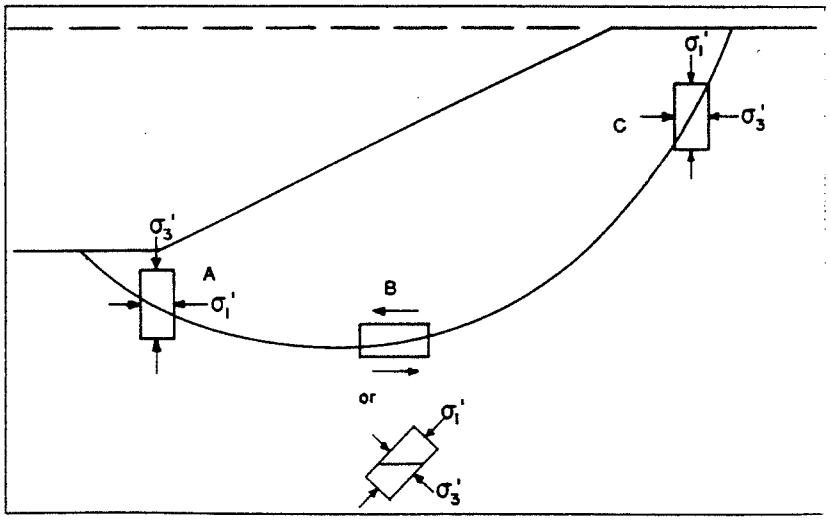

Many soils demonstrate strain-softening behavior, as illustrated by Curve A in Figure 12-3. Any of several mechanisms may be used to explain the strength decrease, but it is important to account for this decrease in design. For strain-softening soils, it is unreasonable to assume that the soil reaches its peak strength simultaneously at all points along a failure surface. In fact, the soil at some points on the rupture surface will suffer displacements greater than Δ_a before the soil at other points reaches this deformation. This phenomenon was called "progressive failure" by Terzaghi and Peck (1948). In the limit of large deformation, the strength at all points will be reduced to that represented by Point c in Figure 12-3. This strength is called the residual strength.

2.5 Effect of Rate of Loading

The difference between the rate of loading applied in a laboratory shear test and that experienced in the slope is usually substantial. Most laboratory and in situ tests bring the soil to failure within several hours or at most a few days. For most slopes the load is permanent, although some dynamic loads may be applied for short durations. The effect of rate of loading on soil strength, excluding effects of consolidation, may be significant. In general, the undrained strength of soils increases as the rate of loading increases; however, this effect depends on the specific material and varies over a wide range (Casagrande and Wilson 1951; Skempton and Hutchinson 1969).

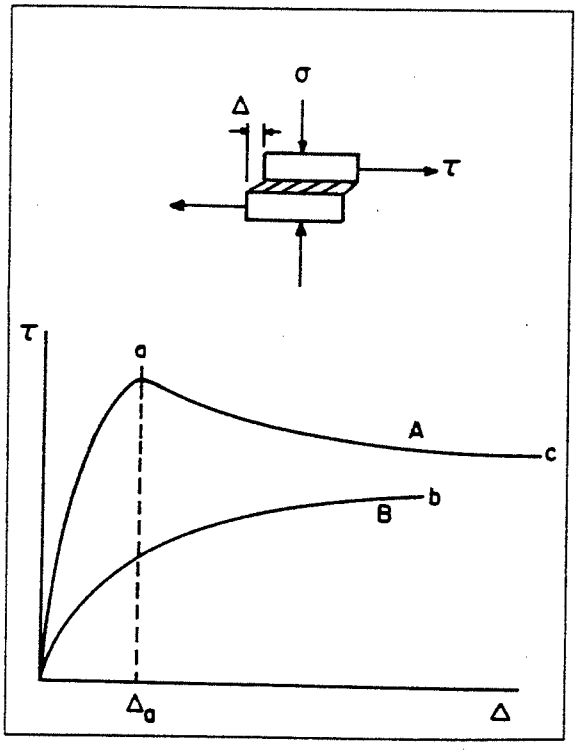

FIGURE 12-3 Typical stress-deformation curves.

3. LABORATORY MEASUREMENT OF SHEAR STRENGTH

Various methods are available for laboratory measurement of shear strength. The simple methods are designed to determine the shear strength of a sample in a particular state, such as the water content of the soil in situ. These methods are most often used to determine the undrained shear strength (s_u) of saturated cohesive soils. More elaborate laboratory tests allow combinations of normal and shear stresses to be employed and pore pressures to be measured or controlled. Then it is possible to establish the shear strength relation defined by Equation 12.4. The most elaborate tests allow simulation of the field stress or deformation conditions. For example, triaxial compression tests simulate the stress state in Figure 12-1(*b*), and triaxial extension tests simulate the stress state in Figure 12-1(*c*) (see Section 3.2). Plane-strain compression and extension tests and simple shear tests can provide better simulation of the stress states in Figure 12-2 (see Section 3.3). A comprehensive summary of stress states in various laboratory tests and constitutive relations that can be deduced from test results was given by Desai and Siriwardane (1984).

3.1 Simple Shear Tests

Three types of simple shear tests are the unconfined compression, cone, and vane shear tests.

The unconfined compression test is usually performed on a cylindrical sample with a diameter-to-length ratio of 1:2. The sample is compressed axially [Figure 12-4(*a*)] until failure occurs; the shear strength is taken as one-half the compressive strength.

In the cone test, a cone with an angle θ is forced into the soil [Figure 12-4(*b*)] under a force (Q), which may be its own weight. The shear strength is obtained from the relation

$$s_u = \frac{KQ}{h^2} \qquad (12.8)$$

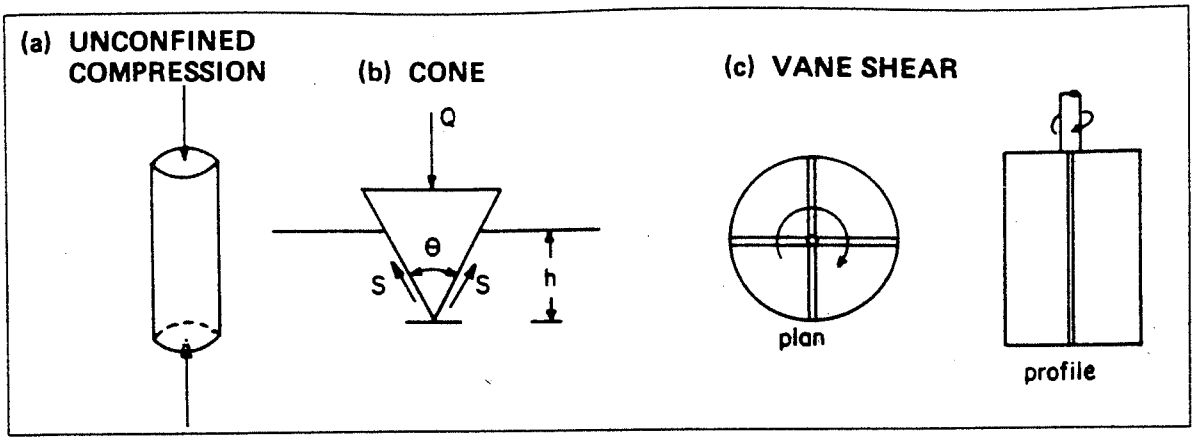

FIGURE 12-4
Simple tests for measurement of soil strength.

where h is the penetration and K is the constant that depends on the angle θ and the weight Q. Calibration curves for K were published by Hansbo (1957).

In the laboratory vane test (Cadling and Odenstad 1950), a vane is pushed into the soil specimen, and a torque is applied to the stem to produce shear failure over a cylindrical surface [Figure 12-4(*c*)]. The shear strength is obtained by equating the torque measured at failure to the moment produced by the shear stresses along the cylindrical surface. According to Cadling and Odenstad, the shear strength for vanes with a diameter-to-height ratio of 1:2 is

$$s = \frac{6}{7}\left(\frac{M}{\pi D^3}\right) \tag{12.9}$$

where M is the torque and D is the diameter of the vane.

Application of the results of these simple tests to the analysis of slope stability should include consideration of the type of soil and loading conditions in situ. The test results are expressed in terms of total stress because pore pressures are not measured. When the soil is brought to failure rapidly under undrained conditions, the shear strength is defined by $s = s_u$. Hence, the application of these test results is commonly limited to saturated cohesive soils under undrained conditions.

It is usually assumed that the measured strength is equal to the in situ strength. However, a major uncertainty is the effect of sampling disturbance on strength. Even "good" samples may suffer strength losses as great as 50 percent (Ladd and Lambe 1964; Clayton et al. 1992; Hight et al. 1992). The effect of sample disturbance is most severe in soft sensitive soils and appears to increase with the depth from which the sample is taken. The state of stress is another factor that should be considered. The directions of the principal stresses and the orientations of rupture surfaces in these simple tests are not the same. They may also be quite different from directions of the principal stresses and the orientation of the failure surface in a slope. Hence, caution should be exercised when the results of these simple strength tests are applied to slope-stability problems (Bjerrum 1973).

3.2 Triaxial Test

The triaxial test is highly versatile; a variety of stress and drainage conditions can be employed (Bishop and Henkel 1962). The cylindrical soil specimen is enclosed within a thin rubber membrane and placed inside a triaxial cell, as shown in Figure 12-5(*a*). The cell is then filled with a fluid. As pressure is applied to the fluid in the cell, the specimen is subjected to a hydrostatic stress (σ_3). Drainage from the specimen is provided through the porous stone at the bottom, and the volume change can be measured. Alternatively, if no drainage is allowed, the pore-water pressure can be measured. For partially saturated soils, the pore-water pressure is measured through a fine ceramic stone that prevents air entry. The pore-air pressure is measured through a screen that permits free air entry. Details on testing of partially saturated soils were given by Fredlund and Rohardjo (1993, 260–282).

In triaxial compression, the axial stress (σ_z) is increased by application of a load through the loading ram. From the known stresses at failure ($\sigma_1 = \sigma_z$ and $\sigma_2 = \sigma_3 = \sigma_r$), Mohr circles or other stress plots can be constructed. Results from several triaxial tests, each using a different cell pressure (σ_3), are

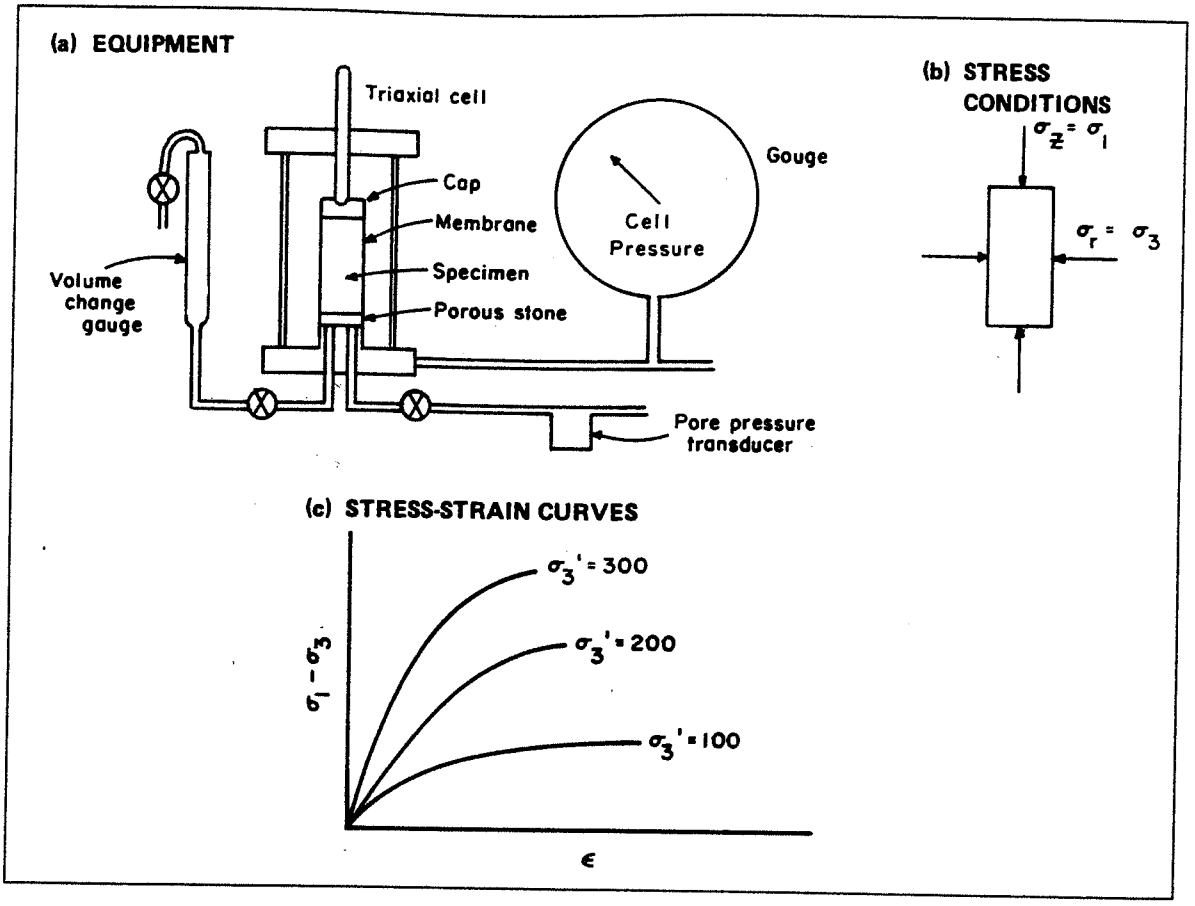

FIGURE 12-5
Triaxial test.

used to obtain the failure envelope. Typical plots of the principal stress difference versus axial strain are shown in Figure 12-5(*c*). The stress-strain behavior is influenced by the confining pressure, the stress history, and other factors. The sample can also be loaded to failure in triaxial extension by increasing the radial stress while maintaining the axial stress constant; then $\sigma_1 = \sigma_2 = \sigma_r$ and $\sigma_3 = \sigma_z$. Triaxial compression and extension simulate, respectively, the stress states beneath a loaded area, as shown in Figure 12-1(*b*), and beneath an excavation, as shown in Figure 12-1(*c*).

Principal stresses and pore pressure at failure are used to construct Mohr circles and to obtain the failure envelope. Figure 12-6 shows a series of failure envelopes. The horizontal axis is $\sigma - u_w$, which is the familar pore pressure for saturated soils. For saturated soils $(u_a - u_w) = 0$. When the soil is partially saturated, $(u_a - u_w)$ is not zero. A series of failure envelopes is obtained for different values of $(u_a - u_w)$, such as those shown in Figure 12-6 for values of $(u_a - u_w)$ equal to *a* and *b*.

Tests with the following drainage conditions can be performed with the triaxial apparatus. Tests on saturated soils are considered first.

In the *consolidated-drained test* (also called a drained test or slow test), the soil is allowed to consolidate completely under an effective cell pressure (σ_3'). In the triaxial compression test, the axial stress is increased at a slow rate, and drainage is permitted. The rate should be slow enough that no excess pore pressure is allowed to build up. Since

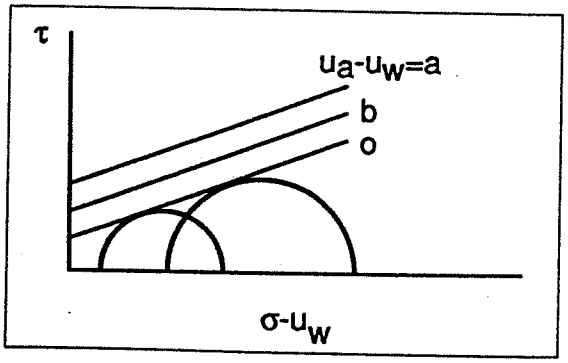

FIGURE 12-6
Failure envelopes.

the excess pore pressure is zero in the drained test, effective stresses are known throughout the test and at failure. The results of a series of drained tests can be used to evaluate the effective stress strength parameters in Equation 12.4.

In the *consolidated-undrained test* with pore-pressure measurement (also called the consolidated-quick test), the drainage valves are closed after the initial consolidation of the sample. The axial stress is increased without drainage, and the excess pore pressure is measured. The pore pressure is subtracted from the total axial and radial stresses to give the effective stresses. The effective stresses at failure from a series of tests are used to define the failure criterion, as in the drained test. The consolidated-undrained test is sometimes performed without pore-pressure measurement. Then the effective stresses at failure cannot be determined. The results could be used to estimate the undrained shear strength after consolidation under σ_3'.

In the *unconsolidated-undrained test* (also called the undrained test or quick test), no drainage is allowed during any part of the test. When the cell pressure is applied, a pore-pressure change occurs in the soil. When the axial stress is applied, additional pore-pressure changes occur. If these pore-pressure changes are not measured, the test results can only be interpreted in terms of total stress. At failure, the undrained shear strength (s_u) is taken to represent the strength at the in situ water content. The unconsolidated-undrained test is then similar to the simple shear tests defined in Section 3.1.

The same three types of triaxial tests can be performed on partially saturated soils. However, because the air voids can be compressed even when there is no drainage, the simplifications derived above for undrained loading do not apply to partially saturated soils. For such soils, the pore-air and pore-water pressures must be measured in all tests in order to construct the failure envelope in terms of effective stress.

Triaxial tests are usually begun by increasing the cell pressure (σ_3) to the desired stress level, thus applying an isotropic or hydrostatic stress to the sample. This initial condition may differ from the initial in situ condition [see Figure 12-1(*a*)], in which the vertical and horizontal principal stresses are different. In situ stresses can be simulated in a triaxial test by using an anisotropic stress state during consolidation. Experimental results that show the effect of stress state on strength properties were reviewed by Ladd et al. (1977).

3.3 Plane-Strain Test

The geometry of many geotechnical problems can be approximated by the condition of plane strain, in which the intermediate principal strain (ε_2) is zero. To simulate this condition, plane-strain tests have been developed (Henkel and Wade 1966) in which the sample is consolidated anisotropically with zero lateral strain ($\varepsilon_x = \varepsilon_y = 0$). Then the sample is loaded to failure by increasing either σ_x or σ_z and maintaining $\varepsilon_y = 0$ to simulate, respectively, the stress conditions at Points A or C of Figure 12-2. Plane-strain tests can be conducted under undrained, consolidated-undrained, or drained conditions as described for triaxial tests.

3.4 Direct Shear Test

The direct shear test is shown in Figure 12-7. The soil specimen is enclosed in a box consisting of upper and lower halves; porous stones on the top and the bottom permit drainage of water from the specimen. If the loading is carried out slowly, no excess pore pressure develops and the drained condition is obtained. The potential plane of failure is *a-a*. A normal stress (σ_z') is applied on plane *a-a*

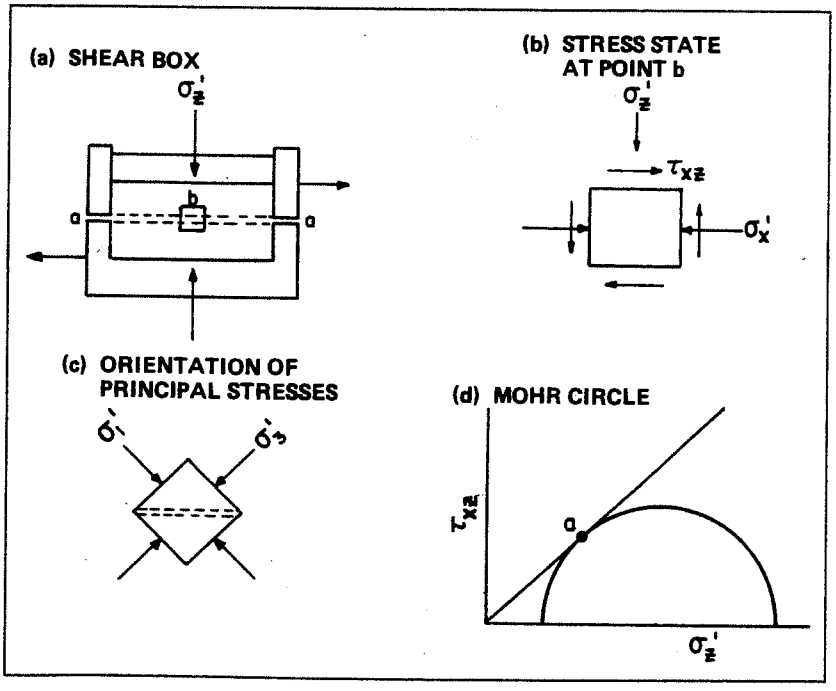

FIGURE 12-7
Direct shear test.

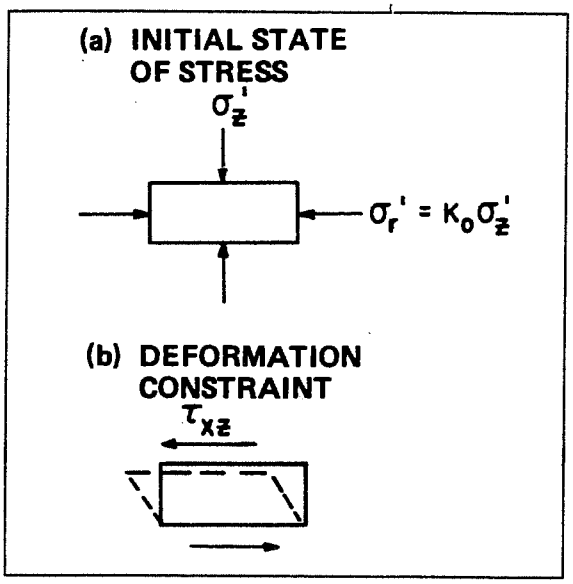

FIGURE 12-8
Simple shear test.

through a loading head, and the shear stress is increased until the specimen fails along plane *a-a*. A stress-deformation curve is obtained by plotting the shear stress versus the displacement. Because the thickness of shear zone *a-a* is not precisely known, the shear strain cannot be determined. The test gives the value of τ_{xz} at failure. The average vertical stress (σ_z') and shear stress (τ_{xz}) are known, but σ_x' is not known. The directions of the principal stresses for Point *b* [Figure 12-7(*b*)] are approximately as shown in Figure 12-7(*c*). Assuming that Point *a* [Figure 12-7(*d*)] represents the conditions at failure, a Mohr circle can be constructed. The failure envelope is obtained from several tests, each using a different effective normal stress, performed on specimens of the same soil. The values of τ_{xz} at failure are plotted against the values of σ_z'. The foregoing represents the common interpretation of the direct shear test. More elaborate analyses were presented by Hill (1950), Morgenstern and Tchalenko (1967), and Jewell and Wroth (1987).

In saturated clays the direct shear test can be performed at a rapid rate so that the test duration is too short for any appreciable amount of water to flow into or out of the sample. This is an undrained condition, and an excess pore pressure of unknown magnitude is developed in the soil. Consequently, this is essentially a simple test, and the shear stress at failure represents the undrained shear strength (s_u). Test procedures for partially saturated soils were given by Fredlund and Rohardjo (1993, 282–254).

3.5 Simple Shear Test

Several simple shear tests have been developed, but the one described by Bjerrum and Landva (1966) is the most commonly used for undisturbed samples. The cylindrical specimen is enclosed in a rubber membrane reinforced by wire. This enclosure allows the shear deformation to be distributed fairly uniformly through the sample, as shown in Figure 12-8(*a*). The sample is consolidated anisotropically under a vertical stress [Figure 12-8(*a*)] and sheared by application of stress τ_{xz} [Figure 12-8(*b*)]. The simple shear test can be performed under undrained, consolidated-undrained, and drained conditions. Zero volume change during shear in an undrained test can be maintained by continuously adjusting the vertical stress σ_z' during the test. In the simple shear test, the initial principal axes are in the vertical and horizontal directions. At failure the horizontal plane becomes the plane of maximum shear strain. This condition approximates that at Point *B* of Figure 12-2.

4. IN SITU MEASUREMENT OF SHEAR STRENGTH

A variety of in situ tests are available for measurement of shear strength. Several of these are described in Chapter 10. Although theories have been proposed to interpret the test results, the stress state in most in situ shear tests is not precisely known. Hence empirical correlation is often relied upon for interpretation of the results. Various correlations have been published for different soils. For a comprehensive review of in situ tests, see the discussions by Orchant et al. (1988) and Lunne et al. (1989).

4.1 Standard Penetration Test

The standard penetration test uses a split-spoon sampler, which is driven with a specified energy into the bottom of a borehole. The number of blows (N) required to advance the sampling spoon through a distance of 30 cm may be used to estimate the angle of internal friction ϕ' of sands (Peck et al. 1974). More data are available on the correlation of N with relative density D_r (Gibbs and Holtz 1957; Marcuson and Bieganousky 1977). Correlation between D_r and ϕ' was given by Schmertmann (1975). Correlation between N and shear strength of cohesive soils is not reliable.

4.2 Cone Penetration Test

In the cone penetration test a cone of specified diameter and shape is attached to the end of a drill rod and advanced at a controlled rate. The force required is measured. This test can provide a continuous record of the resistance. For cohesionless soils, bearing capacity equations can be used to compute ϕ' from the penetration resistance. Empirical correlations between cone resistance and ϕ' are also available. Different correlation equations can give very different values of ϕ' (Mitchell and Lunne 1978; Wu et al. 1987a). The undrained shear strength of cohesive soils can be estimated from the cone resistance by the following relation:

$$s_u = \frac{q_c - \sigma_v}{N_k} \qquad (12.10)$$

where

s_u = undrained shear strength,
q_c = cone resistance,
σ_v = total overburden stress, and
N_k = an empirical constant.

The value of N_k ranges between 10 and 20 and depends on the overconsolidation ratio and plasticity index (Aas et al. 1986).

4.3 Field Vane Test

The field vane test is similar to the laboratory vane test described in Section 3.1. It measures the shear strength along a vertical cylindrical surface and the top and bottom surfaces of the cylinder. An equation similar to Equation 12.9 is used to calculate the shear strength. The coefficient depends on the assumption for stress distribution on the cylindri-cal surface and the top and bottom surfaces (Donald et al. 1977). Since the rupture surface in a stability problem may be quite different from that in a vertical cylinder, the shear strength may also be different from that measured in the vane test because of stress and material anisotropy. Correction factors based on an analysis of the stress state were suggested by Wroth (1984), and empirical correction factors were suggested by Bjerrum (1973).

4.4 Pressuremeter Test

In the pressuremeter test (Menard 1965; Baguelin et al. 1972), the cylindrical instrument is expanded against the wall of the borehole until failure in the surrounding soil occurs. Elastic-plastic solutions for expansion of a cylindrical cavity by Gibson and Anderson (1961) and subsequent modifications are used to obtain the shear strength and stress-strain properties of the soil. Consistent results have been obtained for the undrained shear strength of saturated clays and drained shear strength of cohesionless soils (Wroth 1984).

4.5 Borehole Shear Test

The borehole shear test is analogous to the direct shear test. The two halves of a cylinder, which is split lengthwise, are pressed under a controlled pressure against the opposite walls of a borehole. The cylinder is then pulled vertically, shearing the soil (Handy and Fox 1967). The failure surface is not determined; hence the normal and shear stresses are not accurately known. For cohesionless soils with high permeability, the test may be considered a consolidated-drained test. For cohesive soils, the drainage condition is uncertain. The borehole shear test was analyzed by Lutenegger and Hallberg (1981) and Handy et al. (1985).

4.6 Dilatometer Test

The dilatometer is a flat blade that contains a flexible membrane on one side (Marchetti 1975). The blade is pushed into the soil to reach the desired depth, and the membrane is inflated by pressure and pushes back the adjacent soil. The pressures required to "lift off" the membrane and to displace the soil 1 mm are recorded. These pressures are used to estimate the horizontal in situ stress. Empirical correlation between the horizontal in situ stress and s_u/σ'_v is used to estimate the s_u of clays (Marchetti 1980). The force required to advance the dilatometer is measured and used to estimate the bearing capacity and then ϕ' of cohesionless soils (Schmertmann 1982).

5. SHEAR STRENGTH PROPERTIES OF SOME COMMON SOILS

The strength characteristics of natural soils are strongly influenced by the geologic processes of soil formation. Hence, it is possible to identify strength characteristics that are common to soils within broadly defined groups. Groups with well-defined characteristics include saturated cohesionless soils, soft saturated cohesive soils, heavily overconsoli-

dated clays, sensitive soils, and residual soils and colluvium. More detailed discussions of slopes involving specific soil conditions are given in Chapters 19 through 25.

5.1 Saturated Cohesionless Soils

Cohesionless soils, such as gravel, sand, and nonplastic silts, have effective stress failure envelopes that pass through the origin. This means $c' = 0$ in Equation 12.4. The value of ϕ' ranges from about 27 to 45 degrees or more and depends on several factors. For a given soil the value of ϕ' increases as the relative density increases. For different soils at the same relative density, the value of ϕ' is affected by particle-size distribution and particle shape. The value of ϕ' for a well-graded soil may be several degrees greater than that for a uniform soil of the same average particle size and shape. The same is true when a soil composed of angular grains is compared with one made up of rounded grains. The effect of moisture on ϕ' is small and amounts to no more than 1 or 2 degrees (Lambe and Whitman 1969, 147–149; Holtz and Kovacs 1981, 514–519).

The failure envelope, which is a straight line at low pressures, cannot be extended to high confining pressures. Tests with effective normal stresses above 700 kPa indicate that the failure envelope is curved, as shown in Figure 12-9 (Bishop 1966; Vesic and Clough 1968). The high normal stresses apparently cause crushing of grain contacts and result in a lower friction angle. This factor is particularly important in uncemented carbonate sands (Datta et al. 1982). Another important factor is the difference in the values of ϕ' as measured by different types of tests. The value of ϕ' measured in triaxial tests, which permit change in the radial strain, is 4 to 5 degrees smaller than that measured in plane-strain tests (Ladd et al. 1977).

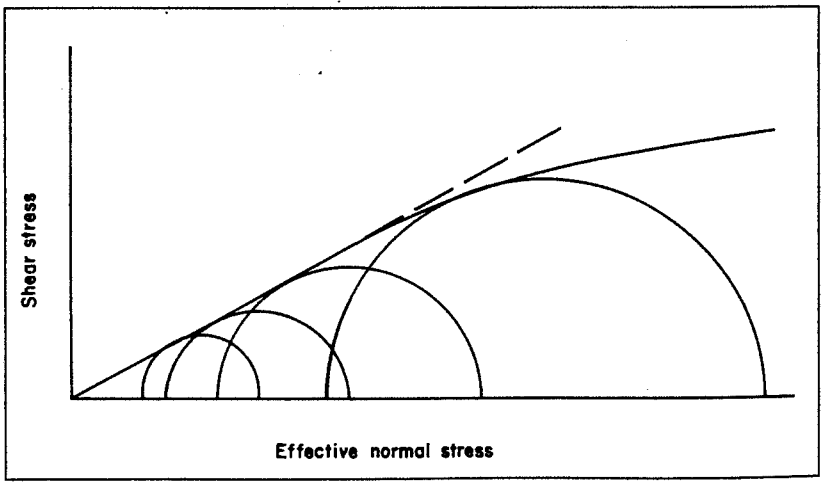

FIGURE 12-9
Failure envelope for cohesionless soils.

In ordinary construction sandy and gravelly soils of high permeability can be considered to be loaded in the drained condition. Volume changes occur rapidly, and no excess pore pressures are developed. Without excess pore pressure, effective stresses can be estimated from the groundwater levels. Stability analyses can be performed by using effective stress strength parameters. For silty soils the permeability may be sufficiently low that excess pore pressure will develop during construction. When this is the case, the pore pressure must be measured or estimated if an effective stress analysis is to be performed.

The undrained response of fine sands and silts is important in some situations. Loose saturated sands and silts may develop large excess pore pressures after reaching peak strength. Because of the large pore pressure, the strength drops and the ultimate strength is well below the peak strength. Large displacements occur as a result of this loss of strength. This phenomenon was called *liquefaction* by Casagrande (1936). Large pore pressures may also develop in saturated sands of medium to high density under cyclic loading. In a triaxial test, if an axial stress is repeated for a number of cycles, the pore pressure may become equal to the confining pressure, thus reducing the effective minor principal stress (σ_3') to 0 (Seed and Lee 1967). Large strain increments will occur with each cycle of stress as the pore pressure approaches σ_3. If the soil dilates with strain, the pore pressure soon drops and the soil becomes stable. This phenomenon is called *cyclic mobility* (Castro 1975). The behavior of a sand under cyclic loading may range from liquefaction to cyclic mobility, depending on whether the sand is contractive or dilative.

Liquefaction and cyclic mobility are important considerations in the evaluation of slope stability under earthquake loadings. Lade (1992) and Sladen et al. (1985) formulated conditions for liquefaction in terms of the yield surface and the critical state, respectively. Methods for assessing the potential for liquefaction and cyclic mobility were reviewed by Casagrande (1976), Seed (1979), Poulos et al. (1985), and Seed et al. (1985).

5.2 Normally Consolidated and Lightly Overconsolidated Clays and Clayey Silts

Because of the low permeability of fine-grained soils, undrained or partially drained conditions are common in normal construction. The general characteristics of normally consolidated to lightly overconsolidated clays are described in this section. Very sensitive normally consolidated clays are described in Section 5.4.

A clay soil is considered to be normally consolidated if the consolidation pressure before shear is equal to or greater than the preconsolidation pressure (σ_p'). When a series of drained triaxial tests is conducted on a normally consolidated soil, the failure envelope is a line that passes through the origin [Figure 12-10(*a*)]; thus, $c' = 0$. If consolidated-undrained tests are performed on a normally consolidated soil, positive excess pore pressures develop. As a result, the undrained shear strength $s_u = {}^1/_2(\sigma_1 - \sigma_3)$ will be less than the drained shear strength of a sample initially consolidated under the same stresses. The respective stress paths of the drained and consolidated-undrained tests are shown as *ca* and *cb* in Figure 12-10(*a*). A typical relation between strength and water content is shown in Figure 12-10(*b*). The results of consolidated-undrained tests can also be used to obtain the ratio s_u/σ_3', which is a constant for normally consolidated soils (Skempton 1948). For lightly overconsolidated soils, s_u/σ_3' is a function of the overconsolidation ratio σ_3'/σ_p' (Ladd and Foott 1974).

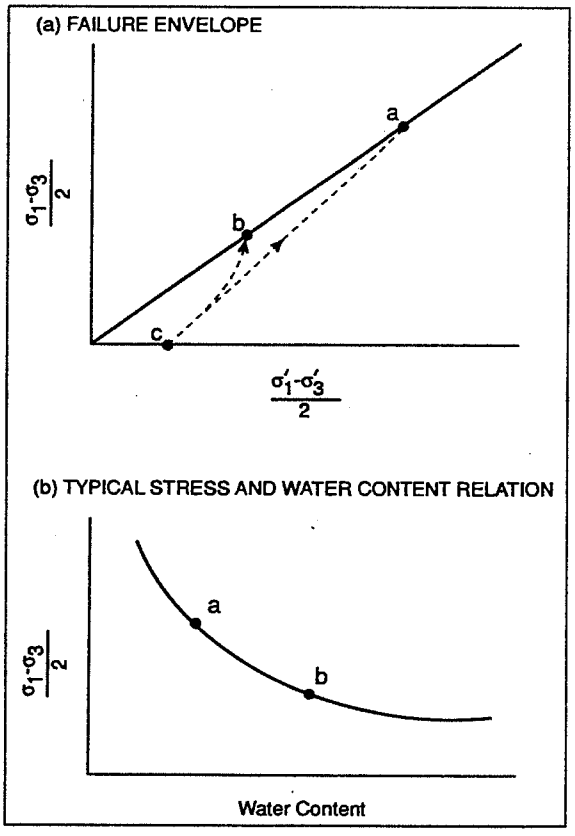

FIGURE 12-10
Strength properties of soft saturated clays.

If the load or stress change in the field induces positive excess pore pressures, as may be the case for a fill, the undrained strength will be lower than the drained strength. A slope based on an initially stable design can be expected to increase in stability with time as the excess pore pressure dissipates and the strength increases. The increase in strength with consolidation makes possible the construction in stages of embankments over soft soils. The strength gained under each stage of loading permits the addition of the next load increment. The ratio s_u/σ_3' is used to estimate the s_u under a given σ_3'. When a slope is made by excavation, there is a simultaneous increase in shear stress due to the slope and a decrease in mean normal stress due to the unloading of the excavation. In a saturated, normally consolidated soil, the increase in shear stress produces a positive excess pore pressure, and the decrease in normal stress produces a negative excess pore pressure. The net excess pore pressure in various parts of the slope depends on the relative values of these two effects. If the excess pore pressure is negative, the strength will decrease with time and drainage. In this case, the long-term or drained stability will be critical for a normally consolidated clay. Bishop and Bjerrum (1960) described several examples.

Failures of real slopes are good sources of information on the reliability of theoretical models. In a number of careful investigations, the factor of safety of the slope that failed was compared with the measured shear strength. If the theory and soil properties used are correct, the computed safety factor of a slope at failure should be unity. Results from many case histories show that for normally consolidated or lightly overconsolidated homogeneous clays of low sensitivity, total stress analysis with undrained shear strength gives a reasonably accurate estimate of immediate stability. For long-term stability under drained conditions, effective stress analysis with c' and ϕ' also gives satisfactory results. Comprehensive reviews and case histories were given by Bishop and Bjerrum (1960) and Bjerrum (1973), and more recent examples were

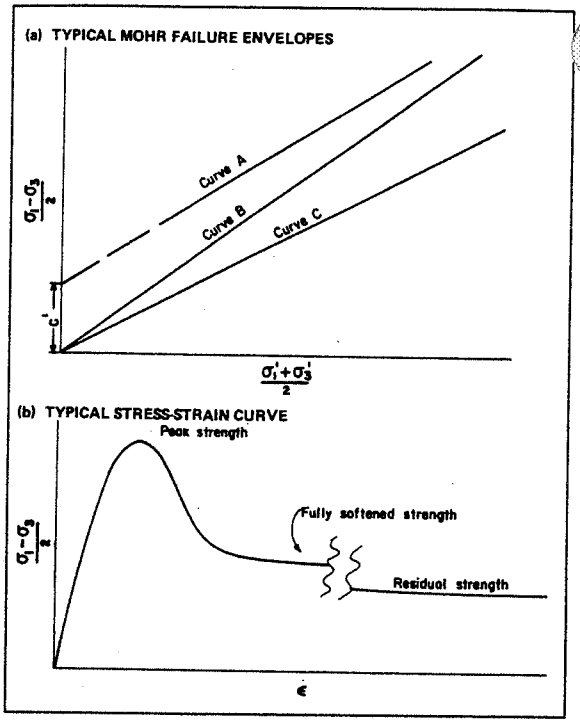

FIGURE 12-11
Strength properties of stiff overconsolidated clays.

presented by Ladd (1991), Pilot et al. (1982), and Tavenas and Leroueil (1980). For most of the reported failures in these case histories, the discrepancy between calculated and observed safety factors is less than 15 percent. Since most of the clays investigated are fairly uniform deposits, an accuracy of ±15 percent may be the best that can be achieved in practice.

It should be noted that earlier studies, such as that by Skempton and Golder (1948), used unconfined compressive strengths obtained from samples of small diameter. These conditions would tend to underestimate the in situ shear strength because of sample disturbance. By comparison, the study by Duncan and Buchignani (1973) used large-diameter samples and unconsolidated-undrained triaxial tests. The computed safety factor was 1.17 for the slope that failed. Various factors that could affect the strength were estimated, and the difference between observed strength and that measured in triaxial tests was attributed to the difference in strain rate. In cases reported by Ladd and Foott (1974), strength anisotropy was accounted for by performing triaxial compression and extension tests and direct simple shear tests. Hence, errors of different nature and magnitude are involved in the estimates of undrained shear strength in the different case histories.

Soft clays may also develop high pore pressures under cyclic loading (Thiers and Seed 1969). Sangrey et al. (1969) showed that a yield surface in effective stress space exists for cyclic stresses. When cyclic stresses reach the yield surface, large strains develop. Measurement and evaluation of strength losses due to complex states of static and cyclic stresses were described by Andersen et al. (1988).

5.3 Heavily Overconsolidated Clays

Most heavily overconsolidated clays show strain softening in their stress-strain curves (Figure 12-3, Curve A). The peak strengths of a series of heavily overconsolidated clay specimens give an effective stress failure envelope shown by Curve A in Figure 12-11(*a*). The failure envelope is approximately a straight line and if extrapolated to the axis at $\sigma' = 0$ gives a cohesion intercept (c'). Laboratory tests should be performed using normal stresses that are close to the normal stresses in the field because research has shown that the failure envelope for the peak strength of heavily overconsolidated clays is curved in the low-stress region and passes through the origin.

When loaded in the drained condition, a heavily overconsolidated clay will absorb water, and the absorbed water leads to a softening of the clay. The water content will increase significantly as the strength is reduced to the fully softened strength [Figure 12-11(*b*)]. The failure envelope for fully softened strength is shown as Curve *B* in Figure 12-11(*a*). The fully softened strength is close to the strength of the same soil in the normally consolidated condition. The strain necessary to develop fully softened strength in a heavily overconsolidated clay varies from one soil to another, but is at least 10 percent.

When much larger shear displacements take place within a narrow zone, the clay particles become oriented along the direction of shear, and a polished surface, or *slickenside*, forms. In natural slopes, slickensides may be developed along rupture surfaces of old landslides, bedding surfaces, or zones of deformation caused by tectonic forces. Along these surfaces the shear strength may approach the residual strength. The failure envelope, Curve C in Figure 12-11(*a*), is a line passing through the origin, and the residual angle of internal friction is ϕ_r'. Results of laboratory direct-shear tests indicate that ϕ_r' is dependent on soil miner-

alogy. As shown in Figure 12-12, "massive minerals," such as quartz, feldspar, and calcite, have high values of ϕ_r' that are close to the values of ϕ' for peak strength. However, clay minerals show significant differences between values of ϕ' and ϕ_r'. The largest difference was found in montmorillonitic clays, for which ϕ_r' was less than 10 degrees (Kenney 1967). The relationship between mineralogical composition and ϕ_r' makes it possible to correlate ϕ_r' with index properties such as plasticity index (Lupini et al. 1981) or liquid limit (Mesri and Cepeda-Diaz 1986). Because of the importance of strain-softening in heavily overconsolidated clays, choice of the strength for a stability analysis of a slope should consider progressive failure as described in Section 2.4. The design strength must be chosen to represent the average of the strengths along the entire rupture surface. For examples of analysis of progressive failure, see studies by Bjerrum (1967) and Duncan and Dunlop (1969).

For most slopes in heavily overconsolidated clays, the excess pore pressure immediately after construction is negative. Thus, the undrained strength will be greater than the drained strength. With drainage, the negative pore pressure dissipates and water is drawn into the sample. As water content increases, strength decreases. The long-term or drained conditions are critical, and there is no assurance that an initially stable slope will remain stable in the long term. Because of the low permeability, the time required to develop the fully drained condition in the field may be several years (Chandler 1984).

In heavily overconsolidated clays and soft shales, fissures and other discontinuities have an important influence on strength (Terzaghi 1936b). The characteristics of discontinuities in some stiff clays were described by Skempton and Petley (1967). The shear strength of laboratory specimens of such clays is strongly dependent on the number, shape, and inclination of discontinuities in the specimen. The presence of discontinuities is less likely in small specimens, which are often trimmed from intact soil between the discontinuities. Hence, the measured strength of laboratory samples tends to be higher than the in situ strength. When the clay contains discontinuities such as fissures and slickensides, the in situ strength will depend on the frequency and orientation of the discontinuities. Skempton and Petley (1967), Skempton and Hutchinson (1969), Chandler (1984), Wu et al. (1987b), and Burland (1990) provided examples of the in situ strength of clays with discontinuities.

5.4 Very Sensitive Soils

Sensitivity is defined as the ratio of the peak undrained shear strength to the undrained shear strength of the same soil after remolding at constant water content. Causes of clay sensitivity were reviewed by Mitchell and Houston (1969). The most dramatic landslides in sensitive soils occur in

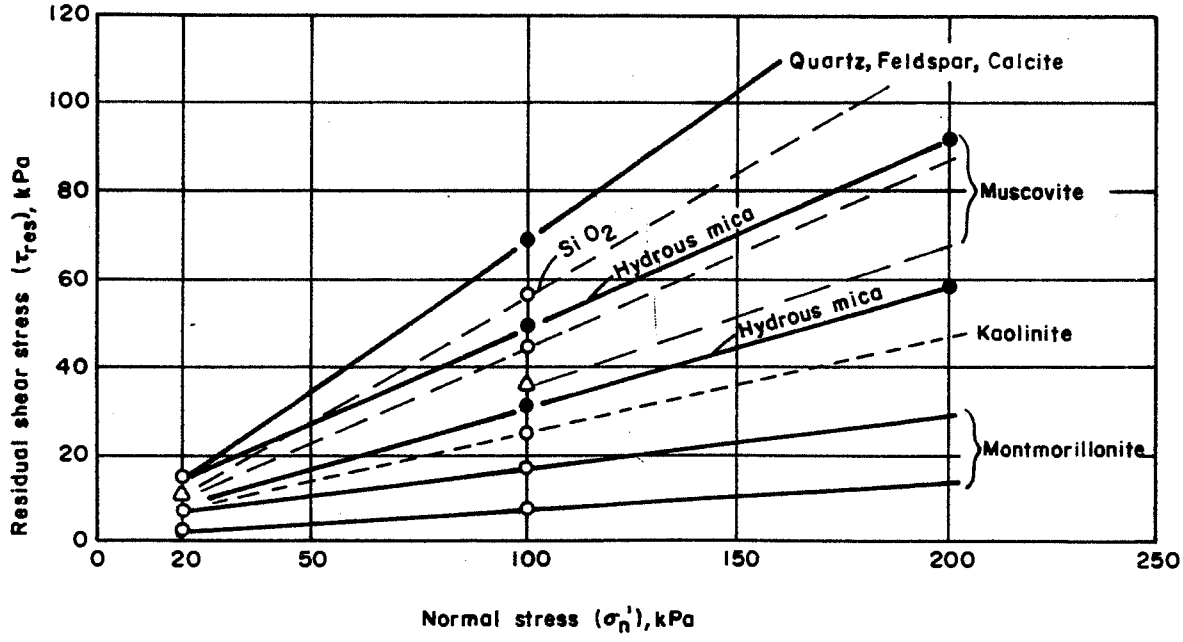

FIGURE 12-12 Residual shear strength of minerals.

Pleistocene marine clays in the Scandinavian countries and in the St. Lawrence River valley of eastern North America. High sensitivity is found in soils that have been subjected to leaching or natural cementation.

Effective stress failure envelopes for sensitive clays differ from those for soft saturated clays, described in Section 5.2. A sensitive clay, consolidated under the K_o condition, has a yield surface Y_o as shown in Figure 12-13. When the stress path for a point reaches the yield curve, such as at Point *P*, the soil structure is destroyed. Then high excess pore pressures are produced, and the shear strength decreases to Point C on the failure envelope for large strains (Tavenas and Leroueil 1977), which corresponds to the critical state (Schofield and Wroth 1968). In the design of slopes in these soils, it is necessary to keep the stresses within the yield curve. Evaluation of slope stability in very sensitive clays is described in Chapter 24.

5.5 Residual Soil and Colluvium

The weathering of rock produces residual soil. In the initial stages of weathering, coarse rock fragments are produced; the ultimate product of weathering is clay. Between these extremes is a soil composed of a mixture of grain sizes. On flat topography residual soil remains where formed. On slopes the weathered material, composed of soil and rock debris, may move down the face of the slope under the force of gravity. The deposit formed by this process is called *colluvium*. Residual soils have a wide range of properties depending on the parent material and the degree of weathering (Deere and Patton 1971; Mitchell and Sitar 1982).

Residual soils frequently exist in the partially saturated state. Some residual soils have high porosity and high permeability. Large changes in moisture content may occur with dry and wet seasons. The shear strength in terms of total stress has been found to be strongly influenced by the moisture content (Foss 1977; O'Rourke and Crespo 1988). Data on shear strength parameters c', ϕ', and ϕ'' are scarce. Tests by Ho and Fredlund (1982) showed that the component $c' + (u_w - u_a)\tan\phi''$ in Equation 12.5 decreases rapidly with decreasing suction, and c' is generally small at saturation. On the other hand, residual soils that are composed of a mineral skeleton held together by cementation may have an undrained shear strength that is unaffected by the water content. Such soils may show appreciable strength in spite of high water content and high porosity (Wallace 1973).

Colluvium presents some particular problems. The extremely heterogeneous nature of the material makes sampling and testing difficult. Results of tests on the finer matrix are likely to underestimate the shear strength.

Failure of slopes on residual soils and colluvium most frequently occurs during wet periods when there is an increase in moisture content and a decrease in suction. Stability of slopes may be determined by means of effective stress analysis and c', ϕ', and ϕ''. It is necessary to estimate the suction $u_w - u_a$ (Anderson and Pope 1984). In many cases in situ measurement of suction is necessary (Brand 1982; Krahn et al. 1989). If the soil is likely to be saturated, an effective stress analysis for the saturated condition provides a conservative estimate of the stability. If a total stress analysis is used, it is necessary to estimate the strength that corresponds to the in situ moisture content.

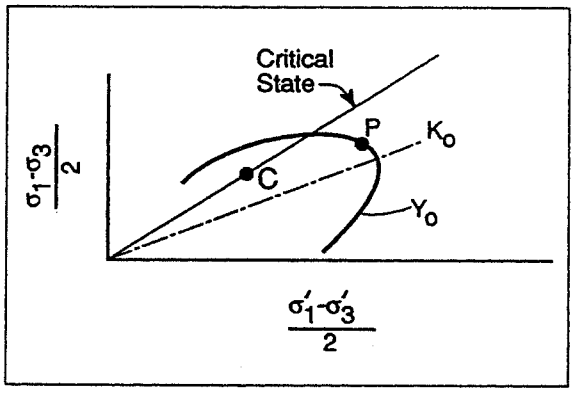

FIGURE 12-13
Strength envelopes of sensitive soils.

REFERENCES

Aas, G., S. Lacasse, T. Lunne, and K. Hoeg. 1986. Use of In Situ Tests for Foundation Design on Clay. In *Use of In Situ Tests in Geotechnical Engineering* (S.P. Clemence, ed.), Geotechnical Special Publication 6, American Society of Civil Engineers, New York, pp. 1–30.

Andersen, K.H., A. Kleven, and D. Heien. 1988. Cyclic Soil Data for Design of Gravity Structures. *Journal of Geotechnical Engineering*, ASCE, Vol. 114, No. 5, pp. 517–539.

Anderson, M.G, and R.G. Pope. 1984. The Incorporation of Soil Physics Models into Geotechnical Studies of Landslide Behavior. In *Proc., Fourth*

International Symposium on Landslides, Canadian Geotechnical Society, Toronto, Vol. 1, pp. 349–353.

Baguelin, F., J.F. Jezequel, E. Le Mee, and A. Le Mehaute. 1972. Expansion of Cylindrical Probes in Cohesive Soils. *Journal of the Soil Mechanics and Foundations Division*, ASCE, Vol. 98, No. SM11, pp. 1129–1142.

Bishop, A.W. 1966. The Strength of Soils as Engineering Materials. *Geotechnique*, Vol. 16, No. 2, pp. 91–128.

Bishop, A.W., and L. Bjerrum. 1960. The Relevance of the Triaxial Test to the Solution of Stability Problems. In *Proc., Research Conference on Shear Strength of Cohesive Soils*, Boulder, Colorado, American Society of Civil Engineers, New York, pp. 437–501.

Bishop, A.W., and D.J. Henkel. 1962. *The Measurement of Soil Properties in the Triaxial Test*. Edward Arnold Publishers, London, 227 pp.

Bjerrum, L. 1967. Progressive Failure in Slopes of Overconsolidated Plastic Clay and Clay Shales. *Journal of the Soil Mechanics and Foundations Division*, ASCE, Vol. 93, No. 5, pp. 1–49.

Bjerrum, L. 1973. Problems of Soil Mechanics and Construction on Soft Clays and Structurally Unstable Soils. In *Proc., Eighth International Conference on Soil Mechanics and Foundation Engineering*, Moscow, Vol. 3, pp. 111–159.

Bjerrum, L., and A. Landva. 1966. Direct Simple-Shear Tests on a Norwegian Quick Clay. *Geotechnique*, Vol. 16, No. 1, pp. 1–20.

Brand, E.W. 1982. Analysis and Design in Residual Soils. In *Engineering and Construction in Tropical and Residual Soils*, American Society of Civil Engineers, New York, pp. 89–143.

Burland, J.B. 1990. On the Compressibility and Shear Strength of Natural Clays. *Geotechnique*, Vol. 40, No. 3, pp. 329–378.

Cadling, L., and S. Odenstad. 1950. The Vane Borer: An Apparatus for Determining the Shear Strength of Clay Soils Directly in the Ground. In *Proc., Swedish Geotechnical Institute*, No. 2, 88 pp.

Casagrande, A. 1936. Characteristics of Cohesionless Soils Affecting the Stability of Earth Fills. *Journal of the Boston Society of Civil Engineers*, Jan., pp. 13–32.

Casagrande, A. 1976. *Liquefaction and Cyclic Deformation of Sands—A Critical Review*. Soil Mechanics Series 88. Harvard University, Cambridge, Mass.

Casagrande, A., and S.D. Wilson. 1951. Effect of Rate of Loading on the Strength of Clays and Shales at Constant Water Content. *Geotechnique*, Vol. 2, No. 3, pp. 251–263.

Castro, G. 1975. Liquefaction and Cyclic Mobility of Saturated Sands. *Journal of the Geotechnical Engineering Division*, ASCE, Vol. 101, No. GT6, pp. 551–569.

Chandler, R.J. 1984. Recent European Experience of Landslides in Heavily Over Consolidated Clays and Soft Rocks. In *Proc., Fourth International Symposium on Landslides*, Canadian Geotechnical Society, Toronto, Vol. 1, pp. 61–81.

Clayton, C.R.I., D.W. Hight, and R.J. Hopper. 1992. Progressive Restructuring of Bothkennar Clay: Implications for Sampling and Reconsolidation Procedures. *Geotechnique*, Vol. 42, No. 2, pp. 219–240.

Datta, M., S.K. Gulhati, and G.V. Rao. 1982. Engineering Behavior of Carbonate Soils of India and Some Observations on Classification of Such Soils. In *Geotechnical Properties, Behavior, and Performance of Calcareous Soils*, Special Technical Publication 777, ASTM, Philadelphia, Pa., pp. 113–140.

Deere, D.U., and F.D. Patton. 1971. Slope Stability in Residual Soils. In *Proc., Fourth Pan-American Conference on Soil Mechanics and Foundation Engineering*, San Juan, Puerto Rico, Vol. 1, pp. 87–170.

Desai, C.S., and H.J. Siriwardane. 1984. *Constitutive Laws for Engineering Materials*. Prentice-Hall, Englewood Cliffs, N.J., 468 pp.

Donald, I.B., D.O. Jordan, R.J. Parker, and C.T. Toh. 1977. The Vane Test—A Critical Appraisal. In *Proc., Ninth International Conference on Soil Mechanics and Foundation Engineering*, Tokyo, Vol. 1, pp. 81–88.

Drucker, D.C., R.E. Gibson, and D.H. Henkel. 1955. Soil Mechanics and Work Hardening Theories of Plasticity. In *Proc., American Society of Civil Engineers*, Vol. 81, No. 798.

Duncan, J.M., and A.L. Buchignani. 1973. Failure of Underwater Slope in San Francisco Bay. *Journal of Soil Mechanics and Foundations Division*, ASCE, Vol. 99, No. SM9, pp. 687–703.

Duncan, J.M., and P. Dunlop. 1969. Slopes in Stiff-Fissured Clays and Shales. *Journal of the Soil Mechanics and Foundations Division*, ASCE, Vol. 95, No. 2, pp. 471–493.

Foss, I. 1977. Red Soil from Kenya as a Foundation Material. In *Proc., Eighth International Conference on Soil Mechanics and Foundation Engineering*, Moscow, Vol. 2, pp. 73–80.

Fredlund, D.G., and H. Rohardjo. 1993. *Soil Mechanics for Unsaturated Soils*. John Wiley & Sons, New York, 517 pp.

Fredlund, D.G., N.R. Morgenstern, and R.A. Widger. 1978. The Shear Strength of Unsaturated Soils. *Canadian Geotechnical Journal*, Vol. 15, No. 3, pp. 313–321.

Gibbs, H.J., and W.H. Holtz. 1957. Research on Determining the Density of Sands by Spoon Penetration Testing. In *Proc., Fourth International Conference on Soil Mechanics and Foundation Engineering*, Butterworths Scientific Publications, London, Vol. 1, pp. 35–39.

Gibson, R.E., and W.F. Anderson. 1961. In Situ Measurement of Soil Properties with the Pressure Meter. *Civil Engineering and Public Works Review*, Vol. 56, pp. 615–618.

Handy, R.L., and N.S. Fox. 1967. A Soil Bore-Hole Direct-Shear Test Device. *Highway Research News*, No. 27, HRB, National Research Council, Washington, D.C., pp. 42–51.

Handy, R.L., J.H. Schmertmann, and A.J. Lutenegger. 1985. Borehole Shear Tests in a Shallow Marine Environment. In *Strength Testing of Marine Sediments*, Special Technical Publication 883, ASTM, Philadelphia, Pa., pp. 140–153.

Hansbo, S. 1957. A New Approach to the Determination of the Shear Strength of Clay by the Fall-Cone Test. In *Proc., Swedish Geotechnical Institute*, No. 14, 47 pp.

Henkel, D.J. 1960. The Shear Strength of Saturated Remolded Clays. In *Proc., Research Conference on Shear Strength of Cohesive Soils*, Boulder, Colorado, American Society of Civil Engineers, New York, pp. 533–554.

Henkel, D.J., and N.H. Wade. 1966. Plane Strain Tests on a Saturated Remolded Clay. *Journal of the Soil Mechanics and Foundations Division*, ASCE, Vol. 92, No. SM6, pp. 67–80.

Hight, D.W., R. Böese, A.P. Butcher, and C.R.I. Clayton. 1992. Disturbance of the Bothkennar Clay Prior to Laboratory Testing. *Geotechnique*, Vol. 42, No. 2, pp. 199–218.

Hill, R. 1950. *The Mathematical Theory of Plasticity*. Oxford University Press, London, 355 pp.

Ho, D.Y.F., and D.G. Fredlund. 1982. Increase in Strength due to Suction for two Hong Kong Soils. In *Engineering and Construction in Tropical and Residual Soils*, American Society of Civil Engineers, New York, pp. 263–295.

Holtz, R.D., and W.D. Kovacs. 1981. *An Introduction to Geotechnical Engineering*. Prentice-Hall, Inc., Englewood Cliffs, N.J., 731 pp.

Jewell, R.A., and C.P. Wroth. 1987. Direct Shear Tests on Reinforced Sand. *Geotechnique*, Vol. 37, No. 1, pp. 53–68.

Kenney, T.C. 1967. The Influence of Mineral Composition on the Residual Strength of Natural Soils. In *Proc., Geotechnical Conference on Shear Strength Properties of Natural Soils and Rocks*, Oslo, Vol. 1, pp. 123–129.

Krahn, J., D.G. Fredlund, and M.J. Klassen. 1989. Effect of Soil Suction on Slope Stability at Notch Hill. *Canadian Geotechnical Journal*, Vol. 26, No. 2, pp. 269–278.

Ladd, C.C. 1991. Stability Evaluation During Staged Construction. *Journal of Geotechnical Engineering*, ASCE, Vol. 117, No. 4, pp. 540–615.

Ladd, C.C., and R. Foott. 1974. New Design Procedure for Stability of Soft Clays. *Journal of the Geotechnical Engineering Division*, ASCE, Vol. 100, No. GT7, pp. 763–786.

Ladd, C.C., R. Foott, K. Ishihara, F. Schlosser, and H.G. Poulos. 1977. Stress-Deformation and Strength Characteristics. In *Proc., Ninth International Conference on Soil Mechanics and Foundation Engineering*, Tokyo, Vol. 2, pp. 421–494.

Ladd, C.C., and T.W. Lambe. 1964. The Strength of "Undisturbed" Clay Determined from Undrained Tests. In *Proc., Symposium on Laboratory Shear Testing of Soils*, Ottawa, Canada, Special Technical Publication 361, ASTM, Philadelphia, Pa., pp. 342–371.

Lade, P.V. 1992. Static Instability and Liquefaction of Loose Fine Sandy Soils. *Journal of Geotechnical Engineering*, ASCE, Vol. 118, No. 1, pp. 51–71.

Lambe, T.W., and R.V. Whitman. 1969. *Soil Mechanics*. John Wiley & Sons, New York, 553 pp.

Lunne, T., S. Lacasse, and N.S. Rad. 1989. SPT, CPT, Pressuremeter Testing and Recent Developments. In *Proc., 12th International Conference on Soil Mechanics and Foundation Engineering*, Rio de Janeiro, A.A. Balkema, Rotterdam, Netherlands, Vol. 4, pp. 2339–2403.

Lupini, J.F., A.E. Skinner, and P.R. Vaughan. 1981. The Drained Residual Strength of Cohesive Soils. *Geotechnique*, Vol. 31, No. 2, pp. 181–214.

Lutenegger, A.J., and G.R. Hallberg. 1981. Borehole Shear Test in Geotechnical Investigations. In *Laboratory Shear Strength of Soil*, Special Technical Publication 740, ASTM, Philadelphia, Pa., pp. 566–578.

Marchetti, S. 1975. A New In Situ Test for the Measurement of Horizontal Soil Deformability. In *Proc., Specialty Conference on In Situ Measurement of Soil Properties*, Raleigh, N.C., American Society of Civil Engineers, New York, Vol. 2, pp. 255–259.

Marchetti, S. 1980. In Situ Tests by Flat Dilatometer. *Journal of the Geotechnical Engineering Division*, ASCE, Vol. 106, No. GT3, pp. 299–321.

Marcuson, W.F. III, and W.A. Bieganousky. 1977. Laboratory Standard Penetration Tests on Fine Sands. *Journal of the Geotechnical Engineering Division*, ASCE, Vol. 103, No. GT6, pp. 565–588.

Menard, L. 1965. Rules for Calculation of Bearing Capacity and Foundation Settlement Based on Pressuremeter Tests. In *Proc., Sixth International Conference on Soil Mechanics and Foundation Engineering*, Montreal, University of Toronto Press, Canada, Vol. 2, pp. 295–299.

Mesri, G., and A.F. Cepeda-Diaz. 1986. Residual Shear Strength of Clays and Shales. *Geotechnique*, Vol. 36, No. 2, pp. 269–274.

Mitchell, J. K., and T. A. Lunne. 1978. Cone Resistance as a Measure of Soil Strength. *Journal of the Geotechnical Engineering Division*, ASCE, Vol. 104, No. GT7, pp. 995–1012.

Mitchell, J.K., and N. Sitar. 1982. Engineering Properties of Tropical Residual Soils. In *Engineering and Construction in Tropical and Residual Soils*, American Society of Civil Engineers, New York, pp. 30–57.

Mitchell, J.K., and W.N. Houston. 1969. Causes of Clay Sensitivity. *Journal of the Soil Mechanics and Foundations Division*, ASCE, Vol. 95, No. SM3, pp. 845–871.

Morgenstern, N.R., and J.S. Tchalenko. 1967. Microscopic Structures in Kaolinite Subjected to Direct Shear. *Geotechnique*, Vol. 17, No. 4, pp. 309–328.

Orchant, C.J., F.H. Kulhawy, and C.H. Trautmann. 1988. *Reliability-Based Foundation Design for Transmission Line Structures*, Vol. 2. Geotechnical Engineering Group, Cornell University, Ithaca, N.Y., 166 pp.

O'Rourke, T.D., and E. Crespo. 1988. Geotechnical Properties of Cemented Volcanic Soil. *Journal of Geotechnical Engineering*, ASCE, Vol. 114, No. 10, pp. 1126–1147.

Peck, R.B., W.E. Hanson, and T.H. Thornburn. 1974. *Foundation Engineering*, 2nd ed. John Wiley & Sons, New York, 514 pp.

Pilot, G., B. Trak, and P. LaRochelle. 1982. Effective Stress Analysis of the Stability of Embankments on Soft Soils. *Canadian Geotechnical Journal*, Vol. 19, No. 4, pp. 433–450.

Poulos, S.J., G. Castro, and J. France. 1985. Liquefaction Evaluation Procedure. *Journal of Geotechnical Engineering*, ASCE, Vol. 111, No. 6, pp. 772–792.

Sangrey, D.A., D.J. Henkel, and M.I. Esrig. 1969. The Effective Stress Response of a Saturated Clay Soil to Repeated Loading. *Canadian Geotechnical Journal*, Vol. 6, No. 3, pp. 241–252.

Schmertmann, J.H. 1975. Measurement of In Situ Shear Strength. In *Proc., Conference on In Situ Measurement of Soil Properties*, Raleigh, N.C., American Society of Civil Engineers, New York, Vol. 2, pp. 57–138.

Schmertmann, J.H. 1982. Method for Determining the Friction Angle in Sands. In *Proc., Second European Symposium on Penetration Testing*, Amsterdam, Vol. 2, pp. 853–862.

Schofield A., and P. Wroth. 1968. *Critical State Soil Mechanics*. McGraw-Hill Book Co., New York, 310 pp.

Seed, H.B. 1979. Considerations in the Earthquake-Resistant Design of Earth and Rockfill Dams. *Geotechnique*, Vol. 29, No. 3, pp. 215–263.

Seed, H.B., and K.L. Lee. 1967. Liquefaction of Saturated Sands During Cyclic Loading. *Journal of the Soil Mechanics and Foundations Division*, ASCE, Vol. 92, No. SM6, pp. 105–134.

Seed, H.B., K. Tokimatsu, L.F. Harder, and R.M. Chung. 1985. Influence of STP Procedures in Soil Liquefaction Resistance Evaluation. *Journal of Geotechnical Engineering*, ASCE, Vol. 111, No. 12, pp. 1425–1445.

Skempton, A.W. 1948. A Study of the Geotechnical Properties of Some Post-Glacial Clays. *Geotechnique*, Vol. 1, No. 1, pp. 7–22.

Skempton, A.W. 1954. The Pore-Pressure Coefficients A and B. *Geotechnique*, Vol. 4, No. 4, pp. 143–147.

Skempton, A.W., and H.Q. Golder. 1948. Practical Examples of the $\phi = 0$ Analysis of Stability of Clays. In *Proc., Second International Conference on Soil Mechanics and Foundation Engineering*, Rotterdam, Vol. 2, pp. 63–70.

Skempton, A.W., and D.J. Petley. 1967. The Strength Along Structural Discontinuities in Stiff Clays. In *Proc., Geotechnical Conference on Shear Strength Properties of Natural Soils and Rocks*, Oslo, Vol. 2, pp. 29–46.

Skempton, A.W., and J.N. Hutchinson. 1969. Stability of Natural Slopes and Embankment Foundations. In *Proc., Seventh International Conference on Soil Mechanics and Foundation Engineering*, Mexico City, pp. 291–340.

Sladen, J.A., R.D. Hollander, and J. Krahn. 1985. The Liquefaction of Sands. *Canadian Geotechnical Journal*, Vol. 22, No. 4, pp. 564–578.

Tavenas, F., and S. Leroueil. 1977. Effects of Stress and Time on Yielding of Clays. In *Proc., Ninth International Conference on Soil Mechanics and Foundation Engineering*, Tokyo, Vol. 1, pp. 319–326.

Tavenas, F., and S. Leroueil. 1980. The Behavior of Embankments on Clay Foundations. *Canadian Geotechnical Journal*, Vol. 17, No. 2, pp. 236–260.

Terzaghi, K. 1936a. The Shearing Resistance of Saturated Soils and the Angle Between Planes of Shear. In *Proc., First International Conference on Soil Mechanics and Foundation Engineering*, Cambridge, Harvard University Press, Vol. 1, pp. 54–56.

Terzaghi, K. 1936b. Stability of Slopes of Natural Clay. In *Proc., First International Conference on Soil Mechanics and Foundation Engineering*, Cambridge, Harvard University Press, Vol. 1, pp. 161–165.

Terzaghi, K., and R.B. Peck. 1948. *Soil Mechanics in Engineering Practice*. John Wiley & Sons, New York, 566 pp.

Thiers, G.R., and H.B. Seed. 1969. Strength and Stress-Strain Characteristics of Clays Subjected to Seismic Loads. In *Symposium on Vibration Effects of Earthquakes on Soils and Foundations*, Special Technical Publication 450, ASTM, Philadelphia, Pa., pp. 3–56.

Vesic, A.S., and G.W. Clough. 1968. Behavior of Granular Materials under High Stresses. *Journal of Soil Mechanics and Foundations Division*, ASCE, Vol. 94, No. SM3, pp. 661–668.

Wallace, K.B. 1973. Structural Behaviour of Residual Soils of the Continually Wet Highlands of Papua New Guinea. *Geotechnique*, Vol. 23, No. 2, pp. 203–218.

Wroth, C.P. 1984. The Interpretation of In Situ Soil Tests. *Geotechnique*, Vol. 34, No. 4, pp. 449–489.

Wu, T.H., I-M. Lee, J.C. Potter, and O. Kjekstad. 1987a. Uncertainities in Evaluation of Strength of Marine Sand. *Journal of Geotechnical Engineering*, ASCE, Vol. 113, No. 7, pp. 719–738.

Wu, T.H., R.L. Williams, J.E. Lynch, and P.H.S.W. Kulatilake. 1987b. Stability of Slopes in Red Conemough Shale of Ohio. *Journal of Geotechnical Engineering*, ASCE, Vol. 113, No. 3, pp. 248–264.

Chapter 13

J. MICHAEL DUNCAN

SOIL SLOPE STABILITY ANALYSIS

Analyses of slopes can be divided into two categories: those used to evaluate the stability of slopes and those used to estimate slope movement. Although stability and movement are closely related, two different and distinct types of analyses are almost always used to evaluate them.

1. INTRODUCTION

Stability of slopes is usually analyzed by methods of limit equilibrium. These analyses require information about the strength of the soil, but do not require information about its stress-strain behavior. They provide no information about the magnitude of movements of the slope.

Movements of slopes are usually analyzed by the finite-element method. Understanding the stress-strain behavior of the soils is required for these analyses, and information regarding the strengths of the soils may also be required. Although these methods define movements and stresses throughout the slope, they do not provide a direct measure of stability, such as the factor of safety calculated by limit equilibrium analyses.

The focus in this chapter is on soil slopes and mechanisms involving shear failure within the soil mass. The methods described are applicable to landslides in weak rocks, where the location of the rupture surface is not controlled by existing discontinuities within the mass (see also Chapter 21). Analyses of slopes in strong rock, where instability mechanisms are controlled by existing discontinuities, are described in Chapter 15. Techniques for evaluating rock strength are discussed in Chapter 14, and those for evaluating soil strength are discussed in Chapter 12.

Limit equilibrium and finite-element analyses are described in subsequent sections of this chapter. Methods that are useful for practical purposes are emphasized, and their uses are illustrated by examples.

2. MECHANICS OF LIMIT EQUILIBRIUM ANALYSES

In limit equilibrium techniques, slope stability is analyzed by first computing the factor of safety. This value must be determined for the surface that is most likely to fail by sliding, the so-called *critical slip surface*. Iterative procedures are used, each involving the selection of a potential sliding mass, subdivision of this mass into a series of slices, and consideration of the equilibrium of each of these slices by one of several possible computational methods. These methods have varying degrees of computational accuracy depending on the suitability of the underlying simplifying assumptions for the situation being analyzed.

2.1 Factor of Safety

The factor of safety is defined as the ratio of the shear strength divided by the shear stress required for equilibrium of the slope:

$$F = \frac{\text{shear strength}}{\text{shear stress required for equilibrium}} \quad (13.1)$$

which can be expressed as

$$F = \frac{c + \sigma\tan\phi}{\tau_{eq}} \quad (13.2)$$

in which

F = factor of safety,
c = cohesion intercept on Mohr-Coulomb strength diagram,
ϕ = angle of internal friction of soil,
σ = normal stress on slip surface, and
τ_{eq} = shear stress required for equilibrium.

The cohesive and frictional components of strength (c and ϕ) are defined in Chapter 12.

The factor of safety defined by Equations 13.1 and 13.2 is an overall measure of the amount by which the strength of the soil would have to fall short of the values described by c and ϕ in order for the slope to fail. This strength-related definition of F is well suited for practical purposes because soil strength is usually the parameter that is most difficult to evaluate, and it usually involves considerable uncertainty.

In discussing equilibrium methods of analysis, it is sometimes said that the factor of safety is assumed to have the same value at all points on the slip surface. It is unlikely that this would ever be true for a real slope. Because the assumption is unlikely to be true, describing this assumption as one of the fundamental premises of limit equilibrium methods seems to cast doubt on their practicality and reliability. It is therefore important to understand that Equation 13.1 defines F, and it does not involve the assumption that F is the same at all points along the slip surface for a slope not at failure. Rather, F is the numerical answer to the question, By what factor would the strength have to be reduced to bring the slope to failure by sliding along a particular potential slip surface? The answer to this question can be determined reliably by limit equilibrium methods and is of considerable practical value.

To calculate a value of F as described above, a potential slip surface must be described. The slip surface is a mechanical idealization of the surface of rupture (see Chapter 3, Section 3.1 and Table 3-3). In general, each potential slip surface results in a different value of F. The smaller the value of F (the smaller the ratio of shear strength to shear stress required for equilibrium), the more likely failure is to occur by sliding along that surface. Of all possible slip surfaces, the one where sliding is most likely to occur is the one with the minimum value of F. This is the *critical slip surface*.

To evaluate the stability of a slope by limit equilibrium methods, it is necessary to perform calculations for a considerable number of possible slip surfaces in order to determine the location of the critical slip surface and the corresponding minimum value of F. This process is described as searching for the critical slip surface. It is an essential part of slope stability analyses.

2.2 Equations and Unknowns

All of the practically useful methods of analysis are methods of slices, so called because they subdivide the potential sliding mass into slices for purposes of analysis. Usually the slice boundaries are vertical, as shown in Figure 13-1. Two useful simplifications are achieved by subdividing the mass into slices:

1. The base of each slice passes through only one type of material, and
2. The slices are narrow enough that the segments of the slip surface at the base of each slice can be accurately represented by a straight line.

The equilibrium conditions can be considered slice by slice. If a condition of equilibrium is sat-

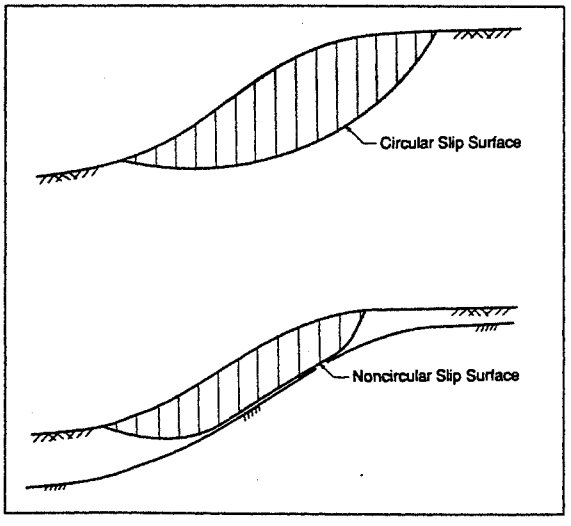

FIGURE 13-1
Division of potential sliding masses into slices (slip surface is idealization of surface of rupture; see Chapter 3, Section 3.1).

isfied for each and every slice, it is also satisfied for the entire mass. The forces on a slice are shown in Figure 13-2.

The number of equations of equilibrium available depends on the number of slices (N) and the number of equilibrium conditions that are used. As shown in Table 13-1, the number of equations available is $2N$ if only force equilibrium is to be satisfied and $3N$ if both force and moment equilibria are to be satisfied. If only force equilibrium is satisfied, the number of unknowns is $3N - 1$. If both force and moment equilibria are satisfied, the number of unknowns is $5N - 2$. In the special case in which $N = 1$, the problem is statically determinate, and the number of equilibrium equations is equal to the number of unknowns. To represent a slip surface with realistic shapes, it is usually necessary to use 10 to 40 slices, and the number of unknowns therefore exceeds the number of equations. The excess of unknowns over equations is $N - 1$ for force equilibrium analyses and $2N - 2$ for analyses that satisfy all conditions of equilibrium. Thus, such problems are statically indeterminate, and assumptions are required to make up the imbalance between equations and unknowns.

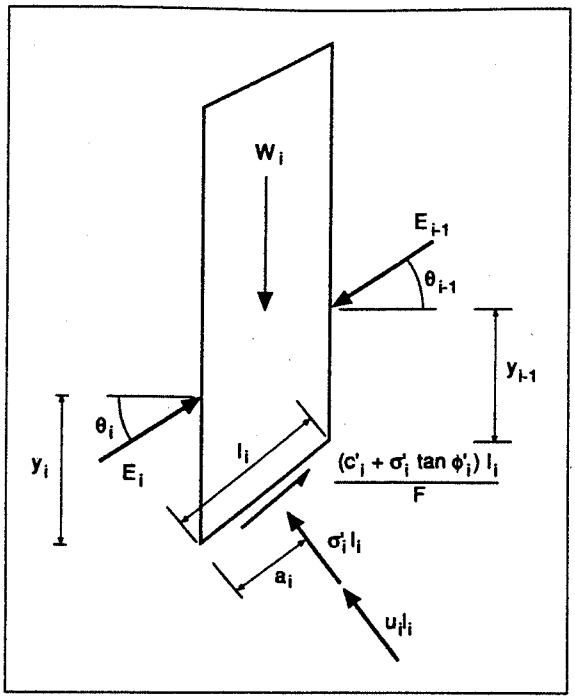

FIGURE 13-2
Forces on slice i.

2.3 Characteristics of Methods

The various methods of limit equilibrium analysis differ from each other in two regards:

1. Different methods use different assumptions to make up the balance between equations and unknowns, and
2. Some methods, such as the ordinary method of slices (Fellenius 1927) and Bishop's modified method (Bishop 1955), do not satisfy all conditions of equilibrium or even the conditions of force equilibrium.

Table 13-1
Equations and Unknowns in Limit Equilibrium Analysis of Slope Stability

EQUATIONS	UNKNOWNS
Methods That Satisfy Only Force Equilibrium	
N = horizontal equilibrium	N = normal forces on bases of slices
N = vertical equilibrium	$N - 1$ = side forces
	$N - 1$ = side force angles, θ
	1 = factor of safety
$2N$ total equations	$3N - 1$ total unknowns
Methods That Satisfy Both Force and Moment Equilibria	
N = horizontal equilibrium	N = normal forces on bases of slices
N = vertical equilibrium	N = locations of normal forces on bases
N = moment equilibrium	$N - 1$ = side forces
	$N - 1$ = side force angles, θ
	$N - 1$ = locations of side forces on slices
	1= factor of safety
$3N$ total equations	$5N - 2$ total unknowns

These methods therefore involve fewer equations and unknowns than those shown in Table 13-1. The characteristics of various practically used methods with regard to the conditions of equilibrium that they satisfy, the assumptions they involve, and their computational accuracies are summarized in Table 13-2.

2.4 Computational Accuracy

"Computational accuracy" here refers to the inherent accuracy with which the various methods handle the mechanics of slope stability and the limitations on accuracy that result from the fact that the equations of equilibrium are too few to solve for the factor of safety without using assumptions. The computational accuracy involves only the accuracy with which the shear stress required for equilibrium (τ_{eq}) and the normal stress σ can be evaluated. Computational accuracy is thus distinct from overall accuracy, which involves also the accuracy with which site conditions and shear strengths can be evaluated. By separating issues that determine computational accuracy from the other issues, it is possible to answer the following important questions:

1. Do any of the various limit equilibrium methods provide accurate values of F, and
2. How are the values of F affected by the assumptions involved in the various methods?

Table 13-2
Characteristics of Commonly Used Methods of Limit Equilibrium Analysis for Slope Stability

Method	Limitations, Assumptions, and Equilibrium Conditions Satisfied
Ordinary method of slices (Fellenius 1927)	Factors of safety low—very inaccurate for flat slopes with high pore pressures; only for circular slip surfaces; assumes that normal force on the base of each slice is $W \cos \alpha$; one equation (moment equilibrium of entire mass), one unknown (factor of safety)
Bishop's modified method (Bishop 1955)	Accurate method; only for circular slip surfaces; satisfies vertical equilibrium and overall moment equilibrium; assumes side forces on slices are horizontal; $N+1$ equations and unknowns
Force equilibrium methods (Section 6.1.3)	Satisfy force equilibrium; applicable to any shape of slip surface; assume side force inclinations, which may be the same for all slices or may vary from slice to slice; small side force inclinations result in values of F less than calculated using methods that satisfy all conditions of equilibrium; large inclinations result in values of F higher than calculated using methods that satisfy all conditions of equilibrium; $2N$ equations and unknowns
Janbu's simplified method (Janbu 1968)	Force equilibrium method; applicable to any shape of slip surface; assumes side forces are horizontal (same for all slices); factors of safety are usually considerably lower than calculated using methods that satisfy all conditions of equilibrium; $2N$ equations and unknowns
Modified Swedish method (U.S. Army Corps of Engineers 1970)	Force equilibrium method, applicable to any shape of slip surface; assumes side force inclinations are equal to the inclination of the slope (same for all slices); factors of safety are often considerably higher than calculated using methods that satisfy all conditions of equilibrium; $2N$ equations and unknowns
Lowe and Karafiath's method (Lowe and Karafiath 1960)	Generally most accurate of the force equilibrium methods; applicable to any shape of slip surface; assumes side force inclinations are average of slope surface and slip surface (varying from slice to slice); satisfies vertical and horizontal force equilibrium; $2N$ equations and unknowns
Janbu's generalized procedure of slices (Janbu 1968)	Satisfies all conditions of equilibrium; applicable to any shape of slip surface; assumes heights of side forces above base of slice (varying from slice to slice); more frequent numerical convergence problems than some other methods; accurate method; $3N$ equations and unknowns
Spencer's method (Spencer 1967)	Satisfies all conditions of equilibrium; applicable to any shape of slip surface; assumes that inclinations of side forces are the same for every slice; side force inclination is calculated in the process of solution so that all conditions of equilibrium are satisfied; accurate method; $3N$ equations and unknowns
Morgenstern and Price's method (Morgenstern and Price 1965)	Satisfies all conditions of equilibrium; applicable to any shape of slip surface; assumes that inclinations of side forces follow a prescribed pattern, called $f(x)$; side force inclinations can be the same or can vary from slice to slice; side force inclinations are calculated in the process of solution so that all conditions of equilibrium are satisfied; accurate method; $3N$ equations and unknowns
Sarma's method (Sarma 1973)	Satisfies all conditions of equilibrium; applicable to any shape of slip surface; assumes that magnitudes of vertical side forces follow prescribed patterns; calculates horizontal acceleration for barely stable equilibrium; by prefactoring strengths and iterating to find the value of the prefactor that results in zero horizontal acceleration for barely stable equilibrium, the value of the conventional factor of safety can be determined; $3N$ equations, $3N$ unknowns

Studies of computational accuracy have shown the following:

1. If the method of analysis satisfies all conditions of equilibrium, the factor of safety will be accurate within ±6 percent. This conclusion is based on the finding that factors of safety calculated using methods that satisfy all conditions of equilibrium never differ by more than 12 percent from each other or ±6 percent from a central value as long as the methods involve reasonable assumptions. The methods of Morgenstern and Price (1965), Spencer (1967), and Sarma (1973) and the generalized procedure of slices (GPS) (Janbu 1968) satisfy all conditions of equilibrium and involve reasonable assumptions. Studies have shown that values of F calculated using these methods differ by no more than 6 percent from values calculated using the log spiral method and the finite-element method, which satisfy all conditions of equilibrium but are not methods of slices.
2. Bishop's modified method is a special case. Although it does not satisfy all conditions of equilibrium, it is as accurate as methods that do. It is limited to circular slip surfaces.
3. No matter what method of analysis is used, it is essential to perform a thorough search for the critical slip surface to ensure that the minimum factor of safety has been calculated.

2.5 Checking Accuracy of Analyses

When slope stability analyses are performed, it is desirable to have an independent check of the results as a guard against mistakes. Unfortunately, computations using methods that satisfy all conditions of equilibrium are lengthy and complex, too involved for hand calculation. It is therefore more practical to use other, simpler types of analyses that can be performed by hand to check computer analyses.

When analyses are performed using circular slip surfaces, the factor of safety for the critical circle can be checked approximately by using the ordinary method of slices or Bishop's modified method. The ordinary method of slices gives values of F that are lower than values calculated by more accurate methods. For total stress analyses the difference is seldom more than 10 percent, but it may reach 50 percent for effective stress analyses under conditions involving high pore pressures. Bishop's modified method, only slightly more time-consuming than the ordinary method of slices, is as accurate as the methods that satisfy all conditions of equilibrium.

Charts provide a simple and effective means of checking slope stability analyses. Although approximations and simplifications are always necessary when charts are used, it is usually possible to calculate the factor of safety with sufficient accuracy to afford a useful check on the results of more detailed analyses. It is also useful to perform chart analyses before detailed computer analyses in order to get the best possible understanding of the problem.

When analyses are performed using noncircular slip surfaces, the results can be checked by hand for the critical slip surface using force equilibrium analyses. If Spencer's method is used for the computer analyses, the results for the critical slip surface can be checked by hand using force equilibrium analyses with the same side force inclination. If Morgenstern and Price's method or Janbu's GPS is used for the computer analyses, the force equilibrium hand calculations can be performed using an average side force inclination determined from the computer analyses.

Another means of checking computer analyses of slope stability is to perform independent analyses using another computer program and completely separate input. It is always desirable to have a different person perform the check analyses to make them as independent as possible.

3. DRAINED AND UNDRAINED CONDITIONS

Slope failures may occur under drained or undrained conditions in the soils that make up the slope. If instability is caused by changes in loading, such as removal of material from the bottom of the slope or increase in loads at the top, soils that have low values of permeability may not have time to drain during the length of time in which the loads are changed; thus they may contain unequalized excess pore pressures leading to slope failure. In that case, these low-permeability soils are said to be undrained. Under the same rates of loading, soils with higher permeabilities may have time to drain and will have no significant excess pore pressures.

One of the most important determinations needed for slope stability analyses is that of the

drainage conditions in the various soils that form the slope. A rational way of making this determination is to calculate the value of the dimensionless time factor T using the following equation:

$$T = \frac{C_v t}{D^2} \tag{13.3}$$

where

T = dimensionless time factor,
C_v = coefficient of consolidation (length squared per unit of time),
t = time for drainage to occur (units of time), and
D = length of drainage path (units of length).

D is the distance water would have to flow to drain from the soil zone. Usually D is defined as half the thickness of the soil layer or zone. If the soil zone is drained on only one side, D is equal to the thickness of the zone.

If the value of T is 3.0 or more, the soil zone will drain as rapidly as the loads are applied, and the soil within the zone can be treated as fully drained in the analysis. If the value of T is 0.01 or less, very little drainage will occur during the loading period, and the soil within the zone can be treated as completely undrained in the analysis. If the value of T is between 0.01 and 3.0, partial drainage will occur during the period of time when the loads are changing. In that case both drained and undrained conditions should be analyzed to bound the problem. For normal rates of loading, involving weeks or months, soils with permeabilities greater than 10^{-4} cm/sec are usually drained, and soils with permeabilities less than 10^{-7} cm/sec are usually undrained. Silts, which have permeabilities between 10^{-4} and 10^{-7} cm/sec, are often partially drained.

If instability in a slope is caused by increasing pore-water pressures *within* the slope, failure occurs under drained conditions by definition because adjustment of internal pore pressures in equilibrium with the flow boundary conditions is drainage. Changes in internal water pressures are often the cause of instability in natural slopes, where landslides almost always occur during wet periods. Such problems should be analyzed as drained conditions.

4. TOTAL STRESS AND EFFECTIVE STRESS ANALYSES

Stability of slopes can be analyzed using either effective stress or total stress methods:

- In effective stress analyses the shear strength of the soil is related to the effective normal stress on the potential slip surface by means of effective stress shear strength parameters. Pore pressures within the soil must be known and are part of the information required for analysis.
- In total stress analyses the shear strength of the soil is related to the total normal stress on the potential slip surface by means of total stress shear strength parameters. Pore pressures within the soil mass need not be known and are not required as input for analysis.

In principle, it is always possible to analyze stability by using effective stress methods because the strengths of soils are governed by effective stresses under both undrained and drained conditions. In practice, however, it is virtually impossible to determine accurately what excess pore pressures will result from changes in external loading on a slope (excavation, fill placement, or change in external water level). Because the excess pore pressures for these loading conditions cannot be estimated accurately, it is not possible to perform accurate analyses of stability for these conditions using effective stress procedures.

Total stress analyses for soils that do not drain during the loading period involve a simple principle: if an element of soil in the laboratory (a laboratory test specimen) is subjected to the same changes in stress under undrained conditions as an element of the same soil would experience in the field, the same excess pore pressures will develop. Thus, if the total stresses in the laboratory and the field are the same, the effective stresses will also be the same. Because soil strength is controlled by effective stresses, the strength measured in laboratory tests should be the same as the strength in the field if the pore pressures and total stresses are also the same. Thus, under undrained conditions, strengths can be related to total stresses, obviating the need to specify undrained excess pore pressures.

Although the principle outlined in the preceding paragraph is reasonably simple, experience has shown that many factors influence the pore pressures that develop under undrained loading. These factors include degree of saturation, density, stress history of the soil, rate of loading, and the magnitudes and orientations of the applied stresses. As a result, determining total stress-related undrained strengths by means of laboratory or in situ testing

is not a simple matter; considerable attention to detail is required if reliable results are to be achieved. Shear strengths for use in undrained total stress analyses must be measured using test specimens and loading conditions that closely duplicate the conditions in the field. Still, using total stress procedures for analysis of undrained conditions is more straightforward and more reliable than trying to predict undrained excess pore pressures for use in effective stress analyses of undrained conditions.

If a slope consists of soils of widely differing permeabilities, it is possible that the more permeable soils would be drained whereas the less permeable soils would be undrained. In such cases it is logical and permissible in the same analysis to treat the drained soils in terms of effective stresses and the undrained soils in terms of total stresses.

4.1 Shear Strengths

Shear strengths for use in drained effective stress analyses can be measured in two ways:

1. In laboratory or field tests in which loads are applied slowly enough so that the soil is drained (there are no excess pore pressures) at failure, or
2. In laboratory tests such as consolidated-undrained (C-U) laboratory triaxial tests in which pore pressures are measured and the effective stresses at failure can be determined.

Effective stress strength envelopes determined using these two methods have been found to be, for all practical purposes, the same (Bishop and Bjerrum 1960).

Studies by Skempton and his colleagues (Skempton 1970, 1977, 1985) showed that peak drained strengths of stiff, overconsolidated clays determined in laboratory tests are larger than the drained strengths that can be mobilized in the field over a long period of time. Skempton recommended the use of "fully softened" strengths for stiff clays in which there has been no previous sliding. The fully softened strength is measured by remolding the clay in the laboratory at a water content near the liquid limit, reconsolidating it in the laboratory, and measuring its strength in a normally consolidated condition.

Once sliding has occurred in a clay, the clay particles become reoriented parallel to the slip surface, and the strength decreases progressively as sliding displacement occurs, eventually reaching a low residual value. Residual shear strengths should be used to analyze clay slopes in which slope failure by sliding has already occurred (Skempton 1970, 1977, 1985).

Morgenstern (1992) and others have pointed out that drained shear may cause structural collapse in certain sensitive or structured soils, resulting in development of excess pore pressures at a rate that is so rapid that drainage cannot occur. As a result, it is not possible to mobilize the full effective stress shearing resistance under drained conditions. These difficult soils (loose sands and sensitive and highly structured clays) deserve special attention (see Chapter 24 for sensitive clays).

For soils that are partly saturated, such as compacted clays or naturally occurring clayey soils from above the water table, undrained strengths should be measured using unconsolidated-undrained tests on specimens with the same void ratio and the same degree of saturation as the soil in the field. The undrained strength envelope for such soils is curved, and as a result the values of total stress c and ϕ from such tests are not unique. It is important therefore to use a range of confining pressures in the laboratory tests that corresponds to the range of pressures to which the soil is subjected in the field and to select values of c and ϕ that provide a reasonable representation of the strength of the soil in this pressure range. Alternatively, with some slope stability computer programs, it is possible to use a nonlinear strength envelope, represented by a series of points, without reference to c and ϕ.

For soils that are completely saturated, the undrained friction angle is zero ($\phi_u = 0$). Undrained strengths for saturated soils can be determined from unconsolidated-undrained tests or from C-U tests by the Stress History and Normalized Soil Engineering Properties (SHANSEP) procedure (Ladd and Foott 1974).

Unconsolidated-undrained tests are performed on undisturbed test specimens from the field. These tests define the undrained strength of the soil in the field at the time and location where the samples were obtained, provided that the samples are undisturbed. Although some procedures provide samples that are called "undisturbed," no sample is completely free of disturbance effects. For saturated clays, these effects usually cause the undrained strengths measured in laboratory tests to be smaller

than the undrained strength in the field. As a result, unconsolidated-undrained triaxial tests usually give conservative values of undrained strengths.

Ladd and Foott (1974) and others have shown that the effects of disturbance on undrained strength can be compensated for by consolidating clay specimens to higher pressures in the laboratory. Because consolidation to higher pressures produces higher undrained shear strengths, the strengths measured using C-U tests are not directly applicable to field conditions. Ladd and Foott described procedures for determining values of S_u/p (the ratio of undrained strength divided by consolidation pressure) from such tests. The undrained strength in the field is estimated by multiplying the value of S_u/p by the field consolidation pressure. The same procedure can be used to estimate current undrained strengths (using current consolidation pressures) or future undrained strengths (using consolidation pressures estimated for some future condition by means of consolidation analysis).

C-U tests should not be used to determine values of c and ϕ from "total stress" Mohr-Coulomb strength envelopes for use in total stress analyses. This procedure is not valid because the normal stresses used to plot the Mohr's circles of stress at failure are not valid total stresses. These stress circles are plotted using the effective stress at the time of consolidation plus the deviator stress at failure. This procedure is not consistent. The method described by Ladd and Foott avoids the inconsistencies of this method by relating undrained strengths measured in C-U tests to consolidation pressure without the use of c- and ϕ-values. The values of undrained strength (S_u), determined as recommended by Ladd and Foott, are combined with $\phi_u = 0$, the correct undrained friction angle for saturated materials.

4.2 Unit Weights and Water Pressures

The primary requirement in slope stability analyses is to satisfy equilibrium *in terms of total stresses*. This is true whether the analysis is an effective stress analysis (in which shear strengths are related to effective stresses) or a total stress analysis (in which shear strengths are related to total stresses). In either case total stress is the prime variable in terms of the fundamental mechanics of the problem because a correct evaluation of equilibrium conditions must include both earth and water forces.

For analyses in terms of effective stress, pore pressures are subtracted from total stresses on the base of each slice to determine the values of effective stress, to which the soil strengths are related. For total stress analyses, it is not necessary to subtract pore pressures because the strengths are related to the total stresses.

Slope stability problems can be correctly formulated so that equilibrium is satisfied in terms of total stresses by using total unit weights and external boundary water pressures. Total unit weights are moist unit weights above the water table and saturated unit weights below the water table. When water pressures act on submerged external slope boundaries, these pressures are a component of total stress, and they must be included for correct evaluation of equilibrium in terms of total stresses.

For hydrostatic (no-flow) water conditions, it is possible to perform effective stress analyses by using bucyant unit weights below the water table and ignoring external boundary water pressures and internal pore pressures. Effective stress analyses of nonhydrostatic conditions can be performed in a similar way if seepage forces are also included. These procedures are not as straightforward as using total unit weights and boundary water pressures, however. They involve essentially the same amount of effort in calculation for hydrostatic conditions and much more calculation when seepage forces have to be evaluated. Thus, these procedures are not useful except for one purpose. Using buoyant unit weights and excluding external boundary water pressures and pore pressures for a hydrostatic condition afford a means of checking some of the functions of a computer program.

5. SLOPE STABILITY CHARTS

The accuracy of charts for slope stability analyses is usually at least as good as the accuracy with which shear strengths can be evaluated. Chart analyses can be accomplished in a few minutes, even when shear strengths and unit weights are carefully averaged to achieve the best possible accuracy. Charts thus provide a rapid and potentially very useful means for slope stability analyses. They can be used to good advantage to perform preliminary analyses, to check detailed analyses, and often to make complete analyses.

5.1 Averaging Slope Profile, Shear Strengths, and Unit Weights

For simplicity, charts are developed for simple homogeneous slopes. To apply them to real conditions, it is necessary to approximate the real slope with an equivalent simple and homogeneous slope.

The most effective method of developing a simple slope profile for chart analysis is to begin with a cross section of the slope drawn to scale. On this cross section, using judgment, the engineer draws a geometrically simple slope that approximates the real slope as closely as possible.

To average the shear strengths for chart analysis, it is useful to know, at least approximately, the location of the critical slip surface. The charts contained in the following sections of this chapter provide a means of estimating the position of the critical circle. Average strength values are calculated by drawing the critical circle, determined from the charts, on the slope. Then the central angle of arc subtended within each layer or zone of soil is measured with a protractor. The central angles are used as weighting factors to calculate weighted average strength parameters, c_{avg} and ϕ_{avg}:

$$c_{avg} = \frac{\Sigma \delta_i c_i}{\Sigma \delta_i} \tag{13.4}$$

$$\phi_{avg} = \frac{\Sigma \delta_i \phi_i}{\Sigma \delta_i} \tag{13.5}$$

where

c_{avg} = average cohesion (stress units);
ϕ_{avg} = average angle of internal friction (degrees);
δ_i = central angle of arc, measured around the center of the estimated critical circle, within zone i (degrees);
c_i = cohesion in zone i (stress units); and
ϕ_i = angle of internal friction in zone i.

The one condition in which it is preferable not to use these straightforward averaging procedures is the case in which an embankment overlies a weak foundation of saturated clay, with $\phi = 0$. Straightforward averaging in such a case would lead to a small value of ϕ_{avg} (perhaps 2 to 5 degrees), and with $\phi_{avg} > 0$, it would be necessary to use a chart like the one in Figure 13-6, which is based entirely on circles that pass through the toe of the slope, often not critical for embankments on weak saturated clays. With $\phi = 0$ foundation soils, the critical circle usually goes as deep as possible in the foundation, passing below the toe of the slope. In these cases it is better to approximate the embankment as a $\phi = 0$ soil and to use a $\phi = 0$ chart of the type shown in Figure 13-3. The equivalent $\phi = 0$ strength of the embankment soil can be estimated by calculating the average normal stress on the part of the slip surface within the embankment (one-half the average vertical stress is usually a reasonable approximation) and determining the corresponding shear strength at that point on the shear strength envelope for the embankment soil. This value of strength is treated as a value of S_u for the embankment, with $\phi = 0$. The average value of S_u is then calculated for both the embankment and the foundation using the same averaging procedure as described above:

$$(S_u)_{avg} = \frac{\Sigma \delta_i (S_u)_i}{\Sigma \delta_i} \tag{13.6}$$

where $(S_u)_{avg}$ is the average undrained shear strength (in stress units), $(S_u)_i$ is S_u in layer i (in stress units), and δ_i is as defined previously. This average value of S_u is then used, with $\phi = 0$, for analysis of the slope.

To average unit weights for use in chart analysis, it is usually sufficient to use layer thickness as a weighting factor, as indicated by the following expression:

$$\gamma_{avg} = \frac{\Sigma \gamma_i h_i}{\Sigma h_i} \tag{13.7}$$

where

γ_{avg} = average unit weight (force per length cubed),
γ_i = unit weight of layer i (force per length cubed), and
h_i = thickness of layer i (in length units).

Unit weights should be averaged only to the depth of the bottom of the critical circle.

If the material below the toe of the slope is a $\phi = 0$ material, the unit weight should be averaged only down to the toe of the slope, since the unit weight of the material below the toe has no effect on stability in this case.

5.2 Soils with $\phi = 0$

Stability charts for slopes in $\phi = 0$ soils are shown in Figure 13-3. These charts, as well as the related

ones in Figures 13-4, 13-5, and 13-6, were developed by Janbu (1968).

The coordinates of the center of the critical circle are given by

$$X_0 = x_0 H \quad (13.8)$$

$$Y_0 = y_0 H \quad (13.9)$$

where

X_0, Y_0 = coordinates of critical circle center measured from toe of slope,

x_0, y_0 = dimensionless numbers determined from charts at bottom of Figure 13-3, and

H = height of slope.

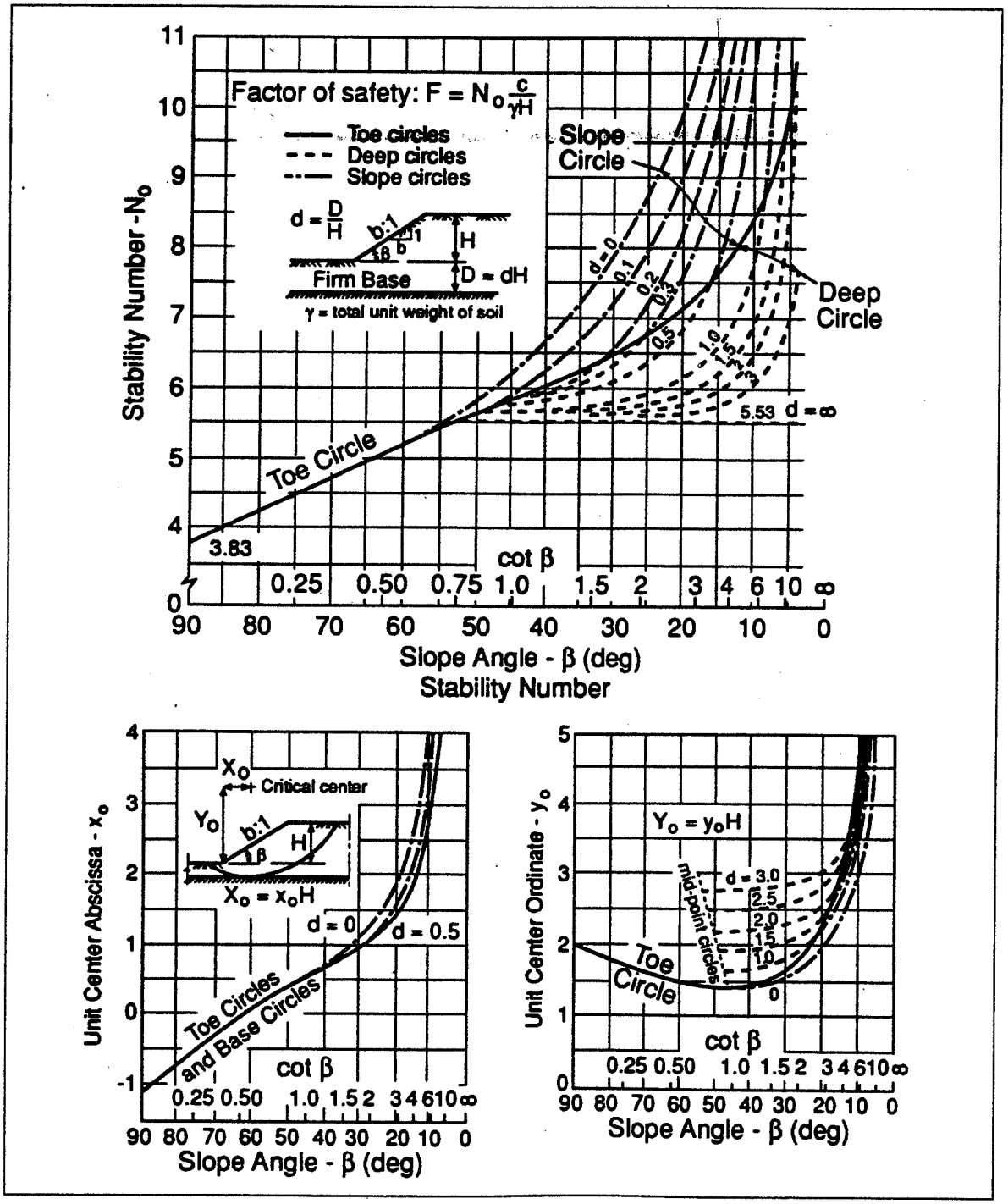

FIGURE 13-3
Slope stability charts for $\phi = 0$ soils (modified from Janbu 1968).

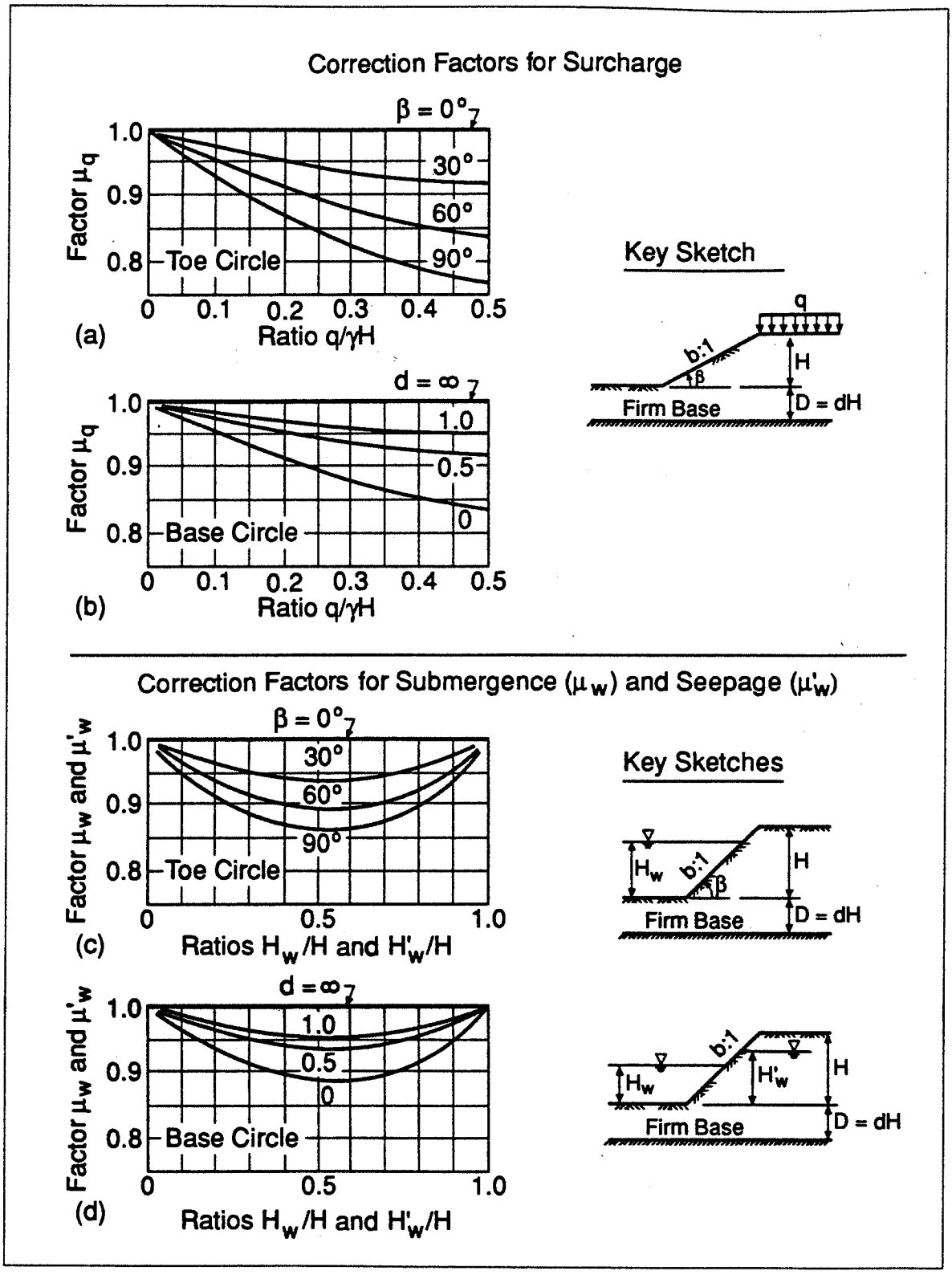

FIGURE 13-4
Correction factors for slope stability charts for $\phi = 0$ and $\phi > 0$ soils for cases with surcharge, submergence, or seepage (modified from Janbu 1968).

FIGURE 13-5
Correction factors for slope stability charts for $\phi = 0$ and $\phi > 0$ soils for cases with tension cracks (modified from Janbu 1968).

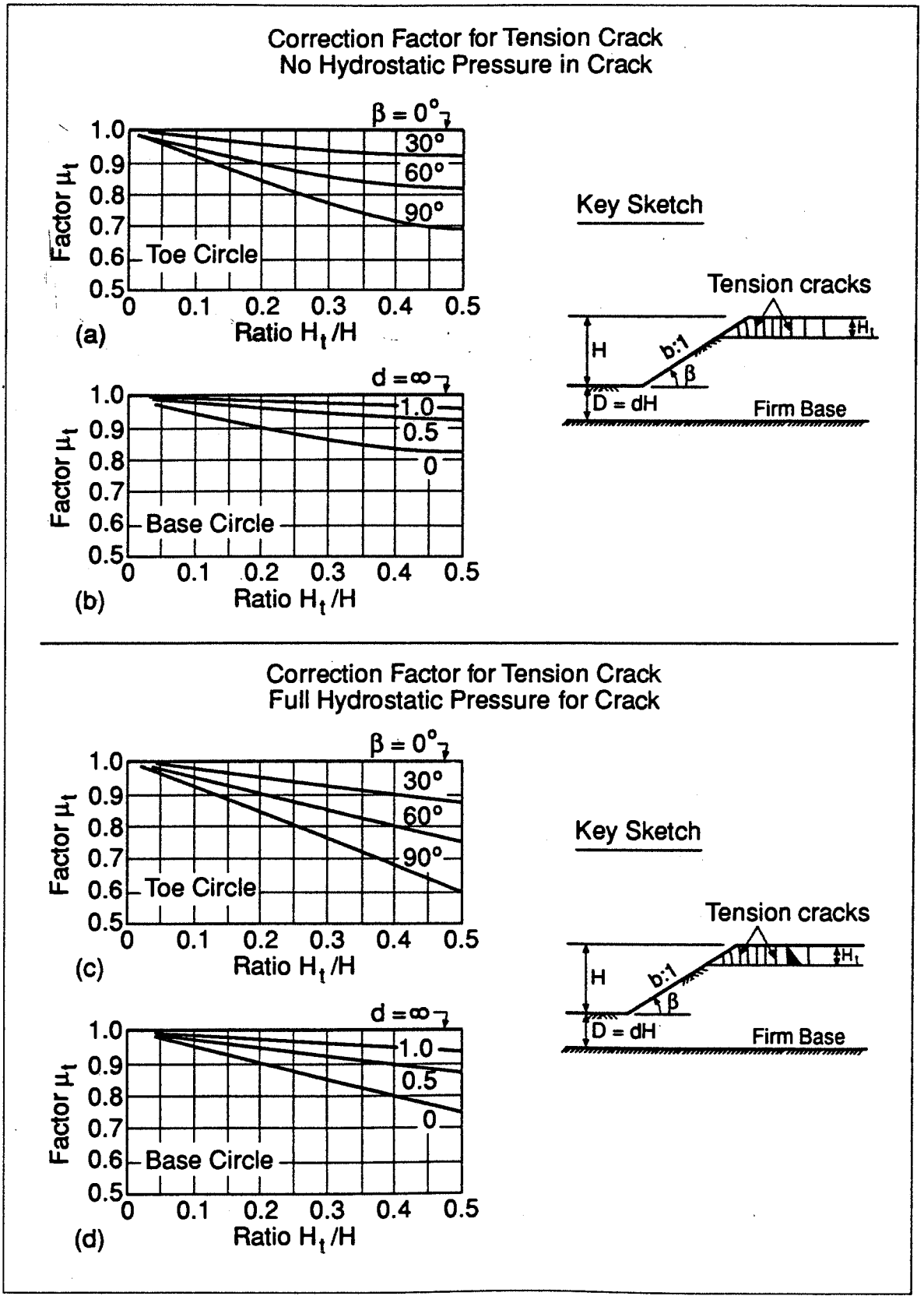

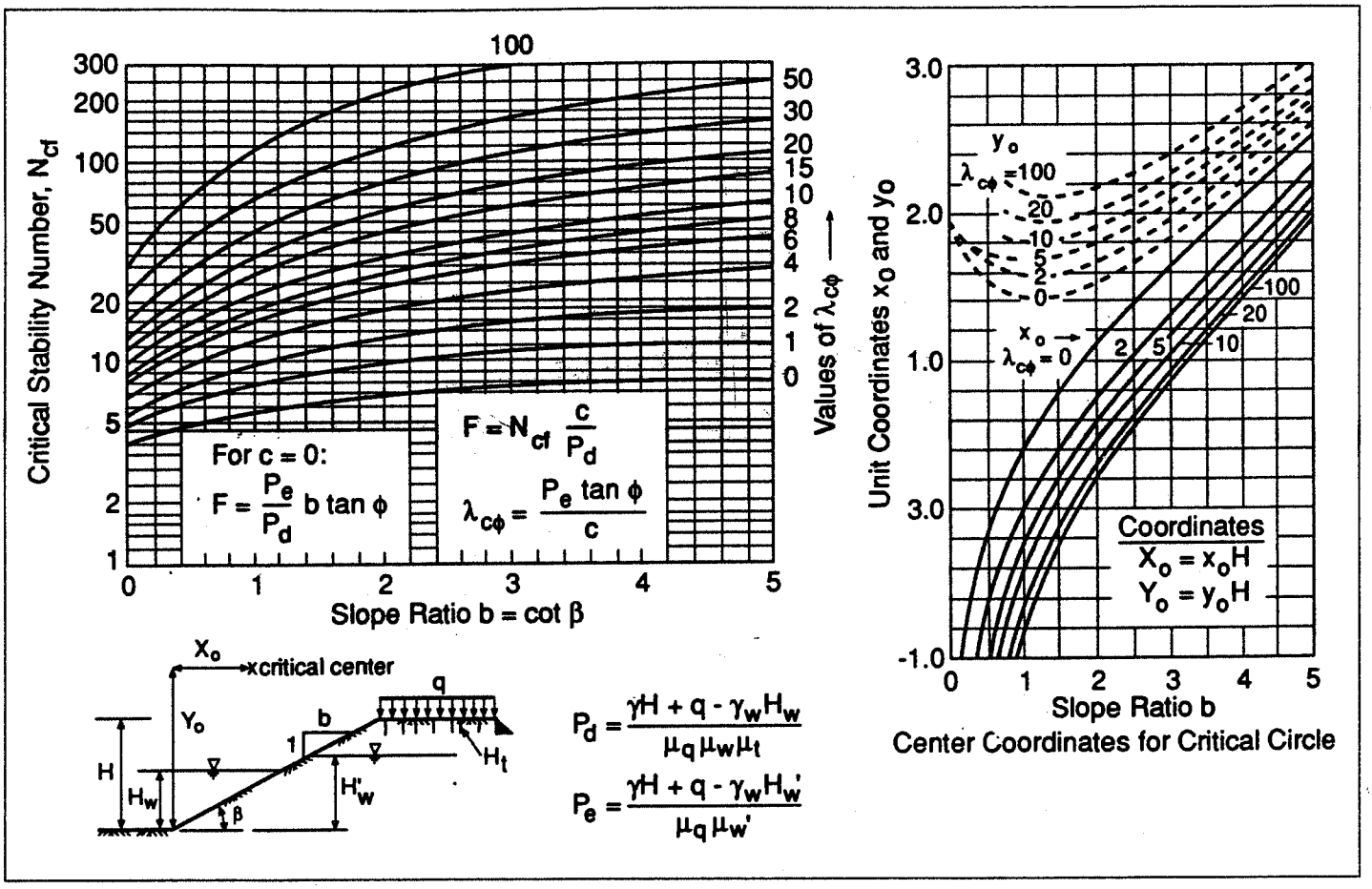

FIGURE 13-6
Slope stability charts for $\phi > 0$ soils (modified from Janbu 1968).

The radius of the critical circle is determined by the position of the center of the circle and the fact that the circle is tangent to a horizontal plane at depth D below the bottom of the slope. Using the chart in Figure 13-3, it is possible to calculate factors of safety for a range of depths (D) to determine which is most critical. If the value of S_u in the foundation does not vary with depth, the critical circle will extend as deep as possible, and only a circle extending through the full depth of the clay layer need be analyzed. If the strength of the foundation clay increases with depth, the critical circle may or may not extend to the base of the layer, and it is necessary to examine various depths to determine which is most critical.

The upper part of Figure 13-3 gives values of the stability number, N_0, which is related to the factor of safety by the expression

$$F = N_0 \frac{c}{P_d} \tag{13.10}$$

where

F = factor of safety (dimensionless),
N_0 = stability number from Figure 13-3 (dimensionless), and
$c = S_u$ = undrained shear strength (in stress units).

The value of P_d is given by the expression

$$P_d = \frac{\gamma H + q - \gamma_w H_w}{\mu_q \mu_w \mu_t} \tag{13.11}$$

where

P_d = driving force term (in pressure units),
γ = unit weight (force per length cubed),
H = slope height (length),
q = surcharge pressure on top of slope (in stress units),
γ_w = unit weight of water (force per length cubed),
H_w = depth of water outside slope, measured above toe (length),
μ_q = surcharge correction factor,
μ_w = water pressure correction factor, and
μ_t = tension crack correction factor.

The correction factors μ_q, μ_w, μ_t are given in Figures 13-4 and 13-5.

5.3 Soils with $\phi > 0$

In most cases for slopes in soils with $\phi > 0$, the critical slip circle passes through the toe of the slope. The stability chart shown in Figure 13-6 is based on the assumption that this is true. The coordinates of the center of the critical toe circle are shown in the chart on the right side of Figure 13-6.

Cohesion values, friction angles, and unit weights are averaged using the procedures described at the beginning of this chapter. The factor of safety is calculated using the expression

$$F = N_{cf}\frac{c}{P_d} \tag{13.12}$$

where N_{cf} is the stability coefficient from the chart on the left-hand side of Figure 13-6 (dimensionless), c is the average cohesion intercept (in stress units), and P_d is defined by Equation 13.11.

The values of N_{cf} shown in Figure 13-6 are determined by the value of b = cotangent of the slope angle = cot ß and the value of the dimensionless parameter, $\lambda_{c\phi}$. The latter is calculated using the expression

$$\lambda_{c\phi} = \frac{P_e \tan\phi}{c} \tag{13.13}$$

where c and $\tan\phi$ are the average values of cohesion intercept and friction angle. The value of P_e is defined as

$$P_e = \frac{\gamma H + q - \gamma_w H_w'}{\mu_q \mu_w'} \tag{13.14}$$

where H_w' is the effective average water level inside the slope measured above the toe of the slope (in length units), μ_w' is the seepage correction factor from the lower part of Figure 13-4, and γ, H, q, and μ_q are as defined previously.

The value of H_w', somewhat difficult to estimate using judgment, is related to H_c, the water level measured below the crest of the slope, as shown in Figure 13-7. When the value of H_c has been determined by field measurements or seepage analyses, the value of H_w' can be determined using the curve given in Figure 13-7.

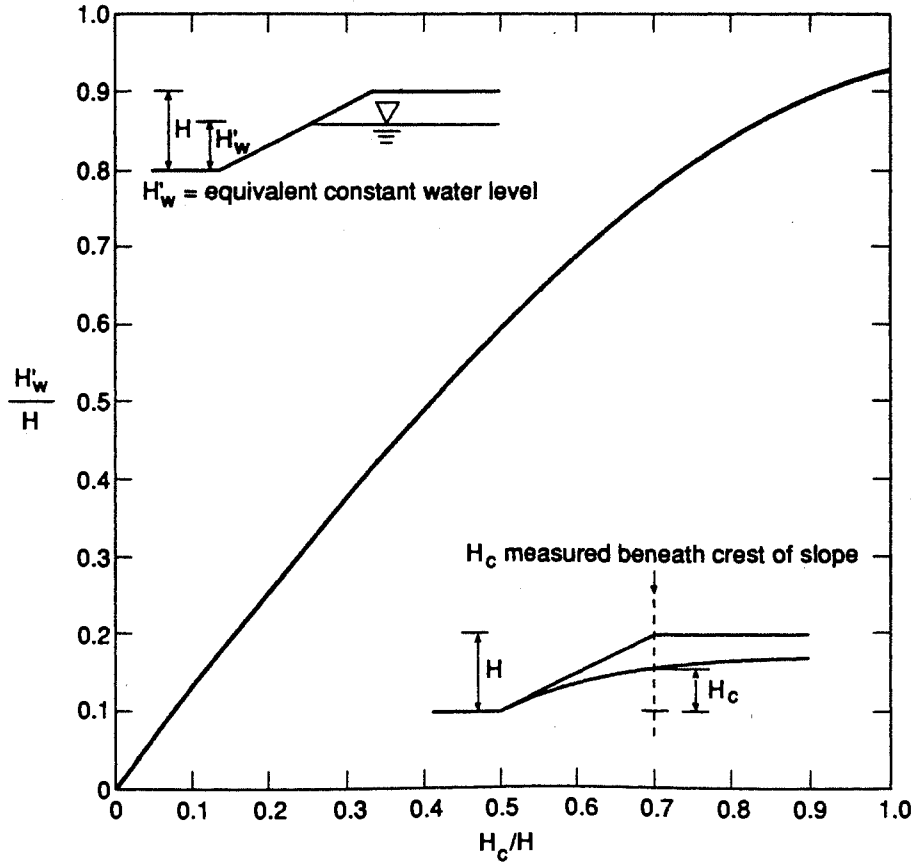

FIGURE 13-7
Chart for determining steady seepage conditions (modified from Duncan et al. 1987).

5.4 Infinite Slope Analyses

Conditions are sometimes encountered in which a layer of firm soil or rock lies parallel to the surface of the slope at shallow depth. In such conditions the slip surface is constrained to parallel the slope, as shown in Figure 13-8. When such slip surfaces are long compared with their depth, they can be approximated accurately by infinite slope analyses. Such analyses ignore the driving force at the upper end of the slide mass and the resisting force at the lower end. The resisting force is ordinarily greater, and infinite slope analyses are therefore somewhat conservative.

The factor of safety for infinite slope analyses can be expressed as

$$F = A\frac{\tan\phi'}{\tan\beta} + B\frac{c'}{\gamma H} \qquad (13.15)$$

where

A, B = dimensionless stability coefficients given in Figure 13-8,
ϕ', c' = effective stress strength parameters for slip surface,
β = slope angle,
γ = unit weight of sliding mass (force per length cubed), and

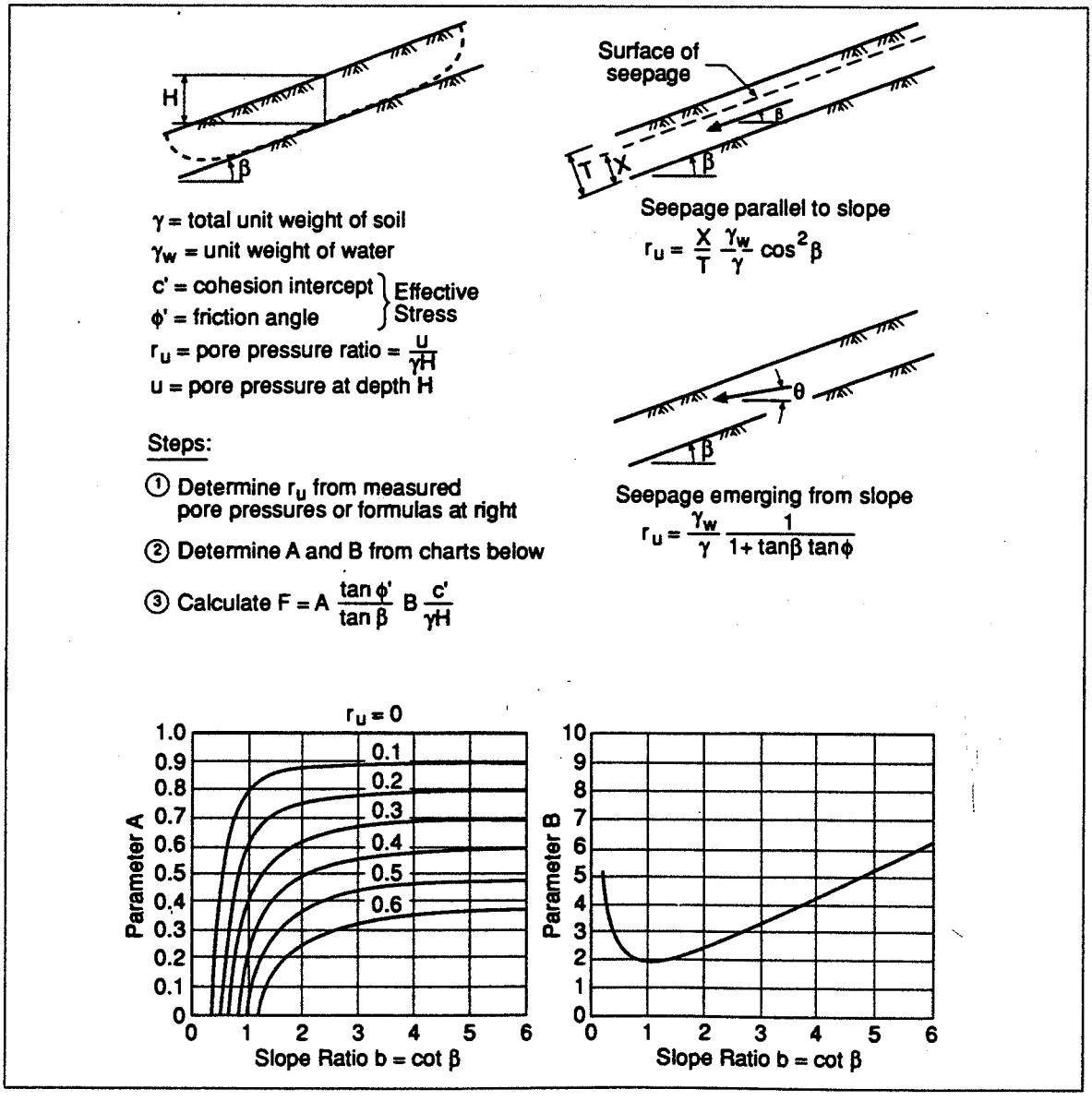

FIGURE 13-8
Stability charts for infinite slopes (modified from Duncan et al. 1987).

H = depth measured vertically from slope surface to slip surface (in length units).

The charts shown in Figure 13-8 can be used for effective stress or total stress analyses. For effective stress analyses, the pore pressures along the slip surface are characterized by the dimensionless pore-pressure ratio, r_u, as indicated in Figure 13-8. For total stress analyses, c and ϕ (total stress shear strength parameters) are used instead of c' and ϕ', and the value of r_u is equal to zero.

5.5 Soils with $\phi = 0$ and Strength Increasing with Depth

The undrained shear strengths of normally consolidated clays usually increase with depth. The strength profile for this condition can often be approximated by a straight line, as shown in Figure 13-9. The factor of safety for slopes in such deposits can be expressed as

$$F = N \frac{c_b}{\gamma (H + H_0)} \tag{13.16}$$

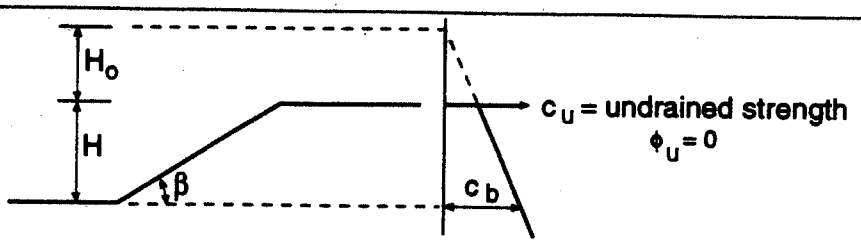

Steps:

1. Extrapolate strength profile upward to determine value of H_o, where strength profile intersects
2. Calculate $M = H_o/H$
3. Determine stability number N from chart below
4. Determine c_b = strength of bottom of slope
5. Calculate $F = N \frac{c_b}{\gamma (H + H_o)}$

Use $\gamma = \gamma_{buoyant}$ for submerged slope

Use $\gamma = \gamma_m$ for no water outside slope

Use reduced value of γ for partly submerged slope:

$$\gamma_r = \frac{\gamma H - \gamma_w H_w}{H}$$

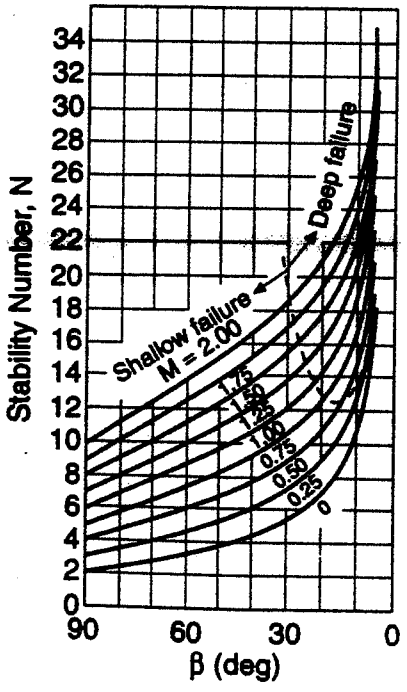

FIGURE 13-9
Slope stability charts for $\phi = 0$ and strength increasing with depth (modified from Hunter and Schuster 1968).

where

N = dimensionless stability coefficient from Figure 13-9,
c_b = undrained shear strength (S_u) at elevation of toe of slope (in stress units),
γ = unit weight of soil (force per length cubed),
H = slope height (length), and
H_0 = height above top of slope where strength profile, projected upward, intersects zero strength (in length units).

Figure 13-9 can be used to analyze subaerial slopes or slopes that are submerged in water. For subaerial slopes the total (moist or saturated) unit weight is used. For submerged slopes the buoyant unit weight ($\gamma_b = \gamma_{sat} - \gamma_w$) is used. A reduced value of γ, calculated using the following expression, can be used for partly submerged slopes:

$$\gamma_r = \frac{\gamma H - \gamma_w H_w}{H} \tag{13.17}$$

where γ_r is the value of unit weight reduced for partial submergence, and the other terms are as defined previously.

6. DETAILED ANALYSES

Detailed analyses of slope stability are needed whenever it is necessary to include details of slope configuration, soil property zonation, or shape of the slip surface that cannot be represented in chart analyses. If a computer and slope stability computer program are available, detailed analyses can be performed efficiently, including a thorough search for the critical slip surface. If a computer is not available, detailed analyses can be performed manually using the procedures described in the following section. Even when analyses are performed using a computer, it is good practice to check the factor of safety for the critical slip surface using manual calculations. The U.S. Army Corps of Engineers (1970) requires such calculations for the critical slip surface for all important slope stability analyses.

6.1 Manual Calculations

It is convenient to use a tabular computation form to perform manual calculations of slope stability. Calculations that are well organized are easy to check. In the following sections, tabular computation forms are given for the ordinary method of slices, Bishop's modified method, and a force equilibrium method with the same side force inclination on all slices.

6.1.1 Ordinary Method of Slices

A tabular form for the ordinary method of slices is presented in Figure 13-10, and example calculations made using this form are given in Figure 13-11. The slope to which the calculations apply is shown in Figure 13-12.

The slice weights in the second column were calculated on the basis of the dimensions of the slices and the unit weights of the soils within them. A simple method of calculating slice weights, shown in Figure 13-12, uses

$$W = b\Sigma(\gamma_i h_i) \tag{13.18}$$

where

W = slice weight (force per unit length),
b = width of slice (length),
γ_i = unit weight of soil i (force per length cubed), and
h_i = height of soil layer i where it is subtended by slice (length).

Values of h_i are measured at the center of the slice. Equation 13.18 can be applied to triangular as well as quadrilateral slices.

The base length l and the base angle α for each slice are measured on a scale drawing of the slope and slip surface. The values of c and ϕ for each slice correspond to the type of soil at the bottom of the slice, and slices are drawn so that the base of each slice is in only one type of soil. The value of u for each slice is the average value at the middle of the base. Slices need not be of equal width.

The quantities in the last two columns (N_1 and N_2) can be calculated using the tabulated values for each slice. These two columns are summed, and the factor of safety is calculated as shown in the bottom right corner of the computation form (Figure 13-11). For the example shown, the ordinary method of slices factor of safety is 1.43.

6.1.2 Bishop's Modified Method

A tabular computation form for Bishop's modified method is shown in Figure 13-13, and calculations

Slice No.	W	l	α	c	ϕ	u	N_1	N_2
1								
2								
3								
4								
5								
6								
7								
8								
9								
10								
11								
12								
13								
14								
15								
						$\Sigma =$		

W = weight of slice - kN/m

c = cohesion intercept - kN/m^2

ϕ = friction angle - degrees

u = pore pressure - kN/m^2

α = angle between base of slice and horizontal - degrees

l = length of slip surface segments measured along base of slice - m

$N_1 = W \sin \alpha$

$N_2 = [W \cos \alpha - ul] \tan \phi + cl$

$F = \Sigma (N_2) / \Sigma (N_1) =$ ____

FIGURE 13-10
Tabular computation form for ordinary method of slices.

for the example slope shown in Figure 13-12 are given in Figure 13-14. The first eight columns in the form are the same as those for the ordinary method of slices.

The value of the quantity N_2 for Bishop's modified method depends on the factor of safety, as shown by the expression for N_2 at the bottom of the form.

Because N_2 depends on the factor of safety and the factor of safety also depends on N_2, it is necessary to use repeated trials to calculate the factor of safety by Bishop's modified method. For this reason, four columns are shown for N_2, each corresponding to a different value of the assumed factor of safety, F_a. The first value assumed for F_a was 1.43, the value calculated using the ordinary method of slices; this value is shown at the top of the ninth column (Figure 13-14). Using the resulting values of N_2 (the values in the ninth column), the value of F_c (the calculated factor of safety) was found to equal 1.51. When this value was used as F_a, F_c was 1.52. When 1.52 was used as the value of F_a, F_c was also 1.52, indicating that the assumed value was correct and no further iteration was needed.

It can be seen that the value of F calculated using Bishop's modified method (1.52) is larger than the value calculated using the ordinary method of slices (1.43), as is usually the case. For effective stress analyses with high pore pressures, the difference may be much larger than the 6 percent difference in this case, indicating significant inaccuracy in the ordinary method of slices for effective stress analyses with high pore pressures.

Slice No.	W	l	α	c	ϕ	u	N_1	N_2
1	112	5.3	-32.0	35.9	0.0	0	-60	191
2	297	4.9	-22.0	35.9	0.0	0	-111	177
3	499	4.7	-13.0	35.9	0.0	0	-112	169
4	726	4.6	-4.0	35.9	0.0	0	-51	165
5	903	4.6	4.0	35.9	0.0	0	63	165
6	1,028	4.7	13.0	35.9	0.0	0	231	169
7	1,003	4.9	22.0	35.9	0.0	0	376	177
8	818	5.3	32.0	35.9	0.0	0	433	191
9	587	6.7	43.0	4.8	35.0	0	400	333
10	128	5.6	55.0	4.8	35.0	0	105	79
11							0	0
12							0	0
13							0	0
14							0	0
15							0	0
						$\Sigma =$	1274	1816

W = weight of slice - kN/m

c = cohesion intercept - kN/m^2

ϕ = friction angle - degrees

u = pore pressure - kN/m^2

α = angle between base of slice and horizontal - degrees

l = length of slip surface segments measured along base of slice - m

$N_1 = W \sin \alpha$

$N_2 = [W \cos \alpha - ul] \tan \phi + cl$

$F = \Sigma (N_2) / \Sigma (N_1) = \underline{1.43}$

FIGURE 13-11
Example computation for ordinary method of slices.

Numerical problems sometimes arise with Bishop's modified method. These difficulties arise at the top or bottom ends of the slip circle, where the bases of the slices are steep. When these numerical problems arise, the value of the factor of safety calculated by Bishop's modified method may be smaller than the value calculated by the ordinary method of slices, rather than larger. When this happens, it is reasonable to use the *F*-value determined by the ordinary method of slices rather than that determined by Bishop's modified method. To check for these numerical problems, it is useful to calculate *F* by the ordinary method of slices to determine whether it is smaller or larger than the value from Bishop's modified method.

6.1.3 Force Equilibrium with Constant Side Force Inclination

The ordinary method of slices and Bishop's modified method can only be used to analyze circular slip surfaces. It is useful to have a method that can be used for manual calculations of noncircular slip surfaces in order to check computer analyses or to perform analyses when a computer is not available. A tabular form for force equilibrium analyses with the same side force inclination on every slice is shown in Figure 13-15, and an example of the use of this form is shown in Figure 13-16. Figure 13-17 shows the slope analyzed in Figure 13-16, a sand embankment on a clay foundation.

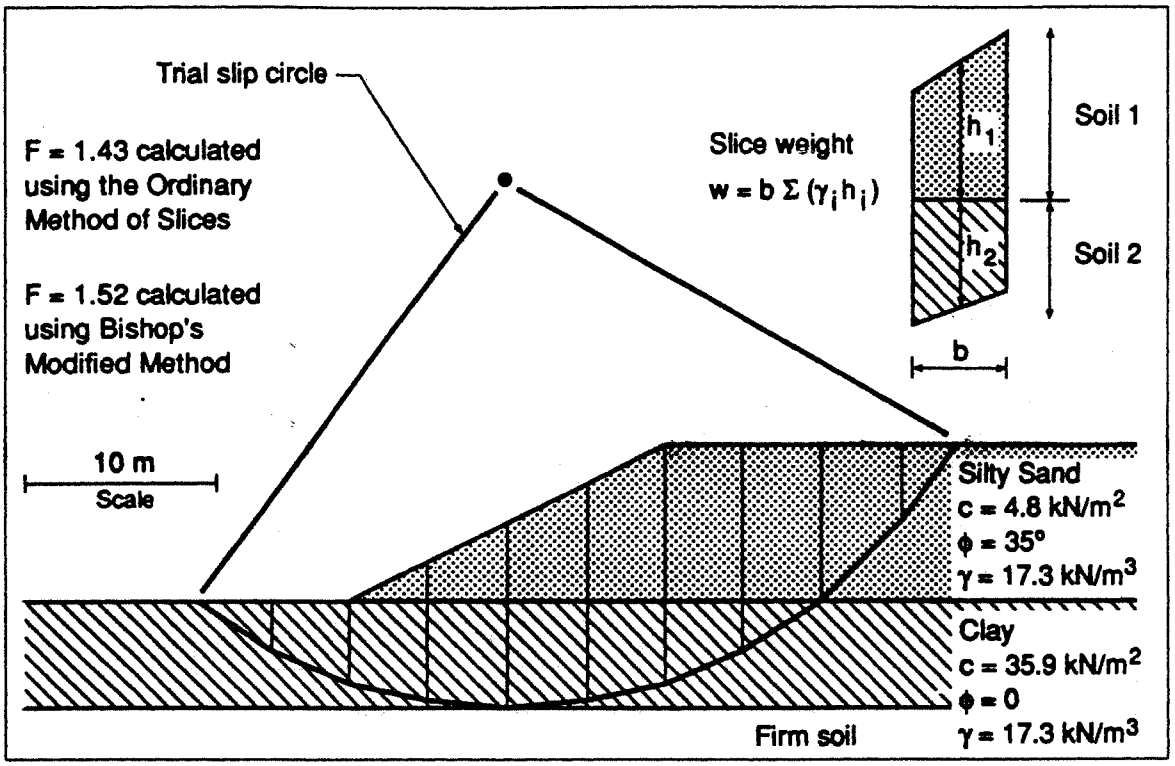

FIGURE 13-12
Example slope: sand embankment over clay foundation.

The seven columns in the upper section of the form contain the same information regarding the slices as shown in the first seven columns of the form for the ordinary method of slices and Bishop's modified method. Note that the assumed value of θ is listed at the top of the upper section of the form. Values of θ must be assumed for all force equilibrium methods.

The calculations for ΔE, the unbalanced force on each slice, involve the five quantities N_0, N_1, N_2, N_3, and N_4. Expressions for these terms are given in the lower part of the form. The values of all of these terms depend on the value of the factor of safety, and iteration is therefore needed to evaluate F. This involves assuming a value for F and checking to see if the forces balance. The forces balance when $\Sigma\Delta E = 0$.

The middle section of the form is labeled Trial 1 and the lower section is labeled Trial 2. Each trial corresponds to a new value of F_a (the assumed value of the factor of safety). The solution is achieved by assuming a value of F_a and using the tabular form to calculate $\Sigma\Delta E$. If $\Sigma\Delta E$ is positive, the assumed factor of safety is too high, and a lower value is assumed for the next trial. If $\Sigma\Delta E$ is negative, a larger value of F_a is assumed for the next trial. The assumed value of F is the correct value when $\Sigma\Delta E = 0$. If more than two trials are needed to find the correct value of F, as is commonly the case, additional copies of the form are used for those calculations.

For the example shown in Figure 13-17, the factor of safety is 2.44 for $\theta = 10$ degrees. This is shown by the calculations in Figure 13-16. Other calculations, not shown, resulted in values of $F = 1.96$ for $\theta = 0$, and $F = 3.38$ for $\theta = 20$ degrees. The variation of F with θ for this example is shown in Figure 13-18.

It is clear from the results shown in Figure 13-18 that the factor of safety from force equilibrium solutions varies significantly with the assumed value of θ. In this particular example, the computed factor of safety increases by 72 percent (from 1.96 to 3.38) as the side force angle θ is varied from zero to 20 degrees. This illustrates the importance of having a reasonable estimate of the value of θ when the force equilibrium method is used.

The best way to determine the value of θ is by use of the condition of moment equilibrium. Spencer's method, like the method of analysis on which the computation form in Figure 13-15 is based, assumes a constant value of θ. However,

Slice No.	W	l	α	c	ϕ	u	N_1	F_a =			
								N_2	N_2	N_2	N_2
1											
2											
3											
4											
5											
6											
7											
8											
9											
10											
11											
12											
13											
14											
15											
						Σ=					
						F_c=					

W = weight of slice - kN/m
ϕ = friction angle - degrees
c = cohesion intercept - kN/m²
u = pore pressure - kN/m²

α = angle between base of slice and horizontal - degrees

l = length of slip surface segments measured along base of slice - m
F_a = assumed F
F_c = calculated F

$$N_1 = W \sin \alpha$$

$$N_2 = \frac{\left\{\left[\frac{W}{\cos \alpha} - ul\right] \tan \phi + cl\right\}}{\left[1 + \frac{\tan \alpha \tan \phi}{F_a}\right]}$$

$$F_c = \Sigma (N_2) / \Sigma (N_1) = ____$$

FIGURE 13-13
Tabular computation form for Bishop's modified method.

Spencer's method satisfies moment equilibrium as well as force equilibrium. Only one value of θ satisfies both force and moment equilibrium. For the example shown in Figure 13-17, the value that satisfies moment equilibrium is θ = 13.5 degrees, and the corresponding factor of safety is F = 2.69. This value of F is the best estimate of the factor of safety for this slope and slip surface. It would differ by no more than about 12 percent from the value of F calculated using any other method that satisfied all conditions of equilibrium and that involved reasonable assumptions.

The trend of F with assumed value of θ shown in Figure 13-18 is typical. As the assumed value of θ for a force equilibrium solution increases, the calculated value of F also increases. It is almost always conservative to assume that θ = 0 degrees, and it is almost always unconservative to assume that θ equals the slope angle. Thus, although the method outlined by the form given in Figure 13-15 can be used to check Spencer's method calculations precisely, it has limited value as an independent method of calculating F because of the strong dependence of the calculated value of F on the assumed value of θ. The same is true of all force equilibrium methods.

6.2 Computer Analyses

As shown in the preceding sections, slope stability analyses involve lengthy calculations. Use of a computer for these calculations has great potential in two respects:

1. Computer analyses make it possible to perform calculations by advanced methods that satisfy all

								F_a =	1.43	1.51	1.52	
Slice No.	W	l	α	c	ϕ	u	N_1		N_2	N_2	N_2	N_2
1	112	5.3	-32.0	35.9	0.0	0	-60		192	192	192	
2	297	4.9	-22.0	35.9	0.0	0	-111		177	177	177	
3	499	4.7	-13.0	35.9	0.0	0	-112		170	170	170	
4	726	4.6	-4.0	35.9	0.0	0	-51		165	165	165	
5	903	4.6	4.0	35.9	0.0	0	63		165	165	165	
6	1,028	4.7	13.0	35.9	0.0	0	231		170	170	170	
7	1,003	4.9	22.0	35.9	0.0	0	376		177	177	177	
8	818	5.3	32.0	35.9	0.0	0	433		192	192	192	
9	587	6.7	43.0	4.8	35.0	0	400		408	415	416	
10	128	5.6	55.0	4.8	35.0	0	105		108	111	111	
11							0		0	0	0	
12							0		0	0	0	
13							0		0	0	0	
14							0		0	0	0	
15							0		0	0	0	
							1,275	Σ=	1,925	1,934	1,935	
								Fc=	1.51	1.52	1.52	

W = weight of slice - kN/m
c = cohesion intercept - kN/m²
ϕ = friction angle - degrees
u = pore pressure - kN/m²

$N_1 = W \sin \alpha$

α = angle between base of slice and horizontal - degrees

$$N_2 = \frac{\left\{\left[\frac{W}{\cos \alpha} - ul\right] \tan \phi + cl\right\}}{\left[1 + \frac{\tan \alpha \tan \phi}{F_a}\right]}$$

l = length of slip surface segments measured along base of slice - m

$F_c = \Sigma (N_2) / \Sigma (N_1) =$ ___

F_a = assumed F
F_c = calculated F

FIGURE 13-14 Example computation for Bishop's modified method.

conditions of equilibrium. This advantage reduces the uncertainty resulting from the method of calculation to ±6 percent. Note that this is only the uncertainty due to the method of analysis. The overall uncertainty, including the uncertainty involved in the estimated values of shear strength, is almost always considerably larger.

2. Computer analyses make it possible to conduct a thorough search for the critical circle or critical noncircular slip surface. Because the calculations for a single slip surface take 1 to 3 hr by hand, it is not feasible to search for these values as thoroughly as it is using computer analyses.

6.2.1 Computer and Computer Program Selection

Practically any personal computer can be used for slope stability analyses. A thorough search for the critical slip surface can be accomplished in 10 min or so using a 286-class personal computer and in 1 min or so using a 486-class personal computer.

The most important aspect of computer analysis is the computer program. Programs are being developed continuously to provide a wider range of capabilities and to offer greater ease of use. The optimum computer program for slope stability analysis should have these features:

- It should be based on an advanced method of analysis that satisfies all conditions of equilibrium. It should also be capable of performing calculations using other methods, such as the ordinary method of slices, Bishop's modified method, and force equilibrium methods if the user needs them.
- It should be efficient in terms of the time required for input and output. The cost of com-

θ =

Slice	Weight	l	α	c	ϕ	u
1						
2						
3						
4						
5						
6						

Trial #1 F_a =

Slice	N_0	N_1	N_2	N_3	N_4	ΔE
1						
2						
3						
4						
5						
6						

$\Sigma\Delta E$ =

Trial #2 F_a =

Slice	N_0	N_1	N_2	N_3	N_4	ΔE
1						
2						
3						
4						
5						
6						

$\Sigma\Delta E$ =

$$N_0 = \frac{\sin\alpha - \cos\alpha \tan\phi / F}{\cos\alpha + \sin\alpha \tan\phi / F} \qquad N_1 = W N_0$$

$$N_2 = \frac{c\,l}{F}(\cos\alpha + N_0 \sin\alpha) \qquad N_3 = u\,l(\sin\alpha - N_0 \cos\alpha)$$

$$N_4 = \cos\theta + N_0 \sin\theta \qquad \Delta E = (N_1 - N_2 + N_3) / N_4$$

θ = side force angle - degrees
W = weight of slice - kN/m
ϕ = friction angle - degrees
α = slice base angle - degrees

F_a = assumed F
c = cohesion intercept - kN/m^2
u = pore pressure - kN/m^2
l = length of slice base - m

FIGURE 13-15
Tabular computation form for force equilibrium method with constant θ.

puter resources for slope stability analyses is usually very small when the cost of equipment and programs is spread over a large number of analyses. The cost of engineering time for input and output is far greater. Therefore it is important that the computer program be designed to minimize the personnel time required for analyses.

- It should be capable of analyzing all the conditions of interest to the user. These will always include undrained conditions, drained conditions, ponded water outside the slope, and internal

FIGURE 13-16
Example computation for force equilibrium.

Theta = 10

Slice	Weight	l	α	c	ϕ	u
1	50.5	3.52	60.00	0.0	30.00	0.00
2	77.1	1.73	45.00	24.0	0.00	0.00
3	189.2	3.66	0.00	24.0	0.00	0.00
4	21.0	1.73	-45.00	24.0	0.00	0.00
5						
6						

Trial #1 F_a = 2.30

Slice	N_0	N_1	N_2	N_3	N_4	ΔE
1	1.03	52.13	0.00	0.00	1.16	44.78
2	1.00	77.10	25.42	0.00	1.16	44.61
3	0.00	0.00	38.11	0.00	0.98	-38.70
4	-1.00	-21.00	25.42	0.00	0.81	-57.22
5						
6						
					ΣΔE =	-6.53

Trial #2 F_a = 2.44

Slice	N_0	N_1	N_2	N_3	N_4	ΔE
1	1.06	53.61	0.00	0.00	1.17	45.86
2	1.00	77.10	23.91	0.00	1.16	45.91
3	0.00	0.00	35.85	0.00	0.98	-36.41
4	-1.00	-21.00	23.91	0.00	0.81	-55.36
5						
6						
					ΣΔE =	0.00

$$N_0 = \frac{\sin\alpha - \cos\alpha \tan\phi / F}{\cos\alpha + \sin\alpha \tan\phi / F}$$

$$N_1 = W N_0$$

$$N_2 = \frac{c\,l}{F}(\cos\alpha + N_0 \sin\alpha)$$

$$N_3 = u\,l\,(\sin\alpha - N_0 \cos\alpha)$$

$$N_4 = \cos\theta + N_0 \sin\theta$$

$$\Delta E = (N_1 - N_2 + N_3) / N_4$$

θ = side force angle - degrees

F_a = assumed F

W = weight of slice - kN/m

c = cohesion intercept - kN/m^2

ϕ = friction angle - degrees

u = pore pressure - kN/m^2

α = slice base angle - degrees

l = length of slice base - m

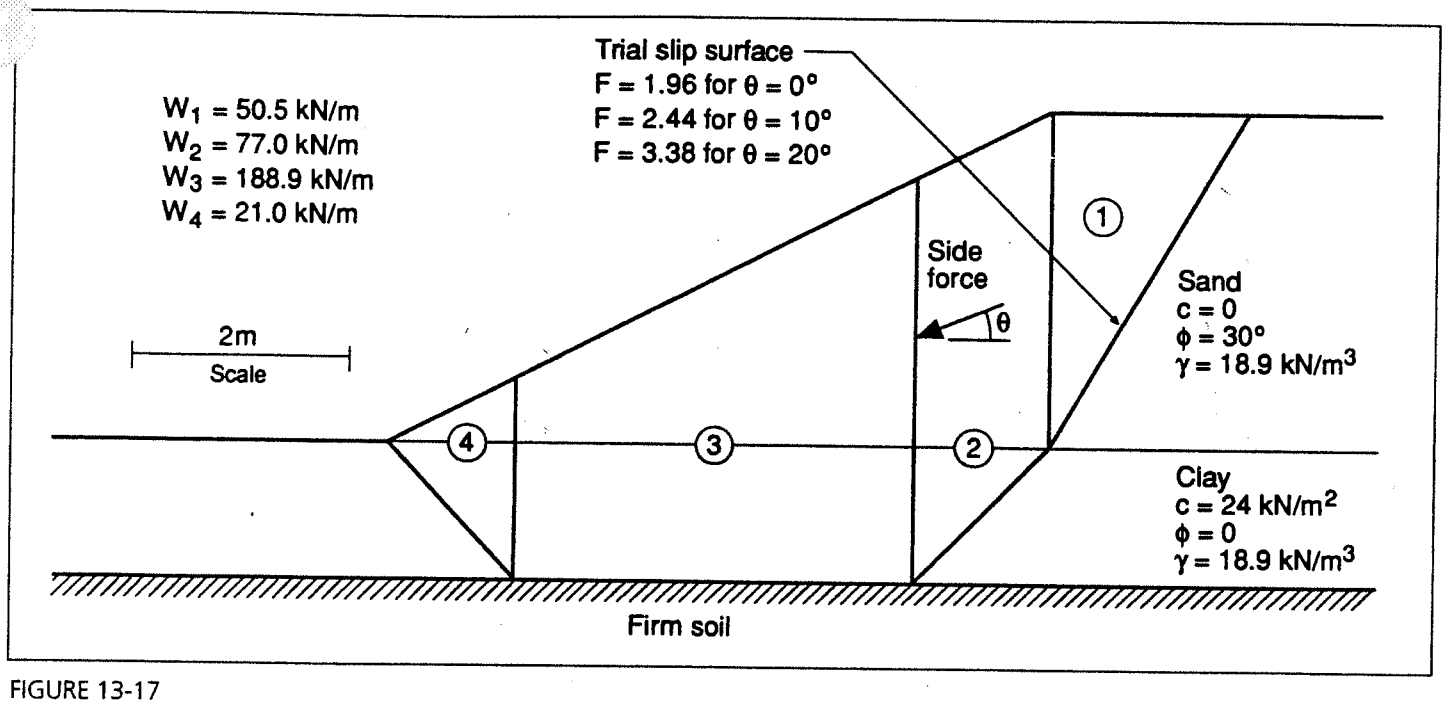

FIGURE 13-17
Noncircular slip surface, force equilibrium analysis.

pore-water pressures. Other conditions that may be of interest include rapid drawdown, slopes with reinforcement, pseudostatic seismic loading, and concentrated or distributed loads on slopes.

Selection of a suitable computer program is an important matter, worthy of careful research and evaluation. It is important to bear in mind that the initial outlay for the computer program is less important than its capabilities, its reliability, and its efficiency as measured in terms of personnel time required to perform analyses. Program distributors and users can provide the information required to make a selection. Because computer programs for slope stability are being improved constantly, acquiring a new program from time to time is a logical method of improving efficiency and effectiveness. Suitable programs may be identified by recommendations of professional colleagues or by review of professional papers and advertisements in technical publications.

6.2.2 Example Computer Analyses

cross section through Waco Dam, in Texas, is own in Figure 13-19. When the embankment

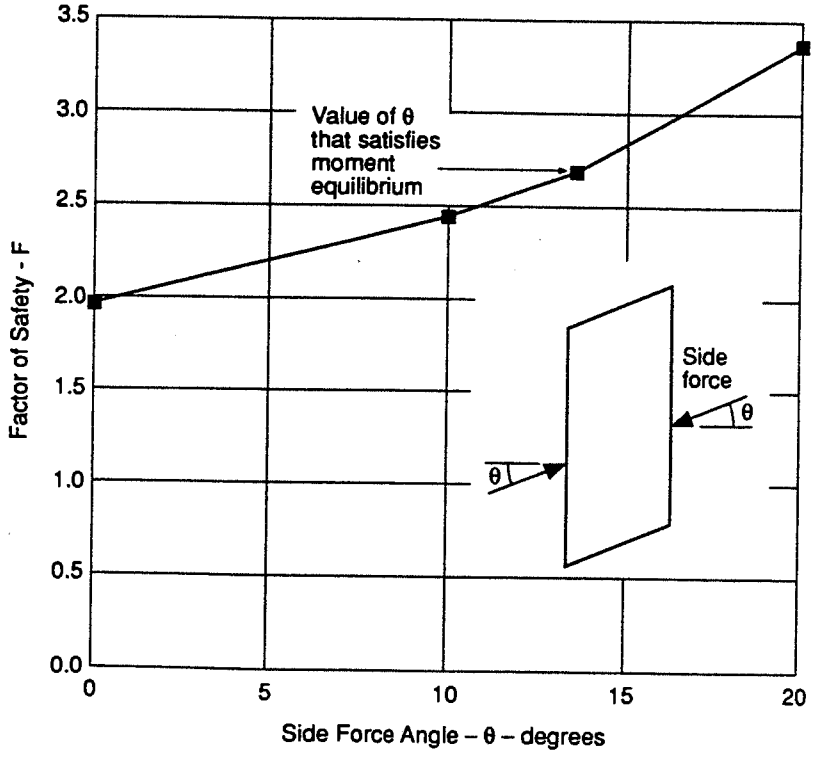

FIGURE 13-18
Variation of F with side force inclination assumed in force equilibrium analyses of sand embankment on clay.

reached the height shown, a slide took place on the downstream slope (Wright and Duncan 1972). The key to the occurrence of the slide was the low undrained shear strength of the Pepper Shale (member of the Woodbine Formation) in the foundation. As shown in Figure 13-19(*a*), the Pepper Shale is highly anisotropic with respect to shear strength. The undrained strength on a horizontal plane (which was measured in laboratory tests using specimens trimmed so that their axes were 30 to 45 degrees from horizontal) was only about 40 percent of the strength measured on conventional vertical test specimens.

The rupture surface of the slide was located in the field by observation of the slide scarp and toe bulge and by inclinometers installed through the slide mass. As a result of the highly anisotropic strength of the Pepper Shale, the slip surface extended horizontally for a considerable distance downstream.

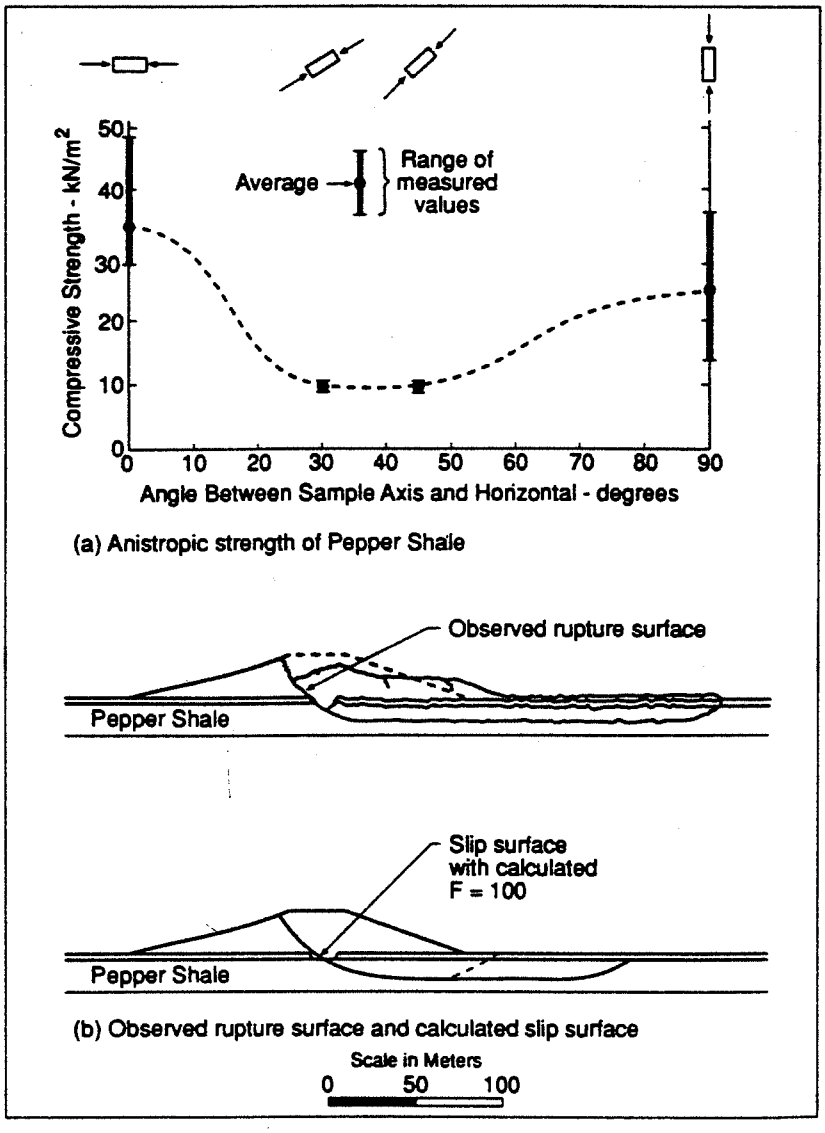

FIGURE 13-19
Analysis of slide in Waco Dam, Texas.

Postfailure analyses of this slide were complicated by two factors: (*a*) the anisotropic strength of the foundation soil and (*b*) the noncircular slip surface. As a result, it was not practical to perform postfailure analyses by hand. With a computer program using Spencer's method, a wide variety of analyses were performed to examine the correspondence among the observed slide, the shear strengths measured in the laboratory, and the most critical slip surface determined by analysis. As shown in Figure 13-19(*b*), the calculated slip surface for $F = 1.00$ was quite similar to the observed slip surface.

A cross section through the Cucaracha landslide at the Panama Canal is shown in Figure 13-20. This slope, which had suffered landslides during excavation of the canal, suffered another slide in 1986 (Berman 1988). The slip surface shown in Figure 13-20 was estimated on the basis of surface observations and inclinometer measurements.

The slide was caused by changes in the groundwater level, with perhaps some influence of loading at the top of the slope, at a location away from the section shown in Figure 13-20. Because the slide was caused by changes in the seepage conditions that resulted in increased pore pressures, it was a drained failure. Therefore the postfailure analyses were performed using drained strengths and the piezometric level that was estimated for the time of the failure.

The slide movement appeared to coincide with bedding surfaces in the Cucaracha shale, which contains numerous slickensides. It therefore seemed appropriate to use residual shear strengths on these bedding surfaces. The residual drained shear strength along the bedding is shown by the lower of the two strength envelopes in Figure 13-20(*a*). The shear strengths on surfaces cutting across bedding were found to be considerably higher, as shown by the upper curve in Figure 13-20(*a*).

The strength envelopes for shear along and across the bedding are nonlinear, and they cannot be represented accurately by single values of c and ϕ. Therefore, each strength envelope was represented by a series of points without reference to values of c and ϕ.

Postfailure analyses of the 1986 Cucaracha landslide involved a number of complications: noncir-

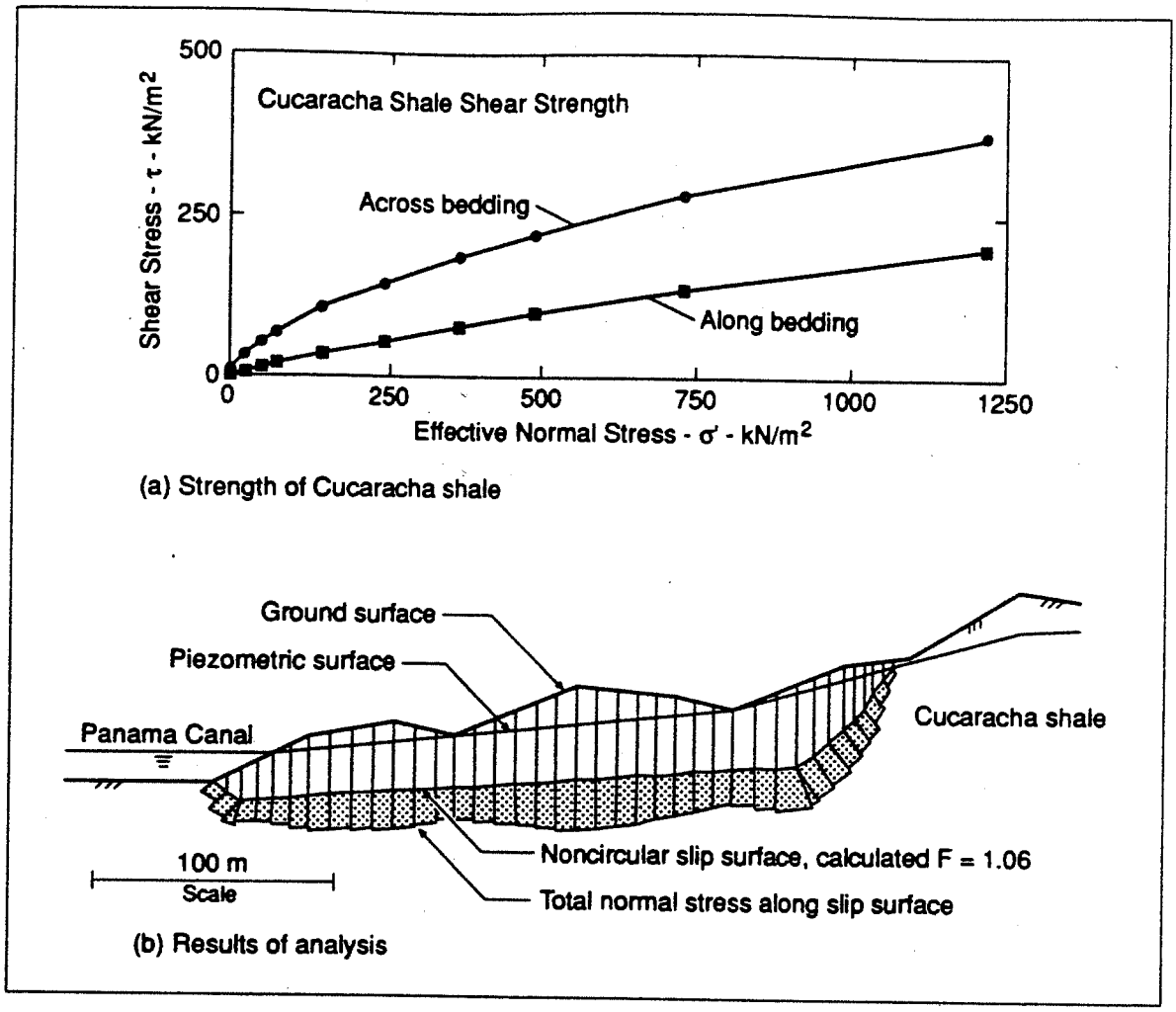

FIGURE 13-20
Analysis of 1986 Cucaracha landslide at Panama Canal.

cular slip surfaces, nonlinear shear strength envelopes, and shear strengths that varied with the orientation of the slip surface. Thorough computer analyses of the slide were performed, confirming the applicability of the shear strengths, and other analyses were made to evaluate the effectiveness of repair schemes (Berman 1988). The results of one of these analyses are shown in Figure 13-20(*b*).

6.2.3 Benefits and Risks of Computer Analyses

Computers afford the most effective means of analysis of slope stability in soil. Computer analyses can be accomplished quickly when a suitable computer program is available; they can accommodate complex conditions of site geometry, seepage, and shear strength; they can be performed using advanced methods that satisfy all conditions of equilibrium; and they can be used to perform thorough analyses to locate the critical slip surface. However, it should be borne in mind that a computer can also propagate mistakes much faster than is possible by hand. Computer analysis must be checked and verified before the results can be relied upon. Analyses can be checked using charts, manual calculations for the critical slip surface, and independent analysis with another computer program using independent input. Common sense and judgment must always be used to ensure that analysis conditions and results are reasonable.

7. BACK ANALYSIS TO DETERMINE SOIL STRENGTHS

The strength properties of many types of natural soil are difficult to determine reliably by means of laboratory tests. In cases where a landslide has

occurred and repair measures are being evaluated, it is often most effective to determine soil strength by back analysis. This process involves three steps:

1. The best estimates possible must be made of the soil strengths and unit weights using the information at hand. Laboratory tests and strength correlations provide an effective basis for these estimates. The slope geometry and phreatic conditions at the time of failure must also be established.
2. The slide should be analyzed using the estimated properties. If the calculated factor of safety is equal to 1.00, the properties and conditions represent a reasonable model of the slide. If the calculated factor of safety is not equal to 1.00, the strengths are adjusted until $F = 1.00$. The adjustment ratio need not be the same for all soils involved in the slide. Logically, larger adjustments should be made for strengths that are considered to involve greater degrees of uncertainty.
3. When values of soil strength have been determined that give $F = 1.00$ for the conditions at the time of failure, these strengths are used to evaluate repair measures.

This process was used to develop mitigative schemes for the Waco Dam slide discussed previously (Figure 13-19) and the 1986 Cucaracha landslide (Figure 13-20). A further example of back analysis is shown by the Olmsted landslide on the Illinois shore of the Ohio River (Filz et al. 1992).

A cross section through the Olmsted landslide is shown in Figure 13-21. The slide occurred on June 4, 1988, when the river dropped to a low level. The location of the rupture surface was known from

Soil	Unit weight (kN/m^3)	Plasticity Index	ϕ'_r (degrees)		
			Lab tests	Correlations	Trial values
Alluvium	18.4	20 to 30	22 to 33	14 to 20	18
Colluvium	17.6	20 to 35	20 to 35	12 to 20	15
McNairy I	18.6	10 to 50	7 to 21	10 to 30	10 and 11 on bedding --- 25 across bedding
Potter's Creek	16.5	50 to 80	5 to 12	6 to 10	8

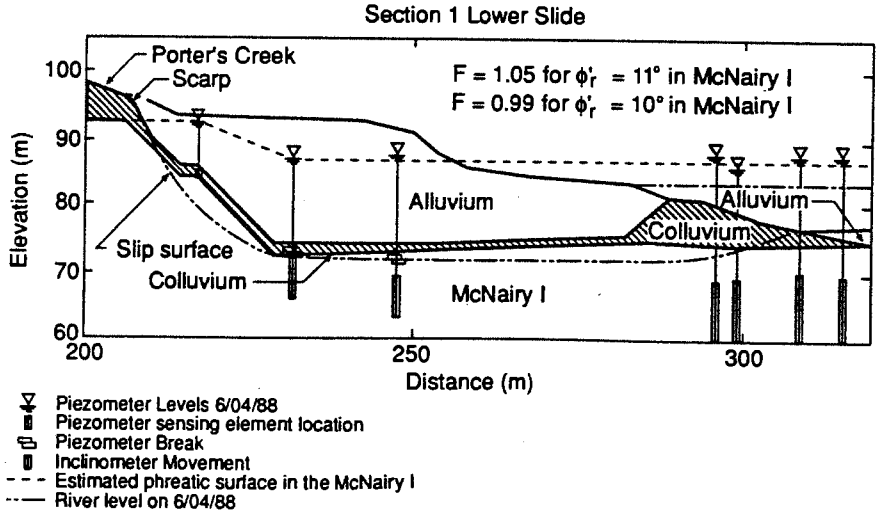

FIGURE 13-21
Back analysis of Olmsted landslide, Illinois.

the position of the scarp at the top of the slide, from movements in inclinometers installed after the slide, and from locations of breaks in piezometer riser tubes. Over most of its length, the rupture surface passed through the McNairy I formation, a sedimentary deposit of flat-lying interbedded sands and clays. The thickness of the individual layers ranged from a few millimeters to nearly a meter.

Laboratory tests were performed on all of the soils involved in the slide, with the results shown in the table at the top of Figure 13-21. It can be seen that there is considerable scatter in the results for all of the soils owing to the variability of the materials, the difficulties involved in obtaining representative and undisturbed specimens for testing, and the layering in McNairy I. On the basis of the results of the tests and correlations with plasticity index, trial values of residual friction angle were established for all of the soils. These are shown in the last column of the table.

The first analysis was performed using Spencer's method with ϕ'_r = 11 degrees in the McNairy I formation. The calculated factor of safety was 1.05. A second analysis, using ϕ'_r = 10 degrees, gave F = 0.99. Only the value of ϕ'_r for McNairy I was changed for the second analysis because it was considered to have the greatest effect on the results and was therefore the most important parameter in the analyses. The same strength parameter values were also used to analyze four other sections through the slide, where the geometry and piezometric levels were different. The calculated values of F, with ϕ'_r = 10 degrees in McNairy I, varied from 0.96 to 1.00 for the five sections. The parameters calculated by back analysis were considered to represent the behavior of the soils quite well and were utilized to analyze the effects of drainage and slope flattening to improve the stability of the slide area.

8. RAPID DRAWDOWN ANALYSIS

When the water level in a lake or stream adjacent to a slope drops, the stabilizing influence of the water pressure on the slope is lost. Many failures of dam slopes and submerged natural slopes have occurred during rapid drawdown. Analysis of rapid drawdown is therefore an important consideration for design of dams and other slopes that will be submerged and subject to such changes in water level.

Methods of analysis of stability during rapid drawdown have been evaluated by Duncan et al. (1990). On the basis of those studies, a method of analysis for rapid drawdown was developed that incorporates these features:

- Undrained strengths are used for soil zones that have values of C_v so low that they are unable to drain during the period of drawdown. Criteria to determine whether a soil zone is drained or undrained are described in Section 3.
- Analyses are performed in three steps:
  - Anisotropic consolidation pressures are determined for each slice using stability and seepage analyses for the predrawdown steady seepage conditions.
  - Values of undrained strength are determined for each slice with its base in a zone of soil that will be undrained, drained strengths are determined for zones of soil that will be drained, and an analysis of stability after drawdown using these strengths is performed.
  - The after-drawdown analyses are repeated using drained strengths for slices where the drained strengths after drawdown are found to be smaller than the undrained strengths.

Thus, the method uses drained or undrained strengths, whichever are lower, for slices where drainage is not expected during drawdown. This technique ensures that the method will not yield unconservative results if the soil drains faster than anticipated.

This method of analysis is logical in its treatment of strengths and stability. Used with Spencer's method for stability computations, it was found to give satisfactory results for Walter Bouldin Dam in Alabama and Pilarcitos Dam in California, both of which suffered embankment slides during rapid drawdown (Duncan et al. 1990).

9. ANALYSIS OF REINFORCED SLOPES

Reinforcing materials, such as geotextiles, geogrids, and steel grids, are widely used to strengthen slopes. Considerable research has been done to evaluate the long-term behavior of these materials and to investigate the mechanisms of interaction by which they improve the stability of slopes. The principal mechanism of reinforcement is limitation of tensile strains at the locations of the reinforcement. Reinforcing materials are commonly placed horizontally within the soil.

Studies of soil reinforcement have shown that the stability of reinforced slopes can be analyzed using the following simple procedure:

1. The long-term ultimate strength of the reinforcing material is determined. This determination involves consideration of short-term strength, creep under load, and the allowable tensile strains considering the type of slope or embankment and the sensitivity of the underlying foundation soil. This long-term limit load is expressed in units of force per unit length of the reinforcement.
2. The long-term limit load is divided by a reinforcement factor of safety, F_R, to produce a factored limit load. The value of F_R logically should depend on the reliability with which the limit load can be evaluated and the possible consequences of failure. Values of F_R near 1.5 are suitable for normal conditions.
3. The factored limit loads are used as known values in conventional limit equilibrium analyses of slope stability. The forces are applied to the bases of slices in which a potential slip surface cuts across the reinforcement. Studies have shown that very flexible types of reinforcement may be reoriented if slip occurs and dragged down so that they parallel the slip surface where they cross it. If a method of analysis is used that satisfies all conditions of equilibrium, the orientation of the reinforcement force (horizontal or parallel to the slip surface) has essentially no effect on the factor of safety computed (Wright and Duncan 1991). The factor of safety computed in this type of analysis is the same as that discussed earlier in this chapter; it is the factor by which the soil strength would have to be divided to bring the soil into a state of barely stable equilibrium.

FIGURE 13-22
Analysis of reinforced St. Alban test embankment.

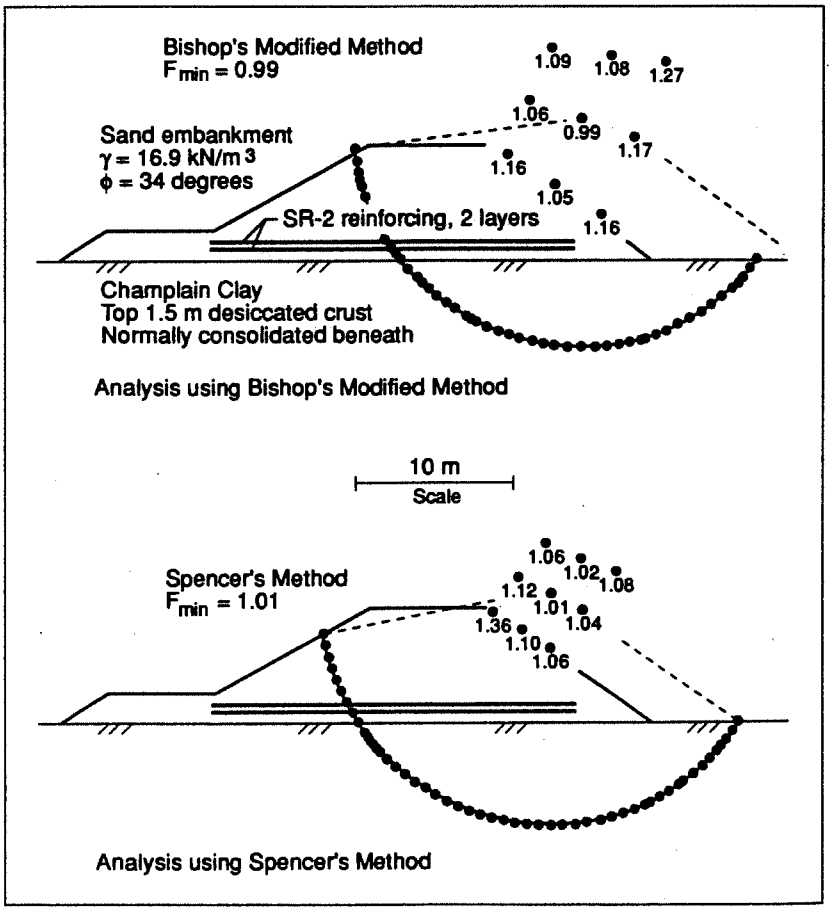

An example analysis of a reinforced slope is shown in Figure 13-22, in which cross sections through the St. Alban test embankment are used; this embankment was constructed on the sensitive Champlain Clay (Schaefer and Duncan 1988). To avoid uncertainties resulting from the sensitivity of the clay, the analyses described here were performed using the postpeak residual undrained shear strength of the crust and the normally consolidated clay beneath the crust. As defined by La Rochelle et al. (1974) and Trak et al. (1980), this "residual" undrained strength is measured at 15 percent axial strain in triaxial tests and is equal to about 90 percent of the undrained strength measured in field vane-shear tests.

The sand embankment was reinforced with two horizontal layers of Tensar SR-2 geogrid. Failure took place as the embankment was being raised about 20 days after construction began. For this load duration, the limit load corresponding to 10 percent strain is about 32 kN/m. Analyses were performed at this reinforcement magnitude using Bishop's modified method and Spencer's method. The results of the analyses are shown in Figure 13-22.

In both analyses the reinforcement force was assumed to act horizontally. It can be seen that both analyses resulted in minimum factors of safety very close to unity. For practical purposes, the values of F calculated by the two analyses were the same. Considering the arbitrary choice of 10 percent strain as the failure strain in the reinforcing, the fact that the calculated factors of safety were so close to unity must be considered somewhat fortuitous.

10. THREE-DIMENSIONAL ANALYSES OF SLOPE STABILITY

Although the methods of slope stability analyses discussed in the previous sections are formulated in two dimensions, actual slope failures are three-dimensional. The question therefore arises as to the accuracy and reliability of two-dimensional (2D) analyses applied to three-dimensional (3D) problems. Research studies [for example, the work by Cavounidis (1987)] have shown clearly that factors of safety calculated using 3D analyses are larger than those calculated using 2D analyses, all other things being equal. Implicit in this conclusion is the notion that the 2D section analyzed is the most critical section through the 3D potential sliding mass.

An example is shown in Figure 13-23, which summarizes 2D and 3D analyses of an ellipsoidal slip surface (Hungr et al. 1989). As shown in Figure 13-23(*a*), the factors of safety for three 2D sections through the sliding mass are F_2 = 1.10, 1.00, and 1.19. The central section (Section 2) is the most critical, and the minimum 2D factor of safety is thus the value calculated for this section, F_2 = 1.00. Figure 13-23(*b*) shows the results of a 3D analysis performed by Hungr et al. (1989) using Bishop's modified method extended to three dimensions (Hungr 1987). The shape of the critical ellipsoidal slip surface is shown in Figure 13-23(*c*). The minimum 3D factor of safety for this case is F_3 = 1.01, which is only 1.0 percent higher than the minimum 2D factor of safety.

It is more difficult to perform 3D analyses than 2D analyses. Because 2D analyses give somewhat conservative results ($F_2 \leq F_3$, all other things being equal), they provide a reasonable and sufficiently accurate approach to most practical problems of stability of soil slopes. Use of 2D analyses requires that the section or sections analyzed be selected using judgment regarding which section will be most critical. In many cases, as in that shown in

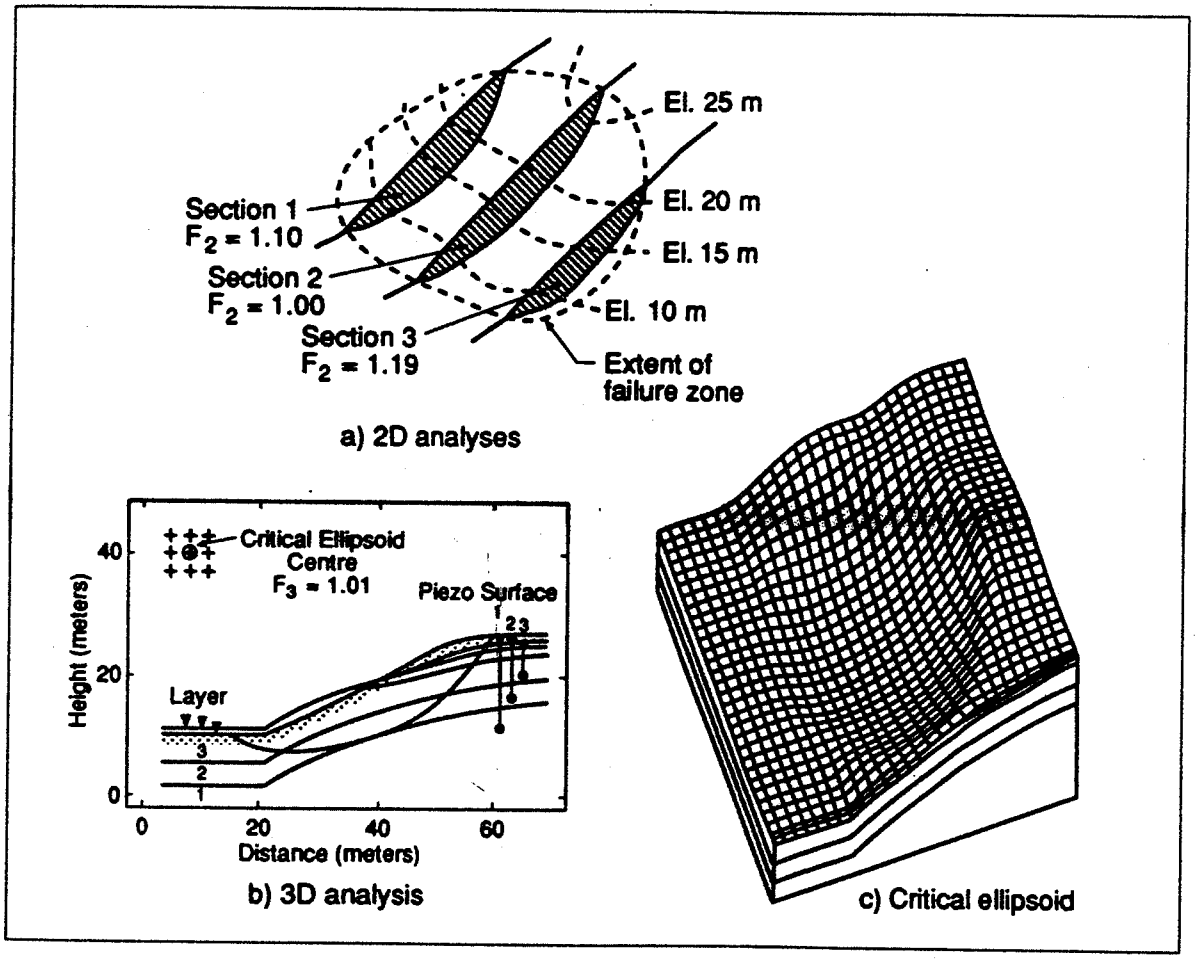

FIGURE 13-23
Comparison of two-dimensional and three-dimensional analyses.

Figure 13-23, the critical 2D section is the one where the slip surface can cut most deeply. In some cases other sections may be more critical. If there is doubt concerning which 2D section is most critical, several should be analyzed.

11. DEFORMATION ANALYSIS

Finite-element analyses have been used since the mid-1960s for analysis of stresses and movements in slopes. A recent review (Duncan 1992) described more than 100 examples of their application. Even though finite-element analyses have been used fairly often in recent years for evaluation of slope deformations, the procedure is not routine. Finite-element analyses are more difficult and time-consuming than slope stability analyses, and they require special expertise if they are to be done successfully and productively.

Experience with finite-element analyses has shown that they are most useful when performed in conjunction with field instrumentation studies. They can be valuable in planning instrumentation programs by showing where the largest movements would be expected to occur and how large they may be. They can also be used for interpreting the results of instrumentation studies. If calculated and measured movements are in agreement at the locations of the instruments, this suggests that the analytical results also may provide reasonable indications of behavior at other locations. Often the more complete finite-element results provide insight into the causes and significance of the measured movements.

An example of a finite-element analysis, summarized in Figure 13-24, concerns Otter Brook Dam in New Hampshire, which deformed considerably during construction (Kulhawy et al. 1969). The embankment, about 40 m high, is essentially homogeneous. It was constructed of compacted silt on a firm foundation of glacial till over rock.

As shown in Figure 13-24, a bridge pier was constructed at about mid-height on the upstream slope of the dam. Because the embankment was constructed above the level of the bridge pier, the embankment deformed under the weight of the added material and the lower part bulged outward. Measurements were made of the movements of the bridge pier as the embankment was constructed. As shown in Figure 13-24(*c*), these measurements reached about 0.15 m vertically and about 0.9 m horizontally by the end of construction. Measurements at other elevations on the upstream slope, also shown in Figure 13-24(*c*), showed that the maximum horizontal movement occurred near mid-height of the embankment.

A finite-element analysis of Otter Brook Dam was performed by Kulhawy et al. (1969) using hyperbolic stress-strain properties determined from conventional laboratory tests. The tests had been performed in support of stability analyses of the dam. The calculated displacements of the upstream slope and the bridge pier are compared with the measured values in Figure 13-24(*c*). It can be seen that agreement is quite good, indicating that the finite-element analyses afford a reasonable representation of the actual behavior of the embankment.

Because engineered fills are water conditioned and compacted with a reasonable degree of control of density and uniformity of the fill, stress-strain properties can be determined for these materials more precisely than for natural soil deposits, which may be less uniform and may have more complex behavior. As a result, the reliability of calculated movements is not as great for natural soil deposits as for embankments. Very often, even in the case of embankments, the agreement between calculated and measured movements is not as close as that shown in Figure 13-24.

12. USE OF CENTRIFUGE EXPERIMENTS

Centrifuge experiments have been used to study problems of slope stability and deformation behavior since the early 1970s (Schofield 1980). Techniques have been developed for constructing model slopes, varying water levels, measuring shear strengths, and measuring displacements in the models while they are rotating. The techniques were applied to studies of levee failures (Kusakabe et al. 1988), highway embankment settlement and stability (Feng and Hu 1988), settlement and cracking in dams (Shcherbina and Olympiev 1991; Zhang and Hu 1991; Zhu et al. 1991), stability of tailings dams (Liu et al. 1988), mechanisms of flow slides (Schofield 1980), and stabilization of slopes by drainage (Resnick and Znidarcic 1990).

The method has the greatest value for qualitative studies of mechanisms of deformation and failure. Because centrifuge models can be constructed so that they simulate the geometry and

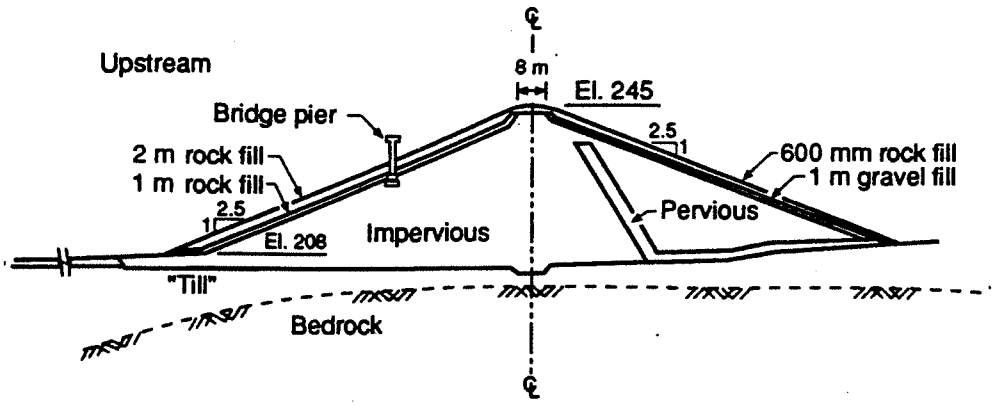

(a) Cross section through Otter Brook Dam

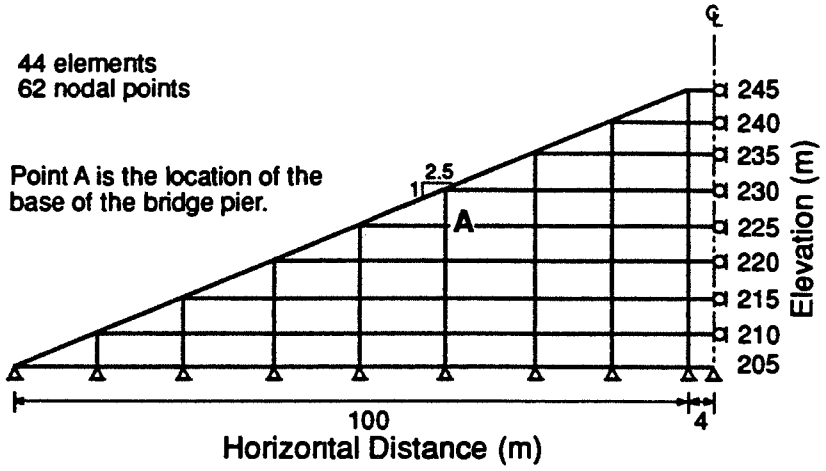

(b) Finite element mesh

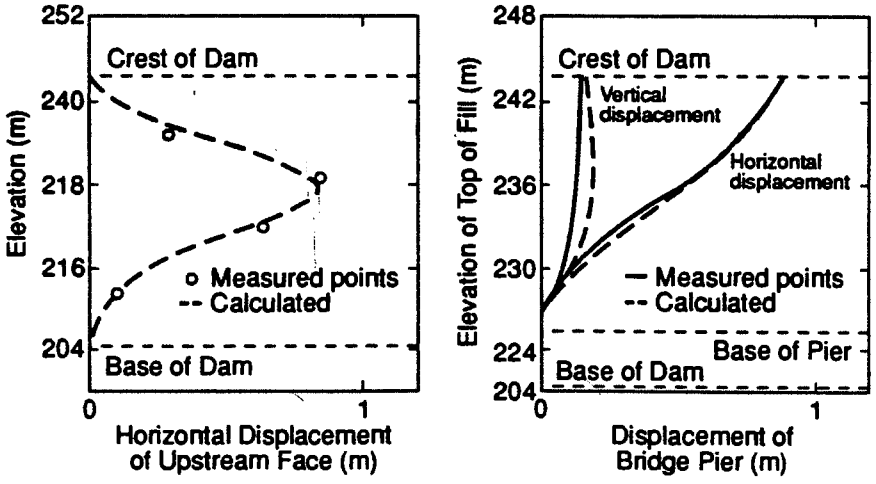

(c) Calculated and measured movements

FIGURE 13-24
Finite-element analysis of Otter Brook Dam, New Hampshire.

stresses in prototype slopes, they are capable, in principle, of simulating the modes of deformation and failure to be expected in the field. Thus, they are useful where mechanisms of deformation and failure are unknown.

Limitations on the use of centrifuge experiments to derive quantitative results stem from the difficulties inherent in constructing centrifuge models that accurately mimic the important details of the full-scale prototype and the loading conditions it will experience. These difficulties, plus the fact that the technique is costly and requires highly specialized equipment, appear to be the principal limitations on its use for practical studies of stability and deformation in soil slopes.

REFERENCES

Berman, G. 1988. *Landslide Control on the Panama Canal: Status Report—1988*. Geotechnical Branch, Engineering Division, Panama Canal Commission, Panama City, 26 pp.

Bishop, A. W. 1955. The Use of the Slip Circle in the Stability Analysis of Slopes. *Geotechnique*, Vol. 5, No. 1, pp. 7–17.

Bishop, A. W., and L. Bjerrum. 1960. The Relevance of the Triaxial Test to the Solution of Stability Problems. In *Proc., ASCE Research Conference on the Shear Strength of Cohesive Soils*, Boulder, Colorado, American Society of Civil Engineers, New York, pp. 437–501.

Cavounidis, S. 1987. On the Ratio of Factors of Safety in Slope Stability Analyses. *Geotechnique*, Vol. 37, No. 2, pp. 207–210.

Duncan, J. M. 1992. State-of-the-Art: Static Stability and Deformation Analysis. In *Proc., ASCE Specialty Conference on Stability and Performance of Slopes and Embankments II*, Berkeley, California, Geotechnical Special Publication 31, American Society of Civil Engineers, New York.

Duncan, J. M., A. L. Buchignani, and M. De Wet. 1987. *An Engineering Manual for Slope Stability Studies*. Virginia Polytechnic Institute and State University, Blacksburg, 80 pp.

Duncan, J. M., S. G. Wright, and K. S. Wong. 1990. Slope Stability During Rapid Drawdown. In *Proc., H. Bolton Seed Memorial Symposium*, Berkeley, California, Bitech Publishers, Vancouver, British Columbia, Canada.

Fellenius, W. 1927. *Erdstatische Berechnungen mit Reibung und Kohasion*. Ernst, Berlin.

Feng, G., and Y. Hu. 1988. Centrifugal Model Test of a Highway Embankment on Soft Clay. In *Proc., First International Conference on Geotechnical Centrifuge Modeling*, Paris, pp. 153–162.

Filz, G. M., T. L. Brandon, and J. M. Duncan. 1992. Back Analysis of the Olmsted Landslide Using Anisotropic Strengths. In *Transportation Research Record 1343*, TRB, National Research Council, Washington, D.C., pp. 72–78.

Hungr, O. 1987. An Extension of Bishop's Simplified Method of Slope Stability Analysis to Three Dimensions. *Geotechnique*, Vol. 37, No. 1, pp. 113–117.

Hungr, O., F. M. Salgado, and P. M. Byrne. 1989. Evaluation of a Three-Dimensional Method of Slope Stability Analysis. *Canadian Geotechnical Journal*, Vol. 26, pp. 679–686.

Hunter, J. H., and R. L. Schuster. 1968. Stability of Simple Cuttings in Normally Consolidated Clays. *Geotechnique*, Vol. 18, No. 3, pp. 372–378.

Janbu, N. 1968. *Slope Stability Computations*. Soil Mechanics and Foundation Engineering Report. Technical University of Norway, Trondheim.

Kulhawy, F. H., J. M. Duncan, and H. B. Seed. 1969. *Finite Element Analyses of Stresses and Movements in Embankments During Construction*. Report TE 69-4. Office of Research Services, University of California, 169 pp.

Kusakabe, O., A. Kawashima, and T. Hagiwara. 1988. Levee Failures Modeled in Drum Centrifuge. In *Proc., First International Conference on Geotechnical Centrifuge Modeling*, Paris, pp. 147–152.

Ladd, C. C., and R. Foott. 1974. New Design Procedure for Stability of Soft Clays. *Journal of the Geotechnical Engineering Division*, ASCE, Vol. 100, No. 7, pp. 763–786.

LaRochelle, P., B. Trak, F. Tavenas, and M. Roy. 1974. Failure of a Test Embankment on a Sensitive Champlain Clay Deposit. *Canadian Geotechnical Journal*, Vol. 11, No. 1, pp. 142–164.

Liu, L., W. Jiang, and W. Han. 1988. Centrifugal Model Tests for Stability of Ash Soil Composite Dams. In *Proc., First International Conference on Geotechnical Centrifuge Modeling*, Paris, pp. 141–146.

Lowe, J., and L. Karafiath. 1960. Stability of Earth Dams upon Drawdown. In *Proc., First Pan-American Conference on Soil Mechanics and Foundation Engineering*, Mexico City, Vol. 2, pp. 537–552.

Morgenstern, N. R. 1992. The Evaluation of Slope Stability—A 25 Year Perspective. In *Proc., ASCE Specialty Conference on Stability and Performance of Slopes and Embankments II*, Berkeley, California,

Geotechnical Special Publication 31, American Society of Civil Engineers, New York, pp. 1–26.

Morgenstern, N. R., and V. E. Price. 1965. The Analysis of the Stability of General Slip Surfaces. *Geotechnique*, Vol. 15, No. 1, pp. 79–93.

Resnick, G. S., and D. Znidarcic. 1990. Centrifugal Modeling of Drains for Slope Stabilization. *Journal of Geotechnical Engineering*, ASCE, Vol. 116, No. 11, pp. 1607–1624.

Sarma, S. K. 1973. Stability Analysis of Embankments and Slopes. *Geotechnique*, Vol. 23, pp. 423–433.

Schaefer, V. R., and J. M. Duncan. 1988. Finite Element Analyses of the St. Alban Test Embankments. In *Proc., Symposium on Geosynthetics for Soil Improvement*, National Convention, Nashville, American Society of Civil Engineers, pp. 158–177.

Schofield, A. N. 1980. Cambridge Geotechnical Centrifuge Operations. *Geotechnique*, Vol. 30, No. 3, pp. 227–268.

Shcherbina, V. I., and D. N. Olympiev. 1991. Numerical and Centrifugal Modeling of Cracking in an Earth-and-Rockfill Dam Core. In *Proc., Second International Conference on Geotechnical Centrifuge Modeling*, Boulder, Colorado, pp. 67–74.

Skempton, A. W. 1970. First-Time Slides in Overconsolidated Clays. *Geotechnique*, Vol. 20, No. 4, pp. 320–324.

Skempton, A. W. 1977. Slope Stability of Cuttings in London Clay. In *Proc., Ninth International Conference on Soil Mechanics and Foundation Engineering*, Tokyo, pp. 261–270.

Skempton, A. W. 1985. Residual Strength of Clays in Landslides, Folded Strata, and the Laboratory. *Geotechnique*, Vol. 35, No. 1, pp. 3–18.

Spencer, E. 1967. A Method of Analysis of the Stability of Embankments Assuming Parallel Interslice Forces. *Geotechnique*, Vol. 17, No. 1, pp. 11–26.

Trak, B., P. LaRochelle, F. Tavenas, S. Leroueil, and M. Roy. 1980. A New Approach to the Stability Analysis of Embankments on Sensitive Clays. *Canadian Geotechnical Journal*, Vol. 17, No. 4, pp. 526–584.

U.S. Army Corps of Engineers. 1970. *Engineering and Design—Stability of Earth and Rockfill Dams*. Engineer Manual EM 1110-2-1902. Department of the Army, Corps of Engineers, Office of the Chief of Engineers, Washington, D.C.

Wright, S. G., and J. M. Duncan. 1972. Analysis of Waco Dam Slide. *Journal of the Soil Mechanics and Foundations Division*, ASCE, Vol. 98, No. SM7, pp. 653–665.

Wright, S. G., and J. M. Duncan. 1991. Limit Equilibrium Stability Analyses for Reinforced Slopes. In *Transportation Research Record 1330*, TRB, National Research Council, Washington, D.C., 1991, pp. 40–46.

Zhang, L., and T. Hu. 1991. Centrifugal Modeling of the Pubugan High-Rise Rockfill Dam. In *Proc., Second International Conference on Geotechnical Centrifuge Modeling*, Boulder, Colorado, pp. 45–50.

Zhu, W., J. Yi, D. Zhu, and S. Liu. 1991. Application of Centrifuge Modeling to Predictions of Earth-Rockfill Dam Core Cracking. In *Proc., Second International Conference on Geotechnical Centrifuge Modeling*, Boulder, Colorado, pp. 59–66.

Appendix B

METRIC CONVERSION TABLE

SI units to inch/pound units

To convert from	To	Multiply by
	LENGTH	
millimeter (mm)	inch (in.)	0.03937
meter (m)	foot (ft)	3.281
	yard (yd)	1.094
kilometer (km)	mile (mi)	0.6214
	mile, nautical (nmi)	0.5400
	AREA	
meter^2 (m^2)	foot^2 (ft^2)	10.76
	yard^2 (yd^2)	1.196
	acre	0.0002471
hectometer^2 (km^2)	acre	2.471
kilometer^2 (km^2)	mile^2 (mi^2)	0.3861
	VOLUME	
centimeter^3 (cm^3)	inch^3 (in.^{3})	0.06102
decimeter^3 (dm^3)	inch^3 (in.^{3})	61.02
	pint (pt)	2.113
	quart (qt)	1.057
	gallon (gal)	0.2642
	foot^3 (ft^3)	0.03531
meter^3 (m^3)	foot^3 (ft^3)	35.31
	yard^3 (yd^3)	1.308
	gallon (gal)	264.2
	barrel (bbl), (petroleum, 1 bbl=42 gal)	6.290
	acre-foot (acre-ft)	0.0008107
hectometer^3 (hm^3)	acre-foot (acre-ft)	810.7
kilometer^3 (km^3)	mile^3 (mi^3)	0.2399

Inch/pound units to SI units

To convert from	To	Multiply by
	LENGTH	
inch (in.)	millimeter (mm)	25.4*
foot (ft)	meter (m)	0.3048
yard (yd)	meter (m)	0.9144*
mile (mi)	kilometer (km)	1.609
mile, nautical (nmi)	kilometer (km)	1.852*
	AREA	
foot^2 (ft^2)	meter^2 (m^2)	0.09290
yard^2 (yd^2)	meter^2 (m^2)	0.8361
acre	meter^2 (m^2)	4,047
	hectometer^2 (hm^2)	0.4047
mile^2 (mi^2)	kilometer^2 (km^2)	2.590
	VOLUME	
inch^3 (in.^{3})	centimeter^3 (cm^3)	16.39
	decimeter^3 (dm^3)	0.01639
foot^3 (ft^3)	decimeter^3 (dm^3)	28.32
	meter^3 (m^3)	0.02832
yard^3 (yd^3)	meter^3 (m^3)	0.7646
pint (pt)	decimeter^3 (dm^3)	0.4732
quart (qt)	decimeter^3 (dm^3)	0.9464
gallon (gal)	decimeter^3 (dm^3)	3.785
	meter^3 (m^3)	0.003785
barrel (bbl), (petroleum, 1bbl=42 gal)	meter^3 (m^3)	0.1590
acre-foot (acre-ft)	meter^3 (m^3)	1,233
	hectometer^3 (hm^3)	0.001233
mile^3 (mi^3)	kilometer^3 (km^3)	4.168

SI units to inch/pound units

To convert from	To	Multiply by
VOLUME PER UNIT TIME (included flow)		
decimeter^3 per second (dm^3/sec)	foot^3 per second (ft^3/sec)	0.03531
	gallon per minute (gal/min)	15.85
	barrel per day (bbl/d), (petroleum)	543.4
meter^3 per second (m^3/sec)	foot^3 per second (ft^3/sec)	35.31
	gallon per minute (gal/min)	15,850
MASS		
gram (g)	ounce avoirdupois (oz avdp)	0.03527
kilogram (kg)	pound avoirdupois (lb avdp)	2.205
megagram (Mg)	ton, short (2,000 lb)	1.102
	ton, long (2,240 lb)	0.9842
PRESSURE		
kilopascal (kPa)	pound-force per inch^2 (lbf/in.^{2})	0.1450
	atmosphere, standard (atm)	0.009869
	bar	0.01*
	inch of mercury at 60°F (in Hg)	0.2961
TEMPERATURE		
kelvin (K)	degreee Fahrenheit (°F)	[1]
degree Celsius (°C)	degree Fahrenheit (°F)	[2]

[1]Temp °F = 1.8 temp K − 459.67. [2]Temp °F = 1.8 temp °C +32.

Inch/pound units to SI units

To convert from	To	Multiply by
VOLUME PER UNIT TIME (included flow)		
foot^3 per second (ft^3/sec)	decimeter^3 per second (dm^3/sec)	28.32
	meter^3 per second (m^3/sec)	0.02832
gallon per minute (gal/min)	decimeter^3 per second (dm^3/sec)	0.06309
	meter^3 per second (m^3/sec)	0.00006309
barrel per day (bbl/d), (petroleum)	decimeter^3 per second (dm^3/sec)	0.001840
MASS		
ounce avoirdupois (oz avdp)	gram (g)	28.35
pound avoirdupois (lb avdp)	kilogram (kg)	0.4536
ton, short (2,000 lb)	megagram (Mg)	0.9072
ton, long (2,240 lb)	megagram (Mg)	1.016
PRESSURE		
pound-force per inch^2 (lbf/in.^{2})	kilopascal (kPa)	6.895
atmosphere, standard (atm)	kilopascal (kPa)	101.3
bar	kilopascal (kPa)	100.*
inch of mercury at 60 F (in Hg)	kilopascal (kPa)	3.377
TEMPERATURE		
degree Fahrenheit (°F)	kelvin (K)	[3]
degree Fahrenheit (°F)	degree Celsius (°C)	[4]

[3]Temp K = (temp °F + 459.67)/1.8. [4]Temp °C = (temp °F − 32)/1.8.

NOTE: The International System of Units (SI) is a modernized metric system of measurement. In this table an asterisk after the last digit of the factor indicates that the conversion factor is exact and that all subsequent digits are zero; all other conversion factors have been rounded to four significant digits. Use of hectare (ha) as an alternative name for square hectometer (hm^2) is restricted to the measurement of small land or water areas. Use of liter (L) as a special name for cubic decimeter (dm^3) is restricted to the measurement of liquids and gases. No prefix other than "milli" should be used with liter.

SOURCE: W.R. Hansen, ed. 1991. *Suggestions to Authors of the Reports of the United States Geological Survey*, 7th ed. Government Printing Office, 289 pp.

TAB 15

Miscellaneous

R. D. Holtz[1]

SI Units in Geotechnical Engineering

REFERENCE: Holtz, R. D., **"SI Units in Geotechnical Engineering,"** *Geotechnical Testing Journal*, GTJODJ, Vol. 3, No. 2, June 1980, pp. 73-79.

ABSTRACT: A brief description is presented of the International System of Units (SI) as it might be applied to geotechnical engineering. Base as well as derived SI units that are of interest to geotechnical engineers are described in detail, and conversion factors for units in common usage are given. A few examples of conversions are also presented.

KEY WORDS: units of measurement, metric system, symbols

Within the scientific and engineering community, there has always been some confusion as to the proper system of units for physical measurements and quantities. Many schemes have been advanced throughout the past few centuries and some, such as the Imperial or British Engineering system, the so-called metric system, and a few hybrids, have achieved moderately wide popular usage. Recently, with the growth of international cooperation and trade, it has become increasingly apparent that one single, commonly accepted system of units would be not only convenient but also of tremendous practical value.

Even though geotechnical engineering may not have the greatest confusion of units, it undoubtedly ranks near the top of all fields in the number of different systems in common usage. Laboratory engineers, following their counterparts in the physical sciences, have attempted to use some sort of metric system, usually the cgs (centimetre-gram-second) system for the simpler laboratory tests. But they also apply the mks (metre-kilogram-second) system to measurements of pressure and stress in consolidation and triaxial tests and use British Engineering units for compaction tests. As any teacher of soil mechanics can testify, the confusion to the uninitiated is tremendous. At least practicing geotechnical engineers in North America have been somewhat consistent in the use of the British Engineering system for laboratory and field densities, stress measurements, and the like, although they commonly alternate between pounds per square foot, kips per square foot, tons per square foot, and pounds per square inch, depending on how they or their clients feel about the subject. Fortunately, 1 ton-force per square foot is within 2% of 1 kgf/cm^2, a common laboratory unit for stress and pressure, and the foundation engineer using consolidation test data can convert directly with little error. Strictly speaking, the use of force as a basic unit is incorrect; mass should be the basic unit, with force derived according to Newton's Second Law of Motion. Use of the kilogram as a unit of force is one of the difficulties with the so-called metric system, a modified version of the mks system that was common among continental European engineers. At least they tried to keep the distinction between mass and force by calling the kilogram-force a "kilopond" (kp).

A modernized version of the metric system has been developing over the past 30 years. The system is known as *SI*, which stands for *le Système International d'Unités* (The International System of Units). It is described in detail in ASTM E 380, the Standard for Metric Practice, available in the back of every part of the *Annual Book of ASTM Standards*. The system may soon become the common system in the United States and the few other countries still using Imperial or British Engineering units. In fact, Great Britain itself converted completely to SI in 1972, and Australia, Canada, and New Zealand are presently well along the way to conversion. Most European countries already have de facto conversion to SI, especially in engineering practice.

The SI Metric System

The SI metric system is a fully coherent and rationalized system. It is founded on seven basic units: for *length* (metre, m), *mass* (kilogram, kg), *time* (second, s), *electric current* (ampere, A), *thermodynamic temperature* (kelvin, K), *luminous intensity* (candela, cd), and *amount of substance* (mole). All of these basic units have precise definitions, names, and symbols. Units for all other physical quantities can be derived in terms of these basic units. Sometimes the derived quantities are given specific names, such as the *newton* (N) for force and the *watt* (W) for power. The derived unit of force replaces the kilogram-force (kgf) of the mks system so that the name of the unit indicates that it is a unit of force, not mass. A great advantage is that *one and only one unit exists for each physical quantity*, and all other mechanical quantities such as velocity, force, work, and so on can be derived from the basic units. In addition, the SI units for force, energy, and power are *independent* of the nature of the physical process, whether mechanical, electrical, or chemical.

Another major advantage of SI is that it is a fully coherent system. This means that a product or quotient of any two unit quantities is a unit of the resulting quantity. For example, unit length squared should be unit area, and unit force should be unit mass times unit acceleration. Obviously, many of the engineering units in common use (for example, acre, pound-force, or kilogram-force), are not coherent units. Also, units that might be related to basic units by powers of ten are not consistent within the SI system. A good example is the litre (L), which is a cubic decimetre. The equivalent volume of the litre has been defined as exactly 10^{-3} m^3 (1000 cm^3). Additional advantages of SI include the use of unique and well-defined symbols and abbreviations and the convenient decimal relation between multiples and submultiples of the basic units.

[1]Associate professor, School of Civil Engineering, Purdue University, W. Lafayette, Ind. 47907. Member of ASTM.

© 1980 by the American Society for Testing and Materials

0149-6115/80/0006-0073$00.40

Basic and Derived SI Metric Units

Base Units

The three base units of interest to geotechnical engineers are length, mass, and time. The SI units for these quantities are the *metre*, the *kilogram*, and the *second*. Temperature, which might also be of interest, is expressed in kelvins, although the system does allow for use of the degree Celsius (°C), which has the same interval. Electric current is expressed in *amperes*. Supplementary units include the *radian* (rad) and *steradian* (sr), the units of plane and solid angle, respectively.

As mentioned, these basic SI units have precise physical definitions. For example, contrary to a popular misconception, the metre is not the distance between two bars in Paris, but rather has been defined as being exactly equal to a certain number of wavelengths of radiation corresponding to a specific transition level in krypton 86. The standard kilogram is equal to the mass of the international prototype kilogram, a cylinder of platinum-iridium alloy preserved in a vault at Le Bureau International des Poids et Mesures at Sèvres, France. Similar standard kilograms can also be found at the U.S. National Bureau of Standards near Washington, D.C. The second has been defined as the duration of a certain number of periods of the radiation corresponding to a specific transition state in cesium 133.

Derived Units

Derived units geotechnical engineers might use are listed in Table 1. Prefixes are used to indicate multiples and submultiples of the basic and derived units. SI prefixes are listed in Table 2. The prefixes should be applied to indicate orders of magnitude of the basic or derived units and to reduce redundant zeros so that numerical values lie between 0.1 and 1000. They should not be applied to the denominator of compound units (kilogram is an exception since it is a basic unit in the SI system). Note that spaces, not commas, should be used to separate groups of zeros. (This latter item was a concession to the Europeans, so that they would stop using a comma where Americans would use a decimal point.)

To maintain the coherence of the system, it is recommended that only basic units be used to form derived units. For example, the unit of force, the newton, is derived according to Newton's Second Law, $F = Ma$, where the mass M is in kilograms, and the acceleration a is in m/s^2, all basic units. For derived combinational units such as pressure or stress (pascals or newtons per square metre), multiples and submultiples of the basic metric units (in this case metres) should be avoided. For example, N/cm^2 and N/mm^2 are wrong; the appropriate prefix should be used with the numerator to indicate larger or smaller quantities, for example, kPa (kN/m^2) or MPa (MN/m^2).

TABLE 2—*Prefixes for SI units.*

Factor	Prefix	Symbol
10^{18}	exa	E
10^{15}	peta	P
10^{12}	tera	T
10^{9}	giga	G
10^{6}	mega	M
10^{3}	kilo	k
10^{2}	hecto	h
10^{1}	deka	da
10^{-1}	deci	d
10^{-2}	centi	c
10^{-3}	milli	m
10^{-6}	micro	μ
10^{-9}	nano	n
10^{-12}	pico	p
10^{-15}	femto	f
10^{-18}	atto	a

SI Units of Interest to Geotechnical Engineers

Length

The SI unit for length, the metre, should already be familiar. (By the way, metre, not meter, is the recommended ASTM spelling.) Useful SI length multiples and submultiples are the kilometre (km), millimetre (mm), micrometre (μm), and nanometre (nm). Conversion factors for common British Engineering and mks units are given in Table 3.

Good SI practice suggests that multiple and submultiple metric units be used in increments of 1000, for example, millimetre, metre, and kilometre. Use of the centimetre, especially for lengths under 300 mm, should be avoided.

TABLE 1—*Derived SI units.*

Quantity	Unit	Symbol	Formula
acceleration	metre per second square	m/s^2	...
area	square metre	m^2	...
area	hectare	ha	$hm^2 = 10^4\ m^2$
density	kilogram per cubic metre	kg/m^3	...
force	newton	N	$kg \cdot m/s^2$
frequency	hertz	Hz	1/s
moment or torque	newton metre	$N \cdot m$	$kg \cdot m^2/s^2$
power	watt	W	J/s
pressure	pascal	Pa	N/m^2
stress	pascal	Pa	N/m^2
unit weight	newton per cubic metre	N/m^3	$kg/s^2 \cdot m^2$
velocity	metre per second	m/s	...
voltage	volt	V	W/A
volume	cubic metre	m^3	...
volume	litre	L	$dm^3 = 10^{-3}\ m^3$
work (energy)	joule	J	$N \cdot m$

TABLE 3—*Conversion factors for units of length.*

Unit	SI Equivalent
1 inch	25.4 mm = 0.0254 m
1 foot	0.3048 m
1 yard	0.9144 m
1 mile (U.S. statute)	1.609×10^3 m = 1.609 km
1 mile (nautical)	1.852×10^3 m = 1.852 km
1 angstrom	1×10^{-10} m = 0.1 nm
1 mil	2.54×10^{-5} m = 0.0254 mm = 25.4 μm

Mass

It will be recalled from physics that the inertia or mass of a physical object, for which the SI unit is the kilogram, is a measure of the property that controls the response of that object to an applied force. It is convenient to measure the mass in terms of the acceleration of an object produced by a unit force, as related by Newton's Second Law of Motion. Thus, a unit force causes a 1-kg mass to accelerate at 1 m/s^2. The mass then is an appropriate measure of the amount of matter an object contains. The mass remains the same even if the object's temperature, shape, or other physical attributes change. Unlike weight, which will be discussed later, the mass of an object does not depend on the local gravitational attraction, and thus it is also independent of the object's location in the universe.

Among all the SI units, the kilogram is the only one whose name, for historical reasons, contains a prefix. The names of multiples and submultiples of the kilogram are formed by attaching prefixes to the word "gram" rather than to "kilogram." In other words, 10^{-6} kg is not a microkilogram, but a milligram, 10^{-3} g. Similarly, 1000 kg is not 1 kilokilogram but is equivalent to 1 megagram (Mg); 1000 kg is also the metric ton, sometimes spelled "tonne" to avoid confusion with the British ton, which is equal to 2000 lb. ASTM recommends that metric ton be restricted to commercial usage, and that the term tonne be avoided altogether. Practical units of mass in engineering practice are the megagram, and in laboratory work, the kilogram and gram.

Some useful relationships and conversion factors for units of mass are given in Table 4.

Time

Although the second is the basic SI time unit, minutes (min), hours (h), days, and the like may be used where convenient, even though they are not decimally related. (Maybe some day we will even have a decimal time system; see Carrigan [*1*].)

Force

As mentioned, the SI unit of force is derived from $F = Ma$, and it is called the newton, equal to 1 kg·m/s^2. Conversion factors for common engineering force units are given in Table 5.

TABLE 4—*Conversion factors for units of mass.*

Unit	SI Equivalent
1 pound mass (avoirdupois)	0.4536 kg
1 British (short) ton (2000 lbm)	907.2 kg
1 gram	10^{-3} kg
1 metric ton	10^3 kg = 10^6 g = 1 Mg
1 slug (1 lb-force per ft/s^2)	14.59 kg

TABLE 5—*Conversion factors for units of force.*

Unit	SI Equivalent
1 lb-force	4.448 N
1 British ton-force	8.896×10^3 N = 8.896 kN
1 kg-force (kp)	9.807 N
1 kip (1000 lb-force)	4.448×10^3 N = 4.448 kN
1 metric ton-force (1000 kg-force)	9.807×10^3 N = 9.807 kN
1 dyne (g·cm/s^2)	10^{-5} N = 10 μN

It is obvious that the numbers in newtons for such items as column loads would be very large indeed and consequently somewhat awkward. Therefore, consistent with the rules for application of prefixes, it is simple to adjust these rather large numbers to more manageable quantities for engineering work. The common prefixes would be kilo-, mega-, and giga-, so that engineering forces would be expressed in kilonewtons, kN, meganewtons, MN, and giganewtons, GN. (The symbol for mega is M to avoid confusion with the symbol for milli, m.) Thus, since 1 ton-force is 8.9 kN, 1000 ton-force would be 8.9 MN. Some useful relationships using these prefixes are:[2]

1 kilonewton (kN) = 10^3 newton
1 meganewton (MN) = 10^6 newton = 10^3 kN
1 figanewton (FN) = 10^8 newton = 10^5 kN = 10^2 MN
1 giganewton (GN) = 10^9 newton = 10^6 kN = 10^3 MN
3 giganewtons = 30 figanewtons = 1 boxafiganewtons[3]
14.4 giganewtons = 1 grossafiganewtons

The correct unit to express the weight of an object is the newton, since weight is the gravitational force that causes a downward acceleration of that object. This can be expressed by saying that weight W equals Mg, where M is the mass of the object and g is the acceleration of gravity. It will be recalled that the acceleration of gravity varies with latitude and elevation; thus SI recommends that weight be avoided and that mass be used instead. If weight must be used, it is suggested that the location and gravitational acceleration also be stated. However, for most ordinary engineering purposes, the difference in acceleration (about 0.5%) can be neglected, and as long as we express the weight in newtons, the units will be consistent.

Another problem with weight is that it is commonly used when we really mean the mass of an object. For example, in the laboratory when we "weigh" an object on a laboratory balance, we really are comparing two masses, that of the unknown object with that of an object of known mass. Even scales or balances that displace linear springs are calibrated against objects of known mass.

Further ambiguity occurs of course because common units of mass, such as the pound or kilogram, are often used in engineering practice as a unit of force. If pound is used as a unit of force, then depending on the resulting accelerations, different mass units are defined. For example, if 1 lbf causes an acceleration of 1 ft/s^2, then the mass is 1 lbf·s^2/ft, which is called a slug. In other words, 1 lbf = 1 slug × 1 ft/s^2. Using slugs as units of mass avoids the confusion with pounds as mass, and this unit has been commonly used in aerodynamics and fluid mechanics.

[2]Kovacs, W. D., "Conversion factors for kilonewtons per square meter and common engineering stress units," Purdue University, 1974 (unpublished).

[3]This unit is only a constant before the box is opened.

If we wanted instead to use a pound-mass system, we would define a unit of force called the *poundal*, where 1 poundal = 1 lb-mass × 1 ft/s^2. Poundals are apparently only found in physics books.

Some examples illustrating conversion between different mass units are given in the Appendix to this paper.

Stress and Pressure

The SI unit for stress and pressure is the *pascal* (Pa), which is exactly equal to 1 N/m^2. There has been some objection, especially in Europe, to the use of the pascal as the basic unit of stress and pressure, because it is so small. The Germans and French, for example, often use the bar, which is exactly 10^5 Pa. However, the pascal is more logical since it is a coherent unit; that is to say, equations involving the pascal with other SI units can be written without coefficients of proportionality being required. Conversion factors for some common engineering units for stress and pressure are given in Table 6.

It is obvious that the pascal is a small unit, but, as with SI units of force, it is easy to add prefixes to make the large numbers more manageable. Thus, 1 psi in the above table is more conveniently expressed as 6.9 kPa than as 6.9 × 10^3 Pa. For ordinary triaxial testing of soils, for example, hydrostatic cell pressures rarely exceed 200 or 300 psi (1379 kPa or 2068 kPa). Or, if all the pressures in a test series are in this range, it might be convenient to use 1.4 MPa or 2.1 MPa. And, as with other systems of units, a rounded or even interval may be more convenient; in this case, 1.5 MPa and 2.0 MPa.

Similar examples could be given for engineering stresses. Either kilopascals or megapascals, kPa or MPa, will become commonly used for foundation stresses, lateral earth pressures, allowable bearing values, and the like. In the laboratory, force is measured by a proving ring or load cell and then converted to stress (for example, in the unconfined compression or direct shear tests), so the computational process will be no more complicated than it is now. Similarly, with electrical pressure transducers, a calibration factor must be used to convert millivolts (mV) of output to pressure in whatever units are used.

A convenient approximation, part of which is already in use in geotechnical engineering practice, is the following:

$$1 \text{ British ton-force/ft}^2 \approx 1 \text{ kgf/cm}^2 \approx 1 \text{ atm}$$
$$\approx 10 \text{ metric ton-force/m}^2 \approx 100 \text{ kPa}$$

The error involved is between 2 and 4% which is certainly less than ordinary engineering accuracy requirements.

TABLE 6—*Conversion factors for units of pressure and stress.*

Unit	SI Equivalent
1 psi (lb-force/in.^{2})	6.895 × 10^3 Pa or 6.895 kPa
1 atm at STP[a]	1.013 × 10^5 Pa or 101.3 kPa
1 kg-force/cm^2	9.807 × 10^4 Pa or 98.07 kPa
1 metric ton-force/m^2	9.807 × 10^3 Pa or 9.807 kPa
1 bar	1 × 10^5 Pa or 100 kPa
1 ksi (kip/in.^{2})	6.895 × 10^6 Pa or 6.895 MPa
1 British ton-force/ft^2	95.76 × 10^3 Pa or 95.76 kPa
1 lb-force/ft^2	47.88 Pa

[a]Standard temperature and pressure, not a motor oil additive or Soil Test Probe.

Density and Unit Weight

Density is defined in physics as mass per unit volume. Its ui in the SI system are kilograms per cubic metre (kg/m^3). In mai cases in geotechnical engineering, it may be more convenient to express density in megagrams per cubic metre. Conversions from the common laboratory and field densities are:

$$1 \text{ lb-mass/ft}^3 = 16.018 \text{ kg/m}^3$$
$$1 \text{ g/cm}^3 = 10^3 \text{ kg/m}^3 = 1 \text{ Mg/m}^3$$

It will be recalled that the density of water ρ_w is exactly 1.000 g/cm^3 at 4°C, and the variation is relatively small over the range of temperatures encountered in ordinary engineering practice. Therefore, it is usually sufficiently accurate to take $\rho_w = 10^3$ kg/m^3 = 1 Mg/m^3, which considerably simplifies phase computations, for example. It is also useful to know that 1000 kg/m^3 is equal to 62.4 lb-mass/ft^3.

Typical densities that might be encountered in geotechnical practice are 1.2 Mg/m^3 (74.8 lb/ft^3), 1.6 Mg/m^3 (100 lb/ft^3), and 2.0 Mg/m^3 (125 lb/ft^3). The commonly used density for concrete, 150 lb/ft^3, is almost exactly 2.4 Mg/m^3.

Note that all mass and volume ratios common in geotechnical engineering practice are not affected by the use of SI units. For example, void ratio or water content of any given soil still has the same numerical value.

So far, unit weight or weight per unit volume has been the common measurement in geotechnical engineering. Since weight should be avoided in technical work for all the reasons discussed earlier, then unit weight also should be avoided. For this reas ASTM Committee D-18 on Soil and Rock recently voted to repla the standard definitions for unit weight with the appropriate definitions of density in ASTM D 653, Definitions of Terms and Symbols Relating to Soil and Rock Mechanics. If density must be converted to unit weight, then simply use $\gamma = \rho g$. Thus the appropriate value for the acceleration of gravity will have to be considered. The "standard" value of g is 9.807 m/s^2 (32.17 ft/s^2), which can be used with sufficient accuracy for ordinary engineering work on the earth. If work is to be carried out on the moon or some other planet, then the local value for g must be used.

For computations of geostatic stresses, the unit weights of the various soil layers can be easily replaced by the ρg of the layers. The usual formula

$$\sigma_v = \sum_{i=1}^{n} \gamma_i z_i$$

then becomes

$$\sigma_v = \sum_{i=1}^{n} \rho_i g z_i$$

where

σ_v = total vertical stress at some depth
ρ_i = density of each layer
z_i = thickness of each layer

If ρg is a constant throughout the depth h, then

$$\sigma_v = \rho g h$$

By analogy, computation of the static pore water pressure u_o at some depth h_w below the ground water table is

$$u_o = \rho_w g h_w$$

nilarly, to obtain the effective vertical overburden stress, the effective or buoyant density ρ' for each layer below the ground water table can be used, or perhaps more simply, $\sigma'_{vo} = \sigma_{vo} - u_o$.

Dimensional analysis of these equations for stress shows that if the densities are expressed in Mg/m^3, then stresses automatically come out in kPa. Or

$$(Mg/m^3)(m/s^2)m = 1000(kg \cdot m)/(s^2 \cdot m^2) = 1000\ N/m^2 = 1\ kPa$$

An example of geostatic stress computations using SI units can be found in the Appendix.

Summary

The SI system is a fully coherent and rational system of units, well suited to the measurements ordinarily made in geotechnical engineering practice. The basic units in the system have precise names, definitions, and symbols, and the units for all other physical quantities can be derived in terms of these basic units. Products or quotients of any two unit quantities are also units of the resulting quantity. Use of prefixes to indicate multiples and submultiples of units helps to make the numbers more manageable. One fact of particular interest to geotechnical engineers is that the SI units of force, stress, and pressure have independent and precisely defined names and symbols. Use of density instead of unit weight is not only more correct physically, but also has the advantage that the density of water is unity (in Mg/m^3). The only nor disadvantage to the use of SI units in geotechnical engineering practice is that a constant value for the acceleration of gravity must be included in the computations of geostatic stresses.

Acknowledgments

This article has been adapted by permission from an appendix to an introductory textbook on geotechnical engineering by R. D. Holtz and W. D. Kovacs, which will be published in 1981 by Prentice-Hall, Inc. The original version was written in 1969 while the author was a graduate student at Northwestern University. The support and encouragement of Prof. R. J. Krizek is gratefully acknowledged. The text was typed by Catherine Minth and the drawings were made by Margaret McFarren.

Reference

[1] Carrigan, R. A., "Decimal Time," *American Scientist*, Vol. 66, No. 3, May-June 1978, pp. 305-313.

Appendix
Computations and Conversions That Use SI Units

Example 1

Given: Neil Armstrong weighs 150 lb on earth.

Required: How much does he weigh on the surface of the moon?

Solution: First, we have to calculate Mr. Armstrong's mass on earth. Unless he had health problems during the voyage, his mass will be the same on the moon.

$$M = W/g = (150\ lbf)/(32.17\ ft/s^2) = 4.66(lbf \cdot s^2)/ft = 4.66\ slugs$$

Since 1 slug = 14.59 kg, his mass is 68.03 kg. Another way to calculate his mass is to convert his weight to newtons; then divide by g:

$$W = 150\ lbf(4.448\ N/1\ lbf) = 667.20\ N \text{ or } 667.2(kg \cdot m)/s^2$$

$$M = W/g = (667.2\ kg \cdot m/s^2)/(9.807\ m/s^2) = 68.03\ kg$$

Next, we have to either ask an astronomer or look up in the *Handbook of Chemistry and Physics* the gravitational acceleration on the surface of the moon. We find that $g_{moon} = 1.67\ m/s^2$. Thus,

$$W_{moon} = Mg_{moon} = 68.03\ kg\ (1.67\ m/s^2) = 113.62\ N$$

Or, since 4.448 N = 1 lbf,

$$W_{moon} = 113.62\ N\ (1\ lbf/4.448\ N) = 25.54\ lbf$$

Check: On earth,

$$667\ N(1.67\ 9.81) = 113.6\ N \text{ on the moon}$$

Example 2

Given: The density of water $\rho_w = 1\ Mg/m^3$.

Required: Calculate the density of water in (a) g/cm^3 and (b) lb/ft^3.

Solution: Set up an equation as follows for Part a.

$$1\ Mg/m^3 = 1\ Mg/m^3 \cdot (10^6\ g/\ 1\ Mg)(1\ m/100\ cm)^3 = 1\ g/cm^3$$

For Part b:

$$1\ Mg/m^3 = 1\ Mg/m^3 \cdot (10^3\ kg/1\ Mg)\ (1\ lbm/0.4536\ kg)(0.3048\ m/1\ ft)^3 = 62.43\ lbm/ft^3$$

where lbm = pound-mass.

Another way to solve Part b is to recall that $1\ lbm/ft^3 = 16.018\ kg/m^3$; so

$$1\ Mg/m^3 = 1\ Mg/m^3 \cdot (10^3\ kg/1\ Mg) \times (1\ lbm/ft^3/16.018\ kg/m^3) = 62.43\ lbm/ft^3$$

Example 3

Given: The density of water $\rho_w = 1\ Mg/m^3$.

Required: Convert this density to unit weight in (a) SI and (b) British Engineering units.

Solution: (a) SI units: We know that $\gamma = \rho g$; so

$$\gamma = 1\ Mg/m^3 \cdot (10^3\ kg/1\ Mg) \cdot 9.807\ m/s^2 = 9807(kg \cdot m)/(m^3 \cdot s^2)$$

Since $1\ N = 1\ kg \cdot m/s^2$, then

$$\gamma = 9807\ N/m^3 = 9.807\ kN/m^3$$

(b) British Engineering units: From Example 2 we know that 1 $Mg/m^3 = 62.43$ lbm/ft^3. Therefore,

$$\gamma = 62.43\ lbm/ft^3 \cdot 32.17\ ft/s^2 = 2008(lbm \cdot ft)/(s^2 \cdot ft^3)$$

$$= 2008\ poundals/ft^3$$

If lbf are used, from Part a,

$$\gamma = 9.807\ kN/m^3 \cdot (1000\ N/1kN)(1\ lbf/4.448\ N)$$

$$\times (0.3048\ m/1\ ft)^3 = 62.43\ lbf/ft^3$$

This is of course the familiar value for the unit weight of water.

Example 4

Given: The soil profile shown in Fig. 1.

Required: Compute and plot the total, neutral, and effective vertical stresses with depth.

Solution: First, calculate the approximate soil densities. For the sand above the water table:

$$\rho_d = \rho_s/(1 + e) = 2.65/(1 + 0.5) = 1.77\ Mg/m^3$$

$$\rho = \rho_d(1 + w) = 1.77(1.06) = 1.87\ Mg/m^3$$

where

ρ_d = dry density,
ρ_s = density of soil solids,
e = void ratio, and
w = water content.

For the sand below the water table:

$$\rho_{sat} = (\rho_s + \rho_w e)/(1 + e)$$

$$= (2.65 + 1.0 \cdot 0.5)/(1 + 0.5) = 2.10\ Mg/m^3$$

where ρ_{sat} = saturated density. For the clay:

$$\rho_{sat} = [\rho_s(1 + w)]/(1 + e) =$$

$$[2.7(1 + 0.37)]/(1 + 1.0) = 1.85\ Mg/m^3$$

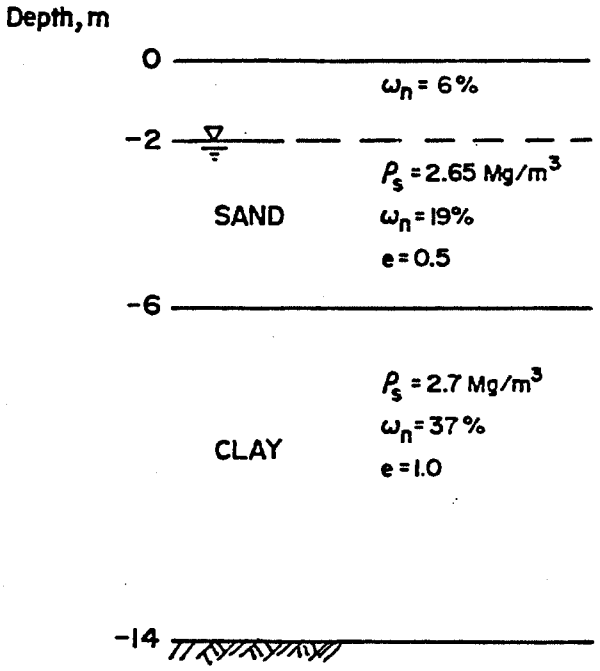

FIG. 1—*Soil profile for Example 4.*

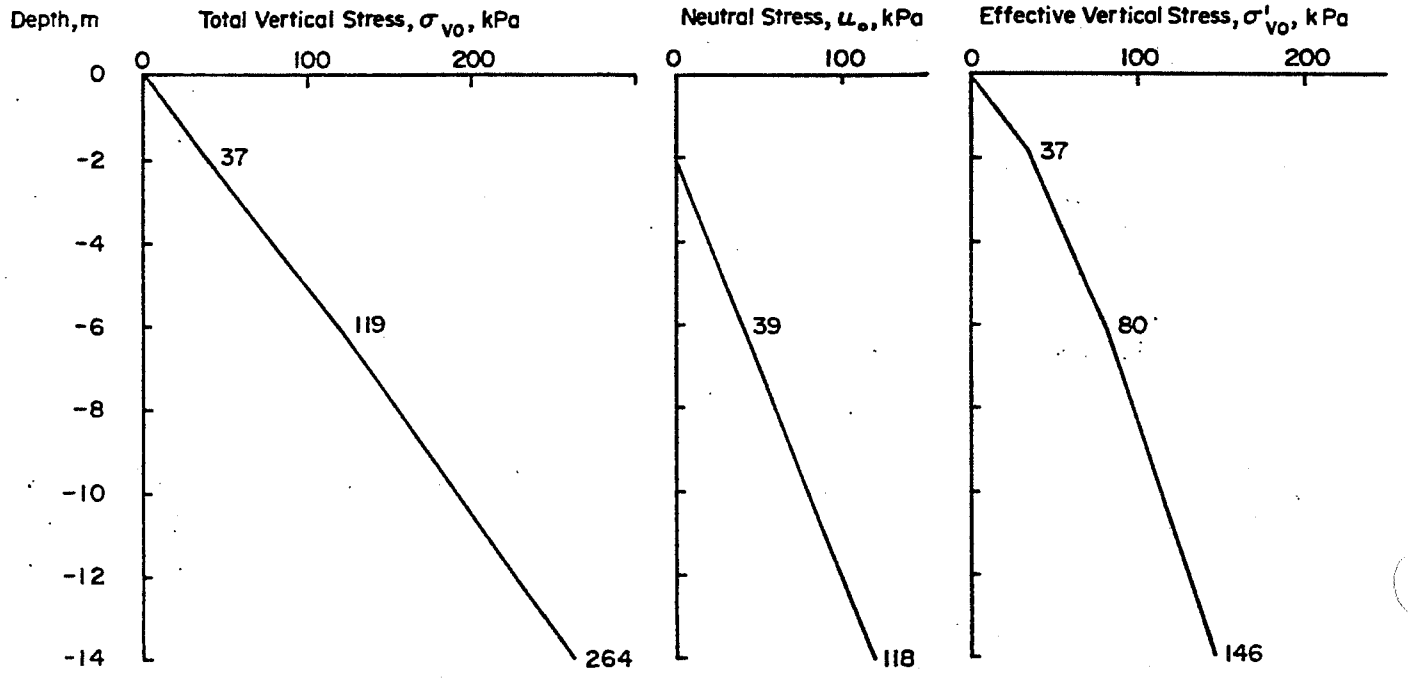

FIG. 2—*Total, neutral, and effective vertical stress profiles for Example 4.*

Second, calculate the total vertical stress σ_{vo} at a few convenient points in the profile. At -2 m:

$$\sigma_{vo} = \rho g z = (1.87\ \text{Mg/m}^3)(9.81\ \text{m/s}^2)2\ \text{m} =$$

$$36.69(\text{Mg} \cdot \text{m})/(\text{s}^2 \cdot \text{m}^2)$$

Recall that 1 $\text{kg}\cdot\text{m/s}^2$ = 1 N and 1 N/m^2 = 1 Pa. So 1 $(\text{Mg}\cdot\text{m})/(\text{s}^2\cdot\text{m}^2)$ = 1 kPa. Therefore, $36.69(\text{Mg}\cdot\text{m})/(\text{s}^2\cdot\text{m}^2)$ = 36.69 kPa or 37 kPa. Note that if densities are expressed in Mg/m^3, vertical stress comes out automatically in kPa. At -6 m: σ_{vo} = 37 kPa + (2.1)(9.81)(4) = 119 kPa, and so on. Pore water pressures are calculated using $u_o = \rho_w g h_w$. For example, at -6 m:

$$u_o = (1\ \text{Mg/m}^3)(9.81\ \text{m/s}^2)(4\ \text{m}) = 39\ \text{kPa}$$

The complete total, neutral, and effective vertical stress profiles are shown in Fig. 2.

SI Metric to US Customary Units

millimeters (mm)	inches (in)	0.03937
centimeters (cm)	inches (in)	0.3937
meters (m)	feet (ft)	3.2808
meters (m)	yards (yd)	1.0936
kilometers (km)	miles (mi)	0.6215
millimeters per meter (mm/m)	inches per yard (in/yd)	0.3600
square centimeters (cm^2)	square inches (sq in)	0.1550
square meters (m^2)	square feet (sq ft)	10.753
cubic centimeters (cm^3)	cubic inches (cu in)	0.0610
cubic meters (m^3)	cubic feet (cu ft)	35.336
kilograms (kg)	pounds (lb)	2.2075
kilograms (kg)	tons (ton)	0.00110
metric tons (mt)	tons (ton)	1.1025
newtons (N)	one pound force (lb)	0.2248
kilonewtons (kN)	one kip (kip)	0.2248
newtons (N)	one kilogram force (kg)	0.1020
kilonewtons per meter (kN/m)	kips per foot (kips/ft)	0.0685
newtons per square meter (N/m^2)	pounds per square foot (psf)	0.0209
kilonewtons per square meter (kN/m^2)	pounds per square inch (psi)	0.1451
meganewtons per square meter (MN/m^2)	pounds per square inch (psi)	145.138
kilograms per square centimeter (kg/cm^2)	pounds per square inch (psi)	14.223
meganewtons per square meter (MN/m^2)	kips per square inch (ksi)	0.1451
kilograms per cubic meter (kg/m^3)	pounds per cubic foot (pcf)	0.0624
Degree Celsius (°C)	Degree Fahrenheit (°F)	1.8018
Temperature Celsius (C)	Temperature Fahrenheit (F)	(1.8)(C°)+32
meters per second	miles per hour (mph)	2.2371
square meters per second (m^2/sec)	square feet per minute (ft^2/min)	645.994
square centimeters per second (cm^2/hr)	square feet per hour (ft^2/hr)	0.00108
watts per square meter ($W\ m^{-2}$)	Btu per hour per square foot ($Btu\ hr^{-1}\ ft^{-2}$)	0.3173
joule per kilogram per degree Celsius ($J\ kg^{-1}\ °C^{-1}$)	Btu per pound per degree Fahrenheit ($Btu\ lb^{-1}\ °F^{-1}$)	0.000239
watts per square meter per degree Celsius ($W\ m^{-2}\ °C^{-1}$)	Btu per hour per square foot per degree Fahrenheit ($Btu\ hr^{-1}\ ft^{-2}\ °F^{-1}$)	0.1761
watts per meter per degree Celsius ($W\ m^{-1}\ °C^{-1}$)	Btu inch per hour per square foot per degree Fahrenheit ($Btu\ in\ hr^{-1}\ ft^{-2}\ °F^{-1}$	6.9348

US Customary to SI Metric Units

To Convert	To	Multiply By
inches (in)	millimeters (mm)	25.40
inches (in)	centimeters (cm)	2.540
feet (ft)	meters (m)	0.3048
yards (yd)	meters (m)	0.9144
miles (mi)	kilometers (km)	1.609
inches per yard (in/yd)	millimeters per meter (mm/m)	27.78
square inches (sq in)	square centimeters (cm^2)	6.45
square feet (sq ft)	square meters (m^2)	0.093
cubic inches (cu in)	cubic centimeters (cm^3)	16.39
cubic feet (cu ft)	cubic meters (m^3)	0.0283
pounds (lb)	kilograms (kg)	0.453
tons (ton)	kilograms (kg)	907.185
tons (ton)	metric tons (mt)	0.907
one pound force (lb)	newtons (N)	4.448
one kip (kip)	kilonewtons (kN)	4.448
one kilogram force (kg)	newtons (N)	9.806
kips per foot (kips/ft)	kilonewtons per meter (kN/m)	14.59
pounds per square foot (psf)	newtons per square meter (N/m^2)	47.88
pounds per square inch (psi)	kilonewtons per square meter (kN/m^2)	6.89
pounds per square inch (psi)	meganewtons per square meter (MN/m^2)	0.00689
pounds per square inch (psi)	kilograms per square centimeter (kg/cm^2)	0.07031
kips per square inch (ksi)	meganewtons per square meter (MN/m^2)	6.89
pounds per cubic foot (pcf)	kilograms per cubic meter (kg/m^3)	16.02
Degree Fahrenheit (°F)	Degree Celsius (°C)	0.555
Temperature Fahrenheit (F)	Temperature Celsius (C)	(°F-32)/1.8
miles per hour (mph)	meters per second	0.4470
square feet per minute (ft^2/min)	square meters per second (m^2/sec)	0.001548
square feet per hour (ft^2/hr)	square centimeters per second (cm^2/hr)	929.03
Btu per hour per square foot (Btu hr^{-1} ft^{-2})	watts per square meter (W m^{-2})	3.152
Btu per pound per degree Fahrenheit (Btu lb^{-1} °F^{-1})	joule per kilogram per degree Celsius (J kg^{-1} °C^{-1})	4186.8
Btu per hour per square foot per degree Fahrenheit (Btu hr^{-1} ft^{-2} °F^{-1}	watts per square meter per degree Celsius (W m^{-2} °C^{-1})	5.678
Btu inch per hour per square foot per degree Fahrenheit (Btu in hr^{-1} ft^{-2} °F^{-1})	watts per meter per degree Celsius (W m^{-1} °C^{-1})	0.1442

San Francisco Chronicle 12/19/00

Underwater Landslides Threaten California Coast

By David Perlman
CHRONICLE SCIENCE EDITOR

When more than 2,200 people died after a 1998 earthquake in Papua New Guinea, it wasn't the earthquake that killed them, but a massive undersea landslide -- triggered by the quake -- that within minutes sent 50-foot waves surging over the shoreline, drowning unwary victims and destroying their villages.

Similar submarine landslides down unstable coastal slopes threaten many California coastal communities, and the slides may not even require earthquakes to touch them off, scientists agreed yesterday at a briefing during the American Geophysical Union meeting in Moscone Center.

A global network of tsunami warning centers are designed to signal whenever major earthquakes occur anywhere around the Pacific's notorious "ring of fire," where the land and sea are marked by almost constant quakes and volcanic eruptions

But predicting the onset of the threatening underwater landslides when quakes are not involved is a science barely in its infancy, and experts are taking the first steps toward understanding the undersea origin of the waves.

A group of geologists and tsunami experts described how their high-tech maps of the offshore sea bottom along coastal areas of California are revealing potential hazards in areas where few have feared major dangers in the past.

Geologist H. Gary Greene of the Moss Landing Marine Laboratories, for example, used two remotely operated submersible vehicles from the Monterey Bay Aquarium Research Institute to map in detail the steep underwater slopes that dip down from the shore facing the Santa Barbara Channel.

He discovered clear evidence that at some unknown time in the past a truly monster slump occurred off Coal Oil Point near Goleta. It was more than six miles wide and nine miles long, and slid in three distinct segments, from a depth of 300 feet down to 2,000 feet.

Whether the slide was triggered by an ancient earthquake on one of the many faults in the region, or on the more distant San Andreas fault, is impossible to tell, Greene said. But his submersible craft recovered samples of chemicals and bacterial mats in the area that indicated the undersea slopes of earth and rock might well have been weakened enough to slide without any earthquake at all to trigger them, he said.

While major earthquakes on either side of the Pacific can cause tsunamis that cross the entire ocean within 12 to 24 hours, undersea landslides can also generate local tsunamis as the surface of the ocean first recedes and then surges forward to crash against the shore.

Such a slump along the Santa Barbara coast could batter the shore with waves as high as 50 feet if it were triggered by even a modest earthquake on one of the many known faults in the Santa Barbara Channel, according to Costas Synolakis, an environmental engineer at the University of Southern California.

Canadian geological engineer Jacques Locat created another scenario affecting the Palos Verdes Peninsula, which stands above the Los Angeles region with its scores of beaches and dense population, based on his calculation of what could happen if a 300-foot-thick rockfall were to slide down the peninsula's escarpment into the sea.

Plunging to a depth of more than 2,000 feet, the rockfall would generate a huge, surging wall of water -- a local tsunami that would batter the coast with a wave at least 100 feet high, Locat said, and give people on the shore at nearby Long Beach just 24 minutes to climb to safety.

What's needed, at least for California if not for all the world's coastal nations, the scientists agreed, is program to map the seabed wherever offshore slopes dip steeply enough to pose the threat of submarine landslides and the deadly tsunamis they are capable of generating.

E-mail David Perlman at
dperlman@sfchronicle.com

Evidence of Underwater Landslides

Using remotely operated submersible vehicles, geologists at the Monterey Bay Aquarium Research Institute have produced high-resolution maps of the sea floor off the coast of Santa Barbara. Their data have produced clear images showing evidence of a massive submarine landslide that occurred at some point in the past. Scientists can use these observations to help determine the causes of potential tsunami-producing landslides in California.

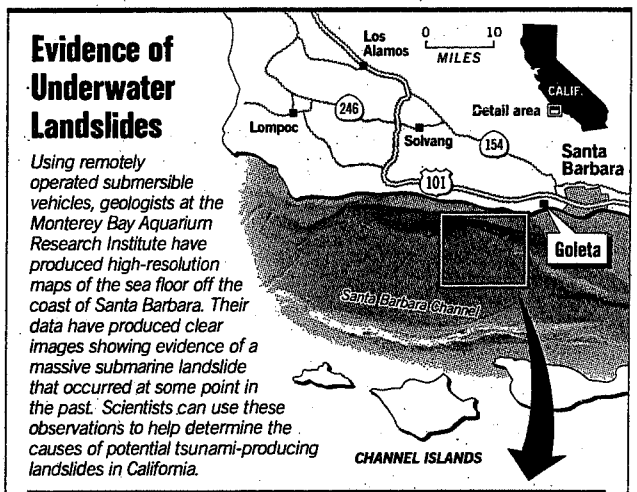

This detailed view of the boxed area in the map reveals evidence of extensive underwater landslides off Coal Oil Point near Goleta.

Source: Monterey Bay Aquarium Research Institute

Chronicle Graphic

Wisconsin State Journal

1/1/01

Earthquake risk may be greater, research says

New underground pictures show dangerous formations in L.A. area.

By Robert Jablon
Associated Press

LOS ANGELES — A new picture of the ground beneath Southern California shows one of its most populous areas could be at greater risk of earthquake damage than previously realized.

A basin of soft sediment beneath the San Gabriel Valley, just east of downtown Los Angeles, is about 3 miles deep — 1½ times deeper than previously estimated. That could lead to more surface shaking during an earthquake, according to a study appearing in January's issue of Geology, the journal of the Geological Society of America.

Such basins shake "like big bowls of Jello," said Gary Fuis, a seismologist with the U.S. Geological Survey in Menlo Park who was the study's lead author.

"The potential damage threat is greater because we've found that the basin is deeper," but specifics will have to await computer modeling of the new data, Fuis said.

The study used data from a series of test explosions in 1994 that created shock waves that were picked up by seismographs as they bounced through underground rock and soil. The area mapped, to a depth of about 12 miles, stretches about 100 miles from Seal Beach through the San Gabriel Valley and across the San Andreas Fault to the Mojave Desert.

Having a detailed picture of the subsurface is important for understanding earthquake hazards.Southern California has long been considered among the places most at risk for earthquakes. Its densely packed cities were built above an area where two plates of the Earth's crust grind together, and it is lined with earthquake faults.

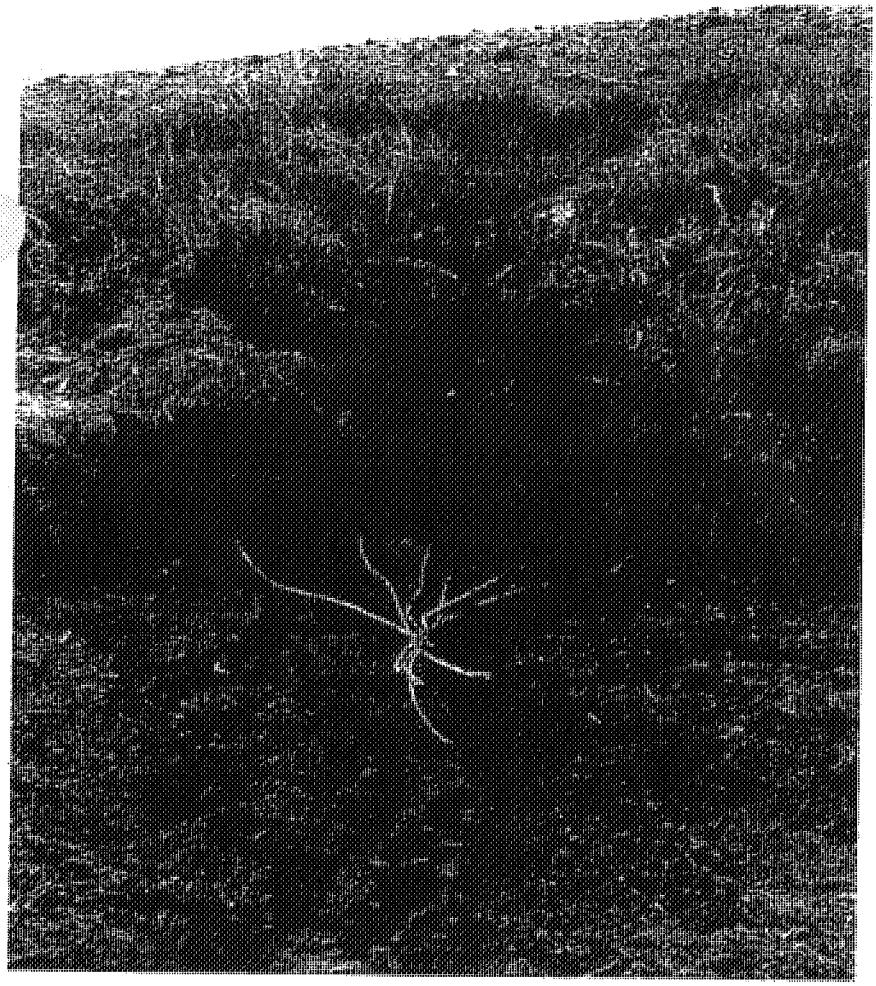

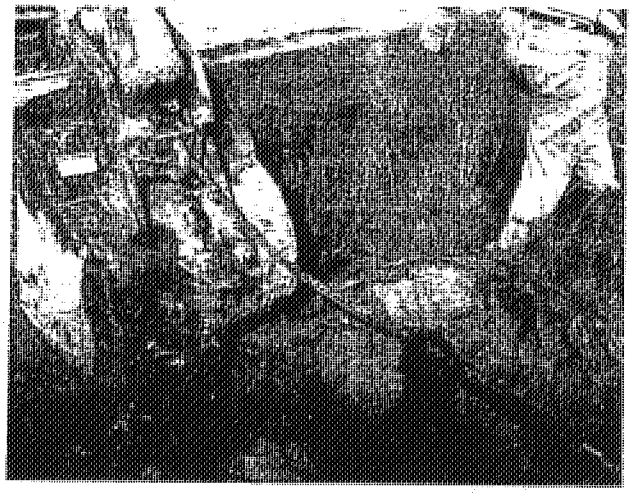

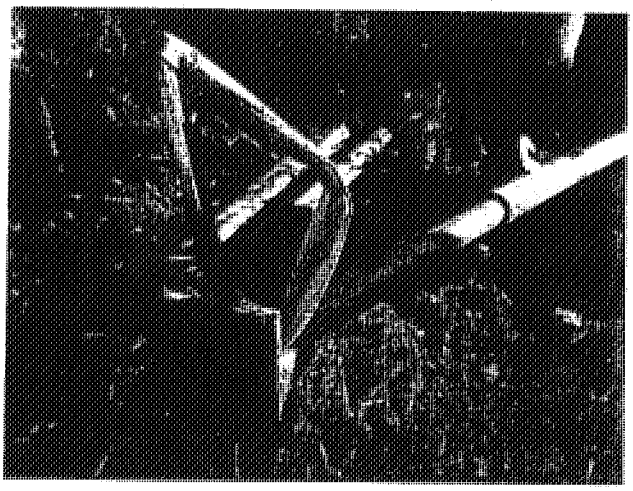

Draining in a New Direction

Wick drains are not new, but in an innovative horizontal application they are proving effective for stabilizing slopes and remediating landslide effects. The horizontal wick drains have several advantages over conventional drains, including lower costs.

By Paul M. Santi, C. Dale Elifrits, James A. Liljegren

Drains can stabilize slopes and landslides by lowering water levels and water pressures. Conventional drilled drains, driven vertically into the ground, tend to clog with fines and need periodic cleaning. Additionally, because they are made of inflexible polyvinyl chloride (PVC), they can be ruptured by landslide movement. Horizontal wick drains alleviate some of these drawbacks.

Horizontal wick drains are encased in a geotextile fabric of fine mesh that reduces clogging, and they may be deformed by as much as 60 to 100 percent before rupturing. The drains are currently being monitored at three test sites in Missouri, four in Colorado, and one in Indiana. So far, the horizontal drains have cost less to install than the drilled types. Following one or two days of training, a crew consisting of an equipment operator and three laborers can install 12 to 21 m of wick drains in as little as one hour.

 0885-7024-/01-0006-00A10/$08.00+50c per page

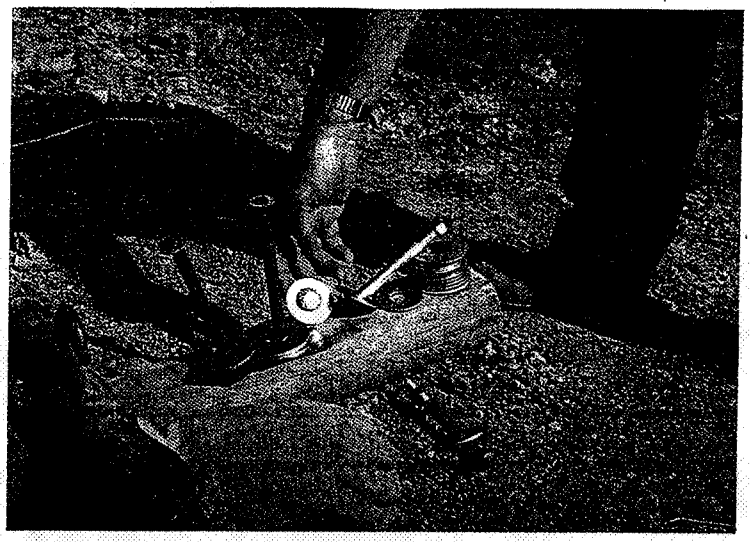

Horizontal wick drains installed in a fan pattern in a landslide at the Meeker, Colorado, test site drained into a puddle, opposite left. *One of the drains produced 20 L/min for several days until the flow slowed to a trickle. The drive head,* opposite below right, *and pulling head,* opposite above right, *protect the drive pipe—which encircles the wick drain—as the pipe is installed and extracted. Drive plates and carriage bolts,* left, *are used in front of the first section of driving pipe during installation.*

Installation is fairly easy. The horizontal wick drains are 4 by 100 mm in cross section and come in 300 m lengths. Installation can be carried out with bulldozers or trackhoe excavators that push a small-diameter steel pipe into the landslide mass. The pipe sections are preloaded with 3 m lengths of wick drain, rolled into long, tight cylinders, and tied at 0.3 m intervals with electrical cable ties. The first pipe has a drive plate attached to the front end of the wick. Next, a drive head is slid over the back end of the first pipe and the wick is folded out of the way. The first pipe is then aligned—usually horizontal or at an angle of less than 5 degrees upward—and pushed into the slope.

Installers drive additional pipes by using a plier/stapler to splice the wick end protruding from the previously placed pipe to the end of the wick in the next pipe. The spliced portion is rolled and tied, the drive pipes are threaded together, and the new piece of pipe is pushed in the same manner as the first. Sections may be added until the drain length is reached or until refusal. Next, workers use a pulling head and a chain to ease each section smoothly out of the ground. The wick remains in the ground because the drive plate anchors the wick in place and resists withdrawal.

The equipment can be purchased from drill pipe vendors or can be readily constructed in a machine shop. The drive plate is modeled after the type used in vertical wick drain installation. The plate is 76 mm² and is cut from 12 to 18 gauge (1.3 to 2.7 mm) sheet steel. A piece of #4 reinforcing bar is welded to the steel, and a washer is welded to the other end of the rebar, which holds the plate in place and forms an attachment point for the wick during withdrawal.

The drive pipe should have a minimum inner diameter of 32 mm to accommodate the rolled wick. The outer diameter is limited only by the pushing force available from the driving machinery. The pipe used for the test sites was able to drive drains 30 m long through materials with stiffnesses—as determined by the standard penetration test (SPT)—requiring up to 28 blows per 0.3 m. Drill pipe of larger diameter can withstand higher driving pressures, but it is significantly more expensive.

A drive head receives and transmits the pushing load induced by the driving equipment while protecting the female threads of the drive pipe and reducing the tendency of the pipe to slide off the equipment or buckle. A pulling head constructed from a short piece of drill pipe to which hooks have been welded simplifies the attachment and removal process. Bulldozers or trackhoe excavators in the 11,000 to 20,000 kg range seem to be best suited for this task, since larger equipment may not provide the fine control needed during driving.

The most common problem encountered during drain installation was flexure of the pipe under driving pressure. The problem was most serious when a new pipe was first being driven and was not yet confined by the hillside soils. The flexure generally subsided once workers drove 1 m of the pipe. However, the pipe would also buckle when hard materials, such as sloping bedrock surfaces or boulders, were encountered. Drill pipe with a larger diameter and a thicker wall than that used in these tests will offer more resistance to buckling. For the tests, buckling was reduced by using a larger pipe as a sleeve. The sleeve may be pushed into the hillside along with the pipe and then pulled out to be reused with the next pipe section. Finally, workers can minimize buckling by supporting the drive pipe from below with timbers and then forcing the flexure downward by controlling the attack angle on the bulldozer blade or trackhoe bucket (see figure 3).

As with drilled drains, the final layout pattern for horizontal wick drains depends on the slope and bedrock geometry

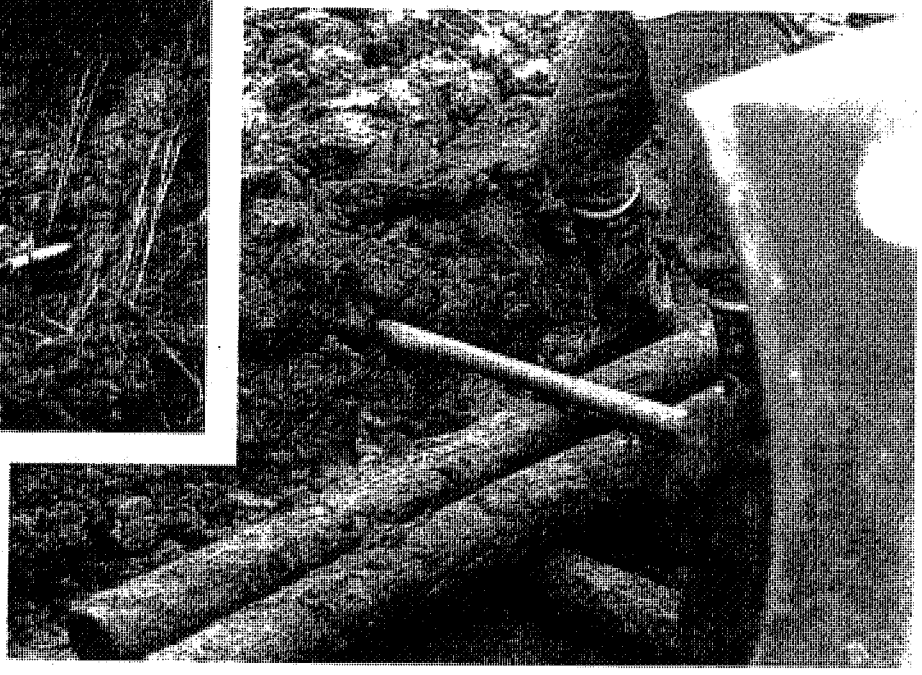

Forty-four drains of the type shown above were installed at the test site in Jasper, Indiana. More than a third of the drains were wet or dripping following installation, but all produced water after a rainstorm two weeks later. Timbers limit buckling as a bulldozer blade pushes a drive pipe into the ground, right.

and the location of water-bearing zones. The initial design should address drain length, angle, spacing, and filter size, with the understanding that these parameters may need to be altered in the field.

In general, longer drains produce more water because there is a greater inlet length along the drain and because a longer drain is more likely to intersect water-producing zones. Researchers recommend that drilled drains extend no more than 3 to 5 m beyond the shear zone, as they may convey water into the landslide mass. Wick drains have been successfully pushed 30 m through materials with stiffnesses requiring 20 to 28 blows per 0.3 m at the test sites. This length would be suitable for a landslide with a sliding plane that is 25 to 27 m back in the hillside. With more robust equipment, drains with lengths of 45 to 60 m could be driven through similar soils.

Drilled drains have typically been installed at a large range of angles above horizontal, from as little as a 2 to 3 percent grade to as much as a 20 percent grade. Wick drains driven at a low angles or no angle appear to be the most effective. The gravitational force pushing the water out of the slope is the same, and low-angle drains will lower the water table and pore-water pressures to a greater degree farther back in the slope. Wick drains with higher angles may be necessary in, for example, a sloping bedrock surface.

There are two general approaches to drain layout: a fan pattern radiating from a single installation point and a parallel layout from a line of evenly spaced installation points. Some research indicates that there is no difference between fan and parallel drain layouts. Based on research presented at the Canadian Geotechnical Conference in 1992, the Canadian National Railways prefers a fan pattern, because installing a

Guidelines to Follow

Based on the tests being conducted in Missouri, Colorado, and Indiana, as well as on the technical literature, the following design guidelines are suggested for the use of horizontal wick drains:

1) Drains should not extend more than 3 to 5 m beyond the potential failure surface.
2) Drains should be installed horizontally or at as low an angle as possible.
3) Drains should be installed in clusters that fan outward, aiming for a typical average drain spacing of 8 m in zones that produce water.
4) For soils with a significant sand component, #70 wick filter fabric is suitable. Finer filter mesh (#100 to #200) should be used for soils that are predominantly silt or clay.
5) The reduction in flow caused by soil smear can be minimized by pushing the pipes containing the drains, rather than pounding or vibrating them into place. The cross-sectional area of the pipes should be kept to a minimum.
6) Finished drains should be protected from root growth by sheathing the drains at the surface with PVC pipes. Drains should be protected from ice in extreme climates by burying the drain outlets in sand or some other highly permeable medium. Drain outlets should be joined through manifolds so that flow can be conveyed to a practical discharge point.

number of drains from a single pad is faster and easier and causes less slope disruption.

The U.S. research so far also suggests that fan patterns are more efficient and just as effective as evenly spaced drains. Drains should be fanned at angles with average spacing of approximately 8 m, measured at approximately half the drain length. Both drain spacing design and slope stability analysis of stabilized landslides require an estimation of new groundwater levels after installation. The groundwater table will coincide with drain elevations near the drains, but it will be higher between them. The calculation depends on drain flow rate, drain length and spacing, and soil permeability. For example, a series of drains 30.5 m long spaced at 7.6 m in sandy soil will have an average water table height that can be up to 0.6 m above the drain height.

Several researchers have investigated soil compaction and smear during vertical wick installation. Pushing or pounding drains displaces soil and creates a zone of disturbance around the wick, in contrast to such nondisplacement methods as drilling. This disturbed zone typically has reduced horizontal permeability. To reduce soil smear during installation, pipes and drive plates should have a small cross-sectional area and should be pushed smoothly into the slope. Clogging can also result from soil pressure compressing the wick filter into the drain channels, constricting water flow along the channels. The best approach at this point is to set the filter permeability and drain discharge capacity higher than expected to counter clogging from the migration of fine particles or the creep of filter fabric.

Drain clogging from fine soil particles can be reduced if the drain filter fabric is properly matched to the soil type. Wick drain types correspond to the size of pore openings and range from #70 to #200 (0.21 to 0.05 mm) sieve mesh sizes. In general, the #70 mesh filter is effective for silt and clay soils with a significant sand component in which 85 percent of the soil is coarser than 0.15 mm. The #100 and #200 mesh filters are more effective for nearly pure silt and clay soils.

The effects of soil smear, fine particle migration, and filter fabric creep can be combined to gauge the long-term performance of wick drains. Previous technical research by others measured the effects of various causes of clogging of vertical wick drains. That research shows that drainage from horizontal wick drains should improve during the first few months of operation as the effects of soil disruption during installation wane and that clogging will occur slowly as a consequence of the fine soil migration and filter fabric compaction over the next several decades.

Horizontal wick drains can be clogged by root growth or ice, as can drilled PVC drains. Root intrusion may be reduced by sheathing the 3 to 5 m of wick closest to the surface in

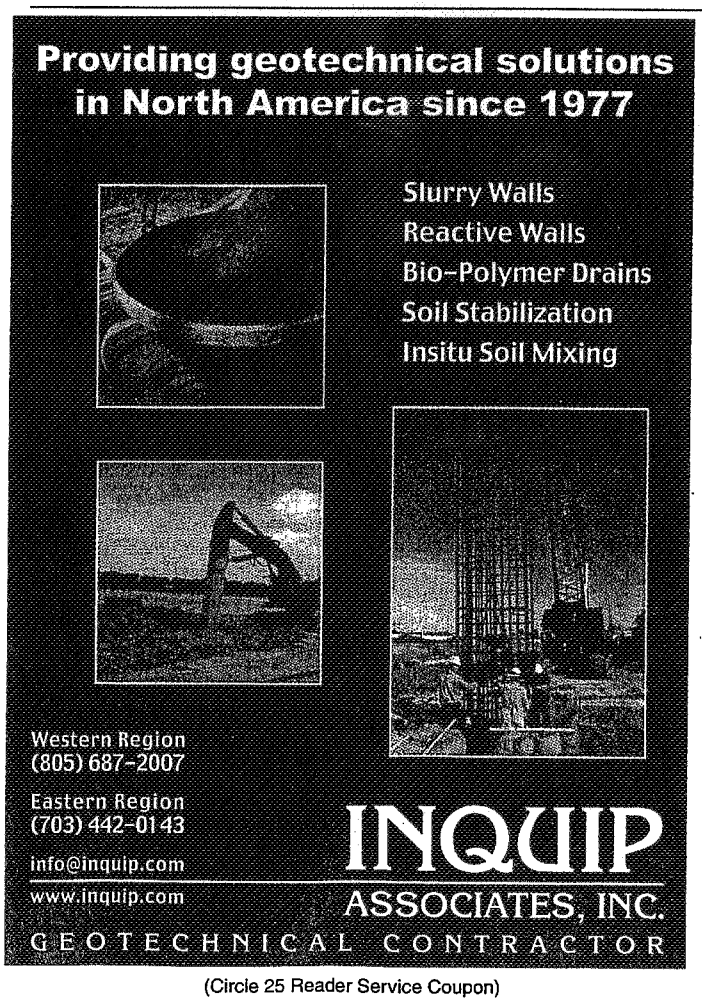

(Circle 25 Reader Service Coupon)

(Circle 26 Reader Service Coupon)

galvanized steel or PVC pipe. The sheath pipe will also work as part of the water collection and conveyance system. Ice buildup may be reduced by burying collection systems and drain outlet points, but according to some research drains tend to thaw out before pore pressures increase to a critical value and the effects of ice on slope drainage are minimal.

Because most landslide masses are heterogeneous, groundwater flow is unpredictable and seems to concentrate in zones. Furthermore, infiltration is strongly influenced by tension cracks caused by slide movement and fissures caused by soil development. Research suggests that landslide groundwater may concentrate in water lenses, which are frequently created as voids caused by dilation of the landslide during slope movement. Water lenses, however, may simply be part of a preferred flow network within the soil. For instance, a horizontal wick drain installed at the Meeker, Colorado, site produced water at a rate of up to 20 L/min for several days before reducing to a trickle. An adjacent drain fanned out from the same drive pad was dry. Both were in a homogeneous silty clay fill. Substantial flow has been observed at the test sites even in clay materials of low permeability. For example, a drain in silty, clayey soil at the Jasper, Indiana, landslide produced over 4 L/min immediately after installation.

As with drilled drains, horizontal wick drains will show varying rates of water production, even within the short horizontal distances between adjacent drains. This is especially true during dry periods. A number of case studies confirm that a significant number—6 to 55 percent—of conventional drilled PVC and steel pipe drains are initially dry. Some turn out to be permanently dry.

When to Think Twice

Horizontal wick drains may not be appropriate in all cases. The tests being conducted around the country show the following potential limitations of horizontal wick drain installation:

1) Wick drains may be driven into material with an SPT value of 30 or less; the ideal material has a value of 20 or less.
2) The maximum drain length is expected to be 30 m for harder soils and 45 to 60 m for soft soils.
3) Drains can be driven through some hard or rocky zones, but bedrock, large rocks, or dense sand or gravel will cause refusal.
4) A significant number of dry drains can be expected on a project (just as for drilled drains), but these drains often become active during wet periods.

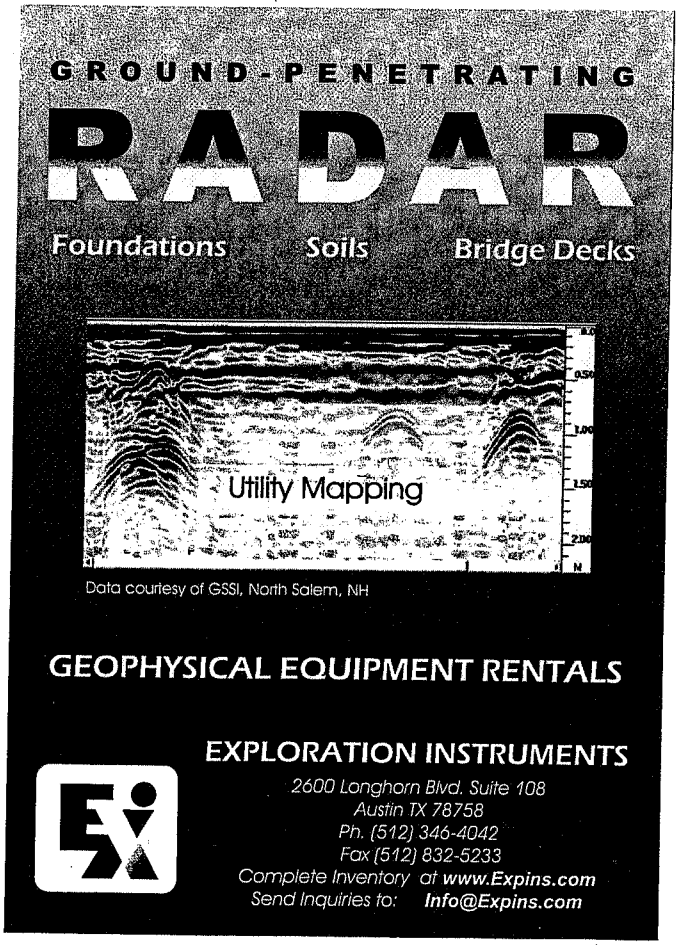

(Circle 27 Reader Service Coupon)

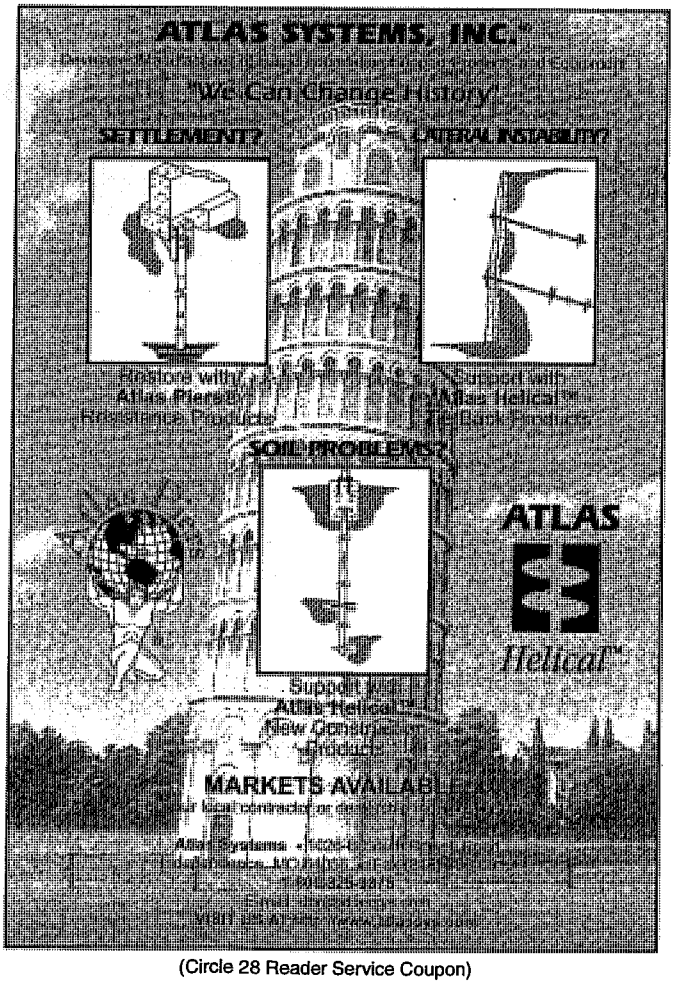

(Circle 28 Reader Service Coupon)

The data from these reports match observations so far regarding horizontal wick drains. Many of the drains will be dry at installation; indeed, a higher percentage have been dry at the test sites because most of the drains have been shorter and shallower than those typically installed by drilling. Nevertheless, dry drains will still serve as water outlet points during the wet season. At the Jasper site, 36 percent of the drains were wet or dripping following installation, but all produced water after a rainstorm two weeks later. Drains should be installed in areas of suspected water accumulation, such as draws or zones where bedrock is deeper, even if the first drains in the area are dry.

One should not judge the success of a drainage program by the water produced. Although large flow volumes are impressive, relatively minor flow tapped from a critical soil unit may be more important for the overall slope stabilization. One researcher concludes that the most successful drains for slope stabilization are those that show decreasing flow rates over time and those that show drainage only after rainfall events. Drains with relatively constant flow rates may be tapping groundwater that has nothing to do with landslide movement.

The first installations of horizontal wick drains in Missouri, in 1998, and Colorado, in 1999, focused on proving the feasibility of the wick drain driving method and on refining the installation technique. The latest installation, which took place last year near Jasper, is a complete landslide remediation project, with drain length and layout sufficient to have an effect on the entire slide mass (see figure 5).

The first site tested, a constructed embankment in Missouri, was approximately 45 m^3 in volume and had a 1:1 front slope face. Instrumentation includes six piezometers, 16 nested soil moisture meters, and 20 survey markers. Half the slope was stabilized with six wick drains, each 6 m long. The other half, which was not stabilized, was used as a control point. Researchers tested the influence of the wick drains by inducing groundwater infiltration through a trench at the back of the slope and then simulating a 100-year, 24-hour rainfall event using sprinklers.

The testing showed that the drains removed a substantial volume of water from the slope (almost 40 L/h apiece), lowering groundwater levels by over 0.3 m. Survey stakes showed substantially less movement within the drained half of the slope.

After installing wick drains at the test embankment, the researchers placed drains at locations with varying geology using various types of driving equipment. They drove the drains through natural and fill materials with SPT values as high as 28 blows per 0.3 m, although 20 blows per 0.3 m appears to be the realistic limit for longer drains. Drains were driven through rocky or hard zones over 1 m in width, although these zones sometimes deflected the drain pipe toward the ground surface or completely halted the driving progress. Wick drains have visibly

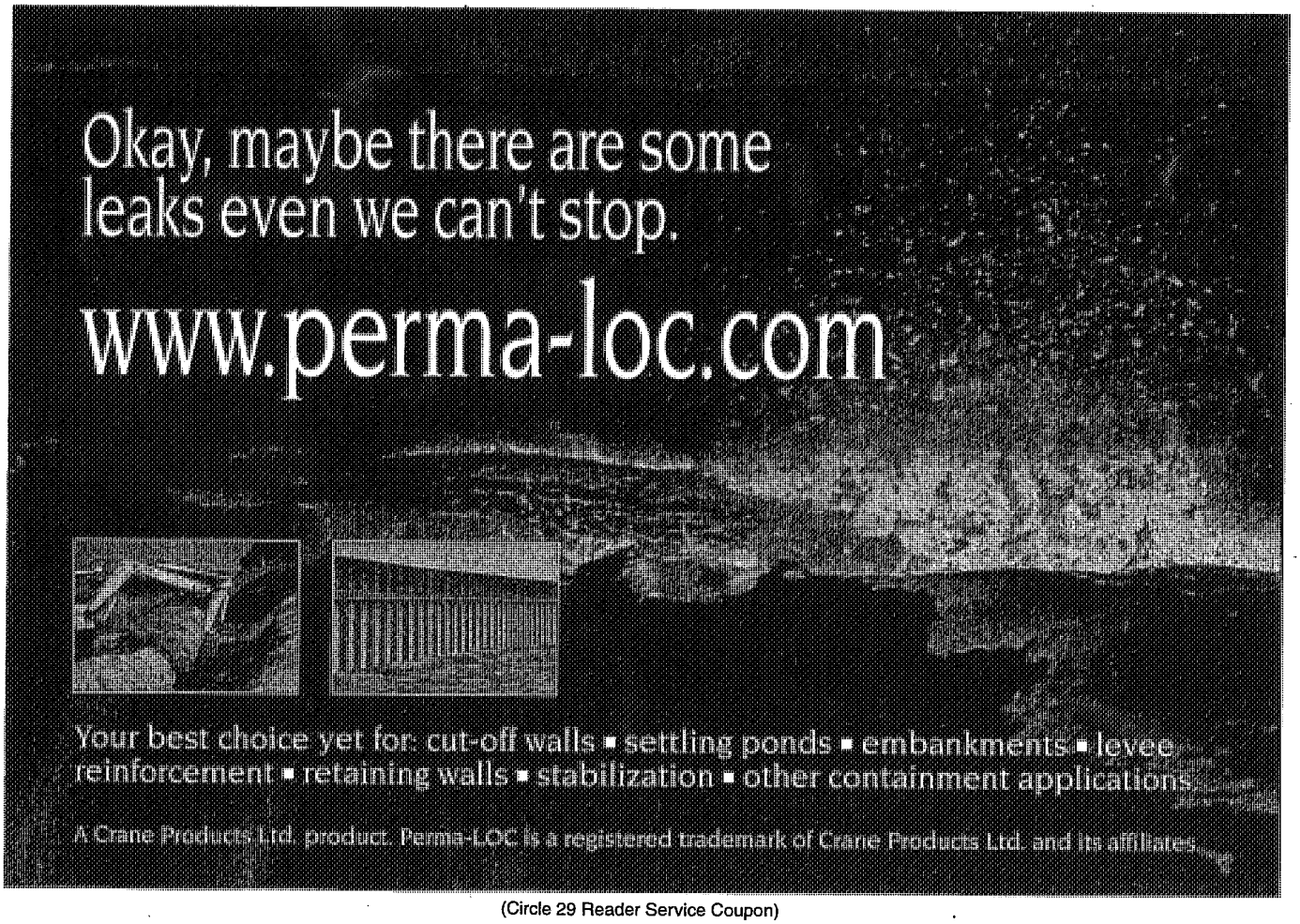

(Circle 29 Reader Service Coupon)

reduced water levels at the south Meeker and Jasper landslides, and water drainage has been observed at the Boonville and St. Joseph sites in Missouri, the north and south Meeker sites, and the Jasper site. Flow rates from a single drain have been as high as 20 L/min at the north Meeker site and 4 L/min at Jasper. Drains at the Rio Blanco landslide, in Colorado, were installed too high to intercept groundwater because of limited access points to the landslide. Drains at the Rye landslide, also in Colorado, were too short to intercept groundwater, and later installation of an uphill cutoff trench lowered the groundwater table below wick levels. The length of the Rye drains was limited to 12 m because a standard wick drain driving crane was used to push the drains horizontally into the hillside.

The drains installed in 1998 and 1999 show no evidence of clogging by dirt or algae, except where the drains lie directly on the ground surface and had been trampled. At locations where a short PVC pipe was used to encase the drain and was inserted a few feet into the soil, the drains were in excellent condition. Continued monitoring of the drains will include periodic observations of drain conditions, water levels, and slope conditions for the Missouri and Colorado sites. The Jasper site will be more closely monitored through eight piezometers and two inclinometers.

Costs for horizontal wick drains are less than for conventional drains. At the Indiana site, a crew with no prior experience installed almost 800 m of wick drains in less than nine working days, for an average cost of approximately $11.50 per meter. These costs will decrease with experienced crews. Conventional drilled drains cost on average from $20 to $36 per meter. Start-up costs to purchase wick driving equipment vary, depending on the size and type of driving rod used. For example, 45 m of drill rod of type AQ—as defined by the Diamond Core Drill Manufacturers Association—and the construction of drive and pulling heads, plus 100 drive plates, would cost between $1,500 and $2,000.

Funding for this work was provided by the National Cooperative Highway Research Programs/Innovations Deserving Exploratory Analysis, a program of the Transportation Research Board, and by the University of Missouri Research Board. Since 1998 more than 100 drains totaling almost 1,500 m have been installed at eight sites. Significant drainage and reductions in the water table have occurred. ■

Paul M. Santi is an assistant professor in the Department of Geological and Petroleum Engineering at the University of Missouri at Rolla, and C. Dale Elifrits is professor emeritus there. James A. Liljegren is a geotechnical engineer with Black and Veatch, Overland Park, Kansas. This article is a summary of a detailed technical paper that will appear later this year in the Transportation Research Record, *published by the Transportation Research Board.*

WATERLOO
BARRIER
SEALABLE JOINT

SHEET PILING

A LOW PERMEABILITY CONTAINMENT WALL FOR GROUNDWATER POLLUTION CONTROL
• rapid, clean installation • long service life
• excellent QA/QC • minimal chemical diffusion

WATERLOO BARRIER INC.
P.O. Box 385, Rockwood, Ontario, Canada N0B 2K0
Tel: (519) 856-1352 Fax: (519) 856-0759
www.waterloo-barrier.com

(Circle 30 Reader Service Coupon)

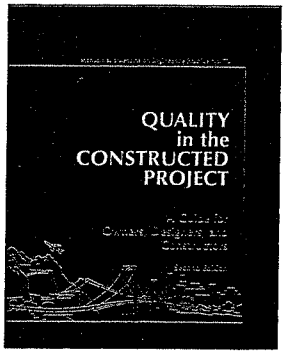

Quality in the Constructed Project
A Guide for Owners, Designers, and Constructors, 2nd Ed.
ASCE Manuals and Reports on Engineering Practice No. 73

Softcover, 288 pp., 2000, Stock #40506
List $40; **ASCE Member $30**

With 90 pages of new material, the revised **Second Edition** of ***ASCE Manual No. 73*** presents the latest thinking from industry experts on the owner's role and selection of a project delivery system, the selection of other team members, design, construction, start-up, and operations and maintenance. ***ASCE Manual No. 73*** provides must-have information on key principles and procedures that are effective in enhancing the quality of constructed projects.

HOW TO ORDER
Call: 800-548-ASCE (2723)
703-295-6300 (Int'l)
Internet: www.pubs.asce.org
ASCE

Slope Stabilization with Recycled Plastic Pins

John J. Bowders
J. Erik Loehr

Introduction

Maintenance costs due to slope failures on public and private transportation routes amount to a significant portion of yearly expenditures for infrastructure maintenance programs (Figure 1). Costs for repair and maintenance of slope failures for U.S. highways alone have been estimated to exceed $100 million annually (TRB 1996).

A new technique for stabilizing slopes is being developed that uses Recycled Plastic Pins (RPPs) in procedures comparable to soil nailing and conventional piling (Figure 2) that will offer a cost-effective alternative to current slope repair techniques.

Figure 1. Slope failure along US Interstate 70 near Emma, Missouri.

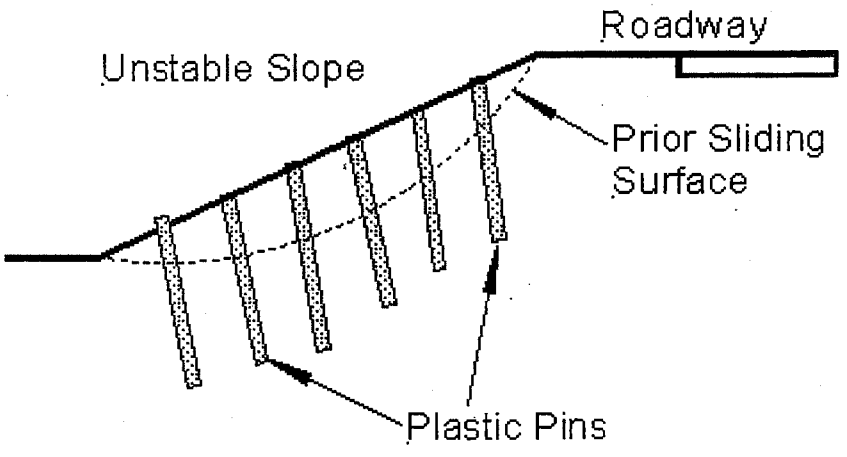

Figure 2. Reinforcement of unstable slope with Recycled Plastic Pins (RPPs).

RPPs are ***non-reinforced*** composite members of recycled plastic, saw dust and other by-products. They are lightweight, produced in various sizes, easily modified with conventional construction equipment, and have excellent resistance against chemical and biological attack.

Unlike fiber-reinforced polymer (FRP) piling discussed by Iskander and Stachula (*Geotechnical News, Vol. 17, No. 4, December 1999, page 27*), RPPs are not intended to compete with conventional structural piling, but rather to function as *weak* reinforcement. In this application, based on parametric studies, the strength of the reinforcement controls the design (Loehr, et. al 2000).

There are benefits to having the RPP capacity control design. Firstly, while the properties of recycled plastic are somewhat variable, they are not as variable as the properties of the soil. By having the reinforcing members control design, the importance of accurately knowing soil properties is diminished, and the reliability of the design is increased. Having the pin capacities control design also reduces the necessity of having a highly accurate theory for predicting the loads imposed by the soil on reinforcing members.

An on-going study is underway to evaluate the constructability of RPP stabilization technology. Toward this end, we report on the recent installation of a full-scale demonstration in which RPPs were used to stabilize two slope failures (one is shown in Figure 1) in a highway embankment located on Interstate 70 (I-70) at Emma, Missouri. The installation was performed during November 1999. The site was instrumented and performance is being monitored. A cost comparison is presented and conclusions are advanced.

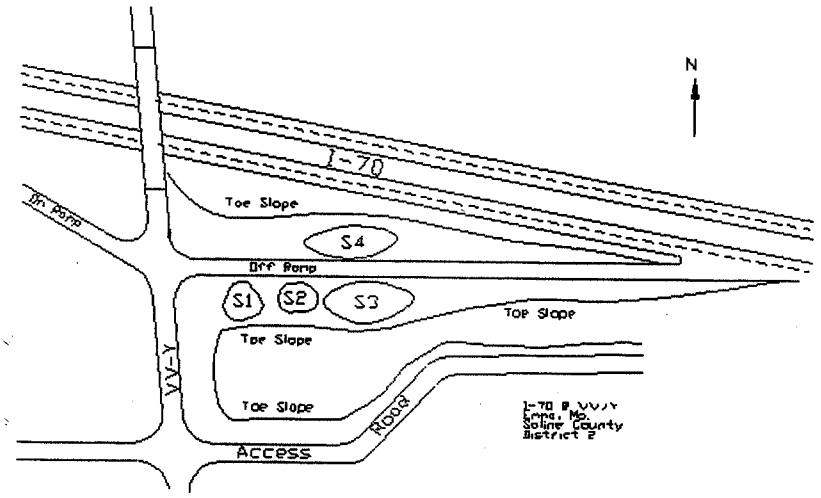

Figure 3. Plan view of the demonstration site located on US Interstate 70, Emma, Missouri, approximately 100 km east of Kansas City, with the four slope failures designated as S1 through S4.

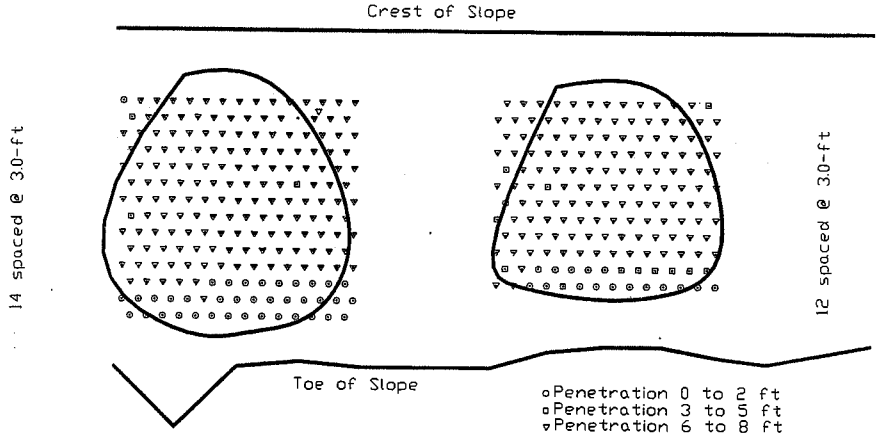

Figure 4. Layout of the RPPs at the Emma demonstration site showing the varying penetration depths.

Material Properties and Design

An extensive program of laboratory testing was conducted to quantify RPP material properties and their durability when exposed to various environments. The tensile strength of the recycled plastic pins is nominally about 13 MPa (1.8 ksi). The compressive strength of the recycled plastic is nominally 21 MPa (3.0 ksi). Specimens of the RPP were subjected to water, acid, freeze-thaw, ultra-violet and hydrocarbon environments for up to one year, and were periodically removed and tested for tensile or compressive strength. Results showed little appreciable change in strength for specimens exposed in various environments except for the hydrocarbon. Specimens submerged in kerosene for 1 year showed up to a 50 percent reduction in tensile strength and up to 30 percent reduction in compressive strength. This is a severe test and is not considered a very probable environment in the application of RPPs.

The fundamental objective for design of stabilization schemes using slender reinforcement is to determine the resistance that can be provided by individual pins and subsequently the number of pins required to increase the stability of a slope to an acceptable level. Given the lateral resistance of individual pins, the mechanics of stability analysis for slopes reinforced with structural members is relatively straightforward and well established. Thus, the primary need for design of RPP stabilization schemes is to determine or estimate the resisting forces provided by each reinforcing member.

A preliminary method for predicting the lateral resistance of individual pins has been developed (Loehr, et. al 2000). The method uses a limit-state design approach wherein a series of potential failure mechanisms are considered in developing the overall distribution of lateral resistance along a reinforcing member. The two general limit states that are considered include: (a) failure

of the soil around or between reinforcing members and (b) failure of the reinforcing members themselves in bending or shear as a result of excessive stresses being imposed by the retained soil. The methodology was used to decide on pin depth (2.4 m (8 ft)) and spacing (0.9 m (3 ft)) at the demonstration site resulting in a 25 percent increase in the factor of safety against sliding.

Field Demonstration

Four general slide areas were observed in the embankment just prior to the field demonstration (Figure 3). Three slide areas, denoted S1, S2, and S3, are located along the south side of the embankment with an additional slide, denoted S4, on the north side of the embankment. Slide areas S1 and S2 were selected as test areas for installation of RPPs; slide area S3 is being used as a control section. The embankment height is nominally 8 m and the slope height varies from 2.5H:1V to 2H:1V.

A total of 317 RPPs were installed in slides S1 and S2 during November 1999. The pins were installed in a 0.9-m (3-ft) staggered grid with every other row offset by 0.5-m (1.5-ft) (Figure 4). Pins were driven perpendicular to the face of the slope in slide S1 and vertically in slide S2. Not all of the RPPs could be driven to the full 2.4-m (8-ft) length due to the presence of concrete rubble from previous repair attempts (Figure 4).

Installation was accomplished using a Davey-Kent DK 100B crawler mounted drilling rig supplied by the Judy Company of Kansas City, Kansas (Figure 5). The rig is equipped with a mast capable of 50-degree tilt from vertical forward, 105-degree tilt backward, and side to side tilt of 32-degrees from vertical. The drilling mast ensures that the hammer and pin remain aligned during driving without requiring any movement of the chassis. The crawler-mounted rig easily maneuvered on the slope thereby keeping set up time between pins to a minimum. The rig is equipped with a hydraulic hammer drill attached to the mast providing a maximum of 400 N-m (295 ft-lbs) of energy at a maximum frequency of 1800 blows/min. The hammer energy is further augmented by a push/pull of 8165 kg (18,000-lbs) supplied by the drill mast.

Penetration rates (not including set up time) and installation rates (including set up time) measured during installation are summarized in Table 1. Penetration rates for pins driven perpendicular to the slope reached 3.0 m/min (10 ft/min) and averaged 1.6 m/min (5.2 ft/min). Penetration rates for pins driven vertically were slightly lower reaching a maximum of 2.9 m/min (9.6 ft/min) and averaging 1.3 m/min (4.1 ft/min). Installation rates reached a maximum of 38 m/hour (124 ft/hour) at peak production for pins installed perpendicular to the slope face. The average installation rate for installation of all pins was 25 m/hour (80 ft/hour). Installation rates generally increased during installation of pins for each slide as experience was developed.

Limitations of the Davey-Kent drilling rig necessitated that pins installed in a vertical alignment were driven with the rig being backed up the slope. While not critical, this feature did result in slightly lower installation rates for pins driven vertically as compared to pins driven perpendicular to the face of the slope (Table 1).

Figure 5a

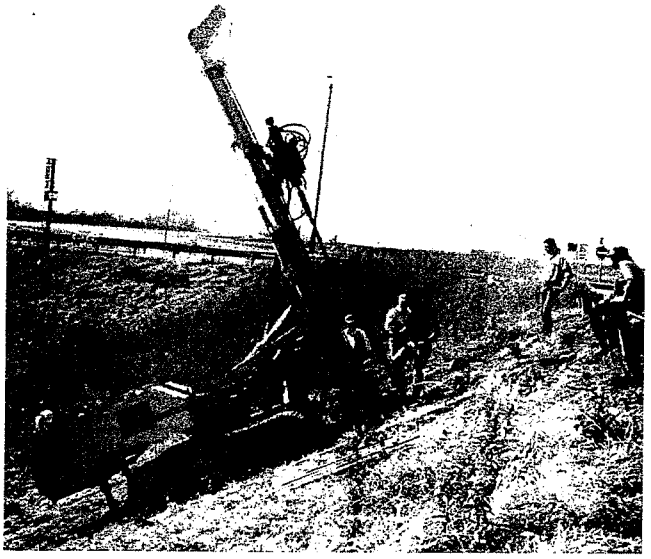

Figure 5b

Figure 5. Drill rig and mast system used for installation of recycled plastic pins at the Emma demonstration site.

Instrumentation and Monitoring

The demonstration site was instrumented to monitor stability of the stabilized slope and measure forces and deformations in reinforcing members (RPPs) to enable improvements to de-

Table 1 - Summary of the RPP penetration and installation rates for slope failures S1 and S2.

	S1		S2	
	Penetration Rate m/min (ft/min)	Installation Rate m/hr (ft/hr)	Penetration Rate m/min (ft/min)	Installation Rate m/hr (ft/hr)
Average Rate	1.6 (5.2)	29.3 (96.0)	1.2 (4.1)	20.7 (68.0)
Maximum Rate	3.1 (10.0)	37.8 (124.0)	2.9 (9.6)	29.9 (98.0)
Minimum Rate	0.1 (0.1)	18.0 (59.0)	0.2 (0.5)	10.1 (33.0)

sign and construction methods. Two inclinometers and two piezometers were installed in each of the RPP stabilized slides (S1 and S2) to monitor lateral movements and locate the phreatic surface (should one exist). The control slide (S3) was instrumented with one inclinometer and one piezometer. Moisture sensors and tensiometers are scheduled for installation.

Ten RPPs were instrumented with 20 strain gages each for measuring strain in the RPPs from which load and moment in the pins can be calculated. Four instrumented pins were installed in slides S1 and S2. Two instrumented pins were installed in the control slide (S3). Strain readings were taken just after installation and in January 2000. Total strains are still very small, e.g., 0.1 percent strain, and are within the variability of the strain gages, indicating that the pins have not picked up substantial loads to date.

As experience is gained and installation technology improved, the unit cost for RPP stabilization is expected to decrease.

Economics

A total of 317 pins were driven in slightly over four days. The RPPs cost approximately $20US per pin (0.1 m x 0.1 m x 2.5 m) or $6340US for the demonstration project. Installation costs (equipment and labor) was $5250US resulting in a total cost of approximately $11590US to stabilize the two failures. The unit cost using RPPs to stabilize the slope was $42/m^2 (cost per unit area of slope face). The estimated unit costs for rock armor was $58/m^2. Clearly, the RPP stabilization method is the least costly. As experience is gained and installation technology improved, the unit cost for RPP stabilization is expected to decrease.

Summary

A developing technology, Recycled Plastic Pins (RPPs) was used to stabilize two slope failures. The RPPs are pressure-molded recycled high-density polyethylene with a compliment of saw dust and other by-products. A total of 317 pins were installed on a 0.9 m grid pattern using a mast-mounted vibratory hammer system that averaged 25 m/hour during installation. The unit cost of RPP stabilization technology was $42/m^2, 25 percent less than for rock armor, the traditional technique. Performance monitoring of the slopes is on-going.

Acknowledgements

The authors greatly appreciate the collaboration and spirit of Kurt DeRuy, Tamko Composite Products (formerly DuraBoard, Inc) for supplying the RPPs and Pat Carr of the Judy Company, Kansas City, Kansas for installation services. Dr. Hani Salim, assistant professor, Dr. Todd Mooney, research assistant professor, and research assistants Warren Khankeo, Willie Liew, Jacob Owen, Lee Sommers, and Zac Thomas accomplished the many tasks. Funding for this effort has been provided through the Research, Development and Technology Division of the Missouri Department of Transportation, Director Jim Murray. The active participation and collaboration of project liaison, Mr. Tom Fennessey of the Soils and Geology section of the MoDOT is especially appreciated. The opinions, findings and conclusions expressed in this publication are not necessarily those of the Missouri Department of Transportation or the Federal Highway Administration. This document does not constitute a standard, specification or regulation.

References

Iskander MG and Stachula A (1999) FRP Composite Polymer Piling: An Alternative to Timber Piling for Water-Front Applications, *Geotechnical News* 17(4):27-31.

Loehr JE, Bowders JJ, Sommers L, Owen JW, and Liew W, (2000) Stabilization of Slopes Using Recycled Plastic Pins, *Presented at the 79th Transportation Research Board Annual Meeting*, Washington, D.C., January 9-13, 2000.

Transportation Research Board (1996), *Landslides: Investigation and Mitigation*, AK Turner and RL Schuster, editors, National Research Council Special Report 247, 673 pp.

John J. Bowders, Ph.D., P.E., Associate Professor of Civil Engineering, University of Missouri Columbia, E 2509 EBE, Columbia, MO 65211-2200 Tel: 573-882-8351, Fax: 573-882-4784, email:bowders@missouri.edu.

J. Erik Loehr, Ph.D, E.I.T., Assistant Professor of Civil Engineering, University of Missouri Columbia, E 2509 EBE, Columbia, MO 65211-2200 Tel: 573-882-6380, Fax: 573-882-4784, email:eloehr@missouri.edu.

Its Causes and Its Remedies

between the void volume to the soil's total volume is called the soil's "porosity." The ratio between the void volume to the solids volume is called the "void ratio." For example, a dense, mixed, dry sand with a porosity of 0.30 and void ratio of 0.43 may have a dry unit weight of 116 pcf. However, when fully saturated, its unit weight may increase to 135 pcf. This represents a 16% increase in weight and a proportional increase in the driving forces leading to slope failure.

The large void zones associated with undermining and karst strata can lead to catastrophic settlement and dislocation of overlying slope structures. Karst strata is defined as natural zones of caverns and large fracture zones. Man-made mining tunnels produce the same effect by removing underlying support from the slope.

Even without large void structures, weak, underlying soils by themselves can greatly destabilize a slope. In this category are purely cohesionless soils, especially when saturated, and organic soils such as peat. The long-term breakdown of soils with a loose or honeycombed structure will have the same effect. This can be a purely mechanical process resulting from accumulative shifting of the loose soils, or from chemical and biochemical deterioration. Deep rooting zones created by adjacent trees can weaken support structures such as retaining walls. A typical slope reinforcement strategy utilizes soil/ cement columns created by auger mixers and pumped grout. However, the long-term deterioration of the cementing material caused by contact with groundwater will create a weak soil zone. Loess soils initially are stiff enough to allow near vertical slopes and excavations, but eventually deteriorate as a result of exposure to weather and precipitation. Even the burrowing activities of humble field rodents can create zones of relatively weak soils.

FIGURE 4 Retaining Wall/Slope Failure

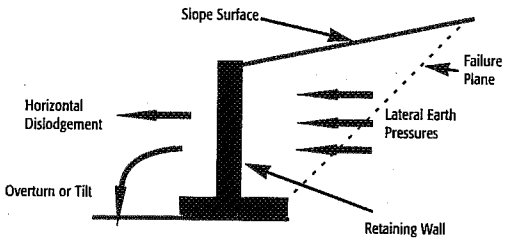

Human activities are on a more impressive scale. Chief among these are the shocks due to blasting and lower level vibrations generated by construction and excavation activities. While singular blasts and short-term excavation may have no apparent

Tensar ADD³ = BIG Savings & Longer Life

ADD³ adds capacity and life to your site.

Years of experience and the development of numerous innovative technologies and design techniques have led to a revolutionary approach for landfill design and closure—the Tensar ADD³ concept.

If you're designing a new site or are faced with closing an existing one, let us show you how to significantly reduce your life cycle costs so you can be more competitive and profitable.

For more information and literature call *1-800-TENSAR-1,* or visit our web site at *www.tensarcorp.com.* For a no-obligation conceptual review call *1-888-4TENSAR.*

TENSAR® Earth Technologies, Inc.

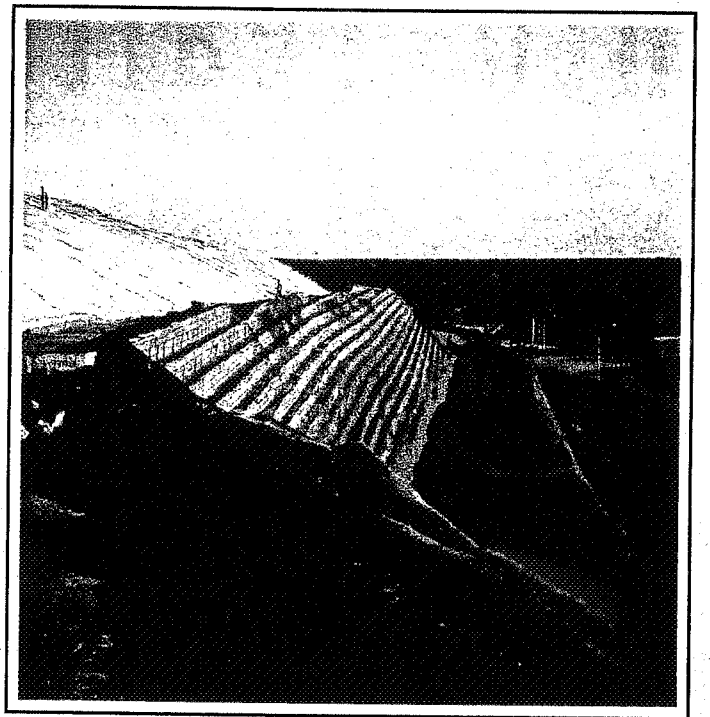

▲ ADD³ at work—an overfilled landfill capped with .5H:1V side slopes.

Circle #30 on Reader Service Card

PORTADAM, INC.
107 Drivers Lane • Laurel Springs, NJ 08021
Toll Free 1-800-346-4793 • In NJ 609-875-4577

INNOVATIVE COFFERDAM WATER DIVERSION & RETENTION STRUCTURES

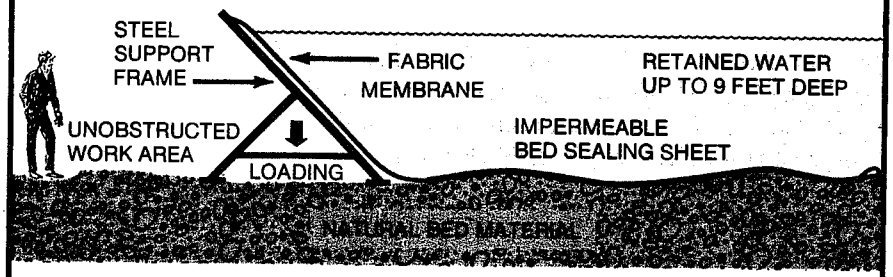

Flexible** temporary retention structures allow construction in rivers, canals, lakes, ponds, and most other waterways to be performed in the **dry!

ENVIRONMENTALLY SAFE — designed to comply with the Federal Clean Water Act, Section 404 as an efficient alternative to illegal earthfill dikes.

COST EFFICIENT — the system utilizes an adaptable free standing design which ends the need for expensive steel sheet piling and heavy equipment.

VERSATILE — can be used in areas where other methods are impossible!

Our Endless Uses Include:

- Bridge Piers and Abutements
- Pipeline and Cable River Crossings
- Boat Ramps
- Raw Water Intake Structures
- Emergency Flood Control
- Stream Diversions

CALL OUR TOLL FREE NUMBER FOR A DEALER NEAR YOU
LICENSES AVAILABLE

Circle #39 on Reader Service Card

Shape your landscaping ideas
into reality

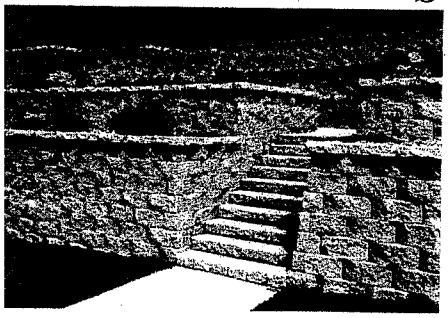

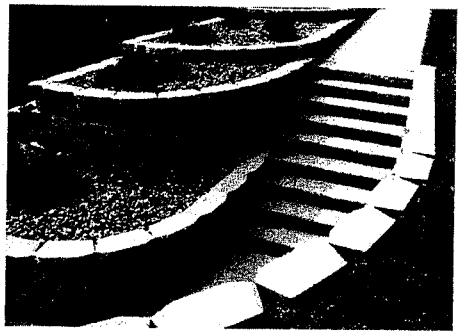

with
ROCKWOOD®
RETAINING WALLS, INC.

• Mortarless and Pinless • Versatile and Attractive • Serpentine or Straight Walls

800-535-2375

7200 N. Hwy 63 Rochester, MN 55906 http://www.retainingwall.com

Circle #42 on Reader Service Card

affect on the slope's structure, continuous activities of this kind adjacent to the slope may greatly weaken its structure by causing localized displacement of underlying soils. Mother Nature's own seismic events tend to be more violent—but of a shorter duration—than human activities. Any structure subject to earthquake forces should be immediately investigated for both major displacements and localized dislocations.

Tension cracks occur when the upper part of a steep slope in a cohesive soil, such as clay, is subjected to a continued state of tension. Under tension, cracks develop which destroy

FIGURE 5 Circular Arc Analysis

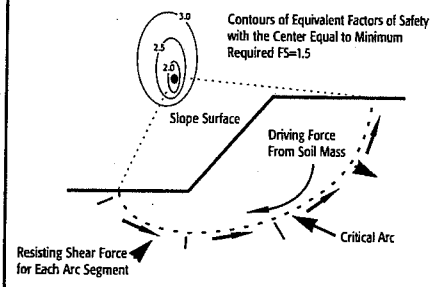

FIGURE 6 Method of Slices

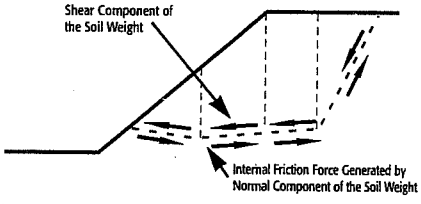

FIGURE 7 Infinite Slope Stability Analysis

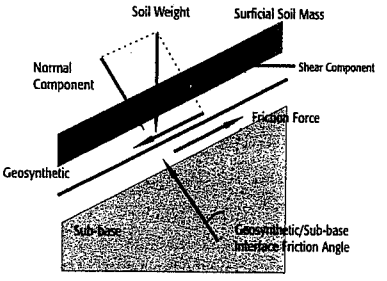

part of the soils' localized shear strength. The depths of the cracks depend upon twice the cohesive strength of the soil divided by its unit weight. For example, a clay soil having a cohesive strength of 500 lb./ft.^{2} and a unit weight of 130 lb./ft.^{2} could develop tension cracks to a depth of 2 m (7 ft.). If water fills the crack, the resultant water pressure in the crack can contribute to overturning forces. These cracks, located at the top of a slope embankment can act as the starting point of a mass block or rotational failure plane. Hair-line cracking from alternate swelling and shrinking or from tension can create similar failure cracks with the slope's

soil mass.

A change in the soil's pore water pressure (neutral stress) due to seepage or drawdown will alter the structure of the soil. The reduction of neutral stress increases the effective stress on the soil generated by its self weight and applied loads. This increase in the effective stress can lead consolidation settlement within the zone of groundwater draw-down. If sandy soil is allowed to completely dry out, steep excavations and slopes can suffer catastrophic collapse due to the loss of capillary tension between the soil particles (a force normally adding to the soil's internal strength). The swelling of clay soils, resulting from excess water and a resultant increase in a clay's void volume, can distort the overall structure of the slope's soils.

The freeze/thaw cycle damages the slope's soils initially by the action of frost heave. Soil in the ground surface freezes after three or four days of freezing temperatures. Since frozen water expands, the ground surface can rise as much as 30 cm (12 in.). Ice layers and lenses form within the soil, creating uneven weak zones. After frost action has altered the structure of the soil, thaw presents its own problems. Warm weather melts soil ice from the top down, leading to temporary perched zones of saturated soils. These soils remain wet until the thaw has penetrated through the underlying frozen zone, allowing the groundwater to drain down through the soil mass. The combination of frost heave dislocation followed by excess neutral stress can severely damage surficial soils. Clay soils are especially susceptible to the effects of the freeze/thaw cycle.

Certain slope structures rely on or incorporate geosynthetics into their construction. These geosynthetics can include woven or nonwoven geotextiles used as filter layers, geomembranes acting as moisture impermeable barriers, geocomposites utilized as wick drains, geogrids used as layers of reinforcement, and geosynthetic clay liners (geotextiles impregnated with bentonite clay). Typically used in landfill engineering, geosynthetics have found wide usage in other geotechnical applications. However, the presence of geosynthetics creates man-made potential failure planes where overlying soils or other geosynthetics can slip. The key factors are the friction forces acting along the interfaces between the geosynthetics and adjacent soils, and the angle of the slope that the geosynthetic was installed on.

Besides the potential for a soil mass to experience mass block failure along its interface with a geosynthetic layer, the geosynthetic itself may experience structural failure due to applied loads

TAYLOR Restoration Nurseries

• 250 Species of Native Seeds/Plants
• Prairie & Wetland Restoration
• Contract Growing
• Planting Design & Installation

A Regional Center for Restoration Ecology

Phone: (608) 897-8641 • Fax: (608) 897-8486 • Rt. 3 Smith Road, P.O. Box 256 • Brodhead, WI 53520

Circle #68 on Reader Service Card

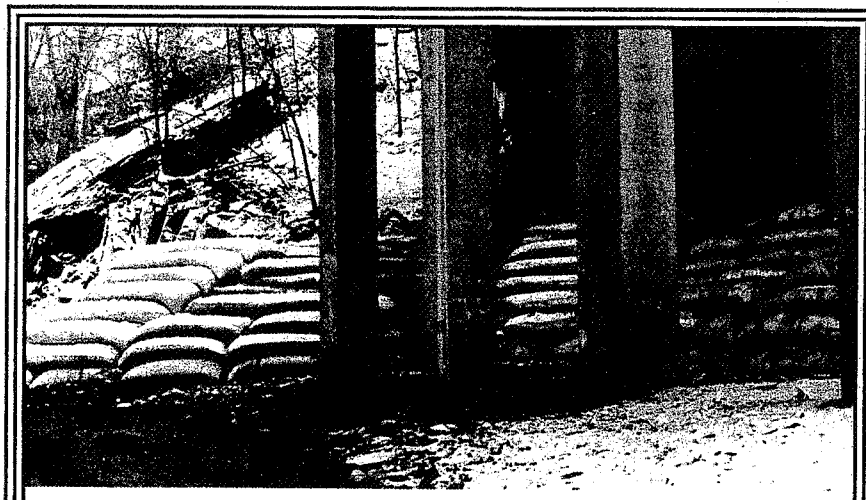

HYDROCAST™

Fabric Formed Concrete -

permanent, fast solutions to bridge scour

HYDROCAST™ Armor Units are a rapid, easy to install method of repairing underscoured bridge abutments and pilings. Filled *in place* by pumping fine aggregate concrete (structural grout) into cylindrical fabric forms, HYDROCAST units can be deployed without dewatering. They allow immediate emergency repair, even for bridge piers near failure.

HYDROCAST Armor Units adapt to bottom and bank contours to prevent further scouring, and their monolithic concrete structure provides a permanent solution, not a temporary fix.

Call us, or visit our web site. Find out why transportation engineers are specifying a better alternative.

Hydrotex Synthetics, Inc.

1-800-225-0023 • Fax (706) 335-1813 • www.hydrotex.com

Distributor and representative inquiries welcome.

HYDROTEX™

Filter Point • Uniform Section • Articulating Block

Hydrotex and Hydrocast are trademarks.

Circle #32 on Reader Service Card

from the soil. It is common for the edges of a geosynthetic layer to be anchored in a back-filled trench located at the top of a slope. If applied loads are severe, the geosynthetic may experience either tensile yield or be pulled out from the anchor. Each type of geosynthetic has its own stress/strain relationship defining its yield and break points. For example, high-density polyethylene geomembranes have yield points equivalent to 13% strain elongation, after which the material does not recover its original dimensions. This deformation can continue to a break point as high as the 300% strain level. Depending on the design and dimensions of the geosynthetic's anchor system, the edges of the geosynthetic can be pulled out of its anchoring, causing the equivalent of a sliding block failure.

Diagnosis

There are several analytical tools for evaluating the potential instability of a slope structure. These analyses can also be used in a post-mortem sense to determine the causes of an actual slope failure. Purely cohesive soils can be analyzed with the circular arc analysis method (Figure 5). Under circular arc analysis, the forces acting to dislodge the soil mass generate turning moments about the failure arc's central pivot point. These moments are equivalent to the product of the magnitude of the force and its distance/radius from the pivot point. The driving forces can be generated by lateral earth pressures, water pressures, the weight of the soil mass, and external applied loads. The sum of all these driving moments is divided into the sum of the resisting moments to determine the overall factor of safety. The resisting moments are generated by the shear forces/cohesive strength of the soils acting along the failure arc. The resisting forces are generated along each segment of the failure arc by the shear strength within the clay soils.

The method of slices is applicable for frictional soils such as sands and sandy clays. In this analysis the frictional forces generated by the weight of each section of the failure mass also act to resist the movement of the slope soils (Figure 6). This method is applicable to both mass block and rotational failure analysis, and can be used to determine potential failure planes or arcs. The bottom of each slice represents a section of the failure plane. A rotational failure arc can be approximated by a series of straight line chords tangent to the arc. Each section is at an angle to the horizontal. The weight of the soil acts in a downward direction. At the bottom of the slice, the weight is resolved into a shear component parallel with the failure plane segment, and a normal component perpendicular to the failure plane. The shear component acts as the driving force to dislodge the soil mass. The normal component generates a friction force based on the internal friction angle of the soil. This friction force and any internal shear/cohesive strength the soil may have act to resist soil movement.

The infinite slope method is used to examine potential sliding block failure involving geosynthetics (Figure 7). The term "infinite" refers to the fact that this analysis is independent of the length of the slope. The resisting friction force acts along the bottom surface of the geosynthetic where it comes into contact with its sub-base. The friction force is a function of both the friction angle of this sub-base/geosynthetic interface and the normal component of the applied surficial soil weight. The shear component

TERRAMAT®
Land Bridge Mats
Made from Recycled Truck Tires

- Cross Streams & Wetlands
- Cross Levees & Dams
- Reusable—Indestructible
- Minimize Erosion
- Prevent Rutting

TERRA MAT
Reinforcing the earth with tires

Patents U.S.A., Australia, & Canada
TERRAMAT Corporation
462 Arbor Circle • Youngstown, Ohio 44505
Phone 330-759-9412 • FAX 330-759-7679

Circle #50 on Reader Service Card

BMP GUIDELINES...
Erosion and Sediment Control Manual with Computer-Ready Drawings

Erosion Draw is now 60% larger with 17 new Best Management Practices (BMPs), including Bioengineering Techniques, Hydraulic Planting, and Gabions. It is filled with "new erosion control" technology, such as Cellular Confinement Systems, and Continuous Berms, along with the industry standards such as: Grass-Lined Channels, Energy Dissipators, Riprap, and Straw Bale Dike.

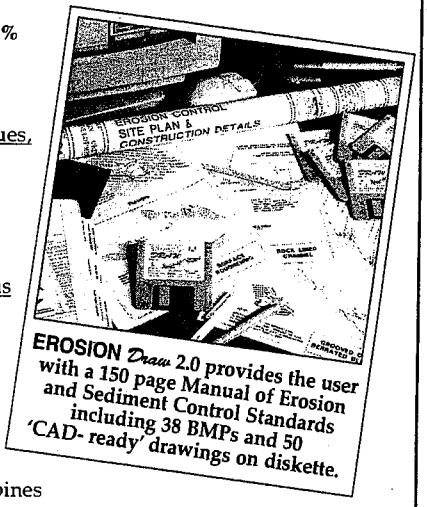

EROSION Draw 2.0 provides the user with a 150 page Manual of Erosion and Sediment Control Standards including 38 BMPs and 50 'CAD- ready' drawings on diskette.

Erosion Draw now combines *"Cutting Edge"* technology and *"Product Awareness"* with an appedix filled with information and manufacturer specifications.

TO ORDER CALL
1-800-403-0474
or 916-224-0878
FAX 916-224-0879
VISA, MC, AMEX accepted

Salix. applied earthcare
3141 Bechelli Ln. • Redding, CA 96002
http://erosiondraw.com
International Erosion Control Association Member

Circle #65 on Reader Service Card

of the applied soil weight acts as the driving force. Calculating the ratio between the resisting force and the driving force results in a factor of safety derived from the slope angle and the interface friction angle. Note that if the friction angle between the geosynthetic and the upper soil layer is less that along the bottom of the geosynthetic, overlaying soil will tend to slide past the geosynthetic rather than generate pull-out or tensile forces within the geosynthetic.

FIGURE 8 Geogrid Slope Reinforcement

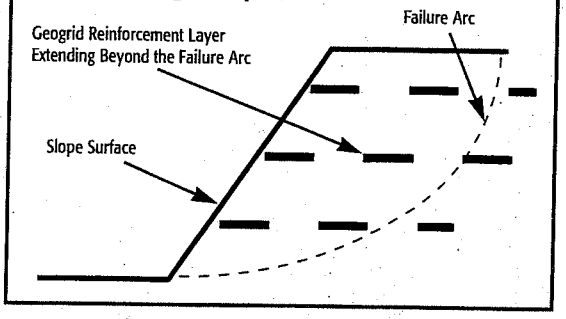

Prevention

A thorough site investigation is the first defense against slope failure. A site investigation should uncover the presence of weak soils, excessive groundwater, fracture zones and other potential structural problems. The site investigation should include a records search as wells direct soil borings, samplings, and tests. Since groundwater is the main cause of most types of the potential slope failures, sufficient drainage is essential for the maintenance of slope stability. As it is very difficult to prevent water from seeping into an embankment or slope backfill, a series of drainage pipes and weep holes should be installed. A system of under drains, wick drains, or trench drains may be needed. However, sudden draw-down or dewatering of the soil mass may also lead to structural problems due to the increase in effective stresses acting on the soil.

The design of the slopes is critical to its stability. Excessive heights (relative to surrounding terrain and the width of the slope embankment) should be avoided, as should excessively steep slopes. Local building codes set limits on these design elements. The allowable applied loads from buildings and structures located at the top of the slope should be limited in both size and weight. Blasting and construction activities should be isolated from the slope by prescribed set back distances.

Geosynthetic reinforcement of slopes is a common solution. Layers of geogrid reinforcement installed at regular horizontal lifts will add their tensile strengths to the slope structure (Figure 8). For the failure arc to propagate through the geogrid layers, it must cause the geogrids to deform by generating forces in excess of the geogrid's tensile strength. Another engineering solution involves the construction of cemented soil zones, or the installation of retaining walls of reinforced concrete, masonry block, or rock-filled gabions. However, no engineered solution is permanent. Cemented soils can degrade as the result of long-term exposure to groundwater. Geogrids may experience long-term weakening and deformation due to creep. Retaining walls of whatever type can be subject to earth pressures leading to overturning. Continuous maintenance is necessary to ensure long-term stability. **EC**

Guest author ***Daniel Duffy****, P.E., is an environmental engineer for Rumpke Waste Inc. in Cincinnati, OH.*

Tension Anchors Stabilize Tieback Projects

For tieback projects, use Chance screw anchors. You can match the anchors to the soils and tension loads you need.

Look at the benefits then use Chance anchors to hold retaining walls, roadways, revetments, dams, levees and buildings.

- ❒ Competitive Installing Costs
- ❒ Immediate Loading
- ❒ Predictable Results
- ❒ Permanent or Temporary
- ❒ Removable
- ❒ Use in Any Weather
- ❒ Use with Available Equipment
- ❒ Labor Saving
- ❒ No Excavation
- ❒ Field Proven

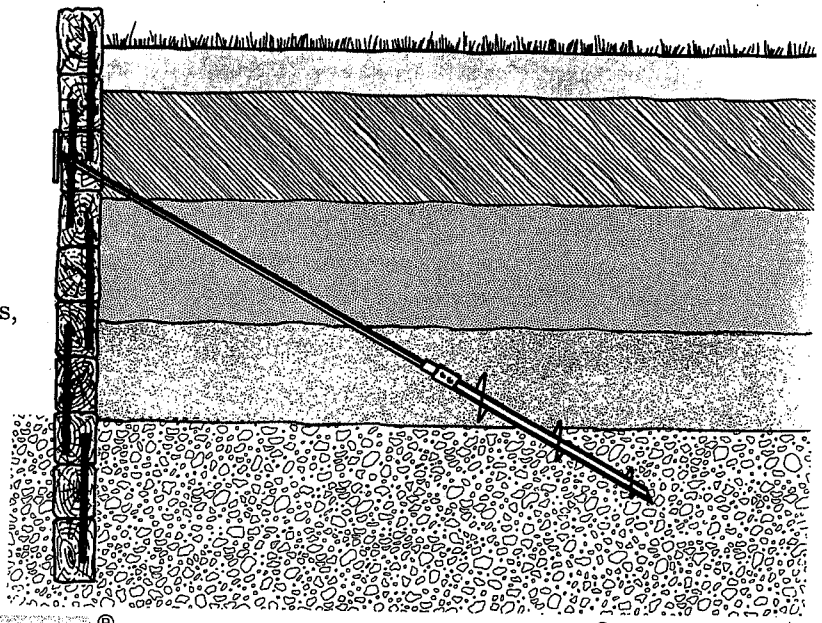

HUBBELL®

CHANCE®

210 North Allen
Centralia, MO 65240
(573) 682-8414
FAX: 573-682-8660

J1-41TFA

Circle #13 on Reader Service Card

Safety in the Workplace:

[illegible]eharst, MIOSHA
Onsite Construction Consultant

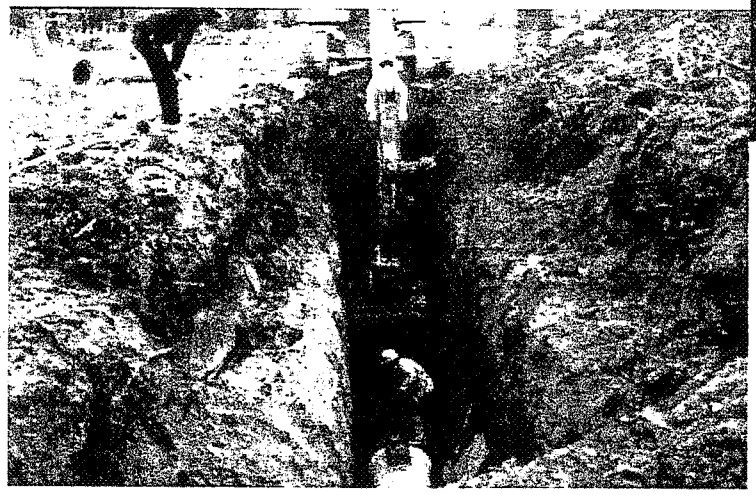

Trenching Excavation

As I'm writing this, spring is here and we're approaching the height of the construction season. There is no better time to prepare for trenching and excavation projects than right now.

In Michigan, employers and employees are subject to the MIOSHA Act. Trenching, excavating and related work, are covered by MIOSHA Construction Safety Standards; more particularly Part 9 - Excavation, Trenching, and Shoring, the scope of which reads as follows: This part pertains to the digging of excavations and trenched which an employee is required to enter and the supporting systems used on construction operations. Public Act 154 states that: An employer of one or more employees must provide a place of employment which is free from recognized hazards which can cause, or are likely to cause, death or serious physical harm to the employee.

Consider that in 1999, four fatal incidents and many serious accidents were reported in Michigan during trenching and excavation activities. It can clearly be seen that trenching and excavation work should be considered a hazardous activity, which requires safety planning and execution. The major causes of death and accidents under Part 9 are:

- Improperly shored and sloped trenches
- Loads too near trenches
- Shocks and vibrations
- Improper or defective shoring material
- Change in soil conditions
- Improper site and trench preparation

Let me take this opportunity to help you who are involved with trenching and excavation projects to have a better understanding of: Who, What, When, Where, and Why the Part 9 Standard would apply. I would also like to remind everyone that the standards are only minimum requirements, and that additional safety measures must be taken when hazards are identified.

Who

As to who, there are really four equally correct answers and many identifying factors for each. Because Michigan has a multi-employer worksite policy, the following employers must be able to identify and correct hazards found in trenching operations. Furthermore, these employers may be cited under this policy by the MIOSHA Construction Safety Division if they are not in compliance.

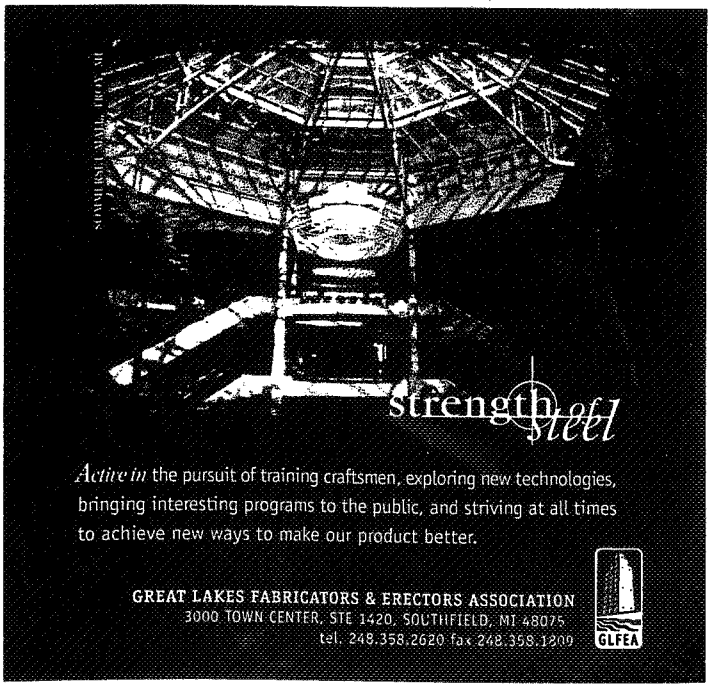

1) The Exposing Employer. The employer of the employees exposed to the hazard.

2) The Creating Employer. The employer that actually creates the hazard.

3) The Controlling Employer. The employer responsible through contract or actual practice for safety at the worksite, i.e., this employer has control and authority for insuring that the hazardous condition is corrected.

4) The Correcting Employer. The employer having the responsibility for correcting and installing safety devices.

What

This basically takes care of the who, so let's talk about what is required to maintain safety in excavation projects. The most vital element is the ability to identify potential problems. In my years as a safety officer, before I joined the consultation staff for MIOSHA, I remember many instances where incidents has occurred and I would hear similar comments. Such as:

"It was only going to take a couple of minutes."

To which I would reply: "It only takes a couple of seconds for a trench side to collapse!"

Or: "I've been doing it this way for 20 years."

To which I would reply: "You've been lucky for 20 years!"

What can be done so that hazard identification becomes a skill you possess? The key to becoming able to identify hazards is: Comprehensive Training. I feel that a review of all trenching "incidents" should be included in a training program.

1) Training in the requirements of MIOSHA Construction Standards, Part 9, and the use of protective systems, including trench boxes, shoring and sheeting.

2) Training in the ability to recognize warning signs that precede trench collapse.

3) Training in the ability to recognize conditions on the site that would enhance the probability of a trench collapse.

4) Training in soil type recognition. Because no two trenches or even any two sections of a trench are the same, recognizing and evaluating soil conditions must be ongoing and relentless to avoid hazardous situations.

5) Training must be presented to all those concerned: Top man, pipe layer, operator, supervisor, and inspector. Without all concerned being acutely aware of potential hazards, the results can be deadly.

When

Constantly. If not, you could miss a change in conditions with disastrous results.

Where

Every excavation is unique, so every trench site needs a competent person in charge and everyone involved must be able to identify all hazards that are possible when you disturb soil by means of excavation. Remember, you're creating an unnatural condition which is constantly trying to return to its natural condition.

Why

Because of the possibility of fatalities and severe injuries involved with trenching! Considering that cubic foot of soil weighs approximately 114 pounds, and a cubic yard can weigh as much as a car, it doesn't take much imagination to see what the results of a trench side collapse, even three feet in depth, could be.

The danger is increased when you add in the location of waste and storm sewer trenching sites i.e., right of ways to streets and highways, and the vibration of traffic and construction equipment. Let's not forget that when repairs are made to existing lines, the principal soil will have been previously disturbed. This presents a situation where there is very little if any soil cohesiveness.

Conclusion

In conclusion, I have repeatedly emphasized the need to train. I feel training is the key which serves as the backbone for competence in trenching safety. An effective trenching safety program should include employee training on the following topics: Other structures involved; Soil type identification; Safe access and egress into trenches; MIOSHA Regulations, Part 9, Trenching, Excavation, and Shoring; Proper use of trench boxes, sheeting and shoring techniques; Mechanics of a trench collapse; Hazardous atmospheres and testing; Machine use in excavation and lifting; the Effects of water and weather; Inspection techniques; Clay soils are heterogeneous; generally, Soil color is not significant factor; and Every trench is different.

And finally, every trench is an unnatural condition and will collapse. It is just a matter of when.

-From MIOSHA News, Spring 2000

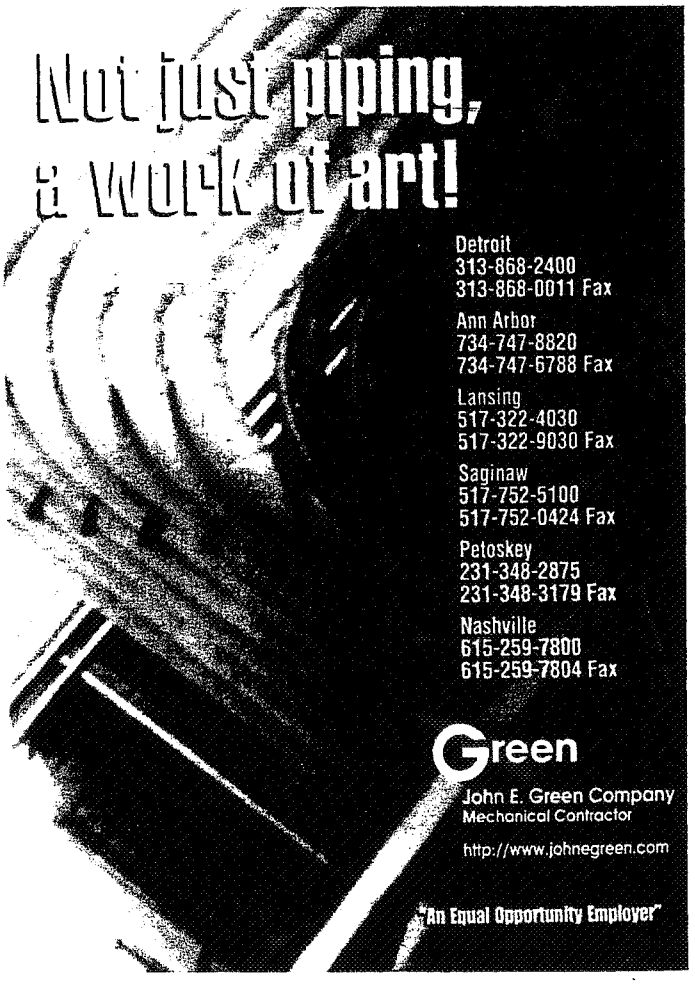

Construction Feature

Dangerous Trenches

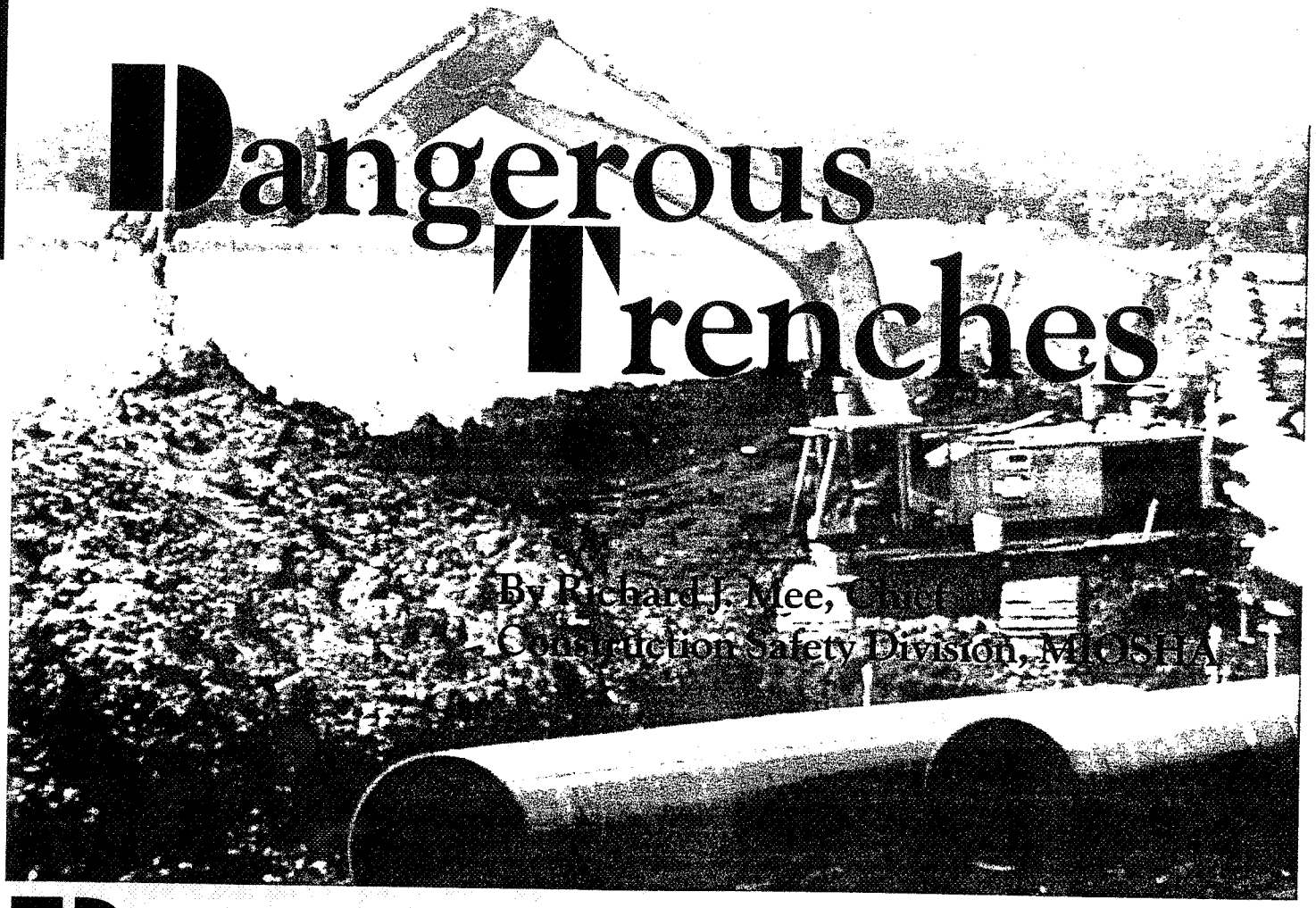

By Richard J. Mee, Chief
Construction Safety Division, MIOSHA

Recently, while reviewing construction fatality statistics, I realized there have been eighty-eight of them. Eighty-eight fathers, sons, grandfathers, brothers, uncles, grandchildren, and friends. Eighty-eight people, not just statistical representations but real people, who no longer live among us. Eight-eight people who left home in the morning for work never to return alive.

Now imagine, for a moment, eight-eight people. Imagine about two busloads of people or about three high school classrooms with every seat filled. Then, imagine them all dead.

Yes, MIOSHA (Michigan Occupational Safety & Health Act) records show that eighty-eight Michigan construction worked have died in excavation cave-in incidents just since the Construction Safety Division has been keeping records. This number, of course, does not include the hundreds or thousands who died before we started keeping records. It does not include the thousands or tens-of-thousands who died in states other than Michigan. Neither does it include the tens-of-thousands or hundreds-of-thousands who were injured, many seriously injured or disabled, in cave-in incidents.

Recent Upturn in Trenching Fatalities

Last year, in 1999, four more workers perished in Michigan trench cave-ins. This tragic upturn in trench deaths came during a period of reduced excavation accidents. In the four previous years, 1995 through 1998, one cave-in death each year was recorded. Statistics reveal a long decline in cave-in deaths with the last several years among the lowest average period.

Dangerous work?

Excavation and trenching work have proven to be very dangerous. Removing soil to create a trench or other cavity disrupts an equilibrium created by nature during hundreds or thousands of years over the surface of the earth. Nature loves an equilibrium and will exert powerful forces to return the earth to that condition. Sometimes, natural forces work slowly and man-made scars in the landscape heal gradually over months or years. All too often, however, natural forces begin the healing process in bursts of great force that have no respect for the unfortunate worker who gets in the way.

These bursts of great force are the cave-ins that kill, maim, and injure workers. Most soils weigh over 100 pounds per cubic foot, so it doesn't take a very large charge of earth falling off the side of a trench to have the effect of a moving automobile striking a person. A slab of trench side only one foot thick, six feet long, and four feet high can weigh as much as a typical mid-size car. Few cave-in deaths are caused by suffocation; most victims are crushed by the weight of the soil chunks.

Underground Work Can Be Done Safely

Is trenching work inherently unsafe? No, if adequate precautions are taken no one need die or suffer serious injuries from a cave-in. Trench sides can be supported by shoring, a trench box, or can be sloped back to an angle appropriate to the type of soil encountered to eliminate the possibility of a large trench-side collapse. Indeed, the death toll could be all but eliminated if current MIOSHA standards were followed.

Most contractors performing underground work devote considerable times and resources to make their trenches safe. If this were not so, the toll of death and injury could be many times greater.

Perhaps the questions to ask is, "Why aren't all trenches made safe if it is possible to do so?" There are many reasons but let's begin by acknowledging the MIOSHA standard. Part 9 of the Construction Safety Standards requires that all excavation and trench sides must be sloped back sufficiently or supported before they are occupied by employees. Training on the recognition and avoidance of excavation and other hazards is required by Part 1, General Rules MIOSHA standard.

Looming large among the reasons hazardous trenches may still exist in this safety-conscious, modern era, is simply the cost. Excavation and trench safety can be very expensive. Trench box use and shoring installation slow down production and in some cases might result in the time required to complete an underground project to double or more. Sloping the excavation sides out to a safe angle can be even more expensive. In most cases, excavated spoil must be hauled away to distant fill sites and the voluminous trench backfilled with sand which must be purchased, trucked to the site, and compacted. Sloping the trench sides out to a safe angle can also mean removing and replacing five times more pavement area, another considerable cost.

Often, unsafe trenches exist because of the lack of a trained, qualified person. The MIOSHA standard requires an ongoing inspection of an excavation or trench shall be made by a qualified person. The qualified person described in the standard is trained to recognize soil types, understand the characteristic hazards of each one, and design shoring and/or soil sloping as dictated by the unique site conditions. The qualified person also monitors the progress of the work to identify hazardous conditions as they develop.

Sometimes, for smaller, less experienced contractors the problem is awareness. Because most soils can support themselves temporarily while a trench is open to install a pipe, inexperienced and uninformed workers may not realize the dangers to which they are exposed. Some clay soils are known to support themselves so well that a mile of vertical-sided trench can be excavated with not even a shovel of soil caving off the sides and then, suddenly, a thousands pounds or more can cave in and crush an unsuspecting worker.

The Real Tragedy

Although the numbers of cave-in fatalities have been at lower levels on average during the six to eight years previous to 1999, last year's trend is alarming and cannot be ignored. Enforcement of the standards that apply to excavation and trenching workplaces will be receiving increased attention consistent with the MIOSHA Strategic Plan as the 2000 construction season is underway. Each employer in the underground industry must pursue the goal of 100 percent compliance with the MIOSHA standards and zero cave-in injuries and fatalities.

As tragic as the 1999 deaths were, the real tragedy would be to repeat history. The real tragedy would be to repeat the agony suffered by the survivors of the workers lost in trenches last year. The real tragedy would be to some day count up to eighty-eight more of them. Even one more is too many.

-From MIOSHA News, Spring 2000

Construction Safety

Only about four percent of Michigan's workforce is employed in construction. Construction fatalities, however, accounted for more than 40 percent of all MIOSHA program-related fatal workplace accidents over the last three years.

1999 Construction Fatalities by Major Cause

Fall	**10**
Caught Between	**11**
(Cave-in - 4)	
Struck By	**3**
(Struck By Traffic - 1)	
Electrocution	**6**
Other (Burns)	**1**
Total	**31**

SPARTAN SPECIALTIES LTD
SOIL STABILIZATION SOLUTIONS
GROUTING TECHNOLOGIES
FOUNDATION GROUTING
COMPACTION GROUTING
CHEMICAL GROUTING
MICRO FINE CEMENT
CONCRETE REPAIR
PREPLACED AGGREGATE
EPOXY INJECTION
FABRIC FORM GROUT BAGS
GUNITE
PILES
MINI PILES
SOIL NAILING
EARTH AND ROCK ANCHORS
(810) 826-8811
6250 SIMS, STERLING HEIGHTS, MICHIGAN 48313

SF Chronicle 1/22/02

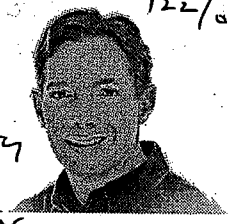

A very good reporter

KEN GARCIA

Rolling stone nothing new on slide site

Condos are built on former quarry

When the builders of a condominium complex up against the hills near the Cow Palace conjured up some alluring names for the site, they came within striking distance of reality.

The developers decided on Stoneridge, perhaps because there were plenty of large stones on that tall ridge. Using history as their guide, however, they could have come up with a more accurate moniker: something like Stonedrop, Falling Rock, Rolling Boulder or Hillside Slides.

And by the time all is said and done and negotiated, it could become known in legal quarters as Lawyers Circle.

A few weeks ago, families living in the 7-year-old complex discovered this for themselves when a batch of winter storms reminded them with some immediacy that rock-laden slopes and heavy rains make for a poor mix.

Twelve of the families were forced to evacuate in early January because of the crumbling cliff that looms over the seven-story structure. It will likely be several weeks before construction crews stabilize the hillside and put in a "catch fence" to protect those below from sliding rocks. But it may take considerably longer to sort out the questions that have tumbled out of the development's recent problems.

The Stoneridge condos, you see, were built on the site of a former quarry, a business enterprise that is based on pulling rocks out of hillsides. That comes as no surprise to the people who were familiar with the site before Stoneridge was built, because the evidence was simply too large to ignore.

"It was always amazing to any of us who spent time there over the years that a housing complex would be built there," said Dave Doran, a local bowling legend who worked for years at Castle Lanes, the bowling alley that occupied the site before the condos went up. "Clearly, anybody who

▶ **GARCIA:** *Page A17 Col. 4*

S.F. slide site has a rocky past

▶ **GARCIA**
From Page A15

was a regular at Castle Lanes knew from experience of the hazard."

Doran said rock slides used to happen on a "relatively regular basis" — to the point that visitors to Castle Lanes knew not to park near the base of the hill. He remembers that in 1974, a rock "the size of a Volkswagen" came crashing down, miraculously avoiding several motorists below.

Anyone who didn't actually see stones sliding off the cliff could easily have figured out there was a problem, Doran says, since a barrier had been erected to catch the falling rocks.

Yet this was all news to the Stoneridge residents who have been forced to find other living quarters while repairs are made to the hillside. They say they never had any idea about the site's shaky past.

"We never heard anything about rockslides," said Danny Udon, who moved with his wife and 10-year-old son into a tiny in-law apartment shortly after he was forced to evacuate. "And certainly no one told us about it when we bought our place."

Udon said the first indication he had there was a problem was when large rocks starting bounding down the hillside several years after he moved in.

Stoneridge resident Chuck Elliot, who is now living with friends in the East Bay, said that rather than being advised of the potential slide problems, just the opposite occurred when he inquired about his property.

"When we first went and looked at it, you could see that there were rocks at the bottom of the hill," he said. "But we were assured how safe the site was. I think basically now they have egg on their face."

> *"Clearly, anybody who was a regular at Castle Lanes knew from experience of the hazard."*
>
> DAVE DORAN
> *local bowling legend*

The question of how San Francisco came to approve development plans for the site remains a mystery — at least to me — because Jim Hutchinson, deputy director of the city's Department of Building Inspection, declined to return my calls.

Stoneridge property manager Kevin Wiley was much more responsive. Wiley said a geology report was turned in to the city last week and that the plans for repairing the hillside have already been approved.

That plan calls for the construction of a 12- to 15-foot, steel-reinforced fence designed to catch rocks that fall from the hill. In some places, the fence will be able to hold back as much as 295 tons of rock, he said.

The work is expected to begin this week and will extend into February. After the fence is complete, residents will also be notified that some of the rocks and loose debris will be removed in case they need to leave the premises for a few hours.

Wiley, whose company, CitiScape Management Group, was not involved in the construction of Stoneridge, said the site's history and any questions about its past were being dealt with by the developer.

"All we know is that it appears that the developer is working with the insurance companies to get this worked out," Wiley said. "Everybody's getting along right now, and we haven't hear any word about lawsuits."

That could change over time, especially as residents begin to ask why they weren't informed of the site's rocky history. For now, most of them would just like to be able to go home.

You can reach Ken Garcia at (415) 777-7152 or e-mail him at kgarcia@sfchronicle.com.